General

SUVI data as an alternative source for EUV imaging data:

SUVI data guide for SDO/AIA users

The book Scientific Debates in Space Science: Discoveries in the Early Space Era was recently published: **https://link.springer.com/book/10.1007/978-3-031-41598-2**

Database for Solar Soft X-ray (Hinode/XRT) and (E)UV (SDO/AIA & PROBA2/SWAP) Irradiance Variability: Solar Cycle-24" - Hinode Science Center, Institute for Space-Earth Environmental Research (ISEE), Nagoya University, Nagoya, Japan.
Database access link:
https://hinode.isee.nagoya-u.ac.jp/xrt_seg/

Space Weather Live

https://www.spaceweatherlive.com/en.html

Next Batch of NISP Data Products

The National Science Foundation's (NSF's) Global Oscillation Network Group (GONG) data products
Solar News 1 Jan 2024 **https://gong2.nso.edu/vmbi_pub_sched.html**

The data center for the Spectrometer and Telescope for Imaging X-rays (STIX) on board Solar Orbiter **https://datacenter.stix.i4ds.net/stix**

The **SOLARNET Virtual Observatory (SVO)**, developed as part of the H2020 SOLARNET project, is now operational with a varied selection of solar physics datasets partially or completely available.
https://solarnet.oma.be/

"Historical Sunspot Records"
The recent article collection of *Living Reviews in Solar Physics* in collaboration with *Solar Phys.* 2023

The special issue inspired by ESPM-16 meeting at Sep 2021
Recent progress in the physics of the Sun and heliosphere
Edited by Istvan Ballai, Eduard P. Kontar
Adv. Space Res. Volume 71, Issue 4, Pages 1855-2058 (15 February **2023**)
https://www.sciencedirect.com/journal/advances-in-space-research/vol/71/issue/4
https://www.astro.gla.ac.uk/users/eduard/cesra/?p=3484

Сборник трудов XXVI Всероссийской ежегодной конференции по физике Солнца «Солнце и солнечно-земная физика – 2022» ГАО РАН.
http://www.gaoran.ru/russian/solphys/2022/book/conf2022.pdf

SOHO CELIAS-PM, CELIAS-SEM, COSTEP-EPHIN, and ERNE data converted to CDF at NASA's Space Physics Data Facility (SPDF)

New SOHO CELIAS-PM, CELIAS-SEM, COSTEP-EPHIN, and ERNE CDF datasets have been archived at NASA's Space Physics Data Facility (SPDF **https://spdf.gsfc.nasa.gov/pub/data/soho**) and are available through CDAWeb (**https://cdaweb.gsfc.nasa.gov**) and its data access methods (**https://cdaweb.gsfc.nasa.gov/alternative_access_methods.html**). The CDF datasets were created from the ASCII datasets at **https://soho.nascom.nasa.gov/data/archive.html** (for CELIAS-PM, CELIAS-SEM, and COSTEP-EPHIN) and **https://srl.utu.fi/export/** (for ERNE), and they cover the period from the beginning of the mission and will continue to be updated. Please note that the new CELIAS-PM ASCII datasets at **https://soho.nascom.nasa.gov/data/archive.html** and the current (version 2) CELIAS-PM CDF datasets were recently fully reprocessed. Thank you to Andriy Koval for curating these data.

New datasets available via the Virtual Solar Observatory

The Virtual Solar Observatory (VSO) is pleased to announce the availability of the following datasets:

- PSP/WISPR data up to and including Encounter 11
- SDO/EVE Level 4 data from 2010 to 2022 (comprising a total of 4424 FITS files)
- All current Solar Orbiter/EUI Level 1 and 2 data (up to April 2022 at time of writing)

If you have any questions about accessing these data using VSO clients please contact the VSO team at **help@virtualsolar.org**

European Solar Physics Meeting – ESPM16

6-10 September 2020, Turin, Italy online
https://indico.ict.inaf.it/e/ESPM-16
https://indico.ict.inaf.it/event/794/overview
Presentations at https://indico.ict.inaf.it/event/794/timetable/#20210906.detailed

---

NMDB - Neutron Monitor Database [http://www01.nmdb.eu]

SILSO/SIDC - Solar Influences Data analysis Center [http://www.sidc.be/silso]

WSO - Wilcox Solar Observatory [http://wso.stanford.edu]

NASA/SPDF - Space Physics Data Facility [https://spdf.gsfc.nasa.gov]

HVO - Heliophysics Virtual Observatory [https://crisp.unipg.it/hvo]

Frontiers in Astronomy and Space Sciences, THE RESEARCH TOPIC**, 2021**
Spectroscopic Instrumentation for Space-borne Solar Observations in the XXI Century
https://www.frontiersin.org/research-topics/15145/spectroscopic-instrumentation-for-space-borne-solar-observations-in-the-xxi-century#articles

NEW MILLENNIUM SOLAR PHYSICS

Reprocessed science-quality data from the Extreme Ultraviolet Sensor (EUVS) on the **GOES-16** satellite is now available. https://www.ngdc.noaa.gov/stp/satellite/goes-r.html

---

The Solar Orbiter mission

Astronomy & Astrophysics Volume 642 **2020** **SPECIAL ISSUES**
https://www.aanda.org/component/toc/?task=topic&id=1082
https://www.aanda.org/articles/aa/abs/2020/10/contents/contents.html

Solar Orbiter First Results (Cruise Phase): many papers on ^{3}He-rich SEPs, near-relativistic electrons, stealth CME, ICMEs, GCR flux, Forbush
Astronomy & Astrophysics Volume 656 (December **2021**)
https://www.aanda.org/articles/aa/abs/2021/12/contents/contents.html

---

LASP Interactive Solar Irradiance Data Center
https://lasp.colorado.edu/lisird/

Table 1. Event catalogs currently implemented in the Interactive Multi-Instrument Database of Solar Flares (https://solarflare.njit.edu/).

Source Name	Dates presented	Source web link
	Primary flare lists	
GOES flare list	Jan, 2002 — current time	ftp://ftp.swpc.noaa.gov/pub/warehouse/
RHESSI flare list	Feb, 2002 — current time	http://hesperia.gsfc.nasa.gov/hessidata/dbase/
HEK flare list	Feb, 2010 — current time	https://www.lmsal.com/isolsearch
	Secondary event catalogs	
IRIS observing logs	Jul, 2013 — current time	http://iris.lmsal.com/search/
Hinode flare catalog	Nov, 2006 — July, 2016	http://st4a.stelab.nagoya-u.ac.jp/hinode_flare/
Fermi GBM flare catalog	Nov, 2008 — current time	https://hesperia.gsfc.nasa.gov/fermi/gbm/qlook/
Nobeyama coverage check	Jan, 2010 — current time	ftp://solar-pub.nao.ac.jp/pub/nsro/norp/xdr/
OVSA flare catalog	Jan, 2002 — Dec, 2003	http://www.ovsa.njit.edu/data/
CACTus CME catalog	Jan, 2002 — current time	http://sidc.oma.be/cactus/
Filament eruption catalog	Apr, 2010 — Oct, 2014	http://aia.cfa.harvard.edu/filament/
Konus-Wind flare catalog	Jan, 2002 — Jul, 2016	http://www.ioffe.ru/LEA/Solar/index.html

---

Aschwanden, Markus J. **Book**
Astrophysics and Space Science Library, Vol. 458
Springer Nature Switzerland AG **2019**
sci-hub.se/10.1007/978-3-030-13956-8

https://link.springer.com/book/10.1007%2F978-3-030-13956-8
1 New Solar Instrumentation 2 Atomic Physics and Spectroscopy 3 The Solar Interior
4 The Photosphere and Sunspots 5 The Chromosphere and Spicules
6 The Quiet-Sun Corona 7 Coronal Holes and Jets 8 Active Regions . 9 Coronal Loops
10 Coronal Loop Oscillations and Waves 11 Filaments and Prominences
12 Flares: Nonthermal Particles 13 Flares: Thermal Emission 14 CME Initiation
15 CME Propagation 16 Sun-Earth Connections

Доступ к книгам Springer Nature
https://link.springer.com/search?query=solar+physics&facet-discipline="Physics"

NASA – Files From the **Heliophysics Advisory Committee December 2018 Meeting** are Available
science.nasa.gov/researchers/nac/science-advisory-committees/hpac

---

Advances in Solar Physics
Solar physics advances from the interior to the heliosphere
Advances in Space Research Volume 63, Issue 4, Pages 1387-1490 (15 February **2019**)
Edited by Manolis K. Georgoulis, Eduard P. Kontar
https://www.sciencedirect.com/journal/advances-in-space-research/vol/63/issue/4

Global solar magnetic field evolution over 4 solar cycles: Use of the McIntosh archive.
Webb, D.F., Gibson, S.E., Hewins, I.M., McFadden, R.H., Emery, B.A., Malanushenko, A., Kuchar, T.A.:
Front. Astron. Space Sci. 5, 23. **2018**, DOI. ADS.
https://www.frontiersin.org/articles/10.3389/fspas.2018.00023/full

========

The Sun as a Guide to Stellar Physics Book
Eds. Oddbjørn Engvold, Jean-Claude Vial, and Andrew Skumanich
Elsevier , November **2018**
https://www.elsevier.com/books/the-sun-as-a-guide-to-stellar-physics/engvold/978-0-12-814334-6
https://www.sciencedirect.com/book/9780128143346/the-sun-as-a-guide-to-stellar-physics

---

Welcome to the Hinode website
http://solarb.mssl.ucl.ac.uk/SolarB/

Open Access Collection of Solar Physics Conference Presentations
http://science-media.org http://science-media.org/showCategoryVideos.php?c=1&s=1

Books **190** Result(s) for **'solar physics'**
https://link.springer.com/search?query=solar+physics&facet-language="En"&just-selected-from-overlay=facet-discipline&facet-content-type="Book"&facet-discipline="Physics"&just-selected-from-overlay-value="Physics"

The Solar Activity Cycle **Book**

Physical Causes and Consequences
André **Balogh**, Hugh Hudson, Kristóf Petrovay…
Space Sciences Series of ISSI (**2015**)
https://link.springer.com/content/pdf/10.1007%2F978-1-4939-2584-1.pdf

---

Solar and Space Physics: A Science for a Technological Society. **Book File**
Washington, The National Academies Press, **2013**,
446 p. DOI: 10.17226/13060.

Solar Storms in Virtual Reality – Public Outreach Material Available at
youtu.be/2uvnyh8ETQc
Alternatively, some explanations can be found on our brochure:
owncloud.ias.u-psud.fr/index.php/s/jUZacqoD3gl58eP
SolarNews 01 March 2017

Textbook I: "Plasma Physics of the Local Cosmos"
Textbook II: "Space Storms and Radiation: Causes and Effects"
Textbook III: "Evolving Solar Activity and the Climates of Space and Earth"
Textbook IV: "Active Stars, their Astrospheres, and Impacts on Planetary Environments"
https://cpaess.ucar.edu/heliophysics/resources-textbook-1

Интересные ролики, если в поиск завести
«The 100 Largest Geomagnetic Storms in the Last 150 Years»

См. http://www.youtube.com/watch?v=QAs73yvZ7eY и представленные там фильмы-лекции

Solar Literature References – Matrix

http://www.lmsal.com/~aschwand/publications/

"Space Weather" Vol. 125 2001 Monograph
http://agupubs.onlinelibrary.wiley.com/hub/journal/10.1002/(ISSN)1542-7390/reprise-of-space-weather-2001-monograph.html

Solar Eruptions and Energetic Particles 2013
http://onlinelibrary.wiley.com/book/10.1029/GM165

Volume on Developing the Solar Probe Plus Mission

Space Science Reviews. Volume 204 Number 1-4, Dec 2016
http://link.springer.com/journal/11214/204/1?wt_mc=alerts.TOCjournals

---

[1] The National Space Weather Strategy, 2015,
www.whitehouse.gov/sites/default/files/microsites/ostp/final_nationalspaceweatherstrategy_20151028.pdf
[2] The National Space Weather Action Plan, 2015,
www.whitehouse.gov/sites/default/files/microsites/ostp/final_nationalspaceweatheractionplan_20151028.pdf
[3] The U.K. "National risk register for civil emergencies" (2015 edition),
www.gov.uk/government/publications/national-risk-register-for-civil-emergencies-2015-edition
[4] Knipp, D. J. et al, 2016, The May 1967 great storm and radio disruption event: Extreme space weather and extraordinary responses, Space Weather, DOI: 10.1002/2016SW001423
[5] **International Space Environment Service (ISES),** www.spaceweather.org

---

Special section on "Effects of solar wind and interplanetary disturbances on the Earth's atmosphere and climate", edited by Katy Georgieva, Alan Aylward, Irina Mironova, Eugene Rozanov, Brian Tinsley
Journal of Atmospheric and Solar-Terrestrial Physics
Volume 149, Pages 1-290, November 2016

CESRA 2016: Solar Radio Physics from the Chromosphere to Near Earth
Abstracts http://cesra2016.sciencesconf.org/conference/cesra2016/pages/CESRA2016_prog_abs_book_v1.pdf

---

"Low-Frequency Waves in Space Plasmas" – New Book
Andreas Keiling, Dong-Hun Lee, Valery Nakariakov
2016
DOI: 10.1002/9781119055006
http://onlinelibrary.wiley.com/book/10.1002/9781119055006
Part IX: Solar Corona
Part X: Solar Photosphere and Chromosphere

Textbook series on "**Heliophysics**"
Edited by Karel Schrijver, George Siscoe, Fran Bagenal, and Jan Sojka.
http://www.vsp.ucar.edu/Heliophysics/science-resources-textbooks.shtml

---

Space Weather Workshops
http://www.swpc.noaa.gov/content/prior-workshops
2016 http://www.swpc.noaa.gov/content/annual-meeting

Management, Search and Analysis of Solar Astronomy Big Data.
A topical issue of Astronomy and Computing, Volume 13, Pages 1-144 (November **2015**)
http://www.sciencedirect.com/science/journal/22131337

Solar and Stellar Flares: Observations, Simulations, and Synergies /
Guest Editors: Lyndsay Fletcher and Petr Heinzel
Solar Phys. Volume 290, Issue 12, December **2015**

http://link.springer.com/journal/11207/290/12/

Probing the Sun: Inside and Out
Guest Editors: **Louise Harra, Deborah Baker, Rachel Howe, John Leibacher…**
Solar Phys. Volume 290, Issue 11, December **2015**
http://link.springer.com/journal/11207/290/11/

Advances in Solar Physics
Advances in Space Research
Volume 56, Issue 12, Pages 2677-2838 (15 December **2015**)
Edited by Manolis K. Georgoulis and Valery M. Nakariakov

Helioseismology and Dynamics of the Solar Interior
Issue Editors: M.J. Thompson, A.S. Brun, J.L. Culhane, Laurent Gizon, M. Roth, T. Sekii
Space Science Reviews Volume 196, Issue 1-4, December **2015**
http://link.springer.com/journal/11214/196/1/page/1

The Sun-climate connection over the last millennium: facts and questions **Book**
Maxim **Ogurtsov**, Risto Jalkanen, Markus Lindholm, Svetlana Veretenenko
2015
http://ebooks.benthamsciencepublisher.org/book/9781608059805/

Rice Space Institute
Current and Predicted Space Weather Conditions
http://mms.rice.edu/realtime/forecast.html

Testing the estimated hypothetical response of a major CME impact on Earth and its implications to space weather
Ramkumar Bala, Patricia Reiff, C. T. Russell
JGR Volume 120, Issue 5 May 2015 Pages 3432–3443

NATIONAL SPACE WEATHER STRATEGY
April **2015**
http://www.dhs.gov/sites/default/files/publications/DRAFT-NSWS-For-Public-Comment-508.pdf
http://www.swpc.noaa.gov/news/national-space-weather-strategy-and-action-plan-released
Comments http://onlinelibrary.wiley.com/doi/10.1002/2015SW001334/full

---

Heliophysics Science and Technology Roadmap for 2014 – 2033
http://science.nasa.gov/heliophysics/
http://science.nasa.gov/media/medialibrary/2015/04/07/2014_HelioRoadmap_Final_Reduced.pdf

---

Solar Storms: 2000 years of human calamity **Book**
Sten **Odenwald, 2015**
tinyurl.com/lzuhenr
It is a companion guide to his previous book '**The 23rd Cycle: Learning to live with a stormy star**'.

Physics of Magnetic Flux Tubes **Book**
Margarita **Ryutova**
2014-2015

Nature's Third Cycle: A Story of Sunspots **Book**
Arnab Rai **Choudhuri**
2015
http://www.amazon.co.uk/Natures-Third-Cycle-Story-Sunspots/dp/0199674752/

The Sun-Climate Connection over the Last Millennium: facts and questions
Maxim **Ogurtsov** , Risto Jalkanen, Markus Lindholm, Svetlana Veretenenko
2015
http://ebooks.benthamsciencepublisher.org/book/9781608059805/

Ground based solar observations in the space instrumentation era

ASP Conference Series, 2016, volume 504:
http://aspbooks.org/a/volumes/table_of_contents/?book_id=570

Recent results from Hinode:
PASJ special issue, Volume 66 Issue SP1 December **2014**
http://pasj.oxfordjournals.org/content/66/SP1.toc

The Solar Activity Cycle: Physical Causes and Consequences
Space Sci. Revs. Volume 186, Issue 1-4, December **2014**
http://link.springer.com/journal/11214/186/1/page/1

Solar Prominences **Book**
Editors: Jean-Claude Vial, Oddbjørn Engvold
Astrophysics and Space Science Library
Volume 415 **2015**
http://link.springer.com/book/10.1007/978-3-319-10416-4#page-1

The Coronas-F Space Mission **Book**
Key Results for Solar Terrestrial Physics
Vladimir **Kuznetsov**
in Astrophysics and Space Science Library (**2014**)
http://link.springer.com/book/10.1007/978-3-642-39268-9

Solar and Space Physics:
A Science for a Technological Society:
An Overview (**2014**)

Popular Summary of the Solar and Space Physics Decadal Survey
http://www.nap.edu/openbook.php?record_id=18974&page=R1

The Many Scales of Solar Activity in Solar Cycle 24 as seen by SDO /
Guest Editors: Aaron Birch, Mark Cheung, Andrew Jones, and W. Dean Pesnell
Solar Phys., Volume 289, Issue 9, September **2014**

Outstanding Problems in Heliophysics: From Coronal Heating to the Edge of the Heliosphere
ASP Conference Series Volume: 484 Year: **2014**
Editors: Hu Q.; Zank G. P.
Synopsis: 12th Annual International Astrophysics Conference
Myrtle Beach, South Carolina, USA, 14–19 April 2013

"Magnetohydrodynamics of the Sun", **Book**
Eric **Priest**
Cambridge University Press, **2014**
http://solarnews.nso.edu/2014/20140415.html

Space Weather Workshop in Boulder, April 8-11, 2014
http://www.swpc.noaa.gov/sww/
Agenda with Presentations:
http://www.swpc.noaa.gov/sww/SWW_Agenda_w_attached_presentations.pdf

- State of the Space Weather Prediction Center
Brent **Gordon**, NOAA/SWPC
- Solar Max – It's Here, Finally
Doug **Biesecker**, NOAA/SWPC
- The Major Solar Eruptive Event in July 2012: Defining Extreme Space Weather Scenarios
Daniel **Baker**, University of Colorado, Boulder

Space Weather and Coronal Mass Ejections **Book**
Timothy A. **Howard**
Springer, **2013**
http://books.google.ru/books?id=ihO4BAAAQBAJ&pg=PA97&lpg=PA97&dq=DeForest,+C.+E.&source=bl&ots=XIvsgYLfFB&sig=525J_9PFZBGda9BsysLsvRRQh34&hl=ru&sa=X&ei=HxlfVOr7HoG6PdDNgegL&ved=0CC4Q6AEwBQ#v=onepage&q=DeForest%2C%20C.%20E.&f=false
25 March 2008, 12-17 Dec 2008, 2010-04-03,

Proceedings of the NSO Workshop # 27, "Fifty Years of Seismology of the Sun and Stars"
Astronomical Society of the Pacific Conference Series, volume 478, **2013**
http://www.aspbooks.org/a/volumes/table_of_contents/478

"Nature of solar prominences and their role in Space Weather", **Book**
Proceedings of IAU Symposion 300Paris, France, June 10-14, **2013**,
B. Schmieder, J.-M. Malherbe & S. T. Wu, eds.
Table of Contents:
http://journals.cambridge.org/action/displayIssue?jid=IAU&volumeId=8&seriesId=0&issueId=S300

Extreme space weather: impacts on engineered systems and infrastructure

Summary report 2013
http://newserver.stil.bas.bg/ISWI/PDFsL/Space_Weather_Summary_Report.PDF

Physics of the Solar Corona. Advanced Course - The Era of RHESSI, STEREO, Hinode, and SDO – 2014
Aschwanden, M.J. 2014, Springer ... (in preparation) **Book**
Chapter 1: **Solar Missions 2000-2015, File**
http://www.lmsal.com/~aschwand/publications/publ.html

Solar Origins of Space Weather and Space Climate **Topical Issues**
Guest Editors: I. González Hernández, R. Komm, and A. Pevtsov
Solar Physics
Volume 289, Issue 2, February **2014**

Coronal Magnetometry **Topical Issues**
Guest Editors: S. Tomczyk, J. Zhang, and T.S. Bastian
Solar Physics, Volume 288, Issue 2, December **2013**
Preface: p. 463–465

The Microphysics of Cosmic Plasmas **Topical Issues**
Space Science Reviews, Volume 178, Number 2-4, **2013**

Radiation Belt Storm Probes
The Van Allen Probes Mission
Space Science Reviews, Volume 179, Number 2-4, **2013**

Presentations at the 2013 SPD meeting now online
The organizers of the 2013 SPD Meeting in Bozeman, Montana, are pleased to announce that the presentation files and audio recordings of the oral presentations are now online. The downloadable presentation files can be accessed directly from http://solar.physics.montana.edu/SPD/SPD2013/all_indexed.html,

or from the meeting webpage at http://solar.physics.montana.edu/SPD/SPD2013

Additionally, the presentations from the Agency Town Hall Meeting are linked from the main meeting webpage, and also at http://solar.physics.montana.edu/SPD/SPD2013/assets/papers/Agency

---

J. Space Weather Space Clim. , Volume 3, 2013
Space Weather and Challenges for Modern Society
http://www.swsc-journal.org/index.php?option=com_toc&task=topic&id=182

Solar Phys, 287(1–2), 2013
Solar Dynamics and Magnetism from the Interior to the Atmosphere
LWS/SDO-3/SOHO-26/GONG-2011 workshop, 31 October – 4 November 2011, at Stanford, California, USA.

i) Local and Global Helioseismology.
ii) Sources of Solar Shape and Irradiance Variations.
iii) Large-Scale Dynamics, Magnetism, and Dynamo.
iv) Emerging Magnetic Flux and Subsurface Dynamics.
v) Formation, Structure, and Evolution of Sunspots and Active Regions.
vi) Magnetic Topology and Dynamics of the Solar Atmosphere.

Влияние космической погоды на человека в космосе и на Земле
Труды Международной конференции
ИКИ РАН, Москва, Россия, 4–8 июня 2012 г. Под ред. А. И. Григорьева, Л. М. Зелёного
В двух томах. См. Файл 2013breus1.pdf

Space Science Reviews
Volume 176, Issue 1-4, June 2013
Cosmic Rays in the Heliosphere - Temporal and Spatial Variations

---

Topical issue – ***PROBA2 – First Two Years of Solar Observation***
Solar Physics, 2013, Volume 286, Issue 1

Topical issue – ***Observations and Modelling of the Inner Heliosphere***
Solar Physics, 2013, Volume 285, Issue 1-2

Probing the Fundamental Physics of the Solar Corona with Lunar Solar Occultation Observations
S. Rifai Habbal, H. Morgan, M. Druckmüller, A. Ding, J. F. Cooper, A. Daw…

Solar Orbiter
D. Müller, R. G. Marsden, O. C. St. Cyr, H. R. Gilbert

MESSENGER Observations of Magnetohydrodynamic Waves in the Solar Corona from Faraday Rotation
E. A. Jensen, M. Nolan, M. M. Bisi, I. Chashei, F. Vilas

Measurements of Faraday Rotation Through the Solar Corona During the 2009 Solar Minimum with the MESSENGER Spacecraft
Elizabeth A. Jensen, Mario M. Bisi, Andrew R. Breen, Carl Heiles

Equatorwards Expansion of Unperturbed, High-Latitude Fast Solar Wind
G. D. Dorrian, A. R. Breen, R. A. Fallows, M. M. Bisi

Observations of Rapid Velocity Variations in the Slow Solar Wind
S. A. Hardwick, M. M. Bisi, J. A. Davies, A. R. Breen, R. A. Fallows…

The Dynamic Spectrum of Interplanetary Scintillation: First Solar Wind Observations on LOFAR
R. A. Fallows, A. Asgekar, M. M. Bisi, A. R. Breen, S. ter-Veen

Results of IPS Observations in the Period Near Solar Activity Minimum
I. V. Chashei, V. I. Shishov, S. A. Tyul'bashev, I. A. Subaev…

Inclusion of Real-Time In-Situ Measurements into the UCSD Time-Dependent Tomography and Its Use as a Forecast Algorithm
B. V. Jackson, J. M. Clover, P. P. Hick, A. Buffington, M. M. Bisi…

Heliolatitude and Time Variations of Solar Wind Structure from in situ Measurements and Interplanetary Scintillation Observations
J. M. Sokół, M. Bzowski, M. Tokumaru, K. Fujiki, D. J. McComas

Study of Corotating Interaction Regions in the Ascending Phase of the Solar Cycle: Multi-spacecraft Observations
J. A. Gonzalez-Esparza, E. Romero-Hernandez, P. Riley

Evolution of the Solar Flare Energetic Electrons in the Inhomogeneous Inner Heliosphere
Hamish A. S. **Reid**, Eduard P. Kontar

и др.

Topical issue – ***ADVANCES IN EUROPEAN SOLAR PHYSICS***
Solar Physics, 2013, Volume 284, Issue 2

Topical issue – ***Flux-Rope Structure of Coronal Mass Ejections***
Solar Physics, 2013, Volume 284, Issue 1

Topical issue – *Solar Image Processing in the Petabyte Era*
Solar Physics, March 2013, Volume 283, Issue 1
The articles are ordered by topic:
i) automated tools,
ii) prediction of solar phenomena,
iii) methods that improve our ability to determine information on solar phenomena, and
iv) three-dimensional structure reconstruction.

Multi-Scale Physics in Coronal Heating and Solar Wind Acceleration
Topical issue
Space Science Reviews, Volume 172, Issue 1-4, November **2012**
http://link.springer.com/journal/11214/172/1/page/1

Self-Organized Criticality in Astrophysics
The Statistics of Nonlinear Processes in the Universe
Markus **Aschwanden**
Springer Praxis Books, **2011**
http://link.springer.com/book/10.1007/978-3-642-15001-2/page/1

National Research Council.
Severe Space Weather Events—Understanding Societal and Economic Impacts: A Workshop Report (The National Academies Press, **2008**).
http://www.nap.edu/openbook.php?record_id=12507&page=R1
1 Introduction 6-15
2 Space Weather Impacts in Retrospect 16-28
3 Space Weather and Society 29-34
4 Current Space Weather Services Infrastructure 35-49
5 User Perspectives on Space Weather Products 50-68
6 Satisfying Space Weather User Needs 69-75
7 Future Solutions, Vulnerabilities, and Risks 76-85
8 Facilitated Open Audience Discussion: The Way Forward 86-90

ФИЗИЧЕСКИЕ ОСНОВЫ ПРОГНОЗИРОВАНИЯ ВОЗМУЩЕНИЙ В ОКОЛОЗЕМНОЙ СРЕДЕ ПО ХАРАКТЕРИСТИКАМ СОЛНЦА
В.Г. Еселевич

обзор, Байкал, 2002
http://www.kosmofizika.ru/irkutsk/eselevich.htm

Солнечно-земная Физика
интернет-учебник
http://www.kosmofizika.ru/

СОЛНЕЧНЫЕ ФАКТОРЫ, ОПРЕДЕЛЯЮЩИЕ СОСТОЯНИЕ КОСМИЧЕСКОЙ ПОГОДЫ,
И ЗАДАЧИ ИХ ПРОГНОЗИРОВАНИЯ
В.П. **Максимов**
http://www.kosmofizika.ru/irkutsk/maksimov.htm
Доклад представлен на Байкальской школе ИСЗФ СО РАН, Иркутск, 2002
и опубликован на сайте http://bsfp.iszf.irk.ru/bsfp2002/articles/

Электронный учебник
Космические исследования и взаимодействия космической среды с системами и материалами космических аппаратов
http://nuclphys.sinp.msu.ru/cosm/index.html

Глава 1. Нейтринная астрофизика (Кузьмичев Л.А.)
Глава 2. **Магнитные бури и магнитосферные суббури** (Калегаев В.В., Алексеев И.И., Кропоткин А.П.)
Глава 3. Проникновение космических лучей в магнитосферу Земли (Юшков Б.Ю.)
Глава 4. **Радиационная опасность на околоземных орбитах и межпланетных траекториях космических аппаратов** (Кузнецов Н.В.)
Глава 5. Взаимодействие заряженных частиц с веществом (Анохина А.М., Галкин В.И., Мурзина Е.А.)
Глава 6. Особенности действия космической радиации на биологические объекты и радиационный риск длительных космических полетов (Шафиркин А.В., Бенгин В.В.)
Глава 7. **Геоэффективность солнечной активности и космическая погода** (Мягкова И.Н.)

М.И. **Панасюк**
Странники Вселенной или эхо Большого взрыва
http://nuclphys.sinp.msu.ru/pilgrims/index.html

Ядерная физика в Интернете
http://nuclphys.sinp.msu.ru/

Магнитные бури и магнитосферные суббури
Калегаев В.В., Алексеев И.И., Кропоткин А.П.
http://nuclphys.sinp.msu.ru/cosm/index-15.htm

Topical issue – Flux Emergence in the Hinode Era / Guest Editor: L. M. Green
Solar Phys. Volume 278, Number 1 / May **2012**

3D MHD Flux Emergence Experiments: Idealised Models and Coronal Interactions
A. W. Hood, V. Archontis and D. MacTaggart

On Signatures of Twisted Magnetic Flux Tube Emergence
S. Vargas Domínguez, D. MacTaggart, L. Green, L. van Driel-Gesztelyi and A. W. Hood

The Creation of Outflowing Plasma in the Corona at Emerging Flux Regions: Comparing Observations and Simulations
L. K. Harra, V. Archontis, E. Pedram, A. W. Hood and D. L. Shelton, et al.
1 – 2 December 2006

Nonlinear Force-Free Extrapolation of Emerging Flux with a Global Twist and Serpentine Fine Structures
G. Valori, L. M. Green, P. Démoulin, S. Vargas Domínguez and L. van Driel-Gesztelyi, et al.

Granular-Scale Elementary Flux Emergence Episodes in a Solar Active Region
S. Vargas Domínguez, L. van Driel-Gesztelyi and L. R. Bellot Rubio

Velocity Characteristics of Rotating Sunspots
C. Zhu, D. Alexander and L. Tian

Quenching of Meridional Circulation in Flux Transport Dynamo Models
Bidya Binay Karak and Arnab Rai Choudhuri

Solar Magnetic Carpet II: Coronal Interactions of Small-Scale Magnetic Fields
K. A. Meyer, D. H. Mackay and A. A. van Ballegooijen

Coronal Seismology Using Transverse Oscillations of Non-planar Coronal Loops
A. Scott and M. S. Ruderman

Spectroscopic Coronal Observations During the Total Solar Eclipse of 11 July 2010
A. G. Voulgaris, P. S. Gaintatzis, J. H. Seiradakis, J. M. Pasachoff and T. E. Economou

Correlations Between CME Parameters and Sunspot Activity
Zhanle Du

Line-of-Sight Observables Algorithms for the Helioseismic and Magnetic Imager (HMI) Instrument Tested with Interferometric Bidimensional Spectrometer (IBIS) Observations
Sébastien Couvidat, S. P. Rajaguru, Richard Wachter, K. Sankarasubramanian and Jesper Schou, et al.

Exploring the Solar Wind

Ed. Marian Lazar
INTECH, **2012**
http://www.intechopen.com/books/exploring-the-solar-wind

Chapter 1
Solar Wind Laws Valid for any Phase of a Solar Cycle, by V.G. Eselevich
Chapter 2
Solar Wind: Origin, Properties and Impact on Earth, by U.L. Visakh Kumar and P.J. Kurian
Chapter 3
Solar Wind Composition Associated with the Solar Activity, by X. Wang, B. Klecker and P. Wurz
Chapter 4
Solar Wind and Solar System Matter After Mission Genesis, by Kurt Marti and Peter Bochsler
Chapter 5

Measuring the Isotopic Composition of Solar Wind Noble Gases, by Alex Meshik, Charles Hohenberg, Olga Pravdivtseva and Donald Burnett

Chapter 6

Solar Wind Noble Gases in Micrometeorites, by Takahito Osawa

Chapter 7

Multifractal Turbulence in the Heliosphere, by Wiesław M. Macek

Chapter 8

Field-Aligned Current Mechanisms of Prominence Destabilization, by Petko Nenovski

Chapter 9

Small Scale Processes in the Solar Wind, by Antonella Greco, Francesco Valentini and Sergio Servidio

Chapter 10

Kinetic Models of Solar Wind Electrons, Protons and Heavy Ions, by Viviane Pierrard

Chapter 11

Suprathermal Particle Populations in the Solar Wind and Corona, by M. Lazar, R. Schlickeiser and S. Poedts

Chapter 12

Impact of the Large-Scale Solar Magnetic Field on the Solar Corona and Solar Wind, by A.G. Tlatov and B.P. Filippov

Chapter 13

Variability of Low Energy Cosmic Rays Near Earth, by Karel Kudela

Chapter 14

Impact of Solar Wind on the Earth Magnetosphere: Recent Progress in the Modeling of Ring Current and Radiation Belts, by Natalia Buzulukova, Mei-Ching Fok and Alex Glocer

Chapter 15

Ground-Based Monitoring of the Solar Wind Geoefficiency, by Oleg Troshichev

Chapter 16

The Polar Cap PC Indices: Relations to Solar Wind and Global Disturbances, by Peter Stauning

Chapter 17

Sudden Impulses in the Magnetosphere and at Ground, by U. Villante and M. Piersanti

Chapter 18

Turbulence in the Magnetosheath and the Problem of Plasma Penetration Inside the Magnetosphere, by Elizaveta E. Antonova, Maria S. Pulinets, Maria O. Riazantseva, Svetlana S. Znatkova, Igor P. Kirpichev and Marina V. Stepanova

Chapter 19

Solar Wind Sails, by Ikkoh Funaki and Hiroshi Yamakawa

Topical Issue

The Solar Dynamics Observatory

W. Dean **Pesnell**, Phillip C. Chamberlin, and Barbara J. Thompson (Eds.)
Solar Phys., (**2012**), volume 275, 3-15

The Solar Dynamics Observatory (SDO)
W. Dean **Pesnell**, B. J. Thompson und P. C. Chamberlin
Solar Phys., (**2012**), volume 275, pp.3-15**; File**

The Atmospheric Imaging Assembly (AIA) on the Solar Dynamics Observatory (SDO)
James R. **Lemen**, Alan M. Title, David J. Akin, Paul F. Boerner und Catherine Chou, et al.
pp.17-40**; File**

Heliophysics Event Knowledgebase for the Solar Dynamics Observatory (SDO) and Beyond
N. **Hurlburt**, M. Cheung, C. Schrijver, L. Chang, S. Freeland, S. Green, C. Heck, A. Jaffey, A. Kobashi und D. Schiff, et al.
pp. 67-78

The Helioseismic and Magnetic Imager (HMI) Investigation for the Solar Dynamics Observatory (SDO)
P. H. **Scherrer**, J. Schou, R. I. Bush, A. G. Kosovichev und R. S. Bogart, et al.
pp. 207-227

Topical Issue

The Sun–Earth Connection near Solar Minimum: Placing it into Context
Mario M. **Bisi**, Barbara J. Thompson, Barbara A. Emery, Sarah E. Gibson, John Leibacher und Lidia van Driel-Gesztelyi (Eds.)
Solar Phys., (**2011**) 274
The Whole Heliosphere Interval (WHI) was an international observing and modeling effort to characterize the 3-D interconnected "heliophysical" system during this solar minimum, centered on Carrington Rotation 2068, **March 20–April 16, 2008.**

Presentations at the
13th European Solar Physics Meeting, Rhodes, Greece, 12-16 September **2011**
http://astro.academyofathens.gr/espm13/program.html

Magnetic Reconnection: Theoretical and Observational Perspectives

Спец выпуск **Space Science Reviews:** Volume 160, Numbers 1-4, October **2011**
http://www.springerlink.com/content/0038-6308/160/1-4/

Observed Aspects of Reconnection in Solar Eruptions **A Review**
Ronald L. **Moore** · Alphonse C. Sterling · G. Allen Gary · JonathanW. Cirtain · David A. Falconer
Space Sci Rev., 160:73–94, **2011, File**

High-Energy Aspects of Solar Flares: A RHESSI-inspired monograph

Спец выпуск **Space Science Reviews**, Volume 159, Numbers 1-4, September **2011**
http://www.springerlink.com/content/0038-6308/159/1-4/

Overview of the Volume **A Review**
B. R. **Dennis**1, A. G. Emslie2, and H. S. Hudso
Space Sci. Rev., 159:3–17, **2011, File**

An Observational Overview of Solar Flares **A Review**
L. **Fletcher**1, B. R. Dennis2, H. S. Hudson3, S. Krucker3, K. Phillips4, A. Veronig5, M. Battaglia1, L. Bone4, A. Caspi3, Q. Chen7 , P. Gallagher8, P. T. Grigis9, · H. Ji10,11, W. Liu2,12, R. O. Milligan2, and M. Temmer5,13,14
Space Sci. Rev., 159:19–106, **2011, File**

Implications of X-ray Observations for Electron Acceleration and Propagation in Solar Flares
G.D. **Holman**1, M. J. Aschwanden2, H. Aurass3, M. Battaglia4, P. C. Grigis5, E. P. Kontar6, W. Liu1, P. Saint-Hilaire7, and V. V. Zharkova8
Space Sci. Rev., 159:107–166, **2011, File** A Review

Properties of Energetic Ions in the Solar Atmosphere from γ-Ray and Neutron Observations
N. **Vilmer**, A. L. MacKinnon and G. J. Hurford
Space Sci. Rev., 159:167– 224, **2011, File** A Review

The Relationship Between Solar Radio and Hard X-ray Emission **A Review**
S. M. **White**1,5, A. O. Benz2, S. Christe3, F. F´arn´ık4, M. R. Kundu5, G. Mann6, Z. Ning7, J.-P. Raulin8, A. V. R. Silva-V´alio8, P. Saint-Hilaire9, N. Vilmer10, and A.Warmuth6
Space Sci. Rev., 159:225–261, **2011, File**

Microflares and the Statistics of X-ray Flares **A Review**
I. G. **Hannah**, H. S. Hudson, M. Battaglia, S. Christe, J. Kašparová, S. Krucker, M. R. Kundu and A. Veronig
Space Sci Rev (**2011**) 159:263–300, **File**

Deducing Electron Properties from Hard X-ray Observations **A Review**
E. P. **Kontar**, J. C. Brown, A. G. Emslie, W. Hajdas, G. D. Holman, G. J. Hurford, J. Kašparová, P. C. V. Mallik, A. M. Massone and M. L. McConnell, et al.
Space Sci Rev (**2011**) 159:301–355, **File**

Recent Advances in Understanding Particle Acceleration Processes in Solar Flares
V.V. **Zharkova** · K. Arzner · A.O. Benz · P. Browning · C. Dauphin · A.G. Emslie · L. Fletcher · E.P. Kontar · G. Mann · M. Onofri · V. Petrosian · R. Turkmani · N. Vilmer · L. Vlahos
Space Sci Rev (**2011**) 159:357–420, **File**

Energy Release and Particle Acceleration in Flares: Summary and Future Prospects
R.P. **Lin**
Space Sci Rev (**2011**) 159:421–445, **File** **A Review**

Physics of Space Storms
From the Solar Surface to the Earth
Hannu E. J. **Koskinen**
2011, ISBN 978-3-642-00310-3 e-ISBN 978-3-642-00319-6
DOI 10.1007/978-3-642-00319-6
Springer Heidelberg Dordrecht London New York
File of Contents
In addition to light and other wavelengths of electromagnetic radiation the Sun affects our environment through complicated plasma physical processes. The study of these interactions is known as solar–terrestrial physics. Already long before the space era there were indications that solar activity and geomagnetic perturbations must somehow be connected. **A remarkable event was the large flare on the Sun observed, independently, by Carrington [1859] and Hodgson [1859] on September 1, 1859, after which a major magnetic storm commenced only 17 hours later.** Today we understand that the storm was caused by a magnetic cloud associated with a coronal mass ejection (CME) that reached the Earth exceptionally quickly. The storm was very strong, evidently much stronger than any event recorded during the present era of space weather sensitive equipment in space and on the ground.

"MHD Waves and Seismology of the Solar Atmosphere"
Space Science Reviews, Volume 158, Numbers 2-4, 365-396, **2011**

>>>Magnetohydrodynamic Waves and Seismology of the Solar Atmosphere<<<
Robertus Erdélyi & Marcel Goossens

>>>Damping Mechanisms for Oscillations in Solar Prominences<<<
Iñigo Arregui & José Luis Ballester

>>>Review Article: MHD Wave Propagation Near Coronal Null Points of Magnetic Fields<<<
J. A. McLaughlin, A. W. Hood & I. Moortel

>>>Filament Thread-like Structures and Their Small-amplitude Oscillations<<<
Yong Lin

>>>Propagating MHD Waves in Coronal Holes<<<
D. Banerjee, G. R. Gupta & L. Teriaca

>>>Resonant MHD Waves in the Solar Atmosphere<<<
Marcel Goossens, Robert Erdélyi & Michael S. Ruderman

>>>Self-consistent Simulations of Alfvén Wave Driven Winds from the Sun and Stars<<<
Takeru K. Suzuki

>>>Large-scale Bright Fronts in the Solar Corona: A Review of “EIT waves”<<<
Peter T. Gallagher & David M. Long

>>>Standing Slow-Mode Waves in Hot Coronal Loops: Observations, Modeling, and Coronal Seismology<<<
Tongjiang Wang

>>>Nonlinear Effects in Resonant Layers in Solar and Space Plasmas<<<
Istvan Ballai & Michael S. Ruderman

>>>Seismic Transients from Flares in Solar Cycle 23<<<
Alina Donea

>>>Effects of Magnetic Fields in the Solar Atmosphere on Global Oscillations<<<
Balázs Pintér & Robert Erdélyi

---

a new book entitled as **“Solar Activity in 1992-2003 : Solar Cycle 23 Observed by Flare Monitoring Telescope” (Authors: Kazunari Shibata, Reizaburo Kitai, Miwako Katoda, et al.)** was published on Feb 28, 2011 from Kyoto University Press.
http://solarnews.nso.edu/2011/20110501.html#section0
http://www.kyoto-up.or.jp/book.php?isbn=9784876989874&lang=en

---

CORONAS-PHOTON solar satellite project
Solar System Research, 42(2), 45(3), **2011**
http://springer.r.delivery.net/r/r?2.1.Ee.2Tp.1gRU2L.B%2asLmQ..T.PDZW.3aHy.bW89MQ%5f%5fCcUCFPO0

Helioseismology
Solar Phys., Volume 268, Number 2 / February **2011**

The RHESSI monograph and the top ten RHESSI flares thus far. See
http://sprg.ssl.berkeley.edu/~tohban/wiki/index.php/The_Flares_of_the_RHESSI_Monograph
2011. a nine-chapter monograph to be published by Space Science Reviews this year

---

Solar Plasma Spectroscopy: Achievements And Future Challenges
DAMTP, University of Cambridge, 13-15 September 2010
http://www.damtp.cam.ac.uk/user/astro/conference_web/talks/index.html
Презентации

Как пока ссылаться на **SDO/AIA**
The Atmospheric Imaging Assembly on the Solar Dynamics Observatory
Title, A. M.; Hoeksema, J. T.; Schrijver, C. J.; The AIA Team
36th COSPAR Scientific Assembly. Held 16 - 23 July 2006, in Beijing, China. Meeting abstract from the CDROM, #260, **2006**
The Atmospheric Imaging Assembly AIA on SDO will provide revolutionary coverage of the entire visible solar hemisphere observed from photospheric to coronal temperatures at 1-arcsecond resolution with a characteristic cadence of 10 seconds for each channel The AIA comprises four dual normal-incidence telescopes that enable it to cycle through a set of EUV channels centered on strong emission lines of iron ranging from Fe IX through XXIII and helium 304A plus two UV channels near 1600A and a broad band visible channel Combined with the vector-

magnetic imagery from SDO HMI the AIA observations will significantly further our understanding of the dynamics of the magnetic field in the solar atmosphere and heliosphere both in quiescent and eruptive stages The comprehensive thermal coverage of the corona will open new avenues of study for coronal energetics and seismology which will benefit from the excellent calibration against the SDO EVE spectral irradiance measurements The AIA data will be easily accessible on the web with a time delay that is expected to be of the order of 15 minutes to 1 hour Users will be able to browse the data through summary web pages that are complemented by a comprehensive metadata catalog Data analysis will be supported through the freely available SolarSoft libraries and through modules in a flexible evolving pipeline data-analysis system to be operated at the AIA-HMI Joint Science Operations Center We plan to incorporate feature recognition software automated movie making coronal field modeling

See Presentation Title (2004), File

The **Heliophysics Summer School** (http://www.vsp.ucar.edu/Heliophysics/)
The **three books and presentations** are subtitled 'Plasma physics of the local cosmos', 'Space storms and radiation: causes and effects', and 'Evolving solar activity and the climates of space and Earth'. Chapter titles and (increasingly) online supporting materials can be accessed at http://www.vsp.ucar.edu/Heliophysics/science-resources-textbooks.shtml

---

Heliophysics II. Space Sotrms and Radiation: Causes and Effects
Schrijver, C.J. and Siscoe,G.L. (eds.) **2010**, Cambridge University Press, Cambridge
www.cambridge.org/9780521760515

Advances in Space Research
Volume 45, Issue 7, Pages 823-948 (1 April **2010**)
Life Sciences in Space

Solar Phys.
Number 2 / Апрель 2010 г.
Solar Image Processing and Analysis | Guest Editors: J. Ireland and C.A. Young

---

The Solar Corona
2nd Edition, 2009
Leon Golub & Jay M. Pasachoff
http://www.cambridge.org/catalogue/catalogue.asp?isbn=9780521882019&ss=res

---

"Three eyes on the Sun – multi-spacecraft studies of the corona and impacts on the heliosphere"
Eds. R. Harrison, J. Luhmann, B. Fleck, C. St Cyr, R. Forsyth
Ann. Geophys., 27, 2771, **2009**

Space solar missions
Jean-Claude Vial
Solar and Stellar Variability: Impact on Earth and Planets, Proceedings IAU Symposium No. 264, **2009**, p. 459-468, A.G. Kosovichev, A.H. Andrei & J.-P. Rozelot, eds.
Y:\obridko\otchet09
In the frame of Symposium 264 which concerns Solar and Stellar Variability we address the space solar missions devoted to the various aspects of solar activity. We describe them in three time categories : missions ready for launch, missions which will operate in the 2012-2015 time frame and ambitious missions to be launched after 2015. We focus on the contributions of these missions according to the following criteria : Understanding mechanisms of

activity, Improving detection and characterisation, Working out some prediction. Major activity contributors and manifestations are addressed : Coronal Mass Ejections, Flares, Solar winds, Magnetism (including dynamo), Irradiance.

Using Virtual Observatories for Heliophysics Research

A number of new virtual observatories have opened their doors to heliophysics researchers, allowing them not only to access and view multiple sources of information at the same time but also to cross-compare data to build new insights.

By R. S. Weigel et al.

http://www.agu.org/journals/eo/eo0947/2009EO470001.pdf#anchor

EOS ONLINE - An AGU Member Service

http://www.agu.org/pubs/eos (Login required)

VOLUME 90 NUMBER 47 24 November **2009**

Solar Physics

Numbers 1-2 / Октябрь 2009 г.

STEREO Science Results at Solar Minimum | Guest Editors: E. R. Christian, M. L. Kaiser, T. A. Kucera, O. C. St. Cyr

---

Proceedings of the International Astronomical Union

Table of Contents - Volume 4 - Symposium S257 (**Universal Heliophysical Processes**) – 2008

http://journals.cambridge.org/action/displayIssue?iid=4866212

Severe Space Weather Events--Understanding Societal and Economic Impacts Workshop Report

The adverse effects of extreme space weather on modern technology--power grid outages, high-frequency communication blackouts, spacecraft anomalies--are well known and well documented, and the physical processes underlying space weather are also generally well understood. Less well documented and understood, however, are the potential economic and societal impacts of the disruption of critical technological systems by severe space weather.

As a first step toward determining the socioeconomic impacts of extreme space weather events and addressing the questions of space weather risk assessment and management, a public workshop was held in **May 2008**. The workshop brought together representatives of industry, the government, and academia to consider both direct and collateral effects of severe space weather events, the current state of the space weather services infrastructure in the United States, the needs of users of space weather data and services, and the ramifications of future technological developments for contemporary society's vulnerability to space weather. The workshop concluded with a discussion of un- or underexplored topics that would yield the greatest benefits in space weather risk management.

http://www.nap.edu/catalog.php?record_id=12507

The Hinode Mission
Sakurai, Takashi (Ed.)
Reprinted from Solar Physics Journal, Vol. 243/1, 2007 and Vol. 249/2, 2008
2009, IV, 208 p. 140 illus., 45 in color., Hardcover
ISBN: 978-0-387-88738-8

The Solar-B satellite was launched in 2006 by the Institute of Space and Astronautical Science, Japan Aerospace Exploration Agency (ISAS/JAXA), and was renamed Hinode ('sunrise' in Japanese). Hinode carries three instruments: the X-ray telescope (XRT), the EUV imaging spectrometer (EIS), and the Solar Optical Telescope (SOT). These instruments were developed by ISAS/JAXA in cooperation with the National Astronomical Observatory of Japan as domestic partner, and NASA and the Science and Technology Facilities Council (UK) as international partners. ESA and the Norwegian Space Center have been providing a downlink station.

The Hinode (Solar-B) Mission gives a comprehensive description of the Hinode mission and its instruments onboard. This book is most useful for researchers, professionals, and graduate students working in the field of solar physics, astronomy, and space instrumentation. This is the only book that carefully describes the details of the Hinode mission; it is richly illustrated with full-color images and figures.

This volume combines the first set of instrumental papers on the mission overview, EIS, XRT, and the database system along with the second set of papers on SOT and XRT.

Hinode Publications
Astronomy and Astrophysics Letters, 2008
http://msslxr.mssl.ucl.ac.uk:8080/SolarB/Publications.jsp

The Sun from Space
Series: Astronomy and Astrophysics Library
Lang, Kenneth R.
2nd ed., **2009**, XXX, 558 p. 124 illus., 67 in color., Hardcover
ISBN: 978-3-540-76952-1
Online version available

This volume is a comprehensive, up-to-date account of solar astrophysics and how our perception and knowledge of this star have evolved as mankind has elucidated ever more of its mysteries. The emphasis of this *second edition* of

The Sun from Space is on the last decade, which includes the findings of the SOHO, Ulysses, and Yohkoh solar spacecraft missions over an entire 11-year cycle of solar activity, the results of the RHESSI solar spacecraft launched during this interval, the early findings of the recently launched Hinode and STEREO solar spacecraft, and the ACE and Wind spacecraft that extend our investigations of the Sun to its varying input to Earth over the past ten years.

Table of Contents - Volume 4 - Symposium S257 (**Universal Heliophysical Processes**) - 2008 Proceedings of the International Astronomical Union
http://journals.cambridge.org/action/displayIssue?jid=IAU&volumeId=4&seriesId=0&issueId=S257

The Sun
A User's Manual
Vita-Finzi, Claudio
2008, Approx. 170 p. 30 illus., 20 in color., Hardcover
The Sun is an account of the many ways in which our nearest star affects our planet, how its influence has changed over the last few centuries and millennia, and the extent to which we can predict its future impact. The Sun's rays foster the formation of Vitamin D by our bodies, but it can also promote skin cancer, cataracts, and mutations in our DNA. Besides providing the warmth and light essential to most animal and plant life, solar energy contributes substantially to global warming. Although the charged particles of the solar wind shield us from harmful cosmic rays, solar storms may damage artificial satellites and cripple communication systems and computer networks. The Sun is the ideal renewable energy source, but its exploitation is still bedevilled by the problems of storage and distribution. Our nearest star, in short, is a complex machine which needs to be treated with caution, and this book will equip every reader with the knowledge that is required to understand the benefits and dangers it can bring.

Links to **textbooks on solar/space/plasma physics** collected by Markus Aschwanden.

Space Weather Euro News (SWEN)
http://esa-spaceweather.net/spweather/SWEN/swen.html

Advances in Space Research, Volume 42, Issue 9, Pages 1445-1618 (3 November **2008**)

SPACE WEATHER: OBSERVATIONS AND MODELING FOR APPLICATIONS AND OPERATIONS

1. **Space weather center in Japan**
   Pages 1445-1449
   S. Watari
2. **Solar activity prediction studies and services in NAOC**
   Pages 1450-1456
   Han He, Huaning Wang, Zhanle Du, Rong Li, Yanmei Cui, Liyun Zhang and Yulin He
3. **A summary of the applications of a weighted average method determining times of solar cycle extrema**
   Pages 1457-1463
   Z.L. Du, H.N. Wang, H. He, L.Y. Zhang, R. Li and Y.M. Cui
4. **Solar flare forecasting model supported with artificial neural network techniques**
   Pages 1464-1468
   H.N. Wang, Y.M. Cui, R. Li, L.Y. Zhang and H. Han
5. **Application of support vector machine combined with K-nearest neighbors in solar flare and solar proton events forecasting**

Pages 1469-1474
Rong Li, Yanmei Cui, Han He and Huaning Wang

6. **Correlation between solar flare productivity and photospheric vector magnetic fields**
   Pages 1475-1479
   Yanmei Cui and Huaning Wang

7. **Observational study of magnetic chirality of solar active regions**
   Pages 1480-1491
   H.Q. Zhang

8. **Comparing proton fluxes of central meridian SEP events with those predicted by SOLPENCO**
   Pages 1492-1499
   A. Aran, B. Sanahuja and D. Lario

9. **Single-event upset in geostationary transfer orbit during solar-activity maximum period measured by the Tsubasa satellite**
   Pages 1500-1503
   H. Koshiishi, H. Matsumoto and T. Goka

10. **Real-time global MHD simulation of the solar wind interaction with the earth's magnetosphere**
    Pages 1504-1509
    H. Shimazu, K. Kitamura, T. Tanaka, S. Fujita, M.S. Nakamura and T. Obara

11. **Geomagnetic effects on mid-latitude railways: A statistical study of anomalies in the operation of signaling and train control equipment on the East-Siberian Railway**
    Pages 1510-1514
    N.G. Ptitsyna, V.V. Kasinskii, G. Villoresi, N.N. Lyahov, L.I. Dorman and N. Iucci

---

STEREO **Space Science Reviews, Volume 136, Number 1-4, 2008**
http://springerlink.com/content/l9161w742658/?p=aabf46ab72a841bf92efb4e20f10c18d&pi=0
http://springerlink.com/content/102996/

The STEREO Mission: An Introduction
M.L. **Kaiser** · T.A. Kucera · J.M. Davila · O.C. St. Cyr · M. Guhathakurta · E. Christian
Space Sci Rev (**2008**) 136: 5–16
DOI 10.1007/s11214-007-9277-0

The STEREO Observatory
Andrew **Driesman** · Shane Hynes · George Cancro
Space Sci Rev (**2008**) 136: 17–44
DOI 10.1007/s11214-007-9286-z

STEREO Space Weather and the Space Weather Beacon
D.A. **Biesecker** · D.F. Webb · O.C. St. Cyr
Space Sci Rev (**2008**) 136: 45–65, **File**
DOI 10.1007/s11214-007-9165-7

Sun Earth Connection Coronal and Heliospheric Investigation (SECCHI)
R.A. **Howard** · J.D. Moses · A. Vourlidas et al.
Space Sci Rev (**2008**) 136: 67–115, File
DOI 10.1007/s11214-008-9341-4

STEREO IMPACT Investigation Goals, Measurements, and Data Products Overview
J.G. **Luhmann** · D.W. Curtis, P. Schroeder et al.
Space Sci Rev (**2008**) 136: 117–184
DOI 10.1007/s11214-007-9170-x

The STEREO IMPACT Boom
The STEREO/IMPACT Magnetic Field Experiment
The IMPACT Solar Wind Electron Analyzer (SWEA)
The STEREO IMPACT Suprathermal Electron (STE) Instrument
The Suprathermal Ion Telescope (SIT) For the IMPACT/SEP Investigation
The Low-Energy Telescope (LET) and SEP Central Electronics for the STEREO Mission
The High Energy Telescope for STEREO
The Plasma and Suprathermal Ion Composition (PLASTIC) Investigation on the STEREO Observatories

S/WAVES: The Radio and Plasma Wave Investigation on the STEREO Mission
J.L. **Bougeret** · K. Goetz · M.L. Kaiser
Space Sci Rev (**2008**) 136: 487–528
DOI 10.1007/s11214-007-9298-8

The Electric Antennas for the STEREO/WAVES Experiment
STEREO/Waves Goniopolarimetry
Theoretical modeling for the stereo mission
STEREO Ground Segment, Science Operations, and Data Archive
The Solar Terrestrial Relations Observatory (STEREO) Education and Outreach (E/PO) Program
---

The Heliospheric Imagers Onboard the STEREO Mission
C. J. **Eyles**, R. A. Harrison, C. J. Davis, N. R. Waltham, B. M. Shaughnessy, H. C. A. Mapson-Menard, D. Bewsher, S. R. Crothers, J. A. Davies, G. M. Simnett, R. A. Howard, J. D. Moses, J. S. Newmark, D. G. Socker, J.-P. Halain, J.-M. Defise, E. Mazy, P. Rochus
Solar Physics, Volume 254 Number 2, Page: 387 – 445, **2009**
DOI: 10.1007/s11207-008-9299-0
URL: http://springer.r.delivery.net/r/r?2.1.Ee.2Tp.1gRU2L.Bxnhyi..T.H3Fo.38KK.DXOEcI00

A Topical Issue on the Hinode Mission
"Solar Physics", Volume 249, Number 2, **2008**
http://springerlink.com/content/hg3825426kx8/?p=0dd9afd47ba747c59caa6b78641b2467&pi=0

- The Solar Optical Telescope for the Hinode Mission: An Overview
- The Solar Optical Telescope of Solar-B (Hinode): The Optical Telescope Assembly
- Image Stabilization System for Hinode (Solar-B) Solar Optical Telescope
- Polarization Calibration of the Solar Optical Telescope onboard Hinode
- The Hinode X-Ray Telescope (XRT): Camera Design, Performance and Operations

---

A Topical Issue on Solar Image Analysis and Visualization

Solar Phys 248(2), (2008).

The third *Solar Image Processing Workshop* (SIPWork III) was held at Trinity College Dublin, Ireland, in September 2006. This meeting brought together researchers in solar physics, image processing, and computer vision, and it focused on preparing for the data analysis and processing needs of new space missions such as the *Solar TErrestrial RElations Observatory* (STEREO), *Hinode*, and the *Solar Dynamics Observatory* (SDO), as well as ground-based instrumentation such as the Advanced Technology Solar Telescope (ATST), the Swedish Solar Telescope (SST), and the Dutch Open Telescope (DOT).

The Solar and Stellar Interior and Dynamo Mechanism
Helioseismology and Solar Interior
Solar Magnetism and Activity Cycle
Advances in Space Research, **Volume 41, Issue 6**, Pages 829-1002 **(2008)**

Energetic Particles and Magnetic Reconnection on the Sun and in the Heliosphere
Advances in Space Research, **Volume 41, Issue 6**, Pages 829-1002 **(2008)**

Handbook of the Solar-Terrestrial Environment
Kamide, Yohsuke; Chian, Abraham C.-L. (Eds.)
2007, XIV, 539 p. 255 illus., 63 in color.,
Springer
http://www.springer.com/east/home/generic/search/results?SGWID=5-40109-22-173682707-0

Stereoscopy basics for the STEREO mission -- Bernd **Inhester**, E-print, Dec **2006**

ILWS Workshop: The Solar Influence on the Heliosphere and Earth's Environment: Recent Progress and Prospects
*February 19-24, **2006**,*
Goa, India
http://cdaw.gsfc.nasa.gov/publications/ilws_goa2006/

Solar Dynamics and its Effects on the Heliosphere and Earth
Space Science Reviews, Volume 124, Number 1-4, **2006**
http://springerlink.com/content/t32wm71r8h6h/?p=450451979925435c9b7f34f5ccf40dce&pi=0

Active Region Dynamics
A. G. Kosovichev, T. L. Duvall, 1 - 12

Sunspot Structure and Dynamics
N. O. Weiss, 13 - 22

Coronal Dynamics and the AIA on SDO
L. Golub, 23 – 33

Solar Wind Sources and Their Variations Over the Solar Cycle
R. Schwenn, 51 – 76

Heliospheric Physics: Linking the Sun to the Magnetosphere

Thomas H. Zurbuchen, 77 – 90

The Evolving Sigmoid: Evidence for Magnetic Flux Ropes in the Corona Before, During, and After CMES

S. E. Gibson, Y. Fan, T. Török, B. Kliem, 131 - 144
Space Science Reviews (2006) 124: 131–144

TOPICAL ISSUE:
>>>**HELIOSEISMOLOGY, ASTEROSEISMOLOGY, AND MHD CONNECTIONS**<<<
"Solar Physics", Volume 251, Number 1-2, **2008**
http://springerlink.com/content/100339/

Special Issue: Initial Results from Hinode
PUBLICATIONS OF THE ASTRONOMICAL SOCIETY OF JAPAN
Vol. 59, No. SP3 (2007 November 30)
http://pasj.asj.or.jp/v59/v59sp3.html

Modern Solar Facilities – Advanced Solar Science
Proceedings of a Workshop held at Göttingen September 27-29, 2006
Franz **Kneer**, Klaus G. Puschmann, Axel D. Wittmann (Eds.); **File 2007**

ANGEO Special Issue
1st European Space Weather Week (ESWW)
Editor(s): J. Lilensten

ANGEO - Volume 23, Number 9, **2005**

"**Solar Extreme Events: Fundamental Science and Applied Aspects**"
ed. A**. Chilingarian** and G. Karapetyan,
Cosmic Ray Division, Alikhanyan Physics Institute, Yerevan, pp. 20-24, **2006**
http://shnet1.stelab.nagoya-u.ac.jp/~ymatsu/etc/see2005/title-pages_foreword.pdf

Energetic Processes on the Sun during the Extreme Events

Magnetospheric Response to the Solar Extreme Events

Space Weather

Solar Extreme Events: Fundamental Science and Applied Aspects
Edited by Helen **Mavromichalaki**
Advances in Space Research
Volume 43, Issue 4, Pages 467-738 (16 February **2009**)
http://www.sciencedirect.com/science/journal/02731177/43/4

++

Solar Neutrino Detection Sensitivity in DARWIN via Electron Scattering
J. **Aalbers**, F. Agostini, S. E. M. Ahmed Maouloud, M. Alfonsi, L. Althueser, …
Eur. Phys. J. C **2020**
https://arxiv.org/pdf/2006.03114.pdf
We detail the sensitivity of the liquid xenon (LXe) DARWIN observatory to solar neutrinos via elastic electron scattering. We find that DARWIN will have the potential to measure the fluxes of five solar neutrino components: pp, 7Be, 13N, 15O and pep. The precision of the 13N, 15O and pep components is hindered by the double-beta decay of 136Xe and, thus, would benefit from a depleted target. A high-statistics observation of pp neutrinos would allow us to infer the values of the weak mixing angle, sin2 θw, and the electron-type neutrino survival probability, Pe, in the electron recoil energy region from a few keV up to 200 keV for the first time, with relative precision of 5% and 4%, respectively, at an exposure of 300 ty. An observation of pp and 7Be neutrinos would constrain the neutrino-inferred solar luminosity down to 0.2%. A combination of all flux measurements would distinguish between the high (GS98) and low metallicity (AGS09) solar models with 2.1-2.5σ significance, independent of external measurements from other experiments or a measurement of 8B neutrinos through coherent elastic neutrino-nucleus scattering in DARWIN. Finally, we demonstrate that with a depleted target DARWIN may be sensitive to the neutrino capture process of 131Xe.

Measurements of the Time-Dependent Cosmic-Ray Sun Shadow with Seven Years of IceCube Data -- Comparison with the Solar Cycle and Magnetic Field Models
M. G. **Aartsen**, R. Abbasi, M. Ackermann, J. Adams, J. A. Aguilar, and many others
2020
https://arxiv.org/pdf/2006.16298.pdf
Observations of the time-dependent cosmic-ray Sun shadow have been proven as a valuable diagnostic for the assessment of solar magnetic field models. In this paper, seven years of IceCube data are compared to solar activity and solar magnetic field models. A quantitative comparison of solar magnetic field models with IceCube data on the event rate level is performed for the first time. Additionally, a first energy-dependent analysis is presented and compared to recent predictions. We use seven years of IceCube data for the Moon and the Sun and compare them to simulations on data rate level. The simulations are performed for the geometrical shadow hypothesis for the Moon and the Sun and for a cosmic-ray propagation model governed by the solar magnetic field for the case of the Sun. We find that a linearly decreasing relationship between Sun shadow strength and solar activity is preferred over a constant relationship at the 6.4sigma level. We test two commonly used models of the coronal magnetic field, both

combined with a Parker spiral, by modeling cosmic-ray propagation in the solar magnetic field. Both models predict a weakening of the shadow in times of high solar activity as it is also visible in the data. We find tensions with the data on the order of 3σ for both models, assuming only statistical uncertainties. The magnetic field model CSSS fits the data slightly better than the PFSS model. This is generally consistent with what is found previously by the Tibet AS-gamma Experiment, a deviation of the data from the two models is, however, not significant at this point. Regarding the energy dependence of the Sun shadow, we find indications that the shadowing effect increases with energy during times of high solar activity, in agreement with theoretical predictions.

IRIS observations of chromospheric heating by acoustic waves in solar quiet and active regions

V. **Abbasvand** (1), M. Sobotka (1), M. Švanda (1 and 2), P. Heinzel (1), W. Liu (1), L. Mravcová (2)
A&A 648, A28 **2021**
https://arxiv.org/pdf/2102.08678.pdf
https://doi.org/10.1051/0004-6361/202140344
https://www.aanda.org/articles/aa/pdf/2021/04/aa40344-21.pdf
Aims: To study the heating of solar chromospheric magnetic and nonmagnetic regions by acoustic and magnetoacoustic waves, the deposited acoustic-energy flux derived from observations of strong chromospheric lines is compared with the total integrated radiative losses. Methods: A set of 23 quiet-Sun and weak-plage regions were observed in the Mg II k and h lines with the Interface Region Imaging Spectrograph (IRIS). The deposited acoustic-energy flux was derived from Doppler velocities observed at two different geometrical heights corresponding to the middle and upper chromosphere. A set of scaled nonlocal thermodynamic equilibrium 1D hydrostatic semi-empirical models (obtained by fitting synthetic to observed line profiles) was applied to compute the radiative losses. The characteristics of observed waves were studied by means of a wavelet analysis. Results: Observed waves propagate upward at supersonic speed. In the quiet chromosphere, the deposited acoustic flux is sufficient to balance the radiative losses and maintain the semi-empirical temperatures in the layers under study. In the active-region chromosphere, the comparison shows that the contribution of acoustic-energy flux to the radiative losses is only 10 - 30 %. Conclusions: Acoustic and magnetoacoustic waves play an important role in the chromospheric heating, depositing a main part of their energy in the chromosphere. Acoustic waves compensate for a substantial fraction of the chromospheric radiative losses in quiet regions. In active regions, their contribution is too small to balance the radiative losses and the chromosphere has to be heated by other mechanisms.
ESPN #1 Jun 2021 https://www.est-east.eu/nuggets/46-espn/1059-heating-of-the-solar-chromosphere-by-acoustic-wave
ESPN #2 Aug **2021** https://www.est-east.eu/nuggets/46-espn/1085-the-challenge-of-constraining-the-properties-and-dynamics-of-the-magnetic-vector-in-the-quiet-solar-photosphere

Observational study of chromospheric heating by acoustic waves

V. **Abbasvand** (1), M. Sobotka (1), M. Švanda (1 and 2), P. Heinzel (1), Marta García Rivas (1 and 2), C. Denker (3), H. Balthasar (3), M. Verma (3), I. Kontogiannis (3), J. Koza (4), D. Korda (2), C. Kuckein (3)
A&A **2020**
https://arxiv.org/pdf/2008.02688.pdf
Aims. To investigate the role of acoustic and magneto-acoustic waves in heating the solar chromosphere, observations in strong chromospheric lines are analyzed by comparing the deposited acoustic-energy flux with the total integrated radiative losses.
Methods. Quiet-Sun and weak-plage regions were observed in the Ca II 854.2 nm and H-alpha lines with the Fast Imaging Solar Spectrograph (FISS) at the 1.6-m Goode Solar Telescope (GST) on 2019 October 3 and in the H-alpha and H-beta lines with the echelle spectrograph attached to the Vacuum Tower Telescope (VTT) on 2018 December 11 and 2019 June 6. The deposited acoustic energy flux at frequencies up to 20 mHz was derived from Doppler velocities observed in line centers and wings. Radiative losses were computed by means of a set of scaled non-LTE 1D hydrostatic semi-empirical models obtained by fitting synthetic to observed line profiles.
Results. In the middle chromosphere (h = 1000-1400 km), the radiative losses can be fully balanced by the deposited acoustic energy flux in a quiet-Sun region. In the upper chromosphere (h > 1400 km), the deposited acoustic flux is small compared to the radiative losses in quiet as well as in plage regions. The crucial parameter determining the amount of deposited acoustic flux is the gas density at a given height.
Conclusions. The acoustic energy flux is efficiently deposited in the middle chromosphere, where the density of gas is sufficiently high. About 90% of the available acoustic energy flux in the quiet-Sun region is deposited in these layers, and thus it is a major contributor to the radiative losses of the middle chromosphere. In the upper chromosphere, the deposited acoustic flux is too low, so that other heating mechanisms have to act to balance the radiative cooling.

Chromospheric Heating by Acoustic Waves Compared to Radiative Cooling: II -- Revised Grid of Models

Vahid **Abbasvand**, Michal Sobotka, Petr Heinzel, Michal Svanda, Jan Jurcák, Dario del Moro, Francesco Berrilli

ApJ **890** 22 **2020**

https://arxiv.org/pdf/2001.03413.pdf

https://doi.org/10.3847/1538-4357/ab665f

Acoustic and magnetoacoustic waves are considered to be possible agents of chromospheric heating. We present a comparison of deposited acoustic energy flux with total integrated radiative losses in the middle chromosphere of the quiet Sun and a weak plage. The comparison is based on a consistent set of high-resolution observations acquired by the IBIS instrument in the Ca II 854.2 nm line. The deposited acoustic-flux energy is derived from Doppler velocities observed in the line core and a set of 1737 non-LTE 1D hydrostatic semi-empirical models, which also provide the radiative losses. The models are obtained by scaling the temperature and column mass of five initial models VAL B-F to get the best fit of synthetic to observed profiles. We find that the deposited acoustic-flux energy in the quiet-Sun chromosphere balances 30-50 % of the energy released by radiation. In the plage, it contributes by 50-60 % in locations with vertical magnetic field and 70-90 % in regions where the magnetic field is inclined more than 50 degrees to the solar surface normal. **2008 October 15**

Seismology of solar spicules based on Hinode/SOT observations

V. **Abbasvand**, H. Ebadi, Z. Fazel

A&A **2015**

http://arxiv.org/pdf/1507.07393v1.pdf

We analyze the time series of Ca ii H-line obtained from Hinode/SOT on the solar limb. The time-distance analysis shows that the axis of spicule undergoes quasi-periodic transverse displacement. We determined the period of transverse displacement as ~40-150 s and the mean amplitude as ~ 0.1-0.5 arcsec. For the oscillation wavelength of λ ~ 1/0.06 arcsec ~ 11500 km, the estimated kink speed is ~ 13-83 km/s. We obtained the magnetic field strength in spicules as B_0 = 2 - 12.5 G and the energy flux as 7 - 227 J/m^-2s. **22 January, 2007**

Deep Learning Based Reconstruction of Total Solar Irradiance

Yasser **Abduallah**, Jason T. L. Wang, Yucong Shen, Khalid A. Alobaid, Serena Criscuoli, Haimin Wang

2021

https://arxiv.org/pdf/2107.11042.pdf

The Earth's primary source of energy is the radiant energy generated by the Sun, which is referred to as solar irradiance, or total solar irradiance (TSI) when all of the radiation is measured. A minor change in the solar irradiance can have a significant impact on the Earth's climate and atmosphere. As a result, studying and measuring solar irradiance is crucial in understanding climate changes and solar variability. Several methods have been developed to reconstruct total solar irradiance for long and short periods of time; however, they are physics-based and rely on the availability of data, which does not go beyond 9,000 years. In this paper we propose a new method, called TSInet, to reconstruct total solar irradiance by deep learning for short and long periods of time that span beyond the physical models' data availability. On the data that are available, our method agrees well with the state-of-the-art physics-based reconstruction models. To our knowledge, this is the first time that deep learning has been used to reconstruct total solar irradiance for more than 9,000 years.

Phase speed and frequency-dependent damping of longitudinal intensity oscillations in coronal loop structures observed with AIA/SDO

A. **Abedini**

Astrophysics and Space Science April **2016**, 361:133

Longitudinal intensity oscillations along coronal loops that are interpreted as signatures of magneto-acoustic waves are observed frequently in different coronal structures. The aim of this paper is to estimate the physical parameters of the slow waves and the quantitative dependence of these parameters on their frequencies in the solar corona loops that are situated above active regions with the Atmospheric Imaging Assembly (AIA) onboard Solar Dynamic Observatory (SDO). The observed data on **2012-Feb-12**, consisting of 300 images with an interval of 24 seconds in the 171 \AA171 \AA and 193 \AA193 \AA passbands is analyzed for evidence of propagating features as slow waves along the loop structures. Signatures of longitudinal intensity oscillations that are damped rapidly as they travel along the loop structures were found, with periods in the range of a few minutes to few tens of minutes. Also, the projected (apparent) phase speeds, projected damping lengths, damping times and damping qualities of filtered

intensities centred on the dominant frequencies are measured in the range of Cs≃38--79 kms−1Cs≃38--79 kms−1, Ld≃23--68 MmLd≃23--68 Mm, τd≃7--21 minτd≃7--21 min and τd/P≃0.34--0.77τd/P≃0.34--0.77, respectively. The theoretical and observational results of this study indicate that the damping times and damping lengths increase with increasing the oscillation periods, and are highly sensitive function of oscillation period, but the projected speeds and the damping qualities are not very sensitive to the oscillation periods. Furthermore, the magnitude values of physical parameters are in good agreement with the prediction of the theoretical dispersion relations of high-frequency MHD waves (>1.1 mHz>1.1 mHz) in a coronal plasma with electron number density in the range of ne≃107--1012 cm−3ne≃107--1012 cm−3.

Magnetic fluxes of solar active regions of different magneto-morphological classes: I. Cyclic variations

Valentina I. **Abramenko**, Regina A. Suleymanova, Anastasija V. Zhukova
MNRAS Volume 518, Issue 3, January **2023**, Pages 4746–4754
https://arxiv.org/pdf/2212.07115.pdf
https://doi.org/10.1093/mnras/stac3338

Data for 3046 solar active regions (ARs) observed since May 12, 1996 to December 27, 2021 were utilized to explore how the magnetic fluxes from ARs of different complexity follow the solar cycle. Magnetograms from the Michelson Doppler Imager instrument on the Solar and Heliospheric Observatory and from the Helioseismic and Magnetic Imager instrument on the Solar Dynamics Observatory were utilized. Each AR was classified as a regular bipolar AR (classes A1 or A2), or as an irregular bipolar AR (class B1), or as a multipolar AR (classes B2 or B3). Unipolar ARs were segregated into a specific class U. We found the following results. Unsigned magnetic fluxes from ARs of different classes evolve synchronously following the cycle, the correlation coefficient between the flux curves varies in a range of (0.70 - 0.99). The deepest solar minimum is observed simultaneously for all classes. Only the most simple ARs were observed during a deepest minimum: A1- and B1-class ARs. The overall shape of a cycle is governed by the regular ARs, whereas the fine structure of a solar maximum is determined by the most complex irregular ARs. Approximately equal amount of flux (45−50% of the total flux) is contributed by the A-class and B-class ARs during a solar maximum. Thus, observations allow us to conclude that the appearance of ARs with the magnetic flux above 1021 Mx is caused by the solar dynamo that operates as a unique process displaying the properties of a non-linear dynamical dissipative system with a cyclic behaviour and unavoidable fluctuations. **April 25, 2001, February 24, 2004**

Signature of the turbulent component of solar dynamo on active region scales and its association with flaring activity

Valentina I. **Abramenko**
MNRAS Volume 507, Issue 3, Pages 3698–3706, **2021**
https://arxiv.org/pdf/2111.04425.pdf
https://watermark.silverchair.com/stab2404.pdf
https://doi.org/10.1093/mnras/stab2404

It is a challenging problem to obtain observational evidence of the turbulent component of solar dynamo operating in the convective zone because the dynamo action is hidden below the photosphere. Here we present results of a statistical study of flaring active regions (ARs) that produced strong solar flares of an X-ray class X1.0 and higher during a time period that covered solar cycles 23 and 24. We introduced a magneto-morphological classification of ARs, which allowed us to estimate the possible contribution of the turbulent component of the dynamo into the structure of an AR. We found that in 72 per cent of cases, flaring ARs do not comply with the empirical laws of the global dynamo (frequently they are not bipolar ARs or, if they are, they violate the Hale polarity law, the Joy law, or the leading sunspot prevalence rule). This can be attributed to the influence of the turbulent dynamo action inside the convective zone on spatial scales of typical ARs. Thus, it appears that the flaring is governed by the turbulent component of the solar dynamo. The contribution into the flaring from these AR ‘violators’ (irregular ARs) is enhanced during the second maximum and the descending phase of a solar cycle, when the toroidal field weakens and the influence of the turbulent component becomes more pronounced. These observational findings are in consensus with a concept of the essential role of non-linearities and turbulent intermittence in the magnetic fields generation inside the convective zone, which follows from dynamo simulations. **16 Oct 1999, 15 Feb 2011, 26 Sep 2011, 27 Oct 2013, 6 Sep 2017**

Table 2. ARs with X-class flares in the 23rd cycle (1996-2006)
Table 3. ARs with X-class flares in the 24th cycle (2011-2017)

Analysis of quiet-sun turbulence on the basis of SDO/HMI and Goode Solar Telescope data

Valentina I. **Abramenko**, Vasyl B. Yurchyshyn
MNRAS Volume 497, Issue 4, October **2020**, Pages 5405–5412,

https://doi.org/10.1093/mnras/staa2427
https://arxiv.org/pdf/2008.06264.pdf
https://sci-hub.st/10.1093/mnras/staa2427
We analysed line-of-sight magnetic fields and magnetic power spectra of an undisturbed photosphere using magnetograms acquired by the Helioseismic and Magnetic Imager (HMI) on-board the Solar Dynamic Observatory (SDO) and the Near InfraRed Imaging Spectrapolarimeter (NIRIS) operating at the Goode Solar Telescope (GST) of the Big Bear Solar Observatory. In the NIRIS data revealed the presence of thin flux tubes of 200-400~km in diameter and of field strength of 1000-2000~G. The HMI power spectra determined for a coronal hole, a quiet sun and a plage areas exhibit the same spectral index of -1 on a broad range of spatial scales from 10-20~Mm down to 2.4~Mm. This implies that the same mechanism(s) of magnetic field generation operate everywhere in the undisturbed photosphere. The most plausible one is the local turbulent dynamo. When compared to the HMI spectra, the -1.2 slope of the NIRIS spectrum appears to be more extended into the short spatial range until the cutoff at 0.8-0.9~Mm, after which it continues with a steeper slope of -2.2. Comparison of the observed and Kolmogorov-type spectra allowed us to infer that the Kolmogorov turbulent cascade cannot account for more than 35\% of the total magnetic energy observed in the scale range of 3.5-0.3~Mm. The energy excess can be attributed to other mechanisms of field generation such as the local turbulent dynamo and magnetic super-diffusivity observed in an undisturbed photosphere that can slow down the rate of the Kolmogorov cascade leading to a shallower resulting spectrum. **2015 February 10**

The multifractal nature of solar magnetism and the solar dynamo problem

Abramenko, V. I.
Geomagnetism and Aeronomy, Volume 54, Issue 7, pp.892-898, **2014**
Based on observation data with a high spatial resolution, the multifractal properties of turbulent magnetized plasma in a nonperturbed solar atmosphere are revealed. It is shown that magnetic fluxes in elements of the magnetic field, as well as the size of elements, are distributed lognormally, which is indicative of multifractality. In coronal holes (CHs), the multifractality of magnetic fields is observed on scales of 10000-400 km; at the same time, it is observed on smaller scales as the resolution improves, and its degree increases. It is shown that two subsets of granules exist: the usual granules, with a characteristic size of 1000-1300 km and Gaussian size distribution, and mini-granules, which do not have a well-pronounced characteristic size and are mostly less than 600 km in diameter. The size distribution function of the mini-granules obeys lognormal law and their multifractal character is seen on small scales down to 50 km, which allows one to make a conclusion about the presence of multifractality of photospheric plasma flows in CHs and in a nonperturbed photosphere. A conclusion is made that multifractality takes place for small-scale magnetic fields of quiet regions, as well as for large-scale fields of active regions. This makes it possible to suppose that solar magnetic fields are generated by a common nonlinear dynamical process.

Response to: “Critical Analysis of a Hypothesis of the Planetary Tidal Influence on Solar Activity” by S. Poluianov and I. Usoskin

J. A. **Abreu**, C. Albert, J. Beer, A. Ferriz-Mas, K. G. McCracken, F. Steinhilber
Solar Physics, June **2014**, Volume 289, Issue 6, pp 2343-2344

A flare sensitive 3 h solar flux radio index for space weather applications

Acebal, Ariel O.; Sojka, Jan J.
Space Weather, Vol. 9, No. 7, S07004, **2011**
http://dx.doi.org/10.1029/2010SW000585
Many space physics models use the F10.7 as their input for solar activity. The F10.7 is a daily index derived from solar radio measurements taken at 2800 MHz, excluding activity from solar flares. In this paper, we compute a 3 h composite index, similar, in part, to the F10.7, using solar radio observations taken at 2695 MHz (11.1 cm) by the United States Air Force's Radio Solar Telescope Network. This index, called the F11.1 index, is similar to the F10.7. But unlike the F10.7 index, which is measured three times each day, at 1700, 2000, and 23 UT, F11.1 consists of eight measurements each day, uniformly distributed over 24 h. These 3 h intervals are aligned in UT with the planetary geomagnetic index Kp's time intervals. Each interval provides an F11.1 value that minimizes solar flare radio emission data. This composite index also provides two additional pieces of quantitative information that the F10.7 does not provide. The first is a factor, ranging from 0 to 1, indicating how representative the single F11.1 value is of this entire 3 h period (representation accuracy parameter). The second is a measure of how much of the 3 h interval can be classified as solar disturbed or as having a flare in progress (duration parameter). These aspects together have relevance for ionospheric modeling/specification for solar conditions in which significant change can occur over a 24 h period.

Extreme value theory applied to the millennial sunspot number series

F.J. **Acero**, M.C. Gallego, J.A. García, I.G. Usoskin, J.M. Vaquero

ApJ **2018**

https://arxiv.org/ftp/arxiv/papers/1801/1801.09776.pdf

In this work, we use two decadal sunspot number series reconstructed from cosmogenic radionuclide data (14C in tree trunks, SN-14C and 10Be in polar ice, SN-10Be) and the Extreme Value Theory to study variability of solar activity during the last 9 millennia. The peaks-over-threshold technique was used to compute, in particular, the shape parameter of the generalized Pareto distribution for different thresholds. Its negative value implies an upper bound of the extreme SN-10Be and SN-14C time series. The return level for 1000 and 10000 years were estimated leading to values lower than the maximum observed values, expected for the 1000-year, but not for the 10000-year return levels, for both series. A comparison of these results with those obtained using the observed sunspot numbers from telescopic observations during the last four centuries suggest that the main characteristics of solar activity have already been recorded in the telescopic period (from 1610 to nowadays) which covers the full range of solar variability from a Grand minimum to a Grand maximum.

Extreme Value Theory and the New Sunspot Number Series

F. J. **Acero**1,2, V. M. S. Carrasco1, M. C. Gallego1,2, J. A. García1,2, and J. M. Vaquero2,

2017 ApJ 839 98 DOI 10.3847/1538-4357/aa69bc

Extreme value theory was employed to study solar activity using the new sunspot number index. The block maxima approach was used at yearly (1700–2015), monthly (1749–2016), and daily (1818–2016) scales, selecting the maximum sunspot number value for each solar cycle, and the peaks-over-threshold (POT) technique was used after a declustering process only for the daily data. Both techniques led to negative values for the shape parameters. This implies that the extreme sunspot number value distribution has an upper bound. The return level (RL) values obtained from the POT approach were greater than when using the block maxima technique. Regarding the POT approach, the 110 year (550 and 1100 year) RLs were lower (higher) than the daily maximum observed sunspot number value of 528. Furthermore, according to the block maxima approach, the 10-cycle RL lay within the block maxima daily sunspot number range, as expected, but it was striking that the 50- and 100-cycle RLs were also within that range. Thus, it would seem that the RL is reaching a plateau, and, although one must be cautious, it would be difficult to attain sunspot number values greater than 550. The extreme value trends from the four series (yearly, monthly, and daily maxima per solar cycle, and POT after declustering the daily data) were analyzed with the Mann–Kendall test and Sen's method. Only the negative trend of the daily data with the POT technique was statistically significant.

Recalibration of the Soft X-Ray TelescopeOnboard Yohkoh

Loren **Acton**

Solar Physics October **2018**, 293:137

We present a new derivation of the X-ray spectral sensitivity of the Soft X-ray Telescope(SXT) experiment onboard Yohkoh. The recalibration is based upon the hypothesis that, during the first 15 months of the mission, an absorbing material gradually built up on the entrance filters of the telescope. We have also re-evaluated the times and sizes of ruptures of the SXT entrance filters. The impact of this recalibration on derived filter-ratio temperature, emission measure, and calculated spectral irradiance is substantial, especially for SXT data prior to November 1992.

On-Orbit Performance and Calibration of the Soft X-ray Telescope on Yohkoh

Loren **Acton**

Solar Phys. Vol. 291, Issue 2 **2016** **Opec Access**

http://ylstone.physics.montana.edu/ylegacy/documents/publication/YLA_SXTcalibration.pdf

This paper documents details of the on-orbit performance, data problem solving, and calibration of the Soft X-ray Telescope (SXT) experiment on Yohkoh. This information is important to a full understanding of the strengths and weaknesses of the SXT data set. The paper begins with summaries of SXT calibration issues and how they have been addressed, operational anomalies experienced during the mission, and a brief discussion of the SXT optical train. The following section on the accuracy of Yohkoh pointing determination provides information important for alignment of SXT images with each other and with other solar data. The remainder of the paper gives details of work by the experiment team to understand and ameliorate the many instrument anomalies and changes which impacted the scientific data.

Solar Soft X-Ray Irradiance Variability, II: Temperature Variations of Coronal X-Ray Features

H. N. **Adithya**, Rangaiah Kariyappa, Kanya Kusano, +++

Solar Physics volume 298, Article number: 99 (**2023**)
https://doi.org/10.1007/s11207-023-02190-x
The temperature variations of the corona and its individual surface features as a function of the solar cycle are an interesting and important aspect of understanding the physics of the Sun. To study the temperature variations, we have used the full-disk soft X-ray images of the corona obtained from Hinode/X-Ray Telescope (XRT) in different filters. A sophisticated algorithm has been developed in Python to segment the different coronal features such as the active regions (ARs), coronal holes (CHs), background regions (BGs), and X-ray bright points (XBPs), derived the total intensity of all the features, and generated the temperature maps of the corona using the filter ratio method. Due to the XRT straylight issue in some filters and unavailability of a good pair of images, we used for our analysis the filter combinations of Ti-poly and Al-mesh for the period from February 01, 2008 to May 08, 2012 and Al-poly and Al-mesh for the period from May 09, 2012 to June 30, 2021, in total for 14 years which covers Solar Cycle 24. The first analysis in using the XRT intensity values of the coronal features from segmented solar disk and their relation to solar activity is presented. We discuss the temperature variations of a full-disk corona and all features (ARs, CHs, BGs, and XBPs). Our time series plots of the average temperature of the full-disk and all the features show temperature fluctuations synchronized with the solar cycle (sunspot number). Although the temperature of all features varies, but the mean temperature estimated for the whole observed period of the full-disk is around 1.29 ± 0.16 MK and active regions (ARs) are around 1.76 ± 0.32 MK, whereas BGs, CHs, and XBPs are 1.27 ± 0.15 MK, 1.23 ± 0.14 MK, and 1.37 ± 0.18 MK, respectively. In addition, we found that the mean temperature contribution estimated of the background regions (BGs) is around 93.2%, whereas ARs, CHs, and XBPs are 3.1%, 1.6% and 2.1%, respectively, to the average coronal temperature of the full-disk. The temperature values and their variations of all the features suggest that the features show a high variability in their temperature and that the heating rate of the emission features may be highly variable on solar cycle timescales. It is evident from the analysis that the filter-ratio method can be directly used for temperature analysis of coronal features and to study their surface temperature variability as a function of solar magnetic activity.

Solar Soft X-ray Irradiance Variability, I: Segmentation of Hinode/XRT Full-Disk Images and Comparison with GOES (1 – 8 Å) X-Ray Flux

H. N. **Adithya**, Rangaiah Kariyappa, Imada Shinsuke, Kusano Kanya, Joe Zender, Luc Damé, Giono Gabriel, Edward DeLuca & Mark Weber
Solar Physics volume 296, Article number: 71 (**2021**)
https://link.springer.com/content/pdf/10.1007/s11207-021-01785-6.pdf
https://doi.org/10.1007/s11207-021-01785-6
It is of great interest and importance to study the variabilities of solar EUV, UV and X-ray irradiance in heliophysics, in Earth's climate, and space weather applications. A careful study is required to identify, track, monitor and segment the different coronal features such as active regions (ARs), coronal holes (CHs), the background regions (BGs) and the X-ray bright points (XBPs) from spatially resolved full-disk images of the Sun. Variability of solar soft X-ray irradiance is studied for a period of 13 years (February 2007–March 2020, covers Solar Cycle 24), using the X-Ray Telescope on board the Hinode (Hinode/XRT) and GOES (1 – 8 Å). The full-disk X-ray images observed in Al_mesh filter from XRT are used, for the first time, to understand the solar X-ray irradiance variability measured, Sun as a star, by GOES instrument. An algorithm in Python has been developed and applied to identify and segment coronal X-ray features (ARs, CHs, BGs, and XBPs) from the full-disk soft X-ray observations of Hinode/XRT. The segmentation process has been carried out automatically based on the intensity level, morphology and sizes of the X-ray features. The total intensity, area, and contribution of ARs/CHs/BGs/XBPs features were estimated and compared with the full-disk integrated intensity (FDI) and GOES (1 – 8 Å) X-ray irradiance measurements. The XBPs have been identified and counted automatically over the full disk to investigate their relation to solar magnetic cycle. The total intensity of ARs/CHs/BGs/XBPs/FD regions are compared with the GOES (1 – 8 Å) X-ray irradiance variations. We present the results obtained from Hinode/XRT full-disk images (in Al_mesh filter) and compare the resulting integrated full-disk intensity (FDI) with GOES X-ray irradiance. The X-ray intensity measured over ARs/CHs/BGs/XBPs/FD is well correlated with GOES X-ray flux. The contributions of the segmented X-ray features to FDI and X-ray irradiance variations are determined. It is found that the background and active regions have a greater impact on the X-ray irradiance fluctuations. The mean contribution estimated for the whole observed period of the background regions (BGs) will be around 65±10.97%65±10.97%, whereas the ARs, XBPs and CHs are 30±11.82%, 4±1.18% and 1±0.52%, respectively, to total solar X-ray flux. We observed that the area and contribution of ARs and CHs varies with the phase of the solar cycle, whereas the BGs and XBPs show an anti-correlation. We find that the area of the coronal features is highly variable suggesting that their area has to be taken into account in irradiance models, in addition to their intensity variations. The time series results of XBPs suggest for an existence of anti-correlation between the number of XBPs and the sunspot numbers. It is also

important to consider both the number variation and the contribution of XBPs in the reconstruction of total solar X-ray irradiance variability.

Unexpected Cyclic Behavior in Cosmic-Ray Protons Observed by PAMELA at 1 au

O. **Adriani**1,2, G. C. Barbarino3,4, G. A. Bazilevskaya5, R. Bellotti6,7, M. Boezio8, E. A. Bogomolov9, M. Bongi1,2, V. Bonvicini8, A. Bruno6, F. Cafagna7 Show full author list

2018 ApJL 852 L28

http://iopscience.iop.org.sci-hub.tw/2041-8205/852/2/L28/

Protons detected by the PAMELA experiment in the period 2006–2014 have been analyzed in the energy range between 0.40 and 50 GV to explore possible periodicities besides the well known solar undecennial modulation. An unexpected clear and regular feature has been found at rigidities below 15 GV, with a quasi-periodicity of ~450 days. A possible Jovian origin of this periodicity has been investigated in different ways. The results seem to favor a small but not negligible contribution to cosmic rays from the Jovian magnetosphere, even if other explanations cannot be excluded.

In the Trenches of the Solar–Stellar Connection. II. Extreme Ultraviolet Flux–Flux Correlations across Solar Cycle 24

Thomas R. Ayres

Slow-Mode MHD Wave Penetration into a Coronal Null Point due to the Mode Transmission

Andrey N. **Afanasyev** , Arkadiy M. Uralov

Solar Phys. **2016**

Recent observations of magnetohydrodynamic oscillations and waves in solar active regions revealed their close link to quasi-periodic pulsations in flaring light curves. The nature of that link has not yet been understood in detail. In our analytical modelling we investigate propagation of slow magnetoacoustic waves in a solar active region, taking into account wave refraction and transmission of the slow magnetoacoustic mode into the fast one. The wave propagation is analysed in the geometrical acoustics approximation. Special attention is paid to the penetration of waves in the vicinity of a magnetic null point. The modelling has shown that the interaction of slow magnetoacoustic waves with the magnetic reconnection site is possible due to the mode transmission at the equipartition level where the sound speed is equal to the Alfvén speed. The efficiency of the transmission is also calculated.

Cut-off period for slow magnetoacoustic waves in coronal plasma structures

A.N. **Afanasyev**, V. M. Nakariakov

A&A **2015**

Context. There is abundant observational evidence of longitudinal compressive waves in plasma structures of the solar corona, which are confidently interpreted in terms of slow magnetoacoustic waves. The uses of coronal slow waves in plasma diagnostics, as well as analysis of their possible contribution to coronal heating and the solar wind acceleration, require detailed theoretical modelling. Aims. We investigate the effects of obliqueness, magnetic field, and non-uniformity of the medium on the evolution of long-wavelength slow magnetoacoustic waves guided by field-aligned plasma non-uniformities, also called tube waves. Special attention is paid to the cut-off effect due to the gravity stratification of the coronal plasma. Methods. We study the behaviour of linear tube waves in a vertical untwisted straight field-aligned isothermal plasma cylinder. We apply the thin flux tube approximation, taking into account effects of stratification caused by gravity. The dispersion due to the finite radius of the flux tube is neglected. We analyse the behaviour of the cut-off period for an exponentially divergent magnetic flux tube filled in with a stratified plasma. The results obtained are compared with the known cases of the constant Alfvén speed and the pure acoustic wave. Results. We derive the wave equation for tube waves and reduce it to the form of the Klein?Gordon equation with varying coefficients, which explicitly contains the cut-off frequency. The cut-off period is found to vary with height, decreasing significantly in the low-beta plasma and in the plasma with the beta of the order of unity. The depressions in the cut-off period profiles can affect the propagation of longitudinal waves along coronal plasma structures towards the higher corona and can form coronal resonators.

Nonlinear slow magnetoacoustic waves in coronal plasma structures

A. N. **Afanasyev**, V.M. Nakariakov
E-print, Nov **2014**; A&A 573, A32 **2015**
http://www2.warwick.ac.uk/fac/sci/physics/research/cfsa/people/valery/research/eprints/aa24516.pdf
Context. There is abundant observational evidence of longitudinal waves in the plasma structures of the solar corona. These essentially compressive waves are confidently interpreted as slow magnetoacoustic waves. The use of the slow waves in plasma diagnostics and estimating their possible contribution to plasma heating and acceleration require detailed theoretical modelling.
Aims. We investigate the role of obliqueness and magnetic effects in the evolution of slow magnetoacoustic waves, also called tube waves, in field-aligned plasma structures. Special attention is paid to the wave damping caused by nonlinear steepening.
Methods. We considered an untwisted straight axisymmetric field-aligned plasma cylinder and analysed the behaviour of the slow magnetoacoustic waves that are guided by this plasma structure. We adopted a thin flux tube approximation. We took into account dissipation caused by viscosity, resistivity and thermal conduction, and nonlinearity. Effects of stratification and dispersion caused by the finite radius of the flux tube were neglected.
Results. We derive the Burgers-type evolutionary equation for tube waves in a uniform plasma cylinder. Compared with a plane acoustic wave, the formation of shock fronts in tube waves is found to occur at a larger distance from the source. In addition, tube waves experience stronger damping. These effects are most pronounced in plasmas with the parameter beta at about or greater than unity. In a low-beta plasma, the evolution of tube waves can satisfactorily be described with the Burgers equation for plane acoustic waves.

Transport of internetwork magnetic flux elements in the solar photosphere

Piyush **Agrawal**, Mark P. Rast, Milan Gosic, Luis R. Bellot Rubio, Matthias Rempel
ApJ **854** 118 **2017**
https://arxiv.org/pdf/1711.01290.pdf
http://sci-hub.tw/http://iopscience.iop.org/0004-637X/854/2/118/
The motions of small-scale magnetic flux elements in the solar photosphere can provide some measure of the Lagrangian properties of the convective flow over the depth which the elements sample. Measurements of these motions have thus been critical in estimating the turbulent diffusion coefficient in flux-transport dynamo models and in determining the Alfven wave excitation spectrum for coronal heating models. We examine the motions of magnetic elements in a 24 hour long Hinode/NFI magnetogram sequence with 90 second cadence, and study both the scaling of their mean squared displacement and the shape of their displacement probability distribution as a function of time. We find, in agreement with previous work, that the mean squared displacement scales super-diffusively with a slope of about 1.48. This is true in other studies even for temporal increments as small as 5 seconds for which ballistic scaling would be expected. Using high cadence MURaM simulations, we show that the observed super-diffusive scaling at short temporal increments is an artifact of interpreting changes in elements' barycenter position as their true motion, as these barycenter positions are subject to random flux evolution. We also find that for long temporal increments, beyond granular lifetimes, the observed displacement distribution deviates from that expected for a diffusive process, changing from Rayleigh to Gaussian. The evolution of the distribution agrees well with an analytic model that accounts for advection by the supergranular flows in addition to the granular motions. These results complicate the interpretation of magnetic element motions on both short and long time scales and suggest that their use in turbulent diffusion or wave excitation models may be problematic. We propose an alternative indirect method of using passive tracers that is likely more robust, in the measured photospheric flow field.

Changes of space weather and space climate at Earth orbit: An update

H.S. **Ahluwalia**
Advances in Space Research Volume 64, Issue 5, 1 September **2019**, Pages 1093-1099
https://sci-hub.se/10.1016/j.asr.2019.05.046
We present an update of the changes in space weather/space climate at Earth orbit using sunspot number (SSN) timeline (1700–2018), geomagnetic indices aa/Ap, solar polar magnetic field, interplanetary magnetic field (IMF) and galactic cosmic ray (GCR) flux in the stratosphere at high latitudes. The Cycle 24 is close to solar minimum, expected in 2020. The baseline of aa index increases monotonically from 1900 to 1986 and declines steeply afterwards, solar polar magnetic field decreases systematically for the last three cycles (22–24) as do SSNs at cycle peaks. Livingston and Penn (2009) note a long term weakening of maximum magnetic field in sunspots since 1992. They expect SSNs for the Cycle 25 to peak at 7 (a steep decline in solar activity) leading to Maunder-like minimum, in contrast to prediction of several colleagues of a Dalton minimum. The North-South asymmetry in solar polar field is pronounced for the decay phase of cycles 23, 24, itseems to change sign after the Cycle 21. GCR flux in the stratosphere is greater that in 1965 and increasing, pointing to an enhanced radiation exposure in future for the passengers on transpolar flights, the astronauts on the space station as well as those travelling to and staying on the Moon and the Mars on prolonged missions; the assets in space would have to be hardened for safety from increased

radiation. We speculate about the connection between the Earth climate and changes in solar activity, inferring that the science of the Earth climate change is not settled yet.

Interplanetary Scintiallation (IPS) of the Radio Source 3C48 During Periods of Low and High Solar Activity

E. **Aguilar-Rodriguez** , S. A. Tyul'bashev , I. V. Chashei , E. Romero-Hernandez
Solar Phys. **2015**

We present a comparative study of three techniques used to estimate the scintillation index using interplanetary scintillation (IPS) observations carried out by the Big Scanning Array (BSA), which operates at a frequency of 111 MHz. These techniques are based on: rms analysis on-source and off-source (classic), Fourier, and wavelet transforms. IPS data are analyzed separately for the period of low solar activity (2007 – 2009), and for the year 2013, near the solar-activity maximum. Our results show that, in general, these methods are equivalent. We analyze the radial dependence of the scintillation index at meter wavelengths during these two periods. It is found that the observed radial dependence of the scintillation index during both periods of U.C. cycle 24 is flatter than the theoretical dependence expected for the case of solar-wind spherical symmetry. This flattening can be explained in terms of the influence of the heliospheric current sheet during the low solar-activity period, and the influence of solar disturbances, such as coronal mass ejections (CMEs), for the high solar-activity period.

Evolution of sunspot number timeline for next several cycles beyond 2016

H.S. **Ahluwalia**
Journal of Atmospheric and Solar-Terrestrial Physics Volume 176, September **2018**, Pages 57-60
http://sci-hub.tw/10.1016/j.jastp.2017.05.007

We explore the evolution of solar activity for next several sunspot cycles beyond 2016 using data for the geomagnetic indices aa/Ap and the solar polar magnetic field intensity for shorter time intervals; the indices are related to the solar windand do not depend on Earth's climate. We find that the baseline of the geomagnetic indices increases monotonically from 1900 to 1986 and declines afterwards. We speculate that a cycle with a period ~86 × 2 = 172y may exist in aa/Ap. If one assumes that solar wind will exhibit the same periodicity for the rest of the twenty-first century, one should expect the next uptick of the aa/Ap timeline to occur in the seventies. In the mean time, the indices Ap/aa may continue to undergo three-cycle-quasi-periodicity (TCQP) to a value lower than in early 1900s, due to a steeper slope during the last few solar cycles compared to that of the period before 1900; it may reach the grand minimum level. Solar polar magnetic field intensity is decreasing systematically for the last three cycles (22–24) as are the sunspot numbers at the cycle peak. Livingston and Penn (2009) note a long term weakening of maximum sunspot magnetic field since 1992. North-South (N-S) asymmetry in the polar field strength is most pronounced for the decay phase of cycles 23, 24; it seems to change sign after cycle 21. These trends have great implications for solar physics and future space weather/climate. We are unable to anticipate the degree and future change of sign of the N-S asymmetry of the solar polar field at present time.

Salient Features of the New Sunspot Number Time Series

H. S. **Ahluwalia**, R. C. Ygbuhay
Solar Phys. Volume 291, Issue 12, pp 3807–3815 **2016**

Recently Clette et al. (Space Sci. Rev. 186, 35, 2014) completed the first revision of the international sunspot number SSN(V2) since its creation by Wolf in 1849 SSN(V1) starting in 1700 and ending in May 2015. The yearly values of SSN(V2) are larger than those of SSN(V1) but the secular trend in their timelines both exhibit a gradual descent after Cycle 21 minimum resulting in greatly reduced activity for Cycle 24. It has two peaks; one in 2012 due to activity in the north hemisphere (NH) and the other in 2014 due to excess activity in the south hemisphere (SH). The N–S excess of hemispheric SSNs is examined for 1950 – 2014, in relation to the time variations of the solar polar field for 1976 – 2015, covering five complete solar cycles (19 – 23) and parts of the bordering two (18, 24). We find that SH tends to become progressively more active in the declining phase of the cycles reaching an extreme value that gave rise to a second higher peak in October 2014 in the smoothed SSNs accompanied by a strong solar polar field in SH. There may be a Gleissberg cyclicity in the asymmetric solar dynamo operation. The continuing descent of the secular trend in SSNs implies that we may be near a Dalton-level grand minimum. The low activity spell may last well past 2060, accompanied by a stable but reduced level of the space weather/climate. Fourier spectrum of the time domain of SSNs shows no evidence of the 208 year/cycle (ypc) (DeVries/Suess cycle) seen in the cosmogenic radionuclide (\({}^{10}\mathrm{Be}\)) concentration in the polar ice cores and \({}^{14}\mathrm{C}\) record in trees indicating that 208 ypc peak may be of non-solar origin. It may arise from the climate process(es) that change(s) the way radionuclides are deposited on polar ice. It should be noted that we only have \({\sim}\,400~\mbox{years}\) of SSN data, so it is possible that DeVries/Suess cycle is really driven by the Sun but for now we do not have any evidence of that; there is no known physical process linking 208 ypc to solar dynamo operation.

Cosmic Ray 11-Year Modulation for Sunspot Cycle 24

H. S. **Ahluwalia**, R. C. Ygbuhay

Solar Phys. February **2015**, Volume 290, Issue 2, pp 635-643

Galactic cosmic-ray (GCR) modulation at 1 AU for sunspot (SSN) Cycle 24 is studied using data from a global network of detectors and balloon measurements of low-energy ions at high latitudes in Russia. The observed modulation is modest compared with previous cycles. The tilt angle of the heliospheric current sheet reached a maximum value for Cycle 24 even though the peak of the interplanetary magnetic-field intensity at 1 AU has a much lower value (≈ 5 nT). The solar polar field in the northern hemisphere reversed in June 2012 and again in March 2014 while that in the southern hemisphere reversed in July 2013. The double field reversal in northern hemisphere after SSN maximum is not expected from dynamo theory. GCR modulation is at maximum phase in 2013. We have also studied the anomalous GCR recovery in 2009 using data from a low-energy proton channel on Payload for Antimatter Matter Exploration and Light-nuclei Astrophysics (PAMELA). The rigidity dependence of the Cycle 24 modulation is computed using data from neutron monitors, directional muon telescopes at Nagoya, Japan, and detectors on balloons at high latitudes in Russia. It is a power law with an exponent −1.29, similar to previous solar cycles (−1.2±0.1); the nearly linear dependence of the modulation on the rigidity over a wide range poses a challenge to the quasi-linear theory (QLT) of GCR modulation.

Sunspot activity and cosmic ray modulation at 1 a.u. for 1900–2013

H.S. **Ahluwalia**

Advances in Space Research, Volume 54, Issue 8, 15 October **2014**, Pages 1704–1716

http://www.sciencedirect.com/science/article/pii/S0273117714004141

The descent of sunspot cycle 23 to an unprecedented minimum of long duration in 2006–2009 led to a prolonged galactic cosmic ray (GCR) recovery to the highest level observed in the instrumental era for a variety of energetic charged particle species on Earth, over a wide range of rigidities. The remarkable GCR increase measured by several ground-based, balloon-borne, and detectors on a satellite is described and discussed. It is accompanied by a decrease in solar wind velocity and interplanetary magnetic field at 1 a.u., reaching the lowest values since measurements of the solar wind began in October 1963; the solar polar field strength (μT) measured at the Wilcox Solar Observatory (WSO) is also significantly reduced compared to prior cycles since the start of the program in 1976, the polar field in the northern hemisphere reversed in June 2012 and again in February 2014, that in the southern hemisphere reversed in July 2013. If updates of WSO data confirm the second reversal in northern solar hemisphere, it would pose a serious challenge to the Dynamo Theory. The long-term change in solar behavior may have begun in 1992, perhaps earlier. The physical underpinnings of these solar changes need to be understood and their effect on GCR modulation processes clarified. The study discusses the recent phenomena in the context of GCR modulation since 1900. These happenings affected our empirical predictions for the key parameters for the next two sunspot cycles (they may be progressively less active than sunspot cycle 24) but it enhanced support for our prediction that solar activity is descending into a Dalton-like grand minimum in the middle of the twentyfirst century, reducing the frequency of the coronal mass ejections; they determine the space weather affecting the quality of life on Earth, radiation dose for hardware and human activities in space as well as the frequency of large Forbush decreases at 1 a.u.

Automatic method for detection of solar coronal width using extreme ultra-violet (EUV) radiation

Najmeh **Ahmadi**, Shervin Parsi

2019

https://arxiv.org/pdf/1904.00104.pdf

Solar corona, the last main layer of the atmosphere of the Sun, is detectable in the EUV and X-ray. The corona is expanding into space up to millions of kilometers and is observable during the eclipse. The temperature is increasing about millions of Kelvin. The investigation of this layer is significant for solar physicists because it is dynamic and features. Active regions (AR) and solar mass ejections (CMEs) are the important features in the solar corona. In this research, the solar limb and coronal width is studied from full-disk images at $284 \AA$ taken by SOHO/EIT during eleven-year period (2000-2010). Next, using image processing methods and by applying region growing function, the corona is segmented and extracted from images in different angles. The radial velocities of CMEs are extracted.

A Curated Image Parameter Dataset from Solar Dynamics Observatory Mission

Azim **Ahmadzadeh**, Dustin J. Kempton, Rafal A. Angryk

ApJ Suppl **243** 18 **2019**
https://arxiv.org/pdf/1906.01062.pdf
We provide a large image parameter dataset extracted from the Solar Dynamics Observatory (SDO) mission's AIA instrument, for the period of January 2011 through the current date, with the cadence of six minutes, for nine wavelength channels. The volume of the dataset for each year is just short of 1 TiB. Towards achieving better results in the region classification of active regions and coronal holes, we improve upon the performance of a set of ten image parameters, through an in depth evaluation of various assumptions that are necessary for calculation of these image parameters. Then, where possible, a method for finding an appropriate settings for the parameter calculations was devised, as well as a validation task to show our improved results. In addition, we include comparisons of JP2 and FITS image formats using supervised classification models, by tuning the parameters specific to the format of the images from which they are extracted, and specific to each wavelength. The results of these comparisons show that utilizing JP2 images, which are significantly smaller files, is not detrimental to the region classification task that these parameters were originally intended for. Finally, we compute the tuned parameters on the AIA images and provide a public API (this http URL) to access the dataset. This dataset can be used in a range of studies on AIA images, such as content-based image retrieval or tracking of solar events, where dimensionality reduction on the images is necessary for feasibility of the tasks.

Calibration of the Instrumental Crosstalk for the Near-IR Imaging Spectropolarimeter at the NST
K. **Ahn** and W. Cao
Solar Polarization 8 ASP Conference Series, **2019**
http://bbso.njit.edu/~ksahn/Ahn_proofs_v2.pdf
The Near-IR Imaging Spectropolarimeter (NIRIS) is a polarimeter that is installed at the New Solar Telescope at Big Bear Solar Observatory. This instrument takes advantages of the highest spatial resolution and flux. The primary mirror is an off-axis type, so it was our interest to evaluate its contribution to the crosstalk among the Stokes parameters since we could not put our calibration optics before the mirror. We would like to present our efforts to compensate for the crosstalk among Stokes profiles caused by the relay optics from the telescope to the detector. The overall data processing pipeline is also introduced.

South Korea's renewed focus on space weather
Byung-Ho **Ahn**
SPACE WEATHER, VOL. 9, S10010, 5 PP., **2011**
This article explains old sunspot and auroral records in Korea.
Space weather activities in four national labs and one vendor are explained.
As a conclusion, the prospect of space weather activity in South Korea is described.

The Possibility of Kelvin-Helmholtz Instability in Solar Spicules
A. **Ajabshirizadeh**, H. Ebadi, R.E. Vekalati, K. Molaverdikhani
Astrophysics and Space science 357:33 **2015**
http://arxiv.org/pdf/1502.04229v1.pdf
Transversal oscillations of spicules axes may be related to the propagation of magnetohydrodynamic waves along them. These waves may become unstable and the instability can be of the Kelvin-Helmholtz type. We use the dispersion relation of kink mode derived from linearized magnetohydrodynamic equations. The input parameters of the derived dispersion equation, namely, spicules and their ambient medium densities ratios as well as their corresponding magnetic fields ratios, are considered to be within the range 0−1. By solving the dispersion equation numerically, we show that for higher densities and lower magnetic fields ratios within the range mentioned, the KHI onset in type II spicules conditions is possible. This possibility decreases with an increase in Alfven velocity inside spicules. A rough criterion for appearing of Kelvin-Helmholtz instability is obtained. We also drive a more reliable and exact criterion for KHI onset of kink waves.

Paradigm transitions in solar-terrestrial physics from 1900: my personal view **Review**
Akasofu, S.-I.
History of Geo- and Space Sciences, Volume 6, Issue 1, **2015**, pp.23-43
http://www.hist-geo-space-sci.net/6/23/2015/hgss-6-23-2015.pdf
Solar-terrestrial physics, like any other scientific field, has evolved and developed by replacing older theories with newer theories. Unfortunately, each generation of young researchers tends to learn naturally only the latest, and perhaps the most popular theory and believes that it is the only useful one to pursue. Therefore, they do not necessarily realize that in the past the theory they chose had struggled to reach its presently acceptable state, and that

eventually it might be replaced with a new theory. Two generations of scientists or in some subjects even more generations tend to be guided by one particular idea or theory. Thus, among us (namely, one or two generations) a high degree of agreement occurs, both on the theoretical assumptions and on the problem to be solved within the framework provided by the theory. Such an idea or theory was termed paradigm by Kuhn (1970). The purpose of this article is to describe several examples of the transition of paradigms and ideas in the subjects of solar-terrestrial physics. The examples are subjects that experienced a paradigm change after prevailing in the field for a few generations and also some that are perhaps on the verge of the transition. The chosen subjects are (1) Stormer's single particle theory to Chapman's plasma theory (1907-1963), (2) the auroral zone to the auroral oval (1860-1971), (3) the closed to open magnetosphere (1931-1971), (4) the current system controversies (1918-1963) and (1964-present), (5) the fixed pattern concept to the concept of auroral/magnetospheric substorms (1935-1982), (6) the importance of the interplanetary magnetic field (IMF) in the development of geomagnetic storms (1905-1966), (7) the ring current: solar wind protons to oxygen ions from the ionosphere (1933-1977), (8) the storm-substorm controversy (1963-present), (9) substorm onset (1964-present), (10) solar flares (1958-present) and (11) sunspots (1961-present).

Single spots, unipolar magnetic regions, and pairs of spots

Akasofu, S.-I.
Geophysical Research Letters, Volume 41, Issue 11, pp. 3698-3700, **2014**
McIntosh (1981) noted that sunspot pairs appear preferentially near the boundary of unipolar magnetic (UM) regions of opposite polarity. A large number of solar magnetograms from the Mount Wilson Observatory and the Kitt Peak Observatory during fairly quiet periods are examined to confirm his finding. In this study, it is also found collaterally that positive single spots appear in a positive UM region and vice versa. It is suggested thus that a pair of spots of opposite polarity is formed because two single spots develop in the vicinity of the boundary (the neutral line) of two UM regions of opposite polarity for polarity arrangement appropriate to the Hale law, namely, the Hale boundary. For these reasons, it is suggested that single spots and UM regions have significant meaning in solar magnetism.

Exploring the Asymmetry of the Solar Corona Electron Density with Very Long Baseline Interferometry

Dan **Aksim**, Alexey Melnikov, Dmitry Pavlov, Sergey Kurdubov
ApJ **2019**
https://arxiv.org/pdf/1910.10529.pdf
The Sun's corona has interested researchers for multiple reasons, including the search for solution for the famous coronal heating problem and a purely practical consideration of predicting geomagnetic storms on Earth. There exist numerous different theories regarding the solar corona; therefore, it is important to be able to perform comparative analysis and validation of those theories. One way that could help us move towards the answers to those problems is the search for observational methods that could obtain information about the physical properties of the solar corona and provide means for comparing different solar corona models.
In this work we present evidence that VLBI observations are, in certain conditions, sensitive to the electron density of the solar corona and are able to distinguish between different electron density models, which makes the technique of VLBI valuable for solar corona investigations. Recent works on the subject used a symmetric power-law model of the electron density in solar plasma; in this work, an improvement is proposed based on a 3D numerical model.
2017-05-01, 2018-05-01

Incorporating Polar Field Data for Improved Solar Flare Prediction

Mehmet **Aktukmak**, Zeyu Sun, Monica Bobra, Tamas Gombosi, Ward B. Manchester, Yang Chen, Alfred Hero
Frontiers **2022**
https://arxiv.org/pdf/2212.01730.pdf
In this paper, we consider incorporating data associated with the sun's north and south polar field strengths to improve solar flare prediction performance using machine learning models. When used to supplement local data from active regions on the photospheric magnetic field of the sun, the polar field data provides global information to the predictor. While such global features have been previously proposed for predicting the next solar cycle's intensity, in this paper we propose using them to help classify individual solar flares. We conduct experiments using HMI data employing four different machine learning algorithms that can exploit polar field information. Additionally, we propose a novel probabilistic mixture of experts model that can simply and effectively incorporate polar field data and provide on-par prediction performance with state-of-the-art solar flare prediction algorithms such as the Recurrent Neural Network (RNN). Our experimental results indicate the usefulness of the polar field data for solar flare prediction, which can improve Heidke Skill Score (HSS2) by as much as 10.1%.

PECULARITIES OF COSMIC RAY MODULATION IN THE SOLAR MINIMUM 23/24.†
M. V. **Alania**1,2,*, R. Modzelewska1 andA. Wawrzynczak
JGR, Volume 119, Issue 6, pages 4164–4174, June **2014**
http://onlinelibrary.wiley.com/doi/10.1002/2013JA019500/abstract
http://arxiv.org/ftp/arxiv/papers/1504/1504.00768.pdf
We study changes of the galactic cosmic ray (GCR) intensity for the ending period of the solar cycle 23 and the beginning of the solar cycle 24 using neutron monitors experimental data. We show that an increase of the GCR intensity in 2009 is generally related with decrease of the solar wind velocity U, the strength B of the interplanetary magnetic field (IMF), and the drift in negative (A < 0) polarity epoch. We present that temporal changes of rigidity dependence of the GCR intensity variation before reaching maximum level in 2009 and after it, do not noticeably differ from each other. The rigidity spectrum of the GCR intensity variations calculated based on neutron monitors data (for rigidities > 10 GV) is hard in the minimum and near minimum epoch. We do not recognize any non-ordinary changes in the physical mechanism of modulation of the GCR intensity in the rigidity range of GCR particles to which neutron monitors respond. We compose 2-D non stationary model of transport equation to describe variations of the GCR intensity for 1996-2012 including the A > 0 (1996-2001) and the A < 0 (2002-2012) periods; diffusion coefficient of cosmic rays for rigidity 10-15 GV is increased by ~ 30% in 2009 (A < 0) comparing with 1996 (A > 0). We believe that the proposed model is relatively realistic and obtained results are satisfactorily compatible with neutron monitors data.

On the relationship of the 27-day variations of the solar wind velocity and galactic cosmic ray intensity in minimum epoch of solar activity

M.V. **Alania**, R. Modzelewska, A. Wawrzynczak
Solar Phys. **2011**
http://arxiv.org/ftp/arxiv/papers/1504/1504.00778.pdf
We study the relationship of the 27-day variation of the galactic cosmic ray intensity with similar changes of the solar wind velocity and the interplanetary magnetic field based on the experimental data for the Bartels rotation period 2379 **of 23 November 2007-19 December 2007**. We develop a three dimensional (3-D) model of the 27-day variation of galactic cosmic ray intensity based on the heliolongitudinally dependent solar wind velocity. A consistent, divergence-free interplanetary magnetic field is derived by solving Maxwells equations with a heliolongitudinally dependent 27-day variation of the solar wind velocity reproducing in situ observations. We consider two types of 3-D models of the 27-day variation of galactic cosmic ray intensity - (1) with a plane heliospheric neutral sheet, and (2)- with the sector structure of the interplanetary magnetic field. The theoretical calculation shows that the sector structure does not influence significantly on the 27-day variation of galactic cosmic ray intensity as it was shown before based on the experimental data. Also a good agreement is found between the time profiles of the theoretically expected and experimentally obtained first harmonic waves of the 27-day variation of the galactic cosmic ray intensity (correlation coefficient equals 0.98 0.02). The expected 27-day variation of the galactic cosmic ray intensity is inversely correlated with the modulation parameter z (correlation coefficient equals -0.91 0.05) which is proportional to the product of the solar wind velocity V and the strength of the interplanetary magnetic field B (z VB). The high anticorrelation between these quantities indicates that the predictable 27-day variation of the galactic cosmic ray intensity mainly is caused by this basic modulation effect.

Modeling and experimental study of the 27-day variation of galactic cosmic-ray intensity for a solar-wind velocity depending on heliolongitude

M.V. **Alania**, R. Modzelewska, A. Wawrzynczak
Advances in Space Research (**2010**)
http://arxiv.org/ftp/arxiv/papers/1504/1504.00767.pdf
We develop a three dimensional (3-D) model of the 27-day variation of galactic cosmic ray (GCR) intensity with a spatial variation of the solar wind velocity. A consistent, divergence-free interplanetary magnetic field is derived by solving the corresponding Maxwell equations with a variable solar wind speed, which reproduces in situ observed experimental data for the time interval to be analyzed (24 August 2007-28 February 2008). We perform model calculations for the GCR intensity using the variable solar wind and the corresponding magnetic field. Results are compatible with experimental data; the correlation coefficient between our model predictions and observed 27-day GCR variation is 0.80 0.05.

New method of enhancement using wavelet transforms applied to SODISM telescope

Amro F.**Alasta** AbdulrazagAlgamudia RamiQahwajia StanleyIpsona AlainHauchecorneb MustaphaMeftahb
Advances in Space Research 63 (**2019**) 606-616
https://www.sciencedirect.com/science/article/pii/S0273117718306112?via%3Dihub

PICARD is a space-based observatory hosting the Solar Diameter Imager and Surface Mapper (SODISM) telescope, which has continuously observed the Sun from July 2010 and up to March 2014. In order to study the fine structure of the solar surface, it is helpful to apply techniques that enhance the images so as to improve the visibility of solar features such as sunspots or faculae. The objective of this work is to develop an innovative technique to enhance the quality of the SODISM images in the five wavelengths monitored by the telescope at 215.0 nm, 393.37 nm, 535.7 nm, 607.1 nm and 782.2 nm. An enhancement technique using interpolation of the high-frequency sub-bands obtained by Discrete Wavelet Transforms (DWT) and the input image is applied to the SODISM images. The input images are decomposed by the DWT as well as Stationary Wavelet Transform (SWT) into four separate sub-bands in horizontal and vertical directions namely, low-low (LL), low–high (LH), high-low (HL) and high–high (HH) frequencies. The DWT high frequency sub-bands are interpolated by a factor 2. The estimated high frequency sub-bands (edges) are enhanced by introducing an intermediate stage using a Stationary Wavelet Transform (SWT), and then all these sub-bands and input image are combined and interpolated with half of the interpolation factor α/2, used to interpolate the high-frequency sub-bands, in order to reach the required size for IDWT processing. Quantitative and visual results show the superiority of the proposed technique over a bicubic image resolution enhancement technique. In addition, filling factors for sunspots are calculated from SODISM images and results are presented in this work.

Accuracy Analysis of the On-board Data Reduction Pipeline for the Polarimetric and Helioseismic Imager on the Solar Orbiter Mission

Kinga **Albert**, Johann Hirzberger, J. Sebastián Castellanos Durán, David Orozco Suárez, Joachim Woch, Harald Michalik & Sami K. Solanki
Solar Physics volume 298, Article number: 58 (**2023**)
https://link.springer.com/content/pdf/10.1007/s11207-023-02149-y.pdf
Context: Scientific data reduction on-board deep space missions is a powerful approach to maximise science return, in the absence of wide telemetry bandwidths. The Polarimetric and Helioseismic Imager (PHI) on-board the Solar Orbiter (SO) is the first solar spectropolarimeter that opted for this solution, and provides the scientific community with science-ready data directly from orbit. This is the first instance of full solar spectropolarimetric data reduction on a spacecraft.
Methods: In this paper, we analyse the accuracy achieved by the on-board data reduction, which is determined by the trade-offs taken to reduce computational demands and ensure autonomous operation of the instrument during the data reduction process. We look at the magnitude and nature of errors introduced in the different pipeline steps of the processing. We use an MHD sunspot simulation to isolate the data processing from other sources of inaccuracy. We process the data set with calibration data obtained from SO/PHI in orbit, and compare results calculated on a representative SO/PHI model on ground with a reference implementation of the same pipeline, without the on-board processing trade-offs.
Results: Our investigation shows that the accuracy in the determination of the Stokes vectors, achieved by the data processing, is at least two orders of magnitude better than what the instrument was designed to achieve as final accuracy. Therefore, the data accuracy and the polarimetric sensitivity are not compromised by the on-board data processing. Furthermore, we also found that the errors in the physical parameters are within the numerical accuracy of typical RTE inversions with a Milne-Eddington approximation of the atmosphere.
Conclusion: This paper demonstrates that the on-board data reduction of the data from SO/PHI does not compromise the accuracy of the processing. This places on-board data processing as a viable alternative for future scientific instruments that would need more telemetry than many missions are able to provide, in particular those in deep space.

Solar Activity from 2006 to 2014 and Short-term Forecasts of Solar Proton Events Using the ESPERTA Model

T. **Alberti**1, M. Laurenza2, E. W. Cliver3, M. Storini2, G. Consolini2, and F. Lepreti
2017 ApJ 838 59 **File**
http://sci-hub.cc/10.3847/1538-4357/aa5cb8
To evaluate the solar energetic proton (SEP) forecast model of Laurenza et al., here termed ESPERTA, we computed the input parameters (soft X-ray (SXR) fluence and ~1 MHz radio fluence) for all ≥M2 SXR flares from 2006 to 2014. This database is outside the 1995–2005 interval on which ESPERTA was developed. To assess the difference in the general level of activity between these two intervals, we compared the occurrence frequencies of SXR flares and SEP events for the first six years of cycles 23 (1996 September–2002 September) and 24 (2008 December–2014 December). We found a reduction of SXR flares and SEP events of 40% and 46%, respectively, in the latter period. Moreover, the numbers of ≥M2 flares with high values of SXR and ~1 MHz fluences (>0.1 J m−2 and >6 × 105 sfu × minute, respectively) are both reduced by ~30%. A somewhat larger percentage decrease of these two parameters (~40% versus ~30%) is obtained for the 2006–2014 interval in comparison with 1995–2005. Despite these differences, ESPERTA performance was comparable for the two intervals. For the 2006–2014 interval, ESPERTA had a probability of detection (POD) of 59% (19/32) and a false alarm rate (FAR) of 30% (8/27), versus a POD = 63% (47/75) and an FAR = 42% (34/81) for the original 1995–2005 data set. In addition, for

the 2006–2014 interval the median (average) warning time was estimated to be ~2 hr (~7 hr), versus ~6 hr (~9 hr), for the 1995–2005 data set.

Table 1 SEP Flare List (2006–2014)

Magnetohydrodynamic Wave Modes of Solar Magnetic Flux Tubes with an Elliptical Cross Section

Anwar A. **Aldhafeeri**1,2, Gary Verth1, Wernher Brevis3, David B. Jess4, Max McMurdo1, and Viktor Fedun5

2021 ApJ 912 50

https://iopscience.iop.org/article/10.3847/1538-4357/abec7a/pdf

https://doi.org/10.3847/1538-4357/abec7a

The purpose of this paper is to study the behavior of magnetohydrodynamic (MHD) wave modes that propagate in compressible magnetic flux tubes with an elliptical cross section embedded in a magnetic environment. The dispersion relation that describes the behavior of MHD wave modes permitted in an elliptical magnetic flux tube is solved numerically. Distortion of the spatial structure of the purely real eigenmodes from the well-known circular flux tube model has been considered. It has been studied under both photospheric and coronal conditions. It has been shown that (i) solutions in the form of even Mathieu functions are more sensitive to the value of eccentricity than solutions with the form of odd Mathieu functions; (ii) if the ellipticity of the cross section of the magnetic flux tube increases, a sausage mode (m = 0) cannot be easily identified; (iii) even solutions that correspond to the fluting mode (m = 3) can be misinterpreted as a kink mode (m = 1) due to their similarities. In contrast to the fluting modes that are polarized along the major axis and strongly depend on the ellipticity of the magnetic flux tube, the kink and sausage surface modes are practically unaffected by ellipticity. Several examples of the spatial structure of the eigenmodes permitted in the pores and sunspots have been visualized. The solutions obtained in the approximation of cylindrical symmetry are in agreement with previous studies.

The impact of limited time resolution on the forward-scattering polarization in the solar Sr I 4607 Å line

T. del Pino **Alemán**, J. Trujillo Bueno

ApJ **2021**

https://arxiv.org/pdf/2101.08485.pdf

Theoretical investigations predicted that high spatio-temporal resolution observations in the Sr I 4607 A line must show a conspicuous scattering polarization pattern at the solar disk-center, which encodes information on the unresolved magnetism of the inter-granular photospheric plasma. Here we present a study of the impact of limited time resolution on the observability of such forward scattering (disk-center) polarization signals. Our investigation is based on three-dimensional radiative transfer calculations in a time-dependent magneto-convection model of the quiet solar photosphere, taking into account anisotropic radiation pumping and the Hanle effect. This type of radiative transfer simulation is computationally costly, reason why the time variation had not been investigated before for this spectral line. We compare our theoretical results with recent disk-center filter polarimetric observations in the Sr I 4607 A line, showing that there is good agreement in the polarization patterns. We also show what we can expect to observe with the Visible Spectro-Polarimeter at the upcoming Daniel K. Inouye Solar Telescope.

The magnetic sensitivity of the resonance and subordinate lines of Mg II in the solar chromosphere

T. del Pino **Alemán**, J. Trujillo Bueno, R. Casini, R. Manso Sainz

2020, The Astrophysical Journal, Volume 891, Issue 1, id.91

https://arxiv.org/pdf/2004.09176.pdf

We carry out a theoretical study of the polarization of the solar Mg II h-k doublet (including its extended wings) and the subordinate UV triplet around 280 nm. These lines are of great diagnostic interest, as they encode information on the physical properties of the solar atmosphere from the upper photosphere to the chromosphere-corona transition region. We base our study on radiative transfer calculations of spectral line polarization in one-dimensional models of quiet and plage regions of the solar atmosphere. Our calculations take into account the combined action of atomic polarization, quantum level interference, frequency redistribution, and magnetic fields of arbitrary strength. In particular, we study the sensitivity of the emergent Stokes profiles to changes in the magnetic field through the Zeeman and Hanle effects. We also study the impact of the chromospheric plasma dynamics on the emergent Stokes profiles, taking into account the angle-dependent frequency redistribution in the h-k resonance transitions. The results presented here are of interest for the interpretation of spectropolarimetric observations in this important region of the solar ultraviolet spectrum.

A novel investigation of the small-scale magnetic activity of the quiet Sun via the Hanle effect in the Sr I 4607 Å line

T. del Pino **Alemán**, J. Trujillo Bueno, J. Štěpán, N. Shchukina

ApJ **2018**

https://arxiv.org/pdf/1806.07293.pdf

One of the key research problems in stellar physics is to decipher the small-scale magnetic activity of the quiet solar atmosphere. Recent magneto-convection simulations that account for small-scale dynamo action have provided three-dimensional (3D) models of the solar photosphere characterized by a high degree of small-scale magnetic activity, similar to that found through theoretical interpretation of the scattering polarization observed in the Sr I 4607 \AA\ line. Here we present the results of a novel investigation of the Hanle effect in this resonance line, based on 3D radiative transfer calculations in a high-resolution magneto-convection model having most of the convection zone magnetized close to the equipartition and a surface mean field strength $\langle B \rangle \approx 170$ G. The Hanle effect produced by the model's magnetic field depolarizes the zero-field scattering polarization signals significantly, to the extent that the center-to-limb variation of the calculated spatially-averaged polarization amplitudes is compatible with the observations. The standard deviation of the horizontal fluctuations of the calculated scattering polarization signals is very sensitive to the model's magnetic field and we find that the predicted spatial variations are sufficiently sizable so as to be able to detect them, especially with the next generation of solar telescopes. We find that at all on-disk positions the theoretical scattering polarization signals are anti-correlated with the continuum intensity. To facilitate reaching new observational breakthroughs, we show how the theoretically predicted polarization signals and spatial variations are modified when deteriorating the signal-to-noise ratio and the spectral and spatial resolutions of the simulated observations.

Magnetic Diagnostics of the Chromosphere with the Mg II h-k Lines

Tanausú del Pino **Alemán** (1), Roberto Casini (1), Rafael Manso Sainz (2)

2016 ApJL 830 L24

http://arxiv.org/pdf/1607.05683v1.pdf

We developed a numerical code for polarized radiative transfer in a plane-parallel geometry that implements a recent formulation of partially coherent scattering by polarized multi-term atoms in arbitrary magnetic field regimes. This code allows the realistic modeling of the scattering polarization of important chromospheric lines, such as the Mg II h-k doublet, the Ca II H-K doublet and IR triplet, and lines of the H I Lyman and Balmer series. We present explicit results of the Mg II h-k doublet in a weakly magnetized atmosphere (20-100 G). These confirm the importance of partial redistribution effects in the formation of these lines, as pointed out by previous work in the non-magnetic case. We show that the presence of a magnetic field can produce measurable modifications of the broadband linear polarization even for relatively small field strengths (~10 G), while the circular polarization remains well represented by the classical magnetograph formula. Both these results open an important new window for the weak-field diagnostics of the upper solar atmosphere.

Seismic Holography of the Solar Interior near the Maximum and Minimum of Solar Activity

M. Díaz **Alfaro** , F. Pérez Hernández, I. González Hernández, T. Hartlep

Solar Phys. Volume 291, Issue 5, pp 1323-1340 **2016**

The base of the convection zone and the tachocline play a major role in the study of the dynamics of the Sun, especially in the solar dynamo. Here, we present a phase-sensitive helioseismic holography method to infer changes in the sound-speed profile of the solar interior. We test the technique using numerically simulated data by Zhao et al. (Astrophys. J. 702, 1150, 2009) with sound-speed perturbations at $0.7R_\odot$. The technique adequately recovers the perturbed sound-speed profile and is seen to be capable of detecting changes in the sound speed as low as 0.05 %. We apply the method to two GONG solar time series of approximately one year, each comprising 13 Bartels rotations, BR2295–BR2307 and BR2387–BR2399, near the maximum and at a minimum of solar activity, respectively. We successfully recover a sound-speed variation with respect to a standard solar model, consistent with previous results. However, we fail to recover a realistic sound-speed variation between maximum and minimum.

Waves in weakly ionised solar plasmas

A. **Alharbi**, I. Ballai, V. Fedun, G. Verth

MNRAS **2022**

https://arxiv.org/pdf/2202.07387.pdf

Here we study the nature and characteristics of waves propagating in partially ionised plasmas in the weakly ionised limit, typical for the lower part of the solar atmosphere. The framework in which the properties of waves are discussed depends on the relative magnitude of collisions between particles, but also on the relative magnitude of the collisional frequencies compared to the gyro-frequency of charged particles. Our investigation shows that the

weakly ionised solar atmospheric plasma can divided into two regions and this division occurs, roughly, at the base of the chromosphere. In the solar photosphere the plasma is non-magnetised and the dynamics can described within the three-fluid framework where acoustic waves associated to each species can propagate. Due to the very high concentration of neutrals, the neutral sound waves propagates with no damping, while for the other two modes the damping rate is determined by collisions with neutrals. The ion and electron-related acoustic modes propagate with a cut-off determined by the collisional frequency of these species with neutrals. In the weakly ionised chromosphere only electrons are magnetised, however, the strong coupling of charged particles reduces the working framework to a two-fluid model. The disassociation of charged particles creates electric currents that can influence the characteristic of waves. The propagation properties of waves with respect to the angle of propagation are studied with the help of polar diagrams.

Microphysical approach to coronal heating problem

Robert **Alicki**, Alejandro Jenkins

2021

https://arxiv.org/pdf/2103.08746.pdf

We show that convection in the stellar photosphere generates plasma waves by an irreversible process akin to Zeldovich superradiance. In the Sun, this mechanism is most efficient in quiet regions with magnetic fields of order one gauss. Most of the energy is carried by Alfven waves with megahertz frequencies, which travel upwards until they reach a height at which they dissipate via mode conversion. A power flux estimate shows that this mechanism offers a plausible explanation of how energy is persistently transported from the colder photosphere to the hotter corona.

Automatic detection of small-scale EUV brightenings observed by the Solar Orbiter/EUI

N. **Alipour**, H. Safari, C. Verbeeck, D. Berghmans, F. Auchère, L. P. Chitta, P. Antolin, K. Barczynski, É. Buchlin, R. Aznar Cuadrado, L. Dolla, M. K. Georgoulis, S. Gissot, L. Harra, A. C. Katsiyannis, D. M. Long, S. Mandal, S. Parenti, O. Podladchikova, E. Petrova, É. Soubrié, U. Schühle, C. Schwanitz, L. Teriaca, M. J. West, A. N. Zhukov

A&A **2022**

https://arxiv.org/pdf/2204.04027.pdf

Context. Accurate detections of frequent small-scale extreme ultraviolet (EUV) brightenings are essential to the investigation of the physical processes heating the corona. Aims. We detected small-scale brightenings, termed campfires, using their morphological and intensity structures as observed in coronal EUV imaging observations for statistical analysis. Methods. We applied a method based on Zernike moments and a support vector machine classifier to automatically identify and track campfires observed by Solar Orbiter/Extreme Ultraviolet Imager (EUI) and SDO/AIA. Results. This method detected 8678 campfires (with length scales between 400 km and 4000 km) from a sequence of 50 High Resolution EUV telescope (HRIEUV) 174Å images. From 21 near co-temporal AIA images covering the same field of view as EUI, we found 1131 campfires, 58% of which were also detected in HRIEUV images. In contrast, about 16% of campfires recognized in HRIEUV were detected by AIA. We obtain a campfire birthrate of 2*10-16m-2s-1. About 40% of campfires show a duration longer than 5 s, having been observed in at least two HRIEUV images. We find that 27% of campfires were found in coronal bright points and the remaining 73% have occurred out of coronal bright points. We detected 23 EUI campfires with a duration greater than 245 s. We found that about 80% of campfires are formed at supergranular boundaries, and the features with the highest total intensities are generated at network junctions and intense H I Lyman-{\alpha} emission regions observed by EUI/HRILya. The probability distribution functions for the total intensity, peak intensity, and projected area of campfires follow a power law behavior with absolute indices between 2 and 3. This self-similar behavior is a possible signature of self-organization, or even self-organized criticality, in the campfire formation process.

Explosive Events in the Quiet Sun Near and Beyond the Solar Limb Observed with the Interface Region Imaging Spectrograph (IRIS)

C. E. **Alissandrakis**, J. -C. Vial

Solar Phys. **298**, Article number: 18 **2023**

https://arxiv.org/pdf/2301.07190.pdf

https://link.springer.com/content/pdf/10.1007/s11207-023-02111-y.pdf

We study point-like explosive events (EE), characterized by emission in the far wings of spectral lines, in a quiet region near the South Pole, using Interface Region Imaging Spectrograph (IRIS) spectra at two slit positions, slit-jaw (SJ) observations and Atmospheric Imaging Assembly (AIA) images. The events were best visible in SiIV spectra; they were weak in SJs, occasionally visible in 1600 A and 304 A AIA images, and invisible in higher temperature AIA images. We identified EEs from position--time images in the far wings of the SiIV lines and measured their distance from the limb. A Gaussian model of the height distribution showed that EEs occur in a narrow (0.9") height range, centered at 3.2" above the continuum limb at 2832.0 A. On the disk, we found that they

occur in network boundaries. Further, we studied the line profiles of two bright EEs above the limb and one on the disk. We found that what appears as broad-band emission, is actually a superposition of 2--3 narrow-band Gaussian components with well-separated line profiles, indicating that material is expelled towards and/or away from the observer in discrete episodes in time and in space. The expelled plasma accelerates quickly, reaching line-of-sight (LOS) velocities up to 90 km/s. Overall, the motion was practically along the LOS, as the velocity on the plane of sky was small. In some cases tilted spectra were observed that could be interpreted in terms of rotating motions of up to 30 km/s. We did not find any strong absorption features in the wing of the SiIV lines, although in one case a very weak absorption feature was detected. No motions, indicative of jets, were detected in SJ or AIA images. Reconnection in an asymmetric magnetic-field geometry, in the middle or near the top of small loops is a plausible explanation of their observational characteristics.

Where is the base of the Transition Region? Evidence from TRACE, SDO, IRIS and ALMA observations

C. E. **Alissandrakis**

Advances in Space Research Volume 71, Issue 4, 15 February **2023**, Pages 1907-1914

https://arxiv.org/pdf/2207.03159.pdf

https://doi.org/10.1016/j.asr.2022.06.053

Classic solar models put the Chromosphere-Corona Transition Region (CCTR} at ∼2Mm above the τ5000=1 level, whereas rMHD models place it in a wider range of heights. Observational verification is scarce. We review and discuss recent results from various instruments and spectral domains. In SDO and TRACE images spicules appear in emission in the 1600, 1700 and 304 A bands and in absorption in the EUV bands; the latter is due to photo-ionization of H and He I. At the shortest available AIA wavelength and taking into account that the photospheric limb is ∼0.34Mm above the τ5000=1 level, we found that CCTR emission starts at ∼3.7Mm; extrapolating to λ=0, where there is no chromospheric absorption, we deduced a height of 3.0±0.5Mm, above the value of 2.14Mm of the Avrett & Loeser model. Another indicator of the extent of the chromosphere is the height of the network structures. Height differences produce a limbward shift of features with respect to their counterparts in magnetograms. Using this approach, we measured heights of 0.14±0.04Mm (at 1700 A), 0.31±0.09Mm (at 1600 A) and 3.31±0.18Mm (at 304 A) for the center of the solar disk. A previously reported possible solar cycle variation is not confirmed. A third indicator is the position of the limb in the UV, where IRIS observations of the Mg II triplet lines show that they extend up to ∼2.1Mm above the 2832 A limb, while AIA/SDO images give a limb height of 1.4±0.2Mm (1600 A) and 5.7±0.2Mm (304 A). Finally, ALMA mm-λ full-disk images provide useful diagnostics, though not very accurate; values of 2.4±0.7Mm at 1.26mm and 4.2±2.5Mm at 3mm were obtained. Putting everything together, we conclude that the average chromosphere extends higher than homogeneous models predict, but within the range of rMHD models.

Structure of the Solar Atmosphere: A Radio Perspective **Review**

Costas E. **Alissandrakis**

Front. Astron. Space Sci. 7:574460 **2020**

https://sci-hub.st/https://www.frontiersin.org/articles/10.3389/fspas.2020.574460/full

Solar radio emission has been providing information about the Sun for over half a century. In order to fully exploit this information, one needs to have a broader view of the solar atmosphere, which cannot be provided by radio observations alone. The purpose of this review is to present this background information, which is necessary to understand the physical processes that determine the solar radio emission and to link the radio domain with the rest of the electromagnetic spectrum. Both classic and modern results are presented in a concise manner. After a brief discussion of the solar interior, the basic physics of the solar atmosphere and some elements of radiative transfer are presented. Subsequently the atmospheric structure as a function of height is examined and one-dimensional models of the photosphere, the chromosphere, the transition region and the corona are presented and discussed. An introduction to basicmagnetohydrodynamics precedes the discussion of the rich fine structure of the solar atmosphere as a 3D object. Active regions are briefly discussed in a separate section, and this is followed by a section on the problem of heating of the chromosphere and the corona. I finish with some thoughts on what to expect from the new instruments currently under development.

Measurement of the Height of the Chromospheric Network Emission from Solar Dynamics Observatory Images

C. E. **Alissandrakis**

Solar Phys. 294:161 **2019**

https://arxiv.org/pdf/1911.00758.pdf

https://link.springer.com/content/pdf/10.1007%2Fs11207-019-1552-1.pdf

We measured the height of the chromospheric network in the 1700, 1600, and 304 A wavelength bands of the Atmospheric Imaging Assembly (AIA) onboard the Solar Dynamics Observatory (SDO) from the shift of features on the disk with respect to corresponding features in SDO/Helioseismic and Magnetic Imager (HMI) images of the

absolute value of the longitudinal magnetic field. We found that near the limb the 304 A network emission forms 3.60±0.24 Mm above the 1600 A emission, which, in turn, forms 0.48±0.10 Mm above the HMI (6173 A) level. At the center of the disk the corresponding height differences are 2.99±0.02 Mm and 0.39±0.06 Mm respectively. We also found that the 1600 A network emission forms 0.25±0.02 Mm above the 1700 A emission near the limb and 0.20±0.02 Mm at the disk center. Finally, we examined possible variations with the solar cycle. Our results can help to check and refine atmospheric models.

Structure of the transition region and the low corona from TRACE and SDO observations near the limb

C. E. **Alissandrakis**, A. Valentino
Solar Phys. 294:96 **2019**
https://arxiv.org/pdf/1906.09497.pdf
sci-hub.se/10.1007/s11207-019-1486-7
We examined the structure near the solar limb in TRACE images of the continuum and in the 1600 and 171 A bands as well as in SDO images in the continuum (from HMI) and all AIA bands. The images in different wavelength bands were carefully coaligned by using the position of Mercury for TRACE and Venus for SDO during their transit in front of the solar disk in 1999 and 2012 respectively. Chromospheric absorbing structures in the TRACE 171 A band are best visible 7" above the white light limb, very close to the inner limb, defined as the inflection point of the rising part of the center-to-limb intensity variation. They are correlated with, but are not identical to spicules in emission, seen in the 1600 A band. Similar results were obtained from AIA and SOT images. Tall spicules in 304 A are not associated with any absorption in the higher temperature bands. Performing azimuthal averaging of the intensity over 15 degree sectors near the N, S, E and W limbs, we measured the height of the limb and of the peak intensity in all AIA bands. We found that the inner limb height in the transition region AIA bands increases with wavelength, consistent with a bound-free origin of the absorption from neutral H and He. From that we computed the column density and the density of neutral hydrogen as a function of height. We estimated a height of (2300 ± 500)km for the base of the transition region. Finally, we measured the scale height of the AIA emission of the corona and associated it with the temperature; we deduced a value of (1.24 ± 0.25) 106 K for the polar corona. **November 15 1999, June 5, 2012**
Correction: Solar Physics October **2019**, 294:146 https://link.springer.com/article/10.1007/s11207-019-1545-0
https://link.springer.com/content/pdf/10.1007%2Fs11207-019-1545-0.pdf

IRIS Observations of Spicules and Structures Near the Solar Limb

C. E. **Alissandrakis**, J.-C. Vial, A. Koukras, E. Buchlin, M. Chane-Yook
Solar Phys. 293:20 **2018**
https://arxiv.org/pdf/1801.02082.pdf
https://link.springer.com/content/pdf/10.1007%2Fs11207-018-1242-4.pdf
We have analyzed IRIS spectral and slit-jaw observations of a quiet region near the South Pole. In this article we present an overview of the observations, the corrections, and the absolute calibration of the intensity. We focus on the average profiles of strong (Mg ii h and k, C ii and Si iv), as well as of weak spectral lines in the near ultraviolet (NUV) and the far ultraviolet (FUV), including the Mg ii triplet, thus probing the solar atmosphere from the low chromosphere to the transition region. We give the radial variation of bulk spectral parameters as well as line ratios and turbulent velocities. We present measurements of the formation height in lines and in the NUV continuum, from which we find a linear relationship between the position of the limb and the intensity scale height. We also find that low forming lines, such as the Mg ii triplet, show no temporal variations above the limb associated with spicules, suggesting that such lines are formed in a homogeneous atmospheric layer and, possibly, that spicules are formed above the height of 2 arc sec. We discuss the spatio-temporal structure near the limb from images of intensity as a function of position and time. In these images, we identify p-mode oscillations in the cores of lines formed at low heights above the photosphere, slow moving bright features in O i and fast moving bright features in C ii. Finally, we compare the Mg ii k and h line profiles, together with intensity values of the Balmer lines from the literature, with computations from the PROM57Mg non-LTE model developed at the Institut d'Astrophysique Spatiale and estimated values of the physical parameters. We obtain electron temperatures in the range of ∼8000 K at small heights to ∼20000 K at large heights, electron densities from 1.1×1011 to 4×1010 cm−3 and a turbulent velocity of ∼24km/s. **24 February 2014**

New approach for analysing dynamical processes on the surface of photospheric vortex tubes

Yasir **Aljohani**, Viktor Fedun, Istvan Ballai, Suzana S. A. Silva, Sergiy Shelyag, Gary Verth
ApJ **928** 3 **2022**
https://arxiv.org/pdf/2202.09332.pdf

https://iopscience.iop.org/article/10.3847/1538-4357/ac56db/pdf
The majority of studies on multi-scale vortex motions employ a two-dimensional geometry by using a variety of observational and numerical data. This approach limits the understanding the nature of physical processes responsible for vortex dynamics. Here we develop a new methodology to extract essential information from the boundary surface of vortex tubes. 3D high-resolution magnetoconvection MURaM numerical data has been used to analyse photospheric intergranular velocity vortices. The Lagrangian Averaged Vorticity Deviation (LAVD) technique was applied to define the centers of vortex structures and their boundary surfaces based on the advection of fluid elements. These surfaces were mapped onto a constructed envelope grid that allows the study of the key plasma parameters as functions of space and time. Quantities that help in understanding the dynamics of the plasma, e.g. Lorentz force, pressure force, plasma-β were also determined. Our results suggest that, while density and pressure have a rather global behaviour, the other physical quantities undergo local changes, with their magnitude and orientation changing in space and time. At the surface, the mixing in the horizontal direction is not efficient, leading to appearance of localized regions with higher/colder temperatures. In addition, the analysis of the MHD Poynting flux confirms that the majority of the energy is directed in the horizontal direction. Our findings also indicate that the pressure and magnetic forces that drive the dynamics of the plasma on vortex surfaces are unbalanced and therefore the vortices do not rotate as a rigid body.

Derivation of the Basic Magnetohydrodynamic Dynamo Equations Obtained by the Vector Potential Averaging in a Time Short-Correlated Turbulence.

Allahverdiyev, R.R., Yushkov, E.V. & Sokoloff, D.D.
Geomagn. Aeron. 63, 882–891 (**2023**).
https://doi.org/10.1134/S0016793223070034
The freezing of a magnetic field into a turbulent flow of a conducting fluid or plasma at high magnetic Reynolds numbers can lead to an exponential increase in magnetic energy due to the accumulated hydrodynamic energy. This process is described by the magnetohydrodynamic dynamo theory and can be conventionally divided into two regimes, in the first of which the average magnetic field increases along with the energy, while in the second, only the energy increases while the average magnetic field remains equal to zero. Both regimes are called a “mean-field dynamo” and a “turbulent dynamo” and are described by the Steenbeck-Krause-Rädler and Kazantsev equations, respectively. These equations are a direct consequence of averaging the magnetic induction equation over a random velocity field; the first moment is calculated in the first case, and the second moment is calculated in the second case. There are many methods of such averaging. However, in this paper, we derive both dynamo models using the method of multiplicative integrals based on the assumption that the random velocity field is short-correlated in time. The main result is that we demonstrate the convenience of averaging not the magnetic field itself, but the vector potential, whose use greatly simplifies the mathematical apparatus of the derivation and, as a result, becomes very promising for generalizing standard models in the case of inhomogeneous and nonisotropic turbulence.

Magnetohydrodynamic Waves in Multi-Layered Asymmetric Waveguides: Solar Magneto-Seismology Theory and Application

Matthew **Allcock**, Daria Shukhobodskaia, Noémi Kinga Zsámberger, and Robert Erdélyi
Front. Astron. Space Sci. **2019**
https://www.frontiersin.org/articles/10.3389/fspas.2019.00048/full?utm_source=F-AAE&utm_medium=EMLF&utm_campaign=MRK_1056122_76_Astron_20190730_arts_A
sci-hub.se/10.3389/fspas.2019.00048
Diagnosing the solar atmospheric plasma is one of the major challenges in solar physics. Magnetohydrodynamic (MHD) waves, by means of applying the powerful concept of solar magneto-seismology (SMS), provide a tool to obtain diagnostic insight into the magnetized solar plasma in MHD waveguides. This paper provides a road-map of simple but applicable models of solar atmospheric waveguides in the framework of Cartesian geometry. We focus on exploiting the diagnostic potential of waveguide asymmetry and consider the effects of steady flow. In particular, the dispersion relation describing linear MHD wave propagation along a multi-layered MHD waveguide is derived. Aiming at lower solar atmospheric applications of SMS, the special case of a single magnetic slab embedded in an asymmetric magnetized plasma environment is revisited. As a proof of concept, the Amplitude Ratio Method is used to make a seismological estimate of the local Alfvén speed in several chromospheric fibrils that exhibit asymmetric oscillations. Absolute ratios of boundary oscillations between 1.29 and 3.42 are detected and, despite the significant errors expected, the local Alfvén speed estimates agree with previously derived estimates from magnetic field extrapolations. Finally, the effects of asymmetric shear flows present in these slab MHD waveguides are considered as a suitable model of Kelvin-Helmholtz instability initiation that is applicable, for example, to coronal mass ejection flanks.

A novel magneto-seismology technique for solar magnetic field diagnostics

Matthew **Allcock** and Robert Erdélyi
UKSP Nugget: 90, June **2018**

http://www.uksolphys.org/uksp-nugget/90-a-novel-magneto-seismology-technique-for-solar-magnetic-field-diagnostics/
The magnetic field in the solar transition region and corona is amongst the least understood but the most significant features in solar physics. As the coronal magnetic field is relatively weak and the plasma is optically thin, it is difficult, and often impossible, to directly measure the magnetic field vector field in the transition region and corona using traditional methods such as Zeeman splitting [1]. Thankfully, we can harness proxy information to do a better job by means of solar magneto-seismology (SMS).
Magnetohydrodynamic (MHD) waves, that permeate almost all solar structures, provide us with one such proxy. Ingenious SMS techniques have utilised observed MHD wave parameters including frequency, period ratio, and damping rates to diagnose the magnetic field in a variety of solar atmospheric structures. One characteristic of MHD waves in magnetic waveguides that has not yet been utilised is how the associated wave power is distributed across the structure (the transverse eigenfunction) – in particular, the (a)symmetry of the waves.

Solar Magnetoseismology with Magnetoacoustic Surface Waves in Asymmetric Magnetic Slab Waveguides

Matthew **Allcock** and Robert Erdélyi
2018 ApJ 855 90
http://iopscience.iop.org/article/10.3847/1538-4357/aaad0c/pdf
Solar magnetoseismology is an indirect method to approximate plasma parameters that are traditionally difficult to measure in the solar atmosphere using observations of magnetohydrodynamic waves. A magnetic slab can act as waveguide for magnetoacoustic waves that approximates magnetic structures in the solar atmosphere. The asymmetry of the slab caused by different plasma parameters in each external region affects both the eigenfrequencies and eigenfunctions differently at each side of the slab, that is, both the temporal and spatial profiles of the eigenmodes of propagation along the slab are influenced by the equilibrium asymmetry. We present two novel diagnostic tools for solar magnetoseismology that use this distortion to estimate the slab magnetic field strength using the spatial distribution of magnetoacoustic surface waves: theamplitude ratio and the minimum perturbation shift techniques. They have the potential to estimate background equilibrium parameters in inhomogeneous solar structures such as elongated magnetic bright points, prominences, and the clusters of magnetic brightenings rooted in sunspot light bridges known as light bridge surges or light walls, which may be locally approximated as slabs.

Magnetohydrodynamic Waves in an Asymmetric Magnetic Slab

Matthew **Allcock**, Robert Erdélyi
Solar Physics February **2017**, 292:35
Analytical models of solar atmospheric magnetic structures have been crucial for our understanding of magnetohydrodynamic (MHD) wave behaviour and in the development of the field of solar magneto-seismology. Here, an analytical approach is used to derive the dispersion relation for MHD waves in a magnetic slab of homogeneous plasma enclosed on its two sides by non-magnetic, semi-infinite plasma with different densities and temperatures. This generalises the classic magnetic slab model, which is symmetric about the slab. The dispersion relation, unlike that governing a symmetric slab, cannot be decoupled into the well-known sausage and kink modes, i.e. the modes have mixed properties. The eigenmodes of an asymmetric magnetic slab are better labelled as quasi-sausage and quasi-kink modes. Given that the solar atmosphere is highly inhomogeneous, this has implications for MHD mode identification in a range of solar structures. A parametric analysis of how the mode properties (in particular the phase speed, eigenfrequencies, and amplitudes) vary in terms of the introduced asymmetry is conducted. In particular, avoided crossings occur between quasi-sausage and quasi-kink surface modes, allowing modes to adopt different properties for different parameters in the external region.

Supervised Neural Networks for Helioseismic Ring-Diagram Inversions

Rasha **Alshehhi**, Chris S. Hanson, Laurent Gizon, Shravan Hanasoge
A&A **2019**
https://arxiv.org/pdf/1901.01505.pdf
The inversion of ring fit parameters to obtain subsurface flow maps in ring-diagram analysis for 8 years of SDO observations is computationally expensive, requiring ~3200 CPU hours. In this paper we apply machine learning techniques to the inversion in order to speed up calculations. Specifically, we train a predictor for subsurface flows using the mode fit parameters and the previous inversion results, to replace future inversion requirements. We utilize Artificial Neural Networks as a supervised learning method for predicting the flows in 15 degree ring tiles. To demonstrate that the machine learning results still contain the subtle signatures key to local helioseismic studies, we use the machine learning results to study the recently discovered solar equatorial Rossby waves. The Artificial Neural Network is computationally efficient, able to make future flow predictions of an entire Carrington rotation in a matter of seconds, which is much faster than the current ~31 CPU hours. Initial training of the networks requires ~3 CPU hours. The trained Artificial Neural Network can achieve a root mean-square error equal to approximately half that reported for the velocity inversions, demonstrating the accuracy of the machine learning (and perhaps the

overestimation of the original errors from the ring-diagram pipeline). We find the signature of equatorial Rossby waves in the machine learning flows covering six years of data, demonstrating that small-amplitude signals are maintained. The recovery of Rossby waves in the machine learning flow maps can be achieved with only one Carrington rotation (27.275 days) of training data. We have shown that machine learning can be applied to, and perform more efficiently than the current ring-diagram inversion. The computation burden of the machine learning includes 3 CPU hours for initial training, then around 0.0001 CPU hours for future predictions.

Helium Abundance Heralds the Onset of Solar Cycle 25

B. L. **Alterman**, Justin C. Kasper, Robert J. Leamon, Scott W. McIntosh
ApJL **2020**
https://arxiv.org/pdf/2006.04669.pdf
We study the solar wind helium-to-hydrogen abundance's (AHe) relationship to solar cycle onset. Using OMNI/Lo data, we show that AHe increases prior to minima of sunspot number (SSN). We also identify a rapid depletion and recovery in AHe that occurs directly prior to cycle onset. This depletion happens at approximately the same time across solar wind speeds (vsw), implying that it is formed by a mechanism distinct from the one that drives AHe's solar cycle scale variation and vsw-dependent phase offset with respect to sunspot number (SSN). As AHe's rapid depletion and recovery have already occurred and AHe is now increasing as it has following previous solar Minima, we infer that solar cycle 25 has already begun.

Helium Variation across Two Solar Cycles Reveals a Speed-dependent Phase Lag

B. L. **Alterman**1,2 and Justin C. Kasper2,3
2019 ApJL 879 L6
https://arxiv.org/pdf/1906.12273.pdf
https://iopscience.iop.org/article/10.3847/2041-8213/ab2391/pdf
We study the relationship between the solar wind helium-to-hydrogen abundance ratio (A He), solar wind speed (v sw), and sunspot number (SSN) over solar cycles 23 and 24. This is the first full 22 year Hale cycle measured with the Wind spacecraft covering a full cycle of the solar dynamo with two polarity reversals. While previous studies have established a strong correlation between A He and SSN, we show that the phase delay between A He and SSN is a monotonic increasing function of v sw. Correcting for this lag, A He returns to the same value at a given SSN over all rising and falling phases and across solar wind speeds. We infer that this speed-dependent lag is a consequence of the mechanism that depletes slow wind A He from its fast wind value during solar wind formation.

Data Mining for Science of the Sun-Earth Connection as a Single System

Nathalia **Alzate**, Simone Di Matteo, Huw Morgan, +++
Front. Astron. Space Sci. 10: 1151785. **2023**
doi: 10.3389/fspas.2023.1151785
https://www.frontiersin.org/articles/10.3389/fspas.2023.1151785/pdf
Establishing the Sun-Earth connection requires overcoming the challenges of exploring the data from past and current missions and leveraging tools and models (data mining) to create an efficient system treatment of the Sun and heliosphere. However, solar and heliospheric environment data constitute a vast source of information whose potential is far from being optimally exploited. In the next decade, the solar and heliospheric community will have to manage the increasing amount of information coming from new missions, improve re-analysis of data from past and current missions, and create new data products from the application of new methodologies. This complex task is further complicated by practical challenges such as different datasets and catalogs in different formats that may require different pre-processing and analysis tools, and the need for numerous analysis approaches that are not all fully optimized for large volumes of data. While several ongoing efforts aim at addressing these problems, the available datasets and tools are not always used to their full potential often due to lack of awareness of available resources. In this paper, we summarize the issues raised and goals discussed by members of the community during recent conference sessions focused on data mining for science.

Tracking Non-Radial Outflows in Extreme Ultraviolet and White Light Solar Images

Nathalia **Alzate**, Huw Morgan, Simone Di Matteo
ApJ **945** 116 **2023**
https://arxiv.org/pdf/2302.04971.pdf
https://iopscience.iop.org/article/10.3847/1538-4357/acba08/pdf
Understanding the solar corona requires knowledge of its dynamics through its various layers and subsequent connectivity to the heliosphere. This requires understanding the nature of the outflows and the physical transitions through the middle corona (~1.5-6.0 Rs). While this region is still inaccessible to in situ measurements, remote sensing observations are available, but their interpretation can be controversial due to line-of-sight effects and the non-radial motion of outflowing structures close to the Sun (<3.0 Rs). In this work, we describe a method to

mitigate these challenges by generating non-radial Height-Time profiles of outflows by using advanced image processing techniques. The North and South boundaries of a large equatorial streamer during the 2008 solar minimum were identified in STEREO/SECCHI solar images, using two different methodologies based on thresholds of brightness and piece-wise polynomial function fitting. To address line-of-sight issues, we used tomographic reconstruction of the 3D distribution of the coronal electron density based on SECCHI/COR2 images. Spectral analysis of the time series of the position angle of the streamer boundary revealed its oscillatory nature at some heights at 36-48 hours and 10.5-14.6 hours. Dividing the distance between the North and South streamer boundaries in equal parts at each height, we obtained non-radial Height-Time paths from which we generated non-radial profiles of corona/solar wind plasma outflow. We tracked outflows as they moved uninterruptedly from the Sun in EUVI, through COR1 and into COR2. Finally, we discuss preliminary results of non-radial plane-of-sky velocities for a CME and two small-scale features. **10-22 Jan 2008**

The Ubiquity of Twisted Flux Ropes in the Quiet Sun

Tahar **Amari**, Aurélien Canou, Marco Velli, Zoran Mikic, Frederic Alauzet, Eric Buchlin, Jean-François Luciani, Jean-Jacques Aly, Lucas A. Tarr
ApJ **2024**
https://arxiv.org/pdf/2411.10563
Models and observations have demonstrated that Twisted Flux Ropes (TFRs) play a significant role in the structure and eruptive dynamics of active regions. Their role in the dynamics of the quiet Sun atmosphere on has remained elusive, their fundamental relevance emerging mainly from theoretical models (Amari et al. 2015), showing that they form and erupt as a result of flux cancellation. Here HINODE high-resolution photospheric vector magnetic field measurements are integrated with advanced environment reconstruction models: TFRs develop on various scales and are associated with the appearance of mesospots. The developing TFRs contain sufficient free magnetic energy to match the requirements of the recently observed "campfires" discovered by Solar Orbiter in the quiet Sun. The free magnetic energy is found to be large enough to trigger eruptions while the magnetic twist large enough to trigger confined eruptions, heating the atmosphere. TFRs are also connected to larger scale magnetic fields such as supergranulation loops, allowing the generation of Alfvén waves at the top of the chromosphere that can propagate along them. High-resolution magnetohydrodynamic simulations, incorporating subsurface dynamo activity at an unprecedented 30 km spatial resolution, confirm that TFRs are ubiquitous products of the permanent small scale dynamo engine that feeds their formation, destabilization, eruption via flux emergence, submergence and cancellation of their chromospheric feet, similar to the dynamics driving large scale eruptive events. Future investigations, especially with the Daniel K. Inouye Solar Telescope (DKIST) and Solar Orbiter will deepen our understanding of TFRs in the context of atmospheric heating.

The solar carbon, nitrogen, and oxygen abundances from a 3D LTE analysis of molecular lines⋆

A. M. **Amarsi**1, N. Grevesse2,3, M. Asplund4 and R. Collet5
A&A 656, A113 (**2021**)
https://www.aanda.org/articles/aa/pdf/2021/12/aa41384-21.pdf
https://doi.org/10.1051/0004-6361/202141384
Carbon, nitrogen, and oxygen are the fourth, sixth, and third most abundant elements in the Sun. Their abundances remain hotly debated due to the so-called solar modelling problem that has persisted for almost 20 years. We revisit this issue by presenting a homogeneous analysis of 408 molecular lines across 12 diagnostic groups, observed in the solar intensity spectrum. Using a realistic 3D radiative-hydrodynamic model solar photosphere and local thermodynamic equilibrium (LTE) line formation, we find log ϵC = 8.47 ± 0.02, log ϵN = 7.89 ± 0.04, and log ϵO = 8.70 ± 0.04. The stipulated uncertainties mainly reflect the sensitivity of the results to the model atmosphere; this sensitivity is correlated between the different diagnostic groups, which all agree with the mean result to within 0.03 dex. For carbon and oxygen, the molecular results are in excellent agreement with our 3D non-LTE analyses of atomic lines. For nitrogen, however, the molecular indicators give a 0.12 dex larger abundance than the atomic indicators, and our best estimate of the solar nitrogen abundance is given by the mean: 7.83 dex. The solar oxygen abundance advocated here is close to our earlier determination of 8.69 dex, and so the present results do not significantly alleviate the solar modelling problem.

3D non-LTE line formation of neutral carbon in the Sun

A. M. **Amarsi**, P. S. Barklem, R. Collet, N. Grevesse, M. Asplund
A&A **2019**
https://arxiv.org/pdf/1903.08838.pdf
Carbon abundances in late-type stars are important in a variety of astrophysical contexts. However C i lines, one of the main abundance diagnostics, are sensitive to departures from local thermodynamic equilibrium (LTE). We present a model atom for non-LTE analyses of C i lines, that uses a new, physically-motivated recipe for the rates of neutral hydrogen impact excitation. We analyse C i lines in the solar spectrum, employing a three-dimensional (3D)

hydrodynamic model solar atmosphere and 3D non-LTE radiative transfer. We find negative non-LTE abundance corrections for C i lines in the solar photosphere, in accordance with previous studies, reaching up to around 0.1 dex in the disk-integrated flux. We also present the first fully consistent 3D non-LTE solar carbon abundance determination: we infer log ϵC = 8.44±0.02, in good agreement with the current standard value. Our models reproduce the observed solar centre-to-limb variations of various C i lines, without any adjustments to the rates of neutral hydrogen impact excitation, suggesting that the proposed recipe may be a solution to the long-standing problem of how to reliably model inelastic collisions with neutral hydrogen in late-type stellar atmospheres.

The PAC2MAN mission: a new tool to understand and predict solar energetic events

Jorge **Amaya**, Sophie Musset, Viktor Andersson, Andrea Diercke, Christian Hoöller, Sergiu Iliev, Lilla Juhász, René Kiefer, Riccardo Lasagni, Solène Lejosne, Mohammad Madi, Mirko Rummelhagen,Markus Scheucher, Arianna Sorba, Stefan Thonhofer

Journal of Space Weather and Space Climate, 5, A5 (16 p) **2015**

http://arxiv.org/pdf/1412.6390v1.pdf

http://www.swsc-journal.org/articles/swsc/pdf/2015/01/swsc140009.pdf

An accurate forecast of flare and CME initiation requires precise measurements of the magnetic energy build up and release in the active regions of the solar atmosphere. We designed **a new space weather mission** that performs such measurements using new optical instruments based on the Hanle and Zeeman effects. The mission consists of two satellites, one orbiting the L1 Lagrangian point (Spacecraft Earth, SCE) and the second in heliocentric orbit at 1AU trailing the Earth by 80∘ (Spacecraft 80, SC80). Optical instruments measure the vector magnetic field in multiple layers of the solar atmosphere. The orbits of the spacecraft allow for a continuous imaging of nearly 73\% of the total solar surface. In-situ plasma instruments detect solar wind conditions at 1AU and ahead of our planet. Earth directed CMEs can be tracked using the stereoscopic view of the spacecraft and the strategic placement of the SC80 satellite. Forecasting of geoeffective space weather events is possible thanks to an accurate surveillance of the magnetic energy build up in the Sun, an optical tracking through the interplanetary space, and in-situ measurements of the near-Earth environment.

Influence of Earth-directed Coronal Mass Ejections on the Sun's Shadow Observed by the Tibet-III Air Shower Array

M. **Amenomori**1, X. J. Bi2, D. Chen3, T. L. Chen4, W. Y. Chen2, S. W. Cui5, Danzengluobu4, L. K. Ding2, C. F. Feng6, Zhaoyang Feng2 .....

2018 ApJ 860 13 DOI 10.3847/1538-4357/aac2e6

We examine the possible influence of Earth-directed coronal mass ejections (ECMEs) on the Sun's shadow in the 3 TeV cosmic-ray intensity observed by the Tibet-III air shower (AS) array. We confirm a clear solar-cycle variation of the intensity deficit in the Sun's shadow during ten years between 2000 and 2009. This solar-cycle variation is overall reproduced by our Monte Carlo (MC) simulations of the Sun's shadow based on the potential field model of the solar magnetic field averaged over each solar rotation period. We find, however, that the magnitude of the observed intensity deficit in the Sun's shadow is significantly less than that predicted by MC simulations, particularly during the period around solar maximum when a significant number of ECMEs is recorded.
The χ 2 tests of the agreement between the observations and the MC simulations show that the difference is larger during the periods when the ECMEs occur, and the difference is reduced if the periods of ECMEs are excluded from the analysis. This suggests the first experimental evidence of the ECMEs affecting the Sun's shadow observed in the 3 TeV cosmic-ray intensity.

Evaluation of the Interplanetary Magnetic Field Strength Using the Cosmic-Ray Shadow of the Sun

M. **Amenomori**,1 X. J. Bi,2 D. Chen,3 …..

Physical Review Letters, Volume 120, Issue 3, id.031101, **2018**

http://sci-hub.tw/10.1103/PhysRevLett.120.031101

We analyze the Sun's shadow observed with the Tibet-III air shower array and find that the shadow's center deviates northward (southward) from the optical solar disk center in the "away" ("toward") interplanetary magnetic field (IMF) sector. By comparing with numerical simulations based on the solar magnetic field model, we find that the average IMF strength in the away (toward) sector is $1.54 \pm 0.21_{stat} \pm 0.20_{svst}$ ($1.62 \pm 0.15_{stat} \pm 0.22_{svst}$) times larger than the model prediction. These demonstrate that the observed Sun's shadow is a useful tool for the quantitative evaluation of the average solar magnetic field.

Solar Reflection of Dark Matter

Haipeng **An**, Haoming Nie, Maxim Pospelov, Josef Pradler, Adam Ritz

2021

https://arxiv.org/pdf/2108.10332.pdf
The scattering of light dark matter off thermal electrons inside the Sun produces a "fast" sub-component of the dark matter flux that may be detectable in underground experiments. We update and extend previous work by analyzing the signatures of dark matter candidates which scatter via light mediators. Using numerical simulations of the dark matter-electron interaction in the solar interior, we determine the energy spectrum of the reflected flux, and calculate the expected rates for direct detection experiments. We find that large Xenon-based experiments (such as XENON1T) provide the strongest direct limits for dark matter masses below a few MeV, reaching a sensitivity to the effective dark matter charge of ∼10−9e.

Measurements of Photospheric and Chromospheric Magnetic Field Structures Associated with Chromospheric Heating over a Solar Plage Region

Tetsu **Anan**, Thomas A. Schad, Reizaburo Kitai, Gabriel I. Dima, Sarah A. Jaeggli, Lucas A. Tarr, Manuel Collados, Carlos Dominguez-Tagle, Lucia Kleint
ApJ **2021**
https://arxiv.org/pdf/2108.07907.pdf
In order to investigate the relation between magnetic structures and the signatures of heating in plage regions, we observed a plage region with the He I 1083.0 nm and Si I 1082.7 nm lines on **2018 October 3** using the integral field unit mode of the GREGOR Infrared Spectrograph (GRIS) installed at the GREGOR telescope. During the GRIS observation, the Interface Region Imaging Spectrograph (IRIS) obtained spectra of the ultraviolet Mg II doublet emitted from the same region. In the periphery of the plage region, within the limited field of view seen by GRIS, we find that the Mg II radiative flux increases with the magnetic field in the chromosphere with a factor of proportionality of 2.38 \times 10^4 erg cm^{-2} s^{-1} G^{-1}. The positive correlation implies that magnetic flux tubes can be heated by Alfv'en wave turbulence or by collisions between ions and neutral atoms relating to Alfv'en waves. Within the plage region itself, the radiative flux was large between patches of strong magnetic field strength in the photosphere, or at the edges of magnetic patches. On the other hand, we do not find any significant spatial correlation between the enhanced radiative flux and the chromospheric magnetic field strength or the electric current. In addition to the Alfv'en wave turbulence or collisions between ions and neutral atoms relating to Alfv'en waves, other heating mechanisms related to magnetic field perturbations produced by interactions of magnetic flux tubes could be at work in the plage chromosphere.

Developments of Multi-wavelength Spectro-Polarimeter on the Domeless Solar Telescope at Hida Observatory

Tetsu **Anan**, Yu Wei Huang, Yoshikazu Nakatani, Kiyoshi Ichimoto, Satoru Ueno, Goichi Kimura,Shota Ninomiya, Sanetaka Okada, Naoki Kaneda
PASJ 70, Issue 6, 102 **2018**
https://arxiv.org/pdf/1803.02094.pdf
To obtain full Stokes spectra in multi-wavelength windows simultaneously, we developed a new spectro-polarimeter on the Domeless Solar Telescope at Hida Observatory. The new polarimeter consists of a 60 cm aperture vacuum telescope on an altazimuth mount, an image rotator, a high dispersion spectrograph, polarization modulator and analyzer composed of a continuously rotating waveplate with a retardation nearly constant around 127^{circ} in 500 - 1100 nm and a polarizing beam splitter located closely behind the focus of the telescope, fast and large format CMOS cameras and an infrared camera. The slit spectrograph allows us to obtain spectra in as many wavelength windows as the number of cameras. We characterized the instrumental polarization of the entire system and established the polarization calibration procedure. The cross-talks among the Stokes Q,U and V are evaluated to be about 0.06% sim 1.2% depending on the degree of the intrinsic polarizations. In a typical observing setup, a sensitivity of 0.03% can be achieved in 20 - 60 second for 500 nm - 1100 nm. The new polarimeter is expected to provide a powerful tool to diagnose the 3D magnetic field and other vector physical quantities in the solar atmosphere.

The Solar Orbiter SPICE instrument
An extreme UV imaging spectrometer

SPICE Consortium
M. **Anderson1**, T. Appourchaux2, F. Auchère2, R. Aznar Cuadrado3, J. Barbay2,
A&A 642, A14 (**2020**)
https://doi.org/10.1051/0004-6361/201935574
https://www.aanda.org/articles/aa/pdf/2020/10/aa35574-19.pdf
Aims. The Spectral Imaging of the Coronal Environment (SPICE) instrument is a high-resolution imaging spectrometer operating at extreme ultraviolet wavelengths. In this paper, we present the concept, design, and pre-launch performance of this facility instrument on the ESA/NASA Solar Orbiter mission.

Methods. The goal of this paper is to give prospective users a better understanding of the possible types of observations, the data acquisition, and the sources that contribute to the instrument's signal.
Results. The paper discusses the science objectives, with a focus on the SPICE-specific aspects, before presenting the instrument's design, including optical, mechanical, thermal, and electronics aspects. This is followed by a characterisation and calibration of the instrument's performance. The paper concludes with descriptions of the operations concept and data processing.
Conclusions. The performance measurements of the various instrument parameters meet the requirements derived from the mission's science objectives. The SPICE instrument is ready to perform measurements that will provide vital contributions to the scientific success of the Solar Orbiter mission.

Oscillations in the Sun with SONG: Setting the scale for asteroseismic investigations

M. Fredslund **Andersen**, P. Pallé, J. Jessen-Hansen, K. Wang, F. Grundahl, T. R. Bedding, T. Roca Cortes, J. Yu, S. Mathur, R. A. Gacia, T. Arentoft, C. Régulo, R. Tronsgaard, H. Kjeldsen, J. Christensen-Dalsgaard

A&A Letters 623, L9 **2019**

https://arxiv.org/pdf/1902.10717.pdf

Context. We present the first high-cadence multi-wavelength radial-velocity observations of the Sun-as-a-star, carried out during 57 consecutive days using the stellar échelle spectrograph at the Hertzsprung SONG Telescope operating at the Teide Observatory.
Aims. The aim was to produce a high-quality data set and reference values for the global helioseismic parameters {\nu_{max}}, and {\Delta \nu} of the solar p-modes using the SONG instrument. The obtained data set or the inferred values should then be used when the scaling relations are applied to other stars showing solar-like oscillations which are observed with SONG or similar instruments.
Methods. We used different approaches to analyse the power spectrum of the time series to determine {\nu_{max}}; simple Gaussian fitting and heavy smoothing of the power spectrum. {\Delta\nu} was determined using the method of autocorrelation of the power spectrum. The amplitude per radial mode was determined using the method described in Kjeldsen et al. (2008).
Results. We found the following values for the solar oscillations using the SONG spectrograph: {\nu_{max}} = 3141 {\pm} 12 {\mu}Hz, {\Delta\nu} = 134.98 {\pm} 0.04 {\mu}Hz and an average amplitude of the strongest radial modes of 16.6 {\pm} 0.4 cm/s. These values are consistent with previous measurements with other techniques.

The Solar Orbiter SPICE instrument -- An extreme UV imaging spectrometer

M. **Anderson**, T. Appourchaux, F. Auchère, R. Aznar Cuadrado, J. Barbay, F. Baudin, ...

A&A **2019**

https://arxiv.org/pdf/1909.01183.pdf

The Spectral Imaging of the Coronal Environment (SPICE) instrument is a high-resolution imaging spectrometer operating at extreme ultraviolet (EUV) wavelengths. In this paper, we present the concept, design, and pre-launch performance of this facility instrument on the ESA/NASA Solar Orbiter mission. The goal of this paper is to give prospective users a better understanding of the possible types of observations, the data acquisition, and the sources that contribute to the instrument's signal. The paper discusses the science objectives, with a focus on the SPICE-specific aspects, before presenting the instrument's design, including optical, mechanical, thermal, and electronics aspects. This is followed by a characterisation and calibration of the instrument's performance. The paper concludes with descriptions of the operations concept and data processing. The performance measurements of the various instrument parameters meet the requirements derived from the mission's science objectives. The SPICE instrument is ready to perform measurements that will provide vital contributions to the scientific success of the Solar Orbiter mission.

Estimates of Active Region Area Coverage through Simultaneous Measurements of He I λλ 5876 and 10830 Lines

V. **Andretta**, M. S. Giampapa, E. Covino, A. Reiners, B. Beeck

ApJ **2017**

https://arxiv.org/pdf/1703.10060.pdf

Simultaneous, high-quality measurements of the neutral helium triplet features at 5876~\AA\ and 10830~\AA, respectively, in a sample of solar-type stars are presented. The observations were made with ESO telescopes at the La Silla Paranal Observatory under program ID 088.D-0028(A) and MPG Utility Run for FEROS 088.A-9029(A). The equivalent widths of these features combined with chromospheric models are utilized to infer the fractional area coverage, or filling factor, of magnetic regions outside of spots. We find that the majority of the sample is characterized by filling factors less than unity. However, discrepancies occur among the coolest K-type and warmest and most rapidly rotating F-type dwarf stars. We discuss these apparently anomalous results and find that in the case of K-type stars they are an artifact of the application of chromospheric models best suited to the Sun than to stars

with significantly lower Teff. The case of the F-type rapid rotators can be explained with the measurement uncertainties of the equivalent widths, but they may also be due to a non-magnetic heating component in their atmospheres. With the exceptions noted above, preliminary results suggest that the average heating rates in the active regions are the same from one star to the other, differing in the spatially integrated, observed level of activity due to the area coverage. Hence, differences in activity in this sample are mainly due to the filling factor of active regions.

The EUV spectrum of the Sun: SOHO CDS NIS radiances during solar cycle 23

V. **Andretta**, G. Del Zanna

E-print, Jan **2014**; A&A, 563, A26 (**2014**)

For the first time, we present and discuss EUV radiances of the solar transition region (TR) and corona obtained during a solar cycle. The measurements were obtained with the SOHO/coronal diagnostic spectrometer (CDS) during the period from 1996 to 2010. We find that limb-brightening significantly affects any characterisation of the solar radiances. We present the limb-brightening function for the main lines and find that it does not change measurably during the cycle. We confirm earlier findings that the radiance histogram of the cooler lines have a well defined, log-normal quiet-Sun component, although our results differ from previous ones. The width of the lowest-radiance log-normal distribution is constant along the cycle. Both the analysis of the centre-to-limb variation and of the radiance statistical distribution point to a constant QS emission along solar cycle 23. Lines formed above 1 MK are dramatically affected by the presence of active regions, and indeed, no "quiet Sun" region can be defined during periods of maximum activity. Much of the irradiance variability in lines formed below 1.5 MK is due to a change in the emitting area. For hotter lines, the emitting area saturates to almost 100% of full solar disk at the maximum of activity, while simultaneously the emission due to active regions increases by more than an order of magnitude. We show that structures around active regions, sometimes referred to as dark halos or dark canopies, are common and discuss their similarities and differences with coronal holes. In particular, we show how they are well visible in TR lines, contrary to coronal holes.

Novel data analysis techniques in coronal seismology **Review**

Sergey A. **Anfinogentov**, Patrick Antolin, Andrew R. Inglis, Dmitrii Kolotkov, Elena G. Kupriyanova, James A. McLaughlin, Giuseppe Nisticò, David J. Pascoe, S. Krishna Prasad, Ding Yuan

Space Science Reviews **volume 218**, Article number: 9 **2022**

https://arxiv.org/pdf/2112.13577.pdf

https://link.springer.com/content/pdf/10.1007/s11214-021-00869-w.pdf

https://doi.org/10.1007/s11214-021-00869-w

We review novel data analysis techniques developed or adapted for the field of coronal seismology. We focus on methods from the last ten years that were developed for extreme ultraviolet (EUV) imaging observations of the solar corona, as well as for light curves from radio and X-ray. The review covers methods for the analysis of transverse and longitudinal waves; spectral analysis of oscillatory signals in time series; automated detection and processing of large data sets; empirical mode decomposition; motion magnification; and reliable detection, including the most common pitfalls causing artefacts and false detections. We also consider techniques for the detailed investigation of MHD waves and seismological inference of physical parameters of the coronal plasma, including restoration of the three-dimensional geometry of oscillating coronal loops, forward modelling and Bayesian parameter inference.

May 9, 2007, June 27, 2007., 2013-01-21

Solar Bayesian Analysis Toolkit -- a new Markov chain Monte Carlo IDL code for Bayesian parameter inference

Sergey A. **Anfinogentov**, Valery M. Nakariakov, David J. Pascoe, Christopher R. Goddard

2021 *ApJS* **252** 11

https://arxiv.org/pdf/2005.05365.pdf

https://doi.org/10.3847/1538-4365/abc5c1

We present the Solar Bayesian Analysis Toolkit (SoBAT) which is a new easy to use tool for Bayesian analysis of observational data, including parameter inference and model comparison. SoBAT is aimed (but not limited) to be used for the analysis of solar observational data. We describe a new Interactive Data Language (IDL) code designed to facilitate the comparison of user-supplied model with data. Bayesian inference allows prior information to be taken into account. The use of Markov chain Monte Carlo (MCMC) sampling allows efficient exploration of large parameter spaces and provides reliable estimation of model parameters and their uncertainties. The Bayesian evidence for different models can be used for quantitative comparison. The code is tested to demonstrate its ability to accurately recover a variety of parameter probability distributions. Its application to practical problems is demonstrated using studies of the structure and oscillation of coronal loops.

Magnetohydrodynamic Seismology of Quiet Solar Active Regions

Sergey A. **Anfinogentov**, Valery. M. Nakariakov
ApJL **884** L40 **2019**
https://arxiv.org/pdf/1910.03809.pdf
https://doi.org/10.3847/2041-8213/ab4792
The ubiquity of recently discovered low-amplitude decayless kink oscillations of plasma loops allows for the seismological probing of the corona on a regular basis. In particular, in contrast to traditionally applied seismology which is based on the large-amplitude decaying kink oscillations excited by flares and eruptions, decayless oscillations can potentially provide the diagnostics necessary for their forecasting. We analysed decayless kink oscillations in several distinct loops belonging to active region NOAA 12107 on **10 July 2010** during its quiet time period, when it was observed on the West limb in EUV by the Atmospheric Imaging Assembly on-board Solar Dynamics Observatory. The oscillation periods were estimated with the use of the motion magnification technique. The lengths of the oscillating loops were determined within the assumption of its semicircular shape by measuring the position of their foot-points. The density contrast in the loops was estimated from the observed intensity contrast accounting for the unknown spatial scale of the background plasma. The combination of those measurements allows us to determine the distribution of kink and Alfvén speeds in the active region. Thus, we demonstrate the possibility to obtain seismological information about coronal active regions during the quiet periods of time.

Motion magnification in coronal seismology

Sergey **Anfinogentov**, Valery M. Nakariakov
Solar Phys. Volume 291, Issue 11, pp 3251–3267 **2016**
https://arxiv.org/pdf/1611.01790v1.pdf
We introduce a new method for the investigation of low-amplitude transverse oscillations of solar plasma non-uniformities, such as coronal loops, individual strands in coronal arcades, jets, prominence fibrils, polar plumes, and other contrast features, observed with imaging instruments. The method is based on the two-dimensional dual tree complex wavelet transform (DTCWT). It allows us to magnify transverse, in the plane-of-the-sky, quasi-periodic motions of contrast features in image sequences. The tests performed on the artificial data cubes imitating exponentially decaying, multi-periodic and frequency-modulated kink oscillations of coronal loops showed the effectiveness, reliability and robustness of this technique. The algorithm was found to give linear scaling of the magnified amplitudes with the original amplitudes provided they are sufficiently small. Also, the magnification is independent of the oscillation period in a broad range of the periods. The application of this technique to SDO/AIA EUV data cubes of a non-flaring active region allowed for the improved detection of low-amplitude decay-less oscillations in the majority of loops. 05 January 2013., 21 January 2013.

The Space Physics Environment Data Analysis System (SPEDAS)

V. **Angelopoulos**1 · P. Cruce1 · A. Drozdov1 · E.W. Grimes1 · N. Hatzigeorgiu2 · D.A. King2 · D. Larson2 · J.W. Lewis2 · J.M. McTiernan2 .....
Space Science Reviews January **2019**, 215:9
https://link.springer.com/content/pdf/10.1007%2Fs11214-018-0576-4.pdf
With the advent of the Heliophysics/Geospace System Observatory (H/GSO), a complement of multi-spacecraft missions and ground-based observatories to study the space environment, data retrieval, analysis, and visualization of space physics data can be daunting. The Space Physics Environment Data Analysis System (SPEDAS), a grass-roots software development platform (www.spedas.org), is now officially supported by NASA Heliophysics as part of its data environment infrastructure. It serves more than a dozen space missions and ground observatories and can integrate the full complement of past and upcoming space physics missions with minimal resources, following clear, simple, and well-proven guidelines. Free, modular and configurable to the needs of individual missions, it works in both command-line (ideal for experienced users) and Graphical User Interface (GUI) mode (reducing the learning curve for first-time users). Both options have “crib-sheets,” user-command sequences in ASCII format that can facilitate record-and-repeat actions, especially for complex operations and plotting. Crib-sheets enhance scientific interactions, as users can move rapidly and accurately from exchanges of technical information on data processing to efficient discussions regarding data interpretation and science. SPEDAS can readily query and ingest all International Solar Terrestrial Physics (ISTP)-compatible products from the Space Physics Data Facility (SPDF), enabling access to a vast collection of historic and current mission data. The planned incorporation of Heliophysics Application Programmer’s Interface (HAPI) standards will facilitate data ingestion from distributed datasets that adhere to these standards. Although SPEDAS is currently Interactive Data Language (IDL)-based (and interfaces to Java-based tools such as Autoplot), efforts are under-way to expand it further to work with python (first as an interface tool and potentially even receiving an under-the-hood replacement). We review the SPEDAS development history, goals, and current implementation. We explain its “modes of use” with examples geared for users and outline its technical implementation and requirements with software developers in mind. We also describe SPEDAS personnel and software management, interfaces with other organizations, resources and support structure available to the community, and future development plans.

Changes in the near-surface shear layer of the Sun

H.M.**Antia**, Sarbani Basu

ApJ **924** 19 **2022**

https://arxiv.org/pdf/2110.13952

https://iopscience.iop.org/article/10.3847/1538-4357/ac32c3/pdf

https://doi.org/10.3847/1538-4357/ac32c3

We use helioseismic data obtained over two solar cycles to determine whether there are changes in the near-surface shear layer (NSSL). We examine this by determining the radial gradient of the solar rotation rate. The radial gradient itself shows a solar-cycle dependence, and the changes are more pronounced in the active latitudes than at adjoining higher latitudes; results at the highest latitudes (greater than about70 degrees) are unreliable. The pattern changes with depth, even within the NSSL. We find that the near-surface shear layer is deeper at lower latitudes than at high latitudes and that the extent of the layer also shows a small solar-cycle related change.

On the magnetic field required for driving the observed angular-velocity variations in the solar convection zone

H. M. **Antia**, S. M. Chitre & D. O. Gough

E-print, Oct **2012**, MNRAS

A putative temporally varying circulation-free magnetic-field configuration is inferred in an equatorial segment of the solar convection zone from the helioseismologically inferred angular-velocity variation, assuming that the predominant dynamics is angular acceleration produced by the azimuthal Maxwell stress exerted by a field whose surface values are consistent with photospheric line-of-sight measurements.

The Structure and Dynamics of the Corona—Heliosphere Connection **Review**

Spiro K. **Antiochos**, Jon A. Linker, Roberto Lionello, Zoran Mikić, Viacheslav Titov, Thomas H. Zurbuchen

Space Science Reviews, November **2012**, Volume 172, Issue 1-4, pp 169-185

Determining how the heliospheric magnetic field and plasma connect to the Sun's corona and photosphere is, perhaps, the central problem in solar and heliospheric physics. For much of the heliosphere, this connection appears to be well understood. It is now generally accepted that so-called coronal holes, which appear dark in X-rays and are predominantly unipolar at the photosphere, are the sources of quasi-steady wind that is generally fast, >500 km/s, but can sometimes be slow. However, the connection to the Sun of the slow, non-steady wind is far from understood and remains a major mystery. We review the existing theories for the sources of the non-steady wind and demonstrate that they have difficulty accounting for both the observed composition of the wind and its large angular extent. A new theory is described in which this wind originates from the continuous opening and closing of narrow open field corridors in the corona, which give rise to a web of separatrices (the S-Web) in the heliosphere. Note that in this theory the corona—heliosphere connection is intrinsically dynamic, at least for this type of wind. Support for the S-Web model is derived from MHD solutions for the corona and wind during the time of the August 1, 2008 eclipse. Additionally, we perform fully dynamic numerical simulations of the corona and heliosphere in order to test the S-Web model as well as the interchange model proposed by Fisk and co-workers. We discuss the implications of our simulations for the competing theories and for understanding the corona—heliosphere connection, in general.

EUV fine structure and variability associated with coronal rain revealed by Solar Orbiter/EUI HRIEUV and SPICE

P. **Antolin**, A. Dolliou, F. Auchère, L. P. Chitta, S. Parenti, D. Berghmans, +++

A&A 676, A112 **2023**

https://arxiv.org/pdf/2305.11691.pdf

https://www.aanda.org/articles/aa/pdf/2023/08/aa46016-23.pdf

Coronal rain is the most dramatic cooling phenomenon of the solar corona and an essential diagnostic tool for the coronal heating properties. A puzzling feature of the solar corona, besides the heating, is its EUV filamentary structure and variability. We aim to identify observable features of the TNE-TI scenario underlying coronal rain at small and large spatial scales, to understand the role it plays in the solar corona. We use EUV datasets at unprecedented spatial resolution of ~240 km from EUI/HRIEUV and SPICE of Solar Orbiter from the spring 2022 perihelion. EUV absorption features produced by coronal rain are detected at scales as small as 260 km. As the rain falls, heating and compression is produced immediately downstream, leading to a small EUV brightening accompanying the fall and producing a "fireball" phenomenon. Just prior to impact, a flash-like EUV brightening downstream of the rain, lasting a few minutes is observed for the fastest events. For the first time, we detect the atmospheric response to the rain's impact on the chromosphere and consists of upward propagating rebound shocks and flows partly reheating the loop. The observed widths of the rain clumps are 500 +- 200 km. They exhibit a broad velocity distribution of 10 - 150 km s^-1, peaking below 50 km s^-1. Coronal strands of similar widths are observed along the same loops co-spatial with cool filamentary structure, which we interpret as the CCTR. Matching with the

expected cooling, prior to the rain appearance sequential loop brightenings are detected in gradually cooler lines from corona to chromospheric temperatures. Despite the large rain showers, most cannot be detected in AIA 171 in quadrature, indicating that LOS effects play a major role in coronal rain visibility. Still, AIA 304 and SPICE observations reveal that only a small fraction of the rain can be captured by HRIEUV. **2022: March 30, April 1**
Solar Orbiter nugget #14 2023 *https://www.cosmos.esa.int/web/solar-orbiter/-/science-nugget-a-sharp-eui-and-spice-look-into-the-euv-variability-and-fine-scale-str*

Multi-Scale Variability of Coronal Loops Set by Thermal Non-Equilibrium and Instability as a Probe for Coronal Heating

Patrick **Antolin**1* and Clara Froment2*
Front. Astron. Space Sci., 9: 820116 **2022** |
https://www.frontiersin.org/articles/10.3389/fspas.2022.820116/full
https://doi.org/10.3389/fspas.2022.820116
Solar coronal loops are the building blocks of the solar corona. These dynamic structures are shaped by the magnetic field that expands into the solar atmosphere. They can be observed in X-ray and extreme ultraviolet (EUV), revealing the high plasma temperature of the corona. However, the dissipation of magnetic energy to heat the plasma to millions of degrees and, more generally, the mechanisms setting the mass and energy circulation in the solar atmosphere are still a matter of debate. Furthermore, multi-dimensional modelling indicates that the very concept of a coronal loop as an individual entity and its identification in EUV images is ill-defined due to the expected stochasticity of the solar atmosphere with continuous magnetic connectivity changes combined with the optically thin nature of the solar corona. In this context, the recent discovery of ubiquitous long-period EUV pulsations, the observed coronal rain properties and their common link in between represent not only major observational constraints for coronal heating theories but also major theoretical puzzles. The mechanisms of thermal non-equilibrium (TNE) and thermal instability (TI) appear in concert to explain these multi-scale phenomena as evaporation-condensation cycles. Recent numerical efforts clearly illustrate the specific but large parameter space involved in the heating and cooling aspects, and the geometry of the loop affecting the onset and properties of such cycles. In this review we will present and discuss this new approach into inferring coronal heating properties and understanding the mass and energy cycle based on the multi-scale intensity variability and cooling properties set by the TNE-TI scenario. We further discuss the major numerical challenges posed by the existence of TNE cycles and coronal rain, and similar phenomena at much larger scales in the Universe.

Reconnection nanojets in the solar corona

Antolin, Patrick; Pagano, Paolo; Testa, Paola; Petralia, Antonino; Reale, Fabio
Nature Astronomy, Volume 5, p. 54-62, **2021**
https://www.nature.com/articles/s41550-020-1199-8#citeas
https://doi.org/10.1038/s41550-020-1199-8
The solar corona is shaped and mysteriously heated to millions of degrees by the Sun's magnetic field. It has long been hypothesized that the heating results from a myriad of tiny magnetic energy outbursts called nanoflares, driven by the fundamental process of magnetic reconnection. Misaligned magnetic field lines can break and reconnect, producing nanoflares in avalanche-like processes. However, no direct and unique observations of such nanoflares exist to date, and the lack of a smoking gun has cast doubt on the possibility of solving the coronal heating problem. From coordinated multi-band high-resolution observations, we report on the discovery of very fast and bursty nanojets, the telltale signature of reconnection-based nanoflares resulting in coronal heating. Using state-of-the-art numerical simulations, we demonstrate that the nanojet is a consequence of the slingshot effect from the magnetically tensed, curved magnetic field lines reconnecting at small angles. Nanojets are therefore the key signature of reconnection-based coronal heating in action.
IRIS Nugget, May **2021**, https://iris.lmsal.com/nugget

In-situ generation of transverse MHD waves from colliding flows in the solar corona

Patrick **Antolin**, Paolo Pagano, Ineke De Moortel, Valery M. Nakariakov
ApJL **861** L15 **2018**
https://arxiv.org/pdf/1807.00395.pdf
Transverse MHD waves permeate the solar atmosphere and are a candidate for coronal heating. However, the origin of these waves is still unclear. In this work, we analyse coordinated observations from \textit{Hinode}/SOT and \textit{IRIS} of a prominence/coronal rain loop-like structure at the limb of the Sun. Cool and dense downflows and upflows are observed along the structure. A collision between a downward and an upward flow with an estimated energy flux of 107−108~erg~cm−2~s−1 is observed to generate oscillatory transverse perturbations of the strands with an estimated ≈40 km~s−1 total amplitude, and a short-lived brightening event with the plasma temperature increasing to at least 105 K. We interpret this response as sausage and kink transverse MHD waves based on 2D MHD simulations of plasma flow collision. The lengths, density and velocity differences between the colliding clumps and the strength of the magnetic field are major parameters defining the response to the collision. The

presence of asymmetry between the clumps (angle of impact surface and/or offset of flowing axis) is crucial to generate a kink mode. Using the observed values we successfully reproduce the observed transverse perturbations and brightening, and show adiabatic heating to coronal temperatures. The numerical modelling indicates that the plasma β in this loop-like structure is confined between 0.09 and 0.36. These results suggest that such collisions from counter-streaming flows can be a source of in-situ transverse MHD waves, and that for cool and dense prominence conditions such waves could have significant amplitudes. **April 3rd, 2014**

Transverse Wave Induced Kelvin-Helmholtz Rolls in Spicules

Patrick **Antolin**, Don Schmit, Tiago M. D. Pereira, Bart De Pontieu, Ineke De Moortel
ApJ **2018**
https://arxiv.org/pdf/1803.00821.pdf
In addition to their jet-like dynamic behaviour, spicules usually exhibit strong transverse speeds, multi-stranded structure and heating from chromospheric to transition region temperatures. In this work we first analyse \textit{Hinode} \& \textit{IRIS} observations of spicules and find different behaviours in terms of their Doppler velocity evolution and collective motion of their sub-structure. Some have a Doppler shift sign change that is rather fixed along the spicule axis, and lack coherence in the oscillatory motion of strand-like structure, matching rotation models or long wavelength torsional Alfv\'en waves. Others exhibit a Doppler shift sign change at maximum displacement and coherent motion of their strands, suggesting a collective MHD wave. By comparing with an idealised 3-D MHD simulation combined with radiative transfer modelling, we analyse the role of transverse MHD waves and associated instabilities in spicule-like features. We find that Transverse Wave Induced Kelvin-Helmholtz (TWIKH) rolls lead to coherence of strand-like structure in imaging and spectral maps, as seen in some observations. The rapid transverse dynamics and the density and temperature gradients at the spicule boundary lead to ring-shaped \ion{Mg}{2} k and \ion{Ca}{2} H source functions in the transverse cross-section, potentially allowing IRIS to capture the KHI dynamics. Twists and currents propagate along the spicule at Alfv\'enic speeds, and the temperature variations within TWIKH rolls produce sudden appearance / disappearance of strands seen in Doppler velocity and in \ion{Ca}{2} H intensity. However, only a mild intensity increase in higher temperature lines is obtained, suggesting there is an additional heating mechanism at work in spicules. **2014-04-29**

Trick or TWIKH Spicules

Patrick **Antolin**, Ineke De Moortel, Don Schmit, Bart De Pontieu, Tiago M. D. Pereira
UKSP Nugget #95 **2018**
http://www.uksolphys.org/uksp-nugget/95-trick-or-twikh-spicules/
The swaying motion of the kink wave induces shear flows at the edges of the flux tube that are expected to lead to Kelvin-Helmholtz instabilities. Despite our very simple spicule model, we have shown that kink modes lead to TWIKH rolls that can successfully explain several aspects of spicules: **2014-04-29**

Observational Signatures of Transverse Magnetohydrodynamic Waves and Associated Dynamic Instabilities in Coronal Flux Tubes

P. **Antolin**1, I. De Moortel1, T. Van Doorsselaere2, and T. Yokoyama
2017 ApJ 836 219
Magnetohydrodynamic (MHD) waves permeate the solar atmosphere and constitute potential coronal heating agents. Yet, the waves detected so far may be but a small subset of the true existing wave power. Detection is limited by instrumental constraints but also by wave processes that localize the wave power in undetectable spatial scales. In this study, we conduct 3D MHD simulations and forward modeling of standing transverse MHD waves in coronal loops with uniform and non-uniform temperature variation in the perpendicular cross-section. The observed signatures are largely dominated by the combination of the Kelvin–Helmholtz instability (KHI), resonant absorption, and phase mixing. In the presence of a cross-loop temperature gradient, we find that emission lines sensitive to the loop core catch different signatures compared to those that are more sensitive to the loop boundary and the surrounding corona, leading to an out-of-phase intensity and Doppler velocity modulation produced by KHI mixing. In all of the considered models, common signatures include an intensity and loop width modulation at half the kink period, a fine strand-like structure, a characteristic arrow-shaped structure in the Doppler maps, and overall line broadening in time but particularly at the loop edges. For our model, most of these features can be captured with a spatial resolution of $0\farcs33$ and a spectral resolution of 25 km s^{-1}, although we do obtain severe over-estimation of the line width. Resonant absorption leads to a significant decrease of the observed kinetic energy from Doppler motions over time, which is not recovered by a corresponding increase in the line width from phase mixing and KHI motions. We estimate this hidden wave energy to be a factor of 5–10 of the observed value.

Modelling observed decay-less oscillations as resonantly enhanced Kelvin-Helmholtz vortices from transverse MHD waves and their seismological application

Patrick **Antolin**, Ineke De Moortel, Tom Van Doorsselaere, Takaaki Yokoyama
ApJL 830 L22 **2016**
https://arxiv.org/pdf/1609.09716v1.pdf
In the highly structured solar corona, resonant absorption is an unavoidable mechanism of energy transfer from global transverse MHD waves to local azimuthal Alfv\'en waves. Due to its localised nature, a direct detection of this mechanism is extremely difficult. Yet, it is the leading theory explaining the observed fast damping of the global transverse waves. However, at odds with this theoretical prediction, recent observations indicate that in the low amplitude regime such transverse MHD waves can also appear decay-less, a yet unsolved phenomenon. Recent numerical work has shown that Kelvin-Helmholtz instabilities (KHI) often accompany transverse MHD waves. In this work, we combine 3D MHD simulations and forward modelling to show that for currently achieved spatial resolution and observed small amplitudes, an apparent decay-less oscillation is obtained. This effect results from the combination of periodic brightenings produced by the KHI and the coherent motion of the KHI vortices amplified by resonant absorption. Such effect is especially clear in emission lines forming at temperatures that capture the boundary dynamics rather than the core, and reflects the low damping character of the local azimuthal Alfv\'en waves resonantly coupled to the kink mode. Due to phase mixing, the detected period can vary depending on the emission line, with those sensitive to the boundary having shorter periods than those sensitive to the loop core. This allows to estimate the density contrast at the boundary.

The multi-thermal and multi-stranded nature of coronal rain

P. **Antolin**, G. Vissers, T. M. D. Pereira, L. Rouppe van der Voort, E. Scullion
ApJ **806** 81 **2015**
http://arxiv.org/pdf/1504.04418v1.pdf
In this work, we analyse coordinated observations spanning chromospheric, TR and coronal temperatures at very high resolution which reveal essential characteristics of thermally unstable plasmas. Coronal rain is found to be a highly multi-thermal phenomenon with a high degree of co-spatiality in the multi-wavelength emission. EUV darkening and quasi-periodic intensity variations are found to be strongly correlated to coronal rain showers. Progressive cooling of coronal rain is observed, leading to a height dependence of the emission. A fast-slow two-step catastrophic cooling progression is found, which may reflect the transition to optically thick plasma states. The intermittent and clumpy appearance of coronal rain at coronal heights becomes more continuous and persistent at chromospheric heights just before impact, mainly due to a funnel effect from the observed expansion of the magnetic field. Strong density inhomogeneities on spatial scales of 0.2"-0.5" are found, in which TR to chromospheric temperature transition occurs at the lowest detectable scales. The shape of the distribution of coronal rain widths is found to be independent of temperature with peaks close to the resolution limit of each telescope, ranging from 0.2" to 0.8". However we find a sharp increase of clump numbers at the coolest wavelengths and especially at higher resolution, suggesting that the bulk of the rain distribution remains undetected. Rain clumps appear organised in strands in both chromospheric and TR temperatures, suggesting an important role of thermal instability in the shaping of fundamental loop substructure. We further find structure reminiscent of the MHD thermal mode. Rain core densities are estimated to vary between 2x10^{10} cm^{-3} and 2.5x10^{11} cm^{-3} leading to significant downward mass fluxes per loop of 1-5x10^{9} g s^{-1}, suggesting a major role in the chromosphere-corona mass cycle. **26 June 2010, 29th November 2013,**

Five Solar Cycles of Solar Corona Investigations

Ester **Antonucci**
Solar Physics volume 297, Article number: 89 (**2022**)
https://link.springer.com/content/pdf/10.1007/s11207-022-02007-3.pdf
These are the **memoirs** of fifty years of research in solar physics, closely related to the history of three of the major solar space missions, from the Solar Maximum Mission, SMM, to Solar Orbiter, at present in navigation toward vantage points closer and closer to the Sun. My interest in solar physics was stimulated by the studies on cosmic rays at the University of Turin, and the research in this field initiated at Stanford University as a postdoctoral fellow in the team of John Wilcox with studies on the large-scale corona and its rotation. Thanks to Alan Gabriel, during my first space mission, SMM, I was involved in the operations and scientific data analysis of the Soft X-ray Polychromator. Together with Giancarlo Noci and Giuseppe Tondello, I participated in the realization of the UltraViolet Coronagraph Spectrometer, NASA/ASI, flown on-board SOHO. After this experience there was the opportunity to participate in the formulation of the proposal of the Solar Orbiter mission, and to guide the team, which for this mission developed the Metis coronagraph, up to the delivery of the instrument to the European Space Agency in 2017.

Observations of the Solar Corona from Space **Review**

Ester **Antonucci**, Louise Harra, Roberto Susino & Daniele Telloni
Space Science Reviews volume 216, Article number: 117 (**2020**)

https://link.springer.com/content/pdf/10.1007/s11214-020-00743-1.pdf
https://link.springer.com/article/10.1007/s11214-020-00743-1
Space observations of the atmosphere of the Sun, obtained in half a century of dedicated space missions, provide a well established picture of the medium and large-scale solar corona, which is highly variable with the level of solar activity through a solar cycle and evolves with the long-term evolution of the magnetic cycles. In this review, we summarize the physical properties and dynamics of the medium and large-scale corona, consisting primarily of ***active regions, streamers and coronal holes***; describe the dependence of coronal patterns on the magnetic field patterns changing through the solar cycle and the properties of the regions of open magnetic flux channeling the solar wind; the ubiquitous presence of fluctuations in the outer corona; the rotational properties of the large-scale corona; and the persistent hemispheric asymmetries in the emergence of magnetic fields and the distribution of the coronal emission. **August 10, 1996, August 19 and September 1, 1996, August 26, 1996, April 18, 2008, 2011-02-14**

Metis: the Solar Orbiter visible light and ultraviolet coronal imager

Ester **Antonucci**, Marco Romoli, Vincenzo Andretta, Silvano Fineschi, Petr Heinzel, et al.
A&A 642, A10 (**2020**)
https://arxiv.org/pdf/1911.08462.pdf
https://www.aanda.org/articles/aa/pdf/2020/10/aa35338-19.pdf
Aims. Metis is the first solar coronagraph designed for a space mission and is capable of performing simultaneous imaging of the off-limb solar corona in both visible and UV light. The observations obtained with Metis aboard the Solar Orbiter ESA-NASA observatory will enable us to diagnose, with unprecedented temporal coverage and spatial resolution, the structures and dynamics of the full corona in a square field of view (FoV) of ±2.9 ◦ in width, with an inner circular FoV at 1.6◦ , thus spanning the solar atmosphere from 1.7 R to about 9 R , owing to the eccentricity of the spacecraft orbit. Due to the uniqueness of the Solar Orbiter mission profile, Metis will be able to observe the solar corona from a close (0.28 AU, at the closest perihelion) vantage point, achieving increasing out-of-ecliptic views with the increase of the orbit inclination over time. Moreover, observations near perihelion, during the phase of lower rotational velocity of the solar surface relative to the spacecraft, allow longer-term studies of the off-limb coronal features, thus finally disentangling their intrinsic evolution from effects due to solar rotation. Methods. Thanks to a novel occultation design and a combination of a UV interference coating of the mirrors and a spectral bandpass filter, Metis images the solar corona simultaneously in the visible light band, between 580 and 640 nm, and in the UV H i Lyman-α line at 121.6 nm. The visible light channel also includes a broadband polarimeter able to observe the linearly polarised component of the K corona. The coronal images in both the UV H i Lyman-α and polarised visible light are obtained at high spatial resolution with a spatial scale down to about 2000 km and 15000 km at perihelion, in the cases of the visible and UV light, respectively. A temporal resolution down to 1 second can be achieved when observing coronal fluctuations in visible light. Results. The Metis measurements, obtained from different latitudes, will allow for complete characterisation of the main physical parameters and dynamics of the electron and neutral hydrogen/proton plasma components of the corona in the region where the solar wind undergoes the acceleration process and where the onset and initial propagation of coronal mass ejections (CMEs) take place. The near-Sun multi-wavelength coronal imaging performed with Metis, combined with the unique opportunities offered by the Solar Orbiter mission, can effectively address crucial issues of solar physics such as: the origin and heating/acceleration of the fast and slow solar wind streams; the origin, acceleration, and transport of the solar energetic particles; and the transient ejection of coronal mass and its evolution in the inner heliosphere, thus significantly improving our understanding of the region connecting the Sun to the heliosphere and of the processes generating and driving the solar wind and coronal mass ejections. Conclusions. This paper presents the scientific objectives and requirements, the overall optical design of the Metis instrument, the thermomechanical design, and the processing and power unit; reports on the results of the campaigns dedicated to integration, alignment, and tests, and to the characterisation of the instrument performance; describes the operation concept, data handling, and software tools; and, finally, the diagnostic techniques to be applied to the data, as well as a brief description of the expected scientific products. The performance of the instrument measured during calibrations ensures that the scientific objectives of Metis can be pursued with success.
2. Scientific objectives

Statistical evolution of quiet-Sun small scale magnetic features using Sunrise observations

L. S. **Anusha**, Sami K. Solanki, Johann Hirzberger, Alex Feller
A&A 598, A47 (**2017**)
http://arxiv.org/pdf/1608.08499v1.pdf
The evolution of small magnetic features in quiet regions of the Sun provides a unique window to probing solar magneto-convection. Here we analyze small scale magnetic features in the quiet Sun, using the high resolution, seeing-free observations from the Sunrise balloon borne solar observatory. Our aim is to understand the contribution of different physical processes, such as splitting, merging, emergence and cancellation of magnetic fields to the rearrangement, addition and removal of magnetic flux in the photosphere. We employ a statistical approach for the analysis and the evolution studies are carried out using a feature tracking technique. In this paper we provide a

detailed description of the feature tracking algorithm that we have newly developed and we present the results of a statistical study of several physical quantities. The results on the fractions of the flux in the emergence, appearance, splitting, merging, disappearance and cancellation qualitatively agrees with other recent studies. To summarize, the total flux gained in unipolar appearance is an order of magnitude larger than the total flux gained in emergence. On the other hand, the bi-polar cancellation contributes nearly an equal amount to the loss of magnetic flux as unipolar disappearance. The total flux lost in cancellation is nearly 6−8times larger than the total flux gained in emergence. One big difference between our study and previous similar studies is that thanks to the higher spatial resolution of Sunrise we can track features with fluxes as low as 9×1014 Mx. This flux is nearly an order of magnitude lower than the smallest fluxes of the features tracked in the highest resolution previous studies based on Hinode data

Prediction of the Maximum Amplitude of Solar Cycle 25 Using the Ascending Inflection Point

A. J. P. **Aparicio**, V. M. S. Carrasco & J. M. Vaquero
Solar Phys. 298, Article number: 100 (**2023**)
https://link.springer.com/content/pdf/10.1007/s11207-023-02194-7.pdf
In this work, we predict the maximum amplitude (using the 13-month smoothed Solar Influences Data Analysis Center (SILSO) Sunspot Number, version 2) of Solar Cycle 25 using as a predictor the slope of the inflection point during the ascending part of the cycle. After a description of the data and methodology employed in this work, we obtain a value of 131 ± 32 for the maximum amplitude of Solar Cycle 25. Finally, we discuss this result in the context of the current debate on the prediction of solar activity and compare it with other predictions of Solar Cycle 25 obtained by other methods.

A Sunspot Catalog for the Period 1952-1986 from Observations Made at the Madrid Astronomical Observatory

A.J.P. **Aparicio**, L. Lefèvre, M.C. Gallego, J.M. Vaquero, F. Clette, N. Bravo-Paredes, P. Galaviz, M.L. Bautista
Solar Phys. 293:164 **2018**
https://arxiv.org/ftp/arxiv/papers/1812/1812.01733.pdf
https://link.springer.com/content/pdf/10.1007%2Fs11207-018-1387-1.pdf
Sunspot catalogs are very useful for studying the solar activity of the recent past. In this context, a catalog covering more than three solar cycles made by the astronomers of the Madrid Astronomical Observatory in Spain (nowadays, the National Astronomical Observatory) from 1952 until 1986 has been recovered. Moreover, a machine-readable version of this catalog has been made available. We have recovered abundant metadata and studied the reliability of this dataset by comparing it with other sunspot catalogs.

Helioseismic Constraints: Past, Current, and Future Observations. Review

Appourchaux, T.
Sol Phys 299, 155 (**2024**).
https://doi.org/10.1007/s11207-024-02403-x
This paper would never have been written without the long support of my beloved wife, Maryse, all the time by my side during my Science career, from University to retirement...hard to believe. I am extremely grateful to Nathalie Esch for proofreading the English; perfection is for tomorrow. I am also grateful to John Leibacher for providing reprints of hard to find papers, and for fruitful discussions. Many thanks to Patrick Boumier for providing me with a scanned version of the GOLF proposal. I am grateful to Hannah Schunker for providing the keys to access HMI and MDI data. Many thanks to Eric Buchlin for giving me the tricks to get the SDO-Sun distance. This work utilizes data from the National Solar Observatory Integrated Synoptic Program, which is operated by the Association of Universities for Research in Astronomy, under a cooperative agreement with the National Science Foundation and with additional financial support from the National Oceanic and Atmospheric Administration, the National Aeronautics and Space Administration, and the United States Air Force. The GONG network of instruments is hosted by the Big Bear Solar Observatory, High Altitude Observatory, Learmonth Solar Observatory, Udaipur Solar Observatory, Instituto de Astrofísica de Canarias, and Cerro Tololo Interamerican Observatory. SoHO is a mission of international collaboration between ESA and NASA. This paper uses data from the HMI instrument aboard SDO. Solar Orbiter is a space mission of international collaboration between ESA and NASA, operated by ESA. I am grateful for the PHI team for their collaboration and contribution especially at IAS, Jean-Jacques Fourmond, Mehdi Bouzit, Claudia Ruiz de Galarreta, Véronique Hervier, Bruno Crane; at Observatoire de Paris-Meudon, the late Régis Le Cocguen; at MPS, Joachim Woch, Achim Gandorfer, Johann Hirzberger and Jesper Schou. The FG contribution to PHI was funded by CNES. This research has made use of the Astrophysics Data System, funded by NASA under Cooperative Agreement 80NSSC21M00561. Comptes rendus de l'Académie des Sciences are gracefully provided by gallica.bnf.fr (Bibliothèque nationale de France).

Searching for g modes: Part II. Unconfirmed g-mode detection in the power spectrum of the time series of round-trip travel time

T.**Appourchaux**, T.Corbard
A&A 624, A106 **2019**
https://arxiv.org/pdf/1903.03791.pdf
https://www.aanda.org/articles/aa/pdf/2019/04/aa35196-19.pdf

Context. The recent claims of g-mode detection have restarted the search for these potentially extremely important modes. The claimed detection of g modes was obtained from the analysis of the power spectrum of the time series of round-trip travel time of p modes.
Aims. The goal of this paper is to reproduce these results on which the claims are based for confirming or invalidating the detection of g modes with the method used to make the claims.
Methods. We computed the time series of round-trip travel time using the procedure given in Fossat et al. (2017), and used different variations of the times series for comparison. We used the recently calibrated GOLF data (published in Paper I) with different sampling, different photomultipliers, different length of data for reproducing the analysis. We also correlated the power spectrum with an asymptotic model of g-mode frequencies in a similar manner to Fossat and Schmider (2018). We devised a scheme for optimising the correlation both for pure noise and for the GOLF data.
Results. We confirm the analysis performed in Fossat et al. (2017) but draw different conclusions. Their claims of detection of g modes cannot be confirmed when changing parameters such as sampling interval, length of time series, or photomultipliers. Other instrument such as GONG and BiSON do not confirm their detection. We also confirm the analysis performed in Fossat and Schmider (2018), but again draw different conclusions. For GOLF, the correlation of the power spectrum with the asymptotic model of g-mode frequencies for l = 1 and l = 2 show a high correlation at lag=0 and at lag corresponding to the rotational splitting νl , but the same occurs for pure noise due to the large number of peaks present in the model. In addition, other very different parameters defining the asymptotic model also provide a high correlation at these lags. We conclude that the detection performed in Fossat and Schmider (2018) is an artefact of the methodology

Searching for g modes
I. A new calibration of the GOLF instrument⋆

T. **Appourchaux**1, P. Boumier1, J. W. Leibacher1,2,3 and T. Corbard4
A&A 617, A108 (**2018**)
https://doi.org/10.1051/0004-6361/201833535

Context. The recent claims of g-mode detection have restarted the search for these potentially extremely important modes. These claims can be reassessed in view of the different data sets available from the SoHO instruments and ground-based instruments.
Aims. We produce a new calibration of the GOLF data with a more consistent p-mode amplitude and a more consistent time shift correction compared to the time series used in the past.
Methods. The calibration of 22 yr of GOLF data is done with a simpler approach that uses only the predictive radial velocity of the SoHO spacecraft as a reference. Using p modes, we measure and correct the time shift between ground- and space-based instruments and the GOLF instrument.
Results. The p-mode velocity calibration is now consistent to within a few percent with other instruments. The remaining time shifts are within ±5 s for 99.8% of the time series.

The quest for the solar g modes

T. **Appourchaux**, K. Belkacem, A.-M. Broomhall, et al.
Astronomy and Astrophysics Review, Volume 18, Numbers 1-2 / Февраль **2010** г., p. 197-277

Solar gravity modes (or g modes)—oscillations of the solar interior on which buoyancy acts as the restoring force—have the potential to provide unprecedented inference on the structure and dynamics of the solar core, inference that is not possible with the well-observed acoustic modes (or p modes). The relative high amplitude of the g-mode eigenfunctions in the core and the evanesence of the modes in the convection zone make the modes particularly sensitive to the physical and dynamical conditions in the core. Owing to the existence of the convection zone, the g modes have very low amplitudes at photospheric levels, which makes the modes extremely hard to detect. In this article, we review the current state of play regarding attempts to detect g modes. We review the theory of g modes, including theoretical estimation of the g-mode frequencies, amplitudes and damping rates. Then we go on to discuss the techniques that have been used to try to detect g modes. We review results in the literature, and finish by looking to the future, and the potential advances that can be made—from both data and data-analysis perspectives—to give unambiguous detections of individual g modes. The review ends by concluding that, at the time of writing, there is indeed a consensus amongst the authors that *there is currently no undisputed detection of solar g modes*.

Alfvén Wave Heating of the Solar Chromosphere: 1.5D models

T.D. **Arber**, C.S. Brady, S. Shelyag

ApJ 817 94 **2016**
http://arxiv.org/pdf/1512.05816v1.pdf
Physical processes which may lead to solar chromospheric heating are analyzed using high-resolution 1.5D non-ideal MHD modelling. We demonstrate that it is possible to heat the chromospheric plasma by direct resistive dissipation of high-frequency Alfv\'en waves through Pedersen resistivity. However this is unlikely to be sufficient to balance radiative and conductive losses unless unrealistic field strengths or photospheric velocities are used. The precise heating profile is determined by the input driving spectrum since in 1.5D there is no possibility of Alfv\'en wave turbulence. The inclusion of the Hall term does not affect the heating rates. If plasma compressibility is taken into account, shocks are produced through the ponderomotive coupling of Alfv\'en waves to slow modes and shock heating dominates the resistive dissipation. In 1.5D shock coalescence amplifies the effects of shocks and for compressible simulations with realistic driver spectra the heating rate exceeds that required to match radiative and conductive losses. Thus while the heating rates for these 1.5D simulations are an overestimate they do show that ponderomotive coupling of Alfv\'en waves to sound waves is more important in chromospheric heating than Pedersen dissipation through ion-neutral collisions.

Magnetic flux emergence in the Sun
V. **Archontis**
JGR, VOL. 113, A03S04, doi:10.1029/2007JA012422, **2008**
http://www.agu.org/pubs/crossref/2008/2007JA012422.shtml
Space weather research is closely connected with the study of the solar magnetic activity. In past years, many solar missions (e.g., YOHKOH, SOHO, TRACE, and RHESSI) have provided outstanding observations, which have been used to improve our understanding of the structure and the dynamical evolution of solar magnetic fields. In addition, the newly launched solar missions (e.g., Hinode and STEREO) will study the interaction between the emerging magnetic field and the preexisting field in the corona (increasing our understanding of the causes of solar variability), and they will also observe the three-dimensional evolution of solar eruptions as they leave the Sun and move into the interplanetary space. One of the most important processes, responsible for many dynamical phenomena observed in the Sun, is the emergence of magnetic flux from the solar interior in active regions and the modification of the coronal magnetic field in response to the emergence. In fact, magnetic flux emergence might be responsible for the appearance of small-scale events (e.g., compact flares, plasmoids, and active-region-associated X-ray brightenings) and large-scale events (e.g., X-class flares and CMEs), which are major drivers of space weather. However, it is clear that the question of how exactly the magnetic fields rise through the convection zone of the Sun and emerge through the photosphere and chromosphere into the corona has still not been solved. It is believed that understanding the process of flux emergence is an important step toward the understanding of the initiation mechanism of eruptive events in the Sun, which is another topic of great debate. **This paper provides a brief review of the theory and the numerical models, which have been used to study the process of magnetic flux emergence into the outer atmosphere of the Sun.** We underline the similarities and differences between these models, and we compare the basic features of the numerical results with observations. Finally, we review the recent progress and discuss what further developments are required in the models to best describe the essential physics in the process of flux emergence.

Measuring solar neutrinos over Gigayear timescales with Paleo Detectors
Natalia Tapia **Arellano**, Shunsaku Horiuchi
2021
https://arxiv.org/pdf/2102.01755.pdf
Measuring the solar neutrino flux over gigayear timescales could provide a new window to inform the Solar Standard Model as well as studies of the Earth's long-term climate. We demonstrate the feasibility of measuring the time-evolution of the 8B solar neutrino flux over gigayear timescales using paleo detectors, naturally occurring minerals which record neutrino-induced recoil tracks over geological times. We explore suitable minerals and identify track lengths of 15--30 nm to be a practical window to detect the 8B solar neutrino flux. A collection of ultra-radiopure minerals of different ages, each some 0.1 kg by mass, can be used to probe the rise of the 8B solar neutrino flux over the recent gigayear of the Sun's evolution. We also show that models of the solar abundance problem can be distinguished based on the time-integrated tracks induced by the 8B solar neutrino flux.

Proposed Resolution to the Solar Open Magnetic Flux Problem
C.Nick **Arge** (1), Andrew Leisner (2), Samantha Wallace (1), Carl J. Henney (3)
A&A **2023**
https://arxiv.org/pdf/2304.07649.pdf
The solar magnetic fields emerging from the photosphere into the chromosphere and corona are comprised of a combination of "closed" and "open" fields. The closed magnetic field lines are defined as those having both ends rooted in the solar surface, while the open field lines are those having one end extending out into interplanetary space and the other rooted at the Sun's surface. Since the early 2000's, the amount of total unsigned open magnetic

flux estimated by coronal models have been in significant disagreement with in situ spacecraft observations, especially during solar maximum. Estimates of total open unsigned magnetic flux using coronal hole observations (e.g., using extreme ultraviolet (EUV) or Helium (He) I) are in general agreement with the coronal model results and thus show similar disagreements with in situ observations. While several possible sources producing these discrepancies have been postulated over the years, there is still no clear resolution to the problem. This paper provides a brief overview of the problem and summarizes some proposed explanations for the discrepancies. In addition, two different ways of estimating the total unsigned open magnetic flux are presented, utilizing the Wang-Sheeley-Arge (WSA) model, and one of the methods produce surprisingly good agreement with in situ observations. The findings presented here suggest that active regions residing near the boundaries of mid-latitude coronal holes are the probable source of the missing open flux. This explanation also brings in line many of the seemly contradictory facts that have made resolving this problem so difficult.

Solar-cycle and Latitude Variations in the Internetwork Magnetism

Juan Carlos Trelles **Arjona**, María Jesús Martínez González, Basilio Ruiz Cobo
Astrophysical Journal, 944:95 **2023**
https://arxiv.org/ftp/arxiv/papers/2302/2302.07780.pdf
https://iopscience.iop.org/article/10.3847/1538-4357/acb64d/pdf
The importance of the quiet-Sun magnetism is that it is always there to a greater or lesser extent, being a constant provider of energy, independently of the solar cycle phase. The open questions about the quiet-Sun magnetism include those related to its origin. Most people claim that the local dynamo action is the mechanism that causes it. This fact would imply that the quiet-Sun magnetism is nearly the same at any location over the solar surface and at any time. Many works claim that the quiet Sun does not have any variation at all, although a few of them raise doubt on this claim and find mild evidence of a cyclic variation in the the quiet-Sun magnetism. In this work, we detect clear variations in the internetwork magnetism both with latitude and solar cycle. In terms of latitude, we find an increase in the averaged magnetic fields toward the solar poles. We also find long-term variations in the averaged magnetic field at the disk center and solar poles, and both variations are almost anticorrelated. These findings do not support the idea that the local dynamo action is the unique factory of the quiet-Sun magnetism.

Mapping the Hidden Magnetic Field of the Quiet Sun

J. C. Trelles **Arjona**1,2, M. J. Martínez González1,2, and B. Ruiz Cobo1,2
2021 ApJL 915 L20
https://doi.org/10.3847/2041-8213/ac0af2
The Sun is the only star where we can resolve the intricate magnetism that all convective stars harbor. Yet, more than 99% of its visible surface along the solar cycle (the so-called quiet Sun) is filled with a tangled, unresolved magnetism. These "hidden" fields are thought to store enough magnetic energy to play a role in the heating of the Sun's outer atmosphere, but its field strength is still not constrained. Previous investigations based on the Hanle effect in atomic lines claim a strong magnetization of about 100 G, while the same effect in molecules show a factor of 10 weaker fields. The discrepancy disappears if the magnetic field strength of the hidden field is not homogeneous in the solar surface. In this Letter, we prove using magnetohydrodynamical simulations that it is possible to infer the average field strength of the hidden quiet-Sun magnetic fields using multiline inversions of intensity profiles in the Zeeman regime. Using this technique with 15 spectral lines in the 1.5 μm spectral range, we reveal that the spatial distribution of the hidden field is strongly correlated with convection motions, and that the average magnetization is about 46 G. Reconciling our findings with the Hanle ones is not obvious and will require future work on both sides, since it implies an increase of the field strength with height, something that is physically questionable.

Extraction of Active Regions and Coronal Holes from EUV Images Using the Unsupervised Segmentation Method in the Bayesian Framework

S. **Arish**, M. Javaherian , H. Safari, A. Amiri
Solar Physics April **2016**, Volume 291, Issue 4, pp 1209-1224
The solar corona is the origin of very dynamic events that are mostly produced in active regions (AR) and coronal holes (CH). The exact location of these large-scale features can be determined by applying image-processing approaches to extreme-ultraviolet (EUV) data.
We here investigate the problem of segmentation of solar EUV images into ARs, CHs, and quiet-Sun (QS) images in a firm Bayesian way. On the basis of Bayes' rule, we need to obtain both prior and likelihood models. To find the prior model of an image, we used a Potts model in non-local mode. To construct the likelihood model, we combined a mixture of a Markov–Gauss model and non-local means. After estimating labels and hyperparameters with the Gibbs estimator, cellular learning automata were employed to determine the label of each pixel.
We applied the proposed method to a Solar Dynamics Observatory/Atmospheric Imaging Assembly (SDO/AIA) dataset recorded during 2011 and found that the mean value of the filling factor of ARs is 0.032 and 0.057 for CHs. The power-law exponents of the size distribution of ARs and CHs were obtained to be −1.597 and −1.508,

respectively, with the maximum likelihood estimator method. When we compare the filling factors of our method with a manual selection approach and the SPoCA algorithm, they are highly compatible.

Superoscillations in solar MHD waves and their possible role in heating coronal loops

A. López **Ariste** and M. Facchin
A&A 614, A145 (**2018**)
Aims. We aim to study the presence of superoscillations in coronal magnetoacoustic (MHD) waves and their possible role in heating coronal loops through the strong and localised gradients that they generate on the wave.
Methods. An analytic model is built for the transition between sausage and kink wave modes propagating along field lines in the corona. We compute in this model the local frequencies, the wave gradients, and the associated heating rates due to compressive viscosity.
Results. We find superoscillations associated with the transition between wave modes accompanying the wave dislocation that shifts through the wave domain. Frequencies ten times higher than the normal frequency are found. This means that a typical three-minute coronal wave will oscillate locally in 10 to 20 s. Such high frequencies bring up strong gradients that efficiently dissipate the wave through compressive viscosity. We compute the associated heating rates; locally, they are very strong, largely compensating typical radiative losses.
Conclusions. We find a new heating mechanism associated to magnetoacoustic waves in the corona. Heating due to superoscillations only happens along particular field lines with small cross sections, comparable in size to coronal loops, inside the much larger magnetic flux tubes and wave propagation domain.

Mapping the hidden magnetic field of the quiet Sun

J. C. Trelles **Arjona**, M. J. Martínez González, B. Ruiz Cobo
ApJ **2021**
https://arxiv.org/pdf/2106.10546.pdf
The Sun is the only star where we can resolve the intricate magnetism that all convective stars harbor. Yet, more than 99% of its visible surface along the solar cycle (the so-called quiet Sun) is filled with a tangled, unresolved magnetism. These "hidden" fields are thought to store enough magnetic energy to play a role in the heating of the Sun's outer atmosphere, but its field strength is still not constrained. Previous investigations based on the Hanle effect in atomic lines claim a strong magnetization of about 100 G, while the same effect in molecules show a factor of 10 weaker fields. The discrepancy disappears if the magnetic field strength of the hidden is not homogeneous in the solar surface. In this letter, we prove using magnetohydrodynamical simulations that it is possible to infer the average field strength of the hidden quiet Sun magnetic fields using multi-line inversions of intensity profiles in the Zeeman regime. Using this technique with 15 spectral lines in the 1.5 μm spectral range, we reveal that the spatial distribution of the hidden field is strongly correlated with convection motions, and that the average magnetization is about 46 G. Reconciling our findings with the Hanle ones is not obvious and will require future work on both sides, since it implies an increase of the field strength with height, something that is physically questionable.

Sunspot positions, areas, and group tilt angles for 1611-1631 from observations by Christoph Scheiner

R. **Arlt**, V. Senthamizh Pavai, C. Schmiel, F. Spada
A&A 595, A104 **2016**
http://arxiv.org/pdf/1608.07172v1.pdf
Digital images of the observations printed in the books "Rosa Ursina sive solis" and "Prodromus pro sole mobili" by Christoph Scheiner as well as the drawings from Scheiner's letters to Marcus Welser are analysed in order to obtain information on positions and sizes of sunspots that appeared before the Maunder minimum. In most cases, the given orientation of the ecliptic is used to set up the heliographic coordinate system for the drawings. Positions and sizes are measured manually on the screen. Very early drawings have no indication of their orientation. A rotational matching using common spots of adjacent days is used in some cases, while in other cases, the assumption of images being aligned with a zenith-horizon coordinate system appeared to be the most probable. In total, 8167 sunspots were measured. A distribution of sunspot latitudes versus time (butterfly diagram) is obtained for Scheiner's observations. The observations of 1611 are very inaccurate, the drawings of 1612 have at least an indication of their orientation, while the remaining part of the spot positions from 1618-1631 have good to very good accuracy. We also computed 697 tilt angles of apparently bipolar sunspot groups observed in the period 1618-1631. We find that the average tilt angle of nearly 4 degrees is not significantly different from 20th-century values.

Solar activity in the past and the chaotic behaviour of the dynamo

R. **Arlt**, N. Weiss
Space Science Reviews, **2014**
http://arxiv.org/pdf/1406.7628v1.pdf

The record of solar activity is reviewed here with emphasis on peculiarities. Since sunspot positions tell us a lot more about the solar dynamo than the various global sunspot numbers, we first focus on the records of telescopic observations of sunspots leading to positional information. Then we turn to the proxy record from cosmogenic isotope abundances, which shows recurrent grand minima over the last 9500 years. The apparent distinction between episodes of strong modulation, and intervening episodes with milder modulation and weaker overall activity, hints at the solar dynamo following a variety of solutions, with different symmetries, over the course of millennia.

Do MURaM and STAGGER Simulations of Solar Faculae Match Observational Signatures from Magnetic Structures?

Melania Cubas **Armas**1,2 and Damian Fabbian5,3,4
2021 ApJ 923 207
https://iopscience.iop.org/article/10.3847/1538-4357/ac2605/pdf
https://doi.org/10.3847/1538-4357/ac2605
We compare results of simulations of solar facular-like conditions performed using the numerical codes MURaM and STAGGER. Both simulation sets have a similar setup, including the initial condition of ≈200 G vertical magnetic flux. After interpolating the output physical quantities to constant optical depth, we compare them and test them against inversion results from solar observations. From the snapshots, we compute the monochromatic continuum in the visible and infrared, and the full Stokes vector of the Fe i spectral line pair around 6301–6302 Å. We compare the predicted spectral lines (at the simulation resolution and after smearing to the HINODE SP/SOT resolution) in terms of their main parameters for the Stokes I line profiles, and of their area and amplitude asymmetry for the Stokes V profiles. The codes produce magnetoconvection with similar appearance and distribution in temperature and velocity. The results also closely match the values from recent relevant solar observations. Although the overall distribution of the magnetic field is similar in both radiation-magnetohydrodynamic (RMHD) simulation sets, a detailed analysis reveals substantial disagreement in the field orientation, which we attribute to the differing boundary conditions. The resulting differences in the synthetic spectra disappear after spatial smearing to the resolution of the observations. We conclude that the two sets of simulations provide robust models of solar faculae. Nevertheless, we also find differences that call for caution when using results from RMHD simulations to interpret solar observational data.

Spatially resolved measurements of the solar photospheric oxygen abundance

Melania Cubas **Armas**, Andrés Asensio Ramos, Héctor Socas-Navarro
A&A 643, A142 **2020**
https://arxiv.org/pdf/2010.02151.pdf
https://doi.org/10.1051/0004-6361/202037849
https://www.aanda.org/articles/aa/pdf/2020/11/aa37849-20.pdf
Aims. We report the results of a novel determination of the solar oxygen abundance using spatially resolved observations and inversions. We seek to derive the photospheric solar oxygen abundance with a method that is robust against uncertainties in the model atmosphere.
Methods. We use observations with spatial resolution obtained at the Vacuum Tower Telescope (VTT) to derive the oxygen abundance at 40 different spatial positions in granules and intergranular lanes. We first obtain a model for each location by inverting the Fe I lines with the NICOLE inversion code. These models are then integrated into a hierarchical Bayesian model that is used to infer the most probable value for the oxygen abundance that is compatible with all the observations. The abundance is derived from the [O I] forbidden line at 6300 Å taking into consideration all possible nuisance parameters that can affect the abundance.
Results. Our results show good agreement in the inferred oxygen abundance for all the pixels analyzed, demonstrating the robustness of the analysis against possible systematic errors in the model. We find a slightly higher oxygen abundance in granules than in intergranular lanes when treated separately (log(\epsilon_O) = 8.83 \pm 0.02 vs log(\epsilon_O) = 8.76 \pm 0.02), which is a difference of approximately 2-{\sigma}. This tension suggests that some systematic errors in the model or the radiative transfer still exist but are small. When taking all pixels together, we obtain an oxygen abundance of log(\epsilon_O)=8.80 \pm 0.03, which is compatible with both granules and lanes within 1-{\sigma}. The spread of results is due to both systematic and random errors. **July 15 2016**

Fast Solar Image Classification Using Deep Learning and its Importance for Automation in Solar Physics

John A. **Armstrong**, Lyndsay Fletcher
Solar Phys. 294:80 **2019**
https://arxiv.org/pdf/1905.13575.pdf
sci-hub.se/10.1007/s11207-019-1473-z
The volume of data being collected in solar physics has exponentially increased over the past decade and with the introduction of the Daniel K. Inouye Solar Telescope (DKIST) we will be entering the age of petabyte solar data.

Automated feature detection will be an invaluable tool for post-processing of solar images to create catalogues of data ready for researchers to use. We propose a deep learning model to accomplish this; a deep convolutional neural network is adept at feature extraction and processing images quickly. We train our network using data from Hinode/Solar Optical Telescope (SOT) Hα images of a small subset of solar features with different geometries: filaments, prominences, flare ribbons, sunspots and the quiet Sun (i.e. the absence of any of the other four features). We achieve near perfect performance on classifying unseen images from SOT (≈99.9\%) in 4.66 seconds. We also for the first time explore transfer learning in a solar context. Transfer learning uses pre-trained deep neural networks to help train new deep learning models i.e. it teaches a new model. We show that our network is robust to changes in resolution by degrading images from SOT resolution (≈0.33″ at λ=6563\AA{}) to Solar Dynamics Observatory/Atmospheric Imaging Assembly (SDO/AIA) resolution (≈1.2″) without a change in performance of our network. However, we also observe where the network fails to generalise to sunspots from SDO/AIA bands 1600/1700\AA{} due to small-scale brightenings around the sunspots and prominences in SDO/AIA 304\AA{} due to coronal emission. **2008/02/07, 2010/09/25, 2011/02/15, 2013/01/01, 2017/07/10, 2017/09/06**

Solar Kaluza-Klein axion search with NEWS-G

NEWS-G collaboration: Q. **Arnaud**, L. Balogh, C. Beaufort, A. Brossard, et al.
2021
https://arxiv.org/pdf/2109.03562.pdf
Kaluza-Klein (KK) axions appear in theories with extra dimensions as higher mass, significantly shorter lifetime, excitations of the Peccei-Quinn axion. When produced in the Sun, they would remain gravitationally trapped in the solar system, and their decay to a pair of photons could provide an explanation of the solar corona heating problem. A low-density detector would discriminate such a signal from the background, by identifying the separation of the interaction point of the two photons. The NEWS-G collaboration uses large volume Spherical Proportional Counters, gas-filled metallic spheres with a spherical anode in their centre. After observation of a single axion-like event in a 42 day long run with the SEDINE detector, a 90% C.L. upper limit of gaγγ<7.76·10−13GeV−1 is set on the axion-photon coupling for a KK axion density on Earth of na=4.07·1013m−3 and two extra dimensions of size R=1eV−1.

Mid-term Periodicities in Solar Radio Emission Corresponding to Sunspot Number During Solar Cycle 23

Mahender **Aroori**, Panditi Vemareddy, Partha Chowdhury & Ganji Yellaiah
Solar Physics volume 296, Article number: 43 (**2021**)
https://doi.org/10.1007/s11207-021-01793-6
We present a systematic time-series analysis of solar radio emission in nine different frequencies to compare with that of daily sunspot number (SSN) during Solar Cycle 23 (1996–2009). Owing to the contribution from quiet-sun emission, the total solar fluxes in microwaves do not decrease as significantly as the sunspot number does during 2006 to 2009. Lomb–Scargle (LS) and wavelet analysis techniques are employed to infer the various periodicities present in the time-series data. False alarm probability (FAP) levels are estimated by the use of background mean power spectrum in the global wavelet spectrum. The LS periodogram contains resolved period peaks, some of which are below FAP levels, for example a well-known rotational period. These peaks are assessed with global significance levels of the wavelet analysis. In all the data sets, the period for solar rotational modulation (26–31 days) is present. The periodogram for the SSN presents Riéger type periods (130–180 days), mid-term periods (300–400 days) and long-term periods (430–850 days). These periods in north and south are not similar, especially long term periods are missing in SSN data of the southern hemisphere. Corresponding to the SSN periodicities, Riéger and near Riéger type of oscillations (130–180 days), quasi-biennial periodicities in the range of 1.2 to 3 years were detected in the time-series data of radio frequencies. Several of these detected periods fall in the range of the periods that are suggested to be connected with magneto-Rossby wave spherical harmonics. Our analysis found reduced power levels in the LS periodograms of low frequencies because of the fact that these low frequency emissions originate higher up in the corona with diminishing contrast to small scale structures.

Study of Local Heliospheric Current Sheet Variations from Multi-Spacecraft Observations

D. **Arrazola**, J. J. Blanco, J. Rodríguez-Pacheco, M. A. Hidalgo
Solar Physics, November **2012**, Volume 281, Issue 1, pp 263-280
The local magnetic structure of the heliospheric current sheet (HCS) is observed as a boundary through which the magnetic field inverts its direction toward or away from Sun. The local variability of the HCS has been studied by means of a comparison of its local orientation estimated from data of different spacecraft. With the aim of determining possible variations in the local orientation, the selected events have been grouped according to their magnetic connection. A rough estimate of the magnetic connection (C) between two observation points has been found by considering the absolute value of the difference between the elapsed and expected times (C=|Δt el – Δt ex|/Δt ex). Lower values of C imply better connections, and smaller variation in the HCS orientation is expected if variations, temporal or spatial, in the HCS shape are negligible. Two periods have been analyzed: the ascending

phase of Solar Cycle 23 and the minimum of the cycle in 2007 – 2008. It has been observed that, during the ascending phase, changes in the local HCS shape are mainly due to spatial variations. During minimum, the results show an increasing trend of the variation of the HCS local inclination with distance between spacecraft up to 5000 Earth radii (R E). For larger distances the results show a downward tendency. This inversion could be related to a continuous interaction of the HCS with the solar wind and with a poor magnetic connection, which could lead to changes in the local HCS shape making it unrecognizable to analyze the evolution of the structure from one observation point to another.

Coronal heating **Review**

Iñigo **Arregui**, Tom Van Doorsselaere

Chapter 10 of "Magnetohydrodynamic Processes in Solar Plasmas", A.K. Srivastava, M. Goossens and I. Arregui (eds). **2024**

https://arxiv.org/pdf/2409.13318

Coronal heating refers to the physical processes that shape and structure the corona of the Sun and are responsible for its multi-million Kelvin temperatures. These processes are revealed in a number of different observational manifestations and have been studied on theoretical grounds in great detail over the last eight decades. The aim of this Chapter is to give an account of some of those manifestations and to discuss relevant physics that we believe is responsible for them. Coronal heating is closely connected to other magnetohydrodynamic (MHD) processes occurring in the solar plasma and described in this book such as waves, shocks, instabilities, and magnetic reconnection.

Bayesian evidence for two slow-wave damping models in hot coronal loops

I. **Arregui**1,2, D. Y. Kolotkov3,4 and V. M. Nakariakov

A&A 677, A23 (**2023**)

https://www.aanda.org/articles/aa/pdf/2023/09/aa46834-23.pdf

We computed the evidence in favour of two models, one based on field-aligned thermal conduction alone and another that includes thermal misbalance as well, to explain the damping of slow magneto-acoustic waves in hot coronal loops. Our analysis is based on the computation of the marginal likelihood and the Bayes factor for the two damping models. We quantified their merit to explain the apparent relationship between slow mode periods and damping times, measured with SOHO/SUMER in a set of hot coronal loops. The results indicate evidence in favour of the model with thermal misbalance in the majority of the sample, with a small population of loops for which thermal conduction alone is more plausible. The apparent possibility of two different regimes of slow-wave damping, if due to differences between the loops of host active regions and/or the photospheric dynamics, may help to reveal the coronal heating mechanism.

Methodology for Predicting the Probability Distribution of the Amplitude of Solar Cycle 25

Iñigo **Arregui**

Solar Physics volume 297, Article number: 21 (**2022**)

https://link.springer.com/content/pdf/10.1007/s11207-022-01960-3.pdf

A number of precursor-type methods for solar-cycle prediction are based on the use of regression models and confidence-level estimates. A drawback of these methods is that they do not permit one to make probability statements, nor do they offer straightforward ways to propagate the uncertainty from observations to the quantities of interest. We suggest a method for calculating the probability of the maximum amplitude of Solar Cycle 25 using Bayesian inference. We illustrate this approach with the predictions made by one particular phenomenological model that relates the time interval between the termination events of preceding cycles to the amplitude of the next cycle. Our results show well-constrained posterior-predictive distributions for the maximum sunspot number. The impact of uncertainty on the sunspot number and the time interval between terminators is quantified. A comparison between the maximum sunspot numbers of the past and the posterior-predictive distributions computed using the method enables us to quantify the quality of the inference and the prediction.

No unique solution to the seismological problem of standing kink MHD waves

Inigo **Arregui**, Marcel Goossens

A&A 622, A44 **2019**

https://arxiv.org/pdf/1812.07266.pdf

The aim of this paper is to point out that the classic seismological problem using observations and theoretical expressions for the periods and damping times of transverse standing magnetohydrodynamic (MHD) waves in coronal loops is better referred to as a reduced seismological problem. Reduced emphasises the fact that only a small number of characteristic quantities of the equilibrium profiles can be determined. Reduced also implies that there is no unique solution to the full seismological problem. Even the reduced seismological problem does not allow a

unique solution. Bayesian inference results support our mathematical arguments and offer insight into the relationship between the algebraic and the probabilistic inversions.

Bayesian Coronal Seismology **Review**

I. **Arregui**

Advances in Space Research **2017**

https://arxiv.org/pdf/1709.08372.pdf

In contrast to the situation in a laboratory, the study of the solar atmosphere has to be pursued without direct access to the physical conditions of interest. Information is therefore incomplete and uncertain and inference methods need to be employed to diagnose the physical conditions and processes. One of such methods, solar atmospheric seismology, makes use of observed and theoretically predicted properties of waves to infer plasma and magnetic field properties. A recent development in solar atmospheric seismology consists in the use of inversion and model comparison methods based on Bayesian analysis. In this paper, the philosophy and methodology of Bayesian analysis are first explained. Then, we provide an account of what has been achieved so far from the application of these techniques to solar atmospheric seismology and a prospect of possible future extensions.

Model comparison for the density structure across solar coronal waveguides

I. **Arregui**, R. Soler, A. Asensio Ramos

2015 ApJ 811 104

http://arxiv.org/pdf/1509.02340v1.pdf

The spatial variation of physical quantities, such as the mass density, across solar atmospheric waveguides governs the timescales and spatial scales for wave damping and energy dissipation. The direct measurement of the spatial distribution of density, however, is difficult and indirect seismology inversion methods have been suggested as an alternative. We applied Bayesian inference, model comparison, and model-averaging techniques to the inference of the cross-field density structuring in solar magnetic waveguides using information on periods and damping times for resonantly damped magnetohydrodynamic (MHD) transverse kink oscillations. Three commonly employed alternative profiles were used to model the variation of the mass density across the waveguide boundary. Parameter inference enabled us to obtain information on physical quantities such as the Alfv\'en travel time, the density contrast, and the transverse inhomogeneity length scale. The inference results from alternative density models were compared and their differences quantified. Then, the relative plausibility of the considered models was assessed by performing model comparison. Our results indicate that the evidence in favor of any of the three models is minimal, unless the oscillations are strongly damped. In such a circumstance, the application of model-averaging techniques enables the computation of an evidence-weighted inference that takes into account the plausibility of each model in the calculation of a combined inversion for the unknown physical parameters.

Wave heating of the solar atmosphere **Review**

I. **Arregui**

Royal Society of London Philosophical Transactions Series A, **2015**

http://arxiv.org/pdf/1501.06708v1.pdf

Magnetic waves are a relevant component in the dynamics of the solar atmosphere. Their significance has increased because of their potential as a remote diagnostic tool and their presumed contribution to plasma heating processes. We discuss our current understanding on coronal heating by magnetic waves, based on recent observational evidence and theoretical advances. The discussion starts with a selection of observational discoveries that have brought magnetic waves to the forefront of the coronal heating discussion. Then, our theoretical understanding on the nature and properties of the observed waves and the physical processes that have been proposed to explain observations are described. Particular attention is given to the sequence of processes that link observed wave characteristics with concealed energy transport, dissipation, and heat conversion. We conclude with a commentary on how the combination of theory and observations should help us understanding and quantifying magnetic wave heating of the solar atmosphere.

Inversion of physical parameters in solar atmospheric seismology

I. **Arregui**

E-print, March **2012**,

Review paper to appear in Astrophysics and Space Science Proceedings

Magnetohydrodynamic (MHD) wave activity is ubiquitous in the solar atmosphere. MHD seismology aims to determine difficult to measure physical parameters in solar atmospheric magnetic and plasma structures by a combination of observed and theoretical properties of MHD waves and oscillations. This technique, similar to seismology or helio-seismology, demands the solution of two problems. The direct problem involves the

computation of wave properties of given theoretical models. The inverse problem implies the calculation of unknown physical parameters, by means of a comparison of observed and theoretical wave properties. Solar atmospheric seismology has been successfully applied to different structures such as coronal loops, prominence fine structures, spicules, or jets. However, it is still in its infancy. Far more is there to come. We present an overview of recent results, with particular emphasis on the inversion procedure.

Universal Constants and Energy Integral in Self-Organized Criticality Systems

Markus J. **Aschwanden**
ApJ **2024**
https://solarpreprint.org/AschwandenDec2024.pdf
The occurrence frequency distributions of fluxes (F) and fluences or energies (E) observed in astrophysical observations are found to be consistent with the predictions of the fractal-diffusive selforganized criticality (FD-SOC) model, which predicts power law slopes with universal constants of $\alpha F = (9/5) = 1.80$ for the flux and $\alpha E = (5/3) \approx 1.67$ for the fluence. The energy integrated over the power law-like (size distribution) energy range is found to be finite for these power law slopes with $\alpha E < 2$, which refutes earlier claims of a divergent energy integral that has been postulated in the energy budget of solar and stellar nanoflare scenarios. The theoretial FD-SOC model approximates the microscopic cellular automaton models satisfactorily with the macroscopic scaling law of classical diffusion. The universal scaling laws predict the size distributions of numerous astrophysical phenomena, such as solar flares, stellar flares, coronal mass ejections (CME), auroras, blazars, galactic fast radio bursts (FRB), active galactic nuclei (AGN), gamma-ray bursts (GRB), soft gamma-ray repeaters (SGB), and black-hole systems (BH), while coherent solar radio bursts, random radio bursts, solar energetic partices (SEP), cosmic rays, and pulsar glitches require non-standard SOC models.

The Universality of Power Law Slopes in the Solar Photosphere and Transition Region Observed with HMI and IRIS

Markus J. **Aschwanden**, Nived Vilangot Nhalil
Front. Astron. Space Sci. 10: 1099346 **2023**
https://arxiv.org/pdf/2211.08323.pdf
https://www.lmsal.com/~aschwand/eprints/2022_iris2.pdf
https://www.frontiersin.org/articles/10.3389/fspas.2023.1099346/full
https://www.frontiersin.org/articles/10.3389/fspas.2023.1099346/pdf
We compare the size distributions of {\sl self-organized criticality (SOC)} systems in the solar photosphere and the transition region, using magnetogram data from {\sl Helioseismic and Magnetic Imager (HMI)} and {\sl Interface Region Imaging Spectrograph (IRIS)} data. For each dataset we fit a combination of a Gaussian and a power law size distribution function, which yields information on four different physical processes: (i) photospheric granulation convection dynamics (explaining the Gaussian random noise distribution in IRIS data); (ii) spicular plage events in the transition region (explaining the power law size distribution in IRIS data); (iii) salt-and-pepper small-scale magnetic structures (explaining the random noise distributions in HMI magnetograms); and (iv) magnetic reconnection processes in flares and nanoflares (explaining the power law size distribution in HMI data). We find a high correlation (CCC=0.97) between IRIS and HMI data. Datasets with magnetic flux balance are found to match the SOC-predicted power law slope $\alpha F=1.80$ for mean fluxes, which confirms the universality of SOC-inferred flux size distributions, and agrees with the results of Parnell et al.~(2009), $\alpha F=1.85\pm0.14$.

Interface Region Imaging Spectrograph (IRIS) Observations of the Fractal Dimension in the Solar Atmosphere

Markus **Aschwanden** and Vilangot Nived
Front. Astron. Space Sci. 9:999319. **2022**
https://arxiv.org/pdf/2207.12894.pdf
https://www.lmsal.com/~aschwand/eprints/2022_iris.pdf
https://doi.org/10.3389/fspas.2022.999319
https://www.frontiersin.org/articles/10.3389/fspas.2022.999319/pdf
We focus here on impulsive phenomena and Quiet-Sun features in the solar transition region, observed with the Interface Region Imaging Spectrograph (IRIS) at 1,400 Å (at formation temperatures of Te ≈ 104–106 K). Summarizing additional literature values we find the following fractal dimensions (in increasing order): DA = 1.23 ± 0.09 for photospheric granulation, DA =1.40 ± 0.09 for chromospheric (network) patterns, DA = 1.54 ± 0.04 for plages in the transition region, DA = 1.56 ± 0.08 for extreme ultra-violet (EUV) nanoflares, DA = 1.59 ± 0.20 for active regions in photospheric magnetograms, and DA = 1.76 ± 0.14 for large solar flares. We interpret low values of the fractal dimension ($1.0 \lesssim DA \lesssim 1.5$) in terms of sparse curvi-linear flow patterns, while high values of the fractal dimension ($1.5 \lesssim DA \lesssim 2.0$) indicate quasi-space-filling transport processes, such as chromospheric evaporation in flares. Phenomena in the solar transition region appear to be consistent with self-organized criticality

(SOC) models, based on their fractality and their size distributions of fractal areas A and (radiative) energies E, which show power law slopes of αobsA=2.51±0.21αAobs=2.51±0.21 (with αtheoA=2.33αAtheo=2.33 predicted), and αobsE=2.03±0.18αEobs=2.03±0.18 (with αtheoE=1.80αEtheo=1.80 predicted). This agreement suggests that brightenings detected with IRIS at 1,400 Å reveal the same nonlinear SOC statistics as their coronal counterparts in EUV.

The Fractality and Size Distributions of Astrophysical Self-Organized Criticality Systems

Markus J. **Aschwanden**

2022

https://arxiv.org/pdf/2203.12484.pdf

The statistics of nonlinear processes in avalanching systems, based on the {\sl self-organized criticality (SOC)} concept of Bak et al.~(1987), predicts power law-like size (or occurrence frequency) distribution functions. Following up on previous work we define a {\sl standard SOC model} in terms of six assumptions: (i) multi-fractality; (ii) the length-area-volume relationship of Mandelbrot (1977); (iii) the flux-volume relationship, (iv) classical diffusion, (v) the Euclidean volume limit at the event peak time, and (vi) the spatio-temporal fluence or energy of an avalanche event. We gather data of the fractal dimension and power law slopes from 162 publications and assemble them in 28 groups (e.g., solar and stellar flare energies), from which we find that 75\% of the groups are consistent with the standard SOC model. Alternative SOC models (Levy-flight, flat-world, non-fractal) are slightly less correlated with the data. The remaining discrepancies are attributed to outliers caused by small-number statistics, background subtraction problems, inadequate fitting ranges, and deviations from ideal power laws.

The Solar Memory From Hours to Decades

Markus J. **Aschwanden**, Jay R. Johnson

ApJ **921** 82 **2021**

https://arxiv.org/pdf/2107.13621.pdf

https://doi.org/10.3847/1538-4357/ac2a29

Waiting time distributions allow us to distinguish at least three different types of dynamical systems, such as (i) linear random processes (with no memory); (ii) nonlinear, avalanche-type, nonstationary Poisson processes (with memory during the exponential growth of the avalanche rise time); and (iii) chaotic systems in the state of a nonlinear limit cycle (with memory during the oscillatory phase). We describe the temporal evolution of the flare rate λ(t)∝tp with a polynomial function, which allows us to distinguish linear (p≈1) from nonlinear ($p \gapprox 2$) events. The power law slopes α of observed waiting times (with full solar cycle coverage) cover a range of α=2.1−2.4, which agrees well with our prediction of α=2.0+1/p=2.3−2.5. The memory time can also be defined with the time evolution of the logistic equation, for which we find a relationship between the nonlinear growth time τG=τrise/(4p) and the nonlinearity index p. We find a nonlinear evolution for most events, in particular for the clustering of solar flares (p=2.2±0.1), partially occulted flare events (p=1.8±0.2), and the solar dynamo (p=2.8±0.5). The Sun exhibits memory on time scales of $\lapprox$2 hours to 3 days (for solar flare clustering), 6 to 23 days (for partially occulted flare events), and 1.5 month to 1 year (for the rise time of the solar dynamo).

Correlation of the sunspot number and the waiting time distribution of solar flares, coronal mass ejections, and solar wind switchback events observed with the Parker Solar Probe

Markus J. **Aschwanden**, Thierry Dudok de Wit

ApJ **2021**

https://arxiv.org/pdf/2102.02305.pdf

Waiting time distributions of solar flares and {\sl coronal mass ejections (CMEs)} exhibit power law-like distribution functions with slopes in the range of ατ≈1.4−3.2, as observed in annual data sets during 4 solar cycles (1974-2012). We find a close correlation between the waiting time power law slope ατ and the {\sl sunspot number (SN)}, i.e., ατ = 1.38 + 0.01 × SN. The waiting time distribution can be fitted with a Pareto-type function of the form N(τ)=N0 (τ0+τ)−ατ, where the offset τ0 depends on the instrumental sensitivity, the detection threshold of events, and pulse pile-up effects. The time-dependent power law slope ατ(t) of waiting time distributions depends only on the global solar magnetic flux (quantified by the sunspot number) or flaring rate, independent of other physical parameters of {\sl self-organized criticality (SOC)} or {\sl magneto-hydrodynamic (MHD)} turbulence models. Power law slopes of ατ≈1.2−1.6 were also found in solar wind switchback events, as observed with the {\sl Parker Solar Probe (PSP)}. We conclude that the annual variability of switchback events in the heliospheric solar wind is modulated by flare and CME rates originating in the photosphere and lower corona.

Order out of randomness: Self-organization processes in astrophysics **Review**

Aschwanden,M.J., Scholkmann,F., Bethune,W., Schmutz,W., Abramenko,W., Cheung,M.C.M., Mueller,D., Benz,A.O., Chernov,G., Kritsuk,A.G., Scargle,J.D., Melatos,A., Wagoner,R.V., Trimble,V., Green,W.

Space Science Reviews 214:55, **2018**

https://link.springer.com/content/pdf/10.1007%2Fs11214-018-0489-2.pdf
Self-organization is a property of dissipative nonlinear processes that are gov- erned by a global driving force and a local positive feedback mechanism, which creates regular geometric and/or temporal patterns, and decreases the entropy locally, in contrast to random processes. Here we investigate for the first time a comprehensive number of (17) self-organization processes that operate in planetary physics, solar physics, stellar physics, galactic physics, and cosmology. Self-organizing systems create spontaneous ?order out of randomness?, during the evolution from an initially disordered system to an ordered quasistationary system, mostly by quasi-periodic limit-cycle dynamics, but also by harmonic (me- chanical or gyromagnetic) resonances. The global driving force can be due to gravity, elec- tromagnetic forces, mechanical forces (e.g., rotation or differential rotation), thermal pres- sure, or acceleration of nonthermal particles, while the positive feedback mechanism is of- ten an instability, such as the magneto-rotational (Balbus-Hawley) instability, the convective (Rayleigh-B?nard) instability, turbulence, vortex attraction, magnetic reconnection, plasma condensation, or a loss-cone instability. Physical models of astrophysical self-organization processes require hydrodynamic, magneto-hydrodynamic (MHD), plasma, or N-body simu- lations. Analytical formulations of self-organizing systems generally involve coupled differ- ential equations with limit-cycle solutions of the Lotka-Volterra or Hopf-bifurcation type.
3 Solar Physics

Convection-driven Generation of Ubiquitous Coronal Waves

Markus J. **Aschwanden**1, Milan Gošic1,2, Neal E. Hurlburt1, and Eamon Scullion
2018 ApJ 866 73
http://www.lmsal.com/~aschwand/eprints/2018_ubi.pdf
We develop a new method to measure the 3D kinematics of the subphotospheric motion of magnetic elements, which is used to study the coupling between the convection-driven vortex motion and the generation of ubiquitous coronal waves. We use the method of decomposing a line-of-sight magnetogram from MDI/SDO into unipolar magnetic charges, which yields the (projected) 2D motion [x(t), y(t)] and the (half) width evolution w(t) of an emerging magnetic element from an initial depth of d $\lesssim$ 1500 km below the photosphere. A simple model of rotational vortex motion with magnetic flux conservation during the emergence process of a magnetic element predicts the width evolution, i.e., w(t)/w 0 = [B(t)/B 0]−1/2, and an upper limit of the depth variation d(t) ≤ 1.3 w(t). While previous 2D tracing of magnetic elements provided information on advection and superdiffusion, our 3D tracing during the emergence process of a magnetic element is consistent with a ballistic trajectory in the upward direction. From the estimated Poynting flux and lifetimes of convective cells, we conclude that the Coronal Multi-channel Polarimeter–detected low-amplitude transverse magnetohydrodynamic waves are generated by the convection-driven vortex motion. Our observational measurements of magnetic elements appear to contradict the theoretical random-walk braiding scenario of Parker.

Order out of Chaos : Self-Organization Processes in Astrophysics **Review**

Markus M. **Aschwanden**
Space Since Rev. 214:55 **2018**
http://www.lmsal.com/~aschwand/eprints/2017_selforg.pdf
Here we investigate for the first time a comprehensive number of 16 self-organization processes that operate in planetary physics, solar physics, stellar physics, galactic physics, and cosmology. Self-organizing systems create spontaneous "order out of chaos", during the evolution from an initially disordered system to an ordered stationary system, via quasi-periodic limit-cycle dynamics, harmonic mechanical resonances, or gyromagnetic resonances. The internal driver can be gravity, rotation, thermal pressure, or acceleration of nonthermal particles, while the positive feedback mechanism is often an instability, such as the magneto-rotational instability, the Rayleigh-Benard convection instability, turbulence, vortex attraction, magnetic reconnection, plasma condensation, or loss-cone instability. Physical models of astrophysical self-organization processes involve hydrodynamic, MHD, and N-body formulations of Lotka-Volterra equation systems.

Harmonic Resonances of Planet and Moon Orbits - From the Titius-Bode Law to Self-Organizing Systems

Markus J. **Aschwanden** and L.A. McFadden
ApJ **2017**
http://www.lmsal.com/~aschwand/eprints/2017_planets.pdf
The geometric arrangement of planet and moon orbits into a regularly spaced pattern of distances is the result of a self-organizing system. The positive feedback mechanism that operates a self-organizing system is accomplished by harmonic orbit resonances, leading to long-term stable planet and moon orbits in solar or stellar systems. The distance pattern of planets was originally described by the empirical Titius-Bode law, and by a generalized version with a constant geometric progression factor (corresponding to logarithmic spacing). We find that the orbital periods Ti and planet distances Ri from the Sun are not consistent with logarithmic spacing, but rather follow the quantized scaling (Ri+1/Ri) = (Ti+1/Ti)2/3 = (Hi+1/Hi)2/3, where the harmonic ratios are given by five dominant resonances,

namely (Hi+1 : Hi) = (3:2), (5:3), (2:1), (5:2), (3:1). We find that the orbital period ratios tend to follow the quantized harmonic ratios in increasing order. We apply this harmonic orbit resonance model to the planets and moons in our solar system, and to the exo-planets of 55 Cnc and HD 10180 planetary systems. The model allows us a prediction of missing planets in each planetary system, based on the quasi-regular self-organizing pattern of harmonic orbit resonance zones. We predict 7 (and 4) missing exo-planets around the star 55 Cnc (and HD 10180). The accuracy of the predicted planet and moon distances amounts to a few percents. All analyzed systems are found to have ≈ 10 resonant zones that can be occupied with planets (or moons) in long-term stable orbits.

The Width Distribution of Loops and Strands in the Solar Corona -- Are we Hitting Rock Bottom ?

Markus J. **Aschwanden**, Hard Peter
ApJ **2017**
https://arxiv.org/pdf/1701.01177v1.pdf
In this study we analyze {\sl Atmospheric Imaging Assembly (AIA)} and Hi-C images in order to investigate absolute limits for the finest loop strands. We develop a model of the occurrence-size distribution function of coronal loop widths, characterized by a lower limit of widths wmin, a peak width wp, a peak occurrence number np, and a power law slope a. Our data analysis includes automated tracing of curvi-linear features with the OCCULT-2 code, automated sampling of the cross-sectional widths of coronal loops, and fitting of the theoretical size distribution to the observed distribution. With Monte-Carlo simulations and variable pixel sizes Δx we derive a first diagnostic criterion to discriminate whether the loop widths are unresolved ($wp/\Delta x \approx 2.5 \pm 0.2$), or fully resolved (if $wp/\Delta x > 2.7$). For images with resolved loop widths we can apply a second diagnostic criterion that predicts the lower limit of loop widths, $wmin \approx 3(\Delta xcrit - 0.37")$ as a function of the critical resolution $\Delta xcrit$. We find that the loop widths are marginally resolved in AIA images, but are fully resolved in Hi-C images, where our model predicts a lower limit of loop widths at wmin≈100 km and a most frequent (peak) value at wp≈300 km, in agreement with recent results of Brooks et al. This result agrees with the statistics of photospheric granulation sizes and thus supports coronal heating mechanisms operating on the macroscopic scale of photospheric magneto-convection, rather than nanoflare heating models with unresolved microscopic scales. **2011 Feb 14**

Preface 25 Years of Self-Organized Criticality

Markus J. **Aschwanden**
Space Sci Rev (**2016**) 198:1–2
http://link.springer.com/journal/11214/198/1?wt_mc=alerts.TOCjournals

THRESHOLDED POWER LAW SIZE DISTRIBUTIONS OF INSTABILITIES IN ASTROPHYSICS

Markus J. **Aschwanden**
2015 ApJ 814 19
Power-law-like size distributions are ubiquitous in astrophysical instabilities. There are at least four natural effects that cause deviations from ideal power law size distributions, which we model here in a generalized way: (1) a physical threshold of an instability; (2) incomplete sampling of the smallest events below a threshold x0; (3) contamination by an event-unrelated background xb; and (4) truncation effects at the largest events due to a finite system size. These effects can be modeled in the simplest terms with a "thresholded power law" distribution function (also called generalized Pareto [type II] or Lomax distribution), where $x0 > 0$ is positive for a threshold effect, while $x0 < 0$ is negative for background contamination. We analytically derive the functional shape of this thresholded power law distribution function from an exponential growth evolution model, which produces avalanches only when a disturbance exceeds a critical threshold x0. We apply the thresholded power law distribution function to terrestrial, solar (HXRBS, BATSE, RHESSI), and stellar flare (Kepler) data sets. We find that the thresholded power law model provides an adequate fit to most of the observed data. Major advantages of this model are the automated choice of the power law fitting range, diagnostics of background contamination, physical instability thresholds, instrumental detection thresholds, and finite system size limits. When testing self-organized criticality models that predict ideal power laws, we suggest including these natural truncation effects.

25 Years of Self-Organized Criticality: Solar and Astrophysics **Review**

Aschwanden, M.J., Crosby, N., Dimitropoulou, M., Geogoulis, M.K., Hergarten, S., McAteer, J., Milovanov, A.V., Mineshige, S., Morales, L., Nishizuka, N., Pruessner, G., Sanchez, R., Sharma, S., Strugarek, A., and Uritsky, V.
Space Science Reviews January **2016**, Volume 198, Issue 1, pp 47-166 **Open Access**
http://www.lmsal.com/~aschwand/eprints/2014_soc25.pdf

http://arxiv.org/pdf/1403.6528v1.pdf
Shortly after the seminal paper ``Self-Organized Criticality: An explanation of 1/f noise" by Bak, Tang, and Wiesenfeld (1987), the idea has been applied to solar physics, in``Avalanches and the Distribution of Solar Flares" by Lu and Hamilton (1991). In the following years, an inspiring cross-fertilization from complexity theory to solar and astrophysics took place, where the SOC concept was initially applied to solar flares, stellar flares, and magnetospheric substorms, and later extended to the radiation belt, the heliosphere, lunar craters, the asteroid belt, the Saturn ring, pulsar glitches, soft X-ray repeaters, blazars, black-hole objects, cosmic rays, and boson clouds. The application of SOC concepts has been performed by numerical cellular automaton simulations, by analytical calculations of statistical (powerlaw-like) distributions based on physical scaling laws, and by observational tests of theoretically predicted size distributions and waiting time distributions. Attempts have been undertaken to import physical models into the numerical SOC toy models, such as the discretization of magneto-hydrodynamics (MHD) processes. The novel applications stimulated also vigorous debates about the discrimination between SOC models, SOC-like, and non-SOC processes, such as phase transitions, turbulence, random-walk diffusion, percolation, branching processes, network theory, chaos theory, fractality, multi-scale, and other complexity phenomena. We review SOC studies from the last 25 years and highlight new trends, open questions, and future challenges, as discussed during two recent ISSI workshops on this theme.

STEREO/ *Extreme Ultraviolet Imager* (EUVI) Event Catalog 2006-2012

Markus J. **Aschwanden**1, Jean-Pierre W.ulser1, Nariaki V. Nitta1, James R. Lemen1, Sam Freeland1, and William T. Thompson2
Solar Physics, March **2014**, Volume 289, Issue 3, pp 919-938; **File**
An event catalog is generated with an automated detection algorithm based on the entire EUVI image database observed with the two STEREO/A and B spacecraft over the first six years of the mission (2006-2012). The event catalog includes the heliographic positions of some 20,000 EUV events, transformed from spacecraft coordinates to Earth coordinates, and information on associated GOES flare events (down to the level of GOES A-class flares). The 304°A wavelength turns out to be most efficient channel for flare detection (79%), while the 171 °A (4%), 195 °A (10%), and the 284 °A channel (7%), retrieve substantially less flare events, partially due to the suppressing effect of EUV dimming, and partially due to the lower cadence they were operated in the later years of the mission. Due to the Sun-circling orbits of STEREO/A and B, a large number of flares have been detected on the back-side of the Sun, invisible from Earth, or seen as partially occulted events. The statistical size distributions of EUV peak fluxes (with a powerlaw slope of $\_P = 2.5 \pm 0.2$) and event durations (with a powerlaw slope of $\_T = 2.4 \pm 0.3$) are found to be consistent with the fractal-diffusive self-organized criticality model. The EUVI event catalog is available on-line at secchi.lmsal.com/EUVI/euvi_autodetection/euvi_events.txt and may serve as a comprehensive tool to identify stereoscopically observed flare events for 3D reconstruction and to study occulted flare events.

Optimization of Curvi-Linear Tracing Applied to Solar Physics and Biophysics

Markus J. **Aschwanden**, Bart De Pontieu, and Eugene A. Katrukha
E-print, July **2013**; Entropy, Special Issue on Advanced Signal Processing in Heliopspheric Physics
We developed an automated pattern recognition code that is particularly well suited to extract one-dimensional curvi-linear features from two-dimensional digital images. A former version of this {sl Oriented Coronal CUrved Loop Tracing (OCCULT)} code was applied to spacecraft images of magnetic loops in the solar corona, recorded with the NASA spacecraft {sl Transition Region And Coronal Explorer (TRACE)} in extreme ultra-violet wavelengths. Here we apply an advanced version of this code ({sl OCCULT-2}) also to similar images from the {sl Solar Dynamics Observatory (SDO)}, to chromospheric H-α images obtained with the {sl Swedish Solar Telescope (SST)}, and to microscopy images of microtubule filaments in live cells in biophysics. We provide a full analytical description of the code, optimize the control parameters, and compare the automated tracing with visual/manual methods. The traced structures differ by up to 16 orders of magnitude in size, which demonstrates the universality of the tracing algorithm.

Self-Organized Criticality Systems –

Dr.Markus J. **Aschwanden** (Ed.)
Open Academic Press, Berlin, Warsaw, **2013**
13 chapters, 439pp, 126 Figures.
http://www.openacademicpress.de/ojs2/index.php/socs,
Contents

Criticality and Self-Organization in Branching Processes: Application to Natural Hazards - Álvaro Corral, Francesc Font-Clos PDF
Power Laws of Recurrence Networks - Yong Zou, Jobst Heitzig, Jürgen Kurths PDF
SOC computer simolations - Gunnar Pruessner PDF
SOC Laboratory Experiments - Gunnar Pruessner PDF
Self-Organizing Complex Earthquakes: Scaling in Data, Models, and Forecasting - Michael K. Sachs et al. PDF
Wildfires and the Forest-Fire Model - Stefan Hergarten PDF
SOC in Landslides - Stefan Hergarten PDF
SOC and Solar Flares - Paul Charbonneau PDF
SOC Systems in Astrophysics - Markus J. Aschwanden PDF

STEREO/EUVI Event Catalog 2006-2012

Markus J. **Aschwanden**1, Jean-Pierre W.ulser1, Nariaki V. Nitta1, James R. Lemen1, Sam Freeland1, and William T. Thompson2
Solar Phys., **2013**
An event catalog is generated with an automated detection algorithm based on the entire EUVI image database observed with the two STEREO/A and B spacecraft over the first six years of the mission (2006-2012). The event catalog includes the heliographic positions of some 20,000 EUV events, transformed from spacecraft coordinates to Earth coordinates, and information on associated GOES flare events (down to the level of GOES A-class flares). The 304°A wavelength turns out to be most efficient channel for flare detection (79%), while the 171 °A (4%), 195 °A (10%), and the 284 °A channel (7%), retrieve substantially less flare events, partially due to the suppressing effect of EUV dimming, and partially due to the lower cadence they were operated in the later years of the mission. Due to the Sun-circling orbits of STEREO/A and B, a large number of flares have been detected on the back-side of the Sun, invisible from Earth, or seen as partially occulted events. The statistical size distributions of EUV peak fluxes (with a powerlaw slope of $\__P = 2.5 \pm 0.2$) and event durations (with a powerlaw slope of $\__T = 2.4 \pm 0.3$) are found to be consistent with the fractal-diffusive self-organized criticality model. The EUVI event catalog is available on-line and may serve as a comprehensive tool to identify stereoscopically observed flare events for 3D reconstruction and to study occulted flare events.

Automated Temperature and Emission Measure Analysis of Coronal Loops and Active Regions Observed with the Atmospheric Imaging Assembly on the Solar Dynamics Observatory (SDO/AIA)

Markus J. **Aschwanden**, Paul Boerner, Carolus J. Schrijver, Anna Malanushenko
Solar Physics, March **2013**, Volume 283, Issue 1, pp 5-30
We developed numerical codes designed for automated analysis of SDO/AIA image datasets in the six coronal filters, including: i) coalignment test between different wavelengths with measurements of the altitude of the EUV-absorbing chromosphere, ii) self-calibration by empirical correction of instrumental response functions, iii) automated generation of differential emission measure [DEM] distributions with peak-temperature maps [T p(x,y)] and emission measure maps [EM p(x,y)] of the full Sun or active region areas, iv) composite DEM distributions [dEM(T)/dT] of active regions or subareas, v) automated detection of coronal loops, and vi) automated background subtraction and thermal analysis of coronal loops, which yields statistics of loop temperatures [T e], temperature widths [σ T], emission measures [EM], electron densities [n e], and loop widths [w]. The combination of these numerical codes allows for automated and objective processing of numerous coronal loops. As an example, we present the results of an application to the active region NOAA 11158, observed on **15 February 2011**, shortly before it produced the largest (X2.2) flare during the current solar cycle. We detect 570 loop segments at temperatures in the entire range of log(T e)=5.7 – 7.0 K and corroborate previous TRACE and AIA results on their near-isothermality and the validity of the Rosner–Tucker–Vaiana (RTV) law at soft X-ray temperatures ($T \gtrsim 2$ MK) and its failure at lower EUV temperatures.

Coronal Seismology with ATST - Advanced Technology Solar Telescope

Markus J. **Aschwanden**
2012, http://www.lmsal.com/~aschwand/eprints/2012_ATST.pdf
We give a brief summary on the current status of coronal seismology and anticipate research opportunities for ATST in this discipline. Given the optical/infrared spectral range and the high-resolution magnetic field capabilities of ATST ($\_ 0.05''_{00} - 0.1''_{00}$), the potential of exploring coronal seismology includes: (1) Optical detection of coronal waves and oscillations, (2) high-resolution magnetic field modeling with accurate determination of Alfv´enic speeds, and (3) correlative studies that investigate the coupling between photospheric waves (detected in optical

wavelengths) and **coronal waves**, which will provide insights into the generation mechanism of coronal waves, the origin and efficiency of coronal heating by waves, and **diagnostics on flare and CME processes by global waves**.

Self-Organized Criticality Systems in Astrophysics (Chapter 13)

Markus J. **Aschwanden**

E-print, July **2012**, e-book - Self-Organized Criticality Systems

Chapter 13: SOC Systems in Astrophysics --- Content list: 13.1 Theory -- 13.1.1 The Sacle-Free Probability Theorem - 13.1.2 The Fractal-Diffusive Spatio-Temporal Relationship - 13.1.3 Size Distributions of Astrophysical Observables - 13.1.4 Scaling Laws for Thermal Emission of Astrophysical Plasmas - 13.1.5 Scaling Laws for Astrophysical Acceleration Mechanisms - 13.2 Observations -- 13.2.1 Lunar Craters - 13.2.2 Asteroid Belt - 13.2.3 Saturn Ring - 13.2.4 Magnetospheric Substorms and Auroras - 13.2.5 Solar Flares - 13.2.6 Stellar Flares - 13.2.7 Pulsars - 13.2.8 Soft Gamma-Ray Repeaters - 13.2.9 Black-Hole Objects - 13.2.10 Blazars - 13.2.11 Cosmic Rays - 13.3 Conclusions

Chapter 2

Theoretical Models of SOC Systems

by Markus J. **Aschwanden**

2012

http://www.lmsal.com/~aschwand/eprints/2012_SOC2.pdf

How can the universe start with a few types of elementary particles at the big bang, and end up with life, history, economics, and literature? The question is screaming out to be answered but it is seldom even asked. Why did the big bang not form a simple gas of particles, or condense into one big crystal? (Bak 1996). The answer to this fundamental question lies in the tendency of the universal evolution towards complexity, which is a property of many nonlinear energy dissipation processes. Dissipative nonlinear systems generally have a source of free energy, which can be partially dissipated whenever an instability occurs. This triggers an avalanche-like energy dissipation event above some threshold level. Such nonlinear processes are observed in astrophysics, magnetospheric physics, geophysics, material sciences, physical laboratories, human activities (stock market, city sizes, internet, brain activity), and in natural hazards and catastrophes (earthquakes, snow avalanches, forest fires). A tentative list of SOC phenomena with the relevant sources of free energy, the physical driver mechanisms, and instabilities that trigger a SOC event are listed in Table 2.1.

Chapter 13

SOC Systems in Astrophysics

by Markus J. **Aschwanden**

2012

http://www.lmsal.com/~aschwand/eprints/2012_SOC13.pdf

The universe is full of nonlinear energy dissipation processes, which occur intermittently, triggered by local instabilities, and can be understood in terms of the **self-organized criticality (SOC) concept.**

The Sun **Review- textbook**

Markus J. **Aschwanden**

2012, File

Solar Stereoscopy and Tomography

Markus J. **Aschwanden**

Living Reviews, PUB.NO. lrsp-2011-5, **2011, File**

http://www.livingreviews.org/lrsp-2011-5

We review stereoscopic and tomographic methods used in the solar corona, including ground-based and space-based measurements, using solar rotation or multiple spacecraft vantage points, in particular from the STEREO mission during 2007-2010. Stereoscopic observations in the solar corona include large-scale structures, streamers, active regions, coronal loops, loop oscillations, acoustic waves in loops, erupting filaments and prominences, bright points, jets, plumes, flares, CME source regions, and CME-triggered global coronal waves. Applications in the solar interior (helioseismic tomography) and in the heliosphere (interplanetary CMEs) are not included.

Movie archive

Image Processing Techniques and Feature Recognition in Solar Physics

Markus J. Aschwanden

Solar Phys (**2010**) 262: 235–275

This review presents a comprehensive and systematic overview of image processing techniques that are used in automated feature-detection algorithms applied to solar data: *i*) image pre-processing procedures, *ii*) automated detection of spatial features, *iii*) automated detection and tracking of temporal features (events), and *iv*) post-processing tasks, such as visualization of solar imagery, cataloguing, statistics, theoretical modeling, prediction, and forecasting. For each aspect the most recent developments and science results are highlighted. We conclude with an outlook on future trends.

Astrophysics in 2006

Markus J. **Aschwanden**

Space Sci Rev (2007) 132: 1–182

http://www.springerlink.com/content/853008743423t452/fulltext.pdf

Observations of Non-thermal Velocity and Comparison with Alfvén Wave Turbulence Model in Solar Active Regions

M. **Asgari-Targhi**, D. H. Brooks, M. Hahn, S. Imada, E. Tajfirouze, D. W. Savin

2024

https://arxiv.org/pdf/2404.17037

We present a study of spectral line width measurements from the Extreme Ultraviolet Imaging Spectrometer (EIS) on {\it Hinode}. We used spectral line profiles of Fe {\sc xvi} 262.984 Å, Fe {\sc xiv} 264.787 Å, Fe {\sc xiv} 270.519 Å, Fe {\sc xiv} 274.203 Å, and Fe {\sc xv} 284.160 Å, and studied 11 active regions. Previous studies of spectral line widths have shown that in hot loops in the cores of active regions, the observed non-thermal velocities are smaller than predicted from models of reconnection jets in the corona or shock heating associated with Alfvén waves. The observed line widths are also inconsistent with models of chromospheric evaporation due to coronal nanoflares. We show that recent advances in higher resolution Alfvén wave turbulence modeling enables us to obtain non-thermal velocities similar to those measured in
active regions. The observed non-thermal velocities for the 11 active regions in our study are in the range of 17−30 km s−1, consistent with the spectral line non-thermal widths predicted from our model of 16 interacting flux tubes, which are in the range of ~15−37 km s−1.

Study of High-temperature Emission in Solar Active Regions

M. **Asgari-Targhi**1, A. A. van Ballegooijen1, and A. R. Davey2

2019 ApJ 881 107

sci-hub.se/10.3847/1538-4357/ab2e01

The high-temperature (T > 4 MK) emissions of nonflaring active regions are investigated in the context of the coronal heating problem. We study the role of emerging flux, nonpotential magnetic fields, and sunspots in the heating of active-region loops. Using extreme ultraviolet images from the Atmospheric Imaging Assembly on the Solar Dynamic Observatory (SDO), we construct intensity maps in Fe xviii 94 Å for 48 active regions. We also use the corresponding magnetograms from the Helioseismic and Magnetic Imager on SDO to measure the total magnetic flux. The Fe xviii 94 Å emission intensity of the brightest loops is found to be correlated with the presence of sunspots and emerging or canceling magnetic flux in the photosphere below. We conclude that sunspots and emerging flux play an important role in the process of coronal heating and the production of high-temperature plasmas. We suggest that energy may be injected into the corona as a result of the dynamics of magnetic fields associated with sunspots and/or emerging flux. These processes may cause the large magnetic disturbances ($\delta B \perp \sim 10$ G) needed to produce strong nanoflare-heating events**. 2011 April 7, 2011 April 15, 2013 November 9 Table** 1 Parameters SP, NP, and EC for the Selected Active Region (2010-2013)

Identification of photospheric activity features from SOHO/MDI data using the ASAP tool

Omar **Ashamari**, Rami Qahwaji, Stan Ipson, Micha Scholl, Omar Nibouche, Margit Haberreiter

Journal of Space Weather and Space Climate **2015**

http://arxiv.org/pdf/1505.02036v1.pdf

The variation of solar irradiance is one of the natural forcing mechanisms of the terrestrial climate. Hence, the time-dependent solar irradiance is an important input parameter for climate modelling. The solar surface magnetic field is a powerful proxy for solar irradiance reconstruction. The analyses of data obtained with the Michelson Doppler Imager (MDI) on board the SOHO mission are therefore useful for the identification of solar surface magnetic features to be used in solar irradiance reconstruction models. However, there is still a need for automated technologies that would enable the identification of solar activity features from large databases. To achieve this we

present a series of enhanced segmentation algorithms developed to detect and calculate the area coverages of specific magnetic features from MDI intensitygrams and magnetograms. These algorithms are part of the Automated Solar Activity Prediction (ASAP) tool. The segmentation algorithms allow us to identify the areas on the solar disk covered by magnetic elements inside and outside boundaries of active regions. Depending on their contrast properties, magnetic features within an active region boundary are classified as sunspot umbra and penumbra, or faculae. Outside an active region boundary magnetic elements are identified as network. We present the detailed steps involved in the segmentation process and provide the area coverages of the segmented MDI intensitygrams and magnetograms. The feature segmentation has been carried out on daily intensitygrams and magnetograms from April 21, 1996 to April 11, 2011. This offers an exciting opportunity to undertake further investigations that benefit from solar features segmentations, such as solar irradiance reconstruction, which we plan to investigate in the future.

Identification of photospheric activity features from SOHO/MDI data using the ASAP tool

Omar **Ashamari**1*, Rami Qahwaji1, Stan Ipson1, Micha Schöll2, Omar Nibouche3 and Margit Haberreiter

J. Space Weather Space Clim., 5, A15 (**2015**)

http://www.swsc-journal.org/articles/swsc/pdf/2015/01/swsc130048.pdf

The variation of solar irradiance is one of the natural forcing mechanisms of the terrestrial climate. Hence, the time-dependent solar irradiance is an important input parameter for climate modelling. The solar surface magnetic field is a powerful proxy for solar irradiance reconstruction. The analyses of data obtained with the Michelson Doppler Imager (MDI) on board the SOHO mission are therefore useful for the identification of solar surface magnetic features to be used in solar irradiance reconstruction models. However, there is still a need for automated technologies that would enable the identification of solar activity features from large databases. To achieve this we present a series of enhanced segmentation algorithms developed to detect and calculate the area coverages of specific magnetic features from MDI intensitygrams and magnetograms. These algorithms are part of the **Automated Solar Activity Prediction (ASAP) tool**. The segmentation algorithms allow us to identify the areas on the solar disk covered by magnetic elements inside and outside boundaries of active regions. Depending on their contrast properties, magnetic features within an active region boundary are classified as sunspot umbra and penumbra, or faculae. Outside an active region boundary magnetic elements are identified as network. We present the detailed steps involved in the segmentation process and provide the area coverages of the segmented MDI intensitygrams and magnetograms. The feature segmentation was carried out on daily intensitygrams and magnetograms from April 21, 1996 to April 11, 2011. This offers an exciting opportunity to undertake further investigations that benefit from solar features segmentations, such as solar irradiance reconstruction, which we plan to investigate in the future. **May 17, 2000**

Full-disk 1,024 · 1,024 pixel intensitygrams and line-of-sight magnetograms data sets are both available to download from the SOHO and JSOC archive: http://soho.nascom.nasa.gov and http://jsoc.stanford.edu

Prediction of even and odd sunspot cycles

Timo **Asikainen**, Jani Mantere

Journal of Space Weather and Space Climate **13**, 25 **2023**

https://arxiv.org/pdf/2309.04208

https://www.swsc-journal.org/articles/swsc/pdf/2023/01/swsc230011.pdf

Here we study the prediction of even and odd numbered sunspot cycles separately, thereby taking into account the Hale cyclicity of solar magnetism. We first show that the temporal evolution and shape of all sunspot cycles are extremely well described by a simple parameterized mathematical expression. We find that the parameters describing even sunspot cycles can be predicted quite accurately using the sunspot number 41 months prior to sunspot minimum as a precursor. We find that the parameters of the odd cycles can be best predicted with maximum geomagnetic aa index close to fall equinox within a 3-year window preceding the sunspot minimum. We use the found precursors to predict all previous sunspot cycles and evaluate the performance with a cross-validation methodology, which indicates that each past cycle is very accurately predicted. For the coming sunspot cycle 25 we predict an amplitude of 171 +/- 23 and the end of the cycle in September 2029 +/- 1.9 years. We are also able to make a rough prediction for cycle 26 based on the predicted cycle 25. While the uncertainty for the cycle amplitude is large we estimate that the cycle 26 will most likely be stronger than cycle 25. These results suggest an increasing trend in solar activity for the next decades.

Modulation of cosmic ray anti-protons in the heliosphere: simulations for a solar cycle

O.P.M. **Aslam**, M.S. Potgieter, Xi Luo, M.D. Ngobeni

ApJ **2023**

https://arxiv.org/pdf/2303.13268.pdf

The precision measurements of galactic cosmic ray protons from PAMELA and AMS are reproduced using a well-established 3D numerical model for the period July 2006 - November 2019. The resulting modulation parameters

are applied to simulate the modulation for cosmic antiprotons over the same period, which includes times of minimum modulation before and after 2009, maximum modulation from 2012 to 2015 including the reversal of the Sun's magnetic field polarity, and the approach to new minimum modulation in 2020. Apart from their local interstellar spectra, the modulation of protons and antiprotons differ only in their charge-sign and consequent drift pattern. The lowest proton flux was in February-March 2014, but the lowest simulated antiproton flux is found to be in March-April 2015. These simulated fluxes are used to predict the proton to anti-proton ratios as a function of rigidity. The trends in these ratios contribute to clarify to a large extent the phenomenon of charge-sign dependence of heliospheric modulation during vastly different phases of the solar activity cycle. This is reiterated and emphasized by displaying so-called hysteresis loops. It is also illustrated how the values of the parallel and perpendicular mean free paths, as well as the drift scale, vary with rigidity over this extensive period. The drift scale is found to be at its lowest level during the polarity reversal period, while the lowest level of the mean free paths are found to be in March-April 2015.

Modeling of Heliospheric Modulation of Cosmic-ray Positrons in a Very Quiet Heliosphere

O.P.M. **Aslam**, D. Bisschoff, M. S. Potgieter, M. Boezio, R. Munini
ApJ **2019**
https://arxiv.org/pdf/1811.10710.pdf
Heliospheric modulation conditions were unusually quite during the last solar minimum activity between Solar Cycles 23/24. Fortunately, the PAMELA space-experiment measured six-month averaged Galactic positron spectra for the period July 2006 to December 2009, over an energy range of 80 MeV to 30 GeV, which is important for solar modulation. The highest level of Galactic positrons was observed at Earth during the July-December 2009 period. A well-established, comprehensive three-dimensional (3D) numerical model is applied to study the modulation of the observed positron spectra. This model had been used previously to understand the modulation of Galactic protons and electrons also measured by PAMELA for the same period. First, a new very local interstellar spectrum for positrons is constructed, using the well-known GALPROP code together with the mentioned PAMELA observations. The 3D model is used to distinguish between the dominant mechanisms responsible for the heliospheric modulation of Galactic positrons, and to understand the effect of particle drift during this unusual minimum in particular, which is considered diffusion dominant, even though particle drift still had a significant role in modulating positrons. Lastly, the expected intensity of Galactic positrons during an A>0 polarity minimum, with similar heliospheric conditions than for 2006-2009, is predicted to be higher than what was observed by PAMELA for the 2006-2009 unusual minimum.

Study of the Geoeffectiveness and Galactic Cosmic-Ray Response of VarSITI-ISEST Campaign Events in Solar Cycle 24

O. P. M. **Aslam**, Badruddin
Solar Physics September **2017**, 292:135
We analyze and compare the geomagnetic and galactic cosmic-ray (GCR) response of selected solar events, particularly the campaign events of the group International Study of Earth-affecting Solar Transients (ISEST) of the program Variability of the Sun and Its Terrestrial Impact (VarSITI). These selected events correspond to Solar Cycle 24, and we identified various of their features during their near-Earth passage. We evaluated the hourly data of geomagnetic indices and ground-based neutron monitors and the concurrent data of interplanetary plasma and field parameters. We recognized distinct features of these events and solar wind parameters when the geomagnetic disturbance was at its peak and when the cosmic-ray intensity was most affected. We also discuss the similarities and differences in the geoeffectiveness and GCR response of the solar and interplanetary structures in the light of plasma and field variations and physical mechanism(s), which play a crucial role in influencing the geomagnetic activity and GCR intensity. **14 July 2012, 8 Oct 2012, 17 March 2013, 31 May 2013, 17 March 2015, 21 June 2015,**

Study of Cosmic-Ray Modulation during the Recent Unusual Minimum and Mini Maximum of Solar Cycle 24

O.P.M. **Aslam**, Badruddin
Solar Phys. **2015**
http://arxiv.org/ftp/arxiv/papers/1507/1507.07917.pdf
After a prolonged and deep solar minimum at the end of Cycle 23, the current Solar Cycle 24 is one of the lowest cycles. These two periods of deep minimum and mini maximum are separated by a period of increasing solar activity. We study the cosmic-ray intensity variation in relation with the solar activity, heliospheric plasma and field parameters, including the heliospheric current sheet, during these three periods (phases) of different activity level and nature: (a) a deep minimum, (b) an increasing activity period and (c) a mini maximum. We use neutron monitor data from stations located around the globe to study the rigidity dependence on modulation during the two extremes, i.e., minimum and maximum. We also study the time lag between the cosmic-ray intensity and various solar and interplanetary parameters separately during the three activity phases. We also analyze the role of various parameters,

including the current sheet tilt, in modulating the cosmic-ray intensity during the three different phases. Their relative importance and the implications of our results are also discussed.

Similarities and Distinctions in Cosmic-Ray Modulation During Different Phases of Solar and Magnetic Activity Cycles

O. P. M. **Aslam**, Badruddin
Solar Physics, June **2014**, Volume 289, Issue 6, pp 2247-2268
http://arxiv.org/pdf/1312.2002v1.pdf

We study the solar-activity and solar-polarity dependence of galactic cosmic-ray intensity (CRI) on the solar and heliospheric parameters playing a significant role in solar modulation. We utilize the data for cosmic-ray intensity as measured by neutron monitors, solar activity as measured by sunspot number (SSN), interplanetary plasma/field parameters, solar-wind velocity [V] and magnetic field [B], as well as the tilt of the heliospheric current sheet [Λ], and we analyze these data for Solar Cycles 20 – 24 (1965 – 2011). We divide individual solar cycles into four phases, i.e. low, high, increasing, and decreasing solar activity. We perform regression analysis to calculate and compare the CRI-response to changes in different solar/interplanetary parameters during different phases of solar activity and similar activity phases but different polarity states.

We find that the CRI-response is different during negative (A<0) as compared to positive (A>0) polarity states not only with SSN and Λ but also with B and V. The relative CRI-response to changes in various parameters, in negative (A<0) as compared to positive (A>0) state, is solar-activity dependent; it is $\approx$ 2 to 3 times higher in low solar activity, $\approx$ 1.5 to 2 times higher in moderate (increasing/decreasing) activity, and it is nearly equal in high solar-activity conditions. Although our results can be ascribed to the preferential entry of charged particles via the equatorial/polar regions of the heliosphere as predicted by drift models, these results also suggest that we should look for any polarity-dependent response of solar-wind and transport parameters in modulating CRI in the heliosphere.

A Near-half-century Simulation of the Solar Corona

Valentin **Aslanyan**1, Karen A. Meyer1, Roger B. Scott2, and Anthony R. Yeates3
2024 ApJL 961 L3
https://iopscience.iop.org/article/10.3847/2041-8213/ad1934/pdf

We present an overview of results from a magnetofrictional model of the entire solar corona over a period of 47 yr. The simulation self-consistently reproduces decades of solar phenomena, varying in duration between rapid eruptions and the long-term solar cycles, from an input of observed active regions emerging at the photosphere. We have developed a geometric approach to use magnetic helicity to identify and localize the frequent eruptions that occur in the simulation. This method allows us to match our results to extreme-ultraviolet observations of transient events. We have analyzed the evolving magnetic topology by computing the squashing factor and segmenting the corona into discrete magnetic domains bounded by the Separatrix-Web. The simulations show a more dynamic structure to the Separatrix-Web than is predicted by potential field models, which may explain solar wind observations.

The chemical make-up of the Sun: A 2020 vision

M. **Asplund**, A. M. Amarsi, N. Grevesse
A&A 653, A141 **2021**
https://arxiv.org/pdf/2105.01661.pdf
https://www.aanda.org/articles/aa/pdf/2021/09/aa40445-21.pdf
https://doi.org/10.1051/0004-6361/202140445

The chemical composition of the Sun is a fundamental yardstick in astronomy, relative to which essentially all cosmic objects are referenced. We reassess the solar abundances of all 83 long-lived elements, using highly realistic solar modelling and state-of-the-art spectroscopic analysis techniques coupled with the best available atomic data and observations. Our new improved analysis confirms the relatively low solar abundances of C, N, and O obtained in our previous 3D-based studies: $\log\epsilon$C=8.46±0.04, $\log\epsilon$N=7.83±0.07, and $\log\epsilon$O=8.69±0.04. The revised solar abundances for the other elements also typically agree well with our previously recommended values with just Li, F, Ne, Mg, Cl, Kr, Rb, Rh, Ba, W, Ir, and Pb differing by more than 0.05 dex. The here advocated present-day photospheric metal mass fraction is only slightly higher than our previous value, mainly due to the revised Ne abundance from Genesis solar wind
measurements: Xsurface=0.7438±0.0054, Ysurface=0.2423±0.0054, Zsurface=0.0139±0.0006, and Zsurface/Xsurface=0.0187±0.0009. Overall the solar abundances agree well with those of CI chondritic meteorites but we identify a correlation with condensation temperature such that moderately volatile elements are enhanced by ≈0.04 dex in the CI chondrites and refractory elements possibly depleted by ≈0.02 dex, conflicting with conventional wisdom of the past half-century. Instead the solar chemical composition resembles more closely that of the fine-grained matrix of CM chondrites. The so-called solar modelling problem remains intact with our revised

solar abundances, suggesting shortcomings with the computed opacities and/or treatment of mixing below the convection zone in existing standard solar models.

Geomagnetic storms, super-storms, and their impacts on GPS-based navigation systems

E. **Astafyeva**1,*, Yu. Yasyukevich2,3, A. Maksikov3 andI. Zhivetiev
Space Weather, Volume 12, Issue 7, pages 508–525, July **2014**
Using data of GPS receivers located worldwide, we analyze the quality of GPS performance during four geomagnetic storms of different intensity: two super-storms and two intense storms. We show that during super-storms the density of GPS Losses-of-Lock (LoL) increases up to 0.25% at L1 frequency and up to 3% at L2 frequency, and up to 0.15% (at L1) and 1% (at L2) during less intense storms. Also, depending on the intensity of the storm time ionospheric disturbances, the total number of total electron content (TEC) slips can exceed from 4 to 40 times the quiet time level. Both GPS LoL and TEC slips occur during abrupt changes of SYM-H index of geomagnetic activity, i.e., during the main phase of geomagnetic storms and during development of ionospheric storms. The main contribution in the total number of GPS LoL was found to be done by GPS sites located at low and high latitudes, whereas the area of numerous TEC slips seemed to mostly correspond to the boundary of the auroral oval, i.e., region with intensive ionospheric irregularities. Our global maps of TEC slips show where the regions with intense irregularities of electron density occur during geomagnetic storms and will let us in future predict appearance of GPS errors for geomagnetically disturbed conditions.

An empirical model of heliospheric cosmic ray modulation on long-term time scale

Eleanna **Asvestari**1* and Ilya G. Usoskin
J. Space Weather Space Clim., 6, A15 (**2016**)
http://www.swsc-journal.org/articles/swsc/pdf/2016/01/swsc150073.pdf
Galactic Cosmic Rays (GCRs) entering the heliosphere are subject to modulation processes due to variable solar magnetic activity. Finding a relationship between cosmic-ray variations and the heliospheric parameters is important for reconstruction of solar activity in the past. Here, we develop a semi-empirical model describing the heliospheric modulation of GCRs in terms of heliospheric parameters such as the open solar magnetic flux, the tilt angle of the heliospheric current sheet and the polarity of the large scale solar magnetic field. Our model is fitted using annual data obtained for the period 1976–2013, which includes the very weak solar minimum during 2008–2010. The model shows a good agreement with the data, and therefore, can be used for reconstructions of the modulation potential at different levels of solar activity. The model's validity is also tested using the cosmogenic radionuclides 14C and 10Be stored in terrestrial archives. The tilt angle used to fit the parameters in our semi-empirical modulation model is reconstructed by a mathematical model described here.

Can Emission Measure Distributions Derived from Extreme-ultraviolet Images Accurately Constrain High-temperature Plasma?

P. S. **Athiray**1,2 and Amy R. Winebarger2
2024 ApJ 961 181
https://iopscience.iop.org/article/10.3847/1538-4357/ad1837/pdf
Measuring the relative amount of high-temperature, low emission measure (EM) plasma is considered to be a smoking-gun observation to constrain the frequency of plasma heating in coronal structures. Often, narrowband, extreme-ultraviolet images, such as those obtained by the Atmospheric Imaging Assembly (AIA) on the Solar Dynamics Observatory (SDO), are used to determine the EM distribution, though the sensitivity to high-temperature plasma is limited. Conversely, the soft X-ray wavelength range offers multiple high-temperature diagnostics, including emission lines of N vii, O vii, O viii, Fe xvii, Ne ix, and Mg xi, which can provide tight constraints to the high-temperature plasma in the log T = 6.1–6.7 (∼1–5+ MK) range. The Marshall Grazing Incidence X-ray Spectrometer (MaGIXS), a slitless spectrograph launched on a NASA sounding rocket on **2021 July 30**, resolved an X-ray-bright point in multiple emission lines in the soft X-ray wavelength range. Using coordinated observations of the same X-ray-bright point from SDO/AIA, we compare and contrast the EM distributions from the EUV image data, the X-ray spectra, and the combined EUV and X-ray data set. In this paper, we demonstrate that EM distributions from SDO/AIA data alone can overestimate the amount of high-temperature (log T > 6.4) plasma in the solar corona by a factor of 3–15. Furthermore, we present our effort to cross-calibrate Hinode/X-ray Telescope (XRT) response functions by comparing the observed XRT fluxes with the predicted ones from combined MaGIXS-1 + AIA EM analysis.

Solar Active Region Heating Diagnostics from High Temperature Emission using the Marshall Grazing Incidence X-ray Spectrometer (MaGIXS)

P.S. **Athiray**, Amy R. Winebarger, Will T. Barnes, Stephen J. Bradshaw, Sabrina Savage, Harry P. Warren, Ken Kobayashi, Patrick Champey, Leon Golub, Lindsay Glesener
ApJ **884** 24 **2019**

https://arxiv.org/pdf/1909.02541.pdf
https://doi.org/10.3847/1538-4357/ab3eb4
The relative amount of high temperature plasma has been found to be a useful diagnostic to determine the frequency of coronal heating on sub-resolution structures. When the loops are infrequently heated, a broad emission measure (EM) over a wider range of temperatures is expected. A narrower EM is expected for high frequency heating where the loops are closer to equilibrium. The soft X-ray spectrum contains many spectral lines that provide high temperature diagnostics, including lines from Fe XVII-XIX. This region of the solar spectrum will be observed by the Marshall Grazing Incidence Spectrometer (MaGIXS) in 2020. In this paper, we derive the expected spectral lines intensity in MaGIXS to varying amounts of high temperature plasma to demonstrate that a simple line ratio of these provides a powerful diagnostic to determine the heating frequency. Similarly, we examine ratios of AIA channel intensities, filter ratios from a XRT, and energy bands from the FOXSI sounding rocket to determine their sensitivity to this parameter. We find that both FOXSI and MaGIXS provide good diagnostic capability for high-temperature plasma. We then compare the predicted line ratios to the output of a numerical model and confirm the MaGIXS ratios provide an excellent diagnostic for heating frequency.

Relationship between supergranulation flows, magnetic cancellation and network flares

R. **Attie**1, D. E. Innes1, S. K. Solanki1,2 and K. H. Glassmeier
A&A 596, A15 (**2016**)
https://arxiv.org/pdf/1705.10389.pdf
Context. Photospheric flows create a network of often mixed-polarity magnetic field in the quiet Sun, where small-scale eruptions and network flares are commonly seen.
Aims. The aim of this paper is (1) to describe the characteristics of the flows that lead to these energy releases, (2) to quantify the energy build up due to photospheric flows acting on the magnetic field, and (3) to assess its contribution to the energy of small-scale, short-lived X-ray flares in the quiet Sun.
Methods. We used photospheric and X-ray data from the SoHO and Hinode spacecraft combined with tracking algorithms to analyse the evolution of five network flares. The energy of the X-ray emitting thermal plasma is compared with an estimate of the energy built up due to converging and sheared flux.
Results. Quiet-Sun network flares occur above sites of converging opposite-polarity magnetic flux that are often found on the outskirts of network cell junctions, sometimes with observable vortex-like motion. In all studied flares the thermal energy was more than an order of magnitude higher than the magnetic free energy of the converging flux model. The energy in the sheared field was always higher than in the converging flux but still lower than the thermal energy.
Conclusions. X-ray network flares occur at sites of magnetic energy dissipation. The energy is probably built up by supergranular flows causing systematic shearing of the magnetic field. This process appears more efficient near the junction of the network lanes. Since this work relies on 11 case studies, our results call for a follow-up statistical analysis to test our hypothesis throughout the quiet Sun.
September 26, 2008

Beyond the disk: EUV coronagraphic observations of the Extreme Ultraviolet Imager on board Solar Orbiter

Auchère, F., Berghmans, D., Dumesnil, C., Halain, J.-P., Mercier, R., +++
A&A 674, A127 **2023**
https://arxiv.org/pdf/2305.15308.pdf
https://www.aanda.org/articles/aa/pdf/2023/06/aa46039-23.pdf
Most observations of the solar corona beyond 2 Rs consist of broadband visible light imagery from coronagraphs. The associated diagnostics mainly consist of kinematics and derivations of the electron number density. While the measurement of the properties of emission lines can provide crucial additional diagnostics of the coronal plasma (temperatures, velocities, abundances, etc.), these observations are comparatively rare. In visible wavelengths, observations at these heights are limited to total eclipses. In the VUV range, very few additional observations have been achieved since the pioneering results of UVCS. One of the objectives of the Full Sun Imager (FSI) channel of the EUI telescope on board the Solar Orbiter mission has been to provide very wide field-of-view EUV diagnostics of the morphology and dynamics of the solar atmosphere in temperature regimes that are typical of the lower transition region and of the corona. FSI carries out observations in two narrowbands of the EUV spectrum centered on 17.4 nm and 30.4 nm that are dominated, respectively, by lines of Fe IX/X (formed in the corona around 1 MK) and by the resonance line of He II (formed around 80 kK in the lower transition region). Unlike previous EUV imagers, FSI includes a moveable occulting disk that can be inserted in the optical path to reduce the amount of instrumental stray light to a minimum. FSI detects signals at 17.4 nm up to the edge of its FOV (7~Rs), which is about twice further than was previously possible. Comparisons with observations by the LASCO and Metis coronagraphs confirm the presence of morphological similarities and differences between the broadband visible light and EUV emissions, as documented on the basis of prior eclipse and space-based observations. The very-wide-

field observations of FSI are paving the way for future dedicated instruments. **2021 March 21, 2021 September 8, 2021 November 1, 3, 4, 2022 February 8, 2022 March 7, 2022 December 5**

Image enhancement with wavelet-optimized whitening⋆

F. **Auchère**, E. Soubrié, G. Pelouze and É. Buchlin
A&A 670, A66 (**2023**)
https://www.aanda.org/articles/aa/pdf/2023/02/aa45345-22.pdf
Context. Due to its physical nature, the solar corona exhibits large spatial variations of intensity that make it difficult to simultaneously visualize the features present at all levels and scales. Many general-purpose and specialized filters have been proposed to enhance coronal images. However, most of them require the ad hoc tweaking of parameters to produce subjectively good results.
Aims. Our aim was to develop a general purpose image enhancement technique that would produce equally good results, but based on an objective criterion.
Methods. The underlying principle of the method is the equalization, or whitening, of power in the à trous wavelet spectrum of the input image at all scales and locations. An edge-avoiding modification of the à trous transform that uses bilateral weighting by the local variance in the wavelet planes is used to suppress the undesirable halos otherwise produced by discontinuities in the data.
Results. Results are presented for a variety of extreme ultraviolet (EUV) and white light images of the solar corona. The proposed filter produces sharp and contrasted output, without requiring the manual adjustment of parameters. Furthermore, the built-in denoising scheme prevents the explosion of high-frequency noise typical of other enhancement methods, without smoothing statistically significant small-scale features. The standard version of the algorithm is about two times faster than the widely used multiscale Gaussian normalization (MGN). The bilateral version is slower, but provides significantly better results in the presence of spikes or edges. Comparisons with other methods suggest that the whitening principle may correspond to the subjective criterion of most users when adjusting free parameters. **2022 March 17, 2022 March 21, 2022 April 2**,

Coordination within the remote sensing payload on the Solar Orbiter mission

F. **Auchère**1, V. Andretta13, E. Antonucci2, N. Bach12, M. Battaglia5, A. Bemporad2,
A&A 642, A6 (**2020**)
https://www.aanda.org/articles/aa/pdf/2020/10/aa37032-19.pdf
https://doi.org/10.1051/0004-6361/201937032
Context. To meet the scientific objectives of the mission, the Solar Orbiter spacecraft carries a suite of in-situ (IS) and remote sensing (RS) instruments designed for joint operations with inter-instrument communication capabilities. Indeed, previous missions have shown that the Sun (imaged by the RS instruments) and the heliosphere (mainly sampled by the IS instruments) should be considered as an integrated system rather than separate entities. Many of the advances expected from Solar Orbiter rely on this synergistic approach between IS and RS measurements.
Aims. Many aspects of hardware development, integration, testing, and operations are common to two or more RS instruments. In this paper, we describe the coordination effort initiated from the early mission phases by the Remote Sensing Working Group. We review the scientific goals and challenges, and give an overview of the technical solutions devised to successfully operate these instruments together.
Methods. A major constraint for the RS instruments is the limited telemetry (TM) bandwidth of the Solar Orbiter deep-space mission compared to missions in Earth orbit. Hence, many of the strategies developed to maximise the scientific return from these instruments revolve around the optimisation of TM usage, relying for example on onboard autonomy for data processing, compression, and selection for downlink. The planning process itself has been optimised to alleviate the dynamic nature of the targets, and an inter-instrument communication scheme has been implemented which can be used to autonomously alter the observing modes. We also outline the plans for in-flight cross-calibration, which will be essential to the joint data reduction and analysis.
Results. The RS instrument package on Solar Orbiter will carry out comprehensive measurements from the solar interior to the inner heliosphere. Thanks to the close coordination between the instrument teams and the European Space Agency, several challenges specific to the RS suite were identified and addressed in a timely manner.

The Coronal Monsoon: Thermal Nonequilibrium Revealed by Periodic Coronal Rain

Frédéric **Auchère**1, Clara Froment2,3, Elie Soubrié1,4, Patrick Antolin5, Ramon Oliver4,6, andGabriel Pelouze1
2018 ApJ 853 176
http://sci-hub.tw/http://iopscience.iop.org/0004-637X/853/2/176/
https://arxiv.org/pdf/1802.01852.pdf
We report on the discovery of periodic coronal rain in an off-limb sequence of Solar Dynamics Observatory/Atmospheric Imaging Assembly images. The showers are co-spatial and in phase with periodic (6.6 hr) intensity pulsations of coronal loops of the sort described by Auchère et al. and Froment et al. These new

observations make possible a unified description of both phenomena. Coronal rain and periodic intensity pulsations of loops are two manifestations of the same physical process: evaporation/condensation cycles resulting from a state of thermal nonequilibrium. The fluctuations around coronal temperatures produce the intensity pulsations of loops, and rain falls along their legs if thermal runaway cools the periodic condensations down and below transition-region temperatures. This scenario is in line with the predictions of numerical models of quasi-steadily and footpoint heated loops. The presence of coronal rain—albeit non-periodic—in several other structures within the studied field of view implies that this type of heating is at play on a large scale. **2012 July 23-25**

On The Fourier And Wavelet Analysis Of Coronal Time Series

F. **Auchère**, C. Froment, K. Bocchialini, E. Buchlin, J. Solomon
2016 ApJ 825 110
http://arxiv.org/pdf/1606.05251v1.pdf
Using Fourier and wavelet analysis, we critically re-assess the significance of our detection of periodic pulsations in coronal loops. We show that the proper identification of the frequency dependence and statistical properties of the different components of the power spectra provies a strong argument against the common practice of data detrending, which tends to produce spurious detections around the cut-off frequency of the filter. In addition, the white and red noise models built into the widely used wavelet code of Torrence & Compo cannot, in most cases, adequately represent the power spectra of coronal time series, thus also possibly causing false positives. Both effects suggest that several reports of periodic phenomena should be re-examined. The Torrence & Compo code nonetheless effectively computes rigorous confidence levels if provided with pertinent models of mean power spectra, and we describe the appropriate manner in which to call its core routines. We recall the meaning of the default confidence levels output from the code, and we propose new Monte-Carlo-derived levels that take into account the total number of degrees of freedom in the wavelet spectra. These improvements allow us to confirm that the power peaks that we detected have a very low probability of being caused by noise.
Erratum: 2017 ApJ 838 166

Long-period intensity pulsations in the solar corona during activity cycle 23⋆

F. **Auchère**, K. Bocchialini, J. Solomon and E. Tison
A&A 563, A8 (**2014**)
We report on the detection (10σ) of 917 events of long-period (3 to 16 h) intensity pulsations in the 19.5 nm passband of the SOHO Extreme ultraviolet Imaging Telescope. The data set spans from January 1997 to July 2010, i.e. the entire solar cycle 23 and the beginning of cycle 24. The events can last for up to six days and have relative amplitudes up to 100%. About half of the events (54%) are found to happen in active regions, and 50% of these have been visually associated with coronal loops. The remaining 46% are localized in the quiet Sun. We performed a comprehensive analysis of the possible instrumental artefacts and we conclude that the observed signal is of solar origin. We discuss several scenarios that could explain the main characteristics of the active region events. The long periods and the amplitudes observed rule out any explanation in terms of magnetohydrodynamic waves. Thermal non-equilibrium could produce the right periods, but it fails to explain all the observed properties of coronal loops and the spatial coherence of the events. We propose that moderate temporal variations of the heating term in the energy equation, so as to avoid a thermal non-equilibrium state, could be sufficient to explain those long-period intensity pulsations. The large number of detections suggests that these pulsations are common in active regions. This would imply that the measurement of their properties could provide new constraints on the heating mechanisms of coronal loops.

Convective Dynamo Simulation with a Grand Minimum

Kyle **Augustson**, Sacha Brun, Mark Miesch, Juri Toomre
Cool Stars 18 Conference Proceedings (**2014**)
http://arxiv.org/pdf/1503.04225v1.pdf
The global-scale dynamo action achieved in a simulation of a Sun-like star rotating at thrice the solar rate is assessed. The 3-D MHD Anelastic Spherical Harmonic (ASH) code, augmented with a viscosity minimization scheme, is employed to capture convection and dynamo processes in this G-type star. The simulation is carried out in a spherical shell that encompasses 3.8 density scale heights of the solar convection zone. It is found that dynamo action with a high degree of time variation occurs, with many periodic polarity reversals occurring roughly every 6.2 years. The magnetic energy also rises and falls with a regular period. The magnetic energy cycles arise from a Lorentz-force feedback on the differential rotation, whereas the processes leading to polarity reversals are more complex, appearing to arise from the interaction of convection with the mean toroidal fields. Moreover, an equatorial migration of toroidal field is found, which is linked to the changing differential rotation, and potentially to a nonlinear dynamo wave. This simulation also enters a grand minimum lasting roughly 20~years, after which the dynamo recovers its regular polarity cycles.

Critical magnetic field strengths for solar coronal plumes in quiet regions and coronal holes?

Ellis A. **Avallone**, Sanjiv K. Tiwari, Navdeep K. Tiwari, Ronald L. Moore, Amy Winebarger

ApJ **861** 111 **2018**
https://arxiv.org/pdf/1805.11188.pdf
http://sci-hub.tw/http://iopscience.iop.org/0004-637X/861/2/111/

Coronal plumes are bright magnetic funnels found in quiet regions (QRs) and coronal holes (CHs). They extend high into the solar corona and last from hours to days. The heating processes of plumes involve dynamics of the magnetic field at their base, but the processes themselves remain mysterious. Recent observations suggest that plume heating is a consequence of magnetic flux cancellation and/or convergence at the plume base. These studies suggest that the base flux in plumes is of mixed polarity, either obvious or hidden in SDO HMI data, but do not quantify it. To investigate the magnetic origins of plume heating, we select ten unipolar network flux concentrations, four in CHs, four in QRs, and two that do not form a plume, and track plume luminosity in SDO AIA 171 A images along with the base flux in SDO HMI magnetograms, over each flux concentrations lifetime. We find that plume heating is triggered when convergence of the base flux surpasses a field strength of 200 to 600 G. The luminosity of both QR and CH plumes respond similarly to the field in the plume base, suggesting that the two have a common formation mechanism. Our examples of non-plume-forming flux concentrations, reaching field strengths of 200 G for a similar number of pixels as for a couple of our plumes, suggest that a critical field might be necessary to form a plume but is not sufficient for it, thus, advocating for other mechanisms, e.g. flux cancellation due to hidden opposite-polarity field, at play. **July 5, 2011, September 8-9, 2011, October 5, 2013, February 1, 2015, August 5, 2015, December 4, 2015, May 12-13, 2016, December 23, 2016, May 12, 2017**

MODELING THE CHROMOSPHERE OF A SUNSPOT AND THE QUIET SUN

E. **Avrett**1, H. Tian1, E. Landi2, W. Curdt3, and J.-P. Wülser

2015 ApJ 811 87

Semiempirical atmospheric modeling attempts to match an observed spectrum by finding the temperature distribution and other physical parameters along the line of sight through the emitting region such that the calculated spectrum agrees with the observed one. In this paper we take the observed spectrum of a sunspot and the quiet Sun in the EUV wavelength range 668–1475 Å from the 2001 SUMER atlas of Curdt et al. to determine models of the two atmospheric regions, extending from the photosphere through the overlying chromosphere into the transition region. We solve the coupled statistical equilibrium and optically thick radiative transfer equations for a set of 32 atoms and ions. The atoms that are part of molecules are treated separately, and are excluded from the atomic abundances and atomic opacities. We compare the Mg ii k line profile observations from the Interface Region Imaging Spectrograph with the profiles calculated from the two models. The calculated profiles for the sunspot are substantially lower than the observed ones, based on the SUMER models. The only way we have found to raise the calculated Mg ii lines to agree with the observations is to introduce illumination of the sunspot from the surrounding active region.

A study of particles acceleration, heating, power deposition, and the damping length of kinetic Alfvén waves in non-Maxwellian coronal plasma

S. **Ayaz**, Gary P. Zank, Imran A. Khan, G. Li, Yeimy J. Rivera

A&A **2024**
https://arxiv.org/pdf/2411.19061

The heating of the solar corona and solar wind, through suprathermal particles and kinetic Alfvén waves within the 0 - 10 RSun range, has been a subject of great interest for many decades. This study investigates the acceleration and heating of charged particles and the role of KAWs in the solar corona. We investigate how KAWs transport energy and accelerate/heat the charged particles, focusing on the behavior of perturbed EM fields, Poynting flux vectors, net power transfer, resonant particle speed, group speed, and the damping length of KAWs. The study examines how these elements are influenced by suprathermal particles \kappa and the electron-to-ion temperature Te/Ti. We use kinetic plasma theory coupled with the Vlasov-Maxwell model to investigate the dynamics of KAWs and particles. We assume a collisionless, homogeneous, and low-beta electron-ion plasma in which Alfvén waves travel in the kinetic limits. The results show the perturbed EM fields are significantly influenced by κ and Te/Ti. We evaluate both the parallel and perpendicular Poynting fluxes and find that the parallel Poynting flux dissipates gradually for lower \kappa values. The perpendicular flux dissipates quickly over shorter distances. Power deposition in solar flux tubes is significantly influenced by \kappa and Te/Ti. We find that particles can heat the solar corona over long distances in the parallel direction and short distances in the perpendicular direction. The group velocity of KAWs increases for lower \kappa values, and the damping length is enhanced under lower \kappa, suggesting longer energy transport distances. These findings offer a comprehensive understanding of particle-wave interactions in the solar corona and wind, with potential applications for missions such as the Parker Solar Probe (PSP), and can also apply to other environments.

Solar Coronal Heating by Kinetic Alfvén Waves

Syed **Ayaz**1, Gang Li1,2, and Imran A. Khan3,4
2024 ApJ 970 140
https://iopscience.iop.org/article/10.3847/1538-4357/ad5bdc/pdf
The utilization of the Cairns distribution serves as a vital tool for characterizing the nonthermal attributes commonly observed in space plasmas. In these intricate plasma environments, extensive measurements have been conducted to monitor the fluctuations inherent in the perturbed electromagnetic (EM) field and the associated Poynting flux, specifically concerning kinetic Alfvén waves (KAWs). Traditionally, these fluctuations have been attributed to gyroradius correction terms within the framework of Maxwellian distributed plasmas. However, our study introduces an innovative perspective grounded in kinetic theory coupled with the Cairns distribution, adept at encapsulating the nonthermal nuances characterized by the index parameter Λ. Within the domain of the solar corona, our investigation centers on the perturbed EM field ratios and the Poynting flux of KAWs, with a foundation in the Cairns distribution function. It is noteworthy that the perpendicular components, although deemed less significant due to the dominance of k⊥ over k∥, remain unquantified regarding their relative insignificance. Similarly, the exploration of the imaginary part of the normalized EM field ratio has been a relatively understudied domain. Furthermore, we delve into the nuanced assessment of the power rate Ix/Iz characterizing the perpendicular and parallel normalized Poynting fluxes (Sx and Sz). Intriguingly, we discern that large values of Λ, compared to their Maxwellian counterparts, manifest advantageous attributes, particularly concerning the energization of the plasma over extended distances along the ambient magnetic field lines. The analytical insights gleaned from this study find practical application in understanding phenomena within the solar atmosphere, particularly shedding light on the significant role played by nonthermal particles in the observed heating processes.

In the Trenches of the Solar–Stellar Connection. II. Extreme Ultraviolet Flux–Flux Correlations across Solar Cycle 24

Thomas R. **Ayres**
2021 ApJ 908 205
https://doi.org/10.3847/1538-4357/abd095
Solar extreme-ultraviolet (EUV: 100–1100 Å) radiation rises in the 104 K upper chromosphere and hotter layers extending into the million-degree corona. Much of the EUV normally is not visible in other stars owing to interstellar H i absorption. The present study derived power-law scaling relations for EUV species based on irradiance spectra from the Extreme Ultraviolet Variability Experiment on board the Solar Dynamics Observatory, over the rise and fall of recent sunspot Cycle 24. These relations not only can test solar models, but also allow "invisible" stellar EUV emissions to be reconstructed from more accessible ultraviolet (UV: 1100–3000 Å) proxies, with implications for heating, ionization, and erosion of exoplanet atmospheres by Sun-like hosts. Hot EUV coronal tracers like Si xii 520 Å (8 MK) show strongly curved power laws relative to chromospheric H i 1025 Å Lyβ, as was seen in Paper I for 0.2–2 keV soft X-rays versus Mg ii 2800 Å. The brightest EUV feature, He ii 303 Å, exhibits a nearly 1:1 correlation with Lyβ (and H i 1215 Lyα, but slightly steeper than 1:1 relative to Mg ii). The second brightest, C iii 977 Å, has a shallower power-law slope of ~0.5. Correlations for low first ionization potential species, such as Mg, Si, and Fe, might be affected by cycle-dependent chemical fractionation. Parameterized flux–flux relations are presented for most of the strong EUV (and selected UV) features, together with fluxes of individual lines and broad EUV wavelength bands at the highs and lows of Cycle 24.

Magnetic field as a tracer for studying the differential rotation of the solar corona

O.G.**Badalyan**, V.N.Obridko
Solar Phys. 293:128 **2018**
https://arxiv.org/pdf/1808.05515.pdf
https://link.springer.com/content/pdf/10.1007%2Fs11207-018-1349-7.pdf
The differential rotation of the solar corona for the period 1976-2004 was studied as a function of the distance from the center of the Sun. For this study, we developed a method using the coronal magnetic field as a tracer. The field in a spherical layer from the base of the corona up to the source surface was determined from photospheric measurements. Calculations were performed for 14 heliocentric distances from the base of the corona up to 2.45 solar radii and from the equator to about 75 degrees of latitude at 5 degrees steps. For each day, we calculated three components, which were then used to obtain the field strength. The coronal rotation periods were determined by the periodogram method for all distances and latitudes under consideration. The variations in the coronal rotation during the time interval 1976-2004 were as follows: the gradient of differential rotation decreased with the increase of heliocentric distance; the rotation remaining differential even in the vicinity of the source surface. The largest rotation rates were recorded at the cycle minimum at small heights in the corona. The lowest rotation rate was observed at the middle of the ascending branch at large distances. At the minimum of the cycle, the differential rotation is most clearly pronounced, especially at small heliocentric distances. As the distance increases, the differential gradient decreases in all phases. The results based on magnetic data and on the brightness of the coronal

green line 530.3nm FeXIV used earlier show a satisfactory agreement. Since the rotation of the magnetic field at the corresponding heights in the corona is probably determined by the conditions in the field generation region, an opportunity arises to use this method for diagnostics of differential rotation in the subphotospheric layers.

North-south asymmetry of solar activity as a superposition of two realizations – the sign and absolute value

O. G. **Badalyan** and V. N. Obridko
A&A 603, A109 (**2017**)
http://www.aanda.org.sci-hub.cc/articles/aa/abs/2017/07/aa27790-15/aa27790-15.html
Context. Since the occurrence of north-south asymmetry (NSA) of alternating sign may be determined by different mechanisms, the frequency and amplitude characteristics of this phenomenon should be considered separately.
Aims. We propose a new approach to the description of the NSA of solar activity.
Methods. The asymmetry defined as A = (N−S)/(N + S) (where N and S are, respectively, the indices of activity of the northern and southern hemispheres) is treated as a superposition of two functions: the sign of asymmetry (signature) and its absolute value (modulus). This approach is applied to the analysis of the NSA of sunspot group areas for the period 1874–2013.
Results. We show that the sign of asymmetry provides information on the behavior of the asymmetry. In particular, it displays quasi-periodic variation with a period of 12 yr and quasi-biennial oscillations as the asymmetry itself. The statistics of the so-called monochrome intervals (long periods of positive or negative asymmetry) are considered and it is shown that the distribution of these intervals is described by the random distribution law. This means that the dynamo mechanisms governing the cyclic variation of solar activity must involve random processes. At the same time, the asymmetry modulus has completely different statistical properties and is probably associated with processes that determine the amplitude of the cycle. One can reliably isolate an 11-yr cycle in the behavior of the asymmetry absolute value shifted by half a period with respect to the Wolf numbers. It is shown that the asymmetry modulus has a significant prognostic value: the higher the maximum of the asymmetry modulus, the lower the following Wolf number maximum.
Conclusions. A fundamental nature of this concept of NSA is discussed in the context of the general methodology of cognizing the world. It is supposed that the proposed description of the NSA will help clarify the nature of this phenomenon.

Spatial distribution of the N-S asymmetry of solar activity and its time variations

O. G. **Badalyan**
Astronomy Letters, Volume 38, Number 1, 51-61, **2012**
Pis'ma v Astronomicheskiĭ Zhurnal, **2012**, Vol. 38, No. 1, pp. 54–64.
The 1943–2001 data on the brightness of the coronal green λ530.3 nm line are used to investigate the surface distribution of the north-south (N-S) asymmetry index A. Synoptic maps of the asymmetry index in 784 successive Carrington rotations have been constructed. The results are presented in the form of a movie that visualizes the time variation in the spatial distribution of the asymmetry. Examination of a series of synoptic maps shows that the time variation in the general distribution of the A index over the solar surface has a number of peculiar features. In particular, the latitude-longitude regions with the dominance of the green line brightness in one of the hemispheres are replaced by similar (in shape) regions with its dominance in the other hemisphere after 14–18 rotations-in other words, the map, as it were, turns into its negative. This may be a manifestation of the quasi-biennial oscillations in the N-S asymmetry. The synodic rotation period of the asymmetry "structures" has been determined. It has turned out to be equal to the period of the fast coronal rotation mode found previously from the large-scale brightness distribution of the coronal green line, i.e., this is 27 days on the equator and slightly more than 28 days at high latitudes. The N-S asymmetry and its characteristics should be taken into account when considering the dynamo mechanism.

The latitude distributions of sunspots and its North-South asymmetry

O. G. **Badalyan**
Astronomy Reports, Volume 55, Number 10, 928-942,
Astronomicheskii Zhurnal, **2011**, Vol. 88, No. 10, pp. 1008–1023.
The temporal variations observed in the monthly mean latitudes of sunspot groups are studied over 1874–2010 using the data of the Greenwich Catalog and its NOAA-USEF extension. The 11-year cycle is quite clear in the temporal variations of the monthly mean latitudes of sunspot groups (i.e., of the centers of spotting) in both the northern and southern hemispheres. The North-South (N-S) asymmetry in the latitudes of sunspot groups defined as the difference between the absolute values of sunspot latitudes observed in the N and S hemispheres is compared with

the N-S asymmetry in the total area of sunspot groups determined on the scales of 11 years and longer. The N-S asymmetry is interpreted as an imbalance in the hemispheres' powers (asymmetry in the total area of sunspot groups) and as spatial imbalance (asymmetry in the latitudes of the centers of spotting). This imbalance is most clearly seen at the solar minima, i.e., in the gradual transition from one cycle to the other, when the absolute values of the asymmetries observed both in the total sunspot area and in the sunspot latitudes reach their maxima. The results obtained here can be helpful for analyses of the solar dynamo.

Solar Event Detection Using Deep-Learning-Based Object Detection Methods

Ji-Hye **Baek**, Sujin Kim, Seonghwan Choi, Jongyeob Park, Jihun Kim, Wonkeun Jo & Dongil Kim
Solar Physics volume 296, Article number: 160 (**2021**)
https://link.springer.com/content/pdf/10.1007/s11207-021-01902-5.pdf

Research on the detection of solar events has been conducted over many years. Recently, deep learning and data-driven approaches have been applied to solar event recognition. In this study, we present solar event detection using deep-learning-based object detection methods for real-time space weather monitoring. First, we construct a new object detection dataset using imaging data obtained by the Solar Dynamics Observatory with bounding boxes as labels for three representative features: coronal holes, sunspots, and prominences. Second, we train two representative object detection models: the Single Shot MultiBox Detector (SSD) and the Faster Region-based Convolutional Neural Network (R-CNN) using the new dataset. The results show that both models perform similarly well for coronal hole and sunspot detection. For prominence detection, the SSD and Faster R-CNN exhibited relatively low performance. This study demonstrates that deep-learning-based object detection can successfully detect multiple types of solar events, and it may be extended to detect other solar events. In addition, we provide the dataset for further achievements of object detection studies in solar physics.

On the Nature of the Kink MHD Waves in Flowing and Twisted Coronal Flux Tubes

Karam **Bahari**
Solar Physics volume 296, Article number: 126 (**2021**)
https://link.springer.com/content/pdf/10.1007/s11207-021-01872-8.pdf
https://doi.org/10.1007/s11207-021-01872-8

We have studied the nature of the magnetohydrodynamic (MHD) kink waves in magnetically twisted flux tubes in the presence of plasma flow. To do this, the eigenfunctions of the kink oscillations have been determined using the dispersion relation and the boundary conditions of the tube. Then the components of the magnetic-tension force and the gradient of the pressure force have been obtained to determine the nature of the waves. For the waves with positive azimuthal wavenumber, the magnetic twist and plasma flow have opposite effects on the ratio of restoring forces and the wave has a mixed nature. However, for the waves with negative azimuthal wavenumber the magnetic twist and plasma flow strengthen the effects of each other in increasing the ratio of the magnetic-tension force to the gradient of the pressure force, and they make the nature of the wave more Alfvénic. In the presence of both plasma flow and magnetic twist, in the case of the waves with negative azimuthal wavenumber, for some specific values of the tube parameters, the magnetic-tension force becomes the dominant restoring force both in the radial and azimuthal directions, and the wave can be considered as an Alfvén wave in the internal region of the tube. However, in the case of the waves with positive azimuthal wavenumber, the nature of the wave remains mixed under all circumstances.

The Effect of Magnetic Twist and Plasma Flow on the Seismology of Oscillating Flux Tubes

Karam **Bahari** and Zeynab Jahan
2020 ApJ 901 28
https://doi.org/10.3847/1538-4357/abafa1

In this paper, we study propagating and standing magnetohydrodynamic kink waves in a magnetically twisted and flowing flux tube. The plasma flow is in the direction of the magnetic field; outside the tube, the magnetic field lines are purely longitudinal. The plasma density is constant both inside and outside the tube, and all stationary quantities vary abruptly at the tube boundary. Using the thin tube and weak twist approximations, the dispersion relation, which determines the dependence of the oscillation frequency on the wavenumber and the stationary quantities of the tube, is found. It is shown that the oscillation frequency of the propagating forward (backward) waves increases (decreases) as the flow speed increases; also, the increase in the magnetic twist increases the oscillation frequency of both forward and backward propagating waves. For very weak magnetic twist, the oscillation frequency of both fundamental mode and first overtone standing waves decreases with increasing flow speed. Our results show that if only the plasma flow or magnetic twist is present in the flux tube, the period ratio P1/P2 of the fundamental mode to the first overtone of the standing kink waves is equal to 2, but if both the plasma flow and magnetic twist are present in the flux tube, the period ratio can be smaller than 2 and support some observational cases. The asymmetry of the wave about the apex point is not affected much by the magnetic twist, but the magnetic twist causes an overestimation of both the flow speed and kink speed of the coronal loop.

The nature of kink MHD waves in the solar corona: magnetic twist and phase mixing

K **Bahari**, Z Ebrahimi

Monthly Notices of the Royal Astronomical Society, Volume 497, Issue 1, September **2020**, Pages 1135–1142,

https://doi.org/10.1093/mnras/staa2019

To study the nature of magnetohydrodynamic (MHD) kink waves, the temporal behaviour of an initial kink perturbation of a typical coronal flux tube has been investigated in this paper. The flux tube has a transitional layer that separates the core region of the tube from the surrounding environment. In the transitional layer, the background density and magnetic field varies continuously from the internal to the external values. The magnetic field is straight and aligned with the tube axis in the internal and external regions of the flux tube, but is assumed to be twisted in the transitional layer. Hence, in the transitional layer the background Alfvén speed is inhomogeneous and perturbations become out of phase due to the process of phase mixing. Our result shows that as the energy of the wave transfers to the local Alfvén waves in the inhomogeneous region, the magnetic tension force becomes the dominant restoring force of the wave. The numerical results show that the nature of the small-scale oscillations in the transitional layer is determined by the ratio of the azimuthal components of the restoring forces.

The Effect of a Twisted Magnetic Field on the Nature of Kink MHD Waves

K. **Bahari**, M. R. Khalvandi

Solar Physics December **2017**, 292:192

https://link.springer.com/content/pdf/10.1007%2Fs11207-017-1215-z.pdf

We consider a pressureless plasma in a thin magnetic-flux tube with a twisted magnetic field. We study the effect of twisted magnetic field on the nature of propagating kink waves. To do this, the restoring forces of oscillations in the linear ideal magnetohydrodynamics (MHD) were obtained. In the presence of a twisted magnetic field, the ratio of the magnetic-tension force to the gradient of the magnetic pressure increases for the mode with negative azimuthal wave number, but it decreases for the mode with positive azimuthal wave number. For the kink mode with positive azimuthal mode number, the ratio of the forces is more affected by the twisted magnetic field in dense loops. For the kink mode with negative azimuthal mode number, the perturbed magnetic pressure is negligible under some conditions. The magnetic twist increases (diminishes) the damping of the kink waves with positive (negative) azimuthal mode number due to resonant absorption. Our conclusion is that introducing a twisted magnetic field breaks the symmetry between the nature of the kink waves with positive and negative azimuthal wave number, and the wave can be a purely Alfvénic wave in the entire loop.

Identifying Acoustic Wave Sources on the Sun. II. Improved Filter Techniques for Source Wavefield Seismology

Shah Mohammad **Bahauddin**, Mark Peter Rast

ApJ **955** 31 **2023**

https://arxiv.org/pdf/2307.05433.pdf

https://iopscience.iop.org/article/10.3847/1538-4357/aced46/pdf

In this paper we refine a previously developed acoustic-source filter (Bahauddin & Rast 2021), improving its reliability and extending its capabilities. We demonstrate how to fine-tune the filter to meet observational constraints and to focus on specific wavefront speeds. This refinement enables discrimination of acoustic-source depths and tracking of local-source wavefronts, thereby facilitating ultra-local helioseismology on very small scales. By utilizing the photospheric Doppler signal from a subsurface source in a MURaM simulation, we demonstrate that robust ultra-local three-dimensional helioseismic inversions for the granular flows and sound speed to depths of at least 80 km below the photosphere are possible. The capabilities of the National Science Foundation's new Daniel K. Inouye Solar Telescope (DKIST) will enable such measurements of the real Sun.

Identifying acoustic wave sources on the Sun I. Two-dimensional waves in a simulated photosphere

Shah Mohammad **Bahauddin**, Mark Peter Rast

ApJ **915** 36 **2021**

https://arxiv.org/pdf/2101.10465.pdf

https://doi.org/10.3847/1538-4357/abfdae

The solar acoustic oscillations are likely stochastically excited by convective dynamics in the solar photosphere, though few direct observations of individual source events have been made and their detailed characteristics are still unknown. Wave source identification requires measurements that can reliably discriminate the local wave signal from the background convective motions and resonant modal power. This is quite challenging as these 'noise' contributions have amplitudes several orders of magnitude greater than the sources and the propagating wave fields they induce. In this paper, we employ a high-temporal-frequency filter to identify sites of acoustic emission in a

radiative magnetohydrodynamic simulation. The properties of the filter were determined from a convolutional neural network trained to identify the two-dimensional acoustic Green's function response of the atmosphere, but once defined, it can be directly applied to an image time series to extract the signal of local wave excitation, bypassing the need for the original neural network. Using the filter developed, we have uncovered previously unknown properties of the acoustic emission process. In the simulation, acoustic events are found to be clustered at mesogranular scales, with peak emission quite deep, about 500 km below the photosphere, and sites of very strong emission can result from the interaction of two supersonic downflows that merge at that depth. We suggest that the method developed, when applied to high-resolution high-cadence observations, such as those forthcoming with Daniel K. Inouye Solar Telescope (DKIST), will have important applications in chromospheric wave-studies and may lead to new investigations in high-resolution local-helioseismology.

Hybrid Detection Algorithm and Study on the Quantity and Brightness Evolution Characteristics of Photospheric Bright Point Groups

Haicheng **Bai**1, Peng Yang7,2, Limin Zhao1, Xiaoying Gong3,4,5,6, Libo Zhong3,4, Yang Yang1, and Changhui Rao3,4,5

2023 ApJ 956 62

https://iopscience.iop.org/article/10.3847/1538-4357/aced94/pdf

Photospheric bright points (BPs), the smallest magnetic elements in the photosphere, are constantly moving and changing. Studying the characteristics of these small-scale strong magnetic fields with kilogauss magnitudes could be of significant importance for investigating the coronal heating problem. Compared to the study of a few specific BPs, investigating the collective features of BP groups can provide us with a better understanding of the overall characteristics of BPs. However, there is still a lack of research on the evolution of BP groups, and the detection algorithm of BPs still has a lot of space for improvement. We propose a hybrid BP detection model (HBD-Model) that combines traditional algorithms and deep learning to improve detection accuracy. Using the HBD-Model, we focus on studying the evolution characteristics of the quantity and brightness of BP groups at different brightness levels and how these characteristics differ between quiet and active regions. Results show that the activity of BP groups is not random or disorderly. In different brightness levels and regions, their quantity and brightness evolution exhibit periodic or complex changes.

A deep learning method to estimate magnetic fields in solar active regions from photospheric continuum images⋆

Xianyong **Bai**1,2, Hui Liu3, Yuanyong Deng1,2, Jie Jiang4, Jingjing Guo1,2, Yi Bi3, Tao Feng5, Zhenyu Jin3, Wenda Cao6, Jiangtao Su1,2 and Kaifan Ji3

A&A 652, A143 (**2021**)

https://www.aanda.org/articles/aa/pdf/2021/08/aa40374-21.pdf

https://doi.org/10.1051/0004-6361/202140374

Context. The magnetic field is the underlying cause of solar activities. Spectropolarimetric Stokes inversions have been routinely used to extract the vector magnetic field from observations for about 40 years. In contrast, the photospheric continuum images have an observational history of more than 100 years.

Aims. We suggest a new method to quickly estimate the unsigned radial component of the magnetic field, |Br|, and the transverse field, Bt, just from photospheric continuum images (I) using deep convolutional neural networks (CNN).

Methods. Two independent models, that is, I versus |Br| and I versus Bt, are trained by the CNN with a residual architecture. A total of 7800 sets of data (I, Br and Bt) covering 17 active region patches from 2011 to 2015 from the Helioseismic and Magnetic Imager are used to train and validate the models.

Results. The CNN models can successfully estimate |Br| as well as Bt maps in sunspot umbra, penumbra, pore, and strong network regions based on the evaluation of four active regions (test datasets). From a series of continuum images, we can also detect the emergence of a transverse magnetic field quantitatively with the trained CNN model. The three-day evolution of the averaged value of the estimated |Br| and Bt from continuum images follows that from Stokes inversions well. Furthermore, our models can reproduce the nonlinear relationships between I and |Br| as well as Bt, explaining why we can estimate these relationships just from continuum images.

Conclusions. Our method provides an effective way to quickly estimate |Br| and Bt maps from photospheric continuum images. The method can be applied to the reconstruction of the historical magnetic fields and to future observations for providing the quick look data of the magnetic fields.

Solar observation with the Fourier transform spectrometer I : Preliminary results of the visible and near-infrared solar spectrum

Xianyong **Bai**, Zhiyong Zhang, Zhiwei Feng, Yuanyong Deng, Xingming Bao, Xiao Yang, Yongliang Song, Liyue Tong, Shuai Jing

Research in Astronomy and Astrophysics **2021**

https://arxiv.org/pdf/2107.07694.pdf
The Fourier transform spectrometer (FTS) is a core instrument for solar observation with high spectral resolution, especially in the infrared. The Infrared System for the Accurate Measurement of Solar Magnetic Field (AIMS), working at 10-13 μm, will use a FTS to observe the solar spectrum. The Bruker IFS-125HR, which meets the spectral resolution requirement of AIMS but just equips with a point source detector, is employed to carry out preliminary experiment for AIMS. A sun-light feeding experimental system is further developed. Several experiments are taken with them during 2018 and 2019 to observe the solar spectrum in the visible and near infrared wavelength, respectively. We also proposed an inversion method to retrieve the solar spectrum from the observed interferogram and compared it with the standard solar spectrum atlas. Although there is a wavelength limitation due to the present sun-light feeding system, the results in the wavelength band from 0.45-1.0 μm and 1.0-2.2 μm show a good consistence with the solar spectrum atlas, indicating the validity of our observing configuration, the data analysis method and the potential to work in longer wavelength. The work provided valuable experience for the AIMS not only for the operation of a FTS but also for the development of its scientific data processing software.

Connection between Sub-surface Layers and Surface Magnetic Activity over Multiple Solar Cycles

Mackenzie A. **Baird**, Sushanta C. Tripathy, Kiran Jain
ApJ **962** 194 **2024**
https://arxiv.org/pdf/2312.12332.pdf
https://iopscience.iop.org/article/10.3847/1538-4357/ad16db/pdf
We investigate spatio-temporal evolution of high-degree acoustic mode frequencies of the Sun and the surface magnetic activity, over the course of multiple solar cycles, to improve our understanding of the connection between the solar interior and atmosphere. We focus on high-degree modes due to their ability to characterize conditions in the shear layer just below the solar surface. Using the full-disk Doppler observations made by the Global Oscillation Network Group (GONG), mode frequencies covering the period from July 2001 to December 2021 are computed through the local helioseismic technique of ring diagrams. Considering 10.7 cm radio flux measurements, the sunspot number, and the local magnetic activity index as solar activity proxies, we note strong correlation between the frequency shifts and each activity index. We further investigate the hemispheric asymmetry in frequency shifts and magnetic activity and find that both the activity and frequencies in the descending phase of cycle 23 were dominant in the southern hemisphere, while in cycle 24 these quantities fluctuated between northern and southern hemispheres. Analyzing the frequency shifts at different latitudes with the progression of solar cycles, we observe that the shifts at mid-latitudes are dominant in the southern hemisphere during the maximum period of solar activity in cycle 24 but the values overlap as the cycle advances towards the minimum activity period. The frequency shifts at the beginning of cycle 25 are found to be dominant in the southern hemisphere following magnetic activity. The analysis presents additional evidence that the variability in oscillation frequencies are caused by both strong and weak magnetic fields.

Searching for Evidence of Subchromospheric Magnetic Reconnection on the Sun

D. **Baker**1, L. van Driel-Gesztelyi1,2,3, A. W. James1, P. Démoulin2,4, A. S. H. To1,5, M. Murabito6,7, D. M. Long8, D. H. Brooks1,9, J. McKevitt1,10, J. M. Laming11
2024 ApJ 970 39
https://iopscience.iop.org/article/10.3847/1538-4357/ad4a6e/pdf
Within the coronae of stars, abundances of those elements with low first ionization potential (FIP) often differ from their photospheric values. The coronae of the Sun and solar-type stars mostly show enhancements of low-FIP elements (the FIP effect) while more active stars such as M dwarfs have coronae generally characterized by the inverse-FIP (I-FIP) effect. Highly localized regions of I-FIP effect solar plasma have been observed by Hinode's EUV Imaging Spectrometer in a number of highly complex active regions (ARs), usually around strong light bridges of the umbrae of coalescing/merging sunspots. These observations can be interpreted in the context of the ponderomotive force fractionation model, which predicts that plasma with I-FIP effect composition is created by the refraction of waves coming from below the plasma fractionation region in the chromosphere. A plausible source of these waves is thought to be reconnection in the (high-plasma-β) subchromospheric magnetic field. In this study, we use the 3D visualization technique of Chintzoglou & Zhang combined with observations of localized I-FIP effect in the corona of AR 11504 to identify potential sites of such reconnection and its possible consequences in the solar atmosphere. We found subtle signatures of episodic heating and reconnection outflows in the expected places, in between magnetic flux tubes forming a light bridge, within the photosphere of the AR. Furthermore, on either side of the light bridge, we observed small antiparallel horizontal magnetic field components, supporting the possibility of reconnection occurring where we observe I-FIP plasma. When taken together with the I-FIP effect observations, these subtle signatures provide a compelling case for indirect observational evidence of reconnection below the fractionation layer of the chromosphere, however direct evidence remains elusive.

Alfvenic Perturbations in a Sunspot Chromosphere Linked to Fractionated Plasma in the Corona

D. **Baker** , M. Stangalini , G. Valori , D. H. Brooks , A. S. H. To , L. van Driel-Gesztelyi (UCL/MSSL), P. Demoulin (LESIA-Meudon), D. Stansby (UCL/MSSL), D. B. Jess (Queen's University Belfast), S. Jafarzadeh (University of Oslo)

2021 *ApJ* **907** 16
https://arxiv.org/pdf/2012.04308.pdf
https://doi.org/10.3847/1538-4357/abcafd

In this study, we investigate the spatial distribution of highly varying plasma composition around one of the largest sunspots of solar cycle 24. Observations of the photosphere, chromosphere, and corona are brought together with magnetic field modelling of the sunspot in order to probe the conditions which regulate the degree of plasma fractionation within loop populations of differing connectivities. We find that in the coronal magnetic field above the sunspot umbra, the plasma has photospheric composition. Coronal loops rooted in the penumbra contain fractionated plasma, with the highest levels observed in the loops that connect within the active region. Tracing field lines from regions of fractionated plasma in the corona to locations of Alfvenic fluctuations detected in the chromosphere shows that they are magnetically linked. These results indicate a connection between sunspot chromospheric activity and observable changes in coronal plasma composition. **20 May 2016**

Can Sub-photospheric Magnetic Reconnection Change the Elemental Composition in the Solar Corona?

Deborah **Baker**, Lidia van Driel-Gesztelyi, David H. Brooks, Pascal Demoulin, Gherardo Valori, David M. Long, J. Martin Laming, Andy S. H. To, Alexander W. James

ApJ **2020**
https://arxiv.org/pdf/2003.03325.pdf

Within the coronae of stars, abundances of those elements with low first ionization potential (FIP) often differ from their photospheric values. The coronae of the Sun and solar-type stars mostly show enhancements of low- FIP elements (the FIP effect) while more active stars such as M-dwarfs have coronae generally characterized by the inverse-FIP effect (I-FIP). Here we observe patches of I-FIP effect solar plasma in AR 12673, a highly complex beta/gamma/delta active region. We argue that the umbrae of coalescing sunspots and more specifically strong light bridges within the umbrae, are preferential locations for observing I-FIP effect plasma. Furthermore, the magnetic complexity of the active region and major episodes of fast flux emergence also lead to repetitive and intense flares. The induced evaporation of the chromospheric plasma in flare ribbons crossing umbrae enables the observation of four localized patches of I-FIP effect plasma in the corona of AR 12673. These observations can be interpreted in the context of the ponderomotive force fractionation model which predicts that plasma with I-FIP effect composition is created by the refraction of waves coming from below the chromosphere. We propose that the waves generating the I-FIP effect plasma in solar active regions are generated by sub-photospheric reconnection of coalescing flux systems. Although we only glimpse signatures of I-FIP effect fractionation produced by this interaction in patches on the Sun, on highly active M-stars it may be the dominant process. **2017 August 28 to September 10.**

Coronal Elemental Abundances in Solar Emerging Flux Regions

Deborah **Baker**1, David H. Brooks2, Lidia van Driel-Gesztelyi1,3,4, Alexander W. James1,3, Pascal Démoulin3, David M. Long1, Harry P. Warren5, and David R. Williams6

2018 ApJ 856 71
http://iopscience.iop.org/article/10.3847/1538-4357/aaadb0/pdf

The chemical composition of solar and stellar atmospheres differs from the composition of their photospheres. Abundances of elements with low first ionization potential (FIP) are enhanced in the corona relative to high-FIP elements with respect to the photosphere. This is known as the FIP effect and it is important for understanding the flow of mass and energy through solar and stellar atmospheres. We used spectroscopic observations from the Extreme-ultraviolet Imaging Spectrometer on board the Hinode observatory to investigate the spatial distribution and temporal evolution of coronal plasma composition within solar emerging flux regions inside a coronal hole. Plasma evolved to values exceeding those of the quiet-Sun corona during the emergence/early-decay phase at a similar rate for two orders of magnitude in magnetic flux, a rate comparable to that observed in large active regions (ARs) containing an order of magnitude more flux. During the late-decay phase, the rate of change was significantly faster than what is observed in large, decaying ARs. Our results suggest that the rate of increase during the emergence/early-decay phase is linked to the fractionation mechanism that leads to the FIP effect, whereas the rate of decrease during the later decay phase depends on the rate of reconnection with the surrounding magnetic field and its plasma composition. **2016 January 7**

Apparent and Intrinsic Evolution of Active Region Upflows

Deborah **Baker**, Miho Janvier, Pascal Demoulin, Cristina Mandrini

Solar Phys. **2017**
https://arxiv.org/pdf/1702.06022.pdf
We analyze the evolution of Fe XII coronal plasma upflows from the edges of ten active regions (ARs) as they cross the solar disk using the Hinode Extreme Ultraviolet Imaging Spectrometer (EIS). Confirming the results of Demoulin et al. (2013, Sol. Phys. 283, 341), we find that for each AR there is an observed long term evolution of the upflows which is largely due to the solar rotation progressively changing the viewpoint of dominantly stationary upflows. From this projection effect, we estimate the unprojected upflow velocity and its inclination to the local vertical. AR upflows typically fan away from the AR core by 40 deg. to near vertical for the following polarity. The span of inclination angles is more spread for the leading polarity with flows angled from -29 deg. (inclined towards the AR center) to 28 deg. (directed away from the AR). In addition to the limb-to-limb apparent evolution, we identify an intrinsic evolution of the upflows due to coronal activity which is AR dependent. Further, line widths are correlated with Doppler velocities only for the few ARs having the largest velocities. We conclude that for the line widths to be affected by the solar rotation, the spatial gradient of the upflow velocities must be large enough such that the line broadening exceeds the thermal line width of Fe XII. Finally, we find that upflows occurring in pairs or multiple pairs is a common feature of ARs observed by Hinode/EIS, with up to four pairs present in AR 11575. This is important for constraining the upflow driving mechanism as it implies that the mechanism is not a local one occurring over a single polarity. AR upflows originating from reconnection along quasi-separatrix layers (QSLs) between over-pressure AR loops and neighboring under-pressure loops is consistent with upflows occurring in pairs, unlike other proposed mechanisms acting locally in one polarity. **Table 1.** ARs included in the limb-to-limb upow study.

Becoming a Space Weather-Ready Nation

Daniel N. **Baker**
Space Weather Quarterly, Vol. 13, Issue 4, **2016**, doi:10.1002/2016SW001555.
http://onlinelibrary.wiley.com/doi/10.1002/swq.12/pdf
This manuscript comments on the new Presidential Executive Order relating to space weather.

"Resource Letter" for Space Weather

Daniel N. **Baker**, Louis J. Lanzerotti
Space Weather Volume 14, Issue 8 August **2016** Pages 528–529
http://onlinelibrary.wiley.com/doi/10.1002/2016SW001485/epdf
This Resource Letter was made open access by the authors and can be accessed at http://scitation.aip.org/content/aapt/journal/ajp/84/3/10.1119/1.4938403.
Space Weather Quarterly Vol. 13, Issue 3, p. 4, **2016**
http://onlinelibrary.wiley.com/doi/10.1002/SWQv13i003/epdf
"Resource Letter describes the phenomena and effects on technological systems that are known collectively as space weather.
Ground-based systems Long conductors Electrical power systems, including economic aspects Long communication conductors Pipelines Radio communications Wireless and GPS issues Radars and geolocation Exploration Radiation effects related to aircraft Space systems Radiation effects on spacecraft: damage, upsets, and charging Satellite drag Spacecraft orientation Dealing with space weather Forecasts, alerts warnings Operational mitigation strategies Engineering solutions Policy implications

FIP Bias Evolution in a Decaying Active Region

D. **Baker**1, D. H. Brooks2, P. Démoulin3, S. L. Yardley1, L. van Driel-Gesztelyi1,3,4, D. M. Long1, and L. M. Green
2015 ApJ 802 104
Solar coronal plasma composition is typically characterized by first ionization potential (FIP) bias. Using spectra obtained byHinode's EUV Imaging Spectrometer instrument, we present a series of large-scale, spatially resolved composition maps of active region (AR)11389. The composition maps show how FIP bias evolves within the decaying AR during the period **2012 January 4–6**. Globally, FIP bias decreases throughout the AR. We analyzed areas of significant plasma composition changes within the decaying AR and found that small-scale evolution in the photospheric magnetic field is closely linked to the FIP bias evolution observed in the corona. During the AR's decay phase, small bipoles emerging within supergranular cells reconnect with the pre-existing AR field, creating a pathway along which photospheric and coronal plasmas can mix. The mixing timescales are shorter than those of plasma enrichment processes. Eruptive activity also results in shifting the FIP bias closer to photospheric in the

affected areas. Finally, the FIP bias still remains dominantly coronal only in a part of the AR's high-flux density core. We conclude that in the decay phase of an AR's lifetime, the FIP bias is becoming increasingly modulated by episodes of small-scale flux emergence, i.e., decreasing the AR's overall FIP bias. Our results show that magnetic field evolution plays an important role in compositional changes during AR development, revealing a more complex relationship than expected from previous well-known Skylab results showing that FIP bias increases almost linearly with age in young ARs.

A major solar eruptive event in July 2012: Defining extreme space weather scenarios.

Baker DN, Li X, Pulkkinen A, Ngwira CM, Mays LL, Galvin AB, Simunac KDC
(**2013**) Space Weather 11:585–591

Insight into how plasma is fractionated in the chromosphere…

Deb **Baker**, Gherardo Valori, Marco Stangalini
Hinode/ EIS Nugget, Feb **2020**
http://solarb.mssl.ucl.ac.uk/SolarB/nuggets/nugget_2020mar.jsp
The simultaneous multi-wavelength polarimetric observations taken by the instruments of DKIST and EST at different heights in the solar atmosphere and at high spatial and temporal resolution will enable us to probe the wave physics of plasma fractionation in the chromosphere in an unprecedent way. **March 6, 2012**

Coronal Elemental Abundances in Solar Emerging Flux Regions

Deborah **Baker**, David H. Brooks, Lidia van Driel-Gesztelyi, Alexander James, Pascal Demoulin, David M. Long, Harry P. Warren, David R. Williams
ApJ **2018**
https://arxiv.org/pdf/1801.08424.pdf
The chemical composition of solar and stellar atmospheres differs from that of their photospheres. Abundances of elements with low first ionization potential (FIP) are enhanced in the corona relative to high FIP elements with respect to the photosphere. This is known as the FIP effect and it is important for understanding the flow of mass and energy through solar and stellar atmospheres. We used spectroscopic observations from the Extreme-ultraviolet Imaging Spectrometer (EIS) onboard the Hinode observatory to investigate the spatial distribution and temporal evolution of coronal plasma composition within solar emerging flux regions inside a coronal hole. Plasma evolved to values exceeding those of the quiet Sun corona during the emergence/early decay phase at a similar rate for two orders of magnitude in magnetic flux, a rate comparable to that observed in large active regions containing an order of magnitude more flux. During the late decay phase, the rate of change was significantly faster than what is observed in large, decaying active regions. Our results suggest that the rate of increase during the emergence/early decay phase is linked to the fractionation mechanism leading to the FIP effect, whereas the rate of decrease during the later decay phase depends on the rate of reconnection with the surrounding magnetic field and its plasma composition.

Apparent and Intrinsic Evolution of Active Region Upflows

Deborah **Baker**, Miho Janvier, Pascal Démoulin, Cristina H. Mandrini
Solar Physics April **2017**, 292:46
http://link.springer.com/article/10.1007/s11207-017-1072-9
We analyze the evolution of Fe xii coronal plasma upflows from the edges of ten active regions (ARs) as they cross the solar disk using the Hinode Extreme Ultraviolet Imaging Spectrometer (EIS) to do this. Confirming the results of Démoulin et al. (Sol. Phys.283, 341, 2013), we find that for each AR there is an observed long-term evolution of the upflows. This evolution is largely due to the solar rotation that progressively changes the viewpoint of dominantly stationary upflows. From this projection effect, we estimate the unprojected upflow velocity and its inclination to the local vertical. AR upflows typically fan away from the AR core by 40° to nearly vertical for the following polarity. The span of inclination angles is more spread out for the leading polarity, with flows angled from −29° (inclined toward the AR center) to 28° (directed away from the AR). In addition to the limb-to-limb apparent evolution, we identify an intrinsic evolution of the upflows that is due to coronal activity, which is AR dependent. Furthermore, line widths are correlated with Doppler velocities only for the few ARs with the highest velocities. We conclude that for the line widths to be affected by the solar rotation, the spatial gradient of the upflow velocities must be large enough such that the line broadening exceeds the thermal line width of Fe xii. Finally, we find that upflows occurring in pairs or multiple pairs are a common feature of ARs observed by Hinode/EIS, with up to four pairs present in AR 11575. This is important for constraining the upflow-driving mechanism as it implies that the mechanism is not local and does not occur over a single polarity. AR upflows originating from reconnection along

quasi-separatrix layers between overpressure AR loops and neighboring underpressure loops is consistent with upflows occurring in pairs, unlike other proposed mechanisms that act locally in one polarity. **30 November- 3 December 2006, 25 April to 6 May 2007, 23 Sept 2012**
Table 1 ARs included in the limb-to-limb upflow study. The minimum age is given for the first observation of the ARs at the east limb or on the far side.
Table 2 Global properties of ARs included in the limb-to-limb upflow study.

Becoming a Space Weather-Ready Nation

Daniel N. **Baker**
Space Weather Volume 14, Issue 11, Version of Record online: 4 NOV **2016**
http://onlinelibrary.wiley.com/doi/10.1002/2016SW001555/pdf

A major solar eruptive event in July 2012: Defining extreme space weather scenarios

D. N. **Baker**, X. Li, A. Pulkkinen, C. M. Ngwira, M. L. Mays, A. B. Galvin and K. D. C. Simunac
Space Weather, Volume 11, Issue 10, pages 585–591, October **2013**
http://onlinelibrary.wiley.com/doi/10.1002/swe.20097/pdf
A key goal for space weather studies is to define severe and extreme conditions that might plausibly afflict human technology. On 23 July 2012, solar active region 1520 (~141°W heliographic longitude) gave rise to a powerful coronal mass ejection (CME) with an initial speed that was determined to be 2500 ± 500 km/s. The eruption was directed away from Earth toward 125°W longitude. STEREO-A sensors detected the CME arrival only about 19 h later and made in situ measurements of the solar wind and interplanetary magnetic field. In this paper, we address the question of what would have happened if this powerful interplanetary event had been Earthward directed. Using a well-proven geomagnetic storm forecast model, we find that the 23–24 July event would certainly have produced a geomagnetic storm that was comparable to the largest events of the twentieth century (Dst ~ −500 nT). Using plausible assumptions about seasonal and time-of-day orientation of the Earth's magnetic dipole, the most extreme modeled value of storm-time disturbance would have been Dst = −1182 nT. This is considerably larger than estimates for the famous Carrington storm of 1859. This finding has far reaching implications because it demonstrates that extreme space weather conditions such as those during March of 1989 or September of 1859 can happen even during a modest solar activity cycle such as the one presently underway. We argue that this extreme event should immediately be employed by the space weather community to model severe space weather effects on technological systems such as the electric power grid.

Science for a Technological Society: The 2013–2022 Decadal Survey in Solar and Space Physics

D. N. **Baker**, A. Charo, T. Zurbuchen
Space Weather, Volume 11, Issue 2, pages 50–51, February **2013**

The Third Electric Infrastructure Security World Summit Meeting,

Baker, D. N.
(**2012**), Space Weather, 10, S07002
Almost 150 scientists, engineers, policy makers, and industry leaders from more than 20 countries met at the Electric Infrastructure Security (EIS) summit meeting in London to iron out recommendations on how to potentially protect power grid infrastructure in the event of an extreme space weather event.

What Does Space Weather Cost Modern Societies?,

Baker, D. N.
Space Weather, *7*, S02003, doi:10.1029/2009SW000465, (**2009**).
How do we avoid the "Chicken Little" syndrome, that the sky is falling, and still make policy makers aware that space weather has large potential societal consequences? A report issued in December 2008 by the Space Studies Board of the U.S. National Academies (http://www.nap.edu) for the first time presents quantitative assessments of some of the impacts of space weather events on human technologies. The report, "Severe space weather events—Understanding societal and economic impacts: A workshop report" (see http://www.nap.edu/catalog.php?record_id=12507), prepared by the Committee on the Societal and Economic Impacts of Severe Space Weather Events operating under the aegis of the National Research Council (NRC), estimates that the economic cost of a severe geomagnetic storm could reach US$1–27 trillion during the first year

alone, with recovery times of 4–10 years. These long recovery times could result from severe damage to large power transformers and other hard-to-replace hardware. Such a scenario would result from a storm of the magnitude of that which struck Earth in September 1859.

A Continuous L1 Presence Required for Space Weather

Baker, Daniel N.; Lanzerotti, Louis J.
Space Weather, Vol. 6, No. 11, S11001, **2008**
http://dx.doi.org/10.1029/2008SW000445
Monitoring and forecasting space weather are essential to the successful operation of technical systems such as civilian and military communications and navigation. The science-driven Advanced Composition Explorer (ACE) spacecraft has monitored the solar wind and energetic particles at the L1 libration point since its launch in 1997; its nearly continuous data set has revolutionized space weather forecasting and alerting functions for the United States.

To ensure long-term space weather monitoring, the United States must develop truly operational data acquisition platforms rather than continue to rely heavily on limited-life science missions.

Impact of nanoflare heating in the lower solar atmosphere

H. **Bakke**
RHESSI Science Nuggets #458 **2023**
https://sprg.ssl.berkeley.edu/~tohban/wiki/index.php/Impact_of_nanoflare_heating_in_the_lower_solar_atmosphere

Accelerated particle beams in a 3D simulation of the quiet Sun.

Lower atmospheric spectral diagnostics

H. **Bakke**, L. Frogner, L. Rouppe van der Voort, B. V. Gudiksen, M. Carlsson
A&A 675, A103 **2023**
https://arxiv.org/pdf/2306.02752.pdf
Nanoflare heating through small-scale magnetic reconnection events is one of the prime candidates to explain heating of the solar corona. However, direct signatures of nanoflares are difficult to determine, and unambiguous observational evidence is still lacking. Numerical models that include accelerated electrons, and can reproduce flaring conditions, are essential in understanding how low-energetic events act as a heating mechanism of the corona, and how such events are able to produce signatures in the spectral lines that can be detected through observations. We investigate the effects of accelerated electrons in synthetic spectra from a 3D radiative magnetohydrodynamics simulation to better understand small-scale heating events and their impact on the solar atmosphere. We synthesised the chromospheric Ca II and Mg II lines and the transition region Si IV resonance lines from a quiet Sun numerical simulation that includes accelerated electrons. We calculated the contribution function to the intensity to better understand how the lines are formed, and what factors are contributing to the detailed shape of the spectral profiles. The synthetic spectra are highly affected by variations in temperature and vertical velocity. Beam heating exceeds conductive heating at the heights where the spectral lines form, indicating that the electrons should contribute to the heating of the lower atmosphere and hence affect the line profiles. However, we find that it is difficult to determine specific signatures from the non-thermal electrons due to the complexity of the atmospheric response to the heating in combination with the relatively low energy output (~1e21 erg/s). Still, our results contribute to the understanding of small-scale heating events in the solar atmosphere, and give further guidance to future observations.
IRIS Nugget Oct **2023** https://iris.lmsal.com/nugget

Chromospheric emission from nanoflare heating in RADYN simulations

H. **Bakke**, M. Carlsson, L. Rouppe van der Voort, B. V. Gudiksen, V. Polito, P. Testa, B. De Pontieu
A&A **2022**
https://arxiv.org/pdf/2201.11961.pdf
Heating signatures from small-scale magnetic reconnection events in the solar atmosphere have proven to be difficult to detect through observations. Numerical models that reproduce flaring conditions are essential in the understanding of how nanoflares may act as a heating mechanism of the corona. We study the effects of non-thermal electrons in synthetic spectra from 1D hydrodynamic RADYN simulations of nanoflare heated loops to investigate the diagnostic potential of chromospheric emission from small-scale events. The Mg II h and k, Ca II H and K, Ca II 854.2 nm, H-alpha and H-beta chromospheric lines were synthesised from various RADYN models of coronal loops subject to electron beams of nanoflare energies. The contribution function to the line intensity was computed to better understand how the atmospheric response to the non-thermal electrons affects the formation of spectral lines and the detailed shape of their spectral profiles. The spectral line signatures arising from the electron beams highly depend on the density of the loop and the lower cutoff energy of the electrons. Low-energy (5 keV) electrons deposit

their energy in the corona and transition region, producing strong plasma flows that cause both redshifts and blueshifts of the chromospheric spectra. Higher-energy (10 and 15 keV) electrons deposit their energy in the lower transition region and chromosphere, resulting in increased emission from local heating. Our results indicate that effects from small-scale events can be observed with ground-based telescopes, expanding the list of possible diagnostics for the presence and properties of nanoflares.

Sunspot Numbers from ISOON: A Ten-Year Data Analysis

K. S. **Balasubramaniam**, T. W. Henry
Solar Physics **2016**
http://arxiv.org/pdf/1602.07741v1.pdf
Sunspot numbers are important tracers of historical solar activity. They are important in the prediction of oncoming solar maximum, in the design of lifetimes of space assets, and in assessing the extent of solar-radiation impact on the space environment. Sunspot numbers were obtained visually from sunspot drawings. The availability of digital images from the US Air Force Improved Solar Optical Observing Network (ISOON) prototype telescope concurrent to observer-dependent sunspot numbers recorded at the National Solar Observatory (NSO) has provided a basis for comparing sunspot numbers determined from the two methods. We compare sunspot numbers from visual and digital methods observed nearly simultaneously. The advantages of digital imagery are illustrated.

A scheme for forecasting severe space weather

N. **Balan**, Y. Ebihara,R. Skoug,K. Shiokawa,I. S. Batista,S. Tulasi Ram,Y. Omura,T. Nakamura, M.-C. Fok
JGR **2017** DOI: 10.1002/2016JA023853
http://sci-hub.cc/doi/10.1002/2016JA023853
A scheme is suggested and tested for forecasting severe space weather (SvSW) using solar wind velocity (V) and the north-south component (Bz) of the interplanetary magnetic field (IMF) measured using the ACE (Advanced Composition Explorer) satellite from 1998 to 2016. SvSW has caused all known electric power outages and telegraph system failures. Earlier SvSW events such as the Carrington event of 1859, Quebec event of 1989 and an event in 1958 are included with information from the literature. Dst storms are used as references to identify 89 major space weather events (DstMin ≤ -100 nT) in 1998-2016. The coincidence of high CME front (or CME shock) velocity ΔV (sudden increase in V over the background by over 275 km/s) and sufficiently large Bz southward at the time of the ΔV increase is associated with SvSW; and their product (ΔV x Bz) is found to exhibit a large negative spike at the speed increase. Such a product (ΔV x Bz) exceeding a threshold seems suitable for forecasting SvSW. However, the coincidence of high V (not containing ΔV) and large Bz southward does not correspond to SvSW, indicating the importance of the impulsive action of large Bz southward and high ΔV coming through when they coincide. The need for the coincidence is verified using the CRCM (Comprehensive Ring Current Model) model, that produces extreme Dst storms (<DstMP > <-250 nT) characterizing SvSW when there is coincidence. **15-16 July 2000, 30-31 March 2001, 03-26 November 2001, 26 Oct-25 Nov 2003, 30-31 October 2003,**

CME front and severe space weather

N. **Balan**1,2,6,*, R. Skoug3, S. Tulasi Ram4, P. K. Rajesh2, K. Shiokawa1, Y. Otsuka1, I. S. Batista5, Y. Ebihara6 andT. Nakamura7
JGR, **201**4
http://onlinelibrary.wiley.com/doi/10.1002/2014JA020151/pdf
Thanks to the work of a number of scientists it is known that severe space weather can cause extensive social and economic disruptions in the modern high-tech society. It is therefore important to understand what determines the severity of space weather, and whether it can be predicted. We present results obtained from the analysis of coronal mass ejections (CME), solar energetic particle (SEP) events, interplanetary magnetic field (IMF), CME-magnetosphere coupling and geomagnetic storms associated with the major space weather events since 1998 by combining data from the ACE and GOES satellites with geomagnetic parameters, and the Carrington event of 1859, the Quebec event of 1989, and an event in 1958. The results seem to indicate that (1) it is the impulsive energy mainly due to the impulsive velocity and orientation of IMF Bz at the leading edge of the CMEs (or CME front) that determine the severity of space weather. (2) CMEs having high impulsive velocity (sudden non-fluctuating increase by over 275 km s−1 over the background) caused severe space weather (SvSW) in the heliosphere (failure of the SWI mode of SWEPAM in ACE) probably by suddenly accelerating the high energy particles in the SEPs ahead directly or through the shocks. (3) The impact of such CMEs which also show the IMF Bz southward from the leading edge caused SvSW at the Earth including extreme geomagnetic storms of mean DstMP < −250 nT during main phases; and the known electric power outages happened during some of these SvSW events. (4) The higher the impulsive velocity, the more severe the space weather, like faster weather fronts and tsunami fronts causing more severe damage through impulsive action. (5) The CMEs having IMF Bz northward at the leading edge do not seem

to cause SvSW on Earth though, later when the IMF Bz turns southward, they can lead to super geomagnetic storms of intensity (DstMin) less than even −400 nT.

Universality in solar flare, magnetic storm and earthquake dynamics using Tsallis statistical mechanics

G. **Balasis**, I. A. Daglis, A. Anastasiadis, C. Papadimitriou, M. Mandea, K. Eftaxias
E-print, Sept 2010; Accepted for publication in : Physica A (**2010**)
The universal character of the dynamics of various extreme phenomena is an outstanding scientific challenge. We show that X-ray flux and Dst time series during powerful solar flares and intense magnetic storms, respectively, obey a nonextensive energy distribution function for earthquake dynamics with similar values for the Tsallis entropic index q. Thus, evidence for uni- versality in solar flares, magnetic storms and earthquakes arise naturally in the framework of Tsallis statistical mechanics. The observed similarity sug- gests a common approach to the interpretation of these diverse phenomena in terms of driving physical mechanisms that have the same character.

Briefing Highlights Vulnerability of GPS to Adverse Space Weather

Balcerak, Ernie
Space Weather, Vol. 9, No. 8, S08003, **2011**
http://dx.doi.org/10.1029/2011SW000712
Through its effects on GPS and other technologies, space weather can affect a variety of industries, including agriculture, commercial air travel, and emergency response. Speakers focused on these topics at a 22 June briefing on Capitol Hill in Washington, D. C. Solar flares can produce radio bursts that directly interfere with GPS signals. Solar activity can also cause ionospheric disturbances that produce distortions and delays in GPS signals, degrading the accuracy of positioning and navigation systems.

Updated verification of the Space Weather Prediction Center's solar energetic particle prediction model

Christopher C. **Balch**
SPACE WEATHER, VOL. 6, S01001, doi:10.1029/2007SW000337, **2008**
This paper evaluates the performance of an operational proton prediction model currently being used at NOAA's Space Weather Prediction Center. The evaluation is based on proton events that occurred between 1986 and 2004. Parameters for the associated solar events determine a set of necessary conditions, which are used to construct a set of control events. Model output is calculated for these events and performance of the model is evaluated using standard verification measures. For probability forecasts we evaluate the accuracy, reliability, and resolution and display these results using a standard attributes diagram. We identify conditions for which the model is systematically inaccurate. The probability forecasts are also evaluated for categorical forecast performance measures. We find an optimal probability and we calculate the false alarm rate and probability of detection at this probability. We also show results for peak flux and rise time predictions. These findings provide an objective basis for measuring future improvements.

EVIDENCE FOR SOLAR FREQUENCY DEPENDENCE ON SUNSPOT TYPE

Charles S. **Baldner**1, Richard S. Bogart2 and Sarbani Basu
2011 ApJ 733 L5
High-degree solar mode frequencies as measured by ring diagrams are known to change in the presence of the strong magnetic fields found in active regions. We examine these changes in frequency for a large sample of active regions analyzed with data from the Michelson Doppler Imager on board the Solar and Heliospheric Observatory spacecraft, spanning most of solar cycle 23. We confirm that the frequencies increase with increasing magnetic field strength, and that this dependence is generally linear. We find that the dependence is slightly but significantly different for active regions with different sunspot types.

The FIELDS Instrument Suite for Solar Probe Plus

Measuring the Coronal Plasma and Magnetic Field, Plasma Waves and Turbulence, and Radio Signatures of Solar Transients
S. D. **Bale**, K. Goetz, P. R. Harvey …
Space Science Reviews December **2016**, Volume 204, Issue 1, pp 49–82
http://link.springer.com/article/10.1007/s11214-016-0244-5
NASA's Solar Probe Plus (SPP) mission will make the first *in situ* measurements of the solar corona and the birthplace of the solar wind. The FIELDS instrument suite on SPP will make direct measurements of electric and magnetic fields, the properties of *in situ* plasma waves, electron density and temperature profiles, and interplanetary radio emissions, amongst other things. Here, we describe the scientific objectives targeted by the

SPP/FIELDS instrument, the instrument design itself, and the instrument concept of operations and planned data products.

Dynamo and the Adiabatic Invariant

Alexander M. **Balk**1
2022 ApJ 926 2
https://iopscience.iop.org/article/10.3847/1538-4357/ac448d/pdf
The paper considers a dynamo generated by a shallow fluid layer in a celestial body (planet or star). This dynamo is based on the extra invariant for interacting magnetic Rossby waves.

Assessing the beginning to end-of-mission sensitivity change of the PREcision MOnitor Sensor total solar irradiance radiometer (PREMOS/PICARD)

William T. **Ball**, Werner Schmutz, André Fehlmann*,a, Wolfgang Finsterle andBenjamin Walter
J. Space Weather Space Clim., 6, A32 (**2016**) **Open access**
The switching of the total solar irradiance (TSI) backup radiometer (PREMOS-B) to a primary role for 2 weeks at the end of the PICARD mission provides a unique opportunity to test the fundamental hypothesis of radiometer experiments in space, which is that the sensitivity change of instruments due to the space environment is identical for the same instrument type as a function of solar-exposure time of the instruments. We verify this hypothesis for the PREMOS TSI radiometers within the PREMOS experiment on the PICARD mission. We confirm that the sensitivity change of the backup instrument, PREMOS-B, is similar to that of the identically-constructed primary radiometer, PREMOS-A. The extended exposure of the backup instrument at the end of the mission allows for the assessment, with an uncertainty estimate, of the sensitivity change of the primary radiometer from the beginning of the PICARD mission compared to the end, and of the degradation of the backup over the mission. We correct six sets of PREMOS-B observations connecting October 2011 with February 2014, using six ratios from simultaneous PREMOS-A and PREMOS-B exposures during the first days of PREMOS-A operation in 2010. These ratios are then used, without indirect estimates or assumptions, to evaluate the stability of SORCE/TIM and SOHO/VIRGO TSI measurements, which have both operated for more than a decade and now show different trends over the time span of the PICARD mission, namely from 2010 to 2014. We find that by February 2014 relative to October 2011 PREMOS-B supports the SORCE/TIM TSI time evolution, which in May 2014 relative to October 2011 is ~0.11 W m−2, or ~84 ppm, higher than SOHO/VIRGO. Such a divergence between SORCE/TIM and SOHO/VIRGO over this period is a significant fraction of the estimated decline of 0.2 W m−2 between the solar minima of 1996 and 2008, and questions the reliability of that estimated trend. Extrapolating the uncertainty indicated by the disagreement of SORCE/TIM and PREMOS with respect to SOHO/VIRGO, we can conclude that it is currently not possible to assess centennial timescale changes in solar irradiance based on any of the presently existing TSI composites. It is imperative to accurately estimate solar irradiance changes from observations in order to extrapolate centennial scale trends important for understanding both long-term solar irradiance changes and the Sun's influence on the Earth's climate.

A new SATIRE-S spectral solar irradiance reconstruction for solar cycles 21--23 and its implications for stratospheric ozone

William T. **Ball**, Natalie A. Krivova, Yvonne C. Unruh, Joanna D. Haigh, Sami K. Solanki
Journal of Atmospheric Sciences, **2014**
http://arxiv.org/pdf/1408.0365v1.pdf
We present a revised and extended total and spectral solar irradiance (SSI) reconstruction, which includes a wavelength-dependent uncertainty estimate, spanning the last three solar cycles using the SATIRE-S model. The SSI reconstruction covers wavelengths between 115 and 160,000 nm and all dates between August 1974 and October 2009. This represents the first full-wavelength SATIRE-S reconstruction to cover the last three solar cycles without data gaps and with an uncertainty estimate. SATIRE-S is compared with the NRLSSI model and SORCE/SOLSTICE ultraviolet (UV) observations. SATIRE-S displays similar cycle behaviour to NRLSSI for wavelengths below 242 nm and almost twice the variability between 242 and 310 nm. During the decline of last solar cycle, between 2003 and 2008, SSI from SORCE/SOLSTICE version 12 and 10 typically displays more than three times the variability of SATIRE-S between 200 and 300 nm. All three datasets are used to model changes in stratospheric ozone within a 2D atmospheric model for a decline from high solar activity to solar minimum. The different flux changes result in different modelled ozone trends. Using NRLSSI leads to a decline in mesospheric ozone, while SATIRE-S and SORCE/SOLSTICE result in an increase. Recent publications have highlighted increases in mesospheric ozone when considering version 10 SORCE/SOLSTICE irradiances. The recalibrated SORCE/SOLSTICE version 12 irradiances result in a much smaller mesospheric ozone response than when using version 10 and now similar in magnitude to SATIRE-S. This shows that current knowledge of variations in spectral irradiance is not sufficient to warrant robust conclusions concerning the impact of solar variability on the atmosphere and climate.

What is our current understanding of solar irradiance variations?

William T. **Ball**
UKSP Nuggets, No. 37, July **2013**
http://www.uksolphys.org/?p=6496
How well are we able to reproduce the observed irradiance variations of the Sun?

Solar irradiance variability: a six-year comparison between SORCE observations and the SATIRE model

W. T. **Ball**1, Y. C. Unruh1, N. A. Krivova2, S. Solanki2,4 and J. W. Harder
A&A 530, A71 (**2011**)
Aims. We investigate how well modeled solar irradiances agree with measurements from the SORCE satellite, both for total solar irradiance and broken down into spectral regions on timescales of several years.
Methods. We use the SATIRE model and compare modeled total solar irradiance (TSI) with TSI measurements over the period 25 February 2003 to 1 November 2009. Spectral solar irradiance over 200−1630 nm is compared with the SIM instrument on SORCE over the period 21 April 2004 to 1 November 2009. We discuss the overall change in flux and the rotational and long-term trends during this period of decline from moderate activity to the recent solar minimum in ~10 nm bands and for three spectral regions of significant interest: the UV integrated over 200−300 nm, the visible over 400−691 nm and the IR between 972−1630 nm.
Results. The model captures 97% of the observed TSI variation. This is on the order at which TSI detectors agree with each other during the period considered. In the spectral comparison, rotational variability is well reproduced, especially between 400 and 1200 nm. The magnitude of change in the long-term trends is many times larger in SIM at almost all wavelengths while trends in SIM oppose SATIRE in the visible between 500 and 700 nm and again between 1000 and 1200 nm. We discuss the remaining issues with both SIM data and the identified limits of the model, particularly with the way facular contributions are dealt with, the limit of flux identification in MDI magnetograms during solar minimum and the model atmospheres in the IR employed by SATIRE. However, it is unlikely that improvements in these areas will significantly enhance the agreement in the long-term trends. This disagreement implies that some mechanism other than surface magnetism is causing SSI variations, in particular between 2004 and 2006, if the SIM data are correct. Since SATIRE was able to reproduce UV irradiance between 1991 and 2002 from UARS, either the solar mechanism for SSI variation fundamentally changed around the peak of cycle 23, or there is an inconsistency between UARS and SORCE UV measurements. We favour the second explanation.

Linear waves in a non-equilibrium ionisation partially ionised plasma

I. **Ballai**
Frontiers in Astronomy **2019**
https://solarpreprint.org/ballai_frontiers.pdf
We aim to investigate the properties of linear Alfvén and slow magnetoacoustic waves in a partially ionised plasma in ionisation non-equilibrium. The propagation characteristics of these 5 waves are studied within the framework of a two-fluid plasma in terms of the collisional strength between heavy particles for different degrees of ionisation. In the ionisation non-equilibrium state the rates of ionisation and recombinations are not equal. For analytical progress we assume a background that is ionisation equilibrium, the non-equilibrium is driven by perturbations in the system, therefore, non-equilibrium effects are related to the perturbed state of the plasma. Using simple analytical methods, we show that ionisation non-equilibrium can provide an additional coupling between ions and neutrals (implicitly a secondary damping mechanism in the collisionless limit) and this process is able to keep the neutrals in the system even in the collisionless limit. Due to the coupling between different species waves become dispersive.
The present study improves our understanding of the complexity of dynamical processes partially ionised plasma in the lower solar atmosphere and solar prominences. Our results clearly show that the problem of partial ionisation and non-equilibrium ionisation introduce new aspects of plasma dynamics with consequences on the evolution waves and their dissipation.

Dispersive shock waves in partially ionised plasmas

I. **Ballai**, E. Forgacs-Dajka, A. Marcu
Advances in Space Research 63 (**2019**) 1472–1482
https://arxiv.org/pdf/1810.07948.pdf

Compressional waves propagating in the partially ionised solar lower atmospheric plasmas can easily steepen into nonlinear waves, including shocks. Here we investigate the effect of weak dispersion generated by Hall currents perpendicular to the ambient magnetic field on the characteristics of shock waves. Our study will also focus on the interplay between weak dispersion and partial ionisation of the plasma. Using a multiple scale technique we derive the governing equation in the form of a Korteweg-de Vries-Burgers equation. The effect of weak dispersion on shock waves is obtained using a perturbation technique. The secular behaviour of second order terms is addressed with the help of a renormalisation technique. Our results show that dispersion modifies the characteristics of shock waves and this change is dependent also on the ionisation degree of the plasma. Dispersion can create short lived oscillations in the shocked plasma. The shock fronts become wider with the increase in the number of neutrals in the plasma.

Nonlinear coupling of Alfvén and slow magnetoacoustic waves in partially ionized solar plasmas

J. L. **Ballester**1,3, R. Soler1,3, J. Terradas1,3 and M. Carbonell2,3
A&A 641, A48 (**2020**)
https://doi.org/10.1051/0004-6361/202038220
Context. Partially ionized plasmas constitute an essential ingredient of the solar atmosphere since layers such as the chromosphere and the photosphere and structures such as prominences and spicules are made of this plasma. On the other hand, ground- and space-based observations have indicated the presence of oscillations in partially ionized layers and structures of the solar atmosphere, which have been interpreted in terms of magnetohydrodynamic (MHD) waves.
Aims. Our aim is to study the temporal behavior of nonlinear Alfvén waves, and the subsequent excitation of field-aligned motions and perturbations, in a partially ionized plasma when dissipative mechanisms such as ambipolar diffusion, radiative losses, and thermal conduction are taken into account.
Methods. First, we applied the regular perturbations method for small-amplitude initial perturbations to obtain the temporal behavior of perturbations. Then we solved the full set of nonlinear MHD equations for larger values of the initial amplitude.
Results. We obtain analytical and numerical solutions to first-, second-, and third-order systems of equations and study the effects produced by ambipolar diffusion and thermal mechanisms on the temporal behavior of Alfvén and slow waves. We also study how the majority of the energy is transferred from the Alfvén waves to plasma internal energy. After numerically solving the full nonlinear equations when a large amplitude is assumed, the profile of the perturbations displays the typical sawtooth profile characteristic of associated shocks.
Conclusions. When ambipolar diffusion is taken into account, first-order Alfvén waves are damped in time, while second-order perturbations are undamped. However, due to the release of heat produced by ambipolar diffusion, other physical effects that modify the physical conditions in the spatial domain under consideration appear. On the other hand, the second-order perturbations are damped by thermal effects with a damping time that can be longer or shorter than that of Afvén waves. Therefore, after the initial excitation, Alfvén waves can be quickly damped, while slow waves remain in the plasma for a longer time, and vice versa.

Magnetic sensitivity in the wing scattering polarization signals of the hydrogen Lyman-alpha line of the solar disk radiation

Ernest Alsina **Ballester**, Luca Belluzzi, Javier Trujillo Bueno
2019 *ApJ* **880** 85
https://arxiv.org/pdf/1901.10994.pdf
The linear polarization produced by scattering processes in the hydrogen Ly{\alpha} line of the solar disk radiation is a key observable for probing the chromosphere-corona transition region (TR) and the underlying chromospheric plasma. While the line-center signal encodes information on the magnetic field and three-dimensional structure of the TR, the sizable scattering polarization signals that the joint action of partial frequency redistribution (PRD) and J-state interference produce in the Ly{\alpha} wings have generally been thought to be sensitive only to the thermal structure of the solar atmosphere. Here we show that the wings of the Q/I and U/I scattering polarization profiles of this line are actually sensitive to the presence of chromospheric magnetic fields, with strengths similar to those that produce the Hanle effect in the line core (i.e., between 5 and 100 gauss, approximately). In spite of the fact that the Zeeman splitting induced by such weak fields is very small compared to the total width of the line, the magneto-optical effects that couple the transfer equations for Stokes Q and U are actually able to produce sizable changes in the Q/I and U/I wings. The theoretical results presented here further expand the diagnostic content of the unprecedented spectropolarimetric observations provided by the Chromospheric Lyman-Alpha Spectropolarimeter (CLASP).

Partially Ionized Plasmas in Astrophysics **Review**

José Luis **Ballester**1 ·Igor Alexeev2 · Manuel Collados3 · Turlough Downes4 · Robert F. Pfaff5 · Holly Gilbert6 · Maxim Khodachenko7 · Elena Khomenko3 · Ildar F. Shaikhislamov8 · Roberto Soler1 · Enrique Vázquez-Semadeni9 · Teimuraz Zaqarashvili7,10
Space Sci Rev (**2018**) 214:58
https://link.springer.com/content/pdf/10.1007%2Fs11214-018-0485-6.pdf
Partially ionized plasmas are found across the Universe in many different astrophysical environments. They constitute an essential ingredient of the solar atmosphere, molecular clouds, planetary ionospheres and protoplanetary disks, among other environments, and display a richness of physical effects which are not present in fully ionized plasmas. This review provides an overview of the physics of partially ionized plasmas, including recent advances in different astrophysical areas in which partial ionization plays a fundamental role. We outline outstanding observational and theoretical questions and discuss possible directions for future progress.
5.1 Solar Atmosphere

The transfer of resonance line polarization with partial frequency redistribution in the general Hanle-Zeeman regime

Ernest Alsina **Ballester**, Luca Belluzzi, Javier Trujillo Bueno
ApJ **2016**
http://arxiv.org/pdf/1609.05723v1.pdf
The spectral line polarization encodes a wealth of information about the thermal and magnetic properties of the solar atmosphere. Modeling the Stokes profiles of strong resonance lines is, however, a complex problem both from the theoretical and computational point of view, especially when partial frequency redistribution (PRD) effects need to be taken into account. In this work, we consider a two-level atom in the presence of magnetic fields of arbitrary intensity (Hanle-Zeeman regime) and orientation, both deterministic and micro-structured. Working within the framework of a rigorous PRD theoretical approach, we have developed a numerical code which solves the full non-LTE radiative transfer problem for polarized radiation, in one-dimensional models of the solar atmosphere, accounting for the combined action of the Hanle and Zeeman effects, as well as for PRD phenomena. After briefly discussing the relevant equations, we describe the iterative method of solution of the problem and the numerical tools that we have developed and implemented. We finally present some illustrative applications to two resonance lines that form at different heights in the solar atmosphere, and provide a detailed physical interpretation of the calculated Stokes profiles. We find that in strong resonance lines sensitive to PRD effects the magneto-optical terms of the Stokes-vector transfer equation produce conspicuous U/I wing signals along with a very interesting magnetic sensitivity in the wings of the linear polarization profiles. We also show that the weak-field approximation has to be used with caution when PRD effects are considered.

Changes in granulation scales over the solar cycle seen with SDO/HMI and Hinode/SOT

J. **Ballot**, T. Roudier, J.M. Malherbe, Z. Frank
A&A 652, A103 **2021**
https://arxiv.org/pdf/2106.03556.pdf
https://www.aanda.org/articles/aa/pdf/2021/08/aa39436-20.pdf
https://doi.org/10.1051/0004-6361/202039436
The Sun is the only star where the superficial turbulent convection can be observed at very high spatial resolution. The Solar Dynamics Observatory (SDO) has continuously observed the full Sun from space with multi-wavelength filters since July 2010. In particular, the Helioseismic and Magnetic Imager (HMI) instrument takes high-cadence frames (45 seconds) of continuum intensity in which solar granulation is visible. We aimed to follow the evolution of the solar granules over an activity cycle and look for changes in their spatial properties. We investigated the density of granules and their mean area derived directly from the segmentation of deconvolved images from SDO/HMI. To perform the segmentation, we define granules as convex elements of images. We measured an approximately 2% variation in the density and the mean area of granules over the cycle, the density of granules being greater at solar maximum with a smaller granule mean area. The maximum density appears to be delayed by about one year compared to classical activity indicators, such as the sunspot number. We complemented this study with high-spatial-resolution observations obtained with Hinode/SOTBFI (Solar Optical Telescope Broadband Filter Imager), which are consistent with our results. The observed variations in solar granulation at the disc centre reveal a direct insight into the change in the physical properties that occur in the upper convective zone during a solar cycle. These variations can be due to interactions between convection and magnetic fields, either at the global scale or, locally, at the granulation scale.
HMI Naggits #161 **2021** http://hmi.stanford.edu/hminuggets/?p=3614

A homogeneous database of sunspot areas covering more than 130 years

Balmaceda, L. A.; Solanki, S. K.; Krivova, N. A.; Foster, S.

J. Geophys. Res., Vol. 114, No. A7, A07104, **2009**
http://dx.doi.org/10.1029/2009JA014299
The historical record of sunspot areas is a valuable and widely used proxy of solar activity and variability. The Royal Greenwich Observatory regularly measured this and other parameters between 1874 and 1976. After that time records from a number of different observatories are available. These, however, show systematic differences and often have significant gaps. Our goal is to obtain a uniform and complete sunspot area time series by combining different data sets. A homogeneous composite of sunspot areas is essential for different applications in solar physics, among others for irradiance reconstructions. Data recorded simultaneously at different observatories are statistically compared in order to determine the intercalibration factors. Using these data we compile a complete and cross-calibrated time series. The Greenwich data set is used as a basis until 1976, the Russian data (a compilation of observations made at stations in the former USSR) are used between 1977 and 1985, and data compiled by the USAF network are used since 1986. Other data sets (Rome, Yunnan, and Catania) are used to fill up the remaining gaps. Using the final sunspot areas record the Photometric Sunspot Index is calculated. We also show that the use of uncalibrated sunspot areas data sets can seriously affect the estimate of irradiance variations. Our analysis implies that there is no basis for the claim that UV irradiance variations have a much smaller influence on climate than total solar irradiance variations.

The Solar Activity Cycle **Book**

Physical Causes and Consequences
André **Balogh**, Hugh Hudson, Kristóf Petrovay…
Space Sciences Series of ISSI (**2015**)
https://link.springer.com/content/pdf/10.1007%2F978-1-4939-2584-1.pdf

Introduction to the Solar Activity Cycle: Overview of Causes and Consequences **Review**

A. **Balogh**, H. S. Hudson, K. Petrovay, R. von Steiger
Space Science Reviews, December **2014**, Volume 186, Issue 1-4, pp 1-15
http://download.springer.com/static/pdf/224/art%253A10.1007%252Fs11214-014-0125-8.pdf?auth66=1420655988_463bc60ba89afe0c01ad5fcdad050639&ext=.pdf
The 11-year activity cycle is a dominant characteristic of the Sun. It is the result of the evolution in time the solar dynamo that generates the solar magnetic field. The nearly periodic variation in the sunspot number has been known since the mid-1800s; as the observations of the Sun broadened to cover an increasing number of phenomena, the same 11-year periodicity was noted in most of them. The discovery of solar magnetic fields introduced a 22-year periodicity, as the magnetic polarities of the polar regions change sign every 11 years. Correlations have been identified and quantified among all the measured parameters, but in most cases such correlations remain empirical rather than grounded in physical processes. This introductory paper and the reviews in the volume describe and discuss the current state of understanding of the causal chains that lead from the variable nature of the solar magnetic fields to the variability of solar phenomena. The solar activity cycle is poorly understood: predictions made for the current Cycle 24 have proved to be generally wrong. However, the re-evaluation of the relationships in the light of unexpected shortcomings is likely to lead to a better physical understanding of solar physics. This will help in the systematic reassessment of solar activity indices and their usefulness in describing and predicting the solar activity cycle.'

"The Heliosphere through the Solar Activity Cycle",

edited by André **Balogh**, Louis J. Lanzerotti, and Steven T. Suess.
Springer-Praxis, **2007**
It provides the definitive discussion of the subject to date and looks forward to discoveries to be made by follow-on missions to Ulysses.

Contents:
1. The heliosphere: Its origin and exploration: A. Balogh & L. J. Lanzerotti.
2. Solar Cycle 23: D.H. Hathaway & S. T. Suess.
3. The solar wind throughout the solar cycle: R. von Steiger.
4. The globa helispheric magnetic field: E. J. Smith.
5. Heliospheric energetic particle variations: D. Lario & M. Pick.
6. Galactic and anomalous cosmic rays through the solar cycle: New insight from Ulysses: B. Heber & M. S. Potgieter.
7. Overview: The heliosphere then and now: S. T. Suess.

Spectropolarimetric Observations of an Arch Filament System with GREGOR

H. **Balthasar**, P. Gömöry, S.J. González Manrique, C. Kuckein, A. Kučera, P. Schwartz, T. Berkefeld, M. Collados, C. Denker, A. Feller, A. Hofmann, D. Schmidt, W. Schmidt, M. Sobotka, S.K.Solanki, D. Soltau, J. Staude, K.G. Strassmeier, O. von der Lühe
in: Solar Polarization 8, ed. L. Belluzzi, ASP Conference Series **2018**
https://arxiv.org/pdf/1804.01789.pdf
We observed an arch filament system (AFS) in a sunspot group with the GREGOR Infrared Spectrograph attached to the GREGOR solar telescope. The AFS was located between the leading sunspot of negative polarity and several pores of positive polarity forming the following part of the sunspot group. We recorded five spectro-polarimetric scans of this region. The spectral range included the spectral lines Si I 1082.7 nm, He I 1083.0 nm, and Ca I 1083.9 nm. In this work we concentrate on the silicon line which is formed in the upper photosphere. The line profiles are inverted with the code `Stokes Inversion based on Response functions' to obtain the magnetic field vector. The line-of-sight velocities are determined independently with a Fourier phase method. Maximum velocities are found close to the ends of AFS fibrils. These maximum values amount to 2.4 km/s next to the pores and to 4 km/s at the sunspot side. Between the following pores, we encounter an area of negative polarity that is decreasing during the five scans. We interpret this by new emerging positive flux in this area canceling out the negative flux. In summary, our findings confirm the scenario that rising magnetic flux tubes cause the AFS. **2015 May 24**

Spectropolarimetric observations of an arch filament system with the GREGOR solar telescope

H. **Balthasar**, P. Gömöry, S.J. González Manrique, C. Kuckein, J. Kavka, A. Kučera, P. Schwartz, R. Vašková, T. Berkefeld, M. Collados Vera, C. Denker, A. Feller, A. Hofmann, A. Lagg, H. Nicklas, D. Orozco Suárez, A. Pastor Yabar, R. Rezaei, R. Schlichenmaier, D. Schmidt, W. Schmidt, M. Sigwarth, M. Sobotka, S.K. Solanki, D. Soltau, J. Staude, K.G. Strassmeier, R. Volkmer, O. von der Lühe, T. Waldmann
Proceedings 12th Potsdam Thinkshop to appear in Astronomische Nachrichten **2016**
http://arxiv.org/pdf/1609.01514v1.pdf
Arch filament systems occur in active sunspot groups, where a fibril structure connects areas of opposite magnetic polarity, in contrast to active region filaments that follow the polarity inversion line. We used the GREGOR Infrared Spectrograph (GRIS) to obtain the full Stokes vector in the spectral lines Si I 1082.7 nm, He I 1083.0 nm, and Ca I 1083.9 nm. We focus on the near-infrared calcium line to investigate the photospheric magnetic field and velocities, and use the line core intensities and velocities of the helium line to study the chromospheric plasma. The individual fibrils of the arch filament system connect the sunspot with patches of magnetic polarity opposite to that of the spot. These patches do not necessarily coincide with pores, where the magnetic field is strongest. Instead, areas are preferred not far from the polarity inversion line. These areas exhibit photospheric downflows of moderate velocity, but significantly higher downflows of up to 30 km/s in the chromospheric helium line. Our findings can be explained with new emerging flux where the matter flows downward along the fieldlines of rising flux tubes, in agreement with earlier results.
2015 May 24

On Dimensionality Reduction for Indexing and Retrieval of Large-Scale Solar Image Data

J. M. **Banda**, R. A. Angryk, P. C. H. Martens
Solar Physics, March **2013**, Volume 283, Issue 1, pp 113-141
This work investigates the applicability of several dimensionality reduction techniques for large-scale solar data analysis. Using a solar benchmark dataset that contains images of multiple types of phenomena, we investigate linear and nonlinear dimensionality reduction methods in order to reduce our storage and processing costs and maintain a good representation of our data in a new vector space. We present a comparative analysis of several dimensionality reduction methods and different numbers of target dimensions by utilizing different classifiers in order to determine the degree of data dimensionality reduction that can be achieved with these methods, and to discover the method that is the most effective for solar images. After determining the optimal number of dimensions, we then present preliminary results on indexing and retrieval of the dimensionally reduced data.

MHD Waves in open coronal structures **Review**

D. **Banerjee**, S. Krishna Prasad, V. Pant, J.A. McLaughlin, P. Antolin, N. Magyar, L. Ofman, H. Tian, T. Van Doorsselaere, I. De Moortel, T. Wang
Space Science Reviews **217**, Article number: 76 (**2021**)
https://arxiv.org/pdf/2012.08802.pdf
https://link.springer.com/content/pdf/10.1007/s11214-021-00849-0.pdf
https://doi.org/10.1007/s11214-021-00849-0

Modern observatories have revealed the ubiquitous presence of magnetohydrodynamic waves in the solar corona. The propagating waves (in contrast to the standing waves) are usually originated in the lower solar atmosphere which makes them particularly relevant for coronal heating. Furthermore, open coronal structures are believed to be the source regions of solar wind, therefore, the detection of MHD waves in these structures is also pertinent to the acceleration of solar wind. Besides, the advanced capabilities of the current generation telescopes have allowed us to extract important coronal properties through MHD seismology. The recent progress made in the detection, origin, and damping of both slow mangetoacoustic waves and Alfvénic waves is presented in this review article especially in the context of open coronal structures. Where appropriate, we give an overview on associated theoretical modelling studies. A few of the important seismological applications of these waves are discussed. The possible role of Aflvénic waves in the acceleration of solar wind is also touched upon. 6 August, 2010, 10 December 2011

Present and Future Observing Trends in Atmospheric Magnetoseismology

D. **Banerjee** · R. Erdélyi · R. Oliver · E. O'Shea
Solar Phys (**2007)** 246: 3–29
http://www.springerlink.com/content/787138343931023t/fulltext.pdf
With modern imaging and spectral instruments observing in the visible, EUV, X-ray, and radio wavelengths, the detection of oscillations in the solar outer atmosphere has become a routine event. These oscillations are considered to be the signatures of a wave phenomenon and are generally interpreted in terms of magnetohydrodynamic (MHD) waves. With multiwavelength observations from ground- and space-based instruments, it has been possible to detect waves in a number of different wavelengths simultaneously and, consequently, to study their propagation properties. Observed MHD waves propagating from the lower solar atmosphere into the higher regions of the magnetized corona have the potential to provide excellent insight into the physical processes at work at the coupling point between these different regions of the Sun. High-resolution wave observations combined with forward MHD modeling can give an unprecedented insight into the connectivity of the magnetized solar atmosphere, which further provides us with a realistic chance to reconstruct the structure of the magnetic field in the solar atmosphere. This type of solar exploration has been termed atmospheric magnetoseismology. In this review we will summarize some new trends in the observational study of waves and oscillations, discussing their origin and their propagation through the atmosphere. In particular, we will focus on waves and oscillations in open magnetic structures (*e.g.*, solar plumes) and closed magnetic structures (*e.g.*, loops and prominences), where there have been a number of observational highlights in the past few years. Furthermore, we will address observations of waves in filament fibrils allied with a better characterization of their propagating and damping properties, the detection of prominence oscillations in UV lines, and the renewed interest in large-amplitude, quickly attenuated, prominence oscillations, caused by flare or explosive phenomena.

Effect of the Solar dark matter wake on planets

Indranil **Banik**, Pavel Kroupa
MNRAS **2019**
https://arxiv.org/pdf/1907.07130.pdf
The Galaxy is conventionally thought to be surrounded by a massive dark matter (DM) halo. As the Sun goes through this halo, it excites a DM wake behind it. This local asymmetry in the DM distribution would gravitationally affect the motions of Solar System planets, potentially allowing the DM wake to be detected or ruled out. Hernandez (2019) recently calculated that the DM-induced perturbation to Saturn's position is 252 metres net of the effect on the Sun. No such anomaly is seen in Saturn's motion despite very accurate tracking of the Cassini spacecraft, which orbited Saturn for >13 years. Here, we revisit the calculation of how much Saturn would deviate from Keplerian motion if we fix its position and velocity at some particular time. The DM wake induces a nearly resonant perturbation whose amplitude grows almost linearly with time. We show that the Hernandez (2019) result applies only for an observing duration comparable to the ≈250 million year period of the Sun's orbit around the Galaxy. Over a 100 year period, the perturbation to Saturn's orbit amounts to <1 cm, which is quite consistent with existing observations. Even smaller perturbations are expected for the terrestrial planets.

Stable Sunspot Area Level of Debrecen Photoheliographic Data and Multivariate Correction Factor of SOON Data

T. **Baranyi**
Solar Physics October **2018**, 293:142
We investigate the spatial and temporal variation of sunspot group areas reported by the Greenwich Photoheliographic Results (GPR), the Solar Optical Observing Network (SOON), the Kislovodsk Mountain Astronomical Station (KMAS), and the Debrecen Photoheliographic Data (DPD) databases. We identify improved

correction factors for reconciling these individual records to a common scale. Our results show that the DPD sunspot group areas are stable over the studied interval (1974 – 2014). We find an improved fit between GPR and DPD sunspot group areas when using a correction factor such that GPR=0.975(±0.006)×DPDGPR=0.975(±0.006)×DPD, independent of the position of the sunspot group on the solar disk. We also find that the scale of KMAS sunspot group areas fits that of DPD well, but has a small position-dependent trend near the limb. However, in order to set SOON sunspot group area records onto the scale of DPD, we find that there is a need for a multivariate correction factor. This multivariate correction factor has a value ranging between 1.1 and 1.9 and is dependent upon the time of the SOON observation, the distance of the group from disk center, and the observatory within the SOON network. Finally, we provide further context to the systematic bias in SOON sunspot group area observations toward lower values relative to those recorded in the GPR and DPD databases that has previously been reported in the literature. We have identified the two main contributors to the SOON area deficit; some penumbral parts are unobserved, and the spot areas are underestimated. Our analysis is vital for studies that require stable, long-term solar activity records such as solar irradiance models that estimate irradiance reduction from records of sunspot group numbers, areas, and locations.

On-line Tools for Solar Data Compiled in the Debrecen Observatory and their Extensions with the Greenwich Sunspot Data

T. **Baranyi**, L. Győri, A. Ludmán
Solar Phys. **2016**
http://arxiv.org/pdf/1606.00669v1.pdf
The primary task of the Debrecen Heliophysical Observatory (DHO) has been the most detailed, reliable, and precise documentation of the solar photospheric activity since 1958. This long-term effort resulted in various solar catalogs based on ground-based and space-borne observations. A series of sunspot databases and on-line tools were compiled at DHO: the Debrecen Photoheliographic Data (DPD, 1974--), the dataset based on the {\it Michelson Doppler Imager} (MDI) of the {\it Solar and Heliospheric Observatory} (SOHO) called SOHO/MDI--Debrecen Data (SDD, 1996--2010), and the dataset based on the {\it Helioseismic and Magnetic Imager} (HMI) of the {\it Solar Dynamics Observatory} (SDO) called SDO/HMI--Debrecen Data (HMIDD, 2010--). User-friendly web-presentations and on-line tools were developed to visualize and search data. As a last step of compilation, the revised version of Greenwich Photoheliographic Results (GPR, 1874--1976) catalog was converted to DPD format, and a homogeneous sunspot database covering more than 140 years was created. The database of images for the GPR era was completed with the full-disc drawings of the Hungarian historical observatories \'Ogyalla and Kalocsa (1872--1919) and with the polarity drawings of Mount Wilson Observatory. We describe the main characteristics of the available data and on-line tools.
See https://arxiv.org/ftp/arxiv/papers/1608/1608.08419.pdf

Software tool for automatic detection of solar plages in the Coimbra Observatory spectroheliograms

T. **Barata**, S. Carvalho, I. Dorotovic, F. Pinheiro, A. Garcia, J. Fernandes, A.M. Lourenco
Astronomy and Computing, Volume 24, **2018**, Pages 70-83
https://arxiv.org/ftp/arxiv/papers/1811/1811.08389.pdf
Full-disk spectroheliograms have been taken in Coimbra on a daily basis since 1926 in the Ca II K-line (K1 and K3). Later, in 1989, with the upgrade of the equipment it was possible to start the observations in the H-alpha line. The spectroheliograms of Coimbra constitutes a huge dataset of solar images, which requires an efficient automatic tool to detect and analyse solar activity features. This work presents a mathematical morphology approach applied to the CaII K3 series. The objective is to create a tool based on the segmentation by watershed transform combined with other morphological operators to detect automatically and analyse chromospheric plages during the solar cycle 24. The tool is validated by comparing its results for cycle 23 with those presented by Dorotovic et al. (2007, 2010). The results obtained are in very good agreement with those, including on images obtained in non-ideal meteorological conditions (eg. some clouds in sky). The results were also qualitatively compared with the results obtained through the application of ASSA model to SDO HMI magnetograms.

Temperature inversion in a gravitationally bound plasma: the case of the solar corona

Luca **Barbieri**, Lapo Casetti, Andrea Verdini, Simone Landi
Physical Review Letters **2023**
https://arxiv.org/pdf/2309.15772.pdf
The temperature of the solar atmosphere increases from thousands to millions of degrees moving from the lower layer, the chromosphere, to the outermost one, the corona, while density drops by several orders of magnitude. Such a phenomenon is called temperature inversion and how it happens is still largely unknown. We argue that temperature fluctuations in the chromosphere play a key role, as suggested by the study of a kinetic model of a plasma confined in a semicircular tube subjected to the gravity of the Sun and in contact with a thermostat at its feet,

mimicking a coronal loop anchored in the chromosphere. Collisions are neglected in the corona, with a sharp transition to a fully collisional chromosphere. Numerical simulations and analytical calculations show that suitable fluctuations of the thermostat temperature drive the plasma towards a non-thermal stationary state with temperature and density profiles strikingly similar to those observed in the atmosphere of the Sun, suggesting this mechanism may significantly contribute to coronal heating.

Propagation of Long-Wavelength Nonlinear Slow Sausage Waves in Stratified Magnetic Flux Tubes

M. **Barbulescu**, R. Erdélyi
Solar Phys. Volume 291, Issue 5, pp 1369–1384 **2016**
The propagation of nonlinear, long-wavelength, slow sausage waves in an expanding magnetic flux tube, embedded in a non-magnetic stratified environment, is discussed. The governing equation for surface waves, which is akin to the Leibovich–Roberts equation, is derived using the method of multiple scales. The solitary wave solution of the equation is obtained numerically. The results obtained are illustrative of a solitary wave whose properties are highly dependent on the degree of stratification.

TomograPy: A Fast, Instrument-Independent, Solar Tomography Software

N. **Barbey**, C. Guennou, F. Auchère
Solar Physics, March **2013**, Volume 283, Issue 1, pp 227-245
Solar tomography has progressed rapidly in recent years thanks to the development of robust algorithms and the availability of more powerful computers. It can today provide crucial insights in solving issues related to the line-of-sight integration present in the data of solar imagers and coronagraphs. However, there remain challenges such as the increase of the available volume of data, the handling of the temporal evolution of the observed structures, and the heterogeneity of the data in multi-spacecraft studies. We present a generic software package that can perform fast tomographic inversions that scales linearly with the number of measurements, linearly with the length of the reconstruction cube (and not the number of voxels), and linearly with the number of cores and can use data from different sources and with a variety of physical models: TomograPy (http://nbarbey.github.com/TomograPy/), an open-source software freely available on the Python Package Index. For performance, TomograPy uses a parallelized-projection algorithm. It relies on the World Coordinate System standard to manage various data sources. A variety of inversion algorithms are provided to perform the tomographic-map estimation. A test suite is provided along with the code to ensure software quality. Since it makes use of the Siddon algorithm it is restricted to rectangular parallelepiped voxels but the spherical geometry of the corona can be handled through proper use of priors. We describe the main features of the code and show three practical examples of multi-spacecraft tomographic inversions using STEREO/EUVI and STEREO/COR1 data. Static and smoothly varying temporal evolution models are presented.

Analysis of geomagnetically induced currents at a low-latitude region over the solar cycles 23 and 24: comparison between measurements and calculations

Cleiton **Barbosa**, Livia Alves, Ramon Caraballo, Gelvam A. Hartmann, Andres R.R. Papa and Risto J. Pirjola
J. Space Weather Space Clim., 5, A35 (**2015**) Open Access
http://www.swsc-journal.org/articles/swsc/pdf/2015/01/swsc150056.pdf
Geomagnetically Induced Currents (GIC) are a space weather effect, which affects ground-based technological structures at all latitudes on the Earth's surface. GIC occurrence and amplitudes have been monitored in power grids located at high and middle latitudes since 1970s and 1980s, respectively. This monitoring provides information about the GIC intensity and the frequency of occurrence during geomagnetic storms. In this paper, we investigate GIC occurrence in a power network at low latitudes (in the central Brazilian region) during the solar cycles 23 and 24. Calculated and measured GIC data are compared for the most intense geomagnetic storms (i.e. $-50 < Dst < -50$ nT) of the solar cycle 24. The results obtained from this comparison show a good agreement. The success of the model employed for the calculation of GIC leads to the possibility of determining GIC for events during the solar cycle 23 as well. Calculated GIC in one transformer reached ca. 30 A during the "Halloween storm" in 2003 whilst most frequent intensities lie below 10 A. The normalized inverse cumulative frequency for GIC data was calculated for the solar cycle 23 in order to perform a statistical analysis. It was found that a q-exponential Tsallis distribution fits the calculated GIC frequency distribution for more than 99% of the data. This analysis provides an overview of the long-term GIC monitoring at low latitudes and suggests new insight into critical phenomena involved in the GIC generation.

Magnetoacoustic Waves and the Kelvin–Helmholtz Instability in a Steady Asymmetric Slab

I: The Effects of Varying Density Ratios

M. **Barbulescu,** R. Erdélyi
Solar Phys (**2018**) 293:86
https://link.springer.com/content/pdf/10.1007%2Fs11207-018-1305-6.pdf
Recent observations have shown that bulk flow motions in structured solar plasmas, most evidently in coronal mass ejections (CMEs), may lead to the formation of Kelvin–Helmholtz instabilities (KHIs). Analytical models are thus essential in understanding both how the flows affect the propagation of magnetohydrodynamic (MHD) waves, and what the critical flow speed is for the formation of the KHI. We investigate both these aspects in a novel way: in a steady magnetic slab embedded in an asymmetric environment. The exterior of the slab is defined as having different equilibrium values of the background density, pressure, and temperature on either side. A steady flow and constant magnetic field are present in the slab interior. Approximate solutions to the dispersion relation are obtained analytically and classified with respect to mode and speed. General solutions and the KHI thresholds are obtained numerically.

Slow solar wind sources. High-resolution observations with a quadrature view

Krzysztof **Barczynski**, Louise Harra, Conrad Schwanitz, Nils Janitzek, et al.
A&A **2023**
https://arxiv.org/pdf/2303.11001.pdf
The origin of the slow solar wind is still an open issue. One possibility that has been suggested is that upflows at the edge of an active region can contribute to the slow solar wind.
We aim to explain how the plasma upflows are generated, which mechanisms are responsible for them, and what the upflow region topology looks like.
We investigated an upflow region using imaging data with the unprecedented temporal (3s) and spatial (2 pixels = 236km) resolution that were obtained on **30 March 2022** with the 174Å of the Extreme-Ultraviolet Imager (EUI)/High Resolution Imager (HRI) on board Solar Orbiter. During this time, the EUI and Earth-orbiting satellites (Solar Dynamics Observatory, Hinode, and the Interface Region Imaging Spectrograph, IRIS) were located in quadrature (92 degrees), which provides a stereoscopic view with high resolution. We used the Hinode/EIS (Fe XII) spectroscopic data to find coronal upflow regions in the active region. The IRIS slit-jaw imager provides a high-resolution view of the transition region and chromosphere.
For the first time, we have data that provide a quadrature view of a coronal upflow region with high spatial resolution. We found extended loops rooted in a coronal upflow region. Plasma upflows at the footpoints of extended loops determined spectroscopically through the Doppler shift are similar to the apparent upward motions seen through imaging in quadrature. The dynamics of small-scale structures in the upflow region can be used to identify two mechanisms of the plasma upflow: Mechanism I is reconnection of the hot coronal loops with open magnetic field lines in the solar corona, and mechanism II is reconnection of the small chromospheric loops with open magnetic field lines in the chromosphere or transition region. We identified the locations in which mechanisms I and II work.

A comparison of the active region upflow and core properties using simultaneous spectroscopic observations from IRIS and Hinode

Krzysztof **Barczynski**, Louise Harra, Lucia Kleint, Brandon Panos, David H. Brooks
A&A **2021**
https://arxiv.org/pdf/2104.10234.pdf
The origin of the slow solar wind is still an open issue. It has been suggested that upflows at the edge of active regions (AR) can contribute to the slow solar wind. Here, we compared the upflow region and the AR core and studied how the plasma properties change from the chromosphere via the transition region to the corona. We studied limb-to-limb observations NOAA 12687 (**14th - 25th Nov 2017**). We analysed spectroscopic data simultaneously obtained from IRIS and Hinode/EIS in six spectral lines. We studied the mutual relationships between the plasma properties for each emission line, as well as comparing the plasma properties between the neighbouring formation temperature lines. To find the most characteristic spectra, we classified the spectra in each wavelength using the machine learning technique k-means. We found that in the upflow region the Doppler velocities of the coronal lines are strongly correlated, but the transition region and coronal lines show no correlation. However, their fluxes are strongly correlated. The upflow region has lower density and lower temperature than the AR core. In the upflow region, the Doppler and non-thermal velocity show a strong correlation in the coronal lines, but the correlation is not seen in the AR core. At the boundary between the upflow region and the AR core, the upflow region shows an increase in the coronal non-thermal velocity, the emission obtained from the DEM, and the domination of the redshifted regions in the chromosphere. The obtained results suggest that at least three parallel mechanisms generate the plasma upflow: (1) the reconnection between closed loops and open magnetic field lines in the lower corona or upper chromosphere; (2) the reconnection between the chromospheric small-scale loops and open magnetic field; (3) the expansion of the magnetic field lines that allows the chromospheric plasma to escape to the solar corona.

Emission of solar chromospheric and transition region features related to the underlying magnetic field

Krzysztof **Barczynski**, Hardi Peter, Lakshmi Pradeep Chitta, Sami K. Solanki

A&A 619, A5 **2018**

https://arxiv.org/pdf/1807.02372.pdf

The emission of the upper atmosphere of the Sun is closely related to magnetic field concentrations at the solar surface.

It is well established that this relation between chromospheric emission and magnetic field is nonlinear. Here we investigate systematically how this relation, characterised by the exponent of a power-law fit, changes through the atmosphere, from the upper photosphere through the temperature minimum region and chromosphere to the transition region.

We used spectral maps from IRIS: MgII and its wings, CII, and SiIV together with magnetograms and UV continuum images from SDO. We performed a power-law fit for the relation between each pair of observables and determine the power-law index (or exponent) for these.

While the correlation between emission and magnetic field drops monotonically with temperature, the power-law index shows a hockey-stick-type variation: from the upper photosphere to the temperature-minimum it drops sharply and then increases through the chromosphere into the transition region. This is even seen through the features of the MgII line, this is, from k1 to k2 and k3. It is irrespective of spatial resolution or feature types on the Sun.

In accordance with the general picture of flux-flux relations from the chromosphere to the corona, above the temperature minimum the sensitivity of the emission to the plasma heating increases with temperature. Below the temperature minimum a different mechanism has to govern the opposite trend of the power-law index with temperature. We suggest four possibilities, in other words, a geometric effect of expanding flux tubes filling the available chromospheric volume, the height of formation of the emitted radiation, the dependence on wavelength of the intensity-temperature relationship, and the dependence of the heating of flux tubes on the magnetic flux density.

Generation of mean flows in rotating anisotropic turbulence: The case of solar near-surface shear layer

A. **Barekat**, M. J. Käpylä, P. J. Käpylä, E. P. Gilson, H. Ji

A&A 655, A79 **2021**

https://arxiv.org/pdf/2012.06343.pdf

https://www.aanda.org/articles/aa/pdf/2021/11/aa40052-20.pdf

https://doi.org/10.1051/0004-6361/202040052

The radial gradient of the rotation rate in the near-surface shear layer (NSSL) of the Sun is independent of latitude and radius. Theoretical mean-field models have been successful in explaining this property of the solar NSSL, while global direct convection models have been unsuccessful. We investigate reason for this discrepancy by measuring the mean flows, Reynolds stress, and turbulent transport coefficients under NSSL conditions. Simulations have minimal ingredients. These ingredients are inhomogeneity due to boundaries, anisotropic turbulence, and rotation. Parameters of the simulations are chosen such they match the weakly rotationally constrained NSSL. The simulations probe locally Cartesian patches of the star at a given depth and latitude. The depth of the patch is varied by changing the rotation rate such that the resulting Coriolis numbers<1. We measure the turbulent transport coefficient relevant for the non-diffusive and diffusive parts of the Reynolds stress and compare them with predictions of current mean-field theories. A negative radial gradient of mean flow similar to the solar NSSL is generated only at the equator where meridional flows are absent. At other latitudes the meridional flow is comparable to the mean flow corresponding to differential rotation. We also find that meridional components of the Reynolds stress cannot be ignored. Additionally, we find that the turbulent viscosity is quenched by rotation by about 50\% from the surface to the bottom of the NSSL. Our local simulations do not validate the explanation for the generation of the NSSL from mean-field theory where meridional stresses are neglected. However, the rotational dependence of turbulent viscosity in our simulations is in good agreement with theoretical prediction. Our results are in qualitative agreement with global convection simulations in that a NSSL obtained near the equator.

Solar-cycle variation of the rotational shear near the solar surface

A. **Barekat**1, J. Schou1 and L. Gizon1

A&A 595, A8 (**2016**)

Context. Helioseismology has revealed that the angular velocity of the Sun increases with depth in the outermost 35 Mm of the Sun. Recently, we have shown that the logarithmic radial gradient (dlnΩ/dlnr) in the upper 10 Mm is close to −1 from the equator to 60° latitude.

Aims. We aim to measure the temporal variation of the rotational shear over solar cycle 23 and the rising phase of cycle 24 (1996−2015).

Methods. We used f mode frequency splitting data spanning 1996 to 2011 from the Michelson Doppler Imager (MDI) and 2010 to 2015 from the Helioseismic Magnetic Imager (HMI). In a first for such studies, the f mode frequency splitting data were obtained from 360-day time series. We used the same method as in our previous work for measuring dlnΩ/dlnr from the equator to 80° latitude in the outer 13 Mm of the Sun. Then, we calculated the variation of the gradient at annual cadence relative to the average over 1996 to 2015.
Results. We found the rotational shear at low latitudes (0° to 30°) to vary in-phase with the solar activity, varying by ~± 10% over the period 1996 to 2015. At high latitudes (60° to 80°), we found rotational shear to vary in anti-phase with the solar activity. By comparing the radial gradient obtained from the splittings of the 360-day and the corresponding 72-day time series of HMI and MDI data, we suggest that the splittings obtained from the 72-day HMI time series suffer from systematic errors.
Conclusions. We provide a quantitative measurement of the temporal variation of the outer part of the near surface shear layer which may provide useful constraints on dynamo models and differential rotation theory.

The radial gradient of the near-surface shear layer of the Sun

Atefeh **Barekat**, Jesper Schou, Laurent Gizon
A&A, **2014**
http://arxiv.org/pdf/1410.3162v1.pdf
Helioseismology has provided unprecedented information about the internal rotation of the Sun. One of the important achievements was the discovery of two radial shear layers: one near the bottom of the convection zone (the tachocline) and one near the surface. These shear layers may be important ingredients for explaining the magnetic cycle of the Sun. We measure the logarithmic radial gradient of the rotation rate (dlnΩ/dlnr) near the surface of the Sun using 15 years of f mode rotational frequency splittings from the Michelson Doppler Imager (MDI) and four years of data from the Helioseismic and Magnetic Imager (HMI). We model the angular velocity of the Sun in the upper ∼10 Mm as changing linearly with depth and use a multiplicative optimally localized averaging inversion to infer the gradient of the rotation rate as a function of latitude. Both the MDI and HMI data show that dlnΩ/dlnr is close to −1 from the equator to 60◦ latitude and stays negative up to 75◦ latitude. However, the value of the gradient is different for MDI and HMI for latitudes above 60◦. Additionally, there is a significant difference between the value of dlnΩ/dlnr using an older and recently reprocessed MDI data for latitudes above 30◦. We could reliably infer the value of dlnΩ/dlnr up to 60◦, but not above this latitude, which will hopefully constrain theories of the near-surface shear layer and dynamo. Furthermore, the recently reprocessed MDI splitting data are more reliable than the older versions which contained clear systematic errors in the high degree f modes.

Periodic behaviour of coronal mass ejections, eruptive events, and solar activity proxies during solar cycles 23 and 24

Tatiana **Barlyaeva**, Julien Wojak, Philippe Lamy, Brice Boclet, Imre Toth
Journal of Atmospheric and Solar-Terrestrial Physics Volume 177, October **2018**, Pages 12-28
https://arxiv.org/pdf/1704.02336.pdf **File**
We report on the parallel analysis of the periodic behaviour of coronal mass ejections (CMEs) based on 21 years [1996-2016] of observations with the SOHO/LASCO-C2 coronagraph, solar flares, prominences, and several proxies of solar activity. We consider values of the rates globally and whenever possible, distinguish solar hemispheres and solar cycles 23 and 24. Periodicities are investigated using both frequency (periodogram) and time-frequency (wavelet) analysis. We find that these different processes, in addition to following the ~11-year Solar Cycle, exhibit diverse statistically significant oscillations with properties common to all solar, coronal, and heliospheric processes: variable periodicity, intermittency, asymmetric development in the northern and southern solar hemispheres, and largest amplitudes during the maximum phase of solar cycles, being more pronounced during solar cycle 23 than the weaker cycle 24. However, our analysis reveals an extremely complex and diverse situation. For instance, there exists very limited commonality for periods of less than one year. The few exceptions are the periods of 3.1-3.2 months found in the global occurrence rates of CMEs and in the sunspot area (SSA) and those of 5.9-6.1 months found in the northern hemisphere. Mid-range periods of ~1 and ~2 years are more wide spread among the studied processes, but exhibit a very distinct behaviour with the first one being present only in the northern hemisphere and the second one only in the southern hemisphere. These periodic behaviours likely results from the complexity of the underlying physical processes, prominently the emergence of magnetic flux.

The State of the Corona During the Weak Solar Cycle 24: the View from LASCO Images

Barlyaeva, T.; Lamy, P.; Llebaria, A.; Boclet, B.
Ground-based Solar Observations in the Space Instrumentation Era
ASP Conference Series, Vol. 504, p. 287, **2016**
http://aspbooks.org/publications/504/287.pdf

The LASCO-C2 coronagraph onboard SOHO continues its white-light imaging of the corona from 1.5 to 6.0 solar radii, thus allowing investigating the consequences of the weak Solar Cycle 24 on the corona and comparing it to the previous cycle (23). Temporal variations of the global radiance of the corona are presented. We pay particular attention to the mid-term variations which are distinctly different between the two cycles and highlight the similarities and differences. Finally, we rely on our ARTEMIS II catalog of coronal mass ejections (CMEs) to compare their global rates during these two cycles.

Cycle Variation of the White-Light Corona from 18.5 Years (1996.0 – 2014.5) of LASCO Observations

T. **Barlyaeva**, P. Lamy, A. Llebaria
Solar Phys. Volume 290, Issue 7, pp 2117-2142 **2015**
http://link.springer.com/content/pdf/10.1007%2Fs11207-015-0736-6.pdf
We report on the analysis of the temporal evolution of the solar corona based on 18.5 years (1996.0 – 2014.5) of white-light observations with the SOHO/LASCO-C2 coronagraph. This evolution is quantified by generating spatially integrated values of the K-corona radiance, first globally, then in latitudinal sectors. The analysis considers time series of monthly values and 13-month running means of the radiance as well as several indices and proxies of solar activity. We study correlation, wavelet time-frequency spectra, and cross-coherence and phase spectra between these quantities. Our results give a detailed insight on how the corona responds to solar activity over timescales ranging from mid-term quasi-periodicities (also known as quasi-biennial oscillations or QBOs) to the long-term 11 year solar cycle. The amplitude of the variation between successive solar maxima and minima (modulation factor) very much depends upon the strength of the cycle and upon the heliographic latitude. An asymmetry is observed during the ascending phase of Solar Cycle 24, prominently in the royal and polar sectors, with north leading. Most prominent QBOs are a quasi-annual period during the maximum phase of Solar Cycle 23 and a shorter period, seven to eight months, in the ascending and maximum phases of Solar Cycle 24. They share the same properties as the solar QBOs: variable periodicity, intermittency, asymmetric development in the northern and southern solar hemispheres, and largest amplitudes during the maximum phase of solar cycles. The strongest correlation of the temporal variations of the coronal radiance – and consequently the coronal electron density – is found with the total magnetic flux. Considering that the morphology of the solar corona is also directly controlled by the topology of the magnetic field, this correlation reinforces the view that they are intimately connected, including their variability at all timescales.

Confinement of the solar tachocline by a cyclic dynamo magnetic field

R. **Barnabé**, A. Strugarek, P. Charbonneau, A. S. Brun, J.-P. Zahn
A&A 601, A47 **2017**
https://arxiv.org/pdf/1703.02374.pdf
The surprising thinness of the solar tachocline is still not understood with certainty today. Among the numerous possible scenarios suggested to explain its radial confinement, one hypothesis is based on Maxwell stresses that are exerted by the cyclic dynamo magnetic field of the Sun penetrating over a skin depth below the turbulent convection zone. Our goal is to assess under which conditions (turbulence level in the tachocline, strength of the dynamo-generated field, spreading mechanism) this scenario can be realized in the solar tachocline. We develop a simplified 1D model of the upper tachocline under the influence of an oscillating magnetic field imposed from above. The turbulent transport is parametrized with enhanced turbulent diffusion (or anti-diffusion) coefficients. Two main processes that thicken the tachocline are considered; either turbulent viscous spreading or radiative spreading. An extensive parameter study is carried out to establish the physical parameter regimes under which magnetic confinement of the tachocline that is due to a surface dynamo field can be realized. We have explored a large range of magnetic field amplitudes, viscosities, ohmic diffusivities and thermal diffusivities. We find that, for large but still realistic magnetic field strengths, the differential rotation can be suppressed in the upper radiative zone (and hence the tachocline confined) if weak turbulence is present (with an enhanced ohmic diffusivity of $\eta > 10^{7-8}$ cm^2/s), even in the presence of radiative spreading. Our results show that a dynamo magnetic field can, in the presence of weak turbulence, prevent the inward burrowing of a tachocline subject to viscous diffusion or radiative spreading.

Testing the current paradigm for space weather prediction with heliospheric imagers

Luke A. **Barnard**, Curt A. de Koning, Christopher J. Scott, Mathew J. Owens, Julia Wilkinson, Jackie A. Davies
Space Weather Volume 15, Issue 6 June **2017** Pages 782–803
http://onlinelibrary.wiley.com/doi/10.1002/2017SW001609/full
http://sci-hub.cc/10.1002/2017SW001609
Predictions of the arrival of four coronal mass ejections (CMEs) in geospace are produced through use of three CME geometric models combined with CME drag modeling, constraining these models with the available Coronagraph and Heliospheric Imager data. The efficacy of these predications is assessed by comparison with the Space Weather

Prediction Center (SWPC) numerical MHD forecasts of these same events. It is found that such a prediction technique cannot outperform the standard SWPC forecast at a statistically meaningful level. We test the Harmonic Mean, Self-Similar Expansion, and Ellipse Evolution geometric models, and find that, for these events at least, the differences between the models are smaller than the observational errors. We present a new method of characterizing CME fronts in the Heliospheric Imager field of view, utilizing the analysis of citizen scientists working with the Solar Stormwatch project, and we demonstrate that this provides a more accurate representation of the CME front than is obtained by experts analyzing elongation time maps for the studied events. Comparison of the CME kinematics estimated independently from the STEREO-A and STEREO-B Heliospheric Imager data reveals inconsistencies that cannot be explained within the observational errors and model assumptions. We argue that these observations imply that the assumptions of the CME geometric models are routinely invalidated and question their utility in a space weather forecasting context. These results argue for the continuing development of more advanced techniques to better exploit the Heliospheric Imager observations for space weather forecasting. **2012-08-31, 2012-09-28, 2012-10-05, 2012-11-20**

Differences between the CME fronts tracked by an expert, an automated algorithm, and the Solar Stormwatch project

L. **Barnard**, C. J. Scott, M. Owens, M. Lockwood, S. R. Crothers, J. A. Davies and R. A. Harrison
Space Weather 13(10) (pages 709–725) **2015**
http://onlinelibrary.wiley.com/doi/10.1002/2015SW001280/epdf
Observations from the Heliospheric Imager (HI) instruments aboard the twin STEREO spacecraft have enabled the compilation of several catalogues of coronal mass ejections (CMEs), each characterizing the propagation of CMEs through the inner heliosphere. Three such catalogues are the Rutherford Appleton Laboratory (RAL)-HI event list, the Solar Stormwatch CME catalogue, and, presented here, the J-tracker catalogue. Each catalogue uses a different method to characterize the location of CME fronts in the HI images: manual identification by an expert, the statistical reduction of the manual identifications of many citizen scientists, and an automated algorithm. We provide a quantitative comparison of the differences between these catalogues and techniques, using 51 CMEs common to each catalogue. The time-elongation profiles of these CME fronts are compared, as are the estimates of the CME kinematics derived from application of three widely used single-spacecraft-fitting techniques. The J-tracker and RAL-HI profiles are most similar, while the Solar Stormwatch profiles display a small systematic offset. Evidence is presented that these differences arise because the RAL-HI and J-tracker profiles follow the sunward edge of CME density enhancements, while Solar Stormwatch profiles track closer to the antisunward (leading) edge. We demonstrate that the method used to produce the time-elongation profile typically introduces more variability into the kinematic estimates than differences between the various single-spacecraft-fitting techniques. This has implications for the repeatability and robustness of these types of analyses, arguably especially so in the context of space weather forecasting, where it could make the results strongly dependent on the methods used by the forecaster.**14-20/12/2009, 9-17/02/2010**

Implications of Different Solar Photospheric Flux-Transport Models for Global Coronal and Heliospheric Modeling

Graham **Barnes**, Marc L. DeRosa, Shaela I. Jones, Charles N. Arge, Carl J. Henney, Mark C. M. Cheung
ApJ **2023**
https://arxiv.org/pdf/2302.06496
The concept of surface-flux transport (SFT) is commonly used in evolving models of the large-scale solar surface magnetic field. These photospheric models are used to determine the large-scale structure of the overlying coronal magnetic field, as well as to make predictions about the fields and flows that structure the solar wind. We compare predictions from two SFT models for the solar wind, open magnetic field footpoints, and the presence of coronal magnetic null points throughout various phases of a solar activity cycle, focusing on the months of April in even-numbered years between 2012 and 2020, inclusive. We find that there is a solar cycle dependence to each of the metrics considered, but there is not a single phase of the cycle in which all the metrics indicate good agreement between the models. The metrics also reveal large, transient differences between the models when a new active region is rotating into the assimilation window. The evolution of the surface flux is governed by a combination of large scale flows and comparatively small scale motions associated with convection. Because the latter flows evolve rapidly, there are intervals during which their impact on the surface flux can only be characterized in a statistical sense, thus their impact is modeled by introducing a random evolution that reproduces the typical surface flux evolution. We find that the differences between the predicted properties are dominated by differences in the model assumptions and implementation, rather than selection of a particular realization of the random evolution.

Understanding Heating in Active Region Cores through Machine Learning II. Classifying Observations

W. T. **Barnes**, S. J. Bradshaw, N. M. Viall
ApJ **919** 132 **2021**
https://arxiv.org/pdf/2107.07612.pdf
https://doi.org/10.3847/1538-4357/ac1514
Constraining the frequency of energy deposition in magnetically-closed active region cores requires sophisticated hydrodynamic simulations of the coronal plasma and detailed forward modeling of the optically-thin line-of-sight integrated emission. However, understanding which set of model inputs best matches a set of observations is complicated by the need for any proposed heating model to simultaneously satisfy multiple observable constraints. In this paper, we train a random forest classification model on a set of forward-modeled observable quantities, namely the emission measure slope, the peak temperature of the emission measure distribution, and the time lag and maximum cross-correlation between multiple pairs of AIA channels. We then use our trained model to classify the heating frequency in every pixel of active region NOAA 1158 using the observed emission measure slopes, peak temperatures, time lags, and maximum cross-correlations and are able to map the heating frequency across the entire active region. We find that high-frequency heating dominates in the inner core of the active region while intermediate frequency dominates closer to the periphery of the active region. Additionally, we assess the importance of each observed quantity in our trained classification model and find that the emission measure slope is the dominant feature in deciding with which heating frequency a given pixel is most consistent. The technique presented here offers a very promising and widely applicable method for assessing observations in terms of detailed forward models given an arbitrary number of observable constraints.

Understanding Heating in Active Region Cores through Machine Learning I. Numerical Modeling and Predicted Observables

W. T. **Barnes**, S. J. Bradshaw, N. M. Viall
ApJ **880** 56 **2019**
https://arxiv.org/pdf/1906.03350.pdf
sci-hub.se/10.3847/1538-4357/ab290c
To adequately constrain the frequency of energy deposition in active region cores in the solar corona, systematic comparisons between detailed models and observational data are needed. In this paper, we describe a pipeline for forward modeling active region emission using magnetic field extrapolations and field-aligned hydrodynamic models. We use this pipeline to predict time-dependent emission from active region NOAA 1158 as observed by SDO/AIA for low-, intermediate-, and high-frequency nanoflares. In each pixel of our predicted multi-wavelength, time-dependent images, we compute two commonly-used diagnostics: the emission measure slope and the time lag. We find that signatures of the heating frequency persist in both of these diagnostics. In particular, our results show that the distribution of emission measure slopes narrows and the mean decreases with decreasing heating frequency and that the range of emission measure slopes is consistent with past observational and modeling work. Furthermore, we find that the time lag becomes increasingly spatially coherent with decreasing heating frequency while the distribution of time lags across the whole active region becomes more broad with increasing heating frequency. In a follow up paper, we train a random forest classifier on these predicted diagnostics and use this model to classify real AIA observations of NOAA 1158 in terms of the underlying heating frequency. **12 February 2011**

The *Sunrise* Mission

P. **Barthol** · A. Gandorfer · S.K. Solanki · M. Schüssler · B. Chares · W. Curdt · W. Deutsch · A. Feller · D. Germerott · B. Grauf · K. Heerlein · J. Hirzberger · M. Kolleck · R. Meller · R. Müller · T.L. Riethmüller · G. Tomasch · M. Knölker · B.W. Lites · G. Card · D. Elmore · J. Fox · A. Lecinski · P. Nelson · R. Summers · A. Watt · V. Martínez Pillet · J.A. Bonet · W. Schmidt · T. Berkefeld · A.M. Title · V. Domingo · J.L. Gasent Blesa · J.C. del Toro Iniesta · A. López Jiménez · A. Álvarez-Herrero · L. Sabau-Graziati · C. Widani · P. Haberler · K. Härtel · D. Kampf · T. Levin · I. Pérez Grande · A. Sanz-Andrés · E. Schmidt
Solar Phys (**2011**) 268: 1–34
The first science flight of the balloon-borne *Sunrise* telescope took place in June 2009 from ESRANGE (near Kiruna/Sweden) to Somerset Island in northern Canada. We describe the scientific aims and mission concept of the project and give an overview and a description of the various hardware components: the 1-m main telescope with its postfocus science instruments (the UV filter imager SuFI and the **imaging vector magnetograph IMaX)** and support instruments (image stabilizing and light distribution system ISLiD and correlating wavefront sensor CWS), the optomechanical support structure and the instrument mounting concept, the gondola structure and the power, pointing, and telemetry systems, and the general electronics architecture. We also explain the optimization of the structural and thermal design of the complete payload. The preparations for the science flight are

described, including AIV and ground calibration of the instruments. The course of events during the science flight is outlined, up to the recovery activities. Finally, the in-flight performance of the instrumentation is discussed.

Constraints on the early luminosity history of the Sun: applications to the Faint Young Sun problem

Connor **Basinger**, Marc Pinsonneault, Sandra T Bastelberger, B Scott Gaudi, Shawn D Domagal-Goldman

MNRAS, Volume 534, Issue 3, November **2024**, Pages 2968–2985,
https://doi.org/10.1093/mnras/stae2280
https://academic.oup.com/mnras/article-pdf/534/3/2968/59811327/stae2280.pdf

Stellar evolution theory predicts that the Sun was fainter in the past, which can pose difficulties for understanding Earth's climate history. One proposed solution to this Faint Young Sun (FYS) problem is a more luminous Sun in the past. In this paper, we address the robustness of the solar luminosity history using the yrec code to compute solar models including rotation, magnetized winds, and the associated mass-loss. We present detailed solar models, including their evolutionary history, which are in excellent agreement with solar observables. Consistent with prior standard models, we infer a high solar metal content. We provide predicted X-ray luminosities and rotation histories for usage in climate reconstructions and activity studies. We find that the Sun's luminosity deviates from the standard solar model trajectory by at most 0.5 per cent during the Archean (corresponding to a radiative forcing of 0.849 W m−2). The total mass-loss experienced by solar models is modest because of strong feedback between mass and angular momentum loss. We find a maximum mass-loss of 1.35×10−3M⊙ since birth, at or below the level predicted by empirical estimates. The associated maximum luminosity increase falls well short of the level necessary to solve the FYS problem. We present compilations of paleotemperature and CO2 reconstructions. One-dimensional 'inverse' climate models demonstrate a mismatch between the solar constant needed to reach high temperatures (e.g. 60–80 ∘C) and the narrow range of plausible solar luminosities determined in this study. Maintaining a temperate Earth, however, is plausible given these conditions.

Spectral resolution effects on the information content in solar spectra

C. J. Díaz **Baso**, I. Milić, L. Rouppe van der Voort, R. Schlichenmaier

A&A **2024**

https://arxiv.org/pdf/2409.13677

When interpreting spectropolarimetric observations of the solar atmosphere, wavelength variations of the emergent intensity and polarization translate into information on the depth stratification of physical parameters. We aim to quantify how the information content contained in a representative set of polarized spectra depends on the spectral resolution and spectral sampling. We use a state-of-the-art numerical simulation of a sunspot to synthesize polarized spectra of magnetically sensitive neutral iron lines. We then apply various degrees of spectral degradation to the synthetic spectra and analyze the impact on its dimensionality using PCA and wavelet decomposition. Finally, we apply the SIR code to the degraded synthetic data, to assess the effect of spectral resolution on the inferred parameters. We find that regions with strong magnetic fields where convection is suppressed produce less complex Stokes profiles. On the other hand, regions with strong gradients give rise to more complex Stokes profiles that are more affected by spectral degradation. The degradation also makes the inversion problem more ill-defined, so inversion models with a larger number of free parameters overfit and give wrong estimates. The impact of spectral degradation depends on multiple factors, including spectral resolution, noise level, line spread function (LSF) shape, complexity of the solar atmosphere, and the degrees of freedom in our inversion methods. Having a finely sampled spectrum may be more beneficial than achieving a higher signal-to-noise ratio per wavelength bin. Considering the inclusion of different spectral lines that can counter these effects, and calibrating the effective degrees of freedom in modeling strategies, are also important considerations. These strategies are crucial for the accurate interpretation and have the potential to offer more cost-effective solutions.

An observationally-constrained 3D model of strong magnetic reconnection in the solar chromosphere. *Atmospheric stratification and estimates of heating rates*

C. J. Díaz **Baso**, J. de la Cruz Rodríguez, J. Leenaarts

A&A 647, A188 (**2021**)

https://arxiv.org/pdf/2012.06229.pdf
https://doi.org/10.1051/0004-6361/202040111
https://www.aanda.org/articles/aa/pdf/2021/03/aa40111-20.pdf

The evolution of the photospheric magnetic field plays a key role in the energy transport into the chromosphere and the corona. In active regions, newly emerging magnetic flux interacts with the pre-existent magnetic field, which can lead to reconnection events that convert magnetic energy to thermal energy. We aim to study the heating caused by a strong reconnection event that was triggered by magnetic flux cancellation. We use imaging-spectropolarimetric data in the Fe I 6301A, Fe I 6302A, Ca II 8542A and Ca II K obtained with the CRISP and

CHROMIS instruments at the Swedish 1-m Solar Telescope. This data was inverted using multi-atom, multi-line non-LTE inversions using the STiC code. The inversion yielded a three-dimensional model of the reconnection event and surrounding atmosphere, including temperature, velocity, microturbulence, magnetic file configuration, and the radiative loss rate. The model atmosphere shows the emergence of magnetic loops with a size of several arcsecs into a pre-existing predominantly unipolar field. Where the reconnection region is expected to be, we see an increase in the chromospheric temperature of roughly 2000 K as well as bidirectional flows of the order of 10 km s−1 emanating from the region. We see bright blobs of roughly 0.2 arcsec diameter in the Ca II K moving at a plane-of-the-sky velocity of order 100 km s−1 and a blueshift of 100 km s−1, which we interpret as plasmoids ejected from the same region. This evidence is consistent with theoretical models of reconnection and we thus conclude that reconnection is taking place. The chromospheric radiative losses at the reconnection site in our inferred model are as high as 160 kW m−2, providing a quantitative constraint on theoretical models that aim to simulate reconnection caused by flux emergence in the chromosphere.

Solar image denoising with convolutional neural networks

C. J. Díaz **Baso**, J. de la Cruz Rodríguez, S. Danilovic
A&A 629, A99 **2019**
https://arxiv.org/pdf/1908.02815.pdf
The topology and dynamics of the solar chromosphere are greatly affected by the presence of magnetic fields. The magnetic field can be inferred by analyzing polarimetric observations of spectral lines. Polarimetric signals induced by chromospheric magnetic fields are, however, particularly weak, and in most cases very close to the detection limit of current instrumentation. Because of this, there are only few observational studies that have successfully reconstructed the three components of the magnetic field vector in the chromosphere. Traditionally, the signal-to-noise ratio of observations has been improved by performing time-averages or spatial averages, but in both cases, some information is lost. More advanced techniques, like principal-component-analysis, have also been employed to take advantage of the sparsity of the observations in the spectral direction. In the present study, we propose to use the spatial coherence of the observations to reduce the noise using deep-learning techniques. We design a neural network that is capable of recovering weak signals under a complex noise corruption (including instrumental artifacts and non-linear post-processing). The training of the network is carried out without a priori knowledge of the clean signals, or an explicit statistical characterization of the noise or other corruption. We only use the same observations as our generative model. The performance of this method is demonstrated on both, synthetic experiments and real data. We show examples of the improvement in typical signals obtained in current telescopes such as the Swedish 1-meter Solar Telescope. The presented method can recover weak signals equally well no matter on what spectral line or spectral sampling is used. It is especially suitable for cases when the wavelength sampling is scarce.

Enhancing SDO/HMI images using deep learning

C.J. Diaz **Baso**, A. Asensio Ramos
A&A 614, A5 **2018**
https://arxiv.org/pdf/1706.02933.pdf
The Helioseismic and Magnetic Imager (HMI) provides continuum images and magnetograms with a cadence better than one every minute. It has been continuously observing the Sun 24 hours a day for the past 7 years. The obvious trade-off between cadence and spatial resolution makes that HMI is not enough to analyze the smallest-scale events in the solar atmosphere. Our aim is developing a new method to enhance HMI data, simultaneously deconvolving and superresolving images and magnetograms. The resulting images will mimick observations with a diffraction-limited telescope twice the diameter of HMI. The method, that we term Enhance, is based on two deep fully convolutional neural networks that input patches of HMI observations and output deconvolved and superresolved data. The neural networks are trained on synthetic data obtained from simulations of the emergence of solar active regions. We have obtained deconvolved and supperresolved HMI images. To solve this ill-defined problem with infinite solutions we have used a neural network approach to add prior information from the simulations. We test Enhance against Hinode data that has been degraded to a 28 cm diameter telescope showing very good consistency. The code is open sourced for the community.
HMI Science Nuggets, #103, June **2018** http://hmi.stanford.edu/hminuggets/?p=2552

Time Variation of the Solar Tachocline

Sarbani **Basu** (Dept. of Astronomy, Yale University), Wesley Antônio Machado Andrade de Aguiar (Dept. of Computer Science, Yale University), Sylvain G. Korzennik
ApJ **975** 276 **2024**
https://arxiv.org/pdf/2410.01895
https://iopscience.iop.org/article/10.3847/1538-4357/ad82e6/pdf
We have used solar oscillation frequencies and frequency splittings obtained over solar cycles 23, 24 and the rising phase of solar cycle 25 to investigate whether the tachocline properties (jump i.e., the change in the rotation rate

across the tachocline, width and position) show any time variation. We confirm that the change in rotation rate across the tachocline changes substantially, however, the change does not show a simple correlation with solar cycle unlike, for instance, changes in mode frequencies. The change during the ascending phase of solar cycle 25 is almost a mirror image of the change during the descending part of solar cycle 24, tempting us to speculate that the tachocline has a much longer period than either the sunspot or the magnetic cycle. We also find that the position of the tachocline, defined as the mid-point of the change in rotation rate, showed significant changes during solar cycle 24. The width of the tachocline, on the other hand, has showed significant changes during solar cycle 23, but not later. The change in the tachocline becomes more visible if we look at the upper and lower extents of the tachocline, defined as (position +/- width). We find that for epochs around solar maxima and minima, the extent decreases before increasing again - a few more years of data should clarify this trend. Our results reinforce the need to continue helioseismic monitoring of the Sun to understand solar activity and its evolution.

Asphericity of the base of the solar convection zone

Sarbani **Basu** (Yale), Sylvain G. Korzennik (CfA)

ApJ **2024**

https://arxiv.org/pdf/2401.12333.pdf

We have used solar oscillation frequencies and frequency splittings obtained over solar cycles 23 and 24 to investigate whether the base of the solar convection zone shows any departure from spherical symmetry. We used the even-order splitting coefficients, a2-a8, and estimated the contributions from each one separately. The average asphericity over the two solar cycles was determined using frequencies and splittings obtained with a 9216-day time-series. We find that evidence of asphericity is, {\em at best}, marginal: the a2 component is consistent with no asphericity, the a4 and a6 components yield results at a level a little greater than 1σ, while the a8 component shows a signature below 1σ. The combined results indicate that the time average of the departure from the spherically symmetric position of the base of the convection zone is $\lesssim 0.0001 R_\odot$. We have also used helioseismic data obtained from time-series of lengths 360 days, 576 days, 1152 days, and 2304 days in order to examine the consistency of the results and evaluate whether there is any time variation. We find that the evidence for time variation is statistically marginal in all cases, except for the a6 component, for which tests consistently yield p values of less than 0.05.

Evidence of solar-cycle related structural changes in the solar convection zone

Sarbani **Basu**

ApJ **917** 45 **2021**

https://arxiv.org/pdf/2106.08383.pdf

https://doi.org/10.3847/1538-4357/ac0c11

While it has been relatively easy to determine solar-cycle related changes in solar dynamics, determining changes in structure in the deeper layers of the Sun has proved to be difficult. By using helioseismic data obtained over two solar cycles, and sacrificing resolution in favour of lower uncertainties, we show that there are significant changes in the solar convection zone, and perhaps even below it. Using MDI data, we find a relative squared sound-speed difference of $(2.56\pm0.71)\times10^{-5}$ at the convection-zone base between the maximum of solar Cycle~23 and the minimum between Cycles~23 and 24. The squared sound-speed difference for the maximum of Cycle~24 obtained with HMI data is $(1.95\pm0.69)\times10^{-5}$. GONG data support these results. We also find that the sound speed in the solar convection zone decreases compared to the sound speed below it as the Sun becomes more active. We find evidence of changes in the radial derivative of the sound-speed difference between the solar minimum and other epochs at the base of the convection zone implying possible small changes in the position of the convection-zone base, however, the results are too noisy to make any definitive estimates of the change.

Changes in the solar rotation over two solar cycles

Sarbani **Basu**, H. M. Antia

ApJ **883** 93 **2019**

https://arxiv.org/pdf/1908.05282.pdf

https://doi.org/10.3847/1538-4357/ab3b57

We use helioseismic data from ground and space-based instruments to analyze how solar rotation has changed since the beginning of solar Cycle 23 with emphasis on studying the differences between Cycles 23 and 24. We find that the nature of solar rotation is indeed different for the two cycles. While the changes in the latitudinally independent component follows solar-cycle indices, some of the other components have a more complicated behavior. There is a substantial change in the behavior of the solar zonal flows and their spatial gradients too. While the zonal flows are in general weaker in Cycle 24 than those in Cycle 23, there are clear signs of the emergence of Cycle 25. We have also investigated the properties of the solar tachocline, in particular, its position, width, and the change (or jump) in the rotation rate across it. We find significant temporal variation in the change of the rotation rate across the tachocline. We also find that the changes in solar Cycle 24 were very different from those of Cycle 23. We do not find any statistically significant change in the position or the width of the tachocline.

Chapter 4 - Helioseismic Inferences on the Internal Structure and Dynamics of the Sun **Review**

Sarbani **Basu** and William J. Chaplin

In: ***The Sun as a Guide to Stellar Physics*** ***Book***

Eds. Oddbjørn Engvold, Jean-Claude Vial, and Andrew Skumanich

Elsevier , November **2018**

https://www.sciencedirect.com/book/9780128143346/the-sun-as-a-guide-to-stellar-physics

Helioseismology has made it possible to peel back the outer layers of the Sun to allow inferences to be made about its internal structure, dynamics, and solar cycle–related changes. In this chapter, we introduce helioseismic analyses, in particular inversion methods, and then discuss knowledge that has been acquired through the application of these analysis techniques to what is now an observational data archive stretching back over a few solar cycles.

Global Seismology of the Sun **Review**

Sarbani **Basu**

Living Reviews of Solar Physics December 2016, 13:2 **2016**

http://arxiv.org/pdf/1606.07071v1.pdf

https://link.springer.com/content/pdf/10.1007%2Fs41116-016-0003-4.pdf

The seismic study of the Sun and other stars offers a unique window into the interior of these stars. Thanks to helioseismology, we know the structure of the Sun to admirable precision. In fact, our knowledge is good enough to use the Sun as a laboratory. We have also been able to study the dynamics of the Sun in great detail. Helioseismic data also allow us to probe the changes that take place in the Sun as solar activity waxes and wanes. The seismic study of stars other than the Sun is a fairly new endeavour, but we are making great strides in this field. In this review I discuss some of the techniques used in helioseismic analyses and the results obtained using those techniques. In this review I focus on results obtained with global helioseismology, i.e., the study of the Sun using its normal modes of oscillation. I also briefly touch upon asteroseismology, the seismic study of stars other than the Sun, and discuss how seismic data of others stars are interpreted.

Understanding the Internal Chemical Composition and Physical Processes of the Solar Interior

Sarbani **Basu**, Nicolas Grevesse, Stephane Mathis, Sylvaine Turck-Chièze

Space Science Reviews, Volume 196, Issue 1, pp 49-77 **2015**

The Sun, the closest and most well studied of stars, is generally used as a standard that other stars are compared to. Models of the Sun are constantly tested with helioseismic data. These data allow us to probe the internal structure and dynamics of the Sun. Among the main sources of the data is the SOHO spacecraft that has been continuously observing the Sun for more than a solar cycle. Current solar models, although good, do not include all the physical processes that are present in the Sun. In this chapter we focus on specific inputs to solar models and discuss generally neglected dynamical physical processes whose inclusion could result in models that are much better representatives of the Sun.

The peculiar solar cycle 24 - where do we stand?

Basu, S.

(**2013**) JPhCS 440: 012001

THINNING OF THE SUN'S MAGNETIC LAYER: THE PECULIAR SOLAR MINIMUM COULD HAVE BEEN PREDICTED

Sarbani **Basu**1, Anne-Marie Broomhall2, William J. Chaplin2, and Yvonne Elsworth

2012 ApJ 758 43

The solar magnetic activity cycle causes changes in the Sun on timescales that are equivalent to human lifetimes. The minimum solar activity that preceded the current solar cycle (cycle 24) was deeper and quieter than any other recent minimum. Using data from the Birmingham Solar Oscillations Network (BiSON), we show that the structure of the solar sub-surface layers during the descending phase of the preceding cycle (cycle 23) was very different from that during cycle 22. This leads us to believe that a detailed examination of the data would have led to the prediction that the cycle 24 minimum would be out of the ordinary. The behavior of the oscillation frequencies allows us to infer that changes in the Sun that affected the oscillation frequencies in cycle 23 were localized mainly to layers above about 0.996 R ⊙, depths shallower than about 3000 km. In cycle 22, on the other hand, the changes must have also occurred in the deeper-lying layers.

High Frequency Waves in Chromospheric Spicules

W. **Bate**, D. B. Jess, V. M. Nakariakov, S. D. T. Grant, S. Jafarzadeh, M. Stangalini, P. H. Keys, D. J. Christian, F. P. Keenan

ApJ **2022**

https://arxiv.org/pdf/2203.04997.pdf

Using high cadence observations from the Hydrogen-alpha Rapid Dynamics camera imaging system on the Dunn Solar Telescope, we present an investigation of the statistical properties of transverse oscillations in spicules captured above the solar limb. At five equally separated atmospheric heights, spanning approximately 4900-7500 km, we have detected a total of 15 959 individual wave events, with a mean displacement amplitude of 151 +/- 124 km, a mean period of 54 +/- 45 s, and a mean projected velocity amplitude of 21 +/- 13 km s^-1. We find that both the displacement and velocity amplitudes increase with height above the solar limb, ranging from 132 +/- 111 km and 17.7 +/- 10.6 km s^-1 at 4900 km, and 168 +/- 125 km and 26.3 +/- 14.1 km s^-1 at 7500 km, respectively. Following the examination of neighboring oscillations in time and space, we find 45% of the waves to be upwardly propagating, 49% to be downwardly propagating, and 6% to be standing, with mean absolute phase velocities for the propagating waves on the order of 75-150 km s^-1. While the energy flux of the waves propagating downwards does not appear to depend on height, we find the energy flux of the upwardly propagating waves decreases with atmospheric height at a rate of -13 200 +/- 6500 W m^-2 /Mm. As a result, this decrease in energy flux as the waves propagate upwards may provide significant thermal input into the local plasma. **2015 July 27**

Hemispheric asymmetry in the sunspot cycle as a nonextensive phenomenon

Leonardo F. G. **Batista**, Thiago M. Santiago, Paulo C. F. da Silva Filho, Cleo V. Silva, Daniel B. de Freitas

Solar Phys. **298**, Article number: 84 **2022**

https://arxiv.org/pdf/2212.02928

https://doi.org/10.1007/s11207-023-02179-6

The appearance of dark sunspots over the solar photosphere is not considered to be symmetric between the northern and southern hemispheres. Among the different conclusions obtained by several authors, we can point out that the North-South asymmetry is a real and systematic phenomenon and is not due to random variability. In the present work, we selected the sunspot area data of a sample of 13 solar cycles divided by hemisphere extracted from the Marshall Space Flight Centre (MSFC) database to investigate the behavior of probability distributions using an out-of-equilibrium statistical model a.k.a non-extensive statistical mechanics. Based on this statistical framework, we obtained that the non-extensive entropic parameter q has a semi-sinusoidal variation with a period of ~22 year (Hale cycle). Among the most important results, we can highlight that the asymmetry index q(A) revealed the dominance of the northern hemisphere against the southern one. Thus, we concluded that the parameter q(A) can be considered an effective measure for diagnosing long-term variations of the solar dynamo. Finally, our study opens a new approach to investigating solar variability from the nonextensive perspective.

The Alfvénic nature of chromospheric swirls

Andrea Francesco **Battaglia**, José Roberto Canivete Cuissa, Flavio Calvo, Aleksi Antoine Bossart, Oskar Steiner

A&A 649, A121 **2021**

https://arxiv.org/pdf/2103.07366.pdf

https://www.aanda.org/articles/aa/pdf/2021/05/aa40110-20.pdf

https://doi.org/10.1051/0004-6361/202040110

We investigate the evolution and origin of small-scale chromospheric swirls by analyzing numerical simulations of the quiet solar atmosphere, using the radiative magnetohydrodynamic code CO5BOLD. We are interested in finding their relation with magnetic field perturbations and in the processes driving their evolution. For the analysis, the swirling strength criterion and its evolution equation are applied in order to identify vortical motions and to study their dynamics. We introduce a new criterion, the magnetic swirling strength, which allows us to recognize torsional perturbations in the magnetic field. We find a strong correlation between swirling strength and magnetic swirling strength, in particular in intense magnetic flux concentrations, which suggests a tight relation between vortical motions and torsional magnetic field perturbations. Furthermore, we find that swirls propagate upward with the local Alfvén speed as unidirectional swirls, in the form of pulses, driven by magnetic tension forces alone. In the photosphere and low chromosphere, the rotation of the plasma co-occurs with a twist in the upwardly directed magnetic field that is in the opposite direction of the plasma flow. All together, these are characteristics of torsional Alfvén waves. We also find indications of an imbalance between the hydrodynamic and magnetohydrodynamic baroclinic effects being at the origin of the swirls. At the base of the chromosphere, we find a net upwardly directed Poynting flux, which is mostly associated with large and complex swirling structures that we interpret as the superposition of various small-scale vortices. We conclude that the ubiquitous swirling events observed in simulations are tightly correlated with perturbations of the magnetic field. At photospheric and chromospheric levels, they form Alfvén pulses that propagate upward and may contribute to chromospheric heating.

The Solar X-Ray Limb

Marina **Battaglia**1, Hugh S. Hudson2,3, Gordon J. Hurford3, Säm Krucker1,3, and Richard A. Schwartz4
2017 ApJ 843 123
http://sci-hub.cc/10.3847/1538-4357/aa76da
We describe a new technique to measure the height of the X-ray limb with observations from occulted X-ray flare sources as observed by the RHESSI (the Reuven Ramaty High-Energy Spectroscopic Imager) satellite. This method has model dependencies different from those present in traditional observations at optical wavelengths, which depend upon detailed modeling involving radiative transfer in a medium with complicated geometry and flows. It thus provides an independent and more rigorous measurement of the "true" solar radius, which means that of the mass distribution. RHESSI's measurement makes use of the flare X-ray source's spatial Fourier components (the visibilities), which are sensitive to the presence of the sharp edge at the lower boundary of the occulted source. We have found a suitable flare event for analysis, **SOL2011-10-20T03**:25 (M1.7), and report a first result from this novel technique here. Using a four-minute integration over the 3–25 keV photon energy range, we find $R_{\text{X-ray}} = 960.11 \pm 0.15 \pm 0.29$ arcsec, at 1 au, where the uncertainties include statistical uncertainties from the method and a systematic error. The standard VAL-C model predicts a value of 959.94 arcsec, which is about 1σ below our value.

The Solar X-ray Limb III

Marina **Battaglia** and Hugh Hudson
RHESSI Science Nugget No. 302 June **2017**
http://sprg.ssl.berkeley.edu/~tohban/wiki/index.php/The_Solar_X-ray_Limb_III
RHESSI succeeds with an entirely new way to measure the solar diameter.
2011-10-20

The Solar X-ray Limb II

Marina **Battaglia** and Hugh Hudson.
RHESSI Science Nugget No. 241, Nov. **2014**
http://sprg.ssl.berkeley.edu/~tohban/wiki/index.php/The_Solar_X-ray_Limb_II
X-raying the mass distribution at the limb of the sun: the true solar radius.

The LASCO Coronal Brightness Index

Karl **Battams**, Russell A. Howard, Hillary A. Dennison, Robert S. Weigel & Judith L. Lean
Solar Physics volume 295, Article number: 20 (**2020**)
https://link.springer.com/content/pdf/10.1007/s11207-020-1589-1.pdf
We present the construction of a new white-light coronal brightness index (CBI) from the entire archive of observations recorded by the Large Angle Spectrometric Coronagraph (LASCO) C2 camera between 1996 and 2017, comprising two full solar cycles. We reduce all fully calibrated daily C2 observations of the white-light corona into a single daily coronal brightness observation for every day of observation recorded by the instrument, with mean daily brightness values binned into 0.1 R⊙ radial ×1×1 degree angular regions from 2.4 – 6.2 R⊙ for a full 360 degrees. As a demonstration of the utility of the CBI, we construct a new solar irradiance proxy that correlates well with a variety of direct solar irradiance observations, with correlations shown to be in the range of 0.77 – 0.89. We also present a correlation mapping technique to show how irradiance correlations depend on, and relate to, coronal structure/locations, and to demonstrate how the LASCO CBI can be used to perform long-term "spatial correlation" studies to investigate relationships between the solar corona and any arbitrary concurrent geophysical index. Using this technique we find possible relationships between coronal brightness and plasma temperature, interplanetary magnetic field magnitude and (very weakly) proton density.

A Global Survey of EUV Corona Power Spectra

Karl **Battams** (1), Brendan M. Gallagher (2), Robert S. Weigel (2) ((1) US Naval Research Laboratory, (2) George Mason University)
Solar Phys. 294 11 **2019**
https://arxiv.org/pdf/1707.02448.pdf
https://link.springer.com/content/pdf/10.1007%2Fs11207-019-1399-5.pdf
We present results of a global survey of single-pixel intensity power spectra from a 12-hour time period on **June 26, 2013** in a 1600x1600 pixel region from five channels of the Solar Dynamics Observatory (SDO) Atmospheric Imaging Assembly (AIA) instrument. We extract single-pixel time series from a derotated image sequence, fit models to the power spectra of these time series, and study the spatial dependence of the model parameters. Two

power spectra models are considered: (1) a 3-parameter power-law + tail model and (2) a power-law + tail model + 3-parameter localized Gaussian, which models a periodicity. In general, spectra are well-described by at least one of these two models for all pixel locations, with an average data/model correlation of 0.93 and a standard deviation of 0.1. The spatial distribution of best-fit parameter values for the models are shown to provide new and unique insights into turbulent, quiescent and periodic features in the EUV solar corona and upper photosphere. Locations where the second model is significantly better than the first model correspond clearly and directly to different visible features in the AIA observations and reveal quasi-periodic 3- and 5-minute oscillations. Other findings include: a method for parameterizing solar EUV observations at pixel-level resolution based on their power spectra; observational identification of concentrated magnetic flux as regions of largest power-law indices; identification of unique spectral features of coronal holes and filaments; identification of sporadic and pervasive 5-minute oscillations throughout the EUV solar corona; a global ~4.0-minute oscillation in 1600A; "Coronal Bullseyes" appearing as radially decaying periodicities over sunspot and sporadic foot-point regions; and "Penumbral Periodic Voids" around sunspots in 1600 and 1700A in which there is no statistically significant Gaussian component.
RHESSI Nuggets #367 December, **2019**
http://sprg.ssl.berkeley.edu/~tohban/wiki/index.php/A_Global_Survey_of_EUV_Coronal_Power_Spectra

An unsupervised machine learning based algorithm for detecting Weak Impulsive Narrowband Quiet Sun Emissions and characterizing their morphology

Shabbir **Bawaji**, Ujjaini Alam, Surajit Mondal, Divya Oberoi, Ayan Biswas
ApJ **2023**
https://arxiv.org/pdf/2306.15104.pdf
The solar corona is extremely dynamic. Every leap in observational capabilities has been accompanied by unexpected revelations of complex dynamic processes. The ever more sensitive instruments now allow us to probe events with increasingly weaker energetics. A recent leap in the low-frequency radio solar imaging ability has led to the discovery of a new class of emissions, namely Weak Impulsive Narrowband Quiet Sun Emissions \citep[WINQSEs;][]{mondal2020}. They are hypothesized to be the radio signatures of coronal nanoflares and could potentially have a bearing on the long standing coronal heating problem. In view of the significance of this discovery, this work has been followed up by multiple independent studies. These include detecting WINQSEs in multiple datasets, using independent detection techniques and software pipelines, and looking for their counterparts at other wavelengths. This work focuses on investigating morphological properties of WINQSEs and also improves upon the methodology used for detecting WINQSEs in earlier works. We present a machine learning based algorithm to detect WINQSEs, classify them based on their morphology and model the isolated ones using 2D Gaussians. We subject multiple datasets to this algorithm to test its veracity. Interestingly, despite the expectations of their arising from intrinsically compact sources, WINQSEs tend to be resolved in our observations. We propose that this angular broadening arises due to coronal scattering. WINQSEs can, hence, provide ubiquitous and ever-present diagnostic of coronal scattering (and, in turn, coronal turbulence) in the quiet sun regions, which has not been possible till date.

Exploring Coronal Heating Using Unsupervised Machine-Learning

Shabbir **Bawaji**, Ujjaini Alam, Surajit Mondal, Divya Oberoi
ADASS 2020 proceedings **2021**
https://arxiv.org/pdf/2103.05371.pdf
The perplexing mystery of what maintains the solar coronal temperature at about a million K, while the visible disc of the Sun is only at 5800 K, has been a long standing problem in solar physics. A recent study by Mondal(2020) has provided the first evidence for the presence of numerous ubiquitous impulsive emissions at low radio frequencies from the quiet sun regions, which could hold the key to solving this mystery. These features occur at rates of about five hundred events per minute, and their strength is only a few percent of the background steady emission. One of the next steps for exploring the feasibility of this resolution to the coronal heating problem is to understand the morphology of these emissions. To meet this objective we have developed a technique based on an unsupervised machine learning approach for characterising the morphology of these impulsive emissions. Here we present the results of application of this technique to over 8000 images spanning 70 minutes of data in which about 34,500 features could robustly be characterised as 2D elliptical Gaussians.

Fizeau Mask Interferometry of Solar Features Using the Multi-application Solar Telescope at the Udaipur Solar Observatory

A. Raja **Bayanna**, P. Venkatakrishnan, Sridharan Rengaswamy, Shibu K. Mathew
Solar Physics volume 295, Article number: 31 (**2020**)
https://link.springer.com/content/pdf/10.1007%2Fs11207-020-1597-1.pdf
The ideal optical system can realize point-to-point imaging, but for an actual observation it is difficult to achieve this ideal phenomenon due to the instrumental effects of imaging system, which is usually described as the instrument profile in the imaging process of a grating spectrometer. The existence of the spectrometer instrument

profiles introduces systematic errors in the observed spectral lines, which make the spectrum of the studied objects degenerate and blur. In this paper, we take the spectral data in the HαHα band observed by the Multi-Band Spectrometer (MBS) of the New Vacuum Solar Telescope (NVST) as an example; according to the characteristics of its acquired spectral data, we calculate the instrument profiles of the MBS in the spatial and the dispersion direction. The results are, respectively, 0.25″0.25″ and 115 mÅ, which might reflect the influence of the MBS optical instruments at that time in the HαHα band. Then the spectral data is deconvolved separately in the two directions by the corresponding IP to obtain the higher spatial and spectral resolution of the NVST spectral data.

Stratospheric Measurements of Magnetospheric Electron Precipitation and Interplanetary Medium Conditions in Solar Activity Cycles 22–24

G. A. **Bazilevskaya**, M. S. Kalinin, M. B. Krainev, V. S. Makhmutov, A. R. Novakova, A. K. Svirzhevskaya, N. S. Svirzhevsky, Yu. I. Stozhkov, B. B. Gvozdevsky
Solar System Research May **2018**, Volume 52, Issue 3, pp 189–194
Astronomicheskii Vestnik, **2018**, Vol. 52, No. 3, pp. 195–200.
http://sci-hub.tw/http://link.springer.com/10.1134/S0038094618030024
High-energy electrons precipitate into the atmosphere under the influence of disturbances of the interplanetary medium on the magnetosphere. Electrons captured from interplanetary space interact in the magnetosphere with waves, resulting in both acceleration and electron energy loss. Some high-energy electrons precipitate into the atmosphere where they generate bremsstrahlung X-rays, which can penetrate deep into the atmosphere to heights of the order of 20 km. The current 11-year cycle is characterized by weak solar activity and a small number of precipitations. The paper discusses the correlation between the parameters of the interplanetary medium and the magnetosphere with the number of precipitations recorded from 1987 to the present during regular measurements of ionizing radiation in the atmosphere in the Murmansk region.

Correlation of the quasi-biennial oscillations in galactic cosmic rays and in the solar activity indices

Bazilevskaya, G. A.; Kalinin, M. S.; Krainev, M. B.; Makhmutov, V. S.; Stozhkov, Y. I.; Svirzhevskaya, A. K.; Svirzhevsky, N. S.
Journal of Physics: Conference Series, Volume 632, Issue 1, article id. 012050 (**2015**).
http://iopscience.iop.org/article/10.1088/1742-6596/632/1/012050/pdf
Quasi-biennial oscillation (QBO) is a well-known variation in solar activity, interplanetary parameters, geomagnetic disturbances and cosmic rays. Solar QBO is translated to the space via open magnetic flux and modulates intensity of cosmic rays. The highest negative correlation exists in the QBO of cosmic rays with QBO in the heliospheric magnetic field strength B as well as with QBO in the scalar product BV, where V is the solar wind velocity, cosmic ray being delayed by ≈ 1 month. During ≈ 50 years of cosmic ray monitoring the QBO periods demonstrated some intermittency. It is argued that the Gnevyshev Gap effect and the step-like changes in the cosmic ray intensity appeared to be a part of QBO in cosmic rays.

Temporal and energy behavior of cosmic ray fluxes in the periods of low solar activity

G. A. **Bazilevskaya**, M. S. Kalinin, M. B. Krainev, V. S. Makhmutov, A. K. Svirzhevskaya, N. S. Svirzhevsky
33-rd International Cosmic Ray Conference, Rio-de-Janeiro, Brasil, 2013
2014
http://arxiv.org/pdf/1411.7534v1.pdf
Modulation of galactic cosmic ray intensity is governed by several mechanisms including diffusion, convection, adiabatic energy losses and drift. Relative roles of these factors change in the course of an 11-year solar cycle. That can result in the changes in the energy dependence of the 11-year cosmic ray modulation. The minimum between the solar cycles 23 and 24 was extremely deep and long-lasting which led to the record high cosmic ray fluxes low-energy particles dominating. This was a signature of unusually soft energy spectrum of the cosmic rays. In this work we examine the energy dependence of the 11-year modulation during the last three solar cycles and argue that a soft energy spectrum was observed in the minimum of each cycle however only for particles below of energy around 10 GeV. From mid 1980s the energy dependence of cosmic rays became softer from minimum to minimum of solar activity. The work is based on the cosmic ray data of the spacecraft, balloon-borne and the ground-based observations.

Solar Cycle in the Heliosphere and Cosmic Rays **Review**

Galina A. **Bazilevskaya**, Edward W. Cliver, Gennady A. Kovaltsov, Alan G. Ling, M. A. Shea, D. F. Smart, Ilya G. Usoskin
Space Science Reviews, December **2014**, Volume 186, Issue 1-4, pp 409-435

Manifestations of the 11-year solar cycle and longer time-scale variability in the heliosphere and cosmic rays are considered. We briefly review the cyclic variability of such heliospheric parameters as solar wind speed and density and heliospheric magnetic field, open magnetic flux and latitude variations of the heliospheric current sheet. It is discussed whether the local in-situ observation near Earth can represent the global 3D heliospheric pattern. Variability of cosmic rays near Earth provides an indirect useful tool to study the heliosphere. We discuss details of the heliospheric modulation of galactic cosmic rays, as recorded at and near Earth, and their relation to the heliospheric conditions in the outer heliosphere. On the other hand, solar energetic particles can serve as probes for explosive phenomena on the Sun and conditions in the corona and inner heliosphere. The occurrence of major solar proton events depicts an overall tendency to follow the solar cycle but individual events may appear at different phases of the solar cycle, as defined by various factors. The solar cycle in the heliosphere and cosmic rays depicts a complex pattern which includes different processes and cannot be described by a simple correlation with sunspot number.

A Combined Analysis of the Observational Aspects of the Quasi-biennial Oscillation in Solar Magnetic Activity **Review**

G. **Bazilevskaya**, A.-M. Broomhall, Y. Elsworth, V. M. Nakariakov
E-print, Nov **2014**,
Space Science Reviews, Volume 186, Issue 1-4, pp 359-386, Dec **2014**
Solar quasi-biennial oscillations (QBOs) with the time scale of 0.6–4 yrs appear to be a basic feature of the Sun's activity. Observational aspects of QBOs are reviewed on the basis of recent publications. Solar QBOs are shown to be ubiquitous and very variable. We demonstrate that many features of QBOs are common to different observations. These features include variable periodicity and intermittence with signs of stochastisity, a presence at all levels of the solar atmosphere and even in the convective zone, independent development in the northern and southern solar hemispheres, most pronounced amplitudes during the maximum phase of the 11-yr cycle and the transition of QBOs into interplanetary space. Temporal weakening of solar activity around the maximum of the 11-yr cycle (Gnevyshev Gap) can be considered an integral part of QBOs. The exact mechanism by which the solar QBO is produced is poorly understood. We describe some of the most plausible theoretical mechanisms and discuss observational features that support/contradict the theory. QBOs have an important meaning as a benchmark of solar activity, not only for investigation of the solar dynamo but also in terms of space weather.

Differential Rotation in Solar-like Convective Envelopes: Influence of Overshoot and Magnetism

Patrice **Beaudoin**1, Antoine Strugarek2, and Paul Charbonneau1
2018 ApJ 859 61
We present a set of four global Eulerian/semi-Lagrangian fluid solver (EULAG) hydrodynamical (HD) and magnetohydrodynamical (MHD) simulations of solar convection, two of which are restricted to the nominal convection zone, and the other two include an underlying stably stratified fluid layer. While all four simulations generate reasonably solar-like latitudinal differential rotation profiles where the equatorial region rotates faster than the polar regions, the rotational isocontours vary significantly among them. In particular, the purely HD simulation with a stable layer alone can break the Taylor–Proudman theorem and produce approximately radially oriented rotational isocontours at medium to high latitudes. We trace this effect to the buildup of a significant latitudinal temperature gradient in the stable fluid immediately beneath the convection zone, which imprints itself on the lower convection zone. It develops naturally in our simulations as a consequence of convective overshoot and rotational influence of rotation on convective energy fluxes. This favors the establishment of a thermal wind balance that allows evading the Taylor–Proudman constraint. A much smaller latitudinal temperature gradient develops in the companion MHD simulation that includes a stable fluid layer, reflecting the tapering of deep convective overshoot that occurs at medium to high latitudes, which is caused by the strong magnetic fields that accumulate across the base of the convection zone. The stable fluid layer also has a profound impact on the large-scale magnetic cycles developing in the two MHD simulations. Even though both simulations operate in the same convective parameter regime, the simulation that includes a stable layer eventually loses cyclicity and transits to a non-solar, steady quadrupolar state.

Center-to-limb Variation of the Inverse Evershed Flow

C. **Beck**1, D. P. Choudhary2, and M. Ranganathan2
2020 ApJ 902 30
https://doi.org/10.3847/1538-4357/abb3bf
We present the properties of the inverse Evershed flow (IEF) based on the center-to-limb variation of the plasma speed and loop geometry of chromospheric superpenumbral fibrils in eleven sunspots that were located at a wide range of heliocentric angles from 12° to 79°. The observations were acquired at the Dunn Solar Telescope in the spectral line of Hα at 656 nm to determine chromospheric flows and the photospheric Si i line at 1082.7 nm to

estimate the photospheric umbral magnetic field strength. All sunspots display opposite line-of-sight (LOS) velocities on the limb and center side with a distinct shock signature near the outer penumbral edge. We developed a simplified flexible sunspot model assuming axisymmetry and prescribing the radial flow speed profile at a known loop geometry to replicate the observed two-dimensional IEF patterns under different viewing angles. The simulated flow maps match the observations for chromospheric loops with 10–20 Mm length starting at 0.8–1.1 sunspot radii, an apex height of 1–3 Mm, and a flow speed of 2–9 km s−1. We find on average a good agreement of the simulated velocities and the observations on elliptical annuli around the sunspot. Individual IEF channels show a significant range of variation in their properties and reach maximal LOS speeds of up to 12 km s−1. Upwards or downwards directed flows do not show a change of sign in the LOS velocities for heliocentric angles above 30°.

Fast Inversion of Solar Ca II Spectra in Non-Local Thermodynamic Equilibrium

C. **Beck**, S. Gosain, C. Kiessner
ApJ **878** 60 **2019**
https://arxiv.org/pdf/1904.11843.pdf
Present day solar imaging spectrometers typically yield a few hundred million spectra in one hour of observing time. This number will increase by an order of magnitude for future instruments with larger 4k x 4k sensors as planned to be used for the upcoming DKIST solar telescope. A fast quantitative analysis of such huge data volumes can be done by comparing the observations to an archive of pre-calculated synthetic spectra to infer the thermodynamic properties of the atmosphere. To analyze intensity spectra of the Ca II IR line at 854 nm in the solar atmosphere, we generated an archive with 2,000,000 spectra under the assumption of non-local thermodynamic equilibrium (NLTE) with the NICOLE code (Socas-Navarro et al, 2015). We tested its performance by inverting 60 spectral scans of Ca II IR at 854 nm in the magnetically quiet Sun with 700,000 profiles each. Based on the inversion results obtained using the full archive, we construct a smaller archive by keeping only the about 70,000 archive profiles that were actually used. We can reproduce the observed intensity spectra to within a few percent using either the full or the small archive. For spectra with 30 wavelength points, this NLTE inversion approach takes 0.02 (0.35) s per profile to obtain a temperature stratification when using the small (full) archive, i.e., it can invert a single spectral scan in about 4 (68) hrs. The code is able to simultaneously deal with an arbitrary number of spectral lines. This makes it a promising tool for deriving thermodynamic properties of the solar atmosphere from current or future solar high-resolution observations of photospheric and chromospheric lines. **September 18, 2015**

High-resolution Observations of Halpha Spectra with a Subtractive Double Pass

C. **Beck**, R. Rezaei, D. Prasad Choudhary, S. Gosain, A. Tritschler, R.E. Louis
Solar Phys. 293:36 **2018**
https://arxiv.org/pdf/1712.07077.pdf
High-resolution imaging spectroscopy in solar physics has relied on Fabry-Perot Interferometers (FPIs) in recent years. FPI systems, however, get technically challenging and expensive for telescopes larger than the 1-m class. A conventional slit spectrograph with a diffraction-limited performance over a large field of view (FOV) can be built at much lower cost and effort. It can be converted to an imaging spectro(polari)meter using the concept of a subtractive double pass (SDP). We demonstrate that an SDP system can reach a similar performance as FPI-based systems with a high spatial and moderate spectral resolution across a FOV of 100"x100" with a spectral coverage of 1 nm. We use Halpha spectra taken with a SDP system at the Dunn Solar Telescope and complementary full-disc data to infer the properties of small-scale superpenumbral filaments. We find that the majority of all filaments end in patches of opposite-polarity fields. The internal fine-structure in the line-core intensity of Halpha at spatial scales of about 0.5" exceeds that in other parameters such as the line width, indicating small-scale opacity effects in a larger-scale structure with common properties. We conclude that SDP systems are a valid alternative to FPI systems when high spatial resolution and a large FOV are required. They also can reach a cadence that is comparable to that of FPI systems, while providing a much larger spectral range. **13 July 2015**

The Polarization Signature of Photospheric Magnetic Fields in 3D MHD Simulations and Observations at Disk Center

C. **Beck**1, D. Fabbian2, R. Rezaei3,4, and K. G. Puschmann
2017 ApJ 842 37
http://sci-hub.cc/10.3847/1538-4357/aa7466
Before using three-dimensional (3D) magnetohydrodynamical (MHD) simulations of the solar photosphere in the determination of elemental abundances, one has to ensure that the correct amount of magnetic flux is present in the simulations. The presence of magnetic flux modifies the thermal structure of the solar photosphere, which affects abundance determinations and the solar spectral irradiance. The amount of magnetic flux in the solar photosphere also constrains any possible heating in the outer solar atmosphere through magnetic reconnection. We compare the polarization signals in disk-center observations of the solar photosphere in quiet-Sun regions with those in Stokes spectra computed on the basis of 3D MHD simulations having average magnetic flux densities of about 20, 56, 112,

and 224 G. This approach allows us to find the simulation run that best matches the observations. The observations were taken with the Hinode SpectroPolarimeter (SP), the Tenerife Infrared Polarimeter (TIP), the Polarimetric Littrow Spectrograph (POLIS), and the GREGOR Fabry–Pèrot Interferometer (GFPI), respectively. We determine characteristic quantities of full Stokes profiles in a few photospheric spectral lines in the visible (630 nm) and near-infrared (1083 and 1565 nm). We find that the appearance of abnormal granulation in intensity maps of degraded simulations can be traced back to an initially regular granulation pattern with numerous bright points in the intergranular lanes before the spatial degradation. The linear polarization signals in the simulations are almost exclusively related to canopies of strong magnetic flux concentrations and not to transient events of magnetic flux emergence. We find that the average vertical magnetic flux density in the simulation should be less than 50 G to reproduce the observed polarization signals in the quiet-Sun internetwork. A value of about 35 G gives the best match across the SP, TIP, POLIS, and GFPI observations.

Spectroscopy at the solar limb: II. Are spicules heated to coronal temperatures ?

C. **Beck**, R. Rezaei, K.G. Puschmann, D. Fabbian
Solar Phys. **2016**
http://arxiv.org/pdf/1606.06132v1.pdf
Spicules of the so-called type II were suggested to be relevant for coronal heating because of their ubiquity on the solar surface and their eventual extension into the corona. We investigate whether solar spicules are heated to transition-region or coronal temperatures and reach coronal heights (>6 Mm) using multi-wavelength observations of limb spicules in different chromospheric spectral lines (Ca II H, Hepsilon, Halpha, Ca II IR at 854.2 nm, He I at 1083 nm). We determine the line width of individual spicules and throughout the field of view and estimate the maximal height that different types of off-limb features reach. We derive estimates of the kinetic temperature and the non-thermal velocity from the line width of spectral lines from different chemical elements. We find that most regular spicules reach a maximal height of about 6 Mm above the solar limb. The majority of features found at larger heights are irregularly shaped with a significantly larger lateral extension than spicules. Both individual and average line profiles in all spectral lines show a decrease in their line width with height above the limb with very few exceptions. Both the kinetic temperature and the non-thermal velocity decrease with height above the limb. We find no indications that the spicules in our data reach coronal heights or transition-region or coronal temperatures.

Fast inversion of solar Ca II spectra

C. **Beck**, D. Prasad Choudhary, R. Rezaei, R.E. Louis
ApJ **798** 100 **2014**
http://arxiv.org/pdf/1410.8451v1.pdf
We present a fast (<< 1 s per profile) inversion code for solar Ca II lines. The code uses an archive of spectra that are synthesized prior to the inversion under the assumption of local thermodynamic equilibrium (LTE). We show that it can be successfully applied to spectrograph data or more sparsely sampled spectra from two-dimensional spectrometers. From a comparison to a non-LTE inversion of the same set of spectra, we derive a first-order non-LTE correction to the temperature stratifications derived in the LTE approach. The correction factor is close to unity up to log tau ~ -3 and increases to values of 2.5 and 4 at log tau = -6 in the quiet Sun and the umbra, respectively.

Evidence for solar forcing: Some selected aspects

J. **Beer** and K. McCracken
Climate and Weather of the Sun-Earth System (CAWSES): Selected Papers from the 2007 Kyoto Symposium,
Edited by T. Tsuda, R. Fujii, K. Shibata, and M. A. Geller, pp. 201-216.

[Full text] (PDF 698 KB)

Space Weather as a Hybrid of Basic Research and Applied Science

Richard A. **Behnke**
SPACE WEATHER, VOL. 6, S09007, doi:10.1029/2008SW000423, 2008
http://www.agu.org/pubs/crossref/2008/2008SW000423.shtml
In 1994, when the National Space Weather Program was being conceived, a small group agreed on what is often thought of as the definition of space weather: "'Space weather' refers to conditions on the sun and in the solar wind, magnetosphere, ionosphere, and thermosphere that can influence the performance and reliability of space-borne and ground-based technological systems and can endanger human life or health. Adverse conditions in the space environment can cause disruption of satellite operations, communications, navigation, and electric power

distribution grids, leading to a variety of socioeconomic losses" (The National Space Weather Program Strategic Plan, *FCM-P30-1995*, p. 1, Washington, D. C., August 1995).

High-resolution Laboratory Measurements of Coronal Lines near the Fe ix Line at 171 Å

Peter **Beiersdorfer** and Elmar Träbert
2018 ApJ 854 114
http://sci-hub.tw/http://iopscience.iop.org/0004-637X/854/2/114/
We present high-resolution laboratory measurements in the spectral region between 165 and 175 Å that focus on the emission from various ions of C, O, F, Ne, S, Ar, Fe, and Ni. This wavelength region is centered on the λ171 Fe ix channel of the Atmospheric Imaging Assembly on the Solar Dynamics Observatory, and we place special emphasis on the weaker emission lines of Fe ix predicted in this region. In general, our measurements show a multitude of weak lines missing in the current databases, where the emission lines of Ni are probably most in need of further identification and reclassification. We also find that the wavelengths of some of the known lines need updating. Using the multi-reference Møller–Plesset method for wavelength predictions and collisional-radiative modeling of the line intensities, we have made tentative assignments of more than a dozen lines to the spectrum of Fe ix, some of which have formerly been identified as Fe vii, Fe xiv, or Fe xvi lines. Several Fe features remain unassigned, although they appear to be either Fe vii or Fe x lines. Further work will be needed to complete and correct the spectral line lists in this wavelength region.

Numerical study of non-toroidal inertial modes with l=m+1 radial vorticity in the Sun's convection zone

Yuto **Bekki**
A&A **2023**
https://arxiv.org/pdf/2311.10414.pdf
Various types of inertial modes have been observed and identified on the Sun, including the equatorial Rossby modes, critical-latitude modes, and high-latitude modes. Recent observations further report a detection of equatorially-antisymmetric radial vorticity modes which propagate in a retrograde direction about three times faster than those of the equatorial Rossby modes when seen in the corotating frame with the Sun. Here, we study the properties of these equatorially-antisymmetric vorticity modes using a realistic linear model of the Sun's convection zone. We find that they are essentially non-toroidal, involving a substantial radial flow at the equator. Thus, the background density stratification plays a critical role in determining their dispersion relation. The solar differential rotation is also found to have a significant impact by introducing the viscous critical layers and confining the modes near the base of the convection zone. Furthermore, we find that their propagation frequencies are strikingly sensitive to the background superadiabaticity δ because the buoyancy force acts as an additional restoring force for these non-toroidal modes. The observed frequencies are compatible with the linear model only when the bulk of the convection zone is weakly subadiabatic ($-5\times10^{-7} \lesssim \delta \lesssim -2.5\times10^{-7}$). Our result is consistent with but tighter than the constraint independently derived in a previous study ($\delta < 2\times10^{-7}$) employing the high-latitude inertial mode. It is implied that, below the strongly superadiabatic near-surface layer, the bulk of the Sun's convection zone might be much closer to adiabatic than typically assumed and may even be weakly subadiabatic.

Theory of solar oscillations in the inertial frequency range: Amplitudes of equatorial modes from a nonlinear rotating convection simulation

Yuto **Bekki**, Robert H. Cameron, Laurent Gizon
A&A 666, A135 **2022**
https://arxiv.org/pdf/2208.11081
https://www.aanda.org/articles/aa/pdf/2022/10/aa44150-22.pdf
Several types of inertial modes have been detected on the Sun. Properties of these inertial modes have been studied in the linear regime but have not been studied in nonlinear simulations of solar rotating convection. Comparing the nonlinear simulations, the linear theory, and the solar observations is important to better understand the differences between the models and the real Sun. We wish to detect and characterize the modes present in a nonlinear numerical simulation of solar convection, in particular to understand the amplitudes and lifetimes of the modes. We developed a code with a Yin-Yang grid to carry out fully-nonlinear numerical simulations of rotating convection in a spherical shell. The stratification is solar-like up to 0.96R. The simulations cover a duration of about 15 solar years. Various large-scale modes at low frequencies are extracted from the simulation. Their characteristics are compared to those from the linear model and to the observations. Among other modes, both the equatorial Rossby modes and the columnar convective modes are seen in the simulation. The columnar convective modes contain most of the large-scale velocity power outside the tangential cylinder and substantially contribute to the heat and angular momentum transport. Equatorial Rossby modes with no radial node (n=0) are also found: They have the same spatial structures as the linear eigenfunctions. They are stochastically excited by convection and have the amplitudes of a few m/s and mode linewidths of about 20-30 nHz, which are comparable to those observed on the Sun. We also confirm the existence of the mixed modes between the equatorial Rossby modes and the columnar convective modes in our

nonlinear simulation, as predicted by the linear eigenmode analysis. We also see the high-latitude mode with m=1 in our nonlinear simulation but its amplitude is much weaker than that observed on the Sun.

Double-Cell Type Solar Meridional Circulation Based on Mean-Field Hydrodynamic Model

Yuto **Bekki**, Takaaki Yokoyama
2017 ApJ 835 9
https://arxiv.org/pdf/1612.00174v1.pdf
The main object of the paper is to present the condition of the non-diffusive part of the Reynolds stress for driving the double-cell structure of the solar meridional circulation, which has been revealed by recent helioseismic observations. By conducting a set of mean-field hydrodynamic simulations, we confirm for the first time that the double-cell meridional circulation can be achieved along with the solar-like differential rotation when the Reynolds stress transports the angular momentum upward in the lower part and downward in the upper part of the convection zone. It is concluded that, in a stationary state, the accumulated angular momentum via the Reynolds stress in the middle layer is advected to both the upper and lower parts of the convection zone by each of the two meridional circulation cells, respectively.

Records of Auroras in Arabic Historical Sources: Additional List and Preliminary Analysis

Mohamed Reda **Bekli**, Ilhem Chadou
Solar Physics January **2020**, 295:3
https://doi.org/10.1007/s11207-019-1567-7
Few studies have collected and analyzed the astronomical events recorded in Arabic literature. In this paper, we present some additional events reported in four Arabic historical sources that could be classified as an aurora. These observations occurred from 9th to 20th century and cover a large geographic area: North Africa, Arabian-Peninsula and Middle-East. Some of them were observed at very low geomagnetic latitude, such as the event seen in Yemen in AD 1919 that can be considered as one of the lowest latitude auroras ever documented by Arabic scholars. In the same Yemenite source, the author describes a twilight phenomenon of 1883 October 03–November 01 which can be considered as an atmospheric-optical phenomenon arising from the major explosive eruptions of Krakatoa in 1883 August 26–27. We also noticed that one of the events which was seen for 7 days coincide probably with the prolonged manifestation of auroras of **1870 September 24–25**.
Including published records, we compiled a so far most complete catalog of potential auroral candidates in the Arabic sources. This data set can be used in order to study the solar activity variations and magnetic storms in the historical past. One of the interesting auroras was seen in Mecca (∼17∘∼17∘ MLAT) in **1872 February 04**. This event is further evidence for the equatorward extension of auroral display and the planetary consequences of the great geomagnetic storm of 1872. Finally, it should be underlined that no aurora observations were recorded during the Maunder minimum (MM).

Analysis of pre-telescopic sunspots and auroras from 8th to 16th century

Mohamed Reda **Bekli**, Ilhem Chadou
Advances in Space Research Volume 64, Issue 4, 15 August **2019**, Pages 1011-1018
sci-hub.se/10.1016/j.asr.2019.05.024
In this paper, we use non-parametric kernel approach to estimate the probability density function (pdf) of auroral-night and naked-eye-sunspot series over multi-century timescale. We selected the events observed in medieval epoch, and auroral records from low geographical latitude (<45°). These astronomical phenomena are recorded mainly in the Oriental historical sources and much less in Occidental sources. The collected events are published in many recent catalogues. The density function are calculated using the Gaussian kernel, including 95% CI obtained by bootstrapping.
Results confirm the existence of strong connection between auroras and sunspot activity, especially from 11th to 16th century. Indeed, a high correlation degree $r = 0.72$ is obtained for the period AD 800–1500 between the two pdf of sunspots (pdfS) and auroras (pdfA) for bandwidth $h = 10$ years, and exceed 0.8 for $h > 43$ years. However, we notice a time-shift between the two density functions. To calculate it, we use the cross-correlation technique, and we find $\tau = -5.9$ years, that is strangely close to the half of solar cycle period. It is very important to note that our results revealed that the high frequency of low latitude auroras occurs before the maximum of naked-eye sunspots activity, and not afterward, on contrary to what is expected.
The pdf curves show multiple peaks occurring at quasi-periodic times and show clearly the three grand minima of solar activity: Oort, Wolf and Spörer. In auroral-night data, the mean period at 95% CI obtained is: $\bar{T} = 61 \pm 7$ years. Using power spectrum analysis, we observe clearly a strong signal of 60 years period that is a new evidence of the existence of such cycle. More importantly, we identified a cycle of 262 years period in the sunspot data, and a new oscillation of 310 years in auroral-night data. These two cycles appear clearly in the pdf curves using optimized bandwidth obtained by the direct plug-in approach of Sheather and Jones.

Variation in solar differential rotation and activity in the period 1964–2016 determined by the Kanzelhöhe data set

I. Poljančić **Beljan**1, R. Jurdana-Šepić1, T. Jurkić1, R. Brajša2, I. Skokić2, D. Sudar2, D. Ruždjak2, D. Hržina3, W. Pötzi4, A. Hanslmeier5 and A. M. Veronig4,5

A&A 663, A24 (**2022**)
https://www.aanda.org/articles/aa/pdf/2022/07/aa40509-21.pdf
https://doi.org/10.1051/0004-6361/202140509

Aims. Theoretical calculations predict an increased equatorial rotation and more pronounced differential rotation (DR) during the minimum of solar magnetic activity. However, the results of observational studies vary, some showing less and some more pronounced DR during the minimum of solar magnetic activity. Our study aims to gain more insight into these discrepancies.
Methods. We determined the DR parameters A and B (corresponding to the equatorial rotation velocity and the gradient of the solar DR, respectively) by tracing sunspot groups in sunspot drawings of the Kanzelhöhe Observatory for Solar and Environmental Research (KSO; 1964–2008, for solar cycles 20–23) and KSO white-light images (2009–2016, for solar cycle 24). We used different statistical methods and approaches to analyse variations in DR parameters related to the cycle and to the phase of the solar cycle, together with long-term related variations.
Results. The comparison of the DR parameters for individual cycles obtained from the KSO and from other sources yield statistically insignificant differences for the years after 1980, meaning that the KSO sunspot group data set is well suited for long-term cycle to cycle studies. The DR parameters A and B show statistically significant periodic variability. The periodicity corresponds to the solar cycle and is correlated with the solar activity. The changes in A related to solar cycle phase are in accordance with previously reported theoretical and experimental results (higher A during solar minimum, lower A during the maximum of activity), while changes in B differ from the theoretical predictions as we observe more negative values of B, that is, a more pronounced differential rotation during activity maximum. The main result of this paper for the long-term variations in A is the detection of a phase shift between the activity flip (in the 1970s) and the equatorial rotation velocity flip (in the early 1990s), during which both A and activity show a secular decreasing trend. This indicates that the two quantities are correlated in between 1970 and 1990. Therefore, the theoretical model fails in the phase-shift time period that occurs after the modern Gleissberg maximum, while in the time period thereafter (after the 1990s), theoretical and experimental results are consistent. The long-term variations in B in general yield an anticorrelation of B and activity, as a rise of B is observed during the entire time period (1964–2016) we analysed, during which activity decreased, with the exception of the end of solar cycle 22 and the beginning of solar cycle 23.
Conclusions. We study for the first time the variation in solar DR and activity based on 53 years of KSO data. Our results agree well with the results related to the solar cycle phase from corona observations. The disagreement of the observational results for B and theoretical studies may be due to the fact that we analysed the period immediately after the modern Gleissberg maximum, where for the phase-shift period, A versus activity also entails a result that differs from theoretical predictions. Therefore, studies of rotation versus activity with data sets encompassing the Gleissberg extremes should include separate analyses of the parts of the data set in between different flips (e.g., before the activity flip, between the activity and the rotation flip, and after the rotation flip).

Amplitudes of Solar Gravity Modes: A Review

Kévin **Belkacem**, Charly Pinçon, Gaël Buldgen

Solar Phys. **297**, Article number: 147 **2022**
https://arxiv.org/pdf/2210.09229
https://doi.org/10.1007/s11207-022-02075-5
https://link.springer.com/epdf/10.1007/s11207-022-02075-5

Solar gravity modes are considered as the {\it Rosetta Stone} for probing and subsequently deciphering the physical properties of the solar inner-most layers. Recent claims of positive detection therefore shed some new light on the long-standing issue of estimating solar gravity mode amplitudes. In this article, our objective is to review the theoretical efforts intended to predict solar gravity mode amplitudes. Because most of these studies assumed analogous driving and damping properties to those for the observed acoustic modes, we also provide a short overview of our current knowledge for these modes in the Sun and solar-type stars (which show solar-like oscillations) before diving into the specific problem of solar gravity modes. Finally, taking recent estimates into account, we conclude and confirm that the low-frequency domain (typically between 10μHz and 100μHz) is certainly more suited to focus on for detecting solar gravity modes. More precisely, around 60μHz, the theoretical estimates are slightly lower than the observational detection threshold as provided by the GOLF (Global Oscillations at Low Frequencies) instrument by about a factor of two only. This is typically within the current uncertainties associated with theoretical estimates and should motivate us for improving our knowledge on turbulence in the whole solar convective region, which is key for improving the accuracy of g-mode amplitude estimates. The recent detection of solar inertial modes (Gizon et al. 2021) combined with the continuous development of numerical simulations provide interesting prospects for future studies.

Towards solar measurements of nuclear reaction rates

Earl Patrick **Bellinger**, Jørgen Christensen-Dalsgaard
MNRAS **2022**
https://arxiv.org/pdf/2206.13570
Nuclear reaction rates are a fundamental yet uncertain ingredient in stellar evolution models. The astrophysical S-factor pertaining to the initial reaction in the proton-proton chain is uncertain at the 1% level, which contributes a systematic but generally unpropagated error of similar order in the theoretical ages of stars. In this work, we study the prospect of improving the measurement of this and other reaction rates in the pp chain and CNO cycle using helioseismology and solar neutrinos. We show that when other aspects of the solar model are improved, then it shall be possible using current solar data to improve the precision of this measurement by nearly an order of magnitude, and hence the corresponding uncertainty on the ages of low-mass stars by a similar amount.

Radiative transfer modeling of the enigmatic scattering polarization in the solar NaI D1 line

Luca **Belluzzi**, Javier Trujillo Bueno, Egidio Landi Degl'Innocenti
ApJ **201**5
http://arxiv.org/pdf/1511.05801v1.pdf
The modeling of the peculiar scattering polarization signals observed in some diagnostically important solar resonance lines requires the consideration of the detailed spectral structure of the incident radiation field as well as the possibility of ground level polarization, along with the atom's hyperfine structure and quantum interference between hyperfine F-levels pertaining either to the same fine structure J-level, or to different J-levels of the same term. Here we present a theoretical and numerical approach suitable for solving this complex non-LTE radiative transfer problem. This approach is based on the density-matrix metalevel theory (where each level is viewed as a continuous distribution of sublevels) and on accurate formal solvers of the transfer equations and efficient iterative methods. We show an application to the D-lines of NaI, with emphasis on the enigmatic D1 line, pointing out the observable signatures of the various physical mechanisms considered. We demonstrate that the linear polarization observed in the core of the D1 line may be explained by the effect that one gets when the detailed spectral structure of the anisotropic radiation responsible for the optical pumping is taken into account. This physical ingredient is capable of introducing significant scattering polarization in the core of the NaI D1 line without the need for ground-level polarization.

Dispersion of Slow Magnetoacoustic Waves in the Active Region Fan Loops Introduced by Thermal Misbalance

S. A. **Belov**, N. E. Molevich & D. I. Zavershinskii
Solar Physics volume 296, Article number: 122 (**2021**)
https://link.springer.com/content/pdf/10.1007/s11207-021-01868-4.pdf
https://doi.org/10.1007/s11207-021-01868-4
Slow magnetoacoustic waves observed in the solar corona are used as seismological probes of plasma parameters. It has been shown that the dispersion properties of such waves can vary significantly under the influence of the wave-induced thermal misbalance. In the current research, we study the effect of misbalance on waves inside the magnetic-flux tube under the second-order thin-flux-tube approximation. Using the parameters of active-region-fan coronal loops, we calculated wave properties such as the phase speed and decrement. It is shown that neglecting thermal misbalance may be the reason for the substantial divergence between seismological and spectrometric estimations of plasma parameters. We also show that the frequency dependence of the phase speed is affected by two features, namely the geometric dispersion and the dispersion caused by the thermal misbalance. In contrast to the phase speed, the wave decrement primarily is affected by the thermal misbalance only. The dependencies of the phase speed and decrement of the slow wave on the magnetic field and tube cross-section are also analysed.

Thermal Misbalance Influence on the Nonlinear Shear Alfvén Waves Under Solar Atmosphere Conditions

S. **Belov**, N. Molevich & D. Zavershinskii
Solar Physics volume 295, Article number: 160 (**2020**)
https://link.springer.com/content/pdf/10.1007/s11207-020-01726-9.pdf
The self-interaction of the Alfvén wave associated with the parametric interaction between the Alfvén wave and longitudinal plasma motion induced by this Alfvén wave is investigated in a dissipative plasma with a thermal misbalance. The thermal misbalance caused by plasma heating and radiation cooling leads to changes in the steepening rate and the resulting amplitude of Alfvén waves. The characteristic times of steepening and changes of amplitude are obtained analytically and subsequently calculated for the initial stage of self-interaction of sinusoidal Alfvén waves applying the upper chromosphere and coronal hole conditions. Comparison with characteristic times

of viscous and Ohmic dissipation is conducted as well. It is revealed that for the chromosphere conditions there are temperature ranges where Alfvén waves can steepen faster and, therefore, the nonlinear Alfvén dissipation observed by Grant et al. (Nat. Phys. 14(5), 480, 2018) could be stronger. Moreover, depending on the temperature range, the steepening of the wave can occur both in front and behind. In addition, temperature ranges were found in which the Alfvén wave can be strongly absorbed due to the thermal misbalance. It should be mentioned that regions of fast steepening and fast damping due to the thermal misbalance intersect. Therefore, in these regions, the damping of Alfvén waves can be most significant. We also show that for coronal hole conditions the thermal misbalance only affects the Alfvén wave steepening.

Magnetohydrodynamic Instabilities of Double Magnetic Bands in a Shallow-water Tachocline Model. I. Cross-equatorial Interactions of Bands

Bernadett **Belucz**1,2,3, Mausumi Dikpati4, Scott W. McIntosh4, Robert J. Leamon5, and Robertus Erdélyi1,2,3

2023 ApJ 945 32

https://iopscience.iop.org/article/10.3847/1538-4357/acb43b/pdf

Along with a butterfly diagram of sunspots, combined observational studies of ephemeral active regions, X-ray and EUV bright points, plage, filaments, faculae, and prominences demonstrate a pattern, which is known as the Extended Solar Cycle. This pattern indicates that the wings of the sunspot butterfly could be extended to much higher latitudes (up to ~60°), to an earlier time than the start of a sunspot cycle, hence yielding a strong overlap between cycles. Thus, during the ongoing cycle's activity near 30° latitude in each hemisphere, the next cycle kicks off at around 60°. By representing these epochs of overlaps by oppositely directed double magnetic bands in each hemisphere, we compute the unstable eigenmodes for MHD Rossby waves at the base of the convection zone and study how the properties of these energetically active Rossby waves change as these band pairs migrate equatorward. We find that in each hemisphere the low-latitude band interacts with the high-latitude band and drives the MHD instability as the solar activity progresses from 35°–15° latitude, which is essentially the rising phase. When the activity proceeds further equatorward from 15°, the interaction between low- and high-latitude bands weakens, and the cross-equatorial interaction between two low-latitude bands in each hemisphere starts. The eigenmodes in the latitude-longitude plane also reflect such changes in their pattern as the bend of the active cycle moves below 15° latitude.

A Babcock-Leighton solar dynamo model with multi-cellular meridional circulation in advection- and diffusion-dominated regimes

Bernadett **Belucz**, Mausumi Dikpati, Emese Forgacs-Dajka

ApJ 806 169 **2015**

http://arxiv.org/pdf/1504.00420v1.pdf

Babcock-Leighton type solar dynamo models with single-celled meridional circulation are successful in reproducing many solar cycle features. Recent observations and theoretical models of meridional circulation do not indicate a single-celled flow pattern. We examine the role of complex multi-cellular circulation patterns in a Babcock-Leighton solar dynamo in advection- and diffusion-dominated regimes. We show from simulations that presence of a weak, second, high-latitude reverse cell speeds up the cycle and slightly enhances the poleward branch in butterfly diagram, whereas the presence of a second cell in depth reverses the tilt of butterfly wing to an anti-solar type. A butterfly diagram constructed from middle of convection zone yields a solar-like pattern, but this may be difficult to realize in the Sun because of magnetic buoyancy effects. Each of the above cases behaves similarly in higher and lower magnetic diffusivity regimes. However, our dynamo with a meridional circulation containing four cells in latitude behaves distinctly differently in the two regimes, producing solar-like butterfly diagrams with fast cycles in the higher diffusivity regime, and complex branches in butterfly diagrams in the lower diffusivity regime. We also find that dynamo solutions for a four-celled pattern, two in radius and two in latitude, prefer to quickly relax to quadrupolar parity if the bottom flow-speed is strong enough, of similar order of magnitude as the surface flow-speed.

Coronal Electron Densities derived with Images acquired during the 21 August 2017 Total Solar Eclipse

Alessandro **Bemporad**

ApJ **904** 178 **2020**

https://arxiv.org/pdf/2010.15005.pdf

https://doi.org/10.3847/1538-4357/abc482

The total solar eclipse of **August 21st, 2017** was observed with a Digital Single Lens Reflex (DSLR) camera equipped with a linear polarizing filter. A method was developed to combine images acquired with 15 different exposure times (from 1/4000 sec to 4 sec), identifying in each pixel the best interval of detector linearity. The

resulting mosaic image of the solar corona extends up to more than 5 solar radii, with a projected pixel size by 3.7 arcsec/pixel, and an effective image resolution by 10.2 arcsecs, as determined with visible α−Leo and ν−Leo stars. Image analysis shows that in the inner corona the intensity gradients are so steep, that nearby pixels shows a relative intensity difference by up to ∼10%; this implies that careful must be taken when analyzing single exposures acquired with polarization cameras.
Images acquired with two different orientations of the polarizer have been analyzed to derive the degree of linear polarization, and the polarized brightness pB in the solar corona. After inter-calibration with pB measurements by the K-Cor instrument on Mauna Loa Solar Observatory (MLSO), data analysis provided the 2D coronal electron density distribution from 1.1 up to ∼3 solar radii. The absolute radiometric calibration was also performed, with the full sun image, and with magnitudes of visible stars. The resulting absolute calibrations show a disagreement by a factor ∼2 with respect to MLSO; interestingly, this is the same disagreement recently found with eclipse predictions provided by MHD numerical simulations.

On the Statistics of Macrospicules

S. M. **Bennett**1 and R. Erdélyi
2015 ApJ 808 135
A new generation of solar telescopes has led to an increase in the resolution of localized features seen on the Sun spatially, temporally, and spectrally, enabling a detailed study of macrospicules. Macrospicules are members of a wide variety of solar ejecta and ascertaining where they belong in this family is vitally important, particularly given that they are chromospheric events which penetrate the transition region and lower corona. We examine the overall properties of macrospicules, both temporal and spatial. We also investigate possible relationships between the macrospicule properties and the sample time period itself, which is selected as a proxy for the ramp from solar minimum to solar maximum. Measurements are taken using the Solar Dynamic Observatory to provide the necessary temporal resolution and coverage. At each point in time, the length of the macrospicule is measured from base to tip and the width is recorded at half the length at each step. The measurements were then applied to determine the statistical properties and relationships between them. It is evident that the properties of maximum velocity, maximum length, and lifetime are all related in specific, established terms. We provide appropriate scaling in terms of the physical properties, which would be a useful test bed for modeling. Also, we note that the maximum lengths and lifetimes of the features show some correlation with the sample epoch and, therefore, by proxy the solar minimum to maximum ramp.

Predicting Space Weather on a Satellite Superhighway

Eric **Betz**, Freelance Writer
Eos, 96, doi:10.1029/2015EO034691. Published on 9 September **2015**.

DOUBLE DYNAMO SIGNATURES IN A GLOBAL MHD SIMULATION AND MEAN-FIELD DYNAMOS

Patrice **Beaudoin**, Corinne Simard, Jean-François Cossette, and Paul Charbonneau
2016 ApJ 826 138
The 11 year solar activity cycle is the most prominent periodic manifestation of the magnetohydrodynamical (MHD) large-scale dynamo operating in the solar interior, yet longer and shorter (quasi-) periodicities are also present. The so-called "quasi-biennial" signal appearing in many proxies of solar activity has been gaining increasing attention since its detection in p-mode frequency shifts, which suggests a subphotospheric origin. A number of candidate mechanisms have been proposed, including beating between co-existing global dynamo modes, dual dynamos operating in spatially separated regions of the solar interior, and Rossby waves driving short-period oscillations in the large-scale solar magnetic field produced by the 11 year activity cycle. In this article, we analyze a global MHD simulation of solar convection producing regular large-scale magnetic cycles, and detect and characterize shorter periodicities developing therein. By constructing kinematic mean-field α 2Ω dynamo models incorporating the turbulent electromotive force (emf) extracted from that same simulation, we find that dual-dynamo behavior materializes in fairly wide regions of the model's parameters space. This suggests that the origin of the similar behavior detected in the MHD simulation lies with the joint complexity of the turbulent emf and differential rotation profile, rather that with dynamical interactions such as those mediated by Rossby waves. Analysis of the simulation also reveals that the dual dynamo operating therein leaves a double-period signature in the temperature field, consistent with a dual-period helioseismic signature. Order-of-magnitude estimates for the magnitude of the expected frequency shifts are commensurate with helioseismic measurements. Taken together, our results support the hypothesis that the solar quasi-biennial oscillations are associated with a secondary dynamo process operating in the outer reaches of the solar convection zone.

A Novel Approach for Forecasting Cycle 25

Katia **Becheker**, Zahir Belhadi, Abdeldjalil Zaidi & Mohamed Reda Bekli

Solar Physics volume 298, Article number: 65 (**2023**)

https://doi.org/10.1007/s11207-023-02156-z

A novel approach to forecast the ongoing solar cycle, Cycle 25, is proposed in this article. The new (Version 2.0) of the smoothed monthly sunspot number is well fitted by our four-parameter function, with a mean correlation coefficient of r=0.984 for all the past cycles. This function can be simplified into different reduced functions, which are more suitable for making predictions. The free parameters of these reduced functions are either B, the key parameter, as it is linked to the amplitude, or both B and α (the parameter linked to the rising time). Three predictions are made. First, relying on the available data (i.e., 25 months) from the sunspot series, we use a two-parameter function to estimate the peak value to be A=172±18 SSN (sunspot number) around 2024.7±0.7. Then, we propose a new model as the foundation of the other two forecasts. A new three-parameter function is introduced to fit the B-parameters of the previous cycles and forecast the ongoing ones. The predictive power of our two functions is added to make two more predictions about the peak of Cycle 25; one that considers the available data (A=147±27SSN around 2024.6±0.72024.6±0.7 year) and another that does not (A=156±31SSN around 2024.3±0.7year). By taking the crossing of the confidence intervals, we estimate Cycle 25 to reach its peak A=164±10SSN around 2024.5±0.7year.

Center-to-Limb Variation of the Inverse Evershed Flow

C. **Beck**, D.P. Choudhary, M. Ranganathan

Ap J. **2020**

https://arxiv.org/pdf/2008.12748.pdf

We present the properties of the inverse Evershed flow (IEF) based on the center-to-limb variation of the plasma speed and loop geometry of chromospheric superpenumbral fibrils in eleven sunspots that were located at a wide range of heliocentric angles from 12 to 79 deg. The observations were acquired at the Dunn Solar Telescope in the spectral lines of Halpha at 656nm, CaII IR at 854 nm and HeI at 1083 nm. All sunspots display opposite line-of-sight (LOS) velocities on the limb and center side with a distinct shock signature near the outer penumbral edge. We developed a simplified flexible sunspot model assuming axisymmetry and prescribing the radial flow speed profile at a known loop geometry to replicate the observed two-dimensional IEF patterns under different viewing angles. The simulated flow maps match the observations for chromospheric loops with 10-20 Mm length starting at 0.8-1.1 sunspot radii, an apex height of 2-3Mm and a true constant flow speed of 2-9km/s. We find on average a good agreement of the simulated velocities and the observations on elliptical annuli around the sunspot. Individual IEF channels show a significant range of variation in their properties and reach maximal LOS speeds of up to 12km/s. Upwards or downwards directed flows do not show a change of sign in the LOS velocities for heliocentric angles above 30 deg. Our results are consistent with the IEF being caused by a siphon flow mechanism driving a flow at a constant sonic speed along elevated loops with a flattened top in the chromosphere.

TABLE 1 List of Observations (2014-2016)

Magnetic Properties and Flow Angle of the Inverse Evershed Flow at Its Downflow Points

C. **Beck**1 and D. P. Choudhary

2019 ApJ 874 6

https://doi.org/10.3847/1538-4357/ab06f9

We determined the direction and strength of the photospheric and lower chromospheric magnetic field in the umbra and penumbra of a sunspot from inversions of spectropolarimetric observations of photospheric lines at 617 nm and 1565 nm and the chromospheric Ca ii IR line at 854 nm, respectively. We compare the magnetic field vector with the direction of 75 flow channels that harbor the chromospheric inverse Evershed effect (IEF) near their downflow points (DFPs) in the sunspot's penumbra. The azimuth and inclination of the IEF channels to the line of sight (LOS) were derived from spatial maps of the LOS velocity and line–core intensity of the Ca ii IR line and a thermal inversion of the Ca ii IR spectra to obtain temperature cubes. We find that the flow direction of the IEF near the DFPs is aligned with the photospheric magnetic field to within about ±15°. The IEF flow fibrils make an angle of 30°–90° to the local vertical with an average value of about 65°. The average field strength at the DFPs is about 1.3 kG. Our findings suggest that the IEF in the lower chromosphere is a field-aligned siphon flow, where the larger field strength at the inner footpoints together with the lower temperature in the penumbra causes the necessary gas pressure difference relative to the outer footpoints in the hotter quiet Sun with lower magnetic field strength. The IEF connects to magnetic field lines that are not, like in the case of the regular Evershed flow, but which continue upward into the chromosphere, indicating an "uncombed" penumbral structure.

Spectroscopy at the Solar Limb: II. Are Spicules Heated to Coronal Temperatures?

C. **Beck**, . Rezaei, K. G. Puschmann, D. Fabbian

Solar Phys. Volume 291, Issue 8, pp 2281–2328 **2016**

Spicules of the so-called type II were suggested to be relevant for coronal heating because of their ubiquity on the solar surface and their eventual extension into the corona. We investigate whether solar spicules are heated to transition-region or coronal temperatures and reach coronal heights (≫6 Mm) using multiwavelength observations of limb spicules in different chromospheric spectral lines (Ca ii H, Hε, Hα, Ca ii IR at 854.2 nm, He i at 1083 nm) taken with slit spectrographs and imaging spectrometers. We determine the line width of spectrally resolved line profiles in individual spicules and throughout the field of view, and estimate the maximal height that different types of off-limb features reach. We derive estimates of the kinetic temperature and the non-thermal velocity from the line width of spectral lines from different chemical elements. We find that most regular, i.e. thin and elongated, spicules reach a height of at most about 6 Mm above the solar limb. The majority of features found at larger heights are irregularly shaped with a significantly larger lateral extension, of up to a few Mm, than spicules. Both individual and average line profiles in all spectral lines show a decrease in their line width with height above the limb with very few exceptions. The kinetic temperature and the non-thermal velocity decrease with height above the limb. We find no indications that the spicules in our data reach coronal heights or transition-region or coronal temperatures.

The Sun's differential rotation is controlled by high-latitude baroclinically unstable inertial modes

Yuto **Bekki**, Robert H. Cameron, Laurent Gizon
Science Advances, 10 (13), eadk5643 (**2024**)
https://arxiv.org/pdf/2403.18986.pdf
Rapidly rotating fluids have a rotation profile which depends only on the distance from the rotation axis, in accordance with the Taylor-Proudman theorem. Although the Sun was expected to be such a body, helioseismology showed that the rotation rate in the convection zone is closer to constant on radii. It has been postulated that this deviation is due to the poles being warmer than the equator by a few degrees. Using numerical simulations, we show that the pole-to-equator temperature difference cannot exceed 7 Kelvin as a result of the back-reaction of the high-latitude baroclinically unstable inertial modes. The observed amplitudes of the modes further indicate that this maximum temperature difference is reached in the Sun. We conclude that the Sun's latitudinal differential rotation reaches its maximum allowed value.

Three-dimensional non-kinematic simulation of the post-emergence evolution of bipolar magnetic regions and the Babcock-Leighton dynamo of the Sun⋆

Yuto **Bekki** and Robert H. Cameron
A&A 670, A101 (**2023**)
https://www.aanda.org/articles/aa/pdf/2023/02/aa44990-22.pdf
Context. The Babcock-Leighton flux-transport model is a widely accepted dynamo model of the Sun that can explain many observational aspects of solar magnetic activity. This dynamo model has been extensively studied in a two-dimensional (2D) mean-field framework in both kinematic and non-kinematic regimes. Recent three-dimensional (3D) models have been restricted to the kinematic regime. In these models, the surface poloidal flux is produced by the emergence of bipolar magnetic regions (BMRs) that are tilted according to Joy's law.
Aims. We investigate the prescription for emergence of a BMR in 3D non-kinematic simulations. In particular, we examine the effect of the radial extent of the BMR. We also report our initial results based on a cyclic Babcock-Leighton dynamo simulation.
Methods. We extended a conventional 2D mean-field model of the Babcock-Leighton flux-transport dynamo into 3D non-kinematic regime, in which a full set of magnetohydrodynamic (MHD) equations are solved in a spherical shell using a Yin-Yang grid. The large-scale mean flows, such as differential rotation and meridional circulation, are not driven by rotationally constrained convection, but rather by the parameterized Λ-effect in this model. For the induction equation, we used a Babcock-Leighton α-effect source term by which the surface BMRs are produced in response to the dynamo-generated toroidal field inside the convection zone.
Results. We find that in the 3D non-kinematic regime, the tilt angle of a newly-emerged BMR is very sensitive to the prescription for the subsurface structure of the BMR (particularly, its radial extent). Anti-Joy tilt angles are found unless the BMR is deeply embedded in the convection zone. We also find that the leading spot tends to become stronger (higher field strengths) than the following spot. The anti-Joy's law trend and the morphological asymmetry of the BMRs can be explained by the Coriolis force acting on the Lorentz-force-driven flows. Furthermore, we demonstrate that the solar-like magnetic cycles can be successfully obtained if Joy's law is explicitly given in the Babcock-Leighton α-effect. In these cyclic dynamo simulations, a strong Lorentz force feedback leads to cycle modulations in the differential rotation (torsional oscillation) and meridional circulation. The simulations, however, do not include radiative effects (e.g., enhanced cooling by faculae) that are required to properly model the torsional oscillations. The non-axisymmetric components of the flows are found to exist as inertial modes such as the equatorial Rossby modes.

Theory of solar oscillations in the inertial frequency range: Linear modes of the convection zone

Yuto **Bekki**, Robert H. Cameron, Laurent Gizon
A&A **2022**
https://arxiv.org/pdf/2203.04442.pdf
On the one hand, several types of global-scale inertial modes of oscillation have been observed on the Sun. They include the equatorial Rossby modes, critical-latitude modes, and high-latitude modes. On the other hand, the columnar convective modes (predicted by simulations; also known as banana cells or thermal Rossby waves) remain elusive. We aim to investigate the influence of turbulent diffusivities, non-adiabatic stratification, differential rotation, and a latitudinal entropy gradient on the linear global modes of the rotating solar convection zone. We solve numerically for the eigenmodes of a rotating compressible fluid inside a spherical shell. We identify modes in the inertial frequency range including the columnar convective modes, as well as modes of mixed character. The corresponding mode dispersion relations and eigenfunctions are computed for azimuthal orders $m \leq 16$. The three main results are as follows. Firstly, we find that, for $m \gtrsim 5$, the radial dependence of the equatorial Rossby modes with no radial node (n=0) is radically changed from the traditional expectation (rm) for turbulent diffusivities $\gtrsim 1012$ cm2 s−1. Secondly, we find mixed modes, i.e. modes that share properties of the equatorial Rossby modes with one radial node (n=1) and the columnar convective modes. Thirdly, we show that the m=1 high-latitude mode in the model is consistent with the solar observations when the latitudinal entropy gradient corresponding to a thermal wind balance is included (baroclinally unstable mode). To our knowledge, this work is the first realistic eigenvalue calculation of the global modes of the rotating solar convection zone. This calculation reveals a rich spectrum of modes in the inertial frequency range, which can be directly compared to the observations. In turn, the observed modes can inform us about the solar convection zone.

Non-parametric Data Analysis of Low-latitude Auroras and Naked-eye Sunspots in the Medieval Epoch

Mohamed Reda **Bekli**, Nabil Zougab, Abdelmoumene Belabbas, Ilhem Chadou
Solar Physics April **2017**, 292:52
http://link.springer.com/content/pdf/10.1007%2Fs11207-017-1084-5.pdf
We have studied solar activity by analyzing naked-eye sunspot observations and aurorae borealis observed at latitudes below 45°. We focused on the medieval epoch by considering the non-telescopic observations of sunspots from AD 974 to 1278 and aurorae borealis from AD 965 to 1273 that are reported in several Far East historical sources, primarily in China and Korea. After setting selection rules, we analyzed the distribution of these individual events following the months of the Gregorian calendar. In December, an unusual peak is observed with data recorded in both China and Japan, but not within Korean data.
In extreme conditions, where the collection of events is reduced and discontinuous in some temporal intervals, we used the non-parametric kernel method. We opted for the plug-in approach of Sheather and Jones instead of cross-validation techniques to estimate the probability density functions (pdf) of the events. We obtained optimized bandwidths of 13.29 years for sunspots and 9.06 years for auroras, and 95% confidence intervals. The pdf curves exhibit multiple peaks occurring at quasi-periodic times with a very high positive correlation, $r_{\mathrm{tt}} = 0.9958$, between the dates of occurrence of the nine extrema of sunspots and auroras. Furthermore, these extrema enabled us to evaluate mean periods at two standard deviations, $66.77 \pm 7.25~\mathrm{years}$ for sunspots and $65.06 \pm 9.36~\mathrm{years}$ for auroras. The accuracy of the average periods, 62.00 years for sunspots and 61.80 years for auroras, was improved by the use of the power spectrum method. The percentage of the total number of non-observed sunspots, using redundant data, from AD 1151 to 1275 was estimated to be greater than or equal to 78%.

Renewed Support Dawns in Europe: An Action to Develop Space Weather Products and Services

Belehaki, Anna; Watermann, Jurgen; Lilensten, Jean; Glover, Alexi; Hapgood, Mike; Messerotti, Mauro; van der Linden, Ronald; Lundstedt, Henrik
Space Weather, Vol. 7, No. 3, S03001, **2009**
http://dx.doi.org/10.1029/2008SW000451
The effects of space weather span a range of sectors. They can cause radio communications problems; can disrupt synthetic aperture radar systems, the Global Positioning System (GPS), and the future European Galileo systems; and can increase radiation risks for aircraft crew and passengers. Electric power network disturbances and enhanced corrosion effects observed in long-distance fuel supply pipelines are other well-known effects of unfavorable space weather. In severe cases, large-scale power outages have also been traced to space weather phenomena (Figure 1).

Variation in solar differential rotation and activity in the period 1964-2016 determined by the Kanzelhöhe data set

I. Poljančić **Beljan** (1), R. Jurdana-Šepić (1), T. Jurkić (1), R. Brajša (2), I. Skokić (2), D. Sudar (2), D. Ruždjak (2), D. Hržina (3), W. Pötzi (4), A. Hanslmeier (5), A. M. Veronig

https://arxiv.org/pdf/2204.07396
A&A **2022**
https://arxiv.org/pdf/2204.07396
We determined the differential rotation (DR) parameters A and B (corresponding to the equatorial rotation velocity and the gradient of the solar DR) by tracing sunspot groups in sunspot drawings of the Kanzelhöhe Observatory for Solar and Environmental Research (KSO; 1964-2008, for solar cycles (SC) 20-23) and KSO white-light images (2009-2016, for SC 24). We used different statistical methods and approaches to analyse cycle related variations, solar cycle phase-related variations and long-term variations of the DR. A and B show statistically significant periodic variability. The changes in A related to solar cycle phase are in accordance with previously reported theoretical and experimental results (higher A during solar minimum, lower A during the maximum of activity), while changes in B differ from the theoretical predictions as we observe more negative values of B, that is, a more pronounced DR during activity maximum. The main result of this paper for the long-term variations in A is the detection of a phase shift between the activity flip (in the 1970s) and the equatorial rotation velocity flip (in the early 1990s). During this time period both A and activity show a secular decreasing trend, indicating their correlation. Therefore, the theoretical model fails in the phase-shift time period that occurs after the modern Gleissberg maximum, while in the time period thereafter (after the 1990s), theoretical and experimental results are consistent. The long-term variations in B in general yield an anticorrelation of B and activity, as a rise of B is observed during the entire time period (1964-2016) we analysed, during which activity decreased. We study for the first time the variation in solar DR and activity based on 53 years of KSO data. Our results agree well with the results related to the solar cycle phase from corona observations.

Solar differential rotation in the period 1964 - 2016 determined by the Kanzelhöhe data set

I. Poljančić **Beljan**, R. Jurdana-Šepić, R. Brajša, D. Sudar, D. Ruždjak, D. Hržina, W. Pötzi, A. Hanslmeier,A. Veronig, I. Skokić, H. Wöhl
A&A 606 A72 **2017**
https://arxiv.org/pdf/1707.07886.pdf
The main aim of this work is to determine the solar differential rotation by tracing sunspot groups during the period 1964-2016, using the Kanzelh{\"o}he Observatory for Solar and Environmental Research (KSO) sunspot drawings and white light images. Two procedures for the determination of the heliographic positions were applied: an interactive procedure on the KSO sunspot drawings (1964 - 2008, solar cycles nos. 20 - 23) and an automatic procedure on the KSO white light images (2009 - 2016, solar cycle no. 24). For the determination of the synodic angular rotation velocities two different methods have been used: a daily shift (DS) method and a robust linear least-squares fit (rLSQ) method. Afterwards, the rotation velocities had to be converted from synodic to sidereal, which were then used in the least-squares fitting for the solar differential rotation law. For the test data from 2014, we found the rLSQ method for calculating rotational velocities to be more reliable than the DS method. The best fit solar differential rotation profile for the whole time period is $\omega(b) = (14.47 \pm 0.01) - (2.66 \pm 0.10) \sin^2 b$ (deg/day) for the DS method and $\omega(b) = (14.50 \pm 0.01) - (2.87 \pm 0.12) \sin^2 b$ (deg/day) for the rLSQ method. A barely noticeable north - south asymmetry is observed for the whole time period 1964 - 2016 in the present paper. Rotation profiles, using different data sets (e.g. Debrecen Photoheliographic Data, Greenwich Photoheliographic Results), presented by other authors for the same time periods and the same tracer types, are in good agreement with our results. Therefore, the KSO data set is suitable for the investigation of the long-term variabilities in the solar rotation profile.

Solar evolution models with a central black hole

Earl P. **Bellinger**, Matt E. Caplan, Taeho Ryu, Deepika Bollimpalli, Warrick H. Ball, Florian Kühnel, R. Farmer, S. E. de Mink, Jørgen Christensen-Dalsgaard
ApJ **959** 113 **2023**
https://arxiv.org/pdf/2312.06782.pdf
https://iopscience.iop.org/article/10.3847/1538-4357/ad04de/pdf
Hawking (1971) proposed that the Sun may harbor a primordial black hole whose accretion supplies some of the solar luminosity. Such an object would have formed within the first 1 s after the Big Bang with the mass of a moon or an asteroid. These light black holes are a candidate solution to the dark matter problem, and could grow to become stellar-mass black holes (BHs) if captured by stars. Here we compute the evolution of stars having such a BH at their center. We find that such objects can be surprisingly long-lived, with the lightest black holes having no influence over stellar evolution, while more massive ones consume the star over time to produce a range of observable consequences. Models of the Sun born about a BH whose mass has since grown to approximately $10^{-6}\,M_\odot$ are compatible with current observations. In this scenario, the Sun would first dim to half its current luminosity over a span of 100 Myr as the accretion starts to generate enough energy to quench nuclear reactions. The Sun would then expand into a fully-convective star, where it would shine luminously for potentially several Gyr with an enriched surface helium abundance, first as a sub-subgiant star, and later as a red straggler, before becoming a sub-solar-mass BH. We also present results for a range of stellar masses and metallicities. The

unique internal structures of stars harboring BHs may make it possible for asteroseismology to discover them, should they exist. We conclude with a list of open problems and predictions.

Longitudinal Plasma Motions Generated by Shear Alfvén Waves in Plasma with Thermal Misbalance

S. **Belov**, S. Vasheghani Farahani, N. Molevich & D. Zavershinskii
Solar Physics volume 296, Article number: 98 (**2021**)
https://link.springer.com/content/pdf/10.1007/s11207-021-01850-0.pdf
https://doi.org/10.1007/s11207-021-01850-0
Compressional plasma perturbations may cause thermal misbalance between plasma-heating and -cooling processes. This misbalance significantly affects the dispersion properties of compressional waves providing a feedback between the perturbations and plasmas. It has been shown that Alfvén waves may induce longitudinal (compressional) plasma motions. In the present study, we analyze the effects of thermal misbalance caused by longitudinal plasma motions induced by shear Alfvén waves. We show that thermal misbalance leads to appearance of exponential bulk flows, which themselves modify the Alfvén-induced plasma motions. In the case of sinusoidal Alfvén waves, we show how the amplitude and phase shift of induced longitudinal motions gain dependence on the Alfvén wave frequency while shedding light on its functionality. This feature has been investigated analytically in application to coronal conditions. We also consider the evolution of longitudinal plasma motions induced by the shear sinusoidal Alfvén wave by numerical methods before comparing the results obtained with our presented analytical predictions to justify the model under consideration in the present study.

Galactic Cosmic Ray Density Variations in Magnetic Clouds

A. **Belov**, A. Abunin, M. Abunina, E.Eroshenko, V. Oleneva, V. Yanke, A. Papaioannou, H. Mavromichalaki
Solar Physics, 290, 1429-1444, **2015**
http://cosray.phys.uoa.gr/publications/D107.pdf
We investigate the characteristics of Galactic cosmic rays in events associated with magnetic clouds that reach Earth. A mathematical model, capable of describing the distribution of the cosmic-ray density in a magnetic cloud is considered. We show that in most cases the behavior of the cosmic-ray density within magnetic clouds at 1 AU can be described accurately by a parabolic function of the distance to the center of the magnetic cloud measured in gyroradii. As expected, the majority of magnetic clouds modulate cosmic rays, resulting in a reduction of their density. However, there is a group of events (about one fifth of the total sample) in which the density of cosmic rays in a magnetic cloud increases. Furthermore, the extremum (a minimum or a maximum) of the cosmic-ray density is found closer to the cloud center and not at its edges. We consider a number of the factors contributing to the model and estimate the effect of each factor.

Synoptic Solar Cycle 24 in Corona, Chromosphere, and Photosphere Seen by the Solar Dynamics Observatory

E. **Benevolenskaya**, G. Slater, J. Lemen
Solar Phys., **2014**
The Solar Dynamics Observatory provides multiwavelength imagery from extreme ultraviolet (EUV) to visible light as well as magnetic-field measurements. These data enable us to study the nature of solar activity in different regions of the Sun, from the interior to the corona. For solar-cycle studies, synoptic maps provide a useful way to represent global activity and evolution by extracting a central meridian band from sequences of full-disk images over a full solar Carrington rotation (≈ 27.3 days). We present the global evolution during Solar Cycle 24 from 20 May 2010 to 31 August 2013 (CR 2097 – CR 2140), using synoptic maps constructed from full-disk, line-of-sight magnetic-field imagery and EUV imagery (171 Å, 193 Å, 211 Å, 304 Å, and 335 Å). The synoptic maps have a resolution of 0.1 degree in longitude and steps of 0.001 in sine of latitude. We studied the axisymmetric and non-axisymmetric structures of solar activity using these synoptic maps. To visualize the axisymmetric development of Cycle 24, we generated time–latitude (also called butterfly) images of the solar cycle in all of the wavelengths, by averaging each synoptic map over all longitudes, thus compressing it to a single vertical strip, and then assembling these strips in time order. From these time–latitude images we observe that during the ascending phase of Cycle 24 there is a very good relationship between the integrated magnetic flux and the EUV intensity inside the zone of sunspot activities. We observe a North–South asymmetry of the EUV intensity in high-latitudes. The North–South asymmetry of the emerging magnetic flux developed and resulted in a consequential asymmetry in the timing of the polar magnetic-field reversals.

The total solar irradiance, UV emission and magnetic flux during the last solar cycle minimum,

Benevolenskaya, E.E. and Kostuchenko, I.G.,

J. Astrophys., **2013**, vol. 2013, pp. 1–9.
https://arxiv.org/ftp/arxiv/papers/1307/1307.6257.pdf
We have analyzed the total solar irradiance (TSI) and the spectral solar irradiance as ultraviolet emission (UV) in the wavelength range 115-180 nm, observed with the instruments TIM and SOLSTICE within the framework of SORCE (The Solar Radiation and Climate Experiment) during the long solar minimum between the 23rd and 24th cycles. The wavelet analysis reveals an increase in the magnetic flux in the latitudinal zone of the sunspot activity, accompanied with an increase in the TSI and UV on the surface rotation timescales of solar activity complexes. In-phase coherent structures between the mid-latitude magnetic flux and TSI/UV appear when the long-lived complexes of the solar activity are present. These complexes, which are related to long- lived sources of magnetic fields under the photosphere, are maintained by magnetic fluxes reappearing in the same longitudinal regions. During the deep solar minimum (the period of the absence of sunspots) a coherent structure has been found, in which the phase between the integrated mid-latitude magnetic flux is ahead of the total solar irradiance on the timescales of the surface rotation.

Synoptic magnetic field in cycle 23 and in the beginning of the cycle 24

E.E. **Benevolenskaya**, Yu.D. Ponyavin
Advances in Space Research, Volume 50, Issue 6, 15 September **2012**, Pages 656–661
The SOHO/MDI data provide the uniform time series of the synoptic magnetic maps which cover the period of the cycle 23 and the beginning of the cycle 24. It is very interesting period because of the long and deep solar minimum between the cycles 23 and 24. Synoptic structure of the solar magnetic field shows variability during solar cycles. It is known that the magnetic activity contributes to the solar irradiance. The axisymmetrical distribution of the magnetic flux (Fig. 3c) is closely associated with the 'butterfly' diagram in the EUV emission (Benevolenskaya et al., 2001). And, also, the magnetic field (B‖) shows the non-uniform distributions of the solar activity with longitude, so-called 'active zones', and 'coronal holes' in the mid-latitude. Polar coronal holes are forming after the solar maxima and they persist during the solar minima. SOHO/EIT data in the emission of Fe XII (195 Å) could be a proxy for the coronal holes tracking. The active longitudinal zones or active longitude exist due to the reappearance of the activity and it is clearly seen in the synoptic structure of the solar cycle. On the descending branch of the solar cycle 23 active zones are less pronounced comparing with previous cycles 20, 21 and 22. Moreover, the weak polar magnetic field precedes the long and deep solar minimum. In this paper we have discussed the development of solar cycles 23 and 24 in details

Forecasting Solar Cycle 25 Using Deep Neural Networks

B. **Benson**, W. D. Pan, A. Prasad, G. A. Gary & Q. Hu
Solar Physics volume 295, Article number: 65 (**2020**)
https://arxiv.org/pdf/2005.12406.pdf
https://link.springer.com/content/pdf/10.1007/s11207-020-01634-y.pdf
With recent advances in the field of machine learning, the use of deep neural networks for time series forecasting has become more prevalent. The quasi-periodic nature of the solar cycle makes it a good candidate for applying time series forecasting methods. We employ a combination of WaveNet and Long Short-Term Memory neural networks to forecast the sunspot number using the years 1749 to 2019 and total sunspot area using the years 1874 to 2019 time series data for the upcoming Solar Cycle 25. Three other models involving the use of LSTMs and 1D ConvNets are also compared with our best model. Our analysis shows that the WaveNet and LSTM model is able to better capture the overall trend and learn the inherent long and short term dependencies in time series data. Using this method we forecast 11 years of monthly averaged data for Solar Cycle 25. Our forecasts show that the upcoming Solar Cycle 25 will have a maximum sunspot number around 106 ± 19.75 and maximum total sunspot area around 1771 ± 381.17. This indicates that the cycle would be slightly weaker than Solar Cycle 24.

Thermodynamics Interpretation of Electron Density and Temperature Description in the Solar Corona

Daniel B. **Berdichevsky**, Jenny M. Rodríguez Gómez, Luis E. Vieira, Allison Dal Lago
2020
https://arxiv.org/ftp/arxiv/papers/2005/2005.07929.pdf
We reach a thermodynamic interpretation of CODET model and its prediction to electrons density and temperature grounded on the physics of hydro magnetism in global equilibrium. The thermodynamic interpretation finds consistency with the model with a magneto-matter medium that is diamagnetic, in the context of ideal magnetohydrodynamics (MHD). It is further noticed that the CODET predicts a polytropic anomalous index for the electron gas of the Sun's corona. It is shown that this unusual characteristic is consistent with assuming that the low quiescent solar corona is a magneto-matter state which possesses an underlying structure that was earlier described to explain the 2-D adsorption process by a surface of a solid of molecules of a gas at a given temperature and pressure by Langmuir. In our case, it is assumed that we are in the presence of a 3-D similar coalescence process, i.e. a Langmuir amorphous lattice in thermodynamic equilibrium. In this way, constitutive properties of the medium

magnetic permeability, the non-dispersive acoustic speed, the expected equilibration time for the 1.1 to 1.3R⊙, and energy density are determined quantitatively for most of the quiescent corona in a near solar minimum that extends for several months from 2008 to 2009.

MHD Turbulence, Turbulent Dynamo and Applications

Andrey **Beresnyak**, Alex Lazarian
"Lecture Notes in Physics", **2014**
http://arxiv.org/pdf/1406.1185v1.pdf
MHD Turbulence is common in many space physics and astrophysics environments. We first discuss the properties of incompressible MHD turbulence. A well-conductive fluid amplifies initial magnetic fields in a process called small-scale dynamo. Below equipartition scale for kinetic and magnetic energies the spectrum is steep (Kolmogorov -5/3) and is represented by critically balanced strong MHD turbulence. In this paper we report the basic reasoning behind universal nonlinear small-scale dynamo and the inertial range of MHD turbulence. We measured the efficiency of the small-scale dynamo CE=0.05, Kolmogorov constant CK=4.2 and anisotropy constant CA=0.63 for MHD turbulence in high-resolution direct numerical simulations. We also discuss so-called imbalanced or cross-helical MHD turbulence which is relevant for in many objects, most prominently in the solar wind. We show that properties of incompressible MHD turbulence are similar to the properties of Alfv\'enic part of MHD cascade in compressible turbulence. The other parts of the cascade evolve according to their own dynamics. The slow modes are being cascaded by Alfv\'enic modes, while fast modes create an independent cascade. We show that different ways of decomposing compressible MHD turbulence into Alfv\'en, slow and fast modes provide consistent results and are useful in understanding not only turbulent cascade, but its interaction with fast particles.

Solar oxygen abundance

Maria **Bergemann**, Richard Hoppe, Ekaterina Semenova, Mats Carlsson, Svetlana A. Yakovleva, Yaroslav V. Voronov, Manuel Bautista, Ahmad Nemer, Andrey K. Belyaev, Jorrit Leenaarts, Lyudmila Mashonkina, Ansgar Reiners, Monika Ellwarth
MNRAS **2021**
https://arxiv.org/pdf/2109.01143
Motivated by the controversy over the surface metallicity of the Sun, we present a re-analysis of the solar photospheric oxygen (O) abundance. New atomic models of O and Ni are used to perform Non-Local Thermodynamic Equilibrium (NLTE) calculations with 1D hydrostatic (MARCS) and 3D hydrodynamical (Stagger and Bifrost) models. The Bifrost 3D MHD simulations are used to quantify the influence of the chromosphere. We compare the 3D NLTE line profiles with new high-resolution, R = 700 000, spatially-resolved spectra of the Sun obtained using the IAG FTS instrument. We find that the O I lines at 777 nm yield the abundance of log A(O) = 8.74 +/- 0.03 dex, which depends on the choice of the H-impact collisional data and oscillator strengths. The forbidden [O I] line at 630 nm is less model-dependent, as it forms nearly in LTE and is only weakly sensitive to convection. However, the oscillator strength for this transition is more uncertain than for the 777 nm lines. Modelled in 3D NLTE with the Ni I blend, the 630 nm line yields an abundance of log A(O) = 8.77 +/- 0.05 dex. We compare our results with previous estimates in the literature and draw a conclusion on the most likely value of the solar photospheric O abundance, which we estimate at log A(O) = 8.75 +/- 0.03 dex.

Solar abundance problem

Maria **Bergemann**, Aldo Serenelli
http://arxiv.org/pdf/1403.3097v1.pdf
The chemical composition of the Sun is among the most important quantities in astrophysics. Solar abundances are needed for modelling stellar atmospheres, stellar structure and evolution, population synthesis, and galaxies as a whole. The solar abundance problem refers to the conflict of observed data from helioseismology and the predictions made by stellar interior models for the Sun, if these models use the newest solar chemical composition obtained with 3D and NLTE models of radiative transfer. Here we take a close look at the problem from observational and theoretical perspective. We also provide a list of possible solutions, which have yet to be tested.

First Perihelion of EUI on the Solar Orbiter mission

D. **Berghmans**, P. Antolin, F. Auchère, R. Aznar Cuadrado, K. Barczynski, +++
A&A 675, A110 **2023**
https://arxiv.org/pdf/2301.05616.pdf
https://www.aanda.org/articles/aa/pdf/2023/07/aa45586-22.pdf
Context. The Extreme Ultraviolet Imager (EUI), onboard Solar Orbiter consists of three telescopes: the two High Resolution Imagers in EUV (HRIEUV) and in Lyman-{\alpha} (HRILya), and the Full Sun Imager (FSI). Solar Orbiter/EUI started its Nominal Mission Phase on 2021 November 27. Aims. EUI images from the largest scales in the extended corona off limb, down to the smallest features at the base of the corona and chromosphere. EUI is

therefore a key instrument for the connection science that is at the heart of the Solar Orbiter mission science goals. Methods. The highest resolution on the Sun is achieved when Solar Orbiter passes through the perihelion part of its orbit. On 2022 March 26, Solar Orbiter reached for the first time a distance to the Sun close to 0.3 au. No other coronal EUV imager has been this close to the Sun. Results. We review the EUI data sets obtained during the period 2022 March-April, when Solar Orbiter quickly moved from alignment with the Earth (2022 March 6), to perihelion (2022 March 26), to quadrature with the Earth (2022 March 29). We highlight the first observational results in these unique data sets and we report on the in-flight instrument performance. Conclusions. EUI has obtained the highest resolution images ever of the solar corona in the quiet Sun and polar coronal holes. Several active regions were imaged at unprecedented cadences and sequence durations. We identify in this paper a broad range of features that require deeper studies. Both FSI and HRIEUV operate at design specifications but HRILya suffered from performance issues near perihelion. We conclude emphasising the EUI open data policy and encouraging further detailed analysis of the events highlighted in this paper. **2022 March 2, 2022 March 4, 7, 8, 10, 2022 March 17, 21, 22, 27, 28, 30, April 1, 2**

Extreme UV quiet Sun brightenings observed by Solar Orbiter/EUI

D. **Berghmans**, F. Auchere, D. M. Long, E. Soubrie, M. Mierla A.N. Zhukov, U. Schuhle, P. Antolin, L. Harra S. Parenti, O. Podladchikova, R. Aznar Cuadrado, E. Buchlin, L. Dolla, C. Verbeeck, S. Gissot, L. Teriaca, M. Haberreiter, A.C. Katsiyannis, L. Rodriguez, E. Kraaikamp, P.J. Smith, K. Stegen, P. Rochus, J. P. Halain, L. Jacques, W.T. Thompson, B. Inhester

A&A Letter **2021**

https://arxiv.org/pdf/2104.03382.pdf

The goal of this paper is to study the smallest brightening events observed in the EUV quiet Sun. We use commissioning data taken by the EUI instrument onboard the recently launched Solar Orbiter mission. On **2020 May 30**, EUI was situated at 0.556AU from the Sun. Its HRIEUV telescope 17.4nm passband reached an exceptionally high two-pixel spatial resolution of 400km. The size and duration of small-scale structures is determined in the HRIEUV data, while their height is estimated from triangulation with the simultaneous SDO/AIA data. This is the first stereoscopy of small scale brightenings at high resolution. We observed small localised brightenings ("campfires") in a quiet Sun region with lengthscales between 400km and 4000km and durations between 10 and 200s. The smallest and weakest of these HRIEUV brightenings have not been observed before. Simultaneous HRILYA observations do not show localised brightening events, but the locations of the HRIEUV events correspond clearly to the chromospheric network. Comparison with simultaneous AIA images shows that most events can also be identified in the 17.1nm, 19.3nm, 21.1nm, and 30.4nm passbands of AIA, although they appear weaker and blurred. DEM analysis indicates coronal temperatures peaking at log(T)~6.1-6.15. We determined the height of a few campfires, which is between 1000 and 5000km above the photosphere. We conclude that "campfires" are mostly coronal in nature and are rooted in the magnetic flux concentrations of the chromospheric network. We interpret these events as a new extension to the flare/microflare/nanoflare family. Given their low height, the EUI "campfires" could be a new element of the fine structure of the transition region/low corona: apexes of small-scale loops that are internally heated to coronal temperatures.

Updated determination of the solar neutrino fluxes from solar neutrino data

Johannes **Bergstrom**, M.C. Gonzalez-Garcia, Michele Maltoni, Carlos Pena-Garay, Aldo M. Serenelli,Ningqiang Song

JHEP **2016**

arXiv admin note: substantial text overlap with arXiv:0910.4584

http://arxiv.org/pdf/1601.00972v1.pdf

We present an update of the determination of the solar neutrino fluxes from a global analysis of the solar and terrestrial neutrino data in the framework of three-neutrino mixing. Using a Bayesian analysis we reconstruct the posterior probability distribution function for the eight normalization parameters of the solar neutrino fluxes plus the relevant masses and mixing, with and without imposing the luminosity constraint. We then use these results to compare the description provided by different Standard Solar Models. Our results show that, at present, both models with low and high metallicity can describe the data with equivalent statistical agreement. We also argue that even with the present experimental precision the solar neutrino data have the potential to improve the accuracy of the solar model predictions.

SunMap: A Solar Image Processing Software for Obtaining Synoptic Maps

Sergio **Bernabé**, Gabriel García, Víctor M. S. Carrasco & José M. Vaquero

Solar Physics volume 297, Article number: 100 (**2022**)

https://link.springer.com/content/pdf/10.1007/s11207-022-02030-4.pdf

A new open-source software, called SunMap, has been developed to obtain synoptic maps in an easy and quick way from multiple full-disc solar images. Our objective is to provide a free and straightforward application for

heliophysicists and geophysicists interested in generating solar synoptic maps. SunMap allows comparison of structures and patterns of solar activity over various periods. Thus, the short- and long-term evolution of solar regions of interest can be studied. To reach this goal, different solar images taken day by day are stored in a single map that uses a sequence of images and allows the positioning of each observable element on it. A simple comparison between a synoptic map generated by SunMap and another previously constructed map is presented to show the versatility of this new available software.

Unexpected frequency of horizontal oscillations of magnetic structures in the solar photosphere

M. **Berretti**, M. Stangalini, G. Verth, S. Jafarzadeh, D. B. Jess, F. Berrilli, S. D. T. Grant, T. Duckenfield, V. Fedun
A&A Letters **2024**
https://arxiv.org/pdf/2407.03950
It is well known that the dominant frequency of oscillations in the solar photosphere is ≈3 mHz, which is the result of global resonant modes pertaining to the whole stellar structure. However, analyses of the horizontal motions of nearly 1 million photospheric magnetic elements spanning the entirety of solar cycle 24 have revealed an unexpected dominant frequency, ≈5 mHz, a frequency typically synonymous with the chromosphere. Given the distinctly different physical properties of the magnetic elements examined in our statistical sample, when compared to largely quiescent solar plasma where ≈3 mHz frequencies are omnipresent, we argue that the dominant ≈5 mHz frequency is not caused by the buffeting of magnetic elements, but instead is due to the nature of the underlying oscillatory driver itself. This novel result was obtained by exploiting the unmatched spatial and temporal coverage of magnetograms acquired by the Helioseismic and Magnetic Imager (HMI) on board NASA's Solar Dynamics Observatory (SDO). Our findings provide a timely avenue for future exploration of the magnetic connectivity between sub-photospheric, photospheric, and chromospheric layers of the Sun's dynamic atmosphere.

Long-term (1749–2015) Variations of Solar UV Spectral Indices

Francesco **Berrilli**, Serena Criscuoli, Valentina Penza & Mija Lovric
Solar Physics volume 295, Article number: 38 (**2020**)
https://link.springer.com/content/pdf/10.1007/s11207-020-01603-5.pdf
Solar radiation variability spans a wide range in time, ranging from seconds to decadal and longer. The nearly 40 years of measurements of solar irradiance from space established that the total solar irradiance varies by ≈0.1%≈0.1% in phase with the Sun’s magnetic cycle. Specific intervals of the solar spectrum, e.g., ultraviolet (UV), vary by orders of magnitude more. These variations can affect the Earth’s climate in a complex non-linear way. Specifically, some of the processes of interaction between solar UV radiation and the Earth’s atmosphere involve threshold processes and do not require a detailed reconstruction of the solar spectrum. For this reason a spectral UV index based on the (FUV-MUV) color has been recently introduced. This color is calculated using SORCE SOLSTICE integrated fluxes in the FUV and MUV bands. We present in this work the reconstructions of the solar (FUV-MUV) color and Ca II K and Mg II indices, from 1749–2015, using a semi-empirical approach based on the reconstruction of the area coverage of different solar magnetic features, i.e., sunspot, faculae and network. We remark that our results are in noteworthy agreement with latest solar UV proxy reconstructions that exploit more sophisticated techniques requiring historical full-disk observations. This makes us confident that our technique can represent an alternative approach which can complement classical solar reconstruction efforts. Moreover, this technique, based on broad-band observations, can be utilized to estimate the activity on Sun-like stars, that cannot be resolved spatially, hosting extra-solar planetary systems.

Cross-helicity in Solar Active Regions

Alexander **Bershadskii**
2020 Res. Notes AAS 4 10
https://iopscience.iop.org/article/10.3847/2515-5172/ab6bd7
Although it is still difficult to compute the cross-helicity from the observations at the solar surface the recently obtained vector magnetograms and Dopplergrams allow reasonable estimates of its finite values to be made. The observed magnetic energy spectra, on the other hand, allow us to make certain conclusions about the contribution of the cross-helicity in the dynamics of the solar active regions. **2012 June 30 to July 6**

Observations and NLTE modeling of Ellerman bombs

Arkadiusz **Berlicki**, Petr Heinzel
A&A 567, A110 (**2014**)
http://arxiv.org/pdf/1406.5702v1.pdf
Ellerman bombs (EBs) are short-lived and compact structures that are observed well in the wings of the hydrogen H-alpha line. EBs are also observed in the chromospheric CaII lines and in UV continua. H-alpha line profiles of EBs

show a deep absorption at the line center and enhanced emission in the line wings. Similar shapes of the line profiles are observed for the CaII IR line at 8542 ang. It is generally accepted that EBs may be considered as compact microflares located in lower solar atmosphere. However, it is still not clear where exactly the emission of EBs is formed in the solar atmosphere. High-resolution spectrophotometric observations of EBs were used for determining of their physical parameters and construction of semi-empirical models. In our analysis we used observations of EBs obtained in the H-alpha and CaII H lines. We also used NLTE numerical codes for the construction of grids of 243 semi-empirical models simulating EBs structures. In this way, the observed emission could be compared with the calculated line spectra. For a specific model we found reasonable agreement between the observed and theoretical emission and thus we consider such model as a good approximation of the EBs atmospheres. This model is characterized by an enhanced temperature in the lower chromosphere and can be considered as a compact structure (hot spot). For the first time the set of two lines H-alpha and CaII H was used to construct semi-empirical models of EBs. Our analysis shows that EBs can be described by a "hot spot" model, with the temperature and/or density increase through a few hundred km atmospheric structure. We confirmed that EBs are located close to the temperature minimum or in the lower chromosphere. Two spectral features, observed simultaneously, significantly strengthen the constraints on a realistic model.

Magnetic pattern at supergranulation scale: the void size distribution

F. **Berrilli**, S. Scardigli and D. Del Moro
A&A 568, A102 (**2014**)
The large-scale magnetic pattern observed in the photosphere of the quiet Sun is dominated by the magnetic network. This network, created by photospheric magnetic fields swept into convective downflows, delineates the boundaries of large-scale cells of overturning plasma and exhibits “voids” in magnetic organization. These voids include internetwork fields, which are mixed-polarity sparse magnetic fields that populate the inner part of network cells. To single out voids and to quantify their intrinsic pattern we applied a fast circle-packing-based algorithm to 511 SOHO/MDI high-resolution magnetograms acquired during the unusually long solar activity minimum between cycles 23 and 24. The computed void distribution function shows a quasi-exponential decay behavior in the range 10–60 Mm. The lack of distinct flow scales in this range corroborates the hypothesis of multi-scale motion flows at the solar surface. In addition to the quasi-exponential decay, we have found that the voids depart from a simple exponential decay at about 35 Mm.

Hamiltonian distributed chaos in long-term solar activity

A. **Bershadskii**
2018
https://arxiv.org/pdf/1803.01806.pdf
It is shown that the long-term solar activity (represented by the dynamically covered monthly time series of the sunspot number for period 1750-2005yy) exhibits spectral properties of the Hamiltonian distributed chaos with spontaneously broken time translational symmetry.

Correlation Between Sunspot Number and Ca II K Emission Index

Luca **Bertello**, Alexei A. Pevtsov, Andrey Tlatov, Jagdev Singh
Solar Phys. **2016**
http://arxiv.org/pdf/1606.01092v1.pdf
Long-term synoptic observations in the resonance line of Ca II K constitute a fundamental database for a variety of retrospective analyses of the state of the solar magnetism. Synoptic Ca II K observations began in late 1904 at the Kodaikanal Observatory, in India. In early 1970s, the National Solar Observatory (NSO) at Sacramento Peak (USA) started a new program of daily Sun-as-a-star observations in the Ca II K line. Today the NSO is continuing these observations through its Synoptic Optical Long-term Investigations of the Sun (SOLIS) facility. These different data sets can be combined into a single disk-integrated Ca II K index time series that describes the average properties of the chromospheric emission over several solar cycles. We present such a Ca II K composite and discuss its correlation with the new entirely revised sunspot number data series. For this preliminary investigation, the scaling factor between pairs of time series was determined assuming a simple linear model for the relationship between the monthly mean values during the duration of overlapping observations.

Spectropolarimetric observations of the solar atmosphere in the Hα 6563 Å line

J. Jaume **Bestard**, J. Trujillo Bueno, M. Bianda, J. Štěpán, R. Ramelli
A&A **2022**
https://arxiv.org/pdf/2201.03815.pdf
We present novel spectropolarimetric observations of the hydrogen Hα line taken with the Zürich Imaging Polarimeter (ZIMPOL) at the Gregory Coudé Telescope of the Istituto Ricerche Solari Locarno (IRSOL). The linear

polarization is clearly dominated by the scattering of anisotropic radiation and the Hanle effect, while the circular polarization by the Zeeman effect. The observed linear polarization signals show a rich spatial variability, the interpretation of which would open a new window for probing the solar chromosphere. We study their spatial variation within coronal holes, finding a different behaviour for the U/I signals near the North and South solar poles. We identify some spatial patterns, which may facilitate the interpretation of the observations. In close-to-the-limb regions with sizable circular polarization signals we find similar asymmetric Q/I profiles. We also show examples of net circular polarization profiles (NCP), along with the corresponding linear polarization signals. The application of the weak field approximation to the observed circular polarization signals gives 10G (40−60G) in close to the limb quiet (plage) regions for the average longitudinal field strength over the spatio-temporal resolution element.

Imprint of the magnetic activity cycle on solar asteroseismic characterisation based on 26 years of GOLF and BiSON data

Jérôme **Bétrisey**, Martin Farnir, Sylvain N. Breton, Rafael A. García, Anne-Marie Broomhall, Anish M. Amarsi, Oleg Kochukhov
A&A Letters 688, L17 **2024**
https://arxiv.org/pdf/2407.15655
https://www.aanda.org/articles/aa/pdf/2024/08/aa51365-24.pdf
Building on the success of previous missions, asteroseismic modelling will play a key role in future space-based missions, such as PLATO, CubeSpec, and Roman. Despite remarkable achievements, asteroseismology has revealed significant discrepancies in the physics of theoretical stellar models, which have the potential to bias stellar characterisation at the precision level demanded by PLATO. The current modelling strategies largely overlook magnetic activity, assuming that its effects are masked by filtering the so-called surface effects. Given the presence of activity cycles in multiple solar-like oscillators, and activity variations in a significant fraction of Kepler observations of main-sequence stars (Santos et al. 2019b, 2021, 2023), we measured the impact of magnetic activity on the asteroseismic characterisation of the Sun based on 26.5 years of GOLF and BiSON observations. While magnetic activity is partially absorbed in the treatment of surface effects, we found a discernible imprint of the activity cycle in the determination of the solar age. Notably, this imprint persists across both BiSON and GOLF datasets, with significant variations of up to 6.5% observed between solar minima and maxima. Considering that the Sun exhibits low levels of activity, our study underscores the looming challenge posed by magnetic activity for future photometry missions, and prompts a potential reevaluation of the asteroseismic characterisation of Kepler's most active targets.

Chromospheric plasma ejection above a pore

L. **Bharti**, B. Shobha, C. Quintero Noda, C. Joshi, U. Pandya
MNRAS Volume 493, Issue 2, Pages 3036–3044 **2020**
https://arxiv.org/pdf/2002.04503.pdf
https://doi.org/10.1093/mnras/staa434
We present high spatial resolution observations of short lived transients, ribbon and jets like events above a pore in Ca II H images where fine structure like umbral dots, lightbridge and penumbral micro filaments are present in the underlying photosphere. We found that current layers are formed at the edges of convective fine structure due to the shear between their horizontal field and the ambient vertical field. High vertical electric current density patches are observed in the photosphere around these events which indicates the formation of a current sheet at the reconnection site. In the framework of past studies, low altitude reconnection could be the mechanism that produces such events. The reconnection is caused by an opposite polarity field produced by the bending of field lines by convective downflows at the edge of the pore fine structures. **May 11, 2007**

Hydraulic effects in a radiative atmosphere with ionization

P. **Bhat**1,2,3 and A. Brandenburg
A&A 587, A90 (**2016**)
Context. In his 1978 paper, Eugene Parker postulated the need for hydraulic downward motion to explain magnetic flux concentrations at the solar surface. A similar process has also recently been seen in simplified (e.g., isothermal) models of flux concentrations from the negative effective magnetic pressure instability (NEMPI).
Aims. We study the effects of partial ionization near the radiative surface on the formation of these magnetic flux concentrations.
Methods. We first obtain one-dimensional (1D) equilibrium solutions using either a Kramers-like opacity or the H− opacity. The resulting atmospheres are then used as initial conditions in two-dimensional (2D) models where flows are driven by an imposed gradient force that resembles a localized negative pressure in the form of a blob. To isolate the effects of partial ionization and radiation, we ignore turbulence and convection.
Results. Because of partial ionization, an unstable stratification always forms near the surface. We show that the extrema in the specific entropy profiles correspond to the extrema in the degree of ionization. In the 2D models without partial ionization, strong flux concentrations form just above the height where the blob is placed.

Interestingly, in models with partial ionization, such flux concentrations always form at the surface well above the blob. This is due to the corresponding negative gradient in specific entropy. Owing to the absence of turbulence, the downflows reach transonic speeds.
Conclusions. We demonstrate that, together with density stratification, the imposed source of negative pressure drives the formation of flux concentrations. We find that the inclusion of partial ionization affects the entropy profile dramatically, causing strong flux concentrations to form closer to the surface. We speculate that turbulence effects are needed to limit the strength of flux concentrations and homogenize the specific entropy to a stratification that is close to marginal.

A unified large/small-scale dynamo in helical turbulence

Pallavi **Bhat**, Kandaswamy Subramanian, Axel Brandenburg
MNRAS **2015**
http://arxiv.org/pdf/1508.02706v1.pdf
We use high resolution direct numerical simulations to show that helical turbulence can generate large-scale fields even in the presence of strong small-scale fields.During the kinematic stage, the unified large/small-scale dynamo grows fields with a shape-invariant eigenfunction, with most power peaked at small scales or large k. Nevertheless, the large-scale field can be clearly detected as an excess power at small k in the negatively polarized component of the energy spectrum for a forcing with positively polarized waves. The strength of such kinematic large-scale field $\overline{B}$ relative to the total rms field Brms decreases with increasing magnetic Reynolds number, ReM. However, as the Lorentz force becomes important, the field orders itself by saturating on successively larger scales. The magnetic power spectrum in the saturated state shows peaks at both the forcing wavenumber k=kf, and at the box scale, k=1. The magnetic integral scale for the positively polarized waves, increases significantly from the kinematic stage to saturation. This implies that the small-scale field becomes as coherent as possible for a given forcing scale. Such an increase in the coherence scale of small-scale fields away from resistive scales averts the ReM-dependent quenching of $\overline{B}$/Brms. The $\overline{B}$, whose energy is measured in terms of the energy at k=1--2, grows from a value of the order of 4% to about 40% of Brms at saturation, aided in the final stages by helicity dissipation. Our results confirm that in helical turbulence, there is a single unified dynamo, with all scales initially growing together at one rate and, as the Lorentz force becomes important, successively larger scales saturate, with the largest scales continuing to grow (aided by small-scale magnetic helicity loss) as the small-scale field saturates.

Magnetic Topology of quiet-Sun Ellerman bombs and associated Ultraviolet brightenings

Aditi **Bhatnagar**, Avijeet Prasad, Luc Rouppe van der Voort, Daniel Nóbrega-Siverio, Jayant Joshi
A&A **2024**
https://arxiv.org/pdf/2412.03211
Quiet-Sun Ellerman bombs (QSEBs) are small-scale magnetic reconnection events in the lower atmosphere of the quiet Sun. Recent work has shown that a small percentage of them can occur co-spatially and co-temporally to ultraviolet (UV) brightenings in the transition region. We aim to understand how the magnetic topologies associated with closely occurring QSEBs and UV brightenings can facilitate energy transport and connect these events. We used high-resolution H-beta observations from the Swedish 1-m Solar Telescope (SST) and detected QSEBs using k-means clustering. We obtained the magnetic field topology from potential field extrapolations using spectro-polarimetric data in the photospheric Fe I 6173 A line. To detect UV brightenings, we used coordinated and co-aligned data from the Interface Region Imaging Spectrograph (IRIS) and imposed a threshold of 5 sigma above the median background on the (IRIS) 1400 A slit-jaw image channel. We identify four distinct magnetic configurations that associate QSEBs with UV brightenings, including a simple dipole configuration and more complex fan-spine topologies with a three-dimensional (3D) magnetic null point. In the fan-spine topology, the UV brightenings occur near the 3D null point, while QSEBs can be found close to the footpoints of the outer spine, the inner spine, and the fan surface. We find that the height of the 3D null varies between 0.2 Mm to 2.6 Mm, depending on the magnetic field strength in the region. We note that some QSEBs and UV brightenings, though occurring close to each other, are not topologically connected with the same reconnection process. We find that the energy released during QSEBs falls in the range of 10^23 to 10^24 ergs. This study shows that magnetic connectivity and topological features, like 3D null points, are crucial in linking QSEBs in the lower atmosphere with UV brightenings in the transition region.
22 June 2021

Transition region response to Quiet Sun Ellerman Bombs

Aditi **Bhatnagar**, Luc Rouppe van der Voort, Jayant Joshi
A&A **2024**
https://arxiv.org/pdf/2406.09585
Quiet Sun Ellerman Bombs (QSEBs) are key indicators of small-scale photospheric magnetic reconnection events. Recent high-resolution observations have shown that they are ubiquitous and that large numbers of QSEBs can be

found in the quiet Sun. We aim to understand the impact of QSEBs on the upper solar atmosphere by analysing their spatial and temporal relationship with the UV brightenings observed in transition region diagnostics. We analyse high-resolution H-beta observations from the Swedish 1-m Solar Telescope and utilise k-means clustering to detect 1423 QSEBs in a 51 min time series. We use coordinated and co-aligned observations from the Interface Region Imaging Spectrograph (IRIS) to search for corresponding signatures in the 1400 A slit-jaw image (SJI) channel and in the Si IV 1394 A and Mg II 2798.8 A triplet spectral lines. We identify UV brightenings from SJI 1400 using a threshold of 5σ above the median background. We focused on 453 long-lived QSEBs (>1 min) and found 67 cases of UV brightenings from SJI 1400 occurring near the QSEBs, both temporally and spatially. Temporal analysis of these events indicates that QSEBs start before UV brightenings in 57 % of cases, while UV brightenings lead in 36 % of instances. The majority of the UV brightenings occur within 1000 km from the QSEBs in the direction of the solar limb. We also identify 21 QSEBs covered by the IRIS slit, with 4 of them showing emissions in both or one of the Si IV 1394 A and Mg II 2798.8 A triplet lines, at distances within 500 km from the QSEBs in the limb direction. We conclude that a small fraction (15 %) of the long-lived QSEBs contribute to localized heating observable in transition region diagnostics, indicating a minimal role in the global heating of the upper solar atmosphere.

Variations in the Solar Coronal Rotation with Altitude - Revisited

Hitaishi **Bhatt**, Rupal Trivedi, Som Kumar Sharma, Hari Om Vats
Solar Phys. 292:55 **2017**
https://arxiv.org/pdf/1702.08297.pdf
http://link.springer.com/content/pdf/10.1007%2Fs11207-017-1071-x.pdf
Here we report in depth reanalysis of a paper by Vats et al. (2001) [Astrophys. J. 548, L87] based on the measurements of differential rotation with altitude as a function of observing frequencies (as lower and higher frequencies indicate higher and lower heights, respectively) in the solar corona. The radial differential rotation of the solar corona is estimated from daily measurements of the disc-integrated solar radio flux at 11 frequencies: (275, 405, 670, 810, 925, 1080, 1215, 1350, 1620, 1755 MHz and 2800 MHz). We use the same data as were used in Vats et al. (2001), but instead of the 12th maxima of autocorrelograms used there, we use the 1st secondary maxima to derive the synodic rotation period. We estimate synodic rotation by Gaussian fit of the 1st secondary maxima. Vats et al. (2001) reported that the sidereal rotation period increases with increasing frequency. The variation found by them was from 23.6 to 24.15 days in this frequency range with a difference of only 0.55 days. The present study finds that sidereal rotation period increases with decreasing frequency. The variation range is from 24.4 to 22.5 days and difference is about three times larger (1.9 days). However, at 925 MHz both studies give similar rotation period. In Vats et al. (2001) the Pearson factor with trend line was 0.86 whereas present analysis obtained a ~ 0.97 Pearson factor with the trend line. Our study shows that the solar corona rotates slower at higher altitudes, which is in contradiction to the findings reported in Vats et al. (2001).

A linear model for inertial modes in a differentially rotating Sun

Jishnu **Bhattacharya**, Chris S. Hanson, Shravan M. Hanasoge, Katepalli R. Sreenivasan
2024 *ApJ* **965** 55
https://arxiv.org/pdf/2308.12766.pdf
https://iopscience.iop.org/article/10.3847/1538-4357/ad226c/pdf
Inertial wave modes in the Sun are of interest owing to their potential to reveal new insight into the solar interior. These predominantly retrograde-propagating modes in the solar subsurface appear to deviate from the thin-shell Rossby-Haurwitz model at high azimuthal orders. We present new measurements of sectoral equatorial inertial modes at m>15 where the modes appear to become progressively less retrograde compared to the canonical Rossby-Haurwitz dispersion relation in a co-rotating frame. We use a spectral eigenvalue solver to compute the spectrum of solar inertial modes in the presence of differential rotation. Focussing specifically on equatorial Rossby modes, we find that the numerically obtained mode frequencies lie along distinct ridges, one of which lies strikingly close to the observed mode frequencies in the Sun. We also find that the n=0 ridge is deflected strongly in the retrograde direction. This suggests that the solar measurements may not correspond to the fundamental n=0 Rossby-Haurwitz solutions as was initially suspected, but to a those for a higher n. The numerically obtained eigenfunctions also appear to sit deep within the convection zone -- unlike those for the n=0 modes -- which differs substantially from solar measurements and complicates inference.

Scale Transfer in 1849 : Heinrich Schwabe to Rudolf Wolf

Shreya **Bhattacharya**, Laure Lefevre, Hisashi Hayakawa, Maarten Jansen, Frederic Clette
Solar Phys. **2022**
https://arxiv.org/ftp/arxiv/papers/2210/2210.03362.pdf
The focus of this study is to reveal the reason behind a scale problem detected around 1849 in the historical version of the International Sunspot Number Series, i.e. version 1 (Leussu et al, Astronomy and Astrophysics, 559, A28, 2013; Friedli, Solar Phys.291, 2505, 2016). From 1826 to 1848 Heinrich Schwabe's observations were considered

primary by Rudolf Wolf, and a shift of primary observer from Schwabe to Wolf in 1849 seems to have led to an inconsistency in the Sunspot Number series. In this study we benefited from various datasets, the most important being Schwabe's raw counts from the Mittheilungen (Prof. Wolf's Journals) that have been digitised at the Royal Observatory of Belgium between 2017 and 2019. We provide a robust quantification of the detected problem by using classic algebraic calculations but also different methods such as a method inspired by Lockwood et al (Journal of Geophysical Research (Space Physics), 119(7), 5172, 2014), hence assigning a modern k-factor to Schwabe's observations before 1849. We also assess the implications of this 1849 inconsistency on the International Sunspot Number series (Versions 1 and 2) before and after 1849.

Numerical evaluation of time-distance helioseismic sensitivity kernels in spherical geometry

Jishnu **Bhattacharya**

A&A **2022**

https://arxiv.org/pdf/2112.13517.pdf

Context: Helioseismic analysis of large-scale flows and structural inhomogeneities in the Sun requires the computation of sensitivity kernels that account for the spherical geometry of the Sun, as well as systematic effects such as line-of-sight projection. Aim: I aim to develop a code to evaluate helioseismic sensitivity kernels for flows using line-of-sight projected measurements. Methods: I decomposed the velocity field in a basis of vector spherical harmonics and computed the kernel components corresponding to the coefficients of velocity in this basis. The kernels thus computed are radial functions that set up a 1.5D inverse problem to infer the flow from surface measurements. I demonstrate that using the angular momentum addition formalism lets us express the angular dependence of the kernels as bipolar spherical harmonics, which may be evaluated accurately and efficiently. Results: Kernels for line-of-sight projected measurements may differ significantly from those that don't account for projection. Including projection in our analysis does not increase the computational time significantly. We demonstrate that it is possible to evaluate kernels for pairs of points that are related through a rotation by linearly transforming the terms that enter the expression of the kernel, and that this result holds even for line-of-sight projected kernels. Conclusion: I developed a Julia code that may be used to evaluate sensitivity kernels for seismic wave travel times computed using line-of-sight projected measurements, which is made freely available under the MIT license.

A modern reconstruction of Carrington's observations (1853-1861)

Shreya **Bhattacharya**, E.T.H Teague, S. Fay, Laure Lefèvre, M. Jansen, F. Clette

Solar Phys. **296**, Article number: 118 **2021**

https://arxiv.org/pdf/2103.05353.pdf

https://link.springer.com/content/pdf/10.1007/s11207-021-01864-8.pdf

https://doi.org/10.1007/s11207-021-01864-8

The focus of this article is a re-count of Richard Carrington's original sunspot observations from his book drawings (Carrington,1863) by an observer from the World data Center-SILSO network, Thomas H. Teague(UK). This modern recount will enable the use of Carrington's observations in the re-computation of the entire Sunspot Number series in a way Carrington's original counts (Casas and Vaquero,2014) did not. here we present comparison studies of the new recounted series with contemporary observations, new data extracted from the Journals of the Zurich Observatory and other sources of Carrington's own observations and conclude that Carrington's group counting is very close to the modern way of counting while his method for counting individual spots lags significantly behind modern counts. We also test the quality and robustness of the new re-count with methods developed in Mathieu et al.,2019.

Helioseismic finite-frequency sensitivity kernels for flows in spherical geometry including systematic effects

Jishnu **Bhattacharya**

ApJ **905** 59 **2020**

https://arxiv.org/pdf/2011.02180.pdf

https://doi.org/10.3847/1538-4357/abc7c0

Helioseismic inferences of large-scale flows in the solar interior necessitate accounting for the curvature of the Sun, both in interpreting systematic trends introduced in measurements as well as the sensitivity kernel that relates photospheric measurements to subsurface flow velocities. Additionally the inverse problem that relates measurements to model parameters needs to be well-posed to obtain accurate inferences, which necessitates a sparse set of parameters. Further, the sensitivity functions need to be computationally easy to evaluate. In this work we address these issues by demonstrating that the sensitivity kernels for flow velocities may be computed efficiently in a basis of vector spherical harmonics. We are also able to account for line-of-sight projections in Doppler measurements, as well as center-to-limb differences in line-formation heights. We show that given the assumed spherical symmetry of the background model, it is often cheap to simultaneously compute the kernels for pairs of

observation points that are related by a rotation. Such an approach is therefore particularly well-suited to inverse problems for large-scale flows in the Sun, such as meridional circulation.

A General Formulation for Computing Spherical Helioseismic Sensitivity Kernels while Incorporating Systematical Effects

Jishnu **Bhattacharya**1, Shravan M. Hanasoge1,2, and Katepalli R. Sreenivasan
2020 ApJ 895 117
https://doi.org/10.3847/1538-4357/ab8eac
https://arxiv.org/pdf/2009.07056
As helioseismology matures and turns into a precision science, modeling finite-frequency, geometric, and systematical effects is becoming increasingly important. Here we introduce a general formulation for treating perturbations of arbitrary tensor rank in spherical geometry using fundamental ideas of quantum mechanics and their extensions in geophysics. We include line-of-sight projections and center-to-limb differences in line formation heights in our analysis. We demonstrate the technique by computing a travel-time sensitivity kernel for sound-speed perturbations. The analysis produces the spherical harmonic coefficients of the sensitivity kernels, which leads to better-posed and computationally efficient inverse problems.

Iterative inversion of synthetic travel times successful at recovering sub-surface profiles of supergranular flows

Recovery of subsurface profiles of supergranular flows via iterative inversion of synthetic travel times

Jishnu **Bhattacharya**, Shravan M. Hanasoge, Aaron C. Birch, Laurent Gizon
A&A 607, A129 **2017**
https://arxiv.org/pdf/1708.03464.pdf
We develop a helioseismic inversion algorithm that can be used to recover sub-surface vertical profiles of 2-dimensional supergranular flows from surface measurements of synthetic wave travel times. We carry out seismic wave-propagation simulations through a 2-dimensional section of a flow profile that resembles an averaged supergranule, and a starting model that has flows only at the surface. We assume that the wave measurements are entirely without realization noise for the purpose of our test. We expand the vertical profile of the supergranule stream function on a basis of B-splines. We iteratively update the B-spline coefficients of the supergranule model to reduce the travel-times differences observed between the two simulations. We carry out the exercise for four different vertical profiles peaking at different depths below the solar surface. We are able to accurately recover depth profiles of four supergranule models at depths up to 8−10Mm below the solar surface using f−p4 modes, under the assumption that there is no realization noise. We are able to obtain the peak depth and the depth of the return flow for each model. A basis-resolved inversion performs significantly better than one where the flow field is inverted for at each point in the radial grid. This is an encouraging result and might act as a guide in developing more realistic inversion strategies that can be applied to supergranular flows in the Sun.

Strategies in seismic inference of supergranular flows on the Sun

Jishnu **Bhattacharya**, Shravan M. Hanasoge
ApJ **826** 105 **2016**
http://arxiv.org/pdf/1605.09315v1.pdf
Observations of the solar surface reveal the presence of flows with length scales of around 35 Mm, commonly referred to as supergranules. Inferring the sub-surface flow profile of supergranules from measurements of the surface and photospheric wavefield is an important challenge faced by helioseismology. Traditionally, the inverse problem has been approached by studying the linear response of seismic waves in a horizontally translationally invariant background to the presence of the supergranule; following an iterative approach that does not depend on horizontal translational invariance might perform better, since the misfit can be analyzed post iterations. In this work, we construct synthetic observations using a reference supergranule, and invert for the flow profile using surface measurements of travel-times of waves belonging to modal ridges f (surface-gravity) and p1 through p7 (acoustic). We study the extent to which individual modes and their combinations contribute to infer the flow. We show that this method of non-linear iterative inversion tends to underestimate the flow velocities as well as inferring a shallower flow profile, with significant deviations from the reference supergranule near the surface. We carry out a similar analysis for a sound-speed perturbation and find that analogous near-surface deviations persist, although the iterations converge faster and more accurately. We conclude that a better approach to inversion would be to expand the supergranule profile in an appropriate basis, thereby reducing the number of parameters being inverted for and appropriately regularizing them.

Frequency shifts of resonant modes of the Sun due to near-surface convective scattering

Jishnu **Bhattacharya**, Shravan. M. Hanasoge, H. M. Antia

ApJ **806** 246 **2015**

http://arxiv.org/pdf/1505.04048v1.pdf

Measurements of oscillation frequencies of the Sun and stars can provide important independent constraints on their internal structure and dynamics. Seismic models of these oscillations are used to connect structure and rotation of the star to its resonant frequencies, which are then compared with observations, the goal being that of minimizing the difference between the two. Even in the case of the Sun, for which structure models are highly tuned, observed frequencies show systematic deviations from modeled frequencies, a phenomenon referred to as the "surface term." The dominant source of this systematic effect is thought to be vigorous near-surface convection, which is not well accounted for in both stellar modeling and mode-oscillation physics. Here we bring to bear the method of homogenization, applicable in the asymptotic limit of large wavelengths (in comparison to the correlation scale of convection), to characterize the effect of small-scale surface convection on resonant-mode frequencies in the Sun. We show that the full oscillation equations, in the presence of temporally stationary 3-D flows, can be reduced to an effective "quiet-Sun" wave equation with altered sound speed, Br\"{u}nt--V\"{a}is\"{a}la frequency and Lamb frequency. We derive the modified equation and relations for the appropriate averaging of three dimensional flows and thermal quantities to obtain the properties of this effective medium. Using flows obtained from three dimensional numerical simulations of near-surface convection, we quantify their effect on solar oscillation frequencies, and find that they are shifted systematically and substantially. We argue therefore that consistent interpretations of resonant frequencies must include modifications to the wave equation that effectively capture the impact of vigorous hydrodynamic convection.

Physical Models for Solar Cycle Predictions **Review**

Prantika **Bhowmik**, Jie Jiang, Lisa Upton, Alexandre Lemerle, Dibyendu Nandy

Space Science Reviews **219**, Article number: 40 **2023**

https://arxiv.org/pdf/2303.12648

https://link.springer.com/content/pdf/10.1007/s11214-023-00983-x.pdf

The dynamic activity of stars such as the Sun influences (exo)planetary space environments through modulation of stellar radiation, plasma wind, particle and magnetic fluxes. Energetic stellar phenomena such as flares and coronal mass ejections act as transient perturbations giving rise to hazardous space weather. Magnetic fields -- the primary driver of stellar activity -- are created via a magnetohydrodynamic dynamo mechanism within stellar convection zones. The dynamo mechanism in our host star -- the Sun -- is manifest in the cyclic appearance of magnetized sunspots on the solar surface. While sunspots have been directly observed for over four centuries, and theories of the origin of solar-stellar magnetism have been explored for over half a century, the inability to converge on the exact mechanism(s) governing cycle to cycle fluctuations and inconsistent predictions for the strength of future sunspot cycles have been challenges for models of solar cycle forecasts. This review discusses observational constraints on the solar magnetic cycle with a focus on those relevant for cycle forecasting, elucidates recent physical insights which aid in understanding solar cycle variability, and presents advances in solar cycle predictions achieved via data-driven, physics-based models. The most successful prediction approaches support the Babcock-Leighton solar dynamo mechanism as the primary driver of solar cycle variability and reinforces the flux transport paradigm as a useful tool for modelling solar-stellar magnetism.

Prediction of the strength and timing of sunspot cycle 25 reveal decadal-scale space environmental conditions

Prantika **Bhowmik**, Dibyendu Nandy

Nature Communications **2019**

https://arxiv.org/pdf/1909.04537.pdf

The Sun's activity cycle governs the radiation, particle and magnetic flux in the heliosphere creating hazardous space weather. Decadal-scale variations define space climate and force the Earth's atmosphere. However, predicting the solar cycle is challenging. Current understanding indicates a short window for prediction best achieved at previous cycle minima. Utilizing magnetic field evolution models for the Sun's surface and interior we perform the first century-scale, data-driven simulations of solar activity and present a scheme for extending the prediction window to a decade. Our ensemble forecast indicates cycle 25 would be similar or slightly stronger than the current cycle and peak around 2024. Sunspot cycle 25 may thus reverse the substantial weakening trend in solar activity which has led to speculation of an imminent Maunder-like grand minimum and cooling global climate. Our simulations demonstrate fluctuation in the tilt angle distribution of sunspots is the dominant mechanism responsible for solar cycle variability.

Polar flux imbalance at the sunspot cycle minimum governs hemispheric asymmetry in the following cycle

Prantika **Bhowmik**1

A&A 632, A117 (**2019**)
https://doi.org/10.1051/0004-6361/201834425

Aims. Hemispheric irregularities of solar magnetic activity is a well-observed phenomenon, the origin of which has been studied through numerical simulations and data analysis techniques. In this work we explore possible causes generating north-south asymmetry in the reversal timing and amplitude of the polar field during cycle minimum. Additionally, we investigate how hemispheric asymmetry is translated from cycle to cycle.
Methods. We pursued a three-step approach. Firstly, we explored the asymmetry present in the observed polar flux and sunspot area by analysing observational data of the last 110 years. Secondly, we investigated the contribution from various factors involved in the Babcock–Leighton mechanism to the evolution and generation of polar flux by performing numerical simulations with a surface flux transport model and synthetic sunspot input profiles. Thirdly, translation of hemispheric asymmetry in the following cycle was estimated by assimilating simulation-generated surface magnetic field maps at cycle minimum in a dynamo simulation. Finally, we assessed our understanding of hemispheric asymmetry in the context of observations by performing additional observational data-driven simulations.
Results. Analysis of observational data shows a profound connection between the hemispheric asymmetry in the polar flux at cycle minimum and the total hemispheric activity during the following cycle. We find that the randomness associated with the tilt angle of sunspots is the most crucial element among diverse components of the Babcock–Leighton mechanism in resulting hemispheric irregularities in the evolution of polar field. Our analyses with dynamo simulations indicate that an asymmetric poloidal field at the solar minimum can introduce significant north-south asymmetry in the amplitude and timing of peak activity during the following cycle. While observational data-driven simulations reproduce salient features of the observed asymmetry in the solar cycles during the last 100 years, we speculate that fluctuations in the mean-field α-effect and meridional circulation can have finite contributions in this regard.

Is hemispheric asymmetry in the sunspot cycle solely governed by polar flux imbalance in the previous cycle?

Prantika **Bhowmik**

2019
https://arxiv.org/pdf/1906.06877.pdf

Hemispheric irregularities of solar magnetic activity is a well-observed phenomenon -- the origin of which has been studied through numerical simulations and data-analysis techniques. In this work we explore possible causes generating north-south asymmetry in the reversal timing and the amplitude of polar field during cycle minimum. Additionally, we investigate how hemispheric asymmetry is translated from cycle to cycle. We pursue a three-step approach. Firstly, we explore the asymmetry present in the observed polar flux and sunspot area by analyzing observational data of the last 110 years. Secondly, we investigate contribution from different factors involved in the Babcock-Leighton mechanism to the evolution and generation of polar flux by performing numerical simulations with a Surface Flux Transport model and synthetic sunspot input profiles. Thirdly, propagation of hemispheric asymmetry in the following cycle is estimated by assimilating simulation-generated surface magnetic field maps at cycle minimum in a dynamo simulation. Finally, we assess our understanding of hemispheric asymmetry while reproducing observed asymmetry in the eight past solar cycles by performing additional observational data-driven simulations.

Morphological evidence for nanoflares heating warm loops in the solar corona⋆

Yi **Bi**1,2, Jia-Yan Yang1, Ying Qin1,2, Zheng-Ping Qiang3, Jun-Chao Hong1, Bo Yang1, Zhe Xu1, Hui Liu1,2 and Kai-Fan Ji1

A&A 679, A9 (**2023**)
https://www.aanda.org/articles/aa/pdf/2023/11/aa46944-23.pdf

Context. Nanoflares are impulsive energy releases that occur due to magnetic reconnection in the braided coronal magnetic field, which is a potential mechanism for heating the corona. However, there are still sporadic observations of the interchange of braiding structure segments and footpoints inside coronal loops, which is predicted to be the morphological evolution of the reconnecting magnetic bundles in the nanoflare picture.
Aims. This work aims to detect the evolutions of the pairs of braiding strands within the apparent single coronal loops observed in Atmospheric Imaging Assembly (AIA) images.
Methods. The loop strands were detected on two kinds of upsampled AIA 193 Å images, which were obtained by upscaling the point spread function matched AIA images via bicubic interpolation and were generated using a super-resolution convolutional neural network. The architecture of the network is designed to map the AIA images to

unprecedentedly high spatial resolution coronal images taken by the High-resolution Coronal Imager (Hi-C) during its brief flight.
Results. At times, pairs of separate strands that appear braided together later evolved into pairs of almost parallel strands with completely exchanged parts. These evolutions offer morphological evidence that magnetic reconnections between the braiding strands have taken place, which is further supported by the appearance of transient hot emissions containing significant high-temperature components (T > 5 MK) at the footpoints of the braiding structures.
Conlusions. The brief appearances of the two rearranging strands support the idea that magnetic reconnections have occurred within what appears to be a single AIA loop.

Variations of helioseismic parameters due to magnetic field generated by a flux transport model

Shaolan **Bi**, Tanda Li, Kang Liu, Jie Jiang, Yaguang Li, Jinghua Zhang, Xianfei Zhang, Yaqian Wu
A&A **2020**
https://arxiv.org/pdf/2011.02676.pdf
The change of sound speed has been found at the base of the convection during the solar cycles, which can be used to constrain the solar internal magnetic field. We aim to check whether the magnetic field generated by the solar dynamo can lead to the cyclic variation of the sound speed detected through helioseismology. The basic configuration of magnetic field in the solar interior was obtained by using a Babcock-Leighton (BL) type flux transport dynamo. We reconstructed one-dimensional solar models by assimilating magnetic field generated by an established dynamo and examined their influences on the structural variables. The results show that magnetic field generated by the dynamo is able to cause noticeable change of the sound speed profile at the base of the convective zone during a solar cycle. Detailed features of this theoretical prediction are also similar to those of the helioseismic results in solar cycle 23 by adjusting the free parameters of the dynamo model.

Dynamics of Descending Knots in a Solar Prominence and Their Possible Contributions to the Heating of the Local Corona

Yi **Bi**1,2,3, Bo Yang1,3, Ting Li2,4, Yan Dong1,3, and Kaifan Ji1,3
2020 ApJL 891 L40
https://doi.org/10.3847/2041-8213/ab79a2
https://arxiv.org/pdf/2003.08075.pdf
The knots in solar prominences are often observed to fall with nearly constant velocity, but the associated physical mechanism is currently not well understood. In this Letter, we present a prominence observed by the New Vacuum Solar Telescope in H α wavelength. Knots that rose within the prominence appear to have been preferentially located at higher altitude, whereas those that fell were found throughout the entire prominence structure. The descending speed of the knots near the solar surface was higher than that far away from the solar surface. We noted that the knots near the solar surface may run along a set of coronal loops observed from the Atmospheric Imaging Assembly. Elsewhere, the majority of knots are interpreted to have descended across more horizontal magnetic fields with a nearly constant speed. This lack of acceleration indicates that the liberated gravitational potential energy may not manifest as an increase in kinetic energy. Assuming instead that the descending knots were capable of exciting Alfvén waves that could then dissipate within the local corona, the gravitational potential energy of the knots may have been converted into thermal energy. Assuming a perfectly elastic system, we therefore estimate that the gravitational energy loss rate of these observed knots amounts to ≈1/2000 of that required to heat the entire quiet Sun, increasing to 1/320 when considering possibly further downward motions of the knots having disappeared in the H α observations. This result suggests such a mechanism may contribute to the heating of the corona local to these prominences. **2017-01-07**

Heating and cooling of coronal loops with turbulent suppression of parallel heat conduction

Bian, Nicolas; Emslie, A. Gordon; Horne, Duncan; Kontar, Eduard P.
ApJ **2017**
https://arxiv.org/pdf/1711.11388.pdf
Using the "enthalpy-based thermal evolution of loops" (EBTEL) model, we investigate the hydrodynamics of the plasma in a flaring coronal loop in which heat conduction is limited by turbulent scattering of the electrons that transport the thermal heat flux. The EBTEL equations are solved analytically in each of the two (conduction-dominated and radiation-dominated) cooling phases. Comparison of the results with typical observed cooling times in solar flares shows that the turbulent mean free-path λ_T lies in a range corresponding to a regime in which classical (collision-dominated) conduction plays at most a limited role. We also consider the magnitude and duration of the heat input that is necessary to account for the enhanced values of temperature and density at the beginning of the cooling phase and for the observed cooling times. We find through numerical modeling that in order to produce a peak temperature $\simeq 1.5 \times 10^7$~K and a 200~s cooling time consistent with

observations, the flare heating profile must extend over a significant period of time; in particular, its lingering role must be taken into consideration in any description of the cooling phase. Comparison with observationally-inferred values of post-flare loop temperatures, densities, and cooling times thus leads to useful constraints on both the magnitude and duration of the magnetic energy release in the loop, as well as on the value of the turbulent mean free-path λ_T.

Spatial variations of the Sr I 4607 Å scattering polarization peak

M. **Bianda**, S. Berdyugina, D. Gisler, R. Ramelli, L. Belluzzi, E. S. Carlin, J. O. Stenflo and T. Berkefeld
A&A 614, A89 (**2018**)
https://doi.org/10.1051/0004-6361/201731887
Context. The scattering polarization signal observed in the photospheric Sr I 4607 Å line is expected to vary at granular spatial scales. This variation can be due to changes in the magnetic field intensity and orientation (Hanle effect), but also to spatial and temporal variations in the plasma properties. Measuring the spatial variation of such polarization signal would allow us to study the properties of the magnetic fields at subgranular scales, but observations are challenging since both high spatial resolution and high spectropolarimetric sensitivity are required.
Aims. We aim to provide observational evidence of the polarization peak spatial variations, and to analyze the correlation they might have with granulation.
Methods. Observations conjugating high spatial resolution and high spectropolarimetric precision were performed with the Zurich IMaging POLarimeter, ZIMPOL, at the GREGOR solar telescope, taking advantage of the adaptive optics system and the newly installed image derotator.
Results. Spatial variations of the scattering polarization in the Sr I 4607 Å line are clearly observed. The spatial scale of these variations is comparable with the granular size. Small correlations between the polarization signal amplitude and the continuum intensity indicate that the polarization is higher at the center of granules than in the intergranular lanes.

Cycle 25 Strikes Again

Kamil **Bicz**
RHESSI Science Nuggets #337 November **2018**
http://sprg.ssl.berkeley.edu/~tohban/wiki/index.php/Cycle_25_Strikes_Again
This Nugget announces that we have seen second clear sign of Cycle 25 sunspot activity. Nugget No. 321 had described first sunspot of Cycle 25, and on November 8 (2018), at a high solar latitude, something interesting again appeared on the Sun. A tiny sunspot with Cycle 25 magnetic orientation appeared, and we believe this to be the second occurrence of the new Cycle. It persisted for about 5 days and appeared to have been bigger than its predecessor. This is interesting because it is already a second sunspot of the new cycle even before the minimum of Cycle 24 has been well established.

Solar Cycle *sic* Maximum
It's Here, Finally

Douglas **Biesecker**
Presentation on Space Weather Workshop in Boulder,
See SOLAR 'MINI-MAX' http://www.spaceweather.com/ of 20-21 May **2014**

STEREO Space Weather and the Space Weather Beacon

D.A. **Biesecker**[1], D.F. Webb[2,3], and O.C. St. Cyr[4]
2008
http://secchi.nrl.navy.mil/spwx/STEREO%20SWx%20chapter.doc
The Solar Terrestrial Relations Observatory (STEREO) is first and foremost a solar and interplanetary research mission, with one of the natural applications being in the area of space weather. The obvious potential for space weather applications is so great that NOAA has worked to incorporate the real-time data into their forecast center as much as possible. A subset of the STEREO data will be continuously downlinked in a real-time broadcast mode, called the Space Weather Beacon. Within the research community there has been considerable interest in conducting space weather related research with STEREO. Some of this research is geared towards making an immediate impact while other work is still very much in the research domain. There are many areas where STEREO might contribute and we cannot predict where all the successes will come. Here we discuss how STEREO will contribute to space weather and many of the specific research projects proposed to address STEREO space weather issues. We also discuss some specific uses of the STEREO data in the NOAA Space Environment Center.

The Relationships between Cyclic Variations of Solar Magnetic Fields of Various Scales in Cycles 21–25.

Bilenko, I.A.

Geomagn. Aeron. 63, 925–936 (**2023**).

https://doi.org/10.1134/S0016793223070058

In this paper, we present the results of a study of cyclic variations in magnetic fields of various scales in cycles 21–25: large-scale magnetic fields reflecting the dynamics of the global magnetic field of the Sun, the number of spots, which characterizes the dynamics of local magnetic fields of spots, and the intensity of radio emissions at a wavelength of 10.7 cm, which reflect variations in the magnetic fields of active regions and faculaes. The results showed that the general cycle changes in local fields and the corresponding oscillation spectra differs from those in the large-scale magnetic field. The dynamic correlation dependences show that the correlation between local and large-scale magnetic fields changes, both in each cycle, and from cycle to cycle. The correlation is at its minimum near the maximum and minimum phases of the solar activity. The correlation has an oscillatory character in the phases of growth and decline. The absence of clearly defined maxima in the general wavelet power spectrum of oscillations with periods from 82 days to 5 years is shown to be explained by the fact that the total spectrum is blurred over large time intervals due to the shift in the region of maximum intensity of individual periods, as well as a change in the width of the maximum intensity range from one Carrington rotation to another.

Meridional Circulations of the Solar Magnetic Fields of Different Strength

Irina A. **Bilenko**

Solar Phys. Volume 299, article number 103, **2024**

https://arxiv.org/pdf/2311.09900.pdf

https://doi.org/10.1007/s11207-024-02332-9

The meridional circulation of the solar magnetic fields in Solar Cycles 21-24 was considered. Data from both ground-based and space observatories were used. Three types of time-latitude distributions of photospheric magnetic fields and their meridional circulations were identified depending on the magnetic field intensity. (i) low-strength magnetic fields. They were distributed evenly across latitude and weakly depended on the magnetic fields of active regions and their cycle variation; (ii) medium-strength magnetic fields. For these fields a wave-like, pole-to-pole, antiphase meridional circulation with a period of approximately 22 years was revealed. The velocities of meridional flows were slower at the minima of solar activity, when they were at high latitudes in the opposite hemispheres, and maximal at the solar maxima, when the positive- and negative-polarity waves crossed the equator. The meridional circulation of these fields reflects the solar global magnetic field dynamics and determines the solar polar field reversal; (iii) high-strength (active region) magnetic fields. They were distributed symmetrically in the Northern and Southern hemispheres. Magnetic fields of both leading and following sunspot polarity migrated from high to low latitudes. The meridional-flow velocities of high-strength magnetic fields were higher at the rising and maxima phases than at the minima. Some of the high-latitude active region magnetic fields were captured by the second type meridional circulation flows and transported along with them to the appropriate pole. But the magnetic fields of active regions are not the main ones in the solar polar field reversal. The results indicate that high-strength magnetic fields were not the main source of weak ones.

Manifestation of Rossby Waves in the Global Magnetic Field of the Sun during Cycles 21–24

Irina A. **Bilenko**

2020 ApJL 897 L24

https://doi.org/10.3847/2041-8213/ab9fa4

The evolution of the solar global magnetic field (GMF) was investigated and compared with oscillations of different periods during cycles 21–24. The data from the Wilcox Solar Observatory were used. The results indicate that GMF structures were associated with certain oscillations. Oscillations of 81.83–163.65 days were associated with structures lasting 10–20 CRs. They occurred as some pulses during solar maxima. Oscillations of 163.652–463.680 days were associated with GMF structures lasting ≈20–50 CRs. They match two peaks in the magnetic-field cycle. Oscillations of 1.270–5.231 yr were formed during the dominance of the sectorial GMF structure. Oscillations of 5.231–13.451 yr were the most intense. From cycle 22 to 24, their intensity decreased, and the range of periods narrowed and shifted to longer periods, determining the corresponding changes in the oscillations of 81.83 days–5.231 yr and associated GMF structures. They match well the evolution of the zonal GMF structure. They are assumed to be a descending part of a period of ≈≥60 yr. A decrease in the magnetic field from cycle 22 to 24 may be due to a decrease in the intensity of these oscillations. Some periodicities of the revealed oscillations are in good agreement with the estimates of the periods for fast magnetic Rossby waves. The GMF structure connection with Rossby waves is discussed.

Relations between Coronal Mass Ejections and the Photospheric Magnetic Field in Cycles 23 and 24

Irina A. **Bilenko**

2020 ApJ 889 1

https://orcid.org/0000-0002-9543-0542

The number of coronal mass ejections (CMEs) and their parameters and cycle variations were investigated and compared to the photospheric magnetic field evolution in cycles 23 and 24. The Coordinated Data Analysis Workshops (CDAW) catalog of white-light CMEs detected by the Solar and Heliospheric Observatory/Large Angle and Spectrometric Coronagraph coronagraphs and the data on the photospheric magnetic fields from the Kitt Peak Vacuum Telescope Spectromagnetograph (KPVT/Spectromagnetograph) and the Synoptic Optical Long-term Investigations of the Sun Vector-Spectromagnetograph (SOLIS/VSM) were used. The results suggest that not only did the number of CMEs increase in cycle 24, but that their parameters, cycle variations, distributions, and dependencies on the photospheric magnetic fields were also different. Various CME categories behave in different ways during solar cycles. The differences in the number and parameters of CMEs and their cycle variations may be related to the differences in the photospheric magnetic fields during the cycles. The strong photospheric magnetic fields maintained approximately the same strength from cycle 23 to cycle 24, whereas the weak fields became weaker and the area they occupied increased. Taking into account that the global magnetic field diminished from cycle 23 to cycle 24, the increase in the number of CMEs in cycle 24 can be understood. A detailed analysis of the similarities and differences in CME parameters and their cycle evolution indicates that, along with the influence of changes in the CME detection mode in 2004 and 2010, the changes in CME rate and parameters were also associated with real differences in the behavior of strong and weak photospheric magnetic fields in cycles 23 and 24.

Coronal Hole and Solar Global Magnetic Field Evolution in 1976 – 2012

Irina A. **Bilenko**, Ksenia S. Tavastsherna

Solar Phys. Volume 291, Issue 8, pp 2329–2352 **2016**

https://arxiv.org/pdf/1805.09543.pdf

We study the spatial-temporal evolution of a coronal hole and compare it with that of the solar global magnetic field in Cycles 21 – 23 (1976 – 2012). We also analyze the latitude-longitude distribution dynamics of coronal holes and the regularities in the global magnetic field associated with the solar polar field reversal. Polar and non-polar coronal hole populations are considered. The investigation reveals some temporal and spatial regularities in coronal hole distributions that match the global magnetic-field cycle evolution well. The results show that the non-polar coronal hole longitudinal distribution follows all configuration changes in the global magnetic-field structure. Reorganizations of the global magnetic field and coronal hole distributions occur simultaneously during a time interval of a few solar rotations. The cycle evolution of the non-polar coronal holes reflects the transition of the solar global magnetic field from the zonal structure to sectorial and *vice versa*. Two different types of waves of non-polar coronal holes are revealed from their latitudinal distribution. The first are short poleward waves. They trace the poleward motion of the unipolar photospheric magnetic fields from approximately 35◦ to the associated pole in each hemisphere and the redevelopment of a new-polarity polar CH. Although they start the poleward movement before the change of the polar magnetic field in the associated hemisphere, they reach the pole after the polar reversal. The other type of non-polar CH wave forms two sinusoidal branches associated with the positive- and negative-polarity magnetic fields. The complete period of the wave is equal to ≈268 CRs (22 years). These wave CHs arrive at high latitudes during declining phases when the new-polarity polar CHs are already completely formed.

Influence of the Solar Global Magnetic-Field Structure Evolution on CMEs

Irina A. **Bilenko**

Solar Physics, July **2014**

We consider the influence of the solar global magnetic-field structure (GMFS) cycle evolution on the occurrence rate and parameters of coronal mass ejections (CMEs) in Solar Cycles 23 – 24. It has been shown that, over solar cycles, CMEs are not distributed randomly, but they are regulated by evolutionary changes in the GMFS. It is proposed that the generation of magnetic Rossby waves in the solar tachocline results in the GMFS cycle changes. Each Rossby wave period favors a particular GMFS. It is proposed that the changes in wave periods result in GMFS reorganization and consequently in CME location, occurrence rate, and parameter changes. The CME rate and parameters depend on the sharpness of the GMFS changes, the strength of the global magnetic field, and the phase of a cycle

SuNeRF: Validation of a 3D Global Reconstruction of the Solar Corona Using Simulated EUV Images

Kyriaki-Margarita **Bintsi**, Robert Jarolim, Benoit Tremblay, Miraflor Santos, Anna Jungbluth, James Paul Mason, Sairam Sundaresan, Angelos Vourlidas, Cooper Downs, Ronald M. Caplan, Andrés Muñoz Jaramillo

Machine Learning and the Physical Sciences workshop, NeurIPS 2022 **2022**
https://arxiv.org/pdf/2211.14879
Extreme Ultraviolet (EUV) light emitted by the Sun impacts satellite operations and communications and affects the habitability of planets. Currently, EUV-observing instruments are constrained to viewing the Sun from its equator (i.e., ecliptic), limiting our ability to forecast EUV emission for other viewpoints (e.g. solar poles), and to generalize our knowledge of the Sun-Earth system to other host stars. In this work, we adapt Neural Radiance Fields (NeRFs) to the physical properties of the Sun and demonstrate that non-ecliptic viewpoints could be reconstructed from observations limited to the solar ecliptic. To validate our approach, we train on simulations of solar EUV emission that provide a ground truth for all viewpoints. Our model accurately reconstructs the simulated 3D structure of the Sun, achieving a peak signal-to-noise ratio of 43.3 dB and a mean absolute relative error of 0.3\% for non-ecliptic viewpoints. Our method provides a consistent 3D reconstruction of the Sun from a limited number of viewpoints, thus highlighting the potential to create a virtual instrument for satellite observations of the Sun. Its extension to real observations will provide the missing link to compare the Sun to other stars and to improve space-weather forecasting.

Average surface flows before the formation of solar active regions and their relationship to the supergranulation pattern

A. C. **Birch**1, H. Schunker1, D. C. Braun2 and L. Gizon
A&A 628, A37 (**2019**)
https://www.aanda.org/articles/aa/pdf/2019/08/aa35591-19.pdf
Context. The emergence of solar active regions is an important but poorly understood aspect of the solar dynamo.
Aims. Knowledge of the flows associated with the rise of active-region-forming magnetic concentrations through the near-surface layers will help determine the mechanisms of active region formation.
Methods. We used helioseismic holography and granulation tracking to measure the horizontal flows at the surface that precede the emergence of active regions. We then averaged these flows over about sixty emerging active regions to reduce the noise, selecting active regions that emerge into relatively quiet Sun. To help interpret the results, we constructed a simple model flow field by generating synthetic “emergence locations” that are probabilistically related to the locations of supergranulation-scale convergence regions in the quiet Sun.
Results. The flow maps obtained from helioseismology and granulation tracking are very similar (correlation coefficients for single maps around 0.96). We find that active region emergence is, on average, preceded by converging horizontal flows of amplitude about 40 m s−1. The convergence region extends over about 40 Mm in the east-west direction and about 20 Mm in the north-south direction and is centered in the retrograde direction relative to the emergence location. This flow pattern is largely reproduced by a model in which active region emergence occurs preferentially in the prograde direction relative to supergranulation inflows.
Conclusions. Averaging over many active regions reveals a statistically significant pattern of near-surface flows prior to emergence. The qualitative success of our simple model suggests that rising flux concentrations and supergranule-scale flows interact during the emergence process.

A low upper limit on the subsurface rise speed of solar active regions

Aaron C. **Birch**, Hannah Schunker, Douglas C. Braun, Robert Cameron, Laurent Gizon, Björn Löptien,Matthias Rempel
Science Advances **2016**
http://arxiv.org/pdf/1607.05250v1.pdf
Magnetic field emerges at the surface of the Sun as sunspots and active regions. This process generates a poloidal magnetic field from a rising toroidal flux tube, it is a crucial but poorly understood aspect of the solar dynamo. The emergence of magnetic field is also important because it is a key driver of solar activity. We show that measurements of horizontal flows at the solar surface around emerging active regions, in combination with numerical simulations of solar magnetoconvection, can constrain the subsurface rise speed of emerging magnetic flux. The observed flows imply that the rise speed of the magnetic field is no larger than 150 m/s at a depth of 20 Mm, that is, well below the prediction of the (standard) thin flux tube model but in the range expected for convective velocities at this depth. We conclude that convective flows control the dynamics of rising flux tubes in the upper layers of the Sun and cannot be neglected in models of flux emergence.

Centrifugal effects and the Kelvin-Helmholtz instability in coronal cavities

R. A. **Bisengaliev**, V. V. Mustsevoi, A. A. Solov’ev
Astronomy Reports, April **2014**, Volume 58, Issue 4, pp 249-259

Astronomicheskii Zhurnal, **2014**, Vol. 91, No. 4, pp. 308–319.
It is proposed that the formation of the morphology of solar magnetic cavities and of the topology of their magnetic fields at a certain stage of their evolution (a decay of a quasi-uniform, rotating, magnetized cylindrical layer into rings, followed by their deformation and the generation of internal fine structure etc.) can be attributed to the excitation of a shear-centrifugal-resonance instability. The calculations show the existence of two families of unstable modes: resonance-gyroscopic modes due to the rotation of the layer and fast magneto acoustic waves propagating outside the layer and resonating in phase with intra-layer perturbations. Both families contain a large number of unstable waveguide harmonics, with the superposition and interaction of these harmonics being responsible for the extremely complex structure of coronal cavities.

Another Mini Solar Maximum in the Offing: A Prediction for the Amplitude of Solar Cycle 25

S. K. **Bisoi**, P. Janardhan, S. Ananthakrishnan
JGR Volume125, Issue7 July **2020** e2019JA027508
https://agupubs.onlinelibrary.wiley.com/doi/pdf/10.1029/2019JA027508
We examine the temporal changes in both solar polar magnetic field (PMF) at latitudes ≥45° and heliospheric magnetic field (HMF) at 1 AU during solar cycles 21–24 with emphasis on the recent activity changes after July 2015, the so called “mini solar maximum” of cycle 24. While unsigned PMF shows solar cycle modulations in cycles 21 and 22, it shows an anti-correlation with solar cycle variation in cycle 24. In addition, the floor level of the HMF (of 4.6 nT), that is, the value that the HMF returns to at each solar minimum, is breached about 2 years prior to cycle 24 minimum, indicating a reduced HMF floor level of 3.2 ± 0.5 nT in the upcoming cycle 24 minimum. In light of the change of unsigned PMF and the availability of a revised smoothed sunspot number (SSN V2.0) after July 2015, we revisit the correlation of unsigned PMF and HMF at solar minimum. The correlation is used to estimate values of the HMF at the cycle 24 minimum and the amplitude of the upcoming cycle 25. The updated prediction is 134 ± 11 or 131 ± 11 on the revised SSN V2.0 scale assuming the cycle 24 minimum to occur in 2020 or 2021, respectively. The SSN values indicate that the cycle 25 will be stronger than cycle 24 and a little weaker than cycle 23, even if the current solar cycle minimum occurs in 2021 instead of 2020. This implies that we will witness another mini solar maximum in the upcoming cycle 25.

A new tool for predicting the solar cycle: Correlation between flux transport at the equator and the poles

Susanta Kumar **Bisoi**, P. Janardhan
Solar Phys. **295**, Article number: 79 **2020**
https://arxiv.org/pdf/1911.03865.pdf
The magnetic flux cancellation on the Sun plays a crucial role in determining the manner in which the net magnetic flux changes in every solar cycle, affecting the large scale evolution of the coronal magnetic fields and heliospheric environment. We investigate, in this paper, the correlation between the solar magnetic flux cancelled at the equator and the solar magnetic flux transported to the poles by comparing the net amount of magnetic flux in the latitude belt 0∘-5∘ and 45∘-60∘, estimated using synoptic magnetograms from National Solar Observatory at Kitt Peak, during Solar Cycles 21-24. We find a good correlation between the net flux in the latitude band 0∘-5∘ and 55∘-60∘ for the Northern as well as for the Southern hemispheres. However, we find a poor correlation if the net flux for the Northern and Southern hemispheres are considered together. In addition, we investigate the correlation between the net flux cancelled at the equator and the strength of solar polar field at cycle minimum, and find a good correlation between the two. We discuss the implication of the correlation of flux transported across the equator and to the poles that has an important bearing in the estimation of the residual polar cap field strength at the cycle minimum. This can be used a predictive tool for estimating the amplitude of subsequent cycles and we use this to estimate maximum smoothed sunspot numbers of 77±5 and 85±5 for the Northern and Southern hemispheres, respectively, for the upcoming Solar Cycle 25.

Another Mini Solar Maximum in the Offing: A Prediction for the Amplitude of Solar Cycle 25

Susanta Kumar **Bisoi**, P. Janardhan, S. Ananthakrishnan
JGR **2019**
https://arxiv.org/pdf/1910.03841.pdf
We examine the temporal changes in both solar polar magnetic field (PMF) at latitudes ≥ 45∘ and heliospheric magnetic field (HMF) at 1 AU during solar cycles 21--24 with emphasis on the recent activity changes after July 2015, the so called "mini solar maximum" of cycle 24. While unsigned PMF shows a solar-cycle-like variation in cycles 21 and 22, it shows an anti-solar-cycle-like variation in cycle 24. In addition, the floor level of the HMF (of 4.6 nT), i.e. the value that the HMF returns to at each solar minimum, is breached about two years prior to cycle 24

minimum, indicating a reduced HMF floor level in the upcoming cycle 24 minimum. In light of the change of unsigned PMF and the availability of a revised smoothed sunspot number (SSN) after July 2015, we have revisited the correlation of unsigned PMF and HMF at solar minimum. The correlation is used to estimate a new value of the HMF of 4.16±0.6 nT at the cycle 24 minimum and the amplitude of the upcoming cycle 25. The updated prediction is 82±8 and 133±11, on the original (V1.0) and revised (V2.0) SSN scales, respectively. These better and more reliable SSN values (due to the larger data set) imply that we will witness another mini solar maximum in the upcoming cycle 25 which will be relatively stronger than cycle 24 and a little weaker than cycle 23, even if the current solar cycle minimum occurs in 2021 instead of 2020.

A study of density modulation index in the inner heliospheric solar wind during solar cycle 23

Susanta Kumar **Bisoi**, P. Janardhan, M. Ingale, P. Subramanian, S. Ananthakrishnan, M. Tokumaru, and K. Fujiki

E-print, Aug **2014**; ApJ

http://arxiv.org/pdf/1408.4199v1.pdf

The ratio of the rms electron density fluctuations to the background density in the solar wind (density modulation index, \epsilonN \equiv \Delta{N}/N) is of vital importance in understanding several problems in heliospheric physics related to solar wind turbulence. In this paper, we have investigated the behavior of \epsilonN in the inner-heliosphere from 0.26 to 0.82 AU. The density fluctuations \Delta{N} have been deduced using extensive ground-based observations of interplanetary scintillation (IPS) at 327 MHz, which probe spatial scales of a few hundred km. The background densities (N) have been derived using near-Earth observations from the Advanced Composition Explorer (\it{ACE}). Our analysis reveals that 0.001 \lesssim \epsilonN \lesssim 0.02 and does not vary appreciably with heliocentric distance. We also find that \epsilonN declines by 8% from 1998 to 2008. We discuss the impact of these findings on problems ranging from our understanding of **Forbush decreases** to the behavior of the solar wind dynamic pressure over the recent peculiar solar minimum at the end of cycle 23.

Exploring the predictability of the solar cycle from the polar field rise rate: Results from observations and simulations

Akash **Biswas**

IAU Symposium 365 **2024**

https://arxiv.org/pdf/2402.01851.pdf

The inherent stochastic and nonlinear nature of the solar dynamo makes the strength of the solar cycles vary in a wide range, making it difficult to predict the strength of an upcoming solar cycle. Recently, our work has shown that by using the observed correlation of the polar field rise rate with the peak of polar field at cycle minimum and amplitude of following cycle, an early prediction can be made. In a follow-up study, we perform SFT simulations to explore the robustness of this correlation against variation of meridional flow speed, and against stochastic fluctuations of BMR tilt properties that give rise to anti-Joy and anti-Hale type anomalous BMRs. The results suggest that the observed correlation is a robust feature of the solar cycle and can be utilized for a reliable prediction of peak strength of a cycle at least 2 to 3 years earlier than the minimum.

The role of nonlinear toroidal flux loss due to flux emergence in the long-term evolution of the solar cycle

Akash **Biswas**

IAU Symposium 365 **2024**

https://arxiv.org/pdf/2402.01853.pdf

A striking feature of the solar cycle is that at the beginning, sunspots appear around mid-latitudes, and over time the latitudes of emergences migrate towards the equator. The maximum level of activity varies from cycle to cycle. For strong cycles, the activity begins early and at higher latitudes with wider sunspot distributions than for weak cycles. The activity and the width of sunspot belts increase rapidly and begin to decline when the belts are still at high latitudes. However, in the late stages of the cycles, the level of activity, and properties of the butterfly wings all have the same statistical properties independent of the peak strength of the cycles. We have modelled these features using Babcock-Leighton type dynamo model and shown that the toroidal flux loss from the solar interior due to magnetic buoyancy is an essential nonlinearity that leads to all the cycles decline in the same way.

Exploring the reliability of polar field rise rate as a precursor for an early prediction of solar cycle

Akash **Biswas**, Bidya Binay Karak, Pawan Kumar

MNRAS Volume 526, Issue 3, December 2023, Pages 3994–4003, **2023**

https://arxiv.org/pdf/2308.01155

https://doi.org/10.1093/mnras/stad2966
The prediction of the strength of an upcoming solar cycle has been a long-standing challenge in the field of solar physics. The inherent stochastic nature of the underlying solar dynamo makes the strength of the solar cycle vary in a wide range. Till now, the polar precursor methods and the dynamo simulations, that use the strength of the polar field at the cycle minimum to predict the strength of the following cycle has gained reasonable consensus by providing convergence in the predictions for solar cycles 24 and 25. Recently, it has been shown that just by using the observed correlation of the polar field rise rate with the peak of the polar field at the cycle minimum and the amplitude of the following cycle, a reliable prediction can be made much earlier than the cycle minimum. In this work, we perform surface flux transport (SFT) simulations to explore the robustness of this correlation against the stochastic fluctuations of BMR tilt properties including anti-Joy and anti-Hale type anomalous BMRs, and against the variation of meridional flow speed. We find that the observed correlation is a robust feature of the solar cycles and thus it can be utilized for a reliable prediction of solar cycle much earlier than the cycle minimum, the usual landmark of the solar cycle prediction.

Long-term modulation of solar cycles

Akash **Biswas**, Bidya Karak, Ilya Usoskin, Eckhard Weisshaar
Space Science Review 219, Article number: 19 **2023**
https://arxiv.org/pdf/2302.14845.pdf
https://link.springer.com/content/pdf/10.1007/s11214-023-00968-w.pdf
https://link.springer.com/article/10.1007/s11214-023-00968-w#Abs1
Solar activity has a cyclic nature with the ~11-year Schwabe cycle dominating its variability on the interannual timescale. However, solar cycles are significantly modulated in length, shape and magnitude, from near-spotless grand minima to very active grand maxima. The ~400-year-long direct sunspot-number series is inhomogeneous in quality and too short to study robust parameters of long-term solar variability. The cosmogenic-isotope proxy extends the timescale to twelve millennia and provides crucial observational constraints of the long-term solar dynamo modulation. Here, we present a brief up-to-date overview of the long-term variability of solar activity at centennial--millennial timescales. The occurrence of grand minima and maxima is discussed as well as the existing quasi-periodicities such as centennial Gleissberg, 210-year Suess/de Vries and 2400-year Hallstatt cycles. It is shown that the solar cycles contain an important random component and have no clock-like phase locking implying a lack of long-term memory. A brief yet comprehensive review of the theoretical perspectives to explain the observed features in the framework of the dynamo models is presented, including the nonlinearity and stochastic fluctuations in the dynamo. We keep gaining knowledge of the processes driving solar variability with the new data acquainted and new models developed.

Toroidal flux loss due to flux emergence explains why solar cycles rise differently but decay in a similar way

Akash **Biswas**, Bidya Binay Karak, Robert Cameron
Phys.Rev.Lett. (PRL) **129**, 24 **2022**
https://arxiv.org/pdf/2210.07061
A striking feature of the solar cycle is that at the beginning, sunspots appear around mid-latitudes, and over time the latitudes of emergences migrate towards the equator.The maximum level of activity (e.g., sunspot number) varies from cycle to cycle.For strong cycles, the activity begins early and at higher latitudes with wider sunspot distributions than for weak cycles. The activity and the width of sunspot belts increase rapidly and begin to decline when the belts are still at high latitudes. Surprisingly, it has been reported that in the late stages of the cycle the level of activity (sunspot number) as well as the widths and centers of the butterfly wings all have the same statistical properties independent of how strong the cycle was during its rise and maximum phases.We have modeled these features using a Babcock--Leighton type dynamo model and show that the flux loss through magnetic buoyancy is an essential nonlinearity in the solar dynamo.Our study shows that the nonlinearity is effective if the flux emergence becomes efficient at the mean-field strength of the order of 104~G in the lower part of the convection zone.
HMI Science Nuggets #191 **2023** http://hmi.stanford.edu/hminuggets/?p=4107

Forecasting the solar cycle 25 using a multistep Bayesian neural network

I **Bizzarri**, D Barghini, S Mancuso, S Alessio, S Rubinetti, C Taricco
MNRAS Volume 515, Issue 4, October **2022**, Pages 5062–5070,
https://doi.org/10.1093/mnras/stac2013
Predicting the solar activity of upcoming cycles is crucial nowadays to anticipate potentially adverse space weather effects on the Earth's environment produced by coronal transients and traveling interplanetary disturbances. The latest advances in deep learning techniques provide new paradigms to obtain effective prediction models that allow to forecast in detail the evolution of cosmogeophysical time series. Because of the underlying complexity of the dynamo mechanism in the solar interior that is at the origin of the solar cycle phenomenon, the predictions offered

by state-of-the-art machine learning algorithms represent valuable tools for our understanding of the cycle progression. As a plus, Bayesian deep learning is particularly compelling thanks to recent advances in the field that provide improvements in both accuracy and uncertainty quantification compared to classical techniques. In this work, a deep learning long short-term memory model is employed to predict the complete profile of Solar Cycle 25, thus forecasting also the advent of the next solar minimum. A rigorous uncertainty estimation of the predicted sunspot number is obtained by applying a Bayesian approach. Two different model validation techniques, namely the Train-Test split and the time series k-fold cross-validation, have been implemented and compared, giving compatible results. The forecasted peak amplitude is lower than that of the preceding cycle. Solar Cycle 25 will last 10.6 ± 0.7 yr, reaching its maximum in the middle of the year 2024. The next solar minimum is predicted in 2030 and will be as deep as the previous one.

Three-dimensional modeling of chromospheric spectral lines in a simulated active region

Johan P. **Bjørgen**, Jorrit Leenaarts, Matthias Rempel, Mark C. M. Cheung, Sanja Danilovic, Jaime de la Cruz Rodríguez, Andrii V. Sukhorukov

A&A 631, A33 **2019**

https://arxiv.org/pdf/1906.01098.pdf

Because of the complex physics that governs the formation of chromospheric lines, interpretation of solar chromospheric observations is difficult. The origin and characteristics of many chromospheric features are, because of this, unresolved. We focus here on studying two prominent features: long fibrils and flare ribbons. To model them, we use a 3D MHD simulation of an active region which self-consistently reproduces both of them. We model the Hα, Mg II k, Ca II K, and Ca II 8542 {\AA} lines using the 3D non-LTE radiative transfer code Multi3D.
This simulation reproduces long fibrils that span between the opposite-polarity sunspots and go up to 4 Mm in height. They can be traced in all lines due to density corrugation. Opposite to previous studies, Hα, Mg II h&k, and Ca II H&K, are formed at similar height in this model. Magnetic field lines are aligned with the Hα fibrils, but the latter holds to a lesser extent for the Ca II 8542 {\AA} line.
The simulation shows structures in the Hα line core that look like flare ribbons. The emission in the ribbons is caused by a dense chromosphere and a transition region at high column mass. The ribbons are visible in all chromospheric lines, but least prominent in Ca II 8542 {\AA} line. In some pixels, broad asymmetric profiles with a single emission peak are produced, similar to the profiles observed in flare ribbons. They are caused by a deep onset of the chromospheric temperature rise and large velocity gradients.
The simulation produces long fibrils similar to what is seen in observations. It also produces structures similar to flare ribbons despite the lack of non-thermal electrons in the simulation. The latter suggests that thermal conduction might be a significant agent in transporting flare energy to the chromosphere in addition to non-thermal electrons.

Three-dimensional modeling of the Ca II H&K lines in the solar atmosphere

Johan P. **Bjørgen**, Andrii V. Sukhorukov, Jorrit Leenaarts, Mats Carlsson, Jaime de la Cruz Rodríguez, Göran B. Scharmer, Viggo H. Hansteen

A&A **2017**

https://arxiv.org/pdf/1712.01045.pdf

CHROMIS, a new imaging spectrometer at the Swedish 1-m Solar Telescope (SST), can observe the chromosphere in the H and K lines of Ca II at high spatial and spectral resolution. Accurate modeling as well as an understanding of the formation of these lines are needed to interpret the SST/CHROMIS observations. Such modeling is computationally challenging because these lines are influenced by strong departures from local thermodynamic equilibrium, three-dimensional radiative transfer, and partially coherent resonance scattering of photons. We aim to model the CaII H&K lines in 3D model atmospheres to understand their formation and to investigate their diagnostic potential for probing the chromosphere. We model the synthetic spectrum of Ca II using the radiative transfer code Multi3D in three different radiation-magnetohydrodynamic model atmospheres computed with the Bifrost code. We classify synthetic intensity profiles according to their shapes and study how their features are related to the physical properties in the model atmospheres. We investigate whether the synthetic data reproduce the observed spatially-averaged line shapes, center-to-limb variation and compare with SST/CHROMIS images. The spatially-averaged synthetic line profiles show too low central emission peaks, and too small separation between the peaks. The trends of the observed center-to-limb variation of the profiles properties are reproduced by the models. The Ca II H&K line profiles provide a temperature diagnostic of the temperature minimum and the temperature at the formation height of the emission peaks. The Doppler shift of the central depression is an excellent probe of the velocity in the upper chromosphere. **October 12, 2016**

Space weather effects on Earth's environment associated to the 24–25 October 2011 geomagnetic storm

E. **Blanch**, S. Marsal, A. Segarra, J. M. Torta, D. Altadill andJ. J. Curto

Space Weather, Volume 11, Issue 4, pages 153–168, April **2013**

Space weather studies have increased due to human society dependence on spaceborne and terrestrial infrastructure vulnerable to its effects. In this paper, we present an interdisciplinary study of the effects of solar activity on the Earth's environment; specifically, we focus on the effects on the ionosphere and the geomagnetic field. A timeline of effects occurring on the Earth produced by one of the first relevant events of the present solar cycle (**24–25 October 2011**) is given. We have analyzed the solar wind shockwave from satellite data, the storm-time development, the ionospheric effects at global and local scales using the National Center for Atmospheric Research Thermosphere-Ionosphere-Electrodynamics General Circulation Model fed with geomagnetic field-aligned current data from the Active Magnetosphere and Planetary Electrodynamics Response Experiment, and ground ionosonde data from both hemispheres, at Ebre Observatory and Port Stanley locations. We have compared observed geomagnetic variations at high latitudes with those modeled by the National Center for Atmospheric Research Thermosphere-Ionosphere-Electrodynamics General Circulation Model. We have analyzed rapid geomagnetic variations (e.g., solar flare effect, storm commencement, Pi2) also on both hemispheres, at Ebre Observatory and Livingston Island locations. Finally, we have estimated geoelectric field and geomagnetically induced currents in the northeast of Spain (Catalonia) produced by this geomagnetic disturbance.

North–South Asymmetry of Solar Meridional Circulation and Synchronization: Two Rings of Four Coupled Oscillators

Elena **Blanter** & Mikhail Shnirman
Solar Physics volume 296, Article number: 86 (**2021**)
https://link.springer.com/content/pdf/10.1007/s11207-021-01821-5.pdf
https://doi.org/10.1007/s11207-021-01821-5
We apply the Kuramoto model with four coupled oscillators to the description of the phase evolution of solar magnetic field proxies at different latitudes. We show that a ring of four coupled oscillators does represent the frequency synchronization of the meridional circulation and the phase evolution of solar proxies. The model allows one to reconstruct the long-term evolution of the meridional flow speed and hemispheric asymmetry at different latitudes. We study the N-S asymmetry of the meridional flow and find a centennial variation of natural frequencies and couplings. Extremes of the north–south asymmetry of the near-equatorial meridional flow correspond to the anomalies of solar activity in Solar Cycles (SC)19–20 and SC23–24. We also find a degeneration of the meridional circulation ring profile in SC23–24, which agrees with helioseismic observations. We show that the N-S asymmetry depends on latitude and is strongly connected with the near-equatorial meridional flow.

Long Term Evolution of Solar Meridional Circulation and Phase Synchronization Viewed Through a Symmetrical Kuramoto Model

E. **Blanter**, J.-L. Le Mouël, M. Shnirman, V. Courtillot
Solar Physics October **2018**, 293:134
https://link.springer.com/content/pdf/10.1007%2Fs11207-018-1355-9.pdf
The solar-cycle oscillations of the toroidal and poloidal components of the solar magnetic field in the northern solar hemisphere have a persistent phase difference of about $\pi\pi$. We propose a symmetrical Kuramoto model with three coupled oscillators as a simple way to understand this anti-synchronization. We solve an inverse problem and reconstruct natural frequencies of the top and bottom oscillators under the conditions of a constant coupling strength and a non-delayed coupling. These natural frequencies are associated with angular velocities of the meridional flow circulation near the solar surface and in the deep layer of the solar convection zone. A relationship between our reconstructions of the shallow and the deep meridional flow speed during recent Solar Cycles 21 – 23 is in agreement with estimates obtained in helioseismology and flux-transport dynamo modeling. The reconstructed top oscillator speed presents significant solar-cycle like variations that agree with recent helioseismical reconstructions. The evolution of reconstructed natural frequencies strongly depends on the coupling strength. We find two stable regimes in the case of strong coupling with a change of regime during anomalous solar cycles. We see the onset of a new transition in Solar Cycle 24. We estimate the admitted range of coupling values and find evidence of cross-equatorial coupling between solar hemispheres not accounted for by the model.

Reconstruction of the North–South Solar Asymmetry with a Kuramoto Model

E. **Blanter**, J.-L. Le Mouël, M. Shnirman, V. Courtillot
Solar Physics April **2017**, 292:54
http://link.springer.com/content/pdf/10.1007%2Fs11207-017-1078-3.pdf
This paper applies a Kuramoto model of coupled oscillators to investigate the north–south (N–S) solar asymmetry and properties of meridional circulation. We focus our study on the asymmetry of the 11-year phase, which is slight but persistent: only two changes of sign (around 1928 and 1968) are observed in the past century. We present a model of two non-linear coupled oscillators that links the hemispheric phase asymmetry of sunspots with the asymmetry of the meridional flow. We use a Kuramoto model with evolving frequencies and constant symmetric coupling to show how asymmetry in meridional circulation could produce a persistent phase lead of one solar hemisphere over the other. We associate the natural frequencies of the two oscillators with the velocities of the

meridional flow cells in the northern and southern hemispheres. We assume the respective circulations to be independent and estimate the value of the relevant cross-equatorial coupling by the coupling coefficient in the Kuramoto model. We find that a persistent N–S asymmetry of sunspots and the change of the leading hemisphere could indeed both be the result of the evolving frequencies of meridional circulation; the necessary asymmetry of the meridional flow may be small; and the cross-equatorial coupling has an intermediate range value. Possible applications of these results in solar dynamo models are discussed.

Kuramoto Model with Non-symmetric Coupling Reconstructs Variations of the Solar-Cycle Period

E. **Blanter** , J.-L. Le Mouël, M. Shnirman, V. Courtillot

Solar Phys. Volume 291, Issue 3, pp 1003-1023 **2016**

We apply a Kuramoto model with two non-linear, coupled oscillators to the simultaneous reconstruction of the phase difference of the two oscillators and instantaneous period (or length) of the solar cycle. The two long series of sunspot numbers [RIRI] and aa geomagnetic indices are considered as proxies of the toroidal and poloidal components of the solar magnetic field, respectively. Variations in the length of the solar cycle are successfully reconstructed when an asymmetry between coupling coefficients is introduced, corresponding to an asymmetry of the αΩαΩ-mechanisms of solar magnetic-field generation. Application of the Kuramoto model to solar indices and comparison with synthetic data series shows the important role of synchronization in allowing one to estimate solar-cycle length. The Kuramoto model reconstruction reveals a ≈30--33≈30--33 year (three solar cycles) quasi-periodicity and the influence of quasi-biennial oscillations present in the aa-index on the determination of solar-cycle length.

The Relative Umbral Area in Spot Groups as an Index of Cyclic Variation of Solar Activity

N. G. **Bludova**, V. N. Obridko, O. G. Badalyan

Solar Physics, March **2014**, Volume 289, Issue 3, pp 1013-1028

The Greenwich series of data was used to study the ratio [q] of the total umbra area to the total area of the sunspot group (for brevity “relative umbral area”) for the period 1874 – 1976. It was revealed that the annual mean value of q varied in time from 0.15 to 0.28 and reached its maximum in the early 1930s. The dependence of q on the sunspot group area [S] was considered to show that the smallest groups, of area less than 100 m.v.h. (millionths of the visible hemisphere), contributed most significantly to the temporal variation of q. In contrast to the earlier results, the dependence obtained proved to be rather complicated. The coefficients of the linear expansion q(S) are themselves dependent on the sunspot-group area and time [t]; i.e. the relation of q to both S and t is nonlinear. Only in sunspot groups with a large area does dependence disappear, and q becomes constant, equal to 0.18. This is the value given in textbooks. The relations obtained show that the relive umbral area and the relative number of small groups are important parameters of the secular variation of solar activity. In particular, they may account for variations in the mean magnetic field in active regions, the complexity of a group according to the magnetic classification, the flare activity of a sunspot group, and its geophysical impact. It is conjectured that the parameter q describes the time-varying relative contribution from the interior and subsurface dynamo mechanisms.

Inertial Waves in a Nonlinear Simulation of the Sun's Convection Zone and Radiative Interior

Catherine C. **Blume**, Bradley W. Hindman, Loren I. Matilsky

ApJ **2024**

https://arxiv.org/pdf/2312.14270.pdf

Recent observations of Rossby waves and other more exotic forms of inertial oscillations in the Sun's convection zone have kindled the hope that such waves might be used as a seismic probe of the Sun's interior. Here we present a 3D numerical simulation in spherical geometry that models the Sun's convection zone and upper radiative interior. This model features a wide variety of inertial oscillations, including both sectoral and tesseral equatorial Rossby waves, retrograde mixed inertial modes, prograde thermal Rossby waves, the recently observed high-frequency retrograde (HFR) vorticity modes, and what may be latitudinal overtones of these HFR modes. With this model, we demonstrate that sectoral and tesseral Rossby waves are ubiquitous within the radiative interior as well as within the convection zone. We suggest that there are two different Rossby-wave families in this simulation that live in different wave cavities: one in the radiative interior and one in the convection zone. Finally, we suggest that many of the retrograde inertial waves that appear in the convection zone, including the HFR modes, are in fact all related, being latitudinal overtones that are mixed modes with the prograde thermal Rossby waves.

Science Platforms for Heliophysics Data Analysis

Monica G. **Bobra**, Will T. Barnes, Thomas Y. Chen, Mark C. M. Cheung, Laura A. Hayes, Jack Ireland, Miho Janvier, Michael S. F. Kirk, James P. Mason, Stuart J. Mumford, Paul J. Wright

Heliophysics 2050 White Paper **2023**
https://arxiv.org/ftp/arxiv/papers/2301/2301.00878.pdf
We recommend that NASA maintain and fund science platforms that enable interactive and scalable data analysis in order to maximize the scientific return of data collected from space-based instruments.

SMARPs and SHARPs: Two Solar Cycles of Active Region Data

Monica G. **Bobra**, Paul J. Wright, Xudong Sun, Michael J. Turmon
ApJS **256** 26 **2021**
https://arxiv.org/pdf/2108.07918.pdf
https://iopscience.iop.org/article/10.3847/1538-4365/ac1f1d/pdf
https://doi.org/10.3847/1538-4365/ac1f1d
We present a new data product, called Space-Weather MDI Active Region Patches (SMARPs), derived from maps of the solar surface magnetic field taken by the Michelson Doppler Imager (MDI) aboard the Solar and Heliospheric Observatory (SoHO). Together with the Space-Weather HMI Active Region Patches (SHARPs), derived from similar maps taken by the Helioseismic and Magnetic Imager (HMI) aboard the Solar Dynamics Observatory, these data provide a continuous and seamless set of maps and keywords that describe every active region observed over the last two solar cycles, from 1996 to the present day. In this paper, we describe the SMARP data and compare it to the SHARP data. **9-20 July 2010, 14 July 2010**

A Survey of Computational Tools in Solar Physics

Monica G. **Bobra**, Stuart J. Mumford, Russell J. Hewett, Steven D. Christe, Kevin Reardon, Sabrina Savage, Jack Ireland, Tiago M. D. Pereira, Bin Chen & David Pérez-Suárez
Solar Physics volume 295, Article number: 57 (**2020**)
https://link.springer.com/content/pdf/10.1007/s11207-020-01622-2.pdf
The SunPy Project developed a 13-question survey to understand the software and hardware usage of the solar-physics community. Of the solar-physics community, 364 members across 35 countries responded to our survey. We found that 99±0.5% of respondents use software in their research and 66% use the Python scientific-software stack. Students are twice as likely as faculty, staff scientists, and researchers to use Python rather than Interactive Data Language (IDL). In this respect, the astrophysics and solar-physics communities differ widely: 78% of solar-physics faculty, staff scientists, and researchers in our sample uses IDL, compared with 44% of astrophysics faculty and scientists sampled by Momcheva and Tollerud (2015). 63±4% of respondents have not taken any computer-science courses at an undergraduate or graduate level. We also found that most respondents use consumer hardware to run software for solar-physics research. Although 82% of respondents work with data from space-based or ground-based missions, some of which (e.g. the Solar Dynamics Observatory and Daniel K. Inouye Solar Telescope) produce terabytes of data a day, 14% use a regional or national cluster, 5% use a commercial cloud provider, and 29% use exclusively a laptop or desktop. Finally, we found that 73±4% of respondents cite scientific software in their research, although only 42±3% do so routinely.

Heliophysics Machine Learning (HelioML): Machine Learning, Statistics, and Data Mining for Heliophysics. Online, Interactive Book Free!

Monica **Bobra** and James Mason
Online, Interactive Book, **2019**
https://helioml.github.io/HelioML/title.html
This book includes a collection of interactive Jupyter notebooks, written in Python, that explicitly shows the reader how to use machine learning, statistics, and data minining techniques on various kinds of heliophysics data sets to reproduce published results.

Analyzing SDO/HMI Data Using Python

Monica G. **Bobra**.
HMI Science Nuggets #50 Apr **2016**
http://hmi.stanford.edu/hminuggets/?p=1428
SDO is six years old now, which means that there is half a solar cycle of data available to study. When SDO launched, most of the solar physics community was using IDL for data analysis. **February 14-15, 2011, March 6, 2012**

Solar Flare Prediction Using SDO/HMI Vector Magnetic Field Data with a Machine-Learning Algorithm

Monica G. **Bobra**, Sebastien Couvidat

ApJ, **798** 135 **2015**
http://arxiv.org/pdf/1411.1405v1.pdf
We attempt to forecast M-and X-class solar flares using a machine-learning algorithm, called Support Vector Machine (SVM), and four years of data from the Solar Dynamics Observatory's Helioseismic and Magnetic Imager, the first instrument to continuously map the full-disk photospheric vector magnetic field from space. Most flare forecasting efforts described in the literature use either line-of-sight magnetograms or a relatively small number of ground-based vector magnetograms. This is the first time a large dataset of vector magnetograms has been used to forecast solar flares. We build a catalog of flaring and non-flaring active regions sampled from a database of 2,071 active regions, comprised of 1.5 million active region patches of vector magnetic field data, and characterize each active region by 25 parameters. We then train and test the machine-learning algorithm and we estimate its performances using forecast verification metrics with an emphasis on the True Skill Statistic (TSS). We obtain relatively high TSS scores and overall predictive abilities. We surmise that this is partly due to fine-tuning the SVM for this purpose and also to an advantageous set of features that can only be calculated from vector magnetic field data. We also apply a feature selection algorithm to determine which of our 25 features are useful for discriminating between flaring and non-flaring active regions and conclude that only a handful are needed for good predictive abilities. **March 7, 2012,**

The Helioseismic and Magnetic Imager (HMI) Vector Magnetic Field Pipeline: SHARPs - Space-weather HMI Active Region Patches

Monica **Bobra**, X. Sun, J.T. Hoeksema, M. Turmon, Y Liu, K. Hayashi, G. Barnes, K.D. Leka
E-print, Apr **2014**, Solar Phys. Volume 289, Issue 9, pp 3549-3578, **2014**
http://sun.stanford.edu/~todd/SHARP.pdf
http://arxiv.org/pdf/1404.1879v1.pdf
A new data product from the Helioseismic and Magnetic Imager (HMI) onboard the Solar Dynamics Observatory (SDO) called Space-weather HMI Active Region Patches (SHARPs) is now available. SDO/HMI is the first space-based instrument to map the full-disk photospheric vector magnetic field with high cadence and continuity. The SHARP data series provide maps in patches that encompass automatically tracked magnetic concentrations for their entire lifetime; map quantities include the photospheric vector magnetic field and its uncertainty, along with Doppler velocity, continuum intensity, and line-of-sight magnetic field. Furthermore, keywords in the SHARP data series provide several parameters that concisely characterize the magnetic-field distribution and its deviation from a potential-field configuration. These indices may be useful for active region event forecasting and for identifying regions of interest. The indices are calculated per patch and are available on a twelve-minute cadence. Quick-look data are available within approximately three hours of observation; definitive science products are produced approximately five weeks later. SHARP data are available at jsoc.stanford.edu and maps are available in either of two different coordinate systems. This article describes the SHARP data products and presents examples of SHARP data and parameters.

The Solar Minimum Eclipse of 2019 July 2. III. Inferring the Coronal Te with a Radiative Differential Emission Measure Inversion

Benjamin **Boe**, Cooper Downs, Shadia Habbal
ApJ **2023**
https://arxiv.org/pdf/2306.04826.pdf
Differential Emission Measure (DEM) inversion methods use the brightness of a set of emission lines to infer the line-of-sight (LOS) distribution of the electron temperature (Te) in the corona. DEM inversions have been traditionally performed with collisionally excited lines at wavelengths in the Extreme Ultraviolet (EUV) and X-ray. However, such emission is difficult to observe beyond the inner corona (1.5 R⊙), particularly in coronal holes. Given the importance of the Te distribution in the corona for exploring the viability of different heating processes, we introduce an analog of the DEM specifically for radiatively excited coronal emission lines, such as those observed during total solar eclipses (TSEs) and with coronagraphs. This Radiative DEM (R-DEM) inversion utilizes visible and infrared emission lines which are excited by photospheric radiation out to at least 3 R⊙. Specifically, we use the Fe X (637 nm), Fe XI (789 nm), and Fe XIV (530 nm) coronal emission lines observed during the 2019 July 2 TSE near solar minimum. We find that despite a large Te spread in the inner corona, the distribution converges to an almost isothermal yet bimodal distribution beyond 1.4 R⊙, with Te ranging from 1.1 to 1.4 in coronal holes, and from 1.4 to 1.65 MK in quiescent streamers. Application of the R-DEM inversion to the Predictive Science Inc. magnetohydrodynamic (MHD) simulation for the 2019 eclipse validates the R-DEM method and yields a similar LOS Te distribution to the eclipse data.

The Solar Minimum Eclipse of 2019 July 2. II. The First Absolute Brightness Measurements and MHD Model Predictions of Fe x, xi, and xiv out to 3.4 R⊙

Benjamin **Boe**1, Shadia Habbal1, Cooper Downs2, and Miloslav Druckmüller3

2022 ApJ 935 173
https://iopscience.iop.org/article/10.3847/1538-4357/ac8101/pdf
We present the spatially resolved absolute brightness of the Fe x, Fe xi, and Fe xiv visible coronal emission lines from 1.08 to 3.4 R⊙, observed during the 2019 July 2 total solar eclipse (TSE). The morphology of the corona was typical of solar minimum, with a dipole field dominance showcased by large polar coronal holes and a broad equatorial streamer belt. The Fe xi line is found to be the brightest, followed by Fe x and Fe xiv (in disk B⊙ units). All lines had brightness variations between streamers and coronal holes, where Fe xiv exhibited the largest variation. However, Fe x remained surprisingly uniform with latitude. The Fe line brightnesses are used to infer the relative ionic abundances and line-of-sight-averaged electron temperature (Te) throughout the corona, yielding values from 1.25 to 1.4 MK in coronal holes and up to 1.65 MK in the core of streamers. The line brightnesses and inferred Te values are then quantitatively compared to the Predictive Science Inc. magnetohydrodynamic model prediction for this TSE. The MHD model predicted the Fe lines rather well in general, while the forward-modeled line ratios slightly underestimated the observationally inferred Te within 5%–10% averaged over the entire corona. Larger discrepancies in the polar coronal holes may point to insufficient heating and/or other limitations in the approach. These comparisons highlight the importance of TSE observations for constraining models of the corona and solar wind formation.

The Color and Brightness of the F-Corona Inferred from the 2019 July 2 Total Solar Eclipse

Benjamin **Boe**, Shadia Habbal, Cooper Downs, Miloslav Druckmuller
ApJ **912** 44 **2021**
https://arxiv.org/pdf/2103.02113.pdf
https://doi.org/10.3847/1538-4357/abea79
Total solar eclipses (TSEs) provide a unique opportunity to quantify the properties of the K-corona (electrons), F-corona (dust) and E-corona (ions) continuously from the solar surface out to a few solar radii. We apply a novel inversion method to separate emission from the K- and F-corona continua using unpolarized total brightness (tB) observations from five 0.5 nm bandpasses acquired during the 2019 July 2 TSE between 529.5 nm and 788.4 nm. The wavelength dependence relative to the photosphere (i.e., color) of the F-corona itself is used to infer the tB of the K- and F-corona for each line-of-sight. We compare our K-corona emission results with the Mauna Loa Solar Observatory (MLSO) K-Cor polarized brightness (pB) observations from the day of the eclipse, and the forward modeled K-corona intensity from the Predictive Science Inc. (PSI) Magnetohydrodynamic (MHD) model prediction. Our results are generally consistent with previous work and match both the MLSO data and PSI-MHD predictions quite well, supporting the validity of our approach and of the PSI-MHD model. However, we find that the tB of the F-corona is higher than expected in the low corona, perhaps indicating that the F-corona is slightly polarized -- challenging the common assumption that the F-corona is entirely unpolarized.

First Empirical Determination of the Fe 10+ and Fe 13+ Freeze-in Distances in the Solar Corona

Benjamin **Boe**, Shadia Habbal, Miloslav Druckmuller, Enrico Landi, Ehsan Kourkchi, Adalbert Ding, Pavel Starha, Joseph Hutton
2018 *ApJ* **859** 155
https://arxiv.org/pdf/1805.03211.pdf
Heavy ions are markers of the physical processes responsible for the density and temperature distribution throughout the fine scale magnetic structures that define the shape of the solar corona. One of their properties, whose empirical determination has remained elusive, is the 'freeze-in' distance (Rf) where they reach fixed ionization states that are adhered to during their expansion with the solar wind. We present the first empirical inference of Rf for Fe10+ and Fe13+ derived from multi-wavelength imaging observations of the corresponding FeXI (Fe10+) 789.2 nm and FeXIV (Fe13+) 530.3 nm emission acquired during the **2015 March 20** total solar eclipse. We find that the two ions freeze-in at different heliocentric distances. In polar coronal holes Rf is around 1.45 Rs for Fe10+ and below 1.25 Rs for Fe13+. Along open field lines in streamer regions Rf ranges from 1.4 to 2 Rs for Fe10+ and from 1.5 to 2.2 Rs for Fe13+. These first empirical Rf values: (1) reflect the differing plasma parameters between coronal holes and streamers and structures within them, including prominences and Coronal Mass Ejections (CMEs); (2) are well below the currently quoted values derived from empirical model studies; and (3) place doubt on the reliability of plasma diagnostics based on the assumption of ionization equilibrium beyond 1.2 Rs.

Evidence of a Quasi-periodic Global-scale Oscillation in the Near-Surface Shear Layer of the Sun

Richard S. **Bogart**, Charles S. Baldner, Sarbani Basu, Rachel Howe, Maria Cristina Rabello Soares
ApJL **2023**
https://arxiv.org/abs/2305.18613

We present evidence of hitherto undiscovered global-scale oscillations in the near-surface shear layer of the Sun. These oscillations are seen as large scale variations of radial shear in both the zonal and meridional flows relative to their mean values. The variations cover all or most of a visible hemisphere, and reverse with a timescale on the order of a solar rotation. A large annual variation in the meridional shear anomaly is understandable in terms of the tilt of the rotation axis, but the rapid oscillations of the shear anomalies in both zonal and the meridional directions appear to be modulated in a more complex, not-quite annual way, although the latter are also strongly modulated by the projected rotational axis angle. Small-scale anomalies in the neighborhood of active regions lend support to their solar origin and physical interpretation. These results were obtained by analyzing ring-diagram fits of low-order modes in high-resolution Doppler data from the Helioseismic and Magnetic Imager on the Solar Dynamics Observatory.

SDO/HMI – Artifact in Images and Processing Delays

Richard **Bogart**
SolarNews Volume 2018 Number 17 01 September **2018**
http://spd.stanford.edu//SolarNews/2018/20180901.html#section_bogart
On 2018.08.17 at 04:52 UT, an artifact appeared in HMI filtergrams from both cameras in the form of a dark stripe across the upper left quadrant of the raw images.

Evolution of Near-surface Flows Inferred from High-resolution Ring-diagram Analysis

Richard S. **Bogart**1, Charles S. Baldner1, and Sarbani Basu
2015 ApJ 807 125
Ring-diagram analysis of acoustic waves observed at the photosphere can provide a relatively robust determination of the sub-surface flows at a particular time under a particular region. The depth of penetration of the waves is related to the size of the region, hence the depth extent of the measured flows is inversely proportional to the spatial resolution. Most ring-diagram analysis has focused on regions of extent ~15° (180 Mm) or more in order to provide reasonable mode sets for inversions. Helioseismic and Magnetic Imager (HMI) data analysis also provides a set of ring fit parameters on a scale three times smaller. These provide flow estimates for the outer 1% (7 Mm) of the Sun only, with very limited depth resolution, but with spatial resolution adequate to map structures potentially associated with the belts and regions of magnetic activity. There are a number of systematic effects affecting the determination of flows from a local helioseismic analysis of regions over different parts of the observable disk, and not all of them are well understood. In this study we characterize those systematic effects with higher spatial resolution so that they may be accounted for more effectively in mapping the temporal and spatial evolution of the flows. Leaving open the question of the mean structure of the global meridional circulation and the differential rotation, we describe the near-surface flow anomalies in time and latitude corresponding to the torsional oscillation pattern in differential rotation and analogous patterns in the meridional cell structure as observed by the Solar Dynamics Observatory/HMI.

New Space Weather Activities in the World Meteorological Organization,

Bogdan, T. J., and T. G. Onsager
(**2010**), Space Weather, 8, S10004, doi:10.1029/2010SW000626.
A new era of enhanced international cooperation in space weather operations has begun with the recent initiation of space weather activities within the World Meteorological Organization (WMO), an agency of the United Nations (U.N.) with a membership of 189 states and territories. These activities aim to standardize and enhance space weather observations and data exchange, coordinate end products and services, and foster dialogue between the research and operational communities. The WMO's role is to foster collaboration among the meteorological and hydrological (and now space weather) service providers and to promote the establishment of networks for making and exchanging geophysical observations and the standardization of data and metadata. It also contributes to policy making and has a lead role in efforts to monitor and protect the environment.

A Reconstruction of Ultraviolet Spectral Irradiance During the Maunder Minimum

C. **Bolduc**, P. Charbonneau, R. Barnabé, M. S. Bourqui
Solar Physics, August **2014**, Volume 289, Issue 8, pp 2891-2906
We present a reconstruction of the solar spectrum in the near and mid-ultraviolet spectral range during the Maunder Minimum, a period of strongly suppressed magnetic activity spanning the second half of the 17th century. This spectral reconstruction is based on an extension of the Monte Carlo Solar Spectral Irradiance Model (MOCASSIM). The new version of the model, documented in this paper, extends its spectral range down to 150 nm, its temporal range back to 1610, includes a secular modulation of the quiet-Sun emissivity based on a total solar irradiance reconstruction, and uses the Atmospheric Laboratory for Applications and Science-3 (ATLAS-3) spectrum as a reconstruction baseline. The model is validated against the ATLAS-1 spectrum for 29 March 1992, showing a general agreement varying from ∼ 1 % in the 300 – 400 nm range, up to 3 – 5 % below 200 nm, the largest

discrepancies occurring in emission lines formed in the chromosphere and transition region. We also reconstruct ultraviolet spectra for May 2008 and March 2009, spanning the extended phase of low activity separating Cycles 23 and 24. Our results suggest that despite the unusually long temporal extent of this activity minimum, the ultraviolet emission still remained slightly higher than during the Maunder Minimum, due to the lingering presence of decay products from active regions having emerged in the late descending phase of Cycle 23.

Comments to the Article by Thuillier et al. "The Infrared Solar Spectrum Measured by the SOLSPEC Spectrometer Onboard the International Space Station" on the Interpretation of Ground-based Measurements at the Izaña Site

D. **Bolsée** , N. Pereira, E. Cuevas, R. García, A. Redondas
Solar Phys. **2016**
Thuillier et al. (Solar Phys. 290, 1581, 2015) article compares ATLAS-3 reference composite solar spectral irradiance (SSI) with more recent spatial measurements, as well as ground-based ones, including IRSPERAD. With respect to the IRSPERAD spectrum of Bolsée et al. (Solar Phys. 289, 2433, 2014), Thuillier et al. (2015) presents an analysis based on a set of meteorological parameters retrieved at the moment of the respective ground-based campaign. This comment is intended to give a new insight to the said analysis which is based upon revised values of the meteorological parameters incorrectly used in Thuillier et al. (2015).

Analytic mean-field α2-dynamo with a force-free corona

Alfio **Bonanno**1 and Fabio Del Sordo
A&A 605, A33 (**2017**)
Context. Stellar dynamos are affected by boundary conditions imposed by stellar coronae. Under some approximations, it is possible to find analytical solutions. Interior dynamo models often consider a current-free corona without taking into account the constraints imposed by the presence of currents in the corona.
Aims. We aim to analytically evaluate the effect of coronal currents and of an outer boundary condition on the efficiency of an α2dynamo. We intend to estimate the change in geometry and dynamo excitation numbers with respect to the current-free case.
Methods. We analytically solved the turbulent dynamo induction equation for a homogeneous, non-mirror symmetric turbulence in a spherical domain surrounded by a linear force-free corona with the mean magnetic field B satisfying $\nabla \times B = \beta B$.
Results. The dynamo number is a decreasing function of β. Moreover, if the current is parallel to the field ($\beta > 0$), the dynamo number is smaller than in the force-free case. In contrast, for ($\beta < 0$), the dynamo number is greater than in the force-free case.
Conclusions. Currents in the corona need to be taken into account because they affect the condition for excitation of a dynamo.

A Bayesian estimation of the helioseismic solar age

Alfio **Bonanno**, Hans-Erich Fröhlich
A&A 580, A130 **2015**
http://arxiv.org/pdf/1507.05847v1.pdf
The helioseismic determination of the solar age has been a subject of several studies because it provides us with an independent estimation of the age of the solar system. We present the Bayesian estimates of the helioseismic age of the Sun, which are determined by means of calibrated solar models that employ different equations of state and nuclear reaction rates. We use 17 frequency separation ratios $r02(n)=(\nu_{n,l=0}-\nu_{n-1,l=2})/(\nu_{n,l=1}-\nu_{n-1,l=1})$ from 8640 days of low-ℓ BiSON frequencies and consider three likelihood functions that depend on the handling of the errors of these r02(n) ratios. Moreover, we employ the 2010 CODATA recommended values for Newton's constant, solar mass, and radius to calibrate a large grid of solar models spanning a conceivable range of solar ages. It is shown that the most constrained posterior distribution of the solar age for models employing Irwin EOS with NACRE reaction rates leads to $t_\odot=4.587\pm0.007$ Gyr, while models employing the Irwin EOS and Adelberger, et al., Reviews of Modern Physics, 83, 195 (2011) reaction rate have $t_\odot=4.569\pm0.006$ Gyr. Implementing OPAL EOS in the solar models results in reduced evidence ratios (Bayes factors) and leads to an age that is not consistent with the meteoritic dating of the solar system. An estimate of the solar age that relies on an helioseismic age indicator such as r02(n) turns out to be essentially independent of the type of likelihood function. However, with respect to model selection, abandoning any information concerning the errors of the r02(n) ratios leads to inconclusive results, and this stresses the importance of evaluating the trustworthiness of error estimates.

Helioseismological determination of the subsurface spatial spectrum of solar convection: Demonstration using numerical simulations

Vincent G. A. **Böning**, Aaron C. Birch, Laurent Gizon, Thomas L. Duvall Jr
A&A 649, A59 **2021**
https://arxiv.org/pdf/2102.08603.pdf
https://www.aanda.org/articles/aa/pdf/2021/05/aa39311-20.pdf
https://doi.org/10.1051/0004-6361/202039311
Understanding convection is important in stellar physics, for example as an input in stellar evolution models. Helioseismic estimates of convective flow amplitudes in deeper regions of the solar interior disagree by orders of magnitude among themselves and with simulations. We aim to assess the validity of an existing upper limit of solar convective flow amplitudes at a depth of 0.96 solar radii obtained using time-distance helioseismology and several simplifying assumptions. We generated synthetic observations for convective flow fields from a magnetohydrodynamic simulation (MURaM) using travel-time sensitivity functions and a noise model. We compared the estimates of the flow with the actual values. For the scales of interest ($\ell<100$), we find that the current procedure for obtaining an upper limit gives the correct order of magnitude of the flow for the given flow fields. We also show that this estimate is not an upper limit in a strict sense because it underestimates the flow amplitude at the largest scales by a factor of about two because the scale dependence of the signal-to-noise ratio has to be taken into account. After correcting for this and after taking the dependence of the measurements on direction in Fourier space into account, we show that the obtained estimate is indeed an upper limit. We conclude that time-distance helioseismology is able to correctly estimate the order of magnitude (or an upper limit) of solar convective flows in the deeper interior when the vertical correlation function of the different flow components is known and the scale dependence of the signal-to-noise ratio is taken into account. We suggest that future work should include information from different target depths to better separate the effect of near-surface flows from those at greater depths. The measurements are sensitive to all three flow directions, which should be taken into account.

Characterizing the spatial pattern of solar supergranulation using the bispectrum A181

Vincent G. A. **Böning**, Aaron C. Birch, Laurent Gizon, Thomas L. Duvall Jr. and Jesper Schou
A&A 635, A181 (**2020**)
https://arxiv.org/pdf/2002.08262.pdf
https://www.aanda.org/articles/aa/pdf/2020/03/aa37331-19.pdf
Context. The spatial power spectrum of supergranulation does not fully characterize the underlying physics of turbulent convection. For example, it does not describe the non-Gaussianity in the horizontal flow divergence.
Aims. Our aim is to statistically characterize the spatial pattern of solar supergranulation beyond the power spectrum. The next-order statistic is the bispectrum. It measures correlations of three Fourier components and is related to the nonlinearities in the underlying physics. It also characterizes how a skewness in the dataset is generated by the coupling of three Fourier components.
Methods. We estimated the bispectrum of supergranular horizontal surface divergence maps that were obtained using local correlation tracking (LCT) and time-distance helioseismology (TD) from one year of data from the helioseismic and magnetic imager on-board the solar dynamics observatory starting in May 2010.
Results. We find significantly nonzero and consistent estimates for the bispectrum using LCT and TD. The strongest nonlinearity is present when the three coupling wave vectors are at the supergranular scale. These are the same wave vectors that are present in regular hexagons, which have been used in analytical studies of solar convection. At these Fourier components, the bispectrum is positive, consistent with the positive skewness in the data and consistent with supergranules preferentially consisting of outflows surrounded by a network of inflows. We use the bispectral estimates to generate synthetic divergence maps that are very similar to the data. This is done by a model that consists of a Gaussian term and a weaker quadratic nonlinear component. Using this method, we estimate the fraction of the variance in the divergence maps from the nonlinear component to be of the order of 4–6%.
Conclusions. We propose that bispectral analysis is useful for understanding the dynamics of solar turbulent convection, for example for comparing observations and numerical models of supergranular flows. This analysis may also be useful to generate synthetic flow fields.

On the signature of solar g modes in first-order p-mode frequency shifts

Vincent G. A. **Böning**, Huanchen Hu, Laurent Gizon
A&A 629, A26 **2019**
https://arxiv.org/pdf/1907.02379.pdf
https://www.aanda.org/articles/aa/pdf/2019/09/aa35434-19.pdf
Context. Solar gravity modes (g modes) are buoyancy waves trapped in the solar radiative zone that have been very difficult to detect at the surface. Solar g modes would complement solar pressure modes (p modes) in probing the central regions of the Sun, for example the core rotation rate.
Aims. A detection of g modes using changes in the large frequency separation of p modes has recently been reported. However, it is unclear how p and g modes interact. The aim of this study is to evaluate to what extent g modes can perturb the frequencies of p modes.
Methods. We computed the first-order perturbation to global p-mode frequencies due to a flow field and

perturbations to solar structure caused by a g mode. We focused on long-period g modes and assumed that the g-mode perturbations are constant in time. The surface amplitude of g modes is assumed to be 1 mm s−1, which is close to the observational limit.
Results. Gravity modes do perturb p-mode frequencies to first order if the harmonic degree of the g mode is even and if its azimuthal order is zero. The effect is extremely small. For dipole and quadrupole p modes, all frequency shifts are smaller than 0.1 nHz, or 2×10−8 in relative numbers. This is because the relative perturbation to solar structure quantities caused by a g mode of realistic amplitude is of the order of 10−6 to 10−5. We find that structural changes dominate over advection. Surprisingly, the interaction of g and p modes takes place to a large part near the surface, where p modes spend most of their propagation times and g modes generate the largest relative changes to solar structure.
Conclusions. It appears to be impossible to detect g modes solely through their signature in p-mode frequency shifts. Whether g modes leave a detectable signature in p-mode travel times under a given observational setup remains an open question.

Inversions for Deep Solar Meridional Flow Using Spherical Born Kernels

Vincent G. A. **Böning**, Markus Roth, Jason Jackiewicz, Shukur Kholikov
ApJ **845** 2 **2017**
https://arxiv.org/pdf/1707.08803.pdf
The solar meridional flow is a crucial ingredient in modern dynamo theory. Seismic estimates of this flow have, however, been contradictory in deeper layers below about 0.9R⊙. Results from time-distance helioseismology have so far been obtained using the ray approximation. Here, we perform inversions using the Born approximation. The initial result is similar to the result previously obtained by Jackiewicz et al. (2015) using ray kernels while using the same set of GONG data and the SOLA inversion technique. However, we show that the assumption of uncorrelated measurements used in earlier studies may lead to inversion errors being underestimated by a factor of about two to four. In a second step, refined inversions are performed using the full covariance matrix and a regularization for cross-talk. As the results are found to depend on the threshold used in the singular value decomposition, they were obtained for a medium threshold (10−7−10−5, about 50% of the values used) and a threshold lower by a factor of 10 (about 70% of the values used). The result obtained with the medium threshold is again similar to the original, with less latitudinal variation. However, using the lower threshold, the inverted flow in the southern hemisphere shows two or three cells stacked radially depending on the associated radial flows. Both the single-cell and the multi-cell profiles are consistent with the measured travel times. All our results confirm a shallow return flow at about 0.9R⊙.

Validation of Spherical Born Approximation Sensitivity Functions for Measuring Deep Solar Meridional Flow

Vincent G. A. **Böning**, Markus Roth, Jason Jackiewicz, Shukur Kholikov
ApJ 838 53 **2017**
https://arxiv.org/pdf/1703.03700.pdf
Accurate measurements of deep solar meridional flow are of vital interest for understanding the solar dynamo. In this paper, we validate a recently developed method for obtaining sensitivity functions (kernels) for travel-time measurements to solar interior flows using the Born approximation in spherical geometry, which is expected to be more accurate than classical ray approximation. Furthermore, we develop a numerical approach to efficiently compute a large number of kernels based on the separability of the eigenfunctions into their horizontal and radial dependence. The validation is performed using a hydrodynamic simulation of linear wave propagation in the Sun, which includes a standard single-cell meridional flow profile. We show that, using the Born approximation, it is possible to accurately model observational quantities relevant for time-distance helioseismology such as the mean power spectrum, disc-averaged cross-covariance functions, and travel times in the presence of a flow field. In order to closely match the model to observations, we show that it is beneficial to use mode frequencies and damping rates which were extracted from the measured power spectrum. Furthermore, the contribution of the radial flow to the total travel time is found to reach 20% of the contribution of the horizontal flow at travel distances over 40◦. Using the Born kernels and a 2D SOLA inversion of travel times, we can recover most features of the input meridional flow profile. The Born approximation is thus a promising method for inferring large-scale solar interior flows.

Sensitivity Kernels for Flows in Time-Distance Helioseismology: Extension to Spherical Geometry

Vincent G. A. **Böning**, Markus Roth, Wolfgang Zima, Aaron C. Birch, Lauren Gizon
ApJ **2016**
http://arxiv.org/pdf/1604.03803v1.pdf

We extend an existing Born approximation method for calculating the linear sensitivity of helioseismic travel times to flows from Cartesian to spherical geometry. This development is necessary for using the Born approximation for inferring large-scale flows in the deep solar interior. In a first sanity check, we compare two f−mode kernels from our spherical method and from an existing Cartesian method. The horizontal and total integrals agree to within 0.3 %. As a second consistency test, we consider a uniformly rotating Sun and a travel distance of 42 degrees. The analytical travel-time difference agrees with the forward-modelled travel-time difference to within 2 %. In addition, we evaluate the impact of different choices of filter functions on the kernels for a meridional travel distance of 42 degrees. For all filters, the sensitivity is found to be distributed over a large fraction of the convection zone. We show that the kernels depend on the filter function employed in the data analysis process. If modes of higher harmonic degree ($90 \lesssim l \lesssim 170$) are permitted, a noisy pattern of a spatial scale corresponding to $l \approx 260$ appears near the surface. When mainly low-degree modes are used ($l \lesssim 70$), the sensitivity is concentrated in the deepest regions and it visually resembles a ray-path-like structure. Among the different low-degree filters used, we find the kernel for phase-speed filtered measurements to be best localized in depth.

Swirls in the solar corona

C. **Breu**1,2, H. Peter1, R. Cameron1 and S. K. Solanki1,3
A&A 675, A94 (**2023**)
https://www.aanda.org/articles/aa/pdf/2023/07/aa45780-22.pdf

Context. Vortex flows have been found in the photosphere, chromosphere, and low corona in observations and simulations. It has been suggested that vortices play an important role in channeling energy and plasma into the corona. However, the impact of vortex flows on the corona has not been studied directly in a realistic setup.
Aims. We investigate the role vortices play for coronal heating using high-resolution simulations of coronal loops. The vortices are not artificially driven and they arise, instead, self-consistently from magnetoconvection.
Methods. We performed 3D resistive (magnetohydrodynamic) MHD simulations with the MURaM code. Studying an isolated coronal loop in a Cartesian geometry allows us to resolve the structure of the loop interior. We conducted a statistical analysis to determine vortex properties as a function of height from the chromosphere into the corona.
Results. We find that the energy injected into the loop is generated by internal coherent motions within strong magnetic elements. A significant part of the resulting Poynting flux is channeled through the chromosphere in vortex tubes forming a magnetic connection between the photosphere and corona. Vortices can form contiguous structures that reach up to coronal heights, but in the corona itself, the vortex tubes get deformed and eventually lose their identity with increasing height. Vortices show increased upward directed Poynting flux and heating rate in both the chromosphere and corona, but their effect becomes less pronounced with increasing height.
Conclusions. While vortices play an important role for the energy transport and structuring in the chromosphere and low corona, their importance higher up in the atmosphere is less clear since the swirls are less distinguishable from their environment. Vortex tubes reaching the corona reveal a complex relationship with the coronal emission.

FarNet-II: An improved solar far-side active region detection method

E. G. **Broock**1,2, A. Asensio Ramos1,2 and T. Felipe1,2
A&A 667, A132 (**2022**)
https://www.aanda.org/articles/aa/pdf/2022/11/aa44206-22.pdf

Context. Activity on the far side of the Sun is routinely studied through the analysis of the seismic oscillations detected on the near side using helioseismic techniques such as phase-shift sensitive holography. Detections made through those methods are limited to strong active regions due to the need for a high signal-to-noise ratio. Recently, the neural network FarNet was developed to improve these detections. This network extracts more information from helioseismic far-side maps, enabling the detection of smaller and weaker active regions.
Aims. We aim to create a new machine learning tool, FarNet-II, which further increases FarNet's scope, and to evaluate its performance in comparison to FarNet and the standard helioseismic method for detecting far-side activity.
Methods. We developed FarNet-II, a neural network that retains some of the general characteristics of FarNet but improves the detections in general, as well as the temporal coherence among successive predictions. The main novelties of the new neural network are the implementation of attention and convolutional long short-term memory (ConvLSTM) modules. A cross-validation approach, training the network 37 times with a different validation set for each run, was employed to leverage the limited amount of data available. We evaluate the performance of FarNet-II using three years of extreme ultraviolet observations of the far side of the Sun acquired with the Solar Terrestrial Relations Observatory (STEREO) as a proxy of activity. The results from FarNet-II were compared with those obtained from FarNet and the standard helioseismic method using the Dice coefficient as a metric. Given that the application of the ConvLSTM modules can affect the accuracy as a function of the position on the sequence, we take this potential dependency into account in the evaluation.
Results. FarNet-II achieves a Dice coefficient that improves that of FarNet by over 0.2 points for every output position on the sequences from the evaluation dates. Its improvement over FarNet is higher than that of FarNet over the standard method.

Conclusions. The new network is a very promising tool for improving the detection of activity on the far side of the Sun given by pure helioseismic techniques. Space weather forecasts can potentially benefit from the higher sensitivity provided by this novel method.

The Solar Minimum Eclipse of 2019 July 2. III. Inferring the Coronal Te with a Radiative Differential Emission Measure Inversion

Benjamin **Boe**1, Cooper Downs2, and Shadia Habbal1
2023 ApJ 951 55
https://iopscience.iop.org/article/10.3847/1538-4357/acd10b/pdf
Differential emission measure (DEM) inversion methods use the brightness of a set of emission lines to infer the line-of-sight (LOS) distribution of the electron temperature (Te) in the corona. DEM inversions have been traditionally performed with collisionally excited lines at wavelengths in the extreme ultraviolet and X-ray. However, such emission is difficult to observe beyond the inner corona (1.5 R⊙), particularly in coronal holes. Given the importance of the Te distribution in the corona for exploring the viability of different heating processes, we introduce an analog of the DEM specifically for radiatively excited coronal emission lines, such as those observed during total solar eclipses (TSEs) and with coronagraphs. This radiative-DEM (R-DEM) inversion utilizes visible and infrared emission lines that are excited by photospheric radiation out to at least 3 R⊙. Specifically, we use the Fe x (637 nm), Fe xi (789 nm), and Fe xiv (530 nm) coronal emission lines observed during the **2019 July 2** TSE near solar minimum. We find that, despite a large Te spread in the inner corona, the distribution converges to an almost isothermal yet bimodal distribution beyond 1.4 R⊙, with Te ranging from 1.1 to 1.4 in coronal holes and from 1.4 to 1.65 MK in quiescent streamers. Application of the R-DEM inversion to the Predictive Science Inc. magnetohydrodynamic simulation for the 2019 eclipse validates the R-DEM method and yields a similar LOS Te distribution to the eclipse data.

Enhanced Phase Mixing of Torsional Alfvén Waves in Stratified and Divergent Solar Coronal Structures, Paper II: Nonlinear Simulations

C.**Boocock** and D.Tsiklauri
MNRAS **2022**
https://arxiv.org/pdf/2112.03724
We use MHD simulations to detect the nonlinear effects of torsional Alfvén wave propagation in a potential magnetic field with exponentially divergent field lines, embedded in a stratified solar corona. In Paper I we considered solutions to the linearised governing equations for torsional Alfvén wave propagation and showed, using a finite difference solver we developed named WiggleWave, that in certain scenarios wave damping is stronger than what would be predicted by our analytic solutions. In this paper we consider whether damping would be further enhanced by the presence of nonlinear effects. We begin by deriving the nonlinear governing equations for torsional Alfvén wave propagation and identifying the terms that cause coupling to magnetosonic perturbations. We then compare simulation outputs from an MHD solver called Lare3d, which solves the full set of nonlinear MHD equations, to the outputs from WiggleWave to detect nonlinear effects such as: the excitation of magnetosonic waves by the Alfvén wave, self-interaction of the Alfvén wave through coupling to the induced magnetosonic waves, and the formation of shock waves higher in the atmosphere caused by the steepening of these compressive perturbations. We suggest that the presence of these nonlinear effects in the solar corona would lead to Alfvén wave heating that exceeds the expectation from the phase mixing alone.

Reply to "Response to 'Limitations in the Hilbert Transform Approach to Locating Solar Cycle Terminators' by R.J. Booth"

R. J. **Booth**
Solar Physics volume 296, Article number: 167 (**2021**)
https://link.springer.com/content/pdf/10.1007/s11207-021-01911-4.pdf
https://doi.org/10.1007/s11207-021-01911-4
This is a reply to Leamon et al., Solar Phys., 2021 (in press, hereinafter L21), which is a response to Booth, Solar Phys. 296, 108, 2021. We agree that, given a fixed constant subtracted from the sunspot counts prior to the Hilbert transform, the L21 algorithm to determine historical sunspot cycle terminators is robust, but add that it has no dependence at all on start and end dates. However, the prediction of a future terminator relies on properties of the transform, which do depend on both start and end dates. For the Cycle 24 terminator, the 95% confidence interval (CI) implied by L21's statistics includes all dates until September 2022. For each new month that the terminator is proven not to occur, the CI's end date will be extended.

Limitations in the Hilbert Transform Approach to Locating Solar Cycle Terminators

R. J. **Booth**
Solar Physics volume 296, Article number: 108 (**2021**)

https://link.springer.com/content/pdf/10.1007/s11207-021-01833-1.pdf
https://doi.org/10.1007/s11207-021-01833-1
This paper studies the method by which Leamon et al. (Solar Phys. 295, 36, 2020) produces predictions for the so-called "terminator" of solar cycles (in particular Solar Cycle 24), which is a novel way of defining the length of a solar cycle. This method involves use of a Hilbert transform of the data and a derived "phase". The present paper both replicates and augments methods and results from that paper, but finds that its claim to have identified a mathematically robust signature of terminators in sunspot records is not well founded. In particular, we demonstrate that the results are significantly sensitive to both the starting point of the data and the centralizing constant used to provide a meaningful Hilbert phase. Some realistic parameter choices, including more recently available data, push the predicted terminator back by about 2 years. This has concomitant implications for predictions of the magnitude of the next cycle (25), which depend on the length of the previous cycle. In particular, an increase by 2 years would reduce the predicted 233 maximum sunspot number in McIntosh et al. (Solar Phys. 295, 163, 2020) to 173.

Combining magneto-hydrostatic constraints with Stokes profiles inversions
II. Application to Hinode/SP observations

J. M. **Borrero**1, A. Pastor Yabar2 and B. Ruiz Cobo3,4
A&A 647, A190 (**2021**)
https://doi.org/10.1051/0004-6361/202039927
https://www.aanda.org/articles/aa/pdf/2021/03/aa39927-20.pdf
Context. Inversion techniques applied to the radiative transfer equation for polarized light are capable of inferring the physical parameters in the solar atmosphere (temperature T, magnetic field B, and line-of-sight velocity vlos) from observations of the Stokes vector (i.e., spectropolarimetric observations) in spectral lines. Inferences are usually performed in the (x, y, τc) domain, where τc refers to the optical-depth scale. Generally, their determination in the (x, y, z) volume is not possible due to the lack of a reliable estimation of the gas pressure, particularly in regions of the solar surface harboring strong magnetic fields.
Aims. We aim to develop a new inversion code capable of reliably inferring the physical parameters in the (x, y, z) domain.
Methods. We combine, in a self-consistent way, an inverse solver for the radiative transfer equation (Firtez-DZ) with a solver for the magneto-hydrostatic equilibrium, which derives realistic values of the gas pressure by taking the magnetic pressure and tension into account.
Results. We test the correct behavior of the newly developed code with spectropolarimetric observations of two sunspots recorded with the spectropolarimeter (SP) instrument on board the Hinode spacecraft, and we show how the physical parameters are inferred in the (x, y, z) domain, with the Wilson depression of the sunspots arising as a natural consequence of the force balance. In particular, our approach significantly improves upon previous determinations that were based on semiempirical models.
Conclusions. Our results open the door for the possibility of calculating reliable electric currents in three dimensions, j(x, y, z), in the solar photosphere. Further consistency checks would include a comparison with other methods that have recently been proposed and which achieve similar goals.

Chromospheric and coronal heating in an active region plage by dissipation of currents from braiding

Bose, Souvik ; De Pontieu, Bart ; Hansteen, Viggo ; +++
Nature Astronomy, Advanced Online Publication **2024**
DOI: 10.1038/s41550-024-02241-8
10.48550/arXiv.2211.08579
IRIS Nugget April **2024** https://iris.lmsal.com/nugget
The question of what heats the outer solar atmosphere remains one of the longstanding mysteries in astrophysics. Statistical studies of Sun-like stars reveal a correlation between global chromospheric and coronal emissions, constraining theoretical models of potential heating mechanisms. However, spatially resolved observations of the Sun have surprisingly failed to show a similar correlation on small spatial scales. Here we use unique coordinated observations of the chromosphere (from the IRIS satellite) and the low corona (from the Hi-C 2.1 sounding rocket), and machine-learning-based inversion techniques, to show a strong correlation on spatial scales of a few hundred kilometres between heating in the chromosphere and emission in the upper transition region in strong magnetic field regions (`plage'). Our observations are compatible with an advanced three-dimensional magnetohydrodynamic simulation in which the dissipation of current sheets caused by magnetic field braiding is responsible for heating the plasma simultaneously to chromospheric and coronal temperatures. Our results provide deep insight into the nature of the heating mechanism in solar active regions. **29 May 2018**

On the dynamics of spicules and mass flows in the solar atmosphere **Thesis**

Souvik **Bose**
PhD dissertation No. 2443 (University of Oslo). **2021**
https://www.duo.uio.no/handle/10852/88981
https://arxiv.org/pdf/2110.10656.pdf
Popular scientific summary -- The atmosphere of the Sun is envisioned as composed of inherently complex, non-homogeneous, and dynamic layers. A detailed understanding of the physical processes involved in these layers is still lacking. For example, it is largely unknown why the outermost layer of the Sun's atmosphere (the solar corona) is so much hotter than the photosphere by millions of degrees. Astrophysicists think that the layer sandwiched between the photosphere and the corona, known as the interface region, may hold the key to a better understanding of the nature of this enigma. With the help of coordinated high-resolution, ground- and space-based observations from the Swedish 1-m Solar Telescope (SST) on La Palma, Spain, and NASA's Interface Region Imaging Spectrograph (IRIS) and Solar Dynamics Observatory (SDO), along with the support from an advanced numerical simulation, I aim to unlock some of the mysteries surrounding the dynamics of the interface region with a focus on small-scale jets, known as "spicules". Spicules are found almost everywhere on the Sun's surface and at any given moment there can be as many as 10 million of them rapidly shooting outwards. They are often found to be heated beyond chromospheric temperatures and appear in the transition region and (even) coronal passbands. Because of their "omnipresence", it is suggested that they play a major role in energizing the outer atmospheric layers of the Sun. This thesis focuses on the physical characteristics and dynamics of spicules, along with their role in mass-balance and heating of the solar atmosphere.

Characterization and formation of on-disk spicules in the Ca II K and Mg II k spectral lines

Souvik **Bose**1,2, Vasco M. J. Henriques1,2, Jayant Joshi1,2 and Luc Rouppe van der Voort1,2
A&A 631, L5 (**2019**)
https://doi.org/10.1051/0004-6361/201936617
We characterize, for the first time, type-II spicules in Ca II K 3934 Å using the CHROMIS instrument at the Swedish 1 m Solar Telescope. We find that their line formation is dominated by opacity shifts with the K3 minimum best representing the velocity of the spicules. The K2 features are either suppressed by the Doppler-shifted K3 or enhanced via increased contribution from the lower layers, leading to strongly enhanced but unshifted K2 peaks, with widening towards the line core as consistent with upper-layer opacity removal via Doppler-shift. We identify spicule spectra in concurrent IRIS Mg II k 2796Å observations with very similar properties. Using our interpretation of spicule chromospheric line formation, we produce synthetic profiles that match observations.
erratum A&A Volume 637, May 2020 C1
https://doi.org/10.1051/0004-6361/201936617e

Enhanced Phase Mixing of Torsional Alfvén Waves in Stratified and Divergent Solar Coronal Structures, Paper II: Nonlinear Simulations

Callum **Boocock**, David Tsiklauri
MNRAS Volume 510, Issue 2, February **2022**, Pages 2618–2627,
https://doi.org/10.1093/mnras/stab3592
https://arxiv.org/pdf/2112.03724
We use MHD simulations to detect the nonlinear effects of torsional Alfvén wave propagation in a potential magnetic field with exponentially divergent field lines, embedded in a stratified solar corona. In Paper I we considered solutions to the linearised governing equations torsional Alfvén wave propagation and showed, using a finite difference solver we developed named WiggleWave, that in certain scenarios wave damping is stronger than what would be predicted by our analytic solutions. In this paper we consider whether damping would be further enhanced by the presence of nonlinear effects. We begin by deriving the nonlinear governing equations for torsional Alfvén wave propagation and identifying the terms that cause coupling to magnetosonic perturbations. We then compare simulation outputs from an MHD solver called Lare3d, which solves the full set of nonlinear MHD equations, to the outputs from WiggleWave to detect nonlinear effects such as: the excitation of magnetosonic waves by the Alfvén wave, self-interaction of the Alfvén wave through coupling to the induced magnetosonic waves, and the formation of shock waves higher in the atmosphere caused by the steepening of these compressive perturbations. We suggest that the presence of these nonlinear effects in the solar corona would lead to Alfvén wave heating that exceeds the expectation from the phase mixing alone.

Enhanced Phase Mixing of Torsional Alfvén Waves in Stratified and Divergent Solar Coronal Structures, Paper I: Linear Solutions

Callum **Boocock**, David Tsiklauri

MNRAS Volume 510, Issue 2, February **2022**, Pages 1910–1922,
https://doi.org/10.1093/mnras/stab3535
https://arxiv.org/pdf/2112.00571
We derive a corrected analytical solution for the propagation and enhanced phase mixing of torsional Alfvén waves, in a potential magnetic field with exponentially divergent field lines, embedded in a stratified solar corona. Further we develop a code named TAWAS which calculates the analytic solution describing torsional Alfvén waves using IDL software language. We then use TAWAS to demonstrate that both our correction to the analytic solution and the inclusion of wave reflection have a significant impact on Alfvén wave damping. We continue to utilise TAWAS by performing a parameter study in order to identify the conditions under which enhanced phase mixing is strongest. We find that phase mixing is the strongest for high frequency Alfvén waves in magnetic fields with highly divergent field lines and without density stratification. We then present a finite difference solver, Wigglewave, which solves the linearised evolution equations for the system directly. Comparing solutions from TAWAS and Wigglewave we see that our analytical solution is accurate within the limits of the WKB approximation but under-reports the wave damping, caused by enhanced phase mixing, beyond the WKB limit. Both TAWAS and Wigglewave solve the linearised governing equations and not the complete nonlinear MHD equations. Paper II will consider simulations that solve the full MHD equations including important nonlinear effects.

Simple magnetic reconnection example

Allen H **Boozer**, Todd Elder
2020
https://arxiv.org/pdf/2011.11822.pdf
In laboratory and natural plasmas of practical interest, the smallest spatial scale Δd over which magnetic field lines are distinguishable on the time scale set by an ideal evolution differs enormously from the scale a of magnetic reconnection across the field lines. In the solar corona, plasma resistivity gives a/Δd~1012, which is the magnetic Reynold number Rm. The standard resolution of the paradox of disparate time scales is for the current density j associated with the reconnecting field Brec to be concentrated by the ideal evolution, so j~Brec/μ0Δd, an amplification by a factor Rm. A second resolution is for the ideal evolution to increase the ratio of the maximum to minimum separation between two arbitrarily chosen magnetic field lines, Δmax/Δmin, when calculated at various points in time. Reconnection becomes inevitable when Δmax/Δmin~Rm. As demonstrated using a simple model of the solar corona, the natural rate of increase in time is linear for the current density but exponential for Δmax/Δmin. Reconnection occurs on a time scale and with a current density enhanced by only ln((a/Δd) from the ideal evolution time and from the current density Brec/μ0a. In both resolutions of the paradox of disparate time scales, once a sufficient region has undergone reconnection, the magnetic field loses force balance and evolves ideally on an Alfvén transit time. This ideal evolution generally expands the region in which Δmax/Δmin is large.

Wavelet-analysis of series of observations of relative sunspot numbers. The dependence of the periods of cyclic activity on the time at different time scales

A.A. **Borisov**, E.A. Bruevich, V.V. Bruevich, I.K. Rozgacheva, E.V. Shimanovskaya
2015
http://arxiv.org/pdf/1512.04098v1.pdf
We applied the method of continuous wavelet-transform to high-quality time-frequency analysis to the sets of observations of relative sunspot numbers. Wavelet analysis of these data reveals the following pattern: at the same time there are several activity cycles whose periods vary widely from the quasi biennial up to the centennial period. These relatively low-frequency periodic variations of the solar activity gradually change the values of periods of different cycles in time. This phenomenon can be observed in every cycle of activity.

Combining magneto-hydrostatic constraints with Stokes profiles inversions III. Uncertainty in the inference of electric currents

J. M. **Borrero**1 and A. Pastor Yabar2
A&A 669, A122 (**2023**)
https://www.aanda.org/articles/aa/pdf/2023/01/aa44716-22.pdf
Context. Electric currents play an important role in the energy balance of the plasma in the solar atmosphere. They are also indicative of non-potential magnetic fields and magnetic reconnection. Unfortunately, the direct measuring of electric currents has traditionally been riddled with inaccuracies.
Aims. We study how accurately we can infer electric currents under different scenarios.
Methods. We carry out increasingly complex inversions of the radiative transfer equation for polarized light applied to Stokes profiles synthesized from radiative three-dimensional magnetohydrodynamic (MHD) simulations. The inversion yields the magnetic field vector, B, from which the electric current density, j, is derived by applying Ampere's law.

Results. We find that the retrieval of the electric current density is only slightly affected by photon noise or spectral resolution. However, the retrieval steadily improves as the Stokes inversion becomes increasingly elaborated. In the least complex case (a Milne-Eddington-like inversion applied to a single spectral region), it is possible to determine the individual components of the electric current density (j_x, j_y, j_z) with an accuracy of $\sigma = 0.90 - 1.00$ dex, whereas the modulus ($\|j\|$) can only be determined with $\sigma = 0.75$ dex. In the most complicated case (with multiple spectral regions, a large number of nodes, Tikhonov vertical regularization, and magnetohydrostatic equilibrium), these numbers improve to $\sigma = 0.70 - 0.75$ dex for the individual components and $\sigma = 0.5$ dex for the modulus. Moreover, in regions where the magnetic field is above 300 gauss, $\|j\|$ can be inferred with an accuracy of $\sigma = 0.3$ dex. In general, the x and y components of the electric current density are retrieved slightly better than the z component. In addition, the modulus of the electric current density is the best retrieved parameter of all, and thus it can potentially be used to detect regions of enhanced Joule heating.
Conclusions. The fact that the accuracy does not worsen with decreasing spectral resolution or increasing photon noise, and instead increases as the Stokes inversion complexity grows, suggests that the main source of errors in the determination of electric currents is the lack of realism in the inversion model employed to determine variations in the magnetic field along the line of sight at scales smaller than the photon mean-free path, along with the intrinsic limitations of the model due to radiative transfer effects.

Combining magneto-hydrostatic constraints with Stokes profile inversions. II. Application to Hinode/SP observations

J.M.**Borrero**, A. Pastor Yabar, B. Ruiz Cobo
A&A **2021**
https://arxiv.org/pdf/2101.04394.pdf
Inversion techniques applied to the radiative transfer equation for polarized light are capable of inferring the physical parameters in the solar atmosphere (temperature T, magnetic field B, and line-of-sight velocity vlos) from observations of the Stokes vector (i.e., spectropolarimetric observations) in spectral lines. Inferences are usually performed in the (x,y,τ_c) domain, where τ_c refers to the optical-depth scale. Generally, their determination in the (x,y,z) volume is not possible due to the lack of a reliable estimation of the gas pressure, particularly in regions of the solar surface harboring strong magnetic fields. We aim to develop a new inversion code capable of reliably inferring the physical parameters in the (x,y,z) domain. We combine, in a self-consistent way, an inverse solver for the radiative transfer equation (Firtez-DZ) with a solver for the magneto-hydrostatic (MHS) equilibrium, which derives realistic values of the gas pressure by taking the magnetic pressure and tension into account. We test the correct behavior of the newly developed code with spectropolarimetric observations of two sunspots recorded with the spectropolarimeter (SP) instrument on board the Hinode spacecraft, and we show how the physical parameters are inferred in the (x,y,z) domain, with the Wilson depression of the sunspots arising as a natural consequence of the force balance. In particular, our approach significantly improves upon previous determinations that were based on semiempirical models. Our results open the door for the possibility of calculating reliable electric currents in three dimensions, j(x,y,z), in the solar photosphere. Further consistency checks would include a comparison with other methods that have recently been proposed and which achieve similar goals. **November 14, 2006**

Combining magnetohydrostatic constraints with Stokes profiles inversions I. Role of boundary conditions

J. M. **Borrero**1, A. Pastor Yabar1, M. Rempel2 and B. Ruiz Cobo
A&A 632, A111 (**2019**)
https://doi.org/10.1051/0004-6361/201936367
Context. Inversion codes for the polarized radiative transfer equation, when applied to spectropolarimetric observations (i.e., Stokes vector) in spectral lines, can be used to infer the temperature T, line-of-sight velocity vlos, and magnetic field B as a function of the continuum optical-depth τ_c. However, they do not directly provide the gas pressure Pg or density ρ. In order to obtain these latter parameters, inversion codes rely instead on the assumption of hydrostatic equilibrium (HE) in addition to the equation of state (EOS). Unfortunately, the assumption of HE is rather unrealistic across magnetic field lines, causing estimations of Pg and ρ to be unreliable. This is because the role of the Lorentz force, among other factors, is neglected. Unreliable gas pressure and density also translate into an inaccurate conversion from optical depth τ_c to geometrical height z.
Aims. We aim at improving the determination of the gas pressure and density via the application of magnetohydrostatic (MHS) equilibrium instead of HE.
Methods. We develop a method to solve the momentum equation under MHS equilibrium (i.e., taking the Lorentz force into account) in three dimensions. The method is based on the iterative solution of a Poisson-like equation. Considering the gas pressure Pg and density ρ from three-dimensional magnetohydrodynamic (MHD) simulations of sunspots as a benchmark, we compare the results from the application of HE and MHS equilibrium using boundary conditions with different degrees of realism. Employing boundary conditions that can be applied to actual observations, we find that HE retrieves the gas pressure and density with an error smaller than one order of magnitude (compared to the MHD values) in only about 47% of the grid points in the three-dimensional domain.

Moreover, the inferred values are within a factor of two of the MHD values in only about 23% of the domain. This translates into an error of about 160 − 200 km in the determination of the z − τc conversion (i.e., Wilson depression). On the other hand, the application of MHS equilibrium with similar boundary conditions allows determination of Pg and ρ with an error smaller than an order of magnitude in 84% of the domain. The inferred values are within a factor of two in more than 55% of the domain. In this latter case, the z − τc conversion is obtained with an accuracy of 30 − 70 km. Inaccuracies are due in equal part to deviations from MHS equilibrium and to inaccuracies in the boundary conditions.
Results. Compared to HE, our new method, based on MHS equilibrium, significantly improves the reliability in the determination of the density, gas pressure, and conversion between geometrical height z and continuum optical depth τc. This method could be used in conjunction with the inversion of the radiative transfer equation for polarized light in order to determine the thermodynamic, kinematic, and magnetic parameters of the solar atmosphere.

Solar magnetoconvection and small-scale dynamo: Recent developments in observation and simulation **Review**

J.M. **Borrero**, S. Jafarzadeh, M. Schüssler, S.K. Solanki
Space Science Reviews September **2017**, Volume 210, Issue 1–4, pp 275–316
http://arxiv.org/pdf/1511.04214v1.pdf
A number of observational and theoretical aspects of solar magnetoconvection are considered in this review. We discuss recent developments in our understanding of the small-scale structure of the magnetic field on the solar surface and its interaction with convective flows, which is at the centre of current research. Topics range from plage areas in active regions over the magnetic network shaped by supergranulation to the ubiquituous `turbulent' internetwork fields. On the theoretical side, we focus upon magnetic field generation by small-scale dynamo action.

Magnetic Structure of Sunspots

Borrero, Juan Manuel and Ichimoto, Kiyoshi
Living Reviews in Solar Physics, PUB.NO. lrsp-**2011**-4
http://www.livingreviews.org/lrsp-2011-4
In this **review** we give an overview about the current state-of-knowledge of the magnetic field in sunspots from an observational point of view. We start by offering a brief description of tools that are most commonly employed to infer the magnetic field in the solar atmosphere with emphasis in the photosphere of sunspots. We then address separately the global and local magnetic structure of sunspots, focusing on the implications of the current observations for the different sunspots models, energy transport mechanisms, extrapolations of the magnetic field towards the corona, and other issues.

The chromosphere underneath a Coronal Bright Point

Souvik **Bose**, Daniel Nóbrega-Siverio, Bart De Pontieu, Luc Rouppe van der Voort
ApJ **2023**
https://arxiv.org/pdf/2301.08596
Coronal Bright Points (CBPs) are sets of small-scale coronal loops, connecting opposite magnetic polarities, primarily characterized by their enhanced extreme-ultraviolet (EUV) and X-ray emission. Being ubiquitous, they are thought to play an important role in heating the solar corona. We aim at characterizing the barely-explored chromosphere underneath CBPs, focusing on the related spicular activity and on the effects of small-scale magnetic flux emergence on CBPs. We used high-resolution observations of a CBP in Hβ and Fe I 617.3 nm from the Swedish 1-m Solar Telescope (SST) in coordination with the Solar Dynamics Observatory (SDO). This work presents the first high-resolution observation of spicules imaged in Hβ. The spicules were automatically detected using advanced image processing techniques, which were applied to the Dopplergrams derived from Hβ. Here we report their abundant occurrence close to the CBP ``footpoints'', and find that the orientation of such spicules is aligned along the EUV loops, indicating that they constitute a fundamental part of the whole CBP magnetic structure. Spatio-temporal analysis across multiple channels indicates that there are coronal propagating disturbances associated with the studied spicules, producing transient EUV intensity variations of the individual CBP loops. Two small-scale flux emergence episodes appearing below the CBP were analyzed; one of them leading to quiet-sun Ellerman bombs and enhancing the nearby spicular activity. This paper presents unique evidence of the tight coupling between the lower and upper atmosphere of a CBP, thus helping to unravel the dynamic phenomena underneath CBPs and their impact on the latter. **4 Aug 2021**

Chromospheric and Coronal heating in active region plage by dissipation of currents from braiding

Souvik **Bose**, Bart De Pontieu, Viggo Hansteen, Alberto Sainz Dalda, Sabrina Savage, Amy Winebarger
2022
https://arxiv.org/pdf/2211.08579.pdf

It remains unclear which physical processes are responsible for the dramatic increase with height of the temperature in stellar atmospheres, known as the chromospheric (~10,000 K) and coronal (several million K) heating problems. Statistical studies of sun-like stars reveal that chromospheric and coronal emissions are correlated on a global scale, constraining, in principle, theoretical models of potential heating mechanisms. However, so far, spatially resolved observations of the Sun have surprisingly failed to show a similar correlation on small spatial scales, leaving models poorly constrained. Here we use unique coordinated high-resolution observations of the chromosphere (from the Interface Region Imaging Spectrograph or IRIS satellite) and low corona (from the Hi-C 2.1 sounding rocket), and machine-learning based inversion techniques to show a strong correlation on spatial scales of a few hundred km between heating in the chromosphere and low corona for regions with strong magnetic field ("plage"). These results are compatible with recent advanced 3D radiative magnetohydrodynamic simulations in which dissipation of current sheets formed due to the braiding of the magnetic field lines deep in the atmosphere is responsible for heating the plasma simultaneously to chromospheric and coronal temperatures. Our results provide deep insight into the nature of the heating mechanism in solar active regions**. 29 May 2018**

Evidence of multithermal nature of spicular downflows. Impact on solar atmospheric heating

Souvik **Bose**, Luc Rouppe van der Voort, Jayant Joshi, Vasco M.J. Henriques, Daniel Nóbrega-Siverio, Juan Martínez-Sykora, Bart De Pontieu

A&A 654, A51 **2021**

https://arxiv.org/pdf/2108.02153.pdf

https://doi.org/10.1051/0004-6361/202141404

Spectroscopic observations of the emission lines formed in the solar transition region (TR) commonly show persistent downflows of the order of 10--15 km/s. The cause of such downflows, however, is still not fully clear and has remained a matter of debate. We aim to understand the cause of such downflows by studying the coronal and TR responses to the recently reported chromospheric downflowing rapid red shifted excursions (RREs), and their impact on heating the solar atmosphere. We have used two sets of coordinated data from SST, IRIS, and SDO for analyzing the response of the downflowing RREs in the TR and corona. To provide theoretical support, we use an already existing 2.5D MHD simulation of spicules performed with the Bifrost code. We find ample occurrences of downflowing RREs and show several examples of their spatio-temporal evolution, sampling multiple wavelength channels ranging from the cooler chromospheric to hotter coronal channels. These downflowing features are thought to be likely associated with the returning components of the previously heated spicular plasma. Furthermore, the TR Doppler shifts associated with them are close to the average red shifts observed in this region which further implies that these flows could (partly) be responsible for the persistent downflows observed in the TR. We also propose two mechanisms (a typical upflow followed by a downflow and downflows along a loop), from the perspective of numerical simulation, that could explain the ubiquitous occurrence of such downflows. A detailed comparison between the synthetic and observed spectral characteristics, reveals a distinctive match, and further suggests an impact on the heating of the solar atmosphere. We present evidence that suggests that at least some of the downflowing RREs are the chromospheric counterparts of the TR and lower coronal downflows.

Spicules and downflows in the solar chromosphere

Souvik **Bose**, Jayant Joshi, Vasco M.J. Henriques, Luc Rouppe van der Voort

A&A 647, A147 **2021**

https://arxiv.org/pdf/2101.07829.pdf

https://www.aanda.org/articles/aa/pdf/2021/03/aa40014-20.pdf

https://doi.org/10.1051/0004-6361/202040014

High-speed downflows have been observed in the solar transition region (TR) and lower corona for many decades. Despite their abundance, it has been hard to find signatures of such downflows in the solar chromosphere. In this work, we target an enhanced network region that shows ample occurrences of rapid spicular downflows in the \halpha\ spectral line that could potentially be linked to high-speed TR downflowing counterparts. We used the k-means algorithm to classify the spectral profiles of on-disk spicules in \halpha{} and \cak{} data observed from the Swedish 1-m Solar Telescope (SST) and employed an automated detection method based on advanced morphological image processing operations to detect such downflowing features, in conjunction with rapid blue-shifted and red-shifted excursions (RBEs and RREs). We report the existence of a new category of RREs (termed as downflowing RRE) for the first time that, contrary to earlier interpretation, are associated with chromospheric field-aligned downflows moving towards the strong magnetic field regions. Statistical analysis performed on nearly 20,000 RBEs and 15,000 RREs (including the downflowing counterparts), detected in our 97~min long dataset, shows that the downflowing RREs are very similar to RBEs and RREs except for their oppositely directed plane-of-sky motion. Furthermore, we also find that RBEs, RREs and downflowing RREs can be represented by a wide range of spectral profiles with varying Doppler offsets, and \halpha{} line core widths, both along and perpendicular to the spicule axis, that causes them to be associated with multiple substructures that evolve together. We speculate that

these rapid plasma downflows could well be the chromospheric counterparts of the commonly observed TR downflows. **25 May 2017**

Characterization and formation of on-disk spicules in the Ca II K and Mg II k spectral lines

Souvik **Bose**, Vasco M.J. Henriques, Jayant Joshi, Luc Rouppe van der Voort
A&A Letter 631, L5 **2019**
https://arxiv.org/pdf/1910.05533.pdf
https://doi.org/10.1051/0004-6361/20193661
We characterize, for the first time, type-II spicules in Ca II K 3934Å\ using the CHROMIS instrument at the Swedish 1-m Solar Telescope. We find that their line formation is dominated by opacity shifts with the K3 minimum best representing the velocity of the spicules. The K2 features are either suppressed by the Doppler-shifted K3 or enhanced via an increased contribution from the lower layers, leading to strongly enhanced but un-shifted K2 peaks, with widening towards the line-core as consistent with upper-layer opacity removal via Doppler-shift. We identify spicule spectra in concurrent IRIS Mg II k 2796Å observations with very similar properties. Using our interpretation of spicule chromospheric line-formation, we produce synthetic profiles that match observations. **25 May 2017**

Space Weather: Physics and Effects,

edited by Volker **Bothmer** and Ioannis A. Daglis,
AGU, **2007**, 438 pages, **Book File**

The Sun as the prime source of space weather

Bothmer, V. and Zhukov, A.:,
in: Space Weather – Physics and Effects, edited by: Bothmer, V. and Daglis, I. A., Springer-Verlag, pp. 31–102, **2007, Book File**.

Sources of magnetic helicity over solar cycle

Bothmer, V.
Proc. ISCS Symp. ESA-SP-535, **2003, File**
The magnetic field characteristics of a sample set of helical magnetic flux rope ICMEs (magnetic clouds) observed by the Wind and ACE satellites in solar cycle 23 and their related space weather effects are investigated. The solar source regions of the magnetic clouds were identified using remote sensing observations of the SOHO, Yohkoh and TRACE spacecraft together with ground-based Hα images. Each cloud observed at 1 AU could be uniquely associated with a well defined frontside halo CME some days before the cloud's arrival at 1 AU. The hemispheric origin is consistent with the expected hemispheric helicity pattern. The space weather effects of the clouds were quite variable, depending on their internal magnetic field configuration and speed of progagation

The structure and origin of magnetic clouds in the solar wind

V. **Bothmer**1* and R. Schwenn
Ann. Geophysicae 16, 1±24 (**1998**), **File**
Plasma and magnetic field data from the Helios 1/2 spacecraft have been used to investigate the structure of magnetic clouds (MCs) in the inner heliosphere. 46 MCs were identified in the Helios data for the period 1974-1981 between 0.3 and 1 AU. 85% of the MCs were associated with fast-forward interplanetary shock waves, supporting the close association between MCs and SMEs (solar mass ejections). Seven MCs were identified as direct consequences of Helios-directed SMEs, and the passage of MCs agreed with that of interplanetary plasma clouds (IPCs) identified as white-light brightness enhancements in the Helios photometer data. The total (plasma and magnetic field) pressure in MCs was higher and the plasma-<beta> lower than in the surrounding solar wind. Minimum variance analysis (MVA) showed that MCs can best be described as large-scale quasi-cylindrical magnetic flux tubes. The axes of the flux tubes usually had a small inclination to the ecliptic plane, with their azimuthal direction close to the east-west direction. The large-scale flux tube model for MCs was validated by the analysis of multi-spacecraft observations. MCs were observed over a range of up to ~60° in solar longitude in the ecliptic having the same magnetic configuration. The Helios observations further showed that over-expansion is a common feature of MCs. From a combined study of Helios, Voyager and IMP data we found that the radial diameter of MCs increases between 0.3 and 4.2 AU proportional to the distance, R, from the Sun as R0.8 (R in AU). The density decrease inside MCs was found to be proportional to R-2.4, thus being stronger compared to the average solar wind. Four different magnetic configurations, as expected from the flux-tube concept, for MCs have been observed in situ by the Helios probes. MCs with left- and right-handed magnetic helicity occurred with about equal

frequencies during 1974-1981, but surprisingly, the majority (74%) of the MCs had a south to north (SN) rotation of the magnetic field vector relative to the ecliptic. In contrast, an investigation of solar wind data obtained near Earth's orbit during 1984-1991 showed a preference for NS-clouds. A direct correlation was found between MCs and large quiescent filament disappearances (disparition brusques, DBs). The magnetic configurations of the filaments, as inferred from the orientation of the prominence axis, the polarity of the overlying field lines and the hemispheric helicity pattern observed for filaments, agreed well with the in situ observed magnetic structure of the associated MCs. The results support the model of MCs as large-scale expanding quasi-cylindrical magnetic flux tubes in the solar wind, most likely caused by SMEs associated with eruptions of large quiescent filaments. We suggest that the hemispheric dependence of the magnetic helicity structure observed for solar filaments can explain the preferred orientation of MCs in interplanetary space as well as their solar cycle behavior. However, the white-light features of SMEs and the measured volumes of their interplanetary counterparts suggest that MCs may not simply be just H<alpha>-prominences, but that SMEs likely convect large-scale coronal loops overlying the prominence axis out of the solar atmosphere.

Spatiotemporal Interpolation Methods for Solar Event Trajectories

Soukaina Filali **Boubrahimi**, Berkay Aydin, Michael A. Schuh, Dustin Kempton, Rafal A. Angryk, and Ruizhe Ma
2018 ApJS 236 23
http://sci-hub.tw/http://iopscience.iop.org/0067-0049/236/1/23/
This paper introduces four spatiotemporal interpolation methods that enrich complex, evolving region trajectories that are reported from a variety of ground-based and space-based solar observatories every day. Our interpolation module takes an existing solar event trajectory as its input and generates an enriched trajectory with any number of additional time–geometry pairs created by the most appropriate method. To this end, we designed four different interpolation techniques: MBR-Interpolation (Minimum Bounding Rectangle Interpolation), CP-Interpolation (Complex Polygon Interpolation), FI-Interpolation (Filament Polygon Interpolation), and Areal-Interpolation, which are presented here in detail. These techniques leverage k-means clustering, centroid shape signature representation, dynamic time warping, linear interpolation, and shape buffering to generate the additional polygons of an enriched trajectory. Using ground-truth objects, interpolation effectiveness is evaluated through a variety of measures based on several important characteristics that include spatial distance, area overlap, and shape (boundary) similarity. To our knowledge, this is the first research effort of this kind that attempts to address the broad problem of spatiotemporal interpolation of solar event trajectories. We conclude with a brief outline of future research directions and opportunities for related work in this area.

Driving solar coronal MHD simulations on high-performance computers

Philippe-A. **Bourdin** (Space Research Institute, Austrian Academy of Sciences, Graz/Austria)
GEOPHYSICAL & ASTROPHYSICAL FLUID DYNAMICS **2019**
https://arxiv.org/pdf/1908.08557.pdf
The quality of today's research is often tightly limited to the available computing power and scalability of codes to many processors. For example, tackling the problem of heating the solar corona requires a most realistic description of the plasma dynamics and the magnetic field. Numerically solving such a magneto-hydrodynamical (MHD) description of a small active region (AR) on the Sun requires millions of computation hours on current high-performance computing (HPC) hardware. The aim of this work is to describe methods for an efficient parallelization of boundary conditions and data input/output (IO) strategies that allow for a better scaling towards thousands of processors (CPUs). The Pencil Code is tested before and after optimization to compare the performance and scalability of a coronal MHD model above an AR. We present a novel boundary condition for non-vertical magnetic fields in the photosphere, where we approach the realistic pressure increase below the photosphere. With that, magnetic flux bundles become narrower with depth and the flux density increases accordingly. The scalability is improved by more than one order of magnitude through the HPC-friendly boundary conditions and IO strategies. This work describes also the necessary nudging methods to drive the MHD model with observed magnetic fields from the Sun's photosphere. In addition, we present the upper and lower atmospheric boundary conditions (photospheric and towards the outer corona), including swamp layers to diminish perturbations before they reach the boundaries. Altogether, these methods enable more realistic 3D MHD simulations than previous models regarding the coronal heating problem above an AR -- simply because of the ability to use a large amount of CPUs efficiently in parallel.

Magnetic Helicity from Multipolar Regions on the Solar Surface

Philippe-A. **Bourdin**1 and Axel Brandenburg
2018 ApJ 869 3
sci-hub.se/10.3847/1538-4357/aae97f
https://arxiv.org/pdf/1804.04160.pdf

The emergence of dipolar magnetic features on the solar surface is an idealization. Most of the magnetic flux emergence occurs in complex multipolar regions. Here, we show that the surface pattern of magnetic structures alone can reveal the sign of the underlying magnetic helicity in the nearly force-free coronal regions above. The sign of the magnetic helicity can be predicted to good accuracy by considering the three-dimensional position vectors of three spots on the sphere ordered by their relative strengths at the surface and compute from them the skew product. This product, which is a pseudoscalar, is shown to be a good proxy for the sign of the coronal magnetic helicity.

Magnetic Helicity Reversal in the Corona at Small Plasma Beta

Philippe **Bourdin**1, Nishant K. Singh2,3, and Axel Brandenburg3,4,5,6
2018 ApJ 869 2
sci-hub.se/10.3847/1538-4357/aae97a
Solar and stellar dynamos shed small-scale and large-scale magnetic helicity of opposite signs. However, solar wind observations and simulations have shown that some distance above the dynamo both the small-scale and large-scale magnetic helicities have reversed signs. With realistic simulations of the solar corona above an active region now being available, we have access to the magnetic field and current density along coronal loops. We show that a sign reversal in the horizontal averages of the magnetic helicity occurs when the local maximum of the plasma beta drops below unity and the field becomes nearly fully force free. Hence, this reversal is expected to occur well within the solar corona and would not directly be accessible to in situ measurements with the Parker Solar Probe or SolarOrbiter. We also show that the reversal is associated with subtle changes in the relative dominance of structures with positive and negative magnetic helicity.

Standard 1D solar atmosphere as initial condition for MHD simulations and switch-on effects

Philippe-A. **Bourdin**
CEAB 38 (**2014**) 1-10
http://arxiv.org/pdf/1507.01218v1.pdf
'Many applications in Solar physics need a 1D atmospheric model as initial condition or as reference for inversions of observational data. The VAL atmospheric models are based on observations and are widely used since decades. Complementary to that, the FAL models implement radiative hydrodynamics and showed the shortcomings of the VAL models since almost equally long time. In this work, we present a new 1D layered atmosphere that spans not only from the photosphere to the transition region, but from the solar interior up to far in the corona. We also discuss typical mistakes that are done when switching on simulations based on such an initial condition and show how the initial condition can be equilibrated so that a simulation can start smoothly. The 1D atmosphere we present here served well as initial condition for HD and MHD simulations and should also be considered as reference data for solving inverse problems.

Quantifying the Influence of Key Physical Processes on the Formation of Emission Lines Observed by IRIS: I. Non-Equilibrium Ionization and Density-Dependent Rates

Stephen J. **Bradshaw**, Paola Testa
2019 *ApJ* **872** 123
https://arxiv.org/pdf/1901.03935.pdf
In the work described here we investigate atomic processes leading to the formation of emission lines within the IRIS wavelength range at temperatures near 105~K. We focus on (1) non-equilibrium and (2) density-dependent effects influencing the formation and radiative properties of S IV and O IV. These two effects have significant impacts on spectroscopic diagnostic measurements of quantities associated with the plasma that emission lines from S IV and O IV provide. We demonstrate this by examining nanoflare-based coronal heating to determine what the detectable signatures are in transition region emission. A detailed comparison between predictions from numerical experiments and several sets of observational data is presented to show how one can ascertain when non-equilibrium ionization and/or density-dependent atomic processes are important for diagnosing nanoflare properties, the magnitude of their contribution, and what information can be reliably extracted from the spectral data. Our key findings are the following. (1) The S/O intensity ratio is a powerful diagnostic of non-equilibrium ionization. (2) Non-equilibrium ionization has a strong effect on the observed line intensities even in the case of relatively weak nanoflare heating. (3) The density-dependence of atomic rate coefficients is only important when the ion population is out of equilibrium. (4) In the sample of active regions we examined, weak nanoflares coupled with non-equilibrium ionization and density-dependent atomic rates were required to explain the observed properties (e.g. the S/O intensity ratios). (5) Enhanced S/O intensity ratios cannot be due solely to the heating strength and must depend on other processes (e.g. heating frequency, non-Maxwellian distributions).

Simulations of Alfven wave driving of the solar chromosphere - efficient heating and spicule launching

C. S. **Brady**, T. D. Arber
2016 *ApJ* **829** 80
http://arxiv.org/pdf/1601.07835v1.pdf
Two of the central problems in our understanding of the solar chromosphere are how the upper chromosphere is heated and what drives spicules. Estmates of the required chromospheric heating, based on radiative and conductive losses suggest a rate of ∼0.1ergcm−3s−1 in the lower chromosphere dropping to ∼10−3ergcm−3s−1 in the upper chromosphere (\citet{Avrett1981}). The chromosphere is also permeated by spicules, higher density plasma from the lower atmosphere propelled upwards at speeds of ∼10−20kms−1, for so called Type-I spicules (\citet {Pereira2012, Zhang2012}, reaching heights of ∼3000−5000km above the photosphere. A clearer understanding of chromospheric dynamics, its heating and the formation of spicules, is thus of central importance to solar atmospheric science. For over thirty years it has been proposed that photospheric driving of MHD waves may be responsible for both heating and spicule formation. This letter presents results from the first high-resolution, self-consistent MHD treatment of photospheric driven Alfv\'en waves propagating upwards into an expanding flux tubes in a realistic chromospheric atmosphere. We show that the ponderomotive coupling from Alfv\'{e}n waves into slow modes generates shocks which both heat the upper chromosphere and drive spicules. These simulations show that Alfv\'{e}n wave driving of the solar chromosphere can give a local heating rate which matches observations and drive spicules consistent with Type-I observations all within a single coherent model.

Two-fluid implementation in MPI-AMRVAC, with applications in the solar chromosphere

B. Popescu **Braileanu**, R. Keppens
A&A **2022**
https://arxiv.org/pdf/2205.05049
The chromosphere is a partially ionized layer of the solar atmosphere, the transition between the photosphere where the gas is almost neutral and the fully ionized corona. As the collisional coupling between neutral and charged particles decreases in the upper part of the chromosphere, the hydrodynamical timescales may become comparable to the collisional timescale, and a two-fluid model is needed. In this paper we describe the implementation and validation of a two-fluid model which simultaneously evolves charges and neutrals, coupled by collisions. The two-fluid equations are implemented in the fully open-source MPI-AMRVAC code. In the photosphere and the lower part of the solar atmosphere, where collisions between charged and neutral particles are very frequent, an explicit time-marching would be too restrictive, since for stability the timestep needs to be proportional to the inverse of the collision frequency. This is overcome by evaluating the collisional terms implicitly using an explicit-implicit (IMEX) scheme. The cases presented cover very different collisional regimes and our results are fully consistent with related literature findings. If collisional time and length scales are smaller than the hydrodynamical scales usually considered in the solar chromosphere, density structures seen in the neutral and charged fluids are similar, with the effect of elastic collisions between charges and neutrals being similar to diffusivity. Otherwise, density structures are different and the decoupling in velocity between the two species increases. The use of IMEX schemes efficiently avoids the small timestep constraints of fully explicit implementations in strongly collisional regimes. Adaptive Mesh Refinement (AMR) greatly decreases the computational cost, compared to uniform grid runs at the same effective resolution.

Effects of ambipolar diffusion on waves in the solar chromosphere

Beatrice Popescu **Braileanu**, Rony Keppens
A&A **2021**
https://arxiv.org/pdf/2105.10285.pdf
The chromosphere is a partially ionized layer of the solar atmosphere, the transition between the photosphere where the gas motion is determined by the gas pressure and the corona dominated by the magnetic field. We study the effect of partial ionization for 2D wave propagation in a gravitationally stratified, magnetized atmosphere with properties similar to the solar chromosphere. We adopt an oblique uniform magnetic field in the plane of propagation with strength suitable for a quiet sun region. The theoretical model used is a single fluid magnetohydrodynamic approximation, where ion-neutral interaction is modeled by the ambipolar diffusion term. Magnetic energy can be converted into internal energy through the dissipation of the electric current produced by the drift between ions and neutrals. We use numerical simulations where we continuously drive fast waves at the bottom of the atmosphere. The collisional coupling between ions and neutrals decreases with the decrease of the density and the ambipolar effect becomes important. Fast waves excited at the base of the atmosphere reach the equipartition layer and reflect or transmit as slow waves. While the waves propagate through the atmosphere and the density drops, the waves steepen into shocks. The main effect of ambipolar diffusion is damping of the waves. We find that for the parameters chosen in this work, the ambipolar diffusion affects the fast wave before it is reflected, with damping being more pronounced for waves which are launched in a direction perpendicular to the magnetic field. Slow waves are less affected by ambipolar effects. The damping increases for shorter periods and larger magnetic field strengths. Small scales produced by the nonlinear effects and the superposition of different types of waves created at the equipartition height are efficiently damped by ambipolar diffusion.

Two-fluid simulations of Rayleigh-Taylor instability in a magnetized solar prominence thread II. Effects of collisionality

B. Popescu **Braileanu**, V. S. Lukin, E. Khomenko, A. de Vicente

A&A **2021**

https://arxiv.org/pdf/2101.12731.pdf

In this work, we explore the dynamical impacts and observable signatures of two-fluid effects in the parameter regimes when ion-neutral collisions do not fully couple the neutral and charged fluids. The purpose of this study is to deepen our understanding of the RTI and the effects of the partial ionization on the development of RTI using non-linear two-fluid numerical simulations. Our two-fluid model takes into account neutral viscosity, thermal conductivity, and collisional interaction between neutrals and charges: ionization/recombination, energy and momentum transfer, and frictional heating. In this paper II, the sensitivity of the RTI dynamics to collisional effects for different magnetic field configurations supporting the prominence thread is explored. This is done by artificially varying, or eliminating, effects of both elastic and inelastic collisions by modifying the model equations. We find that ionization and recombination reactions between ionized and neutral fluids, if in equilibrium prior to the onset of the instability, do not substantially impact the development of the primary RTI. However, such reactions can impact development of secondary structures during mixing of the cold prominence and hotter surrounding coronal material. We find that collisionality within and between ionized and neutral particle populations play an important role in both linear and non-linear development of RTI, with ion-neutral collision frequency as the primary determining factor in development or damping of small scale structures. We also observe that degree and signatures of flow decoupling between ion and neutral fluids can depend both on the inter-particle collisionality and the magnetic field configuration of the prominence thread.

Two-fluid simulations of waves in the solar chromosphere II. Propagation and damping of fast magneto-acoustic waves and shocks

B. Popescu **Braileanu**, V. S. Lukin, E. Khomenko, A. de Vicente

A&A 630, A79 **2019**

https://arxiv.org/pdf/1908.05262.pdf

Waves and shocks traveling through the solar chromospheric plasma are influenced by its partial ionization and weak collisional coupling, and may become susceptible to multi-fluid effects, similar to interstellar shock waves. In this study, we consider fast magneto-acoustic shock wave formation and propagation in a stratified medium, that is permeated by a horizontal magnetic field, with properties similar to that of the solar chromosphere. The evolution of plasma and neutrals is modeled using a two-fluid code that evolves a set of coupled equations for two separate fluids. We observed that waves in neutrals and plasma, initially coupled at the upper photosphere, become uncoupled at higher heights in the chromosphere. This decoupling can be a consequence of either the characteristic spatial scale at the shock front, that becomes similar to the collisional scale, or the change in the relation between the wave frequency, ion cyclotron frequency, and the collisional frequency with height. The decoupling height is a sensitive function of the wave frequency, wave amplitude, and the magnetic field strength. We observed that decoupling causes damping of waves and an increase in the background temperature due to the frictional heating. The comparison between analytical and numerical results allows us to separate the role of the nonlinear effects from the linear ones on the decoupling and damping of waves.

Two-fluid simulations of waves in the solar chromosphere I: numerical code verification

B. Popescu **Braileanu**, V. S. Lukin, E. Khomenko, A. de Vicente

A&A 627, A25 **2019**

https://arxiv.org/pdf/1905.03559.pdf

Solar chromosphere consists of a partially ionized plasma, which makes modeling the solar chromosphere a particularly challenging numerical task. Here we numerically model chromospheric waves using a two-fluid approach with a newly developed numerical code. The code solves two-fluid equations of conservation of mass, momentum and energy, together with the induction equation, for the case of the purely hydrogen plasma with collisional coupling between the charged and neutral fluid components. The implementation of a semi-implicit algorithm allows us to overcome the numerical stability constraints due to the stiff collisional terms. We test the code against analytical solutions of acoustic and Alfvén wave propagation in uniform medium in several regimes of collisional coupling.The results of our simulations are consistent with the analytical estimates, and with other results described in the literature. In the limit of a large collisional frequency, the waves propagate with a common speed of a single fluid. In the other limit of a vanishingly small collisional frequency, the Alfvén waves propagate with an Alfvén speed of the charged fluid only, while the perturbation in neutral fluid is very small. The acoustic waves in these limits propagate with the sound speed corresponding to either the charges or the neutrals, while the perturbation in the other fluid component is very small. Otherwise, when the collision frequency is similar to the real part of the wave frequency, the interaction between charges and neutrals through momentum transfer collisions cause alterations of the waves frequencies and damping of the wave amplitudes.

A prediction for the 25th solar cycle maximum amplitude

R. **Brajša**, G. Verbanac, M. Bandić, A. Hanslmeier, I. Skokić, D. Sudar
Astronomische Nachrichten / Astronomical Notes **2022**
https://arxiv.org/pdf/2203.11293.pdf

The minimum - maximum method, belonging to the precursor class of the solar activity forecasting methods, is based on a linear relationship between relative sunspot number in the minimum and maximum epochs of solar cycles. In the present analysis we apply a modified version of this method using data not only from the minimum year, but also from a couple of years before and after the minimum. The revised 13-month smoothed monthly total sunspot number data set from SILSO/SIDC is used. Using data for solar cycle nos. 1-24 the largest correlation coefficient (CC) is obtained when correlating activity level 3 years before solar cycle minimum with the subsequent maximum (CC = 0.82), independent of inclusion or exclusion of the solar cycle no. 19. For the next solar maximum of the cycle no. 25 we predict: Rmax = 121 +- 33. Our results indicate that the next solar maximum (of the cycle no. 25) will be of the similar amplitude as the previous one, or even something lower. This is in accordance with the general middle-term lowering of the solar activity after the secular maximum in the 20th century and consistent with the Gleissberg period of the solar activity. The reliability of the 3 years before the minimum predictor is experimentally justified by the largest correlation coefficient and verified with the Student t-test. It is satisfactorily explained with the two empirical well-known findings: the extended solar cycle and the Waldmeier effect. Finally, we successfully reproduced the maxima of the last four solar cycles, nos. 21-25, using the 3 years before the minimum method.

Turbulent Processes and Mean-Field Dynamo

Axel **Brandenburg**, Detlef Elstner,Valery Pipin
Space Science Reviews (**2023**) 219 :55
https://doi.org/10.1007/s11214-023-00999-3
https://link.springer.com/content/pdf/10.1007/s11214-023-00999-3.pdf

Mean-field dynamo theory has important applications in solar physics and galactic magnetism. We discuss some of the many turbulence effects relevant to the generation of largescale magnetic fields in the solar convection zone. The mean-field description is then used to illustrate the physics of the α effect, turbulent pumping, turbulent magnetic diffusivity, and other effects on a modern solar dynamo model. We also discuss how turbulence transport coefficients are derived from local simulations of convection and then used in mean-field models.

Turbulent processes and mean-field dynamo **Review**

Axel **Brandenburg**, Detlef Elstner, Youhei Masada, Valery Pipin
Space Science Reviews, special issue "Solar and stellar dynamos: a new era" **2023**
https://arxiv.org/pdf/2303.12425

Mean-field dynamo theory has important applications in solar physics and galactic magnetism. We discuss some of the many turbulence effects relevant to the generation of large-scale magnetic fields in the solar convection zone. The mean-field description is then used to illustrate the physics of the α effect, turbulent pumping, turbulent magnetic diffusivity, and other effects on a modern solar dynamo model. We also discuss how turbulence transport coefficients are derived from local simulations of convection and then used in mean-field models.

Chirality in Astrophysics **Review**

Axel **Brandenburg**
Proceedings to Nobel Symposium 167: Chiral Matter, eds. E. Babaev, D. Kharzeev, M. Larsson, A. Molochkov, & V. Zhaunerchyk, World Scientific, **2021**
https://arxiv.org/pdf/2110.08117

Chirality, or handedness, enters astrophysics in three distinct ways. Magnetic field and vortex lines tend to be helical and have a systematic twist in the northern and southern hemispheres of a star or a galaxy. Helicity is here driven by external factors. Chirality can also enter at the microphysical level and can then be traced back to the parity-breaking weak force. Finally, chirality can arise spontaneously, but this requires not only the presence of an instability, but also the action of nonlinearity. Examples can be found both in magnetohydrodynamics and in astrobiology, where homochirality among biomolecules probably got established at the origin of life. In this review, all three types of chirality production will be explored and compared.

The nature of mean-field generation in three classes of optimal dynamos

Axel **Brandenburg** (Nordita), Long Chen (Durham University)
J. Plasma Phys. **2019**

https://arxiv.org/pdf/1911.01712.pdf
In recent years, several optimal dynamos have been discovered. They minimize the magnetic energy dissipation and the critical magnetic Reynolds number or maximize the growth rate at a fixed magnetic Reynolds number. In the optimal dynamo of Willis (2012, PRL 109, 251101), we find mean-field dynamo action for planar averages. One component of the magnetic field grows exponentially while the other decays in an oscillatory fashion near onset. This behavior is different from that of an alpha^2 dynamo, where the two non-vanishing components of the planar averages are coupled and have the same growth rate. For the Willis dynamo, we find that the mean field is excited by a negative turbulent magnetic diffusivity, which has a non-uniform spatial profile near onset. The temporal oscillations in the decaying component are caused by the corresponding component of the diffusivity tensor being complex when the mean field is decaying and, in this way, time-dependent. The growing mean field can be modeled by a negative magnetic diffusivity combined with a positive magnetic hyperdiffusivity. In two other classes of optimal dynamos of Chen et al. (2015, JFM 783, 23), we find, to some extent, similar mean-field dynamo actions. When the magnetic boundary conditions are mixed, the two components of the planar averaged field grow at different rates when the dynamo is 15% supercritical. When the mean magnetic field satisfies homogeneous boundary conditions, mean-field dynamo action is only found for one-dimensional averages, but not for planar averages. Despite having different spatial profiles, both dynamos show negative turbulent magnetic diffusivities. Our finding suggests negative turbulent magnetic diffusivities may support a broader class of dynamos than previously thought, including these three optimal dynamos.

Magnetic helicity dissipation in an ideal MHD code

Axel **Brandenburg**, Evan Scannapieco
ApJ **2019**
https://arxiv.org/pdf/1910.06074.pdf
We study a turbulent helical dynamo in a periodic domain by solving the ideal magnetohydrodynamic (MHD) equations with the FLASH code using the divergence-cleaning eight-wave method and compare our results with with direct numerical simulations (DNS) using the Pencil Code. At low resolution, FLASH reproduces the DNS results qualitatively by developing the large-scale magnetic field expected from DNS, but at higher resolution, no large-scale magnetic field is obtained. In all those cases in which a large-scale magnetic field is generated, the ideal MHD equations yield too little power at small scales. As a consequence, the small-scale current helicity is too small compared with the DNS. The resulting net current helicity has then always the wrong sign, and it also does not approach zero at late times, as expected from the DNS. Our results have implications for astrophysical dynamo simulations using ideal MHD codes.

Reversed dynamo at small scales and large magnetic Prandtl number

Axel **Brandenburg**, Matthias Rempel
Astrophys. J. 879, 57 (**2019**)
https://arxiv.org/abs/1903.11869
We show that at large magnetic Prandtl numbers, the Lorentz force does work on the flow at small scales and drives fluid motions, whose energy is dissipated viscously. This situation is opposite to that in a normal dynamo, where the flow does work against the Lorentz force. We compute the spectral conversion rates between kinetic and magnetic energies for several magnetic Prandtl numbers and show that normal (forward) dynamo action occurs on large scales over a progressively narrower range of wavenumbers as the magnetic Prandtl number is increased. At higher wavenumbers, reversed dynamo action occurs, i.e., magnetic energy is converted back into kinetic energy at small scales. We demonstrate this in both direct numerical simulations forced by volume stirring and in large eddy simulations of solar convectively driven small-scale dynamos. Low density plasmas such as stellar coronae tend to have large magnetic Prandtl numbers, i.e., the viscosity is large compared with the magnetic diffusivity. The regime in which viscous dissipation dominates over resistive dissipation for large magnetic Prandtl numbers was also previously found in large eddy simulations of the solar corona, i.e., our findings are a more fundamental property of MHD that is not just restricted to dynamos. Viscous energy dissipation is a consequence of positive Lorentz force work, which may partly correspond to particle acceleration in close-to-collisionless plasmas. This is, however, not modeled in the MHD approximation employed. By contrast, resistive energy dissipation on current sheets is expected to be unimportant in stellar coronae.

Magnetic helicity and fluxes in an inhomogeneous alpha squared dynamo

A. **Brandenburg** (Nordita)
Astron. Nachr **2019**
https://arxiv.org/pdf/1901.07552.pdf
Much work on turbulent three-dimensional dynamos has been done using triply periodic domains, in which there are no magnetic helicity fluxes. Here we present simulations where the turbulent intensity is still nearly homogeneous, but now there is a perfect conductor boundary condition on one end and a vertical field or pseudo-vacuum condition on the other. This leads to migratory dynamo waves. Good agreement with a corresponding analytically solvable

alpha^2 dynamo is found. Magnetic helicity fluxes are studied in both types of models. It is found that at moderate magnetic Reynolds numbers, most of the magnetic helicity losses occur at large scales. Whether this changes at even larger magnetic Reynolds numbers, as required for alleviating the catastrophic dynamo quenching problem, remains still unclear.

Strong nonlocality variations in a spherical mean-field dynamo

A. **Brandenburg**, P. Chatterjee

Astron Nachr **2018**

https://arxiv.org/pdf/1802.04231.pdf

To explain the large-scale magnetic field of the Sun and
other bodies, mean-field dynamo theory is commonly applied where one solves the averaged equations for the mean magnetic field. However, the standard approach breaks down when the scale of the turbulent eddies becomes comparable to the scale of the variations of the mean magnetic field. Models showing sharp magnetic field structures have therefore been regarded as unreliable. Our aim is to look for new effects that occur when we relax the restrictions of the standard approach, which becomes particularly important at the bottom of the convection zone where the size of the turbulent eddies is comparable to the depth of the convection zone itself. We approximate the underlying integro-differential equation by a partial differential equation corresponding to a reaction-diffusion type equation for the mean electromotive force, making an approach that is nonlocal in space and time feasible under conditions where spherical geometry and nonlinearity are included. In agreement with earlier findings, spatio-temporal nonlocality lowers the excitation conditions of the dynamo. Sharp structures are now found to be absent. However, in the surface layers the field remains similar to before.

Advances in mean-field dynamo theory and applications to astrophysical turbulence

Axel **Brandenburg**

J. Plasma Phys. 84, 735840404 **2018**

https://arxiv.org/pdf/1801.05384.pdf

Recent advances in mean-field theory are reviewed and applications to the Sun, late-type stars, accretion disks, galaxies, and the early Universe are discussed. We focus particularly on aspects of spatio-temporal nonlocality, which is one of the main insights that emerged from applying the test-field method to magnetic fields of different length and timescales. We also review the status of nonlinear quenching and the relation to magnetic helicity, which is an important observational diagnostic of modern solar dynamo theory. Both solar and some stellar dynamos seem to operate in an intermediate regime that has not yet been possible to model successfully. This regime is bracketed by antisolar-like differential rotation on one end and stellar activity cycles belonging to the superactive stars on the other. The difficulty in modeling this regime may be related to shortcomings in modelling solar/stellar convection. On galactic and extragalactic length scales, the observational constraints are still less stringent and uncertain, but recent advances both in theory and in observations suggest that more conclusive comparisons may soon be possible. The possibility of inversely cascading magnetic helicity throughout all of the early Universe is particularly exciting in explaining the lower limits of magnetic fields on cosmological length scales and the possibility of parity breaking and finite helicity of such a field.

Two-scale analysis of solar magnetic helicity

Axel **Brandenburg** (1,2), Gordon J. D. Petrie (3), Nishant K. Singh

ApJ 836 21 **2017**

https://arxiv.org/pdf/1610.05410v1.pdf

We develop a two-scale formalism to determine global magnetic helicity spectra in systems where the local magnetic helicity has opposite signs on both sides of the equator, giving rise to cancelation with conventional methods. We verify this approach using first synthetic one-dimensional magnetic field and then two-dimensional slices from a three-dimensional alpha effect-type dynamo-generated magnetic field with forced turbulence of opposite helicity above and below the midplane of the domain. We then apply this formalism to global solar synoptic vector magnetograms. To improve the statistics, data from three consecutive Carrington rotations (2161--2163) are combined into a single map. We find that the spectral magnetic helicity representative of the northern hemisphere is negative at all wavenumbers and peaks at ~0.06 Mm^{-1} (scales around 100 Mm). There is no evidence of bihelical magnetic fields that are found in three-dimensional turbulence simulations of helicity-driven alpha effect-type turbulent dynamos.

On Generalized Additive Models for Representation of Solar EUV Irradiance

Daniel A. **Brandt**, Erick F. Vega, Aaron J. Ridley

Space Weather Volume22, Issue3 e2023SW003680 **2024**

https://doi.org/10.1029/2023SW003680

https://agupubs.onlinelibrary.wiley.com/doi/epdf/10.1029/2023SW003680
In the context of space weather forecasting, solar EUV irradiance specification is needed on multiple time scales, with associated uncertainty quantification for determining the accuracy of downstream parameters. Empirical models of irradiance often rely on parametric fits between irradiance in several bands and various solar indices. We build upon these empirical models by using Generalized Additive Models (GAMs) to represent solar irradiance. We apply the GAM approach in two steps: (a) A GAM is fitted between FISM2 irradiance and solar indices F10.7, Revised Sunspot Number, and the Lyman-α solar index. (b) A second GAM is fit to model the residuals of the first GAM with respect to FISM2 irradiance. We evaluate the performance of this approach during Solar Cycle 24 using GAMs driven by known solar indices as well as those forecasted 3 days ahead with an autoregressive modeling approach. We demonstrate negligible dependence of performance on solar cycle and season, and we assess the efficacy of the GAM approach across different wavelengths.

The Contribution of Solar Magnetic Regions to the Residual Meridional and Zonal Flows

D. C. **Braun**
2024 ApJ 972 160
https://iopscience.iop.org/article/10.3847/1538-4357/ad5fea/pdf
We estimate the contributions to the solar-cycle variation of solar meridional and zonal flows near the surface expected solely from local magnetic regions. Maps of flows near magnetic regions are obtained using helioseismic holography and averaged over ensembles of such regions with similar magnetic flux. These averaged flows are assigned to the positions and times of all magnetic regions identified from daily magnetograms over an 11 yr period. Residuals are obtained after averaging both meridional and zonal-flow components over longitude for each Carrington rotation and subtracting the temporal mean at each latitude. Results indicate that magnetic regions produce solar-cycle variations of both components in the active latitude range with peak amplitudes of about 1 m s−1, which represents only a fraction of the known variations in either the residual zonal or meridional flow with amplitudes around 3 and 5 m s−1, respectively. Thus it is unlikely that active regions, and compact magnetic concentrations in general, are the primary source of the 11 yr variation in these global flows. A threshold magnetic flux of 5 × 1020 Mx, below which no significant flows are observed, is identified as a check on the completeness of the set of magnetic regions. We also find that inflows around most magnetic regions are confined to within 10°–12° of their centers, in contrast with recent evidence of more extended inflows.

Probing the Solar Meridional Circulation Using Fourier Legendre Decomposition

D. C. **Braun**1, A. C. Birch2, and Y. Fan3
2021 ApJ 911 54
https://arxiv.org/pdf/2103.02499.pdf
https://doi.org/10.3847/1538-4357/abe7e4
We apply the helioseismic methodology of Fourier Legendre decomposition to 88 months of Dopplergrams obtained by the Helioseismic and Magnetic Imager (HMI) as the basis of inferring the depth variation of the mean meridional flow, as averaged between 20° and 60° latitude and in time, in both the northern and southern hemispheres. We develop and apply control procedures designed to assess and remove center-to-limb artifacts using measurements obtained by performing the analysis with respect to artificial poles at the east and west limbs. Forward modeling is carried out using sensitivity functions proportional to the mode kinetic energy density to evaluate the consistency of the corrected frequency shifts with models of the depth variation of the meridional circulation in the top half of the convection zone. The results, taken at face value, imply substantial differences between the meridional circulation in the northern and southern hemispheres. The inferred presence of a return (equatorward propagating) flow at a depth of approximately 40 Mm below the photosphere in the northern hemisphere is surprising and appears to be inconsistent with many other helioseismic analyses. This discrepancy may be the result of the inadequacy of our methodology to remove systematic errors in HMI data. Our results appear to be at least qualitatively similar to those by Gizon et al., which point to an anomaly in HMI data that is not present in MDI or GONG data.
Erratum **2022** ApJ 924 140 https://iopscience.iop.org/article/10.3847/1538-4357/ac4582/pdf
HMI Science Nuggets #152 March **2021** http://hmi.stanford.edu/hminuggets/?p=3471

Flows around Averaged Solar Active Regions

D.C. **Braun**
2019 *ApJ* **873** 94
https://arxiv.org/pdf/1902.02298.pdf
We explore the general properties of near-surface flows around solar active regions. Helioseismic holography is applied to HMI Dopplergrams yielding nearly 5000 flow measurements of 336 unique active regions observed by the Solar Dynamics Observatory between 2010 and 2014. Ensemble averages of the flows, over subsets of regions sorted on the basis of magnetic flux, are performed. These averages show that converging flows, with speeds about 10 m/s and extending up to 10 degrees from the active region centers, are prevalent and have similar properties for

all regions with magnetic flux above 10^21 Mx. Retrograde flows are also detected, with amplitudes around 10 m/s, which predominantly, but not exclusively, flank the polar side of the active regions. We estimate the expected contribution of these active-region flows to longitudinal averages of zonal and meridional flows and demonstrate the plausibility that they are responsible for at least some component of the time-varying global-scale flows. The reliability of our flow determination is tested using publicly available MHD simulations of both quiet-Sun convection and of a sunspot. While validating the overall methodology in general, the sunspot simulation demonstrates the presence of artifacts which may compromise quantitative flow inferences from some helioseismic measurements.

COCONUT-MF: Two-fluid ion-neutral global coronal modelling

Michaela **Brchnelova**, Błażej Kuźma, Fan Zhang, Andrea Lani, Stefaan Poedts
A&A **2023**
https://arxiv.org/pdf/2308.16043.pdf
The global coronal model COCONUT was originally developed to replace models such as the WSA model in space weather forecasting to improve the physical accuracy of the predictions. This model has, however, several simplifications implemented in its formulation to allow for rapid convergence, one of which includes a single-fluid treatment. In this paper, we have two goals. Firstly, we aim to introduce a novel multi-fluid global coronal model and validate it with simple cases as well as with real data-driven applications. Secondly, we aim to investigate to what extent considering a single-fluid plasma in the global coronal model might affect the resulting plasma dynamics, and thus whether the assumptions on which the single-fluid coronal model is based are justified. We developed a multi-fluid global coronal model, COCONUT-MF, which resolves the ion and neutral fluid equations separately. While this model is still steady-state and thus does not resolve unsteady processes, it can account for charge exchange, chemical and collisional contributions. We present the results of the ion-neutral modelling for a dipole, a minimum of solar activity, and a solar maximum. We demonstrate the higher accuracy of the applied AUSM+ scheme compared to HLL. Subsequently, we also evaluate the effects of the considered ion-neutral coupling terms on the resulting plasma dynamics. Despite the very low concentration of neutrals, these terms still affect the flow field to a limited but non-negligible extent (up to 5 to 10% locally). Even though the coronal plasma is generally assumed to be collisionless, our results show that there is sufficient collisionality in it to couple the two fluids. Follow-up work will include extension of the model to lower atmospheric layers of the Sun and inclusion of more advanced physical terms such as heating and radiation.

The role of plasma beta in global coronal models: Bringing balance back to the force

Michaela **Brchnelova**, Błażej Kuźma, Fan Zhang, Andrea Lani, Stefaan Poedts
A&A **2023**
https://arxiv.org/pdf/2306.08874.pdf
COCONUT is a global coronal magnetohydrodynamic model recently developed. In order to achieve robustness and fast convergence to steady-state, several assumptions have been made during its development, such as prescribing filtered photospheric magnetic maps for representing the magnetic field in the lower corona. This filtering leads to smoothing and lower magnetic field values at the inner boundary, resulting in an unrealistically high plasma this http URL this paper, we examine the effects of prescribing such filtered magnetograms and formulate a method for achieving more realistic plasma beta values without losing computational performance. We demonstrate the effects of the highly pre-processed magnetic maps and the resulting high plasma beta on the features in the domain. Then, in our new approach, we shift the inner boundary to 2 Rs and preserve the prescribed highly filtered magnetic map. This effectively reduces the prescribed plasma beta and leads to a more realistic setup. The method is applied on a magnetic dipole, a minimum (2008) and a maximum (2012) solar activity case, to demonstrate its effects. The results obtained with the proposed approach show significant improvements in the resolved density and radial velocity profiles, and far more realistic values of the plasma \{beta} at the boundary and inside the computational domain. This is also demonstrated via synthetic white light imaging and with the validation against tomography. The computational performance comparison shows similar convergence to a limit residual on the same grid when compared to the original setup. Considering that the grid can be further coarsened with this new setup, the operational performance can be additionally increased if needed. The newly developed method is thus deemed as a good potential replacement of the original setup for operational purposes.

Effects of Mesh Topology on MHD Solution Features in Coronal Simulations

Michaela **Brchnelova**, Fan Zhang, Peter Leitner, Barbara Perri, Andrea Lani, Stefaan Poedts
J. Plasma Phys **2022**
https://arxiv.org/pdf/2202.13696.pdf
Magnetohydrodynamic (MHD) simulations of the solar corona have become more popular with the increased availability of computational power. Modern computational plasma codes, relying upon Computational Fluid Dynamics (CFD) methods, allow for resolving the coronal features using solar surface magnetograms as inputs. These computations are carried out in a full 3D domain and thus selection of the right mesh configuration is

essential to save computational resources and enable/speed up convergence. In addition, it has been observed that for MHD simulations close to the hydrostatic equilibrium, spurious numerical artefacts might appear in the solution following the mesh structure, which makes the selection of the grid also a concern for accuracy. The purpose of this paper is to discuss and trade off two main mesh topologies when applied to global solar corona simulations using the unstructured ideal MHD solver from the COOLFluiD platform. The first topology is based on the geodesic polyhedron and the second on UV mapping. Focus will be placed on aspects such as mesh adaptability, resolution distribution, resulting spurious numerical fluxes and convergence performance. For this purpose, firstly a rotating dipole case is investigated, followed by two simulations using real magnetograms from the solar minima (1995) and solar maxima (1999). It is concluded that the most appropriate mesh topology for the simulation depends on several factors, such as the accuracy requirements, the presence of features near the polar regions and/or strong features in the flow field in general. If convergence is of concern and the simulation contains strong dynamics, then grids which are based on the geodesic polyhedron are recommended compared to more conventionally used UV-mapped meshes.

No swan song for Sun-as-a-star helioseismology: Performances of the Solar-SONG prototype for individual mode characterisation

S. N. **Breton**1, P. L. Pallé2,3, R. A. García1, M. Fredslund Andersen4, F. Grundahl4, J. Christensen-Dalsgaard4, H. Kjeldsen4 and S. Mathur2,3
A&A 658, A27 (**2022**)
https://doi.org/10.1051/0004-6361/202141496
https://www.aanda.org/articles/aa/pdf/2022/02/aa41496-21.pdf
The GOLF instrument on board SoHO has been in operation for almost 25 years, but the ageing of the instrument has now strongly affected its performance, especially in the low-frequency pressure-mode (p-mode) region. At the end of the SoHO mission, the ground-based network BiSON will remain the only facility able to perform Sun-integrated helioseismic observations. Therefore, we want to assess the helioseismic performances of an échelle spectrograph such as SONG. The high precision of such an instrument and the quality of the data acquired for asteroseismic purposes call for an evaluation of the instrument's ability to perform global radial-velocity measurements of the solar disk. Data acquired during the Solar-SONG 2018 observation campaign at the Teide Observatory are used to study mid- and low-frequency p modes. A Solar-SONG time series of 30 days in duration is reduced with a combination of the traditional IDL iSONG pipeline and a new Python pipeline described in this paper. A mode fitting method built around a Bayesian approach is then performed on the Solar-SONG and contemporaneous GOLF, BiSON, and HMI data. For this contemporaneous time series, Solar-SONG is able to characterise p modes at a lower frequency than BiSON or GOLF (1750 μHz versus 1946 and 2157 μHz, respectively), while for HMI it is possible to characterise a mode at 1686 μHz. The decrease in GOLF sensitivity is then evaluated through the evolution of its low-frequency p-mode characterisation abilities over the years: a set of 30-day-long GOLF time series, considered at the same period of the year from 1996 to 2017, is analysed. We show that it is more difficult to accurately characterise p modes in the range 1680 to 2160 μHz when considering the most recent time series. By comparing the global power level of different frequency regions, we also observe that the Solar-SONG noise level in the 1000 to 1500 μHz region is lower than for any GOLF subseries considered in this work. While the global p-mode power-level ratio is larger for GOLF during the first years of the mission, this ratio decreases over the years and is bested by Solar-SONG for every time series after 2000. All these observations strongly suggest that efforts should be made towards deploying more Solar-SONG nodes in order to acquire longer time series with better duty cycles. **27 May-22 July, 2018**

MUSE observations of small-scale heating events

C.A. **Breu**, I. De Moortel, P. Testa
MNRAS **2024**
https://arxiv.org/pdf/2405.01384
Constraining the processes that drive coronal heating from observations is a difficult task due to the complexity of the solar atmosphere. As upcoming missions such as MUSE will provide coronal observations with unprecedented spatial and temporal resolution, numerical simulations are becoming increasingly realistic. Despite the availability of synthetic observations from numerical models, line-of-sight effects and the complexity of the magnetic topology in a realistic setup still complicate the prediction of signatures for specific heating processes. 3D MHD simulations have shown that a significant part of the Poynting flux injected into the solar atmosphere is carried by small-scale motions, such as vortices driven by rotational flows inside intergranular lanes. MHD waves excited by these vortices have been suggested to play an important role in the energy transfer between different atmospheric layers. Using synthetic spectroscopic data generated from a coronal loop model incorporating realistic driving by magnetoconvection, we study whether signatures of energy transport by vortices and eventual dissipation can be identified with future missions such as MUSE.

Swirls in the Solar Corona

C. **Breu**, H. Peter, R. Cameron, S.K. Solanki
A&A **2023**
https://arxiv.org/pdf/2305.03769.pdf
Vortex flows have been found in the photosphere, chromosphere and low corona in observations and simulations. It has been suggested that vortices play an important role for channeling energy and plasma into the corona, but the impact of vortex flows on the corona has not directly been studied in a realistic setup. We investigate the role vortices play for coronal heating using high resolution simulations of coronal loops. The vortices are not artificially driven, but arise self-consistently from magnetoconvection. We perform 3D resistive MHD simulations with the MURaM code. Studying an isolated coronal loop in a Cartesian geometry allows us to resolve the structure of the loop interior. We conduct a statistical analysis to determine vortex properties as a function of height from the chromosphere into the corona. We find that the energy injected into the loop is generated by internal coherent motions within strong magnetic elements. A significant part of the resulting Poynting flux is channeled through the chromosphere in vortex tubes forming a magnetic connection between the photosphere and corona. Vortices can form contiguous structures that reach up to coronal heights, but in the corona itself the vortex tubes get deformed and eventually lose their identity with increasing height. Vortices show increased upward directed Poynting flux and heating rate both in the chromosphere and corona, but their effect becomes less pronounced with increasing height. While vortices play an important role for the energy transport and structuring in the chromosphere and low corona, their importance higher up in the atmosphere is less clear since the swirls are less distinguishable from their environment. Vortex tubes reaching the corona show a complex relationship with the coronal emission.

The return of FarNet-II: Generation of solar far-side magnetograms from helioseismic data

E. G. **Broock**1,2⋆, A. Asensio Ramos1,2 and T. Felipe1,2
A&A, 692, A182 (**2024**)
https://www.aanda.org/articles/aa/pdf/2024/12/aa51625-24.pdf
Context. The far-side activity of the Sun can be inferred by interpreting the near-side wave field using local helioseismic techniques. However, detections are limited to strongly active regions because signal-to-noise ratio of the data is low. Recently, we developed the FarNet and FarNet-II neural networks to improve the identification of active regions on far-side seismic maps.
Aims. We aim to use FarNet-II to leverage seismic data to infer far-side magnetograms, including the magnetic field strength and polarity.
Methods. We used FarNet-II to produce sequences of 11 consecutive binned magnetograms with a 12-hour cadence of a central section of the far side, where each pixel was assigned to one of nine possible classes that define its magnetic field and polarity. The inputs to the network are sequences of phase-shift maps of the same regions, computed using helioseismic holography. We trained the network using a cross-validation approach to estimate its reliability. The targets for the training and the cross-validation were obtained from near-side Helioseismic and Magnetic Imager magnetograms, taken half a rotation later than the seismic data. The metric we used for the evaluation is the volumetric Dice, a newly defined metric that measures the overlap between the outputs and the targets. The results were compared with Solar Orbiter data from a period with far-side coverage between May 2022 and September 2022.
Results. FarNet-II achieves an average volumetric Dice of 0.249, showing a good visual superposition between the targets and outputs of the network. The comparisons of the outputs and the Solar Orbiter magnetograms are also similar.
Conclusions. FarNet-II can correctly predict the level of activity and the polarity of far-side regions using near-side seismic data. This capability can be leveraged in space-weather forecasting.

Plasma composition measurements in an active region from Solar Orbiter/SPICE and Hinode/EIS

David H. **Brooks**, Miho Janvier, Deborah Baker+++
ApJ **940** 66 **2022**
https://arxiv.org/pdf/2210.08899
https://iopscience.iop.org/article/10.3847/1538-4357/ac9b0b/pdf
A key goal of the Solar Orbiter mission is to connect elemental abundance measurements of the solar wind enveloping the spacecraft with EUV spectroscopic observations of their solar sources, but this is not an easy exercise. Observations from previous missions have revealed a highly complex picture of spatial and temporal variations of elemental abundances in the solar corona. We have used coordinated observations from Hinode and Solar Orbiter to attempt new abundance measurements with the SPICE (Spectral Imaging of the Coronal Environment) instrument, and benchmark them against standard analyses from EIS (EUV Imaging Spectrometer). We use observations of several solar features in AR 12781 taken from an Earth-facing view by EIS on **2020 November 10,** and SPICE data obtained one week later on **2020 November 17**; when the AR had rotated into the

Solar Orbiter field-of-view. We identify a range of spectral lines that are useful for determining the transition region and low coronal temperature structure with SPICE, and demonstrate that SPICE measurements are able to differentiate between photospheric and coronal Mg/Ne abundances. The combination of SPICE and EIS is able to establish the atmospheric composition structure of a fan loop/outflow area at the active region edge. We also discuss the problem of resolving the degree of elemental fractionation with SPICE, which is more challenging without further constraints on the temperature structure, and comment on what that can tell us about the sources of the solar wind and solar energetic particles.

Performance of solar far-side active regions neural detection

E. G. **Broock**, T. Felipe, A. Asensio Ramos
A&A 652, A132 **2021**
https://arxiv.org/pdf/2106.09365.pdf
https://www.aanda.org/articles/aa/pdf/2021/08/aa41006-21.pdf
https://doi.org/10.1051/0004-6361/202141006
Context. Far-side helioseismology is a technique used to infer the presence of active regions in the far hemisphere of the Sun based on the interpretation of oscillations measured in the near hemisphere. A neural network has been recently developed to improve the sensitivity of the seismic maps to the presence of far-side active regions. Aims. Our aim is to evaluate the performance of the new neural network approach and to thoroughly compare it with the standard method commonly applied to predict far-side active regions from seismic measurements. Methods. We have computed the predictions of active regions using the neural network and the standard approach from five years of far-side seismic maps as a function of the selected threshold in the signatures of the detections. The results have been compared with direct extreme ultraviolet observations of the far hemisphere acquired with the Solar Terrestrial Relations Observatory (STEREO). Results. We have confirmed the improved sensitivity of the neural network to the presence of far-side active regions. Approximately 96% of the active regions identified by the standard method with a strength above the threshold commonly employed by previous analyses are related to locations with enhanced extreme ultraviolet emission. For this threshold, the false positive ratio is 3.75%. For an equivalent false positive ratio, the neural network produces 47% more true detections. Weaker active regions can be detected by relaxing the threshold in their seismic signature. Conclusions. The neural network is a promising approach to improve the interpretation of the seismic maps provided by local helioseismic techniques.
HMI Science Nuggets, #160, **2021** http://hmi.stanford.edu/hminuggets/?p=3599

The Drivers of Active Region Outflows into the Slow Solar Wind

David H. **Brooks**1,13, Amy R. Winebarger2, Sabrina Savage2, Harry P. Warren3, Bart De Pontieu4,5, Hardi Peter6, Jonathan W. Cirtain7, Leon Golub8, Ken Kobayashi2, Scott W. McIntosh9
2020 ApJ 894 144
https://doi.org/10.3847/1538-4357/ab8a4c
Plasma outflows from the edges of active regions have been suggested as a possible source of the slow solar wind. Spectroscopic measurements show that these outflows have an enhanced elemental composition, which is a distinct signature of the slow wind. Current spectroscopic observations, however, do not have sufficient spatial resolution to distinguish what structures are being measured or determine the driver of the outflows. The High-resolution Coronal Imager (Hi-C) flew on a sounding rocket in **2018 May** and observed areas of active region outflow at the highest spatial resolution ever achieved (250 km). Here we use the Hi-C data to disentangle the outflow composition signatures observed with the Hinode satellite during the flight. We show that there are two components to the outflow emission: a substantial contribution from expanded plasma that appears to have been expelled from closed loops in the active region core and a second contribution from dynamic activity in active region plage, with a composition signature that reflects solar photospheric abundances. The two competing drivers of the outflows may explain the variable composition of the slow solar wind.

Solar cycle observations of the Neon abundance in the Sun-as-a-star

David H. **Brooks**, Deborah Baker, Lidia van Driel-Gesztelyi, Harry P. Warren
ApJ **861** 42 **2018**
https://arxiv.org/pdf/1805.07032.pdf
Properties of the Sun's interior can be determined accurately from helioseismological measurements of solar oscillations. These measurements, however, are in conflict with photospheric elemental abundances derived using 3-D hydrodynamic models of the solar atmosphere. This divergence of theory and helioseismology is known as the "solar modeling problem". One possible solution is that the photospheric neon abundance, which is deduced indirectly by combining the coronal Ne/O ratio with the photospheric O abundance, is larger than generally accepted. There is some support for this idea from observations of cool stars. The Ne/O abundance ratio has also been found to vary with the solar cycle in the slowest solar wind streams and coronal streamers, and the variation

from solar maximum to minimum in streamers (~0.1 to 0.25) is large enough to potentially bring some of the solar models into agreement with the seismic data. Here we use daily-sampled observations from the EUV Variability Experiment (EVE) on the Solar Dynamics Observatory taken in 2010--2014, to investigate whether the coronal Ne/O abundance ratio shows a variation with the solar cycle when the Sun is viewed as a star. We find only a weak dependence on, and moderate anti-correlation with, the solar cycle with the ratio measured around 0.2--0.3 MK falling from 0.17 at solar minimum to 0.11 at solar maximum. The effect is amplified at higher temperatures (0.3--0.6 MK) with a stronger anti-correlation and the ratio falling from 0.16 at solar minimum to 0.08 at solar maximum. The values we find at solar minimum are too low to solve the solar modeling problem.

A Solar cycle correlation of coronal element abundances in Sun-as-a-star observations

David H. **Brooks**, Deborah Baker, Lidia van Driel-Gesztelyi, Harry P. Warren
Nature Communication at this https URL **2018**
https://arxiv.org/ftp/arxiv/papers/1802/1802.00563.pdf
The elemental composition in the coronae of low-activity solar-like stars appears to be related to fundamental stellar properties such as rotation, surface gravity, and spectral type. Here we use full-Sun observations from the Solar Dynamics Observatory, to show that when the Sun is observed as a star, the variation of coronal composition is highly correlated with a proxy for solar activity, the F10.7 cm radio flux, and therefore with the solar cycle phase. Similar cyclic variations should therefore be detectable spectroscopically in X-ray observations of solar analogs. The plasma composition in full-disk observations of the Sun is related to the evolution of coronal magnetic field activity. Our observations therefore introduce an uncertainty into the nature of any relationship between coronal composition and fixed stellar properties. The results highlight the importance of systematic full-cycle observations for understanding the elemental composition of solar-like stellar coronae.

PROPERTIES AND MODELING OF UNRESOLVED FINE STRUCTURE LOOPS OBSERVED IN THE SOLAR TRANSITION REGION BY IRIS

David H. **Brooks**1,3, Jeffrey W. Reep2,4, and Harry P. Warren
2016 ApJ 826 L18
Recent observations from the Interface Region Imaging Spectrograph (IRIS) have discovered a new class of numerous low-lying dynamic loop structures, and it has been argued that they are the long-postulated unresolved fine structures (UFSs) that dominate the emission of the solar transition region. In this letter, we combine IRIS measurements of the properties of a sample of 108 UFSs (intensities, lengths, widths, lifetimes) with one-dimensional non-equilibrium ionization simulations, using the HYDRAD hydrodynamic model to examine whether the UFSs are now truly spatially resolved in the sense of being individual structures rather than being composed of multiple magnetic threads. We find that a simulation of an impulsively heated single strand can reproduce most of the observed properties, suggesting that the UFSs may be resolved, and the distribution of UFS widths implies that they are structured on a spatial scale of 133 km on average. Spatial scales of a few hundred kilometers appear to be typical for a range of chromospheric and coronal structures, and we conjecture that this could be an important clue for understanding the coronal heating process.

Full-Sun observations for identifying the source of the slow solar wind

David H. **Brooks**, Ignacio Ugarte-Urra, Harry P. Warren
Nature Communications, 6, 5947 **2015**
http://www.nature.com/ncomms/2015/150106/ncomms6947/pdf/ncomms6947.pdf
Fast (>700 km s-1) and slow (~400 km s-1) winds stream from the Sun, permeate the heliosphere and influence the near-Earth environment. While the fast wind is known to emanate primarily from polar coronal holes, the source of the slow wind remains unknown. Here we identify possible sites of origin using a slow solar wind source map of the entire Sun, which we construct from specially designed, full-disk observations from the Hinode satellite, and a magnetic field model. Our map provides a full-Sun observation that combines three key ingredients for identifying the sources: velocity, plasma composition and magnetic topology and shows them as solar wind composition plasma outflowing on open magnetic field lines. The area coverage of the identified sources is large enough that the sum of their mass contributions can explain a significant fraction of the mass loss rate of the solar wind. **16–18 January 2013**

Evidence of a Connection Between Active Region Outflows and the Solar Wind

David H. **Brooks** and Harry Warren

EIS Science Nugget, 2 Aug **2011**
http://msslxr.mssl.ucl.ac.uk:8080/SolarB/nuggets/nugget_2011aug.jsp
Hinode has revealed the presence of high temperature (few MK) outflows at the edges of many active regions. These outflows show velocities of tens of km/s and appear to persist for at least several days.
See Brooks & Warren (2011), ApJ, 727, L13

A Helioseismic Perspective on the Depth of the Minimum Between Solar Cycles 23 and 24

A.-M. **Broomhall**
Solar Phys. 292: 67 **2017**
https://arxiv.org/pdf/1702.03149.pdf
The solar-activity-cycle minimum observed between Cycles 23 and 24 is generally regarded as being unusually deep and long. That minimum is being followed by one of the smallest amplitude cycles in recent history. We perform an in-depth analysis of this minimum with helioseismology. We use Global Oscillation Network Group (GONG) data to demonstrate that the frequencies of helioseismic oscillations are a sensitive probe of the Sun's magnetic field: The frequencies of the helioseismic oscillations were found to be systematically lower in the minimum following Cycle 23 than in the minimum preceding it. This difference is statistically significant and may indicate that the Sun's global magnetic field was weaker in the minimum following Cycle 23. The size of the shift in oscillation frequencies between the two minima is dependent on the frequency of the oscillation and takes the same functional form as the frequency dependence observed when the frequencies at cycle maximum are compared with the cycle-minimum frequencies. This implies that the same near-surface magnetic perturbation is responsible. Finally, we determine that the difference in the mean magnetic field between the minimum preceding Cycle 23 and that following it is approximately 1G.

Solar cycle variations in the powers and damping rates of low-degree solar acoustic oscillations

A.-M. **Broomhall**a, b, , , C.E. Pughb, V.M. Nakariakov
Advances in Space Research Volume 56, Issue 12, 15 December **2015**, Pages 2706–2712
http://www.sciencedirect.com/science/article/pii/S027311771500277X
Helioseismology uses the Sun’s natural resonant oscillations to study the solar interior. The properties of the solar oscillations are sensitive to the Sun’s magnetic activity cycle. Here we examine variations in the powers, damping rates, and energy supply rates of the most prominent acoustic oscillations in unresolved, Sun-as-a-star data, obtained by the Birmingham Solar Oscillations Network (BiSON) during solar cycles 22, 23, and the first half of 24. The variations in the helioseismic parameters are compared to the 10.7 cm flux, a well-known global proxy of solar activity. As expected the oscillations are most heavily damped and the mode powers are at a minimum at solar activity maximum. The 10.7 cm flux was linearly regressed using the fractional variations of damping rates and powers observed during cycle 23. In general, good agreement is found between the damping rates and the 10.7 cm flux. However, the linearly regressed 10.7 cm flux and fractional variation in powers diverge in cycles 22 and 24, indicating that the relationship between the mode powers and the 10.7 cm flux is not consistent from one cycle to the next. The energy supply rate of the oscillations, which is usually approximately constant, also decreases at this time. We have determined that this discrepancy is not because of the first-order bias introduced by an increase in the level of background noise or gaps in the data. Although we cannot categorically rule out an instrumental origin, the divergence observed in cycle 24, when the data were of high quality and the data coverage was over 80%, raises the possibility that the effect may be solar in origin.

A Comparison Between Global Proxies of the Sun's Magnetic Activity Cycle: Inferences from Helioseismology

A.-M. **Broomhall**, V.M. Nakariakov
Solar Phys. Volume 290, Issue 11, pp 3095-3111 **2015 File**
http://arxiv.org/pdf/1507.02854v1.pdf
The last solar minimum was, by recent standards, unusually deep and long. We are now close to the maximum of the subsequent solar cycle, which is relatively weak. In this article we make comparisons between different global (unresolved) measures of the Sun's magnetic activity, to investigate how they are responding to this weak-activity epoch. We focus on helioseismic data, which are sensitive to conditions, including the characteristics of the magnetic field, in the solar interior. Also considered are measures of the magnetic field in the photosphere (sunspot number and sunspot area), the chromosphere and corona (10.7cm radio flux and 530.3nm green coronal index), and two measures of the Sun's magnetic activity closer to Earth (the interplanetary magnetic field and the galactic cosmic-ray intensity). Scaled versions of the activity proxies diverge from the helioseismic data around 2000, indicating a change in relationship between the proxies. The degree of divergence varies from proxy to proxy with

sunspot area and 10.7cm flux showing only small deviations, while sunspot number, coronal index, and the two interplanetary proxies show much larger departures. In Cycle 24 the deviations in the solar proxies and the helioseismic data decrease, raising the possibility that the deviations observed in Cycle 23 are just symptomatic of a 22-year Hale cycle. However, the deviations in the helioseismic data and the interplanetary proxies increase in Cycle 24. Interestingly the divergence in the solar proxies and the helioseismic data are not reflected in the shorter-term variations (often referred to as quasi-biennial oscillations) observed on top of the dominant 11-year solar cycle. However, despite being highly correlated in Cycle 22, the short-term variations in the interplanetary proxies show very little correlation with the helioseismic data during Cycles 23 and 24.

The Sun's interior structure and dynamics, and the solar cycle **Review**

A.-M. **Broomhall**, P. Chatterjee, R. Howe, A.A. Norton, M.J. Thompson
Space Science Reviews, Volume 186, Issue 1-4, pp 191-225 Dec **2014**

The Sun's internal structure and dynamics can be studied with helioseismology, which uses the Sun's natural acoustic oscillations to build up a profile of the solar interior. We discuss how solar acoustic oscillations are affected by the Sun's magnetic field. Careful observations of these effects can be inverted to determine the variations in the structure and dynamics of the Sun's interior as the solar cycle progresses. Observed variations in the structure and dynamics can then be used to inform models of the solar dynamo, which are crucial to our understanding of how the Sun's magnetic field is generated and maintained.

Could the unusual solar minimum have been predicted?

A.-M. **Broomhall**1, 2, S. Basu3, W.J. Chaplin2, Y. Elswort
UKSP nuggets, #30, **2012**
http://www.uksolphys.org/?p=5673
Helioseismic warnings of the Sun’s strange behaviour.

The Influence of the Solar Coronal Radiation on Coronal Plasma Structures, I: Determination of the Incident Coronal Radiation

Gerrard M. **Brown**, Nicolas Labrosse
Solar Physics February **2018**, 293:35
https://link.springer.com/content/pdf/10.1007%2Fs11207-018-1255-z.pdf

Coronal structures receive radiation not only from the solar disc, but also from the corona. This height-dependent incident radiation plays a crucial role in the excitation and the ionisation of the illuminated plasma. The aim of this article is to present a method for computing the detailed incident radiation coming from the solar corona, which is perceived at a point located at an arbitrary height. The coronal radiation is calculated by integrating the radiation received at a point in the corona over all of the corona visible from this point. The emission from the corona at all wavelengths of interest is computed using atomic data provided by CHIANTI. We obtain the spectrum illuminating points located at varying heights in the corona at wavelengths between 100 and 912 Å when photons can ionise H or He atoms and ions in their ground states. As expected, individual spectral lines will contribute most at the height within the corona where the local temperature is closest to their formation temperature. As there are many spectral lines produced by many ions, the coronal intensity cannot be assumed to vary in the same way at all wavelengths and so must be calculated for each separate height that is to be considered. This code can be used to compute the spectrum from the corona illuminating a point at any given height above the solar surface. This brings a necessary improvement to models where an accurate determination of the excitation and ionisation states of coronal plasma structures is crucial.

Flux Variations in Lines of Solar EUV Radiation Beyond Flares in Cycle 24

E.A. **Bruevich**, G.V. Yakunina
Geomagnetizm and Aeronomy **2019**
https://arxiv.org/pdf/1912.10736.pdf

Studies in the extreme ultraviolet (EUV) and X-ray ranges of the solar spectrum are important due to the active role of radiation of these ranges in the formation of the Earth's ionosphere. Photons of the EUV range are completely absorbed in the upper layers of the Earth's atmosphere and induce the excitation, dissociation, and ionization of its different components and, finally, the atmospheric heating. From the archive data of the EUV Variability Experiment of the Solar Dynamics Observatory (SDO/EVE), we formed series of diurnal values of the background fluxes radiated beyond flares in the EUV lines HeII (30.4 nm), HeI (58.4 nm), CIII (97.7 nm), and FeXVIII (9.4 nm) in cycle 24 (from 2010 to 2017). These fluxes are compared to the corresponding values of the radio flux F10.7 at a wavelength of 10.7 cm and the background radiation flux F0.1-0.8 in the X-ray range between 0.1 and 0.8 nm measured onboard the GOES-15 satellite of the Geostationary Operational Environmental Satellite system.

Comparative analysis has shown that the solar radiation in individual lines of the EUV range and the fluxes F10.7 and F0.1-0.8 are closely interrelated.

Long-term trends in the solar activity. Variations of solar indices in last 40 years

E.A. **Bruevich**, V.V. Bruevich
Research in Astron. Astrophys. **Vol 19, No 7** **2019**
https://arxiv.org/pdf/1812.11723.pdf
The analysis of long-term variations of several solar activity indices (AI) since in last 40 years has been performed. We studied the AI which characterize the fluxes from different areas in solar atmosphere. Our consideration of mutual correlations between the solar indices is based on the study of relationships between them in the period from 1950 to 1990. This period of time, covering activity cycles 19 -- 22, is characterized by relatively stable relations between the indices. We have studied the normalized variations of these indices in the recent time in relation to their values which have been calculated with help of the radiation of the sun in the radio range at a wavelength of 10.7 cm (F10.7) in 1950 -- 1990. The analysis of time series of variations of the normalized AI (AIFF) in solar cycles 23 -- 24 shows an existence of different trends for different indices in their long-term variations. We assume that variations of normalized SSN, F530.3 and Flare Index, which have shown a sharp decrease in last 40 years is possibly associated with a decrease in the intensity of large-scale magnetic fields in the photosphere (SSN) and in the corona (the coronal index and the Flare Index)

Large flares (M1 - X7) in solar cycle 24

E.A. **Bruevich**, T.V. Kazachevskaya, G.V. Yakunina
2017
https://arxiv.org/pdf/1706.01421.pdf
The large (X-ray class > M1) and very large (X-ray class >X1) flares (according to the observations of GOES-15 and Preliminary data from Current Catalog of Flare Events) in solar activity cycle 24 were analyzed. The monthly average values of optical Flare Index for 2010 - 2016 were calculated. The values of the total energy of the flare E (J m-2) in the 0.1 -- 0.8 nm range at the level of the earth's atmosphere were estimated. The energy spectrum (the dependence of the number of flares with the full energy E from the value of this full energy) for 115 flares of M5 - X7 classes was built. The comparative study of monthly averaged values of several indices of solar activity in current cycle 24: the relative sunspot numbers (SSN), the 10.7 cm radio flux, the radiation flux in the Lyman-alpha line, the solar constant (TSI) and the Flare Index (FI) was made. **9.08.2011**

Evolution of the cycles of magnetic activity of the Sun and Sun-like stars in time

E.A. **Bruevich**, V.V. Bruevich, B.P. Artamonov
2016
http://arxiv.org/pdf/1609.05335v1.pdf
We applied the method of continuous wavelet-transform to the time-frequency analysis to the sets of observations of relative sunspot numbers, sunspot areas and to 6 Mount Wilson HK-project stars with well-defined magnetic cycles. Wavelet analysis of these data reveals the following pattern: at the same time there are several activity cycles whose periods vary widely from the quasi-biennial up to the centennial period for the Sun and vary significant during observations time of the HK-project stars. These relatively low-frequency periodic variations of the solar and stellar activity gradually change the values of periods of different cycles in time. This phenomenon can be observed in every cycles of activity

The histeresis of the indices of solar activity and of the ionospheric indices in 11-yr cycles. The histeresis of the stellar activity indices in the cyclic activity similar to the Sun

E.A. **Bruevich**, G.V. Yakunina, T.V. Kazachevskaya, V.V. Katyushina, A.A. Nusinov
2016
http://arxiv.org/pdf/1607.08543v1.pdf
The analysis of the effect of the hysteresis, which manifests itself in an ambiguous relationship of radiation from the photosphere, chromosphere and corona on the rise and decline phases of the solar and stellar activity cycles have done. Some indices of solar activity: the flux of the hydrogen Lyman-alpha emission, the 10.7 cm flux, the sunspot number SSN, the flux in the coronal green line 530.3 nm, the solar constant TSI and the 280 nm Mg II flux were studied. The stars with the well-determined cycles were examined to detect the effect of hysteresis between the chromosphere's S-index CaII fluxes versus the photosphere's fluxes Fphotosphere.

Magnetic cycles of Sun-like stars with different levels of coronal and chromospheric activity -- comparison with the Sun

E. A. **Bruevich**, V. V. Bruevich, E. V. Shimanovskaya
Research in Astron. Astrophys. **2016**

http://arxiv.org/pdf/1605.08578v1.pdf
The atmospheric activity of the Sun and Sun-like stars is analyzed involving observations from HK-project at the Mount Wilson Observatory, the California and Carnegie Planet Search Program at the Keck and Lick Observatories and the Magellan Planet Search Program at the Las Campanas Observatory. We show that for stars of F, G and K spectral classes, the cyclic activity, similar to the 11-yr solar cycles, is different: it becomes more prominent in K-stars. Comparative study of Sun-like stars with different levels of the chromospheric and coronal activity confirms that the Sun belongs to stars with the low level of the chromospheric activity and stands apart among these stars by the minimum level of its coronal radiation and the minimum level of its variations of the photospheric flux.

General trends in the changes of indices of solar activity in the late XX - early XXI century

E.A. **Bruevich**, G.V. Yakunina
2015
http://arxiv.org/pdf/1504.02226v1.pdf
The analysis of the observations of solar activity indexes SSN (NOAA Sunspot Numbers), the radio flux at a wavelength of 10.7 cm (F10.7) and the solar constant (TSI) during the cycles 22 - 24 is presented. We found a decrease of the observed values of the SSNobs which was calculated with SSNsyn (using regression relationships between SSN and F10.7) after 1990 year on 20 - 25% instead of 35%, as was previously assumed. The changes in characteristics of the most popular index, SSN, such as decrease in the number of sunspots, the reduction of the magnetic field in small and medium-sized spots are not in full compliance with the proposed scenario of solar activity predicted by radio flux F10.7 in the cycles 23 and 24, and cannot be fully explained by the influence on the SSN values of additional minimum of 50 - 70 year cycle. We have also showed that the observed changes of SSN lead to a slight increase of the solar constant TSI during the cycles 23 - 24 compared to the cycle 22.

The Solar-Stellar Connection **Review**

A. S. **Brun**, R. A. Garcia, G. Houdek, D. Nandy, M. Pinsonneault
Space Science Review, Volume 196, Issue 1, pp 303-356 **2015**
http://arxiv.org/pdf/1503.06742v1.pdf
We discuss how recent advances in observations, theory and numerical simulations have allowed the stellar community to progress in its understanding of stellar convection, rotation and magnetism and to assess the degree to which the Sun and other stars share similar dynamical properties. Ensemble asteroseismology has become a reality with the advent of large time domain studies, especially from space missions. This new capability has provided improved constraints on stellar rotation and activity, over and above that obtained via traditional techniques such as spectropolarimetry or CaII H&K observations. New data and surveys covering large mass and age ranges have provided a wide parameter space to confront theories of stellar magnetism. These new empirical databases are complemented by theoretical advances and improved multi-D simulations of stellar dynamos. We trace these pathways through which a lucid and more detailed picture of magnetohydrodynamics of solar-like stars is beginning to emerge and discuss future prospects.
Erratum to: Space Science Reviews December 2015, Volume 196, Issue 1, pp 357-358

Solar-Cycle Variations of South-Atlantic Anomaly Proton Intensities Measured With The PAMELA Mission

A. **Bruno**, M. Martucci, F. S. Cafagna, R. Sparvoli, O. Adriani, G. C. Barbarino, G. A. Bazilevskaya, et al.
Astrophysical Journal Letters **917** L21 **2021**
https://arxiv.org/pdf/2108.06407.pdf
https://doi.org/10.3847/2041-8213/ac1a74
We present a study of the solar-cycle variations of >80 MeV proton flux intensities in the lower edge of the inner radiation belt, based on the measurements of the Payload for Antimatter Matter Exploration and Light-nuclei Astrophysics (PAMELA) mission. The analyzed data sample covers an ~8 year interval from 2006 July to 2014 September, thus spanning from the decaying phase of the 23rd solar cycle to the maximum of the 24th cycle. We explored the intensity temporal variations as a function of drift shell and proton energy, also providing an explicit investigation of the solar-modulation effects at different equatorial pitch angles. PAMELA observations offer new important constraints for the modeling of low-altitude particle radiation environment at the highest trapping energies.

The Solar Wind as a Turbulence Laboratory Review

Roberto **Bruno** and Vincenzo Carbone
Living Reviews in Solar Physics, May **2013**
http://www.livingreviews.org/lrsp-2013-2

In this review we will focus on a topic of fundamental importance for both astrophysics and plasma physics, namely the occurrence of large-amplitude low-frequency fluctuations of the fields that describe the plasma state. This subject will be treated within the context of the expanding solar wind and the most meaningful advances in this research field will be reported emphasizing the results obtained in the past decade or so. As a matter of fact, Helios inner heliosphere and Ulysses' high latitude observations, recent multi-spacecrafts measurements in the solar wind (Cluster four satellites) and new numerical approaches to the problem, based on the dynamics of complex systems, brought new important insights which helped to better understand how turbulent fluctuations behave in the solar wind. In particular, numerical simulations within the realm of magnetohydrodynamic (MHD) turbulence theory unraveled what kind of physical mechanisms are at the basis of turbulence generation and energy transfer across the spectral domain of the fluctuations. In other words, the advances reached in these past years in the investigation of solar wind turbulence now offer a rather complete picture of the phenomenological aspect of the problem to be tentatively presented in a rather organic way.

ON THE CONNECTION BETWEEN PROPAGATING SOLAR CORONAL DISTURBANCES AND CHROMOSPHERIC FOOTPOINTS

P. **Bryans**1, S. W. McIntosh1, I. De Moortel1,2, and B. De Pontieu3
2016 ApJ 829 L18

The Interface Region Imaging Spectrograph (IRIS) provides an unparalleled opportunity to explore the (thermal) interface between the chromosphere, transition region, and the coronal plasma observed by the Atmospheric Imaging Assembly (AIA) of the Solar Dynamics Observatory (SDO). The SDO/AIA observations of coronal loop footpoints show strong recurring upward propagating signals—"propagating coronal disturbances" (PCDs) with apparent speeds of the order of 100–120 km s−1. That signal has a clear signature in the slit-jaw images of IRIS in addition to identifiable spectral signatures and diagnostics in the Mg iih (2803 Å) line. In analyzing the Mg iih line, we are able to observe the presence of magnetoacoustic shock waves that are also present in the vicinity of the coronal loop footpoints. We see there is enough of a correspondence between the shock propagation in Mg iih, the evolution of the Si iv line profiles, and the PCD evolution to indicate that these waves are an important ingredient for PCDs. In addition, the strong flows in the jet-like features in the IRIS Si iv slit-jaw images are also associated with PCDs, such that waves and flows both appear to be contributing to the signals observed at the footpoints of PCDs.

A comparison between solar plage and network properties

D. **Buehler**, A. Lagg, M. van Noort, S.K. Solanki
A&A 630, A86 **2019**
https://arxiv.org/pdf/1908.07464.pdf

We compare the properties of kG magnetic structures in the solar network and in active region plage at high spatial resolution. Our analysis used six SP scans of the solar disc centre aboard Hinode SOT and inverted the obtained spectra of the photospheric 6302 Åline pair using the 2D SPINOR code. Photospheric magnetic field concentrations in network and plage areas are on average 1.5 kG strong with inclinations of 10-20 degrees, and have <400 m/s internal and 2-3 km/s external downflows. At the disc centre, the continuum intensity of magnetic field concentrations in the network are on average 10% brighter than the mean quiet Sun, whilst their plage counterparts are 3% darker. A more detailed analysis revealed that all sizes of individual kG patches in the network have 150 G higher field strengths on average, 5% higher continuum contrasts, and 800 m/s faster surrounding downflows than similarly sized patches in the plage. The speed of the surrounding downflows also correlates with the patch area, and patches containing pores can produce supersonic flows exceeding 11 km/s in individual pixels. Furthermore, the magnetic canopies of kG patches are on average 9 degrees more horizontal in the plage compared to the network. Most of the differences between the network and plage are due to their different patch size distributions, but the intrinsic differences between similarly sized patches is likely results from the modification of the convection photospheric convection with increasing amounts of magnetic flux. **2007 02 18, 2007 04 30, 2007 05 18, 2007 09 10**

Properties of solar plage from a spatially coupled inversion of Hinode SP data

D. **Buehler**1, A. Lagg1, S. K. Solanki1,2 and M. van Noort
A&A 576, A27 (**2015**)

Aims. The properties of magnetic fields forming an extended plage region in **AR 10953** were investigated.

Methods. Stokes spectra of the Fe I line pair at 6302 Å recorded by the spectropolarimeter aboard the Hinode satellite were inverted using the SPINOR code. The code performed a 2D spatially coupled inversion on the Stokes spectra, allowing the retrieval of gradients in optical depth within the atmosphere of each pixel, whilst accounting for the effects of the instrument's PSF. Consequently, no magnetic filling factor was needed.
Results. The inversion results reveal that plage is composed of magnetic flux concentrations (MFCs) with typical field strengths of 1520 G at log (τ) = −0.9 and inclinations of 10°−15°. The MFCs expand by forming magnetic canopies composed of weaker and more inclined magnetic fields. The expansion and average temperature stratification of isolated MFCs can be approximated well with an empirical plage thin flux tube model. The highest temperatures of MFCs are located at their edges in all log (τ) layers. Whilst the plasma inside MFCs is nearly at rest, each is surrounded by a ring of downflows of on average 2.4 km s-1 at log (τ) = 0and peak velocities of up to 10 km s-1, which are supersonic. The downflow ring of an MFC weakens and shifts outwards with height, tracing the MFC's expansion. Such downflow rings often harbour magnetic patches of opposite polarity to that of the main MFC with typical field strengths below 300 G at log (τ) = 0. These opposite polarity patches are situated beneath the canopy of their main MFC. We found evidence of a strong broadening of the Stokes profiles in MFCs and particularly in the downflow rings surrounding MFCs (expressed by a microturbulence in the inversion). This indicates the presence of strong unresolved velocities. Larger magnetic structures such as sunspots cause the field of nearby MFCs to be more inclined.

CLASP Constraints on the Magnetization and Geometrical Complexity of the Chromosphere-Corona Transition Region

J. Trujillo **Bueno**, J. Štěpán, L. Belluzzi, A. Asensio Ramos, R. Manso Sainz, T. del Pino Alemán, R. Casini, R. Ishikawa, R. Kano, A. Winebarger, F. Auchère, N. Narukage, K. Kobayashi, T. Bando, Y. Katsukawa, M. Kubo, S. Ishikawa, G. Giono, H. Hara, Y. Suematsu, T. Shimizu, T. Sakao, S. Tsuneta, K. Ichimoto, J. Cirtain, P. Champey, B. De Pontieu, M. Carlsson

ApJL 866 L15 **2018**

https://arxiv.org/pdf/1809.08865.pdf

The Chromospheric Lyman-Alpha Spectro-Polarimeter (CLASP) is a suborbital rocket experiment that on 3rd September 2015 measured the linear polarization produced by scattering processes in the hydrogen Ly-α line of the solar disk radiation, whose line-center photons stem from the chromosphere-corona transition region (TR). These unprecedented spectropolarimetric observations revealed an interesting surprise, namely that there is practically no center-to-limb variation (CLV) in the Q/I line-center signals. Using an analytical model, we first show that the geometrical complexity of the corrugated surface that delineates the TR has a crucial impact on the CLV of the Q/I and U/I line-center signals. Secondly, we introduce a statistical description of the solar atmosphere based on a three-dimensional (3D) model derived from a state-of-the-art radiation magneto-hydrodynamic simulation. Each realization of the statistical ensemble is a 3D model characterized by a given degree of magnetization and corrugation of the TR, and for each such realization we solve the full 3D radiative transfer problem taking into account the impact of the CLASP instrument degradation on the calculated polarization signals. Finally, we apply the statistical inference method presented in a previous paper to show that the TR of the 3D model that produces the best agreement with the CLASP observations has a relatively weak magnetic field and a relatively high degree of corrugation. We emphasize that a suitable way to validate or refute numerical models of the upper solar chromosphere is by confronting calculations and observations of the scattering polarization in ultraviolet lines sensitive to the Hanle effect.

Seismic Solar Models from Ledoux discriminant inversions

G. **Buldgen**, P. Eggenberger, V.A. Baturin, T. Corbard, J.Christensen-Dalsgaard, S. J. A. J. Salmon, A. Noels, A. V. Oreshina, R. Scuflaire

A&A **2020**

https://arxiv.org/pdf/2007.10222.pdf

The Sun constitutes an excellent laboratory of fundamental physics. With the advent of helioseismology, we were able to probe its internal layers with unprecedented precision. However, the current state of solar modelling is still stained by tedious issues. One of these problems is related to the disagreement between models computed with recent photospheric abundances and helioseismic constraints. We use solar evolutionary models as initial conditions for reintegrations of their structure using Ledoux discriminant inversions. The resulting models are defined as seismic solar models, satisfying the equations of hydrostatic equilibrium. They will allow us to better constrain the internal structure of the Sun and provide complementary information to that of evolutionary models. These seismic models were computed using various reference models with different equations of state, abundances and opacity tables. We check the robustness of our approach by confirming the good agreement of our seismic models in terms of sound speed, density and entropy proxy inversions as well as frequency-separation ratios of low-degree pressure modes. Our method allows us to determine with an excellent accuracy the Ledoux discriminant profile of the Sun and compute full profiles of this quantity. Our models show an agreement with seismic data of ~0.1% in sound speed, density and entropy proxy as well as with the observed frequency-separation ratios. They surpass all standard

and non-standard evolutionary models including ad-hoc changes aiming at reproducing helioseismic constraints. The obtained seismic Ledoux discriminant profile as well as the consistent structure obtained from our procedure paves the way for renewed attempts at constraining the solar modelling problem and the missing physical processes acting in the solar interior by breaking free from the hypotheses of evolutionary models.

From the Sun to solar-like stars: how does the solar modelling problem affect our studies of solar-like oscillators? Review

G. **Buldgen**, C. Pezzotti, M. Farnir, S.J.A.J. Salmon, P. Eggenberger

Proceedings of the conference "Stars and their variability observed from space" held in Vienna in August 2019 **2019**

https://arxiv.org/pdf/1912.01986.pdf

Since the first observations of solar oscillations in 1962, helioseismology has probably been one of the most successful fields of astrophysics. Besides the improvement of observational data, solar seismologists developed sophisticated techniques to infer the internal structure of the Sun. Back in 1990s these comparisons showed a very high agreement between solar models and the Sun. However, the downward revision of the CNO surface abundances in the Sun in 2005, confirmed in 2009, induced a drastic reduction of this agreement leading to the so-called solar modelling problem. More than ten years later, in the era of the space-based photometry missions which have established asteroseismology of solar-like stars as a standard approach to obtain their masses, radii and ages, the solar modelling problem still awaits a solution. We will briefly present the results of new helioseismic inversions, discuss the current uncertainties of solar models and possible solutions to the solar modelling problem. We will also discuss how the solar problem can have significant implications for asteroseismology as a whole by discussing the modelling of the exoplanet-host star Kepler-444, thus impacting the fields requiring a precise and accurate knowledge of stellar masses, radii and ages, such as Galactic archaeology and exoplanetology.

Global Helioseismology Review

G. **Buldgen**

Proceedings of the meeting "How Much do we Trust Stellar Models?" held in Liège in Sept 2018 **2019**

https://arxiv.org/pdf/1912.02003.pdf

Helioseismology is one of the most successful fields of astrophysics. The observation and characterization of solar oscillation has allowed solar seismologists to study the internal structure and dynamics of the Sun with unprecedented thoroughness. Ground-based networks and dedicated space missions have delivered data of exquisite quality, enabling the development of sophisticated inference techniques. The achievements of the fields count, amongst other, the determination of solar photospheric helium abundance, unacessible to spectroscopic constraints, the precise positioning of the base of the convective zone and the demonstration of the importance of microscopic diffusion in stellar radiative regions. Helioseismology played also a key role in validating the framework used to compute solar and stellar models and played an important role in the so-called solar neutrino problem. In the current era of astrophysics, with the increasing importance of asteroseismology to precisely characterize stars, the Sun still plays a crucial calibration role, acting as a benchmark for stellar models. With the revision of the solar abundances and the current discussions related to radiative opacity computations, the role of the Sun as a laboratory of fundamental physics is undisputable. In this brief review, I will discuss some of the inference techniques developed in the field of helioseismology, dedicated to the exploitation of the solar global oscillation modes.

Progress in global helioseismology: a new light on the solar modelling problem and its implications for solar-like stars Review

G. **Buldgen**, A. Noels, S. Salmon

Front. Astron. Space Sci. - 6:42. **2019**

https://arxiv.org/pdf/1906.08213.pdf

https://www.frontiersin.org/articles/10.3389/fspas.2019.00042/full

https://doi.org/10.3389/fspas.2019.00042

sci-hub.ru/10.3389/fspas.2019.00042

Since the first observations of solar oscillations, helioseismology has been one of the most successful fields of astrophysics. Data of high quality were obtained through the implementation of networks of ground-based observatories such as the GONG project or the BiSON network, coupled with space-based telescopes such as SOHO and SDO missions. Besides the improvement of observational data, solar seismologists developed sophisticated techniques to infer the internal structure of the Sun. These methods, then already extensively used in the field of Geophysics, are called inversion techniques. They allowed to determine the position of the solar convective envelope, its helium abundance and the internal radial profiles of thermodynamic quantities. Back in 1990s these comparisons showed a very high agreement between solar models and the Sun. However, the downward revision of the CNO surface abundances in the Sun induced a drastic reduction of this agreement leading to the solar modelling

problem. More than ten years later, in the era of the space-based photometry missions which have established asteroseismology of solar-like stars as a standard approach to obtain their masses, radii and ages, the solar modelling problem still awaits a solution. We will present the results of new helioseismic inversions, discuss the current uncertainties of solar models as well as some possible solutions to the solar problem. We will show how helioseismology can help us grasp what is amiss in our models. We will also show that, far from being an argument about details of solar models, the solar problem has significant implications for seismology of solar-like stars, on the main sequence and beyond, impacting asteroseismology as a whole as well as the fields requiring precise and accurate knowledge of stellar masses, radii and ages, such as Galactic archaeology and exoplanetology.

Combining multiple structural inversions to constrain the Solar modelling problem

G. **Buldgen**, S. J. A. J. Salmon, A. Noels, R. Scuflaire, J. Montalban, V.A. Baturin, P. Eggenberger, V.K. Gryaznov, I.L. Iosilevskiy, G. Meynet, W. J. Chaplin, A. Miglio, A.V. Oreshina, O. Richard, A.N. Starostin

A&A 621, A33 **2019**

https://arxiv.org/pdf/1809.08958.pdf

The Sun is the most studied of all stars. It is a reference for all other observed stars and a laboratory of fundamental physics helping us understand processes occuring in conditions irreproducible on Earth. However, our understanding of the Sun is currently stained by the solar modelling problem which can stem from various causes, such as the opacities, the equation of state and the mixing of chemical elements. We combine inversions of sound speed, an entropy proxy and the Ledoux discriminant with constraints such as the position of the base of the convective zone and the photospheric helium abundance. We test various combinations of standard ingredients for solar modelling such as abundance tables, equation of state, formalism for convection and diffusion and opacity tables and study the diagnostic potential of the inversions to constrain ad-hoc modifications of the opacity profile and additional mixing below the convective envelope. Combining inversions provides stringent constraints on the modifications on the models, far beyond what is achievable only from sound speed inversions. We constrain the form and amplitude of the opacity increase required and show that a 15% increase at log T=6.35 provides a significant improvement but that a more global increase of the opacity, within the uncertainties of current tables, coupled with an additional mixing at the bottom of the convective zone gives the best agreement for low metallicity models. We show that high metallicity models do not satisfy all the inversion results. We conclude that the solar problem likely occurs from various small sources, as ingredients such as the equation of state or the formalism of convection can induce small but significant changes and that using phase shift analyses combined with our approach is the next step for a better understanding of the inaccuracies of solar models just below the convective envelope.

See Proceedings of the PHOST meeting held in Banyuls, France https://arxiv.org/pdf/1902.10390.pdf

Inversions of the Ledoux discriminant: a closer look at the tachocline

Gaël **Buldgen**, S. J. A. J. Salmon, M. Godart, A. Noels, R. Scuflaire, M. A. Dupret, D. R. Reese, J. Colgan, C. J. Fontes, P. Eggenberger, P. Hakel, D. P. Kilcrease, O. Richard

MNRAS **2017**

https://arxiv.org/pdf/1709.00287.pdf

Modelling the base of the solar convective envelope is a tedious problem. Since the first rotation inversions, solar modellers are confronted with the fact that a region of very limited extent has an enormous physical impact on the Sun. Indeed, it is the transition region from differential to solid body rotation, the tachocline, which furthermore is influenced by turbulence and is also supposed to be the seat of the solar magnetic dynamo. Moreover, solar models show significant disagreement with the sound speed profile in this region. In this paper, we show how helioseismology can provide further constraints on this region by carrying out an inversion of the Ledoux discriminant. We compare these inversions for Standard Solar Models built using various opacity tables and chemical abundances and discuss the origins of the discrepancies between Solar Models and the Sun.

Seismic inversion of the solar entropy: A case for improving the Standard Solar Model

G. **Buldgen**, S. J. A. J. Salmon, A. Noels, R. Scuflaire, D. R. Reese, M-A. Dupret, J. Colgan, C. J. Fontes, P. Eggenberger, P. Hakel, D. P. Kilcrease, S. Turck-Chièze

A&A 607, A58 **2017**

https://arxiv.org/pdf/1707.05138.pdf

The Sun is the most constrained and well-studied of all stars. As a consequence, the physical ingredients entering solar models are used as a reference to study all other stars observed in the Universe. However, our understanding of the solar structure is still imperfect, as illustrated by the current debate on the heavy element abundances in the Sun. We wish to provide additional information on the solar structure by carrying out structural inversions of a new physical quantity, a proxy of the entropy of the solar plasma which properties are very sensitive to the temperature

gradient below the convective zone. We use new structural kernels to carry out direct inversions of an entropy proxy of the solar plasma and compare the solar structure to various standard solar models built using various opacity tables and chemical abundances. We also link our results to classical tests commonly found in the literature. Our analysis allows us to probe more efficiently the uncertain regions of the solar models, just below the convective zone, paving the way for new in-depth analyses of the Sun taking into account additional physical uncertainties of solar models beyond the specific question of chemical abundances.

Interpretation of Helioseismic Travel Times **Review**

Sensitivity to Sound Speed, Pressure, Density, and Flows
Raymond **Burston**, Laurent Gizon, Aaron C. Birch
Space Science Reviews Volume 196, Issue 1, pp 201-219 **2015**
http://arxiv.org/pdf/1503.09005v1.pdf
Time-distance helioseismology uses cross-covariances of wave motions on the solar surface to determine the travel times of wave packets moving from one surface location to another. We review the methodology to interpret travel-time measurements in terms of small, localised perturbations to a horizontally homogeneous reference solar model. Using the first Born approximation, we derive and compute 3D travel-time sensitivity (Fréchet) kernels for perturbations in sound-speed, density, pressure, and vector flows. While kernels for sound speed and flows had been computed previously, here we extend the calculation to kernels for density and pressure, hence providing a complete description of the effects of solar dynamics and structure on travel times. We treat three thermodynamic quantities as independent and do not assume hydrostatic equilibrium. We present a convenient approach to computing damped Green's functions using a normal-mode summation. The Green's function must be computed on a wavenumber grid that has sufficient resolution to resolve the longest lived modes. The typical kernel calculations used in this paper are computer intensive and require on the order of 600 CPU hours per kernel. Kernels are validated by computing the travel-time perturbation that results from horizontally-invariant perturbations using two independent approaches. At fixed sound-speed, the density and pressure kernels are approximately related through a negative multiplicative factor, therefore implying that perturbations in density and pressure are difficult to disentangle. Mean travel-times are not only sensitive to sound-speed, density and pressure perturbations, but also to flows, especially vertical flows. Accurate sensitivity kernels are needed to interpret complex flow patterns such as convection.

Measuring the F-corona intensity through time correlation of total and polarized visible light images

A. **Burtovoi** (1), G. Naletto (2,3), S. Dolei (4), D. Spadaro (4), M. Romoli (5,1), F. Landini (6), Y. De Leo (7,8)
A&A 659, A50 **2021**
https://arxiv.org/pdf/2112.11930.pdf
https://www.aanda.org/articles/aa/pdf/2022/03/aa41414-21.pdf
We present a new correlation method for deriving the F-corona intensity distribution, which is based on the analysis of the evolution of the total and polarized visible light (VL) images. We studied the one-month variation profiles of the total and polarized brightness acquired with Large Angle Spectrometric COronagraph (LASCO-C2) and found that in some regions they are highly correlated. Assuming that the F-corona does not vary significantly on a timescale of one month, we estimated its intensity in the high-correlation regions and reconstructed the corresponding intensity maps both during the solar-minimum and solar-maximum periods. Systematic uncertainties were estimated by performing dedicated simulations. We compared the resulting F-corona images with those determined using the inversion technique and found that the correlation method provides a smoother intensity distribution. We also obtained that the F-corona images calculated for consecutive months show no significant variation. Finally, we note that this method can be applied to the future high-cadence VL observations carried out with the Metis/Solar Orbiter coronagraph.

Spotless days and geomagnetic index as the predictors of solar cycle 25

Dipali S. **Burud**, Rajmal Jain, Arun K. Awasthi, Sneha Chaudhari, Sushanta C. Tripathy, N. Gopalswamy, Pramod Chamadia, Subhash C. Kaushik, Rajiv Vhatkar
Research in Astron. Astrophys Volume 21, Issue 9, id.215, **2021**
https://arxiv.org/pdf/2105.11448.pdf
We study the sunspot activity in relation to spotless days (SLDs) during the descending phase of solar cycle 11--24 to predict the amplitude of sunspot cycle 25. For this purpose, in addition to SLD, we also use the geomagnetic activity (aa index) during the descending phase of a given cycle. A very strong correlation of the SLD (R=0.68) and aa index (R=0.86) during the descending phase of a given cycle with the maximum amplitude of next solar cycle has been estimated.The empirical relationship led us to deduce the amplitude of cycle 25 to be 99.13± 14.97 and

104.23± 17.35 using SLD and aa index, respectively as predictors.Both the predictors provide comparable amplitude for solar cycle 25 and reveal that the solar cycle 25 will be weaker than cycle 24. Further we derive that the maximum of cycle 25 is likely to occur between February and March 2024. While the aa index has been used extensively in the past, this work establishes SLDs as another potential candidate for predicting the characteristics of the next cycle.

Twenty-four hour predictions of the solar wind speed peaks by the probability distribution function model

C. D. **Bussy-Virat**, A. J. Ridley
Space Weather Volume 14, Issue 10 October 2016 Pages 861–873
http://sci-hub.cc/10.1002/2016SW001437
Abrupt transitions from slow to fast solar wind represent a concern for the space weather forecasting community. They may cause geomagnetic storms that can eventually affect systems in orbit and on the ground. Therefore, the probability distribution function (PDF) model was improved to predict enhancements in the solar wind speed. New probability distribution functions allow for the prediction of the peak amplitude and the time to the peak while providing an interval of uncertainty on the prediction. It was found that 60% of the positive predictions were correct, while 91% of the negative predictions were correct, and 20% to 33% of the peaks in the speed were found by the model. This represents a considerable improvement upon the first version of the PDF model. A direct comparison with the Wang-Sheeley-Arge model shows that the PDF model is quite similar, except that it leads to fewer false positive predictions and misses fewer events, especially when the peak reaches very high speeds.

Correlation of Long-term Cosmic-Ray Modulation with Solar Activity Parameters

R. A. **Caballero-Lopez**1, N. E. Engelbrecht2,3, and J. D. Richardson4
2019 ApJ 883 73
https://doi.org/10.3847/1538-4357/ab3c57
In this work, we analyze the long-term cosmic-ray modulation observed by the Hermanus neutron monitor, which is the detector with the longest cosmic-ray record, from 1957 July. For our study we use the force-field approximation to the cosmic-ray transport equation, and the newest results on the mean free paths from the scattering theory. We compare the modulation parameter (ϕ) with different rigidity (P) dependences: P, P 2, and P 2/3. We correlate them with solar and interplanetary parameters. We found that (1) these rigidity dependences properly describe the modulation, (2) long-term cosmic-ray variations are better correlated with the magnitude of the heliospheric magnetic field (HMF) than the sunspot number, solar wind speed, and tilt angle of the HMF, and (3) the theoretical dependence of the parallel mean free path on the magnetic field variance is in agreement with the modulation parameter and therefore with the neutron monitor record. We also found that the force-field approximation is not able to take into account the effects of three-dimensional particle transport, showing a poor correlation with the perpendicular mean free path.

Comparison of the Scaling Properties of EUV Intensity Fluctuations in Coronal Hole and Quiet-Sun Regions

Ana Cristina **Cadavid**, Mari Paz Miralles, Kristine Romich
ApJ **2019**
https://arxiv.org/ftp/arxiv/papers/1910/1910.09541.pdf
Using detrended fluctuation analysis (DFA) and rescaled range (R/S) analysis, we investigate the scaling properties of EUV intensity fluctuations of low-latitude coronal holes (CHs) and neighboring quiet-Sun (QS) regions in signals obtained with the Solar Dynamics Observatory/Atmospheric Imaging Assembly (SDO/AIA) instrument. Contemporaneous line-of-sight SDO/Helioseismic and Magnetic Imager (HMI) magnetic fields provide a context for the physical environment. We find that the intensity fluctuations in the time series of EUV images present at each spatial point a scaling symmetry over the range ~20 min to ~ 1 hour. Thus we are able to calculate a generalized Hurst exponent and produce image maps, not of physical quantities like intensity or temperature, but of a single dynamical parameter that sums up the statistical nature of the intensity fluctuations at each pixel. In quiet-Sun (QS) regions and in coronal holes (CHs) with magnetic bipoles, the scaling exponent ($1.0<\alpha\leq1.5$) corresponds to anti-correlated turbulent-like processes. In coronal holes, and in quiet-Sun regions primarily associated with (open) magnetic field of dominant polarity, the generalized exponent ($0.5 <\alpha< 1$) corresponds to positively-correlated (persistent) processes. We identify a tendency for $\alpha \sim 1$ near coronal hole boundaries and in other regions in which open and closed magnetic fields are in proximity. This is a signature of an underlying 1/f type process that is characteristic for self-organized criticality and shot-noise models. **2017 February 27, 2017 April 16, 2017 April 21**

Multifractal Solar EUV Intensity Fluctuations and their Implications for Coronal Heating Models

Ana Cristina Cadavid **Cadavid**, Yeimy J. Rivera, John K. Lawrence, Damian J. Christian, Peter J. Jennings, A. Franco Rappazzo
2016 ApJ 831 186
http://arxiv.org/pdf/1609.02625v1.pdf
We investigate the scaling properties of the long-range temporal evolution and intermittency of SDO/AIA intensity observations in four solar environments: active region core, a weak emission region, and two core loops. We use two approaches: the probability distribution function (PDF) of time series increments, and multifractal detrended fluctuation analysis (MF-DFA). Noise taints the results, so we focus on the 171 Angstrom waveband , which has the highest signal-to-noise ratio. The lags between pairs of wavebands distinguish between coronal versus transition region (TR) emission. In all physical regions studied, scaling in the range 15-45 min is multifractal, and the time series are anti-persistent on the average. The degree of anti-correlation in the TR time series is greater than for coronal emission. The multifractality stems from long term correlations in the data rather than the wide distribution of intensities. Observations in the 335 Angstrom waveband can be described in terms of a multifractal with added noise. The multiscaling of the EUV data agrees qualitatively with the radiance from a phenomenological model of impulsive bursts plus noise, and also from ohmic dissipation in a Reduced Magnetohydrodynamics (RMHD) model for coronal loop heating. The parameter space must be further explored to seek quantitative agreement. Thus, the observational signatures obtained by the combined tests of the PDF of increments and the MF-DFA offer strong constraints which can systematically discriminate among models for coronal heating.

The origin of “Space Weather”

William B. **Cade III** and Christina Chan-Park
Space Weather, Volume 13, Issue 2, pp. 99-103, **2015**
Space Weather Quarterly, Volume 12, Issue 2, pp. 14-18, **2015**
http://onlinelibrary.wiley.com/doi/10.1002/SWQv12i002/epdf
Although "space weather" is a fairly recent term, there is a rich history of similar terms being used beginning in the middle to late 1800s. "Solar meteorology," "magnetic weather," and "cosmic meteorology" all appeared during that time frame. The actual first appearance of space weather can be attributed to the publication Science News Letter in 1957 (with the first modern usage in 1959) and was possibly coined by the editor at the time, Watson Davis.

Solar Temperature Variations Computed from SORCE SIM Irradiances Observed During 2003-2020

Robert F. **Cahalan**, Paulino Ajiquichi, Gaspar Yataz
Solar Physics **volume 297**, Article number: 16 (**2022**)
https://arxiv.org/ftp/arxiv/papers/2109/2109.08736.pdf
For a "reference day" of minimal solar activity between cycles 23 and 24 we compute the brightness temperature from solar spectral irradiance for each wavelength. We consider small variations of irradiance and temperature about the reference day values, and derive linear and quadratic analytic temperature approximations by Taylor expansion about the reference values. To determine approximation accuracy we compare to exact brightness temperatures computed for each day. We find that the linear analytic approximation overestimates, while the quadratic underestimates the exact result. Using R software, we find statistical fit models with minimum root-mean-square-error. We show that the quadratic statistical fit models give the smallest root-mean-square-error, giving results very near the exact.
Correction: Solar Physics volume 297, Article number: 25 (**2022**)
https://link.springer.com/content/pdf/10.1007/s11207-022-01967-w.pdf

Different manifestations of a loop-like transient brightening in solar atmospheres

Qiangwei **Cai**1,2,3,4, Hao Li5, Jincheng Wang6 and Hengqiang Feng1,3⋆
A&A 691, A309 (**2024**)
https://www.aanda.org/articles/aa/pdf/2024/11/aa49396-24.pdf
Context. Small-scale transient brightenings that are the consequence of magnetic reconnection play pivotal roles in the heating process of solar atmospheres. These phenomena contain key information about the dynamic evolution of the solar magnetic field. The fine-scale structures triggered by instabilities in these brightenings are intimately connected with the release of magnetic energy.
Aims. To better understand the conversion and release of magnetic energy in small-scale heating events, we investigated the thermal-dynamical behaviors of a loop-like transient brightening (LTB) with plasma blobs.
Methods. We used the spectroscopic and slit-jaw imaging observations taken from the Interface Region Imaging Spectrograph and the extreme-ultraviolet images taken from the Atmospheric Imaging Assembly on board the Solar Dynamics Observatory to analyze the plasma properties of an LTB that occurred on February 28, 2014. The space-time maps were created to present the spatial evolution of the LTB, and the light curves were calculated to illustrate

the heating process. Additionally, we employed the differential emission measure (DEM) method to compute the temperature and emission measure of the LTB. In order to investigate the plasma motion along the line-of-sight direction, a double-Gaussian function was used to fit the Si IV spectral profiles.
Results. The spectrum and DEM analysis indicate that the LTB was constituted by multithermal plasma with temperatures reaching up to 5.4 × 106 K. The space-time maps of the emission and the Gaussian-fitting results of the Si IV line demonstrate that the LTB not only exhibited bidirectional flows, but was also twisted. Several plasma blobs were identified in the spine of the LTB, suggesting the potential presence of a tearing-mode instability. The low-temperature bands peaked approximately one minute prior to the high-temperature bands, suggesting the occurrence of a heating process driven by magnetic reconnection. The appearance of plasma blobs closely coincided with the sudden increase in the velocity and the quick rise of light curves, providing evidence that plasma blobs facilitate the release of magnetic energy during solar activity.
Conclusions. Based on these findings, we speculate that the LTB was a complex structure that occurred in the upper chromosphere-transition region. These results clearly demonstrate that plasma blobs are important for the conversion and release processes of magnetic energy. **February 28, 2014**

Observational study of intermittent solar jets: p-mode modulation

Qiuzhuo **Cai**, Guiping Ruan, Chenxi Zheng, Brigitte Schmieder, Jinhan Guo, Yao Chen, Jiangtao Su, Yang Liu, Jihong Liu, Wenda Cao
A&A 682, A183 (**2024**)
https://arxiv.org/pdf/2312.03571.pdf
https://www.aanda.org/articles/aa/pdf/2024/02/aa48053-23.pdf
Aims. Recurring jets are observed in the solar atmosphere, which can erupt intermittently. By the observation of intermittent jets, we want to understand the causes of periodic eruption characteristics. Methods. We report intermittent jets observed by the GST. The analysis was aided by 1400 Å and 2796 Å data from IRIS.These observational instruments allowed us to analyze the temporal characteristics of jet events. Results. The jet continued for up to 4 hours. The time distance diagram shows that the peak of the jet has obviously periodic eruption characteristics (5 minutes) during 18:00 UT-18:50 UT. We also found periodic brightening phenomenon (5 minutes) during jets bursts in the observed bands in the Transition Region (1400 Å and 2796 Å), which may be a response to intermittent jets in the upper solar atmosphere.The time lag is 3 minutes. Evolutionary images in the TiO band revealed the horizontal movement of granulation at the location of jet. Compared to the quiet region of the Sun, we found that the footpoint of the jet is enhanced at the center of the H {\alpha} spectral line profile, with no significant changes in the line wings. This suggests the presence of prolonged heating at the footpoint of the jet. In the mixed-polarity magnetic field region of the jet, we observed magnetic flux emergence, cancellation, and shear indicating possible intermittent magnetic reconnection. That is confirmed by the NLFFF model reconstructed using the magneto-friction method. Conclusions. The multi-wavelength analysis indicates that the events we studied were triggered by magnetic reconnection caused by mixed-polarity magnetic fields. We suggest that the horizontal motion of the granulation in the photosphere drives the magnetic reconnection, which is modulated by p-mode oscillations. **August 6, 2016**,

The Co-alignment of Winged Hα Data Observed by the New Vacuum Solar Telescop

Yun-Fang **Cai**, Xu Yang, Yong-Yuang Xiang, Xiao-Li Yan, Zhen-Yu Jin, Hui Liu, Kai-Fan Ji
Research in Astronomy and Astrophysics **2022**
https://arxiv.org/pdf/2201.11913.pdf
The New Vacuum Solar Telescope (NVST) has been releasing its novel winged Ha data (WHD) since April 2021, namely the Ha imaging spectroscopic data. Compared with the prior released version, the new data are further co-aligned among the off-band images and packaged into a standard solar physics community format. In this study, we illustrate the alignment algorithm used by the novel WHD, which is mainly based on the optical flow method to obtain the translation offset between the winged images. To quantitatively evaluate the alignment results of two images with different similarities, we calculate the alignment accuracies between the images of different off-band and line center, respectively. The result shows that our alignment algorithm could reach up to the accuracy of about 0.1 "when the off-band of winged image is lower than 0.6 Å. In addition, we introduce the final product of the WHD in detail, which can provide convenience for the solar physicists to use high-resolution H{\alpha} imaging spectroscopic data of NVST. **26 Feb 2021**

Measurement and Correction of Instrumental Profiles for the Spectral Data of the New Vacuum Solar Telescope

Yunfang **Cai**, Zhi Xu, Kaifan Ji
Solar Physics volume 295, Article number: 31 (**2020**)
https://link.springer.com/content/pdf/10.1007/s11207-020-1598-0.pdf
The ideal optical system can realize point-to-point imaging, but for an actual observation it is difficult to achieve this ideal phenomenon due to the instrumental effects of imaging system, which is usually described as the

instrument profile in the imaging process of a grating spectrometer. The existence of the spectrometer instrument profiles introduces systematic errors in the observed spectral lines, which make the spectrum of the studied objects degenerate and blur. In this paper, we take the spectral data in the HαHα band observed by the Multi-Band Spectrometer (MBS) of the New Vacuum Solar Telescope (NVST) as an example; according to the characteristics of its acquired spectral data, we calculate the instrument profiles of the MBS in the spatial and the dispersion direction. The results are, respectively, 0.25″0.25″ and 115 mÅ, which might reflect the influence of the MBS optical instruments at that time in the HαHα band. Then the spectral data is deconvolved separately in the two directions by the corresponding IP to obtain the higher spatial and spectral resolution of the NVST spectral data.

Precise Reduction of Solar Spectra Observed by the 1-meter New Vacuum Solar Telescope

Yunfang **Cai**, Zhi Xu, Zhenggang Li, Yongyuan Xiang, Yuchao Chen, Yu Fu, Kaifan Ji
Solar Phys. 292:150 **2017**
https://arxiv.org/pdf/1709.09067.pdf
We present a precise and complete procedure for processing spectral data observed by the 1-meter New Vacuum Solar Telescope (NVST). The procedure is suitable for both the sit-and-stare and raster-scan spectra. In this work, the geometric distortions of the spectra are firstly corrected for subsequent processes. Then, considering the temporal changes and the remnants of spectral lines in the flat-field, the original flat-field matrix is split into four independent components for ensuring a high precision flat-fielding correction, consisting of the continuum gradient matrix, slit non-uniform matrix, CCD dust matrix, and interference fringe matrix. Subsequently, the spectral line drifts and intensity fluctuations of the science data are further corrected. After precise reduction with this procedure, the measuring accuracies of the Doppler velocities for different spectral lines and of the oscillation curves of the chromosphere and photosphere are measured. The results show that the highest measuring accuracy of the Doppler velocity is within 100 ms-1, which indicates that the characteristics of the photosphere and chromosphere can be studied co-spatially and co-temporally with the reduced spectra of NVST.

A semi-automated method to reveal the evolution of each sunspot group in a solar cycle

Hikmet **Çakmak**
Astrophysics and Space Science **2018**
https://arxiv.org/pdf/1811.12648.pdf
Sunspots are the most important indicator of the magnetic activity on the solar surface during a cycle. Every sunspot group is formed and shaped by the magnetic field of the Sun. Hence, the magnetic field intensity shows itself as the size of a sunspot group area on the surface. This shows that getting the development or evolution of sunspot groups over time means getting the change of magnetic field intensity during same interval. Here, to reveal the evolution of sunspot groups in a cycle, a method called Solar Cycle Analyzer Tool (SCAT) is presented. This method was developed as a part of Computer-Aided Measurements for Sunspots (CAMS) because the same subroutines and subprograms were used for calculations (Cakmak 2014). The developed software tracks sunspot groups every day and gives them the same group number. The confirmation is made by the user to prevent counting re-formations as a continuation of an old group in the same active region. With this method, the evolution of every sunspot group can be listed for each cycle year besides other cycle features like the daily and monthly sunspot relative numbers and distribution frequency of the sunspot group types. Since 2015, SCAT is being used to get data for the annual reports of Istanbul University Observatory.

Two Practical Methods for Coronal Intensity Determination

Hikmet **Çakmak**
Solar Physics December **2017**, 292:186
https://arxiv.org/pdf/1711.11374.pdf
https://link.springer.com/content/pdf/10.1007%2Fs11207-017-1217-x.pdf
Determining the relative brightness of the solar corona is one of the most critical stages in solar eclipse studies. For this purpose, images taken with different exposures and polarization angles in white-light observations are used. The composite image of each polarization angle is produced by combining the images of different exposures. With the help of the intensity calibration function of these images, the relative intensity of the corona can be calculated. The total brightness of the solar corona is calculated using Stokes parameters obtained from intensity values of three polarization angles. In this study, two methods are presented: the first is used to obtain the intensity calibration function of the photographic material using calibration images, and the second is used to calculate the combined intensity values of images taken with different polarization angles. **24 Oct 1995, 21 June 2001, 29 March 2006**

A New Method for Detecting Solar Atmospheric Gravity Waves

Daniele **Calchetti**, Stuart M. Jefferies, Bernhard Fleck, Francesco Berrilli, Dmitriy V. Shcherbik
Philisophical Transactions A **2020**
https://arxiv.org/pdf/2008.00210.pdf

Internal gravity waves have been observed in the Earth's atmosphere and oceans, on Mars and Jupiter, and in the Sun's atmosphere. Despite ample evidence for the existence of propagating gravity waves in the Sun's atmosphere, we still do not have a full understanding of their characteristics and overall role for the dynamics and energetics of the solar atmosphere. Here we present a new approach to study the propagation of gravity waves in the solar atmosphere. It is based on calculating the three-dimensional cross-correlation function between the vertical velocities measured at different heights. We apply this new method to a time series of co-spatial and co-temporal Doppler images obtained by SOHO/MDI and Hinode/SOT as well as to simulations of upward propagating gravity wave packets. We show some preliminary results and outline future developments.

Differential rotation and radiative equilibrium in the Sun: is the tachocline spreading?

Andrea **Caleo**, Steven Balbus, William Potter

Mon. Not. R. Astron. Soc. **2015**

It is well known that the combination of barotropic rotation and radiative equilibrium are mutually incompatible in stars. The Sun's internal rotation is far from barotropic, however, which allows at least the theoretical possibility that the Sun's thermal balance is one of radiative equilibrium in the region of the tachocline near the outer boundary of the radiative zone. We show here that (i) the constraint of radiative equilibrium leads to a straightforward ordinary differential equation for the Sun's rotation profile, and (ii) solutions of this equation can be found that, to within current levels of accuracy, closely resemble the rotation profile deduced from helioseismology. More generally, we calculate how large a baroclinic deviation from uniform rotation is required to maintain radiative equilibrium without meridional circulation throughout the bulk of the radiative zone. Very little deviation is required, well below detectability. The feasibility of radiative equilibrium for the tachocline suggests that the issue of a spreading boundary layer may be less severe than previously thought.

The KIS Science Data Centre.

Caligari, P., Aghaei, F., Beck, J. et al.

Sol Phys 299, 143 (**2024**).

https://doi.org/10.1007/s11207-024-02388-7

With the steady improvement of the observing capabilities and numerical simulations, an efficient data management of large data volumes has become mandatory. The Institute for Solar Physics (KIS) has developed the Science Data Centre (SDC), a data infrastructure to store, curate, and disseminate science-ready data from the German solar-observing facilities and other partner institutions. The SDC was also conceived to create and disseminate higher-level data products of added value like inversions from spectropolarimetric data. The SDC archive infrastructure consists of a back-end based on the Rucio science data-management and MongoDB systems and a front-end web interface that allows the user to search and discover data based on search parameters like instrument, date, wavelength range, and target. The SDC archive also provides data access via API and TAP services. The SDC currently offers access to 1299 science-ready datasets from the GRIS instrument at the GREGOR telescope (Tenerife) since 2014, a set of 610 spectra from the LARS at the Vacuum Solar Telescope (VTT, Tenerife) and 202 404 full-disc solar images from the Chromospheric Telescope (ChroTel). The SDC also offers to the community Milne–Eddington inversions of the GRIS spectropolarimetric archived data that can be downloaded as well as tools for data visualization and advanced analysis (e.g., GRISView tool). Many SDC activities have been carried out within the framework of large international data projects like the Horizon 2020 ASTERICS and ESCAPE EU-funded projects under the FAIR (Findable, Accessible, Interoperable, Reusable) principles. New and planned SDC activities include the ingestion of solar data from GREGOR context imaging instruments, flare observations from Ondřejov Observatory (Czech Republic), archiving and dissemination of in-house magnetohydrodynamic simulations, and creation of high-level data products using machine learning. The KIS Science Data Centre is a state-of-the-art data-management infrastructure that curates, archives, and provides access to ground-based science-ready spectropolarimetric and imaging solar data. SDC also provides advanced data visualization and analysis tools and invites data providers to publish their data to the solar and broader (astro)physics community via the SDC data archive.

On the Fragility of Alfvén waves in a Stratified Atmosphere

Paul S. **Cally**

MNRAS **2021**

https://arxiv.org/pdf/2111.13435.pdf

Complete asymptotic expansions are developed for slow, Alfvén and fast magnetohydrodynamic waves at the base of an isothermal three-dimensional (3D) plane stratified atmosphere. Together with existing convergent Frobenius series solutions about $z=\infty$, matchings are numerically calculated that illuminate the fates of slow and Alfvén waves injected from below. An Alfvén wave in a two-dimensional model is 2.5D in the sense that the wave propagates in the plane of the magnetic field but its polarization is normal to it in an ignorable horizontal direction, and the wave remains an Alfvén wave throughout. The rotation of the plane of wave propagation away from the vertical plane of the magnetic field pushes the plasma displacement vector away from horizontal, thereby coupling it to stratification.

It is shown that potent slow-Alfvén coupling occurs in such 3D models. It is found that about 50% of direction-averaged Alfvén wave flux generated in the low atmosphere at frequencies comparable to or greater than the acoustic cutoff can reach the top as Alfvén flux for small magnetic field inclinations θ, and this increases to 80% or more with increasing θ. On the other hand, direction-averaged slow waves can be 40% effective in converting to Alfvén waves at small inclination, but this reduces sharply with increasing θ and wave frequency. Together with previously explored fast-slow and fast-Alfvén couplings, this provides valuable insights into which injected transverse waves can reach the upper atmosphere as Alfvén waves, with implications for solar and stellar coronal heating and solar/stellar wind acceleration.

Alfvén Waves in the Structured Solar Corona

Paul S. **Cally**
MNRAS **2016**
https://arxiv.org/pdf/1612.02064v1.pdf
A simple model of a periodic ensemble of closely packed flux tubes sitting atop a vertically stratified layer reveals that an incident fast wave from below preferentially converts almost immediately to Alfv\'en waves in the flux tubes, with kink waves restricted to at most a very few Fourier modes. This suggests that observations of coronal kink modes in such structured systems may greatly underestimate the net wave energy flux being transported into and through the corona, much of which may reside in harder-to-observe Alfv\'en waves. The processes of mode conversion/resonant absorption and Alfv\'en phase mixing are implicated. It is suggested that the Sun's internal p-mode field -- the 5-minute oscillations -- may contribute substantially to the process by supplying incident fast waves in the chromosphere that scatter and mode-convert in the tube ensemble.

Observationally guided models for the solar dynamo and the role of the surface field **Review**

Robert **Cameron**, Manfred Schüssler
Space Science Reviews 219, Article number: 60 **2023**
https://arxiv.org/pdf/2305.02253.pdf
https://link.springer.com/content/pdf/10.1007/s11214-023-01004-7.pdf
Theoretical models for the solar dynamo range from simple low-dimensional ``toy models" to complex 3D-MHD simulations. Here we mainly discuss appproaches that are motivated and guided by solar (and stellar) observations. We give a brief overview of the evolution of solar dynamo models since 1950s, focussing upon the development of the Babcock-Leighton approach between its introduction in the 1960s and its revival in the 1990s after being long overshadowed by mean-field turbulent dynamo theory. We summarize observations and simple theoretical deliberations that demonstrate the crucial role of the surface fields in the dynamo process and and give quantitative analyses of the generation and loss of toroidal flux in the convection zone as well as of the production of poloidal field resulting from flux emergence at the surface. Furthermore, we discuss possible nonlinearities in the dynamo process suggested by observational results and present models for the long-term variability of solar activity motivated by observations of magnetically active stars and the inherent randomness of the dynamo process.

Loss of toroidal magnetic flux by emergence of bipolar magnetic regions

R. H. **Cameron**, M. Schuessler
A&A 636, A7 **2020**
https://arxiv.org/pdf/2002.05436.pdf
https://www.aanda.org/articles/aa/pdf/2020/04/aa37281-19.pdf
The polarity of the toroidal magnetic field in the solar convection zone periodically reverses in the course of the 11/22-year solar cycle. Among the various processes that contribute to the removal of `old-polarity' toroidal magnetic flux is the emergence of flux loops forming bipolar regions at the solar surface. We quantify the loss of subsurface net toroidal flux by this process. To this end, we determine the contribution of an individual emerging bipolar loop and show that it is unaffected by surface flux transport after emergence. Together with the linearity of the diffusion process this means that the total flux loss can be obtained by adding the contributions of all emerging bipolar magnetic regions. The resulting total loss rate of net toroidal flux amounts to 1.3 X 10^{15} Mx/s during activity maxima and 6.1 X 10^{14} Mx/s during activity minima, to which ephemeral regions contribute about 90% and 97%, respectively. This rate is consistent with the observationally inferred loss rate of toroidal flux into interplanetary space and corresponds to a decay time of the subsurface toroidal flux of about 12 years, also consistent with a simple estimate based on turbulent diffusivity. Consequently, toroidal flux loss by flux emergence is a relevant contribution to the budget of net toroidal flux in the solar convection zone. That the toroidal flux loss rate due to flux emergence is consistent with what is expected from turbulent diffusion, and that the corresponding decay time is similar to the length of the solar cycle are important constraints for understanding the solar cycle and the Sun's internal dynamics.

Three years of Sun-as-a-star radial-velocity observations on the approach to solar minimum

A. Collier **Cameron**, A. Mortier, D. Phillips, X. Dumusque, R. D. Haywood, N. Langellier, C. A. Watson, H. M. Cegla, J. Costes, D. Charbonneau, A. Coffinet, D. W. Latham, M. Lopez-Morales, L. Malavolta, J. Maldonado, G. Micela, T. Milbourne, E. Molinari, S. H. Saar, S. Thompson, N. Buchschacher, M. Cecconi, R. Cosentino, A. Ghedina, A. Glenday, M. Gonzalez C.-H. Li, M. Lodi, C. Lovis, F. Pepe, E. Poretti, K. Rice, D. Sasselov, A. Sozzetti, A. Szentgyorgyi, S. Udry, R. Walsworth

MNRAS Volume 487, Issue 1, Pages 1082–1100 **2019**

https://arxiv.org/pdf/1904.12186.pdf

sci-hub.se/10.1093/mnras/stz1215

The time-variable velocity fields of solar-type stars limit the precision of radial-velocity determinations of their planets' masses, obstructing detection of Earth twins. Since 2015 July we have been monitoring disc-integrated sunlight in daytime using a purpose-built solar telescope and fibre feed to the HARPS-N stellar radial-velocity spectrometer. We present and analyse the solar radial-velocity measurements and cross-correlation function (CCF) parameters obtained in the first 3 years of observation, interpreting them in the context of spatially-resolved solar observations. We describe a Bayesian mixture-model approach to automated data-quality monitoring. We provide dynamical and daily differential-extinction corrections to place the radial velocities in the heliocentric reference frame, and the CCF shape parameters in the sidereal frame. We achieve a photon-noise limited radial-velocity precision better than 0.43 m s−1 per 5-minute observation. The day-to-day precision is limited by zero-point calibration uncertainty with an RMS scatter of about 0.4 m s−1. We find significant signals from granulation and solar activity. Within a day, granulation noise dominates, with an amplitude of about 0.4 m s−1 and an autocorrelation half-life of 15 minutes. On longer timescales, activity dominates. Sunspot groups broaden the CCF as they cross the solar disc. Facular regions temporarily reduce the intrinsic asymmetry of the CCF. The radial-velocity increase that accompanies an active-region passage has a typical amplitude of 5 m s−1 and is correlated with the line asymmetry, but leads it by 3 days. Spectral line-shape variability thus shows promise as a proxy for recovering the true radial velocity.

Solar activity: intrinsic periodicities beyond 11 years

Robert **Cameron**, Manfred Schuessler

A&A 625, A28 **2019**

https://arxiv.org/pdf/1903.05398.pdf

https://www.aanda.org/articles/aa/pdf/2019/05/aa35290-19.pdf

Power spectra of solar activity based on historical records of sunspot numbers and on cosmogenic isotopes show peaks with enhanced power apart from the dominant 11-year solar cycle, such as the 90-year Gleissberg cycle or the 210-year de Vries cycle. In a previous paper we have shown that the overall shape of the power spectrum is well represented by the results of the generic normal form model for a noisy and weakly nonlinear limit cycle, with parameters all determined by observations. Using this model as a null case, we show here that all local peaks with enhanced power, apart from the 11-year band, are consistent with realisation noise. Even a 3σ peak is expected to occur with a probability of about 0.25 at least once among the 216 period bins resolved by the cosmogenic isotope data. This casts doubt upon interpretations of such peaks in terms of intrinsic periodicities of the solar dynamo process.

Observing and modeling the poloidal and toroidal fields of the solar dynamo

R. H. **Cameron**, T. L Duvall Jr., M. Schüssler, H. Schunker

A&A 609, A56 (**2018**)

https://arxiv.org/pdf/1710.07126.pdf

https://www.aanda.org/articles/aa/pdf/2018/01/aa31481-17.pdf

Context. The solar dynamo consists of a process that converts poloidal field to toroidal field followed by a process which creates new poloidal field from the toroidal field.

Aims. Our aim is to observe the poloidal and toroidal fields relevant to the global solar dynamo and see if their evolution is captured by a Babcock-Leighton dynamo.

Methods. We use synoptic maps of the surface radial field from the KPNSO/VT and SOLIS observatories to construct the poloidal field as a function of time and latitude, and Wilcox Solar Observatory and SOHO/MDI full disk images to infer the longitudinally averaged surface azimuthal field. We show that the latter is consistent with an estimate of that due to flux emergence and therefore closely related to the subsurface toroidal field.

Results. We present maps of the poloidal and toroidal magnetic field of the global solar dynamo. The longitude-averaged azimuthal field observed at the surface results from flux emergence. At high latitudes this component follows the radial component of the polar fields with a short time lag (1-3 years). The lag increases at lower latitudes. The observed evolution of the poloidal and toroidal magnetic fields is described by the (updated) Babcock-Leighton dynamo model.

The Global Solar Dynamo **Review**

R. H. **Cameron**, M. Dikpati, A. Brandenburg

Space Science Reviews **2017**, Volume 210, Issue 1–4, pp 367–395http://arxiv.org/pdf/1602.01754v1.pdf

A brief summary of the various observations and constraints that underlie solar dynamo research are presented. The arguments that indicate that the solar dynamo is an alpha-omega dynamo of the Babcock-Leighton type are then shortly reviewed. The main open questions that remain are concerned with the subsurface dynamics, including why sunspots emerge at preferred latitudes as seen in the familiar butterfly wings, why the cycle is about 11 years long, and why the sunspot groups emerge tilted with respect to the equator (Joy's law). Next, we turn to magnetic helicity, whose conservation property has been identified with the decline of large-scale magnetic fields found in direct numerical simulations at large magnetic Reynolds numbers. However, magnetic helicity fluxes through the solar surface can alleviate this problem and connect theory with observations, as will be discussed.

Understanding solar cycle variability

Robert **Cameron**, Manfred Schüssler

ApJ **843** 111 **2017**
https://arxiv.org/pdf/1705.10746.pdf

The level of solar magnetic activity, as exemplified by the number of sunspots and by energetic events in the corona, varies on a wide range of time scales. Most prominent is the 11-year solar cycle, which is significantly modulated on longer time scales. Drawing from dynamo theory together with empirical results of past solar activity and of similar phenomena on solar-like stars, we show that the variability of the solar cycle can be essentially understood in terms of a weakly nonlinear limit cycle affected by random noise. In contrast to ad-hoc `toy models' for the solar cycle, this leads to a generic normal-form model, whose parameters are all constrained by observations. The model reproduces the characteristics of the variable solar activity on time scales between decades and millennia, including the occurrence and statistics of extended periods of very low activity (grand minima). Comparison with results obtained with a Babcock-Leighton-type dynamo model confirms the validity of the normal-mode approach.

An update of Leighton's solar dynamo model

R. H. **Cameron**, M. Schuessler

A&A 599, A52 **2017**
https://arxiv.org/pdf/1611.09111v1.pdf

In 1969 Leighton developed a quasi-1D mathematical model of the solar dynamo, building upon the phenomenological scenario of Babcock(1961). Here we present a modification and extension of Leighton's model. Using the axisymmetric component of the magnetic field, we consider the radial field component at the solar surface and the radially integrated toroidal magnetic flux in the convection zone, both as functions of latitude. No assumptions are made with regard to the radial location of the toroidal flux. The model includes the effects of turbulent diffusion at the surface and in the convection zone, poleward meridional flow at the surface and an equatorward return flow affecting the toroidal flux, latitudinal differential rotation and the near-surface layer of radial rotational shear, downward convective pumping of magnetic flux in the shear layer, and flux emergence in the form of tilted bipolar magnetic regions. While the parameters relevant for the transport of the surface field are taken from observations, the model condenses the unknown properties of magnetic field and flow in the convection zone into a few free parameters (turbulent diffusivity, effective return flow, amplitude of the source term, and a parameter describing the effective radial shear). Comparison with the results of two-dimensional flux transport dynamo codes shows that the model captures the essential features of these simulations. We carry out a parameter study over the four-dimensional parameter space and identify the parameter ranges that provide solar-like solutions. Dipole parity is always preferred and solutions with periods around 22 years and a correct phase difference between flux emergence in low latitudes and the strength of the polar fields are found for a return flow speed around 2~m/s, turbulent diffusivity <80~km^2/s, and dynamo excitation not too far above the threshold (linear growth rate <0.1/yr).

The fate of alpha dynamos at large Rm

Alexandre **Cameron**, Alexandros Alexakis

2016
http://arxiv.org/pdf/1607.07294v1.pdf

At the heart of today's solar magnetic field evolution models lies the alpha dynamo description. In this work, we investigate the fate of alpha-dynamos as the magnetic Reynolds number Rm is increased. Using Floquet theory, we are able to precisely quantify mean field effects like the alpha and beta effect (i) by rigorously distinguishing dynamo modes that involve large scale components from the ones that only involve small scales, and by (ii) providing a way to investigate arbitrary large scale separations with minimal computational cost. We apply this framework to helical and non-helical flows as well as to random flows with short correlation time. Our results determine that the alpha-description is valid for Rm smaller than a critical value Rmc at which small scale dynamo instability starts. When Rm is above Rmc the dynamo ceases to follow the mean field description and the growth rate of the large scale modes becomes independent of the scale separation while the energy in the large scale modes is inversely proportional to the square of the scale separation. The results in this second regime do not depend on the presence of helicity. Thus alpha-type modeling for solar and stellar models needs to be reevaluated and new directions for mean field modeling are proposed.

The turbulent diffusion of toroidal magnetic flux as inferred from properties of the sunspot butterfly diagram

R.H. **Cameron**, M. Schuessler
A&A 591, A46 **2016**
http://arxiv.org/pdf/1604.07340v1.pdf
In order to match observed properties of the solar cycle, flux-transport dynamo models require the toroidal magnetic flux to be stored in a region of low magnetic diffusivity, typically located at or below the bottom of the convection zone.
We infer the turbulent magnetic diffusivity affecting the toroidal field on the basis of empirical data.
We consider the time evolution of mean latitude and width of the activity belts of solar cycles 12--23 and their dependence on cycle strength. We interpret the decline phase of the cycles as a diffusion process.
The activity level of a given cycle begins to decline when the centers of its equatorward propagating activity belts come within their width (at half maximum) from the equator. This happens earlier for stronger cycles because their activity belts are wider. From that moment on, the activity and the belt width decrease in the same manner for all cycles, independent of their maximum activity level. In terms of diffusive cancellation of opposite-polarity toroidal flux across the equator, we infer the turbulent diffusivity experienced by the toroidal field, wherever it is located, to be in the range 150--450~km2s−1. Strong diffusive latitudinal spreading of the toroidal flux underneath the activity belts can be inhibited by an inflow towards the toroidal field bands in the convection zone with a magnitude of several meters per second.
The inferred value of the turbulent magnetic diffusivity affecting the toroidal field agrees, to order of magnitude, with estimates based on mixing-length models for the solar convection zone. This is at variance with the requirement of flux-transport dynamo models. The inflows required to keep the toroidal field bands together before they approach the equator are similar to the inflows towards the activity belts observed with local helioseismology.

Solar cycle 25: another moderate cycle?

Robert H. **Cameron**, Jie Jiang, Manfred Schuessler
ApJL **823** L22 **2016**
http://arxiv.org/pdf/1604.05405v1.pdf
Surface flux transport simulations for the descending phase of cycle 24 using random sources (emerging bipolar magnetic regions) with empirically determined scatter of their properties provide a prediction of the axial dipole moment during the upcoming activity minimum together with a realistic uncertainty range. The expectation value for the dipole moment around 2020 (2.5±1.1G) is comparable to that observed at the end of cycle 23 (about 2G). The empirical correlation between the dipole moment during solar minimum and the strength of the subsequent cycle thus suggests that
cycle 25 will be of moderate amplitude, not much higher than that of the current cycle. However, the intrinsic uncertainty of such predictions resulting from the random scatter of the source properties is considerable and fundamentally limits the reliability with which such predictions can be made before activity minimum is reached.

The crucial role of surface magnetic fields for the solar dynamo

Robert **Cameron**, Manfred Schüssler
Science **2015**
http://arxiv.org/pdf/1503.08469v1.pdf
Sunspots and the plethora of other phenomena occuring in the course of the 11-year cycle of solar activity are a consequence of the emergence of magnetic flux at the solar surface. The observed orientations of bipolar sunspot groups imply that they originate from toroidal (azimuthally orientated) magnetic flux in the convective envelope of the Sun. We show that the net toroidal magnetic flux generated by differential rotation within a hemisphere of the convection zone is determined by the emerged magnetic flux at the solar surface and thus can be calculated from the

observed magnetic field distribution. The main source of the toroidal flux is the roughly dipolar surface magnetic field at the polar caps, which peaks around the minima of the activity cycle.

Physical causes of solar cycle amplitude variability

R. H. **Cameron**, J. Jiang, M. Schüssler and L. Gizon
JGR, Volume 119, Issue 2, pages 680–688, February **2014**
The level of solar activity varies from cycle to cycle. This variability is probably caused by a combination of nonlinear and random effects. Based on surface flux transport simulations, we show that the observed inflows into active regions and toward the activity belts provide an important nonlinearity in the framework of Babcock-Leighton model for the solar dynamo. Inclusion of these inflows also leads to a reproduction of the observed proportionality between the open heliospheric flux during activity minima and the maximum sunspot number of the following cycle. A substantial component of the random variability of the cycle strength is associated with the cross-equatorial flux plumes that occur when large, highly tilted sunspot groups emerge close to the equator. We show that the flux transported by these events is important for the amplitude of the polar fields and open flux during activity minima. The combined action of inflows and cross-equatorial flux plumes provides an explanation for the weakness of the polar fields at the end of solar cycle 23 (and hence for the relative weakness of solar cycle 24).

Solar-like to Antisolar Differential Rotation: A Geometric Interpretation

Maria E. **Camisassa**, Nicholas A. Featherstone
ApJ **2022**
https://arxiv.org/pdf/2208.05591
The solar convection zone rotates differentially, with its equatorial region rotating more rapidly than the polar regions. This form of differential rotation, also observed in many other low-mass stars, is understood to arise when Coriolis effects are stronger than those associated with buoyant driving of the convection. When buoyancy dominates, a so-called antisolar state of differential rotation results, characterized by rapidly-rotating poles and a slow equator. The transition between these two states has been shown to occur when the intensity of these two forces is roughly equal or, equivalently, when the convective Rossby number of the system is unity. Here we consider an alternative view of the transition that relates this phenomenon to convective structure and convective-zone depth. Using a series of 3-D rotating convection-zone simulations, we demonstrate that the solar/antisolar transition occurs when the columnar convective structures characteristic of rotating convection attain a diameter roughly equivalent to the shell depth. When the characteristic convective wavelength exceeds twice the shell depth, we find that the coherent convective structures necessary to sustain an equatorward Reynolds stress are lost, and an antisolar state results. We conclude by presenting a force-balance analysis that relates this geometric interpretation of the transition to the convective-Rossby-number criteria identified in previous studies.

An Introduction to Data Analysis in Asteroseismology **Review**

Tiago L. **Campante**
Lecture presented at the IVth Azores International Advanced School in Space Sciences on "Asteroseismology and Exoplanets: Listening to the Stars and Searching for New Worlds" (arXiv:1709.00645), which took place in Horta, Azores Islands, Portugal in July 2016 **(2017)**
https://arxiv.org/pdf/1711.01959.pdf
A practical guide is presented to some of the main data analysis concepts and techniques employed contemporarily in the asteroseismic study of stars exhibiting solar-like oscillations. The subjects of digital signal processing and spectral analysis are introduced first. These concern the acquisition of continuous physical signals to be subsequently digitally analyzed. A number of specific concepts and techniques relevant to asteroseismology are then presented as we follow the typical workflow of the data analysis process, namely, the extraction of global asteroseismic parameters and individual mode parameters (also known as peak-bagging) from the oscillation spectrum.

DKIST unveils the serpentine topology of quiet Sun magnetism in the photosphere

Ryan J. **Campbell**, P H. Keys, M. Mathioudakis, F. Woeger, T. A. Schad, A. Tritschler, A. G. de Wijn . H. N. Smitha, C. A. Beck, D J. Christian, D. B. Jess, R. Erdelyi
ApJL **2023**
https://arxiv.org/pdf/2309.05836.pdf
We present the first quiet Sun spectropolarimetric observations obtained with the Visible SpectroPolarimeter (ViSP) at the 4−m Daniel K. Inouye Solar Telescope (DKIST). We recorded observations in a wavelength range that includes the magnetically sensitive Fe I 6301.5/6302.5 Å doublet. With an estimated spatial resolution of 0.08", this represents the highest spatial resolution full-vector spectropolarimetric observations ever obtained of the quiet Sun.

We identified 53 small-scale magnetic elements, including 47 magnetic loops and 4 unipolar magnetic patches, with linear and circular polarisation detected in all of them. Of particular interest is a magnetic element in which the polarity of the magnetic vector appears to change three times in only 400 km and which has linear polarisation signals throughout. We find complex Stokes V profiles at the polarity inversion lines of magnetic loops and discover degenerate solutions, as we are unable to conclusively determine whether these arise due to gradients in the atmospheric parameters or smearing of opposite polarity signals. We analyse a granule which notably has linear and circular polarisation signals throughout, providing an opportunity to explore its magnetic properties. On this small scale we see the magnetic field strength range from 25 G at the granular boundary to 2 kG in the intergranular lane (IGL), and sanity check the values with the weak and strong field approximations. A value of 2 kG in the IGL is among the highest measurements ever recorded for the internetwork. **26 May 2022**

Constraining the magnetic vector in the quiet solar photosphere and the impact of instrumental degradation

R. J. **Campbell**, S. Shelyag, C. Quintero Noda, M. Mathioudakis, P. H. Keys, A. Reid
A&A 654, A11 **2021**
https://arxiv.org/pdf/2107.01519.pdf
https://www.aanda.org/articles/aa/pdf/2021/10/aa41421-21.pdf
https://doi.org/10.1051/0004-6361/202141421
With the advent of next generation high resolution telescopes, our understanding of how the magnetic field is organized in the internetwork photosphere is likely to advance.We aim to evaluate the extent to which we can retrieve information about the magnetic vector in the internetwork (IN) photosphere using inversions. We use snapshots produced from high resolution 3D magnetohydrodynamic (MHD) simulations and employ the Stokes Inversions based on Response functions (SIR) code to produce synthetic observables in the near infrared spectral window observed by the GREGOR Infrared Spectrograph (GRIS), which contains the highly magnetically sensitive photospheric Fe I line pair at 15648.52 A and 15652.87 A. We perform nearly 14 million inversions to test how well the true MHD atmospheric parameters can be constrained. Finally, we degrade the synthetic Stokes vectors spectrally and spatially to GREGOR resolutions and examine how this influences observations, considering the impact of stray light, spatial resolution and signal-to-noise (S-to-N). We find the depth-averaged parameters can be recovered by the inversions of the undegraded profiles, and by adding gradients to magnetic field strength, inclination and line of sight velocity we show an improvement in the chi squared value is achieved. We evaluate the extent to which we can constrain these parameters at various optical depths, with the kinematic and thermodynamic parameters sensitive deeper in the atmosphere than the magnetic parameters. We find the S-to-N and spatial resolution play a significant role in determining how the atmosphere appears and the magnetic and kinematic parameters are invariant upon inclusion of unpolarized stray light. We studied a linear polarization feature which resembles those recently observed by GRIS, appearing as loop-like structures with similar magnetic flux density.

Temporal evolution of small-scale internetwork magnetic fields in the solar photosphere

Ryan J. **Campbell**, Mihalis Mathioudakis, Manuel Collados, Peter H. Keys, Andrés Asensio Ramos, Chris J. Nelson, David Kuridze, Aaron Reid
A&A 647, A182 **2021**
https://arxiv.org/pdf/2102.00942.pdf
https://doi.org/10.1051/0004-6361/202040028
https://www.aanda.org/articles/aa/pdf/2021/03/aa40028-20.pdf
While the longitudinal field that dominates photospheric network regions has been studied extensively, small scale transverse fields have recently been found to be ubiquitous in the quiet internetwork photosphere. Few observations have captured how this field evolves. We aim to statistically characterise the magnetic properties and observe the temporal evolution of small scale magnetic features. We present two high spatial/temporal resolution observations revealing the dynamics of two disk centre internetwork regions taken by the new GRIS/IFU (GREGOR Infrared Spectrograph Integral Field Unit) with the highly magnetically sensitive Fe I line pair at 15648.52 Å and 15652.87 Å. With the SIR code, we consider two inversion schemes: scheme 1 (S1), where a magnetic atmosphere is embedded in a field free medium, and scheme 2 (S2), with two magnetic models and a fixed stray light component. S1 inversions returned a median magnetic field strength of 200 and 240 G for the two datasets, respectively. We consider the median transverse (horizontal) component, among pixels with Stokes Q or U, and the median unsigned longitudinal (vertical) component, among pixels with Stokes V, above a noise threshold. We determined the former to be 263 G and 267 G, and the latter to be 131 G and 145 G, for the two datasets, respectively. We present three regions of interest (ROIs), tracking the dynamics of small scale magnetic features. We apply S1 and S2 inversions to specific profiles, and find S2 produces better approximations when there is evidence of mixed polarities. We find patches of linear polarization with magnetic flux density between 130 and 150 G, appearing preferentially at granule/intergranular lane (IGL) boundaries. The weak hG magnetic field appears to be organised in terms of complex loop structures, with transverse fields often flanked by opposite polarity longitudinal fields. **5-6 May 2019**
Erratum A&A 652, C2 (**2021**)

https://www.aanda.org/articles/aa/pdf/2021/08/aa40028e-20.pdf
https://doi.org/10.1051/0004-6361/202040028e

Solar cycle variation in radar meteor rates

M D **Campbell-Brown**

Monthly Notices of the Royal Astronomical Society, Volume 485, Issue 3, May **2019**, Pages 4446–4453
https://doi.org/10.1093/mnras/stz697

16 yr of meteor radar data from the Canadian Meteor Orbit Radar (CMOR) were used to investigate the link between observed meteor rates and both solar and geomagnetic activity. Meteor rates were corrected for transmitter power and receiver noise, and seasonal effects were removed. A strong negative correlation is seen between solar activity, as measured with the 10.7 cm flux, and observed meteor rates. This lends support to the idea that heating in the atmosphere at times of elevated solar activity changes the scale height and therefore the length and maximum brightness of meteors; a larger scale height near solar maximum leads to longer, fainter meteors and therefore lower rates. A weaker negative correlation was observed with geomagnetic activity as measured with the K index; this correlation was still present when solar activity effects were removed. Meteor activity at solar maximum is as much as 30 per cent lower than at solar minimum, strictly due to observing biases; geomagnetic activity usually affects meteor rates by less than 10 per cent.

Twisted Magnetic Knots and Links

Simon **Candelaresi**, Celine Beck

2023

https://arxiv.org/pdf/2311.13660.pdf

For magnetic knots and links in plasmas we introduce an internal twist and study their dynamical behavior in numerical simulations. We use a set of helical and non-helical configurations and add an internal twist that cancels the helicity of the helical configurations or makes a non-helical system helical. These fields are then left to relax in a magnetohydrodynamic environment. In line with previous works we confirm the importance of magnetic helicity in field relaxation. However, an internal twist, as could be observed in coronal magnetic loops, does not just add or subtract helicity, but also introduces an alignment of the magnetic field with the electric current, which is the source term for helicity. This source term is strong enough to lead to a significant change of magnetic helicity, which for some cases leads to a loss of the stabilizing properties expressed in the realizability condition. Even a relatively weak internal twist in these magnetic fields leads to a strong enough source term for magnetic helicity that for various cases even in a low diffusion environment we observe an inversion in sign of magnetic helicity within time scales much shorter than the diffusion time. We conclude that in solar and stellar fields an internal twist does not automatically result in a structurally stable configuration and that the alignment of the magnetic field with the electric current must be taken into account.

Estimating the rate of field line braiding in the solar corona by photospheric flows

Simon **Candelaresi**, David Pontin, Anthony Yeates, Paul Bushby, Gunnar Hornig

ApJ **864** 157 **2018**

http://iopscience.iop.org/article/10.3847/1538-4357/aad8bc/pdf

In this paper we seek to understand the timescale on which the photospheric motions on the Sun braid coronal magnetic field lines. This is a crucial ingredient for determining the viability of the braiding mechanism for explaining the high temperatures observed in the corona. We study the topological complexity induced in the coronal magnetic field, primarily using plasma motions extracted from magneto-convection simulations. This topological complexity is quantified using the field line winding, finite time topological entropy and passive scalar mixing. With these measures we contrast mixing efficiencies of the magneto-convection simulation, a benchmark flow known as a ``blinking vortex', and finally photospheric flows inferred from sequences of observed magnetograms using local correlation tracking. While the highly resolved magneto-convection simulations induce a strong degree of field line winding and finite time topological entropy, the values obtained from the observations from the plage region are around an order of magnitude smaller. This behavior is carried over to the finite time topological entropy. Nevertheless, the results suggest that the photospheric motions induce complex tangling of the coronal field on a timescale of hours**. 2006 December 12**

Effects of Fieldline Topology on Energy Propagation in the Corona

Simon **Candelaresi**, David Ian Pontin, Gunnar Hornig

ApJ 832 150 **2016**

https://arxiv.org/pdf/1611.03325v1.pdf

We study the effect of photospheric footpoint motions on magnetic field structures containing magnetic nulls. The footpoint motions are prescribed on the photospheric boundary as a velocity field which entangles the magnetic field. We investigate the propagation of the injected energy, the conversion of energy, emergence of current layers and other consequences of the non-trivial magnetic field topology in this situation. These boundary motions lead initially to an increase in magnetic and kinetic energy. Following this, the energy input from the photosphere is partially dissipated and partially transported out of the domain through the Poynting flux. The presence of separatrix layers and magnetic null-points fundamentally alters the propagation behavior of disturbances from the photosphere into the corona. Depending on the field line topology close to the photosphere, the energy is either trapped or free to propagate into the corona.

Magnetic Field Relaxation and Current Sheets in an Ideal Plasma

S. **Candelaresi**, D. I. Pontin, and G. Hornig
2015 ApJ 808 134.
We investigate the existence of magnetohydrostatic equilibria for topologically complex magnetic fields. The approach employed is to perform ideal numerical relaxation experiments. We use a newly developed Lagrangian relaxation scheme that exactly preserves the magnetic field topology during the relaxation. Our configurations include both twisted and sheared fields, of which some fall into the category for which Parker predicted no force-free equilibrium. The first class of field considered contains no magnetic null points, and field lines connect between two perfectly conducting plates. In these cases, we observe only resolved current layers of finite thickness. In further numerical experiments, we confirm that magnetic null points are loci of singular currents.

Superflare occurrence and energies on G-, K- and M-type dwarfs

Candelaresi, S., Hillier, A., Maehara, H., Brandenburg, A., & Shibata, K.
Astrophys. J. 792, 67 (**2014**)
http://arxiv.org/pdf/1405.1453v3.pdf
Kepler data from G-, K- and M-type stars are used to study conditions that lead to superflares with energies above 1034 {\rm erg}. From the 117,661 stars included, 380 show superflares with a total of 1690 such events. We study whether parameters, like effective temperature or the rotation rate, have any effect on the superflare occurrence rate or energy. With increasing effective temperature we observe a decrease in the superflare rate, which is analogous to the previous findings of a decrease in dynamo activity with increasing effective temperature. For slowly rotating stars, we find a quadratic increase of the mean occurrence rate with the rotation rate up to a critical point, after which the rate decreases linearly. Motivated by standard dynamo theory, we study the behavior of the relative starspot coverage, approximated as the relative brightness variation. For faster rotating stars, an increased fraction of stars shows higher spot coverage, which leads to higher superflare rates. A turbulent dynamo is used to study the dependence of the Ohmic dissipation as a proxy of the flare energy on the differential rotation or shear rate. The resulting statistics of the dissipation energy as a function of dynamo number is similar to the observed flare statistics as a function of the inverse Rossby number and shows similarly strong fluctuations. This supports the idea that superflares might well be possible for solar-type G stars.

It Takes a Village **Memoirs**

Richard C. **Canfield**
Solar Physics volume 297, Article number: 94 (**2022**)
https://link.springer.com/content/pdf/10.1007/s11207-022-02025-1.pdf
My parents taught me the value of a good education. My studies at the state universities of Michigan and Colorado and postgraduate studies at the University of Utrecht built on an interest in astronomy that dated back to high school. These institutions enabled me to have a rewarding fifty-year career focused on the physics of the Sun. My work combined research and education at the High Altitude Observatory, the University of Utrecht, the Sacramento Peak Observatory, the University of California San Diego, the University of Hawaii, and Montana State University. My professional interests ranged from spectroscopic diagnostics and radiative transfer, especially of the flaring solar chromosphere, to the helicity of magnetic fields of active regions in the chromosphere, corona, and interplanetary medium, part of what is now called heliophysics and space weather. I am honored to have been recognized for my efforts as a scientific leader, mentor, and teacher. I am lucky to have lived at a time when access to space led the field of solar physics to grow dramatically, including global studies of solar activity, the heliosphere, and space weather.

Extreme Space Weather: Impacts on Engineered Systems and infrastructure **Review** (for UK)

Cannon, P. S. et al.
Royal Academy of Engineering, **2013**.

http://onlinelibrary.wiley.com/doi/10.1002/swe.20032/pdf
http://www.raeng.org.uk/news/publications/list/reports/Space_Weather_Full_Report_Final.PDF

Extreme Space Weather—A Report Published by the UK Royal Academy of Engineering

Paul S. **Cannon**
Space Weather, 11, 138–139, **2013**
http://onlinelibrary.wiley.com/doi/10.1002/swe.20032/pdf
Кракое изложение.

An Improved Prediction of Solar Cycles 25 and 26 Using the Informer Model: Gnevyshev Peaks and North–South Asymmetry

Jie **Cao**1, Tingting Xu1, Linhua Deng1, Xueliang Zhou1, Shangxi Li1, Yuxia Liu1, Wenhua Wang1, and Weihong Zhou1,2
2024 ApJ 969 120
https://iopscience.iop.org/article/10.3847/1538-4357/ad4551/pdf
Forecasting the amplitude and timing of the sunspot cycle is highly important for solar physics and space weather applications, but high-precision prediction of solar magnetic activity has remained an outstanding challenge. The Informer model, as the most advanced deep learning technique, is an ideal approach for predicting solar activity cycle. Using the whole-disk sunspot numbers (SSNs) between 1749 and 2023 and the hemispheric SSNs between 1992 and 2023, the amplitudes and timings of Solar Cycles 25 and 26 are predicted by the Informer model. The main results are the following: (1) the activity levels of Solar Cycles 25 and 26 continue being weak-moderate cycles with their strengths stronger than Solar Cycle 24, implying that the long-term solar variability is significantly modulated in length and magnitude by the Gleissberg century cycle; (2) the Gnevyshev peaks of Solar Cycles 25 and 26 are clearly observed with a higher value in the second peak, suggesting that the numbers of the large sunspot groups are greater compared to the small sunspot groups in these two cycles; and (3) during Solar Cycle 25, the activity level in the southern hemisphere is predicted to be stronger than that in the northern one, revealing significant asymmetry and asynchronization between the two hemispheres. Our analysis results show that solar cycle predictions can be made more accurate if performed separately for each hemisphere. Furthermore, Solar Cycles 25 and 26 are likely to be weak-moderate cycles, in agreement with the precursor-based and model-based prediction methods.

The impact of composition choices on solar evolution: age, helio- and asteroseismology, and neutrinos

Diogo **Capelo**, Ilídio Lopes
Monthly Notices of the Royal Astronomical Society, 498, 2 (**2020**), 1992-2000
https://arxiv.org/ftp/arxiv/papers/2010/2010.01686.pdf
The Sun is the most studied and well-known star, and as such, solar fundamental parameters are often used to bridge gaps in the knowledge of other stars, when these are required for modelling. However, the two most powerful and precise independent methodologies currently available to infer the internal solar structure are in disagreement. We aim to show the potential impact of composition choices in the overall evolution of a star, using the Sun as an example. To this effect, we create two Standard Solar Models and a comparison model using different combinations of metallicity and relative element abundances and compare evolutionary, helioseismic, and neutrino-related properties for each. We report differences in age for models calibrated to the same point in the HR diagram, in the red giant branch, of more than 1 Gyr, and found that the current precision level of asteroseismic measurements is enough to differentiate these models, which would exhibit differences in priod spacing of 1.30-2.58 per cent. Additionally, we show that the measurement of neutrino fluxes from the carbon-nitrogen-oxygen cycle with a precision of around 17 per cent, which could be achieved by the next generation of solar neutrino experiments, could help resolve the stellar abundance problem.

Is there a black hole in the center of the Sun?

Matthew E. **Caplan**, Earl P. Bellinger, Andrew D. Santarelli
Ap&SS **2023**
https://arxiv.org/pdf/2312.07647.pdf
There is probably not a black hole in the center of the sun. Despite this detail, our goal in this work to convince the reader that this question is interesting and that work studying stars with central black holes is well motivated. If primordial black holes exist then they may exist in sufficiently large numbers to explain the dark matter in the universe. While primordial black holes may form at almost any mass, the asteroid-mass window between 10−16−10−10 M⊙ remains a viable dark matter candidate and these black holes could be captured by stars upon formation. Such a star, partially powered by accretion luminosity from a microscopic black hole in its core, has

been called a `Hawking star.' Stellar evolution of Hawking stars is highly nontrivial and requires detailed stellar evolution models, which were developed in our recent work. We present here full evolutionary models of solar mass Hawking stars using two accretion schemes: one with a constant radiative efficiency, and one that is new in this work that uses an adaptive radiative efficiency to model the effects of photon trapping.

Observational indications of magneto-optical effects in the scattering polarization wings of the Ca I 4227 Å line

E. **Capozzi**, E. Alsina Ballester, L. Belluzzi, M. Bianda, S. K. Dhara, R. Ramelli
A&A 641, A63 **2020**
https://arxiv.org/pdf/2006.13653
https://doi.org/10.1051/0004-6361/202038455
Several strong resonance lines, such as H I Ly-α, Mg II k, Ca II K, Ca I 4227 Å\, which are characterized by deep and broad absorption profiles in the solar intensity spectrum, show conspicuous linear scattering polarization signals when observed in quiet regions close to the solar limb. Such signals show a characteristic triplet-peak structure, with a sharp peak in the line core and extended wing lobes. The line core peak is sensitive to the presence of magnetic fields through the Hanle effect, which however is known not to operate in the line wings. Recent theoretical studies indicate that, contrary to what was previously believed, the wing linear polarization signals are also sensitive to the magnetic field through magneto-optical effects (MO). We search for observational indications of this recently discovered physical mechanism in the scattering polarization wings of the Ca I 4227 Å line. We performed a series of spectropolarimetric observations of this line using the Zurich IMaging POLarimeter (ZIMPOL) camera at the Gregory-Coudé telescope of IRSOL (Switzerland) and at the GREGOR telescope in Tenerife (Spain). Spatial variations of the total linear polarization degree and of the linear polarization angle are clearly appreciable in the wings of the observed line. We provide a detailed discussion of our observational results, showing that the detected variations always take place in regions where longitudinal magnetic fields are present, thus supporting the theoretical prediction that they are produced by MO effects.

DUNE as the Next-Generation Solar Neutrino Experiment

Francesco **Capozzi**, Shirley Weishi Li, Guanying Zhu, John F. Beacom
2018
https://arxiv.org/pdf/1808.08232.pdf
We show that the Deep Underground Neutrino Experiment (DUNE) has the potential to deliver world-leading results in solar neutrinos. Significant but realistic new efforts would be required. With an exposure of 100 kton-year, DUNE could detect ≳105 signal events above 5 MeV. Separate precision measurements of neutrino-mixing parameters and the 8B flux could be made using two detection channels (νe+40Ar and νe,μ,τ+e−) and the day-night effect (>10σ). New particle physics may be revealed through the comparison of solar neutrinos (with matter effects) and reactor neutrinos (without), which is discrepant by ∼2σ (and could become 5.6σ). New astrophysics may be revealed through the most precise measurement of the 8B flux (to 2.5%) and the first detection of the hep flux (to 11%). DUNE is required: No other experiment, even proposed, has been shown capable of fully realizing these discovery opportunities.

Effects of the chromospheric Lyα line profile shape on the determination of the solar wind H I outflow velocity using the Doppler dimming technique

G. E. **Capuano**1, S. Dolei2, D. Spadaro2, S. L. Guglielmino1,2, P. Romano2, R. Ventura2, V. Andretta4, A. Bemporad3, C. Sasso4, R. Susino3, V. Da Deppo5, F. Frassetto5, S. M. Giordano3, F. Landini3, G. Nicolini3, M. Pancrazzi3, M. Romoli6 and L. Zangrilli3
A&A 652, A85 (**2021**)
https://arxiv.org/pdf/2108.05957.pdfhttps://doi.org/10.1051/0004-6361/202039821
https://www.aanda.org/articles/aa/pdf/2021/08/aa39821-20.pdf
Context. The determination of solar wind H I outflow velocity is fundamental to shedding light on the mechanisms of wind acceleration occurring in the corona. Moreover, it has implications in various astrophysical contexts, such as in the heliosphere and in cometary and planetary atmospheres.
Aims. We aim to study the effects of the chromospheric Lyα line profile shape on the determination of the outflow speed of coronal H I atoms via the Doppler dimming technique. This is of particular interest in view of the upcoming measurements of the Metis coronagraph aboard the Solar Orbiter mission.
Methods. The Doppler dimming technique exploits the decrease of coronal Lyα radiation in regions where H I atoms flow out in the solar wind. Starting from UV observations of the coronal Lyα line from the Solar and Heliospheric Observatory (SOHO), aboard the UltraViolet Coronagraph Spectrometer, and simultaneous measurements of coronal electron densities from pB coronagraphic observations, we explored the effect of the profile of the pumping chromospheric Lyα line. We used measurements from the Solar UV Measurement of Emitted Radiation, aboard SOHO, the Ultraviolet Spectrometer and Polarimeter, aboard the Solar Maximum Mission, and the Laboratoire de

Physique Stellaire et Planetaire, aboard the Eight Orbiting Solar Observatory, both from representative on-disc regions, such as coronal holes and quiet Sun and active regions, and as a function of time during the solar activity cycle. In particular, we considered the effect of four chromospheric line parameters: line width, reversal depth, asymmetry, and distance of the peaks.
Results. We find that the range of variability of the four line parameters is of about 50% for the width, 69% for the reversal depth, and 35% and 50% for the asymmetry and distance of the peaks, respectively. We then find that the variability of the pumping Lyα profile affects the estimates of the coronal H I velocity by about 9−12%. This uncertainty is smaller than the uncertainties due to variations of other physical quantities, such as electron density, electron temperature, H I temperature, and integrated chromospheric Lyα radiance.
Conclusions. Our work suggests that the observed variations in the chromospheric Lyα line profile parameters along a cycle and in specific regions negligibly affect the determination of the solar wind speed of H I atoms. Due to this weak dependence, a unique shape of the Lyα profile over the solar disc that is constant in time can be adopted to obtain the values of the solar wind H I outflow velocity. Moreover, the use of an empirical analytical chromospheric profile of the Lyα, assumed uniform over the solar disc and constant in time, is justifiable in order to obtain a good estimate of the coronal wind H I outflow velocity using coronagraphic UV images.

ACE SWICS observations of solar cycle variations of the solar wind

A. **Cardenas-O'Toole**, E. Landi
ApJ **2022**
https://arxiv.org/pdf/2201.05535.pdf
In the present work we utilize ACE/SWICS in-situ measurements of the properties of the solar wind outside ICMEs in order to determine whether, and to what extent are the solar wind properties affected by the solar cycle. We focus on proton temperatures and densities, ion temperatures and differential speeds, charge state distributions and both relative and absolute elemental abundances. We carry out this work dividing the wind in velocity bins to investigate how winds at different speeds react to the solar cycle. We also repeat this study, when possible, to the subset of SWICS measurements less affected by Coulomb collisions. We find that with the only exception of differential speeds (for which we do not have enough measurements) all wind properties change as a function of the solar cycle. Our results point towards a scenario where both the slow and fast solar wind are accelerated by waves, but originate from different sources (open/closed magnetic structures for the fast/slow wind, respectively) whose relative contribution changes along the solar cycle. We also find that the signatures of heating and acceleration on one side, and of the FIP effect on the other, indicate that wave-based plasma heating, acceleration and fractionation remain active throughout the solar cycle, but decrease their effectiveness in all winds, although the slow wind is much affected than the fast one.

Capacity Building: A Tool for Advancing Space Weather Science

M. G. **Cardinal**, A. Yoshikawa, H. Kawano, H. Liu, M. Watanabe, S. Abe, T. Uozumi, G. Maeda, T. Hada, and K. Yumoto
Space Weather Quarterly Volume 12, Issue 1, Article first published online: 30 MAR **2015**
http://onlinelibrary.wiley.com/doi/10.1002/SWQv12i001/pdf

Solar Irradiance Variability Monitor for the Galileo Solar Space Telescope Mission: Concept and Challenges

Franciele **Carlesso**1*, Jenny Marcela Rodríguez Gómez2,3, Adriany Rodrigues Barbosa1, Luis Eduardo Antunes Vieira 1,4 and Alisson Dal Lago1
Front. Phys. V.10 :869738. **2022**
https://www.frontiersin.org/articles/10.3389/fphy.2022.869738/pdf
https://doi.org/10.3389/fphy.2022.869738
Long and reliable total solar irradiance (TSI) time series is one of the essential parameters for understanding solar contributions to climate change. The minor fluctuations of TSI in long timescales could impact the energy balance. Despite the improvement of accurate measurements provided by the instruments, at the time, long-term TSI variability and its effects had not been established. The space-borne radiometer era provided observations in short timescales from minutes to years. Therefore, this study presents an overview of irradiance observations, highlighting the importance of following its variability in different time scales. In this context, the Galileo Solar Space Telescope that has been developed by the Institute for Space Research (INPE), Brazil, includes the Irradiance Monitor Module with a radiometer cavity like the classical design and a next-generation compact radiometer.

Formation and morphology of anomalous solar circular polarization

Edgar S. **Carlin**

A&A 627, A47 **2019**
https://arxiv.org/pdf/1905.08672.pdf
The morphology of spectral line polarization is the most valuable observable to investigate the magnetic and dynamic solar atmosphere. However, in order to develop solar diagnosis, it is fundamental to understand the different kinds of anomalous solar signals that have been routinely found in linear and circular polarization (LP,CP). The goal of this paper has been to explain and characterize the morphology of solar CP signals by understanding the combined effect of magnetic fields, velocity gradients, and atomic orientation in general NLTE regime. To that aim, an analytical two-layer model of the polarized radiative transfer equation is developed and used to solve the NLTE problem with atomic polarization in a semi-parametric way. The formation of polarization is thus insightfully described with certain precision without neither resorting in MHD models nor sacrifying key physical ingredients. The potential of the model for reproducing solar anomalous CP is shown with detailed calculations. The essential physical behavior of dichroism and atomic orientation is described, introducing the concepts of dichroic inversion, neutral and reinforcing medium, critic intensity spectrum, and critic source function. It is shown that the zero-crossings of the CP spectrum are useful to classify its morphology and understand its formation. This led to identify and explain the morphology of the seven most characteristics CP signals that a single (depth-resolved) scattering layer can produce. Futhermore, it is found that a minimal number of two magnetic layers along the LOS is required to fully explain anomalous solar CP signals, and that the morphology and polarity of Stokes V depends on magnetic, radiative and atomic polarities. Some implications of these results are presented through a preliminar modeling of anomalous CP signals in the Na I D and Fe I 1564.8 nm lines.

Spatio-temporal evolution of Hanle and Zeeman synthetic polarization in a chromospheric spectral line

E.S. **Carlin**, M. Bianda
ApJ **2017**
https://arxiv.org/pdf/1706.02381.pdf
Due to the quick evolution of the solar chromosphere, its magnetic field cannot be inferred reliably without accounting for the temporal variations of its polarized light. This has been broadly overlooked in the modelling and interpretation of the polarization due to technical problems (e.g., lack of temporal resolution or of time-dependent MHD solar models) and/or because many polarization measurements can apparently be explained without dynamics. Here, we show that the temporal evolution is critic for explaining the spectral-line scattering polarization because of its sensitivity to rapidly-varying physical quantities and the possibility of signal cancellations and attenuation during extended time integration. For studying the combined effect of time-varying magnetic fields and kinematics, we solved the 1.5D NLTE problem of the second kind in time-dependent 3D R-MHD solar models and we synthesized the Hanle and Zeeman polarization in forward scattering for the chromospheric {\lambda}4227 line. We find that the quiet-sun polarization amplitudes depend on the periodicity and spectral coherence of the signal enhacements produced by kinematics, but that substantially larger linear polarization signals should exist all over the solar disk for short integration times. The spectral morphology of the polarization is discussed as a combination of Hanle, Zeeman, dynamic effects and partial redistribution. We give physical references for observations by degrading and characterizing our slit time-series in different spatio-temporal resolutions. The implications of our results for the interpretation of the second solar spectrum and for the investigation of the solar atmospheric heatings are discussed.

THE KEY ROLE OF SOLAR DYNAMICS IN THE CHROMOSPHERIC HANLE POLARIZATION

E. S. **Carlin** and M. Bianda
2016 ApJL 831 L5
https://arxiv.org/pdf/1610.09860v1.pdf
The quantum theory of polarized light allows one to model scattering in the solar atmosphere for inferring its properties. This powerful approach has revealed two key long-standing problems in solar physics: the puzzling dilemmas between theory and observations in several anomalously polarized spectral lines and the need for inferring the ubiquitous weak chromospheric magnetic fields, which requires discriminating the Hanle effect in dynamic optically thick plasmas. However, the ever-present dynamics, i.e., the temporal evolution of heatings and macroscopic motions, has been widely disregarded when modeling and interpreting the scattering polarization. This has hindered a consistent theoretical solution to the puzzle while falsifying the Hanle diagnosis. Here, we show that the dynamical evolution is a keystone for solving both problems because its systematic impact allows an explanation of the observations from "anomalous" instantaneous polarization signals. Evolution accounted for, we reproduce amplitudes and (spectral and spatial) shapes of the Ca i 4227 Å polarization at solar disk center, identifying a restrictive arrangement of magnetic fields, kinematics, heatings, and spatio-temporal resolution. We find that the joint action of dynamics, Hanle effect, and low temporal resolutions mimics Zeeman linear polarization profiles, the true weak-field Zeeman signals being negligible. Our results allow reinterpretation of many polarization signals of the solar spectra and support time-dependent scattering polarization as a powerful tool for deciphering the spatio-temporal distribution of chromospheric heatings and fields. This approach may be a key aid in developing the Hanle diagnosis for the solar atmosphere.

Chromospheric diagnosis with forward scattering polarization

E.S. **Carlin**

Proceedings of IAU symposium 305 **2015**

https://arxiv.org/pdf/1610.09897v1.pdf

Is it physically feasible to perform chromospheric diagnosis using spatial maps of scattering polarization at the solar disk center? To investigate it we synthesized polarization maps (in 8542 Angstroms) resulting from MHD solar models and NLTE radiative transfer calculations that consider Hanle effect and vertical macroscopic motions. After explaining the physical con- text of forward scattering and presenting our results, we arrive at the definition of Hanle polarity inversion lines. We show how such features can give support for a clearer chromospheric diagnosis in which the magnetic and dynamic effects in the scattering polarization could be disentangled.

Chromospheric diagnosis with Ca II lines: forward modeling in forward scattering (I)

E.S. **Carlin**, A Asensio Ramos

ApJ **801** 16 **2015**

http://arxiv.org/pdf/1412.5386v1.pdf

This paper shows the first synthetic tomography of the quiet solar chromosphere formed by spatial maps of scattering polarization. It has been calculated for the CaII 8498, 8542 and 3934 A lines by solving the NLTE (non-local thermodynamical equilibrium) RT (radiative transfer) problem of the second kind in a 3D atmosphere model obtained from realistic MHD (magneto-hydrodynamical) simulations. Maps of circular polarization were calculated neglecting atomic polarization. Our investigation focuses on the linear polarization signals induced by kinematics, radiation field anisotropy and Hanle effect in forward-scattering geometry. Thus, instead of considering slit profiles at the limb as normally done in the study of the second solar spectrum, we synthetize and analyze spatial maps of polarization at disk center. It allows us to understand the spatial signatures of dynamics and magnetic field in the linear polarization for discriminating them observationally. Our results suggest new ideas for chromospheric diagnosis that will be developed throughout a serie of papers. In particular, Hanle Polarity Inversion Lines and dynamic Hanle diagrams are two concepts introduced in the present work. We find that chromospheric dynamics and magnetic field topology create spatial fingerprints in the polarization maps that trace the dynamic situation of the plasma and the magnetic field. Based on such spatial features we reconstruct the magnetic field intensity in the middle chromosphere along grooves of null linear polarization. We finally address the problems of diagnosing Hanle saturation and kinematic amplification of scattering signals using Hanle diagrams.

New View of the Solar Chromosphere **Review**

Carlsson, Mats ; De Pontieu, Bart , Hansteen, Viggo H.

Annual Review of Astronomy and Astrophysics Vol. 57:189-226 **2019**

DOI: 10.1146/annurev-astro-081817-052044

The solar chromosphere forms a crucial, yet complex and until recently poorly understood, interface between the solar photosphere and the heliosphere. Advances in high-resolution instrumentation, adaptive optics, image reconstruction techniques, and space-based observatories allow unprecedented high-resolution views of the finely structured and highly dynamic chromosphere. Dramatic progress in numerical computations allows 3D radiative magnetohydrodynamic forward models to take the place of the previous generation of 1D semiempirical atmosphere models. These new models provide deep insight into complex nonlocal thermodynamic equilibrium chromospheric diagnostics and enable physics-based interpretations of observations. This combination of modeling and observations has led to new insights into the role of shock waves, transverse magnetic waves, magnetic reconnection and flux emergence in the chromospheric energy balance, the formation of spicules, the impact of ion-neutral interactions, and the connectivity between chromosphere and transition region. During the next few years, the advent of new instrumentation (integral-field-unit spectropolarimetry) and observatories (ALMA, DKIST), coupled with novel inversion codes and expansion of existing numerical models to deal with ever more complex physical processes (including multifluid approaches), is expected to lead to major new insights into the dominant heating processes in the chromosphere and beyond.

A publicly available simulation of an enhanced network region of the Sun

Mats **Carlsson**, Viggo H. Hansteen, Boris V. Gudiksen, Jorrit Leenaarts, Bart De Pontieu

A&A 585, A4 (**2016**) **Open Access**

http://arxiv.org/pdf/1510.07581v1.pdf

Context. The solar chromosphere is the interface between the solar surface and the solar corona. Modelling of this region is difficult because it represents the transition from optically thick to thin radiation escape, from gas-pressure domination to magnetic-pressure domination, from a neutral to an ionised state, from MHD to plasma physics, and from near-equilibrium (LTE) to non-equilibrium conditions.

Aims. Our aim is to provide the community with realistic simulations of the magnetic solar outer atmosphere. This will enable detailed comparison of existing and upcoming observations with synthetic observables from the simulations, thereby elucidating the complex interactions of magnetic fields and plasma that are crucial for our understanding of the dynamic outer atmosphere.
Methods. We used the radiation magnetohydrodynamics code Bifrost to perform simulations of a computational volume with a magnetic field topology similar to an enhanced network area on the Sun.
Results. The full simulation cubes are made available online. The general properties of the simulation are discussed, and limitations are discussed.

What Do IRIS Observations of Mg II k Tell Us about the Solar Plage Chromosphere?

Mats **Carlsson**1, Jorrit Leenaarts2, and Bart De Pontieu
2015 ApJ 809 L30
http://arxiv.org/pdf/1508.04888v1.pdf
We analyze observations from the Interface Region Imaging Spectrograph of the Mg ii k line, the Mg ii UV subordinate lines, and the O i 135.6 nm line to better understand the solar plage chromosphere. We also make comparisons with observations from the Swedish 1-m Solar Telescope of the Hα line, the Ca ii 8542 line, and Solar Dynamics Observatory/Atmospheric Imaging Assembly observations of the coronal 19.3 nm line. To understand the observed Mg ii profiles, we compare these observations to the results of numerical experiments. The single-peaked or flat-topped Mg ii k profiles found in plage imply a transition region at a high column mass and a hot and dense chromosphere of about 6500 K. This scenario is supported by the observed large-scale correlation between moss brightness and filled-in profiles with very little or absent self-reversal. The large wing width found in plage also implies a hot and dense chromosphere with a steep chromospheric temperature rise. The absence of emission in the Mg iisubordinate lines constrain the chromospheric temperature and the height of the temperature rise while the width of the O i 135.6 nm line sets a limit to the non-thermal velocities to around 7 km s−1. **2014 June 11**

Sudden depletion of Alfvénic turbulence in the rarefaction region of corotating solar wind high-speed streams at 1 AU: Possible solar origin?

G. **Carnevale**1,3, R. Bruno2, R. Marino3, E. Pietropaolo1 and J. M. Raines4
A&A 661, A64 (**2022**)
https://doi.org/10.1051/0004-6361/202040006
https://www.aanda.org/articles/aa/pdf/2022/05/aa40006-20.pdf
A canonical description of a corotating solar wind high-speed stream in terms of velocity profile would indicate three main regions: a stream interface or corotating interaction region characterized by a rapid increase in flow speed and by compressive phenomena that are due to dynamical interaction between the fast wind flow and the slower ambient plasma; a fast wind plateau characterized by weak compressive phenomena and large-amplitude fluctuations with a dominant Alfvénic character; and a rarefaction region characterized by a decreasing trend of the flow speed and wind fluctuations that are gradually reduced in amplitude and Alfvénic character, followed by the slow ambient wind. Interesting enough, in some cases, fluctuations are dramatically reduced, and the time window in which the severe reduction of these fluctuations takes place is remarkably short, about some minutes. The region in which the fluctuations are rapidly reduced is located at the flow velocity knee that separates the fast wind plateau from the rarefaction region. The aim of this work is to investigate the physical mechanisms that might be at the origin of this phenomenon. To do this, we searched for any tangential discontinuity that might have inhibited the diffusion of these large-amplitude fluctuations in the rarefaction region as well. We also searched for differences in the composition analysis because minor ions are good tracers of physical conditions in the source regions of the wind under the hypothesis that large differences in the source regions might be linked to the phenomenon observed in situ. We found no positive feedback from these analyses, and finally invoked a mechanism based on interchange reconnection experienced by the field lines at the base of the corona, within the region that separates the open field lines of the coronal hole, which is the source of the fast wind, from the surrounding regions that are mainly characterized by closed field lines. Another possibility clearly is that the observed phenomenon might be due to the turbulent evolution of the fluctuations during the expansion of the wind. However, it is hard to believe that this mechanism would generate a short transition region such as is observed in the phenomenon we discuss. This type of study will greatly benefit from Solar Orbiter observations during the future nominal phase of the mission, when it will be possible to link remote and in-situ data, and from radial alignments between Parker Solar Probe and Solar Orbiter. **28 Feb-15 Mar 2017, 3-9 Aug 2017**

Assessing the Evolution of Solar Cycle 25: A Weak-moderate Cycle

V. M. S. **Carrasco**1, J. M. Vaquero1, and A. J. P. Aparicio1,2
2024 Res. Notes AAS 8 183
https://iopscience.iop.org/article/10.3847/2515-5172/ad62fb

This note aims to analyze the evolution of the sunspot number for Solar Cycle 25, updating our previous findings on this topic. We compare daily, monthly and 13 months smoothed sunspot numbers for Solar Cycle 25 with those from previous cycles since mid-18th century (Solar Cycles 1–25). The highest daily, monthly and 13 months smoothed values for Solar Cycle 25 are significantly lower than the mean and median values considering all cycles. In particular, Solar Cycle 25 ranks 17th in terms of the highest 13 months smoothed sunspot number at this point in the cycle. Based on current data and the progression toward its maximum, we conclude that Solar Cycle 25 is likely to be a weak to moderate cycle, consistent with our earlier analyses. In addition, we find that Solar Cycles 13, 14, and 16 have the most similar behavior to that of Solar Cycle 25. Assuming a cycle length for Solar Cycle 25 similar to those of the above cycles, we estimate that the minimum of Solar Cycle 26 will be in 2030–2031.

Understanding Solar Activity after the Maunder Minimum: Sunspot Records by Rost and Alischer

V. M. S. **Carrasco**1,2, A. J. P. Aparicio1,2,3, T. Chatzistergos4, S. Jamali Jaghdani5, H. Hayakawa6,7,8,9, M. C. Gallego1,2, and J. M. Vaquero1,2
2024 ApJ 968 65
https://iopscience.iop.org/article/10.3847/1538-4357/ad3fb9/pdf
The Maunder Minimum was a period with significantly reduced solar activity between 1645 and 1715, approximately. The transition between the low solar activity in the Maunder Minimum and the subsequent "normal" regime of solar activity was gradual. However, there are discrepancies in the solar activity level from sunspot number indices and solar activity proxies in that period. Among the contemporaneous observers, Johann L. Rost and Sebastian Alischer were two key sunspot observers to understand the solar activity in this transition just after the Maunder Minimum. We have revised all their sunspot records, counting the number of groups and individual sunspots to derive reliable data for the solar activity level for the period 1716–1726. We found significant misinterpretations of the sunspot group counting assigned to these astronomers in the existing group number databases. Our new group sunspot counting significantly reduces the number of groups for Rost and Alischer's observations compared to entries in existing databases. Furthermore, our sunspot number estimates (obtained from the active day fraction methodology) of the maximum amplitude of Solar Cycles −3 and −4 are significantly lower than the amplitudes according to the official sunspot number, but they are compatible with sunspot number values obtained from solar activity proxies such as radioisotopes. Our result would imply that solar activity after the Maunder Minimum recovered more gradually and with a lower intensity than previously considered.

Relationship between the Sunspot Number and Active Day Fraction: An Application for the Maunder Minimum

V. M. S. **Carrasco**1,2, J. Llera1, A. J. P. Aparicio1,2,3, M. C. Gallego1,2, and J. M. Vaquero2,4
2022 ApJ 933 26
https://iopscience.iop.org/article/10.3847/1538-4357/ac7045/pdf
Long-term solar activity can be studied using several parameters. Some of the most used are based on the sunspot counting. The active day fraction (ADF) is the simplest index derived from this counting. It is reliable in periods of low solar activity such as the Maunder minimum (MM). In this work, we study the relationship between the ADF and the sunspot number. We have obtained that the optimal fit of that relationship is an exponential function whose exponent is a degree 3 polynomial including all data except those with ADF equal to 100%. Then, we use that fit to estimate the sunspot number during the MM from the ADF calculated from the most recent sunspot group number database. Our estimations of the annual sunspot numbers are below 15, except that for 1656, which is 40.8, whereas our estimations of the triennial sunspot numbers are below 10 from 1648 to 1714. We have found peaks of the solar cycle in the middle of the 1650s, 1670s, 1680s, and 1700s but no clear evidence of solar cycle in the 1660s and 1690s, likely due to the scarcity of the available data. Our results agree with previous works obtaining values significantly higher than those of the group sunspot number derived by Hoyt and Schatten in 1998 but still fully compatible with a grand minimum period.

An Early Assessment of the Forecast by the Solar Cycle 25 Prediction Panel

V. M. S. **Carrasco**1 and J. M. Vaquero2
2022 Res. Notes AAS 6 121
https://iopscience.iop.org/article/10.3847/2515-5172/ac76ce
The effects of solar activity on technology have increased the interest in solar forecasting both in the scientific community and in society. With two and a half years of data available, we are approximately halfway to the maximum of Solar Cycle 25. Several research groups around the world published their predictions for this cycle. In this work, we assess the forecast made by the Solar Cycle 25 Prediction Panel. Analyzing the sunspot number data available, we conclude that Solar Cycle 25 is one of the weakest cycles since mid-18th century and, however, it is stronger than the initial forecast of the highest range predicted by the Solar Cycle 25 Prediction Panel for the two first years and a half of its ascending phase.

Revisiting Christoph Scheiner's Sunspot Records: A New Perspective on Solar Activity of the Early Telescopic Era

V. M. S. **Carrasco**1,2, A. Muñoz-Jaramillo3, M. C. Gallego1,2, and J. M. Vaquero2,4
2022 ApJ 927 193 2022 ApJ 927 193
https://iopscience.iop.org/article/10.3847/1538-4357/ac52ee/pdf

Christoph Scheiner was one of the most outstanding astronomers in the history of sunspot observations. His book, Rosa Ursina, is the reference work regarding the study of the earliest sunspot records. The sunspot observations compiled by Scheiner in Rosa Ursina and Prodomus, including records made by other observers, forms one of the main references of the observations known for that period—particularly around the 1620s. Thus, his work is crucial to determine the solar activity level of the first solar cycles of the telescopic era. The number of sunspot groups recorded in Scheiner's documentary sources has been included in the existing sunspot group number databases. However, we have detected significant errors in the number of groups currently assigned to Scheiner's records. In this work, we reanalyze the information in Scheiner's source documents. Consequently, the standard 11 yr solar cycle shape for the second solar cycle of the telescopic era, which is not clear in previous studies, now becomes evident. In addition, the highest daily number of groups recorded during this cycle (eight groups) is 20% less than in the one included in the existing sunspot group number databases. Using the hypergeometrical probability distribution, we find that solar minima in 2008–2009 and 2018–2019 are comparable to the most probable solar activity level of the minimum around 1632. In particular, the estimated lower limit for the solar activity in 1632 is even comparable with the solar activity level in 2008 and 2018.

Analyses of Early Sunspot Records by Jean Tarde (1615 – 1617) and Jan Smogulecki (1621 – 1625)

V. M. S. **Carrasco**, M. C. Gallego, J. Villalba Álvarez, J. M. Vaquero & H. Hayakawa
Solar Physics volume 296, Article number: 170 (**2021**)
https://link.springer.com/content/pdf/10.1007/s11207-021-01905-2.pdf
https://doi.org/10.1007/s11207-021-01905-2

Jean Tarde and Jan Smogulecki carried out sunspot observations in the 1610s and 1620s at the dawn of the telescopic era. We analysed their original observational records to revise their sunspot-group numbers in the existing database. In this study, we provide a new counting as a basis for future scientific discussions. Furthermore, we compared Smogulecki's sunspot observations with those of Scheiner and Schönberger on the same observation days. We also detected a big sunspot group on 2 – 3 February 1622 in Smogulecki's sunspot drawings and estimated its area to be approximately 1600 millionths of the solar disc. In addition, we measured the sunspot positions in Tarde's and Smogulecki's sunspot drawings to construct a butterfly diagram for this early period.

Number of Sunspot Groups and Individual Sunspots Recorded by Tevel for the Period 1816–1836 in the Dalton Minimum

V. M. S. **Carrasco**
2021 ApJ 922 58
https://doi.org/10.3847/1538-4357/ac24a5

Cornelis Tevel made sunspot observations during the period 1816–1836, including the Dalton Minimum. In this work, the first revision of these observations since Wolf incorporated them into his database is presented. On the one hand, the number of individual sunspots from Tevel's drawings was counted. This is of special interest for the sunspot number reconstruction because this kind of information is not as common in historical sunspot records as the number of groups. Thus, Tevel could be considered for the future reconstruction of the sunspot number index. On the other hand, the number of groups counted according to modern sunspot group classifications finding significant misinterpretations with the number of groups assigned to Tevel in the existing databases. Tevel was a relevant sunspot observer in the Dalton Minimum. In fact, he was the observer with the highest number of groups observed in Solar Cycles 6 and 7 according to the existing sunspot group number databases. According to the raw group number recount in this work, the maximum amplitudes for Solar Cycles 6 and 7 are, respectively, 27% and 7% lower than those previously determined. Moreover, Solar Cycle 6 is the weakest solar cycle since the Maunder Minimum after applying these new counts. Group counts from Tevel's observations were compared with those from relevant contemporary astronomers, demonstrating that Schwabe and Tevel systematically recorded a higher number of groups than Flaugergues and Derfflinger. In addition, sunspot areas and positions recorded by Tevel should be used with caution for scientific purposes.

A note on the sunspot and prominence records made by Angelo Secchi during the period 1871–1875

Víctor M. S. **Carrasco**, José M. Nogales, José M. Vaquero, Theodosios Chatzistergos and Ilaria Ermolli
J. Space Weather Space Clim. **2021**, 11, 51

https://www.swsc-journal.org/articles/swsc/pdf/2021/01/swsc210057.pdf
https://doi.org/10.1051/swsc/2021033
Angelo Secchi (1818–1878) was an Italian Jesuit who made relevant scientific contributions in geophysics, meteorology, and astrophysics. He was a well-known pioneer in solar physics due to his theories and observations. Secchi published Le Soleil (The Sun) a summary of knowledge about our star in that time. Moreover, he published in this book his sunspot and prominence observations made during the period 1871–1875. In this work, we present a machine-readable version of these observations and a preliminary analysis of them.

Sunspot Catalog (1921–1935) and Area Series (1886–1940) from the Stonyhurst College Observatory

V. M. S. **Carrasco**1,2, A. Muñoz-Jaramillo3, J. M. Nogales4, M. C. Gallego1,2, and J. M. Vaquero2,5
2021 ApJS 256 38
https://doi.org/10.3847/1538-4365/ac24a7
A sunspot observation program was started at the end of the 19th century at the Stonyhurst College Observatory (hereafter SCO) by Father Perry, director of the observatory at that time. A digitization of the daily sunspot area series recorded in this observatory from 1886 to 1940 (with a gap between 1889 and 1897) is provided in this work. This depicts one of the oldest sunspot area series available. A comparison of this series with contemporary area series made in other observatories shows that SCO generally recorded larger areas than those in some of the observatories of that time such as, for example, the Royal Greenwich Observatory (RGO). Furthermore, SCO published a sunspot group catalog for the period 1921–1935. We provide a machine-readable version of this catalog. We compared the SCO group number series with other sunspot data obtained from other observatories. In this case, for example, the RGO systematically recorded more groups than the SCO. We compared SCO and RGO area distribution functions obtaining the calibration constant between both data sets. We also obtained the butterfly diagram from the group latitudes recorded by SCO and compared the percentages of group types computed from the SCO catalog with those from Valencia Observatory (following the Cortie morphological classification of sunspot groups), identifying their similarities and differences.

Solar Cycle 25 is Currently Very Similar to Solar Cycle 24

V. M. S. **Carrasco**1 and J. M. Vaquero2
2021 Res. Notes AAS 5 181
https://iopscience.iop.org/article/10.3847/2515-5172/ac19a2
https://doi.org/10.3847/2515-5172/ac19a2
Solar Cycle 25 started in 2019 December. Different predictions for its amplitude have been published so far without general consensus. We compared the evolution of Solar Cycle 25, using the first available values of the smoothed sunspot number, with past solar cycles. Our analysis shows that Solar Cycle 25 is very similar to Solar Cycles 24 and 7. Therefore, the maximum amplitude for this Solar Cycle 25 could be small-moderate.

Strong evidence of low levels of solar activity during the Maunder Minimum

V M S **Carrasco**, H Hayakawa, C Kuroyanagi, M C Gallego, J M Vaquero
Monthly Notices of the Royal Astronomical Society, Volume 504, Issue 4, July **2021**, Pages 5199–5204,
https://doi.org/10.1093/mnras/stab1155
The Maunder Minimum (MM) was a period of prolonged solar activity minimum between 1645 and 1715. Several works have identified a significant number of problematic spotless days in the MM included in existing data bases. We have found a list of exact spotless (in the second half of 1709) and spot days (January and August 1709) provided by Johann Heinrich Müller. We computed the most probable value and upper/lower limits of the active day fraction (ADF) from Müller's data using the hypergeometrical probability distribution. Our sample is not strictly random because Müller recorded observations in consecutive days when he observed sunspots. Therefore, our result represents an upper threshold of solar activity for 1709. We compared this result with annual values of the ADF calculated for the Dalton Minimum and the most recent solar cycles. We concluded that, although 1709 is one of the most active years in the MM, it was less active than most years both in the Dalton Minimum and in the most recent solar cycles. Therefore, the solar activity level estimated in this work for 1709 represents robust evidence of low solar activity levels in the MM.

A Reanalysis of the Number of Sunspot Groups Recorded by Pierre Gassendi in the Cycle Before the Maunder Minimum

V. M. S. **Carrasco**, M. C. Gallego, J. Villalba Álvarez & J. M. Vaquero
Solar Physics volume 296, Article number: 59 (**2021**)
https://link.springer.com/content/pdf/10.1007/s11207-021-01809-1.pdf
https://doi.org/10.1007/s11207-021-01809-1

Pierre Gassendi (1592 – 1655) carried out sunspot observations during the 1630s. This period is particularly interesting because it occurred a few years before the Maunder Minimum. Gassendi was the second most active sunspot observer in that decade, surpassed only by Christoph Scheiner. Moreover, the sunspot observations made by Gassendi are of interest because most of them were made in days when no other sunspot observations were available. We have analyzed the sunspot drawings included in his Complete Works (Opera Omnia) and the textual reports with sunspot information after translating them from the original Latin. Thus, we have detected mistakes in previous works that studied these observations, such as incorrect dates and incorrect daily number of groups assigned to Gassendi. In addition, we found some observation days recorded by Gassendi not included in the current sunspot-group-number database. In this work, we provide a new account of the number of groups recorded by Gassendi in addition to the translations of his relevant texts on observed sunspots. Our main objective is to include these new recounts into the current sunspot-group-number database, which is the basis of the group-number index, to have a more accurate knowledge of solar activity of the third solar cycle observed with the aid of the telescope.

The Sunspot Drawing Collection of the National Solar Observatory at Sacramento Peak (1947–2004)

V. M. S. **Carrasco**, A. A. Pevtsov, J. M. Nogales & J. M. Vaquero
Solar Physics volume 296, Article number: 3 (**2021**)
https://link.springer.com/content/pdf/10.1007/s11207-020-01746-5.pdf
A complete dataset of sunspot drawings recorded at Sacramento Peak Observatory (SPO) from late 1947 till mid-2004 has been digitized. We present the history of the observations and describe the data included in the drawings. We compare the sunspot number index calculated from the SPO data and the International Sunspot Number (SNv2), and we find that both series exhibit a similar behavior. The ratio of two sunspot numbers is relatively constant at about 1.2 – 1.3 during 1955–1995, with larger variations present at the beginning of the time series. This work represents the first step for the publication of the SPO sunspot catalogue in digital format. More information, such as positions and areas of sunspots, will be included in the next versions in order to provide the space weather and climate community a more complete sunspot catalogue with good quality observations.

On the use of naked-eye sunspot observations during the Maunder Minimum

V.M.S. **Carrasco**, M.C. Gallego, R. Arlt, J.M. Vaquero
ApJ **904** 60 **2020**
https://arxiv.org/ftp/arxiv/papers/2011/2011.00340.pdf
https://doi.org/10.3847/1538-4357/abbd3c
Naked-eye sunspot observations (NESO, hereafter) have been recorded for last two millennia, approximately. This kind of records were made around the world, mainly in Asian civilizations, and they are compiled in several catalogues. In this work, we analyze solar activity in days of the 19th century when NESO were recorded. We found that only more than five sunspot groups were recorded in 39 % of days corresponding to these NESO events. Furthermore, regarding the largest groups observed in days when NESO were reported, we show the uncorrected areas of these groups were below 200 millionths of solar disc (msd hereafter) in 3.2 % of total cases while it is 12.9 % for areas between 200 and 499 msd. Thus, NESO records do not imply high solar activity and big sunspot groups necessarily. Therefore, these results contradict the interpretations of recent works that, using the same NESO set, suggest the solar activity level during the Maunder Minimum is still an open question. NESO records support the Maunder Minimum as a very low solar activity period.

Revisiting the Amplitude of Solar Cycle 9: The Case of Sunspot Observations by W.C. Bond

V. M. S. **Carrasco**, M. C. Gallego, R. Arlt & J. M. Vaquero
Solar Physics volume 295, Article number: 127 (**2020**)
https://link.springer.com/content/pdf/10.1007/s11207-020-01696-y.pdf
William Cranch Bond, director of the Harvard College Observatory in mid-19th century, carried out detailed sunspot observations during the period 1847–1849. We highlight Bond was the observer with the highest daily number of sunspot groups observed in Solar Cycle 9 recording 18 groups on 26 December 1848 according to the current sunspot group database. However, we have detected significant mistakes in these counts due to the use of sunspot position tables instead of solar drawings. Therefore, we have revisited the sunspot observations made by Bond, establishing a new group counting. Our new counts of the sunspot groups from Bond's drawings indicate that solar activity was previously overestimated. Moreover, after this new counting, Bond would not be the astronomer who recorded the highest daily group number for Solar Cycle 9 but Schmidt with 16 groups on 14 February 1849. We have also indicated the new highest annual group numbers recorded by any observer for the period 1847–1849 in order to correct those values applied in the "brightest star" method, which is used as a rough indicator of the solar activity level. Furthermore, a comparison between Bond's sunspot records and the sunspot observations made by

Schwabe and Wolf is shown. We conclude that the statistics of Wolf and Bond are similar as regards the group count. Additionally, Schwabe was able to observe smaller groups than Bond.

Sunspot Records by Antonio Colla Just After the Dalton Minimum

V. M. S. **Carrasco**, C. Bertolin, F. Domínguez-Castro, L. de Ferri, M. C. Gallego & J. M. Vaquero
Solar Physics volume 295, Article number: 112 (**2020**)
https://link.springer.com/content/pdf/10.1007/s11207-020-01678-0.pdf
Antonio Colla was a meteorologist and astronomer who made sunspot observations at the Meteorological Observatory of the Parma University (Italy). He carried out his sunspot observations from 1830 to 1843, just after the Dalton Minimum. We have recovered 71 observation days for this observer. Unfortunately, many of these records are qualitative and we could only obtain the number of sunspot groups and/or single sunspots from 25 observations. However, we highlight the importance of these records because Colla is not included in the sunspot group database as an observer and, therefore, neither are his sunspot observations. With regards to the number of groups, the sunspot observations made by Colla are similar to those of several observers of his time. For common observation days, only Stark recorded significantly more groups than Colla. Moreover, we have calculated the sunspot areas and positions from Colla's sunspot drawings concluding that both areas and positions recorded by this observer seem unreal. Therefore, Colla's drawings can be interpreted such as sketches showing reliable information on the number of groups but the information on sunspot areas and positions should not be used for scientific purposes.

Sunspot Characteristics at the Onset of the Maunder Minimum Based on the Observations of Hevelius

V. M. S. **Carrasco**1,2,3, J. M. Vaquero2,4, M. C. Gallego1,2, A. Muñoz-Jaramillo5, G. de Toma5, P. Galaviz4, R. Arlt6, V. Senthamizh Pavai6, F. Sánchez-Bajo7, J. Villalba Álvarez8 Show full author list
2019 ApJ 886 18
https://doi.org/10.3847/1538-4357/ab4ade
An analysis of the sunspot observations made by Hevelius during 1642–1645 is presented. These records are the only systematic sunspot observations just before the Maunder Minimum (MM). We have studied different phenomena meticulously recorded by Hevelius after translating the original Latin texts. We reevaluate the observations of sunspot groups by Hevelius during this period and obtain an average value 7% greater than that calculated from his observations given in the current group database. Furthermore, the average of the active day fraction obtained in this work from Hevelius's records previous to the MM is significantly greater than the solar activity level obtained from Hevelius's sunspot observations made during the MM (70% versus 30%). We also present the butterfly diagram obtained from the sunspot positions recorded by Hevelius for the period 1642–1645. It can be seen that no hemispheric asymmetry exists during this interval, in contrast with the MM. Hevelius noted a ~3-month period that appeared to lack sunspots in early 1645 that gave the first hint of the impending MM. Recent studies claim that the MM was not a grand minimum period, speculating that astronomers of that time, due to the Aristotelian ideas, did not record all sunspots that they observed, producing thus an underestimation of the solar activity level. However, we show that the good quality of the sunspot records made by Hevelius indicates that his reports of sunspots were true to the observations.

Sunspot observations by Charles Malapert during the period 1618–1626: a key data set to understand solar activity before the Maunder minimum

V M S **Carrasco**, M C Gallego, J Villalba Álvarez, J M Vaquero
MNRAS 488, Issue 3, September **2019**, Pages 3884–3895
sci-hub.se/10.1093/mnras/stz1867
A revision is presented of the sunspot observations made by Charles Malapert from 1618 to 1626, studying several documentary sources that include those observations. The revised accounting of the group numbers recorded by Malapert for that period shows new information unavailable in the current sunspot group data base. The average solar activity level calculated from these revised records of Malapert is by almost one-third greater than that calculated from his records included in the current group data base. Comparison of the sunspot observations made by Malapert and by other astronomers of that time with regard to the number of recorded groups and sunspot positions on the solar disc shows good agreement. Malapert reported that he only recorded one sunspot group in each sunspot drawing presented in Austriaca Sidera Heliocyclia (the documentary source that includes most of the sunspot records made by Malapert), although he sometimes observed several groups. Therefore, the sunspot counts obtained in this work on Malapert's sunspot observations represent the lower limit of the solar activity level corresponding to those records.

Eric Strach: four decades of detailed synoptic solar observations (1969-2008)

V.M.S. **Carrasco**, J.M. Vaquero, V.M. Olmo-Mateos

Space Weather Volume17, Issue6 Pages 796-802 **2019**
https://arxiv.org/ftp/arxiv/papers/2103/2103.09490.pdf
https://doi.org/10.1029/2018SW002147
Eric H. Strach (1914-2011) studied medicine at University of Prague and graduated in 1938. Strach dedicated a great part of his life to astronomy becoming a consistent and meticulous observer. He joined the Liverpool Astronomical Association and British Astronomical Association during the 1960s and obtained two recognitions as proof of his great work in solar physics: the BAA's Merlin Medal and Gift in 1999 and Walter Goodacre Medal and Gift, ten years later. Strach recorded four decades (1969-2008) of systematic solar records in his observation notebooks although he started his observations from the late 1950s. In this work, we document the valuable effort made by Strach in getting four decades of solar records and the importance of this kind of long observation series for studies of space weather and climate. We present the sunspot group number series according to Strach's data and a long observation series of prominences recorded by Strach.

Sunspot Catalogue of the Observatory of the University of Coimbra (1929 – 1941)

V. M. S. **Carrasco**, J. M. Vaquero, M. C. Gallego, A. Lourenço, T. Barata, J. M. Fernandes
Solar Physics November **2018**, 293:153
https://link.springer.com/content/pdf/10.1007%2Fs11207-018-1373-7.pdf
A sunspot catalogue was published by the Coimbra Astronomical Observatory (Portugal), which is now called the Geophysical and Astronomical Observatory of the University of Coimbra, for the period 1929 – 1941. We digitalised data included in that catalogue and provide a machine-readable version. We show the reconstructions for the (total and hemispheric) sunspot number index and sunspot area according to this catalogue and compare it with the sunspot number index (version 2) and the Balmaceda sunspot area series (Balmaceda et al. in J. Geophys. Res.114, A07104, 2009). Moreover, we also compared the Coimbra catalogue with records made at the Royal Greenwich Observatory. The results demonstrate that the historical catalogue compiled by the Coimbra Astronomical Observatory contains reliable sunspot data and can therefore be considered for studies about solar activity.

The umbra-penumbra area ratio of sunspots during the Maunder Minimum

V.M.S. **Carrasco**, J.M. García-Romero, J.M. Vaquero, P.G. Rodríguez, P. Foukal, M.C. Gallego, L. Lefèvre
ApJ **865** 88 **2018**
https://arxiv.org/ftp/arxiv/papers/1809/1809.08670.pdf
The Maunder Minimum (MM) was a prolonged period of low solar activity that occurred between 1645 and 1715. The true level of solar activity corresponding to this epoch is still a matter of debate. In order to compare solar activity during the MM with that of other epochs, we have evaluated the umbra-penumbra area ratio (U/P hereafter) during the MM. Thus, we have analyzed 196 sunspot drawings including 48 different sunspots observed during the period 1660-1709. The mode value of the ratio obtained from the occurrence frequency distribution lies between 0.15 and 0.25. Furthermore, the median and mean values are equal to 0.24 \pm 0.07 and 0.27 \pm 0.08 with a sigma clipping, respectively. These results are consistent with recent research using more modern data. Higher U/P values mean faster sunspot decay rates. From our results, the almost absence of sunspots during the Maunder Minimum could not be explained by changes in the U/P since the values of the ratio obtained in this work are similar to values found for other epochs.

Sunspot Observations Made by Hallaschka during the Dalton Minimum

V.M.S. **Carrasco**, J.M. Vaquero, R. Arlt, M.C. Gallego
Solar Phys. 293:102 **2018**
https://arxiv.org/ftp/arxiv/papers/1807/1807.03014.pdf
https://link.springer.com/content/pdf/10.1007%2Fs11207-018-1322-5.pdf
We present and analyse the sunspot observations performed by Franz I. C. Hallaschka in 1814 and 1816. These solar observations were carried out during the so-called Dalton minimum, around the maximum phase of the Solar Cycle 6. These records are very valuable because they allow us to complete observational gaps in the collection of sunspot group numbers, improving its coverage for this epoch. We have analysed and compared the observations made by Hallaschka with the records made by other contemporary observers. Unfortunately, the analysis of the sunspot areas and positions showed that they are too inaccurate for scientific use. But, we conclude that sunspot counts made by Hallaschka are similar to those made by other astronomers of that time. The observations by Hallaschka confirm a low level of the solar activity during the Dalton minimum.

A Curious History of Sunspot Penumbrae: An Update

V.M.S. **Carrasco**, J.M. Vaquero, R.M. Trigo, M.C. Gallego

Solar Phys. 293 104 **2018**
https://arxiv.org/ftp/arxiv/papers/1807/1807.03017.pdf
The ratio of penumbral to umbral area of sunspots is an important topic for solar and geophysical studies. Hathaway (Solar Physics, 286, 347, 2013) found a curious behaviour in this parameter for small sunspot groups (areas smaller than 100 millionths of solar hemisphere, msh) using records from Royal Greenwich Observatory (RGO). Hathaway showed that penumbra-umbra ratio decreased smoothly from more than 7 in 1905 to lower than 3 by 1930 and then increased to almost 8 in 1961. Thus, Hathaway proposed the existence of a secular variation in the penumbra-umbra area ratio. In order to confirm that secular variation, we employ data of the sunspot catalogue published by the Coimbra Astronomical Observatory (COI) for the period 1929-1941. Our results disagree with the penumbra-umbra ratio found by Hathaway for that period. However, the behaviour of this ratio for large (areas greater or equal than 100 msh) and small groups registered in COI during 1929-1941 is similar to data available from RGO for the periods 1874-1914 and 1950-1976. Nevertheless, while the average values and time evolution of the ratio in large groups is similar to the ratio for small groups according to Coimbra data (1929-1941) it is not analogous for RGO data for the same period. We also found that the behaviour of the penumbra-umbra area ratio for smaller groups in both observatories is significantly different. The main difference between the area measurements made in Coimbra and RGO is associated with the umbra measurements. We would like to stress that the two observatories used different methods of observation and while in COI both methodology and instruments did not change during the study period, some changes were carried out in RGO that could have affected measurements of umbra and penumbra. These facts illustrate the importance of the careful recovery of past solar data.

Could a Hexagonal Sunspot Have Been Observed During the Maunder Minimum?

V.M.S. **Carrasco**, J.M. Vaquero, M.C. Gallego
Solar Phys. 293:51 **2018**
https://arxiv.org/ftp/arxiv/papers/1803/1803.00358.pdf
The Maunder Minimum was the period between 1645 and 1715 whose main characteristic was abnormally low and prolonged solar activity. However, some authors have doubted this low level of solar activity during that period by questioning the accuracy and objectivity of the observers. This work presents a particular case of a sunspot observed during the Maunder Minimum with an unusual shape of its umbra and penumbra: a hexagon. This sunspot was observed by Cassini in November 1676, just at the core of the Maunder Minimum. This historical observation is compared with a twin case that occurred recently in May 2016. The conclusion reached is that Cassini's record is another example of the good quality observations made during the Maunder Minimum, showing the meticulousness of the astronomers of that epoch. This sunspot observation made by Cassini does not support the conclusions of Zolotova and Ponyavin (Astrophys. J. 800, 42, 2015) that professional astronomers in the 17th century only registered round sunspots. Finally, a discussion is given of the importance of this kind of unusual sunspot record for a better assessment of the true level of solar activity in the Maunder Minimum. **22 May 2016**

Analysing the spotless days as predictors of the solar activity from the new sunspot number

V.M.S. **Carrasco**, J.M. Vaquero, M.C. Gallego
Solar Phys. 292:154 **2017**
https://arxiv.org/ftp/arxiv/papers/1708/1708.02202.pdf
The use of the spotless days to predict the future solar activity is here revised based on the new version of the sunspot number index with a 24-month filter. Data from Solar Cycle (SC) 10 are considered because from this solar cycle the temporal coverage of the records is 100 %. The interrelationships of the timing characteristics of spotless days and their comparison with sunspot cycle parameters are explored, in some cases finding very strong correlations. Such is the case for the relationship between the minimum time between spotless days either side of a given solar maximum and the maximum time between spotless days either side in the previous solar minimum, with $r = -0.91$ and a p-value < 0.001. However, the predictions for SC 24 or 23 made by other authors in previous works using the spotless days as a predictor of solar activity are not good since it has not been fulfilled. Although there seems to be a pattern of strong correlation for some relationships between the parameters studied, prediction of future solar cycles from these parameters defined as functions of the spotless days should be made with caution because sometimes the estimated values are far from the observed ones. Finally, SC 23 seems to show a mode change, a break respect to the behavior of their previous solar cycles and more similar to SC 10-15.

The New Sunspot-Number Index and Solar-Cycle Characteristics

V. M. S. **Carrasco**, A. J. P. Aparicio, J. M. Vaquero, M. C. Gallego
Solar Phys. **2016**
http://link.springer.com/article/10.1007/s11207-016-0998-7
We revisit several characteristics of the solar cycle using the new version of the sunspot-number index. Thus, we calculated several correlations, including the recent Solar Cycles 23 and 24 in the analysis. We applied two smoothing methods to the sunspot number: i) the usual 13-month running mean and ii) a 24-month Gaussian filter.

Each of these methods contains two analyses: on the one hand, we consider all of the solar cycles available, and on the other hand, only those from Solar Cycle 10 onward. It can be seen that this new version improves or yields similar results for the correlations with respect to other works using the old version of the sunspot number, except for the amplitude–descending time effect and the linear fit of the secular trend. However, employing the same methodology in the analysis and considering the same solar cycles, it can be seen that the new sunspot number, in general, does not improve the correlations with respect to the old sunspot number and, moreover, the correlations obtained with the Gaussian filter generally are stronger than those with the 13-month running mean. Furthermore, from a sinusoidal fit to the solar-maximum amplitudes of the whole series, we have obtained a periodicity of the Gleissberg cycle equal to 97.7 years (\({\approx}\,8.9\) solar cycles) for the 13-month running mean and 99.8 years (\({\approx}\,9.1\) solar cycles) for the Gaussian filter. Lastly, the Waldmeier effect, the modified Waldmeier effect, the amplitude–period effect, the amplitude–minimum effect, and the even–odd effect are characteristics with high correlation coefficients and significance levels; the sinusoidal fit applied to the solar-maximum amplitudes yields a lower correlation coefficient value but a high significance level; and both the amplitude–descending-time effect and secular trend of the solar activity have weaker correlation coefficients and significance levels.

Revisiting the prediction of solar activity based on the relationship between the solar maximum amplitude and max-max cycle length

V.M.S. **Carrasco**, J.M. Vaquero, M.C. Gallego
Advances in Space Research Volume 59, Issue 1, 1 January 2017, Pages 379–383 **2016**
http://arxiv.org/pdf/1609.01942v1.pdf

It is very important to forecast the future solar activity due to its effect on our planet and near space. Here, we employ the new version of the sunspot number index (version 2) to analyse the relationship between the solar maximum amplitude and max-max cycle length proposed by Du (2006). We show that the correlation between the parameters used by Du (2006) for the prediction of the sunspot number (amplitude of the cycle, Rm, and max-max cycle length for two solar cycles before, Pmax-2) disappears when we use solar cycles prior to solar cycle 9. We conclude that the correlation between these parameters depends on the time interval selected. Thus, the proposal of Du (2006) should definitively not be considered for prediction purposes.

A Normalized Sunspot-Area Series Starting in 1832: an Update

V.M.S. **Carrasco**, J.M. Vaquero, M.C. Gallego, F. Sánchez-Bajo
Solar Phys. **2016**
http://arxiv.org/pdf/1606.04280v1.pdf

A new normalized sunspot-area series has been reconstructed from the series obtained by the Royal Greenwich Observatory and other contemporary institutions for the period 1874 - 2008 and the area series compiled by De la Rue, Stewart, and Loewy from 1832 to 1868. Since the two sets of series do not overlap in time, we used as a link between them the new version of sunspot index number (Version 2) published by SILSO (Sunspot Index and Long-term Solar Observations). We also present a spectral analysis of the normalized area series in search of periodicities beyond the well-known solar cycle of 11 years and a study of the Waldmeier effect in the new version of sunspot-number and the sunspot-area series presented in this study. We conclude that while this effect is significant in the new series of sunspot number, it has a weak relationship with the sunspot-area series.

Sunspot Observations during the Maunder Minimum from the Correspondence of John Flamsteed

V.M.S. **Carrasco**, J.M. Vaquero
Solar Physics Volume 291, Issue 9, pp 2493–2503 **2016**
http://arxiv.org/ftp/arxiv/papers/1601/1601.02851.pdf

We compile and analyze the sunspot observations made by John Flamsteed for the period 1672-1703, corresponding to the second part of the Maunder Minimum, which appear in the correspondence of this famous astronomer. We include in an appendix the original texts of the sunspot records kept by Flamsteed. We compute an estimate of the level of solar activity using these records, and compare the results with the latest reconstructions of solar activity during the Maunder Minimum, obtaining values characteristic of a grand solar minimum. Finally, we discuss a phenomenon observed and described by Stephen Gray in 1705 that has been interpreted as a white-light flare.

Sunspots during the Maunder Minimum from Machina Coelestis by Hevelius

V.M.S. **Carrasco**, J. Villalba Álvarez, J.M. Vaquero
Solar Phys. Volume 290, Issue 10, pp 2719-2732 **2015**
http://arxiv.org/pdf/1502.06270v1.pdf

We revisited the sunspot observations published by Johannes Hevelius in his book Machina Coelestis (1679) corresponding to the period 1653-1675 (just in the middle of the Maunder Minimum). We show detailed translations of the original Latin texts describing the sunspot records and provide the general context of these sunspot observations. From this source only, we present an estimate of the annual values of the Group Sunspot Number based only on the records that explicitly inform about the presence or absence of sunspots. Although we obtain very low values of the Group Sunspot Number, in accordance with a grand minimum of solar activity, these values are significantly higher in general than the values provided by Hoyt and Schatten (1998) for the same period.

Equivalence relations between the Cortie and Zurich sunspot group morphological classifications

V.M.S. **Carrasco**, L. Lefevre, J.M. Vaquero, M.C. Gallego
Solar Phys. May 2015, Volume 290, Issue 5, pp 1445-1455 **2015**
http://arxiv.org/pdf/1503.08724v1.pdf
Catalogues of sunspots have been available with useful information about sunspots or sunspot groups for approximately the last 150 years. However, the task of merging these catalogues is not simple. In this paper, a method is suggested of converting the types of sunspot groups that were proposed by Cortie (1901) into the well-known Zurich types of sunspot groups. To achieve this, the sunspot catalogue of the Valencia University Observatory (from 1920 to 1928) was used in addition to the descriptions proposed by Cortie. To assess the quality of this conversion scheme, the Zurich type was computed from the Valencia catalogue, and the resulting contribution of each group type was compared to what can be found in other catalogues. The results show that the proposed scheme works well within the errors that are found in the different catalogues.

Sunspot Catalogue of the Valencia Observatory (1920 – 1928)

V. M. S. **Carrasco**, J. M. Vaquero, A. J. P. Aparicio, M. C. Gallego
Solar Phys., **2014**
A sunspot catalogue was maintained by the Astronomical Observatory of Valencia University (Spain) from 1920 to 1928. Here we present a machine-readable version of this catalogue (OV catalogue or OVc), including a quality-control analysis. Sunspot number (total and hemispheric) and sunspot area series are constructed using this catalogue. The OV catalogue data are compared with other available solar data, demonstrating that the present contribution provides the scientific community with a reliable catalogue of sunspot data.

The solar rotation in the period 1853-1870 from the sunspot catalogues of Carrington, Peters, and de la Rue

Ricard **Casas**, José M. Vaquero
Solar Phys. Volume 290, Issue 8, pp 2189-2198 **2015**
http://arxiv.org/pdf/1410.8286v1.pdf
R. C. Carrington, C. H. F. Peters, and W. de la Rue observed the sunspots in the second half of the 19th century, determining their heliographic positions between 1853 and 1870, before the establishment of the solar program of the Royal Greenwich Observatory. The large tables of sunspot positions included in the catalogues published by these observers have recently been converted to a machine readable format. The present work analyses this data by calculating the sunspot group velocities for each observer. These results are then fitted with a differential rotation law to compare the data of the three observers with each other and with the results published by other authors. Finally, a study is made of the possible relationship between the sunspot group areas as determined by de la Rue and the corresponding sunspot group velocities.

The Solar Probe Cup on Parker Solar Probe

Anthony W. **Case**, Justin C. Kasper, Michael L. Stevens, Kelly E. Korreck, Kristoff Paulson, Peter Daigneau, Dave Caldwell, Mark Freeman, Thayne Henry, Brianna Klingensmith, Miles Robinson, Peter Berg, Chris Tiu, Kenneth H. Wright Jr., David Curtis, Michael Ludlam, Davin Larson, Phyllis Whittlesey, Roberto Livi, Kristopher G. Klein, Mihailo M. Martinović
ApJ **2019**
https://arxiv.org/pdf/1912.02581.pdf
The Solar Probe Cup (SPC) is a Faraday Cup instrument onboard NASA's Parker Solar Probe (PSP) spacecraft designed to make rapid measurements of thermal coronal and solar wind plasma. The spacecraft is in a heliocentric orbit that takes it closer to the Sun than any previous spacecraft, allowing measurements to be made where the coronal and solar wind plasma is being heated and accelerated. The SPC instrument was designed to be pointed directly at the Sun at all times, allowing the solar wind (which is flowing primarily radially away from the Sun) to

be measured throughout the orbit. The instrument is capable of measuring solar wind ions with an energy/charge between 100 V and 6000 V (protons with speeds from 139−1072 km s−1). It also measures electrons with an energy between 100 V and 1500 V. SPC has been designed to have a wide dynamic range that is capable of measuring protons and alpha particles at the closest perihelion (9.86 solar radii from the center of the Sun) and out to 0.25 AU. Initial observations from the first orbit of PSP indicate that the instrument is functioning well.

Magnetic Energy Powers the Corona: How We Can Understand its 3D Storage & Release

Amir **Caspi**, Daniel B. Seaton, Roberto Casini, Cooper Downs, Sarah E. Gibson, Holly Gilbert, Lindsay Glesener, Silvina E. Guidoni, J. Marcus Hughes, David McKenzie, Joseph Plowman, Katharine K. Reeves, Pascal Saint-Hilaire, Albert Y. Shih, Matthew J. West

White paper to the Decadal Survey for Solar and Space Physics (Heliophysics) 2024-2033 **2023**

https://arxiv.org/pdf/2305.17146.pdf

The coronal magnetic field is the prime driver behind many as-yet unsolved mysteries: solar eruptions, coronal heating, and the solar wind, to name a few. It is, however, still poorly observed and understood. We highlight key questions related to magnetic energy storage, release, and transport in the solar corona, and their relationship to these important problems. We advocate for new and multi-point co-optimized measurements, sensitive to magnetic field and other plasma parameters, spanning from optical to γ-ray wavelengths, to bring closure to these long-standing and fundamental questions. We discuss how our approach can fully describe the 3D magnetic field, embedded plasma, particle energization, and their joint evolution to achieve these objectives.

COMPLETE: A flagship mission for complete understanding of 3D coronal magnetic energy release

Amir **Caspi**, Daniel B. Seaton, Roberto Casini, Cooper Downs, Sarah E. Gibson, Holly Gilbert, Lindsay Glesener, Silvina E. Guidoni, J. Marcus Hughes, David McKenzie, Joseph Plowman, Katharine K. Reeves, Pascal Saint-Hilaire, Albert Y. Shih, Matthew J. West

White paper submitted to the Decadal Survey for Solar and Space Physics (Heliophysics) 2024-2033; **2023**

https://arxiv.org/pdf/2305.16533

COMPLETE is a flagship mission concept combining broadband spectroscopic imaging and comprehensive magnetography from multiple viewpoints around the Sun to enable tomographic reconstruction of 3D coronal magnetic fields and associated dynamic plasma properties, which provide direct diagnostics of energy release. COMPLETE re-imagines the paradigm for solar remote-sensing observations through purposefully co-optimized detectors distributed on multiple spacecraft that operate as a single observatory, linked by a comprehensive data/model assimilation strategy to unify individual observations into a single physical framework. We describe COMPLETE's science goals, instruments, and mission implementation. With targeted investment by NASA, COMPLETE is feasible for launch in 2032 to observe around the maximum of Solar Cycle 26.

A new facility for airborne solar astronomy: NASA's WB-57 at the 2017 total solar eclipse

Amir **Caspi**, Daniel B. Seaton, Constantine C. C. Tsang, Craig E. DeForest, …

ApJ **895** 131 **2020**

https://arxiv.org/pdf/2004.09658.pdf

https://doi.org/10.3847/1538-4357/ab89a8

NASA's WB-57 High Altitude Research Program provides a deployable, mobile, stratospheric platform for scientific research. Airborne platforms are of particular value for making coronal observations during total solar eclipses because of their ability both to follow the Moon's shadow and to get above most of the atmospheric airmass that can interfere with astronomical observations. We used the **2017 Aug 21** eclipse as a pathfinding mission for high-altitude airborne solar astronomy, using the existing high-speed visible-light and near-/mid-wave infrared imaging suite mounted in the WB-57 nose cone. In this paper, we describe the aircraft, the instrument, and the 2017 mission; operations and data acquisition; and preliminary analysis of data quality from the existing instrument suite. We describe benefits and technical limitations of this platform for solar and other astronomical observations. We present a preliminary analysis of the visible-light data quality and discuss the limiting factors that must be overcome with future instrumentation. We conclude with a discussion of lessons learned from this pathfinding mission and prospects for future research at upcoming eclipses, as well as an evaluation of the capabilities of the WB-57 platform for future solar astronomy and general astronomical observation.

Diagnosing Coronal Heating Processes with Spectrally Resolved Soft X-ray Measurements

Amir **Caspi**, Albert Y. Shih, Harry P. Warren, Marek Stęślicki, Janusz Sylwester **White paper**

the Scientific Objectives Team of the Next-Generation Solar Physics Mission **2017**

https://arxiv.org/ftp/arxiv/papers/1701/1701.00619.pdf

Decades of astrophysical observations have convincingly shown that soft X-ray (SXR; ~0.1--10 keV) emission provides unique diagnostics for the high temperature plasmas observed in solar flares and active regions. SXR observations critical for constraining models of energy release in these phenomena can be provided using instruments that have already been flown on sounding rockets and CubeSats, including miniaturized high-resolution photon-counting spectrometers and a novel diffractive spectral imager. These instruments have relatively low cost and high TRL, and would complement a wide range of mission concepts. In this white paper, we detail the scientific background and open questions motivating these instruments, the measurements required, and the instruments themselves that will make groundbreaking progress in answering these questions.

New Observations of the Solar 0.5-5 keV Soft X-ray Spectrum

Amir **Caspi**, Thomas N. Woods, Harry P. Warren
ApJL, 802:L2 **2015**
http://arxiv.org/pdf/1502.01725v1.pdf
http://www.boulder.swri.edu/~amir/eprints/Caspi_Woods_Warren_2015_ApJL.pdf
The solar corona is orders of magnitude hotter than the underlying photosphere, but how the corona attains such high
temperatures is still not understood. Soft X-ray (SXR) emission provides important diagnostics for thermal processes in
the high-temperature corona, and is also an important driver of ionospheric dynamics at Earth. There is a crucial observational gap between ~0.2 and ~4 keV, outside the ranges of existing spectrometers. We present observations from a new SXR spectrometer, the Amptek X123-SDD, which measured the spatially-integrated solar spectral irradiance from
~0.5 to ~5 keV, with ~0.15 keV FWHM resolution, during sounding rocket flights on 2012 June 23 and 2013 October
21. These measurements show that the highly variable SXR emission is orders of magnitude greater than that during the deep minimum of 2009, even with only weak activity. The observed spectra show significant high-temperature (5–
10 MK) emission and are well fit by simple power-law temperature distributions with indices of ~6, close to the predictions of nanoflare models of coronal heating. Observations during the more active 2013 flight indicate an enrichment of low first-ionization potential (FIP) elements of only ~1.6, below the usually-observed value of ~4, suggesting that abundance variations may be related to coronal heating processes. The XUV Photometer System Level 4 data product, a spectral irradiance model derived from integrated broadband measurements, significantly overestimates the spectra from both flights, suggesting a need for revision of its non-flare reference spectra, with important implications for studies of Earth ionospheric dynamics driven by solar SXRs.

Space physics and policy for contemporary society **Review**

P. A. **Cassak**1 , A. G. Emslie2, A. J. Halford3 , D. N. Baker4 , H. E. Spence5 ,
S. K. Avery6,7, and L. A. Fisk8
JGR **2017**
http://onlinelibrary.wiley.com/doi/10.1002/2017JA024219/pdf
Space physics is the study of Earth's home in space. Elements of space physics include how the Sun works from its interior to its atmosphere, the environment between the Sun and planets out to the interstellar medium, and the physics of the magnetic barriers surrounding Earth and other planets. Space physics is highly relevant to society. Space weather, with its goal of predicting how Earth's technological infrastructure responds to activity on the Sun, is an oft-cited example, but there are many more. Space physics has important impacts in formulating public policy.

HATS: A Ground-Based Telescope to Explore the THz Domain

Guillermo Giménez de **Castro**, Jean-Pierre Raulin, Adriana Valio, Guilherme Alaia, Vinicius Alvarenga, …
Solar Physics volume 295, Article number: 56 (**2020**)
https://link.springer.com/content/pdf/10.1007/s11207-020-01621-3.pdf
The almost unexplored frequency window from submillimeter to mid-infrared (mid-IR) may bring new clues about the particle acceleration and transport processes and the atmospheric thermal response during solar flares. Because of its technical complexity and the special atmospheric environment needed, observations at these frequencies are very sparse. The High Altitude THz Solar Photometer (HATS) is a full-Sun ground-based telescope designed to observe the continuum from the submillimeter to the mid-IR. It has a 457-mm spherical mirror with the sensor in its primary focus. The sensor is a Golay cell with high sensitivity in a very wide frequency range. The telescope has a polar mount, and a custom-built data acquisition system based on a 32 ksamples per second, 24 bits (72 dB dynamic range), 8 channels analog-to-digital board. Changing only the composition of the low- and band-pass filters in front of the Golay cell, the telescope can be setup to detect very different frequency bands; making the instrument very

versatile. In this article we describe the telescope characteristics and its development status. Moreover, we give estimates of the expected fluxes during flares.

Periodicities in an active region correlated with Type III radio bursts observed by Parker Solar Probe

Cynthia **Cattell**, Lindsay Glesener, Benjamin Leiran, Keith Goetz, Juan Carlos Martínez Oliveros, Samuel T. Badman, Marc Pulupa, Stuart D. Bale

A&A **2020**

https://arxiv.org/pdf/2009.10899.pdf

Context. Periodicities have frequently been reported across many wavelengths in the solar corona. Correlated periods of ~5 minutes, comparable to solar p-modes, are suggestive of coupling between the photosphere and the corona. Aims. Our study investigates whether there are correlations in the periodic behavior of Type III radio bursts, indicative of non-thermal electron acceleration processes, and coronal EUV emission, assessing heating and cooling, in an active region when there are no large flares. Methods. We use coordinated observations of Type III radio bursts from the FIELDS instrument on Parker Solar Probe (PSP), of extreme ultraviolet emissions by the Solar Dynamics Observatory (SDO)/AIA and white light observations by SDO/HMI, and of solar flare x-rays by Nuclear Spectroscopic Telescope Array (NuSTAR) on **April 12, 2019**. Several methods for assessing periodicities are utilized and compared to validate periods obtained. Results. Periodicities of about 5 minutes in the EUV in several areas of an active region are well correlated with the repetition rate of the Type III radio bursts observed on both PSP and Wind. Detrended 211A and 171A light curves show periodic profiles in multiple locations, with 171A peaks lagging those seen in 211A. This is suggestive of impulsive events that result in heating and then cooling in the lower corona. NuSTAR x-rays provide evidence for at least one microflare during the interval of Type III bursts, but there is not a one-to-one correspondence between the x-rays and the Type-III bursts. Our study provides evidence for periodic acceleration of non-thermal electrons (required to generate Type III radio bursts) when there were no observable flares either in the x-ray data or the EUV. The acceleration process, therefore, must be associated with small impulsive events, perhaps nanoflares.

No evidence for planetary influence on solar activity 330 000 years ago

A. **Cauquoin**1⋆, G. M. Raisbeck2, J. Jouzel1, E. Bard3 and ASTER Team

A&A 561, A132 (**2014**)

Context. Abreu et al. (2012, A&A. 548, A88) have recently compared the periodicities in a 14C – 10Be proxy record of solar variability during the Holocene and found a strong similarity with the periodicities predicted on the basis of a model of the time-dependent torque exerted by the planets on the sun's tachocline. If verified, this effect would represent a dramatic advance not only in the basic understanding of the Sun's variable activity, but also in the potential influence of this variability on the Earth's climate. Cameron and Schussler (2013, A&A. 557, A83) have seriously criticized the statistical treatment used by Abreu et al. to test the significance of the coincidences between the periodicities of their model with the Holocene proxy record.

Aims. If the Abreu et al. hypothesis is correct, it should be possible to find the same periodicities in the records of cosmogenic nuclides at earlier times.

Methods. We present here a high-resolution record of 10Be in the EPICA Dome C (EDC) ice core from Antarctica during the Marine Interglacial Stage 9.3 (MIS 9.3), 325–336 kyr ago, and investigate its spectral properties.

Results. We find very limited similarity with the periodicities seen in the proxy record of solar variability during the Holocene, or with that of the model of Abreu et al.

Conclusions. We find no support for the hypothesis of a planetary influence on solar activity, and raise the question of whether the centennial periodicities of solar activity observed during the Holocene are representative of solar activity variability in general.

A viscous magnetohydrodynamic Kelvin Helmholtz instability in the interface of two fluid layer Part II An application to the atmosphere of the Sun

Huseyin **Cavus**, G.A. Hoshoudy

2019

https://arxiv.org/ftp/arxiv/papers/1907/1907.07419.pdf
The main aim of this submission is to investigate the effects of some parameters like wave number, shear velocity, magnetic field and temperature for the growth rate of the magnetized Kelvin-Helmholtz instability (KHI) with incessant profiles through interface of two viscous fluid layer occurred in the solar atmosphere using the model of Hoshoudy, Cavus and Mahdy (2019). In this examination, the presence of KHI is identified for the various cases of wave number, magnetic field, shear velocity and temperature in the solar atmosphere. The sensible values of these parameters were acquired.

Stellar Surface Magneto-Convection as a Source of Astrophysical Noise III. Sun-as-a-star Simulations and Optimal Noise Diagnostics

H. M. **Cegla**, C. A. Watson, S. Shelyag, M. Mathioudakis, S. Moutari
ApJ **2019**
https://arxiv.org/pdf/1903.08446.pdf
Stellar surface magnetoconvection (granulation) creates asymmetries in the observed stellar absorption lines that can subsequently manifest themselves as spurious radial velocities shifts. In turn, this can then mask the Doppler-reflex motion induced by orbiting planets on their host stars, and represents a particular challenge for determining the masses of low-mass, long-period planets. Herein, we study this impact by creating Sun-as-a-star observations that encapsulate the granulation variability expected from 3D magnetohydrodynamic simulations. These Sun-as-a-star model observations are in good agreement with empirical observations of the Sun, but may underestimate the total variability relative to the quiet Sun due to the increased magnetic field strength in our models. We find numerous line profile characteristics linearly correlate with the disc-integrated convection-induced velocities. Removing the various correlations with the line bisector, equivalent width, and the V_asy indicator may reduce ~50-60% of the granulation noise in the measured velocities. We also find that simultaneous photometry may be a key diagnostic, as our proxy for photometric brightness also allowed us to remove ~50% of the granulation-induced radial velocity noise. These correlations and granulation-noise mitigations breakdown in the presence of low instrumental resolution and/or increased stellar rotation, as both act to smooth the observed line profile asymmetries.

A Tale of Two Emergences: Sunrise II Observations of Emergence Sites in a Solar Active Region

Rebecca **Centeno**, Julian Blanco Rodriguez, Jose Carlos Del Toro Iniesta, Sami K. Solanki, Peter Barthol, Achim Gandorfer, Laurent Gizon, Johann Hirzberger, Tino L. Riethmuller, Michiel van Noort, David Orozco Suarez, Wolfgang Schmidt, Valentin Martinez Pillet, Michael Knolker
the Sunrise II Special Issue in the Astrophysical Journal Supplement Series **2016**
https://arxiv.org/pdf/1610.03531v1.pdf
In June 2013, the two scientific instruments onboard the second Sunrise mission witnessed, in detail, a small-scale magnetic flux emergence event as part of the birth of an active region. The Imaging Magnetograph Experiment (IMaX) recorded two small (~5 arcsec) emerging flux patches in the polarized filtergrams of a photospheric Fe I spectral line. Meanwhile, the Sunrise Filter Imager (SuFI) captured the highly dynamic chromospheric response to the magnetic fields pushing their way through the lower solar atmosphere. The serendipitous capture of this event offers a closer look at the inner workings of active region emergence sites. In particular, it reveals in meticulous detail how the rising magnetic fields interact with the granulation as they push through the Sun's surface, dragging photospheric plasma in their upward travel. The plasma that is burdening the rising field slides along the field lines, creating fast downflowing channels at the footpoints. The weight of this material anchors this field to the surface at semi-regular spatial intervals, shaping it in an undulatory fashion. Finally, magnetic reconnection enables the field to release itself from its photospheric anchors, allowing it to continue its voyage up to higher layers. This process releases energy that lights up the arch-filament systems and heats the surrounding chromosphere. **2013 June 12**

The Helioseismic and Magnetic Imager (HMI) Vector Magnetic Field Pipeline: Optimization of the Spectral Line Inversion Code

R. **Centeno**, J. Schou, K. Hayashi, A. Norton, J.T. Hoeksema, Y. Liu, K.D. Leka, G. Barnes
Solar Phys., **2014**
http://arxiv.org/pdf/1403.3677v1.pdf
The Very Fast Inversion of the Stokes Vector (VFISV) is a Milne-Eddington spectral line inversion code used to determine the magnetic and thermodynamic parameters of the solar photosphere from observations of the Stokes vector in the 6173 A Fe I line by the Helioseismic and Magnetic Imager (HMI) onboard the Solar Dynamics Observatory (SDO). We report on the modifications made to the original VFISV inversion code in order to optimize its operation within the HMI data pipeline and provide the smoothest solution in active regions. The changes either sped up the computation or reduced the frequency with which the algorithm failed to converge to a satisfactory solution. Additionally, coding bugs which were detected and fixed in the original VFISV release, are reported here.

Effect of intense December 2006 solar radio bursts on GPS receivers

Cerruti, Alessandro P.; Kintner, Paul M., Jr.; Gary, Dale E.; Mannucci, Anthony J.; Meyer, Robert F.; Doherty, Patricia; Coster, Anthea J.
Space Weather, Vol. 6, No. 10, S10D07
http://dx.doi.org/10.1029/2007SW000375
http://onlinelibrary.wiley.com/doi/10.1029/2007SW000375/pdf
Solar radio bursts during December 2006 were sufficiently intense to be measurable with GPS receivers. The strongest event occurred on 6 December 2006 and affected the operation of many GPS receivers. This event exceeded 1,000,000 solar flux unit and was about 10 times larger than any previously reported event. The strength of the event was especially surprising since the solar radio bursts occurred near solar minimum. The strongest periods of solar radio burst activity lasted a few minutes to a few tens of minutes and, in some cases, exhibited large intensity differences between L1 (1575.42 MHz) and L2 (1227.60 MHz). Civilian dual frequency GPS receivers were the most severely affected, and these events suggest that continuous, precise positioning services should account for solar radio bursts in their operational plans. This investigation raises the possibility of even more intense solar radio bursts during the next solar maximum that will significantly impact the operation of GPS receivers.

Alfvén Wave Connection between the Chromosphere and the Corona of the Sun: An Analytical Study

Jongchul **Chae**1 and Kyoung-Sun Lee1
2023 ApJ 954 45
https://iopscience.iop.org/article/10.3847/1538-4357/ace771/pdf
Alfvén waves are closely relevant to the three outstanding problems in the solar corona: coronal heating, solar wind acceleration, and the fractionization of low first ionization potential (FIP) elements. There has been increasing observational evidence for the Alfvén waves, not only in the corona, but also in the chromosphere. Here we investigate the Alfvén wave connection between the chromosphere and the corona based on the analytical solution of Alfvén waves in a layer where Alfvén speed varies along magnetic field lines with a constant gradient. The wave transmission of the layer is determined by two parameters: the Alfvénic cutoff frequency and the dimensionless thickness of the layer. It is shown that the ponderomotive acceleration originating from Alfvén waves is always directed upward in the solar atmosphere with the peak occurring in the chromosphere-corona transition region in association with downward low-frequency waves. We also find that some velocity amplitudes observed in the chromosphere of quiet regions and all the velocity amplitudes observed in active regions fall short of the theoretical estimates obtained with the assumption that the Alfvén waves generated below the chromosphere transport upward the energy required for the corona. We suggest considering the possibility that the Alfvén waves responsible for the coronal heating and the FIP fractionization originate from above the chromosphere.

Propagating Alfvénic Waves Observed in the Chromosphere around a Small Sunspot: Tales of 3-minute Waves and 10-minute Waves

Jongchul **Chae**1, Kyuhyoun Cho1,2,3, Eun-Kyung Lim4, and Juhyung Kang1,4
2022 ApJ 933 108
https://iopscience.iop.org/article/10.3847/1538-4357/ac722e/pdf
Recent observations provided evidence that the solar chromosphere of sunspot regions is pervaded by Alfvénic waves—transverse magnetohydrodynamic (MHD) waves (Alfvén waves or kink waves). In order to systematically investigate the physical characteristics of Alfvénic waves over a wide range of periods, we analyzed the time series of line-of-sight velocity maps constructed from the Hα spectral data of a small sunspot region taken by the Fast Imaging Solar Spectrograph of the Goode Solar Telescope at Big Bear. We identified each Alfvénic wave packet by examining the cross-correlation of band-filtered velocity between two points that are located a little apart presumably on the same magnetic field line. As result, we detected a total of 279 wave packets in the superpenumbral region around the sunspot and obtained their statistics of period, velocity amplitude, and propagation speed. An important finding of ours is that the detected Alfvénic waves are clearly separated into two groups: 3-minute period (<7 minutes) waves and 10-minute period (>7 minutes) waves. We propose two tales on the origin of Alfvénic waves in the chromosphere; the 3-minute Alfvénic waves are excited by the upward-propagating slow waves in the chromosphere through the slow-to-Alfvénic mode conversion, and the 10-minute Alfvénic waves represent the chromospheric manifestation of the kink waves driven by convective motions in the photosphere.
2014 June 3

Inference of chromospheric plasma parameters on the Sun

Multilayer spectral inversion of strong absorption lines
Jongchul **Chae**, Maria S. Madjarska, Hannah Kwak, Kyuhyoun Cho

A&A 640, A45 **2020**
https://arxiv.org/pdf/2006.11981.pdf
https://www.aanda.org/articles/aa/pdf/2020/08/aa38141-20.pdf
The solar chromosphere can be observed well through strong absorption lines. We infer the physical parameters of chromospheric plasmas from these lines using a multilayer spectral inversion. This is a new technique of spectral inversion. We assume that the atmosphere consists of a finite number of layers. In each layer the absorption profile is constant and the source function varies with optical depth with a constant gradient. Specifically, we consider a three-layer model of radiative transfer where the lowest layer is identified with the photosphere and the two upper layers are identified with the chromosphere. The absorption profile in the photosphere is described by a Voigt function, and the profile in the chromosphere by a Gaussian function. This three-layer model is fully specified by 13 parameters. Four parameters can be fixed to prescribed values, and one parameter can be determined from the analysis of a satellite photospheric line. The remaining 8 parameters are determined from a constrained least-squares fitting. We applied the multilayer spectral inversion to the spectral data of the Hα and the Ca II 854.21 nm lines taken in a quiet region by the Fast Imaging Solar Spectrograph (FISS) of the Goode Solar Telescope (GST). We find that our model successfully fits most of the observed profiles and produces regular maps of the model parameters. The combination of the inferred Doppler widths of the two lines yields reasonable estimates of temperature and nonthermal speed in the chromosphere. We conclude that our multilayer inversion is useful to infer chromospheric plasma parameters on the Sun.

Nonlinear Effects in Three-minute Oscillations of the Solar Chromosphere. II. Measurement of Nonlinearity Parameters at Different Atmospheric Levels

Jongchul **Chae**1, Kyuhyoun Cho1, Donguk Song2, and Yuri E. Litvinenko
2018 ApJ 854 127
http://sci-hub.tw/http://iopscience.iop.org/0004-637X/854/2/127/
Recent theoretical studies suggest that the nonlinearity of three-minute velocity oscillations at each atmospheric level can be quantified by the two independent parameters—the steepening parameter and the velocity amplitude parameter. For the first time, we measured these two parameters at different atmospheric levels by analyzing a set of spectral lines formed at different heights of sunspots ranging from the temperature minimum to the transition region. The spectral data were taken by the Fast Imaging Solar Spectrograph of the Goode Solar Telescope, and by the Interface Region Imaging Spectrograph. As a result, from the wavelet power spectra of the velocity oscillations at different heights, we clearly identified the growth of the second harmonic oscillations associated with the steepening of the velocity oscillation, indicating that higher-frequency oscillations of periods of 1.2 to 1.5 minutes originate from the nonlinearity of the three-minute oscillations in the upper chromosphere. We also found that the variation of the measured nonlinearity parameters is consistent with the theoretical expectation that the nonlinearity of the three-minute oscillations increases with height, and shock waves form in the upper chromosphere. There are, however, discrepancies as well between theory and observations, suggesting the need to improve both theory and the measurement technique.

Nonlinear Effects in Three-minute Oscillations of the Solar Chromosphere. I. An Analytical Nonlinear Solution and Detection of the Second Harmonic

Chae, J, & Litvinenko, Y.
2017, ApJ, 844, 129
http://sci-hub.tw/10.3847/1538-4357/aa7be9
The vertical propagation of nonlinear acoustic waves in an isothermal atmosphere is considered. A new analytical solution that describes a finite-amplitude wave of an arbitrary wavelength is obtained. Although the short- and long-wavelength limits were previously considered separately, the new solution describes both limiting cases within a common framework and provides a straightforward way of interpolating between the two limits. Physical features of the nonlinear waves in the chromosphere are described, including the dispersive nature of low-frequency waves, the steepening of the wave profile, and the influence of the gravitational field on wavefront breaking and shock formation. The analytical results suggest that observations of three-minute oscillations in the solar chromosphere may reveal the basic nonlinear effect of oscillations with combination frequencies, superposed on the normal oscillations of the system. Explicit expressions for a second-harmonic signal and the ratio of its amplitude to the fundamental harmonic amplitude are derived. Observational evidence of the second harmonic, obtained with the Fast Imaging Solar Spectrograph, installed at the 1.6 m New Solar Telescope of the Big Bear Observatory, is presented. The presented data are based on the time variations of velocity determined from the Na I D2 and Hα lines.

Detection of Shock Merging in the Chromosphere of a Solar Pore

Jongchul **Chae**1, Donguk Song1, Minju Seo1, Kyung-Suk Cho2, Young-Deuk Park2, and Vasyl Yurchyshyn
2015 ApJ 805 L21

It was theoretically demonstrated that a shock propagating in the solar atmosphere can overtake another and merge with it. We provide clear observational evidence that shock merging does occur quite often in the chromosphere of sunspots. Using Hαimaging spectral data taken by the Fast Imaging Solar Spectrograph of the 1.6 m New Solar Telescope at the Big Bear Soar Observatory, we construct time–distance maps of line-of-sight velocities along two appropriately chosen cuts in a pore. The maps show a number of alternating redshift and blueshift ridges, and we identify each interface between a preceding redshift ridge and the following blueshift ridge as a shock ridge. The important finding of ours is that two successive shock ridges often merge with each other. This finding can be theoretically explained by the merging of magneto-acoustic shock waves propagating with lower speeds of about 10 km s−1 and those propagating at higher speeds of about 16–22 km s−1. The shock merging is an important nonlinear dynamical process of the solar chromosphere that can bridge the gap between higher-frequency chromospheric oscillations and lower-frequency dynamic phenomena such as fibrils.

Cycle and Latitudinal Solar-Wind Structure on Co-Rotation Forecasts

Nachiketa **Chakraborty**, Harriet Turner, Mathew Owens & Matthew Lang
Solar Phys. volume 298, Article number: 142 (**2023**)
https://link.springer.com/content/pdf/10.1007/s11207-023-02232-4.pdf
Studying solar-wind conditions is central to forecasting the impact of space weather on Earth. Under the assumption that the structure of this wind is constant in time and co-rotates with the Sun, solar-wind and thereby space-weather forecasts have been made quite effectively. Such co-rotation forecasts are well studied with decades of observations from STEREO and near-Earth spacecraft. Forecast accuracy is primarily determined by three factors: i) the longitudinal separation of spacecraft from Earth determines the corotation time (and hence forecast lead time) [δt] over which the solar wind must be assumed to be constant, ii) the latitudinal separation (or offset) between Earth and spacecraft [δθ]] determines the degree to which the same solar wind is being encountered at both locations, and iii) the solar cycle, via the sunspot number (SSN), acts as a proxy for both how fast the solar-wind structure is evolving and how much it varies in latitude. However, the precise dependencies factoring in uncertainties are a mixture of influences from each of these factors. Furthermore, for high-precision forecasts, it is important to understand what drives the forecast accuracy and its uncertainty. Here we present a causal inference approach based on information-theoretic measures to do this. Our framework can compute not only the direct (linear and nonlinear) dependencies of the forecast mean absolute error (MAE) on SSN, θ, and t, but also how these individual variables combine to enhance or diminish the MAE. We provide an initial assessment of this with the potential of aiding data assimilation in the future.

Solar Ultraviolet Irradiance Observations of the Solar Flares During the Intense September 2017 Storm Period

P. C. **Chamberlin**, T. N. Woods, L. Didkovsky, F. G. Eparvier, A. R. Jones, J. L. Machol, J. P. Mason, M. Snow, E. M. B. Thiemann, R. A. Viereck, D. L. Woodraska
Space Weather **2018**
http://sci-hub.tw/https://agupubs.onlinelibrary.wiley.com/doi/abs/10.1029/2018SW001866
A large outburst of flares occurred between 4-10 September 2017 when new magnetic flux emerged into and strengthened an existing active region, NOAA Region 12673. This intense solar storm period included X9.3 (**6 September**) and X8.2 (**10 September)** flares, the largest flares that have occurred during solar cycle 24, as well as 39 M-class flares and 3 additional X-class flares. Another X-class flare from this active region was observed on the far-side of the Sun from MAVEN prior to the September events, along with other large M-class flares, showing the potential for how far-side irradiance monitoring can improve flare prediction at Earth for 1 to 13 day forecasts. This September 2017 flare period is similar to other famous storm periods such as the *18 October to 5 November 2003* Halloween storm that produced 14 X-class flares and 137 M-class flares and the *6-10 September 2005* period that had 11 X-class and 68 M-class flares. All of these storm periods occurred in the declining phase of the solar cycle when solar activity had decreased significantly from solar maximum levels. This paper focuses on a number of solar irradiance observations at ultraviolet (0-190 nm) wavelengths during the September 2017 storm period and the advantages that an ensemble of measurements and models have for studying solar flares.

Measuring Solar Doppler Velocities in the He II 30.38 nm Emission Using the EUV Variability Experiment (EVE)

Phillip C. **Chamberlin**
Solar Phys. **2016**

The EUV Variability Experiment (EVE) onboard the Solar Dynamics Observatory has provided unprecedented measurements of the solar EUV irradiance at high temporal cadence with good spectral resolution and range since May 2010. The main purpose of EVE was to connect the Sun to the Earth by providing measurements of the EUV irradiance as a driver for space weather and Living With a Star studies, but after launch the instrument has demonstrated the significance of its measurements in contributing to studies looking at the sources of solar variability for pure solar physics purposes. This paper expands upon previous findings that EVE can in fact measure wavelength shifts during solar eruptive events and therefore provide Doppler velocities for plasma at all temperatures throughout the solar atmosphere from the chromosphere to hot flaring temperatures. This process is not straightforward as EVE was not designed or optimized for these types of measurements. In this paper we describe the many detailed instrumental characterizations needed to eliminate the optical effects in order to provide an absolute baseline for the Doppler shift studies. An example is given of a solar eruption on **7 September 2011** (SOL2011-09-07), associated with an X1.2 flare, where EVE Doppler analysis shows plasma ejected from the Sun in the He II 30.38 nm emission at a velocity of almost 120 km s-1 along the line-of-sight.

An approximate analytic solution to the coupled problems of coronal heating and solar-wind acceleration

Benjamin D. G. **Chandran**
Journal of Plasma Physics **2021**
https://arxiv.org/pdf/2101.04156.pdf
Between the base of the solar corona and the Alfven critical point, the solar-wind density decreases by approximately five orders of magnitude, but the temperature varies by a factor of only a few. In this paper, I show that such quasi-isothermal evolution out to the Alfven critical point is a generic property of outflows powered by reflection-driven Alfven-wave (AW) turbulence, in which outward-propagating AWs partially reflect, and counter-propagating AWs interact to produce a cascade of fluctuation energy to small scales, which leads to turbulent heating. Approximating the sub-Alfvenic region as isothermal, I first present a simplified calculation of the mass outflow rate, asymptotic wind speed, and coronal temperature that neglects conductive losses and the wave pressure force. I then develop a more detailed model of the transition region, corona, and solar wind that accounts for the heat flux from the coronal base into the transition region and momentum deposition by AWs. I solve analytically for this heat flux by balancing, within the transition region, conductive heating against internal-energy losses from radiation, pdV work, and advection. The density at the coronal base is determined by locally balancing turbulent heating and radiative cooling. I solve the equations of the model analytically in two different parameter regimes. Analytic and numerical solutions to the model equations agree with a number of observations.

Power spectrum of turbulent convection in the solar photosphere

L. Yelles **Chaouche**, R. H. Cameron, S. K. Solanki, et al.
A&A 644, A44 **2020**
https://arxiv.org/pdf/2010.09037.pdf
https://doi.org/10.1051/0004-6361/202037545
The solar photosphere provides us with a laboratory for understanding turbulence in a layer where the fundamental processes of transport vary rapidly and a strongly superadiabatic region lies very closely to a subadiabatic layer. Our tools for probing the turbulence are high-resolution spectropolarimetric observations such as have recently been obtained with the two sunrise missions, and numerical simulations. Our aim is to study photospheric turbulence with the help of Fourier power spectra that we compute from observations and simulations. We also attempt to explain some properties of the photospheric overshooting flow with the help of its governing equations and simulations. We find that quiet-Sun observations and smeared simulations exhibit a power-law behavior in the subgranular range of their Doppler velocity power spectra with an index of ≈ -2. The unsmeared simulations exhibit a power-law index of ≈ -2.25. The smearing considerably reduces the extent of the power-law-like portion of the spectra. Therefore, the limited spatial resolution in some observations might eventually result in larger uncertainties in the estimation of the power-law indices.
The simulated vertical velocity power spectra as a function of height show a rapid change in the power-law index from the solar surface to 300~km above it. A scale-dependent transport of the vertical momentum occurs. At smaller scales, the vertical momentum is more efficiently transported sideways than at larger scales. This results in less vertical velocity power transported upward at small scales than at larger scales and produces a progressively steeper vertical velocity power law below 180 km. Above this height, the gravity work progressively gains importance at all scales, making the atmosphere progressively more hydrostatic and resulting in a gradually less steep power law.
2009 June 9, 2013 June 12-13

Solar cycle variation of vmax in helioseismic data and its implications for asteroseismology

William J. **Chaplin**, Sarbani Basu, Warrick H. Ball, Guy R. Davies, Yvonne Elsworth, Steven J. Hale, Andrea Miglio, Martin Bo Nielsen, Lucas S. Viani
MNRAS Letters, **2020**, vol 493, pages L49 – 53

https://arxiv.org/pdf/2001.10949.pdf
The frequency, νmax, at which the envelope of pulsation power peaks for solar-like oscillators is an important quantity in asteroseismology. We measure νmax for the Sun using 25 years of Sun-as-a-Star Doppler velocity observations with the Birmingham Solar-Oscillations Network (BiSON), by fitting a simple model to binned power spectra of the data. We also apply the fit to Sun-as-a-Star Doppler velocity data from GONG and GOLF, and photometry data from VIRGO/SPM on the ESA/NASA SOHO spacecraft. We discover a weak but nevertheless significant positive correlation of the solar νmax with solar activity. The uncovered shift between low and high activity, of ≃25μHz, translates to an uncertainty of 0.8 per cent in radius and 2.4 per cent in mass, based on direct use of asteroseismic scaling relations calibrated to the Sun. The mean νmax in the different datasets is also clearly offset in frequency. Our results flag the need for caution when using νmax in asteroseismology.

Sensitivity of low-degree solar p modes to active and ephemeral regions: frequency shifts back to the Maunder Minimum

William J. **Chaplin**, Rachel Howe, Sarbani Basu, Yvonne Elsworth, Timothy W. Milbourne, Raphaëlle D. Haywood, Guy R. Davies, Steven J. Hale, Andrea Miglio, Eddie Ross
MNRAS **2019**
https://arxiv.org/pdf/1908.08755.pdf
We explore the sensitivity of the frequencies of low-degree solar p-modes to near-surface magnetic flux on different spatial scales and strengths, specifically to active regions with strong magnetic fields and ephemeral regions with weak magnetic fields. We also use model reconstructions from the literature to calculate average frequency offsets back to the end of the Maunder minimum. We find that the p-mode frequencies are at least three times less sensitive (at 95% confidence) to the ephemeral-region field than they are to the active-region field. Frequency shifts between activity cycle minima and maxima are controlled predominantly by the change of active region flux. Frequency shifts at cycle minima (with respect to a magnetically quiet Sun) are determined largely by the ephemeral flux, and are estimated to have been 0.1μHz or less over the last few minima. We conclude that at epochs of cycle minimum, frequency shifts due to near-surface magnetic activity are negligible compared to the offsets between observed and model frequencies that arise from inaccurate modelling of the near-surface layers (the so-called surface term). The implication is that this will be the case for other Sun-like stars with similar activity, which has implications for asteroseismic modelling of stars.

Inferences on Stellar Activity and Stellar Cycles from Asteroseismology **Review**

William J. **Chaplin**, Sarbani Basu
Space Science Reviews, December **2014**, Volume 186, Issue 1-4, pp 437-456
The solar activity cycle can be studied using many different types of observations, such as counting sunspots, measuring emission in the Ca II H&K lines, magnetograms, radio emissions, etc. One of the more recent ways of studying solar activity is to use the changing properties of solar oscillations. Stellar activity cycles are generally studied using the Ca II lines, or sometimes using photometry. Asteroseismology is potentially an exciting means of studying these cycles. In this article we examine whether or not asteroseismic data can be used for this purpose, and what the asteroseismic signatures of stellar activity are. We also examine how asteroseismology may help in more indirect ways.

Charting the solar cycle.

Chapman SC
Front. Astron. Space Sci. 9: 1037096 **2023**
https://www.frontiersin.org/articles/10.3389/fspas.2022.1037096/pdf
Sunspot records reveal that whilst the Sun has an approximately 11 year cycle of activity, no two cycles are of the same duration. Since this activity is a direct driver of space weather at Earth, this presents an operational challenge to quantifying space weather risk. We recently showed that the Hilbert transform of the sunspot record can be used to map the variable cycle length onto a regular “clock” where each cycle has the same duration in Hilbert analytic phase. Extreme geomagnetic storms rarely occur within the quiet part of the cycle which is a fixed interval of analytic phase on the clock; there is a clear active-quiet switch-off and quiet-active switch-on of activity. Here we show how the times of the switch-on/off can be determined directly from the sunspot time-series, without requiring a Hilbert transform. We propose a method-charting-that can be used to combine observations, and reports of societal impacts, to improve our understanding of space weather risk.

The Sun's magnetic (Hale) cycle and 27 day recurrences in the aa geomagnetic index

S. C. **Chapman**, S. W. McIntosh, R. J. Leamon, N. W. Watkins
ApJ **917** 54 **2021**
https://arxiv.org/pdf/2101.02569.pdf
https://doi.org/10.3847/1538-4357/ac069e

We construct a new solar cycle phase clock which maps each of the last 18 solar cycles onto a single normalized epoch for the approximately 22 year Hale (magnetic polarity) cycle, using the Hilbert transform of daily sunspot numbers (SSN) since 1818. The occurrences of solar maxima show almost no Hale cycle dependence, confirming that the clock is synchronized to polarity reversals. The odd cycle minima lead the even cycle minima by ~ 1.1 normalized years, whereas the odd cycle terminators (McIntosh et al. (2019)) lag the even cycle terminators by ~ 2.3 normalized years. The mimimum-terminator interval is thus relatively extended for odd cycles and shortened for even ones. We re-engineer the Sargent(1985,2021) R27 index and combine it with our epoch analysis to obtain a high time resolution parameter for 27 day recurrence in aa, <acv(27)>. This reveals that the transition to recurrence, that is, to an ordered solar wind dominated by high speed streams, is fast, occurring within 2-3 solar rotations or less. It resolves an extended late declining phase which is approximately twice as long on even Schwabe cycles as odd. Galactic Cosmic Ray flux rises in step with <acv(27)> but then stays high. Our analysis also identifies a slow timescale trend in SSN that simply tracks the Gleissberg cycle. We find that this trend is in phase with the slow timescale trend in the modulus of sunspot latitudes, and in antiphase with that of the R27 index.

Reproducible Aspects of the Climate of Space Weather Over the Last Five Solar Cycles

S. C. **Chapman**, N. W. Watkins, E. Tindale

Space Weather

Volume16, Issue8 August **2018** Pages 1128-1142

https://agupubs.onlinelibrary.wiley.com/doi/10.1029/2018SW001884

Each solar maximum interval has a different duration and peak activity level, which is reflected in the behavior of key physical variables that characterize solar and solar wind driving and magnetospheric response. The variation in the statistical distributions of the F10.7 index of solar coronal radio emissions, the dynamic pressure PDyn and effective convection electric field Ey in the solar wind observed in situ upstream of Earth, the ring current index DST, and the high-latitude auroral activity index AE are tracked across the last five solar maxima. For each physical variable we find that the distribution tail (the exceedences above a threshold) can be rescaled onto a single master distribution using the mean and variance specific to each solar maximum interval. We provide generalized Pareto distribution fits to the different master distributions for each of the variables. If the mean and variance of the large-to-extreme observations can be predicted for a given solar maximum, then their full distribution is known.

An Observed Decline in the Amplitude of Recent Solar-Cycle Peaks

G. A. **Chapman**, G. de Toma, A. M. Cookson

Solar Phys., Volume 289, Issue 10, pp 3961-3967, **2014**

There has been much speculation about the extended minimum between Solar Cycles 23 and 24. Cycle 24 itself has been unusually weak compared with recent cycles. We present quantitative evidence for the weakness of both Cycles 23 and, particularly, 24. The data are objective indices derived from precision photometric images obtained on a daily basis at the San Fernando Observatory. These data form the longest running, homogeneous photometric record known to us. We show sunspot areas from red images and facular/network areas from Ca ii K-line images. Spot and facular area are a simple and direct measurement of the strength of solar activity. The data clearly show the decline in the amplitude of sunspot maxima for Cycles 23 and 24 compared with Cycle 22. The relative amplitudes of mean spot area for Cycles 22 through 24 are 1.0, 0.74, and 0.37, respectively. There is also an indication that the facular-to-spot area ratio has increased in Cycle 24.

Evolution of solar and stellar dynamo theory **Review**

Paul **Charbonneau**, Dmitry Sokoloff

Space Science Reviews **219**, Article number: 35 **2023**

https://arxiv.org/pdf/2305.16553.pdf

https://link.springer.com/content/pdf/10.1007/s11214-023-00980-0.pdf

In this paper, written as a general historical and technical introduction to the various review papers collected in the special issue ``Solar and Stellar Dynamo: A New Era", we review the evolution and current state of dynamo theory and modelling, with emphasis on the solar dynamo. Starting with a historical survey, we then focus on a set of ``tension points" that are still left unresolved despite the remarkable progress of the past century. In our discussion of these tension points we touch upon the physical well-posedness of mean-field electrodynamics; constraints imposed by magnetic helicity conservation; the troublesome role of differential rotation; meridional flows and flux transpost dynamos; competing inductive mechanisms and Babcock-Leighton dynamos; the ambiguous precursor properties of the solar dipole; cycle amplitude regulation and fluctuation through nonlinear backreaction and stochastic forcing, including Grand Minima; and the promises and puzzles offered by global magnethydrodynamical numerical simulations of convection and dynamo action. We close by considering the potential bridges to be constructed between solar dynamo theory and modelling, and observations of magnetic activity in late-type stars.

External Forcing of the Solar Dynamo

Paul **Charbonneau**

Front. Astron. Space Sci., 9:853676. **2022** |

https://www.frontiersin.org/articles/10.3389/fspas.2022.853676/full

https://doi.org/10.3389/fspas.2022.853676

In this paper I examine whether external forcing of the solar dynamo on long timescales can produce detectable signal in the form of long term modulation of the magnetic cycle. This task is motivated in part by some recent proposals (Abreu et al., 2012; Astron. Ap., 548, A88; Stefani et al., 2021; Solar Phys., 296, 88), whereby modulation of the solar activity cycle on centennial and millennial timescales, as recovered from the cosmogenic radioisotope record, is attributed to perturbation of the tachocline driven by planetary orbital motions. Working with a two-dimensional mean-field-like kinematic dynamo model of the Babcock-Leighton variety, I show that such an external forcing signal may be detectable in principle but is likely to be obliterated by other internal sources of fluctuations, in particular stochastic perturbations of the dynamo associated with convective turbulence, unless a very efficient amplification mechanism is at play. I also examine the ability of external tidal forcing to synchronize an otherwise autonomous, internal dynamo operating at a nearby frequency. Synchronization is readily achieved, and turns out to be very robust to the introduction of stochastic noise, but requires very high forcing amplitudes, again highlighting the critical need for a powerful amplification mechanism.

Dynamo Models of the Solar Cycle **Review**

Paul **Charbonneau**

Living Reviews in Solar Physics, **17**, Article number: 4 , **2020**

https://link.springer.com/content/pdf/10.1007/s41116-020-00025-6.pdf

This paper reviews recent advances and current debates in modeling the solar cycle as a hydromagnetic dynamo process. Emphasis is placed on (relatively) simple dynamo models that are nonetheless detailed enough to be comparable to solar cycle observations. After a brief overview of the dynamo problem and of key observational constraints, I begin by reviewing the various magnetic field regeneration mechanisms that have been proposed in the solar context. I move on to a presentation and critical discussion of extant solar cycle models based on these mechanisms, followed by a discussion of recent magnetohydrodynamical simulations of solar convection generating solar-like large-scale magnetic cycles. I then turn to the origin and consequences of fluctuations in these models and simulations, including amplitude and parity modulation, chaotic behavior, and intermittency. The paper concludes with a discussion of our current state of ignorance regarding various key questions relating to the explanatory framework offered by dynamo models of the solar cycle

Editorial: 50 Years of Solar Physics

Paul **Charbonneau** J. Leibacher, C. Mandrini, L. van Driel-Gesztelyi, M.S. Wheatland

Solar Phys. Volume 291, Issue 12, pp 3461–3465 **2016**

Dynamo Models of the Solar Cycle **Review**

Paul **Charbonneau**

Living Reviews in Solar Physics, **2010**

http://solarphysics.livingreviews.org/Articles/lrsp-2010-3/

ABSTRACT:

This paper reviews recent advances and current debates in modeling the solar cycle as a hydromagnetic dynamo process. Emphasis is placed on (relatively) simple dynamo models that are nonetheless detailed enough to be comparable to solar cycle observations. After a brief overview of the dynamo problem and of key observational constraints, we begin by reviewing the various magnetic field regeneration mechanisms that have been proposed in the solar context. We move on to a presentation and critical discussion of extant solar cycle models based on these mechanisms. We then turn to the origin and consequences of fluctuations in these models, including amplitude and parity modulation, chaotic behavior, intermittency, and predictivity. The paper concludes with a discussion of our current state of ignorance regarding various key questions relating to the explanatory framework offered by dynamo models of the solar cycle.

NOTE ON THE UPDATE:

Besides updates relating to the literature published in the past five years (added about 60 new references), and reworking a few sections of the 2005 version, main major novelties compared to the 2005 version are: 1. Material on turbulent pumping, and its effect in various types of dynamo models. 2. Expanded Section 4.9 on MHD numerical simulations of large-scale dynamo action. 3. Added Section 5.7 on dynamo model-based cycle prediction schemes. 4. Inclusion (and discussion of) animations directly in the text. By appropriate deletions elsewhere in the review, I have managed to retain
its overall length at nearly the same as the 2005 version.

Is the faint young Sun problem for Earth solved?

Benjamin **Charnay**, Eric T. Wolf, Bernard Marty, François Forget
Space Science Reviews. **216**, Article number: 90 **2020**
https://arxiv.org/pdf/2006.06265
https://link.springer.com/content/pdf/10.1007/s11214-020-00711-9.pdf
Stellar evolution models predict that the solar luminosity was lower in the past, typically 20-25 % lower during the Archean (3.8-2.5 Ga). Despite the fainter Sun, there is strong evidence for the presence of liquid water on Earth's surface at that time. This "faint young Sun problem" is a fundamental question in paleoclimatology, with important implications for the habitability of the early Earth, early Mars and exoplanets. Many solutions have been proposed based on the effects of greenhouse gases, atmospheric pressure, clouds, land distribution and Earth's rotation rate. Here we review the faint young Sun problem for Earth, highlighting the latest geological and geochemical constraints on the early Earth's atmosphere, and recent results from 3D global climate models and carbon cycle models. Based on these works, we argue that the faint young Sun problem for Earth has essentially been solved. Unfrozen Archean oceans were likely maintained by higher concentrations of CO2, consistent with the latest geological proxies, potentially helped by additional warming processes. This reinforces the expected key role of the carbon cycle for maintaining the habitability of terrestrial planets. Additional constraints on the Archean atmosphere and 3D fully coupled atmosphere-ocean models are required to validate this conclusion.

Homogenising SoHO/EIT and SDO/AIA 171Å Images: A Deep Learning Approach

Subhamoy **Chatterjee**, Andrés Muñoz-Jaramillo, Maher Dayeh, Hazel M. Bain, Kimberly Moreland
ApJS **268** 33 **2023**
https://arxiv.org/pdf/2308.10322.pdf
https://iopscience.iop.org/article/10.3847/1538-4365/ace9d7/pdf
Extreme Ultraviolet images of the Sun are becoming an integral part of space weather prediction tasks. However, having different surveys requires the development of instrument-specific prediction algorithms. As an alternative, it is possible to combine multiple surveys to create a homogeneous dataset. In this study, we utilize the temporal overlap of SoHO/EIT and SDO/AIA 171~Å ~surveys to train an ensemble of deep learning models for creating a single homogeneous survey of EUV images for 2 solar cycles. Prior applications of deep learning have focused on validating the homogeneity of the output while overlooking the systematic estimation of uncertainty. We use an approach called `Approximate Bayesian Ensembling' to generate an ensemble of models whose uncertainty mimics that of a fully Bayesian neural network at a fraction of the cost. We find that ensemble uncertainty goes down as the training set size increases. Additionally, we show that the model ensemble adds immense value to the prediction by showing higher uncertainty in test data that are not well represented in the training data. **20 Feb 2011**

Editorial: Study of Long-Term Solar Datasets: Exploring Spatio-Temporal Patterns of Solar Variability on Different Time Scales and Implications in Space Weather

Subhamoy **Chatterjee**, Dipankar Banerjee, and Mausumi Dikpati
Front. Astron. Space Sci., 10 :1207120. **2023**
https://doi.org/10.3389/fspas.2023.1207120
https://www.frontiersin.org/articles/10.3389/fspas.2023.1207120/pdf

Efficient labeling of solar flux evolution videos by a deep learning model

Subhamoy **Chatterjee**, Andrés Muñoz-Jaramillo, Derek A. Lamb
Nat.Astron.6(**2022**)796-803
https://arxiv.org/pdf/2308.14976
Machine learning (ML) is becoming a critical tool for interrogation of large complex data. Labeling, defined as the process of adding meaningful annotations, is a crucial step of supervised ML. However, labeling datasets is time consuming. Here we show that convolutional neural networks (CNNs), trained on crudely labeled astronomical videos, can be leveraged to improve the quality of data labeling and reduce the need for human intervention. We use videos of the solar magnetic field, crudely labeled into two classes: emergence or non-emergence of bipolar magnetic regions (BMRs), based on their first detection on the solar disk. We train CNNs using crude labels, manually verify, correct labeling vs. CNN disagreements, and repeat this process until convergence. Traditionally, flux emergence labelling is done manually. We find that a high-quality labeled dataset, derived through this iterative process, reduces the necessary manual verification by 50%. Furthermore, by gradually masking the videos and looking for maximum change in CNN inference, we locate BMR emergence time without retraining the CNN. This demonstrates the versatility of CNNs for simplifying the challenging task of labeling complex dynamic events.

Signature of Extended Solar Cycles as Detected from Ca II K Synoptic Maps of Kodaikanal and Mount Wilson Observatory

Subhamoy **Chatterjee**, Dipankar Banerjee, Scott W. McIntosh, Robert J. Leamon, Mausumi Dikpati, Abhishek K. Srivastava, Luca Bertello
ApJL **874** L4 **2019**
https://arxiv.org/pdf/1903.03598.pdf
In the recent years there has been a resurgence of the study of Extended Solar Cycles (ESCs) through observational proxies mainly in Extreme Ultraviolet. But most of them are limited only to space-based era covering only about two solar cycles. Long-term historical data-sets are worth in examining the consistency of ESCs. Kodaikanal Solar Observatory (KSO) and Mount Wilson Observatory (MWO) are the two major sources of long-term Ca II K digitised spectroheliograms covering the temporal spans 1907-2007 and 1915-1985 respectively. In this study, we detected supergranule boundaries, commonly known as networks, using the Carrington maps from both KSO and MWO datasets. Subsequently we excluded the plage areas to consider only quiet sun (QS) and detected small scale bright features through intensity thresholding over the QS network. Latitudinal density of those features, which we named as `Network Bright Elements' (NBEs), could clearly depict the existence of overlapping cycles with equator-ward branches starting at latitude ≈55∘ and taking about 15±1 years to reach the equator. We performed superposed epoch analysis to depict the similarity of those extended cycles. Knowledge of such equator-ward band interaction, for several cycles, may provide critical constraints on solar dynamo models.

Testing Alfvén wave propagation in a realistic set-up of the solar atmosphere

Piyali **Chatterjee**
Geophysical and Astrophysical Fluid dynamics special issue **2018**
https://arxiv.org/pdf/1806.08166.pdf
We present a radiative magneto-hydrodynamic simulation set-up using the Pencil code to study the generation, propagation and dissipation of Alfv\'en waves in the solar atmosphere which includes a convective layer and photosphere below, and the chromosphere, transition region and the corona above. We outline the procedure to prepare the initial state where the solar convection has reached a steady state and the imposed external magnetic field has reached the final value, gradually increasing from a very small initial value. Any new simulation to study Alfv\'en wave propagation can be started from this state which has been thus prepared. We present first results about the nature of waves excited in this simulation run.

Detecting Prominences from Century-long Disc-blocked C\MakeLowercase{a}~{\sc ii}~K Spectroheliograms of Kodaikanal Observatory

Subhamoy **Chatterjee**, Manjunath Hegde, Dipankar Banerjee, B. Ravindra
ApJ **2018**
https://arxiv.org/pdf/1802.07556.pdf
Kodaikanal Solar Observatory (KoSO) has recently digitised the long-term (1906-2002) disc-blocked Ca~{\sc ii}~K spectroheliograms. This data has been archived at \url{this https URL}. The intriguing features seen in the images are the off-limb prominences which provides a proxy for understanding the solar magnetic activities over a long period of time. To make use of this unique dataset we performed calibration of the raw data and developed an automated technique to identify the prominence locations on daily images. We use the recorded prominence latitudes to generate their time-latitude distribution and find clear signature of poleward migration for about 8 cycles complementing the Ha observation in KoSO. We study the drift rate of polar prominences across solar cycles and latitudes. North-South asymmetries of the drift rates are also computed. We show how latitudinal distribution of prominences vary over a period of 11 years and the dominant latitudes in the aggregate distribution. As one of major sources of coronal mass ejection (CME) is eruptive prominence, the latitudinal distribution of prominences can provide additional input for the understanding of the generation of CMEs, particularly the slow CMEs. Clear depiction of polar rush for multiple cycles presented in this work should be valuable in the study of prediction of solar cycles.

Long term study of the solar filaments from the Synoptic Maps as derived from Hα Spectroheliograms of Kodaikanal Observatory

Subhamoy **Chatterjee**, Manjunath Hegde, Dipankar Banerjee, B. Ravindra
ApJ **849** 44 **2017**
https://arxiv.org/pdf/1707.05658.pdf
The century long (1914-2007) Hα (656.28 nm) spectroheliograms from Kodaikanal Solar Observatory (KSO) have been recently digitised. Using these newly calibrated, processed images we study the evolution of dark elongated on disk structures called filaments, potential representatives of magnetic activities on the Sun. To our knowledge this is the oldest uniform digitised dataset with daily images available today in Hα. We generate Carrington maps for entire time duration and try to find the correspondences with maps of same rotation from Ca II K KSO data. Filaments are segmented from Carrington maps using a semi-automated technique and are studied individually to extract their centroids and tilts. We plot the time-latitude distribution of filament centroids producing Butterfly diagram, which clearly shows presence of poleward migration. We separate polar filaments for each cycle and try to estimate the

delay between the polar filament number cycle and sunspot number cycle peaks. We correlate this delay with the same between polar reversal and sunspot number maxima. This provides new insight on the role of polar filaments on polar reversal.

Variation of Supergranule Parameters With Solar Cycles: Results From Century-Long Kodaikanal Digitized Ca II K Data

Subhamoy **Chatterjee**, Sudip Mandal, Dipankar Banerjee
ApJ 841 70 **2017**
https://arxiv.org/pdf/1705.00175.pdf

The century-long (1907-2007) Ca II K spectroheliograms from Kodaikanal Solar Observatory, India, has recently been digitised and calibrated. Applying a fully-automated algorithm (which includes contrast enhancement and 'Watershed method') on this data, we have identified the supergranules and calculated the associated parameters, such as scale, circularity, fractal dimension. We have segregated the quiet and active regions and obtained the supergranule parameters separately for these two domains. In this way, we have isolated the effect of large and small scale magnetic fields on such structures and find significantly different behavior of the supergranule parameters over solar cycles. Such differences indicate the intrinsic changes in the physical mechanism behind generation and evolution of supergranules in presence of small and large scale magnetic fields. This also highlights the need for further studies using solar dynamo theory along with magneto-convection models.

Butterfly Diagram and Carrington Maps for Century-Long Ca II K Spectroheliograms from Kodaikanal Observatory

Subhamoy **Chatterjee**, Dipankar Banerjee, B. Ravindra
ApJ **827** 87 **2016**
http://arxiv.org/pdf/1605.08219v1.pdf

The century-long (1907-2007) Ca II K spectroheliograms from Kodaikanal Solar Observatory (KSO) are calibrated, processed and analysed in the present study to follow the evolution of bright on disc structures called plages, the possible representatives of magnetic activity on the Sun. This has been the longest dataset studied in Ca II K till date covering about 9.5 cycles of 11 year periods. Plages were segmented with area $\geq$1arcmin^2 using global thresholds for individual full disc images and subsequent application of morphological closing operation. Plage index was calculated and seen to have close positive correlation with fractional disc area covered by plages. The newly generated plage area cycle (from KSO) was compared with the same from Mount Wilson observatory (Correlation~95.6%) for the overlapping years i.e. 1915-2000. Study illustrated time-latitude distribution of plage centroids rendering butterfly diagram (as observed for sunspots). The 3D visualisation of the diagram showed one to one mapping between plage location, time and area. This work further delineated positional correlation between magnetic patches and plage regions through comparison of synoptic maps derived from both Kodaikanal Ca II K images and space based full disc LOS (line of sight) magnetograms. Regular synoptic magnetograms from ground based observatories are available only after 1970s. Thus the long term Ca II K data from KSO can be used as a proxy for estimating magnetic activity locations and their strengths at earlier times.

Wave Reflection in the Solar Atmosphere

Varun **Chaturmutha**, Bernhard Fleck, Stuart Jefferies
ApJ **966** 200 **2024**
https://arxiv.org/pdf/2403.18988.pdf
https://iopscience.iop.org/article/10.3847/1538-4357/ad36c5/pdf

We present evidence supporting wave reflection in the lower solar chromosphere based on helioseismic analysis of multi-height Doppler data. This evidence is derived through a wave propagation model that incorporates both upward- and downward-traveling (reflected) waves. Moreover, we find that the height of the reflecting region varies with magnetic field strengths in a way that suggests a connection with the the plasma $\beta \sim 1$ region. We measure an effective reflection coefficient of 13% in a magnetically quiet region of the Sun.

Discussion of Implausible Total Solar-Irradiance Variations Since 1700.

Chatzistergos, T. A
Sol Phys 299, 21 (**2024**).
https://doi.org/10.1007/s11207-024-02262-6

The Sun plays a role in influencing Earth's climate, making it important to have accurate information about variations in the Sun's radiative output. Models are used to recover total solar-irradiance (TSI) variations in the past when direct space-based measurements are not available. One of the most cryptic such TSI reconstructions is the one by (J. Geophys. Res. 98, 18, 1993, HS93). The rather vague description of the model methodology, the arbitrary selection of solar indices it employs, and the short overlap between the HS93 series and directly measured TSI

values has hindered any evaluation of the performance of this model to this day. Here, we aim at rectifying this by updating the HS93 model with new input data. In this way we are also contributing in the discussion on the possible long-term changes in solar irradiance.
Correction: *Sol Phys* **299**, 35 (**2024**). https://link.springer.com/content/pdf/10.1007/s11207-024-02286-y.pdf

Long-term changes in solar activity and irradiance

Theodosios **Chatzistergos**, Natalie A. Krivova, Kok Leng Yeo
2023
https://arxiv.org/pdf/2303.03046.pdf
The Sun is the main energy source to Earth, and understanding its variability is of direct relevance to climate studies. Measurements of total solar irradiance exist since 1978, but this is too short compared to climate-relevant time scales. Coming from a number of different instruments, these measurements require a cross-calibration, which is not straightforward, and thus several composite records have been created. All of them suggest a marginally decreasing trend since 1996. Most composites also feature a weak decrease over the entire period of observations, which is also seen in observations of the solar surface magnetic field and is further supported by Ca II K data. Some inconsistencies, however, remain and overall the magnitude and even the presence of the long-term trend remain uncertain. Different models have been developed, which are used to understand the irradiance variability over the satellite period and to extend the records of solar irradiance back in time. Differing in their methodologies, all models require proxies of solar magnetic activity as input. The most widely used proxies are sunspot records and cosmogenic isotope data on centennial and millennial time scale, respectively. None of this, however, offers a sufficiently good, independent description of the long-term evolution of faculae and network responsible for solar brightening. This leads to uncertainty in the amplitude of the long-term changes in solar irradiance. Here we review recent efforts to improve irradiance reconstructions on time scales longer than the solar cycle and to reduce the existing uncertainty in the magnitude of the long-term variability. In particular, we highlight the potential of using 3D magnetohydrodynamical simulations of the solar atmosphere as input to more physical irradiance models and of historical full-disc Ca II K observations encrypting direct facular information back to 1892.

Full-disc Ca II K observations - a window to past solar magnetism

Theodosios **Chatzistergos**, Natalie Krivova, and Ilaria Ermolli
Front. Astron. Space Sci. 9:1038949. **2022**
https://doi.org/10.3389/fspas.2022.1038949
https://www.frontiersin.org/articles/10.3389/fspas.2022.1038949/pdf
Full-disc observations of the Sun in the Ca ii K line provide one of the longest collections of solar data. First such observations were made in 1892 and since then various sites around the world have carried out regular observations, with Kodaikanal, Meudon, Mt Wilson, and Coimbra being some of the most prominent ones. By now, Ca ii K observations from over 40 different sites allow an almost complete daily coverage of the last century. Ca ii K images provide direct information on plage and network regions on the Sun and, through their connection to solar surface magnetic field, offer an excellent opportunity to study solar magnetism over more than a century. This makes them also extremely important, among others, for solar irradiance reconstructions and studies of the solar influence on Earth's climate. However, these data also suffer from numerous issues, which for a long time have hampered their analysis. Without properly addressing these issues, Ca ii K data cannot be used to their full potential. Here, we first provide an overview of the currently known Ca ii K data archives and sources of the inhomogeneities in the data, before discussing existing processing techniques, followed by a recap of the main results derived with such data so far.

Full-disc Ca II K observations -- a window to past solar magnetism

Theodosios **Chatzistergos**, Natalie A. Krivova, Ilaria Ermolli
Frontiers in Astronomy and Space Sciences **2022**
https://arxiv.org/pdf/2210.13285
First such observations were made in 1892 and since then various sites around the world have carried out regular observations, with Kodaikanal, Meudon, Mt Wilson, and Coimbra being some of the most prominent ones. By now, Ca II K observations from over 40 different sites allow an almost complete daily coverage of the last century. Ca II K images provide direct information on plage and network regions on the Sun and, through their connection to solar surface magnetic field, offer an excellent opportunity to study solar magnetism over more than a century. This makes them also extremely important, among others, for solar irradiance reconstructions and studies of the solar influence on Earth's climate. However, these data also suffer from numerous issues, which for a long time have hampered their analysis. Without properly addressing these issues, Ca II K data cannot be used to their full potential. Here, we first provide an overview of the currently known Ca II K data archives and sources of the inhomogeneities

in the data, before discussing existing processing techniques, followed by a recap of the main results derived with such data so far.

Scrutinizing the relationship between plage areas and sunspot areas and numbers

Theodosios **Chatzistergos**, Ilaria Ermolli, Natalie A. Krivova, Teresa Barata, Sara Carvalho, Jean-Marie Malherbe

A&A **2022**

https://arxiv.org/pdf/2209.07077

Studies and reconstructions of past solar activity require data on sunspots as well as faculae/plage and network. Such data are also important for understanding the magnetic activity and variability of the Sun and Sun-like stars. The longest available direct faculae/plage datasets are white-light facular and Ca II K observations going back to 1874 and 1892, respectively. Prior to that time, the only direct data available are for sunspots. We reassess the relationship between plage areas and sunspot records (areas and numbers) since 1892, to allow reconstructions of facular/plage areas which can be employed for studies going further back in time, i.e. over the period when solely sunspot observations are available. We use the plage areas derived from 38 consistently processed Ca II K archives as well as the plage area composite based on these archives. We find the relationship between plage and sunspot areas and numbers to be well represented by a power law function. We further find that the relationships depend on the bandwidth and the solar cycle strength. The reconstructions with a power law relationship are in good agreement with the original plage area series, whereas employment of a cycle-strength-dependent relationship improves the reconstructions only marginally. Performing the same analysis on other previously published plage area series, usually derived from a single archive with diverse processing techniques, returns different results when using different time series. This highlights the importance of applying a consistent processing to the various archives and demonstrates the uncertainties introduced by using previously published series. Our results have implications for past solar activity and irradiance reconstructions as well as for stellar activity studies, which sometimes assume a linear dependence between plage and sunspot areas.

Reconstructing solar irradiance from historical Ca II K observations. I. Method and its validation

Theodosios **Chatzistergos** (1,2), Natalie A. Krivova (1), Ilaria Ermolli (2), Kok Leng Yeo (1), Sudip Mandal (1), Sami K. Solanki (1,3), Greg Kopp (4), Jean-Marie Malherbe (5,6)

A&A 656, A104 **2021**

https://arxiv.org/pdf/2109.05844.pdf

https://www.aanda.org/articles/aa/pdf/2021/12/aa41516-21.pdf

https://doi.org/10.1051/0004-6361/202141516

Knowledge of solar irradiance variability is critical to Earth's climate models and understanding the solar influence on Earth's climate. Direct solar irradiance measurements are only available since 1978. Reconstructions of past variability typically rely on sunspot data. These provide only indirect information on the facular and network regions, which are decisive contributors to irradiance variability on timescales of the solar cycle and longer. Our ultimate goal is to reconstruct past solar irradiance variations using historical full-disc Ca II K observations to describe the facular contribution independently of sunspot observations. Here, we develop the method and test it extensively by using modern CCD-based Ca II K observations and carry out initial tests on two photographic archives. We employ carefully reduced and calibrated Ca II K images from 13 datasets, such as those from the Meudon, Mt Wilson, and Rome observatories. We convert them to unsigned magnetograms and then use them as input to the adapted SATIRE model to reconstruct TSI variations over the period 1978-2019, for which direct irradiance measurements are available. The reconstructed TSI from the analysed Ca II K archives agrees well with direct TSI measurements and existing reconstructions. The model also returns good results on data taken with different bandpasses and images with low spatial resolution. Historical Ca II K archives suffer from numerous inconsistencies, but we show that these archives can still be used to reconstruct TSI with reasonable accuracy provided the observations are accurately processed. By using the unsigned magnetograms of the Sun reconstructed from high-quality Ca II K observations as input into the SATIRE model, we can reconstruct solar irradiance variations nearly as accurately as from directly recorded magnetograms.

Modelling solar irradiance from ground-based photometric observations

Theodosios **Chatzistergos**, Ilaria Ermolli, Fabrizio Giorgi, Natalie A. Krivova, Cosmin Constantin Puiu

Journal of Space Weather and Space Climate **10**, 45 **2020**

https://arxiv.org/pdf/2008.10735.pdf

https://www.swsc-journal.org/articles/swsc/pdf/2020/01/swsc200052.pdf

Total solar irradiance (TSI) has been monitored from space since 1978. The measurements show a prominent variability in phase with the solar cycle, as well as fluctuations on timescales shorter than a few days. However, the measurements were done by multiple and usually relatively short-lived missions making the possible long-term trend in the TSI highly uncertain. While the variability in the UV irradiance is clearly in-phase with the solar cycle,

the phase of the variability in the visible range has been debated. In this paper, we aim at getting an insight into the long-term trend of TSI since 1996 and the phase of the solar irradiance variations in the visible part of the spectrum. We use independent ground-based full-disc photometric observations in Ca~II~K and continuum from the Rome and San Fernando observatories to compute the TSI since 1996. We follow the empirical San Fernando approach based on the photometric sum index. We find a weak declining trend in the TSI of -7.8+4.9−0.8×10−3 Wm−2y−1 between the 1996 and 2008 activity minima, while between 2008 and 2019 the reconstructed TSI shows no trend to a marginally decreasing (but statistically insignificant) trend of -0.1+0.25−0.02×10−3 Wm−2y−1. The reference TSI series used for the reconstruction does not significantly affect the determined trend. The variation in the blue continuum (409.2 nm) is rather flat, while the variation in the red continuum (607.1 nm) is marginally in anti-phase, although this result is extremely sensitive to the accurate assessment of the quiet Sun level in the images. These results provide further insights into the long-term variation of the total solar irradiance. The amplitude of the variations in the visible is below the uncertainties of the processing, which prevents an assessment of the phase of the variations.

Analysis of full disc Ca II K spectroheliograms III. Plage area composite series covering 1892-2019

Theodosios **Chatzistergos**, Ilaria Ermolli, Natalie A. Krivova, …, Andrey G. Tlatov
A&A 639, A88 **2020**
https://arxiv.org/pdf/2005.01435.pdf
We derive the plage area evolution over the last 12 solar cycles employing data from all Ca II K archives available publicly in digital form known to us, including several as yet unexplored Ca II K archives. We analyse more than 290,000 full-disc Ca II K observations from 43 datasets spanning the period 1892-2019. All images were consistently processed with an automatic procedure that performs the photometric calibration (if needed) and the limb-darkening compensation. The processing also accounts for artefacts plaguing many of the images, including some very specific artefacts such as bright arcs found in Kyoto and Yerkes data. We have produced a plage area time-series from each analysed dataset. We found that the differences between the plage areas derived from individual archives are mainly due to the differences in the central wavelength and the bandpass used to acquire the data at the various sites. We have empirically cross-calibrated and combined the results obtained from each dataset to produce a composite series of plage areas. "Backbone" series are used to bridge all the series together. We have also shown that the selection of the backbone series has little effect on the final plage area composite. We have quantified the uncertainty of determining the plage areas with our processing due to shifts in the central wavelength and found it to be less than 0.01 in fraction of the solar disc for the average conditions found on historical data. We also found the variable seeing conditions during the observations to slightly increase the plage areas during activity maxima. We provide the so far most complete time series of plage areas based on corrected and calibrated historical and modern Ca II K images. Consistent plage areas are now available on 88% of all days from 1892 onwards and on 98% from 1907 onwards.

Delving into the Historical Ca II K Archive from the Kodaikanal Observatory: the Potential of the Most Recent Digitised Series

Theodosios **Chatzistergos**, Ilaria Ermolli, Sami K. Solanki, Natalie A. Krivova, Dipankar Banerjee, Bibhuti K. Jha, Subhamoy Chatterjee
Solar Phys. 294:145 **2019**
https://arxiv.org/pdf/1908.05493.pdf
https://link.springer.com/content/pdf/10.1007%2Fs11207-019-1532-5.pdf
Full-disc Ca II K photographic observations of the Sun carry direct information about the evolution of solar-plage regions for more than a century and are therefore a unique dataset for solar-activity studies. For a long time Ca II K observations were barely explored, but recent digitisations of multiple archives have allowed their extensive analysis. However, various studies have reported diverse results partly due to the insufficient quality of the digitised data. Furthermore, inhomogeneities have been identified within the individual archives, which, at least partly, could be due to the digitisation. As a result, some of the archives, e.g. that from the Kodaikanal observatory, were re-digitised. The results obtained by different authors who analysed the data from the new digitisation of the Kodaikanal archive differ from each other as well as from those derived from the old digitisation. Since the data were processed and analysed using different techniques, it is not clear, however, whether the differences are due to the digitisation or the processing of the data. To understand the reasons for such discrepancies, we analyse here the data from the two most recent digitisations of this archive. We use the same techniques to consistently process the images from both archives and to derive the plage areas from them. Some issues have been identified in both digitisations, implying that they are intrinsic characteristics of the data. Moreover, errors in timing of the observations plague both digitisations. Overall, the most recent 16-bit digitisation offers an improvement over the earlier 8-bit one. It also includes considerably more data and should be preferred.

Recovering the unsigned photospheric magnetic field from Ca II K observations

Theodosios **Chatzistergos**, Ilaria Ermolli, Sami K. Solanki, Natalie A. Krivova, Fabrizio Giorgi, Kok Leng Yeo
A&A **2019**
https://arxiv.org/pdf/1905.03453.pdf
We reassess the relationship between the photospheric magnetic field strength and the Ca II K intensity for a variety of surface features as a function of the position on the disc and the solar activity level. This relationship can be used to recover the unsigned photospheric magnetic field from images recorded in the core of Ca II K line. We have analysed 131 pairs of high-quality, full-disc, near-co-temporal observations from SDO/HMI and Rome/PSPT spanning half a solar cycle. To analytically describe the observationally-determined relation, we considered three different functions: a power law with an offset, a logarithmic function, and a power law function of the logarithm of the magnetic flux density. We used the obtained relations to reconstruct maps of the line-of-sight component of the unsigned magnetic field (unsigned magnetograms) from Ca II K observations, which were then compared to the original magnetograms. We find that both power-law functions represent the data well, while the logarithmic function is good only for quiet periods. We see no significant variation over the solar cycle or over the disc in the derived fit parameters, independently of the function used. We find that errors in the independent variable, usually not accounted for, introduce attenuation bias. To address this, we binned the data with respect to the magnetic field strength and Ca II K contrast separately and derived the relation for the bisector of the two binned curves. The reconstructed unsigned magnetograms show good agreement with the original ones. RMS differences are less than 90 G. The results were unaffected by the stray-light correction of the SDO/HMI and Rome/PSPT data. Our results imply that Ca~II~K observations, accurately processed and calibrated, can be used to reconstruct unsigned magnetograms by using the relations derived in our study. **07/06/2010, 01/04/2011**

Historical solar Ca II K observations at the Rome and Catania observatories

Theodosios **Chatzistergos**, Ilaria Ermolli, Mariachiara Falco, Fabrizio Giorgi, Salvo L. Guglielmino, Natalie A. Krivova, Paolo Romano, Sami K. Solanki
"Nuovo Cimento C" as proceeding of the Third Meeting of the Italian Solar and Heliospheric Community **2019**
https://arxiv.org/pdf/1902.07483.pdf
Here we present the little explored Ca II K archives from the Rome and the Catania observatories and analyse the digitised images from these archives to derive plage areas. **25/02/1970**

Analysis of full disc Ca II K spectroheliograms. II. Towards an accurate assessment of long-term variations in plage areas

Theodosios **Chatzistergos**, Ilaria Ermolli, Natalie A. Krivova, Sami K. Solanki
A&A 625, A69 **2019**
https://arxiv.org/pdf/1902.07122.pdf
https://www.aanda.org/articles/aa/pdf/2019/05/aa34402-18.pdf
Reconstructions of past irradiance variations require suitable data on solar activity. The longest direct proxy is the sunspot number, and it has been most widely employed for this purpose. These data, however, only provide information on the surface magnetic field emerging in sunspots, while a suitable proxy of the evolution of the bright magnetic features, specifically faculae/plage and network, is missing. This information can potentially be extracted from the historical full-disc observations in the Ca II K line. We have analysed over 100,000 historical images from 8 digitised photographic archives of the Arcetri, Kodaikanal, McMath-Hulbert, Meudon, Mitaka, Mt Wilson, Schauinsland, and Wendelstein observatories, as well as one archive of modern observations from the Rome/PSPT. The analysed data cover the period 1893--2018. We first performed careful photometric calibration and compensation for the centre-to-limb variation, and then segmented the images to identify plage regions. This has been consistently applied to both historical and modern observations. The plage series derived from different archives are generally in good agreement with each other. However, there are also clear deviations that most likely hint at intrinsic differences in the data and their digitisation. We showed that accurate image processing significantly reduces errors in the plage area estimates. Accurate photometric calibration also allows precise plage identification on images from different archives without the need to arbitrarily adjust the segmentation parameters. Finally, by comparing the plage area series from the various records, we found the conversion laws between them. This allowed us to produce a preliminary composite of the plage areas obtained from all the datasets studied here. This is a first step towards an accurate assessment of the long-term variation of plage regions.

Ca II K spectroheliograms for studies of long-term changes in solar irradiance

Theodosios **Chatzistergos**, Ilaria Ermolli, Natalie A. Krivova, Sami K. Solanki
Proceedings IAU Symposium No. 340, **2018**
https://arxiv.org/pdf/1805.03928.pdf

We address the importance of historical full disc Ca II K spectroheliograms for solar activity and irradiance reconstruction studies. We review our work on processing such data to enable them to be used in irradiance reconstructions. We also present our preliminary estimates of the plage areas from five of the longest available historical Ca II K archives.

New reconstruction of the sunspot group number since 1739 using the direct calibration and "backbone" methods

Theodosios **Chatzistergos**, Ilya G. Usoskin, Gennady A. Kovaltsov, Natalie A. Krivova, Sami K. Solanki
A&A 602, A69 **2017**
https://arxiv.org/pdf/1702.06183.pdf

Group sunspot number (GSN) series constitute the longest instrumental astronomical database providing information on solar activity. It is a compilation of observations by many individual observers, and their inter-calibration has usually been performed using linear rescaling. There are multiple published series that show different long-term trends for solar activity. We aim at producing a GSN series, with a non-linear non-parametric calibration. The only underlying assumptions are that the differences between the various series are due to different acuity thresholds of the observers, and that the threshold of each observer remains constant throughout the observing period. We use a daisy chain process with backbone (BB) observers and calibrate all overlapping observers to them. The calibration of each individual observer is performed with a probability distribution function (PDF) matrix, constructed considering all daily values for the overlapping period with the BB. The calibration of the BBs is done in a similar manner. Propagation of errors is modelled with Monte Carlo simulations. The final series extends back to 1739 and includes data from 314 observers. It suggests moderate activity during the 18th and 19th century, which is significantly lower than the high level of solar activity predicted by other recent reconstructions applying linear regressions. The new series provides a robust reconstruction, based on modern and non-parametric methods, of sunspot group numbers since 1739, and it confirms the existence of the Modern grand maximum of solar activity in the second half of the 20th century.

Problems in Observation and Identification of Torsional Waves in the Lower Solar Atmosphere

Andrei **Chelpanov** & Nikolai Kobanov
Solar Physics volume 297, Article number: 154 (**2022**)
https://doi.org/10.1007/s11207-022-02092-4
https://arxiv.org/pdf/2212.13710

The registration of periodic variations of spectral line widths serves as the main method for observing torsional Alfvén waves. Theoretically, the method seems valid, yet it entails a number of caveats when applied to data. For instance, the amplitudes of these observations should vary with changes of the location on the disk and they should be associated with no intensity oscillations. We analyze extensive observational material of periodic non-thermal variations of line widths in coronal holes and facular regions in a number of spectral lines: Hαα, He I 10830 Å, Ca II 8542 Å, Ba II 4554 Å. In most cases, we detected associated intensity oscillations at similar frequencies. Besides, we observed no centre-to-limb dependency. This calls for a discussion on the practical validity of the method and on the alternative explanations for the nature of non-thermal variations of spectral line widths. Based on our observations, we consider registering line profile broadening to be a necessary, but not sufficient, means for unambiguous identification of torsional Alfvén waves in the lower solar atmosphere.

Oscillation Dynamics in Short-Lived Facula Regions during Their Lifetime

Andrei **Chelpanov**, Nikolai Kobanov
ApJ **2022**
https://arxiv.org/pdf/2202.07239.pdf

We performed a multi-wave study of the oscillation dynamic in short-lived facula regions during their lifetime. We studied oscillations in five regions, three of which belonged to the beginning of the current solar activity cycle, and two of them existed at the end of the previous cycle. We found that in the facula regions of the current cycle, low-frequency 1-2 mHz oscillation dominated at the early stages of the faculae formation, while in the regions of the previous cycle, five-minute oscillations dominated at this stage. At the maximal development phase of all the facula regions, the locations of observed low frequencies are closely related to those of the coronal loops. These results support the version that the sources of the low-frequency oscillations in loops lie loops' foot points. **13-15 Feb 2019, 6-14 Jul 2019, 9-12 Dec 2019, 25 Sep-2 Oct 2020, 23-31 Oct 2020**

Multilevel Observations of the Oscillations in the First Active Region of the New Cycle

Andrei **Chelpanov**, Nikolai Kobanov
2020 *Solar Physics* **volume 295**, Article number: 94
https://arxiv.org/pdf/2006.05223.pdf
https://link.springer.com/content/pdf/10.1007/s11207-020-01664-6.pdf

For the first time, a multi-wave research of oscillation dynamics in a solar facula from its birth to decay was carried out. We performed spectral observations of active region NOAA 12744 at Horizontal Solar Telescope of the Sayan Solar Observatory in the Hα, He I 10830 A, and Si I 10827 A lines. We used Solar Dynamics Observatory (SDO) line-of-sight magnetic field data and the 1600 A, 304 A, and 171 A UV channels. At the early stages of the facula evolution, we observed low-frequency (1-2 mHz) oscillations concentrate in the central part of the facula. In the lower solar atmosphere, this is registered in the intensity, line-of-sight velocity, and magnetic field signals. These frequencies were also observed in the transition region and corona (304 A and 171 A channels). At the maximal development phase of the facula evolution, the low frequency oscillations closely reproduce the coronal loop structures forming above the active region. At the decay phase, the spatial distributions of the observed frequencies resemble those found in and above the undisturbed chromosphere network. Our results indicate a direct relation of the low frequency oscillations observed in the lower solar atmosphere with the oscillations in the coronal loops, which is probably implemented through the loop footpoints. **8-14 July 2019**

Influence of the Magnetic Field on Oscillation Spectra in Solar Faculae

A. A. **Chelpanov** N. I. Kobanov D. Y. Kolobov
Solar Physics November **2016**, Volume 291, Issue 11, pp 3329–3338
http://arxiv.org/pdf/1607.01877v1.pdf
We study oscillation parameters in faculae above magnetic knots and in the areas adjacent to them. Using Solar Dynamics Observatory (SDO) data, we analyse oscillations in magnetic field strength, Doppler velocity, and intensity signals for the lower photosphere, and in intensity for the higher levels. We find peaks in the oscillation spectra for the magnetic field strength in magnetic knots at a frequency of about 4.8 mHz, while there are no such frequencies in the adjacent facular patches, which have a moderate field strength. In contrast, the spectra for the Doppler velocity oscillations are similar for these types of regions: in both cases, the significant peaks are in the 2.5 – 4.5 mHz range, although the oscillations in magnetic knots are 2 – 3 times weaker than those at the facular periphery. In the upper photosphere, the dominant frequencies in magnetic knots are 0.5 – 1 mHz higher than in the medium-field regions. The transition region oscillations above magnetic knots are mainly concentrated in the 3 – 6 mHz range, and those above moderate-field patches are concentrated below 3 mHz.

The Long-term Evolution of the Solar Transition Region

W.Q. **Chen**, K.J. Li, J.C. Xu
2024
https://arxiv.org/pdf/2412.08910
Long-term evolution characteristics of the solar transition region have been unclear. In this study, daily images of the solar full disk derived from the observations by the Solar Dynamics Observatory/Atmospheric Imaging Assembly at 304 A wavelength from 2011 January 1 to 2022 December 31 are used to investigate long-term evolution of the solar transition region. It is found that long-term variation in the transition region of the full disk is in phase with the solar activity cycle, and thus the polar brightening should occur in the maximum epoch of the solar cycle. Long-term variation of the background transition region is found to be likely in anti-phase with the solar activity cycle at middle and low latitudes. The entire transition region, especially the active transition region is inferred to be mainly heated by the active-region magnetic fields and the ephemeral-region magnetic fields, while the quieter transition region is believed to be mainly heated by network magnetic fields. Long-term evolution characteristics of various types of the magnetic fields at the solar surface are highly consistent with these findings, and thus provide an explanation for them.

Bidirectional propagating brightenings in arch filament systems observed by Solar Orbiter/EUI

Yajie **Chen**1⋆, Sudip Mandal1, Hardi Peter1,2 and Lakshmi Pradeep Chitta1
A&A, 692, A119 (**2024**)
https://doi.org/10.1051/0004-6361/202451069
https://www.aanda.org/articles/aa/pdf/2024/12/aa51069-24.pdf
Arch filament systems (AFSs) are chromospheric and coronal manifestations of emerging magnetic flux. Using high spatial resolution observations taken at a high cadence by the Extreme Ultraviolet Imager (EUI) on board Solar Orbiter, we identified small-scale elongated brightenings within the AFSs. These brightenings appear as bidirectional flows along the threads of AFSs. For our study, we investigated the coordinated observations of the AFSs acquired by the EUI instrument and the Atmospheric Imaging Assembly (AIA) on board the Solar Dynamics Observatory (SDO) on **2022 March 4 and 17**. We analyzed 15 bidirectional propagating brightenings from EUI 174 Å images. These brightenings reached propagating speeds of 100–150 km s−1. The event observed on March 17 exhibits blob-like structures, which may be signatures of plasmoids and due to magnetic reconnection. In this case, we also observed counterparts in the running difference slit-jaw images in the 1400 Å passbands taken by the Interface Region Imaging Spectrograph (IRIS). Most events show co-temporal intensity variations in all AIA EUV

passbands. Together, this implies that these brightenings in the AFSs are dominated by emission from cool plasma with temperatures well below 1 MK. The Polarimetric and Helioseismic Imager (PHI) on board Solar Orbiter provides photospheric magnetograms at a similar spatial resolution as EUI and from the same viewing angle. The magnetograms taken by PHI show signatures of flux emergence beneath the brightenings. This suggests that the events in the AFSs are triggered by magnetic reconnection that may occur between the newly emerging magnetic flux and the preexisting magnetic field structures in the middle of the AFSs. This would also give a natural explanation for the bidirectional propagation of the brightenings near the apex of the AFSs. The interaction of the preexisting field and the emerging flux may be important for mass and energy transfer within the AFSs.

Investigating explosive events in a 3D quiet-Sun model: Transition region and coronal response

Yajie **Chen**, Hardi Peter, Damien Przybylski

A&A 693, A29 **2024**

https://arxiv.org/pdf/2411.11068

https://doi.org/10.1051/0004-6361/202450862

https://www.aanda.org/articles/aa/pdf/2025/01/aa50862-24.pdf

Context. Transition region explosive events are characterized by non-Gaussian profiles of the emission lines formed at transition region temperatures, and they are believed to be manifestations of small-scale reconnection events in the transition region. Aims. Traditionally, the enhanced emission at the line wings is interpreted as bi-directional outflows generated by reconnection of oppositely directed magnetic field. We investigate whether the 2D picture also holds in a more realistic setup of a 3D radiation magnetohydrodynamics (MHD) quiet-Sun model. We also compare the thermal responses in the transition region and corona of different events. Methods. We took a 3D self-consistent quiet-Sun model extending from the upper convection zone to the lower corona calculated using the MURaM code. We first synthesized the Si iv line profiles from the model and then located the profiles which show signatures of bi-directional flows. These tend to appear along network lanes, and most do not reach coronal temperatures. We isolated two hot (around 1 MK) events and one cool (order of 0.1 MK) event and examined the magnetic field evolution in and around these selected events. Furthermore, we investigated why some explosive events reach coronal temperatures while most remain cool. We also examined the emission of these events as seen in the 174 Å passband of Extreme Ultraviolet Imager (EUI) onboard Solar Orbiter and all coronal passbands of Atmospheric Imaging Assembly (AIA) onboard Solar Dynamics Observatory (SDO). Results. The field lines around two events reconnect at small angles, i.e., they undergo component reconnection. The third case is associated with the relaxation of a highly twisted flux rope. All of the three events reveal signatures in the synthesized EUI 174 Å images. The intensity variations in two events are dominated by variations of the coronal emissions, while the cool component seen in the respective channel contributes significantly to the intensity variation in one case. Comparing to the cool event, one hot event is embedded in regions with higher magnetic field strength and heating rates while the densities are comparable, and the other hot event is heated to coronal temperatures mainly because of the low density. Conclusions. Small-scale heating events seen in EUV channels of AIA or EUI might be hot or cool. Our results imply that the major difference between the events in which coronal counterparts dominate or not is the amount of converted magnetic energy and/or density in and around the reconnection region

The Interaction between Solar Convection and Rotation

Haibin **Chen**, Rong Wu

ApJ **2024**

https://arxiv.org/pdf/2401.10105.pdf

The rotational energy of a fluid parcel changes during isotropic expansion or compression. In solar convection, rotation absorbs energy from convection and inhibits it, causing the motion of fluid parcels larger than a critical size to become vibration. Turbulence and inertial oscillations can cause the deformation of fluid parcels to deviate from isotropic, altering the equilibrium position of the vibration and forming motion larger than the critical size, respectively, the large granules within the granules and probably the mesogranulation. The change in rotational energy of granules during convection causes their rotation speed to differ from the local speed, forming a statistically significant solar radial differential rotation. The meridional circulation driven by radial differential rotation transports angular momentum towards the equator, forming the latitudinal differential rotation. A model constructed by combining mixing length theory explains why granule size and temperature distribution are independent of latitude, and the structure produced by this mechanism is similar to the characteristics of supergranules.

A New Index to Describe the Relationship between Solar Extreme Ultraviolet Variation and Solar Activity

Zhou **Chen**1,2,3,4, Kecheng Zhou1,2, Jing-Song Wang3,4, Qiao Song3,4, Zhihai Ouyang1,2, Haimeng Li1,2, Meng Zhou1,2, and Xiaohua Deng1,2

2023 ApJ 958 69
https://iopscience.iop.org/article/10.3847/1538-4357/acf9f7/pdf
In this paper, a new solar activity index based on a novel disturbance extraction method, the spectral whitening method (SWM), is introduced to process the solar EUV data on the Atmospheric Imaging Assembly (AIA) on board the Solar Dynamics Observatory. Our research suggests that the spatial information derived by SWM can well reflect the location of disturbance extraction, which is consistent with the location of the solar active region. It indicates that the disturbance extraction is effective. From AIA 094 Å to AIA 335 Å, SWM results are strongly correlated with solar radio flux F107 and the sunspot number (SSN), especially at AIA 211 Å, where the correlation coefficient reaches the maximum, while at AIA 1600 Å and AIA 1700 Å there are no detectable correlations. The proposed new solar activity index, Jp(AIA), has the following characteristics: (1) the new index can reflect the main variations of F107 and SSN, indicating that the index is valid; (2) the new index has higher temporal resolution, which is more conducive to the more detailed study of solar activities on short timescales; (3) the new index reveals that the solar atmosphere still has significant variability during solar minimum characterized by low F107 and SSN; (4) the new index can be used in conjunction with the new magnetospheric and ionospheric indices, which are also derived by SWM to deepen the understanding of the causal chain of space weather and promote the improvement of forecasting capabilities.

Inferring Maps of the Sun's Far-side Unsigned Magnetic Flux from Far-side Helioseismic Images using Machine Learning Techniques

Ruizhu **Chen**, Junwei Zhao, Shea Hess Webber, Yang Liu, J. Todd Hoeksema, Marc L. Derosa
ApJ **941** 197 **2022**
https://arxiv.org/pdf/2211.12666.pdf
https://iopscience.iop.org/article/10.3847/1538-4357/aca333/pdf
Accurate modeling of the Sun's coronal magnetic field and solar wind structures require inputs of the solar global magnetic field, including both the near and far sides, but the Sun's far-side magnetic field cannot be directly observed. However, the Sun's far-side active regions are routinely monitored by helioseismic imaging methods, which only require continuous near-side observations. It is therefore both feasible and useful to estimate the far-side magnetic-flux maps using the far-side helioseismic images despite their relatively low spatial resolution and large uncertainties. In this work, we train two machine-learning models to achieve this goal. The first machine-learning training pairs simultaneous SDO/HMI-observed magnetic-flux maps and SDO/AIA-observed EUV 304Å images, and the resulting model can convert 304Å images into magnetic-flux maps. This model is then applied on the STEREO/EUVI-observed far-side 304Å images, available for about 4.3 years, for the far-side magnetic-flux maps. These EUV-converted magnetic-flux maps are then paired with simultaneous far-side helioseismic images for a second machine-learning training, and the resulting model can convert far-side helioseismic images into magnetic-flux maps. These helioseismically derived far-side magnetic-flux maps, despite their limitations in spatial resolution and accuracy, can be routinely available on a daily basis, providing useful magnetic information on the Sun's far side using only the near-side observations.

Rotating Equivalent Temperature and Solar Granulation

Haibin **Chen**, Rong Wu
2022
https://arxiv.org/pdf/2211.08113.pdf
The rotation of the fluid cell generates additional pressure and exhibits properties similar to temperature in isotrotropic expansion, affecting the convection criteria in the form of size, with small fluid cells in a natural convection state and large fluid cells in a forced convection state. This is verified in observational data on solar granulation, which also infer that the critical size of the granule is negatively correlated with the value of the local average vortex.

Oblique Quasi-Kink Modes in Solar Coronal Slabs Embedded in an Asymmetric Magnetic Environment: Resonant Damping, Phase and Group Diagrams

Shao-Xia **Chen**, Bo Li, Mingzhe Guo, Mijie Shi, Hui Yu
ApJ **2022**
https://arxiv.org/pdf/2210.16091
There has been considerable interest in magnetoacoustic waves in static, straight, field-aligned, one-dimensional equilibria where the exteriors of a magnetic slab are different between the two sides. We focus on trapped, transverse fundamental, oblique quasi-kink modes in pressureless setups where the density varies continuously from a uniform interior (with density ρ_i) to a uniform exterior on either side (with density ρ_L or ρ_R), assuming $\rho_L \leq \rho_R \leq \rho_i$. The continuous structuring and oblique propagation make our study new relative to pertinent studies, and lead to wave damping via the Alfve´n resonance. We compute resonantly damped quasi-kink modes as resistive eigenmodes, and isolate the effects of system asymmetry by varying ρ_i/ρ_R from the ``Fully Symmetric'' ($\rho_i/\rho_R=\rho_i/\rho_L$) to the ``Fully Asymmetric'' limit ($\rho_i/\rho_R=1$). We find that the damping rates possess a

nonmonotonic ρi/ρR-dependence as a result of the difference between the two Alfve´n continua, and resonant absorption occurs only in one continuum when ρi/ρR is below some threshold. We also find that the system asymmetry results in two qualitatively different regimes for the phase and group diagrams. The phase and group trajectories lie essentially on the same side (different sides) relative to the equilibrium magnetic field when the configuration is not far from a ``Fully Asymmetric'' (``Fully Symmetric'') one. Our numerical results are understood by making analytical progress in the thin-boundary limit, and discussed for imaging observations of axial standing modes and impulsively excited wavetrains.

Rotating Turbulent Thermal Convection and Solar Differential Rotation

Haibin **Chen**, Rong Wu

2022

https://arxiv.org/pdf/2207.11990.pdf

The expansion of the rotating fluid will change the vorticity and rotational speed of the expanding region and its adjacent regions. In turbulent thermal convection, this microscopic effect is preserved. Tracking the fluid micelles shows that the ststistical vorticity varies with density, producing vorticity transport and angular momentum transport from the low-density area to the high-density area, forming a macroscopic vorticity difference and rotational speed difference, and changing the rotational speed distribution in the convection area of the rotating planet. Taking the axial thermal convection model of the solar polar region, it can generate axial differential rotation, and the centrifugal force difference generated by the axial differential rotation drives the meridional circulation, transporting angular momentum away from the axis of rotation, forming latitudinal differential rotation. The rotation of the fluid cell with the concept of size and shape generates additional pressure. The pressure is related to the rotational speed and size of the fluid cell, which affects the relationship between density and pressure. The convection criterion is no longer determined only by the temperature gradient, the vorticity gradient also affects fluid stability. And the larger the size of the fluid cell, the greater the effect of the vorticity gradient, and a higher temperature gradient is required to drive larger fluid cells convection. The temperature gradient in the solar troposphere is higher than in the non-rotating fluid model, and there is an upper bound on the size of the typical thermal convective fluid cells in the troposphere.

Doppler shifts of spectral lines formed in the solar transition region and corona

Yajie **Chen**, Hardi Peter, Damien Przybylski, Hui Tian, Jiale Zhang

A&A **2022**

https://arxiv.org/pdf/2203.04691

Context. Emission lines formed in the transition region and corona show dominantly redshifts and blueshifts, respectively. Aims. We investigate the Doppler shifts in a 3D radiation MHD model of the quiet Sun and compare these to observed properties. We concentrate on Si IV 1394 A originating in the transition region and examine the Doppler shifts of several other spectral lines at different formation temperatures. Methods. We construct a radiation MHD model extending from the upper convection zone to the lower corona using the MURaM code. In this quiet Sun model the magnetic field is self-consistently maintained by the action of a small-scale dynamo. We synthesize the profiles of several optically thin emission lines, formed at temperatures from the transition region into the corona. We investigate the spatial structure and coverage of red- and blueshifts and how this changes with line-formation temperature. Results. The model successfully reproduces the observed change of average net Doppler shifts from red- to blueshifted from the transition region into the corona. In particular, the model shows a clear imbalance of area coverage of red- vs. blueshifts in the transition region of ca. 80% to 20%. We determine that (at least) four processes generate the systematic Doppler shifts in our model, including pressure enhancement in the transition region, transition region brightenings unrelated to coronal emission, boundaries between cold and hot plasma, and siphon-type flows. Conclusions. We show that there is not a single process that is responsible for the observed net Doppler shifts in the transition region and corona. Because current 3D MHD models do not yet fully capture the evolution of spicules, one of the key ingredients of the chromosphere, most probably these have still to be added to the list of processes responsible for the persistent Doppler shifts.

A Comprehensive Radiative Magnetohydrodynamics Simulation of Active Region Scale Flux Emergence from the Convection Zone to the Corona

Feng **Chen**, Matthias Rempel, Yuhong Fan

2022 *ApJ* **937** 91

https://arxiv.org/pdf/2106.14055.pdf

https://iopscience.iop.org/article/10.3847/1538-4357/ac8f95/pdf

We present a comprehensive radiative magnetohydrodynamic simulation of the quiet Sun and large solar active regions. The 197 Mm wide simulation domain spans from the uppermost convection zone to over 100 Mm in the solar corona. Sophisticated treatments of radiative transfer and conduction transport provide the necessary realism for synthesizing observables to compare with remote sensing observations of the Sun. This model self-consistently reproduces observed features of the quiet Sun, emerging and developed active regions, and solar flares up to M

class. Here, we report an overview on the first results. The surface magnetoconvection yields an upward Poynting flux that is dissipated in the corona and heats the plasma to over one million K. The quiescent corona also presents ubiquitous propagating waves, jets, and bright points with sizes down to 2 Mm. Magnetic flux bundles generated in a solar convective dynamo emerge into the photosphere and gives rise to strong and complex active regions with Over 1023 Mx magnetic flux. The coronal free magnetic energy, which is about 18\% of the total magnetic energy, accumulates to about 1033 erg. The coronal magnetic field is not forcefree, as the Lorentz force needs to balance the pressure force and viscous stress as well as to drive magnetic field evolution. Emission measure from log10T=4.5 to log10T>7 provides a comprehensive view on structures and dynamics in the active region corona, such as coronal loops in various lengths and temperatures, mass circulation by evaporation and condensation, and eruptions from jets to large-scale mass ejections.

Transient small-scale brightenings in the quiet solar corona: a model for campfires observed with Solar Orbiter

Yajie **Chen**, Damien Przybylski, Hardi Peter, Hui Tian, F. Auchère, D. Berghmans
A&A **2021**
https://arxiv.org/pdf/2104.10940.pdf
Context. Recent observations by the Extreme Ultraviolet Imager (EUI) on board Solar Orbiter have characterized prevalent small-scale transient brightenings in the corona above the quiet Sun termed campfires. Aims. In this study we search for comparable brightenings in a numerical model and then investigate their relation to the magnetic field and the processes that drive these events. Methods. We use the MURaM code to solve the 3D radiation MHD equations in a box that stretches from the upper convection zone to the corona. The model self-consistently produces a supergranular network of the magnetic field and a hot corona above this quiet Sun. For the comparison with the model we synthesize the coronal emission as seen by EUI in its 174 Å channel, isolate the seven strongest transient brightenings, and investigate (the changes of) the magnetic field in and around these in detail. Results. The transients we isolate have a lifetime of about 2 minutes and are elongated loop-like features with lengths around 1Mm to 4 Mm. They tend to occur at heights of about 2Mm to 5Mm above the photosphere a bit offset from magnetic concentrations that mark the bright chromospheric network and they reach temperatures of above 1 MK. With this they very much resemble the (larger) campfires found in observations. In our model most events are energised by component reconnection between (bundles of) field lines that interact at coronal heights. In one case we find that untwisting of a highly twisted flux rope initiates the heating. Conclusions. Based on our study we propose that the majority of campfire events found by EUI are driven by component reconnection and our model suggests that this process contributes significantly to the heating of the corona above the quiet Sun.

Coronal Condensation as the Source of Transition Region Supersonic Downflows above a Sunspot

Hechao **Chen**, Hui Tian, Leping Li, Hardi Peter, Lakshmi Pradeep Chitta, Zhenyong Hou
A&A **2021**
https://arxiv.org/pdf/2112.01354.pdf
Plasma loops or plumes rooted in sunspot umbrae often harbor downflows with speeds of 100 km/s. These downflows are supersonic at transition region temperatures of 0.1 MK. The source of these flows is not well understood. We aim to investigate the source of sunspot supersonic downflows (SSDs) in AR 12740 using simultaneous spectroscopic and imaging observations. We identified SSD events from multiple raster scans of a sunspot by the Interface Region Imaging Spectrograph, and calculated the electron densities, mass fluxes and velocities of these SSDs. The EUV images provided by the AIA onboard the SDO and the EUVI onboard the STEREO were employed to investigate the origin of these SSDs and their associated coronal rain. Almost all the identified SSDs appear at the footpoints of sunspot plumes and are temporally associated with appearance of chromospheric bright dots inside the sunspot umbra. Dual-perspective EUV imaging observations reveal a large-scale closed magnetic loop system spanning the sunspot region and a remote region. We observed that the SSDs are caused by repeated coronal rain that forms and flows along these closed magnetic loops toward the sunspot. One episode of coronal rain clearly indicates that reconnection near a coronal X-shaped structure first leads to the formation of a magnetic dip. Subsequently, hot coronal plasma catastrophically cools from 2 MK in the dip region via thermal instability. This results in the formation of a transient prominence in the dip, from which the cool gas mostly slides into the sunspot along inclined magnetic fields under the gravity. This drainage process manifests as a continuous rain flow, which lasts for around 2 hrs and concurrently results in a nearly steady SSD event. Our results demonstrate that coronal condensation in magnetic dips can result in the quasi-steady sunspot supersonic downflows. **2019 May 7-8**

Flare Index Prediction with Machine Learning Algorithms

Anqin **Chen**, Qian Ye & Jingxiu Wang
Solar Physics volume 296, Article number: 150 (**2021**)
https://link.springer.com/content/pdf/10.1007/s11207-021-01895-1.pdf

https://doi.org/10.1007/s11207-021-01895-1
Solar flares are one of the most important sources of disastrous space weather events, leading to negative effects on spacecrafts and living organisms. It is very important to predict solar flares to minimize the potential losses. In this paper, we use three different machine learning algorithms: K-Nearest Neighbors (KNN), Random Forest (RF), and XGBoost (XGB) to predict the total flare index TflareTflare and the maximum flare index MflareMflare of an active region (AR) within the subsequent of 24, 48, and 72 hrs. First, we selected 54514 vector magnetograms of 129 ARs on the visible solar hemisphere in solar cycle 24 whose maximum sunspot groups' area was larger than 400 μh. Then the following four magnetic parameters of each magnetogram were calculated: 1) the total magnetic flux |Φtot|, 2) the total photospheric free magnetic energy density Efree, 3) the gradient-weighted integral length of the neutral line with horizontal magnetic gradient of line-of-sight magnetic field larger than 0.1 G km−1 (WLSG), and 4) the area with magnetic shear angle larger than 40◦ (AΨ), as well as Tflare and Mflare corresponding to each magnetogram. Afterward, we split samples randomly into training (85% of the whole data) and testing (15%) data sets. After hyperparameter tuning and model construction we found that RF is an optimal algorithm for the prediction task and that the coefficients of determination (R2) of test data set via the majority of RF models are beyond 0.97. In addition, the feature importance of RF and XGB models indicates that |Φtot| and Efree are two optimal parameters to predict both Tflare and Mflare, and |Φtot| and Efree are the best parameters for Mflare and Tflare, respectively.

Damping of slow surface kink modes in solar photospheric waveguides modeled by one-dimensional inhomogeneities

Shao-Xia **Chen**, Bo Li, Tom Van Doorsselaere, Marcel Goossens, Hui Yu, Michael Geeraerts
ApJ **2021**
https://arxiv.org/pdf/2012.15426.pdf
Given the recent interest in magnetohydrodynamic (MHD) waves in pores and sunspot umbrae, we examine the damping of slow surface kink modes (SSKMs) by modeling solar photospheric waveguides with a cylindrical inhomogeneity comprising a uniform interior, a uniform exterior, and a continuous transition layer (TL) in between. Performing an eigen-mode analysis in linear, resistive, gravity-free MHD, our approach is idealized in that, among other things, our equilibrium is structured only in the radial direction. We can nonetheless address two damping mechanisms simultaneously, one being the Ohmic resistivity, and the other being the resonant absorption of SSKMs in the cusp and Alfve´n continua. We find that the relative importance of the two mechanisms depends sensitively on the magnetic Reynolds number (Rm). Resonant absorption is the sole damping mechanism for realistically large values of Rm, and the cusp resonance in general dominates the Alfve´n one unless the axial wavenumbers are at the lower end of the observationally relevant range. We also find that the thin-boundary approximation holds only when the TL-width-to-radius ratios are much smaller than nominally expected. The Ohmic resistivity is far more important for realistically small Rm. Even in this case, SSKMs are only marginally damped, with damping-time-to-period-ratios reaching ∼10 in the parameter range we examine.

Flame-like Ellerman Bombs and Their Connection to Solar UV Bursts

Yajie **Chen**, Hui Tian, Hardi Peter, Tanmoy Samanta, Vasyl Yurchyshyn, Haimin Wang, Wenda Cao, Linghua Wang, Jiansen He
ApJL **875** L30 **2019**
https://arxiv.org/pdf/1903.01981.pdf
sci-hub.se/10.3847/2041-8213/ab18a4
Ellerman bombs (EBs) are small-scale intense brightenings in Hα wing images, which are generally believed to be signatures of magnetic reconnection events around the temperature minimum region of the solar atmosphere. They have a flame-like morphology when observed near the solar limb. Recent observations from the Interface Region Imaging Spectrograph (IRIS) reveal another type of small-scale reconnection events, termed UV bursts, in the lower atmosphere. Though previous observations have shown a clear coincidence of some UV bursts and EBs, the exact relationship between these two phenomena is still under debate. We investigate the spatial and temporal relationship between flame-like EBs and UV bursts using joint near-limb observations between the 1.6--meter Goode Solar Telescope (GST) and IRIS. In total 161 EBs have been identified from the GST observations, and 20 of them reveal signatures of UV bursts in the IRIS images. Interestingly, we find that these UV bursts have a tendency to appear at the upper parts of their associated flame-like EBs. The intensity variations of most EB-related UV bursts and their corresponding EBs match well. Our results suggest that these UV bursts and EBs are likely formed at different heights during a common reconnection process. **2015 June 25 , 2017 May 27**

Solar Ultraviolet Bursts in a Coordinated Observation of IRIS, Hinode and SDO

Yajie **Chen**, Hui Tian, Xiaoshuai Zhu, Tanmoy Samanta, Linghua Wang, Jiansen He
Science China, Technological Sciences **2019**
https://arxiv.org/pdf/1902.04226.pdf

Solar ultraviolet (UV) bursts are small-scale compact brightenings in transition region images. The spectral profiles of transition region lines in these bursts are significantly enhanced and broadened, often with chromospheric absorption lines such as Ni~{\sc{ii}} 1335.203 and 1393.330 {\AA} superimposed. We investigate the properties of several UV bursts using a coordinated observation of the Interface Region Imaging Spectrograph (IRIS), Solar Dynamics Observatory (SDO), and \textit{Hinode} on **2015 February 7**. We have identified 12 UV bursts, and 11 of them reveal small blueshifts of the Ni~{\sc{ii}} absorption lines. However, the Ni~{\sc{ii}} lines in one UV burst exhibit obvious redshifts of ∼20 km s−1, which appear to be related to the cold plasma downflows observed in the IRIS slit-jaw images. We also examine the three-dimensional magnetic field topology using a magnetohydrostatic model, and find that some UV bursts are associated with magnetic null points or bald patches. In addition, we find that these UV bursts reveal no obvious coronal signatures from the observations of the Atmospheric Imaging Assembly (AIA) on board SDO and the EUV Imaging Spectrometer (EIS) on board \textit{Hinode}.

Investigating the Transition Region Explosive Events and Their Relationship to Network Jets

Yajie **Chen**, Hui Tian, Zhenghua Huang, Hardi Peter, Tanmoy Samanta

ApJ **873** 79 **2019**

https://arxiv.org/pdf/1901.11215.pdf

Recent imaging observations with the Interface Region Imaging Spectrograp (IRIS) have revealed prevalent intermittent jets with apparent speeds of 80--250 km~s−1from the network lanes in the solar transition region (TR). On the other hand, spectroscopic observations of the TR lines have revealed the frequent presence of highly non-Gaussian line profiles with enhanced emission at the line wings, often referred as explosive events (EEs). Using simultaneous imaging and spectroscopic observations from IRIS, we investigate the relationship between EEs and network jets. We first identify EEs from the Si~{\sc{iv}}~1393.755 {\AA} line profiles in our observations, then examine related features in the 1330 {\AA} slit-jaw images. Our analysis suggests that EEs with double peaks or enhancements in both wings appear to be located at either the footpoints of network jets, or transient compact brightenings. These EEs are most likely produced by magnetic reconnection. We also find that EEs with enhancements only at the blue wing are mainly located on network jets, away from the footpoints. These EEs clearly result from the superposition of the high-speed network jets on the TR background. In addition, EEs showing enhancement only at the red wing of the line are often located around the jet footpoints, possibly caused by the superposition of reconnection downflows on the background emission. Moreover, we find some network jets that are not associated with any detectable EEs. Our analysis suggests that some EEs are related to the birth or propagation of network jets, and that others are not connected to network jets. **2013 Oct 8**

Damping of slow surface sausage modes in photospheric waveguides

Shao-Xia **Chen**, Bo Li, Mijie Shi, Hui Yu

ApJ **2018**

https://arxiv.org/pdf/1810.02051.pdf

There has been considerable interest in sausage modes in photospheric waveguides like pores and sunspots, and slow surface sausage modes (SSSMs) have been suggested to damp ufficiently rapidly to account for chromospheric heating. Working in the framework of linear resistive magnetohydrodynamics, we examine how efficient electric resistivity and resonant absorption in the cusp continuum can be for damping SSSMs in a photospheric waveguide with equilibrium parameters compatible with recent measurements of a photospheric pore. For SSSMs with the measured wavelength, we find that the damping rate due to the cusp resonance is substantially less strong than theoretically expected with the thin-boundary approximation. The damping-time-to-period ratio (τ/P) we derive for standing modes, equivalent to the damping-length-to-wavelength ratio for propagating modes given the extremely weak dispersion, can reach only ∼180. However, the accepted values for electric resistivity (η) correspond to a regime where both the cusp resonance and resistivity play a role. The values for τ/P attained at the largest allowed η may reach ∼30. We conclude that electric resistivity can be considerably more efficient than the cusp resonance for damping SSSMs in the pore in question, and it needs to be incorporated into future studies on the damping of SSSMs in photospheric waveguides in general.

Fast Standing Modes in Transversely Nonuniform Solar Coronal Slabs: Effects of a Finite Plasma Beta

Shao-Xia **Chen**, Bo Li, Sanjay Kumar, Hui Yu, Mijie Shi

ApJ **855** 47 **2018**

https://arxiv.org/pdf/1801.09204.pdf

We examine the dispersive properties of linear fast standing modes in transversely nonuniform solar coronal slabs with finite gas pressure, or, equivalently, finite plasma beta. We derive a generic dispersion relation governing fast

waves in coronal slabs for which the continuous transverse distributions of the physical parameters comprise a uniform core, a uniform external medium, and a transition layer (TL) in between. The profiles in the TL are allowed to be essentially arbitrary. Restricting ourselves to the first several branches of fast modes, which are of most interest from the observational standpoint, we find that a finite plasma beta plays an at most marginal role in influencing the periods (P), damping times (τ), and critical longitudinal wavenumbers (kc), when both P and τ are measured in units of the transverse fast time. However, these parameters are in general significantly affected by how the TL profiles are described. We conclude that, for typical coronal structures, the dispersive properties of the first several branches of fast standing modes can be evaluated with the much simpler theory for cold slabs provided that the transverse profiles are properly addressed and the transverse Alfv\'en time in cold MHD is replaced with the transverse fast time.

Frequency Dependence of Helioseismic Measurements of the Center-to-Limb Effect and Flow-induced Travel-time Shifts

Ruizhu **Chen**1,2 and Junwei Zhao
2018 ApJ 853 161
http://sci-hub.tw/10.3847/1538-4357/aaa3e3
Time–distance helioseismology measures acoustic travel times to infer the structure and flow field of the solar interior; however, both the mean travel times and the travel-time shifts suffer systematic center-to-limb variations, which complicate the interpretation and inversions of the time–distance measurements. In particular, the center-to-limb variation in travel-time shifts (CtoL effect) has a significant impact on the inference of the Sun's meridional circulation, and needs to be removed from the helioseismic measurements, although the observational properties and the physical cause of the CtoL effect have yet to be investigated. In this study, we measure the CtoL effect in the frequency domain using Doppler-velocity data from the Solar Dynamics Observatory/Helioseismic and Magnetic Imager, and study its properties as a function of disk-centric distance, travel distance, and frequency of acoustic waves. It is found that the CtoL effect has a significant frequency dependence—it reverses sign at a frequency around 5.4 mHz and reaches maximum at around 4.0 mHz before the sign reversal. The tendency of frequency dependence varies with disk-centric distance in a way that both the sign-reversal frequency and the maximum-value frequency decrease closer to the limb. The variation tendency does not change with travel distance, but the variation magnitude is approximately proportional to travel distance. For comparison, the flow-induced travel-time shifts show little frequency dependence. These observational properties provide more clues on the nature of the CtoL effect, and also possibly lead to new ways of effect-removal for a more robust determination of the deep meridional flow.
HMI Science Nuggets #86 **2018** http://hmi.stanford.edu/hminuggets/?p=2246

A Comprehensive Method to Measure Solar Meridional Circulation and Center-to-Limb Effect Using Time-Distance Helioseismology

Ruizhu **Chen**, Junwei Zhao
ApJ 849 144 **2017**
https://arxiv.org/pdf/1709.07905.pdf
Meridional circulation is a crucial component of the Sun's internal dynamics, but its inference in the deep interior is complicated by a systematic center-to-limb effect in helioseismic measurement techniques. Previously, an empirical method, removing travel-time shifts measured for east-west traveling waves in the equatorial area from those measured for north-south traveling waves in the central meridian area, was used, but its validity and accuracy need to be assessed. Here we develop a new method to separate the center-to-limb effect, \delta\tau_CtoL, and meridional-flow-induced travel-time shifts, \delta\tau_MF, in a more robust way. Using 7-yr observations of the SDO/HMI, we exhaustively measure travel-time shifts between two surface locations along the solar disk's radial direction for all azimuthal angles and all skip distances. The measured travel-time shifts are a linear combination of \delta\tau_CtoL and \delta\tau_MF, which can be disentangled through solving the linear equation set. The \delta\tau_CtoL is found isotropic relative to the azimuthal angle, and the \delta\tau_MF are then inverted for the meridional circulation. Our inversion results show a three-layer flow structure, with equatorward flow found between about 0.82 and 0.91 R_sun for low latitude areas and between about 0.85 and 0.91 R_sun for higher latitude areas. Poleward flows are found below and above the equatorward flow zones, indicating a double-cell circulation in each hemisphere.
HMI Science Nuggets #76 Dec **2017** http://hmi.stanford.edu/hminuggets/?p=2053

Emergence of Magnetic Flux Generated in a Solar Convective Dynamo. I. The Formation of Sunspots and Active Regions, and The Origin of Their Asymmetries

Feng **Chen**, Matthias Rempel, and Yuhong Fan
2017 ApJ 846 149
https://arxiv.org/pdf/1704.05999.pdf

We present a realistic numerical model of sunspot and active region formation based on the emergence of flux bundles generated in a solar convective dynamo. To this end, we use the magnetic and velocity fields in a horizontal layer near the top boundary of the solar convective dynamo simulation to drive realistic radiative-magnetohydrodynamic simulations of the uppermost layers of the convection zone. The main results are as follows. (1) The emerging flux bundles rise with the mean speed of convective upflows and fragment into small-scale magnetic elements that further rise to the photosphere, where bipolar sunspot pairs are formed through the coalescence of the small-scale magnetic elements. (2) Filamentary penumbral structures form when the sunspot is still growing through ongoing flux emergence. In contrast to the classical Evershed effect, the inflow seems to prevail over the outflow in a large part of the penumbra. (3) A well-formed sunspot is a mostly monolithic magnetic structure that is anchored in a persistent deep-seated downdraft lane. The flow field outside the spot shows a giant vortex ring that comprises an inflow below 15 Mm depth and an outflow above 15 Mm depth. (4) The sunspots successfully reproduce the fundamental properties of the observed solar active regions, including the more coherent leading spots with a stronger field strength, and the correct tilts of bipolar sunspot pairs. These asymmetries can be linked to the intrinsic asymmetries in the magnetic and flow fields adapted from the convective dynamo simulation.

The statistical properties of the solar soft X-ray fluence during 1997–2008

Yulin **Chen**, Guiming Le , Yangping Lu, Minhao Chen, Liuguan Ding, Zhiqiang Yin
Astrophysics and Space Science January **2016**, 361:40

The statistical properties of the solar soft X-ray (SXR) flare fluence, i.e. the time integral of SXR flux of a flare, FSXR, and sum of the FSXR of all flares produced by a solar active region (AR), FAR, during 1997–2008 have been investigated. The results show that FSXR has moderate correlation with the area of the associated AR, while the correlation between FAR and the largest area of the associated AR is also moderate. The total number of ARs that can produce at least one SXR flare during 1997–2008, Nt, is 1408. The sum of FAR produced by 1408 ARs, ∑FAR, is 89 585.81 (erg s cm−2) and the average value of FAR is 63.6 (erg s cm−2). 34 ARs (FAR≥500 ergscm−2) contributed 55.72 % of ∑FAR.
111 ARs (100 (ergscm−2)≤FAR<500 (ergscm−2)) contributed 24.33 % of ∑FAR.
437 ARs (10 (ergscm−2)≤FAR<100 (ergscm−2)) contributed 17.48 % of ∑FAR. The rest 826 ARs only contributed 2.52 % of ∑FAR. The number of ARs decreases dramatically with FAR and the distribution function of FAR is N(FAR)=2840e−0.1286FAR. Finally, the north-south asymmetry of FAR has been investigated. The results show that the solar flare activities dominated in the northern hemisphere during 1997–2000 and the southern hemisphere during 2001–2008 respectively. During 1997–2008, the solar flare activities are stronger in the southern hemisphere than in the northern hemisphere.

Using coronal seismology to estimate the magnetic field strength in a realistic coronal model

Feng **Chen**, Hardi Peter
A&A 581, A137 **2015**
http://arxiv.org/pdf/1508.00593v1.pdf

Coronal seismology is extensively used to estimate properties of the corona, e.g. the coronal magnetic field strength are derived from oscillations observed in coronal loops. We present a three-dimensional coronal simulation including a realistic energy balance in which we observe oscillations of a loop in synthesised coronal emission. We use these results to test the inversions based on coronal seismology.
From the simulation of the corona above an active region we synthesise extreme ultraviolet (EUV) emission from the model corona. From this we derive maps of line intensity and Doppler shift providing synthetic data in the same format as obtained from observations. We fit the (Doppler) oscillation of the loop in the same fashion as done for observations to derive the oscillation period and damping time.
The loop oscillation seen in our model is similar to imaging and spectroscopic observations of the Sun. The velocity disturbance of the kink oscillation shows an oscillation period of 52.5s and a damping time of 125s, both being consistent with the ranges of periods and damping times found in observation. Using standard coronal seismology techniques, we find an average magnetic field strength of Bkink=79G for our loop in the simulation, while in the loop the field strength drops from some 300G at the coronal base to 50G at the apex. Using the data from our simulation we can infer what the average magnetic field derived from coronal seismology actually means. It is close to the magnetic field strength in a constant cross-section flux tube that would give the same wave travel time through the loop.
Our model produced not only a realistic looking loop-dominated corona, but also provides realistic information on the oscillation properties that can be used to calibrate and better understand the result from coronal seismology.

A possible mechanism for the formation of filamentous structures in magneto-plasmas by kinetic Alfvén waves†

L. **Chen**1,2,*, D. J. Wu1, G. Q. Zhao1,3, J. F. Tang4 andJ. Huang
JGR **2015**

Due to having strong anisotropy in their polarization state and spatial structure, it is believed that kinetic Alfvén waves (KAWs) can play an important role in various energization phenomena of plasma particles and the fine-structure formation in magneto-plasma environments. The filamentous fine-structures are a kind of the common density inhomogeneity phenomena in magneto-plasmas, and hence, the density gradient is one of the sources of free energy that can lead to KAWs instabilities. In this paper, based on the two-fluid model in which ions and electrons are treated as separate fluids, we investigate the effect of density gradient inhomogeneous on the dispersion and instability of KAWs in a magneto-plasma. The results show that KAW instability can be excited effectively by the density gradient. Especially, both the real frequency ωR and the growth rate ωI of KAWs are dramatically dependent on the spatial position x in the presence of an inhomogeneous density gradient. The results also show that the real frequency increases with the characteristic spatial scale of inhomogeneity , while the growth rate of KAWs has maximum in the growing ranges of . On the other hand, the excited KAWs are weakly dispersive with λekx < 1. *The results have potential importance for better understanding the microphysics of the filamentous fine-structure formation since the phenomena of density gradient inhomogeneous are ubiquitous in various magneto-plasmas, such as in the laboratory plasma as well as in both the solar coronal and terrestrial auroral plasmas.*

A comparison of the effects of CIR- and CME-induced geomagnetic activity on thermospheric densities and spacecraft orbits: Statistical studies

Guang-ming **Chen**1,*, Jiyao Xu1, Wenbin Wang2 andAlan. G. Burns
JGR, Volume 119, Issue 9, pages 7928–7939, **2014**

Enhanced energy input from the magnetosphere to the upper atmosphere during geomagnetic storms has a profound effect on thermospheric density and consequently near-Earth satellite orbit decay. These geomagnetic storms are caused by two different processes. The first is coronal mass ejections (CMEs) and the second is corotating interaction regions (CIRs). CME-driven storms are characterized by large maximum energy input but relatively short duration, whereas CIR-driven storms have relatively small maximum energy input but are of a considerably longer duration. In this paper we carried out a statistical study to assess the relative importance of each kind of storm to satellite orbital decay. The results demonstrate that CIR storms have a slightly larger effect on total orbital decay than CME storms do in a statistical sense. During the declining phase and the minimum years of a solar cycle, CIR storms occur frequently
and quasiperiodically. These storms have a large effect on thermospheric densities and satellite orbits because of their relatively long duration. Thus, it is important to fully understand their behavior and impact.

Does the F[10.7] index correctly describe solar EUV flux during the deep solar minimum of 2007-2009?

Chen, Yiding; Liu, Libo; Wan, Weixing
J. Geophys. Res., Vol. 116, No. A4, A043046 **2011**

This paper shows that the relationship between solar EUV flux and the F10.7 index during the extended solar minimum (Smin) of 2007–2009 is different from that in the previous Smin. This difference is also seen in the relationship between foF2 and F10.7. We collected SOHO/SEM EUV observations and the F10.7 index, through June 2010, to investigate solar irradiance in the recent Smin. We find that, owing to F10.7 and solar EUV flux decreased from the last Smin to the recent one with different amplitudes (larger in EUV flux), EUV flux is significantly lower in the recent Smin than in the last one for the same F10.7. Namely, F10.7 does not describe solar EUV irradiance in the recent Smin as it did in the last Smin. That caused remarkable responses in ionospheric foF2. For the same F10.7, foF2 in the recent Smin is lower than that in the last one; further, it is also lower than that in other previous Smins. Therefore, F10.7 is not an ideal indicator of foF2 during the recent Smin, which implies that F10.7 is not an ideal proxy for solar EUV irradiance during this period, although it has been adequate during previous Smins. Solar irradiance models and ionospheric models will need to take this into account for solar cycle investigations.

A magnetic reconnection model for the hot explosion with both ultraviolet and Hα wing emissions

Guanchong **Cheng**1,2,3, Lei Ni1,3,4,5, Yajie Chen2 and Jun Lin1,3,4,5
A&A, 685, A2 (**2024**)
https://arxiv.org/pdf/2402.07175.pdf
https://www.aanda.org/articles/aa/pdf/2024/05/aa47012-23.pdf

Context. Ellerman bombs (EBs) with significant Hα wing emissions and ultraviolet bursts (UV bursts) with strong Si IV emissions are two kinds of small transient brightening events that occur in the low solar atmosphere. The statistical observational results indicate that about 20% of the UV bursts connect with EBs. While some promising models exist for the formation mechanism of colder EBs in conjunction with UV bursts, the topic remains an area of ongoing research and investigation.
Aim. We numerically investigated the magnetic reconnection process between the emerging arch magnetic field and the lower atmospheric background magnetic field. We aim to find out if the hot UV emissions and much colder Hα wing emissions can both appear in the same reconnection process and how they are located in the reconnection region.
Methods. The open-source code NIRVANA was applied to perform the 2.5D magnetohydrodynamic (MHD) simulation. We developed the related sub-codes to include the more realistic radiative cooling process for the photosphere and chromosphere and the time-dependent ionization degree of hydrogen. The initial background magnetic field is 600 G, and the emerged magnetic field in the solar atmosphere is of the same magnitude, meaning that it results in a low- β magnetic reconnection environment. We also used the radiative transfer code RH1.5D to synthesize the Si IV and Hα spectral line profiles based on the MHD simulation results.
Results. Magnetic reconnection between emerged and background magnetic fields creates a thin, curved current sheet, which then leads to the formation of plasmoid instability and the nonuniform density distributions. Initially, the temperature is below 8000 K. As the current sheet becomes more vertical, denser plasmas are drained by gravity, and hotter plasmas above 20 000 K appear in regions with lower plasma density. The mix of hot tenuous and much cooler dense plasmas in the turbulent reconnection region can appear at about the same height, or even in the same plasmoid. Through the reconnection region, the synthesized Si IV emission intensity can reach above 106 erg s−1 sr−1 cm−2 Å−1 and the spectral line profile can be wider than 100 km s−1, the synthesized Hα line profile also show the similar characteristics of a typical EB. The turbulent current sheet is always in a dense plasma environment with an optical depth larger than 6.5 × 10−5 due to the emerged magnetic field pushing high-density plasmas upward.
Conclusions. Our simulation results indicate that the cold EB and hot UV burst can both appear in the same reconnection process in the low chromosphere, the EB can either appear several minutes earlier than the UV burst, or they can simultaneously appear at the similar altitude in a turbulent reconnection region below the middle chromosphere.

The Ellerman bomb and Ultraviolet burst triggered successively by an emerging magnetic flux rope

Guanchong **Cheng**, Lei Ni, Yajie Chen, Udo Ziegler, Jun Lin
Research in Astronomy and Astrophysics **2021**
https://arxiv.org/pdf/2105.08995.pdf
Ellerman bombs (EBs) and Ultraviolet (UV) bursts are common brightening phenomena which are usually generated in the low solar atmosphere of emerging flux regions. In this paper, we have investigated the emergence of an initial un-twisted magnetic flux rope based on three-dimensional (3D) magneto-hydrodynamic (MHD) simulations. The EB-like and UV burst-like activities successively appear in the U-shaped part of the undulating magnetic fields triggered by Parker Instability. The EB-like activity starts to appear earlier and lasts for about 80 seconds. Six minutes later, a much hotter UV burst-like event starts to appear and lasts for about 60 seconds. Along the direction vertical to the solar surface, both the EB and UV burst start in the low chromosphere, but the UV burst extends to a higher altitude in the up chromosphere. The regions with apparent temperature increase in the EB and UV burst are both located inside the small twisted flux ropes generated in magnetic reconnection processes, which are consistent with the previous 2D simulations that most hot regions are usually located inside the magnetic islands. However, the twisted flux rope corresponding to the EB is only strongly heated after it floats up to an altitude much higher than the reconnection site during that period. Our analyses show that the EB is heated by the shocks driven by the strong horizontal flows at two sides of the U-shaped magnetic fields. The twisted flux rope corresponding to the UV burst is heated by the driven magnetic reconnection process.

Correcting Doppler Shifts in He II 30.38 nm Line by Using the EVE and AIA data from Solar Dynamics Observatory

Zhixun **Cheng**, Yuming Wang, Rui Liu
2021 *ApJ* **911** 36
https://arxiv.org/ftp/arxiv/papers/2102/2102.13362.pdf
https://doi.org/10.3847/1538-4357/abea1f
The Extreme-ultraviolet Variability Experiment (EVE) onboard the Solar Dynamics Observatory (SDO) detects the solar EUV spectra with high temporal cadence and spectral resolution. The wavelength shifts of emission lines provide key information of the dynamics of the Sun. However, some of EVE spectral observations are influenced by the non-uniformly distributed irradiance on the Sun, which may prevent us from correctly understanding the

physical processes happened in the solar corona. Here, based on the only published on-orbit calibration data of EVE He II 30.38 nm line on **27 Jan 2011** (Chamberlin, 2016), we develop a method to correct the He II 30.38 nm line by using AIA 304 imaging data. This correction method is then applied to EVE He II 30.38 nm data from 29 Oct 2010 to 3 Mar 2011 to study the Doppler oscillations of the solar He II 30.38 nm line, in which we show that the half-month periodic Doppler oscillation is caused by non-uniformly distributed irradiance mainly due to the presence of active regions. Other EVE coronal lines also present similar Doppler oscillations, suggesting that an appropriate correction must be implemented before interpret the oscillation phenomena appearing in these lines.

Incompressible MHD modes in the thin magnetically twisted flux tube

O. K. **Cheremnykh**, V. Fedun, A. N. Kryshtal, G. Verth
A&A 604, A62 **2017**
https://arxiv.org/pdf/1707.03272.pdf
Context. Observations have shown that twisted magnetic fields naturally occur, and indeed are omnipresent in the Sun's atmosphere. It is therefore of great theoretical interest in solar atmospheric waves research to investigate the types of magnetohydrodynamic (MHD) wave modes that can propagate along twisted magnetic flux tubes. Aims. Within the framework of ideal MHD, the main aim of this work is to investigate small amplitude incompressible wave modes of twisted magnetic flux tubes with m more or equal 1. The axial magnetic field strength inside and outside the tube will be allowed to vary, to ensure the results will not be restricted to only cold plasma equilibria conditions. Methods. The dispersion equation for these incompressible linear MHD wave modes was derived analytically by implementing the long wavelength approximation. Results. It is shown, in the long wavelength limit, that both the frequency and radial velocity profile of the m = 1 kink mode are completely unaffected by the choice of internal background magnetic twist. However, fluting modes with m more or equal 2 are sensitive to the particular radial profile of magnetic twist chosen. Furthermore, due to background twist, a low frequency cut-off is introduced for fluting modes that is not present for kink modes. From an observational point of view, although magnetic twist does not affect the propagation of long wavelength kink modes, for fluting modes it will either work for or against the propagation, depending on the direction of wave travel relative to the sign of the background twist.

Long- and Mid-Term Variations of the Soft X-ray Flare Type in Solar Cycles

I.M. **Chertok** (1), A.V. Belov (1),
Solar Phys. 292:144 **2017**
http://www.izmiran.ru/~ichertok/FlareVariations/preprint.pdf
https://arxiv.org/abs/1710.06837
Using data from the GOES spacecraft in the 1-8 A wavelength range for Solar Cycles 23, 24, and part of Cycles 21 and 22, we compare mean temporal parameters (rising, decay times, duration) and the proportion of impulsive short-duration events (SDE) and gradual long-duration events (LDE) among C- and ≥M1.0-class flares. It is found that the fraction of the SDE ≥M1.0-class flares (including spikes) in Cycle 24 exceeds that in Cycle 23 in all three temporal parameters at the maximum phase and in the decay time during the ascending cycle phase. However, Cycles 23 and 24 barely differ in the fraction of the SDE C-class flares. The temporal parameters of SDEs, their fraction, and consequently the relationship between the SDE and LDE flares do not remain constant, but they reveal regular changes within individual cycles and during the transition from one cycle to another. In all phases of all four cycles, these changes have the character of pronounced, large-amplitude "quasi-biennial" oscillations (QBOs). In different cycles and at the separate phases of individual cycles, such QBOs are superimposed on various systematic trends displayed by the analyzed temporal flare parameters. In Cycle 24, the fraction of the SDE ≥M1.0-class flares from the N- and S-hemispheres displays the most pronounced synchronous QBOs. The QBO amplitude and general variability of the intense ≥M1.0-class flares almost always markedly exceeds those of the moderate C-class flares. The ordered quantitative and qualitative variations of the flare type revealed in the course of the solar cycles are discussed within the framework of the concept that the SDE flares are associated mainly with small sunspots (including those in developed active regions) and that small and large sunspots behave differently during cycles and form two distinct populations.

Supergranular turbulence in a quiet Sun: Lagrangian coherent structures

Abraham C.-L. **Chian**, Suzana S. A. Silva, Erico L. Rempel, Milan Gošić, Luis R. Bellot Rubio, Rodrigo A. Miranda, Iker S. Requerey
MNRAS Volume 488, Issue 3, September 2019, Pages 3076–3088, **2019**
https://arxiv.org/pdf/1904.08472.pdf
sci-hub.se/10.1093/mnras/stz1909
The quiet Sun exhibits a wealth of magnetic activities that are fundamental for our understanding of solar and astrophysical magnetism. The magnetic fields in the quiet Sun are observed to evolve coherently, interacting with each other to form distinguished structures as they are advected by the horizontal photospheric flows. We study coherent structures in photospheric flows in a region of quiet Sun consisted of supergranules. Supergranular

turbulence is investigated by detecting hyperbolic and elliptic Lagrangian coherent structures (LCS) using the horizontal velocity fields derived from Hinode intensity maps. Repelling/attracting LCS are found by computing the forward/backward finite-time Lyapunov exponent (FTLE). The Lagrangian centre of a supergranular cell is given by the local maximum of the forward FTLE; the Lagrangian boundaries of supergranular cells are given by the ridges of the backward FTLE. Objective velocity vortices are found by calculating the Lagrangian-averaged vorticity deviation, and false vortices are filtered by applying a criterion given by the displacement vector. The Lagrangian centres of neighboring supergranular cells are interconnected by ridges of the repelling LCS, which provide the transport barriers that allow the formation of vortices and the concentration of strong magnetic fields in the valleys of the repelling LCS. The repelling LCS also reveal the most likely sites for magnetic reconnection. We show that the ridges of the attracting LCS expose the locations of the sinks of photospheric flows at supergranular junctions, which are the preferential sites for the formation of kG magnetic flux tubes and persistent vortices. **2010 Nov 2**
Erratum: MNRAS Volume 489, Issue 1, October **2019**, Page 707 **sci-hub.se/10.1093/mnras/stz2296**

Detection of Coherent Structures in Photospheric Turbulent Flows

Abraham C.-L. **Chian**1,2,3, Erico L. Rempel1,4, Guillaume Aulanier2, Brigitte Schmieder2, Shawn C. Shadden5, Brian T. Welsch6, and Anthony R. Yeates
2014 ApJ 786 51
We study coherent structures in solar photospheric flows in a plage in the vicinity of the active region AR 10930 using the horizontal velocity data derived from Hinode/Solar Optical Telescope magnetograms. Eulerian and Lagrangian coherent structures (LCSs) are detected by computing the Q-criterion and the finite-time Lyapunov exponents of the velocity field, respectively. Our analysis indicates that, on average, the deformation Eulerian coherent structures dominate over the vortical Eulerian coherent structures in the plage region. We demonstrate the correspondence of the network of high magnetic flux concentration to the attracting Lagrangian coherent structures (aLCSs) in the photospheric velocity based on both observations and numerical simulations. In addition, the computation of aLCS provides a measure of the local rate of contraction/expansion of the flow.

Coronal magnetic field evolution over the cycle 24

I. **Chifu**, B. Inhester, T. Wiegelmann
A&A **2022**
https://arxiv.org/pdf/2201.03853.pdf
The photospheric magnetic field vector is continuously derived from measurements, while reconstruction of the three-dimensional (3D) coronal magnetic field requires modelling with photospheric measurements as a boundary condition. For decades the cycle variation of the magnetic field in the photosphere has been investigated. To present, there is no study to show the evolution of the coronal magnetic flux in the corona, nor the evolution of solar cycle magnetic free energy. The paper aims to analyze the temporal variation of the magnetic field and free magnetic energy in the solar corona for the solar cycle 24 and how the magnetic field behaves in the two hemispheres. We investigate if we can obtain better estimates of the magnetic field at Earth using the nonlinear force-free field (NLFFF) extrapolation method. To model the magnetic field over cycle 24 we apply the NLFFF optimization method to the synoptic vector magnetic maps derived from the observations of Heliospheric and Magnetic Imager (HMI) onboard Solar Dynamic Observatory (SDO). We found that during the solar cycle 24, the maximum of the Sun's dynamics is different from the sunspot number (SSN) maximum peak. The major contribution to the total unsigned flux is provided by the flux coming from the magnetic field structures other than sunspots (MSOS) within latitudes between -30 and +30 degrees. The magnetic flux variation during the solar cycle 24 shows a different evolution in the corona than in the photosphere. We found a correlation value of 0.8 between the derived magnetic energy from our model and the flare energy index derived from observations. On average, cycle 24 had a higher number of sunspots in the northern hemisphere (NH) but stronger flux in the southern hemisphere (SH) which could more effectively reach the higher layers of the atmosphere. The coupling between the hemispheres increases with height.

ALMA and IRIS Observations of the Solar Chromosphere II: Structure and Dynamics of Chromospheric Plage

Georgios **Chintzoglou**, Bart De Pontieu, Juan Martínez-Sykora, Viggo Hansteen, Jaime de la Cruz Rodríguez, Mikolaj Szydlarski, Shahin Jafarzadeh, Sven Wedemeyer, Timothy S. Bastian, Alberto Sainz Dalda
2021 *ApJ* **906** 82
https://arxiv.org/pdf/2012.05970.pdf
https://doi.org/10.3847/1538-4357/abc9b1
We propose and employ a novel empirical method for determining chromospheric plage regions, which seems to better isolate plage from its surrounding regions compared to other methods commonly used. We caution that isolating plage from its immediate surroundings must be done with care in order to successfully mitigate statistical

biases that, for instance, can impact quantitative comparisons between different chromospheric observables. Using this methodology, our analysis suggests that 1.25 mm wavelength free-free emission in plage regions observed with ALMA/Band6 may not form in the low chromosphere as previously thought, but rather in the upper chromospheric parts of dynamic plage features (such as spicules and other bright structures), i.e., near geometric heights of transition region temperatures. We investigate the high degree of similarity between chromospheric plage features observed in ALMA/Band6 (at 1.25 mm wavelength) and IRIS/Si IV at 1393Å. We also show that IRIS/Mg II h and k is not as well correlated with ALMA/Band6 as was previously thought, and we discuss the discrepancies with previous works. Lastly, we report indications for chromospheric heating due to propagating shocks supported by the ALMA/Band6 observations. **22-Apr-2017**

IRIS and ALMA Observations Uncovering a Type-II Spicule and the Dynamic Nature of a Chromospheric Plage Region

Georgios **Chintzoglou**, Bart De Pontieu, Juan Martínez-Sykora, Viggo Hansteen, Jaime de la Cruz Rodríguez, Mikolaj Szydlarski, Shahin Jafarzadeh, Sven Wedemeyer, Timothy S. Bastian, Alberto Saínz Dalda

ApJ **2020**

https://arxiv.org/pdf/2005.12717.pdf

We present observations of the solar chromosphere obtained simultaneously with the Atacama Large Millimeter/submillimeter Array (\emph{ALMA}) and the Interface Region Imaging Spectrograph (\emph{IRIS}). The observatories targeted a chromospheric plage region of which the spatial distribution (split between strongly and weakly magnetized regions) allowed the study of linear-like structures in isolation, free of contamination from background emission. Using these observations in conjunction with a radiative magnetohydrodynamic 2.5D model covering the upper convection zone all the way to the corona that considers non-equilibrium ionization effects, we report the detection of an on-disk chromospheric spicule with \emph{ALMA} and confirm its multithermal nature. In addition, we discuss the strikingly high degree of similarity between chromospheric plage features observed in \emph{ALMA}/Band6 and \emph{IRIS}/\ion{Si}{4} (also reproduced in our model) suggesting that \emph{ALMA}/Band6 does not observe in the low chromosphere as previously thought but rather observes the upper chromospheric parts of structures such as spicules and other bright structures above plage at geometric heights near transition region temperatures. We also show that \emph{IRIS}/\ion{Mg}{2} is not as well correlated with \emph{ALMA}/Band6 as was previously thought. For these comparisons, we propose and employ a novel empirical method for the determination of plage regions, which seems to better isolate plage from its surrounding regions as compared to other methods commonly used. We caution that isolating plage from its immediate surroundings must be done with care to mitigate stastistical bias in quantitative comparisons between different chromospheric observables. Lastly, we report indications for chromospheric heating due to traveling shocks supported by the \emph{ALMA}/Band6 observations. **22-Apr-2017**

Bridging the Gap: Capturing the Lyα Counterpart of a Type-II Spicule and its Heating Evolution with VAULT2.0 and IRIS Observations

Georgios **Chintzoglou**, Bart De Pontieu, Juan Martínez-Sykora, Tiago M.D. Pereira, Angelos Vourlidas, Samuel Tun Beltran

ApJ **857** 73 **2018**

https://arxiv.org/pdf/1803.03405.pdf

We present results from an observing campaign in support of the VAULT2.0 sounding rocket launch on **September 30, 2014**. VAULT2.0 is a Lyα (1216 \AA) spectroheliograph capable of providing spectroheliograms at high cadence. Lyα observations are highly complementary to the IRIS observations of the upper chromosphere and the low transition region (TR) but have previously been unavailable. The VAULT2.0 data provide new constraints on upper-chromospheric conditions for numerical models. The observing campaign was closely coordinated with the IRIS mission. Taking advantage of this simultaneous multi-wavelength coverage of target AR 12172 and by using state-of-the-art radiative-MHD simulations of spicules, we investigate in detail a type-II spicule associated with a fast (300 km s−1) network jet recorded in the campaign observations. Our analysis suggests that spicular material exists suspended high in the atmosphere but in lower temperatures (seen in Lyα) until it is heated and becomes visible in TR temperatures as a network jet. The heating begins lower in the spicule and propagates upwards as a rapidly propagating thermal front. The front is then observed as fast, plane-of-the-sky motion typical of a network jet, but contained inside the pre-existing spicule. This work supports that the high speeds reported in network jets should not be taken as real mass upflows but only as apparent speeds of a rapidly propagating heating front along the pre-existing spicule.

Photospheric hot spots at solar coronal loop footpoints revealed by hyperspectral imaging observations

L. P. **Chitta**, M. van Noort, H. N. Smitha, E. R. Priest, L. H. M. Rouppe van der Voort

ApJ **976** 134 **2024**
https://arxiv.org/pdf/2410.04964
https://iopscience.iop.org/article/10.3847/1538-4357/ad8564/pdf
Poynting flux generated by random shuffling of photospheric magnetic footpoints is transferred through the upper atmosphere of the Sun where the plasma is heated to over 1 MK in the corona. High spatiotemporal resolution observations of the lower atmosphere at the base of coronal magnetic loops are crucial to better understand the nature of the footpoint dynamics and the details of magnetic processes that eventually channel energy into the corona. Here we report high spatial resolution (~0.1\arcsec) and cadence (1.33 s) hyperspectral imaging of the solar Hα line, acquired by the Microlensed Hyperspectral Imager prototype installed at the Swedish 1-m Solar Telescope, that reveal photospheric hot spots at the base of solar coronal loops. These hot spots manifest themselves as Hα wing enhancements, occurring on small spatial scales of ~0.2\arcsec, and timescales of less than 100 s. By assuming that the Hα wings and the continuum form under the local thermodynamic equilibrium condition, we inverted the Hα line profiles and found that the hot spots are compatible with a temperature increase of about 1000 K above the ambient quiet-Sun temperature. The Hα wing integrated Stokes V/I maps indicate that hot spots are related to magnetic patches with field strengths comparable to or even stronger than the surrounding network elements. But they do not show the presence of parasitic polarity magnetic field that would support the interpretation that these hot spots are reconnection-driven Ellerman bombs, we interpret these features as proxies of locations where convection-driven magnetic field intensification in the photosphere can lead to energy transfer into higher layers. We suggest that such hot spots at coronal loop footpoints may be indicative of the specific locations and onset of energy flux injection into the upper atmosphere.

Fleeting small-scale surface magnetic fields build the quiet-Sun corona

L. P. **Chitta**, S. K. Solanki, J. C. del Toro Iniesta, J. Woch, +
ApJL **956** L1 **2023**
https://arxiv.org/pdf/2308.10982.pdf
https://iopscience.iop.org/article/10.3847/2041-8213/acf136/pdf
Arch-like loop structures filled with million Kelvin hot plasma form the building blocks of the quiet-Sun corona. Both high-resolution observations and magnetoconvection simulations show the ubiquitous presence of magnetic fields on the solar surface on small spatial scales of ~100\,km. However, the question of how exactly these quiet-Sun coronal loops originate from the photosphere and how the magnetic energy from the surface is channeled to heat the overlying atmosphere is a long-standing puzzle. Here we report high-resolution photospheric magnetic field and coronal data acquired during the second science perihelion of Solar Orbiter that reveal a highly dynamic magnetic landscape underlying the observed quiet-Sun corona. We found that coronal loops often connect to surface regions that harbor fleeting weaker, mixed-polarity magnetic field patches structured on small spatial scales, and that coronal disturbances could emerge from these areas. We suggest that weaker magnetic fields with fluxes as low as 1015\,Mx and or those that evolve on timescales less than 5\,minutes, are crucial to understand the coronal structuring and dynamics. **12 Oct 2022**
Solar Orbiter Nugget #18 2023 *https://www.cosmos.esa.int/web/solar-orbiter/-/science-nugget-fleeting-small-scale-surface-magnetic-fields-build-the-quiet-sun-corona-1*

Solar coronal heating from small-scale magnetic braids

L. P. **Chitta**, H. Peter, S. Parenti, D. Berghmans, F. Auchère, S. K. Solanki, R. Aznar Cuadrado, U. Schühle, L. Teriaca, S. Mandal, K. Barczynski, É. Buchlin, L. Harra, E. Kraaikamp, D. M. Long, L. Rodriguez, C. Schwanitz, P. J. Smith, C. Verbeeck, A. N. Zhukov, W. Liu, M. C. M. Cheung
A&A **2022**
https://arxiv.org/pdf/2209.12203.pdf
Relaxation of braided coronal magnetic fields through reconnection is thought to be a source of energy to heat plasma in active region coronal loops. However, observations of active region coronal heating associated with untangling of magnetic braids remain sparse. One reason for this paucity could be the lack of coronal observations with sufficiently high spatial and temporal resolution to capture this process in action. Using new high spatial resolution (250-270 km on the Sun) and high cadence (3-10 s) observations from the Extreme Ultraviolet Imager (EUI) on board Solar Orbiter we observed untangling of small-scale coronal braids in different active regions. The untangling is associated with impulsive heating of the gas in these braided loops. We assess that coronal magnetic braids overlying cooler chromospheric filamentary structures are perhaps more common. Furthermore, our observations show signatures of both spatially coherent and intermittent coronal heating during relaxation of magnetic braids. Our study reveals the operation of both more gentle and impulsive modes of magnetic reconnection in the solar corona. **2022 March 17, 2022 March 19**

Extreme ultraviolet bursts and nanoflares in the quiet solar transition region and corona

L. P. **Chitta**, H. Peter, P. R. Young

A&A 647, A159 **2021**
https://arxiv.org/pdf/2102.00730.pdf
https://www.aanda.org/articles/aa/pdf/2021/03/aa39969-20.pdf
The quiet solar corona consists of a myriad of loop-like features with magnetic fields originating from network and internetwork regions on the solar surface. Based on HRTS, Yohkoh, SOHO, and TRACE observations, there is a rich literature on a variety of such burst phenomena in the solar atmosphere. However, it remains unclear whether such transients, mostly observed in the extreme ultraviolet (EUV), play a significant role in atmospheric heating. We revisit the issue of these bursts as a prelude to the new high resolution EUV imagery expected from the recently launched Solar Orbiter. We use EUV images recorded by the SDO/AIA to investigate statistical properties of the bursts. We detect the bursts in the 171 Å filter images of AIA in an automated way through a pixel-wise analysis by imposing different intensity thresholds. By exploiting the high cadence (12 s) of the AIA observations, we find that the distribution of lifetime of these events peaks at about 120 s, nevertheless, there are a significant number of events also at timescales shorter than 60 s. The sizes of the detected bursts are limited by the spatial resolution, hinting at a larger number of hidden events in the AIA data. We estimate that there appear about 100 new bursts per second on the whole Sun. The detected bursts have nanoflare-like energies of 1024 erg per event. Based on this we estimate that at least 100 times more events of similar nature would be required to account for energy required to heat the corona. Thus, considering AIA observations alone, the EUV bursts discussed here have no significant role in the quiet-Sun coronal heating. If the quiet-Sun coronal heating is mainly bursty, then the high-resolution EUV observations from the Solar Orbiter may be able to reduce, at least partly, the deficit in the number of EUV bursts seen with SDO/AIA, by detecting more such events. **2011-01-25, 2017-03-21**

Impulsive coronal heating during the interaction of surface magnetic fields in the lower solar atmosphere

L. P. **Chitta**, H. Peter, E. R. Priest, S. K. Solanki
A&A **2020**
https://arxiv.org/pdf/2010.12560.pdf
Coronal plasma in the cores of solar active regions is impulsively heated to more than 5 MK. The nature and location of the magnetic energy source responsible for such impulsive heating is poorly understood. Using observations of seven active regions from the Solar Dynamics Observatory, we found that a majority of coronal loops hosting hot plasma have at least one footpoint rooted in regions of interacting mixed magnetic polarity at the solar surface. In cases when co-temporal observations from the Interface Region Imaging Spectrograph space mission are available, we found spectroscopic evidence for magnetic reconnection at the base of the hot coronal loops. Our analysis suggests that interactions of magnetic patches of opposite polarity at the solar surface and the associated energy release during reconnection are key to impulsive coronal heating. **11 July 2017, 23 Dec 2017, 11 Feb 2018, 27 May-2 June 2018, 17 June 2018, 25 Jan 2019, 12 Apr 2019**
RHESSI Nuggets #395 **2020**
https://sprg.ssl.berkeley.edu/~tohban/wiki/index.php/What_drives_impulsive_coronal_heating%3F

Energetics of magnetic transients in solar active region plage

L. P. **Chitta**, A. R. C. Sukarmadji, L. Rouppe van der Voort, H. Peter
A&A 623, A176 **2019**
https://arxiv.org/pdf/1902.01650.pdf
https://www.aanda.org/articles/aa/pdf/2019/03/aa34548-18.pdf
Densely packed coronal loops are rooted in plages in the vicinity of active regions on the Sun. The photospheric magnetic features underlying these plage areas are patches of mostly unidirectional magnetic field extending several acrsec on the solar surface. To explore the transient nature of magnetic field, its mixed-polarity characteristics and the associated energetics in plages using high spatial resolution observations and numerical simulations. We use photospheric Fe I 6173\,\AA\ spectropolarimetric observations of a decaying active region obtained from the SST. These data are inverted to retrieve the magnetic field underlying the plage as identified in the EUV emission maps obtained from the AIA onboard the SDO. To obtain more insights into the evolution of plages on the Sun, we perform 3D radiation MHD simulations of magnetoconvection using the MURaM code. The observations show transient magnetic flux emergence and cancellation events within the plage, on timescales of a few 100 s, and on spatial scales comparable to granules. These transient events occur at the footpoints of active region plage loops. In one case the coronal response at the footpoints of those loops is clearly associated with the underlying transient. The simulations also reveal similar magnetic flux emergence and cancellation events that extend to even smaller spatial and temporal scales. Individual simulated transient events transfer an energy flux in excess of 1 MW m−2 through the photosphere. We suggest that the magnetic transients could play an important role in the energetics of active region plage. Both in observations and simulations the opposite polarity magnetic field brought up by transient flux emergence cancels with the surrounding plage field. Magnetic reconnection associated with such transient events likely conduits magnetic energy to power the overlying chromosphere and coronal loops. **26 June 2015**

Nature of the energy source powering solar coronal loops driven by nanoflares★

L. P. **Chitta**1, H. Peter1 and S. K. Solanki1,2
A&A 615, L9 (**2018**)
https://www.aanda.org/articles/aa/pdf/2018/07/aa33404-18.pdf
https://arxiv.org/pdf/1806.11045.pdf

Context. Magnetic energy is required to heat the corona, the outer atmosphere of the Sun, to millions of degrees.
Aims. We study the nature of the magnetic energy source that is probably responsible for the brightening of coronal loops driven by nanoflares in the cores of solar active regions.
Methods. We consider observations of two active regions (ARs), 11890 and 12234, in which nanoflares have been detected. To this end, we use ultraviolet (UV) and extreme ultraviolet (EUV) images from the Atmospheric Imaging Assembly (AIA) onboard the Solar Dynamics Observatory (SDO) for coronal loop diagnostics. These images are combined with the co-temporal line-of-sight magnetic field maps from the Helioseismic and Magnetic Imager (HMI) onboard SDO to investigate the connection between coronal loops and their magnetic roots in the photosphere.
Results. The core of these ARs exhibit loop brightening in multiple EUV channels of AIA, particularly in its 9.4 nm filter. The HMI magnetic field maps reveal the presence of a complex mixed polarity magnetic field distribution at the base of these loops. We detect the cancellation of photospheric magnetic flux at these locations at a rate of about 1015 Mx s−1. The associated compact coronal brightenings directly above the cancelling magnetic features are indicative of plasma heating due to chromospheric magnetic reconnection.
Conclusions. We suggest that the complex magnetic topology and the evolution of magnetic field, such as flux cancellation in the photosphere and the resulting chromospheric reconnection, can play an important role in energizing active region coronal loops driven by nanoflares. Our estimate of magnetic energy release during flux cancellation in the quiet Sun suggests that chromospheric reconnection can also power the quiet corona.
9 November 2013, 11 December 2014

A compact solar UV burst triggered in a magnetic field with a fan-spine topology

L. P. **Chitta**, H. Peter, P. R. Young, Y.-M. Huang
A&A 605, A49 **2017**
https://arxiv.org/pdf/1706.08059.pdf

Solar UV bursts are small-scale features that exhibit intermittent brightenings that are thought to be due to magnetic reconnection. They are observed abundantly in the chromosphere and transition region, in particular in active regions. We investigate in detail a UV burst related to a magnetic feature that is advected by the moat flow from a sunspot towards a pore. The moving feature is parasitic in that its magnetic polarity is opposite to that of the spot and the pore. We use UV spectroscopic and slit-jaw observations from the IRIS to identify and study chromospheric and transition region spectral signatures of said UV burst. To investigate the magnetic topology surrounding the UV burst, we use a 2 hrs long time sequence of simultaneous line-of-sight magnetograms from the HMI and perform a data-driven, 3D magnetic field extrapolations by means of a magnetofrictional relaxation technique. We can connect UV burst signatures to the overlying EUV coronal loops observed by the AIA. The UV burst shows a variety of extremely broad line profiles indicating plasma flows in excess of ±200 km s−1 at times. The whole structure is divided into two spatially distinct zones of predominantly up- and downflows. The magnetic field extrapolations show the presence of a persistent fan-spine magnetic topology at the UV burst. The associated 3D magnetic null point exists at a height of about 500 km above the photosphere and evolves co-spatially with the observed UV burst. The EUV emission at the footpoints of coronal loops is correlated with the evolution of the underlying UV burst. The magnetic field around the null point is sheared by photospheric motions, triggering magnetic reconnection that ultimately powers the observed UV burst and energizes the overlying coronal loops. The location of the null point suggests that the burst is triggered low in the solar chromosphere. **2014 July 27**

Numerical simulations of impulsively generated Alfvén waves in solar magnetic arcades

P. **Chmielewski**, K. Murawski, Z.E. Musielak, A.K. Srivastava
ApJ 793 43, **2014**
http://arxiv.org/pdf/1408.0855v1.pdf

We perform numerical simulations of impulsively generated Alfvén waves in an isolated solar arcade, which is gravitationally stratified and magnetically confined. We study numerically the propagation of Alfvén waves along such magnetic structure that extends from the lower chromosphere, where the waves are generated, to the solar corona, and analyze influence of the arcade size and width of the initial pulses on the wave propagation and reflection. Our model of the solar atmosphere is constructed by adopting the temperature distribution based on the semi-empirical VAL-C model and specifying the curved magnetic field lines that constitute the asymmetric magnetic arcade. The propagation and reflection of Alfvén waves in this arcade is described by 2.5D magnetohydrodynamic equations that are numerically solved by the FLASH code. Our numerical simulations reveal that the Alfvén wave amplitude decreases as a result of a partial reflection of Alfvén waves in the solar transition region, and that the waves which are not reflected leak through the transition region and reach the solar corona. We

also find the decrement of the attenuation time of Alfvén waves for wider initial pulses. Moreover, our results show that the propagation of Alfvén waves in the arcade is affected by spatial dependence of the Alfvén speed, which leads to phase-mixing that is stronger for more curved and larger magnetic arcades. We discuss processes that affect the Alfvén wave propagation in an asymmetric solar arcade and conclude that besides phase-mixing in the magnetic field configuration, plasma properties of the arcade and size of the initial pulse as well as structure of the solar transition region all play a vital role in the Alfvén wave propagation.

On the Nature of Propagating Intensity Disturbances in Polar Plumes during the 2017 Total Solar Eclipse

Kyung-Suk **Cho**, Il-Hyun Cho, Maria S. Madjarska, Valery M. Nakariakov, Heesu Yang, Seonghwan Choi, Eun-Kyung Lim, Kyung-Sun Lee, Jung-Jun Seough, Jaeok Lee, Yeon-Han Kim

ApJ **909** 202 **2021**

https://arxiv.org/pdf/2102.02085.pdf

https://doi.org/10.3847/1538-4357/abdfd5

The propagating intensity disturbances (PIDs) in plumes are still poorly understood and their identity (magnetoacoustic waves or flows) remains an open question. We investigate PIDs in five plumes located in the northern polar coronal hole observed during the 2017 total solar eclipse. Three plumes are associated with coronal bright points, jets and macrospicules at their base (active plumes) and the other two plumes are not (quiet plumes). The electron temperature at the base of the plumes is obtained from the filter ratio of images taken with the X-ray Telescope on board Hinode and the passband ratio around 400 nm from an eclipse instrument, the Diagnostic Coronagraph Experiment (DICE). The phase speed (v_r), frequency (omega), and wavenumber (k) of the PIDs in the plumes are obtained by applying a Fourier transformation to the space-time (r-t plane) plots in images taken with the Atmospheric Imaging Assembly (AIA) in three different wavelength channels (171 A, 193 A, and 211 A). We found that the PIDs in the higher temperature AIA channels, 193 and 211 A, are faster than that of the cooler AIA 171 A channel. This tendency is more significant for the active plumes than the quiet ones. The observed speed ratio (~1.3) between the AIA 171 and 193 A channels is similar to the theoretical value (1.25) of a slow magnetoacoustic wave. Our results support the idea that PIDs in plumes represent a superposition of slow magnetoacoustic waves and plasma outflows that consist of dense cool flows and hot coronal jets. **21 Aug 2017**

Toward Next Generation Solar Coronagraph: Diagnostic Coronagraph Experiment

K.-S. **Cho**, H. Yang, J.-O. Lee, S.-C. Bong, J. Kim, S. Choi, J.-Y. Park, K.-H. Cho, J.-H. Baek, Y.-H. Kim, Y.-D. Park

Journal of the Korean Astronomical Society **2020**

https://arxiv.org/pdf/2006.06155.pdf

Korea Astronomy and Space Science Institute (KASI) has been developing a next-generation coronagraph (NGC) in cooperation with NASA to measure the coronal electron density, temperature, and speed simultaneously using four different filters around 400 nm. KASI organized an expedition team to demonstrate the coronagraph measurement scheme and the instrumental technology through the 2017 total solar eclipse (TSE) across the USA. The observation site was in Jackson Hole, Wyoming, USA. We built an eclipse observation system, so-called Diagnostic Coronal Experiment (DICE), which is composed of two identical telescopes to improve a signal to noise ratio. The observation was conducted with 4 wavelengths and 3 linear polarization directions according to the planned schedule in a limited total eclipse time of about 140 seconds. Polarization information of corona from the data was successfully obtained but we were not able to obtain global information of coronal electron temperature and speed in the corona due to a low signal-to-noise ratio of the optical system and a strong emission from the prominence located in the western limb. In this study, we report the development of DICE and observation results from the eclipse expedition. TSE observation and analysis by using our own developed instrument gave an important lesson that a coronagraph should be carefully designed to achieve the scientific purpose of this study. And it was a very useful experience in the way for the success of follow-up NASA-KASI joint missions called the Balloon-borne Investigation of the Temperature and Speed of Electrons in the Corona (BITSE) and COronal Diagnostic EXperiment (CODEX). **August 21, 2017**

The Application of the Filtered Backprojection Algorithm to Solar Rotational Tomography

Kyuhyoun **Cho**, Jongchul Chae, Ryun-Young Kwon, Su-Chan Bong, Kyung-Suk Cho

ApJ **895** 55 **2020**

https://arxiv.org/pdf/2005.06388.pdf

https://doi.org/10.3847/1538-4357/ab88af

Solar rotational tomography (SRT) is an important method to reconstruct the physical parameters of the three-dimensional solar corona. Here we propose an approach to apply the filtered backprojection (FBP) algorithm to the SRT. The FBP algorithm is generally not suitable for SRT due to the several issues with solar extreme ultraviolet (EUV) observations, in particular a problem caused by missing data because of the unobserved back side of corona

hidden behind the Sun. We developed a method to generate a modified sinogram which resolves the blocking problem. The modified sinogram is generated by combining the EUV data at two opposite sites observed by the Atmospheric Imaging Assembly (AIA) onboard the Solar Dynamics Observatory (SDO). We generated the modified sinogram for about one month in **2019 February** and reconstructed the three-dimensional corona under the static state assumption. In order to obtain the physical parameters of the corona, we employed a DEM inversion method. We tested the performance of the FBP algorithm with the modified sinogram by comparing the reconstructed data with the observed EUV image, electron density models, previous studies of electron temperature, and an observed coronagraph image. The results illustrate that the FBP algorithm reasonably reconstructs the bright regions and the coronal holes, and can reproduce their physical parameters. The main advantage of the FBP algorithm is that it is easy to understand and computationally efficient. Thus, it enables us to easily probe the inhomogeneous coronal electron density and temperature distribution of the solar corona.

Seismological determination of the Alfvén speed and plasma-beta in solar photospheric bright points

Il-Hyun **Cho**, Yong-Jae Moon, Valery M. Nakariakov, Dae Jung Yu, Jin-Yi Lee, Su-Chan Bong, Rok-Soon Kim, Kyung-Suk Cho, Yeon-Han Kim, Jae-Ok Lee

ApJLett **871** L14 **2019**

https://arxiv.org/pdf/1901.04144.pdf

sci-hub.tw/10.3847/2041-8213/aafe0a

The Alfvén speed and plasma beta in photospheric bright points observed by the Broadband Filter Imager (BFI) of the Solar Optical Telescope (SOT) on board the \textit{Hinode} satellite, are estimated seismologically. The diagnostics is based on the theory of slow magnetoacoustic waves in a non-isothermally stratified photosphere with a uniform vertical magnetic field. We identify and track bright points in a G-band movie by using the 3D region growing method, and align them with blue continuum images to derive their brightness temperatures. From the Fourier power spectra of 118 continuum light curves made in the bright points, we find that light curves of 91 bright points have oscillations with properties which are significantly different from oscillation in quiet regions, with the periods ranging 2.2--16.2~min. We find that the model gives a moderate value of the plasma beta when γ lies at around 5/3. The calculated Alfvén speed is 9.68±2.02~km~s−1, ranging in 6.3--17.4~km~s−1. The plasma beta is estimated to be of 0.93±0.36, ranging in 0.2--1.9. **2007-Mar-01**

Intensity and Doppler Velocity Oscillations in Pore Atmospheres

K.-S. **Cho**1,2, S.-C. Bong1, V. M. Nakariakov3,4,5, E.-K. Lim1, Y.-D. Park1, J. C. Chae6, H.-S. Yang6, H.-M. Park6, and V. Yurchyshyn

2015 ApJ 802 45

We have investigated chromospheric traveling features running across two merged pores from their centers at speeds of about 55 km s−1, in the active region AR 11828. The pores were observed on 2013 August 24 by using high-time, spatial, and spectral resolution data from the Fast Imaging Solar Spectrograph of the 1.6 m New Solar Telescope. We infer a line-of-sight (LOS) velocity by applying the lambdameter method to the Ca ii 8542 Å band and Hα band, and investigate intensity and LOS velocity changes at different wavelengths and different positions at the pores. We find that they have three-minute oscillations, and the intensity oscillation from the line center (0.0 Å) is preceded by that from the core (−0.3 Å) of the bands. There is no phase difference between the intensity and the LOS velocity oscillations at a given wavelength. The amplitude of LOS velocity from the near core spectra ($\Delta\lambda = 0.10 - 0.21$ Å) is greater than that from the far core spectra ($\Delta\lambda = 0.24 - 0.36$ Å). These results support the interpretation of the observed wave as a slow magnetoacoustic wave propagating along the magnetic field lines in the pores. The apparent horizontal motion and a sudden decrease of its speed beyond the pores can be explained by the projection effect caused by inclination of the magnetic field with a canopy structure. We conclude that the observed wave properties of the pores are quite similar to those from the sunspot observations.

Cycle Length Dependence of Stellar Magnetic Activity and Solar Cycle 23

Hwajin **Choi**1,2, Jeongwoo Lee1,3, Suyeon Oh4, Bogyeong Kim1, Hoonkyu Kim1, and Yu Y

2015 ApJ 802 67

Solar cycle (SC) 23 was extraordinarily long with remarkably low magnetic activity. We have investigated whether this is a common behavior of solar-type stars. From the Ca ii H and K line intensities of 111 stars observed at Mount Wilson Observatory from 1966 to 1991, we have retrieved data of all 23 G-type stars and recalculated their cycle lengths using the damped least-squares method for the chromospheric activity index S as a function of time. A regression analysis was performed to find relations between the derived cycle length, Pavg, and the index for excess chromospheric emission, R'_{HK}. As a noteworthy result, we found a segregation between young and old solar-type stars in the cycle length-activity correlation. We incorporated the relation for the solar-type stars into the previously known rule for stellar chromospheric activity and brightness to estimate the variation of solar brightness from SC 22 to SC 23 as (0.12 ± 0.06)%, much higher than the actual variation of total solar irradiance (TSI) ≤0.02%. We have

then examined solar spectral irradiance (SSI) to find a good phase correlation with a sunspot number in the wavelength range of 170–260 nm, which is close to the spectral range effective in heating the Earth's atmosphere. Therefore, it appears that SSI rather than TSI is a good indicator of the chromospheric activity, and its cycle length dependent variation would be more relevant to the possible role of the Sun in the cyclic variation of the Earth's atmosphere.

Stable solar periodicities: the time stability

Kim **Chol-jun**, Jon Kyong-phyong

Monthly Notices of the Royal Astronomical Society, Volume 511, Issue 1, March **2022**, Pages 1401–1407,

https://doi.org/10.1093/mnras/stac134

We show that while the Fourier transform can figure only an 'intensity' of a periodic signal, there is an additional information embedded, which is a 'coherence' of the signal. Supposing that the periodicity is reflected only on the 'coherence,' we introduce a time stability as a measure of 'coherence' excluding the 'intensity,' i.e. amplitude of signal. In stead of classical strength-based significance, where strength implies the power or amplitude, we adopt a stability-based significance as criterion to choose cycles in a random signal. We inspect the time-stable solar periodicities and show that most periodicities discovered in exterior solar activities such as the solar wind inhere in interior solar activity such as the sunspot and that the time stability can be an effective tool in spectral analysis of stochastic solar activity.

Stability of cycle in samplogram and spurious cycles in solar activity

Kim **Chol-jun**

2020

https://arxiv.org/pdf/2009.09578.pdf

The spectral analysis with stochastic significance cannot distinguish the spurious cycles effectively, because a non-stationary signal can make a significant peak in spectrum. I show that the random separation between the grand extremes such as grand maxima and minima in solar activity can make a spurious but significant peak in spectrum. And it is possible to pick even the weak stable cycle by applying an averaging down-sampling and the differencing to a random signal. This is because both operations variously change the height of peak in spectrum and the spurious cycle is in turn unstable in both operations. I introduce a samplogram showing these operations and stability intuitively.

About 200-Year Cycle of Solar Activity in the Mediaeval Korean Records and Reconstructions from Cosmogenic Radionuclides

Kim **Chol-jun**, Kim Jik-su

MNRAS **2020**

https://arxiv.org/pdf/1912.11226.pdf

We investigated the Korean records of naked-eye sunspot observations and found an implication of periodicity of about 200-year. Adding the Chinese records we showed that the historical naked-eye sunspot observations have the similar periodicity. Recent some works showed that there would be no intrinsic periodicities except 11-year cycle. We adopt the new approach called samplogram to test sampling stability of cycles in terms of power spectra and difference series and show that the Suess/de Vries cycle of about 207-year is a deterministic cycle of the stochastic solar activity. Also we show that occurrences of grand minimum are not necessarily expected with the Suess/de Vries cycle and it is possible to appear double or multiple grand maxima without a grand minimum within them.

The emergence and growth of the flux transport dynamo model of the sunspot cycle **Review**

Arnab Rai **Choudhuri**

Chandrasekhar Prize lecture, Reviews of Modern Plasma Physics **2023**

https://arxiv.org/pdf/2212.14617.pdf

The sunspot cycle is the magnetic cycle of the Sun produced by the dynamo process. A central idea of the solar dynamo is that the toroidal and the poloidal magnetic fields of the Sun sustain each other. We discuss the relevant observational data both for sunspots (which are manifestations of the toroidal field) and for the poloidal field of the Sun. We point out how the differential rotation of the Sun stretches out the poloidal field to produce the toroidal field primarily at the bottom of the convection zone, from where parts of this toroidal field may rise due to magnetic buoyancy to produce sunspots. In the flux transport dynamo model, the decay of tilted bipolar sunspot pairs gives rise to the poloidal field by the Babcock--Leighton mechanism. In this type of model, the meridional circulation of the Sun, which is poleward at the solar surface and equatorward at the bottom of the convection zone, plays a crucial role in the transport of magnetic fluxes. We finally point out that various stochastic fluctuations associated with the dynamo process may play a key role in producing the irregularities of the sunspot cycle.

Temporal and Periodic Analysis of Penumbra–Umbra Ratio for the Last Four Solar Cycles.

Chowdhury, P., Kilcik, A., Saha, A. et al.
Sol Phys 299, 19 (**2024**).
https://doi.org/10.1007/s11207-024-02263-5
https://link.springer.com/content/pdf/10.1007/s11207-024-02263-5.pdf

We investigate the long-term dynamic behavior of the sunspot penumbra to umbra area ratio by analyzing the Debrecen Photoheliographic Data (DPD) of sunspot groups during the period 1976–2017 (Solar Cycles 21–24). We consider all types of spots and find that the average penumbra–umbra ratio does not exhibit any significant variation with spot latitudes, solar-cycle phases as well as sunspot-cycle strengths. However, the behavior of this ratio is different when we consider the latitudinal distribution of the northern and southern hemispheres separately. Our analysis indicates that for daily total sunspot area the average spot ratio varies from 5.5 to 6.5 and for very large sunspots (> 5000 ❖Hem; one ❖Hem is 10−6 the area of visual solar hemisphere) its value rises to about 8.3. In the case of the group-sunspot area, the average spot ratio is ∼6.76. Furthermore, we found that this ratio exhibits a trend for both smaller (area <100 ❖Hem) and large (area > 100 ❖Hem) sunspots. Finally, we report the periodic and quasiperiodic variations present in this ratio time series after applying the multitaper method (MTM) and Morlet-wavelet technique. We found that along with the ∼11-year solar-cycle period, the penumbra to umbra area ratio also shows several midterm variations, specifically, Rieger-type and quasibiennial periodicities. We also found that Rieger-type periods occur in all cycles, but the temporal evolution and the modulation of these types of periodicities are different in different solar cycles.

A non-linear approach to predicting the amplitude and timing of the sunspot area in cycle 25

Partha **Chowdhury**, Volkan Sarp, Ali Kilcik, Pratap Chandra Ray, Jean-Pierre Rozelot, Vladimir N Obridko
Monthly Notices of the Royal Astronomical Society, Volume 513, Issue 3, July **2022**, Pages 4152–4158,
https://doi.org/10.1093/mnras/stac1162

The sunspot cycle waxes and wanes over a period of about 11 years and modulates ‘space weather’. Therefore, predicting the maximum amplitude of the solar cycle is an important goal for both solar physics and space weather. It is clear nowadays that cyclic variations of the Sun are non-linear processes, and thus the above-mentioned goal is difficult to reach with accuracy, albeit several methods currently exist to forecast both long-term and short-term variations. Solar cycle 25 has recently started and knowing the strength and timing of maximum of this cycle in advance is essential. In this study, a non-linear prediction algorithm, non-linear empirical dynamical modelling (EDM), is used to forecast the maximum amplitude and timing of the sunspot area of this cycle. This technique was tested on the last solar cycle 24 (Sarp et al. 2018) and the results obtained are in good agreement with observed values. Our study unveils that the maximum amplitude of the sunspot area of the whole solar disc will be 1606.49 ± 412.78 millionths of the solar hemispheric area (m.s.h.) and is expected to occur around 2025 March. We found that the predicted maximum sunspot areas in the Northern and Southern hemispheres are 731.39 ± 192.7 and 764.89 ± 195.39 m.s.h., respectively, with probable times of maxima around 2023 September and 2024 August, respectively. These results indicate that the strength of the sunspot area in solar cycle 25 will be weaker than or comparable with that in solar cycle 24. Such results are discussed and compared with other recent forecasts.

Variability in Irradiance and Photometric Indices During the Last Two Solar Cycles

Debi Prasad **Choudhary**1 · Ana Cristina Cadavid1 · Angela Cookson1 · Gary A Chapman1
Solar Physics volume 295, Article number: 15 (**2020**)
https://link.springer.com/content/pdf/10.1007/s11207-019-1559-7.pdf

The Total Solar Irradiance (TSI) primarily varies on an 11-year time scale and is governed by features such as sunspots and associated decay products such as plage and faculae. These short-lived physical features can also modulate the solar irradiance at intermediate and short temporal scales. Here we investigate the periodic variations, at solar-surface-rotation time scales, of photometric indices derived from images obtained at the San Fernando Observatory (SFO), and we compare them to the properties of the contemporaneous TSI as measured by the Total Irradiance Monitor (TIM) onboard the SOlar Radiation and Climate Experiment (SORCE) spacecraft. Both the daily ground- and space-based data, which span from early 2003 to late 2018, present missing pixels. We use an autoregressive gap-filling method to construct continuous time series to be analyzed via Fourier and wavelet spectral techniques. Lomb–Scargle periodograms, which can handle time series with missing data, are used for comparison. Both the Fourier spectral power and the periodograms yield compatible results with statistically significant periodicities in the range 25 – 35 days. All of the time series have maximum power at 27 days. Significant secondary periods are found at 29 – 30 days and 34 – 35 days. Wavelet analyses of the full time series show that the photometric index resulting from the red-continuum photometric sum [Σr][Σr] and the TSI exhibit common high

power at surface-solar-rotation scales during the active part of the solar cycle. The phase relation at the surface-solar-rotation scales is not definite. During the solar minimum interval between Solar Cycles (SCs) 23 and 24, variations in the TSI are found to be related to variations both in the photometric index ΣKΣK, calculated from Ca II K-line photometric sums and in the magnetic flux in the solar activity latitudinal band (as found in previous work). This suggests that the TSI changes during the minimum are caused by the reduced line-blanketing effect of diffused magnetic field.

Thermodynamic Properties of the Inverse Evershed Flow at Its Downflow Points

D. P. **Choudhary**1 and C. Beck
2018 ApJ 859 139
http://iopscience.iop.org/article/10.3847/1538-4357/aabf36/pdf
https://arxiv.org/pdf/1804.07326.pdf
We used spectropolarimetric observations of a sunspot in the active region NOAA 11809 in the Ca ii line at 854.2 nm taken with the SpectroPolarimeter for Optical and Infrared Regions at the Dunn Solar Telescope to infer thermodynamic parameters along 100 super-penumbral fibrils that harbor the inverse Evershed flow. The fibrils were identified in line-of-sight (LOS) velocity and line–core intensity maps. The chromospheric LOS velocity abruptly decreases from 3 to 15 km s−1 to zero at the inner footpoints of the fibrils that are located from the mid penumbra to about 1.4 spot radii. The spectra often show multiple absorption components, indicating spatially or vertically unresolved structures. Synthetic spectra with a 100% fill factor of a flow channel in the upper atmosphere yield strongly asymmetric profiles but no multiple separate components. The line–core intensity always peaks slightly closer to the umbra than the LOS velocity. Using the CAlcium Inversion using a Spectral ARchive code, we find that the fibrils make an angle of 30°–60° to the local vertical away from the umbra. The temperature near the downflow points is enhanced by 200 K at log $\tau \sim -2$ and up to 2000 K at log τ ~ (−6) compared to the quiet Sun, without any signature in the low photosphere. Our results are consistent with a critical, i.e., sonic, or supersonic siphon flow along super-penumbral flux tubes in which accelerating plasma abruptly attains subcritical velocity through a standing shock in or near the penumbra. **2013/08/03**

Different Periodicities in the Sunspot Area and the Occurrence of Solar Flares and Coronal Mass Ejections in Solar Cycle 23 – 24

D. P. **Choudhary**, J. K. Lawrence, M. Norris, A. C. Cadavid
Solar Physics, February **2014**, Volume 289, Issue 2, pp 649-656
http://sci-hub.cc/10.1007/s11207-013-0392-7
In order to investigate the relationship between magnetic-flux emergence, solar flares, and coronal mass ejections (CMEs), we study the periodicity in the time series of these quantities. It has been known that solar flares, sunspot area, and photospheric magnetic flux have a dominant periodicity of about 155 days, which is confined to a part of the phase of the solar cycle. These periodicities occur at different phases of the solar cycle during successive phases. We present a time-series analysis of sunspot area, flare and CME occurrence during Cycle 23 and the rising phase of Cycle 24 from 1996 to 2011. We find that the flux emergence, represented by sunspot area, has multiple periodicities. Flares and CMEs, however, do not occur with the same period as the flux emergence. Using the results of this study, we discuss the possible activity sources producing emerging flux.

The Meridional Circulation of the Sun: Observations, Theory and Connections with the Solar Dynamo **Review**

Arnab Rai **Choudhuri**
Science China: Physics, Mechanics & Astronomy **2020**
https://arxiv.org/pdf/2008.09347.pdf
The meridional circulation of the Sun, which is observed to be poleward at the surface, should have a return flow at some depth. Since large-scale flows like the differential rotation and the meridional circulation are driven by turbulent stresses in the convection zone, these flows are expected to remain confined within this zone. Current observational (based on helioseismology) and theoretical (based on dynamo theory) evidences point towards an equatorward return flow of the meridional circulation at the bottom of the convection zone. Assuming the mean values of various quantities averaged over turbulence to be axisymmetric, we study the large-scale flows in solar-like stars on the basis of a 2D mean field theory. Turbulent stresses in a rotating star can transport angular momentum, setting up a differential rotation. The meridional circulation arises from a slight imbalance between two terms which try to drive it in opposite directions: a thermal wind term (arising out of the higher efficiency of convective heat transport in the polar regions) and a centrifugal term (arising out of the differential rotation). To make these terms comparable, the poles of the Sun should be slightly hotter than the equator. We discuss the important role played by the meridional circulation in the flux transport dynamo model. The poloidal field generated by the Babcock--Leighton process at the surface is advected poleward, whereas the toroidal field produced at the bottom of the convection zone is advected equatorward. The fluctuations in the meridional circulation (with coherence time of about 30--40 yr) help in explaining many aspects of the irregularities in the solar cycle. Finally,

we discuss how the Lorentz force of the dynamo-generated magnetic field can cause periodic variations in the large-scale flows with the solar cycle.

A Theoretical Estimate of the Pole-Equator Temperature Difference and a Possible Origin of the Near-Surface Shear Layer

Arnab Rai **Choudhuri**
Solar Physics volume 296, Article number: 37 (**2021**)
https://arxiv.org/pdf/2008.02983.pdf
https://link.springer.com/content/pdf/10.1007/s11207-021-01784-7.pdf

Convective motions in the deep layers of the solar convection zone are affected by rotation, making the convective heat transport latitude-dependent, but this is not the case in the top layers near the surface. We use the thermal wind balance condition in the deeper layers to estimate the pole–equator temperature difference. Surface observations of this temperature difference can be used for estimating the depth of the near-surface layer within which convection is not affected by rotation. If we require that the thermal wind balance holds in this layer also, then we have to conclude that this must be a layer of strong differential rotation and its characteristics which we derive are in broad agreement with the observational data of the near-surface shear layer.

The Sun's polar magnetic field: datasets, proxies and theoretical issues

Arnab Rai **Choudhuri**
Proceedings of IAU Symposium 340 **2018**
https://arxiv.org/pdf/1810.05563.pdf

The polar magnetic field of the Sun is a manifestation of certain aspects of the dynamo process and is a good precursor for predicting a sunspot cycle before its onset. Although actual synoptic measurements of this field exist only from the mid-1970s, it has now been possible to determine its evolution from the beginning of the twentieth century with the help of various proxies. The recently developed 3D kinematic dynamo model can study the build-up of the Sun's polar magnetic field more realistically than the earlier surface flux transport model.

My Life and My Journey through Solar Physics **Review**

Arnab Rai **Choudhuri**
2018
https://arxiv.org/ftp/arxiv/papers/1809/1809.09709.pdf

This is the talk I gave at the workshop "Solar-Stellar Magnetism: Past, Present and Future" held in Jaipur on 18 February 2018 on the occasion of my 60th year.

The Sun as a Laboratory for Plasma Physics **Review**

Arnab Rai **Choudhuri**
The M.N. Saha 125th anniversary issue of "Science and Culture" **2018**
https://arxiv.org/ftp/arxiv/papers/1808/1808.10186.pdf

Several phenomena connected with the magnetic field of the Sun (the cool sunspots, the hot corona, solar flares, the solar wind) are collectively known as solar activity. This paper discusses how one uses the MHD equations to understand how the magnetic field of the Sun is produced by the dynamo process and then gives rise to these diverse activities, making the Sun the best laboratory for plasma physics in the limit of high magnetic Reynolds number (defined at the end of the Introduction).

Predicting a solar cycle before its onset using a flux transport dynamo model

Arnab Rai **Choudhuri**
Proceedings of IAU Symposium 335: Space Weather of the Heliosphere: Processes and Forecasts **2018**
https://arxiv.org/pdf/1808.08543.pdf

We begin with a review of the predictions for cycle~24 before its onset. After summarizing the basics of the flux transport dynamo model, we discuss how this model had been used to make a successful prediction of cycle~24, on the assumption that the irregularities of the solar cycle arise due to the fluctuations in the Babcock--Leighton mechanism. We point out that fluctuations in the meridional circulation can be another cause of irregularities in the cycle.

Flux transport dynamo: From modelling irregularities to making predictions **Review**

Arnab Rai **Choudhuri**
Journal of Atmospheric and Solar-Terrestrial Physics Volume 176, September **2018**, Pages 5-9
http://sci-hub.tw/10.1016/j.jastp.2017.08.002
https://arxiv.org/pdf/1808.08550.pdf
The flux transport dynamo, in which the poloidal magnetic fieldis generated by the Babcock–Leighton mechanism and the meridional circulation plays a crucial role, has emerged as an attractive model for the solar cycle. Based on theoretical calculations done with this model, we argue that the fluctuations in the Babcock–Leighton mechanism and the fluctuations in the meridional circulation are the most likely causes of the irregularities of the solar cycle. With our increased theoretical understanding of how these irregularities arise, it can be possible to predict a future solar cycle by feeding the appropriate observational data in a theoretical dynamo model.

Starspots, Stellar Cycles and Stellar Flares: Lessons from Solar Dynamo Models **Review**

Arnab Rai **Choudhuri**
Science China - Physics, Mechanics & Astronomy **2016**
https://arxiv.org/pdf/1612.02544v1.pdf
In this review, we discuss whether the present solar dynamo models can be extrapolated to explain various aspects of stellar activity. We begin with a summary of the following kinds of data for solar-like stars: (i) data pertaining to stellar cycles from Ca H/K emission over many years; (ii) X-ray data indicating hot coronal activity; (iii) starspot data (especially about giant polar spots); and (iv) data pertaining to stellar superflares. Then we describe the current status of solar dynamo modelling---giving an introduction to the flux transport dynamo model, the currently favoured model for the solar cycle. While an extrapolation of this model to solar-like stars can explain some aspects of observational data, some other aspects of the data still remain to be theoretically explained. It is not clear right now whether we need a different kind of dynamo mechanism for stars having giant starspots or producing very strong superflares.

The treatment of magnetic buoyancy in flux transport dynamo models

Arnab Rai **Choudhuri**, Gopal Hazra
Special issue of Advances in Space Research on "Solar Dynamo Frontiers" **201**5
http://arxiv.org/pdf/1511.03782v1.pdf
One important ingredient of flux transport dynamo models is the rise of the toroidal magnetic field through the convection zone due to magnetic buoyancy to produce bipolar sunspots and then the generation of the poloidal magnetic field from these bipolar sunspots due to the Babcock-Leighton mechanism. Over the years, two methods of treating magnetic buoyancy, a local method and a non-local method have been used widely by different groups in constructing 2D kinematic models of the flux transport dynamo. We review both these methods and conclude that neither of them is fully satisfactory, presumably because magnetic buoyancy is an inherently 3D process. We also point out so far we do not have proper understanding of why sunspot emergence is restricted to rather low latitudes.

A Critical Assessment of the Flux Transport Dynamo

Arnab Rai **Choudhuri**
Journal of Astronomy and Astrophysics, **2014**
http://arxiv.org/pdf/1408.3968v1.pdf
We first discuss how the flux transport dynamo with reasonably high diffusion can explain both the regular and the irregular features of the solar cycle quite well. Then we critically examine the inadequacies of the model and the challenge posed by some recent observational data about meridional circulation, arriving at the conclusion that this model can still work within the bounds of observational data

Effects of partial ionization on magnetic flux emergence in the Sun

Georgios **Chouliaras**, P.Syntelis, V.Archontis
ApJ **2023**
https://arxiv.org/pdf/2305.19883.pdf
We have performed 3-D numerical simulations to investigate the effect of partial ionization on the process of magnetic flux emergence. In our study, we have modified the single-fluid MHD equations to include the presence of neutrals and have performed two basic experiments: one that assumes a fully ionized plasma (FI case) and one that assumes a partially ionized plasma (PI case). We find that the PI case brings less dense plasma to and above the solar surface. Furthermore, we find that partial ionization alters the emerging magnetic field structure, leading to a different shape of the polarities in the emerged bipolar regions compared to the FI case. The amount of emerging flux into the solar atmosphere is larger in the PI case, which has the same initial plasma beta as the FI case, but a larger initial magnetic field strength. The expansion of the field above the photosphere occurs relatively earlier in

the PI case, and we confirm that the inclusion of partial ionization reduces cooling due to adiabatic expansion. However, it does not appear to work as a heating mechanism for the atmospheric plasma. The performance of these experiments in three dimensions shows that PI does not prevent the formation of unstable magnetic structures, which erupt into the outer solar atmosphere.

Analysis of Solar Hemispheric Chromosphere Properties using the Kodaikanal Observatory Ca–K Index

Partha **Chowdhury**1, Ravindra Belur2, Luca Bertello3, and Alexei A. Pevtsov3
2022 ApJ 925 81
https://iopscience.iop.org/article/10.3847/1538-4357/ac3983/pdf
The Kodaikanal Observatory has provided long-term synoptic observations of chromospheric activities in the Ca ii K line (393.34 nm) since 1907. This article investigates temporal and periodic variations of the hemispheric Ca–K-index time series in the low-latitude zone (±40°), utilizing the recently digitized photographic plates of Ca–K images from the Kodaikanal Observatory for the period of 1907–1980. We find that the temporal evolution of the Ca–K index differs from one hemisphere to another, with the solar cycle peaking at different times in the opposite hemisphere, except for cycles 14, 15, and 21, when the phase difference between the two hemispheres was not significant. The monthly averaged data show a higher activity in the northern hemisphere during solar cycles 15, 16, 18, 19, and 20, and in the southern hemisphere during cycles 14, 17, and 21. We notice an exponentially decaying distribution for each hemisphere's Ca–K index and the whole solar disk. We explored different midterm periodicities of the measured Ca–K index using the wavelet technique, including Rieger-type and quasi-biennial oscillations on different timescales present in the time series. We find a clear manifestation of the Waldmeier effect (stronger cycles rise faster than the weaker ones) in both the hemispheres separately and the whole disk in the data. Finally, we have found the presence of the Gnevyshev gap (time interval between two cycle maxmima) in both the hemispheric data during cycles 15 to 20. Possible interpretations of our findings are discussed with the help of existing theoretical models and observations.

Prediction of Amplitude and Timing of Solar Cycle 25

Partha **Chowdhury**, Rajmal Jain, P. C. Ray, Dipali Burud & Amlan Chakrabarti
Solar Physics volume 296, Article number: 69 (**2021**)
https://link.springer.com/content/pdf/10.1007/s11207-021-01791-8.pdf
https://doi.org/10.1007/s11207-021-01791-8
We study the geomagnetic activity Ap-index in relation to sunspot number and area for the interval covering Solar Cycles 17 to 24 (1932 – 2019), in view of the availability of data for the Ap-index from 1932 on, in order to predict the amplitude of Sunspot Cycle 25. We examine the statistical relationship between sunspot-maximum amplitude and Ap-index, and similarly that between sunspot area and Ap-index. We apply the $\chi 2$-test for the best fit between two parameters and obtain the correlation coefficient. We also derive the standard deviation for the error limits in the predicted results. Our study reveals that the amplitude of the Sunspot Cycle 25 is likely to be ≈100.21±15.06 and it may peak in April 2025±6.5 months. On the other hand, the sunspot area will have maximum amplitude ≈1110.62±186.87 μ Hem and may peak in February 2025±5.8 months, which implies that Solar Cycle 25 will be weaker than or comparable to Solar Cycle 24. In view of our results as well as those of other investigators, we propose that the Sun is perhaps approaching a global minimum.

Analysis of the Hemispheric Sunspot Number Time Series for the Solar Cycles 18 to 24

P. **Chowdhury**1 · A. Kilcik2 · V. Yurchyshyn3 · V.N. Obridko4 · J.P. Rozelot5
Solar Physics October **2019**, 294:142
https://link.springer.com/content/pdf/10.1007%2Fs11207-019-1530-7.pdf
In this article, we investigate temporal and periodic variations of the hemispheric sunspot number using sunspot data from Kanzelhöhe Solar Observatory (KSO) for the time period of 1944 – 2017, which covers Solar Cycles 18 to 23 and almost the entire Solar Cycle 24 (2009 – 2017). The KSO data set was verified against the International Sunspot Number (ISSN) data. Temporal and periodic variations in the KSO data were analyzed using cross-correlation analysis, Morlet wavelet and multitaper (MTM) period analysis methods. We find that: i) sunspot numbers, as derived from both KSO and ISSN time series, are highly correlated with one another; ii) the temporal evolution of the sunspot number differs from one hemisphere to another with the solar cycle peaking at different times in each hemisphere; iii) the northern hemisphere showed two- and seven-month lead in Solar Cycles 18 and 19, respectively, while the southern hemisphere was leading in the rest of the cycles with the varying lead time ranging from 2 to 14 months; iv) apart from the fundamental mode of ≈ 11 years, Solar Cycle, the KSO data also show several midterm variations in the opposite hemispheres, specifically, Rieger-type and quasi-biennial periodicities – the detected midterm periodicities also differ in the northern and southern hemispheres; v) our results confirm the Waldmeier effect, which correlates the rise time with the cycle amplitude using the new sunspot data set from KSO.

A Study of Heliospheric Modulation and Periodicities of Galactic Cosmic Rays During Cycle 24

Partha **Chowdhury**, K. Kudela, Y.-J. Moon

Solar Physics Volume 291, Issue 2, pp 581-602 **2016**

Galactic cosmic rays (GCRs) are energetic, charged particles coming from outside the solar system. These particles encounter an outward-moving turbulent solar wind with cyclic magnetic-field fluctuations when entering the heliosphere. This causes convection and diffusion in the heliosphere. The GCR counts detected by the ground-based neutron-monitor stations show intensity changes with a fluctuation of ∼ 11 years and are anti-correlated with the sunspot numbers with some time lags. GCRs experience various types of modulation from different solar activity features and are important components of space weather. The previous solar cycle, Cycle 23, has shown anomalous behavior with a prolonged deep minimum, which was characterized by a record-setting high Galactic cosmic-ray flux observed at Earth. Solar Cycle 24 started much later than expected and progressed sluggishly toward its maxima. In this paper, we study the heliospheric modulation and intermediate-term periodicities of GCRs during the ascending phase of Cycle 24. We utilize simultaneous solar, interplanetary plasma, magnetic field, and geomagnetic activity data including the tilt angle of the heliospheric current sheet, and we study their relation with GCRs. The wavelet power spectrum of GCRs exhibits the presence of a variety of prominent short- and mid-term periodicities including the well-known Rieger and quasi-biennial periodicities. Possible explanations of the observed results are discussed in the light of numerical models.

Short-term periodicities in interplanetary, geomagnetic and solar phenomena during solar cycle 24

Partha **Chowdhury**, D. P. Choudhary, S. Gosain, Y.-J. Moon

Astrophysics and Space Science March **2015**, Volume 356, Issue 1, pp 7-18

In this paper we study the quasi-periodic variations of sunspot area/number, 10.7 cm solar radio flux, Average Photospheric Magnetic Flux, interplanetary magnetic field (B z) and the geomagnetic activity index A p during the ascending phase of the current solar cycle 24. We use both Lomb-Scargle periodogram and wavelet analysis technique and find evidence for a multitude of quasi-periodic oscillations in all the data sets. In high frequency range (10 days to 100 days), both methods yield similar significance periodicities around 20–35 days and 45–60 days in all data sets. In the case of intermediate range, the significant periods were around 100–130 days, 140–170 days and 180–240 days The Morlet wavelet power spectrum shows that all of the above-mentioned periods are intermittent in nature. We find that the well-known “Rieger period” of (150–160 days) and near Rieger periods (130–190 days) were significant in both solar, interplanetary magnetic field and geomagnetic activity data sets during cycle 24. The geomagnetic activity is the result of the solar wind-magnetosphere interaction. Thus the variations in the detected periodicity in variety of solar, interplanetary and geomagnetic indices could be helpful to improve our knowledge of the inter-relationship between various processes in the Sun-Earth-Heliosphere system.

A STUDY OF THE HEMISPHERIC ASYMMETRY OF SUNSPOT AREA DURING SOLAR CYCLES 23 AND 24

Partha **Chowdhury**1, D. P. Choudhary2, and Sanjay Gosain

2013 ApJ 768 188

Solar activity indices vary over the Sun's disk, and various activity parameters are not considered to be symmetric between the northern and southern hemispheres of the Sun. The north-south asymmetry of different solar indices provides an important clue to understanding subphotospheric dynamics and solar dynamo action, especially with regard to nonlinear dynamo models. In the present work, we study the statistical significance of the north-south asymmetry of sunspot areas for the complete solar cycle 23 (1996-2008) and rising branch of cycle 24 (first 45 months). The preferred hemisphere in each year of cycles 23 and 24 has been identified by calculating the probability of hemispheric distribution of sunspot areas. The statistically significant intermediate-term periodicities of the north-south asymmetry of sunspot area data have also been investigated using Lomb-Scargle and wavelet techniques. A number of short- and mid-term periods including the best-known Rieger one (150-160 days) are detected in cycle 23 and near Rieger-type periods during cycle 24, and most of them are found to be time variable. We present our results and discuss their possible explanations with the help of theoretical models and observations.

Solving the Coronal Heating Problem using X-ray Microcalorimeters

Steven **Christe**, Simon Bandler, Edward DeLuca, Amir Caspi, Leon Golub, Randall Smith, Joel Allred, Jeffrey W. Brosius, Brian Dennis, James Klimchuk

Next Generation Solar Physics Mission **2017**
https://arxiv.org/pdf/1701.00795v1.pdf
Even in the absence of resolved flares, the corona is heated to several million degrees. However, despite its importance for the structure, dynamics, and evolution of the solar atmosphere, the origin of this heating remains poorly understood. Several observational and theoretical considerations suggest that the heating is driven by small, impulsive energy bursts which could be Parker-style "nanoflares" (Parker 1988) that arise via reconnection within the tangled and twisted coronal magnetic field. The classical "smoking gun" (Klimchuk 2009; Cargill et al. 2013) for impulsive heating is the direct detection of widespread hot plasma (T > 6 MK) with a low emission measure. In recent years there has been great progress in the development of Transition Edge Sensor (TES) X-ray microcalorimeters that make them more ideal for studying the Sun. When combined with grazing-incidence focusing optics, they provide direct spectroscopic imaging over a broad energy band (0.5 to 10 keV) combined with extremely impressive energy resolution in small pixels, as low as 0.7 eV (FWHM) at 1.5 keV (Lee 2015), and 1.56 eV (FWHM) at 6 keV (Smith 2012), two orders of magnitude better than the current best traditional solid state photon-counting spectrometers. Decisive observations of the hot plasma associated with nanoflare models of coronal heating can be provided by new solar microcalorimeters. These measurements will cover the most important part of the coronal spectrum for searching for the nanoflare-related hot plasma and will characterize how much nanoflares can heat the corona both in active regions and the quiet Sun. Finally, microcalorimeters will enable to study all of this as a function of time and space in each pixel simultaneously a capability never before available.

Solar structure and evolution **Review**

Joergen **Christensen-Dalsgaard**
Living Reviews in Solar Physics **2020**
https://arxiv.org/pdf/2007.06488.pdf
The Sun provides a critical benchmark for the general study of stellar structure and evolution. Also, knowledge about the internal properties of the Sun is important for the understanding of solar atmospheric phenomena, including the solar magnetic cycle. Here I provide a brief overview of the theory of stellar structure and evolution, including the physical processes and parameters that are involved. This is followed by a discussion of solar evolution, extending from the birth to the latest stages. As a background for the interpretation of observations related to the solar interior I provide a rather extensive analysis of the sensitivity of solar models to the assumptions underlying their calculation. I then discuss the detailed information about the solar interior that has become available through helioseismic investigations and the detection of solar neutrinos, with further constraints provided by the observed abundances of the lightest elements. Revisions in the determination of the solar surface abundances have led to increased discrepancies, discussed in some detail, between the observational inferences and solar models. I finally briefly address the relation of the Sun to other similar stars and the prospects for asteroseismic investigations of stellar structure and evolution.

Helioseismology and solar neutrinos **Review**

J. **Christensen-Dalsgaard**
Proceedings of the 5th International Solar Neutrino Conference', eds M. Meyer and K. Zuber, World Scientific **2018**
https://arxiv.org/pdf/1809.03000.pdf
The studies of solar neutrinos and helioseismology have been closely intertwined since the first neutrino experiment and the first observations of solar oscillations in the sixties. Early detailed helioseismic analyses provided strong support for the standard solar model and hence a clear indication that the solution to the discrepancy between the predicted and observed neutrino fluxes had to be found in terms of neutrino physics, as now fully confirmed by direct observations. With the full characterization of neutrino properties we are now in a position to combine neutrino observations and helioseismology to obtain a more complete understanding of conditions in the solar core. Here I provide a personal and largely historical overview of these developments.

Solar differential rotation coefficients fitted from synoptic magnetic maps

Zhe **Chu**, Haihua Gu
MNRAS, Volume 533, Issue 1, September **2024**, Pages 918–924,
https://doi.org/10.1093/mnras/stae1907
https://watermark.silverchair.com/stae1907.pdf

Based on the consecutive synoptic magnetic maps, we devise a new method to calculate the solar differential rotation coefficients. This method is very easy to implement and has a high accuracy. Firstly, based on the two-term or three-term differential rotation formula, we simulate a synoptic map CRn evolves one Carrington Rotation (CR) time only under the effect of the differential rotation, and thereby a stretched synoptic map CRn$*$ is obtained. Then, through searching the maximum covariance between the maps CRn$*$ and CRn+1 by the grid search method, the rotation coefficients can be determined. Based on the synoptic maps of CRs 1625 to 2278 (during the years 1975–

2023), the two-term coefficients A and B for latitude region between ±40◦ are calculated. The rotation coefficient B shows an obvious 11-yr period. From the time series of B, we find that the Sun usually rotates more differentially in the rising phases of the sunspot cycles than in the falling phases. Moreover, the strong magnetic field corresponds to an increasing of B (note that B has a negative sign) or decreasing of differential. The evolutionary trend of B also indicates that there are several years until the maximum value of B will be reached in solar cycle 25, and the coefficient B will be still in the rising phase in the few coming years. The two-term rotation coefficients for the two hemispheres are also calculated separately, and in the studied time-scale, the largest N–S asymmetry of the rotation rate appeared in October 2007.

The Evolution of Multipole Moments for the Global Solar Magnetic Field

Zhe **Chu**, Weihua Wang & Haihua Gu
Solar Physics volume 298, Article number: 71 (**2023**)
https://doi.org/10.1007/s11207-023-02168-9
Based on synoptic magnetic maps, we use spherical harmonic functions to decompose the global magnetic field of the Sun. Through the expansion coefficients, the power spectrum Cl��, and its zonal component CZl��� and sectorial component CSl��� for order l� are defined. Through two sampled synoptic maps, it is easy to show that the multipole moments in solar active years are much stronger than those in the quiet years. We decomposed the synoptic maps for Carrington rotations (CRs) 1625 to 2224, i.e., corresponding Solar Cycles 21 – 24, and studied the evolution of multipole moments. Except for the monopole, the power spectra Cl�� for most moments have an obvious 11-year period. The dipole and octupole in Solar Cycle 22 are much stronger than in the other three cycles. The zonal components of dipole and octupole are opposite to the phases of most modes, while the sectorial components of them are consistent with most phases. In addition, compared to the phase of the yearly sunspot number, the phases of most multipoles are relatively delayed, except for the zonal modes of the quadrupole and 32-pole (l=5). We find that the zonal mode of l=5 is very strong, which leads ahead of the phase of the yearly sunspot number for about 10 CRs. Additionally, unlike the other modes, it has a strong 5.5-year period. Then, the zonal mode of l=5 is mainly induced by the magnetic field of the sunspots, which is further confirmed in this work.

Interplanetary Signatures during the 1972 Early August Solar Storms

Consuelo **Cid**1, Elena Saiz1, Manuel Flores-Soriano1, and Delores J. Knipp2,3
2023 ApJ 958 159
https://iopscience.iop.org/article/10.3847/1538-4357/acf9fd/pdf
In 1972, early August, a series of interplanetary shocks were observed in the heliosphere from 0.8 to 2.2 au. These shocks were attributed to a series of brilliant flares and plasma clouds since at that time coronal mass ejections (CMEs) and their interplanetary counterparts (ICMEs) were unknown to the scientific community. This paper aims to reinterpret the interplanetary data in light of the current understanding about interplanetary transients and to track the evolution of the ICMEs, taking advantage of the alignment of Pioneers 9 and 10 spacecraft. For this purpose, we reanalyze in situ data from these two Pioneers and also from Heos, Prognoz 1 and 2, and Explorer 41 spacecraft searching for ICMEs and high-speed streams. Then we assemble the interplanetary transients and solar activity and analyze the propagation of the ejections through the heliosphere. The evolution of four ICMEs and a high-speed stream from a low-latitude coronal hole is followed using the multipoint in situ observations. The first three ICMEs show clear signatures of ICME–ICME interaction in the interplanetary medium, suggesting the first observations of an ICME which developed into an ICME-in-the-sheath. For a non-perturbed ICME event, we obtain the evolution parameter, ζ, related to the local expansion of ICMEs, getting similar values for Pioneer 9 (ζ = 0.80) and Pioneer 10 (ζ = 0.78). These results support previous findings of ζ being independent of the heliocentric distance and the magnetic field strength decreasing as r−2ζ.

Tidal Forcing on the Sun and the 11-year Solar Activity Cycle

Rodolfo G. **Cionco**, Sergey M. Kudryavtsev, Willie Soon
Solar Phys. **298**, Article number: 70 **2023**
https://arxiv.org/pdf/2304.14168
https://doi.org/10.1007/s11207-023-02167-w
The hypothesis that tidal forces on the Sun are related to the modulations of the solar-activity cycle has gained increasing attention. The works proposing physical mechanisms of planetary action via tidal forcing have in common that quasi-alignments between Venus, Earth, and Jupiter (V-E-J configurations) would provide a basic periodicity of ≈11.0 years able to synchronize the operation of solar dynamo with these planetary configurations. Nevertheless, the evidence behind this particular tidal forcing is still controversial. In this context we develop, for the first time, the complete Sun's tide-generating potential (STGP) in terms of a harmonic series, where the effects of different planets on the STGP are clearly separated and identified. We use a modification of the spectral analysis method devised by Kudryavtsev (J. Geodesy. 77, 829, 2004; Astron. Astrophys. 471, 1069, 2007b) that permits to expand any function of planetary coordinates to a harmonic series over long time intervals. We build a catalog of 713 harmonic terms able to represent the STGP with a high degree of precision. We look for tidal forcings related to

V-E-J configurations and specifically the existence of periodicities around 11.0 years.
Although the obtained tidal periods range from ≈ 1000 years to 1 week, we do not find any ≈ 11.0 years period. The V-E-J configurations do not produce any significant tidal term at this or other periods. The Venus tidal interaction is absent in the 11-year spectral band, which is dominated by Jupiter's orbital motion. The planet that contributes the most to the STGP in three planets configurations, along with Venus and Earth, is Saturn. An ≈11.0 years tidal period with a direct physical relevance on the 11-year-like solar-activity cycle is highly improbable.

Magnetohydrodynamic spectroscopy of a non-adiabatic solar atmosphere

Niels **Claes**, Rony Keppens

Solar Phys. **296**, Article number: 143 **2021**

https://arxiv.org/pdf/2108.09467.pdf
https://link.springer.com/content/pdf/10.1007/s11207-021-01894-2.pdf
https://doi.org/10.1007/s11207-021-01894-2

The quantification of all possible waves and instabilities in a given system is of paramount importance, and knowledge of the full magnetohydrodynamic (MHD) spectrum allows one to predict the (in)stability of a given equilibrium state. This is highly relevant in many (astro)physical disciplines, and when applied to the solar atmosphere it may yield various new insights in processes like prominence formation and coronal loop oscillations. In this work we present a detailed, high-resolution spectroscopic study of the solar atmosphere, where we use our newly developed Legolas code to calculate the full spectrum with corresponding eigenfunctions of equilibrium configurations that are based on fully realistic solar atmospheric models, including gravity, optically thin radiative losses and thermal conduction. Special attention is given to thermal instabilities, known to be responsible for the formation of prominences, together with a new outlook on the thermal and slow continua and how they behave in different chromospheric and coronal regions. We show that thermal instabilities are unavoidable in our solar atmospheric models and that there exist certain regions where both the thermal, slow and fast modes all have unstable wave mode solutions. We also encounter regions where the slow and thermal continua become purely imaginary and merge on the imaginary axis. The spectra discussed in this work illustrate clearly that thermal instabilities (both discrete and continuum modes) and magneto-thermal overstable propagating modes are ubiquitous throughout the solar atmosphere, and may well be responsible for much of the observed fine-structuring and multi-thermal dynamics.

The McNish and Lincoln Solar Activity Predictions: The Method and its Performance

Frédéric **Clette** (1), Shantanu Jain (2), Tatiana Podladchikova (2)

Solar Phys. **299**, 22 **2024**

https://arxiv.org/pdf/2402.09273.pdf
https://doi.org/10.1007/s11207-024-02266-2
https://link.springer.com/content/pdf/10.1007/s11207-024-02266-2.pdf

The McNish and Lincoln (ML) method, introduced in 1949, was one of the first attempts to produce mid-term forecasts of solar activity, up to 12 months ahead. However, it has been poorly described and evaluated in the past literature, in particular its actual operational implementation by NOAA.
Here, we reconstruct the exact formulation of the method, as it was applied since the early 1970s, and we provide a full mathematical derivation of the prediction errors. For bench-marking the method, we also produce monthly predictions over the past 190 years, from 1833 (Cycle 8) to 2023 (Cycle 25), and develop statistics of the differences between the predictions and the observed 13-month smoothed sunspot number (SSN) time series, according to the phase in the solar cycle.
Our analysis shows that the ML method is heavily constrained because it is primarily based on the mean of all past cycles, which imposes a fixed amplitude and length and suffers from a temporal smearing that grows towards the end of the solar cycle. We find that predictions are completely unreliable in the first 12 months of the cycle, and over the last two years preceding the ending minimum (around 130 months), and beyond this minimum. By contrast, in the course of the cycle (months 18 to 65), ML predictions prove to be reliable over a time range of up to 50 months (4.2 years), thus much longer than the 12-month conventional range used so far. However, we find that predictions then suffer from systematic under-(over-)estimates for cycles that have a higher (lower) amplitude than the base mean cycle.
Overall, we conclude that although the ML method provides valid prediction errors, it suffers from strong limitations, with very little room for improvement, as it indifferently merges all past cycles into a single fixed statistics.

Reconstruction of the Sunspot Number Source Database and the 1947 Zurich Discontinuity

Frédéric **Clette**, Laure Lefèvre, Sabrina Bechet, Renzo Ramelli, Marco Cagnotti

Solar Phys. **2023**

https://arxiv.org/pdf/2301.02429.pdf

The recalibration of the sunspot number series, the primary long-term record of the solar cycle, requires the recovery of the entire collection of raw sunspot counts collected by the Zurich Observatory for the production of this index between 1849 and 1980. Here, we report about the major progresses accomplished recently in the construction of this global digital sunspot number database, and we derive global statistics of all the individual observers and professional observatories who provided sunspot data over more than 130 years. First, we can announce the full recovery of long-lost source-data tables covering the last 34 years between 1945 and 1979, and we describe the unique information available in those tables. We then also retrace the evolution of the core observing team in Zurich and of the auxiliary stations. In 1947, we find a major disruption in the composition of both the Zurich team and the international network of auxiliary stations. This sharp transition is unique in the history of the Zurich Observatory and coincides with the main scale-jump found in the original Zurich sunspot number series, the so-called "Waldmeier" jump. This adds key historical evidence explaining why methodological changes introduced progressively in the early 20th century could play a role precisely at that time. We conclude on the remaining steps needed to fully complete this new sunspot data resource.

Re-calibration of the Sunspot Number: Status Report

F. **Clette**, L. Lefèvre, T. Chatzistergos, H. Hayakawa, V. M. Carrasco, R. Arlt, E. W. Cliver, T. Dudok de Wit, T. Friedli, N. Karachik, G. Kopp, M. Lockwood, S. Mathieu, A. Muñoz-Jaramillo, M. Owens, D. Pesnell, A. Pevtsov, L. Svalgaard, I. G. Usoskin, L. van Driel-Gesztelyi, J. M. Vaquero

Solar Phys. **298**, Article number: 44 **2023**

https://arxiv.org/pdf/2301.02084

https://link.springer.com/content/pdf/10.1007/s11207-023-02136-3.pdf

We report progress on the ongoing recalibration of the Wolf sunspot number (SN) and Group sunspot number (GN) following the release of version 2.0 of SN in 2015. This report constitutes both an update of the efforts reported in the 2016 Topical Issue of Solar Physics and a summary of work by the International Space Science Institute (ISSI) International Team formed in 2017 to develop optimal SN and GN re-construction methods while continuing to expand the historical sunspot number database. Significant progress has been made on the database side while more work is needed to bring the various proposed SN and (primarily) GN reconstruction methods closer to maturity, after which the new reconstructions (or combinations thereof) can be compared with (a) ``benchmark" expectations for any normalization scheme (e.g., a general increase in observer normalization factors going back in time), and (b) independent proxy data series such as F10.7 and the daily range of variations of Earth's undisturbed magnetic field. New versions of the underlying databases for SN and GN will shortly become available for years through 2022 and we anticipate the release of next versions of these two time series in 2024.

Reconstruction of the Sunspot Number Source Database and the 1947 Zurich Discontinuity

Frédéric **Clette**, Laure Lefèvre, Sabrina Bechet, Renzo Ramelli & Marco Cagnotti

Solar Physics volume 296, Article number: 137 (**2021**)

https://link.springer.com/content/pdf/10.1007/s11207-021-01882-6.pdf

https://doi.org/10.1007/s11207-021-01882-6

The recalibration of the sunspot number series, the primary long-term record of the solar cycle, requires the recovery of the entire collection of raw sunspot counts collected by the Zurich Observatory for the production of this index between 1849 and 1980.

Here, we report about the major progresses accomplished recently in the construction of this global digital sunspot number database, and we derive global statistics of all the individual observers and professional observatories who provided sunspot data over more than 130 years.

First, we can announce the full recovery of long-lost source-data tables covering the last 34 years between 1945 and 1979, and we describe the unique information available in those tables. We then also retrace the evolution of the core observing team in Zurich and of the auxiliary stations. In 1947, we find a major disruption in the composition of both the Zurich team and the international network of auxiliary stations.

This sharp transition is unique in the history of the Zurich Observatory and coincides with the main scale-jump found in the original Zurich sunspot number series, the so-called “Waldmeier” jump. This adds key historical evidence explaining why methodological changes introduced progressively in the early 20th century could play a role precisely at that time. We conclude on the remaining steps needed to fully complete this new sunspot data resource.

Is the F10.7cm – Sunspot Number relation linear and stable?

Frédéric **Clette***

J. Space Weather Space Clim. **2021**, 11, 2

https://doi.org/10.1051/swsc/2020071

https://arxiv.org/pdf/2301.02588.pdf

https://www.swsc-journal.org/articles/swsc/pdf/2021/01/swsc200021.pdf

The F10.7cm radio flux and the Sunspot Number are the most widely used long-term indices of solar activity. They are strongly correlated, which led to the publication of many proxy relations allowing to convert one index onto the other. However, those existing proxies show significant disagreements, in particular at low solar activity. Moreover, a temporal drift was recently found in the relative scale of those two solar indices. Our aim is to bring a global clarification of those many issues. We compute new polynomial regressions up to degree 4, in order to obtain a more accurate proxy over the whole range of solar activity. We also study the role of temporal averaging on the regression, and we investigate the issue of the all-quiet F10.7 background flux. Finally, we check for any change in the F10.7–Sunspot Number relation over the entire period 1947–2015. We find that, with a 4th-degree polynomial, we obtain a more accurate proxy relation than all previous published ones, and we derive a formula giving standard errors. The relation is different for daily, monthly and yearly mean values, and it proves to be fully linear for raw non-averaged daily data. By a simple two-component model for daily values, we show how temporal averaging leads to non-linear proxy relations. We also show that the quiet-Sun F10.7 background is not absolute and actually depends on the duration of the spotless periods. Finally, we find that the F10.7cm time series is inhomogeneous, with an abrupt 10.5% upward jump occurring between 1980 and 1981, and splitting the series in two stable intervals. Our new proxy relations bring a strong improvement and show the importance of temporal scale for choosing the appropriate proxy and the F10.7 quiet-Sun background level. From historical evidence, we conclude that the 1981 jump is most likely due to a unique change in the F10.7 scientific team and the data processing, and that the newly re-calibrated sunspot number (version 2) will probably provide the only possible reference to correct this inhomogeneity.

Preface to Topical Issue: Recalibration of the Sunspot Number

F. **Clette**, E. W. Cliver, L. Lefèvre, L. Svalgaard, J. M. Vaquero, J. W. Leibacher

Solar Phys. Volume 291, Issue 9, pp 2479–2486 **2016**

This topical issue contains articles on the effort to recalibrate the sunspot number (SN) that was initiated by the Sunspot Number Workshops. These workshops led to a revision of the Wolf sunspot number (WSN) and a new construction of the group sunspot number (GSN), both published herein. In addition, this topical issue includes three independently proposed alternative SN time series (two Wolf and one group), as well as articles providing historical context, critical assessments, correlative analyses, and observational data, both historical and modern, pertaining to the sunspot-number time series. The ongoing effort to understand and reconcile the differences between the various new sunspot number series is briefly discussed.

The new Sunspot Number: assembling all corrections

Frédéric, **Clette**, Laure Lefèvre

Solar Phys. Volume 291, Issue 9, pp 2629–2651 **2015**

http://arxiv.org/pdf/1510.06928v1.pdf

The Sunspot Number, created by R.Wolf in 1849, provides a direct long-term record of solar activity from 1700 to the present. In spite of its central role in multiple studies of the solar dynamo and of the past Sun-Earth relations, it was never submitted to a global critical revision. However, various discrepancies with other solar indices recently motivated a full re-calibration of this series. Based on various diagnostics and corrections established in the framework of several Sunspot Number Workshops and described in Clette et al. 2014, we assembled all corrections in order to produce a new standard version of this reference time series. In this paper, we explain the three main corrections and the criteria used to choose a final optimal version of each correction factor or function, given the available information and published analyses. We then discuss the good agreement obtained with the Group sunspot Number derived from a recent reconstruction. Among the implications emerging from this re-calibrated series, we also discuss the absence of a rising secular trend in the newly-determined solar cycle amplitudes, also in relation with contradictory indications derived from cosmogenic radionuclides. As conclusion, we introduce the new version management scheme now implemented at the World Data Center - SILSO, which reflects a major conceptual transition: beyond the re-scaled numbers, this first revision of the Sunspot Number also transforms the former locked data archive into a living observational series open to future improvements.

The revised Brussels-Locarno Sunspot Number (1981-2015)

Frédéric **Clette**, Laure Lefèvre, Marco Cagnotti, Sergio Cortesi, Andreas Bulling

Solar Phys. Volume 291, Issue 9, pp 2733–2761 **2015**

http://arxiv.org/pdf/1507.07803v1.pdf

In 1981, the production of the international Sunspot Number moved from the Z\"{u}rich Observatory to the Royal Observatory of Belgium, marking a very important transition in the history of the Sunspot Number. Those recent decades are particularly important for linking recent modern solar indices and fluxes and the past Sunspot Number

series. However, large variations have been recently identified in the scale of the Sunspot Number between 1981 and the present.
Here, we reconstruct a new average Sunspot Number series SN using long-duration stations between 1981 and 2015. We also extend this reconstruction using long-time series from 35 stations over 1945-2015, which includes the 1981 transition. In both reconstructions, we also derive a parallel Group Number series GN. Our results confirm the variable trends of the Locarno pilot station. We also verify the scale of the resulting 1981-2015 correction factor relative to the preceding period 1945--1980. By comparing the new SN and GN series, we find that a constant quadratic relation exists between those two indices. This proxy relation leads to a fully constant and cycle-independent SN/GN ratio over cycles 19 to 23, with the exception of cycle 24. We find a very good agreement between our reconstructed GN and the new "backbone" Group Number but inhomogeneities in the original Group Number as well as the F10.7 radio flux and the American sunspot number Ra.
This analysis opens the way to the implementation of a more advanced method for producing the Sunspot Number in the future. In particular, we identify the existence of distinct subsets of observing stations sharing very similar personal k factors, which may be a key element for building a future multi-station reference in place of the past single pilot station.

Revisiting the Sunspot Number **Review**

A 400-year perspective on the solar cycle

Frédéric **Clette**, Leif Svalgaard, José M. Vaquero, Edward W. Cliver
Space Science Reviews December **2014**, Volume 186, Issue 1-4, pp 35-103
http://arxiv.org/pdf/1407.3231v1.pdf
Our knowledge of the long-term evolution of solar activity and of its primary modulation, the 11-year cycle, largely depends on a single direct observational record: the visual sunspot counts that retrace the last 4 centuries, since the invention of the astronomical telescope. Currently, this activity index is available in two main forms: the International Sunspot Number initiated by R. Wolf in 1849 and the Group Number constructed more recently by Hoyt and Schatten (1998a,b). Unfortunately, those two series do not match by various aspects, inducing confusions and contradictions when used in crucial contemporary studies of the solar dynamo or of the solar forcing on the Earth climate. Recently, new efforts have been undertaken to diagnose and correct flaws and biases affecting both sunspot series, in the framework of a series of dedicated Sunspot Number Workshops. Here, we present a global overview of our current understanding of the sunspot number calibration. While the early part of the sunspot record before 1800 is still characterized by large uncertainties due to poorly observed periods, the more recent sunspot numbers are mainly affected by three main inhomogeneities: in 1880-1915 for the Group Number and in 1947 and 1980-2014 for the Sunspot Number. The newly corrected series clearly indicates a progressive decline of solar activity before the onset of the Maunder Minimum, while the slowly rising trend of the activity after the Maunder Minimum is strongly reduced, suggesting that by the mid 18th century, solar activity had already returned to the level of those observed in recent solar cycles in the 20th century. We finally conclude with future prospects opened by this epochal revision of the Sunspot Number, the first one since Wolf himself, and its reconciliation with the Group Number, a long-awaited modernization that will feed solar cycle research into the 21st century.

Extreme solar events **Review**

Edward W. **Cliver**, Carolus J. Schrijver, Kazunari Shibata & Ilya G. Usoskin
Living Reviews in Solar Physics volume 19, Article number: 2 (**2022**)
https://link.springer.com/content/pdf/10.1007/s41116-022-00033-8.pdf
We trace the evolution of research on extreme solar and solar-terrestrial events from the 1859 Carrington event to the rapid development of the last twenty years. Our focus is on the largest observed/inferred/theoretical cases of sunspot groups, flares on the Sun and Sun-like stars, coronal mass ejections, solar proton events, and geomagnetic storms. The reviewed studies are based on modern observations, historical or long-term data including the auroral and cosmogenic radionuclide record, and Kepler observations of Sun-like stars. We compile a table of 100- and 1000-year events based on occurrence frequency distributions for the space weather phenomena listed above. Questions considered include the Sun-like nature of superflare stars and the existence of impactful but unpredictable solar "black swans" and extreme "dragon king" solar phenomena that can involve different physics from that operating in events which are merely large. **774 AD, 17 Sep 1770, 1 September 1859, 4 Feb 1872, 14-15 May 1921, 28 Feb 1942, 5 April 1947, 23 May 1967, 2–11 August 1972 , 29 Apr 1973, 21 Apr 2002, 28 October 2003; 6, 13, 14 Dec 2006, 9 Nov 2011, 28 Oct 2013, 4 Nov 2015**
Table 5 Historical fast transit ICME events

Evolution of the Sunspot Number and Solar Wind B Time Series **Review**

Edward W. **Cliver**, Konstantin Herbst
Space Science Reviews March **2018**, 214:56
http://sci-hub.tw/http://link.springer.com/10.1007/s11214-018-0487-4
The past two decades have witnessed significant changes in our knowledge of long-term solar and solar wind activity. The sunspot number time series (1700-present) developed by Rudolf Wolf during the second half of the 19th century was revised and extended by the group sunspot number series (1610–1995) of Hoyt and Schatten during the 1990s. The group sunspot number is significantly lower than the Wolf series before ~1885. An effort from 2011–2015 to understand and remove differences between these two series via a series of workshops had the unintended consequence of prompting several alternative constructions of the sunspot number. Thus it has been necessary to expand and extend the sunspot number reconciliation process. On the solar wind side, after a decade of controversy, an ISSI International Team used geomagnetic and sunspot data to obtain a high-confidence time series of the solar wind magnetic field strength (BB) from 1750-present that can be compared with two independent long-term (> ~600 year) series of annual BB-values based on cosmogenic nuclides. In this paper, we trace the twists and turns leading to our current understanding of long-term solar and solar wind activity.

Minimal Magnetic States of the Sun and the Solar Wind: Implications for the Origin of the Slow Solar Wind **Review**

E. W. **Cliver**, R. von Steiger
Space Science Reviews September **2017**, Volume 210, Issue 1–4, pp 227–247
During the last decade it has been proposed that both the Sun and the solar wind have minimum magnetic states, lowest order levels of magnetism that underlie the 11-yr cycle as well as longer-term variability. Here we review the literature on basal magnetic states at the Sun and in the heliosphere and draw a connection between the two based on the recent deep 2008–2009 minimum between cycles 23 and 24. In particular, we consider the implications of the low solar activity during the recent minimum for the origin of the slow solar wind.

Sunspot number recalibration: The ~1840–1920 anomaly in the observer normalization factors of the group sunspot number

Edward W. **Cliver**
J. Space Weather Space Clim., 7, A12 (**2017**)
https://www.swsc-journal.org/articles/swsc/pdf/2017/01/swsc160025.pdf
We analyze the normalization factors (k′-factors) used to scale secondary observers to the Royal Greenwich Observatory (RGO) reference series of the Hoyt &' Schatten (1998a, 1998b) group sunspot number (GSN). A time series of these k′-factors exhibits an anomaly from 1841 to 1920, viz., the average k′-factor for all observers who began reporting groups from 1841 to 1883 is 1.075 vs. 1.431 for those who began from 1884 to 1920, with a progressive rise, on average, during the latter period. The 1883–1884 break between the two subintervals occurs precisely at the point where Hoyt and Schatten began to use a complex daisy-chaining method to scale observers to RGO. The 1841–1920 anomaly implies, implausibly, that the average sunspot observer who began from 1841 to 1883 was nearly as proficient at counting groups as mid-20th century RGO (for which k′ = 1.0 by definition) while observers beginning during the 1884–1920 period regressed in group counting capability relative to those from the earlier interval. Instead, as shown elsewhere and substantiated here, RGO group counts increased relative to those of other long-term observers from 1874 to ~1915. This apparent inhomogeneity in the RGO group count series is primarily responsible for the increase in k′-factors from 1884 to 1920 and the suppression, by 44% on average, of the Hoyt and Schatten GSN relative to the original Wolf sunspot number (WSN) before ~1885. Correcting for the early "learning curve" in the RGO reference series and minimizing the use of daisy-chaining rectifies the anomalous behavior of the k′-factor series. The resultant GSN time series (designated GSN*) is in reasonable agreement with the revised WSN (SN*; Clette & Lefèvre 2016) and the backbone-based group sunspot number (RGS; Svalgaard & Schatten 2016) but significantly higher than other recent reconstructions (Friedli, personal communication, 2016; Lockwood et al. 2014a, 2014b; Usoskin et al. 2016a). This result is substantiated by a "correction-factor" (CF) time series defined as the ratio of annual group counts of the Hoyt & Schatten (1998a, 1998b) series to the average raw (unscaled) group counts of all observers, as well as by a comparison of the GSN and GSN* time series with a recent reconstruction of solar wind B from 1845 to the present. The ~1840–1920 k′-factor anomaly and its impact on the Hoyt and Schatten GSN are discussed in the context of the ongoing effort to recalibrate the sunspot number time series.

Comparison of New and Old Sunspot Number Time Series

E. W. **Cliver**
Solar Phys. Volume 291, Issue 9, pp 2891–2916 **2016**
Four new sunspot number time series have been published in this Topical Issue: a backbone-based group number in Svalgaard and Schatten (Solar Phys., 2016; referred to here as SS SS, 1610 – present), a group number series in

Usoskin et al. (Solar Phys., 2016; UEA, 1749 – present) that employs active day fractions from which it derives an observational threshold in group spot area as a measure of observer merit, a provisional group number series in Cliver and Ling (Solar Phys., 2016; CL, 1841 – 1976) that removed flaws in the Hoyt and Schatten (Solar Phys. 179, 189, 1998a; 181, 491, 1998b) normalization scheme for the original relative group sunspot number (RG, 1610 – 1995), and a corrected Wolf (international, RI) number in Clette and Lefèvre (Solar Phys., 2016; SN, 1700 – present). Despite quite different construction methods, the four new series agree well after about 1900. Before 1900, however, the UEA time series is lower than SS, CL, and SN, particularly so before about 1885. Overall, the UEA series most closely resembles the original RG series. Comparison of the UEA and SS series with a new solar wind B time series (Owens et al. in J. Geophys. Res., 2016; 1845 – present) indicates that the UEA time series is too low before 1900. We point out incongruities in the Usoskin et al. (Solar Phys., 2016) observer normalization scheme and present evidence that this method under-estimates group counts before 1900. In general, a correction factor time series, obtained by dividing an annual group count series by the corresponding yearly averages of raw group counts for all observers, can be used to assess the reliability of new sunspot number reconstructions.

The Discontinuity Circa 1885 in the Group Sunspot Number

E. W. **Cliver** , A. G. Ling

Solar Phys. Volume 291, Issue 9, pp 2763–2784 **2016**

On average, the international sunspot number (RI) is 44 % higher than the group sunspot number (RG) from 1885 to the beginning of the RI series in 1700. This is the principal difference between RI and RG. Here we show that this difference is primarily due to an inhomogeneity in the Royal Greenwich Observatory (RGO) record of sunspot groups (1874 – 1976) used to derive observer normalization factors (called k-factors) for RG. Specifically, annual RGO group counts increase relative to those of Wolfer and other long-term observers from 1876 – 1915. A secondary contributing cause is that the k-factors for observers who began observing before 1884 and overlapped with RGO for any years during 1874 – 1883 were not based on direct comparison with RGO but were calculated using one or more intermediary or additional observers. We introduce RGC by rectifying the RGO group counts from 1874 – 1915 and basing k-factors on direct comparison with RGO across the 1885 discontinuity, which brings the RG and RI series into reasonable agreement for the 1841 – 1885 interval (after correcting RI for an inhomogeneity from 1849 – 1867 (to give RIC)). Comparison with an independently derived backbone-based reconstruction of RG (RBB) indicates that RGC over-corrects RBB by 4 % on average from 1841 – 1925. Our analysis suggests that the maxima of Cycles 10 (in 1860), 12 (1883/1884), and 13 (1893) in the RIC series are too low by ≈ 10 %.

Minimal Magnetic States of the Sun and the Solar Wind: Implications for the Origin of the Slow Solar Wind **Review**

E. W. **Cliver** , R. von Steiger

Space Science Reviews **2016**

During the last decade it has been proposed that both the Sun and the solar wind have minimum magnetic states, lowest order levels of magnetism that underlie the 11-yr cycle as well as longer-term variability. Here we review the literature on basal magnetic states at the Sun and in the heliosphere and draw a connection between the two based on the recent deep 2008–2009 minimum between cycles 23 and 24. In particular, we consider the implications of the low solar activity during the recent minimum for the origin of the slow solar wind.

The Extended Cycle of Solar Activity and the Sun's 22-Year Magnetic Cycle **Review**

E. W. **Cliver**

Space Science Reviews, December **2014**, Volume 186, Issue 1-4, pp 169-189

The Sun has two characteristic migrations of surface features—the equatorward movement of sunspots and the poleward movement of high-latitude prominences. The first of these migrations is a defining aspect of the 11-yr Schwabe cycle and the second is a tracer of the process that culminates in solar polarity reversal, signaling the onset of the 22-yr magnetic cycle on the Sun. Zonal flows (torsional oscillations of the Sun's differential rotation) have been identified for both of these migrations. Helioseismology observations of these zonal flows provide support for the extended (>11-yr cycle) of solar activity and offer promise of a long-term precursor for predicting the amplitude of the Schwabe cycle. We review the growth of observational evidence for the extended and 22-yr magnetic cycles and discuss: (1) the significance of latitude ∼50◦ on the Sun; (2) the "over-extended" cycle; and (3) the outlook for solar cycle 25.

Book Review: The Sun Kings: The Unexpected Tragedy of Richard Carrington and the Tale of How Modern Astronomy Began

Cliver, Edward W.
Space Weather, Vol. 6, No. 11, S11003, **2008**
http://dx.doi.org/10.1029/2008SW000433
This acclaimed book, which tells the story of the heroic nineteenth-century astronomers, natural philosophers, and magneticians who established solar-terrestrial science, is a must read for members of the space weather community. *The Sun Kings* recounts the heroic scientific advances—of Alexander von Humboldt, Samuel Schwabe, Edward Sabine, Richard Carrington, Edward Maunder, George Hale, and others—that showed that Earth's magnetic storms originate at the Sun.

The rush to the poles and the role of magnetic buoyancy in the solar dynamo

Simon **Cloutier**, Robert H. Cameron, Laurent Gizon
A&A 693, A11 **2025**
https://arxiv.org/pdf/2411.05623
https://doi.org/10.1051/0004-6361/202450968
https://www.aanda.org/articles/aa/pdf/2025/01/aa50968-24.pdf
The butterfly diagram of the solar cycle exhibits a poleward migration of the diffuse magnetic field resulting from the decay of trailing sunspots. It is one component of what is sometimes referred to as the "rush to the poles". We investigate under which conditions the rush to the poles can be reproduced in flux-transport Babcock-Leighton dynamo models. We identify three main ways to reproduce it: a flux emergence probability that decreases rapidly with latitude; a threshold in subsurface toroidal field strength between slow and fast emergence; and an emergence rate based on magnetic buoyancy. We find that all three mechanisms lead to solar-like butterfly diagrams, but which present notable differences between them. The shape of the butterfly diagram is very sensitive to model parameters for the threshold prescription, while most models incorporating magnetic buoyancy converge to very similar butterfly diagrams, with butterfly wings widths of $\lesssim \pm 30^\circ$, in very good agreement with observations. With turbulent diffusivities above 35 km2/s but below about 40 km2/s, buoyancy models are strikingly solar-like. The threshold and magnetic buoyancy prescriptions make the models non-linear and as such can saturate the dynamo through latitudinal quenching. The period of the models involving buoyancy is independent of the source term amplitude, but emergence loss increases it by $\simeq 60\%$. For the rush to the poles to be visible, a mechanism suppressing (enhancing) emergences at high (low) latitudes must operate. It is not sufficient that the toroidal field be stored at low latitudes for emergences to be limited to low latitudes. From these models we infer that the Sun is not in the advection-dominated regime, but also not in the diffusion-dominated regime. The cycle period is set through a balance between advection, diffusion and flux emergence.

The mean solar butterfly diagram and poloidal field generation rate at the surface of the Sun

Simon **Cloutier**, Robert H. Cameron, Laurent Gizon
A&A 691, A9 **2024**
https://arxiv.org/pdf/2405.17185
https://www.aanda.org/articles/aa/pdf/2024/11/aa50739-24.pdf
The difference between individual solar cycles in the magnetic butterfly diagram can mostly be ascribed to the stochasticity of the emergence process. We aim to obtain the expectation value of the butterfly diagram from observations of four cycles. This allows us to further determine the generation rate of the surface radial magnetic field. We use data from Wilcox Solar Observatory to generate time-latitude diagrams spanning cycles 21 to 24 of the surface radial and toroidal magnetic fields, symmetrize them across the equator and cycle-average them. From the mean butterfly diagram and surface toroidal field we then infer the mean poloidal field generation rate at the surface of the Sun. The averaging procedure removes realization noise from individual cycles. The amount of emerging flux required to account for the evolution of the surface radial field is found to match that provided by the observed surface toroidal field and Joy's law. Cycle-averaging butterfly diagrams removes realization noise and artefacts due to imperfect scale separation, and corresponds to an ensemble average that can be interpreted in the mean-field framework. The result can then be directly compared to $\alpha\Omega$-type dynamo models. The Babcock-Leighton α-effect is consistent with observations, a result that can be appreciated only if the observational data is averaged in some way.

A Babcock-Leighton dynamo model of the Sun incorporating toroidal flux loss and the helioseismically inferred meridional flow

S. **Cloutier**1, R. H. Cameron1 and L. Gizon1,2
A&A 680, A42 (**2023**)

https://www.aanda.org/articles/aa/pdf/2023/12/aa47022-23.pdf
Context. Key elements of the Babcock-Leighton model for the solar dynamo are increasingly constrained by observations.
Aims. We investigate whether the Babcock-Leighton flux-transport dynamo model remains in agreement with observations if the meridional flow profile is taken from helioseismic inversions. Additionally, we investigate the effect of the loss of toroidal flux through the solar surface.
Methods. We employ the two-dimensional flux-transport Babcock-Leighton dynamo framework. We use the helioseismically inferred meridional flow profile, and include toroidal flux loss in a way that is consistent with the amount of poloidal flux generated by Joy's law. Our model does not impose a preference for emergences at low latitudes; however, we do require that the model produces such a preference.
Results. We can find solutions that are in general agreement with observations, including the latitudinal migration of the butterfly wings and the 11 year period of the cycle. The most important free parameters in the model are the depth to which the radial turbulent pumping extends and the turbulent diffusivity in the lower half of the convection zone. We find that the pumping needs to extend to depths of about 0.80 R⊙ and that the bulk turbulent diffusivity needs to be around 10 km2 s−1 or less. We find that the emergences are restricted to low latitudes without the need to impose such a preference.
Conclusions. The flux-transport Babcock-Leighton model, incorporating the helioseismically inferred meridional flow and toroidal field loss term, is compatible with the properties of the observed butterfly diagram and with the observed toroidal loss rate. Reasonably tight constraints are placed on the remaining free parameters. The pumping needs to be just below the depth corresponding to the location where the meridional flow changes direction, and where numerical simulations suggest the convection zone becomes marginally subadiabatic. However, our linear model does not reproduce the observed 'rush to the poles' of the diffuse surface radial field resulting from the decay of sunspots; reproducing this might require the imposition of a preference for flux to emerge near the equator.

The effects of seasonal and diurnal variations in the Earth's magnetic dipole orientation on solar wind–magnetosphere-ionosphere coupling

Cnossen, I., M. Wiltberger, and J. E. Ouellette
J. Geophys. Res., 117, A11211, doi:10.1029/2012JA017825, **2012**
The angle μ between the geomagnetic dipole axis and the geocentric solar magnetospheric (GSM) z axis, sometimes called the "dipole tilt," varies as a function of UT and season. Observations have shown that the cross-polar cap potential tends to maximize near the equinoxes, when on average μ = 0, with smaller values observed near the solstices. This is similar to the well-known semiannual variation in geomagnetic activity. We use numerical model simulations to investigate the role of two possible mechanisms that may be responsible for the influence of μ on the magnetosphere-ionosphere system: variations in the coupling efficiency between the solar wind and the magnetosphere and variations in the ionospheric conductance over the polar caps. Under southward interplanetary magnetic field (IMF) conditions, variations in ionospheric conductance at high magnetic latitudes are responsible for 10–30% of the variations in the cross-polar cap potential associated with μ, but variations in solar wind–magnetosphere coupling are more important and responsible for 70–90%. Variations in viscous processes contribute slightly to this, but variations in the reconnection rate with μ are the dominant cause. The variation in the reconnection rate is primarily the result of a variation in the length of the section of the separator line along which relatively strong reconnection occurs. Changes in solar wind–magnetosphere coupling also affect the field-aligned currents, but these are influenced as well by variations in the conductance associated with variations in μ, more so than the cross-polar cap potential. This may be the case for geomagnetic activity too.

Can Solar Cycle 25 Be a New Dalton Minimum?

Gani Caglar **Coban**, Abd-ur Raheem, Huseyin Cavus & Mahboubeh Asghari-Targhi
Solar Physics volume 296, Article number: 156 (**2021**)
https://link.springer.com/content/pdf/10.1007/s11207-021-01906-1.pdf
The aim of this study is to predict solar activity for the next 10 years (Solar Cycle 25) using a deep learning technique known as a stateful Long Short-Term Memory (LSTM) network. To achieve this goal the number of daily sunspots observed by the American Association of Variable Star Observers (AAVSO) organization from 1945 to 2020 is used as training data for a stateful LSTM model. Time slices are produced by dividing the data between 1945–2020; then data are predicted and examined for the test years of the network trained on these time slices. The mean and smoothed values are calculated from the estimated daily data, compared with the actual mean, and smoothed values, including standard deviations, and the prediction accuracy of the model is examined. Finally, the number of daily sunspots for 10 years of Cycle 25 is estimated. The results are discussed by calculating the mean and smoothed values. The predicted Solar Cycle 25 shows features of a new Dalton Minimum together with Cycle 24. We conclude that Cycle 25 will be the marker of a new Dalton Minimum period.
See **A Critical Comment on "Can Solar Cycle 25 Be a New Dalton Minimum?"**
J. C. **Peguero** & V. M. S. Carrasco
Solar Physics volume 298, Article number: 48 (**2023**)

https://link.springer.com/content/pdf/10.1007/s11207-023-02140-7.pdf

Reimagining Heliophysics: A bold new vision for the next decade and beyond a Review

Ian J. **Cohen**, Dan Baker, Jacob Bortnik, Pontus Brandt, Jim Burch, +++

2023

https://arxiv.org/ftp/arxiv/papers/2308/2308.12308.pdf

The field of Heliophysics has a branding problem. We need an answer to the question: ``What is Heliophysics\?", the answer to which should clearly and succinctly defines our science in a compelling way that simultaneously introduces a sense of wonder and exploration into our science and our missions. Unfortunately, recent over-reliance on space weather to define our field, as opposed to simply using it as a practical and relatable example of applied Heliophysics science, narrows the scope of what solar and space physics is and diminishes its fundamental importance. Moving forward, our community needs to be bold and unabashed in our definition of Heliophysics and its big questions. We should emphasize the general and fundamental importance and excitement of our science with a new mindset that generalizes and expands the definition of Heliophysics to include new ``frontiers" of increasing interest to the community. Heliophysics should be unbound from its current confinement to the Sun-Earth connection and expanded to studies of the fundamental nature of space plasma physics across the solar system and greater cosmos. Finally, we need to come together as a community to advance our science by envisioning, prioritizing, and supporting -- with a unified voice -- a set of bold new missions that target compelling science questions - even if they do not explore the traditional Sun- and Earth-centric aspects of Heliophysics science. Such new, large missions to expand the frontiers and scope of Heliophysics science large missions can be the key to galvanizing the public and policymakers to support the overall Heliophysics program.

Representation of solar features in 3D for creating visual solar catalogues

Tufan **Colak**, a, , Rami Qahwajia, Stan Ipsona and Hassan Ugaila

Advances in Space Research, Volume 47, Issue 12, 15 June **2011**, Pages 2092-2104, **File**

In this study a method for 3D representation of active regions and sunspots that are detected from Solar and Heliospheric Observatory/Michelson Doppler Imager magnetogram and continuum images is provided. This is our first attempt to create a visual solar catalogue. Because of the difficulty of providing a full description of data in text based catalogues, it can be more accurate and effective for scientist to search 3D solar feature models and descriptions at the same time in such a visual solar catalogue. This catalogue would improve interpretation of solar images, since it would allow us to extract data embedded in various solar images and visualize it at the same time. In this work, active regions that are detected from magnetogram images and sunspots that are detected from continuum images are represented in 3D coordinates. Also their properties extracted from text based catalogues are represented at the same time in 3D environment. This is the first step for creating a 3D solar feature catalogue where automatically detected solar features will be presented visually together with their properties.

http://www.spaceweather.inf.brad.ac.uk/3DSolar-View.html

Robustness of oscillatory α2 dynamos in spherical wedges

E. **Cole**1,2, A. Brandenburg2,3,4,5, P. J. Käpylä6,1,2 and M. J. Käpylä7,6

A&A 593, A134 (**2016**)

Context. Large-scale dynamo simulations are sometimes confined to spherical wedge geometries by imposing artificial boundary conditions at high latitudes. This may lead to spatio-temporal behaviours that are not representative of those in full spherical shells.

Aims. We study the connection between spherical wedge and full spherical shell geometries using simple mean-field dynamos.

Methods. We solve the equations for one-dimensional time-dependent α2 and α2Ω mean-field dynamos with only latitudinal extent to examine the effects of varying the polar angle θ0 between the latitudinal boundaries and the poles in spherical coordinates.

Results. In the case of constant α and ηt profiles, we find oscillatory solutions only with the commonly used perfect conductor boundary condition in a wedge geometry, while for full spheres all boundary conditions produce stationary solutions, indicating that perfect conductor conditions lead to unphysical solutions in such a wedge setup. To search for configurations in which this problem can be alleviated we choose a profile of the turbulent magnetic diffusivity that decreases toward the poles, corresponding to high conductivity there. Oscillatory solutions are now achieved with models extending to the poles, but the magnetic field is strongly concentrated near the poles and the oscillation period is very long. By changing both the turbulent magnetic diffusivity and α profiles so that both effects are more concentrated toward the equator, we see oscillatory dynamos with equatorward drift, shorter cycles, and magnetic fields distributed over a wider range of latitudes. Those profiles thus remove the sensitive and unphysical dependence on θ0. When introducing radial shear, we again see oscillatory dynamos, and the direction of drift follows the Parker-Yoshimura rule.

Conclusions. A reduced α effect near the poles with a turbulent diffusivity concentrated toward the equator yields oscillatory dynamos with equatorward migration and reproduces best the solutions in spherical wedges. For weak shear, oscillatory solutions are obtained only for perfect conductor field conditions and negative shear. Oscillatory solutions become preferred at sufficiently strong shear. Recent three-dimensional dynamo simulations producing solar-like magnetic activity are expected to lie in this range.

Modulated cycles in an illustrative solar dynamo model with competing α-effects

L. C. **Cole** and P. J. Bushby
A&A 563, A116 (**2014**)
http://arxiv.org/pdf/1403.6604v1.pdf

Context. The large-scale magnetic field in the Sun varies with a period of approximately 22 years, although the amplitude of the cycle is subject to long-term modulation with recurrent phases of significantly reduced magnetic activity. It is believed that a hydromagnetic dynamo is responsible for producing this large-scale field, although this dynamo process is not well understood.
Aims. Within the framework of mean-field dynamo theory, our aim is to investigate how competing mechanisms for poloidal field regeneration (namely a time-delayed Babcock-Leighton surface α-effect and an interface-type α-effect), can lead to the modulation of magnetic activity in a deep-seated solar dynamo model.
Methods. We solve the standard αΩ dynamo equations in one spatial dimension, including source terms corresponding to both of the competing α-effects in the evolution equation for the poloidal field. This system is solved using two different methods. In addition to solving the one-dimensional partial differential equations directly, using numerical techniques, we also use a local approximation to reduce the governing equations to a set of coupled ordinary differential equations (ODEs), which are studied using a combination of analytical and numerical methods.
Results. In the ODE model, it is straightforward to find parameters such that a series of bifurcations can be identified as the time delay is increased, with the dynamo transitioning from periodic states to chaotic states via multiply periodic solutions. Similar transitions can be observed in the full model, with the chaotically modulated solutions exhibiting solar-like behaviour.
Conclusions. Competing α-effects could explain the observed modulation in the solar cycle.

Lower solar atmosphere and magnetism at ultra-high spatial resolution

A White Paper for the Next Generation Solar Physics Mission
Remo **Collet**, Serena Criscuoli, Ilaria Ermolli, Damian Fabbian, Nuno Guerreiro, Margit Haberreiter, Courtney Peck, Tiago M. D. Pereira, Matthias Rempel, Sami K. Solanki, Sven Wedemeyer-Boehm
(Submitted on 7 Dec **2016**)
https://arxiv.org/pdf/1612.02348v1.pdf

We present the scientific case for a future space-based telescope aimed at very high spatial and temporal resolution imaging of the solar photosphere and chromosphere. Previous missions (e.g., HINODE, SUNRISE) have demonstrated the power of observing the solar photosphere and chromosphere at high spatial resolution without contamination from Earth's atmosphere. We argue here that increased spatial resolution (from currently 70 km to 25 km in the future) and high temporal cadence of the observations will vastly improve our understanding of the physical processes controlling solar magnetism and its characteristic scales. This is particularly important as the Sun's magnetic field drives solar activity and can significantly influence the Sun-Earth system. At the same time a better knowledge of solar magnetism can greatly improve our understanding of other astrophysical objects.

A statistical study of CME properties and of the correlation between flares and CMEs over the solar cycles 23 and 24

A. **Compagnino**, P. Romano, F. Zuccarello
Solar Phys. **2016**
http://arxiv.org/pdf/1609.08943v1.pdf

We investigated some properties of coronal mass ejections (CMEs), such as speed, acceleration, polar angle, angular width and mass, using data acquired by LASCO aboard of SOHO from July 31, 1997, to March 31, 2014, i.e., during the solar cycles 23 and 24. We used two CME catalogs: one provided by the CDAW Data Center and one obtained by the CACTus detection algorithm. For both dataset, we found that the number of CMEs observed during the peak of cycle 24 was higher or comparable to the one during cycle 23, although the photospheric activity during

cycle 24 was weaker than during cycle 23. More precisely, using the CMEs detected by CACTus we noted that the number of events N is of the same order of magnitude during the peaks of the two cycles, but the peak of CME distribution during the cycle 24 is more extended in time (N > 1500 during 2012 and 2013). We ascribe the discrepancy between CDAW and CACTus results to the observer bias for CME definition in the CDAW catalog (Robbrecht et al., 2009; Webb and Howard, 2012; Yashiro et al., 2008). We also used a dataset containing 19811 flares of C, M, and X class, observed by GOES during the same period. Using both dataset, we studied the relationship between the mass ejected by the CMEs and the flux emitted during the corresponding flares: we found 11441 flares that were temporally-correlated with CMEs for CDAW and 9120 for CACTus. Moreover, we found a log-linear relationship between the flux of the flares integrated from the start to end in the 0.1-0.8 nm range and the CME mass: log(CME mass) proportional to 0.23 x log(flare flux). We also found some differences in the mean CMEs velocity and acceleration between the events associated with flares and those that were not. In particular, the CMEs associated with flares are on average 100 km/s faster than the ones not associated with flares.

NuSTAR observations of a repeatedly microflaring active region

Kristopher **Cooper**, Iain G. Hannah, Brian W. Grefenstette, Lindsay Glesener, Säm Krucker, Hugh S. Hudson, Stephen M. White, David M. Smith, Jessie Duncan
MNRAS **2021**
https://arxiv.org/pdf/2109.00263
We investigate the spatial, temporal, and spectral properties of 10 microflares from AR12721 on **2018 September 9 and 10** observed in X-rays using the Nuclear Spectroscopic Telescope ARray (NuSTAR) and the Solar Dynamic Observatory's Atmospheric Imaging Assembly and Helioseismic and Magnetic Imager (SDO/AIA and HMI). We find GOES sub-A class equivalent microflare energies of 1026-1028 erg reaching temperatures up to 10 MK with consistent quiescent or hot active region core plasma temperatures of 3-4 MK. One microflare (SOL2018-09-09T10:33), with an equivalent GOES class of A0.1, has non-thermal HXR emission during its impulsive phase (of non-thermal power ∼7×1024 erg s−1) making it one of the faintest X-ray microflares to have direct evidence for accelerated electrons. In 4 of the 10 microflares, we find that the X-ray time profile matches fainter and more transient sources in the EUV, highlighting the need for observations sensitive to only the hottest material that reaches temperatures higher than those of the active region core (>5 MK). Evidence for corresponding photospheric magnetic flux cancellation/emergence present at the footpoints of 8 microflares is also observed.

Cosmic radiation exposure of aircraft occupants on simulated high-latitude flights during solar proton events from 1 January 1986 through 1 January 2008

Kyle **Copeland**, Herbert H. Sauer[b], Frances E. Duke[a] and Wallace Friedberg[a]
Advances in Space Research, Volume 42, Issue 6, **2008**, Pages 1008-1029

Future perspectives in solar hot plasma observations in the soft X-rays

Alain Jody **Corso**, Giulio Del Zanna, Vanessa Polito
Experimental Astronomy **2021**
https://arxiv.org/pdf/2105.05549.pdf
The soft X-rays (SXRs: 90--150 Å) are among the most interesting spectral ranges to be investigated in the next generation of solar missions due to their unique capability of diagnosing phenomena involving hot plasma with temperatures up to 15~MK. Multilayer (ML) coatings are crucial for developing SXR instrumentation, as so far they represent the only viable option for the development of high-efficiency mirrors in this spectral range. However, the current standard MLs are characterized by a very narrow spectral band which is incompatible with the science requirements expected for a SXR spectrometer. Nevertheless, recent advancement in the ML technology has made the development of non-periodic stacks repeatable and reliable, enabling the manufacturing of SXR mirrors with a valuable efficiency over a large range of wavelengths.
In this work, after reviewing the state-of-the-art ML coatings for the SXR range, we investigate the possibility of using M-fold and aperiodic stacks for the development of multiband SXR spectrometers. After selecting a possible choice of key spectral lines, some trade-off studies for an eight-bands spectrometer are also presented and discussed, giving an evaluation of their feasibility and potential performance.

Sunspot Observations and Counting at Specola Solare Ticinese in Locarno since 1957

Sergio **Cortesi**, Marco Cagnotti, Michele Bianda, Renzo Ramelli, Andrea Manna
Solar Phys. **2016**
http://arxiv.org/pdf/1602.07998v1.pdf
Specola Solare Ticinese is an observatory dedicated to Sunspot Number counting, which was constructed in 1957 in Locarno, Southern Switzerland, as an external observing station of the Zurich Federal Observatory. When in 1981 the responsibility of the determination of the International Sunspot Number was assumed by the Royal Observatory

of Belgium, Specola Solare Ticinese was given the role of pilot station, with the aim of preserving the continuity in the counting method. We report the observing procedure and counting rules applied in Locarno.

Numerical Modeling of Galactic Cosmic-Ray Proton and Helium Observed by AMS-02 during the Solar Maximum of Solar Cycle 24

Claudio **Corti**1, Marius S. Potgieter2, Veronica Bindi1, Cristina Consolandi1, Christopher Light1, Matteo Palermo1, and Alexis Popkow
2019 ApJ 871 253
https://doi.org/10.3847/1538-4357/aafac4
Galactic cosmic rays (GCRs) are affected by solar modulation while they propagate through the heliosphere. The study of the time variation of GCR spectra observed at Earth can shed light on the underlying physical processes, specifically diffusion and particle drifts. Recently, the AMS-02 experiment measured with very high accuracy the time variation of the cosmic-ray proton and helium flux between 2011 May and 2017 May in the rigidity range from 1 to 60 GV. In this work, a comprehensive three-dimensional steady-state numerical model is used to solve Parker's transport equation and reproduce the monthly proton fluxes observed by AMS-02. We find that the rigidity slope of the perpendicular mean free path above 4 GV remains constant, while below 4 GV, it increases during solar maximum. Assuming the same mean free paths for helium and protons, the models are able to reproduce the time behavior of the p/He ratio observed by AMS-02. The dependence of the diffusion tensor on the particle mass-to-charge ratio, A/Z, is found to be the main cause of the time dependence of p/He below 3 GV.

Supergranulation as the largest buoyantly driven convective scale of the Sun

Jean-Francois **Cossette**, Mark Peter Rast
ApJ 829 L17 **2016**
http://arxiv.org/pdf/1606.04041v1.pdf
Supergranulation is characterized by horizontally divergent flows with typical length scales of 32 Mm in the solar photosphere. Unlike granulation, the size of which is comparable to both the thickness of the radiative boundary layer and local scale height of the plasma in the photosphere, supergranulation does not reflect any obvious length scale of the solar convection zone. Early suggestions that the depth of second helium ionization is important are not supported by numerical simulations. Thus the origin of the solar supergranulation remains largely a mystery. Moreover, observations of flows in the photosphere using either Doppler imaging or correlation or feature tracking show a monotonic decrease in power at scales larger than supergranulation. Both local area and global spherical shell simulations of solar convection by contrast show the opposite, a power law increase in horizontal flow amplitudes to low wavenumber. Here we examine this disparity, and investigate how the solar supergranulation may arise as a consequence of strong photospheric driving and non-local heat transport by cool diving plumes. Using three dimensional anelastic simulations with surface driving, we show that the kinetic energy of largest convective scales in the upper layers of a stratified domain reflects the depth of transition from strong buoyant driving to adiabatic stratification below. We interpret the observed monotonic decrease in solar convective power at scales larger than supergranulation to be a consequence of this rapid transition, and show how the supergranular scale can be understood as the largest buoyantly driven mode of convection in the Sun.

Slow magnetoacoustic gravity waves in an equilibrium stratified solar atmosphere: cut-off periods through the transition region

A. **Costa**, M. Schneiter, E. Zurbriggen
MNRAS Volume 480, Issue 1, p.623-628 **2018**
https://arxiv.org/pdf/1807.02141.pdf
Assuming the thin flux tube approximation, we introduce an analytical model that contemplates the presence of: a non-isothermal temperature; a varying magnetic field and a non-uniform stratified medium in hydrostatic equilibrium due to a constant gravity acceleration. This allows the study of slow magnetoacoustic cut-off periods across the solar transition region, from the base of the solar chromosphere to the lower corona. The used temperature profile approaches the VAC solar atmospheric model. The periods obtained are consistent with observations. Similar to the acoustic cut-off periods, the resulting magnetoacoustic gravity ones follow the sharp temperature profile, but shifted towards larger heights; in other words, at a given height the magnetoacoustic cut-off period is significantly lower than the corresponding acoustic one. Along a given longitude of an inclined thin magnetic tube, the greater its inclination the softener the temperature gradient it crosses. Changes in the magnetic field intensity do not significantly modify the periods at the coronal level but modulate the values below the transition region within periods between ~[2−6]min. Within the limitations of our model, we show that monochromatic oscillations of the solar atmosphere are the atmospheric response at its natural frequency to random or impulsive perturbations, and not a consequence of the forcing from the photosphere.

See Solar slow magneto-acoustic-gravity waves: an erratum correction and a revisited scenario

E. **Zurbriggen**, M. V. Sieyra, A. Costa, A. Esquivel, G. Stenborg
MNRAS **2020**
https://arxiv.org/pdf/2004.09609.pdf

An on Orbit Determination of Point Spread Functions for the Interface Region Imaging Spectrograph

Hans **Courrier**, Charles Kankelborg, Bart De Pontieu, Jean-Pierre Wülser
Solar Physics September **2018**, 293:125
Using the 2016 Mercury transit of the Sun, we characterize on orbit spatial point spread functions (PSFs) for the Near- (NUV) and Far- (FUV) Ultra-Violet spectrograph channels of NASA's Interface Region Imaging Spectrograph (IRIS). A semi-blind Richardson–Lucy deconvolution method is used to estimate PSFs for each channel. Corresponding estimates of Modulation Transfer Functions (MTFs) indicate resolution of 2.47 cycles/arcsec in the NUV channel near 2796 Å and 2.55 cycles/arcsec near 2814 Å. In the short (≈1336 A˚≈1336 A˚) and long (≈1394 A˚≈1394 A˚) wavelength FUV channels, our MTFs show pixel-limited resolution (3.0 cycles/arcsec). The PSF estimates perform well under deconvolution, removing or significantly reducing instrument artifacts in the Mercury transit spectra. The usefulness of the PSFs is demonstrated in a case study of an isolated explosive event. PSF estimates and deconvolution routines are provided through a SolarSoft module.

On the Prediction of Solar Cycles

V. **Courtillot**, F. Lopes & J. L. Le Mouël
Solar Physics volume 296, Article number: 21 (**2021**)
https://link.springer.com/content/pdf/10.1007/s11207-020-01760-7.pdf
The series of observations of sunspots is one of the longest available; it is considered as a valuable proxy of solar activity at the centennial time scale. The series is a useful tool to study solar physics, and also the influence of solar variability on space weather, satellite orbits, the well being of astronauts, long distance communications and terrestrial climate, to name a few. Mankind is particularly keen to be able to predict the evolution of solar activity and its bearing on space weather and terrestrial climate. Upon a first look at the time series of sunspots (Figure 1), the ≈ 11 year repetition of an otherwise rather irregular solar cycle, the Schwabe cycle, immediately jumps to the eye. The series is generally considered reliable since the end of the quasi-spotless Maunder minimum (Maunder 1894; Maunder and Maunder 1905), that is the early 1700s. We are currently (2020) entering Solar Cycle 25.

Neural network forecast of the sunspot diagram

Eurico **Covas**, Nuno Peixinho, Joao Fernandes
Solar Phys. **2019**, 294:24
https://arxiv.org/pdf/1801.04435.pdf
https://link.springer.com/content/pdf/10.1007%2Fs11207-019-1412-z.pdf
We attempt to forecast the Sun's sunspot butterfly diagram using neural networks as a prediction method. We use this approach to forecast in both latitude (space) and time, using a full spatial-temporal series of the sunspot diagram from 1874 to 2015 that trains the neural network. The analysis of the results show that it is indeed possible to reconstruct the overall shape and amplitude of the spatial-temporal pattern of sunspots using these feed-forward neural networks. However, we conclude that more data and/or improved neural network techniques are probably necessary for this approach to have real predictive power.

Spatial-temporal forecasting the sunspot diagram

Eurico **Covas**
2017, A&A, 605, A44
https://arxiv.org/pdf/1709.02796.pdf
We attempt to forecast the Sun's sunspot butterfly diagram in both space (i.e. in latitude) and time, instead of the usual one-dimensional time series forecasts prevalent in the scientific literature. We use a prediction method based on the non-linear embedding of data series in high dimensions. We use this method to forecast both in latitude (space) and in time, using a full spatial-temporal series of the sunspot diagram from 1874 to 2015. The analysis of the results shows that it is indeed possible to reconstruct the overall shape and amplitude of the spatial-temporal pattern of sunspots, but that the method in its current form does not have real predictive power. We also apply a metric called structural similarity to compare the forecasted and the observed butterfly cycles, showing that this metric can be a useful addition to the usual root mean square error metric when analysing the efficiency of different prediction methods.

Coronal energy release by MHD avalanches

II. EUV line emission from a multi-threaded coronal loop

G. **Cozzo**, J. Reid, P. Pagano, F. Reale, P. Testa, A. W. Hood, C. Argiroffi, A. Petralia, E. Alaimo, F. D'Anca, L. Sciortino, M. Todaro, U. Lo Cicero, M. Barbera, B. De Pontieu, J. Martinez-Sykora

A&A **2024**

https://arxiv.org/pdf/2406.11701

MHD kink instability can trigger the fragmentation of a twisted magnetic flux tube into small-scale current sheets that dissipate as aperiodic impulsive heating events. This instability propagates as an avalanche to nearby flux tubes and leads to a nanoflare storm. Our previous work was devoted to related 3D MHD numerical modeling with a stratified and realistic atmosphere. This work addresses predictions for the EUV imaging spectroscopy of such structure and evolution of a loop, with an average temperature of 2.5 MK in the solar corona. We set a particular focus on the forthcoming MUSE mission. From the output of the numerical simulations, we synthesized the intensities, Doppler shifts, and non-thermal line broadening in 3 EUV spectral lines in the MUSE passbands: Fe IX 171A, Fe XV 284 A, and Fe XIX 108 A, at 1 MK, 2 MK, and 10 MK, respectively, according to the MUSE expected pixel size, temporal resolution, and temperature response functions. We provide maps showing different view angles and realistic spectra. Finally, we discuss the relevant evolutionary processes from the perspective of possible observations. We find that the MUSE observations might be able to detect the fine structure determined by tube fragmentation. In particular, the Fe IX line is mostly emitted at the loop footpoints, where we track the motions that drive the magnetic stressing and detect the upward motion of evaporating plasma from the chromosphere. In Fe XV, we see the bulk of the loop with increasing intensity. The Fe XIX line is very faint within the chosen simulation parameters; thus, any transient brightening around the loop apex may possibly be emphasized by the folding of sheet-like structure. In conclusion, we show that coronal loop observations with MUSE can pinpoint some crucial features of MHD-modeled ignition processes, such as the related dynamics, helping to identify the heating processes.

Coronal energy release by MHD avalanches. Effects on a structured, active region, multi-threaded coronal loop

G. **Cozzo**, J. Reid, P. Pagano, F. Reale, A. W. Hood

A&A **2023**

https://arxiv.org/pdf/2306.06047.pdf

A possible key element for large-scale energy release in the solar corona is an MHD kink instability in a single twisted magnetic flux tube. An initial helical current sheet fragments in a turbulent way into smaller-scale sheets, similarly to a nanoflare storm. As the loop expands in the radial direction during the relaxation process, an unstable loop can disrupt nearby stable loops and trigger an MHD avalanche. Exploratory investigations have been conducted in previous works with relatively simplified loop configurations. Here, we address a more realistic environment that comprehensively accounts for most of the physical effects involved in a stratified atmosphere, typical of an active region. The question is whether the avalanche process will be triggered, with what timescales, and how it will develop, as compared with the original, simpler approach. Three-dimensional MHD simulations describe the interaction of magnetic flux tubes, which have a stratified atmosphere, including chromospheric layers, the thin transition region to the corona, and the related transition from high-beta to low-beta regions. The model also includes the effects of thermal conduction and of optically thin radiation. Our simulations address the case where one flux tube among a few is twisted at the footpoints faster than its neighbours. We show that this flux tube becomes kink unstable first, in conditions in agreement with those predicted by analytical models. It rapidly involves nearby stable tubes, instigating significant magnetic reconnection and dissipation of energy as heat. The heating determines the development of chromospheric evaporation, while the temperature rises up to about 10 MK, close to microflares observations. This work confirms that avalanches are a viable mechanism for the storing and release of magnetic energy in plasma confined in closed coronal loops, as a result of photospheric motions.

Magnetohydrodynamic Mode Conversion in the Solar Corona: Insights from Fresnel-like Models of Waves at Sharp Interfaces

Steven R. **Cranmer** , Momchil E. Molnar

ApJ **2023**

https://arxiv.org/pdf/2308.04394.pdf

The solar atmosphere is known to contain many different types of wavelike oscillation. Waves and other fluctuations (e.g., turbulent eddies) are believed to be responsible for at least some of the energy transport and dissipation that heats the corona and accelerates the solar wind. Thus, it is important to understand the behavior of magnetohydrodynamic (MHD) waves as they propagate and evolve in different regions of the Sun's atmosphere. In this paper, we investigate how MHD waves can affect the overall plasma state when they reflect and refract at sharp, planar interfaces in density. First, we correct an error in a foundational paper (Stein 1971) that affects the calculation of wave energy-flux conservation. Second, we apply this model to reflection-driven MHD turbulence in the solar wind, where the presence of density fluctuations can enhance the generation of inward-propagating Alfven waves. This model reproduces the time-averaged Elsasser imbalance fraction (i.e., ratio of inward to outward Alfvenic

power) from several published numerical simulations. Lastly, we model how the complex magnetic field threading the transition region between the chromosphere and corona helps convert a fraction of upward-propagating Alfven waves into fast-mode and slow-mode MHD waves. These magnetosonic waves dissipate in a narrow region around the transition region and produce a sharp peak in the heating rate. This newly found source of heating sometimes exceeds the expected heating rate from Alfvenic turbulence by an order of magnitude. It may explain why some earlier models seemed to require an additional ad-hoc heat source at this location.

Inward Propagating Plasma Parcels in the Solar Corona: Models with Aerodynamic Drag, Ablation, and Snowplow Accretion

Steven R. **Cranmer** (CU Boulder), Craig E. DeForest (SwRI), Sarah E. Gibson (HAO/NCAR)
ApJ **2021**
https://arxiv.org/pdf/2103.12039.pdf
Although the solar wind flows primarily outward from the Sun to interplanetary space, there are times when small-scale plasma inflows are observed. Inward-propagating density fluctuations in polar coronal holes were detected by the COR2 coronagraph on board the STEREO-A spacecraft at heliocentric distances of 7 to 12 solar radii, and these fluctuations appear to undergo substantial deceleration as they move closer to the Sun. Models of linear magnetohydrodynamic waves have not been able to explain these deceleration patterns, so they have been interpreted more recently as jets from coronal sites of magnetic reconnection. In this paper, we develop a range of dynamical models of discrete plasma parcels with the goal of better understanding the observed deceleration trend. We found that parcels with a constant mass do not behave like the observed flows, and neither do parcels undergoing ablative mass loss. However, parcels that accrete mass in a snowplow-like fashion can become decelerated as observed. We also extrapolated OMNI in situ data down to the so-called Alfven surface and found that the initial launch-point for the observed parcels may often be above this critical radius. In other words, in order for the parcels to flow back down to the Sun, their initial speeds are probably somewhat nonlinear (i.e., supra-Alfvenic) and thus the parcels may be associated with structures such as shocks, jets, or shear instabilities.

The Properties of the Solar Corona and Its Connection to the Solar Wind **Review**

Steven R. **Cranmer** (CU Boulder), Amy R. Winebarger (NASA/MSFC)
Annual Review of Astronomy and Astrophysics, volume 57 (**2019**)
https://arxiv.org/pdf/1811.00461.pdf
The corona is a layer of hot plasma that surrounds the Sun, traces out its complex magnetic field, and ultimately expands into interplanetary space as the supersonic solar wind. Although much has been learned in recent decades from advances in observations, theory, and computer simulations, we still have not identified definitively the physical processes that heat the corona and accelerate the solar wind. In this review, we summarize these recent advances and speculate about what else is required to finally understand the fundamental physics of this complex system. Specifically: (1) We discuss recent sub-arcsecond observations of the corona, some of which appear to provide evidence for tangled and braided magnetic fields, and some of which do not. (2) We review results from three-dimensional numerical simulations that, despite limitations in dynamic range, reliably contain sufficient heating to produce and maintain the corona. (3) We provide a new tabulation of scaling relations for a number of proposed coronal heating theories that involve waves, turbulence, braiding, nanoflares, and helicity conservation. An understanding of these processes is important not only for improving our ability to forecast hazardous space-weather events, but also for establishing a baseline of knowledge about a well-resolved star that is relevant to other astrophysical systems. **2012 July 11, 2014 July 25**

Some Turbulent Predictions for Parker Solar Probe

Steven R. **Cranmer** (CU Boulder)
Research Notes of the AAS **2** 158 **2018**
https://arxiv.org/pdf/1808.09477.pdf
http://iopscience.iop.org/article/10.3847/2515-5172/aadd98
From the the solar photosphere to the outer heliosphere, the Sun's plasma properties are fluctuating with a broad range of temporal and spatial scales. In fact, a turbulent cascade of energy from large to small scales is a frequently invoked explanation for heating the corona and accelerating the solar wind. NASA's Parker Solar Probe (PSP) is expected to revolutionize our understanding of coronal heating and magnetohydrodynamic (MHD) turbulence by performing in situ sampling closer to the Sun than any other prior space mission. This research note presents theoretical predictions for some properties of MHD turbulence (e.g., spacecraft-frame power spectra and variance anisotropies) in the regions to be explored by PSP. These results are derived from a previously published semi-empirical model of coupled Alfvenic and fast-mode turbulence in the fast solar wind. The primary reason for this research note is to show how straightforward it can be to extract useful predictions from existing theoretical models about measurable quantities that were not even considered when creating the models initially. The variance anisotropy, for example, may be an important quantity for distinguishing between different theoretical models for coronal heating and solar wind acceleration.

Low-frequency Alfven Waves Produced by Magnetic Reconnection in the Sun's Magnetic Carpet

Steven R. **Cranmer** (CU Boulder)
ApJ **2018**
https://arxiv.org/pdf/1805.12184.pdf
The solar corona is a hot, dynamic, and highly magnetized plasma environment whose source of energy is not yet well understood. One leading contender for that energy source is the dissipation of magnetohydrodynamic (MHD) waves or turbulent fluctuations. Many wave-heating models for the corona and the solar wind presume that these fluctuations originate at or below the Sun's photosphere. However, this paper investigates the idea that magnetic reconnection may generate an additional source of MHD waves over a gradual range of heights in the low corona. A time-dependent Monte Carlo simulation of the mixed-polarity magnetic field is used to predict the properties of reconnection-driven coronal MHD waves. The total power in these waves is typically small in comparison to that of photosphere-driven waves, but their frequencies are much lower. Reconnection-driven waves begin to dominate the total power spectrum at periods longer than about 30 minutes. Thus, they may need to be taken into account in order to understand the low-frequency power-law spectra observed by both coronal spectropolarimetry and in-situ particle/field instruments. These low-frequency Alfven waves should carry more magnetic energy than kinetic energy, and thus they may produce less nonthermal Doppler broadening (in comparison to photosphere-driven high-frequency waves) in emission lines observed above the solar limb.

Origins of the Ambient Solar Wind: Implications for Space Weather **Review**

Steven R. **Cranmer** (CU Boulder), Sarah E. Gibson (HAO), Pete Riley (PSI)
Space Science Reviews. Special issue connected with a 2016 ISSI workshop on "The Scientific Foundations of Space Weather." **2017**
https://arxiv.org/pdf/1708.07169.pdf
The Sun's outer atmosphere is heated to temperatures of millions of degrees, and solar plasma flows out into interplanetary space at supersonic speeds. This paper reviews our current understanding of these interrelated problems: coronal heating and the acceleration of the ambient solar wind. We also discuss where the community stands in its ability to forecast how variations in the solar wind (i.e., fast and slow wind streams) impact the Earth. Although the last few decades have seen significant progress in observations and modeling, we still do not have a complete understanding of the relevant physical processes, nor do we have a quantitatively precise census of which coronal structures contribute to specific types of solar wind. Fast streams are known to be connected to the central regions of large coronal holes. Slow streams, however, appear to come from a wide range of sources, including streamers, pseudostreamers, coronal loops, active regions, and coronal hole boundaries. Complicating our understanding even more is the fact that processes such as turbulence, stream-stream interactions, and Coulomb collisions can make it difficult to unambiguously map a parcel measured at 1 AU back down to its coronal source. We also review recent progress -- in theoretical modeling, observational data analysis, and forecasting techniques that sit at the interface between data and theory -- that gives us hope that the above problems are indeed solvable.

Driving Solar Spicules and Jets with Magnetohydrodynamic Turbulence: Testing a Persistent Idea

Steven R. **Cranmer**, Lauren N. Woolsey
ApJ **2015**
http://arxiv.org/pdf/1509.03263v1.pdf
The solar chromosphere contains thin, highly dynamic strands of plasma known as spicules. Recently, it has been suggested that the smallest and fastest (Type II) spicules are identical to intermittent jets observed by the Interface Region Imaging Spectrograph. These jets appear to expand out along open magnetic field lines rooted in unipolar network regions of coronal holes. In this paper we revisit a thirty-year-old idea that spicules may be caused by upward forces associated with Alfven waves. These forces involve the conversion of transverse Alfven waves into compressive acoustic-like waves that steepen into shocks. The repeated buffeting due to upward shock propagation causes nonthermal expansion of the chromosphere and a transient levitation of the transition region. Some older models of wave-driven spicules assumed sinusoidal wave inputs, but the solar atmosphere is highly turbulent and stochastic. Thus, we model this process using the output of a time-dependent simulation of reduced magnetohydrodynamic turbulence. The resulting mode-converted compressive waves are strongly variable in time, with a higher transition region occurring when the amplitudes are large and a lower transition region when the amplitudes are small. In this picture, the transition region bobs up and down by several Mm on timescales less than a minute. These motions produce narrow, intermittent extensions of the chromosphere that have similar properties as the observed jets and Type II spicules.

The Role of Turbulence in Coronal Heating and Solar Wind Expansion **Review**

S. R. **Cranmer**, M. Asgari-Targhi, M. P. Miralles, J. C. Raymond, L. Strachan, H. Tian, L. N. Woolsey
Phil. Trans. Royal Soc. A, theme issue on "Dissipation and Heating in Solar Wind Plasma Turbulence," edited by K. Kiyani, K. Osman, and S. Chapman
2014
http://arxiv.org/pdf/1412.2307v1.pdf

Plasma in the Sun's hot corona expands into the heliosphere as a supersonic and highly magnetized solar wind. This paper provides an overview of our current understanding of how the corona is heated and how the solar wind is accelerated. Recent models of magnetohydrodynamic turbulence have progressed to the point of successfully predicting many observed properties of this complex, multi-scale system. However, it is not clear whether the heating in open-field regions comes mainly from the dissipation of turbulent fluctuations that are launched from the solar surface, or whether the chaotic "magnetic carpet" in the low corona energizes the system via magnetic reconnection. To help pin down the physics, we also review some key observational results from ultraviolet spectroscopy of the collisionless outer corona.

Suprathermal Electrons in the Solar Corona: Can Nonlocal Transport Explain Heliospheric Charge States?

Steven R. **Cranmer**
ApJ Letters, 791, L31 **2014**
http://arxiv.org/pdf/1407.5941v1.pdf

There have been several ideas proposed to explain how the Sun's corona is heated and how the solar wind is accelerated. Some models assume that open magnetic field lines are heated by Alfvén waves driven by photospheric motions and dissipated after undergoing a turbulent cascade. Other models posit that much of the solar wind's mass and energy is injected via magnetic reconnection from closed coronal loops. The latter idea is motivated by observations of reconnecting jets and also by similarities of ion composition between closed loops and the slow wind. Wave/turbulence models have also succeeded in reproducing observed trends in ion composition signatures versus wind speed. However, the absolute values of the charge-state ratios predicted by those models tended to be too low in comparison with observations. This letter refines these predictions by taking better account of weak Coulomb collisions for coronal electrons, whose thermodynamic properties determine the ion charge states in the low corona. A perturbative description of nonlocal electron transport is applied to an existing set of wave/turbulence models. The resulting electron velocity distributions in the low corona exhibit mild suprathermal tails characterized by "kappa" exponents between 10 and 25. These suprathermal electrons are found to be sufficiently energetic to enhance the charge states of oxygen ions, while maintaining the same relative trend with wind speed that was found when the distribution was assumed to be Maxwellian. The updated wave/turbulence models are in excellent agreement with solar wind ion composition measurements.

Challenges and advances in modeling of the solar atmosphere **Review**

Serena **Criscuoli**, Irina Kitashvili, Viacheslav Sadykov, Alan Wray, Maria Kazachenko, Alexander Kosovichev, Gelu Nita, Valentín Martínez Pillet
2021
https://arxiv.org/pdf/2101.00011.pdf

The next decade will be a new exciting period for solar astrophysics, as new ground- and space-based instrumentation will provide unprecedented observations of the solar atmosphere and heliosphere. The synergy between modeling effort and comprehensive analysis of observations has great potential to shed light on the physical processes behind the observed phenomena. However, as we approach smaller scales in models and observations, challenges emerge that require the development of new approaches in both data analysis and numerical modeling. In this white paper, we summarize recent numerical achievements to reproduce structure, dynamics, and observed phenomena from the photosphere to the low corona and outline challenges we expect to face for the interpretation of future observations.

Comparing Radiative Transfer Codes and Opacity Samplings for Solar Irradiance Reconstructions

Serena **Criscuoli**, Matthias Rempel, Margit Haberreiter, Tiago M. D. Pereira, Han Uitenbroek & Damian Fabbian
Solar Physics volume 295, Article number: 50 (**2020**)
https://link.springer.com/content/pdf/10.1007/s11207-020-01614-2.pdf

Some techniques developed to reproduce solar irradiance variations make use of synthetic radiative fluxes of quiet and magnetic features. The synthesis of radiative fluxes of astronomical objects is likely to be affected by uncertainties resulting from approximations and specific input employed for the synthesis. In this work we compare spectra obtained with three radiative transfer codes with the purpose of investigating differences in reproducing

solar irradiance variations. Specifically, we compare spectral synthesis produced in non-local thermodynamic equilibrium obtained with COSI and RH using 1-D atmosphere models. We also compare local thermodynamic equilibrium syntheses emerging from 3-D MURaM simulations of the solar atmosphere obtained with two sets of opacity tables generated with the ATLAS9 package and with the RH code, and test the effects of opacity sampling on the emergent spectra. We find that, although the different codes and methodologies employed to synthesize the spectrum reproduce overall the observed solar spectrum with a similar degree of accuracy, subtle differences in quiet Sun spectra may translate into larger differences in the computation of the contrasts of magnetic features, which, in turn, critically affect the estimates of solar variability.

The correlation of synthetic UV color vs Mg II index along the solar cycle

Serena **Criscuoli**, Valentina Penza, Mija Lovric, Francesco Berrilli

ApJ **865** 22 **2018**

https://arxiv.org/pdf/1808.08439.pdf

Modeling of planets' climate and habitability requires as fundamental input the UV emission of the hosting star. \citet{lovric2017} employed SORCE/SOLSTICE solar observations to introduce a UV color index which is a descriptor of the UV radiation that modulates the photochemistry of planets atmospheres. After correcting the SOLSTICE data for residual instrumental effects that produced asymmetric signals during different phases of the cycles analyzed, the authors found that the UV color index is linearly correlated with the Mg II index.In this paper we employ an irradiance reconstruction technique to synthetize the UV color and Mg II index with the purpose of investigating whether the correction applied by \citet{lovric2017} to SORCE/SOLSTICE data might have compensated for solar variations, and to investigate the physical mechanisms that produce such a strong correlation between the UV color index and the solar activity. Reconstructed indices reproduce very well the observations and present the same strong linear dependence. Moreover our reconstruction, which extends back to 1989, shows that the UV color - Mg II index relation can be described by the same linear relation for almost three cycles, thus ruling out an overcompensation of SORCE/SOLTICE data in the analysis of \citet{lovric2017}. We suggest that the strong correlation between the indices results from the fact that most of the Far- and Middle- UV radiation originates in the chromosphere, where atmosphere models of quiet and magnetic features present similar temperature and density gradients.

Photometric Properties of Network and Faculae Derived from HMI Data Compensated for Scattered-Light

Serena **Criscuoli**, Aimee Norton, Taylor Whitney

ApJ **847** 93 **2017**

https://arxiv.org/pdf/1709.01593.pdf

We report on the photometric properties of faculae and network as observed in full-disk, scattered-light corrected images from the Helioseismic Magnetic Imager. We use a Lucy-Richardson deconvolution routine that corrects an image in less than one second. Faculae are distinguished from network through proximity to active regions. This is the first report that full-disk observations, including center-to-limb variations, reproduce the photometric properties of faculae and network observed previously only in sub-arcsecond resolution, small field-of-view studies, i.e. that network, as defined by distance from active regions, exhibit higher photometric contrasts. Specifically, for magnetic flux values larger than approximately 300 G, the network is brighter than faculae and the contrast differences increases toward the limb, where the network contrast is about twice the facular one. For lower magnetic flux values, network appear darker than faculae. Contrary to reports from previous full-disk observations, we also found that network exhibits a higher center-to-limb variation. Our results are in agreement with reports from simulations that indicate magnetic flux alone is a poor proxy of the photometric properties of magnetic features. We estimate that the contribution of faculae and network to Total Solar Irradiance variability of the current Cycle 24 is overestimated by at least 11\% due to the photometric properties of network and faculae not being recognized as different. This estimate is specific to the method employed in this study to reconstruct irradiance variations, so caution should be paid when extending it to other techniques.

A study of solar photospheric temperature gradient variation using limb darkening measurements

Serena **Criscuoli**, Peter Foukal

ApJ **835** 99 **2017**

https://arxiv.org/ftp/arxiv/papers/1611/1611.10201.pdf

The variation in area of quiet magnetic network measured over the sunspot cycle should modulate the spatially averaged photospheric temperature gradient, since temperature declines with optical depth more gradually in magnetic flux tube atmospheres. Yet, limb darkening measurements show no dependence upon activity level, even

at an rms precision of 0.04%. We study the sensitivity of limb darkening to changes in area filling factor using a 3D MHD model of the magnetized photosphere. The limb darkening change expected from the measured 11 yr area variation lies below the level of measured limb darkening variations, for a reasonable range of magnetic flux in quiet network and internetwork regions. So the remarkably constant limb darkening observed over the solar activity cycle is not inconsistent with the measured 11 year change in area of quiet magnetic network. Our findings offer an independent constraint on photospheric temperature gradient changes reported from measurements of the solar spectral irradiance from the Spectral Irradiance Monitor (SIM), and recently, from wavelength differential spectrophotometry using the Solar Optical Telescope (SOT) aboard the HINODE spacecraft.

Angular dependence of the facular-sunspot coverage relation as derived by MDI magnetograms

Serena **Criscuoli**
Solar Phys. Volume 291, Issue 7, pp 1957–1975 **2016**
http://arxiv.org/pdf/1606.04851v1.pdf
Previous studies have shown that the variation over the solar magnetic activity cycle of the area of facular/network features identified on broad band and narrow band imagery is positively correlated with the sunspot area and number, the relation between the area coverages being described as either linear or quadratic. On the other hand, the temporal variation of the spatial distributions of faculae, network and sunspots follows patterns that are less obviously correlated, so that we expect the relation that describes variation of the area coverage of different types of magnetic features to vary with the position over the disk. In this work we employ MDI full-disk magnetograms acquired during Cycle 23 and at the beginning of Cycle 24 to investigate the relation between the coverage of magnetic elements characterized by different amounts of magnetic flux and located at different angular distances from disk center with the sunspot number. In agreement with some previous studies we find that daily data are best described by a quadratic function while data averaged over 6-months are best described by a linear function. In both cases the coefficients of the fits show large dependence on the position over the disk and the magnetic flux. We also find that toward disk center 6-months averaged data show asymmetries between the ascending and the descending phase. Implications for solar irradiance modeling are discussed.

Interpretation of Solar Irradiance Monitor measurements through analysis of 3D MHD simulations

Serena **Criscuoli**, Han Uitenbroek
ApJ 788 151 **2014**
http://arxiv.org/pdf/1404.4651v1.pdf
Measurements from the Solar Irradiance Monitor (SIM) onboard the SORCE mission indicate that solar spectral irradiance at Visible and IR wavelengths varies in counter phase with the solar activity cycle. The sign of these variations is not reproduced by most of the irradiance reconstruction techniques based on variations of surface magnetism employed so far, and it is not clear yet whether SIM calibration procedures need to be improved, or if instead new physical mechanisms must be invoked to explain such variations. We employ three-dimensional magneto hydrodynamic simulations of the solar photosphere to investigate the dependence of solar radiance in SIM Visible and IR spectral ranges on variations of the filling factor of surface magnetic fields. We find that the contribution of magnetic features to solar radiance is strongly dependent on the location on the disk of the features, being negative close to disk center and positive toward the limb. If features are homogeneously distributed over a region around the equator (activity belt) then their contribution to irradiance is positive with respect to the contribution of HD snapshots, but decreases with the increase of their magnetic flux for average magnetic flux larger than 50 G in at least two of the Visible and IR spectral bands monitored by SIM. Under the assumption that the 50 G snapshots are representative of quiet Sun regions we find thus that the Spectral Irradiance can be in counter-phase with the solar magnetic activity cycle.

1D atmosphere models from inversion of Fe I 630 nm observations with an application to solar irradiance studies

A. **Cristaldi**, I. Ermolli
ApJ **2017**
https://arxiv.org/pdf/1705.02915.pdf
Present-day semi-empirical models of solar irradiance (SI) variations employ spectra computed on one-dimensional atmosphere models (1D models) representative of various solar surface features to reconstruct SI changes measured on timescales greater than a day. Various recent studies have, however, pointed out that the spectra synthesized on 1D models do not reflect the radiative emission of the inhomogenous atmosphere revealed by high-resolution solar observations. We aimed to derive observational-based atmospheres from such observations and test their accuracy

for SI estimates. We analysed spectro-polarimetric data of the Fe I 630 nm line pair on photospheric regions representative of the granular, quiet Sun pattern (QS) and of small- and large-scale magnetic features, both bright and dark with respect to the QS. The data were taken on 2011 August 6, with the CRISP at the Swedish Solar Telescope, under excellent seeing conditions. We derived atmosphere models of the observed regions from data inversion with the SIR code. We studied the sensitivity of results to spatial resolution and temporal evolution, and discussed the obtained atmospheres with respect to several 1D models. The atmospheres derived from our study agree well with most of the compared 1D models, both qualitatively and quantitatively (differences are within 10%), but for pore regions. Spectral synthesis computations on the atmosphere obtained from the QS observations return SI between 400 nm and 2400 nm that agrees, on average, within 2.2% with standard reference measurements, and within -0.14% with the SI computed on the quiet Sun atmosphere employed by the most advanced semi-empirical model of SI variations.

Solar structure and evolution **Review**

Jørgen **Christensen-Dalsgaard**
Living Reviews in Solar Physics volume 18, Article number: 2 (**2021**)
https://link.springer.com/content/pdf/10.1007/s41116-020-00028-3.pdf
https://doi.org/10.1007/s41116-020-00028-3
The Sun provides a critical benchmark for the general study of stellar structure and evolution. Also, knowledge about the internal properties of the Sun is important for the understanding of solar atmospheric phenomena, including the solar magnetic cycle. Here I provide a brief overview of the theory of stellar structure and evolution, including the physical processes and parameters that are involved. This is followed by a discussion of solar evolution, extending from the birth to the latest stages. As a background for the interpretation of observations related to the solar interior I provide a rather extensive analysis of the sensitivity of solar models to the assumptions underlying their calculation. I then discuss the detailed information about the solar interior that has become available through helioseismic investigations and the detection of solar neutrinos, with further constraints provided by the observed abundances of the lightest elements. Revisions in the determination of the solar surface abundances have led to increased discrepancies, discussed in some detail, between the observational inferences and solar models. I finally briefly address the relation of the Sun to other similar stars and the prospects for asteroseismic investigations of stellar structure and evolution.

On the hydrostatic stratification of the solar tachocline

J **Christensen-Dalsgaard** D O Gough E Knudstrup
Monthly Notices of the Royal Astronomical Society, Volume 477, Issue 3, 1 July **2018**, Pages 3845–3852,
https://sci-hub.tw/10.1093/mnras/sty752
We present an attempt to reconcile the solar tachocline glitch, a thin layer immediately beneath the convection zone in which the seismically inferred sound speed in the Sun exceeds corresponding values in standard solar models, with a degree of partial material mixing which we presume to have resulted from a combination of convective overshoot, wave transport, and tachocline circulation. We first summarize the effects either of modifying in the models the opacity in the radiative interior or of incorporating either slow or fast tachocline circulation. Neither alone is successful. We then consider, without physical justification, incomplete material redistribution immediately beneath the convection zone which is slow enough not to disturb radiative equilibrium. It is modelled simply as a diffusion process. We find that, in combination with an appropriate opacity modification, it is possible to find a density-dependent diffusion coefficient that removes the glitch almost entirely, with a radiative envelope that is consistent with seismology.

Multiple New or Updated Satellite Total Solar Irradiance (TSI) Composites (1978–2023)

Ronan **Connolly**1,2, Willie Soon1,3, Michael Connolly1,2, Rodolfo Gustavo Cionco4,5, Ana G. Elias6,7, Gregory W. Henry8, Nicola Scafetta9, and Víctor M. Velasco Herrera10
2024 ApJ 975 102
https://iopscience.iop.org/article/10.3847/1538-4357/ad7794/pdf
Several total solar irradiance (TSI) satellite missions have been carried out since 1978. None of these missions have lasted more than one to two solar cycles (SCs), and each mission implies a slightly different absolute TSI baseline. Nonetheless, several satellite composites have been developed by compositing satellite data from different missions to form an almost continuous daily record for the satellite era. However, disconcertingly, each mission has implied slightly different changes in TSI between consecutive solar minima and solar maxima. Some groups have developed adjustments to individual missions that have substantially reduced these differences. Others prefer to use the original data published by the satellite science teams. Some TSI composites average together conflicting records, while others prioritize specific records over others. Here, we compare four existing composites to 17 new alternative series based on the available satellite data. These 21 TSI series are statistically sorted into six groups of three to four series each. We found that the six groups suggest different intercycle trends between solar minima. We compare the

groups to eight daily resolved solar proxy-based TSI reconstructions and to daily sunspot numbers. Excellent agreement is obtained over one to two SCs, but significant differences are observed over longer timescales for each group. Therefore, we have assembled all these time series (old and new) into a large and new TSI data set for use by the scientific community. Versions scaled to 1 au (for studying solar variability) or in situ values at Earth (for studying solar/terrestrial interactions) are provided at daily, monthly, and yearly resolutions.

Interchange Reconnection: Remote Sensing of Solar Signature and Role in Heliospheric Magnetic Flux Budget **Review**

N. U. **Crooker**, M. J. Owens

Space Science Reviews, November **2012**, Volume 172, Issue 1-4, pp 201-208

Interchange reconnection at the Sun, that is, reconnection between a doubly-connected field loop and singly-connected or open field line that extends to infinity, has important implications for the heliospheric magnetic flux budget. Recent work on the topic is reviewed, with emphasis on two aspects. The first is a possible heliospheric signature of interchange reconnection at the coronal hole boundary, where open fields meet closed loops. The second aspect concerns the means by which the heliospheric magnetic field strength reached record-lows during the recent solar minimum period. A new implication of this work is that interchange reconnection may be responsible for the puzzling, occasional coincidence of the heliospheric current sheet and the interface between fast and slow flow in the solar wind.

Vortices evolution in the solar atmosphere: A dynamical equation for the swirling strength

J.R. Canivete **Cuissa**, O. Steiner

A&A 639, A118 **2020**

https://arxiv.org/pdf/2005.12871.pdf

https://www.aanda.org/articles/aa/pdf/2020/07/aa38060-20.pdf

We study vortex dynamics in the solar atmosphere by employing and deriving the analytical evolution equations of two vortex identification criteria. The two criteria used are vorticity and the swirling strength. Vorticity can be biased in the presence of shear flows, but its dynamical equation is well known; the swirling strength is a more precise criterion for the identification of vortical flows, but its evolution equation is not known yet. Therefore, we explore the possibility of deriving a dynamical equation for the swirling strength. We then apply the two equations to analyze radiative MHD simulations of the solar atmosphere produced with the CO5BOLD code. We present a detailed review of the swirling strength criterion and the mathematical derivation of its evolution equation. This equation did not exist in the literature before and it constitutes a novel tool that is suitable for the analysis of a wide range of problems in (magneto-)hydrodynamics. By applying this equation to numerical models, we find that hydrodynamical and magnetic baroclinicities are the driving physical processes responsible for vortex generation in the convection zone and the photosphere. Higher up in the chromosphere, the magnetic terms alone dominate. Moreover, we find that the swirling strength is produced at small scales in a chaotic fashion, especially inside magnetic flux concentrations. The swirling strength represents an appropriate criterion for the identification of vortices in turbulent flows, such as those in the solar atmosphere. Moreover, its evolution equation, which is derived in this paper, is pivotal for obtaining precise information about the dynamics of these vortices and the physical mechanisms responsible for their production and evolution. Since this equation is available, the swirling strength is now the ideal quantity to study the dynamics of vortices in (magneto-)hydrodynamics.

Innovative and automated method for vortex identification
II. Application to numerical simulations of the solar atmosphere

J. R. Canivete **Cuissa**1,2 and O. Steiner2,3

A&A 682, A181 (**2024**)

https://www.aanda.org/articles/aa/pdf/2024/02/aa46217-23.pdf

Context. Ubiquitous small-scale vortical motions are seen to occur in the solar atmosphere both in simulations and observations. They are thought to play a significant role in the local heating of the quiet chromosphere and corona. In a previous paper, we proposed a new method for the automated identification of vortices based on the accurate estimation of curvature centers; this method was implemented in the SWIRL algorithm.

Aims. We aim to assess the applicability of the SWIRL algorithm to self-consistent numerical simulations of the solar atmosphere. The highly turbulent and dynamical solar flow poses a challenge to any vortex-detection method. We also conduct a statistical analysis of the properties and characteristics of photospheric and chromospheric small-scale swirling motions in numerical simulations.

Methods. We applied the SWIRL algorithm to realistic, three-dimensional, radiative, magneto-hydrodynamical simulations of the solar atmosphere carried out with the CO5BOLD code. In order to achieve statistical validity, we analyzed 30 time instances of the simulation covering 2 h of physical time.

Results. The SWIRL algorithm accurately identified most of the photospheric and chromospheric swirls, which are perceived as spiraling instantaneous streamlines of the horizontal component of the flow. Part of the identified swirls form three-dimensional coherent structures that are generally rooted in magnetically dominated intergranular

lanes and extend vertically into the chromospheric layers. From a statistical analysis, we find that the average number densities of swirls in the photosphere and chromosphere are 1 Mm−2 and 4 Mm−2, respectively, while the average radius is 50 − 60 km throughout the simulated atmosphere. We also find an approximately linear correlation between the rotational speed of chromospheric swirls and the local Alfvén speed. We find evidence that more than 80% of the identified, coherent, vortical structures may be Alfvénic in nature.
Conclusions. The SWIRL algorithm is a reliable tool for the identification of vortical motions in magnetized, turbulent, and complex astrophysical flows. It can serve to expand our understanding of the nature and properties of swirls in the solar atmosphere. A statistical analysis shows that swirling structures may be smaller, more numerous, and may rotate faster than previously thought, and also suggests a tight relation between swirls and the propagation of Alfvénic waves in the solar atmosphere.

Tracking Solar Active Region Outflow Plasma from its Source to the near-Earth Environment

Len **Culhane**
Hinode/EIS Nuggets, Sept **2014**
http://solarb.mssl.ucl.ac.uk/SolarB/nuggets/nugget_2014sep.jsp
Following the discovery of persistent hot plasma upflows from the edges of solar active regions (ARs) by Hinode/XRT (Sakao et al., 2007) and EIS (Harra et al. 2008), much effort has been devoted to their study given the possibility that they may in fact be outflows and therefore contributors to the slow solar wind (SSW).
AR expansion drives reconnection at QSLs between the AR closed loops and the large-scale network fields East of the AR.
Additional diffusion of the photospheric AR field forces interchange reconnection at null N1 of the large-scale field lines anchored to the North-West of the AR with the open ones in the neighborhood of the northern negative CH.

A Poynting-Robertson-like drag at the Sun's surface

Ian **Cunnyngham**, Marcelo Emilio, Jeff Kuhn, Isabelle Scholl, Rock Bush
Physical Review Letters **2016**
https://arxiv.org/pdf/1612.00873v1.pdf
The Sun's internal rotation {\Omega}(r,{\Theta}) has previously been measured using helioseismology techniques and found to be a complex function of co-latitude, {\theta}, and radius, r. From helioseismology and observations of apparently "rooted" solar magnetic tracers we know that the surface rotates more slowly than much of the interior. The cause of this slow-down is not understood but it is important for understanding stellar rotation generally and any plausible theory of the solar interior. A new analysis using 5-min solar p-mode limb oscillations as a rotation "tracer" finds an even larger velocity gradient in a thin region at the top of the photosphere. This shear occurs where the solar atmosphere radiates energy and angular momentum. We suggest that the net effect of the photospheric angular momentum loss is similar to Poynting-Robertson "photon braking" on, for example, Sun-orbiting dust. The resultant photospheric torque is readily computed and, over the Sun's lifetime, is found to be comparable to the apparent angular momentum deficit in the near-surface shear layer.

Historical Heliophysical Series of the Ebro Observatory

J. J. **Curto**, J. G. Solé, M. Genescà, M. J. Blanca, J. M. Vaquero
Solar Phys. Volume 291, Issue 9, pp 2587–2607 **2016**
We present the contents of the historical heliophysical series collected at the Ebro Observatory, as well as the actions carried out to restore and save these data and to conserve the physical media containing the data and the telescopes that helped to obtain them. We also discuss the results obtained with these measurements, describe how we disseminated them, and report on the investigations that we have carried out with this information. We show the evolution of the local solar indices such as the Ebro Sunspot Number (ESN), the Ebro Group Sunspot Number (EGSN), or the Ebro Sunspot Area (ESA), which are derived directly from our data. For verification purposes, these local solar indices have been compared to the international sunspot numbers published by SILSO. Our data are reliable and correlate well with the respective international series. Finally, as an example of the possibilities that the Ebro series offer, we explain the use of these data to elucidate one of the recent problems in solar physics: the discontinuity in international data known as the Waldmeier discontinuity and, in general, the ratio between sunspots and sunspot groups. In the Ebro Observatory series, no discontinuity such as this is detected. We instead observe a rather stable ratio in the spot or group rates. This result is in agreement with the hypothesis of Svalgaard (2010, ASP CS-428, 297) that the Waldmeier discontinuity is produced only on a procedural level, perhaps by a change in the criteria used in Zürich by Waldmeier or by changing external conditions.

Using eigenmode-mixing to measure or constrain the Sun's interior B-field

Curt **Cutler**

ApJ **2017**
https://arxiv.org/pdf/1706.07404.pdf
Understanding the generation and distribution of the Sun's interior magnetic (B-) field is a longstanding challenge. Here we describe how measurements of the Sun's oscillation eigenfunctions might be used to measure the Sun's interior B-field. The B-field induces mode-mode couplings, causing the angular patterns of the eigenfunctions to differ from simple Y_{lm}'s We concentrate on the magnetic coupling between modes with the same (n,l) values and different but nearby m-values, since these non-axisymmetric couplings clearly cannot be due to the Sun's axisymmetric rotation and since for these cases, mode mixing is enhanced by the near-degeneracy of the mode frequencies. We analyze magnetically-induced mode mixing in two stages of increasing complexity: first neglecting mode damping, and then incorporating realistic damping rates. We introduce a novel detection statistic that tests for the presence of non-axisymmetric mode-mixing in Solar Doppler data. We show that our detection statistic is naturally robust against spatial aliasing. We estimate our statistic's signal-to-noise ratio (SNR) as a function of the mode-mixing amplitude. While B-induced mode-mixing is probably not detectable in a single mode pair, we argue that the phase of the B-induced mixing should be approximately the same across a wide range of modes. The total SNR then grows roughly as Np^{1/2}, where Np is the number of mode pairs. We conclude that B-induced mode-mixing should be detectable for a fairly wide range of B-field magnitudes and geometries.

Solar energetic particle warnings from a coronagraph

O. C. St. **Cyr**, A. Posner, J. T. Burkepile
Space Weather Volume 15, Issue 1 January **2017** Pages 240–257
http://sci-hub.cc/10.1002/2016SW001545
We report here the concept of using near-real time observations from a coronagraph to provide early warning of a fast coronal mass ejection (CME) and the possible onset of a solar energetic particle (SEP) event. The **1 January 2016**, fast CME, and its associated SEP event are cited as an example. The CME was detected by the ground-based K-Cor coronagraph at Mauna Loa Solar Observatory and by the SOHO Large Angle and Spectrometric Coronagraph. The near-real-time availability of the high-cadence K-Cor observations in the low corona leads to an obvious question: "Why has no one attempted to use a coronagraph as an early warning device for SEP events?" The answer is that the low image cadence and the long latency of existing spaceborne coronagraphs make them valid for archival studies but typically unsuitable for near-real-time forecasting. The January 2016 event provided favorable CME viewing geometry and demonstrated that the primary component of a prototype ground-based system for SEP warnings is available several hours on most days. We discuss how a conceptual CME-based warning system relates to other techniques, including an estimate of the relative SEP warning times, and how such a system might be realized.

2. Existing SEP Forecasting Techniques

Complex Network for Solar Active Regions

Farhad **Daei**, Hossein Safari, Neda Dadashi
2017
https://arxiv.org/pdf/1707.02371.pdf
Here, we developed a complex network of solar active regions (ARs) to study various local and global properties of the network. The values of the Hurst exponent (0.8−0.9) were evaluated by both the detrended fluctuation analysis and the rescaled range analysis applied on the time series of the AR numbers. The findings suggest that ARs can be considered as a system of self-organized criticality. We constructed a growing network based on locations, occurrence times, and the lifetimes of 4,227 ARs recorded from 1 January 1999 to 14 April 2017. The behaviour of the clustering coefficient shows that the ARs network is not a random network. The logarithmic behaviour of the length scale has the characteristics of a so-called \textquotedblleft small-world network\textquotedblright. It is found that the probability distribution of the node degrees for undirected networks follows the power-law with exponents of about 3.7 to 4.2. This indicates the scale-free nature of the ARs network. The scale-free and small-world properties of the ARs network confirm that the system of ARs forms a system of self-organized criticality. Our results show that the occurrence probability of flares (classified by GOES class C >5, M, and X flares) in the position of the ARs network hubs take values greater than that obtained for other nodes.

Intercycle and intracycle variation of halo CME rate obtained from SOHO/LASCO observations

Fithanegest Kassa **Dagnew**, Nat Gopalswamy, Solomon Belay Tessema, Sachiko Akiyama, Seiji Yashiro, Tesfay Yemane Tesfu
ApJ **903** 118 **2020**
https://arxiv.org/ftp/arxiv/papers/2009/2009.06033.pdf

https://doi.org/10.3847/1538-4357/abb887
We report on the properties of halo coronal mass ejections (HCMEs) in solar cycles 23 and 24. We compare the HCMEs properties between the corresponding phases (rise, maximum, and declining) in cycles 23 and 24 in addition to comparing those between the whole cycles. Despite the significant decline in the sunspot number (SSN) in cycle 24, which dropped by 46% with respect to cycle 23, the abundance of HCMEs is similar in the two cycles. The HCME rate per SSN is 44% higher in cycle 24. In the maximum phase, cycle-24 rate normalized to SSN increased by 127% while the SSN dropped by 43%. The source longitudes of cycle-24 HCMEs are more uniformly distributed than those in cycle 23. We found that the average sky-plane speed in cycle 23 is ~16% higher than that in cycle 24. The size distributions of the associated flares between the two cycles and the corresponding phases are similar. The average speed at a central meridian distance (CMD) = 600 for cycle 23 is ~28% higher than that of cycle 24. We discuss the unusual bump in HCME activity in the declining phase of cycle 23 as due to exceptional active regions that produced many CMEs during October 2003 to October 2005. The differing HCME properties in the two cycles can be attributed to the anomalous expansion of cycle-24 CMEs. Considering the HCMEs in the rise, maximum and declining phases, we find that the maximum phase shows the highest contrast between the two cycles.

PONDEROMOTIVE ACCELERATION IN CORONAL LOOPS

R. B. **Dahlburg**[1], J. M. Laming[2], B. D. Taylor[3], and K. Obenschain
2016 *ApJ* **831** 160
Ponderomotive acceleration has been asserted to be a cause of the first ionization potential (FIP) effect, the well-known enhancement in abundance by a factor of 3–4 over photospheric values of elements in the solar corona with FIP less than about 10 eV. It is shown here by means of numerical simulations that ponderomotive acceleration occurs in solar coronal loops, with the appropriate magnitude and direction, as a "by-product" of coronal heating. The numerical simulations are performed with the HYPERION code, which solves the fully compressible three-dimensional magnetohydrodynamic equations including nonlinear thermal conduction and optically thin radiation. Numerical simulations of coronal loops with an axial magnetic field from 0.005 to 0.02 T and lengths from 25,000 to 75,000 km are presented. In the simulations the footpoints of the axial loop magnetic field are convected by random, large-scale motions. There is a continuous formation and dissipation of field-aligned current sheets, which act to heat the loop. As a consequence of coronal magnetic reconnection, small-scale, high-speed jets form. The familiar vortex quadrupoles form at reconnection sites. Between the magnetic footpoints and the corona the reconnection flow merges with the boundary flow. It is in this region that the ponderomotive acceleration occurs. Mirroring the character of the coronal reconnection, the ponderomotive acceleration is also found to be intermittent.

Electron acceleration and small-scale coherent structure formation by an Alfvén wave propagating in coronal interplume region

K. **Daiffallah**, F. Mottez
Astronomische Nachrichten **2017, 2019**
http://sci-hub.cc/10.1002/asna.201713364
https://arxiv.org/pdf/1904.12224.pdf
We use the 2.5-D electromagnetic particle-in-cell simulation code to investigate the acceleration of electrons in solar coronal holes through the interaction of Alfvén waves with an interplume region. The interplume is modeled by cavity density gradients that are perpendicular to the background magnetic field. The aim is to help explain the observation of suprathermal electrons under a relatively quiet Sun. Simulations show that Alfvén waves interacting with the interplume region give rise to a strong local electric field that accelerates electrons in the direction parallel to the background magnetic field. Suprathermal electron beams and small-scale coherent structures are observed within interplume of strong density gradients. These features result from the nonlinear evolution of the electron beam plasma instability.

f-mode interaction with models of sunspot : near-field scattering and multi-frequency effects

Khalil **Daiffallah**
MNRAS Volume 460, Issue 1, p.1077-1085 **2016**
http://arxiv.org/pdf/1605.01248v1.pdf
We use numerical simulations to investigate the interaction of an f-mode wave packet with small and large models of a sunspot in a stratified atmosphere. While a loose cluster model has been largely studied before, we focus in this study on the scattering from an ensemble of tightly compact tubes. We showed that the small compact cluster produces a slight distorted scattered wave field in the transverse direction, which can be attributed to the simultaneous oscillations of the pairs of tubes within the cluster aligned in a perpendicular direction to the incoming wave. However, no signature of a multiple-scattering regime has been observed from this model, while it has been clearly observable for the large compact cluster model. Furthermore, we pointed out the importance of the

geometrical shape of the monolithic model on the interaction of f-mode waves with a sunspot in a high frequency range (ν= 5 mHz). These results are a contribution to the observational effort to distinguish seismically between different configurations of magnetic flux tubes within sunspots and plage.

Chromospheric swirls

I. Automated detection in Hα observations and their statistical properties⋆

I. **Dakanalis**1,2, G. Tsiropoula2, K. Tziotziou2 and I. Kontogiannis3
A&A 663, A94 (**2022**)
https://www.aanda.org/articles/aa/pdf/2022/07/aa43236-22.pdf
Context. Chromospheric swirls are related to convectively driven vortex flows and considered to play a significant role in the dynamics and heating of the upper solar atmosphere. It is important to automatically detect and track them in chromospheric observations and determine their properties.
Aims. We aim to detect and track chromospheric swirls both in space and time by applying a newly developed novel automated method on high quality time series of Hα observations and to conduct a statistical analysis to determine their properties.
Methods. We applied a recently developed automated chromospheric swirl detection method to time-series observations of a quiet region of the solar chromosphere obtained in the Hα-0.2 Å wavelength of the Hα spectral line by the CRISP instrument at the Swedish 1-m Solar Telescope. The algorithm exploits the morphological characteristics of swirling events in high contrast chromospheric observations and results in the detection of these structures in each frame of the time series and their tracking over time. We conducted a statistical analysis to determine their various properties, including a survival analysis for deriving the mean lifetime.
Results. A mean number of 146 ± 9 swirls was detected within the Hα-0.2 Å field of view at any given time. The mean surface density is found equal to ∼0.08 swirls Mm−2 and the occurrence rate is ∼10−2 swirls Mm−2 min−1. These values are much higher than those previously reported from chromospheric observations. The radii of the detected swirls range between 0.5 and 2.5 Mm, with a mean value equal to 1.3 ± 0.3 Mm, which is slightly higher than previous reports. The lifetimes range between 1.5 min and 33.7 min (equal to the duration of the observations) with an arithmetic mean value of ∼8.5 min. A survival analysis of the lifetimes, however, using the Kaplan-Meier estimator in combination with a parametric model results in a mean lifetime of 10.3 ± 0.6 min.
Conclusions. Swirls are ubiquitous in the solar chromosphere. An automated method sheds more light on their abundance than visual inspection, while higher cadence, higher resolution observations will most probably result in the detection of a higher number of such features on smaller scales and with shorter lifetimes. **August 13, 2019**

Automated Detection of Chromospheric Swirls Based on Their Morphological Characteristics

Ioannis **Dakanalis**, Georgia Tsiropoula, Kostas Tziotziou & Konstantinos Koutroumbas
Solar Physics volume 296, Article number: 17 (**2021**)
https://link.springer.com/content/pdf/10.1007/s11207-020-01748-3.pdf
High-resolution observations have revealed that rotating structures known as “chromospheric swirls” are ubiquitous in the solar chromosphere. These structures have circular or spiral shapes, are present across a broad range of spatial and temporal scales and are considered as viable candidates for providing an alternative mechanism for the heating of the chromosphere and corona. Therefore, an accurate determination of their number and a statistical study of their physical properties are deemed necessary. In this work we present a novel, automated swirl detection method, which utilizes image pre-processing, curved structure tracing and machine learning techniques that allow for the detection of swirling events based on their morphological features as they appear in chromosphere filtergrams. The method is applied to Hαα chromospheric spectral line images obtained by the CRisp Imaging Spectropolarimeter (CRISP) at the Swedish 1-m Solar Telescope (SST). It is also tested on grayscale images of vortical sea current flows represented/visualized by synthetic streamlines from the NASA/Goddard Space Flight Center Scientific Visualization Studio. The results are rather encouraging since swirling events are successfully identified. Further improvements of the algorithm, its prospects for the detection and statistical studies of the properties of these events using a wide range of imaging data and its potential application in other scientific fields for the detection of rotating motions are discussed. **June 7, 2014**

IRIS2+: A comprehensive database of stratified thermodynamic models in the low solar atmosphere

Alberto Sainz **Dalda**, Aaryan Agrawal, Bart De Pontieu, M. Gosic
ApJ **2022**
https://arxiv.org/pdf/2211.09103.pdf
Our knowledge of the low solar atmosphere, i.e., the photosphere and chromosphere, is based on the knowledge gained from the observations and the theoretical and numerical modeling of these layers. In this sense, the thermodynamical and magnetic semi-empirical models of the solar atmosphere have significantly contributed to the advance in the understanding of the physics of the Sun. In the past, many of these models have been used as a

reference that helps us to, e.g., constrain the theoretical and numerical modeling, or to verify the goodness of physical parameters obtained from the inversion of the spectral lines. Nevertheless, semi-empirical models are quite limited by the assumptions that are inherent to the approach and do not necessarily provide an accurate view of the instantaneous and local thermodynamic conditions in the solar atmosphere. In this work, we provide an extensive collection of thermodynamic model atmospheres for active regions (ARs) obtained from the simultaneous inversion of 6 lines sensitive to changes in the thermodynamical conditions in the chromosphere, and another 6 lines sensitive to changes in the thermodynamical conditions in the photospere. These inversions were made using 320 representative profiles (RP) obtained by clustering the profiles in the umbra, penumbra, pore-like, plage, and surrounding quiet-sun in 126 active regions. Due to the simultaneous inversion of the selected lines, the resulting representative model atmosphere (RMA) samples the thermodynamics from the bottom of the photosphere to the top of the chromosphere. As a result, this database, named IRIS2+ and formed by 40,320 RP-RMA pairs, represents the most comprehensive collection of stratified-in-optical-depth thermodynamic models of the low solar atmosphere.

Recovering Thermodynamics from Spectral Profiles observed by IRIS: A Machine and Deep Learning Approach

Alberto Sainz **Dalda**, Jaime de la Cruz Rodríguez, Bart De Pontieu, Milan Gošić
ApJL 875 L18 **2019**
https://arxiv.org/pdf/1904.08390.pdf
Inversion codes allow reconstructing a model atmosphere from observations. With the inclusion of optically thick lines that form in the solar chromosphere, such modelling is computationally very expensive because a non-LTE evaluation of the radiation field is required. In this study, we combine the results provided by these traditional methods with machine and deep learning techniques to obtain similar-quality results in an easy-touse, much faster way. We have applied these new methods to Mg II h&k lines observed by IRIS. As a result, we are able to reconstruct the thermodynamic state (temperature, line-of-sight velocity, non-thermal velocities, electron density, etc.) in the chromosphere and upper photosphere of an area equivalent to an active region in a few CPU minutes, speeding up the process by a factor of 105-106. The open-source code accompanying this paper will allow the community to use IRIS observations to open a new window to a host of solar phenomena. **January 14, 2016**

Heating and cooling in stellar coronae: coronal rain on a young Sun

Simon **Daley-Yates**, Moira M Jardine, Craig D Johnston
MNRAS, Volume 526, Issue 2, **2023**, Pages 1646–1656,
https://doi.org/10.1093/mnras/stad2752
https://watermark.silverchair.com/stad2752.pdf
Recent observations of rapidly rotating cool dwarfs have revealed H α line asymmetries indicative of clumps of cool, dense plasma in the stars' coronae. These clumps may be either long-lived (persisting for more than one stellar rotation) or dynamic. The fastest dynamic features show velocities greater than the escape speed, suggesting that they may be centrifugally ejected from the star, contributing to the stellar angular momentum loss. Many, however, show lower velocities, similar to coronal rain observed on the Sun. We present 2.5D magnetohydrodynamic simulations of the formation and dynamics of these condensations in a rapidly rotating (Prot = 1 d) young Sun. Formation is triggered by excess surface heating. This pushes the system out of thermal equilibrium and triggers a thermal instability. The resulting condensations fall back towards the surface. They exhibit quasi-periodic behaviour, with periods longer than typical periods for solar coronal rain. We find line-of-sight velocities for these clumps in the range of 50 km s−1 (blueshifted) to 250 km s−1 (redshifted). These are typical of those inferred from stellar H α line asymmetries, but the inferred clump masses of 3.6 × 1014 g are significantly smaller. We find that a maximum of 3 per cent of the coronal mass is cool clumps. We conclude that coronal rain may be common in solar-like stars, but may appear on much larger scales in rapid rotators.

A comparative study of non-deep learning, deep learning, and ensemble learning methods for sunspot number prediction

Yuchen **Dang**, Ziqi Chen, Heng Li, Hai Shu
2022
https://arxiv.org/pdf/2203.05757.pdf
Solar activity has significant impacts on human activities and health. One most commonly used measure of solar activity is the sunspot number. This paper compares three important non-deep learning models, four popular deep learning models, and their five ensemble models in forecasting sunspot numbers. Our proposed ensemble model XGBoost-DL, which uses XGBoost as a two-level nonlinear ensemble method to combine the deep learning models, achieves the best forecasting performance among all considered models and the NASA's forecast. Our XGBoost-DL forecasts a peak sunspot number of 133.47 in May 2025 for Solar Cycle 25 and 164.62 in November 2035 for Solar Cycle 26, similar to but later than the NASA's at 137.7 in October 2024 and 161.2 in December 2034.

Ludendorff Coronal Flattening Index of the Total Solar Eclipse on March 9, 2016

Tiar **Dani**, Rhorom Priyatikanto, Abdul Rachman
International Symposium on Sun, Earth, and Life **2016**
https://arxiv.org/pdf/1610.07704v1.pdf

Ludendorff coronal flattening index of the Total Solar Eclipse (TSE) on March 9, 2016, was calculated at various distances in solar radius. As a result, we obtained the coronal flattening index (ϵ=a+b) at a distance of 2 solar radii is 0.16. The 24th solar cycle phase based on the 2016 TSE event obtained -0.64 which showed the corona is pre-minimum type. Resulted coronal flattening index value gives a predicted maximum amplitude of the monthly sunspot number (W
max) for the 25th solar cycle to be 70±65. Therefore, the solar activity for 25th solar cycle predicted to be lower than the current solar cycle, which has a maximum sunspot number value of 146 in February 2014

Modeling of Chromospheric Features and Dynamics in Solar Plage

Sanja **Danilovic**
Adv. Space Res. **2022**
https://arxiv.org/pdf/2208.03744.pdf

The chromosphere is a dynamic and complex layer where all the relevant physical processes happen on very small spatio-temporal scales. A few spectral lines that can be used as chromospheric diagnostics give us convoluted information that is hard to interpret without realistic theoretical models. What are the key ingredients that these models need to contain? The magnetic field has a paramount effect on chromospheric structuring. This is obvious from the ubiquitous presence of chromospheric dynamic fibrilar structures visible on the solar disk and at the limb. The numerical experiments presented in this manuscript illustrate the present state of modeling. They showcase to what extent our models reproduce various chromospheric features and their dynamics. The publication describes the effect different ingredients have on chromospheric models and provides a recipe for building one-to-one models. Combining these models with observations will provide insight into the physical processes that take place in the solar atmosphere.

Simulating Ellerman bomb-like events

S. **Danilovic**
A&A 601, A122 (**2017**)
https://www.aanda.org/articles/aa/pdf/2017/05/aa30403-17.pdf

Context. Ellerman bombs (EB) seem to be a part of a whole spectrum of phenomena that might have the same underlying physical mechanism: magnetic reconnection.
Aims. The aim of this study is to investigate whether the proposed mechanism, applied to the circumstances of EBs, produces the observed characteristics.
Methods. To this end, comprehensive three-dimensional magnetohydrodynamic (3D MHD) simulations were used. Two different cases are presented: the quiet Sun and an active region.
Results. Both runs confirm that EB-like brightenings coincide with hot and dense plasma, which is in agreement with predictions of 1D and 2D modellings. The simulated EB-like phenomena assume the observed flame-like form which depends on the complexity of the ongoing reconnection and the viewing angle. At the layers sampled by Hα-wings, near temperature minimum and below, the magnetic field topology seems always to be the same. The field lines there trace the base of the current sheet and the reconnected Ω-loops.
Conclusions. The EB features are caused by reconnection of strong-field patches of opposite polarity in the regions where the surface flows are the strongest. The weakest cases among them can be reproduced quantitatively by the current simulations.

Observed and simulated power spectra of kinetic and magnetic energy retrieved with 2D inversions

S. **Danilovic**1, M. Rempel2, M. van Noort1 and R. Cameron
A&A 594, A103 (**2016**)

Context. Information on the origin of internetwork magnetic field is hidden at the smallest spatial scales.
Aims. We try to retrieve the power spectra with certainty to the highest spatial frequencies allowed by current instrumentation.
Methods. To accomplish this, we use a 2D inversion code that is able to recover information up to the instrumental diffraction limit.
Results. The retrieved power spectra have shallow slopes that extend further down to much smaller scales than has been found before. They do not seem to show any power law. The observed slopes at subgranular scales agree with

those obtained from recent local dynamo simulations. Small differences are found for the vertical component of kinetic energy that suggest that observations suffer from an instrumental effect that is not taken into account. Conclusions. Local dynamo simulations quantitatively reproduce the observed magnetic energy power spectra on the scales of granulation down to the resolution limit of Hinode/SP, within the error bars inflicted by the method used and the instrumental effects replicated.

Photospheric response to EB-like event

S. **Danilovic**, S. K. Solanki, P. Barthol, A. Gandorfer, L. Gizon, J. Hirzberger, T. L. Riethmüller M. van Noort, J. Blanco Rodríguez, J. C. Del Toro Iniesta, D. Orozco Suárez, W. Schmidt, V. Martínez Pillet, M. Knölker

ApJS **2016**

http://arxiv.org/pdf/1609.03817v1.pdf

Ellerman Bombs are signatures of magnetic reconnection, which is an important physical process in the solar atmosphere. How and where they occur is a subject of debate. In this paper we analyse Sunrise/IMaX data together with 3D MHD simulations that aim to reproduce the exact scenario proposed for the formation of these features. Although the observed event seems to be more dynamic and violent than the simulated one, simulations clearly confirm the basic scenario for the production of EBs. The simulations also reveal the full complexity of the underlying process. The simulated observations show that the Fe I 525.02 nm line gives no information on the height where reconnection takes place. It can only give clues about the heating in the aftermath of the reconnection. The information on the magnetic field vector and velocity at this spatial resolution is, however, extremely valuable because it shows what numerical models miss and how they can be improved. **June 12th 2013**

Variation of the Mn I 539.4 nm line with the solar cycle

S. **Danilovic**, S.K. Solanki, W. Livingston, N. Krivova, I. Vince

A&A **2015**

http://arxiv.org/pdf/1511.01286v1.pdf

As a part of the long-term program at Kitt Peak National Observatory (KPNO), the Mn I 539.4 nm line has been observed for nearly three solar cycles using the McMath telescope and the 13.5 m spectrograph in double-pass mode. These full-disk spectrophotometric observations revealed an unusually strong change of this line's parameters over the solar cycle. Optical pumping by the Mg II k line was originally proposed to explain these variations. More recent studies have proposed that this is not required and that the magnetic variability might explain it. Magnetic variability is also the mechanism that drives the changes in total solar irradiance variations (TSI). With this work we investigate this proposition quantitatively by using using the model SATIRE-S. We applied exactly the same model atmospheres and value of the free parameter as were used in previous solar irradiance reconstructions to now model the variation in the Mn I 539.4 nm line profile and in neighboring Fe I lines. We compared the results of the theoretical model with KPNO observations. Our result confirms that optical pumping of the Mn I 539.4 nm line by Mg II k is not the main cause of its solar cycle change. It also provides independent confirmation of solar irradiance models which are based on the assumption that irradiance variations are caused by the evolution of the solar surface magnetic flux. The result obtained here also supports the spectral irradiance variations computed by these models.

Simulated magnetic flows in the solar photosphere⋆

S. **Danilovic**1, R. H. Cameron1 and S. K. Solanki

A&A 574, A28 (**2015**)

Context. Recent Sunrise/IMaX observations have revealed supersonic magnetic flows.
Aims. Our aim is to determine the origin of these flows by using realistic magnetohydrodynamics simulations.
Methods. We simulated cancellation and emergence of magnetic flux through the solar photosphere. Our first numerical experiment started with a magnetic field of both polarities. To simulate emergence into a region with pre-existing field, we introduced a large-scale horizontally uniform sheet of a horizontal field. We followed the subsequent evolution and created synthetic polarimetric observations, including known instrumental effects of the Sunrise/IMaX and Hinode/SP instruments. We compared the simulated and observed spectropolarimetric signals.
Results. Strongly blue- and redshifted Stokes V signals are produced in locations where strong line-of-sight velocities coincide with the strong line-of-sight component of the magnetic field. The size and strength of simulated events is smaller than observed, and they are mostly associated with downflows, contrary to observations. In a few cases where they appear above a granule, single blue-lobed Stokes V are produced by strong gradients in magnetic field and velocity. No change of magnetic field sign is detected along the line of sight in these instances. More high-speed magnetised flows occurred when an emergence was simulated than when no horizontal field was added.
Conclusions. The simulations indicate that the observed events result from magnetic flux emergences in which reconnection may take place, but does not seem to be necessary.
The movies are available in electronic form at http://www.aanda.org

The GOES-R Solar UltraViolet Imager

Jonathan M. **Darnel**,Daniel B. Seaton,Christian Bethge,Laurel Rachmeler,Alison Jarvis,Steven M. Hill,Courtney L. Peck,J. Marcus Hughes,Jason Shapiro … See all authors

Space Weather **Volume20, Issue4** e2022SW003044 **2022**

https://doi.org/10.1029/2022SW003044

https://agupubs.onlinelibrary.wiley.com/doi/epdf/10.1029/2022SW003044

The four Solar UltraViolet Imagers on board the GOES-16 and GOES-17 and the upcoming GOES-T and GOES-U weather satellites serve as NOAA's operational solar coronal imagers. These four identically designed solar EUV instruments are similar in design and capability to the SDO-AIA suite of solar telescopes, and are planned to operationally span two solar cycles or more, from 2017 through 2040. We present the concept of operations for the SUVI instruments, operational requirements, and constraints. The reader is also introduced to the instrument design, testing, and performance characteristics. Finally, the various data products are described along with their potential utility to the operational user or researcher. **21 Aug 2017, 10 Sep 2017, 29 Nov 2020, 29 Apr 2021**

A theoretic analysis of magnetoactive GES-based turbulent solar plasma instability

Souvik **Das**, Ahmed Atteya, Pralay Kumar Karmakar

MNRAS, Volume 523, Issue 4, August **2023**, Pages 5635–5660,

https://doi.org/10.1093/mnras/stad1664

A recently reported gravito-electrostatic sheath (GES) model is procedurally applied to study the turbumagnetoactive helioseismic oscillation features in the entire bi-fluidic solar plasma system. The bounded solar interior plasma (SIP, internally self-gravitating), and the unbounded solar wind plasma (SWP, externally point-gravitating) are coupled through the interfacial diffused solar surface boundary (SSB) due to an exact gravito-electrostatic interplay. A numerical platform on the developed theoretic formalism reveals the evolution of both dispersive and non-dispersive features of the modified GES mode fluctuations in new parametric windows. Different colourspectral profiles exhibit important features of the GES-based SIP–SWP perturbations elaborately. It is illustratively shown that the thermostatistical GES stability depends mainly on the radial distance, magnetic field, equilibrium plasma density, and plasma temperature. We see that their dispersive features are more pertinently pronounced in the self-gravitational domains (SIP) than the electrostatic counterparts (SWP). Besides, different characteristic parameters with accelerating (or decelerating) and stabilizing (or destabilizing) effects influencing the entire solar plasma stability are illustratively portrayed. We speculate that, in the SIP, the long-wave (gravitational-like) helioseismic fluctuations become highly dispersive showing more propagatory nature than the shorter ones (acoustic-like). The short waves show more propagatory propensity than the longer ones in the SSB and SWP regime. The reliability of our proposed investigation is bolstered along with the tentative applicability and future scope in light of the current solar observational scenarios, such as SOHO, STEREO, SDO, PSP, and SolO.

Minuscule corrections to near-surface solar internal rotation using mode-coupling

Srijan Bharati **Das**, Samarth G. Kashyap, Deniz Oktay, Shravan M. Hanasoge, Jeroen Tromp

Astrophysical Journal Supplement Series **2023**

https://arxiv.org/pdf/2303.13699.pdf

The observed solar oscillation spectrum is influenced by internal perturbations such as flows and structural asphericities. These features induce splitting of characteristic frequencies and distort the resonant-mode eigenfunctions. Global axisymmertric flow -- differential rotation -- is a very prominent perturbation. Tightly constrained rotation profiles as a function of latitude and radius are products of established helioseismic pipelines that use observed Dopplergrams to generate frequency-splitting measurements at high precision. However, the inference of rotation using frequency-splittings do not consider the effect of mode-coupling. This approximation worsens for high-angular-degree modes, as they become increasingly proximal in frequency. Since modes with high angular degrees probe the near-surface layers of the Sun, inversions considering coupled modes could potentially lead to more accurate estimates of rotation very close to the surface. In order to investigate if this is indeed the case, we perform inversions for solar differential rotation, considering coupling of modes for angular degrees $160 \leq \ell \leq 300$ in the surface gravity f-branch and first-overtone p modes. In keeping with the character of mode coupling, we carry out a non-linear inversion using an eigenvalue solver. Differences in inverted profiles for frequency splitting measurements from MDI and HMI are compared and discussed. We find that corrections to the near-surface differential rotation profile, when accounting for mode-coupling effects, are smaller than 0.003 nHz and hence are insignificant. These minuscule corrections are found to be correlated with the solar cycle. We also present corrections to even-order splitting coefficients, which could consequently impact inversions for structure and magnetic fields.

Non-planar magnetoactive GES-based solar plasma stability

Souvik **Das**, Pralay Kumar Karmakar
A&A **2022**
https://arxiv.org/pdf/2207.14618
A laboratory plasma-wall interaction-based astrophysical gravito-electrostatic sheath (GES) model is methodologically applied to study the dynamic stability of the magnetoactive bi-fluidic solar plasma system in the presence of turbulence effect. The spherically symmetric GES-model formalism couples the solar interior plasma (SIP, internally self-gravitating, bounded) and the solar wind plasma (SWP, externally point-gravitating, unbounded) through the diffused solar surface boundary (SSB). A normal spherical mode ansatz results in a generalized linear quadratic dispersion relation depicting the modal fluctuations on both the SIP and SWP scales. A constructive numerical platform reveals the evolution of both dispersive and non-dispersive modal features of the modified-GES mode excitations. The reliability of the derived non-planar dispersion laws is concretized with the help of an exact analytic shape matching the previously reported results founded on the plane-wave approximation. It is found that the thermo-statistical GES stability depends mainly on the magnetic field, equilibrium plasma density, and plasma temperature. It is speculated that the dispersive features are more pronounced in the self-gravitational domains against the electrostatic ones. The magneto-thermal interplay introduces decelerating (accelerating) and destabilizing (stabilizing) influences on the SIP (SWP), and so forth. At last, we briefly indicate the applicability of the proposed analysis to understand diverse helioseismic activities from the collective plasma dynamical viewpoint in accordance with the recent astronomical observational scenarios reported in the literature.

Is the Hemispheric Asymmetry of Monthly Sunspot Area an Irregular Process with Long-Term Memory?

Ratul **Das**, Aparup Ghosh, Bidya Binay Karak
MNRAS Volume 511, Issue 1, March **2022**, Pages 472–479,
https://doi.org/10.1093/mnras/stac035
https://arxiv.org/pdf/2111.06332.pdf
The hemispheric asymmetry of the sunspot cycle is a real feature of the Sun. However, its origin is still not well understood. Here we perform nonlinear time series analysis of the sunspot area (and number) asymmetry to explore its dynamics. By measuring the correlation dimension of the sunspot area asymmetry, we conclude that there is no strange attractor in the data. Further computing Higuchi's dimension, we conclude that the hemispheric asymmetry is largely governed by stochastic noise. However, the behaviour of Hurst exponent reveals that the time series is not completely determined by a memory-less stochastic noise, rather there is a long-term persistence, which can go beyond two solar cycles. Therefore, our study suggests that the hemispheric asymmetry of the sunspot cycle is predominantly originated due to some irregular process in the solar dynamo. The long-term persistence in the solar cycle asymmetry suggests that the solar magnetic field has some memory in the convection zone.

Sensitivity kernels for inferring Lorentz stresses from normal-mode frequency splittings in the Sun

Srijan Bharati **Das**, Tuneer Chakraborty, Shravan M. Hanasoge, Jeroen Tromp
ApJ **897** 38 **2020**
https://arxiv.org/pdf/2004.14536.pdf
https://doi.org/10.3847/1538-4357/ab8e3a
Departures from standard spherically symmetric solar models, in the form of perturbations such as global and local-scale flows and structural asphericities, result in the splitting of eigenfrequencies in the observed spectrum of solar oscillations. Drawing from prevalent ideas in normal-mode coupling theory in geophysical literature, we devise a procedure that enables the computation of sensitivity kernels for general Lorentz stress fields in the Sun. Mode coupling due to any perturbation requires careful consideration of self- and cross-coupling of multiplets. Invoking the isolated-multiplet approximation allows for limiting the treatment to purely self-coupling, requiring significantly less computational resources. We identify the presence of such isolated multiplets under the effect of Lorentz stresses in the Sun. Currently, solar missions allow precise measurements of self-coupling of multiplets via "a-coefficients" and the cross-spectral correlation signal which enables the estimation of the "structure coefficients". We demonstrate the forward problem for both self-coupling (a-coefficients) and cross-coupling (structure coefficients). In doing so, we plot the self-coupling kernels and estimate a-coefficients arising from a combination of deep-toroidal and surface-dipolar axisymmetric fields. We also compute the structure coefficients for an arbitrary general magnetic field (real and solenoidal) and plot the corresponding "splitting function", a convenient way to visualize the splitting of multiplets under 3D internal perturbations. The results discussed in this paper pave the way to formally pose an inverse problem, and infer solar internal magnetic fields.

Long-term forcing of Sun's coronal field, open flux and cosmic ray modulation potential during grand minima, maxima and regular activity phases by the solar dynamo mechanism

Soumyaranjan **Dash**, Dibyendu Nandy, Ilya Usoskin

MNRAS Volume 525, Issue 4, November **2023**, Pages 4801–4814,
https://doi.org/10.1093/mnras/stad1807
https://arxiv.org/pdf/2208.12103.pdf
Magnetic fields generated in the Sun's interior by the solar dynamo mechanism drive solar activity over a range of time-scales. While space-based observations of the Sun's corona exist only for few decades, direct sunspot observations exist for a few centuries, solar open flux and cosmic ray flux variations can be reconstructed through studies of cosmogenic isotopes over thousands of years. While such reconstructions indicate the presence of extreme solar activity fluctuations in the past, causal links between millennia scale dynamo activity, consequent coronal field, solar open flux and cosmic ray modulation remain elusive. By utilizing a stochastically forced solar dynamo model we perform long-term simulations to illuminate how the dynamo generated magnetic fields govern the structure of the solar corona and the state of the heliosphere -- as indicated by variations in the open flux and cosmic ray modulation potential. We establish differences in the nature of the large-scale structuring of the solar corona during grand maximum, minimum, and regular solar activity phases and simulate how the open flux and cosmic ray modulation potential varies over time scales encompassing these different phases of solar activity. We demonstrate that the power spectrum of simulated and reconstructed solar open flux are consistent with each other. Our study provides the theoretical basis for interpreting long-term solar cycle variability based on reconstructions relying on cosmogenic isotopes and connects solar internal variations to the forcing of the state of the heliosphere.

Reconstruction of spectral solar irradiance since 1700 from simulated magnetograms

M. **Dasi-Espuig**, J. Jiang, N. A. Krivova, S. K. Solanki, Y. C. Unruh, K. L. Yeo
A&A 590, A63 **2016**
http://arxiv.org/pdf/1605.02039v1.pdf
We present a reconstruction of the spectral solar irradiance since 1700 using the SATIRE-T2 (Spectral And Total Irradiance REconstructions for the Telescope era version 2) model. This model uses as input magnetograms simulated with a surface flux transport model fed with semi-synthetic records of emerging sunspot groups. We used statistical relationships between the properties of sunspot group emergence, such as the latitude, area, and tilt angle, and the sunspot cycle strength and phase to produce semi-synthetic sunspot group records starting in the year 1700. The semisynthetic records are fed into a surface flux transport model to obtain daily simulated magnetograms that map the distribution of the magnetic flux in active regions (sunspots and faculae) and their decay products on the solar surface. The magnetic flux emerging in ephemeral regions is accounted for separately based on the concept of extended cycles whose length and amplitude are linked to those of the sunspot cycles through the sunspot number. The magnetic flux in each surface component (sunspots, faculae and network, and ephemeral regions) was used to compute the spectral and total solar irradiance between the years 1700 and 2009. This reconstruction is aimed at timescales of months or longer although the model returns daily values. We found that SATIRE-T2, besides reproducing other relevant observations such as the total magnetic flux, reconstructs the total solar irradiance (TSI) on timescales of months or longer in good agreement with the PMOD composite of observations, as well as with the reconstruction starting in 1878 based on the RGO-SOON data. The model predicts an increase in the TSI of 1.2[+0.2, -0.3] Wm-2 between 1700 and the present. The spectral irradiance reconstruction is in good agreement with the UARS/SUSIM measurements as well as the Lyman-alpha composite.

Modelling total solar irradiance since 1878 from simulated magnetograms

M. **Dasi-Espuig**1, J. Jiang2, N. A. Krivova1 and S. K. Solanki
A&A 570, A23 (**2014**)
http://www.aanda.org/articles/aa/pdf/2014/10/aa24290-14.pdf
Aims. We present a new model of total solar irradiance (TSI) based on magnetograms simulated with a surface flux transport model (SFTM) and the Spectral And Total Irradiance REconstructions (SATIRE) model. Our model provides daily maps of the distribution of the photospheric field and the TSI starting from 1878.
Methods. The modelling is done in two main steps. We first calculate the magnetic flux on the solar surface emerging in active and ephemeral regions. The evolution of the magnetic flux in active regions (sunspots and faculae) is computed using a surface flux transport model fed with the observed record of sunspot group areas and positions. The magnetic flux in ephemeral regions is treated separately using the concept of overlapping cycles. We then use a version of the SATIRE model to compute the TSI. The area coverage and the distribution of different magnetic features as a function of time, which are required by SATIRE, are extracted from the simulated magnetograms and the modelled ephemeral region magnetic flux. Previously computed intensity spectra of the various types of magnetic features are employed.
Results. Our model reproduces the PMOD composite of TSI measurements starting from 1978 at daily and rotational timescales more accurately than the previous version of the SATIRE model computing TSI over this period of time. The simulated magnetograms provide a more realistic representation of the evolution of the magnetic field on the photosphere and also allow us to make use of information on the spatial distribution of the magnetic

fields before the times when observed magnetograms were available. We find that the secular increase in TSI since 1878 is fairly stable to modifications of the treatment of the ephemeral region magnetic flux.

Sunspot group tilt angles and the strength of the solar cycle

M. **Dasi-Espuig**1, S. K. Solanki1,2, N. A. Krivova1, R. Cameron1 and T. Peñuela
A&A 556, C3 (**2013**)
Erratum to: A&A 518, A7 (**2010**), DOI: 10.1051/0004-6361/201014301

Slitless Solar Imaging Spectroscopy

Joseph M. **Davila**1, Figen S. Oktem2, and Farzad Kamalabadi3
2019 ApJ 883 7
https://doi.org/10.3847/1538-4357/ab372a
Spectrometers provide our most detailed diagnostics of the solar coronal plasma, and spectral data is routinely used to measure the temperature, density, and flow velocity in coronal features. However, spectrographs suffer from a limited instantaneous field of view (IFOV). Conversely, imaging instruments can provide a relatively large IFOV, but extreme-ultraviolet (EUV) multilayer imaging offers very limited spectral resolution. In this paper, we suggest an instrument concept that combines the large IFOV of an imager with the diagnostic capability of a spectrograph, develop a new parametric model to describe the instrument, and evaluate a new method for "deconvolving" the data from such an instrument. To demonstrate the operating principle of this new slitless spectroscopy instrument, actual spectroscopic raster data from the Hinode/EUV Imaging Spectrometer (EIS) spectrometer is used. We assume that observations in multiple spectral orders are obtained, and then use a new inverse problem method to infer the spectral properties. Unlike previous methods, physical constraints and regularization derived from prior knowledge can be naturally incorporated as part of the solution process. We find that the fidelity of the solution is vastly improved compared to previous methods. The errors are typically only a few km s−1 over a large IFOV, with a width of a few hundred pixels and an arbitrarily large height. These errors are not much larger than the errors in current slit spectroscopic instruments with limited IFOV. A further benefit is that the performance of candidate instruments can be optimized for specific scientific objectives. We demonstrate this by deriving optimum values for the spectral dispersion and signal-to-noise ratio.

Universal processes in heliophysics

Joseph M. **Davila**1, Nat Gopalswamy2 and Barbara J. Thompson3
*Universal Heliophysical Processe, Proceedings IAU Symposium No. 257, **2008**, N. Gopalswamy & D.F. Webb, eds.*
http://journals.cambridge.org/action/displayIssue?iid=4866212
The structure of the Universe is determined primarily by the interplay of gravity which is dominant in condensed objects, and the magnetic force which is dominant in the rarefied medium between condensed objects. Each of these forces orders the matter into a set of characteristic structures each with the ability to store and release energy in response to changes in the external environment. For the most part, the storage and release of energy proceeds through a number of Universal Processes. The coordinated study of these processes in different settings provides a deeper understanding of the underlying physics governing Universal Processes in astrophysics.

The polarization of the Lyman-α lines of H I and He II as a tool for exploring the solar corona

Supriya Hebbur **Dayananda**, Javier Trujillo Bueno, Ángel de Vicente, Tanausú del Pino Alemán
ApJ **2021**
https://arxiv.org/pdf/2107.01015.pdf
The near-Earth space weather is driven by the quick release of magnetic free energy in the solar corona. Probing this extremely hot and rarified region of the extended solar atmosphere requires modeling the polarization of forbidden and permitted coronal lines. To this end, it is important to develop efficient codes to calculate the Stokes profiles that emerge from given three-dimensional (3D) coronal models, and this should be done taking into account the symmetry breaking produced by the presence of magnetic fields and non-radial solar wind velocities. We have developed such a tool with the aim of theoretically predicting and interpreting spectropolarimetric observations of the solar corona in permitted and forbidden lines. In this paper we show the results of a theoretical investigation of the linear polarization signals produced by scattering processes in the H I Ly-α line at 1216 A and in the He II Ly-α line at 304 A using 3D coronal models by Predictive Science Inc. These spectral lines have very different critical magnetic fields for the onset of the Hanle effect (53 G and 850 G, respectively), as well as different sensitivities to the Doppler effect caused by the solar wind velocities. We study under which circumstances simultaneous observations of the scattering polarization in these Ly-α lines can facilitate the determination of magnetic fields and macroscopic velocities in the solar corona.

Modeling proton intensity gradients and radiation dose equivalents in the inner heliosphere using EMMREM: May 2003 solar events,

Dayeh, M. A., M. I. Desai, K. Kozarev, N. A. Schwadron, L. W. Townsend, M. PourArsalan, C. Zeitlin, and R. B. Hatcher
(**2010**), Space Weather, 8, S00E07, doi:10.1029/2009SW000566.

Solar energetic particles (SEPs) provide a significant radiation hazard for manned and unmanned interplanetary (IP) space missions. In order to estimate these hazards, it is essential to quantify the gradients of SEP intensities in the IP medium. The Earth-Moon-Mars Radiation Exposure Module (EMMREM) is a new project aimed at characterizing the time-dependent radiation exposure in IP space. In this paper, we utilize EMMREM to study the radial dependence of proton peak intensities, event fluences, and radiation dose equivalents of 27–31 May 2003 SEP events at eight different locations between 1 and 4.91 AU at energies between ~1.5 MeV and ~130 MeV. We have modeled onset times and intensity profiles of the SEP events at Mars and Ulysses and found very good agreement at different energies. We report observations of energetic particles at locations with magnetic field line footprints that are separated by ~90° in heliolongitude, possibly indicating very large coronal mass ejection sizes and/or high cross-field diffusion at large radial distances. Our results show that radial dependencies of proton peak intensities exhibit a broken power law between 1 to 2.5 AU and 2.5 to 4.91 AU, ranging between $R^{-2.52 \pm 0.42}$ and $R^{-5.97 \pm 0.32}$ for 25 MeV and between $R^{-2.13 \pm 0.36}$ and $R^{-5.21 \pm 0.29}$ for 52 MeV, where R is the radial distance from the Sun in units of AU. Event fluences exhibit a similar behavior but with a harder spectra. Radiation dose calculations show that these events did not pose a short-term radiation hazard to humans in the IP space.

The Highly Structured Outer Solar Corona

C. E. **DeForest**1, R. A. Howard2, M. Velli3, N. Viall4, and A. Vourlidas
2018 ApJ 862 18
http://iopscience.iop.org/article/10.3847/1538-4357/aac8e3/pdf

We report on the observation of fine-scale structure in the outer corona at solar maximum, using deep-exposure campaign data from the Solar Terrestrial Relations Observatory-A (STEREO-A)/COR2 coronagraph coupled with postprocessing to further reduce noise and thereby improve effective spatial resolution. The processed images reveal radial structure with high density contrast at all observable scales down to the optical limit of the instrument, giving the corona a "woodgrain" appearance. Inferred density varies by an order of magnitude on spatial scales of 50 Mm and follows an f^{-1} spatial spectrum. The variations belie the notion of a smooth outer corona. They are inconsistent with a well-defined "Alfvén surface," indicating instead a more nuanced "Alfvén zone"—a broad trans-Alfvénic region rather than a simple boundary. Intermittent compact structures are also present at all observable scales, forming a size spectrum with the familiar "Sheeley blobs" at the large-scale end. We use these structures to track overall flow and acceleration, finding that it is highly inhomogeneous and accelerates gradually out to the limit of the COR2 field of view. Lagged autocorrelation of the corona has an enigmatic dip around 10 $R_\odot$, perhaps pointing to new phenomena near this altitude. These results point toward a highly complex outer corona with far more structure and local dynamics than has been apparent. We discuss the impact of these results on solar and solar-wind physics and what future studies and measurements are necessary to build upon them.

ERRATUM: "FEASIBILITY OF HELIOSPHERIC IMAGING FROM NEAR EARTH" (2015, ApJ, 804, 126)

C. E. **DeForest** and T. A. Howard
2015 ApJ 813 139

Validating Forward Modeling and Inversions of Helioseismic Holography Measurements

K. **DeGrave**1, D. C. Braun1, A. C. Birch2, A. D. Crouch1, and B. Javornik1
2018 ApJ 863 34
http://sci-hub.tw/http://iopscience.iop.org/article/10.3847/1538-4357/aacffd/meta

Here, we use synthetic data to explore the performance of forward models and inverse methods for helioseismic holography. Specifically, this work presents the first comprehensive test of inverse modeling for flows using lateral-vantage (deep-focus) holography. We derive sensitivity functions in the Born approximation. We then use these sensitivity functions in a series of forward models and inversions of flows from a publicly available magnetohydrodynamic quiet-Sun simulation. The forward travel times computed using the kernels generally compare favorably with measurements obtained by applying holography, in a lateral-vantage configuration, on a 15 hr time series of artificial Dopplergrams extracted from the simulation. Inversions for the horizontal flow components are able to reproduce the flows in the upper 3 Mm of the domain, but are compromised by noise at greater depths.

Time-distance Helioseismology of Two Realistic Sunspot Simulations

K. **DeGrave**1, J. Jackiewicz1, and M. Rempel
2014 ApJ 794 18.
Linear time-distance helioseismic inversions are carried out using several filtering schemes to determine vector flow velocities within two ~1002 Mm2 × 20 Mm realistic magnetohydrodynamic sunspot simulations of 25 hr. One simulation domain contains a model of a full sunspot (i.e., one with both an umbra and penumbra), while the other contains a pore (i.e., a spot without a penumbra). The goal is to test current helioseismic methods using these state-of-the-art simulations of magnetic structures. We find that horizontal flow correlations between inversion and simulation flow maps are reasonably high (~0.5-0.8) in the upper 3 Mm at distances exceeding 25-30 Mm from spot center, but are substantially lower at smaller distances and larger depths. Inversions of forward-modeled travel times consistently outperform those of our measured travel times in terms of horizontal flow correlations, suggesting that our inability to recover flow structure near these active regions is largely due to the fact that we are unable to accurately measure travel times near strong magnetic features. In many cases the velocity amplitudes from the inversions underestimate those of the simulations by up to 50%, possibly indicating nonlinearity of the forward problem. In every case, we find that our inversions are unable to recover the vertical flow structure of the simulations at any depth.

A Remarkable Recent Transition in the Solar Dynamo **Review**

C. **de Jager**, S.-I. Akasofu, S. Duhau, W. C. Livingston, H. Nieuwenhuijzen, M. S. Potgiete
Space Science Reviews Volume 201, Issue 1, pp 109–145 **2016**
http://link.springer.com/article/10.1007/s11214-016-0293-9
We summarize the major aspects of the remarkable, fairly long lasting period (\(\sim 2005\) to \(\sim 2010\)) of low solar activity, that we will call the Transition. It is the transitional stage between the Grand Maximum of the 20th century and a forthcoming (most probably Regular) episode of solar activity. The various kinds of activity in the functioning of the equatorial components of the solar dynamo before and during the Transition are summarized. While the behavior of unipolar magnetic regions and their rest-latitudes already gave very early indications – mid 20th century – of the forthcoming Transition, more such indications became available around 1995 and the main part of it occurred between 2005 and 2010. Some of the inferences are discussed. We submit the hypothesis that the solar tachocline undergoes pulsations and we present some helioseismic evidences. In that scenario we find that its equatorial part has moved downward over a fairly small semi-amplitude (\(\sim 0.03\) solar radii) during the time of the Transition. There are several indications, apart from this 'pulsation', that the tachocline may even be pulsating with still smaller amplitudes in more modes. We speculate about the physical mechanism(s).

(When) Can Wave Heating Balance Optically Thin Radiative Losses in the Corona?

I. **De Moortel**1,2 and T. A. Howson1
2022 ApJ 941 85
https://iopscience.iop.org/article/10.3847/1538-4357/aca072/pdf
Why the atmosphere of the Sun is orders of magnitudes hotter than its surface is a long standing question in solar physics. Over the years, many studies have looked at the potential role of magnetohydrodynamic (MHD) waves in sustaining these high temperatures. In this study, we use 3D MHD simulations to investigate (driven) transverse waves in a coronal loop. As the boundary-driven transverse waves propagate along the flux tube, the radial density profile leads to resonant absorption (or mode coupling) and phase mixing in the boundaries of the flux tube and the large velocity shears are subject to the Kelvin–Helmholtz instability (KHI). The combination of these effects leads to enhanced energy dissipation and wave heating. Considering both resonant and nonresonant boundary driving as well as different densities for the flux tube, we show that only wave heating associated with a resonant driver in a lower-density loop (with a loop core density ∼5 × 10−13 kg m−3) is able to balance radiative losses in the loop shell. Changing the model parameters to consider a denser loop or a driver with a nonresonant frequency, or both, leads to cooling of the coronal loop as the energy losses are greater than the energy injection and dissipation rates.

Observational Signatures of Waves and Flows in the Solar Corona

I. **De Moortel**, P. Antolin, T. Van Doorsselaere
Solar Phys. February **2015**, Volume 290, Issue 2, pp 399-421
Propagating perturbations have been observed in extended coronal loop structures for a number of years, but the interpretation in terms of slow (propagating) magneto-acoustic waves and/or as quasi-periodic upflows remains unresolved. We used forward-modelling to construct observational signatures associated with a simple slow magneto-acoustic wave or periodic flow model. Observational signatures were computed for the 171 Å Fe ix and the 193 Å Fe xii spectral lines. Although there are many differences between the flow and wave models, we did not find any clear, robust observational characteristics that can be used in isolation (i.e. that do not rely on a comparison between the models). For the waves model, a relatively rapid change of the average line widths as a function of (shallow) line-of-sight angles was found, whereas the ratio of the line width amplitudes to the Doppler velocity amplitudes is relatively high for the flow model. The most robust observational signature found is that the ratio of the mean to the amplitudes of the Doppler velocity is always higher than one for the flow model. This ratio is

substantially higher for flows than for waves, and for the flows model used in the study is exactly the same in the 171 Å Fe ix and the 193 Å Fe xii spectral lines. However, these potential observational signatures need to be treated cautiously because they are likely to be model-dependent.

3D ELECTRON DENSITY DISTRIBUTIONS IN THE SOLAR CORONA DURING SOLAR MINIMA: ASSESSMENT FOR MORE REALISTIC SOLAR WIND MODELING

Judith **de Patoul**1,2, Claire Foullon1, and Pete Riley
2015 ApJ 814 68

Knowledge of the electron density distribution in the solar corona put constraints on the magnetic field configurations for coronal modeling and on initial conditions for solar wind modeling. We work with polarized SOHO/LASCO-C2 images from the last two recent minima of solar activity (1996–1997 and 2008–2010), devoid of coronal mass ejections. The goals are to derive the 4D electron density distributions in the corona by applying a newly developed time-dependent tomographic reconstruction method and to compare the results between the two solar minima and with two magnetohydrodynamic models. First, we confirm that the values of the density distribution in thermodynamic models are more realistic than in polytropic ones. The tomography provides more accurate distributions in the polar regions, and we find that the density in tomographic and thermodynamic solutions varies with the solar cycle in both polar and equatorial regions. Second, we find that the highest-density structures do not always correspond to the predicted large-scale heliospheric current sheet or its helmet streamer but can follow the locations of pseudo-streamers. We deduce that tomography offers reliable density distributions in the corona, reproducing the slow time evolution of coronal structures, without prior knowledge of the coronal magnetic field over a full rotation. Finally, we suggest that the highest-density structures show a differential rotation well above the surface depending on how they are magnetically connected to the surface. Such valuable information on the rotation of large-scale structures could help to connect the sources of the solar wind to their in situ counterparts in future missions such as Solar Orbiter and Solar Probe Plus.

The cyclic behaviour in the N-S asymmetry of sunspots and solar plages for the period 1910 to 1937 using data from Ebro catalogues

V. **de Paula**, J.J. Curto, R. Oliver
MNRAS **2022**
https://arxiv.org/pdf/2202.08628.pdf

The heliophysics catalogues published by the Ebro Observatory during 1910--1937 have been converted into a digital format in order to provide the data for computational processing. This has allowed us to study in detail the North-South (N-S) asymmetry of solar activity in that period, focusing on two different structures located at two different layers of the solar atmosphere: sunspots (Photosphere) and solar plages (Chromosphere). The examination of the absolute and normalised N-S asymmetry indices in terms of their monthly sum of occurrences and areas has made possible to find out a cyclic behaviour in the solar activity, in which the preferred hemisphere changes systematically with a global period of 7.9 ± 0.2 yr. In order to verify and quantify accurately this periodicity and study its prevalence in time, we employed the RGO-USAF/NOAA sunspot data series during 1874--2016. Then, we examined each absolute asymmetry index time series through different techniques as the power spectrum analysis, the Complete Ensemble Empirical Mode Decomposition With Adaptive Noise algorithm, or the Morlet wavelet transform. The combined results reveal a cyclic behaviour at different time scales, consisting in two quite stable periodicities of 1.47 ± 0.02 yr and 3.83 ± 0.06 yr, which coexist with another three discontinuous components with more marked time-varying periods with means of 5.4 ± 0.2 yr, 9.0 ± 0.2 yr, and 12.7 ± 0.3 yr. Moreover, during 1910--1937, only two dominant signals with averaged periods of 4.10 ± 0.04 yr and 7.57 ± 0.03 yr can be clearly observed. Finally, in both signals, periods are slightly longer for plages in comparison with sunspots.

Application of the Markov Chain Model to Sunspots and Solar Plages for the Period 1910 to 1937 Using Data from Ebro Catalogues

V. **de Paula**, J. J. Curto & T. Sole
Solar Physics volume 296, Article number: 92 (**2021**)
https://link.springer.com/content/pdf/10.1007/s11207-021-01838-w.pdf
https://doi.org/10.1007/s11207-021-01838-w

In this article, we analyzed the morphological evolution of the sunspot and solar calcium plage groups recorded at the Ebro Observatory in the period 1910–1937 to make predictions about several properties of these solar structures by using Markov chain models. For this purpose, we first checked the applicability of first and second order models to all the data series by carrying out dependency tests, which ensure that the current morphological type presented by the structures has a dependence with the morphology presented in previous observations. Next, as a first approximation, we applied the first order Markov chain model to the total number of transitions between the different morphological types of sunspots and solar plage groups to estimate the probability of occurrence associated with each transition, the prevalence time that these structures spend within each morphological type, the extinction-

occultation forecast, the expectation of these structures converting into a determined morphological type, and the occurrence daily rate associated to each type after a certain number of transitions. In addition, we also analyzed the observed morphology of the structures at the time of their appearance and extinction. Our main results show that both sunspots and solar plage groups become morphologically stable after their transition to a new type. Nevertheless, this stability seems to decrease once the decay phase starts and their morphology changes to the observed type during the last stage of their evolution sequence. Finally, we also studied the temporal and spatial homogeneity of the data, concluding that the two solar structures evolve with similar patterns in the northern and southern hemispheres, but both Solar Cycles 15 and 16 as well as each solar cycle phase, i.e. solar minimum, ascending phase, solar maximum and descending phase, present small deviations in all the analyzed properties. These deviations may affect some aspects of the morphological evolution of both sunspots and solar plage groups.

The Evolution over Time and North–South Asymmetry of Sunspots and Solar Plages for the Period 1910 to 1937 Using Data from Ebro Catalogues

V. **de Paula** & J. J. Curto

Solar Physics volume 295, Article number: 99 (**2020**)

https://link.springer.com/content/pdf/10.1007/s11207-020-01648-6.pdf

In this work, we analysed both the evolution over time and the north–south (N-S) asymmetry of certain solar features with regards to their morphological type and area. We examined and compared simultaneously 4212 photospheric sunspot groups and 5781 chromospheric solar plage groups using data from the Ebro Observatory catalogues for the period 1910–1937. We found that the most frequently recorded groups of sunspots and solar plages are the smallest ones, and the total number of occurrences of these groups is, on average, about 23% higher for solar plages than for sunspots. Concerning the N-S asymmetry, when the northern hemisphere becomes predominant, it dominates the other hemisphere for a longer time than the opposite case and shows a higher asymmetry. In addition, we found that the normalized N-S asymmetry index, δδ, of solar activity in terms of the occurrence of sunspots and solar plage groups follows approximately the same behaviour regardless of the morphological type, but presents a slight dependence on their area, since sunspot and solar plage groups show higher values of the δδ index, the larger their areas are. Furthermore, we noticed three highly significant extremes in the N-S asymmetry, located around the minima of the 14th, 15th and 16th solar cycles (1912 [S]; 1924 [N]; 1933 [N]). However, the general trend is not equal in both structures, since in contrast to sunspots, solar plage groups present lower values of asymmetry throughout practically all the period under consideration. These facts could be interpreted in terms of magnetic cancellation processes and/or merging of close-by faculae.

The Solar Rotation in the 1930s from the Sunspot and Flocculi Catalogs of the Ebro Observatory

V. **de Paula**, J. J. Curto, R. Casas

Solar Phys. Volume 291, Issue 8, pp 2269–2279 **2016**

The tables of sunspot and flocculi heliographic positions included in the catalogs published by the Ebro Observatory in the 1930s have recently been recovered and converted into digital format by using optical character recognition (OCR) technology. We here analyzed these data by computing the angular velocity of several sunspot and flocculi groups. A difference was found in the rotational velocity for sunspots and flocculi groups at high latitudes, and we also detected an asymmetry between the northern and southern hemispheres, which is especially marked for the flocculi groups. The results were then fitted with a differential-rotation law [\(\omega=a+b \sin^{2} B\)] to compare the data obtained with the results published by other authors. A dependence on the latitude that is consistent with former studies was found. Finally, we studied the possible relationship between the sunspot/flocculi group areas and their corresponding angular velocity. There are strong indications that the rotational velocity of a sunspot/flocculi group is reduced (in relation to the differential rotation law) when its maximum area is larger.

Probing the physics of the solar atmosphere with the Multi-slit Solar Explorer (MUSE): I. Coronal Heating

Bart De Pontieu, Paola Testa, Juan Martinez-Sykora, Patrick Antolin, …..

ApJ **2021**

https://arxiv.org/pdf/2106.15584.pdf

The Multi-slit Solar Explorer (MUSE) is a proposed NASA MIDEX mission, currently in Phase A, composed of a multi-slit EUV spectrograph (in three narrow spectral bands centered around 171A, 284A, and 108A) and an EUV context imager (in two narrow passbands around 195A and 304A). MUSE will provide unprecedented spectral and imaging diagnostics of the solar corona at high spatial (<0.5 arcsec), and temporal resolution (down to ~0.5s) thanks to its innovative multi-slit design. By obtaining spectra in 4 bright EUV lines (Fe IX 171A , Fe XV 284A, Fe XIX-Fe XXI 108A) covering a wide range of transition region and coronal temperatures along 37 slits simultaneously, MUSE will for the first time be able to "freeze" (at a cadence as short as 10 seconds) with a spectroscopic raster the evolution of the dynamic coronal plasma over a wide range of scales: from the spatial scales on which energy is

released (~0.5 arcsec) to the large-scale often active-region size (170 arcsec x 170 arcsec) atmospheric response. We use advanced numerical modeling to showcase how MUSE will constrain the properties of the solar atmosphere on the spatio-temporal scales (~0.5 arcsec, ~20 seconds) and large field-of-view on which various state-of-the-art models of the physical processes that drive coronal heating, solar flares and coronal mass ejections (CMEs) make distinguishing and testable predictions. We describe how the synergy between MUSE, the single-slit, high-resolution Solar-C EUVST spectrograph, and ground-based observatories (DKIST and others) can address how the solar atmosphere is energized, and the critical role MUSE plays because of the multi-scale nature of the physical processes involved. In this first paper, we focus on how comparisons between MUSE observations and theoretical models will significantly further our understanding of coronal heating mechanisms.

A new view of the solar interface region from the Interface Region Imaging Spectrograph (IRIS) Review

B. **De Pontieu**, V. Polito, V. Hansteen, P. Testa, K.K. Reeves, P. Antolin, D. Nobrega-Siverio, A. Kowalski, J. Martinez-Sykora, M. Carlsson, S.W. McIntosh, W. Liu, A. Daw, C.C. Kankelborg
Solar Phys. **2021**
https://arxiv.org/pdf/2103.16109.pdf

The Interface Region Imaging Spectrograph (IRIS) has been obtaining near- and far-ultraviolet images and spectra of the solar atmosphere since July 2013. The unique combination of near and far-ultraviolet spectra and images at subarcsecond resolution and high cadence allows the tracing of mass and energy through the critical interface between the solar surface and the corona or solar wind. IRIS has enabled research into the fundamental physical processes thought to play a role in the low solar atmosphere such as ion-neutral interactions, magnetic reconnection, the generation, propagation, and dissipation of various types of waves, the acceleration of non-thermal particles, and various small-scale instabilities. These new findings have helped provide novel insights into a wide range of phenomena including the discovery of non-thermal particles in coronal nanoflares, the formation and impact of spicules and other jets, resonant absorption and dissipation of Alfvenic waves, energy release associated with braiding of magnetic field lines, the thermal instability in the chromosphere-corona mass and energy cycle, the contribution of waves, turbulence, and non-thermal particles in the energy deposition during flares and smaller-scale events such as UV bursts, and the role of flux ropes and other mechanisms in triggering CMEs. IRIS observations have also advanced studies of the connections between solar and stellar physics. Advances in numerical modeling, inversion codes, and machine learning techniques have played a key role in driving these new insights. With the advent of exciting new instrumentation both on the ground (e.g., DKIST, ALMA) and space-based (e.g., Parker Solar Probe, Solar Orbiter), we aim to review new insights based on IRIS observations or related modeling, and highlight some of the outstanding challenges that have been brought to the fore.

The Multi-slit Approach to Coronal Spectroscopy with the Multi-slit Solar Explorer (MUSE)

Bart **De Pontieu**1,2,3, Juan Martínez-Sykora1,2,4, Paola Testa5, Amy R. Winebarger6, Adrian Daw7, Viggo Hansteen1,2,3,4, Mark C. M. Cheung1,8, and Patrick Antolin9
2020 ApJ 888 3
https://iopscience.iop.org/article/10.3847/1538-4357/ab5b03/pdf

The Multi-slit Solar Explorer (MUSE) is a proposed mission aimed at understanding the physical mechanisms driving the heating of the solar corona and the eruptions that are at the foundation of space weather. MUSE contains two instruments, a multi-slit extreme ultraviolet (EUV) spectrograph and a context imager. It will simultaneously obtain EUV spectra (along 37 slits) and context images with the highest resolution in space ($0\farcs33$–$0\farcs4$) and time (1–4 s) ever achieved for the transition region (TR) and corona. The MUSE science investigation will exploit major advances in numerical modeling, and observe at the spatial and temporal scales on which competing models make testable and distinguishable predictions, thereby leading to a breakthrough in our understanding of coronal heating and the drivers of space weather. By obtaining spectra in four bright EUV lines (Fe ix 171 Å, Fe xv 284 Å, Fe xix 108Å, Fe xxi 108 Å) covering a wide range of TR and coronal temperatures along 37 slits simultaneously, MUSE will be able to "freeze" the evolution of the dynamic coronal plasma. We describe MUSE's multi-slit approach and show that the optimization of the design minimizes the impact of spectral lines from neighboring slits, generally allowing line parameters to be accurately determined. We also describe a Spectral Disambiguation Code to resolve multi-slit ambiguity in locations where secondary lines are bright. We use simulations of the corona and eruptions to perform validation tests and show that the multi-slit disambiguation approach allows accurate determination of MUSE observables in locations where significant multi-slit contamination occurs.

What causes the high apparent speeds in chromospheric and transition region spicules on the Sun?

Bart **De Pontieu**, Juan Martinez-Sykora, Georgios Chintzoglou
ApJL **849** L7 **2017**

https://arxiv.org/pdf/1710.06803.pdf
http://sci-hub.cc/http://iopscience.iop.org/2041-8205/849/1/L7/
Spicules are the most ubuiquitous type of jets in the solar atmosphere. The advent of high-resolution imaging and spectroscopy from the Interface Region Imaging Spectrograph (IRIS) and ground-based observatories has revealed the presence of very high apparent motions of order 100-300 km/s in spicules, as measured in the plane of the sky. However, line-of-sight measurements of such high speeds have been difficult to obtain, with values deduced from Doppler shifts in spectral lines typically of order 30-70 km/s. In this work we resolve this long-standing discrepancy using recent 2.5D radiative MHD simulations. This simulation has revealed a novel driving mechanism for spicules in which ambipolar diffusion resulting from ion-neutral interactions plays a key role. In our simulation we often see that the upward propagation of magnetic waves and electrical currents from the low chromosphere into already existing spicules can lead to rapid heating when the currents are rapidly dissipated by ambipolar diffusion. The combination of rapid heating and the propagation of these currents at Alfv\'enic speeds in excess of 100 km/s leads to the very rapid apparent motions, and often wholesale appearance, of spicules at chromospheric and transition region temperatures. In our simulation, the observed fast apparent motions in such jets are actually a signature of a heating front, and much higher than the mass flows, which are of order 30-70 km/s. Our results can explain the behavior of transition region "network jets" and the very high apparent speeds reported for some chromospheric spicules. **04-Aug-2013**

Observations and Numerical Models of Solar Coronal Heating Associated with Spicules

B. **De Pontieu**1,2, I. De Moortel3, J. Martinez-Sykora1,4, and S. W. McIntosh
2017 ApJL 845 L18
https://arxiv.org/pdf/1710.06790.pdf
Spicules have been proposed as significant contributors to the mass and energy balance of the corona. While previous observations have provided a glimpse of short-lived transient brightenings in the corona that are associated with spicules, these observations have been contested and are the subject of a vigorous debate both on the modeling and the observational side. Therefore, it remains unclear whether plasma is heated to coronal temperatures in association with spicules. We use high-resolution observations of the chromosphere and transition region (TR) with the Interface Region Imaging Spectrograph and of the corona with the Atmospheric Imaging Assembly on board the Solar Dynamics Observatory to show evidence of the formation of coronal structures associated with spicular mass ejections and heating of plasma to TR and coronal temperatures. Our observations suggest that a significant fraction of the highly dynamic loop fan environment associated with plage regions may be the result of the formation of such new coronal strands, a process that previously had been interpreted as the propagation of transient propagating coronal disturbances. Our observations are supported by 2.5D radiative MHD simulations that show heating to coronal temperatures in association with spicules. Our results suggest that heating and strong flows play an important role in maintaining the substructure of loop fans, in addition to the waves that permeate this low coronal environment.

Why is Non-Thermal Line Broadening of Spectral Lines in the Lower Transition Region of the Sun Independent of Spatial Resolution?

B. **De Pontieu**1,2, S. McIntosh3, J. Martinez-Sykora1,4, H. Peter5, and T. M. D. Pereira
2015 ApJ 799 L12
Spectral observations of the solar transition region (TR) and corona show broadening of spectral lines beyond what is expected from thermal and instrumental broadening. The remaining non-thermal broadening is significant (5–30 km s−1) and correlated with intensity. Here we study spectra of the TR Si iv 1403 Å line obtained at high resolution with the Interface Region Imaging Spectrograph (IRIS). We find that the large improvement in spatial resolution ($0\farcs33$) of IRIS compared to previous spectrographs (2") does not resolve the non-thermal line broadening which, in most regions, remains at pre-IRIS levels of about 20 km s−1. This invariance to spatial resolution indicates that the processes behind the broadening occur along the line-of-sight (LOS) and/or on spatial scales (perpendicular to the LOS) smaller than 250 km. Both effects appear to play a role. Comparison with IRIS chromospheric observations shows that, in regions where the LOS is more parallel to the field, magneto-acoustic shocks driven from below impact the TR and can lead to significant non-thermal line broadening. This scenario is supported by MHD simulations. While these do not show enough non-thermal line broadening, they do reproduce the long-known puzzling correlation between non-thermal line broadening and intensity. This correlation is caused by the shocks, but only if non-equilibrium ionization is taken into account. In regions where the LOS is more perpendicular to the field, the prevalence of small-scale twist is likely to play a significant role in explaining the invariance and correlation with intensity.

On the prevalence of small-scale twist in the solar chromosphere and transition region

B. **De Pontieu**, L. Rouppe van der Voort, S.W. McIntosh, T.M.D. Pereira, M. Carlsson, V. Hansteen, H. Skogsrud, J. Lemen, A. Title, P. Boerner, N. Hurlburt, T.D. Tarbell, J.P. Wuelser, E.E. De Luca, L.

Golub, S. McKillop, K. Reeves, S. Saar, P. Testa, H. Tian, C. Kankelborg, S. Jaeggli, L. Kleint, J. Martinez-Sykora
Science, **2014**
http://arxiv.org/pdf/1410.6862v1.pdf
The solar chromosphere and transition region (TR) form an interface between the Sun's surface and its hot outer atmosphere. Here most of the non-thermal energy that powers the solar atmosphere is transformed into heat, although the detailed mechanism remains elusive. High-resolution (0.33-arcsec) observations with NASA's Interface Region Imaging Spectrograph (IRIS) reveal a chromosphere and TR that are replete with twist or torsional motions on sub-arcsecond scales, occurring in active regions, quiet Sun regions, and coronal holes alike. We coordinated observations with the Swedish 1-m Solar Telescope (SST) to quantify these twisting motions and their association with rapid heating to at least TR temperatures. This view of the interface region provides insight into what heats the low solar atmosphere. **10-27 Sept 2013, 9 Oct 2013, 13 Oct 2013**

The Interface Region Imaging Spectrograph (IRIS)

B. **De Pontieu**, A. M. Title, J. R. Lemen, G. D. Kushner, D. J. Akin…
Solar Physics, July **2014**, Volume 289, Issue 7, pp 2733-2779,
The Interface Region Imaging Spectrograph (IRIS) small explorer spacecraft provides simultaneous spectra and images of the photosphere, chromosphere, transition region, and corona with 0.33 – 0.4 arcsec spatial resolution, two-second temporal resolution, and 1 km s−1 velocity resolution over a field-of-view of up to 175 arcsec × 175 arcsec. IRIS was launched into a Sun-synchronous orbit on 27 June 2013 using a Pegasus-XL rocket and consists of a 19-cm UV telescope that feeds a slit-based dual-bandpass imaging spectrograph. IRIS obtains spectra in passbands from 1332 – 1358 Å, 1389 – 1407 Å, and 2783 – 2834 Å, including bright spectral lines formed in the chromosphere (Mg ii h 2803 Å and Mg ii k 2796 Å) and transition region (C ii 1334/1335 Å and Si iv 1394/1403 Å). Slit-jaw images in four different passbands (C ii 1330, Si iv 1400, Mg ii k 2796, and Mg ii wing 2830 Å) can be taken simultaneously with spectral rasters that sample regions up to 130 arcsec × 175 arcsec at a variety of spatial samplings (from 0.33 arcsec and up). IRIS is sensitive to emission from plasma at temperatures between 5000 K and 10 MK and will advance our understanding of the flow of mass and energy through an interface region, formed by the chromosphere and transition region, between the photosphere and corona. This highly structured and dynamic region not only acts as the conduit of all mass and energy feeding into the corona and solar wind, it also requires an order of magnitude more energy to heat than the corona and solar wind combined. The IRIS investigation includes a strong numerical modeling component based on advanced radiative–MHD codes to facilitate interpretation of observations of this complex region. Approximately eight Gbytes of data (after compression) are acquired by IRIS each day and made available for unrestricted use within a few days of the observation.

Collisional Depolarization of the Solar Ca, Mg, and Ba Levels

M. **Derouich**
2019 ApJ 880 10
sci-hub.se/10.3847/1538-4357/ab26b4
We study the depolarization of the p-states of the Mg, Ca, and Ba atoms by isotropic collisions with neutral hydrogen. We show that the main source of error in calculating the collisional depolarization is the inaccuracy of the interaction potentials. To better investigate this problem, we determine the region of the interaction potential that is decisive in the calculation of the depolarization rates. We conclude that semiclassical and quantum potentials should be combined in view of obtaining the so-called hybrid potentials, which are the most precise ones. The depolarization rates of the p-states of the Ca i, Mg i, and Ba i are inferred by using hybrid potentials and compared to previously obtained quantum and semiclassical rates. Insights are also given for treating the effects of the spin. Our results should be useful for interpreting the second solar spectrum.

ANALYSIS OF SUNSPOT AREA OVER TWO SOLAR CYCLES

G. **de Toma**1, G. A. Chapman2, D. G. Preminger2, and A. M. Cookson
2013 ApJ 770 89
We examine changes in sunspots and faculae and their effect on total solar irradiance during solar cycles 22 and 23 using photometric images from the San Fernando Observatory. We find important differences in the very large spots between the two cycles, both in their number and time of appearance. In particular, there is a noticeable lack of very large spots in cycle 23 with areas larger than 700 millionths of a solar hemisphere which corresponds to a decrease of about 40% relative to cycle 22. We do not find large differences in the frequencies of small to medium spots between the two cycles. There is a decrease in the number of pores and very small spots during the maximum phase of cycle 23 which is largely compensated by an increase during other phases of the solar cycle. The decrease of the very large spots, in spite of the fact that they represent only a few percent of all spots in a cycle, is primarily

responsible for the observed changes in total sunspot area and total sunspot deficit during cycle 23 maximum. The cumulative effect of the decrease in the very small spots is an order of magnitude smaller than the decrease caused by the lack of large spots. These data demonstrate that the main difference between cycles 22 and 23 was in the frequency of very large spots and not in the very small spots, as previously concluded. Analysis of the USAF/NOAA and Debrecen sunspot areas confirms these findings.

Long characteristics vs. short characteristics in 3D radiative transfer simulations of polarized radiation

A. **de Vicente**, T. del Pino Alemán, J. Trujillo Bueno
ApJ **2021**
https://arxiv.org/pdf/2103.04065
We compare maps of scattering polarization signals obtained from three-dimensional (3D) radiation transfer calculations in a magneto-convection model of the solar atmosphere using formal solvers based on the "short characteristics" (SC) and the "long characteristics" (LC) methods. The SC method requires less computational work, but it is known to introduce spatial blurring in the emergent radiation for inclined lines of sight. For polarized radiation this effect is generally more severe due to it being a signed quantity and to the sensitivity of the scattering polarization to the model's inhomogeneities. We study the differences in the polarization signals of the emergent spectral line radiation calculated with such formal solvers. We take as a case study already published results of the scattering polarization in the Sr I 4607 Å line obtained with the SC method, demonstrating that in high-resolution grids it is accurate enough for that type of study. In general, the LC method is the preferred one for accurate calculations of the emergent radiation, reason why it is now one of the options in the public version of the 3D radiative transfer code PORTA.

Supervised classification of solar features using prior information

Ruben **De Visscher**1*, Véronique Delouille1, Pierre Dupont2 and Charles-Alban Deledalle
J. Space Weather Space Clim., 5, A34 (**2015**)
http://www.swsc-journal.org/articles/swsc/pdf/2015/01/swsc140058.pdf
Context: The Sun as seen by Extreme Ultraviolet (EUV) telescopes exhibits a variety of large-scale structures. Of particular interest for space-weather applications is the extraction of active regions (AR) and coronal holes (CH). The next generation of GOES-R satellites will provide continuous monitoring of the solar corona in six EUV bandpasses that are similar to the ones provided by the SDO-AIA EUV telescope since May 2010. Supervised segmentations of EUV images that are consistent with manual segmentations by for example space-weather forecasters help in extracting useful information from the raw data.
Aims: We present a supervised segmentation method that is based on the Maximum A Posteriori rule. Our method allows integrating both manually segmented images as well as other type of information. It is applied on SDO-AIA images to segment them into AR, CH, and the remaining Quiet Sun (QS) part.
Methods: A Bayesian classifier is applied on training masks provided by the user. The noise structure in EUV images is non-trivial, and this suggests the use of a non-parametric kernel density estimator to fit the intensity distribution within each class. Under the Naive Bayes assumption we can add information such as latitude distribution and total coverage of each class in a consistent manner. Those information can be prescribed by an expert or estimated with an Expectation-Maximization algorithm.
Results: The segmentation masks are in line with the training masks given as input and show consistency over time. Introduction of additional information besides pixel intensity improves upon the quality of the final segmentation.
Conclusions: Such a tool can aid in building automated segmentations that are consistent with some ground truth' defined by the users.

Detecting undocumented trends in solar irradiance observations

Thierry Dudok **de Wit***
J. Space Weather Space Clim. **2022**, 12, 10
https://www.swsc-journal.org/articles/swsc/pdf/2022/01/swsc200095.pdf
Quantifying the long-term stability of solar irradiance observations is crucial for determining how the Sun varies in time and detecting decadal climate change signals. The stability of irradiance observations is challenged by the degradation of instrumental sensitivity in space and by the post-launch corrections needed to mitigate this degradation. We propose a new framework for detecting instrumental trends based on the existing idea of comparing the solar irradiance at pairs of dates for which a proxy quantity reaches the same level. Using a parametric model, we then reconstruct the trend and its confidence interval at all times. While this method cannot formally prove the instrumental origin of the trends, the observation of similar trends with different proxies provides strong evidence for a non-solar origin. We illustrate the method with spectral irradiance observations from the Solar Radiation and Climate Experiment (SORCE) mission, using various solar proxies such as sunspot number, MgII index, F10.7 index. The results support the existence of non-solar trends that exceed the level of solar cycle variability. After

correcting the spectral irradiance for these trends, we find the difference between the levels observed at solar maximum and at solar minimum to be in good agreement with irradiance models.

Response of Solar Irradiance to Sunspot-area Variations

T. Dudok **de Wit**1, G. Kopp2,3, A. Shapiro3, V. Witzke3, and M. Kretzschmar1
2018 ApJ 853 197
http://sci-hub.tw/10.3847/1538-4357/aa9f19
https://arxiv.org/pdf/1805.04350.pdf
One of the important open questions in solar irradiance studies is whether long-term variability (i.e., on timescales of years and beyond) can be reconstructed by means of models that describe short-term variability (i.e., days) using solar proxies as inputs. Preminger & Walton showed that the relationship between spectral solar irradiance and proxies of magnetic-flux emergence, such as the daily sunspot area, can be described in the framework of linear system theory by means of the impulse response. We significantly refine that empirical model by removing spurious solar-rotational effects and by including an additional term that captures long-term variations. Our results show that long-term variability cannot be reconstructed from the short-term response of the spectral irradiance, which questions the extension of solar proxy models to these timescales. In addition, we find that the solar response is nonlinear in a way that cannot be corrected simply by applying a rescaling to a sunspot area.

Uncertainties in the Sunspot Numbers: Estimation and Implications

Thierry Dudok **de Wit**, Laure Lefèvre, Frédéric Clette
Solar Phys. Volume 291, Issue 9, pp 2709–2731 **2016**
http://arxiv.org/pdf/1608.05261v1.pdf
Sunspot number series are subject to various uncertainties, which are still poorly known. The need for their better understanding was recently highlighted by the major makeover of the international Sunspot Number [Clette et al., Space Science Reviews, 2014]. We present the first thorough estimation of these uncertainties, which behave as Poisson-like random variables with a multiplicative coefficient that is time- and observatory-dependent. We provide a simple expression for these uncertainties, and reveal how their evolution in time coincides with changes in the observations, and processing of the data. Knowing their value is essential for properly building composites out of multiple observations, and for preserving the stability of the composites in time.

Synoptic observations at centimetric wavelengths are needed for a better description of solar forcing on the upper atmosphere

Thierry Dudok **De Wit**_y1, Sean Bruinsma2, Louis Hecker , Cl_emence Le F_evre , Pascal Perrachon , and Philippe Yaya
CESRA **2016**, p.80
http://cesra2016.sciencesconf.org/conference/cesra2016/pages/CESRA2016_prog_abs_book_v3.pdf
While the F10.7 index (ux at 10.7 cm) is probably the most widely used proxy for solar activity, radio emissions at other centimetric wavelengths are also good tracers. In particu-lar, the radio ux at 30 cm has an important contribution from thermal emissions, making it more sensitive to solar features such as plages an faculae. In contrast, the F10.7 index has a strong contribution from gyroemissions, and is a better proxy for the energetic part of the UV spectrum.
By replacing the F10.7 index by the 30 cm ux, we recently found that the performance of the **DTM2013 model for satellite drag** improves. By using blind source separation, we showed how the solar rotational variability in these centimetric wavelengths is made out of three contributions, one of which is thermal.
These properties of the 30 cm ux have motivated us to set up a prototype service that col-lects daily values at several wavelengths from the Nobeyama radio observatory, pre-processes them, and _nally delivers them in near real-time (with a forecast) for upper atmospheric mod-elling.
Here we discuss the di_erences between the F10.7 index and other centimetric wavelengths, and show why it is essential to consider multi-wavelength observations for achieving a better description of solar forcing on the upper atmosphere.

Three-polarizer Treatment of Linear Polarization in Coronagraphs and Heliospheric Imagers

Craig E. **DeForest**1, Daniel B. Seaton1, and Matthew J. West1
2022 ApJ 927 98
https://iopscience.iop.org/article/10.3847/1538-4357/ac43b6/pdf

Linearly polarized light has been used to view the solar corona for over 150 years. While the familiar Stokes representation for polarimetry is complete, it is best matched to a laboratory setting and therefore is not the most convenient representation either for coronal instrument design or for coronal data analysis. Over the last 100 years of development of coronagraphs and heliospheric imagers, various representations have been used for both direct measurement and analysis. These systems include famous representations such as the (B, pB) system, which is analogous to the Stokes system in solar observing coordinates, and also internal representations such as in-instrument Stokes parameters with fixed or variable "vertical" direction, and brightness values through a particular polarizing optic or set thereof. Many polarimetric instruments currently use a symmetric three-polarizer measurement and representation system (which we refer to as "(M, Z, P)") to derive the (B, pB) or Stokes parameters. We present a symmetric derivation of (B, pB) and Stokes parameters from (M, Z, P), analyze the noise properties of (M, Z, P) in the context of instrument design, develop (M, Z, P) as a useful intermediate system for data analysis including background subtraction, and draw a helpful analogy between linear polarimetric systems and the large existing body of work on photometric colorimetry.

FADING CORONAL STRUCTURE AND THE ONSET OF TURBULENCE IN THE YOUNG SOLAR WIND

C. E. **DeForest**1, W. H. Matthaeus2, N. M. Viall3, and S. R. Cranmer
2016 ApJ 828 66 DOI 10.3847/0004-637X/828/2/66
Above the top of the solar corona, the young, slow solar wind transitions from low-β, magnetically structured flow dominated by radial structures to high-β, less structured flow dominated by hydrodynamics. This transition, long inferred via theory, is readily apparent in the sky region close to 10° from the Sun in processed, background-subtracted solar wind images. We present image sequences collected by the inner Heliospheric Imager instrument on board theSolar-Terrestrial Relations Observatory (STEREO/HI1) in 2008 December, covering apparent distances from approximately 4° to 24° from the center of the Sun and spanning this transition in the large-scale morphology of the wind. We describe the observation and novel techniques to extract evolving image structure from the images, and we use those data and techniques to present and quantify the clear textural shift in the apparent structure of the corona and solar wind in this altitude range. We demonstrate that the change in apparent texture is due both to anomalous fading of the radial striae that characterize the corona and to anomalous relative brightening of locally dense puffs of solar wind that we term "flocculae." We show that these phenomena are inconsistent with smooth radial flow, but consistent with the onset of hydrodynamic or magnetohydrodynamic instabilities leading to a turbulent cascade in the young solar wind.
2008 December 16

Validating Forward Modeling and Inversions of Helioseismic Holography Measurements

K. **DeGrave** (1), D. C. Braun (1), A. C. Birch (2), A. D. Crouch, (1), B. Javornik (1)
ApJ **2018**
https://arxiv.org/pdf/1807.03841.pdf
Here we use synthetic data to explore the performance of forward models and inverse methods for helioseismic holography. Specifically, this work presents the first comprehensive test of inverse modeling for flows using lateral-vantage (deep-focus) holography. We derive sensitivity functions in the Born approximation. We then use these sensitivity functions in a series of forward models and inversions of flows from a publicly available magnetohydrodynamic quiet-Sun simulation. The forward travel times computed using the kernels generally compare favorably with measurements obtained by applying holography, in a lateral-vantage configuration, on a 15-hour time series of artificial Dopplergrams extracted from the simulation. Inversions for the horizontal flow components are able to reproduce the flows in the upper 3Mm of the domain, but are compromised by noise at greater depths.

Helioseismic Investigation of Modeled and Observed Supergranule Structure

K. **DeGrave**, J. Jackiewicz
Solar Phys. **2015**
http://arxiv.org/pdf/1504.01422v1.pdf
The subsurface structure of an "average" supergranule is derived from existing HMI pipeline time-distance data products and compared to the best helioseismic flow model detailed in Duvall and Hanasoge (2013). We find that significant differences exist between them. Unlike the shallow structure predicted by the model, the average HMI supergranule is very extended in depth, exhibiting horizontal outflow down to 7--10~Mm, followed by a weak inflow reaching a depth of ∼20~Mm below the photosphere. The maximal velocities in the horizontal direction for the average supergranule are much smaller than the model, and its near-surface flow field RMS value is about an order of magnitude smaller than the often-quoted values of ∼250−350~ms−1 for supergranulation. Much of the overall HMI supergranule structure and its weak flow amplitudes can be explained by examining the HMI pipeline averaging kernels for the near-surface inversions, which are found to be very broad in depth, and nearly identical to one another in terms of sensitivity along the z-direction. We also show that forward-modeled travel times in the

Born approximation using the model (derived from a ray theory approach) are inconsistent with measured travel times for an average supergranule at any distance. Our findings suggest systematic inaccuracies in the typical techniques used to study supergranulation, confirming some of the results in Duvall and Hanasoge (2013).

Time-Distance Helioseismology of Two Realistic Sunspot Simulations

K. **DeGrave**, J. Jackiewicz, M. Rempel

2014

http://arxiv.org/pdf/1408.2262v2.pdf

Linear time-distance helioseismic inversions are carried out using several filtering schemes to determine vector flow velocities within two ∼1002Mm2×20Mm realistic magnetohydrodynamic sunspot simulations of 25~hr. One simulation domain contains a model of a full sunspot (i.e. one with both an umbra and penumbra), while the other contains a pore (i.e. a spot without a penumbra). The goal is to test current helioseismic methods using these state-of-the-art simulations of magnetic structures. We find that horizontal flow correlations between inversion and simulation flow maps are reasonably high (~0.5--0.8) in the upper 3~Mm at distances exceeding 25--30~Mm from spot center, but are substantially lower at smaller distances and larger depths. Inversions of forward-modeled travel times consistently outperform those of our measured travel times in terms of horizontal flow correlations, suggesting that our inability to recover flow structure near these active regions is largely due to the fact that we are unable to accurately measure travel times near strong magnetic features. In many cases the velocity amplitudes from the inversions underestimate those of the simulations by up to 50\%, possibly indicating nonlinearity of the forward problem. In every case, we find that our inversions are unable to recover the vertical flow structure of the simulations at any depth.

Validating Time-Distance Helioseismology With Realistic Quiet Sun Simulations

K. **DeGrave**, J. Jackiewicz, M. Rempel

2014

http://arxiv.org/pdf/1404.4645v1.pdf

Linear time-distance helioseismic inversions are carried out for vector flow velocities using travel times measured from two ∼100^2 M m 2×20Mm realistic magnetohydrodynamic quiet-Sun simulations of about 20 hr. The goal is to test current seismic methods on these state-of-the-art simulations. Using recent three-dimensional inversion schemes, we find that inverted horizontal flow maps correlate well with the simulations in the upper ∼3 Mm of the domains for
several filtering schemes, including phase-speed, ridge, and combined phase-speed and ridge measurements. In several cases, however, the velocity amplitudes from the inversions severely underestimate those of the simulations, possibly indicating nonlinearity of the forward problem. We also find that, while near-surface inversions of the vertical velocites are best using phase-speed filters, in almost all other example cases these flows are irretrievable due to noise, suggesting a need for statistical averaging to obtain better inferences.

A Parabolic Equation Approach to Modeling Acousto-Gravity Waves for Local Helioseismology

Kevin **Del Bene**, Joseph Lingevitch , George Doschek

Solar Phys. Volume 291, Issue 6, pp 1581-1598 **2016**

A wide-angle parabolic-wave-equation algorithm is developed and validated for local-helioseismic wave propagation. The parabolic equation is derived from a factorization of the linearized acousto-gravity wave equation. We apply the parabolic-wave equation to modeling acoustic propagation in a plane-parallel waveguide with physical properties derived from helioseismic data. The wavenumber power spectrum and wave-packet arrival-time structure for receivers in the photosphere with separation up to 30∘30∘ is computed, and good agreement is demonstrated with measured values and a reference spectral model.

JP3D compression of solar data-cubes: photospheric imaging and spectropolarimetry

Dario **Del Moro**, Luca Giovannelli, Ermanno Pietropaolo, Francesco Berrilli

Exp Astron (**2017**) 43: 23. doi:10.1007/s10686-016-9518-x

https://arxiv.org/pdf/1705.06611.pdf

Hyperspectral imaging is an ubiquitous technique in solar physics observations and the recent advances in solar instrumentation enabled us to acquire and record data at an unprecedented rate. The huge amount of data which will be archived in the upcoming solar observatories press us to compress the data in order to reduce the storage space and transfer times. The correlation present over all dimensions, spatial, temporal and spectral, of solar data-sets

suggests the use of a 3D base wavelet decomposition, to achieve higher compression rates. In this work, we evaluate the performance of the recent JPEG2000 Part 10 standard, known as JP3D, for the lossless compression of several types of solar data-cubes. We explore the differences in: a) The compressibility of broad-band or narrow-band time-sequence; I or V stokes profiles in spectropolarimetric data-sets; b) Compressing data in [x,y,λ] packages at different times or data in [x,y,t] packages of different wavelength; c) Compressing a single large data-cube or several smaller data-cubes; d) Compressing data which is under-sampled or super-sampled with respect to the diffraction cut-off.

A Novel Investigation of the Small-scale Magnetic Activity of the Quiet Sun via the Hanle Effect in the Sr i 4607 Å Line

T. **del Pino Alemán**1, J. Trujillo Bueno1,2,3,6, J. Štěpán4, and N. Shchukina5
2018 ApJ 863 164
One of the key research problems in stellar physics is to decipher the small-scale magnetic activity of the quiet solar atmosphere. Recent magneto-convection simulations that account for small-scale dynamo action have provided three-dimensional (3D) models of the solar photosphere characterized by a high degree of small-scale magnetic activity, similar to that found through theoretical interpretation of the scattering polarization observed in the Sr i 4607 Å line. Here we present the results of a novel investigation of the Hanle effect in this resonance line based on 3D radiative transfer calculations in a high-resolution magneto-convection model having most of the convection zone magnetized close to the equipartition and a surface mean field strength G. The Hanle effect produced by the model's magnetic field depolarizes the zero-field scattering polarization signals significantly, to the extent that the center-to-limb variation (CLV) of the calculated spatially averaged polarization amplitudes is compatible with the observations. The standard deviation of the horizontal fluctuations of the calculated scattering polarization signals is very sensitive to the model's magnetic field, and we find that the predicted spatial variations are sufficiently sizable so as to be able to detect them, especially with the next generation of solar telescopes. We find that at all on-disk positions, the theoretical scattering polarization signals are anticorrelated with the continuum intensity. To facilitate reaching new observational breakthroughs, we show how the theoretically predicted polarization signals and spatial variations are modified when deteriorating the signal-to-noise ratio and the spectral and spatial resolutions of the simulated observations.

Multiwavelength Observations by XSM, Hinode, and SDO of an Active Region. Chemical Abundances and Temperatures

G**. Del Zanna**1, B. Mondal2,3, Y. K. Rao1, N. P. S. Mithun2, S. V. Vadawale2, K. K. Reeves4, H. E. Mason1, A. Sarkar2, P. Janardhan2, and A. Bhardwaj2
2022 ApJ 934 159
https://iopscience.iop.org/article/10.3847/1538-4357/ac7a9a/pdf
We have reviewed the first year of observations of the Solar X-ray Monitor (XSM) on board Chandrayaan-2 and the available multiwavelength observations to complement the XSM data, focusing on the Solar Dynamics Observatory AIA and Hinode XRT and EIS observations. XSM has provided disk-integrated solar spectra in the 1–15 keV energy range, observing a large number of microflares. We present an analysis of multiwavelength observations of AR 12759 during its disk crossing. We use a new radiometric calibration of EIS to find that the quiescent active region (AR) core emission during its disk crossing has a distribution of temperatures and chemical abundances that does not change significantly over time. An analysis of the XSM spectra confirms the EIS results and shows that the low first ionization potential (FIP) elements are enhanced compared to their photospheric values. The frequent microflares produced by the AR did not affect the abundances of the quiescent AR core. We also present an analysis of one of the flares it produced, SOL2020-04-09T09:32. The XSM analysis indicates isothermal temperatures reaching 6 MK. The lack of very high-T emission is confirmed by AIA. We find excellent agreement between the observed XSM spectrum and the one predicted using an AIA DEM analysis. In contrast, the XRT Al-poly/Be-thin filter ratio gives lower temperatures for the quiescent and flaring phases. We show that this is due to the sensitivity of this ratio to low temperatures, as the XRT filter ratios predicted with a DEM analysis based on EIS and AIA give values in good agreement with the observed ones. **29 Mar-12 Apr 2020, 8-9 Apr 2020**

High resolution soft X-ray spectroscopy and the quest for the hot (5-10 MK) plasma in solar active regions

G. **Del Zanna**, V. Andretta, P.J. Cargill, A.J.Corso, A.N. Daw, L. Golub, J.A. Klimchuk, H.E. Mason
Frontiers in Astronomy and Space Sciences, section Stellar and Solar Physics **2021**
https://arxiv.org/pdf/2103.06156
https://www.frontiersin.org/articles/10.3389/fspas.2021.638489/full
https://doi.org/10.3389/fspas.2021.638489
We discuss the diagnostics available to study the 5-10 MK plasma in the solar corona, which is key to understanding the heating in the cores of solar active regions. We present several simulated spectra, and show that excellent

diagnostics are available in the soft X-rays, around 100 Angstroms, as six ionisation stages of Fe can simultaneously be observed, and electron densities derived, within a narrow spectral region. As this spectral range is almost unexplored, we present an analysis of available and simulated spectra, to compare the hot emission with the cooler component. We adopt recently designed multilayers to present estimates of count rates in the hot lines, with a baseline spectrometer design. Excellent count rates are found, opening up the exciting opportunity to obtain high-resolution spectroscopy of hot plasma.

Helium line emissivities in the solar corona

G. **Del Zanna**, P.J. Storey, N.R. Badnell, V. Andretta
ApJ **898** 72 **2020**
https://arxiv.org/pdf/2006.08971.pdf
https://doi.org/10.3847/1538-4357/ab9d84
We present new collisional-radiative models (CRMs) for helium in the quiescent solar corona, and predict the emissivities of the He and He+ lines to be observed by DKIST, Solar Orbiter, and Proba-3. We discuss in detail the rates we selected for these models, highlighting several shortcomings we have found in previous work. As no previous complete and self-consistent coronal CRM for helium existed, we have benchmarked our largest model at a density of 106 cm−3 and temperature of 20,000 K against recent CRMs developed for photoionised nebulae. We then present results for the outer solar corona, using new dielectronic recombination rates we have calculated, which increase the abundance of neutral helium by about a factor of two. We also find that all the optical triplet He I lines, and in particular the well known He I 10830 and 5876 A lines are strongly affected by both photo-excitation and photo-ionisation from the disk radiation, and that extensive CRM models are required to obtain correct estimates. Close to the Sun, at an electron density of 108 cm−3 and temperature of 1 MK, we predict the emissivity of the He I 10830 A to be comparable to that of the strong Fe XIII coronal line at 10798 A. However, we expect the He I emissivity to sharply fall in the outer corona, with respect to Fe XIII. We confirm that the He+ Lyman α at 304 A is also significantly affected by photo-excitation and is expected to be detectable as a strong coronal line up to several solar radii.

Hinode EIS line widths in the quiet corona up to 1.5 Rsun

G. **Del Zanna**, G.R. Gupta, H.E. Mason
A&A 631, A163 **2019**
https://arxiv.org/pdf/1905.09783.pdf
https://doi.org/10.1051/0004-6361/201834625
We present an analysis of several Hinode EIS observations of coronal line widths in the quiet Sun, up to 1.5 Rsun radial distances. No significant variations are found, which indicates no damping of Alfvén waves in the quiescent corona. However, the uncertainties in estimating the instrumental width mean that a firm conclusion cannot be reached. We present a discussion of various EIS instrumental issues and suggest that the strongest lines, from Fe XII at 193.5 and 195.1 A, have anomalous instrumental widths. We show how line widths in EIS are uncertain when the signal is low, and that the instrumental variation along the slit is also uncertain. We also found an anomalous decrease (up to 40%) in the intensities of these lines in many off-limb and active region observations, and suggest that this is due to opacity effects. We find that the most reliable measurements are obtained from the weaker lines.

The EUV spectrum of the Sun: quiet and active Sun irradiances and chemical composition

G. **Del Zanna**
A&A 624, A36 **2019**
https://arxiv.org/pdf/1901.08841.pdf
We benchmark new atomic data against a selection of irradiances obtained from medium-resolution quiet Sun spectra in the EUV, from 60 to 1040 \AA. We use as a baseline the irradiances measured during solar minimum on **2008 April 14** by the prototype (PEVE) of the Solar Dynamics Observatory Extreme ultraviolet Variability Experiment (EVE). We take into account some inconsistencies in the PEVE data, using flight EVE data and irradiances we obtained from Solar & Heliospheric Observatory (SoHO) Coronal Diagnostics Spectrometer (CDS) data. We perform a differential emission measure and find overall excellent agreement (to within the accuracy of the observations, about 20%) between predicted and measured irradiances in most cases, although we point out several problems with the currently available ion charge state distributions. We used the photospheric chemical abundances of Asplund et al. (2009). The new atomic data are nearly complete in this spectral range, for medium-resolution irradiance spectra. Finally, we use observations of the active Sun in 1969 to show that also in that case the composition of the solar corona up to 1 MK is nearly photospheric. Variations of a factor of 2 are present for higher-temperature plasma, which is emitted within active regions.These results are in excellent agreement with our previous findings.

Solar UV and X-ray spectral diagnostics **Review**

Del Zanna, G. & Mason, H.E.

Living Rev Sol Phys 15: 5 (**2018**)
https://arxiv.org/pdf/1809.01618.pdf
https://link.springer.com/content/pdf/10.1007%2Fs41116-018-0015-3.pdf
X-ray and ultraviolet (UV) observations of the outer solar atmosphere have been used for many decades to measure the fundamental parameters of the solar plasma. This review focuses on the optically thin emission from the solar atmosphere, mostly found at UV and X-ray (XUV) wavelengths, and discusses some of the diagnostic methods that have been used to measure electron densities, electron temperatures, differential emission measure (DEM), and relative chemical abundances. We mainly focus on methods and results obtained from high-resolution spectroscopy, rather than broad-band imaging. However, we note that the best results are often obtained by combining imaging and spectroscopic observations. We also mainly focus the review on measurements of electron densities and temperatures obtained from single ion diagnostics, to avoid issues related to the ionisation state of the plasma. We start the review with a short historical introduction on the main XUV high-resolution spectrometers, then review the basics of optically thin emission and the main processes that affect the formation of a spectral line. We mainly discuss plasma in equilibrium, but briefly mention non-equilibrium ionisation and non-thermal electron distributions. We also summarise the status of atomic data, which are an essential part of the diagnostic process. We then review the methods used to measure electron densities, electron temperatures, the DEM, and relative chemical abundances, and the results obtained for the lower solar atmosphere (within a fraction of the solar radii), for coronal holes, the quiet Sun, active regions and flares.

Predicting the COSIE-C Signal from the Outer Corona up to 3 Solar Radii

Giulio **Del Zanna**, John Raymond, Vincenzo Andretta, Daniele Telloni, Leon Golub
ApJ **865** 132 **2018**
https://arxiv.org/pdf/1808.07951.pdf
sci-hub.tw/10.3847/1538-4357/aadcf1
We present estimates of the signal to be expected in quiescent solar conditions, as would be obtained with the COronal Spectrographic Imager in the EUV in its coronagraphic mode (COSIE-C). COSIE-C has been proposed to routinely observe the relatively unexplored outer corona, where we know that many fundamental processes affecting both the lower corona and the solar wind are taking place. The COSIE-C spectral band, 186--205 A, is well-known as it has been observed with Hinode EIS. We present Hinode EIS observations that we obtained in 2007 out to 1.5 Rsun, to show that this spectral band in quiescent streamers is dominated by Fe XII and Fe XI and that the ionization temperature is nearly constant. To estimate the COSIE-C signal in the 1.5--3.1 Rsun region we use a model based on CHIANTI atomic data and SoHO UVCS observations in the Si XII and Mg X coronal lines of two quiescent 1996 streamers. We reproduce the observed EUV radiances with a simple density model, photospheric abundances, and a constant temperature of 1.4 MK. We show that other theoretical or semi-empirical models fail to reproduce the observations. We find that the coronal COSIE-C signal at 3 Rsun should be about 5 counts/s per 3.1" pixel in quiescent streamers. This is unprecedented and opens up a significant discovery space. We also briefly discuss stray light and the visibility of other solar features. In particular, we present UVCS observations of an active region streamer, indicating increased signal compared to the quiet Sun cases.

Solar coronal lines in the visible and infrared. A rough guide **Review**

Giulio **Del Zanna**, Edward E. DeLuca
2018 ApJ 852 52
https://arxiv.org/pdf/1708.03626.pdf
We review the coronal visible and infrared lines, collecting previous observations, and comparing, whenever available, observed radiances with those predicted by various models: the quiet Sun, a moderately active Sun, and an active region as observed near the limb, around 1.1R⊙. We also model the off-limb radiances for the quiet Sun case. We used the most up-to-date atomic data in CHIANTI version 8. The comparison is satisfactory, in that all of the strong visible lines now have a firm identification. We revise several previous identifications and suggest some new ones. We also list the large number of observed lines for which we do not currently have atomic data, and therefore still await firm identifications. We also show that a significant number of coronal lines should be observable in the near-infrared region of the spectrum by the upcoming Daniel K. Inouye Solar Telescope (DKIST) and the AIR-Spec instrument, which will observe the corona during the **2017 August 21** solar eclipse. We also briefly discuss the many potential spectroscopic diagnostics available to the visible and infrared, with particular emphasis on measurements of electron densities and chemical abundances. We briefly point out some of the potential diagnostics that could be available with the future infrared instrumentation that is being built for DKIST. Finally, we highlight the need for further improvements in the atomic data.

EUV irradiances across a solar cycle

G. **Del Zanna**
UKSP Nugget #65, Feb **2016**
http://www.uksolphys.org/uksp-nugget/65-euv-irradiances-across-a-solar-cycle/

The analysis of the various EUV irradiances has allowed us to quantify how the irradiances of lines formed at temperatures above 1 MK are affected by the solar cycle. We have also shown that the irradiances of transition-region lines (e.g. O IV) are nearly unaffected by the solar cycle, with the exception of the helium lines.
In addition our results indicate that the CDS/NIS irradiances are the most reliable ones for Cycles 23 and 24, and that the SDO/EVE v.5 data, at least up to 2012, are in good agreement with CDS. However, the calibration of TIMED/EGS data, which are very limited after 2011, is clearly in need of revision. The solar minimum PEVE irradiances of 2008 have also been overestimated in several cases.

The EUV spectrum of the Sun: Irradiances during 1998–2014

G. **Del Zanna**1 and V. Andretta
A&A 584, A29 (**2015**)
We present calibrated EUV spectral irradiances obtained from observations with the Solar and Heliospheric Observatory (SOHO) Coronal Diagnostics Spectrometer (CDS) Normal Incidence Spectrometer (NIS) during the 1998–2014 period, which spans the cycle 23 maximum and minimum and the cycle 24 maximum. We revise the corrections for the burn-in of the strong lines and our previous long-term calibration of the NIS. We find no indications of further overall degradation of the instrument responsivities after 2010. We compare the CDS irradiances with those obtained by the prototype and flight instruments aboard the Solar Dynamics Observatory (SDO) Extreme ultraviolet Variability Experiment (EVE) and the Thermosphere Ionosphere Mesosphere Energetics Dynamics (TIMED) Solar EUV Experiment (SEE) EUV Grating Spectrograph (EGS). We find overall excellent agreement (to within a relative 10–20%) with the EVE data (especially during 2010–2012), but point out inconsistencies in some of the prototype and flight EVE irradiances. There is overall agreement with some of the TIMED SEE EGS data. We confirm the small variations in the irradiances of low-temperature lines (except the helium lines) and show that the irradiances in the hot (2–3 MK) lines are significantly lower for the cycle 24 maximum compared to the previous one.

The EUV spectrum of the Sun: SOHO, SEM, and CDS irradiances

G**. Del Zanna**1, S. R. Wieman2, V. Andretta3 and L. Didkovsky
A&A 581, A25 (**2015**)
http://www.aanda.org/articles/aa/pdf/2015/09/aa26227-15.pdf
We use calibrated extreme-UV (EUV) spectral irradiances obtained from observations with the Solar & Heliospheric Observatory (SOHO) Coronal Diagnostics Spectrometer Normal Incidence Spectrometer (NIS) to estimate the signal measured by the Solar EUV Monitor (SEM) first-order band, 260 to 340 Å (SEM 1). The NIS observes the resonance lines He ii 304 Å and Si xi 303 Å directly in second order. The irradiances of the other lines in the band are estimated with a differential emission measure (DEM) modelling, using updated atomic data. The observations analysed here were obtained during 1998–2011, which means that they span the maximum and minimum of Cycle 23. The current knowledge of the SEM 1 degradation is used to find effective areas during the dates of the NIS observations and to predict the SEM 1 count rates across the band. The total count rates, estimated by folding the NIS-based spectra with the SEM 1 effective areas, agree very well (within 10–20%) with the observed ones during solar minimum conditions, when the He ii 304 Å is the dominant contribution to the band. Excellent agreement with the Solar Dynamics Observatory (SDO) Extreme ultraviolet Variability Experiment (EVE) observations is also found. On the other hand, the predicted SEM 1 count rates during the Cycle-23 maximum are significantly (by about 30%) lower than the observed ones. The solar spectrum in the SEM 1 band changes significantly during maximum conditions, with the He ii 304 Å only contributing about 40%. A significant fraction of the observed count rates comes from coronal emission in an off-band spectral region that has recently been discovered. An explanation for the discrepancy needs further investigation.

Editorial: Active Experiments in Space: Past, Present, and Future
Gian Luca **Delzanno**, Joseph E. Borovsky, and Evgeny Mishin
Front. Astron. Space Sci., 06 March **2020** | https://doi.org/10.3389/fspas.2020.00005
https://www.frontiersin.org/articles/10.3389/fspas.2020.00005/pdf
THIS ARTICLE IS PART OF THE RESEARCH TOPIC
Active Experiments in Space: Past, Present, and Future **View all 20 Articles**

Improving the Spatial Resolution of Solar Images Using Generative Adversarial Network and Self-attention Mechanism*

Junlan **Deng**1, Wei Song1,2,3, Dan Liu1, Qin Li4,5, Ganghua Lin2,6, and Haimin Wang4,5,7
2021 ApJ 923 76
https://doi.org/10.3847/1538-4357/ac2aa2

In recent years, the new physics of the Sun has been revealed using advanced data with high spatial and temporal resolutions. The Helioseismic and Magnetic Imager (HMI) on board the Solar Dynamic Observatory has accumulated abundant observation data for the study of solar activity with sufficient cadence, but their spatial resolution (about 1") is not enough to analyze the subarcsecond structure of the Sun. On the other hand, high-resolution observation from large-aperture ground-based telescopes, such as the 1.6 m Goode Solar Telescope (GST) at the Big Bear Solar Observatory, can achieve a much higher resolution on the order of $0\farcs1$ (about 70 km). However, these high-resolution data only became available in the past 10 yr, with a limited time period during the day and with a very limited field of view. The Generative Adversarial Network (GAN) has greatly improved the perceptual quality of images in image translation tasks, and the self-attention mechanism can retrieve rich information from images. This paper uses HMI and GST images to construct a precisely aligned data set based on the scale-invariant feature transform algorithm and t0 reconstruct the HMI continuum images with four times better resolution. Neural networks based on the conditional GAN and self-attention mechanism are trained to restore the details of solar active regions and to predict the reconstruction error. The experimental results show that the reconstructed images are in good agreement with GST images, demonstrating the success of resolution improvement using machine learning.

The spatial distribution of quasi-biennial oscillations in the high-latitude solar activity

L. H. **Deng**, Y. Fei, H. Deng, Y. Mei, F. Wang

MNRAS Volume 494, Issue 4, June 2020, Pages 4930–4938, **2020**

https://arxiv.org/pdf/2004.08331.pdf

https://doi.org/10.1093/mnras/staa1061

Magnetic activity at low latitudes (≤50◦). However, the evolutionary aspect and the hemispheric distribution of solar QBOs at high latitudes (≥60◦) are rarely studied. Here, a relatively novel time-frequency analysis technique, named the synchrosqueezed wavelet transform, is applied to extract the main components of the polar faculae in the northern and southern hemispheres for the time interval from August 1951 to December 1998. It is found as the following: (1) Apart from the 22-year Hale cycle, the 17-year extended activity cycle, and the 11-year Schwabe cycle, the QBOs have been estimated as a prominent timescale of solar magnetic activity at high latitudes; (2) the QBOs of the polar faculae are coherent in the two hemispheres, but the temporal (phase) and the spatial (amplitude) variations of solar QBOs occur unevenly on both hemispheres; and (3) for the 11-year period mode, the northern hemisphere begins three months earlier than that in the southern one. Moreover, the spatial and temporal distributions of the hemispheric QBOs differ from those of the 11-year Schwabe cycle mode in the two hemispheres. Our findings could be helpful to improve our knowledge on the physical origin of the spatial distribution of solar QBOs at high latitudes, and could also provide more constraints on solar dynamo models introduced to characterize the different components of the solar magnetic activity cycle.

Systematic Regularity of Solar Coronal Rotation During the Time Interval 1939-2019

L. H. **Deng**, X. J. Zhang, H. Deng, Y. Mei, F. Wang

MNRAS **2019**

https://arxiv.org/pdf/1911.08131.pdf

Temporal variation of the solar coronal rotation appears to be very complex and its relevances to the eleven-year solar activity cycle are still unclear. Using the modified coronal index for the time interval from 1939 January 1 to 2019 May 31, the systematic regularities of the solar coronal rotation are investigated. Our main findings are as follows: (1) from a global point of view, the synodic coronal rotation period with a value of 27.5 days is the only significant period at the periodic scales shorter than 64 days; (2) the coronal rotation period exhibit an obviously decreasing trend during the considered time interval, implying the solar corona accelerates its global rotation rate in the long run; (3) there exist significant periods of 3.25, 6.13, 9.53, and 11.13 years in the period length of the coronal rotation, providing an evidence that the coronal rotation should be connected with the quasi-biennial oscillation, the eleven-year solar cycle, and the 22-year Hale cycle (or the magnetic activity reversal); and (4) the phase relationship between the coronal rotation period and the solar magnetic activity is not only time-dependent but also frequency-dependent. For a small range around the 11- year cycle band, there is a systematic trend in the phase, and the small mismatch in this band brings out the phase to drift. The possible mechanism for the above analysis results is discussed.

Periodic variation and phase analysis of grouped solar flare with sunspot activity

Hui **Deng**, Ying Mei, Feng Wang

Research in Astronomy and Astrophysics **2019**

https://arxiv.org/pdf/1910.02671.pdf

Studies on the periodic variation and the phase relationship between different solar activity indicators are useful for understanding the long-term evolution of solar activity cycle. Here we report the statistical analysis of grouped solar flare (GSF) and sunspot number (SN) during the time interval from January 1965 to March 2009. We find that, 1) the significant periodicities of both GSF and SN are related to the differential rotation periodicity, the quasi-biennial

oscillation (QBO), and the eleven-year Schwabe cycle (ESC), but the specific values are not absolutely identical; 2) the ESC signal of GSF lags behind that of SN with an average of 7.8 months during the considered time interval, implying that the systematic phase delays between GSF and SN originate from the inter-solar-cycle signal. Our results may provide evidence about the storage of magnetic energy in the corona.

Phase and amplitude asymmetry in the quasi-biennial oscillation of solar Halpha flare activity

L. H. **Deng**, X. J. Zhang, G. Y. Li, H. Deng, F. Wang
MNRAS **2019**
https://arxiv.org/pdf/1910.02891.pdf
Quasi-biennial oscillation (QBO) of solar magnetic activities is intrinsic to dynamo mechanism, but still far from fully understood. In this work, the phase and amplitude asymmetry of solar QBO of Halpha flare activity in the northern and southern hemispheres is studied by the ensemble empirical mode decomposition, the cross-correlation analysis, and the wavelet transform technique. The following results are found: (1) solar QBO of Halpha flare index in the two hemispheres has a complicated phase relationship, but does not show any systematic regularity; (2) the solar cycle mode of solar Halpha flare index in the northern hemisphere generally leads that in the southern one by 9 months for the time interval from 1966 to 2014. The possible origin of these results is discussed.

Statistical properties of solar Hα flare activity

Linhua **Deng**, Xiaojuan Zhang, Jianmei An and Yunfang Cai
J. Space Weather Space Clim. **2017**, 7, A34
https://www.swsc-journal.org/articles/swsc/pdf/2017/01/swsc170008.pdf
Magnetic field structures on the solar atmosphere are not symmetric distribution in the northern and southern hemispheres, which is an important aspect of quasi-cyclical evolution of magnetic activity indicators that are related to solar dynamo theories. Three standard analysis techniques are applied to analyze the hemispheric coupling (north-south asymmetry and phase asynchrony) of monthly averaged values of solar Hα flare activity over the past 49 years (from 1966 January to 2014 December). The prominent results are as follows: (1) from a global point of view, solar Hα flare activity on both hemispheres are strongly correlated with each other, but the northern hemisphere precedes the southern one with a phase shift of 7 months; (2) the long-range persistence indeed exists in solar Hα flare activity, but the dynamical complexities in the two hemispheres are not identical; (3) the prominent periodicities of Hα flare activity are 17 years full-disk activity cycle and 11 years Schwabe solar cycle, but the short- and mid-term periodicities cannot determined by monthly time series; (4) by comparing the non-parametric rescaling behavior on a point-by-point basis, the hemispheric asynchrony of solar Hα flare activity are estimated to be ranging from several months to tens of months with an average value of 8.7 months. The analysis results could promote our knowledge on the long-range persistence, the quasi-periodic variation, and the hemispheric asynchrony of solar Hα flare activity on both hemispheres, and possibly provide valuable information for the hemispheric interrelation of solar magnetic activity.

Multi-wavelength Study of Transition Region Penumbral Subarcsecond Bright Dots Using IRIS and NST

Na **Deng**, Vasyl Yurchyshyn, Hui Tian, Lucia Kleint, Chang Liu, Yan Xu, Haimin Wang
ApJ 829 103 **2016**
http://arxiv.org/pdf/1607.00306v1.pdf
Using high-resolution transition region (TR) observations taken by the Interface Region Imaging Spectrograph (IRIS) mission, Tian et al. (2014b) revealed numerous short-lived subarcsecond bright dots (BDs) above sunspots (mostly located in the penumbrae), which indicate yet unexplained small-scale energy releases. Moreover, whether these subarcsecond TR brightenings have any signature in the lower atmosphere and how they are formed are still not fully resolved. This paper presents a multi-wavelength study of the TR penumbral BDs using a coordinated observation of a near disk-center sunspot with IRIS and the 1.6 m New Solar Telescope (NST) at the Big Bear Solar Observatory. NST provides high-resolution chromospheric and photospheric observations with narrow-band H-alpha imaging spectroscopy and broad-band TiO images, respectively, complementary to IRIS TR observations. A total of 2692 TR penumbral BDs are identified from a 37-minute time series of IRIS 1400 A slitjaw images. Their locations tend to be associated more with downflowing and darker fibrils in the chromosphere, and weakly associated with bright penumbral features in the photosphere. However, temporal evolution analyses of the BDs show that there is no consistent and convincing brightening response in the chromosphere. These results are compatible with a formation mechanism of the TR penumbral BDs by falling plasma from coronal heights along more vertical and dense magnetic loops. The BDs may also be produced by small-scale impulsive magnetic reconnection taking place sufficiently high in the atmosphere that has no energy release in the chromosphere.

Objective Image-Quality Assessment for High-Resolution Photospheric Images by Median Filter-Gradient Similarity

Hui **Deng**, Dandan Zhang, Tianyu Wang, Kaifan Ji, Feng Wang, Zhong Liu, Yongyuan Xiang,Zhenyu Jin,
Wenda Cao
Solar Phys. **2015**

All next-generation ground-based and space-based solar telescopes require a good quality-assessment metric to evaluate their imaging performance. In this paper, a new image quality metric, the median filter-gradient similarity (MFGS) is proposed for photospheric images. MFGS is a no-reference/blind objective image-quality metric (IQM) by a measurement result between 0 and 1 and has been performed on short-exposure photospheric images captured by the New Vacuum Solar Telescope (NVST) of the Fuxian Solar Observatory and by the Solar Optical Telescope (SOT) onboard the Hinode satellite, respectively. The results show that (1) the measured value of the MFGS changes monotonically from 1 to 0 with degradation of image quality; (2) there exists a linear correlation between the measured values of the MFGS and the root-mean-square contrast (RMS-contrast) of the granulation; (3) the MFGS is less affected by the image contents than the granular RMS-contrast. Overall, the MFGS is a good alternative for the quality assessment of photospheric images.

Chromospheric Rapid Blueshifted Excursions Observed with IBIS and Their Association with Photospheric Magnetic Field Evolution

Na **Deng**, Xin Chen, Chang Liu, Ju Jing, Alexandra Tritschler, Kevin P. Reardon, Derek A. Lamb, Craig E. Deforest, Carsten Denker, Shuo Wang, Rui Liu, Haimin Wang
ApJ, **799** 219 **2015**
http://arxiv.org/pdf/1412.4038v1.pdf

Chromospheric rapid blueshifted excursions (RBEs) are suggested to be the disk counterparts of type II spicules at the limb and believed to contribute to the coronal heating process. Previous identification of RBEs was mainly based on feature detection using Dopplergrams. In this paper, we study RBEs on **2011 October 21** in a very quiet region at the disk center, which were observed with the high-cadence imaging spectroscopy of the Ca II 8542 A line from the Interferometric Bidimensional Spectrometer (IBIS). By using an automatic spectral analysis algorithm, a total of 98 RBEs are identified during a 11 minute period. Most of these RBEs have either a round or elongated shape, with an average area of 1.2 arcsec^2. The detailed temporal evolution of spectra from IBIS makes possible a quantitative determination of the velocity (~16 km/s) and acceleration (~400 m/s^2) of Ca II 8542 RBEs, and reveal an additional deceleration (~-160 m/s^2) phase that usually follows the initial acceleration. In addition, we also investigate the association of RBEs with the concomitant photospheric magnetic field evolution, using coordinated high-resolution and high-sensitivity magnetograms made by Hinode. Clear examples are found where RBEs appear to be associated with the preceding magnetic flux emergence and/or the subsequent flux cancellation. However, a further analysis with the aid of the Southwest Automatic Magnetic Identification Suite does not yield a significant statistical association between these RBEs and magnetic field evolution. We discuss the implications of our results in the context of understanding the driving mechanism of RBEs.

Multi-scale analysis of coronal Fe xiv emission: The role of mid-range periodicities in the Sun–heliosphere connection

L.H. **Deng**, B. Li, Y.Y. Xiang, G.T. Dun
JASTP, Volume 122, January **2015**, Pages 18–25

Two relatively modern analysis techniques, including the empirical mode decomposition and Morlet wavelet transform, are combined to investigate the short- and mid-term periodicities of daily coronal index from 1 January 1939 to 31 December 2008. Apart from the well-known periodicities of annual-oscillation variation, 11-year Schwabe cycle, 17-year full-disk activity cycle and 22-year magnetic cycle, the combined procedure reveals a variety of mid-term quasi-periodicities (MTQPs) in this solar-activity indicator, especially the periodicities near the 1.3 and 1.7 years. The prominent results show the followings: (1) the synodic rotation periodicities of 26 and 29 days correspond to the two principal components (the fast and slow types) of differential rotation in the solar corona; (2) the Rieger-type periodicity near 150 days is not found in time series of coronal index, which may be due to the intermittent character of its quasi-periodic pattern; (3) the MTQPs with a shorter periodicity around 1.3 years and a longer one around 1.7 years indeed exist in the solar coronal region. Our analysis results suggest that the coronal dynamics should be a connecting agent among the oscillations in the tachocline layer (Howe et al., 2000), in the lower atmospheric layers (Krivova and Solanki, 2002) and in the interplanetary space (Mursula and Vilppola, 2004).

On mid-term periodicities of high-latitude solar activity

L.H. **Deng**, B. Li, , , Y.Y. Xiang, G.T. Dun
Advances in Space Research, **2014**
The mid-term periodicities of polar faculae are studied separately for the total disk, northern and southern hemispheres of the Sun for a time interval from 1951 August to 1998 December. Apart from the 11-year Schwabe cycle which is the fundamental period and is found in all of the three time series, the following prominent results are found: (1) the rotational periodicity of solar activity at high latitudes is approximately from 28 to 32 days; (2) a large number of quasi-periods appearing in low-latitude solar activity (annual variation, 1.3-1.7 years, quasi-biennial oscillation, and 4-5 years) also exist in polar faculae; (3) the periodicities on both hemispheres are not identical.

Phase asynchrony between coronal index and sunspot numbers

L.H. **Deng**, Z.Q. Qu, K.R. Wang, X.B. Li
Adv. Space Res., 50(10), 1425-1433, **2012**
In this paper, the phase asynchrony between coronal index and sunspot numbers is investigated. It is found that, (1) the sunspot numbers begin one month earlier than coronal index, which should mathematically lead to phase asynchrony between them but with a slight effect; (2) the 11-year Schwabe cycle is the only one period with statistical significance for coronal index and sunspot numbers, and the difference between the length of the Schwabe cycle of them should also lead to phase asynchrony between them; (3) although coronal index and sunspot numbers are coherent in low-frequency components corresponding to the 11-year Schwabe cycle, they are asynchronous in phase in high-frequency components; (4) their different definitions and physical meanings may be a major reason why there is a phase asynchrony between them.

Background-subtracted Solar Activity Maps

Carsten **Denker**, Meetu Verma
Solar Phys. 294:71 **2019**
https://arxiv.org/pdf/1905.06057.pdf
https://link.springer.com/content/pdf/10.1007%2Fs11207-019-1459-x.pdf
We introduce the concept of a Background-subtracted Solar Activity Map (BaSAM) as a new quantitative tool to assess and visualize the temporal variation of the photospheric magnetic field and the UV 160 nm intensity. The method utilizes data of the Solar Dynamics Observatory (SDO) and is applicable to both full-disk observations and regions-of-interest. We illustrate and discuss the potential of BaSAM resorting to datasets representing solar minimum and maximum conditions: (1) Contributions of quiet-Sun magnetic fields, i.e. the network and (decaying) plage, to solar activity can be better determined when their variation is measured with respect to the background given by "deep" magnetograms. (2) Flaring and intermittent brightenings are easily appraised in BaSAMs of the UV intensity. (3) Both magnetic-field and intensity variations demonstrated that the flux system of sunspots is well connected to the surrounding supergranular cells. In addition, producing daily full-disk BaSAMs for the entire mission time of SDO provides a unique tool to analyze solar cycle variations, showing how vigorous or frail are the variations of magnetic-field and intensity features. **2018 February 19** , **2014 April 17**

High-Cadence Imaging and Imaging Spectroscopy at the GREGOR Solar Telescope – A Collaborative Research Environment for High-Resolution Solar Physics

C. **Denker**, C. Kuckein, M. Verma, S. J. González Manrique, A. Diercke, H. Enke, J. Klar, H. Balthasar, R. E. Louis, E. Dineva
Astrophysical Journal Supplement Series **236** 5 **2018**
https://arxiv.org/pdf/1802.10146.pdf
In high-resolution solar physics, the volume and complexity of photometric, spectroscopic, and polarimetric ground-based data significantly increased in the last decade reaching data acquisition rates of terabytes per hour. This is driven by the desire to capture fast processes on the Sun and by the necessity for short exposure times "freezing" the atmospheric seeing, thus enabling post-facto image restoration. Consequently, large-format and high-cadence detectors are nowadays used in solar observations to facilitate image restoration. Based on our experience during the "early science" phase with the 1.5-meter GREGOR solar telescope (2014-2015) and the subsequent transition to routine observations in 2016, we describe data collection and data management tailored towards image restoration and imaging spectroscopy. We outline our approaches regarding data processing, analysis, and archiving for two of GREGOR's post-focus instruments (see this http URL), i.e., the GREGOR Fabry-Perot Interferometer (GFPI) and the newly installed High-Resolution Fast Imager (HiFI). The heterogeneous and complex nature of multi-dimensional data arising from high-resolution solar observations provides an intriguing but also a challenging example for "big data" in astronomy. The big data challenge has two aspects: (1) establishing a workflow for publishing the data for the whole community and beyond and (2) creating a Collaborative Research Environment (CRE), where computationally intense data and post-processing tools are co-located and collaborative work is enabled for scientists of multiple institutes. This requires either collaboration with a data center or frameworks and databases capable of dealing with huge data sets based on Virtual Observatory (VO) and other community standards and procedures. **2014 August 14, 2016 April 11., 2016 September 24, 2017 March 25.**

Image Quality in High-resolution and High-cadence Solar Imaging

C. **Denker**, E. Dineva, H. Balthasar, M. Verma, C. Kuckein, A. Diercke, S.J. González Manrique
Solar Phys. 293:44 **2018**
https://arxiv.org/pdf/1802.00760.pdf
https://link.springer.com/content/pdf/10.1007%2Fs11207-018-1261-1.pdf
Broad-band imaging and even imaging with a moderate bandpass (about 1 nm) provides a "photon-rich" environment, where frame selection ("lucky imaging") becomes a helpful tool in image restoration allowing us to perform a cost-benefit analysis on how to design observing sequences for high-spatial resolution imaging in combination with real-time correction provided by an adaptive optics (AO) system. This study presents high-cadence (160 Hz) G-band and blue continuum image sequences obtained with the High-resolution Fast Imager (HiFI) at the 1.5-meter GREGOR solar telescope, where the speckle masking technique is used to restore images with nearly diffraction-limited resolution. HiFI employs two synchronized large-format and high-cadence sCMOS detectors. The Median Filter Gradient Similarity (MFGS) image quality metric is applied, among others, to AO-corrected image sequences of a pore and a small sunspot observed on **2017 June 4 and 5**. A small region-of-interest, which was selected for fast imaging performance, covered these contrast-rich features and their neighborhood, which were part of active region NOAA 12661. Modifications of the MFGS algorithm uncover the field- and structure-dependency of this image quality metric. However, MFGS still remains a good choice for determining image quality without a priori knowledge, which is an important characteristic when classifying the huge number of high-resolution images contained in data archives. In addition, this investigation demonstrates that a fast cadence and millisecond exposure times are still insufficient to reach the coherence time of daytime seeing. Nonetheless, the analysis shows that data acquisition rates exceeding 50 Hz are required to capture a substantial fraction of the best seeing moments, significantly boosting the performance of post-facto image restoration.

Emission Measures Demystified.

Dennis, B.R., Phillips, K.J.H.
Sol Phys 299, 48 (**2024**).
https://doi.org/10.1007/s11207-024-02291-1
We review the terms spectral radiance and spectral irradiance, and show how their precise definitions are crucial for interpreting observations made with different instruments covering widely different energy or wavelength ranges. We show how the use of column and volume emission measures in different solar physics and astrophysics communities has led to confusion in relating measured extreme-ultraviolet and soft-X-ray spectra with theoretical spectra generated, in particular, using CHIANTI. We describe a method for obtaining spatially integrated X-ray line and continuum spectra using CHIANTI that requires a column emission measure when only the plasma temperature and volume emission measure, but not the source area, are known from observations.

Quiet Sun electron densities and their uncertainties derived from spectral emission line intensities

Kenneth **Dere**
MNRAS Volume 496, Issue 2, Pages 2334–2345 **2020**
https://arxiv.org/pdf/2006.04184.pdf
https://doi.org/10.1093/mnras/staa1645
The goal of this paper is to apply statistical methods to determine electrons densities and their errors from measurements of density-sensitive line intensities in the quiet Sun. Three methods are employed. The first is the use of L-function plots to provide a quick visual assessment of the likelihood that a set of line intensities can provide a robust estimate of these quantities. A second methods involves a chi-squared minimization together with a prescription for determining the regions of statistical confidence in addition to the best-fitting value. A third method uses a Bayesian inference technique that employs a Monte-Carlo Markov-chain (MCMC) calculation from which an analysis of the posterior distributions provide estimates of the mean and regions of high probability density. Using these three methods, observations of extreme-ultraviolet spectral lines originating from regions of the quiet Sun have been analyzed. The quantitative chi-squared minimization and MCMC sampling provide results that are generally in good agreement, especially for sets of lines of ions that have L-function plots that suggest that a robust analysis might be possible.

Probing the Sunspot Atmosphere with Three-Minute Oscillations

Anastasiia **Deres**, Sergey Anfinogentov
Solar Physics January **2018**, 293:2
https://link.springer.com/content/pdf/10.1007%2Fs11207-017-1222-0.pdf
https://arxiv.org/pdf/1710.11552.pdf

We present a seismological method for probing the solar atmosphere above sunspot umbrae with three-minute oscillations. Our technique allows us to estimate both the vertical distance between atmospheric layers and the wave-propagation speed, without specifying any additional parameters, in particular, the phase speed of the wave or the emission formation heights. Our method uses the projected wave paths of slow magnetohydrodynamic waves that propagate through the atmospheric layers of different heights and are guided by the magnetic field. The length of the projected wave path depends upon the distance between the layers and the inclination angle of the magnetic field with respect to the line of sight, allowing us to estimate the distance between the layers from measured projected wave paths and the local magnetic-field vector. In turn, the wave-propagation delay registered at different heights allows for the calculation of the phase speed. We estimated the vertical distance between the emission layers at the temperature minimum (1600 Å) and transition region (304 Å), as well as the average phase speed above the sunspot umbrae, for three active regions. We found that the distance between the 1600 Å emission layer and the transition region above the sunspot umbrae lies in the range of 500 – 800 km. The average phase speed between these layers was found to be about 30 $km\,s^{-1}$, giving a sound speed of 6 $km\,s^{-1}$. The temperature between the layers has been roughly estimated as 3000 K and corresponds to the region of the temperature minimum. The results obtained are consistent with the semiempirical model of the sunspot-umbrae atmosphere by Fontenla *et al.* (*Astrophys. J.***707**, 482, 2009). **8 December 2010, 2 October 2012, 6 April 2013**

Acoustic Waves in a High-Temperature Plasma III. Two-Periodic Disturbances.

Derteev, S.B., Sapraliev, M.E., Shividov, N.K. et al.
Sol Phys 299, 141 (**2024**).
https://doi.org/10.1007/s11207-024-02381-0
The aim of this work is to study the dispersion of acoustic waves in the rarefied high-temperature plasma of the solar corona and its role in propagating intensity disturbances (PDs) occurring in this region. We believe that a multi-periodicity in wavelet spectra, recorded when observing PDs in coronal holes and loops, is due to a result of the combined effect of dispersion and damping of compression waves. Observations show the presence of continuous spectra, where periods are distinguished by suitable maxima. The shape of the spectra is characteristic of localized disturbances. This study is based on our previously proposed clear model of nonadiabatic waves in high-temperature plasma, which takes into account the properties of thermal conduction, radiative cooling, and constant heating. Thermal conduction forms a local minimum of group speed, separating groups of waves with short and long periods. Waves of the first group have strong dispersion and weak damping while waves of the second group have the opposite properties. This effect leads to the fact that the initial pulse disturbance eventually acquires a form in which the indicated groups are clearly separated. Two maxima appear in the wavelet spectrum which determine the short period Ps and the long period Pl. Two groups of waves with dominant periods propagate at the same speed, which is less than the sound speed. We assume that the form of PDs can indeed arise in the corona under the influence of small-scale disturbances in the lower atmosphere. The speed of the observed disturbances is also less than the sound speed. This is usually explained by the projection effect, but can also be explained by the fact that PDs propagate with a group speed. The time signals in the corona recorded by observing PDs bear little resemblance to the superposition of just a few harmonic components. The observed periods are not regular, they can change several times during the entire observation time (often 2 – 3 hours). We propose to consider PDs as a sequence of independent pulse disturbances. Two periods occur only in a given pulse, the duration of which is on the order of a long period Pl, often 20 – 30 minutes. They may change in the next pulse, since they depend on the length of the initial pulse formed at the boundary of the corona and the lower atmosphere.

Variation of Chromospheric Features as a Function of Latitude and Time using Ca-K Spectroheliograms for Solar Cycles 15-23: Implications for Meridional Flow

Pooja **Devi**, Jagdev Singh, Ramesh Chandra, Muthu Priyal, Reetika Joshi
Solar Phys. **296**, Article number: 49 **2021**
https://arxiv.org/pdf/2102.04864.pdf
https://link.springer.com/content/pdf/10.1007/s11207-021-01798-1.pdf
https://doi.org/10.1007/s11207-021-01798-1
We have analysed the Ca-K images obtained at Kodaikanal Observatory as a function of latitude and time for the period of 1913 - 2004 covering the Solar Cycle 15 to 23. We have classified the chromospheric activity into plage, Enhanced Network (EN), Active Network (AN), and Quiet Network (QN) areas to differentiate between large strong active and small weak active regions. The strong active regions represent toroidal and weak active regions poloidal component of the magnetic field. We find that plages areas mostly up to 50 deg latitude belt vary with about 11-year Solar Cycle. We also find that weak activity represented by EN, AN and QN varies with about 11-year with significant amplitude up to about 50 deg latitude in both the hemispheres. The amplitude of variation is minimum around 50 deg latitude and again increases by small amount in the polar region. In addition, the plots of plages, EN, AN and QN as a function of time indicate the maximum of activity at different latitude occur at different epoch. To determine the phase difference for the different latitude belts, we have computed the cross-correlation coefficients of other latitude belts with 35 deg latitude belt. We find that activity shifts from mid-latitude belts

towards equatorial belts at fast speed at the beginning of Solar Cycle and at slower speed as the cycle progresses. The speed of shift varies between approximately 19 and 3 m/s considering all the data for the observed period. This speed can be linked with speed of meridional flows those believed to occur between convection zone and the surface of the Sun.

Validating time-distance helioseismic inversions for non-separable subsurface profiles of an average supergranule

Vedant **Dhruv**, Jishnu Bhattacharya, Shravan Hanasoge
ApJ 883 136 **2019**
https://arxiv.org/pdf/1908.08456.pdf
https://doi.org/10.3847/1538-4357/ab3a95
Supergranules are divergent 30-Mm sized cellular flows observed everywhere at the solar photosphere. Their place in the hierarchy of convective structures and their origin remain poorly understood (Rincon et al., 2018). Estimating supergranular depth is of particular interest since this may help point to the underlying physics. However, their subsurface velocity profiles have proven difficult to ascertain. Birch et al. (2006) had suggested that helioseismic inferences would benefit from an ensemble average over multiple realizations of supergranules due to the reduction in realization noise. Bhattacharya et al. (2017) used synthetic forward-modelled seismic wave travel times and demonstrated the potential of helioseismic inversions at recovering the flow profile of an average supergranule that is separable in the horizontal and vertical directions, although the premise of this calculation has since been challenged by Ferret (2019). In this work we avoid this assumption and carry out a validation test of helioseismic travel-time inversions starting from plausible synthetic non-separable profiles of an average supergranule. We compute seismic wave travel times and sensitivity kernels by simulating wave propagation through this background. We find that, while the ability to recover the exact profile degrades based on the number of parameters involved, we are nevertheless able to recover the peak depth of our models in a few iterations where the measurements are presumably above the noise cutoff. This represents an important step towards unraveling the physics behind supergranules, as we start appreciating the parameters that we may reliably infer from a time-distance helioseismic inversion.

The Effect of Limited Sample Sizes on the Accuracy of the Estimated Scaling Parameter for Power-Law-Distributed Solar Data

Elke **D'Huys**, David Berghmans, Daniel B. Seaton, Stefaan Poedts
Solar Phys. Volume 291, Issue 5, pp 1561-1576 **2016**
http://arxiv.org/pdf/1605.06972v1.pdf
Many natural processes exhibit power-law behavior. The power-law exponent is linked to the underlying physical process and therefore its precise value is of interest. With respect to the energy content of nanoflares, for example, a power-law exponent steeper than 2 is believed to be a necessary condition to solve the enigmatic coronal heating problem. Studying power-law distributions over several orders of magnitudes requires sufficient data and appropriate methodology. In this paper we demonstrate the shortcomings of some popular methods in solar physics that are applied to data of typical sample sizes. We use synthetic data to study the effect of the sample size on the performance of different estimation methods and show that vast amounts of data are needed to obtain a reliable result with graphical methods (where the power-law exponent is estimated by a linear fit on a log-transformed histogram of the data). We **revisit published results on power laws for the angular width of solar coronal mass ejections and the radiative losses of nanoflares.** We demonstrate the benefits of the maximum likelihood estimator and advocate its use.

Connectivity between the solar photosphere and chromosphere in a vortical structure. Observations of multi-phase, small-scale magnetic field amplification

S.M. **Díaz-Castillo**, C.E. Fischer, R. Rezaei, O. Steiner, S. Berdyugina
A&A **2024**
https://arxiv.org/pdf/2409.05769
High-resolution solar observations have revealed the existence of small-scale vortices, as seen in chromospheric intensity maps and velocity diagnostics. Frequently, these vortices have been observed near magnetic flux concentrations, indicating a link between swirls and the evolution of the small-scale magnetic fields. Vortices have also been studied with magneto-hydrodynamic (MHD) numerical simulations of the solar atmosphere, revealing their complexity, dynamics, and magnetic nature. In particular, it has been proposed that a rotating magnetic field structure driven by a photospheric vortex flow at its footprint produces the chromospheric swirling plasma motion. We present a complete and comprehensive description of the time evolution of a small-scale magnetic flux concentration interacting with the intergranular vortex flow and affected by processes of intensification and

weakening of its magnetic field. In addition, we study the chromospheric dynamics associated with the interaction, including the analysis of a chromospheric swirl and an impulsive chromospheric jet.

Overdense Threads in the Solar Corona Induced by Torsional Alfvén Waves

Sergio **Díaz-Suárez**1,2 and Roberto Soler1,2
2021 ApJL 922 L26
https://iopscience.iop.org/article/10.3847/2041-8213/ac39a3/pdf
https://doi.org/10.3847/2041-8213/ac39a3
High-resolution and high-cadence observations have shown that Alfvén waves are ubiquitous in the solar atmosphere. Theoretical works suggest their ability to transfer large energy fluxes from the photosphere to the corona and solar wind. In this proof-of-concept Letter we show that torsional Alfvén waves can induce the formation of filamentary plasma structures in the solar corona. We perform high-resolution 3D ideal MHD simulations in an initially uniform coronal plasma permeated by a line-tied twisted magnetic field. We find that torsional Alfvén waves develop Kelvin–Helmholtz instabilities as a result of the phase mixing process. The Kelvin–Helmholtz instability drives plasma compression that breaks the uniformity of density, creating elongated overdense threads aligned with the direction of the magnetic field. With synthetic modeling of SDO/AIA imaging we show that the overdense filaments could be seen in observations as fine strands that illuminate the underlying magnetic structure.

Transition to turbulence in nonuniform coronal loops driven by torsional Alfven waves

S. **Díaz-Suárez**, R. Soler
A&A 648, A22 **2021**
https://arxiv.org/pdf/2102.06464.pdf
https://doi.org/10.1051/0004-6361/202040161
https://www.aanda.org/articles/aa/pdf/2021/04/aa40161-20.pdf
Both observations and numerical simulations suggest that Alfvenic waves may carry sufficient energy to sustain the hot temperatures of the solar atmospheric plasma. However, the thermalization of wave energy is inefficient unless very short spatial scales are considered. Phase mixing is a mechanism that can take energy down to dissipation lengths, but it operates over too long a timescale. Here, we study how turbulence, driven by the nonlinear evolution of phase-mixed torsional Alfven waves in coronal loops, is able to take wave energy down to the dissipative scales much faster than the theory of linear phase mixing predicts. We consider a simple model of a transversely nonuniform cylindrical flux tube with a constant axial magnetic field. The flux tube is perturbed by the fundamental mode of standing torsional Alfven waves. We solved the three-dimensional (3D) ideal magnetohydrodynamics equations numerically to study the temporal evolution. Initially, torsional Alfven waves undergo the process of phase mixing because of the transverse variation of density. After only few periods of torsional waves, azimuthal shear flows generated by phase mixing eventually trigger the Kelvin-Helmholtz instability (KHi), and the flux tube is subsequently driven to a turbulent state. Turbulence is very anisotropic and develops transversely only to the background magnetic field. The obtained power law for the energy cascade to small scales is compatible with theoretical predictions of nearly 2D weak Alfvenic turbulence. After the onset of turbulence, the effective Reynolds number decreases in the flux tube much faster than in the initial linear stage governed by phase mixing alone. We conclude that the nonlinear evolution of torsional Alfven waves, and the associated KHi, is a viable mechanism for the onset of turbulence in coronal loops.

Quiet-Sun EUV He ii (30.4 nm) Spatial Power Ratios and Network Dissipation Trend for 2010 – 2018

Leonid **Didkovsky**
Solar Physics July **2019**, 294:98
We explore a significant change of the trend of the transition region network scale variation that occurred around of 2016 when a series of spotless days in 2018, with similar radiative characteristics, were added to previously analyzed days in 2017. We find that a mean per six-year spatial power ratio for 2016 vs. 2010 shows a 29% yearly increase of the dissipation of the network scale, reaching a ratio of 1.74 in 2016. A similar comparison of power ratios for 2018 vs. 2017 gives almost an order of magnitude drop in the previous yearly-mean increase, a yearly ratio of 3%. To study the dynamics of this change, which is consistent with the change of the mean He ii network radius around 2016 mentioned by McIntosh (2019, private communication) based on the method of "watershed segmentation" by McIntosh et al.(Astrophys. J.730, L3, 2011a), the monthly-mean ratios (MMRs) were analyzed. The MMR profile for 2010 – 2018 calculated for near-a-year time intervals is consistent with the decrease of the dissipation rates during the last couple of years. Such dynamics of the MMRs demonstrates a solar nature of the network scale variation in the transition region and may be used as a new sensitive prediction tool for some existing and future changes of solar activity. The network structure dissipation ratio of about 1.8 for 2018 to 2010 reported in this article may be a signature of such changes, expected, in part, to demonstrate a further decrease of the minimum between Solar Cycles 24 and 25 compared to the two previous minima and a lower solar activity during Solar Cycle

(SC) 25. With the current extension of the data to near the next SC minimum, the suggestion expressed by Didkovsky and Gurman (Solar Phys.289, 153, 2014) that "if spatially resolved measurements of He ii emission are maintained through several solar minima, we should be able to conclude whether the spatial distribution of that emission provides a proxy for predicting cycles with anomalously prolonged minima" has new supporting evidence.

A Long-Term Dissipation of the EUV He ii (30.4 nm) Segmentation in Full-Disk Solar Images

Leonid **Didkovsky**
Solar Physics June **2018**, 293:87
Some quiet-Sun days observed by the Atmospheric Imaging Assembly (AIA) on-board the Solar Dynamics Observatory (SDO) during the time interval in 2010 – 2017 were used to continue our previous analyses reported by Didkovsky and Gurman (Solar Phys.289, 153, 2014a) and Didkovsky, Wieman, and Korogodina (Solar Phys.292, 32, 2017). The analysis consists of determining and comparing spatial spectral ratios (spectral densities over some time interval) from spatial (segmentation-cell length) power spectra. The ratios were compared using modeled compatible spatial frequencies for spectra from the Extreme ultraviolet Imaging Telescope (EIT) on-board the Solar and Heliospheric Observatory(SOHO) and from AIA images. With the new AIA data added to the EIT data we analyzed previously, the whole time interval from 1996 to 2017 reported here is approximately the length of two "standard" solar cycles (SC). The spectral ratios of segmentation-cell dimension structures show a significant and steady increase with no detected indication of SC-related returns to the values that characterize the SC minima. This increase in spatial power at high spatial frequencies is interpreted as a dissipation of medium-size EUV network structures to smaller-size structures in the transition region. Each of the latest ratio changes for 2010 through 2017 spectra calculated for a number of consecutive short-term intervals has been converted into monthly mean ratio (MMR) changes. The MMR values demonstrate variable sign and magnitudes, thus confirming the solar nature of the changes. These changes do not follow a "typical" trend of instrumental degradation or a long-term activity profile from the He ii (30.4 nm) irradiance measured by the Extreme ultraviolet Spectrophotometer (ESP) either. The ESP is a channel of the Extreme ultraviolet Variability Experiment (EVE) on-board SDO.

A Long-Term Decrease of the Mid-Size Segmentation Lengths Observed in the HeII 30.4 nm Solar EUV Emission

Leonid **Didkovsky**, Seth Wieman, Elena Korogodina
Solar Phys. February 2017, 292:32 **2017**
https://arxiv.org/pdf/1701.04729v1.pdf
Power spectra of segmentation-cell length (a dominant length scale of EUV emission in the transition region) from full-disk HeII extreme ultraviolet (EUV) images observed by the Extreme ultraviolet Imaging Telescope (EIT) onboard the Solar and Heliospheric Observatory (SOHO) and the Atmospheric Imaging Assembly (AIA) onboard the Solar Dynamics Observatory (SDO) during periods of quiet Sun conditions for a time interval from 1996 to 2015 were analyzed. The spatial power as a function of the spatial frequency from about 0.04 to 0.27 (EIT) or up to 0.48 (AIA) 1/Mm depends on the distribution of the observed segmentation-cell dimensions, -- a structure of the solar EUV network. The temporal variations of the spatial power reported by Didkovsky and Gurman (Solar Phys., 289, 153) were suggested as decreases at the mid-spatial frequencies for the compared spectra when the power curves at the highest spatial frequencies of 0.5 1/pix were adjusted to match each other. That approach has been extended in this work to compare spectral ratios at high spatial frequencies expressed in the solar spatial frequency units of 1/Mm. Based on this approach we represent these ratio changes as a long-term network transformation which may be interpreted as a continuous dissipation of mid-size network structures to the smaller-size structures in the transition region. In contrast to expected cycling of the segmentation-cell dimension structures and associated spatial power in the spectra with the solar cycle, the spectra demonstrate a significant and steady change of the EUV network. The temporal trend across these structural spectra is not critically sensitive to any long-term instrumental changes, e.g. degradation of sensitivity, but to the change of the segmentation-cell dimensions of the EUV network structure.

Geomagnetic activity recurrences for predicting the amplitude and shape of solar cycle n. 25

Piero **Diego*** and Monica Laurenza
J. Space Weather Space Clim. **2021**, 11, 52
https://www.swsc-journal.org/articles/swsc/pdf/2021/01/swsc210010.pdf
https://doi.org/10.1051/swsc/2021036
Predicting solar activity is one of the most challenging topics among the various Space Weather and Space Climate issues. In the last decades, the constant enhancement of Space Climate data improved the comprehension of the related physical phenomena and the statistical bases for prediction algorithms. For this purpose, we used

geomagnetic indices to provide a powerful algorithm (see Diego et al. [2010. J Geophys Res 115: A06103]) for the solar activity prediction, based on evaluating the recurrence rate in the geomagnetic activity. This paper aims to present the validation of our algorithm over solar cycle n. 24, for which a successful prediction was made, and upgrade it to forecast the shape and time as well as the amplitude of the upcoming cycle n. 25. Contrary to the consensus, we predict it to be quite high, with a maximum sunspot number of 205 ± 29, which should be reached in the first half of 2023. This prediction is consistent with the scenario in which the long-term Gleissberg cycle has reached its minimum in cycle n. 24, and the rising phase is beginning.

Solar Hα excess during Solar Cycle 24 from full-disk filtergrams of the Chromospheric Telescope

A. **Diercke**, C. Kuckein, P. W. Cauley, K. Poppenhäger, J. D. Alvarado-Gómez, E. Dineva, C. Denker
A&A 661, A107 **2022**
https://arxiv.org/pdf/2203.04357.pdf
https://www.aanda.org/articles/aa/pdf/2022/05/aa40091-20.pdf
The chromospheric H-alpha spectral line is a strong line in the spectrum of the Sun and other stars. In the stellar regime, this spectral line is already used as a powerful tracer of stellar activity. For the Sun, other tracers (i.e, CaII K) are typically used to monitor solar activity. We used observations of full-disk H-alpha filtergrams of the Chromospheric Telescope (ChroTel) to extract the imaging H-alpha excess and deficit, which are related to bright features (plage regions) and dark absorption features (filaments and sunspots), respectively. The aim of this study is to introduce the imaging H-alpha excess and deficit as tracers of solar activity and compare them to other established indicators: the relative sunspot number, the F10.7cm radio flux, and the MgII index. The H-alpha excess and deficit follow the behavior of the solar activity over the course of the cycle, whereby the peak of the H-alpha deficit is shortly after the solar maximum. The H-alpha excess is closely correlated to the chromospheric MgII index. The highest correlation of the H-alpha deficit is found with the F10.7cm radio flux. The H-alpha deficit reflects the cyclic behavior of polar crown filaments and their disappearance shortly before the solar maximum. We investigated the mean intensity distribution for H-alpha excess regions for solar minimum and maximum, whereby the shape of the distributions is very similar, but with different amplitudes. Furthermore, we investigate whether the area coverage fraction or the changing H-alpha excess in the active regions dominates temporal variability in solar H-alpha observations. The area coverage fraction and the H-alpha excess are strongly correlated, whereas the weak correlation between the area coverage fraction and mean intensity leaves us pessimistic that the degeneracy between these two quantities can be broken for the modeling of unresolved stellar surfaces.

Dynamics and connectivity of an extended arch filament system

Andrea **Diercke**, Christoph Kuckein, Carsten Denker
A&A 629, A48 **2019**
https://arxiv.org/pdf/1908.01510.pdf
In this study, we analyzed a filament system, which expanded between moving magnetic features (MMFs) of a decaying sunspot and opposite flux outside of the active region from the nearby quiet-Sun network. This configuration deviated from a classical arch filament system (AFS), which typically connects two pores in an emerging flux region. Thus, we called this system an extended AFS. We contrasted classical and extended AFSs with an emphasis on the complex magnetic structure of the latter. Furthermore, we examined the physical properties of the extended AFS and described its dynamics and connectivity. At the southern footpoint, we measured that the flux decreases over time. We find strong downflow velocities at the footpoints of the extended AFS, which increase in a time period of 30 minutes. The velocities are asymmetric at both footpoints with higher velocities at the southern footpoint.
The extended AFS was observed with two instruments at the Dunn Solar Telescope (DST). The Rapid Oscillations in the Solar Atmosphere (ROSA) imager provided images in three different wavelength regions. The Interferometric Bidimensional Spectropolarimeter (IBIS) provided spectroscopic Hα data and spectropolarimetric data that was obtained in the near-infrared Ca II 8542 \AA\ line. We used He II 304 \AA\ extreme ultraviolet images of the Atmospheric Imaging Assembly (AIA) and LOS magnetograms of the Helioseismic and Magnetic Imager (HMI) on board the Solar Dynamics Observatory (SDO) as context data. **2013 January 20**

Digitization of sunspot drawings by Spörer made in 1861-1894

Andrea **Diercke** (1 and 2), Rainer Arlt (1), Carsten Denker
Astronomische Nachrichten/Astronomical Notes, **201**4
http://arxiv.org/pdf/1411.7790v1.pdf
Most of our knowledge about the Sun's activity cycle arises from sunspot observations over the last centuries since telescopes have been used for astronomy. The German astronomer Gustav Sp\"orer observed almost daily the Sun from 1861 until the beginning of 1894 and assembled a 33-year collection of sunspot data covering a total of 445 solar rotation periods. These sunspot drawings were carefully placed on an equidistant grid of heliographic longitude and latitude for each rotation period, which were then copied to copper plates for a lithographic reproduction of the

drawings in astronomical journals. In this article, we describe in detail the process of capturing these data as digital images, correcting for various effects of the aging print materials, and preparing the data for contemporary scientific analysis based on advanced image processing techniques. With the processed data we create a butterfly diagram aggregating sunspot areas, and we present methods to measure the size of sunspots (umbra and penumbra) and to determine tilt angles of active regions. A probability density function of the sunspot area is computed, which conforms to contemporary data after rescaling.

Magnetohydrodynamic Instabilities of Double Magnetic Bands in a Shallow-water Tachocline Model. II. Teleconnection Between High- and Low-latitude Bands and Across Equator

Mausumi **Dikpati**, Bernadett Belucz, Robertus Erdélyi, Peter A. Gilman, Scott W. McIntosh, and Breno Raphaldini
2024 ApJ 977 99
https://iopscience.iop.org/article/10.3847/1538-4357/ad8b50/pdf
The "extended solar cycle" indicates that there are two deeply seated toroidal magnetic field bands in each hemisphere. Both bands migrate equatorward as a sunspot cycle progresses. Here, we examine the consequences of global MHD instability of this migrating double-band system in tachocline on the latitudinal structure of unstable modes, which are essentially MHD Rossby waves. We find that latitude-location, latitude-separation, and the amplitude of the bands strongly influence the latitudinal structure and growth rates of the unstable modes of both symmetries about the equator. These properties can lead to "teleconnections" between low- and high-latitudes in each hemisphere and across the equator. High-latitude bands can destabilize low-latitude bands that would otherwise be stable. Stronger high-latitude bands lead to strong interactions between low and high latitude in each hemisphere, but inhibit cross-equatorial band-interaction. Strong cross-equatorial interactions of modes can synchronize cycle minima in north and south. Symmetric and antisymmetric modes of similar amplitudes can lead to substantial asymmetries between north and south. As a solar cycle progresses, excited MHD Rossby waves go through a sequence of changes in latitude structure and growth rate, while maintaining strong links in latitude. These changes and links are theoretical evidence of teleconnections between widely separated latitudes and longitudes in the Sun, which may explain many of the evolving surface magnetic patterns observed as a solar cycle progresses. The wider the separation between high- and low-latitude bands, the earlier the cross-equatorial teleconnection starts in a cycle, and hence the earlier the cycle starts declining.

Simulating Properties of “Seasonal” Variability in Solar Activity And Space Weather Impacts

Mausumi **Dikpati,** Scott McIntosh, and Simon Wing
Front. Astron. Space Sci., 11 May **2021** |
https://doi.org/10.3389/fspas.2021.688604
https://www.frontiersin.org/articles/10.3389/fspas.2021.688604/full
Solar short-term, quasi-annual variability within a decadal sunspot-cycle has recently been observed to strongly correlate with major class solar flares, resulting into quasi-periodic space weather “seasons.” In search for the origin of this quasi-periodic enhanced activity bursts, significant researches are going on. In this article we show, by employing a 3D thin-shell shallow-water type model, that magnetically modified Rossby waves can interact with spot-producing toroidal fields and create certain quasi-periodic spatio-temporal patterns, which plausibly cause a season of enhanced solar activity followed by a relatively quiet period. This is analogous to the Earth’s lower atmosphere, where Rossby waves and jet streams are produced and drive global terrestrial weather. Shallow-water models have been applied to study terrestrial Rossby waves, because their generation layer in the Earth’s lower atmospheric region has a much larger horizontal than vertical scale, one of the model-requirements. In the Sun, though Rossby waves can be generated at various locations, particularly favorable locations are the subadiabatic layers at/near the base of the convection zone where the horizontal scale of the fluid and disturbances in it can be much larger than the vertical scale. However, one important difference with respect to terrestrial waves is that solar Rossby waves are magnetically modified due to presence of strong magnetic fields in the Sun. We consider plausible magnetic field configurations at the base of the convection zone during different phases of the cycle and describe the properties of energetically active Rossby waves generated in our model. We also discuss their influence in causing short-term spatio-temporal variability in solar activity and how this variability could have space weather impacts. An example of a possible space weather impact on the Earth’s radiation belts are presented.

Physics of Magnetohydrodynamic Rossby Waves in the Sun

Mausumi **Dikpati**1, Peter A. Gilman1, Subhamoy Chatterjee2, Scott W. McIntosh1, and Teimuraz V. Zaqarashvili3
2020 ApJ 896 141
https://doi.org/10.3847/1538-4357/ab8b63

Evidence of the existence of hydrodynamic and MHD Rossby waves in the Sun is accumulating rapidly. We employ an MHD Rossby wave model for the Sun in simplified Cartesian geometry, with a uniform toroidal field and no differential rotation, to analyze the role of each force that contributes to Rossby wave dynamics, and compute fluid particle trajectories followed in these waves. This analysis goes well beyond the traditional formulation of Rossby waves in terms of conservation of vorticity. Hydrodynamic Rossby waves propagate retrograde relative to the rotation of the reference frame, while MHD Rossby waves can be both prograde and retrograde. Fluid particle trajectories are either clockwise or counterclockwise spirals, depending on where in the wave pattern they are initiated, that track generally in the direction of wave propagation. Retrograde propagating MHD Rossby waves move faster than their hydrodynamic counterparts of the same wavelength, becoming Alfvén waves at very high field strengths. Prograde MHD Rossby waves, which have no hydrodynamic counterpart, move more slowly eastward than retrograde MHD Rossby waves for the same toroidal field, but with a speed that increases with toroidal field, in the high field limit again becoming Alfvén waves. The longitude and latitude structures of all these waves, as seen in their velocity streamlines and perturbation field lines as well as fluid particle trajectories, are remarkably similar for different toroidal fields, rotation, longitudinal wavelength, and direction of propagation.

Phase Speed of Magnetized Rossby Waves that Cause Solar Seasons

Mausumi **Dikpati**1, Bernadett Belucz1,2,3, Peter A. Gilman1, and Scott W. McIntosh
2018 ApJ 862 159
http://sci-hub.tw/http://iopscience.iop.org/article/10.3847/1538-4357/aacefa/meta
Motivated by recent analysis of solar observations that show evidence of propagating Rossby waves in coronal holes and bright points, we compute the longitudinal phase velocities of unstable MHD Rossby waves found in an MHD shallow-water model of the solar tachocline (both overshoot and radiative parts). We demonstrate that phase propagation is a typical characteristic of tachocline nonlinear oscillations that are created by unstable MHD Rossby waves, responsible for producing solar seasons. For toroidal field bands placed at latitudes between 5° and 75°, we find that phase velocities occur in a range similar to the observations, with more retrograde speeds (relative to the solar core rotation rate) for bands placed at higher latitudes, just as coronal holes have at high latitudes compared to low ones. The phase speeds of these waves are relatively insensitive to the toroidal field peak amplitude. Rossby waves for single bands at 25° are slightly prograde. However, at latitudes lower than 25° they are very retrograde, but much less so if a second band is included at a much higher latitude. This double-band configuration is suggested by evidence of an extended solar cycle, containing a high-latitude band in its early stages that does not yet produce spots, while the spot-producing low-latitude band is active. Collectively, our results indicate a strong connection between longitudinally propagating MHD Rossby waves in the tachocline and surface manifestations in the form of similarly propagating coronal holes and patterns of bright points.

Role of Interaction between Magnetic Rossby Waves and Tachocline Differential Rotation in Producing Solar Seasons

Mausumi **Dikpati**1, Scott W. McIntosh1, Gregory Bothun2, Paul S. Cally3,Siddhartha S. Ghosh4, Peter A. Gilman1, and Orkan M. Umurhan5
2018 ApJ 853 144
http://sci-hub.tw/http://iopscience.iop.org/0004-637X/853/2/144/
We present a nonlinear magnetohydrodynamic shallow-water model for the solar tachocline (MHD-SWT) that generates quasi-periodic tachocline nonlinear oscillations (TNOs) that can be identified with the recently discovered solar "seasons." We discuss the properties of the hydrodynamic and magnetohydrodynamic Rossby waves that interact with the differential rotation and toroidal fields to sustain these oscillations, which occur due to back-and-forth energy exchanges among potential, kinetic, and magnetic energies. We perform model simulations for a few years, for selected example cases, in both hydrodynamic and magnetohydrodynamic regimes and show that the TNOs are robust features of the MHD-SWT model, occurring with periods of 2–20 months. We find that in certain cases multiple unstable shallow-water modes govern the dynamics, and TNO periods vary with time. In hydrodynamically governed TNOs, the energy exchange mechanism is simple, occurring between the Rossby waves and differential rotation. But in MHD cases, energy exchange becomes much more complex, involving energy flow among six energy reservoirs by means of eight different energy conversion processes. For toroidal magnetic bands of 5 and 35 kG peak amplitudes, both placed at 45° latitude and oppositely directed in north and south hemispheres, we show that the energy transfers responsible for TNO, as well as westward phase propagation, are evident in synoptic maps of the flow, magnetic field, and tachocline top-surface deformations. Nonlinear mode–mode interaction is particularly dramatic in the strong-field case. We also find that the TNO period increases with a decrease in rotation rate, implying that the younger Sun had more frequent seasons.

DATA ASSIMILATION IN A SOLAR DYNAMO MODEL USING ENSEMBLE KALMAN FILTERS: SENSITIVITY AND ROBUSTNESS IN RECONSTRUCTION OF MERIDIONAL FLOW SPEED

Mausumi **Dikpati**1,4, Jeffrey L. Anderson2, and Dhrubaditya Mitra

2016 ApJ 828 91
We implement an Ensemble Kalman Filter procedure using the Data Assimilation Research Testbed for assimilating "synthetic" meridional flow-speed data in a Babcock–Leighton-type flux-transport solar dynamo model. By performing several "observing system simulation experiments," we reconstruct time variation in meridional flow speed and analyze sensitivity and robustness of reconstruction. Using 192 ensemble members including 10 observations, each with 4% error, we find that flow speed is reconstructed best if observations of near-surface poloidal fields from low latitudes and tachocline toroidal fields from midlatitudes are assimilated. If observations include a mixture of poloidal and toroidal fields from different latitude locations, reconstruction is reasonably good for error in low-latitude data, even if observational error in polar region data becomes 200%, but deteriorates when observational error increases in low- and midlatitude data. Solar polar region observations are known to contain larger errors than those in low latitudes; our forward operator (a flux-transport dynamo model here) can sustain larger errors in polar region data, but is more sensitive to errors in low-latitude data. An optimal reconstruction is obtained if an assimilation interval of 15 days is used; 10- and 20-day assimilation intervals also give reasonably good results. Assimilation intervals days do not produce faithful reconstructions of flow speed, because the system requires a minimum time to develop dynamics to respond to flow variations. Reconstruction also deteriorates if an assimilation interval days is used, because the system's inherent memory interferes with its short-term dynamics during a substantially long run without updating.

Cyclic Evolution of Coronal Fields from a Coupled Dynamo Potential-Field Source-Surface Model

Mausumi **Dikpati** , Akshaya Suresh, Joan Burkepile
Solar Phys. Volume 291, Issue 2, pp 339-355 **2016** **Open Access**
The structure of the Sun’s corona varies with the solar-cycle phase, from a near spherical symmetry at solar maximum to an axial dipole at solar minimum. It is widely accepted that the large-scale coronal structure is governed by magnetic fields that are most likely generated by dynamo action in the solar interior. In order to understand the variation in coronal structure, we couple a potential-field source-surface model with a cyclic dynamo model. In this coupled model, the magnetic field inside the convection zone is governed by the dynamo equation; these dynamo-generated fields are extended from the photosphere to the corona using a potential-field source-surface model. Assuming axisymmetry, we take linear combinations of associated Legendre polynomials that match the more complex coronal structures. Choosing images of the global corona from the Mauna Loa Solar Observatory at each Carrington rotation over half a cycle (1986 – 1991), we compute the coefficients of the associated Legendre polynomials up to degree eight and compare with observations. We show that at minimum the dipole term dominates, but it fades as the cycle progresses; higher-order multipolar terms begin to dominate. The amplitudes of these terms are not exactly the same for the two limbs, indicating that there is a longitude dependence. While both the 1986 and the 1996 minimum coronas were dipolar, the minimum in 2008 was unusual, since there was a substantial departure from a dipole. We investigate the physical cause of this departure by including a North–South asymmetry in the surface source of the magnetic fields in our flux-transport dynamo model, and find that this asymmetry could be one of the reasons for departure from the dipole in the 2008 minimum.

SDO/HMI Observations Create New Challenge to Solar Meridional Circulation Theories

M. **Dikpati**
HMI Science Nuggets, Feb **2014**
http://hmi.stanford.edu/hminuggets/?p=467
Solar meridional circulation, if mechanically driven and thermally braked, contains two cells in latitude; generating two cells in depth, recently observed by SDO/HMI, is a new challenge to theory.

Simulating solar 'climate' (введение/обзор по солнечному **динамо**)

M. **Dikpati**
Climate and Weather of the Sun-Earth System (CAWSES): Selected Papers from the 2007 Kyoto Symposium, Edited by T. Tsuda, R. Fujii, K. Shibata, and M. A. Geller, pp. 171-199.
© by TERRAPUB, Tokyo, **2009**.
[Full text] (PDF 3.2 MB)

Coronagraphic Observations of Si x λ14301 and Fe xiiiλ10747 Linearly Polarized Spectra Using the SOLARC Telescope

Gabriel I. **Dima**1, Jeffrey R. Kuhn2, and Thomas A. Schad1
2019 ApJ 877 144
sci-hub.se/10.3847/1538-4357/ab1d4f

The forbidden Si x emission line at 14301 Å has been identified as a potentially valuable polarized diagnostic for solar coronal magnetic fields; however, the only polarized Si x measurements achieved to date have been during eclipses and at comparatively low spatial and spectral resolution. Here we report spectropolarimetric observations of both the Si x 14301 Å and more well-established Fe xiii 10747 Å coronal lines acquired with the 0.45 m aperture SOLARC coronagraph atop Haleakalā. Using its fiber-based integral field spectropolarimeter, we derive observations sampled at radial intervals of 0.05 (i.e., ~50") with a spectral resolving power of ≈36,000. Results for both lines, which represent averages over different active and nonactive regions of the corona, indicate a relatively flat radial variation for the line widths and line centers and a factor of ≈2–3 decrease in polarized brightness between 1.05 and 1.45 . Averaging over all the measurements the mean and standard deviations of line properties for Si x 14301 Å and Fe xiii 10747 Å are, respectively, FWHM of 3.0 ± 0.4 Å and 1.6 ± 0.1 Å, line-integrated polarized brightness of 0.07 ± 0.03 and 0.3 ± 0.3 erg s−2 cm−2 sr−1, where the uncertainty quoted reflects a large sample variance, and line center wavelengths 14300.7 ± 0.2 Å and 10746.3 ± 0.1 Å. The polarized brightness for both lines may be underestimated by up to a factor of 5 due to limitations in the photometric calibration. When accounting for this uncertainty we find consistency between our observations and previous measurements of the two lines as well as theoretical calculations and affirm the potential of the Si x line as a polarized diagnostic of the solar corona.

Cloud model inversions of strong chromospheric absorption lines using principal component analysis

Ekaterina **Dineva** (1 and 2), Meetu Verma (1), Sergio Javier González Manrique (3), Pavol Schwartz (3), Carsten Denker (1)
Astronomische Nachrichten/Astronomical Notes **2020**
https://arxiv.org/pdf/1912.10476.pdf
High-resolution spectroscopy of strong chromospheric absorption lines delivers nowadays several millions of spectra per observing day, when using fast scanning devices to cover large regions on the solar surface. Therefore, fast and robust inversion schemes are needed to explore the large data volume. Cloud Model (CM) inversions of the chromospheric Hα line are commonly employed to investigate various solar features including filaments, prominences, surges, jets, mottles, and (macro-)spicules. The choice of the CM was governed by its intuitive description of complex chromospheric structures as clouds suspended above the solar surface by magnetic fields. This study is based on observations of active region NOAA 11126 in Hα, which were obtained **2010 November 18-23** with the echelle spectrograph of the Vacuum Tower Telescope (VTT) at the Observatorio del Teide, Spain. Principal Component Analysis (PCA) reduces the dimensionality of spectra and conditions noise-stripped spectra for CM inversions. Modeled Hα intensity and contrast profiles as well as CM parameters are collected in a database, which facilitates efficient processing of the observed spectra. Physical maps are computed representing the line-core and continuum intensity, absolute contrast, equivalent width, and Doppler velocities, among others. Noise-free spectra expedite the analysis of bisectors. The data processing is evaluated in the context of "big data", in particular with respect to automatic classification of spectra.

Effect of the non-uniform solar chromospheric Lyα radiation on determining the coronal H I outflow velocity

S. **Dolei**, D. Spadaro, R. Ventura, A. Bemporad, V. Andretta, C. Sasso, R. Susino, E. Antonucci, V. Da D eppo, S. Fineschi et al. (6 more)
A&A 627, A18 (**2019**)
DOI: https://doi.org/10.1051/0004-6361/201935048
We derived maps of the solar wind outflow velocity of coronal neutral hydrogen atoms at solar minimum in the altitude range 1.5–4.0 R⊙. We applied the Doppler dimming technique to coronagraphic observations in the UV H I Lyα line at 121.6 nm. The technique exploits the intensity reduction in the coronal line with increasing velocities of the outflowing plasma to determine the solar wind velocity by iterative modelling. The Lyα line intensity is sensitive to the wind outflow velocity and also depends on the physical properties of coronal particles and underlying chromospheric emission. Measurements of irradiance by the chromospheric Lyα radiation in the corona are required for a rigorous application of the Doppler dimming technique, but they are not provided by past and current instrumentations. A correlation function between the H I 121.6 nm and He II 30.4 nm line intensities was used to construct Carrington rotation maps of the non-uniform solar chromospheric Lyα radiation and thus to compute the Lyα line irradiance throughout the outer corona. Approximations concerning the temperature of the scattering H I atoms and exciting solar disc radiation were also adopted to significantly reduce the computational time and obtain a faster procedure for a quick-look data analysis of future coronagraphic observations. The effect of the chromospheric Lyα brightness distribution on the resulting H I outflow velocities was quantified. In particular, we found that the usual uniform-disc approximation systematically leads to an overestimated velocity in the polar and mid-latitude coronal regions up to a maximum of about 50−60 km s−1 closer to the Sun. This difference decreases at higher altitudes, where an increasingly larger chromospheric portion, including both brighter and darker

disc features, contributes to illuminate the solar corona, and the non-uniform radiation condition progressively approaches the uniform-disc approximation.

Temperature of Solar Orbiter/EUI quiet Sun small scale brightenings: evidence for a cooler component

A. **Dolliou**, S. Parenti, F. Auchère, K. Bocchialini, G. Pelouze, P. Antolin, D. Berghmans, L. Harra, D. M. Long, U. Schühle, E. Kraaikamp, K. Stegen, C. Verbeeck, S. Gissot, R. Aznar Cuadrado, E. Buchlin, M. Mierla, L. Teriaca, A. N. Zhukov

A&A 671, A64 **2023**

https://arxiv.org/pdf/2301.02040.pdf

https://www.aanda.org/articles/aa/pdf/2023/03/aa44914-22.pdf

Context: On **2020 May 30**, small and short-lived EUV brightenings were observed in the Quiet Sun (QS) during a four minutes sequence by EUI/HRIEUV on board Solar Orbiter. Their physical origin and possible impact on coronal or Transition Region (TR) heating are still to be determined. Aims: Our aim is to derive the statistical thermal evolution of these events in order to establish their coronal or TR origin. Methods. Our thermal analysis takes advantage of the multithermal sensitivity of the Atmospheric Imaging Assembly (AIA) imager on board the Solar Dynamics Observatory (SDO). We first identified these HRIEUV events in the six coronal bands of AIA. We then performed a statistical time lag analysis, which quantifies the delays between the light curves from different bands. These time lags can give significant insights into the temperature evolution of these events. The analysis is performed taking into account the possible contribution to the results from the background and foreground emissions. Results: The events are characterized by time lags inferior to the AIA cadence of 12 s, for all nine couples of AIA bands analyzed. Our interpretation is the possible co-presence of events which reach or do not reach coronal temperatures (≈ 1MK). We believe that the cool population dominates the events analyzed in this work.

Solar Orbiter Nugget #43 2024 *https://www.cosmos.esa.int/web/solar-orbiter/-/science-nugget-the-role-of-small-scale-euv-brightenings-in-the-quiet-sun-coronal-heating*

Seismic Transients from Flares in Solar Cycle 23

Donea, Alina

Space Science Reviews, Volume 158, Issue 2-4, pp. 451-469, **2011**

Some solar flares are known to drive seismic waves into the sub-photospheres of the magnetic regions that host them. Sunquakes, which are identified as a wave-packet of ripples are observed on the solar surface emanating from a focal region, known as seismic source or sometimes as a transient. Not all seismic transients from flares generate sunquakes. How these are produced is still a puzzle. In this paper, I will give an overview of the observed properties of sunquakes and efforts to understanding physics underlying them, including numerical modelling of flare-driven oscillations.

Editorial: Magnetohydrodynamic Waves in the Solar Atmosphere: Heating and Seismology **Review**

Tom Van **Doorsselaere**, Valery M. Nakariakov, Bo Li, and Patrick Antolin

Front. Astron. Space Sci., 6:79.**2020** |

https://www.frontiersin.org/articles/10.3389/fspas.2019.00079/full

https://doi.org/10.3389/fspas.2019.00079

Solar differential rotation profile estimation using coronal bright points data derived from the SDO/AIA images

Ivan **Dorotovič**, A. Coelho, J. Rybak, A. Mora, R. Ribeiro, W. Kusa

Sun and Geosphere, **2018**; 13/2: 129 - 133

http://newserver.stil.bas.bg/SUNGEO//00SGArhiv/SG_v13_No2_2018-pp-129-133.pdf

The AIA instrument, on-board the SDO satellite, provides high-resolution and high-cadence solar images since 2010. To extract scientific knowledge about coronal bright points (CBPs) from those high-resolution images there is a need for efficient automatic algorithms to detect and/or track the CBPs. In the last decade other research teams have developed algorithms to obtain more precise estimations of the solar rotation profile. However, it is a difficult task because CBPs may change shape and size over time, yielding great difficulty to track them. In this work we discuss the usage of two automatic segmentation algorithms to detect CBPs in SDO/AIA images: (1) using SunPy and OpenCV in Python and (2) using a Gradient Path Labeling (GPL) algorithm. Our preliminary tests and results, with a three-day dataset, show that these algorithms are promising tools to help refine the solar rotational profile.

Modified Homogeneous Data Set of Coronal Intensities

I. **Dorotovič**, M. Minarovjech, M. Lorenc, M. Rybanský
Solar Physics, July **2014**, Volume 289, Issue 7, pp 2697-2703
The Astronomical Institute of the Slovak Academy of Sciences has published the intensities, recalibrated with respect to a common intensity scale, of the 530.3 nm (Fe xiv) green coronal line observed at ground-based stations up to the year 2008. The name of this publication is Homogeneous Data Set (HDS). We have developed a method that allows one to successfully substitute the ground-based observations by satellite observations and, thus, continue with the publication of the HDS. For this purpose, the observations of the Extreme-ultraviolet Imaging Telescope (EIT), onboard the Solar and Heliospheric Observatory (SOHO) satellite, were exploited. Among other data the EIT instrument provides almost daily 28.4 nm (Fe xv) emission-line snapshots of the corona. The Fe xiv and Fe xv data (4051 observation days) taken in the period 1996 – 2008 have been compared and good agreement was found. The method to obtain the individual data for the HDS follows from the correlation analysis described in this article. The resulting data, now under the name of Modified Homogeneous Data Set (MHDS), are identical up to 1996 to those in the HDS. The MHDS can be used further for studies of the coronal solar activity and its cycle. These data are available at http://www.suh.sk .

Adventures in Space Science

George **Doschek**
Solar Physics volume 296, Article number: 123 (**2021**)
https://link.springer.com/content/pdf/10.1007/s11207-021-01851-z.pdf
https://doi.org/10.1007/s11207-021-01851-z
This **memoir** is a summary of my early childhood, education, and research career at the Naval Research Laboratory (NRL) in Washington, DC. I describe my early interest in astronomy and how I wound up working in the fields of solar physics and X-ray-UV spectroscopy of high temperature plasmas. I describe some of my home life and other interests, my education at the University of Pittsburgh, and the various projects and management activities that I have been fortunate to work on at NRL. I have been blessed with being able to work at a first-class research laboratory populated by outstanding scientists. I am particularly blessed to have worked with my many friends and colleagues in the NRL Space Science Division. Perhaps I am most blessed by having had wonderful parents that gave me the interests I have in life and the passion to pursue them, and an outstanding wife that has been my partner through good and bad times for over 50 years. I am now retired but for three years I was a participant in the NRL Voluntary Emeritus Program (VEP). However, this memoir is a personal account, and not work done as a VEP.

The Variability of Solar Coronal Abundances in Active Regions and the Quiet Sun

G. A. **Doschek**1 and H. P. Warren2
2019 ApJ 884 158
sci-hub.se/10.3847/1538-4357/ab426e
Measurements of elemental abundances hold important clues to how mass and energy flow through the solar atmosphere. Variations in abundances are organized by an element's first ionization potential (FIP), and many previous studies have assumed that low FIP (less than 10 eV) elements are enriched by a factor of 3–4 in the corona. In this paper, we use spatially resolved observations from the Extreme-ultraviolet Imaging Telescope on board the Hinode spacecraft to examine the spatial variability of elemental abundance in and around active regions. We find substantial variations within some active regions. In general, however, we find that the enrichment of low FIP elements is limited to bright, active region structures. In faint active region structures and in the dark, quiet regions around active regions, the measured abundances are close to photospheric. These measurements use the ratio of low FIP Si to high FIP S. Similar conclusions concerning quiet Sun regions have been reached recently by Del Zanna using full-Sun spectra. He has found that the coronal quiet Sun (at temperatures greater than 1 MK) has photospheric abundances. Transition region abundances (at temperatures less than 1 MK in the solar atmosphere) have been found to be photospheric. These results and results from this paper suggest that a coronal composition is not a general property of million-degree plasma, but is limited to bright active region loops, and is variable.

Sunspots, Starspots, and Elemental Abundances

G. A. **Doschek** and H. P. Warren
2017 ApJ 844 52
http://sci-hub.cc/10.3847/1538-4357/aa7bea
Element abundances in the solar photosphere, chromosphere, transition region, and corona are key parameters for investigating sources of the solar wind and for estimating radiative losses in the quiet corona and in dynamical events such as solar flares. Abundances in the solar corona and photosphere differ from each other depending on the first ionization potential (FIP) of the element. Normally, abundances with FIP values less than about 10 eV are about 3–4 times more abundant in the corona than in the photosphere. However, recently, an inverse FIP effect was found in small regions near sunspots where elements with FIP less than 10 eV are less abundant relative to high FIP elements ($\geqslant 10$ eV) than they are in the photosphere. This is similar to fully convective stars with large starspots. The inverse FIP effect is predicted to occur in the vicinity of sunspots/starspots. Up to now, the solar anomalous

abundances have only been found in very spatially small areas. In this paper, we show that in the vicinity of sunspots there can be substantially larger areas with abundances that are between coronal and photospheric abundances and sometimes just photospheric abundances. In some cases, the FIP effect tends to shut down near sunspots. We examine several active regions with relatively large sunspots that were observed with the Extreme-ultraviolet Imaging Spectrometer on the Hinodespacecraft in cycle 24. **2012 March 9, 2014 February 1–5, 2014 October 24, 2016 February 15**
Table 1 Regions Observed

THE ELECTRON DENSITY IN EXPLOSIVE TRANSITION REGION EVENTS OBSERVED BY IRIS

G. A. **Doschek**1, H. P. Warren1, and P. R. Young
2016 ApJ 832 77
We discuss the intensity ratio of the O iv line at 1401.16 Å to the Si iv line at 1402.77 Å in Interface Region Imaging Spectrograph (IRIS) spectra. This intensity ratio is important if it can be used to measure high electron densities that cannot be measured using line intensity ratios of two different O iv lines from the multiplet within the IRIS wavelength range. Our discussion is in terms of considerably earlier observations made from the Skylab manned space station and other spectrometers on orbiting spacecraft. The earlier data on the O iv and Si iv ratio and other intersystem line ratios not available to IRIS are complementary to IRIS data. In this paper, we adopt a simple interpretation based on electron density. We adopt a set of assumptions and calculate the electron density as a function of velocity in the Si iv line profiles of two explosive events. At zero velocity the densities are about 2–3 × 1011 cm−3, and near 200 km s−1 outflow speed the densities are about 1012 cm−3. The densities increase with outflow speed up to about 150 km s−1 after which they level off. Because of the difference in the temperature of formation of the two lines and other possible effects such as non-ionization equilibrium, these density measurements do not have the precision that would be available if there were some additional lines near the formation temperature of O iv.

Magnetohydrodynamic Simulations of Spicular Jet Propagation Applied to Lower Solar Atmosphere Model

Fionnlagh Mackenzie **Dover**1, Rahul Sharma2, and Robertus Erdélyi1,3,4
2021 ApJ 913 19
https://doi.org/10.3847/1538-4357/abefd1
We report a series of numerical experiments for the propagation of a momentum pulse representing a chromospheric jet, simulated using an idealized magnetohydrodynamic model. The jet in a stratified lower solar atmosphere is subjected to a varied initial driver (amplitude, period) and magnetic field conditions to examine the parameter influence over jet morphology and kinematics. The simulated jet captured key observed spicule characteristics including maximum heights, field-aligned mass motions/trajectories, and cross-sectional width deformations. Next, the jet features also show a prominent bright, bulb-like apex, similar to reported observed chromospheric jets, formed due to the higher density of plasma and/or waves. Furthermore, the simulations highlight the presence of not yet observed internal crisscross/knots substructures generated by shock waves reflected within the jet structure. Therefore we suggest verifying these predicted fine-scale structures in highly localized lower solar atmospheric jets, e.g., in spicules or fibrils by high-resolution observations, offered by the Daniel K. Inoyue Solar Telescope or otherwise.

Signatures of Cross-sectional Width Modulation in Solar Spicules due to Field-aligned Flows

Fionnlagh Mackenzie **Dover**1, Rahul Sharma2, Marianna B. Korsós3,4,5, and Robertus Erdélyi1,4,5
2020 ApJ 905 72
https://doi.org/10.3847/1538-4357/abc349
We report the first observational detection of frequency modulation in the cross-sectional width of spicule structures due to field-aligned plasma flows. Cross-sectional width variations were estimated for the least superimposed off-limb spicules observed in high-resolution Hα imaging spectroscopy data. Analysis of estimated cross-sectional widths suggest periodic oscillations, concurrent with 2D numerical modeling for a jet structure in a stratified solar atmosphere. Spectral analysis for both observed and simulated cross-sectional widths indicate frequency modulation as noticeable shifts in estimated periodicities during rise and fall phases of field-aligned plasma flows in the jet structure. Furthermore, the presence of the first overtone in a dynamic/spicular waveguide is also evident in both the observed and the simulated jet structures. These harmonics can be an important tool for future chromospheric magnetoseismology investigations and applications to dynamic waveguides (like spicules).

Closed-Field Coronal Heating Driven by Wave Turbulence

Cooper **Downs**, Roberto Lionello, Zoran Mikić, Jon A. Linker, Marco Velli

ApJ **832** 180 **2016**
https://arxiv.org/pdf/1610.02113v1.pdf
To simulate the energy balance of coronal plasmas on macroscopic scales, we often require the specification of the coronal heating mechanism in some functional form. To go beyond empirical formulations and to build a more physically motivated heating function, we investigate the wave-turbulence-driven (WTD) phenomenology for the heating of closed coronal loops. Our implementation is designed to capture the large-scale propagation, reflection, and dissipation of wave turbulence along a loop. The parameter space of this model is explored by solving the coupled WTD and hydrodynamic evolution in 1D for an idealized loop. The relevance to a range of solar conditions is also established by computing solutions for over one hundred loops extracted from a realistic 3D coronal field. Due to the implicit dependence of the WTD heating model on loop geometry and plasma properties along the loop and at the footpoints, we find that this model can significantly reduce the number of free parameters when compared to traditional empirical heating models, and still robustly describe a broad range of quiet-sun and active region conditions. The importance of the self-reflection term in producing relatively short heating scale heights and thermal nonequilibrium cycles is also discussed.

A NOISE ADAPTIVE FUZZY EQUALIZATION METHOD FOR PROCESSING SOLAR EXTREME ULTRAVIOLET IMAGES

M. **Druckmülle**r
2013 ApJS 207 25
A new image enhancement tool ideally suited for the visualization of fine structures in extreme ultraviolet images of the corona is presented in this paper. The Noise Adaptive Fuzzy Equalization method is particularly suited for the exceptionally high dynamic range images from the **Atmospheric Imaging Assembly** instrument on the Solar Dynamics Observatory. This method produces artifact-free images and gives significantly better results than methods based on convolution or Fourier transform which are often used for that purpose.

The formation and heating of chromospheric fibrils in a radiation-MHD simulation

M. K. **Druett**, J. Leenaarts, M. Carlsson, M. Szydlarski
A&A **2021**
https://arxiv.org/pdf/2112.08245.pdf
Aims: We examine the movements of mass elements within dense fibrils using passive tracer particles (corks) in order to understand fibril creation and destruction processes.
Methods: Simulated fibrils were selected at times when they were visible in an Hα image proxy. The corks were selected within fibril Hα formation regions. From this set, a cork was selected, and the field line passing through it was constructed. Other fibrilar corks close to this fieldline were also selected. Pathlines were constructed, revealing the locations of the mass elements forward and backward in time. The forces acting on these mass elements were analysed.
Results: The main process of fibrilar loading in the simulation is different to the mass loading scenario in which waves steepen into shocks and push material upwards along the fieldlines from near their footpoints. Twisted low lying fieldlines were destabilised and then they untwisted, lifting the material trapped above their apexes via the Lorentz force. Subsequently, the majority of the mass drained down the fieldlines towards one or both footpoints under gravity. Material with large horizontal velocities could also elevated in rising fieldlines, creating somewhat parabolic motions, but material was not generally moving upward along a stationary magnetic fieldline during loading.
Conclusions: The processes observed in the simulation are plausible additional scenarios. Criteria for observing such events are described. It is desirable that our simulations can also form more densely-packed fibrils from material fed from the base of field footpoints. Experimental parameters required to achieve this are discussed.

New eyes and ideas for the chromosphere **Review**

Malcolm **Druett**, Ben Snow
Astronomy & Geophysics, Volume 62, Issue 2, April **2021**, Pages 2.34–2.39,
https://doi.org/10.1093/astrogeo/atab058
An RAS Specialist Discussion Meeting organized by Malcolm Druett and Ben Snow on 13 November 2020 drew a broad international audience to explore a tricky layer of the Sun

Evolution of the Correlation Between the Amplitude of the Solar Cycle and the Sunspot Number Since the Previous Declining Phase in Both Hemispheres

Zhanle **Du**
Solar Physics volume 297, Article number: 117 (**2022**)
https://doi.org/10.1007/s11207-022-02051-z
Analyzing the variation in the correlation between the maximum amplitude [RmaxRmax] of the solar cycle and the hemispheric sunspot number [RHRH], since the previous declining phase, is helpful in understanding the temporal

evolution of the cycle and the possible different mechanisms at work in the two hemispheres. The correlation coefficient [rr] between RmaxRmax and the smoothed monthly mean RHRH as a function of m=−50,−49,…,50m=−50,−49,…,50 months from the solar minimum [RminRmin] is studied, and it is found that rr is maximum about three years before RminRmin at the declining phase, falls to a minimum value around RminRmin, and increases with mm during the rising phase in both hemispheres. Based on the highest correlations at the declining phase, the maximum amplitudes of Cycle 25 in the northern [NH] and southern hemisphere [SH] are predicted to be Rmax,N(25)=85.6±21.9Rmax,N(25)=85.6±21.9 and Rmax,S(25)=74.4±17.9Rmax,S(25)=74.4±17.9, respectively. Using data at the rising phase, Rmax,N(25)=84.0±26.7Rmax,N(25)=84.0±26.7 and Rmax,S(25)=88.3±16.8Rmax,S(25)=88.3±16.8. The average values are R¯¯¯¯¯max,N(25)=84.8±24.3R¯max,N(25)=84.8±24.3 and R¯¯¯¯¯max,S(25)=81.4±17.4R¯max,S(25)=81.4±17.4. According to the weak correlation between the rise time and RmaxRmax, the peak times of Cycle 25 in the NH and SH are predicted to be November 2023 ±10±10 months and July 2024 ±10±10 months, respectively. Employing the strong correlation between the amplitude of the total sunspot number [Rmax,TRmax,T] and those of RHRH in both hemispheres (r=0.99r=0.99), the amplitude of Cycle 25 is predicted to be Rmax,T(25)=139.7±28.7Rmax,T(25)=139.7±28.7 and 152.3±31.5152.3±31.5 using data at the declining and rising phases, respectively, with an average value of 146.0±30.1146.0±30.1.

Comparing the Correlations Between Solar Cycle Parameters in the Northern and Southern Hemispheres

Zhanle **Du**

Solar Physics volume 297, Article number: 70 (**2022**)
https://doi.org/10.1007/s11207-022-02005-5

The correlations between the parameters of Solar Cycles 12 – 24 for the smoothed monthly mean sunspot numbers of the total [RTRT], northern [RNRN], and southern [RSRS] hemispheres are compared using the newly reconstructed hemispheric sunspot numbers. The main conclusions are as follows: i) the maximum amplitude [RmaxRmax] is inversely correlated [r=−0.54r=−0.54] with the rise time [TaTa] of the cycle in the southern hemisphere [SH], while in the northern hemisphere [NH], they are positively correlated [r=0.36r=0.36], not satisfying the Waldmeier effect; ii) the positive correlation between RmaxRmax and the preceding cycle minimum [RminRmin] in the SH [r=0.51r=0.51] is much stronger than that in the NH [r=0.21r=0.21]; iii) the decay time [TdTd] is found to be strongly anti-correlated with TaTa in the NH [r=−0.83r=−0.83], and this correlation is weaker in the SH [r=−0.50r=−0.50]; iv) the negative correlation between RmaxRmax and the cycle length [P=Ta+TdP=Ta+Td] in the NH [r=−0.51r=−0.51] is much stronger than that in the SH [r=−0.18r=−0.18]; and v) the correlation in even-numbered cycles tends to be much stronger than in odd-numbered ones. These seem to imply that the solar activity in the northern hemisphere evolves partially differently from that in the southern hemisphere. These results might provide constraints on dynamo models in both hemispheres. However, the correlations depend on the timings of solar minima and maxima, which are related to the smoothing method.

Predicting the Maximum Amplitude of Solar Cycle 25 Using the Early Value of the Rising Phase

Zhanle **Du**

Solar Physics volume 297, Article number: 61 (**2022**)
https://doi.org/10.1007/s11207-022-01991-w

The rising rate [βaβa] of a solar cycle is a good indicator for the subsequent maximum amplitude [SmSm] of sunspot numbers. We compared the correlation between SmSm and βaβa and that between SmSm and the early value of the smoothed monthly mean sunspot number [SNSN] ΔmΔm months after the solar minimum. Our main conclusions are as follows: i) The correlation coefficient [rr] between SmSm and SNSN is slightly higher than that between SmSm and βaβa, and both increase with ΔmΔm as the cycle progresses; ii) In the first year of the cycle, the correlation is weak [r∼r∼ 0.56]. At the inflection point [Δm=21Δm=21], the correlation is stronger [r=0.83r=0.83]. After the inflection point, rr increases slowly with ΔmΔm. Three years after the solar minimum, r⩾0.90r⩾0.90. Around the average rise time [52 months], r=0.95r=0.95; iii) The correlation between SmSm and SNSN (or βaβa) in even-numbered cycles is stronger than that in odd-numbered ones, and the latter is slightly weaker than that for all the cycles; iv) The mean relative error [ηη] of SmSm decreases and the MSE (Mean Square Error) skill score [ScSc] increases with ΔmΔm. One, two, three, and four years after the solar minimum: η⩽19%η⩽19%, 14%14%, 10%10%, and 6.5%6.5%, Sc⩾0.24Sc⩾0.24, 0.68, 0.86, and 0.97, respectively; v) Currently [Δm=20Δm=20], the maximum amplitude of Cycle 25 is predicted to be 135.5±33.2135.5±33.2 and to occur around December 2024 (± 11 months).

Variations in the Correlations of Acceleration and Force of Slow and Fast CMEs with Solar Activity during Solar Cycles 23 – 24

Zhanle **Du**
Solar Physics volume 296, Article number: 34 (**2021**)
https://link.springer.com/content/pdf/10.1007/s11207-021-01778-5.pdf
Studying the behavior of coronal mass ejections (CMEs) is important for both solar physics and space weather. The correlations of smoothed monthly mean daily integrated CME acceleration [a], mass [M], and the force [Ma] to drive CMEs with sunspot activity [RI] are analyzed for both slow and fast CMEs and for both Solar Cycles 23 and 24 separately. It is found that aa is inversely related to both RI and M. The correlation between Ma and RI for both slow and fast CMEs is negative at the rising phase of Solar Cycle 23 and positive otherwise. There is a sharp peak in γ=Ma/RI near the solar minimum (December 2008) for both slow and fast CMEs. However, for fast CMEs, there is a sharp negative peak near the previous solar minimum (August 1996) and another positive peak near the current solar minimum (2019). The positive (negative) peak tends to be related to the solar minimum from a stronger (weaker) to a weaker (stronger) solar cycle. These results suggest that the CME acceleration depends more on the strength of solar activity than on the CME's speed. Stronger magnetic activity may slow down the CMEs that are too massive or too fast and weaker activity may speed up the CMEs that are less massive or too slow. During a few years' period of magnetic-field polarity reversal around the solar minimum, the force provided by large-scale magnetic-field structures may not be strong enough to constrain CME motions, leading to the "escape" of CMEs with large $|\gamma|$.

Predicting the Amplitude of Solar Cycle 25 Using the Value 39 Months Before the Solar Minimum

Zhanle **Du**
Solar Physics volume 295, Article number: 147 (**2020**)
https://link.springer.com/content/pdf/10.1007/s11207-020-01720-1.pdf
Yoshida and Yamagishi (Ann. Geophys. 28, 417, 2010) found that the rate of decrease in the smoothed monthly mean sunspot number [RI] over the final three years of a solar cycle or RIRI itself at three years before the solar minimum [Rmin] can be used as a precursor for the ensuing maximum amplitude [Rm] if the time of RminRmin can be predicted in advance. The RI series of the new version is employed to carefully analyze the decrease rate [β] at different months [mm] before RminRmin and over different time intervals [Δm] in this study. It is found that Rm(n) of Solar Cycle nn is best correlated (r=0.831) with the preceding $\beta(n-1,m,\Delta m)$ over the final $\Delta m=m=39$months. In addition, Rm is found to be best correlated (r=0.834) with the RI value 39 months before the preceding minimum. For the even- (odd-)numbered cycles, Rm is best correlated, r=0.956 (0.747), with the rate of decrease over $\Delta m=38(43)$ months interval from m=39(47) months before the solar minimum, and RmRm is best correlated, r=0.964(0.739) with the RIRI-value 39 (46) months before the solar minimum. Based on this method and the inferred end time of Solar Cycle 24, the amplitude of Solar Cycle 25 is predicted to be Rm=130.0±31.9, occurring around October 2024 ±13 (months).

Predicting the Shape of Solar Cycle 25 Using a Similar-Cycle Method

Zhanle **Du**
Solar Physics volume 295, Article number: 134 (**2020**)
https://link.springer.com/content/pdf/10.1007/s11207-020-01701-4.pdf
A similar-cycle method is applied in predicting the shape of Solar Cycle 25, through a more scientific definition to select similar cycles. Using the current solar minimum Rmin(25)Rmin(25) as a reference, the six most similar cycles to Solar Cycle 25 are found to be Cycles 24, 15, 12, 14, 17, and 10 (in that order). The monthly values of sunspot-number series for the whole of Cycle 25 are predicted by weighted averaging the corresponding ones in the six similar cycles. As a result, Solar Cycle 25 is predicted to peak around October 2024 with an amplitude of about Rm=137.8±31.3Rm=137.8±31.3 and to end around September 2030. As a by-product, there might be a secondary peak eight months earlier. The similar-cycle method considers only the solar cycles with similar parameters rather than all ones as for regression methods. It has an advantage that it does not depend so much on the accuracy of the observation.

Forecasting the Daily 10.7 cm Solar Radio Flux Using an Autoregressive Model

Zhanle **Du**
Solar Physics volume 295, Article number: 125 (**2020**)
https://link.springer.com/content/pdf/10.1007/s11207-020-01689-x.pdf
As an important proxy of the solar extreme ultraviolet radiation from the upper chromosphere and lower corona, the 10.7 cm solar radio flux (F10.7) has a wide range of applications in models of the thermosphere and ionosphere. Forecasting F10.7 has already become a routine business in space weather services. In this study, we analyzed the predictive power of autoregressive (AR) models with orders p=15p=15 – 1005, a training sample length L=22L=22 years, and a running time window w=50w=50 days on the daily F10.7, during the last two solar cycles (Solar Cycles 23 and 24) at the forecast steps n=1n=1 – 81 days. The main conclusions are as follows. (i) The mean forecast error ($\delta\bar{\ }\delta\bar{\ }$) at the nnth day or over NN days is minimum at an optimal order popo, which tends to

increase as nn or NN increases. (ii) $\bar{\delta}\bar{\delta}$ is positively related to both nn and F10.7. The large error during the maximum period is the result of the large daily variation in F10.7, mainly due to the appearance and decay of active regions, especially the eruptions of solar flares. (iii) The solar cycle can be divided into six parts in the rising order of $\bar{\delta}\bar{\delta}$: (a) closing part of the declining phase, (b) initial rising phase, (c) middle declining phase, (iv) closing rising phase, (v) middle rising phase, and (f) initial declining phase. (iv) The AR model at popo is not inferior to other techniques. (v) popo is uncorrelated to the autocorrelation coefficient, and (vi) $\bar{\delta}\bar{\delta}$ is minimum at a certain LL.

Bimodal Structure of the Solar Cycle

Z. L. **Du**

ApJ 804 3 **2015**

Some properties of the 11 yr solar cycle can be explained by the current solar dynamo models. However, some other features remain not well understood such as the asymmetry of the cycle, the double-peaked structure, and the "Waldmeier effect" that a stronger cycle tends to have less rise time and a shorter cycle length. We speculate that the solar cycle is governed by a bi-dynamo model forming two stochastic processes depicted by a bimodal Gaussian function with a time gap of about 2 yr, from which the above features can be reasonably explained. The first one describes the main properties of the cycle dominated by the current solar dynamo models, and the second one occurs either in the rising phase as a short weak explosive perturbation or in the declining phase as a long stochastic perturbation. The above function is the best one selected from several in terms of the Akaike information criterion. Through analyzing different distributions, one might speculate about the dominant physical process inside the convection zone. The secondary (main) process is found to be closely associated with complicated (simple) active ranges. In effect, the bi-dynamo model is a reduced form of a multi-dynamo model, which could occur from the base of the convection zone through its envelope and from low to high heliographic latitude, reflecting the active belts in the convection zone. These results are insensitive to the hemispheric asymmetry, smoothing filters, and distribution functions selected and are expected to be helpful in understanding the formation of solar and stellar cycles.

Ubiquitous Small-scale EUV Upflow-Like Events above Network Regions Observed by the Solar Orbiter/Extreme Ultraviolet Imager

Yadan **Duan**, Hechao Chen, Zhenyong Hou, Zheng Sun, Yuandeng Shen

ApJ **2024**

https://arxiv.org/pdf/2412.13444

Universal small-scale solar activity in quiet region are suggested to be a potential source of solar wind and the upper solar atmosphere. Here, with the high-resoltion 174 Å~imaging observations from the Solar Orbiter/Extreme Ultraviolet Imager (EUI), we investigate 59 EUV upflow-like events observed in the quiet Sun. Their average apparent (plane-of-sky) velocity, lifetime, and propagation distance are measured as 62 $\speed$, 68.6 s and 3.94 Mm, respectively. These upflow-like events exhibit dynamic characteristics but lack base brightening, featuring a hot front and subsequent cold plasma ejection. 39\% of the EUV upflow-like events exhibit recurrent characteristics. Unprecedented high-resolution 174 Å~observations reveal that some EUV upflow-like events exhibit blob-like fine structures and multi-strand evolutionary features, and some upflow-like events can cause localized haze-like plasma heating ahead of their spire region during the ejection process. A subset of the EUV upflow-like events covered by the Solar Dynamics Observatory reveals that they appear at the chromospheric networks. Through emission measure analysis, we found that these upflow-like events eject hot plasma of transient region or coronal temperature (an average of ~105.5K). We suggest that EUV upflow-like events may be EUV counterparts of chromospheric spicules and/or transition region network jets, and play a role in heating localized corona above the network regions.
2020 May 30, 2021 February 23,

On the Lorentz Force and Torque of Solar Photospheric Emerging Magnetic Fields

Aiying **Duan**1, Chaowei Jiang2, Shin Toriumi3, and Petros Syntelis4

2020 ApJL 896 L9

https://doi.org/10.3847/2041-8213/ab961e

Magnetic flux generated and intensified by the solar dynamo emerges into the solar atmosphere, forming active regions (ARs) including sunspots. Existing theories of flux emergence suggest that the magnetic flux can rise buoyantly through the convection zone but is trapped at the photosphere, while its further rising into the atmosphere resorts to the Parker buoyancy instability. To trigger such an instability, the Lorentz force in the photosphere needs to be as large as the gas pressure gradient to hold up an extra amount of mass against gravity. This naturally results in a strongly non-force-free photosphere, which is indeed shown in typical idealized numerical simulations of flux tube buoyancy from below the photosphere into the corona. Here we conduct a statistical study of the extents of normalized Lorentz forces and torques in the emerging photospheric magnetic field with a substantially large sample of Solar Dynamics Observatory/Helioseismic and Magnetic Imager vector magnetograms. We found that the photospheric field has a rather small Lorentz force and torque on average, and thus is very close to a force-free state, which is not consistent with theories as well as idealized simulations of flux emergence. Furthermore, the small

extents of forces and torques seem not to be influenced by the emerging AR's size, the emergence rate, or the nonpotentiality of the field. This result puts an important constraint on future development of theories and simulations of flux emergence.

Helicity inversion in spherical convection as a means for equatorward dynamo wave propagation

Lúcia D. V. **Duarte**, Johannes Wicht, Matthew K. Browning, Thomas Gastine
MNRAS **201**5
http://arxiv.org/pdf/1511.05813v1.pdf
We discuss here a purely hydrodynamical mechanism to invert the sign of the kinetic helicity, which plays a key role in determining the direction of propagation of cyclical magnetism in most models of dynamo action by rotating convection. Such propagation provides a prominent, and puzzling constraint on dynamo models. In the Sun, active regions emerge first at mid-latitudes, then appear nearer the equator over the course of a cycle, but most previous global-scale dynamo simulations have exhibited poleward propagation (if they were cyclical at all). Here, we highlight some simulations in which the direction of propagation of dynamo waves is altered primarily by an inversion of the kinetic helicity throughout much of the interior, rather than by changes in the differential rotation. This tends to occur in cases with a low Prandtl number and internal heating, in regions where the local density gradient is relatively small. We analyse how this inversion arises, and contrast it to the case of convection that is either highly columnar (i.e., rapidly rotating) or locally very stratified; in both of those situations, the typical profile of kinetic helicity (negative throughout most of the northern hemisphere) instead prevails.

The effect of magnetic field on the damping of slow waves in the solar corona

T. J. **Duckenfield**, D. Y. Kolotkov, V. M. Nakariakov
A&A 646, A155 (**2021**)
https://arxiv.org/pdf/2011.10437.pdf
https://doi.org/10.1051/0004-6361/202039791
https://www.aanda.org/articles/aa/pdf/2021/02/aa39791-20.pdf
Slow magnetoacoustic waves are routinely observed in astrophysical plasma systems such as the solar corona. As a slow wave propagates through a plasma, it modifies the equilibrium quantities of density, temperature, and magnetic field. In the corona and other plasma systems, the thermal equilibrium is comprised of a balance between continuous heating and cooling processes, the magnitudes of which vary with density, temperature and magnetic field. Thus the wave may induce a misbalance between these competing processes. Its back reaction on the wave has been shown to lead to dispersion, and amplification or damping, of the wave. In this work the importance of the effect of magnetic field in the rapid damping of slow waves in the solar corona by heating/cooling misbalance is evaluated and compared to the effects of thermal conduction. The two timescales characterising the effect of misbalance are derived and calculated for plasma systems with a range of typical coronal conditions. The predicted damping times of slow waves from thermal misbalance in the solar corona are found to be of the order of 10-100 minutes, coinciding with the wave periods and damping times observed. Moreover the slow wave damping by thermal misbalance is found to be comparable to the damping by field-aligned thermal conduction. We show that in the infinite field limit, the wave dynamics is insensitive to the dependence of the heating function on the magnetic field, and this approximation is found to be valid in the corona so long as the magnetic field strength is greater than 10G for quiescent loops and plumes and 100G for hot and dense loops. In summary thermal misbalance may damp slow magnetoacoustic waves rapidly in much of the corona, and its inclusion in our understanding of slow mode damping may resolve discrepancies between observations and theory relying on compressive viscosity and thermal conduction alone.

Electron Densities in the Solar Corona Measured Simultaneously in the Extreme-Ultraviolet and Infra-Red

Jaroslav **Dudík**, Giulio Del Zanna, Ján Rybák, Juraj Lörinčík, Elena Dzifčáková, Helen E. Mason, Steven Tomczyk, Michael Galloy
2021 *ApJ* **906** 118
https://arxiv.org/pdf/2011.09175.pdf
https://doi.org/10.3847/1538-4357/abcd91
Accurate measurements of electron density are critical for determination of the plasma properties in the solar corona. We compare the electron densities diagnosed from Fe XIII lines observed by the Extreme-Ultraviolet Imaging Spectrometer (EIS) onboard the Hinode mission with the near infra-red (NIR) measurements provided by the ground-based Coronal Multichannel Polarimeter (COMP). To do that, the emissivity-ratio method based on all available observed lines of Fe XIII is used for both EIS and CoMP. The EIS diagnostics is further supplemented by the results from Fe XII lines. We find excellent agreement, within 10%, between the electron densities measured from both EUV and NIR lines. In the five regions selected for detailed analysis, we obtain electron densities of log(Ne [cm-3]) = 8.2-8.6. Where available, the background subtraction has a significant impact on the diagnostics,

especially on the NIR lines, where the loop contributes less than a quarter of the intensity measured along the line of sight. For the NIR lines, we find that the line center intensities are not affected by stray light within the instrument, and recommend using these for density diagnostics. The measurements of the Fe XIII NIR lines represent a viable method for density diagnostics using ground-based instrumentation. **2016 August 30**

Signatures of the non-Maxwellian κ-distributions in optically thin line spectra. II. Synthetic Fe XVII--XVIII X-ray coronal spectra and predictions for the Marshall Grazing-Incidence X-ray Spectrometer (MaGIXS)

Jaroslav **Dudik**, Elena Dzifcakova, Giulio Del Zanna, Helen E. Mason, Leon L. Golub, Amy R. Winebarger, Sabrina L. Savage
A&A **2019**
https://arxiv.org/pdf/1905.10356.pdf
We investigated the possibility of diagnosing the degree of departure from the Maxwellian distribution using the Fe XVII - Fe XVIII spectra originating in plasmas in collisional ionization equilibrium, such as in the cores of solar active regions or microflares. The original collision strengths for excitation are integrated over the non-Maxwellian electron κ-distributions characterized by a high-energy tail. Synthetic X-ray emission line spectra were calculated for a range of temperatures and κ. We focus on the 6-24 A spectral range to be observed by the upcoming Marshall Grazing-Incidence X-ray Spectrometer MaGIXS. We find that many line intensity ratios are sensitive to both T and κ. Best diagnostic options are provided if a ratio involving both Fe XVII and Fe XVIII is combined with another ratio involving lines formed within a single ion. The sensitivity of such diagnostics to κ is typically a few tens of per cent. Much larger sensitivity, of about a factor of two to three, can be obtained if the Fe XVIII 93.93 A line observed by SDO/AIA is used in conjuction with the X-ray lines. We conclude that the MaGIXS instrument is well-suited for detection of departures from the Maxwellian distribution, especially in active region cores.

Non-Equilibrium Processes in the Solar Corona, Transition Region, Flares, and Solar Wind \textit{(Invited Review)}

Jaroslav **Dudík**, Elena Dzifčáková, Nicole Meyer-Vernet, Giulio Del Zanna, Peter R. Young, Alessandra Giunta, Barbara Sylwester, Janusz Sylwester, Mitsuo Oka, Helen E. Mason, Christian Vocks, Lorenzo Matteini, Säm Krucker, David R. Williams, Šimon Mackovjak
Solar Physics 292:100 **2017**
https://arxiv.org/pdf/1706.03396.pdf
We review the presence and signatures of the non-equilibrium processes, both non-Maxwellian distributions and non-equilibrium ionization, in the solar transition region, corona, solar wind, and flares. Basic properties of the non-Maxwellian distributions are described together with their influence on the heat flux as well as on the rates of individual collisional processes and the resulting optically thin synthetic spectra. Constraints on the presence of high-energy electrons from observations are reviewed, including positive detection of non-Maxwellian distributions in the solar corona, transition region, flares, and wind. Occurrence of non-equilibrium ionization is reviewed as well, especially in connection to hydrodynamic and generalized collisional-radiative modelling. Predicted spectroscopic signatures of non-equilibrium ionization depending on the assumed plasma conditions are summarized. Finally, we discuss the future remote-sensing instrumentation that can be used for detection of these non-equilibrium phenomena in various spectral ranges. **2012-07-19**

Non-Maxwellian analysis of the transition-region line profiles observed by the Interface Region Imaging Spectrograph

Jaroslav **Dudik**, Vanessa Polito, Elena Dzifcakova, Giulio Del Zanna, Paola Testa
ApJ 842 19 **2017**
https://arxiv.org/pdf/1705.02104.pdf
We investigate the nature of the spectral line profiles for transition region ions observed with the Interface Region Imaging Spectrograph (IRIS). In this context, we have analyzed an active-region observation performed by IRIS in its 1400 A spectral window. The transition-region lines are found to exhibit significant wings in their spectral profiles, which can be well-fitted with non-Maxwellian kappa-distribution. The fit with a kappa-distribution can perform better than a double Gaussian fit, especially for the strongest line, Si IV 1402.8 A. Typical values of κ found are about 2, occurring in a majority of spatial pixels where the transition region lines are symmetric, i.e., the fit can be performed. Furthermore, all five spectral lines studied (from Si IV, O IV and S IV) appear to have the same FWHM irrespective of whether the line is an allowed or an intercombination transition. A similar value of kappa is obtained for the electron distribution by fitting of the line intensities relative to Si IV 1402.8 A, if photospheric abundances are assumed. The kappa-distributions however do not remove the presence of non-thermal broadening. Instead, they actually increase the non-thermal width. This is because for kappa-distributions the

transition-region ions are formed at lower temperatures. The large observed non-thermal width lowers the opacity of the Si IV line sufficiently enough for this line to become optically thin.

Modelling Ion Populations in Astrophysical Plasmas: Carbon in the Solar Transition Region

R.P. **Dufresne**, G. Del Zanna
A&A **2019**
https://arxiv.org/pdf/1901.08992.pdf
A collisional-radiative model for carbon has been developed to determine ion populations in lower-temperature, higher-density plasmas, such as the solar transition region. These conditions mean the often-used coronal approximation no longer holds for the modelling. The most up-to-date atomic rates have been employed for the processes which influence the populations in these regions. In the absence of level-resolved rates for electron-impact direct ionisation and excitation-autoionisation, new calculations have been made using atomic codes. Comparison with laboratory cross-sections and previous studies, where available, show satisfactory agreement. The ion populations resulting from the modelling are presented, demonstrating the influence each atomic process has as density and temperature vary. An initial investigation into the influence of photo-ionisation has also been investigated. Tests against observations have been made by comparing the ratio of predicted to observed intensities using differential emission measure modelling in the quiet-Sun transition region, showing noticeable improvements and particularly for the anomalous ion, C IV.

Shear-driven magnetic buoyancy in the solar tachocline: the mean electromotive force due to rotation

Craig D **Duguid**, Paul J Bushby, Toby S Wood
Monthly Notices of the Royal Astronomical Society, Volume 520, Issue 1, March **2023**, Pages 527–541,
https://doi.org/10.1093/mnras/stad158
The leading theoretical paradigm for the Sun's magnetic cycle is an αω-dynamo process, in which a combination of differential rotation and turbulent, helical flows produces a large-scale magnetic field that reverses every 11 yr. Most αω solar dynamo models rely on differential rotation in the solar tachocline to generate a strong toroidal field. The most problematic part of such models is then the production of the large-scale poloidal field, via a process known as the α-effect. Whilst this is usually attributed to small-scale convective motions under the influence of rotation, the efficiency of this regenerative process has been called into question by some numerical simulations. Motivated by likely conditions within the tachocline, the aim of this paper is to investigate an alternative mechanism for the poloidal field regeneration, namely the magnetic buoyancy instability in a shear-generated, rotating magnetic layer. We use a local, fully compressible model in which an imposed vertical shear winds up an initially vertical magnetic field. The field ultimately becomes buoyantly unstable, and we measure the resulting mean electromotive force (EMF). For sufficiently rapid rotation, we find that a significant component of the mean EMF is aligned with the direction of the mean magnetic field, which is the characteristic feature of the classical αω-dynamo model. Our results therefore suggest that magnetic buoyancy could contribute directly to the generation of large-scale poloidal field in the Sun.

Eigenspectra of solar active region long-period oscillations

G. **Dumbadze**1,2,3, B. M. Shergelashvili2,3,4,5, S. Poedts1,9, T. V. Zaqarashvili3,6,7, M. Khodachenko4,8,10 and P. De Causmaecker5
A&A 653, A39 (**2021**)
https://arxiv.org/pdf/2109.04189.pdf
https://www.aanda.org/articles/aa/pdf/2021/09/aa38124-20.pdf
https://doi.org/10.1051/0004-6361/202038124
Context. We studied the low-frequency $\lesssim$0.5 h−1 (long-period $\gtrsim$2 h) oscillations of active regions (ARs). The investigation is based on an analysis of a time series built from Solar Dynamics Observatory/Helioseismic and Magnetic Imager photospheric magnetograms and comprises case studies of several types of AR structures.
Aims. The main goals are to investigate whether ARs can be engaged in long-period oscillations as unified oscillatory entities and, if so, to determine the spectral pattern of such oscillations.
Methods. Time series of characteristic parameters of the ARs, such as, the total area, total unsigned radial magnetic flux, and tilt angle, were measured and recorded using the image moment method. The power spectra were built out of Gaussian-apodised and zero-padded datasets.
Results. There are long-period oscillations ranging from 2 to 20 h, similarly to the characteristic lifetimes of super-granulation, determined from the datasets of the AR total area and radial magnetic flux, respectively. However, no periodicity in tilt angle data was found.
Conclusions. Whatever nature these oscillations have, they must be energetically supported by convective motions beneath the solar surface. The possible interpretations can be related to different types of magnetohydrodynamic oscillations of the multi-scale structure of the AR magnetic field, which is probably linked with the characteristic

turnover timescales of the super-granulation cells. The presence of oscillations in the radial magnetic flux data may be connected to periodic flux emergence or cancellation processes.

Long-period oscillations of active region patterns: least-squares mapping on second-order curves

G. **Dumbadze**, B.M. Shergelashvili, V. Kukhianidze, G. Ramishvili, T.V. Zaqarashvili, M. Khodachenko, E. Gurgenashvili, S. Poedts, P. De Causmaecker

A&A 597, A93 **2017**

https://arxiv.org/pdf/1610.01509v1.pdf

Active regions (ARs) are the main sources of variety in solar dynamic events. Automated detection and identification tools need to be developed for solar features for a deeper understanding of the solar cycle. Of particular interest here are the dynamical properties of the ARs, regardless of their internal structure and sunspot distribution. We studied the oscillatory dynamics of two ARs: NOAA 11327 and NOAA 11726 using two different methods of pattern recognition. We developed a novel method of automated AR border detection and compared it to an existing method for the proof-of-concept. The first method uses least-squares fitting on the smallest ellipse enclosing the AR, while the second method applies regression on the convex hull.} After processing the data, we found that the axes and the inclination angle of the ellipse and the convex hull oscillate in time. These oscillations are interpreted as the second harmonic of the standing long-period kink oscillations (with the node at the apex) of the magnetic flux tube connecting the two main sunspots of the ARs. In both ARs we have estimated the distribution of the phase speed magnitude along the magnetic tubes (along the two main spots) by interpreting the obtained oscillation of the inclination angle as the standing second harmonic kink mode. After comparing the obtained results for fast and slow kink modes, we conclude that both of these modes are good candidates to explain the observed oscillations of the AR inclination angles, as in the high plasma β regime the phase speeds of these modes are comparable and on the order of the Alfv\'{e}n speed. Based on the properties of the observed oscillations, we detected the appropriate depth of the sunspot patterns, which coincides with estimations made by helioseismic methods. The latter analysis can be used as a basis for developing a magneto-seismological tool for ARs. **20-22.10.2011, 20-22.04.2013**

Anticorrelated temperature-density profiles in the quiet solar corona and coronal mass ejections: Approach based on the spine-type Hamiltonians

Yu.V. **Dumin**

A&A **2020**

https://arxiv.org/pdf/2002.08624.pdf

Context: The mechanism of the solar corona heating remains one of key problems in astrophysics for a few decades; but none of the proposed mechanisms can give a definitive answer to this question. As a result, the novel scenarios are still suggested. Aims: Here, we perform a critical consideration of the recently-proposed mechanism for the formation of the anticorrelated temperature and density profiles due to specific features of relaxation in the strongly non-equilibrium plasmas described by the so-called spin-type Hamiltonians [L. Casetti and S. Gupta, 2014, Eur. Phys. J. B 87, 91; T.N. Teles et al., 2015, Phys. Rev. E 92, 020101(R)]. Methods: We employ the universal property of the above-mentioned systems to produce the long-lived anticorrelated temperature-density distributions and analyse their most important qualitative features that should be expected in the context of the coronal plasmas. Results: As follows from our consideration, the anticorrelated profiles predicted by the spine-type Hamiltonians can be hardly relevant to explanation of the temperature distribution in the quiet solar corona. However, they might be interesting for the interpretation of the large-scale inhomogeneity of the powerful coronal mass ejections, possessing the filament-type structure.

Three Years of HARPS-N High-Resolution Spectroscopy and Precise Radial Velocity Data for the Sun

X. **Dumusque**, M. Cretignier, D. Sosnowska, N. Buchschacher, C. Lovis, D. F. Phillips, F. Pepe, F. Alesina, L. A. Buchhave, J. Burnier, M. Cecconi, H. M. Cegla, R. Cloutier, A. Collier Cameron, R. Cosentino, A. Ghedina, M. Gonzalez, R. D. Haywood, D. W. Latham, M. Lodi, M. Lopez-Morales, J. Maldonado, L. Malavolta, G. Micela, E. Molinari, A. Mortier, H. Perez Ventura, M. Pinamonti, E. Poretti, K. Rice, L. Riverol, C. Riverol, J. San Juan, D. Segransan, A. Sozzetti, S. J.Thompson, S. Udry, T. G Wilson

A&A **2020**

https://arxiv.org/pdf/2009.01945.pdf

The solar telescope connected to HARPS-N has observed the Sun since the summer of 2015. Such high-cadence, long-baseline data set is crucial for understanding spurious radial-velocity (RV) signals induced by our Sun and by the instrument.

This manuscript describes the data reduction performed to obtain unprecedented RV precision for the three years of

solar data released along with this paper.
The nearly continuous observation of our Sun has allowed us to detect sub-\ms\,systematics in the HARPS-N solar data reduced by the current HARPS-N data reduction software (DRS). To improve the RV precision of the solar data, we reduced them using the new ESPRESSO DRS and developed new recipes to mitigate the detected systematics.
The most significant improvement brought by the new data reduction is a strong decrease in the day-to-day RV scatter, from 1.28 to 1.09\ms; this is thanks to a more stable method to derive wavelength solutions, but also to the use of calibrations closer in time. We also demonstrate that the current HARPS-N DRS induces a long-term drift of ∼1.2\ms, due to the use of non-stable thorium lines. As a result, the old solar RVs are weakly correlated to the solar magnetic cycle, which is not expected. On the contrary, the newly derived RVs are much more correlated, with a Pearson correlation coefficient of 0.93. We also discuss a special correction for ghost contamination, to extract a calcium activity index free from instrument systematics.
Our work leads toward a better understanding of the instrumental and data reduction systematics affecting the HARPS-N spectrograph. The new solar data released, representing an unprecedented time-series of 34550 high-resolution spectra and precise RVs will be crucial to understanding stellar activity signals of solar-type stars, with the goal of enabling the detection of other Earths. **2017-04- 12**

Additional Evidence Supporting a Model of Shallow, High-Speed Supergranulation

T.L. **Duvall** Jr., S.M. Hanasoge, S. Chakraborty
Solar Phys., Volume 289, Issue 9, pp 3421-3433, **2014**
http://arxiv.org/pdf/1404.2533v1.pdf
Recently, Duvall and Hanasoge ({\it Solar Phys.} {\bf 287}, 71-83, 2013) found that large distance [Δ] separation travel-time differences from a center to an annulus [δtoi] implied a model of the average supergranular cell that has a peak upflow of 240ms −1 at a depth of 2.3Mm and a corresponding peak outward horizontal flow of 700ms −1 at a depth of 1.6Mm. In the present work, this effect is further studied by measuring and modeling center-to-quadrant travel-time differences [δtqu], which roughly agree with this model. Simulations are analyzed that show that such a model flow would lead to the expected travel-time differences. As a check for possible systematic errors, the center-to-annulus travel-time differences [δtoi] are found not to vary with heliocentric angle. A consistency check finds an increase of δtoi with the temporal frequency [ν] by a factor of two, which is not predicted by the ray theory.

Solar hard X-ray imaging by means of Compressed Sensing and Finite Isotropic Wavelet Transform

M. A. **Duval-Poo**, M. Piana, A. M. Massone
A&A **2017**
https://arxiv.org/pdf/1708.03877.pdf
This paper shows that compressed sensing realized by means of regularized deconvolution and the Finite Isotropic Wavelet Transform is effective and reliable in hard X-ray solar imaging.
The method utilizes the Finite Isotropic Wavelet Transform with Meyer function as the mother wavelet. Further, compressed sensing is realized by optimizing a sparsity-promoting regularized objective function by means of the Fast Iterative Shrinkage-Thresholding Algorithm. Eventually, the regularization parameter is selected by means of the Miller criterion.
The method is applied against both synthetic data mimicking the Spectrometer/Telescope Imaging X-rays (STIX) measurements and experimental observations provided by the Reuven Ramaty High Energy Solar Spectroscopic Imager (RHESSI). The performances of the method are compared with the results provided by standard visibility-based reconstruction methods.
The results show that the application of the sparsity constraint and the use of a continuous, isotropic framework for the wavelet transform provide a notable spatial accuracy and significantly reduce the ringing effects due to the instrument point spread functions**. February 20, 2002, April 15, 2002, July 23, 2002, December 02, 2003, August 31, 2004, May 13, 2013**

Solar coronal plumes and the fast solar wind

B.N. **Dwivedi**, K. Wilhelm
A&A **2015**
http://arxiv.org/pdf/1506.01700v1.pdf
The spectral profiles of the coronal Ne viii line at 77 nm have different shapes in quiet-Sun regions and coronal holes (CHs). A single Gaussian fit of the line profile provides an adequate approximation in quiet-Sun areas, whereas a strong shoulder on the long-wavelength side is a systematic feature in CHs. Although this has been noticed since 1999, no physical reason for the peculiar shape could be given. In an attempt to identify the cause of this peculiarity, we address three problems that could not be conclusively resolved in a review article by a study team of the International Space Science Institute (ISSI; Wilhelm et al. 2011) : (1) The physical processes operating

at the base and inside of plumes as well as their interaction with the solar wind (SW). (2) The possible contribution of plume plasma to the fast SW streams. (3) The signature of the first-ionization potential (FIP) effect between plumes and inter-plume regions (IPRs). Before the spectroscopic peculiarities in IPRs and plumes in polar coronal holes (PCHs) can be further investigated with the instrument Solar Ultraviolet Measurements of Emitted Radiation (SUMER) aboard the Solar and Heliospheric Observatory (SOHO), it is mandatory to summarize the results of the review to place the spectroscopic observations into context. Finally, a plume model is proposed that satisfactorily explains the plasma flows up and down the plume field lines and leads to the shape of the neon line in PCHs.

Possible signature of Alfv .en wave dissipation in the localized magnetic funnels of the equatorial solar corona

Bhola N. **DWIVEDI**,∗ Abhishek Kumar SRIVASTAVA, and Anita MOHAN
Publ. Astron. Soc. Japan (**2014**) 66 (SP1), S13 (1–11)
http://pasj.oxfordjournals.org/content/66/SP1/S13.full.pdf+html
We analyse the Hinode/EIS 2__-spectroscopic scan data containing the spectral line formed at typical inner coronal temperature. The strong Fe XII 195.120 °A line shows the existence of funnel-like expanding flux-tubes which exhibit the signature of blue-/red-shifted plasma motions in the off-limb equatorial corona. These coronal funnels expand in the form of open magnetic field channels up to inner coronal heights. They are most likely the parts of large-scale and closed magnetic fields (loops) which exist at higher heights in the diffused equatorial corona. We also find the signature of decreasing line-widths with altitude in observed coronal funnels (e.g., funnel 1), which is the lower part of a curved loop system. This provides the most likely signature of Alfve.n wave dissipation in lower part of this loop system. We also examine the blue-shifted and diffused coronal loop boundary and interfaced region (funnel 3) which shows increasing Fe XII 195.120 °A line-width along it. Therefore, it exhibits the most likely signature of Alfve.n wave growth in this region which is slightly curved and rising higher in the corona. Density measurements in these funnels show that it falls off with height, but more rapidly in the second funnel. We conjecture the almost constant line-width trend as a most likely signature of Alfve.n wave dissipation in this density-stratified second coronal funnel, which is also the lower part of a large-scale closed loop system. Both dissipative and growing Alfve.nwaves can change the non-thermal component and thus the full width at half-maximum of the Fe XII 195.120 °A line. We find the clues of Alfve.n wave dissipation along the expanding field lines of the coronal funnel (lower parts of the loop system) imparting its energy to the outflowing plasma and thereby contributing to the formation of the nascent solar wind in the inner corona.

Local stability of differential rotation in magnetised radiation zones and the solar tachocline

Robert W. **Dymott**, Adrian J. Barker, Chris A. Jones, Steven M. Tobias
MNRAS **2024**
https://arxiv.org/pdf/2410.06989
We study local magnetohydrodynamical (MHD) instabilities of differential rotation in magnetised, stably-stratified regions of stars and planets using a Cartesian Boussinesq model. We consider arbitrary latitudes and general shears (with gravity direction misaligned from this by an angle ϕ), to model radial (ϕ=0), latitudinal (ϕ=±90∘), and mixed differential rotations, and study both non-diffusive (including magnetorotational, MRI, and Solberg-Høiland instabilities) and diffusive instabilities (including Goldreich-Schubert-Fricke, GSF, and MRI with diffusion). These instabilities could drive turbulent transport and mixing in radiative regions, including the solar tachocline and the cores of red giant stars, but their dynamics are incompletely understood. We revisit linear axisymmetric instabilities with and without diffusion and analyse their properties in the presence of magnetic fields, including deriving stability criteria and computing growth rates, wavevectors and energetics, both analytically and numerically. We present a more comprehensive analysis of axisymmetric local instabilities than prior work, exploring arbitrary differential rotations and diffusive processes. The presence of a magnetic field leads to stability criteria depending upon angular velocity rather than angular momentum gradients. We find MRI operates for much weaker differential rotations than the hydrodynamic GSF instability, and that it typically prefers much larger lengthscales, while the GSF instability is impeded by realistic strength magnetic fields. We anticipate MRI to be more important for turbulent transport in the solar tachocline than the GSF instability when ϕ>0 in the northern (and vice versa in the southern) hemisphere, though the latter could operate just below the convection zone when MRI is absent for ϕ<0

Non-equilibrium ionization by a periodic electron beam
II. Synthetic Si IV and O IV transition region spectra★

Elena **Dzifčáková** and Jaroslav Dudík

A&A 610, A67 (**2018**)
Context. Transition region (TR) spectra typically show the Si IV 1402.8 Å line to be enhanced by a factor of 5 or more compared to the neighboring O IV 1401.2 Å, contrary to predictions of ionization equilibrium models and the Maxwellian distribution of particle energies. Non-equilibrium effects in TR spectra are therefore expected.
Aims. To investigate the combination of non-equilibrium ionization and high-energy particles, we apply the model of the periodic electron beam, represented by a κ-distribution that recurs at periods of several seconds, to plasma at chromospheric temperatures of 104 K. This simple model can approximate a burst of energy release involving accelerated particles.
Methods. Instantaneous time-dependent charge states of silicon and oxygen were calculated and used to synthesize the instantaneous and period-averaged spectra of Si IV and O IV.
Results. The electron beam drives the plasma out of equilibrium. At electron densities of Ne = 1010 cm−3, the plasma is out of ionization equilibrium at all times in all cases we considered, while for a higher density of Ne = 1011 cm−3, ionization equilibrium can be reached toward the end of each period, depending on the conditions. In turn, the character of the period-averaged synthetic spectra also depends on the properties of the beam. While the case of κ = 2 results in spectra with strong or even dominant O IV, higher values of κ can approximate a range of observed TR spectra. Spectra similar to typically observed spectra, with the Si IV 1402.8 Å line about a factor 5 higher than O IV 1401.2 Å, are obtained for κ = 3. An even higher value ofκ = 5 results in spectra that are exclusively dominated by Si IV, with negligible O IV emission. This is a possible interpretation of the TR spectra of UV (Ellerman) bursts, although an interpretation that requires a density that is 1–3 orders of magnitude lower than for equilibrium estimates.

Elena Dzifčáková and Jaroslav Dudík

Synthetic IRIS spectra of the solar transition region: Effect of high-energy tails

E. **Dzifcakova**, C. Vocks, J. Dudik
A&A 603, A14 **2017**
https://arxiv.org/pdf/1705.08728.pdf

The solar transition region satisfies the conditions for presence of non-Maxwellian electron energy distributions with high-energy tails at energies corresponding to the ionization potentials of many ions emitting in the EUV and UV portions of the spectrum. We calculate the synthetic Si IV, O IV, and S IV spectra in the far ultra-violet (FUV) channel of the Interface Region Imaging Spectrograph (IRIS). Ionization, recombination, and excitation rates are obtained by integration of the cross-sections or their approximations over the model electron distributions considering particle propagation from the hotter corona. The ionization rates are significantly affected by the presence of high-energy tails. This leads to the peaks of the relative abundance of individual ions to be broadened with pronounced low-temperature shoulders. As a result, the contribution functions of individual lines observable by IRIS also exhibit low-temperature shoulders, or their peaks are shifted to temperatures an order of magnitude lower than for the Maxwellian distribution. The integrated emergent spectra can show enhancements of Si IV compared toO IV by more than a factor of two. The high-energy particles can have significant impact on the emergent spectra and their presence needs to be considered even in situations without strong local acceleration.

What Controls the Structure and Dynamics of Earth's Magnetosphere? **Review**

J. P. **Eastwood**, H. Hietala, G. Toth, T. D. Phan, M. Fujimoto
Space Science Reviews May **2015**, Volume 188, Issue 1-4, pp 251-286,
http://download.springer.com/static/pdf/335/art%253A10.1007%252Fs11214-014-0050-x.pdf?originUrl=http%3A%2F%2Flink.springer.com%2Farticle%2F10.1007%2Fs11214-014-0050-x&token2=exp=1433750748~acl=%2Fstatic%2Fpdf%2F335%2Fart%25253A10.1007%25252Fs11214-014-0050-x.pdf%3ForiginUrl%3Dhttp%253A%252F%252Flink.springer.com%252Farticle%252F10.1007%252Fs11214-014-0050-x*~hmac=110a0cb4332030e3df0431ef78fe8208fb18f113b7cc05867e9fb372cc1ec34d

Unlike most cosmic plasma structures, planetary magnetospheres can be extensively studied in situ. In particular, studies of the Earth's magnetosphere over the past few decades have resulted in a relatively good experimental understanding of both its basic structural properties and its response to changes in the impinging solar wind. In this article we provide a broad overview, designed for researchers unfamiliar with magnetospheric physics, of the main processes and parameters that control the structure and dynamics of planetary magnetospheres, especially the Earth's. In particular, we concentrate on the structure and dynamics of three important regions: the bow shock, the magnetopause and the magnetotail. In the final part of this review we describe the current status of global magnetospheric modelling, which is crucial to placing in situ observations in the proper context and providing a better understanding of magnetospheric structure and dynamics under all possible input conditions. Although the parameter regime experienced in the solar system is limited, the plasma physics that is learned by studying planetary magnetospheres can, in principle, be translated to more general studies of cosmic plasma structures. Conversely,

studies of cosmic plasma under a wide range of conditions should be used to understand Earth's magnetosphere under extreme conditions. We conclude the review by discussing this and summarizing some general properties and principles that may be applied to studies of other cosmic plasma structures.

The period ratio P_1/P_2 of torsional Alfvén waves with steady flows in spicules

H. **Ebadi**, S. Shahmorad, S. Vasheghani Farahani
Astrophysics and Space Science 361(4) **2016**
http://arxiv.org/pdf/1603.05370v1.pdf
The aim here is to model the standing torsional oscillations in solar spicules in the presence of density stratification, magnetic field expansion, and steady flows. By implementing cylindrical geometry, the eigenfrequencies, eigenfunctions, and the period ratio P_1/P_2 of these waves is obtained for finite plasma-beta. The shifts created by the steady flow justifies the divergence of the observed period ratio for the first and second periods from the number 2.

Observation of the period ratio P_1/P_2 of transversal oscillations in solar macro-spicules

H. **Ebadi**, M. Khoshrangbaf
Astrophysics and Space Science, **2014**
http://arxiv.org/pdf/1404.5806v1.pdf
We analyze the time series of oxygen line profiles (O vi 1031.93 A and O vi 1037.61 A obtained from SUMER/SOHO on the solar south limb. We calculated Doppler shifts and consequently Doppler velocities in three heights 4", 14", and 24" from the limb on a coronal hole region. Then, we performed wavelet analysis with Morlet wavelet transform to determine the periods of fundamental mode and its first harmonic mode. The calculated period ratios have departures from its canonical value of 2. The density stratification and magnetic twist are two main factors which may cause these departures.

Phase Mixing of Kink MHD Waves in the Solar Corona: Viscous Dissipation and Heating

Zanyar **Ebrahimi**1, Roberto Soler2,3, and Kayoomars Karami4
2020 ApJ 893 157
https://doi.org/10.3847/1538-4357/ab80ca
https://arxiv.org/pdf/2005.04389.pdf
Magnetohydrodynamic (MHD) kink waves have been observed frequently in solar coronal flux tubes, which makes them a great tool for seismology of the solar corona. Here, the effect of viscosity is studied on the evolution of kink waves. To this aim, we solve the initial value problem for the incompressible linearized viscous MHD equations in a radially inhomogeneous flux tube in the limit of long wavelengths. Using a modal expansion technique the spatio-temporal behavior of the perturbations is obtained. We confirm that for large Reynolds numbers representative of the coronal plasma the decrement in the amplitude of the kink oscillations is due to the resonant absorption mechanism that converts the global transverse oscillation to rotational motions in the inhomogeneous layer of the flux tube. We show that viscosity suppresses the rate of phase mixing of the perturbations in the inhomogeneous region of the flux tube and prevents the continuous building up of small scales in the system once a sufficiently small scale is reached. The viscous dissipation function is calculated to investigate plasma heating by viscosity in the inhomogeneous layer of the flux tube. For Reynolds numbers of the order of 106–108, the energy of the kink wave is transformed into heat in two to eight periods of the kink oscillation. For larger and more realistic Reynolds numbers, heating happens, predominantly, after the global kink oscillation is damped, and no significant heating occurs during the observable transverse motion of the flux tube.

Resonant absorption of kink oscillations in coronal flux tubes with continuous magnetic twist

Zanyar **Ebrahimi**, Karam Bahari
2019
https://arxiv.org/pdf/1909.09787.pdf
There are observational evidences for the existence of twisted magnetic field in the solar corona. Here, we have investigated resonant damping of the magnetohydrodynamic (MHD) kink waves in magnetic flux tubes. A realistic model of the tube with continuous magnetic twist and radially inhomogeneous density profile has been considered. We have obtained the dispersion relation of the kink wave using the solution to the linear MHD equations outside the density inhomogeneity and the appropriate connection formula to the solutions across the thin transitional boundary layer. The dependence of the oscillation frequency and damping rate of the waves on the twist parameter and longitudinal wavenumber has been investigated. For the flux tube parameters considered in this paper, we obtain rapid damping of the kink waves comparable to the observations. In order to justify this rapid damping, depending on the sign of the azimuthal kink mode number, m=+1 or m=−1, the background magnetic field must have left handed or right handed twisted profile, respectively. For the model considered here, the resonant absorption occurs only when the twist parameter is in a range specified by the density contrast.

Multiscale Aspects of the Solar Indexes Mg II, F10.7 and Sunspot Number.

de Souza **Echer**, M.P., Domingues, M.O., Yamashita, C.S. et al.
Sol Phys 299, 107 (**2024**).
https://doi.org/10.1007/s11207-024-02348-1

The Sun is a major source of energy for the planetary system in our solar system. The solar output shows variations in timescales from a few days (Bartel's 27-day solar rotation cycle) to several years (the 11-year solar cycle and longer timescales). This variability can be seen in the magnetic field, particle flux, and electromagnetic radiation flux behavior. Several indicators, such as the sunspot number and the Mg II index, have been used as solar activity proxies. Further, direct measurements in radio at centimeter wavelengths have been conducted since 1947 (the F10.7 index). This work uses multiscale techniques to study the relations between these solar indexes and their long-term variations through multiscale techniques. The monthly averages of these indexes from 1979 to 2022 are analyzed using wavelet scalogram, global wavelet spectrum, wavelet cross-correlation, and wavelet entropy techniques. As a result, some nonlinear multiscale aspects in the long-term variations of these solar indexes are identified. The major scales at which these indexes vary are found to be, in order of decreasing energy: sunspots (130.1, 253.9, 11.7, 5.0, and 2.0 months); F10.7 (130.1, 253.9, 39.1, 10.9, 9.9, and 5.4 months), and Mg II (132.9, 39.0, and 10.3 months). Thus, all three indexes present the nearly 11-year solar cycle period as the strongest signal. The three indexes are correlated with a coefficient higher than 0.85 and vary in phase for scales near the 11-year solar cycle, with slight and large deviations from it for longer and shorter scales, respectively. The wavelet entropy analysis shows that the F10.7 and sunspot number values are comparable, while Mg II entropy values are much lower. The entropy also indicates that the minimum values for all the indexes occur close to the solar minimum. However, after the last solar maximum in 2014, the entropy increased even in the declining phase of the cycle, during the 2015 – 2020.

Solar Atmospheric Oscillations as Measured by the GOES-R Series EXIS EUVS-C Instrument

Thomas D. **Eden Jr**.1, Francis. G. Eparvier1, Andrew R. Jones1, William E. McClintock1, Donald L. Woodraska1, Tom Woods1, and Martin Snow2
2024 ApJL 973 L18
https://iopscience.iop.org/article/10.3847/2041-8213/ad73d9/pdf

This Letter presents first observations of distinct solar atmospheric oscillations from signals collected by the Extreme Ultraviolet and X-ray Irradiance Sensors EUVS-C instrument, which is part of each Geostationary Observational Environmental Satellite R-Series instrument payload. The EUVS-C instrument is a full-disk, normal-incidence spectrograph that covers a narrow band in the mid-ultraviolet between 276 and 284 nm, where it can measure the magnesium ii emission doublet at ∼280 nm and the photospheric continuum. The primary goal of EUVS-C data is to construct the well-known Mg ii index, which is often used as a proxy for chromospheric activity. Because of the high temporal and spectral resolution of EUVS-C measurements, the data provide a unique opportunity to observe discernible solar atmospheric waves that have definite signatures of 3 and 5 minute oscillation periods, where the frequency response of these signals is dependent on what part of the spectrum is analyzed (e.g., Mg emission lines). Furthermore, both photospheric and chromospheric waves can simultaneously be examined. With the recent increase in solar activity for Solar Cycle 25, these waves exhibit enhanced amplitudes and phase shifts during the impulsive shock of strong solar flares. This Letter will discuss the analysis for deriving these waves, and results from both a quiescent Sun and an X-class solar flare event will be presented. **17 Jul 2017, 2023 January 9**

Evidence that 1.6-year solar quasi-biennial oscillations are synchronous with maximum Sun-planet alignments

Ian R. **Edmonds**
2021
https://arxiv.org/ftp/arxiv/papers/2110/2110.13143.pdf

Solar quasi-biennial oscillations with period range 0.6 to 4 years, are prominent in records of solar activity. Here we show that the 1.6 year quasi-biennial oscillation in solar activity has the exceptional feature of phase inversion between each solar cycle in the sequence of four solar cycles, 20 to 23. The hypothesis advanced is that this feature is due to synchronicity between solar activity and planetary alignment. An index of alignment between Earth and Mercury, Venus, Jupiter and Saturn is shown to have dominant peaks of alignment separated by 1.6 years in each solar cycle with, however, peak alignments shifting by half a period, 0.8 years, between alternate solar cycles. Accepting that solar activity increases when planets align would explain the phase inversion in alternate solar cycles observed in the 1.6 year quasi-biennial oscillation. Two new methods were developed to test this hypothesis: (a) Narrow band filtering of solar activity with the pass band based on the frequency content of the planetary alignment index. (b) Superposing intervals of raw solar activity data centered on times of maximum planet alignment. Both methods provided strong support for the hypothesis. Planetary alignment is complex but predictable enabling the forecasting of solar oscillation intermittency and future oscillation spectral content.

Assessment of a planetary model to predict Rieger periodicity in sunspots and flares

Ian R. **Edmonds**

2018

https://arxiv.org/ftp/arxiv/papers/1811/1811.10703.pdf

This paper develops a planetary model to predict the occurrence of intermediate range periodicity in solar activity, in particular the ~155 day Rieger periodicity in flare activity. It is shown that periodicity at half integer multiples of the period of Mercury occurs consistently in indices of solar activity. For this reason the planetary model is based on the triggering of sunspot emergence when planetary tides peak at times of conjunction of Mercury with Venus, Earth and/or Jupiter. The periodicity of components in the planetary model match reasonably well the observed intermediate periodicity in sunspot and flare activity with the strongest model component occurring at 155 day period. A comparison of filtered versions of the model and the N.O.A.A. flare index at 155 day periodicity demonstrates the potential for both short term, (within a solar cycle), and longer term, (over several solar cycles), predictive capability of the model. However, this assessment finds that prediction of 155 day periodicity in flare activity is effective only when the north and south hemispheric components of flare activity are in-phase.

Planetary model of sunspot emergence: A spectral and autocorrelation analysis

Ian **Edmonds**

2016

https://arxiv.org/pdf/1610.02632v1.pdf

This paper is concerned with intermediate range periodicity in the sunspot area spectrum. An empirical model of sunspot area emergence based on Mercury planet conjunctions was developed and the spectra of the model variation and the sunspot area variation compared. By including solar cycle amplitude modulation and the effect of solar magnetic field reversal the model was able to predict fine detail in the sunspot area spectrum. As Mercury planet conjunctions occur predictably it was possible to compare the time variation of band limited components of sunspot area with the corresponding component variations in the model. When the model component variation was stable corresponding components of sunspot area lagged the model variation by a few tens of days. When a 180 degree phase change occurred in the model variation the corresponding component of sunspot area followed the change over an interval of a few hundred days, first by decreasing to zero and then emerging in phase with the model variation. Where periodicities in sunspot area did not match periods of Fourier components of the model the autocorrelation function of the model variation provided an indirect numerical link to these periodicities. Included in these indirect periodicities were components at periods of about 138, 235, 355, 472, 530, 605, 833, 1190 and 2020 days. Direct periodicities in the model, those linked directly to Fourier components of sunspot area, included components at about 88, 116, 176, 200, 292 and 405 days. The model was developed without allowing for a variable threshold for sunspot emergence. However, it was found that with a variable threshold above which the model variation is effective in triggering sunspots, weak Fourier components at the indirect periods were generated. The model with threshold then encompasses all of the significant intermediate range periodicities in sunspot area.

Are intermediate range periodicities in sunspot area associated with planetary motion?

Ian **Edmonds**

2016

http://arxiv.org/pdf/1605.05028v1.pdf

Rieger quasi-periodicities have been reported numerous times. However, no accepted explanation of the quasi-periodicities has emerged. We examine the possibility that the some of the reported periodicities are associated with a Mercury to Sun interaction of base period 88 days. To test this idea we filter the daily sunspot area record with band pass filters centred on the 88 day period and 176 day sub harmonic period of Mercury. We observed that the time variation of the amplitude of the components was comprised of episodes that varied in duration from 1.5 to 4 years, with successive episodes usually overlapping in time but, for significant intervals in the record, the episodes were discrete, i.e. not overlapping. The time variation of the filtered components was compared with the time variation of the tidal effect of Mercury. We were able to show that when episodes were discrete the time variation of the component of sunspot area during the episode was either in-phase or in anti-phase with the tidal effect. We interpret this result as an indication of a connection between planetary motion and sunspot emergence. When several discrete episodes of the 88 day or the 176 day period components occurred during a solar cycle the spectrum of sunspot area exhibited periodicities at sidebands to the 88 day or 176 day periods with the periodicity of the sidebands dependent on the duration of the episodes. A model based on amplitude modulation of 88 day and 176 day period sinusoids was able to consistently reproduce periodicities observed in the spectra of sunspot area. It is proposed that the observed connection between planetary motion and sunspot emergence involves magnetic Rossby waves with mode periods close to the sub harmonic periods associated with Mercury and the triggering of sunspot emergence by those Rossby waves.

On the Role of Interchange Reconnection in the Generation of the Slow Solar Wind Review

J. K. **Edmondson**

Space Science Reviews, November **2012**, Volume 172, Issue 1-4, pp 209-225

The heating of the solar corona and therefore the generation of the solar wind, remain an active area of solar and heliophysics research. Several decades of in situ solar wind plasma observations have revealed a rich bimodal solar wind structure, well correlated with coronal magnetic field activity. Therefore, the reconnection processes associated with the large-scale dynamics of the corona likely play a major role in the generation of the slow solar wind flow regime. In order to elucidate the relationship between reconnection-driven coronal magnetic field structure and dynamics and the generation of the slow solar wind, this paper reviews the observations and phenomenology of the solar wind and coronal magnetic field structure. The geometry and topology of nested flux systems, and the (interchange) reconnection process, in the context of coronal physics is then explained. Once these foundations are laid out, the paper summarizes several fully dynamic, 3D MHD calculations of the global coronal system. Finally, the results of these calculations justify a number of important implications and conclusions on the role of reconnection in the structural dynamics of the coronal magnetic field and the generation of the solar wind.

Derived Electron Densities from Linear Polarization Observations of the Visible-Light Corona During the 14 December 2020 Total Solar Eclipse

Liam **Edwards**1 · Kaine A. Bunting1 · Brad Ramsey1 · Matthew Gunn1 · Tomos Fearn2 · Thomas Knight1 ·Gabriel Domingo Muro1,3 ·Huw Morgan1

Solar Physics (**2023**) 298:140

https://doi.org/10.1007/s11207-023-02231-5

https://link.springer.com/content/pdf/10.1007/s11207-023-02231-5.pdf

A new instrument was designed to take visible-light (VL) polarized brightness (pB) observations of the solar corona during the 14 December 2020 total solar eclipse. The instrument, called the Coronal Imaging Polarizer (CIP), consisted of a 16 MP CMOS detector, a linear polarizer housed within a piezoelectric rotation mount, and an f-5.6, 200 mm DSLR lens. Observations were successfully obtained, despite poor weather conditions, for five different exposure times (0.001 s, 0.01 s, 0.1 s, 1 s, and 3 s) at six different orientation angles of the linear polarizer (0◦, 30◦, 60◦, 90◦, 120◦, and 150◦). The images were manually aligned using the drift of background stars in the sky and images of different exposure times were combined using a simple signal-to-noise ratio cut. The polarization and brightness of the local sky were also estimated and the observations were subsequently corrected. The pB of the K-corona was determined using least-squares fitting and radiometric calibration was done relative to the Mauna Loa Solar Observatory (MLSO) K-Cor pB observations from the day of the eclipse. The pB data was then inverted to acquire the coronal electron density, ne, for an equatorial streamer and a polar coronal hole, which agreed very well with previous studies. The effect of changing the number of polarizer angles used to compute the pB is also discussed and it is found that the results vary by up to ≈ 13% when using all six polarizer angles versus only a select of three angles.

A solar-cycle study of coronal rotation: large variations, rapid changes, and implications for solar wind models

Liam T. **Edwards**, David Kuridze, Thomas Williams, Huw Morgan

2022 *ApJ* **928** 42

https://arxiv.org/pdf/2203.03447.pdf

https://iopscience.iop.org/article/10.3847/1538-4357/ac54ba/pdf

Information on the rotation rate of the corona, and its variation over latitude and solar cycle, is valuable for making global connections between the corona and the Sun, for global estimates of reconnection rates, and as a basic parameter for solar wind modelling. Here, we use a time series of tomographical maps gained from coronagraph observations between 2007 - 2020 to directly measure the longitudinal drift of high-density streamers over time. The method reveals abrupt changes in rotation rates, revealing a complex relationship between the coronal rotation and the underlying photosphere. The majority of rates are between -1.0 to +0.5∘/day relative to the standard Carrington rate of 14.18∘/day, although rates are measured as low as -2.2∘/day and as high as 1.6∘/day. Equatorial rotation rates during the 2008 solar minimum are slightly faster than the Carrington rate, with an abrupt switch to slow rotation in 2009, then a return to faster rates in 2017. Abrupt changes and large variations in rates are seen at all latitudes. Comparison with a magnetic model suggests that periods of equatorial fast rotation are associated with times when a large proportion of the magnetic footpoints of equatorial streamers are near the equator, and we interpret the abrupt

changes in terms of the latitudinal distribution of the streamer photospheric footpoints. The coronal rotation rate is a key parameter for solar wind models, and variations of up to a degree per day or more can lead to large systematic errors over forecasting periods of longer than a few days. The approach described in this paper gives corrected values that can form a part of future forecasting efforts.

A Comparison of Global Magnetic Field Skeletons and Active-Region Upflows

S. J. **Edwards**, C. E. Parnell , L. K. Harra, J. L. Culhane, D. H. Brooks
Solar Phys. **201**5
Plasma upflows have been detected in active regions using Doppler velocity maps. The origin and nature of these upflows is not well known with many of their characteristics determined from the examination of single events. In particular, some studies suggest these upflows occur along open field lines and, hence, are linked to sources of the solar wind. To investigate the relationship these upflows may have with the solar wind, and to probe what may be driving them, this paper considers seven active regions observed on the solar disc using the Extreme ultraviolet Imaging Spectrometer aboard Hinode between August 2011 and September 2012. Plasma upflows are observed in all these active regions. The locations of these upflows are compared to the global potential magnetic field extrapolated from the Solar Dynamics Observatory, Helioseismic and Magnetic Imager daily synoptic magnetogram taken on the day the upflows were observed. The structure of the magnetic field is determined by constructing its magnetic skeleton in order to help identify open-field regions and also sites where magnetic reconnection at global features is likely to occur. As a further comparison, measurements of the temperature, density and composition of the plasma are taken from regions with active-region upflows. In most cases the locations of the upflows in the active regions do not correspond to areas of open field, as predicted by a global coronal potential-field model, and therefore these upflows are not always sources of the slow solar wind. The locations of the upflows are, in general, intersected by separatrix surfaces associated with null points located high in the corona; these could be important sites of reconnection with global consequences.

The global oscillations of the sun from tsi, soho and sdo data

V.I. **Efremov**, L.D. Parfinenko, A. A. Soloviev
2018
https://arxiv.org/ftp/arxiv/papers/1805/1805.08856.pdf
The global oscillations of the Sun are investigated on the base of three independent sets of data: 1. Records of Total Solar Irradiance (TSI). 2. The average brightness of the photosphere in MDI (SOHO) and HMI (SDO) images. 3. Records of the time variations of sunlight reflected from the planets during their passage in the field of view of the LASCO C3 coronagraph. It is found that in the low-frequency spectrum of solar oscillations as a star there are modes of 8-10, 36-38 hours and the main stable 9-day mode. The last mode can be regarded as a reflection of oscillatory processes near the fast rotating core of the Sun according to Fossat et al. (2017).

Global oscillations of the Sun according to the data of coronagraph SOHO LASCO C3

V.I. **Efremov**, L.D. Parfinenko, A.A. Soloviev
2017
https://arxiv.org/ftp/arxiv/papers/1708/1708.00837.pdf
We investigate the long-period fluctuations in the brightness of the Sun as a star using the measurements of sunlight reflected from the planets (Jupiter, Mars) when the light hits the field of view of the LASCO C3 coronagraph (Large Angle and Spectrometric Coronagraph Experiment).

Identification of large-scale cellular structures on the Sun based on the SDO and PSPT data

V. I. **Efremov**, L. D. Parfinenko, A. A. Solovev
Astrophys Space Sci March **2015**, Volume 356, Issue 1, pp 1-6
http://arxiv.org/pdf/1412.1612v1.pdf
Three independent sets of data: i). series of filtergrams obtained in line CaII K (393.416 nm) with the ground-based telescope Precision Solar Photometric Telescope (PSPT) of Mauna Loa Solar Observatory; ii). series of filtergrams of Atmospheric Imaging Assembly (AIA) of the Solar Dynamics Observatory (SDO) in {\lambda}160 nm and iii). series of magnetograms of Helioseismic and Magnetic Imager (HMI) of SDO have been processed to reveal reliably the existence of spatial cellular structures on the solar photosphere at scale about of 300 arcsec. This scale is intermediate between supergranules and giant cells (~30,000 and ~300,000 kilometers across, respectively). To

identify the different spatial structures the tens of two-dimensional power spectra (2DFFT) have been averaged. For one-dimensional photometric cross sections of frames, the Fourier power spectra (FFT) and wavelet transforms (Morlet 5-th order) have been calculated.

sunstardb: A Database for the Study of Stellar Magnetism and the Solar-stellar Connection

Ricky **Egeland**
2018 ApJS 236 19
http://sci-hub.tw/10.3847/1538-4365/aab771
The "solar-stellar connection" began as a relatively small field of research focused on understanding the processes that generate magnetic fields in stars and sometimes lead to a cyclic pattern of long-term variability in activity, as demonstrated by our Sun. This area of study has recently become more broadly pertinent to questions of exoplanet habitability and exo-space weather, as well as stellar evolution. In contrast to other areas of stellar research, individual stars in the solar-stellar connection often have a distinct identity and character in the literature, due primarily to the rarity of the decades-long time-series that are necessary for studying stellar activity cycles. Furthermore, the underlying stellar dynamo is not well understood theoretically, and is thought to be sensitive to several stellar properties, e.g., luminosity, differential rotation, and the depth of the convection zone, which in turn are often parameterized by other more readily available properties. Relevant observations are scattered throughout the literature and existing stellar databases, and consolidating information for new studies is a tedious and laborious exercise. To accelerate research in this area I developed sunstardb, a relational database of stellar properties and magnetic activity proxy time-series keyed by individual named stars. The organization of the data eliminates the need for the problematic catalog cross-matching operations inherent when building an analysis data set from heterogeneous sources. In this article I describe the principles behind sunstardb, the data structures and programming interfaces, as well as use cases from solar-stellar connection research.

The Mount Wilson Observatory S-index of the Sun

Ricky **Egeland**, Willie Soon, Sallie Baliunas, Jeffrey C. Hall, Alexei A. Pevtsov, Luca Bertello
ApJ **2016**
https://arxiv.org/pdf/1611.04540v1.pdf
The most commonly used index of stellar magnetic activity is the instrumental flux scale of singly-ionized calcium H & K line core emission, S, developed by the Mount Wilson Observatory (MWO) HK Project, or the derivative index R'_HK. Accurately placing the Sun on the S scale is important for comparing solar activity to that of the Sun-like stars. We present previously unpublished measurements of the reflected sunlight from the Moon using the second-generation MWO HK photometer during solar cycle 23 and determine cycle minimum S_min,23 = 0.1634 +/- 0.0008, amplitude Delta S_23 = 0.0143 +/- 0.0015, and mean <S_23> = 0.1701 +/- 0.0005. By establishing a proxy relationship with the closely related National Solar Observatory Sacramento Peak calcium K emission index, itself well-correlated with the Kodaikanal Observatory plage index, we extend the MWO S time series to cover cycles 15-24 and find on average <S_min> = 0.1621 +/- 0.0008, <Delta S_cyc> = 0.0145 +/- 0.0012, <S_cyc> = 0.1694 +/- 0.0005. Our measurements represent an improvement over previous estimates which relied on stellar measurements or solar proxies with non-overlapping time series. We find good agreement from these results with measurements by the Solar-Stellar Spectrograph at Lowell Observatory, an independently calibrated instrument, which gives us additional confidence that we have accurately placed the Sun on the S-index flux scale.

Revised historical solar irradiance forcing

T. **Egorova**, W. Schmutz, E. Rozanov, A. I. Shapiro, I. Usoskin, J. Beer, R. V. Tagirov, T. Peter
A&A 615, A85 **2018**
https://arxiv.org/pdf/1804.00287.pdf
Context. There is no consensus on the amplitude of the historical solar forcing. The estimated magnitude of the total solar irradiance difference between Maunder minimum and present time ranges from 0.1 to 6 W/m2 making uncertain the simulation of the past and future climate. One reason for this disagreement is the applied evolution of the quiet Sun brightness in the solar irradiance reconstruction models. This work addresses the role of the quiet Sun model choice and updated solar magnetic activity proxies on the solar forcing reconstruction.
Aims. We aim to establish a plausible range of the solar irradiance variability on decadal to millennial time scales.
Methods. The spectral solar irradiance (SSI) is calculated as a weighted sum of the contributions from sunspot umbra/penumbra, fac- ulae and quiet Sun, which are pre-calculated with the spectral synthesis code NESSY. We introduce activity belts of the contributions from sunspots and faculae and a new structure model for the quietest state of the Sun. We assume that the brightness of the quiet Sun varies in time proportionally to the secular (22-year smoothed) variation of the solar modulation potential.
Results. A new reconstruction of the TSI and SSI covering the period 6000 BCE - 2015 CE is presented. The model simulates solar irradiance variability during the satellite era well. The TSI change between the Maunder and recent minima ranges between 3.7 and 4.5 W/m2 depending on the applied solar modulation potential. The implementation of a new quietest Sun model reduces, by approximately a factor of two, the relative solar forcing compared to the

largest previous estimation, while the application of updated solar modulation potential increases the forcing difference between Maunder minimum and the present by 25-40 %.

Energetics and 3-D Structure of Elementary Events in Solar Coronal Heating

G. **Einaudi**, R.B. Dahlburg, I. Ugarte-Urra, J.W. Reep, A.F. Rappazzo, M. Velli

ApJ **910** 84 **2021**
https://arxiv.org/pdf/2103.13499.pdf
https://doi.org/10.3847/1538-4357/abe464

Parker (1972) first proposed that coronal heating was the necessary outcome of an energy flux caused by the tangling of coronal magnetic field lines by photospheric flows. In this paper we discuss how this model has been modified by subsequent numerical simulations outlining in particular the substantial differences between the "nanoflares" introduced by Parker and "elementary events", defined here as small-scale spatially and temporally isolated heating events resulting from the continuous formation and dissipation of field-aligned current sheets within a coronal loop. We present numerical simulations of the compressible 3-D MHD equations using the HYPERION code. We use two clustering algorithms to investigate the properties of the simulated elementary events: an IDL implementation of a Density-Based Spatial Clustering of Applications with Noise (DBSCAN) technique; and our own Physical Distance Clustering (PDC) algorithm. We identify and track elementary heating events in time, both in temperature and in Joule heating space. For every event we characterize properties such as: density, temperature, volume, aspect ratio, length, thickness, duration and energy. The energies of the events are in the range 1018−1021 ergs, with durations shorter than 100 seconds. A few events last up to 200 seconds and release energies up to 1023 ergs. While high temperature are typically located at the flux tube apex, the currents extend all the way to the footpoints. Hence a single elementary event cannot at present be detected. The observed emission is due to the superposition of many elementary events distributed randomly in space and time within the loop.

Deep solar ALMA neural network estimator for image refinement and estimates of small-scale dynamics

Henrik **Eklund**1,2,3

A&A 669, A106 (**2023**)
https://www.aanda.org/articles/aa/pdf/2023/01/aa44484-22.pdf

Context. The solar atmosphere is highly dynamic, and observing the small-scale features is valuable for interpretations of the underlying physical processes. The contrasts and magnitude of the observable signatures of small-scale features degrade as angular resolution decreases.
Aims. The estimates of the degradation associated with the observational angular resolution allows a more accurate analysis of the data.
Methods. High-cadence time-series of synthetic observable maps at $\lambda = 1.25$ mm were produced from three-dimensional magnetohydrodynamic Bifrost simulations of the solar atmosphere and degraded to the angular resolution corresponding to observational data with the Atacama Large Millimeter/sub-millimeter Array (ALMA). The deep solar ALMA neural network estimator (Deep-SANNE) is an artificial neural network trained to improve the resolution and contrast of solar observations. This is done by recognizing dynamic patterns in both the spatial and temporal domains of small-scale features at an angular resolution corresponding to observational data and correlated them to highly resolved nondegraded data from the magnetohydrodynamic simulations. A second simulation, previously never seen by Deep-SANNE, was used to validate the performance.
Results. Deep-SANNE provides maps of the estimated degradation of the brightness temperature across the field of view, which can be used to filter for locations that most probably show a high accuracy and as correction factors in order to construct refined images that show higher contrast and more accurate brightness temperatures than at the observational resolution. Deep-SANNE reveals more small-scale features in the data and achieves a good performance in estimating the excess temperature of brightening events with an average of 94.0% relative to the highly resolved data, compared to 43.7% at the observational resolution. By using the additional information of the temporal domain, Deep-SANNE can restore high contrasts better than a standard two-dimensional deconvolver technique. In addition, Deep-SANNE is applied on observational solar ALMA data, for which it also reveals eventual artifacts that were introduced during the image reconstruction process, in addition to improving the contrast. It is important to account for eventual artifacts in the analysis.
Conclusions. The Deep-SANNE estimates and refined images are useful for an analysis of small-scale and dynamic features. They can identify locations in the data with high accuracy for an in-depth analysis and allow a more meaningful interpretation of solar observations.

The Influence of Asymmetrical Distribution of Hemispheric Sunspot Areas on Some Solar Parameters' Periodicities during the Period 1945–2017: Wavelet Analysis

M. A. **El-Borie**1, A. M. El-Taher2, A. A. Thabet3, S. F. Ibrahim2, N. S. Aly2, and A. A. Bishara1

2020 ApJ 898 73
https://doi.org/10.3847/1538-4357/ab9d21

Monthly data of some solar parameters (the solar radio flux F10.7, the plage area PA, the coronal index CI, the solar mean magnetic field B , and the solar flare index SFI) during the period 1945–2017 have been classified into two groups (northern and southern) based on the distribution of the monthly averages of the hemispheric sunspot areas (SSAs). This has been done to investigate the symmetry and/or asymmetry in periodicities between the hemispheric groups for these parameters by utilizing the Morlet wavelet technique. For each of the considered parameters except B , it is observed that the most dominant and significant period (above the 95% confidence level) in both the wavelet spectra (WPS and GWS) for both hemispheric groups is the solar activity cycle at 10.7 yr during the entire time interval. The power values for other periods appeared to be quite small relative to that of the 10.7 yr period, and of less significance (below the 95% confidence level). For B , the most remarkable sign is the disappearance of the prominent peak of the solar activity cycle. The Hale cycle is clearly seen in both hemispheric groups of B , with a slight shift in time between the two hemispheric groups, and it increased through the entire considered duration. Periodicities of 10.7, 3.5, 1.5, and 0.8 yr have been observed in the northern hemispheric group of the parameters SSAs, F10.7, PA, CI, and SFI, indicating a possible correlation between them. For the southern hemispheric group, however, periodicities of 10.7, 5.4, and 0.8 yr have been revealed for the parameters F10.7, PA, and CI.

The Dependence of Solar, Plasma, and Geomagnetic Parameters' Oscillations on the Heliospheric Magnetic Field Polarities: Wavelet Analysis

M. A. **El-Borie**1, A. M. El-Taher2,4, A. A. Thabet3, and A. A. Bishara
2019 ApJ 880 86
sci-hub.se/10.3847/1538-4357/ab12d8
We investigate the dependence of solar, plasma, and geomagnetic parameters' periodicities on the heliospheric magnetic field polarities for the past five solar activity cycles (1967–2016). For this purpose, the Morlet wavelet technique has been performed to extract information about significant periods. The monthly averages of toward (T) and away (A) polarity groups have been calculated for each parameter. The solar and plasma parameters used in this work are the interplanetary magnetic field (B), sunspot numbers (R), and solar plasma speed (V), and the geomagnetic indices aa, Kp, and Ap. We found that the wavelet power spectra (WPS) for the monthly averages of BT and BA nearly showed a symmetrical power spectra distribution. The global wavelet spectra (GWS) for BT and BA displayed a coupling at some level between 3.2–3.5, 10.7, and 18.3 yr of variations. The GWS for VA provided two significant peaks, within the 95% confidence level, at 9.8 and 15.2 yr, as well as at 1 and 9.8 yr, for VT . In addition, the existence of a periodicity of 1 yr is obvious for VT spectra and it shifted to a 1.5 yr variation in VA spectra. Both the WPS and GWS for RT and RA reflect symmetric power spectra for both groups in the northern and southern hemispheres. The aa spectra exhibited prominent periodicities at 10.7 yr for aaA and 9.8 yr for aaT . Also, the well-known 9.8 yr periodicity variation is a dominant variation in both the spectra of ApT and ApA. On the other hand, within the cone of influence, the periodicities of 10.7 and 13.9 yr are observed for the KpA spectra and 9.8 yr for KpT spectra. The GWS showed double-peak structure for the spectrum of KpA.

Spatial Inhomogeneity In Solar Faculae

A. **Elek**, N. Gyenge, M B. Korsós, R. Erdélyi
Space Weather of the Heliosphere: Processes and Forecasts Proceedings IAU Symposium No. 335, **2017** C. Foullon & O. Malandraki **2018**
https://arxiv.org/pdf/1801.01716.pdf
In this paper, we investigate the inhomogeneous spatial distribution of solar faculae. The focus is on the latitudinal and longitudinal distributions of these highly localised features covering ubiquitously the solar surface. The statistical analysis is based on white light observations of the Solar and Heliospheric Observatory (SOHO) and Solar Dynamics Observatory (SDO) between 1996 and 2014. We found that the fine structure of the latitudinal distribution of faculae displays a quasi-biennial oscillatory pattern. Furthermore, the longitudinal distribution of photospheric solar faculae does not show homogeneous behaviour either. In particular, the non-axisymmetric behaviour of these events show similar properties as that of the active longitude (AL) found in the distribution of sunspots. Our results, preliminary though, may provide a valuable observational constrain for developing the next-generation solar dynamo model.

The IAG spectral atlas of the spatially resolved Sun: Centre-to-limb observations⋆

M. **Ellwarth**, S. Schäfer, A. Reiners and M. Zechmeister
A&A 673, A19 (**2023**)
https://www.aanda.org/articles/aa/pdf/2023/05/aa45612-22.pdf
Context. Solar surface magneto-convection appears as granulation pattern that impacts spectral lines in terms of both shape and wavelength. Such induced effects also tend to vary over the observed solar disc because of the changing observation angle and, thus, the changing observation height as well. Centre-to-limb observations of the resolved Sun offer an insight into the variable spectral behaviour across different heliocentric observing positions, providing crucial information about limb darkening, convective velocities, and line profile variability relevant to radial

velocity (RV) calculations. Thus, RV measurements and exoplanet transit spectroscopy depend on precise reference templates.
Aims. We want to provide a spectroscopic centre-to-limb solar atlas at high spectral resolution and high-frequency accuracy. The atlas shall help improve the understanding of the solar atmosphere and convection processes.
Methods. We performed high-resolution observations of the resolved quiet Sun with a Fourier transform spectrograph at the Institut für Astrophysik und Geophysik in Göttingen. Our dataset contains a wavelength range from 4200 Å to 8000 Å. We obtained 165 spectra in total, with a spectral resolution of $\Delta\nu = 0.024$ cm−1, corresponding to a resolving power R of 700 000 at ∼6000 Å.
Results. We present a centre-to-limb solar atlas containing 14 heliocentric positions. To check for consistency, we investigated the Fe I 6175 Å absorption line and compared our line profiles with previous centre-to-limb observations and also with simulations. The line profile and also the bisector profiles are generally consistent with previous observations, but we have identified differences to model line profiles, especially close to the solar limb.

Newly formed downflow lanes in exploding granules in the solar photosphere

M. **Ellwarth**, C. E. Fischer, N. Vitas, S. Schmiz, W. Schmidt
A&A 653, A96 **2021**
https://arxiv.org/pdf/2107.00582.pdf
https://www.aanda.org/articles/aa/pdf/2021/09/aa38252-20.pdf
Exploding granules have drawn renewed interest because of their interaction with the magnetic field. Especially the newly forming downflow lanes developing in their centre seem to be eligible candidates for the intensification of magnetic fields. We analyse spectroscopic data from two different instruments in order to study the intricate velocity pattern within the newly forming downflow lanes in detail. We aim to examine general properties of a number of exploding granules. To gain a better understanding of the formation process of the developing intergranular lane in exploding granules, we study the temporal evolution and height dependence of the line-of-sight velocities at their formation location. Additionally, we search for evidence that exploding granules act as acoustic sources. We investigated the evolution of several exploding granules using data taken with the Interferometric Bidimensional Spectrometer and the Imaging Magnetograph eXperiment. Velocities for different heights of the solar atmosphere were determined by computing bisectors of the Fe I 6173.0Å and the Fe I 5250.2Å lines. We performed a wavelet analysis to study the intensity and velocity oscillations within and around exploding granules. We also compared our findings with predictions of numerical simulations. We found that exploding granules have significantly longer lifetimes than regular granules. Exploding granules larger than 3.8 arcsec form an independent intergranular lane during their decay phase, while smaller granules usually fade away or disappear into the intergranular area. For all exploding granules that form a new intergranular downflow lane, we find a temporal height-dependent shift with respect to the maximum of the downflow velocity. Our suggestion that this results from a complex atmospheric structure within the newly forming downflow lane is supported by the simulations. **10 June 2009, 12 and 14 October 2016**

Various scenarios for the equatorward migration of sunspots

Detlef **Elstner**, Yori Fournier, Rainer Arlt
Proceedings IAU Symposium No. 354, 2019 **2020**
https://arxiv.org/pdf/2003.08131.pdf
The profile of the differential rotation together with the sign of the alpha-effect determine the dynamo wave direction. In early models of the solar dynamo the dynamo wave often leads to a poleward migration of the activity belts. Flux transport by the meridional flow or the effect of the surface shear layer are possible solutions. In a model including the corona, we show that various migrations can be obtained by varying the properties of the corona. A new dynamo of Babcock-Leighton type also leads to the correct equatorward migration by the non-linear relation between flux density and rise time of the flux.

The Importance of Long-Term Synoptic Observations and Data Sets for Solar Physics and Helioseismology **Review**

Yvonne **Elsworth**, Anne-Marie Broomhall, Sanjay Gosain, Markus Roth, Stuart M. Jefferies, Frank Hill
Space Science Reviews **201**5
A casual single glance at the Sun would not lead an observer to conclude that it varies. The discovery of the 11-year sunspot cycle was only made possible through systematic daily observations of the Sun over 150 years and even today historic sunspot drawings are used to study the behavior of past solar cycles. The origin of solar activity is still poorly understood as shown by the number of different models that give widely different predictions for the strength and timing of future cycles. Our understanding of the rapid transient phenomena related to solar activity, such as flares and coronal mass ejections (CMEs) is also insufficient and making reliable predictions of these events, which can adversely impact technology, remains elusive. There is thus still much to learn about the Sun and its activity that requires observations over many solar cycles. In particular, modern helioseismic observations of the solar interior currently span only 1.5 cycles, which is far too short to adequately sample the characteristics of the plasma flows

that govern the dynamo mechanism underlying solar activity. In this paper, we review some of the long-term solar and helioseismic observations and outline some future directions.

Latitude Variations in Primary and Secondary Polar Crown Polarity Inversion Lines and Polar Coronal Hole Boundaries over Five Solar Cycles

B. A. **Emery**, D. F. Webb, S. E. Gibson, I. M. Hewins, R. H. McFadden & T. A. Kuchar
Solar Physics volume 296, Article number: 119 (**2021**)
https://link.springer.com/content/pdf/10.1007/s11207-021-01857-7.pdf
https://doi.org/10.1007/s11207-021-01857-7

We undertake a five solar-cycle (SC 19 - 23) ≈55-year (December 1954 to August 2009) study of the high latitude polarity inversion lines (PILs) using the recently digitized McIntosh Archive (McA) of solar synoptic (Carrington) maps. We looked at the evolution of the median solar latitudes of primary and secondary PILs, and of the polar coronal hole (CH) boundary for all 732 Carrington Rotations (CRs). We found hemispheric differences in the "Rush to the Poles" (RttP) where the polar CH gaps are often longer in the southern hemisphere (SH), and the secondary PIL reaches its polemost latitude at the end of its RttP later and more poleward than in the northern hemisphere (NH). The latitude oscillations found after this poleward peak are also stronger and often longer in the SH than in the NH, and exhibit a 22-year variation. The location variations in the CH boundaries and PILs appear to be at least partly associated with similar variations in the magnetic field. We also found equatorward expansions of the polar CHs by ≈50% and equatorward shifts in the PILs that were part of a disturbance that propagated ≈15°/CR from the SH to the NH in the descending phase of SC 23.

Measuring the Solar Radius from Space during the 2012 Venus Transit

M. **Emilio**1,2, S. Couvidat3, R. I. Bush3, J. R. Kuhn2, and I. F. Scholl
2015 ApJ 798 48

We report in this work the determination of the solar radius from observations by the Helioseismic and Magnetic Imager (HMI) and the Atmospheric Imaging Assembly (AIA) instruments on board the Solar Dynamics Observatory during the 2012 June Venus transit of the Sun. Two different methods were utilized to determine the solar radius using images of Sun taken by the HMI instrument. The first technique fit the measured trajectory of Venus in front of the Sun for seven wavelengths across the Fe I absorption line at 6173 Å. The solar radius determined from this method varies with the measurement wavelength, reflecting the variation in the height of line formation. The second method measured the area of the Sun obscured by Venus to determine the transit duration from which the solar radius was derived. This analysis focused on measurements taken in the continuum wing of the line, and applied a correction for the instrumental point spread function (PSF) of the HMI images. Measurements taken in the continuum wing of the 6173 Å line, resulted in a derived solar radius at 1 AU of 959."57 ± 0."02 (695, 946 ± 15 km). The AIA instrument observed the Venus transit at ultraviolet wavelengths. Using the solar disk obscuration technique, similar to that applied to the HMI images, analysis of the AIA data resulted in values of $R_\odot$ = 963."04 ± 0."03 at 1600 Å and $R_\odot$ = 961."76 ± 0."03 at 1700 Å.

Identifying Alfvén wave modes in the solar corona

E. **Enerhaug**1,2, T. A. Howson3,1 and I. De Moortel1,2
A&A 681, L11 (**2024**)
https://www.aanda.org/articles/aa/pdf/2024/01/aa47790-23.pdf

Context. Oscillations are observed to be pervasive throughout the solar corona, but it remains challenging to positively identify different wave modes. Improving this identification would provide a powerful tool for investigating coronal wave heating and improving seismological inversions.

Aims. We aim to establish whether theoretical methods used to identify magnetohydrodynamical wave modes in numerical simulations can be employed on observational datasets.

Methods. We applied wave identifiers based on fundamental wave characteristics such as compressibility and direction of propagation to a fully 3D numerical simulation of a transversely oscillating coronal loop. The same wave identifiers were applied to the line-of-sight integrated synthetic emission derived from the numerical simulation data to investigate whether this method could feasibly be useful for observational studies.

Results. We established that for particular line(s) of sight and assumptions about the magnetic field, we can correctly identify the properties of the Alfvén mode in synthetic observations of a transversely oscillating loop. Under suitable conditions, there is a strong agreement between the simulation and synthetic emission results.

Conclusions. For the first time, we have provided a proof of concept that this theoretically derived classification of magnetohydrodynamic wave modes can be applied to observational data.

Chapter 12.2 - High-Resolution Ground-Based Observations of the Sun

Oddbjørn **Engvold** and Jack B. Zirker
In: ***The Sun as a Guide to Stellar Physics*** ***Book***
Eds. Oddbjørn Engvold, Jean-Claude Vial, and Andrew Skumanich
Elsevier , November **2018**
https://www.sciencedirect.com/book/9780128143346/the-sun-as-a-guide-to-stellar-physics
To investigate the small-scale interactions between magnetic and velocity fields that underlie many solar phenomena, solar physicists need higher spatial and temporal resolution. As a result, they are gradually introducing telescopes with meter-class mirrors and instruments with more sensitivity. Adaptive optics systems have been developed to minimize, in real time, the image distortions caused by the Earth's atmosphere. Post facto image correcting techniques facilitate further reduction of the distortions. Combinations of instruments now observe simultaneously and record the many aspects of a dynamic solar feature. The infrared spectrum, out to 2 μm and beyond to submillimeters, is used to a greater extent. The first of a new generation of 4-m telescopes is being built and 8-m telescopes are being designed. The future beckons for ground-based solar research. In this chapter, we survey these developments.

The Solar Activity Monitor Network – SAMNet

Robertus **Erdélyi**1,2,3*, Marianna B. Korsós2,3,4, Xin Huang5, Yong Yang6, Danielle Pizzey7, Steven A. Wrathmall7, et al.
J. Space Weather Space Clim. **2022**, 12, 2
https://www.swsc-journal.org/articles/swsc/pdf/2022/01/swsc200065.pdf
https://doi.org/10.1051/swsc/2021025
The Solar Activity Magnetic Monitor (SAMM) Network (SAMNet) is a future UK-led international network of ground-based solar telescope stations. SAMNet, at its full capacity, will continuously monitor the Sun's intensity, magnetic, and Doppler velocity fields at multiple heights in the solar atmosphere (from photosphere to upper chromosphere). Each SAMM sentinel will be equipped with a cluster of identical telescopes each with a different magneto-optical filter (MOFs) to take observations in K I, Na D, and Ca I spectral bands. A subset of SAMM stations will have white-light coronagraphs and emission line coronal spectropolarimeters. The objectives of SAMNet are to provide observational data for space weather research and forecast. The goal is to achieve an operationally sufficient lead time of e.g., flare warning of 2–8 h and provide many sought-after continuous synoptic maps (e.g., LoS magnetic and velocity fields, intensity) of the lower solar atmosphere with a spatial resolution limited only by seeing or diffraction limit, and with a cadence of 10 min. The individual SAMM sentinels will be connected to their master HQ hub where data received from all the slave stations will be automatically processed and flare warning issued up to 26 h in advance.

Exploring the Temporal Variation of the Solar Quadrupole Moment J2

Saliha **Eren**1 and Jean-Pierre Rozelot2
2023 ApJ 942 90
https://iopscience.iop.org/article/10.3847/1538-4357/aca8a4/pdf
Recently, Rozelot & Eren pointed out that the first solar gravitational moment (J2) might exhibit a temporal variation. The suggested explanation is through the temporal variation of the solar rotation with latitude. This issue is deeper developed due to an accurate knowledge of the long-term variations in solar differential rotation regarding solar activity. Here we analyze solar cycles 12–24, investigating the long-term temporal variations in solar differential rotation. It is shown that J2 exhibits a net modulation over the 13 studied cycles of $\approx(89.6 \pm 0.1)$ yr, with a peak-to-peak amplitude of $\approx 0.1 \times 10^{-7}$ for a reference value of 2.07×10^{-7}). Moreover, J2 exhibits a positive linear trend in the period of minima solar activity (sunspot number up to around 40) and a marked declining trend in the period of maxima (sunspot number above 50). In absolute magnitude, the mean value of J2 is more significant during periods of minimum than in periods of maximum. These findings are based on observational results that are not free of errors and can be refined further by considering torsional oscillations for example. They are comforted by identifying a periodic variation of the J2 term evidenced through the analysis of the perihelion precession of planetary orbits either deduced from ephemerides or computed in the solar equatorial coordinate system instead of the ecliptic coordinate one usually used.

Rome Precision Solar Photometric Telescope: precision solar full-disk photometry during solar cycles 23–25.

Ermolli I, Giorgi F and Chatzistergos T
(**2022**) Front. Astron. Space Sci. 9: 1042740.
doi: 10.3389/fspas.2022.1042740
https://www.frontiersin.org/articles/10.3389/fspas.2022.1042740/pdf
The Rome Precision Solar Photometric Telescope (Rome/PSPT) is a ground-based telescope engaged in precision solar photometry. It has a 27-year database of full-disk images of the photosphere and chromosphere beginning in 1996 and continuing to 2022. The solar images have been obtained daily, weather permitting, with approximately 2 arcsec/pixel scale in Ca II K line at 393.3 nm, G-band at 430.6 nm, and continuum in the blue and red parts of the spectrum at 409.4 nm and 607.2 nm, respectively. Regular observations were also performed at the green continuum at 535.7 nm for a period of about 18 months. Since the first-light, Rome/PSPT operations have been directed at understanding the source of short-and long-term solar irradiance changes, spanning from 1 min to several months, and from 1 year to a few solar cycles, respectively. However, Rome/PSPT data have also served to study a variety of other topics, including the photometric properties of solar disk features and of the supergranulation manifested by the chromospheric network. Moreover, they have been unique in allowing to connect series of historical and modern full-disk solar observations, especially the Ca II K line data. Here, we provide an overview of the Rome/PSPT telescope and of the solar monitoring carried out with it from its first light to the present, across solar cycles 23–25. We also briefly describe the main results achieved with Rome/PSPT data, and give an overview of new results being derived with the whole time series of observations covering the period 1996–2022.

IBIS-A: The IBIS data Archive. High resolution observations of the solar photosphere and chromosphere with contextual data

Ilaria **Ermolli**, Fabrizio Giorgi, Mariarita Murabito, Marco Stangalini, Vincenzo Guido, Marco Molinaro, Paolo Romano, Salvatore L. Guglielmino, Giorgio Viavattene, Gianna Cauzzi, Serena Criscuoli, Kevin P. Reardon, Alexandra Tritschler
A&A **2022**
https://arxiv.org/pdf/2202.09946.pdf
The IBIS data Archive (IBIS-A) stores data acquired with the Interferometric BIdimensional Spectropolarimeter (IBIS), which was operated at the Dunn Solar Telescope of the US National Solar Observatory from 2003 to 2019. The instrument provided series of high-resolution narrowband spectropolarimetric imaging observations of the photosphere and chromosphere in the range 5800−8600 Å~ and co-temporal broadband observations in the same spectral range and with the same field of view of the polarimetric data. We present the data currently stored in IBIS-A, as well as the interface utilized to explore such data and facilitate its scientific exploitation. To this purpose we also describe the use of IBIS-A data in recent and undergoing studies relevant to solar physics and space weather research. IBIS-A includes raw and calibrated observations, as well as science-ready data. The latter comprise maps of the circular, linear, and net circular polarization, and of the magnetic and velocity fields derived for a significant fraction of the series available in the archive. IBIS-A furthermore contains links to observations complementary to the IBIS data, such as co-temporal high-resolution observations of the solar atmosphere available from the instruments onboard the Hinode and IRIS satellites, and full-disc multiband images from INAF solar telescopes. IBIS-A currently consists of 30 TB of data taken with IBIS during 28 observing campaigns performed in 2008 and from 2012 to 2019 on 159 days. Metadata and movies of each calibrated and science-ready series are also available to help users evaluating observing conditions. IBIS-A represents a unique resource for investigating the plasma processes in the solar atmosphere and the solar origin of space weather events. **25 October 2014, 13 May 2016**

The potential of Ca II K observations for solar activity and variability studies

Ilaria **Ermolli**, Theodosios Chatzistergos, Natalie A. Krivova, Sami K. Solanki
Proceedings IAU Symposium No. xxx, **2018**
https://arxiv.org/pdf/1805.04483.pdf
Several observatories around the globe started regular full-disc imaging of the solar atmosphere in the Ca II K line in the early decades of the 20th century. These observations are continued today at a few sites with either old spectroheliographs or modern telescopes equipped with narrow-band filters. The Ca II K time series are unique in representing long-term variations of the Sun's chromospheric magnetic field. However, meaningful results from their analysis require accurate processing of the available data and robust merging of the information stored in different archives. This paper provides an overview of the historical and modern full-disc Ca II K observations, with focus on their quality and the main results obtained from their analysis over the last decade.

Plasma flows and magnetic field interplay during the formation of a pore A102

I. **Ermolli**, A. Cristaldi, F. Giorgi, F. Giannattasio, M. Stangalini, P. Romano, A. Tritschler and F. Zuccarello
A&A 600, A102 (**2017**)

Aims. Recent simulations of solar magneto-convection have offered new levels of understanding of the interplay between plasma motions and magnetic fields in evolving active regions. We aim at verifying some aspects of the formation of magnetic regions derived from recent numerical studies in observational data.
Methods. We studied the formation of a pore in the active region (AR) NOAA 11462. We analysed data obtained with the Interferometric Bidimensional Spectrometer (IBIS) at the Dunn Solar Telescope on April 17, 2012, consisting of full Stokes measurements of the Fe I 617.3 nm lines. Furthermore, we analysed SDO/HMI observations in the continuum and vector magnetograms derived from the Fe I 617.3 nm line data taken from April 15 to 19, 2012. We estimated the magnetic field strength and vector components and the line-of-sight (LOS) and horizontal motions in the photospheric region hosting the pore formation. We discuss our results in light of other observational studies and recent advances of numerical simulations.
Results. The pore formation occurs in less than 1 h in the leading region of the AR. We observe that the evolution of the flux patch in the leading part of the AR is faster (<12 h) than the evolution (20–30 h) of the more diffuse and smaller scale flux patches in the trailing region. During the pore formation, the ratio between magnetic and dark area decreases from 5 to 2. We observe strong downflows at the forming pore boundary and diverging proper motions of plasma in the vicinity of the evolving feature that are directed towards the forming pore. The average values and trends of the various quantities estimated in the AR are in agreement with results of former observational studies of steady pores and with their modelled counterparts, as seen in recent numerical simulations of a rising-tube process. The agreement with the outcomes of the numerical studies holds for both the signatures of the flux emergence process (e.g. appearance of small-scale mixed polarity patterns and elongated granules) and the evolution of the region. The processes driving the formation of the pore are identified with the emergence of a magnetic flux concentration and the subsequent reorganization of the emerged flux, by the combined effect of velocity and magnetic field, in and around the evolving structure. **April 15-19, 2012**

Solar Cycle Indices from the Photosphere to the Corona: Measurements and Underlying Physics **Review**

Ilaria **Ermolli**, Kiyoto Shibasaki, Andrey Tlatov, Lidia van Driel-Gesztelyi
Space Science Reviews December **2014**, Volume 186, Issue 1-4, pp 105-135
https://arxiv.org/pdf/1705.07054.pdf

A variety of indices have been proposed in order to represent the many different observables modulated by the solar cycle. Most of these indices are highly correlated with each other owing to their intrinsic link with the solar magnetism and the dominant eleven year cycle, but their variations may differ in fine details, as well as on short- and long-term trends. In this paper we present an overview of the indices that are often employed to describe the many features of the solar cycle, moving from the ones referring to direct observations of the inner solar atmosphere, the photosphere and chromosphere, to those deriving from measurements of the transition region and solar corona. For each index, we summarize existing measurements and typical use, and for those that quantify physical observables, we describe the underlying physics.

Recent variability of the solar spectral irradiance and its impact on climate modelling

I. **Ermolli**, K. Matthes, T. Dudok de Wit, N. A. Krivova, K. Tourpali, M. Weber, Y. C. Unruh, L. Gray, U. Langematz, P. Pilewskie, E. Rozanov, W. Schmutz, A. Shapiro, S. K. Solanki, and T. N. Woods
E-print, March **2013**; ACP (Atmospheric Chemistry and Physics)

The lack of long and reliable time series of solar spectral irradiance (SSI) measurements makes an accurate quantification of solar contributions to recent climate change difficult. Whereas earlier SSI observations and models provided a qualitatively consistent picture of the SSI variability, recent measurements by the SORCE satellite suggest a significantly stronger variability in the ultraviolet (UV) spectral range and changes in the visible and near-infrared (NIR) bands in anti-phase with the solar cycle. A number of recent chemistry-climate model (CCM) simulations have shown that this might have significant implications on the Earth's atmosphere. Motivated by these results, we summarize here our current knowledge of SSI variability and its impact on Earth's climate. We present a detailed overview of existing SSI measurements and provide thorough comparison of models available to date. SSI changes influence the Earth's atmosphere, both directly, through changes in shortwave (SW) heating and therefore, temperature and ozone distributions in the stratosphere, and indirectly, through dynamical feedbacks. We investigate these direct and indirect effects using several state-of-the art CCM simulations forced with measured and modeled SSI changes. A unique asset of this study is the use of a common comprehensive approach for an issue that is usually addressed separately by different communities. We show that the SORCE measurements are difficult to reconcile with earlier observations and with SSI models. Of the five SSI models discussed here, specifically NRLSSI, SATIRE-S, COSI, SRPM, and OAR, only one shows a behaviour of the UV and visible irradiance qualitatively resembling that of the recent SORCE measurements. However, the integral of the SSI computed with this model over the entire spectral range does not reproduce the measured cyclical changes of the total solar irradiance, which is an essential requisite for realistic evaluations of solar effects on the Earth's climate in CCMs.

We show that within the range provided by the recent SSI observations and semi-empirical models discussed here, the NRLSSI model and SORCE observations represent the lower and upper limits in the magnitude of the SSI solar cycle variation. The results of the CCM simulations, forced with the SSI solar cycle variations estimated from the NRLSSI model and from SORCE measurements, show that the direct solar response in the stratosphere is larger for the SORCE than for the NRLSSI data. Correspondingly, larger UV forcing also leads to a larger surface response. Finally, we discuss the reliability of the available data and we propose additional coordinated work, first to build composite SSI datasets out of scattered observations and to refine current SSI models, and second, to run coordinated CCM experiments.

Wavefunction Properties of a Single and a System of Magnetic Flux Tube(s) Oscillations

Shahriar **Esmaeili**, Mojtaba Nasiri, Neda Dadashi, Hossein Safari
2015
http://arxiv.org/pdf/1511.05472v1.pdf
In this study, the properties of wavefunctions of the MHD oscillations for a single and a system of straight flux tubes are investigated. Magnetic flux tubes with a straight magnetic field and longitudinally density stratification under coronal conditions were considered. With repect to the density inhomogeneity in the radial direction of the flux tube, a smoothed step function at the lateral surface is employed. A single three-dimensional wave equation for longitudinal component of the perturbed magnetic field is solved using the finite element method (FEM). Wavefunctions of the MHD oscillations are categorized into kink, sausage, and torsional modes. Concerning the amplitude location of the waves which are arisen from the flux tube, those waves identified as body, surface, and leaky waves and appeared in both a single and a system of flux tubes cases. Exact recognition of the wavefunctions can be used in coronal seismology and also helps to future the high resolution instruments that would be designed for studying the detailed properties of the solar loops.

A model-free, data-based forecast for sunspot cycle 25

Aleix **Espuña-Fontcuberta** (NORDITA), Saikat Chatterjee (KTH), Dhrubaditya Mitra (NORDITA), Dibyendu Nandy
2020 ApJ
https://arxiv.org/pdf/2005.12166.pdf
The dynamic activity of the Sun, governed by its cycle of sunspots -- strongly magnetized regions that are observed on its surface -- modulate our solar system space environment creating space weather. Severe space weather leads to disruptions in satellite operations, telecommunications, electric power grids and air-traffic on polar routes. Forecasting the cycle of sunspots, however, has remained a challenging problem. We use reservoir computing -- a model-free, neural--network based machine-learning technique -- to forecast the upcoming solar cycle, sunspot cycle 25. The standard algorithm forecasts that solar cycle 25 is going to last about ten years, the maxima is going to appear in the year 2024 and the maximum number of sunspots is going to be 113 (±15). We also develop a novel variation of the standard algorithm whose forecasts for duration and peak timing matches that of the standard algorithm, but whose peak amplitude forecast is 124 (±2) -- within the upper bound of the standard reservoir computing algorithm. We conclude that sunspot cycle 25 is likely to be a weak, lower than average solar cycle, somewhat similar in strength to sunspot cycle 24.

Multi-fluid Simulation of Solar Chromospheric Turbulence and Heating Due to the Thermal Farley-Buneman Instability

Samuel **Evans**, Meers Oppenheim, Juan Martínez-Sykora, Yakov Dimant, Richard Xiao
ApJ **2022**
https://arxiv.org/pdf/2211.03644.pdf
Models fail to reproduce observations of the coldest parts of the Sun's atmosphere, where interactions between multiple ionized and neutral species prevent an accurate MHD representation. This paper argues that a meter-scale electrostatic plasma instability develops in these regions and causes heating. We refer to this instability as the Thermal Farley-Buneman instability, or TFBI. Using parameters from a 2.5D radiative MHD Bifrost simulation, we show that the TFBI develops in many of the colder regions in the chromosphere. This paper also presents the first multi-fluid simulation of the TFBI and validates this new result by demonstrating close agreement with theory during the linear regime. The simulation eventually develops turbulence, and we characterize the resulting wave-driven heating, plasma transport, and random motions. These results all contend that effects of the TFBI contribute to the discrepancies between solar observations and radiative MHD models.

Continuum intensity and [O I] spectral line profiles in solar 3D photospheric models: the effect of magnetic fields

D. **Fabbian**, F. Moreno-Insertis
ApJ **802** 96 **2015**

http://arxiv.org/pdf/1501.06916v1.pdf
The importance of magnetic fields in three-dimensional magnetoconvection models of the Sun's photosphere is investigated in terms of their influence on the continuum intensity at different viewing inclination angles, and on the intensity profile of two [O I] spectral lines. We use the RH numerical radiative transfer code to perform a posteriori spectral synthesis on the same time-series of magnetoconvection models used in our publications on the effect of magnetic fields on abundance determination. We obtain a good match of the synthetic disc-centre continuum intensity to the absolute continuum values from the FTS observational spectrum; the match of the centre-to-limb variation (CLV) synthetic data to observations is also good, thanks, in part, to the 3D radiation transfer capabilities of the RH code. The different levels of magnetic flux in the numerical time-series do not modify the quality of the match. Concerning the targetted [O I] spectral lines, we find, instead, that magnetic fields lead to non-negligible changes in the synthetic spectrum, with larger average magnetic flux causing the line to become noticeably weaker. The photospheric oxygen abundance that one would derive if instead using non-magnetic numerical models would thus be lower by a few to several centidexes. The inclusion of magnetic fields is confirmed to be important for improving the current modelling of the Sun, here in particular in terms of spectral line formation and of deriving consistent chemical abundances. These results may shed further light on the still controversial issue regarding the precise value of the solar oxygen abundance.

Comparison of different populations of granular features in the solar photosphere

M. **Falco**1, G. Puglisi2, S. L. Guglielmino3, P. Romano4, I. Ermolli1 and F. Zuccarello3
A&A 605, A87 (**2017**)
Context. The granulation is the most visible manifestation of convective motions occurring in the uppermost layers of the solar convection zone. Strong magnetic fields hinder these motions, but the appearance of bright structures such as umbral dots (UDs) and light bridges (LBs) in sunspots also shows that in strong magnetic field regions, the convection is not completely suppressed.
Aims. We aim to investigate the properties of the granules identified by a new segmentation algorithm in regions characterized by different magnetic field strength, in order to improve the current knowledge of the mechanism behind the appearance of the different bright structures in sunspots.
Methods. We analyzed data acquired by the CRisp Imaging SpectroPolarimeter at the Swedish Solar Telescope on 6 August 2011 relevant to a large sunspot with a LB observed in NOAA AR 11263. We applied a new segmentation algorithm to the data acquired along the Fe I 630.15 nm line.
Results. We found that the granules in the LB have a diameter between 0.″22 and 0.″99, that is, smaller than the granules in a nearby plage region (PL) and similar to those of the UDs. We observed values of the mean continuum intensity between 0.42 Icand 0.98 Ic for the LB granules, which are similar to those of the UDs. PL granules have higher values, probably reflecting different conditions of the plasma convection. Mean Doppler velocity and mean magnetic field strength have been studied and even for these physical parameters we found similar values between LB granules and UDs.
Conclusions. Different values for the physical properties analyzed have been found between the granules of the PL and LB granules of the three analyzed solar regions. In particular, we show that the granules in PL and sunspot regions have different physical properties. This clearly depends on the different physical conditions of the regions where these two kind of granular structures are embedded. We also confirm the recent findings on the similarity between granules in PL and quiet Sun regions. We show values of the various physical quantities analyzed in PL granules in agreement with those reported in the literature for quiet Sun granules. Finally, a noteworthy result is that the granules observed in the faint LB have physical properties similar to those found for UDs.

Magnetic fields in the solar convection zone

Yuhong **Fan**
Living Reviews in Solar Physics volume 18, Article number: 5 (**2021**)
https://link.springer.com/content/pdf/10.1007/s41116-021-00031-2.pdf
https://doi.org/10.1007/s41116-021-00031-2
It has been a prevailing picture that active regions on the solar surface originate from a strong toroidal magnetic field stored in the overshoot region at the base of the solar convection zone, generated by a deep seated solar dynamo mechanism. This article reviews the studies in regard to how the toroidal magnetic field can destabilize and rise through the convection zone to form the observed solar active regions at the surface. Furthermore, new results from the global simulations of the convective dynamos, and from the near-surface layer simulations of active region formation, together with helioseismic investigations of the pre-emergence active regions, are calling into question the picture of active regions as buoyantly rising flux tubes originating from the bottom of the convection zone. This article also gives a review on these new developments.

Differential Rotation in Solar Convective Dynamo Simulations

Yuhong **Fan**, Fang Fang
Advances in Space Research **2016**

http://arxiv.org/pdf/1512.08038v1.pdf
We carry out a magneto-hydrodynamic (MHD) simulation of convective dynamo in the rotating solar convective envelope driven by the solar radiative diffusive heat flux. The simulation is similar to that reported in Fan & Fang (2014) but with further reduced viscosity and magnetic diffusion. The resulting convective dynamo produces a large scale mean field that exhibits similar irregular cyclic behavior and polarity reversals, and self-consistently maintains a solar-like differential rotation. The main driver for the solar-like differential rotation (with faster rotating equator) is a net outward transport of angular momentum away from the rotation axis by the Reynolds stress, and we found that this transport is enhanced with reduced viscosity and magnetic diffusion.

A Simulation of Convective Dynamo in the Solar Convective Envelope: Maintenance of the Solar-like Differential Rotation and Emerging Flux

Yuhong **Fan** and Fang Fang
2014 ApJ 789 35
We report the results of a magnetohydrodynamic (MHD) simulation of a convective dynamo in a model solar convective envelope driven by the solar radiative diffusive heat flux. The convective dynamo produces a large-scale mean magnetic field that exhibits irregular cyclic behavior with oscillation time scales ranging from about 5 to 15 yr and undergoes irregular polarity reversals. The mean axisymmetric toroidal magnetic field is of opposite signs in the two hemispheres and is concentrated at the bottom of the convection zone. The presence of the magnetic fields is found to play an important role in the self-consistent maintenance of a solar-like differential rotation in the convective dynamo model. Without the magnetic fields, the convective flows drive a differential rotation with a faster rotating polar region. In the midst of magneto-convection, we found the emergence of strong super-equipartition flux bundles at the surface, exhibiting properties that are similar to emerging solar active regions.

Can the temperature of Ellerman Bombs be more than 10000K?

C. **Fang**, Q. Hao, M. D. Ding, Z. Li
Research in Astron. Astrophys. RAA **2017**
https://arxiv.org/pdf/1702.01905.pdf
Ellerman bombs (EBs) are small brightening events in the solar lower atmosphere. By original definition, the main EB's characteristic is the two emission bumps in both wings of chromospheric lines, such as Hα and Ca II 8542 {\AA} lines. Up to now, most authors found that the temperature increase of EBs around the temperature minimum region is in the range of 600K-3000K. However, with recent IRIS observations, some authors proposed that the temperature increase of EBs could be more than 10000K. Using non-LTE semi-empirical modeling, we investigate the line profiles, continuum emission and the radiative losses for the EB models with different temperature increases, and compare them with observations. Our result indicates that if the EB maximum temperature attains more than 10000K around the temperature minimum region, then the resulted Hα and Ca II 8542 {\AA} line profiles and the continuum emission would be much stronger than that of EB observations. Moreover, due to the high radiative losses, the high temperature EB would have a very short lifetime, which is not comparable with the observations. Thus, our study does not support the proposal that the EB temperatures are higher than 10000K.

Total Solar Irradiance Monitor for Chinese FY-3A and FY-3B Satellites – Instrument Design

Wei **Fang**, Hongrui Wang, Huiduan Li, Yupeng Wang
Solar Phys. **2014**
The Total Solar Irradiance Monitor (TSIM) instrument is designed to perform daily observations of total solar irradiance (TSI) in space on the Chinese FY-3A and FY-3B satellites. Three absolute radiometers are constructed for the TSIM to achieve measurements with traceability to SI with an absolute accuracy better than 550 ppm. The absolute radiometers are implemented based on the principle of electrical substitution. The design of the absolute radiometers and their electrical system, operation modes in space, and uncertainty evaluation are described. A method for calculating the electrical power in the observation and reference phases is proposed to maintain the primary cavity at a nearly constant temperature.

A new multi-wavelength solar telescope: Optical and Near-infrared Solar Eruption Tracer (ONSET)

Fang, Cheng; Chen, Peng-Fei; Li, Zhen; Ding, Ming-De; Dai, Yu; Zhang, Xiao-Yu; Mao, Wei-Jun; Zhang, Jun-Ping; Li, Ting; Liang, Yong-Jun; Lu, Hai-Tian
Research in Astronomy and Astrophysics, Volume 13, Issue 12, article id. 1509-1517 (**2013**).
https://arxiv.org/pdf/1307.4533.pdf
A new multi-wavelength solar telescope, the Optical and Near-infrared Solar Eruption Tracer (ONSET) of Nanjing University, has been constructed. It was fabricated at the Nanjing Institute of Astronomical Optics & Technology, and the operation is jointly administered with Yunnan Astronomical Observatory. ONSET is able to observe the Sun

in three wavelength windows: He I 10830 Å, Hα and white-light at 3600 Å and 4250 Å, which are selected in order to simultaneously record the dynamics of the corona, chromosphere and photosphere respectively. Full-disk or partial-disk solar images with a field of 10' at three wavelengths can be obtained nearly simultaneously. It is designed to trace solar eruptions with high spatial and temporal resolutions. This telescope was installed at a new solar observing site near Fuxian Lake in Yunnan Province, southwest China. The site is located at E102N24, with an altitude of 1722 m. The seeing is stable and has high quality. We give a brief description of the scientific objectives and the basic structure of ONSET. Some preliminary results are also presented. **21 April 2011, 2012 March 9, 13 March 2013, 30 April 2013**

Torsional wave propagation in solar tornadoes

S. Vasheghani **Farahani**1, E. Ghanbari2, G. Ghaffari1 and H. Safari
A&A 599, A19 (**2017**) 10.1051/0004-6361/201629563
https://www.aanda.org/articles/aa/pdf/2017/03/aa29563-16.pdf

Aims. We investigate the propagation of torsional waves in coronal structures together with their collimation effects in the context of magnetohydrodynamic (MHD) theory. The interplay of the equilibrium twist and rotation of the structure, e.g. jet or tornado, together with the density contrast of its internal and external media is studied to shed light on the nature of torsional waves.
Methods. We consider a rotating magnetic cylinder embedded in a plasma with a straight magnetic field. This resembles a solar tornado. In order to express the dispersion relations and phase speeds of the axisymmetric magnetohydrodynamic waves, the second-order thin flux tube approximation is implemented for the internal medium and the ideal MHD equations are implemented for the external medium.
Results. The explicit expressions for the phase speed of the torsional wave show the modification of the torsional wave speed due to the equilibrium twist, rotation, and density contrast of the tornado. The speeds could be either sub-Alfvénic or ultra-Alfvénic depending on whether the equilibrium twist or rotation is dominant. The equilibrium twist increases the phase speed while the equilibrium rotation decreases it. The good agreement between the explicit versions for the phase speed and that obtained numerically proves adequate for the robustness of the model and method. The density ratio of the internal and external media also play a significant role in the speed and dispersion.

Conclusions. The dispersion of the torsional wave is an indication of the compressibility of the oscillations. When the cylinder is rotating or twisted, in contrast to when it only possesses a straight magnetic field, the torsional wave is a collective mode. In this case its phase speed is determined by the Alfvén waves inside and outside the tornado.

EUV observables of simulated plasmoid-mediated reconnection in the solar corona

Ø. H. **Færder**, D. Nóbrega-Siverio, M. Carlsson, J. Martínez-Sykora
A&A **2024**
https://arxiv.org/pdf/2404.07327.pdf

Context. Understanding the role of magnetic reconnection in the heating and dynamics of the solar atmosphere requires detailed observational data of any observable aspect of the reconnection process, including small-scale features such as plasmoids. Aims. We aim to examine the capability of active and upcoming instruments to detect plasmoids generated by reconnection in the corona including low-density regimes. Methods. We used the Bifrost code to perform simulations of plasmoid-mediated reconnection in the corona based on a 2D idealised setup: a fan-spine topology with uniform density including thermal conduction. Through forward-modelling of extreme-ultraviolet (EUV) observables, we checked whether the plasmoids in our simulations could be detected with the instruments of Solar Dynamics Observatory (SDO) and Solar Orbiter (SO), as well as the upcoming Multi-Slit Solar Explorer (MUSE) and Solar-C missions. Results. Short-lived (∼ 10 − 20 s) small-scale (∼ 0.2 − 0.5 Mm) coronal plasmoids are not resolvable with the Atmospheric Imaging Assembly (AIA) onboard SDO. In contrast, they could be captured with the EUV High-Resolution Imager at the Extreme Ultraviolet Imager (EUI-HRIEUV) of SO. The spatial and temporal high-resolution planned for the MUSE spectrograph (SG) is adequate to obtain full spectral information of these plasmoids. To achieve a sufficient signal-to-noise ratio for ∼0.8 MK plasmoids in the MUSE/SG 171 Å channel, this should work on full-raster mode in regions with electron densities above 109 cm−3 whereas on sit-and-stare mode for lower-density regions. The future Solar-C mission could also capture these coronal plasmoids using the EUV High-Throughput Spectroscopic Telescope (EUVST), through rapid changes in Doppler shift and line width in different EUV lines caused by plasmoid motions along the current sheet. Conclusions. With combined spectra of MUSE/SG and Solar-C/EUVST in multiple emission lines, along with high-resolution images from SO/EUI-HRIEUV and MUSE/CI, it should be possible to gain new insights about plasmoid formation in the corona.

A comparative study of resistivity models for simulations of magnetic reconnection in the solar atmosphere. II. Plasmoid formation

Øystein Håvard **Færder**, Daniel Nóbrega-Siverio, Mats Carlsson

A&A **2024**
https://arxiv.org/pdf/2401.01177.pdf
Plasmoid-mediated reconnection plays a fundamental role in different solar atmospheric phenomena. Numerical reproduction of this process is therefore essential for developing robust solar models. Our goal is to assess plasmoid-mediated reconnection across various numerical resistivity models in order to investigate how plasmoid numbers and reconnection rates depend on the Lundquist number. We used the Bifrost code to drive magnetic reconnection in a 2D coronal fan-spine topology, carrying out a parametric study of several experiments with different numerical resolution and resistivity models. We employed three anomalous resistivity models: (1) the original hyper-diffusion from Bifrost, (2) a resistivity proportional to current density, and (3) a resistivity quadratically proportional to electron drift velocity. For comparisons, experiments with uniform resistivity were also run. Plasmoid-mediated reconnection is obtained in most of the experiments. With uniform resistivity, increasing the resolution reveals higher plasmoid frequency with weaker scaling to the Lundquist number, obtaining 7.9-12 plasmoids per minute for SL∈[1.8×104,2.6×105] with a scaling of S0.210L in the highest-resolution resistivity cases, transcending into Petschek reconnection in the high-SL limit and Sweet-Parker reconnection in the low-SL limit. Anomalous resistivity leads to similar results even with lower resolution. The drift-velocity-dependent resistivity excellently reproduces Petschek reconnection for any Lundquist number, and similar results are seen with resistivity proportional to current-density. Among the different resistivity models applied on the given numerical resolution, the hyper-diffusion model reproduced plasmoid characteristics in closest resemblance to those obtained with uniform resistivity at a significantly higher resolution.

The size of the Sun
Marc-Antoine **Fardin**, Mathieu Hautefeuille
2024
https://arxiv.org/pdf/2401.17105.pdf
Why does the Sun have a radius around 696000~km? We will see in this article that dimensional arguments can be used to understand the size of the Sun and of a few other things along the way. These arguments are not new and can be found scattered in textbooks. They are presented here in a succinct way in order to better confront the kinematic and mechanical viewpoints on size. We derive and compare a number of expressions for the size of the Sun and relate large and small scales. We hope that such presentation will be useful to students, instructors and researchers alike.

Embedding Cyclical Information in Solar Irradiance Forecasting
T. A. **Fathima**, Vasudevan Nedumpozhimana, Yee Hui Lee, Soumyabrata Dev
Proc. IEEE AP-S Symposium on Antennas and Propagation and USNC-URSI Radio Science Meeting, **2021**
https://arxiv.org/pdf/2110.09761.pdf
In this paper, we demonstrate the importance of embedding temporal information for an accurate prediction of solar irradiance. We have used two sets of models for forecasting solar irradiance. The first one uses only time series data of solar irradiance for predicting future values. The second one uses the historical solar irradiance values, together with the corresponding timestamps. We employ data from the weather station located at Nanyang Technological University (NTU) Singapore. The solar irradiance values are recorded with a temporal resolution of 1 minute, for a period of 1 year. We use Multilayer Perceptron Regression (MLP) technique for forecasting solar irradiance. We obtained significant better prediction accuracy when the time stamp information is embedded in the forecasting framework, as compared to solely using historical solar irradiance values.

Spectral atlases of the Sun from 3980 to 7100 Å at the center and at the limb
Hassan **Fathivavsari**, Ali Ajabshirizadeh, Serge Koutchmy
Ap&SS, **2014**
http://arxiv.org/pdf/1407.5727v1.pdf
In this work, we present digital and graphical atlases of spectra of both the solar disk-center and of the limb near the Solar poles using data taken at the UTS-IAP & RIAAM (the University of Tabriz Siderostat, telescope and spectrograph jointly developed with the Institut d'Astrophysique de Paris and Research Institute for Astronomy and Astrophysics of Maragha). High resolution and high signal-to-noise ratio (SNR)CCD-slit spectra of the sun for 2 different parts of the disk, namely for μ~=~1.0 (solar center) \& for ~=~ 0.3 solar limb) are provided and discussed. While there are several spectral atlases of the solar disk-center, this is the first spectral atlas ever produced for the solar limb at this spectral range. The resolution of the spectra is about \emph{R}~~~70 000 (Δλ~~~0.09 {\AA} with the signal-to-noise ratio (SNR) of 400−600. The full atlas covers the 3980 to 7100 {\AA} spectral regions and contains 44 pages with three partial spectra of the solar spectrum put on each page to make it compact. The difference spectrum of the normalized solar disk-center and the solar limb is also included in the graphic presentation of the atlas to show the difference of line profiles, including far wings. The identification of the most significant solar lines is included in the graphic presentation of the atlas. Telluric lines are producing a definite

signature on the difference spectra which is easy to notice. At the end of this paper we present only two sample pages of the whole atlas while the graphic presentation of the whole atlas along with its ASCII file can be accessed via the ftp server of the CDS in Strasbourg via anonymous ftp to cdsarc.u-strasbg.fr (130.79.128.5) or via this link \footnote{\url{this http URL}}.

C2 representations of the solar background coefficients for the model S-AtmoI

Florian **Faucher**, Damien Fournier, Ha Pham
2020
https://arxiv.org/pdf/2009.01587.pdf
We construct C2 representations of the background quantities that characterize the interior of the Sun and its atmosphere starting from the data-points of the standard solar model S. This model is further extended considering an isothermal atmosphere, that we refer to as model AtmoI. It is not trivial to build the C2 representations of the parameters from a discrete set of values, in particular in the transition region between the end of model S and the atmosphere. This technical work is needed as a crucial building block to study theoretically and numerically the propagation of waves in the Sun, using the equations of solar oscillations (also referred to as Galbrun's equation in aeroacoustics). The constructed models are available at this http URL.

Rotational radial shear in the low solar photosphere

M. **Faurobert**1, T. Corbard1, B. Gelly2, R. Douet2 and D. Laforgue2
A&A Letter 676, L4 (**2023**)
https://www.aanda.org/articles/aa/pdf/2023/08/aa46610-23.pdf
Context. Radial differential rotation is an important physical ingredient in stellar dynamo theory. In the case of the Sun, heliosismology techniques have revealed the existence of a near-surface shear layer covering 15–20% of the upper convection zone. It was recently shown that the rotation velocity gradient is not uniform in this layer and that it displays a steep increase in a shallow layer near the surface.
Aims. We report the detection of a rotation velocity depth-gradient in the low photosphere that is not accessible to heliosismology techniques.
Methods. We applied differential interferometric methods to spectroscopic data obtained with the solar telescope THEMIS, which is equipped with an efficient adaptative optics system. The detection was based on the measurement of a systematic east-west shift between images of the solar granulation at different depths in the FeI 630.15 nm at the center of the solar disk. The same technique was applied to obtain the depth-difference between the images from their perspective shift when they are observed away from the disk center. Both THEMIS and HINODE/SOT data were used for the height-difference measurement, giving similar results.
Results. At the center of the solar disk, we measured a systematic retrograde shift of the photospheric granular structures on the east-west axis and with no shift in the north-south direction. The retrograde shift increases linearly with height. We interpret these findings as a signature of a steep decrease in the angular velocity in the low photosphere.
Conclusions. The rotational radial shear in the low solar photosphere is likely related to the dynamics of the subsurface shear layer. Its measurement yields a valuable constraint on the numerical simulations of the solar upper convection zone. **July 19-22, 2022**

Magnetic flux structuring of the quiet Sun internetwork. Center-to-limb analysis of solar-cycle variations

Marianne **Faurobert**, Gilbert Ricort
A&A 651, A21 **2021**
https://arxiv.org/pdf/2105.08657.pdf
https://www.aanda.org/articles/aa/pdf/2021/07/aa40705-21.pdf
https://doi.org/10.1051/0004-6361/202140705
It is now well established that the quiet Sun contains in total more magnetic flux than active regions and represents an important reservoir of magnetic energy. But the nature and evolution of these fields remain largely unknown. We investigate the solar-cycle and center-to-limb variations of magnetic-flux structures at small scales in internetwork regions of the quiet Sun.
We used Hinode SOT/SP data from the irradiance program between 2008 and 2016. Maps of the magnetic-flux density are derived from the center-of gravity method applied to the FeI 630.15 nm and FeI 630.25 nm lines. To correct the maps from the instrumental smearing, we applied a deconvolution method based on a principal component analysis of the line profiles and on a Richardson-Lucy deconvolution of their coefficients. We then performed a spectral analysis of the spatial fluctuations of the magnetic-flux density in 10" x 10" internetwork regions spanning a wide range of latitudes.
At low and mid latitudes the power spectra do not vary significantly with the solar cycle. However at solar maximum for one scan in the activity belt showing an enhanced network, a marginal increase in the power of the magnetic fluctuations is observed at granular and larger scales in the internetwork. At high latitudes, we observe

variations at granular and larger scales where the power decreases at solar maximum. At all the latitudes the power of the magnetic fluctuations at scales smaller than 0.5"remain constant throughout the solar cycle.
Our results favor a small-scale dynamo that operates in the internetwork, but they show that the global dynamo also contributes to the internetwork fields.

A new spectroscopic method for measuring the temperature gradient in the solar photosphere *Generalized application in magnetized regions*

M. **Faurobert**1, S. Criscuoli2, M. Carbillet1 and G. Contursi1
A&A 642, A186 (**2020**)
https://www.aanda.org/articles/aa/pdf/2020/10/aa37736-20.pdf
Context. The contribution of quiet-Sun regions to the solar irradiance variability is currently unclear. Certain solar-cycle variations of the quiet-Sun's physical structure, such as the temperature gradient, might affect the irradiance. Accurate measurements of this quantity over the course of the activity cycle would improve our understanding of long-term irradiance variations.
Aims. In a previous work, we introduced and successfully tested a new spectroscopic method for measuring the photospheric temperature gradient directly on a geometric scale in the case of non-magnetic regions. In this paper, we generalize this method for moderately magnetized regions that may be encountered in the quiet solar photosphere.
Methods. To simulate spectroscopic observations, we used synthetic Stokes profiles I and V of the magnetic FeI 630.15 nm line and intensity profiles of the non-magnetic FeI 709 nm line computed from realistic three-dimensional magneto-hydrodynamical simulations of the photospheric granulation and line radiative transfer under local thermodynamical equilibrium conditions. We then obtained maps at different levels in the line-wings by convolution with the instrumental point spread function (PSF) under various conditions of atmospheric turbulence – with and without correction by an adaptive optics (AO) system. The PSF were obtained with the PAOLA software and the AO performance is inspired by the system that will be operating on the Daniel K. Inouye Solar Telescope.
Results. We considered different conditions of atmospheric turbulence and photospheric regions with different mean magnetic strengths of 100 G and 200 G. As in non-magnetic cases studied in our previous work, the image correction by the AO system is mandatory for obtaining accurate measurements of the temperature gradient. We show that the non-magnetic line at 709 nm may be safely used in all the cases we have investigated. However, the intensity profile of the magnetic-sensitive line is broadened by the Zeeman effect, which would bias our temperature-gradient measurement. We thus implemented a correction procedure of the line profile for this magnetic broadening in the case of weakly magnetized regions. In doing so, we remarked that in the weak-field regime, the right- and left-hand (I + V and I − V) components have similar shapes, however, they are shifted in opposite directions due to the Zeeman effect. We thus reconstructed the intensity profile by shifting back the I + V and I − V profiles and by adding the re-centered profiles. The measurement then proceeds as in the non-magnetic case. We find that this correction procedure is efficient in regions where the mean magnetic strength is smaller or on the order of 100 G.
Conclusions. The new method we implement here may be used to measure the temperature gradient in the quiet Sun from ground-based telescopes equipped with an efficient AO system. We stress that we derive the gradient on a geometrical scale and not on an optical-depth scale as we would do with other standard methods. This allows us to avoid any confusion due to the effect of temperature variations on the continuum opacity in the solar photosphere.

Chapter 8 - Solar and Stellar Variability **Review**

Marianne **Faurobert**
In: ***The Sun as a Guide to Stellar Physics*** ***Book***
Eds. Oddbjørn Engvold, Jean-Claude Vial, and Andrew Skumanich
Elsevier , November **2018**
https://www.sciencedirect.com/book/9780128143346/the-sun-as-a-guide-to-stellar-physics
The Sun, like many cool stars on the main sequence, is variable. Changing dark and bright features, sunspots, and faculae appear and disappear on its surface. These variations are cyclic and related to a dynamo mechanism operating in the solar interior. The basic principles of the dynamo theories were presented in the previous chapter within the formalism of the mean field theory and its two branches, the flux-transport dynamos and the tachocline dynamos. However, many important problems remain to be solved to understand the magnetic activity of the Sun and stars.
In this chapter, we focus on observational studies of solar and stellar variability. This subject has been evolving quickly within the past decades thanks to the development of new space-borne and ground-based instruments, which have provided us with a wealth of data of unprecedented quality for both the Sun and stars. We will emphasize how knowledge and methods developed in the context of solar physics can serve as guides for stellar investigations and how, in turn, observation of stellar activity offers us a unique possibility of testing the dynamo theories through varying stellar parameters.

Because magnetic activity affects the radiative output of stars, we will examine variations in solar and stellar irradiance and discuss their modeling. This problem is related to the hotly debated subject of the impact of solar activity on the terrestrial climate and also to stars hosting exoplanets regarding the issue of accessing their habitability conditions.

Temperature gradient in the solar photosphere. Test of a new spectroscopic method and study of its feasibility for ground-based telescopes

M. **Faurobert**1, M. Carbillet1, L. Marquis2, A. Chiavassa1 and G. Ricort1
A&A 616, A133 (**2018**)
https://arxiv.org/pdf/1809.00893.pdf

Context. The contribution of quiet-Sun regions to the solar irradiance variability is currently unclear. Some solar-cycle variations of the quiet-Sun physical structure, such as the temperature gradient, might affect the irradiance. The synoptic measurement of this quantity along the activity cycle would improve our understanding of long-term irradiance variations.
Aims. We intend to test a method previously introduced for measuring the photospheric temperature gradient from high-resolution spectroscopic observation and to study its feasibility with ground-based instruments with and without adaptative optics.
Methods. We used synthetic profiles of the FeI 630.15 nm obtained from realistic three-dimensional hydrodynamical simulations of the photospheric granulation and line radiative transfer computations under local thermodynamical equilibrium conditions. Synthetic granulation images at different levels in the line are obtained by convolution with the instrumental point spread function (PSF) under various conditions of atmospheric turbulence, with and without correction by an adaptative optics (AO) system. The PSF are obtained with the PAOLA software, and the AO performances are inspired by the system that will be operating on the Daniel K. Inouye Solar Telescope.
Results. We consider two different conditions of atmospheric turbulence, with Fried parameters of 7 cm and 5 cm, respectively. We show that the degraded images lead to both a bias and a loss of precision in the temperature-gradient measurement, and that the correction with the AO system allows us to drastically improve the measurement quality.
Conclusions. Long-term synoptic observations of the temperature gradient in the solar photosphere can be undertaken by implementing this method on ground-based solar telescopes that are equipped with an AO correction system.

Variation of the temperature gradient in the solar photosphere with magnetic activity

M. **Faurobert**1, R. Balasubramanian2 and G. Ricort
A&A 595, A71 (**2016**)

Context. The contribution of quiet-Sun regions to the solar irradiance variability is currently unclear. Some solar-cycle variations of the quiet-Sun physical structure, such as the temperature gradient or the photospheric radius, might affect the irradiance.
Aims. We intend to investigate possible variations of the photospheric temperature gradient with magnetic activity.
Methods. We used high-resolution center-to-limb observations of the FeI 630.15 nm line profile in the quiet Sun performed onboard the Hinode satellite on 2007, December 19, and on 2013, December 7, that is, close to a minimum and a maximum of magnetic activity, respectively. We analyzed samples of 10″ × 10″ internetwork regions. The wings of the FeI 630.15 nm line were used in a non-standard way to recover images at roughly constant continuum optical depths above the continuum formation level. The image formation height is derived from measuring its perspective shift with respect to the continuum image, both observed away from disk center. The measurement relies on a cross-spectral method that is not limited by the spatial resolution of the SOT telescope and does not rely on any radiative transfer computation. The radiation temperature measured in the images is related to the photospheric temperature at their respective formation height.
Results. The method allows us to investigate the temperature gradient in the low photosphere at altitudes of between 0 and 60 km above the 500 nm continuum formation height. In this layer the internetwork temperature gradient appears steeper in our 2013 sample than in the sample of 2007 in the northern hemisphere, whereas we detect no significant change in the southern hemisphere. We argue that this might be related to some strong hemispheric asymmetry of the magnetic activity at the solar maximum of cycle 24.
Conclusions. Structural changes have been observed in numerical simulations of the magneto-convection at the surface of the Sun where the increase of the ambient sub-surface magnetic fields leads to some steepening of the temperature gradient in the internetwork. Hemispheric asymmetry of the activity has been reported for the last solar cycles with successive dominant north and south hemisphere during the activity maximum. Our results seem consistent with this global physical picture, but need to be confirmed by additional studies.

The Emergence of Solar Supergranulation as a Natural Consequence of Rotationally-Constrained Interior Convection

Nicholas A. **Featherstone**, Bradley W. Hindman

ApJ Letters **830** L15 **2016**

http://arxiv.org/pdf/1609.05153v1.pdf

We investigate how rotationally-constrained, deep convection might give rise to supergranulation, the largest distinct spatial scale of convection observed in the solar photosphere. While supergranulation is only weakly influenced by rotation, larger spatial scales of convection sample the deep convection zone and are presumably rotationally influenced. We present numerical results from a series of nonlinear, 3-D simulations of rotating convection and examine the velocity power distribution realized under a range of Rossby numbers. When rotation is present, the convective power distribution possesses a pronounced peak, at characteristic wavenumber ℓ peak, whose value increases as the Rossby number is decreased. This distribution of power contrasts with that realized in non-rotating convection, where power increases monotonically from high to low wavenumbers. We find that spatial scales smaller than ℓ peak behave in analogy to non-rotating convection. Spatial scales larger than ℓ peak are rotationally-constrained and possess substantially reduced power relative to the non-rotating system. We argue that the supergranular scale emerges due to a suppression of power on spatial scales larger than $\ell \approx 100$ owing to the presence of deep, rotationally-constrained convection. Supergranulation thus represents the largest non-rotationally-constrained mode of solar convection. We conclude that the characteristic spatial scale of supergranulation bounds that of the deep convective motions from above, making supergranulation an indirect measure of the deep-seated dynamics at work in the solar dynamo. Using the spatial scale of supergranulation in conjunction with our numerical results, we estimate an upper bound of 10 m s$-$1 for the Sun's bulk rms convective velocity.

Meridional Circulation in Solar and Stellar Convection Zones

Nicholas A. **Featherstone**, Mark S. Miesch

ApJ **2015**

http://arxiv.org/pdf/1501.06501v1.pdf

We present a series of 3-D nonlinear simulations of solar-like convection, carried out using the Anelastic Spherical Harmonic (ASH) code, that are designed to isolate those processes that drive and shape meridional circulations within stellar convection zones. These simulations have been constructed so as to span the transition between solar-like differential rotation (fast equator/slow poles) and ``anti-solar' differential rotation (slow equator/fast poles). Solar-like states of differential rotation, arising when convection is rotationally constrained, are characterized by a very different convective Reynolds stress than anti-solar regimes, wherein convection only weakly senses the Coriolis force. We find that the angular momentum transport by convective Reynolds stress plays a central role in establishing the meridional flow profiles in these simulations. We find that the transition from single-celled to multi-celled meridional circulation profiles in strong and weak regimes of rotational constraint is linked to a change in the convective Reynolds stress, a clear demonstration of gyroscopic pumping. Latitudinal thermal variations differ between these different regimes, with those in the solar-like regime conspiring to suppress a single cell of meridional circulation, whereas the cool poles and warm equator established in the anti-solar states tend to promote single-celled circulations. Though the convective angular momentum transport becomes radially inward at mid-latitudes in anti-solar regimes, it is the meridional circulation that is primarily responsible for establishing a rapidly-rotating pole. We conclude with a discussion of how these results relate to the Sun, and suggest that the Sun may lie near the transition between rapidly-rotating and slowly-rotating regimes.

Chromospheric resonances above sunspots and potential seismological applications

T. **Felipe**, C. Kuckein, S. J. González Manrique, I. Milic, C. R. Sangeetha

ApJL **2020**

https://arxiv.org/pdf/2008.10623.pdf

Oscillations in sunspot umbrae exhibit remarkable differences between the photosphere and chromosphere. We evaluate two competing scenarios proposed for explaining those observations: a chromospheric resonant cavity and waves traveling from the photosphere to upper atmospheric layers. We have employed numerical simulations to analyze the oscillations in both models. They have been compared with observations in the low (Na I D2) and high (He I 10830 Å) chromosphere. The nodes of the resonant cavity can be detected as phase jumps or power dips, although the identification of the latter is not sufficient to claim the existence of resonances. In contrast, phase differences between velocity and temperature fluctuations reveal standing waves and unequivocally prove the presence of an acoustic resonator above umbrae. Our findings offer a new seismic method to probe active region chromospheres through the detection of resonant nodes. **2000 Oct 01, 2001 May 09, 2007 Aug 29, 2017 Jun 17-18, 2018 May 09**

Table 1. Details of the six data sets obtained with VTT and GREGOR telescopes

Numerical determination of the cutoff frequency in solar models

T. **Felipe**, C. R. Sangeetha

A&A 640, A4 **2020**

https://arxiv.org/pdf/2006.00526.pdf

https://www.aanda.org/articles/aa/pdf/2020/08/aa38387-20.pdf

In stratified atmospheres, acoustic waves can only propagate if their frequency is above the cutoff value. Different theories provide different cutoff values. We developed an alternative method to derive the cutoff frequency in several standard solar models, including various quiet-Sun and umbral atmospheres. We performed numerical simulations of wave propagation in the solar atmosphere. The cutoff frequency is determined from the inspection of phase difference spectra computed between the velocity signal at two atmospheric heights. The process is performed by choosing pairs of heights across all the layers between the photosphere and the chromosphere, to derive the vertical stratification of the cutoff in the solar models. The cutoff frequency predicted by the theoretical calculations departs significantly from our measurements. In quiet-Sun atmospheres, the cutoff shows a strong dependence on the magnetic field for adiabatic wave propagation. When radiative losses are taken into account, the cutoff frequency is greatly reduced and the variation of the cutoff with the strength of the magnetic field is lower. The effect of the radiative losses in the cutoff is necessary to understand recent quiet-Sun and sunspot observations. In the presence of inclined magnetic fields, our numerical calculations confirm the reduction of the cutoff frequency due to the reduced gravity experienced by waves propagating along field lines. An additional reduction is also found in regions with significant changes in the temperature, due to the lower temperature gradient along the path of field-guided waves. Our results show that the cutoff values are not correctly captured by theoretical estimates. In addition, most of the widely-used analytical cutoff formulae neglect the impact of magnetic fields and radiative losses, whose role is critical to determine the evanescent or propagating nature of the waves.

Improved detection of farside solar active regions using deep learning

T. **Felipe**, A. Asensio Ramos

A&A 632, A82 **2019**

https://arxiv.org/pdf/1911.01099.pdf

https://doi.org/10.1051/0004-6361/201936838

The analysis of waves in the visible side of the Sun allows the detection of active regions in the farside through local helioseismology techniques. The knowledge of the magnetism in the whole Sun, including the non-visible hemisphere, is fundamental for several space weather forecasting applications. Seismic identification of farside active regions is challenged by the reduced signal-to-noise, and only large and strong active regions can be reliable detected. Here we develop a new methodology to improve the identification of active region signatures in farside seismic maps. We have constructed a deep neural network that associates the farside seismic maps obtained from helioseismic holography with the probability of presence of active regions in the farside. The network has been trained with pairs of helioseismic phase shift maps and Helioseismic and Magnetic Imager magnetograms acquired half a solar rotation later, which were used as a proxy for the presence of active regions in the farside. The method has been validated using a set of artificial data, and it has also been applied to actual solar observations during the period of minimum activity of the solar cycle 24. Our approach shows a higher sensitivity to the presence of farside active regions than standard methods applied up to date. The neural network can significantly increase the number of detected farside active regions, and will potentially improve the application of farside seismology to space weather forecasting. **2015 December 10, 2018-12-18/19, 2019-02-04/09**

Inversions of synthetic umbral flashes: effects of the scanning time on the inferred atmospheres

T. **Felipe**, H. Socas-Navarro, D. Przybylski

A&A **2018**

https://arxiv.org/pdf/1802.05028.pdf

The use of instruments that record narrow band images at selected wavelengths is a common approach in solar observations. They allow the scanning of a spectral line by sampling the Stokes profiles with 2D images at each line position, but require a compromise between spectral resolution and temporal cadence. We evaluate the impact of the time-dependent acquisition of different wavelengths on the inversion of spectropolarimetric profiles from chromospheric lines during umbral flashes. Simulations of non-linear wave propagation in a sunspot were performed with the code MANCHA. Synthetic Stokes parameters in the Ca II 8542 A line in NLTE were computed for an umbral flash using the code NICOLE. Artificial profiles with the same wavelength coverage and temporal cadence from reported observations were constructed and inverted. The inferred atmospheric stratifications were compared with the original models. The inferred atmospheres provide a reasonable characterization of the thermodynamic properties of the atmosphere during most of the phases of the umbral flash. Only at the early stages of the flash, when the shock wave reaches the formation height of the line, the Stokes profiles present apparent wavelength shifts and other spurious deformations. These features are misinterpreted by the inversion code, which can return unrealistic atmospheric models from a good fit of the Stokes profiles. The misguided results include

flashed atmospheres with strong downflows, even though the simulation exhibits upflows during the umbral flash, and large variations in the magnetic field strength. Our analyses validate the inversion of Stokes profiles acquired by sequentially scanning certain selected wavelengths of a line profile, even in the case of rapidly-changing events such as umbral flashes. However, the inversions are unreliable during a short period at the development phase of the flash.

Helioseismic holography of simulated sunspots: dependence of the travel time on magnetic field strength and Wilson depression

T. **Felipe**1,2, D. C. Braun3 and A. C. Birch4
A&A 604, A126 (**2017**)
http://www.aanda.org.sci-hub.cc/articles/aa/abs/2017/08/aa30798-17/aa30798-17.html
Improving methods for determining the subsurface structure of sunspots from their seismic signature requires a better understanding of the interaction of waves with magnetic field concentrations. We aim to quantify the impact of changes in the internal structure of sunspots on local helioseismic signals. We have numerically simulated the propagation of a stochastic wave field through sunspot models with different properties, accounting for changes in the Wilson depression between 250 and 550 km and in the photospheric umbral magnetic field between 1500 and 3500 G. The results show that travel-time shifts at frequencies above approximately 3.50 mHz (depending on the phase-speed filter) are insensitive to the magnetic field strength. The travel time of these waves is determined exclusively by the Wilson depression and sound-speed perturbation. The travel time of waves with lower frequencies is affected by the direct effect of the magnetic field, although photospheric field strengths below 1500 G do not leave a significant trace on the travel-time measurements. These results could potentially be used to develop simplified travel-time inversion methods.

HELIOSEISMIC HOLOGRAPHY OF SIMULATED SUNSPOTS: MAGNETIC AND THERMAL CONTRIBUTIONS TO TRAVEL TIMES

T. **Felipe**1,2,3, D. C. Braun3, A. D. Crouch3, and A. C. Birch4
2016 ApJ 829 67
Wave propagation through sunspots involves conversion between waves of acoustic and magnetic character. In addition, the thermal structure of sunspots is very different than that of the quiet Sun. As a consequence, the interpretation of local helioseismic measurements of sunspots has long been a challenge. With the aim of understanding these measurements, we carry out numerical simulations of wave propagation through sunspots. Helioseismic holography measurements made from the resulting simulated wavefields show qualitative agreement with observations of real sunspots. We use additional numerical experiments to determine, separately, the influence of the thermal structure of the sunspot and the direct effect of the sunspot magnetic field. We use the ray approximation to show that the travel-time shifts in the thermal (non-magnetic) sunspot model are primarily produced by changes in the wave path due to the Wilson depression rather than variations in the wave speed. This shows that inversions for the subsurface structure of sunspots must account for local changes in the density. In some ranges of horizontal phase speed and frequency there is agreement (within the noise level in the simulations) between the travel times measured in the full magnetic sunspot model and the thermal model. If this conclusion proves to be robust for a wide range of models, it would suggest a path toward inversions for sunspot structure.

Midterm Periodicity Analysis of the Mount Wilson Magnetic Indices Using the Synchrosqueezing Transform

Song **Feng**, Lan Yu, Feng Wang, Hui Deng, Yunfei Yang
Astrophysical Journal, 845:11 (8pp), **2017** August 10
https://arxiv.org/pdf/1803.07893.pdf
A novel time--frequency technique, called the synchrosqueezing transform (SST), is used to investigate the midterm periodic variations of magnetic fields on the solar surface. The Magnetic Plage Strength Index (MPSI) and the Mount Wilson Sunspot Index (MWSI), measured daily by the Mount Wilson Observatory between 1970 January 19 and 2012 January 22, are selected. The short-, mid, and longer-term periodicities are represented and decomposed by the SST with hardly any mode mixing. This demonstrates that the SST is a useful time--frequency analysis technique to characterize the periodic modes of helioseismic data. Apart from the fundamental modes of the annual periodicity, ~27 day rotational cycle and ~11 year solar cycle, the SST reveals several midterm periodicities in the two magnetic activity indices, specifically, ~157 day (i.e., Rieger-type periodicity), and ~1.3 and 1.7 years. The periodic modes, with 116.4 and 276.2 day periodicity in the MPSI, with 108.5 and 251.6 day periodicity in the MWSI, and the 157.7 day periodicity in the two indices, are in better accord with those significant periodicities derived from the Rossby waves theoretical model. This study suggests that the modes are caused by the Rossby waves. For the 1.30 and 1.71 year periodicity of the MPSI, and the 1.33 and 1.67 year periodicity of the MWSI, our

analysis infers that they are related to those periodicity with the same timescale in the interior of the Sun and in the high atmospheric layers.

Data-driven modeling of the solar wind from 1 Rs to 1 AU

Xueshang **Feng**, Xiaopeng Ma, Changqing Xiang

JGR **2016**

We present here a time-dependent three-dimensional magnetohydrodynamic (MHD) solar wind simulation from the solar surface to the Earth's orbit driven by time-varying line-of-sight solar magnetic field data. The simulation is based on the three-dimensional (3-D) solar-interplanetary (SIP) adaptive mesh refinement (AMR) space-time conservation element and solution element (CESE) MHD (SIP-AMR-CESE MHD) model. In this simulation, we first achieve the initial solar wind background with the time-relaxation method by inputting a potential field obtained from the synoptic photospheric magnetic field and then generate the time-evolving solar wind by advancing the initial 3-D solar wind background with continuously varying photospheric magnetic field. The model updates the inner boundary conditions by using the projected normal characteristic method, inputting the high-cadence photospheric magnetic field data corrected by solar differential rotation, and limiting the mass flux escaping from the solar photosphere. We investigate the solar wind evolution from **1 July to 11 August 2008** with the model driven by the consecutive synoptic maps from the Global Oscillation Network Group. We compare the numerical results with the previous studies on the solar wind, the solar coronal observations from the Extreme ultraviolet Imaging Telescope board on Solar and Heliospheric Observatory, and the measurements from OMNI at 1 astronomical unit (AU). Comparisons show that the present data-driven MHD model's results have overall good agreement with the large-scale dynamical coronal and interplanetary structures, including the sizes and distributions of the coronal holes, the positions and shapes of the streamer belts, the heliocentric distances of the Alfvénic surface, and the transitions of the solar wind speeds. However, the model fails to capture the small-sized equatorial holes, and the modeled solar wind near 1 AU has a somewhat higher density and weaker magnetic field strength than observed. Perhaps better preprocessing of high-cadence observed photospheric magnetic field (particularly 3-D global measurements), combined with plasma measurements and higher resolution grids, will enable the data-driven model to more accurately capture the time-dependent changes of the ambient solar wind for further improvements. In addition, other measures may also be needed when the model is employed in the period of high solar activity.

Automated Detection of Low-Contrast Solar Features Using the Phase-Congruency Algorithm

Song **Feng**, Zhi Xu, Feng Wang, Hui Deng, Yunfei Yang, Kaifan Ji

Solar Physics, Volume 289, Issue 10, pp 3985-3994, **2014**

We propose a new feature-detection technique based on phase-congruency (PC) measurements to automatically recognize or enhance faint features in solar observations, such as off-limb coronal loops and umbral dots. Compared with other feature-detection methods that are based on gradient illuminance and imaging filtering, PC-based measurements are particular efficient for recognizing faint features, which generally have a low-intensity contrast to their surroundings. In the present article, we carry out a PC-based measurement of the local weighted mean phase angle (LWMPA) at each point in an image to indicate or highlight low-contrast features. We first used artificial images to check the detection accuracy and sensitivity to the noise of this approach. Subsequently, we applied this approach to an EUV observation obtained by the Solar Dynamics Observatory/Atmospheric Imaging Assembly to highlight off-limb coronal loops, and a photospheric observation obtained by the Hinode/Solar Optical Telescope to recognize faint dots within the cores of sunspots and pores. The results illustrate that this PC-based measurement of the LWMPA is a robust detection method for faint structures in solar observations.

SDO/HMI observations of the average supergranule are not compatible with separable flow models

R. Z. **Ferret**

A&A 623, A98 (**2019**)

sci-hub.tw/10.1051/0004-6361/201833742

Aims. Despite extensive studies carried out since its discovery half a century ago, the nature of supergranulation remains an open question in solar physics. Separability of flow models is a common assumption made in the literature to shed light on the properties of supergranules. This paper studies the ability of separable mass-conserving flow models to reproduce photospheric observations from the Helioseismic Magnetic Imager (HMI) on board of the Solar Dynamics Observatory (SDO) spacecraft corresponding to an average supergranule.
Methods. For a steady mass-conserving separable flow model to be compatible with the observations, there is an integral relation between the horizontal and vertical components of the flow. We test this relation directly on observations and compare the results with the proportionality relationship for a separable model.

Results. Observations of an average supergranule do not satisfy the condition for separability. Selecting a narrower range of horizontal scales of supergranules when performing the average does not change this result. Separable models are not consistent with observations of an average supergranule.

A correlation between sunspot observations and solar Ca ii H&K activity proxies

R R **Ferreira**, B F O Gonçalves, J -D do Nascimento, Jr, M Castro
MNRAS Volume 535, Issue 3, December **2024**, Pages 2394–2403,
https://doi.org/10.1093/mnras/stae2381
https://academic.oup.com/mnras/article-pdf/535/3/2394/60766889/stae2381.pdf

The magnetic phenomena on the solar surface have been the subject of several investigations over the last 400 yr. An early indicator of solar magnetic activity was sunspot counting. Currently, the main sunspot indicators are the international sunspot number, the sunspot group number, the total sunspot area, and the photometric sunspot index. Several improvements in observational techniques have allowed magnetic activity to be measured using solar/stellar spectra. Standard spectroscopic activity indicators are the SMW index, based on the Ca ii H&K emission lines, and the chromospheric component RHK′ index. In this context, we present a correlation between sunspot observations and solar Ca ii H&K activity proxies. We present our comparisons between the spectroscopic chromospheric activity proxies (SMW and RHK′) and the sunspot indicators over the last decades, using solar measurements (spectroscopic and spot proxy) performed on the same day. In general, our results indicate a linear fit between the chromospheric proxies and sunspot indicators. In addition, using the long-term sunspot group number records, we estimate an average spectroscopic proxy along the solar Maunder minimum (MM) phase, corresponding to ⟨SMW⟩=0.167±0.013 and $\log_{10}$⟨RHK′⟩=−4.913±0.363. The estimated variability is σSMW=1.137×10−7 and σ$\log_{10}$RHK′=2.704×10−6. Our linear regression analysis, applied annually, suggests that the variability level of the chromospheric activity in the MM phase is significantly lower than in the normal period of activity and that this could be the result of linear regression on annually averaged data, combined with minimal sunspot activity during the solar MM phase. Further observations of MM analogues will be needed to test this hypothesis

.

The Centennial Gleissberg Cycle and its Association with Extended Minima†

J. **Feynman*** andA. Ruzmaikin
JGR, Volume 119, Issue 8, pages 6027–6041, August **2014**

The recent extended minimum of solar and geomagnetic variability (XSM) mirrors the XSMs in the 19th and 20th centuries: 1810–1830 and 1900–1910. Such extended minima also were evident in aurorae reported from 450 AD to 1450 AD. This paper argues that these minima are consistent with minima of the Centennial Gleissberg Cycles (CGC), a 90–100 year variation observed on the Sun, in the solar wind, at the Earth and throughout the Heliosphere. The occurrence of the recent XSM is consistent with the existence of the CGC as a quasi-periodic variation of the solar dynamo. Evidence of CGC's is provided by the multi-century sunspot record, by the almost 150-year record of indexes of geomagnetic activity (1868-present), by 1,000 years of observations of aurorae (from 450 to 1450 AD) and millennial records of radionuclides in ice cores. The aa index of geomagnetic activity carries information about the two components of the solar magnetic field (toroidal and poloidal), one driven by flares and CMEs (related to the toroidal field) the other driven by co-rotating interaction regions in the solar wind (related to the poloidal field). These two components systematically vary in their intensity and relative phase giving us information about centennial changes of the sources of solar dynamo during the recent CGC over the last century. The dipole and quadrupole modes of the solar magnetic field changed in relative amplitude and phase; the quadrupole mode became more important as the XSM was approached. Some implications for the solar dynamo theory are discussed.

Nested active regions anchor the heliospheric current sheet and stall the reversal of the coronal magnetic field

Adam J. **Finley**
A&A **2024**
https://arxiv.org/pdf/2410.18244

During the solar cycle, the Sun's magnetic field polarity reverses due to the emergence, cancellation, and advection of magnetic flux towards the rotational poles. Flux emergence events occasionally cluster together, although it is unclear if this is due to the underlying solar dynamo or simply by chance. Regardless of the cause, we aim to characterise how the reversal of the Sun's magnetic field and the structure of the solar corona are influenced by nested flux emergence. From the spherical harmonic decomposition of the Sun's photospheric magnetic field, we identify times when the reversal of the dipole component stalls for several solar rotations. Using observations from sunspot cycle 23 to present, we locate the nested active regions responsible for each stalling and explore their impact on the coronal magnetic field using potential field source surface extrapolations. Nested flux emergence has a more significant impact on the topology of the coronal magnetic field than isolated emergences as it produces a coherent (low spherical harmonic order) contribution to the photospheric magnetic field. The heliospheric current sheet (HCS), that separates oppositely directed coronal magnetic field, can become anchored above these regions due to the formation of strong opposing magnetic fluxes. Further flux emergence, cancellation, differential rotation, and

diffusion, then effectively advects the HCS and shifts the dipole axis. Nested flux emergence can restrict the evolution of the HCS and impede the reversal of the coronal magnetic field. The sources of the solar wind can be more consistently identified around nested active regions as the magnetic field topology remains self-similar for multiple solar rotations. This highlights the importance of identifying nested active regions to guide the remote-sensing observations of modern heliophysics missions.

Evolution of solar wind sources and coronal rotation driven by the cyclic variation of the Sun's large-scale magnetic field

Adam J. **Finley**, Allan Sacha Brun
A&A 679, A29 **2023**
https://arxiv.org/pdf/2309.10850.pdf
https://www.aanda.org/articles/aa/pdf/2023/11/aa47445-23.pdf
The strength and morphology of the Sun's magnetic field evolves significantly during the solar cycle, with the overall polarity of the Sun's magnetic field reversing during the maximum of solar activity. Long-term changes are also observed in sunspot and geomagnetic records, however systematic magnetic field observations are limited to the last four cycles. We investigate the long-term evolution of the Sun's magnetic field, and the influence this has on the topology and rotation of the solar corona. The Sun's photospheric magnetic field was decomposed into spherical harmonics using synoptic Carrington magnetograms from 1) WSO, 2) MDI onboard the SOHO, and 3) HMI onboard the SDO. The time-evolution of the spherical harmonic coefficients was used to explore the variation of the Sun's magnetic field, focusing on the large-scale modes. PFSS extrapolations of the photospheric field were computed to follow topological changes in the corona. The footpoints of the Sun's open magnetic field vary between the polar coronal holes and activity driven features such as active regions, and equatorial coronal holes. Consequently, the mean rotation rate of the solar wind is modulated during each cycle by the latitudinal variation of open field footpoints, with slower rotation during minima and faster (Carrington-like) rotation during maxima. Thisc variation is sensitive to cycle to cycle differences in the polar field strengths and hemispherical flux emergence rates, with the ratio of quadrupole to dipole energy following a similar variation. Cycle 23 maintained a larger fraction of quadrupolar energy in the declining phase, which kept the sources of open magnetic flux closer to the equator, extending the period of faster equator-ward connectivity. The ratio of quadrupole to dipole energy could be a useful proxy when examining the impact of differential rotation on the coronae of other Sun-like stars.

Accounting for differential rotation in calculations of the Sun’s angular momentum-loss rate

A. J. **Finley** and A. S. Brun
A&A 674, A42 (**2023**)
https://www.aanda.org/articles/aa/pdf/2023/06/aa45642-22.pdf
Context. Sun-like stars shed angular momentum due to the presence of magnetised stellar winds. Magnetohydrodynamic models have been successful in exploring the dependence of this ‘wind-braking torque’ on various stellar properties; however the influence of surface differential rotation is largely unexplored. As the wind-braking torque depends on the rotation rate of the escaping wind, the inclusion of differential rotation should effectively modulate the angular momentum-loss rate based on the latitudinal variation of wind source regions.
Aims. Here we aim to quantify the influence of surface differential rotation on the angular momentum-loss rate of the Sun, in comparison to the typical assumption of solid-body rotation.
Methods. To do this, we exploited the dependence of the wind-braking torque on the effective rotation rate of the coronal magnetic field, which is known to be vitally important in magnetohydrodynamic models. This quantity has been evaluated by tracing field lines through a potential field source surface (PFSS) model, driven by ADAPT-GONG magnetograms. The surface rotation rates of the open magnetic field lines were then used to construct an open-flux weighted rotation rate, from which the influence on the wind-braking torque could be estimated.
Results. During solar minima, the rotation rate of the corona decreases with respect to the typical solid-body rate (the Carrington rotation period is 25.4 days), as the sources of the solar wind are confined towards the slowly rotating poles. With increasing activity, more solar wind emerges from the Sun’s active latitudes which enforces a Carrington-like rotation. Coronal rotation often displays a north-south asymmetry driven by differences in active region emergence rates (and consequently latitudinal connectivity) in each hemisphere.
Conclusions. The effect of differential rotation on the Sun’s current wind-braking torque is limited. The solar wind-braking torque is $\sim 10-15\%$ lower during solar minimum, (compared with the typical solid body rate), and a few percent larger during solar maximum (as some field lines connect to more rapidly rotating equatorial latitudes). For more rapidly rotating Sun-like stars, differential rotation may play a more significant role, depending on the configuration of the large-scale magnetic field.

Stirring the base of the solar wind: On heat transfer and vortex formation

A. J. **Finley**1, A. S. Brun1, M. Carlsson2,3, M. Szydlarski2,3, V. Hansteen2,3,4,5 and M. Shoda6
A&A 665, A118 (**2022**)

https://www.aanda.org/articles/aa/pdf/2022/09/aa43947-22.pdf
Context. Current models of the solar wind must approximate (or ignore) the small-scale dynamics within the solar atmosphere; however, these are likely important in shaping the emerging wave-turbulence spectrum that ultimately heats and accelerates the coronal plasma.
Aims. This study strives to make connections between small-scale vortex motions at the base of the solar wind and the resulting heating and acceleration of the coronal plasma.
Methods. The Bifrost code produces realistic simulations of the solar atmosphere which facilitate the analysis of spatial and temporal scales which are currently at, or beyond, the limit of modern solar telescopes. For this study, the Bifrost simulation is configured to represent the solar atmosphere in a coronal hole region, from which the fast solar wind emerges. The simulation extends from the upper-convection zone (2.5 Mm below the photosphere) to the low corona (14.5 Mm above the photosphere), with a horizontal extent of 24 Mm × 24 Mm. The network of magnetic funnels in the computational domain influence the movement of plasma, as well as the propagation of magnetohydrodynamic waves into the low corona.
Results. The twisting of the coronal magnetic field by photospheric flows efficiently injects energy into the low corona. Poynting fluxes of up to 2 − 4 kWm−2 are commonly observed inside twisted magnetic structures with diameters in the low corona of 1–5 Mm. Torsional Alfvén waves are favourably transmitted along these structures, and subsequently escape into the solar wind. However, reflections of these waves from the upper boundary condition make it difficult to unambiguously quantify the emerging Alfvén wave-energy flux.
Conclusions. This study represents a first step in quantifying the conditions at the base of the solar wind using Bifrost simulations. It is shown that the coronal magnetic field is readily braided and twisted by photospheric flows. Temperature and density contrasts form between regions with active stirring motions and those without. Stronger whirlpool-like flows in the convection, concurrent with magnetic concentrations, launch torsional Alfvén waves up through the magnetic funnel network, which are expected to enhance the turbulent generation of magnetic switchbacks in the solar wind.

Direct Detection of Solar Angular Momentum Loss with the Wind Spacecraft

Adam J. **Finley**, Amy L. Hewitt, Sean P. Matt, Mathew Owens, Rui F. Pinto, Victor Réville
ApJL **2019**
https://arxiv.org/pdf/1910.10177.pdf
The rate at which the solar wind extracts angular momentum from the Sun has been predicted by theoretical models for many decades, and yet we lack a conclusive measurement from in-situ observations. In this letter we present a new estimate of the time-varying angular momentum flux in the equatorial solar wind, as observed by the \textit{Wind} spacecraft from 1994-2019. We separate the angular momentum flux into contributions from the protons, alpha particles, and magnetic stresses, showing that the mechanical flux in the protons is ∼3 times larger than the magnetic field stresses. We observe the tendency for the angular momentum flux of fast wind streams to be oppositely signed to the slow wind streams, as noted by previous authors. From the average total flux, we estimate the global angular momentum loss rate of the Sun to be 3.3×1030erg, which lies within the range of various MHD wind models in the literature. This angular momentum loss rate is a factor of ∼2 weaker than required for a Skumanich-like rotation period evolution ($\Omega_* \propto$ stellar age$^{-1/2}$), which should be considered in studies of the rotation period evolution of Sun-like stars.

Direct Detection of Solar Angular Momentum Loss with the Wind Spacecraft

Adam J. **Finley**1, Amy L. Hewitt1, Sean P. Matt1, Mathew Owens2, Rui F. Pinto3, and Victor Réville3
2019 ApJL 885 L30
sci-hub.se/10.3847/2041-8213/ab4ff4
The rate at which the solar wind extracts angular momentum (AM) from the Sun has been predicted by theoretical models for many decades, and yet we lack a conclusive measurement from in situ observations. In this Letter we present a new estimate of the time-varying AM flux in the equatorial solar wind, as observed by the Wind spacecraft from 1994 to 2019. We separate the AM flux into contributions from the protons, alpha particles, and magnetic stresses, showing that the mechanical flux in the protons is ~3 times larger than the magnetic field stresses. We observe the tendency for the AM flux of fast wind streams to be oppositely signed to the slow wind streams, as noted by previous authors. From the average total flux, we estimate the global AM loss rate of the Sun to be 3.3 × 1030 erg, which lies within the range of various magnetohydrodynamic wind models in the literature. This AM loss rate is a factor of ~2 weaker than required for a Skumanich-like rotation period evolution ($\Omega_* \propto$ stellar age$^{-1/2}$), which should be considered in studies of the rotation period evolution of Sun-like stars.

Solar Angular Momentum Loss Over the Past Several Millennia

Adam J. **Finley**, Siddhant Deshmukh, Sean P. Matt, Mathew Owens, Chi-Ju Wu
ApJ **883** 67 **2019**
https://arxiv.org/pdf/1907.13143.pdf
https://doi.org/10.3847/1538-4357/ab3729

The Sun and Sun-like stars lose angular momentum to their magnetised stellar winds. This braking torque is coupled to the stellar magnetic field, such that changes in the strength and/or geometry of the field modifies the efficiency of this process. Since the space-age, we have been able to directly measure solar wind properties using in-situ spacecraft. Furthermore, indirect proxies such as sunspot number, geomagnetic indices, and cosmogenic radionuclides, constrain the variation of solar wind properties on centennial, and millennial timescales. We use near-Earth measurements of the solar wind plasma and magnetic field to calculate the torque on the Sun throughout the space-age. Then, reconstructions of the solar open magnetic flux are used to estimate the time-varying braking torque during the last nine millennia. We assume a relationship for the solar mass loss rate based on observations during the space-age which, due to the weak dependence of the torque on mass loss rate, does not strongly affect our predicted torque. The average torque during the last nine millennia is found to be 2.2×1030erg, which is comparable to the average value from the last two decades. Our dataset includes grand minima (such as the Maunder Minimum), and maxima in solar activity, where the torque varies from ∼1−5×1030erg (averaged on decadal timescales), respectively. We find no evidence for any secular variation of the torque on timescales of less than 9000 years.
UKSP Nugget: #104 Sept **2019**
http://www.uksolphys.org/uksp-nugget/104-comparing-different-methods-for-computing-solar-angular-momentum-loss/

The Dipole, Quadrupole, and Octupole Components of the Solar Magnetic Field Over 22 Years

Adam James **Finley**
HMI Science Nuggets #81 **2018** http://hmi.stanford.edu/hminuggets/?p=2129
As shown previously, the Solar magnetic field can be decomposed into its spherical harmonic components (see work in Ref. 1).
The Solar magnetic field has now been continuously observed by space-borne instruments (SOHO/MDI and SDO/HMI) for 22 years, the length of the magnetic solar cycle. We choose to use these data to observe how the lowest order component fluctuate over decadal timescales.

Interaction of magnetic fields with a vortex tube at solar subgranular scale

C.E.**Fischer**, G.Vigeesh, P.Lindner, J.M.Borrero, F.Calvo, O.Steiner
ApJL **903** L10 **2020**
https://arxiv.org/pdf/2010.05577.pdf
https://iopscience.iop.org/article/10.3847/2041-8213/abbada/pdf
Using high-resolution spectropolarimetric data recorded with the Swedish 1 m Solar Telescope, we have identified several instances of granular lanes traveling into granules. These are believed to be the observational signature of underlying tubes of vortical flow with their axis oriented parallel to the solar surface. Associated with these horizontal vortex tubes, we detect in some cases a significant signal in linear polarization, located at the trailing dark edge of the granular lane. The linear polarization appears at a later stage of the granular lane development, and is flanked by patches of circular polarization. Stokes inversions show that the elongated patch of linear polarization signal arises from the horizontal magnetic field aligned with the granular lane. We analyze snapshots of a magnetohydrodynamic numerical simulation and find cases in which the horizontal vortex tube of the granular lane redistributes and transports the magnetic field to the solar surface causing a polarimetric signature similar to what is observed. We thus witness a mechanism capable of transporting magnetic flux to the solar surface within granules. This mechanism is probably an important component of the small-scale dynamo supposedly acting at the solar surface and generating the quiet-Sun magnetic field. **2019 April**
European Solar Physics Nuggets (ESPN) **#3** Oct **2021** https://www.est-east.eu/nuggets/46-espn/1098-espn-3-high-resolution-data-reveals-the-interaction-of-magnetic-fields-with-a-vortex-tube

Observations of solar small-scale magnetic flux-sheet emergence

C.E. **Fischer**, J.M. Borrero, N. Bello González, A.J. Kaithakkal
A&A 622, L12 **2019**
https://arxiv.org/pdf/1901.05870.pdf
Aims. Moreno-Insertis et al. (2018) recently discovered two types of flux emergence in their numerical simulations: magnetic loops and magnetic sheet emergence. Whereas magnetic loop emergence has been documented well in the last years, by utilising high-resolution full Stokes data from ground-based telescopes as well as satellites, magnetic sheet emergence is still an understudied process. We report here on the first clear observational evidence of a magnetic sheet emergence and characterise its development.
Methods. Full Stokes spectra from the Hinode spectropolarimeter were inverted with the SIR code to obtain solar atmospheric parameters such as temperature, line-of-sight velocities and full magnetic field vector information.
Results. We analyse a magnetic flux emergence event observed in the quiet-sun internetwork. After a large scale appearance of linear polarisation, a magnetic sheet with horizontal magnetic flux density of up to 194

Mx/cm2 hovers in the low photosphere spanning a region of 2 to 3 arcsec. The magnetic field azimuth obtained through Stokes inversions clearly shows an organised structure of transversal magnetic flux density emerging. The granule below the magnetic flux-sheet tears the structure apart leaving the emerged flux to form several magnetic loops at the edges of the granule.
Conclusions. A large amount of flux with strong horizontal magnetic fields surfaces through the interplay of buried magnetic flux and convective motions. The magnetic flux emerges within 10 minutes and we find a longitudinal magnetic flux at the foot points of the order of ∼1018 Mx. This is one to two orders of magnitude larger than what has been reported for small-scale magnetic loops. The convective flows feed the newly emerged flux into the pre-existing magnetic population on a granular scale. **28 April 2014**

Chromospheric impact of an exploding solar granule

Catherine E. **Fischer**, Nazaret Bello González, Reza Rezaei
A&A 602, L12 **2017**
https://arxiv.org/pdf/1706.00770.pdf
Observations of multi-wavelength and therefore height-dependent information following events throughout the solar atmosphere and unambiguously assigning a relation between these rapidly evolving layers are rare and difficult to obtain. Yet, they are crucial for our understanding of the physical processes that couple the different regimes in the solar atmosphere. We characterize the exploding granule event with simultaneous observations of Hinode spectroplarimetric data in the solar photosphere and Hinode broadband CaIIH images combined with Interface Region Imaging Spectrograph (IRIS) slit spectra. We follow the evolution of an exploding granule and its connectivity throughout the atmosphere and analyze the dynamics of a magnetic element that has been affected by the abnormal granule. In addition to magnetic flux maps we use a local correlation tracking method to infer the horizontal velocity flows in the photosphere and apply a wavelet analysis on several IRIS chromospheric emission features such as MgIIk2v and MgIIk3 to detect oscillatory phenomena indicating wave propagation. During the vigorous expansion of the abnormal granule we detect radially outward horizontal flows, causing, together with the horizontal flows from the surrounding granules, the magnetic elements in the bordering intergranular lanes to be squeezed and elongated. In reaction to the squeezing, we detect a chromospheric intensity and velocity oscillation pulse which we identify as an upward traveling hot shock front propagating clearly through the IRIS spectral line diagnostics of MgIIh&k. Conclusion: Exploding granules can trigger upward-propagating shock fronts that dissipate in the chromosphere. **28 April 2014**

JPEG2000 Image Compression on Solar EUV Images

Catherine E. **Fischer**, Daniel Müller, Ineke De Moortel
Solar Physics January **2017**, 292:16
http://link.springer.com/article/10.1007/s11207-016-1038-3
https://arxiv.org/pdf/1702.01946.pdf
For future solar missions as well as ground-based telescopes, efficient ways to return and process data have become increasingly important. Solar Orbiter, which is the next ESA/NASA mission to explore the Sun and the heliosphere, is a deep-space mission, which implies a limited telemetry rate that makes efficient onboard data compression a necessity to achieve the mission science goals. Missions like the Solar Dynamics Observatory (SDO) and future ground-based telescopes such as the Daniel K. Inouye Solar Telescope, on the other hand, face the challenge of making petabyte-sized solar data archives accessible to the solar community. New image compression standards address these challenges by implementing efficient and flexible compression algorithms that can be tailored to user requirements. We analyse solar images from the Atmospheric Imaging Assembly (AIA) instrument onboard SDO to study the effect of lossy JPEG2000 (from the Joint Photographic Experts Group 2000) image compression at different bitrates. To assess the quality of compressed images, we use the mean structural similarity (MSSIM) index as well as the widely used peak signal-to-noise ratio (PSNR) as metrics and compare the two in the context of solar EUV images. In addition, we perform tests to validate the scientific use of the lossily compressed images by analysing examples of an on-disc and off-limb coronal-loop oscillation time-series observed by AIA/SDO.

Global Circulation of the Open Magnetic Flux of the Sun

L. A. **Fisk** and J. C. Kasper
2020 ApJL 894 L4
https://doi.org/10.3847/2041-8213/ab8acd
The global circulation of the open magnetic flux of the Sun, the component of the solar magnetic field that opens into the heliosphere, and the consequences of the global circulation were proposed by Fisk and coworkers in the early 2000s. The Parker Solar Probe, on its initial encounters with the Sun, has provided direct confirmation of both the global circulation and the physical mechanism by which the circulation occurs, transport by interchange reconnection between open magnetic flux and large coronal loops. The implications of this confirmation of the global circulation of open magnetic flux and the importance of interchange reconnection is discussed.

The Temperature Dependence of Hot Prograde Flows in Solar Active Regions

Jimmy C. **Fitzpatrick** & Hugh S. Hudson

Solar Physics volume 298, Article number: 2 (**2023**)

https://link.springer.com/content/pdf/10.1007/s11207-022-02093-3.pdf

Using simultaneous observations from the EUV Variability Experiment (EVE) and imaging from the Atmospheric Imaging Assembly (AIA), we characterise the temperature dependence of apparent hot flows in solar active regions. The EVE instrument performs Sun-as-a-star spectroscopy and is composed of two spectrographs: MEGS-A and MEGS-B (Multiple EUV Grating Spectrograph-A, -B). It is known that EVE can measure wavelength shifts and thus can observe relative Doppler velocities in solar atmospheric plasmas over an extended temperature range. However, MEGS-A is affected by a known astigmatism effect (Chamberlin: Solar Phys. 291, 1665, 2016); inhomogeneities in EUV brightness on the solar surface result in purely instrumental wavelength errors. We validate our methods by independently quantifying this effect and comparing to Chamberlin's results, and we explore the wavelength dependence as an extension of his formula as derived for He II 304 Å. MEGS-B is unaffected by this instrumental effect in any case, and this has allowed us to find evidence of hot prograde flows in active regions. Using our image-based models for the astigmatism and flows, we independently confirm our original MEGS-B result. We now extend our knowledge of the temperature dependence of these flows via the additional Fe emission lines available in MEGS-A. We find a monotonic increase of apparent flow speed with temperature up through lines of Fe XVI, nominally formed at about 6.4 MK.

Photospheric Temperature Gradient

Martin **Fivian**, Hugh Hudson

RHESSI Science Nugget No. 186, Oct **2012**

A simple telescope in space, rapidly rotating around its line of sight to the Sun, has provided very tight limits on the possible latitudinal variation of solar effective temperature. Since this initial look used only a few percent of the available data, and since analysis procedures continually improve, this limit will get better and/or RHESSI will actually begin to see real effects. This mapping of mean temperature structures on the surface of the Sun, we hope, will complement the results obtained from helioseismology, and teach us basically new things about the nature of convection and the solar cycle.

A prediction for 25th solar cycle using visibility graph and Hathaway function

Eduardo **Flandez**, Victor Munoz

2024

https://arxiv.org/pdf/2412.12924

We apply a complex network approach to analyse the time series of five solar parameters, and propose an strategy to predict the number of sunspots for the next solar maximum, and when will this maximum will occur. The approach is based on the Visibility Graph (VG) algorithm, and a slightly modified version of it, the Horizontal Visibility Graph (HVG), which map a time series into a complex network. Various network metrics exhibit either an exponential or a scale-free behavior, and we find that the evolution of the characteristic decay exponents is consistent with variations of the sunspots number along solar cycles. During solar minimum, the sunspots number and the solar index time series have characteristic decay exponents that correlate well with the next maximum sunspots number, suggesting that they may be good precursors of the intensity of the next solar maximum. Based on this observation, we find that, based on current data, the algorithm predicts a number of 179 sunspots for cycle 25. Combining this with the Hathaway function, adjusted to yield such maximum sunspots number, we find that the maximum for solar cycle 25 will occur in December 2024/January 2025.

A 22-Year Cycle of the Network Topology for Solar Active Regions

Eduardo **Flández**, Alejandro Zamorano, Víctor Muñoz

ApJ **2024**

https://arxiv.org/pdf/2412.12047

In this paper, solar cycles 21 to 24 were compared using complex network analysis. A network was constructed for these four solar cycles to facilitate the comparison. In these networks, the nodes represent the active regions of the Sun that emit flares, and the connections correspond to the sequence of solar flares over time. This resulted in a directed network with self-connections allowed. The model proposed by Abe and Suzuki for earthquake networks was followed. The incoming degree for each node was calculated, and the degree distribution was analyzed. It was found that for each solar cycle, the degree distribution follows a power law, indicating that solar flares tend to appear in correlated active zones rather than being evenly distributed. Additionally, a variation in the characteristic exponent {\gamma} for each cycle was observed, with higher values in even cycles compared to odd cycles. A more detailed analysis was performed by constructing 11-year networks and shifting them in one-year intervals. This

revealed that the characteristic exponent shows a period of approximately 22 years coincident with the Hale cycle, suggesting that the complex networks provide information about the solar magnetic activity.

Acoustic-gravity wave propagation characteristics in 3D radiation hydrodynamic simulations of the solar atmosphere

B. **Fleck**, M. Carlsson, E. Khomenko, M. Rempel, O. Steiner, G. Vigeesh
Philosophical Transactions A **Volume 379 Issue 2190 2021**
https://arxiv.org/pdf/2007.05847.pdf
There has been tremendous progress in the degree of realism of three-dimensional radiation magneto-hydrodynamic simulations of the solar atmosphere in the past decades. Four of the most frequently used numerical codes are Bifrost, CO5BOLD, MANCHA3D, and MURaM. Here we test and compare the wave propagation characteristics in model runs from these four codes by measuring the dispersion relation of acoustic-gravity waves at various heights. We find considerable differences between the various models. The height dependence of wave power, in particular of high-frequency waves, varies by up to two orders of magnitude between the models, and the phase difference spectra of several models show unexpected features, including ±180∘ phase jumps.

Coronal Heating Law Constrained by Microwave Gyroresonant Emission

Gregory D. **Fleishman**, Sergey A. Anfinogentov, Alexey G. Stupishin, Alexey A. Kuznetsov, Gelu M. Nita
ApJ **909** 89 **2021**
https://arxiv.org/pdf/2101.03651.pdf
https://doi.org/10.3847/1538-4357/abdab1
The question why the solar corona is much hotter than the visible solar surface still puzzles solar researchers. Most theories of the coronal heating involve a tight coupling between the coronal magnetic field and the associated thermal structure. This coupling is based on two facts: (i) the magnetic field is the main source of the energy in the corona and (ii) the heat transfer preferentially happens along the magnetic field, while is suppressed across it. However, most of the information about the coronal heating is derived from analysis of EUV or soft X-ray emissions, which are not explicitly sensitive to the magnetic field. This paper employs another electromagnetic channel -- the sunspot-associated microwave gyroresonant emission, which is explicitly sensitive to both the magnetic field and thermal plasma. We use nonlinear force-free field reconstructions of the magnetic skeleton dressed with a thermal structure as prescribed by a field-aligned hydrodynamics to constrain the coronal heating model. We demonstrate that the microwave gyroresonant emission is extraordinarily sensitive to details of the coronal heating. We infer heating model parameters consistent with observations. **2012 Jul 12**

Ion Traps at the Sun: Implications for Elemental Fractionation

Gregory **Fleishman**, Sophie Musset, Véronique Bommier, Lindsay Glesener
ApJ **857** 85 **2018**
https://arxiv.org/pdf/1803.02851.pdf
http://sci-hub.tw/http://iopscience.iop.org/0004-637X/857/2/85/
Why the tenuous solar outer atmosphere, or corona, is much hotter than the underlying layers remains one of the greatest challenge for solar modeling. Detailed diagnostics of the coronal thermal structure come from extreme ultraviolet (EUV) emission. The EUV emission is produced by heavy ions in various ionization states and depends on the amount of these ions and on plasma temperature and density. Any nonuniformity of the elemental distribution in space or variability in time affects thermal diagnostics of the corona. Here we theoretically predict ionized chemical element concentrations in some areas of the solar atmosphere, where the electric current is directed upward. We then detect these areas observationally, by comparing the electric current density with the EUV brightness in an active region. We found a significant excess in EUV brightness in the areas with positive current density rather than negative. Therefore, we report the observational discovery of substantial concentrations of heavy ions in current-carrying magnetic flux tubes, which might have important implications for the elemental fractionation in the solar corona known as the first ionization potential (FIP) effect. We call such areas of heavy ion concentration the "ion traps." These traps hold enhanced ion levels until they are disrupted by a flare whether large or small. **February 15 2011, March 9 2011, September 6 2011 and July 12 2012.**

Cosmic Electrodynamics **Book**

Electrodynamics and Magnetic Hydrodynamics of Cosmic Plasmas
Gregory D. **Fleishman** • Igor N. Toptygin
Springer Science+Business Media New York **2013**
https://link.springer.com/content/pdf/10.1007%2F978-1-4614-5782-4.pdf

The UK in DKIST (Daniel K. Inouye Solar Telescope)

Lyndsay **Fletcher** (Glasgow), Mihalis Mathioudakis (Queen's University Belfast) and Erwin Verwichte
UKSP Nugget #60, Aug **2015**
http://www.uksolphys.org/uksp-nugget/60-the-uk-in-dkist/
The Daniel K. Inouye Solar Telescope is a 4m ground-based solar telescope currently under construction on the Haleakala mountain on the island of Maui, Hawai'i. It will be the largest solar telescope in the world by some way. The UK has now joined the DKIST project, providing the cameras for four of the DKIST instruments. This nugget gives an overview of the DKIST, the UK's contribution, and the opportunities for all UK solar physicists to get involved.

Structures in the outer solar atmosphere **Review**

Lyndsay **Fletcher**, Peter J. Cargill, Spiro K. Antiochos, Boris V. Gudiksen
Space Science Reviews Volume 188, Issue 1-4, pp 211-249 **2015**
http://arxiv.org/pdf/1412.7378v1.pdf **File**
The structure and dynamics of the outer solar atmosphere are reviewed with emphasis on the role played by the magnetic field. Contemporary observations that focus on high resolution imaging over a range of temperatures, as well as UV, EUV and hard X-ray spectroscopy, demonstrate the presence of a vast range of temporal and spatial scales, mass motions, and particle energies present. By focussing on recent developments in the chromosphere, corona and solar wind, it is shown that small scale processes, in particular magnetic reconnection, play a central role in determining the large-scale structure and properties of all regions. This coupling of scales is central to understanding the atmosphere, yet poses formidable challenges for theoretical models**. 15-07-202,** 9th March 2012**,**

First observations from the SPICE EUV spectrometer on Solar Orbiter

A. **Fludra**, M. Caldwell, A. Giunta, T. Grundy, S. Guest, S. Leeks, S. Sidher, F. Auchère, M. Carlsson, D. Hassler, H. Peter, R. Aznar Cuadrado, É. Buchlin, S. Caminade, C. DeForest, T. Fredvik, M. Haberreiter, L. Harra, M. Janvier, T. Kucera, D. Müller, S. Parenti, W. Schmutz, U. Schühle, S.K. Solanki, L. Teriaca, W.T. Thompson, S. Tustain, D. Williams, P.R. Young, L.P. Chitta
A&A **2021**
https://arxiv.org/pdf/2110.11252.pdf
We present first science observations taken during the commissioning activities of the Spectral Imaging of the Coronal Environment (SPICE) instrument on the ESA/NASA Solar Orbiter mission. SPICE is a high-resolution imaging spectrometer operating at extreme ultraviolet (EUV) wavelengths. In this paper we illustrate the possible types of observations to give prospective users a better understanding of the science capabilities of SPICE. The paper discusses the first observations of the Sun on different targets and presents an example of the full spectra from the quiet Sun, identifying over 40 spectral lines from neutral hydrogen and ions of carbon, oxygen, nitrogen, neon, sulphur, magnesium, and iron. These lines cover the temperature range between 20,000 K and 1 million K (10MK in flares), providing slices of the Sun's atmosphere in narrow temperature intervals. We provide a list of count rates for the 23 brightest spectral lines. We show examples of raster images of the quiet Sun in several strong transition region lines, where we have found unusually bright, compact structures in the quiet Sun network, with extreme intensities up to 25 times greater than the average intensity across the image. The lifetimes of these structures can exceed 2.5 hours. We identify them as a transition region signature of coronal bright points and compare their areas and intensity enhancements. We also show the first above-limb measurements with SPICE above the polar limb in C III, O VI, and Ne VIII lines, and far off limb measurements in the equatorial plane in Mg IX, Ne VIII, and O VI lines. We discuss the potential to use abundance diagnostics methods to study the variability of the elemental composition that can be compared with in situ measurements to help confirm the magnetic connection between the spacecraft location and the Sun's surface, and locate the sources of the solar wind. **21 April 2020, 14 May 2020, 28 May 2020, 17 June 2020, 26 March 2021**

DIAGNOSTICS OF CORONAL HEATING IN ACTIVE-REGION LOOPS

A. **Fludra**1, C. Hornsey1,2, and V. M. Nakariakov
2017 ApJ 834 100
Understanding coronal heating remains a central problem in solar physics. Many mechanisms have been proposed to explain how energy is transferred to and deposited in the corona. We summarize past observational studies that attempted to identify the heating mechanism and point out the difficulties in reproducing the observations of the solar corona from the heating models. The aim of this paper is to study whether the observed extreme ultraviolet (EUV) emission in individual coronal loops in solar active regions can provide constraints on the volumetric heating function, and to develop a diagnostic for the heating function for a subset of loops that are found close to static thermal equilibrium. We reconstruct the coronal magnetic field from Solar Dynamics Observatory/HMI data using a

nonlinear force-free magnetic field model. We model selected loops using a one-dimensional stationary model, with a heating rate dependent locally on the magnetic field strength along the loop, and we calculate the emission from these loops in various EUV wavelengths for different heating rates. We present a method to measure a power index β defining the dependence of the volumetric heating rate E H on the magnetic field, $E_H \propto B^{\beta}$, and controlling also the shape of the heating function: concentrated near the loop top, uniform and concentrated near the footpoints. The diagnostic is based on the dependence of the electron density on the index β. This method is free from the assumptions of the loop filling factor but requires spectroscopic measurements of the density-sensitive lines. The range of applicability for loops of different length and heating distributions is discussed, and the steps to solving the coronal heating problem are outlined.

Forecasting Solar Cycle 25 with Physical Model-Validated Recurrent Neural Networks

Aleix Espuña **Fontcuberta**, Anubhab Ghosh, Saikat Chatterjee, Dhrubaditya Mitra & Dibyendu Nandy
Solar Physics volume 298, Article number: 8 (**2023**)
https://link.springer.com/content/pdf/10.1007/s11207-022-02104-3.pdf
The Sun's activity, which is associated with the solar magnetic cycle, creates a dynamic environment in space known as space weather. Severe space weather can disrupt space-based and Earth-based technologies. Slow decadal-scale variations on solar-cycle timescales are important for radiative forcing of the Earth's atmosphere and impact satellite lifetimes and atmospheric dynamics. Predicting the solar magnetic cycle is therefore of critical importance for humanity. In this context, a novel development is the application of machine-learning algorithms for solar-cycle forecasting. Diverse approaches have been developed for this purpose; however, with no consensus across different techniques and physics-based approaches. Here, we first explore the performance of four different machine-learning algorithms – all of them belonging to a class called Recurrent Neural Networks (RNNs) – in predicting simulated sunspot cycles based on a widely studied, stochastically forced, nonlinear time-delay solar dynamo model. We conclude that the algorithm Echo State Network (ESN) performs the best, but predictability is limited to only one future sunspot cycle, in agreement with recent physical insights. Subsequently, we train the ESN algorithm and a modified version of it (MESN) with solar-cycle observations to forecast Cycles 22 – 25. We obtain accurate hindcasts for Solar Cycles 22 – 24. For Solar Cycle 25 the ESN algorithm forecasts a peak amplitude of 131 ± 14 sunspots around July 2024 and indicates a cycle length of approximately 10 years. The MESN forecasts a peak of 137 ± 2 sunspots around April 2024, with the same cycle length. Qualitatively, both forecasts indicate that Cycle 25 will be slightly stronger than Cycle 24 but weaker than Cycle 23. Our novel approach bridges physical model-based forecasts with machine-learning-based approaches, achieving consistency across these diverse techniques.

Bright Network, UVA, and the Physical Modeling of Solar Spectral and Total Irradiance in Recent Solar Cycles

J. M. **Fontenla**1,2 and E. Landi3
2018 ApJ 861 120
http://sci-hub.tw/http://iopscience.iop.org/0004-637X/861/2/120/
In this paper we study the total solar irradiance (TSI) and the spectral solar irradiance (SSI) by applying the solar disk image decomposition algorithm (SDIDA) and solar irradiance synthesis algorithm (SISA) methods. These methods were applied to space-based observations in previous works, but in this work, they are applied to ground-based observations from various observatories, which allows for a long-term determination of TSI and SSI. We discuss the results of the SDIDA and SISA methods for the areas of solar features and the synthesized TSI and SSI. We find that SDIDA decompositions based on Ca ii K line images from various sources are all in good agreement between them and with previous space results when cross-calibration is performed, and consequently yield essentially the same TSI and SSI when SISA is applied. This paper shows the synthesized TSI and SSI, as well as the contributions from various feature types, during the recent solar cycles 23 and 24 and suggest further work can provide historical extended coverage using archival ground-based observations. The results demonstrate the presence of a significant variable bright network contribution during the cycle maximum, and of a reduced one at solar minimum, and that such a presence and variability affect both the SSI and TSI. We also find that all activity features are loosely correlated over solar cycle variations, but this correlation is nonlinear, and we show differences between cycles 23 and 24. Furthermore, we find that the SISA method can be successfully applied to determine the TSI and SSI for any particular state of the solar disk, and that the results depend not only on the total areas on the disk for each feature, but also on the relative distances from disk center of the active region features.

FIVE YEARS OF SYNTHESIS OF SOLAR SPECTRAL IRRADIANCE FROM SDID/SISA AND SDO/AIA IMAGES

J. M. **Fontenla**1, M. Codrescu2, M. Fedrizzi3, T. Fuller-Rowell3, F. Hill4, E. Landi5, and T. Woods6
2017 ApJ 834 54
In this paper we describe the synthetic solar spectral irradiance (SSI) calculated from 2010 to 2015 using data from the Atmospheric Imaging Assembly (AIA) instrument, on board the Solar Dynamics Observatory spacecraft. We used the algorithms for solar disk image decomposition (SDID) and the spectral irradiance synthesis algorithm

(SISA) that we had developed over several years. The SDID algorithm decomposes the images of the solar disk into areas occupied by nine types of chromospheric and 5 types of coronal physical structures. With this decomposition and a set of pre-computed angle-dependent spectra for each of the features, the SISA algorithm is used to calculate the SSI. We discuss the application of the basic SDID/SISA algorithm to a subset of the AIA images and the observed variation occurring in the 2010–2015 period of the relative areas of the solar disk covered by the various solar surface features. Our results consist of the SSI and total solar irradiance variations over the 2010–2015 period. The SSI results include soft X-ray, ultraviolet, visible, infrared, and far-infrared observations and can be used for studies of the solar radiative forcing of the Earth's atmosphere. These SSI estimates were used to drive a thermosphere–ionosphere physical simulation model. Predictions of neutral mass density at low Earth orbit altitudes in the thermosphere and peak plasma densities at mid-latitudes are in reasonable agreement with the observations. The correlation between the simulation results and the observations was consistently better when fluxes computed by SDID/SISA procedures were used.

Solar Spectral Irradiance, Solar Activity, and the Near-ultra-violet

J. M. **Fontenla**1, P. C. Stancil2, and E. Landi
2015 ApJ 809 157
The previous calculations of the Solar Spectral Irradiance (SSI) by the Solar Radiation Physical Modeling, version 2 system, are updated in this work by including new molecular photodissociation cross-sections of important species, and many more levels and lines in its treatment of non-LTE radiative transfer. The current calculations including the new molecular photodissociation opacities produce a reduced over-ionizaton of heavy elements in the lower chromosphere and solve the problems with prior studies of the UV SSI in the wavelength range 160–400 nm and now reproduce the available observations with much greater accuracy. Calculations and observations of the near-UV at 0.1 nm resolution and higher are compared. The current set of physical models includes four quiet-Sun and five active-region components, from which radiance is computed for ten observing angles. These radiances are combined with images of the solar disk to obtain the SSI and Total Solar Irradiance and their variations. The computed SSI is compared with measurements from space at several nm resolution and agreement is found within the accuracy level of these measurements. An important result is that the near-UV SSI increase with solar activity is significant for the photodissociation of ozone in the terrestrial atmosphere because a number of highly variable upper chromospheric lines overlap the ozone Hartley band.

Data reduction pipeline for MOF-based synoptic telescopes

Roberta **Forte**1,2,3, Francesco Berrilli1, Daniele Calchetti1, Dario Del Moro1, Bernhard Fleck, +
J. Space Weather Space Clim. **2020**, 10, 63
https://www.swsc-journal.org/articles/swsc/pdf/2020/01/swsc200064.pdf
There are strong scientific cases and practical reasons for building ground-based solar synoptic telescopes. Some issues, like the study of solar dynamics and the forecasting of solar flares, benefit from the 3D reconstruction of the Sun’s atmosphere and magnetic field. Others, like the monitoring and prediction of space weather, require full disk observations, at the proper sampling rate, combining H-alpha images and Doppler velocity and magnetic field. The synoptic telescopes based on Magneto Optical Filters (MOF) using different lines are capable of measuring the line-of-sight Doppler velocity and magnetic field over the full solar disk at different ranges of height in the Sun’s photosphere and low chromosphere. Instruments like the MOTH (Magneto-Optical filters at Two Heights), using a dual-channel based on MOFs operating at 589.0 nm (Na D2 line) and 769.9 nm (K D1 line), the VAMOS instrument (Velocity And Magnetic Observations of the Sun), operating at 769.9 nm (K D1 line), and the future TSST (Tor Vergata Synoptic Solar Telescope), using a dual-channel telescope operating at 656.28 nm (H-alpha line) and at 769.9 nm (K D1 line), allow to face both aspects, the scientific and the operative related to Space Weather applications. The MOTH, VAMOS and TSST data enable a wide variety of studies of the Sun, from seismic probing of the solar interior (sound speed, rotation, details of the tachocline, sub-surface structure of active regions), to the dynamics and magnetic evolution of the lower part of the solar atmosphere (heating of the solar atmosphere, identification of the signatures of solar eruptive events, atmospheric gravity waves, etc.), to the 3D reconstruction of the solar atmosphere and flare locations. However, the use of MOF filters requires special care in calibrating the data for scientific or operational use. This work presents a systematic pipeline that derives from the decennial use of MOF’s technology. More in detail, the pipeline is based on data reduction procedures tested and validated on MOTH data acquired at Mees Solar Observatory of the University of Hawaii Haleakala Observatories and at South Pole Solar Observatory (SPSO), at the Amundsen-Scott South Pole Station in Antarctica, during Antarctica Summer Campaign 2016/17.

More about solar g modes

E. **Fossat** and F. X. Schmider
A&A 612, L1 (**2018**)
https://www.aanda.org/articles/aa/pdf/2018/04/aa32626-18.pdf

Context. The detection of asymptotic solar g-mode parameters was the main goal of the GOLF instrument onboard the SOHO space observatory. This detection has recently been reported and has identified a rapid mean rotation of the solar core, with a one-week period, nearly four times faster than all the rest of the solar body, from the surface to the bottom of the radiative zone.
Aim. We present here the detection of more g modes of higher degree, and a more precise estimation of all their parameters, which will have to be exploited as additional constraints in modeling the solar core.
Methods. Having identified the period equidistance and the splitting of a large number of asymptotic g modes of degrees 1 and 2, we test a model of frequencies of these modes by a cross-correlation with the power spectrum from which they have been detected. It shows a high correlation peak at lag zero, showing that the model is hidden but present in the real spectrum. The model parameters can then be adjusted to optimize the position (at exactly zero lag) and the height of this correlation peak. The same method is then extended to the search for modes of degrees 3 and 4, which were not detected in the previous analysis.
Results. g-mode parameters are optimally measured in similar-frequency bandwidths, ranging from 7 to 8 μHz at one end and all close to 30 μHz at the other end, for the degrees 1 to 4. They include the four asymptotic period equidistances, the slight departure from equidistance of the detected periods for l = 1 and l = 2, the measured amplitudes, functions of the degree and the tesseral order, and the splittings that will possibly constrain the estimated sharpness of the transition between the one-week mean rotation of the core and the almost four-week rotation of the radiative envelope. The g-mode periods themselves are crucial inputs in the solar core structure helioseismic investigation.

Asymptotic g modes: Evidence for a rapid rotation of the solar core

E. **Fossat**1, P. Boumier2, T. Corbard1, J. Provost1, D. Salabert3, F. X. Schmider1, A. H. Gabriel2, G. Grec1, C. Renaud1, J. M. Robillot4, T. Roca-Cortés5,6, S. Turck-Chièze7, R. K. Ulrich8 and M. Lazrek9
A&A 604, A40 (**2017**)
https://www.aanda.org/articles/aa/pdf/2017/08/aa30460-17.pdf
https://arxiv.org/pdf/1708.00259.pdf
Context. Over the past 40 years, helioseismology has been enormously successful in the study of the solar interior. A shortcoming has been the lack of a convincing detection of the solar gmodes, which are oscillations driven by gravity and are hidden in the deepest part of the solar body – its hydrogen-burning core. The detection of g modes is expected to dramatically improve our ability to model this core, the rotational characteristics of which have, until now, remained unknown.
Aims. We present the identification of very low frequency g modes in the asymptotic regime and two important parameters that have long been waited for: the core rotation rate, and the asymptotic equidistant period spacing of these g modes.
Methods. The GOLF instrument on board the SOHO space observatory has provided two decades of full-disk helioseismic data. The search for g modes in GOLF measurements has been extremely difficult because of solar and instrumental noise. In the present study, the p modes of the GOLF signal are analyzed differently: we search for possible collective frequency modulations that are produced by periodic changes in the deep solar structure. Such modulations provide access to only very low frequency g modes, thus allowing statistical methods to take advantage of their asymptotic properties.
Results. For oscillatory periods in the range between 9 and nearly 48 h, almost 100 g modes of spherical harmonic degree 1 and more than 100 g modes of degree 2 are predicted. They are not observed individually, but when combined, they unambiguously provide their asymptotic period equidistance and rotational splittings, in excellent agreement with the requirements of the asymptotic approximations. When the period equidistance has been measured, all of the individual frequencies of each mode can be determined. Previously, p-mode helioseismology allowed the g-mode period equidistance parameter P0 to be bracketed inside a narrow range, between approximately 34 and 35 min. Here, P0 is measured to be 34 min 01 s, with a 1 s uncertainty. The previously unknown g-mode splittings have now been measured from a non-synodic reference with very high accuracy, and they imply a mean weighted rotation of 1277 ± 10 nHz (9-day period) of their kernels, resulting in a rapid rotation frequency of 1644 ± 23 nHz (period of one week) of the solar core itself, which is a factor 3.8 ± 0.1faster than the rotation of the radiative envelope.
Conclusions. The g modes are known to be the keys to a better understanding of the structure and dynamics of the solar core. Their detection with these precise parameters will certainly stimulate a new era of research in this field.
See **A Critical Evaluation of Recent Claims Concerning Solar Rotation**
P.H. **Scherrer**, D.O. Gough
ApJ **2019**
https://arxiv.org/pdf/1904.02820.pdf

Large-Scale Spatial Cross-Calibration of Hinode/SOT-SP and SDO/HMI

David F. **Fouhey**, Richard E. L. Higgins, Spiro K. Antiochos, Graham Barnes, Marc L. DeRosa, J. Todd Hoeksema, K. D. Leka, Yang Liu, Peter W. Schuck, Tamas I. Gombosi
ApJS **264** 49 **2023**
https://arxiv.org/pdf/2209.15036
https://iopscience.iop.org/article/10.3847/1538-4365/aca539/pdf
We investigate the cross-calibration of the Hinode/SOT-SP and SDO/HMI instrument meta-data, specifically the correspondence of the scaling and pointing information. Accurate calibration of these datasets gives the correspondence needed by inter-instrument studies and learning-based magnetogram systems, and is required for physically-meaningful photospheric magnetic field vectors. We approach the problem by robustly fitting geometric models on correspondences between images from each instrument's pipeline. This technique is common in computer vision, but several critical details are required when using scanning slit spectrograph data like Hinode/SOT-SP. We apply this technique to data spanning a decade of the Hinode mission. Our results suggest corrections to the published Level 2 Hinode/SOT-SP data. First, an analysis on approximately 2,700 scans suggests that the reported pixel size in Hinode/SOT-SP Level 2 data is incorrect by around 1%. Second, analysis of over 12,000 scans show that the pointing information is often incorrect by dozens of arcseconds with a strong bias. Regression of these corrections indicates that thermal effects have caused secular and cyclic drift in Hinode/SOT-SP pointing data over its mission. We offer two solutions. First, direct co-alignment with SDO/HMI data via our procedure can improve alignments for many Hinode/SOT-SP scans. Second, since the pointing errors are predictable, simple post-hoc corrections can substantially improve the pointing. We conclude by illustrating the impact of this updated calibration on derived physical data products needed for research and interpretation. Among other things, our results suggest that the pointing errors induce a hemispheric bias in estimates of radial current density.

A Remarkably Accurate Predictor of Sunspot Cycle Amplitude

Peter **Foukal**
2023
https://arxiv.org/ftp/arxiv/papers/2307/2307.03047.pdf
The area ratios of sunspots to white light faculae in the first two years of sunspot cycles 12-21 correlate remarkably well with the peak amplitudes of those cycles between 1878-1980 (Brown and Evans, 1980). This finding could not be used to predict subsequent cycle amplitudes because the Royal Greenwich Observatory program of facular area measurements was discontinued in 1976. We use continuum images from the Michelson Doppler Imager (MDI) and the Heliospheric and Magnetic Imager (HMI) to show that the close relation holds also for cycle 24, and we predict an amplitude of approximately 185 for the current cycle 25.

Learned infinite elements for helioseismology -- Learning transparent boundary conditions for the solar atmosphere

Damien **Fournier**, Janosch Preuss, Thorsten Hohage, Laurent Gizon
A&A **2024**
https://arxiv.org/pdf/2402.08059.pdf
Context. Acoustic waves in the Sun are affected by the atmospheric layers, but this region is often ignored in forward models due to the increase in computational cost. Aims. The purpose of this work is to take into account the solar atmosphere without increasing significantly the computational cost. Methods. We solve a scalar wave equation that describes the propagation of acoustic modes inside the Sun using a finite element method. The boundary conditions used to truncate the computational domain are learned from the Dirichlet-to-Neumann operator, that is the relation between the solution and its normal derivative at the computational boundary. These boundary conditions may be applied at any height above which the background medium is assumed to be radially symmetric. Results. Taking into account the atmosphere is important even for wave frequencies below the acoustic cut-off. In particular, the mode frequencies computed for an isothermal atmosphere differ by up 10 {\mu}Hz from those computed for the VAL-C atmospheric model. We show that learned infinite elements lead to a numerical accuracy similar to that obtained for a traditional radiation boundary condition. Its main advantage is to reproduce the solution for any radially symmetric atmosphere to a very good accuracy at a low computational cost. Conclusions. This work emphasizes the importance of including atmospheric layers in helioseismology and proposes a computationally efficient method to do so.

Viscous inertial modes on a differentially rotating sphere: Comparison with solar observations⋆

Damien **Fournier**1, Laurent Gizon1,2,3 and Laura Hyest1,4
A&A 664, A6 (**2022**)
https://www.aanda.org/articles/aa/pdf/2022/08/aa43473-22.pdf

Context. In a previous paper, we studied the effect of latitudinal rotation on solar equatorial Rossby modes in the β-plane approximation. Since then, a rich spectrum of inertial modes has been observed on the Sun, which is not limited to the equatorial Rossby modes and includes high-latitude modes.
Aims. Here we extend the computation of toroidal modes in 2D to spherical geometry using realistic solar differential rotation and including viscous damping. The aim is to compare the computed mode spectra with the observations and to study mode stability.
Methods. At a fixed radius, we solved the eigenvalue problem numerically using a spherical harmonics decomposition of the velocity stream function.
Results. Due to the presence of viscous critical layers, the spectrum consists of four different families: Rossby modes, high-latitude modes, critical-latitude modes, and strongly damped modes. For each longitudinal wavenumber $m \leq 3$, up to three Rossby-like modes are present on the sphere, in contrast to the equatorial β plane where only the equatorial Rossby mode is present. The least damped modes in the model have eigenfrequencies and eigenfunctions that resemble the observed modes; the comparison improves when the radius is taken in the lower half of the convection zone. For radii above $0.75\,R_\odot$ and Ekman numbers $E < 10^{-4}$, at least one mode is unstable. For either $m = 1$ or $m = 2$, up to two Rossby modes (one symmetric and one antisymmetric) are unstable when the radial dependence of the Ekman number follows a quenched diffusivity model ($E \approx 2 \times 10^{-5}$ at the base of the convection zone). For $m = 3$, up to two Rossby modes can be unstable, including the equatorial Rossby mode.
Conclusions. Although the 2D model discussed here is highly simplified, the spectrum of toroidal modes appears to include many of the observed solar inertial modes. The self-excited modes in the model have frequencies close to those of the observed modes with the largest amplitudes.

Delayed Babcock-Leighton dynamos in the diffusion-dominated regime

Y. **Fournier**, R. Arlt, D. Elstner
A&A **2018**
https://arxiv.org/pdf/1808.08135.pdf
Context. Solar dynamo models of Babcock-Leighton type typically assume the rise of magnetic flux tubes to be instantaneous. Solutions with high-magnetic-diffusivity have too short periods and a wrong migration of their active belts. Only the low-diffusivity regime with advective meridional flows is usually considered.
Aims. In the present paper we discuss these assumptions and applied a time delay in the source term of the azimuthally averaged induction equation. This delay is set to be the rise time of magnetic flux tubes which supposedly form at the tachocline. We study the effect of the delay, which adds to the spacial non-locality a non-linear temporal one, in the advective but particularly in the diffusive regime.
Methods. Fournier et al. (2017) obtained the rise time according to stellar parameters such as rotation, and the magnetic field strength at the bottom of the convection zone. These results allowed us to constrain the delay in the mean-field model used in a parameter study.
Results. We identify an unknown family of solutions. These solutions self-quench, and exhibit longer periods than their non-delayed counterparts. Additionally, we demonstrate that the non-linear delay is responsible for the recover of the equatorward migration of the active belts at high turbulent diffusivities.
Conclusions. By introducing a non-linear temporal non-locality (the delay) in a Babcock-Leighton dynamo model, we could obtain solutions quantitatively comparable to the solar butterfly diagram in the diffusion-dominated regime.

Sensitivity kernels for time-distance helioseismology: efficient computation for spherically-symmetric solar models

Damien **Fournier**, Chris S. Hanson, Laurent Gizon, Helene Barucq
2018
https://arxiv.org/pdf/1805.06141.pdf
The interpretation of helioseismic measurements, such as wave travel-time, is based on the computation of kernels that give the sensitivity of the measurements to localized changes in the solar interior. These are computed using the ray or the Born approximation. The Born approximation is preferable as it takes finite-wavelength effects into account, but can be computationally expensive. We propose a fast algorithm to compute travel-time sensitivity kernels under the assumption that the background solar medium is spherically symmetric. Kernels are typically expressed as products of Green's functions that depend upon depth, latitude and longitude. Here, we compute the spherical harmonic decomposition of the kernels and show that the integrals in latitude and longitude can be performed analytically. In particular, the integrals of the product of three associated Legendre polynomials can be computed thanks to the algorithm of Dong and Lemus (2002). The computations are fast and accurate and only require the knowledge of the Green's function where the source is at the pole. The computation time is reduced by two orders of magnitude compared to other recent computational frameworks. This new method allows for flexible and computationally efficient calculations of a large number of kernels, required in addressing key helioseismic problems. For example, the computation of all the kernels required for meridional flow inversion takes less than two hours on 100 cores.

Atmospheric radiation boundary conditions for high frequency waves in time-distance helioseismology

Damien **Fournier**, Michael Leguebe, Chris S. Hanson, Laurent Gizon, Helene Barucq, Juliette Chabassier, Marc Durufle

A&A 608, A109 **2017**

https://arxiv.org/pdf/1709.02156.pdf

The temporal covariance between seismic waves measured at two locations on the solar surface is the fundamental observable in time-distance helioseismology. Above the acoustic cut-off frequency (~5.3~mHz), waves are not trapped in the solar interior and the covariance function can be used to probe the upper atmosphere. We wish to implement appropriate radiative boundary conditions for computing the propagation of high-frequency waves in the solar atmosphere. We consider the radiative boundary conditions recently developed by Barucq et al. (2017) for atmospheres in which sound-speed is constant and density decreases exponentially with radius. We compute the cross-covariance function using a finite element method in spherical geometry and in the frequency domain. The ratio between first- and second-skip amplitudes in the time-distance diagram is used as a diagnostic to compare boundary conditions and to compare with observations. We find that a boundary condition applied 500 km above the photosphere and derived under the approximation of small angles of incidence accurately reproduces the `infinite atmosphere' solution for high-frequency waves. When the radiative boundary condition is applied 2 Mm above the photosphere, we find that the choice of atmospheric model affects the time-distance diagram. In particular, the time-distance diagram exhibits double-ridge structure when using a VAL atmospheric model.

3D simulations of rising magnetic flux tubes in a compressible rotating interior: The effect of magnetic tension

Yori **Fournier**, Rainer Arlt, Udo Ziegler, Klaus G. Strassmeier

A&A **2017**

https://arxiv.org/pdf/1707.06781.pdf

Context: Long-term variability in solar cycles represents a challenging constraint for theoretical models. Mean-field Babcock-Leighton dynamos that consider non-instantaneous rising flux tubes have been shown to exhibit long-term variability in their magnetic cycle. However a relation that parameterizes the rise-time of non-axisymmetric magnetic flux tubes in terms of stellar parameters is still missing. Aims: We aim to find a general parameterization of the rise-time of magnetic flux tubes for solar-like stars. Methods: By considering the influence of magnetic tension on the rise of non-axisymmetric flux tubes, we predict the existence of a control parameter referred as Γα2α1. This parameter is a measure of the balance between rotational effects and magnetic effects (buoyancy and tension) acting on the magnetic flux tube. We carry out two series of numerical experiments (one for axisymmetric rise and one for non-axisymmetric rise) and demonstrate that Γα2α1 indeed controls the rise-time of magnetic flux tubes. Results: We find that the rise-time follows a power law of Γα2α1 with an exponent that depends on the azimuthal wavenumber of the magnetic flux loop. Conclusions: Compressibility does not impact the rise of magnetic flux tubes, while non-axisymmetry does. In the case of non-axisymmetric rise, the tension force modifies the force balance acting on the magnetic flux tube. We identified the three independent parameters required to predict the rise-time of magnetic flux tubes, that is, the stellar rotation rate, the magnetic flux density of the flux tube, and its azimuthal wavenumber. We combined these into one single relation that is valid for any solar-like star. We suggest using this generalized relation to constrain the rise-time of magnetic flux tubes in Babcock-Leighton dynamo models.

Generalization of the noise model for time-distance helioseismology

Damien **Fournier**, Laurent Gizon, Thorsten Hohage, Aaron C. Birch

A&A, 567, A137, **2014**,

http://arxiv.org/pdf/1406.5335v1.pdf

In time-distance helioseismology, information about the solar interior is encoded in measurements of travel times between pairs of points on the solar surface. Travel times are deduced from the cross-covariance of the random wave field. Here we consider travel times and also products of travel times as observables. They contain information about e.g. the statistical properties of convection in the Sun. The basic assumption of the model is that noise is the result of the stochastic excitation of solar waves, a random process which is stationary and Gaussian. We generalize the existing noise model (Gizon and Birch 2004) by dropping the assumption of horizontal spatial homogeneity. Using a recurrence relation, we calculate the noise covariance matrices for the moments of order 4, 6, and 8 of the observed wave field, for the moments of order 2, 3 and 4 of the cross-covariance, and for the moments of order 2, 3 and 4 of the travel times. All noise covariance matrices depend only on the expectation value of the cross-covariance of the observed wave field. For products of travel times, the noise covariance matrix consists of three terms proportional to 1/T, 1/T2, and 1/T3, where T is the duration of the observations. For typical observation times of a

few hours, the term proportional to 1/T2 dominates and Cov[τ1τ2,τ3τ4]≈Cov[τ1,τ3]Cov[τ2,τ4]+Cov[τ1,τ4]Cov[τ2,τ3], where the τi are arbitrary travel times. This result is confirmed for p1 travel times by Monte Carlo simulations and comparisons with SDO/HMI observations. General and accurate formulae have been derived to model the noise covariance matrix of helioseismic travel times and products of travel times. These results could easily be generalized to other methods of local helioseismology, such as helioseismic holography and ring diagram analysis.

The 2020 Senior Review of the Heliophysics Operating Missions

Nicola J. **Fox**

2020

https://science.nasa.gov/science-pink/s3fs-public/atoms/files/SeniorReview2020_Final_TAGGED.pdf

Editorial: Topical Volume on Developing the Solar Probe Plus Mission

Nicola J. **Fox**, David J. McComas

Space Science Reviews Volume 204, Issue 1, pp 1–6 **2016**

http://link.springer.com/article/10.1007/s11214-016-0323-7

The Solar Probe Plus Mission: Humanity's First Visit to Our Star

N. J. **Fox** , M. C. Velli, S. D. Bale, R. Decker, A. Driesman, R. A. Howard, J. C. Kasper, J. Kinnison, M. Kusterer and 5 more

Space Science Reviews Volume 204, Issue 1, pp 7–48 **2016** **Open Access**

Solar Probe Plus (SPP) will be the first spacecraft to fly into the low solar corona. SPP's main science goal is to determine the structure and dynamics of the Sun's coronal magnetic field, understand how the solar corona and wind are heated and accelerated, and determine what processes accelerate energetic particles. Understanding these fundamental phenomena has been a top-priority science goal for over five decades, dating back to the 1958 Simpson Committee Report. The scale and concept of such a mission has been revised at intervals since that time, yet the core has always been a close encounter with the Sun. The mission design and the technology and engineering developments enable SPP to meet its science objectives to: (1) Trace the flow of energy that heats and accelerates the solar corona and solar wind; (2) Determine the structure and dynamics of the plasma and magnetic fields at the sources of the solar wind; and (3) Explore mechanisms that accelerate and transport energetic particles. The SPP mission was confirmed in March 2014 and is under development as a part of NASA's Living with a Star (LWS) Program. SPP is scheduled for launch in mid-2018, and will perform 24 orbits over a 7-year nominal mission duration. Seven Venus gravity assists gradually reduce SPP's perihelion from 35 solar radii (RS) for the first orbit to <10 RS for the final three orbits. In this paper we present the science, mission concept and the baseline vehicle for SPP, and examine how the mission will address the key science questions

Segmentation of spectroscopic images of the low solar atmosphere by the Self Organizing Map technique

Schillirò **Francesco**, Romano Paolo

MNRAS **2021**

https://arxiv.org/pdf/2102.11595

We describe the application of Semantic Segmentation by using the Self Organizing Map technique to an high spatial and spectral resolution dataset acquired along the Hα line at 656.28 nm by the Interferometric Bi-dimensional Spectrometer installed at the focus plane of the Dunn Solar Telescope. This machine learning approach allowed us to identify several features corresponding to the main structures of the solar photosphere and chromosphere. The obtained results show the capability and flexibility of this method to identifying and analyzing the fine structures which characterize the solar activity in the low atmosphere. This is a first successful application of the SOM technique to astrophysical data sets.

Travel time classification of extreme solar events: Two families and an outlier,

Freed, A. J., and C. T. Russell (**2014**),

*Geophys. Res. Lett., Volume 41, Issue 19, pages 6590–6594, **2014***

Extreme solar events are of great interest because of the extensive damage that could be experienced by technological systems such as electrical transformers during such periods. In studying geophysical phenomena, it is helpful to have a quantitative measure of event strength so that similar events can be intercompared. Such a measure also allows the calculation of the occurrence rates of events with varying strength. We use historical fast travel time

solar events to develop a measure of strength based on the Sun-Earth trip time. We find that these fast events can be grouped into two distinct families with one even faster outlier. That outlier is not the Carrington event of 1859 but the extremely intense solar particle event of August 1972.

Predicting relationships between solar jet variables

Leonard A **Freeman**

2019

https://arxiv.org/ftp/arxiv/papers/1904/1904.08289.pdf

Studies of spicules and similar solar jets have revealed a strong correlation between some of the kinematic variables, particularly between the initial velocity V, and the subsequent deceleration, a. It has been proposed that this is caused by, and offers proof for a shock wave mechanism acting on the spicules. However it is shown here that these correlations arise simply from the statistics of the sample of spicules being studied, for example in the range of spicule heights. The relationship between two kinematic variables has been expressed as a linear equation but there is no general agreement on the actual linear equation, which shows wide variations. The reason for these variations is analysed and it is shown how the different linear equations can be derived from the co-ordinates of a single point: the mean spicule height and deceleration of the group of spicules being studied. Another method sometimes used is to determine the correlation coefficient of two of the kinematic variables from their scatter plots . It is shown how this too can be calculated from the sample statistics. The problems of the linear equations for the (a,V) correlation disappear if a square law relationship is used instead, which also provides a simple physical interpretation of the results. The implications of these results and the possibility that spicule behaviour is partly due to magnetic fields are discussed.

Spicules: velocity, acceleration and scatter plots

Leonard A **Freeman**

2017

https://arxiv.org/pdf/1704.07925.pdf

Spicules and other solar jets such as bright points and fibrils generally show a parabolic height-time relationship, which means that each spicule has a constant deceleration. However the deceleration is only constant for a particular spicule and varies widely from one spicule or jet to another. Nonetheless the careful observations of a number of researchers show that the distance - time relationship is parabolic to a high level of precision. The measurements for heights, maximum velocities, decelerations and flight times are normally presented as histograms or scatter plots, which allow some general trends to be observed. The published results show a clear correlation between the maximum velocity and the deceleration of spicules on scatter plots. This correlation has been claimed to show a linear relation between the acceleration and the maximum velocity of a jet. This linear relationship has been used to help model the mechanisms responsible for the jets. However it is proposed here that the relation between velocity and acceleration is given by the normal equations of motion for constant acceleration and consequently the relationship is non-linear. Other correlations are also examined and the implications for spicule mechanisms are considered.

On the properties of slow mhd sausage waves within small-scale photospheric magnetic structures

N. **Freij**, I. Dorotovic, R. J. Morton, M. S. Ruderman, V. Karlovsky, R. Erdekyi

ApJ **2015**

http://arxiv.org/pdf/1509.08680v1.pdf

The presence of magneto-acoustic waves in magnetic structures in the solar atmosphere is well-documented. Applying the technique of solar magneto-seismology (SMS) allows us to infer the background properties of these structures. Here, we aim to identify properties of the observed magneto-acoustic waves and study the background properties of magnetic structures within the lower solar atmosphere. Using the Dutch Open Telescope (DOT) and Rapid Oscillations in the Solar Atmosphere (ROSA) instruments, we captured two series of high-resolution intensity images with short cadence of two isolated magnetic pores. Combining wavelet analysis and empirical mode decomposition (EMD), we determined characteristic periods within the cross-sectional (i.e., area) and intensity time series. Then, by applying the theory of linear magnetohydrodynamics (MHD), we identified the mode of these oscillations within the MHD framework. Several oscillations have been detected within these two magnetic pores. Their periods range from 3 to 20 minutes. Combining wavelet analysis and EMD enables us to confidently find the phase difference between the area and intensity oscillations. From these observed features, we concluded that the detected oscillations can be classified as slow sausage MHD waves. Further, we determined several key properties of these oscillations such as the radial velocity perturbation, magnetic field perturbation and vertical wavenumber using solar magnetoseismology. The estimated range of the related wavenumbers reveals that these oscillations are trapped within these magnetic structures. Our results suggest that the detected oscillations are standing harmonics, and, this allows us to estimate the expansion factor of the waveguides by employing SMS. The calculated expansion factor ranges from 4-12. **12th August 2007, 22nd August 2008**

The Detection of Upwardly Propagating Waves Channeling Energy from the Chromosphere to the Low Corona

N. **Freij**1, E. M. Scullion2,3, C. J. Nelson1,4, S. Mumford1, S. Wedemeyer2, and R. Erdélyi
2014 ApJ 791 61
http://arxiv.org/pdf/1408.4621v1.pdf

There have been ubiquitous observations of wave-like motions in the solar atmosphere for decades. Recent improvements to space- and ground-based observatories have allowed the focus to shift to smaller magnetic structures on the solar surface. In this paper, high-resolution ground-based data taken using the Swedish 1 m Solar Telescope is combined with co-spatial and co-temporal data from the Atmospheric Imaging Assembly (AIA) on board the Solar Dynamics Observatory (SDO) satellite to analyze running penumbral waves (RPWs). RPWs have always been thought to be radial wave propagation that occurs within sunspots. Recent research has suggested that they are in fact upwardly propagating field-aligned waves (UPWs). Here, RPWs within a solar pore are observed for the first time and are interpreted as UPWs due to the lack of a penumbra that is required to support RPWs. These UPWs are also observed co-spatially and co-temporally within several SDO/AIA elemental lines that sample the transition region and low corona. The observed UPWs are traveling at a horizontal velocity of around 17 ± 0.5 km s–1 and a minimum vertical velocity of 42 ± 21 km s–1. The estimated energy of the waves is around 150 W m–2, which is on the lower bound required to heat the quiet-Sun corona. This is a new, yet unconsidered source of wave energy within the solar chromosphere and low corona.

Spectral characteristic of mid-term quasi-periodicities in sunspots data

P. **Frick**, D. Sokoloff, R. Stepanov, V. Pipin, I. Usoskin
MNRAS Volume 491, Issue 4, February **2020**, Pages 5572–5578, https://doi.org/10.1093/mnras/stz3238
https://arxiv.org/pdf/1911.06881.pdf

Numerous analyses suggest the existence of various quasi-periodicities in solar activity. The power spectrum of solar activity recorded in sunspot data is dominated by the ∼11-year quasi-periodicity, known as the Schwabe cycle. In the mid-term range (1 month -- 11 years) a pronounced variability known as a quasi-biennial oscillation (QBO) is widely discussed. In the shorter time scale a pronounced peak, corresponding to the synodic solar rotation period (∼ 27 days) is observed. Here we revisited the mid-term solar variability in terms of statistical dynamic of fully turbulent systems, where solid arguments are required to accept an isolated dominant frequency in a continuous (smooth) spectrum. For that, we first undertook an unbiased analysis of the standard solar data, sunspot numbers and the F10.7 solar radioflux index, by applying a wavelet tool, which allows one to perform a frequency-time analysis of the signal. Considering the spectral dynamics of solar activity cycle by cycle, we showed that no single periodicity can be separated, in a statistically significant manner, in the specified range of periods. We examine whether a model of solar dynamo can reproduce the mid-term oscillation pattern observed in solar data. We found that a realistically observed spectrum can be explained if small spatial (but not temporal) scales are effectively smoothed. This result is important because solar activity is a it global feature, although monitored via small-scale tracers like sunspots.

Recalculation of the Wolf Series from 1877 to 1893

Thomas K. **Friedli**
Solar Physics volume 295, Article number: 72 (**2020**)
https://link.springer.com/content/pdf/10.1007/s11207-020-01637-9.pdf

Homogeneity is considered as the most important property of the Wolf series of sunspot relative numbers, or Wolf numbers, since without a stable scale no valid conclusions about variations in the long-term progress of solar activity can be drawn. However, the homogeneity testing of the Wolf series is a difficult task, since the raw data entering the series and the methods of data-reduction and interpolation used to compile the series are largely unknown. In this article we reconstruct the data-reduction algorithms based on hitherto unpublished original sources from the archives of the former Swiss Federal Observatory in Zürich and discuss their impact on the homogeneity of the Wolf series. Based on Alfred Wolfer as reference, we recalculate the progress of the Wolf series from 1877 to 1893, correcting for the widely disregarded diminishing of Wolf's eyesight, for the change of Wolf's main instrument from the 40/700 mm Parisian refractor to the 42/800 mm Fraunhofer refractor, and for the inhomogeneities in the data-reduction procedure during the same time period. The maxima of Cycle 12 in 1884 and of Cycle 13 in 1893 are roughly 10% higher in the recalculated and corrected Wolf series than in the original Wolf series as provided by WDC-SILSO version 1.0. From 1877 to 1883 the smoothed monthly means of the recalculated and corrected Wolf series are up to a factor of 0.76 lower than the original values.

Sunspot Observations of Rudolf Wolf from 1849 – 1893

Thomas K. **Friedli**

Solar Phys. **2016**

The sunspot observations of Rudolf Wolf form the core of the Wolf series of sunspot relative numbers, or Wolf numbers, since his observations define the original scale of the series and also the main course of solar activity from 1849 to 1893. Unfortunately, the raw data for the years 1856 to 1869 were never published in full detail. The heritage group of the Rudolf Wolf Society in Switzerland digitized parts of the hitherto unpublished original source book of the Wolf series and put it on its website www.wolfinstitute.ch . Now, the Wolf numbers from 1849 to 1876, as provided by the World Data Center for Solar Index and Long-term Solar Observations (WDC-SILSO), can be reconstructed in every detail, since the source book contains all the raw sunspot group and individual spot numbers as well as the implemented calibration and interpolation methods. Thus, the observations made by Rudolf Wolf with the 83/1320 mm Fraunhofer refractor and with the 40/700 mm Parisian refractor as well as those made by Heinrich Schwabe can be identified and separated now. In this article, we describe Wolf's instruments and methods of observation. An inspection of the source book and other published sources reveals that the calibration factor of the 40/700 mm Parisian refractor should probably be lowered. Since no appropriate comparison observations are available, the scale transfer from Heinrich Schwabe to Rudolf Wolf has to be analyzed further.

Accelerated particle beams in a 3D simulation of the quiet Sun. Effects of advanced beam propagation modelling

L. **Frogner**, B. V. Gudiksen

A&A **2023**

https://arxiv.org/pdf/2311.00490.pdf

683, A195 (**2024**)

https://www.aanda.org/articles/aa/pdf/2024/03/aa48457-23.pdf

Context. Charged particles are constantly accelerated to non-thermal energies by the reconnecting magnetic field in the solar atmosphere. Our understanding of the interactions between the accelerated particles and their environment can benefit considerably from three-dimensional atmospheric simulations that account for non-thermal particle beam generation and propagation. In a previous publication, we presented the first results from such a simulation, which considers quiet Sun conditions. However, the original treatment of beam propagation ignores potentially important phenomena such as the magnetic gradient forces associated with a converging or diverging magnetic field.

Aims. Here we present a more general beam propagation model incorporating magnetic gradient forces, the return current, acceleration by the ambient electric field, corrected collision rates due to the ambient temperature, and collisions with heavier elements than hydrogen and the free electrons they contribute. Neglecting collisional velocity randomisation makes the model sufficiently lightweight to simulate millions of beams. We investigate how each new physical effect in the model changes the non-thermal energy transport in a realistic three-dimensional atmosphere.

Methods. We applied the method of characteristics to the steady-state continuity equation for electron flux to derive ordinary differential equations for the mean evolution of energy, pitch angle, and flux with distance. For each beam, we solved these numerically for a range of initial energies to obtain the evolving flux spectrum, from which we computed the energy deposited into the ambient plasma.

Results. Magnetic gradient forces significantly influence the spatial distribution of deposited beam energy. The magnetic field converges strongly with depth in the corona above loop footpoints. This convergence leads to a small coronal peak in deposited energy followed by a heavy dip caused by the onset of magnetic mirroring. Magnetically reflected electrons carry away 5 to 10% of the injected beam energy on average. The remaining electrons are relatively energetic and produce a peak in deposited energy below the transition region a few hundred kilometres deeper than they would in a uniform magnetic field. A diverging magnetic field at the beginning of the trajectory, which is common in the simulation, enhances the subsequent impact of magnetic mirroring. The other new physical effects do not qualitatively alter the picture of non-thermal energy transport for the atmospheric conditions under consideration.

Accelerated particle beams in a 3D simulation of the quiet Sun

L. **Frogner**, B. V. Gudiksen, H. Bakke

A&A 643, A27 **2020**

https://arxiv.org/pdf/2005.14483.pdf

https://doi.org/10.1051/0004-6361/202038529

Observational and theoretical evidence suggests that beams of accelerated particles are produced in flaring events of all sizes in the solar atmosphere, from X-class flares to nanoflares. Current models of such particles in flaring loops assume an isolated 1D atmosphere. A more realistic environment for modelling accelerated particles can be provided by 3D radiative magnetohydrodynamics codes. Here we present a simple model for particle acceleration and propagation in the context of a 3D simulation of the quiet solar atmosphere spanning from convection zone to corona. We then examine the additional transport of energy introduced by the particle beams. Locations of particle acceleration associated with magnetic reconnection are identified by detecting changes in magnetic topology. At each location, the parameters of the accelerated particle distribution are estimated from local conditions. The particle

distributions are then propagated along the magnetic field, and the energy deposition due to Coulomb collisions with the ambient plasma is computed. We find that particle beams originate in extended acceleration regions distributed across the corona. Upon reaching the transition region, they converge and produce strands of intense heating penetrating the chromosphere. Within these strands, beam heating consistently dominates conductive heating below the bottom of the transition region. This indicates that particle beams will qualitatively alter the energy transport even outside of active regions.
RHESSI Science Nugget #380 June **2020**
http://sprg.ssl.berkeley.edu/~tohban/wiki/index.php/Energy_transport_by_accelerated_particles_in_the_quiet_solar_atmosphere

Determination of time-dependent uncertainty of the total solar irradiance records from 1978 to present

Claus **Fröhlich**
J. Space Weather Space Clim. Volume 6, **2016** A18 **Open access**
Aims. The existing records of total solar irradiance (TSI) since 1978 differ not only in absolute values, but also show different trends. For the study of TSI variability these records need to be combined and three composites have been devised; however, the results depend on the choice of the records and the way they are combined. A new composite should be based on all existing records with an individual qualification. It is proposed to use a time-dependent uncertainty for weighting of the individual records.
Methods. The determination of the time-dependent deviation of the TSI records is performed by comparison with the square root of the sunspot number (SSN). However, this correlation is only valid for timescales of the order of a year or more because TSI and SSN react quite differently to solar activity changes on shorter timescales. Hence the results concern only periods longer than the one-year-low-pass filter used in the analysis.
Results. Besides the main objective to determine an investigator-independent uncertainty, the comparison of TSI with √SSN turns out to be a powerful tool for the study of the TSI long-term changes. The correlation of √SSN with TSI replicates very well the TSI minima, especially the very low value of the recent minimum. The results of the uncertainty determination confirm not only the need for adequate corrections for degradation, but also show that a rather detailed analysis is needed. The daily average of all TSI values available on that day, weighted with the correspondingly determined uncertainty, is used to construct a "new" composite, which, overall, compares well with the Physikalisch-Meteorologisches Observatorium Davos (PMOD) composite. Finally, the TSI − √SSN comparison proves to be an important diagnostic tool not only for estimating uncertainties of observations, but also for a better understanding of the long-term variability of TSI.

Total solar irradiance variability: What have we learned about its variability from the record of the last three solar cycles?

C. **Fröhlich**
Climate and Weather of the Sun-Earth System (CAWSES): Selected Papers from the 2007 Kyoto Symposium,
Edited by T. Tsuda, R. Fujii, K. Shibata, and M. A. Geller, pp. 217-230.

[Full text] (PDF 1.7 MB)

Implementing accelerated particle beams in a 3D simulation of the quiet Sun

L. **Frogner**, B. V. Gudiksen
A&A **2022**
https://arxiv.org/pdf/2210.01609
Context. The magnetic field in the solar atmosphere continually reconnects and accelerates charged particles to high energies. Simulations of the atmosphere in three dimensions that include the effects of accelerated particles can aid our understanding of the interplay between energetic particle beams and the environment where they emerge and propagate. We presented the first attempt at such a simulation in a previous paper, emphasising the physical model of particle beams. However, the numerical implementation of this model is not straightforward due to the diverse conditions in the atmosphere and the way we must distribute computation between multiple CPU cores. Aims. Here, we describe and verify our numerical implementation of energy transport by electron beams in a 3D magnetohydrodynamics code parallelised by domain decomposition. Methods. We trace beam trajectories using a Runge-Kutta scheme with adaptive step length control and integrate deposited beam energy along the trajectories with a hybrid analytical and numerical approach. To parallelise this, we coordinate beam transport across subdomains owned by separate processes using a buffering system designed to optimise data flow. Results. Using an ad hoc magnetic field with analytical field lines as a test scenario, we show that our parallel implementation of adaptive tracing efficiently follows a challenging trajectory with high precision. By timing executions of electron

beam transport with different numbers of processes, we found that the processes communicate with minimal overhead but that the parallel scalability is still sublinear due to workload imbalance caused by the uneven spatial distribution of beams.

Measurement of outflow velocities in plumes from EIS observations

Hui **Fu**, Lidong Xia, Bo Li, Zhenghua Huang, Fangran Jiao and Chaozhou MouLen
EIS Nugget, Oct **2014**
Following the discovery of persistent hot plasma upflows from the edges of solar active regions (ARs) by Hinode/XRT (Sakao et al., 2007) and EIS (Harra et al. 2008), much effort has been devoted to their study given the possibility that they may in fact be outflows and therefore contributors to the slow solar wind (SSW). Since the original observations, it has been shown that the plasma has temperature (Te) of 1 MK ² Te ² 2.5 MK, coronal AR composition, morphology differing from fan-loops where plasma is downflowing with Te ~ 0.6 MK and origin mainly at sites of Quasi-Separatrix Layers (QSLs) where magnetic reconnection between loops of high and low plasma density can drive the plasma upwards.

Measurements of Outflow Velocities in On-Disk Plumes from EIS Hinode Observations

Hui **Fu**, Lidong Xia, Bo Li, Zhenghua Huang, Fangran Jiao, Chaozhou Mou
ApJ, 794 109 **2014**
http://arxiv.org/pdf/1408.5473v1.pdf
The contribution of plumes to the solar wind has been subject to hot debate in the past decades. The EUV Imaging Spectrometer (EIS) on board Hinode provides a unique means to deduce outflow velocities at coronal heights via direct Doppler shift measurements of coronal emission lines. Such direct Doppler shift measurements were not possible with previous spectrometers. We measure the outflow velocity at coronal heights in several on-disk long-duration plumes, which are located in coronal holes and show significant blue shifts throughout the entire observational period. In one case, a plume is measured 4 hours apart. The deduced outflow velocities are consistent, suggesting that the flows are quasi-steady. Furthermore, we provide an outflow velocity profile along the plumes, finding that the velocity corrected for the line-of-sight effect can reach 10 km s−1 at 1.02R⊙, 15 km s−1 at 1.03 R⊙, and 25 km s−1 at 1.05 R⊙. This clear signature of steady acceleration, combined with the fact that there is no significant blue shift at the base of plumes, provides an important constraint on plume models. At the height of 1.03 R⊙, EIS also deduced a density of 1.3
×108 cm−3, resulting in a proton flux of about 4.2×109 cm−2s−1 scaled to 1AU, which is an order of magnitude higher than the proton input to a typical solar wind if a radial expansion is assumed. This suggests that, coronal hole plumes may be an important source of the solar wind.

Assessing the Observability of Deep Meridional Flow Cells in the Solar Interior

J. R. **Fuentes**1, Bradley W. Hindman1,2, Junwei Zhao3, Catherine C. Blume2, Maria E. Camisassa4, Nicholas A. Featherstone5, Thomas Hartlep6, Lydia Korre1, and Loren I. Matilsky7
2024 ApJ 961 78
https://iopscience.iop.org/article/10.3847/1538-4357/ad13f3/pdf
Meridional circulation regulates the Sun's interior dynamics and magnetism. While it is well accepted that meridional flows are poleward at the Sun's surface, helioseismic observations have yet to provide a definitive answer for the depth at which those flows return to the equator, or the number of circulation cells in depth. Here, we explore the observability of multiple circulation cells stacked in radius. Specifically, we examine the seismic signature of several meridional flow profiles by convolving time–distance averaging kernels with mean flows obtained from a suite of 3D hydrodynamic simulations. At mid and high latitudes, we find that weak flow structures in the deep convection zone can be obscured by signals from the much stronger surface flows. This contamination of 1–2 m s−1 is caused by extended side lobes in the averaging kernels, which produce a spurious equatorward signal with flow speeds that are 1 order of magnitude stronger than the original flow speeds in the simulations. At low latitudes, the flows in the deep layers of the simulations are stronger (>2 m s−1) and multiple cells across the convection zone can produce a sufficiently strong signal to survive the convolution process. Now that meridional flows can be measured over two decades of data, the uncertainties arising from convective noise have fallen to a level where they are comparable in magnitude to the systematic biases caused by nonlocal features in the averaging kernels. Hence, these systematic errors are beginning to influence current helioseismic deductions and need broader consideration.

The effect of nanoflare flows on EUV spectral lines

Marcelo López **Fuentes** , James A. Klimchuk
ApJ **939** 17 **2022**
https://arxiv.org/abs/2210.01896

https://iopscience.iop.org/article/10.3847/1538-4357/ac90c8/pdf
The nanoflare model of coronal heating is one of the most successful scenarios to explain, within a single framework, the diverse set of coronal observations available with the present instrument resolutions. The model is based on the idea that the coronal structure is formed by elementary magnetic strands which are tangled and twisted by the displacement of their photospheric footpoints by convective motions. These displacements inject magnetic stress between neighbor strands that promotes current sheet formation, reconnection, plasma heating, and possibly also particle acceleration. Among other features, the model predicts the ubiquitous presence of plasma flows at different temperatures. These flows should, in principle, produce measurable effects on observed spectral lines in the form of Doppler-shifts, line asymmetries and non-thermal broadenings. In this work we use a Two-Dimensional Cellular Automaton Model (2DCAM) developed in previous works, in combination with the Enthalpy Based Thermal Evolution of Loops (EBTEL) model, to analyze the effect of nanoflare heating on a set of known EUV spectral lines. We find that the complex combination of the emission from plasmas at different temperatures, densities and velocities, in simultaneously evolving unresolved strands, produces characteristic properties in the constructed synthetic lines, such as Doppler-shifts and non-thermal velocities up to tens of km s^{-1} for the higher analyzed temperatures. Our results might prove useful to guide future modeling and observations, in particular, regarding the new generation of proposed instruments designed to diagnose plasmas in the 5 to 10 MK temperature range.

LONG-TERM TREND OF SOLAR CORONAL HOLE DISTRIBUTION FROM 1975 TO 2014

K. **Fujiki**1, M. Tokumaru1, K. Hayashi1, D. Satonaka1, and K. Hakamada
2016 ApJ 827 L41
We developed an automated prediction technique for coronal holes using potential magnetic field extrapolation in the solar corona to construct a database of coronal holes appearing from 1975 February to 2015 July (Carrington rotations from 1625 to 2165). Coronal holes are labeled with the location, size, and average magnetic field of each coronal hole on the photosphere and source surface. As a result, we identified 3335 coronal holes and found that the long-term distribution of coronal holes shows a similar pattern known as the magnetic butterfly diagram, and polar/low-latitude coronal holes tend to decrease/increase in the last solar minimum relative to the previous two minima.

Relationship Between Solar Wind Speed and Coronal Magnetic Field Properties

Ken'ichi **Fujiki**, Munetoshi Tokumaru, Tomoya Iju, Kazuyuki Hakamada, Masayoshi Kojima
Solar Phys. **2015**
http://arxiv.org/pdf/1507.03301v2.pdf
We have studied the relationship between the solar-wind speed [V] and the coronal magnetic-field properties (a flux expansion factor [f] and photospheric magnetic-field strength [Bs]) at all latitudes using data of interplanetary scintillation and solar magnetic field obtained for 24 years from 1986 to 2009. Using a cross-correlation analyses, we verified that V is inversely proportional to f and found that V tends to increase with Bs if f is the same. As a consequence, we find that V has extremely good linear correlation with Bs/f. However, this linear relation of V and Bs/f cannot be used for predicting the solar-wind velocity without information on the solar-wind mass flux. We discuss why the inverse relation between V and f has been successfully used for solar-wind velocity prediction, even though it does not explicitly include the mass flux and magnetic-field strength, which are important physical parameters for solar-wind acceleration.

Revisiting Kunitomo's Sunspot Drawings during 1835-1836 in Japan

Masashi **Fujiyama**, Hisashi Hayakawa, Tomoya Iju, Toshiki Kawai, Shin Toriumi, Kenichi Otsuji, Katsuya Kondo, Yusaku Watanabe, Satoshi Nozawa, Shinsuke Imada
Solar Physics 294:43 **2019**
https://arxiv.org/ftp/arxiv/papers/1903/1903.03092.pdf
We revisit the sunspot drawings made by the Japanese astronomer Kunitomo Toubei during 1835-1836 and recount the sunspot group number for each image. There are two series of drawings, preliminary (P, containing 17 days with observations) and summary (S, covering 156 days with observations), all made using brush and ink. S is a compilation of drawings for the period from February 1835, to March 1836. Presently, the P drawings are available only for one month, September 1835; those of other periods have presumably been lost. Another drawing (I) lets us recover the raw group count (RGC) for 25 September 1836, on which the RGC has not been registered in the existing catalogs. We also revise the RGCs from P and S using the Zurich classification and determine that Kunitomo's results tend to yield smaller RGCs than those of other contemporary observers. In addition, we find that Kunitomo's RGCs and spot areas have a correlation (0.71) that is not very different from the contemporary observer Schwabe (0.82). Although Kunitomo's spot areas are much larger than those determined by Schwabe due to skill and instrument limitations, Kunitomo at least captured the growing trend of the spot activity in the early phase of the Solar Cycle 8. We also determine the solar rotation axis to estimate the accurate position (latitude and longitude) of the sunspot groups in Kunitomo's drawings.

Forward modelling of heating within a coronal arcade

L. E. **Fyfe**1, T. A. Howson1 and I. De Moortel1,2

A&A 656, A120 (**2021**)
https://www.aanda.org/articles/aa/pdf/2021/12/aa42028-21.pdf
https://doi.org/10.1051/0004-6361/202142028

Aims. We investigate the synthetic observational signatures generated from numerical models of coronal heating in an arcade in order to determine what features are associated with such heating and what tools can be used to identify them.
Methods. We consider two simulations of coronal arcades driven by footpoint motions with different characteristic timescales. Forward modelling is then conducted, and the synthetic emission data are analysed (e.g., intensities, Doppler shifts, line widths and estimated kinetic energies).
Results. The total intensity and Doppler shift perturbations clearly show the magnetic structure of the coronal arcade. Contrasts in the local Doppler velocity also highlight the locations of separatrix surfaces. The distinguishing feature of the models with short and long timescale photospheric motions (in comparison to the Alfvén travel time along a loop) is that of the frequencies. Through fast Fourier transform analysis of the Doppler velocities, it is clear that when short timescale footpoint motions are present, higher frequency perturbations are observed. For longer timescale footpoint motions, the dominant signal is that of lower frequencies; however, higher (but less powerful) frequencies were also detected, which matched the natural Alfvén frequency of the background magnetic field. Signatures of Alfvénic waves were identified in both models, with fast wave signatures observable when short timescale driving is present. Finally, we examine the estimates of the kinetic energy using the Doppler velocities and find it to be significantly underestimated within these models.
Conclusions. All of the observables within this article behave as one would expect, given the evolution of the plasma parameters. Such features were, for example, Alfvén waves, fast waves, the arcade structure and separatrix surfaces. We were able to differentiate between the two models by examining the frequencies present. The Doppler velocities cannot provide accurate estimates of the total kinetic energy or even the component parallel to the line-of-sight (LOS). This is due to some of the plasma being outside the formation temperature of the ion, the multi-directional driver limiting the proportion of the velocity aligned along the LOS, and cancellation of the velocity along the LOS. The exact impact each factor has on the estimation is dependent on the setup of the model and the emission line under investigation.

Investigating coronal wave energy estimates using synthetic non-thermal line widths

L. E. **Fyfe**1, T. A. Howson1, I. De Moortel1,2, V. Pant3 and T. Van Doorsselaere4

A&A 656, A56 (**2021**)
https://www.aanda.org/articles/aa/pdf/2021/12/aa41749-21.pdf
https://doi.org/10.1051/0004-6361/202141749

Aims. Estimates of coronal wave energy remain uncertain as a large fraction of the energy is likely hidden in the non-thermal line widths of emission lines. In order to estimate these wave energies, many previous studies have considered the root mean squared wave amplitudes to be a factor of $\sqrt{2}$ greater than the non-thermal line widths. However, other studies have used different factors. To investigate this problem, we consider the relation between wave amplitudes and the non-thermal line widths within a variety of 3D magnetohydrodynamic (MHD) simulations.
Methods. We consider the following 3D numerical models: Alfvén waves in a uniform magnetic field, transverse waves in a complex braided magnetic field, and two simulations of coronal heating in an arcade. We applied the forward modelling code FoMo to generate the synthetic emission data required to analyse the non-thermal line widths.
Results. Determining a single value for the ratio between the non-thermal line widths and the root mean squared wave amplitudes is not possible across multiple simulations. It was found to depend on a variety of factors, including line-of-sight angles, velocity magnitudes, wave interference, and exposure time. Indeed, some of our models achieved the values claimed in recent articles while other more complex models deviated from these ratios.
Conclusions. To estimate wave energies, an appropriate relation between the non-thermal line widths and root mean squared wave amplitudes is required. However, evaluating this ratio to be a singular value, or even providing a lower or upper bound on it, is not realistically possible given its sensitivity to various MHD models and factors. As the ratio between wave amplitudes and non-thermal line widths is not constant across our models, we suggest that this widely used method for estimating wave energy is not robust.

Forward modelling of MHD waves in braided magnetic fields⋆

L. E. **Fyfe**1, T. A. Howson1 and I. De Moortel1,2

A&A 643, A86 (**2020**)
https://doi.org/10.1051/0004-6361/202038945

Aims. We investigate synthetic observational signatures generated from numerical models of transverse waves propagating in complex (braided) magnetic fields.
Methods. We consider two simulations with different levels of magnetic field braiding and impose periodic, transverse velocity perturbations at the lower boundary. As the waves reflect off the top boundary, a complex pattern of wave interference occurs. We applied the forward modelling code FoMo and analysed the synthetic emission data. We examined the line intensity, Doppler shifts, and kinetic energy along several line-of-sight (LOS) angles.
Results. The Doppler shift perturbations clearly show the presence of the transverse (Alfvénic) waves. However, in the total intensity, and running difference, the waves are less easily observed for more complex magnetic fields and may be indistinguishable from background noise. Depending on the LOS angle, the observable signatures of the waves reflect some of the magnetic field braiding, particularly when multiple emission lines are available, although it is not possible to deduce the actual level of complexity. In the more braided simulation, signatures of phase mixing can be identified. We highlight possible ambiguities in the interpretation of the wave modes based on the synthetic emission signatures.
Conclusions. Most of the observables discussed in this article behave in the manner expected, given knowledge of the evolution of the parameters in the 3D simulations. Nevertheless, some intriguing observational signatures are present. Identifying regions of magnetic field complexity is somewhat possible when waves are present; although, even then, simultaneous spectroscopic imaging from different lines is important in order to identify these locations. Care needs to be taken when interpreting intensity and Doppler velocity signatures as torsional motions, as is done in our setup. These types of signatures are a consequence of the complex nature of the magnetic field, rather than real torsional waves. Finally, we investigate the kinetic energy, which was estimated from the Doppler velocities and is highly dependent on the polarisation of the wave, the complexity of the background field, and the LOS angles.

Magneto-Rossby Waves in the Solar Tachocline and the Annual Variations in Solar Activity

Tamar **Gachechiladze**1, Teimuraz V. Zaqarashvili1,2,3, Eka Gurgenashvili1,4, Giorgi Ramishvili1, Marc Carbonell5,6, Ramon Oliver6,7, and Jose Luis Ballester
2019 ApJ 874 162
sci-hub.se/10.3847/1538-4357/ab0955
https://arxiv.org/pdf/1904.12788.pdf
Annual oscillations have been detected in many indices of solar activity during many cycles. Recent multi-spacecraft observations of coronal bright points revealed slow retrograde toroidal phase drift (with the speed of ~3 m s−1) of 1 yr oscillations, which naturally suggested their connection with Rossby-type waves in the interior. We have studied, from a theoretical point of view, the dynamics of global magneto-Kelvin and magneto-Rossby waves in the solar tachocline with toroidal magnetic field. Using spherical coordinates, the dispersion relations of the waves and latitudinal structure of solutions were obtained analytically. We have also obtained the spectrum of unstable magneto-Rossby wave harmonics in the presence of the latitudinal differential rotation. Estimated periods and phase speeds show that the magneto-Rossby waves rather than the Kelvin waves match with the observations of 1 yr oscillations. On the other hand, Morlet wavelet analysis of Greenwich Royal Observatory sunspot areas for the solar cycle 23 has revealed multiple periodicities with periods of 450–460, 370–380, 310–320, 240–270, and 150–175 days in hemispheric and full disk data. Comparison of theoretical results with the observations allow us to conclude that the global magneto-Kelvin waves in the upper overshoot tachocline may be responsible for the periodicity of 450–460 days (~1.3 yr), while the remaining periods can be connected with different harmonics of global fast magneto-Rossby waves.
Erratum: **2020** ApJ 895 149 https://iopscience.iop.org/article/10.3847/1538-4357/ab9367/pdf

Exploring the Sun's core with BabyIAXO

Javier **Galan**
TAUP 2021 Proceedings **2021**
https://arxiv.org/pdf/2110.15668
Axions are a natural consequence of the Peccei-Quinn mechanism, the most compelling solution to the strong-CP problem. Similar axion-like particles (ALPs) also appear in a number of possible extensions of the Standard Model, notably in string theories. Both, axions and ALPs, are very well motivated candidates for Dark Matter (DM), and they would be copiously produced at the suns core. A relevant effort during the last two decades has been the CAST experiment at CERN, the most sensitive axion helioscope to date. The International Axion Observatory (IAXO) is a large-scale 4th generation helioscope, and its primary physics goal is to extend further the search for solar axions or ALPs with a final signal to background ratio of about 5 orders of magnitude higher.
We briefly review here the astrophysical hints and models that will be at reach while searching for solar axions within the context of the IAXO helioscope search program, and in particular the physics under reach for BabyIAXO, an intermediate helioscope stage towards the full IAXO.

Active region upflows II. Data driven magnetohydrodynamic modelling⋆

K. **Galsgaard**1, M. S. Madjarska2, K. Vanninathan3, Z. Huang4 and M. Presmann
A&A 584, A39 (**2015**)

Context. Observations of many active regions show a slow systematic outflow/upflow from their edges lasting from hours to days. At present no physical explanation has been proven, while several suggestions have been put forward.
Aims. This paper investigates one possible method for maintaining these upflows assuming, that convective motions drive the magnetic field to initiate them through magnetic reconnection.
Methods. We use Helioseismic and Magnetic Imager (HMI) data to provide an initial potential 3D magnetic field of the active region NOAA 11123 on 2010 November 13 where the characteristic upflow velocities are observed. A simple 1D hydrostatic atmospheric model covering the region from the photosphere to the corona is derived. Local correlation tracking of the magnetic features in the HMI data is used to derive a proxy for the time dependent velocity field. The time dependent evolution of the system is solved using a resistive 3D magnetohydrodynamic code.
Results. The magnetic field contains several null points located well above the photosphere, with their fan planes dividing the magnetic field into independent open and closed flux domains. The stressing of the interfaces between the different flux domains is expected to provide locations where magnetic reconnection can take place and drive systematic flows. In this case, the region between the closed and open flux is identified as the region where observations find the systematic upflows.
Conclusions. In the present experiment, the driving only initiates magneto-acoustic waves without driving any systematic upflows at any of the flux interfaces.

A Machine Learning Dataset Prepared From the NASA Solar Dynamics Observatory Mission

Richard **Galvez**, David F. Fouhey, Meng Jin, Alexandre Szenicer, Andrés Muñoz-Jaramillo, Mark C. M. Cheung, Paul J. Wright, Monica G. Bobra, Yang Liu, James Mason, Rajat Thomas
ApJ Supplement Series **242** 7 **2019**
https://arxiv.org/pdf/1903.04538.pdf
https://iopscience.iop.org/article/10.3847/1538-4365/ab1005/pdf

In this paper we present a curated dataset from the NASA Solar Dynamics Observatory (SDO) mission in a format suitable for machine learning research. Beginning from level 1 scientific products we have processed various instrumental corrections, downsampled to manageable spatial and temporal resolutions, and synchronized observations spatially and temporally. We illustrate the use of this dataset with two example applications: forecasting future EVE irradiance from present EVE irradiance and translating HMI observations into AIA observations. For each application we provide metrics and baselines for future model comparison. We anticipate this curated dataset will facilitate machine learning research in heliophysics and the physical sciences generally, increasing the scientific return of the SDO mission. This work is a direct result of the 2018 NASA Frontier Development Laboratory Program. Please see the appendix for access to the dataset. **2014-February-25**
Erratum 2020 ApJS 250 38 https://iopscience.iop.org/article/10.3847/1538-4365/aba82f/pdf

Multiscale statistical analysis of coronal solar activity

Diana **Gamborino**, Diego del-Castillo-Negrete, Julio J. Martinell
2016
http://arxiv.org/pdf/1601.07681v1.pdf

Multi-filter images from the solar corona are used to obtain temperature maps which are analyzed using techniques based on proper orthogonal decomposition (POD) in order to extract dynamical and structural information at various scales. Exploring active regions before and after a solar flare and comparing them with quiet regions we show that the multiscale behavior presents distinct statistical properties for each case that can be used to characterize the level of activity in a region. Information about the nature of heat transport is also be extracted from the analysis.

The Advanced Space-Based Solar Observatory (ASO-S)

Weiqun **Gan**, Cheng Zhu, Yuanyong Deng, Zhe Zhang, Bo Chen, +++
Solar Physics volume 298, Article number: 68 (**2023**)
https://doi.org/10.1007/s11207-023-02166-x

The Advanced Space-based Solar Observatory (ASO-S) was successfully launched at 23:43 UT on 8 October 2022. Here we describe the final technical status of the whole mission right before the launch, including the spacecraft platform and the three onboard payloads. The mission's science goals, organizations, preliminary performance in the commissioning phase, and the first-light results of the three payloads are briefly presented.
See http://aso-s.pmo.ac.cn/en_index.jsp

China's First Comprehensive Space Solar Observatory

Gan, W. Q. ; Zhu, C. ; Chen, B. ; Huang, Y.

Acta Astronomica Sinica, vol. 63, no. 6, article id. 60 **2022**

Being China's first comprehensive space solar observatory, ASO-S (Advanced Space-based Solar Observatory) has been launched into orbit at 7:43 on October 9, 2022. A brief introduction on ASO-S is presented here, including the background, scientific goals, payload deployments, mission assembly, and organizations. A short prospect is made for the operation of the mission and the future scientific output.

A Chinese solar observatory in space

W. Q. **Gan**, L. Feng & Y. Su

Nature Astronomy volume 6, page165 (**2022**)

https://www.nature.com/articles/s41550-021-01593-9.pdf

https://doi.org/10.1038/s41550-021-01593-9

https://www.nature.com/articles/s41550-021-01593-9

http://www.raa-journal.org/issues/all/2019/v19n11/

http://aso-s.pmo.ac.cn/en_index.jsp

Advanced Space-based Solar Observatory (ASO-S): an overview

Wei-Qun **Gan**, Cheng Zhu, Yuan-Yong Deng, Hui Li, Yang Su, Hai-Ying Zhang, Bo Chen, Zhe Zhang, Jian Wu, Lei Deng, ...

Research in Astronomy and Astrophysics (RAA) **2019** Vol. 19 No. 11, 156(8pp)

http://www.raa-journal.org/raa/index.php/raa/article/view/4428/4955

The Advanced Space-based Solar Observatory (ASO-S) is a mission proposed for the 25th solar maximum by the Chinese solar community. The scientific objectives are to study the relationships between the solar magnetic field, solar flares and coronal mass ejections (CMEs). Three payloads are deployed: the Full-disk vector MagnetoGraph (FMG), the Lyman-α Solar Telescope (LST) and the Hard X-ray Imager (HXI). ASO-S will perform the first simultaneous observations of the photospheric vector magnetic field, non-thermal imaging of solar flares, and the initiation and early propagation of CMEs on a single platform. ASO-S is scheduled to be launched into a 720 km Sun-synchronous orbit in 2022. This paper presents an overview of the mission till the end of Phase-B and the beginning of Phase-C.

ASO-S: Advanced Space-based Solar Observatory

Weiqun **Gan**, Yuanyong Deng, Hui Li, Jian Wu, Haiying Zhang, +++

Proceedings Volume 9604, Solar Physics and Space Weather Instrumentation VI; 96040T **2015**

https://doi.org/10.1117/12.2189062

https://sci-hub.ru/10.1117/12.2189062

ASO-S is a mission proposed for the 25th solar maximum by the Chinese solar community. The scientific objectives are to study the relationships among solar magnetic field, solar flares, and coronal mass ejections (CMEs). ASO-S consists of three payloads: Full-disk Magnetograph (FMG), Lyman-alpha Solar Telescope (LST), and Hard X-ray Imager (HXI), to measure solar magnetic field, to observe CMEs and solar flares, respectively. ASO-S is now under the phase-B studies. This paper makes a brief introduction to the mission.

The Future of Solar Neutrinos **Review**

G. D. Orebi **Gann**, K. Zuber, D. Bemmerer, A. Serenelli

Annu. Rev. Nucl. Part. Sci. **2021**. 71:1–39

https://doi.org/10.1146/annurev-nucl011921-061243

https://arxiv.org/pdf/2107.08613.pdf

In this article we review the current state of the field of solar neutrinos, including flavour oscillations, non-standard effects, solar models, cross section measurements, and the broad experimental program thus motivated and enabled. We discuss the historical discoveries that contributed to current knowledge, and define critical open questions to be addressed in the next decade. We discuss the state of the art of standard solar models, including uncertainties and problems related to the solar composition, and review experimental and model solar neutrino fluxes, including future prospects. We review the state of the art of the nuclear reaction data relevant for solar fusion in the proton-proton chain and carbon-nitrogen-oxygen cycle. Finally, we review the current and future experimental program that can address outstanding questions in this field.

Temporal evolution of axially standing kink motions in solar coronal slabs: An eigenfunction expansion approach

Yuhong **Gao**, Bo Li, Mijie Shi, Shaoxia Chen, Hui Yu
A&A 692, A259 **2024**
https://arxiv.org/pdf/2411.10011
https://www.aanda.org/articles/aa/pdf/2024/12/aa52139-24.pdf

We aim to provide more insights into the applicability to solar coronal seismology of the much-studied discrete leaky modes (DLMs) in classic analyses. Under linear ideal pressureless MHD, we examine two-dimensional (2D) axial fundamental kink motions that arise when localized velocity exciters impact some symmetric slab equilibria. Continuous structuring is allowed for. A 1D initial value problem (IVP) is formulated in conjunction with an eigenvalue problem (EVP) for laterally open systems, with no strict boundary conditions (BCs) at infinity. The IVP is solved by eigenfunction expansion, allowing a clear distinction between the contributions from proper eigenmodes and improper continuum eigenmodes. Example solutions are offered for parameters typical of active region loops. Our solutions show that the system evolves towards long periodicities due to proper eigenmodes (of order the axial Alfven time), whereas the interference of the improper continuum may lead to short periodicities initially (of order the lateral Alfven time). Specializing to the slab axis, we demonstrate that the proper contribution strengthens with the density contrast, but may occasionally be stronger for less steep density profiles. Short periodicities are not guaranteed in the improper contribution, the details of the initial exciter being key. When identifiable, these periodicities tend to agree with the oscillation frequencies expected for DLMs, despite the differences in the BCs between our EVP and classic analyses. The eigenfunction expansion approach enables all qualitative features to be interpreted as the interplay between the initial exciter and some response function, the latter solely determined by the equilibria. Classic theories for DLMs can find seismological applications, with time-dependent studies offering additional ways for constraining initial exciters.

Measurements of the solar coronal magnetic field based on coronal seismology with propagating Alfvenic waves: forward modeling

Yuhang **Gao**, Hui Tian, Tom Van Doorsselaere, Zihao Yang, Mingzhe Guo, Konstantinos Karampelas
Research in Astron. Astrophys. **2024**
https://arxiv.org/pdf/2411.08310

Recent observations have demonstrated the capability of mapping the solar coronal magnetic field using the technique of coronal seismology based on the ubiquitous propagating Alfvenic/kink waves through imaging spectroscopy. We established a magnetohydrodynamic (MHD) model of a gravitationally stratified open magnetic flux tube, exciting kink waves propagating upwards along the tube. Forward modeling was performed to synthesize the Fe XIII 1074.7 and 1079.8 nm spectral line profiles, which were then used to determine the wave phase speed, plasma density, and magnetic field with seismology method. A comparison between the seismologically inferred results and the corresponding input values verifies the reliability of the seismology method. In addition, we also identified some factors that could lead to errors during magnetic field measurements. Our results may serve as a valuable reference for current and future coronal magnetic field measurements based on observations of propagating kink waves.

Relationship between the Tilt Angles of Sunspot Groups and the Properties of the Next Solar Cycle

P. X. **Gao**1,2 and J. C. Xu1,2
2024 ApJ 974 268
https://iopscience.iop.org/article/10.3847/1538-4357/ad7118/pdf

Based on the data from the Kodaikanal and Mount Wilson observatories, we investigate the relationships of the tilt angles of sunspot groups, including the mean tilt angle and the tilt-angle scatter, during the declining phase with the parameters of the next solar cycle (SC). The main findings are summarized in the following three points. (1) During the declining phase, the correlation between the mean tilt angle and the tilt-angle scatter is statistically insignificant. (2) Six quantities measured during the declining phase show significant anticorrelations with the strength and amplitude of the next SC and positive correlations with the duration of the ascending phase of the next SC: the standard deviation of the tilt angles, the rms tilt angle, the mean absolute value of the tilt angles, the area-weighted absolute value of the tilt angles, the latitude-weighted absolute value of the tilt angles, and the area- and latitude-weighted absolute value of the tilt angles. (3) The correlations of the mean tilt angle, the area-weighted tilt angle, the latitude-weighted tilt angle, and the area- and latitude-weighted tilt angle during the declining phase with the strength, amplitude, and duration of the ascending phase of the next SC are statistically insignificant. These findings demonstrate that the modulation of the parameters of the next SC by the tilt-angle scatter during the declining phase plays a vital role in regulating SC variability.

Propagating kink waves in an open coronal magnetic flux tube with gravitational stratification: Magnetohydrodynamic simulation and forward modelling

Yuhang **Gao**1,2,⋆, Tom Van Doorsselaere2, Hui Tian1,⋆, Mingzhe Guo2,3 and Konstantinos Karampelas2

A&A, 689, A195 (**2024**)

https://www.aanda.org/articles/aa/pdf/2024/09/aa50769-24.pdf

Context. In coronal open-field regions, such as coronal holes, there are many transverse waves propagating along magnetic flux tubes, which are generally interpreted as kink waves. Previous studies have highlighted their potential role in coronal heating, solar wind acceleration, and seismological diagnostics of various physical parameters.
Aims. This study aims to investigate propagating kink waves, considering both vertical and horizontal density inhomogeneity, using 3D magnetohydrodynamic (MHD) simulations.
Methods. We established a 3D MHD model of a gravitationally stratified open flux tube, incorporating a velocity driver at the lower boundary to excite propagating kink waves. Forward modelling was conducted to synthesise observational signatures of the Fe IX 17.1 nm line.
Results. Resonant absorption and density stratification both affect the wave amplitude. When diagnosing the relative density profile with velocity amplitude, resonant damping needs to be properly considered to avoid a possible underestimation. In addition, unlike standing modes, propagating waves are believed to be Kelvin-Helmholtz stable. In the presence of vertical stratification, however, the phase mixing of transverse motions around the tube boundary can still induce small-scale structures, partially dissipating wave energy and leading to a temperature increase, especially at higher altitudes. Moreover, we conducted forward modeling to synthesise observational signatures, which revealed the promising potential of future coronal imaging spectrometers such as MUSE in resolving these wave-induced signatures. Also, the synthesised intensity signals exhibit apparent periodic variations, offering a potential method for indirectly observing propagating kink waves with current extreme ultraviolet imagers.

Detection of decayless oscillations in solar transition region loops L4

Yuhang **Gao**, Zhenyong Hou, Tom Van Doorsselaere and Mingzhe Guo

A&A Letter Volume 681, L4, January **2024**

https://doi.org/10.1051/0004-6361/202348702

https://www.aanda.org/articles/aa/pdf/2024/01/aa48702-23.pdf

Context. Decayless kink oscillations have been frequently observed in coronal loops, serving as a valuable diagnostic tool for the coronal magnetic field. Such oscillations have never before been reported in low-lying loops of the transition region (TR).
Aims. The aim of this study is to detect decayless kink oscillations in TR loops for the first time.
Methods. We used the SI IV 1400 Å imaging data obtained from the Interface Region Imaging Spectrograph. We applied the Multiscale Gaussian Normalization method to highlight the TR loops, and generated time–distance maps to analyse the oscillation signals.
Results. Seven oscillation events detected here exhibit a small but sustained displacement amplitude (0.04–0.10 Mm) for more than three cycles. Their periods range from 3 to 5 min. The phase speed is found to increase with loop length, which is consistent with the decrease in Alfvén speed with height. With these newly detected oscillations, we obtain a rough estimate of the magnetic field in the transition region, which is about 5–10 G.
Conclusions. Our results further reveal the ubiquity of decayless kink oscillations in the solar atmosphere. These oscillations in TR loops have the potential to be a diagnostic tool for the TR magnetic field. **2013/09/24, 2013/09/25&26, 2013/10/25, 2013/11/07, 2013/12/27**

Modelling of transverse oscillations driven by p-modes in short coronal loops

Yuhang **Gao**, Mingzhe Guo, Tom Van Doorsselaere, Hui Tian, Samuel J. Skirvin

ApJ **955** 73 **2023**

https://arxiv.org/pdf/2308.13813.pdf

https://iopscience.iop.org/article/10.3847/1538-4357/acf454/pdf

Recent observations have revealed two types of decayless transverse oscillations in short coronalloops: one with short periods scaling with loop lengths, and the other with longer periods that exhibit a peak at around 5 min in the period distribution. To understand such a difference in period, we work in the framework of ideal MHD and model a short coronal loop embedded in an atmosphere with density stratification from the chromosphere to the corona. An inclined p-mode-like driver with a period of 5 min is launched at one loop footpoint. It is discovered that two types of decayless transverse oscillations can be excited in the loop. We interpret the 5 min periodicity as being directly driven by the footpoint driver, while the others, with periods of several tens of seconds, are regarded as kink eigenmodes of different harmonics. Therefore, our simulation shows that both types of decayless oscillations found in observations can be excited by p-modes in one short coronal loop. This study extends our understanding of ubiquitous decayless transverse oscillations in the corona. Furthermore, it suggests that p-modes could be an important energy source for coronal heating by driving decayless transverse oscillations.

Cyclical Behaviors of Sunspot-Group Tilt Angles in Solar Cycles 21 – 23

Peng-Xin **Gao**

Solar Physics volume 298, Article number: 21 (**2023**)

https://doi.org/10.1007/s11207-023-02117-6

Based on the Debrecen Photoheliographic Data (DPD) sunspot catalog, we investigate the cyclical behaviors of tilt angles of all sunspot groups (SGs) and SGs with angular separation constraint S>2.5∘ in Solar Cycles (SCs) 21 – 23. It is found that, the cyclical behaviors of tilt angles during SC 23 are different from those of SCs 21 and 22, confirmed by using the SDD sunspot catalog where possible, which are embodied in the following five aspects: (i) For all SGs (SGs with separation constraint), the percentage of SGs with larger absolute values of tilt angles in the declining phase than during the maximum phase is about 80% (60%) in SCs 21 and 22. In SC 23, the percentage of SGs with larger absolute values of tilt angles during the declining phase is about 1.10 times (at least not lower than) that during the maximum. (ii) During SCs 21 – 23, the yearly mean of tilt angles decreases with time for all SGs (SGs with separation constraint) and the slopes of the linear regression lines are negative: −0.404, −0.910, and −0.740/−1.005 (−0.500, −1.138, and −0.764/−0.576). (iii) During SCs 21 and 22, the yearly mean of the absolute value of tilt angles generally decreases with time for all SGs (SGs with separation constraint) and the slopes of the linear regression lines also are negative: −0.347 and −0.451 (−0.504 and −0.397). (iv) During SC 23, for all SGs, the yearly mean of the absolute value of tilt angles generally increases with time and the slope of the linear regression line is positive: 0.281/0.429. For SGs with separation constraint, the linear regression line to the yearly mean of the absolute value of tilt angles is almost horizontal and its slope is −0.008/0.014. (v) The yearly mean of latitude of SGs decreases steadily with time during each SC.

Cyclical Behavior of Magnetically Complex Sunspot Groups and Major Flares in Solar Cycles 22 – 24

Peng-Xin **Gao** & Jing-Lan Xie

Solar Physics volume 297, Article number: 31 (**2022**)

https://link.springer.com/content/pdf/10.1007/s11207-022-01965-y.pdf

To better study the importance of the collision of different magnetic systems in generating magnetically complex sunspot groups and major (M- and X-class) flares, we define the index ALW: Area/LWArea/LW, where LW represents the latitudinal width of the sunspot group band, and AreaArea represents the total area of sunspot groups within the latitudinal width. Then, using the sunspot-group data collected by the United States Air Force/Mount Wilson Observatory and the flare data recorded by the Geostationary Operational Environmental Satellites, we investigate the variations of the ALW-index, the percentage of complex sunspot groups, and the percentage of major flares in the northern and southern hemispheres during Solar Cycles 22, 23, and 24. The main findings are reported as follows: First, in most cases, the maximum percentage of complex sunspot groups occurs after the maximum ALW is reached, and ALW starts to decrease. The result suggests that the collision of different magnetic systems cannot affect directly whether more complex sunspot groups are produced or more complex sunspot groups may be produced when there is a lower probability of the collision of different magnetic-flux systems, which does not support the suggestion of Jaeggli and Norton (Astrophys. J. Lett. 820, L11, 2016). Second, in most cases, the maximum percentage of complex sunspot groups occurs after the maximum percentage of major flares is reached, and the percentage of major flares starts to decrease, supporting the suggestion of Nikbakhsh et al. (Astron. Astrophys. 629, A45, 2019) – the large-scale dynamo peaks before the small-scale dynamo starts increasing, and the complex sunspot groups are linked to the small-scale dynamo taking over after the large-scale dynamo starts decreasing.

Curious Changes in Association of Complex Sunspot Groups with X-Ray Flares (≥M 1) in Solar Cycles 22–24

P. X. **Gao**1

2020 ApJ 894 77

https://doi.org/10.3847/1538-4357/ab8466

We investigate the variations in the probabilities of complex sunspot groups (SGs)—large, asymmetric, or δ-type SGs—producing X-ray flares (≥M 1) in solar cycles (SCs) 22, 23, and 24 based on the SG data collected by the United States Air Force/Mount Wilson Observatory and the flare data recorded by Geostationary Operational Environmental Satellites. The following are the main findings. (1) For complex SGs in the whole disk as well as the northern and southern hemispheres during SC 22, their numbers and probabilities of producing flares change almost synchronously. (2) For complex SGs during SC 23, probabilities of producing flares during the early declining phase in the whole disk do not decrease with decreasing complex SG number; in the northern hemisphere, the probability of producing flares during the declining phase is significantly higher than that during the maximum phase; in the southern hemisphere, there is no definite variation trend in the probabilities of producing flares during the maximum and declining phases. (3) For complex SGs during SC 24, the probabilities of producing flares during the later rising and early declining phases are significantly higher than or comparable to those during the maximum phase no matter how their numbers change; in the northern hemisphere, the probability of producing flares during the rising phase is

significantly higher than or at least comparable to that during the maximum phase; in the southern hemisphere, there is no definite variation trend in the probabilities of producing flares during the maximum and declining phases.

Phase Relation Between Large and Simple Sunspot Groups in Solar Cycles 22 – 24

Peng-Xin **Gao**
Solar Physics February **2020**, 295:23
https://doi.org/10.1007/s11207-020-1592-6
In order to investigate the phase relation between the temporal variations of sunspot groups of various classes, firstly we use the separation scheme that was introduced by Kilcik et al. (Solar Phys.289, 4365, 2014b) to separate sunspot groups into large sunspot groups (D, E, and F classes in the modified Zurich classification) and simple sunspot groups (A and B classes) in Solar Cycles 22 – 24 collected by the United States Air Force/Mount Wilson Observatory (USAF/MWL). Then, using lagged-cross-correlation analysis and the block-bootstrap method, we calculate the correlation coefficients against time lags and determine the statistical significance of phase relation between large and simple sunspot groups in Solar Cycles 22 – 24, respectively. The main results that we obtained are summarized as follows: i) During Solar Cycles 22 and 24, the results – large sunspot groups lead or lag simple sunspot groups – are statistically insignificant and large sunspot groups should be in phase with simple sunspot groups. ii) During Solar Cycle 23, large sunspot groups statistically significantly lag simple sunspot groups in temporal phase.

A High-Precision Flat Field Method Based on Image Stitching for Short Wavelength Instruments

XingJun **Gao**, Bo Chen, LingPing He & Xin Zheng
Solar Physics volume 295, Article number: 12 (**2020**)
https://link.springer.com/content/pdf/10.1007/s11207-020-1583-7.pdf
We present a method to obtain a large-scale flat field using only small offsets. The method is derived from the Kuhn, Lin, and Loranz (KLL) algorithm (Publ. Astron. Soc. Pacific103, 1097, 1991), but combined with the image stitching technique. Due to complementary images, which optimize and replace the bad edges, the accuracy is better than 0.1 root mean square across the full field of view, and the pixel-level relative error is also better than 0.1%. Another significant advantage is that its small sampling interval provides a rapid sampling time, while maintaining a large-scale and high-precision flat field (beyond 95% proportion). We have proved its high efficiency and robustness by simulating a cosine and a Gaussian CCD response and comparing the results with the KLL algorithm. Finally, a visible non-uniform target experiment with a uniform response was performed to prepare for the upcoming solar X-ray Extreme Ultraviolet Imager (X-EUVI) instrument on the FengYun-3 (FY-3) weather satellite series.

Variations and Regularities in the Hemispheric Distributions in Sunspot Groups of Various Classes

Peng-Xin **Gao**
Solar Physics May **2018**, 293:79
http://sci-hub.tw/http://link.springer.com/10.1007/s11207-018-1298-1
The present study investigates the variations and regularities in the distributions in sunspot groups (SGs) of various classes in the northern and southern hemispheres from Solar Cycles (SCs) 12 to 23. Here, we use the separation scheme that was introduced by Gao, Li, and Li (Solar Phys.292, 124, 2017), which is based on A/UA/U (A is the corrected area of the SG, and Uis the corrected umbral area of the SG), in order to separate SGs into simple SGs (A/U≤4.5A/U≤4.5) and complex SGs (A/U>6.2A/U>6.2). The time series of Greenwich photoheliographic results from 1875 to 1976 (corresponding to complete SCs 12 – 20) and Debrecen photoheliographic data during the period 1974 – 2015 (corresponding to complete SCs 21 – 23) are used to show the distributions of simple and complex SGs in the northern and southern hemispheres. The main results we obtain are reported as follows: i) the larger of the maximum annual simple SG numbers in the two hemispheres and the larger of the maximum annual complex SG numbers in the two hemispheres occur in different hemispheres during SCs 12, 14, 18, and 19; ii) the relative changing trends of two curves – cumulative SG numbers in the northern and southern hemispheres – for simple SGs are different from those for complex SGs during SCs 12, 14, 18, and 21; and iii) there are discrepancies between the dominant hemispheres of simple and complex SGs for SCs 12, 14, 18, and 21.

A Quantity Characterising Variation of Observed Magnetic Twist of Solar Active Regions

Yu **Gao**
Research in Astron. Astrophys **2017**
https://arxiv.org/pdf/1712.07833.pdf

An alternative parameter RJz is introduced as the ratio of one of two kinds of opposite-sign current to the total current and investigate the relationship between the quantity and the hemispheric sign rule of helicity (HSR) that is established by a series of previous statistical studies. The classification of current in each hemisphere is according to the following rule: If the product of the current and the corresponding longitudinal field component contributes a consistent sign with reference to the HSR, it is called "HSR-compliant" current, or else it is called "HSR-noncompliant" current. Firstly, the consistence between the butterfly diagram of the RJz and the current helicity was obtained in a statistical study. Active regions with RJz smaller than 0.5 tend to obey the HSR whereas those with RJz greater than 0.5 tend to disobey the HSR. The "HSRcompliant" current systems have 60% probability of realization compared to 40% of "HSR-noncompliant" current systems. Overall, the HSR is violated for active regions in which the "HSR-noncompliant" current is greater than the "HSR-compliant" current. Secondly, the RJz parameter was subsequently used to study the evolution of current systems in the case analyses of flare-productive active regions NOAA AR 11158 and 11283. It is found that there were "RJz -quasi-stationary" phase that is relatively flare quiescent and "RJz -dynamic" phase that is covered by the occurrence of large flares. **13-17 Feb 2011, 3-8 Sept 2011**

Possible Explanation of the Different Temporal Behaviors of Various Classes of Sunspot Groups

Peng-Xin **Gao**, Ke-Jun Li, Fu-Yu Li
Solar Physics September **2017**, 292:124
In order to investigate the periodicity and long-term trends of various classes of sunspot groups (SGs), we separated SGs into two categories: simple SGs (A/U≤4.5A/U≤4.5, where AArepresents the total corrected whole spot area of the group in millionths of the solar hemisphere (msh), and UU represents the total corrected umbral area of the group in msh); and complex SGs (A/U>6.2A/U>6.2). Based on the revised version of the Greenwich Photoheliographic Results sunspot catalogue, we investigated the periodic behaviors and long-term trends of simple and complex SGs from 1875 to 1976 using the Hilbert-Huang Transform method, and we confirm that the temporal behaviors of simple and complex SGs are quite different. Our main findings are as follows. i) For simple and complex SGs, the values of the Schwabe cycle wax and wane, following the solar activity cycle. ii) There are significant phase differences (almost antiphase) between the periodicity of 53.50±3.7953.50±3.79 years extracted from yearly simple SG numbers and the periodicity of 56.21±2.9256.21±2.92 years extracted from yearly complex SG numbers. iii) The adaptive trends of yearly simple and complex SG numbers are also quite different: for simple SGs, the values of the adaptive trend gradually increase during the time period of 1875 – 1949, then they decrease gradually from 1949 to 1976, similar to the rise and the maximum phase of a sine curve; for complex SGs, the values of the adaptive trend first slowly increase and then quickly increase, similar to the minimum and rise phase of a sine curve.

LONG-TERM TREND OF SUNSPOT NUMBERS

P. X. **Gao**
2016 ApJ 830 140
Using the Hilbert–Huang Transform method, we investigate the long-term trend of yearly mean total sunspot numbers in the time interval of 1700–2015, which come from the World Data Center—the sunspot Index and long-term solar observations. The main findings of this study are summarized below. (1) From the adaptive trend, which is extracted from the yearly mean total sunspot numbers, we can find that the value gradually increases during the time period 1700–1975, then decreases gradually from 1975 to 2015. (2) The Centennial Gleissberg Cycle is extracted from the yearly mean total sunspot numbers and confirms that a new grand minimum is in progress; the Dalton Minimum, the Gleissberg Minimum, and low level of solar activity during solar cycle 24 (the part of the new grand minimum) all can be understood as minima of the Centennial Gleissberg Cycle. (3) Based on the adaptive (overall) trend, and the 100-year and longer timescale trend of yearly mean total sunspot numbers, we can infer that the level of solar activity during the new grand minimum may be close to that during the Gleissberg Minimum, slightly higher than that during the Dalton Minimum, and significantly higher than that during the Maunder Minimum. Our results do not support the suggestion that a new grand minimum, somewhat resembling the Maunder Minimum, is in progress.

Phase Relationships Between the CME-Energy Cycle, the Sunspot-Area Cycle and the Flare-Index Cycle

P. X. **Gao**, J. L. Xie, J. Zhong
Solar Phys., Volume 289, Issue 5, pp 1831-1841. **2014**

We study the phase relationships between the coronal-mass-ejection (CME) energy cycle, the sunspot-area cycle, and the flare-index cycle from 1996 to 2010. The results show the following: i) The activity cycle of the flare index significantly leads the activity cycle of the sunspot area. ii) The activity cycle of the CME energy is inferred to be almost in phase with the activity cycle of the sunspot area; the activity cycle of the CME energy at low latitudes slightly leads the activity cycle of the sunspot area; the CME energy at high latitudes is shown to significantly lag behind the sunspot area. iii) The CME energy is shown to significantly lag behind the flare index; the CME energy at low latitudes is shown to slightly lag behind the flare index; the CME energy at high latitudes is shown to significantly lag behind the flare index.

The tachocline revisited **Review**

Pascale **Garaud**

Invited review for the meeting Dynamics of the Sun and Stars: Honoring the Life and Work of Michael J. Thompson (Boulder, Colorado, 24-26 September 2019 **2020**

https://arxiv.org/pdf/2004.02341.pdf

The solar tachocline is a shear layer located at the base of the solar convection zone. The horizontal shear in the tachocline is likely turbulent, and it is often assumed that this turbulence would be strongly anisotropic as a result of the local stratification. What role this turbulence plays in the tachocline dynamics, however, remains to be determined. In particular, it is not clear whether it would result in a turbulent eddy diffusivity, or anti-diffusivity, or something else entirely. In this paper, we present the first direct numerical simulations of turbulence in horizontal shear flows at low Prandtl number, in an idealized model that ignores rotation and magnetic fields. We find that several regimes exist, depending on the relative importance of the stratification, viscosity and thermal diffusivity. Our results suggest that the tachocline is in the stratified turbulence regime, which has very specific properties controlled by a balance between buoyancy, inertia, and thermal diffusion.

Seismic differences between solar magnetic cycles 23 and 24 for low-degree modes

R. A. **García1**⋆, S. N. Breton2,3, D. Salabert4, S. C. Tripathy5, K. Jain5, S. Mathur6,7 and E. Panetier3

A&A 691, L20 (**2024**)

https://www.aanda.org/articles/aa/pdf/2024/11/aa51949-24.pdf

Solar magnetic activity follows regular cycles of about 11 years with an inversion of polarity in the poles every ∼22 years. This changing surface magnetism impacts the properties of the acoustic modes. The acoustic mode frequency shifts are a good proxy of the magnetic cycle. In this Letter we investigate solar magnetic activity cycles 23 and 24 through the evolution of the frequency shifts of low-degree modes ($\ell = 0$, 1, and 2) in three frequency bands. These bands probe properties between 74 and 1575 km beneath the surface. The analysis was carried out using observations from the space instrument Global Oscillations at Low Frequency and the ground-based Birmingham Solar Oscillations Network and Global Oscillation Network Group. The frequency shifts of radial modes suggest that changes in the magnetic field amplitude and configuration likely occur near the Sun's surface rather than near its core. The maximum shifts of solar cycle 24 occurred earlier at mid and high latitudes (relative to the equator) and about 1550 km beneath the photosphere. At this depth but near the equator, this maximum aligns with the surface activity but has a stronger magnitude. At around 74 km deep, the behaviour near the equator mirrors the behaviour at the surface, while at higher latitudes, it matches the strength of cycle 23.

Asteroseismology of solar-type stars **Review**

Rafael A. **García**, Jérôme Ballot

Living Reviews in Solar Physics December **2019**, 16:4

https://link.springer.com/content/pdf/10.1007%2Fs41116-019-0020-1.pdf

Until the last few decades, investigations of stellar interiors had been restricted to theoretical studies only constrained by observations of their global properties and external characteristics. However, in the last 30 years the field has been revolutionized by the ability to perform seismic investigations of stellar interiors. This revolution begun with the Sun, where helioseismology has been yielding information competing with what can be inferred about the Earth's interior from geoseismology. The last two decades have witnessed the advent of asteroseismology of solar-like stars, thanks to a dramatic development of new observing facilities providing the first reliable results on the interiors of distant stars. The coming years will see a huge development in this field. In this review we focus on solar-type stars, i.e., cool main-sequence stars where oscillations are stochastically excited by surface convection. After a short introduction and a historical overview of the discipline, we review the observational techniques generally used, and we describe the theory behind stellar oscillations in cool main-sequence stars. We continue with a complete description of the normal mode analyses through which it is possible to extract the physical information about the structure and dynamics of the stars. We then summarize the lessons that we have learned and discuss unsolved issues and questions that are still unanswered.

Magnetic properties on the boundary of an evolving pore

M. **García-Rivas**1,2, J. Jurčák1 and N. Bello González3

A&A 649, A129 (**2021**)
https://www.aanda.org/articles/aa/pdf/2021/05/aa39661-20.pdf
https://doi.org/10.1051/0004-6361/202039661
Context. Analyses of the magnetic properties on umbrae boundaries have led to the Jurčák criterion, which states that umbra-penumbra boundaries in stable sunspots are equally defined by a constant value of the vertical magnetic field, Bvercrit, and by a 50% continuum intensity of the quiet Sun, IQS. Umbrae with vertical magnetic fields stronger than Bvercrit are stable, whereas umbrae with vertical magnetic fields weaker than Bvercrit are unstable and prone to vanishing.
Aims. We aim to investigate the existence of a critical value of the vertical magnetic field on a pore boundary and its role in the evolution of the magnetic structure.
Methods. We analysed SDO/HMI vector field maps corrected for scattered light and with a temporal cadence of 12 min during a 26.5-hour period. A continuum intensity threshold (Ic = 0.55 IQS) is used to define the pore boundary and we study the temporal evolution of the magnetic properties there.
Results. We observe well-defined stages in the pore evolution: (1) during the initial formation phase, total magnetic field strength (B) and vertical magnetic field (Bver) increase to their maximum values of ∼1920 G and ∼1730 G, respectively; (2) then the pore reaches a stable phase; (3) in a second formation phase, the pore undergoes a rapid growth in terms of size, along with a decrease in B and Bver on its boundary. In the newly formed area of the pore, Bver remains mostly below 1731 G and B remains everywhere below 1921 G; (4) ultimately, pore decay starts. We find overall that pore areas with Bver < 1731 G, or equivalently B < 1921 G, disintegrate faster than regions that fulfil this criteria.
Conclusions. We find that the most stable regions of the pore, similarly to the case of umbral boundaries, are defined by a critical value of the vertical component of the magnetic field that is comparable to that found in stable sunspots. In addition, in this case study, the same pore areas can be similarly well-defined by a critical value of the total magnetic field strength.

Energy Loss of Solar p Modes due to the Excitation of Magnetic Sausage Tube Waves: Importance of Coupling the Upper Atmosphere

A. **Gascoyne**1, R. Jain1, and B. W. Hindman
2014 ApJ 789 109
We consider damping and absorption of solar p modes due to their energy loss to magnetic tube waves that can freely carry energy out of the acoustic cavity. The coupling of p modes and sausage tube waves is studied in a model atmosphere composed of a polytropic interior above which lies an isothermal upper atmosphere. The sausage tube waves, excited by p modes, propagate along a magnetic fibril which is assumed to be a vertically aligned, stratified, thin magnetic flux tube. The deficit of p-mode energy is quantified through the damping rate, Γ, and absorption coefficient, α. The variation of Γ and α as a function of frequency and the tube's plasma properties is studied in detail. Previous similar studies have considered only a subphotospheric layer, modeled as a polytrope that has been truncated at the photosphere. Such studies have found that the resulting energy loss by the p modes is very sensitive to the upper boundary condition, which, due to the lack of an upper atmosphere, have been imposed in a somewhat ad hoc manner. The model presented here avoids such problems by using an isothermal layer to model the overlying atmosphere (chromosphere, and, consequently, allows us to analyze the propagation of p-mode-driven sausage waves above the photosphere. In this paper, we restrict our attention to frequencies below the acoustic cut off frequency. We demonstrate the importance of coupling all waves (acoustic, magnetic) in the subsurface solar atmosphere with the overlying atmosphere in order to accurately model the interaction of solar f and p modes with sausage tube waves. In calculating the absorption and damping of p modes, we find that for low frequencies, below 3.5 mHz, the isothermal atmosphere, for the two-region model, behaves like a stress-free boundary condition applied at the interface (z = –z 0).

Automated detection and analysis of coronal active region structures across Solar Cycle 24

Daniel Gordon **Gass**, Robert William Walsh
MNRAS Volume 532, Issue 1, July **2024**, Pages 965–981,
https://doi.org/10.1093/mnras/stae1528
https://arxiv.org/pdf/2305.11066.pdf
https://academic.oup.com/mnras/article-pdf/532/1/965/58389789/stae1528.pdf
Observations from the NASA Solar Dynamic Observatory Atmospheric Imaging Assembly were employed to investigate targeted physical properties of coronal active region structures across the entirety of Solar Cycle 24 (dates). This is the largest consistent study to date which analyses emergent trends in structural width, location, and occurrence rate by performing an automatic and long-term examination of observable coronal limb features within equatorial active region belts across four extreme ultraviolet wavelengths (171, 193, 211, and 304 angstroms). This has resulted in over thirty thousand observed coronal structures and hence allows for the production of spatial and temporal distributions focused upon the rise, peak and decay activity phases of Solar Cycle 24. Employing a self-organized-criticality approach as a descriptor of coronal structure formation, power law slopes of structural widths

versus frequency are determined, ranging from -1.6 to -3.3 with variations of up to 0.7 found between differing periods of the solar cycle, compared to a predicted Fractal Diffusive Self Organized Criticality (FD-SOC) value of -1.5. The North-South hemispheric asymmetry of these structures was also examined with the northern hemisphere exhibiting activity that is peaking earlier and decaying slower than the southern hemisphere, with a characteristic "butterfly" pattern of coronal structures detected. This represents the first survey of coronal structures performed across an entire solar cycle, demonstrating new techniques available to examine the composition of the corona by latitude in varying wavelengths at selected altitudes.

Solar Cycle Dependence of the Turbulence Cascade Rate at 1 au

Sujan Prasad **Gautam**1,2, Laxman Adhikari1,2, Gary P Zank1,2, Ashok Silwal1,2, and Lingling Zhao1,2
2024 ApJ 968 12
https://iopscience.iop.org/article/10.3847/1538-4357/ad4797/pdf
We study the solar cycle dependence of various turbulence cascade rates based on the methodology developed by Adhikari et al. that utilizes Kolmogorov phenomenology. This approach is extended to derive the heating rates for an Iroshnikov–Kriachnan (IK) phenomenology. The observed turbulence cascade rates corresponding to the total turbulence energy, fluctuating magnetic energy density, fluctuating kinetic energy, and the normalized cross helicity are derived from WIND spacecraft plasma and magnetometer data from 1995 through 2020. We find that (i) the turbulence cascade rate derived from a Kolmogorov phenomenology and an IK phenomenology changes with solar cycle, such that the cascade rate is largest during solar maximum and smallest during solar minimum; (ii) the turbulence energy Kolmogorov cascade rate increases from θUB (angle between mean magnetic field and velocity) = 0° to 90° and peaks near θUB = 90°, and then decreases as θUB tends to 180°; (iii) the 2D turbulence heating rate is larger than the slab heating rate; (iv) the 2D and slab fluctuating magnetic energy density cascade rates are larger than the corresponding cascade rates of the fluctuating kinetic energy; and (v) the total turbulence energy cascade rate is positively correlated with the solar wind speed and temperature and the normalized cross-helicity cascade rate. Finally, we find that the total turbulent energy Kolmogorov cascade rate is larger than the IK cascade rate.

Latitudinal Dynamics and Sectoral Structure of the Solar Magnetic Field

Elena **Gavryuseva**
2023 in Russian language
https://arxiv.org/ftp/arxiv/papers/2302/2302.04943.pdf
The study of the global structure of the large-scale magnetic field of the Sun is extremely important for creating a theoretical model of the dynamics of the Sun and predictions of the real situation in the helio- and geomagnetosphere. The purpose of the present study was to calculate the differential rotation period of a large-scale photospheric magnetic field, to study its behavior over time and to find out whether there is a sectoral structure of this field along the longitude. However, the choice of the coordinate system in which to search for it is far from unambiguous. This is closely related to the fact that the rotation of the Sun is differential in latitude and varies with depth and over time. Based on the observational data of the J. Wilcox Solar Observatory for three complete cycles of solar activity 21, 22 and 23, the period of rotation of the magnetic field at various latitudes and its change in time were calculated. A uniquely stable over 30 years longitude structure was found. It was determined that its speed of rotation coincides with the one with which the base of the convective shell rotates, that is, the structuring of the magnetic field of the Sun occurs in tachocline. This result clearly demonstrates the close connection of solar activity processes with the topology of magnetic fields, with their dynamics and depth stratification.

Relations between variability of the photospheric and interplanetary magnetic fields, solar wind and geomagnetic characteristics

E. A. **Gavryuseva** (Institute for Nuclear Research RAS)
2018
https://arxiv.org/pdf/1802.03135.pdf
Large scale solar magnetic field topology has a great influence on the structure of the corona, heliosphera and geomagnetic perturbations.
Data obtained over the last three solar cycles have been analysed to reveal the relationships between the photospheric field measured along the line of sight by the WSO group at 30 levels of heliolatitudes from -75 to 75 degrees and the interplanetary magnetic field The main aim of this first paper is to make a direct comparison between the basic structure and dynamics of the photospheric magnetic field and components and intensity of the interplanetary magnetic field % solar wind and geomagnetic parameters without using theoretical assumptions, models, physical expectations, etc.
The second paper by Gavryuseva, 2018d presents the raports between different characteristics of the solar wind at the Earth orbit, and geomagnetic parameters provided by the OMNI team. % Data obtained over the last three solar cycles have been analysed % to reveal the relationships % between the photospheric field measured along the line of sight % by the WSO group % at heliolatitudes from -75 to 75 degrees averaged over one year % and the interplanetary magnetic field, different characteristics % of the solar wind at the Earth orbit, and geomagnetic

parameters. % provided by the OMNI team.
The heliospheric and geomagnetic data are found to be divided into two groups characterized by their response to variability of the solar magnetic field latitudinal structures on short and on long time scales.

Longitudinal structure of the photospheric magnetic field in the Carrington system

E. A. **Gavryuseva** (Institute for Nuclear Research RAS)
2018
https://arxiv.org/pdf/1802.02692.pdf
The observations of the Sun have been performed over the years, even centuries- Whether are there active longitudes? If yes how stable are they? One of the first The Wilcox Solar Observatory data taken over three cycles N 21, N 22, N 23 have been used to reveal the longitudinal structure of the photospheric magnetic field. Mean over three cycles magnetic field distribution has been calculated in the North and in the South hemispheres as well as at 30 levels of latitude from -75 to 75 degrees. This study was performed using observations of the magnetic field taking into account its polarity or only intensity. The longitudinal structure of the magnetic field was calculated in the coordinate system rotating with Carrington rate. These structures were compared with a model of random longitudinal distribution of the magnetic field. Random character of the longitudinal structure was refused. The results agree with the presence of two active meridians seen in different phenomena of solar activity at longitudes separated by 150-170 degrees in the Carrington coordinate system.

Latitudinal structure and dynamic of the photospheric magnetic field

E. A. **Gavryuseva** (Institute for Nuclear Research RAS)
2018
https://arxiv.org/pdf/1802.02450.pdf
Analysis of the structure and dynamics of the magnetic field of the Sun is fundamental for understanding of the origin of solar activity and variability as well as for the study of solar-terrestrial relations. Observations of the large scale magnetic field in the photosphere taken at the Wilcox Solar Observatory from 1976 up to 2007 have been analysed to deduce its latitudinal and longitudinal structures, its differential rotation, and their variability in time. This paper is dedicated to the analysis and dynamics of the latitudinal structure of the solar magnetic field over three solar cycles 21, 22, 23. The main results discussed in this paper are the following: the large scale latitudinal structure is antisymmetric and composed of four zones with boundaries located at the equator, -25 and + 25 degrees, stable over 10-11 years with a time delay of about 5-6 years in near-equatorial zones. The variability and North-South asymmetry of polarity waves running from the equator to the poles with 2-3 - year period was studied in detail.

Rotation of the photospheric magnetic field through solar cycles 21, 22, 23

E. A. **Gavryuseva** (Institute for Nuclear Research RAS)
2018
https://arxiv.org/pdf/1802.02461.pdf
Rotation of the large scale solar magnetic field has a great importance for the understanding of solar dynamic, for the search of longitidinal structure and for the study of solar-terrestrial relations. 30-year long observations taken at the Wilcox Solar Observatory (USA) in 21-23 cycles have been analysed carefully to deduce magnetic field rotation rate at different latitudes in both hemispheres and its variability in time. The WSO data appear to indicate that additionally to the differential rotation along the latitudes there are running waves of fast rotation of the magnetic field. These torsional waves are running from the poles to the equator with a period of 11 years. The rotation of the magnetic field (RMF) is almost rigid at latitudes above 55 degrees in both hemispheres. The rotation rate in the sub-polar regions is slower when the magnetic field is strong there (during minima of solar activity), and faster when the magnetic field changes polarity (during maxima of solar activity).

Breaking Boundaries: A Universal Wavefront Reconstruction Approach for High-resolution Solar Imaging

Xinlan **Ge**1,2,3,4, Licheng Zhu1,2,3, Zeyu Gao1,2,3, Shiqing Ma1,2,3, Ao Li1,2,3,4, Shuai Wang1,2,3, and Ping Yang1,2,3
2024 ApJL 970 L1
https://iopscience.iop.org/article/10.3847/2041-8213/ad5b53/pdf
This Letter proposes a universal wavefront reconstruction approach based on a coupled data set and neural network, aiming to overcome the limitations of current algorithms in terms of universality and wavefront sensing accuracy for variable imaging objects. First, a novel data set, Multi-Object Wavefront Coupling Dataset (MOCD-Dataset), is developed to provide diverse data and enable the network to learn universal wavefront features. Next, a new universal wavefront reconstruction network called Object-Independent Wavefront Decoupling Network (OIWD-Net) is introduced, aiming to separate imaging object information from multiple variable images. Our algorithm eliminates the need for specialized wavefront sensors, has a simple system, high light energy utilization, and does

not require customized models for each different type of imaging objects, making it highly practical. By combining the MOCD-Dataset and the OIWD-Net, excellent accuracy in wavefront reconstruction of different imaging objects has been achieved. This research provides a new solution for high-resolution image restoration in fields such as solar structure observation and astronomical high-resolution imaging.

Quasimodes in the cusp continuum in nonuniform magnetic flux tubes

Michaël **Geeraerts**, Pieter Vanmechelen, Tom Van Doorsselaere, Roberto Soler
A&A **2022**
https://arxiv.org/pdf/2203.02359.pdf
The study of MHD waves is important both for understanding heating in the solar atmosphere and for solar atmospheric seismology. The analytical investigation of wave mode properties in a cylinder is of particular interest in this domain, as many atmospheric structures can be modeled as such in a first approximation. We use linearized ideal MHD to study quasimodes (global modes that are damped through resonant absorption) with a frequency in the cusp continuum, in a straight cylinder with a circular base and an inhomogeneous layer at its boundary which separates two homogeneous plasma regions inside and outside. We are in particular interested in the damping of these modes, and shall hence try to determine their frequency as a function of background parameters. After linearizing the ideal MHD equations, we find solutions to the second-order differential equation for the perturbed total pressure in the inhomogeneous layer in the form of Frobenius series around the regular singular points that are the Alfvén and cusp resonant positions, as well as power series around regular points. By connecting these solutions appropriately through the inhomogeneous layer and with the solutions of the homogeneous regions inside and outside the cylinder, we derive a dispersion relation for the frequency of the eigenmodes of the system. From the dispersion relation, it is also possible to find the frequency of quasimodes even though they are not eigenmodes. As an example, we find the frequency of the slow surface sausage quasimode as a function of the inhomogeneous layer's width, for values of the longitudinal wavenumber relevant for photospheric conditions. The results were found to match well the results found in another paper which studied the resistive slow surface sausage eigenmode. We also discuss the perturbation profiles of the quasimode and the eigenfunctions of continuum modes.

Stability of solar atmospheric structures harboring standing slow waves
An analytical model in a compressible plasma

M. **Geeraerts** and T. Van Doorsselaere
A&A 650, A144 (**2021**)
https://www.aanda.org/articles/aa/pdf/2021/06/aa40534-21.pdf
https://doi.org/10.1051/0004-6361/202140534
Context. In the context of the solar coronal heating problem, one possible explanation for the high coronal temperature is the release of energy by magnetohydrodynamic (MHD) waves. The energy transfer is believed to be possible, among others, by the development of the Kelvin-Helmholtz instability (KHI) in coronal loops.
Aims. Our aim is to determine if standing slow waves in solar atmospheric structures such as coronal loops, and also prominence threads, sunspots, and pores, can trigger the KHI due to the oscillating shear flow at the structure’s boundary.
Methods. We used linearized nonstationary MHD to work out an analytical model in a cartesian reference frame. The model describes a compressible plasma near a discontinuous interface separating two regions of homogeneous plasma, each harboring an oscillating velocity field with a constant amplitude which is parallel to the background magnetic field and aligned with the interface. The obtained analytical results were then used to determine the stability of said interface, both in coronal and photospheric conditions.
Results. We find that the stability of the interface is determined by a Mathieu equation. In function of the parameters of this equation, the interface can either be stable or unstable. For coronal as well as photospheric conditions, we find that the interface is stable with respect to the KHI. Theoretically, it can, however, be unstable with respect to a parametric resonance instability, although it seems physically unlikely. We conclude that, in this simplified setup, a standing slow wave does not trigger the KHI without the involvement of additional physical processes.

Effect of Electrical Resistivity on the Damping of Slow Sausage Modes

Michaël **Geeraerts**1, Tom Van Doorsselaere1, Shao-Xia Chen2, and Bo Li2
2020 ApJ 897 120
https://doi.org/10.3847/1538-4357/ab9b28
Recent observations of slow surface sausage modes in a photospheric magnetic pore have been shown to be heavily damped. Numerical calculations have shown that electrical resistivity plays a significant role in this damping process. The aim of the present paper is to make an independent analytical derivation that would confirm the importance of electrical resistivity in the damping of these modes. An analytical dispersion relation in the framework of resistive magnetohydrodynamics is derived for sausage modes in a straight cylinder with a circular cross section and a discontinuous boundary. The effect of electrical resistivity on the damping of slow sausage

modes in photospheric pore conditions is then studied, by solving the obtained dispersion relation numerically. The obtained results agree with those from the numerical calculations.

Modelling 3D magnetic networks in a realistic solar atmosphere

Frederick A. **Gent**, Ben Snow, Robertus Erdelyi, Viktor Fedun
MNRAS **2019**
https://arxiv.org/pdf/1904.11421.pdf
The magnetic network extending from the photosphere (solar radius \simeq R_\odot) to lower corona (R_\odot + 10 Mm) plays an important role in the heating mechanisms of the solar atmosphere. Here we further develop the models with realistic open magnetic flux tubes of Gent et al. (2013, 2014) in order to model more complicated configurations. Closed magnetic loops, and combinations of closed and open magnetic flux tubes are modelled. These are embedded within a realistic stratified atmosphere, subject to solar gravity and including the Interface Region. Constructing a magnetic field comprising self-similar magnetic flux tubes, an analytic solution for the kinetic pressure and plasma density is derived following Gent et al. (2014).
Combining flux tubes of opposite polarity it is possible to create a steady background magnetic field configuration modelling realistic solar atmosphere. The result can be applied to SOHO/MDI and SDO/HMI and other magnetograms from the solar surface, upon which realistic photospheric motions can be simulated to explore the mechanism of energy transport. We demonstrate this powerful and versatile method with an application to Helioseismic and Magnetic Imager data.

Solar Influences on the Earth's Atmosphere: Solved and Unsolved Questions **Review**

Katya **Georgieva**, and Svetlana Veretenenko
Front. Astron. Space Sci., 22 December **2023**, Volume 10 - 2023 , 1244402
https://doi.org/10.3389/fspas.2023.1244402
https://www.frontiersin.org/articles/10.3389/fspas.2023.1244402/pdf
The influence of the Sun on the Earth’s atmosphere and climate has been a matter of hot debate for more than two centuries. In spite of the correlations found between the sunspot numbers and various atmospheric parameters, the mechanisms for such influences are not quite clear yet. Though great progress has been recently made, a major problem remains: the correlations are not stable, they may strengthen, weaken, disappear, and even change sign depending on the time period. None of the proposed so far mechanisms explains this temporal variability. The basis of all solar activity is the solar magnetic field which cyclically oscillates between its two components—poloidal and toroidal. We first briefly describe the operation of the solar dynamo transforming the poloidal field into toroidal and back, the evaluated relative variations of these two components, and their geoeffective manifestations. We pay special attention to the reconstruction of the solar irradiance as the key natural driver of climate. We point at some problems in reconstructing the long-term irradiance variations and the implications of the different irradiance composite series on the estimation of the role of the Sun in climate change. We also comment on the recent recalibration of the sunspot number as the only instrumentally measured parameter before 1874, and therefore of crucial importance for reconstructing the solar irradiance variations and their role in climate change. We summarize the main proposed mechanisms of solar influences on the atmosphere, and list some of the modelling and experimental results either confirming or questioning them. Two irradiance-driven mechanisms have been proposed. The “bottom-up” mechanism is based on the enhanced absorption of solar irradiance by the oceans in relatively cloud-free equatorial and subtropical regions, amplified by changes in the temperature gradients, circulation, and cloudiness. The “top-down” mechanism involves absorption by the stratospheric ozone of solar UV radiation whose variability is much greater than that of the visible one, and changes of large-scale circulation patterns like the stratospheric polar vortex and the tropospheric North Atlantic Oscillation. The positive phase of the tropospheric North Atlantic Oscillation indicative of a strong vortex is found to lag by a couple of years the enhanced UV in Smax. It was however shown that this positive response is not due to lagged UV effects but instead to precipitating energetic particles which also peak a couple of years after Smax. The solar wind and its transients modulate the flux of galactic cosmic rays which are the main source of ionization of the Earth’s atmosphere below ∼50 km. This modulation leads to modulation of the production of aerosols which are cloud condensation nuclei, and to modulation of cloudiness. Increased cloudiness decreases the solar irradiance reaching the low atmosphere and the Earth’s surface. Variations of the galactic cosmic rays also lead to variations of the electric currents and the ionospheric potential in the polar caps which may intensify microphysical processes in clouds and thus also cause cloudiness variations. Solar energetic particles are produced during eruptive events at the Sun. They produce reactive odd hydrogen HOx and nitrogen NOx which catalytically destroy ozone in the mesosphere and upper stratosphere—“direct effect.” NOx which are long-lived in the lack of photoionization during the polar night, can descend to lower altitudes and destroy ozone there producing a delayed “indirect effect.” In the absence of sunlight ozone absorbs longwave outgoing radiation emitted by the Earth and atmosphere. Ozone depletion associated with ionization increases leads to cooling of the polar middle atmosphere, enhancing the temperature contrast between polar and midlatitudes and, thus, the strength of the stratospheric polar vortex. Solar energetic particles are powerful but sporadic and rare events. An additional source of energetic particles are the electrons trapped in the Earth’s magnetosphere which during geomagnetic disturbances are accelerated and precipitate into the atmosphere. They are

less energetic but are always present. Their effects are the same as that of the solar energetic particles: additional production of reactive HOx and NOx which destroy ozone resulting in a stronger vortex and a positive phase of the North Atlantic Oscillation. It has been shown that the reversals of the correlations between solar activity and atmospheric parameters have a periodicity of ~60 years and are related to the evolution of the main forms of large-scale atmospheric circulation whose occurrence has a similar periodicity. The large-scale circulation forms are in turn influenced by the state of the polar vortex which can affect the troposphere-stratosphere interaction via the propagation of planetary waves. Two solar activity agents are supposed to affect the stratospheric polar vortex: spectral solar irradiance through the "top-down" mechanism, and energetic particles. Increased UV irradiance was found to lead to a negative phase of the North Atlantic Oscillation, while increased energetic particles result in a positive phase. Solar irradiance, like sunspots, is related to the solar toroidal field, and energetic particle precipitation is related to the solar poloidal field. In the course of the solar cycle the irradiance is maximum in sunspot maximum, and particle precipitation peaks strongly in the cycle's declining phase. The solar poloidal and toroidal fields are the two faces of the solar large-scale magnetic field. They are closely connected, but because they are generated in different domains and because of the randomness involved in the generation of the poloidal field from the toroidal field, on longer time-scales their variations differ. As a result, in some periods poloidal field-related solar drivers prevail, in other periods toroidal field-related drivers prevail. These periods vary cyclically. When the poloidal field-related drivers prevail, the stratospheric polar vortex is stronger, and the correlation between solar activity and atmospheric parameters is positive. When toroidal field-related drivers prevail, the vortex is weaker and the correlations are negative.

The ratio between the number of sunspot and the number of sunspot groups

K. **Georgieva**, A. Kilcik, Yu. Nagovitsyn, B. Kirov
Geomagnetism and Aeronomy, **2017**, Vol. 57, No. 7, pp. 1–7
https://arxiv.org/ftp/arxiv/papers/1710/1710.01775.pdf
Data from three solar observatories, Learmonth, Holloman, and San Vito, are used to study the variations in the average number of sunspots per sunspot group. It is found that the different types of sunspot groups and the number of sunspots in these groups have different solar cycle and cycle to cycle variations. The varying ratio between the average number of sunspots and the number of sunspot groups is shown to be a real feature and not a result of changing observational instruments, observers experience, calculation schemes, etc., and is a result of variations in the solar magnetic fields. Therefore, the attempts to minimize the discrepancies between the sunspot number and sunspot group series are not justified, and lead to the loss of important information about the variability of the solar dynamo.

About the recalibration of the sunspot record

Katya **Georgieva**, Ali Kilcik, Yury Nagovitsyn, Boian Kirov
Proceedings of the XX Conference "Solar and solar-terrestrial Physics", pp. 61-66, **2016**,
«Солнечная и солнечно-земная физика – 2016», Санкт-Петербург, Пулково, 10 – 14 октября
https://arxiv.org/pdf/1701.06165v1.pdf
In 2015 the calculation of the International (Zurich) sunspot number was cancelled, and it was replaced by a new "recalibrated" series. A new data series was proposed also for the Group sunspot number. As a result, these two series which originally differed mainly in their long-term trends, were "reconciled", and the long-term trends in both of them were minimized. These changes led to new reconstructions of the long-term variations of solar irradiance, and to reconsidering the impact of the solar activity variations on climate change. Here we use data for the number of sunspots and the number of sunspot groups from a single observatory with continuous and homogeneous observations in order to evaluate how justified these recalibrations are.

Solar magnetic fields and terrestrial climate

Katya **Georgieva**, Yury Nagovitsyn, Boian Kirovregions
Proceedings of the XVIII conference "Solar and Solar-Terrestrial Physics 2014", Pulkovo, Russia, 20-25 October **2014**
http://arxiv.org/pdf/1411.6030v1.pdf
Solar irradiance is considered one of the main natural factors affecting terrestrial climate, and its variations are included in most numerical models estimating the effects of natural versus anthropogenic factors for climate change. Solar wind causing geomagnetic disturbances is another solar activity agent whose role in climate change is not yet fully estimated but is a subject of intense research. For the purposes of climate modeling, it is essential to evaluate both the past and the future variations of solar irradiance and geomagnetic activity which are ultimately due to the variations of solar magnetic fields. Direct measurements of solar magnetic fields are available for a limited period, but can be reconstructed from geomagnetic activity records. Here we present a reconstruction of total solar irradiance based on geomagnetic data, and a forecast of the future irradiance and geomagnetic activity relevant for the expected climate change.

A new signal of the solar magnetic cycle: Opposite shifts of weak magnetic field distributions in the two hemispheres

Tibebu **Getachew,** Ilpo Virtanen, Kalevi Mursula

2019

https://arxiv.org/pdf/1907.11001.pdf

We study the asymmetric distribution of weak photospheric magnetic field values in the two hemispheres separately using synoptic maps from SDO/HMI, SOLIS/VSM and WSO during solar cycles 21-24. We calculate the weak-field asymmetry (shift) by fitting the distributions of weak-field values to a shifted Gaussian. Hemispheric shifts derived from the three data sets agree very well, and increase systematically when reducing the spatial resolution of the map. Shifts of the northern and southern hemisphere are typically opposite to each other. Shifts follow the evolution of the trailing flux and have a strong solar cycle variation with maxima in the early to mid-declining phase of the solar cycle. The sign of the hemispheric weak-field shift is always the same as the polarity of the polar field in the respective hemisphere and solar cycle. We also find that shifts in the south are systematically larger in absolute value than in the north.

Asymmetric distribution of weak photospheric magnetic field values

Tibebu **Getachew**, Ilpo Virtanen, Kalevi Mursula

ApJ 874, 116, **2019**

https://arxiv.org/pdf/1904.10866.pdf

sci-hub.se/10.3847/1538-4357/ab0749

We use the synoptic maps of the photospheric magnetic field observed at Wilcox Solar Observatory, Mount Wilson Observatory, Kitt Peak, SOHO/MDI, SOLIS/VSM, and SDO/HMI to study the distribution of weak photospheric magnetic field values in 1974-2018. We fit the histogram distribution of weak field values for each synoptic map of the six data-sets separately with a parametrized Gaussian function in order to calculate the possible shift (to be called here the weak-field asymmetry) of the maximum of the Gaussian distribution from zero. We estimate the statistical significance of the weak-field asymmetry for each rotation. We also calculate several versions of lower-resolution synoptic maps from the high-resolution maps and calculate their rotational weak-field asymmetries. We find that the weak-field asymmetries increase with decreasing map resolution. A very large fraction of weak-field asymmetries are statistically significant, with the fraction of significant weak-field asymmetries increasing with decreasing resolution. Significant weak-field asymmetries of high- and low-resolution maps mainly occur at the same times and have the same sign. Weak-field asymmetries for the different data-sets and resolutions vary quite similarly in time, and their mutual correlations are very high, especially for low-resolution maps. These results give strong evidence for weak-field asymmetries reflecting a real feature of weak field values, which is best seen in medium- and low-resolution synoptic maps and is most likely related to the supergranulation scale of the photospheric field.

Structure of the Photospheric Magnetic Field During Sector Crossings of the Heliospheric Magnetic Field

Tibebu **Getachew,** Ilpo Virtanen, Kalevi Mursula

Solar Physics November **2017**, 292:174

The photospheric magnetic field is the source of the coronal and heliospheric magnetic fields (HMF), but their mutual correspondence is non-trivial and depends on the phase of the solar cycle. The photospheric field during the HMF sector crossings observed at 1 AU has been found to contain enhanced field intensities and definite polarity ordering, forming regions called Hale boundaries. Here we separately study the structure of the photospheric field during the HMF sector crossings during Solar Cycles 21 – 24 for the four phases of each solar cycle. We use a refined version of Svalgaard's list of major HMF sector crossings, mapped to the Sun using the solar wind speed observed at Earth, and the daily level-3 magnetograms of the photospheric field measured at the Wilcox Solar Observatory in 1976 – 2016. We find that the structure of the photospheric field corresponding to the HMF sector crossings and the existence and properties of the corresponding Hale bipolar regions varies significantly with solar cycle, solar cycle phase, and hemisphere. The Hale boundaries in more than half of the ascending, maximum, and declining phases are clear and statistically significant. The clearest Hale boundaries are found during the (+,−) HMF crossings in the northern hemisphere of odd Cycles 21 and 23, but less systematical during the (+,−) crossings in the southern hemisphere of even Cycles 22 and 24. No similar difference between odd and even cycles is found for the (−,+) crossings. This shows that the northern hemisphere has a more organized Hale pattern overall. The photospheric field distribution also depicts a larger area for the field of the northern hemisphere during the declining and minimum phases, in a good agreement with the bashful ballerina phenomenon.

The Ten-Rotation Quasi-periodicity in Sunspot Areas

R. **Getko**

Solar Physics, June **2014**, Volume 289, Issue 6, pp 2269-228

Sunspot-area fluctuations over an epoch of 12 solar cycles (12 – 23) are investigated in detail using wavelets. Getko (Universal Heliophysical Processes, IAU Symp. 257, 169, 2009) found three significant quasi-periodicities at 10, 17, and 23 solar rotations, but two longer periods could be treated as subharmonics of the ten-rotation quasi-periodicity. Therefore we focused the analysis on the occurrence of this quasi-periodicity during the low- and high-activity periods of each solar cycle. Because of the N – S asymmetry, each solar hemisphere was considered separately. The skewness of each fluctuation-probability distribution suggests that the positive and negative fluctuations could be examined separately. To avoid the problem that occurs when a few strong fluctuations create a wavelet peak, we applied fluctuation transformations for which the amplitudes at the high- and the low-activity periods are almost the same. The wavelet analyses show that the ten-rotation quasi-periodicity is mainly detected during the high-activity periods, but it also exists during a few low-activity periods. The division of each solar hemisphere into 30∘-wide longitude bins and the wavelet calculations for the areas of sunspot clusters belonging to these 30∘ bins enable one to detect longitude zones in which the ten-rotation quasi-periodicity exists. These zones are present during the whole high-activity periods and dominate the integrated spectra.

Spatial Scales and Time Variation of Solar Subsurface Convection

Alexander V. **Getling**, Alexander G. Kosovichev

ApJ **937** 41 **2022**

https://arxiv.org/pdf/2208.04642.pdf

https://iopscience.iop.org/article/10.3847/1538-4357/ac8870/pdf

Spectral analysis of the spatial structure of solar subphotospheric convection is carried out for subsurface flow maps constructed using the time--distance helioseismological technique. The source data are obtained from the Helioseismic and Magnetic Imager (HMI) onboard Solar Dynamics Observatory (SDO) from 2010 May to 2020 September. A spherical-harmonic transform is applied to the horizontal-velocity-divergence field at depths from 0 to 19~Mm. The range of flow scales is fairly broad in shallow layers and narrows as the depth increases. The horizontal flow scales rapidly increase with depth, from supergranulation to giant-cell values, and indicate the existence of large-scale convective motions in the near-surface shear layer. The results can naturally be interpreted in terms of a superposition of differently scaled flows localized in different depth intervals. There is some tendency toward the emergence of meridionally elongated (banana-shaped) convection structures in the deep layers. The total power of convective flows is anticorrelated with the sunspot-number variation over the solar activity cycle in shallow subsurface layers and positively correlated at larger depths, which is suggestive of the depth redistribution of the convective-flow energy due to the action of magnetic fields.

HMI Nuggets #189 **2022** http://hmi.stanford.edu/hminuggets/?p=4047

Spatial Spectrum of Solar Convection from Helioseismic Data: Flow Scales and Time Variations

Alexander V. **Getling**, Alexander G. Kosovichev

ApJ **2022**

https://arxiv.org/pdf/2201.00638.pdf

We analyze spectral properties of solar convection in the range of depths from 0 to 19~Mm using subsurface flow maps obtained by the time-distance heiioseismology analysis of solar-oscillation data from the Helioseismic and Magnetic Imager (HMI) onboard Solar Dynamics Observatory (SDO) from May 2010 to September 2020. The results reveal a rapid increase of the horizontal flow scales with the depth, from supergranulation to giant-cell scales, and support the evidence of large-scale convection, previously detected by tracking the motion of supergranular cells on the surface. The total power of convective flows correlates with the solar activity cycle. During the solar maximum, the total power decreases in shallow subsurface layers and increases in the deeper layers.

Evolution of Subsurface Zonal and Meridional Flows in Solar Cycle 24 from Helioseismological Data

Alexander V. **Getling**, Alexander G. Kosovichev, Junwei Zhao

ApJL **2021**

https://arxiv.org/pdf/2012.15555.pdf

The results of determinations of the azimuthal and meridional velocities by time-distance helioseismology from Helioseismic and Magnetic Imager (HMI) onboard Solar Dynamics Observatory (SDO) from May 2010 to September 2020 at latitudes from -60° to +60° and depths to about 19 Mm below the photosphere are used to analyze spatiotemporal variations of the solar differential rotation and meridional circulation. The pattern of torsional oscillations, or latitudinal belts of alternating `fast' and `slow' zonal flows migrating from high latitudes towards the equator, is found to extend in the time--latitude diagrams over the whole time interval. The oscillation period is comparable with a doubled solar-activity-cycle and can be described as an extended solar cycle. The zonal-velocity variations are related to the solar-activity level, the local-velocity increases corresponding to the sunspot-number increases and being localized at latitudes where the strongest magnetic fields are recorded. The dramatic

growth of the zonal velocities in 2018 appears to be a precursor of the beginning of activity Cycle 25. The strong symmetrization of the zonal-velocity field by 2020 can be considered another precursor. The general pattern of poleward meridional flows is modulated by latitudinal variations that are similar to the extended-solar-cycle behavior of the zonal flows. During the activity maximum, these variations are superposed with a higher harmonic corresponding to meridional flows converging to the spot-formation latitudes. Our results indicate that variations of both the zonal and meridional flows exhibit the extended solar-cycle behavior, which is an intrinsic feature of the solar dynamo.

Properties of Nonlinear Torsional Waves Effective on Solar Swirling Plasma Motions

A. Mozafari **Ghoraba**1 and S. Vasheghani Farahani
2018 ApJ 869 93
https://iopscience.iop.org/article/10.3847/1538-4357/aaec81/pdf
We model the evolution of solar helical structures: swirling motions, tornadoes, and spirals in the context of nonlinear magnetohydrodynamic waves. By considering vorticity and magnetic twist, the nonlinear forces that confine and shape helical or swirling plasma motions are incorporated in nonlinear partial differential equations. The solution to the governing equations provides insight on the significance of the equilibrium conditions. The key in providing explicit expressions for the compressive perturbations in the presence of equilibrium twist and vorticity is the second-order thin flux tube approximation. Nonlinear differential equations for the perturbations of the density, tube cross sectional area, and longitudinal speed are obtained in terms of the characteristics of the torsional wave, which itself is determined by the magnetic twist and vorticity. The analytic nonlinear solutions enable measurement of the efficiency of the equilibrium magnetic twist and vorticity, which confine and shape swirling motions differently as they evolve up the solar atmosphere. For chromospheric and coronal conditions, the nonlinear induced density perturbations increase with vorticity and decrease with magnetic twist. Regarding confinement, the nonlinear forces prove that the vorticity is predominant compared to the twist. The vorticity acts similarly to the shear flow in confining plasma swirling motions. It features in the compressive perturbations due to the ponderomotive force. We conclude that weak vorticities and twists are easily dominated by the plasma-β. For observing swirling plasma motions and tornadoes, focus must be on regions with high vorticity.

Helical and rotating plasma structures in the solar atmosphere

A. Mozafari **Ghoraba**1, A. Abedi1, S. Vasheghani Farahani2 and S. M. Khorashadizadeh1
A&A 618, A82 (**2018**)
https://www.aanda.org/articles/aa/pdf/2018/10/aa32620-18.pdf
Aims. We model helical or rotating signatures in the solar atmosphere to further understand the efficiency of the equilibrium conditions, for example magnetic twist, rotation, plasma-β, and viscous effects on the life of solar helical structures.
Methods. Solar rotating structures, such as tornadoes, spirals, and whirls are modelled by considering a rotating and twisted magnetic cylinder residing in an environment with a straight magnetic field. A macroscopic approach proves adequate for working on the phase speed and damping of waves in solar atmospheric structures; as such, the magnetohydrodynamic theory is implemented. In this way the second order thin flux tube approximation is used for obtaining expressions for the frequency, deceleration, and damping of torsional waves in solar plasma structures in the presence of equilibrium rotation, magnetic twist, viscosity, and gravity.
Results. The dependency of the dissipation effects regarding the torsional wave in the linear regime is highlighted. The dispersion relation for axisymmetric oscillations propagating along a rotating and twisted solar cylindrical plasma structure in the presence of plasma viscosity and gravity is obtained. In this way we present explicit expressions for the oscillation and damping of torsional waves. The explicit expressions shed light on the influence of the equilibrium and environmental conditions on the speed deceleration, frequency, and damping of the torsional wave that exists in various layers of the solar atmosphere. The dispersion of the torsional wave is highly controlled by the combined effects of the rotation and the plasma-β, where when both are zero, the magnetic twist becomes significant only when the plasma resistivity comes into play. Regarding damping, the dominant actor for coronal conditions is the magnetic twist. However, since the damping time is highly dependent on the plasma-β, for photospheric conditions, the rotation becomes very significant. The damping of torsional waves is inversely proportional to the elevation of the rotating structure. This means that if the torsional wave survives through the photosphere and chromosphere, the chance for it to extend through the corona and solar wind is very high by gradually dissipating energy, which gives more opportunity for it to be observed.

Non-thermal Velocity in the Transition Region of Active Regions and its Centre-to-Limb Variation

Avyarthana **Ghosh**, Durgesh Tripathi, James A. Klimchuk
ApJ **913** 151 **2021**
https://arxiv.org/pdf/2103.15081.pdf
https://doi.org/10.3847/1538-4357/abf244

We derive the non-thermal velocities (NTVs) in the transition region of an active region using the \ion{Si}{4}~1393.78~Å line observed by the Interface Region Imaging Spectrograph (IRIS) and compare them with the line-of-sight photospheric magnetic fields obtained by the Helioseismic and Magnetic Imager (HMI) onboard the Solar Dynamics Observatory (SDO). The active region consists of two strong field regions with opposite polarity, separated by a weak field corridor, that widened as the active region evolved. The means of the NTV distributions in strong-field regions (weak field corridors) range between ~18{--}20 (16{--}18)~km~s−1, albeit the NTV maps show much larger range. In addition, we identify a narrow lane in the middle of the corridor with significantly reduced NTV. The NTVs do not show a strong center-to-limb variation, albeit somewhat larger values near the disk center. The NTVs are well correlated with redshifts as well as line intensities. The results obtained here and those presented in our companion paper on Doppler shifts suggest two populations of plasma in the active region emitting in \ion{Si}{4}. The first population exists in the strong field regions and extends partway into the weak field corridor between them. We attribute this plasma to spicules heated to ~0.1 MK (often called type II spicules). They have a range of inclinations relative to vertical. The second population exists in the center of the corridor, is relatively faint, and has smaller velocities, likely horizontal. These results provide further insights into the heating of the transition region. **1-8 March 2017**

On Doppler shift and its Center-to-Limb Variation in Active Regions in the Transition Region

Avyarthana **Ghosh**, James A. Klimchuk, Durgesh Tripathi
2019 *ApJ* **886** 46
https://arxiv.org/pdf/1910.12033.pdf
https://doi.org/10.3847/1538-4357/ab43c4
A comprehensive understanding of the structure of Doppler motions in transition region including the center-to-limb variation and its relationship with the magnetic field structure is vital for the understanding of mass and energy transfer in the solar atmosphere. In this paper, we have performed such a study in an active region using the Si IV 1394~Å emission line recorded by the Interface Region Imaging Spectrograph (IRIS) and the line-of-sight photospheric magnetic field obtained by the Helioseismic and Magnetic Imager (HMI) on-board the Solar Dynamics Observatory (SDO). The active region has two opposite polarity strong field regions separated by a weak field corridor, which widened as the active region evolved. On average the strong field regions (corridor) show(s) redshifts of 5{--}10 (3{--}9)~km~s−1 (depending on the date of observation). There is, however, a narrow lane in the middle of the corridor with near-zero Doppler shifts at all disk positions, suggesting that any flows there are very slow. The Doppler velocity distributions in the corridor seem to have two components---a low velocity component centered near 0 km/s and a high velocity component centered near 10~km~s−1. The high velocity component is similar to the velocity distributions in the strong field regions, which have just one component. Both exhibit a small center-to limb variation and seem to come from the same population of flows. To explain these results, we suggest that the emission from the lower transition region comes primarily from warm type II spicules, and we introduce the idea of a `chromospheric wall'---associated with classical cold spicules---to account for a diminished center-to-limb variation. **March 1–8, 2017**

On the Signature of Chaotic Dynamics in 10.7 cm Daily Solar Radio Flux

Oindrilla **Ghosh** , T. N. Chatterjee
Solar Phys. **201**5
We examine the properties of the time-series of daily values of the 10.7-cm solar radio flux and sunspot-number activity indices, and their relative behavior. The analysis and the comparisons are based upon the estimation of the embedded dimension and the use of recurrence plots. The result shows higher-order chaos in 10.7-cm radio flux, and a similar but not identical chaotic nature in the sunspot number indicative of a change in the phase space of the Sun. Both data series show a stochastic behavior only during the rising and peak phase of Solar Cycle 23.

Multi-technique Analysis of the Solar 10.7 cm Radio Flux Time-Series in Relation to Predictability

Oindrilla **Ghosh**, Tanushree Ghosh, T. N. Chatterjee
Solar Physics, June **2014**, Volume 289, Issue 6, pp 2297-2315
We studied the predictability of the 10.7 cm solar radio flux by using stationary and non-stationary time-series analysis techniques of fractal theory to find the correlation exponent, the spectral exponent, the Hurst exponent, and the fluctuation exponent of the time series. The Hurst exponent was determined, from which the fractal dimension and consequently the predictability was evaluated. The results suggest that stationary methods of analysis yield inconsistent result, that is, amongst the four techniques used, the values of the exponents show great disparity. While two of the techniques, namely the auto-correlation function analysis and the spectral analysis, indicate long-term positive correlation, the other two methods, specifically the Hurst rescaled range-analysis and the fluctuation analysis, clearly exhibit the anti-correlated nature of the time series. The two non-stationary methods, that is, the discrete wavelet transform and the centered moving-average analysis, yielded values of the Hurst exponent that are

indicative of positive correlation, of persistent behavior, and also showed that the time series is predictable to a certain extent.

Vortex Flows in the Solar Atmoshpere: Automated Identification and Statistical Analysis

Ioannis **Giagkiozis**, Viktor Fedun, Eamon Scullion, Gary Verth
2018 ApJ 869 169
https://arxiv.org/pdf/1706.05428.pdf
http://iopscience.iop.org/article/10.3847/1538-4357/aaf797/pdf
Vortices on the photosphere are fundamentally important as these coherent flows have the potential to form coherent magnetic field structures in the solar atmosphere, e.g., twisted magnetic flux tubes. These flows have traditionally been identified by tracking magnetic bright points (BPs) using primarily visual inspection. This approach has the shortcoming that it introduces bias into the statistical analyses. In this work we fully automate the process of vortex identification using an established method from hydrodynamics for the study of eddies in turbulent flows. For the first time, we apply this to detect intergranular photospheric intensity vortices. Using this automated approach, we find that the expected lifetime of intensity vortices is much shorter (≈17 s) compared with previously observed magnetic BP swirls. We suggest that at any time there are 1.48 × 106 such small-scale intensity vortices covering about 2.8% of the total surface of the solar photosphere. Lastly, we compare our results with previous works and speculate what this could imply with regards to estimating the global energy flux due magnetic tornadoes in the solar atmosphere with future higher resolution instrumentation. **2012 June 21**

RESONANT ABSORPTION OF AXISYMMETRIC MODES IN TWISTED MAGNETIC FLUX TUBES

I. **Giagkiozis**1, M. Goossens2, G. Verth1, V. Fedun3, and T. Van Doorsselaere
2016 ApJ 823 71
https://arxiv.org/pdf/1706.09665.pdf
It has been shown recently that magnetic twist and axisymmetric MHD modes are ubiquitous in the solar atmosphere, and therefore the study of resonant absorption for these modes has become a pressing issue because it can have important consequences for heating magnetic flux tubes in the solar atmosphere and the observed damping. In this investigation, for the first time, we calculate the damping rate for axisymmetric MHD waves in weakly twisted magnetic flux tubes. Our aim is to investigate the impact of resonant damping of these modes for solar atmospheric conditions. This analytical study is based on an idealized configuration of a straight magnetic flux tube with a weak magnetic twist inside as well as outside the tube. By implementing the conservation laws derived by Sakurai et al. and the analytic solutions for weakly twisted flux tubes obtained recently by Giagkiozis et al. we derive a dispersion relation for resonantly damped axisymmetric modes in the spectrum of the Alfvén continuum. We also obtain an insightful analytical expression for the damping rate in the long wavelength limit. Furthermore, it is shown that both the longitudinal magnetic field and the density, which are allowed to vary continuously in the inhomogeneous layer, have a significant impact on the damping time. Given the conditions in the solar atmosphere, resonantly damped axisymmetric modes are highly likely to be ubiquitous and play an important role in energy dissipation. We also suggest that, given the character of these waves, it is likely that they have already been observed in the guise of Alfvén waves.

AXISYMMETRIC MODES IN MAGNETIC FLUX TUBES WITH INTERNAL AND EXTERNAL MAGNETIC TWIST

I. **Giagkiozis**1,2, V. Fedun2, R. Erdélyi1,3, and G. Verth
ApJ Volume 810, Number 1 53 **2015**
https://arxiv.org/pdf/1706.09669.pdf
Observations suggest that twisted magnetic flux tubes are ubiquitous in the Sun's atmosphere. The main aim of this work is to advance the study of axisymmetric modes of magnetic flux tubes by modeling both twisted internal and external magnetic fields, when the magnetic twist is weak. In this work, we solve the derived wave equations numerically assuming that the twist outside the tube is inversely proportional to the distance from its boundary. We also study the case of a constant magnetic twist outside the tube and solve these equations analytically. We show that the solution for a constant twist outside the tube is a good approximation for the case where the magnetic twist is proportional to $1/r$, namely, the error is in all cases less than 5.4%. The solution is in excellent agreement with solutions to simpler models of twisted magnetic flux tubes, i.e., without external magnetic twist. It is shown that axisymmetric Alfvén waves are naturally coupled with magnetic twist as the azimuthal component of the velocity perturbation is nonzero. We compared our theoretical results with observations and comment on what the Doppler signature of these modes is expected to be. Lastly, we argue that the character of axisymmetric waves in twisted magnetic flux tubes can lead to false positives in identifying observations with axisymmetric Alfvén waves.

3D Visualisation of the Eigenmodes of a Straight Magnetic Flux Tube

Ioannis **Giagkiozis**, Viktor Fedun, Robertus Erdélyi, and Gary Verth at the Solar Physics and Space Plasma Research Centre (SP2RC), Solar WAve Theory Group (SWAT) and Space Systems Laboratory (SSL) at the University of Sheffield
UKSP Nugget: #50, **2014**
http://www.uksolphys.org/uksp-nugget/50-3d-visualisation-of-the-eigenmodes-of-a-straight-magnetic-flux-tube/

Magnetic Energy Balance in the Quiet Sun on Supergranular Spatial and Temporal Scales

Fabio **Giannattasio**1, Giuseppe Consolini2, Francesco Berrilli3, and Dario Del Moro3
2020 ApJ 904 7
https://doi.org/10.3847/1538-4357/abbb36
Small-scale magnetic fields are ubiquitous in the quiet solar photosphere and may store and transfer huge amounts of energy to the upper atmospheric layers. For this reason, it is fundamental to constrain the energetics of the quiet Sun. By taking advantage of a 24 hr long magnetogram time series acquired by the Hinode mission without interruption, we computed, for the first time, the average rate of change of magnetic energy density on supergranular spatial and temporal scales. We found that the regions where this quantity is positive correspond with the longest magnetic field decorrelation times, with the latter being consistent with the timescales of magnetic energy density variation. This suggests that, on average, the energy provided by photospheric electric and magnetic fields and current density is effective in sustaining the magnetic fields in the network.

The Complex Nature of Magnetic Element Transport in the Quiet Sun: The Lévy-walk Character

F. **Giannattasio**1, G. Consolini2, F. Berrilli3, and D. Del Moro
2019 ApJ 878 33
sci-hub.se/10.3847/1538-4357/ab1be2
The study of the dynamic properties of small-scale magnetic fields in the solar photosphere (magnetic elements, MEs) provides a fundamental tool to investigate some still unknown aspects of turbulent convection, and gain information on the spatial and temporal scales of evolution of the magnetic field in the quiet Sun. We track the MEs in a set of magnetogram long-time series acquired by the Hinode mission, and take advantage of a method based on entropy (the diffusion entropy analysis, DEA) to detect their dynamic regime, under the assumption that MEs are passively transported by the photospheric plasma flow. DEA has been proven to perform better than other standard techniques, and for the first time it is successfully used to provide the scaling properties of the displacement of MEs in the quiet Sun. The main results of this work, which represents an extension of the analysis presented in previous literature, can be summarized as two points: (i) MEs in the quiet Sun undergo a common dynamic turbulent regime independent of the local environment; (ii) the displacement of MEs exhibits a complex transport dynamics that is consistent with a Lévy walk.

Occurrence and persistence of magnetic elements in the quiet Sun

F. **Giannattasio**, F. Berrilli, G. Consolini, D. Del Moro, M. Gosic, L. Bellot Rubio
A&A **2018**
https://arxiv.org/pdf/1801.03871.pdf
Turbulent convection efficiently transports energy up to the solar photosphere, but its multi-scale nature and dynamic properties are still not fully understood. Several works in the literature have investigated the emergence of patterns of convective and magnetic nature in the quiet Sun at spatial and temporal scales from granular to global. Aims. To shed light on the scales of organisation at which turbulent convection operates, and its relationship with the magnetic flux therein, we studied characteristic spatial and temporal scales of magnetic features in the quiet Sun. Methods. Thanks to an unprecedented data set entirely enclosing a supergranule, occurrence and persistence analysis of magnetogram time series were used to detect spatial and long-lived temporal correlations in the quiet Sun and to investigate their nature. Results. A relation between occurrence and persistence representative for the quiet Sun was found. In particular, highly recurrent and persistent patterns were detected especially in the boundary of the supergranular cell. These are due to moving magnetic elements undergoing motion that behaves like a random walk together with longer decorrelations (∼2 h) with respect to regions inside the supergranule. In the vertices of the supegranular cell the maximum observed occurrence is not associated with the maximum persistence, suggesting that there are different dynamic regimes affecting the magnetic

Solar Physics from Unconventional Viewpoints **Review**

Sarah E. **Gibson**, Angelos Vourlidas, Donald M. Hassler, Laurel A. Rachmeler, Michael J Thompson, Jeffrey Newmark, Marco Velli, Alan Title, Scott W. McIntosh
Front. Astron. Space Sci. 5:32. **2018**
https://arxiv.org/pdf/1805.09452.pdf **File**
https://www.frontiersin.org/articles/10.3389/fspas.2018.00032/full
https://doi.org/10.3389/fspas.2018.00032
We explore new opportunities for solar physics that could be realized by future missions providing sustained observations from vantage points away from the Sun-Earth line. These include observations from the far side of the Sun, at high latitudes including over the solar poles, or from near-quadrature angles relative to the Earth (e.g., the Sun-Earth L4 and L5 Lagrangian points). Such observations fill known holes in our scientific understanding of the three-dimensional, time-evolving Sun and heliosphere, and have the potential to open new frontiers through discoveries enabled by novel viewpoints.
2 EXTRA-SUN-EARTH-LINE OBSERVATIONS TO DATE
3 SCIENCE ENABLED BY EXTRA-SUN-EARTH-LINE OBSERVATIONS
4 SPACE-WEATHER SIGNIFICANCE OF EXTRA-SUN-EARTH-LINE OBSERVATIONS
5 DISCOVERY SPACE
6 FUTURE MISSIONS AND GAP ANALYSIS

Coronal Magnetometry. Ebook

Gibson, S. E., Rachmeler, L. A., White, S. M., eds. (**2017**).
Lausanne: Frontiers Media. doi: 10.3389/978-2-88945-220-0
http://www.frontiersin.org/books/Coronal_Magnetometry_5/1259#nogo

Data-model comparison using FORWARD and CoMP

Sarah **Gibson**
Proceedings of the International Astronomical Union, Volume 305, pp. 245-250, **2015**
http://arxiv.org/pdf/1511.04416v1.pdf
The FORWARD SolarSoft IDL package is a community resource for model-data comparison, with a particular emphasis on analyzing coronal magnetic fields. FORWARD allows the synthesis of coronal polarimetric signals at visible, infrared, and radio frequencies, and will soon be augmented for ultraviolet polarimetry. In this paper we focus on observations of the infrared (IR) forbidden lines of Fe XIII, and describe how FORWARD may be used to directly access these data from the Mauna Loa Solar Observatory Coronal Multi-channel Polarimeter (MLSO/CoMP), to put them in the context of other space- and ground-based observations, and to compare them to synthetic observables generated from magnetohydrodynamic (MHD) models.

Reanalysis of Solar Observing Optical Network Sunspot Areas

Owen **Giersch**, John Kennewell, Mervyn Lynch
Solar Physics October **2018**, 293:138
https://link.springer.com/content/pdf/10.1007%2Fs11207-018-1358-6.pdf
We address recent concerns that the sunspot-area measurements performed by the United States Air Force (USAF) Solar Observing Optical Network (SOON) have been underestimating sunspot areas. We examine briefly the history of SOON, and we perform an analysis of a three-decade time series of SOON measurements. By remeasuring USAF sunspot areas, we find that sunspot areas are being underestimated by between 8% and 17% due to the measuring techniques employed by SOON analysts. In particular, the SOON practice of rounding down limb-area correction factors results in some individual regions having areas reported by up to 50% less than their true values. This does not, however, account for the full discrepancy in sunspot areas between SOON and other observatories, which, in recent years, may be as high as a 50% discrepancy.

Investigation of N–S asymmetry of solar differential rotation by various patterns for solar cycles 20 and 21

M.Sh. **Gigolashvili**, , D.R. Japaridze, T.G. Mdzinarishvili
Advances in Space Research, **2013**
For solar cycles 20 and 21 the latitudinal variations of the solar rotation rates are found using data of the Hα filaments and the long-lived magnetic features of negative and positive polarities. Analysis of the data showed that: (a) there is N–S asymmetry in the equatorial rotation of the Hα filaments and the long-lived magnetic features; (b) for both solar cycles the long-lived magnetic features of both polarities have similar behavior; (c) in the solar cycle

20 the long-lived magnetic features of both polarities vary in phase to each other but show some difference during cycle 21. For the long-lived magnetic features of positive polarity the confidence level is lower than for those of negative one.

Comparing two intervals of exceptionally strong solar rotation recurrence of galactic cosmic rays

A. **Gil** and K. Mursula

JGR v. 123 Pages 6148-6160 **2018**

http://sci-hub.tw/https://onlinelibrary.wiley.com/doi/abs/10.1029/2018JA025523

Two intervals of exceptionally strong recurrence of galactic cosmic ray (GCR) intensity at solar rotation period stand out in recent history, one in 2007-2008, the other in 2014-2015. We use neutron monitor data from Oulu and Hermanus, solar wind (SW) data and coronal images to study these intervals. We find that in both cases the source of solar rotation period recurrence was a coronal hole (CH), but CH structures were different. While a large, longitudinally asymmetric CH existed at high southern latitudes in 2014-2015, a low-latitude CH caused the recurrence in 2007-2008. Spectral properties of GCR and SW parameters reflect these differences. In 2014-2015 the GCR power spectrum density was broad and peaked at a period of 28.9 days, longer than the simultaneous recurrence period of SW speed. In 2007-2008 the GCR power spectrum was narrow and peaked at 27.5 days, exactly the same as for SW speed. The effect of CHs to GCRs was somewhat different in the two cases because of opposite solar polarities in the two intervals. In 2014-2015, during positive polarity when GCRs drift inward from high latitudes, the convection of fast SW from CH reduces the inward GCR drift over a wide range of high heliolatitudes at certain heliolongitudes. In 2007-2008, during negative polarity when GCRs drift inward via the heliospheric current sheet (HCS), a low-latitude CH depletes the GCR flux not only by convection but also by deflecting HCS away from the ecliptic, whence GCR drift to higher latitudes in a limited longitude range.
25 September 2007, 30 January 2015

Hale cycle and long-term trend in variation of galactic cosmic rays related to solar rotation

A. **Gil**1,2 and K. Mursula

A&A 599, A112 (**2017**)

Context. Galactic cosmic ray (GCR) intensities around solar minimum times are modulated by magnetic drifts that depend on the overall solar polarity. GCR intensities reach a higher but more narrow peak during negative minima than during positive minima. However, despite these higher intensities, the variation of GCRs over timescales of solar rotation is smaller during negative minima than during positive minima.

Aims. We study the variation of GCR intensity over the 27-day synodic solar rotation and over the 14-day half-rotation, in particular the long-term trend and cyclic pattern of this variation, and propose a unifying explanation for the observations.

Methods. We used two high-latitude neutron monitors, Oulu and Apatity, which are most sensitive to the low-energy part of the GCR spectrum and thereby more strongly affected by the changes in the conditions of the local heliosphere. We calculated the yearly mean amplitudes of the GCR intensity variation during the full solar rotation (A27) and half-rotation (A14) in 1964–2016.

Results. We verify that the A27 and A14 amplitudes exhibit a clear 22-yr Hale cycle during solar minima at both stations, with larger amplitudes in positive minima. We find that the mean amplitude of the Hale cycle is about 30–45% of the mean amplitude for A14, while is only about 15–30% for A27. We also find that all amplitudes depict a declining long-term trend, which we suggest is due to the weakening of solar polar magnetic fields during the last four solar cycles and the ensuing latitudinal widening of the heliospheric current sheet (HCS) region. An exceptionally wide HCS region during the last solar minimum, when A14 reached its all-time minimum, is demonstrated by Ulysses probe observations.

Conclusions. Our results emphasize the effect of polarity-dependent drift and the properties of the HCS in modulating the variation of GCR intensity during solar rotation in solar minimum times. The second rotation harmonic yields a larger Hale amplitude than the first because it is more probable for the Earth to be outside the HCS only once during the rotation than twice or more, which more strongly reduces A14 during negative polarity times than A27. With the HCS region widening from minimum to minimum, the decrease in A14 is relatively faster than in A27.

Energy Spectrum of the Recurrent Variation of Galactic Cosmic Rays During the Solar Minimum of Cycles 23/24

Agnieszka **Gil**, Michael V. Alania

Solar Phys. Volume 291, Issue 6, pp 1877–1886 **2016**

The Sun during the recent epoch of solar activity operated in a different way than during the last 60 years, being less active. We study temporal changes of the energy spectrum of the first three harmonics of the 27-day variation of the galactic cosmic rays (GCR) intensity during the unusual, recent solar minimum, between Solar Cycles 23 and 24

(SC 23/24) and compare with four previous minima. We show that the energy spectrum of the amplitudes of the recurrent variation of the GCR intensity is hard in the maximum epochs and is soft in the minimum epochs during Solar Cycles 20 – 24, but with peculiarities during the Solar Minimum 23/24. In particular, while the energy/rigidity spectrum of the amplitudes of the first harmonic of the recurrent variation of the GCR intensity behaves practically the same as for previous epochs, the energy/rigidity spectrum of the amplitudes of the second and the third harmonics demonstrates a pronounced softening. We attribute this phenomenon to the decrease of the extension of the heliosphere caused by the decrease of the solar-wind dynamic pressure during the unusual Solar Minimum 23/24.

Magnetoacoustic Wave Energy Dissipation in the Atmosphere of Solar Pores

Caitlin A. **Gilchrist-Millar**, David B. Jess, Samuel D. T. Grant, Peter H. Keys, Christian Beck, Shahin Jafarzadeh, Julia M. Rield, Tom Van Doorselaere, Basilio Ruiz Cobo

Philoophical Transactions A **2020**

https://arxiv.org/pdf/2007.11594.pdf

The suitability of solar pores as magnetic wave guides has been a key topic of discussion in recent years. Here we present observational evidence of propagating magnetohydrodynamic wave activity in a group of five photospheric solar pores. Employing data obtained by the Facility Infrared Spectropolarimeter at the Dunn Solar Telescope, oscillations with periods on the order of 5 minutes were detected at varying atmospheric heights by examining Si I 10827 Å line bisector velocities. Spectropolarimetric inversions, coupled with the spatially resolved root mean square bisector velocities, allowed the wave energy fluxes to be estimated as a function of atmospheric height for each pore. We find propagating magnetoacoustic sausage mode waves with energy fluxes on the order of 30 kW/m2 at an atmospheric height of 100 km, dropping to approximately 2 kW/m2 at an atmospheric height of around 500 km. The cross-sectional structuring of the energy fluxes reveals the presence of both body- and surface-mode sausage waves. Examination of the energy flux decay with atmospheric height provides an estimate of the damping length, found to have an average value across all 5 pores of Ld≈268km, similar to the photospheric density scale height. We find the damping lengths are longer for body mode waves, suggesting that surface mode sausage oscillations are able to more readily dissipate their embedded wave energies. This work verifies the suitability of solar pores to act as efficient conduits when guiding magnetoacoustic wave energy upwards into the outer solar atmosphere. **2016 July 12**

The Effect of Solar Wind Expansion and Non-Equilibrium Ionization on the Broadening of Coronal Emission Lines

Chris R. **Gilly**, Steven R. Cranmer

ApJ **901** 150 **2020**

https://arxiv.org/pdf/2008.09580.pdf

https://doi.org/10.3847/1538-4357/abb1ad

When observing spectral lines in the optically-thin corona, line-of-sight (LOS) effects can strongly affect the interpretation of the data, especially in regions just above the limb. We present a semi-empirical forward model, called GHOSTS, to characterize these effects. GHOSTS uses inputs from several other models to compute non-equilibrium ionization states (which include the solar-wind freezing-in effect) for many ions. These are used to generate ensembles of simulated spectral lines that are examined in detail, with emphasis on: (1) relationships between quantities derived from observables and the radial variation of the observed quantities, (2) the behavior of thermal and non-thermal components of the line width, and (3) relative contributions of collisionally excited and radiatively scattered photons. We find that rapidly changing temperatures in the low corona can cause ion populations to vary dramatically with height. This can lead to line-width measurements that are constant with height (a "plateau" effect) even when the temperature is increasing rapidly, as the plane-of-sky becomes evacuated and the foreground/background plasma dominates the observation. We find that LOS effects often drive the velocity width to be close to the plane-of-sky value of the wind speed, despite it flowing perpendicularly to the LOS there. The plateau effect can also cause the non-thermal component of the line width to greatly exceed the solar wind velocity at the observation height. Lastly, we study how much of the LOS is significant to the observation, and the importance of including continuum in the solar spectrum when computing the radiatively scattered emission.

Magnetic Buoyancy and Magnetorotational Instabilities in Stellar Tachoclines for Solar- and Antisolar-type Differential Rotation

Peter A. **Gilman**

2018 ApJ 867 45

sci-hub.tw/10.3847/1538-4357/aae08e

We present results from an analytical model for magnetic buoyancy and rotational instabilities in full spherical shell stellar tachoclines that include rotation, differential rotation of either solar or antisolar type, and toroidal field. We find that in all cases, for latitudes where the tachocline vertical rotation gradient is positive, toroidal fields can be

stored against magnetic buoyancy up to a limit that is proportional to the square root of the local vertical rotation gradient. For solar magnitude differential rotation, this limit is about 9 kG. For fixed percentage differential rotation, storage capacity varies linearly with the rotation rate. Faster rotators with the same percentage differential rotation can store larger fields, and slower rotators can store smaller fields. At latitudes where the vertical rotation gradient is negative, vigorous magnetorotational instability for even weak ($\ll$1 kG) toroidal fields prevents such storage. We infer from these results that for stars with solar-type latitudinal differential rotation (fast equator, slow poles), any starspots present should be found in low latitudes, similar to the Sun. For antisolar differential rotation, any spots present should be found in mid- and high latitudes, perhaps with a peak of occurrence near 55°. These results hopefully provide some guidance for making and interpreting observations of stellar activity and differential rotation on stars with convection zones and tachoclines.

Magnetic Buoyancy and Rotational Instabilities in the Tachocline

Peter A. **Gilman**

2018 ApJ 853 65 10.3847/1538-4357/aaa4f4

We present results from an analytical model for magnetic buoyancy and rotational instabilities in a full spherical shell tachocline that includes rotation, differential rotation close to that observed helioseismically, and toroidal field. Perturbation solutions are found for the limit of large latitudinal wave number, a limit commonly used to maximize instability due to magnetic buoyancy. We find that at all middle and high latitudes vigorous rotational instability is induced by weak toroidal fields, particularly for high longitudinal wave number, even when the vertical rotation gradient is marginally stable without toroidal field. We infer that this instability will prevent much storage of toroidal fields in the tachocline at these latitudes, but could be responsible for the appearance of ephemeral active regions there. By contrast, the low-latitude vertical rotation gradient, opposite in sign to that at high latitudes, is not only stable itself but also prevents magnetic buoyancy instability until the peak toroidal field is raised above a threshold of about 9 kG at the equator, declining to zero where the vertical rotation gradient changes sign, at $32^\circ.3$ in our model. Thus this rotation gradient provides a previously unnoticed mechanism for storage of toroidal fields until they amplify by dynamo action to order 10 kG, whereupon they can overcome the rotation gradient to emerge as sunspots. These results provide a new explanation for why sunspots are seen only at low latitudes. The purely rotational instability at latitudes above 50°, even without toroidal fields, also suggests that the high-latitude tachocline should be much thicker, due to HD turbulence, than has been inferred for lower latitudes from helioseismic measurements.

Baroclinic Instability in the Solar Tachocline for Continuous Vertical Profiles of Rotation, Effective Gravity, and Toroidal Field

Peter A. **Gilman**

2017 ApJ 842 130

We present results from an MHD model for baroclinic instability in the solar tachocline that includes rotation, effective gravity, and toroidal field that vary continuously with height. We solve the perturbation equations using a shooting method. Without toroidal fields but with an effective gravity declining linearly from a maximum at the bottom to much smaller values at the top, we find instability at all latitudes except at the poles, at the equator, and where the vertical rotation gradient vanishes ($32^\circ.3$) for longitude wavenumbers m from 1 to >10. High latitudes are much more unstable than low latitudes, but both have e-folding times that are much shorter than a sunspot cycle. The higher the m and the steeper the decline in effective gravity, the closer the unstable mode peak to the top boundary, where the energy available to drive instability is greatest. The effect of the toroidal field is always stabilizing, shrinking the latitude ranges of instability as the toroidal field is increased. The larger the toroidal field, the smaller the longitudinal wavenumber of the most unstable disturbance. All latitudes become stable for a toroidal field exceeding about 4 kG. The results imply that baroclinic instability should occur in the tachocline at latitudes where the toroidal field is weak or is changing sign, but not where the field is strong.

Effect of Toroidal Fields On Baroclinic Instability in the Solar Tachocline

Peter A. **Gilman**

2015 ApJ 801 22

Using an MHD generalization of a two-layer hydrostatic but non-geostrophic model, we show that a toroidal field tends to stabilize baroclinically unstable modes in the solar tachocline. In the hydrodynamic (HD) case, baroclinic instability occurs at almost all latitudes in both the radiative and overshoot tachoclines. The toroidal field creates stable bands of latitude near where the vertical rotation gradient changes sign, as well as near the equator and pole, which widen with increasing field until, by ~2.25 kG, all latitudes are stable. The stable bands center on where the local latitudinal entropy gradient is smallest. This result is independent of how subadiabatic the local stratification is, provided it is not so subadiabatic that baroclinic instability is absent in the HD case. Growth rates and most unstable longitudinal wavenumbers remain close to their HD values until the toroidal field gets within $\sim 20\%$ of the value that totally suppresses the instability. The results are similar to those found in the 1960s from an MHD geostrophic model, but apply to a much wider range of latitudes and subadiabatic stratifications. Where tachocline toroidal fields

are weak enough to allow baroclinic instability, magnetic patterns in longitude should be produced that could be transmitted through the convection zone to be seen in the photosphere. The results also show it should be possible to construct a baroclinic wave dynamo for the solar tachocline.

Baroclinic Instability in the Solar Tachocline

Peter **Gilman** and Mausumi Dikpati
2014 ApJ 787 60
The solar tachocline is likely to be close to a geostrophic "thermal wind," for which the Coriolis force associated with differential rotation is closely balanced by a latitudinal pressure gradient, leading to a tight relation between the vertical gradient of rotation and the latitudinal entropy gradient. Using a hydrostatic but nongeostrophic spherical shell model, we examine baroclinic instability of the tachocline thermal wind. We find that both the overshoot and radiative parts of the tachocline should be baroclinicly unstable at most latitudes. Growth rates are roughly five times higher in middle and high latitudes compared to low latitudes, and much higher in the overshoot than in the radiative tachocline. They range in e-folding amplification from 10 days in the high latitude overshoot tachocline, down to 20 yr for the low latitude radiative tachocline. In the radiative tachocline only, longitudinal wavenumbers m = 1, 2 are unstable, while in the overshoot tachocline a much broader range of m are unstable. At all latitudes and with all stratifications, the longitudinal scale of the most unstable mode is comparable to the Rossby deformation radius, while the growth rate is set by the local latitudinal entropy gradient. Baroclinic instability in the tachocline competing with instability of the latitude rotation gradient established in earlier studies should be important for the workings of the solar dynamo and should be expected to be found in most stars that contain an interface between radiative and convective domains.

Origin of the Solar Rotation Harmonics Seen in the EUV and UV Irradiance

G. **Giono**, J. J. Zender, R. Kariyappa & L. Damé
Solar Physics volume 296, Article number: 172 (**2021**)
https://link.springer.com/content/pdf/10.1007/s11207-021-01918-x.pdf
https://doi.org/10.1007/s11207-021-01918-x
Long-term periodicities in the solar irradiance are often observed with periods proportional to the solar rotational period of 27 days. These periods are linked either to some internal mechanism in the Sun or said to be higher harmonics of the rotation without further discussion of their origin. In this article, the origin of the peaks in periodicities seen in the solar extreme ultraviolet (EUV) and ultraviolet (UV) irradiance around the 7, 9, and 14 days periods is discussed. Maps of the active regions and coronal holes are produced from six images per day using the Spatial Possibilistic Clustering Algorithm (SPoCA), a segmentation algorithm. Spectral irradiance at coronal, transition-region/chromospheric, and photospheric levels are extracted for each feature as well as for the full disk by applying the maps to full-disk images (at 19.3, 30.4, and 170 nm sampling in the corona/hot flare plasma, the chromosphere/transition region, and the photosphere, respectively) from the Atmospheric Imaging Assembly (AIA) on board the Solar Dynamics Observatory (SDO) from January 2011 to December 2018. The peaks in periodicities at 7, 9, and 14 days as well as the solar rotation around 27 days can be seen in almost all of the solar irradiance time series. The segmentation also provided time series of the active regions and coronal holes visible area (i.e. in the area observed in the AIA images, not corrected for the line-of-sight effect with respect to the solar surface), which also show similar peaks in periodicities, indicating that the periodicities are due to the change in area of the features on the solar disk rather than to their absolute irradiance. A simple model was created to reproduce the power spectral density of the area covered by active regions also showing the same peaks in periodicities. Segmentation of solar images allows us to determine that the peaks in periodicities seen in solar EUV/UV irradiance from a few days to a month are due to the change in area of the solar features, in particular, active regions, as they are the main contributors to the total full-disk irradiance variability. The higher harmonics of the solar rotation are caused by the clipping of the area signal as the regions rotate behind the solar limb.

Probing the Solar Wind Acceleration Region with the Sun--Grazing Comet C/2002 S2

Silvio **Giordano**, John C. Raymond, Philippe Lamy, Michael Uzzo, Danuta Dobrzycka
ApJ, 2014
http://arxiv.org/pdf/1411.1300v1.pdf
Comet C/2002 S2, a member of the Kreutz family of Sungrazing comets, was discovered in white light images of the SOHO/LASCO coronagraph on **2002 September 18** and observed in \hi\, \lya\, emission by the SOHO/UVCS instrument at four different heights as it approached the Sun. The \hi\, \lya\, line profiles detected by UVCS are analyzed to determine the spectral parameters: line intensity, width and Doppler shift with respect to the coronal background. Two dimensional comet images of these parameters are reconstructed at the different heights. A novel aspect of the observations of this sungrazing comet data is that, whereas the emission from the most of the tail is blue--shifted, that along one edge of the tail is red--shifted. We attribute these shifts to a combination of solar wind speed and interaction with the magnetic field. In order to use the comet to probe the density, temperature and speed of the corona and solar wind through which it passes, as well as to determine the outgassing rate of the comet, we develop a Monte Carlo simulation of the \hi\, \lya\, emission of a comet moving through a coronal plasma. From the

outgassing rate, we estimate a nucleus diameter of about 9 meters. This rate steadily increases as the comet approaches the Sun while the optical brightness decreases by more than a factor of ten and suddenly recovers. This indicates that the optical brightness is determined by the lifetimes of the grains, sodium atoms and molecules produced by the comet.

The Tor Vergata Synoptic Solar Telescope (TSST): A robotic, compact facility for solar full disk imaging

Luca **Giovannelli**, et al.
J. Space Weather Space Clim. **2020**, 10, 58
https://doi.org/10.1051/swsc/2020061
https://www.swsc-journal.org/articles/swsc/pdf/2020/01/swsc200063.pdf
By the continuous multi-line observation of the solar atmosphere, it is possible to infer the magnetic and dynamical status of the Sun. This activity is essential to identify the possible precursors of space weather events, such as flare or coronal mass ejections. We describe the design and assembly of TSST (Tor Vergata Synoptic Solar Telescope), a robotic synoptic telescope currently composed of two main full-disk instruments, a Hα telescope and a Potassium (KI D1) magneto-optical filter (MOF)-based telescope operating at 769.9 nm. TSST is designed to be later upgraded with a second MOF channel. This paper describes the TSST concepts and presents the first light observation carried out in February 2020. We show that TSST is a low-cost robotic facility able to achieve the necessary data for the study of precursors of space weather events (using the magnetic and velocity maps by the MOF telescope) and fast flare detection (by the Hα telescope) to support Space Weather investigation and services.

On Extreme-ultraviolet Helium Line Intensity Enhancement Factors on the Sun

A. S. **Giunta**1, A. Fludra1, A. C. Lanzafame2, M. G. O'Mullane3, H. P. Summers3, and W. Curdt
2015 ApJ 803 66
Helium lines in the solar EUV spectrum provide useful diagnostics of the solar atmosphere plasma. Helium is one of the few elements that exhibits strong emission lines formed in the lower transition region, and it is the second most abundant element in the Sun. However, the analysis of helium lines is complicated by their optical thickness and the unusual behavior of their intensities, with enhancements by a factor of up to 15 reported in the literature. Detailed study requires spatially and spectrally resolved observations in the EUV range, as well as sophisticated atomic modeling. The present work focuses on the application of the differential emission measure distribution to reproduce the observed fluxes of the He i and He ii lines observed by the Solar and Heliospheric Observatory (SOHO)/Coronal Diagnostic Spectrometer and Hinode/EIS spectrometers, using the latest atomic data. It is found that the comparison between observed and reconstructed intensities for He i resonance lines λλ537.03, 522.21, and 515.62 and the intercombination line λ591.41 does not show a real enhancement. By contrast, He i λ584.33, the first line of the $1s^2\ ^1S - 1s\,np\ ^1P$ resonance series, shows a depletion of a factor ~2, due to the opacity effect, as supported by non-LTE radiative transfer calculations. For single ionized helium lines 303.78 and 256.32 Å, the enhancement factors obtained are higher and agree with those of previous work. The different behavior of He i and He ii lines suggests a mechanism that affects ionized helium only.

Solar Inertial Modes

Laurent **Gizon**, Yuto Bekki, Aaron C. Birch, Robert H. Cameron, Damien Fournier, Jordan Philidet, B. Lekshmi, Zhi-Chao Liang
Procs. IAU Symp 365, Eds. A. Getling and L. Kitchatinov **2024**
https://arxiv.org/pdf/2409.04309
The Sun's global inertial modes are very sensitive to the solar differential rotation and to properties of the deep solar convection zone which are currently poorly constrained. These properties include the superadiabatic temperature gradient, the latitudinal entropy gradient, and the turbulent viscosity. The inertial modes also play a key role in controlling the Sun's large-scale structure and dynamics, in particular the solar differential rotation. This paper summarizes recent observations and advances in the (linear and nonlinear) modeling of the solar inertial modes.

Solar inertial modes: Observations, identification, and diagnostic promise

Laurent **Gizon**, Robert H. Cameron, Yuto Bekki, Aaron C. Birch, Richard S. Bogart, Allan Sacha Brun, Cilia Damiani, Damien Fournier, Laura Hyest, Kiran Jain, B. Lekshmi, Zhi-Chao Liang, Bastian Proxauf
A&A 652, L6 **2021**
https://arxiv.org/pdf/2107.09499
https://www.aanda.org/articles/aa/pdf/2021/08/aa41462-21.pdf
https://doi.org/10.1051/0004-6361/202141462
The oscillations of a slowly rotating star have long been classified into spheroidal and toroidal modes. The spheroidal modes include the well-known 5-min acoustic modes used in helioseismology. Here we report

observations of the Sun's toroidal modes, for which the restoring force is the Coriolis force and whose periods are on the order of the solar rotation period. By comparing the observations with the normal modes of a differentially rotating spherical shell, we are able to identify many of the observed modes. These are the high-latitude inertial modes, the critical-latitude inertial modes, and the equatorial Rossby modes. In the model, the high-latitude and critical-latitude modes have maximum kinetic energy density at the base of the convection zone, and the high-latitude modes are baroclinically unstable due to the latitudinal entropy gradient. As a first application of inertial-mode helioseismology, we constrain the superadiabaticity and the turbulent viscosity in the deep convection zone.

Effect of latitudinal differential rotation on solar Rossby waves: Critical layers, eigenfunctions, and momentum fluxes in the equatorial β plane

L. **Gizon**, D. Fournier, M. Albekioni
A&A **2020**
https://arxiv.org/pdf/2008.02185.pdf
Retrograde-propagating waves of vertical vorticity with longitudinal wavenumbers between 3 and 15 have been observed on the Sun with a dispersion relation close to that of classical sectoral Rossby waves. The observed vorticity eigenfunctions are symmetric in latitude, peak at the equator, switch sign near 20∘-30∘, and decrease at higher latitudes. We search for an explanation that takes into account solar latitudinal differential rotation. In the equatorial β plane, we study the propagation of linear Rossby waves (phase speed $c<0$) in a parabolic zonal shear flow, $U=-\overline{U}\,\xi 2<0$, where $\overline{U}=244$ m/s and ξ is the sine of latitude. In the inviscid case, the eigenvalue spectrum is real and continuous and the velocity stream functions are singular at the critical latitudes where $U=c$. We add eddy viscosity in the problem to account for wave attenuation. In the viscous case, the stream functions are solution of a fourth-order modified Orr-Sommerfeld equation. Eigenvalues are complex and discrete. For reasonable values of the eddy viscosity corresponding to supergranular scales and above (Reynolds number $100\leq Re\leq 700$), all modes are stable. At fixed longitudinal wavenumber, the least damped mode is a symmetric mode with a real frequency close to that of the classical Rossby mode, which we call the R mode. For $Re\approx 300$, the attenuation and the real part of the eigenfunction is in qualitative agreement with the observations (unlike the imaginary part of the eigenfunction, which has a larger amplitude in the model. Conclusion: Each longitudinal wavenumber is associated with a latitudinally symmetric R mode trapped at low latitudes by solar differential rotation. In the viscous model, R modes transport significant angular momentum from the dissipation layers towards the equator.

Meridional flow in the Sun's convection zone is a single cell in each hemisphere

Laurent **Gizon**[1,2,3,*], Robert H. Cameron[1], Majid Pourabdian[1,2], Zhi-Chao Liang[1], …
Science 26 Jun **2020**: Vol. 368, Issue 6498, pp. 1469-1472 DOI: 10.1126/science.aaz7119
sci-hub.tw/10.1126/science.aaz7119
The activity of the Sun, including the occurrence of sunspots, is driven by magnetic fields that originate from the motion of charged plasma beneath the surface. Helioseismology uses acoustic oscillations to probe the Sun's interior, analogous to seismology's use of earthquakes to investigate Earth's interior. Gizon et al. analyzed helioseismology data from 1996 to 2019, covering two 11-year solar cycles. They measured the latitudinal and radial flow of plasma as a function of depth within the Sun and how it varies with time. The results support magnetic flux-transport dynamo models, which can explain the distribution of sunspots over each solar cycle.

Signal and noise in helioseismic holography

Laurent **Gizon**, Damien Fournier, Dan Yang, Aaron C. Birch, Hélène Barucq
A&A 620, A136 **2018**
https://arxiv.org/pdf/1810.00402.pdf
Helioseismic holography is an imaging technique used to study heterogeneities and flows in the solar interior from observations of solar oscillations at the surface. Holograms contain noise due to the stochastic nature of solar oscillations. We provide a theoretical framework for modeling signal and noise in Porter-Bojarski helioseismic holography. The wave equation may be recast into a Helmholtz-like equation, so as to connect with the acoustics literature and define the holography Green's function in a meaningful way. Sources of wave excitation are assumed to be stationary, horizontally homogeneous, and spatially uncorrelated. Using the first Born approximation we calculate holograms in the presence of perturbations in sound-speed, density, flows, and source covariance, as well as the noise level as a function of position. This work is a direct extension of the methods used in time-distance helioseismology to model signal and noise. To illustrate the theory, we compute the hologram intensity numerically for a buried sound-speed perturbation at different depths in the solar interior. The reference Green's function is obtained for a spherically-symmetric solar model using a finite-element solver in the frequency domain. Below the pupil area on the surface, we find that the spatial resolution of the hologram intensity is very close to half the local wavelength. For a sound-speed perturbation of size comparable to the local spatial resolution, the signal-to-noise ratio is approximately constant with depth. Averaging the hologram intensity over a number N of frequencies above 3 mHz increases the signal-to-noise ratio by a factor nearly equal to the square root of N. This may not be the case at

lower frequencies, where large variations in the holographic signal are due to the individual contributions of the long-lived modes of oscillation.

Problems in computational helioseismology

Laurent **Gizon**, Damien Fournier, Thorsten Hohage
2017
https://arxiv.org/pdf/1707.08566.pdf
We discuss current advances in forward and inverse modeling for local helioseismology. We report theoretical uniqueness results, in particular the Novikov-Agaltsov reconstruction algorithm, which is relevant to solving the non-linear inverse problem of time-distance helioseismology (finite amplitude pertubations to the medium). Numerical experiments were conducted to determine the number of frequencies required to reconstruct density and sound speed in the solar interior.

Computational helioseismology in the frequency domain: acoustic waves in axisymmetric solar models with flows

Laurent **Gizon**, Hélène Barucq, Marc Duruflé, Chris S. Hanson, Michael Leguèbe, Aaron C. Birch, Juliette Chabassier, Damien Fournier, Thorsten Hohage, Emanuele Papini
A&A **2016**
https://arxiv.org/pdf/1611.01666v1.pdf
Local helioseismology has so far relied on semi-analytical methods to compute the spatial sensitivity of wave travel times to perturbations in the solar interior. These methods are cumbersome and lack flexibility. Here we propose a convenient framework for numerically solving the forward problem of time-distance helioseismology in the frequency domain. The fundamental quantity to be computed is the cross-covariance of the seismic wavefield. We choose sources of wave excitation that enable us to relate the cross-covariance of the oscillations to the Green's function in a straightforward manner. We illustrate the method by considering the 3D acoustic wave equation in an axisymmetric reference solar model, ignoring the effects of gravity on the waves. The symmetry of the background model around the rotation axis implies that the Green's function can be written as a sum of longitudinal Fourier modes, leading to a set of independent 2D problems. We use a high-order finite-element method to solve the 2D wave equation in frequency space. The computation is `embarrassingly parallel', with each frequency and each azimuthal order solved independently on a computer cluster. We compute travel-time sensitivity kernels in spherical geometry for flows, sound speed, and density perturbations under the first Born approximation. Convergence tests show that travel times can be computed with a numerical precision better than one millisecond, as required by the most precise travel-time measurements. The method presented here is computationally efficient and will be used to interpret travel-time measurements in order to infer, e.g., the large-scale meridional flow in the solar convection zone. It allows the implementation of (full-waveform) iterative inversions, whereby the axisymmetric background model is updated at each iteration.

Re-evaluation of Predictive Models in Light of New Data: Sunspot Number Version 2.0

A. **Gkana**, L. Zachilas
Solar Phys. **2016**, Volume 291, Issue 8, pp 2457–2472
The original version of the Zürich sunspot number (Sunspot Number Version 1.0) has been revised by an entirely new series (Sunspot Number Version 2.0). We re-evaluate the performance of our previously proposed models for predicting solar activity in the light of the revised data. We perform new monthly and yearly predictions using the Sunspot Number Version 2.0 as input data and compare them with our original predictions (using the Sunspot Number Version 1.0 series as input data). We show that our previously proposed models are still able to produce quite accurate solar-activity predictions despite the full revision of the Zürich Sunspot Number, indicating that there is no significant degradation in their performance. Extending our new monthly predictions (July 2013 – August 2015) by 50 time-steps (months) ahead in time (from September 2015 to October 2019), we provide evidence that we are heading into a period of dramatically low solar activity. Finally, our new future long-term predictions endorse our previous claim that a prolonged solar activity minimum is expected to occur, lasting up to the year \(\approx 2100\).

Mysterious High Energy Gamma Rays Might Help Explain What Drives Solar Cycles

Gregory S **Glenn**
2019
https://arxiv.org/ftp/arxiv/papers/1901/1901.10574.pdf
This paper is in response to a technical paper, entitled "Evidence for a New Component of High-Energy Solar Gamma-Ray Production" (Linden, et al., 2018). An article in Scientific American entitled "The Sun Is Spitting Out Strange Patterns of Gamma Rays-and No One Knows Why" is a discussion of Linden's paper. It may be summarized as follows: The Sun has been observed to be emitting gamma ray bursts. The weaker gamma rays tend to be less

than 50 GeV, emitted during the most active energetic period of the solar cycle and towards the poles. The gamma-ray emission is most intense during Solar Minimum, reaching >100 GeV and those emissions are near the equator: "Most strikingly, although 6 gamma rays above 100 GeV are observed during the 1.4 years of solar minimum, none are observed during the next 7.8 years (Linden, et al., 2018)." Pease and Glenn, in the conclusion of a recent paper, suggested that solar cycles are regulated by planetary orbital positions, influencing the Sun through transfer of gravitational or electromagnetic forces, or both (Pease & Glenn, 2016). This paper will describe a working hypothesis that points strongly to electromagnetic connections between Jupiter, Saturn, and the Sun during Solar Minimum which contribute to the high gamma-ray energy observed being emitted by the Sun. The hypothesis further suggests that the electromagnetic connections between the Sun and Jupiter, Saturn, and other planets with magnetospheres, namely Neptune, Earth, and Uranus, are responsible over billions of years for modulating a dual electromagnetic field resonance internal to the Sun. These major periodic cycles are known as the 11-year Schwabe and 22-year Hale solar cycles.

The flight of FOXSI-3

Lindsay **Glesener** and Noriyuki Narukage
RHESSI Science Nuggets No. 340, **2018**
http://sprg.ssl.berkeley.edu/~tohban/wiki/index.php/The_flight_of_FOXSI-3
The FOXSI-3 sounding rocket flew for a successful 6-minute observation of the Sun on **September 7, 2018** from the White Sands Missile Range. FOXSI stands for the Focusing Optics X-ray Solar Imager, and it is the first experiment to optimize direct-focusing optics for the Sun in hard X-rays (HXRs).

A New Python Module for Accessing HMI and AIA Data

K. **Glogowski** & M. G. Bobra
HMI Science Nuggets – #63 Oct **2016**
http://hmi.stanford.edu/hminuggets/?p=1757
There are many different ways to obtain data from the Solar Dynamics Observatory's (SDO) Helioseismic and Magnetic Imager (HMI) and Atmospheric Imaging Assembly (AIA) instruments. Two of the most popular methods, aside from a direct web interface, use the SolarSoft library in IDL and the SunPy library in Python. We have released a new Python module, called drms, to access the HMI and AIA data provided by the Joint Science Operations Center (JSOC).

The Solar Internetwork. I. Contribution to the Network Magnetic Flux

M. **Go**, L. R. Bellot Rubio1, D. Orozco Su?rez2, Y. Katsukawa3, and J. C. del Toro Iniesta
2014 ApJ 797 49
The magnetic network (NE) observed on the solar surface harbors a sizable fraction of the total quiet Sun flux. However, its origin and maintenance are not well known. Here we investigate the contribution of internetwork (IN) magnetic fields to the NE flux. IN fields permeate the interior of supergranular cells and show large emergence rates. We use long-duration sequences of magnetograms acquired by Hinode and an automatic feature tracking algorithm to follow the evolution of NE and IN flux elements. We find that 14% of the quiet Sun (QS) flux is in the form of IN fields with little temporal variations. IN elements interact with NE patches and modify the flux budget of the NE either by adding flux (through merging processes) or by removing it (through cancellation events). Mergings appear to be dominant, so the net flux contribution of the IN is positive. The observed rate of flux transfer to the NE is 1.5 × 1024 Mx day?1 over the entire solar surface. Thus, the IN supplies as much flux as is present in the NE in only 9-13 hr. Taking into account that not all the transferred flux is incorporated into the NE, we find that the IN would be able to replace the entire NE flux in approximately 18-24 hr. This renders the IN the most important contributor to the NE, challenging the view that ephemeral regions are the main source of flux in the QS. About 40% of the total IN flux eventually ends up in the NE.

Predicting frequency changes of global-scale solar Rossby modes due to solar cycle changes in internal rotation

C. R. **Goddard**, A. C. Birch, D. Fournier, L. Gizon
A&A 640, L10 **2020**
https://arxiv.org/pdf/2007.14387.pdf
https://www.aanda.org/articles/aa/pdf/2020/08/aa38539-20.pdf
Context. Large-scale equatorial Rossby modes have been observed on the Sun over the last two solar cycles. Aims. We investigate the impact of the time-varying zonal flows on the frequencies of Rossby modes. Methods. A first-order perturbation theory approach is used to obtain an expression for the expected shift in the mode frequencies due to perturbations in the internal rotation rate. Results. Using the time-varying rotation from helioseismic inversions we predict the changes in Rossby mode frequencies with azimuthal orders from m = 1 to m = 15 over the last two solar cycles. The peak-to-peak frequency change is less than 1 nHz for the m = 1 mode, grows with m, and reaches

25 nHz for m = 15. Conclusions. Given the observational uncertainties on mode frequencies due to the finite mode lifetimes, we find that the predicted frequency shifts are near the limit of detectability.

Fast Magnetoacoustic Wave Trains with Time-dependent Drivers

C. R. **Goddard**1 , V. M. Nakariakov1, 2 , and D. J. Pascoe3
A&A 624, L4 **2019**
https://warwick.ac.uk/fac/sci/physics/research/cfsa/people/goddard/wave_trains_crg.pdf
https://www.aanda.org/articles/aa/pdf/2019/04/aa35401-19.pdf
Context. Frequent observations of quasi-periodic rapidly-propagating wave trains in coronal structures have been made in the last decade. The dispersive evolution of fast magnetohydrodynamic waves propagating in coronal waveguides can provide a physical interpretation for many of these observations. Aims. Previous studies have considered the generation of fast wave trains by impulsive drivers which deposit energy instantaneously. The signatures of dispersively formed wave trains must depend on the temporal nature of the driver. We investigate the effect of varying the temporal width of the driving perturbation. Methods. 2D magnetohydrodynamic numerical simulations of impulsively generated wave trains in a guiding field-aligned density enhancement were performed with the novel addition of a time-dependant driver. Results. The final spatial and spectral signatures of the guided wave trains are found to depend strongly on the temporal duration of the initial perturbation. In particular, the wavelength (or frequency) of highest spectral amplitude is found to increase (decrease) with increasing temporal duration, whereas the spectral width decreases. Additionally, the efficiency of generation of fast wave trains is found to decrease strongly with increasing temporal width of the driver, with a cut-off at twice the internal Alfvén crossing time.

An Analysis of Alfvén Radius Based on Sunspot Number from 1749 to Today†

Molly L. **Goelzer**1,2, Nathan A. Schwadron2, Charles W. Smith
JGR, **2014,** Volume 119, Issue 1, 115–120
http://onlinelibrary.wiley.com/doi/10.1002/2013JA019420/pdf
The Solar Probe Plus mission now under construction will provide the first in situ measurements from inside the orbit of Mercury. The most critical part of that mission will be measurements from inside the Alfvén radius where the Alfvén speed exceeds the wind speed and the physics of the solar wind changes fundamentally due, in part, to the multidirectionality of wave propagation. In this region waves from both Sunward and anti-Sunward of the observation point can effect the local dynamics including the turbulent evolution, heating and acceleration of the plasma. While the location of this point can change with solar wind conditions, we ask the question of whether there is a systematic dependence on the solar cycle that moves the average Alfvén radius to different locations depending upon solar activity. We show that the average Alfvén radius is correlated with the sunspot number and moves systematically from ~ 15 at solar minimum to 30 solar radii at solar maximum. The analysis shown here does not predict movement of the Alfvén radius during the recent protracted solar minimum. We project the average Alfvén radius backward and forward in time using the monthly sunspot record to attempt a better understanding of the historical record and predict the behavior of this point during the coming solar cycle.

An Analysis of Heliospheric Magnetic Field Flux Based on Sunspot Number from 1749 to Today and Prediction for the Coming Solar Minimum

Molly L. **Goelzer**, Charles W. Smith, Nathan A. Schwadron and K. G. McCracken
JGR, 2013-**2014**
It is now well-established that many bulk properties of the solar wind rise and fall with the solar cycle and the heliospheric magnetic field (HMF) intensity is no exception. The HMF intensity is seen to be maximum around the time of solar maximum, lowest during solar minimum, and lower still during the recent protracted solar minimum 2006-2009. One explanation of this behavior can be found in the theory of Schwadron et al. (2010) that argues magnetic flux is injected into interplanetary space by coronal mass ejection (CME) eruptions and removed by reconnection in the low solar atmosphere. This produces an HMF intensity that is correlated with sunspot number and the rapid injection of flux followed by the slow removal by reconnection results in a hysteresis effect that is readily evident in the observations. Here for the first time we apply this theory to the sunspot record going back to 1749 and compare favorably our predictions to the results derived from 10Be observations. We also make a prediction for the coming solar minimum based on results from the Dalton Minimum.

A Statistical Analysis of Solar Surface Indices Through the Solar Activity Cycles 21-23

Umit Deniz **Goker**, Jagdev Singh, Ferhat Nutku, Muthu Priyal
MNRAS **2016**
http://arxiv.org/pdf/1604.03011v1.pdf
Variations of total solar irradiance (TSI), magnetic field, Ca II K-flux, faculae and plage areas due to the number and the type of sunspots/sunspot groups (SGs) are well established by using ground based data from various centers such as Solar Irradiance Platform, Stanford Data (SFO), Kodaikanal data (KKL) and National Geographical Data Center (NGDC) Homepage, respectively. We applied time series analysis for extracting the data over the descending phases of solar activity cycles (SACs) 21, 22 and 23, and the ascending phases 22 and 23 of SACs, and analyzed the

selected data using the Python programming language. Our detailed analysis results suggest that there is a stronger correlation between solar surface indices and the changes in the relative portion of the small and large SGs. This somewhat unexpected finding suggest that plage regions decreased in a lower values in spite of the higher number of large SGs in SAC 23 while Ca II K-flux did not decrease by large amount or it was comparable with SAC 22 for some years and relates with C type and DEF type SGs. Thus, increase of facular areas which are influenced by large SGs caused a small percentage decrease in TSI while decrement of plage areas triggered a higher decrease in the flux of magnetic field. Our results thus reveal the potential of such detailed comparison of SG analysis with solar surface indices for understanding and predicting future trends in the SAC.

Formation of the helium extreme-UV resonance lines

T. P. **Golding**1, J. Leenaarts2 and M. Carlsson
A&A 597, A102 (**2017**)
Context. While classical models successfully reproduce intensities of many transition region lines, they predict helium extreme-UV (EUV) line intensities roughly an order of magnitude lower than the observed value.

Aims. Our aim is to determine the relevant formation mechanism(s) of the helium EUV resonance lines capable of explaining the high intensities under quiet Sun conditions.
Methods. We synthesised and studied the emergent spectra from a 3D radiation-magnetohydrodynamics simulation model. The effects of coronal illumination and non-equilibrium ionisation of hydrogen and helium are included self-consistently in the numerical simulation.
Results. Radiative transfer calculations result in helium EUV line intensities that are an order of magnitude larger than the intensities calculated under the classical assumptions. The enhanced intensity of He iλ584 is primarily caused by He ii recombination cascades. The enhanced intensity of He iiλ304 and He iiλ256 is caused primarily by non-equilibrium helium ionisation.
Conclusions. The analysis shows that the long standing problem of the high helium EUV line intensities disappears when taking into account optically thick radiative transfer and non-equilibrium ionisation effects.

Non-equilibrium helium ionization in an MHD simulation of the solar atmosphere

Thomas Peter **Golding**, Jorrit Leenaarts, Mats Carlsson
ApJ 817 125 **2016**
http://arxiv.org/pdf/1512.04738v1.pdf
The ionization state of the gas in the dynamic solar chromosphere can depart strongly from the instantaneous statistical equilibrium commonly assumed in numerical modeling. We improve on earlier simulations of the solar atmosphere that only included non-equilbrium hydrogen ionization by performing a 2D radiation-magneto-hydrodynamics simulation featuring non-equilibrium ionization of both hydrogen and helium. The simulation includes the effect of hydrogen Lyman-α and the EUV radiation from the corona on the ionization and heating of the atmosphere. Details on code implementation are given. We obtain helium ion fractions that are far from their equilibrium values. Comparison with models with LTE ionization shows that non-equilibrium helium ionization leads to higher temperatures in wave fronts and lower temperatures in the gas between shocks. Assuming LTE ionization results in a thermostat-like behaviour with matter accumulating around the temperatures where the LTE ionization fractions change rapidly. Comparison of DEM curves computed from our models shows that non-equilibrium ionization leads to more radiating material in the temperature range 11-18 kK compared to models with LTE helium ionization. We conclude that non-equilbrium helium ionization is important for the dynamics and thermal structure of the upper chromosphere and transition region. It might also help resolve the problem that intensities of chromospheric lines computed from current models are smaller than those observed.

Detailed and Simplified Nonequilibrium Helium Ionization in the Solar Atmosphere

Thomas Peter **Golding**, Mats Carlsson, and Jorrit Leenaarts
2014 ApJ 784 30
Helium ionization plays an important role in the energy balance of the upper chromosphere and transition region. Helium spectral lines are also often used as diagnostics of these regions. We carry out one-dimensional radiation-hydrodynamics simulations of the solar atmosphere and find that the helium ionization is set mostly by photoionization and direct collisional ionization, counteracted by radiative recombination cascades. By introducing an additional recombination rate mimicking the recombination cascades, we construct a simplified three-level helium model atom consisting of only the ground states. This model atom is suitable for modeling nonequilibrium helium ionization in three-dimensional numerical models. We perform a brief investigation of the **formation of the He I 10830 and He II 304 spectral lines**. Both lines show nonequilibrium features that are not recovered with statistical equilibrium models, and caution should therefore be exercised when such models are used as a basis for interpretating observations.

Interpretation of the power spectrum of the quiet Sun photospheric turbulence

Itzhak **Goldman**

Volume 499, Issue 4, December **2020**, Pages 5363–5365,

https://arxiv.org/pdf/2010.07598.pdf

https://doi.org/10.1093/mnras/staa3238

Observational power spectra of the photospheric magnetic field turbulence, of the quiet-sun, were presented in a recent paper by Abramenko and Yurchyshyn. Here I focus on the power spectrum derived from the observations of the Near InfraRed Imaging Spectrapolarimeter (NIRIS) operating at the Goode Solar Telescope. The latter exhibits a transition from a power law with index −1.2 to a steeper power law with index −2.2, for smaller spatial scales. The present paper presents an interpretation of this change. Furthermore, this interpretation provides an estimate for the effective width of the turbulent layer probed by the observations. The latter turns out to be practically equal to the depth of the photosphere.

Solar Coronal Structure: Loops, Clouds, or Both?

Leon **Golub**1, Mahboubeh Asgari-Targhi1, Bruno Coppi2, and Bamandas Basu

2019 *Res. Notes AAS* **3** 4

http://iopscience.iop.org/article/10.3847/2515-5172/aafb75

In summary, based on the observation presented here, there is a diffuse or unresolved component to the X-ray corona, in addition to the well-defined loops. We will be conducting further observational analysis of these diffusive emission structures such as density and temperature measurements to provide a better understanding of these structures. Using estimates of density, temperature, magnetic field strength and their variations with height, we will develop further the theory. **2007 January 24.**

Probing the variations in the timing of the Sun's polar magnetic field reversals through observations and surface flux transport simulations

Elena M. **Golubeva**, Akash Biswas, Anna I. Khlystova, Pawan Kumar, Bidya Binay Karak

MNRAS **2023**

https://arxiv.org/pdf/2307.13452

The polar field reversal is a crucial process in the cyclic evolution of the large-scale magnetic field of the Sun.Various important characteristics of a solar cycle, such as its duration and strength, and also the cycle predictability, are determined by the polar field reversal time. While the regular measurements of solar magnetic field have been accumulated for more than half a century, there is no consensus in the heliophysics community concerning the interpretation of the Sun's polar field measurements and especially the determination of polar field reversal time. There exists a severe problem of non-reproducibility in the reported results even from studies of the same observational dataset, and this causes an obstacle to make more accurate forecasts of solar cycle. Here, we analyze the solar magnetograms from four instruments for the last four cycles, to provide a more correct interpretation of the polar field observations and to find more accurate time of the reversals. We show the absence of triple (multipolar) reversals in Cycles 21 - 24, significant variations in the time interval between reversals in the hemispheres and in the time interval between a reversal and a cycle beginning. In order to understand the origin of the reversal time variation, we perform Surface Flux Transport (SFT) simulations and find out that the presence of the 'anomalous' bipolar magnetic regions (BMRs) in different phases of a cycle can cause cycle-to-cycle variations of the reversal time within the similar range found in observations.

Rearrangements of Open Magnetic Flux and Formation of Polar Coronal Holes in Cycle 24

E.M. **Golubeva**, A.V.Mordvinov

Solar Phys. **2017**

https://arxiv.org/pdf/1711.01044.pdf

A method of synoptic map assimilation has been developed to study global rearrangements of open magnetic flux and formation of polar coronal holes (PCHs) in the current cycle. The analysis reveals ensembles of coronal holes (ECHs) which appear within unipolar magnetic regions associated with decaying activity complexes (ACs). The cause-effect relations between them explain asynchronous PCH formation observed at the northern and southern hemispheres of the Sun. Thus, the decay of large ACs, that were observed in 2014, led to formation of an extensive ECH, which then became the south PCH in mid-2015. Intricate structure of magnetic fields in the northern polar zone has impeded the north PCH formation, despite the fact that the dominant polarity at the North Pole reversed two years earlier than at the South Pole. The north PCH formed only by mid-2016 as the result of gradual merger of high-latitudinal ECHs associated with several decaying ACs.

Variations in Ratio and Correlation of Solar Magnetic Fields in the Fe i 525.02 nm and Na i 589.59 nm Lines According to Mount Wilson Measurements During 2000 – 2012

Elena **Golubeva**

Solar Phys. **2016**

Variations in the solar magnetic-field ratio over 13 years are analyzed, relying on the comparison of simultaneous measurements in two spectral lines at the Mount Wilson Observatory (MWO). The ratio and correlation coefficient are calculated over the general working range of measured magnetic-field values and in various ranges of the field magnitudes. Variations in both parameters are considered. We found the following tendencies: i) the parameters show changes with the cycle of solar activity in the general case; ii) their dependence on magnetic-field magnitude is a nonlinear function of time, and this is especially pronounced in the ratio behavior; iii) several separate ranges of the field magnitudes can be distinguished based on the behavioral patterns of the ratio variations. Correspondences between these ranges and the known structural objects of the solar atmosphere are discussed. This permits us to reach the conclusion that the dependence of parameters considered on the magnetic-field magnitude and time is connected with the variety of magnetic structural components and their cyclic rearrangements. The results represented may be useful for solving interpretation problems of solar magnetic-field measurements and for the cross-calibration of applicable instruments. They can also be of interest for tasks related to the creation of a uniform long temporal series of solar magnetic-field data from various sources.

Extended MHD modeling of the steady solar corona and the solar wind **Review**

Tamas I. **Gombosi**, Bart van der Holst, Ward B. Manchester, Igor V. Sokolov

Living Reviews in Solar Physics, **2018**

https://arxiv.org/pdf/1807.00417.pdf

The history and present state of large-scale magnetohydrodynamic (MHD) modeling of the solar corona and the solar wind with steady or quasi-steady coronal physics is reviewed. We put the evolution of ideas leading to the recognition of the existence of an expanding solar atmosphere into historical context. The development and main features of the first generation of global corona and solar wind models are described in detail. This historical perspective is also applied to the present suite of global corona and solar wind models. We discuss the evolution of new ideas and their implementation into numerical simulation codes. We point out the scientific and computational challenges facing these models and discuss the ways various groups tried to overcome these challenges. Next, we discuss the latest, state-of-the art models and point to the expected next steps in modeling the corona and the interplanetary medium.

High-frequency oscillations in small chromospheric bright features observed with ALMA

Juan Camilo Guevara **Gómez**, Shahin Jafarzadeh, Sven Wedemeyer, Mikolaj Szydlarski, Marco Stangalini, Bernhard Fleck, Peter Keys

Philosophical Transactions of the Royal Society A **2020**

https://arxiv.org/pdf/2008.04179.pdf

We report detection of oscillations in brightness temperature, size, and horizontal velocity of three small bright features in the chromosphere of a plage/enhanced-network region. The observations, which were taken with high temporal resolution (i.e., 2-sec cadence) with the Atacama Large Millimeter/submillimeter Array (ALMA) in Band 3 (centred at 3 mm; 100 GHz), exhibit three small-scale features with oscillatory behaviour with different, but overlapping, distributions of period on the order of, on average, 90±22 s, 110±12 s and 66±23 s, respectively. We find anti-correlations between perturbations in brightness temperature and size of the three features, which suggest the presence of fast sausage-mode waves in these small structures. In addition, the detection of transverse oscillations (although with a larger uncertainty) may suggest as well the presence of Alfvénic oscillations which are likely representative of kink waves. This work demonstrates the diagnostic potential of high-cadence observations with ALMA for detecting high-frequency magnetohydrodynamic waves in the solar chromosphere. Such waves can potentially channel a vast amount of energy into the outer atmosphere of the Sun. **2017 April 22**

The plasma β evolution through the solar corona during solar cycles 23 and 24

Jenny Marcela Rodríguez **Gómez**, Judith Palacios, Luis E. A. Vieira, Alisson Dal Lago

2019 *ApJ* **884** 88

https://arxiv.org/ftp/arxiv/papers/1910/1910.00894.pdf

https://doi.org/10.3847/1538-4357/ab40af

The plasma β is important to investigate the interchanging roles of plasma and magnetic pressure in the solar atmosphere. It can help to describe features over the photosphere and their changes at different heights. The goal is to obtain the plasma β variations through the solar corona during the solar cycles 23 and 24. The plasma β is reconstructed in different layers of the solar atmosphere. For this purpose, we use an updated version of COronal DEnsity and Temperature (CODET) model. In this version, we selected different features in the solar atmosphere such as Quiet Sun (QS), faculae and Active Regions (ARs). We calculate the β variations at different layers in the

solar corona (R= 1.14, 1.19, 1.23, 1.28, 1.34, 1.40, 1.46, 1.53, 1.61, 1.74, 1.79, 1.84 and 1.90 R). In the photosphere, we use temperature values from FALC model to obtain plasma β in QS and faculae. Additionally, variations of the magnetic and kinetic pressure were modelled during the last solar cycles at coronal heights.

Coronal Electron Density Temperature and Solar Spectral Irradiance during Solar Cycles 23 and 24

J. M Rodríguez **Gómez**1, L. Vieira1, A. Dal Lago1, and J. Palacios2
2018 ApJ 852 137
http://sci-hub.tw/http://iopscience.iop.org/0004-637X/852/2/137/
https://arxiv.org/ftp/arxiv/papers/1804/1804.04089.pdf
Plasma parameters such as the electron density and temperature play a key role in the dynamics of the solar atmosphere. These characteristics are important in solar physics because they can help us to understand the physics of the solar corona, the ultimate goal being the reconstruction of the electron density and temperature distributions in the solar corona. The relations between emission and plasma parameters in different timescales are studied. We present a physics-based model to reconstruct the density, temperature, and emission in the EUV band. This model, called COronal DEnsity and Temperature (CODET), is composed of a flux transport model, an extrapolation model, an emission model, and an optimization algorithm. The CODET model parameters were constrained by comparing the model's output to the TIMED/SEE record instead of direct observations because it covers a longer time interval than the direct solar observations currently available. The most important results of the current work are the recovery of SSI variability in specific wavelengths in the EUV band, as well as the variations in density and temperature during large timescales through the solar atmosphere with the CODET model. The evolution of the electron density and temperature profiles through the solar corona in different layers during solar cycles 23 and 24 will be presented. The emission maps were obtained and they are in accordance with the observations. Additionally, the density and temperature maps are related to the variations of the magnetic field in different layers through the solar atmosphere.

North and South Hemispheric Solar Activity for Cycles 21 – 23: Asymmetry and Conditional Volatility of Plage Region Areas

E. **Gonçalves**, N. Mendes-Lopes, I. Dorotovič, J. M. Fernandes, A. Garcia
Solar Physics, June **2014**, Volume 289, Issue 6, pp 2283-2296
We study the dynamic evolution of the time series describing the plage regions areas observed daily at the Observatório Astronómico da Universidade de Coimbra, in each one of the solar hemispheres during solar cycles 21 – 23. The classical ARMA model has proven to be insufficient to describe the time variations seen in the data because of the strong conditional variability. We found that the data are well fitted by ARMA mixed with power-δ TGARCH error models. The power index δ is non-integer; this property has recently been introduced in the literature on time-series analyses and indicates the presence of strong volatility and long memory in the data series. We also detected dynamic asymmetry in the plage region areas observed in the two hemispheres when two different temporal models were obtained to fit them. The finding of a dynamic asymmetry is also supported by the dynamic evolution of the daily difference (north–south) time series, which is significantly different from white noise. This statistical modeling of time series, taking into account new and different characteristics of the solar activity, will be very useful in subsequent forecast developments.

Temporal Correlation between Positive-Charged Cosmic Ray Flux and Solar Magnetic Field Variation: Insights from Delayed Modulation Analysis

Shaokun **Gong**, Linjing Duan, Jiawei Zhao, Xueyu Wei, Jie Feng, Zhibing Li
ApJ **2024**
https://arxiv.org/pdf/2409.17646
We present an analysis of the time-dependent modulation of galactic cosmic rays near Earth, with a focus on the cosmic proton flux and solar magnetic field strength. Using data from the Alpha Magnetic Spectrometer (AMS) and the Wilcox Solar Observatory, we identify a significant time-lagged relationship between the observation of two missions. Our model incorporates a weighted magnetic field parameter to address the hemispheric asymmetry in solar magnetic fields and captures the temporal evolution of cosmic-ray proton spectra in relation to solar activity. We find a time lag of approximately 10 months, varying with cosmic ray rigidity. At 1 GV, the time lag is 360 days, while it is 300 days above 3 GV. This offers predictive insights into cosmic ray modulation within the heliosphere. These results enhance the accuracy of space weather forecasting models, with significant implications for the safety of space missions and aviation.

Effects of resonant scattering of the Si IV doublet near 140 nm in a solar active region⋆

C. **Gontikakis**1 and J.-C. Vial2,3
A&A 619, A64 (**2018**)

http://sci-hub.tw/https://www.aanda.org/articles/aa/abs/2018/11/aa32563-17/aa32563-17.html
Aims. In a previous study we analysed the C IV 1548.189 Å and 1550.775 Å lines observed with the Solar Ultraviolet Measurements of Emitted Radiation (SUMER), showing cases where the 1548.189 Å spectral profile was noticeably different from the 1550.775 Å one, profiles that we dubbed differentially shaped profiles. We explained this differential behaviour by an important radiative contribution, affecting multiple plasma motions happening at the instrument sub-resolution scale. In the present study we examine more general cases where radiative effects may contribute to the emission from the transition region of an active region. Here we analyse the lines Si IV 1393.757 Å and 1402.772 Å observed with the Interface Region Imaging Spectrograph (IRIS).
Methods. We study active region NOAA 12529, observed with IRIS on **18 April 2016**. Using sorting techniques we selected individual profiles for which the intensity line ratio 1393.757 Å/1402.772 Å is significantly higher or lower than 2 and we also tracked differentially shaped profiles. We analyse the physical conditions that create these profiles and in some cases we estimate electron densities.
Results. We found more than 4000 individual profiles with line ratios higher than 2, about 500 profiles for which the line ratio is in the range 1.3–1.6, and 15 differentially shaped profiles. Line ratios higher than 2, are found along loops, and mostly at the y = 250 to 300″ part of the plage. There, we estimated the incident radiation and derived electron densities that can vary from 109 to a few times 1011 cm−3, depending on the plasma temperature. For the low line ratios, the sources are concentrated at the periphery of the active region plage, mostly along fibrils and present optical depths, τ, between 1.5 and 3. in most cases. The electron densities calculated from these Si IV profiles are comparable with electron densities derived using the O IV 1399.766 Å-1401.163 Å ratios.
Conclusions. We found that about 2.4% of the individual profiles for which we can perform a Gaussian fit present a line ratio higher than 2. In profiles with a high line ratio, the resonant scattering appears to be due to the combination of an average incident radiation field with a relatively low local electron density and not due to the vicinity of an ephemeral strong light source. As far as low intensity ratios are concerned, non-negligible optical depths are found at the edge of the plage, near the footpoints of fibrils that are oriented towards quiet Sun areas, where the electron density can be as high as (7 − 9) × 1011 cm−3 if we assume a plasma in ionization equilibrium.

On the Magnetic Nature of Quiet-Sun Chromospheric Grains

María Jesús Martínez **González**1,2, Tanausú del Pino Alemán1,2, Adur Pastor Yabar3, Carlos Quintero Noda1,2, and Andrés Asensio Ramos1,2
2023 ApJL 955 L40
https://iopscience.iop.org/article/10.3847/2041-8213/acfa97/pdf
Ca ii K grains, i.e., intermittent, short-lived (about 1 minute), periodic (2–4 minutes), pointlike chromospheric brightenings, are considered to be the manifestations of acoustic waves propagating upward from the solar surface and developing into shocks in the chromosphere. After the simulations of Carlsson and Stein, we know that hot shocked gas moving upward interacting with the downflowing chromospheric gas (falling down after having been displaced upward by a previous shock) nicely reproduces the spectral features of the Ca ii K profiles observed in such grains, i.e., a narrowband emission-like feature at the blue side of the line core. However, these simulations are one-dimensional and cannot explain the location or the pointlike shape of the grains. Here, we report on the magnetic nature of these events. Furthermore, we report on similar events occurring at the largest flux concentrations, though they are longer-lived (up to 8 minutes) and exhibit the typical signature of steep velocity gradients traveling across the atmosphere. The spectral signatures of the studied events resemble their counterparts in sunspots, the umbral flashes. We then propose that magnetohydrodynamical waves are not only channeled through the magnetic field in sunspots, but they pervade the whole atmosphere. The propagation along magnetic fields can explain the pointlike appearance of the calcium grains observed in the quiet chromosphere. **2015 Aug 19**

Numerical simulations of macrospicule jets under energy imbalance conditions in the solar atmosphere

J. J. **González-Avilés**, K. Murawski, A. K. Srivastava, T. V. Zaqarashvili, J. A. González-Esparza
MNRAS **2021**
https://arxiv.org/pdf/2104.14605.pdf
Using numerical simulations, we study the effects of thermal conduction and radiative cooling on the formation and evolution of solar jets with some macrospicules features. We initially assume that the solar atmosphere is rarely in equilibrium through energy imbalance. Therefore, we test whether the background flows resulting from an imbalance between thermal conduction and radiative cooling influence the jets' behavior. In this particular scenario, we trigger the formation of the jets by launching a vertical velocity pulse localized at the upper chromosphere for the following test cases: i) adiabatic case; ii) thermal conduction case; iii) radiative cooling case; iv) thermal conduction + radiative cooling case. According to the test results, the addition of the thermal conduction results in smaller and hotter jets than in the adiabatic case. On the other hand, the radiative cooling dissipates the jet after reaching the maximum height (≈ 5.5 Mm), making it shorter and colder than in the adiabatic and thermal conduction cases. Besides, the flow generated by the radiative cooling is more substantial than the caused by thermal conduction. Despite the energy imbalance of the solar atmosphere background, the simulated jet shows morphological features of macrospicules. Furthermore, the velocity pulse steepens into a shock that propagates

upward into a solar corona that maintains its initial temperature. The shocks generate the jets with a quasi-periodical behavior that follows a parabolic path on time-distance plots consistent with macrospicule jets' observed dynamics.

Joint action of Hall and ambipolar effects in 3D magneto-convection simulations of the quiet Sun. I. Dissipation and generation of waves

P. A. **Gonzalez-Morales**, E. Khomenko, N. Vitas, M. Collados

A&A **2020**

https://arxiv.org/pdf/2008.10429.pdf

The partial ionization of the solar plasma causes several nonideal effects such as the ambipolar diffusion, the Hall effect, and the Biermann battery effect. Here we report on the first three-dimensional realistic simulations of solar local dynamo where all three effects were taken into account. The simulations started with a snapshot of already saturated battery-seeded dynamo, where two new series were developed: one with solely ambipolar diffusion and another one also taking into account the Hall term in the generalized Ohm's law. The simulations were then run for about 4 hours of solar time to reach the stationary regime and improve the statistics. In parallel, a purely MHD dynamo simulation was also run for the same amount of time. The simulations are compared in a statistical way. The results show that, with the inclusion of the ambipolar diffusion, the amplitudes of the incompressible perturbations related to Alfven waves are reduced, and the Poynting flux is absorbed, with a frequency dependence. The Hall effect causes the opposite action: significant excess of incompressible perturbations is generated and an excess of the Poynting flux is observed in the chromospheric layers. The model with ambipolar diffusion shows, on average, sharper current sheets and slightly more abundant fast magneto-acoustic shocks in the chromosphere. The model with the Hall effect has higher temperatures at the lower chromosphere and stronger and more vertical magnetic field concentrations all over the chromosphere. The study of high-frequency waves reveals that significant power of incompressible perturbations is associated with areas with intense and more vertical magnetic fields and larger temperatures. We find a positive correlation between the magnitude of the ambipolar heating and the temperature increase at the same location after a characteristic time of 10^2 sec.

Spicule jets in the solar atmosphere modeled with resistive MHD and thermal conduction

J. J. **González-Avilés**, F. S. Guzmán, V. Fedun, G. Verth

ApJ 897:153 **2020**

https://arxiv.org/pdf/2005.13647.pdf

https://iopscience.iop.org/article/10.3847/1538-4357/ab97b8/pdf

Using numerical simulations, we study the effects of magnetic resistivity and thermal conductivity in the dynamics and properties of solar jets with characteristics of Type II spicules and cool coronal jets. The dynamic evolution of the jets is governed by the resistive MHD equations with thermal conduction along the magnetic field lines on a 2.5D slice. The magnetic field configuration consists of two symmetric neighboring loops with opposite polarity, used to support reconnection and followed by the plasma jet formation. In total 10 simulations were carried out with different values of resistivity and thermal conductivity, that produce jets with different morphological and thermal properties we quantify. We find that an increase in magnetic resistivity does not produce significant effects on the morphology, velocity and temperature of the jets. However, thermal conductivity affects both temperature and morphology of the jets. In particular, thermal conductivity causes jets to reach greater heights and increases the temperature of the jet-apex. Also, heat flux maps indicate the jet-apex and corona interchange energy more efficiently than the body of the jet. These results could potentially open a new avenue for plasma diagnostics in the Sun's atmosphere.

In situ generation of coronal Alfvén waves by jets

J J **González-Avilés** F S Guzmán V Fedun G Verth R Sharma S Shelyag S Regnier

MNRAS, Volume 484, Issue 2, 1 April **2019**, Pages 1936–1945,

https://doi.org/10.1093/mnras/stz087

Within the framework of 3D resistive magnetohydrodynamic, we simulate the formation of a plasma jet with the morphology, upward velocity up to 130 km s−1, and time-scale formation between 60 and 90 s after beginning of simulation, similar to those expected for type II spicules. Initial results of this simulation were published in paper by, e.g. González-Avilés et al. (2018), and present paper is devoted to the analysis of transverse displacements and rotational-type motion of the jet. Our results suggest that 3D magnetic reconnection may be responsible for the formation of the jet in paper by González-Avilés et al. (2018). In this paper, by calculating times series of the velocity components vvx and vvy in different points near to the jet for various heights we find transverse oscillations in agreement with spicule observations. We also obtain a time-distance plot of the temperature in a cross-cut at the plane x = 0.1 Mm and find significant transverse displacements of the jet. By analysing temperature isosurfaces of 104 K with the distribution of vvx, we find that if the line-of-sight (LOS) is approximately perpendicular to the jet axis then there is both motion towards and away from the observer across the width of the jet. This red–blue shift pattern of the jet is caused by rotational motion, initially clockwise and anti-clockwise afterwards, which could be interpreted as torsional motion and may generate torsional Alfvén waves in the corona region. From a nearly vertical

perspective of the jet the LOS velocity component shows a central blue-shift region surrounded by red-shifted plasma.

Fast-to-Alfvén mode conversion mediated by Hall current. II Application to the solar atmosphere

P. A. **González-Morales**, E. Khomenko, P. S. Cally
2019 *ApJ* **870** 94
https://arxiv.org/pdf/1811.06565.pdf
Coupling between fast magneto-acoustic and Alfvén waves can be observe in fully ionized plasmas mediated by stratification and 3D geometrical effects. In Paper I, Cally & Khomenko (2015) have shown that in a weakly ionized plasma, such as the solar photosphere and chromosphere, the Hall current introduces a new coupling mechanism. The present study extends the results from Paper I to the case of warm plasma. We report on numerical experiments where mode transformation is studied using quasi-realistic stratification in thermodynamic parameters resembling the solar atmosphere. This redresses the limitation of the cold plasma approximation assumed in Paper I, in particular allowing the complete process of coupling between fast and slow magneto-acoustic modes and subsequent coupling of the fast mode to the Alfvén mode through the Hall current. Our results confirm the efficacy of the mechanism proposed in Paper I for the solar case. We observe that the efficiency of the transformation is a sensitive function of the angle between the wave propagation direction and the magnetic field, and of the wave frequency. The efficiency increases when the field direction and the wave direction are aligned for increasing wave frequencies. After scaling our results to typical solar values, the maximum amplitude of the transformed Alfvén waves, for a frequency of 1 Hz, corresponds to an energy flux (measured above the height of peak Hall coupling) of ∼103 Wm−2, based on an amplitude of 500 ms−1 at β=1, which is sufficient to play a major role in both quiet and active region coronal heating.

MHDSTS: a new explicit numerical scheme for simulations of partially ionised solar plasma

P. A. **González-Morales**, E. Khomenko, T. P. Downes, A. de Vicente
A&A **2018**
https://arxiv.org/pdf/1803.04891.pdf
The interaction of plasma with magnetic field in the partially ionised solar atmosphere is frequently modelled via a single-fluid approximation, which is valid for the case of a strongly coupled collisional media, such as solar photosphere and low chromosphere. Under the single-fluid formalism the main non-ideal effects are described by a series of extra terms in the generalised induction equation and in the energy conservation equation. These effects are: Ohmic diffusion, ambipolar diffusion, the Hall effect, and the Biermann battery effect. From the point of view of the numerical solution of the single-fluid equations, when ambipolar diffusion or Hall effects dominate can introduce severe restrictions on the integration time step and can compromise the stability of the numerical scheme. In this paper we introduce two numerical schemes to overcome those limitations. The first of them is known as Super Time-Stepping (STS) and it is designed to overcome the limitations imposed when the ambipolar diffusion term is dominant. The second scheme is called the Hall Diffusion Scheme (HDS) and it is used when the Hall term becomes dominant. These two numerical techniques can be used together by applying Strang operator splitting. This paper describes the implementation of the STS and HDS schemes in the single-fluid code Mancha3D. The validation for each of these schemes is provided by comparing the analytical solution with the numerical one for a suite of numerical tests.

I. Jet Formation and Evolution due to 3D Magnetic Reconnection

J. J. **González-Avilés**, F. S. Guzmán, V. Fedun, G. Verth, S. Shelyag, S. Regnier
ApJ **2017**
https://arxiv.org/pdf/1709.05066.pdf
Using simulated data-driven three-dimensional resistive MHD simulations of the solar atmosphere, we show that magnetic reconnection can be responsible of the formation of jets with characteristic of Type II spicules. For this, we numerically model the photosphere-corona region using the C7 equilibrium atmosphere model. The initial magnetic configuration is a 3D potential magnetic field, extrapolated up to the solar corona region from a dynamic realistic simulation of solar photospheric magnetoconvection model which is mimicking quiet-Sun. In this case we consider a uniform and constant value of the magnetic resistivity of 12.56 Ω m. We have found that formation of the jets depends on the Lorentz force, which helps to accelerate the plasma upwards. Analyzing various properties of the jet dynamics, we found that the jet structure shows Doppler shift near to regions with high vorticity. The morphology, upward velocity, covering a range up to 100 km s−1, and life-time of the estructure, bigger than 100 s, are similar to those expected for Type II spicules.

Non-parametric PSF estimation from celestial transit solar images using blind deconvolution

Adriana **Gonzalez**, Véronique Delouille, Laurent Jacques

2015

http://arxiv.org/pdf/1412.6279v1.pdf

Context: Characterization of instrumental effects in astronomical imaging is important in order to extract accurate physical information from the observations. Optics are never perfect and the non-ideal path through the telescope is usually represented by the convolution of an ideal image with a Point Spread Function (PSF). Other sources of noise (read-out, Photon) also contaminate the image acquisition process. The problem of estimating both the PSF filter and a denoised image is called blind deconvolution and is ill-posed.
Aims: We propose a blind deconvolution scheme that relies on image regularization. Contrarily to most methods presented in the literature, it does not assume a parametric model of the PSF and can thus be applied to any telescope.
Methods: Our scheme uses a wavelet analysis image prior model and weak assumptions on the PSF filter's response. We use the observations from a celestial body transit where such object can be assumed to be a black disk. Such constraints limits the interchangeability between the filter and the image in the blind deconvolution problem.
Results: Our method is applied on synthetic and experimental data. We compute the PSF for SECCHI/EUVI instrument using the 2007 Lunar transit, and for SDO/AIA with the 2012 Venus transit. Results show that the proposed non-parametric blind deconvolution method is able to estimate the core of the PSF with a similar quality than parametric methods proposed in the literature. We also show that, if these parametric estimations are incorporated in the acquisition model, the resulting PSF outperforms both the parametric and non-parametric methods.

Key Processes in Solar-Terrestrial Physics

Walter D. **Gonzalez** · James L. Burch

Space Sci Rev (**2011**) 158: 1–3

During the week of October 4–9, 2009, about 160 participants from 19 countries met at the Itamambuca resort area of Ubatuba, Sao Paulo, Brazil to discuss the influence of solar variability on geophysical and heliospheric phenomena at a conference organized by the International Living With a Star (ILWS) Program of NASA and by the National Institute of Space Research (INPE) of Brazil.
Five of the invited review papers of this Conference appear in this **special issue.**

CAFE-PakalMPI: a new model to study the solar chromosphere in the NLTE approximation

J. J. **González-Avilés**, V. De la Luz

ApJ Supplement Series **2018**

https://arxiv.org/pdf/1808.07817.pdf

We present a new numerical model called CAFE-PakalMPI with the capability to solve the equations of classical magnetohydrodynamic (MHD) and to obtain the multispecies whose ionization states are calculated through statistical equilibrium, using the approximation of non-local thermodynamic equilibrium (NLTE) in three dimensions with the multiprocessor environment. For this, we couple the Newtonian CAFE MHD code introduced in Gonz\'alez-Avil\'es et al. (2015) with PakalMPI presented in De la Luz et al. (2010). In this model, Newtonian CAFE solves the equations of ideal MHD under the effects of magnetic resistivity and heat transfer considering a fully ionized plasma. On the other hand, PakalMPI calculates the density of ionization states using the NLTE approximation for Hydrogen, electronic densities and H-, the other species are computed by the classical local thermodynamic equilibrium (LTE) approximation. The main purpose of the model focuses on the analysis of solar phenomena within the chromospheric region. As an application of the model, we study the stability of the C7 equilibrium atmospheric model with a constant magnetic field in a 3D environment. According to the results of the test, the C7 model remains stable in the low chromosphere, while in the range $z \in [1.5,2.1]$ Mm we can observe the propagation of a wave produced by the changes in the ionization rate of H.

Newtonian CAFE: a new ideal MHD code to study the solar atmosphere

J.J.**Gonzalez-Aviles**, A.Cruz-Osorio, F.D.Lora-Clavijo, F.S.Guzman

MNRAS **2015**

http://arxiv.org/pdf/1509.00225v1.pdf

We present a new code designed to solve the equations of classical ideal magneto-hydrodynamics (MHD) in three dimensions, submitted to a constant gravitational field. The purpose of the code centers on the analysis of solar phenomena within the photosphere-corona region. We present 1D and 2D standard tests to demonstrate the quality of the numerical results obtained with our code. As solar tests we present the transverse oscillations of Alfvenic

pulses in coronal loops using a 2.5D model, and as 3D tests we present the propagation of impulsively generated MHD-gravity waves and vortices in the solar atmosphere. The code is based on high-resolution shock-capturing methods, uses the HLLE flux formula combined with Minmod, MC and WENO5 reconstructors. The divergence free magnetic field constraint is controlled using the Flux Constrained Transport method.

Estimating the contribution of Alfvén waves to the process of heating the quiet solar corona

J. J. **Gonzalez-Aviles**, F. S. Guzman
MNRAS **2015**
http://arxiv.org/pdf/1505.01401v1.pdf
We solve numerically the ideal MHD equations with an external gravitational field in 2D in order to study the effects of impulsively generated linear and non-linear Alfv\'en waves into isolated solar arcades and coronal funnels. We analyze the region containing the interface between the photosphere and the corona. The main interest is to study the possibility that Alfv\'en waves triggers the energy flux transfer toward the quiet solar corona and heat it, including the case that two consecutive waves can occur. We find that in the case of arcades, short or large, the transferred fluxes by Alfv\'en waves are sufficient to heat the quiet corona only during a small lapse of time and in a certain region. In the case of funnels the threshold is achieved only when the wave is faster than 10 km/s, which is extremely high. We conclude from our analysis, that Alfv\'en waves, even in the optimistic scenario of having two consecutive Alfv\'en wave pulses, cannot transport enough energy as to heat the quiet corona.

Improved SOT (Hinode mission) high resolution solar imaging observations

Hadis **Goodarzi**, Serge Koutchmy, Ali Adjabshirizadeh
Astrophysics and Space Science , 358:25 **2015**
http://arxiv.org/pdf/1506.08265v1.pdf
We consider the best today available observations of the Sun free of turbulent Earth atmospheric effects, taken with the Solar Optical Telescope (SOT) onboard the Hinode spacecraft. Both the instrumental smearing and the observed stray light are analyzed in order to improve the resolution. The Point Spread Function (PSF) corresponding to the blue continuum Broadband Filter Imager (BFI) near 450 nm is deduced by analyzing i/ the limb of the Sun and ii/ images taken during the transit of the planet Venus in 2012. A combination of Gaussian and Lorentzian functions is selected to construct a PSF in order to remove both smearing due to the instrumental diffraction effects (PSF core) and the large-angle stray light due to the spiders and central obscuration (wings of the PSF) that are responsible for the parasitic stray light. A Max-likelihood deconvolution procedure based on an optimum number of iterations is discussed. It is applied to several solar field images, including the granulation near the limb. The normal non-magnetic granulation is compared to the abnormal granulation which we call magnetic. A new feature appearing for the first time at the extreme- limb of the disk (the last 100 km) is discussed in the context of the definition of the solar edge and of the solar diameter. A single sunspot is considered in order to illustrate how effectively the restoration works on the sunspot core. A set of 125 consecutive deconvolved images is assembled in a 45 min long movie illustrating the complexity of the dynamical behavior inside and around the sunspot. **Febr. 28- March 1, 2007, 6th July 2012**

Conditions for Photospherically Driven Alfvenic Oscillations to Heat the Solar Chromosphere by Pedersen Current Dissipation

Michael L. **Goodman**
2011, Astrophysical Journal, 735, 45
http://arxiv.org/pdf/1410.8519v1.pdf
A magnetohydrodynamic model that includes a complete electrical conductivity tensor is used to estimate conditions for photospherically driven, linear, non-plane Alfvenic oscillations extending from the photosphere to the lower corona to drive a chromospheric heating rate due to Pedersen current dissipation that is comparable to the net chromospheric net radiative loss of ~107 ergs-cm−2-sec−1. The heating rates due to electron current dissipation in the photosphere and corona are also computed. The wave amplitudes are computed self-consistently as functions of an inhomogeneous background (BG) atmosphere. The effects of the conductivity tensor are resolved numerically using a resolution of 3.33 m. The oscillations drive a chromospheric heating flux FCh~107−108 ergs-cm−2-sec−1 at frequencies ν~102−103 mHz for BG magnetic field strengths B≳700 G and magnetic field perturbation amplitudes ~0.01−0.1 B. The total resistive heating flux increases with ν. Most heating occurs in the photosphere. Thermalization of Poynting flux in the photosphere due to electron current dissipation regulates the Poynting flux into the chromosphere, limiting FCh. FCh initially increases with ν, reaches a maximum, and then decreases with increasing ν due to increasing electron current dissipation in the photosphere. The resolution needed to resolve the oscillations increases from ~10 m in the photosphere to ~10 km in the upper chromosphere, and is proportional to ν−1/2. Estimates suggest that these oscillations are normal modes of photospheric flux tubes with diameters ~10−20 km, excited by magnetic reconnection in current sheets with thicknesses ~0.1 km.

Acceleration of Type 2 Spicules in the Solar Chromosphere. II. Viscous Braking and Upper Bounds on Coronal Energy Input

Michael L. **Goodman**

2014 ApJ 785 87

A magnetohydrodynamic model is used to determine conditions under which the Lorentz force accelerates plasma to type 2 spicule speeds in the chromosphere. The model generalizes a previous model to include a more realistic pre-spicule state, and the vertical viscous force. Two cases of acceleration under upper chromospheric conditions are considered. The magnetic field strength for these cases is ≤12.5 and 25 G. Plasma is accelerated to terminal vertical speeds of 66 and 78 km s–1 in 100 s, compared with 124 and 397 km s–1 for the case of zero viscosity. The flows are localized within horizontal diameters ~80 and 50 km. The total thermal energy generated by viscous dissipation is ~10 times larger than that due to Joule dissipation, but the magnitude of the total cooling due to rarefaction is this energy. Compressive heating dominates during the early phase of acceleration. The maximum energy injected into the corona by type 2 spicules, defined as the energy flux in the upper chromosphere, may largely balance total coronal energy losses in quiet regions, possibly also in coronal holes, but not in active regions. It is proposed that magnetic flux emergence in intergranular regions drives type 2 spicules.

The Persistent Mystery of Collisionless Shocks

Katherine **Goodrich**, Steven Schwartz, Lynn Wilson III, Ian Cohen, Drew Turner, Amir Caspi, Keith Smith, Randall Rose, Phyllis Whittlesey, Ferdinand Plaschke, Jasper Halekas, George Hospodarsky, James Burch, Imogen Gingell, Li-Jen Chen, Alessandro Retino, Yuri Khotyaintsev

White paper submitted to the Decadal Survey for Solar and Space Physics (Heliophysics) 2024-2033; **2023**

https://arxiv.org/pdf/2306.05491.pdf

Collisionless shock waves are one of the main forms of energy conversion in space plasmas. They can directly or indirectly drive other universal plasma processes such as magnetic reconnection, turbulence, particle acceleration and wave phenomena. Collisionless shocks employ a myriad of kinetic plasma mechanisms to convert the kinetic energy of supersonic flows in space to other forms of energy (e.g., thermal plasma, energetic particles, or Poynting flux) in order for the flow to pass an immovable obstacle. The partitioning of energy downstream of collisionless shocks is not well understood, nor are the processes which perform energy conversion. While we, as the heliophysics community, have collected an abundance of observations of the terrestrial bow shock, instrument and mission-level limitations have made it impossible to quantify this partition, to establish the physics within the shock layer responsible for it, and to understand its dependence on upstream conditions. This paper stresses the need for the first ever spacecraft mission specifically designed and dedicated to the observation of both the terrestrial bow shock as well as Interplanetary shocks in the solar wind.

Multi-point Assessment of the Kinematics of Shocks (MAKOS): A Heliophysics Mission Concept Study

Katherine A. **Goodrich**, Lynn B. Wilson III, Steven Schwartz, Ian J. Cohen, Drew L. Turner, Phyllis Whittlesey, Amir Caspi, Randall Rose, Keith Smith

White paper submitted to the Decadal Survey for Solar and Space Physics (Heliophysics) 2024-2033; **2023**

https://arxiv.org/ftp/arxiv/papers/2306/2306.05496.pdf

Collisionless shocks are fundamental processes that are ubiquitous in space plasma physics throughout the Heliosphere and most astrophysical environments. Earth's bow shock and interplanetary shocks at 1 AU offer the most readily accessible opportunities to advance our understanding of the nature of collisionless shocks via fully-instrumented, in situ observations. One major outstanding question pertains to the energy budget of collisionless shocks, particularly how exactly collisionless shocks convert incident kinetic bulk flow energy into thermalization (heating), suprathermal particle acceleration, and a variety of plasma waves, including nonlinear structures. Furthermore, it remains unknown how those energy conversion processes change for different shock orientations (e.g., quasi-parallel vs. quasi-perpendicular) and driving conditions (upstream Alfvénic and fast Mach numbers, plasma beta, etc.). Required to address these questions are multipoint observations enabling direct measurement of the necessary plasmas, energetic particles, and electric and magnetic fields and waves, all simultaneously from upstream, downstream, and at the shock transition layer with observatory separations at ion to magnetohydrodynamic (MHD) scales. Such a configuration of spacecraft with specifically-designed instruments has never been available, and this white paper describes a conceptual mission design -- MAKOS -- to address these outstanding questions and advance our knowledge of the nature of collisionless shocks.

Impacts of Training Windows, Data Volumes, and the Solar Cycle

Griffin T. **Goodwin**, Viacheslav M. Sadykov, Petrus C. Martens

ApJ **2024**
https://arxiv.org/pdf/2402.05288.pdf
This study explores the behavior of machine learning-based flare forecasting models deployed in a simulated operational environment. Using Georgia State University's Space Weather Analytics for Solar Flares benchmark dataset (Angryk et al. 2020a,b), we examine the impacts of training methodology and the solar cycle on decision tree, support vector machine, and multilayer perceptron performance. We implement our classifiers using three temporal training windows: stationary, rolling, and expanding. The stationary window trains models using a single set of data available before the first forecasting instance, which remains constant throughout the solar cycle. The rolling window trains models using data from a constant time interval before the forecasting instance, which moves with the solar cycle. Finally, the expanding window trains models using all available data before the forecasting instance. For each window, a number of input features (1, 5, 10, 25, 50, 120) and temporal sizes (5, 8, 11, 14, 17, 20 months) were tested. To our surprise, we found that for a 20-month window, skill scores were comparable regardless of the window type, feature count, and classifier selected. Furthermore, reducing the size of this window only marginally decreased stationary and rolling window performance. This implies that, given enough data, a stationary window can be chosen over other window types, eliminating the need for model retraining. Lastly, a moderately strong positive correlation was found to exist between a model's false positive rate and the solar X-ray background flux. This suggests that the solar cycle phase has a considerable influence on forecasting.

Mixed properties of magnetohydrodynamic waves undergoing resonant absorption in the cusp continuum

Marcel **Goossens**, Shao-Xia Chen, Michaël Geeraerts, Bo Li, Tom Van Doorsselaere
A&A 646, A86 (**2021**)
https://arxiv.org/pdf/2012.06303.pdf
Observations of magnetohydrodynamic (MHD) waves in the structured solar atmosphere have shown that these waves are damped and can thus contribute to atmospheric heating. In this paper, we focus on the damping mechanism of resonant absorption in the cusp continuum. This process takes places when waves travel through an inhomogeneous plasma. Our aim is to determine the properties of MHD waves undergoing resonant absorption in the cusp continuum in the transition layer of a cylindrical solar atmospheric structure, such as a photospheric pore or a coronal loop. Depending on which quantities dominate, one can assess what type of classical MHD wave the modes in question resemble most. In order to study the properties of these waves, we analytically determine the spatial profiles of compression, displacement, and vorticity for waves with frequencies in the cusp continuum, which undergo resonant absorption. We confirm these analytical derivations via numerical calculations of the profiles in the resistive MHD framework. We show that the dominant quantities for the modes in the cusp continuum are the displacement parallel to the background magnetic field and the vorticity component in the azimuthal direction (i.e. perpendicular to the background magnetic field and along the loop boundary).

Resonant absorption: transformation of compressive motions into vortical motions

M. **Goossens**, I. Arregui, R. Soler, T. Van Doorsselaere
A&A, 641, A106 (**2020**)
https://arxiv.org/pdf/2009.08152.pdf
This paper investigates the changes in spatial properties when magnetohydrodynamic (MHD) waves undergo resonant damping in the Alfvén continuum. The analysis is carried out for a 1D cylindrical pressure-less plasma with a straight magnetic field. The effect of the damping on the spatial wave variables is determined by using complex frequencies that arise as a result of the resonant damping. Compression and vorticity are used to characterise the spatial evolution of the MHD wave. The most striking result is the huge spatial variation in the vorticity component parallel to the magnetic field. Parallel vorticity vanishes in the uniform part of the equilibrium. However, when the MHD wave moves into the non-uniform part, parallel vorticity explodes to values that are orders of magnitude higher than those attained by the transverse components in planes normal to the straight magnetic field. In the non-uniform part of the equilibrium plasma, the MHD wave is controlled by parallel vorticity and resembles an Alfvén wave, with the unfamiliar property that it has pressure variations even in the linear regime.

The Transverse and Rotational Motions of Magnetohydrodynamic Kink Waves in the Solar Atmosphere

M. **Goossens**1, R. Soler2, J. Terradas2, T. Van Doorsselaere1, and G. Verth
2014 ApJ 788 9
Magnetohydrodynamic (MHD) kink waves have now been observed to be ubiquitous throughout the solar atmosphere. With modern instruments, they have now been detected in the chromosphere, interface region, and corona. The key purpose of this paper is to show that kink waves do not only involve purely transverse motions of solar magnetic flux tubes, but the velocity field is a spatially and temporally varying sum of both transverse and rotational motion. Taking this fact into account is particularly important for the accurate interpretation of varying Doppler velocity profiles across oscillating structures such as spicules. It has now been shown that, as well as bulk

transverse motions, spicules have omnipresent rotational motions. Here we emphasize that caution should be used before interpreting the particular MHD wave mode/s responsible for these rotational motions. The rotational motions are not necessarily signatures of the classic axisymmetric torsional Alfvén wave alone, because kink motion itself can also contribute substantially to varying Doppler velocity profiles observed across these structures. In this paper, the displacement field of the kink wave is demonstrated to be a sum of its transverse and rotational components, both for a flux tube with a discontinuous density profile at its boundary, and one with a more realistic density continuum between the internal and external plasma. Furthermore, the Doppler velocity profile of the kink wave is forward modeled to demonstrate that, depending on the line of sight, it can either be quite distinct or very similar to that expected from a torsional Alfvén wave.

Implications of the abundance of halo coronal mass ejections for the strength of solar cycle 25

Nat **Gopalswamy**, Grzegorz Michalek, Seiji Yashiro, Pertti Makela, Sachiko Akiyama, Hong Xie
Proceedings of IAU Symposium 388 **2024**
https://arxiv.org/pdf/2407.04548
We assess the relative strength of solar cycle (SC) 25 with respect to SCs 23 and 24 based on the abundance of halo coronal mass ejections (CMEs). We make use of the halo CME database (this https URL) to compare the halo CME abundance during the first four years in each of SCs 23 to 25. The main result is that in several aspects such as the abundance, occurrence rate, source locations, and halo heights, halo CMEs are similar between SCs 24 and 25 but different from SC 23. This result follows from the fact that weaker cycles have low heliospheric total pressure, whose backreaction on CMEs allows them to expand more and hence enhancing the chance of becoming a halo. The solar cycle variation of halo CME properties is consistent with the precursor-based cycle prediction methods that indicate SC 25 is similar to or only slightly stronger than SC 24.

What do halo CMEs tell us about solar cycle 25?

Nat **Gopalswamy**, Grzegorz Michalek, Seiji Yashiro, Pertti Mäkelä, Sachiko Akiyama, Hong Xie
ApJL **952** L13 **2023**
https://arxiv.org/ftp/arxiv/papers/2306/2306.06633.pdf
https://iopscience.iop.org/article/10.3847/2041-8213/acdde2/pdf
It is known that the weak state of the heliosphere due to diminished solar activity in cycle 24 back-reacted on coronal mass ejections (CMEs) to make them appear wider for a given speed. One of the consequences of the weak state of the heliosphere is that more CMEs appear as halo CMEs (HCMEs), and halos are formed at shorter heliocentric distances. Current predictions for the strength of solar cycle (SC) 25 range from half to twice the strength of SC 24. We compare the HCME occurrence rate and other properties during the rise phase of cycles 23, 24, and 25 to weigh in on the strength of SC 25. We find that HCME and solar wind properties in SC 25 are intermediate between SCs 23 and 24, but closer to SC 24. The HCME occurrence rate, normalized to the sunspot number, is higher in SCs 24 and 25 than in SC 23. The solar wind total pressure in SC 25 is ~35% smaller than that in SC 23. Furthermore, the occurrence rates of high-energy solar energetic particle events and intense geomagnetic storms are well below the corresponding values in SC 23, but similar to those in SC 24. We conclude that cycle 25 is likely to be similar to or slightly stronger than cycle 24, in agreement with polar-field precursor methods for cycle 25 prediction.

Solar Activity and Space Weather **Review**

Nat **Gopalswamy**, Pertti Mäkelä, Seiji Yashiro, Sachiko Akiyama, Hong Xie
Journal of Physics: Conference Series, Proc. 2nd International Symposium on Space Science 2021, LAPAN, Indonesia **2022**
https://arxiv.org/ftp/arxiv/papers/2201/2201.02724.pdf **File**
After providing an overview of solar activity as measured by the sunspot number (SSN) and space weather events during solar cycles (SCs) 21-24, we focus on the weak solar activity in SC 24. The weak solar activity reduces the number of energetic eruptions from the Sun and hence the number of space weather events. The speeds of coronal mass ejections (CMEs), interplanetary (IP) shocks, and the background solar wind all declined in SC 24. One of the main heliospheric consequences of weak solar activity is the reduced total (magnetic + gas) pressure, magnetic field strength, and Alfvén speed. There are three groups of phenomena that decline to different degrees in SC 24 relative to the corresponding ones in SC 23: (i) those that decline more than SSN does, (ii) those that decline like SSN, and (iii) those that decline less than SSN does. The decrease in the number of severe space weather events such as high-energy solar energetic particle (SEP) events and intense geomagnetic storms is deeper than the decline in SSN. CMEs expand anomalously and hence their magnetic content is diluted resulting in weaker geomagnetic storms. The reduction in the number of intense geomagnetic storms caused by corotating interaction regions is also drastic. The diminished heliospheric magnetic field in SC 24 reduces the efficiency of particle acceleration, resulting in fewer high-energy SEP events. The numbers of IP type II radio bursts, IP socks, and high-intensity energetic storm particle events closely follow the number of fast and wide CMEs (and approximately SSN). The number of halo CMEs in

SC 24 declines less than SSN does, mainly due to the weak heliospheric state. Phenomena such as IP CMEs and magnetic clouds related to frontside halos also do not decline significantly. The mild space weather is likely to continue in SC 25, whose strength has been predicted to be not too different from that of SC 24.
Table 1. Comparison of various parameters between solar cycles 23 and 24
Table 2. List of intense storms in cycle 23 and 24 and the associated coronal hole properties

The Multiview Observatory for Solar Terrestrial Science (MOST)

Gopalswamy, Nat ; Kucera, Therese ; Leake, James ; MacDowall, Robert ; Wilson, Lynn ; et al.
AGU Fall Meeting 2021, held in New Orleans, LA, 13-17 December 2021, id. SH12A-07. **2022**
The Multiview Observatory for Solar Terrestrial Science (MOST) is a comprehensive mission concept targeting the magnetic coupling between the solar interior and the heliosphere. The wide-ranging imagery and time series data from MOST will help understand the solar drivers and the heliospheric responses as a system, discerning and tracking 3D magnetic field structures, both transient and quiescent in the inner heliosphere. MOST will have seven remote-sensing and three in-situ instruments: (1) Magnetic and Doppler Imager (MaDI) to investigate surface and subsurface magnetism by exploiting the combination of helioseismic and magnetic-field measurements in the photosphere; (2) Inner Coronal Imager in EUV (ICIE) to study large-scale structures such as active regions, coronal holes and eruptive structures by capturing the magnetic connection between the photosphere and the corona to about 3 solar radii; (3) Hard X-ray Imager (HXI) to image the non-thermal flare structure; (4) White-light Coronagraph (WCOR) to seamlessly study transient and quiescent large-scale coronal structures extending from the ICIE field of view (FOV); (5) Faraday Effect Tracker of Coronal and Heliospheric structures (FETCH), a novel radio package to determine the magnetic field structure and plasma column density, and their evolution within 0.5 au; (6) Heliospheric Imager with Polarization (HIP) to track solar features beyond the WCOR FOV, study their impact on Earth, and provide important context for FETCH; (7) Radio and Plasma Wave instrument (M/WAVES) to study electron beams and shocks propagating into the heliosphere via passive radio emission; (8) Solar High-energy Ion Velocity Analyzer (SHIVA) to determine spectra of electrons, and ions from H to Fe at multiple spatial locations and use energetic particles as tracers of magnetic connectivity; (9) Solar Wind Magnetometer (MAG) to characterize magnetic structures at 1 au; (10) Solar Wind Plasma Instrument (SWPI) to characterize plasma structures at 1 au. MOST will have two large spacecraft with identical payloads deployed at L4 and L5 and two smaller spacecraft ahead of L4 and behind L5 to carry additional FETCH elements. MOST will build upon SOHO and STEREO achievements to expand the multiview observational approach into the first half of the 21st Century.

The Balloon-borne Investigation of Temperature and Speed of Electrons in the corona (BITSE): Mission Description and Preliminary Results

N. **Gopalswamy**, J. Newmark, S. Yashiro, P. Mäkelä, N. Reginald, N. Thakur, Q. Gong, Y-H. Kim, K-S. Cho, S-H. Choi, J-H. Baek, S-C. Bong, H-S. Yang, J-Y. Park, J-H. Kim, Y-D. Park, J.-O. Lee, R.-S. Kim, E.-K. Lim
Solar Phys. **296**, Article number: 15 (**2021**)
https://arxiv.org/ftp/arxiv/papers/2011/2011.06111.pdf
https://link.springer.com/content/pdf/10.1007/s11207-020-01751-8.pdf
We report on the Balloonborne Investigation of Temperature and Speed of Electrons in the corona (BITSE) mission launched recently to observe the solar corona from about 3 Rs to 15 Rs at four wavelengths (393.5, 405.0, 398.7, and 423.4 nm). The BITSE instrument is an externally occulted single stage coronagraph developed at NASA's Goddard Space Flight Center in collaboration with the Korea Astronomy and Space Science Institute (KASI). BITSE used a polarization camera that provided polarization and total brightness images of size 1024 x 1024 pixels. The Wallops Arc Second Pointing (WASP) system developed at NASA's Wallops Flight Facility (WFF) was used for Sun-pointing. The coronagraph and WASP were mounted on a gondola provided by WFF and launched from the Fort Sumner, New Mexico station of Columbia Scientific Balloon Facility (CSBF) on **September 18, 2019**. BITSE obtained 17,060 coronal images at a float altitude of about 128,000 feet (39 km) over a period of about 4 hrs. BITSE flight software was based on NASA's core Flight System, which was designed to help develop flight quality software. We used EVTM (Ethernet Via Telemetry) to download science data during operations; all images were stored onboard using flash storage. At the end of the mission, all data were recovered and analyzed. Preliminary analysis shows that BITSE imaged the solar minimum corona with the equatorial streamers on the east and west limbs. The narrow streamers observed by BITSE are in good agreement with the geometric properties obtained by SOHO coronagraphs in the overlapping physical domain. In spite of the small signal-to-noise ratio (about 14) we were able to obtain the temperature and flow speed of the western steamer region in the range 4 to 7 Rs as: For the equatorial streamer on the west limb, we obtained a temperature of 1.0 +/- 0.3 MK and a flow speed of about 260 km/s with a large uncertainty interval.

Long-term Solar Activity Studies using Microwave Imaging Observations and Prediction for Cycle 25

N. **Gopalswamy**, P. Makela, S. Yashiro, S. Akiyama
Journal of Atmospheric and Solar-Terrestrial Physics Volume 176, Pages 26-33 **2018**
https://arxiv.org/ftp/arxiv/papers/1804/1804.02544.pdf
We use microwave imaging observations from the Nobeyama Radioheliograph at 17 GHz for long-term studies of solar activity. In particular, we use the polar and low-latitude brightness temperatures as proxies to the polar magnetic field and the active-regions, respectively. We also use the location of prominence eruptions as a proxy to the filament locations as a function of time. We show that the polar microwave brightness temperature is highly correlated with the polar magnetic field strength and the fast solar wind speed. We also show that the polar microwave brightness at one cycle is correlated with the low latitude brightness with a lag of about half a solar cycle. We use this correlation to predict the strength of the solar cycle: the smoothed sunspot numbers in the southern and northern hemispheres can be predicted as 89 and 59, respectively. These values indicate that cycle 25 will not be too different from cycle 24 in its strength. We also combined the rush to the pole data from Nobeyama prominences with historical data going back to 1860 to study the north-south asymmetry of sign reversal at solar poles. We find that the reversal asymmetry has a quasi-periodicity of 3-5 cycles.

Unusual Polar Conditions in Solar Cycle 24 and their Implications for Cycle 25

Nat **Gopalswamy**, Seiji Yashiro, Sachiko Akiyama
ApJ Lett. 823 L15 **2016**
https://arxiv.org/ftp/arxiv/papers/1605/1605.02217.pdf
We report on the prolonged solar-maximum conditions until late 2015 at the north-polar region of the Sun indicated by the occurrence of high-latitude prominence eruptions and microwave brightness temperature close to the quiet Sun level. These two aspects of solar activity indicate that the polarity reversal was completed by mid-2014 in the south and late 2015 in the north. . The microwave brightness in the south-polar region has increased to a level exceeding the level of cycle 23/24 minimum, but just started to increase in the north. The north-south asymmetry in the polarity reversal has switched from that in cycle 23. These observations lead us to the hypothesis that the onset of cycle 25 in the northern hemisphere is likely to be delayed with respect to that in the southern hemisphere. We find that the unusual condition in the north is a direct consequence of the arrival of poleward surges of opposite polarity from the active region belt. We also find that multiple rush-to-the-pole episodes were indicated by the prominence eruption locations that lined up at the boundary between opposite polarity surges. The high-latitude prominence eruptions occurred in the boundary between the incumbent polar flux and the insurgent flux of opposite polarity.

Solar Activity Studies using Microwave Imaging Observations

Nat **Gopalswamy**
URSI Asia-Pacific Radio Science Conference in Seoul, August 21-25, 2016 **2016**
2016)
http://arxiv.org/pdf/1605.02221v1.pdf
We report on the status of solar cycle 24 based on polar prominence eruptions (PEs) and microwave brightness enhancement (MBE) information obtained by the Nobeyama radioheliograph. The north polar region of the Sun had near-zero field strength for more than three years (2012 to 2015) and ended only in September 2015 as indicated by the presence of polar PEs and the lack of MBE. The zero-polar-field condition in the south started only around 2013, but it ended by June 2014. Thus the asymmetry in the times of polarity reversal switched between cycle 23 and 24. The polar MBE is a good proxy for the polar magnetic field strength as indicated by the high degree of correlation between the two. The cross-correlation between the high- and low-latitude MBEs is significant for a lag of ~5.5 to 7.3 years, suggesting that the polar field of one cycle indicates the sunspot number of the next cycle in agreement with the Babcock-Leighton mechanism of solar cycles. The extended period of near-zero field in the north-polar region should result in a weak and delayed sunspot activity in the northern hemisphere in cycle 25. **11 Dec 2014, 30 Aug 2015**

CMEs during the Two Activity Peaks in Cycle 24 and their Space Weather Consequences

N. **Gopalswamy**, P. Mäkelä, S. Akiyama, S. Yashiro, N. Thakur
Sun and Geosphere, **2015**
http://arxiv.org/pdf/1509.04216v1.pdf **File**
We report on a comparison between space weather events that occurred around the two peaks in the sunspot number (SSN) during solar cycle 24. The two SSN peaks occurred in the years 2012 and 2014. Even though SSN was larger during the second peak, we find that there were more space weather events during the first peak. The space weather events we considered are large solar energetic particle (SEP) events and major geomagnetic storms associated with coronal mass ejections (CMEs). We also considered interplanetary type II radio bursts, which are indicative of

energetic CMEs driving shocks. When we compared the CME properties between the two SSN peaks, we find that more energetic CMEs occurred during the 2012 peak. In particular, we find that CMEs accompanying IP type II bursts had an average speed of 1543 km/s during the 2012 peak compared to 1201 km/s during the 2014 peak. This result is consistent with the reduction in the average speed of the general population of CMEs during the second peak. All SEP events were associated with the interplanetary type II bursts, which are better than halo CMEs as indicators of space weather. The comparison between the two peaks also revealed the discordant behavior CME rate and SSN is more pronounced during the second peak. None of the 14 disk-center halo CMEs was associated with a major storm in 2014. The lone major storm in 2014 was due to the intensification of the (southward) magnetic field in the associated magnetic cloud by a shock that caught up and propagated into the magnetic cloud. **23-24 Apr 2012; 18-19 Feb 2014**

Table 2. List of DH-km type II bursts in 2012, the associated CMEs and SEP events

Table 3. List of DH-km type II bursts in 2014, the associated CMEs and SEP events

The Mild Space Weather in Solar Cycle 24

Nat **Gopalswamy**, Sachiko Akiyama, Seiji Yashiro, Hong Xie, Pertti Makela, Grzegorz Michalek
Proc. 14th International Ionospheric Effects Symposium on 'Bridging the gap between applications and research involving ionospheric and space weather disciplines' May 12-14, **2015**, Alexandria, VA
http://arxiv.org/ftp/arxiv/papers/1508/1508.01603.pdf

The space weather is extremely mild during solar cycle 24: the number of major geomagnetic storms and high-energy solar energetic particle events are at the lowest since the dawn of the space age. Solar wind measurements at 1 AU using Wind and ACE instruments have shown that there is a significant drop in the density, magnetic field, total pressure, and Alfven speed in the inner heliosphere as a result of the low solar activity. The drop in large space weather events is disproportionately high because the number of energetic coronal mass ejections that cause these events has not decreased significantly. For example, the rate of halo CMEs, which is a good indicator of energetic CMEs, is similar to that in cycle 23, even though the sunspot number has declined by about 40%. The mild space weather seems to be a consequence of the anomalous expansion of CMEs due to the low ambient pressure in the heliosphere. The anomalous expansion results in the dilution of the magnetic contents of CMEs, so the geomagnetic storms are generally weak. CME driven shocks propagating through the weak heliospheric field are less efficient in accelerating energetic particles, so the particles do not attain high energies. Finally, we would like to point out that extreme events such as the 2012 July 23 CMEs that occurred on the backside of the Sun and did not affect Earth except for a small proton event. **March 17, 2015**

Short term Variability of the Sun Earth System: An Overview of Progress Made during the CAWSES II Period **Review**

Nat **Gopalswamy**, Bruce Tsurutani, Yihua Yan
Progress in Earth and Planetary Science, v. 2, 13, **2015, File**
http://arxiv.org/pdf/1504.06332v1.pdf

This paper presents an overview of results obtained during the CAWSES II period on the short term variability of the Sun and how it affects the near Earth space environment. CAWSES II was planned to examine the behavior of the solar terrestrial system as the solar activity climbed to its maximum phase in solar cycle 24. After a deep minimum following cycle 23, the Sun climbed to a very weak maximum in terms of the sunspot number in cycle 24 (MiniMax24), so many of the results presented here refer to this weak activity in comparison with cycle 23. The short term variability that has immediate consequence to Earth and geospace manifests as solar eruptions from closed field regions and high speed streams from coronal holes. Both electromagnetic (flares) and mass emissions (coronal mass ejections, CMEs) are involved in solar eruptions, while coronal holes result in high speed streams that collide with slow wind forming the so called corotating interaction regions (CIRs). Fast CMEs affect Earth via leading shocks accelerating energetic particles and creating large geomagnetic storms. CIRs and their trailing high speed streams (HSSs), on the other hand, are responsible for recurrent small geomagnetic storms and extended (days) of auroral zone activity, respectively. The latter lead to the acceleration of relativistic magnetospheric killer electrons. One of the major consequences of the weak solar activity is the altered physical state of the heliosphere that has serious implications for the shock-driving and storm causing properties of CMEs. Finally, a discussion is presented on extreme space weather events prompted by the 2012 July 23 super storm event that occurred on the backside of the Sun. Many of these studies were enabled by the simultaneous availability of remote-sensing and in situ observations from multiple vantage points with respect to the Sun Earth line.

TABLE 2 Major geomagnetic storms of cycle 24 (Dst < -100 nT)

Anomalous Expansion of Coronal Mass Ejections during Solar Cycle 24 and its Space Weather Implications

Nat **Gopalswamy**, Sachiko Akiyama, Seiji Yashiro, Hong Xie, and Pertti M?kel?, Grzegorz Michalek
E-print, April **2014**; GRL

The familiar correlation between the speed and angular width of coronal mass ejections (CMEs) is also found in solar cycle 24, but the regression line has a larger slope: for a given CME speed, cycle 24 CMEs are significantly wider than those in cycle 23. The slope change indicates a significant change in the physical state of the heliosphere, due to the weak solar activity. The total pressure in the heliosphere (magnetic + plasma) is reduced by ~40%, which leads to the anomalous expansion of CMEs explaining the increased slope. The excess CME expansion contributes to the diminished effectiveness of CMEs in producing magnetic storms during cycle 24, both because the magnetic content of the CMEs is diluted and also because of the weaker ambient fields. The reduced magnetic field in the heliosphere may contribute to the lack of solar energetic particles accelerated to very high energies during this cycle.

Testing the empirical shock arrival model using quadrature observations

N. **Gopalswamy**1,*, P. Mäkelä, 1,2, H. Xie1,2, S. Yashiro
Space Weather, Volume 11, Issue 11, pages 661–669, November **2013**
http://cdaw.gsfc.nasa.gov/publications/gopal/gopal2013SW_testESA.pdf

The empirical shock arrival (ESA) model was developed based on quadrature data from Helios (in situ) and P-78 (remote sensing) to predict the Sun-Earth travel time of coronal mass ejections (CMEs). The ESA model requires earthward CME speed as input, which is not directly measurable from coronagraphs along the Sun-Earth line. The Solar Terrestrial Relations Observatory (STEREO) and the Solar and Heliospheric Observatory (SOHO) were in quadrature during 2010–2012, so the speeds of Earth-directed CMEs were observed with minimal projection effects. We identified a set of 20 full halo CMEs in the field of view of SOHO that were also observed in quadrature by STEREO. We used the earthward speed from STEREO measurements as input to the ESA model and compared the resulting travel times with the observed ones from L1 monitors. We find that the model predicts the CME travel time within about 7.3 h, which is similar to the predictions by the ENLIL model. We also find that CME-CME and CME-coronal hole interaction can lead to large deviations from model predictions. **2011 February 15, 2012 July 12**

Table 1. List of shocks detected at L1 and the corresponding halo CMEs observed by SOHO
Table 2. List of events with coronal holes visible on the disk.
Table 3. The number of preceding CMEs within a 24 h interval preceding the CMEs in Table 1

Energetic Particle and Other Space Weather Events of Solar Cycle 24

N. **Gopalswamy**
E-print, Jan 2013, **File**; In Space Weather: The space Radiation Environment, Ed. Q. Hu, G. Li, G. P. Zank, X. Ao, O. Verkhoglyadova, J. H. Adama, AIP Conf Proc. 1500, pp. 14-19, **2012**

We report on the space weather events of solar cycle 24 in comparison with those during a similar epoch in cycle 23. We find major differences in all space weather events: solar energetic particles, geomagnetic storms, and interplanetary shocks. Dearth of ground level enhancement (GLE) events and major geomagnetic storms during cycle 24 clearly standout. The space weather events seem to reflect the less frequent solar eruptions and the overall weakness of solar cycle 24.

TABLE 1. List of large SEP events from solar cycle 24.

2010/08/14; 2011/03/08; 2011/03/21; 2011/06/07; 2011/08/04; 2011/08/09; 2011/09/23; 2011/11/26; 2012/01/23; 2012/01/27; 2012/03/07; 2012/03/13; 2012/05/17; 2012/05/27; 2012/06/16; 2012/07/07; 2012/07/09; 2012/07/12; 2012/07/17; 2012/07/19; 2012/07/23

TABLE 2. Major geomagnetic storms of cycle 24 (Dst < -100 nT)

2011/09/27; 2011/10/25; 2012/03/09; 2012/04/24; 2012/07/15

Solar Radio Bursts and Space Weather

N. **Gopalswamy**
ISWI Workshop, Oct **2012**, Presentation, **File**

Earth-Affecting Solar Causes Observatory (EASCO): A potential International Living with a Star Mission from Sun–Earth L5 ☆

N. **Gopalswamy**, J.M. Davilaa, O.C. St. Cyra, E.C. Sittlera, F. Auchèreb, T.L. Duvall Jr.a, J.T. Hoeksemac, M. Maksimovicd, R.J. MacDowalla, A. Szaboa, M.R. Colliera
Journal of Atmospheric and Solar-Terrestrial Physics, Volume 73, Issues 5–6, April 2011, Pages 658–663
http://www.sciencedirect.com/science/article/pii/S1364682611000149
This paper describes the scientific rationale for an L5 mission and a partial list of key scientific instruments the mission should carry. The L5 vantage point provides an unprecedented view of the solar disturbances and their solar sources that can greatly advance the science behind space weather. A coronagraph and a heliospheric imager at L5 will be able to view CMEs broadsided, so space speed of the Earth-directed CMEs can be measured accurately and their radial structure discerned. In addition, an inner coronal imager and a magnetograph from L5 can give advance information on active regions and coronal holes that will soon rotate on to the solar disk. Radio remote sensing at low frequencies can provide information on shock-driving CMEs, the most dangerous of all CMEs. Coordinated helioseismic measurements from the Sun–Earth line and L5 provide information on the physical conditions at the base of the convection zone, where solar magnetism originates. Finally, in situ measurements at L5 can provide information on the large-scale solar wind structures (corotating interaction regions (CIRs)) heading towards Earth that potentially result in adverse space weather.

Universal Heliophysical Processes

Gopalswamy, N.
In: The Sun, the Solar Wind, and the Heliosphere, ed. M. P. Miralles and J. Sanchez Almeida, IAGA Special Sopron Book Series, Vol 4, Chapter 2, Springer, pp 9-20, **2011, File,** DOI: 10.1007/978/90-481-9787-3_2
The physical processes in the heliospace are a direct consequence of the influenced by Sun's mass and electromagnetic emissions. There has been enormous progress in studying these processes since the dawn of the space age half a century ago. The heliospace serves as a great laboratory to study numerous physical processes, using the vast array of ground and space-based measurements of various physical quantities. The observational capabilities collectively form the Great Observatory to make scientific investigations not envisioned by individual instrument teams. The International Heliophysical Year (IHY) program has been promoting scientific investigations on the universality of physical processes such as shocks, particle acceleration, dynamo, magnetic reconnection, magnetic flux ropes, plasma-neutral matter interactions, turbulence, and so on. This paper highlights scientific deliberations on these and related topics that took place during the IAGA sessionon "Universal Heliophysical Processes" in Sopron, Hungary. The session featured several invited and contributed papers that focused on observations, theory and modeling of the universal heliophysical processes.

Energetic Phenomena on the Sun

Nat **Gopalswamy**
E-print, Nov. **2007**
AIP Conf. Proc. , Kodai School on Solar Physics, edited by S. S. Hasan and D. Banerjee, V. 919, pp. 275-313, 2007; File
Solar flares, coronal mass ejections (CMEs), solar energetic particles (SEPs), and fast solar wind represent the energetic phenomena on the Sun.
This paper provides an **over view** of the energetic phenomena on the Sun including their origin interplanetary propagation and space weather consequences.

Empirical relations between the intensities of Lyman lines of H and He+

M. **Gordino**1, F. Auchère1, J.-C. Vial1, K. Bocchialini1, D. M. Hassler2, T. Bando3, R. Ishikawa4, R. Kano3, K. Kobayashi5, N. Narukage3, J. Trujillo Bueno6 and A. Winebarger5
A&A 657, A86 (**2022**)
https://www.aanda.org/articles/aa/pdf/2022/01/aa41960-21.pdf
Context. Empirical relations between major UV and extreme UV spectral lines are one of the inputs for models of chromospheric and coronal spectral radiances and irradiances. They are also needed for the interpretation of some of the observations of the Solar Orbiter mission.
Aims. We aim to determine an empirical relation between the intensities of the H I 121.6 nm and He II 30.4 nm Ly-α lines.
Methods. Images at 121.6 nm from the Chromospheric Lyman-Alpha Spectro Polarimeter (CLASP) and Multiple XUV Imager (MXUVI) sounding rockets were co-registered with simultaneous images at 30.4 nm from the EIT and AIA orbital telescopes in order to derive a spatially resolved relationship between the intensities.
Results. We have obtained a relationship between the H I 121.6 nm and He II 30.4 nm intensities that is valid for a wide range of solar features, intensities, and activity levels. Additional SUMER data have allowed the derivation of

another relation between the H I 102.5 nm (Ly-β) and He II 30.4 nm lines for quiet-Sun regions. We combined these two relationships to obtain a Ly-α/Ly-β intensity ratio that is comparable to the few previously published results. Conclusions. The relationship between the H I 121.6 nm and He II 30.4 nm lines is consistent with the one previously obtained using irradiance data. We have also observed that this relation is stable in time but that its accuracy depends on the spatial resolution of the observations. The derived Ly-α/Ly-β intensity ratio is also compatible with previous results.

Beyond small-scale transients: a closer look at the diffuse quiet solar corona

J. **Gorman**, L. P. Chitta, H. Peter, D. Berghmans, F. Auchère, R. Aznar Cuadrado, L. Teriaca, S.K. Solanki, C. Verbeeck, E. Kraaikamp, K. Stegen, S. Gissot

A&A 678, A188 **2023**

https://arxiv.org/pdf/2308.01640.pdf

https://www.aanda.org/articles/aa/pdf/2023/10/aa45892-23.pdf

Within the quiet Sun corona imaged at 1 MK, much of the field of view consists of diffuse emission that appears to lack the spatial structuring that is so evident in coronal loops or bright points. We seek to determine if these diffuse regions are categorically different in terms of their intensity fluctuations and spatial configuration from the more well-studied dynamic coronal features. We analyze a time series of observations from Solar Orbiter's High Resolution Imager in the Extreme Ultraviolet to quantify the characterization of the diffuse corona at high spatial and temporal resolutions. We then compare this to the dynamic features within the field of view, mainly a coronal bright point. We find that the diffuse corona lacks visible structuring, such as small embedded loops, and that this is persistent over the 25 min duration of the observation. The intensity fluctuations of the diffuse corona, which are within +/-5%, are significantly smaller in comparison to the coronal bright point. Yet, the total intensity observed in the diffuse corona is of the same order as the bright point. It seems inconsistent with our data that the diffuse corona is a composition of small loops or jets or that it is driven by discrete small heating events that follow a power-law-like distribution. We speculate that small-scale processes like MHD turbulence might be energizing the diffuse regions, but at this point we cannot offer a conclusive explanation for the nature of this feature**. March 26, 2021**

Ground-based Synoptic Studies of the Sun

Sanjay **Gosain**, V. Martinez Pillet, A. Pevtsov, H. Gilbert, S. Gibson, A. G. de Wijn, J. Burkepile, A. Asai, H. M. Bain, C. J. Henney, Y. Katsukawa, H. Lin, W. Manchester, J. McAteer, K. Muglach, M. Rast, M. Roth, J. Zhang

White paper submitted to Heliodecadal 2024, **2022**

https://arxiv.org/ftp/arxiv/papers/2212/2212.03247.pdf

Ground-based synoptic solar observations provide critical contextual data used to model the large-scale state of the heliosphere. The next decade will see a combination of ground-based telescopes and space missions that will study our Sun's atmosphere microscopic processes with unprecedented detail. This white paper describes contextual observations from a ground-based network needed to fully exploit this new knowledge of the underlying physics that leads to the magnetic linkages between the heliosphere and the Sun. This combination of a better understanding of small-scale processes and the appropriate global context will enable a physics-based approach to Space Weather comparable to Terrestrial Weather forecasting.

Spectral Magnetic Helicity of Solar Active Regions between 2006 and 2017

Sanjay **Gosain**1 and Axel Brandenburg

2019 ApJ 882 80

https://doi.org/10.3847/1538-4357/ab32ef

We compute magnetic helicity and energy spectra from about 2485 patches of about 100 Mm side length on the solar surface using data from Hinode during 2006–2017. An extensive database is assembled where we list the magnetic energy and helicity, large- and small-scale magnetic helicity, mean current helicity density, fractional magnetic helicity, and correlation length along with the Hinode map identification number (MapID), as well as the Carrington latitude and longitude for each MapID. While there are departures from the hemispheric sign rule for magnetic and current helicities, the weak trend reported here is in agreement with the previous results. This is argued to be a physical effect associated with the dominance of individual active regions that contribute more strongly in the better-resolved Hinode maps. In comparison with earlier work, the typical correlation length is found to be 6–8 Mm, while the length scale relating the magnetic and current helicities to each other is around 1.4 Mm.

Global impact of emerging internetwork fields on the low solar atmosphere

Milan **Gošić**, Bart De Pontieu, Alberto Sainz Dalda

ApJ **964** 175 **2022**

https://arxiv.org/pdf/2211.09111.pdf

https://iopscience.iop.org/article/10.3847/1538-4357/ad2e03/pdf

Small-scale, newly emerging internetwork (IN) magnetic fields are considered a viable source of energy and mass for the solar chromosphere and possibly the corona. Multiple studies show that single events of flux emergence can indeed locally heat the low solar atmosphere through interactions of the upward propagating magnetic loops and the preexisting ambient field lines. However, the global impact of the newly emerging IN fields on the solar atmosphere is still unknown. In this letter we study the spatio-temporal evolution of IN bipolar flux features and analyze their impact on the energetics and dynamics of the quiet Sun (QS) atmosphere. We use high resolution, multi-wavelength, coordinated observations obtained with the Interface Region Imaging Spectrograph (IRIS), Hinode and the Atmospheric Imaging Assembly (AIA) to identify emerging IN magnetic fields and follow their evolution. Our observational results suggest that only the largest IN bipoles are capable of heating locally the low solar atmosphere, while the global contribution of these bipoles appears to be marginal. However, the total number of bipoles detected and their impact estimated in this work is limited by the sensitivity level, spatial resolution, and duration of our observations. To detect smaller and weaker IN fields that would maintain the basal flux, and examine their contribution to the chromospheric heating, we will need higher resolution, higher sensitivity and longer time series obtained with current and next-generation ground- and space-based telescopes.

The solar internetwork. III. Unipolar versus bipolar flux appearance

Milan **Gošić**, Luis R. Bellot Rubio, Mark C. M. Cheung, David Orozco Suárez, Yukio Katsukawa, Jose Carlos Del Toro Iniesta

ApJ **925** 188 **2021**

https://arxiv.org/pdf/2111.03208.pdf

https://iopscience.iop.org/article/10.3847/1538-4357/ac37be/pdf

Small-scale internetwork (IN) magnetic fields are considered to be the main building blocks of the quiet Sun magnetism. For this reason, it is crucial to understand how they appear on the solar surface. Here, we employ a high-resolution, high-sensitivity, long-duration Hinode/NFI magnetogram sequence to analyze the appearance modes and spatio-temporal evolution of individual IN magnetic elements inside a supergranular cell at the disk center. From identification of flux patches and magnetofrictional simulations, we show that there are two distinct populations of IN flux concentrations: unipolar and bipolar features. Bipolar features tend to be bigger and stronger than unipolar features. They also live longer and carry more flux per feature. Both types of flux concentrations appear uniformly over the solar surface. However, we argue that bipolar features truly represent the emergence of new flux on the solar surface, while unipolar features seem to be formed by coalescence of background flux. Magnetic bipoles appear at a faster rate than unipolar features (68 as opposed to 55 Mx cm−2 day−1), and provide about 70% of the total instantaneous IN flux detected in the interior of the supergranule. **2010 Nov 2–3**

Emergence of Internetwork Magnetic Fields through the Solar Atmosphere

M. **Gošić**1,2, B. De Pontieu1,3,4, L. R. Bellot Rubio5, A. Sainz Dalda1,2, and S. Esteban Pozuelo5,6,7

2021 ApJ 911 41

https://doi.org/10.3847/1538-4357/abe7e0

Internetwork (IN) magnetic fields are highly dynamic, short-lived magnetic structures that populate the interior of supergranular cells. Since they emerge all over the Sun, these small-scale fields bring a substantial amount of flux, and therefore energy, to the solar surface. Because of this, IN fields are crucial for understanding the quiet Sun (QS) magnetism. However, they are weak and produce very small polarization signals, which is the reason why their properties and impact on the energetics and dynamics of the solar atmosphere are poorly known. Here we use coordinated, high-resolution, multiwavelength observations obtained with the Swedish 1 m Solar Telescope and the Interface Region Imaging Spectrograph (IRIS) to follow the evolution of IN magnetic loops as they emerge into the photosphere and reach the chromosphere and transition region. We studied in this paper three flux emergence events having total unsigned magnetic fluxes of 1.9 × 1018, 2.5 × 1018, and 5.3 × 1018 Mx. The footpoints of the emerging IN bipoles are clearly seen to appear in the photosphere and to rise up through the solar atmosphere, as observed in Fe i 6173 Å and Mg i b2 5173 Å magnetograms, respectively. For the first time, our polarimetric measurements taken in the chromospheric Ca ii 8542 Å line provide direct observational evidence that IN fields are capable of reaching the chromosphere. Moreover, using IRIS data, we study the effects of these weak fields on the heating of the chromosphere and transition region.

IRIS Science Nuggets Nov **2021** https://iris.lmsal.com/nugget

Chromospheric heating due to cancellation of quiet Sun internetwork fields

Milan **Gošić**, Jaime de la Cruz Rodríguez, Bart De Pontieu, Luis R. Bellot Rubio, Mats Carlsson, Sara Esteban Pozuelo, Ada Ortiz, Vanessa Polito

ApJ **857** 48 **2018**

https://arxiv.org/pdf/1802.07392.pdf'

The heating of the solar chromosphere remains one of the most important questions in solar physics. Our current understanding is that small-scale internetwork (IN) magnetic fields play an important role as a heating agent. Indeed,

cancellations of IN magnetic elements in the photosphere can produce transient brightenings in the chromosphere and transition region. These bright structures might be the signature of energy release and plasma heating, probably driven by magnetic reconnection of IN field lines. Although single events are not expected to release large amounts of energy, their global contribution to the chromosphere may be significant due to their ubiquitous presence in quiet Sun regions. In this paper we study cancellations of IN elements and analyze their impact on the energetics and dynamics of the quiet Sun atmosphere. We use high resolution, multiwavelength, coordinated observations obtained with the Interface Region Imaging Spectrograph (IRIS) and the Swedish 1-m Solar Telescope (SST) to identify cancellations of IN magnetic flux patches and follow their evolution. We find that, on average, these events live for ~3 minutes in the photosphere and ~12 minutes in the chromosphere and/or transition region. Employing multi-line inversions of the Mg II h & k lines we show that cancellations produce clear signatures of heating in the upper atmospheric layers. However, at the resolution and sensitivity accessible to the SST, their number density still seems to be one order of magnitude too low to explain the global chromospheric heating. **2014-05-16**

The Solar Internetwork. II. Magnetic Flux Appearance and Disappearance Rates

Milan **Gošić**, Luis R. Bellot Rubio, Jose Carlos Del Toro Iniesta, David Orozco Suárez, Yukio Katsukawa

ApJ 820 35 **2016**

Small-scale internetwork magnetic fields are important ingredients of the quiet Sun. In this paper we analyze how they appear and disappear on the solar surface. Using high resolution \textit{Hinode} magnetograms, we follow the evolution of individual magnetic elements in the interior of two supergranular cells at the disk center. From up to 38 hr of continuous measurements, we show that magnetic flux appears in internetwork regions at a rate of 120±3~Mx~cm−2~day−1 (7.3±0.2×10 24~Mx~day−1 over the entire solar surface). Flux disappears from the internetwork at a rate of 125±6~Mx~cm−2~day−1 (7.6±0.4×1024~Mx~day−1) through fading of magnetic elements, cancellation between opposite-polarity features, and interactions with network patches, which converts internetwork elements into network features. Most of the flux is lost through fading and interactions with the network, at nearly the same rate of about 50~Mx~cm−2~day−1. Our results demonstrate that the sources and sinks of internetwork magnetic flux are well balanced. Using the instantaneous flux appearance and disappearance rates, we successfully reproduce the time evolution of the total unsigned flux in the two supergranular cells.

Magnetic Reconnection in the Solar Wind **Review**

J. T. **Gosling**

Space Science Reviews, November **2012**, Volume 172, Issue 1-4, pp 187-200

It is only within the last 5 years that we have learned how to recognize the unambiguous signature of magnetic reconnection in the solar wind in the form of roughly Alfvénic accelerated plasma flows embedded within bifurcated magnetic field reversal regions (current sheets). This paper provides a brief overview of what has since been learned about reconnection in the solar wind from both single and multi-spacecraft observations of these so-called reconnection exhausts.

Testing solar surface flux transport models in the first days after active region emergence

Nils **Gottschling**, Hannah Schunker, Aaron C. Birch, Robert Cameron, Laurent Gizon

A&A **2021**

https://arxiv.org/pdf/2111.01896.pdf

Active regions (ARs) play an important role in the magnetic dynamics of the Sun. Solar surface flux transport models (SFTMs) are used to describe the evolution of the radial magnetic field at the solar surface. There is however uncertainty about using these models in the early stage of AR evolution. We aim to test the applicability of SFTMs in the first days after the emergence of ARs by comparing them with observations. The models we employ range from passive evolution to models where the inflows around ARs are included. We simulate the evolution of the surface magnetic field of 17 emerging active regions using a local surface flux transport simulation. We selected regions that do not form fully-fledged sunspots that exhibit moat flows. The simulation includes diffusion and advection. We use observed flows from local correlation tracking of solar granulation, as well as parametrizations of the inflows around ARs. To evaluate our simulations, we measure the cross correlation between the observed and the simulated magnetic field, as well as the total unsigned flux of the ARs, over time. We also test the validity of our simulations by varying the starting time relative to the emergence of flux. We find that the simulations using observed surface flows can reproduce the evolution of the observed magnetic flux. The effect of buffeting of the field by supergranulation can be described as a diffusion process. The SFTM is applicable after 90% of the peak total unsigned flux of the AR has emerged. Diffusivities in the range between D=250 to 720 km2/s are consistent with the evolution of the AR flux in the first five days after this time. We find that the converging flows around emerging ARs are not important for the evolution of the total flux of the AR in these first five days; their effect of increasing flux cancellation is balanced by the decrease of flux transport away from the AR.

Evolution of solar surface inflows around emerging active regions⋆

N. **Gottschling**1, H. Schunker1,2, A. C. Birch1, B. Löptien1 and L. Gizon1,3,4
A&A 652, A148 (**2021**)
https://www.aanda.org/articles/aa/pdf/2021/08/aa40324-21.pdf
https://doi.org/10.1051/0004-6361/202140324
Context. Solar active regions are associated with Evershed outflows in sunspot penumbrae, moat outflows surrounding sunspots, and extended inflows surrounding active regions. Extended inflows have been identified around established active regions with various methods. The evolution of these inflows and their dependence on active region properties as well as their effect on the global magnetic field are not yet understood.
Aims. We aim to understand the evolution of the average inflows around emerging active regions and to derive an empirical model for these inflows. We expect that this can be used to better understand how the inflows act on the diffusion of the magnetic field in active regions.
Methods. We analyzed horizontal flows at the surface of the Sun using local correlation tracking of solar granules observed in continuum images of the Helioseismic and Magnetic Imager on board the Solar Dynamics Observatory. We measured average flows of a sample of 182 isolated active regions up to seven days before and after their emergence onto the solar surface with a cadence of 12 h. About half of the active regions in the sample developed sunspots with moat flows in addition to the surrounding inflows. We investigated the average inflow properties with respect to active region characteristics of total flux and latitude. We fit a model to these observed inflows for a quantitative analysis.
Results. We find that converging flows of about 20–30 m s−1 are first visible one day prior to emergence, in agreement with recent results. These converging flows are present regardless of the active region properties of latitude or flux. We confirm a recently found prograde flow of about 40 m s−1 at the leading polarity during emergence. We find that the time after emergence when the latitudinal inflows increase in amplitude depends on the flux of the active region, ranging from one to four days after emergence and increasing with flux. The largest extent of the inflows is up to about 7 ± 1° away from the center of the active region within the first six days after emergence. The inflow velocities have amplitudes of about 50 m s−1.

Anticipating the Sun's heavy-element abundance

Douglas **Gough**
MNRAS **2019**
https://arxiv.org/pdf/1904.00301.pdf
Much of our understanding of the internal structure of the Sun derives from so-called standard theoretical solar models. Unfortunately, none of those models agrees completely with observation. The discrepancy is commonly associated with chemical abundance, and has led to what is now called the solar abundance problem, the resolution of which has previously been out of sight. But now the Borexino Collaboration, who recently announced measurements of the pp-chain solar neutrinos, are optimistic that %in future they will be able to measure the flux ΦCNO of the neutrinos emitted by the relatively weak CNO cycle. Since C, N and O constitute the majority of the heavy elements, that measurement will permit a crucial determination of the heavy-element abundance Zc in the Sun's energy-generating core, thereby shedding important light on the problem. To accomplish that determination, a robust relation between Zc and ΦCNO will be required. That relation is Zc=0.400ΦCNO, where ΦCNO is in units of 1010cm−2s−1.

Is the Sun a Magnet?

Gough, D.O.
Sol Phys (**2017**) 292: 70.
http://link.springer.com/content/pdf/10.1007%2Fs11207-017-1088-1.pdf
It has been argued (Gough and McIntyre in Nature394, 755, 1998) that the only way for the radiative interior of the Sun to be rotating uniformly in the face of the differentially rotating convection zone is for it to be pervaded by a large-scale magnetic field, a field which is responsible also for the thinness of the tachocline. It is most likely that this field is the predominantly dipolar residual component of a tangled primordial field that was present in the interstellar medium from which the Sun condensed (Braithwaite and Spruit in Nature431, 819, 2004), and that advection by the meridional flow in the tachocline has caused the dipole axis to be inclined from the axis of rotation by about \(60^{\circ}\) (Gough in Geophys. Astrophys. Fluid Dyn., 106, 429, 2012). It is suggested here that, notwithstanding its turbulent passage through the convection zone, a vestige of that field is transmitted by the solar wind to Earth, where it modulates the geomagnetic field in a periodic way. The field variation reflects the inner rotation of the Sun, and, unlike turbulent-dynamo-generated fields, must maintain phase. I report here a new look at an earlier analysis of the geomagnetic field by Svalgaard and Wilcox (Solar Phys.41, 461, 1975), which reveals evidence for appropriate phase coherence, thereby adding support to the tachocline theory.

Some glimpses from helioseismology at the dynamics of the deep solar interior **Review**

D. O. **Gough**
Space Science Reviews Volume 196, Issue 1, pp 15-47 **2015**

http://arxiv.org/pdf/1505.04881v1.pdf
Helioseismology has taught us a great deal about the stratification and kinematics of the solar interior, sufficient for us to embark upon dynamical studies more detailed than have been possible before. The most sophisticated studies to date have been the very impressive numerical simulations of the convection zone, from which, especially in recent years, a great deal has been learnt. Those simulations, and the seismological evidence with which they are being confronted, are reviewed elsewhere in this volume. Our understanding of the global dynamics of the radiative interior of the Sun is in a much more primitive state. Nevertheless, some progress has been made, and seismological inference has provided us with evidence of more to come. Some of that I summarize here, mentioning in passing hints that are pointing the way to the future.

Heliophysics gleaned from seismology **Review**

D. O. **Gough**
E-print, Oct **2012**
in Progress in solar/stellar Physics with Helio- and Asteroseismology; Proc. 65th Fujihara Seminar, (ed. H. Shibahashi & M. Takata), Astron. Soc. Pacific Conf. Ser., vol. 462, pp 429--454 (**2011**)
Some of the principal heliophysical inferences that have been drawn from, or refined by, seismology, and the manner in which those inferences have been made, are very briefly described. Prominence is given to the use of simple formulae, derived either from simple toy models or from asymptotic approximations to more realistic situations, for tailoring procedures to be used for analysing observations in such a way as to answer specific questions about physics. It is emphasized that precision is not accuracy, and that confusing the two can be quite misleading.

Turbulent Gravito-Electrostatic Sheath (GES) Structure with Kappa-Distributed Electrons for Solar Plasma Characterization

H. P. **Goutam**, P. K. Karmakar
Solar Physics December **2017**, 292:182
We report on new characteristic features of the plasma-based gravito-electrostatic sheath (GES) model for solar plasma equilibrium characterization through nonthermal (κκ-distributed) electrons composed of both a thermal halo (low-speed) and a suprathermal (high-speed) energy tail. The constituent ions are treated collectively as inertial species. The presence of intrinsic fluid turbulence is included with the help of a proper logatropic equation of state in the ionic momentum conservation law. The analysis is based on the basic physics of space-charge polarization effects, collectively evolving as a plasma sheath, but previously known only for laboratory plasma-scales. We show that the radial location of the solar surface boundary (SSB, inner boundary, diffused), formed by the counteracting GES force balancing, becomes slightly enhanced (by 0.5 on the Jeans scale). The net electric current densities, in both the solar interior and exterior, confirm the universal law of total charge conservation in the presence of geometrical curvature effects. The relevant properties of the new κκ-modified equilibrium GES structure are numerically illustrated and discussed. The results are finally compared in the light of existing reports based on the Maxwell–Boltzmann electron distribution. The new outcomes can be extensively expanded to analyze the realistic thermostatistical dynamics of the Sun and its ambient atmosphere, as predicted earlier from various space-based observations.

Automated Detection of Rapid Variability of Moss Using SDO/AIA and Its Connection to the Solar Corona

David R. **Graham**1, Bart De Pontieu2,3,4, and Paola Testa5
2019 ApJL 880 L12
https://doi.org/10.3847/2041-8213/ab2f91
Active region moss—the upper transition region of hot loops—was observed exhibiting rapid intensity variability on timescales of order 15 s by Testa et al. in a short time series (~150 s) data set from Hi-C (High-resolution Coronal Imager). The intensity fluctuations in the subarcsecond 193A images (~1.5 MK plasma) were uncharacteristic of steadily heated moss and were considered an indication of heating events connected to the corona. Intriguingly, these brightenings displayed a connection to the ends of transient hot loops seen in the corona. Following the same active region, AR11520, for 6 days, we demonstrate an algorithm designed to detect the same temporal variability in lower resolution Atmospheric Imaging Assembly (AIA) data, significantly expanding the number of events detected. Multiple analogous regions to the Hi-C data are successfully detected, showing moss that appears to "sparkle" prior to clear brightening of connected high-temperature loops; this is confirmed by the hot AIA channels and the isolated Fe xviii emission. The result is illuminating, as the same behavior has recently been shown by Polito et al. while simulating nanoflares with a beam of electrons depositing their energy in the lower atmosphere. Furthermore, the variability is localized mostly to the hot core of the region, hence we reinforce the diagnostic

potential of moss variability as the driver of energy release in the corona. The ubiquitous nature of this phenomenon, and the ability to detect it in data with extended time series, and large fields of view, opens a new window into investigating the coronal heating mechanism.

Alfvén Wave Dissipation in the Solar Chromosphere

S. D. T. **Grant**, D. B. Jess, T. V. Zaqarashvili, C. Beck, H. Socas-Navarro, M. J. Aschwanden, P. H. Keys, D. J. Christian, S. J. Houston, R. L. Hewitt
Nature Physics, 14, 480-483 (**2018**)
https://arxiv.org/ftp/arxiv/papers/1810/1810.07712.pdf
Magneto-hydrodynamic (MHD) Alfv\'en waves have been a focus of laboratory plasma physics and astrophysics for over half a century. Their unique nature makes them ideal energy transporters, and while the solar atmosphere provides preferential conditions for their existence, direct detection has proved difficult as a result of their evolving and dynamic observational signatures. The viability of Alfv\'en waves as a heating mechanism relies upon the efficient dissipation and thermalization of the wave energy, with direct evidence remaining elusive until now. Here we provide the first observational evidence of Alfv\'en waves heating chromospheric plasma in a sunspot umbra through the formation of shock fronts. The magnetic field configuration of the shock environment, alongside the tangential velocity signatures, distinguish them from conventional umbral flashes. Observed local temperature enhancements of 5% are consistent with the dissipation of mode-converted Alfv\'en waves driven by upwardly propagating magneto-acoustic oscillations, providing an unprecedented insight into the behaviour of Alfv\'en waves in the solar atmosphere and beyond. **24 August 2014**

Wave Damping Observed in Upwardly Propagating Sausage-mode Oscillations contained within a Magnetic Pore

S.D.T. **Grant**, D.B. Jess, M.G. Moreels, R.J. Morton, D.J. Christian, I. Giagkiozis, G. Verth, V. Fedun, P.H. Keys, T. Van Doorsselaere, R. Erdelyi
ApJ **2015**
http://arxiv.org/pdf/1505.01484v1.pdf
We present observational evidence of compressible magnetohydrodynamic wave modes propagating from the solar photosphere through to the base of the transition region in a solar magnetic pore. High cadence images were obtained simultaneously across four wavelength bands using the Dunn Solar Telescope. Employing Fourier and wavelet techniques, sausage-mode oscillations displaying significant power were detected in both intensity and area fluctuations. The intensity and area fluctuations exhibit a range of periods from 181-412s, with an average period ~290s, consistent with the global p-mode spectrum. Intensity and area oscillations present in adjacent bandpasses were found to be out-of-phase with one another, displaying phase angles of 6.12 degrees, 5.82 degrees and 15.97 degrees between 4170 Angstrom continuum - G-band, G-band - Na I D1 and Na I D1 - Ca II K heights, respectively, reiterating the presence of upwardly-propagating sausage-mode waves. A phase relationship of ~0 degrees between same-bandpass emission and area perturbations of the pore best categorises the waves as belonging to the `slow' regime of a dispersion diagram. Theoretical calculations reveal that the waves are surface modes, with initial photospheric energies in excess of 35000 W/m^2. The wave energetics indicate a substantial decrease in energy with atmospheric height, confirming that magnetic pores are able to transport waves that exhibit appreciable energy damping, which may release considerable energy into the local chromospheric plasma.
See UKSP Nugget #59, July **2015**
http://www.uksolphys.org/uksp-nugget/59-propagating-sausage-mode-waves-damping-in-the-chromosphere/

The Solar-flux Third Granulation Signature

David F. **Gray**1 and Benjamin Oostra
2018 ApJ 852 42
The velocity shifts of spectral lines as a function of line strength, so-called the third signature of granulation, are investigated using three published solar-flux atlases. We use flux atlases because we wish to treat the Sun as a star, against which stellar observations can be compared and judged. The atlases are critiqued and compared to the lower-resolution observations taken with the Elginfield stellar spectrograph. Third-signature plots are constructed for the 6020–6340 Å region. No dependence on excitation potential or wavelength is found over this wavelength span. The shape of the plots from the three solar atlases is essentially the same, with rms line-core velocity differences of 30–35 m s−1. High-resolution atlas data are degraded to the level of the Elginfield spectrograph and compared to direct observations taken with that spectrograph. The line-core velocities show good agreement, with rms differences of 38 m s−1. A new standard curve is derived and compared with the previously published one. Only small differences in shape are found, but a significant (+97 m s−1) change in the zero point is indicated. The bisector of the Fe i 6253

line is mapped onto the third-signature plots and flux deficits are derived, which measure the granule/lane flux imbalance. The lower spectral resolution lowers the flux deficit area slightly and moves the peak of the deficit 0.3–0.5 km s−1 toward higher velocities. These differences, while significant, are not large compared to measurement errors for stellar data.

The 2013 February 17 Sunquake in the Context of the Active Region's Magnetic Field Configuration

L. M. **Green**1, G. Valori1, F. P. Zuccarello1,2, S. Zharkov3, S. A. Matthews1, and S. L. Guglielmino
2017 ApJ 849 40
https://arxiv.org/pdf/1709.04874.pdf
Sunquakes are created by the hydrodynamic response of the lower atmosphere to a sudden deposition of energy and momentum. In this study, we investigate a sunquake that occurred in NOAA active region 11675 on **2013 February 17**. Observations of the corona, chromosphere, and photosphere are brought together for the first time with a nonlinear force-free model of the active region's magnetic field in order to probe the magnetic environment in which the sunquake was initiated. We find that the sunquake was associated with the destabilization of a flux rope and an associated M-class GOES flare. Active region 11675 was in its emergence phase at the time of the sunquake and photospheric motions caused by the emergence heavily modified the flux rope and its associated quasi-separatrix layers, eventually triggering the flux rope's instability. The flux rope was surrounded by an extended envelope of field lines rooted in a small area at the approximate position of the sunquake. We argue that the configuration of the envelope, by interacting with the expanding flux rope, created a "magnetic lens" that may have focussed energy on one particular location of the photosphere, creating the necessary conditions for the initiation of the sunquake.
UKSP Nugget: **#85 Nov 2017** http://www.uksolphys.org/uksp-nugget/85-the-role-of-the-magnetic-field-in-sunquakes/

Impact of space weather on the satellite industry **Review**

J. C. **Green**, J. Likar, Yuri Shprits
Space Weather, Volume 15, Issue 6 June **2017** Pages 804–818
http://onlinelibrary.wiley.com/doi/10.1002/2017SW001646/full
http://sci-hub.cc/10.1002/2017SW001646
This paper describes space weather impacts to the satellite infrastructure as perceived by satellite industry stakeholders. The information was gathered through in-person and remote meetings with both satellite operators and manufacturers. The paper describes current impacts, industry processes for managing and mitigating impacts, costs, and industry needs and requirements. Lastly, we suggest potential improvements and solutions to problem areas based on our observation of the industry processes including (1) improved tools for quick anomaly attribution, (2) training, and (3) coordinated information sharing.

Observations of flux rope formation prior to coronal mass ejections (invited), **Review**

Green, Lucie M., Kliem, Bernhard:
Nature of Prominences and Their Role in Space Weather, Proc. IAU Symp. 300, 209, **2014**
http://arxiv.org/pdf/1312.4388v1.pdf
Understanding the magnetic configuration of the source regions of coronal mass ejections (CMEs) is vital in order to determine the trigger and driver of these events. Observations of four CME productive active regions are presented here, which indicate that the pre-eruption magnetic configuration is that of a magnetic flux rope. The flux ropes are formed in the solar atmosphere by the process known as flux cancellation and are stable for several hours before the eruption. The observations also indicate that the magnetic structure that erupts is not the entire flux rope as initially formed, raising the question of whether the flux rope is able to undergo a partial eruption or whether it undergoes a transition in specific flux rope configuration shortly before the CME.

A Comparison of the 10.7-cm Radio Flux Values and the International Sunspot Numbers for Solar Activity Cycles 19, 20, and 21

Robert A. **Greenkorn**
Solar Physics, Volume 280, Number 1 (**2012**), 205-221
A nonlinear analysis of the daily 10.7-cm radio flux values for each of Solar Cycles 19, 20, and 21 is used to determine if the results match those of the International Sunspot Numbers for each of these cycles. Fractals and chaos are described and a brief review of utilizing fractals and chaos is given. The origin of the 10.7-cm radio flux is discussed and a short review of recent work discussing its measurement and its relation to the international sunspot

number and other proxies for solar activity cycles given. The parameters used to describe chaos for the 10.7-cm radio flux are discussed. The length of the data sets for either statistical analysis or nonlinear analysis of the 10.7-cm radio flux values is considered. These results indicate that the 10.7-cm radio flux values appear to be stochastic for Cycle 19 and chaotic for Cycles 20 and 21. The International Sunspot Numbers show similar behavior for these three cycles. A day-by-day comparison of the dimensionless 10.7-cm radio flux values and the dimensionless International Sunspot Numbers differences shows a linear trend. The results remain consistent in that the 10.7-cm radio flux values indicate, as did the International Sunspot Numbers, that there is a transition from stochastic behavior for Cycle 19 to chaotic behavior in Cycles 20 and 21. The day-by-day comparison of the 10.7-cm radio flux values and the International Sunspot Numbers emphasizes that the 10.7 cm radio flux values are responding to the magnetic field associated with the sunspots.

HELIOSEISMIC IMAGING OF SUPERGRANULATION THROUGHOUT THE SUN'S NEAR-SURFACE SHEAR LAYER

Benjamin J. **Greer**, Bradley W. Hindman, and Juri Toomre
2016 ApJ 824 128
We present measurements of the Sun's sub-surface convective flows and provide evidence that the pattern of supergranulation is driven at the surface. The pattern subsequently descends slowly throughout the near-surface shear layer in a manner that is inconsistent with a 3D cellular structure. The flow measurements are obtained through the application of a new helioseismic technique based on traditional ring analysis. We measure the flow field over the course of eleven days and perform a correlation analysis between all possible pairs of depths and temporal separations. In congruence with previous studies, we find that the supergranulation pattern remains coherent at the surface for slightly less than two days and the instantaneous surface pattern is imprinted to a depth of 7 Mm. However, these correlation times and depths are deceptive. When we admit a potential time lag in the correlation, we find that peak correlation in the convective flows descends at a rate of 10–40 m s−1 (or equivalently 1–3 Mm per day). Furthermore, the correlation extends throughout all depths of the near-surface shear layer. This pattern-propagation rate is well matched by estimates of the speed of downflows obtained through the anelastic approximation. Direct integration of the measured speed indicates that the supergranulation pattern that first appears at the surface eventually reaches the bottom of the near-surface shear layer a month later. Thus, the downflows have a Rossby radius of deformation equal to the depth of the shear layer and we suggest that this equality may not be coincidental.

Helioseismic Imaging of Fast Convective Flows Throughout the Near-Surface Shear Layer

Benjamin J. **Greer**, Bradley W. Hindman, Nicholas A. Featherstone, Juri Toomre
2015 *ApJ* **803** L17
http://arxiv.org/pdf/1504.00699v1.pdf
Using a new implementation of ring-diagram helioseismology, we ascertain the strength and spatial scale of convective flows throughout the near-surface shear layer. Our ring-diagram technique employs highly overlapped analysis regions and an efficient method of 3D inversion to measure convective motions with a resolution that ranges from 3 Mm at the surface to 80 Mm at the base of the layer. We find the rms horizontal flow speed to peak at 427 m s−1 at the photosphere and fall to a minimum of 124 m s−1between 20 Mm and 30 Mm. From the velocity amplitude and the dominant horizontal scales seen at each depth, we infer the level of rotational influence on convection to be low near the surface, but transition to a significant level at the base of the near-surface shear layer with a Rossby number varying between 2.2 to as low as 0.1.

Multi-Ridge Fitting for Ring-Diagram Helioseismology

Benjamin J. **Greer**, Bradley W. Hindman, Juri Toomre
Solar Physics, Volume 289, Issue 8, pp 2823-2843, **2014**
Inferences of subsurface flow velocities using local domain ring-diagram helioseismology depend on measuring the frequency shifts of oscillation modes seen in acoustic power spectra. Current methods for making these measurements use maximum-likelihood fitting techniques to match a model of modal power to the spectra. The model typically describes a single oscillation mode, and each mode in a given power spectrum is fit independently. We present a new method that produces measurements with higher reliability and accuracy by fitting multiple modes simultaneously. We demonstrate that this method permits measuring sub-surface flows deeper into the Sun while providing higher uniformity in data coverage and velocity response closer to the limb of the solar disk. While the previous fitting method performs better for some measurements of low phase-speed modes, we find this new method to be particularly useful for high phase-speed modes and small spatial areas.

Stability of solar atmospheric structures harboring standing slow waves: An analytical model in a compressible plasma

Michaël **Geeraerts**, Tom Van Doorsselaere

A&A **2021**
https://arxiv.org/pdf/2104.13064.pdf
Context: In the context of the solar coronal heating problem, one possible explanation for the high coronal temperature is the release of energy by magnetohydrodynamic (MHD) waves. The energy transfer is believed to be possible, among others, by the development of the Kelvin-Helmholtz instability (KHI) in coronal loops. Aims: Our aim is to determine if standing slow waves in solar atmospheric structures such as coronal loops, and also prominence threads, sunspots, and pores, can trigger the KHI due to the oscillating shear flow at the structure's boundary. Methods: We used linearized nonstationary MHD to work out an analytical model in a cartesian reference frame. The model describes a compressible plasma near a discontinuous interface separating two regions of homogeneous plasma, each harboring an oscillating velocity field with a constant amplitude which is parallel to the background magnetic field and aligned with the interface. The obtained analytical results were then used to determine the stability of said interface, both in coronal and photospheric conditions. Results: We find that the stability of the interface is determined by a Mathieu equation. In function of the parameters of this equation, the interface can either be stable or unstable. For coronal as well as photospheric conditions, we find that the interface is stable with respect to the KHI. Theoretically, it can, however, be unstable with respect to a parametric resonance instability, although it seems physically unlikely. We conclude that, in this simplified setup, a standing slow wave does not trigger the KHI without the involvement of additional physical processes.

A prototype of a large tunable Fabry-Perot interferometer for solar spectroscopy

V. **Greco**, A. Sordini, G. Cauzzi, F. Cavallini, C. Del Vecchio, L. Giovannelli, F. Berrilli, D. Del Moro, K. Reardon, K. Pietraszewski
PASP **2021**
https://arxiv.org/pdf/2112.02224.pdf
Large Fabry-Perot Interferometers are used in a variety of astronomical instrumentation, including spectro-polarimeters for 4-meter class solar telescopes. In this work we comprehensively characterize the cavity of a prototype 150 mm Fabry-Perot interferometer, sporting a novel, fully symmetric design. Of note, we define a new method to properly assess the gravity effects on the interferometer's cavity when the system is used in either the vertical or horizontal configuration, both typical of solar observations.
We show that the symmetric design very effectively limits the combined effects of pre-load and gravity forces to only a few nm over a 120 mm diameter illuminated surface, with gravity contributing about 2 nm peak-to-valley (0.3 nm rms) in either configuration. We confirm a variation of the tilt between the plates of the interferometer during the spectral scan, which can be mitigated with appropriate corrections to the spacing commands. Finally, we show that the dynamical response of the new system fully satisfies typical operational scenarios. We conclude that large, fully symmetric Fabry-Perot interferometers can be safely used within solar instrumentation in both, horizontal and vertical position, with the latter better suited to limiting the overall volume occupied by such an instrument.

Solar atmosphere wave dynamics generated by solar global oscillating eigenmodes

M.K.**Griffiths**, V.FeduncR.ErdélyiadR.Zhenge
Advances in Space Research Volume 61, Issue 2, 15 January **2018**, Pages 720-737
The solar atmosphere exhibits a diverse range of wave phenomena, where one of the earliest discovered was the five-minute global acoustic oscillation, also referred to as the p-mode. The analysis of wave propagation in the solar atmosphere may be used as a diagnostic tool to estimate accurately the physical characteristics of the Sun’s atmospheric layers.
In this paper, we investigate the dynamics and upward propagation of waves which are generated by the solar global eigenmodes. We report on a series of hydrodynamic simulations of a realistically stratified model of the solar atmosphere representing its lower region from the photosphere to low corona. With the objective of modelling atmospheric perturbations, propagating from the photosphere into the chromosphere, transition region and low corona, generated by the photospheric global oscillations the simulations use photospheric drivers mimicking the solar p-modes. The drivers are spatially structured harmonics across the computational box parallel to the solar surface. The drivers perturb the atmosphere at 0.5 Mm above the bottom boundary of the model and are placed coincident with the location of the temperature minimum. A combination of the VALIIIC and McWhirter solar atmospheres are used as the background equilibrium model.
We report how synthetic photospheric oscillations may manifest in a magnetic field free model of the quiet Sun. To carry out the simulations, we employed the magnetohydrodynamics code, SMAUG (Sheffield MHD Accelerated Using GPUs).
Our results show that the amount of energy propagating into the solar atmosphere is consistent with a model of solar global oscillations described by Taroyan and Erdélyi (2008) using the Klein-Gordon equation. The computed results indicate a power law which is compared to observations reported by Ireland et al. (2015) using data from the Solar Dynamics Observatory/Atmospheric Imaging Assembly.

The Space Physics Environment Data Analysis System in Python (PySPEDAS)

Eric **Grimes**, Bryan Harter, Nick Hatzigeorgiu, Alexander Drozdov, +++
Front. Astron. Space Sci., 9: 1020815 **2022**
https://doi.org/10.3389/fspas.2022.1020815
https://www.frontiersin.org/articles/10.3389/fspas.2022.1020815/pdf

In this article, we describe the free, open-source Python-based Space Physics Environment Data Analysis System (PySPEDAS), a platform for multi-mission, multi-instrument retrieval, analysis, and visualization of Heliophysics data. PySPEDAS currently contains load routines for data from 23 space missions, as well as a variety of data from ground-based observatories. The load routines are built from a common set of general routines that provide access to datasets in different ways (e.g., downloading and caching CDF files or accessing data hosted on web services), making the process of adding additional datasets simple. In addition to load routines, PySPEDAS contains numerous analysis tools for working with the dataset once it is loaded. We describe how these load routines and analysis tools are built by utilizing other free, open-source Python projects (e.g., PyTplot, cdflib, hapiclient, etc.) to make tools for space and solar physicists that are extremely powerful, yet easy-to-use. After discussing the code in detail, we show numerous examples of code using PySPEDAS, and discuss limitations and future plans.

Improvement of the Helioseismic and Magnetic Imager (HMI) Vector Magnetic Field Inversion Code

Ana Belén **Griñón-Marín**, Adur Pastor Yabar, Yang Liu, J. Todd Hoeksema, Aimee Norton
2021 *ApJ* **923** 84
https://arxiv.org/pdf/2109.09131.pdf
https://iopscience.iop.org/article/10.3847/1538-4357/ac2aa8/pdf
https://doi.org/10.3847/1538-4357/ac2aa8

A spectral line inversion code, Very Fast Inversion of the Stokes Vector (VFISV), has been used since May 2010 to infer the solar atmospheric parameters from the spectropolarimetric observations taken by the Helioseismic and Magnetic Imager (HMI) aboard the Solar Dynamics Observatory (SDO). The magnetic filling factor, the fraction of the surface with a resolution element occupied by magnetic field, is set to have a constant value of one in the current version of VFISV. This report describes an improved inversion strategy for the spectropolarimetric data observed with HMI for magnetic field strengths of intermediate values in areas spatially not fully resolved. The VFISV inversion code has been modified to enable inversion of the Stokes profiles with two different components: one magnetic and one non-magnetic. In this scheme, both components share the atmospheric components except for the magnetic field strength, inclination, and azimuth. In order to determine whether the new strategy is useful, we evaluate the inferred parameters inverted with one magnetic component (the original version of the HMI inversion) and with two components (the improved version) using a Bayesian analysis. In pixels with intermediate magnetic field strengths (e.g. plages), the new version provides statistically significant values of filling fraction and magnetic field vector. Not only does the fitting of the Stokes profile improve, but the inference of the magnetic parameters and line-of-sight velocity are obtained uniquely. The new strategy is also proven to be effective for mitigating the anomalous hemispheric bias in the east-west magnetic field component in moderate field regions.

Height formation of bright points observed by IRIS in Mg II line wings during flux emergence

M. **Grubecka**1, B. Schmieder2, A. Berlicki3,1, P. Heinzel3, K. Dalmasse4 and P. Mein
A&A 593, A32 (**2016**)

Context. A flux emergence in the active region AR 111850 was observed on September 24, 2013 with the Interface Region Imaging Spectrograph (IRIS). Many bright points are associated with the new emerging flux and show enhancement brightening in the UV spectra.
Aims. The aim of this work is to compute the altitude formation of the compact bright points (CBs) observed in Mg II lines in the context of searching Ellerman bombs (EBs).
Methods. IRIS provided two large dense rasters of spectra in Mg II h and k lines, Mg II triplet, C II and Si IV lines covering all the active region and slit jaws in the two bandpasses (1400 Å and 2796 Å) starting at 11:44 UT and 15:39 UT, and lasting 20 min each. Synthetic profiles of Mg II and Hα lines are computed with non-local thermodynamic equlibrium (NLTE) radiative transfer treatment in 1D solar atmosphere model including a hotspot region defined by three parameters: temperature, altitude, and width.
Results. Within the two IRIS rasters, 74 CBs are detected in the far wings of the Mg II lines (at +/−1 Å and 3.5 Å). Around 10% of CBs have a signature in Si IV and CII. NLTE models with a hotspot located in the low atmosphere were found to fit a sample of Mg II profiles in CBs. The Hα profiles computed with these Mg II CB models are consistent with typical EB profiles observed from ground based telescopes e.g. THEMIS. A 2D NLTE modelling of fibrils (canopy) demonstrates that the Mg II line centres can be significantly affected but not the peaks and the wings of Mg II lines.

Conclusions. We conclude that the bright points observed in Mg II lines can be formed in an extended domain of altitudes in the photosphere and/or the chromosphere (400 to 750 km). Our results are consistent with the theory of heating by Joule dissipation in the atmosphere produced by magnetic field reconnection during flux emergence.

Desaturating SDO/AIA Observations of Solar Flaring Storms

Sabrina **Guastavino**1, Michele Piana1,2, Anna Maria Massone1,2, Richard Schwartz3, and Federico Benvenuto1
2019 ApJ 882 109
https://doi.org/10.3847/1538-4357/ab35d8
Image saturation has been an issue for several instruments in solar astronomy, mainly at EUV wavelengths. However, with the launch of the Atmospheric Imaging Assembly (AIA) as part of the payload of the Solar Dynamic Observatory image saturation has become a big data issue, involving around 105 frames of the impressive data set the telescope has been providing every year since 2010 February. This paper introduces a novel desaturation method that utilizes a sparsity constraint to solve the inverse scattering problem of determining the signal in the primary saturation region from the knowledge of the diffraction fringes produced by the instrument point-spread function. The method works without any need of a priori information on the image background and therefore can be applied even for desaturation of several consecutively deteriorated frames recorded during long-lasting intense solar storms. This peculiar methodological property could make this algorithm a possible tool for the realization of an automatic pipeline for the processing of the whole AIA data archive.

The Sun Through Time

Manuel **Güdel**
Space Science Reviews volume 216, Article number: 143 (**2020**)
https://link.springer.com/content/pdf/10.1007/s11214-020-00773-9.pdf
Magnetic activity of stars like the Sun evolves in time because of spin-down owing to angular momentum removal by a magnetized stellar wind. These magnetic fields are generated by an internal dynamo driven by convection and differential rotation. Spin-down therefore converges at an age of about 700 Myr for solar-mass stars to values uniquely determined by the stellar mass and age. Before that time, however, rotation periods and their evolution depend on the initial rotation period of a star after it has lost its protostellar/protoplanetary disk. This non-unique rotational evolution implies similar non-unique evolutions for stellar winds and for the stellar high-energy output. I present a summary of evolutionary trends for stellar rotation, stellar wind mass loss and stellar high-energy output based on observations and models.

Wavelet analysis of CME, X-ray flare, and sunspot series

M. R. G. **Guedes**, E. S. Pereira and J. R. Cecatto
A&A 573, A64 (**2015**)
http://www.aanda.org/articles/aa/pdf/2015/01/aa23080-13.pdf
Context. Coronal mass ejections (CMEs) and solar flares are the most energetic transient phenomena taking place at the Sun. Together they are principally responsible for disturbances in outer geospace. Coronal mass ejections and solar flares are believed to be correlated with the solar cycle, which is mainly characterized by sunspot numbers.
Aims. Here, we search for pattern identification in CMEs, X-ray solar flares, and sunspot number time series using a new data mining process and a quantitative procedure to correlate these series.
Methods. This new process consists of the combination of a decomposition method with the wavelet transform technique applied to the series ranging from 2000 until 2012. A simple moving average is used for the time-series decomposition as a high-pass filter. A continuous wavelet transform is applied to the series in sequence, which permits us to uncover signals previously masked by the original time series. We made use of the wavelet coherence to find some correlation between the data.
Results. The results have shown the existence of periodic and intermittent signals in the CMEs, flares, and sunspot time series. For the CME and flare series, few and relatively short time intervals without any signal were observed. Signals with an intermittent character take place during some epochs of the maximum and descending phases of the solar cycle 23 and rising phase of solar cycle 24. A comparison among X-ray flares, sunspots, and CME time series shows a stronger relation between flare and CMEs, although during some short intervals (four–eight months) and in a relatively narrow band. Yet, in contrast we have obtained a fainter or even absent relation between the X-ray flares and sunspot number series as well as between the CMEs and sunspot number series.

Relative Abundance Measurements in Plumes and Interplumes

C. **Guennou**1,2, M. Hahn1, and D. W. Savin
2015 ApJ 807 145
We present measurements of relative elemental abundances in plumes and interplumes. Plumes are bright, narrow structures in coronal holes that extend along open magnetic field lines far out into the corona. Previous work has found that in some coronal structures the abundances of elements with a low first ionization potential (FIP) <10 eV

are enhanced relative to their photospheric abundances. This coronal-to-photospheric abundance ratio, commonly called the FIP bias, is typically 1 for elements with a high-FIP (>10 eV). We have used Extreme Ultraviolet Imaging Spectrometer observations made on **2007 March 13 and 14** over a ≈24 hr period to characterize abundance variations in plumes and interplumes. To assess their elemental composition, we used a differential emission measure analysis, which accounts for the thermal structure of the observed plasma. We used lines from ions of iron, silicon, and sulfur. From these we estimated the ratio of the iron and silicon FIP bias relative to that for sulfur. From the results, we have created FIP-bias-ratio maps. We find that the FIP-bias ratio is sometimes higher in plumes than in interplumes and that this enhancement can be time dependent. These results may help to identify whether plumes or interplumes contribute to the fast solar wind observed in situ and may also provide constraints on the formation and heating mechanisms of plumes.

See **Hinode/EIS Nugget, August 2015**
http://solarb.mssl.ucl.ac.uk/SolarB/nuggets/nugget_2015aug.jsp

SMALL-SCALE HEATING EVENTS IN THE SOLAR ATMOSPHERE. I. IDENTIFICATION, SELECTION, AND IMPLICATIONS FOR CORONAL HEATING

N. **Guerreiro**1, M. Haberreiter1, V. Hansteen2, and W. Schmutz1
2015 ApJ 813 61
We present a comprehensive method to analyze small-scale heating events in detail in a 3D magnetohydrodynamics simulation for quiet-Sun conditions. The method determines the number, volume, and some general geometric properties of the small-scale heating events at different instants in a simulation with a volume of 16 × 8 × 16 Mm3, spanning from the top of the convection zone to the corona. We found that there are about 104 small-scale heating events at any instant above the simulated area of 128 Mm2. They occur mainly at heights between 1.5 and 3.0 Mm. We determine the average value of their projected vertical extent, which ranges from 375 to 519 km over time, and we show that height, volume, and energy distribution of the events at any instant resemble power laws. Finally, we demonstrate that larger heating structures are a combination of much smaller heating events and that small-scale heating events dissipate enough energy to maintain the coronal energetic balance at any instant.

Implicit large eddy simulations of global solar convection: effects of numerical resolution in non-rotating and rotating cases

G. **Guerrero**, A.M. Stejko, A.G. Kosovichev, P.K Smolarkiewicz, A. Strugarek
ApJ **2022**
https://arxiv.org/pdf/2208.05738.pdf
Simulating deep solar convection and its coupled mean-field motions is a formidable challenge where few observational results constrain models that suffer from the non-physical influence of the grid resolution. We present hydrodynamic global Implicit Large-Eddy simulations (ILES) of deep solar convection performed with the EULAG-MHD code, and explore the effects of grid resolution on the properties of rotating and non-rotating convection. The results, based on low-order moments and turbulent spectra reveal that convergence could be achieved in non-rotating simulations provided sufficient resolution in the radial direction. The flow is highly anisotropic, with the energy contained in horizontal divergent motions exceeding by more than three orders of magnitude their radial counterpart. By contrast, in rotating simulations the largest energy is in the toroidal part of the horizontal motions. As the grid resolution increases, the turbulent correlations change in such a way that a solar-like differential rotation, obtained in the simulation with the coarser grid, transitions to the anti-solar differential rotation. The reason for this change is the contribution of the effective viscosity to the balance of the forces driving large-scale flows. As the effective viscosity decreases, the angular momentum balance improves, yet the force balance in the meridional direction lessens, favoring a strong meridional flow that advects angular momentum towards the poles. The results suggest that obtaining the correct distribution of angular momentum may not be a mere issue of numerical resolution. Accounting for additional physics, such as magnetism or the near-surface shear layer, may be necessary in simulating the solar interior.

Understanding solar torsional oscillations from global dynamo models

G. **Guerrero**, P. K. Smolarkiewicz, E. M. de Gouveia Dal Pino, A. G. Kosovichev, N. N. Mansour
ApJL **828** L3 **2016**
http://arxiv.org/pdf/1608.02278v1.pdf
The phenomenon of solar "torsional oscillations" (TO) represents migratory zonal flows associated with the solar cycle. These flows are observed on the solar surface and, according to helioseismology, extend through the convection zone. We study the origin of the TO using results of a global MHD simulation of the solar interior that reproduces several of the observed characteristics of the mean-flows and magnetic fields. Our results indicate that the magnetic tension (MT) in the tachocline region is a key factor for the periodic changes in the angular momentum transport that causes the TO. The torque induced by the magnetic tension at the base of the convection zone is positive at the poles and negative at the equator. A rising MT torque at higher latitudes causes the poles to speed-up, whereas a declining negative MT torque at the lower latitudes causes the equator to slow-down. These changes in

the zonal flows propagate through the convection zone up to the surface. Also, our results suggest that it is the magnetic field at the tachocline that modulates the amplitude of the surface meridional flow rather than the opposite as assumed by flux-transport dynamo models of the solar cycle.

On the role of tachoclines in solar and stellar dynamos

G. **Guerrero**, P. K. Smolarkiewicz, E. M. de Gouveia Dal Pino, A. G. Kosovichev, N. N. Mansour
ApJ 819 104 **2015**
http://arxiv.org/pdf/1507.04434v1.pdf
Rotational shear layers at the boundary between radiative and convective zones, tachoclines, play a key role in the dynamo process of magnetic field generation in the Sun and solar-like stars. We present two sets of global simulations of rotating turbulent convection and dynamo. The first set considers a stellar convective envelope only; the second one, aiming at the formation of a tachocline, considers also the upper part of the radiative zone. Our results indicate that dynamo properties like the growth rate, the saturation energy and mode depend on the Rossby (Ro) number. The models with slow rotation in the first set of simulations reproduce remarkably well the solar differential rotation in the convection zone. Depending on the value of Ro either oscillatory (with ~2 yr period) or steady dynamo solutions are obtained. The models in the second set naturally develop a tachocline which, in turn, leads to the generation of strong mean magnetic field (~1 Tesla). Since the field is also deposited into the stable deeper layer, its evolutionary time-scale is much longer than in the models without a tachocline. Surprisingly, the magnetic field in the upper turbulent convection zone evolves in the same time scale as the deep field. These models result in either an oscillatory dynamo with ~30 yr period or in a steady dynamo depending on the value of Ro. Finally, we study the evolution of the magnetic field in terms of the mean-field dynamo source terms with the dynamo coefficients computed using the FOSA approximation. For the oscillatory models without a tachocline the evolution of the fields seems to be consistent with a pattern of dynamo waves propagating according to the Parker-Yoshimura sign rule. In the models with tachocline the dynamics is more complex and could involve other transport mechanisms due to the longer time-scale.

Solar and stellar differential rotation and dynamo, mean-field vs. global models

G. **Guerrero**1, P. K. Smolarkiewicz2, A. G. Kosovichev3 & N. N. Mansour
HMI Science Nuggets #24, 2014
http://hmi.stanford.edu/hminuggets/?p=893

Five-Minute Solar Oscillations and Ion-Cyclotron Waves in the Solar Wind

A. **Guglielmi**, A. Potapov, B. Dovbnya
Solar Phys. Volume 290, Issue 10, pp 3023-3032 **2015**
We study the possible impact of the photospheric five-minute oscillations on the ion-cyclotron waves in the solar wind. We proceed from the assumption that the ion-cyclotron waves in the solar wind experience a modulation with a characteristic period of five minutes under the influence of Alfvén waves driven by photospheric motions. The theory presented in this article predicts a deep frequency modulation. This modulation is expected mainly from variations in the orientation of the interplanetary magnetic field lines, which, in turn, are caused by the Alfvén waves propagating from the Sun. To test the theoretical predictions, we analyzed records of the ultra-low-frequency (ULF) geoelectromagnetic waves to find the permanent quasi-monochromatic oscillations of natural origin in the Pc1 – 2 frequency band (0.1 – 5 Hz), the carrier frequency of which varies with time in a wide range. As a result, we found the so-called serpentine emission (SE), which was observed in Antarctica at the Vostok station near the South Geomagnetic Pole. The permanency, range of frequencies, and the deep frequency modulation of the SE correspond to the qualitative properties of ion-cyclotron waves in the solar wind. In the context of this work, one of the most important features of the SE is a clearly expressed five-minute modulation of the carrier frequency. We assume that we have found non-trivial manifestations of the solar five-minute oscillations on the Earth.

On the Magnetic Nature of an Exploding Granule as Revealed by Sunrise/IMaX

Salvo L. **Guglielmino**1, Valentín Martínez Pillet2, Basilio Ruiz Cobo3,4, Luis R. Bellot Rubio5, José Carlos del Toro Iniesta5, Sami K. Solanki6,7, Tino L. Riethmüller6, and Francesca Zuccarello1
2020 ApJ 896 62
https://iopscience.iop.org/article/10.3847/1538-4357/ab917b/pdf
We study the photospheric evolution of an exploding granule observed in the quiet Sun at high spatial (~0.″3) and temporal (31.5 s) resolution by the imaging magnetograph Sunrise/IMaX in 2009 June. These observations show that the exploding granule is cospatial to a magnetic flux emergence event occurring at mesogranular scale (up to ~12 Mm2 area). Using a modified version of the SIR code for inverting the IMaX spectropolarimetric measurements, we obtain information about the magnetic configuration of this photospheric feature. In particular,

we find evidence of highly inclined emerging fields in the structure, carrying a magnetic flux content up to ~4 × 1018 Mx. The balance between gas and magnetic pressure in the region of flux emergence, compared with a very quiet region of the Sun, indicates that the additional pressure carried by the emerging flux increases the total pressure by about 5% and appears to allow the granulation to be modified, as predicted by numerical simulations. The overall characteristics suggest that a multipolar structure emerges into the photosphere, resembling an almost horizontal flux sheet. This seems to be associated with exploding granules. Finally, we discuss the origin of such flux emergence events. **2009 June 10**

Long-term optical monitoring of the solar atmosphere in Italy

S.L. **Guglielmino**, I. Ermolli, P. Romano, F. Zuccarello, F. Giorgi, M. Falco, R. Piazzesi, M. Stangalini, M. Murabito, M. Ferrucci, A. Mangano

IAU Symposium 340 **2019**

https://arxiv.org/pdf/1901.01050.pdf

Probably, the long-term monitoring of the solar atmosphere started in Italy with the first telescopic observations of the Sun made by Galileo Galilei in the early 17thcentury. His recorded observations and science results, as well as the work carried out by other following outstanding Italian astronomers inspired the start of institutional programs of regular solar observations at the Arcetri, Catania, and Rome Observatories. These programs have accumulated daily images of the solar photosphere and chromosphere taken at various spectral bands over a time span greater than 80 years. In the last two decades, regular solar observations were continued with digital cameras only at the Catania and Rome Observatories, which are now part of the INAF National Institute for Astrophysics. At the two sites, daily solar images are taken at the photospheric G-band, Blue (λ=409.4 nm), and Red (λ=606.9 nm) continua spectral ranges and at the chromospheric Ca II K and Hα lines, with a 2″ spatial resolution. Solar observation in Italy, which benefits from over 2500 hours of yearly sunshine, currently aims at the operational monitoring of solar activity and long-term variability and at the continuation of the historical series as well. Existing instruments will be soon enriched by the SAMM double channel telescope equipped with magneto-optical filters that will enable the tomography of the solar atmosphere with simultaneous observations at the K I 769.9 nm and Na I D 589.0 nm lines. In this contribution, we present the available observations and outline their scientific relevance.

Satellite observations of reconnection between emerging and pre-existing small-scale magnetic fields

S.L. **Guglielmino**, F. Zuccarello, P.R. Young, P. Romano, M. Murabito

Nuovo Cimento C" as proceeding of the Third Meeting of the Italian Solar and Heliospheric Community **2019**

https://arxiv.org/pdf/1901.01056.pdf

We report multi-wavelength ultraviolet observations taken with the IRIS satellite, concerning the emergence phase in the upper chromosphere and transition region of an emerging flux region (EFR) embedded in the unipolar plage of active region NOAA 12529. The photospheric configuration of the EFR is analyzed in detail benefitting from measurements taken with the spectropolarimeter aboard the Hinode satellite, when the EFR was fully developed. In addition, these data are complemented by full-disk, simultaneous observations of the SDO satellite, relevant to the photosphere and the corona. In the photosphere, magnetic flux emergence signatures are recognized in the fuzzy granulation, with dark alignments between the emerging polarities, cospatial with highly inclined fields. In the upper atmospheric layers, we identify recurrent brightenings that resemble UV bursts, with counterparts in all coronal passbands. These occur at the edges of the EFR and in the region of the arch filament system (AFS) cospatial to the EFR. Jet activity is also found at chromospheric and coronal levels, near the AFS and the observed brightness enhancement sites. The analysis of the IRIS line profiles reveals the heating of dense plasma in the low solar atmosphere and the driving of bi-directional high-velocity flows with speeds up to 100 km/s at the same locations. Furthermore, we detect a correlation between the Doppler velocity and line width of the Si IV 1394 and 1402 Å line profiles in the UV burst pixels and their skewness. Comparing these findings with previous observations and numerical models, we suggest evidence of several long-lasting, small-scale magnetic reconnection episodes between the emerging bipole and the ambient field. This process leads to the cancellation of a pre-existing photospheric flux concentration of the plage with the opposite polarity flux patch of the EFR. The reconnection appears to occur higher in the atmosphere than usually observed. **13 April 2016**

IRIS observations of magnetic interactions in the solar atmosphere between pre-existing and emerging magnetic fields. II. UV emission properties

Salvo L. **Guglielmino**, Peter R. Young, Francesca Zuccarello

ApJ **871**:82 **2018**

https://arxiv.org/pdf/1812.07285.pdf

http://iopscience.iop.org/article/10.3847/1538-4357/aaf79d/pdf

Multi-wavelength ultraviolet (UV) observations by the IRIS satellite in active region NOAA 12529 have recently pointed out the presence of long-lasting brightenings, akin to UV bursts, and simultaneous plasma ejections occurring in the upper chromosphere and transition region during secondary flux emergence. These signatures have been interpreted as evidence of small-scale, recurrent magnetic reconnection episodes between the emerging flux region (EFR) and the pre-existing plage field. Here, we characterize the UV emission of these strong, intermittent brightenings and we study the surge activity above the chromospheric arch filament system (AFS) overlying the EFR. We analyze the surges and the cospatial brightenings observed at different wavelengths. We find an asymmetry in the emission between the blue and red wings of the Si IV 1402 Å and Mg II k 2796.3 Å lines, which clearly outlines the dynamics of the structures above the AFS that form during the small-scale eruptive phenomena. We also detect a correlation between the Doppler velocity and skewness of the Si IV 1394 Å and 1402 Å line profiles in the UV burst pixels. Finally, we show that genuine emission in the Fe XII 1349.4 Å line is cospatial to the Si IV brightenings. This definitely reveals a pure coronal counterpart to the reconnection event. **13-14 April 2016**

Quiet-Sun hydrogen Lyman-alpha line profile derived from SOHO/SUMER solar-disk observations

S. **Gunar** (1), P. Schwartz (2), J. Koza (2), P. Heinzel (1)
A&A 644, A109 **2020**
https://arxiv.org/pdf/2011.01299.pdf
https://doi.org/10.1051/0004-6361/202039348
The solar radiation in the Lyman-alpha spectral line of hydrogen plays a significant role in the illumination of chromospheric and coronal structures, such as prominences, spicules, chromospheric fibrils, cores of coronal mass ejections, and solar wind. Moreover, it is important for the investigation of the heliosphere, Earth's ionosphere, and the atmospheres of planets, moons, and comets. We derive a reference quiet-Sun Lyman-alpha spectral profile that is representative of the Lyman-alpha radiation from the solar disk during a minimum of solar activity. This profile can serve as an incident radiation boundary condition for the radiative transfer modelling of chromospheric and coronal structures. Because the solar radiation in the Lyman lines is not constant over time but varies significantly with the solar cycle, we provide a method for the adaptation of the incident radiation Lyman line profiles (Lyman-alpha and higher lines) to a specific date. Moreover, we analyse how the change in the incident radiation influences the synthetic spectra produced by the radiative transfer modelling. To take into account the Lyman-alpha variation with the solar cycle, we used the LISIRD composite Lyman-alpha$ index. To estimate the influence of the change in the incident radiation in the Lyman lines on the results of radiative transfer models, we used a 2D prominence fine structure model. The analysis of the influence of the change in the incident radiation shows that the synthetic spectra are strongly affected by the modification of the incident radiation boundary condition. The hydrogen H alpha line can also be considerably affected, despite the fact that the H alpha radiation from the solar disk does not vary with the solar cycle.

A model of solar equilibrium: the hydrodynamic limit

Lee **Gunderson**, Amitava Bhattacharjee
2019 *ApJ* **870** 47
https://arxiv.org/pdf/1712.08069.pdf
Helioseismology has revealed the internal density and rotation profile of the Sun. Yet, knowledge of its magnetic fields and meridional circulation is confined much closer to the surface, and mean entropy gradients at the surface are below detectable limits. Numerical simulations can offer insight into the interior dynamics, and help identify which ingredients are necessary to produce particular features. However, several gross features of the Sun can be understood analytically from an equilibrium perspective, for example the 1-D density profile arising from steady-state energy transport from the core to the surface, or the tilting of isorotation contours in the convection zone due to baroclinic forcing. To help answer the question of which features can be qualitatively explained by equilibrium, we propose analyzing stationary axisymmetric ideal MHD flows in the solar regime. By choosing an appropriate latitudinal entropy profile, we recover a rotation profile that reasonably matches observations in the bulk of the convection zone. Furthermore, we include the effects of poloidal flow, developing a feature reminiscent of the near surface shear layer. No tachocline-like feature is seen in hydrodynamic equilibrium, suggesting the importance of either dynamics or magnetic fields in any description.

Horizontally and vertically polarized kink oscillations in curved solar coronal loops⋆

Mingzhe **Guo**1,2, Tom Van Doorsselaere1, Bo Li2 and Marcel Goossens1
A&A, 687, A30 (**2024**)
https://www.aanda.org/articles/aa/pdf/2024/07/aa49991-24.pdf
Aims. Kink oscillations are frequently observed in coronal loops. This work aims to numerically clarify the influence of the loop curvature on horizontally and vertically polarized kink oscillations.

Methods. Working within the framework of ideal magnetohydrodynamics (MHD), we conduct three-dimensional (3D) simulations of axial fundamental kink oscillations in curved density-enhanced loops embedded in a potential magnetic field. Both horizontal and vertical polarizations are examined, and their oscillation frequencies are compared with Wentzel-Kramers-Brillouin (WKB) expectations. We discriminate between two different density specifications. In the first (dubbed "uniform density"), the density is axially uniform and varies continuously in the transverse direction toward a uniform ambient corona. Some further stratification is implemented in the second specification (dubbed "stratified"), allowing us to address the effect of evanescent barriers.
Results. Examining the oscillating profiles of the initially perturbed uniform-density loops, we found that the frequencies for both polarizations deviate from the WKB expectation by ∼10%. In the stratified loop, however, the frequency of the horizontal polarization deviates to a larger extent (∼25%). We illustrate the lateral leakage of kink modes through wave tunneling in 3D simulations, for the first time. Despite this, in the uniform density and the stratified loops, the damping time-to-period ratios are similar and are close to the analytical predictions for straight configurations under the thin-tube-thin-boundary (TTTB) assumption.
Conclusions. The WKB expectation for straight configurations can reasonably describe the eigenfrequency of kink oscillations only in loops without an asymmetrical cross-loop density profile perpendicular to the oscillating direction. Lateral leakage via wave tunneling is found to be less efficient than resonant absorption, meaning that the latter remains a robust damping mechanism for kink motions even when loop curvature is included.

Estimating the energy flux of transverse waves associated with Kelvin-Helmholtz instability in solar coronal loops

Mingzhe **Guo**1, Yuhang Gao2,1, Tom Van Doorsselaere1 and Marcel Goossens1
A&A 676, L7 (**2023**)
https://www.aanda.org/articles/aa/pdf/2023/08/aa46816-23.pdf
Context. The energy flux of kink waves in coronal loops has been estimated in previous studies. Recent numerical simulations have revealed that kink oscillations can induce a Kelvin-Helmholtz Instability (KHI) in magnetic flux tubes. This non-linear process breaks the assumptions that have typically been included in previous eigenmode analyses. Therefore, the current analytical expressions of energy flux need to be re-examined.
Aims. In the present work, we aim to compare our numerical energy flux with previous analytical formulae and establish modifications to the estimation of the energy flux of kink waves in coronal loops.
Methods. Working within the framework of ideal magnetohydrodynamics (MHD), we conducted three-dimensional (3D) simulations of kink oscillations in coronal cylinders. Forward models were also employed to translate our numerical results into observables using the FoMo code.
Results. We find that the previous estimation of the energy flux of kink waves is reasonable up to the point before the KHI is fully developed. However, as small vortices develop, the energy flux derived from the analytical formula becomes smaller than the total Poynting flux calculated from our numerical results. Furthermore, when degrading the original numerical resolution to match a realistic instrumental resolution, for instance, the Extreme Ultraviolet Imager (EUI) on board the Solar Orbiter (SO), the energy flux becomes much smaller than the numerical value.
Conclusions. The energy flux calculated from the analytical formula should be modified by multiplying it by a factor of about 2. When it comes to the energy flux estimation based on SO/EUI observations, this factor should be between about 3 and 4.

Impulsively Generated Kink Wave Trains in Solar Coronal Slabs

Mingzhe **Guo**, Bo Li, Tom Van Doorsselaere, Mijie Shi
MNRAS Volume 515, Issue 3, Pages 4055–4064 **2022**
https://arxiv.org/pdf/2207.07249.pdf
https://doi.org/10.1093/mnras/stac2006
We numerically follow the response of density-enhanced slabs to impulsive, localized, transverse velocity perturbations by working in the framework of ideal magnetohydrodynamics (MHD). Both linear and nonlinear regimes are addressed. Kink wave trains are seen to develop along the examined slabs, sharing the characteristics that more oscillatory patterns emerge with time and that the apparent wavelength increases with distance at a given instant. Two features nonetheless arise due to nonlinearity, one being a density cavity close to the exciter and the other being the appearance of shocks both outside and inside the nominal slab. These features may be relevant for understanding the interaction between magnetic structures and such explosive events as coronal mass ejections. Our numerical findings on kink wave trains in solar coronal slabs are discussed in connection with typical measurements of streamer waves.

A dynamo-based prediction of solar cycle 25

Wei **Guo**, Jie Jiang, Jing-Xiu Wang
Solar Phys. **296**, Article number: 136 **2021**
https://arxiv.org/pdf/2108.01412.pdf **File**
https://link.springer.com/content/pdf/10.1007/s11207-021-01878-2.pdf

https://doi.org/10.1007/s11207-021-01878-2
Solar activity cycle varies in amplitude. The last Cycle 24 is the weakest in the past century. Sun's activity dominates Earth's space environment. The frequency and intensity of the Sun's activity are accordant with the solar cycle. Hence there are practical needs to know the amplitude of the upcoming Cycle 25. The dynamo-based solar cycle predictions not only provide predictions, but also offer an effective way to evaluate our understanding of the solar cycle. In this article we apply the method of the first successful dynamo-based prediction developed for Cycle 24 to the prediction of Cycle 25, so that we can verify whether the previous success is repeatable. The prediction shows that Cycle 25 would be about 10% stronger than Cycle 24 with an amplitude of 126 (international sunspot number version 2.0). The result suggests that Cycle 25 will not enter the Maunder-like grand solar minimum as suggested by some publications. Solar behavior in about four to five years will give a verdict whether the prediction method captures the key mechanism for solar cycle variability, which is assumed as the polar field around the cycle minimum in the model.

Shock Propagation and Associated Particle Acceleration in the Presence of Ambient Solar-Wind Turbulence

Fan **Guo**, Joe Giacalone, Lulu Zhao
Frontier in Astronomy and Space Sciences **2021**
https://arxiv.org/pdf/2102.06054.pdf
The topic of this review paper is on the influence of solar wind turbulence on shock propagation and its consequence on the acceleration and transport of energetic particles at shocks. As the interplanetary shocks sweep through the turbulent solar wind, the shock surfaces fluctuate and ripple in a range of different scales. We discuss particle acceleration at rippled shocks in the presence of ambient solar-wind turbulence. This strongly affects particle acceleration and transport of energetic particles (both ions and electrons) at shock fronts. In particular, we point out that the effects of upstream turbulence is critical for understanding the variability of energetic particles at shocks. Moreover, the presence of pre-existing upstream turbulence significantly enhances the trapping near the shock of low-energy charged particles, including near the thermal energy of the incident plasma, even when the shock propagates normal to the average magnetic field. Pre-existing turbulence, always present in space plasmas, provides a means for the efficient acceleration of low-energy particles and overcoming the well known injection problem at shocks.

Kink Oscillations in Solar Coronal Loops with Elliptical Cross-Sections. I. the linear regime

Mingzhe **Guo**, Bo Li, Tom Van Doorsselaere
ApJ **2020**
https://arxiv.org/pdf/2010.06991.pdf
The cross sections of solar coronal loops are suggested to be rarely circular. We examine linear kink oscillations in straight, density-enhanced, magnetic cylinders with elliptical cross-sections by solving the three-dimensional magnetohydrodynamic equations from an initial-value-problem perspective. Motivated by relevant eigen-mode analyses, we distinguish between two independent polarizations, one along the major axis (the M-modes) and the other along the minor one (the m-modes). We find that, as happens for coronal loops with circular cross-sections, the apparent damping of the transverse displacement of the loop axis is accompanied by the accumulation of transverse Alfvénic motions and the consequent development of small-scales therein, suggesting the robustness of the concepts of resonant absorption and phase-mixing. In addition, two stages can in general be told apart in the temporal evolution of the loop displacement; a Gaussian time dependence precedes an exponential one. For the two examined density ratios between loops and their surroundings, the periods of the M-modes (m-modes) tend to increase (decrease) with the major-to-minor-half-axis ratio, and the damping times in the exponential stage for the M-modes tend to exceed their m-mode counterparts. This is true for the two transverse profiles we examine. However, the relative magnitudes of the damping times in the exponential stage for different polarizations depend on the specification of the transverse profile and/or the density contrast. The applications of our numerical findings are discussed in the context of coronal seismology.

Heating effects from driven transverse and Alfvén waves in coronal loops

Mingzhe **Guo**, Tom Van Doorsselaere, Kostas Karampelas, Bo Li, Patrick Antolin, Ineke De Moortel
2019 *ApJ* **870** 55
https://arxiv.org/pdf/1811.07608.pdf
Recent numerical studies revealed that transverse motions of coronal loops can induce the Kelvin-Helmholtz Instability (KHI). This process could be important in coronal heating because it leads to dissipation of energy at small spatial-scale plasma interactions. Meanwhile, small amplitude decayless oscillations in coronal loops have been discovered recently in observations of SDO/AIA. We model such oscillations in coronal loops and study wave

heating effects, considering a kink and Alfv{é}n driver separately and a mixed driver at the bottom of flux tubes. Both the transverse and Alfv{é}n oscillations can lead to the KHI. Meanwhile, the Alfv{é}n oscillations established in loops will experience phase mixing. Both processes will generate small spatial-scale structures, which can help the dissipation of wave energy. Indeed, we observe the increase of internal energy and temperature in loop regions. The heating is more pronounced for the simulation containing the mixed kink and Alfv{é}n driver. This means that the mixed wave modes can lead to a more efficient energy dissipation in the turbulent state of the plasma and that the KHI eddies act as an agent to dissipate energy in other wave modes. Furthermore, we also obtained forward modelling results using the FoMo code. We obtained forward models which are very similar to the observations of decayless oscillations. Due to the limited resolution of instruments, neither Alfv{é}n modes nor the fine structures are observable. Therefore, this numerical study shows that Alfv{é}n modes probably can co-exist with kink modes, leading to enhanced heating.

Magnetic Helicity Estimations in Models and Observations of the Solar Magnetic Field. Part III: Twist Number Method

Y. **Guo**, E. Pariat , G. Valori , S. Anfinogentov , F. Chen , M. Georgoulis , Y. Liu , K. Moraitis , J. K. Thalmann , S. Yang
A&A **2017**
http://www.issibern.ch/teams/magnetichelicity/guoyang_20170326.pdf
We study the writhe, twist and magnetic helicity of different magnetic flux ropes, based on models of the solar coronal magnetic field structure. These include an analytical force-free Titov"D"moulin equilibrium solution, non force-free magnetohydrodynamic simulations, and nonlinear force-free magnetic field models. The geometrical boundary of the magnetic flux rope is determined by the quasi-separatrix layer and the bottom surface, and the axis curve of the flux rope is determined by its overall orientation. The twist is computed by the Berger?Prior formula that is suitable for arbitrary geometry and both force-free and non-force-free models. The magnetic helicity is estimated by the twist multiplied by the square of the axial magnetic flux. We compare the obtained values with those derived by a finite volume helicity estimation method. We find that the magnetic helicity obtained with the twist method agrees with the helicity carried by the purely current-carrying part of the field within uncertainties for most test cases. It is also found that the current-carrying part of the model field is relatively significant at the very location of the magnetic flux rope. This qualitatively explains the agreement between the magnetic helicity computed by the twist method and the helicity contributed purely by the current-carrying magnetic field.
2007 February 12, 20100807

Spatial damping of propagating sausage waves in coronal cylinders

Ming-Zhe **Guo**, Shao-Xia Chen, Bo Li, Li-Dong Xia, Hui Yu
A&A 581, A130 **2015**
http://arxiv.org/pdf/1507.07724v1.pdf
Sausage modes are important in coronal seismology. Spatially damped propagating sausage waves were recently observed in the solar atmosphere. We examine how wave leakage influences the spatial damping of sausage waves propagating along coronal structures modeled by a cylindrical density enhancement embedded in a uniform magnetic field. Working in the framework of cold magnetohydrodynamics, we solve the dispersion relation (DR) governing sausage waves for complex-valued longitudinal wavenumber k at given real angular frequencies ω. For validation purposes, we also provide analytical approximations to the DR in the low-frequency limit and in the vicinity of ωc, the critical angular frequency separating trapped from leaky waves. In contrast to the standing case, propagating sausage waves are allowed for ω much lower than ωc. However, while able to direct their energy upwards, these low-frequency waves are subject to substantial spatial attenuation. The spatial damping length shows little dependence on the density contrast between the cylinder and its surroundings, and depends only weakly on frequency. This spatial damping length is of the order of the cylinder radius for ω≲1.5vAi/a, where a and vAi are the cylinder radius and the Alfv\'en speed in the cylinder, respectively. We conclude that if a coronal cylinder is perturbed by symmetric boundary drivers (e.g., granular motions) with a broadband spectrum, wave leakage efficiently filters out the low-frequency components.

A study of global magnetic helicity in self-consistent spherical dynamos

Parag **Gupta**, Radostin D. Simitev, David MacTaggart
Geophysical and Astrophysical Fluid Dynamics **2022**
https://arxiv.org/pdf/2211.01356
Magnetic helicity is a fundamental constraint in both ideal and resistive magnetohydrodynamics. Measurements of magnetic helicity density on the Sun and other stars are used to interpret the internal behaviour of the dynamo generating the global magnetic field. In this note, we study the behaviour of the global relative magnetic helicity in three self-consistent spherical dynamo solutions of increasing complexity. Magnetic helicity describes the global linkage of the poloidal and toroidal magnetic fields (weighted by magnetic flux), and our results indicate that there

are preferred states of this linkage. This leads us to propose that global magnetic reversals are, perhaps, a means of preserving this linkage, since, when only one of the poloidal or toroidal fields reverses, the preferred state of linkage is lost. It is shown that magnetic helicity indicates the onset of reversals and that this signature may be observed at the outer surface.

Spectroscopic evidence of damping of Alfvén waves in the off-limb solar corona

G. R. **Gupta**

ApJ **836** 4 **2017**

https://arxiv.org/pdf/1612.09551v1.pdf

We investigate off-limb active region and quiet Sun corona using spectroscopic data. Active region is clearly visible in several spectral lines formed in the temperature range of 1.1--2.8 MK. We derive electron number density using line ratio method, and non-thermal velocity in the off-limb region up to the distance of 140 Mm. We compare density scale heights derived from several spectral line pairs with expected scale heights as per hydrostatic equilibrium model. Using several isolated and unblended spectral line profiles, we estimate non-thermal velocities in active region and quiet Sun. Non-thermal velocities obtained from warm lines in active region first show increase and later show either decrease or almost constant value with height in the far off-limb region, whereas hot lines show consistent decrease. However, in the quiet Sun region, non-thermal velocities obtained from various spectral lines show either gradual decrease or remain almost constant with height. Using these obtained parameters, we further calculate Alfv\'en wave energy flux in the both active and quiet Sun regions. We find significant decrease in wave energy fluxes with height, and hence provide evidence of Alfv\'en wave damping. Furthermore, we derive damping lengths of Alfv\'en waves in the both regions and find them to be in the range of 25-170 Mm. Different damping lengths obtained at different temperatures may be explained as either possible temperature dependent damping or measurements obtained in different coronal structures formed at different temperatures along the line-of-sight. Temperature dependent damping may suggest some role of thermal conduction in the damping of Alfv\'en waves in the lower corona.

Rieger-type periodicity in the total irradiance of the Sun as a star during solar cycles 23-24

Gurgenashvili, E., Zaqarashvili, T.V., Kukhianidze, V., Reiners, A., Oliver, R., Lanza, A.F., Reinhold, T

A&A 653, A146 **2021**

https://arxiv.org/pdf/2108.04006.pdf

https://www.aanda.org/articles/aa/pdf/2021/09/aa41370-21.pdf

https://doi.org/10.1051/0004-6361/202141370

Context. Total solar irradiance allows for the use of the Sun as a star for studying observations of stellar light curves from recent space missions. Aims. We aim to study how the mid-range periodicity observed in solar activity indices influences the total solar irradiance. Methods. We studied periodic variations of total solar irradiance based on SATIRE-S and SOHO/VIRGO data during solar cycles 23-24 on timescales of Rieger-type periodicity. Then we compared the power spectrum of oscillations in the total solar irradiance to those of sunspot and faculae data to determine their contributions. Results. Wavelet analyses of TSI data reveal strong peaks at 180 days and 115 days in cycle 23, while cycle 24 showed periods of 170 days and 145 days. There are several periods in the sunspot and faculae data that are not seen in total solar irradiance as they probably cancel each other out through simultaneous brightening (in faculae) and darkening (in sunspots). Rieger-type periodicity is probably caused by magneto-Rossby waves in the internal dynamo layer, where the solar cyclic magnetic field is generated. Therefore, the observed periods in the total solar irradiance and the wave dispersion relation allow us to estimate the dynamo magnetic field strength as 10-15 kG. Conclusions. Total solar irradiance can be used to estimate the magnetic field strength in the dynamo layer. This tool can be of importance in estimating the dynamo magnetic field strength of solar-like stars using light curves obtained by space missions.

North-south asymmetry in Rieger-type periodicity during solar cycles 19-23

Eka **Gurgenashvili**, Teimuraz V. Zaqarashvili, Vasil Kukhianidze, Ramon Oliver, Jose Luis Ballester,Mausumi Dikpati, Scott W. McIntosh

2017 *ApJ* **845** 137

https://arxiv.org/pdf/1707.08615.pdf

Rieger-type periodicity has been detected in different activity indices over many solar cycles. It was recently shown that the periodicity correlates with solar activity having a shorter period during stronger cycles. Solar activity level is generally asymmetric between northern and southern hemispheres, which could suggest the presence of a similar behavior in the Rieger-type periodicity. We analyse the sunspot area/number and the total magnetic flux data for northern and southern hemispheres during solar cycles 19-23 which had remarkable north-south asymmetry. Using wavelet analysis of sunspot area and number during the north-dominated cycles (19-20) we obtained the periodicity of 160-165 days in the stronger northern hemisphere and 180-190 days in the weaker southern hemisphere. On the other hand, south-dominated cycles (21-23) display the periodicity of 155-160 days in the stronger southern hemisphere and 175-188 days in the weaker northern hemisphere. Therefore, the Rieger-type periodicity has the

north-south asymmetry in sunspot area/number data during solar cycles with strong hemispheric asymmetry. We suggest that the periodicity is caused by magnetic Rossby waves in the internal dynamo layer. Using the dispersion relation of magnetic Rossby waves and observed Rieger periodicity we estimated the magnetic field strength in the layer as 45-49 kG in more active hemispheres (north during the cycles 19-20 and south during the cycles 21-23) and 33-40 kG in weaker hemispheres. The estimated difference in the hemispheric field strength is around 10 kG, which provides a challenge for dynamo models. Total magnetic flux data during the cycle 20-23 reveals no clear north-south asymmetry which needs to be explained in the future.

Rieger-type periodicity during solar cycles 14-24: estimation of dynamo magnetic field strength in the solar interior

Eka **Gurgenashvili**, Teimuraz Zaqarashvili, Vasil Kukhianidze, Ramon Oliver, Jose Luis Ballester, Giorgi Ramishvili, Bidzina Shergelashvili, Arnold Hanslmeier, Stefaan Poedts

ApJ **826** 55 **2016**

http://arxiv.org/pdf/1605.04162v1.pdf

Solar activity undergoes a variation over time scales of several months known as Rieger-type periodicity, which usually occurs near maxima of sunspot cycles. An early analysis showed that the periodicity appears only in some cycles, and is absent in other cycles. But the appearance/absence during different cycles has not been explained. We performed a wavelet analysis of sunspot data from the Greenwich Royal Observatory and the Royal Observatory of Belgium during cycles 14-24. We found that the Rieger-type periods occur in all cycles, but they are cycle-dependent: shorter periods occur during stronger cycles. Our analysis revealed a periodicity of 185-195 days during the weak cycles 14-15 and 24, and a periodicity of 155-165 days during the stronger cycles 16-23. We derived the dispersion relation of the spherical harmonics of the magnetic Rossby waves in the presence of differential rotation and a toroidal magnetic field in the dynamo layer near the base of the convection zone. This showed that the harmonic of fast Rossby waves with m=1 and n=4, where m (n) indicate the toroidal (poloidal) wavenumbers, respectively, perfectly fit with the observed periodicity. The variation of the toroidal field strength from weaker to stronger cycles may lead to the different periods found in those cycles, which explains the observed enigmatic feature of the Rieger-type periodicity. Finally, we used the observed periodicity to estimate the dynamo field strength during cycles 14-24. Our estimations suggest a field strength of 40 kG for the stronger cycles, and 20 kG for the weaker cycles.

The Solar Disk at High Energies

Miguel **Gutiérrez**1, Manuel Masip1, and Sergio Muñoz1

2022 ApJ 941 86

https://iopscience.iop.org/article/10.3847/1538-4357/aca020/pdf

High energy cosmic rays illuminate the Sun and produce an image that could be observed in up to five different channels: a cosmic-ray shadow (whose energy dependence has been studied by HAWC); a gamma-ray flux (observed at $E \leq 200$ GeV by Fermi-LAT); a muon shadow (detected by ANTARES and IceCube); a neutron flux (undetected, as there are no hadronic calorimeters in space); a flux of high energy neutrinos. Since these signals are correlated, the ones already observed can be used to reduce the uncertainty in the still undetected ones. Here we define a simple setup that uses the Fermi-LAT and HAWC observations to imply very definite fluxes of neutrons and neutrinos from the solar disk. In particular, we provide a fit of the neutrino flux at 10 GeV–10 TeV that includes its dependence on the zenith angle and on the period of the solar cycle. This flux represents a neutrino floor in indirect dark matter searches. We show that in some benchmark models the current bounds on the dark matter–nucleon cross section push the solar signal below this neutrino floor.

Predicting the Loci of Solar Eruptions

N. **Gyenge**, R. Erdélyi

2017 Space Weather of the Heliosphere: Processes and Forecasts Proceedings IAU Symposium No. 335

https://arxiv.org/pdf/1710.06196.pdf

The longitudinal distribution of solar active regions shows non-homogeneous spatial behaviour, which is often referred to as Active Longitude (AL). Evidence for a significant statistical relationships between the AL and the longitudinal distribution of flare and coronal mass ejections (CME) occurrences is found in Gyenge et al, 2017 (ApJ, 838, 18). The present work forecasts the spatial position of AL, hence the most flare/CME capable active regions are also predictable. Our forecast method applies Autoregressive Integrated Moving Average model for the next 2 years time period. We estimated the dates when the solar flare/CME capable longitudinal belts face towards Earth.

Active longitude and CME occurrences

N. **Gyenge**, T. Singh, T. S. Kiss, A. K. Srivastava, R. Erdélyi

2017
https://arxiv.org/pdf/1702.06664.pdf
The spatial inhomogeneity of the distribution of coronal mass ejection (CME) occurrences in the solar atmosphere could provide a tool to estimate the longitudinal position of the most probable CME-capable active regions in the Sun. The anomaly in the longitudinal distribution of active regions themselves is often referred to as active longitude (AL). In order to reveal the connection between the AL and CME spatial occurrences, here we investigate the morphological properties of active regions. The first morphological property studied is the separateness parameter, which is able to characterise the probability of the occurrence of an energetic event, such as solar flare or CME. The second morphological property is the sunspot tilt angle. The tilt angle of sunspot groups allows us to estimate the helicity of active regions. The increased helicity leads to a more complex built-up of the magnetic structure and also can cause CME eruption. We found that the most complex active regions appear near to the AL and the AL itself is associated with the most tilted active regions. Therefore, the number of CME occurrences is higher within the AL. The origin of the fast CMEs is also found to be associated with this region. We concluded that the source of the most probably CME-capable active regions is at the AL. By applying this method we can potentially forecast a flare and/or CME source several Carrington rotations in advance. This finding also provides new information for solar dynamo modelling.
0/03/2011, 25/06/2011, 07/03/2012

Active Longitude and Solar Flare Occurrences

N. **Gyenge**, A. Ludmány, T. Baranyi
2016
http://arxiv.org/pdf/1512.08124v1.pdf
The aim of the present work is to specify the spatio-temporal characteristics of flare activity observed by the Reuven Ramaty High Energy Solar Spectroscopic Imager (RHESSI) and Geostationary Operational Environmental Satellite (GOES) satellites in connection with the behaviour of the longitudinal domain of enhanced sunspot activity known as active longitude (AL). By using our method developed for this purpose, we identified the AL in every Carrington Rotation provided by the Debrecen Photoheliographic Data (DPD). The spatial probability of flare occurrence has been estimated depending on the longitudinal distance from AL in the northern and southern hemispheres separately. We have found that more than the 60\% of the RHESSI and GOES flares is located within ±36∘ from the active longitude. Hence, the most flare-productive active regions tend to be located in or close to the active longitudinal belt. This observed feature may allow predicting the geo-effective position of the domain of enhanced flaring probability. Furthermore, we studied the temporal properties of flare occurrence near the active longitude and several significant fluctuations were found. More precisely, the results of the method are the following fluctuations: 0.8 years, 1.3 years and 1.8 years. These temporal and spatial properties of the solar flare occurrence within the active longitudinal belts could provide us enhanced solar flare forecasting opportunity.

Migration and Extension of Solar Active Longitudinal Zones

N. **Gyenge**, T. Baranyi, A. Ludmány
Solar Physics, February **2014**, Volume 289, Issue 2, pp 579-591
Solar active longitudes show a characteristic migration pattern in the Carrington coordinate system if they can be identified at all. By following this migration, the longitudinal activity distribution around the center of the band can be determined. The half-width of the distribution is found to be varying in Cycles 21 – 23, and in some time intervals it was as narrow as 20 – 30 degrees. It was more extended around a maximum but it was also narrow when the activity jumped to the opposite longitude. Flux emergence exhibited a quasi-periodic variation within the active zone with a period of about 1.3 years. The path of the active-longitude migration does not support the view that it might be associated with the 11-year solar cycle. These results were obtained for a limited time interval of a few solar cycles and, bearing in mind uncertainties of the migration-path definition, are only indicative. For the major fraction of the dataset no systematic active longitudes were found. Sporadic migration of active longitudes was identified only for Cycles 21 – 22 in the northern hemisphere and Cycle 23 in the southern hemisphere.

Comparative analysis of Debrecen sunspot catalogues

L. **Győri**, A. Ludmány, T. Baranyi
MNRAS **465,** 1259–1273 (**2017**)
https://arxiv.org/pdf/1612.03274v1.pdf
Sunspot area data are important for studying solar activity and its long term variations. At the Debrecen Heliophysical Observatory, we compiled three sunspot catalogues: the Debrecen Photoheliographic Data (DPD), the SDO/HMI Debrecen Data (HMIDD), and the SOHO/MDI Debrecen Data. For comparison, we also compiled an additional sunspot catalogue, the Greenwich Photoheliographic Data, from the digitized Royal Greenwich Observatory images for the 1974-76. By comparing these catalogues when they overlap in time, we can investigate how various factors influence the measured area of the sunspots, and, in addition, we can derive area cross-calibration factors for these catalogues.The main findings are as follows. The poorer seeing increases the individual

corrected spot areas and decreases the number of the small spots. Interestingly, the net result of these two effects for the total corrected spot area is zero. DPD daily total corrected sunspot areas are 5 per cent smaller than the HMIDD ones. Revised DPD daily total corrected umbra areas are 9 per cent smaller than those of HMIDD. The Greenwich Photoheliographic Result areas are only a few per cent smaller than DPD areas. A 0.2∘ difference between the North directions of the DPD and MDI images is found. This value is nearly the same as that was found (0.22∘) by us in a previous paper comparing HMI and MDI images. The Solar Observing Optical Network area measurement practice (spots smaller than 10mh were not directly measured but an area of 2mh were assigned to each) can not explain the large area deficit of the Solar Observing Optical Network.

Precise Determination of the Orientation of the Solar Image

L. **Gy˝ori**

Solar Phys (**2010**) 267: 445–461; **File**

Accurate heliographic coordinates of objects on the Sun have to be known in several fields of solar physics. One of the factors that affect the accuracy of the measurements of the heliographic coordinates is the accuracy of the orientation of a solar image. In this paper the well-known drift method for determining the orientation of the solar image is applied to data taken with a solar telescope equipped with a CCD camera. The factors that influence the accuracy of the method are systematically discussed, and the necessary corrections are determined. These factors are as follows: the trajectory of the center of the solar disk on the CCD with the telescope drive turned off, the astronomical refraction, the change of the declination of the Sun, and the optical distortion of the telescope. The method can be used on any solar telescope that is equipped with a CCD camera and is capable of taking solar fulldisk images. As an example to illustrate the method and its application, the orientation of solar images taken with the Gyula heliograph is determined. As a byproduct, a new method to determine the optical distortion of a solar telescope is proposed.

A Total Solar Eclipse Earth-Based Mission: Multi-wavelength Observations from Land, Sea and Air to Probe the Critical middle Corona

Shadia R **Habbal**, Benjamin Boe, Colby Haggerty, Adalbert Ding

White Paper was submitted to the 2024 Solar and Space Physics (Heliophysics) Decadal Survey **2023**

https://arxiv.org/ftp/arxiv/papers/2302/2302.11781.pdf

There has been an unfortunate gap in coronal emission line observations from space in the visible and near IR (V+NIR). Their distinct scientific advantage stems from the dominance of radiative excitation in their formation, whereby their emission can be detected out to several solar radii above the limb. V+NIR emission lines can thus yield the only inferences of the physical properties of the coronal plasma, such as species temperatures, densities, elemental abundances, and speeds along and perpendicular to the line of sight in this critical spatial span. These diagnostics have been demonstrated with decades of unsurpassed high-resolution imaging and spectroscopic observations during total solar eclipses. This white paper calls for dedicated funding for a Total Solar Eclipse Earth-Based Mission for ground, airborne and seaborne observations of the corona during totality for the next decade starting in 2024. The proposed Mission capitalizes on the unique diagnostic potential offered by the V+NIR coronal emission lines for the inference of key plasma parameters over a distance range of at least 5 Rs from the solar surface. This critical coronal space is currently missing from existing and to-be launched coronagraphic instrumentation in the proposed time frame. Multi-site observing platforms for each eclipse would further capture the temporal variability of coronal plasmas over a time span of at least 1 hour, with a temporal resolution of a fraction of a minute. Furthermore, this Mission offers unsurpassed opportunities for the exploration of new technologies for future implementation with coronagraphs. This Mission has a unique significant broader impact for outreach opportunities to engage the public and the younger generations in heliospheric science from an awe-inspiring cosmic event. **2012/11/13**

Solar Atmosphere Radiative Transfer Model Comparison based on 3D MHD simulations

M. **Haberreiter**, S. Criscuoli, M. Rempel, T.M.D. Pereira

A&A 653, A161 **2021**

https://arxiv.org/pdf/2109.02681.pdf

https://www.aanda.org/articles/aa/pdf/2021/09/aa39237-20.pdf

https://doi.org/10.1051/0004-6361/202039237

The reconstruction of the solar spectral irradiance (SSI) on various time scales is essential for the understanding of the Earth's climate response to the SSI variability. The driver of the SSI variability is understood to be the intensity contrast of magnetic features present on the Sun with respect to the largely non-magnetic quiet Sun. However, different spectral synthesis codes lead to diverging projections of SSI variability. In this study we compare three

different radiative transfer codes and carry out a detailed analysis of their performance. We perform the spectral synthesis at the continuum wavelength of 665 nm with the Code for Solar Irradiance (COSI), and the Rybicki-Hummer (RH), and Max Planck University of Chicago Radiative MHD (MURaM) codes for three 3D MHD simulations snapshots, a non-magnetic case, and MHD simulations with 100 G, and 200 G magnetic field strength. We determine the intensity distributions, the intensity differences and ratios for the spectral synthesis codes. We identify that the largest discrepancies originate in the intergranular lanes where the most field concentration occurs. Overall, the applied radiative transfer codes give consistent intensity distributions. Also, the intensity variation as a function of magnetic field strength for the particular 100 G and 200 G snapshots agree within the 2-3% range.

A new observational solar irradiance composite

Margit **Haberreiter**, Micha Schöll, Thierry Dudok de Wit, Matthieu Kretzschmar, Stergios Misios, Kleareti Tourpali and Werner Schmutz

JGR **2017** Volume 122, Issue 6 Pages 5910–5930 DOI: 10.1002/2016JA023492

Variations in the solar spectral irradiance (SSI) are an important driver of the chemistry, temperature, and dynamics of the Earth's atmosphere, and ultimately the Earth's climate. To investigate the detailed response of the Earth's atmosphere to SSI variations, a reliable SSI dataset is needed. We present an observational SSI composite dataset that is based on 20 instruments, and has been built by using probabilistic approach that takes into account the scale-dependent uncertainty of each available SSI observation. We compare the variability of this new composite with available SSI reconstructions and discuss the respective modelled responses in the Earth's atmosphere. As the composite is based on purely statistical means we consider it as a valuable independent dataset.

Reconstruction of the solar EUV irradiance from 1996 to 2010 based on SOHO/EIT images

Margit **Haberreiter**1*, Véronique Delouille2, Benjamin Mampaey2, Cis Verbeeck2, Giulio Del Zanna3 and Seth Wieman

J. Space Weather Space Clim. 4 (**2014**) A30

http://www.swsc-journal.org/articles/swsc/pdf/2014/01/swsc130045.pdf

The solar Extreme UltraViolet (EUV) spectrum has important effects on the Earth’s upper atmosphere. For a detailed investigation of these effects it is important to have a consistent data series of the EUV spectral irradiance available. We present a reconstruction of the solar EUV irradiance based on SOHO/EIT images, along with synthetic spectra calculated using different coronal features which represent the brightness variation of the solar atmosphere. The EIT images are segmented with the SPoCA2 tool which separates the features based on a fixed brightness classification scheme. With the SOLMOD code we then calculate intensity spectra for the 10–100 nm wavelength range and each of the coronal features. Weighting the intensity spectra with the area covered by each of the features yields the temporal variation of the EUV spectrum. The reconstructed spectrum is then validated against the spectral irradiance as observed with SOHO/SEM. Our approach leads to good agreement between the reconstructed and the observed spectral irradiance. This study is an important step toward understanding variations in the solar EUV spectrum and ultimately its effect on the Earth’s upper atmosphere.

Buoyancy-driven Magnetohydrodynamic Waves in a Partially Ionized Plasma

Hague1 and R. Erdélyi

2018 ApJ, 866 2

http://iopscience.iop.org/article/10.3847/1538-4357/aae25f/meta

A magnetohydrodynamic (MHD) fluid description is typically employed to study the magnetized plasma comprising the solar atmosphere. This approach has had many successes in modeling and explaining solar phenomena. Most often, the plasma is assumed to be fully ionized. While this approach is justified in the higher atmosphere, i.e., the solar corona; the temperature in the lower solar atmosphere is such that a large proportion of the fluid may be electrically neutral. This begs the question: to what degree are the results derived from a fully ionized MHD description valid? In this article, we investigate the effect of partial ionization on buoyancy-driven MHD waves (the MHD analog of internal gravity waves) by applying a simplified two-fluid description. We show that previously derived results may be applied, when the fluid is weakly ionized, if the ion–neutral collision frequency is high. We derive dispersion relations for buoyancy-driven MHD waves, which include correction factors and damping rates due to ion–neutral collisions.

Evidence for Parametric Decay Instability in the Lower Solar Atmosphere

Michael **Hahn**1, Xiangrong Fu2, and Daniel Wolf Savin1

2022 ApJ 933 52

https://iopscience.iop.org/article/10.3847/1538-4357/ac7147/pdf

We find evidence for the first observation of the parametric decay instability (PDI) in the lower solar atmosphere. In particular, we find that the power spectrum of density fluctuations near the solar transition region resembles the power spectrum of the velocity fluctuations but with the frequency axis scaled up by about a factor of 2. These

results are from an analysis of the Si iv lines observed by the Interface Region Imaging Spectrometer in the transition region of a polar coronal hole. We also find that the density fluctuations have radial velocity of about 75 km s−1 and that the velocity fluctuations are much faster with an estimated speed of 250 km s−1, as is expected for sound waves and Alfvén waves, respectively, in the transition region. Theoretical calculations show that this frequency relationship is consistent with those expected from PDI for the plasma conditions of the observed region. These measurements suggest an interaction between sound waves and Alfvén waves in the transition region, which is evidence for the parametric decay instability**. 2016 October 31**

Inferring the Coronal Density Irregularity from EUV Spectra

Michael **Hahn**, Daniel Wolf Savin

ApJ **2016**

http://arxiv.org/pdf/1606.06247v1.pdf

Understanding the density structure of the solar corona is important for modeling both coronal heating and the solar wind. Direct measurements are difficult because of line-of-sight integration and possible unresolved structures. We present a new method for quantifying such structure using density-sensitive EUV line intensities to derive a density irregularity parameter, a relative measure of the amount of structure along the line of sight. We also present a simple model to relate the inferred irregularities to physical quantities, such as the filling factor and density contrast. For quiet Sun regions and interplume regions of coronal holes, we find a density contrast of at least a factor of three to ten and corresponding filling factors of about 10-20%. Our results are in rough agreement with other estimates of the density structures in these regions. The irregularity diagnostic provides a useful relative measure of unresolved structure in various regions of the corona.

Weakest Solar Cycle of the Space Age: A Study on Solar Wind–Magnetosphere Energy Coupling and Geomagnetic Activity

Rajkumar **Hajra**

Solar Physics volume 296, Article number: 33 (**2021**)

https://link.springer.com/content/pdf/10.1007/s11207-021-01774-9.pdf

Solar Cycle 24, from December 2008 to December 2019, is recorded to be the weakest in magnitude in the space age (after 1957). A comparative study of this cycle with Solar Cycles 20 through 23 is presented. It is found that Solar Cycle 24 is not only the weakest in solar activity, but also in average solar wind parameters and solar wind–magnetosphere energy coupling. This resulted in lower geomagnetic activity, lower numbers of high-intensity long-duration continuous auroral electrojet (AEAE) activity (HILDCAA) events and geomagnetic storms. The Solar Cycle 24 exhibited a ≈54≈54 – 61%61% reduction in HILDCAA occurrence rate (per year), ≈15≈15 – 34%34% reduction in moderate storms (−50 nT≥Dst>−100 nT), ≈49≈49 – 75%75% reduction in intense storms (−100 nT≥Dst>−250 nT) compared to previous cycles, and no superstorms (Dst≤−250). Implications of the solar and geomagnetic weakening to space weather science and operations are discussed.

Straylight-Rejection Performance of the STEREO HI Instruments

J.-P. **Halain**, C. J. Eyles, A. Mazzoli, D. Bewsher and J. A. Davies, et al.

Solar Physics, Volume 271, Numbers 1-2, 197-218, **2011**

The SECCHI Heliospheric Imager (HI) instruments on-board the STEREO spacecraft have been collecting images of solar wind transients, including coronal mass ejections, as they propagate through the inner heliosphere since the beginning of 2007.

The scientific use of the images depends critically on the performance of the instruments and its evolution over time. One of the most important factors affecting the performance of the instrument is the rejection of straylight from the Sun and from other bright objects located both within and outside the HI fields of view.

This paper presents an analysis of the evolution of the straylight-rejection performance of the HI instrument on each of the two STEREO spacecraft over the three first years of the mission. The straylight level has been evaluated and expressed in mean solar brightness units, in which such scientific observations are usually quoted, using photometric conversion factors.

Detector bandwidth and polarisation switching rates: spectrophotometric observations of the Sun by the Birmingham Solar Oscillations Network (BiSON)

S. J. **Hale**, W. J. Chaplin, G. R. Davies, Y. P. Elsworth, R. Howe

RAS Techniques and Instruments: **2023**

https://arxiv.org/pdf/2303.00518

The Birmingham Solar Oscillations Network (BiSON) observes acoustic oscillations of the Sun. The dominant noise source is caused by fluctuations of Earth's atmosphere, and BiSON seeks to mitigate this effect by combining

multiple rapid observations in alternating polarisation states. Current instrumentation uses bespoke Pockels-effect cells to select the polarisation state. Here, we investigate an alternative off-the-shelf solution, a liquid crystal retarder, and discuss the potential impact of differences in performance. We show through electrical simulation of the photodiode-based detectors, and assessment of both types of polarisation device, that although the switching rate is slower the off-the-shelf LCD retarder is a viable replacement for a bespoke Pockels-effect cell. The simplifications arising from the use of off-the-shelf components allows easier and quicker instrumentation deployment.

The next generation Birmingham Solar Oscillations Network (BiSON) spectrophotometer: a new miniaturised instrument for helioseismology

S. J. **Hale**, W. J. Chaplin, G. R. Davies, Y. P. Elsworth, R. Howe
RAS Techniques and Instruments **2022**
https://arxiv.org/pdf/2210.11293.pdf
We describe a new spectrophotometer for the Birmingham Solar Oscillations Network (BiSON), based on a next generation observation platform, BiSON:NG, a significantly miniaturised system making use of inexpensive consumer-grade hardware and off-the-shelf components, where possible. We show through system modelling and simulation, along with a summer observing campaign, that the prototype instrument produces data on the Sun's low-degree acoustic (p-mode) oscillations that are of equal quality and can be seamlessly integrated into the existing network. Refreshing the existing ageing hardware, and the extended observational network potential of BiSON:NG, will secure our ongoing programme of high-quality synoptic observations of the Sun's low-degree oscillations (e.g., for seismic monitoring of the solar cycle at a "whole Sun" level).

A next generation upgraded observing platform for the automated Birmingham Solar Oscillations Network (BiSON)

S J **Hale**, W J Chaplin, G R Davies, Y P Elsworth
SPIE Software and Cyberinfrastructure for Astronomy VI **2021**
https://arxiv.org/pdf/2101.10205.pdf
The Birmingham Solar Oscillations Network (BiSON) is a collection of ground-based automated telescopes observing oscillations of the Sun. The network has been operating since the early 1990s. We present development work on a prototype next generation observation platform, BiSON:NG, based almost entirely on inexpensive off-the-shelf components, and where the footprint is reduced to a size that can be inexpensively installed on the roof of an existing building. Continuous development is essential in ensuring that automated networks such as BiSON are well placed to observe the next solar cycle and beyond.

Performance of the Birmingham Solar-Oscillations Network (BiSON)

S.J. **Hale**, R. Howe, W.J. Chaplin, G.R. Davies, Y.P. Elsworth
Solar Phys. January **2016**, Volume 291, Issue 1, pp 1-28 Open Access
http://arxiv.org/pdf/1510.07085v1.pdf
The Birmingham Solar-Oscillations Network (BiSON) has been operating with a full complement of six stations since 1992. Over 20 years later, we look back on the network history. The meta-data from the sites have been analysed to assess performance in terms of site insolation, with a brief look at the challenges that have been encountered over the years. We explain how the international community can gain easy access to the ever-growing dataset produced by the network, and finally look to the future of the network and the potential impact of nearly 25 years of technology miniaturisation.

The Sunward Electron Deficit: A Telltale Sign of the Sun's Electric Potential

J. S. **Halekas**1, L. Berčič2, P. Whittlesey3, D. E. Larson3, R. Livi3, M. Berthomier4, J. C. Kasper5,6, A. W. Case6, M. L. Stevens6, S. D. Bale3,7Show full author list
2021 ApJ 916 16
https://doi.org/10.3847/1538-4357/ac096e
As the Parker Solar Probe explores new regions of the inner heliosphere, it travels ever deeper into the electric potential of the Sun. In the near-Sun environment, a new feature of the electron distribution emerges, in the form of a deficit in the sunward suprathermal population. The lower boundary of this deficit forms a cutoff in phase space, at an energy determined by the electric potential drop between the observation point and the outer heliosphere. We explore the characteristics of the sunward deficit and the associated cutoff, as well as the properties of the plasma in which we observe them. The deficit occurs in ~60%–80% of electron observations within ~0.2 au, and even more frequently in plasma with low β, low collisional age, and a more anisotropic electron core population. At greater distances, the deficit rapidly disappears, as the suprathermal halo grows, with these two trends likely related. The cutoff energy varies linearly with the local electron core temperature, confirming a direct relationship to the ambipolar electric potential. Meanwhile, the cutoff width varies with β and collisional age, suggesting that energy diffusion plays a role in erasing the deficit. The nearly ubiquitous occurrence of the sunward deficit in the inner

heliosphere suggests that we may need to reconsider the functional forms commonly used to represent electron distributions in this environment.

Far-side Active Regions Based on Helioseismic and EUV Measurements: A New Data Set for Heliospheric Machine Learning Advancements

Amr **Hamada**1, Kiran Jain1, Charles Lindsey2, Mitchell Creelman1, and Niles Oien1
2024 ApJ 977 85
https://iopscience.iop.org/article/10.3847/1538-4357/ad8636/pdf
Active Regions (ARs) are regions of strong magnetic flux in the solar atmosphere. Understanding the global evolution of ARs is critical for solar magnetism as well as for accurate space-weather forecasting. We present the first far-side AR data set based on EUV observation and helioseismic measurements. For the EUV observations, we use synchronic maps at 304 Å comprised of observations from the Solar Dynamics Observatory/Atmospheric Imaging Assembly and the Solar TErrestrial RElations Observatory/Extreme UltraViolet Imager, in heliocentric orbit with direct vantages into the Sun's far hemisphere. We used the brightening of the solar transition region in EUV/304 Å maps as a proxy for the magnetic regions. For the far-side helioseismic measurements, we used seismic phase-shift maps of the Sun's far hemisphere, computed from helioseismic Dopplergrams observed by NSO/Global Oscillations Network Group (GONG). In this study, we present the first global EUV AR data set of the whole Sun, providing several basic parameters, such as location, area, tilt angle, EUV brightness, and latitudinal/longitudinal extents of the identified ARs. We also present a similar data set for the far-side GONG ARs where the helioseismic phase shift parameters are included. Helioseismic far-side GONG ARs are examined, and their success at predicting strong ARs is assessed. We discuss the temporal and spatial evolution for the EUV AR signatures and far-side GONG AR signatures during the ascending and maximum phases of Solar Cycle 24 (2010 May–2016 May). We examine the correlation between the helioseismic signatures and the respective EUV source distributions in the Sun's far hemisphere. We present the first far-side AR butterfly diagram based on helioseismic measurements.

New Homogeneous Dataset of Solar EUV synoptic maps from SOHO/EIT and SDO/AIA

Amr **Hamada**, Timo Asikainen, Kalevi Mursula
Solar Phys. January **2020**, 295:2
https://arxiv.org/pdf/1910.13720.pdf
https://link.springer.com/content/pdf/10.1007%2Fs11207-019-1563-y.pdf
https://doi.org/10.1007/s11207-019-1563-y
Synoptic maps of solar EUV intensities have been constructed for many decades in order to display the distribution of the different EUV emissions across the solar surface, with each map representing one Carrington rotation (i.e., one rotation of the Sun). This paper presents a new solar EUV synoptic map dataset based on full-disk images from Solar and Heliospheric Observatory/Extreme Ultraviolet Imaging Telescope (SOHO/EIT) and Solar Dynamics Observatory/Atmospheric Imaging Assembly (SDO/AIA). In order to remove the significant and complicated drift of EIT and AIA EUV intensities due to sensor degradation, we construct the synoptic maps in standardized intensity scale. We describe a method of homogenizing the SOHO/EIT maps with SDO/AIA maps by transforming the EIT intensity histograms to AIA level. The new maps cover the years from 1996 to 2018 with 307 SOHO/EIT and 116 SDO/AIA synoptic maps, respectively. These maps provide a systematic and homogenous view of the entire solar surface in four EUV wavelengths, and are well suited, e.g., for studying long-term coronal hole evolution.

Effects of Magnetic Perturbation on Reconnection and Heating in the Solar Corona

Mostafa M. **Hammoud**1, Ghassan Y. Antar1, Maher A. Dayeh2,3, Marwan S. Darwish4, and Mounib F. El Eid1
2020 ApJ 903 95
https://doi.org/10.3847/1538-4357/abb807
The solar corona exhibits unusually high temperatures (~106 K) compared to the photosphere (~5800 K). This coronal heating is one of the fundamental problems in solar physics that has yet to be resolved. Magnetic reconnection is thought to play a critical role in driving this enigmatic heating process. We address the interplay between reconnection in the solar corona and the photospheric footpoint motion. The effect of the latter is modeled to generate an external magnetic perturbation that is added to the main coronal field. Resistive magnetohydrodynamics is used where sources and sinks terms due to the perturbation are explicitly obtained in the equations. We set the perturbation to be sinusoidal in space while remaining time independent. The equations are solved using openFOAM. Our results show that magnetic reconnection with perturbation, even with a very small amplitude, leads to (1) more complex formation and evolution of X-points and plasmoids, (2) a transition from slow to fast reconnection rate, (3) a stronger increase of the temperature, and (4) a quicker formation of high-speed jets driving the hot plasma outside the simulation domain with a Mach number that is six times greater compared to the case without perturbation. Moreover, we also find that a magnetic perturbation with shorter wavelength promotes even a faster temporal evolution of the reconnection process than for the longer wavelength. Therefore, the heating

and the dynamics of plasma particles in the solar corona are significantly enhanced when the reconnection process is externally disturbed by even a very small perturbation.

A Decline Phase Modeling for the Prediction of Solar Cycle 25

Y. B. **Han**, Z. Q. Yin
Solar Physics August **2019**, 294:107
sci-hub.se/10.1007/s11207-019-1494-7
We use the Vondrak smoothing method and the V2.0 version of the monthly mean sunspot number (SSN) to produce a series of smoothed SSN (denoted SSN-VS), which closely mimics the 13-month running mean SSN. SSN-VS is then used to determine the characteristics of solar cycles. In particular, we find that our simulations for the past seven solar cycles yield predictions with relatively small errors. Applying the technique to the descending portion (i.e.the 20 months following SSN-VS = 70) of the present Solar Cycle 24, we make predictions for the next Solar Cycle 25. In particular, we find, assuming that Solar Cycle 25 is not a statistical outlier, that: 1) the sunspot minimum occurrence is expected around 2019.188±0.982019.188±0.98 years, 2) the sunspot maximum occurrence is expected around 2023.918±1.642023.918±1.64 years, and 3) a sunspot maximum value of about 228.8±40.5228.8±40.5 units of sunspot number is expected.

Internetwork Magnetic Fields Seen in Fe i 1564.8 nm Full-disk Images

Yoichiro **Hanaoka** and Takashi Sakurai
2020 ApJ 904 63
https://doi.org/10.3847/1538-4357/abbc07
We studied the properties of internetwork magnetic fields in the solar photosphere, taking advantage of full-disk Stokes V/I maps of the Fe i 1564.8 nm line, which were obtained during 2010–2019. In contrast to most previous studies, we used data with moderate spatial and spectral resolutions. Nonetheless, we were able to distinguish the internetwork field components and the active region/network boundary components using large Zeeman splitting of the Fe i 1564.8 nm line. Thus, our analysis provides a point of view quite different from that of previous studies. We analyzed the data statistically without ordinary inversions, yet we successfully derived some properties of internetwork fields; the internetwork is filled with small-scale magnetic fields, their strength is within the weak field regime of the Fe i 1564.8 nm line (300–400 G or less), and the internetwork fields are highly inclined. Although the results were obtained from the analysis performed from a different perspective, they are consistent with the majority of previous findings. In addition, no notable variation in the properties of the internetwork fields was found during the period covering most of solar cycle 24.

Synoptic solar observations of the Solar Flare Telescope focusing on space weather

Yoichiro **Hanaoka**, Takashi Sakurai, Ken'ichi Otsuji, Isao Suzuki, Satoshi Morita
Journal of Space Weather and Space Climate **10**, 41 **2020**
https://arxiv.org/pdf/2007.14054.pdf
https://doi.org/10.1051/swsc/2020044
https://www.swsc-journal.org/articles/swsc/pdf/2020/01/swsc200039.pdf
The solar group at the National Astronomical Observatory of Japan is conducting synoptic solar observations with the Solar Flare Telescope. While it is a part of a long-term solar monitoring, contributing to the study of solar dynamo governing solar activity cycles, it is also an attempt at contributing to space weather research. The observations include imaging with filters for Hα, Ca K, G-band, and continuum, and spectropolarimetry at the wavelength bands including the He I 1083.0 nm / Si I 1082.7 nm and the Fe I 1564.8 nm lines. Data for the brightness, Doppler signal, and magnetic field information of the photosphere and the chromosphere are obtained. In addition to monitoring dynamic phenomena like flares and filament eruptions, we can track the evolution of the magnetic fields that drive them on the basis of these data. Furthermore, the magnetic field in solar filaments, which develops into a part of the interplanetary magnetic cloud after their eruption and occasionally hits the Earth, can be inferred in its pre-eruption configuration. Such observations beyond mere classical monitoring of the Sun will hereafter become crucially important from the viewpoint of the prediction of space weather phenomena. The current synoptic observations with the Solar Flare Telescope is considered to be a pioneering one for future synoptic observations of the Sun with advanced instruments. **August 6–8, 2012, July 9, 2013, October 19, 2015**

Statistical Study of the Magnetic Field Orientation in Solar Filaments

Yoichiro **Hanaoka**, Takashi Sakurai
2017
https://arxiv.org/pdf/1711.07735.pdf
We have carried out a statistical study of the average orientation of the magnetic field in solar filaments with respect to their axes for more than 400 samples, based on data taken with daily full-Sun, full-Stokes spectropolarimetric observations using the He I 1083.0 nm line. The major part of the samples are the filaments in the quiet areas, but those in the active areas are included as well. The average orientation of the magnetic field in filaments shows a

systematic property depending on the hemisphere; the direction of the magnetic field in filaments in the northern (southern) hemisphere mostly deviates clockwise (counterclockwise) from their axes, which run along the magnetic polarity inversion line. The deviation angles of the magnetic field from the axes, are concentrated between 10--30 deg. This hemispheric pattern is consistent with that revealed for chirality of filament barbs, filament channels and for other solar features found to possess chirality. For some filaments it was confirmed that their magnetic field direction is locally parallel to their structure seen in Halpha images. Our results for the first time confirmed this hemispheric pattern with the direct observation of the magnetic field in filaments. Interestingly, the filaments which show the opposite magnetic field deviation to the hemispheric pattern, are in many cases found above the polarity inversion line whose ambient photospheric magnetic field has the polarity alignment being opposite to that of active regions following the Hale-Nicholson law. **2014 November 23, 2015 October 27.**

Surface and interior meridional circulation in the Sun **Review**

Shravan M. **Hanasoge**

Living Reviews in Solar Physics volume 19, Article number: 3 (**2022**)

https://link.springer.com/content/pdf/10.1007/s41116-022-00034-7.pdf

Solar meridional circulation is an axisymmetric flow system, extending from the equator to the poles (∼∼20 m/s at the surface, ≈≈1% of the mean solar rotation rate), plunging inwards and subsequently completing the circuit in the interior through an equatorward return flow and a radially outward flow back up to the surface. This article reviews the profound role that meridional circulation plays in maintaining global dynamics and regulating large-scale solar magnetism. Because it is relatively weak in comparison to differential rotation (∼∼300 m/s, ≈≈7% of the mean solar rotation rate) and owing to numerous systematical errors, accurate surface measurements were only first made in 1978 and initial inferences of interior meridional circulation were obtained using helioseismology two decades later. However, systematical biases have made it very challenging to reliably recover flow in the deep interior. Despite numerous advances that have served to improve the accuracy of inferences, the location of the return flow and the full extent of the circulation are still open problems. This article follows the historical developments and summarises contemporary advances that have led to modern inferences of surface and interior meridional flow.

Detection of Rossby waves in the Sun using normal-mode coupling

Shravan **Hanasoge**, Krishnendu Mandal

ApJL **871** L32 **2019**

https://arxiv.org/pdf/1901.06479.pdf

Rossby waves play a fundamental role in angular momentum processes in rotating fluids. In addition to the potential to shed light on physical mechanisms operating in the solar convection zone, the recent detection of Rossby waves in the Sun (Löptien et al. 2018; Liang et al. 2018) also serves as a means of comparison between different helioseismic methods. Time-distance helioseismology, ring-diagram analysis and other techniques have all proven successful in recovering the Rossby-wave dispersion relation from analyses of Helioseismic and Magnetic Imager data (HMI; Schou et al. 2012). In this article, we demonstrate that analyses of two years of HMI global-mode-oscillation data using the technique of normal-mode coupling also show signatures of Rossby waves. In addition to providing an independent means of inferring Rossby waves, this detection lends credence to the methodology of mode coupling and encourages a more complete exploration of its possibilities.

Measurement process and inversions using helioseismic normal-mode coupling

Shravan **Hanasoge**

ApJ **2018**

https://arxiv.org/pdf/1802.02776.pdf

Normal modes are coupled by the presence of perturbations in the Sun, providing a unique and little-explored helioseismic technique with which to image the solar interior. The process of measuring coupling between normal modes is straightforward, much more so when compared with other prevalent helioseismic techniques. The theoretical framework to interpret these measurements is well developed with the caveat that it applies only in the case where the entire surface of the Sun is observed. In practice however, the limited visibility of the Sun and line-of-sight related effects diminish the resolution of the technique. Here, we compute realistic sensitivities of normal-mode coupling measurements to flows in the solar interior and describe how to mitigate the sometimes overwhelming effect of leakage. The importance of being able to isolate individual spherical harmonics and observe the full Sun, to which future solar observatories may aspire, is thus highlighted in our results. In the latter part of the article, we describe the noise model for the variance of coupling coefficients, a critical component to the process of inference.

Seismic sensitivity of Normal-mode Coupling to Lorentz stresses in the Sun

Shravan M. **Hanasoge**

MNRAS **2017**
https://arxiv.org/pdf/1705.09431.pdf
Understanding the governing mechanism of solar magnetism remains an outstanding challenge in astrophysics. Seismology is the most compelling technique with which to infer the internal properties of the Sun and stars. Waves in the Sun, nominally acoustic, are sensitive to the emergence and cyclical strengthening of magnetic field, evidenced by measured changes in resonant oscillation frequencies that are correlated with the solar cycle. The inference of internal Lorentz stresses from these measurements has the potential to significantly advance our appreciation of the dynamo. Indeed, seismological inverse theory for the Sun is well understood for perturbations in composition, thermal structure and flows but, is not fully developed for magnetism, owing to the complexity of the ideal magnetohydrodynamic (MHD) equation. Invoking first-Born perturbation theory to characterize departures from spherically symmetric hydrostatic models of the Sun and applying the notation of generalized spherical harmonics, we calculate sensitivity functions of seismic measurements to the general time-varying Lorentz stress tensor. We find that eigenstates of isotropic (i.e. acoustic only) background models are dominantly sensitive to isotropic deviations in the stress tensor and much more weakly so to anisotropic stresses (and therefore challenging to infer). The apple cannot fall far from the tree.

Sensitivity of Helioseismic Measurements of Normal-mode Coupling to Flows and Sound-speed Perturbations

Shravan M. **Hanasoge**, Martin Woodard, H. M. Antia, Laurent Gizon, Katepalli R. Sreenivasan
MNRAS **2017**
https://arxiv.org/pdf/1705.08204.pdf
In this article, we derive and compute the sensitivity of measurements of coupling between normal modes of oscillation in the Sun to underlying flows. The theory is based on first-Born perturbation theory, and the analysis is carried out using the formalism described by \citet{lavely92}. Albeit tedious, we detail the derivation and compute the sensitivity of specific pairs of coupled normal modes to anomalies in the interior. Indeed, these kernels are critical for the accurate inference of convective flow amplitudes and large-scale circulations in the solar interior. We resolve some inconsistencies in the derivation of \citet{lavely92} and reformulate the fluid-continuity condition. We also derive and compute sound-speed kernels, paving the way for inverting for thermal anomalies alongside flows.

Seismic Sounding of Convection in the Sun

Shravan **Hanasoge**, Laurent Gizon, Katepalli R. Sreenivasan
Annual Reviews of Fluid Mechanics **2015**
http://arxiv.org/pdf/1503.07961v1.pdf
Our Sun, primarily composed of ionized hydrogen and helium, has a surface temperature of 5777~K and a radius R⊙≈696,000 km. In the outer R⊙/3, energy transport is accomplished primarily by convection. Using typical convective velocities u∼100ms−1 and kinematic viscosities of order 10−4 m2s−1, we obtain a Reynolds number Re∼1014. Convection is thus turbulent, causing a vast range of scales to be excited. The Prandtl number, Pr, of the convecting fluid is very low, of order 10−7\,--\,10−4, so that the Rayleigh number (∼Re2Pr) is on the order of 1021−1024. Solar convection thus lies in extraordinary regime of dynamical parameters, highly untypical of fluid flows on Earth. Convective processes in the Sun drive global fluid circulations and magnetic fields, which in turn affect its visible outer layers ("solar activity") and, more broadly, the heliosphere ("space weather"). The precise determination of the depth of solar convection zone, departures from adiabaticity of the temperature gradient, and the internal rotation rate as a function of latitude and depth are among the seminal contributions of helioseismology towards understanding convection in the Sun. Contemporary helioseismology, which is focused on inferring the properties of three-dimensional convective features, suggests that transport velocities are substantially smaller than theoretical predictions. Furthermore, helioseismology provides important constraints on the anisotropic Reynolds stresses that control the global dynamics of the solar convection zone. This review discusses the state of our understanding of convection in the Sun, with a focus on helioseismic diagnostics. We present our considerations with the interests of fluid dynamicists in mind.

Solar Dynamics, Rotation, Convection and Overshoot **Review**

S. **Hanasoge**, M. S. Miesch, M. Roth, J. Schou, M. Schüssler, M. J. Thompson
Space Sci. Rev. Volume 196, Issue 1, pp 79-99 **2015**
http://arxiv.org/pdf/1503.08539v1.pdf
We discuss recent observational, theoretical and modeling progress made in understanding the Sun's internal dynamics, including its rotation, meridional flow, convection and overshoot. Over the past few decades, substantial theoretical and observational effort has gone into appreciating these aspects of solar dynamics. A review of these observations, related helioseismic methodology and inference and computational results in relation to these problems is undertaken here.

Full Waveform Inversion of Solar Interior Flows

Shravan M **Hanasoge**

ApJ, **2014**

http://arxiv.org/pdf/1410.1981v1.pdf

The inference of flows of material in the interior of the Sun is a subject of major interest in helioseismology. Here we apply techniques of Full Waveform Inversion (FWI) to synthetic data to test flow inversions. In this idealized setup, we do not model seismic realization noise, training the focus entirely on the problem of whether a chosen supergranulation flow model can be seismically recovered. We define the misfit functional as a sum of L_2 norm deviations in travel times between prediction and observation, as measured using short-distance f and p_1 filtered and large-distance unfiltered p modes. FWI allows for the introduction of measurements of choice and iteratively improving the background model, while monitoring the evolution of the misfit in all desired categories. Although the misfit is seen to uniformly reduce in all categories, convergence to the true model is very slow, possibly because it is trapped in a local minimum. The primary source of error is inaccurate depth localization, which, owing to density stratification, leads to wrong ratios of horizontal and vertical flow velocities (`cross talk'). In the present formulation, the lack of sufficient temporal frequency and spatial resolution makes it difficult to accurately localise flow profiles at depth. We therefore suggest that the most efficient way to discover the global minimum is to perform a probabilistic forward search, involving calculating the misfit associated with a broad range of models (generated, for instance, by a Monte-Carlo algorithm) and locating the deepest minimum. Such techniques possess the added advantage of being able to quantify model uncertainty as well as realization noise (data uncertainty).

Anomalously Weak Convection on Large Scales in the Sun

Shravan M **Hanasoge**

HMI Science Nuggets, #27, Sept **2014**

http://hmi.stanford.edu/hminuggets/?p=946

The Quest to Understand Supergranulation and Large-Scale Convection in the Sun

Shravan M. **Hanasoge**, Katepalli R. Sreenivasan

Solar Physics, September **2014**, Volume 289, Issue 9, pp 3403-3419

Surface granulation of the Sun is primarily a consequence of thermal transport in the outer 1 % of the radius. Its typical scale of about $1-2$ Mm is set by the balance between convection, free-streaming radiation, and the strong density stratification in the surface layers. The physics of granulation is well understood, as demonstrated by the close agreement between numerical simulation, theory, and observation. Superimposed on the energetic granular structure comprising high-speed flows, are larger-scale long-lived flow systems (≈ 300 m s^{-1}) called supergranules. Supergranulation has a typical scale of $24-36$ Mm. It is not clear if supergranulation results from the interaction of granules or is causally linked to deep convection or a consequence of magneto–convection. Other outstanding questions remain: how deep are supergranules? How do they participate in global dynamics of the Sun? Further challenges are posed by our lack of insight into the dynamics of larger scales in the deep convection region. Recent helioseismic constraints have suggested that convective-velocity amplitudes on large scales may be overestimated by an order of magnitude or more, implying that Reynolds stresses associated with large-scale convection, thought to play a significant role in the sustenance of differential rotation and meridional circulation, might be two orders of magnitude weaker than theory and computation predict. While basic understanding on the nature of convection on global scales and the maintenance of global circulations is incomplete, progress is imminent, given substantial improvements in computation, theory, and helioseismic inferences.

Full Waveform Inversion for Time-Distance Helioseismology

Shravan M. **Hanasoge**1,2,3 and Jeroen Tromp

2014 ApJ 784 69

Inferring interior properties of the Sun from photospheric measurements of the seismic wavefield constitutes the helioseismic inverse problem. Deviations in seismic measurements (such as wave travel times) from their fiducial values estimated for a given model of the solar interior imply that the model is inaccurate. Contemporary inversions in local helioseismology assume that properties of the solar interior are linearly related to measured travel-time deviations. It is widely known, however, that this assumption is invalid for sunspots and active regions and is likely for supergranular flows. Here, we introduce nonlinear optimization, executed iteratively, as a means of inverting for the subsurface structure of large-amplitude perturbations. Defining the penalty functional as the L 2 norm of wave travel-time deviations, we compute the total misfit gradient of this functional with respect to the relevant model parameters at each iteration around the corresponding model. The model is successively improved using either steepest descent, conjugate gradient, or the quasi-Newton limited-memory Broyden-Fletcher-Goldfarb-Shanno

algorithm. Performing nonlinear iterations requires privileging pixels (such as those in the near field of the scatterer), a practice that is not compliant with the standard assumption of translational invariance. Measurements for these inversions, although similar in principle to those used in time-distance helioseismology, require some retooling. For the sake of simplicity in illustrating the method, we consider a two-dimensional inverse problem with only a sound-speed perturbation.

The First X-ray Imaging Spectroscopy of Quiescent Solar Active Regions with NuSTAR

Iain G. **Hannah**, Brian W. Grefenstette, David M. Smith, Lindsay Glesener, Säm Krucker, Hugh S. Hudson, Kristin K. Madsen, Andrew Marsh, Stephen M. White, Amir Caspi, Albert Y. Shih, Fiona A. Harrison, Daniel Stern, Steven E. Boggs, Finn E. Christensen, William W. Craig, Charles J. Hailey, William W. Zhang

2016, ApJL, 820, L4

http://arxiv.org/pdf/1603.01069v1.pdf

We present the first observations of quiescent active regions (ARs) using the Nuclear Spectroscopic Telescope Array (NuSTAR), a focusing hard X-ray telescope capable of studying faint solar emission from high-temperature and non-thermal sources. We analyze the first directly imaged and spectrally resolved X-rays above 2 keV from non-flaring ARs, observed near the west limb on **2014 November 1**. The NuSTAR X-ray images match bright features seen in extreme ultraviolet and soft X-rays. The NuSTAR imaging spectroscopy is consistent with isothermal emission of temperatures 3.1-4.4 MK and emission measures 1-8 x 10^{46} cm^{-3}. We do not observe emission above 5 MK, but our short effective exposure times restrict the spectral dynamic range. With few counts above 6 keV, we can place constraints on the presence of an additional hotter component between 5 and 12 MK of ~10^{46} cm^{-3} and ~10^{43} cm^{-3}, respectively, at least an order of magnitude stricter than previous limits. With longer duration observations and a weakening solar cycle (resulting in an increased livetime), future NuSTAR observations will have sensitivity to a wider range of temperatures as well as possible non-thermal emission.

Discovery of high-frequency vorticity waves in the Sun

Chris S. **Hanson**1, Shravan Hanasoge2,1, & Katepalli R. Sreenivasan1,3

HMI Science Nuggets #181 Jun **2022**

http://hmi.stanford.edu/hminuggets/?p=3922

Analyzing supergranular power spectra using helioseismic normal-mode coupling

Chris S. **Hanson**, Shravan Hanasoge, Katepalli R. Sreenivasan

ApJ **910** 156 **2021**

https://arxiv.org/pdf/2102.08715.pdf

https://doi.org/10.3847/1538-4357/abe770

Normal-mode coupling is a technique applied to probe the solar interior using surface observations of oscillations. The technique, which is straightforward to implement, makes more use of the seismic information in the wavefield than other comparable local imaging techniques and therefore has the potential to significantly improve current capabilities. Here, we examine supergranulation power spectra using mode-coupling analyses of intermediate-to-high-degree modes by invoking a Cartesian-geometric description of wave propagation under the assumption that the localized patches are much smaller in size than the solar radius. We extract the supergranular power spectrum and compare the results with prior helioseismic studies. Measurements of the dispersion relation and life times of supergranulation, obtained using near surface modes (f and p1), are in accord with the literature. We show that the cross-coupling between the p2 and p3 acoustic modes, which are capable of probing greater depths, are also sensitive to supergranulation.

Solar east-west flow correlations that persist for months at low latitudes are dominated by active region inflows

Chris S. **Hanson**, Thomas L. Duvall Jr., Aaron C. Birch, Laurent Gizon, Katepalli R. Sreenivasan

A&A 644, A103 **2020**

https://arxiv.org/pdf/2010.13052.pdf

Context: Giant-cell convection is believed to be an important component of solar dynamics. For example, it is expected to play a crucial role in maintaining the Sun's differential rotation.

Aims: We re-examine early reports of giant convective cells detected using correlation analysis of Dopplergrams. We extend this analysis using 19 years of space and ground-based observations of near-surface horizontal flows.

Method: Flow maps are derived through local correlation tracking of granules and helioseismic ring-diagram analysis. We compute temporal auto-correlation functions of the east-west flows at fixed latitude.

Results: Correlations in the east-west velocity can be clearly seen up to five rotation periods. The signal consists of

features with longitudinal wavenumbers up to m=9 at low latitudes. Comparison with magnetic images indicates that these flow features are associated with magnetic activity. The signal is not seen above the noise level during solar minimum.
Conclusions: Our results show that the long-term correlations in east-west flows at low latitudes are dominantly due to inflows into active regions and not to giant convective cells.

Solar Rossby waves observed in GONG++ ring-diagram flow maps

Chris S. **Hanson**, Laurent Gizon, Zhi-Chao Liang
A&A 635, A109 **2020**
https://arxiv.org/pdf/2002.01194.pdf
Context: Solar sectoral Rossby waves have only recently been unambiguously identified in Helioseimsic and Magnetic Imager (HMI) and Michelson Doppler Imager (MDI) maps of flows near the solar surface. So far this has not been done with the Global Oscillation Network Group (GONG) ground-based observations, which have different noise properties.
Aims: We utilize 17 years of GONG++ data, to identify and characterize solar Rossby waves using ring-diagram helioseismology. We compare directly with HMI ring-diagram analysis.
Methods: Maps of the radial vorticity are obtained for flows within the top 2 Mm of the surface for 17 years of GONG++. The data is corrected for systematic effects including the annual periodicity related to the B0 angle. We then compute the Fourier components of the radial vorticity of the flows in the co-rotating frame. We perform the same analysis on the HMI data that overlap in time.
Results: We find that the solar Rossby waves have measurable amplitudes in the GONG++ sectoral power spectra for azimuthal orders between m=3 and m=15. The measured mode characteristics (frequencies, lifetimes and amplitudes) from GONG++ are consistent with the HMI measurements in the overlap period from 2010 to 2018 for $m \leq 9$. For higher-m modes the amplitudes and frequencies agree within two sigmas. The signal-to-noise ratio of modes in GONG++ power spectra is comparable to HMI for $8 \leq m \leq 11$, but is lower by a factor of two for other modes.
Conclusions: The GONG++ data provide a long and uniform data set to study solar global-scale Rossby waves from 2001.

Enhanced Acoustic Emission in Relation to the Acoustic Halo Surrounding Active Region 11429

Chris S. **Hanson**, Alina C. Donea, K.D. Leka
Solar Phys., Volume 290, Issue 8, pp 2171-2187 **2015**
http://arxiv.org/pdf/1507.03447v1.pdf
The use of acoustic holography in the high-frequency p-mode spectrum can resolve the source distributions of enhanced acoustic emissions within halo structures surrounding active regions. In doing so, statistical methods can then be applied to ascertain relationships with the magnetic field. This is the focus of this study. The mechanism responsible for the detected enhancement of acoustic sources around solar active regions has not yet been explained. Furthermore the relationship between the magnetic field and enhanced acoustic emission has not yet been comprehensively examined. We have used vector magnetograms from the \Helioseismic and Magnetic Imager (HMI) on-board the Solar Dynamics Observatory (SDO) to image the magnetic-field properties in the halo. We have studied the acoustic morphology of an active region, with a complex halo and "glories," and we have linked some acoustic properties to the magnetic-field configuration. In particular, we find that acoustic sources are significantly enhanced in regions of intermediate field strength with inclinations no different from the distributions found in the quiet Sun. Additionally we have identified a transition region between the active region and the halo, in which the acoustic source power is hindered by inclined fields of intermediate field strength. Finally, we have compared the results of acoustic emission maps, calculated from holography, and the commonly used local acoustic maps, finding that the two types of maps have similar properties with respect to the magnetic field but lack spatial correlation when examining the highest-powered regions.

Multiple Scattering of Seismic Waves from Ensembles of Upwardly Lossy Thin Flux Tubes

Chris S. **Hanson**, Paul S. Cally
Solar Phys., Volume 290, Issue 7, pp 1889-1896 **2015**
http://arxiv.org/pdf/1506.07638v1.pdf
Our previous semi-analytic treatment of f- and p-mode multiple scattering from ensembles of thin flux tubes (Hanson and Cally, Astrophys. J. 781, 125; 791, 129, 2014) is extended by allowing both sausage and kink waves to freely escape at the top of the model using a radiative boundary condition there. As expected, this additional avenue of escape, supplementing downward loss into the deep solar interior, results in substantially greater absorption of

incident f- and p-modes. However, less intuitively, it also yields mildly to substantially smaller phase shifts in waves emerging from the ensemble. This may have implications for the interpretation of seismic data for solar plage regions, and in particular their small measured phase shifts.
Erratum Solar Phys. 291(2) 2016

Time-Distance Seismology and the Solar Transition Region

Shelley C. **Hansen**, Paul S. Cally
Solar Phys., **2014**
Time-Distance 'travel time' perturbations (as inferred from wave phase) are calculated relative to the quiet-Sun as a function of wave orientation and field inclination in a uniform inclined magnetic field. Modelling indicates that the chromosphere-corona Transition Region (TR) profoundly alters travel times at inclinations from the vertical θ for which the ramp-reduced acoustic cutoff frequency ω c cosθ is similar to the wave frequency ω. At smaller inclinations phase shifts are much smaller as the waves are largely reflected before reaching the TR. At larger inclinations, the shifts resume their quiet-Sun values, although with some resonant oscillatory behaviour. Changing the height of the TR in the model atmosphere has some effect, but the thickness and temperature jump do not change the results substantially. There is a strong correspondence between travel-time shifts and the Alfvén flux that emerges at the top of the modelled region as a result of fast/Alfvén mode conversion. We confirm that the TR transmission coefficient for Alfvén waves generated by mode conversion in the chromosphere is far larger (typically 30 % or more) than for Alfvén waves injected from the photosphere.

Ellerman bombs and UV bursts: transient events in chromospheric current sheets

V. **Hansteen**, A. Ortiz, V. Archontis, M. Carlsson, T. M. D. Pereira, J. P. Bjørgen
A&A 626, A33 **2019**
https://arxiv.org/pdf/1904.11524.pdf
Ellerman bombs (EBs) and UV bursts are both brightenings related to flux emergence regions and specifically to magnetic flux of opposite polarity that meet in the photosphere. These two reconnection-related phenomena, nominally formed far apart, occasionally occur in the same location and at the same time, thus challenging our understanding of reconnection and heating of the lower solar atmosphere. We consider the formation of an active region, including long fibrils and hot and dense coronal plasma. The emergence of a untwisted magnetic flux sheet, injected 2.5~Mm below the photosphere, is studied as it pierces the photosphere and interacts with the preexisting ambient field. Specifically, we aim to study whether EBs and UV bursts are generated as a result of such flux emergence and examine their physical relationship. The Bifrost radiative magnetohydrodynamics code was used to model flux emerging into a model atmosphere that contained a fairly strong ambient field, constraining the emerging field to a limited volume wherein multiple reconnection events occur as the field breaks through the photosphere and expands into the outer atmosphere. Synthetic spectra of the different reconnection events were computed using the 1.5D RH code and the fully 3D MULTI3D code. The formation of UV bursts and EBs at intensities and with line profiles that are highly reminiscent of observed spectra are understood to be a result of the reconnection of emerging flux with itself in a long-lasting current sheet that extends over several scale heights through the chromosphere. Synthetic diagnostics suggest that there are no compelling reasons to assume that UV bursts occur in the photosphere. Instead, EBs and UV bursts are occasionally formed at opposite ends of a long current sheet that resides in an extended bubble of cool gas.

Numerical Simulations of Coronal Heating through Footpoint Braiding

Viggo **Hansteen**, Nuno Guerreiro, Bart De Pontieu, Mats Carlsson
ApJ 811 106 **2015**
http://arxiv.org/pdf/1508.07234v1.pdf
Advanced 3D radiative MHD simulations now reproduce many properties of the outer solar atmosphere. When including a domain from the convection zone into the corona, a hot chromosphere and corona are self-consistently maintained. Here we study two realistic models, with different simulated area, magnetic field strength and topology, and numerical resolution. These are compared in order to characterize the heating in the 3D-MHD simulations which self-consistently maintains the structure of the atmosphere. We analyze the heating at both large and small scales and find that heating is episodic and highly structured in space, but occurs along loop shaped structures, and moves along with the magnetic field. On large scales we find that the heating per particle is maximal near the transition region and that widely distributed opposite-polarity field in the photosphere leads to a greater heating scale height in the corona. On smaller scales, heating is concentrated in current sheets, the thicknesses of which are set by the numerical resolution. Some current sheets fragment in time, this process occurring more readily in the higher-resolution model leading to spatially highly intermittent heating. The large scale heating structures are found to fade in less than about five minutes, while the smaller, local, heating shows time scales of the order of 2 minutes in one model and 1 minutes in the other, higher-resolution, model.

The Unresolved Fine Structure Resolved - IRIS observations of the Solar Transition Region

V. **Hansteen**, B. De Pontieu, M. Carlsson, J. Lemen, A. Title, P. Boerner, N. Hurlburt, T.D. Tarbell,J.P. Wuelser, T.M.D. Pereira, E.E. De Luca, L. Golub, S. McKillop, K. Reeves, S. Saar, P. Testa, H. Tian, C. Kankelborg, S. Jaeggli, L. Kleint, J. Martinez-Sykora

Science , Vol. 346 no. 6207 1255757 **2014**

http://arxiv.org/ftp/arxiv/papers/1412/1412.3611.pdf

The heating of the outer solar atmospheric layers, i.e., the transition region and corona, to high temperatures is a long standing problem in solar (and stellar) physics. Solutions have been hampered by an incomplete understanding of the magnetically controlled structure of these regions. The high spatial and temporal resolution observations with the Interface Region Imaging Spectrograph (IRIS) at the solar limb reveal a plethora of short, low lying loops or loop segments at transition-region temperatures that vary rapidly, on the timescales of minutes. We argue that the existence of these loops solves a long standing observational mystery. At the same time, based on comparison with numerical models, this detection sheds light on a critical piece of the coronal heating puzzle.
Movies are available at this http URL

Solar Wind Models from the Chromosphere to 1 AU

Viggo H. **Hansteen** and Marco Velli

Space Science Reviews, **2012**, DOI: 10.1007/s11214-012-9887-z

Recent models of the fast solar wind are characterized by low coronal electron temperatures while proton, α-particle, and minor ion temperatures are expected to be quite high and generally anisotropic, including large temperatures perpendicular to the magnetic field and parallel beams. This entails that the electric field should be relatively unimportant and that solar wind outflows with both high asymptotic flow speeds but maintaining a low mass flux should be a natural outcome of plasma expansion along open polar magnetic field lines. In this chapter we will explain why such changes with respect to the classical, electron thermally driven solar wind have come about and outline the most important remaining concerning the astrophysics of coronal winds.
The progress we have seen in the last decade is largely due observations made with instruments onboard Ulysses (McComas et al. in Space Sci. Rev. 72:93, 1995) and SOHO (Fleck et al. in The SOHO Mission, Kluwer, Dordrecht, 1995). These observations have spawned a new understanding of solar wind energetics, and the consideration of the chromosphere, corona, and solar wind as a unified system.
We will begin by giving our own, highly biased, "pocket history" of solar wind theory highlighting the problems that had to be resolved in order to make the original Parker formulation of thermally driven winds conform with observational results. Central to this discussion are questions of how the wind's asymptotic flow speed and mass flux are set, but we will also touch upon higher order moments such as the ion and electron temperatures and heat fluxes as well as the possible role of Alfvén waves and particle effects in driving the solar wind outflow. Solar wind scaling laws will be discussed in the context of the origin of slow and fast wind streams.

Automated Detection Methods for Solar Activities and an Application for Statistic Analysis of Solar Filament

Q. **Hao**, P. F. Chen, C. Fang

Proceedings IAU Symposium No. 340, **2018**

https://arxiv.org/pdf/1804.03320.pdf

With the rapid development of telescopes, both temporal cadence and the spatial resolution of observations are increasing. This in turn generates vast amount of data, which can be efficiently searched only with automated detections in order to derive the features of interest in the observations. A number of automated detection methods and algorithms have been developed for solar activities, based on the image processing and machine learning techniques. In this paper, after briefly reviewing some automated detection methods, we describe our efficient and versatile automated detection method for solar filaments. It is able not only to recognize filaments, determine the features such as the position, area, spine, and other relevant parameters, but also to trace the daily evolution of the filaments. It is applied to process the full disk H-alpha data observed in nearly three solar cycles, and some statistic results are presented.

Statistical Analysis of Filament Features Based on the Hα Solar Images from 1988 to 2013 by Computer Automated Detection Method

Q. **Hao**, C. Fang, W. Cao, P. F. Chen

ApJS **201**5

http://arxiv.org/pdf/1511.04692v1.pdf

We improve our filament automated detection method which was proposed in our previous works. It is then applied to process the full disk Hα data mainly obtained by Big Bear Solar Observatory (BBSO) from 1988 to 2013, spanning nearly 3 solar cycles. The butterfly diagrams of the filaments, showing the information of the filament

area, spine length, tilt angle, and the barb number, are obtained. The variations of these features with the calendar year and the latitude band are analyzed. The drift velocities of the filaments in different latitude bands are calculated and studied. We also investigate the north-south (N-S) asymmetries of the filament numbers in total and in each subclass classified according to the filament area, spine length, and tilt angle. The latitudinal distribution of the filament number is found to be bimodal. About 80% of all the filaments have tilt angles within [0{\deg}, 60{\deg}]. For the filaments within latitudes lower (higher) than 50{\deg} the northeast (northwest) direction is dominant in the northern hemisphere and the southeast (southwest) direction is dominant in the southern hemisphere. The latitudinal migrations of the filaments experience three stages with declining drift velocities in each of solar cycles 22 and 23, and it seems that the drift velocity is faster in shorter solar cycles. Most filaments in latitudes lower (higher) than 50{\deg} migrate toward the equator (polar region). The N-S asymmetry indices indicate that the southern hemisphere is the dominant hemisphere in solar cycle 22 and the northern hemisphere is the dominant one in solar cycle 23. ftp://ftp.bbso.njit.edu/pub/archive

HEMISPHERIC HELICITY TREND FOR SOLAR CYCLE 24
Juan **Hao** and Mei Zhang
2011 ApJ 733 L27
Using vector magnetograms obtained with the Spectro-polarimeter (SP) on board Hinode satellite, we studied two helicity parameters (local twist and current helicity) of 64 active regions that occurred in the descending phase of solar cycle 23 and the ascending phase of solar cycle 24. Our analysis gives the following results. (1) The 34 active regions of the solar cycle 24 follow the so-called hemispheric helicity rule, whereas the 30 active regions of the solar cycle 23 do not. (2) When combining all 64 active regions as one sample, they follow the hemispheric helicity sign rule as in most other observations. (3) Despite the so-far most accurate measurement of vector magnetic field given by SP/Hinode, the rule is still weak with large scatters. (4) The data show evidence of different helicity signs between strong and weak fields, confirming previous result from a large sample of ground-based observations. (5) With two example sunspots we show that the helicity parameters change sign from the inner umbra to the outer penumbra, where the sign of penumbra agrees with the sign of the active region as a whole. From these results, we speculate that both the Σ-effect (turbulent convection) and the dynamo have contributed in the generation of helicity, whereas in both cases turbulence in the convection zone has played a significant role.

Long-Term Trend Analysis in the Solar Radiation and Climate Experiment (SORCE)/Spectral Irradiance Monitor (SIM)

Jerald W. **Harder**, Stéphane Béland, Steven Penton & Thomas N. Woods
Solar Physics volume 297, Article number: 69 (**2022**)
https://link.springer.com/content/pdf/10.1007/s11207-022-02001-9.pdf
The Solar Radiation and Climate Experiment/Spectral Irradiance Monitor (SORCE/SIM) instrument was launched on 25 January 2003 with mission termination occurring on 25 February 2020. The SORCE/SIM provides a unique data set of the variability in solar spectral irradiance (SSI) during the descending phase of Solar Cycle 23 (SC23) from April 2003 to February 2009, the weaker solar-maximum conditions of SC24, and the quiescent SC24/SC25 minimum. The determination of the magnitude and phase of SSI variations rely on the unambiguous determination of the effects of the space environment and solar-exposure-related degradation mechanisms. The instrument-only corrections for SIM are based on a comparison of two functionally identical (mirror image) prism spectrometers with four independent detectors in each spectrometer channel. The degradation correction is strictly instrumental in its methodology and makes no assumptions about the magnitude, slope, or wavelength dependence of the SSI variability.

Offset Power-law Dependence of the Sun's Radial Electron Density Profile: Evidence and Implications

J. C. **Harding**, Iver H. Cairns, and V. V. Lobzin
2019 ApJ 877 25
sci-hub.se/10.3847/1538-4357/ab19a0
The radial electron density profile n e (r) of the Sun's corona and solar wind contains information on the sources, heating, and acceleration of the coronal and solar wind plasma. Currently, several empirically derived density models are used to describe the corona, with varying degrees of success and little physical justification or predictive power. The offset power-law (OPL) profile $n_e(r) = A(r - r_0)^{-\alpha}$, with radial offset r 0 and power-law index α, models radial outflow from r 0 that conserves total electron number and may be accelerated and heated (affecting α), thus having physical significance and predictive power. We fit the OPL model to multiple sets of published radial density profiles obtained from spectroscopic, white light, and radio data from different regions on the Sun and during different periods of solar activity. The spectroscopic and white light data yield r0 = (1.02 ± 0.06) R S , where the uncertainties are standard errors of the mean, and $\langle \alpha \rangle = -2.4 \pm 0.2$, consistent with plasma originating near the chromosphere and acceleration similar to the nominal Parker solar wind model. Comparisons with time-lapse

coronagraph and spectroscopic observations are favorable and show evidence for significant variations with position and time. These are expected given the corona's well-known asymmetries, three-dimensional structures, and time variability. Radio burst data yield flatter profiles $\alpha < 2$, suggesting that pre-flare activity alters the density profile by increasing the coronal density at large heights. We discuss the possible interpretations and implications for coronal physics and solar radio bursts.

Auroral radio absorption: The prediction question

J.K. **Hargreaves**

Adv. Space Res. Volume 45, Issue 9, Pages 1075-1092, **2010**.

The paper summarises key facts and figures about the phenomenon of auroral radio absorption which are relevant to the problem of predicting its occurrence and intensity. The regions most affected are well known in terms of magnetic latitude (or L-value) and local time. The greater difficulty comes from its highly variable character. Exact predictions are never likely to be possible, but statistical forecasts, which would give the likelihood that some critical level will be reached or exceeded, may well be possible. At the present time it is suggested that they might be based on magnetic indices, since their prediction is already well established. Direct measurements of the solar wind, now available in real time, offer another possibility, perhaps to be considered in parallel. The substorm character of the absorption might also be applied, using the observed duration of absorption events and their known dynamics over the Earth's surface, as an early warning. A comprehensive reference list is included.

The source of unusual coronal upflows with photospheric abundance in a solar active region⋆

L. K. **Harra**1,2, C. H. Mandrini3, D. H. Brooks4, K. Barczynski1,2, C. Mac Cormack, +++

A&A 675, A20 (**2023**)

https://www.aanda.org/articles/aa/pdf/2023/07/aa45747-22.pdf

Context. Upflows in the corona are of importance, as they may contribute to the solar wind. There has been considerable interest in upflows from active regions (ARs). The coronal upflows that are seen at the edges of active regions have coronal elemental composition and can contribute to the slow solar wind. The sources of the upflows have been challenging to determine because they may be multiple, and the spatial resolution of previous observations is not yet high enough.

Aims. In this article, we analyse coronal upflows in AR 12960 that are unusually close to the sunspot umbra. We analyse their properties, and we attempt to determine if it is possible that they feed into the slow solar wind.

Methods. We analysed the activity in the upflow region in detail using a combination of Solar Orbiter EUV images at high spatial and temporal resolution, Hinode/EUV Imaging Spectrometer data, and observations from instruments on board the Solar Dynamics Observatory. This combined dataset was acquired during the first Solar Orbiter perihelion of the science phase, which provided a spatial resolution of 356 km for two pixels. Doppler velocity, density, and plasma composition determinations, as well as coronal magnetic field modelling, were carried out to understand the source of the upflows.

Results. We observed small magnetic fragments, called moving magnetic features (MMFs), moving away from the sunspot in the active region. Specifically, they moved towards the sunspot from the edge of the penumbra where a small positive polarity connects to the umbra via small-scale and very dynamic coronal loops. At this location, small dark grains are evident and flow along penumbral filaments in continuum images. The magnetic field modelling showed small low-lying loops anchored close to the umbral magnetic field. The high-resolution data of the Solar Orbiter EUV Imagers showed the dynamics of these small loops, which last on time scales of only minutes. The edges of these small loops are the location of the coronal upflow that has photospheric abundance. **7 Mar 2022**

Getting it all from spectra! Measuring velocities in the early stages of an eruption using the wide slot data from Hinode EIS

Louise **Harra**, George Doschek, Sarah Matthews, Harry Warren, Len Culhane, Magnus Woods

Hinode/EIS Nugget Jan **2018**

http://solarb.mssl.ucl.ac.uk/SolarB/nuggets/nugget_2018jan.jsp

31 Dec 2013

A study of the long term evolution in active region upflows

Louise K. **Harra** Ignacio Ugarte-Urra Marc De Rosa Cristina MandriniLidia van Driel-Gesztelyi Deborah Baker J. Leonard Culhane Pascal Démoulin

Publications of the Astronomical Society of Japan, Volume 69, Issue 3, 1 June **2017**, 47,

Since their discovery, upflows at the edges of active regions have attracted a lot of interest, primarily as they could potentially contribute to the slow solar wind. One aspect that has not been studied yet is how the long term evolution

of active regions impacts the upflows. In this work, we analyze one active region that survives three solar rotations. We track how the flows change with time. We use local and global modeling of the decaying active region to determine how the age of the active region will impact the extent of the open magnetic fields, and then how some of the upflows could become outflows. We finish with a discussion of how these results, set in a broader context, can be further developed with the Solar Orbiter mission.

Preface: Probing the Sun Inside and Out

Louise **Harra**, Deborah Baker , Rachel Howe, John Leibacher, Lidia van Driel-Gesztelyi
Solar Physics, November **2015**, Volume 290, Issue 11, pp 3091-3094
http://link.springer.com/article/10.1007/s11207-015-0816-7
The results that we have obtained concentrate on this activity cycle (inside and outside the Sun) and also on solar flares. This Topical Issue highlights some of the key results from this network (the Birmingham Solar-Oscillations Network (BiSON; Hale et al., 2015) and Global Oscillation Network Group (GONG: Harvey et al., 1996)).

A Study of the Coronal Non-thermal Velocity in Polar Regions During the Rise from Solar Minimum to Solar Maximum in Cycle 24

Velocity in Polar Regions During the Rise from Solar Minimum to Solar Maximum in Cycle 24

L. **Harra**, D. Baker, S. J. Edwards, H. Hara, R. Howe, L. van Driel-Gesztelyi
Solar Phys. Volume 290, Issue 11, pp 3203-3220 **2015**
We explore the changes in coronal non-thermal velocity (V nt) measurements at the poles from solar minimum to solar maximum using Hinode EUV Imaging Spectrometer data. We find that although the intensity in the corona at the poles does tend to increase with the cycle, there are no significant changes in the V nt values. The locations of enhanced V nt values measured do not always have a counterpart in intensity, and they are sometimes located in weak emission regions. Unipolar magnetic streams, created through diffusion of the following polarity of the decaying active regions, slowly progress towards the poles. These streams are expected to be related to magnetic nulls as locations that indicate an increased likelihood for magnetic reconnection to occur. Through global potential field source-surface modelling, we determine how the number of nulls varied during the cycle and find that those that lie at < 1.1 solar radii vary significantly. We search for a correlation between the variation of the magnetic nulls and the V nt values, as it may be expected that with an increasing number of nulls, the V nt values in the corona increase as well. There is no correlation with the V nt values, however. This indicates that the magnetic structures that create the enhanced V nt behaviour are small-scale features and hence not easily measurable at the poles. Because they do not change during the solar cycle, they are likely to be created by a local dynamo. The variation of the upper range of V nt is reduced, which highlights that strongly dynamic behaviour is reduced as the solar maximum approaches. This is likely to be due to the reduced area of the polar coronal hole, which allows fewer opportunities for reconnection to occur between open and closed magnetic fields.

Computing Helioseismic Sensitivity Kernels for the Sun's Large-Scale Internal Flows using Global-Scale Wave-Propagation Simulations

Thomas **Hartlep**, Junwei Zhao
ApJ **909** 66 **2021**
https://arxiv.org/pdf/2102.06411.pdf
https://doi.org/10.3847/1538-4357/abd0f7
Helioseismic waves observable at the solar surface can be used to probe the properties of the Sun's interior. By measuring helioseismic travel times between different location on the surface, flows and other interior properties can be inferred using so-called sensitivity kernels which relate the amount of travel-time shift with variations in interior proporties. In particular, sensitivity kernels for flows have been developed in the past, using either ray or Born approximation, and have been used to infer solar interior flows such as the meridional circulation which is of particular interest for understanding the structure and dynamics of the Sun. Here we introduce a new method for deriving three-dimensional sensitivity kernels for large-scale horizontal flows in the solar interior. We perform global-Sun wave-propagation simulations through 784 small flow perturbations placed individually in the interior of a simulated Sun, and measure the shifts in helioseismic travel times caused by these perturbations. Each measurement corresponds to a linear equation connecting the flow perturbation velocities and the sensitivity kernels. By solving the resulting large set of coupled linear equations, we derive three-dimensional sensitivity kernels for horizontal flows which have a longitudinal component (parallel to the wave's travel direction) and a transverse component (perpendicular to the wave's travel direction). The kernels exhibit a "banana" shape, similar to kernels derived using Born approximation methods, and show that transverse components are not negligible in inversions for interior flows.
HMI Science Nuggets #153 March **2021** **http://hmi.stanford.edu/hminuggets/?p=3483**

Deconstructing Sunlight – A Community Enterprise MEMOIRS

J. W. **Harvey**

Solar Physics volume 295, Article number: 70 (**2020**)

https://link.springer.com/content/pdf/10.1007/s11207-020-01633-z.pdf

Good fortune allowed me to have a career in solar research. With the aid of many generous and gifted colleagues, I have tried to learn more about the Sun's magnetic and velocity fields through observation and instrumentation development. These interests captured me early and remain strong. In this memoir I describe my path through 60 years of solar research that was sometimes random but did not deviate much from my core interests. The chromospheric magnetic field and helioseismology have been especially intriguing and frequently rewarding topics.

Under the Lens: Investigating the Sun`s Mysteries

Harwood, William; Klotz, Irene

Space Weather, Vol. 6, No. 11, S11005, **2008**

http://dx.doi.org/10.1029/2008SW000449

To help give space weather applications new predictive capabilities, NASA's **Solar Dynamics Observator**y spacecraft will image the Sun in unprecedented detail.

Preface: Probing the Sun Inside and Out **Topical Issue**

Louise **Harra**1 · Deborah Baker1 · Rachel Howe2 · John Leibacher3,4 · Lidia van Driel-Gesztelyi1,5,6

Solar Phys **201**5 DOI 10.1007/s11207-015-0816-7

Atomic Transition Probabilities for UV and Blue Lines of Fe iiand Abundance Determinations in the Photospheres of the Sun and Metal-poor Star HD 84937

E. A. Den **Hartog**1, J. E. Lawler1, C. Sneden2, J. J. Cowan3, and A. Brukhovesky1

2019 ApJS 243 33

sci-hub.se/10.3847/1538-4365/ab322e

We report new branching fractions (BFs) for 121 UV lines from the low-lying odd-parity levels of Fe ii belonging to the z6Do, z6Fo, z6Po, z4Fo, z4Do, and z4Po terms of the 3d6(5D)4p configuration. These lines range in wavelength from 2250 to 3280 Å and originate in levels ranging in energy from 38,459 to 47,626 cm−1. In addition, we report BFs for 10 weak blue lines connecting to the z4Do term that range in wavelength from 4173 to 4584 Å. The BFs are combined with radiative lifetimes from the literature to determine transition probabilities and log(gf) values. Comparison is made to selected experimental and theoretical data from the literature. Our new data are applied to iron abundance determinations in the Sun and in metal-poor star HD 84937. For the Sun, eight blue lines yield $\log \varepsilon(\mathrm{Fe}) = 7.46 \pm 0.03$, in agreement with standard solar abundance estimates. For HD 84937 the observable wavelength range extends to the vacuum UV ($\lambda \geq 2327$ Å), and from 75 lines we derive $\log \varepsilon(\mathrm{Fe}) = 5.26 \pm 0.01$ ($\sigma = 0.07$), near to the metallicity estimates of past HD 84937 studies.

Locating heating channels of the solar corona in a plage region with the aid of high-resolution 10830 Å filtergrams

Parida **Hashim**, Fangyu Xu, Ya Wang, Weijie Men, Jinhua Shen, Yingna Su, Jianping Li, Zhenyu Jin, Haisheng Ji

ApJ **964** 157 **2024**

https://arxiv.org/pdf/2402.18077.pdf

https://iopscience.iop.org/article/10.3847/1538-4357/ad2e9d/pdf

In this paper, with a set of high-resolution He I 10830 Å filtergrams, we select an area in a plage, very likely an EUV moss area, as an interface layer to follow the clues of coronal heating channels down to the photosphere. The filtergrams are obtained from the 1-meter aperture New Vacuum Solar Telescope (NVST). We make a distinction between the darker and the brighter regions in the selected area and name the two regions enhanced absorption patches (EAPs) and low absorption patches (LAPs). With well-aligned, nearly simultaneous data from multiple channels of the AIA and the continuum of the HMI on board SDO, we compare the EUV/UV emissions, emission measure, mean temperature, and continuum intensity in the two kinds of regions. The following progress is made: 1) The mean EUV emissions over EAPs are mostly stronger than the corresponding emissions over LAPs except for the emission at 335 Å. The UV emissions at 1600 and 1700 Å fail to capture the difference between the two regions. 2) In the logarithmic temperature range of 5.6-6.2, EAPs have higher EUV emission measure than LAPs, but they have lower mean coronal temperature. 3) The mean continuum intensity over EAPs is lower. Based on the above progress, we suggest that the energy for coronal heating in the moss region can be traced down to some areas in intergranular lanes with enhanced density of both cool and hot material. The lower temperature over the EAPs is due to the greater fraction of cool material over there.

Observation of solar coronal heating powered by magneto-acoustic oscillations in a moss region

Parida **Hashim**, Zhenxiang Hong, Haisheng Ji, Jinhua Shen, Kaifan Ji, Wenda Cao
Research in Astron. Astrophys. **2020**
https://arxiv.org/pdf/2010.06787.pdf
In this paper, we report the observed temporal correlation between extreme-violet (EUV) emission and magneto-acoustic oscillations in a EUV moss region, which is the footpoint region only connected by magnetic loops with million-degree plasma. The result is obtained from a detailed multi-wavelength data analysis to the region with the purpose of resolving fine-scale mass and energy flows that come from the photosphere, pass through the chromosphere and finally heat solar transition region or the corona. The data set covers three atmospheric levels on the Sun, consisting of high-resolution broad-band imaging at TiO 7057 Å and the line of sight magnetograms for the photosphere, high-resolution narrow-band images at Helium \textsc{i} 10830 Å for the chromosphere and EUV images at 171 Å for the corona. We report following new phenomena: 1) Repeated injections of chromospheric material shown as 10830 Å\ absorption are squirted out from inter-granular lanes with the period of ∼ 5 minutes. 2) EUV emissions are found to be periodically modulated with the similar periods of ∼ 5 minutes. 3) Around the injection area where 10830 Å absorption is enhanced, both EUV emissions and the strength of magnetic field are remarkably stronger. 4) The peaks on the time profile of the EUV emissions are found to be in sync with oscillatory peaks of the stronger magnetic field in the region. These findings may give a series of strong evidences supporting the scenario that coronal heating is powered by magneto-acoustic waves. **July 22, 2012**

Solaris: A Focused Solar Polar Discovery-class Mission to achieve the Highest Priority Heliophysics Science Now

Donald M. **Hassler**, Sarah E Gibson, Jeffrey S Newmark, Nicholas A. Featherstone, +++
White Paper **2023**
https://arxiv.org/ftp/arxiv/papers/2301/2301.07647.pdf
Solaris is a transformative Solar Polar Discovery-class mission concept to address crucial outstanding questions that can only be answered from a polar vantage. Solaris will image the Sun's poles from ~**75 degree latitude**, providing new insight into the workings of the solar dynamo and the solar cycle, which are at the foundation of our understanding of space weather and space climate. Solaris will also provide enabling observations for improved space weather research, modeling and prediction, revealing a unique, new view of the corona, coronal dynamics and CME eruptions from above.

Variations in Differential Rotation and Meridional Flow within the Sun's Surface Shear Layer 1996-2022

David H. **Hathaway**, Lisa A. Upton, Sushant S. Mahajan
Frontiers **2022**
https://arxiv.org/pdf/2212.10619.pdf
We measure differential rotation and meridional flow in the Sun's surface shear layer by tracking the motions of the magnetic network seen in magnetograms from SOHO/MDI and SDO/HMI over solar cycles 23, 24, and the start of 25 (1996-2022). We examine the axisymmetric flows derived from 15-24 daily measurements averaged over individual 27-day Carrington rotations. Variations in the differential rotation include the equatorial torsional oscillation - cyclonic flows centered on the active latitudes with slower flows on the poleward sides of the active latitudes and faster flows equatorward. The fast flow band starts at ∼45◦ latitude during the declining phase of the previous cycle and drifts equatorward, terminating at the equator at about the time of cycle minimum. Variations in the differential rotation also include a polar oscillation above 45◦ with faster rotation at cycle maxima and slower rotation at cycle minima. The equatorial variations were stronger in cycle 24 than in cycle 23 but the polar variations were weaker. Variations in the meridional flow include a slowing of the poleward flow in the active latitudes during cycle rise and maximum and a speeding up of the poleward flow during cycle decline and minimum. The slowing in the active latitudes was less pronounced in cycle 24 than in cycle 23. Polar countercells (equatorward flow) extend from the poles down to ∼60◦ latitude from time to time (1996-2000 and 2016-2022 in the south and 2001-2011 and 2017-2022 in the north). Both axisymmetric flows vary in strength with depth. The rotation rate increases inward while the meridional flow weakens inward.

Hydrodynamic Properties of the Sun's Giant Cellular Flows

David H. **Hathaway**1 and Lisa A. Upton2
2021 ApJ 908 160
https://doi.org/10.3847/1538-4357/abcbfa
Measurements of the large cellular flows on the Sun were made by local correlation tracking of features (supergranules) seen in full-disk Doppler images obtained by the Helioseismic and Magnetic Imager (HMI) instrument on the NASA Solar Dynamics Observatory (SDO) satellite. Several improvements made to the local

correlation tracking method allowed for more precise measurements of these flows. Measurements were made hourly over the nearly ten years of the mission-to-date. A four-hour time-lag between images was determined to give the best results as a compromise between increased feature displacement and decreased feature evolution. The hourly measurements were averaged over the 34 days that it takes to observe all longitudes at all latitudes to produce daily maps of the latitudinal and longitudinal velocities. Analyses of these flow maps reveal many interesting characteristics of these large cellular flows. While flows at all latitudes are largely in the form of vortices with left-handed helicity in the north and right-handed helicity in the south, there are key distinctions between the low-latitude and high-latitude cells. The low-latitude cells have roughly circular shapes, lifetimes of about one month, rotate nearly rigidly, do not drift in latitude, and do not exhibit any correlation between longitudinal and latitudinal flow. The high-latitude cells have long extensions that spiral inward toward the poles and can wrap nearly completely around the Sun. They have lifetimes of several months, rotate differentially with latitude, drift poleward at speeds approaching 2 m s−1, and have a strong correlation between prograde and equatorward flows. Spherical harmonic spectral analyses of maps of the divergence and curl of the flows confirm that the flows are dominated by the curl component with rms velocities of about 12 m s−1 at wavenumber $\ell = 10$. Fourier transforms in time over 1024 daily records of the spherical harmonic spectra indicate two notable components—an $m = \pm\ell$ feature representing the low-latitude component and an $m = \pm 1$ feature representing the high-latitude component. The dispersion relation for the low-latitude component is well represented by that derived for Rossby waves or r-modes. The high-latitude component has a constant temporal frequency for all ℓ indicating features advected by differential rotation at rates representative of the base of the convection zone high latitudes. The poleward motions of these features further suggest that the high-latitude meridional flow at the base of the convection zone is poleward—not equatorward.
HMI Science Nuggets #155 May **2021** http://hmi.stanford.edu/hminuggets/?p=3518

Predicting the Amplitude and Hemispheric Asymmetry of Solar Cycle 25 with Surface Flux Transport

David H. **Hathaway**, Lisa A. Upton
JGR Vol: 121, Pages: 10,744–10,753 **2016**
https://arxiv.org/pdf/1611.05106v1.pdf

Evidence strongly indicates that the strength of the Sun's polar fields near the time of a sunspot cycle minimum determines the strength of the following solar activity cycle. We use our Advective Flux Transport (AFT) code, with flows well constrained by observations, to simulate the evolution of the Sun's polar magnetic fields from early 2016 to the end of 2019 --- near the expected time of Cycle 24/25 minimum. We run a series of simulations in which the uncertain conditions (convective motion details, active region tilt, and meridional flow profile) are varied within expected ranges. We find that the average strength of the polar fields near the end of Cycle 24 will be similar to that measured near the end of Cycle 23, indicating that Cycle 25 will be similar in strength to the current cycle. In all cases the polar fields are asymmetric with fields in the south stronger than those in the north. This asymmetry would be more pronounced if not for the predicted weakening of the southern polar fields in late 2016 and through 2017. After just four years of simulation the variability across our ensemble indicates an accumulated uncertainty of about 15\%. This accumulated uncertainty arises from stochastic variations in the convective motion details, the active region tilt, and changes in the meridional flow profile. These variations limit the ultimate predictability of the solar cycle.

The Sun's Photospheric Convection Spectrum

David H. **Hathaway**, Thibaud Teil, Aimee A. Norton, Irina Kitiashvili
ApJ 811 105 **2015**
http://arxiv.org/pdf/1508.03022v1.pdf

Spectra of the cellular photospheric flows are determined from full-disk Doppler velocity observations acquired by the Helioseismic and Magnetic Imager (HMI) instrument on the Solar Dynamics Observatory (SDO) spacecraft. Three different analysis methods are used to separately determine spectral coefficients representing the poloidal flows, the toroidal flows, and the radial flows. The amplitudes of these spectral coefficients are constrained by simulated data analyzed with the same procedures as the HMI data. We find that the total velocity spectrum rises smoothly to a peak at a wavenumber of about 120 (wavelength of about 35 Mm), which is typical of supergranules. The spectrum levels off out to wavenumbers of about 400, and then rises again to a peak at a wavenumber of about 3500 (wavelength of about 1200 km), which is typical of granules. The velocity spectrum is dominated by the poloidal flow component (horizontal flows with divergence but no curl) at wavenumbers above 30. The toroidal flow component (horizontal flows with curl but no divergence) dominates at wavenumbers less than 30. The radial flow velocity is only about 3\% of the total flow velocity at the lowest wavenumbers, but increases in strength to become about 50\% at wavenumbers near 4000. The spectrum compares well with the spectrum of giant cell flows at the lowest wavenumbers and with the spectrum of granulation from a 3D radiative-hydrodynamic simulation at the highest wavenumbers.

The Solar Cycle **Review**

David H. **Hathaway**
Living Reviews in Solar Physics, 12 (**2015**), 4
http://arxiv.org/pdf/1502.07020v1.pdf
http://solarphysics.livingreviews.org/Articles/lrsp-2015-4/
https://link.springer.com/content/pdf/10.1007/lrsp-2015-4.pdf
The Solar Cycle is reviewed. The 11-year cycle of solar activity is characterized by the rise and fall in the numbers and surface area of sunspots. A number of other solar activity indicators also vary in association with the sunspots including; the 10.7cm radio flux, the total solar irradiance, the magnetic field, flares and coronal mass ejections, geomagnetic activity, galactic cosmic ray fluxes, and radioisotopes in tree rings and ice cores. Individual solar cycles are characterized by their maxima and minima, cycle periods and amplitudes, cycle shape, the equatorward drift of the active latitudes, hemispheric asymmetries, and active longitudes. Cycle-to-cycle variability includes the Maunder Minimum, the Gleissberg Cycle, and the Gnevyshev-Ohl (even-odd) Rule. Short-term variability includes the 154-day periodicity, quasi-biennial variations, and double-peaked maxima. We conclude with an examination of prediction techniques for the solar cycle and a closer look at cycles 23 and 24.

How to keep the Sun's equator rotating faster than its poles: Giant Cells

David H. **Hathaway**, Lisa Upton
HMI Science Nuggets, #14, **2014**
http://hmi.stanford.edu/hminuggets/?p=715
The Sun’s equator rotates more rapidly than its polar regions – once every 24 days at the equator and once every 35 days at the poles. This behavior is the opposite to what we might expect from the conservation of angular momentum. If we take fluid from the Sun’s equator and move to the poles then it should spin up the same way an ice skater spins faster when she pulls her arms in closer to her rotation axis.

The Solar Meridional Circulation and Sunspot Cycle Variability

David H. **Hathaway**, Lisa Upton
JGR, Volume 119, Issue 5, pages 3316–3324, May **2014**
http://arxiv.org/pdf/1404.5893v1.pdf
We have measured the meridional motions of the magnetic elements in the Sun's surface layers since 1996 and find systematic and substantial variations. In general the meridional flow speed is fast at cycle minima and slow at cycle maxima. We find that these systematic variations are characterized by a weakening of the meridional flow on the poleward sides of the active (sunspot) latitudes. This can be interpreted as a inflow toward the sunspot zones superimposed on a more general poleward meridional flow profile. We also find variations in the meridional flow which vary from cycle-to-cycle. The meridional flow was slower at both the minimum and maximum of cycle 23 compared to similar phases of cycles 21, 22, and 24. Models of the magnetic flux transport by a variable meridional flow suggest that it can significantly modulate the size and timing of the following sunspot cycle through its impact on the Sun's polar magnetic fields. We suggest that the meridional flow variations observed in cycle 23 contributed to the weak polar fields at the end of the cycle which then produced a weak cycle 24 and the extraordinary cycle 23/24 minimum.

The Solar Cycle (обзор) **Review**

David H. **Hathaway**
Living Reviews in Solar Phys., 7, (**2010**), 1
http://www.livingreviews.org/lrsp-2010-1
sci-hub.tw/10.1007/lrsp-2015-4
The Solar Cycle is reviewed. The 11-year cycle of solar activity is characterized by the rise and fall in the numbers and surface area of sunspots. We examine a number of other solar activity indicators including the 10.7 cm radio flux, the total solar irradiance, the magnetic field, flares and coronal mass ejections, geomagnetic activity, galactic cosmic ray fluxes, and radioisotopes in tree rings and ice cores that vary in association with the sunspots. We examine the characteristics of individual solar cycles including their maxima and minima, cycle periods and amplitudes, cycle shape, and the nature of active latitudes, hemispheres, and

longitudes. We examine long-term variability including the Maunder Minimum, the Gleissberg Cycle, and the Gnevyshev–Ohl Rule. Short-term variability includes the 154-day periodicity, quasi-biennial variations, and double peaked maxima. We conclude with an examination of prediction techniques for the solar cycle.

Inversion for Inferring Solar Meridional Circulation: The Case with Constraints on Angular Momentum Transport inside the Sun

Yoshiki **Hatta**1,2, Hideyuki Hotta1, and Takashi Sekii2,3
2024 ApJ 972 79
https://iopscience.iop.org/article/10.3847/1538-4357/ad596c/pdf
We have carried out inversions of travel times as measured by Gizon et al. to infer the internal profile of the solar meridional circulation (MC). A linear inverse problem has been solved by the regularized least-squares method with a constraint that the angular momentum (AM) transport by MC should be equatorward (HK21-type constraint). Our motivation for using this constraint is based on the result by Hotta & Kusano (hereafter HK21), where the solar equator-fast rotation was reproduced successfully without any manipulation. The inversion result indicates that the MC profile is a double-cell structure if the so-called HK21 regime, in which AM transported by MC sustains the equator-fast rotation, correctly describes the physics inside the solar convective zone. The sum of the squared residuals computed with the inferred double-cell MC profile is comparable to that computed with the single-cell MC profile obtained when we exclude the HK21-type constraint, showing that both profiles can explain the data more or less at the same level. However, we also find that adding the HK21-type constraint degrades the resolution of the averaging kernels. Although it is difficult for us to determine the large-scale morphology of the solar MC at the moment, our attempt highlights the relevance of investigating the solar MC profile from both theoretical and observational perspectives
HMI Science Nuggets #205 **2024** http://hmi.stanford.edu/hminuggets/?p=4302

Solar Radius Determination from Sodism/Picard and HMI/SDO Observations of the Decrease of the Spectral Solar Radiance during the 2012 June Venus Transit

A. **Hauchecorne**1, M. Meftah1, A. Irbah1, S. Couvidat2, R. Bush2, and J.-F. Hochedez
2014 ApJ 783 127
On **2012 June 5-6, the transit of Venus** provided a rare opportunity to determine the radius of the Sun using solar imagers observing a well-defined object, namely, the planet and its atmosphere, partially occulting the Sun. A new method has been developed to estimate the solar radius during a planetary transit. It is based on the estimation of the spectral solar radiance decrease in a region around the contact between the planet and the Sun at the beginning of the ingress and at the end of the egress. The extrapolation to zero of the radiance decrease versus the Sun-to-Venus apparent angular distance allows estimation of the solar radius at the time of first and fourth contacts. This method presents the advantage of being almost independent on the plate scale, the distortion, the refraction by the planetary atmosphere, and on the point-spread function of the imager. It has been applied to two space solar visible imagers, SODISM/PICARD and HMI/SDO. The found results are mutually consistent, despite their different error budgets: 959."85 ± 0."19 (1σ) for SODISM at 607.1 nm and 959."90 ± 0."06 (1σ) for HMI at 617.3 nm.

SOLARNET Metadata Recommendations for Simulated Data

Stein Vidar **Haugan**, Terje Fredvik
2024
https://arxiv.org/ftp/arxiv/papers/2403/2403.12241.pdf
Until the advent of the SOLARNET recommendations, metadata sharing of simulated data within the Solar Physics community has been mostly on a "private communication" basis, with the description of the data format and content conveyed in an ad hoc manner. This document aims to amend this situation by establishing recommendations for representing such data and the associated metadata, based on the SOLARNET Metadata Recommendations for Solar Observations (arXiv:2011.12139)

SOLARNET Metadata Recommendations for Solar Observations **Explanations**

Stein Vidar Hagfors **Haugan**, Terje Fredvik
2020
https://arxiv.org/ftp/arxiv/papers/2011/2011.12139.pdf
Metadata descriptions of Solar observations have so far only been standardized for space-based observations, but the standards have been mostly within a single space mission at a time, at times with significant differences between different mission standards. In the context of ground-based Solar observations, data has typically not been made freely available to the general research community, resulting in an even greater lack of standards for metadata

descriptions. This situation makes it difficult to construct multi-instrument archives/virtual observatories with anything more than the most basic metadata available for searching, as well as making it difficult to write generic software for instrument-agnostic data analysis. This document describes the metadata recommendations developed under the SOLARNET EU project, which aims foster more collaboration and data sharing between both ground-based and space-based Solar observatories. The recommendations will be followed by data pipelines developed under the SOLARNET project as well as e.g. the Solar Orbiter SPICE pipeline and the SST CHROMIS/CRISP common pipeline. These recommendations are meant to function as a common reference to which even existing diverse data sets may be related, for ingestion into solar virtual observatories and for analysis by generic software.
1. An ideal Solar Virtual Observatory (SVO)
5. The World Coordinate System (WCS) and related keywords

Hemispheric injection of magnetic helicity by surface flux transport

G. **Hawkes**1 and A. R. Yeates2
A&A 631, A138 (**2019**)
https://doi.org/10.1051/0004-6361/201936475
Aims. We estimate the injection of relative magnetic helicity into the solar atmosphere by surface flux transport over 27 solar cycles (1700–2009).
Methods. We determine the radial magnetic field evolution using two separate surface flux transport models: one driven by magnetogram inputs and another by statistical active region insertion guided by the sunspot number record. The injection of relative magnetic helicity is then computed from this radial magnetic field together with the known electric field in the flux transport models.
Results. Neglecting flux emergence, solar rotation is the dominant contributor to the helicity injection. At high latitudes, the injection is always negative/positive in the northern/southern hemisphere, while at low latitudes the injection tends to have the opposite sign when integrated over the full solar cycle. The overall helicity injection in a given solar cycle depends on the balance between these two contributions. This net injected helicity correlates well with the end-of-cycle axial dipole moment.

Magnetic Helicity as a Predictor of the Solar Cycle

G. **Hawkes**, M. A. Berger
Solar Physics July **2018**, 293:109
It is well known that the polar magnetic field is at its maximum during solar minima, and that the behaviour during this time acts as a strong predictor of the strength of the following solar cycle. This relationship relies on the action of differential rotation (the Omega effect) on the poloidal field, which generates the toroidal flux observed in sunspots and active regions. We measure the helicity flux into both the northern and the southern hemispheres using a model that takes account of the Omega effect, which we apply to data sets covering a total of 60 years. We find that the helicity flux offers a strong prediction of solar activity up to five years in advance of the next solar cycle. We also hazard an early guess as to the strength of Solar Cycle 25, which we believe will be of similar amplitude and strength to Cycle 24.
UKSP Nugget #96 2018 http://www.uksolphys.org/uksp-nugget/96-magnetic-helicity-sunspot-number-and-solar-activity/

Analyses of Johannes Kepler's Sunspot Drawings in 1607: A Revised Scenario for the Solar Cycles in the Early 17th Century

Hisashi **Hayakawa**1,2,3,4, Koji Murata5, E. Thomas H. Teague6, Sabrina Bechet7, and Mitsuru Sôma8
2024 ApJL 970 L31
https://iopscience.iop.org/article/10.3847/2041-8213/ad57c9/pdf
Telescopic sunspot observations began in 1610 and captured subsequent solar cycles. In combination with proxy reconstructions on an annual scale, these data sets indicate a gradual transition between regular solar cycles and the Maunder Minimum. The telescopic sunspot observations missed the beginning of the first telescopic solar cycle (Solar Cycle −13), leaving room for considerable uncertainty as to its temporal evolution. Before these early telescopic observations, however, Kepler made solar observations using camerae obscurae and recorded a sunspot group in three solar drawings in 1607. Here, we make use of Kepler's sunspot drawings and descriptive texts to identify his observational sites and time stamps. We have deprojected his sunspot drawings and compared the reported positions with our calculations of the inclination of the solar equator as seen from these sites at that time. These results locate the reported sunspot group near the solar equator eastward from the central meridian. This contrasts with telescopic sunspot drawings from the 1610s that show sunspot groups in the higher heliographic latitudes. Therefore, what Kepler saw was probably a sunspot group from Solar Cycle −14, rather than one from Solar Cycle −13. These records allow us to place the beginning of Solar Cycle −13 between 1607 and 1610. In comparison with the 14C-based solar-cycle reconstructions, our result supports regular solar-cycle durations around the 1610s, rather than any suggested extreme extensions of the solar-cycle duration(s) around the 1610s.

An Overview of Sunspot Observations in the Early Maunder Minimum: 1645–1659

Hisashi **Hayakawa**, Víctor M S Carrasco, Alejandro J P Aparicio, Joaquín Villalba Álvarez, José M Vaquero

MNRAS Volume 528, Issue 4, March **2024**, Pages 6280–6291,
https://academic.oup.com/mnras/article-pdf/528/4/6280/56719311/stad3922.pdf

Within four centuries of sunspot observations, the Maunder Minimum (MM) in 1645–1715 has been considered a unique grand minimum with weak solar cycles in group numbers of sunspots and hemispheric asymmetry in sunspot positions. However, the early part of the MM (1645–1659) is poorly understood in terms of its source records and has accommodated diverse reconstructions of the contemporaneous group number. This study identified their source records, classidied them in three different categories (datable observations, general descriptions, and misinterpreted records), and revised their data. On this basis, we estimated the yearly mean group number using the brightest star method, derived the active day fraction (ADF), reconstructed the sunspot number based on ADF, and compared them with proxy reconstructions from the tree-ring data sets. Our results revised the solar activity in the early MM downward in yearly mean group numbers using the brightest star method and upward in the active day fraction and sunspot number estimates. Our results are consistent with the proxy reconstruction for 1645–1654 and show more realistic values for 1657–1659 (against the unphysical negative sunspot number). These records have paid little attention to sunspot positions, except for Hevelius' report on a sunspot group in the northern solar hemisphere in 1652 April. Therefore, slight caveats are required to discuss if the sunspot positions are located purely in the southern solar hemisphere throughout the MM.

An Overview of Sunspot Observations in 1727–1748

Hisashi **Hayakawa**1,2,3,4, Kentaro Hattori5, Mitsuru Sôma6, Tomoya Iju6, Bruno P. Besser7,8, and Shunsuke Kosaka1,9,10

2022 ApJ 941 151
https://iopscience.iop.org/article/10.3847/1538-4357/ac6671/pdf

Solar activity generally exhibits cyclic behavior in terms of sunspot group number and sunspot positions every ≈11 yr. These sunspot data have therefore played key roles in numerous analyses of solar–terrestrial physics. However, their reconstructions prior to the 1830s have remained controversial and included significant data gaps, especially from the 1720s to the 1740s. Therefore, this study reviewed contemporary sunspot observations for 1727–1748 to add several forgotten records by Van Coesfelt in 1728–1729, Dû clos in 1736, Martin in 1737, and Cassini and Maraldi in 1748. On the basis of these records, this study revised the sunspot group number and newly derived the sunspot positions in this interval. The results show clearer solar cycles in sunspot group number than those of previous studies and indicate regular solar cycles with limited hemispheric asymmetry over Solar Cycles 0 to −2. The sunspot positions also show sunspot groups mostly at heliographic latitude φ fulfilling $|\varphi| < 35°$ in both solar hemispheres, with slight equatorward motions. Furthermore, the solar minima between Solar Cycles −2 and −1 and between Solar Cycles −1 and 0 have been located around 1733.5 ± 0.5 and 1743 ± 0.5, indicating cycle lengths of 11.7 ± 0.5 yr and 10.0 ± 1.0 yr, respectively. Our results provide a chronological missing link between the Maunder Minimum and the regular solar cycles observed since Staudach's observations from 1749 onward. This lets us better understand the transition of solar activity from the grand minimum to the regular solar cycles.

Johann Christoph Müller's Sunspot Observations in 1719 – 1720: Snapshots of the Immediate Aftermath of the Maunder Minimum

Hisashi **Hayakawa**, Tomoya Iju, Chiaki Kuroyanagi, Víctor M. S. Carrasco, Bruno P. Besser, Shoma Uneme & Shinsuke Imada

Solar Physics volume 296, Article number: 154 (**2021**)
https://link.springer.com/content/pdf/10.1007/s11207-021-01880-8.pdf
https://doi.org/10.1007/s11207-021-01880-8

The Maunder Minimum (1645 – 1715) was unique in terms of solar-cycle amplitudes and sunspot-position distributions registered in the last four centuries; however, little is known for its recovery and transition to the regular solar cycles until 1749 and the existing reconstructions vary from one to another here. This article presents a snapshot of Solar Cycle −3 including sunspot observations by Johann Christoph Müller (hereafter, JCM) in 1719 – 1720. We identified his sunspot drawings in the manuscript department of the National Library of Russia in St. Petersburg and compiled his biographical profile and observational expertise. Subsequently, we analysed his sunspot drawings and derived the group number and positions of the observed sunspots. The results and comparative analyses with contemporary observations revealed that JCM reported up to five sunspot groups, corresponding well with Sebastian Alischer's records but contrasting with Johann Rost's records in the existing databases. These comparisons indicated that Rost's extremely large values recorded in 1719 – 1720 probably represented individual sunspot numbers instead of sunspot group numbers, unlike the understanding in the existing databases. Accordingly, JCM's group number forms a robust reference for representing the solar activity in 1719 – 1720 and exhibits relatively moderate solar cycle amplitude in the immediate aftermath of the Maunder Minimum. Moreover, JCM's

sunspot drawings provide significantly detailed information on sunspot positions. Our analyses could locate the reported sunspot groups in both solar hemispheres, unlike those in the Maunder Minimum, which support the suggested transition between Solar Cycles −4 and −3.

Stephan Prantner's Sunspot Observations during the Dalton Minimum

Hisashi **Hayakawa**, Shoma Uneme, Bruno P. Besser, Tomoya Iju, Shinsuke Imada

ApJ **919** 1 **2021**

https://arxiv.org/ftp/arxiv/papers/2105/2105.05405.pdf

https://doi.org/10.3847/1538-4357/abee1b

In addition to regular Schwabe cycles (~ 11 years), solar activity also shows longer periods of enhanced or reduced activity. Of these, reconstructions of the Dalton Minimum provide controversial sunspot group numbers and limited sunspot positions, partially due to limited source record accessibility. We analysed Stephan Prantner's sunspot observations from 1804--1844, the values of which had only been known through estimates despite their notable chronological coverage during the Dalton Minimum. We identified his original manuscript in Stiftsarchiv Wilten, near Innsbruck, Austria. We reviewed his biography (1782--1873) and located his observational sites at Wilten and Waidring, which housed the principal telescopes for his early and late observations: a 3.5-inch astronomical telescope and a Reichenbach 4-feet achromatic erecting telescope, respectively. We identified 215 days of datable sunspot observations, which are twice as much data as his estimated data in the existing database (= 115 days). Prantner counted up to 7--9 sunspot groups per day and measured sunspot positions, which show their distributions in both solar hemispheres. These results strikingly emphasise the difference between the Dalton Minimum and the Maunder Minimum as well as the similarity between the Dalton Minimum and the modern solar cycles.

Sunspot Observations at the Eimmart Observatory and in Its Neighborhood during the Late Maunder Minimum (1681–1718)

Hisashi **Hayakawa**1,2,3,4, Chiaki Kuroyanagi5, Víctor M. S. Carrasco6,7, Shoma Uneme1, Bruno P. Besser8,9, Mitsuru Sôma10, and Shinsuke Imada1

2021 ApJ 909 166

https://doi.org/10.3847/1538-4357/abd949

The Maunder Minimum (1645–1715; hereafter MM) is generally considered as the only grand minimum in the chronological coverage of telescopic sunspot observations. Characterized by scarce sunspot occurrences and their asymmetric concentrations in the southern solar hemisphere, the MM has frequently been associated with a special state of solar dynamo activity. As such, it is important to analyze contemporary observational records and improve our understanding of this peculiar interval, whereas the original records are frequently preserved in historical archives and can be difficult to access. In this study, we consult historical archives in the National Library of Russia, St. Petersburg, and analyze a series of sunspot observations conducted at the Eimmart Observatory from 1681 to 1709, which is the second-richest sunspot data set produced during the MM, following La Hire's series, among existing data sets. We have further extended our analyses to neighboring observations to extend our investigations up to 1718. We first analyze source documents and descriptions of observational instruments. Our analyses have significantly revised the existing data set, removed contaminations, and updated and labeled them as Eimmart Observatory (78 days), Altdorf Observatory (4 days), Hoffmann (22 days), and Wideburg (25 days). The revisions have updated the temporal coverage of the contemporary sunspot observations from 73.4% to 66.9% from 1677 to 1709. We have also derived the positions of the observed sunspot groups in comparison with contemporary observations. Our results indicate hemispheric asymmetry in the MM and recovery of sunspot groups in both hemispheres after 1716, supporting the common paradigm of the MM.

Candidate Auroral Observations Indicating a Major Solar–Terrestrial Storm in 1680: Implication for Space Weather Events during the Maunder Minimum

Hisashi **Hayakawa**1,2,3, Kristian Schlegel4, Bruno P. Besser5, and Yusuke Ebihara6,7

2021 ApJ 909 29

https://doi.org/10.3847/1538-4357/abb3c2

https://arxiv.org/ftp/arxiv/papers/2008/2008.13739.pdf

The Maunder Minimum (MM; 1645–1715) is currently considered the only grand minimum within telescopic sunspot observations since 1610. During this epoch, the Sun was extremely quiet and unusually free from sunspots. However, despite a reduced frequency, candidate aurorae were reported in the mid-European sector during this period and have been associated with occurrences of interplanetary coronal mass ejections (ICMEs), although some of them have been identified as misinterpretations. Here, we have analyzed reports of candidate aurorae on 1680 June 1 with simultaneous observations in central Europe, and compared their descriptions with visual accounts of early modern aurorae. Contemporary sunspot drawings on 1680 May 22, 24, and 27 have shown a sunspot. This sunspot may have been a source of ICMEs, which caused the reported candidate aurorae. On the other hand, its intensity estimate shows that the geomagnetic storm during this candidate aurora was probably within the capability of the storms derived from the corotating interaction region (CIR). Therefore, we accommodate both ICMEs and

CIRs as its possible origin. This interpretation is probably applicable to a number of candidate aurorae in the oft-cited Hungarian catalog, on the basis of the reconstructed margin of their equatorward auroral boundary. Moreover, this catalog itself has clarified that the considerable candidates during the MM were probably misinterpretations. Therefore, the frequency of the auroral visibility in Hungary was probably lower than previously considered and agrees more with the generally slow solar wind in the existing reconstructions, whereas sporadic occurrences of sunspots and coronal holes still caused occasional geomagnetic storms.

Daniel Mögling's sunspot observations in 1626 - 1629: A manuscript reference for the solar activity before the Maunder Minimum

Hisashi **Hayakawa**, Tomoya Iju, Koji Murata, Bruno P. Besser

ApJ **909** 194 **2021**

https://arxiv.org/ftp/arxiv/papers/2102/2102.04047.pdf

https://doi.org/10.3847/1538-4357/abdd34

The sunspot groups have been observed since 1610 and their numbers have been used for evaluating the amplitude of solar activity. Daniel Mögling recorded his sunspot observations for more than 100 days in 1626 - 1629 and formed a significant dataset of sunspot records before the Maunder Minimum. Here, we have analysed his original manuscripts in the Universitäts- und Landesbibliothek Darmstadt (ULBD) to review Mögling's personal profile and observational instruments and derive number and positions of the sunspot groups. In his manuscript, we have identified 134 days with an exact sunspot group number and 3 days of additional descriptions. Our analyses have completely revised their observational dates and group number, added 19 days of hitherto overlooked observations, and removed 8 days of misinterpreted observations. We have also revisited sunspot observations of Schickard and Hortensius and revised their data. These results have been compared with the contemporary observations. Moreover, we have derived the sunspot positions from his sunspot drawings and located them at 2°-23° in the heliographic latitude in both solar hemispheres. Contextualised with contemporary observations, these results indicate their temporal migration to lower heliographic latitudes and emphasise its location in the declining phase of Solar Cycle -12 in the 1620s. His observations were probably conducted using a pinhole and camera obscura, which made Mögling likely underestimate the sunspot group number by >~ 33% - 52 %. This underestimation should be noted upon their comparison with the modern datasets.

Graphical evidence for the solar coronal structure during the Maunder minimum: comparative study of the total eclipse drawings in 1706 and 1715

Hisashi **Hayakawa**, Mike Lockwood, Matthew J. Owens, Mitsuru Sôma, Bruno P. Besser and Lidia van Driel-Gesztelyi

J. Space Weather Space Clim. **2021**, 11, 1

https://doi.org/10.1051/swsc/2020035

https://www.swsc-journal.org/articles/swsc/pdf/2021/01/swsc190067.pdf

We discuss the significant implications of three eye-witness drawings of the total solar eclipse on 1706 May 12 in comparison with two on 1715 May 3, for our understanding of space climate change. These events took place just after what has been termed the “deep Maunder Minimum” but fall within the “extended Maunder Minimum” being in an interval when the sunspot numbers start to recover. Maria Clara Eimmert’s image in 1706 is particularly important because she was both a highly accomplished astronomical observer and an excellent artist: it was thought lost and was only re-discovered in 2012. Being the earliest coronal drawings of observational value yet identified, these drawings corroborate verbal accounts a corona without significant streamers, seen at totality of this and another eclipse event in 1652 during the Maunder Minimum. The graphical evidence implies that the coronal solar magnetic field was not lost but significantly weakened and the lack of coronal structure means there was little discernable open flux (either polar or at lower latitudes) even during the recovery phase of the Maunder Minimum. These observations provide evidence for a different state of oscillation of the solar dynamo, and hence behaviour of the Sun, in comparison with that during normal solar cycle minima (when a streamer belt between two polar coronal holes is visible) or near normal sunspot maxima (when coronal structure is caused by coronal holes at all latitudes) even to observers without a telescope.

Reanalyses of the Sunspot Observations of Fogelius and Siverus: Two "Long-Term" Observers during the Maunder Minimum

Hisashi **Hayakawa**, Tomoya Iju, Shoma Uneme, Bruno P. Besser, Shunsuke Kosaka, Shinsuke Imada

MNRAS Volume 506, Issue 1, September **2021**, Pages 650–658,

https://doi.org/10.1093/mnras/staa2965

https://arxiv.org/pdf/2009.14369

The solar activity during the Maunder Minimum (MM; 1645 -- 1715) has been considered significantly different from the one captured in modern observations, in terms of sunspot group number and sunspot positions, whereas its

actual amplitudes and distributions is still under active discussions. In its core period (1650/1660 -- 1700), Martin Fogelius and Henrich Siverus have formed significant long-term series in the existing databases with numerous spotless days, as the 13th and 7th most active observers before the end of the MM. In this study, we have analysed their original archival records, revised their data, have removed significant contaminations of the apparent "spotless days" in the existing databases, and cast caveats on the potential underestimation of the solar-cycle amplitude in the core MM. Still, they reported at best one sunspot group throughout their observational period and confirm the significant suppressed the solar cycles during the MM, which is also supported from the contemporary observations of Hook and Willoughby. Based on the revised data, we have also derived positions of notable sunspot groups, which Siverus recorded in 1671 (~ N7.5° +/- 2.5°), in comparison with those of Cassini's drawings (~ N10° +/- 1°). Their coincidence in position and chronology in corrected dates indicates these sunspot groups were probably the same recurrent active region (AR) and its significantly long lifespan (>~ 35 days) even during the MM.

The Solar Corona during the Total Eclipse on 16 June 1806: Graphical Evidence of the Coronal Structure during the Dalton Minimum

Hisashi **Hayakawa**, Mathew J. Owens, Michael Lockwood, Mitsuru Sôma
ApJ **900** 114 **2020**
https://arxiv.org/ftp/arxiv/papers/2006/2006.02868.pdf
https://doi.org/10.3847/1538-4357/ab9807
Visible coronal structure, in particular the spatial evolution of coronal streamers, provides indirect information about solar magnetic activity and the underlying solar dynamo. Their apparent absence of structure observed during the total eclipses of throughout the Maunder Minimum has been interpreted as evidence of a significant change in the solar magnetic field from that during modern cycles. Eclipse observations available from the more recent Dalton Minimum may be able to provide further information, sunspot activity being between the levels seen during recent cycles and in the Maunder Minimum. Here, we show and examine two graphical records of the total solar eclipse on 1806 June 16, during the Dalton Minimum. These records show significant rays and streamers around an inner ring. The ring is estimated to be ~ 0.44 R_S in width and the streamers in excess of 11.88 R_S in length. In combination with records of spicules or prominences, these eclipse records visually contrast the Dalton Minimum with the Maunder Minimum in terms of their coronal structure and support the existing discussions based on the sunspot observations. These eclipse records are broadly consistent with the solar cycle phase in the modelled open solar flux and the reconstructed slow solar wind at most latitudes.

Thaddäus Derfflinger's sunspot observations during 1802-1824: A primary reference to understand the Dalton Minimum

Hisashi **Hayakawa**, Bruno P. Besser, Tomoya Iju, Rainer Arlt, Shoma Uneme, Shinsuke Imada, Philippe-A. Bourdin, Amand Kraml
ApJ **890** 98 **2020**
https://arxiv.org/ftp/arxiv/papers/2001/2001.02367.pdf
https://doi.org/10.3847/1538-4357/ab65c9
As we are heading towards the next solar cycle, presumably with a relatively small amplitude, it is of significant interest to reconstruct and describe the past grand minima on the basis of actual observations of the time. The Dalton Minimum is often considered one of the grand minima captured in the coverage of telescopic observations. Nevertheless, the reconstructions of the sunspot group number vary significantly, and the existing butterfly diagrams have a large data gap during the period. This is partially because most long-term observations have remained unexplored in historical archives. Therefore, to improve our understanding on the Dalton Minimum, we have located two series of Thaddäus Derfflinger's observational records (a summary manuscript and logbooks) as well as his Brander's 5.5-feet azimuthal-quadrant preserved in the Kremsmünster Observatory. We have revised the existing Derfflinger's sunspot group number with Waldmeier classification and eliminated all the existing 'spotless days' to remove contaminations from solar meridian observations. We have reconstructed the butterfly diagram on the basis of his observations and illustrated sunspot distributions in both solar hemispheres. Our article aims to revise the trend of Derfflinger's sunspot group number and to bridge a data gap of the existing butterfly diagrams around the Dalton Minimum. Our results confirm that the Dalton Minimum is significantly different from the Maunder Minimum, both in terms of cycle amplitudes and sunspot distributions. Therefore, the Dalton Minimum is more likely a secular minimum in the long-term solar activity, while further investigations for the observations at that time are required.

Sunspot Observations by Hisako Koyama: 1945-1996

Hisashi **Hayakawa**, Frédéric Clette, Toshihiro Horaguchi, Tomoya Iju, Delores J. Knipp, Huixin Liu, Takashi Nakajima
MNRAS Volume 492, Issue 3, March **2020**, Pages 4513–4527
https://arxiv.org/ftp/arxiv/papers/1911/1911.12702.pdf
https://doi.org/10.1093/mnras/stz3345

The sunspot record is the only observational tracer of solar activity that provides a fundamental, multi-century reference. Its homogeneity has been largely maintained with a succession of long-duration visual observers. In this paper, we examine observations of one of the primary reference sunspot observers, Hisako Koyama. By consulting original archives of the National Museum of Nature and Science of Japan (hereafter, NMNS), we retrace the main steps of her solar-observing career, from 1945 to 1996. We also present the reconstruction of a full digital database of her sunspot observations at the NMNS, with her original drawings and logbooks. Here, we extend the availability of her observational data from 1947-1984 to 1945-1996. Comparisons with the international sunspot number (version 2) and with the group sunspot number series show a good global stability of Koyama's observations, with only temporary fluctuations over the main interval 1947-1982. Identifying drawings made by alternate observers throughout the series, we find that a single downward baseline shift in the record coincides with the partial contribution of replacement observers mostly after 1983. We determine the correction factor to bring the second part (1983-1996) to the same scale with Koyama's main interval (1947-1982). We find a downward jump by 9% after 1983, which then remains stable until 1996. Overall, the high quality of Koyama's observations with her life-long dedication leaves a lasting legacy of this exceptional personal achievement. With this comprehensive recovery, we now make the totality of this legacy directly accessible and exploitable for future research.

The Earliest Candidates of Auroral Observations in Assyrian Astrological Reports: Insights on Solar Activity around 660 BCE

Hisashi **Hayakawa**, Yasuyuki Mitsuma, Yusuke Ebihara, Fusa Miyake

ApJL **2019**

https://arxiv.org/ftp/arxiv/papers/1909/1909.05498.pdf

Auroral records found in historical archives and cosmogenic isotopes found in natural archives have served as sound proxies of coronal mass ejections (CMEs) and solar energetic particles (SEPs), respectively, for dates prior to the onset of telescopic sunspot observations in 1610. These space weather events constitute a significant threat to a modern civilization, because of its increasing dependency on an electronic infrastructure. Recent studies have identified multiple extreme space weather events derived from solar energetic particles (SEPs) in natural archives, such as the event in 660 BCE. While the level of solar activity around 660 BCE is of great interest, this had not been within the coverage of the hitherto-known datable auroral records in historical documents that extend back to the 6th century BCE. Therefore, we have examined Assyrian astrological reports in the 8th and 7th centuries BCE, identified three observational reports of candidate aurorae, and dated these reports to approximately 680 BCE -- 650 BCE. The Assyrian cuneiform tablets let us extend the history of auroral records and solar activity by a century. These cuneiform reports are considered to be the earliest datable records of candidate aurorae and they support the concept of enhanced solar activity suggested by the cosmogenic isotopes from natural archives.

A Transit of Venus Possibly Misinterpreted as an Unaided-Eye Sunspot Observation in China on 9 December 1874

Hisashi **Hayakawa**, Mitsuru Sôma, Kiyotaka Tanikawa, David M. Willis, Matthew N. Wild, Lee T. Macdonald, Shinsuke Imada, Kentaro Hattori, F. Richard Stephenson

Solar Phys. **2019**

https://arxiv.org/ftp/arxiv/papers/1908/1908.02452.pdf

Large sunspots can be observed with the unaided eye under suitable atmospheric seeing conditions. Such observations are of particular value because the frequency of their appearance provides an approximate indication of the prevailing level of solar activity. Unaided-eye sunspot (UES) observations can be traced back well before the start of telescopic observations of the Sun, especially in the East Asian historical records. It is therefore important to compare more modern, UES observations with the results of telescopic sunspot observations, to gain a better understanding of the nature of the UES records. A previous comparison of Chinese UES records and Greenwich photo-heliographic results between 1874 and 1918 indicated that a few of the UES were apparently not supported by direct photographic evidence of at least one sunspot with a large area. This article reveals that one of the Chinese unaided-eye observations had possibly captured the transit of Venus on 9 December 1874. The Chinese sunspot records on this date are compared with Western sunspot observations on the same day. It is concluded that sunspots on the solar disk were quite small and the transit of Venus was probably misinterpreted as a sunspot by the Chinese local scholars. This case indicates that sunspots or comparable "obscuring" objects with an area as large as 1000 millionths of the solar disk could easily have been seen with the unaided eye under suitable seeing conditions. It also confirms the visibility of sunspots near the solar limb with the unaided eye. This study provides an explanation of the apparent discrepancy between the Chinese UES observation on 9 December 1874 and the Western sunspot observations using telescopes, as well as a basis for further discussion on the negative pairs in 1900 and 1911, apparently without sufficiently large area.

Unaided-eye Sunspot Observations in 1769 November: A Comparison of Graphical Records in the East and the West

Hisashi **Hayakawa**, David M. Willis, Kentaro Hattori, Yuta Notsu, Matthew N. Wild, Christoffer Karoff
Solar Physics July **2019**, 294:95
sci-hub.se/10.1007/s11207-019-1488-5
Sunspots can be seen with the unaided eye when they are sufficiently large. Due to the known correlation between the occurrence of unaided-eye sunspot observations and the phase of the solar cycle, these observations frequently provide some insight into the level of solar activity in the past. In this context, we have identified a few unaided-eye sunspot observations in late 1769 in East Asia, analyzed their observational conditions, and compared them with contemporary telescopic sunspot observations. The East Asian records indicate that large sunspots were seen with the aid of a temporary coverage of cloud mist on 1769 November 18 and 20. The contemporary sunspot drawings by Christian Horrebow show extremely large sunspot groups near the disk centre for each occasion. These unaided-eye sunspot observations occurred immediately after the maximum of Solar Cycle 2 and provide a snapshot of the enhanced level of solar activity at that time.

The Celestial Sign in the Anglo-Saxon Chronicle in the 770s: Insights on Contemporary Solar Activity

Hisashi **Hayakawa**, F. Richard Stephenson, Yuta Uchikawa, Yusuke Ebihara, Christopher J. Scott, Matthew N. Wild, Julia Wilkinson, David M. Willis
Solar Physics April **2019**, 294:42
https://link.springer.com/content/pdf/10.1007%2Fs11207-019-1424-8.pdf
The anomalous concentration of radiocarbon in 774/775 attracted intense discussion on its origin, including the possible extreme solar event(s) exceeding any events in observational history. Anticipating such extreme solar events, auroral records were also surveyed in historical documents and those including the red celestial sign after sunset in the Anglo-Saxon Chronicle (ASC) were subjected to consideration. Usoskin et al. (Astron. Astrophys. 55, L3, 2013: U13) interpreted this record as an aurora and suggested enhanced solar activity around 774/775. Conversely, Neuhäuser and Neuhäuser (Astron. Nachr. 336, 225, 2015a: N15a; Astron. Nachr. 336, 913, 2015b: N15b) interpreted "after sunset" as during sunset or twilight; they considered this sign as a halo display and suggested a solar minimum around 774. However, so far these records have not been discussed in comparison with eyewitness auroral records during the known extreme space weather events, although they were discussed in relationship with potential extreme events in 774/775. Therefore, we reconstruct the observational details based on the original records in the ASC and philological references, compare them with eyewitness auroral observations during known extreme space weather events, and consider contemporary solar activity. We clarify the observation was indeed "after sunset", reject the solar-halo hypothesis, define the observational time span between 25 March 775 and 25 December 777, and note that the parallel "drawing of lunar halo display" in 806 in the ASC shown in N15b was not based on the original observation in England. We show examples of eyewitness auroral observations during twilight in known space weather events, and this celestial sign does not contradict the observational evidence. Accordingly, we consider this event to have happened after the onset of the event in 774/775, but to have shown relatively enhanced solar activity, with regard to other historical auroral records in the mid-770s, as also confirmed by the 10Be data from ice cores.

Sunspot drawings by Japanese official astronomers in 1749–1750

Hisashi **Hayakawa**; Kiyomi Iwahashi; Masashi Fujiyama; Toshiki Kawai; Shin Toriumi ...
http://sci-hub.tw/10.1093/pasj/psy066
Publications of the Astronomical Society of Japan, Volume 70, Issue 4, 1 August **2018**, 63,
Sunspot observations with telescopes in the 18th century were carried out in Japan as well as elsewhere. One of these sunspot observations is recorded in an account called Sansaizusetsu narabini Kansei irai Jissoku Zusetsu (Charts of Three Worlds and Diagrams of Actual Observations since Kansei Era). We have analyzed manuscripts of this account to show a total of 15 sunspot drawings during 1749–1750. These observations are considered to be carried out by contemporary official astronomers in Japan, with telescopes covered by zongurasus (< zonglas in Dutch, corresponding to "sunglass" in English). We counted their group number of sunspots to locate them in long-term solar activity and show that their observations were situated near the solar maximum in 1750. We also computed their locations and areas, while we have to admit differences of the variant manuscripts with one another. These observational records show the spread of sunspot observations not only in Europe, but also in Japan, and hence may contribute to crosscheck, or possibly to improve the known sunspot indices.

Records of auroral candidates and sunspots in Rikkokushi, chronicles of ancient Japan from early 7th century to 887

Hisashi **Hayakawa**; Kiyomi Iwahashi; Harufumi Tamazawa; Yusuke Ebihara; Akito Davis Kawamura ...
Publications of the Astronomical Society of Japan, Volume 69, Issue 6, 1 December **2017**, 86,

https://doi.org/10.1093/pasj/psx087
We present the results of the surveys on sunspots and auroral candidates inRikkokushi, Japanese official histories from the early 7th century to 887, to review the solar and auroral activities. In total, we found one sunspot record and 13 auroral candidates in Rikkokushi. We then examine the records of the sunspots and auroral candidates, compare the auroral candidates with the lunar phase to estimate their reliability, and compare the records of the sunspots and auroral candidates with the contemporary total solar irradiance reconstructed from radioisotope data. We also identify the locations of the observational sites to review possible equatorward expansion of the auroral oval. These discussions suggest a major gap in auroral candidates from the late 7th to early 9th centuries, which includes the candidate of the grand minimum reconstructed from the radioisotope data, a similar tendency as the distributions of sunspot records in contemporary China, and a relatively high magnetic latitude of observational sites with a higher potential for observing aurorae more frequently than at present.

Records of Sunspots and Aurora Candidates in the Chinese Official Histories of the Yuán and Míng Dynasties during 1261-1644

Hisashi **Hayakawa**, Harufumi Tamazawa, Yusuke Ebihara, Hiroko Miyahara, Akito Davis Kawamura, Tadanobu Aoyama, Hiroaki Isobe

PASJ **2017**

https://arxiv.org/ftp/arxiv/papers/1705/1705.02238.pdf

Records of observations of sunspots and auroras in pre-telescopic historical documents provide useful information about past solar activity both in long-term trends and short-term space weather events. In this study, we present the results of a comprehensive survey of the records of sunspots and aurora candidates in the Yu\'ansh\v{i} and M\'ingsh\v{i}, Chinese Official Histories spanning 1261-1368 and 1368-1644, based on continuous observations with well-formatted reportds conducted by contemporary professional astronomers. We then provide a brief comparison of these data with Total Solar Irradiance (TSI) as an indicator of the solar activity during the corresponding periods to show significant active phases between 1350s-80s and 1610s-30s. We then compared the former with contemporary Russian reports for naked-eye sunspots and the latter with contemporary sunspot drawings based on Western telescopic observations. Especially some of the latter are consistent with nitrate signals preserved in ice cores. These results show us some insights on not only minima and maxima of solar activity during 13th - 17th century.

East Asian Observations of Low Latitude Aurora during the Carrington Magnetic Storm

Hisashi **Hayakawa**, Kiyomi Iwahashi, Harufumi Tamazawa, Hiroaki Isobe, Ryuho Kataoka, Yusuke Ebihara, Hiroko Miyahara, Akito Davis Kawamura, Kazunari Shibata

PASJ **2016**

https://arxiv.org/ftp/arxiv/papers/1608/1608.07702.pdf

The magnetic storm around **1859 September 2**, caused by so-called Carrington flare, was the most intense in the history of modern scientific observations, and hence is considered to be the benchmark event for space weather. The magnetic storm caused worldwide observations of auroras even at very low latitudes such as Hawaii, Panama, or Santiago, and the available magnetic field measurement at Bombay, India, showed two peaks: the main was the Carrington event which occurred in day time in East Asia, and a second storm after the Carrington event which occurred at night in East Asia. In this paper, we present a result from surveys of aurora records in East Asia, which provides new information of the aurora activity of this important event. We found some new East Asian records of low latitude aurora observations caused by the storm which occurred after the Carrington event. The size of the aurora belt of the second peak of the Carrington magnetic storm was even wider than usual low-latitude aurora events.

Historical Auroras in the 990s: Evidence of Great Magnetic Storms

Hisashi **Hayakawa** , Harufumi Tamazawa, Yurina Uchiyama, Yusuke Ebihara, Hiroko Miyahara, Shunsuke Kosaka, Kiyomi Iwahashi, Hiroaki Isobe

Solar Physics January **2017**, 292:12

A significant carbon-14 enhancement has recently been found in tree rings for the year 994, suggesting an extremely strong and brief cosmic ray flux event. The origin of this particular cosmic ray event has not been confirmed, but one possibility is that it might be of solar origin. Contemporary historical records of low-latitude auroras can be used as supporting evidence of intense solar activity around that time. We investigate previously reported as well as new records that have been found in contemporary observations from the 990s to determine potential auroras. Records of potential red auroras in late 992 and early 993 were found around the world, i.e. in the Korean Peninsula, Saxonian cities in modern Germany, and the Island of Ireland, suggesting the occurrence of an intense geomagnetic storm driven by solar activity.

See: **New sunspots and aurorae in the historical Chinese text corpus? Comments on uncritical digital search applications**

D.L. **Neuhaeuser**, R. Neuhaeuser , J. Chapman
Astron. Nachr. / AN 999, No. 88, 1 – 20 (**2018**)
https://arxiv.org/pdf/1711.05132.pdf

"Unusual Rainbow and White Rainbow" A new auroral candidate in oriental historical sources

Hisashi **Hayakawa**, Hiroaki Isobe, Akito Davis Kawamura, Harufumi Tamazawa, Hiroko Miyahara, Ryuho Kataoka
Publ. Astron. Soc. Japan **2016**
http://arxiv.org/pdf/1603.02374v1.pdf
Solar activity has been recorded as auroras or sunspots in various historical sources. These records are of much importance for investigating both long-term solar activities and extremely intense solar flares. In previous studies, they were recorded as "vapor," "cloud," or "light," especially in oriental historical sources; however, the terminology was not discussed adequately and is still quite vague. In this paper, we suggest the possibility of "unusual rainbow" and "white rainbow" as candidates of historical auroras in oriental historical sources and examine if it is probable. This discovery will help us to make more comprehensive historical auroral catalogues and require us to add these terms to auroral candidates in oriental historical sources.

Records of sunspot and aurora during CE 960-1279 in the Chinese chronicle of the Song dynasty

Hisashi **Hayakawa**, Harufumi Tamazawa, Akito D Kawamura, Hiroaki Isobe
Earth, Planets and Space **2015**
http://arxiv.org/ftp/arxiv/papers/1506/1506.03715.pdf
Records of sunspots and aurora observations in pre-telescopic historical documents can provide useful information about solar activity in the past. This is also true for extreme space weather events, as they may have been recorded as large sunspots observed by the naked eye or as low-latitude auroras. In this paper, we present the results of a comprehensive survey of records of sunspots and auroras in the Songshi, a Chinese formal chronicle spanning the tenth to the thirteenth century. This chronicle contains a record of continuous observations with well-formatted reports conducted as a policy of the government. A brief comparison of the frequency of observations of sunspots and auroras and the observations of radioisotopes as an indicator of the solar activity during corresponding periods is provided. This paper is the first step of our project in which we survey and compile the records of sunspots and aurora in historical documents from various locations and languages, ultimately providing it to the science community as online data.

The Nonpotentiality of Steady-state Coronal Magnetic Field Derived with Time-relaxation Magnetohydrodynamics Simulations Using Helioseismic and Magnetic Imager Three-component Magnetic Field Data

Keiji **Hayashi**1, Chin-Chun Wu2, and Kan Liou3
2022 ApJ 940 82
https://iopscience.iop.org/article/10.3847/1538-4357/ac9b25/pdf
The steady states of the coronal magnetic field obtained with the magnetohydrodynamic (MHD) time-relaxation simulation model are examined. Our electric-field-driven model can introduce the three components of the solar surface magnetic field data maps as the boundary values of an MHD simulation, without violating the divergence-free condition of the magnetic field. The magnetic field in the simulated steady-state solar corona exhibits substantial nonpotentiality in the closed-field streamers. A few choices are allowed in our model, such as the criteria for determining whether or not the horizontal components at the weak-field region are included. The initial magnetic field configuration can be arbitrarily determined. In this work, we examined the differences between the steady states obtained with the information on the horizontal components and with several choices of the simulation setting, and compared the new steady states with those obtained without using the horizontal magnetic field components. We found that nonpotential magnetic structures in the derived steady states well correspond to the observed solar filament structures during a selected period of Carrington Rotation 2106. The difference in the steady state with different boundary treatments is found to be large. The difference caused by the initial magnetic configuration is found to be small. **2011 January 20 - February 16**

Coupling a Global Heliospheric Magnetohydrodynamic Model to a Magnetofrictional Model of the Low Corona

Keiji **Hayashi**1, William P. Abbett2, Mark C. M. Cheung3, and George H. Fisher2
2021 ApJS 254 1

https://doi.org/10.3847/1538-4365/abe9b5
Recent efforts coupling our Sun-to-Earth magnetohydrodynamics (MHD) model and lower-corona magnetofrictional (MF) model are described. Our Global Heliospheric MHD (GHM) model uses time-dependent three-component magnetic field data from the lower-corona MF model as time-dependent boundary values. The MF model uses data-assimilation techniques to introduce the vector magnetic field data from the Solar Dynamics Observatory/Helioseismic and Magnetic Imager, hence as a whole this simulation coupling structure is driven with actual observations. The GHM model employs a newly developed interface boundary treatment that is based on the concept of characteristics, and it properly treats the interface boundary sphere set at a height of the sub-Alfvénic lower corona (1.15 R⊙ in this work). The coupled model framework numerically produces twisted nonpotential magnetic features and consequent eruption events in the solar corona in response to the time-dependent boundary values. The combination of our two originally independently developed models presented here is a model framework toward achieving further capabilities of modeling the nonlinear time-dependent nature of magnetic field and plasma, from small-scale solar active regions to large-scale solar wind structures. This work is a part of the Coronal Global Evolutionary Model project for enhancing our understanding of Sun–Earth physics to help improve space weather capabilities.
HMI Science Nuggets #180 May **2022** http://hmi.stanford.edu/hminuggets/?p=3911

Unsigned magnetic flux as a proxy for radial-velocity variations in Sun-like stars

R.D. **Haywood**, T.W. Milbourne, S.H. Saar, A. Mortier, D. Phillips, D. Charbonneau, A. Collier Cameron, H.M. Cegla, N. Meunier, M.L. Palumbo III
ApJ **2020**
https://arxiv.org/pdf/2005.13386.pdf
We estimate disc-averaged RV variations of the Sun over the last magnetic cycle, from the single Fe I line observed by SDO/HMI, using a physical model for rotationally modulated magnetic activity that was previously validated against HARPS-N solar observations. We estimate the disc-averaged, unsigned magnetic flux and show that a simple linear fit to it reduces the RMS of RV variations by 62%, i.e. a factor of 2.6. We additionally apply the FF' method, which predicts RV variations based on a star's photometric variations. At cycle maximum, we find that additional physical processes must be at play beyond suppression of convective blueshift and velocity imablances resulting from brightness inhomogeneities, in agreement with recent studies of solar RV variations. By modelling RV variations over the magnetic cycle using a linear fit to the unsigned magnetic flux, we recover injected planets at an orbital period of about 300 days with RV semi-amplitudes down to 0.3 m/s. To reach semi-amplitudes of 0.1 m/s, we will need to identify and model additional physical phenomena that are not well traced by the unsigned magnetic flux or FF'. The unsigned magnetic flux is an excellent proxy for rotationally modulated, activity-induced RV variations, and could become a key tool in confirming and characterising Earth analogs orbiting Sun-like stars. The present study motivates ongoing and future efforts to develop observation and analysis techniques to measure the unsigned magnetic flux at high precision in slowly rotating, relatively inactive stars like the Sun. **2015 Nov 28**

Mean field models of flux transport dynamo and meridional circulation in the Sun and stars **Review**

Gopal **Hazra**, Dibyendu Nandy, Leonid Kitchatinov, Arnab Rai Choudhuri
Space Science Reviews 219, Article number: 39 **2023**
https://arxiv.org/pdf/2302.09390.pdf
https://link.springer.com/content/pdf/10.1007/s11214-023-00982-y.pdf
The most widely accepted model of the solar cycle is the flux transport dynamo model. This model evolved out of the traditional αΩ dynamo model which was first developed at a time when the existence of the Sun's meridional circulation was not known. In these models, the toroidal magnetic field (which gives rise to sunspots) is generated by the stretching of the poloidal field by solar differential rotation. The primary source of the poloidal field in the flux transport models is attributed to the Babcock--Leighton mechanism, in contrast to the mean-field α-effect used in earlier models. With the realization that the Sun has a meridional circulation, which is poleward at the surface and is expected to be equatorward at the bottom of the convection zone, its importance for transporting the magnetic fields in the dynamo process was recognized. Much of our understanding about the physics of both the meridional circulation and the flux transport dynamo has come from the mean field theory obtained by averaging the equations of MHD over turbulent fluctuations. The mean field theory of meridional circulation makes clear how it arises out of an interplay between the centrifugal and thermal wind terms. We provide a broad review of mean field theories for solar magnetic fields and flows, the flux transport dynamo modeling paradigm and highlight some of their applications to solar and stellar magnetic cycles. We also discuss how the dynamo-generated magnetic field acts on the meridional circulation of the Sun and how the fluctuations in the meridional circulation, in turn, affect the solar dynamo. We conclude with some remarks on how the synergy of mean field theories, flux transport dynamo models, and direct numerical simulations can inspire the future of this field.

Recent advances in the 3D kinematic Babcock-Leighton solar dynamo modeling **Review**

Gopal **Hazra**
A&A **2020**
https://arxiv.org/pdf/2009.03810
In this review, we explain recent progress made in the Babcock-Leighton dynamo models for the Sun, which have been most successful to explain various properties of the solar cycle. In general, these models are 2D axisymmetric and the mean-field dynamo equations are solved in the meriodional plane of the Sun. Various physical processes (e.g., magnetic buoyancy and Babcock-Leighton mechanism) involved in these models are inherently 3D process and could not be modeled properly in a 2D framework. After pointing out limitations of 2D models (e.g., Mean-field Babcock-Leighton dynamo models and Surface Flux Transport models), we describe recently developed next-generation 3D dynamo models that implement more sophisticated flux emergence algorithm of buoyant flux tube rise through the convection zone and capture Babcock-Leighton process more realistically than previous 2D models. The detailed results from these 3D dynamo models including surface flux transport counterpart are presented. We explain the cycle irregularities that are reproduced in 3D dynamo models by introducing scattering around the tilt angle only. Some results by assimilating observed photospheric convective velocity fields into the 3D models are also discussed, pointing out the wide opportunity that these 3D models hold to deliver.

Mean-Field Alpha Effect impacts Memory of the Solar Cycle

Soumitra **Hazra**, Allan Sacha Brun, Dibyendu Nandy
A&A **2020**
https://arxiv.org/pdf/2003.02776.pdf
Predictions of solar cycle 24 obtained from the advection-dominated and diffusion-dominated kinematic dynamo model are different if we consider only the Babcock-Leighton mechanism as a poloidal field generation source term. Yeates et al (2008) argue that the discrepancy between the results is due to the different memory of solar dynamo for advection- and diffusion-dominated solar convection zones. We aim to investigate the discrepancy between the solar cycle memory obtained from advection-dominated and diffusion-dominated kinematic solar dynamo models. Specifically, we want to investigate whether another poloidal field generation mechanism, namely, Parker's mean-field alpha effect has any impact on the memory of the solar cycle. We used a kinematic flux transport solar dynamo model where poloidal field generation takes place due to both the Babcock-Leighton mechanism and mean-field alpha effect. The addition of a mean-field alpha effect reduces the memory of the Babcock Leighton solar dynamo to within one cycle for both advection-and diffusion-dominated dynamo regimes. Our result provides an alternative resolution to the discrepancy in memory of advection- and diffusion-dominated kinematic dynamo models. We also find a moderate decrease in the correlation between the radial flux at the cycle minima and the toroidal flux at the maxima of the next cycle with the increase of mean-field alpha amplitude. We confirm the conclusions of Yeates et al (2008) and Karak and Nandy (2012) regarding the short, one-cycle memory of the solar cycle. We establish that the mean-field alpha effect impacts the memory of the solar cycle. However, correlation coefficients are highly dependent on the assumed amplitude and fluctuation levels of the mean-field alpha

The Origin of Parity Changes in the Solar Cycle

Soumitra **Hazra**, Dibyendu Nandy
MNRAS **2019**
https://arxiv.org/pdf/1906.06780.pdf
Although sunspots have been systematically observed on the Sun's surface over the last four centuries, their magnetic properties have been revealed and documented only since the early 1900s. Sunspots typically appear in pairs of opposite magnetic polarities which have a systematic orientation. This polarity orientation is opposite across the equator -- a trend that has persisted over the last century over which magnetic field observations exist. Taken together with the configuration of the global poloidal field of the Sun -- that governs the heliospheric open flux and cosmic ray flux at Earth -- this phenomenon is consistent with the dipolar parity state of an underlying magnetohydrodynamic dynamo. Although hemispheric asymmetry in the emergence of sunspots is observed in the Sun, a parity shift has never been observed. We simulate hemispheric asymmetry through the introduction of random fluctuations in a computational dynamo model of the solar cycle and demonstrate that changes in parity are indeed possible in long-term simulations covering thousands of years. Quadrupolar modes are found to exist over a significant fraction of the simulated time. In particular, we find that a parity shift in the underlying nature of the sunspot cycle is more likely to occur when sunspot activity dominates in any one hemisphere for a time which is significantly longer than the cycle period. We establish causal pathways connecting hemispheric asymmetry and cross-equatorial phase-shifts to parity flips in the underlying dynamo mechanism. Our findings indicate that the solar cycle may have resided in quadrupolar parity states in the distant past, and provides a possible pathway for predicting parity flips in the future.

A New Formula for Predicting Solar Cycles

Gopal **Hazra**, Arnab Rai Choudhuri
ApJ **880** 113 **2018**

https://arxiv.org/pdf/1811.01363.pdf
sci-hub.se/10.3847/1538-4357/ab2718
A new formula for predicting solar cycles based on the current theoretical understanding of the solar cycle from flux transport dynamo is presented. Two important processes -- Babcock-Leighton mechanism and variation in meridional circulation, which are believed to be responsible for irregularities of the solar cycle, are constrained using observational data. We take the polar field near minima of the cycle as a measure of the randomness in the Babcock-Leighton process, and the decay rate near the minima as a consequence of the change in meridional circulation. We couple these two observationally derived quantities into a single formula to predict the amplitude of the future solar cycle. Whether this formula is reasonable to predict future solar cycle is also discussed using simulation from the flux transport dynamo model.

A Three- dimensional Babcock-Leighton Solar Dynamo Model with Non-axisymmetric Convective Flows

Gopal **Hazra**, Mark Miesch
Proceedings of IAU Symposium No. 340, **2018**
https://arxiv.org/pdf/1809.06595.pdf
The observed convective flows on the photosphere (e.g., supergranulation, granulation) play a key role in the Babcock-Leighton (BL) process to generate large-scale polar fields from sunspots fields. In most surface flux transport (SFT) and BL dynamo models, the dispersal and migration of surface fields are modeled as an effective turbulent diffusion. We present the first kinematic 3D FT/BL model to explicitly incorporate realistic convective flows based on solar observations. The results obtained are generally in good agreement with the observed surface flux evolution and with non-convective models that have a turbulent diffusivity on the order of 3×1012 cm2 s−1(300 km2 s−1). However, we find that the use of a turbulent diffusivity underestimates the dynamo efficiency, producing weaker mean fields and shorter cycle.

Explaining the variation of the meridional circulation with the solar cycle

Gopal **Hazra**, Arnab Rai Choudhuri
Proceedings of IAU Symposium No. 340, **2018**
https://arxiv.org/pdf/1809.06600.pdf
The meridional circulation of the Sun is observationally found to vary with the solar cycle, becoming slower during the solar maxima. We explain this by constructing a theoretical model in which the equation of the meridional circulation (the ϕ component of the vorticity equation) is coupled with the equations of the flux transport dynamo model. We find that the Lorentz force of the dynamo-generated magnetic fields can slow down the \MC\ during the solar maxima in broad conformity with the observations.

Incorporating Surface Convection into a 3D Babcock-Leighton Solar Dynamo Model

Gopal **Hazra**, Mark Miesch
ApJ **864** 110 **2018**
https://arxiv.org/pdf/1804.03100.pdf
The observed convective flows on the photosphere (e.g., supergranulation, granulation) play a key role in the Babcock-Leighton (BL) process to generate large-scale polar fields from sunspots fields. In most surface flux transport (SFT) and BL dynamo models, the dispersal and migration of surface fields is modeled as an effective turbulent diffusion. Recent SFT models have incorporated explicit, realistic convective flows in order to improve the fidelity of convective transport but, to our knowledge, this has not yet been implemented in previous BL models. Since most Flux-Transport (FT)/BL models are axisymmetric, they do not have the capacity to include such flows. We present the first kinematic 3D FT/BL model to explicitly incorporate realistic convective flows based on solar observations. Though we describe a means to generalize these flows to 3D, we find that the kinematic small-scale dynamo action they produce disrupts the operation of the cyclic dynamo. Cyclic solution is found by limiting the convective flow to act only on the vertical radial component of the magnetic field. The results obtained are generally in good agreement with the observed surface flux evolution and with non-convective models that have a turbulent diffusivity on the order of 3×1012 cm2 s−1 (300 km2 s−1). However, we find that the use of a turbulent diffusivity underestimates the dynamo efficiency, producing weaker mean fields and shorter cycle than in the convective models. Also, the convective models exhibit mixed polarity bands in the polar regions that have no counterpart in solar observations. Also, the explicitly computed turbulent electromotive force (emf) bears little resemblance to a diffusive flux. We also find that the poleward migration speed of poloidal flux is determined mainly by the meridional flow and the vertical diffusion.

Hemispheric Preference and Cyclic Variation of Solar Filament Chirality from 2000 to 2016

Soumitra **Hazra**, Sushant S. Mahajan, William Keith Douglas Jr., Petrus C. H. Martens

2018 ApJ 865 108
https://arxiv.org/pdf/1711.05758.pdf
It is well known that solar filaments are features in the solar atmosphere which show a hemispheric preference in their chirality. The hemispheric preference is such that the dextral chirality dominates in the northern hemisphere while the sinistral chirality dominates in the southern. Determining the strength and cyclic variation of the degree of this hemispheric preference, however, is challenging and tedious and thus needs to be automated. In this paper, we follow Dr. Pietro Bernasconi's algorithm (Bernasconi et al. 2005) to detect filament chirality with two parallel channels of application. The algorithm is applied to H-alpha images by "Advanced Automated Filament Detection and Characterization Code" (AAFDCC) (Bernasconi et al. 2005) or the algorithm is explained to a human and the human determines the chirality of the solar filament. We have conducted this exercise on data during the month of August from years 2000 to 2016 and we found that 83 % of our visually determined filaments follow the hemispheric chirality preference, while 58 % of automatically determined filaments follow it. Our visually compiled results have over 90 % agreement with those of Pevtsov et al. (2003), yet the visually determined chiralities of filaments disagree with automated determinations significantly. We find that the hemispheric preference remained the same between solar cycles 23 and 24 but the preference is very difficult to determine during the solar minimum of 2008-2010 primarily due to the absence of filaments.

A theoretical model of the variation of the meridional circulation with the solar cycle

Gopal **Hazra**, Arnab Rai Choudhuri
MNRAS **2017**
https://arxiv.org/pdf/1708.05204.pdf
Observations of the meridional circulation of the Sun, which plays a key role in the operation of the solar dynamo, indicate that its speed varies with the solar cycle, becoming faster during the solar minima and slower during the solar maxima. To explain this variation of the meridional circulation with the solar cycle, we construct a theoretical model by coupling the equation of the meridional circulation (the ϕ component of the vorticity equation within the solar convection zone) with the equations of the flux transport dynamo model. We consider the back reaction due to the Lorentz force of the dynamo-generated magnetic fields and study the perturbations produced in the meridional circulation due to it. This enables us to model the variations of the meridional circulation without developing a full theory of the meridional circulation itself. We obtain results which reproduce the observational data of solar cycle variations of the meridional circulation reasonably well. We get the best results on assuming the turbulent viscosity acting on the velocity field to be comparable to the magnetic diffusivity (i.e. on assuming the magnetic Prandtl number to be close to unity). We have to assume an appropriate bottom boundary condition to ensure that the Lorentz force cannot drive a flow in the subadiabatic layers below the bottom of the tachocline. Our results are sensitive to this bottom boundary condition. We also suggest a hypothesis how the observed inward flow towards the active regions may be produced.
HMI Science Nuggets #80 **2018** http://hmi.stanford.edu/hminuggets/?p=2098

A theoretical study of the build-up of the Sun's polar magnetic field by using a 3D kinematic dynamo model

Gopal **Hazra**, Arnab Rai Choudhuri, Mark S. Miesch
2017 ApJ 835 39
https://arxiv.org/pdf/1610.02726v1.pdf
https://iopscience.iop.org/article/10.3847/1538-4357/835/1/39/pdf
We develop a three-dimensional kinematic self-sustaining model of the solar dynamo in which the poloidal field generation is from tilted bipolar sunspot pairs placed on the solar surface above regions of strong toroidal field by using the SpotMaker algorithm and then the transport of this poloidal field to the tachocline is primarily caused by turbulent diffusion. We obtain a dipolar solution within a certain range of parameters. We use this model to study the build-up of the polar magnetic field and show that some insights obtained from surface flux transport (SFT) models have to be revised. We present results obtained by putting a single bipolar sunspot pair in a hemisphere and two symmetrical sunspot pairs in two hemispheres. We find that the polar fields produced by them disappear due to subduction by the meridional circulation sinking underneath the surface in the polar region, which is not included in the SFT models. We also study the effect that a large sunspot pair violating Hale's polarity law would have on the polar field. We find that there would be some effect---especially if the anti-Hale pair appears at high latitudes in the mid-phase of the cycle---though the effect is not very dramatic.

A proposed paradigm for solar cycle dynamics mediated via turbulent pumping of magnetic flux in Babcock-Leighton type solar dynamos

Soumitra **Hazra**, Dibyendu Nandy
ApJ 832 9 **2016**

http://arxiv.org/pdf/1608.08167v1.pdf
At present, Babcock-Leighton flux transport solar dynamo models appear as the most promising model for explaining diverse observational aspects of the sunspot cycle. The success of these flux transport dynamo models is largely dependent upon a single-cell meridional circulation with a deep equatorward component at the base of the Sun's convection zone. However, recent observations suggest that the meridional flow may in fact be very shallow (confined to the top 10 % of the Sun) and more complex than previously thought. Taken together these observations raise serious concerns on the validity of the flux transport paradigm. By accounting for the turbulent pumping of magnetic flux as evidenced in magnetohydrodynamic simulations of solar convection, we demonstrate that flux transport dynamo models can generate solar-like magnetic cycles even if the meridional flow is shallow. Solar-like periodic reversals is recovered even when meridional circulation is altogether absent, however, in this case the solar surface magnetic field dynamics does not extend all the way to the polar regions. Very importantly, our results demonstrate that the Parker-Yoshimura sign rule for dynamo wave propagation can be circumvented in Babcock-Leighton dynamo models by the latitudinal component of turbulent pumping -- which can generate equatorward propagating sunspot belts in the absence of a deep, equatorward meridional flow. We also show that variations in turbulent pumping coefficients can modulate the solar cycle amplitude and periodicity. Our results suggest the viability of an alternate magnetic flux transport paradigm -- mediated via turbulent pumping -- for sustaining solar-stellar dynamo action.

Exploring the Origin and Dynamics of Solar Magnetic Fields

Soumitra **Hazra**
PhD Thesis, IISER Kolkata, **2015**
http://arxiv.org/pdf/1604.00563v1.pdf
The Sun is a magnetically active star and is the source of the solar wind, electromagnetic radiation and energetic particles which affect the heliosphere and the Earths atmosphere. The magnetic field of the Sun is responsible for most of the dynamic activity of the Sun. This thesis research seeks to understand solar magnetic field generation and the role that magnetic fields play in the dynamics of the solar atmosphere. Specifically, this thesis focuses on two themes: in the first part, we study the origin and behaviour of solar magnetic fields using magnetohydrodynamic dynamo theory and modelling, and in the second part, utilizing observations and data analysis we study two major problems in solar physics, namely, the coronal heating problem and initiation mechanisms of solar flares.

Correlation Between Decay Rate and Amplitude of Solar Cycles as Revealed from Observations and Dynamo Theory

Gopal **Hazra**, Bidya Binay Karak, Dipankar Banerjee, Arnab Rai Choudhuri
Solar Phys. Volume 290, Issue 6, pp 1851-1870 **2015**
Using different proxies of solar activity, we have studied the following features of the solar cycle: i) The linear correlation between the amplitude of cycle and its decay rate, ii) the linear correlation between the amplitude of cycle n and the decay rate of cycle (n−1), and iii) the anti-correlation between the amplitude of cycle n and the period of cycle (n−1). Features ii) and iii) are very useful because they provide precursors for future cycles. We have reproduced these features using a flux-transport dynamo model with stochastic fluctuations in the Babcock–Leighton α effect and in
the meridional circulation. Only when we introduce fluctuations in meridional circulation, are we able to reproduce different observed features of the solar cycle. We discuss the possible reasons for these correlations.

A Stochastically Forced Time Delay Solar Dynamo Model: Self-consistent Recovery from a Maunder-like Grand Minimum Necessitates a Mean-field Alpha Effect

Soumitra **Hazra**1, Dário Passos2,3,4, and Dibyendu Nandy
2014 ApJ 789 5
Fluctuations in the Sun's magnetic activity, including episodes of grand minima such as the Maunder minimum have important consequences for space and planetary environments. However, the underlying dynamics of such extreme fluctuations remain ill-understood. Here, we use a novel mathematical model based on stochastically forced, non-linear delay differential equations to study solar cycle fluctuations in which time delays capture the physics of magnetic flux transport between spatially segregated dynamo source regions in the solar interior. Using this model, we explicitly demonstrate that the Babcock-Leighton poloidal field source based on dispersal of tilted bipolar sunspot flux, alone, cannot recover the sunspot cycle from a grand minimum. We find that an additional poloidal field source effective on weak fields—e.g., the mean-field α effect driven by helical turbulence—is necessary for self-consistent recovery of the sunspot cycle from grand minima episodes.

Parametric instabilities and particles heating of circularly polarized Alfvén waves with an incoherent spectrum: two-dimensional hybrid simulations

Peng **He**

2021

https://arxiv.org/ftp/arxiv/papers/2108/2108.07016.pdf

Plasma ions heating (especially minor heavy ions preferential heating) in fast solar wind and solar corona is an open question in space physics. However, Alfvén waves have been always considered as a candidate of energy source for corona heating. In this paper, by using a two-dimensional (2-D) hybrid simulation model in a low beta electron-proton-alpha plasma system, we have investigated the relationships between plasma ions heating and power spectra evolution of density and magnetic field fluctuations excited from the parametric instabilities of initial pump Alfvén waves with an incoherent spectrum at different propagation angles theta_k0B0 (an oblique angle between the initial pump wave vector k0 and the background magnetic field B0). It is found that, the wave-wave coupling as well as wave-particle interaction play key roles in ions heating, and an Alfvén spectrum with small propagation angle (e.g. theta_k0B0=15degree) can most effectively heat alpha particles in perpendicular direction as well as in parallel direction for both proton and alpha particle than the case of a monochromatic Alfvén wave or an Alfvén spectrum with larger propagation angle.

Born Kernels for the Helioseismic Fourier–Legendre Analysis Method

Emanuel **Hecht** and Markus Roth

2018 ApJ 862 145

Measuring large-scale flows like the meridional flow with helioseismic methods plays a crucial role for understanding solar dynamics. In this work, we develop a detailed forward model for the Fourier–Legendre analysis method. This method has initially been applied for measuring the meridional flow by Braun & Fan, who observed frequency shifts between poleward and equatorward traveling p-modes. However, a detailed theoretical model based on a description of the solar internal wavefield is lacking. We therefore describe the effect of advection on the acoustic wavefronts in the first Born approximation following the framework of Gizon & Birch. We derive 2D sensitivity kernels for a suitable and unified definition of the frequency shift, and validate them on the example of a meridional flow. Finally, an inversion technique to estimate the meridional flow is developed on the basis of synthetic data from a simulation of linear wave propagation.

Disparity among low first ionization potential elements

Verena **Heidrich-Meisner**, Lars Berger and Robert F. Wimmer-Schweingruber

A&A 619, A79 (**2018**)

https://www.aanda.org/articles/aa/pdf/2018/11/aa33454-18.pdf

Context. The elemental composition of the solar wind differs from the solar photospheric composition. Elements with low first ionization potential (FIP) appear enhanced compared to O in the solar wind relative to the respective photospheric abundances. This so-called FIP effect is different in the slow solar wind and the coronal hole wind. However, under the same plasma conditions, for elements with similar FIPs such as Mg, Si, and Fe, comparable enhancements are expected.

Aims. We scrutinize the assumption that the FIP effect is always similar for different low FIP elements, namely Mg, Si, and Fe.

Methods. Here we investigate the dependency of the FIP effect of low FIP elements on the O7+/O6+ charge state ratio depending on time, that is the solar activity cycle, and solar wind type. In addition, we order the observed FIP ratios with respect to the O7+/O6+ charge state ratio into bins and analyze separately the respective distributions of the FIP ratio of Mg, Si, and Fe for each O7+/O6+ charge state ratio bin.

Results. We observe that the FIP effect shows the same qualitative yearly behavior for Mg and Si, while Fe shows significant differences during the solar activity maximum and its declining phase. In each year, the FIP effect for Mg and Si always increases with increasing O7+/O6+charge state ratio, but for high O7+/O6+ charge state ratios the FIP effect for Fe shows a qualitatively different behavior. During the years 2001–2006, instead of increasing with the O7+/O6+ charge state ratio, the Fe FIP ratio exhibits a broad peak or plateau. In addition, the FIP distribution per O7+/O6+ charge state bin is significantly broader for Fe than for Mg and Si.

Conclusions. These observations support the conclusion that the elemental fractionation is only partly determined by FIP. In particular, the qualitative difference in behavior with increasing O7+/O6+ charge state ratio between Fe on the one hand and Mg and Si on the other hand is not yet well explained by models of fractionation.

On the Origin of the sudden Heliospheric Open Magnetic Flux Enhancement during the 2014 Pole Reversal

Stephan G. **Heinemann**, Mathew J. Owens, Manuela Temmer, James A. Turtle, +++

ApJ **965** 151 **2024**

https://arxiv.org/pdf/2402.12805.pdf

https://iopscience.iop.org/article/10.3847/1538-4357/ad2b69/pdf
Coronal holes are recognized as the primary sources of heliospheric open magnetic flux (OMF). However, a noticeable gap exists between in-situ measured OMF and that derived from remote sensing observations of the Sun. In this study, we investigate the OMF evolution and its connection to solar structures throughout 2014, with special emphasis on the period from September to October, where a sudden and significant OMF increase was reported. By deriving the OMF evolution at 1au, modeling it at the source surface, and analyzing solar photospheric data, we provide a comprehensive analysis of the observed phenomenon. First, we establish a strong correlation between the OMF increase and the solar magnetic field derived from a Potential Field Source Surface (PFSS) model (ccPearson=0.94). Moreover, we find a good correlation between the OMF and the open flux derived from solar coronal holes (ccPearson=0.88), although the coronal holes only contain 14−32% of the Sun's total open flux. However, we note that while the OMF evolution correlates with coronal hole open flux, there is no correlation with the coronal hole area evolution (ccPearson=0.0). The temporal increase in OMF correlates with the vanishing remnant magnetic field at the southern pole, caused by poleward flux circulations from the decay of numerous active regions months earlier. Additionally, our analysis suggests a potential link between the OMF enhancement and the concurrent emergence of the largest active region in solar cycle 24.

Forecasting solar extreme and far ultraviolet irradiance

C. J. **Henney**, R. A. Hock, A. K. Schooley, W. A. Toussaint, S. M. White, C. N. Arge
Space Weather Volume 13, Issue 3 March **2015** Pages 141–153
Space Weather Quarterly Volume 12, Issue 2 **2015** Pages 19–31
http://onlinelibrary.wiley.com/doi/10.1002/SWQv12i002/epdf
A new method is presented to forecast the solar irradiance of selected wavelength ranges within the extreme ultraviolet (EUV) and far ultraviolet (FUV) bands. The technique is similar to a method recently published by Henney et al. (2012) to predict solar 10.7 cm (2.8 GHz) radio flux, abbreviated $F_{10.7}$, utilizing advanced predictions of the global solar magnetic field generated by a flux transport model. In this and the previous study, we find good correlation between the absolute value of the observed photospheric magnetic field and selected EUV/FUV spectral bands. By evolving solar magnetic maps forward 1 to 7 days with a flux transport model, estimations of the Earth side solar magnetic field distribution are generated and used to forecast irradiance. For example, Pearson correlation coefficient values of 0.99, 0.99, and 0.98 are found for 1 day, 3 day, and 7 day predictions, respectively, of the EUV band from 29 to 32 nm. In the FUV, for example, the 160 to 165 nm spectral band, correlation values of 0.98, 0.97, and 0.96 are found for 1 day, 3 day, and 7 day predictions, respectively. In the previous study, the observed $F_{10.7}$ signal is found to correlate well with strong magnetic field (i.e., sunspot) regions. Here we find that solar EUV and FUV signals are significantly correlated with the weaker magnetic fields associated with plage regions, suggesting that solar magnetic indices may provide an improved indicator (relative to the widely used $F_{10.7}$signal) of EUV and FUV nonflaring irradiance variability as input to ionospheric and thermospheric models.

Quiet Sun Hα Transients and Corresponding Small-Scale Transition Region and Coronal Heating

V. M. J. **Henriques**, D. Kuridze, M. Mathioudakis, F. P. Keenan
ApJ **820** 124 **2016**
http://arxiv.org/pdf/1602.04820v1.pdf
Rapid Blue- and Red-shifted Excursions (RBEs and RREs) are likely to be the on-disk counterparts of Type II spicules. Recently, heating signatures from RBEs/RREs have been detected in IRIS slit-jaw images dominated by transition-region lines around network patches. Additionally, signatures of Type II spicules have been observed in AIA diagnostics. The full-disk, ever-present nature of the AIA diagnostics should provide us with sufficient statistics to directly determine how important RBEs and RREs are to the heating of the transition region and corona. We find, with high statistical significance, that at least 11% of the low-coronal brightenings detected in a quiet-Sun region in 304, can be attributed to either RBEs or RREs as observed in H\alpha, and a 6% match of 171 detected events to RBEs or RREs with very similar statistics for both types of H\alpha\ features. We took a statistical approach that allows for noisy detections in the coronal channels and provides us with a lower, but statistical significant, bound. Further, we consider matches based on overlapping features in both time and space, and find strong visual indications of further correspondence between coronal events and co-evolving but non-overlapping, RBEs and RREs**. 3 May 2013**

Stable Umbral Chromospheric Structures

V. M. J. **Henriques**, E. Scullion, M. Mathioudakis, D. Kiselman, P. T. Gallagher, F. P. Keenan
A&A **2015**

http://arxiv.org/pdf/1412.6100v1.pdf
Aims. To understand the morphology of the chromosphere in sunspot umbra. We investigate if the horizontal structures observed in the spectral core of the Ca II H line are ephemeral visuals caused by the shock dynamics of more stable structures, and examine their relationship with observables in the H-alpha line.
Methods. Filtergrams in the core of the Ca II H and H-alpha lines as observed with the Swedish 1-m Solar Telescope are employed. We utilise a technique that creates composite images and tracks the flash propagation horizontally.
Results. We find 0"15 wide horizontal structures, in all of the three target sunspots, for every flash where the seeing was moderate to good. Discrete dark structures are identified that are stable for at least two umbral flashes, as well as systems of structures that live for up to 24 minutes. We find cases of extremely extended structures with similar stability, with one such structure showing an extent of 5". Some of these structures have a correspondence in H-alpha but we were unable to find a one to one correspondence for every occurrence. If the dark streaks are formed at the same heights as umbral flashes then there are systems of structures with strong departures from the vertical for all three analysed sunspots.
Conclusions. Long-lived Ca II H filamentary horizontal structures are a common and likely ever-present feature in the umbra of sunspots. If the magnetic field in the chromosphere of the umbra is indeed aligned with the structures, then the present theoretical understanding of the typical umbra needs to be revisited.

Inferring the Solar Meridional Circulation Flow Profile by Applying Bayesian Methods to Time–Distance Helioseismology

Aleczander **Herczeg**1 and Jason Jackiewicz1
2023 ApJ 954 187
https://iopscience.iop.org/article/10.3847/1538-4357/acea7b/pdf
Mapping the large-scale subsurface plasma flow profile within the Sun has been attempted using various methods for several decades. One such flow in particular is the meridional circulation, for which numerous studies have been published. However, such studies often show disagreement in structure. In an effort to constrain the flow profile from the data, a Bayesian Markov chain Monte Carlo framework has been developed to take advantage of the advances in computing power that allow for the efficient exploration of high-dimensional parameter spaces. This study utilizes helioseismic travel-time difference data covering a span of 21 years and a parameterized model of the meridional circulation to find the most likely flow profiles. Tests were carried out on artificial data to determine the ability of this method to recover expected solar-like flow profiles, as well as a few extreme cases. We find that this method is capable of recovering the input flows of both single- and double-cell flow structures. Some inversion results indicate potential differences in meridional circulation between the two solar cycles in terms of both magnitude and morphology, in particular in the mid-convection zone. Of these, the most likely solutions show that solar cycle 23 has a large single-celled profile, while cycle 24 shows weaker flows in general and hints toward a double-celled structure.

The Solar eruptioN Integral Field Spectrograph

Vicki L. **Herde**, Phillip C. Chamberlin, Don Schmit, +++
Solar Phys. **299**, 120 **2024**
https://arxiv.org/pdf/2407.08834
https://doi.org/10.1007/s11207-024-02367-y
https://link.springer.com/content/pdf/10.1007/s11207-024-02367-y.pdf
The Solar eruptioN Integral Field Spectrograph (SNIFS) is a solar-gazing spectrograph scheduled to fly in the summer of 2025 on a NASA sounding rocket. Its goal is to view the solar chromosphere and transition region at a high cadence (1s) both spatially (0.5") and spectrally (33 mÅ) viewing wavelengths around Lyman Alpha (1216 Å), Si iii (1206 Å) and O v (1218 Å) to observe spicules, nanoflares, and possibly a solar flare. This time cadence will provide yet-unobserved detail about fast-changing features of the Sun. The instrument is comprised of a Gregorian-style reflecting telescope combined with a spectrograph via a specialized mirrorlet array that focuses the light from each spatial location in the image so that it may be spectrally dispersed without overlap from neighboring locations. This paper discusses the driving science, detailed instrument and subsystem design, and pre-integration testing of the SNIFS instrument.

Spicules in IRIS Mg II Observations: Automated Identification

Vicki L. **Herde**, Phillip C. Chamberlin, Don Schmit, Souvik Bose, Adrian Daw, Ryan O. Milligan, Vanessa Polito
AAS Journal **2022**
https://arxiv.org/pdf/2212.04990.pdf
We have developed an algorithm to identify solar spicules in the first-ever systematic survey of on-disk spicules using exclusively Mg II spectral observations. Using this algorithm we identify 2219 events in three IRIS datasets with unique solar feature targets spanning a total of 300 minutes: 1) an active region, 2) decayed active region/active

network, and 3) a coronal hole. We present event statistics and relate occurrence rates to underlying photospheric magnetic field strength. This method identifies spicule event densities and occurrence rates similar to previous studies performed using H{\alpha} and Ca II observations of active regions. Additionally, this study identifies spicule-like events at very low rates at magnetic field intensities below 20 Gauss and increasing significantly between 100-200 Gauss in active regions and above 20 Gauss in coronal holes, which can be used to inform future observation campaigns. This information can be be used to help characterize spicules over their full lifetime, and compliments existing H-{\alpha} spectral capabilities and upcoming Ly-{\alpha} spectral observations on the SNIFS Sounding Rocket. In total, this study presents a method for detecting solar spicules using exclusively Mg II spectra, and provides statistics for spicule occurrence in Mg II wavelengths with respect to magnetic field strength for the purpose of predicting spicule occurrences. **14 Feb 2015, 24 Sept 2014, 24 Sep 2021**
IRIS Nuggets 8 Mar **2023** https://iris.lmsal.com/nugget

The New Composite Solar Flare Index from Solar Cycle 17 to Cycle 24 (1937 – 2020)

Victor Manuel Velasco **Herrera**, Willie Soon, Štefan Knoška, et al.
Solar Physics volume 297, Article number: 108 (**2022**)
https://doi.org/10.1007/s11207-022-02035-z
The chromosphere is a highly dynamic outer plasma layer of the Sun. Its physical processes accounting for the variability are poorly understood. We reconstructed the solar chromospheric flare index (SFI) to study the solar chromospheric variability from 1937 to 2020. The new SFI database is a composite record of the Astronomical Institute Ondřejov Observatory of the Czech Academy of Sciences from 1937 – 1976 and the records of the Kandilli Observatory of Istanbul, Turkey from 1977 – 2020. The SFI records are available in daily, monthly, and yearly resolutions. We carried out the time-frequency analyses of the new 84-year long SFI records using the wavelet transform. We report the periodicities of 21.88 (Hale cycle), 10.94 (Schwabe cycle), 5.2 (quasi-quinquennial cycle), 3.5, 1.7, 1, 0.41 (or 149.7 days, Rieger cycle), 0.17 (62.1 days), 0.07 (25.9 days, solar rotational modulation) years. All these periodicities seem always present and persistent throughout the observational interval. Thus, we suggest that there is no reason to assume these solar periodicities are absent from other solar cycles. Time variations of the amplitude of each oscillation or periodicity were also studied using the inverse wavelet transform. We found that for the SFI the most active flare cycles over the record were Cycles 17, 19, and 21, while Cycles 20, 22, 23, and 24 were the weakest ones with Cycle 18 was intermediate in flare activity. This shows several differences to the equivalent relationships for solar activity implied by sunspot number records. Furthermore, this confirms that solar activity trends and variability in the chromosphere as captured by SFI are not necessarily the same as those of the Sun's photosphere, as implied by the sunspot number activity records, for instance. We have also introduced a new signal/noise wavelet coherence metric to analyze two different chromospheric indices available (i.e. the SFI and the disk-integrated chromospheric Ca II K activity indices) and to quantify the differences and similarities of the oscillations within the solar chromosphere. Our findings suggest the importance of carrying out additional co-analyses with other solar activity records to find physical inter-relations and connections between the different solar layers from the photosphere, the chromosphere to the corona.

Group Sunspot Numbers: A New Reconstruction of Sunspot Activity Variations from Historical Sunspot Records Using Algorithms from Machine Learning

Víctor Manuel Velasco **Herrera**, Willie Soon, Douglas V. Hoyt & Judit Muraközy
Solar Physics volume 297, Article number: 8 (**2022**)
https://link.springer.com/content/pdf/10.1007/s11207-021-01926-x.pdf
https://doi.org/10.1007/s11207-021-01926-x
Historical sunspot records and the construction of a comprehensive database are among the most sought after research activities in solar physics. Here, we revisit the issues and remaining questions on the reconstruction of the so-called group sunspot numbers (GSN) that was pioneered by D. Hoyt and colleagues. We use the modern tools of artificial intelligence (AI) by applying various algorithms based on machine learning (ML) to GSN records. The goal is to offer a new vision in the reconstruction of sunspot activity variations, i.e. a Bayesian reconstruction, in order to obtain a complete probabilistic GSN record from 1610 to 2020. This new GSN reconstruction is consistent with the historical GSN records. In addition, we perform a comparison between our new probabilistic GSN record and the most recent GSN reconstructions produced by several solar researchers under various assumptions and constraints. Our AI algorithms are able to reveal various new underlying patterns and channels of variations that can fully account for the complete GSN time variability, including intervals with extremely low or weak sunspot activity like the Maunder Minimum from 1645 – 1715. Our results show that the GSN records are not strictly represented by the 11-year cycles alone, but that other important timescales for a fuller reconstruction of GSN activity history are the 5.5-year, 22-year, 30-year, 60-year, and 120-year oscillations. The comprehensive GSN reconstruction by AI/ML is able to shed new insights on the nature and characteristics of not only the underlying 11-year-like sunspot cycles but also on the 22-year Hale's polarity cycles during the Maunder Minimum, among other results previously hidden so far. In the early 1850s, Wolf multiplied his original sunspot number reconstruction by a factor of 1.25 to

arrive at the canonical Wolf sunspot numbers (WSN). Removing this multiplicative factor, we find that the GSN and WSN differ by only a few percent for the period 1700 to 1879. In a comparison to the international sunspot number (ISN) recently recommended by Clette et al. (Space Sci. Rev. 186, 35, 2014), several differences are found and discussed. More sunspot observations are still required. Our article points to observers that are not yet included in the GSN database.

The Evolution of Coronal Holes over Three Solar Cycles Using the McIntosh Archive

Ian M. **Hewins**, Sarah E. Gibson, David F. Webb, Robert H. McFadden, Thomas A. Kuchar, Barbara A. Emery & Scott W. McIntosh
Solar Physics volume 295, Article number: 161 (**2020**)
https://link.springer.com/content/pdf/10.1007/s11207-020-01731-y.pdf
Using the McIntosh Archive of solar features, we analyze the evolution of coronal holes over more than three solar cycles. We demonstrate that coronal-hole positions and lifetimes change significantly on time scales from months to years, and that the pattern of these changes is clearly linked to the solar-activity cycle. We demonstrate that the lifetimes of low-latitude coronal holes are usually less than one rotation but may extend to almost three years. When plotted over time, the positions of low-latitude coronal holes that remain visible for over one rotation track the sunspot butterfly diagram in terms of their positions on the Sun over a solar cycle. Finally, we confirm that coronal holes do not in general rigidly rotate.

Data Assimilation in the ADAPT Photospheric Flux Transport Model

Kyle S. **Hickmann**, Humberto C. Godinez, Carl J. Henney, C. Nick Arge
Solar Physics April **2015**, Volume 290, Issue 4, pp 1105-1118
Global maps of the solar photospheric magnetic flux are fundamental drivers for simulations of the corona and solar wind and therefore are important predictors of geoeffective events. However, observations of the solar photosphere are only made intermittently over approximately half of the solar surface. The Air Force Data Assimilative Photospheric Flux Transport (ADAPT) model uses localized ensemble Kalman filtering techniques to adjust a set of photospheric simulations to agree with the available observations. At the same time, this information is propagated to areas of the simulation that have not been observed. ADAPT implements a local ensemble transform Kalman filter (LETKF) to accomplish data assimilation, allowing the covariance structure of the flux-transport model to influence assimilation of photosphere observations while eliminating spurious correlations between ensemble members arising from a limited ensemble size. We give a detailed account of the implementation of the LETKF into ADAPT. Advantages of the LETKF scheme over previously implemented assimilation methods are highlighted.

Fast and Accurate Emulation of the SDO/HMI Stokes Inversion with Uncertainty Quantification

Richard E.L. **Higgins**, David F. Fouhey, Dichang Zhang, Spiro K. Antiochos, Graham Barnes, Todd Hoeksema, KD Leka, Yang Liu Peter W. Schuck, Tamas I. Gombosi
ApJ **911** 130 **2021**
https://arxiv.org/pdf/2103.17273.pdf
https://doi.org/10.3847/1538-4357/abd7fe
The Helioseismic and Magnetic Imager (HMI) onboard NASA's Solar Dynamics Observatory (SDO) produces estimates of the photospheric magnetic field which are a critical input to many space weather modelling and forecasting systems. The magnetogram products produced by HMI and its analysis pipeline are the result of a per-pixel optimization that estimates solar atmospheric parameters and minimizes disagreement between a synthesized and observed Stokes vector. In this paper, we introduce a deep learning-based approach that can emulate the existing HMI pipeline results two orders of magnitude faster than the current pipeline algorithms. Our system is a U-Net trained on input Stokes vectors and their accompanying optimization-based VFISV inversions. We demonstrate that our system, once trained, can produce high-fidelity estimates of the magnetic field and kinematic and thermodynamic parameters while also producing meaningful confidence intervals. We additionally show that despite penalizing only per-pixel loss terms, our system is able to faithfully reproduce known systematic oscillations in full-disk statistics produced by the pipeline. This emulation system could serve as an initialization for the full Stokes inversion or as an ultra-fast proxy inversion. This work is part of the NASA Heliophysics DRIVE Science Center (SOLSTICE) at the University of Michigan, under grant NASA 80NSSC20K0600E, and has been open sourced. **2016/01/15, 2016/02/10, 2016/03/05, 2016/03/11, 2016/06/13, 2016/05/10, 2016/08/10**
HMI Science Nuggets # 156 May **2021** http://hmi.stanford.edu/hminuggets/?p=3530

Sun's Magnetic Fields Best at Forecasting Solar Cycle Peaks

Aleida K. **Higginson**
EOS 97 23 Feb **2016**
https://eos.org/research-spotlights/suns-magnetic-fields-best-at-forecasting-solar-cycle-peaks

Models based on the Sun's polar magnetic fields performed best in simulating the solar cycle and predicting solar behavior.

The New SCIAMACHY Reference Solar Spectral Irradiance and Its Validation

T. **Hilbig**, M. Weber, K. Bramstedt, S. Noël, J. P. Burrows, J. M. Krijger…
Solar Physics August **2018**, 293:121
This paper describes a new reference solar spectrum retrieved from measurements of the satellite instrument SCIAMACHY in the wavelength region from 0.24 µm0.24 µm to 2.4 µm2.4 µm and its comparison with several other established solar reference spectra. The SCIAMACHY reference spectrum was recorded early in the mission before substantial optical degradation due to the harsh space environment sets in. The radiometric calibration of SCIAMACHY, applied in this study, includes a physical model of the scanner unit. Furthermore, SCIAMACHY's internal white light source (WLS) is used to correct for on-ground to in-flight changes. The resultant calibrated solar spectrum from SCIAMACHY is in good agreement with several available solar spectral irradiance (SSI) references in the visible spectral range. Strong throughput losses due to detector icing in the near infrared (NIR) are now adequately accounted for. Nevertheless, a deficit with respect to the ATLAS-3 composite and SORCE/SIM SSI is observed in the NIR. However, the SCIAMACHY solar reference spectrum agrees well with the recently re-evaluated SOLAR/SOLSPEC-ISS and recent ground measurements taken at Mauna Loa in the NIR.

The Global Oscillation Network Group Facility—An Example of Research to Operations in Space Weather

Frank **Hill**
Space Weather Volume16, Issue10 October **2018** Pages 1488-1497
https://doi.org/10.1029/2018SW002001
The Global Oscillation Network Group (GONG) is a system of ground-based solar observing stations distributed geographically so that the Sun is visible nearly continuously at all times. Originally developed to provide data for research into the solar interior via helioseismology, GONG is now also providing data for operational space weather forecasting as a cost-effective and reliable alternative to space missions. The data comprise full-disk magnetograms, H-α intensity images, and helioseismic maps of activity on the solar far side. These data are provided in near real time to the NOAA Space Weather Prediction Center, the US Air Force, and NASA. GONG is a successful example of transitioning a research facility funded by the NSF into an operational asset.

Nonlinear wave damping by Kelvin-Helmholtz instability induced turbulence

Andrew **Hillier**, Iñigo Arregui, Takeshi Matsumoto
ApJ **2023**
https://arxiv.org/pdf/2308.02217.pdf
Magnetohydrodynamic kink waves naturally form as a consequence of perturbations to a structured medium, for example transverse oscillations of coronal loops. Linear theory has provided many insights in the evolution of linear oscillations, and results from these models are often applied to infer information about the solar corona from observed wave periods and damping times. However, simulations show that nonlinear kink waves can host the Kelvin-Helmholtz instability (KHi) which subsequently creates turbulence in the loop, dynamics which are beyond linear models. In this paper we investigate the evolution of KHi-induced turbulence on the surface of a flux tube where a non-linear fundamental kink-mode has been excited. We control our numerical experiment so that we induce the KHi without exciting resonant absorption. We find two stages in the KHi turbulence dynamics. In the first stage, we show that the classic model of a KHi turbulent layer growing ∝tis applicable. We adapt this model to make accurate predictions for damping of the oscillation and turbulent heating as a consequence of the KHi dynamics. In the second stage, the now dominant turbulent motions are undergoing decay. We find that the classic model of energy decay proportional to t−2 approximately holds and provides an accurate prediction of the heating in this phase. Our results show that we can develop simple models for the turbulent evolution of a non-linear kink wave, but the damping profiles produced are distinct from those of linear theory that are commonly used to confront theory and observations.

Shocks and instabilities in the partially ionised solar atmosphere

Andrew **Hillier**, Ben Snow
Advances in Space Research Volume 71, Issue 4, 15 February **2023**, Pages 1962-1983
https://arxiv.org/ftp/arxiv/papers/2302/2302.07362.pdf
https://reader.elsevier.com/reader/sd/pii/S0273117722008158
The low solar atmosphere is composed of mostly neutral particles, but the importance of the magnetic field for understanding observed dynamics means that interactions between charged and neutral particles play a very important role in controlling the macroscopic fluid motions. As the exchange of momentum between fluids, essential for the neutral fluid to effectively feel the Lorentz force, is through collisional interactions, the relative

timescale of these interactions to the dynamic timescale determines whether a single-fluid model or, when the dynamic frequency is higher, the more detailed two-fluid model is the more appropriate. However, as many MHD phenomena fundamentally contain multi-time-scale processes, even large-scale, long-timescale motions can have an important physical contribution from two-fluid processes. In this review we will focus on two-fluid models, looking in detail at two areas where the multi-time-scale nature of the solar atmosphere means that two-fluid physics can easily develop: shock-waves and instabilities. We then connect these ideas to observations attempting to diagnose two-fluid behaviour in the solar atmosphere, suggesting some ways forward to bring observations and simulations closer together.

The role of cooling induced by mixing in the mass and energy cycles of the solar atmosphere

Andrew **Hillier**, Ben Snow, Inigo Arregui
MNRAS **2023**, Volume 520, Issue 2, pp.1738-1747
https://arxiv.org/pdf/2302.07364
In many astrophysical systems, mixing between cool and hot temperature gas/plasma through Kelvin-Helmholtz-instability-driven turbulence leads to the formation of an intermediate temperature phase with increased radiative losses that drive efficient cooling. The solar atmosphere is a potential site for this process to occur with interaction between either prominence or spicule material and the solar corona allowing the development of transition region material with enhanced radiative losses. In this paper, we derive a set of equations to model the evolution of such a mixing layer and make predictions for the mixing-driven cooling rate and the rate at which mixing can lead to the condensation of the coronal material. These theoretical predictions are benchmarked against 2.5D MHD simulations. Applying the theoretical scalings to prominence threads or fading spicules, we found that as a mixing layer grows on their boundaries this would lead to the creation of transition region material with a cooling time of ~100 s, explaining the warm emission observed as prominence threads or spicules fade in cool spectral lines without the requirement for any heating. For quiescent prominences, dynamic condensation driven by the mixing process could restore ~18 per cent of the mass lost from a prominence through downflows. Overall, this mechanism of thermal energy loss through radiative losses induced by mixing highlights the importance for considering dynamical interaction between material at different temperatures when trying to understand the thermodynamic evolution of the cool material in the solar corona.

Estimating the Energy Dissipation from Kelvin–Helmholtz Instability Induced Turbulence in Oscillating Coronal Loops

Andrew **Hillier**1, Tom Van Doorsselaere2, and Konstantinos Karampelas2
2020 ApJL 897 L13
https://doi.org/10.3847/2041-8213/ab9ca3
https://arxiv.org/pdf/2007.09068.pdf
Kelvin–Helmholtz instability induced turbulence is one promising mechanism by which loops in the solar corona can be heated by MHD waves. In this Letter we present an analytical model of the dissipation rate of Kelvin–Helmholtz instability induced turbulence ε D, finding it scales as the wave amplitude (d) to the third power (ε D ∝ d 3). Based on the concept of steady-state turbulence, we expect the turbulence heating throughout the volume of the loop to match the total energy injected through its footpoints. In situations where this holds, the wave amplitude has to vary as the cube-root of the injected energy. Comparing the analytic results with those of simulations shows that our analytic formulation captures the key aspects of the turbulent dissipation from the numerical work. Applying this model to the observed characteristics of decayless kink waves we predict that the amplitudes of these observed waves are insufficient to turbulently heat the solar corona.

Coronal cooling as a result of mixing by the nonlinear Kelvin--Helmholtz instability

Andrew **Hillier**, Inigo Arregui
ApJ **885** 101 **2019**
https://arxiv.org/pdf/1909.11351.pdf
https://doi.org/10.3847/1538-4357/ab4795
Recent observations show cool, oscillating prominence threads fading when observed in cool spectral lines and appearing in warm spectral lines. A proposed mechanism to explain this evolution is that the threads were heated by turbulence driven by the Kelvin--Helmholtz instability that developed as a result of wave-driven shear flows on the surface of the thread. As the Kelvin--Helmholtz instability is an instability that works to mix the fluids, in the solar corona it can be expected to work by mixing the cool prominence material with that of the hot corona to form a warm boundary layer. In this paper we develop a simple phenomenological model of nonlinear Kelvin--Helmholtz mixing, using it to determine the characteristic density and temperature of the mixing layer, which for the case under study with constant pressure across the two fluids are ρmixed=ρ1ρ2−−−−√ and Tmixed=T1T2−−−−√. One result from the model is that it provides an accurate, as determined by comparison with simulation results, determination of the kinetic energy in the mean velocity field. A consequence of this is that the magnitude of turbulence, and with

it the energy that can be dissipated on fast time-scales, as driven by this instability can be determined. For the prominence-corona system, the mean temperature rise possible from turbulent heating is estimated to be less than 1\% of the characteristic temperature (which is found to be 105\,K). These results highlight that mixing, and not heating, are likely to be the cause of the observed transition between cool to warm material in Okamoto et. al (2015). One consequence of this result is that the mixing creates a region with higher radiative loss rates on average than either of the original fluids, meaning that this instability could contribute a net loss of thermal energy from the corona, i.e. coronal cooling.

On Kelvin–Helmholtz and parametric instabilities driven by coronal waves

Andrew **Hillier** Adrian Barker Iñigo Arregui Henrik Latter

MNRAS 482, Issue 1, 1 January **2019**, Pages 1143–1153

The Kelvin–Helmholtz instability has been proposed as a mechanism to extract energy from magnetohydrodynamic (MHD) kink waves in flux tubes, and to drive dissipation of this wave energy through turbulence. It is therefore a potentially important process in heating the solar corona. However, it is unclear how the instability is influenced by the oscillatory shear flow associated with an MHD wave. We investigate the linear stability of a discontinuous oscillatory shear flow in the presence of a horizontal magnetic field within a Cartesian framework that captures the essential features of MHD oscillations in flux tubes. We derive a Mathieu equation for the Lagrangian displacement of the interface and analyse its properties, identifying two different instabilities: a Kelvin–Helmholtz instability and a parametric instability involving resonance between the oscillatory shear flow and two surface Alfvén waves. The latter occurs when the system is Kelvin–Helmholtz stable, thus favouring modes that vary along the flux tube, and as a consequence provides an important and additional mechanism to extract energy. When applied to flows with the characteristic properties of kink waves in the solar corona, both instabilities can grow, with the parametric instability capable of generating smaller scale disturbances along the magnetic field than possible via the Kelvin–Helmholtz instability. The characteristic time-scale for these instabilities is ∼100 s, for wavelengths of 200 km. The parametric instability is more likely to occur for smaller density contrasts and larger velocity shears, making its development more likely on coronal loops than on prominence threads.

A Novel Approach to Resonant Absorption of the Fast MHD Eigenmodes of a Coronal Arcade

Bradley W. **Hindman**, Rekha Jain

ApJ **2018**

https://arxiv.org/pdf/1803.08948.pdf

The arched field lines forming coronal arcades are often observed to undulate as magnetohydrodynamic (MHD) waves propagate both across and along the magnetic field. These waves are most likely a combination of resonantly coupled fast magnetoacoustic waves and Alfv\'en waves. The coupling results in resonant absorption of the fast waves, converting fast wave energy into Alfv\'en waves. The fast eigenmodes of the arcade have proven difficult to compute or derive analytically, largely because of the mathematical complexity that the coupling introduces. When a traditional spectral decomposition is employed, the discrete spectrum associated with the fast eigenmodes is often subsumed into the continuous Alfv\'en spectrum. Thus fast eigenmodes, become collective modes or quasi-modes. Here we present a spectral decomposition that treats the eigenmodes as having real frequencies but complex wavenumbers. Using this procedure we derive dispersion relations, spatial damping rates, and eigenfunctions for the resonant, fast eigenmodes of the arcade. We demonstrate that resonant absorption introduces a fast mode that would not exist otherwise. This new mode is heavily damped by resonant absorption, only travelling a few wavelengths before losing most of its energy.

Forecast and backcast of the solar cycles

K M **Hiremath**

2022

https://arxiv.org/pdf/2204.04818.pdf

Solar cycle is modeled as a forced and damped harmonic oscillator and the amplitudes, frequencies, phases and decay factors of such a harmonic oscillator are estimated by non-linear fitting the equation of sinusoidal and transient parts to the sunspot and irradiance (proxy for the sunspot) data for the years 1700-2008. We find that:(i) amplitude and frequency (or period of ∼11 yr) of the sinusoidal part remain constant for all the solar cycles; (ii) the amplitude of the transient part is phase locked with the phase of the sinusoidal part; (iii) for all the cycles, the period and decay factor (that is much less than 1) of the transient part remain approximately constant. The constancy of the amplitudes and the frequencies of the sinusoidal part and a very small decay factor from the transient part suggests that the solar activity cycle mainly consists of a persistent oscillatory part that might be compatible with long-period (∼22 yr) Alfven oscillations. For all the cycles, with the estimated physical parameters (amplitudes, phases and periods) and, by an autoregressive model, we forecast (especially for coming solar cycle 25) and backcast (to check whether Maunder minimum type solar activity exists or not) the solar cycles. We find that amplitude of coming solar cycle 25 is almost same as the amplitude of the previous solar cycle 24. We also find that sun might not have

experienced a deep Maunder minimum (MM) type of activity during 1645-1700 AD corroborating some of the paleoclimatic inferences and, MM type of activity will not be imminent in near future, until at least 200 years.

Nearly Century-scale Variation of the Sun's Radius

K. M. **Hiremath**1, J. P. Rozelot2, V. Sarp3, A. Kilcik3, Pavan D. G.1, and Shashanka R. Gurumath4
2020 ApJ 891 151
https://doi.org/10.3847/1538-4357/ab6d08
https://arxiv.org/ftp/arxiv/papers/2003/2003.08676.pdf
The Kodaikanal Archive Program (India) is now available to the scientific community in digital form as daily digitized solar white light pictures, from 1923 to 2011. We present here the solar radius data, obtained after a painstaking effort to remove all effects that contribute to the error in their measurements (limb darkening, distortion of the objective lens, refraction, other instrumental effects, etc.). These data were analyzed to reveal any significant periodic variations, after applying a multi-taper method with red noise approximation and the Morlet wavelet transform analysis. After removing obvious periodic variations (such as solar rotation and Earth annual rotation), we found a possible cycle variation at 11.4 yr, quasi biennial oscillations at 1.5 and 3.8 yr, and Rieger-type periodicity at ≈159, 91, and 63 days. Another yr periodicity (as a mean) resulting from two other main periodicities detected at 6.3–7.8 yr can be identified as an atmospheric component. The detrending data show, over a mean radius of , a residual of less than ≈(−)1 mas over the time period of analysis: if not spurious, this estimate indicates a faint decline, but probably confirms more the constancy of the solar diameter during the considered ranging time, within instrumental and methodological limits. The Kodaikanal long quality observations contribute to international efforts to bring past solar data measurements to the community to further explore issues, for instance, those of the luminosity/radius properties that could be used to pinpoint the "seat of the solar cycle."

Kodaikanal calcium images: Detection of plages, Fixing the heliographic coordinates and Estimation of Area

K. M. **Hiremath**, Shreyam Krishna, Adithya H. N, S. R. Chinmaya, Shashanka R Gurumath
2019
https://arxiv.org/pdf/1909.00406.pdf
Kodaikanal Observatory is a veritable treasure trove of data, with the data repository covering almost 100 years of observations. For the years 1909-2007, we use calibrated Ca II K spectroheliograms from the Kodaikanal Observatory to detect the plages, fix their heliographic coordinates and also estimate the plage areas. We adopt the following procedure. After ensuring that, for all the years, Kodai calcium images have very negligible ellipcity, a circle is fitted and two central coordinates and radius of calcium images are determined uniquely. For each pixel of the calcium image, we then fix heliographic coordinates and extract plages along with their weighted average coordinates. The heliographic coordinates of these extracted plages are then compared with the heliographic coordinates of photospheric sunspots from the Greenwich sunspot database and chromospheric magnetic plages detected from the SOHO/MDI magnetograms. We find that the heliographic coordinates of calcium plages match very well with the heliographic coordinates of sunspots and magnetic plages authenticating our method of detection of plages and computation of positional coordinates. A code is developed in Python and all the nearly century scale plages data, with accurately estimated heliographic coordinates and areas, is available to the public.

Physics of the Solar Cycle: New Views

K. M. **Hiremath**
Sun and Geosphere, **2010**; 5(1): 17 – 22, **File**
Presently there are two schools of thought viz., *turbulent dynamo* and *MHD oscillation* mechanisms that explain the solar cycle and activity phenomena. Both the mechanisms are critically examined and fundamental difficulties are presented. By keeping in mind the more advantages of having MHD oscillation mechanism, compared to the turbulent dynamo mechanism, the following new ideas on the genesis of the solar cycle and activity phenomena are presented. The inevitability of the most likely existence of a combined poloidal and toroidal magnetic field structure in the solar interior is proposed. Owing to the suitable poloidal part of the steady field structure, the Alfven wave perturbations of long periods (~22 years) that excite in the solar core travel first to the poles in both the hemispheres and later reach the equator. While traveling towards the surface, the Alfven wave perturbations along the weak poloidal field structure in turn perturb the embedded strong toroidal field structure producing sunspots, especially in the convective envelope, that travel to the surface due to buoyancy along isorotational contours. With a realistic density structure of the solar interior, the computation of Alfven wave travel times along different field lines of the poloidal field structure [1] yields almost similar periods (~22 years) explaining the constancy of 22 years periodicity of the odd degree modes obtained from the Spherical Harmonic Fourier analysis of the surface magnetic field. The observed quasi-periodicities of solar activity indices in the range of 1-5 years are explained as due to the Alfven wave perturbation of the strong toroidal field structure. The variation of the long period solar cycle and activity

phenomena such as the Maunder and the grand minima is explained to be due to the coupling of long period poloidal and toroidal MHD oscillations.

Cross-Calibration of TIMED SEE and SOHO EIT Irradiances

R.A. **Hock** · F.G. Eparvier
Solar Phys (**2008**) 250: 207–219, **File**
http://www.springerlink.com/content/p7l5p76352505730/fulltext.pdf
Absolutely calibrated solar images are necessary for a variety of solar physics problems, such as the identification of solar variability sources and the derivation of differential emission measure (DEM) maps. SOHO EIT is absolutely calibrated by using TIMED SEE spectra to provide a method of determining physical values of irradiance for EIT images. EIT images from 1 April 2002 to 15 March 2005 in the **28.4- and 30.4-nm** channels are compared to SEE daily spectra from the same time period. The resulting fitted EIT irradiances are well correlated to SEE irradiance measurements and are within the uncertainties of both instruments. The new cross-calibration results are compared to the currently used calibration based on the UARS SUSIM Mg II index.

On-Orbit Performance of the Helioseismic and Magnetic Imager Instrument onboard the Solar Dynamics Observatory

J. Todd **Hoeksema**, Charles S. Baldner, Rock I. Bush, Jesper Schou, Philip H. Scherrer
Solar Phys. 293:45 **2018**
https://arxiv.org/pdf/1802.01731.pdf
http://sun.stanford.edu/~todd/Perfpaper/HMI_Performance.pdf
https://link.springer.com/content/pdf/10.1007%2Fs11207-018-1259-8.pdf
The Helioseismic and Magnetic Imager (HMI) instrument is a major component of NASA's Solar Dynamics Observatory (SDO) spacecraft. Since beginning normal science operations on 1 May 2010, HMI has operated with remarkable continuity, e.g. during the more than five years of the SDO prime mission that ended 30 September 2015, HMI collected 98.4% of all possible 45-second velocity maps; minimizing gaps in these full-disk Dopplergrams is crucial for helioseismology. HMI velocity, intensity, and magnetic-field measurements are used in numerous investigations, so understanding the quality of the data is important. We describe the calibration measurements used to track HMI performance and detail trends in important instrument parameters during the mission. Regular calibration sequences provide information used to improve and update the HMI data calibration. The set-point temperature of the instrument front window and optical bench is adjusted regularly to maintain instrument focus, and changes in the temperature-control scheme have been made to improve stability in the observable quantities. The exposure time has been changed to compensate for a 15% decrease in instrument throughput. Measurements of the performance of the shutter and tuning mechanisms show that they are aging as expected and continue to perform according to specification. Parameters of the tunable-optical-filter elements are regularly adjusted to account for drifts in the central wavelength. Frequent measurements of changing CCD-camera characteristics, such as gain and flat field, are used to calibrate the observations. Infrequent expected events, such as eclipses, transits, and spacecraft off-points, interrupt regular instrument operations and provide the opportunity to perform additional calibration. Onboard instrument anomalies are rare and seem to occur quite uniformly in time. The instrument continues to perform very well.

Scientific considerations for future spectroscopic measurements from space of activity on the Sun **Review**

Gordon D. **Holman**
JGR **2016**
http://sci-hub.cc/10.1002/2016JA022651
High-resolution UV and X-ray spectroscopy are important to understanding the origin and evolution of magnetic energy release in the solar atmosphere, as well as the subsequent evolution of heated plasma and accelerated particles. Electromagnetic radiation is observed from plasma heated to temperatures ranging from about 10 kK to above 10 MK, from accelerated electrons emitting photons primarily at X-ray energies, and from ions emitting in γ rays. These observations require space-based instruments sensitive to emissions at wavelengths shorter than the near UV. This article reviews some recent observations with emphasis on solar eruptive events, the models that describe them, and the measurements they indicate are needed for substantial progress in the future. Specific examples are discussed demonstrating that imaging spectroscopy with a cadence of seconds or better is needed to follow, understand, and predict the evolution of solar activity. Critical to substantial progress is the combination of a

judicious choice of UV, EUV, and soft X-ray imaging spectroscopy sensitive to the evolution of this thermal plasma combined with hard X-ray imaging spectroscopy sensitive to suprathermal electrons. The major challenge will be to conceive instruments that, within the bounds of possible technologies and funding, have the flexibility and field of view to obtain spectroscopic observations where and when events occur while providing an optimum balance of dynamic range, spectral resolution and range, and spatial resolution.

Revisiting the Spectral Features of Ellerman Bombs and UV Bursts. I. Radiative Hydrodynamic Simulations

Jie **Hong**, Ying Li, M. D. Ding, Qi Hao
ApJ **921** 50 **2021**
https://arxiv.org/pdf/2108.02699.pdf
https://doi.org/10.3847/1538-4357/ac1ba0
Ellerman bombs (EBs) and UV bursts are both small-scale solar activities that occur in active regions. They are now believed to form at different heights in the lower atmosphere. In this paper, we use one-dimensional radiative hydrodynamic simulations to calculate various line profiles in response to heating in different atmospheric layers. We confirm that heating in the upper photosphere to the lower chromosphere can generate spectral features of typical EBs, while heating in the mid to upper chromosphere can generate spectral features of typical UV bursts. The intensity evolution of the Hα line wing in EBs shows a rise--plateau pattern, while that of the Si IV 1403 Å line center in UV bursts shows a rise--fall pattern. However, the predicted enhancement of FUV continuum near 1400 Å for EBs is rarely reported and requires further observations to check it. With two heating sources or an extended heating source in the atmosphere, both EB and UV burst features could be reproduced simultaneously.

Mapping Solar X-Ray Images from SDO/AIA EUV Images by Deep Learning

Junchao **Hong**1,2,3, Hui Liu1,2, Yi Bi1,2, Zhe Xu2,4, Bo Yang1,2, Jiayan Yang1,2, Yang Su5,6, Yuehan Xia5,6, and Kaifan Ji1,
2021 ApJ 915 96
https://doi.org/10.3847/1538-4357/ac01d5
The full-Sun corona is now imaged every 12 s in extreme ultraviolet (EUV) passbands by Solar Dynamics Observatory/Atmospheric Imaging Assembly (AIA), whereas it is only observed several times a day at X-ray wavelengths by Hinode/X-Ray Telescope (XRT). In this paper, we apply a deep-learning method, i.e., the convolution neural network (CNN), to establish data-driven models to generate full-Sun X-ray images in XRT filters from AIA EUV images. The CNN models are trained using a number of data pairs of AIA six-passband (171, 193, 211, 335, 131, and 94 Å) images and the corresponding XRT images in three filters: "Al_mesh," "Ti_poly," and "Be_thin." It is found that the CNN models predict X-ray images in good consistency with the corresponding well-observed XRT data. In addition, the purely data-driven CNN models are better than the conventional analysis method of the coronal differential emission measure (DEM) in predicting XRT-like observations from AIA data. Therefore, under conditions where AIA provides coronal EUV data well, the CNN models can be applied to fill the gap in limited full-Sun coronal X-ray observations and improve pool-observed XRT data. It is also found that DEM inversions using AIA data and our deep-learning-predicted X-ray data jointly are better than those using AIA data alone. This work indicates that deep-learning methods provide the opportunity to study the Sun based on virtual solar observation in future.

Non-LTE Calculations of the Mg i 12.32 μm Line in a Flaring Atmosphere

Jie **Hong**1,2,3, Xianyong Bai2,4, Ying Li5, M. D. Ding1,3, and Yuanyong Deng2,4
2020 ApJ 898 134
https://doi.org/10.3847/1538-4357/ab9c21
The infrared Mg i lines near 12 μm are a pair of emission lines that are magnetically sensitive and have been used to measure solar magnetic fields. Here we calculate the response of the Mg i 12.32 μm line during a flare and find that in our modeling this line has a complicated behavior. At the beginning of the flare heating, this line shows an intensity dimming at the line center. The intensity then increases when heating continues, with increasing contributions from the heated layers in the chromosphere. The line formation height and the line width also increase as a result. As for the polarized line profiles, we find that flare heating tends to decrease the Zeeman splitting width and attenuates the Stokes V lobe intensity. The wider features in the Stokes V profiles are more pronounced during flare heating, which should be considered when performing magnetic field inversions.

Non-LTE Calculations of the Fe I 6173 Å Line in a Flaring Atmosphere

Jie **Hong**, M. D. Ding, Ying Li, Mats Carlsson
ApJL **2018**
https://arxiv.org/pdf/1803.09912.pdf

The Fe I 6173 {\AA} line is widely used in the measurements of vector magnetic fields by instruments including the Helioseismic and Magnetic Imager (HMI). We perform non-local thermodynamic equilibrium calculations of this line based on radiative hydrodynamic simulations in a flaring atmosphere. We employ both a quiet-Sun atmosphere and a penumbral atmosphere as the initial one in our simulations. We find that, in the quiet-Sun atmosphere, the line center is obviously enhanced during an intermediate flare. The enhanced emission is contributed from both radiative backwarming in the photosphere and particle beam heating in the lower chromosphere. A blue asymmetry of the line profile also appears due to an upward mass motion in the lower chromosphere. If we take a penumbral atmosphere as the initial atmosphere, the line has a more significant response to the flare heating, showing a central emission and an obvious asymmetry. The low spectral resolution of HMI would indicate some loss of information but the enhancement and line asymmetry are still kept. By calculating polarized line profiles, we find that the Stokes I and V profiles can be altered as a result of flare heating. Thus the distortion of this line has a crucial influence on the magnetic field measured from this line, and one should be cautious in interpreting the magnetic transients observed frequently in solar flares.

RADYN simulations of non-thermal and thermal models of Ellerman bombs

Jie **Hong**, Mats Carlsson, M. D. Ding

ApJ **2017**

https://arxiv.org/pdf/1707.05514.pdf

Ellerman bombs (EBs) are brightenings in the Hα line wings that are believed to be caused by magnetic reconnection in the lower atmosphere. To study the response and evolution of the chromospheric line profiles, we perform radiative hydrodynamic simulations of EBs using both non-thermal and thermal models. Overall, these models can generate line profiles that are similar to observations. However, in non-thermal models we find dimming in the Hα line wings and continuum when the heating begins, while for the thermal models dimming occurs only in the Hα line core, and with a longer lifetime. This difference in line profiles can be used to determine whether an EB is dominated by non-thermal heating or thermal heating. In our simulations, if a higher heating rate is applied, the Hα line will be unrealistically strong, while there are still no clear UV burst signatures.

Multi-wavelength Spectral Analysis of Ellerman Bombs Observed by FISS and IRIS

Jie **Hong**, M. D. Ding, Wenda Cao

ApJ **838** 101 **2017**

https://arxiv.org/pdf/1703.04268.pdf

http://iopscience.iop.org/article/10.3847/1538-4357/aa671e/pdf

Ellerman bombs (EBs) are a kind of solar activities that is suggested to occur in the lower atmosphere. Recent observations using the Interface Region Imaging Spectrograph (IRIS) show connections of EBs and IRIS bombs (IBs), implying that EBs might be heated to a much higher temperature (8×104 K) than previous results. Here we perform a spectral analysis of the EBs simultaneously observed by the Fast Imaging Solar Spectrograph (FISS) and IRIS. The observational results show clear evidence of heating in the lower atmosphere, indicated by the wing enhancement in Hα, Ca II 8542 \r{A} and Mg II triplet lines, and also by brightenings in the images of 1700 \r{A} and 2832 \r{A} ultraviolet continuum channels. Additionally, the Mg II triplet line intensity is correlated with that of Hα when the EB occurs, indicating the possibility to use the triplet as an alternative way to identify EBs. However, we do not find any signal in IRIS hotter lines (C II and Si IV). For further analysis, we employ a two-cloud model to fit the two chromospheric lines (Hα and Ca II 8542 \r{A}) simultaneously, and obtain a temperature enhancement of 2300 K for a strong EB. This temperature is among the highest of previous modeling results while still insufficient to produce IB signatures at ultraviolet wavelengths**. 2015 August 16**

Spectral observations of Ellerman bombs and fitting with a two-cloud model

Jie **Hong**, M. D. Ding, Ying Li, Cheng Fang, Wenda Cao

ApJ, 792 13, **2014**

http://arxiv.org/pdf/1407.3048v1.pdf

We study the Hα and Ca II 8542 \r{A} line spectra of four typical Ellerman bombs (EBs) in active region NOAA 11765 on **2013 June 6**, observed with the Fast Imaging Solar Spectrograph installed at the 1.6 meter New Solar Telescope at Big Bear Solar Observatory. Considering that EBs may occur in a restricted region in the lower atmosphere, and that their spectral lines show particular features, we propose a two-cloud model to fit the observed line profiles. The lower cloud can account for the wing emission, and the upper cloud is mainly responsible for the absorption at line center. After choosing carefully the free parameters, we get satisfactory fitting results. As expected, the lower cloud shows an increase of the source function, corresponding to a temperature increase of 400--1000 K in EBs relative to the quiet Sun. This is consistent with previous results deduced from semi-empirical models and confirms that a local heating occurs in the lower atmosphere during the appearance of EBs. We also find that the optical depths can increase to some extent in both the lower and upper clouds, which may result from either a direct heating in the lower cloud, or illumination by an enhanced radiation on the upper cloud. The velocities derived from this method, however, are different from those obtained using the traditional bisector method, implying

that one should be cautious when interpreting this parameter. The two-cloud model can thus be used as an efficient method to deduce the basic physical parameters of EBs.

An MHD avalanche model of multi-threaded coronal loop

A. W. **Hood**, P. J. Cargill, P. K. Browning, K. V. Tam
2016 ApJ 817 5
http://arxiv.org/pdf/1512.00628v1.pdf
For the first time, we demonstrate how an MHD avalanche might occur in a multi-threaded coronal loop. Considering 23 non-potential magnetic threads within a loop, we use 3D MHD simulations to show that only one thread needs to be unstable in order to start an avalanche even when the others are below marginal stability. This has significant implications for coronal heating in that it provides for energy dissipation with a trigger mechanism. The instability of the unstable thread follows the evolution determined in many earlier investigations. However, once one stable thread is disrupted, it coalesces with a neighbouring thread and this process disrupts other nearby threads. Coalescence with these disrupted threads then occurs leading to the disruption of yet more threads as the avalanche develops. Magnetic energy is released in discrete bursts as the surrounding stable threads are disrupted. The volume integrated heating, as a function of time, shows short spikes suggesting that the temporal form of the heating is more like that of \textit{nanoflares} than of constant heating.

The Solar Orbiter magnetometer

T. S. **Horbury**1, H. O'Brien1, I. Carrasco Blazquez1, M. Bendyk1, P. Brown1 …
A&A 642, A9 (**2020**)
https://doi.org/10.1051/0004-6361/201937257
https://www.aanda.org/articles/aa/pdf/2020/10/aa37257-19.pdf
The magnetometer instrument on the Solar Orbiter mission is designed to measure the magnetic field local to the spacecraft continuously for the entire mission duration. The need to characterise not only the background magnetic field but also its variations on scales from far above to well below the proton gyroscale result in challenging requirements on stability, precision, and noise, as well as magnetic and operational limitations on both the spacecraft and other instruments. The challenging vibration and thermal environment has led to significant development of the mechanical sensor design. The overall instrument design, performance, data products, and operational strategy are described.

Dynamics of Large-Scale Solar Flows **Review**

Hideyuki **Hotta**, Yuto Bekki, Laurent Gizon, Quentin Noraz & Mark Rast
Space Science Reviews 219, Article number: 77 (**2023**)
https://link.springer.com/content/pdf/10.1007/s11214-023-01021-6.pdf
The Sun's axisymmetric large-scale flows, differential rotation and meridional circulation, are thought to be maintained by the influence of rotation on the thermal-convective motions in the solar convection zone. These large-scale flows are crucial for maintaining the Sun's global magnetic field. Over the last several decades, our understanding of large-scale motions in the Sun has significantly improved, both through observational and theoretical efforts. Helioseismology has constrained the flow topology in the solar interior, and the growth of supercomputers has enabled simulations that can self-consistently generate large-scale flows in rotating spherical convective shells. In this article, we review our current understanding of solar convection and the large-scale flows present in the Sun, including those associated with the recently discovered inertial modes of oscillation. We discuss some issues still outstanding, and provide an outline of future efforts needed to address these.

Dynamics of solar large-scale flows **Review**

Hideyuki **Hotta**, Yuto Bekki, Laurent Gizon, Quentin Noraz, Mark P. Rast
Nature **2023**
https://arxiv.org/pdf/2307.06481.pdf
The Sun's axisymmetric large-scale flows, differential rotation and meridional circulation, are thought to be maintained by the influence of rotation on the thermal-convective motions in the solar convection zone. These large-scale flows are crucial for maintaining the Sun's global magnetic field. Over the last several decades, our understanding of large-scale motions in the Sun has significantly improved, both through observational and theoretical efforts. Helioseismology has constrained the flow topology in the solar interior, and the growth of supercomputers has enabled simulations that can self-consistently generate large scale flows in rotating spherical convective shells. In this chapter, we review our current understanding of solar convection and the large-scale flows present in the Sun, including those associated with the recently discovered inertial modes of oscillation. We discuss some issues still outstanding, and provide an outline of future efforts needed to address these.

Generation of Solar-like Differential Rotation

H. **Hotta**1, K. Kusano2, and R. Shimada3
2022 ApJ 933 199
https://iopscience.iop.org/article/10.3847/1538-4357/ac7395/pdf
We analyze the simulation result shown in Hotta & Kusano (2021) in which the solar-like differential rotation is reproduced. The Sun is rotating differentially with the fast equator and the slow pole. It is widely thought that the thermal convection maintains the differential rotation, but recent high-resolution simulations tend to fail to reproduce the fast equator. This fact is an aspect of one of the biggest problems in solar physics called the convective conundrum. Hotta & Kusano succeed in reproducing the solar-like differential rotation without using any manipulation with an unprecedentedly high-resolution simulation. In this study, we analyze the simulation data to understand the maintenance mechanism of the fast equator. Our analyses lead to conclusions that are summarized as follows. (1) The superequipatition magnetic field is generated by the compression, which can indirectly convert the massive internal energy to magnetic energy. (2) The efficient small-scale energy transport suppresses large-scale convection energy. (3) Non-Taylor–Proudman differential rotation is maintained by the entropy gradient caused by the anisotropic latitudinal energy transport enhanced by the magnetic field. (4) The fast equator is maintained by the meridional flow mainly caused by the Maxwell stress. The Maxwell stress itself also has a role in the angular momentum transport for the fast near-surface equator (we call it the Punching ball effect). The fast equator in the simulation is reproduced not due to the low Rossby number regime but due to the strong magnetic field. This study newly finds the role of the magnetic field in the maintenance of differential rotation.

Solar differential rotation reproduced with high-resolution simulation

H. **Hotta**, K. Kusano
Nature Astronomy (**2021**)
https://arxiv.org/pdf/2109.06280.pdf
The Sun rotates differentially with a fast equator and slow pole. Convection in the solar interior is thought to maintain the differential rotation. However, although many numerical simulations have been conducted to reproduce the solar differential rotation, previous high-resolution calculations with solar parameters fall into the anti-solar (fast pole) differential rotation regime. Consequently, we still do not know the true reason why the Sun has a fast-rotating equator. While the construction of the fast equator requires a strong rotational influence on the convection, the previous calculations have not been able to achieve the situation without any manipulations. The problem is called convective conundrum. The convection and the differential rotation in numerical simulations were different from the observations. Here, we show that a high-resolution calculation succeeds in reproducing the solar-like differential rotation. Our calculations indicate that the strong magnetic field generated by a small-scale dynamo has a significant impact on thermal convection. The successful reproduction of the differential rotation, convection, and magnetic field achieved in our calculation is an essential step to understanding the cause of the most basic nature of solar activity, specifically, the 11-year cycle of sunspot activity.

On rising magnetic flux tube and formation of sunspots in a deep domain

H. **Hotta**, H. Iijima
MNRAS **2020**
https://arxiv.org/pdf/2003.10583.pdf
We investigate the rising flux tube and the formation of sunspots in an unprecedentedly deep computational domain that covers the whole convection zone with a radiative magnetohydrodynamics simulation. Previous calculations had shallow computational boxes (< 30 Mm) and convection zones at a depth of 200 Mm. By using our new numerical code R2D2, we succeed in covering the whole convection zone and reproduce the formation of the sunspot from a simple horizontal flux tube because of the turbulent thermal convection. The main findings are (1) The rising speed of the flux tube is larger than the upward convection velocity because of the low density caused by the magnetic pressure and the suppression of the mixing. (2) The rising speed of the flux tube exceeds 250 m/s at a depth of 18 Mm, while we do not see any clear evidence of the divergent flow 3 hr before the emergence at the solar surface. (3) Initially, the root of the flux tube is filled with the downflows and then the upflow fills the center of the flux tube during the formation of the sunspot. (4) The essential mechanisms for the formation of the sunspot are the coherent inflow and the turbulent transport. (5) The low-temperature region is extended to a depth of at least 40 Mm in the matured sunspot, with the high-temperature region in the center of the flux tube. Some of the findings indicate the importance of the deep computational domain for the flux emergence simulations.

Solar overshoot region and small-scale dynamo with realistic energy flux

H. **Hotta**
ApJ **843** 52 **2017**
https://arxiv.org/pdf/1706.06413.pdf

We carry out high resolution calculations of the solar overshoot region with unprecedentedly realistic parameters, especially the small energy flux compared with ρc3s, where ρ and cs are density and speed of sound. Our main purpose is to investigate behavior of the overshoot and the
small-scale dynamo with parameters as close as possible to those of the Sun. Our calculations show that the bottom part of the convection zone becomes subadiabatic, which efficiently suppresses downflows. As a result we see a steep transition from the CZ to the RZ whose width is estimated 0.4% of the local pressure scale height. This result is consistent with a semi-analytic convection/overshoot model. We also find that the small-scale dynamo becomes efficient with a smaller energy flux. The sudden suppression of the downflows around the base of the convection zone increases the efficiency of the small-scale dynamo.

Efficient small-scale dynamo in solar convection zone

H. **Hotta**, M. Rempel, T. Yokoyama
ApJ **803** 42 **2015**
http://arxiv.org/pdf/1502.03846v1.pdf
We investigate small-scale dynamo action in the solar convection zone through a series of high resolution MHD simulations in a local Cartesian domain with 1R⊙ (solar radius) of horizontal extent and a radial extent from 0.715 to 0.96R⊙. The dependence of the solution on resolution and diffusivity is studied. For a grid spacing of less than 350 km, the root mean square magnetic field strength near the base of the convection zone reaches 95% of the equipartition field strength (i.e. magnetic and kinetic energy are comparable). For these solutions the Lorentz force feedback on the convection velocity is found to be significant. The velocity near the base of the convection zone is reduced to 50% of the hydrodynamic one. In spite of a significant decrease of the convection velocity, the reduction in the enthalpy flux is relatively small, since the magnetic field also suppresses the horizontal mixing of the entropy between up- and downflow regions. This effect increases the amplitude of the entropy perturbation and makes convective energy transport more efficient. We discuss potential implications of these results for solar global convection and dynamo simulations.

High-resolution calculation of the solar global convection with the reduced speed of sound technique: II. Near surface shear layer with the rotation

H. **Hotta**, M. Rempel, T. Yokoyama
ApJ, **2014**
http://arxiv.org/pdf/1410.7093v1.pdf
We present a high-resolution, highly stratified numerical simulation of rotating thermal convection in a spherical shell. Our aim is to study in detail the processes that can maintain a near surface shear layer (NSSL) as inferred from helioseismology. Using the reduced speed of sound technique we can extend our global convection simulation to 0.99R⊙ and include near the top of our domain small-scale convection with short time scales that is only weakly influenced by rotation. We find the formation of a NSSL preferentially in high latitudes in the depth range r=0.95−0.975R⊙. The maintenance mechanisms are summarized as follows. Convection under
weak influence of rotation leads to Reynolds stresses that transport angular momentum radially inward in all latitudes. This leads to the formation of a strong poleward directed meridional flow and a NSSL, which is balanced in the meridional plane by forces resulting from the ⟨v′rv′θ⟩ correlation of turbulent velocities. The origin of the required correlations depends to some degree on latitude. In high latitudes a positive correlation ⟨v′rv′θ⟩ is induced in the NSSL by the poleward meridional flow whose amplitude increases with the radius, while a negative correlation is generated by the Coriolis force in bulk of the convection zone. In low latitudes a positive correlation ⟨v′rv′θ⟩ results from rotationally aligned convection cells ("banana cells"). The force caused by these Reynolds stresses is in balance with the Coriolis force in the NSSL.

Coronal Microjets in Quiet-Sun Regions Observed with the Extreme Ultraviolet Imager on Board the Solar Orbiter

Zhenyong **Hou**1, Hui Tian1,2, David Berghmans3, Hechao Chen1, Luca Teriaca4, Udo Schühle4, Yuhang Gao1, Yajie Chen1, Jiansen He1, Linghua Wang1Show full author list
2021 ApJL 918 L20
https://doi.org/10.3847/2041-8213/ac1f30
We report the smallest coronal jets ever observed in the quiet Sun with recent high-resolution observations from the High Resolution Telescopes (HRIEUV and HRILyα) of the Extreme Ultraviolet Imager on board the Solar Orbiter (SO). In the HRIEUV (174 Å) images, these microjets usually appear as nearly collimated structures with brightenings at their footpoints. Their average lifetime, projected speed, width, and maximum length are 4.6 minutes, 62 km s−1, 1.0 Mm, and 7.7 Mm, respectively. Inverted-Y shaped structures and moving blobs can be identified in some events. A subset of these events also reveal signatures in the HRILyα (H i Lyα at 1216 Å) images and the extreme ultraviolet images taken by the Atmospheric Imaging Assembly (AIA) on board the Solar Dynamics Observatory (SDO). Our differential emission-measure (EM) analysis suggests a multithermal nature and

an average density of ∼1.4 × 109 cm−3 for these microjets. Their thermal and kinetic energies were estimated to be ∼3.9 × 1024 erg and ∼2.9 × 1023 erg, respectively, which are of the same order of the released energy predicted by the nanoflare theory. Most events appear to be located at the edges of network lanes and magnetic flux concentrations, suggesting that these coronal microjets are likely generated by magnetic reconnection between small-scale magnetic loops and the adjacent network field.

Spectro-polarimetric Observations at the NVST: I. Instrumental Polarization Calibration and Primary Measurements

Jun-Feng **Hou**, Zhi Xu, Shu Yuan, Yu-Chao Chen, Jian-Guo Peng, Dong-Guang Wang, Jun Xu, Yuan-Yong Deng, Zhen-Yu Jin, Kai-Fan Ji, Zhong Liu
Research in Astronomy and Astrophysics **2019**
https://arxiv.org/pdf/1911.07397.pdf
This paper is devoted to the primary spectro-polarimetric observation performed at the New Vacuum Solar Telescope of China since 2017, and our aim is to precisely evaluate the real polarimetric accuracy and sensitivity of this polarimetry by using full Stokes spectro-polarimetric observations of the photospheric line Fe I 532.4 nm. In the work, we briefly describe the salient characteristic of the NVST as a polarimeter in technology and then characterize its instrumental polarization based on the operation in 2017 and 2019. It is verified that the calibration method making use of the instrumental polarization calibration unit (ICU) is stable and credible. The calibration accuracy can reach up to 3×10−3 . Based on the scientific observation of the NOAA 12645 on April 5th, 2017, we estimate that the residual cross-talk from Stokes I to Stokes Q, U and V, after the instrumental polarization calibration, is about 4×10−3 on average, which is consistent with the calibration accuracy and close to the photon noise. The polarimetric sensitivity (i.e., the detection limit) for polarized light is of the order of 10−3 with an integration time over 20 seconds. Slow modulation rate is indeed an issue for the present system. The present NVST polarimeter is expected to be integrated with an high-order adaptive optics system and a field scanner to realize 2D magnetic field vector measurements in the following instrumentation update. **April 5th, 2017**

Narrow-line-width UV bursts in the transition region above Sunspots observed by IRIS

Zhenyong **Hou**, Zhenghua Huang, Lidong Xia, Bo Li, Maria S. Madjarska, Hui Fu, Chaozhou Mou, Haixia Xie
ApJL 829 L30 **2016**
http://arxiv.org/pdf/1608.04892v1.pdf
Various small-scale structures abound in the solar atmosphere above active regions, playing an important role in the dynamics and evolution therein. We report on a new class of small-scale transition region structures in active regions, characterized by strong emissions but extremely narrow Si IV line profiles as found in observations taken with the Interface Region Imaging Spectrograph (IRIS). Tentatively named as Narrow-line-width UV bursts (NUBs), these structures are located above sunspots and comprise of one or multiple compact bright cores at sub-arcsecond scales. We found six NUBs in two datasets (a raster and a sit-and-stare dataset). Among these, four events are short-living with a duration of ∼10 mins while two last for more than 36 mins. All NUBs have Doppler shifts of 15--18 km/s, while the NUB found in sit-and-stare data possesses an additional component at ∼50 km/s found only in the C II and Mg II lines. Given that these events are found to play a role in the local dynamics, it is important to further investigate the physical mechanisms that generate these phenomena and their role in the mass transport in sunspots. **2014 February 16**

Light Walls Around Sunspots Observed by the Interface Region Imaging Spectrograph

Y. J. **Hou**, T. Li, S. H. Yang, J. Zhang
A&A Letters **2016**
http://arxiv.org/pdf/1604.00485v1.pdf
The Interface Region Imaging Spectrograph (IRIS) mission provides high-resolution observations of the chromosphere and transition region. We try to determine whether the light walls exist somewhere else in active regions besides light bridges. Employing half-year high tempo-spatial data from the IRIS, we find lots of light walls either around sunspots or above light bridges. For the first time, we report one light wall near an umbral-penumbral boundary and another along a neutral line between two small sunspots. These new observations reveal that these light walls are multi-layer and multi-thermal structures which occur along magnetic neutral lines in active regions.

On the surface physics affecting solar oscillation frequencies

G. **Houdek**, R. Trampedach, M. J. Aarslev, J. Christensen-Dalsgaard
MNRAS **2016**
http://arxiv.org/pdf/1609.06129v1.pdf
Adiabatic oscillation frequencies of stellar models, computed with the standard mixing-length formulation for convection, increasingly deviate with radial order from observations in solar-like stars. Standard solar models

overestimate adiabatic frequencies by as much as ~ 20 {\mu}Hz. In this letter, we address the physical processes of turbulent convection that are predominantly responsible for the frequency differences between standard models and observations, also called `surface effects'. We compare measured solar frequencies from the MDI instrument on the SOHO spacecraft with frequency calculations that include three-dimensional (3D) hydrodynamical simulation results in the equilibrium model, nonadiabatic effects, and a consistent treatment of the turbulent pressure in both the equilibrium and stability computations. With the consistent inclusion of the above physics in our model computation we are able to reproduce the observed solar frequencies to < 3 {\mu}Hz without the need of any additional ad-hoc functional corrections.

"Interaction Between Convection and Pulsation" Review

Günter **Houdek** and Marc-Antoine Dupret
Living Reviews in Solar Physics, PUB.NO. lrsp-**2015**-8
www.livingreviews.org/lrsp-2015-8
This article reviews our current understanding of modelling convection dynamics in stars. Several semi-analytical time-dependent convection models have been proposed for pulsating one-dimensional stellar structures with different formulations for how the convective turbulent velocity field couples with the global stellar oscillations. In this review we put emphasis on two, widely used, time-dependent convection formulations for estimating pulsation properties in one-dimensional stellar models. Applications to pulsating stars are presented with results for oscillation properties, such as the effects of convection dynamics on the oscillation frequencies, or the stability of pulsation modes, in classical pulsators and in stars supporting solar-type oscillations.

Magnetohydrodynamic Non-linearities in Sunspot Atmospheres: Chromospheric Detections of Intermediate Shocks

S.J. **Houston**, D.B. Jess, R. Keppens, M. Stangalini, P.H. Keys, S.D.T. Grant, S. Jafarzadeh, L.M. McFetridge, M. Murabito, I. Ermolli, F. Giorgi
ApJ **2020**
https://arxiv.org/pdf/2002.12368.pdf
The formation of shocks within the solar atmosphere remains one of the few observable signatures of energy dissipation arising from the plethora of magnetohydrodynamic waves generated close to the solar surface. Active region observations offer exceptional views of wave behavior and its impact on the surrounding atmosphere. The stratified plasma gradients present in the lower solar atmosphere allow for the potential formation of many theorized shock phenomena. In this study, using chromospheric Ca II 854.2nm spectropolarimetric data of a large sunspot, we examine fluctuations in the plasma parameters in the aftermath of powerful shock events that demonstrate polarimetric reversals during their evolution. Modern inversion techniques are employed to uncover perturbations in the temperatures, line-of-sight velocities, and vector magnetic fields occurring across a range of optical depths synonymous with the shock formation. Classification of these non-linear signatures is carried out by comparing the observationally-derived slow, fast, and Alfvén shock solutions to the theoretical Rankine-Hugoniot relations. Employing over 200,000 independent measurements, we reveal that the Alfvén (intermediate) shock solution provides the closest match between theory and observations at optical depths of log(tau) = -4, consistent with a geometric height at the boundary between the upper photosphere and lower chromosphere. This work uncovers first-time evidence of the manifestation of chromospheric intermediate shocks in sunspot umbrae, providing a new method for the potential thermalization of wave energy in a range of magnetic structures, including pores, magnetic flux ropes, and magnetic bright points. **2016 May 20**,

A new solar neutrino channel for grand-unification monopole searches

Nick **Houston**, Tianjun Li, Chen Sun
2018
https://arxiv.org/pdf/1803.02835.pdf
We identify a previously untapped discovery channel for grand-unification monopoles, arising from their ability to catalyse the direct decay of protons into monoenergetic 459 MeV antineutrinos within the Sun. Previous analyses omit this possibility as it necessarily involves an electroweak suppression factor, and instead search for the unsuppressed 20-50 MeV neutrinos produced via two-stage proton decays. By accounting for the relative difference in interaction cross section and experimental background at typical neutrino detection experiments, we demonstrate that this new channel in fact possesses greater discovery potential. As a case in point, using 5326 live days of Super-Kamiokande exposure we find that $2\;\sigma$ ($3\;\sigma$) deviations in the 20-50 MeV channel are amplified to $3\;\sigma$ ($4.6\;\sigma$) deviations in the 459 MeV case. Exploiting correlations between these two channels may also offer even greater statistical power.

Two New Methods for Counting and Tracking the Evolution of Polar Faculae

B. **Hovis-Afflerbach** & W. Dean Pesnell

Solar Physics volume 297, Article number: 48 (**2022**)
https://link.springer.com/content/pdf/10.1007/s11207-022-01977-8.pdf
Polar faculae are the footpoints of magnetic-field lines near the Sun's poles that are seen as bright regions along the edges of granules. The time variation in the number of polar faculae has been shown to correlate with the strength of the polar magnetic field and to be a predictor of the subsequent solar cycle. Due to the small size and transient nature of these features, combined with different techniques and observational factors, previous counts of polar faculae differ in magnitude. Further, there were no scalable techniques to measure the statistical properties of the faculae, such as the variation of the facular lifetime with time or solar activity. Using data from the Helioseismic and Magnetic Imager (HMI) onboard the Solar Dynamics Observatory (SDO), we present two new methods for tracking faculae and measuring their properties. In the first, we calculate the pixel-by-pixel standard deviation of the HMI continuum intensity images over one day, visualizing the faculae as streaks. The lifetime of the facula is found by dividing the angular length of the streaks by the latitude-dependent rotation rate. We apply this method to the more visible pole each day for a week every six months, from September 2010 to March 2021. Combining all of the measured facular lifetimes provides a statistical distribution with a mean of 6.0 hours, a FWHM of 5.4 hours, and a skew towards longer lifetimes, with some faculae lasting up to 1 day. In the second method, we overlay images of the progressive standard deviation with the HMI magnetogram to show the close relationship between the facular candidates and the magnetic field. The results of this method allow us to distinguish between motion due to the Sun's rotation and "proper motion" due to faculae moving across the Sun's surface, confirming that faculae participate in convective motions at the poles. Counts of polar faculae using both methods agree with previous counts in their variation with the solar cycle and the polar magnetic field. These methods can be extended to automate the identification and measurement of other properties of polar faculae, which would allow for daily measurements of all faculae since SDO began operation in 2010.

The Solar Orbiter Heliospheric Imager (SoloHI)

R. A. **Howard**1, A. Vourlidas2, R. C. Colaninno1, C. M. Korendyke1, S. P. Plunkett1 …
A&A 642, A13 (**2020**)
https://doi.org/10.1051/0004-6361/201935202
https://www.aanda.org/articles/aa/pdf/2020/10/aa35202-19.pdf
Aims. We present the design and pre-launch performance of the Solar Orbiter Heliospheric Imager (SoloHI) which is an instrument prepared for inclusion in the ESA/NASA Solar Orbiter mission, currently scheduled for launch in 2020.
Methods. The goal of this paper is to provide details of the SoloHI instrument concept, design, and pre-flight performance to give the potential user of the data a better understanding of how the observations are collected and the sources that contribute to the signal.
Results. The paper discusses the science objectives, including the SoloHI-specific aspects, before presenting the design concepts, which include the optics, mechanical, thermal, electrical, and ground processing. Finally, a list of planned data products is also presented.
Conclusions. The performance measurements of the various instrument parameters meet or exceed the requirements derived from the mission science objectives. SoloHI is poised to take its place as a vital contributor to the science success of the Solar Orbiter mission.

Near-Sun observations of an F-corona decrease and K-corona fine structure

R. A. **Howard**, A. Vourlidas, […] N. M. Viall
Nature volume 576, pages232–236 (**2019**)
https://www.nature.com/articles/s41586-019-1807-x.pdf
Remote observations of the solar photospheric light scattered by electrons (the K-corona) and dust (the F-corona or zodiacal light) have been made from the ground during eclipses1 and from space at distances as small as 0.3 astronomical units2,3,4,5 to the Sun. Previous observations6,7,8 of dust scattering have not confirmed the existence of the theoretically predicted dust-free zone near the Sun9,10,11. The transient nature of the corona has been well characterized for large events, but questions still remain (for example, about the initiation of the corona12 and the production of solar energetic particles13) and for small events even its structure is uncertain14. Here we report imaging of the solar corona15 during the first two perihelion passes (0.16–0.25 astronomical units) of the Parker Solar Probe spacecraft13, each lasting ten days. The view from these distances is qualitatively similar to the historical views from ground and space, but there are some notable differences. At short elongations, we observe a decrease in the intensity of the F-coronal intensity, which is suggestive of the long-sought dust free zone9,10,11. We also resolve the fine-scale plasma structure of very small eruptions, which are frequently ejected from the Sun. These take two forms: the frequently observed magnetic flux ropes12,16 and the predicted, but not yet observed, magnetic islands17,18 arising from the tearing-mode instability in the current sheet. Our observations of the coronal streamer evolution confirm the large-scale topology of the solar corona, but also reveal that, as recently predicted19, streamers are composed of yet smaller substreamers channelling continual density fluctuations at all visible scales.

The Solar Orbiter Heliospheric Imager (SoloHI)

R. A. **Howard**1, A. Vourlidas2 , R. C. Colaninno1 , C. M. Korendyke1 , S. P. Plunkett1 , M. T. Carter1 , D. Wang1 ...

A&A **2019**

https://www.aanda.org/articles/aa/pdf/forth/aa35202-19.pdf

Aims. We present the design and pre-launch performance of the Solar Orbiter Heliospheric Imager (SoloHI) which is an instrument prepared for inclusion in the ESA/NASA Solar Orbiter mission, currently scheduled for launch in 2020. Methods. The goal of this paper is to provide details of the SoloHI instrument concept, design, and pre-flight performance to give the potential user of the data a better understanding of how the observations are collected and the sources that contribute to the signal. Results. The paper discusses the science objectives, including the SoloHI-specific aspects, before presenting the design concepts, which include the optics, mechanical, thermal, electrical, and ground processing. Finally, a list of planned data products is also presented. Conclusions. The performance measurements of the various instrument parameters meet or exceed the requirements derived from the mission science objectives. SoloHI is poised to take its place as a vital contributor to the science success of the Solar Orbiter mission. **2007-04-29**

2. Science objectives **Review**

Update on Global Helioseismic Observations of the Solar Torsional Oscillation

Rachel **Howe**1, W. J. Chaplin1, J. Christensen-Dalsgaard2, Y. P. Elsworth1, and J. Schou3

Res. Notes AAS 6 261 **2022**

https://iopscience.iop.org/article/10.3847/2515-5172/aca97d

We present an up-to-date latitude–time map of the solar zonal flows at 0.99 R⊙ from global helioseismology using data from the Global Oscillation Network Group, the Michelson Doppler Imager, and the Helioseismic and Magnetic Imager.

Unexpected solar-cycle variation of acoustic mode power in Sun-as-a-star observations

Rachel **Howe**, W. J. Chaplin, Y. P. Elsworth, S. J. Hale, M. B. Nielsen

MNRAS Volume 514, Issue 3, August **2022**, Pages 3821–3827,

https://doi.org/10.1093/mnras/stac1534

https://arxiv.org/pdf/2205.15655

We examine the solar-cycle variation of the power in the low-degree helioseismic modes by looking at binned power spectra from 45 years of observations with the Birmingham Solar Oscillations Network, which provides a more robust estimate of the mode power than that obtained by peak fitting. The solar-cycle variation of acoustic mode power in the five-minute band is clearly seen. Unusually, even though Cycle 24 was substantially weaker in terms of surface magnetic activity than Cycle 23, the reduction in mode power at solar maximum is very similar for the two cycles, suggesting that the relationship between mode power and magnetic activity is more complex than has previously been thought. This is in contrast to the mode frequencies, which show a strong correlation with activity with only subtle differences between in the response across different solar cycles.

Signatures of Solar Cycle 25 in Subsurface Zonal Flows

R. **Howe**, F. Hill, R. Komm, W. J. Chaplin, Y. Elsworth, G. R. Davies, J. Schou, M. J. Thompson

ApJL **862** L5 **2018**

https://arxiv.org/pdf/1807.02398.pdf

The pattern of migrating zonal flow bands associated with the solar cycle, known as the torsional oscillation, has been monitored with continuous global helioseismic observations by the Global Oscillations Network Group, together with those made by the Michelson Doppler Imager onboard the Solar and Heliospheric Observatory and its successor the Helioseismic and Magnetic Imager onboard the Solar Dynamics Observatory, since 1995, giving us nearly two full solar cycles of observations. We report that the flows now show traces of the mid-latitude acceleration that is expected to become the main equatorward-moving branch of the zonal flow pattern for Cycle 25. Based on the current position of this branch, we speculate that the onset of widespread activity for Cycle 25 is unlikely to be earlier than the middle of 2019.

HMI Science Nuggets #108 **2018** http://hmi.stanford.edu/hminuggets/?p=2626

Changes in the sensitivity of solar p-mode frequency shifts to activity over three solar cycles

R. **Howe**, W.J. Chaplin, G.R. Davies, Y. Elsworth, S. Basu, A.-M. Broomhall

MNRAS **2018**

https://arxiv.org/pdf/1807.01504.pdf

Low-degree solar p-mode observations from the long-lived Birmingham Solar Oscillations Network (BiSON) stretch back further than any other single helioseismic data set. Results from BiSON have suggested that the response of the mode frequency to solar activity levels may be different in different cycles. In order to check whether such changes can also be seen at higher degrees, we compare the response of medium-degree solar p-modes to activity levels across three solar cycles using data from Big Bear Solar Observatory (BBSO), Global Oscillation Network Group (GONG), Michelson Doppler Imager (MDI) and Helioseismic and Magnetic Imager (HMI), by examining the shifts in the mode frequencies and their sensitivity to solar activity levels. We compare these shifts and sensitivities with those from radial modes from BiSON. We find that the medium-degree data show small but significant systematic differences between the cycles, with solar cycle 24 showing a frequency shift about 10 per cent larger than cycle 23 for the same change in activity as determined by the 10.7 cm radio flux. This may support the idea that there have been changes in the magnetic properties of the shallow subsurface layers of the Sun that have the strongest influence on the frequency shifts.

The Sun in transition? Persistence of near-surface structural changes through Cycle 24

R. **Howe**, G. R. Davies, W. J. Chaplin, Y. Elsworth, S. Basu, S. J. Hale, W. H. Ball, R. W. Komm
MNRAS **2017**
https://arxiv.org/pdf/1705.09099.pdf

We examine the frequency shifts in low-degree helioseismic modes from the Birmingham Solar-Oscillations Network (BiSON) covering the period from 1985 - 2016, and compare them with a number of global activity proxies well as a latitudinally-resolved magnetic index. As well as looking at frequency shifts in different frequency bands, we look at a parametrization of the shift as a cubic function of frequency. While the shifts in the medium- and highfrequency bands are very well correlated with all of the activity indices (with the best correlation being with the 10.7 cm radio flux), we confirm earlier findings that there appears to have been a change in the frequency response to activity during solar cycle 23, and the low frequency shifts are less correlated with activity in the last two cycles than they were in Cycle 22. At the same time, the more recent cycles show a slight increase in their sensitivity to activity levels at medium and higher frequencies, perhaps because a greater proportion of activity is composed of weaker or more ephemeral regions. This lends weight to the speculation that a fundamental change in the nature of the solar dynamo may be in progress.

Validation of solar-cycle changes in low-degree helioseismic parameters from the Birmingham Solar-Oscillations Network

R. **Howe**, G.R. Davies, W.J. Chaplin, Y.P. Elsworth, S.J. Hale
MNRAS **2015**
http://arxiv.org/pdf/1509.06894v1.pdf

We present a new and up-to-date analysis of the solar low-degree p-mode parameter shifts from the Birmingham Solar-Oscillations Network (BiSON) over the past 22 years, up to the end of 2014. We aim to demonstrate that they are not dominated by changes in the asymmetry of the resonant peak profiles of the modes and that the previously published results on the solar-cycle variations of mode parameters are reliable. We compare the results obtained using a conventional maximum likelihood estimation algorithm and a new one based on the Markov Chain Monte Carlo (MCMC) technique, both taking into account mode asymmetry. We assess the reliability of the solar-cycle trends seen in the data by applying the same analysis to artificially generated spectra. We find that the two methods are in good agreement. Both methods accurately reproduce the input frequency shifts in the artificial data and underestimate the amplitude and width changes by a small amount, around 10 per cent. We confirm earlier findings that the frequency and line width are positively correlated, and the mode amplitude anticorrelated, with the level of solar activity, with the energy supplied to the modes remaining essentially unchanged. For the mode asymmetry the correlation with activity is marginal, but the MCMC algorithm gives more robust results than the MLE. The magnitude of the parameter shifts is consistent with earlier work. There is no evidence that the frequency changes we see arise from changes in the asymmetry, which would need to be much larger than those observed in order to give the observed frequency shift.

Persistent Near-Surface Flow Structures from Local Helioseismology

R. **Howe**, R.W. Komm, D. Baker, L. Harra, L. van Driel-Gesztelyi, R.S. Bogart
Solar Phys. Volume 290, Issue 11, pp 3137-3149 **2015**
http://arxiv.org/pdf/1507.06525v1.pdf

Near-surface flows measured by the ring-diagram technique of local helioseismology show structures that persist over multiple rotations. We examine these phenomena using data from the {\em Global Oscillation Network Group} (GONG) and the {\em Helioseismic and Magnetic Imager} (HMI) and show that a correlation analysis of the structures can be used to estimate the rotation rate as a function of latitude, giving a result consistent with the near-surface rate from global helioseismology and slightly slower than that obtained from a similar analysis of the surface

magnetic field strength. At latitudes of 60◦ and above the HMI flow data reveal a strong signature of a two-sided zonal flow structure. This signature may be related to recent reports of "giant cells" in solar convection.

A Prospectus on Kinetic Heliophysics

Gregory G. **Howes**
Physics of Plasmas **2017**
https://arxiv.org/pdf/1705.07840.pdf

Under the low density and high temperature conditions typical of heliospheric plasmas, the macroscopic evolution of the heliosphere is strongly affected by the kinetic plasma physics governing fundamental microphysical mechanisms. Kinetic turbulence, collision less magnetic reconnection, particle acceleration, and kinetic instabilities are four poorly understood, grand-challenge problems that lie at the new frontier of kinetic heliophysics. The increasing availability of high cadence and high phase-space resolution measurements of particle velocity distributions by current and upcoming spacecraft missions and of massively parallel nonlinear kinetic simulations of weakly collisional heliospheric plasmas provides the opportunity to transform our understanding of these kinetic mechanisms through the full utilization of the information contained in the particle velocity distributions. Several major considerations for future investigations of kinetic heliophysics are examined. Turbulent dissipation followed by particle heating is highlighted as an inherently two-step process in weakly collisional plasmas, distinct from the more familiar case in fluid theory. Concerted efforts must be made to tackle the big-data challenge of visualizing the high-dimensional (3D-3V) phase space of kinetic plasma theory through physics-based reductions. Furthermore, the development of innovative analysis methods that utilize full velocity-space measurements, such as the field-particle correlation technique, will enable us to gain deeper insight into these four grand-challenge problems of kinetic heliophysics. A systems approach to tackle the multi-scale problem of heliophysics through a rigorous connection between the kinetic physics at microscales and the self-consistent evolution of the heliosphere at macro scales will propel the field of kinetic heliophysics into the future.

The effects of driving time scales on coronal heating in a stratified atmosphere⋆

T. A. **Howson**1 and I. De Moortel1,2
A&A 661, A144 (**2022**)
https://www.aanda.org/articles/aa/pdf/2022/05/aa42872-21.pdf

Aims. We investigate the atmospheric response to coronal heating driven by random velocity fields with different characteristic time scales and amplitudes.
Methods. We conducted a series of three-dimensional magnetohydrodynamic simulations of random driving imposed on a gravitationally stratified model of the solar atmosphere. In order to understand differences between alternating current (AC) and direct current (DC) heating, we considered the effects of changing the characteristic time scales of the imposed velocities. We also investigated the effects of the magnitude of the velocity driving.
Results. In all cases, complex foot point motions lead to a proliferation of current sheets and energy dissipation throughout the coronal volume. For a given driving amplitude, DC driving typically leads to a greater rate of energy injection when compared to AC driving. This ultimately leads to the formation of larger currents, increased heating rates, and higher coronal temperatures in DC simulations. There is no difference in the spatial distribution of energy dissipation across simulations; however, energy release events in AC cases tend to be more frequent and last for less time than in DC cases. This results in more asymmetric temperature profiles for field lines heated by AC drivers. Higher velocity driving is associated with larger currents, higher temperatures, and the corona occupying a larger fraction of the simulation volume. In all cases, the majority of heating is associated with small energy release events, which occur much more frequently than larger events.
Conclusions. When combined with observational results that highlight a greater abundance of oscillatory power in lower frequency modes, these findings suggest that energy release in the corona is more likely to be driven by longer time scale motions. In the corona, AC and DC driving occur concurrently and their effects remain difficult to isolate. The distribution of field line temperatures and the asymmetry of temperature profiles may reveal the frequency and longevity of energy release events and therefore the relative importance of AC and DC heating.

Magnetic reconnection and the Kelvin-Helmholtz instability in the solar corona

T. A. **Howson**1, I. De Moortel1,2 and D. I. Pontin3
A&A 656, A112 (**2021**)
https://www.aanda.org/articles/aa/pdf/2021/12/aa41620-21.pdf
https://doi.org/10.1051/0004-6361/202141620

Context. The magnetic Kelvin-Helmholtz instability (KHI) has been proposed as a means of generating magnetohydrodynamic turbulence and encouraging wave energy dissipation in the solar corona, particularly within transversely oscillating loops.
Aims. Our goal is to determine whether the KHI encourages magnetic reconnection in oscillating flux tubes in the solar corona. This will establish whether the instability enhances the dissipation rate of energy stored in the magnetic field.

Methods. We conducted a series of three-dimensional magnetohydrodynamic simulations of the KHI excited by an oscillating velocity shear. We investigated the effects of numerical resolution, field line length, and background currents on the growth rate of the KHI and on the subsequent rate of magnetic reconnection.
Results. The KHI is able to trigger magnetic reconnection in all cases, with the highest rates occurring during the initial growth phase. Reconnection is found to occur preferentially along the boundaries of Kelvin-Helmholtz vortices, where the shear in the velocity and magnetic fields is greatest. The estimated rate of reconnection is found to be lowest in simulations where the KHI growth rate is reduced. For example, this is the case for shorter field lines or due to shear in the background field.
Conclusions. In non-ideal regimes, the onset of the instability causes the local reconnection of magnetic field lines and enhances the rate of coronal wave heating. However, we found that if the equilibrium magnetic field is sheared across the Kelvin-Helmholtz mixing layer, the instability does not significantly enhance the rate of reconnection of the background field, despite the free energy associated with the non-potential field.

The effects of driving time scales on heating in a coronal arcade

Thomas **Howson**, Ineke De Moortel, Lianne Fyfe
A&A 643, A85 **2020**
https://arxiv.org/pdf/2009.07535.pdf
https://doi.org/10.1051/0004-6361/202038869
Context. The relative importance of AC and DC heating in maintaining the temperature of the corona is not well constrained. Aims. Investigate the effects of the characteristic time scales of photospheric driving on the injection and dissipation of energy within a coronal arcade. Methods. We have conducted three dimensional MHD simulations of foot point driving imposed on an arcade. We modified the typical driving time scales to understand the efficiency of heating obtained using AC and DC drivers. We considered the implications for the injected Poynting flux and the nature of the energy release in dissipative regimes. Results. For the same driver amplitude and complexity, long time scale motions are able to inject a much greater Poynting flux into the corona. Consequently, in non-ideal regimes, slow stressing motions result in a greater increase in plasma temperature than for wave-like driving. In dissipative simulations, Ohmic heating is found to be much more significant than viscous heating. For all drivers in our parameter space, energy dissipation is greatest close to the base of the arcade where the magnetic field strength is strongest and at separatrix surfaces, where the field connectivity changes. Across all simulations, the background field is stressed with random foot point motions (in a manner typical of DC heating studies) and even for short time scale driving, the injected Poynting flux is large given the small amplitude flows considered. For long time scale driving, the rate of energy injection was comparable to the expected requirements in active regions. The heating rates were found to scale with the perturbed magnetic field strength and not the total field strength. Conclusions. Alongside recent studies which show power within the corona is dominated by low frequency motions, our results suggest that in the closed corona, DC heating is more significant than AC heating.

Phase mixing and wave heating in a complex coronal plasma

Thomas **Howson**, Ineke De Moortel, Jack Reid
A&A 636, A40 **2020**
https://arxiv.org/pdf/2003.05226.pdf
https://www.aanda.org/articles/aa/pdf/2020/04/aa37332-19.pdf
Aims. We investigate the formation of small scales and the dissipation of MHD wave energy through non-linear interactions of counter-propagating, phase-mixed Alfvenic waves in a complex magnetic field. Methods. We conducted fully 3-D, non-ideal MHD simulations of transverse waves in complex magnetic fields. Continuous wave drivers were imposed on the foot points of magnetic field lines and the system was evolved for several Alfven travel times. Phase-mixed waves were allowed to reflect off the upper boundary and the interactions between the resultant counter-streaming wave packets were analysed. Results. The complex nature of the background magnetic field encourages the development of phase mixing, leading to a growth in currents and vorticities. Counter-propagating phase-mixed waves induce a cascade of energy to small scales and result in more efficient energy dissipation. This effect is enhanced in simulations with more complex magnetic fields. High-frequency drivers excite localised field line resonances and produce efficient wave heating. However, this relies on the formation of large amplitude oscillations on resonant field lines. Drivers with smaller frequencies than the fundamental frequencies of field lines are not able to excite resonances and thus do not inject sufficient Poynting flux to power coronal heating. Even in the case of high-frequency oscillations, the rate of dissipation is likely too slow to balance coronal energy losses, even within the quiet Sun. Conclusions. For the generalised phase-mixing presented here, complex background field structures enhance the rate of wave energy dissipation. However, it remains difficult for realistic wave drivers to inject sufficient Poynting flux to heat the corona. Indeed, significant heating only occurs in cases which exhibit amplitudes that are much larger than those currently observed in the solar atmosphere.

Resonant absorption in expanding coronal magnetic flux tubes with uniform density

Thomas **Howson**, Ineke De Moortel, Patrick Antolin, Tom Van Doorsselaere, Andrew Wright

A&A 631, A105 **2019**
https://arxiv.org/pdf/1909.10781.pdf
https://doi.org/10.1051/0004-6361/201936146
Aims. We investigate the transfer of energy between a standing kink mode and azimuthal Alfven waves within an expanding flux tube. We consider the process of resonant absorption in a loop with a non-uniform Alfven frequency profile but in the absence of a radial density gradient. Methods. Using the MHD code, Lare3d, we model an oscillating magnetic flux tube that expands radially with height. An initially straight loop structure with a magnetic field enhancement is relaxed towards a force-free state before a standing kink mode is introduced. Results. We demonstrate that the transverse gradient in Alfven frequency required for the existence of resonant field lines can be associated with the expansion of a high field-strength flux tube from concentrated flux patches. This allows for the conversion of energy between wave modes even in the absence of the density profile typically assumed in wave heating models. As with standing modes in straight flux tubes, small scales are dominated by the vorticity at the loop apex and by currents at the foot points. The azimuthal wave exhibits the structure of the expanded flux tube and is therefore associated with smaller length scales close to the foot points of the flux tube. Conclusions. Resonant absorption can proceed throughout the corona, even in the absence of dense loop structures. The flux tube and MHD waves considered are difficult to observe and our model highlights how estimating hidden wave power within the solar atmosphere can be problematic. We highlight that, for standing modes, the global properties of field lines are important for resonant absorption and coronal conditions at a single altitude will not fully determine the nature of MHD resonances. We provide a new model in partial response to the criticism that wave heating models cannot self-consistently generate or sustain the density profile upon which they typically rely.

Magnetohydrodynamic waves in braided magnetic fields

Thomas **Howson**, Ineke De Moortel, Jack Reid, Alan Hood
A&A 629, A60 **2019**
https://arxiv.org/pdf/1908.03089.pdf
We consider a series of MHD simulations in which a small amplitude, transverse velocity perturbation is introduced into a complex magnetic field. We analysed the deformation of the wave fronts as the perturbation propagates through the braided magnetic structures and explore the nature of Alfvénic wave phase mixing in this regime. Spatial gradients in the local Alfvén speed and variations in the length of magnetic field lines ensure that small scales form throughout the propagating wave front due to phase mixing. Additionally, the presence of complex, intricate current sheets associated with the background field locally modifies the polarisation of the wave front. The combination of these two effects enhances the rate of viscous dissipation, particularly in more complex field configurations. Unlike in classical phase mixing configurations, the greater spatial extent of Alfvén speed gradients ensures that wave energy is deposited over a larger cross-section of the magnetic structure. Further, the complexity of the background magnetic field ensures that small gradients in a wave driver can map to large gradients within the coronal plasma. The phase mixing of MHD waves in a complex magnetic field will progress throughout the braided volume. As a result, in a non-ideal regime wave energy will be dissipated over a greater cross-section than in classical phase mixing models. The formation rate of small spatial scales in a propagating wave front is a function of the complexity of the background magnetic field. As such, if the coronal field is sufficiently complex it remains plausible that phase mixing induced wave heating can contribute to maintaining observed temperatures. Furthermore, the weak compressibility of the transverse wave and the observed phase mixing pattern may provide seismological information about the nature of the background plasma.

Measuring Solar Differential Rotation with an Iterative Phase Correlation Method

Zdeněk **Hrazdíra**1, Miloslav Druckmüller1, and Shadia Habbal2
2021 ApJS 252 6
https://doi.org/10.3847/1538-4365/abc702
A reliable inference of the differential rotation rate of the solar photosphere is essential for models of the solar interior. The work presented here is based on a novel iterative phase correlation technique, which relies on the measurement of the local shift, at the central meridian, between two images separated by a given time interval. Consequently, it does not require any specific reference features, such as sunspots or supergranules, nor extended observations spanning several months. The reliability of the method is demonstrated by applying it to high spatial and temporal resolution continuum images of the solar photosphere, at 6173 Å, acquired by the Solar Dynamics Observatory Helioseismic and Magnetic Imager over one complete Carrington rotation. The data selected covers the time period of **2020 January 1 to February 2**. The method was applied to one day, and to the full time interval. The differential rotation rate derived using this feature-independent technique yields values that fall in the middle of the range of those published to date. Most importantly, the method is suited for the production of detailed rotation maps of the solar photosphere. It also enables the visual and quantitative identification of the north–south asymmetry in the solar differential rotation rate, when present.

Fabry–Pérot Interferometer-Based Tunable Narrow-Band Imager for Solar Chromospheric Observation: First Results

Xingcheng **Hu**, Jinsheng Yang, Xuejun Rao & Changhui Rao
Solar Physics volume 297, Article number: 74 (**2022**)
https://link.springer.com/content/pdf/10.1007/s11207-022-01995-6.pdf
Recently, we have developed a tunable narrow-band imager (NBI) with high spectral resolution based on a Fabry–Pérot (FP) interferometer to observe the solar chromosphere. The NBI system is designed for imaging the Sun at the Hαα wavelength (6563 Å). The FP interferometer has a bandpass (FWHM) of 0.09 Å and a free spectral range (FSR) of 3.85 Å at λ=628λ=628 nm, working in combination with a prefilter with a bandpass of 1.6 Å and a center wavelength at 656.3 nm to achieve narrow-band imaging. We have successfully tested the NBI system on the 65-cm Educational Adaptive-optics Solar Telescope (EAST) in the Shanghai Astronomy Museum, and observed the sunspots in active region (AR) 12880 of the Sun on October 2 and 3, 2021. In this paper, we briefly present a description of the instrument, experimental observations, data processing, and the first observational results.

In situ Remnants of Solar Surface Structures from Jensen-Shannon Scalogram

Zesen **Huang**, Chen Shi, Marco Velli, Nikos Sioulas, Olga Panasenco, Trevor Bowen, Lorenzo Matteini, Mingtao Xia, Xiaofei Shi, Sheng Huang, Jia Huang, Lizet Casillas
ApJ **2023**
https://arxiv.org/pdf/2312.08669.pdf
The heliosphere is permeated with highly structured solar wind originating from the sun. One of the primary science objectives of Parker Solar Probe (PSP) is to determine the structures and dynamics of the plasma and magnetic fields at the sources of the solar wind. However, establishing the connection between in situ measurements and structures and dynamics in the solar atmosphere is challenging: most of the magnetic footpoint mapping techniques have significant uncertainties in the source localization of a plasma parcel observed in situ, and the PSP plasma measurements suffer from a limited field of view. Therefore it lacks a universal tool to self-contextualize the in situ measurements. Here we develop a novel time series visualization method named Jensen-Shannon Scalogram. Utilizing this method, by analyzing the magnetic magnitude data from both PSP and Ulysses, we successfully identify in situ remnants of solar atmospheric and magnetic structures spanning more than seven orders of magnitude, from years to seconds, including polar and mid-latitude coronal holes, as well as structures compatible with super-granulation, ``jetlets" and very small scale flaring activity. Furthermore, computer simulations of Alfvénic turbulence support key features of the observed magnetic magnitude distribution. Building upon these discoveries, the Jensen-Shannon Scalogram therefore not only enables us to reveal the fractal fine structures in the solar wind time series from both PSP and decades-old data archive, but will also serve as a general-purpose data visualization method applicable to all time series

Imaging and spectroscopic observations of extreme-ultraviolet brightenings using EUI and SPICE on board Solar Orbiter

Ziwen **Huang**, L. Teriaca, R. Aznar Cuadrado, L. P. Chitta, S. Mandal, H. Peter, U. Schühle, S.K. Solanki, F. Auchère, D. Berghmans, É. Buchlin, M. Carlsson, A. Fludra, T. Fredvik, A. Giunta, T. Grundy, D. Hassler, S. Parenti, F. Plaschke
A&A **2023**
https://arxiv.org/pdf/2303.15979.pdf
The smallest extreme-ultraviolet (EUV) brightening events that were detected so far, called campfires, have recently been uncovered by the High Resolution EUV telescope (HRIEUV), which is part of the Extreme Ultraviolet Imager (EUI) on board Solar Orbiter. HRIEUV has a broad bandpass centered at 17.4 nm that is dominated by Fe ix and Fe x emission at about 1 MK. We study the thermal properties of EUI brightening events by simultaneously observing their responses at different wavelengths using spectral data from the Spectral Imaging of the Coronal Environment (SPICE) also on board Solar Orbiter and imaging data from EUI. We studied three EUI brightenings that were identified in HRIEUV data that lie within the small areas covered by the slit of the SPICE EUV spectrometer. We obtained the line intensities of the spectral profiles by Gaussian fitting. These diagnostics were used to study the evolution of the EUI brightenings over time at the different line-formation temperatures. We find that (i) the detection of these EUI brightenings is at the limit of the SPICE capabilities. They could not have been independently identified in the data without the aid of HRIEUV observations. (ii) Two of these EUI brightenings with longer lifetimes are observed up to Ne viii temperatures (0.6 MK). (iii) All of the events are detectable in O vi (0.3 MK), and the two longer-lived events are also detected in other transition region (TR) lines. (iv) In one case, we observe two peaks in the intensity light curve of the TR lines that are separated by 2.7 min for C iii and 1.2 min for O vi. The Ne viii intensity shows a single peak between the two peak times of the TR line intensity. Spectral data from SPICE allow us to follow the thermal properties of EUI brightenings. Our results indicate that at least some EUI brightenings barely reach coronal temperatures. **23 February 2021, 12-13 September 2021**
Solar Orbiter nugget #6 **2023** https://www.cosmos.esa.int/web/solar-orbiter/science-nuggets/euv-brightenings-using-eui-and-spice-on-board-solar-orbiter

Do chaotic field lines cause fast reconnection in coronal loops?

Yi-Min **Huang**, Amitava Bhattacharjee

2022

https://arxiv.org/pdf/2208.06965.pdf

Over the past decade, Boozer has argued that three-dimensional (3D) magnetic reconnection fundamentally differs from two-dimensional (2D) reconnection due to the fact that the separation between any pair of neighboring field lines almost always increases exponentially over distance in a 3D magnetic field. This feature makes 3D field-line mapping chaotic and exponentially sensitive to small non-ideal effects; consequently, 3D reconnection can occur without intense current sheets. We test Boozer's theory via ideal and resistive reduced magnetohydrodynamic simulations of the Boozer-Elder coronal loop model driven by sub-Alfvénic footpoint motions. Our simulation results do not support Boozer's theory. The ideal simulation shows that Boozer and Elder significantly under-predict the intensity of current density due to missing terms in their reduced model equations. Furthermore, resistive simulations of varying Lundquist numbers show that the maximal current density scales linearly with the Lundquist number, as opposed to Boozer's prediction of a logarithmic dependence.

Dynamics in the transition region beneath active region upflows viewed by IRIS

Zhenghua **Huang**, Lidong Xia, Hui Fu, Zhenyong Hou, Ziyuan Wang

ApJ **918** 33 **2021**

https://arxiv.org/pdf/2107.01577.pdf

https://iopscience.iop.org/article/10.3847/1538-4357/ac0dbe/pdf

https://doi.org/10.3847/1538-4357/ac0dbe

Coronal upflows at the edges of active regions (AR), which are a possible source of slow solar wind, have been found to connect with dynamics in the transition region. To infer at what scale transition region dynamics connect to AR upflows, we investigate the statistical properties of the small-scale dynamics in the transition region underneath the upflows at the edge of AR NOAA 11934. With observations from the Interface Region Imaging Spectragraph (IRIS), we found that the Si IV 1403\,Å Doppler map consists of numerous blue-shifted and red-shifted patches mostly with sizes less than 1\,Mm2. The blue-shifted structures in the transition region tend to be brighter than the red-shifted ones, but their nonthermal velocities have no significant difference. With the SWAMIS feature tracking procedure, in IRIS slit-jaw 1400\,Å images we found that dynamic bright dots with an average size of about 0.3\,Mm2 and lifetimes mostly less than 200\,s spread all over the region. Most of the bright dots appear to be localised, without clear signature of propagation of plasma to a long distance on the projection plane. Surge-like motions with speeds about 15 km/s could be seen in some events at the boundaries of the upflow region, where the magnetic field appear to be inclined. We conclude that the transition region dynamics connecting to coronal upflows should occur in very fine scale, suggesting that the corresponding coronal upflows should also be highly-structured. It is also plausible that the transition region dynamics might just act as stimulation at the coronal base that then drives the upflows in the corona. **27 December 2013**

Transition region loops in the very late phase of flux-emergence in IRIS sit-and-stare observations

Zhenghua **Huang**, Bo Li, Lidong Xia, Mijie Shi, Hui Fu, Zhenyong Hou

ApJ **2019**

https://arxiv.org/pdf/1911.02199.pdf

Loops are one of the fundamental structures that trace the geometry of the magnetic field in the solar atmosphere. Their evolution and dynamics provide a crucial proxy for studying how the magnetized structures are formed and heated in the solar atmosphere. Here, we report on spectroscopic observations of a set of transition region loops taken by the Interface Region Imaging Spectrograph (IRIS) at Si IV 1394 Å with a sit-and-stare mode. The loops are corresponding to the flux emergence at its very late phase when the emerged magentic features in the photosphere have fully developed. We find the transition region loops are still expanding and moving upward with a velocity of a few kilometers per second ($\lesssim$10 km/s) at this stage. The expansion of the loops leads to interactions between themselves and the ambient field, which can drive magnetic reconnection evidenced by multiple intense brightenings, including transition region explosive events and IRIS bombs in the footpoint region associated with the moving polarity. A set of quasi-periodic brightenings with a period of about 130 s is found at the loop apex, from which the Si IV 1394 Å profiles are significantly non-Gaussian with enhancements at both blue and red wings at Doppler velocities of about 50 km/s. We suggest that the transition region loops in the very late phase of flux emergence can be powered by heating events generated by the interactions between the expanding loops and the ambient fields and also by (quasi-)periodic processes, such as oscillation-modulated braiding reconnection. **2017 August 26**

OBSERVATIONS OF SMALL-SCALE ENERGETIC EVENTS IN THE SOLAR TRANSITION REGION: EXPLOSIVE EVENTS, UV BURSTS, AND NETWORK JETS

Zhenghua **Huang**, Bo Li, Lidong Xia.

Solar-Terrestrial Physics. **2019**. Vol. 5. Iss. 2, pp. 58–68

Solnechno-zemnaya fizika, 2019, Vol. 5. Iss. 2. P. 63–73

https://naukaru.ru/en/storage/view/36901

In this paper, we review observational aspects of three common small-scale energetic events in the solar transition region (TR), namely TR explosive events, ultraviolet bursts and jets. These events are defined in either (both) spectral or (and) imaging data. The development of multiple instruments capable of observing the TR has allowed researchers to gain numerous insights into these phenomena in recent years. These events have provided a proxy to study how mass and energy are transported between the solar chromosphere and the corona. As the physical mechanisms responsible for these small-scale events might be similar to the mechanisms responsible for large-scale phenomena, such as flares and coronal mass ejections, analysis of these events could also help our understanding of the solar atmosphere from small to large scales. The observations of these small-scale energetic events demonstrate that the TR is extremely dynamic and is a crucial layer in the solar atmosphere between the chromosphere and the corona. **June 27, 2013, 2014-01-23, 14 Feb 2014, December 4, 2015**

Perception Evaluation -- A new solar image quality metric based on the multi-fractal property of texture features

Yi **Huang**, Peng Jia, Dongmei Cai, Bojun Cai

Solar Phys. 294:133 **2019**

https://arxiv.org/pdf/1905.09980.pdf

https://doi.org/10.1007/s11207-019-1524-5

Next-generation ground-based solar observations require good image quality metrics for post-facto processing techniques. Based on the assumption that texture features in solar images are multi-fractal which can be extracted by a trained deep neural network as feature maps, a new reduced-reference objective image quality metric, the perception evaluation is proposed. The perception evaluation is defined as cosine distance of Gram matrix between feature maps extracted from high resolution reference image and that from blurred images. We evaluate performance of the perception evaluation with simulated and real observation images. The results show that with a high resolution image as reference, the perception evaluation can give robust estimate of image quality for solar images of different scenes.

Observations of small-scale energetic events in the solar transition region: explosive events, UV bursts and network jets **Review**

Zhenghua **Huang**, Bo Li, Lidong Xia

2019

https://arxiv.org/ftp/arxiv/papers/1904/1904.06688.pdf

In this paper, we review observational aspects of three common small-scale energetic events in the solar transition region (TR), namely: TR explosive events, ultraviolet bursts and jets. These events are defined in either (both) spectral or (and) imaging data. The development of multiple instruments capable of observing the TR has allowed researchers to gain numerous insights into these phenomena in recent years. These events have provided a proxy to study how mass and energy are transported between the solar chromosphere and the corona. As the physical mechanisms responsible for these small-scale events might be similar to the mechanisms responsible for large-scale phenomena, such as flares and coronal mass ejections, analysis of these events could also help our understanding of the solar atmosphere from small to large scales. The observations of these small-scale energetic events demonstrate that the TR is extremely dynamic and is a crucial layer in the solar atmosphere between the chromosphere and the corona.

A magnetic reconnection event in the solar atmosphere driven by relaxation of a twisted arch filament system

Zhenghua **Huang**, Chaozhou Mou, Hui Fu, Linhua Deng, Bo Li, Lidong Xia

ApJL **853** L26 **2018**

https://arxiv.org/pdf/1801.05983.pdf

http://sci-hub.tw/http://iopscience.iop.org/2041-8205/853/2/L26/

We present high-resolution observations of a magnetic reconnection event in the solar atmosphere taken with the New Vacuum Solar Telescope, AIA and HMI. The reconnection event occurred between the threads of a twisted arch filament system (AFS) and coronal loops. Our observations reveal that the relaxation of the twisted AFS drives some of its threads to encounter the coronal loops, providing inflows of the reconnection. The reconnection is evidenced by flared X-shape features in the AIA images, a current-sheet-like feature apparently connecting post-reconnection loops in the \halpha+1 \AA\ images, small-scale magnetic cancellation in the HMI magnetograms and

flows with speeds of 40--80 km/s along the coronal loops. The post-reconnection coronal loops seen in AIA 94 \AA\ passband appear to remain bright for a relatively long time, suggesting that they have been heated and/or filled up by dense plasmas previously stored in the AFS threads. Our observations suggest that the twisted magnetic system could release its free magnetic energy into the upper solar atmosphere through reconnection processes. While the plasma pressure in the reconnecting flux tubes are significantly different, the reconfiguration of field lines could result in transferring of mass among them and induce heating therein. **September 25 2016**

Solar Open Flux Migration from Pole to Pole: Magnetic Field Reversal

Huang, G.-H., Lin, C.-H., and Lee, L.C.
SCIENTIfIC REPORTS | 7: 9488 **2017**
http://www.nature.com.sci-hub.cc/articles/s41598-017-09862-2
Coronal holes are solar regions with low soft X-ray or low extreme ultraviolet intensities. The magnetic fields from coronal holes extend far away from the Sun, and thus they are identified as regions with open magnetic field lines. Coronal holes are concentrated in the polar regions during the sunspot minimum phase, and spread to lower latitude during the rising phase of solar activity. In this work, we identify coronal holes with outward and inward open magnetic fluxes being in the opposite poles during solar quiet period. We find that during the sunspot rising phase, the outward and inward open fluxes perform pole-to-pole trans-equatorial migrations in opposite directions. The migration of the open fluxes consists of three parts: open flux areas migrating across the equator, new open flux areas generated in the low latitude and migrating poleward, and new open flux areas locally generated in the polar region. All three components contribute to the reversal of magnetic polarity. The percentage of contribution from each component is different for different solar cycle. Our results also show that the sunspot number is positively correlated with the lower-latitude open magnetic flux area, but negatively correlated with the total open flux area.

Explosive events in active region observed by IRIS and SST/CRISP

Z. **Huang**, M. S. Madjarska, E. M. Scullion, L.-D. Xia, J. G. Doyle, T. Ray
MNRAS **2016**
Transition-region explosive events (EEs) are characterized by non-Gaussian line profiles with enhanced wings at Doppler velocities of 50-150 km/s. They are believed to be the signature of solar phenomena that are one of the main contributors to coronal heating. The aim of this study is to investigate the link of EEs to dynamic phenomena in the transition region and chromosphere in an active region. We analyze observations simultaneously taken by the Interface Region Imaging Spectrograph (IRIS) in the Si IV 1394\AA\ line and the slit-jaw (SJ) 1400\AA\ images, and the Swedish 1-m Solar Telescope (SST) in the Hα line. In total 24 events were found. They are associated with small-scale loop brightenings in SJ 1400\AA\ images. Only four events show a counterpart in the Hα-35 km/s and Hα+35 km/s images. Two of them represent brightenings in the conjunction region of several loops that are also related to a bright region (granular lane) in the Hα-35km/s and Hα+35 km/s images. Sixteen are general loop brightenings that do not show any discernible response in the Hαimages. Six EEs appear as propagating loop brightenings, from which two are associated with dark jet-like features clearly seen in the Hα-35 km/s images. We found that chromospheric events with jet-like appearance seen in the wings of the Hα line can trigger EEs in the transition region and in this case the IRIS Si IV 1394\AA\ line profiles are seeded with absorption components resulting from Fe II and Ni II. Our study indicates that EEs occurring in active regions have mostly upper-chromosphere/transition-region origin. We suggest that magnetic reconnection resulting from the braidings of small-scale transition region loops is one of the possible mechanisms of energy release that are responsible for the EEs reported in this paper. **2014 June 10**

Pitfalls of Periodograms: The Nonstationarity Bias in the Analysis of Quasiperiodic Oscillations

Moritz **Hübner**1,2, Daniela Huppenkothen3, Paul D. Lasky1,2, and Andrew R. Inglis4,5
2022 ApJS 259 32
https://iopscience.iop.org/article/10.3847/1538-4365/ac49ec/pdf
Quasiperiodic oscillations (QPOs) are an important key to understand the dynamic behavior of astrophysical objects during transient events like gamma-ray bursts, solar flares, and magnetar flares. Searches for QPOs often use the periodogram of the time series and perform spectral density estimation using a Whittle likelihood function. However, the Whittle likelihood is only valid if the time series is stationary since the frequency bins are otherwise not statistically independent. We show that if time series are nonstationary, the significance of QPOs can be highly overestimated and estimates of the central frequencies and QPO widths can be overconstrained. The effect occurs if the QPO is only present for a fraction of the time series and the noise level is varying throughout the time series. This can occur, for example, if background noise from before or after the transient is included in the time series or if the low-frequency noise profile varies strongly over the time series. Thus, we highlight the importance of careful segment selection prior to the analysis. We confirm the presence of this bias in previously reported results from

solar flare data and show that significance can be highly overstated. Finally, we provide some suggestions that help identify whether an analysis is affected by this bias. **2013 May 12**

Introducing SunSketcher

Hugh **HUDSON**, Gordon EMSLIE
RHESSI Nuggets, #455 **2023**
https://sprg.ssl.berkeley.edu/~tohban/wiki/index.php/Introducing_SunSketcher
Solar eclipses fascinate us with their drama and beauty, and their scientific credentials go way back before the word "scientific" actually existed. In this modern space age, actual observations from the surface of the Earth no longer have so much cutting-edge research impact, but in this Nugget we introduce the SunSketcher project. SunSketcher takes advantage of modern technology and crowdsourced help to tackle a basic astronomical question: How round is the Sun? We discussed the history of this question in an earlier Nugget.

Fast Coronal Flows in Solar Active Regions

Hugh S. **Hudson**, Sargam M. Mulay, Lyndsay Fletcher, Jennifer Docherty, Jimmy Fitzpatrick, Eleanor Pike, Morven Strong, Phillip C. Chamberlin, Thomas N. Woods
MNRAS **2022**
https://arxiv.org/pdf/2207.13461.pdf
We report the discovery and characterization of high-speed (>100 km/s) horizontal flows in solar active regions, making use of the Sun-as-a-star spectroscopy in the range 5-105 nm provided by the EVE (Extreme Ultraviolet Variability Experiment) spectrometers on the Solar Dynamics Observatory. These apparent flows are persistent on time scales of days, and are well observed in lines of Mg X, Si XII and Fe XVI for example. They are prograde, as evidenced directly by blueshifts/redshifts peaking at the east/west limb passages of isolated active regions. The high-speed flow behavior does not depend upon active-region latitude or solar cycle, with similar behavior in Cycles 24 and 25.
RHESSI Nuggets #433 Jul **2022**
https://sprg.ssl.berkeley.edu/~tohban/wiki/index.php/Fast_Prograde_Flows_in_Solar_Active_Regions

Disk Occultation of a Lopsided Sun

Hugh **HUDSON**, Stephen WHITE and Säm KRUCKER
RHESSI Nuggets #424 Jan **2022**
https://sprg.ssl.berkeley.edu/~tohban/wiki/index.php/Disk_Occultation_of_a_Lopsided_Sun
As solar magnetic activity increases with the beginning of Solar Cycle 25, we are seeing extreme variations of solar activity on the time scale of the period of roughly one month (Carrington determed the sidereal period from sunspot motions to be 25.38 days). The general behavior of solar rotation is interestingly complicated. This lopsided behavior may be a common feature of early and late phases of solar cycles, in which one face of the Sun may have multiple active regions while the other face does not. We are unaware of any actual literature on this topic, but it is clearly a manifestation of the highly non-random nature of all aspects of solar magnetic activity.

The Interesting RHESSI/SAS Archive

Hugh **HUDSON** and Martin FIVIAN
RHESSI Nuggets #342 Jan **2019**
http://sprg.ssl.berkeley.edu/~tohban/wiki/index.php/The_Interesting_RHESSI/SAS_Archive
The full mission database shows RHESSI to have been very stable geometrically.

Chapter 9 - High-Energy Solar Physics **Review**

H.S. **Hudson** and A.L. MacKinnon
In: ***The Sun as a Guide to Stellar Physics*** ***Book***
Eds. Oddbjørn Engvold, Jean-Claude Vial, and Andrew Skumanich
Elsevier , November **2018**
https://www.sciencedirect.com/book/9780128143346/the-sun-as-a-guide-to-stellar-physics
This chapter deals generally with the high-energy astrophysics of the Sun, specifically with solar flares and coronal mass ejections (CMEs), but it also touches on the whole range of nonthermality or departures from Maxwellian distributions in solar plasmas. Radio, x-ray, and γ-ray observations provide primary remote-sensing observations of these departures, but such signatures can be hidden by brighter thermal emissions that may not be as fundamental in physics events. The solar paradigm for flare/CME development appears to match many of the new stellar observations of similar phenomena, but the limitations of observational sensitivity mean that we have few direct observations of the expected hard x-rays and none at all of the γ-rays that could confirm this.

The true dawn of multimessenger astronomy

Hugh **Hudson**
RHESSI Science Nugget No. 328, **2018**
http://sprg.ssl.berkeley.edu/~tohban/wiki/index.php/The_true_dawn_of_multimessenger_astronomy

RHESSI and the Megamovie

Hugh **Hudson**, Laura Peticolas, and Juan Carlos Martinez Oliver's:
RHESSI Science Nugget No. 304, Aug **2017**
http://sprg.ssl.berkeley.edu/~tohban/wiki/index.php/RHESSI_and_the_Megamovie
A wholly new way to observe a solar eclipse, and to do solar astrometry

Spotlessness returns

Hugh **Hudson**
RHESSI Nugget No. 277, June 27: **2016**
http://sprg.ssl.berkeley.edu/~tohban/wiki/index.php/Spotlessness_returns

Ionospheric Effects, Flare History, and Dick Donnelly

Hugh **Hudson** and Peter Gallagher:
RHESSI Nugget No. 251, April **2015**
http://sprg.ssl.berkeley.edu/~tohban/wiki/index.php/Ionospheric_Effects,_Flare_History,_and_Dick_Donnelly
Recogning the world's largest X-ray detector, its ionosphere.
This Nugget notes the existence of the ionospheric effects of solar flares, which have had a substantial influence on our understanding of both the ionosphere and the perturbing flares themselves. This began with Carrington and continues to the present, with major contributions by late friend Richard Donnelly.

Solar extreme events **Review**

Hugh S. **Hudson**
24th European Cosmic Ray Symposium, Kiel, September 2014, **2015**
http://arxiv.org/pdf/1504.04755v1.pdf
Solar flares and CMEs have a broad range of magnitudes. This review discusses the possibility of "extreme events," defined as those with magnitudes greater than have been seen in the existing historical record. For most quantitative measures, this direct information does not extend more than a century and a half into the recent past. The magnitude distributions (occurrence frequencies) of solar events (flares/CMEs) typically decrease with the parameter measured or inferred (peak flux, mass, energy etc. Flare radiation fluxes tend to follow a power law slightly flatter than S−2, where S represents a peak flux; solar particle events (SPEs) follow a still flatter power law up to a limiting magnitude, and then appear to roll over to a steeper distribution, which may take an exponential form or follow a broken power law. This inference comes from the terrestrial 14C record and from the depth dependence of various radioisotope proxies in the lunar regolith and in meteorites. Recently major new observational results have impacted our use of the relatively limited historical record in new ways: the detection of actual events in the 14C tree-ring records, and the systematic observations of flares and "superflares" by the Kepler spacecraft. I discuss how these new findings may affect our understanding of the distribution function expected for extreme solar events. 2003-11-04,

The IAU Solar Target Identifier

Hugh **Hudson** and John Leibacher.
RHESSI Science Nuggets, #243, December **2014**
http://sprg.ssl.berkeley.edu/~tohban/wiki/index.php/The_IAU_Solar_Target_Identifier_-_A_Good_Thing
Standardized names for flares help a lot.

Cycle 23 Variation in Solar Flare Productivity

Hugh **Hudson**, Lyndsay Fletcher, Jim McTiernan
Solar Physics, April **2014**, Volume 289, Issue 4, pp 1341-1347
The NOAA listings of solar flares in cycles 21 – 24, including the GOES soft X-ray magnitudes, enable a simple determination of the number of flares each flaring active region produces over its lifetime. We have studied this measure of flare productivity over the interval 1975 – 2012. The annual averages of flare productivity remained approximately constant during cycles 21 and 22, at about two reported M- or X-flares per region, but then increased

significantly in the declining phase of cycle 23 (the years 2004 – 2005). We have confirmed this by using the independent RHESSI flare catalog to check the NOAA events listings where possible. We note that this measure of solar activity does not correlate with the solar cycle. The anomalous peak in flare productivity immediately preceded the long solar minimum between cycles 23 and 24.

Flares and the Chromosphere

Hugh S. **Hudson**1 and Lyndsay Fletcher2
E-print, Aug **2008, File**; *Earth Planets Space*,
The chromosphere (the link between the photosphere and the corona) plays a crucial role in flare and CME development. In analogies between flares and magnetic substorms, it is normally identified with the ionosphere, but we argue that the correspondence is not exact. Much of the important physics of this interesting region remains to be explored. We discuss chromospheric flares in the context of recent observations of white-light flares and hard X-rays as observed by TRACE and RHESSI, respectively. We interpret key features of these observations as results of the stepwise changes a flare produces in the photospheric magnetic field.

Pitfalls of periodograms: The non-stationarity bias in the analysis of quasi-periodic oscillations

Moritz **Huebner**, Daniela Huppenkothen, Paul D. Lasky, Andrew R. Inglis
ApJ **2021**
https://arxiv.org/pdf/2108.07418.pdf
Quasi-periodic oscillations (QPOs) are an important key to understand the dynamic behavior of astrophysical objects during transient events like gamma-ray bursts, solar flares, and magnetar flares. Searches for QPOs often use the periodogram of the time series and perform spectral density estimation using a Whittle likelihood function. However, the Whittle likelihood is only valid if the time series is stationary since the frequency bins are otherwise not statistically independent. We show that if time series are non-stationary, the significance of QPOs can be highly overestimated and estimates of the central frequencies and QPO widths can be overconstrained. The effect occurs if the QPO is only present for a fraction of the time series and the noise level is varying throughout the time series. This can occur for example if background noise from before or after the transient is included in the time series or if the low-frequency noise profile varies strongly over the time series. We confirm the presence of this bias in previously reported results from solar flare data and show that significance can be highly overstated. Finally, we provide some suggestions that help identify if an analysis is affected by this bias.

Real-time solar image classification: assessing spectral, pixel-based approaches

J. Marcus **Hughes**, Vicki W. Hsu, Daniel B. Seaton, Hazel M. Bain, Jonathan M. Darnel, Larisza Krista
Journal of Space Weather and Space Climate 9, A38 **2019**
https://arxiv.org/pdf/1910.00144.pdf
https://www.swsc-journal.org/articles/swsc/pdf/2019/01/swsc180074.pdf
In order to utilize solar imagery for real-time feature identification and large-scale data science investigations of solar structures, we need maps of the Sun where phenomena, or themes, are labeled. Since solar imagers produce observations every few minutes, it is not feasible to label all images by hand. Here, we compare three machine learning algorithms performing solar image classification using extreme ultraviolet and Hydrogen-alpha images: a maximum likelihood model assuming a single normal probability distribution for each theme from Rigler et al. (2012), a maximum-likelihood model with an underlying Gaussian mixtures distribution, and a random forest model. We create a small database of expert-labeled maps to train and test these algorithms. Due to the ambiguity between the labels created by different experts, a collaborative labeling is used to include all inputs. We find the random forest algorithm performs the best amongst the three algorithms. The advantages of this algorithm are best highlighted in: comparison of outputs to hand-drawn maps; response to short-term variability; and tracking long-term changes on the Sun. Our work indicates that the next generation of solar image classification algorithms would benefit significantly from using spatial structure recognition, compared to only using spectral, pixel-by-pixel brightness distributions. **2017 Sep 6, 2018-09-06**

HMI Synoptic Maps Produced by NSO/NISP

Anna L. H. **Hughes**, Luca Bertello, Andrew R. Marble, Niles A. Oien, Gordon Petrie, Alexei A. Pevtsov
Technical Report No. NSO/NISP-2016-002 **2016**
http://arxiv.org/pdf/1605.03500v1.pdf
Recently, the National Solar Observatory (NSO) Solar-atmosphere Pipeline Working Group has undertaken the production of synoptic maps from Helioseismic and Magnetic Imager (HMI) magnetograms. A set of maps has been processed spanning the data available for **2010-2015** using twice daily images (taken at UT midnight and noon) and

running them through the same algorithms used to produce SOLIS/VSM 6302l mean-magnetic and spatial-variance maps. The contents of this document provide an overview of what these maps look like, and the processing steps used to generate them from the original HMI input data.

A multi-wavelength analysis of small-scale brightenings observed by IRIS

Llŷr Dafydd **Humphries**, Huw Morgan

2021

https://arxiv.org/pdf/2109.14736.pdf

Small-scale brightenings in solar atmospheric observations are a manifestation of heating and/or energy transport events. We present statistical characteristics of brightenings from a new detection method applied to 1330, 1400, and 2796 Å IRIS slitjaw image time series. 2377 events are recorded which coexist in all three channels, giving high confidence that they are real. ≈1800 of these are spatially coherent, equating to event densities of ∼9.7×10−5arcsec−2s−1 within a $90\arcsec\times100\arcsec$ FOV over 34.5 minutes. Power Law indices estimates are determined for total brightness (2.78<α<3.71), maximum brightness (3.84<α<4.70), and average area (4.31<α<5.70) distributions. Duration and speed distributions do not obey a power law. A correlation is found between the events' spatial fragmentation, area, and duration, and a weak relationship with total brightness, showing that larger/longer-lasting events are more likely to fragment during their lifetime. Speed distributions show that all events are in motion, with an average speed of ∼7\kms. The events' spatial trajectories suggest that cooler 2796 Å events tend to appear slightly later, and occupy a different position/trajectory to the hotter channel results. This suggests that either many of these are impulsive events caused by reconnection, with subsequent rapid cooling, or that the triggering event occurs near the TR, with a subsequent propagating disturbance to cooler atmospheric layers. The spatial distribution of events is not uniform, with broad regions devoid of events. A comparison of spatial distribution with properties of other atmospheric layers shows a tentative connection between high magnetic field strength, the corona's multithermality, and high IRIS brightening activity.

Detecting and characterising small-scale brightenings in solar imaging data

Llŷr Dafydd **Humphries**, Huw Morgan, David Kuridze

ApJ **296**, Article number: 140 **2021**

https://arxiv.org/pdf/2107.13635.pdf

https://link.springer.com/content/pdf/10.1007/s11207-021-01885-3.pdf

https://doi.org/10.1007/s11207-021-01885-3

Observations of small-scale brightenings in the low solar atmosphere can provide valuable constraints on possible heating/heat-transport mechanisms. We present a method for the detection and analysis of brightenings and demonstrate its application to IRIS EUV time-series imagery. The method uses band-pass filtering, adaptive thresholding and centroid tracking, and records an event's position, duration, and total/maximum brightness. Area, brightness, and position are also recorded as functions of time throughout their lifetime. Detected brightenings can fragment or merge over time, thus the number of distinct regions constituting a brightening event is recorded over time and the maximum number of regions are recorded as a simple measure of an event's coherence/complexity. A test is made on a synthetic datacube composed of a static background based on IRIS data, Poisson noise and ≈104 randomly-distributed, moving, small-scale Gaussian brightenings. Maximum brightness, total brightness, area, and duration follow power-law distributions and the results show the range over which the method can extract information. The recorded maximum brightness is a reliable measure for the brightest and most accurately detected events with an error of 6%. Area, duration, and speed are generally underestimated by 15% with an uncertainty of 20-30%. Total brightness is underestimated by 30% with an uncertainty of 30%. Applying this method to real IRIS QS data spanning 19 minutes over a 54.40"×55.23" FOV yields 2997 detections. 1340 of these either remain un-fragmented or fragment to two distinct regions at least once during their lifetime equating to an event density of 3.96×10−4arcsec−2s−1. The method will be used for a future large-scale statistical analysis of several QS data sets from IRIS, other EUV imagers, as well as H-α and visible photospheric imagery.

Multiwavelength Imaging and Spectral Analysis of Jet-like Phenomena in a Solar Active Region Using IRIS and AIA

Ll̂r Dafydd **Humphries**1, Erwin Verwichte2, David Kuridzé1, and Huw Morgan1

2020 ApJ 898 17

https://doi.org/10.3847/1538-4357/ab974d

https://sci-hub.tw/https://iopscience.iop.org/article/10.3847/1538-4357/ab974d

https://arxiv.org/pdf/2010.04042.pdf

High-resolution observations of dynamic phenomena give insight into properties and processes that govern the low solar atmosphere. We present the analysis of jet-like phenomena emanating from a penumbral foot-point in active region (AR) 12192 using imaging and spectral observations from the Interface Region Imaging Spectrograph (IRIS) and the Atmospheric Imaging Assembly (AIA) on board the Solar Dynamics Observatory. These jets are associated

with line-of-sight (LoS) Doppler speeds of ± 10-22 km s−1 and bright fronts which seem to move across the Plane-of-Sky (PoS) at speeds of 23-130 km s−1. Such speeds are considerably higher than the expected sound speed in the chromosphere. The jets have signatures which are visible both in the cool and hot channels of IRIS and AIA. Each jet lasts on average 15 minutes and occur 5-7 times over a period of 2 hours. Possible mechanisms to explain this phenomenon are suggested, the most likely of which involve p-mode or Alfv\' en wave shock trains impinging on the transition region (TR) and corona as a result of steepening photospheric wavefronts or gravity waves. **Oct. 25, 2014**

Variational estimation of the large scale time dependent meridional circulation in the Sun: proofs of concept with a solar mean field dynamo model

Ching Pui **Hung**, Allan Sacha Brun, Alexandre Fournier, Laurène Jouve, Olivier Talagrand, Mustapha Zakari

ApJ **849** 160 **2017**

https://arxiv.org/pdf/1710.02114.pdf

We present in this work the development of a solar data assimilation method based on an axisymmetric mean field dynamo model and magnetic surface data, our mid-term goal is to predict the solar quasi cyclic activity. Here we focus on the ability of our algorithm to constrain the deep meridional circulation of the Sun based on solar magnetic observations. To that end, we develop a variational data assimilation technique. Within a given assimilation window, the assimilation procedure minimizes the differences between data and the forecast from the model, by finding an optimal meridional circulation in the convection zone, and an optimal initial magnetic field, via a quasi-Newton algorithm. We demonstrate the capability of the technique to estimate the meridional flow by a closed-loop experiment involving 40 years of synthetic, solar-like data. By assimilating the synthetic magnetic proxies annually, we are able to reconstruct a (stochastic) time-varying meridional circulation which is also slightly equatorially asymmetric. We show that the method is robust in estimating a flow whose level of fluctuation can reach 30% about the average, and that the horizon of predictive capability of the method is of the order of 1 cycle length.

Estimating the deep solar meridional circulation using magnetic observations and a dynamo model: a variational approach

Ching Pui **Hung**, Laurène Jouve, Allan Sacha Brun, Alexandre Fournier, Olivier Talagrand

(ApJ 814, 151, **2015**) **2017**

https://arxiv.org/pdf/1710.02084.pdf

We show how magnetic observations of the Sun can be used in conjunction with an axisymmetric flux-transport solar dynamo model in order to estimate the large-scale meridional circulation throughout the convection zone. Our innovative approach rests on variational data assimilation, whereby the distance between predictions and observations (measured by an objective function) is iteratively minimized by means of an optimization algorithm seeking the meridional flow which best accounts for the data. The minimization is performed using a quasi-Newton technique, which requires the knowledge of the sensitivity of the objective function to the meridional flow. That sensitivity is efficiently computed via the integration of the adjoint flux-transport dynamo model. Closed-loop (also known as twin) experiments using synthetic data demonstrate the validity and accuracy of this technique, for a variety of meridional flow configurations, ranging from unicellular and equatorially symmetric to multicellular and equatorially asymmetric. In this well-controlled synthetic context, we perform a systematic study of the behavior of our variational approach under different observational configurations, by varying their spatial density, temporal density, noise level, as well as the width of the assimilation window. We find that the method is remarkably robust, leading in most cases to a recovery of the true meridional flow to within better than 1%. These encouraging results are a first step towards using this technique to i) better constrain the physical processes occurring inside the Sun and ii) better predict solar activity on decadal time scales.

Chapter 13 - Solar Data and Simulations **Review**

Neal **Hurlburt**

In: ***The Sun as a Guide to Stellar Physics*** ***Book***

Eds. Oddbjørn Engvold, Jean-Claude Vial, and Andrew Skumanich

Elsevier , November **2018**

https://www.sciencedirect.com/book/9780128143346/the-sun-as-a-guide-to-stellar-physics

Data collected from instruments observing the Sun and simulations of solar phenomenon have historically been difficult to connect owing to the richness of the observations. Here we review the progress that has been made in bringing them together. We begin by reviewing the life cycle of solar data, from the initial collection, calibration, and processing through the discovery and retrieval of archival data, recent applications of modern statistical and machine learning methods. We then review the evolution of numerical simulations from idealized investigations that could only give general guidance on interpreting solar data to high-resolution simulations that are hard to distinguish

from reality. Here we focus on simulations that attempt to capture the essential (magneto-)hydrodynamics of solar phenomena from first principles rather than models based on more heuristic assumptions. With that constraint, the range of simulations is still broad, so we have concentrated on those addressing observations of the Sun and corona while neglecting those focused on stellar evolution and the solar cycle or focused on the solar wind and heliospheric dynamics.

Heliophysics Event Knowledgebase for the *Solar Dynamics Observatory* and Beyond

N. **Hurlburt**, M. Cheung, C. Schrijver, L. Chang, S. Freeland, S. Green, C. Heck, A. Jaffey, A. Kobashi, D. Schiff, J.Serafin, R. Seguin, G. Slater, A. Somani and R. Timmons
to appear in *Solar Physics*, SDO special issue. **2010, File**
The immense volume of data generated by the suite of instruments on **SDO** requires new tools for efficient identifying and accessing data that is most relevant to research investigations. We have developed the **Heliophysics Events Knowledgebase (HEK)** to fill this need. The HEK system combines automated data mining using feature-detection methods and high-performance visualization systems for data markup. In addition, web services and clients are provided for searching the resulting metadata, reviewing results, and efficiently accessing the data. We review these components and present examples of their use with SDO data.
http://www.lmsal.com/sungate

A relaxation model of coronal heating in multiple interacting flux ropes

A. S. **Hussain**1, P. K. Browning2 and A. W. Hood3
A&A 600, A5 (**2017**)
http://www.aanda.org/articles/aa/pdf/2017/04/aa29589-16.pdf
Context. Heating the solar corona requires dissipation of stored magnetic energy, which may occur in twisted magnetic fields. Recently published numerical simulations show that the ideal kink instability in a twisted magnetic thread may trigger energy release in stable twisted neighbours, and demonstrate an avalanche of heating events.
Aims. We aim to construct a Taylor relaxation model for the energy release from two flux ropes and compare this with the outcomes of the simulations. We then aim to extend the model to large numbers of flux ropes, allowing the possibility of modelling a heating avalanche, and calculation of the energy release for ensembles of twisted threads with varying twist profiles.
Methods. The final state is calculated by assuming a helicity-conserving relaxation to a minimum energy state. Multiple scenarios are examined, which include kink-unstable flux ropes relaxing on their own, as well as stable and unstable flux ropes merging into a single rope as a result of magnetic reconnection. We consider alternative constraints that determine the spatial extent of the final relaxed state.
Results. Good agreement is found between the relaxation model and the magnetohydrodynamic simulations, both for interactions of two twisted threads and for a multi-thread avalanche. The model can predict the energy release for flux ropes of varying degrees of twist, which relax individually or which merge through reconnection into a single flux rope. It is found that the energy output of merging flux ropes is dominated by the energy of the most strongly twisted rope.
Conclusions. The relaxation approach provides a very good estimate of the energy release in an ensemble of twisted threads of which one is kink-unstable.

Modeling the scattering polarization of the solar Ca I 4227 Å line with angle-dependent partial frequency redistribution

Gioele **Janett**1,2, Ernest Alsina Ballester1,3, Nuno Guerreiro1,2, Simone Riva1,2, Luca Belluzzi1,4,2, Tanausú del Pino Alemán3 and Javier Trujillo Bueno3,5,6
A&A 655, A13 (**2021**)
https://www.aanda.org/articles/aa/pdf/2021/11/aa41549-21.pdf
https://doi.org/10.1051/0004-6361/202141549
Context. The correct modeling of the scattering polarization signals observed in several strong resonance lines requires taking partial frequency redistribution (PRD) phenomena into account. Modeling scattering polarization with PRD effects is very computationally demanding and the simplifying angle-averaged (AA) approximation is therefore commonly applied.
Aims. This work aims to assess the impact and the range of validity of the AA approximation with respect to the general angle-dependent (AD) treatment of PRD effects in the modeling of scattering polarization in strong resonance lines, with a focus on the solar Ca I 4227 Å line.
Methods. Spectral line polarization was modeled by solving the radiative transfer problem for polarized radiation, under nonlocal thermodynamic equilibrium conditions, taking PRD effects into account in static one-dimensional

semi-empirical atmospheric models presenting arbitrary magnetic fields. The problem was solved through a two-step approach. In step 1, the problem was solved for the intensity only, considering a multilevel atom. In step 2, the problem was solved including polarization, considering a two-level atom with an unpolarized and infinitely sharp lower level, and fixing the lower level population calculated at step 1.
Results. The results for the Ca I 4227 Å line show a good agreement between the AA and AD calculations for the Q/I and U/I wings' signals. However, AA calculations reveal an artificial trough in the line-core peak of the linear polarization profiles, whereas AD calculations show a sharper peak in agreement with the observations.
Conclusions. An AD treatment of PRD effects is essential to correctly model the line-core peak of the scattering polarization signal of the Ca I 4227 Å line. By contrast, in the considered static case, the AA approximation seems to be suitable to model the wing scattering polarization lobes and their magnetic sensitivity through magneto-optical effects.

Instrumentation for solar spectropolarimetry: state of the art and prospects **Review**
Francisco A. **Iglesias**, Alex Feller
Journal-ref: Opt. Eng. 58(8), 082417 **2019**
https://arxiv.org/pdf/1911.01368.pdf
Given its unchallenged capabilities in terms of sensitivity and spatial resolution, the combination of imaging spectropolarimetry and numeric Stokes inversion represents the dominant technique currently used to remotely sense the physical properties of the solar atmosphere and, in particular, its important driving magnetic field. Solar magnetism manifests itself in a wide range of spatial, temporal, and energetic scales. The ubiquitous but relatively small and weak fields of the so-called quiet Sun are believed today to be crucial for answering many open questions in solar physics, some of which have substantial practical relevance due to the strong Sun-Earth connection. However, such fields are very challenging to detect because they require spectropolarimetric measurements with high spatial (sub-arcsec), spectral (<100 mA), and temporal (<10 s) resolution along with high polarimetric sensitivity (<0.001 of the intensity). We collect and discuss both well-established and upcoming instrumental solutions developed during the last decades to push solar observations toward the above-mentioned parameter regime. This typically involves design trade-offs due to the high dimensionality of the data and signal-to-noise-ratio considerations, among others. We focus on the main three components that form a spectro-polarimeter, namely, wavelength discriminators, the devices employed to encode the incoming polarization state into intensity images (polarization modulators), and the sensor technologies used to register them. We consider the instrumental solutions introduced to perform this kind of measurements at different optical wavelengths and from various observing locations, i.e., ground-based, from the stratosphere or near space.

High-resolution, high-sensitivity, ground-based solar spectropolarimetry with a new fast imaging polarimeter
F. A. **Iglesias**, A. Feller, K. Nagaraju, S. K. Solanki
A&A **2016**
http://arxiv.org/pdf/1604.01521v1.pdf
Context. Remote sensing of weak and small-scale solar magnetic fields is of utmost relevance for a number of important open questions in solar physics. This requires the acquisition of spectropolarimetric data with high spatial resolution (0.1 arcsec) and low noise (1e-3 to 1e-5 of the continuum intensity). The main limitations to obtain these measurements from the ground, are the degradation of the image resolution produced by atmospheric seeing and the seeing-induced crosstalk (SIC). Aims. We introduce the prototype of the Fast Solar Polarimeter (FSP), a new ground-based, high-cadence polarimeter that tackles the above-mentioned limitations by producing data that are optimally suited for the application of post-facto image restoration, and by operating at a modulation frequency of 100 Hz to reduce SIC. Results. The pnCCD camera reaches 400 fps while keeping a high duty cycle (98.6 %) and very low noise (4.94 erms). The modulator is optimized to have high (> 80%) total polarimetric efficiency in the visible spectral range. This allows FSP to acquire 100 photon-noise-limited, full-Stokes measurements per second. We found that the seeing induced signals present in narrow-band, non-modulated, quiet-sun measurements are (a) lower than the noise (7e-5) after integrating 7.66 min, (b) lower than the noise (2.3e-4) after integrating 1.16 min and (c) slightly above the noise (4e-3) after restoring case (b) by means of a multi-object multi-frame blind

deconvolution. In addition, we demonstrate that by using only narrow-band images (with low SNR of 13.9) of an active region, we can obtain one complete set of high-quality restored measurements about every 2 s.

The effects of solar wind on galactic cosmic ray flux at Earth

G. D. **Ihongo** , C. H.-T. Wang

Astrophysics and Space Science January **2016**, 361:44 **Open Access**

The amount of solar wind produced continuously by the sun is not constant due to changes in solar activity. This unsteady nature of the solar wind seems to be responsible for galactic cosmic ray flux modulation, hence the flux of incoming galactic cosmic rays observed at the top of the Earth's atmosphere varies with the solar wind reflecting the solar activity. The aforementioned reasons have lead to attempts by several researchers to study correlations between galactic cosmic rays and the solar wind. However, most of the correlation studies carried out by authors earlier are based on the analyses of observational data from neutron monitors. In this context, we study the effects of solar wind on galactic cosmic ray flux observed at r≈1 AU, using a theoretical approach and found that the solar wind causes significant decreases in galactic cosmic ray flux at r≈1 AU. A short time variation of the calculated flux is also checked and the result is reflected by exposing a negative correlation of the solar wind with the corresponding galactic cosmic ray flux. This means that the higher the solar wind the lower the galactic cosmic rays flux and vice-versa. To obtain a better understanding, the calculated flux and its short time variation at 1 AU are compared to data that shows a good fit to the model making it possible to establish a statistically significant negative correlation of −0.988±0.001 between solar wind variation and galactic cosmic rays flux variation theoretically.

Tracking of magnetic flux concentrations over a five-day observation and an insight into surface magnetic flux transport

Y. **Iida**

Space Weather and Space Climate **2016**

http://arxiv.org/pdf/1605.02533v1.pdf

The solar dynamo problem is the question of how the cyclic variation in the solar magnetic field is maintained. One of the important processes is the transport of magnetic flux by surface convection. To reveal this process, the dependence of the squared displacement of magnetic flux concentrations upon the elapsed time is investigated in this paper via a feature-recognition technique and a continual five-day magnetogram. This represents the longest time scale over which a satellite observation has ever been performed for this problem. The dependence is found to follow a power-law and differ significantly from that of diffusion transport. Furthermore there is a change in the behavior at a spatial scale of 10^{3.8} km. A super-diffusion behavior with an index of 1.4 is found on smaller scales, while changing to a sub-diffusion behavior with an index of 0.6 on larger ones. I interpret this difference in the transport regime as coming from the network-flow pattern.

A Comprehensive Simulation of Solar Wind Formation from the Solar Interior: Significant Cross-field Energy Transport by Interchange Reconnection near the Sun

H. **Iijima**, T. Matsumoto, H. Hotta, S. Imada

ApJL **2023**

https://arxiv.org/pdf/2306.17324

The physical connection between thermal convection in the solar interior and the solar wind remains unclear due to their significant scale separation. Using an extended version of the three-dimensional radiative magnetohydrodynamic code RAMENS, we perform the first comprehensive simulation of the solar wind formation, starting from the wave excitation and the small-scale dynamo below the photosphere. The simulation satisfies various observational constraints as a slow solar wind emanating from the coronal hole boundary. The magnetic energy is persistently released in the simulated corona, showing a hot upward flow at the interface between open and closed fields. To evaluate the energetic contributions from Alfvén wave and interchange reconnection, we develop a new method to quantify the cross-field energy transport in the simulated atmosphere. The measured energy transport from closed coronal loops to open field accounts for approximately half of the total. These findings suggest a significant role of the supergranular-scale interchange reconnection in solar wind formation.

Effect of morphological asymmetry between leading and following sunspots on the prediction of solar cycle activity

H. **Iijima**, H. Hotta, S. Imada

ApJ **883** 24 **2019**

https://arxiv.org/pdf/1908.04474.pdf

https://doi.org/10.3847/1538-4357/ab3b04

The morphological asymmetry of leading and following sunspots is a well-known characteristic of the solar surface. In the context of large-scale evolution of the surface magnetic field, the asymmetry has been assumed to have only a negligible effect. Using the surface flux transport model, we show that the morphological asymmetry of leading and following sunspots has a significant impact on the evolution of the large-scale magnetic field on the solar surface. By evaluating the effect of the morphological asymmetry of each bipolar magnetic region (BMR), we observe that the introduction of the asymmetry in the BMR model significantly reduces its contribution to the polar magnetic field, especially for large and high-latitude BMRs. Strongly asymmetric BMRs can even reverse the regular polar field formation. The surface flux transport simulations based on the observed sunspot record shows that the introduction of the morphological asymmetry reduces the root-mean-square difference from the observed axial dipole strength by 30--40 percent. These results indicate that the morphological asymmetry of leading and following sunspots has a significant effect on the solar cycle prediction.

Improvement of solar cycle prediction: Plateau of solar axial dipole moment

H. **Iijima**, H. Hotta, S. Imada, K. Kusano, D. Shiota

A&A 607, L2 **2017**

https://arxiv.org/pdf/1710.06528.pdf

Aims. We report the small temporal variation of the axial dipole moment near the solar minimum and its application to the solar cycle prediction by the surface flux transport (SFT) model. Methods. We measure the axial dipole moment using the photospheric synoptic magnetogram observed by the Wilcox Solar Observatory (WSO), the ESA/NASA Solar and Heliospheric Observatory Michelson Doppler Imager (MDI), and the NASA Solar Dynamics Observatory Helioseismic and Magnetic Imager (HMI). We also use the surface flux transport model for the interpretation and prediction of the observed axial dipole moment. Results. We find that the observed axial dipole moment becomes approximately constant during the period of several years before each cycle minimum, which we call the axial dipole moment plateau. The cross-equatorial magnetic flux transport is found to be small during the period, although the significant number of sunspots are still emerging. The results indicates that the newly emerged magnetic flux does not contributes to the build up of the axial dipole moment near the end of each cycle. This is confirmed by showing that the time variation of the observed axial dipole moment agrees well with that predicted by the SFT model without introducing new emergence of magnetic flux. These results allows us to predict the axial dipole moment in Cycle 24/25 minimum using the SFT model without introducing new flux emergence. The predicted axial dipole moment of Cycle 24/25 minimum is 60--80 percent of Cycle 23/24 minimum, which suggests the amplitude of Cycle 25 even weaker than the current Cycle 24. Conclusions. The plateau of the solar axial dipole moment is an important feature for the longer prediction of the solar cycle based on the SFT model.

Reconstruction of the Solar Activity from the Catalogs of the Zurich Observatory

Egor **Illarionov**, Rainer Arlt

Solar Phys. **297**, Article number: 79 **2022**

https://arxiv.org/pdf/2205.10167

https://doi.org/10.1007/s11207-022-02015-3

Catalogs of the Zurich Observatory contain positional information on sunspots, prominences and faculae in late 19th and early 20th centuries. This database is given in handwritten tabular form and was not systematically analysed earlier. It is different from the sunspot number time series made in Zurich and was obtained with a larger telescope. We trained a neural-network model for handwritten text recognition and present the database of reconstructed coordinates. The database obtained connects the earlier observations by Spörer with later programs of the 20th century and supplements the sunspot-group catalogs of the Royal Greenwich Observatory. We also expect that the presented machine-learning approach and its deep capabilities will motivate the processing of a wide bulk of astronomical data, which is still given in non-digitized form or as plain scanned images.

Finite memory time and anisotropy effects for initial magnetic energy growth in random flow of conducting media

E. A. **Illarionov**, D. D. Sokoloff

2021

https://arxiv.org/pdf/2107.06387.pdf

The dynamo mechanism is a process of magnetic field self-excitation in a moving electrically conducting fluid. One of the most interesting applications of this mechanism related to the astrophysical systems is the case of a random motion of plasma. For the very first stage of the process, the governing dynamo equation can be reduced to a system of first order ordinary differential equations. For this case we suggest a regular method to calculate the growth rate of magnetic energy. Based on this method we calculate the growth rate for random flow with finite memory time and anisotropic statistical distribution of the stretching matrix and compare the results with corresponding ones for isotropic case and for short-correlated approximation. We find that for moderate Strouhal numbers and moderate anisotropy the analytical results reproduce the numerically estimated growth rates reasonably well, while for larger governing parameters the quantitative difference becomes substantial. In particular, analytical approximation is

applicable for the Strouhal numbers s<0.6 and we find some numerical models and observational examples for which this region might be relevant. Rather unexpectedly, we find that the mirror asymmetry does not contribute to the growth rates obtained, although the mirror asymmetry effects are known to be crucial for later stages of dynamo action.

New Website Showing Past and Present Solar Activity

Egor **Illarionov**

Would you like to know how active the Sun is today? Or how did it look like 100 years ago? You can explore this by visiting our new website atwww.observethesun.com The main features of the website:

- a 3D map of the tracers of solar activity (sunspots, filaments, plages, coronal holes, corona, prominences), updated daily
- large-scale datasets of sunspots (1918 – present), plages (from 1907), filaments and prominences (1919 – present) and variety of solar activity indices
- you can see solar activity from different vantage points, select objects to be displayed and download the data.

A detailed information about features of the website and a tutorial are available at medium.com/@egor.mypost/observe-the-sun-in-3d-from-the-past-hundred-years-up-to-the-present-day-c4b198568d6e.

Effect of Magnetic Field Strength on Solar Differential Rotation and Meridional Circulation

Shinsuke **Imada**, Masashi Fujiyama

ApJL **864** L5 **2018**

https://arxiv.org/pdf/1808.03005.pdf

http://sci-hub.tw/http://iopscience.iop.org/article/10.3847/2041-8213/aad904/meta

We studied the solar surface flows (differential rotation and meridional circulation) using a magnetic element feature tracking technique by which the surface velocity is obtained using magnetic field data. We used the line-of-sight magnetograms obtained by the Helioseismic and Magnetic Imager aboard the Solar Dynamics Observatory from 01 May 2010 to 16 August 2017 (Carrington rotations 2096 to 2193) and tracked the magnetic element features every hour. Using our method, we estimated the differential rotation velocity profile. We found rotation velocities of ∼ 30 and -170 m s−1 at latitudes of 0∘ and 60∘ in the Carrington rotation frame, respectively. Our results are consistent with previous results obtained by other methods, such as direct Doppler, time-distance helioseismology, or cross correlation analyses. We also estimated the meridional circulation velocity profile and found that it peaked at ∼12 m s−1 at a latitude of 45∘, which is also consistent with previous results. The dependence of the surface flow velocity on the magnetic field strength was also studied. In our analysis, the magnetic elements having stronger and weaker magnetic fields largely represent the characteristics of the active region remnants and solar magnetic networks, respectively. We found that magnetic elements having a strong (weak) magnetic field show faster (slower) rotation speed. On the other hand, magnetic elements having a strong (weak) magnetic field show slower (faster) meridional circulation velocity. These results might be related to the Sun's internal dynamics.

UV/EUV High-Throughput Spectroscopic Telescope: A Next Generation Solar Physics Mission white paper **Review**

S. **Imada**, T. Shimizu, T. Kawate, H. Hara, T. Watanabe

2017

https://arxiv.org/pdf/1701.04972v1.pdf

The origin of the activity in the solar corona is a long-standing problem in solar physics. Recent satellite observations, such as Hinode, Solar Dynamics Observatory (SDO), Interface Region Imaging Spectrograph (IRIS), show the detail characteristics of the solar atmosphere and try to reveal the energy transfer from the photosphere to the corona through the magnetic fields and its energy conversion by various processes. However, quantitative estimation of energy transfer along the magnetic field is not enough. There are mainly two reason why it is difficult to observe the energy transfer from photosphere to corona; 1) spatial resolution gap between photosphere (a few 0.1 arcsec) and corona (a few arcsec), 2) lack in temperature coverage. Furthermore, there is not enough observational knowledge of the physical parameters in the energy dissipation region. There are mainly three reason why it is difficult to observe in the vicinity of the energy dissipation region; 1) small spatial scale, 2) short time scale, 3) low emission. It is generally believed that the energy dissipation occurs in the very small scale and its duration is very short (10 second). Further, the density in the dissipation region might be very low. Therefore, the high spatial and

temporal resolution UV/EUV spectroscopic observation with wide temperature coverage is crucial to estimate the energy transport from photosphere to corona quantitatively and diagnose the plasma dynamics in the vicinity of the energy dissipation region. Main Science Target for the telescope is quantitative estimation for the energy transfer from the photosphere to the corona, and clarification of the plasma dynamics in the vicinity of the energy dissipation region, where is the key region for coronal heating, solar wind acceleration, and/or solar flare, by the high spatial and temporal resolution UV/EUV spectroscopy.

Outflow Structure of the Quiet Sun Corona Probed by Spacecraft Radio Scintillations in Strong Scattering

Takeshi **Imamura**1, Munetoshi Tokumaru2, Hiroaki Isobe3, Daikou Shiota2, Hiroki Ando1, Mayu Miyamoto4, Tomoaki Toda1, Bernd Häusler5, Martin Pätzold6, Alexander Nabatov7, Ayumi Asai3, Kentaro Yaji8, Manabu Yamada9, and Masato Nakamura
2014 ApJ 788 117

Radio scintillation observations have been unable to probe flow speeds in the low corona where the scattering of radio waves is exceedingly strong. Here we estimate outflow speeds continuously from the vicinity of the Sun to the outer corona (heliocentric distances of 1.5-20.5 solar radii) by applying the strong scattering theory to radio scintillations for the first time, using the Akatsuki spacecraft as the radio source. Small, nonzero outflow speeds were observed over a wide latitudinal range in the quiet-Sun low corona, suggesting that the supply of plasma from closed loops to the solar wind occurs over an extended area. The existence of power-law density fluctuations down to the scale of 100 m was suggested, which is indicative of well-developed turbulence which can play a key role in heating the corona. At higher altitudes, a rapid acceleration typical of radial open fields is observed, and the temperatures derived from the speed profile show a distinct maximum in the outer corona. This study opened up a possibility of observing detailed flow structures near the Sun from a vast amount of existing interplanetary scintillation data.

Causal Interaction between the Subsurface Rotation Rate Residuals and Radial Magnetic Field in Different Timescales

Fadil **Inceoglu**1, Rachel Howe2,3, and Paul T. M. Loto'aniu4,5
2022 ApJ 925 170
https://iopscience.iop.org/article/10.3847/1538-4357/ac4096/pdf

We studied the presence and spatiotemporal characteristics and evolution of the variations in the differential rotation rates and radial magnetic fields in the Schwabe and quasi-biennial-oscillation (QBO) timescales. To achieve these objectives, we used rotation rate residuals and radial magnetic field data from the Michelson Doppler Imager on the Solar and Heliospheric Observatory and the Helioseismic and Magnetic Imager on the Solar Dynamics Observatory, extending from 1996 May to 2020 August, covering solar cycles 23 and 24, respectively. Under the assumption that the radial surface magnetic field is nonlocal and the differential rotation is symmetric around the equator, our results suggest that the source region of the Schwabe cycle is confined between ∼30° N and S throughout the convection zone. As for the source region of the QBO, our results suggest that it is below 0.78 R⊙.

The Quasi-biennial-oscillation-type Signals in the Subsurface Flow Fields during Solar Cycles 23 and 24

Fadil **Inceoglu**1,2,3, Rachel Howe4,5, and Paul T. M. Loto'aniu1,2
2021 ApJ 920 49
https://doi.org/10.3847/1538-4357/ac16de

We studied the presence and spatiotemporal evolution of quasi-biennial oscillations (QBOs) in the rotation-rate residuals at target depths of 0.90R⊙, 0.95R⊙, and 0.99R⊙ and at low- (0°–30°), mid- (30°–50°), and high-latitudinal (50°–70°) bands. To achieve these objectives we used data from the Michelson Doppler Imager on the Solar and Heliospheric Observatory and the Helioseismic and Magnetic Imager on the Solar Dynamics Observatory, covering solar cycles 23 and 24, respectively. The results show that there are QBO-like signals in each latitudinal band and depth; however, they are affected by higher-amplitude and longer-timescale variations. The QBO-like signals found in each target depth and latitudinal bands show different spatiotemporal evolution. The amplitudes of variations of the rotation-rate residuals in the QBO timescale increase with increasing depth.
HMI Science Nuggets #169 **2021** http://hmi.stanford.edu/hminuggets/?p=3747

Constraining non-linear dynamo models using quasi-biennial oscillations from sunspot area data

Fadil **Inceoglu**, Rosaria Simoniello, Rainer Arlt, Matthias Rempel

A&A 625, A117 **2019**
https://arxiv.org/pdf/1904.03724.pdf
sci-hub.se/10.1051/0004-6361/201935272
Contex: Solar magnetic activity exhibits variations with periods between 1.5--4 years, the so-called quasi-biennial oscillations (QBOs), in addition to the well-known 11-year Schwabe cycles. Solar dynamo is thought to be the responsible mechanism for generation of the QBOs.
Aims: In this work, we analyse sunspot areas to investigate the spatial and temporal behaviour of the QBO signal and study the responsible physical mechanisms using simulations from fully nonlinear mean-field flux-transport dynamos.
Methods: We investigated the behaviour of the QBOs in the sunspot area data in full disk, and northern and southern hemispheres, using wavelet and Fourier analyses. We also ran solar dynamos with two different approaches to generating a poloidal field from an existing toroidal field, Babcock-Leighton and turbulent α mechanisms. We then studied the simulated magnetic field strengths as well as meridional circulation and differential rotation rates using the same methods.
Results: The results from the sunspot areas show that the QBOs are present in the full disk and hemispheric sunspot areas and they show slightly different spatial and temporal behaviours, indicating a slightly decoupled solar hemispheres. The QBO signal is generally intermittent and in-phase with the sunspot area data, surfacing when the solar activity is in maximum. The results from the BL-dynamos showed that they are neither capable of generating the slightly decoupled behaviour of solar hemispheres nor can they generate QBO-like signals. The turbulent α-dynamos, on the other hand, generated decoupled hemispheres and some QBO-like shorter cycles.
Conclusions: In conclusion, our simulations show that the turbulent α-dynamos with the Lorentz force seems more efficient in generating the observed temporal and spatial behaviour of the QBO signal compared with those from the BL-dynamos.

The Nature of Grand Minima and Maxima from Fully Nonlinear Flux Transport Dynamos

Fadil **Inceoglu**1, Rainer Arlt1, and Matthias Rempel2
2017 ApJ 848 93
We aim to investigate the nature and occurrence characteristics of grand solar minimum and maximum periods, which are observed in the solar proxy records such as 10Be and 14C, using a fully nonlinear Babcock–Leighton type flux transport dynamo including momentum and entropy equations. The differential rotation and meridional circulation are generated from the effect of turbulent Reynolds stress and are subjected to back-reaction from the magnetic field. To generate grand minimum- and maximum-like periods in our simulations, we used random fluctuations in the angular momentum transport process, namely the Λ-mechanism, and in the Babcock–Leighton mechanism. To characterize the nature and occurrences of the identified grand minima and maxima in our simulations, we used the waiting time distribution analyses, which reflect whether the underlying distribution arises from a random or a memory-bearing process. The results show that, in the majority of the cases, the distributions of grand minima and maxima reveal that the nature of these events originates from memoryless processes. We also found that in our simulations the meridional circulation speed tends to be smaller during grand maximum, while it is faster during grand minimum periods. The radial differential rotation tends to be larger during grand maxima, while it is smaller during grand minima. The latitudinal differential rotation, on the other hand, is found to be larger during grand minima.
See https://arxiv.org/pdf/1710.08644.pdf

Hemispheric progression of solar cycles in solar magnetic field data and its relation to the solar dynamo models

F. **Inceoglu**1, R. Simoniello2, M. F. Knudsen3 and C. Karoff
A&A 601, A51 (**2017**)
Aims. We aim to characterise the solar cycle progression simultaneously at different latitudes in each solar hemisphere using solar magnetic field data provided by the Wilcox Solar Observatory (WSO). We also investigate whether the features observed in the WSO data are best explained by the Babcock-Leighton (BL) mechanism and/or turbulent helicity as the α-effect in solar dynamos.
Methods. We analysed the hemispheric solar-cycle progression of the Sun's magnetic field in different 15° latitudinal bands, which allow us to explore the extent of cycle overlap. We also investigated the Waldmeier Rule, and the relationship between decay rates and peak amplitudes of the same cycle. These aspects of the solar-cycle progression can be explained in different ways by solar dynamo models depending on the source of the α-effect.
Results. The progression of the last four solar cycles in different latitudinal bands reveals that the degree of overlap between consecutive cycles is small and is more likely to be confined to low solar latitudes. We also found that the southern and northern solar hemispheres behave differently for the last four solar cycles, suggesting a slight

decoupling between the hemispheres. The results also reveal a strong correlation between the decay rates and the peak amplitudes of the solar cycles.

On the current solar magnetic activity in the light of its behaviour during the Holocene

F. **Inceoglu**, R. Simoniello, M. F. Knudsen, C. Karoff, J. Olsen, S. Turck-Chièze
Solar Phys. January **2016**, Volume 291, Issue 1, pp 303-315
http://arxiv.org/pdf/1509.06182v1.pdf

Solar modulation potential (SMP) reconstructions based on cosmogenic nuclide records reflect changes in the open solar magnetic field and can therefore help us obtain information on the behaviour of the open solar magnetic field over the Holocene period. We aim at comparing the Sun's large-scale magnetic field behaviour over the last three solar cycles with variations in the SMP reconstruction through the Holocene epoch. To achieve these objectives, we use the IntCal13 14C data to investigate distinct patterns in the occurrences of grand minima and maxima during the Holocene period. We then check whether these patterns might mimic the recent solar magnetic activity by investigating the evolution of the energy in the Sun's large-scale dipolar magnetic field using the Wilcox Solar Observatory data. The cosmogenic radionuclide data analysis shows that ~71\% of grand maxima during the period from 6600 BC to 1650 AD were followed by a grand minimum. The occurrence characteristics of grand maxima and minima are consistent with the scenario in which the dynamical non-linearity induced by the Lorentz force leads the Sun to act as a relaxation oscillator. This finding implies that the probability for these events to occur is non-uniformly distributed in time, as there is a memory in their driving mechanism, which can be identified via the back reaction of the Lorentz force.

Grand solar minima and maxima deduced from 10Be and 14C: magnetic dynamo configuration and polarity reversal

F. **Inceoglu** 1,3, R. Simoniello2, M. F. Knudsen3, C. Karoff1,3, J. Olsen4, S. Turck-Chiéze2 and B. H. Jacobsen3
A&A 577, A20 (**2015**)

Aims. This study aims to improve our understanding of the occurrence and origin of grand solar maxima and minima.
Methods. We first investigate the statistics of peaks and dips simultaneously occurring in the solar modulation potentials reconstructed using the Greenland Ice Core Project (GRIP) 10Be and IntCal13 14C records for the overlapping time period spanning between ~1650 AD to 6600 BC. Based on the distribution of these events, we propose a method to identify grand minima and maxima periods. By using waiting time distribution analysis, we investigate the nature of grand minima and maxima periods identified based on the criteria as well as the variance and significance of the Hale cycle during these kinds of events throughout the Holocene epoch.
Results. Analysis of grand minima and maxima events occurring simultaneously in the solar modulation potentials, reconstructed based on the 14C and the 10Be records, shows that the majority of events characterized by periods of moderate activity levels tend to last less than 50 years: grand maxima periods do not last longer than 100 years, while grand minima can persist slightly longer. The power and the variance of the 22-year Hale cycle increases during grand maxima and decreases during grand minima, compared to periods characterized by moderate activity levels.
Conclusions. We present the first reconstruction of the occurrence of grand solar maxima and minima during the Holocene based on simultaneous changes in records of past solar variability derived from tree-ring 14C and ice-core 10Be, respectively. This robust determination of the occurrence of grand solar minima and maxima periods will enable systematic investigations of the influence of grand solar minima and maxima episodes on Earth's climate.

Reconstruction of Subdecadal Changes in Sunspot Numbers Based on the NGRIP 10Be Record

F. **Inceoglu**, M. F. Knudsen, C. Karoff, J. Olsen
Solar Physics, Volume 289, Issue 11, pp 4377-4392 **2014**

Sunspot observations since 1610 A.D. show that the solar magnetic activity displays long-term changes, from Maunder Minimum-like low-activity states to Modern Maximum-like high-activity episodes, as well as short-term variations, such as the pronounced 11-year periodicity. Information on changes in solar activity levels before 1610 relies on proxy records of solar activity stored in natural archives, such as 10Be in ice cores and 14C in tree rings. These cosmogenic radionuclides are produced by the interaction between Galactic cosmic rays (GCRs) and atoms in the Earth's atmosphere; their production rates are anti-correlated with the solar magnetic activity. The GCR intensity displays a distinct 11-year periodicity due to solar modulation of the GCRs in the heliosphere, which is inversely proportional to, but out of phase with, the 11-year solar cycle. This implies a time lag between the actual solar

cycles and the GCR intensity, which is known as the hysteresis effect. In this study, we use the North Greenland Ice Core Project (NGRIP) records of the 10Be flux to reconstruct the solar modulation strength (Φ), which describes the modulation of GCRs throughout the heliosphere, to reconstruct both long-term and subdecadal changes in sunspot numbers (SSNs). We compare three different approaches for reconstructing subdecadal-scale changes in SSNs, including a linear approach and two approaches based on the hysteresis effect, i.e. models with ellipse–linear and ellipse relationships between Φ and SSNs. We find that the ellipse approach provides an amplitude-sensitive reconstruction and the highest cross-correlation coefficients in comparison with the ellipse–linear and linear approaches. The long-term trend in the reconstructed SSNs is computed using a physics-based model and agrees well with the other group SSN reconstructions. The new empirical approach, combining a physics-based model with ellipse-modeling of the 11-year cycle, therefore provides a method for reconstructing SSNs during individual solar cycles based on 10Be in ice cores. This, in turn, represents a new window for studying short-term changes in solar activity on unprecedented timescales, which may help improve our understanding of the solar dynamo.

Modeling the Relationship Between Neutron Counting Rates and Sunspot Numbers Using the Hysteresis Effect

F. **Inceoglu**, M. F. Knudsen, C. Karoff, J. Olsen

Solar Physics, April **2014**, Volume 289, Issue 4, pp 1387-1402

Several studies show that temporal variations in the Galactic cosmic ray (GCR) intensity display a distinct 11-year periodicity due to solar modulation of the galactic cosmic rays in the heliosphere. The 11-year periodicity of GCRs is inversely proportional to, but out of phase with, the 11-year solar cycle, implying that there is a time lag between actual solar cycle and the GCR intensity, which is known as the hysteresis effect. In this study, we use the hysteresis effect to model the relationship between neutron counting rates (NCRs), an indicator of the GCR intensity, and sunspot numbers (SSNs) over the period that covers the last four solar cycles (20, 21, 22, and 23). Both linear and ellipse models were applied to SSNs during odd and even cycles in order to calculate temporal variations of NCRs. We find that ellipse modeling provides higher correlation coefficients for odd cycles compared to linear models, e.g. 0.97, 0.97, 0.92, and 0.97 compared to 0.69, 0.72, 0.53, and 0.68 for data from McMurdo, Swarthmore, South Pole, and Thule neutron monitors, respectively, during solar cycle 21 with overall improvement of 31 % for odd cycles. When combined to a continuous model, the better correlation observed for the odd cycles increases the overall correlation between observed and modeled NCRs. The new empirical model therefore provides a better representation of the relationship between NCRs and SSNs. A major goal of the ongoing research is to use the new non-linear empirical model to reconstruct SSNs on annual time scales prior to 1610, where we do not have observational records of SSNs, based on changes in NCRs reconstructed from 10Be in ice cores.

Virtual EVE: a Deep Learning Model for Solar Irradiance Prediction

Manuel **Indaco**, Daniel Gass, William James Fawcett, Richard Galvez, Paul J. Wright, Andrés Muñoz-Jaramillo

Submission to Machine Learning and the Physical Sciences Workshop, NeurIPS **2023**

https://arxiv.org/pdf/2408.17430

Understanding space weather is vital for the protection of our terrestrial and space infrastructure. In order to predict space weather accurately, large amounts of data are required, particularly in the extreme ultraviolet (EUV) spectrum. An exquisite source of information for such data is provided by the Solar Dynamic Observatory (SDO), which has been gathering solar measurements for the past 13 years. However, after a malfunction in 2014 affecting the onboard Multiple EUV Grating Spectrograph A (MEGS-A) instrument, the scientific output in terms of EUV measurements has been significantly degraded. Building upon existing research, we propose to utilize deep learning for the virtualization of the defective instrument. Our architecture features a linear component and a convolutional neural network (CNN) -- with EfficientNet as a backbone. The architecture utilizes as input grayscale images of the Sun at multiple frequencies -- provided by the Atmospheric Imaging Assembly (AIA) -- as well as solar magnetograms produced by the Helioseismic and Magnetic Imager (HMI). Our findings highlight how AIA data are all that is needed for accurate predictions of solar irradiance. Additionally, our model constitutes an improvement with respect to the state-of-the-art in the field, further promoting the idea of deep learning as a viable option for the virtualization of scientific instruments.

Beyond the mini-solar maximum of solar cycle 24: Declining solar magnetic fields and the response of the terrestrial magnetosphere

M. **Ingale**, P. Janardhan, S. K. Bisoi

JGR **2019**

https://arxiv.org/pdf/1908.02576.pdf

The present study examines the response of the terrestrial magnetosphere to the long-term steady declining trends observed in solar magnetic fields and solar wind micro-turbulence levels since mid-1990's that has been continuing beyond the mini-solar maximum of cycle 24. A detailed analysis of the response of the terrestrial magnetosphere has been carried out by studying the extent and shape of the Earth's magnetopause and bow shock over the past four

solar cycles. We estimate sub-solar stand-off distance of the magnetopause and bow shock, and the shape of the magnetopause using numerical as well as empirical models. The computed magnetopause and bow shock stand-off distances have been found to be increasing steadily since around mid-1990's, consistent with the steady declining trend seen in solar magnetic fields and solar wind micro-turbulence levels. Similarly, we find an expansion in the shape of the magnetopause since 1996. The implications of the increasing trend seen in the magnetopause and bow shock stand-off distances are discussed and a forecast of the shape of the magnetopause in 2020, the minimum of cycle 24, has been made. Importantly, we also find two instances between 1968 and 1991 when the magnetopause stand-off distance dropped to values close to 6.6 earth radii, the geostationary orbit, for duration ranging from 9−11 hours and one event in 2005, post 1995 when the decline in photospheric fields began. Though there have been no such events since 2005, it represents a clear and present danger to our satellite systems.

Error Estimation of Linear Polarization Data from Coronagraphs – Application to STEREO-A/SECCHI-COR1 Observations

Bernd **Inhester**, Marilena Mierla, Sergei Shestov & Andrei N. Zhukov
Solar Physics volume 296, Article number: 72 (**2021**)
https://link.springer.com/content/pdf/10.1007/s11207-021-01815-3.pdf
https://doi.org/10.1007/s11207-021-01815-3

We attempt to quantitatively study the uncertainties of the polarized brightness and for the polarization angle which are to be expected for measurements from noisy image detectors in classical coronagraphs. We derive the probability density functions (PDF) which apply to polarization observations with polarization filters at 0∘, 60∘ and 120∘. The noise in the directly observed image intensities is assumed to be normally distributed. We find that for low and medium signal-to-noise ratios the polarized brightness obeys a distribution with a strongly biased mean which, if not taken account of, leads to an overestimation of the polarized brightness and degree of polarization. The PDFs are compared with data from the SECCHI-COR1 coronagraph onboard STEREO-A in order to detect systematic or random perturbations of the polarized brightness and the polarization angle beyond the unavoidable photon and detector hardware noise. This noise is estimated from two successive filter sequences taken in-flight during calm coronal conditions on **18 May 2008** and is expressed in the form of an intensity–variance relation. Two small deviations between the measured distributions and the predicted PDF for the polarization angle were found. The standard deviation of the polarization angle error decreases with increasing signal-to-noise ratio of the polarized brightness. For ratios larger than about 8 this decrease was found not as steep anymore as predicted which could hint to a small additional noise source. Next, we found a systematic constant deviation of the polarization angle by −1∘ for all signal-to-noise ratios of the polarized brightness. Besides these small discrepancies, our theoretically derived PDFs agree quite well with the distributions of measured brightnesses in test regions of the images. The PDFs we present here can equally be applied to similarly measured data from other coronagraphs and may help to quantify uncertainty limits of the derived polarization. They can be used for in-flight health checks of an instrument, are useful when separating unpolarized stray light from the polarized K-corona and when comparing the observed polarization data with results from model simulations.

Are the planetary orbital effects of the solar dark matter wake detectable?

Lorenzo **Iorio**
MNRAS Volume 489, Issue 1, October **2019**, Pages 723–726,
sci-hub.se/10.1093/mnras/stz2175

Recently, there has been some discussion in the literature about the effects of the anisotropy in the spatial density of dark matter in the Solar neighbourhood arising from the motion of the Sun through the Galactic halo. In particular, questions have been asked about the orbital motions of the Solar system's planets and whether these motions can be effectively constrained by the radiotechnical observations collected by Cassini. I show that the semilatus rectum p, the eccentricity e, the inclination I, the longitude of the ascending node Ω, the longitude of perihelion ϖ, and the mean anomaly at epoch η of a test particle of a restricted two-body system affected by the gravity of a dark matter wake undergo secular rates of change. In the case of Saturn, they are completely negligible, being at the order of ≃0.1 millimetres per century and ≃0.05–2 nanoarcseconds per century: the current (formal) accuracy level in constraining any anomalous orbital precessions is of the order of ≃0.002–2 milliarcseconds per century for Saturn. I also numerically simulate the Earth–Saturn range signature Δρ(t) arising from the dark matter wake over the same time span (2004–2017) as covered by the Cassini data record. I find that it is as low as ≃0.1−0.2m, while the existing range residuals, computed by astronomers without modelling any dark matter wake effect, are of the order of ≃ 30 m. The local dark matter density ϱDM would need to be larger than the currently accepted value of ϱDM=0.018M⊙pc−3 by a factor of 2.5 × 106 in order to induce a geocentric Kronian range signature large enough to make it discernible in the present-day residuals.

Variations of Solar Oblateness with the 22 yr Magnetic Cycle Explain Apparently Inconsistent Measurements

Abdanour **Irbah**1, Redouane Mecheri2, Luc Damé1, and Djelloul Djafer3

2019 ApJL 875 L26
sci-hub.se/10.3847/2041-8213/ab16e2
Solar oblateness results from distortion processes due to several phenomena inside of the Sun, but it can also be induced by the centrifugal potential of surface rotation. This fundamental parameter is of great scientific interest, yet for more than a century its measurements have remained a controversial topic, whether because of its average value or its variations observed (or not) over time. Special images acquired for almost the whole of Cycle 24 by the Helioseismic and Magnetic Imager on board the Solar Dynamic Observatory are used for calculating solar oblateness. The average oblateness obtained is 8.8 ± 0.8 mas, in good agreement with measurements over the last two decades. Variations are observed in anti-phase with the solar activity during Cycle 24, whereas they were in phase with activity during Cycle 23. More generally, the trend of both in-phase variation during odd cycles and anti-phase variation during even cycles is confirmed when revisiting past measurements. Therefore, it is possible that the Sun initiates a physical process resulting in a pulsation with the 22 yr magnetic cycle; it has extreme values during the polarity reversals, with a maximum swelling during odd cycles and the opposite for even ones. This oscillation could resolve the controversy surrounding past measurements.
HMI Science Nuggets # 126 **2019** http://hmi.stanford.edu/hminuggets/?p=2923

Multi-Scale Deep Learning for Estimating Horizontal Velocity Fields on the Solar Surface

Ryohtaroh T. **Ishikawa**, Motoki Nakata, Yukio Katsukawa, Youhei Masada, Tino L. Riethmüller
A&A **2021**
https://arxiv.org/pdf/2111.12518.pdf
The dynamics in the photosphere is governed by the multi-scale turbulent convection termed as granulation and supergranulation. It is important to derive 3-dimensional velocity vectors to understand the nature of the turbulent convection. However, it is difficult to obtain the velocity component perpendicular to the line-of-sight, which corresponds to the horizontal velocity in disk center observations. We developed a convolutional neural network model with a multi-scale deep learning architecture. The method consists of multiple convolutional kernels with various sizes of the receptive fields, and it performs convolution for spatial and temporal axes. The network is trained with data from three different numerical simulations of turbulent convection, and we introduced a coherence spectrum to assess the horizontal velocity fields that were derived at each spatial scale. The multi-scale deep learning method successfully predicts the horizontal velocities for each convection simulation in terms of the global-correlation-coefficient, which is often used for evaluating the prediction accuracy of the methods. The coherence spectrum reveals the strong dependence of the correlation coefficients on the spatial scales. Although coherence spectra are higher than 0.9 for large-scale structures, they drastically decrease to less than 0.3 for small-scale structures wherein the global-correlation-coefficient indicates a high value of approximately 0.95. We determined that this decrease in the coherence spectrum occurs around the energy injection scales. The accuracy for the small-scale structures is not guaranteed solely by the global-correlation-coefficient. To improve the accuracy in small-scales, it is important to improve the loss function for enhancing the small-scale structures and to utilize other physical quantities related to the non-linear cascade of convective eddies as input data.

Temporal and Spatial Scales in Coronal Rain Revealed by UV Imaging and Spectroscopic Observations

Ryohtaroh T. **Ishikawa**, Yukio Katsukawa, Patrick Antolin, Shin Toriumi
Solar Phys. **295**, Article number: 53 **2020**
https://arxiv.org/pdf/2003.13214.pdf
https://link.springer.com/content/pdf/10.1007/s11207-020-01617-z.pdf
Coronal rain corresponds to cool and dense clumps in the corona accreting towards the solar surface, and is often observed above solar active regions. They are generally thought to be produced by thermal instability in the corona and their lifetime is limited by the time they take to reach the chromosphere. Although the rain usually fragments into smaller clumps while falling down, their specific spatial and temporal scales remain unclear. In addition, the observational signatures of the impact of the rain with the chromosphere have not been clarified yet. In this study, we investigate the time evolution of velocity and intensity of coronal rain above a sunspot by analyzing coronal images obtained by the AIA onboard the SDO satellite as well as the Slit-Jaw Images (SJIs) and spectral data taken by the IRIS satellite. We identify dark and bright threads moving towards the umbra in AIA images and in SJIs, respectively, and co-spatial chromospheric intensity enhancements and redshifts in three IRIS spectra, Mg II k 2796 Angstrom, Si IV 1394 Angstrom, and C II 1336 Angstrom. The intensity enhancements and coronal rain redshifts occur almost concurrently in all the three lines, which clearly demonstrates the causal relationship with coronal rain. Furthermore, we detect bursty intensity variation with a timescale shorter than 1 minute in Mg II k, Si IV and C II spectra, indicating that a length scale of rain clumps is about 2.7 Mm if we multiply the typical time scale of the busty intensity variation at 30 sec by the rain velocity at 90 km s−1. Such rapid enhancements in the IRIS lines are excited within a time lag of 5.6 sec limited by the temporal resolution. These temporal and spatial scales may reflect the physical processes responsible for the rain morphology, and are suggestive of instabilities such as Kelvin-Helmholtz. **24 April 2014,**

Study of the Dynamics of Convective Turbulence in the Solar Granulation by Spectral Line Broadening and Asymmetry

Ryohtaroh T. **Ishikawa**, Yukio Katsukawa, Takayoshi Oba, Motoki Nakata, Kenichi Nagaoka, Tatsuya Kobayashi

ApJ **890** 138 **2020**

https://arxiv.org/pdf/2001.04632.pdf

https://doi.org/10.3847/1538-4357/ab6bce

In the quiet regions on the solar surface, turbulent convective motions of granulation play an important role in creating small-scale magnetic structures, as well as in energy injection into the upper atmosphere. The turbulent nature of granulation can be studied using spectral line profiles, especially line broadening, which contains information on the flow field smaller than the spatial resolution of an instrument. Moreover, the Doppler velocity gradient along a line-of-sight (LOS) causes line broadening as well. However, the quantitative relationship between velocity gradient and line broadening has not been understood well. In this study, we perform bisector analyses using the spectral profiles obtained using the Spectro-Polarimeter of the Hinode/Solar Optical Telescope to investigate the relationship of line broadening and bisector velocities with the granulation flows. The results indicate that line broadening has a positive correlation with the Doppler velocity gradients along the LOS. We found excessive line broadening in fading granules, that cannot be explained only by the LOS velocity gradient, although the velocity gradient is enhanced in the process of fading. If this excessive line broadening is attributed to small-scale turbulent motions, the averaged turbulent velocity is obtained as 0.9 km/s. **22 Nov. 2006, 25 Aug. 2009, 08 Nov. 2018**

Hot plasma in a quiescent solar active region as measured by RHESSI, XRT, and AIA

Shin-nosuke **Ishikawa**, Sam Krucker

ApJ **2019**

https://arxiv.org/pdf/1903.11293.pdf

This paper investigates a quiescent (non-flaring) active region observed on **July 13, 2010** in EUV, SXR, and HXRs to search for a hot component that is speculated to be a key signature of coronal heating. We use a combination of RHESSI imaging and long-duration time integration (up to 40 min) to detect the active regions in the 3-8 keV range during apparently non-flaring times. The RHESSI imaging reveals a hot component that originates from the entire active region, as speculated for a nanoflare scenario where the entire active region is filled with a large number of unresolved small energy releases. An isothermal fit to the RHESSI data gives temperatures around ~7 MK with emission measure of several times 10^46 cm^-3. Adding EUV and SXR observations taken by AIA and XRT, respectively, we derive a differential emission measure (DEM) that shows a peak between 2 and 3 MK with a steeply decreasing high-temperature tail, similar to what has been previously reported. The derived DEM reveals that a wide range of temperatures contributes to the RHESSI flux (e.g. 40 % of the 4 keV emission being produced by plasma below 5 MK, while emission at 7 keV is almost exclusively from plasmas above 5 MK) indicating that the RHESSI spectrum should not be fitted with an isothermal. The hot component has a rather small emission measure (~0.1 % of the total EM is above 5 MK), and the derived thermal energy content is of the order of 10 % for a filling factor of unity, or potentially below 1 % for smaller filling factors.

Detection of nanoflare-heated plasma in the solar corona by the FOXSI-2 sounding rocket

Shin-nosuke **Ishikawa**, Lindsay Glesener, Säm Krucker, Steven Christe, Juan Camilo Buitrago-Casas, Noriyuki Narukage & Juliana Vievering

Nature Astronomyvolume 1, pages771–774 (**2017**)

https://www.nature.com/articles/s41550-017-0269-z

The processes that heat the solar and stellar coronae to several million kelvins, compared with the much cooler photosphere (5,800 K for the Sun), are still not well known1. One proposed mechanism is heating via a large number of small, unresolved, impulsive heating events called nanoflares2. Each event would heat and cool quickly, and the average effect would be a broad range of temperatures including a small amount of extremely hot plasma. However, detecting these faint, hot traces in the presence of brighter, cooler emission is observationally challenging. Here we present hard X-ray data from the second flight of the Focusing Optics X-ray Solar Imager (FOXSI-2), which detected emission above 7 keV from an active region of the Sun with no obvious individual X-ray flare emission. Through differential emission measure computations, we ascribe this emission to plasma heated above 10 MK, providing evidence for the existence of solar nanoflares. The quantitative evaluation of the hot plasma strongly constrains the coronal heating models. **11 December 2014**,

CLASP/SJ Observations of Rapid Time Variations in the Lyα Emission in a Solar Active Region

Shin-nosuke **Ishikawa**1, Masahito Kubo2, Yukio Katsukawa2, Ryouhei Kano2, Noriyuki Narukage2, Ryohko Ishikawa2, Takamasa Bando2, Amy Winebarger3, Ken Kobayashi3, Javier Trujillo Bueno4
2017 ApJ 846 127
The Chromospheric Lyα SpectroPolarimeter (CLASP) is a sounding rocket experiment launched on **2015 September 3** to investigate the solar chromosphere and transition region. The slit-jaw (SJ) optical system captured Lyα images with a high time cadence of 0.6 s. From the CLASP/SJ observations, many variations in the solar chromosphere and transition region emission with a timescale of <1 minute were discovered. In this paper, we focus on the active region within the SJ field of view and investigate the relationship between short (<30 s) temporal variations in the Lyα emission and the coronal structures observed by Solar Dynamics Observatory/Atmospheric Imaging Assembly (AIA). We compare the Lyα temporal variations at the coronal loop footpoints observed in the AIA 211 Å (≈2 MK) and AIA 171 Å (≈0.6 MK) channels with those in the regions with bright Lyα features without a clear association with the coronal loop footpoints. We find more short (<30 s) temporal variations in the Lyα intensity in the footpoint regions. Those variations did not depend on the temperature of the coronal loops. Therefore, the temporal variations in the Lyα intensity at this timescale range could be related to the heating of the coronal structures up to temperatures around the sensitivity peak of 171 Å. No signature was found to support the scenario that these Lyα intensity variations were related to the nanoflares. Waves or jets from the lower layers (lower chromosphere or photosphere) are possible causes for this phenomenon.

Electroweak Hall Effect of Neutrino and Coronal Heating
Kenzo **Ishikawa**, Yutaka Tobita
2015
http://arxiv.org/pdf/1503.07285v1.pdf
The inversion of temperature at the solar corona is hard to understand from classical physics, and the coronal heating mechanism remains unclear. The heating in the quiet region seems contradicting with the thermodynamics and is a keen problem for physicists. A new mechanism for the coronal heating based on the neutrino radiative transition unique in the corona region is studied. The probability is enormously amplified by an electroweak Chern-Simons form and overlapping waves, and the sufficient energy is transfered. Thus the coronal heating is understood from the quantum effects of the solar neutrino.

Strategy for Realizing High-Precision VUV Spectro-Polarimeter
R. **Ishikawa**, N. Narukage, M. Kubo, S. Ishikawa, R. Kano, S. Tsuneta
Solar phys., **2014**
Spectro-polarimetric observations in the vacuum ultraviolet (VUV) range are currently the only means to measure magnetic fields in the upper chromosphere and transition region of the solar atmosphere. The Chromospheric Lyman-Alpha Spectro-Polarimeter (CLASP) aims to measure linear polarization at the hydrogen Lyman-α line (121.6 nm). This measurement requires a polarization sensitivity better than 0.1 %, which is unprecedented in the VUV range. We here present a strategy with which to realize such high-precision spectro-polarimetry. This involves the optimization of instrument design, testing of optical components, extensive analyses of polarization errors, polarization calibration of the instrument, and calibration with onboard data. We expect that this strategy will aid the development of other advanced high-precision polarimeters in the UV as well as in other wavelength ranges.

Medium-Sized Solar Cycles in Different Epochs of Solar Activity.
Ishkov, V.N.
Geomagn. Aeron. 63, 1024–1030 (**2023**).
https://doi.org/10.1134/S0016793223070101
The study of a reliable series of sunspot observations has allowed formulation of a scenario for the sustainable development of solar cyclicity over the past ~190 years. This scenario predicts a change in the level of sunspot activity in epochs of increased or lowered solar activity with selected transition periods, which gives three different modes of the total magnetic field generation of the Sun with a duration of approximately five cycles. Since January 2020, the 25th solar cycle has begun with the expected average magnitude according to the development of the first 3 years and the Gnevyshev-Ol' rule. Therefore, an attempt has been made to study the observational characteristics of a family of average solar cycles in different epochs of solar activity, i.e., the 13th, 15th, and 25th epochs of lowered solar activity, the 10th and 20th epochs of increased solar activity, and the 17th and 23rd transitional periods between the epochs.

A MECHANISM FOR THE DEPENDENCE OF SUNSPOT GROUP TILT ANGLES ON CYCLE STRENGTH

Emre **Işık**

2015 ApJ 813 L13

The average tilt angle of sunspot groups emerging throughout the solar cycle determines the net magnetic flux crossing the equator, which is correlated with the strength of the subsequent cycle. I suggest that a deep-seated, non-local process can account for the observed cycle-dependent changes in the average tilt angle. Motivated by helioseismic observations indicating cycle-scale variations in the sound speed near the base of the convection zone, I determined the effect of a thermally perturbed overshoot region on the stability of flux tubes and on the tilt angles of emerging flux loops. I found that 5–20 K of cooling is sufficient for emerging flux loops to reproduce the reported amplitude of cycle-averaged tilt angle variations, suggesting that it is a plausible effect responsible for the nonlinearity of the solar activity cycle.

Data on Solar Activity for Science

Ishkov V. 1,2, Sergeyeva N. 2 , Zabarinskaya L. 2 , Nisilevich M. 2 , Kedrov E. 2 , Krylova T. 2

Sun and Geosphere, **2019**; 14/1: 7 -11

http://newserver.stil.bas.bg/SUNGEO//00SGArhiv/SG_v14_No1_2019-pp-07-11.pdf

Solar activity has a huge impact on our planet and surrounding space causing various physical phenomena and processes. Observational and experimental data on solar activity are widely used in basic and applied research. Studying of the phenomena occurring on the Sun and in interplanetary space and their influence on the processes in the outer envelopes and inner shells of the Earth is very important. The data of long-term observations are the most valuable. The World Data Center for Solar-Terrestrial Physics in Moscow has a representative collection of the Sun's observation results obtained by the global network of solar and astronomical observatories and instruments installed on spacecrafts. The article describes the solar activity data stored in the Center and available on the website in open access. The Center is constantly improving and expanding its information resources; new information technologies providing free convenient access to data are applied. Activities on the preservation and efficient use of historical data, as well as a new approach to the data publication with the assignment of digital object identifier (DOI) convenient for citing data are presented in this article.

Experimental Investigation of the Delay Time in Galactic Cosmic Ray Flux in Different Epochs of Solar Magnetic Cycles: 1959 – 2014

Krzysztof **Iskra**, Marek Siluszyk, Michael Alania, Witold Wozniak

Solar Physics September **2019**, 294:115

https://link.springer.com/content/pdf/10.1007%2Fs11207-019-1509-4.pdf

sci-hub.se/10.1007/s11207-019-1509-4

In the present article, we analyze long-term changes in the intensity of galactic cosmic rays (GCRs) in different polarity epochs of the solar magnetic cycles from 1959 to 2014. Our purpose is to carry out a study of the delay time (DT) between the changes of the GCR intensity and various parameters characterizing the conditions in the heliosphere. We prove the existence of varying DTs between the changes of GCR intensity and the parameters characterizing solar activity, such as sunspot number and tilt angle. Based on our investigation, we obtained different DTs in epochs with different global solar magnetic field polarities. We conclude that the observed DTs are very important parameters for the study of GCR transport in the heliosphere.

Links between Adjacent 11-Year Solar Cycles and Their Mutual Conditioning.

Ivanov, V.G., Nagovitsyn, Y.A.

Geomagn. Aeron. 63, 920–924 (**2023**).

https://doi.org/10.1134/S0016793223070113

Study of general statistical relationships of the 11-year sunspot cycles including: (a) 'the length-amplitude rule', or LAR (anticorrelation between the length of the current cycle from minimum to minimum and the amplitude of the next one), (b) 'the rule of the 3rd year', or R3 (correlation between the activity about 3 years before the first minimum of the cycle and its amplitude), (c) 'the rule of the 7th year', or R7 (correlation between the activity about 7 years before the maximum of the cycle and its amplitude), (d) the Waldmeier rule, or WR (anticorrelation between the length of the ascending phase of the cycle and its amplitude) was performed for the Wolf numbers. Analysis of the mutual conditionality of these rules showed that LAR, R3, R7 and WR are not independent effects. In particular, R3 and R7 hold in a series if WR and LAR hold in it.

Solar cycle 25 prediction using length-to-amplitude relations

Vladimir G. **Ivanov**

Solar Physics **volume 297**, Article number: 92 **2022**

https://arxiv.org/pdf/2203.02028.pdf

https://doi.org/10.1007/s11207-022-02031-3
We propose a simple method for prediction of the 11-year solar cycle maximum that is based on two relations. One of them is well known Waldmeier's rule that binds the amplitude of a cycle and the length of its ascending phase. The second rule relates the length of a given cycle from minimum to minimum and the amplitude of the next one. Using corresponding linear regressions we obtain for the amplitide of cycle 25 in the scale of 13-month smoothed monthly total revised sunspot number SNmax(25)=181±46 and for the moment of the maximum Tmax(25)=2024.2±1.0. Therefore, according to the prediction, cycle 25 will be higher than the previous one (SNmax(24)=116) with probability 0.92.

Solar activity classification based on Mg II spectra: towards classification on compressed data

Sergey **Ivanov**, Maksym Tsizh, Denis Ullmann, Brandon Panos, Slava Voloshynovskiy
2020
https://arxiv.org/pdf/2009.07156.pdf
Although large volumes of solar data are available for investigation, the majority of these data remain unlabeled and are therefore unsuited to modern supervised machine learning methods. Having a way to automatically classify spectra into categories related to the degree of solar activity is highly desirable and will assist and speed up future research efforts in solar physics. At the same time, the large volume of raw observational data is a serious bottleneck for machine learning, requiring powerful computational means. Additionally, the raw data communication imposes restrictions on real time data observations and requires considerable bandwidth and energy for the onboard solar observation systems. To solve mentioned issues, we propose a framework to classify solar activity on compressed data. To this end, we used a labeling scheme from a clustering technique in conjunction with several machine learning algorithms to categorize Mg II spectra measured by NASA's satellite IRIS into groups characterizing solar activity. Our training data set is a human-annotated list of 85 IRIS observations containing 29097 frames in total or equivalently 9 million Mg II spectra. The annotated types of Solar activity are active region, pre-flare activity, Solar flare, Sunspot and quiet Sun. We used the vector quantization to compress these data before training classifiers. We found that the XGBoost classifier produced the most accurate results on the compressed data, yielding over a 0.95 prediction rate, and outperforming other ML methods: convolution neural networks, K-nearest neighbors, naive Bayes classifiers and support vector machines. A principle finding of this research is that the classification performance on compressed and uncompressed data is comparable under our particular architecture, implying the possibility of large compression rates for relatively low degrees of information loss.

Latitude and power characteristics of solar activity in the end of the Maunder minimum

V. G. **Ivanov**, E. V. Miletsky
Geomagnetism and Aeronomy **2016**
https://arxiv.org/pdf/1611.08189v1.pdf
Two important sources of information about sunspots in the Maunder minimum are the Sp\"orer catalog and observations of the Paris observatory, which cover in total the last quarter of the 17th and the first two decades of the 18th century.
These data, in particular, contain information about sunspot latitudes. As we showed in previous papers, dispersions of sunspot latitude distributions are tightly related to sunspot indices, so we can estimate the level of solar activity in this epoch by a method which is not based on direct calculation of sunspots and is weakly affected by loss of observational data.
The latitude distributions of sunspots in the time of transition from the Maunder minimum to the common regime of solar activity proved to be wide enough. It gives evidences in favor of, first, not very low cycle No. -3 (1712-1723) with the Wolf number in maximum W=100±50, and, second, nonzero activity in the maximum of cycle No. -4 (1700-1711) W=60±45.
Therefore, the latitude distributions in the end of the Maunder minimum are in better agreement with the traditional Wolf number and new revisited indices of activity SN and GN than with the GSN; the latter provide much lower level of activity in this epoch.

Characteristics of latitude distribution of sunspots and their links to solar activity in pre-Greenwich data

V. G. **Ivanov**, E. V. Miletsky
Geomagnetism and Aeronomy **2016**
http://arxiv.org/pdf/1603.03297v1.pdf
We study and compare characteristics of sunspot group latitude distribution in two catalogs: the extended Greenwich (1874--2014) and Schwabe ones (1825--1867). We demonstrate that both datasets reveal similar links between latitude and amplitude characteristics of the 11-year cycle: the latitude dispersion correlates with the

current activity and the mean latitude of sunspots in the cycle's maximum is proportional to its amplitude, It agrees with conclusions that we made in previous papers for the Greenwich catalog.
We show that the latitude properties of sunspot distribution are much more stable against loss of observational data than traditional amplitude indices of activity. Therefore, the found links can be used for estimates of quality of observations and independent normalizing of activity levels in a gappy pre-Greenwich data. We demonstrate it using the Schwabe catalog as an example.
In addition, we show that the first part of the Schwabe data probably contains errors in determination of sunspot latitudes that lead to overestimation of the sunspot latitude dispersions.

Form of the latitude distribution of sunspot activity

V. G. **Ivanov**, E. V. Miletskii and Yu. A. Nagovitsyn
Astronomy Reports, Volume 55, Number 10, 911-917,
Astronomicheskii Zhurnal, **2011**, Vol. 88, No. 10, pp. 989–996.
The spatial (latitude) distribution of sunspots is studied, including its dependence on solar activity. It is shown that the latitude distributions of sunspots for a given year can be approximately described by the normal law, with its variance being a linear function of the current level of solar activity. Thus, an increase in activity is accompanied by an expansion of the zone of solar activity, in good agreement with earlier results. As the solar activity increases, the width of the zone of sunspot generation and the latitude maximum of the sunspot density grow somewhat more slowly than the number of sunspots, in agreement with observations. The results obtained can be used to reconstruct the spatial distributions of sunspots in the past, interpret the magnetic activity of stars, and address the requirements of the dynamo theory in the form of constraints imposed on models of cyclicity.

Sharp magnetic structures from dynamos with density stratification

Sarah **Jabbari**, Axel Brandenburg, Nathan Kleeorin, Igor Rogachevskii
MNRAS **2016**
http://arxiv.org/pdf/1607.08897v1.pdf
Recent direct numerical simulations (DNS) of large-scale turbulent dynamos in strongly stratified layers have resulted in surprisingly sharp bipolar structures at the surface. Here we present new DNS of helically and non-helically forced turbulence with and without rotation and compare with corresponding mean-field simulations (MFS) to show that these structures are a generic outcome of a broader class of dynamos in density-stratified layers. The MFS agree qualitatively with the DNS, but the period of oscillations tends to be longer in the DNS. In both DNS and MFS, the sharp structures are produced by converging flows at the surface and are driven by the Lorentz force associated with the large-scale dynamo-driven magnetic field if the dynamo number is at least 5 times supercritical.

Magnetic flux concentrations from dynamo-generated fields

S. **Jabbari**1,2, A. Brandenburg1,2, I. R. Losada1,2, N. Kleeorin3,1,4 and I. Rogachevskii
A&A 568, A112 (**2014**)
http://arxiv.org/pdf/1401.6107v3.pdf
Context. The mean-field theory of magnetized stellar convection gives rise to two distinct instabilities: the large-scale dynamo instability, operating in the bulk of the convection zone and a negative effective magnetic pressure instability (NEMPI) operating in the strongly stratified surface layers. The latter might be important in connection with magnetic spot formation. However, as follows from theoretical analysis, the growth rate of NEMPI is suppressed with increasing rotation rates. On the other hand, recent direct numerical simulations (DNS) have shown a subsequent increase in the growth rate.
Aims. We examine quantitatively whether this increase in the growth rate of NEMPI can be explained by an $\alpha 2$ mean-field dynamo, and whether both NEMPI and the dynamo instability can operate at the same time.
Methods. We use both DNS and mean-field simulations (MFS) to solve the underlying equations numerically either with or without an imposed horizontal field. We use the test-field method to compute relevant dynamo coefficients.
Results. DNS show that magnetic flux concentrations are still possible up to rotation rates above which the large-scale dynamo effect produces mean magnetic fields. The resulting DNS growth rates are quantitatively reproduced with MFS. As expected for weak or vanishing rotation, the growth rate of NEMPI increases with increasing gravity, but there is a correction term for strong gravity and large turbulent magnetic diffusivity.
Conclusions. Magnetic flux concentrations are still possible for rotation rates above which dynamo action takes over. For the solar rotation rate, the corresponding turbulent turnover time is about 5 h, with dynamo action commencing in the layers beneath.

Probabilistic Inversions for Time-Distance Helioseismology

Jason **Jackiewicz**
Solar Phys. **2020**

https://arxiv.org/pdf/2007.01432.pdf

Time-distance helioseismology is a set of powerful tools to study features below the Sun's surface. Inverse methods are needed to interpret time-distance measurements, with many examples in the literature. However, techniques that utilize a more statistical approach to inferences, and broadly used in the astronomical community, are less-commonly found in helioseismology. This article aims to introduce a potentially powerful inversion scheme based on Bayesian probability theory and Monte Carlo sampling that is suitable for local helioseismology. We describe the probabilistic method and how it is conceptually different from standard inversions used in local helioseismology. Several example calculations are carried out to compare and contrast the setup of the problems and the results that are obtained. The examples focus on two important phenomena studied with helioseismology: meridional circulation and supergranulation. Numerical models are used to compute synthetic observations, providing the added benefit of knowing the solution against which the results can be tested. For demonstration purposes, the problems are formulated in two and three dimensions, using both ray- and Born-theoretical approaches. The results seem to indicate that the probabilistic inversions not only find a better solution with much more realistic estimation of the uncertainties, but they also provide a broader view of the range of solutions possible for any given model, making the interpretation of the inversion more quantitative in nature. Unlike the progress being made in fundamental measurement schemes in local helioseismology that image the far side of the Sun, or have detected signatures of global Rossby waves, among many others, inversions of those measurements have had significantly less success. Such statistical methods may help overcome some of these barriers to move the field forward.

A Determination of the North–South Heliospheric Magnetic Field Component from Inner Corona Closed-loop Propagation

B. V. **Jackson**1, P. P. Hick1, A. Buffington1, H.-S. Yu1, M. M. Bisi2, M. Tokumaru3, and X. Zhao

2015 ApJ 803 L1

A component of the magnetic field measured in situ near the Earth in the solar wind is present from north–south fields from the low solar corona. Using the Current-sheet Source Surface model, these fields can be extrapolated upward from near the solar surface to 1 AU. Global velocities inferred from a combination of interplanetary scintillation observations matched to in situ velocities and densities provide the extrapolation to 1 AU assuming mass and mass flux conservation. The north–south field component is compared with the same ACE in situ magnetic field component—the Normal (Radial Tangential Normal) Bn coordinate—for three years throughout the solar minimum of the current solar cycle. We find a significant positive correlation throughout this period between this method of determining the Bn field compared with in situ measurements. Given this result from a study during the latest solar minimum, this indicates that a small fraction of the low-coronal Bn component flux regularly escapes from closed field regions. The prospects for Space Weather, where the knowledge of a Bz field at Earth is important for its geomagnetic field effects, is also now enhanced. This is because the Bn field provides the major portion of the Geocentric Solar Magnetospheric Bz field coordinate that couples most closely to the Earth's geomagnetic field.

Transverse oscillations in slender Ca II H fibrils observed with Sunrise/SuFI

Shahin **Jafarzadeh**, S. K. Solanki, R. Gafeira, M. van Noort, P. Barthol, J. Blanco Rodriguez, J. C. del Toro Iniesta, A. Gandorfer, L. Gizon, J. Hirzberger, M. Knoelker, D. Orozco Suarez, T. L. Riethmueller, W. Schmidt

Astrophysical Journal Supplement Series **2016**

https://arxiv.org/pdf/1610.07449v1.pdf

We present observations of transverse oscillations in slender Ca II H fibrils (SCFs) in the lower solar chromosphere. We use a 1-hour long time series of high (spatial and temporal) resolution, seeing-free observations in a 0.11 nm wide passband covering the line core of Ca II H 396.9 nm from the second flight of the Sunrise balloon-borne solar observatory. The entire field of view, spanning the polarity inversion line of an active region close to the solar disk center, is covered with bright, thin, and very dynamic fine structures. Our analysis reveals the prevalence of transverse waves in SCFs with median amplitudes and periods on the order of 2.4+-0.8 km/s and 83+-29 s, respectively (with standard deviations given as uncertainties). We find that the transverse waves often propagate along (parts of) the SCFs with median phase speeds of 9+-14 km/s. While the propagation is only in one direction along the axis in some of the SCFs, propagating waves in both directions, as well as standing waves are also observed. The transverse oscillations are likely Alfvenic and are thought to be representative of magnetohydrodynamic kink waves. The wave propagation suggests that the rapid, high-frequency transverse waves, often produced in the lower photosphere, can penetrate into the chromosphere, with an estimated energy flux of ~ 15 kW/m^2. Characteristics of these waves differ from those reported for other fibrillar structures, which, however, were observed mainly in the upper solar chromosphere. **2013 June 12-13**

Helioseismic Investigation of Quasi-biennial Oscillation Source Regions

Kiran **Jain**, Partha Chowdhury, Sushanta C. Tripathy

ApJ **959** 16 **2023**

https://arxiv.org/pdf/2311.16331.pdf

https://iopscience.iop.org/article/10.3847/1538-4357/ad045c/pdf
We studied the temporal evolution of quasi-biennial oscillations (QBOs) using acoustic mode oscillation frequencies from the Global Oscillation Network Group. The data used here span over more than 25 yr, covering solar cycles 23 and 24 and the ascending phase of cycle 25. The analysis reveals that the QBO-like signals are present in both the cycles, but with different periods. The dominant QBO period in cycle 23 is found to be about 2 yr while it is about 3 yr in cycle 24. Furthermore, the quasi-biennial oscillatory signals are present only during the ascending and high-activity phases of cycle 23 and quickly weaken around 2005 during the declining phase. In comparison, the QBO signals are present throughout the cycle 24, starting from 2009 to 2017. We also explored the depth dependence in QBO signals and obtained a close agreement at all depths, except in the near-surface shear layer. A detailed analysis of the near-surface shear layer suggests that the source region of QBOs is probably within a few thousand kilometers just below the surface.

Divergent Horizontal Sub-surface Flows within Active Region 11158

Kiran **Jain**, S. C. Tripathy, and F. Hill
2015 ApJ 808 60
We measure the horizontal subsurface flow in a fast emerging active region (AR; NOAA 11158) using the ring-diagram technique and the Helioseismic and Magnetic Imager high spatial resolution Dopplergrams. This AR had a complex magnetic structure and displayed significant changes in morphology during its disk passage. Over a period of six days from **2011 February 11 to 16**, the temporal variation in the magnitude of the total velocity is found to follow the trend of magnetic field strength. We further analyze regions of individual magnetic polarity within AR 11158 and find that the horizontal velocity components in these sub-regions have significant variation with time and depth. The leading and trailing polarity regions move faster than the mixed-polarity region. Furthermore, both zonal and meridional components have opposite signs for trailing and leading polarity regions at all depths showing divergent flows within the AR. We also find a sharp decrease in the magnitude of total horizontal velocity in deeper layers around major flares. It is suggested that the re-organization of magnetic fields during flares, combined with the sunspot rotation, decreases the magnitude of horizontal flows or that the flow kinetic energy has been converted into the energy released by flares. After the decline in flare activity and sunspot rotation, the flows tend to follow the pattern of magnetic activity. We also observe less variation in the velocity components near the surface but these tend to increase with depth, further demonstrating that the deeper layers are more affected by the topology of ARs.

Five-minute Oscillation Power within Magnetic Elements in the Solar Atmosphere

Rekha **Jain**1, Andrew Gascoyne1, Bradley W. Hindman2, and Benjamin Gree
2014 ApJ 796 72
It has long been known that magnetic plage and sunspots are regions in which the power of acoustic waves is reduced within the photospheric layers. Recent observations now suggest that this suppression of power extends into the low chromosphere and is also present in small magnetic elements far from active regions. In this paper we investigate the observed power suppression in plage and magnetic elements, by modeling each as a collection of vertically aligned magnetic fibrils and presuming that the velocity within each fibril is the response to buffeting by incident p modes in the surrounding field-free atmosphere. We restrict our attention to modeling observations made near the solar disk center, where the line-of-sight velocity is nearly vertical and hence, only the longitudinal component of the motion within the fibril contributes. Therefore, we only consider the excitation of axisymmetric sausage waves and ignore kink oscillations as their motions are primarily horizontal. We compare the vertical motion within the fibril with the vertical motion of the incident p mode by constructing the ratio of their powers. In agreement with observational measurements we find that the total power is suppressed within strong magnetic elements for frequencies below the acoustic cut-off frequency. However, further physical effects need to be examined for understanding the observed power ratios for stronger magnetic field strengths and higher frequencies. We also find that the magnitude of the power deficit increases with the height above the photosphere at which the measurement is made. Furthermore, we argue that the area of the solar disk over which the power suppression extends increases as a function of height.

Probabilistic Inversions for Time–Distance Helioseismology

Jason **Jackiewicz**
Solar Physics volume 295, Article number: 137 (**2020**)
https://link.springer.com/content/pdf/10.1007/s11207-020-01667-3.pdf
Time–distance helioseismology is a set of powerful tools to study localized features below the Sun's surface. Inverse methods are needed to robustly interpret time–distance measurements, with many examples in the literature.

However, techniques that utilize a more statistical approach to inferences, and that are broadly used in the astronomical community, are less-commonly found in helioseismology. This article aims to introduce a potentially powerful inversion scheme based on Bayesian probability theory and Monte Carlo sampling that is suitable for local helioseismology. We first describe the probabilistic method and how it is conceptually different from standard inversions used in local helioseismology. Several example calculations are carried out to compare and contrast the setup of the problems and the results that are obtained. The examples focus on two important phenomena that are currently outstanding issues in helioseismology: meridional circulation and supergranulation. Numerical models are used to compute synthetic observations, providing the added benefit of knowing the solution against which the results can be tested. For demonstration purposes, the problems are formulated in two and three dimensions, using both ray- and Born-theoretical approaches. The results seem to indicate that the probabilistic inversions not only find a better solution with much more realistic estimation of the uncertainties, but they also provide a broader view of the range of solutions possible for any given model, making the interpretation of the inversion more quantitative in nature. The probabilistic inversions are also easy to set up for a broad range of problems, and they can take advantage of software that is publicly available. Unlike the progress being made in fundamental measurement schemes in local helioseismology that image the far side of the Sun, or have detected signatures of global Rossby waves, among many others, inversions of those measurements have had significantly less success. Such statistical methods may help overcome some of these barriers to move the field forward.

Meridional Flow in the Solar Convection Zone II: Helioseismic Inversions of GONG Data

J. **Jackiewicz**, A. Serebryanskiy, S. Kholikov

ApJ **805** 133 **2015**

http://arxiv.org/pdf/1504.08071v1.pdf

Meridional flow is thought to play a very important role in the dynamics of the solar convection zone; however, because of its relatively small amplitude, precisely measuring it poses a significant challenge. Here we present a complete time-distance helioseismic analysis of about two years of ground-based GONG Doppler data to retrieve the meridional circulation profile for modest latitudes, in an attempt to corroborate results from other studies. We use an empirical correction to the travel times due to an unknown center-to-limb systematic effect. The helioseismic inversion procedure is first tested and reasonably validated on artificial data from a large-scale numerical simulation, followed by a test to broadly recover the solar differential rotation found from global seismology.

From GONG data, we measure poleward photospheric flows at all latitudes with properties that are comparable with earlier studies, and a shallow equatorward flow about 65\,Mm beneath the surface, in agreement with recent findings from HMI data. No strong evidence of multiple circulation cells in depth nor latitude is found, yet the whole phase space has not yet been explored. Tests of mass flux conservation are then carried out on the inferred GONG and HMI flows and compared to a fiducial numerical baseline from models, and we find that the continuity equation is poorly satisfied.

While the two disparate data sets do give similar results for about the outer 15% of the interior radius, the total inverted circulation pattern appears to be unphysical in terms of mass conservation when interpreted over modest time scales. We can likely attribute this to both the influence of realization noise and subtle effects in the data and measurement procedure.

Axions as a probe of solar metals

Joerg **Jaeckel**, Lennert J. Thormaehlen

2019

https://arxiv.org/pdf/1908.10878.pdf

If axions or axion-like particles exist and are detected, they will not only extend the standard model of particle physics but will also open a new way to probe their sources. Axion helioscopes aim to detect axions which are produced in the core of the sun. Their spectrum contains information about the solar interior and could in principle help to solve the conflict between high and low metallicity solar models. Using the planned International Axion Observatory (IAXO) as an example, we show that helioscopes could measure the strength of characteristic emission peaks caused by the presence of heavier elements with good precision. In order to determine unambiguously the elemental abundances from this information, an improved modelling of the states of atoms inside the solar plasma is required.

Formation of the UV Spectrum of Molecular Hydrogen in the Sun

Sarah A. **Jaeggli**, Philip G. Judge, Adrian N. Daw

ApJ **855** 134 **2018**

https://arxiv.org/pdf/1802.03779.pdf

Ultraviolet lines of molecular hydrogen have been observed in solar spectra for almost four decades, but the behavior of the molecular spectrum and its implications for solar atmospheric structure are not fully understood. Data from the HRTS instrument revealed that H2 emission forms in particular regions, selectively excited by bright UV transition region and chromospheric lines. We test the conditions under which H2 emission can originate by

studying non-LTE models sampling a broad range of temperature stratifications and radiation conditions. Stratification plays the dominant role in determining the population densities of H2, which forms in greatest abundance near the continuum photosphere. However, opacity due to photoionization of silicon and other neutrals determines the depth to which UV radiation can penetrate to excite the H2. Thus the majority of H2 emission forms in a narrow region, at about 650 km in standard 1D models of the quiet-Sun, near the tau=1 opacity surface for the exciting UV radiation, generally coming from above. When irradiated from above using observed intensities of bright UV emission lines, detailed non-LTE calculations show that the spectrum of H2 seen in the quiet-Sun SUMER atlas spectrum and HRTS light bridge spectrum can be satisfactorily reproduced in 1D stratified atmospheres, without including 3D or time dependent thermal structures. A detailed comparison to observations from 1205 to 1550 Angstroms is presented, and the success of this 1D approach to modeling solar UV H2 emission is illustrated by the identification of previously unidentified lines and upper levels in HRTS spectra.

The Magnetic Classification of Solar Active Regions 1992 - 2015

Sarah A. **Jaeggli**, Aimee A. Norton
ApJL **2016**
http://arxiv.org/pdf/1603.02552v1.pdf
The purpose of this letter is to address a blind-spot in our knowledge of solar active region statistics. To the best of our knowledge there are no published results showing the variation of the Mount Wilson magnetic classifications as a function of solar cycle based on modern observations. We show statistics for all active regions reported in the daily Solar Region Summary from 1992 January 1 to 2015 December 31. We find that the α and β class active regions (including all sub-groups e.g. βγ, βδ) make up fractions of approximately 20% and 80% of the sample respectively. This fraction is relatively constant during high levels of activity, however, an increase in the α fraction to about 35% and and a decrease in the β fraction to about 65% can be seen near each solar minimum and is statistically significant at the 2-σ level. Over 30% of all active regions observed during the years of solar maxima were appended with the classifications γ and/or δ, while these classifications account for only a fraction of a percent during the years near the solar minima. This variation in the active region types indicates that the formation of complex active regions may be due to the pileup of frequent emergence of magnetic flux during solar maximum, rather than the emergence of complex, monolithic flux structures.

Nanoflare Theory Revisited

Amir **Jafari**1, Ethan T. Vishniac2, and Siyao Xu3
2021 ApJ 906 109
https://doi.org/10.3847/1538-4357/abca47
At any scale l in the turbulent inertial range, the magnetic field can be divided up into a large-scale component and a small-scale, high spatial frequency component which undergoes magnetic reversals. Such local reconnections, i.e., on any inertial scale l, seem to be an inseparable part of magnetohydrodynamic (MHD) turbulence, whose collective outcome can lead to global reconnection with a rate independent of the small-scale physics dominant at dissipative scales. We show that this picture, known as stochastic reconnection, is intimately related to nanoflare theory, proposed long ago to explain solar coronal heating. We argue that, due to stochastic flux freezing, a generalized version of magnetic flux freezing in turbulence, the field follows the flow in a statistical sense. Turbulence bends and stretches the field, increasing its spatial complexity. Strong magnetic shears associated with such a highly tangled field can trigger local reversals and field annihilations on a wide range of inertial scales which convert magnetic energy into kinetic and thermal energy. The former may efficiently enhance turbulence and the latter heat generation. We support this theoretical picture using scaling laws of MHD turbulence and also recent analytical and numerical studies which suggest a statistical correlation between magnetic spatial complexity and energy dissipation. Finally, using an MHD numerical simulation, we show that the time evolution of the magnetic complexity is statistically correlated with the rate of kinetic energy injection and/or magnetic-to-thermal energy conversion, in agreement with our proposed theoretical picture.

An overall view of temperature oscillations in the solar chromosphere with ALMA

Shahin **Jafarzadeh**, Sven Wedemeyer, Bernhard Fleck, Marco Stangalini, David B. Jess, Richard J. Morton, Mikolaj Szydlarski, Vasco M. J. Henriques, Xiaoshuai Zhu, Thomas Wiegelmann, Juan C. Guevara Gómez, Samuel D. T. Grant, Bin Chen, Kevin Reardon, Stephen M. White
Philosophical Transactions of the Royal Society A **2020**
https://arxiv.org/pdf/2010.01918.pdf
By direct measurements of the gas temperature, the Atacama Large Millimeter/sub-millimeter Array (ALMA) has yielded a new diagnostic tool to study the solar chromosphere. Here we present an overview of the brightness-temperature fluctuations from several high-quality and high-temporal-resolution (i.e., 1 and 2 sec cadence) time series of images obtained during the first two years of solar observations with ALMA, in Band 3 and Band 6, centred at around 3 mm (100 GHz) and 1.25 mm (239 GHz), respectively. The various datasets represent solar

regions with different levels of magnetic flux. We perform Fast Fourier and Lomb-Scargle transforms to measure both the spatial structuring of dominant frequencies and the average global frequency distributions of the oscillations (i.e., averaged over the entire field of view). We find that the observed frequencies significantly vary from one dataset to another, which is discussed in terms of the solar regions captured by the observations (i.e., linked to their underlying magnetic topology). While the presence of enhanced power within the frequency range 3-5 mHz is found for the most magnetically quiescent datasets, lower frequencies dominate when there is significant influence from strong underlying magnetic field concentrations (present inside and/or in the immediate vicinity of the observed field of view). We discuss here a number of reasons which could possibly contribute to the power suppression at around 5.5 mHz in the ALMA observations. However, it remains unclear how other chromospheric diagnostics (with an exception of Halpha line-core intensity) are unaffected by similar effects, i.e., they show very pronounced 3-min oscillations dominating the dynamics of the chromosphere, whereas only a very small fraction of all the pixels in the ten ALMA data sets analysed here show peak power near 5.5 mHz. **2017 April 18, 2017 April 22, 2017 April 23, 2018 April 12, 2018 August 23**
Table 1. Summary of the ALMA datasets employed in this study.

Kinematics of magnetic bright features in the solar photosphere

Shahin **Jafarzadeh**, S. K. Solanki, R. H. Cameron, P. Barthol, J. Blanco Rodriguez, J. C. del Toro Iniesta, A. Gandorfer, L. Gizon, J. Hirzberger, M. Knoelker, V. Martinez Pillet, D. Orozco Suarez, T. L. Riethmueller, W. Schmidt, M. van Noort

ApJS **2016**

https://arxiv.org/pdf/1610.07634v1.pdf

Convective flows are known as the prime means of transporting magnetic fields on the solar surface. Thus, small magnetic structures are good tracers of the turbulent flows. We study the migration and dispersal of magnetic bright features (MBFs) in intergranular areas observed at high-spatial resolution with Sunrise/IMaX. We describe the flux dispersal of individual MBFs as a diffusion process whose parameters are computed for various areas in the quiet Sun and the vicinity of active regions from seeing-free data. We find that magnetic concentrations are best described as random walkers close to network areas (diffusion index, gamma=1.0), travelers with constant speeds over a supergranule (gamma=1.9-2.0), and decelerating movers in the vicinity of flux-emergence and/or within active regions (gamma=1.4-1.5). The three types of regions host MBFs with mean diffusion coefficients of 130 km^2/s, 80-90 km^2/s, and 25-70 km^2/s, respectively. The MBFs in these three types of regions are found to display a distinct kinematic behavior at a confidence level in excess of 95%.

Slender Ca II H fibrils mapping magnetic fields in the low solar chromosphere

Shahin **Jafarzadeh**, R. J. Rutten, S. K. Solanki, T. Wiegelmann, T. Riethmueller, M. van Noort, M. Szydlarski, J. Blanco Rodriguez, P. Barthol, J. C. del Toro Iniesta, A. Gandorfer, L. Gizon, J. Hirzberger, M. Knoelker, V. Martinez Pillet, D. Orozco Suarez, W. Schmidt

ApJS **2016**

https://arxiv.org/pdf/1610.03104v1.pdf

A dense forest of slender bright fibrils near a small solar active region is seen in high-quality narrow-band Ca II H images from the SuFI instrument onboard the Sunrise balloon-borne solar observatory. The orientation of these slender Ca II H fibrils (SCF) overlaps with the magnetic field configuration in the low solar chromosphere derived by magnetostatic extrapolation of the photospheric field observed with Sunrise/IMaX and SDO/HMI. In addition, many observed SCFs are qualitatively aligned with small-scale loops computed from a novel inversion approach based on best-fit numerical MHD simulation. Such loops are organized in canopy-like arches over quiet areas that differ in height depending on the field strength near their roots.

Magnetic upflow events in the quiet-Sun photosphere. I. Observations

S. **Jafarzadeh**, L. Rouppe van der Voort, J. de la Cruz Rodriguez

ApJ 810 54 **2015**

http://arxiv.org/pdf/1507.07355v1.pdf

Rapid magnetic upflows in the quiet-Sun photosphere were recently uncovered from both SUNRISE/IMaX and Hinode/SOT observations. Here, we study magnetic upflow events (MUEs) from high-quality, high (spatial, temporal, and spectral) resolution, and full Stokes observations in four photospheric magnetically sensitive Fe I lines centered at 525.021 nm, 617.334 nm, 630.151 nm, and 630.250 nm acquired with SST/CRISP. We detect MUEs by subtracting in-line Stokes V signals from those in far-blue-wing whose signal-to-noise ratio >= 7. We find a larger number of MUEs at any given time (0.02 per square arcsec), larger by one to two orders of magnitude, than previously reported. The MUEs appear to fall into four classes presenting different shapes of Stokes V profiles with (I) asymmetric double lobes, (II) single lobes, (III) double-humped (two same-polarity lobes), and (IV) three lobes (extra blue-shifted bump in addition to a double-lobes), from which, only less than half of them are single-lobed. We also find that MUEs are almost equally distributed in network and internetwork areas and they appear in the interior

or at the edge of granules in both regions. Distributions of physical properties, except that of horizontal velocity, of the MUEs (namely, Stokes V signal, size, line-of-sight velocity, and lifetime) are almost identical for the different spectral lines in our data. A bisector analysis of our spectrally resolved observations shows that these events host modest upflows, and do not show direct indication of the presence of supersonic upflows reported earlier. Our findings reveal that number, type (class), and properties of MUEs can strongly depend on detection techniques and properties of the employed data, namely, signal-to-noise ratio, resolutions, and wavelength.

How Does the Critical Torus Instability Height Vary with the Solar Cycle?

Alexander W. **James**1, Lucie M. Green1, Graham Barnes2, Lidia van Driel-Gesztelyi1,3,4, and David R. Williams5
2024 ApJ 975 52
https://iopscience.iop.org/article/10.3847/1538-4357/ad77a0/pdf
The ideal magnetohydrodynamic torus instability can drive the eruption of coronal mass ejections. The critical threshold of magnetic field strength decay for the onset of the torus instability occurs at different heights in different solar active regions, and understanding this variation could therefore improve space weather prediction. In this work, we aim to find out how the critical torus instability height evolves throughout the solar activity cycle. We study a significant subset of Helioseismic and Magnetic Imager (HMI) and Michelson Doppler Imager Space-Weather HMI Active Region Patches (SHARPs and SMARPs) from 1996 to 2023, totaling 21,584 magnetograms from 4436 unique active-region patches. For each magnetogram, we compute the critical height averaged across the main polarity inversion line, the total unsigned magnetic flux, and the separation between the positive and negative magnetic polarities. We find the critical height in active regions varies with the solar cycle, with higher (lower) average critical heights observed around solar maximum (minimum). We conclude that this is because the critical height is proportional to the separation between opposite magnetic polarities, which in turn is proportional to the total magnetic flux in a region, and more magnetic regions with larger fluxes and larger sizes are observed at solar maximum. This result is noteworthy because, despite the higher critical heights, more coronal mass ejections are observed around solar maximum than at solar minimum.

A Unifying Model of Mixed Inertial Modes in the Sun

Rekha **Jain**1, Bradley W. Hindman2,3, and Catherine Blume2
2024 ApJL 965 L8
https://iopscience.iop.org/article/10.3847/2041-8213/ad35c6/pdf
We present an analytical model that unifies many of the inertial waves that have been recently observed on the surface of the Sun, as well as many other modes that have been theoretically predicted—but have yet to be observed—into a single family of mixed inertial modes. By mixed, we mean that the prograde- and retrograde-propagating members of this family have different restoring forces and hence different behavior. Thermal Rossby waves exist as prograde-propagating waves, while the high-frequency retrograde (HFR) wave is one example of a member of the retrograde branch. This family of mixed modes has fully 3D motions that satisfy the anelastic form of the continuity condition. As such, the horizontal velocity is both vortical and divergent with the later flow component associated with a dynamically important radial velocity. The modes are differentiated by the number of nodes in latitude, with the lowest latitudinal order corresponding to the traditional thermal Rossby wave of Busse, the first latitudinal overtone to the mixed mode of Bekki et al., and the second overtone to the HFR wave discovered by Hanson et al. There also exist infinitely more modes of higher latitudinal order whose frequencies increase as the order increases. These higher overtones may correspond to many of the inertial modes that have been recently identified by numerical eigenmode solvers.

Subsurface Flows in Active Regions with Peculiar Magnetic Configurations

Kiran **Jain**, Sushanta C. Tripathy
Proceedings of the IAU Symposium 365 - Dynamics of Solar and Stellar Convection Zones and Atmospheres, 2023 August 21-25, Yerevan, Armenia **2023**
https://arxiv.org/pdf/2310.07271.pdf
We present analysis of the evolution of subsurface flows in and around active regions with peculiar magnetic configurations and compare their characteristics with the normal active regions. We also study the zonal and meridional components of subsurface flows separately in different polarity regions separately to better understand their role in flux migration. We use the techniques of local correlation tracking and ring diagrams for computing surface and subsurface flows, respectively. Our study manifests an evidence that the meridional component of the flows near anti-Hale active regions is predominantly equatorward which disagrees with the poleward flow pattern seen in pro-Hale active regions. We also find clockwise or anti-clockwise flows surrounding the anti-Joy active regions depending on their locations in the Southern or Northern hemispheres, respectively.

Editorial: Connecting solar flows and fields to understand surface magnetism

Kiran **Jain**1*, Mausumi Dikpati2 and J. Todd Hoeksema3
Front. Astron. Space Sci., 10 :1202706 **2023**
https://www.frontiersin.org/articles/10.3389/fspas.2023.1202706/pdf
https://doi.org/10.3389/fspas.2023.1202706

Seismic Monitoring of the Sun's Far Hemisphere: A Crucial Component in Future Space Weather Forecasting (A White Paper Submitted to the Decadal Survey for Solar and Space Physics (Heliophysics) -- SSPH 2024-2033) Review

Kiran **Jain**, C. Lindsey, E. Adamson, C. N. Arge, T. E. Berger, D. C. Braun, R. Chen, Y. M. Collado-Vega, M. Dikpati, T. Felipe, C. J. Henney, J. T. Hoeksema, R. W. Komm, K. D. Leka, A. R. Marble, V. Martinez Pillet, M. Miesch, L. J. Nickisch, A. A. Pevtsov, V. J. Pizzo, W. K. Tobiska, S. C. Tripathy, J. Zhao
A White Paper Submitted to Decadal Survey for Solar and Space Physics (Heliophysics) – SSPH 2024-2033 **2022**
https://arxiv.org/ftp/arxiv/papers/2210/2210.01291.pdf
The purpose of this white paper is to put together a coherent vision for the role of helioseismic monitoring of magnetic activity in the Sun's far hemisphere that will contribute to improving space weather forecasting as well as fundamental research in the coming decade. Our goal fits into the broader context of helioseismology in solar research for any number of endeavors when helioseismic monitors may be the sole synoptic view of the Sun's far hemisphere. It is intended to foster a growing understanding of solar activity, as realistically monitored in both hemispheres, and its relationship to all known aspects of the near-Earth and terrestrial environment. Some of the questions and goals that can be fruitfully pursued through seismic monitoring of farside solar activity in the coming decade include: What is the relationship between helioseismic signatures and their associated magnetic configurations, and how is this relationship connected to the solar EUV irradiance over the period of a solar rotation?; How can helioseismic monitoring contribute to data-driven global magnetic-field models for precise space weather forecasting?; What can helioseismic monitors tell us about prospects of a flare, CME or high-speed stream that impacts the terrestrial environment over the period of a solar rotation?; How does the inclusion of farside information contribute to forecasts of interplanetary space weather and the environments to be encountered by human crews in interplanetary space? Thus, it is crucial for the development of farside monitoring of the Sun be continued into the next decade either through ground-based or space-borne observations. **2020-11-29, 2022 Jan 29 and Feb 25**

A study on the solar coronal dynamics during the post-maxima phase of the solar cycle 24 using S-band radio signals from the Indian Mars Orbiter Mission

Richa N **Jain**, R K Choudhary, Anil Bhardwaj, Umang Parikh, Bijoy K Dai, M V Roopa
Monthly Notices of the Royal Astronomical Society, Volume 511, Issue 2, April **2022**, Pages 1750–1756,
https://doi.org/10.1093/mnras/stac056
Radio signals from India's Mars Orbiter Mission (MOM) have been used to study turbulence in the solar plasma during the post-maximum phase of solar cycle 24. S-band (2.29 GHz) radio carrier downlink signals from MOM were received at the Indian Deep Space Network, Bangalore, and frequency residuals were spectrally analysed to obtain coronal turbulence spectra at heliocentric distances ranging between 4 and 20 R⊙, corresponding to coronal regions where the solar wind is primarily accelerated. The frequency fluctuation spectrum relates to the turbulence regime in the near-Sun region. The turbulence power spectrum (the temporal spectrum of frequency fluctuations) at smaller heliocentric distances (<10 R⊙) reveals flattening in lower-frequency regions, with a spectral index $\alpha f \sim 0.3-0.5$, which corresponds to the solar wind acceleration region. For larger heliocentric distances (>10 R⊙), the curve steepens with a spectral index $\alpha f \sim 0.7-0.8$, a value close to 2/3 and indicative of a developed Kolmogorov-type turbulence spectrum. The findings are consistent with earlier results. Plausible explanations to support the theory of coronal heating by magnetohydrodynamic waves and the acceleration of the solar wind are presented. An insight into the feeble maximum of solar cycle 24 is discussed.

What Seismic Minimum Reveals About Solar Magnetism Below the Surface?

Kiran **Jain**, Niket Jain, Sushanta C. Tripathy, Mausumi Dikpati
ApJL **924** L20 **2022**
https://arxiv.org/pdf/2111.14323.pdf
https://iopscience.iop.org/article/10.3847/2041-8213/ac3de9/pdf
https://doi.org/10.3847/2041-8213/ac3de9

The Sun's magnetic field varies in multiple time scales. Observations show that the minimum between cycles 24 and 25 was the second consecutive minimum which was deeper and wider than several earlier minima. Since the active regions observed at the Sun's surface are manifestations of the magnetic field generated in the interior, it is crucial to investigate/understand the dynamics below the surface. In this context, we report, by probing the solar interior with helioseismic techniques applied to long-term oscillations data from the Global Oscillation Network Group (GONG), that the seismic minima in deeper layers have been occurring about a year earlier than that at the surface for the last two consecutive solar cycles. Our findings also demonstrate a decrease in strong magnetic fields at the base of the convection zone, the primary driver of the surface magnetic activity. We conclude that the magnetic fields located in the core and near-surface shear layers, in addition to the tachocline fields, play an important role in modifying the oscillation frequencies. This provides evidence that further strengthens the existence of a relic magnetic field in the Sun's core since its formation.

What is Exceptional about Solar Activity in the Early Phase of Cycle 25?

Kiran **Jain**1, Charles Lindsey2, and Sushanta C. Tripathy1
2021 Res. Notes AAS 5 253
https://iopscience.iop.org/article/10.3847/2515-5172/ac3429
https://doi.org/10.3847/2515-5172/ac3429
Solar Cycle 25 began in 2019 December and has been progressing nominally since. However, a closely associated pair of strong active regions, NOAA 12786 and 12785, emerged in 2020 November. The greater, northern component, 12786, attained a maximum sunspot area of 1000 μHemi. The sudden, uncharacteristic emergence of such a large concentration of intense magnetic flux in the early phase of the solar cycle has not been seen in previous cycles. Although the active region pair survived for two Carrington rotations, it did not produce any X- or M-class flares. Here we remark on the evolution of NOAA 12786 and 12785, first in the Sun's invisible and subsequently the visible hemispheres, and compare the irradiance and other characteristic profiles it manifested in the early ascending phase of cycle 25 with those of previous solar cycles. **13-27 Nov 2020**

Continuous Solar Observations from the Ground -- Assessing Duty Cycle from GONG Observations

Kiran **Jain**, Sushant C. Tripathy, Frank Hill, Alexei A. Pevtsov
Pub. Astron. Soc. Pacific **2021**
https://arxiv.org/pdf/2110.06319.pdf
Continuous observations play an important role in the studies of solar variability. While such observations can be achieved from space with almost 100% duty cycle, it is difficult to accomplish very high duty cycle from the ground. In this context, we assess the duty cycle that has been achieved from the ground by analyzing the observations of a six station network of identical instruments, Global Oscillation Network Group (GONG). We provide a detailed analysis of the duty cycle using GONG observations spanning over 18 years. We also discuss duty cycle of individual sites and point out various factors that may impact individual site or network duty cycle. The mean duty cycle of the network is 93%, however it reduces by about 5% after all images pass through the stringent quality-control checks. The standard deviations in monthly and yearly duty cycle values are found to be 1.9% and 2.2%, respectively. These results provide a baseline that can be used in the planning of future ground-based networks.

The Sun's Seismic Radius as Measured from the Fundamental Modes of Oscillations and Its Implications for the TSI Variations

Kiran **Jain**, S. C. Tripathy, and F. Hill
2018 ApJL 859 L9
http://sci-hub.tw/http://iopscience.iop.org/2041-8205/859/1/L9/
In this Letter we explore the relationship between the solar seismic radius and total solar irradiance (TSI) during the last two solar cycles using the uninterrupted data from space-borne instruments on board the Solar and Heliospheric Observatory (SoHO) and the Solar Dynamics Observatory (SDO). The seismic radius is calculated from the fundamental (f) modes of solar oscillations utilizing the observations from SoHO/Michelson Doppler Imager (MDI) and SDO/Helioseismic and Magnetic Imager (HMI), and the TSI measurements are obtained from SoHO/VIRGO. Our study suggests that the major contribution to the TSI variation arises from the changes in magnetic field, while the radius variation plays a secondary role. We find that the solar irradiance increases with decreasing seismic radius; however, the anti-correlation between them is moderately weak. The estimated maximum change in seismic radius during a solar cycle is about 5 km, and is consistent in both solar cycles 23 and 24. Previous studies ;suggest a radius change at the surface of the order of 0.06 arcsec to explain the 0.1% variation in the TSI values during the solar cycle; however, our inferred seismic radius change is significantly smaller, hence the TSI variations cannot be fully explained by the temporal changes in seismic radius.

22 Year Solar Magnetic Cycle and its relation to Convection Zone Dynamics

Kiran **Jain**, Sushanta Tripathy, Rudolf Komm, Frank Hill, Rosaria Simoniello

Proceedings of IAU Symposium 340 **2018**

https://arxiv.org/pdf/1805.05371.pdf

Using continuous observations for 22 years from ground-based network GONG and space-borne instruments MDI onboard {\it SoHO} and HMI onboard {\it SDO}, we report both global and local properties of the convection zone and their variations with time.

The effect of a dynamo-generated field on the Parker wind

P. **Jakab**, A. Brandenburg

A&A **2020**

https://arxiv.org/pdf/2006.02971

Stellar winds are an integral part of the underlying dynamo, the motor of stellar activity. The wind controls the star's angular momentum loss, which depends on the magnetic field geometry which, in turn, varies significantly in time and latitude. Here we study basic properties of a self-consistent model that includes simple representations of both the global stellar dynamo in a spherical shell and the exterior in which the wind accelerates and becomes supersonic. We numerically solve an axisymmetric mean-field model for the induction, momentum, and continuity equations using an isothermal equation of state. The model allows for the simultaneous generation of a mean magnetic field and the development of a Parker wind. The resulting flow is transonic at the critical point, which we arrange to be between the inner and outer radii of the model. The boundary conditions are assumed to be such that the magnetic field is antisymmetric about the equator, i.e., dipolar. At the solar rotation rate, the dynamo is oscillatory and of $\alpha 2$ type. In most of the domain, the magnetic field corresponds to that of a split monopole. The magnetic energy flux is largest between the stellar surface and the critical point. At rapid rotation of up to 50 times the solar value, most of the magnetic field is lost along the axis within the inner tangential cylinder of the model. The model reveals unexpected features that are not generally anticipated from models that are designed to reproduce the solar wind: highly variable angular momentum flux fluxes even from just an $\alpha 2$ dynamo in the star. For rapid rotation, magnetic fields are ejected mostly along the axis, where the wind speed is reduced.

How does the critical torus instability height vary with the solar cycle?

Alexander W. **James**, Lucie M. Green, Graham Barnes, Lidia van Driel-Gesztelyi, David R. Williams

ApJ **2024**

https://arxiv.org/pdf/2409.02695

The ideal magnetohydrodynamic torus instability can drive the eruption of coronal mass ejections. The critical threshold of magnetic field strength decay for the onset of the torus instability occurs at different heights in different solar active regions, and understanding this variation could therefore improve space weather prediction. In this work, we aim to find out how the critical torus instability height evolves throughout the solar activity cycle. We study a significant subset of HMI and MDI Space-Weather HMI Active Region Patches (SHARPs and SMARPs) from 1996-2023, totalling 21584 magnetograms from 4436 unique active region patches. For each magnetogram, we compute the critical height averaged across the main polarity inversion line, the total unsigned magnetic flux and the separation between the positive and negative magnetic polarities. We find the critical height in active regions varies with the solar cycle, with higher (lower) average critical heights observed around solar maximum (minimum). We conclude this is because the critical height is proportional to the separation between opposite magnetic polarities, which in turn is proportional to the total magnetic flux in a region, and more magnetic regions with larger fluxes and larger sizes are observed at solar maximum. This result is noteworthy because, despite the higher critical heights, more CMEs are observed around solar maximum than at solar minimum. **4 Jun 2012**

Solar cycle 24: an unusual polar field reversal

P. **Janardhan**, K. Fujiki, M. Ingale, Susanta Kumar Bisoi, Diptiranjan Rout

A&A 618, A148 **2018**

https://arxiv.org/pdf/1805.06654.pdf

Aims: To investigate solar polar fields during cycle 24, using measurements of solar magnetic fields in the latitude range 55 - 90 degree and 78 - 90 degree, to report a prolonged and unusual hemispheric asymmetry in the polar field reversal pattern in solar cycle 24.

Methods: This study was carried out using medium resolution line-of-sight synoptic magnetograms from the magnetic database of the National Solar Observatory at Kitt Peak (NSO/KP), USA for the period between February 1975 and October 2017, covering solar cycles 21-24 and high-resolution line-of-sight synoptic magnetograms from the Michaelson Doppler Imager instrument onboard the Solar Heliospheric Observatory. Synoptic magnetograms using radial measurements from the Heliospheric Magnetic Imager instrument onboard the Solar Dynamics Observatory, covering solar cycle 23 and 24, were also used.

Results: We show that the Southern solar hemisphere unambiguously reversed polarity in mid-2013 while the reversal in the field in the Northern solar hemisphere started as early as June 2012, was followed by a sustained

period of near-zero field strength lasting until the end of 2014, after which the field began to show a clear rise from its near-zero value. While this study compliments a similar study carried out using microwave brightness measurements (Gopalswamy et al. 2016) which claimed that the field reversal process in cycle 24 was completed by the end of 2015, our results show that the field reversal in cycle 24 was completed earlier i.e. in late 2014. Signatures of this unusual field reversal pattern were also clearly identifiable in the solar wind, using our observations of interplanetary scintillation at 327 MHz which supported our magnetic field observations and confirmed that the field reversal process was completed at the end of 2014.

A 20 year decline in solar photospheric magnetic fields: Inner-heliospheric signatures and possible implications

P. **Janardhan**, Susanta Kumar Bisoi, S. Ananthakrishnan, M. Tokumaru, K. Fujiki, L. Jose, R. Sridharan
JGR Volume 120, Issue 7 July **2015** Pages 5306–5317
We report observations of a steady 20 year decline of solar photospheric fields at latitudes ≥45° starting from ~1995. This prolonged and continuing decline, combined with the fact that cycle 24 is already past its peak, implies that magnetic fields are likely to continue to decline until ~2020, the expected minimum of the ongoing solar cycle 24. In addition, interplanetary scintillation observations of the inner heliosphere for the period 1983–2013 and in the distance range 0.2–0.8 AU have also shown a similar and steady decline in solar wind microturbulence levels, in sync with the declining photospheric fields. Using the correlation between the polar field and heliospheric magnetic field (HMF) at solar minimum, we have estimated the value of the HMF in 2020 to be 3.9 (±0.6) nT and a floor value of the HMF of ~3.2 (±0.4) nT. Given this floor value for the HMF, our analysis suggests that the estimated peak sunspot number for solar cycle 25 is likely to be 62 (±12).

Coronal Dynamic Activities in the Declining Phase of a Solar Cycle

Minhwan **Jang**, T. N. Woods, Sunhak Hong, G. S. Choe
2016
https://arxiv.org/pdf/1610.02944v1.pdf
It has been known that some solar activity indicators show a double-peak feature in their evolution through a solar cycle, which is not conspicuous in sunspot number. In this letter, we investigate the high solar dynamic activity in the declining phase of the sunspot cycle by examining the evolution of polar and low latitude coronal hole areas and the statistics of splitting and merging events of coronal holes and coronal mass ejections detected by SOHO/LASCO C3 in solar cycle 23. Although the total coronal hole area is at its maximum near the sunspot minimum, in which polar coronal holes prevail, it shows a comparable second maximum in the declining phase of the cycle, in which low latitude coronal holes are dominant. The events of coronal hole splitting or merging, which are attributed to surface motions of magnetic fluxes, are also mostly populated in the declining phase of the cycle. The far-reaching C3 coronal mass ejections are also over-populated in the declining phase of the cycle. From these results we suggest that solar dynamic activities due to the horizontal motions of magnetic fluxes extend far in the declining phase of the sunspot cycle. **Хорошее Введение**.

Prediction of the amplitude of solar cycle 25 using polar faculae observations

Jan **Janssens***
J. Space Weather Space Clim. **2021**, 11, 3
https://doi.org/10.1051/swsc/2020081
Prediction of the amplitude of solar cycle 25 using polar faculae observations (swsc-journal.org)
Based on the monthly number of polar faculae, a forecast of the amplitude of solar cycle 25 (SC25) is provided, as well as a prediction of the number of solar flares. Faculae near both solar poles have been visually observed using a commercial off-the-shelf 20 cm Schmidt-Cassegrain telescope since 1995. The monthly averages were corrected for varying seeing conditions and the heliographic latitude of the center of the solar disk B0. From the deduced relationship between the smoothed number of monthly polar faculae during the solar cycle minimum, and the subsequent maximum of the monthly sunspot number, a prediction has been made for the amplitude of the next solar cycle. The methodology used can be considered as a precursor technique. The expected number of M- and X-class flares was calculated based on a statistical approach. The maximum of SC25 is predicted to be 118 ± 29, of similar strength than the previous SC24. Also the number of M5 or stronger flares is expected to be comparable to that of the previous solar cycle.

SuNeRF: 3D Reconstruction of the Solar EUV Corona Using Neural Radiance Fields

Robert **Jarolim**1, Benoit Tremblay2, Andrés Muñoz-Jaramillo3, Kyriaki-Margarita Bintsi, +++
2024 ApJL 961 L31
https://iopscience.iop.org/article/10.3847/2041-8213/ad12d2/pdf
To understand its evolution and the effects of its eruptive events, the Sun is permanently monitored by multiple satellite missions. The optically thin emission of the solar plasma and the limited number of viewpoints make it

challenging to reconstruct the geometry and structure of the solar atmosphere; however, this information is the missing link to understand the Sun as it is: a 3D evolving star. We present a method that enables a complete 3D representation of the uppermost solar layer (corona) observed in extreme ultraviolet (EUV) light. We use a deep-learning approach for 3D scene representation that accounts for radiative transfer to map the entire solar atmosphere from three simultaneous observations. We demonstrate that our approach provides unprecedented reconstructions of the solar poles and directly enables height estimates of coronal structures, solar filaments, coronal hole profiles, and coronal mass ejections. We validate the approach using model-generated synthetic EUV images, finding that our method accurately captures the 3D geometry of the Sun even from a limited number of 32 ecliptic viewpoints ($|\text{latitude}| \leq 7°$). We quantify the uncertainties of our model using an ensemble approach that allows us to estimate the model performance in the absence of a ground truth. Our method enables a novel view of our closest star and is a breakthrough technology for the efficient use of multi-instrument data sets, which paves the way for future cluster missions.

Discovery of a relation between the decay rate of the Sun's magnetic dipole and the growth rate of the following sunspot cycle: a new precursor for solar cycle prediction

Priyansh **Jaswal**, Chitradeep Saha, Dibyendu Nandy
MNRAS Letter Volume 528, Issue 1, February **2024**, Pages L27–L32,
https://arxiv.org/pdf/2307.00520
https://academic.oup.com/mnrasl/article-pdf/528/1/L27/53679679/slad122.pdf
https://doi.org/10.1093/mnrasl/slad122
Sunspots have been observed for over four centuries and the magnetic nature of sunspot cycles has been known for about a century: however, some of its underlying physics still remain elusive. It is known that the solar magnetic cycle involves a recycling of magnetic flux between the poloidal and toroidal components of the magnetic field, that manifests as the solar dipole and sunspots, respectively. Here we report the discovery of a new relationship between the rise rate of the sunspot cycle and the decay rate of the solar (axial) dipole moment. We argue that this points to the existence of a causal connection between the aforementioned physical quantities -- providing an extension to the Waldmeier effect: namely, the decay rate of the Sun's dipole moment is related to the rate of rise and eventual amplitude of the following sunspot cycle. We demonstrate how one may take advantage of this new relationship to predict the amplitude and timing of the sunspot cycle. Our analysis indicates solar cycle 25 is going to be a weak-moderate cycle, peaking in \(2024.00_{-0.49}^{+0.68} \).

Review of Image Processing Methods in Solar Photospheric Data Analyzes

Mohsen **Javaherian**, Zahra Eskandari
Iranian Journal of Astronomy and Astrophysics, 10(1), 77-109 (**2023**)
https://arxiv.org/pdf/2310.00380.pdf
With the exponential growth in data volume, especially in recent decades, the demand for data processing has surged across all scientific fields. Within astronomical datasets, the combination of solar space missions and ground-based telescopes has yielded high spatial and temporal resolutions for observing the Sun, thus fueling an increase in the utilization of automatic image processing approaches. Image processing methodologies play a pivotal role in analyzing solar data, a critical component in comprehending the Sun's behavior and its influence on Earth. This paper provides an overview of the utilization of diverse processing techniques applied to images captured from the solar photosphere. The introduction of our manuscript furnishes a description of the solar photosphere along with its primary characteristics. Subsequently, we endeavor to outline the significance of preprocessing photospheric images, a crucial prerequisite before engaging in any form of analysis. The subsequent section delves into an examination of numerous reputable sources that have employed image processing methodologies in their research pertaining to the Sun's surface. This section also encompasses discussions concerning recent advancements in image processing techniques for solar data analysis and their potential implications for future solar research. The final section deliberates on post-processing procedures as supplementary steps that are essential for deriving meaningful results from raw data. Effectively, this paper imparts vital information, offering concise explanations regarding the Sun's surface, the application of image processing techniques to various types of photospheric images, indispensable image preprocessing stages, and post-processing procedures aimed at transforming raw data into coherent and comprehensive insights. **9 June 2009, 14 February 2011, November 3 to 5, 2015, 30 December 2015**

Long-term Variations in Solar Activity: Predictions for Amplitude and North--South Asymmetry of Solar Cycle 25

J. **Javaraiah**
Solar Phys. **2022**
https://arxiv.org/pdf/2202.13838.pdf

We analysed the sunspot group data from Greenwich Photoheliographic Results (GPR) during 1874-1976 and Debrecen Photoheliographic Data (DPD) during 1977-2017 and studied the cycle-to-cycle variations in the values of 13-month smoothed monthly mean sunspot-group area in whole sphere (WSGA), northern hemisphere (NSGA), and southern hemisphere (SSGA) at the epochs of maxima of Sunspot Cycles 12-24, and at the epochs of maxima of WSGA, NSGA, and SSGA Cycles 12-24. The cosine fits to the values of WSGA, NSGA, and SSGA at the maxima of the sunspot number, WSGA, NSGA, and SSGA Cycles 12-24, and to the values of the corresponding north-south asymmetry, suggest the existence of a ~132-year periodicity in the activity of northern hemisphere, a 54-66-year periodicity in the activity of southern hemisphere, and a 50-66 year periodicity in the north-south asymmetry in activity at all the aforementioned epochs. By extrapolating the best-fit cosine curves we predicted the amplitudes and the corresponding north-south asymmetry of the 25th WSGA, NSGA, and SSGA cycles. We find that on average Solar Cycle 25 in sunspot-group area would be to some extent smaller than Solar Cycle 24 in sunspot-group area. However, by inputting the predicted amplitudes of the 25th WSGA, NSGA, and SSGA cycles in the linear relationship between sunspot-group area and sunspot number we find that the amplitude (130 +or- 12) of Sunspot Cycle 25 would be slightly larger than that of reasonably small Sunspot Cycle 24. Still it confirms that the beginning of the upcoming Gleissberg cycle would take place around Solar Cycle 25. We also find that except at the maximum of NSGA Cycle 25 where the strength of activity in northern hemisphere would be dominant, the strength of activity in the southern hemisphere would be dominant at the maximum epochs of the 25th sunspot, WSGA, and SSGA cycles.

A Study of Variations in Correlation Between Rotation Residual and Meridional Velocity of Sunspot Groups

J. **Javaraiah**

Solar Physics volume 296, Article number: 152 (**2021**)

https://link.springer.com/content/pdf/10.1007/s11207-021-01883-5.pdf

https://doi.org/10.1007/s11207-021-01883-5

We analyzed the combined 142 years sunspot-group data from Greenwich Photoheliograpic Results (GPR) and Debrecen Photoheliographic Data (DPD) and determined the yearly mean residual rotation rate and the meridional velocity of sunspot groups in different 5∘5∘ latitude intervals. We find that there exists a considerable latitude–time dependence in both the residual rotation and the meridional motion. The residual rotation rate is found to be −120 m s−1 to 80 m s−1. In a large number of solar cycles, the rotation is to some extent weaker during maxima than that of during minima. There exist alternate bands of equatorward and poleward meridional motions. The equatorward motion is dominant mostly around the maxima of solar cycles with velocity 8–12 m s−1, whereas the poleward motion is dominant mostly around the minima but with a relatively weak velocity, only 4–6 m s−1. The analysis of the data during Solar Cycles 12–24 that are folded according to the years from their respective epochs of maxima suggests the existence of equatorward migrating alternate bands of slower and faster than average rotation within the activity belt. This analysis suggests no clear equatorward or poleward migrating bands of meridional motions. A statistically significant anticorrelation exists between the meridional motion and residual rotation. The corresponding linear-least-squares best-fit is found to be reasonably good (slope, −0.028±0.008−0.028±0.008, is about 3.5 times larger than its standard deviation). As per the sign convention used for the meridional motions, the significant negative value of the slope indicates the existence of a strong angular momentum transport toward the equator. The cross-correlation between the slopes determined from the data in 3-year moving time intervals and yearly mean sunspot number (SN) suggests that the slope leads SN by about 4 and 9 years. The Morlet wavelet spectrum of the slope suggests the existence of ≈11-year periodicity in the slope almost throughout the data window, but it was very weak during 1920–1940. We have also done cross-wavelet, wavelet-coherence, and wavelet-phase difference analyses of the slope and SN. Overall the results suggest there exists a strong relationship between the slope and amount of activity during a solar cycle. However, the correlation between the cycle-to-cycle modulations in the slope and the amplitude of solar cycle is found to be insignificant, indicating that there is no relationship between the slope and strength of activity on a long-time scale (longer than 11-year period).

North-South Asymmetry in Solar Activity and Solar Cycle Prediction, V: Prediction for the North-South Asymmetry in the Amplitude of Solar Cycle 25

J. **Javaraiah**

Astrophysics and Space Science **2021**

https://arxiv.org/pdf/2101.10126.pdf

We analyzed the daily sunspot-group data reported by the Greenwich Photoheliographic Results (GPR) during the period 1874-1976 and Debrecen Photoheligraphic Data (DPD) during the period 1977-2017, and the revised Version-2 of ISSN during the period 1874-2017. We determined the amplitude of the Solar Cycles 12-24 and the 13-month smoothed monthly mean corrected areas of the sunspot groups in the Sun's whole-sphere (WSGA), northern hemisphere (NSGA), and southern hemisphere (SSGA) at the epochs of the maxima of the Solar Cycles 12-24. Using all these we obtained the relations similar to that found in our earlier analyzes -- i.e., the existence of a high correlation between the sum of the areas of sunspot groups in the southern-hemisphere near-equatorial band during a small interval (7-9 months) just after a maximum epoch of a solar cycle and the amplitude of next solar

cycle -- separately for the Sun's whole-sphere and northern- and southern-hemispheres. By using these relations we predicted ~701 msh (millionth of solar hemisphere), ~429 msh, and ~366 msh for the values of WSGA, NSGA, and SSGA, respectively, at the maximum epoch of the Solar Cycle 25. We predicted 86 + or - 18 for the amplitude of Solar Cycle 25. The 13-month smoothed monthly mean sunspot-group area highly correlate with that of ISSN. Using this relation and the predicted values of WSGA, NSGA, and SSGA we have obtained 68 + or -11 for the amplitude of Solar Cycle 25, which is slightly lower than the aforementioned predicted value, and 39 + or - 4 and 31 + or - 6 for the values of northern- and southern-hemispheres' sunspot numbers at the maximum epoch of Solar Cycle 25. Overall, our results suggest that the amplitude of Solar Cycle 25 would be 25%-40% smaller, and the corresponding north-south asymmetry would be much smaller, than those of Solar Cycle 24.

Long-Term Variations in Solar Differential Rotation and Sunspot Activity, II: Differential Rotation Around the Maxima and Minima of Solar Cycles 12-24

J. **Javaraiah**

Solar Phys. **295**, Article number: 170 **2020**

https://arxiv.org/pdf/2012.01421.pdf

https://link.springer.com/content/pdf/10.1007/s11207-020-01740-x.pdf

We analyzed the sunspot-group daily data that were reported by Greenwich Photoheliogrphic Results (GPR) during the period 1874-1976 and Debrecen Photoheliographic Data (DPD) during the period 1977-2017. We determined the equatorial rotation rate [A] and the latitude gradient [B] components of the solar differential rotation by fitting the data in each of the 3-year moving time intervals (3-year MTIs) successively shifted by one year during the period 1874-2017 to the standard law of differential rotation. The values of A and B around the years of maxima and minima of Solar Cycles 12-24 are obtained from the 3-year MTIs series of A and B and studied the long-term cycle-to-cycle modulations in these coefficients. Here we have used the epochs of the maxima and minima of Solar Cycles 12-24 that were recently determined from the revised Version-2 international sunspot-number series. We find that there exits a considerably significant secular decreasing-trend in A around the maxima of solar cycles. There exist no secular trends in both A and B around the minima of solar cycles. The secular trend in B around the maxima of solar cycles is also found to be statistically insignificant. We fitted a cosine function to the values of A, and also to those of B, after removing the corresponding linear trends. The cosine-fits suggest that there exist ~54-year (~94-year) and ~82-year (~79-year) periodicities in A (B) around the maxima and minima of solar cycles, respectively. The amplitude of the cosine-profile of A (B) around the minima of solar cycles is about 41% (65%) larger than that of A (B) around the maxima. In addition, the cosine profiles of A and B suggest a large (up to 180 degree) phase difference between the long-term variations of A, and also between those of B, around maxima and minima of solar cycles.

Long-term Periodicities in North–south Asymmetry of Solar Activity and Alignments of the Giant Planets

J. **Javaraiah**

Solar Physics January **2020**, 295:8

https://doi.org/10.1007/s11207-019-1575-7

https://link.springer.com/content/pdf/10.1007%2Fs11207-019-1575-7.pdf

https://arxiv.org/pdf/2001.05879.pdf

The existence of ≈ 12-year and ≈ 51-year periodicities in the north–south asymmetry of solar activity is well known. However, the origin of these as well as the well-known relatively short periodicities in the north–south asymmetry is not yet clear. Here we have analyzed the combined daily data of sunspot groups reported in Greenwich Photoheliographic Results (GPR) and Debrecen Photoheliographic Data (DPD) during the period 1874 – 2017 and the data of the orbital positions (ecliptic longitudes) of the giant planets in ten-day intervals during the period 1600 – 2099. Our analysis suggests that ≈ 12-year and ≈ 51-year periodicities in the north–south asymmetry of solar activity are the manifestations of the differences in the strengths of ≈ 11-year and ≈ 51-year periodicities of activity in the northern- and southern-hemispheres. During the period 1874 – 2017 the Morlet wavelet power spectrum of the north–south asymmetry of sunspot-group area and that of the mean absolute difference (ψDof the orbital positions of the giant planets are found to be similar. Particularly, there is a suggestion that the ≈ 12-year and ≈ 51-year periodicities in the north–south asymmetry of sunspot-group area occurred during approximately the same times as the corresponding periodicities in ψD. Therefore, we suggest that there could be influence of some specific configurations of the giant planets in the origin of the ≈ 12-year and ≈ 50-year periodicities of the north–south asymmetry of solar activity.

North--South Asymmetry in Solar Activity and Solar Cycle Prediction, IV: Prediction for Lengths of Upcoming Solar Cycles

J. **Javaraiah**

Solar Phys. 294:64 **2019**

https://arxiv.org/pdf/1904.11500.pdf
https://link.springer.com/content/pdf/10.1007%2Fs11207-019-1442-6.pdf
We analyzed the daily sunspot-group data reported by the Greenwich Photoheliographic Results (GPR) during the period 1874-1976 and Debrecen Photoheliographic Data (DPD) during the period 1977-2017 and studied North-South asymmetry in the maxima and minima of the Solar Cycles 12-24. We derived the time series of the 13-month smoothed monthly mean corrected whole-spot areas of the sunspot groups in the Sun's whole sphere (WSGA), northern hemisphere (NSGA), and southern hemisphere (SSGA). From these smoothed time series we obtained the values of the maxima and minima, and the corresponding epochs, of the WSGA, NSGA, and SSGA Cycles 12-24. We find that there exists a 44-66 years periodicity in the North-South asymmetry of the minimum. A long periodicity (130-140 years) may exist in the asymmetry of the maximum. A statistically significant correlation exists between the maximum of SSGA Cycle n and the rise time of WSGA Cycle n + 2. A reasonably significant correlation also exists between the maximum of WSGA Cycle n and the decline time of WSGA Cycle n + 2. These relations suggest that the solar dynamo carries memory over at least three solar cycles. Using these relations we obtained the values 11.7 + or - 0.15 years, 11.2 + or - 0.2 years, and 11.45 + or - 0.3 years for the lengths of WSGA Cycles 24, 25, and 26, respectively, and hence, July 2020, October 2031, and March 2043 for the minimum epochs (start dates) of WSGA Cycles 25, 26, and 27, respectively. We also obtained May 2025 and March 2036 for the maximum epochs of WSGA Cycles 25 and 26, respectively. It seems during the late Maunder minimum sunspot activity was absent around the epochs of the maxima of the NSGA-cycles and the minima of the SSGA-cycles, and some activity was present at the epochs of the maxima of some SSGA-cycles and the minima of some NSGA-cycles.

Will Solar Cycles 25 and 26 Be Weaker than Cycle 24?

J. **Javaraiah**
Solar Physics November **2017**, 292:172
https://link.springer.com/content/pdf/10.1007%2Fs11207-017-1197-x.pdf
https://arxiv.org/pdf/1711.04117.pdf
The study of variations in solar activity is important for understanding the underlying mechanism of solar activity and for predicting the level of activity in view of the activity impact on space weather and global climate. Here we have used the amplitudes (the peak values of the 13-month smoothed international sunspot number) of Solar Cycles 1 – 24 to predict the relative amplitudes of the solar cycles during the rising phase of the upcoming Gleissberg cycle. We fitted a cosine function to the amplitudes and times of the solar cycles after subtracting a linear fit of the amplitudes. The best cosine fit shows overall properties (periods, maxima, minima,etc.) of Gleissberg cycles, but with large uncertainties. We obtain a pattern of the rising phase of the upcoming Gleissberg cycle, but there is considerable ambiguity. Using the epochs of violations of the Gnevyshev–Ohl rule (G–O rule) and the 'tentative inverse G–O rule' of solar cycles during the period 1610 – 2015, and also using the epochs where the orbital angular momentum of the Sun is steeply decreased during the period 1600 – 2099, we infer that Solar Cycle 25 will be weaker than Cycle 24. Cycles 25 and 26 will have almost same strength, and their epochs are at the minimum between the current and upcoming Gleissberg cycles. In addition, Cycle 27 is expected to be stronger than Cycle 26 and weaker than Cycle 28, and Cycle 29 is expected to be stronger than both Cycles 28 and 30. The maximum of Cycle 29 is expected to represent the next Gleissberg maximum. Our analysis also suggests a much lower value (30 – 40) for the maximum amplitude of the upcoming Cycle 25.

Short-Term Variations in the Equatorial Rotation Rate of Sunspot Groups

J. **Javaraiah** L. Bertello
Solar Phys. **2016** Volume 291, Issue 12, pp 3485–3500
We have detected several periodicities in the solar equatorial rotation rate of sunspot groups in the catalog Greenwich Photoheliographic Results (GPR) during the period 1931 – 1976, the Solar Optical Observing Network (SOON) during the period 1977 – 2014, and the Debrecen Photoheliographic Data (DPD) during the period 1974 – 2014. We have compared the results from the fast Fourier transform (FFT), the maximum entropy method (MEM), and the Morlet wavelet power-spectra of the equatorial rotation rates determined from SOON and DPD sunspot-group data during the period 1986 – 2007 with those of the Mount Wilson Doppler-velocity data during the same period determined by Javaraiah et al. (Solar Phys.257, 61, 2009). We have also compared the power-spectra computed from the DPD and the combined GPR and SOON sunspot-group data during the period 1974 – 2014 to those from the GPR sunspot-group data during the period 1931 – 1973. Our results suggest a ~ 250-day period in the equatorial rotation rate determined from both the Mt. Wilson Doppler-velocity data and the sunspot-group data during 1986 – 2007. However, a wavelet analysis reveals that this periodicity appears mostly around 1991 in the velocity data, while it is present in most of the solar cycles covered by the sunspot-group data, mainly near the minimum epochs of the solar cycles. We also found the signature of a period of ~ 1.4 years in the velocity data during 1990 – 1995, and in the equatorial rotation rate of sunspot groups mostly around the year 1956. The equatorial rotation rate of sunspot groups reveals a strong ~ 1.6-year periodicity around 1933 and 1955, a weaker one around 1976, and a strong ~ 1.8-year periodicity around 1943. Our analysis also suggests periodicities of ~ 5

years, ~ 7 years, and ~ 17 years, as well as some other short-term periodicities. However, short-term periodicities are mostly present at the time of solar minima. Hence, short-term periodicities cannot be confirmed because of the larger uncertainty in the data.

North-south asymmetry in small and large sunspot group activity and violation of even-odd solar cycle rule

J. **Javaraiah**
Astrophysics and Space Science **2016**
http://arxiv.org/pdf/1605.07361v1.pdf

According to Gnevyshev-Ohl (G-O) rule an odd-numbered cycle is stronger than its preceding even-numbered cycle. In the modern time the cycle pair (22, 23) violated this rule. By using the combined Greenwich Photoheliographic Results (GPR) and Solar Optical Observing Network (SOON) sunspot group data during the period 1874-2015, and Debrecen Photoheliographic Data (DPD) of sunspot groups during the period 1974-2015, here we have found that the solar cycle pair (22, 23) violated the G-O rule because, besides during cycle 23 a large deficiency of small sunspot groups in both the northern and the southern hemispheres, during cycle 22 a large abundance of small sunspot groups in the southern hemisphere. In the case of large and small sunspot groups the cycle pair (22, 23) violated the G-O rule in the northern and southern hemispheres, respectively, suggesting the north-south asymmetry in solar activity has a significant contribution in the violation of G-O rule. The amplitude of solar cycle 24 is smaller than that of solar cycle 23. However, Coronal Mass Ejections (CMEs) rate in the rising phases of the cycles 23 and 24 are almost same (even slightly large in cycle 24). From both the SOON and the DPD sunspot group data here we have also found that on the average the ratio of the number (counts) of large sunspot groups to the number of small sunspot groups is larger in the rising phase of cycle 24 than that in the corresponding phase of cycle 23. We suggest this could be a potential reason for the aforesaid discrepancy in the CME rates during the rising phases of cycles 23 and 24. These results have significant implication on solar cycle mechanism

Long-term variations in the north-south asymmetry of solar activity and solar cycle prediction, III: Prediction for the amplitude of solar cycle 25.

Javaraiah J (**2015**) NewA 34: 54-64

Un-interrupted Sun-as-a-star Helioseismic Observations over Multiple Solar Cycles

Kiran **Jain**, Sushanta Tripathy, Frank Hill, David Salabert, Rafael A. Garcia, Anne-Marie Broomhall
Proceedings of IAU Symposium 340 **2018**
https://arxiv.org/pdf/1805.05298.pdf

We analyze Sun-as-a-star observations spanning over solar cycles 22 -- 24 from the ground-based network BiSON and solar cycles 23 -- 24 collected by the space-based VIRGO and GOLF instruments on board the {\it SoHO} satellite. Using simultaneous observations from all three instruments, our analysis suggests that the structural and magnetic changes responsible for modifying the frequencies remained comparable between cycle 23 and cycle 24 but differ from cycle 22. Thus we infer that the magnetic layer of the Sun has become thinner since the beginning of cycle 23 and continues during the current cycle.

Sun's Seismic Radius as Measured from the Fundamental Modes of Oscillations and its Implications for the TSI Variations

Kiran **Jain**, S.C. Tripathy, F. Hill
ApJL **2018**
https://arxiv.org/pdf/1805.05307.pdf

In this letter, we explore the relationship between the solar seismic radius and total solar irradiance (TSI) during last two solar cycles using the uninterrupted data from space-borne instruments onboard {\it SoHO} and {\it SDO}. The seismic radius is calculated from the fundamental ({\it f}) modes of solar oscillations utilizing the observations from {\it SoHO}/MDI and {\it SDO}/HMI, and the total solar irradiance measurements are obtained from {\it SoHO}/VIRGO. Our study suggests that the major contribution to the TSI variation arises from the changes in magnetic field while the radius variation plays a secondary role. We find that the solar irradiance increases with decreasing seismic radius, however the anti-correlation between them is moderately weak. The estimated maximum change in seismic radius during a solar cycle is about 5 kilometers, and is consistent in both solar cycles 23 and 24. Previous studies suggest a radius change at the surface of the order of 0.06 arcsecond to explain the 0.1\% variation in the TSI values during the solar cycle, however our inferred seismic radius change is significantly smaller, hence the TSI variations can not be fully explained by the temporal changes in seismic radius.

Probing Subsurface Flows in Active Region NOAA 12192 - Comparison with NOAA 10486

Kiran **Jain**, S.C. Tripathy, F. Hill

ApJ **2017**
https://arxiv.org/pdf/1710.02137.pdf
Active Region (AR) 12192 is the biggest AR observed in solar cycle 24 so far. This was a long-lived AR which survived for four Carrington rotations (CR) and exhibited several unusual phenomena. We measure the horizontal subsurface flows in this active region in multiple rotation using the ring-diagram technique of local helioseismology and the Global Oscillation Network Group (GONG+) Dopplergrams, and investigate how different was the plasma flow in AR 12192 from that in AR 10486. Both regions produced several high M- and X-class flares but had different CME productivity. Our analysis suggests that these ARs had unusually large horizontal flow amplitude with distinctly different directions. While meridional flow in AR 12192 was poleward that supports the flux transport to poles, it was equatorward in AR 10486. Furthermore, there was a sudden increase in the magnitude of estimated zonal flow in shallow layers in AR 12192 during the X3.1 flare, however, it reversed direction in AR 10486 with X17.2 flare. These flow patterns produced strong twists in horizontal velocity with depth in AR 10486 that persisted throughout the disk passage as opposed to AR 12192, which produced a twist only after the eruption of the X3.1 flare that disappeared soon after. Our study indicates that the sunspot rotation combined with the re-organization of magnetic field in AR 10486 was not sufficient to decrease the flow energy even after several large flares that might have triggered CMEs. Furthermore, in the absence of sunspot rotation in AR 12192, this re-organization of magnetic field contributed significantly to the substantial release of flow energy after the X3.1 flare.
2014/10/18-26, 2003/10/26-11/02

Horizontal Flows in Active Regions from Ring-diagram and Local Correlation Tracking Methods

Kiran **Jain**, S.C. Tripathy, B. Ravindra, R. Komm, F. Hill
ApJ **201**5
http://arxiv.org/pdf/1511.03208v1.pdf
Continuous high-cadence and high-spatial resolution Dopplergrams allow us to study sub-surface dynamics that may be further extended to explore precursors of visible solar activity on the surface. Since the p-mode power is absorbed in the regions of high magnetic field, the inferences in these regions are often presumed to have large uncertainties. In this paper, using the Dopplergrams from space-borne Helioseismic Magnetic Imager (HMI), we compare horizontal flows in a shear layer below the surface and the photospheric layer in and around active regions. The photospheric flows are calculated using local correlation tracking (LCT) method while the ring-diagram (RD) technique of helioseismology is used to infer flows in the sub-photospheric shear layer. We find a strong positive correlation between flows from both methods near the surface. This implies that despite the absorption of acoustic power in the regions of strong magnetic field, the flows inferred from the helioseismology are comparable to those from the surface measurements. However, the magnitudes are significantly different; the flows from the LCT method are smaller by a factor of 2 than the helioseismic measurements. Also, the median difference between direction of corresponding vectors is 49 degree.

Five-minute oscillation power within magnetic elements in the solar atmosphere

Rekha **Jain**, Andrew Gascoyne, Bradley W. Hindman, Benjamin Greer
2014
http://arxiv.org/pdf/1405.0695v2.pdf
It has long been known that magnetic plage and sunspots are regions in which the power of acoustic waves is reduced within the photospheric layers. Recent observations now suggest that this suppression of power extends into the low chromosphere and is also present in small magnetic elements far from active regions. In this paper we investigate the observed power supression in plage and magnetic elements, by modelling each as a collection of vertically aligned magnetic fibrils and presuming that the velocity within each fibril is the response to buffeting by incident p modes in the surrounding field-free atmosphere. We restrict our
attention to modeling observations made near solar disk center, where the line-of-sight velocity is nearly vertical and hence, only the longitudinal component of the motion within the fibril contributes. Therefore, we only consider the excitation of axisymmetric sausage waves and ignore kink oscillations as their motions are primarily horizontal. We compare the vertical motion within the fibril with the vertical motion of the incident p
mode by constructing the ratio of their powers. In agreement with observational measurements we find that the total power is suppressed within strong magnetic elements for frequencies below the acoustic cut-off frequency. We also find that the magnitude of the power deficit increases with the height above the photosphere at which the measurement is made. Further, we argue that the area of the solar disk over which the power suppression extends increases as a function of height.

Variation of solar oscillation frequencies in solar cycle 23 and their relation to sunspot area and number

R. **Jain**1, S. C. Tripathy2, F. T. Watson2, L. Fletcher3, K. Jain2 and F. Hill
A&A 545, A73 (**2012**)

Aims. Studying the long term evolution of the solar acoustic oscillations is necessary for understanding how the large-scale solar dynamo operates. In particular, an understanding of the solar cycle variation in the frequencies of solar oscillations can provide a powerful diagnostic tool for constraining various dynamo models. In this work, we report the temporal evolution of solar oscillations for the solar cycle 23, and correlate with solar magnetic activity indices.
Methods. We use solar oscillation frequencies obtained from the Michelson Doppler Imager on board the Solar and Heliospheric Observatory, correlate them with the sunspot number provided by the international sunspot number, RI, and compare them with the sunspot number calculated with the Sunspot Tracking And Recognition Algorithm (STARA).
Results. We find that the mean frequency shifts correlate very well with the sunspot numbers obtained from two different datasets. We also find a hysteresis-type behaviour for the STARA sunspot area and mean magnetic field strength for the different phases of the solar cycle. The increase in solar oscillation frequencies precedes slightly the increase in total sunspot area and the mean magnetic field strength for the solar cycle 23. We briefly discuss the cyclic behaviour in the context of p-mode frequencies.
Erratum: A&A 560, C1 (**2013**)

A Twenty Year Decline in Solar Photospheric Magnetic Fields: Inner-Heliospheric Signatures and Possible Implications?

P. **Janardhan**, Susanta Kumar Bisoi, S. Ananthakrishnan, M. Tokumaru, K. Fujiki, L. Jose, R. Sridharan
JGR **2015**
http://arxiv.org/pdf/1506.03589v1.pdf
We report observations of a steady 20 year decline of solar photospheric fields at latitudes ≥45o starting from ~1995. This prolonged and continuing decline, combined with the fact that Cycle 24 is already past its peak, implies that magnetic fields are likely to continue to decline until ~2020, the expected minimum of the ongoing solar Cycle 24. In addition, interplanetary scintillation (IPS) observations of the inner heliosphere for the period 1983--2013 and in the distance range 0.2--0.8 AU, have also shown a similar and steady decline in solar wind micro-turbulence levels, in sync with the declining photospheric fields. Using the correlation between the polar field and heliospheric magnetic field (HMF) at solar minimum, we have estimated the value of the HMF in 2020 to be 3.9 (±0.6) and a floor value of the HMF of ~3.2 (±0.4) nT. Given this floor value for the HMF, our analysis suggests that the estimated peak sunspot number for solar Cycle 25 is likely to be ~ 62 (±12).

Development of a Deep Learning Model for Inversion of Rotational Coronagraphic Images Into 3D Electron Density

Soojeong **Jang**1, Ryun-Young Kwon1,2, Jon A. Linker3, Pete Riley3, Gyungin Shin4, Cooper Downs3, and Yeon-Han Kim1
2021 ApJL 920 L30
https://iopscience.iop.org/article/10.3847/2041-8213/ac2a46/pdf
https://doi.org/10.3847/2041-8213/ac2a46
We present, for the first time, a deep learning model that returns the three-dimensional (3D) coronal electron density from coronagraphic images. The intensity of coronagraphic observations arises from the Thomson scattering of photospheric light by the coronal electrons. We use MHD numerical simulations to obtain realistic 3D electron density and construct error-free training sets consisting of input (observation) and target (electron density) images. In the training sets, the input images are directly synthesized from the target 3D electron density by applying the Thomson scattering theory. The input and target images are in the form of latitude–longitude maps given at a radius, often referred to as synoptic maps. Using synoptic maps reduces a tomographic method to an image translation problem. We use pix2pixHD, one of the well-established supervised image translation methods and develop models for six selected heights: 2.0, 2.2, 2.5, 4.0, 6.0, and 12.0 solar radii. All six models have similar performance and the mean absolute percent error of the generated density images is less than 7% with respect to the ground-truth simulated data sets.

CORONAL DYNAMIC ACTIVITIES IN THE DECLINING PHASE OF A SOLAR CYCLE

Minhwan **Jang**1,2, T. N. Woods3, Sunhak Hong2,4, and G. S. Choe
2016 ApJL 833 L11
https://arxiv.org/pdf/1610.02944v2.pdf
It has been known that some solar activity indicators show a double-peak feature in their evolution through a solar cycle, which is not conspicuous in sunspot number. In this Letter, we investigate the high solar dynamic activity in the declining phase of the sunspot cycle by examining the evolution of polar and low-latitude coronal hole (CH) areas, splitting and merging events of CHs, and coronal mass ejections (CMEs) detected by SOHO/LASCO C3 in solar cycle 23. Although the total CH area is at its maximum near the sunspot minimum, in which polar CHs prevail, it shows a comparable second maximum in the declining phase of the cycle, in which low-latitude CHs are

dominant. The events of CH splitting or merging, which are attributed to surface motions of magnetic fluxes, are also mostly populated in the declining phase of the cycle. The far-reaching C3 CMEs are also overpopulated in the declining phase of the cycle. From these results we suggest that solar dynamic activities due to the horizontal surface motions of magnetic fluxes extend far in the declining phase of the sunspot cycle. Хорошее Введение.

Generic Magnetic Field Intensity Profiles of Interplanetary Coronal Mass Ejections at Mercury, Venus, and Earth From Superposed Epoch Analyses

Miho **Janvier**, Reka M. Winslow, Simon Good, Elise Bonhomme, Pascal Démoulin, Sergio Dasso, Christian Möstl, Noé Lugaz, Tanja Amerstorfer, Elie Soubrié, Peter D. Boakes
JGR Volume124, Issue2, February **2019**, Pages 812-836
sci-hub.tw/10.1029/2018JA025949
https://arxiv.org/pdf/1901.09921.pdf
We study interplanetary coronal mass ejections (ICMEs) measured by probes at different heliocentric distances (0.3–1 AU) to investigate the propagation of ICMEs in the inner heliosphere and determine how the generic features of ICMEs change with heliospheric distance. Using data from the MErcury Surface, Space ENvironment, GEochemistry, and Ranging (MESSENGER), Venus Express and ACE spacecraft, we analyze with the superposed epoch technique the profiles of ICME substructures, namely, the sheath and the magnetic ejecta. We determine that the median magnetic field magnitude in the sheath correlates well with ICME speeds at 1 AU, and we use this proxy to order the ICMEs at all spacecraft. We then investigate the typical ICME profiles for three categories equivalent to slow, intermediate, and fast ICMEs. Contrary to fast ICMEs, slow ICMEs have a weaker solar wind field at the front and a more symmetric magnetic field profile. We find the asymmetry to be less pronounced at Earth than at Mercury, indicating a relaxation taking place as ICMEs propagate. We also find that the magnetic field intensities in the wake region of the ICMEs do not go back to the pre-ICME solar wind intensities, suggesting that the effects of ICMEs on the ambient solar wind last longer than the duration of the transient event. Such results provide an indication of physical processes that need to be reproduced by numerical simulations of ICME propagation. The samples studied here will be greatly improved by future missions dedicated to the exploration of the inner heliosphere, such as Parker Solar Probe and Solar Orbiter. **08.01.2013**

Self-organization of solar magnetic fields **Review**

T.R. **Jarboe**, T.E. Benedett, C.J. Everson, C.J. Hansen, A.C. Hossack, K.D. Morgan, B.A. Nelson, J.M. Penna, D.A. Sutherland
2018
https://arxiv.org/pdf/1807.09593.pdf
Self-organization properties of sustained magnetized plasma are applied to selected solar data to understand solar magnetic fields. Torsional oscillations are speed-up and slow-down bands of the azimuthal flow that correlate with the solar cycle, and they imply the existence of a symmetric solar dynamo with a measured polar flux of 3x10^14 Wb. It is shown that the solar dynamo is thin (~0.1 Mm gradient scale size) and powerful (~10^23 W). These properties are found from the amplitude of the torsional oscillations and the relationship of their velocity contours to solar magnetograms supports the result. The dynamo has enough power to heat the chromosphere and to power the corona and the solar wind. The dynamo also causes a rigid rotation of the heliosphere out to at least the corona and the relationship of the rotation of the corona to solar magnetograms supports this result as well. The thin solar dynamo sustains a thin stable minimum energy state that seems to be covering most of the solar surface just below the photosphere. The magnetic field lines of the minimum energy state should be parallel to the solar surface and rotate with distance from the surface with 2{\pi} radians of rotation in ~1 Mm Resistive diffusion helps to push the magnetic fields to the surface and the global magnetic structure (GMS) seems to lose {\pi} radians every 11 years, causing the observed 180 degree flipping of the solar magnetic field. The thin sheets of magnetized plasma in solar prominences may be the lost thin sheets of the GMS. For completeness, the formation of sunspots, CMEs and flares is discussed.

Evidence for a shallow thin magnetic structure and solar dynamo: the driver of torsional oscillations

T.R. **Jarboe**, T.E. Benedett, C.J. Everson, C.J. Hansen, A.C. Hossack, K.D. Morgan, B.A. Nelson, J.M. Penna, D.A. Sutherland
2017
https://arxiv.org/pdf/1712.01247.pdf
The solar dynamo and the solar Global internal Magnetic Structure (GMS) appear to be a thin (~2 Mm thick) structure near (~1 Mm below) the solar surface. Evidence for these properties are found from the amplitude of the torsional oscillations and in their velocity contours relationship to solar magnetogram; the power to the chromosphere; power to the corona and the solar wind; the current in the helio-current-sheet measured at the radius

of the orbit of Earth; the calculated size (∼1 Mm) of the expanding polar flux when it enters the photosphere; and from the observation that solar magnetic activity is generated near the surface. A thin stable minimum energy state seems to be covering most of the solar surface just below the photosphere. The magnetic field lines should be parallel to the solar surface and rotate with distance from the surface for 2π radians in ∼2 Mm. Resistive diffusion helps to push the magnetic fields to the surface and the GMS seems to lose π radians every 11 years, causing the observed 180◦ flipping of the solar magnetic fields including the flipping of the polar flux. Further evidence for this GMS and its loss is that solar prominences are made of thin sheets of magnetized plasma, which are, likely, remnants of the lost thin sheet of the GMS. The loss process is consistent with the butterfly pattern of the sunspots and with the differences observed between solar maximum and solar minimum in the corona. The solar dynamo drives current parallel to the polar flux, which, in turn, sustains the GMS using cross-field current drive. For completeness, the formation of sunspots, CMEs and flares is discussed.

Image Quality Assessment for Full-Disk Solar Observations with Generative Adversarial Networks

Robert **Jarolim**, Astrid Veronig, Werner Pötzi, Tatiana Podladchikova
Instrumentation and Methods for Astrophysics **2020**
arXiv:2008.12030

Prediction of the amplitude of solar cycle 25 from the ratio of sunspot number to sunspot-group area, low latitude activity, and 130-year solar cycle

J. **Javaraiah**
Advances in Space Research **2024**
https://arxiv.org/pdf/2405.03441
We analysed the combined data of sunspot groups from Greenwich Photoheliographic Results (GPR) during the period 1874-1976 and Debrecen Photoheliographic Data (DPD) during 1977-2017 and determined the monthly mean, annual mean, and 13-month smoothed monthly mean whole sphere sunspot-group area (WSGA). We have also analysed the monthly mean, annual mean, and 13-month smoothed monthly mean version 2 of international sunspot number (SN) during the period 1874-2017. We fitted the annual mean WSGA and SN data during each of Solar Cycles 12-24 separately to the linear and nonlinear (parabola) forms. In the cases of Solar Cycles 14, 17, and 24 the nonlinear fits are found better than the linear fits. We find that there exists a secular decreasing trend in the slope of the WSGA-SN linear relation during Solar Cycles 12-24. A secular decreasing trend is also seen in the coefficient of the first order term of the nonlinear relation. The existence of ~77-year variation is seen in the ratio of the amplitude to WSGA at the maximum epoch of solar cycle. From the pattern of this long-term variation of the ratio we inferred that Solar Cycle 25 will be larger than both Solar Cycles 24 and 26. Using an our earlier method (now slightly revised) we predicted 127 (plus or minus 26) and 141 (plus or minus 19) for the amplitude of Solar Cycle~25. Based on ~130-year periodicity found in the cycle-to-cycle variation of the amplitudes of Solar Cycles 12-24 we find the shape of Solar Cycle 25 would be similar to that of Solar Cycle 13 and predicted for Solar Cycle 25 the amplitude 135 (plus or minus 8), maximum epoch 2024.21 (March 2024) plus or minus 6-month, and end epoch 2032.21 (March 2032) plus or minus 6-month with SN ~4.

Dependence of North--South Difference in the Slope of Joy's Law on Amplitude of Solar Cycle

J. **Javaraiah**
Solar Phys. **2023**
https://arxiv.org/pdf/2309.03650
Study of the tilt angles of solar bipolar magnetic regions is important because the tilt angles have an important role in the solar dynamo. We analysed the data on tilt angles of sunspot groups measured at the Mt. Wilson Observatory (MWOB) during the period 1917-1986 and Kodaikanal Observatory (KOB) during the period 1906-1986. We binned the daily tilt-angle data during each of the Solar Cycles 15-21 into different 5-deg. latitude intervals and calculated the mean value of the tilt angles in each latitude interval and the corresponding standard error. We fitted these binned data to Joy's Law (increase of the tilt angle with latitude), i.e. the linear relationship between tilt angle and latitude of an active region. The linear-least-square fit calculations were done by taking into account the uncertainties in both the abscissa (latitude) and ordinate (mean tilt angle). The calculations were carried out by using both the tilt-angle and area weighted tilt-angle data in the whole sphere, northern hemisphere, and southern hemisphere during the whole period and during each individual solar cycle. We find a significant difference (absolute north--south asymmetry) between the slopes of Joy's Law recovered from northern and southern hemispheres' whole period MWOB data of area-weighted tilt angles. Only the slope obtained from the southern hemisphere's MWOB data of a solar cycle is found to be reasonably well anti-correlated to the amplitude of the solar cycle. In the case of area weighted tilt-angle data, a good correlation is found between the absolute north--south asymmetry in the slope of a solar cycle and the amplitude of the solar cycle. The corresponding best-fit linear equations are found to be statistically significant.

Prediction for the amplitude and second maximum of Solar Cycle 25 and a comparison of the predictions based on strength of polar magnetic field and low-latitude sunspot area

J **Javaraiah**

MNRAS, Volume 520, Issue 4, April **2023**, Pages 5586–5599,
https://doi.org/10.1093/mnras/stad479

The maximum of a solar cycle contains two or more peaks, known as Gnevyshev peaks. Studies of this property of solar cycles may help in better understanding the solar dynamo mechanism. We analysed the 13-month smoothed monthly mean Version-2 international sunspot number (SN) during the period 1874–2017 and found that there exists a good correlation between the amplitude (value of the main and highest peak) and the value of the second maximum (value of the second highest peak) during the maximum of a solar cycle. Using this relationship and the earlier predicted value 86 ± 18 (92 ± 11) of the amplitude of Solar Cycle 25, here we predict a value 73 ± 15 (79 ± 15) for the second maximum of Solar Cycle 25. The ratio of the predicted second maximum to the amplitude is found to be 0.85, almost the same as that of Solar Cycle 24. The least-square cosine fits to the values of the peaks that occurred first and second during the maxima of Solar Cycles 12–24 suggest that in Solar Cycle 25 the second maximum would occur before the main maximum, the same as in Solar Cycle 24. However, these fits suggest ≈106 and ≈119 for the second maximum and the amplitude of Solar Cycle 25, respectively. Earlier, we analysed the combined Greenwich and Debrecen sunspot-group data during 1874–2017 and predicted the amplitude of Solar Cycle 25 from the activity just after the maximum of Solar Cycle 24 in the equatorial latitudes of the Sun's Southern hemisphere. Here, from the hindsight of the results we found the earlier prediction is reasonably reliable. We analysed the polar-fields data measured in Wilcox Observatory during Solar Cycles 20–24 and obtained a value 125 ± 7 for the amplitude of Solar Cycle 25. This is slightly larger – whereas the value ≈86 (≈92) predicted from the activity in the equatorial latitudes is slightly smaller – than the observed amplitude of Solar Cycle 24. This difference is discussed briefly.

Long-Term Variations in Solar Activity: Predictions for Amplitude and North–South Asymmetry of Solar Cycle 25

J. **Javaraiah**

Solar Physics volume 297, Article number: 33 (**2022**)
https://link.springer.com/content/pdf/10.1007/s11207-022-01956-z.pdf

In most of the solar cycles, activity in the northern and southern hemispheres peaks at different times. One hemisphere peaks well before the other, and at least one of the hemispheric maxima frequently does not coincide with the whole sphere maximum. Prediction of the maximum of a hemisphere and the corresponding north–south asymmetry of a solar cycle may help to understand the mechanisms of the solar cycle, the solar-terrestrial relationship, and solar-activity influences on space weather. Here we analysed the sunspot-group data from the Greenwich Photoheliographic Results (GPR) during 1874 – 1976 and Debrecen Photoheliographic Data (DPD) during 1977 – 2017 and studied the cycle-to-cycle variations in the values of 13-month smoothed monthly mean sunspot-group area in the whole sphere (WSGA), northern hemisphere (NSGA), and southern hemisphere (SSGA) at the epochs of maxima of Sunspot Cycles 12 – 24 and at the epochs of maxima of WSGA, NSGA, and SSGA Cycles 12 – 24 (note that solar-cycle variation of a parameter is expressed as a cycle of that parameter). The cosine fits to the values of WSGA, NSGA, and SSGA at the maxima of sunspot, WSGA, NSGA, and SSGA Cycles 12 – 24, and to the values of the corresponding north–south asymmetry, suggest the existence of a ≈132-year periodicity in the activity of the northern hemisphere, a 54 – 66-year periodicity in the activity of the southern hemisphere, and a 50 – 66 year periodicity in the north–south asymmetry in activity at all the aforementioned epochs. By extrapolating the best-fit cosine curves we predicted the amplitudes and the corresponding north–south asymmetry of the 25th WSGA, NSGA, and SSGA cycles. We find that on average Solar Cycle 25 in sunspot-group area would be to some extent smaller than Solar Cycle 24 in sunspot-group area. However, by inputting the predicted amplitudes of the 25th WSGA, NSGA, and SSGA cycles relationship between sunspot-group area and sunspot number we find that the amplitude (130±12130±12) of Sunspot Cycle 25 would be slightly larger than that of reasonably small Sunspot Cycle 24. Still it confirms that the beginning of the upcoming Gleissberg cycle would take place around Solar Cycle 25. We also find that except at the maximum of NSGA Cycle 25 where the strength of activity in the northern hemisphere would be dominant, the strength of activity in the southern hemisphere would be dominant at the maximum epochs of the 25th sunspot, WSGA, and SSGA cycles.

A Study of Variations in Correlation Between Rotation Residual and Meridional Velocity of Sunspot Groups

J. **Javaraiah**

Solar Physics volume 296, Article number: 152 (**2021**)
https://link.springer.com/content/pdf/10.1007/s11207-021-01883-5.pdf
https://doi.org/10.1007/s11207-021-01883-5

We analyzed the combined 142 years sunspot-group data from Greenwich Photoheliograpic Results (GPR) and Debrecen Photoheliographic Data (DPD) and determined the yearly mean residual rotation rate and the meridional velocity of sunspot groups in different 5∘5∘ latitude intervals. We find that there exists a considerable latitude–time dependence in both the residual rotation and the meridional motion. The residual rotation rate is found to be −120 m s−1 to 80 m s−1. In a large number of solar cycles, the rotation is to some extent weaker during maxima than that of during minima. There exist alternate bands of equatorward and poleward meridional motions. The equatorward motion is dominant mostly around the maxima of solar cycles with velocity 8–12 m s−1, whereas the poleward motion is dominant mostly around the minima but with a relatively weak velocity, only 4–6 m s−1. The analysis of the data during Solar Cycles 12–24 that are folded according to the years from their respective epochs of maxima suggests the existence of equatorward migrating alternate bands of slower and faster than average rotation within the activity belt. This analysis suggests no clear equatorward or poleward migrating bands of meridional motions. A statistically significant anticorrelation exists between the meridional motion and residual rotation. The corresponding linear-least-squares best-fit is found to be reasonably good (slope, −0.028±0.008−0.028±0.008, is about 3.5 times larger than its standard deviation). As per the sign convention used for the meridional motions, the significant negative value of the slope indicates the existence of a strong angular momentum transport toward the equator. The cross-correlation between the slopes determined from the data in 3-year moving time intervals and yearly mean sunspot number (SN) suggests that the slope leads SN by about 4 and 9 years. The Morlet wavelet spectrum of the slope suggests the existence of ≈11-year periodicity in the slope almost throughout the data window, but it was very weak during 1920–1940. We have also done cross-wavelet, wavelet-coherence, and wavelet-phase difference analyses of the slope and SN. Overall the results suggest there exists a strong relationship between the slope and amount of activity during a solar cycle. However, the correlation between the cycle-to-cycle modulations in the slope and the amplitude of solar cycle is found to be insignificant, indicating that there is no relationship between the slope and strength of activity on a long-time scale (longer than 11-year period).

North--South Asymmetry in Solar Activity and Solar Cycle Prediction, IV: Prediction for Lengths of Upcoming Solar Cycles

J. **Javaraiah**

Solar Phys. **2019**

https://arxiv.org/pdf/1904.11500.pdf

We analyzed the daily sunspot-group data reported by the Greenwich Photoheliographic Results (GPR) during the period 1874-1976 and Debrecen Photoheliographic Data (DPD) during the period 1977-2017 and studied North-South asymmetry in the maxima and minima of the Solar Cycles 12-24. We derived the time series of the 13-month smoothed monthly mean corrected whole-spot areas of the sunspot groups in the Sun's whole sphere (WSGA), northern hemisphere (NSGA), and southern hemisphere (SSGA). From these smoothed time series we obtained the values of the maxima and minima, and the corresponding epochs, of the WSGA, NSGA, and SSGA Cycles 12-24. We find that there exists a 44-66 years periodicity in the North-South asymmetry of the minimum. A long periodicity (130-140 years) may exist in the asymmetry of the maximum. A statistically significant correlation exists between the maximum of SSGA Cycle n and the rise time of WSGA Cycle n + 2. A reasonably significant correlation also exists between the maximum of WSGA Cycle n and the decline time of WSGA Cycle n + 2. These relations suggest that the solar dynamo carries memory over at least three solar cycles. Using these relations we obtained the values 11.7 + or - 0.15 years, 11.2 + or - 0.2 years, and 11.45 + or - 0.3 years for the lengths of WSGA Cycles 24, 25, and 26, respectively, and hence, July 2020, October 2031, and March 2043 for the minimum epochs (start dates) of WSGA Cycles 25, 26, and 27, respectively. We also obtained May 2025 and March 2036 for the maximum epochs of WSGA Cycles 25 and 26, respectively. It seems during the late Maunder minimum sunspot activity was absent around the epochs of the maxima of the NSGA-cycles and the minima of the SSGA-cycles, and some activity was present at the epochs of the maxima of some SSGA-cycles and the minima of some NSGA-cycles.

Short-Term Variations in the Equatorial Rotation Rate of Sunspot Groups

J. **Javaraiah**, L. Bertello

Solar Phys. **2016**

https://arxiv.org/pdf/1610.06710v1.pdf

We have detected several periodicities in the solar equatorial rotation rate of sunspot groups in the Greenwich Photoheliographic Results (GPR) during the period 1931-1976, the Solar Optical Observing Network (SOON) during the period 1977-2014, and the Debrecen Photoheliographic Data (DPD) during the period 1974-2014. Our results suggest a ~250-day period in the equatorial rotation rate determined from both the Mt. Wilson Doppler-velocity data and the sunspot-group data during 1986-2007. However, a wavelet analysis reveals that this periodicity appears mostly around 1991 in the velocity data, while it is present in most of the solar cycles covered by the sunspot-group data, mainly near the minimum epochs of the solar cycles. We also found the signature of a period of ~1.4 years period in the velocity data during 1990-1995, and in the equatorial rotation rate of sunspot groups mostly

around the year 1956. The equatorial rotation rate of sunspot groups reveals a strong ~1.6-year periodicity around 1933 and 1955 and a weaker one around 1976, and a strong ~1.8-year periodicity around 1943. Our analysis also suggests periodicities of ~5 years, ~7 years, and ~17 years as well as some other short-term periodicities. However, short-term periodicities are mostly present at the time of solar minima. Hence, short-term periodicities cannot be confirmed because of the larger uncertainty in the data.

Long-term variations in the north-south asymmetry of solar activity and solar cycle prediction, III: prediction for the amplitude of solar cycle 25

J. **Javaraiah**

New Astronomy 34, 54-64 (**2015**)

http://arxiv.org/pdf/1407.0554v1.pdf

The combined Greenwich and Solar Optical Observing Network (SOON) sunspot group data during 1874-2013 are analyzed and studied the relatively long-term variations in the annual sums of the areas of sunspot groups in 0-10 deg, 10-20 deg, and 20-30 deg latitude intervals of the Sun's northern and southern hemispheres. The variations in the corresponding north-south differences are also studied. Long periodicities in these parameters are determined from the fast Fourier transform (FFT), maximum entropy method (MEM), and Morlet wavelet analysis. It is found that in the difference between the sums of the areas of the sunspot groups in 0-10 deg latitude intervals of northern and southern hemispheres, there exist ~9-year periodicity during the high activity period 1940-1980 and ~12-year periodicity during the low activity period 1890-1939. It is also found that there exists a high correlation (85% from 128 data points) between the sum of the areas of the sunspot groups in 0-10 deg latitude interval of the southern hemisphere during a Qth year (middle year of 3-year smoothed time series) and the annual mean International Sunspot Number (Rz) of (Q+9)th year. Implication of these results is discussed in the context of solar activity prediction and predicted 50 + or - 10 for the amplitude of solar cycle 25, which is about 31% lower than the amplitude of cycle 24.

The G–O Rule and Waldmeier Effect in the Variations of the Numbers of Large and Small Sunspot Groups

J. **Javaraiah**

Solar Physics, December **2012**, Volume 281, Issue 2, pp 827-837

We have analyzed the combined Greenwich and Solar Optical Observing Network (SOON) sunspot group data during the period of 1874 – 2011 and determined variations in the annual numbers (counts) of the small (maximum area A M<100 millionth of solar hemisphere, msh), large (100≤A M<300 msh), and big (A M≥300 msh) spot groups. We found that the amplitude of an even-numbered cycle of the number of large groups is smaller than that of its immediately following odd-numbered cycle. This is consistent with the well known Gnevyshev and Ohl rule (G–O rule) of solar cycles, generally described by using the Zurich sunspot number (R Z). During cycles 12 – 21 the G–O rule holds good for the variation in the number of small groups also, but it is violated by cycle pair (22, 23) as in the case of R Z. This behavior of the variations in the small groups is largely responsible for the anomalous behavior of R Z in cycle pair (22, 23). It is also found that the amplitude of an odd-numbered cycle of the number of small groups is larger than that of its immediately following even-numbered cycle. This might be called the 'reverse G–O rule'. In the case of the number of the big groups, both cycle pairs (12, 13) and (22, 23) violated the G–O rule. In many cycles the positions of the peaks of the small, large, and big groups are different, and considerably differ with respect to the corresponding positions of the R Z peaks. In the case of cycle 23, the corresponding cycles of the small and large groups are largely symmetric/less asymmetric (the Waldmeier effect is weak/absent) with their maxima taking place two years later than that of R Z. The corresponding cycle of the big groups is more asymmetric (strong Waldmeier effect) with its maximum epoch taking place at the same time as that of R Z.

Quasi 9 and 30–40 days periodicities in the solar differential rotation

J. **Javaraiah**

Advances in Space Research, Volume 48, Issue 6, 15 September **2011**, Pages 1032-1040

Using the daily Mt. Wilson Doppler velocity data during 1986–1994 (solar cycle 22), we studied the short-term variations of the order of a few days to a month timescales in the solar differential rotation. We represent the differential rotation in the form: , using a set of Gegenbauer polynomials, where $\omega(\lambda)$ is the angular velocity at latitude λ. The coefficients , and are free of crosstalk. We found that ≈9-day periodicity is statistically highly significant in the variations of at the maximum of solar cycle 22. A similar periodicity is found in the variations of during the descending phase of the cycle 22 with significant on 99.9% confidence level. At this cycle maximum, a 30–40 day periodicity is found to be dominant among the variations in , and this periodicity is found in during almost throughout the period 1986–1994. The ≈9-day periodicity in the variation of the differential rotation

approximately matches with the known quasi 10-day periodicity in the total solar irradiance (TSI) variability. Hence, we speculate that there exists a relationship between the differential rotation and TSI variability. We suggest that the 9–10 day periodicities of the differential rotation and TSI have a relationship with the production and the emergence rates of the large-scale solar magnetic flux.

Sunspot-Cycle Evolution of Major Periodicities of Solar Activity

G. L. **Jayalekshmi**, Tarun Kumar Pant & P. R. Prince
Solar Physics volume 297, Article number: 85 (**2022**)
https://doi.org/10.1007/s11207-022-02017-1

Solar activity is generally periodic in nature, having a main periodicity of ≈ 11 years, known as the solar cycle. Sunspots are one of the visible indicators of this cycle, and its different characteristics have been known for many years. Due to the presence of irregularities – long and short-term trends, stochasticity, etc. – it is difficult to predict solar activity. In sunspot cycles, amplitude and duration are highly varying parameters, making their prediction challenging. In this study, wavelet analysis of sunspot numbers for the period 1819 – 2019 is carried out to find the long- and short-term periodic variations in different cycles and changes in cycle duration. The assumptions of the flux-transport dynamo model of the sunspot cycle are used as the basis for the interpretation of the results. The results bring out 10.1-, 10.8-, and 11.6-year periods as the basic periodicities of the sunspot cycle and the ones having the highest strength in a sunspot cycle. Further, their amplitudes have been found to depend on whether the solar cycle belongs to a grand episode or a regular one. Solar-cycle duration is mainly determined by the length of the basic periodicities of the sunspot cycle, and major irregularities in the duration of Solar Cycles 9, 20, and 23 are caused by modulation of periodic trends. Since all the types of variations shown by the duration of the sunspot cycle appear related to the meridional-flow circulation, the results of the study explain the characteristic changes of this circulation postulated by the flux-transport dynamo model.

Dependence of North–South Difference in the Slope of Joy's Law on the Amplitude of Solar Cycle

J. **Javaraiah**
Solar Physics volume 298, Article number: 106 (**2023**)
https://doi.org/10.1007/s11207-023-02201-x

Study of the tilt angles of solar bipolar magnetic regions is important because the tilt angles have an important role in the solar dynamo. We analyzed the data on tilt angles of sunspot groups measured at the Mt. Wilson Observatory (MWOB) during the period 1917 – 1986 and Kodaikanal Observatory (KOB) during the period 1906 – 1986. We binned the daily tilt-angle data during each of the Solar Cycles 15 – 21 into different 5∘5∘-latitude intervals and calculated the mean value of the tilt angles in each latitude interval and the corresponding standard error. We fitted these binned data to Joy's law (increase of the tilt angle with latitude), i.e. the linear relationship between tilt angle and latitude of an active region. The linear least-square fit calculations were carried out by taking into account the uncertainties in both the abscissa (latitude) and ordinate (mean tilt angle). The calculations were carried out by using both the tilt-angle and area-weighted tilt-angle data in the whole sphere, northern hemisphere, and southern hemisphere during the whole period and during each individual solar cycle. We find a significant difference (north–south asymmetry) between the slopes of Joy's laws recovered from northern and southern hemispheres' whole-period MWOB data of area-weighted tilt angles. Only the slope obtained from the southern hemisphere's MWOB data of a solar cycle is found to be reasonably well anticorrelated to the amplitude of the solar cycle. In the case of area-weighted tilt-angle data, a good correlation is found between the north–south asymmetry in the slope of a solar cycle and the amplitude of the solar cycle. The corresponding best-fit linear equations are found to be statistically significant.

Prediction for the amplitude and second maximum of Solar Cycle 25 and a comparison of the predictions based on strength of polar magnetic field and low latitude sunspot area

J. **Javaraiah**
MNRAS **2023**
https://arxiv.org/pdf/2302.12615

The maximum of a solar cycle contain two or more peaks, known as Gnevyshev peaks. Studies of this property of solar cycles may help for better understanding the solar dynamo mechanism. We analysed the 13-month smoothed monthly mean Version-2 international sunspot number (SN) during the period 1874-2017 and found that there exists a good correlation between the amplitude (value of the main and highest peak) and the value of the second maximum (value of the second highest peak) during the maximum of a solar cycle.Using this relationship and the earlier predicted value 86 (~92) of the amplitude of Solar Cycle 25, here we predict a value ~73 (~79) for the second maximum of Solar Cycle 25. The ratio of the predicted second maximum to the amplitude is found to be 0.85, almost the same as that of Solar Cycle 24.The cosine fits to the values of the peaks that occurred first and second during the maxima of Solar Cycles 12-24 suggests that in Solar Cycle 25 the second maximum would occur before the main maximum, the same as in Solar Cycle 24. However, these fits suggest ~106 and ~119 for the second

maximum and the amplitude of Solar Cycle 25, respectively. We analysed the polar-fields data measured in Wilcox Observatory during Solar Cycles 20-24 and obtained a value ~125 for the amplitude of Solar Cycle 25. This is slightly larger-whereas the value ~86 (~92) predicted from the aforementioned relationship is slightly smaller-than the observed amplitude of Solar Cycle~24. This difference is discussed briefly.

Observed local dispersion relations for magneto-acoustic-gravity waves in the Sun's atmosphere: Mapping the acoustic cut-off frequency

Stuart M. **Jefferies**, Bernhard Fleck, Neil Murphy, Francesco Berrilli
2019 ApJL 884 L8
https://arxiv.org/pdf/1910.03198.pdf
We present the observed local dispersion relations for magneto-acoustic-gravity waves in the Sun's atmosphere for different levels of magnetic field strength. We model these data with a theoretical local dispersion relation to produce spatial maps of the acoustic cut-off frequency in the Sun's photosphere. These maps have implications for the mechanical heating of the Sun's upper atmosphere, by magneto-acoustic-gravity waves, at different phases of the solar magnetic activity cycle.

Numerical Simulations of Oscillations in Solar Corona Excited by Vortex Shedding

Petr **Jelínek**1, Sofya Belov1, and Marian Karlický2
2022 ApJ 941 124
https://iopscience.iop.org/article/10.3847/1538-4357/aca40d/pdf
We study transverse oscillations of plasma structures in the solar corona excited by vortex shedding solving the full set of the 3D ideal time-dependent magnetohydrodynamic equations. To present how the creation of vortices and excited oscillations depend on the initial flow speed and various values of the magnetic field, we performed a parametric study for two cases, an interaction of a steady flow with a rigid and spatially fixed cylindrical obstacle, and with a cylinder fixed at the boundaries. We show that generated vortices can excite oscillations, e.g., transverse (kink), in the solar corona, for example in coronal loops, filaments, flux ropes, or similar magnetic structures. It has been found that the oscillation period is close to the theoretically predicted value. Moreover, we study the dependence of the Strouhal number with respect to the magnetic field under the conditions of the solar atmosphere.

Energy Budget of the Solar Cycle

Adam S. **Jermyn**1, Shashikumar M. Chitre2, and Christopher A. Tout3
2019 Res. Notes AAS 3 124
https://iopscience.iop.org/article/10.3847/2515-5172/ab3fae
During the solar cycle the Sun exhibits variations in rotation (Howe 2009), gravitational moments (Antia et al. 2008), total luminosity, or irradiance measured at the Earth (Willson & Hudson 1988), and magnetic field (Clette & Lefèvre 2012). Each of these phenomena corresponds to a reservoir or sink of energy and so a key question in understanding the solar cycle is how energy is transferred between them. To begin to understand that question we construct an order of magnitude energy budget (Table 1) for the solar cycle. In doing so we assume that the solar cycle is principally a phenomenon of the solar convection zone and not of the radiative interior.
Erratum 2019 Res. Notes AAS 3 124

Waves in the lower solar atmosphere: the dawn of next-generation solar telescopes

Review

David B. **Jess**, Shahin Jafarzadeh, Samuel D. T. Grant +
Living Reviews in Solar Physics Article: 1 **2023**
https://link.springer.com/content/pdf/10.1007/s41116-022-00035-6.pdf
Waves and oscillations have been observed in the Sun’s atmosphere for over half a century. While such phenomena have readily been observed across the entire electromagnetic spectrum, spanning radio to gamma-ray sources, the underlying role of waves in the supply of energy to the outermost extremities of the Sun’s corona has yet to be uncovered. Of particular interest is the lower solar atmosphere, including the photosphere and chromosphere, since these regions harbor the footpoints of powerful magnetic flux bundles that are able to guide oscillatory motion upwards from the solar surface. As a result, many of the current- and next-generation ground-based and space-borne observing facilities are focusing their attention on these tenuous layers of the lower solar atmosphere in an attempt to study, at the highest spatial and temporal scales possible, the mechanisms responsible for the generation, propagation, and ultimate dissipation of energetic wave phenomena. Here, we present a two-fold review that is designed to overview both the wave analyses techniques the solar physics community currently have at their disposal, as well as highlight scientific advancements made over the last decade. Importantly, while many ground-breaking studies will address and answer key problems in solar physics, the cutting-edge nature of their investigations will naturally pose yet more outstanding observational and/or theoretical questions that require subsequent follow-up work. This is not only to be expected, but should be embraced as a reminder of the era of

rapid discovery we currently find ourselves in. We will highlight these open questions and suggest ways in which the solar physics community can address these in the years and decades to come.

Theo Murphy meeting issue'High-resolution wave dynamics in the lower solar atmosphere'organised and edited by Dr David B. **Jess**, Dr Peter H. Keys, Dr Marco Stangalini and Dr Shahin Jafarzadeh

The magnetic and convective nature of the Sun's photosphere provides a unique platform from which generated waves can be modelled, observed, and interpreted across a wide breadth of spatial and temporal scales. As oscillations are generated, the interplay between the rapidly evolving densities, temperatures, and magnetic field strengths provides dynamic evolution of the embedded wave modes as they propagate into the tenuous solar chromosphere. A focused scientific team was assembled to discuss the current challenges faced in wave studies in the lower solar atmosphere, including those related to the observation and modelling of the dynamic regions, culminating in 15 independent publications within the theme of high-resolution wave dynamics in the lower solar atmosphere.

Waves in the lower solar atmosphere: the dawn of next-generation solar telescopes **Review**

David B. **Jess**, Shahin Jafarzadeh, Peter H. Keys, Marco Stangalini, Gary Verth, Samuel D. T. Grant
Living Review in Solar Physics (LRSP) **2022**
https://arxiv.org/pdf/2212.09788.pdf

Waves and oscillations have been observed in the Sun's atmosphere for over half a century. While such phenomena have readily been observed across the entire electromagnetic spectrum, spanning radio to gamma-ray sources, the underlying role of waves in the supply of energy to the outermost extremities of the Sun's corona has yet to be uncovered. Of particular interest is the lower solar atmosphere, including the photosphere and chromosphere, since these regions harbor the footpoints of powerful magnetic flux bundles that are able to guide oscillatory motion upwards from the solar surface. As a result, many of the current- and next-generation ground-based and space-borne observing facilities are focusing their attention on these tenuous layers of the lower solar atmosphere in an attempt to study, at the highest spatial and temporal scales possible, the mechanisms responsible for the generation, propagation, and ultimate dissipation of energetic wave phenomena. Here, we present a two-fold review that is designed to overview both the wave analyses techniques the solar physics community currently have at their disposal, as well as highlight scientific advancements made over the last decade. Importantly, while many ground-breaking studies will address and answer key problems in solar physics, the cutting-edge nature of their investigations will naturally pose yet more outstanding observational and/or theoretical questions that require subsequent follow-up work. This is not only to be expected, but should be embraced as a reminder of the era of rapid discovery we currently find ourselves in. We will highlight these open questions and suggest ways in which the solar physics community can address these in the years and decades to come.

High-resolution wave dynamics in the lower solar atmosphere

David B. **Jess**, Peter H. Keys, Marco Stangalini, Shahin Jafarzadeh
Philosophical Transactions A: **Volume 379 Issue 2190** **2021** https://walsa.team/u/rsta
https://arxiv.org/pdf/2011.13940.pdf

The magnetic and convective nature of the Sun's photosphere provides a unique platform from which generated waves can be modelled, observed, and interpreted across a wide breadth of spatial and temporal scales. As oscillations are generated in-situ or emerge through the photospheric layers, the interplay between the rapidly evolving densities, temperatures, and magnetic field strengths provides dynamic evolution of the embedded wave modes as they propagate into the tenuous solar chromosphere. A focused science team was assembled to discuss the current challenges faced in wave studies in the lower solar atmosphere, including those related to spectropolarimetry and radiative transfer in the optically thick regions. Following the Theo Murphy international scientific meeting held at Chicheley Hall during February 2020, the scientific team worked collaboratively to produce 15 independent publications for the current Special Issue, which are introduced here. Implications from the current research efforts are discussed in terms of upcoming next-generation observing and high performance computing facilities.
Theo Murphy **meeting issue** https://royalsocietypublishing.org/toc/rsta/2021/379/2190

Statistical Signatures of Nanoflare Activity. I. Monte Carlo Simulations and Parameter Space Exploration

David B. **Jess** , Chris J. Dillon, Michael S. Kirk, Fabio Reale, Mihalis Mathioudakis, Samuel D. T. Grant, Damian J. Christian, Peter H. Keys, S. Krishna Prasad, Scott J. Houston
ApJ **871** 133 **2019**
https://arxiv.org/pdf/1812.06978.pdf

Small-scale magnetic reconnection processes, in the form of nanoflares, have become increasingly hypothesized as important mechanisms for the heating of the solar atmosphere, for driving propagating disturbances along magnetic

field lines in the Sun's corona, and for instigating rapid jet-like bursts in the chromosphere. Unfortunately, the relatively weak signatures associated with nanoflares places them below the sensitivities of current observational instrumentation. Here, we employ Monte Carlo techniques to synthesize realistic nanoflare intensity time series from a dense grid of power-law indices and decay timescales. Employing statistical techniques, which examine the modeled intensity fluctuations with more than 10^7 discrete measurements, we show how it is possible to extract and quantify nanoflare characteristics throughout the solar atmosphere, even in the presence of significant photon noise. A comparison between the statistical parameters (derived through examination of the associated intensity fluctuation histograms) extracted from the Monte Carlo simulations and SDO/AIA 171Å and 94Å observations of active region NOAA 11366 reveals evidence for a flaring power-law index within the range of 1.82 - 1.90, combined with e-folding timescales of 385 +/- 26 s and 262 +/- 17 s for the SDO/AIA 171Å and 94Å channels, respectively. These results suggest that nanoflare activity is not the dominant heating source for the active region under investigation. This opens the door for future dedicated observational campaigns to not only unequivocally search for the presence of small-scale reconnection in solar and stellar environments, but also quantify key characteristics related to such nanoflare activity. **2011 December 10**

Multiwavelength studies of MHD waves in the solar chromosphere: An overview of recent results **Review**

D.B. **Jess**, R.J. Morton, G. Verth, V. Fedun, S.D.T. Grant, I. Giagkiozis

Space Science Reviews Volume 190, Issue 1-4, pp 103-161 **2015**

The chromosphere is a thin layer of the solar atmosphere that bridges the relatively cool photosphere and the intensely heated transition region and corona. Compressible and incompressible waves propagating through the chromosphere can supply significant amounts of energy to the interface region and corona. In recent years an abundance of high-resolution observations from state-of-the-art facilities have provided new and exciting ways of disentangling the characteristics of oscillatory phenomena propagating through the dynamic chromosphere. Coupled with rapid advancements in magnetohydrodynamic wave theory, we are now in an ideal position to thoroughly investigate the role waves play in supplying energy to sustain chromospheric and coronal heating. Here, we review the recent progress made in characterising, categorising and interpreting oscillations manifesting in the solar chromosphere, with an impetus placed on their intrinsic energetics.

Ultra-high-resolution Observations of MHD Waves in Photospheric Magnetic Structures

David B. **Jess**, Gary Verth

AGU/Wiley book "Low-frequency Waves in Space Plasmas" **2015**

http://arxiv.org/pdf/1502.06960v1.pdf

Here we review the recent progress made in the detection, examination, characterisation and interpretation of oscillations manifesting in small-scale magnetic elements in the solar photosphere. This region of the Sun's atmosphere is especially dynamic, and importantly, permeated with an abundance of magnetic field concentrations. Such magnetic features can span diameters of hundreds to many tens of thousands of km, and are thus commonly referred to as the `building blocks' of the magnetic solar atmosphere. However, it is the smallest magnetic elements that have risen to the forefront of solar physics research in recent years. Structures, which include magnetic bright points, are often at the diffraction limit of even the largest of solar telescopes. Importantly, it is the improvements in facilities, instrumentation, imaging techniques and processing algorithms during recent years that have allowed researchers to examine the motions, dynamics and evolution of such features on the smallest spatial and temporal scales to date. It is clear that while these structures may demonstrate significant magnetic field strengths, their small sizes make them prone to the buffeting supplied by the ubiquitous surrounding convective plasma motions. Here, it is believed that magnetohydrodynamic waves can be induced, which propagate along the field lines, carrying energy upwards to the outermost extremities of the solar corona. Such wave phenomena can exist in a variety of guises, including fast and slow magneto-acoustic modes, in addition to Alfven waves. Coupled with rapid advancements in magnetohydrodynamic wave theory, we are now in an ideal position to thoroughly investigate how wave motion is generated in the solar photosphere, which oscillatory modes are most prevalent, and the role that these waves play in supplying energy to various layers of the solar atmosphere.

Sunspot cycles are connected to the Earth and Jupiter

Lauri **Jetsu**

ApJ **2023**

https://arxiv.org/pdf/2311.08317.pdf

The sunspot number record covers over three centuries.These numbers measure the activity of the Sun. This activity follows the solar cycle of about eleven years. In the dynamo-theory, the interaction between differential rotation and convection produces the solar magnetic field. On the surface of Sun, this field concentrates to the sunspots. The dynamo-theory predicts that the period, the amplitude and the phase of the solar cycle are stochastic. Here we show that the solar cycle is deterministic, and connected to the orbital motions of the Earth and Jupiter. This planetary-influence theory allows us to model the whole sunspot record, as well as the near past and the near future of sunspot

numbers. We may never be able to predict the exact times of exceptionally strong solar flares, like the catastrophic Carrington event in September 1859, but we can estimate when such events are more probable. Our results also indicate that during the next decades the Sun will no longer help us to cope with the climate change. The inability to find predictability in some phenomenon does not prove that this phenomenon itself is stochastic.

Predicting the Timing of the the Solar Cycle 25 Polar Field Reversal

Bibhuti Kumar **Jha**, Lisa A. Upton

ApJL **962** L15 **2024**

https://arxiv.org/pdf/2401.10502.pdf

https://iopscience.iop.org/article/10.3847/2041-8213/ad20d2/pdf

The process of the Sun's polar field cancellation reversal commences with the emergence of new cycle Hale's polarity active regions. Once the Sun undergoes polarity reversal, typically occurring near the peak of solar activity, it begins the process of accumulating the seed field for the forthcoming solar cycle. In recent years, the Advective Flux Transport (AFT) model has proven highly effective in forecasting the progression of polar fields by leveraging observations of surface flows and magnetic flux emergence. In this study, we make use of the predictive capability of the AFT model to simulate the evolution of the polar fields and estimate the timing of the Solar Cycle 25 polarity reversal in both hemispheres of the Sun. We use the statistical properties of active regions along with Solar Cycle~13, which closely resembles the current solar cycle (Cycle~25), to generate synthetic active regions in order to simulate future magnetic flux emergence in AFT to predict the evolution of the polar field. Based on our simulations, we anticipate that the Northern hemisphere of the Sun will undergo a polarity reversal between June 2024 and November 2024, with the center of our distribution at August 2024. In the Southern hemisphere, we anticipate a polarity reversal between November 2024 and July 2025, centered around February 2025. Additionally, assuming that the reversal of the axial dipole moment coincides with the peak of the solar cycle, our findings indicate that Cycle 25 is expected to peak in 2024 (likely between April to August 2024).

HMI Science Nuggets #199 Mar **2024** http://hmi.stanford.edu/hminuggets/?p=4204

Exploring the Quenching of Bipolar Magnetic Region Tilts using AutoTAB

Bibhuti Kumar **Jha**, Anu B. Sreedevi, Bidya Binay Karak, Dipankar Banerjee

IAUS 365 Proceedings Series **2024**

https://arxiv.org/pdf/2401.04255.pdf

The tilt of the bipolar magnetic region (BMR) is crucial in the Babcock-Leighton process for the generation of the poloidal magnetic field in the Sun. We extend the work of Jha et al. (2020) and analyze the recently reported tracked BMR catalogue based on AutoTAB Sreedevi et al. (2023) from Michelson Doppler Imager (1996-2011) and Helioseismic and Magnetic Imager (2010-2018). Using the tracked information of BMRs based on AutoTAB, we confirm that the distribution of bmax reported by Jha et al. (2020) is not because of the BMRs are picked multiple times at the different phases of their evolution instead it is also present if we consider each BMRs only once. Moreover, we find that the slope of Joy's law initially increases slowly with the increase of bmax. However, when bmax>2.5 kG, gamma_0 decreases. The decrease of observed gamma0 with bmax provides a hint to a nonlinear tilt quenching in the Babcock-Leighton process.

Long-term Study of the Sun and Its Implications to Solar Dynamo Models

Bibhuti Kumar **Jha**

Thesis, Pondicherry University **2022**

https://arxiv.org/pdf/2210.09072

The Sun shows a wide range of temporal variations, from a few seconds to decades and even centuries, broadly classified into two classes short-term and Long-term. The solar dynamo mechanism is believed to be responsible for these global changes happening in the Sun. Hence, many dynamo models have been proposed to explain the observed behaviour of the Sun. This thesis is primarily focused on studying the \lt\ variation of the Sun and provides various inputs to the solar dynamo models. With a renewed interest in the subject, several automatic techniques have been developed for extensive data analysis as applied to long-term datasets and presented in this thesis. This approach provides better consistency and eliminates human subjectivity, which has been a normal practice in the past. The variation of penumbra to umbra area ratio, q, observed here, will provide constraints in sunspot simulations. In addition, the absence of any difference in the behaviour of small and big spots does not support the idea of the global and local dynamo. Two classes of BMRs observed in the magnetograms further verify this behaviour. The importance of the NSSL is not studied so well in the context of solar dynamo models, but it will be worth waiting to see its significance for understanding solar dynamo. Finally, the indication of tilt quenching presented here needs to be further verified using the more comprehensive data set, including stronger cycles.

A Theoretical Model of the Near Surface Shear Layer of the Sun

Bibhuti Kumar **Jha**, Arnab Rai Choudhuri

MNRAS **2021**
https://arxiv.org/pdf/2105.14266.pdf
The Sun has a Near-Surface Shear Layer (NSSL), within which the angular velocity decreases rapidly with radius. We provide an explanation of this layer based on the thermal wind balance equation. Since convective motions are not affected by solar rotation in the top layer of the convection zone, we argue that the temperature falls at the same rate at all latitudes in this layer. This makes the thermal wind term very large in this layer and the centrifugal term has also to become very large to balance it, giving rise to the NSSL. From the values of differential rotation $\Omega(r<rc,\theta)$ at radii less than a radius rc, we can calculate the temperature difference $\Delta T(r,\theta)$ with respect to the standard solar model at different points of the convection zone, by making use of the thermal wind balance equation. Then we again use this equation in the top layer to calculate $\Omega(r>rc,\theta)$ there from $\Delta T(r,\theta)$. We carry on this exercise using both an analytical expression of the differential rotation and the actual data provided by helioseismology. We find that our theoretical results of the NSSL match the observational data reasonably well for $rc \approx 0.96\ R_\odot$, giving an estimate of the radius till which the convective motions are affected by the solar rotation.

Measurements of Solar Differential Rotation Using the Century Long Kodaikanal Sunspot Data

Bibhuti Kumar **Jha**, Aditya Priyadarshi, Sudip Mandal, Subhamoy Chaterjee, Dipankar Banerjee
Solar Phys. **296**, Article number: 25 **2021**
https://arxiv.org/pdf/2101.01941.pdf
https://link.springer.com/content/pdf/10.1007/s11207-021-01767-8.pdf
The rotational profile of the Sun is considered to be one of the key inputs in a solar dynamo model. Hence, precise and long-term measurements of this quantity is important for our understanding of solar magnetism and its variability. In this study, we use the newly digitized, white light sunspot data (1923 -- 2011) from Kodaikanal Solar Observatory (KoSO) to derive the solar rotation profile. An automated correlation based sunspot tracking algorithm is implemented to measure the rotation parameters, A, the equatorial rotation rate and B, the latitudinal gradient. Our measurements of $A=14.381\pm0.004$ and $B=-2.72\pm0.04$ compare well with previous studies. In our analysis, we find that the bigger sunspots (with area >400~μHem) rotate slower than the smaller ones. At the same time, we do not find any variation in the rotation rates between activity extremes, i.e solar maxima and minima. Lastly, we employ our tracking algorithm on the Michelson Doppler Imager (MDI) data and compare the MDI results with our KoSO values.

Magnetic field dependence of bipolar magnetic region tilts on the Sun: Indication of tilt quenching

Bibhuti Kumar **Jha**, Bidya Binay Karak, Sudip Mandal, Dipankar Banerjee
ApJL **889** L19 **2020**
https://arxiv.org/pdf/1912.13223.pdf
https://doi.org/10.3847/2041-8213/ab665c
The tilt of bipolar magnetic region (BMR) is crucial in the Babcock--Leighton process for the generation of the poloidal magnetic field in Sun. Based on the thin flux tube model of the BMR formation, the tilt is believed to be caused by the Coriolis force acting on the rising flux tube of the strong toroidal magnetic field from the base of the convection zone (BCZ). We analyze the magnetic field dependence of BMR tilts using the magnetograms of Michelson Doppler Imager (MDI) (1996-2011) and Helioseismic and Magnetic Imager (HMI) (2010-2018). We observe that the distribution of the maximum magnetic field (Bmax) of BMRs is bimodal. Its first peak at the low field corresponds to BMRs which do not have sunspots as counterparts in the white light images, whereas the second peak corresponds to sunspots as recorded in both types of images. We find that the slope of Joy's law ($\gamma 0$) initially increases slowly with the increase of Bmax. However, when $Bmax \gtrsim 2$ kG, $\gamma 0$ decreases. Scatter of BMR tilt around Joy's law systematically decreases with the increase of Bmax. The decrease of observed $\gamma 0$ with Bmax provides a hint to a nonlinear tilt quenching in the Babcock--Leighton process. We finally discuss how our results may be used to make a connection with the thin flux tube model.
HMI Science Nuggets, #159, **2021** http://hmi.stanford.edu/hminuggets/?p=3574

Magneto-acoustic oscillations observed in a solar plage region

Haisheng **Ji**, Parida Hashim, Zhenxiang Hong, Zhe Xu, Jinhua Shen, Kaifan Ji, Wenda Cao
Research in Astronomy and Astrophysics **2021**
https://arxiv.org/pdf/2101.11998.pdf
We gave an extensive study for the quasi-periodic perturbations on the time profiles of the line of sight (LOS) magnetic field in 10x10 sub-areas in a solar plage region (corresponds to a facula on the photosphere). The perturbations are found to be associated with enhancement of He I 10830 A absorption in a moss region, which is connected to loops with million-degree plasma. FFT analysis to the perturbations gives a kind of spectrum similar to that of Doppler velocity: a number of discrete periods around 5 minutes. The amplitudes of the magnetic perturbations are found to be proportional to magnetic field strength over these sub-areas. In addition, magnetic

perturbations lag behind a quarter of cycle in phase with respect to the p-mode Doppler velocity. We show that the relationships can be well explained with an MHD solution for the magneto-acoustic oscillations in high-\b{eta} plasma. Observational analysis also shows that, for the two regions with the stronger and weaker magnetic field, the perturbations are always anti-phased. All findings show that the magnetic perturbations are actually magneto-acoustic oscillations on the solar surface, the photosphere, powered by p-mode oscillations. The findings may provide a new diagnostic tool for exploring the relationship between magneto-acoustic oscillations and the heating of solar upper atmosphere, as well as their role in helioseismology.

Forecast of solar proton flux profiles for well-connected events†

Eun-Young **Ji**1, Yong-Jae Moon2,* and Jinhye Park
JGR, **201**4
http://onlinelibrary.wiley.com/doi/10.1002/2014JA020333/pdf
We have developed a forecast model of solar proton flux profiles (>10 MeV channel) for well-connected events. Among 136 solar proton events (SPEs) from 1986 to 2006, we select **49 well-connected ones** that are all associated with single X-ray flares stronger than M1 class and start to increase within four hours after their X-ray peak times. These events show rapid increments in proton flux. By comparing several empirical functions, we select a modified Weibull curve function to approximate a SPE flux profile, which is not far from the particle injection rate. The parameters (peak flux, rise time, and decay time) of this function are determined by the relationship between X-ray flare parameters (peak flux, impulsive time, and emission measure) and SPE parameters. For 49 well-connected SPEs, the linear correlation coefficient between the predicted and the observed proton peak fluxes is 0.65 with the RMS error of 0.55 log10(pfu). In addition, we determine another forecast model based on flare and CME parameters using 22 SPEs. The used CME parameters are linear speed and angular width. As a result, we find that the linear correlation coefficient between the predicted and the observed proton peak fluxes is 0.83 with the RMS error of 0.35 log10(pfu). From the relationship between error of model and CME acceleration, we find that CME acceleration is an important factor for predicting proton flux profiles. **Table**

Solar Image Restoration with the Cycle-GAN Based on Multi-Fractal Properties of Texture Features

Peng **Jia**, Yi Huang, Bojun Cai, Dongmei Cai
ApJL **881** L30 **2019**
https://arxiv.org/pdf/1907.12192.pdf
Texture is one of the most obvious characteristics in solar images and it is normally described by texture features. Because textures from solar images of the same wavelength are similar, we assume texture features of solar images are multi-fractals. Based on this assumption, we propose a pure data-based image restoration method: with several high resolution solar images as references, we use the Cycle-Consistent Adversarial Network to restore burred images of the same steady physical process, in the same wavelength obtained by the same telescope. We test our method with simulated and real observation data and find that our method can improve the spatial resolution of solar images, without loss of any frames. Because our method does not need paired training set or additional instruments, it can be used as a post-processing method for solar images obtained by either seeing limited telescopes or telescopes with ground layer adaptive optic system.

Multi-fluid Model of a Sun-grazing Comet in the Rapidly Ionizing, Magnetized Low Corona

Y.-D. **Jia**1, C. T. Russell1, W. Liu2, and Y. S. Shou
2014 ApJ 796 42
Two Sun-grazing comets were recently imaged in the low solar corona by space telescopes in unprecedented detail, revealing a wide range of new phenomena. This sparked growing interest in the interaction of comets with the coronal plasma and magnetic field and their diagnostic potential as solar probes. However, interpretation of such rich observational data requires profound understanding of relevant physical processes in an unexplored regime. Here advanced numerical modeling can provide critical clues. To this end, we present a prototype, multi-fluid, magnetohydrodynamic model of a steady-state comet in the low solar corona. These simulation results are compared with previously modeled comets in the solar wind environment. By inspecting their projection and column densities, we find a dominance of O6 + ions in the cometary tail, which can explain the observed extreme ultraviolet emission. The tail is found to be comparable to recent EUV images of these comets. In addition, the comet tail appears wider when the observer's line of sight is perpendicular rather than parallel to the local magnetic field. This is opposite to the trend in the interplanetary space permeated in the solar wind, because the ratio between dynamic pressure and magnetic pressure is an order of magnitude smaller than at 1 AU. On the other hand, we find that iron ions in the comet head build up to a density comparable to that of oxygen ions, but are unlikely to form a visible tail because of the shorter mean free paths of the neutrals.

Free Energy Sources in Current Sheets Formed in Collisionless Plasma Turbulence

Neeraj **Jain**1, Jörg Büchner1,4, Horia Comişel2, and Uwe Motschmann3,5
2021 ApJ 919 103
https://doi.org/10.3847/1538-4357/ac106c
Collisionless dissipation of macroscopic energy into heat is an unsolved problem of space and astrophysical plasmas, e.g., solar wind and Earth's magnetosheath. The most viable process under consideration is the turbulent cascade of macroscopic energy to kinetic scales where collisionless plasma processes dissipate the energy. Space observations and numerical simulations show the formation of kinetic scale current sheets in turbulent plasmas. Instabilities in these current sheets (CS) can provide collisionless dissipation and influence the turbulence. Spatial gradients of physical quantities and non-Maxwellian velocity distribution functions provide the free energy sources for CS plasma instabilities. To determine the free energy sources provided by the spatial gradients of plasma density and electron/ion bulk velocities in CS formed in collisionless turbulent plasmas with an external magnetic field B0, we carried out two-dimensional particle-in-cell-hybrid simulations and interpret the results within the limitations of the simulation model. We found that ion-scale CS in a collisionless turbulent plasma are formed primarily by electron shear flows, i.e., electron bulk velocity inside CS is much larger than ion bulk velocity while the density variations through the CS are relatively small (<10%). The electron bulk velocity and, thus, the current density inside the sheets are directed mainly parallel to B0. The shear in the perpendicular electron and ion bulk velocities generates parallel electron and ion flow vorticities. Inside CS, parallel electron flow vorticity exceeds the parallel ion flow vorticity, changes sign around the CS centers, and peaks near the CS edges. An ion temperature anisotropy develops near CS during the CS formation. It has a positive correlation with the parallel ion and electron flow vorticities. Theoretical estimates support the simulation results.

A New Scenario of Solar Modulation Model during the Polarity Reversing

Jieteng **Jiang**1,2, Sujie Lin1,2, and Lili Yang1,2,3
2023 ApJ 957 72
https://iopscience.iop.org/article/10.3847/1538-4357/acf719/pdf
When entering the heliosphere, galactic cosmic rays (GCRs) will encounter the solar wind plasma, reducing their intensity. This solar modulation effect is strongly affected by the structure of the solar wind and the heliospheric magnetic field (HMF). To address the effect during the solar maximum of cycle 24, we study the solar modulation under a scenario in which the weights for $A = \pm 1$ are determined by the structure of HMF, and the traveling time of GCRs simulated by SOLARPROP is taken into account. We then fit the cosmic-ray proton data provided by AMS-02 and Voyager in the energy range 4 MeV–30 GeV, and confirm that the modulation time lag in this model is about 9 months, which is consistent with the previous studies. This model incorporates a more realistic description of the polarity reversing and provides a more reliable estimation of the solar modulation effect during the maximum activity period.

Comparison of physics-based prediction models of solar cycle 25 **Review**

Jie **Jiang**, Zebin Zhang, Kristóf Petrovay
JASTP **2022**
https://arxiv.org/pdf/2212.01158
Physics-based solar cycle predictions provide an effective way to verify our understanding of the solar cycle. Before the start of cycle 25, several physics-based solar cycle predictions were developed. These predictions use flux transport dynamo (FTD) models, surface flux transport (SFT) models, or a combination of the two kinds of models. The common physics behind these predictions is that the surface poloidal fields around cycle minimum dominate the subsequent cycle strength. In the review, we first give short introductions to SFT and FTD models. Then we compare 7 physics-based prediction models from 4 aspects, which are what the predictor is, how to get the predictor, how to use the predictor, and what to predict. Finally, we demonstrate the large effect of assimilated magnetograms on predictions by two SFT numerical tests. We suggest that uncertainties in both initial magnetograms and sunspot emergence should be included in such physics-based predictions because of their large effects on the results. In addition, in the review we put emphasis on what we can learn from different predictions, rather than an assessment of prediction results.

Tracing Hα Fibrils through Bayesian Deep Learning

Haodi **Jiang**1,2, Ju Jing1,3,4, Jiasheng Wang1,3,4, Chang Liu1,3,4, Qin Li1,3,4, Yan Xu1,3,4, Jason T. L. Wang1,2, and Haimin Wang1,3,4
2021 ApJS 256 20
https://doi.org/10.3847/1538-4365/ac14b7
We present a new deep-learning method, named FibrilNet, for tracing chromospheric fibrils in Hα images of solar observations. Our method consists of a data preprocessing component that prepares training data from a threshold-based tool, a deep-learning model implemented as a Bayesian convolutional neural network for probabilistic image segmentation with uncertainty quantification to predict fibrils, and a post-processing component containing a fibril-

fitting algorithm to determine fibril orientations. The FibrilNet tool is applied to high-resolution Hα images from an active region (AR 12665) collected by the 1.6 m Goode Solar Telescope (GST) equipped with high-order adaptive optics at the Big Bear Solar Observatory (BBSO). We quantitatively assess the FibrilNet tool, comparing its image segmentation algorithm and fibril-fitting algorithm with those employed by the threshold-based tool. Our experimental results and major findings are summarized as follows. First, the image segmentation results (i.e., the detected fibrils) of the two tools are quite similar, demonstrating the good learning capability of FibrilNet. Second, FibrilNet finds more accurate and smoother fibril orientation angles than the threshold-based tool. Third, FibrilNet is faster than the threshold-based tool and the uncertainty maps produced by FibrilNet not only provide a quantitative way to measure the confidence on each detected fibril, but also help identify fibril structures that are not detected by the threshold-based tool but are inferred through machine learning. Finally, we apply FibrilNet to full-disk Hα images from other solar observatories and additional high-resolution Hα images collected by BBSO/GST, demonstrating the tool's usability in diverse data sets.

MHD Modeling of Solar Coronal Magnetic Evolution Driven by Photospheric Flow

Chaowei **Jiang***, Xinkai Bian, Tingting Sun and Xueshang Feng

Front. Phys., May **2021** |

https://doi.org/10.3389/fphy.2021.646750

https://www.frontiersin.org/articles/10.3389/fphy.2021.646750/full

It is well-known that magnetic fields dominate the dynamics in the solar corona, and new generation of numerical modeling of the evolution of coronal magnetic fields, as featured with boundary conditions driven directly by observation data, are being developed. This paper describes a new approach of data-driven magnetohydrodynamic (MHD) simulation of solar active region (AR) magnetic field evolution, which is for the first time that a data-driven full-MHD model utilizes directly the photospheric velocity field from DAVE4VM. We constructed a well-established MHD equilibrium based on a single vector magnetogram by employing an MHD-relaxation approach with sufficiently small kinetic viscosity, and used this MHD equilibrium as the initial conditions for subsequent data-driven evolution. Then we derived the photospheric surface flows from a time series of observed magentograms based on the DAVE4VM method. The surface flows are finally inputted in time sequence to the bottom boundary of the MHD model to self-consistently update the magnetic field at every time step by solving directly the magnetic induction equation at the bottom boundary. We applied this data-driven model to study the magnetic field evolution of AR 12158 with SDO/HMI vector magnetograms. Our model reproduced a quasi-static stress of the field lines through mainly the rotational flow of the AR's leading sunspot, which makes the core field lines to form a coherent S shape consistent with the sigmoid structure as seen in the SDO/AIA images. The total magnetic energy obtained in the simulation matches closely the accumulated magnetic energy as calculated directly from the original vector magnetogram with the DAVE4VM derived flow field. Such a data-driven model will be used to study how the coronal field, as driven by the slow photospheric motions, reaches a unstable state and runs into eruptions. **2014 September 8**

Non-linear mechanisms that regulate the solar cycle amplitude

Jie **Jiang**

ApJ **900** 19 **2020**

https://arxiv.org/pdf/2007.07069.pdf

https://doi.org/10.3847/1538-4357/abaa4b

The solar magnetic activity cycle has an amplitude that varies within a wide, but limited range of values. This implies that there are non-linear mechanisms that prevent runaway solutions. The purpose of this paper is to propose the observable non-linear mechanisms in the framework of the Babcock-Leighton(BL)-type dynamo. Sunspot emergences show systematic properties that strong cycles tend to have higher mean latitudes and lower tilt angle coefficients. We use the surface flux transport model to investigate effects of the systematic properties on the expected final total dipolar moment, i.e. cancellation plus generation of dipole moment by a whole solar cycle. We demonstrate that the systematic change in latitude has similar nonlinear feedback on the solar cycle (latitudinal quenching) as tilt does (tilt quenching). Both forms of quenching lead to that the expected final total dipolar moment is enhanced for weak cycles and saturates to a nearly constant value for normal and strong cycles. This explains observed long-term solar cycle variability, e.g., the Gnevyshev-Ohl rule, which, in turn, justifies the non-linear mechanisms inherent in the BL-type dynamo. Our work paves the way for understanding magnetic cycles of cool stars, especially how the properties of stellar spots may determine their properties.

Predicting solar surface large-scale magnetic field of Cycle 24

Jie **Jiang** JinbinCaoa

Journal of Atmospheric and Solar-Terrestrial Physics Volume 176, September **2018**, Pages 34-41

http://sci-hub.tw/10.1016/j.jastp.2017.06.019

The Sun's surface field, especially the polar field, sets the boundary condition for the coronal and heliospheric magnetic fields, but also provides us insight into the dynamo process. The evolution of the polar fields

results from the emergence and subsequent evolution of magnetic flux through the solar surface. In this paper we use a Monte Carlo approach to investigate the evolution of the fields during the decay phase of cycle 24. Our simulations include the emergence of flux through the solar surface with statistical properties derived from previous cycles. The well-calibrated surface flux transport model is used to follow the evolution of the large-scale field. We find the polar field can be well reproduced one year in advance using the observed synoptic magnetograms as the initial condition. The temporary variation of the polar field measured by Wilcox Solar Observatory (WSO), e.g., the strong decrease of the south polar field during 2016–2017 which is not shown by SDO/HMI and NSO/SOLIS data usually is not well reproduced. We suggest observational effects, such as the effect of the large gradient of the magnetic field around the southern polar capand the low resolution of WSO might be responsible. The northern hemisphere polar field is predicted to increase during 2017. The southern polar field is predicted to be stable during 2017–2018. At the end of 2017, the magnetic field in two poles is predicted to be similar (although of opposite polarities). The expected value for the dipole moment around 2020 is 1.76 ±0.68 G and 2.11±0.69 G based on the initial conditions from SDO/HMI and NSO/SOLIS synoptic magnetograms, respectively. It is comparable to that observed one at the end of Cycle 23 (about 1.6G based on SOHO/MDI).

Predictability of the solar cycle over one cycle

Jie **Jiang**, Jing-Xiu Wang, Qi-Rong Jiao, Jin-Bin Cao

ApJ **863** 159 **2018**

https://arxiv.org/pdf/1807.01543.pdf

http://iopscience.iop.org/article/10.3847/1538-4357/aad197/pdf

The prediction of the strength of future solar cycles is of interest because of its practical significance for space weather and as a test of our theoretical understanding of the solar cycle. The Babcock-Leighton mechanism allows predictions by assimilating the observed magnetic field on the surface. But the emergence of sunspot groups has the random properties, which make it impossible to accurately predict the solar cycle and also strongly limit the scope of cycle predictions. Hence we develop the scheme to investigate the predictability of the solar cycle over one cycle. When a cycle has been ongoing for more than 3 years, the sunspot group emergence can be predicted along with its uncertainty during the rest time of the cycle. The method for doing this is to start by generating a set of random realizations which obey the statistical relations of the sunspot emergence. We then use a surface flux transport model to calculate the possible axial dipole moment evolutions. The correlation between the axial dipole moment at cycle minimum and the subsequent cycle strength and other empirical properties of solar cycles are used to predict the possible profiles of the subsequent cycle. We apply this scheme to predict the large-scale field evolution from 2018 to the end of cycle 25, whose maximum strength is expected to lie in the range from 93 to 155 with a probability of 95\%.

Predicting solar surface large-scale magnetic field of Cycle 24

Jie **Jiang**, Jinbin Cao

JASTP **2017**

https://arxiv.org/pdf/1707.00268.pdf

The Sun's surface field, especially the polar field, sets the boundary condition for the coronal and heliospheric magnetic fields, but also provides us insight into the dynamo process. The evolution of the polar fields results from the emergence and subsequent evolution of magnetic flux through the solar surface. In this paper we use a Monte Carlo approach to investigate the evolution of the fields during the decay phase of cycle 24. Our simulations include the emergence of flux through the solar surface with statistical properties derived from previous cycles. The well-calibrated surface flux transport model is used to follow the evolution of the large-scale field. We find the polar field can be well reproduced one year in advance using the observed synoptic magnetograms as the initial condition. The temporary variation of the polar field measured by Wilcox Solar Observatory (WSO), e.g., the strong decrease of the south polar field during 2016-2017 which is not shown by SDO/HMI and NSO/SOLIS data usually is not well reproduced. We suggest observational effects, such as the effect of the large gradient of the magnetic field around the southern polar cap and the low resolution of WSO might be responsible. The northern hemisphere polar field is predicted to increase during 2017. The southern polar field is predicted to be stable during 2017-2018. At the end of 2017, the magnetic field in two poles is predicted to be similar (although of opposite polarities). The expected value for the dipole moment around 2020 is 1.76±0.68 G and 2.11±0.69 G based on the initial conditions from SDO/HMI and NSO/SOLIS synoptic magnetograms, respectively. It is comparable to that observed one at the end of Cycle 23 (about 1.6G based on SOHO/MDI).

The cause of the weak solar cycle 24

Jie **Jiang**, Robert H. Cameron, Manfred Schuessler

ApJL **808** L28 **2015**

http://arxiv.org/pdf/1507.01764v1.pdf

The ongoing 11-year cycle of solar activity is considerably less vigorous than the three cycles before. It was preceded by a very deep activity minimum with a low polar magnetic flux, the source of the toroidal field responsible for solar magnetic activity in the subsequent cycle. Simulation of the evolution of the solar surface field shows that the weak polar fields and thus the weakness of the present cycle 24 are mainly caused by a number of bigger bipolar regions emerging at low latitudes with a `wrong' (i.e., opposite to the majority for this cycle) orientation of their magnetic polarities in the North-South direction, which impaired the growth of the polar field. These regions had a particularly strong effect since they emerged within ±10◦ latitude from the solar equator.
See **HMI Science Nugget #41**
http://hmi.stanford.edu/hminuggets/?p=1234

Magnetic Flux Transport at the Solar Surface **Review**

J. **Jiang**, D. H. Hathaway, R. H. Cameron, S. K. Solanki, L. Gizon, L. Upton
Space Sci. Rev., **2014**
http://arxiv.org/pdf/1408.3186v1.pdf
After emerging to the solar surface, the Sun's magnetic field displays a complex and intricate evolution. The evolution of the surface field is important for several reasons. One is that the surface field, and its dynamics, sets the boundary condition for the coronal and heliospheric magnetic fields. Another is that the surface evolution gives us insight into the dynamo process. In particular, it plays an essential role in the Babcock-Leighton model of the solar dynamo. Describing this evolution is the aim of the surface flux transport model. The model starts from the emergence of magnetic bipoles. Thereafter, the model is based on the induction equation and the fact that after emergence the magnetic field is observed to evolve as if it were purely radial. The induction equation then describes how the surface flows -- differential rotation, meridional circulation, granular, supergranular flows, and active region inflows -- determine the evolution of the field (now taken to be purely radial). In this paper, we review the modeling of the various processes that determine the evolution of the surface field. We restrict our attention to their role in the surface flux transport model. We also discuss the success of the model and some of the results that have been obtained using this model.

Sunspot tilt angles revisited: Dependence on the solar cycle strength

Qirong **Jiao**, Jie Jiang, Zi-Fan Wang
A&A 653, A27 **2021**
https://arxiv.org/pdf/2106.11615.pdf
https://www.aanda.org/articles/aa/pdf/2021/09/aa41215-21.pdf
https://doi.org/10.1051/0004-6361/202141215
The tilt angle of sunspot groups is crucial in the BL type dynamo. Some studies have shown that the tilt coefficient is anti-correlated with the cycle strength. If the anti-correlation exists, it will be shown to act as an effective nonlinearity of the BL-type dynamo to modulate the solar cycle. However, some studies have shown that the anti-correlation has no statistical significance. We aim to investigate the causes behind the controversial results of tilt angle studies and to establish whether the tilt coefficient is indeed anti-correlated with the cycle strength. We first analyzed the tilt angles from DPD. Based on the methods applied in previous studies, we took two criteria to select the data, along with the linear and square-root functions to describe Joy's law, and three methods to derive the tilt coefficients for cycles 21-24. This allowed us to evaluate different methods based on comparisons of the differences among the tilt coefficients and the tilt coefficient uncertainties. Then we utilized Monte Carlo experiments to verify the results. Finally, we extended these methods to analyze the separate hemispheric DPD data and the tilt angle data from Kodaikanal and Mount Wilson. The tilt angles exhibit an extremely wide scatter due to both the intrinsic mechanism for its generation and measurement errors, for instance, the unipolar regions included in data sets. Different methods to deal with the uncertainties are mainly responsible for the controversial character of the previous results. The linear fit to the tilt-latitude relation of sunspot groups with $\Delta s>2.5$ of a cycle carried out without binning the data can minimize the effect of the tilt scatter on the uncertainty of the tilt coefficient. Based on this method the tilt angle coefficient is anti-correlated with the cycle strength with strong statistical significance.

Magnetic outbreak associated with exploding granulations

Chunlan **Jin**, Guiping Zhou, Guiping Ruan, T. Baildon, Wenda Cao, Jingxiu Wang
ApJL **2022**
https://arxiv.org/pdf/2212.04149.pdf
Diagnosing the spatial-temporal pattern of magnetic flux on the Sun is vital for understanding the origin of solar magnetism and activity. Here, we report a new form of flux appearance, magnetic outbreak, using observations with an extremely high spatial resolution of 0.16 arcsec from the 1.6-m Goode Solar Telescope (GST) at the Big Bear Solar Observatory. Magnetic outbreak refers to an early growth of unipolar magnetic flux and its later explosion into fragments, in association with plasma upflow and exploding granulations; each individual fragment has flux of 1016-1017 Mx, moving apart with velocity of 0.5-2.2 km/s. The magnetic outbreak takes place in the hecto-Gauss

region of pore moats. In this study, we identify six events of magnetic outbreak during 6-hour observations over an approximate 40×40 arcsec2 field of view. The newly discovered magnetic outbreak might be the first evidence of the long-anticipated convective blowup. **25 August 2016**

Magnetic flux participation in solar surface magnetism during solar cycle 24

Chun-Lan **Jin**, Jing-Xiu Wang

Vol 19, No 5, 69 (**2019**)

This study aims at investigating surface magnetic flux participation among different types of magnetic features during solar cycle 24. State-of-the-art observations from SDO/HMI and Hinode/SOT are combined to form a unique database in the interval from April 2010 to October 2015. Unlike previous studies, the statistics presented in this paper are feature-detection-based. More than 20 million magnetic features with relatively large scale, such as sunspot/pore cases, and enhanced and quiet networks, are automatically detected and categorized from HMI observations, and the internetwork features are identified from SOT/SP observations. The total flux from these magnetic features reaches 5.9×1022 Mx during solar minimum and 2.4 × 1023 Mx in solar maximum. Flux occupation from the sunspot/pore region is 29% in solar maximum. Enhanced and quiet networks contribute 18% and 21% flux during the solar minimum, and 50% and 9% flux in the solar maximum respectively. The internetwork field contributes over 55% of flux in the solar minimum, and its flux contribution exceeds that of sunspot/pore features in the solar maximum. During the solar active condition, the sunspot field increases its area but maintains the flux density of about 150 G, while the enhanced network follows the sunspot number variation showing increasing flux density and area, but the quiet network displays decreasing area and somewhat increasing flux density of about 6%. The origin of the quiet network is not known exactly, but is suggestive of representing the interplay between mean-field and local dynamos. The source, magnitude and possible importance of 'hidden flux' are discussed in some detail.

Does the Variation of Solar Intra-network Horizontal Field Follow Sunspot Cycle?

C. L. **Jin** and J. X. Wang

2015 ApJ 807 70

The ubiquitousness of the solar inter-network horizontal magnetic field has been revealed by space-borne observations with high spatial resolution and polarization sensitivity. However, no consensus has been achieved on the origin of the horizontal field among solar physicists. For a better understanding, in this study, we analyze the cyclic variation of the inter-network horizontal field by using the spectro-polarimeter observations provided by the Solar Optical Telescope on board Hinode, covering the interval from 2008 April to 2015 February. The method of wavelength integration is adopted to achieve a high signal-to-noise ratio. It is found that from 2008 to 2015 the inter-network horizontal field does not vary when solar activity increases, and the average flux density of the inter-network horizontal field is 87 ± 1 G, In addition, the imbalance between horizontal and vertical fields also keeps invariant within the scope of deviation, i.e., 8.7 ± 0.5, from the solar minimum to maximum of solar cycle 24. This result confirms that the inter-network horizontal field is independent of the sunspot cycle. The revelation favors the idea that a local dynamo is creating and maintaining the solar inter-network horizontal field.

Variation of the solar magnetic flux spectrum during solar cycle 23†

C. L. **Jin**, J. X. Wang

E-print, Dec **2013**; JGR, Volume 119, Issue 1, pages 11–17, January **2014**

http://onlinelibrary.wiley.com/doi/10.1002/2013JA019291/pdf

By using the unique database of SOHO/MDI full disk magnetograms from 1996 September to 2011 January, covering the entire solar cycle 23, we analyze the time-variability of the solar magnetic flux spectrum and study the properties of extended minimum of cycle 23. We totally identify 11.5 million magnetic structures. It has been revealed that magnetic features with different magnetic fluxes exhibit different cycle behaviors. The magnetic features with flux larger than 4.0 × 1019 Mx, which cover solar active regions and strong network features, show exactly the same variation as sunspots; However, the remaining 82% magnetic features which cover the majority of network elements show anti-phase variation with sunspots. We select a criterion that the monthly sunspot number is less than 20 to represent the Sun's low activity status. Then we find the extended minimum of cycle 23 is characterized by the long duration of low activity status, but the magnitude of magnetic flux in this period is not lower than previous cycle. Both the duration of low activity status and the minimum activity level defined by minimum sunspot number show a century period approximately. The extended minimum of cycle 23 shows similarities with solar cycle 11, which preceded the mini-maxima in later solar cycles. This similarity is suggestive that the solar cycles following cycle 23 are likely to have low activity.

NONPOTENTIALITY OF CHROMOSPHERIC FIBRILS IN NOAA ACTIVE REGIONS 11092 AND 9661

Ju **Jing**1, Yuan Yuan1, Kevin Reardon2,3, Thomas Wiegelmann4, Yan Xu1, and Haimin Wang
2011 ApJ 739 67
http://iopscience.iop.org/article/10.1088/0004-637X/739/2/67/pdf
In this paper, we present a method to automatically segment chromospheric fibrils from Hα observations and further identify their orientation. We assume that chromospheric fibrils are aligned with the magnetic field. By comparing the orientation of the fibrils with the azimuth of the embedding chromospheric magnetic field extrapolated from a potential field model, the shear angle, a measure of nonpotentiality, along the fibrils is readily deduced. Following this approach, we make a quantitative assessment of the nonpotentiality of fibrils in two NOAA active regions (ARs): (1) the relatively simple AR 11092, observed with very high resolution by Interferometric Bidimensional Spectrometer, and (2) a β-γ-δ AR 9661, observed with median resolution by Big Bear Solar Observatory before and after an X1.6 flare.

Information Horizon of Solar Active Regions

Jay R. **Johnson**1, Simon Wing2, Carson O'ffill1, and Bishwa Neupane1
2023 ApJL 947 L8
https://iopscience.iop.org/article/10.3847/2041-8213/acc58e/pdf
Information theory is used to characterize the solar active region periodicities and memories from the Carrington map images 1974–2021. The active regions typically evolve and move from one map to the next. In order to track these active region structures in sequences of images, an innovative method based on information theory is developed. Image entropy provides a measure of the organization of structures in the images. The entropy can also be used as a filter to identify structures and partition the active regions, which are then registered for each image. The partitions are used to compute the mutual information and measure the information flow from the active regions from one image to the next. Finally, conditional mutual information is used to give a measure of the information flow from one image to another given the third image. The results suggest the following: (1) there is a long-term memory of two cycles or more; (2) the coherence time of the active regions is ∼2 yr; and (3) the average active region structure scale size carrying the most information is approximately 118 × 103–236 × 103 Mm2. The study has implications to the short- and long-term predictability of active regions and sunspots as well as the nature of flux transport at the Sun. Finally, our innovative method can be similarly applied to stellar data to determine the dynamics of the active regions of stars.

Solar Sail Propulsion by 2050 : An Enabling Capability for Heliophysics Missions

Les **Johnson**, Nathan Barnes, Matteo Ceriotti, Thomas Y. Chen, Artur Davoyan, Louis Friedman, Darren Garber, Roman Kezerashvili, Ken Kobayashi, Greg Matloff, Colin McInnes, Pat Mulligan, Grover Swartzlander, Slava G. Turyshev
Heliophysics 2050 White Paper **2023**
https://arxiv.org/ftp/arxiv/papers/2301/2301.01297.pdf
Solar sails enable missions to observe the solar environment from unique vantage points, such as sustained observations away from the Sun-Earth line; sub-L1 station keeping; high inclination solar orbits; Earth polar-sitting and polar-viewing observatories; fast transit missions to study heliosphere to interstellar medium transition, as well as missions of interest across a broad user community. Recent and planned demonstration missions make this technology ready for use on near-term science missions.

A fast multi-dimensional magnetohydrodynamic formulation of the transition region adaptive conduction (TRAC) method⋆

C. D. **Johnston**1,2,3, A. W. Hood1, I. De Moortel1,4, P. Pagano5,6 and T. A. Howson1
A&A 654, A2 (**2021**)
https://www.aanda.org/articles/aa/pdf/2021/10/aa40987-21.pdf
https://doi.org/10.1051/0004-6361/202140987
We have demonstrated that the transition region adaptive conduction (TRAC) method permits fast and accurate numerical solutions of the field-aligned hydrodynamic equations, successfully removing the influence of numerical resolution on the coronal density response to impulsive heating. This is achieved by adjusting the parallel thermal conductivity, radiative loss, and heating rates to broaden the transition region (TR), below a global cutoff temperature, so that the steep gradients are spatially resolved even when using coarse numerical grids. Implementing the original 1D formulation of TRAC in multi-dimensional magnetohydrodynamic (MHD) models would require tracing a large number of magnetic field lines at every time step in order to prescribe a global cutoff temperature to each field line. In this paper, we present a highly efficient formulation of the TRAC method for use in multi-dimensional MHD simulations, which does not rely on field line tracing. In the TR, adaptive local cutoff temperatures are used instead of global cutoff temperatures to broaden any unresolved parts of the atmosphere. These local cutoff temperatures are calculated using only local grid cell quantities, enabling the MHD extension of

TRAC to efficiently account for the magnetic field evolution, without tracing field lines. Consistent with analytical predictions, we show that this approach successfully preserves the properties of the original TRAC method. In particular, the total radiative losses and heating remain conserved under the MHD formulation. Results from 2D MHD simulations of impulsive heating in unsheared and sheared arcades of coronal loops are also presented. These simulations benchmark the MHD TRAC method against a series of 1D models and demonstrate the versatility and robustness of the method in multi-dimensional magnetic fields. We show, for the first time, that pressure differences, generated during the evaporation phase of impulsive heating events, can produce current layers that are significantly narrower than the transverse energy deposition.

Modelling the solar transition region using an adaptive conduction method

C. D. **Johnston**, P. J. Cargill, A. W. Hood, I. De Moortel, S. J. Bradshaw, A. C. Vaseekar
A&A 635, A168 **2020**
https://arxiv.org/pdf/2002.01887.pdf
https://doi.org/10.1051/0004-6361/201936979

In Johnston & Bradshaw (2019), we proposed that modelling the solar Transition Region with the use of an Adaptive Conduction method permits fast and accurate numerical solutions of the field-aligned hydrodynamic equations, capturing the corona/transition region enthalpy exchange when the corona undergoes impulsive heating. This approach, referred to as TRAC, eliminates the need for highly resolved numerical grids in the transition region (TR) and the commensurate very short time steps that are required for numerical stability. When employed with coarse spatial resolutions, typically achieved in multi-dimensional magnetohydrodynamic (MHD) codes, the errors at peak density are less than 5% and the computation time is three orders of magnitude faster than fully resolved field-aligned models. This paper presents further examples that demonstrate the versatility and robustness of the method over a range of heating events, including impulsive and quasi-steady footpoint heating. A detailed analytical assessment of the TRAC method is also presented showing that the approach works through all phases of an impulsive heating event because (i) the total radiative losses and (ii) the total heating when integrated over the TR are both preserved at all temperatures under the broadening modifications of the method. The results from the numerical simulations complement this conclusion.

A Fast and Accurate Method to Capture the Solar Corona/Transition Region Enthalpy Exchange

C. D. **Johnston**, S. J. Bradshaw
ApJL **873** L22 **2019**
https://arxiv.org/pdf/1903.01132.pdf
https://doi.org/10.3847/2041-8213/ab0c1f

The brightness of the emission from coronal loops in the solar atmosphere is strongly dependent on the temperature and density of the confined plasma. After a release of energy, these loops undergo a heating and upflow phase, followed by a cooling and downflow cycle. Throughout, there are significant variations in the properties of the coronal plasma. In particular, the increased coronal temperature leads to an excess downward heat flux that the transition region is unable to radiate. This generates an enthalpy flux from the transition region to the corona, increasing the coronal density. The enthalpy exchange is highly sensitive to the transition region resolution in numerical simulations. With a numerically under-resolved transition region, major errors occur in simulating the coronal density evolution and, thus, the predicted loop emission. This Letter presents a new method that addresses the difficulty of obtaining the correct interaction between the corona and corona/chromosphere interface. In the transition region, an adaptive thermal conduction approach is used that broadens any unresolved parts of the atmosphere. We show that this approach, referred to as TRAC, successfully removes the influence of numerical resolution on the coronal density response to heating while maintaining high levels of agreement with fully resolved models. When employed with coarse spatial resolutions, typically achieved in multi-dimensional MHD codes, the peak density errors are less than 3% and the computation time is three orders of magnitude faster than fully resolved field-aligned models. The advantages of using TRAC in field-aligned hydrodynamic and multi-dimensional magnetohydrodynamic simulations are discussed.

A new approach for modelling chromospheric evaporation in response to enhanced coronal heating: II Non-uniform heating

C. D. **Johnston**, A. W. Hood, P. J. Cargill, I. De Moortel
A&A **2017**
https://arxiv.org/pdf/1705.04054.pdf

We proposed that the use of an approximate \lq jump condition\rq\ at the solar transition region permits fast and accurate numerical solutions of the one dimensional hydrodynamic equations when the corona undergoes impulsive heating. In particular, it eliminates the need for the very short timesteps imposed by a highly resolved numerical

grid. This paper presents further examples of the applicability of the method for cases of non-uniform heating, in particular, nanoflare trains (uniform in space but non-uniform in time) and spatially localised impulsive heating, including at the loop apex and base of the transition region. In all cases the overall behaviour of the coronal density and temperature shows good agreement with a fully resolved one dimensional model and is significantly better than the equivalent results from a 1D code run without using the jump condition but with the same coarse grid. A detailed assessment of the errors introduced by the jump condition is presented showing that the causes of discrepancy with the fully resolved code are (i) the neglect of the terms corresponding to the rate of change of total energy in the unresolved atmsophere, (ii) mass motions at the base of the transition region and (iii) for some cases with footpoint heating, an over-estimation of the radiative losses in the transition region.

A new approach for modelling chromospheric evaporation in response to enhanced coronal heating
I. The method

C. D. **Johnston**1, A. W. Hood1, P. J. Cargill1, 2 and I. De Moortel1
A&A 597, A81 (**2017**)
We present a new computational approach that addresses the difficulty of obtaining the correct interaction between the solar corona and the transition region, in response to rapid heating events. In the coupled corona, transition region, and chromosphere system, an enhanced downward conductive flux results in an upflow (chromospheric evaporation). However, obtaining the correct upflow generally requires high spatial resolution in order to resolve the transition region. With an unresolved transition region, artificially low coronal densities are obtained because the downward heat flux "jumps" across the unresolved region to the chromosphere, underestimating the upflows. Here, we treat the lower transition region as a discontinuity that responds to changing coronal conditions through the imposition of a jump condition that is derived from an integrated form of energy conservation. To illustrate and benchmark this approach against a fully resolved one-dimensional model, we present field-aligned simulations of coronal loops in response to a range of impulsive (spatially uniform) heating events. We show that our approach leads to a significant improvement in the coronal density evolution than just when using coarse spatial resolutions insufficient to resolve the lower transition region. Our approach compensates for the jumping of the heat flux by imposing a velocity correction that ensures that the energy from the heat flux goes into driving the transition region dynamics, rather than being lost through radiation. Hence, it is possible to obtain improved coronal densities. The advantages of using this approach in both one-dimensional hydrodynamic and three-dimensional magnetohydrodynamic simulations are discussed.

Recent U.S. policy developments designed to address the effects of geomagnetically induced currents (GICs)

Seth **Jonas** and Eoin D. McCarron
SWQuarterly Volume 13, Issue 1, **2016**
http://onlinelibrary.wiley.com/doi/10.1002/SWQv13i001/epdf

The Science of Sungrazers, Sunskirters, and Other Near-Sun Comets **Review**

Geraint H. **Jones**, Matthew M. Knight, Karl Battams, …
Space Science Reviews February **2018**, 214:20
https://link.springer.com/content/pdf/10.1007%2Fs11214-017-0446-5.pdf
This review addresses our current understanding of comets that venture close to the Sun, and are hence exposed to much more extreme conditions than comets that are typically studied from Earth. The extreme solar heating and plasma environments that these objects encounter change many aspects of their behaviour, thus yielding valuable information on both the comets themselves that complements other data we have on primitive solar system bodies, as well as on the near-solar environment which they traverse. We propose clear definitions for these comets: We use the term near-Sun comets to encompass all objects that pass sunward of the perihelion distance of planet Mercury (0.307 AU). Sunskirters are defined as objects that pass within 33 solar radii of the Sun's centre, equal to half of Mercury's perihelion distance, and the commonly-used phrase sungrazers to be objects that reach perihelion within 3.45 solar radii, i.e. the fluid Roche limit. Finally, comets with orbits that intersect the solar photosphere are termed sundivers. We summarize past studies of these objects, as well as the instruments and facilities used to study them, including space-based platforms that have led to a recent revolution in the quantity and quality of relevant observations. Relevant comet populations are described, including the Kreutz, Marsden, Kracht, and Meyer groups, near-Sun asteroids, and a brief discussion of their origins. The importance of light curves and the clues they provide on cometary composition are emphasized, together with what information has been gleaned about nucleus parameters, including the sizes and masses of objects and their families, and their tensile strengths. The physical processes occurring at these objects are considered in some detail, including the disruption of nuclei, sublimation, and ionisation, and we consider the mass, momentum, and energy loss of comets in the corona and those that

venture to lower altitudes. The different components of comae and tails are described, including dust, neutral and ionised gases, their chemical reactions, and their contributions to the near-Sun environment. Comet-solar wind interactions are discussed, including the use of comets as probes of solar wind and coronal conditions in their vicinities. We address the relevance of work on comets near the Sun to similar objects orbiting other stars, and conclude with a discussion of future directions for the field and the planned ground- and space-based facilities that will allow us to address those science topics.

Christian Horrebow's Sunspot Observations -- I. Life and Published Writings

Carsten Sønderskov **Jørgensen**, Christoffer Karoff, V. Senthamizh Pavai, Rainer Arlt
Solar Phys. **2019**
https://arxiv.org/pdf/1906.10884.pdf
Between 1761 and 1776, Christian Horrebow made regular observations of sunspots from Rundetaarn in Copenhagen. Based on these observations he writes in 1775 that "it appears that after the course of a certain number of years, the appearance of the Sun repeats itself with respect to the number and size of the spots". Thus, Horrebow hypothesized the idea of a cyclic Sun several decades before Heinrich Schwabe discovered the solar cycle and estimated its period. This proves the ability of Horrebow as a sunspot observer. In this article, we present a general overview of the work of Christian Horrebow, including a brief biography and a complete bibliography. We also present a translation from Danish to English of his writings on sunspots in the Dansk Historisk Almanak. These writings include tables of daily sunspot measurements of which we discuss the completeness.

A Semi-Analytical Computation of the Theoretical Uncertainties of the Solar Neutrino Flux

Andreas Christ Sølvsten **Jørgensen**, Jørgen Christensen-Dalsgaard
MNRAS **2018**
https://arxiv.org/pdf/1808.09153.pdf
We present a comparison between Monte Carlo simulations and a semi-analytical approach that reproduces the theoretical probability distribution functions of the solar neutrino fluxes, stemming from the pp, pep, hep, 7Be, 8B, 13N, 15O, and 17F source reactions. We obtain good agreement between the two approaches. Thus, the semi-analytical method yields confidence intervals that closely match those found, based on Monte Carlo simulations, and points towards the same general symmetries of the investigated probability distribution functions. Furthermore, the negligible computational cost of this method is a clear advantage over Monte Carlo simulations, making it trivial to take new observational constraints on the input parameters into account.

Properties of ubiquitous magnetic reconnection events in the lower solar atmosphere

Jayant **Joshi**, Luc H. M. Rouppe van der Voort
A&A 664, A72 **2022**
https://arxiv.org/pdf/2203.08172.pdf
https://www.aanda.org/articles/aa/pdf/2022/08/aa43051-22.pdf
Magnetic reconnection in the deep solar atmosphere can give rise to enhanced emission in the Balmer hydrogen lines, a phenomenon referred to as Ellerman bombs. Recent high quality Hβ observations indicate that Ellerman bombs are more common than previously thought and it was estimated that at any time about half a million Ellerman bombs are present in the quiet Sun. We performed an extensive statistical characterization of the quiet Sun Ellerman bombs (QSEBs) in these new Hβ observations. We analyzed a 1 h dataset of quiet Sun observed with the Swedish 1-m Solar Telescope that consists of spectral imaging in the Hβ and Hα lines, as well as spectropolarimetric imaging in Fe I 617.3 nm. We detected a total of 2809 QSEBs. The lifetime varies between 9 s and 20.5 min with a median of 1.14 min. The maximum area ranges between 0.0016 and 0.2603 Mm2 with a median of 0.018 Mm2. A subset (14%) of the QSEBs display enhancement of the Hβ line core. On average, the line core brightening appears 0.88 min after the onset of brightening in the wings, and the distance between these brightenings is 243 km. This gives rise to an apparent propagation speed ranging between −14.3 and +23.5 km s−1, with an average that is upward propagating at +4.4 km −1. The average orientation is nearly parallel to the limbward direction. QSEBs are nearly uniformly distributed over the field of view but we find empty areas with the size of mesogranulation. QSEBs are located more frequent near the magnetic network where they are often bigger, longer lived and brighter. We conclude that QSEBs are ubiquitous in quiet Sun and appear everywhere except in areas of mesogranular size with weakest magnetic field (BLOS≲50~G). Our observations support the interpretation of reconnection along vertically extended current sheets. **6 June 2019.**

Signatures of ubiquitous magnetic reconnection in the lower solar atmosphere⋆

Jayant **Joshi**1,2, Luc H. M. Rouppe van der Voort1,2 and Jaime de la Cruz Rodríguez3
A&A 641, L5 (**2020**)
https://www.aanda.org/articles/aa/pdf/2020/09/aa38769-20.pdf

https://arxiv.org/pdf/2006.14975.pdf
Ellerman Bomb-like brightenings of the hydrogen Balmer line wings in the quiet Sun, also known as quiet Sun Ellerman bombs (QSEBs), are a signature of the fundamental process of magnetic reconnection at the smallest observable scale in the lower solar atmosphere. We analyze high spatial resolution observations (0.″1) obtained with the Swedish 1-m Solar Telescope to explore signatures of QSEBs in the Hβ line. We find that QSEBs are ubiquitous and uniformly distributed throughout the quiet Sun, predominantly occurring in intergranular lanes. We find up to 120 QSEBs in the field of view for a single moment in time; this is more than an order of magnitude higher than the number of QSEBs found in earlier Hα observations. This suggests that about half a million QSEBs could be present in the lower solar atmosphere at any given time. The QSEB brightenings found in the Hβ line wings also persist in the line core with a temporal delay and spatial offset toward the nearest solar limb. Our results suggest that QSEBs emanate through magnetic reconnection along vertically extended current sheets in the lower solar atmosphere. The apparent omnipresence of small-scale magnetic reconnection may play an important role in the energy balance of the solar chromosphere. **6 June 2019**

North-South Distribution and Asymmetry of GOES SXR Flares during Solar Cycle 24

Anita **Joshi**, Ramesh Chandra
Open Astron. 28, 228-235 (**2019**)
https://arxiv.org/ftp/arxiv/papers/2007/2007.06998.pdf
Here we present the results of the study of the north-south (N-S) distribution and asymmetry of GOES soft X-ray (SXR) flares during solar cycle 24. The period of study includes ascending, maximum and descending phases of the cycle. During the cycle double-peaked (2011, 2014) solar maximum has occurred. The cycle peak in the year 2011 is due to B-class flares excess activity in the northern hemisphere (NH) whereas C and M class flares excess activity in the southern hemisphere (SH) supported the second peak of the cycle in 2014. The data analysis shows that the SXR flares are more pronounced in 11 to 20 degree latitudes for each hemisphere. Cumulative values of SXR flare count show northern excess during the ascending phase of the cycle. However, in the descending phase of the cycle, southern excess occurred. In the cycle a significant SH dominated asymmetry exists. Near the maximum of the cycle, the asymmetry enhances pronouncedly and reverses in sign.

Evolutionary aspects and north-south asymmetry of soft X-ray flare index during solar cycles 21, 22, and 23

B. **Joshi**1,3, R. Bhattacharyya1, K. K. Pandey2, U. Kushwaha1 and Yong-Jae Moon
A&A 582, A4 (**2015**) (**2017**)
https://arxiv.org/pdf/1705.02107.pdf
Aims. In this paper, we investigate the temporal evolution and north–south (N–S) asymmetry in the occurrence of solar flares during cycle 21, 22, and 23, and compare the results with traditional solar activity indices.
Methods. The flare activity is characterized by a soft X-ray (SXR) flare index, which incorporates information about flare occurrences during a selected interval along with the peak intensity of individual events.
Results. The SXR flare index correlates well with other conventional parameters of solar activity. Further, it exhibits a significantly higher correlation with sunspot area over sunspot number, which suggests the variations in sunspot area to be more closely linked with the transient energy release in the solar corona. The cumulative plots of the flare index indicate a slight excess of activity in the northern hemisphere during cycle 21, while a southern excess clearly prevails for cycles 22 and 23. The study reveals a significant N–S asymmetry, which exhibits variations with the phases of solar cycle. The reliability and persistency of this asymmetry significantly increases when the data is averaged over longer periods, while an optimal level is achieved when data is binned for 13 Carrington rotations. The time evolution of the flare index further confirms evolution of dual peaks in solar cycles during the solar maxima and violation of Gnevyshev-Ohl rule for the pair of solar cycles 22 and 23.
Conclusions. The SXR flare index in the northern and the southern hemispheres of the Sun exhibits significant asymmetry during the evolutionary phases of the solar cycle, which implies that N–S asymmetry of solar flares is manifested in terms of the flare counts as well as the intensity of flare events.

Energetic characterisation and statistics of solar coronal brightenings

Vincent **Joulin**, Éric Buchlin, Jacques Solomon, Chloé Guennou
A&A 591, A148 **2016**
http://arxiv.org/pdf/1605.02780v1.pdf
To explain the high temperature of the corona, much attention has been paid to the distribution of energy in dissipation events. Indeed, if the event energy distribution is steep enough, the smallest, unobservable events could be the largest contributors to the total energy dissipation in the corona. Previous observations have shown a wide distribution of energies but remain inconclusive about the precise slope. Furthermore, these results rely on a very crude estimate of the energy. On the other hand, more detailed spectroscopic studies of structures such as coronal bright points do not provide enough statistical information to derive their total contribution to heating. We aim at getting a better estimate of the distributions of the energy dissipated in coronal heating events using high-resolution,

multi-channel Extreme Ultra-Violet (EUV) data. To estimate the energies corresponding to heating events and deduce their distribution, we detect brightenings in five EUV channels of the Atmospheric Imaging Assembly (AIA) on-board the Solar Dynamics Observatory (SDO). We combine the results of these detections and we use maps of temperature and emission measure derived from the same observations to compute the energies. We obtain distributions of areas, durations, intensities, and energies (thermal, radiative, and conductive) of events. These distributions are power-laws, and we find also power-law correlations between event parameters. The energy distributions indicate that the energy from a population of events like the ones we detect represents a small contribution to the total coronal heating, even when extrapolating to smaller scales. The main explanations for this are how heating events can be extracted from observational data, and the incomplete knowledge of the thermal structure and processes in the coronal plasma attainable from available observations.

Interactions of twisted Ω-loops in a model solar convection zone

L. **Jouve**, A.S. Brun, G. Aulanier
ApJ **857** 83 2018
https://arxiv.org/pdf/1803.04709.pdf
http://sci-hub.tw/http://iopscience.iop.org/0004-637X/857/2/83/
This study aims at investigating the ability of strong interactions between magnetic field concentrations during their rise through the convection zone to produce complex active regions at the solar surface. To do so, we perform numerical simulations of buoyant magnetic structures evolving and interacting in a model solar convection zone. We first produce a 3D model of rotating convection and then introduce idealized magnetic structures close to the bottom of the computational domain. These structures possess a certain degree of field line twist and they are made buoyant on a particular extension in longitude. The resulting twisted Ω-loops will thus evolve inside a spherical convective shell possessing large-scale mean flows. We present results on the interaction between two such loops with various initial parameters (mainly buoyancy and twist) and on the complexity of the emerging magnetic field. In agreement with analytical predictions, we find that if the loops are introduced with opposite handedness and same axial field direction or same handedness but opposite axial field, they bounce against each other. The emerging region is then constituted of two separated bipolar structures. On the contrary, if the loops are introduced with the same direction of axial and peripheral magnetic fields and if sufficiently close, they merge while rising. This more interesting case produces complex magnetic structures, with a high degree of non-neutralized currents, especially when the convective motions act significantly on the magnetic field. This indicates that those interactions could be good candidates to produce eruptive events like flares or CMEs.

Reflection Properties of Gravito-MHD Waves in an Inhomogeneous Horizontal Magnetic Field

G. **Jovanović**
Solar Phys. Volume 289, Issue 11, pp 4085-4104 **2014**
We derive the dispersion equation for gravito-magnetohydrodynamical (MHD) waves in an isothermal, gravitationally stratified plasma with a horizontal inhomogeneous magnetic field. Sound and Alfvén speeds are constant. Under these conditions, it is possible to derive analytically the equations for gravito-MHD waves. The high values of the viscous and magnetic Reynolds numbers in the solar atmosphere imply that the dissipative terms in the MHD equations are negligible, except in layers around the positions where the frequency of the MHD wave equals the local Alfvén or slow wave frequency. Outside these layers the MHD waves are accurately described by the equations of ideal MHD.
We consider waves that propagate energy upward in the atmosphere. For the plane boundary, z=0, between two isothermal plasma regions with horizontal but different magnetic fields, we discuss the boundary conditions and derive the equations for the reflection and transmission coefficients.
In the simpler case of a gravitationally stratified plasma without magnetic field, these coefficients describe the reflection and transmission properties of gravito-acoustic waves.

Magnetic fields beneath active region coronal loops

Philip **Judge**, Lucia Kleint, Christoph Kuckein
ApJ **2024**
https://arxiv.org/pdf/2405.05391
We examine the hypothesis that multipolar magnetic fields advected by photospheric granules can contribute heating to the active chromosphere and corona. On **28 September 2020** the GRIS and HiFI+ instruments at the GREGOR telescope obtained data of NOAA 12773. We analyze Stokes profiles of spectral lines of Si I and He I, to study magnetic fields from photosphere to the upper chromosphere. Magnetogram and EUV data from the HMI and AIA instruments on the SDO spacecraft are co-aligned and studied in relation to the GRIS data. At coronal loop footpoints, minor polarity fields comprise just 0.2% and 0.02% of the flux measured over the 40" x 60" area observed in the photosphere and upper chromosphere, centered 320" from disk center. Significantly, the minority

fields are situated >~ 12" from bright footpoints. We use physical arguments to show that any unresolved minority flux cannot reach coronal footpoints adjacent to the upper chromosphere. Even if it did, the most optimistic estimate of the energy released through chromospheric reconnection is barely sufficient to account for the coronal energy losses. Further, dynamical changes accompanying reconnection between uni- and multi- polar fields are seen neither in the He I data nor in narrow-band movies of the H alpha line core. We conclude that the hypothesis must be rejected. Bright chromospheric, transition region and coronal loop plasmas must be heated by mechanisms involving unipolar fields.

Magnetic fields and plasma heating in the Sun's atmosphere

Philip **Judge**, Lucia Kleint, Roberto Casini, Alfred de Wijn, Tom Schad, Alexandra Tritschler
ApJ **2023**
https://arxiv.org/pdf/2311.01286.pdf

We use the first publically available data from the Daniel K. Inouye Solar Telescope (DKIST) to track magnetic connections from the solar photosphere into the corona. We scrutinize relationships between chromospheric magnetism and bright chromospheric, transition region and coronal plasmas. In June 2022, the Visible Spectro-Polarimeter (ViSP) instrument targeted unipolar network within a decaying active region. ViSP acquired rastered scans with longitudinal Zeeman sensitivities of 0.25 Mx/cm2 (Fe I 630.2 nm) and 0.5 Mx/cm2 (Ca II 854.2 nm). ViSP was operated in a "low" resolution mode (0.214" slit width, spectral resolution R ~ 70,000) to produce polarization maps over a common area of 105" x 50". Data from SDO and IRIS are combined to ask: Why is only a fraction of emerging flux filled with heated plasma? What is the elemental nature of the plasmas? No correlations were found between heated plasma and properties of chromospheric magnetic fields derived from the WFA, on scales below supergranules. Processes hidden from our observations control plasma heating. While improved magnetic measurements are needed, these data indicate that "the corona is a self-regulating forced system" (Einaudi et al. 2021). Heating depends on the state of the corona, not simply on boundary conditions. Heating models based upon identifiable bipolar fields, including cool loops, tectonics and observable magnetic reconnection, are refuted for these regions with unipolar chromospheric magnetic fields. **2-3 Jun 2022**

Steadiness of coronal heating

Philip G. **Judge**
ApJ 957 25 **2023**
https://arxiv.org/pdf/2309.05164.pdf
https://iopscience.iop.org/article/10.3847/1538-4357/acf83a/pdf

The EUI instrument on the Solar Orbiter spacecraft has obtained the most stable, high-resolution images of the solar corona from its orbit with a perihelion near 0.4 AU. A sequence of 360 images obtained at 17.1 nm, between **25-Oct-2022** 19:00 and 19:30 UT is scrutinized. One image pixel corresponds to 148 km at the solar surface. The widely-held belief that the outer atmosphere of the Sun is in a continuous state of magnetic turmoil is pitted against the EUI data. The observed plasma variations appear to fall into two classes. By far the dominant behavior is a very low amplitude variation in brightness (1%) in the coronal loops, with larger variations in some footpoint regions. No hints of observable changes in magnetic topology are associated with such small variations. The larger amplitude, more rapid, rarer and less-well organized changes are associated with flux emergence. It is suggested therefore that while magnetic reconnection drives the latter, most of the active corona is heated with no evidence of a role for large-scale (observable) reconnection. Since most coronal emission line widths are subsonic, the bulk of coronal heating, if driven by reconnection, can only be of tangentially discontinuous magnetic fields, with angles below about $0.5c_S/c_A \sim 0.3\beta$, with β the plasma beta parameter (~ 0.01), and c_S and c_A sound and Alfvén speeds. If heated by multiple small flare-like events, then these must be $\lesssim 10^{21}$ erg, i.e. pico-flares. But processes other than reconnection have yet to be ruled out, such as viscous dissipation, which may contribute to the steady heating of coronal loops over active regions.
SO Nuggets #22 **2023** https://www.cosmos.esa.int/web/solar-orbiter/-/science-nugget-eui-data-reveal-a-steady-mode-of-coronal-heating

The enduring mystery of the solar corona **Review**

Philip G. **Judge**
Physics World, Volume 34, Issue 9, pp.38-42 **2021**
https://arxiv.org/ftp/arxiv/papers/2211/2211.17098.pdf

Physicists have long known that the Sun's magnetic fields make its corona much hotter than the surface of the star itself. But how -- and why -- those fields transport and deposit their energy is still a mystery, as Philip G Judge explains

Magnetic Connections across the Chromosphere–Corona Transition Region

Philip **Judge**1

2021 ApJ 914 70
https://doi.org/10.3847/1538-4357/abf8ad
The plasma contributing to emission from the Sun between the cool chromosphere (≤104 K) and hot corona (≥106 K) has been subjected to many different interpretations. Here we look at the magnetic structure of this transition region (TR) plasma, based upon the implications of CLASP2 data of an active region recently published by Ishikawa et al., and earlier Interface Region Imaging Spectrograph (IRIS) and Solar Dynamics Observatory (SDO) data of quiet regions. Ishikawa et al. found that large areas of sunspot plages are magnetically unipolar as measured in the cores of Mg ii resonance lines, formed in the lower TR under low plasma-β conditions. Here we show that IRIS images in the line cores have fibrils that are well aligned with the overlying coronal loop segments seen in the 171 Å channel of SDO. When the TR emission in active regions arises from plasma magnetically and thermally connected to the corona, then the line cores can provide the first credible magnetic boundary conditions for force-free calculations extended to the corona. We also re-examine IRIS images of dynamic TR cool loops previously reported as a major contributor to TR emission from the quiet Sun. Dynamic cool loops contribute only a small fraction of the total TR emission from the quiet Sun.

On single-point inversions of magnetic dipole lines in the corona

Philip **Judge**, Roberto Casini, Alin Paraschiv
ApJ **2021**
https://arxiv.org/pdf/2103.03824
Prompted by a recent paper by Dima and Schad, we re-consider the problem of inferring magnetic properties of the corona using polarimetric observations of magnetic dipole (M1) lines. Dima and Schad point to a potential source of degeneracy in a formalism developed by Plowman, which under some circumstances can lead to the solution being under-determined. Here we clarify the nature of the problem. Its resolution lies in solving for the scattering geometry using the elongation of the observed region of the corona. We discuss some conceptual problems that arise when casting the problem for inversion in the observer's reference frame, and satisfactorily resolve difficulties identified by Plowman, Dima and Schad.

New light on an old problem of the cores of solar resonance lines

Philip **Judge**, Lucia Kleint, Jorrit Leenaarts, Andrii Sukhorukov, Jean-Claude Vial
ApJ **901** 32 **2020**
https://arxiv.org/pdf/2008.01250.pdf
https://iopscience.iop.org/article/10.3847/1538-4357/abadf4/pdf
We re-examine a 50+ year-old problem of deep central reversals predicted for strong solar spectral lines, in contrast to the smaller reversals seen in observations. We examine data and calculations for the resonance lines of H I, Mg II and Ca II, the self-reversed cores of which form in the upper chromosphere. Based on 3D simulations as well as data for the Mg II lines from IRIS, we argue that the resolution lies not in velocity fields on scales in either of the micro- or macro-turbulent limits. Macro-turbulence is ruled out using observations of optically thin lines formed in the upper chromosphere, and by showing that it would need to have unreasonably special properties to account for critical observations of the Mg II resonance lines from the IRIS mission. The power in turbulence in the upper chromosphere may therefore be substantially lower than earlier analyses have inferred. Instead, in 3D calculations horizontal radiative transfer produces smoother source functions, smoothing out intensity gradients in wavelength and in space. These effects increase in stronger lines. Our work will have consequences for understanding the onset of the transition region, the energy in motions available for heating the corona, and for the interpretation of polarization data in terms of the Hanle effect applied to resonance line profiles.

Sun-like Stars Shed Light on Solar Climate Forcing

P. G. **Judge**1, R. Egeland1, and G. W. Henry2
2020 ApJ 891 96
https://doi.org/10.3847/1538-4357/ab72a9
Recently published precise stellar photometry of 72 Sun-like stars obtained at the Fairborn Observatory between 1993 and 2017 is used to set limits on the solar forcing of Earth's atmosphere of ±4.5 W m−2 since 1750. This compares with the +2.2 ± 1.1 W m−2 IPCC estimate for anthropogenic forcing. Three critical assumptions are made. In decreasing order of importance they are: (a) most of the brightness variations occur within the average time series length of ≈17 yr; (b) the Sun seen from the ecliptic behaves as an ensemble of middle-aged solar-like stars; and (c) narrowband photometry in the Strömgren b and y bands are linearly proportional to the total solar irradiance. Assumption (a) can best be relaxed and tested by obtaining more photometric data of Sun-like stars, especially those already observed. Eight stars with near-solar parameters have been observed from 1999, and two since 1993. Our work reveals the importance of continuing and expanding ground-based photometry, to complement expensive solar irradiance measurements from space.

Solar Eclipse Observations from the Ground and Air from 0.31 to 5.5 Microns

Philip **Judge**, Ben Berkey, Alyssa Boll, Paul Bryans, Joan Burkepile…
Solar Physics November **2019**, 294:166
https://link.springer.com/content/pdf/10.1007%2Fs11207-019-1550-3.pdf
We present spectra and broad-band polarized light data from a novel suite of instruments deployed during the 21st August 2017 total solar eclipse. Our goals were to survey solar spectra at thermal infrared wavelengths during eclipse, and to test new technology for measuring polarized coronal light. An infrared coronal imaging spectrometer, flown at 14.3 km altitude above Kentucky, was supported on the ground by observations from Madras, Oregon (elevation 683 m) and Camp Wyoba on Casper Mountain, Wyoming (2402 m). In Wyoming we deployed a new infrared Fourier Transform Spectrometer (FTS), three low-dispersion spectrometers loaned to us by Avantes, a novel visible-light camera PolarCam, sensitive to linear polarization, and one of two infrared cameras from FLIR Systems, the other operated at Madras. Circumstances of eclipse demanded that the observations spanned 17:19 to 18:26 UT. We analyze spectra of the limb photosphere, the chromosphere, prominences, and coronal lines from 310 nm to 5.5 μm. We calibrated data photometrically using the solar disk as a source. Between different spectrometers, the calibrations were consistent to better than 13%. But the sensitivities achieved were insufficient to detect coronal lines from the ground. The PolarCam data are in remarkable agreement with polarization data from the K-Cor synoptic instrument on Mauna Loa, and with FLIR intensity data acquired in Madras. We discuss new results, including a detection of the He i 1083 nm multiplet in emission during the whole of totality. The combination of the FTS and AIR-Spec spectra reveals for the first time the effects of the telluric extinction on the infrared coronal emission lines, to be observed with upcoming Daniel K. Inouye Solar Telescope.

High-cadence Visible and Infrared Spectra of the Sun during Eclipse

P. **Judge**1, S. Tomczyk1, J. Hannigan2, and S. Sewell1
Astrophysical Journal, 877:10 (11pp), **2019**
https://iopscience.iop.org/article/10.3847/1538-4357/ab0e04/pdf
We study novel spectra from 310 nm to 5.5 μm obtained during the **2017 August 21** eclipse. Four spectrometers were deployed at Camp Wyoba (altitude 2402 m) on Casper Mountain, WY. Three low-resolution ($\mathcal{R} \lesssim 1000$) Avantes spectrometers obtained useful spectra from 310 nm to 2.3 μm, at cadences from 8 to 500 ms. To maximize photometric precision, these instruments were fed with optical fibers placed in the pupil planes of two small (D = 5 cm) telescopes, thereby integrating all light from the field of view. We also acquired higher-resolution ($\mathcal{R} \approx 30000$) spectra with a new infrared Fourier Transform Spectrometer, fed by a Sun-tracking heliostat, at a 2.5 s cadence. We calibrate the fluxes using counts obtained during partial eclipse, with known limb-darkened photospheric intensities. Fluxes of chromospheric lines, including Ca ii H, K, and Hα, obtained near third contact, were measured every 20 ms, a sampling in height above the limb of 5.6 km. The behavior found corresponds to that found in traditional (image-plane) flash spectra. Two unknown chromospheric emission lines are noted. Based upon our measurements and earlier calculations, we propose new eclipse experiments to uncover clues to the origin and structure of spicules.

UV spectra, bombs, and the solar atmosphere

Philip G. **Judge**
ApJ **808** 116 **2015**
http://arxiv.org/pdf/1506.08336v1.pdf
A recent analysis of UV data from the Interface Region Imaging Spectrograph {\em IRIS} reports plasma "bombs" with temperatures near \hot{} within the solar photosphere. This is a curious result, firstly because most bomb plasma pressures p (the largest reported case exceeds 103 dyn~cm−2) fall well below photospheric pressures (>7×103), and secondly, UV radiation cannot easily escape from the photosphere. In the present paper the {\em IRIS} data is independently analyzed. I find that the bombs arise from plasma originally at pressures between $\lta80$ and 800 dyne~cm−2 before explosion, i.e. between $\lta850$ and 550 km above τ500=1. This places the phenomenon's origin in the low-mid chromosphere or above. I suggest that bomb spectra are more compatible with Alfv\'enic turbulence than with bi-directional reconnection jets.

Photon Mean Free Paths, Scattering, and Ever-Increasing Telescope Resolution

P. G. **Judge**, L. Kleint, H. Uitenbroek, M. Rempel, Y. Suematsu, S. Tsuneta
Solar Phys. **2015**
We revisit an old question: what are the effects of observing stratified atmospheres on scales below a photon mean free path λ? The mean free path of photons emerging from the solar photosphere and chromosphere is ≈ 102 km. Using current 1 m-class telescopes, λ is on the order of the angular resolution. But the Daniel K. Inoue Solar Telescope will have a diffraction limit of 0.020″ near the atmospheric cutoff at 310 nm, corresponding to 14 km at the solar surface. Even a small amount of scattering in the source function leads to physical smearing due to this solar “fog”, with effects similar to a degradation of the telescope point spread function. We discuss a unified picture that depends simply on the nature and amount of scattering in the source function. Scalings are derived from which the scattering in the solar atmosphere can be transcribed into an effective Strehl ratio, a quantity useful to observers.

Observations in both permitted (e.g., Fe i630.2 nm) and forbidden (Fe i 525.0 nm) lines will shed light on both instrumental performance as well as on small-scale structures in the solar atmosphere.

EVIDENCE FOR SHEET-LIKE ELEMENTARY STRUCTURES IN THE SUN'S ATMOSPHERE?

Philip G. **Judge**1,3, Kevin Reardon2, and Gianna Cauzzi
2012 ApJ 755 L11

Narrow, thread-like structures in the Sun's chromosphere are currently understood to be plasma guided along narrow tubes of magnetic flux. We report on 1 s cadence imaging spectroscopic measurements of the Hα line with the IBIS Fabry-Pérot instrument at the Dunn Solar Telescope, obtained +0.11 nm from line center. Rapid changes grossly exceeding the Alfvén speed are commonly seen along the full extent of many chromospheric threads. We argue that only an optical superposition effect can reasonably explain the data, analogous to striations of curtains blowing in the wind. Otherexplanations appear to require significant contrivances to avoid contradicting various aspects of the data. We infer that the absorbing plasma exists in two-dimensional sheet-like structures within the three-dimensional magnetofluid, related perhaps to magnetic tangential discontinuities. This interpretation demands a re-evaluation of basic assumptions about low-β solar plasmas, as advocated by Parker, with broader implications in astrophysics and plasma physics. Diverse, high-cadence observations are needed to further define the relationship between magnetic field and thermal fine structure.

Recent advancements in the EST project

Jan **Jurcak**, Manuel Collados, Jorrit Leenaarts, Michiel van Noort, Rolf Schlichenmaier
Advances in Space Research Volume 63, Issue 4, 15 February **2019**, Pages 1389-1395
https://arxiv.org/pdf/1811.00851.pdf

The European Solar Telescope (EST) is a project of a new-generation solar telescope. It has a large aperture of 4~m, which is necessary for achieving high spatial and temporal resolution. The high polarimetric sensitivity of the EST will allow to measure the magnetic field in the solar atmosphere with unprecedented precision. Here, we summarise the recent advancements in the realisation of the EST project regarding the hardware development and the refinement of the science requirements.

Comparison of theoretical and observed Ca~{\sc ii}~8542 Stokes profiles in quiet regions at the centre of the solar disc

Jan **Jurcak**, Jiri Stepan, Javier Trujillo Bueno, Michele Bianda
A&A 619, A60 **2018**
https://arxiv.org/pdf/1808.09470.pdf

Interpreting the Stokes profiles observed in quiet regions of the solar chromosphere is a challenging task. The Stokes Q and U profiles are dominated by the scattering polarisation and the Hanle effect, and these processes can only be correctly quantified if 3D radiative transfer effects are taken into account. Forward-modelling of the intensity and polarisation of spectral lines using a 3D model atmosphere is a suitable approach in order to statistically compare the theoretical and observed line profiles. Our aim is to present novel observations of the Ca 8542 line profiles in a quiet region at the centre of the solar disc and to quantitatively compare them with the theoretical Stokes profiles. We aim at estimating the reliability of the 3D model atmosphere using not only the line intensity but the full vector of Stokes parameters. We used data obtained with the ZIMPOL instrument at the IRSOL and compared the observations with the theoretical profiles computed with the PORTA radiative transfer code, using as solar model atmosphere a 3D snapshot taken from a radiation-magnetohydrodynamics simulation. The synthetic profiles were degraded to match the instrument and observing conditions. The degraded theoretical profiles of the Ca 8542 line are qualitatively similar to the observed ones. We confirm that there is a fundamental difference in the widths of all Stokes profiles: the observed lines are wider than the theoretical lines. We find that the amplitudes of the observed profiles are larger than those of the theoretical ones, which suggests that the symmetry breaking effects in the solar chromosphere are stronger than in the model atmosphere. This means that the isosurfaces of temperature, velocity, and magnetic field strength and orientation are more corrugated in the solar chromosphere than in the currently available 3D radiation-magnetohydrodynamics simulation. **September 2, 2015**

A relationship between the solar rotation and activity in the period 1998–2006 analysed by tracing small bright coronal structures in SOHO-EIT images

R. **Jurdana-Šepić**1, R. Brajša2, H. Wöhl3, A. Hanslmeier4, I. Poljančić1, L. Svalgaard5 and S. F. Gissot
A&A 534, A17 (**2011**)

Aims. The study aims to find a relationship between the rotation of the small bright coronal structures (SBCS) described by the solar rotation parameters and indices of solar activity on monthly and yearly temporal scales. Methods. We analyse precise measurements of the solar differential rotation determined by tracing SBCS in SOHO-EIT images and compare the derived solar rotation parameters with the status of solar activity in the period 1998 − 2006. Full-disc solar images obtained with the Extreme ultraviolet Imaging Telescope (EIT) on board the Solar and

Heliospheric Observatory (SOHO) were used to analyse solar differential rotation determined by tracing SBCS. An automatic method to identify and track the SBCS in EIT full-disc images with a six hour cadence is applied. We performed a statistical analysis of the monthly and yearly values of solar sidereal rotation velocity parameters A and B (corresponding to the equatorial rotation velocity and the gradient of the solar differential rotation, respectively) as a function of various solar activity indices.
Results. The dependence of the solar rotation on the phase of the solar cycle was found. It is clearly visible for the solar rotation parameter A, whilst the results are not conclusive for parameter B. The relationship between the solar rotation and activity, expressed by the monthly relative sunspot number, the smoothed monthly relative sunspot number, the yearly relative sunspot number, and the interdiurnal variability (IDV) index was investigated. The statistically significant correlation was found for the solar rotation parameter A, whilst a very low and insignificant correlation was obtained for the rotation parameter B.
Conclusions. Dring the maximum of the solar cycle 23 and just after it, the equatorial solar rotation velocity was lower than in other phases of the cycle, when there was less activity. This is consistent with other observational findings, obtained by different tracers and methods.

The Role of the Magnetorotational Instability in the Sun

Daniel **Kagan** and J. Craig Wheeler
2014 ApJ 787 21
http://arxiv.org/pdf/1407.4654v1.pdf
We calculate growth rates for nonaxisymmetric instabilities including the magnetorotational instability (MRI) throughout the Sun. We first derive a dispersion relation for nonaxisymmetric instability including the effects of shear, convective buoyancy, and three diffusivities (thermal conductivity, resistivity, and viscosity). We then use a solar model evolved with the stellar evolution code MESA and angular velocity profiles determined by Global Oscillations Network Group helioseismology to determine the unstable modes present at each location in the Sun and the associated growth rates. The overall instability has unstable modes throughout the convection zone and also slightly below it at middle and high latitudes. It contains three classes of modes: large-scale hydrodynamic convective modes, large-scale hydrodynamic shear modes, and small-scale magnetohydrodynamic shear modes, which may be properly called MRI modes. While large-scale convective modes are the most rapidly growing modes in most of the convective zone, MRI modes are important in both stably stratified and convectively unstable locations near the tachocline at colatitudes $\theta < 53°$. Nonaxisymmetric MRI modes grow faster than the corresponding axisymmetric modes; for some poloidal magnetic fields, the nonaxisymmetric MRI growth rates are similar to the angular rotation frequency Ω, while axisymmetric modes are stabilized. We briefly discuss the saturation of the field produced by MRI modes, finding that the implied field at the base of the convective zone in the Sun is comparable to that derived based on dynamos active in the tachocline and that the saturation of field resulting from the MRI may be of importance even in the upper convection zone.

The magnetic drivers of campfires seen by the Polarimetric and Helioseismic Imager (PHI) on Solar Orbiter

F. **Kahil** (1), J. Hirzberger (1), S.K. Solanki (1 and 10), L. P. Chitta (1), H. Peter (1), F. Auchère (3), +++
A&A 660, A143 **2022**
https://arxiv.org/pdf/2202.13859.pdf
https://doi.org/10.1051/0004-6361/202142873
https://www.aanda.org/articles/aa/pdf/2022/04/aa42873-21.pdf
The Extreme Ultraviolet Imager (EUI) on board the Solar Orbiter (SO) spacecraft observed small extreme ultraviolet (EUV) bursts, termed campfires, that have been proposed to be brightenings near the apexes of low-lying loops in the quiet-Sun atmosphere. The underlying magnetic processes driving these campfires are not understood. During the cruise phase of SO and at a distance of 0.523\,AU from the Sun, the Polarimetric and Helioseismic Imager on Solar Orbiter (SO/PHI) observed a quiet-Sun region jointly with SO/EUI, offering the possibility to investigate the surface magnetic field dynamics underlying campfires at a spatial resolution of about 380~km.
In 71\% of the 38 isolated events, campfires are confined between bipolar magnetic features, which seem to exhibit signatures of magnetic flux cancellation. The flux cancellation occurs either between the two main footpoints, or between one of the footpoints of the loop housing the campfire and a nearby opposite polarity patch. In one particularly clear-cut case, we detected the emergence of a small-scale magnetic loop in the internetwork followed soon afterwards by a campfire brightening adjacent to the location of the linear polarisation signal in the photosphere, that is to say near where the apex of the emerging loop lays. The rest of the events were observed over small scattered magnetic features, which could not be identified as magnetic footpoints of the campfire hosting loops. The majority of campfires could be driven by magnetic reconnection triggered at the footpoints, similar to the physical processes occurring in the burst-like EUV events discussed in the literature. About a quarter of all analysed campfires, however, are not associated to such magnetic activity in the photosphere, which implies that other heating mechanisms are energising these small-scale EUV brightenings. **February 23, 2021,**

Brightness Contrast of Solar Magnetic Elements Observed by Sunrise Thesis

Fatima **Kahil**

Thesis **2019**

https://arxiv.org/pdf/2109.00057

The irradiance of the Sun is modulated on all time scales. Small-scale solar magnetic elements composed of quiet-Sun network and active region plages contribute to this modulation on solar cycle time scales. The evaluation of their contrast as a function of their magnetic field strength is an important constraint for models of solar irradiance variation. In this thesis, we improve and extend the results of earlier contrast studies taking advantage of the high resolution data delivered by the balloon-borne solar observatory Sunrise during its science flights in 2009 and 2013. In addition to the high quality of the Sunrise data, access to the UV wavelengths makes these data unique in this kind of study. In the first two parts of this thesis, we find that the contrast variation with the magnetic field strength agrees qualitatively with radiative magnetohydrodynamic simulations of the quiet Sun. In particular, at a continuum wavelength around 500\,nm, the contrast does not decrease at large field strengths, indicative of having resolved these features. In addition, the contrast at all wavelengths in the quiet-Sun network is found to be higher than in solar plage, and the difference decreases with atmospheric height in accordance with empirical models of flux tubes. In the last part of this thesis, we make use of solar limb data observed by Sunrise to evaluate the contribution of stray light to the total point spread function of the telescope.

Intensity contrast of solar plage as a function of magnetic flux at high spatial resolution

F. **Kahil**1, T. L. Riethmüller1 and S. K. Solanki

A&A 621, A78 (**2019**)

sci-hub.tw/10.1051/0004-6361/201833722

Magnetic elements have an intensity contrast that depends on the type of region they are located in (for example quiet Sun, or active region plage). Observed values also depend on the spatial resolution of the data. Here we investigate the contrast-magnetic field dependence in active region plage observed near disk center with SUNRISE during its second flight in 2013. The wavelengths under study range from the visible at 525 nm to the near ultraviolet (NUV) at 300 nm and 397 nm. We use quasi-simultaneous spectropolarimetric and photometric data from the Imaging Magnetograph eXperiment (IMaX) and the Sunrise Filter Imager (SuFI), respectively. We find that in all wavelength bands, the contrast exhibits a qualitatively similar dependence on the line-of-sight magnetic field, BLOS, as found in the quiet Sun, with the exception of the continuum at 525 nm. There, the contrast of plage magnetic elements peaks for intermediate values of BLOS and decreases at higher field strengths. By comparison, the contrast of magnetic elements in the quiet Sun saturates at its maximum value at large BLOS. We find that the explanation of the turnover in contrast in terms of the effect of finite spatial resolution of the data is incorrect with the evidence provided by the high-spatial resolution SUNRISE data, as the plage magnetic elements are larger than the quiet Sun magnetic elements and are well-resolved. The turnover comes from the fact that the core pixels of these larger magnetic elements are darker than the quiet Sun. We find that plages reach lower contrast than the quiet Sun at disk center at wavelength bands formed deep in the photosphere, such as the visible continuum and the 300 nm band. This difference decreases with formation height and disappears in the Ca II H core, in agreement with empirical models of magnetic element atmospheres.

Brightness of Solar Magnetic Elements as a Function of Magnetic Flux at High Spatial Resolution

F. **Kahil**, T. L. Riethmüller, S. K. Solanki

2017

https://arxiv.org/pdf/1701.00759v1.pdf

We investigate the relationship between the photospheric magnetic field of small-scale magnetic elements in the quiet Sun (QS) at disc centre, and the brightness at 214 nm, 300 nm, 313 nm, 388 nm, 397 nm, and at 525.02 nm. To this end we analysed spectropolarimetric and imaging time series acquired simultaneously by the IMaX magnetograph and the SuFI filter imager on-board the balloon-borne observatory Sunrise during its first science flight in 2009, with high spatial and temporal resolution.

We find a clear dependence of the contrast in the near ultraviolet (NUV) and the visible on the line-of-sight component of the magnetic field, BLOS, which is best described by a logarithmic model. This function represents well the relationship between the Ca II H-line emission and BLOS, and works better than a power-law fit adopted by previous studies. This, along with the high contrast reached at these wavelengths, will help with determining the contribution of small-scale elements in the QS to the irradiance changes for wavelengths below 388 nm. At all wavelengths including the continuum at 525.40 nm the intensity contrast does not decrease with increasing BLOS. This result also strongly supports that Sunrise has resolved small strong magnetic field elements in the internetwork, resulting in constant contrasts for large magnetic fields in our continuum contrast at 525.40 nm s. BLOS scatterplot, unlike the turnover obtained in previous observational studies. This turnover is due to the intermixing of the bright magnetic features with the dark intergranular lanes surrounding them. **2009 June 9**

Validating the proton prediction system (PPS)

S.W. **Kahler,** E.W. Cliver, A.G. Ling

Journal of Atmospheric and Solar-Terrestrial Physics 69 (**2007**) 43–49, **File**

The proton prediction system (PPS) is a program developed at the Air Force Research Laboratory (AFRL) to predict solar energetic Ep>5 MeV proton (SEP) intensities at 1AU following solar flares. It is based on average observed SEP intensity-time profiles, peak intensities, and event durations. The input parameters are solar flare peak or time-integrated X-ra or radio fluxes and their times of onsets and maxima, and solar flare locations. We do a limited validation of the PPS using 78 GOES solar X-ray flares of peak intensity XM5 with well associated Ha flare locations. Predicted peak proton intensities Jp>10 MeV and event onset and rise times are compared with SEP events observed by GOES. We also select all GOES >10MeV SEP events above 10 proton flux units (pfu) during the same time period to compare with those predicted by the PPS. With our M5 X-ray flare threshold the PPS yields approximately equal numbers of correct predictions, false predictions, and missed 10-pfu SEP events.

A reconnection driven magnetic flux cancellation and a quiet Sun Ellerman bomb

Anjali. J. **Kaithakkal**, J. M. Borrero, A. Pastor Yabar, J. de la Cruz Rodríguez

MNRAS Volume 521, Issue 3, May 2023, Pages 3882–3897,

https://doi.org/10.1093/mnras/stad759

https://arxiv.org/pdf/2303.06331.pdf

The focus of this investigation is to quantify the conversion of magnetic to thermal energy initiated by a quiet Sun cancellation event and to explore the resulting dynamics from the interaction of the opposite polarity magnetic features. We used imaging spectroscopy in the Hα line, along with spectropolarimetry in the \ion{Fe}{I} 6173~Å and \ion{Ca}{II} 8542~Å lines from the Swedish Solar Telescope (SST) to study a reconnection-related cancellation and the appearance of a quiet Sun Ellerman bomb (QSEB). We observed, for the first time, QSEB signature in both the wings and core of the \ion{Fe}{I} 6173~Å line. We also found that, at times, the \ion{Fe}{I} line-core intensity reaches higher values than the quiet Sun continuum intensity. From FIRTEZ-dz inversions of the Stokes profiles in \ion{Fe}{I} and \ion{Ca}{II} lines, we found enhanced temperature, with respect to the quiet Sun values, at the photospheric (logτc = -1.5; ∼1000 K) and lower chromospheric heights (logτc = -4.5; ∼360 K). From the calculation of total magnetic energy and thermal energy within these two layers it was confirmed that the magnetic energy released during the flux cancellation can support heating in the aforesaid height range. Further, the temperature stratification maps enabled us to identify cumulative effects of successive reconnection on temperature pattern, including recurring temperature enhancements. Similarly, Doppler velocity stratification maps revealed impacts on plasma flow pattern, such as a sudden change in the flow direction. **2019 April 24**

Evolution of Stokes V area asymmetry related to a quiet Sun cancelation observed with GRIS/IFU

Anjali. J. **Kaithakkal**, J. M. Borrero, C. E. Fischer, C. Dominguez-Tagle, M. Collados

A&A 634, A131 **2020**

https://arxiv.org/pdf/2001.05465.pdf

A quiet Sun magnetic flux cancelation event at the disk centre was recorded using the Integral Field Unit (IFU) mounted on the GREGOR Infrared Spectrograph (GRIS). GRIS sampled the event in the photospheric Si I 10827 Å spectral line. The cancelation is preceded by a significant rise in line core intensity and excitation temperature, which is inferred from Stokes inversions under local thermodynamic equilibrium (LTE). The opposite polarity features seem to undergo reconnection above the photosphere. We also found that the border pixels neighboring the polarity inversion line of one of the polarities exhibit a systematic variation of area asymmetry. Area asymmetry peaks right after the line core intensity enhancement and gradually declines thereafter. Analyzing Stokes profiles recorded from either side of the polarity inversion line could therefore potentially provide additional information on the reconnection process related to magnetic flux cancelation. Further analysis without assuming LTE will be required to fully characterize this event. **2018 November 02**

Randomness in Sunspot Number: A Clue to Predict Solar Cycle 25

Bharati **Kakad**, Raj Kumar & Amar Kakad

Solar Physics volume 295, Article number: 88 (**2020**)

https://link.springer.com/content/pdf/10.1007/s11207-020-01655-7.pdf

Forecasting of solar activity is extremely important, due to its impact on our space-based technology. In recent years, we have observed a continuous decline in the peak sunspot number for Solar Cycles (SCs) 21 to 24. We are more curious about peak activity of SC 25 because if the solar activity weakens further, then it may be an indication of new extended minima. So far, the daily sunspot-number data make up the longest observational series of the solar activity available, and recently this has been replaced with the corrected new Version 2.0 sunspot-number series. In general, different prediction models are available to forecast the peak smoothed sunspot number (SSN) of the upcoming SC but they are based on the older Version 1.0 sunspot data. Therefore, it is necessary to check the

applicability of earlier proposed models to predict the peak SSN using the Version 2.0 sunspot-number series. Here, we re-evaluate one such earlier proposed prediction model, which is based on the estimates of the Shannon entropy, a measure of randomness, for Version 2.0 sunspot data. We find that this prediction model is applicable to the Version 2.0 sunspot-number series. To verify the robustness of the prediction model, we used the histogram and additionally the kernel density estimator (KDE) method to calculate the probability distribution function (PDF). The estimate of the PDF is a prerequisite to compute the Shannon entropy. We found that the prediction model is robust and the correlation coefficients between model parameters are 0.93 and 0.92, respectively, for these two approaches. This exercise provides a new prediction model for the peak SSN based on the Version 2.0 sunspot-number series. The model forecasts the peak smoothed sunspot number of 136.9±24136.9±24 using a histogram-derived PDF and 150.7±25150.7±25 using a KDE-derived PDF for the upcoming SC 25. These predictions for SC 25 are more reliable as up to date (December 2020) sunspot-number data have been utilized to get the entropy in the end phase of SC 24. It suggests that SC 25 would be similar or slightly stronger than SC 24.

Diminishing activity of recent solar cycles (22–24) and their impact on geospace

Bharati **Kakad**, Amar Kakad, Durbha Sai Ramesh and Gurbax S. Lakhina
J. Space Weather Space Clim. **2019**, 9, A01
https://www.swsc-journal.org/articles/swsc/pdf/2019/01/swsc180016.pdf
sci-hub.se/10.1051/swsc/2018048
This study examines the variation of different energies linked with the Sun and the Earth's magnetosphere-ionosphere systems for solar cycles (SCs) 22–24 for which the gradual decrease in the solar activity is noticed. Firstly, we investigated the variation of solar magnetic energy density (SMED) for SCs 21–24 and its relation to the solar activity. We observed distinct double peak structures in SMED for the past four SCs, 21–24. This feature is consistent with noticeable asymmetry in their two peaks. For SCs 22–24 a significant decrease is observed in the integrated SMED of each SC. This reduction is 37% from SCs 22 to 23 and 51% from SCs 23 to 24, which indicates substantial weakening of Sun's magnetic field for SC 24. Also, the magnetic, kinetic, and thermal energy densities at the Earth's bow-shock nose are found to be considerably low for the SC 24. We examined the solar wind Alfven speed, magnetosonic Mach number, solar wind-magnetosphere energy coupling parameter (ε), and the Chapman-Ferraro magnetopause distance (LCF) for the SCs 22–24. The estimated maximum stand-off magnetopause distance is larger for SC 24 (LCF ≤ 10.6 RE) as compared to SC 23 (LCF ≤ 10.2 RE) and SC 22 (LCF ≤ 9.8 RE). The solar wind Alfven speeds during SCs 22 and 23 are in the same range and do not exceed ≈73 km/s whereas, it is below 57 km/s for SC 24. A lower bound of solar wind magnetosonic Mach number for SC 24 is larger (M ≥ 6.9) as compared to SC 22 (M ≥ 5.9) and SC 23 (M ≥ 6). We noticed weakening in the energy coupling parameter for SC 24, which resulted in substantial (15%–38%) decrease in average strength of high latitude ionospheric (AE), low latitude magnetospheric (Dst) and equatorial ionospheric (EEJ) current systems in comparison with SC 23. Subsequently, a reduction of ≈30% is manifested in the high latitude Joule heating for SC 24. Overall this study indicates the significant step down in various energies at Sun, Earth's bow-shock, and near Earth environment for current SC 24, which will have important implication on our Earth's atmosphere-ionosphere-magnetosphere system.

Prediction of the Length of Upcoming Solar Cycles

Bharati **Kakad**, Amar Kakad, Durbha Sai Ramesh
Solar Physics December **2017**, 292:181
https://link.springer.com/content/pdf/10.1007%2Fs11207-017-1207-z.pdf
The forecast of solar cycle (SC) characteristics is crucial particularly for several space-based missions. In the present study, we propose a new model for predicting the length of the SC. The model uses the information of the width of an autocorrelation function that is derived from the daily sunspot data for each SC. We tested the model on Versions 1 and 2 of the daily international sunspot number data for SCs 10 – 24. We found that the autocorrelation width AnwAwn of SC nn during the second half of its ascending phase correlates well with the modified length that is defined as Tn+2cy−TnaTcyn+2−Tan. Here Tn+2cyTcyn+2 and TnaTan are the length and ascent time of SCs n+2n+2 and nn, respectively. The estimated correlation coefficient between the model parameters is 0.93 (0.91) for Version 1 (Version 2) sunspot series. The standard errors in the observed and predicted lengths of the SCs for Version 1 and Version 2 data are 0.38 and 0.44 years, respectively. The advantage of the proposed model is that the predictions of the length of the upcoming two SCs (i.e., n+1n+1, n+2n+2) are readily available at the time of the peak of SC nn. The present model gives a forecast of 11.01, 10.52, and 11.91 years (11.01, 12.20, and 11.68 years) for the length of SCs 24, 25, and 26, respectively, for Version 1 (Version 2).

Shannon Entropy-Based Prediction of Solar Cycle 25

Bharati **Kakad**, Amar Kakad, Durbha Sai Ramesh
Solar Physics July **2017**, 292:95
A new model is proposed to forecast the peak sunspot activity of the upcoming solar cycle (SC) using Shannon entropy estimates related to the declining phase of the preceding SC. Daily and monthly smoothed international

sunspot numbers are used in the present study. The Shannon entropy is the measure of inherent randomness in the SC and is found to vary with the phase of an SC as it progresses. In this model each SC with length TcyTcy is divided into five equal parts of duration Tcy/5Tcy/5. Each part is considered as one phase, and they are sequentially termed P1, P2, P3, P4, and P5. The Shannon entropy estimates for each of these five phases are obtained for the nnth SC starting from n=10--23n=10--23. We find that the Shannon entropy during the ending phase (P5) of the nnth SC can be efficiently used to predict the peak smoothed sunspot number of the (n+1)(n+1)th SC, i.e.Sn+1maxSmaxn+1. The prediction equation derived in this study has a good correlation coefficient of 0.94. A noticeable decrease in entropy from 4.66 to 3.89 is encountered during P5 of SCs 22 to 23. The entropy value for P5 of the present SC 24 is not available as it has not yet ceased. However, if we assume that the fall in entropy continues for SC 24 at the same rate as that for SC 23, then we predict the peak smoothed sunspot number of 63±11.3 for SC 25. It is suggested that the upcoming SC 25 will be significantly weaker and comparable to the solar activity observed during the Dalton minimum in the past.

A new method for forecasting the solar cycle descent time

Bharati **Kakad***, Amar Kakad and Durbha Sai Ramesh
J. Space Weather Space Clim., 5, A29 (**2015**)
http://www.swsc-journal.org/articles/swsc/pdf/2015/01/swsc140052.pdf
The prediction of an extended solar minimum is extremely important because of the severity of its impact on the near-earth space. Here, we present a new method for predicting the descent time of the forthcoming solar cycle (SC); the method is based on the estimation of the Shannon entropy. We use the daily and monthly smoothed international sunspot number. For each nth SC, we compute the parameter [Tpre]n by using information on the descent and ascent times of then − 3th and nth SCs, respectively. We find that [Tpre] of nth SC and entropy can be effectively used to predict the descent time of the n + 2th SC. The correlation coefficient between [Td]n+2 − [Tpre]n and [E]n is found to be 0.95. Using these parameters the prediction model is developed. Solar magnetic field and F10.7 flux data are available for SCs 21–22 and 19–23, respectively, and they are also utilized to get estimates of the Shannon entropy. It is found that the Shannon entropy, a measure of randomness inherent in the SC, is reflected well in the various proxies of the solar activity (viz sunspot, magnetic field, F10.7 flux). The applicability and accuracy of the prediction model equation is verified by way of association of least entropy values with the Dalton minimum. The prediction model equation also provides possible criteria for the occurrence of unusually longer solar minima.

A Novel Technique for the Extraction of Dynamic Events in Extreme Ultraviolet Solar Images

Petra Kosová **Kalenská**1 , Pavel Rajmic2 , Karolína Gebrtová1 , and Miloslav Druckmüller1
Astrophysical Journal Supplement Series, 275:15 (10pp), **2024**
https://iopscience.iop.org/article/10.3847/1538-4365/ad8633/pdf
High-spatial-resolution images of the solar corona acquired in the extreme ultraviolet (EUV), most notably with the Atmospheric Imaging Assembly (AIA) instrument on the Solar Dynamics Observatory (SDO) reveal the abundance of dynamic events which range from flaring bright points and jets to erupting prominences and coronal mass ejections (CMEs). In this work we present novel techniques to extract such dynamic events from the more steady background corona using 17.1 nm SDO-AIA images. The techniques presented here treat any time series of coronal images as a matrix that can be decomposed into two matrices representing the background and the dynamic component, respectively. The latter has the properties of a so-called sparse matrix, and the proposed methods are classified as methods based on sparse representations. The proposed methods are the median-filter method, the principal component pursuit, and the dynamic-mode decomposition, all of which include data pre-processing using the noise-adaptive fuzzy equalization method. The study reveals that the median-filter method and the dynamicmode decomposition enhance all motions in the time series and produce similar results. On the other hand, the principal component pursuit enables the clear differentiation of CMEs from the background corona, thus providing a valuable tool for the characterization of their acceleration profiles in the low corona as seen in the EUV.

Resonances in Spherical Dynamos and Super-Flares

A. O. **Kalinin**, D. D. Sokoloff
Astronomy Reports October **2018**, Volume 62, Issue 10, pp 689–695
Astronomicheskii Zhurnal, 2018, Vol. 95, No. 10, pp. 728–734.
https://link.springer.com/content/pdf/10.1134%2FS1063772918100050.pdf
Stars similar to the Sun demonstrate super-flares, which are considerably more powerful than solar flares. It is believed that the magneticfield energies of these stars are much higher than that of the Sun. The present study attempts to explain such an anomalously high magnetic energy by resonance phenomena related to the stellar

dynamo, which involve significant changes in the behavior of the solutions subject to certain external effects and satisfy certain parametric relationships. These resonance phenomena are studied using low-mode models for a dynamo occurring in two or one spherical shells. It is shown that resonance effects arising in these models can result in increases of the magnetic energies by one and a half orders of magnitude compared with nonresonance cases. It is also shown that resonance dynamo conditions can differ considerably from the simple resonance conditions used for oscillating systems. This can probably be explained by the fact that the excitation and propagation of magnetic waves in dynamo problems are closely connected with each other, so that the resonance equations remain nonlinear even when they are maximally simplified.

On the description of the GCR intensity in the last three solar minima

M. S. **Kalinin**, G. A. Bazilevskaya, M. B. Krainev, A. K. Svirzhevskaya, N. S. Svirzhevsky
33-rd International Cosmic Ray Conference, Rio-de-Janeiro, Brasil, 2013
2014
http://arxiv.org/pdf/1411.7519v1.pdf
We discuss the main characteristic features in the heliospheric parameters important for the GCR intensity modulation for the last three solar minima (1986--1987, 1996--1997 and 2008--2009). The model for the GCR intensity modulation is considered and the set of the model parameters is chosen which allows the description of the observed GCR intensity distributions at the moments of the maximum GCR intensity in two solar minima (1987 and 1997) normal for the second half of the last century. Then we try to describe with the above model and set of parameters the unusually soft GCR energy spectra at the moments of the maximum GCR intensity in the last solar minimum between cycles 23 and 24 (2009). Our main conclusion is that the most simple way to do so is to reduce the size of the modulation region and, probably, change the rigidity dependence of the diffusion coefficient. The change of both parameters is substantiated by the observations of the solar wind and heliospheric magnetic field.

Predictions of solar activity cycles 25 and 26 using non-linear autoregressive exogenous neural networks

Mirkan Y **Kalkan**, Diaa E Fawzy, A Talat Saygac
MNRAS, Volume 523, Issue 1, July **2023**, Pages 1175–1181,
https://doi.org/10.1093/mnras/stad1460
This study presents new prediction models of the 11-yr solar activity cycles (SC) 25 and 26 based on multiple activity indicator parameters. The developed models are based on the use of non-linear autoregressive exogenous (NARX) neural network approach. The training period of the NARX model is from July 1749 to December 2019. The considered activity indicator parameters are the monthly sunspot number time series (SSN), the flare occurence frequency, the 10.7-cm solar radio flux, and the total solar irradiance (TSI). The neural network models are fed by these parameters independently and the prediction results are compared and verified. The obtained training, validation, and prediction results show that our models are accurate with an accuracy of about 90 per cent in the prediction of peak activity values. The current models produce the dual-peak maximum (Gnevyshev gap) very well. Based on the obtained results, the expected solar peaks in terms of SSN (monthly averaged smoothed) of the solar cycles 25 and 26 are RSSN = 116.6 (February 2025) and RSSN = 113.25 (October 2036), respectively. The expected time durations of SC 25 and SC 26 cycles are 9.2 and 11 yr, respectively. The activity levels of SC 25 and 26 are expected to be very close and similar to or weaker than SC 24. This suggests that these two cycles are at the minimum level of the Gleissberg cycle. A comparison with other reported studies shows that our results based on the NARX model are in good agreement.

Wavelength Dependence of Image Quality Metrics and Seeing Parameters and Their Relation to Adaptive Optics Performance

R. **Kamlah**,M. Verma, A. Diercke & C. Denker
Solar Physics volume 296, Article number: 29 (**2021**)
https://link.springer.com/content/pdf/10.1007/s11207-021-01771-y.pdf
Ground-based solar observations are severely affected by Earth's turbulent atmosphere. As a consequence, observed image quality and prevailing seeing conditions are closely related. Partial correction of image degradation is nowadays provided in real time by adaptive optics (AO) systems. In this study, different metrics of image quality are compared with parameters characterizing the prevailing seeing conditions, i.e. Median Filter Gradient Similarity (MFGS), Median Filter Laplacian Similarity (MFLS), Helmli–Scherer mean, granular rms-contrast, differential image motion, and Fried-parameter r0r0. The quiet-Sun observations at disk center were carried out at the Vacuum Tower Telescope (VTT), Observatorio del Teide (OT), Izaña, Tenerife, Spain. In July and August 2016, time series of short-exposure images were recorded with the High-resolution Fast Imager (HiFI) at various wavelengths in the visible and near-infrared parts of the spectrum. Correlation analysis yields the wavelength dependence of the image quality metrics and seeing parameters, and Uniform Manifold Approximation and Projection (UMAP) is employed to characterize the seeing on a particular observing day. In addition, the image quality metrics and seeing parameters are used to determine the field dependence of the correction provided by the AO system. Management of high-

resolution imaging data from large-aperture, ground-based telescopes demands reliable image quality metrics and meaningful characterization of prevailing seeing conditions and AO performance. The present study offers guidance on how retrieving such information ex post facto.

Lags and Hysteresis Loops of Cosmic Ray Intensity *Versus* Sunspot Numbers: Quantitative Estimates for Cycles 19 – 23 and a Preliminary Indication for Cycle 24

R.P. **Kane**

Solar Phys., **2014,** Volume 289, Issue 7, pp 2727-2732

Hysteresis plots between cosmic-ray (CR) intensity (recorded at the Climax station) and sunspot relative number *R*z show broad loops in odd cycles (19, 21, and 23) and narrow loops in even cycles (20 and 22). However, in the even cycles, the loops are not narrow throughout the whole cycle; around the sunspot-maximum period, a broad loop is seen. Only in the rising and declining phases, the loops are narrow in even cycles. The CR modulation is known to have a delay with respect to *R*z, and the delay was believed to be longer in odd cycles (19, 21, and 23; about 10 months) than the delay in even cycles (20 and 22; about 3 – 5 months). When this was reexamined, it was found that the delays are different during the sunspot-minimum periods (2, 6, and 14 months for odd cycles and 7 and 9 months for even cycles) and sunspot-maximum periods (0, 4, and 7 months for odd cycles and 5 and 8 months for even cycles). Thus, the differences between odd and even cycles are not significant throughout the whole cycle. In the recent even cycle 24, hysteresis plots show a preliminary broadening near the sunspot maximum, which occurred recently (February 2012). The CR level (recorded at Newark station) is still high in 2013, indicating a long lag (exceeding 10 months) with respect to the sunspot maximum.

Apparent cross-field superslow propagation of magnetohydrodynamic waves in solar plasmas

T. **Kaneko**, M. Goossens, R. Soler, J. Terradas, T. Van Doorsselaere, T. Yokoyama, A. N. Wright

ApJ **2015**

http://arxiv.org/pdf/1509.03042v1.pdf

In this paper we show that the phase mixing of continuum Alfv\'{e}n waves and/or continuum slow waves in magnetic structures of the solar atmosphere as, e.g., coronal arcades, can create the illusion of wave propagation across the magnetic field. This phenomenon could be erroneously interpreted as fast magnetosonic waves. The cross-field propagation due to phase mixing of continuum waves is apparent because there is no real propagation of energy across the magnetic surfaces. We investigate the continuous Alfv\'{e}n and slow spectra in 2D Cartesian equilibrium models with a purely poloidal magnetic field. We show that apparent superslow propagation across the magnetic surfaces in solar coronal structures is a consequence of the existence of continuum Alfv\'{e}n waves and continuum slow waves that naturally live on those structures and phase mix as time evolves. The apparent cross-field phase velocity is related to the spatial variation of the local Alfv\'{e}n/slow frequency across the magnetic surfaces and is slower than the Alfv\'{e}n/sound velocities for typical coronal conditions. Understanding the nature of the apparent cross-field propagation is important for the correct analysis of numerical simulations and the correct interpretation of observations.

Emission of Joule heating events in simulations of the solar corona

Charalambos **Kanella**1,2 and Boris V. Gudiksen

A&A 621, A95 (**2019**)

Context. Nanoscale events in cooperation with steady heating from a slow heating mechanism, such as slow-burning current-sheets, could be able to heat the corona; however, their observational traces are hard to detect via current instrumentation. After we locate heating events in magnetohydrodynamic (MHD) simulations and synthesise observational data, we extract observational signatures of small-scale events.

Aims. Our mission is threefold. The first goal is to observe the manifestation of small-scale events via three observational tools: intensity maps of three extreme ultraviolet (EUV) filters in the Atmospheric Imaging Assembly (AIA) instrument with resolution better than that in AIA images, emission measure (EM) analysis, and time-lag maps. The second goal is to identify the reason why we cannot quantify the energy release from observed events. The third goal is to study the differences between the radiation from isolated heating events and that from the whole corona.

Methods. We employed a three-dimensional magnetohydrodynamic (3D-MHD) simulation using the Bifrost code. We simulated the atmosphere of a network embedded in the quiet Sun (QS), and we identified 3D heating events in the corona in several time-steps. Then we synthesised the three observational tools for two cases. First, we considered information from the total column mass in the corona, and then we considered only regions that exhibit heating events.

Results. We report on the differences between the two regions of investigation, which also consist of the evidence to justify why observers cannot identify small-scale heating events in observations. We found that the combination of multiple heating events at different cooling phases along the line of sight gives the impression of thin elongated threads of events. For this reason, the EM as a function of temperature has a multi-thermal distribution. Both the radiation and the emission measure of the isolated heating events have values at least ten times lower than the signal

calculated from the total corona. We also found that heating events move together with diffuse emission from the slow heating mechanism, and for this reason we cannot differentiate between the two. In addition, we find that the frequency of heating events and their intensity affect the EM distribution as a function of temperature. We also find that the filter's intensity, EM, and time-lag maps of heating events are different to those incorporating information from the total column mass of the corona. However, the two regions have, on average, comparable values, which are slightly smaller than the analytical cooling timescales calculated for an optically thin and radiation-dominated atmosphere.

Investigating 4D Coronal Heating Events In MHD Simulations

Charalambos **Kanella**, Boris V. Gudiksen
A&A 617, A50 **2018**
https://arxiv.org/pdf/1806.04495.pdf
One candidate-model for heating the solar corona is magnetic reconnection that embodies Ohmic dissipation of current sheets. When numerous small-scaled magnetic reconnection occur, then it is possible to heat the corona. Due to the limitations of current instrumentation, nanoflares cannot be resolved. But their importance is evaluated via statistics by finding the power-law index of the energy distribution. This method is however biased due to technical and physical reasons. We aim to overcome limitations imposed by observations and statistical analysis. This way, we will identify, and study the small scale impulsive events. We employ a three-dimensional magnetohydrodynamic (3D-MHD) simulation using the \bifrost code. We also employ a new technique to identify the evolution of 3D Joule heating events in the corona. Then, we derive parameters describing the heating events in these locations. We report on the identification of heating events. We obtain the distribution of duration, released energy, and volume. We also find weak power-law correlation between these parameters. In addition, we extract information about geometrical parameters of 2D slices of 3D events, and about the evolution of resolved Joule heating compared to the total Joule heating and the magnetic energy in the corona. Even though the energy power index is less than 2, when classifying the energy release into three categories regarding with respect to the energy release (pico-, nano-, and micro-events), we find that nano-events release 82 % of the resolved energy. This fraction corresponds to an energy flux larger than the one needed to heat the corona. It seems that the most popular population is the one containing short-lived, with small spatial extend events.

Identification of coronal heating events in 3D simulations

Charalambos **Kanella**, Boris V. Gudiksen
2017
https://arxiv.org/pdf/1703.02808.pdf
The solar coronal heating problem is an open question. One model for the transport and release of mechanical energy generated in the sub-phorospheric layers and photosphere is the nanoflare model that incorporates Ohmic heating which releases a part of the energy stored in the magnetic field. The problem with the verification of this model is that we cannot resolve small scale events. Histograms of observable characteristics of flares, show powerlaw behavior, for both energy release rate, size and total energy. Depending on the powerlaw index of the energy release, nanoflares might be an important candidate for coronal heating; we seek to find that index. In this paper we employ a numerical 3D-MHD simulation produce by the numerical code {\it{Bifrost}}, and a new technique to identify the 3D heating events at a specific instant. The quantity we explore is the Joule heating, which is explicitly correlated with the magnetic reconnection because depends on the curl of the magnetic field. We are able to identify 4136 events in a volume 24×24×9.5 Mm3 (i.e. 768×786×331 grid cells) of a specific snapshot. We find a powerlaw slope of the released energy per second, and two powerlaw slopes of the identified volume. The identified energy events do not represent all the released energy, but of the identified events, the total energy of the largest events dominate the energy release. Most of the energy release happens in the lower corona, while heating drops with height. We find that with a specific identification method that large events can be resolved into smaller ones, but at the expense of the total identified energy releases. The energy release which cannot be identified as an event favours a low energy release mechanism.

Discovery of Scattering Polarization in the Hydrogen Lyman-α Line of the Solar Disk Radiation

R. **Kano**, J. Trujillo Bueno, A. Winebarger, F. Auchère, N. Narukage, R. Ishikawa, K. Kobayashi, T. Bando, Y. Katsukawa, M. Kubo, S. Ishikawa, G. Giono, H. Hara, Y. Suematsu, T. Shimizu, T. Sakao, S. Tsuneta, K. Ichimoto, M. Goto, L. Belluzzi, J. Štěpán, A. Asensio Ramos, R. Manso Sainz, P. Champey, J. Cirtain, B. De Pontieu, R. Casini, M. Carlsson
Astrophysical Journal Letters, Volume 839, Number 1, L10, **2017**
https://arxiv.org/pdf/1704.03228.pdf

There is a thin transition region (TR) in the solar atmosphere where the temperature rises from 10,000 K in the chromosphere to millions of degrees in the corona. Little is known about the mechanisms that dominate this enigmatic region other than the magnetic field plays a key role. The magnetism of the TR can only be detected by polarimetric measurements of a few ultraviolet (UV) spectral lines, the Lyman-α line of neutral hydrogen at 121.6 nm (the strongest line of the solar UV spectrum) being of particular interest given its sensitivity to the Hanle effect (the magnetic-field-induced modification of the scattering line polarization). We report the discovery of linear polarization produced by scattering processes in the Lyman-α line, obtained with the Chromospheric Lyman-Alpha Spectro-Polarimeter (CLASP) rocket experiment. The Stokes profiles observed by CLASP in quiet regions of the solar disk show that the Q/I and U/I linear polarization signals are of the order of 0.1 % in the line core and up to a few percent in the nearby wings, and that both have conspicuous spatial variations with scales of ∼10 arcsec. These observations help constrain theoretical models of the chromosphere-corona TR and extrapolations of the magnetic field from photospheric magnetograms. In fact, the observed spatial variation from disk to limb of polarization at the line core and wings already challenge the predictions from three-dimensional magnetohydrodynamical models of the upper solar chromosphere. **2015 September 3**

High-Resolution 10Be and 36Cl Data From the Antarctic Dome Fuji Ice Core (∼100 Years Around 5480 BCE): An Unusual Grand Solar Minimum Occurrence?

K. **Kanzawa**, F. Miyake, K. Horiuchi, K. Sasa, K. Takano, M. Matsumura, T. Takahashi, Y. Motizuki, K. Takahashi, Y. Nakai, K. Ohtani, Y. Tada, Y. Ochiai, H. Motoyama, H. Matsuzaki, A. Yamazaki, Y. Muramatsu, T. Yamagata

JGR Volume126, Issue10 October **2021** e2021JA029378

https://doi.org/10.1029/2021JA029378

https://agupubs.onlinelibrary.wiley.com/doi/epdf/10.1029/2021JA029378

Cosmogenic nuclides in tree rings and polar ice cores record the information of past cosmic ray intensities and solar activities. A large 14C increase over 10 years has been discovered around 5480 BCE. The 14C variations in this event differ from those of other short-term cosmic ray events and typical grand solar minima. To elucidate the cause of the 14C increase around 5480 BCE, we measured the 10Be and 36Cl concentrations in the Antarctic Dome Fuji ice core at quasi-annual and 4–5 years resolutions, respectively. Based on the combined 14C, 10Be, and 36Cl data, the 5480 BCE event was probably not caused by a solar proton event (SPE) or a gamma-ray event, because the 36Cl concentration did not significantly increase as expected in these events. The incremented 10Be data were enhanced similarly to those of recent grand solar minima, but more rapidly increased (over ∼10 years). These results suggest that an unusual grand solar minimum occurred around 5480 BCE, characterized by a rapidly decreasing solar activity.

Simulations of solar and stellar dynamos and their theoretical interpretation **Review**

Petri J. **Käpylä**, Matthew K. Browning, Allan Sacha Brun, Gustavo Guerrero, Jörn Warnecke

Space Science Reviews 219, Article number: 58 **2023** 70 pages

https://arxiv.org/pdf/2305.16790

https://link.springer.com/content/pdf/10.1007/s11214-023-01005-6.pdf

We review the state of the art of three dimensional numerical simulations of solar and stellar dynamos. We summarize fundamental constraints of numerical modelling and the techniques to alleviate these restrictions. Brief summary of the relevant observations that the simulations seek to capture is given. We survey the current progress of simulations of solar convection and the resulting large-scale dynamo. We continue to studies that model the Sun at different ages and to studies of stars of different masses and evolutionary stages. Both simulations and observations indicate that rotation, measured by the Rossby number which is the ratio of rotation period and convective turnover time, is a key ingredient in setting the overall level and characteristics of magnetic activity. Finally, efforts to understand global 3D simulations in terms of mean-field dynamo theory are discussed.

Transition from anti-solar to solar-like differential rotation: Dependence on Prandtl number

Petri J. **Käpylä**

A&A **2022**

https://arxiv.org/pdf/2207.00302

Context: Late-type stars such as the Sun rotate differentially due to the interaction of turbulent convection and rotation. Aims: The aim of the study is to investigate the effects of the thermal Prandtl number on the transition from anti-solar (slow equator, fast poles) to solar-like (fast equator, slow poles) differential rotation. Methods: Three-dimensional hydrodynamic and magnetohydrodynamic simulations in semi-global spherical wedge geometry are used to model convection zones of solar-like stars. Results: The overall convective velocity amplitude increases as the Prandtl number decreases in accordance with earlier studies. The transition from anti-solar to solar-like

differential rotation is insensitive to the Prandtl number for Prandtl numbers below unity but for Prandtl numbers greater than unity, solar-like differential rotation becomes significantly harder to excite. Magnetic fields and more turbulent regimes with higher fluid and magnetic Reynolds numbers help in achieving solar-like differential rotation in near-transition cases. Solar-like differential rotation occurs only in cases with radially outward angular momentum transport at the equator. The dominant contribution to such outward transport near the equator is due to prograde propagating thermal Rossby waves. Conclusions: The differential rotation is sensitive to the Prandtl number only for large Prandtl numbers in the parameter regime explored in the current study. Magnetic fields have a greater effect on the differential rotation, although the inferred presence of a small-scale dynamo does not lead to drastically different results in the present study. The dominance of the thermal Rossby waves in the simulations is puzzling given the non-detection in the Sun. The current simulations are shown to be incompatible with the currently prevailing mean-field theory of differential rotation.

Effects of small-scale dynamo and compressibility on the Λ effect

Petri J. **Käpylä**
Astron. Nachr **2019**
https://arxiv.org/pdf/1903.04363.pdf
The Λ effect describes a rotation-induced non-diffusive contribution to the Reynolds stress. It is commonly held responsible for maintaining the observed differential rotation of the Sun and other late-type stars. Here the sensitivity of the Λ effect to small-scale magnetic fields and compressibility is studied by means of forced turbulence simulations either with anisotropic forcing in fully periodic cubes or in density-stratified domains with isotropic forcing. Effects of small-scale magnetic fields are studied in cases where the magnetic fields are self-consistently generated by a small-scale dynamo. The results show that small-scale magnetic fields lead to a quenching of the Λ effect which is milder than in cases where also a large-scale field is present. The effect of compressibility on the Λ effect is negligible in the range of Mach numbers from 0.015 to 0.8. Density stratification induces a marked anisotropy in the turbulence and a vertical Λ effect if the forcing scale is roughly two times larger than the density scale height.

Magnetic flux concentrations from turbulent stratified convection

P. J. **Käpylä** (1,2,3), A. Brandenburg (3,4,5,6), N. Kleeorin (7,3), M. J. Käpylä (1), I. Rogachevskii
A&A **201**5
http://arxiv.org/pdf/1511.03718v1.pdf
Context: The mechanisms that cause the formation of sunspots are still unclear. Aims: We study the self-organisation of initially uniform sub-equipartition magnetic fields by highly stratified turbulent convection. Methods: We perform simulations of magnetoconvection in Cartesian domains that are 8.5-24 Mm deep and 34-96 Mm wide. We impose either a vertical or a horizontal uniform magnetic field in a convection-driven turbulent flow. Results: We find that super-equipartition magnetic flux concentrations are formed near the surface with domain depths of 12.5 and 24 Mm. The size of the concentrations increases as the box size increases and the largest structures (20 Mm horizontally) are obtained in the 24 Mm deep models. The field strength in the concentrations is in the range of 3-5 kG. The concentrations grow approximately linearly in time. The effective magnetic pressure measured in the simulations is positive near the surface and negative in the bulk of the convection zone. Its derivative with respect to the mean magnetic field, however, is positive in the majority of the domain, which is unfavourable for the negative effective magnetic pressure instability (NEMPI). Furthermore, we find that magnetic flux is concentrated in regions of converging flow corresponding to large-scale supergranulation convection pattern. Conclusions: The linear growth of large-scale flux concentrations implies that their dominant formation process is tangling of the large-scale field rather than an instability. One plausible mechanism explaining both the linear growth and the concentrate on of the flux in the regions of converging flow pattern is flux expulsion. Possible reasons for the absence of NEMPI are that the derivative of the effective magnetic pressure with respect to the mean magnetic field has an unfavourable sign and that there may not be sufficient scale separation.

Multiple dynamo modes as a mechanism for long-term solar activity variations

Maarit J. **Käpylä** (1), Petri J. Käpylä (1,2,3), Nigul Olspert (1), Axel Brandenburg (3,4), Jörn Warnecke (5,1),Bidya B. Karak (3), Jaan Pelt
A&A 589, A56 **2015**
http://arxiv.org/pdf/1507.05417v1.pdf
Solar magnetic activity shows both smooth secular changes, such as the Grand Modern Maximum, and quite abrupt drops that are denoted as Grand Minima. Direct numerical simulations (DNS) of convection driven dynamos offer one way of examining the mechanisms behind these events. In this work, we analyze a solution of a solar-like DNS that has been evolved for roughly 80 magnetic cycles of 5.4 years, during which epochs of irregular behavior are

detected. The emphasis of our analysis is to find physical causes for such behavior. The DNS employed is a semi-global (wedge) magnetoconvection model. For data analysis we use Ensemble Empirical Mode Decomposition (EEMD) and phase dispersion (D^2) methods. A special property of the DNS is the existence of multiple dynamo modes at different depths and latitudes. The dominant mode is solar-like. This mode is accompanied by a higher frequency mode near the surface and a low-frequency mode in the bottom of the convection zone. The overall behavior of the dynamo solution is very complex exhibiting variable cycle lengths, epochs of disturbed and even ceased surface activity, and strong short-term hemispherical asymmetries. Surprisingly, the suppressed surface activity epochs are global magnetic energy maxima, as during them the toroidal magnetic field at the bottom obtains a maximum. We interpret the overall irregular behavior to be due to the interplay of the different dynamo modes showing different equatorial symmetries, especially the smoother part of the irregular variations being related to the variations of the mode strengths, evolving with different and variable cycle lengths. The abrupt low activity epochs in the dominant dynamo mode near the surface have a relation with the extrema and polarity reversals of the bottom dynamo mode, which causes abrupt disturbances in the differential rotation profile through suppressing the Reynolds stresses.

The effect of telescope aperture, scattered light, and human vision on early measurements of sunspot and group numbers

Nina V. **Karachik**, Alexei A. Pevtsov, Yury A. Nagovitsyn
MNRAS **2019**
https://arxiv.org/pdf/1907.04932.pdf
Early telescopic observations of sunspots were conducted with instruments of relatively small aperture. These instruments also suffered from a higher level of scattered light, and the human eye served as a "detector". The eye's ability to resolve small details depends on image contrast, and on average the intensity variations smaller than ≈ 3\% contrast relative to background are not detected even if they are resolved by the telescope. Here we study the effect of these three parameters (telescope aperture, scattered light, and detection threshold of human vision) on sunspot number, group number, and area of sunspots. As an "ideal" dataset, we employ white-light (pseudo-continuum) observations from Helioseismic and Magnetic Imager (HMI) onboard of Solar Dynamics Observatory, and we model the appearance of sunspots by degrading the HMI images to corresponding telescope apertures with an added scattered light. We discuss the effects of different parameters on sunspot counts and derive functional dependencies, which could be used to normalize historical observations of sunspot counts to common denominator.

Recent Developments in the Babcock-Leighton Solar Dynamo Theory **Review**

Bidya Binay **Karak**
IAU Symposium 365 in Yerevan **2024**
https://arxiv.org/pdf/2401.06410.pdf
Babcock-Leighton process, in which the poloidal field is generated through the decay and dispersal of tilted bipolar magnetic regions (BMRs), is observed to be the major process behind the generating poloidal field in the Sun. Based on this process, the Babcock-Leighton dynamo models have been a promising tool for explaining various aspects of solar and stellar magnetic cycles. In recent years, in the toroidal to poloidal part of this dynamo loop, various nonlinear mechanisms, namely the flux loss through the magnetic buoyancy in the formation of BMRs, latitude quenching, tilt quenching, and inflows around BMRs, have been identified. While these nonlinearities tend to produce a stable magnetic cycle, the irregular properties of BMR, mainly the scatter around Joy's law tilt, make a considerable variation in the solar cycle, including grand minima and maxima. After reviewing recent developments in these topics, I end the presentation by discussing the recent progress in making the early prediction of the solar cycle.

Models for the long-term variations of solar activity **Review**

Bidya Binay **Karak**
Living Reviews in Solar Physics **20**, Article number: 3 **2023**
https://arxiv.org/pdf/2305.17188
https://link.springer.com/content/pdf/10.1007/s41116-023-00037-y.pdf
One obvious feature of the solar cycle is its variation from one cycle to another. In this article, we review the dynamo models for the long-term variations of the solar cycle. By long-term variations, we mean the cycle modulations beyond the 11-year periodicity and these include, the Gnevyshev-Ohl/Even-Odd rule, grand minima, grand maxima, Gleissberg cycle, and Suess cycles. After a brief review of the observed data, we present the dynamo models for the solar cycle. By carefully analyzing the dynamo models and the observed data, we identify the following broad causes for the modulation: (i) magnetic feedback on the flow, (ii) stochastic forcing, and (iii) time delays in various processes of the dynamo. To demonstrate each of these causes, we present the results from some illustrative models for the cycle modulations and discuss their strengths and weakness. We also discuss a few critical issues and their current trends. The article ends with a discussion of our current state of ignorance about comparing

detailed features of the magnetic cycle and the large-scale velocity from the dynamo models with robust observations.

Dynamo saturation through the latitudinal variation of bipolar magnetic regions in the Sun

Bidya Binay **Karak**
ApJL **2020**
https://arxiv.org/pdf/2009.06969.pdf
Observations of the solar magnetic cycle showed that the amplitude of the cycle did not grow all the time in the past. Thus, there must be a mechanism to halt the growth of the magnetic field in the Sun. We demonstrate a recently proposed mechanism for this under the Babcock-Leighton dynamo framework which is believed to be the most promising paradigm for the generation of the solar magnetic field at present. This mechanism is based on the observational fact that the stronger solar cycles produce Bipolar Magnetic Regions (BMRs) at higher latitudes and thus have higher mean latitudes than the weaker ones. We capture this effect in our three-dimensional Babcock-Leighton solar dynamo model and show that when the toroidal magnetic field tries to grow, it produce BMRs at higher latitudes. The BMRs at higher latitudes generate a less poloidal field, which consequently limits the overall growth of the magnetic field in our model. Thus, our study suggests that the latitudinal variation of BMRs is a potential mechanism for limiting the magnetic field growth in the Sun.

Double-peaks of the solar cycle: An explanation from a dynamo model

Bidya Binay **Karak**, Sudip Mandal, Dipankar Banerjee
ApJ **866** 17 **2018**
https://arxiv.org/pdf/1808.03922.pdf
sci-hub.tw/10.3847/1538-4357/aada0d
One peculiar feature of the solar cycle which is yet to be understood properly is the frequent occurrence of double peaks (also known as the Gnevyshev peaks). Not only the double peaks but also multiple peaks and spikes are often observed in any phase of the cycle. We propose that these peaks and spikes are generated due to fluctuations in the Babcock-Leighton process (the poloidal field generation from tilted bipolar magnetic regions). When the polar field develops, large negative fluctuations in the Babcock-Leighton process can reduce the net polar field abruptly. As these fluctuations in the polar field are propagated to the new toroidal field, these can promote double peaks in the next solar cycle. When fluctuations in the polar field occur outside the solar maximum, we observe their effects as spikes or dips in the following sunspot cycle. Using an axisymmetric Babcock-Leighton dynamo model we first demonstrate this idea. Later, we perform a long simulation by including random scatter in the poloidal field generation process and successfully reproduce the double-peaked solar cycles. These results are robust under reasonable changes in the model parameters as long as the diffusivity is not too larger than 1012 cm2s−1. Finally, we analyze the observed polar field data to show a close connection between the short-term fluctuations in the polar field and the double peaks/spikes in the next cycle. Thereby, this supports our theoretical idea that the fluctuations in the Babcock-Leighton process can be responsible for the double peaks/spikes in the observed solar cycle.
HMI Science Nuggets #112 September **2018** http://hmi.stanford.edu/hminuggets/?p=2685

Solar magnetic cycle and its variability in a 3D Babcock-Leighton dynamo model

Bidya Binay **Karak** and Mark Miesch
HMI Science Nuggets, #**102**, June **2018** http://hmi.stanford.edu/hminuggets/?p=2529

Recovery from Maunder-like Grand Minima in a Babcock–Leighton Solar Dynamo Model

Bidya Binay **Karak**1,2,3 and Mark Miesch
2018 ApJL 860 L26
https://doi.org/10.3847/2041-8213/aaca97
The Sun occasionally goes through Maunder-like extended grand minima when its magnetic activity drops considerably from the normal activity level for several decades. Many possible theories have been proposed to explain the origin of these minima. However, how the Sun managed to recover from such inactive phases every time is even more enigmatic. The Babcock–Leighton type dynamos, which are successful in explaining many features of the solar cycle remarkably well, are not expected to operate during grand minima due to the lack of a sufficient number of sunspots. In this Letter, we explore the question of how the Sun could recover from grand minima through the Babcock–Leighton dynamo. In our three-dimensional dynamo model, grand minima are produced spontaneously as a result of random variations in the tilt angle of emerging active regions. We find that the Babcock–Leighton process can still operate during grand minima with only a minimal number of sunspots, and that the model can emerge from such phases without the need for an additional generation mechanism for the poloidal field. The essential ingredient in our model is a downward magnetic pumping, which inhibits the diffusion of the magnetic flux across the solar surface.

Long-term variability of the solar cycle in the Babcock-Leighton dynamo framework

Bidya Binay **Karak**, Mark Miesch

Proceedings IAU Symposium No. xxx, 2015 **2018**

https://arxiv.org/pdf/1805.04821.pdf

We explore the cause of the solar cycle variabilities using a novel 3D Babcock--Leighton dynamo model. In this model, based on the toroidal flux at the base of the convection zone, bipolar magnetic regions (BMRs) are produced with statistical properties obtained from observed distributions. We find that a little quenching in BMR tilt is sufficient to stabilize the dynamo growth. The randomness and nonlinearity in the BMR emergences make the poloidal field unequal and cause some variability in the solar cycle. However, when observed scatter of BMR tilts around Joy's law with a standard deviation of 15∘, is considered, our model produces a variation in the solar cycle, including north-south asymmetry comparable to the observations. The morphology of magnetic fields closely resembles observations, in particular the surface radial field possesses a more mixed polarity field. Observed scatter also produces grand minima. In 11,650 years of simulation, 17 grand minima are detected and 11% of its time the model remained in these grand minima. When we double the tilt scatter, the model produces correct statistics of grand minima. Importantly, the dynamo continues even during grand minima with only a few BMRs, without requiring any additional alpha effect. The reason for this is the downward magnetic pumping which suppresses the diffusion of the magnetic flux across the surface. The magnetic pumping also helps to achieve 11-year magnetic cycle using the observed BMR flux distribution, even at the high diffusivity.

Solar Cycle Variability Induced by Tilt Angle Scatter in a Babcock--Leighton Solar Dynamo Model

Bidya Binay **Karak**, Mark Miesch

ApJ **847** 69 **2017**

https://arxiv.org/pdf/1706.08933.pdf

We present results from a three-dimensional Babcock--Leighton dynamo model that is sustained by the explicit emergence and dispersal of bipolar magnetic regions (BMRs). On average, each BMR has a systematic tilt given by Joy's law. Randomness and nonlinearity in the BMR emergence of our model produce variable magnetic cycles. However, when we allow for a random scatter in the tilt angle to mimic the observed departures from Joy's law, we find more variability in the magnetic cycles. We find that the observed standard deviation in Joy's law of σδ=15∘ produces a variability comparable to observed solar cycle variability of ∼ 32%, as quantified by the sunspot number maxima between 1755--2008. We also find that tilt angle scatter can promote grand minima and grand maxima. The time spent in grand minima for σδ=15∘ is somewhat less than that inferred for the Sun from cosmogenic isotopes (about 9% compared to 17%). However, when we double the tilt scatter to σδ=30∘, the simulation statistics are comparable to the Sun (∼18% of the time in grand minima and ∼10% in grand maxima). Though the Babcock--Leighton mechanism is the only source of poloidal field, we find that our simulations always maintain magnetic cycles even at large fluctuations in the tilt angle. We also demonstrate that tilt quenching is a viable and efficient mechanism for dynamo saturation; a suppression of the tilt by only 1-2∘ is sufficient to limit the dynamo growth. Thus, any potential observational signatures of tilt quenching in the Sun may be subtle.

Babcock-Leighton solar dynamo: the role of downward pumping and the equatorward propagation of activity

Bidya Binay **Karak**, Robert Cameron

ApJ **832** 94 **2016**

http://arxiv.org/pdf/1605.06224v1.pdf

The key elements of the Babcock-Leighton dynamo are the generation of poloidal field through the decay of tilted bipolar active regions and the generation of toroidal field through the observed differential rotation. There are two classes of Babcock-Leighton models: flux transport dynamos where an equatorward flow at the bottom of the convection zone (CZ) is responsible for the equatorial propagation of the butterfly wings, and dynamo waves where the radial gradient of differential rotation and the α effect act in conjunction to produce the equatorial propagation. Here we investigate the role of
downward magnetic pumping near the surface using a kinematic Babcock-Leighton model. We find that the pumping causes the poloidal field to become predominately radial in the near-surface shear layer. This allows the negative radial shear in the near-surface layer to effectively act on the radial field to produce a toroidal field. Consequently, we observe a clear equatorward migration of the toroidal field at low latitudes even when there is no meridional flow in the deep CZ. Both the dynamo wave and flux transport dynamo are thus able to reproduce some of the observed features of solar cycle including the 11-year periodicity. The main difference between the two types of dynamo is the value of α required to produce dynamo action. In flux transport
dynamo the equatorward flow near the bottom of CZ advects toroidal field to cause the equatorward migration in butterfly wings and this advection makes the dynamo easier by transporting strong toroidal field to low latitudes where α effect works. Second conclusion of this paper is that the magnetic

pumping suppresses the diffusion of fields through the photospheric surface which helps to achieve the 11-year dynamo cycle at a moderately larger value of magnetic diffusivity η than has previously been used.

IS THE SMALL-SCALE MAGNETIC FIELD CORRELATED WITH THE DYNAMO CYCLE?
Bidya Binay **Karak**1,2 and Axel Brandenburg
2016 ApJ 816 28
'The small-scale magnetic field is ubiquitous at the solar surface?even at high latitudes. From observations we know that this field is uncorrelated (or perhaps even weakly anticorrelated) with the global sunspot cycle. Our aim is to explore the origin, and particularly the cycle dependence, of such a phenomenon using three-dimensional dynamo simulations. We adopt a simple model of a turbulent dynamo in a shearing box driven by helically forced turbulence. Depending on the dynamo parameters, large-scale (global) and small-scale (local) dynamos can be excited independently in this model. Based on simulations in different parameter regimes, we find that, when only the large-scale dynamo is operating in the system, the small-scale magnetic field generated through shredding and tangling of the large-scale magnetic field is positively correlated with the global magnetic cycle. However, when both dynamos are operating, the small-scale field is produced from both the small-scale dynamo and the tangling of the large-scale field. In this situation, when the large-scale field is weaker than the equipartition value of the turbulence, the small-scale field is almost uncorrelated with the large-scale magnetic cycle. On the other hand, when the large-scale field is stronger than the equipartition value, we observe an anticorrelation between the small-scale field and the large-scale magnetic cycle. This anticorrelation can be interpreted as a suppression of the small-scale dynamo. Based on our studies we conclude that the observed small-scale magnetic field in the Sun is generated by the combined mechanisms of a small-scale dynamo and tangling of the large-scale field.

Hysteresis between distinct modes of turbulent dynamos
Bidya Binay **Karak**, Leonid L. Kitchatinov, Axel Brandenburg
ApJ, **803** 95 **2014**
Nonlinear mean-field models for the solar dynamo show long-term variability, which may be relevant to different states of activity inferred from long-term radiocarbon data. This paper is aimed to probe the dynamo hysteresis predicted by the recent mean-field models of Kitchatinov & Olemskoy (2010) with direct numerical simulations. We perform three-dimensional simulations of large-scale dynamos in a shearing box with helically forced turbulence. As initial condition, we either take a weak random magnetic field or we start from a snapshot of an earlier simulation. Two quasi-stable states are found to coexist in a certain range of parameters close to onset of the large-scale dynamo. The simulations converge to one of these states in dependence on the initial conditions. When either the fractional helicity or the magnetic Prandtl number is increased between successive runs above the critical value for onset of the dynamo, the field strength jumps to a finite value. However, when the fractional helicity or the magnetic Prandtl number is then decreased again, the field strength stays at a similar value (strong field branch) even below the original onset. We also observe intermittent decaying phases away from the strong field branch close to the point where large-scale dynamo action is just possible. The dynamo hysteresis seen previously in mean-field models is thus reproduced by 3D simulations. Its possible relation to distinct modes of solar activity such as grand minima is discussed.

Is the recent discovery of the multi-cell meridional circulation a threat to the flux-transport dynamo?
Bidya Binay **Karak**
HMI Science Nuggets, #17, **2014**
In recent years the flux-transport dynamo model has become popular due to its success in reproducing many important observational features of the solar cycle. However, in spite of this success, some recent observations raise doubts about the validity of the flux-transport dynamo model. The meridional circulation of the Sun is a crucial component of this model and some recent analyses of observational data suggest that this circulation may be quite different from what had been assumed in the early models of the flux-transport dynamo. We now show that the attractive features of the flux-transport dynamo can be retained even with meridional circulations more complicated than what had so far been assumed in theoretical models, provided some conditions are satisfied.

TURBULENT PUMPING OF MAGNETIC FLUX REDUCES SOLAR CYCLE MEMORY AND THUS IMPACTS PREDICTABILITY OF THE SUN'S ACTIVITY
Bidya Binay **Karak**1 and Dibyendu Nandy
2012 ApJ 761 L13

Prediction of the Sun's magnetic activity is important because of its effect on space environment and climate. However, recent efforts to predict the amplitude of the solar cycle have resulted in diverging forecasts with no consensus. Yeates et al. have shown that the dynamical memory of the solar dynamo mechanism governs predictability, and this memory is different for advection- and diffusion-dominated solar convection zones. By utilizing stochastically forced, kinematic dynamo simulations, we demonstrate that the inclusion of downward turbulent pumping of magnetic flux reduces the memory of both advection- and diffusion-dominated solar dynamos to only one cycle; stronger pumping degrades this memory further. Thus, our results reconcile the diverging dynamo-model-based forecasts for the amplitude of solar cycle 24. We conclude that reliable predictions for the maximum of solar activity can be made only at the preceding minimum—allowing about five years of advance planning for space weather. For more accurate predictions, sequential data assimilation would be necessary in forecasting models to account for the Sun's short memory.

Characteristics of Magnetoacoustic Waves and Coronal Seismology

M. R. **Karamimehr**1, S. Vasheghani Farahani2, and H. Ebadi1
2019 ApJ 886 112
https://doi.org/10.3847/1538-4357/ab4b4e
We model fast magnetohydrodynamic sausage and kink wave characteristics propagating in solar slab-like plasma structures. By implementing Cartesian coordinates, explicit expressions are provided governing the dependence of the frequency, damping, damping time, phase, and group speeds of fast sausage and kink waves on the wavenumber and density contrasts of solar slab-like plasmas. Explicit expressions are presented through equilibrium conditions and physical parameters controlling the plasma structure. Solutions of the explicit expressions are compared with numerical results. The overlap of curves proves adequate for the robustness of the explicit expressions. Kink modes possess higher frequencies compared to sausage modes in the leaky regime, while the sausage mode phase speed increases more rapidly compared to the kink speed. This explains the higher group speeds of sausage waves compared to kink waves around the cutoff. Sausage waves damp quicker compared with kink waves. The damping is inversely proportional to the mode number. As the damping time is directly proportional with the wavenumber, the damping time is much higher around the cutoff frequency compared to the long wavelength limit. The presented expressions prove adequate for coronal seismology, where, as the magnetoacoustic oscillations damp and disappear, the local and neighboring physical parameters and conditions could be estimated. As leaky kink modes live longer than sausage modes, they have a higher chance of being observed while transporting energy to a broader region. Sausage modes penetrate less due to fast damping providing higher heating rates in shorter ranges. Both modes contribute to coronal heating in various scales.

Kelvin-Helmholtz instability and heating in oscillating loops perturbed by power-law transverse wave drivers

Konstantinos **Karampelas**, Tom Van Doorsselaere, Mingzhe Guo, Timothy Duckenfield, Gabriel Pelouze
A&A **2024**
https://arxiv.org/pdf/2406.11700
Instabilities in oscillating loops are believed to be essential for dissipating the wave energy and heating the solar coronal plasma. Our aim is to study the development of the Kelvin-Helmholtz (KH) instability in an oscillating loop that is driven by random footpoint motions. Using the PLUTO code, we performed 3D simulations of a straight gravitationally stratified flux tube. The loop footpoints are embedded in chromospheric plasma, in the presence of thermal conduction and an artificially broadened transition region. Using drivers with a power-law spectrum, one with a red noise spectrum and one with the low-frequency part subtracted, we excited standing oscillations and the KH instability in our loops, after one-and-a-half periods of the oscillation. We see that our broadband drivers lead to fully deformed, turbulent loop cross-sections over the entire coronal part of the loop due to the spatially extended KH instability. The low RMS velocity of our driver without the low-frequency components supports the working hypothesis that the KH instability can easily manifest in oscillating coronal loops. We report for the first time in driven transverse oscillations of loops the apparent propagation of density perturbations due to the onset of the KH instability, from the apex towards the footpoints. Both drivers input sufficient energy to drive enthalpy and mass flux fluctuations along the loop, while also causing heating near the driven footpoint of the oscillating loop, which becomes more prominent when a low-frequency component is included in the velocity driver. Finally, our power-law driver with the low-frequency component provides a RMS input Poynting flux of the same order as the radiative losses of the quiet-Sun corona, giving us promising prospects for the contribution of decayless oscillations in coronal heating.

Oscillatory reconnection as a plasma diagnostic in the solar corona

Konstantinos **Karampelas**, James A. McLaughlin, Gert J. J. Botha, Stéphane Régnier
ApJ **943** 131 **2023**
https://arxiv.org/pdf/2301.02452.pdf

https://iopscience.iop.org/article/10.3847/1538-4357/acac90/pdf
Oscillatory reconnection is a relaxation process in magnetised plasma, with an inherent periodicity that is exclusively dependent on the properties of the background plasma. This study focuses on the seismological prospects of oscillatory reconnection in the solar corona. We perform three sets of parameter studies (for characteristic coronal values of the background magnetic field, density and temperature) using the PLUTO code to solve the fully compressive, resistive MHD equations for a 2D magnetic X-point. From each parameter study, we derive the period of the oscillatory reconnection. We find that this period is inversely proportional to the characteristic strength of the background magnetic field and the square root of the initial plasma temperature, while following a square root dependency upon the equilibrium plasma density. These results reveal an inverse proportionality between the magnitude of the Alfvén speed and the period, as well as the background sound speed and the period. Furthermore, we note that the addition of anisotropic thermal conduction only leads to a small increase in the mean value for the period. Finally, we establish an empirical formula that gives the value for the period in relation to the background magnetic field, density and temperature. This gives us a quantified relation for oscillatory reconnection, to be used as a plasma diagnostic in the solar corona, opening up the possibility of using oscillatory reconnection for coronal seismology.

The independence of oscillatory reconnection periodicity from the initial pulse

Konstantinos **Karampelas**, James A. McLaughlin, Gert J. J. Botha, Stéphane Régnier

ApJ **933** 142 **2022**

https://arxiv.org/pdf/2207.01980.pdf
https://iopscience.iop.org/article/10.3847/1538-4357/ac746a/pdf
Oscillatory reconnection can manifest through the interaction between the ubiquitous MHD waves and omnipresent null points in the solar atmosphere and is characterized by an inherent periodicity. In the current study, we focus on the relationship between the period of oscillatory reconnection and the strength of the wave pulse initially perturbing the null point, in a hot coronal plasma. We use the PLUTO code to solve the fully compressive, resistive MHD equations for a 2D magnetic X-point. Using wave pulses with a wide range of amplitudes, we perform a parameter study to obtain values for the period, considering the presence and absence of anisotropic thermal conduction separately. In both cases, we find that the resulting period is independent of the strength of the initial perturbation. The addition of anisotropic thermal conduction only leads to an increase in the mean value for the period, in agreement with our previous study. We also consider a different type of initial driver and we obtain an oscillation period matching the independent trend previously mentioned. Thus, we report for the first time on the independence between the type and strength of the initializing wave pulse and the resulting period of oscillatory reconnection in a hot coronal plasma. This makes oscillatory reconnection a promising mechanism to be used within the context of coronal seismology.

Transverse loop oscillations via vortex shedding: a self oscillating process

Konstantinos **Karampelas**, Tom Van Doorsselaere

ApJL **908** L7 **2021**

https://arxiv.org/pdf/2102.03332.pdf
https://doi.org/10.3847/2041-8213/abdc2b
Identifying the underlying mechanisms behind the excitation of transverse oscillations in coronal loops is essential for their role as diagnostic tools in coronal seismology and their potential use as wave heating mechanisms of the solar corona. In this paper, we explore the concept of these transverse oscillations being excited through a self-sustaining process, caused by Alfvénic vortex shedding from strong background flows interacting with coronal loops. We show for the first time in 3D simulations that vortex shedding can generate transverse oscillations in coronal loops, in the direction perpendicular to the flow due to periodic "pushing" by the vortices. By plotting the power spectral density we identify the excited frequencies of these oscillations. We see that these frequencies are dependent both on the speed of the flow, as well as the characteristics of the oscillating loop. This, in addition to the fact that the background flow is constant and not periodic, makes us treat this as a self-oscillating process. Finally, the amplitudes of the excited oscillations are near constant in amplitude, and are comparable with the observations of decay-less oscillations. This makes the mechanism under consideration a possible interpretation of these undamped waves in coronal loops.

Amplitudes and energy fluxes of simulated decayless kink oscillations

K. **Karampelas**, T. Van Doorsselaere, D. J. Pascoe, M. Guo, P. Antolin

Frontiers in Astronomy and Space Sciences (**2019**), 6, 38

https://arxiv.org/pdf/1906.02001.pdf
Recent observations with the Atmospheric Imaging Assembly (AIA) instrument on the SDO spacecraft have revealed the existence of decayless coronal kink oscillations. These transverse oscillations are not connected to any external phenomena like flares or coronal mass ejections, and show significantly lower amplitudes than the externally excited decaying oscillations. Numerical studies have managed to reproduce such decayless oscillations

in the form of footpoint driven standing waves in coronal loops, and to treat them as a possible mechanism for wave heating of the solar corona. Our aim is to investigate the correlation between the observed amplitudes of the oscillations and input the energy flux from different drivers. We perform 3D MHD simulations in single, straight, density-enhanced coronal flux tubes for different drivers, in the presence of gravity. Synthetic images at different spectral lines are constructed with the use of the FoMo code. The development of the Kelvin-Helmholtz instability leads to mixing of plasma between the flux tube and the hot corona. Once the KHI is fully developed, the amplitudes of the decayless oscillations show only a weak correlation with the driver strength. We find that low amplitude decayless kink oscillations may correspond to significant energy fluxes of the order of the radiative losses for the Quiet Sun. A clear correlation between the input energy flux and the observed amplitudes from our synthetic imaging data cannot be established. Stronger drivers lead to higher vales of the line width estimated energy fluxes. Finally, estimations of the energy fluxes by spectroscopic data are affected by the LOS angle, favoring combined analysis of imaging and spectroscopic data for single oscillating loops.

Wave heating in gravitationally stratified coronal loops in the presence of resistivity and viscosity

K. **Karampelas**, T. Van Doorsselaere, M. Guo
A&A 2019
https://arxiv.org/pdf/1901.02676.pdf
In recent years, coronal loops have been the focus of studies related to the damping of different magnetohydrodynamic (MHD) surface waves and their connection with coronal seismology and wave heating. For a better understanding of wave heating, we need to take into account the effects of different dissipation coefficients such as resistivity and viscosity, the importance of the loop physical characteristics, and the ways gravity can factor into the evolution of these phenomena. We aim to map the sites of energy dissipation from transverse waves in coronal loops in the presence and absence of gravitational stratification and to compare ideal, resistive, and viscous MHD. Using the PLUTO code, we performed 3D MHD simulations of kink waves in single, straight, density-enhanced coronal flux tubes of multiple temperatures. We see the creation of spatially expanded Kelvin-Helmholtz eddies along the loop, which deform the initial monolithic loop profile. For the case of driven oscillations, the Kelvin-Helmholtz instability develops despite physical dissipation, unless very high values of shear viscosity are used. Energy dissipation gets its highest values near the apex, but is present all along the loop. We observe an increased efficiency of wave heating once the kinetic energy saturates at the later stages of the simulation and a turbulent density profile has developed. The inclusion of gravity greatly alters the dynamic evolution of our systems and should not be ignored in future studies. Stronger physical dissipation leads to stronger wave heating in our set-ups. Finally, once the kinetic energy of the oscillating loop starts saturating, all the excess input energy turns into internal energy, resulting in more efficient wave heating.

Solar Soft X-ray Irradiance Variability III: Magnetic Field Variations of Coronal X-ray Features.

Kariyappa, R., Adithya, H.N., Masuda, S. et al.
Sol Phys 299, 46 (**2024**).
https://doi.org/10.1007/s11207-024-02289-9
The magnetic field changes the radiative output of the Sun and is the main source for all the solar surface features. To study the role of the underlying photospheric magnetic field in relation to emission features observed in the solar corona, we have used the full-disk soft X-ray images from Hinode/X-Ray Telescope (Hinode/XRT) and the magnetograms obtained from the Helioseismic and Magnetic Imager (HMI) on board the Solar Dynamics Observatory (SDO) for a period of about 13 years (May 2010 – June 2023), which covers Solar Cycle 24 and the ascending phase of Solar Cycle 25. A sophisticated and established algorithm developed in Python is applied to the X-ray observations from Hinode/XRT to segment the different coronal features by creating segmentation maps of the active regions (ARs), coronal holes (CHs), background regions (BGs), and X-ray bright points (XBPs). Further, these maps have been applied to the full-disk (FD) line-of-sight (LOS) magnetograms from HMI to isolate the X-ray coronal features and photospheric magnetic counterparts, respectively. We computed full-disk and featurewise averages of X-ray intensity and LOS magnetic field (MF) over ARs, CHs, BGs, XBPs, and FD regions. Variations in the quantities resulting from the segmentation, namely the mean intensity, temperature from the filter ratio method, and the unsigned magnetic field of ARs, CHs, BGs, XBPs, and FD regions, are intercompared and compared with the sunspot number (SSN). We find that the X-ray intensity and temperature over ARs, CHs, BGs, XBPs, and FD regions are well correlated with the underlying magnetic field. We discuss the intensity, temperature, and magnetic field variations of the full-disk corona and of all the features. The time series plots of the unsigned magnetic field of the full disk and all the features show magnetic field fluctuations synchronized with the solar cycle (sunspot number). Although

the magnetic field of all features varies, the mean, spatially smoothed magnitude of the magnetic field values estimated for the whole observed period of the full disk is around 8.9 ± 2.60 G, active regions (ARs) are around 34.4 ± 18.42 G, whereas BGs, CHs, and XBPs are 7.7 ± 1.72 G, 6.6 ± 1.04 G, and 15.62 ± 8.76 G, respectively. In addition, we find that the mean magnetic field contribution of the background regions (BGs) is around 85%, whereas ARs, CHs, and XBPs are 11%, 2%, and 2%, respectively, to the average magnetic field of the full disk. The magnetic field time series of all the features suggest that the features show a high variability in their magnetic field and the fluctuations in magnetic field are correlated to fluctuations in intensity and temperature, suggesting that the magnetic field is important in producing different emission features, which are associated with different intensity and temperature values. The magnetic field is responsible for the heating rate of the emission features, which are highly variable on solar cycle timescales. We conclude from the full-disk intensity-temperature-magnetogram analysis that the magnetic field plays a crucial role in driving the different brightenings, emissions, and temperature and heating of the corona at the sites of these magnetic features. In this study, we demonstrate that the segmented coronal features observed in the soft X-ray wavelength can be used as proxies to isolate the corresponding underlying magnetic structures.

Magnetic Reconnection between a Solar Jet and a Filament Channel

Garima **Karki**, Brigitte Schmieder, Pooja Devi, Ramesh Chandra, Nicolas Labrosse, Reetika Joshi, Bernard Gelly

2024

https://arxiv.org/pdf/2412.09206

The solar corona is highly structured by bunches of magnetic field lines forming either loops, or twisted flux ropes representing prominences/filaments, or very dynamic structures such as jets. The aim of this paper is to understand the interaction between filament channels and jets. We use high-resolution Hα spectra obtained by the ground-based Telescope Heliographique pour lEtude du Magnetisme et des Instabilites Solaires (THEMIS) in Canary Islands, and data from Helioseismic Magnetic Imager (HMI) and Atmospheric Imaging Assembly (AIA) aboard the Solar Dynamics Observatory (SDO). In this paper we present a multi-wavelength study of the interaction of filaments and jets. They both consist of cool plasma embedded in magnetic structures. A jet is particularly well studied in all the AIA channels with a flow reaching 100-180 km s−1. Its origin is linked to cancelling flux at the edge of the active region. Large Dopplershifts in Hα are derived in a typical area for a short time (order of min). They correspond to flows around 140 km s−1. In conclusion we conjecture that these flows correspond to some interchange of magnetic field lines between the filament channel and the jets leading to cool plasmoid ejections or reconnection jets perpendicularly to the jet trajectory. **2023 September 25**

Hot-cold plasma transition region: collisionless case

Marian **Karlicky**, Frantisek Karlicky

A&A **2017**

https://arxiv.org/pdf/1709.07622.pdf

We study processes at the transition region between hot (rare) and cold (dense) plasma in the collisionless regime. We use a 3-dimensional electromagnetic particle-in-cell (3-D PIC) relativistic code. Motivated by the transition region in the solar atmosphere the temperature and density ratio of the plasmas is chosen as 100 and 0.01, respectively. For better understanding of studied processes we make two types of computations: a) without any interactions among plasma particles (free expansion) and b) with the full electromagnetic interactions. In both the cases we found that the flux of cold plasma electrons and protons from colder plasma to hotter one dominates over the flux of hot plasma electrons and protons in the opposite direction. Thus, the plasma in the hotter part of the system becomes colder and denser during time evolution. In the case without any interactions among particles the cold plasma electrons and protons freely penetrate into the hot plasma. But, the cold plasma electrons are faster than cold plasma protons and therefore they penetrate deeper into the hotter part of the system than the protons. Thus, the cooling of the electron and proton components of the plasma in the hotter part of the system is different. On the other hand, in the case with the electromagnetic interactions, owing to the plasma property, which tries to keep the total electric current constant everywhere (close to zero in our case), the cold plasma electrons penetrate into the hotter part of the system together with the cold plasma protons. The plasma waves generated at the transition region during these processes reduce the number of electrons escaping from the hot plasma into the colder one. Therefore these waves support a temperature jump between hot and cold plasma.

The Formation and Maintenance of the Dominant Southern Polar Crown Cavity of Cycle 24

N. **Karna**1,2, J. Zhang2, and W. D. Pesnell

2017 ApJ 835 13

In this article, we report a study of the longest-lived polar crown cavity of Solar Cycle 24, using an observation from 2013, and propose a physical mechanism to explain its sustained existence. We used high temporal and spatial resolution observations from the Atmospheric Imaging Assembly (AIA) and the Helioseismic Magnetic Imager (HMI) instruments on board the Solar Dynamics Observatory (SDO) to explore the structure and evolution of the cavity. Although it existed for more than a year, we examined the circumpolar cavity in great detail from 2013 March 21 to 2013 October 31. Our study reinforces the existing theory of formation of polar crown filaments that involves two basic processes to form any polar crown cavity as well as the long-lived cavity that we studied here. First, the underlying polarity inversion line (PIL) of the circumpolar cavity is formed between (1) the trailing part of dozens of decayed active regions distributed in different longitudes and (2) the unipolar magnetic field in the polar coronal hole. Second, the long life of the cavity is sustained by the continuing flux cancellation along the PIL. The flux is persistently transported toward the polar region through surface meridional flow and diffusion. The continuing flux cancellation leads to the shrinking of the polar coronal hole.

STUDY OF THE 3D GEOMETRIC STRUCTURE AND TEMPERATURE OF A CORONAL CAVITY USING THE LIMB SYNOPTIC MAP METHOD

N. **Karna**1,2, J. Zhang2, W. Dean Pesnell1, and S. A. Hess Webbe

2015 ApJ 810 124

We present the three-dimensional geometric structure and thermal properties of a coronal cavity deduced from limb synoptic maps. The observations are extreme ultraviolet images from the Atmospheric Imager Assembly (AIA) and magnetic images from the Helioseismic Magnetic Imager instruments on board the Solar Dynamics Observatory. We describe a limb synoptic-map method used to effectively identify and measure cavities from annuli of radiance above the solar limb. We find that cavities are best seen in the 211, 193, and 171 Å passbands. The prominence associated with each cavity is best seen in the 304 Å synoptic maps. We also estimate the thermal properties of the cavity and surrounding plasma by combining the AIA radiances with a differential emission measure analysis. This paper focuses on one long cavity from a catalog of coronal cavities that we are developing. Cavities in this catalog are designated by a coded name using the Carrington Rotation number and position. Cavity C211347177N was observed during Carrington Rotation 2113 at the northwestern limb of the solar disk with an average latitude of 47° N and a central longitude of 177°. We showed the following. (1) The cavity is a long tube with an elliptical cross-section with ratios of the length to width and the length to height of 11:1 and 7:1, respectively. (2) The cavity is about 1360 Mm long, or 170° in longitude. (3) It is tilted in latitude. (4) And it is slightly hotter than its surroundings.

APPEARANCES AND STATISTICS OF CORONAL CAVITIES DURING THE ASCENDING PHASE OF SOLAR CYCLE 24

N. **Karna**1,2, W. D. Pesnell1, and J. Zhang

2015 ApJ 810 123

We present a survey of 429 coronal prominence cavities found between 2010 May and 2015 February using the Solar Dynamics Observatory (SDO)/Atmospheric Imaging Assembly limb synoptic maps. We examined correlations between each cavity's height, width, and length. Our findings showed that around 38% of the cavities were prolate, 27% oblate, and 35% circular in shape. The lengths of the cavities ranged from 0.06 to 2.9 . When a cavity is longer than 1.5 , it has a narrower height range (0.1–0.3), whereas when the cavity was shorter than 1.5 , it had a wider height range (0.07–0.5). We find that the overall three-dimensional topology of the long, stable cavities can be characterized as a long tube with an elliptical cross section. We also noted that the circular and oblate cavities are longer in length than the prolate cavities. We also studied the physical mechanisms behind the cavity drift toward the pole and found it to be tied to the meridional flow. Finally, by observing the evolution of the cavity regions using SDO/Helioseismic Magnetic Imager (HMI) surface magnetic field observations, we found that the cavities formed a belt near the polar coronal hole boundary; we call this the cavity belt. Our results showed that the cavity belt migrated toward higher latitude over time and the cavity belt disappeared after the polar magnetic field reversal. This result shows that cavity evolution provides new insight into the solar cycle.

Using Polar Coronal Hole Area Measurements to Determine the Solar Polar Magnetic Field Reversal in Solar Cycle 24

N. **Karna**, S. A. Hess Webber, W. D. Pesnell

Solar Phys., **2014**

An analysis of solar polar coronal hole (PCH) areas since the launch of the Solar Dynamics Observatory (SDO) shows how the polar regions have evolved during Solar Cycle 24. We present PCH areas from mid-2010 through 2013 using data from the Atmospheric Imager Assembly (AIA) and Helioseismic and Magnetic Imager (HMI)

instruments onboard SDO. Our analysis shows that both the northern and southern PCH areas have decreased significantly in size since 2010. Linear fits to the areas derived from the magnetic-field properties indicate that, although the northern hemisphere went through polar-field reversal and reached solar-maximum conditions in mid-2012, the southern hemisphere had not reached solar-maximum conditions in the polar regions by the end of 2013. Our results show that solar-maximum conditions in each hemisphere, as measured by the area of the polar coronal holes and polar magnetic field, will be offset in time.

Christian Horrebow's Sunspot Observations – II. Construction of a Record of Sunspot Positions

Christoffer **Karoff**, Carsten Sønderskov Jørgensen, V. Senthamizh Pavai, Rainer Arlt
Solar Phys. **2019**
https://arxiv.org/pdf/1906.10895.pdf
The number of spots on the surface of the Sun is one of the best tracers of solar variability we have. The sunspot number is not only known to change in phase with the 11-year solar cycles, but also to show variability on longer time scales. It is, however, not only the sunspot number that changes in connection with solar variability. The location of the spots on the solar surface is also known to change in phase with the 11-year solar cycle. This has traditionally been visualised in the so-called butterfly diagram, but this is only well constrained from the beginning of the 19th century. This is unfortunate, as knowledge about the butterfly diagram could aid our understanding of the variability and the Sun-Earth connection. As part of a larger review of the work done on sunspots by the Danish astronomer Christian Horrebow, we here present a reanalysis of Christian Horrebow's notebooks covering the years 1761 and 1764 - 1777. These notebooks have been analysed in at least three earlier studies by Thiele (Astron. Nachr. 50, 257, 1859), d'Arrest (published in Wolf, Astron. Mitt. Eidgenoss. Sternwarte Zur. 4, 77, 1873) and Hoyt and Schatten (Solar Phys. 160, 387, 1995). In this article, we construct a complete record of sunspot positions covering the years 1761 and 1764 - 1777. The resulting butterfly diagram shows the characteristic structure known from observations in the 19th and 20th century. We do see some indications of equatorial sunspots in the observations we have from Cycle 1. However, in Cycle 2, which has much better coverage, we do not see such indications.

The lost sunspot cycle: New support from Be10 measurements

C. **Karoff**, F. Inceoglu, M. F. Knudsen, J. Olsen, A. Fogtmann-Schulz
A&A, 575, A77 **2015**
http://arxiv.org/pdf/1412.2931v1.pdf
It has been suggested that the deficit in the number of spots on the surface of the Sun between 1790 and 1830, known as the Dalton minimum, contained an extra cycle that was not identified in the original sunspot record by Wolf. Though this cycle would be shorter and weaker than the average solar cycle, it would shift the magnetic parity of the solar magnetic field of the earlier cycles. This extra cycle is sometimes referred to as the 'lost solar cycle' or 'cycle 4b'. Here we reanalyse Be10 measurements with annual resolution from the NGRIP ice core in Greenland in order to investigate if the hypothesis regarding a lost sunspot cycle is supported by these measurements. Specifically, we make use of the fact that the Galactic cosmic rays, responsible for forming Be10 in the Earth's atmosphere, are affected differently by the open solar magnetic field during even and odd solar cycles. This fact enables us to evaluate if the numbering of cycles earlier than cycle 5 is correct. For the evaluation, we use Bayesian analysis, which reveals that the lost sunspot cycle hypothesis is likely to be correct. We also discuss if this cycle 4b is a real cycle, or a phase catastrophe, and what implications this has for our understanding of stellar activity cycles in general.

Predicting the Emergence of Solar Active Regions Using Machine Learning

Spiridon **Kasapis**, Irina N. Kitiashvili, Alexander G. Kosovichev, John T. Stefan, Bhairavi Apte
IAU Symposium 365 Proceedings **2024**
https://arxiv.org/pdf/2402.08890.pdf
To create early warning capabilities for upcoming Space Weather disturbances, we have selected a dataset of 61 emerging active regions, which allows us to identify characteristic features in the evolution of acoustic power density to predict continuum intensity emergence. For our study, we have utilized Doppler shift and continuum intensity observations from the Helioseismic and Magnetic Imager (HMI) onboard the Solar Dynamics Observatory (SDO). The local tracking of 30.66 x 30.66-degree patches in the vicinity of active regions allowed us to trace the evolution of active regions starting from the pre-emergence state. We have developed a machine learning model to capture the acoustic power flux density variations associated with upcoming magnetic flux emergence. The trained Long Short-Term Memory (LSTM) model is able to predict 5 hours ahead whether, in a given area of the solar surface, continuum intensity values will decrease. The performed study allows us to investigate the potential of the machine learning approach to predict the emergence of active regions using acoustic power maps as input.

Modeling the Center-to-limb Systematic in Normal-mode Coupling Measurements

Samarth G. **Kashyap** and Shravan M. Hanasoge

2025 ApJ 978 78

https://iopscience.iop.org/article/10.3847/1538-4357/ad9476/pdf

Solar meridional circulation (MC), which manifests as poleward flow near the surface, is a relatively weak flow. While MC has been measured through various local helioseismic techniques, there is a lack of consensus about the nature of the depth profile and location of return flow, owing to its small amplitude and poor signal-to-noise ratio in observations. The measurements are strongly hampered by systematic effects whose amplitudes are comparable to the signal induced by the flow, and modeling them is therefore crucial. The removal of the center-to-limb (C2L) systematic, which is the largest known feature hampering the inference of meridional flow, has been heuristically performed in helioseismic analyses, but its effect on global modes is not fully understood or modeled. Here, we propose both a way to model the C2L systematic and a method for estimation of meridional flow using global helioseismic cross-spectral analysis. We demonstrate that the systematic cannot be ignored while modeling the mode-coupling cross-spectral measurement, and thus is critical for the inference of MC. We also show that inclusion of a model for the C2L systematic improves shallow MC estimates from cross-spectral analysis.

Center-to-limb Variations in Solar Plage Using IRIS Observations

Pradeep **Kayshap** and Peter R. Young

2024 ApJ 977 141

https://iopscience.iop.org/article/10.3847/1538-4357/ad901d/pdf

The center-to-limb variations (CLV) of transition region line Gaussian fit parameters in solar plage are reported for the first time. The Si iv 1402.77 Å line observed by the Interface Region Imaging Spectrograph is used. The spectral intensity increases linearly from the disk center to the solar limb. Similarly, the nonthermal velocity also increases linearly from 23.6 (at the disk center) to 30.9 km s−1 (at the solar limb). On the other hand, the Doppler velocity decreases from 8.9 ± 1.0 at the disk center to 0.0 km s−1 at the limb. This CLV pattern in solar plages is consistent with the CLV pattern reported in the quiet Sun (QS). However, the average values of the parameters in the solar plage are significantly higher than in the QS. The intensity and nonthermal velocity increase linearly with the magnetic field at the disk center, while the Doppler velocity does not depend on the magnetic field. Due to the line-of-sight effect, the plasma column depth increases toward the solar limb, which leads to a linear increase in the spectral intensity. Further, the increasing plasma column depth toward the solar limb adds more and more unresolved motions, and as a result, the nonthermal velocity increases from the disk center to the solar limb. In the solar plages, the higher plasma density due to the strong magnetic field leads to higher intensity and nonthermal velocity compared to the QS and coronal hole. **(2014 December 14), 2015 February 15**

Characterising solar surface convection using Doppler measurements

Samarth G **Kashyap**, Shravan M Hanasoge

ApJ **916** 87 **2021**

https://arxiv.org/pdf/2105.12055.pdf

https://doi.org/10.3847/1538-4357/ac05bc

The Helioseismic Magnetic Imager (HMI) onboard the Solar Dynamics Observatory (SDO) records line-of-sight Dopplergram images of convective flows on the surface. These images are used to obtain the multi-scale convective spectrum. We design a pipeline to process the raw images to remove large-scale features like differential rotation, meridional circulation, limb shift and imaging artefacts. The Hierarchical Equal Area Pixelization scheme (HEALPix) is used to perform spherical harmonic transforms on the cleaned image. Because we only have access to line-of-sight velocities on half the solar surface, we define a "mixing matrix" to relate the observed and true spectra. This enables the inference of poloidal and toroidal flow spectra in a single step through the inversion of the mixing matrix. Performing inversions on a number of flow profiles, we find that the poloidal flow recovery is most reliable among all the components. We also find that the poloidal spectrum is in qualitative agreement with inferences from Local Correlation Tracking (LCT) of granules. The fraction of power in vertical motions increases as a function of wavenumber and is at 8% level for ℓ=1500. In contrast to seismic results and LCT, the flows show nearly no temporal-frequency dependence. Poloidal flow power peaks in the range of $\ell - |m| \approx 150-250$ which may potentially hint at a latitudinal preference for convective flows.

HMI Science Nuggets, #164, **2021** http://hmi.stanford.edu/hminuggets/?p=3646

Inferring Solar Differential Rotation through Normal-mode Coupling Using Bayesian Statistics

Samarth G. **Kashyap**5,1, Srijan Bharati Das5,2, Shravan M. Hanasoge1, Martin F. Woodard3, and Jeroen Tromp4

2021 ApJS 253 47

https://doi.org/10.3847/1538-4365/abdf5e

Normal-mode helioseismic data analysis uses observed solar oscillation spectra to infer perturbations in the solar interior due to global and local-scale flows and structural asphericity. Differential rotation, the dominant global-scale axisymmetric perturbation, has been tightly constrained primarily using measurements of frequency splittings via "a-coefficients." However, the frequency-splitting formalism invokes the approximation that multiplets are isolated. This assumption is inaccurate for modes at high angular degrees. Analyzing eigenfunction corrections, which respect cross-coupling of modes across multiplets, is a more accurate approach. However, applying standard inversion techniques using these cross-spectral measurements yields a-coefficients with a significantly wider spread than the well-constrained results from frequency splittings. In this study, we apply Bayesian statistics to infer a-coefficients due to differential rotation from cross-spectra for both f-modes and p-modes. We demonstrate that this technique works reasonably well for modes with angular degrees $\ell = 50–291$. The inferred a3-coefficients are found to be within 1 nHz of the frequency-splitting values for $\ell > 200$. We also show that the technique fails at $\ell < 50$ owing to the insensitivity of the measurement to the perturbation. These results serve to further establish mode-coupling as an important helioseismic technique with which to infer internal structure and dynamics, both axisymmetric (e.g., meridional circulation) and non-axisymmetric perturbations.

A zone of preferential ion heating extends tens of solar radii from Sun

Justin C. **Kasper**, Kris G. Klein, Tristan Weber, Milan Maksimovic, Arnaud Zaslavsky, Stuart D. Bale, Ben A. Maruca, Michael L. Stevens, Anthony W. Case

ApJ **2017**

https://arxiv.org/pdf/1708.05683.pdf

The extreme temperatures and non-thermal nature of the solar corona and solar wind arise from an unidentified physical mechanism that preferentially heats certain ion species relative to others. Spectroscopic indicators of unequal temperatures commence within a fraction of a solar radius above the surface of the Sun, but the outer reach of this mechanism has yet to be determined. Here we present an empirical procedure for combining interplanetary solar wind measurements and a modeled energy equation including Coulomb relaxation to solve for the typical outer boundary of this zone of preferential heating. Applied to two decades of observations by the Wind spacecraft, our results are consistent with preferential heating being active in a zone extending from the transition region in the lower corona to an outer boundary 20-40 solar radii from the Sun, producing a steady state super-mass-proportional α-to-proton temperature ratio of 5.2−5.3. Preferential ion heating continues far beyond the transition region and is important for the evolution of both the outer corona and the solar wind. The outer boundary of this zone is well below the orbits of spacecraft at 1 AU and even closer missions such as Helios and MESSENGER, meaning it is likely that no existing mission has directly observed intense preferential heating, just residual signatures. We predict that {Parker Solar Probe} will be the first spacecraft with a perihelia sufficiently close to the Sun to pass through the outer boundary, enter the zone of preferential heating, and directly observe the physical mechanism in action.

Vortex Flows in the Solar Chromosphere -- I. Automatic detection method

Yoshiaki **Kato**, Sven Wedemeyer

A&A 601, A135 **2017**

https://arxiv.org/pdf/1702.06032.pdf

https://www.aanda.org/articles/aa/pdf/2017/05/aa30082-16.pdf

Solar "magnetic tornadoes" are produced by rotating magnetic field structures that extend from the upper convection zone and the photosphere to the corona of the Sun. Recent studies show that such rotating features are an integral part of atmospheric dynamics and occur on a large range of spatial scales. A systematic statistical study of magnetic tornadoes is a necessary next step towards understanding their formation and their role for the mass and energy transport in the solar atmosphere. For this purpose, we have developed a new automatic detection method for chromospheric swirls, i.e. the observable signature of solar tornadoes or, more generally, chromospheric vortex flows and rotating motions. Unlike the previous studies that relied on visual inspections, our new method combines a line integral convolution (LIC) imaging technique and a scalar quantity which represents a vortex flow on a two-dimensional plane. We have tested two detection algorithms, based on the enhanced vorticity and vorticity strength quantities, by applying them to 3D numerical simulations of the solar atmosphere with CO5BOLD. We conclude that the vorticity strength method is superior compared to the enhanced vorticity method in all aspects. Applying the method to a numerical simulation of the solar atmosphere revealed very abundant small-scale, short-lived chromospheric vortex flows that had not been found by visual inspection before.

Chromospheric and Coronal Wave Generation in a Magnetic Flux Sheath

Yoshiaki **Kato**, Osker Steiner, Viggo Hansteen, Boris Gudiksen, Sven Wedemeyer, Mats Carlsson

ApJ **2016**

http://arxiv.org/pdf/1606.08826v1.pdf

Using radiation magnetohydrodynamic simulations of the solar atmospheric layers from the upper convection zone to the lower corona, we investigate the self-consistent excitation of slow magneto-acoustic body waves (slow modes) in a magnetic flux concentration. We find that the convective downdrafts in the close surroundings of a two-dimensional flux slab "pump" the plasma inside it in the downward direction. This action produces a downflow inside the flux slab, which encompasses ever higher layers, causing an upwardly propagating rarefaction wave. The slow mode, excited by the adiabatic compression of the downflow near the optical surface, travels along the magnetic field in the upward direction at the tube speed. It develops into a shock wave at chromospheric heights, where it dissipates, lifts the transition region, and produces an offspring in the form of a compressive wave that propagates further into the corona. In the wake of downflows and propagating shock waves, the atmosphere inside the flux slab in the chromosphere and higher tends to oscillate with a period of $\nu \approx 4$~mHz. We conclude that this process of "magnetic pumping" is a most plausible mechanism for the direct generation of longitudinal chromospheric and coronal compressive waves within magnetic flux concentrations, and it may provide an important heat source in the chromosphere. It may also be responsible for certain types of dynamic fibrils.

Inferring solar differential rotation through normal-mode coupling using Bayesian statistics

Samarth G. **Kashyap**, Srijan Bharati Das, Shravan M. Hanasoge, Martin F. Woodard, Jeroen Tromp
ApJ **2021**
https://arxiv.org/pdf/2101.08933.pdf
Normal-mode helioseismic data analysis uses observed solar oscillation spectra to infer perturbations in the solar interior due to global and local-scale flows and structural asphericity. Differential rotation, the dominant global-scale axisymmetric perturbation, has been tightly constrained primarily using measurements of frequency splittings via "a-coefficients". However, the frequency-splitting formalism invokes the approximation that multiplets are isolated. This assumption is inaccurate for modes at high angular degrees. Analysing eigenfunction corrections, which respect cross coupling of modes across multiplets, is a more accurate approach. However, applying standard inversion techniques using these cross-spectral measurements yields a-coefficients with a significantly wider spread than the well-constrained results from frequency splittings. In this study, we apply Bayesian statistics to infer a-coefficients due to differential rotation from cross spectra for both f-modes and p-modes. We demonstrate that this technique works reasonably well for modes with angular degrees $\ell = 50-291$. The inferred a_3−coefficients are found to be within 1 nHz of the frequency splitting values for $\ell > 200$. We also show that the technique fails at $\ell < 50$ owing to the insensitivity of the measurement to the perturbation. These results serve to further establish mode coupling as an important helioseismic technique with which to infer internal structure and dynamics, both axisymmetric (e.g., meridional circulation) and non-axisymmetric perturbations.

Energy conversion rate of an active region transient brightening estimated by a spectroscopic observation of Hinode

Toshiki **Kawai**, Shinsuke Imada
ApJ **918** 51 **2021**
https://arxiv.org/pdf/2106.06208.pdf
https://doi.org/10.3847/1538-4357/ac09eb
We statistically estimate the conversion rate of the energy released during an active-region transient brightening to Doppler motion and thermal and non-thermal energies. We used two types of datasets for the energy estimation and detection of transient brightenings. One includes spectroscopic images of Fe xiv, Fe xv, and Fe xvi lines observed by the Hinode/EUV Imaging Spectrometer. The other includes images obtained from the 211 Åchannel of the Solar Dynamics Observatory/Atmospheric Imaging Assembly (AIA). The observed active region was NOAA 11890 on **November 09, 2013**, and the day after that. As a result, the released Doppler motion and non-thermal energies were found to be approximately 0.1 \-- 1% and 10 \-- 100% of the change in the amount of thermal energy in each enhancement, respectively. Using this conversion rate, we estimated the contribution of the total energy flux of AIA transient brightenings to the active region heating to be at most 2% of the conduction and radiative losses.

Energy Distribution of Small-scale Flares Derived Using a Genetic Algorithm

Toshiki **Kawai** and Shinsuke Imada
2021 ApJ 906 2
https://doi.org/10.3847/1538-4357/abc9ae
https://arxiv.org/pdf/2011.06390.pdf
To understand the mechanism of coronal heating, it is crucial to derive the contribution of small-scale flares, the so-called nanoflares, to the heating up of the solar corona. To date, several studies have tried to derive the occurrence frequency distribution of flares as a function of energy to reveal the contribution of small-scale flares. However, there are no studies that derive the distribution with considering the following conditions: (1) evolution of the

coronal loop plasma heated by small-scale flares, (2) loops smaller than the spatial resolution of the observed image, and (3) multiwavelength observation. To take into account these conditions, we introduce a new method to analyze small-scale flares statistically based on a one-dimensional loop simulation and a machine learning technique, that is, genetic algorithm. First, we obtain six channels of SDO/AIA light curves of the active-region coronal loops. Second, we carry out many coronal loop simulations and obtain the SDO/AIA light curves for each simulation in a pseudo-manner. Third, using the genetic algorithm, we estimate the best combination of simulated light curves that reproduce the observation. Consequently, the observed coronal loops are heated by small-scale flares with energy flux larger than that typically required to heat up an active region intermittently. Moreover, we derive the occurrence frequency distribution which have various power-law indices in the range from 1 to 3, which partially supports the nanoflare heating model. In contrast, we find that 90% of the coronal heating is done by flares that have energy larger than 1025 erg. **30 May 2018**

Propagation of Waves above a Plage as Observed by IRIS and SDO

P. **Kayshap**, A.K. Srivastava, S.K. Tiwari, P. Jelinek, M. Mathioudakis
A&A 634, A63 **2020**
https://arxiv.org/pdf/1910.11557.pdf
sci-hub.si/10.1051/0004-6361/201936070
Context. MHD waves are proposed to transport sufficient energy from the photosphere to heat the transition-region (TR) and corona. However, various aspects of these waves such as their nature, propagation characteristics and role in the atmospheric heating process remain poorly understood and are a matter of further investigation. Aims. We aim to investigate wave propagation within an active-region (AR) plage using IRIS and AIA observations. The main motivation is to understand the relationship between photospheric and TR oscillations. We plan to identify the locations in the plage region where magnetic flux tubes are essentially vertical, and further our understanding of the propagation and nature of these waves. Methods. We have used photospheric observations from AIA (i.e., AIA 1700 Å) as well as TR imaging observations (IRIS/SJI Si iv 1400.0 Å). We have investigated propagation of the waves into the TR from the photosphere using wavelet analysis (e.g., cross power, coherence and phase difference) with inclusion of a customized noise model. Results. Fast Fourier Transform(FFT) shows the distribution of wave power at photospheric & TR heights. Waves with periods between 2.0- and 9.0-minutes appear to be correlated between the photosphere and TR. We exploited a customized noise model to estimate 95% confidence levels for IRIS observations. On the basis of the sound speed in the TR and estimated propagation speed, these waves are best interpreted as the slow magneto acoustic waves (SMAW). It is found that almost all locations show correlation/propagation of waves over broad range of period from photosphere to TR. It suggests the wave's correlation/propagation spatial occurrence frequency is very high within the plage area. **28 July 2014**

Vertical Propagation of Acoustic Waves in the Solar Inter-Network as Observed by IRIS

P.**Kayshap**, K. Murawski, A.K. Srivastava, Z.E. Musielak, B.N. Dwivedi
MNRAS 479, Issue 4, 1 October **2018**, Pages 5512–5521
https://arxiv.org/pdf/1807.01449.pdf
We investigate the Interface Region Imaging Spectrograph (IRIS) observations of the quiet-Sun (QS) to understand the propagation of acoustic waves in transition region (TR) from photosphere. We selected a few IRIS spectral lines, which include the photospheric (Mn~{\sc i} 2801.25~{\AA}), chromospheric (Mg~{\sc ii} k 2796.35~{\AA}) and TR (C~{\sc ii} 1334.53~{\AA}), to investigate the acoustic wave propagation.The wavelet cross-spectrum reveals significant coherence (about 70\% locations) between photosphere and chromosphere. Few minutes oscillations (i.e., period range from 1.6 to 4.0 minutes) successfully propagate into chromosphere from photosphere, which is confirmed by dominance of positive phase lags. However, in higher period regime (i.e., greater than $\approx$ 4.5 minutes), the downward propagation dominates is evident by negative phase lags. The broad spectrum of waves (i.e., 2.5-6.0 minutes) propagates freely upwards from chromosphere to TR. We find that only about 45\% locations (out of 70\%) show correlation between chromosphere and TR. Our results indicate that roots of 3 minutes oscillations observed within chromosphere/TR are located in photosphere. Observations also demonstrate that 5 minute oscillations propagate downward from chromosphere. \textbf{However, some locations within QS also show successful propagation of 5 minute oscillations as revealed by positive phase lags, which might be the result of magnetic field}. In addition, our results clearly show that a significant power, within period ranging from 2.5 to 6.0 minutes, of solar chromosphere is freely transmitted into TR triggering atmospheric oscillations. Theoretical implications of our observational results are discussed.

Active Region Irradiance During Quiescent Periods: New Insights from Sun-as-a-star Spectra

Maria D. **Kazachenko**, Hugh Hudson
ApJ **901** 64 **2020**
https://arxiv.org/pdf/2008.02702.pdf
https://doi.org/10.3847/1538-4357/abada6

How much energy do solar active regions (ARs) typically radiate during quiescent periods? This is a fundamental question for storage and release models of flares and ARs, yet it is presently poorly answered by observations. Here we use the "Sun-as-a-point-source" spectra from the EUV Variability Experiment (EVE) on the Solar Dynamics Observatory (SDO) to provide a novel estimate of radiative energy losses of an evolving active region. Although EVE provides excellent spectral (5-105nm) and temperature (2-25MK) coverage for AR analysis, to our knowledge, these data have not been used for this purpose due to the lack of spatial resolution and the likelihood of source confusion. Here we present a way around this problem. We analyze EVE data time series, when only one large AR 11520 was present on the disk. By subtracting the quiet Sun background, we estimate the radiative contribution in EUV from the AR alone. We estimate the mean AR irradiance and cumulative AR radiative energy losses in the 1-300A and astronomical standard ROSAT-PSPC, 3-124A, passbands and compare these to the magnetic energy injection rate through the photosphere, and to variations of the solar cycle luminosity. We find that while AR radiative energy losses are ~100 times smaller than typical magnetic energy injection rates at the photosphere, they are an order of magnitude larger or similar to the bolometric radiated energies associated with large flares. This study is the first detailed analysis of AR thermal properties using EVE Sun-as-a-star observations, opening doors to AR studies on other stars. **~11 July 2012**

Modeling the Effects of Observational Gaps on p-mode Oscillation Parameters

J. Z. **Keith-Hardy**1,2, S. C. Tripathy3, and K. Jain
2019 ApJ 877 148
sci-hub.se/10.3847/1538-4357/ab1b3b
We investigate the effect of the window function on the parameters of solar acoustic oscillations, namely frequency, amplitude, and width, using the data from Global Oscillation Network Group (GONG). This is carried out by simulating 108 new time series from a base time series by modifying the window functions. In order to minimize the effect of solar activity, the base time series was chosen during the activity minimum period. The new window functions were randomly chosen from a set of 30 observed window functions to incorporate the reported duty cycles of the GONG network. The modified time series were processed through the standard GONG p-mode pipeline to extract the mode parameters that were fitted to a linear model as a function of the duty cycle to yield the correction factor. We find significant changes between the observed and corrected amplitudes and widths while the change in mode frequencies was found to be insignificant. We also analyze the variation of the corrected mode parameters over the solar cycles 23 and 24 and compare their correlations with 10.7 cm radio flux, which represents a proxy of the solar activity.

Tracking Solar Phenomena from the SDO

Dustin J. **Kempton**, Michael A. Schuh, and Rafal A. Angryk
2018 ApJ 869 54
sci-hub.tw/10.3847/1538-4357/aae9e9
This paper focuses on the problem of tracking solar phenomena by creating spatiotemporal trajectories from solar event detection reports. Though tracking of multiple objects in video sequences has seen much research and improvement in recent years, there has been relatively little focus on the domain of tracking solar phenomena (events). In this work, we improve on our previous endeavors by eliminating offline model training requirements and utilizing crowd-sourced human labels to evaluate our performance. We apply our method to the metadata of two solar event types spanning 4 yr of detection reports from the automated detection modules for the Solar Dynamics Observatory mission. We compare our results with those produced by the detection module for active regions and coronal holes by using a crowd-sourced trajectory database as the ground truth. We show that our results are as good as or better than the event-specific detection module for these two event types. This is especially promising because our tracking algorithm is a generalized module for all solar events, and not specific to a single event type, allowing it to be applied to other solar event types reported to the Heliophysics Event Knowledgebase that do not contain tracking information**. 2012-01-20**

Scale Selection in the Stratified Convection of the Solar Photosphere

M. **Kessar**, D.W. Hughes, E. Kersale, K.A. Mizerski, S.M. Tobias
2019 *ApJ* **874** 103
https://arxiv.org/pdf/1802.01309.pdf
sci-hub.se/10.3847/1538-4357/ab07bf
We examine the role of stratification in determining the length scales of turbulent anelastic convection. Motivated by the range of scales observed in convection at the solar photosphere, we perform local numerical simulations of convection for a range of density contrasts in large domains, analyzing both the Eulerian and Lagrangian statistics of the flow. We consider the two cases of constant dynamic viscosity and constant kinematic viscosity. We discuss the implications of our results to the issue of solar mesogranulation.

Application of Mutual Information Methods in Time-Distance Helioseismology

Dustin **Keys**, Shukur Kholikov, Alexei Pevtsov
Solar Phys. Volume 290, Issue 3, pp 659-671 **2015**
http://arxiv.org/pdf/1501.05597v1.pdf
We apply a new technique, the mutual information (MI) from information theory, to time-distance helioseismology, and demonstrate that it can successfully reproduce several classic results based on the widely used cross-covariance method. MI quantifies the deviation of two random variables from complete independence, and represents a more general method for detecting dependencies in time series than the cross-covariance function, which only detects linear relationships. We provide a brief description of the MI-based technique and discuss the results of the application of MI to derive the solar differential profile, a travel-time deviation map for a sunspot and a time-distance diagram from quiet Sun measurements.
See HMI Science Nuggets, #36, March 2015
http://hmi.stanford.edu/hminuggets/?p=1142

Equator to Pole Solar Chromospheric Differential Rotation using Ca-K Features Derived from Kodaikanal Data

Hema **Kharayat**, Jagdev Singh, Muthu Priyal, B. Ravindra
ApJL **2024**
https://arxiv.org/pdf/2405.07532
Differential rotation is one of the basic characteristics of the Sun, and it plays an important role in generating the magnetic fields and its activities. We investigated rotation rate using chromospheric features such as plages, enhanced network, active network, and quiet network separately (for the first time). The digitized Ca-K images from Kodaikanal Observatory for 1907-1996 are used to study rotation over 0-80 degrees latitudes at an interval of 10∘ . We find that plages and all types of networks exhibit the differential rotation of the chromosphere. Furthermore, the rotation rate shows a decreasing pattern as one move from the equator to the higher polar latitudes for all the features used in the study. By analyzing how the area of chromospheric features varies over time, we can effectively map the Sun's rotation rate at all latitudes, including the polar regions. Interestingly, both plages and small-scale networks exhibit similar differential rotation rate. This suggests these features likely rooted at the same layer below the visible surface of the Sun. Therefore, the long-term Ca-K data is very useful to study the solar rotation rate at all latitudes including the polar regions.

Association of solar flares with coronal mass ejections accompanied by Deca-Hectometric type II radio burst for two solar cycles 23 and 24

Hema **Kharayat**, Lalan Prasad & Sumit Pant
Astrophysics and Space Science May **2018**, 363:87
http://sci-hub.tw/10.1007/s10509-018-3309-y
The aim of present study is to find the association of solar flares with coronal mass ejections (CMEs) accompanied by Deca-Hectometric (DH) type II radio burst for the period 1997–2014 (solar cycle 23 and ascending phase of solar cycle 24). We have used a statistical analysis and found that 10–20∘ latitudinal belt of northern region and 80–90∘ longitudinal belts of western region of the sun are more effective for flare-CME accompanied by DH type II radio burst events. M-class flares (52%) are in good association with the CMEs accompanied by DH type II radio burst. Further, we have calculated the flare position and found that most frequent flare site is at the center of the CME span. However, the occurrence probability of all flares is maximum outside the CME span. X-class flare associated CMEs have maximum speed than that of M, C, and B-class flare associated CMEs. We have also found a good correlation between flare position and central position angle of CMEs accompanied by DH type II radio burst.

Study of cosmic ray intensity and geomagnetic storms with solar wind parameters during the period 1998–2005

Hema **Kharayat**, Lalan Prasad
Astrophysics and Space Science January **2017**, 362:20
http://link.springer.com/article/10.1007/s10509-016-2996-5?wt_mc=alerts.TOCjournals
The aim of this paper is to study the effect of solar wind parameters (solar wind speed VV, plasma flow pressure, and plasma density) on cosmic ray intensity and on geomagnetic storms for the period 1998–2005 (solar cycle 23). A Chree analysis by the superposed epoch method has been done for the study. From the present study we have found that the solar wind speed is a highly effective parameter in producing cosmic ray intensity decreases and geomagnetic storms. No time lag is found between cosmic ray intensity decreases, geomagnetic storms, and peak value of solar wind speed. Further, we have found that the plasma flow pressure is effectively correlated with geomagnetic storms but it is weakly correlated with cosmic ray intensity. The cosmic ray intensity and geomagnetic storms are found to be weakly correlated with plasma density. The decrease in cosmic ray intensity and geomagnetic storms takes place one day after the peak values of plasma flow pressure and plasma density. There is a time lag of one day between solar wind parameters (plasma flow pressure and plasma density) and

cosmic ray intensity decrease, geomagnetic storms. Also, we have found a high correlation of cosmic ray intensity and geomagnetic storms with the product of interplanetary magnetic field BB and solar wind speed VV i.e. B·VB·V. This study may be useful in predicting the space-weather phenomena.

Photospheric Velocity Structures during the Emergence of Small Active Regions on the Sun

Anna **Khlystova**, Shin Toriumi
2017 ApJ 839 63
http://iopscience.iop.org.sci-hub.cc/0004-637X/839/1/63/
https://arxiv.org/pdf/1704.02482.pdf
We study the plasma flows in the solar photosphere during the emergence of two small active regions, NOAA 9021 and 10768. Using SOHO/MDI data, we find that the strong plasma upflows appear at the initial stage of active region formation, with maximum upflow velocities of -1650 and -1320 m/s. The structures with enhanced upflows have size about 8 Mm in diameter, and they exist for 1-2 hr. The parameters of the enhanced upflows are consistent with those of the large active region NOAA 10488, which may suggest the possibility that the elementary emerging magnetic loops that appear at the earliest phase of active region formation have similar properties, irrespective of scales of active regions. Comparison between the observations and a numerical simulation of magnetic flux emergence shows a striking consistency. We find that the driving force of the plasma upflow is at first the gas pressure gradient and later the magnetic pressure gradient. **2000.05.27-31, 2003.10.26 , 2005.05.25-28**,

Photospheric Velocity Structures during the Emergence of Small Active Regions on the Sun

Anna **Khlystova**, Shin Toriumi
ApJ **2017**
https://arxiv.org/pdf/1704.02482.pdf
We study the plasma flows in the solar photosphere during the emergence of two small active regions, NOAA 9021 and 10768. Using SOHO/MDI data, we find that the strong plasma upflows appear at the initial stage of active region formation, with maximum upflow velocities of -1650 and -1320 m/s. The structures with enhanced upflows have size about 8 Mm in diameter, and they exist for 1-2 hr. The parameters of the enhanced upflows are consistent with those of the large active region NOAA 10488, which may suggest the possibility that the elementary emerging magnetic loops that appear at the earliest phase of active region formation have similar properties, irrespective of scales of active regions. Comparison between the observations and a numerical simulation of magnetic flux emergence shows a striking consistency. We find that the driving force of the plasma upflow is at first the gas pressure gradient and later the magnetic pressure gradient. **2000.05.27 , 2003.10.26, 2005.05.25,**

Meridional Flow in the Solar Convection Zone I: Measurements from GONG Data

Shukur **Kholikov**, Alexander Serebryanskiy, Jason Jackiewicz
2014 ApJ 784 145
http://arxiv.org/pdf/1403.5026v1.pdf
Large-scale plasma flows in the Sun's convection zone likely play a major role in solar dynamics on decadal timescales. In particular, quantifying meridional motions is a critical ingredient for understanding the solar cycle and the transport of magnetic flux. Because the signal of such features can be quite small in deep solar layers and be buried in systematics or noise, the true meridional velocity profile has remained elusive. We perform time-distance helioseismology measurements on several years worth of GONG Doppler data. A spherical harmonic decomposition technique is applied to a subset of acoustic modes to measure travel-time differences to try to obtain signatures of meridional flows throughout the solar convection zone. Center-to-limb systematics are taken into account in an intuitive, yet ad hoc manner. Travel-time differences near the surface that are consistent with a poleward flow in each hemisphere and are similar to previous work are measured. Additionally, measurements in deep layers near the base of the convection zone suggest a possible equatorward flow, as well as partial evidence of a sign change in the travel-time differences at mid-convection zone depths. This analysis on an independent data set using different measurement techniques strengthens recent conclusions that the convection zone may have multiple "cells" of meridional flow. The results may challenge the common understanding of one large conveyor belt operating in the solar convection zone. Further work with helioseismic inversions and a careful study of systematic effects are needed before firm conclusions of these large-scale flow structures can be made.

Influence of ambipolar and Hall effects on vorticity in 3D simulations of magneto-convection

E. Khomenko, M. Collados, N. Vitas, P. A. Gonzalez-Morales
Philosophical Transactions of the Royal Society A **2020**

https://arxiv.org/pdf/2009.09753.pdf
This paper presents the results of the analysis of 3D simulations of solar magneto-convection that include the joint action of the ambipolar diffusion and the Hall effect. Three simulation-runs are compared: one including both ambipolar diffusion and Hall effect; one including only ambipolar diffusion; and one without any of these two effects. The magnetic field is amplified from initial field to saturation level by the action of turbulent local dynamo. In each of these cases, we study 2 hours of simulated solar time after the local dynamo reaches the saturation regime. We analyze the power spectra of vorticity, of magnetic field fluctuations and of the different components of the magnetic Poynting flux responsible for the transport of vertical or horizontal perturbations. Our preliminary results show that the ambipolar diffusion produces a strong reduction of vorticity in the upper chromospheric layers and that it dissipates the vortical perturbations converting them into thermal energy. The Hall effect acts in the opposite way, strongly enhancing the vorticity. When the Hall effect is included, the magnetic field in the simulations becomes, on average, more vertical and long-lived flux tube-like structures are produced. We trace a single magnetic structure to study its evolution pattern and the magnetic field intensification, and their possible relation to the Hall effect.

Three-dimensional simulations of solar magneto-convection including effects of partial ionization

E. **Khomenko**, N. Vitas, M. Collados, A. de Vicente
A&A 618, A87 **2018**
https://arxiv.org/pdf/1807.01061.pdf
Over the last decades, realistic 3D radiative-MHD simulations have become the dominant theoretical tool for understanding the complex interactions between the plasma and the magnetic field on the Sun. Most of such simulations are based on approximations of magnetohydrodynamics, without directly considering the consequences of the very low degree of ionization of the solar plasma in the photosphere and bottom chromosphere. The presence of large amount of neutrals leads to a partial decoupling of the plasma and the magnetic field. As a consequence of that, a series of non-ideal effects (ambipolar diffusion, Hall effect and battery effect) arises. The ambipolar effect is the dominant one in the solar chromosphere. Here we report on the first three-dimensional realistic simulations of magneto-convection including ambipolar diffusion and battery effects. The simulations are done using the newly developed Mancha3D code. Our results reveal that ambipolar diffusion causes measurable effects on the amplitudes of waves excited by convection in the simulations, on the absorption of Poynting flux and heating and on the formation of chromospheric structures. We provide a low limit on the chromospheric temperature increase due to the ambipolar effect using the simulations with battery-excited dynamo fields.

Numerical simulations of quiet Sun magnetic fields seeded by Biermann battery

E. **Khomenko**, N. Vitas, M. Collados, A. de Vicente
A&A 604, A66 **2017**
https://arxiv.org/pdf/1706.06037.pdf
The magnetic fields of the quiet Sun cover at any time more than 90\% of its surface and their magnetic energy budget is crucial to explain the thermal structure of the solar atmosphere. One of the possible origins of these fields is due to the action of local dynamo in the upper convection zone of the Sun. Existing simulations of the local solar dynamo require an initial seed field, and sufficiently high spatial resolution, in order to achieve the amplification of the seed field to the observed values in the quiet Sun. Here we report an alternative model of seeding based on the action of the Bierman battery effect. This effect generates a magnetic field due to the local imbalances in electron pressure in the partially ionized solar plasma. We show that the battery effect self-consistently creates from zero an initial seed field of a strength of the order of micro G, and together with dynamo amplification, allows the generation of quiet Sun magnetic fields of a similar strength to those from solar observations.

On the effects of ion-neutral interactions in solar plasmas

Elena **Khomenko**
Plasma Physics and Controlled Fusion", Volume 59, Number 1, **2016**
https://arxiv.org/pdf/1611.06063v1.pdf
Solar photosphere and chromosphere are composed of weakly ionized plasma for which collisional coupling decreases with height. This implies a breakdown of some hypotheses underlying magnetohydrodynamics at low altitudes and gives rise to non-ideal MHD effects such as ambipolar diffusion, Hall effect, etc. Recently, there has been progress in understanding the role of these effects for the dynamics and energetics of the solar atmosphere. There are evidences that such phenomena as wave propagation and damping, magnetic reconnection, formation of stable magnetic field concentrations, magnetic flux emergence, etc. can be affected. This paper reviews the current state-of-the-art of multi-fluid MHD modeling of the coupled solar atmosphere.

Oscillations and Waves in Sunspots Review

Elena **Khomenko** and Manuel Collados Vera

Living Reviews in Solar Physics PUB.NO. lrsp-**2015**-6

http://solarphysics.livingreviews.org/Articles/lrsp-2015-6/download/lrsp-2015-6Color.pdf

A magnetic field modifies the properties of waves in a complex way. Significant advances have been made recently in our understanding of the physics of sunspot waves with the help of high-resolution observations, analytical theories, as well as numerical simulations. We review the current ideas in the field, providing the most coherent picture of sunspot oscillations as by present understanding. 20-28 Jan 2002

Evershed flow observed in neutral and singly ionized iron lines

E. **Khomenko**1,2, M. Collados1,2, N. Shchukina1,3 and A. Díaz

A&A 584, A66 (**2015**)

The amplitudes of the Evershed flow are measured using pairs of carefully selected Fe i and Fe ii spectral lines that are close in wavelength and registered simultaneously. A sunspot belonging to the NOAA 11582 group was scanned using the spectrograph of the German Vacuum Tower Telescope (Observatorio del Teide, Tenerife). Velocities were extracted from intensity profiles using the λ-meter technique. The formation heights of the observed spectral lines were calculated using semi-empirical models of a bright and dark penumbral filament taking into account the sunspot location at the limb. Our objective is to compare azimuthally averaged amplitudes of the Evershed flow extracted from neutral and ion lines. We find measurable differences in the radial component of the flow. All five pairs of lines show the same tendency; the flow measured from the Fe i lines has an amplitude that is a few hundred ms-1 larger than that of the Fe ii lines. This tendency is preserved at all photospheric heights and radial distances in the penumbra. We discuss the possible origin of this effect.

Beyond MHD: modeling and observation of partially ionized solar plasma processes

Elena **Khomenko**

Proceedings of the XI Scientific Meeting of the Spanish Astronomical Society, Teruel, Spain (**2014**)

http://arxiv.org/pdf/1504.01578v1.pdf

The temperature and density conditions in the magnetized photosphere and chromosphere of the Sun lead to a very small degree of atomic ionization. In addition, at particular height, the magnetic field may be strong enough to give rise to a cyclotron frequency larger than the collisional frequency for some species, while for others the opposite may happen. These circumstances influence the collective behavior of the particles and some of the hypotheses of magnetohydrodynamics may be relaxed, giving rise to non-ideal MHD effects. In this paper we discuss our recent developments in modeling non-ideal plasma effects derived from the presence of a large amount of neutrals in the solar photosphere and the chromosphere, as well as observational consequences of these effects.

Context-Aware Neural Video Compression on Solar Dynamics Observatory

Atefeh **Khoshkhahtinat**, Ali Zafari, Piyush M. Mehta, Nasser M. Nasrabadi, Barbara J. Thompson, Michael S. F. Kirk, Daniel da Silva

IEEE 22nd International Conference on Machine Learning and Applications **2023**

https://arxiv.org/pdf/2309.10784.pdf

NASA's Solar Dynamics Observatory (SDO) mission collects large data volumes of the Sun's daily activity. Data compression is crucial for space missions to reduce data storage and video bandwidth requirements by eliminating redundancies in the data. In this paper, we present a novel neural Transformer-based video compression approach specifically designed for the SDO images. Our primary objective is to efficiently exploit the temporal and spatial redundancies inherent in solar images to obtain a high compression ratio. Our proposed architecture benefits from a novel Transformer block called Fused Local-aware Window (FLaWin), which incorporates window-based self-attention modules and an efficient fused local-aware feed-forward (FLaFF) network. This architectural design allows us to simultaneously capture short-range and long-range information while facilitating the extraction of rich and diverse contextual representations. Moreover, this design choice results in reduced computational complexity. Experimental results demonstrate the significant contribution of the FLaWin Transformer block to the compression performance, outperforming conventional hand-engineered video codecs such as H.264 and H.265 in terms of rate-distortion trade-off.

Collisionless Magnetic Reconnection and Waves: Progress Review.

Khotyaintsev YV, Graham DB, Norgren C and Vaivads A

(**2019**) Front. Astron. Space Sci. 6:70. doi: 10.3389/fspas.2019.00070

sci-hub.se/10.3389/fspas.2019.00070

Magnetic reconnection is a fundamental process whereby microscopic plasma processes cause macroscopic changes in magnetic field topology, leading to explosive energy release. Waves and turbulence generated during the reconnection process can produce particle diffusion and anomalous resistivity, as well as heat the plasma and accelerate plasma particles, all of which can impact the reconnection process. We review progress on waves related to reconnection achieved using high resolution multi-point in situ observations over the last decade, since early Cluster and THEMIS observations and ending with recent Magnetospheric Multiscale results. In particular, we focus on the waves most frequently observed in relation to reconnection, ranging from low-frequency kinetic Alfvén waves (KAW), to intermediate frequency lower hybrid and whistler-mode waves, electrostatic broadband and solitary waves, as well as the high-frequency upper hybrid, Langmuir, and electron Bernstein waves. Significant progress has been made in understanding localization of the different wave modes in the context of the reconnection picture, better quantification of generation mechanisms and wave-particle interactions, including anomalous resistivity. Examples include: temperature anisotropy driven whistlers in the flux pileup region, anomalous effects due to lower-hybrid waves, upper hybrid wave generation within the electron diffusion region, wave-particle interaction of electrostatic solitary waves. While being clearly identified in observations, some of the wave processes remain challenging for reconnection simulations (electron Bernstein, upper hybrid, Langmuir, whistler), as the instabilities (streaming, loss-cone, shell) which drive these waves require high resolution of distribution functions in phase space, and realistic ratio of Debye to electron inertia scales. We discuss how reconnection configuration, i.e., symmetric vs. asymmetric, guide-field vs. antiparallel, affect wave occurrence, generation, effect on particles, and feedback on the overall reconnection process. Finally, we outline some of the major open questions, such as generation of electromagnetic radiation by reconnection sites and role of waves in triggering/onset of reconnection.

Anti-phase oscillations of Hα line Doppler velocity and width in solar limb spicules

D. **Khutsishvili** , T. V. Zaqarashvili, E. Khutsishvili, T. Kvernadze, V. Kulidzanishvili, V. Kakhiani, M. Sikharulidze

Astrophysics and Space Science December **2017**, 362:235

https://link.springer.com/content/pdf/10.1007%2Fs10509-017-3213-x.pdf

Spectroscopic observations of limb spicules were carried out during **September 25 and October 17–19, 2012** in Hαα line using large 53-cm non-eclipsing coronagraph of Abastumani Astrophysical Observatory (Georgia). The spectrograph slit was located at the height of about 7500 km above the solar limb. Spectrograms in Hαα line were obtained in a second order of the spectrograph, where reversed dispersion equal to 0.96 Å/mm. Doppler velocities and FWHM of 35 spicules were measured with the average cadence of 4.5 s and standard error equal to ±0.3 km/s and 0.03 Å, respectively. Lifetimes of almost all measured spicules were 12–16 min, therefore they resemble type I spicules. We studied the temporal variations of Doppler shift and width of Hαα line using the Lomb periodogram algorithm for unevenly distributed time series. We found the oscillations in both, velocity and width, with periods of 4–9 min (240–540 s) at confidence levels of 95% and clear anti-phase relations (stronger Doppler velocity–weaker Doppler width and vice versa) between Doppler velocity and FWHM in all 35 spicules. The observed anti-phase oscillation with long periods can be explained by up and down motions of turbulent plasma in type I spicules, but the oscillations with shorter periods can be caused by helical motion of spicule axis formed after superposition of two linearly polarised magnetohydrodynamic kink waves.

Quasi-periodic variations in Doppler velocities of Hα spicules

E. **Khutshishvili**, V. Kulidzanishvili, T. Kvernadze, T. V. Zaqarashvili, V. Kakhiani, D. Khutsishvili, M. Sikharulidze

Astrophysics and Space Science October **2014**, 354:2100

New series of CCD spectral observations of spicules were obtained using 53-cm Lyot coronagraph of Abastumani Astrophysical Observatory (Georgia) at 5500 km height above the solar limb on **October 17, 2012** in Hα spectral line. The line-of-sight Doppler velocities of 34 spicules were measured with the cadence of 4.5 s and standard error equal to ±0.3 km/s. Life times of almost all measured spicules were 5–6 min (and longer), therefore they resemble the type I spicules. No short lived structures (similar to type II spicules) were identified during the time series neither inside nor outside the observed spicules. The Doppler velocity time series were processed using Lomb Periodogram Algorithm revealing 4 types of dominating period intervals centered around: 254 s, 136 s, 94 s and 65 s having confidence levels over 95 %. The oscillations with periods around 254 s can be caused by quasi-periodic rebound shocks after the propagation of photospheric pulses. The oscillations with periods around 136 s can be caused by the oscillation of spicules axis at the kink cut-off frequency in gravitationally stratified magnetic tubes. In this case, seismological estimations give the density scale height as 380–540 km for the kink wave speed of 70–100 km/s in spicules. Shorter period oscillations are probably caused by propagating kink waves in spicules.

Transverse oscillations in 3D along Ca II K bright fibrils in the Solar chromosphere

Sepideh **Kianfar**, Jorrit Leenaarts, Sara Esteban Pozuelo, João M. da Silva Santos, Jaime de la Cruz Rodríguez, Sanja Danilovic
A&A **2022**
https://arxiv.org/pdf/2210.14089.pdf
Fibrils in the solar chromosphere carry transverse oscillations as determined from non-spectroscopic imaging data. They are estimated to carry an energy flux of several kW m−2, which is a significant fraction of the average chromospheric radiative energy losses. We aim to determine oscillation properties of fibrils not only in the plane-of-the-sky (horizontal) direction, but also along the line-of-sight (vertical) direction. We obtained imaging-spectroscopy data in Fe I 6173, Ca II 8542, and Ca II K obtained with the Swedish 1-m Solar Telescope. We created a sample of 120 bright Ca II K fibrils and measured their horizontal motions. Their vertical motion was determined through non-LTE inversion of the observed spectra. We determined the periods and velocity amplitudes of the fibril oscillations, as well as phase differences between vertical and horizontal oscillations in the fibrils. The bright Ca II K fibrils carry transverse waves with a mean period of 2.2×102 s, and a horizontal velocity amplitude of 2 km s−1, consistent with earlier results. The mean vertical velocity amplitude is 1 km s−1. We find that 118 out of the 120 fibrils carry waves in both the vertical and horizontal directions, and 55 of those have identical periods. For those 55, we find that all phase differences between 0 and 2π occur, with a mild but significant preference for linearly polarized waves (phase difference of 0 or π). The results are consistent with the scenario where transverse waves are excited by granular buffeting at the photospheric footpoints of the fibrils. Estimates of transverse wave flux based on imaging data only are too low because they ignore the contribution of the vertical velocity.

Physical properties of bright Ca II K fibrils in the solar chromosphere

Sepideh **Kianfar**, Jorrit Leenaarts, Sanja Danilovic, Jaime de la Cruz Rodríguez, Carlos José Díaz Baso
A&A 637, A1 **2020**
https://arxiv.org/pdf/2003.11302.pdf
https://www.aanda.org/articles/aa/pdf/2020/05/aa37572-20.pdf
Broad-band images of the solar chromosphere in the Ca II H&K line cores around active regions are covered with fine bright elongated structures called bright fibrils. The mechanisms that form these structures and cause them to appear bright are still unknown. We aim to investigate the physical properties, such as temperature, line-of-sight velocity, and microturbulence, in the atmosphere that produces bright fibrils and to compare those to the properties of their surrounding atmosphere. We used simultaneous observations of a plage region in Fe I 6301-2 Å, Ca II 8542 Å, Ca II K, and Hα acquired by the CRISP and CHROMIS instruments on the Swedish 1-m Solar Telescope. We manually selected a sample of 282 Ca II K bright fibrils. We compared the appearance of the fibrils in our sample to the Ca II 8542 Å and Hα data. We performed non-local thermodynamic equilibrium (non-LTE) inversions using the inversion code STiC on the Fe I 6301-2 Å, Ca II 8542 Å, Ca II K lines to infer the physical properties of the atmosphere. The line profiles in bright fibrils have a higher intensity in their K2 peaks compared to profiles formed in the surrounding atmosphere. The inversion results show that the atmosphere in fibrils is on average 100−200~K hotter at an optical depth log(τ)=−4.3 compared to their surroundings. The line-of-sight velocity at chromospheric heights in the fibrils does not show any preference towards upflows or downflows. The microturbulence in the fibrils is on average 0.5 km s−1 higher compared to their surroundings. Our results suggest that the fibrils have a limited extent in height, and they should be viewed as hot threads pervading the chromosphere. **2016-09-15**

Linear Polarization Features in the Quiet-Sun Photosphere: Structure and Dynamics

S. **Kianfar**, S. Jafarzadeh, M. T. Mirtorabi, T. L. Riethmüller
Solar Phys. 293:123 **2018**
https://arxiv.org/pdf/1807.04633.pdf
https://link.springer.com/content/pdf/10.1007%2Fs11207-018-1341-2.pdf
We present detailed characteristics of linear polarization features (LPFs) in the quiet-Sun photosphere from high resolution observations obtained with Sunrise/IMaX. We explore differently treated data with various noise levels in linear polarization signals, from which structure and dynamics of the LPFs are studied. Physical properties of the detected LPFs are also obtained from the results of Stokes inversions. The number of LPFs, as well as their sizes and polarization signals, are found to be strongly dependent on the noise level, and on the spatial resolution. While the linear polarization with signal-to-noise ratio ≥4.5 covers about 26% of the entire area in the least noisy data in our study (with a noise level of 1.7×10−4 in the unit of Stokes I continuum), the detected (spatially resolved) LPFs cover about 10% of the area at any given time, with an occurrence rate on the order of 8×10−3 s−1 arcsec−2. The LPFs were found to be short lived (in the range of 30−300 s), relatively small structures (radii of ≈0.1−1.5 arcsec), highly inclined, posing hG fields, and move with an average horizontal speed of 1.2 km s−1. The LPFs were observed (almost) equally on both upflow and downflow regions, with intensity contrast always larger than that of the the average quiet-Sun.

They Do Change After All: 25 Years of GONG Data Reveal Variation of p-Mode Energy Supply Rates

René **Kiefer**, Anne-Marie Broomhall
MNRAS **2020**
https://arxiv.org/pdf/2010.06287.pdf
It has been shown over and over again that the parameters of solar p modes vary through the solar activity cycle: frequencies, amplitudes, lifetimes, energies. However, so far, the rates at which energy is supplied to the p modes have not been detected to be sensitive to the level of magnetic activity. We set out to re-inspect their temporal behaviour over the course of the last two Schwabe cycles. For this, we use Global Oscillation Network Group (GONG) p-mode parameter tables. We analyse the energy supply rates for modes of harmonic degrees l=0-150 and average over the azimuthal orders and, subsequently, over modes in different parameter ranges. This averaging greatly helps in reducing the noise in the data.We find that energy supply rates are anti-correlated with the level of solar activity, for which we use the F10.7 index as a proxy. Modes of different mode frequency and harmonic degrees show varying strengths of anti-correlation with the F10.7 index, reaching as low as r=−0.82 for low frequency modes with l=101-150. In this first dedicated study of solar p-mode energy supply rates in GONG data, we find that they do indeed vary through the solar cycle. Earlier investigations with data from other instruments were hindered by being limited to low harmonic degrees or by the data sets being too short. We provide tables of time-averaged energy supply rates for individual modes as well as for averages over disjunct frequency bins.

GONG p-mode parameters through two solar cycles

René **Kiefer**, Rudi Komm, Frank Hill, Anne-Marie Broomhall, Markus Roth
Solar Phys. 293:151 **2018**
https://arxiv.org/pdf/1810.09324.pdf
We investigate the parameters of global solar p-mode oscillations, namely damping width Γ, amplitude A, mean squared velocity ⟨v2⟩, energy E, and energy supply rate dE/dt, derived from two solar cycles' worth (1996 - 2018) of Global Oscillation Network Group (GONG) time series for harmonic degrees l=0−150. We correct for the effect of fill factor, apparent solar radius, and spurious jumps in the mode amplitudes. We find that the amplitude of the activity related changes of Γ and A depends on both frequency and harmonic degree of the modes, with the largest variations of Γ for modes with 2400μHz≤ν≤3300μHz and 31≤l≤60 with a min-to-max variation of 26.6±0.3% and of A for modes with 2400μHz≤ν≤3300μHz and 61≤l≤100 with a min-to-max variation of 27.4±0.4%. The level of correlation between the solar radio flux F10.7 and mode parameters also depends on mode frequency and harmonic degree. As a function of mode frequency, the mode amplitudes are found to follow an asymmetric Voigt profile with νmax=3073.59±0.18μHz. From the mode parameters, we calculate physical mode quantities and average them over specific mode frequency ranges. This way, we find that the mean squared velocities ⟨v2⟩ and energies E of p modes are anti-correlated with the level of activity, varying by 14.7±0.3% and 18.4±0.3%, respectively, and that the mode energy supply rates show no significant correlation with activity. With this study we expand previously published results on the temporal variation of solar p-mode parameters. Our results will be helpful to future studies of the excitation and damping of p modes, i.e., the interplay between convection, magnetic field, and resonant acoustic oscillations.

The Effect of Toroidal Magnetic Fields on Solar Oscillation Frequencies

René **Kiefer**, Markus Roth
ApJ **854** 74 **2018**
https://arxiv.org/pdf/1801.07932.pdf
http://iopscience.iop.org/article/10.3847/1538-4357/aaa3f7/pdf
Solar oscillation frequencies change with the level of magnetic activity. Localizing subsurface magnetic field concentrations in the Sun with helioseismology will help us to understand the solar dynamo. Because the magnetic fields are not considered in standard solar models, adding them to the basic equations of stellar structure changes the eigenfunctions and eigenfrequencies. We use quasi-degenerate perturbation theory to calculate the effect of toroidal magnetic fields on solar oscillation mean multiplet frequencies for six field configurations. In our calculations, we consider both the direct effect of the magnetic field, which describes the coupling of modes, and the indirect effect, which accounts for changes in stellar structure due to the magnetic field. We limit our calculations to self-coupling of modes. We find that the magnetic field affects the multiplet frequencies in a way that depends on the location and the geometry of the field inside the Sun. Comparing our theoretical results with observed shifts, we find that strong tachocline fields cannot be responsible for the observed frequency shifts of p modes over the solar cycle. We also find that part of the surface effect in helioseismic oscillation frequencies might be attributed to magnetic fields in the outer layers of the Sun. The theory presented here is also applicable to models of solar-like stars and their oscillation frequencies.

Three-lobed near-infrared Stokes V profiles in the quiet Sun

Christoph **Kiess**, Juan Manuel Borrero and Wolgang Schmidt
A&A 616, A109 (**2018**)

http://sci-hub.tw/https://www.aanda.org/articles/aa/abs/2018/08/aa32267-17/aa32267-17.html
Context. The 1.5-m GREGOR solar telescope can resolve structures as small as 0.4″ at near-infrared wavelengths on the Sun. At this spatial resolution the polarized solar spectrum shows complex patterns, such as large horizontal and/or vertical variations of the physical parameters in the solar photosphere.
Aims. We investigate a region of the quiet solar photosphere exhibiting three-lobed Stokes V profiles in the Fe I spectral line at 15 648 Å. The data were acquired with the GRIS spectropolarimeter attached to the GREGOR telescope. We aim at investigating the thermal, kinematic and magnetic properties of the atmosphere responsible for these measured complex signals.
Methods. The SIR inversion code is employed to retrieve the physical parameters of the lower solar photosphere from the observed polarization signals. We follow two different approaches. On the one hand, we consider that the multi-lobe circular polarization signals are only produced by the line-of-sight variation of the physical parameters. We therefore invert the data assuming a single atmospheric component that occupies the entire resolution element in the horizontal plane and where the physical parameters vary with optical depth τ (i.e., line-of-sight). On the other hand, we consider that the multi-lobe circular polarization signals are produced not by the optical depth variations of the physical parameters but instead by their horizontal variations. Here we invert the data assuming that the resolution element is occupied by two different atmospheric components where the kinematic and magnetic properties are constant along the line-of-sight.
Results. Both approaches reveal some common features about the topology responsible for the observed three-lobed Stokes Vsignals: both a strong (>1000 Gauss) and a very weak (<10 Gauss) magnetic field with opposite polarities and harboring flows directed in opposite directions must co-exist (either vertically or horizontally interlaced) within the resolution element.
Conclusions.

Properties of sunspot umbrae observed in cycle 24

Christoph **Kiess**, Reza Rezaei and Wolfgang Schmidt
A&A 565, A52 (**2014**)
Aims. There is an ongoing debate whether the solar activity cycle is overlaid with a long-term decline that may lead to another grand minimum in the near future. We used the size, intensity, and magnetic field strength of sunspot umbrae to compare the present cycle 24 with the previous one.
Methods. We used data of the Helioseismic and Magnetic Imager on board the Solar Dynamics Observatory and selected all sunspots between May 2010 and October 2012, using one image per day. We created two subsets of this dataset with a manual tracking algorithm, both without duplication. One contains each sunspot (910 umbrae within 488 spots) and was used to analyze the distribution of umbral areas, selected with an automated thresholding method. The other subset contains 205 fully evolved sunspots. We estimated their magnetic field and the total magnetic flux and discuss the relations between umbral size, minimum continuum intensity, maximum field strength, and total magnetic flux.
Results. We find non-linear relations between umbral minimum intensity and size and between maximum magnetic field strength and size. The field strength scales linearly with the intensity and the umbral size scales roughly linearly with the total magnetic flux, while the size and field strength level off with stronger flux. When separated into hemispheres and averaged temporally, the southern umbrae show a temporal increase in size and the northern umbrae remain constant. We detected no temporal variation in the umbral mean intensity. The probability density function of the umbral area in the ascending phase of the current solar cycle is similar to that of the last solar cycle.
Conclusions. From our investigation of umbral area, magnetic field, magnetic flux, and umbral intensity of the sunspots of the rising phase of cycle 24, we do not find a significant difference to the previous cycle, and hence no indication for a long-term decline of solar activity.

Temporal and Periodic Variation of the MCMESI for the Last Two Solar Cycles; Comparison with the Number of Different Class X-ray Solar Flares

Ali **Kilcik**, Partha Chowdhury, Volkan Sarp, Vasyl Yurchyshyn, Burcin Donmez, Jean-Pierre Rozelot & Atila Ozguc
Solar Physics volume 295, Article number: 159 (**2020**)
https://link.springer.com/content/pdf/10.1007/s11207-020-01711-2.pdf
In this study we compared the temporal and periodic variations of the Maximum CME Speed Index (MCMESI) and the the number of different class (C, M, and X) solar X-ray flares for the last two solar cycles (Solar Cycles 23 and 24). To obtain the correlation between the MCMESI and solar flare numbers the cross-correlation analysis was applied to monthly data sets. Also to investigate the periodic behavior of all data sets the Multi Taper Method (MTM) and the Morlet wavelet analysis method were performed with daily data from 2009 to 2018. To evaluate our wavelet analysis Cross Wavelet Transform (XWT) and Wavelet Transform Coherence (WTC) methods were performed. Causal relationship between data sets were further examined by Convergence Cross Mapping (CCM) method. As results of our analysis we found the following: i) The C class X-ray flare numbers increased about 16%

during the Solar Cycle 24 compared to Cycle 23, while all other data sets decreased; the MCMESI decreased about 16% and the number of M and X class flares decreased about 32%. ii) All the X-ray solar flare classes show remarkable positive correlation with the MCMESI. While the correlation between the MCMESI and C class flares comes from the general solar cycle trend, it mainly results from the fluctuations in the data in case of the X class flares. iii) In general, all class flare numbers and the MCMESI show similar periodic behavior. iv) The 546-day periodicity detected in the MCMESI may not be of solar origin or at least the solar flares are not the source of this periodicity. v) C and M class solar flares have a stronger causative effect on the MCMESI compared to X class solar flares. However, the only bidirectional causal relationship is obtained between the MCMESI and C class flare numbers.

Temporal and Periodic Variations of Sunspot Counts in Flaring and Non-flaring Active Regions

A. **Kilcik**, V. Yurchyshyn, B. Donmez, V.N. Obridko, A. Ozguc, J.P. Rozelot
Solar Phys. **2017**
https://arxiv.org/pdf/1705.09065.pdf

We analyzed temporal and periodic behavior of sunspot counts (SSCs) in flaring (C, M, or X class flares), and non-flaring active regions (ARs) for the almost two solar cycles (1996 through 2016). Our main findings are as follows: i) The temporal variation of monthly means of daily total SSCs in flaring and non-flaring ARs are different and these differences are also varying from cycle to cycle; temporal profile of non-flaring ARs are wider than the flaring ones during the solar cycle 23, while they are almost the same during the current cycle 24. The second peak (second maximum) of flaring ARs are strongly dominate during current cycle 24, while this difference is not such a remarkable during cycle 23. The amplitude of SSCs in the non-flaring ARs are comparable during the first and second peaks (maxima) of the current solar cycle, while the first peak is almost not existent in case of the flaring ARs. ii) Periodic variations observed in SSCs of flaring and non-flaring ARs are quite different in both MTM spectrum and wavelet scalograms and these variations are also different from one cycle to another; the largest detected period in the flaring ARs is 113 days, while there are much higher periodicities (327, 312, and 256 days) in non-flaring ARs. There are no meaningful periodicities in MTM spectrum of flaring ARs exceeding 45 days during solar cycle 24, while a 113 days periodicity detected from flaring ARs of solar cycle 23. For the non-flaring ARs the largest period is 72 days during solar cycle 24, while the largest period is 327 days during current cycle.

Active Latitude Oscillations Observed on the Sun

A. **Kilcik**, V. Yurchyshyn, F. Clette, A. Ozguc, J.-P. Rozelot
Solar Phys. Volume 291, Issue 4, pp 1077-1087 **2016**
http://arxiv.org/pdf/1604.00831v1.pdf

We investigate periodicities in mean heliographic latitudes of sunspot groups, called active latitudes, for the last six complete solar cycles (1945-2008). For this purpose, the Multi Taper Method and Morlet Wavelet analysis methods were used. We found the following: 1) Solar rotation periodicities (26-38 days) are present in active latitudes of both hemispheres for all the investigated cycles (18 to 23). 2) Both in the northern and southern hemispheres, active latitudes drifted towards the equator starting from the beginning to the end of each cycle by following an oscillating path. These motions are well described by a second order polynomial. 3) There are no meaningful periods between 55 and about 300 days in either hemisphere for all cycles. 4) A 300 to 370 day periodicity appears in both hemispheres for Cycle 23, in the northern hemisphere for Cycle 20, and in the southern hemisphere for Cycle 18.

Solar Cycle 24: Curious Changes in the Relative Numbers of Sunspot Group Types

A. **Kilcik**1, V. B. Yurchyshyn2,3, A. Ozguc4, and J. P. Rozelot
2014 ApJ 794 L2

Here, we analyze different sunspot group (SG) behaviors from the points of view of both the sunspot counts (SSCs) and the number of SGs, in four categories, for the time period of 1982 January-2014 May. These categories include data from simple (A and B), medium (C), large (D, E, and F), and decaying (H) SGs. We investigate temporal variations of all data sets used in this study and find the following results. (1) There is a very significant decrease in the large groups' SSCs and the number of SGs in solar cycle 24 (cycle 24) compared to cycles 21-23. (2) There is no strong variation in the decaying groups' data sets for the entire investigated time interval. (3) Medium group data show a gradual decrease for the last three cycles. (4) A significant decrease occurred in the small groups during solar cycle 23, while no strong changes show in the current cycle (cycle 24) compared to the previous ones. We confirm that the temporal behavior of all categories is quite different from cycle to cycle and it is especially flagrant in solar cycle 24. Thus, we argue that the reduced absolute number of the large SGs is largely, if not solely, responsible for the weak cycle 24. These results might be important for long-term space weather predictions to understand the rate of formation of different groups of sunspots during a solar cycle and the possible consequences for the long-term geomagnetic activity.

Sunspot Count Periodicities in Different Zurich Sunspot Group Classes Since 1986

A. **Kilcik**, A. Ozguc, V. Yurchyshyn, J. P. Rozelot

Solar Phys., **2014**

We used two methods to investigate the periodic behavior of sunspot counts in four categories for the time period January 1986 – October 2013. These categories include the counts from simple (A and B), medium (C), large (D, E, and F), and final (final-stage; H) sunspot groups. We used i) the multitaper method with red noise approximation, and ii) the Morlet wavelet transform for periodicity analysis. Our main findings are that 1) the solar rotation periodicity of about 25 to 37 days, which is of obvious significance, is found in all groups with at least a 95 % significance level; 2) the periodic behavior of a cycle is strongly related to its amplitude and group distribution during the cycle; 3) the appearance of periods follows the amplitude of the investigated solar cycles; and that 4) meaningful periods do not appear during the minimum phases of the investigated cycles.
We would like to underline that the cyclic behavior of all categories is not exactly the same; there are some differences between these groups. This result can provide a clue for the better understanding of solar cycles.

One Possible Reason for Double-Peaked Maxima in Solar Cycles: Is a Second Maximum of Solar Cycle 24 Expected?

A. **Kilcik**, A. Ozguc

Solar Physics, April **2014**, Volume 289, Issue 4, pp 1379-1386

We investigate solar activity by focusing on double maxima in solar cycles and try to estimate the shape of the current solar cycle (Cycle 24) during its maximum. We analyzed data for Solar Cycle 24 by using Learmonth Solar Observatory sunspot-group data collected since 2008. All sunspot groups (SGs) recorded during this time interval were separated into two groups: The first group includes small SGs [A, B, C, and H classes according to the Zurich classification], the second group consists of large SGs [D, E, and F]. We then calculated how many small and large sunspot groups occurred, their sunspot numbers [SSN], and the Zurich numbers [Rz] from their daily mean numbers as observed on the solar disk during a given month. We found that the temporal variations for these three different separations behave similarly. We also analyzed the general shape of solar cycles from Cycle 1 to 23 by using monthly International Sunspot Number [ISSN] data and found that the durations of maxima were about 2.9 years. Finally, we used the ascending time and SSN relationship and found that the maximum of Solar Cycle 24 is expected to occur later than 2011. Thus, we conclude that i) one possible reason for a double maximum in solar cycles is the different behavior of large and small sunspot groups, and ii) a double maximum is expected for Solar Cycle 24.

A Statistical Study of the Relationship Between the Sunspot Number, Maximum CME Speed and Geomagnetic Indices

A **Kilcik**, V.B. Yurchyshyn, V. Abramenko, P.R. Goode, N. Gopalswamy, A. Ozguc and J.P. Rozelot

BBSO Preprint #1424, **2010; File**

We investigated the relationship between the monthly averaged maximal speeds of coronal mass ejections (CMEs), sunspot number (SSN) and the geomagnetic Dst and Ap indices covering the 1996-2008 time interval. The study was carried out using frequency and correlation analyses. Frequency analysis of the maximum speed of CMEs (or CME speed index) shows a cyclic behavior similar to that found for SSN and the Ap index. Our new findings are as follows. 1) Unlike the SSN, the CME speed index does not exhibit a double peak maximum. 2) The CME speed index has a correlative relationship with SSN and Dst and Ap indices (correlation coefficients are 0.76, -0.53, 0.68 respectively). Various peculiarities in the monthly Dst index are better correlated with the fine structures in the CME speed profile than that in the SSN data. 3) Similar to the Ap index, both CME speed and the Dst indices lag behind the sunspot numbers by several months. We thus conclude that CME speed index may be a good parameter to describe the geo-effectiveness of solar activity.

Sources of the Slow Solar Wind During the Solar Cycle 23/24 Minimum

E. K. J. **Kilpua**, M. S. Madjarska, N. Karna, T. Wiegelmann, C. Farrugia, W. Yu, K. Andreeova

Solar Phys. Volume 291, Issue 8, pp 2441–2456 **2016**

We investigate the characteristics and the sources of the slow (\({<}\,450~\mbox{km}\,\mbox{s}^{-1}\)) solar wind during the four years (2006 – 2009) of low solar activity between Solar Cycles 23 and 24. We used a comprehensive set of in-situ observations in the near-Earth solar wind (Wind and ACE) and removed the periods when large-scale interplanetary coronal mass ejections were present. The investigated period features significant variations in the global coronal structure, including the frequent presence of low-latitude active regions in 2006 – 2007, long-lived low- and mid-latitude coronal holes in 2006 – mid-2008 and mostly the quiet Sun in 2009. We examined Carrington rotation averages of selected solar plasma, charge state, and compositional parameters and distributions of these

parameters related to the quiet Sun, active region Sun, and the coronal hole Sun. While some of the investigated parameters (e.g. speed, the C+6/C+4 and He/H ratios) show clear variations over our study period and with solar wind source type, some (Fe/O) exhibit very little changes. Our results highlight the difficulty of distinguishing between the slow solar wind sources based on the inspection of solar wind conditions.

Statistical Study of Strong and Extreme Geomagnetic Disturbances and Solar Cycle Characteristics

E. K. J. **Kilpua**1, N. Olspert2, A. Grigorievskiy2, M. J. Käpylä2, E. I. Tanskanen2, H. Miyahara3, R. Kataoka4,5, J. Pelt2,6, and Y. D. Liu

2015 ApJ 806 272

We study the relation between strong and extreme geomagnetic storms and solar cycle characteristics. The analysis uses an extensive geomagnetic index AA data set spanning over 150 yr complemented by the Kakioka magnetometer recordings. We apply Pearson correlation statistics and estimate the significance of the correlation with a bootstrapping technique. We show that the correlation between the storm occurrence and the strength of the solar cycle decreases from a clear positive correlation with increasing storm magnitude toward a negligible relationship. Hence, the quieter Sun can also launch superstorms that may lead to significant societal and economic impact. Our results show that while weaker storms occur most frequently in the declining phase, the stronger storms have the tendency to occur near solar maximum. Our analysis suggests that the most extreme solar eruptions do not have a direct connection between the solar large-scale dynamo-generated magnetic field, but are rather associated with smaller-scale dynamo and resulting turbulent magnetic fields. The phase distributions of sunspots and storms becoming increasingly in phase with increasing storm strength, on the other hand, may indicate that the extreme storms are related to the toroidal component of the solar large-scale field.

Temporal and Periodic Variation of the MCMESI for the Last Two Solar Cycles; Comparison with the Number of Different Class X-Ray Solar Flares

A. **Kilcik**, P. Chowdhury, V. Sarp, V. Yurchyshyn, B. Donmez, J.P. Rozelot, A. Ozguc

Solar Phys. **2020**

https://arxiv.org/ftp/arxiv/papers/2008/2008.11506.pdf

In this study we compared the temporal and periodic variations of the Maximum CME Speed Index (MCMESI) and the number of different class (C, M, and X) solar X-Ray flares for the last two solar cycles (Cycle 23 and 24). To obtain the correlation between the MCMESI and solar flare numbers the cross correlation analysis was applied to monthly data sets. Also to investigate the periodic behavior of all data sets the Multi Taper Method (MTM) and the Morlet wavelet analysis method were performed with daily data from 2009 to 2018. To evaluate our wavelet analysis Cross Wavelet Transform (XWT) and Wavelet Transform Coherence (WTC) methods were performed. Causal relationships between datasets were further examined by Convergence Cross Mapping (CCM) method. In results of our analysis we found followings; 1) The C class X-Ray flare numbers increased about 16 % during the solar cycle 24 compared to cycle 23, while all other data sets decreased; the MCMESI decreased about 16 % and the number of M and X class flares decreased about 32 %. 2) All the X-Ray solar flare classes show remarkable positive correlation with the MCMESI. While the correlation between the MCMESI and C class flares comes from the general solar cycle trend, it mainly results from the fluctuations in the data in case of the X class flares. 3) In general, all class flare numbers and the MCMESI show similar periodic behavior. 4) The 546 days periodicity detected in the MCMESI may not be of solar origin or at least the solar flares are not the source of this periodicity. 5) C and M Class solar flares have a stronger causative effect on the MCMESI compared to X class solar flares. However the only bidirectional causal relationship is obtained between the MCMESI and C class flare numbers.

Stable solar cylces

Kim Chol-jun

2020

https://arxiv.org/pdf/2011.14564.pdf

The question on the long-term solar cycles is still open. I choose the stable solar cycles in terms of the sampling and differencing stability in samplogram, the time stability or stationarity in wavelet scalogram and the modulation analysis. The short-term solar cycles are also little known due to the strong randomness of solar activity. I found the stable cycles near to the orbital cycles of all major planets upto the Saturn. This may imply a possible planetary forcing of solar activity.

Solar Farside Magnetograms from Deep Learning Analysis of STEREO/EUVI Data

Kim, T., Park, E., Lee, H., et al.

2019, Nature Astronomy,

http://sci-hub.se/10.1038/s41550-019-0711-5

Solar magnetograms are important for studying solar activity and predicting space weather disturbances1 . Farside magnetograms can be constructed from local helioseismology without any farside data2-4, but their quality is lower than that of typical frontside magnetograms. Here we generate farside solar magnetograms from STEREO/Extreme UltraViolet Imager (EUVI) 304-Å images using a deep learning model based on conditional generative adversarial networks (cGANs). We train the model using pairs of Solar Dynamics Observatory (SDO)/Atmospheric Imaging Assembly (AIA) 304-Å images and SDO/Helioseismic and Magnetic Imager (HMI) magnetograms taken from 2011 to 2017 except for September and October each year. We evaluate the model by comparing pairs of SDO/HMI magnetograms and cGAN-generated magnetograms in September and October. Our method successfully generates frontside solar magnetograms from SDO/AIA 304-Å images and these are similar to those of the SDO/HMI, with Hale-patterned active regions being well replicated. Thus we can monitor the temporal evolution of magnetic fields from the farside to the frontside of the Sun using SDO/HMI and farside magnetograms generated by our model when farside extreme-ultraviolet data are available. This study presents an application of image-to-image translation based on cGANs to scientific data. **4-13, 2014, 1-7 September 2017,**
HMI Science Nuggets #125 Apr **2019** http://hmi.stanford.edu/hminuggets/?p=2890

Imaging the Structure of the Low K-corona

I. S. **Kim**, L. P. Nasonova, D. V. Lisin, V. V. Popov, N. L. Krusanova
JGR Volume 122, Issue 1 January **2017** Pages 77–88
The first 2D distributions of the polarization angle and of the relative color index for the K-corona of March 29, 2006 are presented. The distributions illustrate the efficiency of the total solar eclipse approach for high-precision measurements of the K-corona continuum in the range < 1.4 R⊙. Natural ground and space total solar eclipses caused by external occulting the bright solar-disk light by the Moon or Earth group planets are discussed. Calculations of the eclipse magnitude m are carried out to show ideal conditions for total solar eclipse observations in space from Lagrange point L2 for Mars (m ≈ 1.025). The illumination in Mars' shadow is estimated to equal 5.6 × 10-11 for the wavelength of 550 nm. No internal or external occulting coronagraphs are needed. Partial solar eclipses with m > 0.91 can be observed from Lagrange points L2 for Mercury, Venus, and Earth.

Variations of solar, interplanetary, and geomagnetic parameters with solar magnetic multipole fields during Solar Cycles 21–24

Bogyeong **Kim**, Jeongwoo Leea, b, Yu Yia, Suyeon Oh
Advances in Space Research, Volume 55, Issue 1, 1 January **2015**, Pages 401–406
http://www.sciencedirect.com/science/article/pii/S0273117714005912
In this study we compare the temporal variations of the solar, interplanetary, and geomagnetic (SIG) parameters with that of open solar magnetic flux from 1976 to 2012 (from Solar Cycle 21 to the early phase of Cycle 24) for a purpose of identifying their possible relationships. By the open flux, we mean the average magnetic field over the source surface (2.5 solar radii) times the source area as defined by the potential field source surface (PFSS) model of the Wilcox Solar Observatory (WSO). In our result, most SIG parameters except the solar wind dynamic pressure show rather poor correlations with the open solar magnetic field. Good correlations are recovered when the contributions from individual multipole components are counted separately. As expected, solar activity indices such as sunspot number, total solar irradiance, 10.7 cm radio flux, and solar flare occurrence are highly correlated with the flux of magnetic quadrupole component. The dynamic pressure of solar wind is strongly correlated with the dipole flux, which is in anti-phase with Solar Cycle (SC). The geomagnetic activity represented by the Ap index is correlated with higher order multipole components, which show relatively a slow time variation with SC. We also found that the unusually low geomagnetic activity during SC 23 is accompanied by the weak open solar fields compared with those in other SCs. It is argued that such dependences of the SIG parameters on the individual multipole components of the open solar magnetic flux may clarify why some SIG parameters vary in phase with SC and others show seemingly delayed responses to SC variation.

Relationships Between Sequential Chromospheric Brightening and the Corona **Review**

Michael S. **Kirk**, K. S. Balasubramaniam, Jason Jackiewicz, Holly R. Gilbert
Proceedings IAU Symposium No. xxx, **2017**
https://arxiv.org/pdf/1704.03835.pdf
The chromosphere is a complex region that acts as an intermediary between the magnetic flux emergence in the photosphere and the magnetic features seen in the corona. Large eruptions in the chromosphere of flares and filaments are often accompanied by ejections of coronal mass off the sun. Several studies have observed fast-moving progressive trains of compact bright points (called Sequential Chromospheric Brightenings or SCBs) streaming away from chromospheric flares that also produce a coronal mass ejection (CME). In this work, we review studies of SCBs and search for commonalties between them. We place these findings into a larger context with contemporary chromospheric and coronal observations. SCBs are fleeting indicators of the solar atmospheric environment as it existed before their associated eruption. Since they appear at the very outset of a flare eruption, SCBs are good early indication of a CME measured in the chromosphere. **2010-11-06,**

Table 1. A summary of the events used to investigate the evolution of SCBs.

The Origin of Sequential Chromospheric Brightenings

Michael S. **Kirk**, K.S. Balasubramaniam, Jason Jackiewicz, Holly R. Gilbert
Solar Phys. 292: 72 **2017**
https://arxiv.org/pdf/1704.03828.pdf

Sequential chromospheric brightenings (SCBs) are often observed in the immediate vicinity of erupting flares and are associated with coronal mass ejections. Since their initial discovery in 2005, there have been several subsequent investigations of SCBs. These studies have used differing detection and analysis techniques, making it difficult to compare results between studies. This work employs the automated detection algorithm of Kirk et al. (Solar Phys. 283, 97, 2013) to extract the physical characteristics of SCBs in 11 flares of varying size and intensity. We demonstrate that the magnetic substructure within the SCB appears to have a significantly smaller area than the corresponding H-alpha emission. We conclude that SCBs originate in the lower corona around 0.1 R_sun above the photosphere, propagate away from the flare center at speeds of 35 - 85 km/s, and have peak photosphere magnetic intensities of 148 +/- 2.9 G. In light of these measurements, we infer SCBs to be distinctive chromospheric signatures of erupting coronal mass ejections. 19 December 2002, 6 November 2010

Table 1. The events used in this work to investigate the automated identi_cation and tracking of SCBs and are ribbons.

Forecasting the sunspot maximum through an analysis of geomagnetic activity

B.**Kirov** S.AsenovskiaK.GeorgievaaV.N.ObridkobG.Maris-Munteanc
Journal of Atmospheric and Solar-Terrestrial Physics Volume 176, September **2018**, Pages 42-50
http://sci-hub.tw/10.1016/j.jastp.2017.12.016

In the present work we show that it is possible to predict the maximum sunspot number for a particular solar cycle from the maximum value of the solar dipole magnetic field of the previous cycle. Based on the measured dipole field maximum, we determine the geomagnetic activity in the upcoming solar minimum during the intervals when the Earth is not exposed to CME and HSS influences. The physical meaning of the relationship between the geomagnetic activity in the solar activity minimum and the maximum value of the solar dipole magnetic field is that the basic factor determining the geomagnetic activity during the minimum is not the heliospheric current sheet thickness but the physical parameters of the slow solar wind in this period.
Then, based on the established relationship between the average geomagnetic activity at the specified minimum and the next solar maximum, we can predict the sunspot maximum of the next solar cycle.

Machine learning for reconstruction of polarity inversion lines from solar filaments

V. **Kisielius**, E. Illarionov
Solar Phys. **2024**
https://arxiv.org/pdf/2405.06293

Solar filaments are well-known tracers of polarity inversion lines that separate two opposite magnetic polarities on the solar photosphere. Because observations of filaments began long before the systematic observations of solar magnetic fields, historical filament catalogs can facilitate the reconstruction of magnetic polarity maps at times when direct magnetic observations were not yet available. In practice, this reconstruction is often ambiguous and typically performed manually. We propose an automatic approach based on a machine-learning model that generates a variety of magnetic polarity maps consistent with filament observations. To evaluate the model and discuss the results we use the catalog of solar filaments and polarity maps compiled by McIntosh. We realize that the process of manual compilation of polarity maps includes not only information on filaments, but also a large amount of prior information, which is difficult to formalize. In order to compensate for the lack of prior knowledge for the machine-learning model, we provide it with polarity information at several reference points. We demonstrate that this process, which can be considered as the user-guided reconstruction or super-resolution, leads to polarity maps that are reasonably close to hand-drawn ones, and additionally allows for uncertainty estimation.

On Quasi-biennial oscillations in chromospheric macrospicules and their potential relation to global solar magnetic field

T. S. **Kiss**, R. Erdelyi
2018
https://arxiv.org/pdf/1804.01513.pdf

This study aims to provide further evidence for the potential influence of the global solar magnetic field on localised chromospheric jets, the macrospicules (MS). To find a connection between the long-term variation of properties of MS and other solar activity proxies, including e.g. the temporal variation of the frequency shift of solar global

oscillations, sunspot area, etc., a database overarching seven years of observations was built up. This database contains 362 MS, based on observations at the 30.4 nm of the Atmospheric Imaging Assembly (AIA) on-board the Solar Dynamics Observatory (SDO). Three of the five investigated physical properties of MS show a clear long-term temporal variation after smoothing the raw data. Wavelet analysis of the temporal variation of maximum length, maximum area and average velocity is carried out. The results reveal a strong pattern of periodicities at around 2-year (also referred to as Quasi-Biennial Oscillations -- QBOs). Comparison to solar activity proxies, that also possess the properties of QBOs, provides some interesting features: the minima and maxima of QBOs of MS properties occur at around the same epoch as the minima and maxima of these activity proxies. For most of the time span investigated, the oscillations are out-of-phase. This out-of-phase behaviour was also corroborated by a cross-correlation analysis. These results suggest that the physical processes, that generate and drive the long-term evolution of the global solar activity proxies, may be coupled to the short-term local physical processes driving the macrospicules, and, therefore modulate the properties of local dynamics.

Quasi-biennial oscillations in the cross-correlation of properties of macrospicules

T. S. **Kiss**, N. Gyenge, R. Erdelyi

Advances in Space Research Volume 61, Issue 2, 15 January **2018**, Pages 611-616

https://arxiv.org/pdf/1706.00275.pdf

Jets, whatever small (e.g. spicules) or large (e.g. macrospicules) their size, may play a key role in momentum and energy transport from photosphere to chromosphere and at least to the low corona. Here, we investigate the properties of abundant, large-scale dynamic jets observable in the solar atmosphere: the macrospicules (MS). These jets are observationally more distinct phenomena than their little, and perhaps more ubiquitous, cousins, the spicules. Investigation of long-term variation of the properties of macrospicules may help to a better understanding of their underlying physics of generation and role in coronal heating. Taking advantage of the high temporal and spatial resolution of the Solar Dynamics Observatory, a new dataset, with several hundreds of macrospicules, was constructed encompassing a period of observations over six years. Here, we analyse the measured properties and relations between these properties of macrospicules as function of time during the observed time interval. We found that cross-correlations of several of these macrospicule properties display a strong oscillatory pattern. Next, wavelet analysis is used to provide more detailed information about the temporal behaviour of the various properties of MS. For coronal hole macrospicules, a significant peak is found at around 2-year period. This peak also exists partially or is shifted to longer period, in the case of quiet Sun macrospicules. These observed findings may be rooted in the underlying mechanism generating the solar magnetic field, i.e. the global solar dynamo.

Systematic variations of macrospicule properties observed by SDO/AIA over half a decade

T. S. **Kiss**, N. Gyenge, R. Erdelyi

2017 ApJ 835 47

https://arxiv.org/pdf/1612.02224v1.pdf

Macrospicules (MS) are localised small-scale jet-like phenomena in the solar atmosphere, which have the potential to transport considerable amount of momentum and energy from the lower solar atmospheric regions to the Transition Region and the low corona. A detailed statistical analysis of their temporal behaviour and spatial properties is carried out in this work. By means of state-of-the-art spatial and temporal resolution observations, yielded by the Atmospheric Imaging Assembly (AIA) of Solar Dynamics Observatory (SDO), we constructed a database covering a 5.5-year long period, containing 301 macrospicules that occurred between June 2010 and December 2015 detected at 30.4 nm wavelength. Here, we report the long-term variation of the height, length, average speed and width of MS in Coronal Holes and Quiet Sun areas both in the northern and southern hemisphere of the Sun. This new database helps to refine our knowledge about the physical properties of MS. Cross-correlation of these properties show a relatively strong correlation, but not always a dominant one. However, a more detailed analysis indicates a wave-like signature in the behaviour of MS properties in time. The period of these long-term oscillatory behaviours are just under two years. Also, in terms of solar north/south hemispheres, a strong asymmetry was found in the spatial distribution of MS properties, which may be accounted for the solar dynamo. This latter feature may then indicate a strong and rather intrinsic link between global internal and local atmospheric phenomena in the Sun. 03. 07. 2012

Doppler shift of the quiet region measured by meridional scans with the EUV Imaging Spectrometer onboard Hinode

N. **Kitagawa**, H. Hara, T. Yokoyama

ApJ **201**5

http://arxiv.org/pdf/1511.05213v1.pdf

Spatially averaged (> 50") EUV spectral lines in the transition region of solar quiet regions are known to be redshifted. Because the mechanism underlying this phenomenon is unclear, we require additional physical information on the lower corona for limiting the theoretical models. To acquire this information, we measured the Doppler shifts over a wide coronal temperature range (log T[K]=5.7--6.3) using the spectroscopic data taken by the

Hinode EUV Imaging Spectrometer. By analyzing the data over the center-to-limb variations covering the meridian from the south to the north pole, we successfully measured the velocity to an accuracy of 3 km/s. Below log T[K] = 6.0, the Doppler shifts of the emission lines were almost zero with an error of 1--3 km/s; above this temperature, they were blueshifted with a gradually increasing magnitude, reaching - 6.3 +/- 2.1 km/s at log T[K]=6.25.

Origin of the Near-Surface Shear Layer of Solar Rotation

Leonid **Kitchatinov**
ApJL **2024**
https://arxiv.org/pdf/2402.07421.pdf
Helioseismology has revealed an increase in the rotation rate with depth in a thin (∼30 Mm) near-surface layer. The normalized rotational shear in this layer is independent of latitude. This rotational state is shown to be a consequence of the short characteristic time of near-surface convection compared to the rotation period, and the radial anisotropy of the convective turbulence. Analytical derivations within mean-field hydrodynamics reproduce the observed normalized rotational shear and are in agreement with numerical experiments on the radiative hydrodynamics of solar convection. The near-surface shear layer is the source of the global meridional flow important for the solar dynamo.

Near-surface shear layer of solar rotation: origin and significance

Leonid **Kitchatinov**
Proceedings of IAUS 365, **2023**
https://arxiv.org/pdf/2311.07875.pdf
Helioseismology has discovered a thin layer beneath the solar surface where the rotation rate increases rapidly with depth. The normalized rotational shear in the upper 10 Mm of the layer is constant with latitude. Differential rotation theory explains such a rotational state by a radial-type anisotropy of the near-surface convection and a short correlation time of convective turbulence compared to the rotation period. The shear layer is the main driver of the global meridional circulation.

Inferring Quadrupolar Dynamo Mode from Sunspot Statistics

Leonid **Kitchatinov**
Geomagnetism & Aeronomy, **2022**, vol.62, No.7
https://arxiv.org/pdf/2205.13747.pdf
Observations of long-term north-south asymmetry in solar activity demand the equator-symmetric (quadrupolar) mode be present in the solar magnetic field in line with the dominant antisymmetric (dipolar) mode. This paper proposes treating the sunspot area as a proxy for subsurface toroidal magnetic flux to infer the quadrupolar mode of the solar dynamo from sunspot data. Toroidal pseudo-fluxes (PF) in the northern and southern hemispheres are defined as a signed sunspot area with plus or minus sign prescribed to them in accord with the Hale's sunspot polarity rules. Statistical correlation analysis and wavelet analysis of so-defined PFs reveal quadrupolar oscillations with a period of about 16 yr and amplitude of about 0.17 relative to the amplitude of the dominant 22-yr dipolar mode.

Dynamo Model for North-South Asymmetry of Solar Activity

Leonid **Kitchatinov**, Anna Khlystova
ApJ **2021**
https://arxiv.org/pdf/2107.00865
Observations reveal a relatively small but statistically significant North-South (NS) asymmetry in sunspot activity varying on a time scale of several solar cycles. This paper proposes a dynamo model for the phenomenon of long-term NS asymmetry. The model separates dynamo equations for magnetic fields of dipolar and quadrupolar equatorial parity. The NS asymmetry results from the superposition of dipolar and quadrupolar fields. Model computations confirm the formerly proposed excitation of the quadrupolar dynamo mode by a dominant dipolar mode mediated by the equator-symmetric fluctuations in the α-effect as a mechanism for the long-term NS asymmetry. An analytically solvable example of oscillations excited by short-term random forcing is given to justify the numerical result of NS asymmetry coherent on a time scale of several (about 6 in the present model) solar cycles resulting from random variations in the α-effect on a time scale of one solar rotation. The model computations show the phase locking phenomenon of dipolar and quadrupolar fields oscillating predominantly in phase (northern type asymmetry) or in antiphase (southern type asymmetry) with relatively short irregular transitions between these two states. Large asymmetry in the simulated Grand minima is found and explained by weak magnetic quenching of the α-effect during the minima. The possibility of polar field asymmetry in activity minima as a precursor of sunspot asymmetry in the following activity cycles is discussed based on the dynamo model and observations.

Flux-tubes forming instability near the base of the rotating convection zone: A possible explanation for low latitudes of sunspots

Leonid **Kitchatinov**

ApJ **893** 131 **2020**

https://arxiv.org/pdf/2003.09068.pdf

sci-hub.tw/10.3847/1538-4357/ab7fa8

The rise of flux-tubes with intense magnetic fields from the base of the convection zone to the solar surface has been substantiated as a probable mechanism for sunspot formation. The origin of flux-tubes of sufficient strength (~10^5 G) is however uncertain. This paper considers the instability of a large-scale toroidal magnetic field caused by the magnetic suppression of convective heat transport as a candidate for the flux tube forming mechanism. The consideration employs the analytical dependence of the eddy diffusion on the magnetic field supplied by mean-field magnetohydrodynamics. The instability tends to produce regions of increased field strength with spatial scales of an order of 100 Mm at the base of the convection zone. Characteristic growth times of the instability are short compared to the 11-year cycle. The threshold field strength for the onset of the instability increases from several hundred Gauss in the vicinity of the equator to some kilo-Gauss at middle latitudes. Growth rates of unstable disturbances decrease with latitude. These latitudinal trends can be the reason for the observed confinement of sunspot activity to a near-equatorial belt.

Stability of a force-free Hall equilibrium and release of magnetic energy

Leonid **Kitchatinov**

AN **2019**

https://arxiv.org/pdf/1906.07936.pdf

Conservation of magnetic helicity by the Hall drift does not prevent Hall instability of helical fields. This conclusion follows from stability analysis of a force-free spatially-periodic Hall equilibrium. The growth rates of the instability scale as $\sigma \propto B^{3/4}\eta^{1/4}$ with the field strength B and magnetic diffusivity η and can be large compared to the rate of resistive decay of the background field. The instability deviates the magnetic field from the force-free configuration. The unstable eigenmodes include a fine spatial structure which evolves into current sheets at the nonlinear stage of the instability. The instability catalyses the resistive release of magnetic energy. The energy is released in a sequence of spikes, every spike emits several percent of the total energy. A numerically defined scaling for the energy released in a single spike permits an extrapolation to astrophysically relevant values of the Hall number. The instability can be relevant to magnetic energy release in a neutron star crust and, possibly, in stellar coronae.

Solar cycle asymmetry as a consequence of fluctuations in dynamo parameters

Leonid **Kitchatinov**, Alexander Nepomnyashchikh

Astronomy Letters Vol. 44, No. 10 **2018**

https://arxiv.org/pdf/1806.05384.pdf

The duration of activity growths in solar cycles is on average shorter than the duration of its declines. This asymmetry can result from fluctuations in dynamo parameters. A solar dynamo model with fluctuations in the α-effect shows the statistical asymmetry which increases with both fluctuation amplitude and coherence time. An interpretation for the asymmetry origin is suggested, which predicts a correlation between the asymmetry measure and delay of the polar field reversals relative to the activity maxima. Data on the twelve latest solar cycles confirm such a correlation.

Modelling variability of solar activity cycles

L. L. **Kitchatinov**, A. V. Mordvinov, A. A. Nepomnyashchikh

A&A 615, A38 **2018**

https://arxiv.org/pdf/1804.02833.pdf

Context. Solar activity cycles vary in amplitude and duration. The variations can be at least partly explained by fluctuations in dynamo parameters. Aims. We want to restrict uncertainty in fluctuating dynamo parameters and find out which properties of the fluctuations control the amplitudes of the magnetic field and energy in variable dynamo cycles. Methods. A flux-transport model for the solar dynamo with fluctuations of the Babcock-Leighton type α-effect was applied to generate statistics of magnetic cycles for our purposes. The statistics were compared with data on solar cycle periods to restrict the correlation time of dynamo fluctuations. Results. A characteristic time of fluctuations in the α-effect is estimated to be close to the solar rotation period. The fluctuations produce asymmetry between the times of rise and descent of dynamo cycles, the rise time being on average shorter. The affect of the fluctuations on cycle amplitudes depends on the phase of the cycle in which the fluctuations occur. Negative fluctuations (decrease in α) in the rise phase delay decay of poloidal field and increase the cycle amplitude in toroidal field and magnetic energy. Negative fluctuation in the decline phase reduces the polar field at the end of a cycle and the amplitude of the next cycle. The low amplitude of the 24th solar cycle compared to the preceding 23rd cycle can be explained by this effect. Positive fluctuations in the descent phase enhance the magnetic energy of the

next cycle by increasing the seed poloidal field for the next cycle. The statistics of the computed energies of the cycles suggest that superflares of ≥1034 erg are not possible on the Sun.

A joined model for solar dynamo and differential rotation

L. L. **Kitchatinov**, A. A. Nepomnyashchikh
Astronomy Letters **2017**
https://arxiv.org/pdf/1612.07503v1.pdf
A model for the solar dynamo, consistent in global flow and numerical method employed with the differential rotation model, is developed. The magnetic turbulent diffusivity is expressed in terms of the entropy gradient, which is controlled by the model equations. The magnetic Prandtl number and latitudinal profile of the alpha-effect are specified by fitting the computed period of the activity cycle and the equatorial symmetry of magnetic fields to observations. Then, the instants of polar field reversals and time-latitude diagrams of the fields also come into agreement with observations. The poloidal field has a maximum amplitude of about 10 Gs in the polar regions. The toroidal field of several thousand Gauss concentrates near the base of the convection zone and is transported towards the equator by the meridional flow. The model predicts a value of about 10^37 erg for the total magnetic energy of large-scale fields in the solar convection zone.

Diamagnetic pumping in a rotating convection zone

L. **Kitchatinov**, A. Nepomnyashchikh
AdSR **2016**
http://arxiv.org/pdf/1604.07942v1.pdf
Solar dynamo models require some mechanism for magnetic field concentration near the base of the convection zone in order to generate super-kilogauss toroidal fields with sufficiently large (~10^{24} Mx) magnetic flux. We consider the downward diamagnetic pumping near the base of the convection zone as a possible concentration mechanism and derive the pumping velocities with allowance for the effect of rotation. Transport velocities for poloidal and toroidal fields differ in rotating fluid. The toroidal field is transported downward along the radius only but the pumping velocity for the poloidal field has an equatorward meridional component also. Previous results for cases of slow and rapid rotation are reproduced and the diamagnetic pumping expressions adapted for use in dynamo models are presented.

Meridional circulation in the Sun and stars **Review**

L. L. **Kitchatinov**
Geomagnetism & Aeronomy **2016**
Mean-field hydrodynamics advanced to clear explanations for the origin and properties of the global meridional flow in stellar convection zones. Qualitative arguments and analysis of basic equations both show that the meridional circulation is driven by non-conservative centrifugal and buoyancy forces and results from a slight disbalance between these two drivers. The deviations from the thermal wind balance are relatively large near the boundaries of convection zones. Accordingly, the meridional flow attains its largest velocities in the boundary layers and decreases inside the convection zone. This picture, however, is neither supported nor dismissed by the conflicting results of recent helioseismic soundings or 3D numerical experiments. The relevant physics of the differential temperature and its possible relation to the solar oblateness are briefly discussed.

Dynamo model for grand maxima of solar activity: can superflares occur on the Sun?

L. L. **Kitchatinov**, S. V. Olemskoy
MNRAS **2016**
http://arxiv.org/pdf/1602.08840v1.pdf
Recent data on superflares on sun-like stars and radiocarbon data on solar activity in the past are both indicative of transient epochs of unusually high magnetic activity. We propose an explanation for the grand activity maxima in the framework of a solar dynamo model with fluctuating parameters. Solar-type dynamos are oscillatory because of the combination of the solar-type differential rotation with positive (in the northern hemisphere) alpha-effect. An artificial reversal of the sign in the alpha-effect changes the dynamo to a steady regime with hundreds of times larger magnetic energy compared to the amplitude of the cyclic dynamo. Sufficiently large and durable fluctuations reversing the sign of the alpha-effect during the growth phase of a magnetic cycle can, therefore, cause a transient change to a steady dynamo with considerably increased magnetic energy. This qualitative scenario for grand activity maxima is supported by computations of the dynamo model with a fluctuating alpha-effect. The computed statistics of several thousand magnetic cycles gives examples of cycles with very high magnetic energy. Our preliminary estimations however suggest that the probability of solar superflares is extremely low.

Parametric Modulation of Dynamo Waves

Leonid **Kitchatinov**, Alexander Nepomnyashchikh
Astronomy Letters, **2015**
http://arxiv.org/pdf/1504.01837v1.pdf
Long-term variations of solar activity, including the Grand minima, are believed to result from temporal variations of dynamo parameters. The simplest approximation of dynamo waves is applied to show that cyclic variations of the parameters can lead to an exponential growth or decay of magnetic oscillations depending on the variations frequency. There is no parametric resonance in a dynamo, however: the selective sensitivity to distinct frequencies, characteristic of resonant phenomena, is absent. A qualitative explanation for this finding is suggested. Nonlinear analysis of dynamo-waves reveals the hysteresis phenomenon found earlier in more advanced models. However, the simplified model allows a computation of a sufficiently large number of dynamo-cycles for constructing the distribution function of their amplitudes to reproduce qualitatively two modes of solar activity inferred recently from cosmogenic isotope content in natural archives.

North-south asymmetry of solar dynamo in the current activity cycle

L. L. **Kitchatinov**, A. I. Khlystova
Astronomy Letters, **2014**
http://arxiv.org/pdf/1406.7072v1.pdf
An explanation is suggested for the north-south asymmetry of the polar magnetic field reversal in the current cycle of solar activity. The contribution of the Babcock-Leighton mechanism to the poloidal field generation is estimated using sunspot data for the current activity cycle. Estimations are performed separately for the northern and southern hemispheres. The contribution of the northern hemisphere exceeded considerably that of the southern hemisphere during the initial stage of the cycle. This is the probable reason for the earlier reversal of the northern polar field. The estimated contributions of the Babcock-Leighton mechanism are considerably smaller than similar estimations for the previous activity cycles. A relatively weak (<1G) large-scale polar field can be expected for the next activity minimum.

The solar dynamo: inferences from observations and modeling **Review**

L. L. **Kitchatinov**
Geomagnetism & Aeronomy (a review), **2014**
http://arxiv.org/pdf/1404.4126v1.pdf
It can be shown on observational grounds that two basic effects of dynamo theory for solar activity - production of the toroidal field from the poloidal one by differential rotation and reverse conversion of the toroidal field to the poloidal configuration by helical motions - are operating in the Sun. These two effects, however, do not suffice for constructing a realistic model for the solar dynamo. Only when a non-local version of the alpha-effect is applied, is downward diamagnetic pumping included and field advection by the equatorward meridional flow near the base of the convection zone allowed for, can the observed activity cycles be closely reproduced. Fluctuations in the alpha-effect can be estimated from sunspot data. Dynamo models with fluctuating parameters reproduce irregularities of solar cycles including the grand activity minima. The physics of parametric excitation of irregularities remains, however, to be understood.

Global Evolution of Solar Magnetic Fields and Prediction of Activity Cycles

Irina N. **Kitiashvili**
Proceedings of IAUS #354 **2020**
https://arxiv.org/pdf/2003.04563.pdf
Prediction of solar activity cycles is challenging because physical processes inside the Sun involve a broad range of multiscale dynamics that no model can reproduce and because the available observations are highly limited and cover mostly surface layers. Helioseismology makes it possible to probe solar dynamics in the convective zone, but variations in differential rotation and meridional circulation are currently available for only two solar activity cycles. It has been demonstrated that sunspot observations, which cover over 400 years, can be used to calibrate the Parker-Kleeorin-Ruzmaikin dynamo model, and that the Ensemble Kalman Filter (EnKF) method can be used to link the modeled magnetic fields to sunspot observations and make reliable predictions of a following activity cycle. However, for more accurate predictions, it is necessary to use actual observations of the solar magnetic fields, which are available only for the last four solar cycles. In this paper I briefly discuss the influence of the limited number of available observations on the accuracy of EnKF estimates of solar cycle parameters, the criteria to evaluate the predictions, and application of synoptic magnetograms to the prediction of solar activity.

Effects of Observational Data Shortage on Accuracy of Global Solar Activity Forecast

Irina N. **Kitiashvili**

MNRAS , Volume 505, Issue 4, August **2021**, Pages 6085–6102,

https://scholar.google.com/scholar_url?url=https://academic.oup.com/mnras/advance-article-pdf/

https://doi.org/10.1093/mnras/stab1605

https://arxiv.org/pdf/2001.09376.pdf

Building a reliable forecast of solar activity is a long-standing problem that requires to accurately describe past and current global dynamics. However, synoptic observations of magnetic fields and subsurface flows became available relatively recently. In this paper, we present an investigation of effects of short observational data series on accuracy of solar cycle prediction. This analysis is performed using the annual sunspot number time-series applied to the Parker-Kleeorin-Ruzmaikin dynamo model and employing the Ensemble Kalman Filter (EnKF) data assimilation method. The testing of the cycle prediction accuracy is performed for the last six cycles (from Solar Cycle 19 to 24) by sequentially shortening the observational data series that are used for prediction of a target cycle, and evaluating the prediction accuracy according to specified criteria. According to the analysis, reliable activity predictions can be made using relatively short time-series of the sunspot number. It demonstrated that even two cycles of available observations allow us to obtain reasonable forecasts.

Application of Synoptic Magnetograms to Global Solar Activity Forecast

Irina N. **Kitiashvili**

2020 *ApJ* **890** 36

https://arxiv.org/pdf/1910.00820.pdf

https://doi.org/10.3847/1538-4357/ab64e7

sci-hub.tw/10.3847/1538-4357/ab64e7

Synoptic magnetograms provide us with knowledge about the evolution of magnetic fields on the solar surface and present important information for forecasting future solar activity. In this work, poloidal and toroidal magnetic field components derived from synoptic magnetograms are assimilated, using the Ensemble Kalman Filter method, into a mean-field dynamo model based on Parker's migratory dynamo theory complemented by magnetic helicity conservation. It was found that the predicted toroidal field is in good agreement with observations for almost the entire following solar cycle. However, poloidal field predictions agree with observations only for the first 2 - 3 years of the predicted cycle. The results indicate that the upcoming Solar Maximum of Cycle 25 (SC25) is expected to be weaker than the current Cycle 24. The model results show that a deep extended solar activity minimum is expected during 2019 - 2021, and that the next solar maximum will occur in 2024 - 2025. The sunspot number at the maximum will be about 50 with an error estimate of 15 - 30 %. The maximum will likely have a double peak or show extended periods (for 2 - 2.5 years) of high activity. According to the hemispheric prediction results, SC25 will start in 2020 in the Southern hemisphere, and will have a maximum in 2024 with a sunspot number of about 28. In the Northern hemisphere the cycle will be delayed for about 1 year (with an error of ±0.5 year), and reach a maximum in 2025 with a sunspot number of about 23.

HMI Science Nuggets #139 March **2020** http://hmi.stanford.edu/hminuggets/?p=3255

The Origin of Deep Acoustic Sources Associated with Solar Magnetic Structures

I. N. **Kitiashvili**1, A. G. Kosovichev2, N. N. Mansour1, A. A. Wray1, and T. A. Sandstrom

2019 ApJ 872 34

It is generally accepted that solar acoustic (p) modes are excited by near-surface turbulent motions, in particular by downdrafts and interacting vortices in intergranular lanes. Recent analysis of Solar Dynamics Observatory data by Zhao et al. (2015) revealed fast-moving waves around sunspots, which are consistent with magnetoacoustic waves excited approximately 5 Mm beneath the sunspot. We analyzed 3D radiative MHD simulations of solar magnetoconvection with a self-organized pore-like magnetic structure, and identified more than 600 individual acoustic events both inside and outside this structure. By performing a case-by-case study, we found that acoustic sources surrounding the magnetic structure are associated with downdrafts. Their depth correlates with downdraft speed and magnetic field strength. The sources often can be transported into deeper layers by downdrafts. The wave front shape, in the case of a strong or inclined downdraft, can be stretched along the downdraft. Inside the magnetic structure, excitation of acoustic waves is driven by converging flows. Frequently, strong converging plasma streams hit the structure boundaries, causing compressions in its interior that excite acoustic waves. Analysis of the depth distribution of acoustic events shows the strongest concentration at 0.2–1 Mm beneath the surface for the outside sources and mostly below 1 Mm inside the magnetic region, that is, deeper than their counterparts outside the magnetic region.

DATA ASSIMILATION APPROACH FOR FORECAST OF SOLAR ACTIVITY CYCLES

Irina N. **Kitiashvili**

2016 ApJ 831 15

Numerous attempts to predict future solar cycles are mostly based on empirical relations derived from observations of previous cycles, and they yield a wide range of predicted strengths and durations of the cycles. Results obtained with current dynamo models also deviate strongly from each other, thus raising questions about criteria to quantify the reliability of such predictions. The primary difficulties in modeling future solar activity are shortcomings of both the dynamo models and observations that do not allow us to determine the current and past states of the global solar magnetic structure and its dynamics. Data assimilation is a relatively new approach to develop physics-based predictions and estimate their uncertainties in situations where the physical properties of a system are not well-known. This paper presents an application of the ensemble Kalman filter method for modeling and prediction of solar cycles through use of a low-order nonlinear dynamo model that includes the essential physics and can describe general properties of the sunspot cycles. Despite the simplicity of this model, the data assimilation approach provides reasonable estimates for the strengths of future solar cycles. In particular, the prediction of Cycle 24 calculated and published in 2008 is so far holding up quite well. In this paper, I will present my first attempt to predict Cycle 25 using the data assimilation approach, and discuss the uncertainties of that prediction.

Realistic modeling of local dynamo processes on the Sun

I.N. **Kitiashvili**, A.G. Kosovichev, N.N. Mansour, A.A. Wray
ApJ **809** 84 **2015**
http://arxiv.org/pdf/1506.08924v1.pdf
Magnetic fields are usually observed in the quiet Sun as small-scale elements that cover the entire solar surface (the `salt and pepper' patterns in line-of-sight magnetograms). By using 3D radiative MHD numerical simulations we find that these fields result from a local dynamo action in the top layers of the convection zone, where extremely weak 'seed' magnetic fields (e.g., from a 10−6 G) can locally grow above the mean equipartition field, to a stronger than 2000~G field localized in magnetic structures. Our results reveal that the magnetic flux is predominantly generated in regions of small-scale helical downflows. We find that the local dynamo action takes place mostly in a shallow, about 500~km deep, subsurface layer, from which the generated field is transported into the deeper layers by convective downdrafts. We demonstrate that the observed dominance of vertical magnetic fields at the photosphere and horizontal fields above the photosphere can be explained by small-scale magnetic loops produced by the dynamo. Such small-scale loops play an important role in the structure and dynamics of the solar atmosphere and that their detection in observations is critical for understanding the local dynamo action on the Sun.

Using Realistic MHD Simulations for Modeling and Interpretation of Quiet-Sun Observations with the Solar Dynamics Observatory Helioseismic and Magnetic Imager

Irina N. **Kitiashvili**, Sebastien Couvidat, Andreas Lagg
2015 *ApJ* 808 59
http://arxiv.org/pdf/1407.2663v1.pdf
The solar atmosphere is extremely dynamic, and many important phenomena develop on small scales that are unresolved in observations with the Helioseismic and Magnetic Imager (HMI) instrument on the Solar Dynamics Observatory (SDO). For correct calibration and interpretation, it is very important to investigate the effects of small-scale structures and dynamics on the HMI observables, such as Doppler shift, continuum intensity, spectral line depth, and width. We use 3D radiative hydrodynamics simulations of the upper turbulent convective layer and the atmosphere of the Sun, and a spectro-polarimetric radiative transfer code to study observational characteristics of the Fe I 6173A line observed by HMI in quiet-Sun regions. We use the modeling results to investigate the sensitivity of the line Doppler shift to plasma velocity, and also sensitivities of the line parameters to plasma temperature and density, and determine effective line formation heights for observations of solar regions located at different distances from the disc center. These estimates are important for the interpretation of helioseismology measurements. In addition, we consider various center-to-limb effects, such as convective blue-shift, variations of helioseismic travel-times, and the 'concave' Sun effect, and show that the simulations can qualitatively reproduce the observed phenomena, indicating that these are related to a complex interaction of solar dynamics and radiative transfer.

Forecast of solar activity based on mean-field dynamo model and neural network

Nathan **Kleeorin**, Kirill Kuzanyan, Nikolai Safiullin, Igor Rogachevskii, Vladimir Obridko, Sergey Porshnev, Rodion Stepanov
ApJ **2024**
https://arxiv.org/pdf/2411.10380
We discuss a prediction of the solar activity on a short time-scale applying the method based on a combination of a nonlinear mean-field dynamo model and the artificial neural network. The artificial neural network which serves as a correction scheme for the forecast, uses the currently available observational data (e.g., the 13 month running

average of the observed solar sunspot numbers) and the dynamo model output. The nonlinear mean-field αΩ dynamo produces the large-scale magnetic flux which is redistributed by negative effective magnetic pressure instability (NEMPI) producing sunspots and active regions. The nonlinear mean-field dynamo model includes algebraic nonlinearity (caused by the feedback of the growing magnetic field on the plasma motion) and dynamic nonlinearities (related to the dynamics of the magnetic helicity of small-scale magnetic field). We compare the forecast errors with a horizon of 1, 6, 12 and 18 months, for different forecast methods, with the same corrections on the current monthly observations. Our forecast is in good agreement with the observed solar activity, the forecast error is almost stably small over short-medium ranges of forecasting windows. Despite a strong level of chaotic component in the solar magnetic activity we present quantitative evidence that the solar activity on a short range can be stably well predicted, by the joint use of the physically based model with the neural network. This result may have an immediate practical implementation for predictions of various phenomena of solar activity and other astrophysical processes, so may be of interest to a broad community.

Turbulent magnetic helicity fluxes in solar convective zone

N. **Kleeorin**, I. Rogachevskii
Mon. Not. R. Astron. Soc. Volume 515, Issue 4, Pages 5437–5448, **2022**
https://arxiv.org/pdf/2206.14152.pdf
https://doi.org/10.1093/mnras/stac2141
Combined action of helical motions of plasma (the α effect) and non-uniform (differential) rotation is a key dynamo mechanism of solar and galactic large-scale magnetic fields. Dynamics of magnetic helicity of small-scale fields is a crucial mechanism in a nonlinear dynamo saturation where turbulent magnetic helicity fluxes allow to avoid catastrophic quenching of the α effect. The convective zone of the Sun and solar-like stars as well as galactic discs are the source for production of turbulent magnetic helicity fluxes. In the framework of the mean-field approach and the spectral τ approximation, we derive turbulent magnetic helicity fluxes using the Coulomb gauge in a density-stratified turbulence. The turbulent magnetic helicity fluxes include non-gradient and gradient contributions. The non-gradient magnetic helicity flux is proportional to a nonlinear effective velocity (which vanishes in the absence of the density stratification) multiplied by small-scale magnetic helicity, while the gradient contributions describe turbulent magnetic diffusion of the small-scale magnetic helicity. In addition, the turbulent magnetic helicity fluxes contain source terms proportional to the kinetic α effect or its gradients, and also contributions caused by the large-scale shear (solar differential rotation). We have demonstrated that the turbulent magnetic helicity fluxes due to the kinetic α effect and its radial derivative in combination with the nonlinear magnetic diffusion of the small-scale magnetic helicity are dominant in the solar convective zone.

The mean tilt of sunspot bipolar regions: theory, simulations and comparison with observations

N. **Kleeorin**, N. Safiullin, K. Kuzanyan, I. Rogachevskii, A. Tlatov, S. Porshnev
MNRAS Volume 495, Issue 1, June **2020**, Pages 238–248,
https://doi.org/10.1093/mnras/staa1047
https://arxiv.org/pdf/2001.01932.pdf
A theory of the mean tilt of sunspot bipolar regions (the angle between a line connecting the leading and following sunspots and the solar equator) is developed. A mechanism of formation of the mean tilt is related to the effect of Coriolis force on meso-scale motions of super-granular convection and large-scale meridional circulation. The balance between the Coriolis force and the Lorentz force (the magnetic tension) determines a contribution of the large-scale magnetic field to the mean tilt of the sunspot bipolar regions at low latitudes. In addition, the latitudinal dependence of the solar differential rotation affects the mean tilt which can explain deviations from the Joy's law for the sunspot bipolar regions at high latitudes. The obtained theoretical results and performed numerical simulations based on the nonlinear mean-field dynamo theory which takes into account conservation of the total magnetic helicity are in agreement with observational data of the mean tilt of sunspot bipolar regions over individual solar cycles 15 - 24.

The dynamics of Wolf numbers based on nonlinear dynamo with magnetic helicity: comparisons with observations

Ya. **Kleeorin** (1), N. Safiullin (2), N. Kleeorin (1,3), S. Porshnev (2), I. Rogachevskii (1,3), D. Sokoloff
Mon. Not. R. Astron. Soc. **2015**
http://arxiv.org/pdf/1512.04363v1.pdf
We investigated the dynamics of solar activity using the nonlinear one-dimensional dynamo model and phenomenological equation for evolution of Wolf numbers. This system of equations was solved numerically. We took into account the algebraic and dynamical nonlinearities of the alpha effect. The dynamic nonlinearity is related to the evolution of small-scale magnetic helicity and leads to complicated behavior of the solar activity. The evolutionary equation for the Wolf number is based on the mechanism of formation of magnetic spots caused by the

negative effective magnetic pressure instability (NEMPI). This phenomenon was predicted 25 years ago and investigated intensively in recent years in direct numerical simulations and mean-field simulations. The evolutionary equation for the Wolf number includes the production and decay of sunspots. Comparison of numerical simulations and observational data of Wolf numbers shows 70 \% correlations in all interval of observations (about 270 years). We determined the dependence of the maximum value of the Wolf number versus the period of the cycle and asymmetry of the solar cycles versus the amplitude of the cycle. These dependencies are in good agreement with observations.

HelioSwarm: A Multipoint, Multiscale Mission to Characterize Turbulence. Review

Klein, K.G., Spence, H., Alexandrova, O. et al.
Space Sci Rev 219, 74 (**2023**).
https://doi.org/10.1007/s11214-023-01019-0
HelioSwarm (HS) is a NASA Medium-Class Explorer mission of the Heliophysics Division designed to explore the dynamic three-dimensional mechanisms controlling the physics of plasma turbulence, a ubiquitous process occurring in the heliosphere and in plasmas throughout the universe. This will be accomplished by making simultaneous measurements at nine spacecraft with separations spanning magnetohydrodynamic and sub-ion spatial scales in a variety of near-Earth plasmas. In this paper, we describe the scientific background for the HS investigation, the mission goals and objectives, the observatory reference trajectory and instrumentation implementation before the start of Phase B. Through multipoint, multiscale measurements, HS promises to reveal how energy is transferred across scales and boundaries in plasmas throughout the universe.

A Modified Version of Taylor's Hypothesis for Solar Probe Plus Observations

Kristopher G. **Klein**, Jean C. Perez, Daniel Verscharen, Alfred Mallet, Benjamin D.G. Chandran
ApJL **2015**
http://arxiv.org/pdf/1412.3786v1.pdf
The Solar Probe Plus (SPP) spacecraft will explore the near-Sun environment, reaching heliocentric distances as small as~9.5R⊙. Near Earth, spacecraft measurements of fluctuating velocities and magnetic fields taken in the time domain are translated into information about the spatial structure of the solar wind via Taylor's "frozen turbulence" hypothesis. Near the perihelion of SPP, however, the solar-wind speed is comparable to the Alfv\'en speed, and Taylor's hypothesis in its usual form does not apply. In this paper, we show that a modified version of Taylor's hypothesis can be recovered in the near-Sun region. In particular, we show that transverse, non-compressive fluctuations propagating away from the Sun in the plasma frame obey a relation analogous to Taylor's hypothesis when$V_{\rm sc,\perp} \gg |\bm{z}^-|$ and $|\bm{z}^+| \gg |\bm{z}^-|$, where Vsc,⊥ is the component of the spacecraft velocity perpendicular to the mean magnetic field and $\bm{z}^+$ ($\bm{z}^-$) is the Els\"asser variable corresponding to transverse, non-compressive fluctuations propagating away from (towards) the Sun in the plasma frame. Observations and simulations indicate that $\bm{z}^+$ fluctuations account for most of the fluctuation energy in the near-Sun solar wind. This modified form of Taylor's hypothesis will thus make it possible to characterize the spatial structure of the energetically dominant component of the turbulence encountered by~SPP.

Occurrence and Statistics of IRIS Bursts

Lucia **Kleint**, Brandon Panos
A&A 657, A132 **2021**
https://arxiv.org/pdf/2110.12957.pdf
https://doi.org/10.1051/0004-6361/202142235
https://www.aanda.org/articles/aa/pdf/2022/01/aa42235-21.pdf
Small reconnection events in the lower solar atmosphere can lead to its heating, but whether such heating can propagate into higher atmospheric layers and potentially contribute to coronal heating is an open question. We carry out a large statistical analysis of all IRIS observations from 2013 and 2014. We identified "IRIS burst" (IB) spectra via a k-means analysis by classifying and selecting Si IV spectra with superimposed blend lines on top of bursts, which indicate low atmospheric heating. We found that ~8% of all observations show IBs with about 0.01% of all recorded IRIS spectra being IB spectra. We found varying blend absorption levels, which may indicate different depths of the reconnection event and heating. IBs are statistically visible with similar properties and timings in the spectral lines Mg II, C II, and Si IV, but invisible in Fe XXI. By statistically analyzing co-spatial AIA lightcurves, we found systematic enhancements in AIA 1600 and AIA 1700, but no clear response to bursts in all other AIA wavelengths (94, 131, 171, 193, 211, 304, 335) in a timeframe of ±6 minutes around the burst. This may indicate that heating due to IBs is confined within the lower atmosphere and dissipates before reaching temperatures or formation heights covered by the hotter AIA lines. Our developed methods are applicable for statistical analyses of any co-observed data sets and allow us to efficiently analyze millions of spectra and lightcurves simultaneously.

A synchronized two-dimensional α−Ω model of the solar dynamo

M. **Klevs**, F. Stefani, L. Jouve
Solar. Phys. **298**, Article number: 90 **2023**
https://arxiv.org/pdf/2301.05452.pdf
https://link.springer.com/content/pdf/10.1007/s11207-023-02173-y.pdf
We consider a conventional α−Ω-dynamo model with meridional circulation that exhibits typical features of the solar dynamo, including a Hale cycle period of around 20 years and a reasonable shape of the butterfly diagram. With regard to recent ideas of a tidal synchronization of the solar cycle, we complement this model by an additional time-periodic α-term that is localized in the tachocline region. It is shown that amplitudes of some dm/s are sufficient for this α-term to become capable of entraining the underlying dynamo. We argue that such amplitudes of α may indeed be realistic, since velocities in the range of m/s are reachable, e.g., for tidally excited magneto-Rossby waves.

The Thickness of Electric Current Sheets and Implications for Coronal Heating

James A. **Klimchuk**, James E. Leake, Lars K. S. Daldorff, Craig D. Johnston
Frontiers in Physics 11: 1198194 **2023**
https://arxiv.org/ftp/arxiv/papers/2307/2307.13825.pdf
https://www.frontiersin.org/articles/10.3389/fphy.2023.1198194/pdf
The thickness of current sheets is extremely important, especially as it relates to the onset of fast magnetic reconnection. Onset determines how much magnetic free energy can build up in a field before it is explosively released. This has implications for many phenomena on the Sun and throughout the universe, including the heating of the solar corona. Significant effort has been devoted to the question of whether equilibrium current sheets in realistic geometries have finite or zero thickness. Using a simple force balance analysis, we show why current sheets without a guide field (2D) and with a guide field that is invariant in the guide field direction (2.5D) cannot be in equilibrium if they have both finite thickness and finite length. We then estimate the conditions under which the tension of a curved line-tied guide field can facilitate equilibrium in 3D sheets that are finite in all dimensions. Finally, we argue that some quasi-statically evolving current sheets undergoing slow stressing (e.g., when the coronal magnetic field is subjected to photospheric boundary driving) may reach a critical shear, at which point they lose equilibrium, spontaneously collapse, and reconnect. The critical shear is generally consistent with the heating requirements of solar active regions.

Observational Signatures of Coronal Heating in MHD Simulations Without Radiation or a Lower Atmosphere

James A. **Klimchuk**, Kalman J. Knizhnik, Vadim M. Uritsky
ApJ *ApJ* **942** 10 **2023**
https://arxiv.org/pdf/2211.00104
https://iopscience.iop.org/article/10.3847/1538-4357/ac9f41/pdf
It is extremely difficult to simulate the details of coronal heating and also make meaningful predictions of the emitted radiation. Thus, testing realistic models with observations is a major challenge. Observational signatures of coronal heating depend crucially on radiation, thermal conduction, and the exchange of mass and energy with the transition region and chromosphere below. Many magnetohydrodynamic simulation studies do not include these effects, opting instead to devote computational resources to the magnetic aspects of the problem. We have developed a simple method of accounting approximately for the missing effects. It is applied to the simulation output post facto and therefore may be a valuable tool for many studies. We have used it to predict the emission from a model corona that is driven by vortical boundary motions meant to represent photospheric convection. We find that individual magnetic strands experience short-term brightenings, both scattered throughout the computational volume and in localized clusters. The former may explain the diffuse component of the observed corona, while the latter may explain bright coronal loops. Several observed properties of loops are reproduced reasonably well: width, lifetime, and quasi-circular cross-section (aspect ratio not large). Our results lend support to the idea that loops are multi-stranded structures heated by "storms" of nanoflares.

How Turbulent is the Magnetically Closed Corona?

James A. **Klimchuk**, Spiro K. Antiochos
Frontiers in Astronomy and Space Sciences **2021**
https://arxiv.org/ftp/arxiv/papers/2105/2105.12212.pdf
https://doi.org/10.3389/fspas.2021.662861
https://www.frontiersin.org/articles/10.3389/fspas.2021.662861/full
We argue that the magnetically closed corona evolves primarily quasi-statically, punctuated by many localized bursts of activity associated with magnetic reconnection at a myriad of small current sheets. The sheets form by various processes that do not involve a traditional turbulent cascade whereby energy flows losslessly through a continuum of spatial scales starting from the large scale of the photospheric driving. If such an inertial range is a

defining characteristic of turbulence, then the magnetically closed corona is not a turbulent system. It nonetheless has a complex structure that bears no direct relationship to the pattern of driving.

Heating of the Magnetically Closed Corona

Jim **Klimchuk**
Fleishman's Webinar Jan **2021** https://www.youtube.com/watch?v=K_MyQb6U-XM&feature=youtu.be

Intensity Conserving Spectral Fitting

J. A. **Klimchuk** , S. Patsourakos, D. Tripathi
Solar Phys. January **2016**, Volume 291, Issue 1, pp 55-65
The detailed shapes of spectral-line profiles provide valuable information about the emitting plasma, especially when the plasma contains an unresolved mixture of velocities, temperatures, and densities. As a result of finite spectral resolution, the intensity measured by a spectrometer is the average intensity across a wavelength bin of non-zero size. It is assigned to the wavelength position at the center of the bin. However, the actual intensity at that discrete position will be different if the profile is curved, as it invariably is. Standard fitting routines (spline, Gaussian, etc.) do not account for this difference, and this can result in significant errors when making sensitive measurements. We have developed an iterative procedure that corrects for this effect. It converges rapidly and is very flexible in that it can be used with any fitting function. We present examples of cubic-spline and Gaussian fits and give special attention to measurements of blue–red asymmetries of coronal emission lines.

Intensity Conserving Spline Interpolation (ICSI): A New Tool for Spectroscopic Analysis

J. A. **Klimchuk**, S. Patsourakos, D. Tripathi
ApJ **2015**
http://lanl.arxiv.org/ftp/arxiv/papers/1506/1506.08102.pdf
The detailed shapes of spectral line profiles provide valuable information about the emitting plasma, especially when the plasma contains an unresolved mixture of velocities, temperatures, and densities. As a result of finite spectral resolution, the intensity measured by a spectrometer is the average intensity across a wavelength bin of non-zero size. It is assigned to the wavelength position at the center of the bin. However, the actual intensity at that discrete position will be different if the profile is curved, as it invariably is. Standard fitting routines (spline, Gaussian, etc.) do not account for this difference, and this can result in significant errors when making sensitive measurements. Detection of asymmetries in solar coronal emission lines is one example. Removal of line blends is another. We have developed an iterative procedure called Intensity Conserving Spline Interpolation (ICSI) that corrects for this effect. As its name implies, it conserves the observed intensity within each wavelength bin, which ordinary fits do not. Given the rapid convergence, speed of computation, and ease of use, we suggest that ICSI be made a standard component of the processing pipeline for spectroscopic data. **2007 December 11**

Key Aspects of Coronal Heating **Review**

James A. **Klimchuk**
Phil. Trans. Royal Soc. A, **2014**
http://arxiv.org/pdf/1410.5660v1.pdf
We highlight ten key aspects of coronal heating that must be understood before we can consider the problem to be solved. (1) All coronal heating is impulsive. (2) The details of coronal heating matter. (3) The corona is filled with elemental magnetic stands. (4) The corona is densely populated with current sheets. (5) The strands must reconnect to prevent an infinite buildup of stress. (6) What determines the nanoflare frequency? (7) What is the quantum of energy release? (8) What causes the collective behavior responsible for loops? (9) What are the onset conditions for energy release? (10) Chromospheric nanoflares are not a primary source of coronal plasma. Significant progress in solving the coronal heating problem will require a coordination of approaches: observational studies, 1D hydro simulations, large-scale and localized 3D MHD simulations, and possibly also kinetic simulations. There is a unique value to each of these approaches, and the community must strive to coordinate better.

Corrugation Instability of a Coronal Arcade

D. Y. **Klimushkin**, V. M. Nakariakov, P. N. Mager, O. K. Cheremnykh
Solar Physics December **2017**, 292:184
https://link.springer.com/content/pdf/10.1007%2Fs11207-017-1209-x.pdf
We analyse the behaviour of linear magnetohydrodynamic perturbations of a coronal arcade modelled by a half-cylinder with an azimuthal magnetic field and non-uniform radial profiles of the plasma pressure, temperature, and the field. Attention is paid to the perturbations with short longitudinal (in the direction along the arcade) wavelengths. The radial structure of the perturbations, either oscillatory or evanescent, is prescribed by the radial profiles of the equilibrium quantities. Conditions for the corrugation instability of the arcade are determined. It is

established that the instability growth rate increases with decreases in the longitudinal wavelength and the radial wave number. In the unstable mode, the radial perturbations of the magnetic field are stronger than the longitudinal perturbations, creating an almost circularly corrugated rippling of the arcade in the longitudinal direction. For coronal conditions, the growth time of the instability is shorter than one minute, decreasing with an increase in the temperature. Implications of the developed theory for the dynamics of coronal active regions are discussed.

Nowcasting Solar EUV Irradiance With Photospheric Magnetic Fields and the Mg II Index

Kara L. **Kniezewski**, Samuel J. Schonfeld, Carl J. Henney
Space Weather Volume22, Issue4 April **2024** e2023SW003772
https://doi.org/10.1029/2023SW003772
https://agupubs.onlinelibrary.wiley.com/doi/epdf/10.1029/2023SW003772
A new method to nowcast spectral irradiance in extreme ultraviolet (EUV) and far ultraviolet (FUV) bands is presented here, utilizing only solar photospheric magnetograms and the Mg II index (i.e., the core-to-wing ratio). The EUV and FUV modeling outlined here is a direct extension of the SIFT (Solar Indices Forecasting Tool) model, based on Henney et al. (2015, https://doi.org/10.1002/2014sw001118). SIFT estimates solar activity indices using the earth-side solar photospheric magnetic field sums from global magnetic maps generated by the ADAPT (Air Force Data Assimilative Photospheric Flux Transport) model. Utilizing strong and weak magnetic field sums from ADAPT maps, Henney et al. (2015, https://doi.org/10.1002/2014sw001118) showed that EUV & FUV observations can also be well modeled using this technique. However, the original forecasting method required a recent observation of each SIFT model output to determine and apply a 0-day offset. The new method described here expands the SIFT and ADAPT modeling to nowcast the observed Mg II index with a Pearson correlation coefficient of 0.982. By correlating the Mg II model-observation difference with the model-observation difference in the EUV & FUV channels, Mg II can be used to apply the 0-day offset correction yielding improvements in modeling each of the 37 studied EUV & FUV bands. With daily global photospheric magnetic maps and Mg II index observations, this study provides an improved method of nowcasting EUV & FUV bands used to drive thermospheric and ionospheric modeling.

The Rise and Emergence of Untwisted Toroidal Flux Ropes on the Sun

Kalman J. **Knizhnik**, James E. Leake, Mark G. Linton, Sally Dacie
ApJ **2021**
https://arxiv.org/pdf/2101.01020.pdf
Magnetic flux ropes (MFRs) rising buoyantly through the Sun's convection zone are thought to be subject to viscous forces preventing them from rising coherently. Numerous studies have suggested that MFRs require a minimum twist in order to remain coherent during their rise. Furthermore, even MFRs that get to the photosphere may be unable to successfully emerge into the corona unless they are at least moderately twisted, since the magnetic pressure gradient needs to overcome the weight of the photospheric plasma. To date, however, no lower limit has been placed on the critical minimum twist required for an MFR to rise coherently through the convection zone or emerge through the photosphere. In this paper, we simulate an untwisted toroidal MFR which is able to rise from the convection zone and emerge through the photosphere as an active region that resembles those observed on the Sun. We show that untwisted MFRs can remain coherent during their rise and then pile-up near the photosphere, triggering the undular instability, allowing the MFR to emerge through the photosphere. We propose that the toroidal geometry of our MFR is critical for its coherent rise. Upon emerging, a pair of lobes rises into the corona which interact and reconnect, resulting in a localized high speed jet. The resulting photospheric magnetogram displays the characteristic salt-and-pepper structure often seen in observations. Our major result is that MFRs need not be twisted to rise coherently through the convection zone and emerge through the photosphere.

Nanoflare Diagnostics from Magnetohydrodynamic Heating Profiles

K. J. **Knizhnik**1, W. T. Barnes2, J. W. Reep1, and V. M. Uritsky3,4
2020 ApJ 899 156
https://doi.org/10.3847/1538-4357/aba959
https://arxiv.org/pdf/2009.00132.pdf
The nanoflare paradigm of coronal heating has proven extremely promising for explaining the presence of hot, multi-million degree loops in the solar corona. In this paradigm, localized heating events supply enough energy to heat the solar atmosphere to its observed temperatures. Rigorously modeling this process, however, has proven difficult because it requires an accurate treatment of both the magnetic field dynamics and reconnection as well as the plasma response to magnetic perturbations. In this paper, we combine fully 3D magnetohydrodynamic (MHD) simulations of coronal active region plasma driven by photospheric motions with spatially averaged, time-dependent hydrodynamic (HD) modeling of coronal loops to obtain physically motivated observables that can be quantitatively compared with observational measurements of active region cores. We take the behavior of reconnected field lines from the MHD simulation and use them to populate the HD model to obtain the thermodynamic evolution of the plasma and subsequently the emission measure distribution. We find that the photospheric driving of the MHD

model produces only very low-frequency nanoflare heating that cannot account for the full range of active region core observations as measured by the low-temperature emission measure slope. Additionally, we calculate the spatial and temporal distributions of field lines exhibiting collective behavior, and argue that loops occur due to random energization occurring on clusters of adjacent field lines.

The Distribution of Time Delays Between Nanoflares in Magnetohydrodynamic Simulations

Kalman J. **Knizhnik** & Jeffrey W. Reep
Solar Physics volume 295, Article number: 21 (**2020**)
https://link.springer.com/content/pdf/10.1007/s11207-020-1588-2.pdf
Nanoflares are thought to be an important energy source for heating the solar corona. The exact amount of heating contributed by nanoflares depends, in part, on the frequency of the heating and the time interval between nanoflares. Several numerical models have attempted to constrain the frequency of the heating by fitting to observed emission measures. To date, however, no physically motivated value for the time interval between nanoflares has been obtained. In this paper, we calculate a physically motivated distribution of time intervals between successive “nanoflare” reconnection events in driven magnetohydrodynamic simulations. We show that this distribution follows a power law with a slope near −1, much shallower than previously inferred from observations and determined from loop model comparisons with observations. We show that the energy flux injected into the corona in our model is of order 107 ergcm−2s−1107 ergcm−2s−1, and that the heating rate due to these reconnection events reaches values of order 1--10 ergcm−3s−11--10 ergcm−3s−1. Additionally, we show that this power law slope is dependent only weakly on the amount of magnetic helicity injected into the solar magnetic field by the photospheric motions, but the rate of reconnection is about 45%45% higher if no magnetic helicity is injected.

The Role of Magnetic Helicity in Coronal Heating

Kalman J. **Knizhnik**, Spiro K. Antiochos, James A. Klimchuk, C. Richard DeVore
ApJ **883** 26 **2019**
https://arxiv.org/pdf/1909.03768.pdf
https://doi.org/10.3847/1538-4357/ab3afd
One of the greatest challenges in solar physics is understanding the heating of the Sun's corona. Most theories for coronal heating postulate that free energy in the form of magnetic twist/stress is injected by the photosphere into the corona where the free energy is converted into heat either through reconnection or wave dissipation. The magnetic helicity associated with the twist/stress, however, is expected to be conserved and appear in the corona. In previous work we showed that helicity associated with the small-scale twists undergoes an inverse cascade via stochastic reconnection in the corona, and ends up as the observed large-scale shear of filament channels. Our ``helicity condensation" model accounts for both the formation of filament channels and the observed smooth, laminar structure of coronal loops. In this paper, we demonstrate, using helicity- and energy-conserving numerical simulations of a coronal system driven by photospheric motions, that the model also provides a natural mechanism for heating the corona. We show that the heat generated by the reconnection responsible for the helicity condensation process is sufficient to account for the observed coronal heating. We study the role that helicity injection plays in determining coronal heating and find that, crucially, the heating rate is only weakly dependent on the net helicity preference of the photospheric driving. Our calculations demonstrate that motions with 100\% helicity preference are least efficient at heating the corona; those with 0\% preference are most efficient. We discuss the physical origins of this result and its implications for the observed corona.
Erratum **2019** ApJ 887 270 https://iopscience.iop.org/article/10.3847/1538-4357/ab57fe/pdf

Power-Law Statistics Of Driven Reconnection In The Magnetically Closed Corona

Kalman J. **Knizhnik**, Vadim M. Uritsky, James A. Klimchuk, C. Richard DeVore
ApJ 2018 ApJ 853 82 **2018**
https://arxiv.org/pdf/1801.05245.pdf
Numerous observations have revealed that power-law distributions are ubiquitous in energetic solar processes. Hard X-rays, soft X-rays, extreme ultraviolet radiation, and radio waves all display power-law frequency distributions. Since magnetic reconnection is the driving mechanism for many energetic solar phenomena, it is likely that reconnection events themselves display such power-law distributions. In this work, we perform numerical simulations of the solar corona driven by simple convective motions at the photospheric level. Using temperature changes, current distributions, and Poynting fluxes as proxies for heating, we demonstrate that energetic events occurring in our simulation display power-law frequency distributions, with slopes in good agreement with observations. We suggest that the braiding-associated reconnection in the corona can be understood in terms of a self-organized criticality model driven by convective rotational motions similar to those observed at the photosphere.

The Role of Magnetic Helicity in Structuring the Solar Corona

Kalman J. **Knizhnik**, Spiro K. Antiochos, C. Richard DeVore

ApJ **835** 85 **2017**

http://arxiv.org/pdf/1607.06756v1.pdf

Two of the most widely observed and yet most puzzling features of the Sun's magnetic field are coronal loops that are smooth and laminar and prominences/filaments that are strongly sheared. These two features would seem to be quite unrelated in that the loops are near their minimum-energy current-free state, whereas filaments are regions of high magnetic stress and intense electric currents. We argue that, in fact, these two features are inextricably linked in that both are due to a single process: the injection of magnetic helicity into the corona by photospheric motions and the subsequent evolution of this helicity by coronal reconnection. In this paper, we present numerical simulations of the response of a \citet{Parker72} corona to photospheric driving motions that have varying degrees of helicity preference. We obtain four main conclusions: 1) in agreement with the helicity condensation model of \citet{Antiochos13}, the inverse cascade of helicity by magnetic reconnection results in the formation of prominences/filaments localized about polarity inversion lines (PILs); 2) this same process removes most structure from the rest of the corona, resulting in smooth and laminar coronal loops; 3) the amount of remnant tangling in coronal loops is inversely dependent on the net helicity injected by the driving motions; and 4) the structure of the solar corona depends only on the helicity preference of the driving motions and not on their detailed time dependence. We discuss the implications of our results for high-resolution observations of the corona.

The Role of Magnetic Helicity in the Structure and Heating of the Sun's Corona

Kalman J. **Knizhnik**

2016 **Thesis**

http://arxiv.org/pdf/1606.09196v1.pdf

Two of the most important features of the solar atmosphere are its hot, smooth coronal loops and the concentrations of magnetic shear, known as filament channels, that reside above photospheric polarity inversion lines (PILs). The shear observed in filament channels represents magnetic helicity, while the smoothness of the coronal loops indicates an apparent lack of magnetic helicity in the rest of the corona. At the same time, models that attempt to explain the high temperatures observed in these coronal loops require magnetic energy, in the form of twist, to be injected at the photosphere. In addition to magnetic energy, this twist also represents magnetic helicity. Unlike magnetic energy, magnetic helicity is conserved under reconnection, and is consequently expected to accumulate and be observed in the corona. However, filament channels, rather than the coronal loops, are the locations in the corona where magnetic helicity is observed, and it manifests itself in the form of shear, rather than twist. This naturally raises the question: if magnetic helicity needs to be injected to heat coronal loops, why is it only observed in filament channels, while coronal loops are observed to be laminar and smooth? This thesis addresses this question using a series of numerical simulations that demonstrate that magnetic helicity is transported throughout the solar corona by magnetic reconnection in such a way that it accumulates above PILs, forming filament channels, and leaving the rest of the corona generally smooth. In the process, it converts magnetic energy into heat, accounting for the large observed temperatures. This thesis presents a model for the formation of filament channels in the solar corona and the presence of smooth, hot coronal loops, and shows how the transport of magnetic helicity throughout the solar corona by magnetic reconnection is responsible for both of these phenomena.

Waves and Magnetism in the Solar Atmosphere (WAMIS)

Yuan-Kuen **Ko**, John M. Laming, Leonard Strachan, Samuel Tun Beltran, Steven Tomczyk, Sarah E. Gibson, Frédéric Auchère, Roberto Casini, Silvano Fineschi, Michael Knoelker, Clarence Korendyke, Scott W. McIntosh, Marco Romoli, Jan Rybak, Dennis G. Socker, Angelos Vourlidas, and Qian Wu Front. Astron. Space Sci., 3:1. **2016** |

https://www.frontiersin.org/articles/10.3389/fspas.2016.00001/full

https://doi.org/10.3389/fspas.2016.00001

Comprehensive measurements of magnetic fields in the solar corona have a long history as an important scientific goal. Besides being crucial to understanding coronal structures and the Sun's generation of space weather, direct measurements of their strength and direction are also crucial steps in understanding observed wave motions. In this regard, the remote sensing instrumentation used to make coronal magnetic field measurements is well suited to measuring the Doppler signature of waves in the solar structures. In this paper, we describe the design and scientific values of the Waves and Magnetism in the Solar Atmosphere (WAMIS) investigation. WAMIS, taking advantage of greatly improved infrared filters and detectors, forward models, advanced diagnostic tools and inversion codes, is a long-duration high-altitude balloon payload designed to obtain a breakthrough in the measurement of coronal magnetic fields and in advancing the understanding of the interaction of these fields with space plasmas. It consists of a 20 cm aperture coronagraph with a visible-IR spectro-polarimeter focal plane assembly. The balloon altitude would provide minimum sky background and atmospheric scattering at the wavelengths in which these observations are made. It would also enable continuous measurements of the strength and direction of coronal magnetic fields without interruptions from the day–night cycle and weather. These measurements will be made over a large field-of-

view allowing one to distinguish the magnetic signatures of different coronal structures, and at the spatial and temporal resolutions required to address outstanding problems in coronal physics. Additionally, WAMIS could obtain near simultaneous observations of the electron scattered K-corona for context and to obtain the electron density. These comprehensive observations are not provided by any current single ground-based or space observatory. The fundamental advancements achieved by the near-space observations of WAMIS on coronal field would point the way for future ground based and orbital instrumentation.

CORRELATION OF CORONAL PLASMA PROPERTIES AND SOLAR MAGNETIC FIELD IN A DECAYING ACTIVE REGION

Yuan-Kuen **Ko**1, Peter R. Young2,3, Karin Muglach4,5, Harry P. Warren1, and Ignacio Ugarte-Urra1
2016 ApJ 826 126

We present the analysis of a decaying active region observed by the EUV Imaging Spectrometer on Hinode during **2009 December 7–11**. We investigated the temporal evolution of its structure exhibited by plasma at temperatures from 300,000 to 2.8 million degrees, and derived the electron density, differential emission measure, effective electron temperature, and elemental abundance ratios of Si/S and Fe/S (as a measure of the First Ionization Potential (FIP) Effect). We compared these coronal properties to the temporal evolution of the photospheric magnetic field strength obtained from the Solar and Heliospheric Observatory Michelson Doppler Imager magnetograms. We find that, while these coronal properties all decreased with time during this decay phase, the largest change was at plasma above 1.5 million degrees. The photospheric magnetic field strength also decreased with time but mainly for field strengths lower than about 70 Gauss. The effective electron temperature and the FIP bias seem to reach a "basal" state (at 1.5× 106 K and 1.5, respectively) into the quiet Sun when the mean photospheric magnetic field (excluding all areas <10 G) weakened to below 35 G, while the electron density continued to decrease with the weakening field. These physical properties are all positively correlated with each other and the correlation is the strongest in the high-temperature plasma. Such correlation properties should be considered in the quest for our understanding of how the corona is heated. The variations in the elemental abundance should especially be considered together with the electron temperature and density.

Oscillations Above Sunspots and Faculae: Height Stratification and Relation to Coronal Fan Structure

N.I. **Kobanov**, D.Y. Kolobov, A.A. Chelpanov
Solar Phys. February **2015**, Volume 290, Issue 2, pp 363-380
http://arxiv.org/pdf/1411.6258v1.pdf

Oscillation properties in two sunspots and two facular regions are studied using Solar Dynamics Observatory (SDO) data and ground-based observations in the SiI 10827 and HeI 10830 lines. The aim is to study different-frequency spatial distribution characteristics above sunspots and faculae and their dependence on magnetic-field features and to detect the oscillations that reach the corona from the deep photosphere most effectively. We used Fast-Fourier-Transform and frequency filtration of the intensity and Doppler-velocity variations with Morlet wavelet to trace the wave propagating from the photosphere to the chromosphere and corona. Spatial distribution of low-frequency (1-2 mHz) oscillations outlines well the fan-loop structures in the corona (the Fe IX 171 line) above sunspots and faculae. High-frequency oscillations (5-7 mHz) are concentrated in fragments inside the photospheric umbra boundaries and close to facular-region centers. This implies that the upper parts of most coronal loops, which transfer low-frequency oscillations from the photosphere, sit in the Fe IX 171 line-formation layer. We used dominant frequency vs. distance from barycenter relations to estimate magnetic-tube inclination angle in the higher layers, which poses difficulties for direct magnetic-field measurements. According to our calculations, this angle is about 40 degrees in the transition region around umbra borders. Phase velocities measured in the coronal loops' upper parts in the Fe IX 171 line-formation layer reach 100-150 km/s for sunspots and 50-100 km/s for faculae.

A publicly available multi-observatory data set of an enhanced network patch from the Photosphere to Corona

Adam R. **Kobelski**, 1, 2 Lucas A. Tarr, 3 Sarah A. Jaeggli, 3 Nicholas Luber,2 Harry P. Warren, 4 and Sabrina Savage1
ApJ **2022**
https://arxiv.org/pdf/2205.01766.pdf

New instruments sensitive to chromospheric radiation at X-ray, UV, Visible, IR, and sub-mm wavelengths have become available that significantly enhance our ability to understand the bi-directional flow of energy through the chromosphere. We describe the calibration, co-alignment, initial results, and public release of a new data set combining a large number of these instruments to obtain multiwavelength photospheric, chromospheric, and coronal observations capable of improving our understanding of the connectivity between the photosphere and the corona via transient brightenings and wave signatures. The observations center on a bipolar region of enhanced network magnetic flux near disk center on SOL**2017-03-17**T14:00-17:00. The comprehensive data set provides one of the most complete views of chromospheric activity related to small scale brightenings in the corona and chromosphere

to date. Our initial analysis shows strong spatial correspondence between the areas of broadest width of the Hydrogen-α spectral line and the hottest temperatures observed in ALMA Band 3 radio data, with a linear coefficient of 6.12 × 10−5˚A/K. The correspondence persists for the duration of co-temporal observations (≈ 60 m). Numerous transient brightenings were observed in multiple data series. We highlight a single, well observed transient brightening along a set of thin filamentary features with a duration of 20 minutes. The timing of the peak intensity transitions from the cooler (ALMA, 7000 K) to hotter (XRT, 3 MK) data series.

Calibrating Data from the Hinode/X-Ray Telescope and Associated Uncertainties

Adam R. **Kobelski**, Steven H. Saar, Mark A. Weber, David E. McKenzie…
Solar Physics, July **2014**, Volume 289, Issue 7, pp 2781-2802
The X-Ray Telescope (XRT) onboard the Hinode satellite, launched 23 September 2006 by the Japan Aerospace Exploration Agency (JAXA), is a joint mission of Japan, the United States, and the United Kingdom to study the solar corona. In particular, XRT was designed to study solar plasmas with temperatures between 1 and 10 MK with ≈1″ pixels (≈2″ resolution). Prior to analysis, the data product from this instrument must be properly calibrated and data values quantified to accurately assess the information contained within. We present here the standard methods of calibration for these data. The calibration was performed on an empirical basis that uses the least complicated correction that accurately describes the data while suppressing spurious features. By analyzing the uncertainties remaining in the data after calibration, we conclude that the procedure is successful, because the remaining uncertainty after calibration is dominated by photon noise. This calibration software is available in the SolarSoft software library.

Solar survey at Pic du Midi: Calibrated data and improved images

Laurent **Koechlin**1, Luc Dettwiller2, Maurice Audejean3, Maël Valais1 and Arturo López Ariste1
A&A 631, A55 (**2019**)
sci-hub.se/10.1051/0004-6361/201732504
https://www.aanda.org/articles/aa/pdf/2019/11/aa32504-17.pdf
Context. We carry out a solar survey with images of the photosphere, prominences, and corona at Pic du Midi observatory. This survey, named CLIMSO (for CLIchés Multiples du SOleil), is in the following spectral lines: Fe XIII corona (1.075 μm), Hα (656.3 nm), and He I (1.083 μm) prominences, and Hα and Ca II (393.4 nm) photosphere. All frames cover 1.3 times the diameter of the Sun with an angular resolution approaching one arcsecond. The frame rate is one per minute per channel (weather permitting) for the prominences and chromosphere, and one per hour for the Fe XIII corona. This survey started in 2007 for the disk and prominences and in 2015 for the corona. We have almost completed one solar cycle and hope to cover several more, keeping the same wavelengths or adding others.
Aims. We seek to make the CLIMSO images easier to use and more profitable for the scientific community.
Methods. At the beginning of the survey, the images that we sent to the CLIMSO database were not calibrated. We have implemented a photometric calibration for the present and future images, in order to provide "science-ready" data. The old images have been calibrated. We have also improved the contrast capabilities of our coronagraphs, which now provide images of the Fe XIII corona, in addition to previous spectral channels. We also implemented an autoguiding system based on a diffractive Fresnel array for precise positioning of the Sun behind coronagraphic masks.
Results. The data, including the images and films, are publicly available and downloadable through virtual observatories and dedicated websites (use "CLIMSO" and "IRAP" keywords to find them). For the Hα and Ca II channels we calibrate the data into physical units, independent of atmospheric or instrumental conditions; we provide solar maps of spectral radiances in W m−2 sr−1 nm−1. The instrumental improvements and calibration process are presented in this paper. **2015-03-20, 2015-03-27**

The Coronal Physics Investigator (CPI) Experiment for ISS: A New Vision for Understanding Solar Wind Acceleration

J. L. **Kohl**, S. R. Cranmer, J. C. Raymond, T. J. Norton, P. J. Cucchiaro, D. B. Reisenfeld, P. H. Janzen, B. D. G. Chandran, T. G. Forbes, P. A. Isenberg, A. V. Panasyuk, A. A. van Ballegooijen
E-print, April **2011**; White paper describing a proposed NASA mission of opportunity for ISS
In February 2011 we proposed a NASA Explorer Mission of Opportunity program to develop and operate a large-aperture ultraviolet coronagraph spectrometer called the Coronal Physics Investigator (CPI) as an attached International Space Station (ISS) payload. The primary goal of this program is to identify and characterize the physical processes that heat and accelerate the primary and secondary components of the fast and slow solar wind. In addition, CPI can make key measurements needed to understand CMEs. UVCS/SOHO allowed us to identify what additional measurements need to be made to answer the fundamental questions about how solar wind streams are produced, and CPI's next-generation capabilities were designed specifically to make those measurements. Compared to previous instruments, CPI provides unprecedented sensitivity, a wavelength range extending from 25.7 to 126 nm, higher temporal resolution, and the capability to measure line profiles of He II, N V, Ne VII, Ne VIII, Si

VIII, S IX, Ar VIII, Ca IX, and Fe X, never before seen in coronal holes above 1.3 solar radii. CPI will constrain the properties and effects of coronal MHD waves by (1) observing many ions over a large range of charge and mass, (2) providing simultaneous measurements of proton and electron temperatures to probe turbulent dissipation mechanisms, and (3) measuring amplitudes of low-frequency compressive fluctuations. CPI is an internally occulted ultraviolet coronagraph that provides the required high sensitivity without the need for a deployable boom, and with all technically mature hardware including an ICCD detector. A highly experienced Explorer and ISS contractor, L-3 Com Integrated Optical Systems and Com Systems East, will provide the tracking and pointing system as well as the instrument, and the integration to the ISS.

Can we rely on EUV emission to identify coronal waveguides?

P. **Kohutova**1,2,⋆, P. Antolin3, M. Szydlarski1,2 and N. Poirier1,2
A&A, 690, A202 (**2024**)
https://www.aanda.org/articles/aa/pdf/2024/10/aa51196-24.pdf

Context. Traditional models of coronal oscillations rely on a modelling of the coronal structures that support them as compact cylindrical waveguides. An alternative model of the structure of the corona has recently been proposed, in which the thin strand-like coronal loops, that are observed in the extreme-UV (EUV) emission are the result of the line-of-sight integration of warps in more complex coronal structures. This is referred to as the coronal veil model.
Aims. We extend the implications of the coronal veil model of the solar corona to models of coronal oscillations.
Methods. Using convection-zone-to-corona simulations with the radiation-magnetohydrodynamics (rMHD) code Bifrost, we analysed the structure of the self-consistently formed simulated corona. We focused on the spatial variability of the volumetric emissivity of the Fe IX 171.073 Å EUV line and on the variability of the Alfvén speed, which captures the density and magnetic structuring of the simulated corona. We traced features associated with large magnitudes of the Alfvén speed gradient, which trap MHD waves and act as coronal waveguides. We searched for the correspondence with emitting regions, which appear as strand-like loops in the line-of-sight-integrated EUV emission.
Results. We find that the cross sections of the waveguides bounded by large Alfvén speed gradients become less circular and more distorted with increasing height in the solar atmosphere. The waveguide filling factors corresponding to the fraction of the waveguides filled with plasma that emits in the given EUV wavelength range from 0.09–0.44. This suggests that we can only observe a small fraction of the waveguide. Similarly, the projected waveguide widths in the plane of the sky are several times larger than the widths of the apparent loops that are observed in the EUV.
Conclusions. We conclude that the coronal veil structure is independent of the model. As a result, we find a lack of straightforward correspondence between peaks in the integrated emission profile that constitute apparent coronal loops and regions of plasma bound by a large Alfvén speed gradient that act as waveguides. Coronal waveguides cannot be reliably identified based on emission in a single EUV wavelength is not reliable in the simulated corona formed in convection-zone-to-corona models.

Excitation and evolution of coronal oscillations in self-consistent 3D radiative MHD simulations of the solar atmosphere

P. **Kohutova**, A. Popovas
A&A 647, A81 **2021**
https://arxiv.org/pdf/2101.06430.pdf
https://doi.org/10.1051/0004-6361/202039491

Solar coronal loops are commonly subject to oscillations. Observations of coronal oscillations are used to infer physical properties of the coronal plasma using coronal seismology. Excitation and evolution of oscillations in coronal loops is typically studied using highly idealised models of magnetic flux-tubes. In order to improve our understanding of coronal oscillations, it is necessary to consider the effect of realistic magnetic field topology and evolution. We study excitation and evolution of coronal oscillations in three-dimensional self-consistent simulations of solar atmosphere spanning from convection zone to solar corona using radiation-MHD code Bifrost. We use forward-modelled EUV emission and three-dimensional tracing of magnetic field to analyse oscillatory behaviour of individual magnetic loops. We further analyse the evolution of individual plasma velocity components along the loops using wavelet power spectra to capture changes in the oscillation periods. Various types of oscillations commonly observed in the corona are present in the simulation. We detect standing oscillations in both transverse and longitudinal velocity components, including higher order oscillation harmonics. We also show that self-consistent simulations reproduce existence of two distinct regimes of transverse coronal oscillations: rapidly decaying oscillations triggered by impulsive events and sustained small-scale oscillations showing no observable damping. No harmonic drivers are detected at the footpoints of oscillating loops. We show that coronal loop oscillations are abundant in self-consistent 3D MHD simulations of the solar atmosphere. The dynamic evolution and variability of individual magnetic loops suggest we need to reevaluate our models of monolithic and static coronal loops with constant lengths in favour of more realistic models.

Self-consistent 3D radiative MHD simulations of coronal rain formation and evolution

P. **Kohutova**, P. Antolin, A. Popovas, M. Szydlarski, V. H. Hansteen
A&A 639, A20 **2020**
https://arxiv.org/pdf/2005.03317.pdf
https://www.aanda.org/articles/aa/pdf/2020/07/aa37899-20.pdf
Coronal rain consists of cool and dense plasma condensations formed in coronal loops as a result of thermal instability. Previous numerical simulations of thermal instability and coronal rain formation have relied on artificially adding a coronal heating term to the energy equation. To reproduce large-scale characteristics of the corona, using more realistic coronal heating prescription is necessary. We analyse coronal rain formation and evolution in a 3-dimensional radiative magnetohydrodynamic simulation spanning from convection zone to corona which is self-consistently heated by magnetic field braiding as a result of convective motions. We investigate the spatial and temporal evolution of energy dissipation along coronal loops which become thermally unstable. Ohmic dissipation in the model leads to the heating events capable of inducing sufficient chromospheric evaporation into the loop to trigger thermal instability and condensation formation. The cooling of the thermally unstable plasma occurs on timescales comparable to the duration of the individual impulsive heating events. The impulsive heating has sufficient duration to trigger thermal instability in the loop but does not last long enough to lead to coronal rain limit cycles. We show that condensations can either survive and fall into the chromosphere or be destroyed by strong bursts of Joule heating associated with a magnetic reconnection events. In addition, we find that condensations can also form along open magnetic field lines.

First direct observation of a torsional Alfvén oscillation at coronal heights

P. **Kohutova**, E. Verwichte, C. Froment
A&A 633, L6 (**2020**)
https://arxiv.org/pdf/1912.03954.pdf
https://www.aanda.org/articles/aa/pdf/2020/01/aa37144-19.pdf
Torsional Alfvén waves are promising candidates for transport of energy across different layers of the solar atmosphere and have been theoretically predicted for decades. Previous detections of Alfvén waves so far have however mostly relied on indirect signatures. We present a first direct observational evidence of a fully resolved torsional Alfvén oscillation of a large-scale structure occurring at coronal heights. We analyse IRIS imaging and spectral observation of a surge resulting from magnetic reconnection between active region prominence threads and surrounding magnetic fieldlines. The IRIS spectral data provides clear evidence of an oscillation in the line-of-sight velocity with a 180° phase difference between the oscillation signatures at opposite edges of the surge flux tube. This together with an alternating tilt in the Si IV and Mg II k spectra across the flux tube and the trajectories traced by the individual threads of the surge material provides clear evidence of torsional oscillation of the flux tube. Our observation shows that magnetic reconnection leads to the generation of large-scale torsional Alfvén waves. **9 December 2015**

Formation of coronal rain triggered by impulsive heating associated with magnetic reconnection

P. **Kohutova**, E. Verwichte, C. Froment
A&A Volume 630, id.A123 **2019**
https://arxiv.org/pdf/1910.07746.pdf
Context. Coronal rain consists of cool plasma condensations formed in coronal loops as a result of thermal instability. The standard models of coronal rain formation assume that the heating is quasi-steady and localised at the coronal loop footpoints.
Aims. We present an observation of magnetic reconnection in the corona and the associated impulsive heating triggering formation of coronal rain condensations. Methods. We analyse combined SDO/AIA and IRIS observations of a coronal rain event following a reconnection between threads of a low-lying prominence flux rope and surrounding coronal field lines.
Results. The reconnection of the twisted flux rope and open field lines leads to a release of magnetic twist. Evolution of the emission of one of the coronal loops involved in the reconnection process in different AIA bandpasses suggests that the loop becomes thermally unstable and is subject to the formation of coronal rain condensations following the reconnection and that the associated heating is localised in the upper part of the loop leg.
Conclusions. In addition to the standard models of thermally unstable coronal loops with heating localised exclusively in the footpoints, thermal instability and subsequent formation of condensations can be triggered by the impulsive heating associated with magnetic reconnection occurring anywhere along a magnetic field line.
9 December 2015
RHESSI Science Nugget, No. **362**, Nov **2019**
http://sprg.ssl.berkeley.edu/~tohban/wiki/index.php/Can_magnetic_reconnection_cause_solar_rainstorms%3F

Excitation of coronal loop oscillations by coronal rain

Petra **Kohutova** and Erwin Verwichte
UKSP Nugget: 88, June **2018**
http://www.uksolphys.org/uksp-nugget/88-excitation-of-coronal-loop-oscillations-by-coronal-rain/
Coronal rain is a common phenomenon occurring in active region coronal loops. As the name suggests, it shares many parallels with its terrestrial counterpart; it consists of cool plasma condensations falling from coronal heights towards the solar surface guided by magnetic field lines. Coronal rain is formed as a direct consequence of thermal instability. A coronal loop is likely to become thermally unstable if it is heated predominantly at the footpoints. If the thermal conduction along the loop is not efficient enough, the radiative losses from the plasma at the loop top can overcome the heating input from the footpoints, resulting in onset of a thermally unstable regime and in the runway cooling of the plasma at the loop top. This leads to the formation of cool and dense plasma condensations, which then fall towards the solar surface in the form of coronal rain showers. Recent high resolution observations have shown that coronal rain is much more common than previously thought [1], suggesting it has an important role in the chromosphere-corona mass cycle. Due to its origin, coronal rain also provides us with physical insight into the atmospheric thermal cycle. **2014/08/27**

Dynamics of plasma condensations in a gravitationally stratified coronal loop A23

P. **Kohutova** and E. Verwichte
A&A 602, A23 (**2017**)
https://www.aanda.org/articles/aa/pdf/2017/06/aa29912-16.pdf
Context. Coronal rain composed of cool plasma condensations falling from coronal heights is a phenomenon occurring in footpoint-heated coronal loops as a result of thermal instability. High-resolution coronal rain observations suggest that condensations move with less than free-fall speed and can sometimes undergo longitudinal oscillations.
Aims. We investigate the evolution and dynamics of plasma condensations in a gravitationally stratified coronal loop.
Methods. We carried out 2.5 dimensional magnetohydrodynamic simulations of a cool plasma condensation in a gravitationally stratified coronal loop and analysed its evolution, kinematics, and the evolution of the forces acting on the condensation. We further propose a one-dimensional analytical model of the condensation dynamics.
Results. The motion of plasma condensations is found to be strongly affected by the pressure of the coronal loop plasma. Maximum downward velocities are in agreement with recent coronal rain observations. A high coronal magnetic field or low condensation mass can lead to damped oscillatory motion of the condensations that are caused by the pressure gradient force and magnetic tension force that results from bending of the magnetic field in the lower part of the coronal loop. Period and damping scaling time of the oscillatory motion seen in the simulations are consistent with values predicted by the model.
Conclusions. The combined effect of pressure gradients in the coronal loop plasma and magnetic tension force that results from changes in magnetic field geometry can explain observed sub-ballistic motion and longitudinal oscillations of coronal rain.

Time Lag Between Cosmic-Ray and Solar Variability: Sunspot Numbers and Open Solar Magnetic Flux

Sergey A. **Koldobskiy**, Riikka Kähkönen, Bernhard Hofer, Natalie A. Krivova, Gennady A. Kovaltsov & Ilya G. Usoskin
Solar Physics volume 297, Article number: 38 (**2022**)
https://link.springer.com/content/pdf/10.1007/s11207-022-01970-1.pdf
Solar magnetic activity drives the dominant 11-year cyclic variability of different space environmental indices, but they can be delayed with respect to the original variations due to the different physical processes involved. Here, we analyzed the pairwise time lags between three global solar and heliospheric indices: sunspot numbers (SSN), representing the solar surface magnetic activity, the open solar flux (OSF), representing the heliospheric magnetic variability, and the galactic cosmic-ray (GCR) intensity near Earth, using the standard cross-correlation and the more detailed wavelet-coherence methods. All the three indices appear highly coherent at a timescale longer than a few years with persistent high coherence at the timescale of the 11-year solar cycle. The GCR variability is delayed with respect to the inverted SSN by about eight 27-day Bartels rotations on average, but the delay varies greatly with the 22-year cycle, being shorter or longer around positive A+A+ or negative A−A− solar polarity epochs, respectively. The 22-year cyclicity of the time lag is determined by the global heliospheric drift effects, in agreement with theoretical models. The OSF lags by about one year behind SSN, and is likely determined by a combination of the short lifetime of active regions and a longer (≈3 years) transport time of the surface magnetic field to the poles. GCRs covary nearly in antiphase with the OSF, also depicting a strong 22-year cycle in the delay, confirming that the OSF is a good index of the heliospheric modulation of GCRs. This provides an important observational constraint for solar and heliospheric physics.

Validation of the Neutron Monitor Yield Function Using Data From AMS-02 Experiment, 2011–2017

Sergey A. **Koldobskiy**, Veronica Bindi, Claudio Corti, Gennady A. Kovaltsov, Ilya G. Usoskin
JGR Volume124, Issue4 April **2019** Pages: 2367-2379 |
sci-hub.se/10.1029/2018JA026340

The newly published spectra of protons and helium over time directly measured in space by the Alpha Magnetic Spectrometer (AMS-02) experiment for the period 2011–2017 provide a unique opportunity to calibrate ground-based neutron monitors (NMs). Here, calibration of several stable sea level NMs (Inuvik, Apatity, Oulu, Newark, Moscow, Hermanus, and Athens) was performed using these spectra. Four modern NM yield functions were verified: Mi13 (Mishev et al., 2013, https://doi.org/10.1002/jgra.50325), Ma16 (Mangeard et al., 2016, https://doi.org/10.1002/2016JA023515), CM12 (Caballero-Lopez & Moraal, 2012, https://doi.org/10.1029/2012JA017794), and CD00 (Clem & Dorman, 2000, https://doi.org/10.1023/A:1026508915269), on the basis of the cosmic ray spectra measured by AMS-02. The Mi13 yield function was found to realistically represent the NM response to galactic cosmic rays. CM12 yield function leads to a small skew in the solar cycle dependence of the scaling factor. In contrast, Ma16 and CD00 yield functions tend to overestimate the NM sensitivity to low-rigidity (<10 GV) cosmic rays. This effect may be important for an analysis of ground level enhancements, leading to a potential underestimate of fluxes of solar energetic particles as based on NM data. The Mi13 yield function is recommended for quantitative analyses of NM data, especially for ground level enhancements. The validity of the force field approximation was studied, and it was found that it fits well the directly measured proton spectra, within a few percent for periods of low to moderate activity and up to ≈10% for active periods. The results of this work strengthen and validate the method of the cosmic ray variability analysis based on the NM data and yield function formalism and improve its accuracy.

A solar cycle of cosmic-ray fluxes for 2006–2014: Comparison between PAMELA and neutron monitors

Sergey A **Koldobskiy**, Gennady A. Kovaltsov, Ilya G. Usoskin
JGR Volume123, Issue6 Pages 4479-4487 **2018**
https://agupubs.onlinelibrary.wiley.com/doi/pdf/10.1029/2018JA025516
http://sci-hub.tw/https://onlinelibrary.wiley.com/doi/abs/10.1029/2018JA025516

A comparison of cosmic proton spectra directly measured by the PAMELA experiment during 2006–2014 with data of polar neutron monitors for the same time interval is presented. It is shown that the measured spectra are well described by the force-field model for the modulation potential range 350 – 750 MV. The obtained modulation potential agrees with that calculated from the data of the world neutron monitor network for low solar activity between 2006 and 2012 but diverges during the maximum of solar cycle. The empirical relation between the modulation potential and the (inverted) NM count rate appears somewhat steeper than the modelled one, as confirmed also by data from fragmentary balloon-borne measurements. A reason for the discrepancy is unclear and calls for additional study using independent datasets.

Coronal seismology by slow waves in non-adiabatic conditions

Dmitrii **Kolotkov**
Front. Astron. Space Sci. 9: 1073664. **2022**
https://doi.org/10.3389/fspas.2022.1073664
https://www.frontiersin.org/articles/10.3389/fspas.2022.1073664/pdf

Slow magnetoacoustic waves represent an important tool for probing the solar coronal plasma. The majority of seismological methods with slow waves are based on a weakly non-adiabatic approach, which assumes the coronal energy transport has only weak effects on the wave dynamics. Despite it significantly simplifies the application of coronal seismology by slow waves, this assumption omits a number of important and confidently observed effects and thus puts strong limitations on the reliability of seismological estimations. We quantitatively assess the applicability of the weak thermal conduction theory to coronal seismology by slow waves. We numerically model the linear standing slow wave in a 1D coronal loop, with field-aligned thermal conduction $\kappa_\parallel$ as a free parameter and no restrictions on its efficiency. The time variations of the perturbed plasma parameters, obtained numerically with full conductivity, are treated as potential observables and analysed with the standard data processing techniques. The slow wave oscillation period is found to increase with $\kappa_\parallel$ by about 30%, indicating the corresponding modification in the effective wave speed, which is missing from the weak conduction theory. Phase shifts between plasma temperature and density perturbations are found to be well consistent with the approximate weakly conductive solution for all considered values of $\kappa_\parallel$. In contrast, the comparison of the numerically obtained ratio of temperature and density perturbation amplitudes with the weak theory revealed relative errors up to 30–40%. We use these parameters to measure the effective adiabatic index of the coronal plasma directly as the ratio of the effective slow wave speed to the standard sound speed and in the polytropic assumption, which is found to be justified in a weakly conductive regime only, with relative errors up to 14% otherwise. The damping of the initial perturbation is found to

be of a non-exponential form during the first cycle of oscillation, which could be considered as an indirect signature of entropy waves in the corona, also not described by weak conduction theory. The performed analysis and obtained results offer a more robust scheme of coronal seismology by slow waves, with reasonable simplifications and without the loss of accuracy.

A new look at the frequency-dependent damping of slow-mode waves in the solar corona

Dmitrii Y. **Kolotkov**, Valery M. Nakariakov
MNRAS Lett **2022**
https://arxiv.org/pdf/2205.05346.pdf
Being directly observed in the Doppler shift and imaging data and indirectly as quasi-periodic pulsations in solar and stellar flares, slow magnetoacoustic waves offer an important seismological tool for probing many vital parameters of the coronal plasma. A recently understood active nature of the solar corona for magnetoacoustic waves, manifested through the phenomenon of wave-induced thermal misbalance, led to the identification of new natural mechanisms for the interpretation of observed properties of waves. A frequency-dependent damping of slow waves in various coronal plasma structures remains an open question, as traditional wave damping theories fail to match observations. We demonstrate that accounting for the back-reaction caused by thermal misbalance on the wave dynamics leads to a modification of the relationship between the damping time and oscillation period of standing slow waves, prescribed by the linear theory. The modified relationship is not of a power-law form and has the equilibrium plasma conditions and properties of the coronal heating/cooling processes as free parameters. It is shown to readily explain the observed scaling of the damping time with period of standing slow waves in hot coronal loops. Functional forms of the unknown coronal heating process, consistent with the observed frequency-dependent damping, are seismologically revealed.

Fast magnetoacoustic wave trains: from tadpoles to boomerangs

Dmitrii Y. **Kolotkov**, Valery M. Nakariakov, Guy Moss, Paul Shellard
MNRAS **2021**
https://arxiv.org/pdf/2105.13696.pdf
Rapidly propagating fast magnetoacoustic wave trains guided by field-aligned plasma non-uniformities are confidently observed in the Sun's corona. Observations at large heights suggest that fast wave trains can travel long distances from the excitation locations. We study characteristic time signatures of fully developed, dispersive fast magnetoacoustic wave trains in field-aligned zero-β plasma slabs in the linear regime. Fast wave trains are excited by a spatially localised impulsive driver and propagate along the waveguide as prescribed by the waveguide-caused dispersion. In slabs with steeper transverse density profiles, developed wave trains are shown to consist of three distinct phases: a long-period quasi-periodic phase with the oscillation period shortening with time, a multi-periodic (peloton) phase in which distinctly different periods co-exist, and a short-lived periodic Airy phase. The appearance of these phases is attributed to a non-monotonic dependence of the fast wave group speed on the parallel wavenumber due to the waveguide dispersion, and is shown to be different for axisymmetric (sausage) and non-axisymmetric (kink) modes. In wavelet analysis, this corresponds to the transition from the previously known tadpole shape to a new boomerang shape of the wave train spectrum, with two well-pronounced arms at shorter and longer periods. We describe a specific previously published radio observation of a coronal fast wave train, highly suggestive of a change of the wavelet spectrum from a tadpole to a boomerang, broadly consistent with our modelling. The applicability of these boomerang-shaped fast wave trains for probing the transverse structuring of the waveguiding coronal plasma is discussed.

Seismological constraints on the solar coronal heating function

D. Y. **Kolotkov**1, 2?, T. J. Duckenfield1 , and V. M. Nakariakov1, 3
A&A 644, A33 **2020**
https://warwick.ac.uk/fac/sci/physics/research/cfsa/people/kolotkov/eprints/heating_slow_kolotkov_ana_r2.pdf
https://arxiv.org/pdf/2010.03364.pdf
https://doi.org/10.1051/0004-6361/202039095
The hot solar corona exists because of the balance between radiative and conductive cooling and some counteracting heating mechanism which remains one of the major puzzles in solar physics. The coronal thermal equilibrium is perturbed by magnetoacoustic waves which are abundantly present in the corona, causing a misbalance between the heating and cooling rates. Due to this misbalance, the wave experiences a back-reaction, either losing or gaining energy from the energy supply that heats the plasma, at the time scales comparable to the wave period. In particular, the plasma can be subject to wave-induced instability or over-stability, depending on the specific choice of the coronal heating function. In the unstable case, the coronal thermal equilibrium would be violently destroyed, which does not allow for the existence of long-lived plasma structures typical for the corona. Based on this, we constrained the coronal heating function using observations of slow magnetoacoustic waves in various coronal plasma structures.

RHESSI Nuggets #394 **2020**
https://sprg.ssl.berkeley.edu/~tohban/wiki/index.php/Probing_the_solar_coronal_heating_function_with_slow_magnetoacoustic_waves

Damping of slow magnetoacoustic oscillations by the misbalance between heating and cooling processes in the solar corona

D. Y. **Kolotkov**1?, V. M. Nakariakov1, 2 , and D. I. Zavershinskii3, 4
A&A 628, A133 **2019**
https://warwick.ac.uk/fac/sci/physics/research/cfsa/people/kolotkov/eprints/kolotkov_aanda_slow_r2.pdf
sci-hub.se/10.1051/0004-6361/201936072

Context. Rapidly decaying slow magnetoacoustic waves are regularly observed in the solar coronal structures, offering a promising tool for a seismological diagnostics of the coronal plasma, including its thermodynamical properties. Aims. The effect of damping of standing slow magnetoacoustic oscillations in the solar coronal loops is investigated accounting for the field-aligned thermal conductivity and a wave-induced misbalance between radiative cooling and some unspecified heating rates. Methods. The non-adiabatic terms were allowed to be arbitrarily large, corresponding to the observed values. The thermal conductivity was taken in its classical form, and a power-law dependence of the heating function on the density and temperature was assumed. The analysis was conducted in the linear regime and in the infinite magnetic field approximation. Results. The wave dynamics is found to be highly sensitive to the characteristic time scales of the thermal misbalance. Depending on certain values of the misbalance time scales three regimes of the wave evolution were identified, namely the regime of a suppressed damping, enhanced damping where the damping rate drops down to the observational values, and acoustic over-stability. The specific regime is determined by the dependences of the radiative cooling and heating functions on thermodynamical parameters of the plasma in the vicinity of the perturbed thermal equilibrium. Conclusions. The comparison of the observed and theoretically derived decay times and oscillation periods allows us to constrain the coronal heating function. For typical coronal parameters, the observed properties of standing slow magnetoacoustic oscillations could be readily reproduced with a reasonable choice of the heating function.

Peculiarity of the Oscillation Stratification in Sunspot Penumbrae

D. Y. **Kolobov**, A. A. Chelpanov, N. I. Kobanov
Solar Phys. **2016**

Spatial distributions of the dominant oscillation frequency obtained for four sunspots show a feature shared by all the analysed levels of the solar atmosphere in these sunspots. This feature located in the inner penumbrae indicates that this region has favourable conditions for 2.5 – 4 mHz oscillation propagation. This agrees with the fact that the spectral composition of the oscillations at three atmospheric heights (Fe i 6173 Å, 1700 Å, and He ii 304 Å) in this region are similar. There has been previous evidence of particular similarities along the height of the photospheric magnetic field strength, line-of-sight velocity, and temperature profile in the inner penumbra, where the internal boundary of the Evershed flow is located. The finding of the same dominant oscillation frequency at a range of altitudes from the chromosphere up to the transition region extends the height range, suggesting similarities in physical conditions.

The centroid speed as a characteristic of the group speed of solar coronal fast magnetoacoustic wave trains

Dmitrii Y. **Kolotkov**, Valery M. Nakariakov, Maximilien Cloesen
MNRAS **2023**
https://arxiv.org/pdf/2311.14512.pdf

The highly-filamented nature of the coronal plasma significantly influences dynamic processes in the corona such as magnetohydrodynamic waves and oscillations. Fast magnetoacoustic waves, guided by coronal plasma non-uniformities, exhibit strong geometric dispersion, forming quasi-periodic fast-propagating (QFP) wave trains. QFP wave trains are observed in extreme-ultraviolet imaging data and indirectly in microwaves and low-frequency radio, aiding in understanding the magnetic connectivity, energy, and mass transport in the corona. However, measuring the field-aligned group speed of QFP wave trains, as a key parameter for seismological analysis, is challenging due to strong dispersion and associated rapid evolution of the wave train envelope. We demonstrate that the group speed of QFP wave trains formed in plane low-β coronal plasma non-uniformities can be assessed through the propagation of the wave train's effective centre of mass, referred to as the wave train's centroid speed. This centroid speed, as a potential observable, is shown empirically to correspond to the group speed of the most energetic Fourier harmonic in the wave train. The centroid speed is found to be almost insensitive to the waveguide density contrast with the ambient corona, and to vary with the steepness of the transverse density profile. The discrepancy between the centroid speed as the group speed measure and the phase speed at the corresponding wavelength is shown to reach 70\%, which is crucial for the energy flux estimation and interpretation of observations.

Magnetohydrodynamic (MHD) Waves and Oscillations in the Sun's Corona and MHD Coronal Seismology: Editorial as a Review

Dmitrii Y. **Kolotkov**, Bo Li & John Leibacher
Solar Physics volume 298, Article number: 40 (**2023**)
https://link.springer.com/content/pdf/10.1007/s11207-023-02132-7.pdf
https://link.springer.com/article/10.1007/s11207-023-02132-7#Abs1

Established in the late 1990s, solar MHD seismology has rapidly grown into a unique tool for diagnostics of the solar atmospheric plasma. This **Topical Collection** presents the current state-of-the-art in the field, addressing both observational and theoretical aspects: from oscillations in coronal loops and filaments to quasi-periodic pulsations in flares, MHD wave dynamics in non-adiabatic coronal conditions, waves in the lower atmosphere, and novel techniques and approaches to theoretical modelling and data analysis.

Stability of slow magnetoacoustic and entropy waves in the solar coronal plasma with thermal misbalance

Dmitrii Y. **Kolotkov**, Valery M. Nakariakov, Joseph B. Fihosy
Physics journal **2023**
https://arxiv.org/pdf/2301.09012.pdf

The back-reaction of the perturbed thermal equilibrium in the solar corona on compressive perturbations, also known as the effect of wave-induced thermal misbalance, is known to result in thermal instabilities chiefly responsible for the formation of fine thermal structuring of the corona. We study the role of the magnetic field and field-aligned thermal conduction in triggering instabilities of slow magnetoacoustic and entropy waves in quiescent and hot active region loops, caused by thermal misbalance. Effects of the magnetic field are accounted for by including it in the parametrisation of a guessed coronal heating function, and the finite plasma parameter β, in terms of the first-order thin flux tube approximation. Thermal conduction tends to stabilise both slow and entropy modes, broadening the interval of plausible coronal heating functions allowing for the existence of a thermodynamically stable corona. This effect is most pronounced for hot loops. In contrast to entropy waves, the stability of which is found to be insensitive to the possible dependence of the coronal heating function on the magnetic field, slow waves remain stable only for certain functional forms of this dependence, opening up perspectives for its seismological diagnostics in future.

The solar corona as an active medium for magnetoacoustic waves

D. Y. **Kolotkov**, D. I. Zavershinskii, V. M. Nakariakov
Plasma Phys. Control. Fusion **2021**
https://arxiv.org/pdf/2111.02370.pdf

The presence and interplay of continuous cooling and heating processes maintaining the corona of the Sun at the observed one million K temperature were recently understood to have crucial effects on the dynamics and stability of magnetoacoustic waves. These essentially compressive waves perturb the coronal thermal equilibrium, leading to the phenomenon of a wave-induced thermal misbalance. Representing an additional natural mechanism for the exchange of energy between the plasma and the wave, thermal misbalance makes the corona an active medium for magnetoacoustic waves, so that the wave can not only lose but also gain energy from the coronal heating source (similarly to burning gases, lasers and masers). We review recent achievements in this newly emerging research field, focussing on the effects that slow-mode magnetoacoustic waves experience as a back-reaction of this perturbed coronal thermal equilibrium. The new effects include enhanced frequency-dependent damping or amplification of slow waves, and effective, not associated with the coronal plasma non-uniformity, dispersion. We also discuss the possibility to probe the unknown coronal heating function by observations of slow waves and linear theory of thermal instabilities. The manifold of the new properties that slow waves acquire from a thermodynamically active nature of the solar corona indicate a clear need for accounting for the effects of combined coronal heating/cooling processes not only for traditional problems of the formation and evolution of prominences and coronal rain, but also for an adequate modelling and interpretation of magnetohydrodynamic waves.

Long-period quasi-periodic oscillations of a small-scale magnetic structure on the Sun

D. Y. **Kolotkov**, V. V. Smirnova, P. V. Strekalova, A. Riehokainen, and V. M. Nakariakov
A&A letters **2017**
http://www2.warwick.ac.uk/fac/sci/physics/research/cfsa/people/kolotkov/eprints/facula_letter_r2.pdf

Long-period quasi-periodic variations of the average magnetic field in a small-scale magnetic structure on the Sun are analysed. The structure is situated at the photospheric level and is involved in a facula formation in the chromosphere. The observational signal obtained from the SDO/HMI line-of-sight magnetograms of the target structure has a non-stationary behaviour, and is therefore processed with the Hilbert-Huang Transform spectral technique. The empirical decomposition of the original signal and subsequent testing of the statistical significance of its intrinsic modes reveal the presence of the white and pink noisy components for the periods shorter and longer than 10 min, respectively, and a significant oscillatory mode. The oscillation is found to have a non-stationary

period growing from about 80 to 230 min and an increasing relative amplitude, while the mean magnetic field in the oscillating structure is seen to decrease. The observed behaviour could be interpreted either by the dynamical interaction of the structure with the boundaries of supergranula cells in the region of interest or in terms of the vortex shedding appearing during the magnetic flux emergence. **6 July 2013**

Empirical mode decomposition analysis of random processes in the solar atmosphere

D. Y. **Kolotkov**, S. A. Anfinogentov, and V. M. Nakariakov
A&A 592, A153 **2016**
http://www2.warwick.ac.uk/fac/sci/physics/research/cfsa/people/kolotkov/eprints/kolotkov_noise_2016_r2.pdf
Solar signals of various types often show appearance of coloured noisy components with a power law spectral energy distribution. Such a frequency-dependent noise may indicate the operation of various randomly distributed dynamical processes in the solar atmosphere. We develop a recipe for the correct usage of the empirical mode decomposition (EMD) technique in the presence of coloured noise, allowing for the clear distinguishing between quasi-periodic oscillatory phenomena in the solar atmosphere and superimposed random background processes. For illustration, we statistically investigate EUV emission intensity variations observed with SDO/AIA in the coronal (171 Å), chromospheric (304 Å), and upper photospheric (1600 Å) layers of the solar atmosphere, from a quiet sun and a sunspot umbrae regions. EMD has been used for analysis due to its adaptive nature and essential applicability to the processing non-stationary and amplitude-modulated time series. For the comparison of the results obtained with EMD, we use the Fourier transform technique as an etalon. We empirically revealed statistical properties of synthetic coloured noises in EMD, and suggested a scheme allowing for the detection of noisy components among the intrinsic modes obtained with EMD in real signals. Application of the method to the solar EUV signals showed that they indeed behave randomly and could be represented as a combination of different coloured noises characterised by a specific value of the power law indices in their spectral energy distributions. On the other hand, 3-min oscillations in the analysed sunspot were detected to have energies significantly above the corresponding noise level. The correct accounting for the background frequency-dependent random processes is essential when using EMD for analysis of oscillations in the solar atmosphere. For the quiet sun region the power law index was found to increase with height above the photosphere, indicating that the higher frequency processes are trapped deeper in the quiet sun atmosphere. In contrast, lower levels of the sunspot umbrae were found to be characterised by higher values of the power law index, meaning the domination of lower frequencies deep inside the sunspot atmosphere. Comparison of the EMD results with those obtained with the Fourier transform showed good consistency, justifying the applicability of EMD.

The sunspot cycle no. 24 in relation to long term solar activity variation

Boris **Komitov**, Vladimir Kaftanb
Journal of Advanced Research Volume 4, Issue 3, May **2013**, Pages 279-282
sci-hub.tw/10.1016/j.jare.2013.02.001
The solar minimum between solar cycles 23 and 24 during the period 2007–2009 has been the longest and deepest one at least since for the last 100 years. We suggest that the Sun is going to his next supercenturial minimum. The main aim of this paper is to tell about arguments concerning this statement. They are based on series of studies, which have been provided during the period since 1997 up to 2010. The progress of solar cycle 24 since its minimum at the end of 2008 up to the end of October 2011 in the light of long term solar activity dynamics is analyzed.

Long-Term Trends in Subsurface Flows of Solar Cycle 23 to 25.

Komm, R.
Sol Phys 299, 150 (**2024**).
https://doi.org/10.1007/s11207-024-02397-6
We study the long-term variation of the zonal and meridional flows from Solar Cycle 23 to 25 derived with ring-diagram analysis applied to Global Oscillation Network Group (GONG) and Helioseismic and Magnetic Imager (HMI) Dopplergrams. We focus mainly on the subsurface flows averaged over depths from 2.0 Mm to 11.6 Mm since their long-term variations are sufficiently similar. First, we examine their temporal variations for systematic artifacts. We find that the GONG-derived zonal flows increase almost linearly with time until about 2020, which we correct with a linear regression. Then we determine the average differences between the GONG- and HMI-derived flows. The average offset is 0.15±0.53 m s−1 for the zonal flow and 0.65±0.08 m s−1 for the meridional flow within ±30.0∘ latitude. The average difference of the meridional flow is nearly constant with latitude in this range, whereas that of the zonal flow varies similarly to that of the magnetic activity. At latitudes of 45.0∘ and higher, the differences increase and are larger than those at lower latitudes, which is most likely due to the combined effect of different spatial resolution between GONG and HMI and geometric projection effects. Finally, we combine the GONG- and HMI-derived flows and find, as expected, that the solar-cycle variation is the dominant long-term variation. At each latitude within ±30.0∘, the meridional-flow pattern appears ahead of the zonal-flow pattern by an average lag of 0.926±0.126 years. The equatorward and poleward branches of the solar-cycle variation

occur at 52.5∘ with the poleward branches present near 60.0∘ and the equatorward ones at lower latitudes. The zonal flows at 52.5∘ and 60.0∘ show an additional trend and decrease by 2.9±0.3 m s−1 over 11 years. This decrease might nevertheless be related to the solar cycle and imply that the flow amplitudes are anticorrelated with the strength of the associated solar cycle.

Is the Subsurface Meridional Flow Zero at the Equator?

R. **Komm**

Solar Physics volume 297, Article number: 99 (**2022**)

https://doi.org/10.1007/s11207-022-02027-z

We study the subsurface meridional flow and its divergence from the surface to a depth of about 16 Mm at the equator and its variation with the solar cycle derived with ring-diagram analysis applied to Michelson Doppler Imager (MDI) Dynamics Program, Global Oscillation Network Group (GONG), and Helioseismic and Magnetic Imager (HMI) Dopplergrams. The meridional flow at the equator is small but nonzero and is mainly negative (southward) during Solar Cycle 23 with an average of −1.1±0.2 ms−1−1.1±0.2 ms−1 at depths shallower than 7 Mm and positive (northward) during Solar Cycle 24 with an average of +1.3±0.1 ms−1+1.3±0.1 ms−1 over the same depth range derived from supersynoptic maps of combined HMI and GONG data (scaled to match HMI flow amplitudes). The divergence in supersynoptic maps is positive at all times and clearly varies with the solar cycle with large values during cycle maxima and small values during minima. On time scales of synoptic maps, we found that at depths shallower than 10 Mm the cross-equatorial flow is, on average, toward the hemisphere with the larger amount of flux. The meridional flow at the equator has broad distributions with widths that are at least five times larger than the mean values. The distributions of Solar Cycles 23 and 24 overlap but are distinguishable. For a high-activity subset, the cross-equatorial flow is predominantly toward locations with high activity and the divergence is greater than average. The nonzero cross-equatorial flow is in this case a consequence of the inflows present near active regions and the imbalance of activity between the hemispheres. For a quiet-region subset, the cross-equatorial flow is, on average, in the same direction as the average flow over a solar cycle with a similar broad distribution, while the quiet-region divergence is smaller than the grand average.

Subsurface Horizontal Flows During Solar Cycles 24 and 25 with Large-Tile Ring-Diagram Analysis

R. **Komm**

Solar Physics volume 296, Article number: 174 (**2021**)

https://link.springer.com/content/pdf/10.1007/s11207-021-01923-0.pdf

https://doi.org/10.1007/s11207-021-01923-0

We study the large-scale subsurface flows to a depth of about 32 Mm covering the near-surface shear layer (NSSL). The flows were derived with a ring-diagram analysis applied to Helioseismic and Magnetic Imager (HMI) Dopplergrams using tiles with 30∘ diameter instead of the commonly used 15∘ ones. This allows us to determine flows at greater depths in exchange for coarser spatial resolution. We confirm that the average zonal flow increases with increasing depth and reaches a plateau in the NSSL. There is a hint of a local maximum or saddle point much closer to the surface at about 8 Mm. The average meridional flow is poleward at all depths in both hemispheres. The average amplitude is 14.3±0.214.3±0.2 m s−1 at 30∘ and 12.4±0.212.4±0.2 m s−1 at 15∘ latitude at depths of 20 Mm and shallower, while amplitudes at these latitudes decrease at greater depths. The solar-cycle variation of the zonal and meridional flow are clearly noticeable from the surface throughout the NSSL. The dominant features of the zonal flow are bands of faster-than-average flow associated with Solar Cycles 24 and 25. The onset of the fast bands happens almost simultaneously at all depths. For Cycle 25, the fast bands appear in the southern hemisphere about one year before those in the northern one and both fast bands appear several years before magnetic activity appeared at the surface in either hemisphere. The meridional flow shows a similar pattern after subtracting the temporal mean at each latitude. The bands of converging residual meridional flow move from mid- to low latitudes during a solar cycle. These bands appear at low latitudes almost at the same time at all depths, similar to the fast bands of the zonal flow. However, at 45∘ latitude they appear first in layers near 32 Mm and about two years later at the solar surface, as if the pattern were rising through the outer layers.

Divergence and Vorticity of Subsurface Flows During Solar Cycles 23 and 24

R. **Komm**, R. Howe & F. Hill

Solar Physics volume 296, Article number: 73 (**2021**)

https://link.springer.com/content/pdf/10.1007/s11207-021-01799-0.pdf

We study the solar-cycle variation of the divergence and vorticity of subsurface horizontal flows from the surface to a depth of 16 Mm. The flows were derived with ring-diagram analysis applied to Michelson Doppler Imager (MDI) Dynamics Program, Global Oscillation Network Group (GONG), and Helioseismic and Magnetic Imager (HMI) Dopplergrams. We study their variation for the complete data set and for two subsets representing active and quiet regions. All three data sets show alternating bands of diverging and converging flows and bands of cyclonic and anticyclonic flows moving from mid-latitudes toward the equator during a solar cycle. For Solar Cycle 24, these

bands are precursors of the magnetic activity appearing several years before magnetic activity is present at a given latitude even leading the fast bands of the flows. The amplitude differences between the cyclonic and anticyclonic and the converging and diverging bands during a solar cycle agree within the error bars between the complete data set and the two subsets. For Solar Cycle 24, the amplitude differences are 6.0±0.710−8 s−1for the bands of vorticity and −4.9±0.610−8 s−1for those of divergence averaged over 2.0 – 11.6 Mm using the complete data set. The amplitude differences of Solar Cycle 23 are 26±3% smaller than those of Solar Cycle 24. The flows of the active-region subset are more converging and cyclonic than those of the quiet-region subset with an extra vorticity of 1.3±0.110−8 s−1and an extra divergence of −6.7±0.310−8 s−1averaged over 7.5∘ – 30∘ and all depths and epochs. The amplitude of the extra divergence of active regions is about a factor of 1.3 larger at depths shallower than 6 Mm and decreases with increasing depth, while the extra vorticity is nearly constant with depth.

Solar-Cycle Variation of the Subsurface Flows of Active- and Quiet-Region Subsets.

Komm, R., Howe, R. & Hill, F.
Sol Phys 295, 47 (**2020**).
https://doi.org/10.1007/s11207-020-01611-5
We study the solar-cycle variation of subsurface flows for both active and quiet solar regions. We derive flows from the surface to a depth of 16 Mm using ring-diagram analysis applied to Dopplergrams obtained with the Michelson Doppler Imager (MDI) Dynamics Program, the Global Oscillation Network Group (GONG), and the Helioseismic and Magnetic Imager (HMI) instrument. We derive the temporal variation of the zonal and meridional flows in a consistent manner for Solar Cycles 23 and 24 combining the flows from the three data sources scaled to match HMI-derived flows. The subsurface flows associated with active and quiet regions show the same variation with the solar cycle with alternating bands of faster- and slower-than-average zonal and meridional flows moving from mid-latitudes toward the equator during the course of a cycle. We derive the differences between the amplitudes of the extrema of the fast and the slow flows. For Cycle 24, the average difference between the fast- and slow-flow amplitude is 9.5±0.5 ms−19.5±0.5 ms−1 for the zonal flows and 7.0±0.4 ms−17.0±0.4 ms−1 for the meridional flows of the quiet-region subset averaged over 2 to 12 Mm within ±30∘±30∘ latitude. For the active-region subset, the average difference is 10.4±0.9 ms−110.4±0.9 ms−1 for the zonal flows and 9.3±0.7 ms−19.3±0.7 ms−1 for the meridional flows. We subtract the flows of the quiet-region subset from those of the active-region one to determine the contribution of active regions to the long-term flow pattern. The resulting meridional flow associated with active regions has a maximum amplitude near 3.1 Mm and its amplitude decreases with depth. This implies that the converging flows attributed to active regions are a shallow-layer phenomenon.

Kinetic Helicity and Lifetime of Activity Complexes During Solar Cycle 24

R. **Komm** and S. Gosain
2019 ApJ 887 192
sci-hub.se/10.3847/1538-4357/ab58ca
We study magnetic features on the solar surface that exist for several rotations during solar cycle 24. To identify them, we average synoptic maps over a range in latitude and stack the resulting longitudinal strips in time. We use synoptic maps of magnetograms obtained with the NSO/Synoptic Optical Long-term Investigations of the Sun instrument and create synoptic maps of the kinetic helicity of subsurface flows integrated over 2.0–7.1 Mm based on Solar Dynamics Observatory/Helioseismic and Magnetic Imager Dopplergrams. To distinguish between active and quiet regions, we sort the grid points of the synoptic maps by their activity level and divide the data into four subsets with 25% of activity each and into two subsets with the highest or lowest 12.5% of activity values. The kinetic helicity of these six subsets follows the hemispheric helicity rule with, on average, positive values in the southern and negative values in the northern hemisphere. However, the helicity of the subset with the highest activity is about four times higher than that of the other subsets, and the mid-quartile subsets show the weakest hemispheric helicity rule. We define the lifetime of complexes in each subset and find that for the high-activity subset, the amplitude of magnetic activity and kinetic helicity increases almost linearly with the lifetime of complexes. The distribution of flares closely resembles that of the high-activity subset. The flare-productive locations in long-lived complexes produce, on average, the same number of flares as those of short-lived complexes. However, long-lived complexes have a higher fractional number of these locations than the short-lived complexes and thus produce more flares not just because they live longer.

Subsurface Zonal and Meridional Flow During Cycles 23 and 24

R. **Komm**, R. Howe, F. Hill
Solar Physics October **2018**, 293:145
We study the solar-cycle variation of subsurface flows from the surface to a depth of 16 Mm. We have used ring-diagram analysis to analyze Dopplergrams obtained with the Michelson Doppler Imager (MDI) Dynamics Program, the Global Oscillation Network Group (GONG), and the Helioseismic and Magnetic Imager (HMI) instrument. We combined the zonal and meridional flows from the three data sources and scaled the flows derived from MDI and GONG to match those from HMI observations. In this way, we derived their temporal variation in a consistent

manner for Solar Cycles 23 and 24. We have corrected the measured flows for systematic effects that vary with disk positions. Using time-depth slices of the corrected subsurface flows, we derived the amplitudes and times of the extrema of the fast and slow zonal and meridional flows during Cycles 23 and 24 at every depth and latitude. We find an average difference between maximum and minimum amplitudes of 8.6±0.4 ms−18.6±0.4 ms−1 for the zonal flows and 7.9±0.3 ms−17.9±0.3 ms−1 for the meridional flows associated with Cycle 24 averaged over a depth range from 2 to 12 Mm. The corresponding values derived from GONG data alone are 10.5±0.3 ms−110.5±0.3 ms−1 for the zonal and 10.8±0.3 ms−110.8±0.3 ms−1 for the meridional flow. For Cycle 24, the flow patterns are precursors of the magnetic activity. The timing difference between the occurrence of the flow pattern and the magnetic one increases almost linearly with increasing latitude. For example, the fast zonal and meridional flow appear 2.1±0.62.1±0.6 years and 2.5±0.62.5±0.6 years, respectively, before the magnetic pattern at 30∘30∘ latitude in the northern hemisphere, while in the southern hemisphere, the differences are 3.2±1.23.2±1.2 years and 2.6±0.62.6±0.6 years. The flow patterns of Cycle 25 are present and have reached 30∘30∘ latitude. The amplitude differences of Cycle 25 are about 22% smaller than those of Cycle 24, but are comparable to those of Cycle 23. Moreover, polynomial fits of meridional flows suggest that equatorward meridional flows (counter-cells) might exist at about 80∘80∘ latitude except during the declining phase of the solar cycle.

Solar-Cycle Variation of Subsurface-Flow Divergence: A Proxy of Magnetic Activity?

R. **Komm**, R. Howe, F. Hill

Solar Physics September **2017**, 292:122

We study the solar-cycle variation of subsurface flows from the surface to a depth of 16 Mm. We have analyzed Global Oscillation Network Group (GONG) Dopplergrams with a ring-diagram analysis covering about 15 years and Helioseismic and Magnetic Imager (HMI) Dopplergrams covering more than 6 years. After subtracting the average rotation rate and meridional flow, we have calculated the divergence of the horizontal residual flows from the maximum of Solar Cycle 23 through the declining phase of Cycle 24. The subsurface flows are mainly divergent at quiet regions and convergent at locations of high magnetic activity. The relationship is essentially linear between divergence and magnetic activity at all activity levels at depths shallower than about 10 Mm. At greater depths, the relationship changes sign at locations of high activity; the flows are increasingly divergent at locations with a magnetic activity index (MAI) greater than about 24 G. The flows are more convergent by about a factor of two during the rising phase of Cycle 24 than during the declining phase of Cycle 23 at locations of medium and high activity (about 10 to 40 G MAI) from the surface to at least 10 Mm. The subsurface divergence pattern of Solar Cycle 24 first appears during the declining phase of Cycle 23 and is present during the extended minimum. It appears several years before the magnetic pattern of the new cycle is noticeable in synoptic maps. Using linear regression, we estimate the amount of magnetic activity that would be required to generate the precursor pattern and find that it should be almost twice the amount of activity that is observed.

Solar-Cycle Variation of Subsurface Meridional Flow Derived with Ring-Diagram Analysis

R. **Komm**, I. González Hernández, R. Howe, F. Hill

Solar Phys. Volume 290, Issue 11, pp 3113-3136 **2015**

We study the solar-cycle variation of the meridional flow in the near-surface layers of the solar convection zone from the surface to a depth of 16 Mm. We have analyzed Global Oscillation Network Group (GONG) Dopplergrams with a ring-diagram analysis covering about 13 years (July 2001 – October 2014), from the maximum of Cycle 23 through the rising phase of Cycle 24, and Helioseismic and Magnetic Imager (HMI) Dopplergrams covering more than four years (May 2010 – January 2015). GONG and HMI lead to similar meridional flows during common epochs and latitudes. The meridional flow averaged over a Carrington rotation is poleward up to about 70∘ in both hemispheres at all depths after correcting for systematic effects. The flow amplitude peaks at about 40∘ latitude with an amplitude of about 16 to 20 ms−1 depending on depth. The meridional flow varies with the solar cycle; the flow amplitudes are larger during cycle minimum than during maximum at low- and mid-latitudes. The flows are mainly faster or more-poleward-than-average on the equatorward side of the mean latitude of activity and slower or less-poleward-than-average on its poleward side. The residual meridional flow converges near the mean latitude of activity. A comparison with the corresponding zonal flow derived from GONG and HMI data shows that the bands of more-poleward-than-average meridional flow coincide with the bands of faster-than-average zonal flow and that the bands of less-poleward-than-average meridional flow coincide with the bands of slower-than-average zonal flow. This implies that the residual flows are cyclonic. The bands of fast meridional flow appear at mid-latitudes about three years before magnetic activity of Cycle 24 is present in synoptic maps.

Sub-photosphere to Solar Atmosphere Connection **Review**

Rudolf **Komm**, Ineke De Moortel, Yuhong Fan, Stathis Ilonidis, Oskar Steiner

Space Science Reviews, Volume 196, Issue 1, pp 167-199 **2015**

Magnetic fields extend from the solar interior through the atmosphere. The formation and evolution of active regions can be studied by measuring subsurface flows with local helioseismology. The emergence of magnetic flux

from the solar convection zone is associated with acoustic perturbation signatures. In near-surface layers, the average dynamics can be determined for emerging regions. MHD simulations of the emergence of a twisted flux tube show how magnetic twist and free energy are transported from the interior into the corona and the dynamic signatures associated with such transport in the photospheric and sub-photospheric layers. The subsurface twisted flux tube does not emerge into the corona as a whole in emerging active regions. Shear flows at the polarity inversion line and coherent vortical motions in the subsurface flux tubes are the major means by which twist is transported into the corona, leading to the formation of sigmoid-shaped coronal magnetic fields capable of driving solar eruptions. The transport of twist can be followed from the interior by using the kinetic helicity of subsurface flows as a proxy of magnetic helicity; this quantity holds great promise for improving the understanding of eruptive phenomena. Waves are not only vital for studying the link between the solar interior and the surface but for linking the photosphere with the corona as well. Acoustic waves that propagate from the surface into the magnetically structured, dynamic atmosphere undergo mode conversion and refraction. These effects enable atmospheric seismology to determine the topography of magnetic canopies in the solar atmosphere. Inclined magnetic fields lower the cut-off frequency so that low frequency waves can leak into the outer atmosphere. Recent high resolution, high cadence observations of waves and oscillations in the solar atmosphere, have lead to a renewed interest in the potential role of waves as a heating mechanism. In light of their potential contribution to the heating of the solar atmosphere, some of the recent observations of waves and oscillations and ongoing modelling efforts are reviewed.

Subsurface Zonal and Meridional Flow Derived from GONG and SDO/HMI: A Comparison of Systematics

R. **Komm**, I. González Hernández, R. Howe, F. Hill
Solar Phys. 290, Issue 4, pp 1081-1104 **2015**
We study the subsurface flows in the near-surface layers of the solar convection zone from the surface to a depth of 16 Mm derived from Global Oscillation Network Group (GONG) andHelioseismic and Magnetic Imager (HMI) Dopplergrams using a ring-diagram analysis. We characterize the systematic east–west and north–south variations present in the zonal and meridional flows and compare flows derived from GONG and HMI data before and after the correction. The average east–west variation with depth of one flow component resembles the average north–south variation with depth of the other component. The east–west variation of the zonal flow together with the north–south variation of the meridional flow can be modeled as a systematic radial velocity. This indicates a solar center-to-limb variation as the underlying cause. The north–south variation of the zonal flow and the east–west variation of the meridional flow require two separate functions. The east–west variation of the meridional flow consists mainly of an annual variation with the B 0 angle, while the north–south trend of the zonal flow consists of a constant non-zero component in addition to an annual variation. This indicates a geometric projection artifact. After compensating for these systematic effects, the meridional and zonal flows derived from HMI data agree well with those derived from GONG data. An offset remains between the zonal flow derived from GONG and HMI data. The equatorward meridional flows at high latitude that appear episodically depending on the B 0 angle are absent from the corrected flows.

Current and Kinetic Helicity of Long-lived Activity Complexes

Rudolf **Komm** and Sanjay Gosain
2015 ApJ 798 20
We study long-lived activity complexes and their current helicity at the solar surface and their kinetic helicity below the surface. The current helicity has been determined from synoptic vector magnetograms from the NSO/SOLIS facility, and the kinetic helicity of subsurface flows has been determined with ring-diagram analysis applied to full-disk Dopplergrams from NSO/GONG andSDO/HMI. Current and kinetic helicity of activity complexes follow the hemispheric helicity rule with mainly positive values (78%; 78%, respectively, with a 95% confidence level of 31%) in the southern hemisphere and negative ones (80%; 93%, respectively, with a 95% confidence level of 22% and 14%, respectively) in the northern hemisphere. The locations with the dominant sign of kinetic helicity derived from Global Oscillation Network Group (GONG) and SDO/HMI data are more organized than those of the secondary sign even if they are not part of an activity complex, while locations with the secondary sign are more fragmented. This is the case for both hemispheres even for the northern one where it is not as obvious visually due to the large amount of magnetic activity present as compared to the southern hemisphere. The current helicity shows a similar behavior. The dominant sign of current helicity is the same as that of kinetic helicity for the majority of the activity complexes (83% with a 95% confidence level of 15%). During the 24 Carrington rotations analyzed here, there is at least one longitude in each hemisphere where activity complexes occur repeatedly throughout the epoch. These "active" longitudes are identifiable as locations of strong current and kinetic helicity of the same sign.

Solar-Cycle Variation of Subsurface Zonal Flow

R. **Komm**, R. Howe, I. González Hernández, F. Hill
Solar Physics, September **2014**, Volume 289, Issue 9, pp 3435-3455

We study the solar-cycle variation of the zonal flow in the near-surface layers of the solar convection zone from the surface to a depth of 16 Mm covering the period from mid-2001 to mid-2013 or from the maximum of Cycle 23 through the rising phase of Cycle 24. We have analyzed Global Oscillation Network Group (GONG) and Helioseismic and Magnetic Imager (HMI) Dopplergrams with a ring-diagram analysis. The zonal flow varies with the solar cycle showing bands of faster-than-average flows equatorward of the mean latitude of activity and slower-than-average flows on the poleward side. The fast band of the zonal flow and the magnetic activity appear first in the northern hemisphere during the beginning of Cycle 24. The bands of fast zonal flow appear at mid-latitudes about three years in the southern and four years in the northern hemisphere before magnetic activity of Cycle 24 is present. This implies that the flow pattern is a direct precursor of magnetic activity. The solar-cycle variation of the zonal flow also has a poleward branch, which is visible as bands of faster-than-average zonal flow near 50° latitude. This band appears first in the southern hemisphere during the rising phase of the Cycle 24 and migrates slowly poleward. These results are in good agreement with corresponding results from global helioseismology.

Investigation on the solar spectrum using Blackbody Radiation Inversion

Koustav **Konar**, Kingshuk Bose, R.K. Paul

2021

https://arxiv.org/ftp/arxiv/papers/2104/2104.03548.pdf

The probability distribution of temperature of a blackbody can be determined from its power spectrum. This technique is called blackbody radiation inversion. In the present paper blackbody radiation inversion is applied on the spectrum of the Sun. The probability distribution of temperature and the mean temperature of the Sun are calculated without assuming a homogenous temperature and without using Stefan-Boltzmann law. Different properties of this distribution are characterized. This paper presents the very first mention and investigation of the distortions present within the Sun's spectrum.

Emergence of small-scale magnetic flux in the quiet Sun

I. **Kontogiannis**, G. Tsiropoula, K. Tziotziou, C. Gontikakis, C. Kuckein, M. Verma, C. Denker

A&A 633, A67 **2020**

https://arxiv.org/pdf/1912.02496.pdf

https://doi.org/10.1051/0004-6361/201936778

We study the evolution of a small-scale emerging flux region (EFR) in the quiet Sun, from its emergence to its decay. We track processes and phenomena across all atmospheric layers, explore their interrelations and compare our findings with recent numerical modelling studies. We used imaging, spectral and spectropolarimetric observations from space-borne and ground-based instruments. The EFR appears next to the chromospheric network and shows all characteristics predicted by numerical simulations. The total magnetic flux of the EFR exhibits distinct evolutionary phases, namely an initial subtle increase, a fast increase and expansion of the region area, a more gradual increase, and a slow decay. During the initial stages, bright points coalesce, forming clusters of positive- and negative-polarity in a largely bipolar configuration. During the fast expansion, flux tubes make their way to the chromosphere, producing pressure-driven absorption fronts, visible as blueshifted chromospheric features. The connectivity of the quiet-Sun network gradually changes and part of the existing network forms new connections with the EFR. A few minutes after the bipole has reached its maximum magnetic flux, it brightens in soft X-rays forming a coronal bright point, exhibiting episodic brightenings on top of a long smooth increase. These coronal brightenings are also associated with surge-like chromospheric features, which can be attributed to reconnection with adjacent small-scale magnetic fields and the ambient magnetic field. The emergence of magnetic flux even at the smallest scales can be the driver of a series of energetic phenomena visible at various atmospheric heights and temperature regimes. Multi-wavelength observations reveal a wealth of mechanisms which produce diverse observable effects during the different evolutionary stages of these small-scale structures. **15 October, 2007**

Probing the quiet solar atmosphere from the photosphere to the corona

Ioannis **Kontogiannis**, Costis Gontikakis, Georgia Tsiropoula, Kostas Tziotzou

Solar Phys. 293:56 **2018**

https://arxiv.org/pdf/1803.07934.pdf

We investigate the morphology and temporal variability of a quiet Sun network region in different solar layers. The emission in several EUV spectral lines through both raster and slot time series, recorded by EIS/Hinode is studied along with Hα observations and high resolution spectropolarimetric observations of the photospheric magnetic field. The photospheric magnetic field is extrapolated up to the corona showing a multitude of large and small scale structures. We show for the first time that the smallest magnetic structures both at the network and the internetwork contribute significantly to the emission in EUV lines, with temperatures ranging from 8 104 K to 6 105 K. Two components of transition region emission are present, one associated with small-scale loops that do not reach coronal temperatures and another one acting as an interface between coronal and chromospheric plasma. Both components are associated with persistent chromospheric structures. The temporal variability of the EUV intensity at the network region is also associated with chromospheric motions, pointing to a connection between transition

region and chromospheric features. Intensity enhancements in the EUV transition region lines are preferentially produced by Hα upflows. Examination of two individual chromospheric jets shows that their evolution is associated with intensity variations in transition region and coronal temperatures.

Wave propagation in a solar quiet region and the influence of the magnetic canopy

Ioannis **Kontogiannis**, Georgia Tsiropoula, Kostas Tziotziou
A&A 585, A110 (**2016**)
http://arxiv.org/pdf/1511.08618v1.pdf
Aims. We seek indications or evidence of transmission/conversion of magnetoacoustic waves at the magnetic canopy, as a result of its impact on the properties of the wave field of the photosphere and chromosphere. Methods. We use cross-wavelet analysis to measure phase differences between intensity and Doppler signal oscillations in the Halpha, CaII H, and G-band.We use the height of the magnetic canopy to create appropriate masks to separate internetwork (IN) and magnetic canopy regions. We study wave propagation and differences between these two regions. Results. The magnetic canopy affects wave propagation by lowering the phase differences of progressive waves and allowing the propagation of waves with frequencies lower than the acoustic cut-off. We also find indications in the Doppler signals of Halpha of a response to the acoustic waves at the IN, observed in the CaII H line. This response is affected by the presence of the magnetic canopy. Conclusions. Phase difference analysis indicates the existence of a complicated wave field in the quiet Sun, which is composed of a mixture of progressive and standing waves. There are clear imprints of mode conversion and transmission due to the interaction between the p-modes and small-scale magnetic fields of the network and internetwork.

Transmission and conversion of magnetoacoustic waves on the magnetic canopy in a quiet Sun region

I. **Kontogiannis**, G. Tsiropoula and K. Tziotziou
A&A 567, A62 (**2014**)
Context. We present evidence for the conversion and transmission of wave modes on the magnetic flux tubes that constitute mottles and form the magnetic canopy in a quiet Sun region.
Aims. Our aim is to highlight the details and the key parameters of the mechanism that produces power halos and magnetic shadows around the magnetic network observed in Hα.
Methods. We use our previous calculations of the magnetic field vector and the height of the magnetic canopy, and based on simple assumptions, we determine the turning height, i.e., the height at which the fast magnetoacoustic waves reflect at the chromosphere. We compare the variation of 3, 5, and 7 min power in the magnetic shadow and the power halo with the results of a two-dimensional model on mode conversion and transmission. The key parameter of the model is the attack angle, which is related to the inclination of the magnetic field vector at the canopy height. Our analysis takes also into account that 1) there are projection effects on the propagation of waves; 2) the magnetic canopy and the turning height are curved layers; 3) waves with periods longer than 3 min only reach the chromosphere in the presence of inclined magnetic fields (ramp effect); 4) mottles in Hα are canopy structures; and 5) the wings of Hα contain mixed signal from low- and high-β plasma.
Results. The dependence of the measured power on the attack angle follows the anticipated by the two-dimensional model very well. Long-period slow waves are channeled to the upper chromospheric layers following the magnetic field lines of mottles, while short-period fast waves penetrate the magnetic canopy and are reflected back higher, at the turning height.
Conclusions. Although both magnetoacoustic modes contribute to velocity signals, making the interpretation of observations a challenging task, we conclude that conversion and transmission of the acoustic waves into fast and slow magnetoacoustic waves are responsible for forming power halos and magnetic shadows in the quiet Sun region.

Correlations between Total and Spectral Solar Irradiance Variations

Greg **Kopp**1, Nina-Elisabeth Nèmec2, and Alexander Shapiro3
2024 ApJ 964 60
https://iopscience.iop.org/article/10.3847/1538-4357/ad24e5/pdf
We compare short-term (seven solar rotations), wavelength-dependent temporal variations in spectral solar irradiance (SSI) with those from the total solar irradiance (TSI). Using space-based measurements, we empirically find good correlations across most of the visible and near-infrared (NIR) spectral range, suggesting that the TSI time variability can provide a useful estimate of SSI variability. These empirically determined correlations are consistent with physics-based bolometric variations, providing a straightforward wavelength-dependent parameterization of the SSI variability given a known change in the TSI. Using a solar-irradiance model to distinguish the facular and sunspot contributions, which are responsible for nearly all the irradiance variability on timescales longer than a day, we confirm these results and determine the correlation contributions due to each magnetic activity type individually.

The correlations determined from the model agree in functional form to those of the empirical data, although we do note differences near opacity minimum (1.6 μm). Our results provide a simple TSI-based estimate of the time dependence of the spectral solar variability across the ultraviolet to NIR spectral regions, with the TSI accounting for 94% of the variability in the SSI over the 400–1200 nm range.

Science Highlights and Final Updates from 17 Years of Total Solar Irradiance Measurements from the SOlar Radiation and Climate Experiment/Total Irradiance Monitor (SORCE/TIM)

Greg **Kopp**
Solar Physics volume 296, Article number: 133 (**2021**)
https://link.springer.com/content/pdf/10.1007/s11207-021-01853-x.pdf
https://doi.org/10.1007/s11207-021-01853-x
The final version (V.19) of the total solar irradiance data from the SOlar Radiation and Climate Experiment (SORCE) Total Irradiance Monitor has been released. This version includes all calibrations updated to the end of the mission and provides irradiance data from 25 February 2003 through 25 February 2020. These final calibrations are presented along with the resulting final data products. An overview of the on-orbit operations timeline is provided as well as the associated changes in the time-dependent uncertainties. Scientific highlights from the instrument are also presented. These include the establishment of a new, lower TSI value; accuracy improvements to other TSI instruments via a new calibration facility; the lowest on-orbit noise (for high sensitivity to solar variability) of any TSI instrument; the best inherent stability of any on-orbit TSI instrument; a lengthy (17-year) measurement record benefitting from these stable, low-noise measurements; the first reported detection of a solar flare in TSI; and observations of two Venus transits and four Mercury transits.

Irradiance Variations of the Sun and Sun-Like Stars -- Overview of Topical Collection **Review**

Greg **Kopp**, Alexander Shapiro
Solar Phys. **296**, Article number: 60 **2021**
https://arxiv.org/pdf/2102.06913.pdf
https://link.springer.com/content/pdf/10.1007/s11207-021-01802-8.pdf
https://doi.org/10.1007/s11207-021-01802-8
This topical collection summarizes recent advances in observing and modeling irradiance variations of the Sun and Sun-like stars, emphasizing the links between surface magnetic fields and the resulting solar and stellar variability. In particular, the articles composing this collection summarize recent progress in i) solar-irradiance measurements; ii) modeling of solar- and stellar-irradiance variability; and iii) understanding of the effects of such variability on Earth's climate and exoplanet environments. This topical-collection overview article gives background and more details on these aspects of variability.

Magnitudes and Timescales of Total Solar Irradiance Variability **Review**

Greg **Kopp**
Journal of Space Weather and Space Climate **6**, A30 **2016**
http://arxiv.org/pdf/1606.05258v1.pdf
http://www.swsc-journal.org/articles/swsc/pdf/2016/01/swsc160010.pdf
The Sun's net radiative output varies on timescales of minutes to gigayears. Direct measurements of the total solar irradiance (TSI) show changes in the spatially- and spectrally-integrated radiant energy on timescales as short as minutes to as long as a solar cycle. Variations of ~0.01 % over a few minutes are caused by the ever-present superposition of convection and oscillations with very large solar flares on rare occasion causing slightly-larger measureable signals. On timescales of days to weeks, changing photospheric magnetic activity affects solar brightness at the ~0.1 % level. The 11-year solar cycle shows variations of comparable magnitude with irradiances peaking near solar maximum. Secular variations are more difficult to discern, being limited by instrument stability and the relatively short duration of the space-borne record. Historical reconstructions of the Sun's irradiance based on indicators of solar-surface magnetic activity, such as sunspots, faculae, and cosmogenic isotope records, suggest solar brightness changes over decades to millennia, although the magnitudes of these variations have high uncertainties due to the indirect historical records on which they rely. Stellar evolution affects yet longer timescales and is responsible for the greatest solar variabilities. In this manuscript I summarize the Sun's variability magnitudes over different temporal regimes and discuss the irradiance record's relevance for solar and climate studies as well as for detections of exo-solar planets transiting Sun-like stars.

The Impact of the Revised Sunspot Record on Solar Irradiance Reconstructions

G. **Kopp**, N. Krivova, J. Lean, C.J. Wu
Solar Physics, **2016**

http://arxiv.org/pdf/1601.05397v1.pdf
Reliable historical records of total solar irradiance (TSI) are needed for climate change attribution and research to assess the extent to which long-term variations in the Sun's radiant energy incident on the Earth may exacerbate (or mitigate) the more dominant warming in recent centuries due to increasing concentrations of greenhouse gases. We investigate potential impacts of the new Sunspot Index and Long-term Solar Observations (SILSO) sunspot-number time series on model reconstructions of TSI. In contemporary TSI records, variations on time scales longer than about a day are dominated by the opposing effects of sunspot darkening and facular brightening. These two surface magnetic features, retrieved either from direct observations or from solar activity proxies, are combined in TSI models to reproduce the current TSI observational record. Indices that manifest solar-surface magnetic activity, in particular the sunspot-number record, then enable the reconstruction of historical TSI. Revisions to the sunspot-number record therefore affect the magnitude and temporal structure of TSI variability on centennial time scales according to the model reconstruction methodologies. We estimate the effects of the new SILSO record on two widely used TSI reconstructions, namely the NRLTSI2 and the SATIRE models. We find that the SILSO record has little effect on either model after 1885 but leads to greater amplitude solar-cycle fluctuations in TSI reconstructions prior, suggesting many 18th and 19th century cycles could be similar in amplitude to those of the current Modern Maximum. TSI records based on the revised sunspot data do not suggest a significant change in Maunder Minimum TSI values, and comparing that era to the present we find only very small potential differences in estimated solar contributions to climate with this new sunspot record.

An assessment of the solar irradiance record for climate studies

Greg **Kopp**
J. Space Weather Space Clim. 4 (**2014**) A14
http://www.swsc-journal.org/articles/swsc/pdf/2014/01/swsc130036.pdf
Total solar irradiance, the spatially and spectrally integrated radiant output from the Sun at a mean Sun-Earth distance of 1 astronomical unit, provides nearly all the energy driving the Earth's climate system. Variations in this energy, particularly over long time scales, contribute to changes in Earth's climate and have been linked to historical glaciation and inter-glacial periods as well as having a small effect on more recent global warming. Accurate measurements of solar irradiances require measurements above the Earth's atmosphere. The total solar irradiance spaceborne record began in 1978 and has been uninterrupted since, with over a dozen instruments contributing to the present solar climate data record. I assess the required and achieved accuracies of this record with a focus on its value for climate studies.

One-sided arc averaging geometries in time-distance local helioseismology

David **Korda**, Michal Švanda, Thierry Roudier
A&A 654, A84 **2021**
https://arxiv.org/pdf/2108.00872.pdf
https://www.aanda.org/articles/aa/pdf/2021/10/aa40580-21.pdf
https://doi.org/10.1051/0004-6361/202140580
The study of solar oscillations (helioseismology) has been a very successful method of researching the Sun. Helioseismology teaches us about the structure and mean properties of the Sun. Together with mid-resolution data, the local properties were uncovered in quiet-Sun regions. However, magnetic fields affect the oscillations and prevent us from studying the properties of magnetically active regions with helioseismology. We aim to create a new methodology to suppress the negative effects of magnetic fields on solar oscillations and measure plasma properties close to active regions. The methodology consists of new averaging geometries, a non-linear approach to travel-time measurements, and a consistent inversion method that combines plasma flows and sound-speed perturbations. We constructed the one-sided arc averaging geometries and applied them to the non-linear approach of travel-time measurements. Using the one-sided arc travel times, we reconstructed the annulus travel times in a quiet-Sun region. We tested the methodology against the validated helioseismic inversion pipeline. We applied the new methodology for an inversion for surface horizontal flows in a region with a circular H-type sunspot. The inverted surface horizontal flows are comparable with the output of the coherent structure tracking, which is not strongly affected by the presence of the magnetic field. We show that the new methodology suppresses the negative effects of magnetic fields up to outer penumbra. We measure divergent flows with properties comparable to the moat flow. The new methodology can teach us about the depth structure of active regions and physical conditions that contribute to the evolution of the active regions.
HMI Science Nuggets #166 Oct **2021** http://hmi.stanford.edu/hminuggets/?p=3703

Plasma flows and sound-speed perturbations in the average supergranule

David **Korda**, Michal Švanda
A&A 646, A184 **2021**

https://arxiv.org/pdf/2101.05731.pdf
https://doi.org/10.1051/0004-6361/202039928

Supergranules create a peak in the spatial spectrum of photospheric velocity features. They have some properties of convection cells but their origin is still being debated in the literature. The time-distance helioseismology constitutes a method that is suitable for investigating the deep structure of supergranules. Our aim is to construct the model of the flows in the average supergranular cell using fully consistent time-distance inverse methodology. We used the Multi-Channel Subtractive Optimally Localised Averaging inversion method with regularisation of the cross-talk. We combined the difference and the mean travel-time averaging geometries. We applied this methodology to travel-time maps averaged over more than 10000 individual supergranular cells. These cells were detected automatically in travel-time maps computed for 64 quiet days around the disc centre. The ensemble averaging method allows us to significantly improve the signal-to-noise ratio and to obtain a clear picture of the flows in the average supergranule. We found near-surface divergent horizontal flows which quickly and monotonously weakened with depth; they became particularly weak at the depth of about 7 Mm, where they even apparently switched sign. To learn about the vertical component, we integrated the continuity equation from the surface. The derived estimates of the vertical flow depicted a sub-surface increase from about 5 m/s at the surface to about 35 m/s at the depth of about 3 Mm followed by a monotonous decrease to greater depths. The vertical flow remained positive (an upflow) and became indistinguishable from the background at the depth of about 15 Mm. We further detected a systematic flow in the longitudinal direction. The course of this systematic flow with depth agrees well with the model of the solar rotation in the sub-surface layers.

Comparison of time-distance inversion methods applied to SDO/HMI Dopplergrams

David **Korda**, Michal Švanda, Junwei Zhao
A&A 629, A55 **2019**
https://arxiv.org/pdf/1908.03950.pdf

We compared the results from the JSOC pipeline for horizontal flow components and the perturbations of the speed of sound at set of depths with equivalent results from an independently implemented pipeline using a different time-distance inversion scheme. Our inversion pipeline allows inversion for all quantities at once while allowing minimisation of the crosstalk between them. This gives us an opportunity to discuss the possible biases present in the JSOC data products. For the tests we used the subtractive optimally localised averaging (SOLA) method with a minimisation of the cross-talk. We compared three test inversions for each quantity at each target depth. At first, we used the JSOC setup to reproduce the JSOC results. Subsequently, we used the extended pipeline to improve these results by incorporating more independent travel-time measurements but keeping the JSOC-indicated localisation in the Sun. Finally, we inverted for flow components and sound-speed perturbations using a localisation kernel with properties advertised in the JSOC metadata. We successfully reproduced the horizontal flow components. The sound-speed perturbations are strongly affected by the high level of the cross-talk in JSOC products. This leads to larger amplitudes in the inversions for the sound-speed perturbations. Different results were obtained when a target function localised around the target depth was used. This is a consequence of non-localised JSOC averaging kernels. We add that our methodology also allows inversion for the vertical flow.

Combined helioseismic inversions for 3D vector flows and sound-speed perturbations

David **Korda**, Michal Švanda
A&A 622, A163 **2019**
https://arxiv.org/pdf/1901.01293.pdf

Time-distance helioseismology is the method of the study of the propagation of waves through the solar interior via the travel times of those waves. The travel times of wave packets contain information about the conditions in the interior integrated along the propagation path of the wave. We introduce an improved methodology of the time-distance helioseismology which allows us to invert for a full 3D vector of flows and the sound-speed perturbations at once. Using this methodology one can also derive the mean value of the vertical component of flows and the cross-talk between the flows and the sound-speed perturbations. We used the SOLA method with a minimisation of the cross-talk as a tool for inverse modelling. In the forward model, we use Born approximation travel-time sensitivity kernels with the Model S as a background. The methodology was validated using forward-modelled travel times with both mean and difference point-to-annulus averaging geometries applied to a snapshot of fully self-consistent simulation of the convection. We tested the methodology on synthetic data. We demonstrate that we are able to recover flows and sound-speed perturbations in the near-surface layers. We have taken the advantage of the sensitivity of our methodology to entire vertical velocity, and not only to its variations as in other available methodologies. The cross-talk from both the vertical flow component and the sound-speed perturbation has only a negligible effect for inversions for the horizontal flow components. The inversions for the vertical component of the vector flows or for the sound-speed perturbations are affected by the cross-talk from the horizontal components, which needs to be minimised in order to provide valid results. It seems that there is a nearly constant cross-talk between the vertical component of the vector flows and the sound-speed perturbations.
HMI Science Nuggets #122, Apr 2019 http://hmi.stanford.edu/hminuggets/?p=2858

Solar-cycle variation of quiet-Sun magnetism and surface gravity oscillation mode

M. J. **Korpi-Lagg**1,3, A. Korpi-Lagg1,2, N. Olspert1 and H.-L. Truong1
A&A 665, A141 (**2022**)
https://www.aanda.org/articles/aa/pdf/2022/09/aa43979-22.pdf

Context. The origins of quiet-Sun magnetism (QS) is still under debate and investigating the solar cycle variation observationally in greater detail can provide clues on how to resolve the ensuing controversies.
Aims. We investigate the solar cycle variation of the most magnetically quiet regions and their surface gravity oscillation (f-) mode-integrated energy, Ef.
Methods. We used 12 years of Helioseismic and Magnetic Imager (HMI) data and applied a stringent selection criteria based on spatial and temporal quietness to avoid any influence from active regions (ARs). We developed an automated high-throughput pipeline to go through all available magnetogram data and to compute the value of Ef for the selected quiet regions.
Results. We observed a clear solar cycle dependence of the magnetic field strength in the most quiet regions containing several supergranular cells. For patch sizes smaller than a supergranular cell, no significant cycle dependence was detected. The Ef at the supergranular scale is not constant over time. During the late ascending phase of Cycle 24 (SC24, 2011-2012), it is roughly constant, but starts diminishing in 2013, as the maximum of SC24 is approached. This trend continues until mid-2017, when hints of strengthening at higher southern latitudes are seen. Slow strengthening continues, stronger at higher latitudes than at the equatorial regions, but Ef never returns to the values seen in 2011-2012. In addition, the strengthening trend continues past the solar minimum, to the years when SC25 is already clearly ascending. Hence, the Ef behavior is not in phase with the solar cycle.
Conclusions. The dependence of Ef on the solar cycle at supergranular scales is indicative of the fluctuating magnetic field being replenished by tangling from the large-scale magnetic field – and not solely due to the action of a fluctuation dynamo process in the surface regions. The absence of variations on smaller scales might be an effect of the limited spatial resolution and magnetic sensitivity of HMI. The anticorrelation of Ef with the solar cycle in gross terms is expected, but the phase shift of several years indicates a connection to the large-scale poloidal magnetic field component rather than the toroidal one. Calibrating AR signals with the QS Ef does not reveal significant enhancement of the f-mode prior to AR emergence.

HMI Nuggets #186 **2022** http://hmi.stanford.edu/hminuggets/?p=4005

On the dynamical interaction between overshooting convection and an underlying dipole magnetic field -- I. The non-dynamo regime

Lydia **Korre**, Nicholas H. Brummell, Pascale Garaud, Celine Guervilly
MNRAS **2020**
https://arxiv.org/pdf/2008.01857.pdf

Motivated by the dynamics in the deep interiors of many stars, we study the interaction between overshooting convection and the large-scale poloidal fields residing in radiative zones. We have run a suite of 3D Boussinesq numerical calculations in a spherical shell that consists of a convection zone with an underlying stable region that initially compactly contains a dipole field. By varying the strength of the convective driving, we find that, in the less turbulent regime, convection acts as turbulent diffusion that removes the field faster than solely molecular diffusion would do. However, in the more turbulent regime, turbulent pumping becomes more efficient and partially counteracts turbulent diffusion, leading to a local accumulation of the field below the overshoot region. These simulations suggest that dipole fields might be confined in underlying stable regions by highly turbulent convective motions at stellar parameters. The confinement is of large-scale field in an average sense and we show that it is reasonably modeled by mean-field ideas. Our findings are particularly interesting for certain models of the Sun, which require a large-scale, poloidal magnetic field to be confined in the solar radiative zone in order to explain simultaneously the uniform rotation of the latter and the thinness of the solar tachocline.

On the Connection between Rieger-type and Magneto-Rossby Waves Driving the Frequency of the Large Solar Eruptions during Solar Cycles 19–25

Marianna B. **Korsós**1,2,3,4, Mausumi Dikpati5, Robertus Erdélyi2,4,6, Jiajia Liu7, and Francesca Zuccarello1,8
2023 ApJ 944 180
https://iopscience.iop.org/article/10.3847/1538-4357/acb64f/pdf

Global solar activity variation mainly occurs over about an 11 yr cycle. However, both longer and shorter periodicities than the solar cycle are also present in many different solar activity indices. The longer timescales may be up to hundreds of years, while the shorter timescales for global solar variability could be within 0.5–2 yr, which include, e.g., from the Rieger-type periods (150–160 days) to quasi-biennial oscillations of 2 yr. The most likely origin of this short-timescale quasi-periodicity is attributed to magnetic Rossby waves, which have periods of 0.8–2.4 yr. In this work, we present findings of a unique evolution of identified shorter periodicities, like the Rieger-

type, arising from magnetic Rossby waves, throughout Solar Cycles 19–25. We report further observational evidence of the strong relationship between the Rieger-type periodicity, magneto-Rossby waves, and major solar flare activity. Moreover, this study also reveals that the global solar magnetic field has a continuous periodic longitudinal conveyor belt motion along the solar equator, together with an up-and-down movement in the latitudinal directions. We found that when these longitudinal and latitudinal movements have Rieger-type periodicity and magneto-Rossby waves during the same period of a solar cycle, major flare activity is present.

A SART-Based Iterative Inversion Methodology to Infer the Solar Rotation Rate from Global Helioseismic Data

Sylvain G. **Korzennik**, Antonio Eff-Darwich
Solar Phys. **299**, 86 **2024**
https://arxiv.org/pdf/2406.10183
https://doi.org/10.1007/s11207-024-02334-7
We present a new iterative rotation inversion technique based on the Simultaneous Algebraic Reconstruction Technique developed for image reconstruction. We describe in detail our algorithmic implementation and compare it to the classical inversion techniques like the Regularized Least Squares (RLS) and the Optimally Localized Averages (OLA) methods. In our implementation, we are able to estimate the formal uncertainty on the inferred solution using standard error propagation, and derive the averaging kernels without recourse to any Monte-Carlo simulation. We present the potential of this new technique using simulated rotational frequency splittings. We use noiseless sets that cover the range of observed modes and associate to these artificial splittings observational uncertainties. We also add random noise to present the noise magnification immunity of the method. Since the technique is iterative we also show its potential when using an apriori solution. With the right regularization this new method can outperform our RLS implementation in precision, scope and resolution. Since it results in very different averaging kernels where the solution is poorly constrained, this technique infers different values. Adding such a technique to our compendium of inversion methods will allow us to improve the robustness of our inferences when inverting real observations and better understand where they might be biased and/or unreliable, as we push our techniques to maximize the diagnostic potential of our observations.

Initial Results from Fitting pp-Modes Using Intensity Observations from the Helioseismic and Magnetic Imager

Sylvain G. **Korzennik**
Solar Physics September **2017**, 292:138
The Helioseismic and Magnetic Imager project recently started processing the continuum-intensity images following global helioseismology procedures similar to those used to process the velocity images. The spatial decomposition of these images has produced time series of spherical harmonic coefficients for degrees up to ℓ=300ℓ=300, using a different apodization than the one used for velocity observations. The first 360 days of observations were processed and are made available. I present initial results from fitting these time series using my fitting method and compare the derived mode characteristics to those estimated using coeval velocity observations.

A Multi-Instrument Investigation of the Frequency Stability of Oscillations Above the Acoustic Cut-Off Frequency with Solar Activity

K. **Kosak**, R. Kiefer, A.M. Broomhall
MNRAS **2022**
https://arxiv.org/pdf/2203.03685.pdf
Below the acoustic cut-off frequency, oscillations are trapped within the solar interior and become resonant. However, signatures of oscillations persist above the acoustic cut-off frequency, and these travelling waves are known as pseudomodes. Acoustic oscillation frequencies are known to be correlated with the solar cycle, but the pseudomode frequencies are predicted to vary in anti-phase. We have studied the variation in pseudomode frequencies with time systematically through the solar cycle. We analyzed Sun-as-a-star data from Variability of Solar Irradiance and Gravity Oscillations (VIRGO), and Global Oscillations at Low Frequencies (GOLF), as well as the decomposed data from Global Oscillation Network (GONG) for harmonic degrees $0 \leq l \leq 200$. The data cover over two solar cycles (1996--2021, depending on instrument). We split them into overlapping 100-day long segments and focused on two frequency ranges, namely 5600--6800μHz and 5600--7800μHz. The frequency shifts between segments were then obtained by fitting the cross-correlation function between the segments' periodograms. For VIRGO and GOLF, we found no significant variation of pseudomode frequencies with solar activity. However, in agreement with previous studies, we found that the pseudomode frequency variations are in anti-phase with the solar cycle for GONG data. Furthermore, the pseudomode frequency shifts showed a double-peak feature at their maximum, which corresponds to solar activity minimum, and is not seen in solar activity proxies. An, as yet unexplained, pseudo-periodicity in the amplitude of the variation with harmonic degree l is also observed in the GONG data.

Southward shift of the coronal neutral line and the heliospheric current sheet: Evidence for radial evolution of hemispheric asymmetry

J. S. **Koskela**, I. I. Virtanen and K. Mursula
A& A 618, A105 (**2018**)
sci-hub.tw/10.1051/0004-6361/201832609

Aims. The heliospheric current sheet (HCS) has been observed to be southward shifted in the late declining to minimum phase of the solar cycle. Here we study the existence of a simultaneous shift in the heliosphere and in the corona using a robust new method.
Methods. We use the synoptic maps of the photospheric field of the Wilcox Solar Observatory (WSO) and the Mount Wilson Observatory (MWO) together with the potential field source surface (PFSS) model to calculate the coronal magnetic field and compare it with the simultaneous heliospheric magnetic field of the NASA/NSSDC OMNI 2 dataset. We divide the magnetic field into the two sectors, towards (T) and away (A) from the Sun, and calculate how often the sector polarities at 1 AU and in the corona match each other. We divide the sectors both at 1 AU and in the corona. We also calculate the annual (T − A)/(T + A) ratios of sector occurrence both at 1 AU and in the corona.
Results. We verify that the HCS/neutral line is southward shifted both in the corona and heliosphere. We find that the coronal shift is systematically larger than the simultaneous heliospheric shift.
Conclusions. The fact that the southward shift of the coronal neutral line is larger than the simultaneous shift of the heliospheric current sheet at 1 AU implies that the radial evolution of the magnetic field between the two sites is different between the northern and southern hemispheres.

Advances and Challenges in Observations and Modeling of the Global-Sun Dynamics and Dynamo **Review**

A.G. **Kosovichev**, G. Guerrero, A.M. Stejko, V.V. Pipin, A.V. Getling
Proceedings of IAU Symposium 362 "Predictive Power of Computational Astrophysics as a Discovery Tool" **2022**
https://arxiv.org/pdf/2203.10721.pdf

Computational heliophysics has shed light on the fundamental physical processes inside the Sun, such as the differential rotation, meridional circulation, and dynamo-generation of magnetic fields. However, despite the substantial advances, the current results of 3D MHD simulations are still far from reproducing helioseismic inferences and surface observations. The reason is the multi-scale nature of the solar dynamics, covering a vast range of scales, which cannot be solved with the current computational resources. In such a situation, significant progress has been achieved by the mean-field approach, based on the separation of small-scale turbulence and large-scale dynamics. The mean-field simulations can reproduce solar observations, qualitatively and quantitatively, and uncover new phenomena. However, they do not reveal the complex physics of large-scale convection, solar magnetic cycles, and the magnetic self-organization that causes sunspots and solar eruptions. Thus, developing a synergy of these approaches seems to be a necessary but very challenging task.

Dynamo Wave Patterns Inside the Sun Revealed by Torsional Oscillations

Alexander G. **Kosovichev**, Valery V. Pipin
2019 *ApJL* **871** L20
https://arxiv.org/pdf/1809.10776.pdf

Torsional oscillations represent bands of fast and slow zonal flows around the Sun, which extend into the deep convection zone and migrate during solar cycles towards the equator following the sunspot butterfly diagram. Principal component analysis of helioseismology data obtained in 1996-2018 for almost two solar cycles reveals zones of deceleration of the torsional oscillations inside the Sun due to back reaction of dynamo-generated magnetic field. The zonal deceleration originates in the solar tachocline at high latitudes, and migrates through the convection zone revealing patterns of magnetic dynamo waves predicted by the Parker's dynamo theory. The analysis reveals that the primary seat of the solar dynamo is located in a high-latitude zone of the tachocline. It explains the phenomenon of the extended solar cycle observed in the evolving shape of the solar corona, and why the polar magnetic field strength predicts the solar maxima. The results show a substantial decrease of the zonal acceleration in the current solar cycle and predict further decline of sunspot activity in the next solar cycle.
HMI Science Nuggets #118 **2019** hmi.stanford.edu/hminuggets/?p=2781

Acoustic tomography of solar convective flows and structures

A.G. **Kosovichev**, T.L. Duvall Jr

SCORe'96: Solar Convection and Oscillations and their Relationship, Eds.: F.P. Pijpers, J. Christensen-Dalsgaard, and C.S. Rosenthal, Kluwer (Astrophysics and Space Science Library Vol. 225), p. 241-260, **1997** **2018**
https://arxiv.org/pdf/1806.03273.pdf
We present a new method for helioseismic diagnostics of the three-dimensional structure of sound speed, magnetic fields and flow velocities in the convection zone by inversion of acoustic travel-time data. The data are measurements of the time for acoustic waves to travel between points on the solar surface and surrounding annuli obtained from continuous observations at the South Pole in 1991 and from high-resolution observations from the Solar and Heliospheric Observatory (SOHO) in 1996. The travel time of the waves depends primarily on the sound speed perturbations and the velocity of flow along the ray paths. The effects of the sound speed perturbations and flows can be separated by measuring the travel time of waves propagating in opposite directions along the same ray paths. Magnetic fields result in anisotropy of the wave speed. A 3D inversion method based on Fermat's Principle and a regularized least-squares technique have been applied to infer the properties of convection in the quiet Sun and in active regions.

Cyclic Changes of the Sun's Seismic Radius
Alexander **Kosovichev**, Jean-Pierre Rozelot
ApJ **861** 90 **2018**
https://arxiv.org/pdf/1805.09385.pdf
http://sci-hub.tw/http://iopscience.iop.org/0004-637X/861/2/90/
The questions whether the Sun shrinks with the solar activity and what causes this have been a subject of debate. Helioseismology provides means to measure with high precision the radial displacement of subsurface layers, co-called "seismic radius", through analysis of oscillation frequencies of surface gravity (f) modes. Here, we present results of a new analysis of twenty one years of helioseismology data from two space missions, Solar and Heliospheric Observatory (SoHO) and Solar Dynamics Observatory (SDO), which allow us to resolve previous uncertainties and compare variations of the seismic radius in two solar cycles. After removing the f-mode frequency changes associated with the surface activity we find that the mean seismic radius is reduced by 1-2 km during the solar maxima, and that most significant variations of the solar radius occur beneath the visible surface of the Sun at the depth of about 5 Mm, where the radius is reduced by 5-8 km. These variations can be interpreted as changes in the solar subsurface structure caused by predominately vertical ~10 kG magnetic field.
HMI Science Nuggets #107 **2018** http://hmi.stanford.edu/hminuggets/?p=2605

Solar Cycle Variations of Rotation and Asphericity in the Near-Surface Shear Layer
A.G. **Kosovichev**, J.-P. Rozelot
JASTP Volume 176, Pages 21-25 **2018**
https://arxiv.org/pdf/1804.05081.pdf
The precise shape of the Sun is sensitive to the influence of gravity, differential rotation, local turbulence and magnetic fields. It has been previously shown that the solar shape exhibits asphericity that evolves with the 11-year cycle. Thanks to the capability of the SoHO/MDI and SDO/HMI instruments to observe with an unprecedented accuracy the surface gravity oscillation (f) modes, it is possible to extract information concerning the coefficients of rotational frequency splitting, a1, a3 and a5, that measure the differential rotation, together with the a2, a4 and a6 asphericity coefficients. Analysis of these helioseismology data for almost two solar cycles, from 1996 to 2017, reveals a close correlation of the a1 and a5 coefficients with the solar activity, whilst a3 exhibits a long-term trend and a weak correlation in the current cycle indicating a substantial change of the global rotation, potentially associated with a long-term evolution of the solar cycles. Looking in more details, the asphericity coefficients, a2, a4 and a6 are more strongly associated with the solar cycle when applying a time lag of respectively 0.1, 1.6 and -1.6 years. The magnitude of a6-coefficient varies in phase with the sunspot number (SN), but its amplitude is ahead of the SN variation. The last measurements made in mid 2017 indicate that the magnitude of a6-coefficient has probably reached its minimum; therefore, the next solar minimum can be expected by the end of 2018 or in the beginning of 2019. The so-called seismic radius in the range of f-mode angular degree: l=137-299 exhibits a temporal variability in anti-phase with the solar activity; its relative value decreased by 2.3E-05 in Solar Cycle 23 and 1.7E-05 in Cycle 24. Such results will be useful for better understanding the physical mechanisms which act inside the Sun, and so, better constrain dynamo models for forecasting the solar cycles.

Unusual sunquakes caused by the X9.3 flare on September 6, 2017
Alexander **Kosovichev**
HMI Science Nuggets #73 Sept **2017**
http://hmi.stanford.edu/hminuggets/?p=2010

A powerful impact on the surface of Sun caused by the flare explosion excited helioseismic acoustic waves that travel through the solar interior and after reflection displayed a set of wave ripples on the surface. Such events are called "sunquakes" (Ref. 1). The sunquake ripples are usually observed 15-20 min after the impact, when the seismic acoustic waves emerge on the surface after reflection from the high-temperature interior layers of the Sun. This time delay depends on the wave speed beneath the surface. Sunquakes were excited by the X9.3 flare that occurred in AR 12673 on September 6, 2017. The unusual feature of this event was that initially the flare impact excited several relatively small sunquake waves, and then a much large wave traveling to much longer distances from the flare impact.

Formation of Large-Scale Inflows Into Active Regions

Alexander **Kosovichev**1 and Junwei Zhao
HMI Science Nugget #576 July **2016**
http://hmi.stanford.edu/hminuggets/?p=1641
These results show that the subsurface flows that develop in and around emerging active regions have a complex multi-scale structure, which is important for the understanding of how the active regions are formed and how they affect the global Sun's dynamics and magnetic activity.

Reconstruction of Solar Subsurfaces by Local Helioseismology **Review**

in "Cartography of the Sun and the Stars", Editors: Rozelot, Jean-Pierre, Neiner, Coralie **2016**
http://arxiv.org/pdf/1607.05681v1.pdf
Local helioseismology has opened new frontiers in our quest for understanding of the internal dynamics and dynamo on the Sun. Local helioseismology reconstructs subsurface structures and flows by extracting coherent signals of acoustic waves traveling through the interior and carrying information about subsurface perturbations and flows, from stochastic oscillations observed on the surface. The initial analysis of the subsurface flow maps reconstructed from the 5 years of SDO/HMI data by time-distance helioseismology reveals the great potential for studying and understanding of the dynamics of the quiet Sun and active regions, and the evolution with the solar cycle. In particular, our results show that the emergence and evolution of active regions are accompanied by multi-scale flow patterns, and that the meridional flows display the North-South asymmetry closely correlating with the magnetic activity. The latitudinal variations of the meridional circulation speed, which are probably related to the large-scale converging flows, are mostly confined in shallow subsurface layers. Therefore, these variations do not necessarily affect the magnetic flux transport. The North-South asymmetry is also pronounced in the variations of the differential rotation ("torsional oscillations"). The calculations of a proxy of the subsurface kinetic helicity density show that the helicity does not vary during the solar cycle, and that supergranulation is a likely source of the near-surface helicity.

Local Helioseismology of Emerging Active Regions: A Case Study

Alexander G. **Kosovichev**, Junwei Zhao, Stathis Ilonidis
Lecture Notes in Physics **2016**
http://arxiv.org/pdf/1607.04987v1.pdf
Local helioseismology provides a unique opportunity to investigate the subsurface structure and dynamics of active regions and their effect on the large-scale flows and global circulation of the Sun. We use measurements of plasma flows in the upper convection zone, provided by the Time-Distance Helioseismology Pipeline developed for analysis of solar oscillation data obtained by Helioseismic and Magnetic Imager (HMI) on Solar Dynamics Observatory (SDO), to investigate the subsurface dynamics of emerging active region NOAA 11726. The active region emergence was detected in deep layers of the convection zone about 12 hours before the first bipolar magnetic structure appeared on the surface, and 2 days before the emergence of most of the magnetic flux. The speed of emergence determined by tracking the flow divergence with depth is about 1.4 km/s, very close to the emergence speed in the deep layers. As the emerging magnetic flux becomes concentrated in sunspots local converging flows are observed beneath the forming sunspots. These flows are most prominent in the depth range 1-3 Mm, and remain converging after the formation process is completed. On the larger scale converging flows around active region appear as a diversion of the zonal shearing flows towards the active region, accompanied by formation of a large-scale vortex structure. This process occurs when a substantial amount of the magnetic flux emerged on the surface, and the converging flow pattern remains stable during the following evolution of the active region. The Carrington synoptic flow maps show that the large-scale subsurface inflows are typical for active regions. In the deeper layers (10-13 Mm) the flows become diverging, and surprisingly strong beneath some active regions. In

addition, the synoptic maps reveal a complex evolving pattern of large-scale flows on the scale much larger than supergranulation. **19 Apr 2013**

Helioseismic Constraints and Paradigm Shift in Solar Dynamo

Alexander G. **Kosovichev**, Valery V. Pipin, Junwei Zhao

E-print, Feb **2014**; Progress in Physics of the Sun and Stars: A New Era in Helio- and Asteroseismology. Edited by H. Shibahashi and A.E. Lynas-Gray. ASP Conf. Proc. Vol. 479. **2013**, p.395

http://arxiv.org/pdf/1402.1901v1.pdf

Helioseismology provides important constraints for the solar dynamo problem. However, the basic properties and even the depth of the dynamo process, which operates also in other stars, are unknown. Most of the dynamo models suggest that the toroidal magnetic field that emerges on the surface and forms sunspots is generated near the bottom of the convection zone, in the tachocline. However, there is a number of theoretical and observational problems with justifying the deep-seated dynamo models. This leads to the idea that the subsurface angular velocity shear may play an important role in the solar dynamo. Using helioseismology measurements of the internal rotation and meridional circulation, we investigate a mean-field MHD model of dynamo distributed in the bulk of the convection zone but shaped in a near-surface layer. We show that if the boundary conditions at the top of the dynamo region allow the large-scale toroidal magnetic fields to penetrate into the surface, then the dynamo wave propagates along the isosurface of angular velocity in the subsurface shear layer, forming the butterfly diagram in agreement with the Parker-Yoshimura rule and solar-cycle observations. Unlike the flux-transport dynamo models, this model does not depend on the transport of magnetic field by meridional circulation at the bottom of the convection zone, and works well when the meridional circulation forms two cells in radius, as recently indicated by deep-focus time-distance helioseismology analysis of the SDO/HMI and SOHO/MDI data. We compare the new dynamo model with various characteristics if the solar magnetic cycles, including the cycle asymmetry (Waldmeier's relations) and magnetic `butterfly' diagrams.

Astrophysical processes on the Sun

Alexander G. **Kosovichev**

Geophysical & Astrophysical Fluid Dynamics, vol. 107, issue 6, pp. 717-719, **2013**

http://www.tandfonline.com/doi/abs/10.1080/03091929.2013.792633

Local Helioseismology of Sunspots: Current Status and Perspectives **A Review**

Alexander G. **Kosovichev**

Solar Physics,Volume 279, Number 2 (**2012**), 323-348

Mechanisms of the formation and stability of sunspots are among the longest-standing and intriguing puzzles of solar physics and astrophysics. Sunspots are controlled by subsurface dynamics, hidden from direct observations. Recently, substantial progress in our understanding of the physics of the turbulent magnetized plasma in strong-field regions has been made by using numerical simulations and local helioseismology. Both the simulations and helioseismic measurements are extremely challenging, but it is becoming clear that the key to understanding the enigma of sunspots is a synergy between models and observations. Recent observations and radiative MHD numerical models have provided a convincing explanation for the Evershed flows in sunspot penumbrae. Also, they lead to the understanding of sunspots as self-organized magnetic structures in the turbulent plasma of the upper convection zone, which are maintained by a large-scale dynamics. Local helioseismic diagnostics of sunspots still have many uncertainties, some of which are discussed in this review. However, there have been significant achievements in resolving these uncertainties, verifying the basic results by new high-resolution observations, testing the helioseismic techniques by numerical simulations, and comparing results obtained by different methods. For instance, a recent analysis of helioseismology data from the Hinode space mission has successfully resolved several uncertainties and concerns (such as the inclined-field and phase-speed filtering effects) that might affect the inferences of the subsurface wave-speed structure of sunspots and the flow pattern. It is becoming clear that for the understanding of the phenomenon of sunspots it is important to further improve the helioseismology methods and investigate the whole life cycle of active regions, from magnetic flux emergence to dissipation. The Solar Dynamics Observatory mission has started to provide data for such investigations.

Advances in Global and Local Helioseismology: an Introductory Review

Alexander **Kosovichev**

E-print, March **2011**; Lecture Notes in Physics v.831 (in press)

Helioseismology studies the structure and dynamics of the Sun's interior by observing oscillations on the surface. These studies provide information about the physical processes that control the evolution and magnetic activity of the Sun. In recent years, helioseismology has made substantial progress towards the understanding of the physics of solar oscillations and the physical processes inside the Sun, thanks to observational, theoretical and modeling efforts. In addition to the global seismology of the Sun based on measurements of global oscillation modes, a new field of local helioseismology, which studies oscillation travel times and local frequency shifts, has been developed. It is capable of providing 3D images of the subsurface structures and flows. The basic principles, recent advances and perspectives of global and local helioseismology are reviewed in this article.

The possible origin of facular brightness in the solar atmosphere

R. **Kostik**1 and E. Khomenko

A&A 589, A6 (**2016**)

This paper studies the dependence of the Ca ii H line core brightness on the strength and inclination of the photospheric magnetic field, and on the parameters of convective and wave motions in a facular region at the center of the solar disc. We use three simultaneous data sets that were obtained at the German Vacuum Tower Telescope (Observatorio del Teide, Tenerife): (1) spectra of Ba ii 4554 Å line, registered with the instrument TESOS to measure the variations of intensity and velocity through the photosphere up to the temperature minimum; (2) spectropolarimetric data in Fe i 1.56 μm lines (registered with the instrument TIP II) to measure photospheric magnetic fields; (3) filtergrams in Ca ii H that give information about brightness fluctuations in the chromosphere. The results show that the Ca ii H brightness in the facula strongly depends on the power of waves with periods in the 5-min range, which propagate upwards, and also on the phase shift between velocity oscillations at the bottom photosphere and around the temperature minimum height that is measured from Ba ii line. The Ca ii H brightness is maximum at locations where the phase shift between temperature and velocity oscillations lies within 0°–100°. There is an indirect influence of convective motions on the Ca ii H brightness. The higher the amplitude of convective velocities is and the greater the height is where they change their direction of motion, the brighter the facula. In summary, our results lead to conclusions that facular regions appear bright not only because of the Wilson depression in magnetic structures, but also owing to real heating.

Modelling continuum intensity perturbations caused by solar acoustic oscillations

N.M.**Kostogryz**, D.Fournier, L. Gizon

A&A 654, A1 **2021**

https://arxiv.org/pdf/2107.07220

https://www.aanda.org/articles/aa/pdf/2021/10/aa40264-20.pdf

https://doi.org/10.1051/0004-6361/202040264

Helioseismology is the study of the solar interior using observations of oscillations at the surface. It suffers from systematic errors, such as a center-to-limb error in travel-time measurements. Understanding these errors requires a good understanding of the nontrivial relationship between wave displacement and helioseismic observables. The wave displacement causes perturbations in the atmospheric thermodynamical quantities which perturb the opacity, the optical depth, the source function, and the local ray geometry, thus affecting the emergent intensity. We aim to establish the most complete relationship up to now between the displacement and the intensity perturbation by solving the radiative transfer problem in the atmosphere. We derive an expression for the intensity perturbation caused by acoustic oscillations at any point on the solar disk by applying the first-order perturbation theory. As input, we consider adiabatic modes of oscillation of different degrees. The background and the perturbed intensities are computed considering the main sources of opacity in the continuum. We find that, for all modes, the perturbations to the thermodynamical quantities are not sufficient to model the intensity. In addition, the geometrical effects due to the displacement must be taken into account as they lead to a difference in amplitude and a phase shift between the temperature at the surface and intensity perturbations. The closer to the limb, the larger the differences. This work presents improvements for the computation of the intensity perturbations, in particular for high-degree modes, and explains differences in intensity computations in earlier works. The phase shifts and amplitude differences between the temperature and intensity perturbations increase towards the limb. This should help to interpret some of the systematic center-to-limb effects observed in local helioseismology.

Accurate Short-Characteristics Radiative Transfer in A Numerical Tool for Astrophysical RESearch (ANTARES)

Nadiia M. **Kostogryz**, Friedrich Kupka, Nikolai Piskunov, Damian Fabbian, Daniel Krüger & Laurent Gizon

Solar Physics volume 296, Article number: 46 (**2021**)

https://link.springer.com/content/pdf/10.1007/s11207-021-01777-6.pdf

https://doi.org/10.1007/s11207-021-01777-6

We aim to improve the accuracy of radiative energy transport in three-dimensional radiation hydrodynamical simulations in ANTARES (A Numerical Tool for Astrophysical RESearch). We implement in the ANTARES short-

characteristics numerical schemes a modification of the Bézier interpolant solver. This method yields a smoother surface structure in simulations of solar convection and reduces the artifacts appearing due to the limited number of rays along which the integration is done. Reducing such artifacts leads to increased stability of the code. We show that our new implementation achieves a better agreement of the temperature structure and its gradient with a semi-empirical model derived from observations, as well as of synthetic spectral-line profiles with the observed solar spectrum.

The features of longitudinal distribution of solar spots during the last 13 solar activity minima

I. G. **Kostuchenko** & E. E. Benevolenskaya
Geomagnetism and Aeronomy volume 55, pages1039–1044(**2015**)
https://link.springer.com/content/pdf/10.1134/S0016793215080162.pdf
We analyzed the features of the longitudinal distribution of the areas of solar spots during the solar activity minima, from the 11th cycle to the last minimum, based on data provided by the Greenwich Observatory and the Marshall Research Center. We discovered that the solar spots evolved in one or two neighboring bands (in terms of longitude), the Carrington longitude of which smoothly displaced from the east to the west, in the phase of the deep minimum in all of the considered cases. The spots at the high latitudes associated with a “new” cycle evolved on the same longitude bands. All of this led to the noticeable longitudinal asymmetry of magnetic fluxes related to the spots and flocculi. Based on our research, we propose the hypothesis that a nonaxisymmetric component of the total magnetic flux of the Sun is generated, together with the dipole component, by the solar dynamo mechanism, which is a typical feature of the phase of a minimum between the solar activity cycles.

Thermodynamic properties of small flares in the quiet Sun observed by Hα and EUV: plasma motion of the chromosphere and time evolution of temperature/emission measure

Yuji **Kotani**, T T Ishii, D Yamasaki, K Otsuji, K Ichimoto, A Asai, K Shibata
Monthly Notices of the Royal Astronomical Society, Volume 522, Issue 3, **2023**, Pages 4148–4160,
https://doi.org/10.1093/mnras/stad1232
https://arxiv.org/pdf/2304.12037.pdf
Small flares frequently occur in the quiet Sun. Previous studies have noted that they share many common characteristics with typical solar flares in active regions. However, their similarities and differences are not fully understood, especially their thermal properties. In this study, we performed imaging spectroscopic observations in the Hα line taken with the Solar Dynamics Doppler Imager on the Solar Magnetic Activity Research Telescope (SMART/SDDI) at the Hida Observatory and imaging observations with the Atmospheric Imaging Assembly onboard Solar Dynamics Observatory (SDO/AIA). We analysed 25 cases of small flares in the quiet Sun over the thermal energy range of 1024−1027erg1024−1027erg , paying particular attention to their thermal properties. Our main results are as follows: (1) We observe a redshift together with line centre brightening in the Hα line associated with more than half of the small flares. (2) We employ differential emission measure analysis using AIA multitemperature (channel) observations to obtain the emission measure and temperature of the small flares. The results are consistent with the Shibata & Yokoyama (1999, 2002) scaling law. From the scaling law, we estimated the coronal magnetic field strength of small flares to be 5–15 G. (3) The temporal evolution of the temperature and the density shows that the temperature peaks precede the density peaks in more than half of the events. These results suggest that chromospheric evaporations/condensations play an essential role in the thermal properties of some of the small flares in the quiet Sun, as does for large flares. **2019-09-07**

Numerical simulation of solar photospheric jet-like phenomena caused by magnetic reconnection

Yuji **Kotani**, Kazunari Shibata
PASJ **2020**
https://arxiv.org/pdf/2006.12511.pdf
Jet phenomena with a bright loop in their footpoint, called anemone jets, have been observed in the solar corona and chromosphere. These jets are formed as a consequence of magnetic reconnection, and from the scale universality of magnetohydrodynamics (MHD), it can be expected that anemone jets exist even in the solar photosphere. However, it is not necessarily apparent that jets can be generated as a result of magnetic reconnection in the photosphere, where the magnetic energy is not dominant. Furthermore, MHD waves generated from the photospheric jets could contribute to chromospheric heating and spicule formation; however, this hypothesis has not yet been thoroughly investigated. In this study, we perform 3D MHD simulation including gravity with the solar photospheric parameter to investigate anemone jets in the solar photosphere. In the simulation, jet-like structures were induced by magnetic reconnection in the solar photosphere. We determined that these jet-like structures were caused by slow shocks formed by the reconnection and were propagated approximately in the direction of the background magnetic field. We also suggested that MHD waves from the jet-like structures could influence local atmospheric heating and spicule formation.

Is the Earth's orbital motion linked to the spin rotation of the Sun?

V.A.**Kotov**

Advances in Space Research Volume 63, Issue 10, 15 May **2019**, Pages 3385-3389

sci-hub.se/10.1016/j.asr.2019.01.018

Time variations of the magnetic field of the Sun, seen as a star (the data 1968–2018, with more than 27 thousand daily measurements of the solar mean magnetic field), allowed to specify the rotation period of the gravitating solar mass: 27.027(6) days, synodic. This indicates a presumably unknown physical connection between motions of the Sun and the Earth: in the course of a year our star accomplishes nearly 27 half-revolutions, while the planet itself performs an identical number of its spinnings during one complete axial revolution of the Sun. True origin of this strange Sun–Earth resonance is unknown, but it is supposed the phenomenon might be caused by slight coherent perturbations of gravity within the solar system.

Rotation of the Solar Equator

V.A. **Kotov**

Solar Physics June **2017**, 292:76

Regular measurements of the general magnetic field of the Sun, performed over about half a century at the Crimean Astrophysical Observatory, the J. Wilcox Solar Observatory, and five other observatories, are considered in detail for the time 1968 – 2016. They include more than twenty-six thousand daily values of the mean line-of-sight field strength of the visible solar hemisphere. On the basis of these values, the equatorial rotation period of the Sun is found to be 26.926(9) d (synodic). It is shown that its half-value coincides within error limits with both the main period of the magnetic four-sector structure, 13.4577(25) d, and the best-commensurate period of the slow motions of the major solar system bodies, 13.479(22) d (sidereal). The probability that the two periods coincide by chance is estimated to be about 10−710−7. The true origin of this odd resonance is unknown.

Solar 22 years cycle

Valery A. **Kotov**, Francis M. Sanchez

Astrophysics and Space Science January **2017**, 362:6

Seven observatories performed in 1968–2015 numerous daily measurements of general magnetic field of the Sun seen as a star (of a mean line-of-sight field component of the visible solar hemisphere). The new data 2013–2015 confirmed the recent prediction about saw-edged profile of the mean curve of the Hale's 22 years magnetic cycle and, thus, a hypothesis about its cosmological (partial) origin. This is supported by a special analysis of epochs of extrema of Wolf's sunspot number, demonstrating a remarkable stability, since Galileo's time, of the initial phase of the cycle, which can hardly be explained by dynamo theory exclusively.

On the origin of the 22 years solar cycle

V.A. **Kotov**

Advances in Space Research, Volume 55, Issue 3, 1 February **2015**, Pages 979–981

http://www.sciencedirect.com/science/article/pii/S0273117714007662

Measurements of the general magnetic field of the Sun seen as a star were performed over last 45 years by the CrAO and five other observatories (1968–2012, nearly 23 thousand daily strengths B). Analysis of the B time series showed that the most substantial long-term period of the field variation is the Hale's cycle 22 years, which cannot be explained by dynamo theory. It reveals a saw-edged profile, indicating perhaps a cosmic origin of the cycle.

Rieger Periodicity Behaviour in Solar Mg II 280 nm Spectral Emission

P. B. **Kotzé**

Solar Physics volume 296, Article number: 44 (**2021**)

https://doi.org/10.1007/s11207-021-01786-5

The temporal variation of the approximately 155-day Rieger solar periodicity, first detected in solar-flare data, is investigated in the Mg II spectral emission as observed at 280 nm during the interval between 1980 and 2019. Daily mean values of Mg II at each annual interval are spectrally analysed using Lomb–Scargle and Morlet wavelet techniques to obtain the temporal behaviour of particularly the ≈ 155-day Rieger as well as the ≈27≈27-day solar-rotation periodicities. Results obtained indicate substantial power in the Rieger periodicity that varies on an annual basis. In particular we found that the power of the Rieger periodicity exceeds that of the 27-day period during the maxima of Solar Cycles 21 (1981), 22 (1992), and 23 (2001), with the power of the 27-day periodicity dominating during the minima of these cycles. In contrast to these findings, we observe a substantial increase in power of the Rieger periodicity in comparison to that of the ≈ 27-day solar-rotation period during the minima of Solar Cycles 23 (2006, 2007) and 24 (2018, 2019). We report the first detection of the ≈ 1.3-year period as well as the temporal behaviour of the ≈ 155-day Rieger periodicity in Mg II at 280 nm.

Fourth Harmonic Behaviour of the 27-Day Periodicity in Galactic Cosmic Rays During Different Solar Magnetic Polarity Intervals

P. B. **Kotzé**

Solar Physics volume 295, Article number: 158 (**2020**)

https://link.springer.com/content/pdf/10.1007/s11207-020-01708-x.pdf

Galactic cosmic rays as observed by the Hermanus and Jungfraujoch Neutron Monitors between 1960 and 2018 have been analysed using various spectral analysis techniques. Daily mean neutron monitor measurements are used to identify how several harmonics of the roughly 27-day synodic rotation period change during each of these years. Spectral analysis using Lomb-Scargle and Morlet wavelet techniques of Hermanus and Jungfraujoch data revealed in particular that the fourth harmonic (~7-day) of the solar rotation period is exceptionally strong during the minima of solar cycles when A < 0 (solar dipole pointing south) in comparison to the minima of cycles when A > 0 (solar dipole pointing north). The power spectrum results obtained in this investigation showed that galactic cosmic rays at both Hermanus and Jungfraujoch exhibit peculiar short-term periodicity behaviour as a result of solar polarity dependent magnetic drifts during negative minima.

Polar regions activity and the prediction of the height of the solar cycle 25

S. **Koutchmy**, B. Filippov, E. Tavabi, J-C. Noens, O. Wurmser

ACTAASTROPHYSICA TAURICA **2022**

https://arxiv.org/pdf/2205.09089

The forthcoming solar cycle (SC) 25 was beleived to be rather low when using the sunspot number (SN) as a measurement of the level of activity. The most popular prediction was made by the panel of NASA in 2019, including works based on extrapolations of dynamo-type models. We however discovered that using different observations to measure the level of polar regions activity several years before the start of SC25 and also after the start of the SC25 in 2020, the height of the SC25 could be high. The polar regions activity we considered seems related to the polar coronal holes (CH) activity and it is found significantly higher before the SC25 that it was before the SC24 and accordingly, we suggest that the SN cycle could indeed be much higher than during the SC24 that was a low SN height cycle.

Update of the Solar Lyα Profile Line Model

Izabela **Kowalska-Leszczynska**1, Maciej Bzowski1, Marzena A. Kubiak1, and Justyna M. Sokół1,2

2020 ApJS 247 62

https://doi.org/10.3847/1538-4365/ab7b77

We present a modification of a model of solar cycle evolution of the solar Lyα line profile, along with a sensitivity study of interstellar neutral hydrogen to uncertainties in radiation pressure level. The line profile model, originally developed by Kowalska-Leszczynska et al., is parameterized by the composite solar Lyα flux, which recently was revised. We present modified parameters of the previously developed model of solar radiation pressure for neutral hydrogen and deuterium atoms in the heliosphere. The mathematical function used in the model, as well as the fitting procedure, remain unchanged. We show selected effects of the model modification on interstellar neutral H properties in the heliosphere, and we discuss the sensitivity of these quantities to uncertainties in the calibration of the composite Lyα series.

Evolution of the Solar Lyα Line Profile during the Solar Cycle. II. How Accurate Is the Present Radiation Pressure Paradigm for Interstellar Neutral H in the Heliosphere?

Izabela **Kowalska-Leszczynska**, Maciej Bzowski, Justyna M. Sokół, Marzena A. Kubiak

2018 ApJ 868 49

sci-hub.tw/10.3847/1538-4357/aae70b

Following the derivation of a more accurate model of the evolution of the solar Lyα line with the changing solar activity by Kowalska-Leszczynska et al. (IKL18) than the formerly used model by Tarnopolski & Bzowski (ST09), we investigate the potential consequences that adoption of the resulting refined model of radiation pressure has for the model distribution of interstellar neutral (ISN) H in the inner heliosphere and on the interpretation of selected observations. We simulated the ISN H densities using the two alternative radiation pressure models and identical models of all other factors affecting the ISN H distribution. We found that during most of the solar cycle, the IKL18 model predicts larger densities of ISN H and pickup ions than ST09 in the inner heliosphere, especially in the downwind hemisphere. However, the density of ISN H at the termination shock estimated by Bzowski et al. obtained using ST09 does not need revision, and the detection of ISN D by IBEX is supported. However, we point out the existence of a considerable absorption of a portion of the solar Lyα spectral flux inside the heliosphere. Therefore, the model of radiation pressure for ISN H is still likely to need revision, and hence the available models of ISN H are not self-consistent.

Evolution of the Solar Lyman-Alpha line profile during the solar cycle

Izabela **Kowalska-Leszczynska**, Maciej Bzowski, Justyna M. Sokół, Marzena A. Kubiak
ApJ **852** 115 **2018**
https://arxiv.org/pdf/1710.06602.pdf
Recent studies of interstellar neutral (ISN) hydrogen observed by the Interstellar Boundary Explorer (IBEX) suggested that the present understanding of the radiation pressure acting on hydrogen atoms in the heliosphere should be revised. There is a significant discrepancy between theoretical predictions of the ISN H signal using the currently used model of the solar Lyman-alpha profile by Tarnopolski et al. 2009 (TB09) and the signal due to ISN H observed by IBEX-Lo. We developed a new model of evolution of the solar Lyman-alpha profile that takes into account all available observations of the full-disk solar Lyman-alpha profiles from SUMER/SOHO, provided by Lemaire et al. 2015 (L15), covering practically the entire 23rd solar cycle. The model has three components that reproduce different features of the profile. The main shape of the emission line that is produced in the chromosphere is modeled by the kappa function; the central reversal due to absorption in the transition region is modeled by the Gauss function; the spectral background is represented by the linear function. The coefficients of all those components are linear functions of the line-integrated full-disk Lyman-alpha irradiance, which is the only free parameter of the model. The new model features potentially important differences in comparison with the model by TB09, which was based on a limited set of observations. This change in the understanding of radiation pressure, especially during low solar activity, may significantly affect the interstellar H and D distributions in the inner heliosphere and their derivative populations.
Erratum 2018 *ApJ* **856** 87

Solar chromospheric heating by magnetohydrodynamic waves: dependence on magnetic field inclination

Mayu **Koyama**, Toshifumi Shimizu
ApJ **965** 136 **2024**
https://arxiv.org/pdf/2403.11419
https://iopscience.iop.org/article/10.3847/1538-4357/ad343f/pdf
A proposed mechanism for solar chromospheric heating is that magnetohydrodynamic waves propagate upward along magnetic field lines and dissipate their energy in the chromosphere. In particular, compressible magneto-acoustic waves may contribute to the heating. Theoretically, the components below the cutoff frequency cannot propagate into the chromosphere; however, the cutoff frequency depends on the inclination of the magnetic field lines. In this study, using high temporal cadence spectral data of IRIS and Hinode SOT spectropolarimeter (SP) in plages, we investigated the dependence of the low-frequency waves on magnetic-field properties and quantitatively estimated the amount of energy dissipation in the chromosphere. The following results were obtained: (a) The amount of energy dissipated by the low-frequency component (3--6 mHz) increases with the field inclination below 40 degrees, whereas it is decreased as a function of the field inclination above 40 degrees. (b) The amount of the energy is enhanced toward 104W/m2, which is the energy required for heating in the chromospheric plage regions, when the magnetic field is higher than 600 G and inclined more than 40 degree. (c) In the photosphere, the low-frequency component has much more power in the magnetic field inclined more and weaker than 400 G. The results suggest that the observed low-frequency components can bring the energy along the magnetic field lines and that only a specific range of the field inclination angles and field strength may allow the low-frequency component to bring the sufficient amount of the energy into the chromosphere.

The Coronal Analysis of SHocks and Waves (CASHeW) Framework

K. **Kozarev**, A. Davey, A. Kendrick, M. Hammer, C. Keith
Journal of Space Weather and Space Climate (SWSC) **2017**
https://arxiv.org/pdf/1710.05302.pdf
Coronal Bright Fronts (CBF) are large-scale wavelike disturbances in the solar corona, related to solar eruptions. They are observed in extreme ultraviolet (EUV) light as transient bright fronts of finite width, propagating away from the eruption source. Recent studies of individual solar eruptive events have used EUV observations of CBFs and metric radio type II burst observations to show the intimate connection between low coronal waves and coronal mass ejection (CME)-driven shocks. EUV imaging with the Atmospheric Imaging Assembly(AIA) instrument on the Solar Dynamics Observatory (SDO) has proven particularly useful for detecting CBFs, which, combined with radio and in situ observations, holds great promise for early CME-driven shock characterization capability. This characterization can further be automated, and related to models of particle acceleration to produce estimates of particle fluxes in the corona and in the near Earth environment early in events. We present a framework for the Coronal Analysis of SHocks and Waves (CASHeW). It combines analysis of NASA Heliophysics System Observatory data products and relevant data-driven models, into an automated system for the characterization of off-limb coronal waves and shocks and the evaluation of their capability to accelerate solar energetic particles (SEPs). The system utilizes EUV observations and models written in the Interactive Data Language (IDL). In addition, it leverages analysis tools from the SolarSoft package of libraries, as well as third party libraries. We have tested the CASHeW framework on a representative list of coronal bright front events. Here we present its features, as well as

initial results. With this framework, we hope to contribute to the overall understanding of coronal shock waves, their importance for energetic particle acceleration, as well as to the better ability to forecast SEP events fluxes.
2011-05-11, June 7, 2011, December 12, 2013

Modeling the time and energy behavior of the GCR intensity in the periods of low activity around the last three solar minima

M. B. **Krainev**, G. A. Bazilevskaya, M. S. Kalinin, A. K. Svirzhevskaya, N. S. Svirzhevsky
33-rd International Cosmic Ray Conference, Rio-de-Janeiro, Brasil, 2013
2014
http://arxiv.org/pdf/1411.7526v1.pdf
Using the simple model for the description of the GCR modulation in the heliosphere and the sets of parameters discussed in the accompanying paper we model some features of the time and energy behavior of the GCR intensity near the Earth observed during periods of low solar activity around three last solar minima. In order to understand the mechanisms underlying these features in the GCR behavior, we use the suggested earlier decomposition of the calculated intensity into the partial intensities corresponding to the main processes (diffusion, adiabatic losses, convection and drifts).

GCR intensity during the sunspot maximum phase and the inversion of the heliospheric magnetic field

M. **Krainev**, G. Bazilevskaya, M. Kalinin, A. Svirzhevskaya, N. Svirzhevsky
34th International Cosmic Ray Conference, The Hague, The Netherlands, 30 July - 6 August, **2015**, paper ID 437
http://arxiv.org/pdf/1509.00613v1.pdf
The maximum phase of the solar cycle is characterized by several interesting features in the solar activity, heliospheric characteristics and the galactic cosmic ray (GCR) intensity. Recently the maximum phase of the current solar cycle (SC) 24, in many relations anomalous when compared with solar cycles of the second half of the 20-th century, came to the end. The corresponding phase in the GCR intensity cycle is also in progress. In this paper we study different aspects of the sunspot, heliospheric and GCR behavior around this phase. Our main conclusions are as follows: 1) The maximum phase of the sunspot SC 24 ended in 06.2014, the development of the sunspot cycle being similar to those of SC 14, 15 (the Glaisberg minimum). The maximum phase of SC 24 in the GCR intensity is still in progress. 2) The inversion of the heliospheric magnetic field consists of three stages, characterized by the appearance of the global heliospheric current sheet (HCS), connecting all longitudes. In two transition dipole stages beside the global HCS there are additional local HCSs, while the inversion stage lies between two transition dipole ones and there is no global HCS in this stage. The inversion stage of the current SC 24 is the longest when compared with those for SC 21-23. The second transition dipole stage and hence the whole inversion period of the heliospheric magnetic field in SC 24 provisionally ended in 08.2014. 3) The behavior of the GCR intensity in the period of the sunspot maximum phase and the inversion of the heliospheric magnetic fields for SC 21-23 demonstrates all the characteristic features for this period: the two-gap structure corresponding to two-peak structure in the sunspot activity, and the energy hysteresis. In the current SC 24 the GCR intensity shows rather unusual features and we should wait for one or even two years to see the whole picture.

On the causes and mechanisms of the long-term variations in the GCR characteristics

M. **Krainev**, J. Kóta, M.S. Potgieter
34th International Cosmic Ray Conference, The Hague, The Netherlands, 30 July - 6 August, **2015**, paper ID 198
http://arxiv.org/pdf/1509.00614v1.pdf
We argue that the degree of understanding the causes and mechanisms of the long-term variations (11-year and 22-year) in the galactic cosmic rays (GCR) characteristics is still insufficient and to improve it we need new approaches and methods. For the time being there is a long-lasting controversy on how these long-term variations, observed for more than 50 years in the inner heliosphere, are formed. It is widely believed that the 11-year variation is due entirely to the toroidal branch of solar activity (the area and number of sunspots, the strength of the heliospheric magnetic field etc) because of the diffusion, convection and adiabatic energy loss, while the much smaller 22-year variation is caused by the particle drifts connected with the poloidal branch of solar activity (the high-latitude solar magnetic fields). At the same time, both past and more recent numerical simulations indicate that the contribution of particle drifts could be significant for both 22- and 11-year variations in the GCR intensities. However, even those who agree on the significant influence of drifts appear to have different perceptions on the mechanisms of this influence. In this paper, we present an analysis of the possible causes of the first point of view (small role of drifts in the 11-year GCR variation) and the reasons why one can expect the significant contri- bution of the processes connected with the poloidal branch of solar activity in both types of the long-term variations of the GCR

characteristics. Then we briefly discuss some numerical methods suggested in the past and recently and the approaches and perspectives for the sought-for methods are considered.

On the mechanisms of the quasi-biennial oscillations in the GCR intensity

M. **Krainev**, G. Bazilevskaya, M. Kalinin, A. Svirzhevskaya, N. Svirzhevsky
34th International Cosmic Ray Conference, The Hague, The Netherlands, 30 July - 6 August, **2015**, paper ID 439
http://arxiv.org/pdf/1509.00625v1.pdf
Quasi-biennial oscillation (QBO) is a well-known quasi-periodical variation with characteristic time 0.5-4 years in different solar, heliospheric and cosmic ray characteristics. In this paper a hypothesis is checked on the causes of the apparent lack of correlation between solar and heliospheric QBOs, then the possible mechanisms of QBO in the GCR intensity are discussed as well as the idea of the same nature of the step-like changes and Gnevyshev Gap effects in the GCR intensity.
Our main conclusions are as follows: 1) In the first approximation the hypothesis is justified that the change in the sunspot and QBO cycles in the transition from the Sun to the heliosphere is due to 1) the different magnitude and time behavior of the large-scale and small-scale photospheric solar magnetic fields and 2) the stronger attenuation of the small-scale fields in this transition. 2) As the QBO in the HMF strength influences both the diffusion coefficients and drift velocity, it can give rise to the complex QBO in the GCR intensity with respect to the dominating HMF polarity. The description of drift velocity field for the periods of the HMF inversion is suggested, although it has drawbacks. 3) As the conditions in the heliosphere are quite different around the sunspot maximum and during the periods of low solar activity (both with respect to the HMF polarity distribution and with the presence or absence of the large-scale barriers), the suggestion that both the step-like changes of the GCR intensity and Gnevyshev Gap effect could have the same nature, looks questionable.

On the GCR intensity and the inversion of the heliospheric magnetic field during the periods of the high solar activity

M. B. **Krainev**, M. S. Kalinin
33-rd International Cosmic Ray Conference, Rio-de-Janeiro, Brasil, 2013
2014
http://arxiv.org/pdf/1411.7532v1.pdf
We consider the long-term behavior of the solar and heliospheric parameters and the GCR intensity in the periods of high solar activity and the inversions of heliospheric magnetic field (HMF). The classification of the HMF polarity structures and the meaning of the HMF inversion are discussed. The procedure is considered how to use the known HMF polarity distribution for the GCR intensity modeling during the periods of high solar activity. We also briefly discuss the development and the nearest future of the sunspot activity and the GCR intensity in the current unusual solar cycle 24.

Monochromatic Two-Fluid Alfvén Waves in the Partially Ionised Solar Chromosphere

J. **Kraskiewicz**, K. Murawski, F. Zhang & S. Poedts
Solar Physics volume 298, Article number: 11 (**2023**)
https://link.springer.com/content/pdf/10.1007/s11207-022-02095-1.pdf
We present new results towards the explanation of the chromospheric-heating problem and the solar-wind origin, using a two-fluid model that takes into account the collisional interaction between ions (protons) and neutrals (hydrogen atoms). Our aim is to further reveal the mechanism behind chromospheric heating and plasma outflows. We simulate and analyse the propagation and evolution of Alfvén waves in the partially ionised solar chromosphere, consisting of ions + electrons and neutral fluids. The simplified model chromosphere is permeated by a vertical, uniform magnetic field. We perform numerical simulations in the framework of a quasi-1.5-dimensional (1.5D), two-fluid model in which Alfvén waves are excited by a harmonic driver in the transverse component of the ion and neutral velocities, operating in the chromosphere. In the case of a small-amplitude driver, Alfvén waves are weakly damped, and for the chosen wave periods of a few seconds, Alfvén waves manage to propagate through the chromosphere and enter the solar corona. Non-linear Alfvén waves excited by a large-amplitude driver cause significant chromospheric heating and plasma outflows. We thus conclude that two-fluid Alfvén waves with larger amplitudes can contribute to chromospheric heating and plasma outflows, which may result higher up in the solar-wind origin.

Cutoff periods of magnetoacoustic waves in the solar atmosphere

J. **Kraśkiewicz**1, K. Murawski1 and Z. E. Musielak2,3
A&A 623, A62 (**2019**)
https://doi.org/10.1051/0004-6361/20183318

We perform numerical simulations of magnetoacoustic waves (MAWs) in the solar atmosphere, which is gravitationally stratified and structured by either vertical or horizontal uniform magnetic fields. These waves are excited by a monochromatic driver that operates in the photosphere. We show that the gradients of the atmospheric parameters lead to filtering of the waves through the solar atmosphere and to variations of the dominant wave period with height. We use these variations to determine a local cutoff period, which shows a good agreement with the previously obtained analytical and numerical results in an isothermal solar atmosphere. In our numerical simulations, the propagation of MAWs in a more realistic model of the solar atmosphere is considered, and the obtained results demonstrate that the waves with periods higher than a local cutoff wave period are strongly reflected and become evanescent with height, while the waves with shorter wave periods are propagating, and may even reach the solar corona. Some of the evanescent waves may also tunnel and reach the atmospheric heights that would not be otherwise accessible to them. An important result of our study is excitation of chromospheric oscillations with periods equal to the period that is comparable to the observed solar chromospheric oscillations. Implications of our theoretical predictions are discussed.

SOLAR OPACITY CALCULATIONS USING THE SUPER-TRANSITION-ARRAY METHOD

M. **Krief**, A. Feigel, and D. Gazit
2016 ApJ 821 45
A new opacity model has been developed based on the Super-Transition-Array (STA) method for the calculation of monochromatic opacities of plasmas in local thermodynamic equilibrium. The atomic code, named STAR (STA-Revised), is described and used to calculate spectral opacities for a solar model implementing the recent AGSS09 composition. Calculations are carried out throughout the solar radiative zone. The relative contributions of different chemical elements and atomic processes to the total Rosseland mean opacity are analyzed in detail. Monochromatic opacities and charge-state distributions are compared with the widely used Opacity Project (OP) code, for several elements near the radiation–convection interface. STAR Rosseland opacities for the solar mixture show a very good agreement with OP and the OPAL opacity code throughout the radiation zone. Finally, an explicit STA calculation was performed of the full AGSS09 photospheric mixture, including all heavy metals. It was shown that, due to their extremely low abundance, and despite being very good photon absorbers, the heavy elements do not affect the Rosseland opacity.

On the magnetic and thermodynamic properties of dark fibrils in the chromosphere

Matheus **Kriginsky**, Ramon Oliver
ApJ **2024**
https://arxiv.org/pdf/2411.05532
Fibrillar structures are ubiquitous in the solar chromosphere and their potential for mediating the mass and energy transport in the solar atmosphere is undeniable. An accurate determination of their properties requires the use of advanced high-resolution observations which are now becoming broadly available from different observatories. We exploit the capabilities of multi-atom, multi-line spectropolarimetric inversions using the Stockholm Inversion Code (STiC). Non-local thermodynamic equilibrium inversions of a fibril-rich area are performed using spectropolarimetric observations in the Ca II 854.2 nm line obtained with the CRISP imaging spectropolarimeter and spectroscopic observations in the Ca II H line obtained with the CHROMospheric Imaging Spectrometer (CHROMIS) at the Swedish 1-meter Solar Telescope (SST). Additionally, coobservations in the Mg II h & k lines obtained with the Interface Region Imaging Spectrograph (IRIS) are used in the inversions to better constrain the thermodynamic properties of the fibrils. The incorporation of multiple atomic species and spectral lines proves to better constrain the properties of the plasma constituting the fibrils. In particular, the tracing of a large number of fibrils allowed for the study of the variation of the temperature and magnetic field along their projected length over the field of view. The results provide a view of fibrils possessing hot footpoints of about 5 900 K. The temperature drop away from the footpoints is on average 250 K, with a larger drop of around 500 K for the longer fibrils. The magnetic field is also reported to be larger at the footpoints, being almost twice as large as the minimum value reported at the middle point of the fibrils

Magnetic field inference in active region coronal loops using coronal rain clumps

M. **Kriginsky**, R. Oliver, P. Antolin, D. Kuridze, N. Freij
A&A 650, A71 **2021**
https://arxiv.org/pdf/2104.03089.pdf
https://www.aanda.org/articles/aa/pdf/2021/06/aa40611-21.pdf
https://doi.org/10.1051/0004-6361/202140611
Aims. We aim to infer information about the magnetic field in the low solar corona from coronal rain clumps using high-resolution spectropolarimetric observations in the Ca ii 8542 A line obtained with the Swedish 1-m Solar Telescope. Methods. The weak-field approximation (WFA) provides a simple tool to obtain the line-of-sight component of the magnetic field from spectropolarimetric observations. We adapted a method developed in a

previous paper in order to assess the different conditions that must be satisfied in order to properly use the WFA for the data at hand. We also made use of velocity measurements in order to estimate the plane-of-the-sky magnetic field component, so that the magnetic field vector could be inferred. Results. We have inferred the magnetic field vector from a data set totalling 100 spectral scans in the Ca ii 8542 A line, containing an off-limb view of the lower portion of catastrophically cooled coronal loops in an active region. Our results, albeit limited by the cadence and signal-to-noise ratio of the data, suggest that magnetic field strengths of hundreds of Gauss, even reaching up to 1000 G, are omnipresent at coronal heights below 9 Mm from the visible limb. Our results are also compatible with the presence of larger magnetic field values such as those reported by previous works. However, for large magnetic fields, the Doppler width from coronal rain is not that much larger than the Zeeman width, thwarting the application of the WFA. Furthermore, we have determined the temperature, T , and microturbulent velocity, ξ, of coronal rain clumps and off-limb spicules present in the same data set, and we have found that the former ones have narrower T and ξ distributions, their average temperature is similar, and coronal rain has microturbulent velocities smaller than those of spicules. **03 June 2016**

Ubiquitous hundred-Gauss magnetic fields in solar spicules

M. **Kriginsky**, R. Oliver, N. Freij, D. Kuridze, A. Asensio Ramos, P. Antolin
A&A 642, A61 **2020**
https://arxiv.org/pdf/2006.01809.pdf
https://doi.org/10.1051/0004-6361/202038546
Aims. We use high-resolution spectropolarimetric observations in the Ca ii 8542 A line obtained with the SST to study the magnetic field in solar spicules. Methods. The equations that result from the application of the Weak Field Approximation (WFA) to the radiative transfer equations are used to infer the LOS component of the magnetic field (BLOS). Two restrictive conditions are imposed on the Stokes I and V profiles at each pixel before they can be used in a Bayesian inversion to compute its BLOS. Results. The LOS magnetic field component has been inferred in six data sets totalling 448 spectral scans in the Ca ii 8542 A line and containing both active region and quiet Sun areas, with values of hundreds of G being abundantly inferred. There seems to be no difference, from the statistical point of view, between the magnetic field strength of spicules in the quiet Sun or near an active region. On the other hand, the BLOS distributions present smaller values on the disk than off-limb, a fact that can be explained by the effect of superposition on the chromosphere of on-disk structures. We find that spicules in the vicinity of a sunspot have a magnetic field polarity (i.e. north or south) equal to that of the sunspot. This paper also contains an analysis of the effect of off-limb overlapping structures on the observed Stokes I and V parameters and the BLOS obtained from the WFA. It is found that this value is equal to or smaller than the largest LOS magnetic field components of the two structures. In addition, using random BLOS, Doppler velocities and line intensities of these two structures leads in ~ 50% of the cases to Stokes I and V parameters unsuitable to be used with the WFA. Conclusions. Our results present a scarcity of LOS magnetic field components smaller than some 50 G, which must not be taken as evidence against the existence of these magnetic field strengths in spicules. **3 June 2016**

The Standardisation and Sequencing of Solar Eclipse Images for the Eclipse Megamovie Project

Larisza D. **Krista**, Scott W. McIntosh
Solar Phys. Volume 290, Issue 8, pp 2381-2391 **2015**
http://arxiv.org/pdf/1510.08941v1.pdf
We present a new tool, the Solar Eclipse Image Standardisation and Sequencing (SEISS), developed to process multi-source total solar eclipse images by adjusting them to the same standard of size, resolution, and orientation. Furthermore, by analysing the eclipse images, we can determine the relative time between the observations and order them to create a movie of the observed total solar eclipse sequence. We successfully processed images taken at the **14 November 2012** total solar eclipse that occurred in Queensland, Australia, and created a short eclipse proto-movie. The SEISS tool was developed for the Eclipse Megamovie Project (EMP:www.eclipsemegamovie.org), with the goal of processing thousands of images taken by the public during solar eclipse events. EMP is a collaboration among multiple institutes aiming to engage and advance the public interest in solar eclipses and the science of the Sun–Earth connection.

Modelling the evolution of the Sun's open and total magnetic flux

N. A. **Krivova**, S. K. Solanki, B. Hofer, C.-J. Wu, I. G. Usoskin, R. Cameron
A&A 650, A70 **2021**
https://arxiv.org/pdf/2103.15603.pdf
https://www.aanda.org/articles/aa/pdf/2021/06/aa40504-21.pdf
https://doi.org/10.1051/0004-6361/202140504
Solar activity in all its varied manifestations is driven by the magnetic field. Particularly important for many purposes are two global quantities, the Sun's total and open magnetic flux, which can be computed from sunspot number records using models. Such sunspot-driven models, however, do not take into account the presence of

magnetic flux during grand minima, such as the Maunder minimum. Here we present a major update of a widely used simple model, which now takes into account the observation that the distribution of all magnetic features on the Sun follows a single power law. The exponent of the power law changes over the solar cycle. This allows for the emergence of small-scale magnetic flux even when no sunspots are present for multiple decades and leads to non-zero total and open magnetic flux also in the deepest grand minima, such as the Maunder minimum, thus overcoming a major shortcoming of the earlier models. The results of the updated model compare well with the available observations and reconstructions of the solar total and open magnetic flux. This opens up the possibility of improved reconstructions of sunspot number from time series of cosmogenic isotope production rate.

The Spectrometer/Telescope for Imaging X-rays (STIX)

Säm **Krucker**1,2, G. J. Hurford1,2, O. Grimm1,3, S. Kögl1, H.-P Gröbelbauer1,
A&A 642, A15 (**2020**)
https://doi.org/10.1051/0004-6361/201937362
https://www.aanda.org/articles/aa/pdf/2020/10/aa37362-19.pdf

Aims. The Spectrometer Telescope for Imaging X-rays (STIX) on **Solar Orbiter** is a hard X-ray imaging spectrometer, which covers the energy range from 4 to 150 keV. STIX observes hard X-ray bremsstrahlung emissions from solar flares and therefore provides diagnostics of the hottest (≳10 MK) flare plasma while quantifying the location, spectrum, and energy content of flare-accelerated nonthermal electrons.
Methods. To accomplish this, STIX applies an indirect bigrid Fourier imaging technique using a set of tungsten grids (at pitches from 0.038 to 1 mm) in front of 32 coarsely pixelated CdTe detectors to provide information on angular scales from 7 to 180 arcsec with 1 keV energy resolution (at 6 keV). The imaging concept of STIX has intrinsically low telemetry and it is therefore well-suited to the limited resources available to the Solar Orbiter payload. To further reduce the downlinked data volume, STIX data are binned on board into 32 selectable energy bins and dynamically-adjusted time bins with a typical duration of 1 s during flares.
Results. Through hard X-ray diagnostics, STIX provides critical information for understanding the acceleration of electrons at the Sun and their transport into interplanetary space and for determining the magnetic connection of Solar Orbiter back to the Sun. In this way, STIX serves to link Solar Orbiter's remote and in-situ measurements.

RHESSI Heliophysics Senior Review 2013

Samuel **Krucker**, Brian Dennis, Manfred Bester, Laura Peticolas
http://hesperia.gsfc.nasa.gov/senior_review/2013/senior_review_proposal_2013.pdf**, 2013, File**

RHESSI was given an excellent rating by the Heliophysics Senior Review panel for both "overall scientific merit of the proposed extended mission" and for "Value to the Heliophysics System Observatory." The Panel recommends "the continued operation of the RHESSI extended mission," and states in its report that "RHESSI plays a unique role within the HSO, enabling system-wide studies of energy release and particle acceleration in flares/CMEs and their effects on the interplanetary medium, magnetosphere, and ITM."

Generation of low-frequency kinetic waves at the footpoints of pre-flare coronal loops

Kryshtal Alexandr, Voitsekhovska Anna, Cheremnykh Oleg, Ballai Istvan, Verth Gary, Fedun Viktor
Solar Phys. **2020**
https://arxiv.org/pdf/2010.10167.pdf

In this study we discuss the excitation of low frequency plasma waves in the lower-middle chromosphere region of loop footpoints for the case when the plasma can be considered in a pre-flare state. It is shown, that among the known semi-empirical models of the solar atmosphere, only the VAL (F) model together with a particular set of basic plasma parameters and amplitudes of the electric and magnetic fields supports generation of low frequency wave instability. Our results show that it is possible to predict the onset of the flare process in the active region by using the interaction of kinetic Alfven and kinetic ion-acoustic waves, which are solutions of the derived dispersion equation. The VAL (F) model allows situations when the main source of the aforementioned instability can be a sub-Dreicer electric field and drift plasma movements due to the presence of spatial inhomogeneities. We also show that the generation of kinetic Alfven and kinetic ion-acoustic waves can occur both, in plasma with a purely Coulomb conductivity and in the presence of small-scale Bernstein turbulence. The excitation of the small amplitude kinetic waves due to development of low threshold instability in plasma with relatively low values of the magnetic field strength is also discussed.

DISCOVERY OF UBIQUITOUS FAST-PROPAGATING INTENSITY DISTURBANCES BY THE CHROMOSPHERIC LYMAN ALPHA SPECTROPOLARIMETER (CLASP)

M. **Kubo**1, Y. Katsukawa1, Y. Suematsu1, R. Kano1, T. Bando1, N. Narukage1, R. Ishikawa1, H. Hara1, G. Giono1, S. Tsuneta…
2016 ApJ 832 141

High-cadence observations by the slit-jaw (SJ) optics system of the sounding rocket experiment known as the Chromospheric Lyman Alpha Spectropolarimeter (CLASP) reveal ubiquitous intensity disturbances that recurrently propagate in either the chromosphere or the transition region or both at a speed much higher than the speed of sound. The CLASP/SJ instrument provides a time series of two-dimensional images taken with broadband filters centered on the Lyα line at a 0.6 s cadence. The multiple fast-propagating intensity disturbances appear in the quiet Sun and in an active region, and they are clearly detected in at least 20 areas in a field of view of 527" × 527" during the 5 minute observing time. The apparent speeds of the intensity disturbances range from 150 to 350 km s−1, and they are comparable to the local Alfvén speed in the transition region. The intensity disturbances tend to propagate along bright elongated structures away from areas with strong photospheric magnetic fields. This suggests that the observed fast-propagating intensity disturbances are related to the magnetic canopy structures. The maximum distance traveled by the intensity disturbances is about 10", and the widths are a few arcseconds, which are almost determined by a pixel size of 103. The timescale of each intensity pulse is shorter than 30 s. One possible explanation for the fast-propagating intensity disturbances observed by CLASP is magnetohydrodynamic fast-mode waves.

Multiple Stokes I inversions for inferring magnetic fields in the spectral range around Cr I 5782 Å

C. **Kuckein**1, H. Balthasar1, C. Quintero Noda2,3, A. Diercke1,4, J. C. Trelles Arjona2,3, B. Ruiz Cobo2,3, T. Felipe2,3, C. Denker1, M. Verma1, I. Kontogiannis1 and M. Sobotka5
A&A 653, A165 (**2021**)
https://www.aanda.org/articles/aa/pdf/2021/09/aa40596-21.pdf
https://doi.org/10.1051/0004-6361/202140596
Aims. In this work, we explore the spectral window containing Fraunhofer lines formed in the solar photosphere, around the magnetically sensitive Cr I lines at 5780.9, 5781.1, 5781.7, 5783.0, and 5783.8 Å, with Landé g-factors between 1.6 and 2.5. The goal is to simultaneously analyze 15 spectral lines, comprising Cr I, Cu I, Fe I, Mn I, and Si I lines, without the use of polarimetry, to infer the thermodynamic and magnetic properties in strongly magnetized plasmas using an inversion code.
Methods. Our study is based on a new setup at the Vacuum Tower Telescope (VTT, Tenerife), which includes fast spectroscopic scans in the wavelength range around the Cr I 5781.75 Å line. The oscillator strengths log(gf) of all spectral lines, as well as their response functions to temperature, magnetic field, and Doppler velocity, were determined using the Stokes Inversion based on Response functions (SIR) code. Snapshot 385 of the enhanced network simulation from the Bifrost code serves to synthesize all the lines, which are, in turn, inverted simultaneously with SIR to establish the best inversion strategy. We applied this strategy to VTT observations of a sunspot belonging to NOAA 12723 on 2018 September 30 and compared the results to full-disk vector field data obtained with the Helioseismic and Magnetic Imager (HMI).
Results. The 15 simultaneously inverted intensity profiles (Stokes I) delivered accurate temperatures and Doppler velocities when compared with the simulations. The derived magnetic fields and inclinations achieve the best level of accuracy when the fields are oriented along the line-of-sight (LOS) and less accurate when the fields are transverse to the LOS. In general, the results appear similar to what is reported in the HMI vector-field data, although some discrepancies exist.
Conclusions. The analyzed spectral range has the potential to deliver thermal, dynamic, and magnetic information for strongly magnetized features on the Sun, such as pores and sunspots, even without the use of polarimetry. The highest sensitivity of the lines is found in the lower photosphere, on average, around log $\tau = -1$. The multiple-line inversions provide smooth results across the whole field of view (FOV). The presented spectral range and inversion strategy will be used for future VTT observing campaigns.

Tools - a data reduction pipeline for the GREGOR Fabry-Pérot Interferometer and the High-resolution Fast Imager at the GREGOR solar telescope

C. **Kuckein** (1), C. Denker (1), M. Verma (1), H. Balthasar (1), S. J. González Manrique (1 and 2), R. E. Louis (1), A. Diercke (1 and 2) ((1) Leibniz-Institut für Astrophysik Potsdam, (2) Universität Potsdam, Institut für Physik and Astronomie)
Fine Structure and Dynamics of the Solar Atmosphere Proceedings IAU Symposium No. 327, **2017**
https://arxiv.org/pdf/1701.01670v1.pdf
A huge amount of data has been acquired with the GREGOR Fabry-P\'erot Interferometer (GFPI), large-format facility cameras, and since 2016 with the High-resolution Fast Imager (HiFI). These data are processed in standardized procedures with the aim of providing science-ready data for the solar physics community. For this purpose, we have developed a user-friendly data reduction pipeline called "sTools" based on the Interactive Data Language (IDL) and licensed under creative commons license. The pipeline delivers reduced and image-reconstructed data with a minimum of user interaction. Furthermore, quick-look data are generated as well as a webpage with an overview of the observations and their statistics. All the processed data are stored online at the

GREGOR GFPI and HiFI data archive of the Leibniz Institute for Astrophysics Potsdam (AIP). The principles of the pipeline are presented together with selected high-resolution spectral scans and images processed with sTools.
2014 July 27

NuSTAR Detection of X-Ray Heating Events in the Quiet Sun

Matej **Kuhar**1,2, Säm Krucker1,3, Lindsay Glesener4, Iain G. Hannah5, Brian W. Grefenstette6, David M. Smith7, Hugh S. Hudson3,5, and Stephen M. White8
2018 ApJL 856 L32
https://arxiv.org/pdf/1803.08365.pdf
In this Letter, we present the first imaging spectroscopy X-ray observations of three quiet Sun flares during the Nuclear Spectroscopic Telescope ARray (NuSTAR) solar campaigns on **2016 July 26 and 2017 March 21**, concurrent with the Solar Dynamics Observatory/Atmospheric Imaging Assembly (SDO/AIA) observations. Two of the three events showed time lags of a few minutes between peak X-ray and extreme ultraviolet emissions. Isothermal fits with rather low temperatures in the range 3.2–4.1 MK and emission measures of (0.6–15) × 1044 cm−3 describe their spectra well, resulting in thermal energies in the range (2–6) × 1026 erg. NuSTAR spectra did not show any signs of a nonthermal or higher temperature component. However, as the estimated upper limits of (hidden) nonthermal energy are comparable to the thermal energy estimates, the lack of a nonthermal component in the observed spectra is not a constraining result. The estimated Geostationary Operational Environmental Satellite (GOES) classes from the fitted values of temperature and emission measure fall between 1/1000 and 1/100 A class level, making them eight orders of magnitude fainter in soft X-ray flux than the largest solar flares.

Annual Cosmic Ray Spectra from 250 MeV up to 1.6 GeV from 1995 – 2014 Measured with the Electron Proton Helium Instrument onboard SOHO

P. **Kühl** , R. Gómez-Herrero, B. Heber
Solar Phys. Volume 291, Issue 3, pp 965-974 **2016**
The solar modulation of galactic cosmic rays (GCR) can be studied in detail by examining long-term variations of the GCR energy spectrum (e.g. on the scales of a solar cycle). With almost 20 years of data, the Electron Proton Helium INstrument (EPHIN) onboard the SOlar and Heliospheric Observatory (SOHO) is well suited for this kind of investigation. Although the design of the instrument is optimised to measure proton and helium isotope spectra up to 50 MeVnucleon−1, the capability exists to determine proton energy spectra from 250 MeV up to above 1.6 GeV. Therefore we developed a sophisticated inversion method to calculate such proton spectra. The method relies on a GEANT4 Monte Carlo simulation of the instrument and a simplified spacecraft model that calculates the energy-response function of EPHIN for electrons, protons, and heavier ions. For validation purposes, proton spectra based on this method are compared to various balloon missions and space instrumentation. As a result we present annual galactic cosmic-ray spectra from 1995 to 2014.

A Poynting-Robertson-Like Drag at the Sun's Surface

HMI Science Nuggets # 66, Feb. **2017**
Jeff **Kuhn**
http://hmi.stanford.edu/hminuggets/?p=1802

Enhancing Solar Cycle 25 and 26 Forecasting with Vipin-Deep-Decomposed-Recomposed Rolling-window (vD2R2w) Model on Sunspot Number Observations.

Kumar, V.
Sol Phys 299, 147 (**2024**).
https://doi.org/10.1007/s11207-024-02389-6
Effective predicting sunspot numbers (SSN) is the complex task of studying space weather, solar activity, satellite communication, and Earth's climate. Developing a reliable SSN forecasting model is difficult because SSN time series exhibit complex patterns, nonlinearity, and nonstationarity characteristics. The state-of-the-art shows that deep-learning models often need help capturing SSN data's intricate dynamics and long-term dependencies. The SSN time series' decomposed trend and seasonal and residual characteristics may provide better information on long-term dependencies and associated dynamics for effective learning. In this research, the vipin-deep-decomposed-recomposed rolling-window (vD2R2w) models have been proposed with a combination of time-series decomposition, deep-learning models, and a rolling-window method to predict the SSN accurately. The proposed vD2R2w models have been evaluated over four datasets and consistently outperform traditional deep-learning models. The model improves the performance in terms of RMSE, MAPE, and R2 over the datasets as SSN_Daily: 84.18% (RMSE), 10.38% (MAPE), and 3.504% (R2); SSN_Monthly: 39.5% (RMSE), 26.06% (MAPE), and 7.258% (R2); SSN_MonthlyMean: 178.32% (RMSE), 54.83% (MAPE), and 1.56% (R2); and SSN_Yearly: 6.06% (RMSE), 10.36% (MAPE), and 1.366% (R2). Further, the superiority of the vD2R2w models is validated through AIC & BIC, Diebold Mariano test, and Friedman ranking statistical tests. Additionally, the vD2R2w model has

forecasted the peak value of Solar Cycles (SC) and time, i.e., SC25: 127.16 (± 6.83) in 2025 and SC26: 191.71 (± 43.37) in 2035. The analysis of proposed model performances and statistical validation over various measures with four SSNs have concluded that the vD2R2w model outperforms the traditional models and is a reliable framework for SSN time series forecasting. Implementing the proposed model may benefit domains such as space-weather monitoring, satellite communication planning, and solar energy forecasting that rely on accurate SSN predictions.

Comparative Study of Solar Rotation of Transition Region and Corona using Solar Irradiance and Radio Flux.

Kumar, A., Kumar, N. & Vats, H.O.
Sol Phys 299, 130 (**2024**).
https://doi.org/10.1007/s11207-024-02375-y
We study the temporal variation of solar rotation profiles based on solar irradiance at 93.5 nm and solar radio flux at 10.7 cm originating from the transition region and lower corona, respectively. The autocorrelation technique is used to calculate the period in periodic time series data. The sidereal rotation periods for normalized and detrended data are studied for 2011 – 2021. The sidereal rotation periods for solar irradiance and radio flux for 2011 – 2021 vary from 22.75 to 26.17 days and 19.42 to 28.14 days, respectively. The mean of the sidereal rotation periods for solar irradiance and radio flux are 24.76 and 23.76 days, respectively. The mean sidereal rotation period for solar irradiance is higher than the mean sidereal rotation period for solar radio flux. The sidereal rotation period for solar irradiance is greater than or equal to the sidereal rotation period for solar radio flux for almost all the years between 2011 and 2021. It is found that the lower corona rotates faster than the transition region during 2011 – 2021, i.e., the lower corona is found to be moving 4% faster than the transition region during 2011 – 2021. We found a linear relationship between the normalized daily irradiance and radio flux with a correlation coefficient of 0.986. Using cross-correlation analysis, we investigated a phase relationship between solar irradiance and radio flux and found no time lag between solar irradiance and radio flux.

Variabilities in the polar field and solar cycle due to irregular properties of Bipolar Magnetic Regions

Pawan **Kumar**, Bidya Binay Karak, Anu Sreedevi
MNRAS Volume 530, Issue 3, May **2024**, Pages 2895–2905,
https://doi.org/10.1093/mnras/stae1052
https://arxiv.org/pdf/2404.10526.pdf
https://watermark.silverchair.com/stae1052.pdf
Decay and dispersal of the tilted Bipolar Magnetic Regions (BMRs) on the solar surface are observed to produce large-scale poloidal field, which acts as the seed for the toroidal field and, thus, the next sunspot cycle. However, various properties of BMR, namely, the tilt, time delay between successive emergences, location, and flux, all have irregular variations. Previous studies show that these variations can lead to changes in the polar field. In this study, we first demonstrate that our 3D kinematic dynamo model, STABLE, reproduces the robust feature of the surface flux transport (SFT) model, namely the variation of the generated dipole moment with the latitude of the BMR position. Using STABLE in both SFT and dynamo modes, we perform simulations by varying the individual properties of BMR and keeping their distributions the same in all the cycles as inspired by the observations. We find that randomness due to the distribution in either the time delay or the BMR latitude produces negligible variation in the polar field and the solar cycle. However, randomness due to BMR flux distribution produces substantial effects, while the scatter in the tilt around Joy law produces the largest variation. Our comparative analyses suggest that the scatter of BMR tilt around Joy law is the major cause of variation in the solar cycle. Furthermore, our simulations also show that the magnetic field-dependent time delay of BMR emergence produces more realistic features of the magnetic cycle, consistent with observation.
Correction: MNRAS Volume 531, Issue 2, June 2024, Page 2531, https://doi.org/10.1093/mnras/stae1308

Solar cycle variability induced by stochastic fluctuations of BMR properties and at different amounts of dynamo supercriticality

Pawan **Kumar**
Proceedings IAU Symposium No.365, 2023 **2024**
https://arxiv.org/pdf/2401.11159.pdf
Understanding the irregular variation of the solar cycle is crucial due to its significant impact on global climates and the heliosphere. Since the polar magnetic field determines the amplitude of the next solar cycle, variations in the polar field can lead to fluctuations in the solar cycle. We have explored the variability of the solar cycle at different levels of dynamo supercriticality. We observe that the variability depends on the dynamo operation regime, with the near-critical regime exhibiting more variability than the supercritical regime. Furthermore, we have explored the effects of the irregular BMR properties (emergence rate, latitude, tilt, and flux) on the polar field and the solar cycle.

We find that they all produce considerable variation in the solar cycle; however, the variation due to the tilt scatter is the largest.

Impulsively generated waves in two-fluid plasma in the solar chromosphere: Heating and generation of plasma outflows

M. **Kumar**1,2, K. Murawski1, L. Kadowaki1, B. Kuźma3,4 and E. K. J. Kilpua2
A&A 681, A60 (**2024**)
https://www.aanda.org/articles/aa/pdf/2024/01/aa45638-22.pdf
Context. We present new insights into impulsively generated Alfvén and magneto-acoustic waves in the partially ionized two-fluid plasma of the solar atmosphere and their contribution to chromospheric heating and plasma outflows.
Aims. Our study attempts to elucidate the mechanisms responsible for chromospheric heating and excitation of plasma outflows that may contribute to the generation of the solar wind in the upper atmospheric layers. The main aim of this work is to investigate the impulsively generated waves by taking into account two-fluid effects. These effects may alter the wave propagation leading to attenuation and collisional plasma heating.
Methods. The two-fluid equations were solved by the JOint ANalytical Numerical Approach (JOANNA) code in a 2.5-dimensional (2.5D) framework to simulate the dynamics of the solar atmosphere. Here, electrons + ions (protons) and neutrals (hydrogen atoms) are treated as separate fluids, which are coupled via ion-neutral collisions. The latter acts as a dissipation mechanism for the energy carried by the waves in two-fluid plasma and may ultimately lead to the frictional heating of the partially ionized plasma. The waves in two-fluid plasma, which are launched from the top of the photosphere, are excited by perturbations induced by localized Gaussian pulses in the horizontal components of the ion and neutral velocities.
Results. In the middle and upper chromosphere, a substantial fraction of the energy carried by large amplitude waves in the two-fluid plasma is dissipated in ion-neutral collisions, resulting in the thermalization of wave energy and generation of plasma outflows. We find that coupled Alfvén and magneto-acoustic waves are more effective in heating the chromosphere than magneto-acoustic waves.
Conclusions. Large-amplitude waves in the two-fluid plasma may be responsible for heating the chromosphere. The net flow of ions is directed outward, leading to plasma outflows in the lower solar corona, which may contribute to the solar wind at higher altitudes The primary source of wave energy dissipation in the current paradigm comes from collisions between ions and neutrals.

Stacked 1D Convolutional LSTM (sConvLSTM1D) Model for Effective Prediction of Sunspot Time Series

Abhijeet **Kumar** & Vipin Kumar
Solar Physics volume 298, Article number: 121 (**2023**)
https://doi.org/10.1007/s11207-023-02209-3
A multi-layer, deep-learning (DL) architecture consisting of stacked Convolutional Long Short Term Memory (sConvLSTM1D) layers is proposed to forecast the sunspot number (SSN) more effectively. The proposed model with optimized hyper-parameters performs efficiently on four kinds of sunspot data with different frequencies of time that are yearly, monthly, daily, and 13-month smoothed provided by the World Data Center-Sunspot Index and Long Term Solar Observation (WDC-SILSO), the Royal Observatory of Belgium (SILSO World Data Center). The model was contrasted with other traditional DL models on different performance metrics, namely root-mean-square error (RMSE), mean-absolute error (MAE), mean-absolute-percentage error (MAPE), and mean-absolute-scaled error (MASE). A non-parametric statistical test has also been carried out to confirm the model's effectiveness. The prediction of the highest yearly mean of total sunspot number (SSN) in Solar Cycle 25 (SC25) has also been performed. The proposed sConvLSTM1D model suggests that the solar cycle exhibits the characteristics of a weak cycle. However, it is anticipated to be stronger than the preceding Solar Cycle 24 (SC24). The year of peak sunspot number will be 2024, as per the prediction, with the peak value of yearly mean sunspot number as 140.84, which is 24.3% higher than the peak value of the yearly mean of total sunspot number, which was 113.3 in the Solar Cycle 24 in the year 2014.

A study of the propagation of magnetoacoustic waves in small-scale magnetic fields using solar photospheric and chromospheric Dopplergrams: HMI/SDO and MAST observations

Hirdesh **Kumar**, Brajesh Kumar, S. P. Rajaguru, Shibu K. Mathew, Ankala Raja Bayanna
Journal of Atmospheric and Solar-Terrestrial Physics (Special Issue of STP-15) **2023**
https://arxiv.org/pdf/2304.13492.pdf
In this work, we present a study of the propagation of low-frequency magneto-acoustic waves into the solar chromosphere within small-scale inclined magnetic fields over a quiet-magnetic network region utilizing near-simultaneous photospheric and chromospheric Dopplergrams obtained from the HMI instrument onboard SDO

spacecraft and the Multi-Application Solar Telescope (MAST) operational at the Udaipur Solar Observatory, respectively. Acoustic waves are stochastically excited inside the convection zone of the Sun and intermittently interact with the background magnetic fields resulting into episodic signals. In order to detect these episodic signals, we apply the wavelet transform technique to the photospheric and chromospheric velocity oscillations in magnetic network regions. The wavelet power spectrum over photospheric and chromospheric velocity signals show a one-to-one correspondence between the presence of power in the 2.5-4 mHz band. Further, we notice that power in the 2.5-4 mHz band is not consistently present in the chromospheric wavelet power spectrum despite its presence in the photospheric wavelet power spectrum. This indicates that leakage of photospheric oscillations (2.5-4 mHz band) into the higher atmosphere is not a continuous process. The average phase and coherence spectra estimated from these photospheric and chromospheric velocity oscillations illustrate the propagation of photospheric oscillations (2.5-4 mHz) into the solar chromosphere along the inclined magnetic fields. Additionally, chromospheric power maps estimated from the MAST Dopplergrams also show the presence of high-frequency acoustic halos around relatively high magnetic concentrations, depicting the refraction of high-frequency fast mode waves around vA ~ vs layer in the solar atmosphere. **May 21, 2020**

Physical link of the polar field build-up with the Waldmeier effect broadens the scope of early solar cycle prediction: Cycle 25 is likely to be stronger than Cycle 24

Pawan **Kumar**, Akash Biswas, Bidya Binay Karak
MNRAS **2022**
https://arxiv.org/pdf/2203.11494
Prediction of the solar cycle is challenging but essential because it drives space weather. Several predictions with varying amplitudes of the ongoing Cycle~25 have been made. We show that an aspect of the Waldmeier effect, i.e., a strong positive correlation between the rise rate and the amplitude of the cycle, has a physical link with the build-up of the previous cycle's polar field after its reversal. We find that the rise rate of the polar field is highly correlated with the rise rate and the amplitude of the next solar cycle. Thus, the prediction of the amplitude of the solar cycle can be made just a few years after the reversal of the previous cycle's polar field, thereby extending the scope of the solar cycle prediction to much earlier than the usual time. Our prediction of Cycle 25 based on the rise rate of the previous polar field is 137±23, which is quite close to the prediction 138±26 based on the WE2 computed from the available 2 years sunspot data of the ongoing cycle.
HMI Nuggets # 178 Apr **2022** http://hmi.stanford.edu/hminuggets/?p=3889

Super-criticality of dynamo limits the memory of polar field to one cycle

Pawan **Kumar**, Bidya Binay Karak, Vindya Vashishth
ApJ **913** 65 **2021**
https://arxiv.org/pdf/2103.11754.pdf
https://doi.org/10.3847/1538-4357/abf0a1
The polar magnetic field precursor is considered to be the most robust and physics-based method for the prediction of the next solar cycle strength. However, to make a reliable prediction of a cycle, is the polar field at the solar minimum of the previous cycle enough or we need the polar field of many previous cycles? To answer this question, we performed several simulations using Babcock-Leighton type flux transport dynamo models with the stochastically forced source for the poloidal field (α term). We show that when the dynamo is operating near the critical dynamo transition or only weakly supercritical, the polar field of the cycle n determines the amplitude of the next several cycles (at least three). However, when the dynamo is substantially supercritical, this correlation of the polar field is reduced to one cycle. This change in the memory of the polar field from multi- to one-cycle with the increase of the super-criticality of the dynamo is independent of the importance of various turbulent transport processes in the model. We further show that when the dynamo operates near the critical, it produces frequent extended episodes of weaker activity, resembling the solar grand minima. The occurrence of grand minima is accompanied by the multi-cycle correlation of polar field. The frequency of grand minima decreases with the increase of supercriticality of the dynamo.

The polar precursor method for solar cycle prediction: comparison of predictors and their temporal range

Pawan **Kumar**, Melinda Nagy, Alexandre Lemerle, Bidya Binay Karak, Kristof Petrovay
ApJ **909** 87 **2021**
https://arxiv.org/pdf/2101.05013.pdf
https://doi.org/10.3847/1538-4357/abdbb4
The polar precursor method is widely considered to be the most robust physically motivated method to predict the amplitude of an upcoming solar this http URL uses indicators of the magnetic field concentrated near the poles around sunspot minimum. Here, we present an extensive performance analysis of various such predictors, based on both observational data (WSO magnetograms, MWO polar faculae counts and Pulkovo A(t) index) and outputs (polar cap magnetic flux and global dipole moment) of various existing flux transport dynamo models.We calculate

Pearson correlation coefficients (r) of the predictors with the next cycle amplitude as a function of time measured from several solar cycle landmarks: setting r=0.8 as a lower limit for acceptable predictions, we find that observations and models alike indicate that the earliest time when the polar predictor can be safely used is 4 years after polar field reversal. This is typically 2--3 years before solar minimum and about 7~years before the predicted maximum, considerably extending the {usual} temporal scope of the polar precursor method. Re-evaluating the predictors another 3 years later, at the time of solar minimum, further increases the correlation level to $r\ga 0.9$. As an illustration of the result, we determine the predicted amplitude of Cycle 25 based on the value of the WSO polar field at the now official minimum date of December 2019 as 126±3. A forecast based on the value in early 2017, 4~years after polar reversal would have only differed from this final prediction by 3.1±14.7\%.

A 3D kinematic Babcock Leighton solar dynamo model sustained by dynamic magnetic buoyancy and flux transport processes

R. **Kumar**, L. Jouve, D. Nandy
A&A 623, A54 **2019**
https://arxiv.org/pdf/1901.04251.pdf
https://www.aanda.org/articles/aa/pdf/2019/03/aa34705-18.pdf
Magnetohydrodynamic interactions between plasma flows and magnetic fields is fundamental to the origin and sustenance of the 11-year sunspot cycle. These processes are intrinsically three-dimensional (3D) in nature. Our goal is to construct a 3D solar dynamo model that on the one hand captures the buoyant emergence of tilted bipolar sunspot pairs, and on the other hand produces cyclic large-scale field reversals mediated via surface flux-transport processes -- that is, the Babcock-Leighton mechanism. We perform kinematic dynamo simulations where the prescribed velocity field is a combination of solar-like differential rotation and meridional circulation, along with a parametrized turbulent diffusivity. We use a novel methodology for modeling magnetic buoyancy through field-strength-dependent 3D helical up-flows that results in the formation of tilted bipolar sunspots. The bipolar spots produced in our simulations participate in the process of poloidal-field generation through the Babcock-Leighton mechanism, resulting in self-sustained and periodic large-scale magnetic field reversal. Our parameter space study varying the amplitude of the meridional flow, the convection zone diffusivity, and parameters governing the efficiency of the magnetic buoyancy mechanism reveal their relative roles in determining properties of the sunspot cycle such as amplitude, period, and dynamical memory relevant to solar cycle prediction. We also derive a new dynamo number for the Babcock-Leighton solar dynamo mechanism which reasonably captures our model dynamics. This study elucidates the relative roles of different flux-transport processes in the Sun's convection zone in determining the properties and physics of the sunspot cycle and could potentially lead to realistic, data-driven 3D dynamo models for solar-activity predictions and exploration of stellar magnetism and starspot formation in other stars.

Production of sunspots and their effects on the corona and solar wind: Insights from a new 3D flux-transport dynamo model

Rohit **Kumar**, Laurène Jouve, Rui F. Pinto, Alexis P. Rouillard
Front. Astron. Space Sci., 5:4 **2018**
https://arxiv.org/pdf/1801.09625.pdf
https://doi.org/10.3389/fspas.2018.00004
https://www.frontiersin.org/articles/10.3389/fspas.2018.00004/full
We present a three-dimensional numerical model for the generation and evolution of the magnetic field in the solar convection zone, in which sunspots are produced and contribute to the cyclic reversal of the large-scale magnetic field. We then assess the impact of this dynamo-generated field on the structure of the solar corona and solar wind. This model solves the induction equation in which the velocity field is prescribed. This velocity field is a combination of a solar-like differential rotation and meridional circulation. We develop an algorithm that enables the magnetic flux produced in the interior to be buoyantly transported towards the surface to produce bipolar spots. We find that those tilted bipolar magnetic regions contain a sufficient amount of flux to periodically reverse the polar magnetic field and sustain dynamo action. We then track the evolution of these magnetic features at the surface during a few consecutive magnetic cycles and analyze their effects on the topology of the corona and on properties of the solar wind (distribution of streamers and coronal holes, and of slow and fast wind streams) in connection with current observations of the Sun.

On the signatures of flare-induced global waves in the Sun: GOLF and VIRGO observations

Brajesh **Kumar**, Savita Mathur, Rafael A. Garcia, Antonio Jimenez
MNRAS, Vol. 471, Issue 4, November **2017**
https://arxiv.org/pdf/1710.06245.pdf

Recently, several efforts have been made to identify the seismic signatures of flares and magnetic activity in the Sun and Sun-like stars. In this work, we have analyzed the disk-integrated velocity and intensity observations of the Sun obtained from the GOLF and VIRGO/SPM instruments, respectively, on board the SOHO space mission covering several successive flare events, for the period from **11 February 2011 to 17 February 2011**, of which 11 February 2011 remained a relatively quiet day and served as a "null test" for the investigation. Application of the spectral analysis to these disk-integrated Sun-as-a-star velocity and intensity signals indicates that there is enhanced power of the global modes of oscillations in the Sun during the flares, as compared to the quiet day. The GOLF instrument obtains velocity observations using the Na I D lines which are formed in the upper solar photosphere, while the intensity data used in our analysis are obtained by VIRGO/SPM instrument at 862~nm, which is formed within the solar photosphere. Despite the fact that the two instruments sample different layers of the solar atmosphere using two different parameters (velocity v/s intensity), we have found that both these observations show the signatures of flare-induced global waves in the Sun. These results could suffice in identifying the asteroseismic signatures of stellar flares and magnetic activity in the Sun-like stars.

Propagation and damping of slow MHD waves in a flowing viscous coronal plasma

Nagendra **Kumar**, Anil Kumar , K. Murawski

Astrophysics and Space Science April **2016**, 361:143

We investigate the propagation of slow MHD waves in a flowing viscous solar coronal plasma. The compressive viscosity and steady flow along and opposite to the wave propagation are taken into account to study the damping of slow waves. We numerically solve the MHD equations by MacCormack method to examine the effect of steady flow on the damping of slow MHD waves in viscous solar coronal plasma. Amplitude of velocity perturbation and damping time of slow waves decrease with the increase in the value of Mach number. Flow causes a phase shift in the perturbed velocity amplitude and an increase in wave period. The damping of slow waves in flowing viscous plasma is stronger than the damping of waves in viscous plasma. Slow wave in backward flow damps earlier than the wave in forward flow.

Segmentation of coronal features to understand the solar EUV and UV irradiance variability

S. T. **Kumara**1,2,7, R. Kariyappa2, J. J. Zender3, G. Giono4, V. Delouille5, L. P. Chitta2,8, L. Damé6, J.-F. Hochedez6,5, C. Verbeeck5, B. Mampaey5 and V. H. Doddamani

A&A 561, A9 (**2014**)

Context. The study of solar irradiance variability is of great importance in heliophysics, the Earth's climate, and space weather applications. These studies require careful identifying, tracking and monitoring of active regions (ARs), coronal holes (CHs), and the quiet Sun (QS).

Aims. We studied the variability of solar irradiance for a period of two years (January 2011–December 2012) using the Large Yield Radiometer (LYRA), the Sun Watcher using APS and image Processing (SWAP) on board PROBA2, and the Atmospheric Imaging Assembly (AIA) on board the Solar Dynamics Observatory (SDO).

Methods. We used the spatial possibilistic clustering algorithm (SPoCA) to identify and segment coronal features from the EUV observations of AIA. The AIA segmentation maps were then applied on SWAP images, and parameters such as the intensity, fractional area, and contribution of ARs/CHs/QS features were computed and compared with the full-disk integrated intensity and LYRA irradiance measurements.

Results. We report the results obtained from SDO/AIA and PROBA2/SWAP images taken from January 2011 to December 2012 and compare the resulting integrated full-disk intensity with PROBA2/LYRA irradiance. We determine the contributions of the segmented features to EUV and UV irradiance variations. The variations of the parameters resulting from the segmentation, namely the area, integrated intensity, and relative contribution to the solar irradiance, are compared with LYRA irradiance. We find that the active regions have a great impact on the irradiance fluctuations. In the EUV passbands considered in this study, the QS is the greatest contributor to the solar irradiance, with up to 63% of total intensity values. Active regions, on the other hand, contribute to about 10%, and off-limb structures to about 24%. We also find that the area of the features is highly variable suggesting that their area has to be taken into account in irradiance models, in addition to their intensity variations.

Conclusions. We successfully show that the feature extraction allows us to use EUV telescopes to measure irradiance fluctuations and to quantify the contribution of each part to the EUV spectral solar irradiance observed with a calibrated radiometer. This study also shows that SPoCA is viable, and that the segmentation of images can be a useful tool. We also provide the measurement correlation between SWAP and AIA during this analysis.

Coupled macro spin model with two variables for polarity reversals in the Earth and the Sun

Ariyoshi **Kunitomo**, Akika Nakamichi, Tetsuya Hara

2020
https://arxiv.org/ftp/arxiv/papers/2006/2006.15902.pdf
The structure of geomagnetism is very complex, and there are still some problems left in magnetohydrodynamics (MHD) simulations. Recently, the macro spin model has been suggested. This is the idea that geomagnetism is described by interaction with many local dynamo elements (macro-spins). This model can reproduce some features of geomagnetism by solving equations of motion with only one variable. In this paper, we study this model to make more general by adding one variable. In this result, our model becomes possible for several things that are not treated in the previous study, for example, migration of the North (or South) Magnetic Pole, comparison with observed data of magnetic field distributions expressed in two directions, etc. Moreover, as a result of an application to the sun, we could reproduce periodic polarity reversals and the power index of the power spectrum, etc. In addition, we investigate the statistical properties of the pole migration.

Comprehensive Synthesis of Magnetic Tornado: Co-spatial Incidence of Chromospheric Swirls and EUV Brightening

Hidetaka **Kuniyoshi**, Souvik Bose, Takaaki Yokoyama
2024 *ApJL* **969** L34
https://iopscience.iop.org/article/10.3847/2041-8213/ad5a0e/pdf
https://arxiv.org/pdf/2404.18892
Magnetic tornadoes, characterized as impulsive Alfven waves initiated by photospheric vortices in intergranular lanes, are considered efficient energy channels to the corona. Despite their acknowledged importance for solar coronal heating, their observational counterparts from the corona have not been well understood. To address this issue, we use a radiative MHD simulation of a coronal loop with footpoints rooted in the upper convection zone, and synthesize the chromospheric and coronal emissions corresponding to a magnetic tornado. Considering SDO/AIA 171 A and Solar Orbiter/EUI 174 A channels, our synthesis reveals that the coronal response to magnetic tornadoes can be observed as an EUV brightening of which width is ~2 Mm. This brightening is located above the synthesized chromospheric swirl observed in Ca II 8542 A, Ca II K, and Mg II k lines, which can be detected by instruments such as SST/CRISP, GST/FISS, and IRIS. Considering the height correspondence of the synthesized brightening, magnetic tornadoes can be an alternative mechanism for the small-scale EUV brightenings such as the solar "campfires". Our findings indicate that coordinated observations encompassing the chromosphere to the corona are indispensable for comprehending the origin of coronal EUV brightenings.

Can the solar p-modes contribute to the high-frequency transverse oscillations of spicules?

Hidetaka **Kuniyoshi**, Munehito Shoda, Richard J. Morton, Takaaki Yokoyama
ApJ **960** 118 **2024**
https://arxiv.org/pdf/2311.16461.pdf
https://iopscience.iop.org/article/10.3847/1538-4357/ad1038/pdf
Lateral motions of spicules serve as vital indicators of transverse waves in the solar atmosphere, and their study is crucial for understanding the wave heating process of the corona. Recent observations have focused on "high-frequency" transverse waves (periods < 100 s), which have the potential to transport sufficient energy for coronal heating. These high-frequency spicule oscillations are distinct from granular motions, which have much longer time scales of 5-10 min. Instead, it is proposed that they are generated through the mode conversion from high-frequency longitudinal waves that arise from a shock steepening process. Therefore, these oscillations may not solely be produced by the horizontal buffeting motions of granulation but also by the leakage of p-mode oscillations. To investigate the contribution of p-modes, our study employs a two-dimensional magneto-convection simulation spanning from the upper convection zone to the corona. During the course of the simulation, we introduce a p-mode-like driver at the bottom boundary. We reveal a notable increase in the mean velocity amplitude of the transverse oscillations in spicules, ranging from 10% to 30%, and attribute this to the energy transfer from longitudinal to transverse waves. This effect results in an enhancement of the estimated energy flux by 30-80%.

Magnetic Tornado Properties: A Substantial Contribution to the Solar Coronal Heating via Efficient Energy Transfer

Hidetaka **Kuniyoshi**, Munehito Shoda, Haruhisa Iijima, Takaaki Yokoyama
ApJ **949** 8 **2023**
https://arxiv.org/pdf/2304.03010.pdf
https://iopscience.iop.org/article/10.3847/1538-4357/accbb8/pdf
In solving the solar coronal heating problem, it is crucial to comprehend the mechanisms by which energy is conveyed from the photosphere to the corona. Recently, magnetic tornadoes, characterized as coherent, rotating magnetic field structures extending from the photosphere to the corona, have drawn growing interest as a possible means of efficient energy transfer. Despite its acknowledged importance, the underlying physics of magnetic tornadoes remains still elusive. In this study, we conduct a three-dimensional radiative magnetohydrodynamic

simulation that encompasses the upper convective layer and extends into the corona, with a view to investigating how magnetic tornadoes are generated and efficiently transfer energy into the corona. We find that a single event of magnetic flux concentration merger on the photosphere gives rise to the formation of a single magnetic tornado. The Poynting flux transferred into the corona is found to be four times greater in the presence of the magnetic tornado, as compared to its absence. This increase is attributed to a reduction in energy loss in the chromosphere, resulting from the weakened magnetic energy cascade. Based on an evaluation of the fraction of the merging events, our results suggest that magnetic tornadoes contribute approximately 50% of the Poynting flux into the corona in regions where the coronal magnetic field strength is 10 G. Potentially, the contribution could be even greater in areas with a stronger coronal magnetic field.

Semi-empirical models of spicule from inversion of Ca II 8542 Å line

D. **Kuridze**, H. Socas-Navarro, J. Koza, R. Oliver

ApJ **908** 168 **2020**

https://arxiv.org/pdf/2012.03702.pdf

We study a solar spicule observed off-limb using high-resolution imaging spectroscopy in the Ca II 8542 Å line obtained with the CRisp Imaging SpectroPolarimeter (CRISP) on the Swedish 1-m Solar Telescope. Using a new version of the non-LTE code NICOLE specifically developed for this problem we invert the spicule single- and double-peak line profiles. This new version considers off-limb geometry and computes atomic populations by solving the 1D radiative transfer assuming a vertical stratification. The inversion proceeds by fitting the observed spectral profiles at 14 different heights with synthetic profiles computed in the model by solving the radiative transfer problem along its length. Motivated by the appearance of double-peak Ca II 8542 Å spicule profiles, which exhibit two distinct emission features well separated in wavelength, we adopt a double-component scenario. We start from the ansatz that the spicule parameters are practically constant along the spicule axis for each component, except for a density drop. Our results support this ansatz by attaining very good fits to the entire set of 14×4 profiles (14 heights and 4 times). We show that the double-component model with uniform temperature of 9560 K, exponential decrease of density with a height scale of 1000−2000 km, and the counter-oriented line-of-sight velocities of components reproduce the double-peak line profiles at all spicule segments well. Analyses of the numerical response function reveals the necessity of the inversions of spectra at multiple height positions to obtain height-dependent, degeneracy-free reliable model with a limited number of free parameters. **2018 June 22**

Kelvin-Helmholtz instability in solar chromospheric jets: theory and observation

D. **Kuridze**, T. V. Zaqarashvili, V. Henriques, M. Mathioudakis, F. P. Keenan, A. Hanslmeier

ApJ **2016**

http://arxiv.org/pdf/1608.01497v1.pdf

Using data obtained by the high resolution CRisp Imaging SpectroPolarimeter instrument on the Swedish 1-m Solar Telescope, we investigate the dynamics and stability of quiet-Sun chromospheric jets observed at disk center. Small-scale features, such as Rapid Redshifted and Blueshifted Excursions, appearing as high speed jets in the wings of the Hα line, are characterized by short lifetimes and rapid fading without any descending behavior. To study the theoretical aspects of their stability without considering their formation mechanism, we model chromospheric jets as twisted magnetic flux tubes moving along their axis, and use the ideal linear incompressible magnetohydrodynamic approximation to derive the governing dispersion equation. Analytical solutions of the dispersion equation indicate that this type of jet is unstable to Kelvin-Helmholtz instability (KHI), with a very short (few seconds) instability growth time at high upflow speeds. The generated vortices and unresolved turbulent flows associated with the KHI could be observed as broadening of chromospheric spectral lines. Analysis of the Hα line profiles shows that the detected structures have enhanced line widths with respect to the background. We also investigate the stability of a larger scale Hα jet that was ejected along the line-of-sight. Vortex-like features, rapidly developing around the jet's boundary, are considered as evidence of the KHI. The analysis of the energy equation in the partially ionized plasma shows that the ion-neutral collisions may lead to the fast heating of the KH vortices over timescales comparable to the lifetime of chromospheric jets.

The Dynamics of Rapid Redshifted and Blueshifted Excursions in the Solar Halpha line

D. **Kuridze**, V. Henriques, M. Mathioudakis, R. Erdélyi, T. V. Zaqarashvili, S. Shelyag, P. H. Keys, F. P. Keenan

ApJ **802** 26 **2015**

http://arxiv.org/pdf/1501.06205v1.pdf

We analyse high temporal and spatial resolution time-series of spectral scans of the Halpha line obtained with the CRisp Imaging SpectroPolarimeter (CRISP) instrument mounted on the Swedish Solar Telescope. The data reveal highly dynamic, dark, short-lived structures known as Rapid Redshifted and Blueshifted Excursions (RREs, RBEs) that are on-disk absorption features observed in the red and blue wings of spectral lines formed in the chromosphere. We study the dynamics of RREs and RBEs by tracking their evolution in space and time, measuring the speed of the

apparent motion, line-of-sight Doppler velocity, and transverse velocity of individual structures. A statistical study of their measured properties shows that RREs and RBEs have similar occurrence rates, lifetimes, lengths, and widths. They also display non-periodic, non-linear transverse motions perpendicular to their axes at speeds of 4 - 31 km/s. Furthermore, both types of structures either appear as high speed jets and blobs that are directed outwardly from a magnetic bright point with speeds of 50 - 150 km/s, or emerge within a few seconds. A study of the different velocity components suggests that the transverse motions along the line-of-sight of the chromospheric flux tubes are responsible for the formation and appearance of these redshifted/blueshifted structures. The short lifetime and fast disappearance of the RREs/RBEs suggests that, similar to type II spicules, they are rapidly heated to transition region or even coronal temperatures. We speculate that the Kelvin-Helmholtz instability triggered by observed transverse motions of these structures may be a viable mechanism for their heating.

The rotation rate of solar active and ephemeral regions – II. Temporal variations of the rotation rates

Alexander S **Kutsenko**, Valentina I Abramenko, Daria V Litvishko
MNRAS Volume 519, Issue 4, March **2023**, Pages 5315–5323,
https://doi.org/10.1093/mnras/stac3826
Systematic studies of the rotation rate of sunspot groups using white light images yield controversial results on the variations of the rotation rate: sunspot groups were found to either accelerate or decelerate systematically. This disagreement might be related to shortcomings of the method used to probe the rotation rate of sunspot groups. In contrast to previous works, in this study we use magnetic field maps to analyse the variations of the rotation rate of active regions. We found that an active region may exhibit either acceleration or deceleration during the emergence, while the rotation rate remains almost unchanged during decay. Hence, we suppose that there is no systematic geometrical inclination to the radial direction of the apex of the subsurface magnetic flux loop forming an active region. A thorough comparison of the rotation rate of unipolar and bi/multipolar active regions revealed no significant changes in the rotation rate of decaying active regions. In contrast to previous works, we presume the rotation rate to remain constant (within the expected uncertainties) during the evolution of an active region after emergence.

The rotation rate of solar active and ephemeral regions – I. Dependence on morphology and peak magnetic flux

Alexander S **Kutsenko**
Monthly Notices of the Royal Astronomical Society, Volume 500, Issue 4, February **2021**, Pages 5159–5166,
https://doi.org/10.1093/mnras/staa3616
Using magnetic field maps acquired by the Helioseismic and Magnetic Imager on board the Solar Dynamics Observatory, we measured rotation rates of 864 active and 322 ephemeral regions observed between 2010 and 2016. We found smaller magnetic tracers to show a tendency to rotate faster as compared to larger ones. Thus, ephemeral regions exhibit on average the fastest rotation rate. We further divided active regions into three classes. Class A comprised magnetic bipoles obeying Hale's polarity law, Joy's law, and exhibiting more coherent leading polarity in comparison with the following one. The second class B included active regions violating at least one of the aforementioned empirical laws. The third class U comprised unipolar active regions. We found no significant difference between the rotation rates of active regions of classes A and B. In contrast, unipolar active regions exhibited on average lower rotation rate and narrower distribution of the rotation rate differences. Assuming the rotation rate to indicate the anchoring depth of the magnetic structure within the convection zone, we supposed that active regions of classes A and B might be anchored throughout the entire convective envelope while unipolar active regions a rooted within a thin layer located either near the base of the convection zone or at a shallow near-surface depth.

Intermittency spectra of current helicity in solar active regions

A. S. **Kutsenko**, V. I. Abramenko, K. M. Kuzanyan, Haiqing Xu, Hongqi Zhang
MNRAS **2018**
https://arxiv.org/pdf/1802.02323.pdf
We intend to analyse the intermittency spectra of current helicity in solar active regions. We made a pixel-by-pixel comparison of current helicity maps derived from three different instruments, namely by Helioseismic and Magnetc Imager on board the Solar Dynamics Observatory (SDO/HMI), Spectro-Polarimeter on board the Hinode, and Solar Magnetic Field Telescope at the Huairou Solar Observing Station, China (HSOS/SMFT). The comparison showed an excellent correlation between the maps derived from the spaceborne instruments and moderate correlation between the maps derived from SDO/HMI and HSOS/SMFT vector magnetograms. The results suggest that the obtained maps characterize real spatial distribution of current helicity over an active region. To analyse the multifractality and intermittency of current helicity, we traditionally use the high-order structure function and flatness function approach. The slope of a flatness function within some range of scales - the flatness exponent - is a

measure of the degree of intermittency. We used SDO/HMI vector magnetograms to calculate the flatness exponent variations of current helicity of three active regions: NOAA 11158, 12494, and 12673. The flatness exponents were determined within the scale range of 2-10 Mm. All three regions exhibited emergence of a new magnetic flux during the observational interval. Interestingly, the flatness exponent increased rapidly 12-20 hours before the emergence of a new flux and restored its previous value by the beginning of the emergence. We suppose that this behaviour can be explained by subphotospheric fragmentation or distortion of the existed current system by emerging magnetic flux. During the imperturbable development of active region, the flatness exponent of current helicity remains relatively low and the intermittency range shifts toward higher values up to 20-40 Mm. **2011.02.12-17, 2015.01.19, 2016.02.03-08, 2017.09.01-05**

Estimates of current helicity and tilt of solar active regions and Joy's law

K. **Kuzanyan**, N. Kleeorin, I. Rogachevskii, D. Sokoloff, H. Zhang
Geomagnetism and Aeronomy **2020**
https://arxiv.org/pdf/2006.10197.pdf
The tilt angle, current helicity and twist of solar magnetic fields can be observed in solar active regions. We carried out estimates of these parameters by two ways. Firstly, we consider the model of turbulent convective cells (super-granules) which have a loop floating structure towards the surface of the Sun. Their helical properties are attained during the rising process in the rotating stratified convective zone. The other estimate is obtained from a simple mean-field dynamo model that accounts magnetic helicity conservation. The both values are shown to be capable to give important contributions to the observable tilt, helicity and twist.

Large Scale Properties of Tilt of Sunspot Groups and Joy's Law Near The Solar Equator

K.M. **Kuzanyan**, N. Safiullin, N. Kleeorin, I. Rogachevskii, S. Porshnev
Astrophysics[Armenia] **2019**
https://arxiv.org/ftp/arxiv/papers/1810/1810.05200.pdf
https://arxiv.org/abs/1810.05200
We present a physical mechanism of formation of tilt angles of sunspots due to the process of formation of active regions below the solar photosphere. The contribution of Coriolis force factors on large-scale flows of super-granular convection in turbulent media has been investigated in details. On the basis of earlier works by Kleeorin et al. (2016) and Safiullin et al. (2018) we give physical estimates of orders of magnitude of the effect and estimate the tilt angles near the solar equator, in the "Royal" zone of solar activity. The above model is based on the balance of the small-scale and large scale magnetic helicities and describes in details the sunspot formation process over the last five solar cycles (since 1964). We adopt this model for a wider class of manifestations of solar activity. We present latitudinal dependence of the mean tilt on these five solar cycles and time-latitudinal diagrams over a limited range of latitudes and phases of the solar cycle.

The TESIS experiment on the CORONAS-PHOTON spacecraft<<<

S. V. **Kuzin**, I. A. Zhitnik, S. V. Shestov, S. A. Bogachev, O. I. Bugaenko, A. P. Ignat'ev, A. A. Pertsov, A. S. Ulyanov, A. A. Reva, V. A. Slemzin, N. K. Sukhodrev, Yu. S. Ivanov, L. A. Goncharov, A. V. Mitrofanov, S. G. Popov, T. A. Shergina, V. A. Solov'ev, S. N. Oparin & A. M. Zykov
Solar System Research, 42(2), **2011**

Processing method of images obtained during the TESIS/CORONAS-PHOTON experiment

S. V. **Kuzin**, S. V. Shestov, S. A. Bogachev, A. A. Pertsov, A. S. Ulyanov & A. A. Reva
Solar System Research, 42(2), **2011**

3D numerical simulations of propagating two-fluid, torsional Alfvén waves and heating of a partially-ionized solar chromosphere

B. **Kuźma**, K. Murawski, S. Poedts
MNRAS Volume 506, Issue 1, September **2021**, Pages 989–996,
https://doi.org/10.1093/mnras/stab1780
https://arxiv.org/pdf/2106.10537.pdf
We present a new insight into the propagation, attenuation and dissipation of two-fluid, torsional Alfvén waves in the context of heating of the lower solar atmosphere. By means of numerical simulations of the partially-ionized plasma, we solve the set of two-fluid equations for ion plus electron and neutral fluids in three-dimensional (3D) Cartesian geometry. We implement initially a current-free magnetic field configuration, corresponding to a magnetic flux-tube that is rooted in the solar photosphere and expands into the chromosphere and corona. We put the lower

boundary of our simulation region in the low chromosphere, where ions and neutrals begin to decouple, and implement there a monochromatic driver that directly generates Alfvén waves with a wave period of 30 s. As the ion-neutral drift increases with height, the two-fluid effects become more significant and the energy carried by both Alfvén and magneto-acoustic waves can be thermalized in the process of ion-neutral collisions there. In fact, we observe a significant increase in plasma temperature along the magnetic flux-tube. In conclusion, the two-fluid torsional Alfvén waves can potentially play a role in the heating of the solar chromosphere.

Spatial variation of periods of ion and neutral waves in a solar magnetic arcade

Błażej **Kuźma**, Kris Murawski, Zdzisław E. Musielak, Stefaan Poedts, Dariusz Wójcik
A&A 652, A88 **2021**
https://arxiv.org/pdf/2105.09882.pdf
https://doi.org/10.1051/0004-6361/202038003
https://www.aanda.org/articles/aa/pdf/2021/08/aa38003-20.pdf
We present a new insight into the propagation of ion magnetoacoustic and neutral acoustic waves in a magnetic arcade in the lower solar atmosphere. By means of numerical simulations, we aim to: (a) study two-fluid waves propagating in a magnetic arcade embedded in the partially-ionized, lower solar atmosphere; and (b) investigate the impact of the background magnetic field configuration on the observed wave-periods. We consider a 2D approximation of the gravitationally stratified and partially-ionized lower solar atmosphere consisting of ion+electron and neutral fluids that are coupled by ion-neutral collisions. In this model, the convection below the photosphere is responsible for the excitation of ion magnetoacoustic-gravity and neutral acoustic-gravity waves. We find that in the solar photosphere, where ions and neutrals are strongly coupled by collisions, ion magnetoacoustic-gravity and neutral acoustic-gravity waves have periods ranging from 250 s to 350 s. In the chromosphere, where the collisional coupling is weak, the wave characteristics strongly depend on the magnetic field configuration. Above the foot-points of the considered arcade, the plasma is dominated by a vertical magnetic field along which ion magnetoacoustic-gravity waves propagate. These waves exhibit a broad range of periods with the most prominent periods of 180 s, 220 s, and 300 s. Above the main loop of the solar arcade, where mostly horizontal magnetic field lines guide ion magnetoacoustic-gravity waves, the main spectral power reduces to the period of about 180 s and longer wave-periods do not exist. Our results are in agreement with the recent observational data reported by Wiśniewska et al. (2016) and Kayshap et al. (2018).

Numerical simulations of the lower solar atmosphere heating by two-fluid nonlinear Alfvén waves

B. **Kuźma**1, D. Wójcik1, K. Murawski1, D. Yuan2 and S. Poedts3,1
A&A 639, A45 (**2020**)
https://www.aanda.org/articles/aa/pdf/2020/07/aa37260-19.pdf
Context. We present new insight into the long-standing problem of plasma heating in the lower solar atmosphere in terms of collisional dissipation caused by two-fluid Alfvén waves.
Aims. Using numerical simulations, we study Alfvén wave propagation and dissipation in a magnetic flux tube and their heating effect.
Methods. We set up 2.5-dimensional numerical simulations with a semi-empirical model of a stratified solar atmosphere and a force-free magnetic field mimicking a magnetic flux tube. We consider a partially ionized plasma consisting of ion + electron and neutral fluids, which are coupled by ion-neutral collisions.
Results. We find that Alfvén waves, which are directly generated by a monochromatic driver at the bottom of the photosphere, experience strong damping. Low-amplitude waves do not thermalize sufficient wave energy to heat the solar atmospheric plasma. However, Alfvén waves with amplitudes greater than 0.1 km s−1 drive through ponderomotive force magneto-acoustic waves in higher atmospheric layers. These waves are damped by ion-neutral collisions, and the thermal energy released in this process leads to heating of the upper photosphere and the chromosphere.
Conclusions. We infer that, as a result of ion-neutral collisions, the energy carried initially by Alfvén waves is thermalized in the upper photosphere and the chromosphere, and the corresponding heating rate is large enough to compensate radiative and thermal-conduction energy losses therein.

Heating of a Quiet Region of the Solar Chromosphere by Ion and Neutral Acoustic Waves

B. **Kuźma**, D. Wójcik, K. Murawski
2019 *ApJ* **878** 81
https://arxiv.org/pdf/1906.01746.pdf
Using high-resolution numerical simulations we investigate the plasma heating driven by periodic two-fluid acoustic waves that originate at the bottom of the photosphere and propagate into the gravitationally stratified and partially ionized solar atmosphere. We consider ions+electrons and neutrals as separate fluids that interact between themselves via collision forces. The latter play an important role in the chromosphere, leading to significant

damping of short-period waves. Long-period waves do not essentially alter the photospheric temperatures, but they exhibit the capability of depositing a part of their energy in the chromosphere. This results in up about a five times increase of ion temperature that takes place there on a time-scale of a few minutes. The most effective heating corresponds to waveperiods within the range of about 30-200 s with a peak value located at 80 s. However, we conclude that for the amplitude of the driver chosen to be equal to 0.1 km s−1, this heating is too low to balance the radiative losses in the chromosphere.

Numerical Simulations of Transverse Oscillations of a Finely Structured Solar Flux Tube

Błażej **Kuźma** and Kris Murawski
2018 ApJ 866 50
https://doi.org/10.3847/1538-4357/aadd00
In the light of recent CRISP/SST observations we aim to study transverse oscillations of a finely structured flux tube. With the use of PLUTO code, we numerically solve ideal magnetohydrodynamic equations in three-dimensional Cartesian geometry. With a pressure signal we generate a finely structured magnetic flux tube that consists of a central strand and four off-central strands. This flux tube is perturbed by a periodic driver in the azimuthal component of velocity. This driver results in transverse oscillations that propagate upward along these strands. The central strand experiences torsional Alfvén waves, while the off-central strands exhibit fast magnetoacoustic kink oscillations. The latter are guided by the off-central strands, which are regions of depression in Alfvén speed.

Two-fluid Numerical Simulations of Solar Spicules

Błażej **Kuźma**1, Kris Murawski1, Pradeep Kayshap1, Darek Wójcik1, Abhishek Kumar Srivastava2, and Bhola N. Dwivedi2
2017 ApJ 849 78
https://arxiv.org/pdf/1711.01383.pdf
We aim to study the formation and evolution of solar spicules by means of numerical simulations of the solar atmosphere. With the use of newly developed JOANNA code, we numerically solve two-fluid (for ions + electrons and neutrals) equations in 2D Cartesian geometry. We follow the evolution of a spicule triggered by the time-dependent signal in ion and neutral components of gas pressure launched in the upper chromosphere. We use the potential magnetic field, which evolves self-consistently, but mainly plays a passive role in the dynamics. Our numerical results reveal that the signal is steepened into a shock that propagates upward into the corona. The chromospheric cold and dense plasma lags behind this shock and rises into the corona with a mean speed of 20–25 km s−1. The formed spicule exhibits the upflow/downfall of plasma during its total lifetime of around 3–4 minutes, and it follows the typical characteristics of a classical spicule, which is modeled by magnetohydrodynamics. The simulated spicule consists of a dense and cold core that is dominated by neutrals. The general dynamics of ion and neutral spicules are very similar to each other. Minor differences in those dynamics result in different widths of both spicules with increasing rarefaction of the ion spicule in time.

Numerical simulations of solar spicules: Adiabatic and non-adiabatic studies

B. **Kuźma** , K. Murawski, T.V. Zaqarashvili, P. Konkol, and A. Mignone
A&A 597, A133 (**2017**)
http://kft.umcs.lublin.pl/kmur/download/papers/2016/spicule_non-adiab_2016.pdf
Aims. We aim to study the formation and evolution of solar spicules using numerical simulations of vertical velocity pulse launched from upper chromosphere.
Methods. With the use of the PLUTO code we numerically solve adiabatic and non-adiabatic magnetohydrodynamic (MHD) equations in 2D cylindrical geometry. We follow the evolution of spicules triggered by pulses in a vertical component of velocity in the upper chromosphere. Then we compare the results obtained with and without non-adiabatic terms in the MHD equations.
Results. Our numerical results reveal that the velocity pulse is steepened into a shock which propagates upwards into the corona.The chromospheric cold and dense plasma follows the shock and rises into the corona with the mean speed of 20-25 km s-1. The nonlinear wake behind the pulse in the stratified atmosphere leads to quasi-periodic rebound shocks, which lead to quasi-periodic rising of chromospheric plasma into the corona with the period close to the acoustic cut-off period of the chromosphere. We found that the effect of non-adiabatic terms on spicule evolution is minor; the general properties of spicules such as their heights and rising-time remain slightly affected by these terms.
Conclusions. In the framework of the axisymmetric model we devised, we show that the solar spicules can be triggered by the vertical velocity pulses and the thermal conduction and radiative cooling terms do not exert any significant influence on the dynamics of these spicules.

Empirical model of long-time variations of galactic cosmic ray particle fluxes

N. V. **Kuznetsov**, H. Popova and M. I. Panasyuk
JGR (pages 1463–1472) **2017** DOI: 10.1002/2016JA022920
The GCR particle flux model is developed by using a wide range of experimental data obtained during the 21–24 solar cycles
GCR proton fluxes in interplanetary space depending on calendar time are calculated and discussed for 25th and 26th predicted solar cycles
This forecast indicates a continuing trend of solar activity reduction starting since the 23rd solar cycle

Solar and heliospheric space missions **Review**

V.D. **Kuznetsov**
Advances in Space Research, Volume 55, Issue 3, 1 February **2015**, Pages 879–885
http://www.sciencedirect.com/science/article/pii/S0273117714004906
The paper provides a review of the state of the art and prospects of space research in heliophysics, in which a pivotal role belongs to magnetic measurements in the Sun and heliosphere. New space missions, such as the Interhelioprobe, Solar Orbiter, Solar Probe Plus, etc., will follow the currently operating ones (Hinode, SDO, STEREO, etc.) to observe the Sun from short distances and from out-of-ecliptic positions, as well as to conduct in situ measurements in the vicinity of the Sun and outside the ecliptic. The planned coordinated observations within the framework of these missions will allow us to explore the structure and dynamics of magnetic fields in the polar regions of the Sun, to study the mechanisms of the solar dynamo and solar cycle, to gain a deeper insight into the process of corona heating and acceleration of the solar wind, and to get a response to a number of other pressing issues of heliophysics.

The Coronas-F Space Mission **Book**

Key Results for Solar Terrestrial Physics
V.D. **Kuznetsov**
Springer-Verlag Berlin Heidelberg **2014**
https://link.springer.com/content/pdf/10.1007%2F978-3-642-39268-9.pdf

Results of solar observations by the CORONAS-F payload

V.D. **Kuznetsov** a,⇑, I.I. Sobelman b, I.A. Zhitnik b, S.V. Kuzin b, Yu.D. Kotov c,
Yu.E. Charikov d, S.N. Kuznetsov e, E.P. Mazets d, A.A. Nusinov f,
A.M. Pankov g, J. Sylwester
Advances in Space Research 47 (**2011**) 1538–1543
The CORONAS-F mission experiments and results have been reviewed. The observations with the DIFOS multi-channel photometer in a broad spectral range from 350 to 1500 nm have revealed the dependence of the relative amplitudes of p-modes of the global solar oscillations on the wavelength that agrees perfectly well with the earlier data obtained in a narrower spectral ranges. The SPIRIT EUV observations have enabled the study of various manifestations of solar activity and high-temperature events on the Sun. The data from the X-ray spectrometer RESIK, gamma spectrometer HELICON, flare spectrometer IRIS, amplitude–temporal spectrometer AVS-F, and X-ray spectrometer RPS-1 have been used to analyze the X- and gamma-ray emission from solar flares and for diagnostics of the flaring plasma. The absolute and relative content of various elements (such as potassium, argon, and sulfur) of solar plasma in flares has been determined for the first time with the X-ray spectrometer RESIK. The Solar Cosmic Ray Complex monitored the solar flare effects in the Earth's environment. The UV emission variations recorded during solar flares in the vicinity of the 120-nm wavelength have been analyzed and the amplitude of relative variations has been determined.

Spectroscopic Detection of Alfvénic Waves in the Chromospheric Fibrils of a Solar-quiet Region

Hannah **Kwak**1, Jongchul Chae2, Eun-Kyung Lim1, Kyoung-Sun Lee2, Donguk Song1,3, and Heesu Yang1
2023 ApJ 958 131
https://iopscience.iop.org/article/10.3847/1538-4357/ad06b5/pdf
We report the detection of transverse magnetohydrodynamic waves, also known as Alfvénic waves, in the chromospheric fibrils of a solar-quiet region. Unlike previous studies that measured transversal displacements of fibrils in imaging data, we investigate the line-of-sight (LOS) velocity oscillations of the fibrils in spectral data. The observations were carried out with the Fast Imaging Solar Spectrograph of the 1.6 m Goode Solar Telescope at the

Big Bear Solar Observatory. By applying spectral inversion to the Hα and Ca ii 8542 Å line profiles, we determine various physical parameters, including the LOS velocity in the chromosphere of the quiet Sun. In the Hα data, we select two adjacent points along the fibrils and analyze the LOS velocities at those points. For the time series of the velocities that show high cross-correlation between the two points and do not exhibit any correlation with intensity, we interpret them as propagating Alfvénic wave packets. We identify a total of 385 Alfvénic wave packets in the quiet-Sun fibrils. The mean values of the period, velocity amplitude, and propagation speed are 7.5 minutes, 1.33 km s−1, and 123 km s−1, respectively. We find that the detected waves are classified into three groups based on their periods, namely, 3, 5, and 10 minute bands. Each group of waves exhibits distinct wave properties, indicating a possible connection to their generation mechanism. Based on our results, we expect that the identification of Alfvénic waves in various regions will provide clues to their origin and the underlying physical processes in the solar atmosphere. **2020 July 30**

Impulsive wave excitation by rapidly changing granules

Hannah **Kwak**, Jongchul Chae, Maria S. Madjarska, Kyuhyoun Cho, Donguk Song
A&A 642, A154 **2020**
https://arxiv.org/pdf/2008.12779.pdf
https://doi.org/10.1051/0004-6361/202038288
It is not yet fully understood how magnetohydrodynamic waves in the interior and atmosphere of the Sun are excited. Traditionally, turbulent convection in the interior is considered to be the source of wave excitation in the quiet Sun. Over the last few decades, acoustic events observed in the intergranular lanes in the photosphere have emerged as a strong candidate for a wave excitation source. Here we report our observations of wave excitation by a new type of event: rapidly changing granules. Our observations were carried out with the Fast Imaging Solar Spectrograph in the Hα and Ca II 8542 Å lines and the TiO 7057 Å broadband filter imager of the 1.6 m Goode Solar Telescope at the Big Bear Solar Observatory. We identify granules in the internetwork region that undergo rapid dynamic changes such as collapse (event 1), fragmentation (event 2), or submergence (event 3). In the photospheric images, these granules become significantly darker than neighboring granules. Following the granules' rapid changes, transient oscillations are detected in the photospheric and chromospheric layers. In the case of event 1, the dominant period of the oscillations is close to 4.2 min in the photosphere and 3.8 min in the chromosphere. Moreover, in the Ca II−0.5 Å raster image, we observe repetitive brightenings in the location of the rapidly changing granules that are considered the manifestation of shock waves. Based on our results, we suggest that dynamic changes of granules can generate upward-propagating acoustic waves in the quiet Sun that ultimately develop into shocks. **June 14, 2017**

Oscillatory Response of the Solar Chromosphere to a Strong Downflow above a Sunspot

Hannah **Kwak**, Jongchul Chae, Donguk Song, Yeon-Han Kim, Eun-Kyung Lim, Maria S. Madjarska
ApJ Letters **821** L30 **2016**
http://arxiv.org/pdf/1604.02252v1.pdf
We report three-minute oscillations in the solar chromosphere driven by a strong downflow event in a sunspot. We used the Fast Imaging Solar Spectrograph of the 1.6 m New Solar Telescope and the Interface Region Imaging Spectrograph (IRIS). The strong downflow event is identified in the chromospheric and transition region lines above the sunspot umbra. After the event, oscillations occur at the same region. The amplitude of the Doppler velocity oscillations is 2 km/s, and gradually decreases with time. In addition, the period of the oscillations gradually increases from 2.7 minutes to 3.3 minutes. In the IRIS 1330 slit-jaw images, we identify a transient brightening near the footpoint of the downflow detected in the Ha+0.5A image. The characteristics of the downflowing material are consistent with those of sunspot plumes. Based on our findings, we suggest that the gravitationally stratified atmosphere came to oscillate with three minute period in response to the impulsive downflow event as was theoretically investigated by Chae & Goode(2015). **2014 September 27**

A Dynamo-based Forecast of Solar Cycle 25

Francois **Labonville**, Paul Charbonneau, Alexandre Lemerle
Solar Physics June **2019**, 294:82
sci-hub.se/10.1007/s11207-019-1480-0
We present a data-driven version of the solar cycle model of Lemerle and Charbonneau (Astrophys. J.834, 133; 2017), which we use to forecast properties of the upcoming sunspot Cycle 25. The two free parameters of the model are fixed by requiring the model to reproduce Cycle 24 upon being driven by active region data for Cycle 23. Our forecasting model incorporates self-consistently the expected fluctuations associated with stochastic variations in properties of emerging active regions, most notably the scatter in the tilt angle of the line segment joining the opposite polarity focii of bipolar magnetic regions, as embodied in Joy's law. By carrying out ensemble forecasts with statistically independent realizations of active region parameters, we can produce error bars that capture the impact of this physical source of fluctuations. We forecast a smoothed monthly international sunspot number (version 2.0) peaking at 89+29−1489−14+29 in year 2025.3+0.89−1.052025.3−1.05+0.89, with a 6 month onset delay in the northern hemisphere, but a peak amplitude 20% higher than in the southern hemisphere.

Radiative transfer in cylindrical threads with incident radiation VII. Multi-thread models

N. **Labrosse** and A.S. Rodger

A&A **2016**

http://arxiv.org/pdf/1601.02392v1.pdf

We solved the radiative transfer and statistical equilibrium equations in a two-dimensional cross-section of a cylindrical structure oriented horizontally and lying above the solar surface. The cylinder is filled with a mixture of hydrogen and helium and is illuminated at a given altitude from the solar disc. We constructed simple models made from a single thread or from an ensemble of several threads along the line of sight. This first use of two-dimensional, multi-thread fine structure modelling combining hydrogen and helium radiative transfer allowed us to compute synthetic emergent spectra from cylindrical structures and to study the effect of line-of-sight integration of an ensemble of threads under a range of physical conditions. We analysed the effects of variations in temperature distribution and in gas pressure. We considered the effect of multi-thread structures within a given field of view and the effect of peculiar velocities between the structures in a multi-thread model. We compared these new models to the single thread model and tested them with varying parameters. These new computations show, for the first time, the effect of integrating the radiation emitted in H and He lines by several cylindrical threads that are static or moving along the line of sight. They can be used to interpret high-spatial and spectral resolutions of cylindrical structures found in the solar atmosphere, such as cool coronal loops or prominence threads.

An Explanation of Remarkable Emission-line Profiles in Post-flare Coronal Rain

Daniela A. **Lacatus**1, Philip G. Judge2, and Alina Donea

2017 ApJ 842 15

http://sci-hub.cc/10.3847/1538-4357/aa725d

We study broad redshifted emission in chromospheric and transition region lines that appears to correspond to a form of post-flare coronal rain. Profiles of Mg ii, C ii, and Si iv lines were obtained using IRIS before, during, and after the X2.1 flare of **2015 March 11** (SOL2015-03-11T16:22). We analyze the profiles of the five transitions of Mg ii (the h and k transitions, and three lines belonging to the transitions). We use analytical methods to understand the unusual profiles, together with higher-resolution observational data of similar phenomena observed by Jing et al. The peculiar line ratios indicate anisotropic emission from the strands that have cross-strand line center optical depths (k line) of between 1 and 10. The lines are broadened by unresolved Alfvénic motions whose energy exceeds the radiation losses in the Mg ii lines by an order of magnitude. The decay of the line widths is accompanied by a decay in the brightness, suggesting a causal connection. If the plasma is 99% ionized, ion–neutral collisions can account for the dissipation; otherwise, a dynamical process seems necessary. Our work implies that the motions are initiated during the impulsive phase, to be dissipated as radiation over a period of an hour, predominantly by strong chromospheric lines. The coronal "rain" we observe is far more turbulent than most earlier reports have indicated, with implications for plasma heating mechanisms.

Probing deep photospheric layers of the quiet Sun with high magnetic sensitivity

A. **Lagg**, S. K. Solanki, H.-P. Doerr, M. J.Martínez González, T. Riethmüller, M. Collados Vera, R. Schlichenmaier, D. Orozco Suárez, M. Franz, A. Feller, C. Kuckein, W. Schmidt, A. Asensio Ramos, A. Pastor Yabar, O. von der Lühe, C. Denker, H. Balthasar, R. Volkmer, J. Staude, A. Hofmann, K. Strassmeier, F. Kneer, T. Waldmann, J. M. Borrero, M. Sobotka, M. Verma, R. E. Louis, R. Rezaei, D. Soltau, T. Berkefeld, M. Sigwarth, D. Schmidt, C. Kiess, H. Nicklas

A&A **2016**

http://arxiv.org/pdf/1605.06324v1.pdf

Context. Investigations of the magnetism of the quiet Sun are hindered by extremely weak polarization signals in Fraunhofer spectral lines. Photon noise, straylight, and the systematically different sensitivity of the Zeeman effect to longitudinal and transversal magnetic fields result in controversial results in terms of the strength and angular distribution of the magnetic field vector.

Aims. The information content of Stokes measurements close to the diffraction limit of the 1.5 m GREGOR telescope is analyzed. We took the effects of spatial straylight and photon noise into account.

Methods. Highly sensitive full Stokes measurements of a quiet-Sun region at disk center in the deep photospheric Fe I lines in the 1.56 {\mu}m region were obtained with the infrared spectropolarimeter GRIS at the GREGOR telescope. Noise statistics and Stokes V asymmetries were analyzed and compared to a similar data set of the Hinode spectropolarimeter (SOT/SP). Simple diagnostics based directly on the shape and strength of the profiles were applied to the GRIS data. We made use of the magnetic line ratio technique, which was tested against MHD simulations.

Results. About 80% of the GRIS spectra of a very quiet solar region show polarimetric signals above a 3{\sigma} level. Area and amplitude asymmetries agree well with small-scale surface dynamo MHD simulations. The

magnetic line ratio analysis reveals ubiquitous magnetic regions in the ten to hundred Gauss range with some concentrations of kilo-Gauss fields.
Conclusions. The GRIS spectropolarimetric data at a spatial resolution of 0.40" are so far unique in the combination of high spatial resolution scans and high magnetic field sensitivity. Nevertheless, the unavoidable effect of spatial straylight and the resulting dilution of the weak Stokes profiles means that inversion techniques still bear a high risk of misinterpretating the data.

Effect of Radiation on Chromospheric Magnetic Reconnection: Reactive and Collisional Multi-fluid Simulations

A. Alvarez **Laguna**1,2, A. Lani2, N. N. Mansour3, H. Deconinck2, and S. Poedts
2017 ApJ 842 117
We study magnetic reconnection under chromospheric conditions in five different ionization levels from 0.5% to 50% using a self-consistent two-fluid (ions + neutrals) model that accounts for compressibility, collisional effects, chemical inequilibrium, and anisotropic heat conduction. Results with and without radiation are compared, using two models for the radiative losses: an optically thin radiation loss function, and an approximation of the radiative losses of a plasma with photospheric abundances. The results without radiation show that reconnection occurs faster for the weakly ionized cases as a result of the effect of ambipolar diffusion and fast recombination. The tearing mode instability appears earlier in the low ionized cases and grows rapidly. We find that radiative losses have a stronger effect than was found in previous results as the cooling changes the plasma pressure and the concentration of ions inside the current sheet. This affects the ambipolar diffusion and the chemical equilibrium, resulting in thin current sheets and enhanced reconnection. The results quantify this complex nonlinear interaction by showing that a strong cooling produces faster reconnections than have been found in models without radiation. The results accounting for radiation show timescales and outflows comparable to spicules and chromospheric jets.

The magnetically quiet solar surface dominates HARPS-N solar RVs during low activity

Ben S. **Lakeland**, Tim Naylor, Raphaëlle Haywood, Nadège Meunier, +++
MNRAS **2023**
https://arxiv.org/pdf/2311.16076.pdf
Using images from the Helioseismic and Magnetic Imager aboard the \textit{Solar Dynamics Observatory} (SDO/HMI), we extract the radial-velocity (RV) signal arising from the suppression of convective blue-shift and from bright faculae and dark sunspots transiting the rotating solar disc. We remove these rotationally modulated magnetic-activity contributions from simultaneous radial velocities observed by the HARPS-N solar feed to produce a radial-velocity time series arising from the magnetically quiet solar surface (the 'inactive-region radial velocities'). We find that the level of variability in the inactive-region radial velocities remains constant over the almost 7 year baseline and shows no correlation with well-known activity indicators. With an RMS of roughly 1 m/s, the inactive-region radial-velocity time series dominates the total RV variability budget during the decline of solar cycle 24. Finally, we compare the variability amplitude and timescale of the inactive-region radial velocities with simulations of supergranulation. We find consistency between the inactive-region radial-velocity and simulated time series, indicating that supergranulation is a significant contribution to the overall solar radial velocity variability, and may be the main source of variability towards solar minimum. This work highlights supergranulation as a key barrier to detecting Earth twins.

Measurements of Solar Differential Rotation and Meridional Circulation from Tracking of Photospheric Magnetic Features

Derek A. **Lamb**
ApJ **836** 10 **2017**
https://arxiv.org/pdf/1701.02723v1.pdf
Long-lived rotational and meridional flows are important ingredients of the solar cycle. Magnetic field images have typically been used to measure these flows on the solar surface by cross-correlating thin longitudinal strips or square patches across sufficiently long time gaps. Here, I use one month of SDO/HMI line-of-sight magnetic field observations, combined with the SWAMIS magnetic feature tracking algorithm to measure the motion of individual features in these magnetograms. By controlling for perturbations due to short-lived flows and due to false motions from feature interactions, I effectively isolate the long-lived flows traced by the magnetic features. This allows me to produce high-fidelity differential rotation measurements with well-characterized variances and covariances of the fit parameters.I find a sidereal rotational profile of $(14.296\pm0.006)+(-1.847\pm0.056)\sin2b+(-2.615\pm0.093)\sin4b$, with units of deg d$-1$, and a large covariance $\sigma 2BC=-4.87\times10-3(\text{ deg d}-1)2$. I also produce medium-fidelity measurements of the much weaker meridional flow that is broadly consistent with previous results. This measurement shows a peak flow of 16.7 ± 0.6 m s-1 at latitude $b=45\circ$ but is insufficiently characterized at higher latitudes to ascertain whether the chosen functional form 2cosbsinb is appropriate. This work shows that measuring the motions of individual features in photospheric magnetograms can produce high precision results in relatively short time spans, and suggests that high resolution non-longitudinally averaged photospheric velocity residual

measurements could be produced to compare with coronal results, and to provide other diagnostics of the solar dynamo.
HMI Science Nuggets #69, **2017** http://hmi.stanford.edu/hminuggets/?p=1918

The FIP and Inverse FIP Effects in Solar Flares

J. Martin **Laming**
ApJ **2021**
https://arxiv.org/pdf/2101.03038.pdf
The Inverse First Ionization Potential (FIP) Effect, the depletion in coronal abundance of elements like Fe, Mg, and Si that are ionized in the solar chromosphere relative to those that are neutral, has been identified in several solar flares. We give a more detailed discussion of the mechanism of fractionation by the ponderomotive force associated with magnetohydrodynamic waves, paying special attention to the conditions in which Inverse FIP fractionation arises in order to better understand its relation to the usual FIP Effect, i.e. the enhancement of coronal abundance of Fe, Mg, Si, etc. The FIP Effect is generated by parallel propagating Alfvén waves, with either photospheric, or more likely coronal, origins. The Inverse FIP Effect arises as upward propagating fast mode waves with an origin in the photosphere or below, refract back downwards in the chromosphere where the Alfvén speed is increasing with altitude. We give a more physically motivated picture of the FIP fractionation, based on the wave refraction around inhomogeneities in the solar atmosphere, and inspired by previous discussions of analogous phenomena in the optical trapping of particles by laser beams. We apply these insights to modeling the fractionation and find good agreement with the observations of Katsuda et al. (2020; arXiv:2001.10643) and Dennis et al. (2015; arXiv:1503.01602).

Element Abundances: A New Diagnostic for the Solar Wind

J. Martin **Laming**, Angelos Vourlidas, Clarence Korendyke, Damien Chua, Steven R. Cranmer, Yuan-Kuen Ko, Natsuha Kuroda, Elena Provornikova, John C. Raymond, Nour-Eddine Raouafi, Leonard Strachan, Samuel Tun-Beltran, Micah Weberg, Brian E. Wood
ApJ **2019**
https://arxiv.org/pdf/1905.09319.pdf
We examine the different element abundances exhibited by the closed loop solar corona and the slow speed solar wind. Both are subject to the First Ionization Potential (FIP) Effect, the enhancement in coronal abundance of elements with FIP below 10 eV (e.g. Mg, Si, Fe) with respect to high FIP elements (e.g. O, Ne, Ar), but with subtle differences. Intermediate elements, S, P, and C, with FIP just above 10 eV, behave as high FIP elements in closed loops, but are fractionated more like low FIP elements in the solar wind. On the basis of FIP fractionation by the ponderomotive force in the chromosphere, we discuss fractionation scenarios where this difference might originate. Fractionation low in the chromosphere where hydrogen is neutral enhances the S, P and C abundances. This arises with nonresonant waves, which are ubiquitous in open field regions, and is also stronger with torsional Alfven waves, as opposed to shear (i.e. planar) waves. We discuss the bearing these findings have on models of interchange reconnection as the source of the slow speed solar wind. The outflowing solar wind must ultimately be a mixture of the plasma in the originally open and closed fields, and the proportions and degree of mixing should depend on details of the reconnection process. We also describe novel diagnostics in ultraviolet and extreme ultraviolet spectroscopy now available with these new insights, with the prospect of investigating slow speed solar wind origins and the contribution of interchange reconnection by remote sensing.

The First Ionization Potential Effect from the Ponderomotive Force: On the Polarization and Coronal Origin of Alfvén Waves

J. Martin **Laming**
2017 ApJ 844 153
We investigate in more detail the origin of chromospheric Alfvén waves that give rise to the separation of ions and neutrals—the first ionization potential (FIP) effect—through the action of the ponderomotive force. In open field regions, we model the dependence of fractionation on the plasma upflow velocity through the chromosphere for both shear (or planar) and torsional Alfvén waves of photospheric origin. These differ mainly in their parametric coupling to slow mode waves. Shear Alfvén waves appear to reproduce observed fractionations for a wider range of model parameters and present less of a "fine-tuning" problem than do torsional waves. In closed field regions, we study the fractionations produced by Alfvén waves with photospheric and coronal origins. Waves with a coronal origin, at or close to resonance with the coronal loop, offer a significantly better match to observed abundances than do photospheric waves, with shear and torsional waves in such a case giving essentially indistinguishable fractionations. Such coronal waves are likely the result of a nanoflare coronal heating mechanism that, as well as heating coronal plasmas, releases Alfvén waves that can travel down to loop footpoints and cause FIP fractionation through the ponderomotive force as they reflect from the chromosphere back into the corona.

Possible Estimation of the Solar Cycle Characteristic Parameters by the 10.7 cm Solar Radio Flux

George **Lampropoulos**, Helen Mavromichalaki, Vasilis Tritakis
Solar Phys. Volume 291, Issue 3, pp 989-1002 **2016**
http://cosray.phys.uoa.gr/publications/D108.pdf
Two independent methods for estimating basic parameters of the solar cycle are presented. The first of them, the ascending-descending triangle method, is based on a previous work by Tritakis (Astrophys. Space Sci. 82, 463, 1982), which described how the fundamental parameters of a certain solar cycle could be predicted from the shape of the previous one. The relation between the two cycles before and after a specific 11-year solar cycle is tighter than between the two cycles belonging to the same 22-year solar cycle (even-odd cycle). The second is the MinimaxX method, which uses a significant relation in the international sunspot number between the maximum value of a solar cycle and its value 2.5 or 3 years (depending on the enumeration of the even or odd cycle) before the preceding minimum. The tests applied to Cycles 12 to 24 indicate that both methods can estimate the peak of the 11-year solar radio flux at a high confidence level. The data used in this study are the 10.7 cm solar radio flux since 1947, which have been extrapolated back to 1848 from the strong correlation between the monthly international sunspot numbers and the adjusted values of the 10.7 cm radio flux.

Observation of the Solar F-corona from Space

Philippe **Lamy** (1), Hugo Gilardy (1), Antoine Llebaria (1)
2022
https://arxiv.org/pdf/2202.11533.pdf
We present a review of the observations of the solar F-corona from space with a special emphasis of the 25 years of continuous monitoring achieved by the LASCO-C2 and C3 coronagraphs. Our work includes images obtained by the navigation cameras of the Clementine spacecraft, the SECCHI/HI-1A heliospheric imager onboard STEREO-A, and the Wide Field Imager for Solar Probe onboard the Parker Solar Probe. The connection to the zodiacal light is considered based on ground- and space-based observations, prominently from the past Helios, IRAS, COBE, and IRAKI missions. The characteristic radiance profiles along the equatorial and polar directions follow power laws in the 5°-50° range of elongation, with constant power exponents of -2.33 and -2.55. Both profiles connect extremely well to the corresponding standard profiles of the zodiacal light. The LASCO equatorial profile exhibits a shoulder implying a 17% decrease of the radiance within 10Rsun that may be explained by the disappearance of organic materials within 0.3 AU. LASCO detected for the first time a secular variation of the F-corona, an increase at a rate of 0.46% per year of the integrated radiance in the LASCO-C3 FoV. This is likely the first observational evidence of the role of collisions in the inner zodiacal cloud. A composite of C2 and C3 images produced the LASCO reference map of the radiance of the F-corona from 2 to 30Rsun and, by combining with ground-based measurements, the LASCO extended map from 1 to 6 Rsun. The plane of symmetry of the inner zodiacal cloud is strongly warped, its inclination increasing towards the planes of the inner planets and ultimately the solar equator. In contrast, its longitude of ascending node is found to be constant and equal to 87.6°. LASCO did not detect any small scale structures such as putative rings occasionally reported during solar eclipses.

Coronal Photopolarimetry with the LASCO-C3 Coronagraph over 24 Years [1996-2019] -- Application to the K/F Separation and to the Determination of the Electron Density

Philippe **Lamy** (1), Hugo Gilardy (1), Antoine Llebaria (2), Eric Quemerais (1), Fabrice Ernandes (2)
Solr Phys. **2020**
https://arxiv.org/pdf/2009.04820.pdf
We present an in-depth characterization of the polarimetric channel of the Large-Angle Spectrometric COronagraph/LASCO-C3 onboard SOHO. The polarimetric analysis of the white-light images makes use of polarized sequences composed of three images obtained through three polarizers oriented at +60∘, 0∘, and -60∘, complemented by a neighboring unpolarized image. However, the degradation of the 0∘ polarizer noticed in 1999 compelled us to reconstruct the corresponding images from the other ones thereafter. The analysis closely follows the method developed for LASCO-C2 (Lamy, et al. Solar Physics 295, 89, 2020 and arXiv:2001.05925) and implements the formalism of Mueller, albeit with additional difficulties notably the presence of a non-axially symmetric component of stray light. Critical corrections were derived from a SOHO roll sequence and from consistency criteria (e.g., the tangential direction of polarization). The quasi-uninterrupted photopolarimetric analysis of the outer corona over two complete Solar Cycles 23 and 24 was successfully achieved and our final results encompass the characterization of its polarization, of its polarized radiance, of the two-dimensional electron density, and of the K-corona. Comparison between the C3 and C2 results where their field of view overlaps shows an overall agreement. The C3 results are further in agreement with those of eclipses and radio ranging measurements to an elongation of about 10 solar radii but tend to diverge further out. Whereas the coronal polarization out to 20 solar radii is still highly correlated with the temporal variation of the total magnetic field, this divergence probably results from the increasing polarization of the F-corona.

Coronal Photopolarimetry with the LASCO-C2 Coronagraph over 24 Years [1996-2019] -- Application to the K/F Separation and to the Determination of the Electron Density

Philippe **Lamy** (1), Antoine Llebaria (2), Brice Boclet (2), Hugo Gilardy (1), Michael Burtin (2 and 3), Olivier Floyd (1)

Solar Phys. **295**, Article number: 89 **2020**
https://arxiv.org/pdf/2001.05925.pdf
https://link.springer.com/content/pdf/10.1007/s11207-020-01650-y.pdf

We present an in-depth characterization of the polarimetric channel of the Large-Angle Spectrometric COronagraph LASCO-C2 onboard the Solar and Heliospheric Observatory (SoHO). The polarimetric analysis of the white-light images makes use of polarized sequences composed of three images obtained though three polarizers oriented at +60°, 0° and -60°, complemented by a neighboring unpolarized image, and relies on the formalism of Mueller. The Mueller matrix characterizing the C2 instrument was obtained through extensive ground-based calibrations of the optical components and global laboratory tests. Additional critical corrections were derived from in-flight tests relying prominently on roll sequences and on consistency criteria, mainly the tangential direction of polarization. Our final results encompass the characterization of the polarization of the white-light corona, of its polarized radiance, of the two-dimensional electron density, and of the K-corona over two solar cycles. They are in excellent agreement with measurements obtained at several solar eclipses except for slight discrepancies affecting the innermost part of the C2 field-of-view, probably resulting from an imperfect removal of the bright diffraction fringe surrounding the occulter. **11 August 1999, 29 March 2006, 21 August 2017**

Coronal Mass Ejections over Solar Cycles 23 and 24 **Review**

P. L. **Lamy**, O. Floyd, B. Boclet, J. Wojak, H. Gilardy…

Space Science Reviews August **2019**, 215:39
https://link.springer.com/content/pdf/10.1007%2Fs11214-019-0605-y.pdf

We present a statistical analysis of solar coronal mass ejections (CMEs) based on 23 years of quasi-continuous observations with the LASCO coronagraph, thus covering two complete Solar Cycles (23 and 24). We make use of five catalogs, one manual (CDAW) and four automated (ARTEMIS, CACTus, SEEDS, and CORIMP), to characterize the temporal evolutions and distributions of their properties: occurrence and mass rates, waiting times, periodicities, angular width, latitude, speed, acceleration and kinetic energy. Our analysis points to inevitable discrepancies between catalogs due to the complex nature of CMEs and to the different techniques implemented to detect them, but also to large areas of convergence that are critically important to ascertain the reliability of the results. The temporal variations of these properties are compared to four indices/proxies of solar activity: the radio flux at 10.7 cm (F10.7), the international sunspot number (SSN), the sunspot area (SSA), and the total magnetic field (TMF), either globally or separately in the northern and southern hemispheres in the case of the last three. We investigate the association of CMEs with flares, erupting prominences, active regions and streamers. We find that the CME occurrence and mass rates globally track the indices/proxies of solar activity with no time lag, prominently the radio flux F10.7, but the linear relationships were different during the two solar cycles, implying that the CME rates were relatively larger during SC 24 than during SC 23. However, there exists a pronounced divergence of the CME rates in the northern hemisphere during SC 24 as these rates were substantially larger than predicted by the temporal variation of the sunspot number. The distribution of kinetic energy follows a log-normal law and that of angular width follows an exponential law implying that they are random and independent. The distribution of waiting time (WTD) has a long power-law tail extending from 3 to 100 hr with a power-law index which varies with the solar cycle, thus reflecting the temporal variability of the process of CME formation. There is very limited evidence for periodicities in the occurrence and mass rates of CMEs, a striking feature being the dichotomy between the two hemispheres. Rather weak correlations are present among the various CME parameters and particularly none between speed and acceleration. The association of CMEs with flares and erupting prominences involves only a few percents of the overall population of CMEs but the associated CMEs have distinctly larger mass, speed, kinetic energy and angular width. A more pronounced association is found with active regions but the overwhelming one is with streamers further confirmed by the similarity between the heliolatitudinal distribution of CMEs and that of the electron density reconstructed from time-dependent tomographic inversion. We find no evidence of bimodality in the distributions of physical parameters that would support the existence of two classes, particularly that based on speed and acceleration, the distributions thus favoring a continuum of properties. There exists an excess of narrows CMEs which however does not define a special class. These narrow CMEs are likely associated with the ubiquitous mini-filaments eruptions and with mini flux ropes originating from small magnetic bipoles, the disruption mechanisms being similar to those launching larger CMEs. This supports the concept that CMEs at large arise from closed-field coronal regions at both large and small scales.

Anomalous Surge of the White-Light Corona at the Onset of the Declining Phase of Solar Cycle 24

P. **Lamy**, B. Boclet, J. Wojak, D. Vibert

Solar Physics April **2017**, 292:60

http://link.springer.com/content/pdf/10.1007%2Fs11207-017-1085-4.pdf
In late 2014, when the current Solar Cycle 24 entered its declining phase, the white-light corona as observed by the LASCO-C2 coronagraph underwent an unexpected surge that increased its global radiance by 60%, reaching a peak value comparable to the peak values of the more active Solar Cycle 23. A comparison of the temporal variation of the white-light corona with the variations of several indices and proxies of solar activity indicate that it best matches the variation of the total magnetic field. The daily variations point to a localized enhancement or bulge in the electron density that persisted for several months. Carrington maps of the radiance and of the HMI photospheric field allow connecting this bulge to the emergence of the large sunspot complex AR 12192 in October 2014, the largest since AR 6368 observed in November 1990. The resulting unusually high increase of the magnetic field and the distortion of the neutral sheet in a characteristic inverse S-shape caused the coronal plasma to be trapped along a similar pattern. A 3D reconstruction of the electron density based on time-dependent solar rotational tomography supplemented by 2D inversion of the coronal radiance confirms the morphology of the bulge and reveals that its level was well above the standard models of a corona of the maximum type, by typically a factor of 3. A rather satisfactory agreement is found with the results of the thermodynamic MHD model produced by Predictive Sciences, although discrepancies are noted. The specific configuration of the magnetic field that led to the coronal surge resulted from the interplay of various factors prevailing at the onset of the declining phase of the solar cycles, which was particularly efficient in the case of Solar Cycle 24. **18-28 November 2014.**

A Novel Technique for Measuring the Solar Radius from Eclipse Light Curves – Results for 2010, 2012, 2013, and 2015

Philippe **Lamy** , Jean-Yves Prado, Olivier Floyd, Patrick Rocher, Guillaume Faury, Serge Koutchmy
Solar Phys. Volume 290, Issue 10, pp 2617-2648 **2015**
We report on a novel technique for measuring the solar radius during total solar eclipses that exploits light curves recorded just before and after second and third contacts. The measurements are performed by pre-programmed photometers that are deployed over the eclipse paths and are operated without supervision. The recorded light curves are compared to synthetic light curves calculated from high-accuracy ephemerides and lunar-limb profiles constructed from the topographic model of the Moon provided by the Kaguya lunar space mission. A minimization process between the two sets of curves yields the solar radius. Altogether, seventeen determinations have been obtained during the past four total eclipses with the following averages (at a wavelength of 540 nm and scaled to 1 AU): 959.94±0.02 arcsec on 11 July 2010, 960.02±0.04 arcsec on 13 November 2012, 959.99±0.09 arcsec on 3 November 2013, and 960.01±0.09 arcsec on 20 March 2015. Part of the differences between these four values may be attributed to weather conditions. Averaging the whole set of measurements yields a radius of 959.99±0.06 arcsec (696,246±45 km), which agrees excellently well with the most recent data and supports an upward revision of the standard IAU value, as previously suggested.

Comparing the solar minima of cycles 22/23 and 23/24: The view from LASCO white light coronal images

P. **Lamy**, T. Barlyaeva, A. Llebaria and O. Floyd
JGR, Volume 119, Issue 1, pages 47–58, January **2014**
http://onlinelibrary.wiley.com/doi/10.1002/2013JA019468/pdf
The Large Angle and Spectrometric Coronagraph LASCO-C2 aboard SOHO has now completed 17 years (1996–2012) of quasi-continuous white-light imaging of the corona from 2.2 to 6.5 solar radii, thus allowing an unprecedented view of its evolution over a solar cycle and a half including the minima of solar cycles 22/23 and 23/24. The corrected and calibrated polarization sequences produce images of the radiance (B), the polarized radiance (pB), and the electron density Ne of the K corona, and, in turn, of their synoptic maps. Their temporal variations are quantified by integration first globally, then in the north and south hemispheres, and finally, in sectors of 30° latitudinal extent centered along the equatorial and polar directions. The global radiance of the K corona follows well the solar activity as described by the sunspot number and the radio flux and was 24% fainter during the minimum of solar cycle 23/24 than during that of cycle 22/23. However, the two hemispheres experienced different reductions, 17% for the north one and 29% for the south one. The equatorial sector suffered a drastic reduction of 44%, in remarkable agreement with the in situ measurements of Wind and ACE at 1 AU, whereas the north and south polar sectors did not experience much variation. Cycle 23 is estimated to have lasted 12 years and 3 months. Maximum conditions have been reached in the northern region, whereas the southern region is still lagging. Finally, the rate of coronal mass ejections follows well the solar activity.

Coronal plasma diagnostics from ground-based observations **Review**

E. **Landi**, S. R. Habbal, S. Tomczyk
JGR Volume 121, Issue 9 September **2016** Pages 8237–8249
http://sci-hub.cc/doi/10.1002/2016JA022598

In this paper we discuss the potential of ground-based visible observations of the solar corona to address the key open problems in the physics of the solar atmosphere and of solar activity. We first compare the diagnostic potential of visible observations with those of high-resolution spectrometers and narrowband imagers working in the EUV and X-ray wavelength ranges. We then review the main diagnostic techniques (and introduce a few new ones) that can be applied to line and continuum emission in the solar atmosphere, and the physical problems that they enable us to address. Finally, we briefly review the main features of ground-based coronographic instrumentation currently being developed and planned.

The Temperature of Quiescent Streamers during Solar Cycles 23 and 24

E. **Landi**1 and P. Testa

2014 ApJ 787 33

Recent in-situ determinations of the temporal evolution of the charge state distribution in the fast and slow solar wind have shown a general decrease in the degree of ionization of all the elements in the solar wind along solar cycles 23 and 24. Such a decrease has been interpreted as a cooling of the solar corona which occurred during the decline and minimum phase of solar cycle 23 from 2000 to 2010. In the present work, we investigate whether spectroscopic determinations of the temperature of the quiescent streamers show signatures of coronal plasma cooling during cycles 23 and 24. We measure the coronal electron density and thermal structure at the base of 60 quiescent streamers observed from 1996 to 2013 by SOHO/SUMER and Hinode/EIS and find that both quantities do now show any significant dependence on the solar cycle. We argue that if the slow solar wind is accelerated from the solar photosphere or chromosphere, the measured decrease in the in-situ wind charge state distribution might be due to an increased efficiency in the wind acceleration mechanism at low altitudes. If the slow wind originates from the corona, a combination of density and wind acceleration changes may be responsible for the in-situ results.

Evolution and wave-like properties of the average solar supergranule

J. **Langfellner**, A. C. Birch, L. Gizon

A&A **2018**

https://arxiv.org/pdf/1805.12522.pdf

Solar supergranulation presents us with many mysteries. For example, previous studies in spectral space found that supergranulation has wave-like properties. Here we study, in real space, the wave-like evolution of the average supergranule over a range of spatial scales (from 10 to 80 Mm). We complement this by characterizing the evolution of the associated network magnetic field. We use one year of data from the Helioseismic and Magnetic Imager (HMI) to measure horizontal near-surface flows near the solar equator by applying time-distance helioseismology on Dopplergrams and granulation tracking on intensity images. The average supergranule outflow (or inflow) is constructed by averaging over 10000 individual outflows (or inflows). The contemporaneous evolution of the magnetic field is studied with HMI line-of-sight observations. We confirm and extend previous measurements of the supergranular wave dispersion relation to angular wavenumbers in the range $50<kR<270$. We find a plateau for $kR>120$. In real space, larger supergranules undergo oscillations with longer periods and lifetimes than smaller cells. We find excellent agreement between TD and LCT and obtain wave properties that are independent of the tracking rate. The observed network magnetic field follows the oscillations of the supergranular flows with a six-hour time lag. This behavior can be explained by computing the motions of corks carried by the supergranular flows. Signatures of supergranular waves in surface horizontal flows near the solar equator can be observed in real space. These oscillatory flows control the evolution of the network magnetic field, in particular they explain the recently discovered east-west anisotropy of the magnetic field around the average supergranule. Background flow measurements that we obtain from Doppler frequency shifts do not favor shallow models of supergranulation.

Intensity contrast of the average supergranule

J. **Langfellner**, A. C. Birch, L. Gizon

A&A **2016**

https://arxiv.org/pdf/1609.09308v1.pdf

While the velocity fluctuations of supergranulation dominate the spectrum of solar convection at the solar surface, very little is known about the fluctuations in other physical quantities like temperature or density at supergranulation scale. Using SDO/HMI observations, we characterize the intensity contrast of solar supergranulation at the solar surface. We identify the positions of ∼104 outflow and inflow regions at supergranulation scales, from which we construct average flow maps and co-aligned intensity and magnetic field maps. In the average outflow center, the maximum intensity contrast is $(7.8\pm0.6)\times10-4$ (there is no corresponding feature in the line-of-sight magnetic field). This corresponds to a temperature perturbation of about 1.1 ± 0.1 K, in agreement with previous studies. We discover an east-west anisotropy, with a slightly deeper intensity minimum east of the outflow center. The evolution is asymmetric in time: the intensity excess is larger 8 hours before the reference time (the time of maximum outflow), while it has almost disappeared 8 hours after the reference time. In the average inflow region, the intensity contrast mostly follows the magnetic field distribution, except for an east-west anisotropic component that dominates 8 hours before the reference time. We suggest that the east-west anisotropy in the intensity is related to the wave-like properties of supergranulation.

Anisotropy of the solar network magnetic field around the average supergranule

J. **Langfellner**, L. Gizon, A. C. Birch

A&A **2015**

http://arxiv.org/pdf/1505.01427v1.pdf

Supergranules in the quiet Sun are outlined by a web-like structure of enhanced magnetic field strength, the so-called magnetic network. We aim to map the magnetic network field around the average supergranule near disk center. We use observations of the line-of-sight component of the magnetic field from the Helioseismic and Magnetic Imager (HMI) onboard the Solar Dynamics Observatory (SDO). The average supergranule is constructed by coaligning and averaging over 3000 individual supergranules. We determine the positions of the supergranules with an image segmentation algorithm that we apply on maps of the horizontal flow divergence measured using time-distance helioseismology. In the center of the average supergranule the magnetic (intranetwork) field is weaker by about 2.2 Gauss than the background value (3.5 Gauss), whereas it is enhanced in the surrounding ring of horizontal inflows (by about 0.6 Gauss on average). We find that this network field is significantly stronger west (prograde) of the average supergranule than in the east (by about 0.3 Gauss). With time-distance helioseismology, we find a similar anisotropy. The observed anisotropy of the magnetic field adds to the mysterious dynamical properties of solar supergranulation. 2 May 2010

Spatially resolved vertical vorticity in solar supergranulation using helioseismology and local correlation tracking

J. **Langfellner**, L. Gizon, A. C. Birch

A&A 581, A67 **2015**

http://arxiv.org/pdf/1504.00223v1.pdf

Flow vorticity is a fundamental property of turbulent convection in rotating systems. Solar supergranules exhibit a preferred sense of rotation, which depends on the hemisphere. This is due to the Coriolis force acting on the diverging horizontal flows. We aim to spatially resolve the vertical flow vorticity of the average supergranule at different latitudes, both for outflow and inflow regions. To measure the vertical vorticity, we use two independent techniques: time-distance helioseismology (TD) and local correlation tracking of granules in intensity images (LCT) using data from the Helioseismic and Magnetic Imager (HMI) onboard the Solar Dynamics Observatory (SDO). Both maps are corrected for center-to-limb systematic errors. We find that 8-h TD and LCT maps of vertical vorticity are highly correlated at large spatial scales. Associated with the average supergranule outflow, we find tangential (vortical) flows that reach about 10 m/s in the clockwise direction at 40{\deg} latitude. In average inflow regions, the tangential flow reaches the same magnitude, but in the anti-clockwise direction. These tangential velocities are much smaller than the radial (diverging) flow component (300 m/s for the average outflow and 200 m/s for the average inflow). The results for TD and LCT as measured from HMI are in excellent agreement for latitudes between −60{\deg} and 60{\deg}. From HMI LCT, we measure the vorticity peak of the average supergranule to have a full width at half maximum of about 13 Mm for outflows and 8 Mm for inflows. This is larger than the spatial resolution of the LCT measurements (about 3 Mm). On the other hand, the vorticity peak in outflows is about half the value measured at inflows (e.g. 4/(10^6 s) clockwise compared to 8/(10^6 s) anti-clockwise at 40{\deg} latitude). Results from MDI/SOHO obtained in 2010 are biased compared to the HMI/SDO results for the same period.

Time-distance helioseismology: A new averaging scheme for measuring flow vorticity

Jan **Langfellner**, Laurent Gizon, Aaron C. Birch

A&A, 570, A90 **2014**

http://arxiv.org/pdf/1408.4669v1.pdf

Time-distance helioseismology provides information about vector flows in the near-surface layers of the Sun by measuring wave travel times between points on the solar surface. Specific spatial averages of travel times have been proposed for distinguishing between flows in the east-west and north-south directions and measuring the horizontal divergence of the flows. No specific measurement technique has, however, been developed to measure flow vorticity. Here we propose a new measurement technique tailored to measuring the vertical component of vorticity. Fluid vorticity is a fundamental property of solar convection zone dynamics and of rotating turbulent convection in particular. The method consists of measuring the travel time of waves along a closed contour on the solar surface in order to approximate the circulation of the flow along this contour. Vertical vorticity is related to the difference between clockwise and counter-clockwise travel times. We applied the method to characterize the vortical motions of solar convection using helioseismic data from the Helioseismic and Magnetic Imager onboard the Solar Dynamics Observatory (SDO/HMI) and from the Michelson Doppler Imager onboard the Solar and Heliospheric Observatory (SOHO/MDI). Away from the equator, a clear correlation between vertical vorticity and horizontal divergence is detected. Horizontal outflows are associated with negative vorticity in the northern hemisphere and

positive vorticity in the southern hemisphere. The signal is much stronger for HMI than for MDI observations. We characterize the spatial power spectrum of the signal by comparison with a noise model. Vertical vorticity at horizontal wavenumbers below 250/R_Sun can be probed with this helioseismic technique.

Reducing activity-induced variations in a radial-velocity time series of the Sun as a star

A. F. **Lanza**, A. Collier Cameron, R. D. Haywood
MNRAS **2019**
https://arxiv.org/pdf/1904.05608.pdf
The radial velocity of the Sun as a star is affected by its surface convection and magnetic activity. The moments of the cross-correlation function between the solar spectrum and a binary line mask contain information about the stellar radial velocity and line-profile distortions caused by stellar activity. As additional indicators, we consider the disc-averaged magnetic flux and the filling factor of the magnetic regions. Here we show that the activity-induced radial-velocity fluctuations are reduced when we apply a kernel regression to these activity indicators. The disc-averaged magnetic flux proves to be the best activity proxy over a timescale of one month and gives a standard deviation of the regression residuals of 1.04 m/s, more than a factor of 2.8 smaller than the standard deviation of the original radial velocity fluctuations. This result has been achieved thanks to the high-cadence and time continuity of the observations that simultaneously sample both the radial velocity and the activity proxies.

Global-Mode Analysis of Full-Disk Data from theMichelson Doppler Imager and the Helioseismic and Magnetic Imager

Timothy P. **Larson** , Jesper Schou
Solar Physics February **2018**, 293:29
https://link.springer.com/content/pdf/10.1007%2Fs11207-017-1201-5.pdf
Building upon our previous work, in which we analyzed smoothed and subsampled velocity data from the Michelson Doppler Imager (MDI), we extend our analysis to unsmoothed, full-resolution MDI data. We also present results from the Helioseismic and Magnetic Imager(HMI), in both full resolution and processed to be a proxy for the low-resolution MDI data. We find that the systematic errors that we saw previously, namely peaks in both the high-latitude rotation rate and the normalized residuals of odd aa-coefficients, are almost entirely absent in the two full-resolution analyses. Furthermore, we find that both systematic errors seem to depend almost entirely on how the input images are apodized, rather than on resolution or smoothing. Using the full-resolution HMI data, we confirm our previous findings regarding the effect of using asymmetric profiles on mode parameters, and also find that they occasionally result in more stable fits. We also confirm our previous findings regarding discrepancies between 360-day and 72-day analyses. We further investigate a six-month period previously seen in ff-mode frequency shifts using the low-resolution datasets, this time accounting for solar-cycle dependence using magnetic-field data. Both HMI and MDI saw prominent six-month signals in the frequency shifts, but we were surprised to discover that the strongest signal at that frequency occurred in the mode coverage for the low-resolution proxy. Finally, a comparison of mode parameters from HMI and MDI shows that the frequencies and aa-coefficients agree closely, encouraging the concatenation of the two datasets.

Improved Helioseismic Analysis of Medium-ℓ Data from the Michelson Doppler Imager

Timothy P. **Larson** , Jesper Schou
Solar Phys. Volume 290, Issue 11, pp 3221-3256 **201**5
http://arxiv.org/pdf/1511.05217v1.pdf
We present a comprehensive study of one method for measuring various parameters of global modes of oscillation of the Sun. Using velocity data taken by the Michelson Doppler Imager (MDI), we analyze spherical harmonic degrees $\ell \leq 300$. Both current and historical methodologies are explained, and the various differences between the two are investigated to determine their effects on global-mode parameters and systematic errors in the analysis. These differences include a number of geometric corrections made during spherical harmonic decomposition; updated routines for generating window functions, detrending time series, and filling gaps; and consideration of physical effects such as mode-profile asymmetry, horizontal displacement at the solar surface, and distortion of eigenfunctions by differential rotation. We apply these changes one by one to three years of data, and then reanalyze the entire MDI mission applying all of them, using both the original 72-day long time series and 360-day long time series. We find significant changes in mode parameters, both as a result of the various changes to the processing, as well as between the 72-day and 360-day analyses. We find reduced residuals of inversions for internal rotation, but seeming artifacts remain, such as the peak in the rotation rate near the surface at high latitudes. An annual periodicity in the f-mode frequencies is also investigated.

Generation of Solar Coronal White-light Images from SDO/AIA EUV Images by Deep Learning

Bendict **Lawrance**1, Harim Lee1, Eunsu Park2, Il-Hyun Cho1, Yong-Jae Moon1,3, Jin-Yi Lee1, Shanmugaraju A4, and Sumiaya Rahman2
2022 ApJ 937 111
https://iopscience.iop.org/article/10.3847/1538-4357/ac8c24/pdf
Low coronal white-light observations are very important to understand low coronal features of the Sun, but they are rarely made. We generate Mauna Loa Solar Observatory (MLSO) K-coronagraph like white-light images from the Solar Dynamics Observatory/Atmospheric Imaging Assembly (SDO/AIA) EUV images using a deep learning model based on conditional generative adversarial networks. In this study, we used pairs of SDO/AIA EUV (171, 193, and 211 Å) images and their corresponding MLSO K-coronagraph images between 1.11 and 1.25 solar radii from 2014 to 2019 (January to September) to train the model. For this we made seven (three using single channels and four using multiple channels) deep learning models for image translation. We evaluate the models by comparing the pairs of target white-light images and those of corresponding artificial intelligence (AI)–generated ones in October and November. Our results from the study are summarized as follows. First, the multiple channel AIA 193 and 211 Å model is the best among the seven models in view of the correlation coefficient (CC = 0.938). Second, the major low coronal features like helmet streamers, pseudostreamers, and polar coronal holes are well identified in the AI-generated ones by this model. The positions and sizes of the polar coronal holes of the AI-generated images are very consistent with those of the target ones. Third, from AI-generated images we successfully identified a few interesting solar eruptions such as major coronal mass ejections and jets. We hope that our model provides us with complementary data to study the low coronal features in white light, especially for nonobservable cases (during nighttime, poor atmospheric conditions, and instrumental maintenance).

Evidence of active MHD instability in EULAG-MHD simulations of solar convection

N. **Lawson**, A. Strugarek, P. Charbonneau
ApJ **2015**
http://arxiv.org/pdf/1509.07447v1.pdf
We investigate the possible development of magnetohydrodynamical instabilities in the EULAG-MHD "millenium simulation" of Passos & Charbonneau (2014). This simulation sustains a large-scale magnetic cycle characterized by solar-like polarity reversals taking place on a regular multidecadal cadence, and in which zonally-oriented bands of strong magnetic field accumulate below the convective layers, in response to turbulent pumping from above in successive magnetic half-cycles. Key aspects of this simulation include low numerical dissipation and a strongly subadiabatic fluid layer underlying the convectively unstable layers corresponding to the modeled solar convection zone. These properties are conducive to the growth and development of two-dimensional instabilities otherwise suppressed by stronger dissipation. We find evidence for the action of a non-axisymmetric magnetoshear instability operating in the upper portions of the stably stratified fluid layers. We also investigate the possibility that the Tayler instability may be contributing to the destabilization of the large-scale axisymmetric magnetic component at high latitudes. On the basis of our analyses, we propose a global dynamo scenario whereby the magnetic cycle is driven primarily by turbulent dynamo action in the convecting layers, but MHD instabilities accelerate the dissipation of the magnetic field pumped down into the overshoot and stable layers, thus perhaps significantly influencing the magnetic cycle period. Support for this scenario is found in the distinct global dynamo behaviors observed in an otherwise identical EULAG-MHD simulations, using a different degree of subadiabaticity in the stable fluid layers underlying the convection zone.

On the interpretation and applicability of κ-distributions

M. **Lazar**1,2,3, H. Fichtner3,4 and P. H. Yoon
A&A 589, A39 (**2016**)
Context. The generally accepted representation of κ-distributions in space plasma physics allows for two different alternatives, namely assuming either the temperature or the thermal velocity to be κ-independent.
Aims. The present paper aims to clarify the issue concerning which of the two possible choices and the related physical interpretation is correct.
Methods. A quantitative comparison of the consequences of the use of both distributions for specific physical systems leads to their correct interpretation.
Results. It is found that both alternatives can be realized, but they are valid for principally different physical systems.
Conclusions. The investigation demonstrates that, before employing one of the two alternatives, one should be conscious about the nature of the physical system one intends to describe, otherwise one would possibly obtain unphysical results.

3D turbulent reconnection: Theory, tests, and astrophysical implications **Review**

Lazarian, Alex; Eyink, Gregory L.; Jafari, Amir; Kowal, Grzegorz; Li, Hui; Xu, Siyao; Vishniac, Ethan T.
Physics of Plasmas 27, 012305 (**2020**); https://doi.org/10.1063/1.5110603

https://arxiv.org/pdf/2001.00868.pdf
https://aip.scitation.org/doi/pdf/10.1063/1.5110603
Magnetic reconnection, topological changes in magnetic fields, is a fundamental process in magnetized plasmas. It is associated with energy release in regions of magnetic field annihilation, but this is only one facet of this process. Astrophysical fluid flows normally have very large Reynolds numbers and are expected to be turbulent, in agreement with observations. In strong turbulence, magnetic field lines constantly reconnect everywhere and on all scales, thus making magnetic reconnection an intrinsic part of the turbulent cascade. We note in particular that this is inconsistent with the usual practice of magnetic field lines as persistent dynamical elements. A number of theoretical, numerical, and observational studies starting with the paper done by Lazarian and Vishniac [Astrophys. J. 517, 700-718 (1999)] proposed that 3D turbulence makes magnetic reconnection fast and that magnetic reconnection and turbulence are intrinsically connected. In particular, we discuss the dramatic violation of the textbook concept of magnetic flux-freezing in the presence of turbulence. We demonstrate that in the presence of turbulence, the plasma effects are subdominant to turbulence as far as the magnetic reconnection is concerned. The latter fact justifies a magnetohydrodynamiclike treatment of magnetic reconnection on all scales much larger than the relevant plasma scales. We discuss the numerical and observational evidence supporting the turbulent reconnection model. In particular, we demonstrate that the tearing reconnection is suppressed in 3D, and unlike the 2D settings, 3D reconnection induces turbulence that makes magnetic reconnection independent of resistivity. We show that turbulent reconnection dramatically affects key astrophysical processes, e.g., star formation, turbulent dynamo, and acceleration of cosmic rays. We provide criticism of the concept of "reconnection-mediated turbulence" and explain why turbulent reconnection is very different from enhanced turbulent resistivity and hyper-resistivity and why the latter have fatal conceptual flaws.

3D Turbulent Reconnection: 20 Years After **Review**

Lazarian, A.; Kowal, Grzegorz; Xu, Siyao; Jafari, Amir
Journal of Physics: Conference Series, Volume 1332, Issue 1, article id. 012009 (**2019**).
https://iopscience.iop.org/article/10.1088/1742-6596/1332/1/012009/pdf
A theory of 3D turbulent reconnection was published 20 years ago. At that time it was suggested that the fast reconnection requires X-point Petschek-type configuration of magnetic field in the reconnection region, as well as plasma effects that would stabilize this configuration. On the contrary, the turbulent reconnection theory (i) identified 3D Alfvenic turbulence as the cause of fast reconnection, (ii) postulated the ubiquitous nature of turbulent reconnection in astrophysical high-Reynolds number environments, and (iii) identified Y-point volume reconnection as the typical magnetic reconnection on length scales where the magnetohydrodynamic (MHD) approximation is valid. In this article we briefly summarize the status of the 3D turbulent reconnection theory. We show that other alternative models of reconnection have evolved toward supporting the essential features of the original turbulent reconnection theory. We also provide numerical and observational evidence supporting the turbulent reconnection and its consequences, e.g., the breakdown of classical magnetic flux freezing in highly conducting turbulent fluids.

Identification of Gleissberg Cycles and a Rising Trend in a 315-Year-Long Series of Sunspot Numbers

Jean-Louis **Le Mouël**, Fernand Lopes, Vincent Courtillot
Solar Physics March **2017**, 292:43
We show in this short note that the method of singular spectrum analysis (SSA) is able to clearly extract a strong, clean, and clear component from the longest available sunspot (International Sunspot Number, ISN) time series (1700 – 2015) that cannot be an artifact of the method and that can be safely identified as the Gleissberg cycle. This is not a small component, as it accounts for 13% of the total variance of the total original signal. Almost three and a half clear Gleissberg cycles are identified in the sunspot number series. Four extended solar minima (XSM) are determined by SSA, the latest around 2000 (Cycle 23/24 minimum). Several authors have argued in favor of a double-peaked structure for the Gleissberg cycle, with one peak between 55 and 59 years and another between 88 and 97 years. We find no evidence of the former: solar activity contains an important component that has undergone clear oscillations of ≈90≈90 years over the past three centuries, with some small but systematic longer-term evolution of “instantaneous” period and amplitude. Half of the variance of solar activity on these time scales can be satisfactorily reproduced as the sum of a monotonous multi-secular increase, a ≈90≈90-year Gleissberg cycle, and a double-peaked (≈10.0≈10.0 and 11.0 years) Schwabe cycle (the sum amounts to 46% of the total variance of the signal). The Gleissberg-cycle component definitely needs to be addressed when attempting to build dynamo models of solar activity. The first SSA component offers evidence of an increasing long-term trend in sunspot numbers, which is compatible with the existence of the modern grand maximum.

3D turbulent reconnection: Theory, tests, and astrophysical implications **Review**

Alex **Lazarian**1,a), Gregory L. Eyink2,3, Amir Jafari3, Grzegorz Kowal4, Hui Li5, Siyao Xu1, and Ethan T. Vishniac3
Physics of Plasmas 27, 012305 (**2020**); https://doi.org/10.1063/1.5110603

Magnetic reconnection, topological changes in magnetic fields, is a fundamental process in magnetized plasmas. It is associated with energy release in regions of magnetic field annihilation, but this is only one facet of this process. Astrophysical fluid flows normally have very large Reynolds numbers and are expected to be turbulent, in agreement with observations. In strong turbulence, magnetic field lines constantly reconnect everywhere and on all scales, thus making magnetic reconnection an intrinsic part of the turbulent cascade. We note in particular that this is inconsistent with the usual practice of magnetic field lines as persistent dynamical elements. A number of theoretical, numerical, and observational studies starting with the paper done by Lazarian and Vishniac [Astrophys. J. 517, 700–718 (1999)] proposed that 3D turbulence makes magnetic reconnection fast and that magnetic reconnection and turbulence are intrinsically connected. In particular, we discuss the dramatic violation of the textbook concept of magnetic flux-freezing in the presence of turbulence. We demonstrate that in the presence of turbulence, the plasma effects are subdominant to turbulence as far as the magnetic reconnection is concerned. The latter fact justifies a magnetohydrodynamiclike treatment of magnetic reconnection on all scales much larger than the relevant plasma scales. We discuss the numerical and observational evidence supporting the turbulent reconnection model. In particular, we demonstrate that the tearing reconnection is suppressed in 3D, and unlike the 2D settings, 3D reconnection induces turbulence that makes magnetic reconnection independent of resistivity. We show that turbulent reconnection dramatically affects key astrophysical processes, e.g., star formation, turbulent dynamo, and acceleration of cosmic rays. We provide criticism of the concept of "reconnection-mediated turbulence" and explain why turbulent reconnection is very different from enhanced turbulent resistivity and hyper-resistivity and why the latter have fatal conceptual flaws.
CESRA #2520 March **2020** http://www.astro.gla.ac.uk/users/eduard/cesra/?p=2520

Extreme space weather events caused by super active regions during solar cycles 21-24

Gui-Ming **Le**, Gui-Ang Liu, Ming-Xian Zhao, Tian Mao, Ping-Guo Xu
Research in Astronomy and Astrophysics **2021**
https://arxiv.org/pdf/2103.00670.pdf **File**
Extreme space weather events including ≥X5.0 flares, ground level enhancement (GLE) events and super geomagnetic storms (Dst ≤ -250 nT) caused by super active regions (SARs) during solar cycles 21-24 were studied. The total number of ≥X5.0 solar flares was 62, 41 of them were X5.0-X9.9 flares and 21 of them were ≥X10.0 flares. We found that 83.9\% of the ≥X5.0 flares were produced by SARs. 78.05\% of the X5.0-X9.9 and 95.24\% of the ≥X10.0 solar flares were produced by SARs. 46 GLEs registered during solar cycles 21-24, and 25 GLEs were caused by SARs, indicating that 54.3\% of the GLEs were caused by SARs. 24 super geomagnetic storms were recorded during solar cycles 21-24, and 12 of them were caused by SARs, namely 50\% of the super geomagnetic storms are caused by SARs. It is found that only 29 SARs can produce ≥X5.0 flares, 15 SARs can produce GLEs and 10 SARs can produce super geomagnetic storms. Of the 51 SARs, only 33 SARs can produce at least one extreme space weather event, while none of the rest 18 SARs can produce an extreme space weather event. There were only 4 SARs, each of them can produce not only a ≥X5.0 flare, but also a GLE event and a super geomagnetic storm. Most of the extreme space weather events caused by the SARs appeared during solar cycles 22 and 23, especially for GLE events and super geomagnetic storms. The longitudinal distributions of source locations for the extreme space weather events caused by SARs were also studied. **28-30, October 2003**
Table 1: The flares with intensities ≥X5.0 caused by SARs during solar cycles 21-24.
Table 2: The GLE events caused by SARs during solar cycles 21-24.
Table 3: The SGSs and the related ARs during solar cycles 21-24.

FIRST NEW SOLAR MODELS WITH OPAS OPACITY TABLES

M. **Le Pennec**1, S. Turck-Chièze1, S. Salmon1, C. Blancard2, P. Cossé2, G. Faussurier2, and G. Monde
2015 ApJ 813 L42
Stellar seismology appears more and more as a powerful tool for a better determination of the fundamental properties of solar-type stars. However, the particular case of the Sun is still challenging. For about a decade now, the helioseismic sound-speed determination has continued to disagree with the standard solar model (SSM) prediction, questioning the reliability of this model. One of the sources of uncertainty could be in the treatment of the transport of radiation from the solar core to the surface. In this Letter, we use the new OPAS opacity tables, recently available for solar modeling, to address this issue. We discuss first the peculiarities of these tables, then we quantify their impact on the solar sound-speed and density profiles using the reduced OPAS tables taken on the grids of the OPAL ones. We use the two evolution codes, Modules for Experiments in Stellar Astrophysics and Code Liégeois d'Evolution Stellaire, that led to similar conclusions in the solar radiative zone. In comparison to commonly used OPAL opacity tables, the new solar models are computed for the most recent photospheric composition with OPAS tables and present improvements to the location of the base of the convective zone and to the description of the solar radiative zone in comparison to the helioseismic observations, even if the differences in the Rosseland mean opacity do not exceed 6%. We finally carry out a comparison to a solar model computed with the OP opacity tables.

The Onset of 3D Magnetic Reconnection and Heating in the Solar Corona

James **Leake**, Lars Daldorff, James Klimchuk

2020 *ApJ* **891** 62

https://arxiv.org/pdf/2001.02971.pdf

Magnetic reconnection, a fundamentally important process in many aspects of astrophysics, is believed to be initiated by the tearing instability of an electric current sheet, a region where magnetic field abruptly changes direction and electric currents build up. Recent studies have suggested that the amount of magnetic shear in these structures is a critical parameter for the switch-on nature of magnetic reconnection in the solar atmosphere, at fluid spatial scales much larger than kinetic scales. We present results of simulations of reconnection in 3D current sheets with conditions appropriate to the solar corona. Using high-fidelity simulations, we follow the evolution of the linear and non-linear 3D tearing instability, leading to reconnection. We find that, depending on the parameter space, magnetic shear can play a vital role in the onset of significant energy release and heating via non-linear tearing. Two regimes in our study exist, dependent on whether the current sheet is longer or shorter than the wavelength of the fastest growing parallel mode (in the corresponding infinite system), thus determining whether sub-harmonics are present in the actual system. In one regime, where the fastest growing parallel mode has sub-harmonics, the non-linear interaction of these sub-harmonics and the coalescence of 3D plasmoids dominates the non-linear evolution, with magnetic shear playing only a weak role in the amount of energy released. In the second regime, where the fastest growing parallel mode has no-sub-harmonics, then only strongly sheared current sheets, where oblique mode are strong enough to compete with the dominant parallel mode, show any significant energy release. We expect both regimes to exist on the Sun, and so our results have important consequences for the the question of reconnection onset in different solar physics applications.

Deciphering Solar Magnetic Activity: The Solar Cycle Clock

Robert J. **Leamon1**,2*, Scott W. McIntosh3 and Alan M. Title4

Front. Astron. Space Sci., 9:886670 **2022** |

https://doi.org/10.3389/fspas.2022.886670

https://www.frontiersin.org/articles/10.3389/fspas.2022.886670/full

The Sun's variability is controlled by the progression and interaction of the magnetized systems that form the 22-year magnetic activity cycle (the "Hale Cycle") as they march from their origin at ∼55° latitude to the equator, over ∼19 years. We will discuss the end point of that progression, dubbed "terminator" events, and our means of diagnosing them. In this paper we expand on the Extended Solar Cycle framework to construct a new solar activity "clock" which maps all solar magnetic activity onto a single normalized epoch based on the terminations of Hale Magnetic Cycles. Defining phase 0*2π on this clock as the Terminators, then solar polar field reversals occur at ∼ 0.2*2π, and the geomagnetically quiet intervals centered around solar minimum start at ∼ 0.6*2π and end at the terminator, thus lasting 40% of the cycle length. At this onset of quiescence, dubbed a "pre-terminator," the Sun shows a radical reduction in active region complexity and, like the terminator events, is associated with the time when the solar radio flux crosses F10.7 = 90 sfu. We use the terminator-based clock to illustrate a range of phenomena that further emphasize the strong interaction of the global-scale magnetic systems of the Hale Cycle: the vast majority, 96%, of all X-flares happen between the Terminator and pre-Terminator. In addition to the X-rays from violent flares, rapid changes in the number of energetic photons—EUV spectral emission from a hot corona and the F10.7 solar radio flux—impinging on the atmosphere are predictable from the Terminator-normalized unit cycle, which has implications for improving the fidelity of atmospheric modelling.

Response to "Limitations in the Hilbert Transform Approach to Locating Solar Cycle Terminators" by R. Booth

Robert J. **Leamon**, Scott W. McIntosh, Sandra C. Chapman & Nicholas W. Watkins

Solar Physics volume 296, Article number: 151 (**2021**)

https://link.springer.com/content/pdf/10.1007/s11207-021-01897-z.pdf

https://doi.org/10.1007/s11207-021-01897-z

Booth (Solar Phys. 296, 108, 2021; hereafter B21) is essentially a critique of the Hilbert transform techniques used in our paper (Leamon et al., Solar Phys. 295, 36, 2020; hereafter L20) to predict the termination of solar cycles. Here we respond to his arguments; our methodology and parameter choices do extract a mathematically robust signature of terminators from the historical sunspot record. We agree that the attempt in L20 to extrapolate beyond the sunspot record gives a failed prediction for the next terminator of May 2020, and we identify both a possible cause and remedy here. However, we disagree with the B21 assessment that the likely termination of Solar Cycle 24 is two years after the date predicted in L20, and we show why.

Deciphering Solar Magnetic Activity. II. The Solar Cycle Clock and the Onset of Solar Minimum Conditions

Robert **Leamon**, Scott McIntosh, Sandra Chapman, Nicholas Watkins, Subhamoy Chatterjee, Alan Title

Solar Phys. **2021**
https://arxiv.org/pdf/2012.15186.pdf
The Sun's variability is controlled by the progression and interaction of the magnetized systems that form the 22-year magnetic activity cycle (the "Hale Cycle") as they march from their origin at ∼55 degrees latitude to the equator, over ∼19 years. We will discuss the end point of that progression, dubbed "terminator" events, and our means of diagnosing them. Based on the terminations of Hale Magnetic Cycles, we construct a new solar activity "clock" which maps all solar magnetic activity onto a single normalized epoch. The Terminators appear at phase $0*2\pi$ on this clock (by definition), then solar polar field reversals commence at $0.2*2\pi$, and the geomagnetically quiet intervals centered around solar minimum, start at $0.6*2\pi$ and end at the terminator, lasting 40% of the normalized cycle length. With this onset of quiescence, dubbed a "pre-terminator," the Sun shows a radical reduction in active region complexity and (like the terminator events) is associated with the time when the solar radio flux crosses F10.7=90 sfu -- effectively marking the commencement of solar minimum conditions. In this paper we use the terminator-based clock to illustrate a range of phenomena associated with the pre-terminator "event" that further emphasize the strong interaction of the global-scale magnetic systems of the Hale Cycle.

Timing Terminators: Forecasting Sunspot Cycle 25 Onset

Leamon, Robert J. , McIntosh, Scott W. , Chapman, Sandra C. , Watkins, Nicholas W.
Solar Physics, Volume 295, Issue 2, article id.36, **2020**
https://arxiv.org/pdf/1909.06603.pdf
Recent research has demonstrated the existence of a new type of solar event, the "terminator." Unlike the Sun's signature events, flares and coronal mass ejections, the terminator most likely originates in the solar interior, at or near the tachocline. The terminator signals the end of a magnetic activity cycle at the Sun's equator and the start of a sunspot cycle at mid-latitudes. Observations indicate that the time difference between these events is very short, less than a solar rotation, in the context of the sunspot cycle. As the (definitive) start and end point of solar activity cycles the precise timing of terminators should permit new investigations into the meteorology of our star's atmosphere. In this article we use a standard method in signal processing, the Hilbert transform, to identify a mathematically robust signature of terminators in sunspot records and in radiative proxies. Using a linear extrapolation of the Hilbert phase of the sunspot number and F10.7 cm solar radio flux time series we can achieve higher fidelity historical terminator timing than previous estimates have permitted. Further, this method presents a unique opportunity to project, from analysis of sunspot data, when the next terminator will occur, May 2020 (+4 , -1.5 months), and trigger the growth of Sunspot Cycle 25.

Solar Chromospheric Network as a Source for Solar Wind Switchbacks

Jeongwoo **Lee**1,2,3, Vasyl Yurchyshyn1,2,3, Haimin Wang1,2,3, Xu Yang1,2,3, Wenda Cao1,2,3, and Juan Carlos Martínez Oliveros4
2022 ApJL 935 L27
https://iopscience.iop.org/article/10.3847/2041-8213/ac86bf/pdf
Recent studies suggest that the magnetic switchbacks (SBs) detected by the Parker Solar Probe carry information on the scales of solar supergranulation (large scale) and granulation (medium scale). We test this claim using high-resolution Hα images obtained with the visible spectropolarimeters of the Goode Solar Telescope in Big Bear Solar Observatory. As possible solar sources, we count all the spicule-like features standing along the chromospheric networks near the coronal hole boundary visible in the Hα blue-wing but absent in the red-wing images and measure the geometric parameters of dense sections of individual flux tubes. Intervals between adjacent spicules located along the chromospheric networks are found in the range of 0.4–1.5 Mm (0.″03–0.″12) tending to be smaller than the medium scale of SBs. Interdistances between all pairs of the flux tubes are also counted and they appear in a single peak distribution around 0.7 Mm (0.″06) unlike the waiting-time distribution of SBs in a scale-free single power-law form. The length-to-diameter ratio of the dense section of flux tubes is as high as 6–40, similar to the aspect ratio of SBs. The number of spicules along a network can be as high as 40–100, consistent with numerous SBs within a patch. With these numbers, it is argued that the medium scale of SBs can be understood as an equilibrium distance resulting from a random walk within each diverging magnetic field funnel connected to the chromospheric networks. **2020 June 17**

Comparison of LOS Doppler Velocities and Non-thermal Line Widths in the Off-limb Solar Corona Measured Simultaneously by CoMP and Ninode/EIS

Lee, Jae-Ok ; Lee, Kyoung-Sun ; Seough, Jungjoon ; Cho, Kyung-Suk
Journal of the Korean Astronomical Society, vol. 54, pp. 49-60 (**2021**)
http://jkas.kas.org/journal/article.php?code=78212&list.php?m=1&ckattempt=1
https://doi.org/10.5303/JKAS.2021.54.2.49
Observations of line of sight (LOS) Doppler velocity and non-thermal line width in the off-limb solar corona are often used for investigating the Alfvén wave signatures in the corona. In this study, we compare LOS Doppler velocities and non-thermal line widths obtained simultaneously from two different instruments, Coronal

Multichannel Polarimeter (CoMP) and Hinode/EUV Imaging Spectrometer (EIS), on various off-limb coronal regions: flaring and quiescent active regions, equatorial quiet region, and polar prominence and plume regions observed in 2012-2014. CoMP provides the polarization at the Fe XIII 10747 Å coronal forbidden lines which allows their spectral line intensity, LOS Doppler velocity, and line width to be measured with a low spectral resolution of 1.2 Å in 2-D off limb corona between 1.05 and 1.40 R_Sun, while Hinode/EIS gives us the EUV spectral information with a high spectral resolution (0.025 Å) in a limited field of view raster scan. In order to compare them, we make pseudo raster scan CoMP maps using information of each EIS scan slit time and position. We compare the CoMP and EIS spectroscopic maps by visual inspection, and examine their pixel to pixel correlations and percentages of pixel numbers satisfying the condition that the differences between CoMP and EIS spectroscopic quantities are within the EIS measurement accuracy: ±3 km/s for LOS Doppler velocity and ±9 km/s for non-thermal width. The main results are summarized as follows. By comparing CoMP and EIS Doppler velocity distributions, we find that they are consistent with each other overall in the active regions and equatorial quiet region ($0.25 \leq CC \leq 0.7$), while they are partially similar to each other in the overlying loops of prominences and near the bottom of the polar plume ($0.02 \leq CC \leq 0.18$). CoMP Doppler velocities are consistent with the EIS ones within the EIS measurement accuracy in most regions (≥ 87% of pixels) except for the polar region (45% of pixels). We find that CoMP and EIS non-thermal width distributions are similar overall in the active regions ($0.06 \leq CC \leq 0.61$), while they seem to be different in the others ($-0.1 \leq CC \leq 0.00$). CoMP non-thermal widths are similar to EIS ones within the EIS measurement accuracy in a quiescent active region (79% of pixels), while they do not match in the other regions (≤ 61% of pixels); the CoMP observations tend to underestimate the widths by about 20% to 40% compared to the EIS ones. Our results demonstrate that CoMP observations can provide reliable 2-D LOS Doppler velocity distributions on active regions and might provide their non-thermal width distributions.
Hinode/EIS Nuggets Nov **2021** http://solarb.mssl.ucl.ac.uk/SolarB/nuggets/nugget_2021nov_a.jsp

EMD and LSTM Hybrid Deep Learning Model for Predicting Sunspot Number Time Series with a Cyclic Pattern

Taesam **Lee**
Solar Physics volume 295, Article number: 82 (**2020**)
https://link.springer.com/content/pdf/10.1007/s11207-020-01653-9.pdf
The prediction of a time series such as climate indices and the sunspot number (SSN) with long-term oscillatory behaviors has been a challenging task due to the complex combination of oscillations. Frequency extraction algorithms have been developed to separate a time series into different oscillation components according to frequency, such as empirical model decomposition (EMD) and wavelet analysis. In the current study, the deep learning long short-term memory (LSTM) model was employed to predict the oscillation components extracted using EMD. The SSN series was modeled with the hybrid EMD-LSTM model. The simulation study results indicate that the LSTM model reproduces the smooth cyclic pattern of the sine function, and only a few hidden units are needed to model it. The EMD-LSTM model achieves better performance than does the LSTM model for mid-range SSN predictions while the LSTM achieves better performance within the first few time lags. However, the cyclic prediction of the SSN requires mid-range lags; thus, the superior performance of the EMD-LSTM model for these lags cannot be ignored. Furthermore, the remaining components from the significant EMD signals can be modeled to reveal the variability (or uncertainty) in the prediction. The summed residual is fitted by k-nearest neighbor resampling. The final SSN prediction results show that the EMD-LSTM model predicts a later and larger SSN for Solar Cycle 25 than does the LSTM model. Overall, the results lead to the conclusion that the EMD-LSTM model might be a suitable alternative for modeling complex sunspot time series with cyclic patterns.

Timing Terminators: Forecasting Sunspot Cycle 25 Onset

Robert J **Leamon**, Scott W. McIntosh, Sandra C. Chapman, Nicholas W. Watkins
Solar Phys. **295**, Article number: 36 (**2020**)
https://arxiv.org/pdf/1909.06603.pdf
Recent research has demonstrated the existence of a new type of solar event, the "terminator". Unlike the Sun's signature events: flares and Coronal Mass Ejections the terminator takes place in the solar interior. The terminator signals the end of a magnetic activity cycle at the Sun's equator and the start of a sunspot cycle at mid latitudes. Observations indicate that the time difference between these events is very short, less than a solar rotation, in the context of the sunspot cycle. As the (definitive) start and end point of solar activity cycles the precise timing of terminators should permit new investigations into the meteorology of our star's atmosphere. In this letter we use a standard method in signal processing, the Hilbert transform, to identify a mathematically robust signature of terminators in sunspot records and in radiative proxies. Using this technique we can achieve higher fidelity terminator timing than previous estimates have permitted. Further, this method presents a unique opportunity to project when the next terminator will occur, 2020.33(\pm0.16), and trigger the growth of sunspot cycle 25.

Quantifying Properties of Photospheric Magnetic Cancellations in the Quiet Sun Internetwork

Vincent E. **Ledvina**, Maria D. Kazachenko, Serena Criscuoli, Dennis Tilipman, Ilaria Ermolli, Mariachiara Falco, Salvatore Guglielmino, Shahin Jafarzadeh, Luc Rouppe van der Voort, Francesca Zuccarello

ApJ **2022**

https://arxiv.org/pdf/2206.04644.pdf

We analyzed spectropolarimetric data from the Swedish 1-meter Solar Telescope to investigate physical properties of small-scale magnetic cancellations in the quiet Sun photosphere. Specifically, we looked at the full Stokes polarization profiles along the Fe I 557.6 nm and of the Fe I 630.1 nm lines measured by CRisp Imaging SpectroPolarimeter (CRISP) to study temporal evolution of the line-of-sight (LOS) magnetic field during 42.5 minutes of quiet Sun evolution. From this magnetogram sequence, we visually identified 38 cancellation events. We then used Yet Another Feature Tracking Algorithm (YAFTA) to characterize physical properties of these magnetic cancellations. We found on average 1.6×1016 Mx of magnetic flux cancelled in each event with an average cancellation rate of 3.8×1014 Mx s−1. The derived cancelled flux is associated with strong downflows, with an average speed of VLOS≈1.1 km s−1. Our results show that the average lifetime of each event is 9.2 minutes with an average 44.8% of initial magnetic flux being cancelled. Our estimates of magnetic fluxes provide a lower limit since studied magnetic cancellation events have magnetic field values that are very close to the instrument noise level. We observed no horizontal magnetic fields at the cancellation sites and therefore can not conclude whether the events are associated structures that could cause magnetic reconnection.

Visibility Analysis of the Sun as Viewed from Multiple Spacecraft at the Sun-Earth Lagrange Points

Jinsung **Lee**, Sung-Hong Park, Arik Posner, Kyung-Suk Cho, Jaemyung Ahn

Space Weather **2024**

https://arxiv.org/pdf/2408.04208

Beyond the Sun-Earth line, spacecraft equipped with various solar telescopes are intended to be deployed at several different vantage points in the heliosphere to carry out coordinated, multi-view observations of the Sun and its dynamic activities. In this context, we investigate solar visibility by imaging instruments onboard the spacecraft orbiting the Sun-Earth Lagrange points L1, L4 and L5, respectively. An optimal arrival time for vertical periodic orbits stationed at L4 and L5 is determined based on geometric considerations that ensure maximum visibility of solar poles or higher latitudes per year. For a different set of orbits around the three Lagrange points (L1, L4 and L5), we calculate the visibility of the solar surface (i.e., observation days per year) as a function of the solar latitude. We also analyze where the solar limb viewed from one of the three Sun-Earth Lagrange points under consideration is projected onto the solar surface visible to the other two. This analysis particularly aims at determining the feasibility of studying solar eruptions, such as flares and coronal mass ejections, with coordinated observations of off-limb erupting coronal structures and their on-disk magnetic footpoints. In addition, visibility analysis of a feature (such as sunspots) on the solar surface is made for multiple spacecraft in various types of orbits with different inclinations to quantify the improvement in continuous tracking of the target feature for studying its long-term evolution from emergence, growth and to decay. A comprehensive comparison of observations from single (L1), double (L1 and L4) and multi-space missions (L1, L4 and L5) is carried out through our solar visibility analysis, and this may help us to design future space missions of constructing multiple solar observatories at the Sun-Earth Lagrange points.

Solar Spicules, Filigrees, and Solar Wind Switchbacks

Jeongwoo **Lee**1,2,3, Haimin Wang1,2,3, Jiasheng Wang1,2,3, and Meiqi Wang1,2

2024 ApJ 963 79

https://iopscience.iop.org/article/10.3847/1538-4357/ad23e0/pdf

Spicules, the smallest observable jetlike dynamic features ubiquitous in the chromosphere, are supposedly an important potential source for small-scale solar wind transients, with supporting evidence yet needed. We studied the high-resolution Hα images ($0\farcs10$) and magnetograms ($0\farcs29$) from the Big Bear Solar Observatory to find that spicules are an ideal candidate for the solar wind magnetic switchbacks detected by the Parker Solar Probe (PSP). It is not that spicules are a miniature of coronal jets, but that they have unique properties not found in other solar candidates in explaining solar origin of switchbacks. (1) The spicules under this study originate from filigrees, all in a single magnetic polarity. Since filigrees are known as footpoints of open fields, the spicule guiding field lines can form a unipolar funnel, which is needed to create an SB patch, a group of field lines that switch from one common base polarity to the other polarity. (2) The spicules come in a cluster lined up along a supergranulation boundary, and the simulated waiting times from their spatial intervals exhibit a number distribution continuously decreasing from a few seconds to ∼30 minutes, similar to that of switchbacks. (3) From a time–distance map for spicules, we estimate their occurrence rate as 0.55 spicules Mm−2 s−1, which is sufficiently high for detection by PSP. In

addition, the dissimilarity of spicules with coronal jets, including the absence of base brightening and low correlation with EUV emission, is briefly discussed. **2018 July 29**,

Heating and Eruption of a Solar Circular Ribbon Flare

Jeongwoo **Lee**, Judith T. Karpen, Chang Liu, Haimin Wang
2020 ApJ 893 158
https://arxiv.org/pdf/2008.05020.pdf
https://doi.org/10.3847/1538-4357/ab80c4
We studied a circular-ribbon flare, SOL**2014-12-17**T04:51, with emphasis on its thermal evolution as determined by the Differential Emission Measure (DEM) inversion analysis of the extreme ultraviolet (EUV) images of the Atmospheric Imaging Assembly (AIA) instrument onboard the Solar Dynamics Observatory (SDO). Both temperature and emission measure start to rise much earlier than the flare, along with an eruption and formation of a hot halo over the fan structure. In the main flare phase, another set of ribbons forms inside the circular ribbon, and expands as expected for ribbons at the footpoints of a postflare arcade. An additional heating event further extends the decay phase, which is also characteristic of some eruptive flares. The basic magnetic configuration appears to be a fan-spine topology, rooted in a minority-polarity patch surrounded by majority-polarity flux. We suggest that reconnection at the null point begins well before the impulsive phase, when the null is distorted into a breakout current sheet, and that both flare and breakout reconnection are necessary in order to explain the subsequent local thermal evolution and the eruptive activities in this confined magnetic structure. Using local DEMs, we found a postflare temperature increase inside the fan surface, indicating that the so-called EUV late phase is due to continued heating in the flare loops.

DEPENDENCE OF OCCURRENCE RATES OF SOLAR FLARES AND CORONAL MASS EJECTIONS ON THE SOLAR CYCLE PHASE AND THE IMPORTANCE OF LARGE-SCALE CONNECTIVITY

Kangjin **Lee**1, Y.-J. Moon1, and V. M. Nakariakov1,2
2016 ApJ 831 131 DOI 10.3847/0004-637X/831/2/131
http://sci-hub.cc/10.3847/0004-637X/831/2/131
We investigate the dependence of the occurrence rates of major solar flares (M- and X-class) and front-side halo coronal mass ejections (FHCMEs), observed from 1996 to 2013, on the solar cycle (SC) phase for six active McIntosh sunspot group classes: Fkc, Ekc, Dkc, Fki, Eki, and Dki. We classify SC phases as follows: (1) ascending phase of SC 23 (1996–1999), (2) maximum phase of SC 23 (2000–2002), (3) descending phase of SC 23 (2003–2008), and (4) ascending phase of SC 24 (2009–2013). We find that the occurrence rates of major flares and FHCMEs during the descending phase are noticeably higher than those during the other phases for most sunspot group classes. For the most active sunspot group class, Fkc, the occurrence rate of FHCMEs during the descending phase of SC 23 is three times as high as that during the ascending phase of SC 23. The potential of each McIntosh sunspot group class to produce major flares or FHCMEs is found to depend on the SC phase. The occurrence rates (R) of major flares and FHCMEs are strongly anti-correlated with the annual average latitude of the sunspot groups (L): for major flares and for FHCMEs. This finding indicates the possible role of large-scale coronal connectivity, e.g., trans-equatorial loops, in powerful energy releases. Interestingly, this relationship is very similar to that between the volumetric coronal heating rate and X-ray loop lengths, indicating common energy release mechanisms.

Solar rotational modulations of spectral irradiance and correlations with the variability of total solar irradiance

Jae N. **Lee**1,2*, Robert F. Cahalan2 and Dong L. Wu
J. Space Weather Space Clim., 6, A33 (**2016**)
http://www.swsc-journal.org/articles/swsc/pdf/2016/01/swsc160008.pdf
Aims: We characterize the solar rotational modulations of spectral solar irradiance (SSI) and compare them with the corresponding changes of total solar irradiance (TSI). Solar rotational modulations of TSI and SSI at wavelengths between 120 and 1600 nm are identified over one hundred Carrington rotational cycles during 2003–2013.
Methods: The SORCE (Solar Radiation and Climate Experiment) and TIMED (Thermosphere Ionosphere Mesosphere Energetics and Dynamics)/SEE (Solar EUV Experiment) measured and SATIRE-S modeled solar irradiances are analyzed using the EEMD (Ensemble Empirical Mode Decomposition) method to determine the phase and amplitude of 27-day solar rotational variation in TSI and SSI.
Results: The mode decomposition clearly identifies 27-day solar rotational variations in SSI between 120 and 1600 nm, and there is a robust wavelength dependence in the phase of the rotational mode relative to that of TSI. The rotational modes of visible (VIS) and near infrared (NIR) are in phase with the mode of TSI, but the phase of the rotational mode of ultraviolet (UV) exhibits differences from that of TSI. While it is questionable that the VIS to NIR portion of the solar spectrum has yet been observed with sufficient accuracy and precision to determine the 11-year solar cycle variations, the temporal variations over one hundred cycles of 27-day solar rotation, independent of the two solar cycles in which they are embedded, show distinct solar rotational modulations at each wavelength.

Radiation hydrodynamics in simulations of the solar atmosphere **Review**

Jorrit **Leenaarts**

Living Reviews in Solar Physics **17,** 3 **2020**

https://arxiv.org/pdf/2002.03623.pdf

https://link.springer.com/content/pdf/10.1007/s41116-020-0024-x.pdf

Nearly all energy generated by fusion in the solar core is ultimately radiated away into space in the solar atmosphere, while the remaining energy is carried away in the form of neutrinos. The exchange of energy between the solar gas and the radiation field is thus an essential ingredient of atmospheric modeling. The equations describing these interactions are known, but their solution is so computationally expensive that they can only be solved in approximate form in multi-dimensional radiation-MHD modeling. In this review, I discuss the most commonly used approximations for energy exchange between gas and radiation in the photosphere, chromosphere, and corona. **2013 August 6**

Tracing the evolution of radiation-MHD simulations of solar and stellar atmospheres in the Lagrangrian frame

Jorrit **Leenaarts**

A&A **2018**

https://arxiv.org/pdf/1805.06666.pdf

Context: Radiation-MHD simulations have become a standard tool to investigate the physics of solar and stellar atmospheres. Aims: The aim of this paper to present a method that allows efficient and accurate analysis of flows in such simulations in the Lagrangian frame. Methods: This paper presents a method that allows the construction of pathlines given a seed point that can be chosen freely at any location and at any time during the simulation where the simulation state is stored. The method is based on passive tracer particles. Through injection of particles in expanding regions the occurrence of particle-free volumes is avoided, even in the case of strongly compressive flows. Results:The method was implemented in the solar and stellar atmosphere simulation code Bifrost. It is efficient and accurate. As examples I present an analysis of a gas parcel in the convection zone and a particle in the solar transition region.}

On chromospheric heating during flux emergence in the solar atmosphere

Jorrit **Leenaarts**, Jaime de la Cruz Rodríguez, Sanja Danilovic, Göran Scharmer, Mats Carlsson

A&A 612, A28 **2017**

https://arxiv.org/pdf/1712.00474.pdf

Context. The radiative losses in the solar chromosphere vary from 4~kW~m−2 in the quiet Sun, to 20~kW~m−2 in active regions. The mechanisms that transport non-thermal energy to and deposit it in the chromosphere are still not understood. Aims. We aim to investigate the atmospheric structure and heating of the solar chromosphere in an emerging flux region. Methods. We use observations taken with the CHROMIS and CRISP instruments on the Swedish 1-m Solar Telescope in the Ca II K, Ca II 854.2 nm, Hα, and Fe I 630.1 nm and 630.2 nm lines. We analyse the various line profiles and in addition perform multi-line, multi-species, non-Local Thermodynamic Equilibrium (non-LTE) inversions to estimate the spatial and temporal variation of the chromospheric structure. Results. We investigate which spectral features of Ca II K contribute to the frequency-integrated Ca II K brightness, which we use as a tracer of chromospheric radiative losses. The majority of the radiative losses are not associated with localized high-Ca II K-brightness events, but instead with a more gentle, spatially extended, and persistent heating. The frequency-integrated Ca II K brightness correlates strongly with the total linear polarization in the Ca II 854.2 nm line, while the Ca II K profile shapes indicate that the bulk of the radiative losses occur in the lower chromosphere.

Non-LTE inversions indicate a transition from heating concentrated around photospheric magnetic elements below logτ500=−3 to a more space-filling and time-persistent heating above logτ500=−4. The inferred gas temperature at logτ500=−3.8 correlates strongly with the total linear polarization in the Ca II 854.2 nm line, suggesting that that the heating rate correlates with the strength of the horizontal magnetic field in the low chromosphere. **2016-09-19**

The cause of spatial structure in solar He I 1083 nm multiplet images

Jorrit **Leenaarts**, Thomas Golding, Mats Carlsson, Tine Libbrecht, Jayant Joshi

A&A 594, A104 **2016**

http://arxiv.org/pdf/1608.00838v1.pdf

Context. The He i 1083 nm is a powerful diagnostic for inferring properties of the upper solar chromosphere, in particular for the magnetic field. The basic formation of the line in one-dimensional models is well understood, but the influence of the complex 3D structure of the chromosphere and corona has however never been investigated. This structure must play an essential role because images taken in He i 1083 nm show structures with widths down

to 100 km. Aims. To understand the effect of the three-dimensional temperature and density structure in the solar atmosphere on the formation of the He i 1083 nm line. Methods. We solve the non-LTE radiative transfer problem assuming statistical equilibrium for a simple 9-level helium atom that nevertheless captures all essential physics. As a model atmosphere we use a snapshot from a 3D radiation-MHD simulation computed with the Bifrost code. Ionising radiation from the corona is self-consistently taken into account. Results. The emergent intensity in the He i 1083 nm is set by the source function and the opacity in the upper chromosphere. The former is dominated by scattering of photospheric radiation and does not vary much with spatial location. The latter is determined by the photonionisation rate in the He i ground state continuum, as well as the electron density in the chromosphere. The spatial variation of the flux of ionising radiation is caused by the spatially-structured emissivity of the ionising photons from material at T = 100 kK in the transition region. The hotter coronal material produces more ionising photons, but the resulting radiation field is smooth and does not lead to small-scale variation of the UV flux. The corrugation of the transition region further increases the spatial variation of the amount of UV radiation in the chromosphere.

On Fibrils and Field Lines: the Nature of Hα Fibrils in the Solar Chromosphere

Jorrit **Leenaarts**1, Mats Carlsson2, and Luc Rouppe van der Voort
2015 ApJ 802 136
Observations of the solar chromosphere in the line core of the Hα line show dark elongated structures called fibrils that show swaying motion. We performed a three-dimensional radiation-MHD simulation of a network region and computed synthetic Hαimages from this simulation to investigate the relation between fibrils and the magnetic field lines in the chromosphere. The periods, amplitudes, and phase speeds of the simulated fibrils are consistent with observations. We find that some fibrils trace out the same field line along the fibril's length, while other fibrils sample different field lines at different locations along their length. Fibrils sample the same field lines on a timescale of ~200 s. This is shorter than their own lifetime. Fibril-threading field lines carry slow-mode waves, as well as transverse waves propagating with the Alfvén speed. Transverse waves propagating in opposite directions cause an interference pattern with complex apparent phase speeds. The relationship between fibrils and field lines is governed by constant migration and swaying of the field lines, their mass loading and draining, and their visibility in Hα. Field lines are visible where they lie close to the optical depth unity surface. The location of the latter is at a height at which the column mass reaches a certain fixed value. The visibility of the field line is thus determined by its own mass density and by the mass density of the material above it. Using the swaying motion of fibrils as a tracer of chromospheric transverse oscillations must be done with caution.

An Early Sunspot Catalog by Miguel Aguilar for the Period 1914 – 1920

L. **Lefèvre** , A. J. P. Aparicio, M. C. Gallego, J. M. Vaquero
Solar Phys. Volume 291, Issue 9, pp 2609–2628 **2016**
We provide a source of detailed solar parameters spanning the years 1914 – 1920. Although various catalogs containing information on sunspots and sunspot groups have been available for almost 150 years, the contents and conventions can vary greatly from one source to another. Thus, the availability of multiple sources is very important to assess the relative uncertainties in the identified quantities. We provide here a machine-readable version of the sunspot catalog made by M. Aguilar from 1914 to 1920. We show and explain the structure and possible errors found in this catalog. We also try to understand the specific differences of this catalog, i.e. explain the shortcomings and benefits of this catalog versus other available sources of solar information. This catalog, combined with the Valencia catalog, presents a valuable source of comparison with the Royal Greenwich Observatory (RGO or GPR for Greenwich Photoheliographic Results) data, and it helps shed more light on the link between the RGO classification and the more modern classifications of sunspot groups found in the Zürich or McIntosh classifications. We also extend the work started by Carrasco et al. (Solar Phys. 290, 1445, 2015) on the mapping of Cortie types.

Survey and Merging of Sunspot Catalogs

Laure **Lefevre**, Frédéric Clette
Solar Physics, February **2014**, Volume 289, Issue 2, pp 545-561
In view of the construction of new sunspot-based activity indices and proxies, we conducted a comprehensive survey of all existing catalogs providing detailed parameters of photospheric features over long time intervals. Although there are a fair number of such catalogs, a global evaluation showed that they suffer from multiple limitations: finite or fragmented time coverage, limited temporal overlap between catalogs, and, more importantly, a mismatch in contents and conventions. Starting from the existing material, we demonstrate how the information from parallel catalogs can be merged to form a much more comprehensive record of sunspots and sunspot groups. To do this, we use the uniquely detailed Debrecen Photoheliographic Data (DPD), which is already a composite of several ground-based observatories and of SOHO data, and the USAF/Mount Wilson catalog from the Solar Observing Optical Network (SOON). We also outline our cross-identification method, which was needed to match the non-overlapping solar active-region nomenclature. This proved to be the most critical and subtle step when

working with multiple catalogs. This effort, focused here first on the last two solar cycles, should lead to a better central database that collects all available sunspot group parameters to address future solar-cycle studies beyond the traditional sunspot-index time series [R i].

Solar Observation Target Identification Convention for use in *Solar Physics*

John **Leibacher,** Takashi Sakurai, Karel Schrijver (Editorial Board Chair), and Lidia van Driel-Gesztelyi
Solar Phys (**2010**) 263: 1–2

Structure of the solar photosphere studied from the radiation hydrodynamics code ANTARES

P. **Leitner**, B. Lemmerer, A. Hanslmeier, T. Zaqarashvili, A. Veronig, H. Grimm-Strele, H.J. Muthsam
Astrophysics and Space Science 362:181 **2017**
https://arxiv.org/pdf/1708.01156.pdf
https://link.springer.com/content/pdf/10.1007%2Fs10509-017-3151-7.pdf
The ANTARES radiation hydrodynamics code is capable of simulating the solar granulation in detail unequaled by direct observation. We introduce a state-of-the-art numerical tool to the solar physics community and demonstrate its applicability to model the solar granulation. The code is based on the weighted essentially non-oscillatory finite volume method and by its implementation of local mesh refinement is also capable of simulating turbulent fluids. While the ANTARES code already provides promising insights into small-scale dynamical processes occurring in the quiet-Sun photosphere, it will soon be capable of modeling the latter in the scope of radiation magnetohydrodynamics. In this first preliminary study we focus on the vertical photospheric stratification by examining a 3-D model photosphere with an evolution time much larger than the dynamical timescales of the solar granulation and of particular large horizontal extent corresponding to 25"×25" on the solar surface to smooth out horizontal spatial inhomogeneities separately for up- and downflows. The highly resolved Cartesian grid thereby covers ∼4 Mm of the upper convection zone and the adjacent photosphere. Correlation analysis, both local and two-point, provides a suitable means to probe the photospheric structure and thereby to identify several layers of characteristic dynamics: The thermal convection zone is found to reach some ten kilometers above the solar surface, while convectively overshooting gas penetrates even higher into the low photosphere. An ∼145km-wide transition layer separates the convective from the oscillatory layers in the higher photosphere.

Hemispheric asymmetry in meridional flow and the sunspot cycle

B **Lekshmi**, Dibyendu Nandy, H M Antia
MNRAS Volume 489, Issue 1, October **2019**, Pages 714–722
sci-hub.se/10.1093/mnras/stz2168
Magnetohydrodynamic dynamo modelling shows that the large-scale solar meridional plasma flow plays an important role in governing the dynamics of the sunspot cycle. Observations indicate that meridional flow velocities at each solar latitude and depth vary over time and are asymmetric across the equator. Here, using helioseismic observations we explore the temporal variation in the hemispherical asymmetry of near-surface residual (time-varying) component of the Sun's meridional flow velocity. The meridional flow velocities obtained from Global Oscillation Network Group (GONG) and Helioseismic and Magnetic Imager (HMI) onboard Solar Dynamics Observatory (SDO) ring-diagram pipelines are used in this work. Our data set covers the declining phase of cycle 23 and cycle 24 (from July 2001 till December 2018) and the flow velocities are poleward for the observed depth range. We observe a time delayed anticorrelation between the hemispherical asymmetry in near-surface meridional flow velocities and the sunspot cycle quantified in terms of magnetic flux and sunspot number. Interestingly, asymmetry in meridional flow velocity precedes the asymmetry in sunspot cycle by 3.1–3.5 yr. We propose that meridional flow asymmetry is a precursor of asymmetry in hemispherical cycle strength. The symmetric component of meridional flow is observed to be positively correlated with the corresponding symmetric components of the magnetic cycle, also with a time delay. Our analysis sets important constraints on theories for the origin of meridional plasma flow asymmetries and its temporal variations and is relevant for understanding the role of plasma flux transport processes in determining hemispheric asymmetry in the sunspot cycle.
HMI Science Nuggets, #133 Oct **2019** http://hmi.stanford.edu/hminuggets/?p=3125

Asymmetry in Solar Torsional Oscillation and the Sunspot Cycle

Lekshmi B, Dibyendu Nandy, H M Antia
ApJ **861** 121 **2018**
https://arxiv.org/pdf/1807.03588.pdf

Solar torsional oscillations are migrating bands of slower- and faster-than-average rotation, which are strongly related to the Sun's magnetic cycle. We perform a long-term study (16 yr) of hemispherical asymmetry in solar torsional oscillation velocity using helioseismic data for the first time. We study the north-south asymmetry in the velocity using the zonal flow velocities obtained by ring diagram analysis of the Global Oscillation Network Group (GONG) Doppler images. We find significant hemispherical asymmetry in the torsional oscillation velocity and explore its variation with respect to depth, time, and latitude. We also calculate the hemispherical asymmetry in the surface velocity measurements from the Mount Wilson Observatory and the zonal flow velocities obtained from the Helioseismic and Magnetic Imager ring diagram pipeline. These asymmetries are found to be consistent with the asymmetry obtained from GONG observations. We show that the asymmetry in near-surface torsional oscillation velocity is correlated with the asymmetry in magnetic flux and sunspot number at the solar surface, with the velocity asymmetry preceding the flux and sunspot number asymmetries. We speculate that the asymmetry in torsional oscillation velocity may help in predicting the hemispherical asymmetry in sunspot cycles.

Radial Distributions of Coronal Electron Temperatures: Specificities of the DYN Model

Joseph F. **Lemaire** & Athanassios C. Katsiyannis
Solar Physics volume 296, Article number: 64 (**2021**)
https://link.springer.com/content/pdf/10.1007/s11207-021-01814-4.pdf
https://doi.org/10.1007/s11207-021-01814-4
This paper is a follow up of the article where Lemaire and Stegen (Solar Phys. 291(12), 3659, 2016) introduced their DYN method to calculate coronal temperature profiles from given radial distributions of the coronal and solar wind (SW) electron densities. Several such temperature profiles are calculated and presented corresponding to a set of given empirical density models derived from eclipse observations and in-situ measurements of the electron density and bulk velocity at 1 AU. The DYN temperature profiles obtained for the equatorial and polar regions of the corona challenge the results deduced since 1958 from singular hydrodynamical models of the SW. In these models—where the expansion velocity transits through a singular saddle point—the maximum coronal temperature is predicted to be located at the base of the corona, while in all DYN models the altitude of the maximum temperature is found at significantly higher altitudes in the mid-corona. Furthermore, the maximum of the DYN-estimated temperatures is found at much higher altitudes over the polar regions and coronal holes, than over the equator. However, at low altitudes, in the inner corona, the DYN temperatures are always smaller at high latitudes, than at low equatorial latitudes. This appears well in agreement with existing coronal hole observations. These findings have serious implications on the open questions: what is the actual source of the coronal heating, and where is the maximum energy deposited within the solar corona?

Radial distributions of coronal electron densities and temperatures linked to solar wind streams

Joseph F. **Lemaire** (1 and 2), Athanassios C. Katsiyannis (3)
Solar Phys. **2020**
https://arxiv.org/pdf/2002.07495.pdf
This paper is a follow up of the article where Lemaire & Stegen (2016) introduced the novel method to calculate coronal temperature distribution when the Solar Corona is not assumed to be in hydrostatic equilibrium as it has been assumed until 1957. In their study as well as in the present paper it is considered that the corona plasma is expanding with supersonic speeds u_E, and with electron densities n_E, at 1AU is given by the average values determined from the statistical study of the Solar Wind parameters reported by Ebert et al. (2009). In inner coronal altitudes n_e(r) is taken from Saito's (1970) empirical electron density model. It is found that, at high altitudes, the radial profile of the dyn-temperature distributions differ significantly from those obtained by the scale-height method shm-method generally used in the past. It is also found that, at the base of the Corona, the dyn-temperature is smaller over the polar regions (and CHs) than in the equatorial plane. The temperature gradient dT_e/dr has very small and positive values at altitudes above the transition region, between 0.001 R_S and 0.02 R_S. We confirm also that larger Solar Wind (SW) velocities, u(r), observed in fast speed SW streams imply larger temperatures in the solar Corona. Furthermore, the maximum temperature T_{e,max} is always located significantly above the altitude of the transition region.

Improved Determination of the Location of the Temperature Maximum in the Corona

Lemaire, J.F. & Stegen, K.
Sol Phys (**2016**) 291: 3659.
The most used method to calculate the coronal electron temperature [*Te(r)*] from a coronal density distribution [*ne(r)*] is the scale-height method (SHM). We introduce a novel method that is a generalization of a method introduced by Alfven (*Ark. Mat. Astron.Fys.* **27**, 1, 1941) to calculate *Te(r)* for a corona in hydrostatic equilibrium: the “HST” method. All of the methods discussed here require given electron-density distributions [*ne(r)*] which can be derived from white-light (WL) eclipse observations. The new “DYN” method determines the unique solution of

Te(r) for which *Te(r→∞)*→0 when the solar corona expands radially as realized in hydrodynamical solar-wind models. The applications of the SHM method and DYN method give comparable distributions for *Te(r)*. Both have a maximum [*T*max] whose value ranges between 1 – 3 MK. However, the peak of temperature is located at a different altitude in both cases. Close to the Sun where the expansion velocity is subsonic (r < 1.3R_) the DYN method gives the same results as the HST method. The effects of the other free parameters on the DYN temperature distribution are presented in the last part of this study. Our DYN method is a new tool to evaluate the range of altitudes where the heating rate is maximum in the sola

A coupled 2×2D Babcock-Leighton solar dynamo model. II. Reference dynamo solutions

Alexandre **Lemerle**, Paul Charbonneau

ApJ **834** 133 **2017**

http://arxiv.org/pdf/1606.07375v1.pdf

In this paper we complete the presentation of a new hybrid 2×2D flux transport dynamo (FTD) model of the solar cycle based on the Babcock-Leighton mechanism of poloidal magnetic field regeneration via the surface decay of bipolar magnetic regions (BMRs). This hybrid model is constructed by allowing the surface flux transport (SFT) simulation described in Lemerle et al. 2015 to provide the poloidal source term to an axisymmetric FTD simulation defined in a meridional plane, which in turn generates the BMRs required by the SFT. A key aspect of this coupling is the definition of an emergence function describing the probability of BMR emergence as a function of the spatial distribution of the internal axisymmetric magnetic field. We use a genetic algorithm to calibrate this function, together with other model parameters, against observed cycle 21 emergence data. We present a reference dynamo solution reproducing many solar cycle characteristics, including good hemispheric coupling, phase relationship between the surface dipole and the BMR-generating internal field, and correlation between dipole strength at cycle maximum and peak amplitude of the next cycle. The saturation of the cycle amplitude takes place through the quenching of the BMR tilt as a function of the internal field. The observed statistical scatter about the mean BMR tilt, built into the model, acts as a source of stochasticity which dominates amplitude fluctuations. The model thus can produce Dalton-like epochs of strongly suppressed cycle amplitude lasting a few cycles and can even shut off entirely following an unfavorable sequence of emergence events.

A COUPLED 2 × 2D BABCOCK–LEIGHTON SOLAR DYNAMO MODEL. I. SURFACE MAGNETIC FLUX EVOLUTION

Alexandre **Lemerle**1,2, Paul Charbonneau1, and Arnaud Carignan-Dugas

2015 ApJ 810 78

http://arxiv.org/pdf/1511.08548v1.pdf

The need for reliable predictions of the solar activity cycle motivates the development of dynamo models incorporating a representation of surface processes sufficiently detailed to allow assimilation of magnetographic data. In this series of papers we present one such dynamo model, and document its behavior and properties. This first paper focuses on one of the model's key components, namely surface magnetic flux evolution. Using a genetic algorithm, we obtain best-fit parameters of the transport model by least-squares minimization of the differences between the associated synthetic synoptic magnetogram and real magnetographic data for activity cycle 21. Our fitting procedure also returns Monte Carlo-like error estimates. We show that the range of acceptable surface meridional flow profiles is in good agreement with Doppler measurements, even though the latter are not used in the fitting process. Using a synthetic database of bipolar magnetic region (BMR) emergences reproducing the statistical properties of observed emergences, we also ascertain the sensitivity of global cycle properties, such as the strength of the dipole moment and timing of polarity reversal, to distinct realizations of BMR emergence, and on this basis argue that this stochasticity represents a primary source of uncertainty for predicting solar cycle characteristics.

The Göttingen Solar Radial Velocity Project: Sub-m/s Doppler precision from FTS observations of the Sun as a star

Ulrike **Lemke**, Ansgar Reiners

PASP (Publications of the Astronomical Society of the Pacific) **2016**

http://arxiv.org/pdf/1603.00470v1.pdf

Radial velocity observations of stars are entering the sub-m/s domain revealing fundamental barriers for Doppler precision experiments. Observations of the Sun as a star can easily overcome the m/s photon limit but face other obstacles. We introduce the G\"ottingen Solar Radial Velocity Project with the goal to obtain high precision (cm/s) radial velocity measurements of the Sun as a star with a Fourier Transform Spectrograph. In this first paper, we present the project and first results. The photon limit of our 2 min observations is at the 2 cm/s level but currently

limited by strong instrumental systematics. A drift of a few m/s per h is visible in all observing days probably caused by vignetting of the solar disk in our fiber coupled setup, and imperfections of our guiding system adds further offsets in our data. Binning the data into 30 min groups shows m/s stability after correcting for a daily and linear instrumental trend. Our results show the potential of Sun-as-a-star radial velocity measurements that can possibly be achieved after a substantial upgrade of our spectrograph coupling strategy. Sun-as-a-star observations can provide crucial empirical information about the radial velocity signal of convective motion and stellar activity, and on the wavelength dependence of radial velocity signals caused by stellar line profile variations.

Dynamics of small-scale convective motions

Birgit **Lemmerer**, Arnold Hanslmeier, Herbert Muthsam, Isabell Piantschitsch
A&A **2016**
https://arxiv.org/pdf/1611.06786v1.pdf
Previous studies have discovered a population of small granules with diameters less than 800 km showing differing physical properties. High resolution simulations and observations of the solar granulation, in combination with automated segmentation and tracking algorithms, allow us to study the evolution of the structural and physical properties of these granules and surrounding vortex motions with high temporal and spatial accuracy. We focus on the dynamics of granules (lifetime, fragmentation, size, position, intensity, vertical velocity) over time and the influence of strong vortex motions. Of special interest are the dynamics of small granules compared to regular-sized granules. We developed a temporal tracking algorithm based on our developed segmentation algorithm for solar granulation. This was applied to radiation hydrodynamics simulations and high resolution observations of the quiet Sun by SUNRISE/IMaX. The dynamics of small granules differ in regard to their diameter, intensity and depth evolution compared to regular granules. The tracked granules in the simulation and observations reveal similar dynamics (lifetime, evolution of size, vertical velocity and intensity). The fragmentation analysis shows that the majority of granules in simulations do not fragment, while the opposite was found in observations. Strong vortex motions were detected at the location of small granules. Regions of strong vertical vorticity show high intensities and downflow velocities, and live up to several minutes. The analysis of granules separated according to their diameter in different groups reveals strongly differing behaviors. The largest discrepancies can be found within the groups of small, medium-sized and large granules and have to be analyzed independently. The predominant location of vortex motions on and close to small granules indicates a strong influence on the dynamics of granules.

Varying Driver Velocity Fields in Photospheric MHD Wave Simulations

A. J. **Leonard**, S. J. Mumford, V. Fedun, R. Erdelyi
MNRAS **2018**
https://arxiv.org/pdf/1807.10049.pdf
Torsional motions are ubiquitous in the solar atmosphere. In this work, we perform 3D numerical simulations which mimic a vortex-type photospheric driver with a Gaussian spatial profile. This driver is implemented to excite MHD waves in an axially symmetric, 3D magnetic flux tube embedded in a realistic solar atmosphere. The Gaussian width of the driver is varied and the resulting perturbations are compared. Velocity vectors were decomposed into parallel, perpendicular and azimuthal components with respect to pre-defined magnetic flux surfaces. These components correspond broadly to the fast, slow and Alfven modes, respectively. From these velocities the corresponding wave energy fluxes are calculated, allowing us to estimate the contribution of each mode to the energy flux. For the narrowest driver (0.15 Mm) the parallel component accounts for ∼55−65%of the flux. This contribution increases smoothly with driver width up to nearly 90% for the widest driver (0.35Mm). The relative importance of the perpendicular and azimuthal components decrease at similar rates. The azimuthal energy flux varied between ∼35% for the narrowest driver and <10% for the widest one. Similarly, the perpendicular flux was ∼25−10%. We also demonstrate that the fast mode corresponds to the sausage wave in our simulations. Our results therefore show that the fast sausage wave is easily excited by this driver and that it carries the majority of the energy transported. For this vortex-type driver the Alfven wave does not contribute a significant amount of energy.

Temperature diagnostics of the solar atmosphere using SunPy

Andrew **Leonard**, Huw Morgan
Proceedings of the 7th European Conference on Python in Science (EuroSciPy 2014), Pierre de Buyl and Nelle Varoquaux editors, (**2014**)
http://arxiv.org/pdf/1412.6483v1.pdf
The solar atmosphere is a hot (about 1MK), magnetised plasma of great interest to physicists. There have been many previous studies of the temperature of the Sun's atmosphere (Plowman2012, Wit2012, Hannah2012, Aschwanden2013, etc.). Almost all of these studies use the SolarSoft software package written in the commercial Interactive Data Language (IDL), which has been the standard language for solar physics. The SunPy project aims to provide an open-source library for solar physics. This work presents (to the authors' knowledge) the first study of its type to use SunPy rather than SolarSoft. This work uses SunPy to process multi-wavelength solar observations made by the Atmospheric Imaging Assembly (AIA) instrument aboard the Solar Dynamics Observatory (SDO) and

produce temperature maps of the Sun's atmosphere. The method uses SunPy's utilities for querying databases of solar events, downloading solar image data, storing and processing images as spatially aware Map objects, and tracking solar features as the Sun rotates. An essential consideration in developing this software is computational efficiency due to the large amount of data collected by AIA/SDO, and in anticipating new solar missions which will result in even larger sets of data. An overview of the method and implementation is given, along with tests involving synthetic data and examples of results using real data for various regions in the Sun's atmosphere.

Wings of the butterfly: Sunspot groups for 1826–2015⋆

R. **Leussu**1, I. G. Usoskin1,2, V. Senthamizh Pavai3,4, A. Diercke3,4, R. Arlt3, C. Denker3 and K. Mursula1

A&A 599, A131 (**2017**)

The spatio-temporal evolution of sunspot activity, the so-called Maunder butterfly diagram, has been continously available since 1874 using data from the Royal Greenwich Observatory, extended by SOON network data after 1976. Here we present a new extended butterfly diagram of sunspot group occurrence since 1826, using the recently digitized data from Schwabe (1826–1867) and Spörer (1866–1880). The wings of the diagram are separated using a recently developed method based on an analysis of long gaps in sunspot group occurrence in different latitude bands. We define characteristic latitudes, corresponding to the start, end, and the largest extent of the wings (the F, L, and H latitudes). The H latitudes (30°–45°) are highly significantly correlated with the strength of the wings (quantified by the total sum of the monthly numbers of sunspot groups). The F latitudes (20°–30°) depict a weak tendency, especially in the southern hemisphere, to follow the wing strength. The L latitudes (2°–10°) show no clear relation to the wing strength. Overall, stronger cycle wings tend to start at higher latitudes and have a greater wing extent. A strong (5–6)-cycle periodic oscillation is found in the start and end times of the wings and in the overlap and gaps between successive wings of one hemisphere. While the average wing overlap is zero in the southern hemisphere, it is two to three months in the north. A marginally significant oscillation of about ten solar cycles is found in the asymmetry of the L latitudes. The new long database of butterfly wings provides new observational constraints to solar dynamo models that discuss the spatio-temporal distribution of sunspot occurrence over the solar cycle and longer.

Properties of sunspot cycles and hemispheric wings since the 19th century

Raisa **Leussu**1, Ilya G. Usoskin1,2, Rainer Arlt3 and Kalevi Mursula1

A&A 592, A160 (**2016**)

Aims. The latitudinal evolution of sunspot emergence over the course of the solar cycle, the so-called butterfly diagram, is a fundamental property of the solar dynamo. Here we present a study of the butterfly diagram of sunspot group occurrence for cycles 7–10 and 11–23 using data from a recently digitized sunspot drawings by Samuel Heinrich Schwabe in 1825–1867, and from RGO/USAF/NOAA(SOON) compilation of sunspot groups in 1874–2015.

Methods. We developed a new, robust method of hemispheric wing separation based on an analysis of long gaps in sunspot group occurrence in different latitude bands. The method makes it possible to ascribe each sunspot group to a certain wing (solar cycle and hemisphere), and separate the old and new cycle during their overlap. This allows for an improved study of solar cycles compared to the common way of separating the cycles.

Results. We separated each hemispheric wing of the butterfly diagram and analysed them with respect to the number of groups appearing in each wing, their lengths, hemispheric differences, and overlaps.

Conclusions. The overlaps of successive wings were found to be systematically longer in the northern hemisphere for cycles 7–10, but in the southern hemisphere for cycles 16–22. The occurrence of sunspot groups depicts a systematic long-term variation between the two hemispheres. During Schwabe time, the hemispheric asymmetry was north-dominated during cycle 9 and south-dominated during cycle 10.

The Effect of Missing Groups in the Calculation of the Solar Irradiance Deficit
Analysis of the Sunspot Areas from the SOON Network

Luis **Leuzzi**, Laura A. Balmaceda & Carlos Francile

Solar Physics volume 296, Article number: 149 (**2021**)

https://link.springer.com/content/pdf/10.1007/s11207-021-01893-3.pdf

https://doi.org/10.1007/s11207-021-01893-3

Sunspot areas are one of the most important indices of solar activity. To obtain an extended time series covering multiple solar cycles, one must combine data from different observatories after a proper comparison and calibration of the individual datasets. We compare the daily and group values of sunspot areas provided by the different stations from the Solar Optical Observing Network, SOON, which are determined using similar instruments and techniques. We investigate if there are systematic differences among the stations and whether the differences in the daily values can be attributed to missing groups in the records or errors in the measurements. We find significant differences among the stations of the SOON network in terms of sizes (average daily and group values), quality of observations and coverage (considering the number of missing groups and data gaps). Our results indicate that calibration factors

for daily values can be used with confidence to combine datasets from different stations. However, for some applications which require the location of the sunspot groups, the same correction factors should not be used. We estimate the irradiance deficit due to sunspot through the Photometric Sunspot Index and compare the output from similar datasets to quantify the effect of missing groups. We find differences as high as 150 ppm during the maximum of solar cycle. The effect increases for sunspot groups near the center of the disk accounting for about 80% of the observed differences.

A solar tornado observed by EIS: Plasma diagnostics

Peter **Levens**, Nicolas Labrosse, Lyndsay Fletcher, Brigitte Schmieder
A&A 582, A27 **2015**
http://arxiv.org/pdf/1508.01377v1.pdf
https://www.aanda.org/articles/aa/pdf/2015/10/aa25586-14.pdf
The term `solar tornadoes' has been used to describe apparently rotating magnetic structures above the solar limb, as seen in high resolution images and movies from the Atmospheric Imaging Assembly (AIA) aboard the Solar Dynamics Observatory (SDO). These often form part of the larger magnetic structure of a prominence, however the links between them remain unclear. Here we present plasma diagnostics on a tornado-like structure and its surroundings, seen above the limb by the Extreme-ultraviolet Imaging Spectrometer (EIS) aboard the Hinode satellite. We aim to extend our view of the velocity patterns seen in tornado-like structures with EIS to a wider range of temperatures and to provide insight into the physical characteristics of the plasma. Using Gaussian fitting to fit and de-blend the spectral lines seen by EIS, we calculated line-of-sight velocities and non-thermal line widths. Along with information from the CHIANTI database, we used line intensity ratios to calculate electron densities at each pixel. Using a regularised inversion code we also calculated the differential emission measure (DEM) at different locations in the prominence. The split Doppler-shift pattern is found to be visible down to a temperature of around log(T) = 6.0. At temperatures lower than this, the pattern is unclear in this data set. We obtain an electron density of log(n_e) = 8.5 when looking towards the centre of the tornado structure at a plasma temperature of log(T) = 6.2, as compared to the surroundings of the tornado structure where we find log(n_e) to be nearer 9. Non-thermal line widths show broader profiles at the tornado location when compared to the surrounding corona. We discuss the differential emission measure in both the tornado and the prominence body, which suggests that there is more contribution in the tornado at temperatures below log(T) = 6.0 than in the prominence. **14 September 2013**

First Solar Orbiter observation of a dark halo in the solar atmosphere

Serena Maria **Lezzi**, David M. Long, Vincenzo Andretta, Deborah Baker, Antoine Dolliou, Mariarita Murabito, Susanna Parenti, Natalia Zambrana Prado
A&A Letter 690, A342 **2024**
https://arxiv.org/pdf/2408.17172
Solar active regions (ARs) are often surrounded by dark large areas of reduced emission compared to the quiet Sun, observed at various wavelengths corresponding to chromosphere, transition region (TR) and corona, and known as Dark Halos (DHs). DHs have been insufficiently studied, and the mechanisms behind their darker emission remain unclear. This study aims to investigate for the first time the fine structure of a DH observed by the EUV High Resolution Imager (HRIEUV) onboard the ESA's Solar Orbiter (SO) mission and its appearance in the TR. We utilized the extensive 1-hour dataset from SO on **19 March 2022**, which includes high-resolution observations of NOAA 12967 and part of the surrounding DH. We analyzed the dynamics of the HRIEUV DH fine structure and its appearance in the HRILyα image and the Spectral Imaging of the Coronal Environment (SPICE) Lyβ, C III, N VI, O VI and Ne VIII lines, which sample the TR in the logT (K) ∼ 4.0 - 5.8 range. This analysis was complemented with a simultaneous BLOS magnetogram taken by the High Resolution Telescope (HRT). We report the presence of a peculiar fine structure which is not observed in the quiet Sun, characterized by combined bright EUV bundles and dark regions, arranged and interconnected in such a way that they cannot be clearly separated. They form a spatial continuum extending approximately radially from the AR core, suggesting a deep connection between the DH and the AR. Additionally, we find that the bright EUV bundles are observed in all the SPICE TR lines and the HRILyα band and present photospheric BLOS footprints in the HRT magnetogram. This spatial correlation indicates that the origin of the 174 Å DH may lie in the low atmosphere, i.e. photosphere/chromosphere.

Dark halos around solar active regions. I. Emission properties of the dark halo around NOAA 12706

Serena M. **Lezzi** [1,2], Vincenzo Andretta [2], Mariarita Murabito [3,4] & Giulio Del Zanna [5]
Astronomy & Astrophysics, Volume 680, id.A61, **2023**
https://www.aanda.org/articles/aa/pdf/2023/12/aa47414-23.pdf
Context. Dark areas around active regions (ARs) were first observed in chromospheric lines more than a century ago and are now associated with the Hα fibril vortex around ARs. Nowadays, large areas surrounding ARs with reduced emission relative to the quiet Sun (QS) are also observed in spectral lines emitted in the transition region (TR) and the low corona. For example, they are clearly seen in the SDO/AIA 171 Å images. We name these chromospheric

and TR-coronal dark regions "dark halos" (DHs). Coronal DHs are poorly studied and, because their origin is still unknown, to date it is not clear if they are related to the chromospheric fibrillar ones. Furthermore, they are often mistaken for coronal holes (CHs).
Aims: Our goal is to characterize the emission properties of a DH by combining, for the first time, chromospheric, TR, and coronal observations in order to provide observational constraints for future studies on the origin of DHs. This study also aims to investigate the different properties of DHs and CHs and provide a quick-look recipe to distinguish between them.
Methods: We studied the DH around AR NOAA 12706 and the southern CH that were on the disk on **April 22, 2018** by analyzing IRIS full-disk mosaics and SDO/AIA filtergrams to evaluate their average intensities, normalized to the QS. In addition, we used the AIA images to derive the DH and CH emission measure (EM) and the IRIS Si IV 1393.7 Å line to estimate the nonthermal velocities of plasma in the TR. We also employed SDO/HMI magnetograms to study the average magnetic field strength inside the DH and the CH.
Results: Fibrils are observed all around the AR core in the chromospheric Mg II h&k IRIS mosaics, most clearly in the h3 and k3 features. The TR emission in the DH is much lower than in the QS area, unlike in the CH. Moreover, the DH is much more extended in the low corona than in the chromospheric Mg II h3 and k3 images. Finally, the intensities, EM, spectral profile, nonthermal velocity, and average magnetic field strength measurements clearly show that DHs and CHs exhibit different characteristics, and therefore should be considered as distinct types of structures on the Sun.
IRIS Nugget Jan **2024** https://iris.lmsal.com/nugget

The differential rotation of the chromosphere and the quiet chromosphere in the falling and rising period of a solar cycle

KJ **Li**, JC Xu
MNRAS Volume 528, Issue 2, February **2024**, Pages 1438–1444,
https://arxiv.org/pdf/2401.02613.pdf
https://academic.oup.com/mnras/article-pdf/528/2/1438/56409461/stae044.pdf
The full-disk chromosphere was routinely monitored in the He I 10830Å\, line at the National Solar Observatory/Kitt Peak from 2004 Nov. to 2013 March, and thereby, synoptic maps of He I line intensity from Carrington rotations 2032 to 2135 were acquired. They are utilized to investigate the differential rotation of the chromosphere and the quiet chromosphere during the one falling (descending part of solar cycle 23) and the one rising (ascending part of solar cycle 24) period of a solar cycle. Both the quiet chromosphere and the chromosphere are found to rotate slower and have a more prominent differential rotation, in the rising period of solar cycle 24 than in the falling period of solar cycle 23, and an illustration is offered.

How are the abnormally hot chromosphere and corona heated by the solar magnetic fields?

K. J. **Li**, J. C. Xu, W. F eng, J. L. Xie, X. J. Shi, L. H. Deng
ApJ **962** 144 **2024**
https://arxiv.org/pdf/2401.02617.pdf
https://iopscience.iop.org/article/10.3847/1538-4357/ad1ab3/pdf
The corona is a structure possessed by stars, including the sun. The abnormal heating of the solar corona and chromosphere is one of the greatest mysteries in modern astronomy. While state-of-the-art observations have identified some candidates of magnetic activity events that could be responsible for this abnormal heating, and theoretical studies have proposed various heating modes, a complete physical picture of how they are heated as a whole remains elusive. In this study, the characteristics of the heated corona and chromosphere are investigated, and for the first time, the question of how they are abnormally heated is explicitly answered by analyzing the long-term observations of the global chromosphere in the Ca II K line and the global corona in the coronal green line. The findings reveal that both the quiet chromosphere and corona are in anti-phase with the solar cycle, whereas the active chromosphere and corona are in phase with it. Different parts of the solar corona and chromosphere exhibit significantly different variation characteristics, and are found to be heated by different magnetic categories and probably in different modes. This study posits that unraveling the heating mystery is best approached through the lens of magnetic categories, rather than magnetic activity events.

Study of Global Photospheric and Chromospheric Flows Using Local Correlation Tracking and Machine Learning Methods I: Methodology and Uncertainty Estimates

Qin **Li**, Yan Xu,Meetu Verma, Carsten Denker, Junwei Zhao & Haimin Wang
Solar Physics volume 298, Article number: 62 (**2023**)
https://link.springer.com/content/pdf/10.1007/s11207-023-02158-x.pdf

Cyclical variations of the solar magnetic fields, and hence the level of solar activity, are among the top interests of space weather research. Surface flows in global-scale, in particular differential rotation and meridional flows, play important roles in the solar dynamo that describes the origin and variation of solar magnetic fields. In principle, differential rotation is the fundamental cause of dipole field formation and emergence, and meridional flows are the surface component of a longitudinal circulation that brings decayed field from low latitudes to polar regions. Such flows are key inputs and constraints of observational and modeling studies of solar cycles. Here, we present two methods, local correlation tracking (LCT) and machine learning-based self-supervised optical flow methods, to measure differential rotation and meridional flows from full-disk magnetograms that probe the photosphere and Hα images that probe the chromosphere, respectively. LCT is robust in deriving photospheric flows using magnetograms. However, we found that it failed to trace flows using time-sequence Hα data because of the strong dynamics of traceable features. The optical flow methods handle Hα data better to measure the chromospheric flow fields. We found that the differential rotation from photospheric and chromospheric measurements shows a strong correlation with a maximum of 2.85 μrads−1 at the equator and the accuracy holds until 60◦60◦ for the MDI and Hα, 75◦ for the HMI dataset. On the other hand, the meridional flow deduced from the chromospheric measurement shows a similar trend as the concurrent photospheric measurement within 60◦60◦ with a maximum of 20 ms−1 at 40◦ in latitude. Furthermore, the measurement uncertainties are discussed.

The quiet chromosphere: differential rotation

K J **Li**, M Wan, W Feng

MNRAS, Volume 520, Issue 4, April **2023**, Pages 5928–5937,

https://doi.org/10.1093/mnras/stad478

The solar chromosphere was daily observed in the Ca II K line at the Mount Wilson Observatory from 1915 August to 1985 July. A digitized data base was created, which includes synoptical maps of the chromosphere in Ca II intensity from Carrington rotations 827 to 1764. We have used the data base to investigate rotation and its differential of the chromosphere and the quiet chromosphere. The chromosphere is found to rotate faster than sunspots, but the difference in their rotation rates decreases with decreasing latitude, and near the equator they rotate at nearly the same speed. The chromosphere is obviously faster than the quiet photosphere and slightly faster than the quiet chromosphere at low latitudes, but slightly slower than the quiet chromosphere at middle latitudes. The differential degree of the rotation rate at low latitudes, ranging from largest to smallest in order, is found to be: sunspots, the chromosphere, the quiet photosphere, and the quiet chromosphere. The differential of the rotation rate is found to be different in different solar cycles for the chromosphere and the quiet chromosphere. Helioseismology observations suggest that these findings are plausible.

Three-Dimensional Propagation of Kink Wave Trains in Solar Coronal Slabs

Bo **Li**, Mingzhe Guo, Hui Yu, Shao-Xia Chen, Mijie Shi

MNRAS Letters **2022**

https://arxiv.org/pdf/2210.16104

Impulsively excited wave trains are of considerable interest in solar coronal seismology. To our knowledge, however, it remains to examine the three-dimensional (3D) dispersive propagation of impulsive kink waves in straight, field-aligned, symmetric, low-beta, slab equilibria that are structured only in one transverse direction. We offer a study here, starting with an analysis of linear oblique kink modes from an eigenvalue problem perspective. Two features are numerically found for continuous and step structuring alike, one being that the group and phase velocities may lie on opposite sides of the equilibrium magnetic field ($\vec{B}_0$), and the other being that the group trajectories extend only to a limited angle from $\vec{B}_0$. We justify these features by making analytical progress for the step structuring. More importantly, we demonstrate by a 3D time-dependent simulation that these features show up in the intricate interference patterns of kink wave trains that arise from a localized initial perturbation. In a plane perpendicular to the direction of inhomogeneity, the large-time slab-guided patterns are confined to a narrow sector about $\vec{B}_0$, with some wavefronts propagating toward $\vec{B}_0$. We conclude that the phase and group diagrams lay the necessary framework for understanding the complicated time-dependent behavior of impulsive waves.

The role and contribution of magnetic fields, characterized via their magnetic flux, to the statistical structuring of the solar atmosphere

K.J. **Li**, J.C. Xu, W. Feng

Scientifc Reports | (**2022**) 12:15877 | https://www.nature.com/srep/

https://doi.org/10.1038/s41598-022-20094-x

https://arxiv.org/ftp/arxiv/papers/2209/2209.13789.pdf

https://www.nature.com/articles/s41598-022-20094-x.pdf

The anomalous heating of the solar upper atmosphere is one of the eight key problems in modern astronomy. Moreover, the stratification of the solar atmosphere is an outstanding key-problem in solar physics. In this study, a hot butterfly-like pattern is found to run through the chromosphere to the corona lying right on top of the magnetic butterfly pattern of sunspots in the photosphere. We thus propose to introduce the term butterfly body to describe the

butterfly diagram in the 3-dimensional atmosphere. Besides, we discuss the so-called polar brightening in different layers. It is found to be statistically in anti-phase with the solar cycle in the photosphere and the chromosphere, while in phase with the solar cycle in the corona. Accordingly, we describe the role and relationship of solar magnetic elements of different magnetic flux strengths to explain the statistical structuring of the solar atmosphere with the butterfly body over the solar cycle.

On the Energy Dispersion of Magnetic Rossby Waves

Yaokun **Li**
2022 ApJ 934 40
https://iopscience.iop.org/article/10.3847/1538-4357/ac778d/pdf
The energy dispersion of magnetic Rossby waves has been investigated by applying the two-dimensional incompressible magnetohydrodynamic (MHD) equations in both uniform basic flow and basic magnetic field. The dispersion relation suggests that the magnetic Rossby waves can be divided into fast- and slow-propagating modes, respectively. The fast-propagating mode propagates eastward and is similar to the fast Alfvén waves. The energy dispersion speed is faster than the phase speed, which means the perturbation energy can lead the perturbations themselves to arrive downstream. The slow-propagating waves with smaller (larger) horizontal scales are similar to those of the slow Alfvén waves (Rossby waves). The zonal group velocity is slower than the zonal phase speed for the slow-propagating magnetic Rossby waves. For the slow-propagating waves that propagate eastward, this means that the perturbation energy may trigger new perturbations that are located upstream of the perturbations themselves. The group velocity vector is basically same as (opposite of) the wavevector for the fast-propagating (slow-propagating) magnetic Rossby waves that propagate eastward. The endpoints of the group velocity vectors and the wavevector multiplying a factor are located on a cycle in the wavenumber space. Due to the uniform basic flow and the uniform basic magnetic field, the energy dispersion paths (called rays) are straight lines. Along the straight-line rays, the wave action, wave energy, and amplitude keep their initial values, and the wave neither develops nor decays.

The Chinese H{\alpha} Solar Explorer (CHASE) Mission: An overview,

C. **Li**, C. Fang, Z. Li, M. D. Ding, P. F. Chen, Y. Qiu, et al.,
Sci. China-Phys. Mech. Astron. 65, 289602 (**2022**)
https://arxiv.org/pdf/2205.05962
The Chinese H{\alpha} Solar Explorer (CHASE), dubbed "Xihe" - Goddess of the Sun, was launched on October 14, 2021 as the first solar space mission of China National Space Administration (CNSA). The CHASE mission is designed to test a newly developed satellite platform and to acquire the spectroscopic observations in the H{\alpha} waveband. The H{\alpha} Imaging Spectrograph (HIS) is the scientific payload of the CHASE satellite. It consists of two observational modes: raster scanning mode and continuum imaging mode. The raster scanning mode obtains full-Sun or region-of-interest spectral images from 6559.7 to 6565.9 Å and from 6567.8 to 6570.6 Å with 0.024 Å pixel spectral resolution and 1 minute temporal resolution. The continuum imaging mode obtains photospheric images in continuum around 6689 Å with the full width at half maximum of 13.4 Å. The CHASE mission will advance our understanding of the dynamics of solar activity in the photosphere and chromosphere. In this paper, we present an overview of the CHASE mission including the scientific objectives, HIS instrument overview, data calibration flow, and first results of on-orbit observations.

Coronal rain in randomly heated arcades

Xiaohong **Li** , 1 Rony Keppens , 1 and Yuhao Zhou
ApJ **2021**
https://arxiv.org/pdf/2112.02702.pdf
Adopting the MPI-AMRVAC code, we present a 2.5-dimensional magnetohydrodynamic (MHD) simulation, which includes thermal conduction and radiative cooling, to investigate the formation and evolution of the coronal rain phenomenon. We perform the simulation in initially linear force-free magnetic fields which host chromospheric, transition region, and coronal plasma, with turbulent heating localized on their footpoints. Due to thermal instability, condensations start to occur at the loop top, and rebound shocks are generated by the siphon inflows. Condensations fragment into smaller blobs moving downwards and as they hit the lower atmosphere, concurrent upflows are triggered. Larger clumps show us clear “coronal rain showers” as dark structures in synthetic EUV hot channels and bright blobs with cool cores in the 304 ˚A channel, well resembling real observations. Following coronal rain dynamics for more than 10 hours, we carry out a statistical study of all coronal rain blobs to quantify their widths, lengths, areas, velocity distributions, and other properties. The coronal rain shows us continuous heating-condensation cycles, as well as cycles in EUV emissions. Compared to previous studies adopting steady heating, the rain happens faster and in more erratic cycles. Although most blobs are falling downward, upward-moving blobs exist at basically every moment. We also track the movement of individual blobs to study their dynamics and the forces driving their movements. The blobs have a prominence-corona transition-region-like structure surrounding them, and their movements are dominated by the pressure evolution in the very dynamic loop system.

Three-dimensional magnetic reconnection in astrophysical plasmas Review

Li, Ting ; Priest, Eric ; Guo, Ruilong

Proceedings of the Royal Society A, Volume 477, Issue 2249, article id.20200949, **2021**

https://arxiv.org/pdf/2104.05174.pdf

https://royalsocietypublishing.org/doi/pdf/10.1098/rspa.2020.0949

https://doi.org/10.1098/rspa.2020.0949

Magnetic reconnection is a fundamental process in laboratory, magnetospheric, solar and astrophysical plasmas, whereby magnetic energy is converted into heat, bulk kinetic energy and fast particle energy. Its nature in two dimensions is much better understood than that in three dimensions, where its character is completely different and has many diverse aspects that are currently being explored. Here, we focus on the magnetohydrodynamics of three-dimensional reconnection in the plasma environment of the Solar System, especially solar flares. The theory of reconnection at null points, separators and quasi-separators is described, together with accounts of numerical simulations and observations of these three types of reconnection. The distinction between separator and quasi-separator reconnection is a theoretical one that is unimportant for the observations of energy release. A new paradigm for solar flares, in which three-dimensional reconnection plays a central role, is proposed.

Is Solar Minimum 24/25 Another Unusual One?

Huichao **Li**, Xueshang Feng, Fengsi Wei

ApJL **917** L26 **2021**

https://arxiv.org/pdf/2107.04944.pdf

https://doi.org/10.3847/2041-8213/ac13a6

The solar minimum 23/24 is considered to be unusual because it exhibits features that differ notably from those commonly seen in pervious minima. In this letter, we analyze the solar polar magnetic field, the potential-field solution of the solar corona, and the in-situ solar wind measurements to see whether the recent solar minimum 24/25 is another unusual one. While the dipolar configuration that are commonly seen during minimum 22/23 and earlier minima persist for about half a year after the absolute minimum of solar cycle 24, the corona has a morphology more complex than a simple dipole before the absolute minimum. The fast solar wind streams are less dominant than minimum 23/24. The IMF strength, density and mass flux that are historically low in the minimum 23/24 are regained during minimum 24/25, but still do not reach the minimum 22/23 level. From the analysis of this Letter, it seems that the minimum 24/25 is only partially unusual, and the recovery of the commonly minimum features may result from the enhancement of the polar field.

Revisiting the formation mechanism for coronal rain from previous studies

Leping **Li**, Hardi Peter, Lakshmi Pradeep Chitta, Hongqiang Song

Research in Astronomy and Astrophysics **21** 255 **2021**

https://arxiv.org/pdf/2107.01339.pdf

https://doi.org/10.1088/1674-4527/21/10/255

Solar coronal rain is classified generally into two categories: flare-driven and quiescent coronal rain. The latter is observed to form along both closed and open magnetic field structures. Recently, we proposed that some of the quiescent coronal rain events, detected in the transition region and chromospheric diagnostics, along loop-like paths could be explained by the formation mechanism for quiescent coronal rain facilitated by interchange magnetic reconnection between open and closed field lines. In this study, we revisited 38 coronal rain reports from the literature. From these earlier works, we picked 15 quiescent coronal rain events out of the solar limb, mostly suggested to occur in active region closed loops due to thermal nonequilibrium, to scrutinize their formation mechanism. Employing the extreme ultraviolet images and line-of-sight magnetograms, the evolution of the quiescent coronal rain events and their magnetic fields and context coronal structures is examined. We find that 6, comprising 40%, of the 15 quiescent coronal rain events could be totally or partially interpreted by the formation mechanism for quiescent coronal rain along open structures facilitated by interchange reconnection. The results suggest that the quiescent coronal rain facilitated by interchange reconnection between open and closed field lines deserves more attention. **2010 October 31, 2010 November 26, 2012 February 22, 2012 July 24, 2014 May 1, 2015 December 9**

!!! Table 1: General information of the coronal rain events from previous studies.

Can small-scale magnetic fields be the major cause for the near-surface effect of the solar p-mode frequencies?

Yan **Li**, Qian-sheng Zhang, Tao Wu, Jie Su, Xing-hao Chen, Gui-fang Lin, Jian-heng Guo, Jie-ying Liu

ApJ **916** 107 **2021**

https://arxiv.org/pdf/2106.03294.pdf

https://doi.org/10.3847/1538-4357/ac0882

Small-scale magnetic fields are not only the fundamental element of the solar magnetism, but also closely related to the structure of the solar atmosphere. The observations have shown that there is a ubiquitous tangled small-scale magnetic field with a strength of 60 ~ 130\,G in the canopy forming layer of the quiet solar photosphere. On the other hand, the multi-dimensional MHD simulations show that the convective overshooting expels the magnetic field to form the magnetic canopies at a height of about 500\,km in the upper photosphere. However, the distribution of such small-scale ``canopies" in the solar photosphere cannot be rigorously constrained by either observations and numerical simulations. Based on stellar standard models, we identify that these magnetic canopies can act as a global magnetic-arch splicing layer, and find that the reflections of the solar p-mode oscillations at this magnetic-arch splicing layer results in significant improvement on the discrepancy between the observed and calculated p-mode frequencies. The location of the magnetic-arch splicing layer is determined at a height of about 630\,km, and the inferred strength of the magnetic field is about 90\,G. These features of the magnetic-arch splicing layer derived independently in the present study are quantitatively in agreement with the presence of small-scale magnetic canopies as those obtained by the observations and 3-D MHD simulations.

A Theoretical Investigation of the Magnetic-field-induced Transition in Fe X, of Importance for Measuring Magnetic Field Strengths in the Solar Corona

W. **Li**6,1, M. Li2, K. Wang3, T. Brage1, R. Hutton4, and E. Landi5
2021 ApJ 913 135
https://doi.org/10.3847/1538-4357/abfa97

The use of the magnetic-field-induced transition (MIT) $3p^4 3d\ {}^4D_{7/2} \rightarrow 3p^5\ {}^2P^o_{3/2}$ in Fe X for the measurement of the magnetic field strength in the solar corona has been discussed and demonstrated in a number of recent studies. This diagnostic technique depends on, among other conditions, the accuracy of the atomic data for Fe X. In the present work, we carry out a large-scale calculation for the atomic properties needed for the determination of the MIT rate using the multiconfiguration Dirac–Hartree–Fock method. Four computational schemes are employed to study the convergence of the atomic properties of interest. Comparison with other experimental and theoretical sources are performed and recommended values are suggested for important properties, e.g., the magnetic induced transition probabilities as a function of magnetic field strengths. The present calculations affect magnetic field measurements by decreasing the magnetic field strengths by 10%–15%, leading to differences in magnetic energy up to 30%. We recommend that the current data should be employed in magnetic field measurements in the future.

On-disk solar coronal condensations facilitated by magnetic reconnection between open and closed magnetic structures

Leping **Li**, Hardi Peter, Lakshmi Pradeep Chitta, Hongqiang Song
ApJ **910** 82 **2021**
https://arxiv.org/pdf/2102.04605.pdf
https://doi.org/10.3847/1538-4357/abe537
Coronal condensation and rain are a crucial part of the mass cycle between the corona and chromosphere. In some cases, condensation and subsequent rain originate in the magnetic dips formed during magnetic reconnection. This provides a new and alternative formation mechanism for coronal rain. Until now, only off-limb, rather than on-disk, condensation events during reconnection have been reported. In this paper, employing extreme-ultraviolet (EUV) images of the Solar Terrestrial Relations Observatory (STEREO) and Solar Dynamics Observatory (SDO), we investigate the condensations facilitated by reconnection from **2011 July 14 to 15**, when STEREO was in quadrature with respect to the Sun-Earth line. Above the limb, in STEREO/EUV Imager (EUVI) 171 Å~images, higher-lying open structures move downward, reconnect with the lower-lying closed loops, and form dips. Two sets of newly reconnected structures then form. In the dips, bright condensations occur in EUVI 304 Å~images repeatedly which then flow downward to the surface. In the on-disk observations by SDO/Atmospheric Imaging Assembly (AIA) in the 171 Å~channel, these magnetic structures are difficult to identify. Dark condensations appear in AIA 304 Å~images, and then move to the surface as on-disk coronal rain. The cooling and condensation of coronal plasma is revealed by the EUV light curves. If only the on-disk observations would be available, the relation between the condensations and reconnection, shown clearly by the off-limb observations, would not be identified. Thus, we suggest that some on-disk condensation events seen in transition region and chromospheric lines may be facilitated by reconnection.

Differential rotation of the chromosphere in the He I absorption line

KJ **Li**, JC Xu, JL Xie, W Feng
ApJL **905** L11 **2020**
https://arxiv.org/pdf/2011.14055.pdf
https://doi.org/10.3847/2041-8213/abcb84
Differential rotation is the basis of the solar dynamo theory. Synoptic maps of He I intensity from Carrington rotations 2032 to 2135 are utilized to investigate the differential rotation of the solar chromosphere in the He I

absorption line. The chromosphere is surprisingly found to rotate faster than the photosphere below it. The anomalous heating of the chromosphere and corona has been a big problem in modern astronomy. It is speculated that the small-scale magnetic elements with magnetic flux in the range of (2.9−32.0)×1018 Mx which are anchored in the leptocline, heat the quiet chromosphere to present the anomalous temperature increase, causing it to rotate at the same rate as the leptocline. The differential of rotation rate in the chromosphere is found to be strengthened by strong magnetic fields, but in stark contrast, at the photosphere strong magnetic fields repress the differential of rotation rate. A plausible explanation is given for these findings.

Relation of coronal rain originating from coronal condensations to interchange magnetic reconnection

Leping **Li**, Hardi Peter, Lakshmi Pradeep Chitta, Hongqiang Song
ApJ **2020**
https://arxiv.org/pdf/2011.00709.pdf
Using extreme-ultraviolet images, we recently proposed a new and alternative formation mechanism for coronal rain along magnetically open field lines due to interchange magnetic reconnection. In this paper we report coronal rain at chromospheric and transition region temperatures originating from the coronal condensations facilitated by reconnection between open and closed coronal loops. For this, we employ the Interface Region Imaging Spectrograph (IRIS) and the Atmospheric Imaging Assembly (AIA) of the Solar Dynamics Observatory (SDO). Around 2013 October 19, a coronal rain along curved paths was recorded by IRIS over the southeastern solar limb. Related to this, we found reconnection between a system of higher-lying open features and lower-lying closed loops that occurs repeatedly in AIA images. In this process, the higher-lying features form magnetic dips. In response, two sets of newly reconnected loops appear and retract away from the reconnection region. In the dips, seven events of cooling and condensation of coronal plasma repeatedly occur due to thermal instability over several days, from October 18 to 20. The condensations flow downward to the surface as coronal rain, with a mean interval between condensations of 6.6 hr. In the cases where IRIS data were available we found the condensations to cool all the way down to chromospheric temperatures. Based on our observations we suggest that some of the coronal rain events observed at chromospheric temperatures could be explained by the new and alternative scenario for the formation of coronal rain, where the condensation is facilitated by interchange reconnection. **2013 October 18-20**

Magnetohydrodynamic Fast Sausage Waves in the Solar Corona **Review**

B. **Li**, P. Antolin, M.-Z. Guo, A. A. Kuznetsov, D. J. Pascoe, T. Van Doorsselaere, S. Vasheghani Farahani
Space Sci. Rev. **216**, Article number: 136 **2020**
https://arxiv.org/pdf/2010.16023.pdf
https://link.springer.com/content/pdf/10.1007/s11214-020-00761-z.pdf
Characterized by cyclic axisymmetric perturbations to both the magnetic and fluid parameters, magnetohydrodynamic fast sausage modes (FSMs) have proven useful for solar coronal seismology given their strong dispersion. This review starts by summarizing the dispersive properties of the FSMs in the canonical configuration where the equilibrium quantities are transversely structured in a step fashion. With this preparation we then review the recent theoretical studies on coronal FSMs, showing that the canonical dispersion features have been better understood physically, and further exploited seismologically. In addition, we show that departures from the canonical equilibrium configuration have led to qualitatively different dispersion features, thereby substantially broadening the range of observations that FSMs can be invoked to account for. We also summarize the advances in forward modeling studies, emphasizing the intricacies in interpreting observed oscillatory signals in terms of FSMs. All these advances notwithstanding, we offer a list of aspects that remain to be better addressed, with the physical connection of coronal FSMs to the quasi-periodic pulsations in solar flares particularly noteworthy.

On the Fast Propagating Ultra-hot Disturbance Captured by SDO/AIA: An In-depth Insight into the Coronal Nonlinear Dynamics

Hongbo **Li**1,2, Hengqiang Feng1,2, Yu Liu1,3, Yuandeng Shen1,3, Zhanjun Tian1,2, Guoqing Zhao1,2, and Ake Zhao
2020 ApJL 898 L8
https://doi.org/10.3847/2041-8213/aba128
The impulsive heating events and their corresponding nonlinear dynamics remain one of the most obscure physical processes in solar atmospheric physics. The complicacy of these processes together with limited observations have greatly hampered our understanding of them. Here, we present, for the first time, an unambiguous example of a nonlinear acoustic wave in a closed coronal loop or loop segment, which appeared as a fast propagating ultra-hot disturbance cohesively in an indistinguishable corona loop with a highly evolving emission intensity profile. Based on the theory of propagating nonlinear waves, we argue that this type of observation can provide further information for the disturbance during its propagation. With this information, we conclude that the propagating nonlinear

disturbance can quickly heat the corona through the rarefaction wave, and the disturbance-induced magnetic reconnection should not happen in our observation. Besides, a convenient criterion has also been deduced for the existence of the disturbance-induced reconnection mechanism. All of this provides us with a new insight into the accompanying nonlinear dynamics of solar impulsive heating events, which can not only shed light on problems including coronal heating and the fast formation of hot coronal loops, but also show us a very novel and prospective seismology scheme for the diagnosis of coronal plasma properties.

Why Does the Solar Corona Abnormally Rotate Faster Than the Photosphere?

KJ **Li**, JC Xu, ZQ Yin, W Feng
2019 *ApJ* **875** 90
https://arxiv.org/pdf/1904.07465.pdf
sci-hub.se/10.3847/1538-4357/ab0f3a
Coronal heating is a big question for modern astronomy. Daily measurement of 985 solar spectral irradiances (SSIs) at the spectral intervals 1-39 nm and 116-2416 nm during March 1 2003 to October 28 2017 is utilized to investigate characteristics of solar rotation in the solar atmosphere by means of the Lomb \,-\, Scargle periodogram method to calculate their power spectra. The rotation period of coronal plasma is obtained to be 26.3 days, and that of the solar atmosphere at the bottom of the photosphere modulated by magnetic structures is 27.5 days. Here we report for the first time that unexpectedly the coronal atmosphere is found to rotate faster than the underlying photosphere. When time series of SSIs are divided into different cycles, and the ascending and descending periods of a solar cycle, rotation rate in the corona is also found to be larger than that in the photosphere, and this actually gives hidden evidence: it is small-scale magnetic activity that heats the corona.

The Present Special Solar Cycle 24: Casting a Shadow over Periodicity of the North–South Hemispherical Asymmetry

F. Y. **Li**1,2,3,4, N. B. Xiang1,3,4, J. L. Xie1,3,4, and J. C. Xu1,3,4
2019 ApJ 873 121
https://doi.org/10.3847/1538-4357/ab06bf
The N–S asymmetry (the north–south hemispheric asymmetry) of sunspot areas for each of the cycles 7–24 have been investigated, and a trend of a long-term characteristic timescale of about eight cycles is inferred, which is confirmed again by studying the fitted lines of the yearly values of the N–S asymmetry of sunspot numbers and sunspot group numbers at solar cycle 24. Then, a periodic behavior of about 12 solar cycles is found in the cumulative counts of yearly sunspot areas for each of the cycles 7–24. Nevertheless, the cumulative counts of sunspot numbers and sunspot group numbers for cycle 24 have different behaviors. Moreover, the dominant hemispheres for cycles 7–23 show a trend of a long-term characteristic timescale of about 12 cycles. However, we cannot determine the dominant hemisphere of cycle 24, as these three parameters give different results for the dominant hemisphere. Cycle 24 is a particular solar activity cycle, as sunspot areas suggest a long characteristic timescale of about 12-cycle length, while sunspot numbers and sunspot group numbers support an eight-cycle period of the N–S asymmetry.

Transition-region explosive events produced by plasmoid instability

Dong **Li**
RAA Vol 19, No 5 (**2019**) , 67
Magnetic reconnection is thought to be a key process in most solar eruptions. Thanks to high-resolution observations and simulations, the studied scale of the reconnection process has become smaller and smaller. Spectroscopic observations show that the reconnection site can be very small, which always exhibits a bright core and two extended wings with fast speeds, i.e., transition-region explosive events. In this paper, using the PLUTO code, we perform a 2-D magnetohydrodynamic simulation to investigate small-scale reconnection in double current sheets. Based on our simulation results, such as the line-of-sight velocity, number density and plasma temperature, we can synthesize the line profile of Si IV 1402.77 Å which is a well known emission line used to study transition-region explosive events on the Sun. The synthetic line profile of Si IV 1402.77 Å is complex with a bright core and two broad wings which can extend to nearly 200 km s−1. Our simulation results suggest that the transition-region explosive events on the Sun are produced by plasmoid instability during small-scale magnetic reconnection.

Solar cycle characteristics and their application in the prediction of cycle 25

F.Y.**Li**, D.F.Kong, J.L.Xie, N.B.Xiang, J.C.Xu
Journal of Atmospheric and Solar-Terrestrial Physics Volume 181, Part B, December **2018**, Pages 110-115
sci-hub.tw/10.1016/j.jastp.2018.10.014
The Solar Influences Data Analysis Center (SIDC) issued a new version (version 2) of the sunspot number data in July 2015. The 13-month smoothed monthly sunspot number from the new version is used for the first time to

research the relations among the feature parameters of solar cycles under the bimodal distribution for the modern era cycles (10–23), and, their physical implications are discussed. These relations are utilized to predict the maximum amplitude of solar cycle 25. Cycle 25 is predicted to start in October 2020 and reach its maximum amplitude of 168.5±16.3 in October 2024, thus, it should be stronger than cycle 24 but weaker than cycle 23.

A Systematic Study of Hale and Anti-Hale Sunspot Physical Parameters

Jing **Li**

ApJ **867** 89 **2018**

https://arxiv.org/pdf/1809.08980.pdf

https://iopscience.iop.org/article/10.3847/1538-4357/aae31a/pdf

We present a systematic study of sunspot physical parameters using full disk magnetograms from MDI/SoHO and HMI/SDO. Our aim is to use uniform datasets and analysis procedures to characterize the sunspots, paying particular attention to the differences and similarities between "Hale" and "anti-Hale" spots. Included are measurements of the magnetic tilt angles, areas, fluxes and polarity pole separations for 4385 sunspot groups in Cycles 23 and 24 each measured, on average, at ∼66 epochs centered on meridian-crossing. The sunspots are classified as either "Hale" or "anti-Hale", depending on whether their polarities align or anti-align with Hale's hemispheric polarity rule. We find that (1) The "anti-Hale" sunspots constitute a fraction (8.1±0.4)\% of all sunspots, and this fraction is the same in both hemispheres and cycles, (2) "Hale" sunspots obey Joy's law in both hemispheres and cycles but "anti-Hale" sunspots do not. Three equivalent forms of Joy's law are derived, $\sin\gamma=(0.38\pm0.05)\sin\phi$, $\gamma=(0.39\pm0.06)\phi$, and $\gamma=(23.80\pm3.51)\sin\phi$, where γ is the tilt angle and ϕ is the heliospheric latitude, (3) The average Hale sunspot tilt angle is $\bar{\gamma}=5.49^{\circ}\pm0.09$, (4) The tilt angles, magnetic fluxes and pole separations of sunspots are interrelated, with larger fluxes correlated with larger pole separations and smaller tilt angles. We present empirical relations between these quantities. Cycle 24 is a much weaker cycle than Cycle 23 in sunspot numbers, cumulative magnetic flux, and average sunspot magnetic flux. The "anti-Hale" sunspots are also much weaker than "Hale" sunspots in those parameters, but they share similar magnetic flux distributions and average latitudes. We characterize the two populations, and aim to shed light on the origin of "anti-Hale" sunspots.

HMI Science Nuggets #114 Dec **2018** http://hmi.stanford.edu/hminuggets/?p=2707

Is It Small-scale, Weak Magnetic Activity That Effectively Heats the Upper Solar Atmosphere?

K. J. **Li**1,2,3, J. C. Xu1,2,3, and W. Feng4

2018 ApJ Supplement Series 237 7

http://sci-hub.tw/http://iopscience.iop.org/0067-0049/237/1/7/

https://arxiv.org/pdf/1807.02902.pdf

Solar chromosphere and coronal heating are big questions for astrophysics. Daily measurement of 985 solar spectral irradiances (SSIs) at the spectral intervals 1–39 nm and 116–2416 nm during 2003 March 1 to 2017 October 28 are utilized to investigate phase relation with respect to daily sunspot number, the Mount Wilson sunspot Index, and the Magnetic Plage Strength Index. All the SSIs form in the abnormally heated layer; the upper photosphere, chromosphere, transition region, and corona are found to be significantly more correlated to weak magnetic activity than to strong magnetic activity, and are found to dance in step with weak magnetic activity. All the SSIs that form in the low photosphere, which indicate the "energy" leaked from the solar subsurface, are found to be more related to strong magnetic activity instead and in anti-phase with weak magnetic activity. In the upper photosphere and chromosphere, strong magnetic activity should lead SSI by about a solar rotation, which also implies that weak magnetic activity should take effect from heating there. It is thus small-scale weak magnetic activity that effectively heats the upper solar atmosphere.

Spectroscopic and imaging observations of small-scale reconnection events

Dong **Li**, Leping Li, Zongjun Ning

MNRAS **2018**

https://arxiv.org/pdf/1806.10205.pdf

We present spectroscopic and imaging observations of small-scale reconnection events on the Sun. Using the Interface Region Imaging Spectrograph (IRIS) observations, one reconnection event is first detected as IRIS jets with fast bi-directional velocities in the chromosphere and transition region, which are identified as non-Gaussian broadenings with two extended wings in the line profiles of Si iv, C ii, and Mg ii k. The magnetograms under the IRIS jets from Helioseismic and Magnetic Images exhibit magnetic flux cancellation simultaneously, supporting that the IRIS jets are driven by magnetic reconnection. The Atmospheric Imaging Assembly images also show an extreme ultraviolet (EUV) brightening which is shortly after the underlying IRIS jets, i.e., in the 131 A, 171 A, 193 A, 211 A, and 94 A channels, implying that the over-lying EUV brightening in the corona is caused by the IRIS jets in the chromosphere and transition region. We also find another three reconnection events which show the same features during this IRIS observation. Our observational results suggest that the small-scale reconnection events

might contribute to the coronal heating. The new result is that the process of magnetic reconnection is detected from the photosphere through chromosphere and transition region to the corona. **2017 September 18**

Impulsively generated wave trains in coronal structures: II. Effects of transverse structuring on sausage waves in pressureless slabs

Bo **Li**, Ming-Zhe Guo, Hui Yu, Shao-Xia Chen
ApJ **855** 53 **2018**
https://arxiv.org/pdf/1802.04651.pdf
Impulsively generated sausage wave trains in coronal structures are important for interpreting a substantial number of observations of quasi-periodic signals with quasi-periods of order seconds. We have previously shown that the Morlet spectra of these wave trains in coronal tubes depend crucially on the dispersive properties of trapped sausage waves, the existence of cutoff axial wavenumbers and the monotonicity of the dependence of the axial group speed on the axial wavenumber in particular. This study examines the difference a slab geometry may introduce, for which purpose we conduct a comprehensive eigenmode analysis, both analytically and numerically, on trapped sausage modes in coronal slabs with a considerable number of density profiles. For the profile descriptions examined, coronal slabs can trap sausage waves with longer axial wavelengths, and the group speed approaches the internal Alfv\'en speed more rapidly at large wavenumbers in the cylindrical case. However, common to both geometries, cutoff wavenumbers exist only when the density profile falls sufficiently rapidly at distances far from coronal structures. Likewise, the monotonicity of the group speed curves depends critically on the profile steepness right at the structure axis. Furthermore, the Morlet spectra of the wave trains are shaped by the group speed curves for coronal slabs and tubes alike. Consequently, we conclude that these spectra have the potential for telling the sub-resolution density structuring inside coronal structures, although their detection requires an instrumental cadence of better than ~1 second.

Solar Spectral Lines with Special Polarization Properties for the Calibration of Instrument Polarization

W. **Li**, R. Casini, T. del Pino Alemán, and P. G. Judge
2017 ApJ 848 82
http://sci-hub.cc/http://iopscience.iop.org/0004-637X/848/2/82/
We investigate atomic transitions that have previously been identified as having zero polarization from the Zeeman effect. Our goal is to identify spectral lines that can be used for the calibration of instrumental polarization of large astronomical and solar telescopes, such as the Daniel K. Inouye Solar Telescope, which is currently under construction on Haleakala. We use a numerical model that takes into account the generation of scattering polarization and its modification by the presence of a magnetic field of arbitrary strength. We adopt values for the Landé factors from spectroscopic measurements or semi-empirical results, thus relaxing the common assumption of LS-coupling previously used in the literature. The mechanisms dominating the polarization of particular transitions are identified, and we summarize groups of various spectral lines useful for the calibration of spectropolarimetric instruments, classified according to their polarization properties.

Polarization of Coronal Forbidden Lines

Hao **Li**1,2, Egidio Landi Degl'Innocenti3, and Zhongquan Qu1
2017 ApJ 838 69
Since the magnetic field is responsible for most manifestations of solar activity, one of the most challenging problems in solar physics is the diagnostics of solar magnetic fields, particularly in the outer atmosphere. To this end, it is important to develop rigorous diagnostic tools to interpret polarimetric observations in suitable spectral lines. This paper is devoted to analyzing the diagnostic content of linear polarization imaging observations in coronal forbidden lines. Although this technique is restricted to off-limb observations, it represents a significant tool to diagnose the magnetic field structure in the solar corona, where the magnetic field is intrinsically weak and still poorly known. We adopt the quantum theory of polarized line formation developed in the framework of the density matrix formalism, and synthesize images of the emergent linear polarization signal in coronal forbidden lines using potential-field source-surface magnetic field models. The influence of electronic collisions, active regions, and Thomson scattering on the linear polarization of coronal forbidden lines is also examined. It is found that active regions and Thomson scattering are capable of conspicuously influencing the orientation of the linear polarization. These effects have to be carefully taken into account to increase the accuracy of the field diagnostics. We also found that linear polarization observation in suitable lines can give valuable information on the long-term evolution of the magnetic field in the solar corona.

THE SHAPE OF SOLAR CYCLES DESCRIBED BY A SIMPLIFIED BINARY MIXTURE OF GAUSSIAN FUNCTIONS

F. Y. **Li**1,2,3,4, N. B. Xiang1,3,4, D. F. Kong1,3,4, and J. L. Xie

2017 ApJ 834 192

Sunspot cycles usually present a double-peak structure. This work is devoted to using a function to describe the shape of sunspot cycles, including bimodal cycles, and we find that the shape of sunspot cycles can be described by a binary mixture of Gaussian functions with six parameters, two amplitudes, two gradients of curve, and two rising times, and the parameters could be reduced to three. The fitting result of this binary mixture of Gaussian functions is compared with some other functions used previously in the literature, and this function works pretty well, especially at cycle peaks. It is worth mentioning that the function can describe well the shape of those sunspot cycles that show double peaks, and it is superior to the binary mixture of the Laplace functions that was once utilized. The Solar Influences Data Analysis Center, on behalf of the World Data Center, recently issued a new version (version 2) of sunspot number. The characteristics of sunspot cycles are investigated, based on the function description of the new version.

Statistical properties of the Bipolar Magnetic Regions

Dong **Li**

Research in Astron. Astrophys. **2016**

https://arxiv.org/pdf/1612.02610v1.pdf

Using the observations from Michelson Doppler Imager (MDI) onboard Solar and Heliospheric Observatory (SOHO), we develop a computational algorithm to automatically identify the bipolar magnetic regions (BMRs) in the active regions, and then study their statistical properties. The individual magnetic (positive or negative) pole of the BMR is determined from the region with an absolute strength above 55 G and with an area above 250 pixel^2 (495 Mm^2), while a BMR is identified as a pair of positive and negative poles with a shortest area-weight distance between them. Based on this method, 2234 BMRs are identified from the MDI synoptic magnetograms between the Carrington Rotation 1909 (1996 May 06) and 2104 (2010 December 10). 1005 of them are located in the northern hemisphere, while the other 1229 are in the southern hemisphere.We find that the BMR paraments (e.g., latitudes, separations, fragments, and strength) are similar to those of active regions (ARs). Moreover, based on the maximum likelihood estimation (MLE)method, the frequency distributions of these BMRs occurrence as functions of area size and magnetic flux exhibit a power-law behavior. We also find that their orientation angles follow the Hale's Polarity Laws and deviate slightly to the solar equator direction. Consistent with the previous findings, we obtain the orientation angles dependence on the latitudes for the normal BMRs during the 23rd solar cycle. The north-south asymmetry of these BMRs is also detected here.

Investigation of Sunspot Area Varying with Sunspot Number

K. J. **Li**, F. Y. Li, J. Zhang, W. Feng

Solar Phys. Volume 291, Issue 9-10, pp. 2917-2930 **2016**

http://link.springer.com/journal/11207/291/9/page/2

The statistical relationship between sunspot area (SA) and sunspot number (SN) is investigated through analysis of their daily observation records from May 1874 to April 2015. For a total of 1607 days, representing \(3~\%\) of the total interval considered, either SA or SN had a value of zero while the other parameter did not. These occurrences most likely reflect the report of short-lived spots by a single observatory and subsequent averaging of zero values over multiple stations. The main results obtained are as follows: i) The number of spotless days around the minimum of a solar cycle is statistically negatively correlated with the maximum strength of solar activity of that cycle. ii) The probability distribution of SA generally decreases monotonically with SA, but the distribution of SN generally increases first, then it decreases as a whole. The different probability distribution of SA and SN should strengthen their non-linear relation, and the correction factor [\(k\)] in the definition of SN may be one of the factors that cause the non-linearity. iii) The non-linear relation of SA and SN indeed exists statistically, and it is clearer during the maximum epoch of a solar cycle.

Slipping Magnetic Reconnection of Flux Rope Structures as a Precursor to an Eruptive X-class Solar Flare

Ting **Li**, Kai Yang, Yijun Hou, Jun Zhang

ApJ **2016**

We present the quasi-periodic slipping motion of flux rope structures prior to the onset of an eruptive X-class flare on **2015 March 11**, obtained by the \emph{Interface Region Imaging Spectrograph} (\emph{IRIS}) and the \emph{Solar Dynamics Observatory} (\emph{SDO}). The slipping motion occurred at the north part of the flux rope and seemed to successively peel off the flux rope. The speed of the slippage was 30−40 km s−1, with an average period of 130±30 s. The Si {\sc iv} 1402.77 {\AA} line showed a redshift of 10−30 km s−1 and a line width of 50−120 km s−1 at the west legs of slipping structures, indicative of reconnection downflow. The slipping motion

lasted about 40 min and the flux rope started to rise up slowly at the late stage of the slippage. Then an X2.1 flare was initiated and the flux rope was impulsively accelerated. One of the flare ribbons swept across a negative-polarity sunspot and the penumbral segments of the sunspot decayed rapidly after the flare. We studied the magnetic topology at the flaring region and the results showed the existence of a twisted flux rope, together with quasi-separatrix layers (QSLs) structures binding the flux rope. Our observations imply that quasi-periodic slipping magnetic reconnection occurs along the flux-rope-related QSLs in the preflare stage, which drives the later eruption of the flux rope and the associated flare.

Mass motion in upper solar chromosphere detected from solar eclipse observation

Zhi **Li** , Zhongquan Qu, Xiaoli Yan, Guangtao Dun,
Astrophysics and Space Science May **2016**, 361:159
The eclipse-observed emission lines formed in the upper solar atmosphere can be used to diagnose the atmosphere dynamics which provides an insight to the energy balance of the outer atmosphere. In this paper, we analyze the spectra formed in the upper chromospheric region by a new instrument called Fiber Arrayed Solar Optic Telescope (FASOT) around the Gabon total solar eclipse on **November 3, 2013**. The double Gaussian fits of the observed profiles are adopted to show enhanced emission in line wings, while red-blue (RB) asymmetry analysis informs that the cool line (about 104 K) profiles can be decomposed into two components and the secondary component is revealed to have a relative velocity of about 16--45 kms−1 s. The other profiles can be reproduced approximately with single Gaussian fits. From these fittings, it is found that the matter in the upper solar chromosphere is highly dynamic. The motion component along the line-of-sight has a pattern asymmetric about the local solar radius. Most materials undergo significant red shift motions while a little matter show blue shift. Despite the discrepancy of the motion in different lines, we find that the width and the Doppler shifts both are function of the wavelength. These results may help us to understand the complex mass cycle between chromosphere and corona.

Conversion from mutual helicity to self-helicity observed with IRIS

Leping **Li**, Hardi Peter, Feng Chen, Jun Zhang
A&A, 570, A93 **2014**
http://arxiv.org/pdf/1410.5597v1.pdf
Context. In the upper atmosphere of the Sun observations show convincing evidence for crossing and twisted structures, which are interpreted as mutual helicity and self-helicity.
Aims. We use observations with the new Interface Region Imaging Spectrograph (IRIS) to show the conversion of mutual helicity into self-helicity in coronal structures on the Sun.
Methods. Using far UV spectra and slit-jaw images from IRIS and coronal images and magnetograms from SDO, we investigated the evolution of two crossing loops in an active region, in particular, the properties of the Si IV line profile in cool loops.
Results. In the early stage two cool loops cross each other and accordingly have mutual helicity. The Doppler shifts in the loops indicate that they wind around each other. As a consequence, near the crossing point of the loops (interchange) reconnection sets in, which heats the plasma. This is consistent with the observed increase of the line width and of the appearance of the loops at higher temperatures. After this interaction, the two new loops run in parallel, and in one of them shows a clear spectral tilt of the Si IV line profile. This is indicative of a helical (twisting) motion, which is the same as to say that the loop has self-helicity.
Conclusions. The high spatial and spectral resolution of IRIS allowed us to see the conversion of mutual helicity to self-helicity in the (interchange) reconnection of two loops. This is observational evidence for earlier theoretical speculations. **2013-09-27**

INTERNAL-CYCLE VARIATION OF SOLAR DIFFERENTIAL ROTATION

K. J. **Li** 1,2, J. L. Xie1,3, and X. J. Shi
2013 ApJS 206 15
The latitudinal distributions of the yearly mean rotation rates measured by Suzuki in 1998 and 2012 and Pulkkinen & Tuominen in 1998 are utilized to investigate internal-cycle variation of solar differential rotation. The rotation rate at the solar equator seems to have decreased since cycle 10 onward. The coefficient B of solar differential rotation, which represents the latitudinal gradient of rotation, is found to be smaller in the several years after the minimum of a solar cycle than in the several years after the maximum time of the cycle, and it peaks several years after the maximum time of the solar cycle. The internal-cycle variation of the solar rotation rates looks similar in profile to that of the coefficient B. A new explanation is proposed to address such a solar-cycle-related variation of the solar rotation rates. Weak magnetic fields may more effectively reflect differentiation at low latitudes with high rotation rates than at high latitudes with low rotation rates, and strong magnetic fields may more effectively repress differentiation at relatively low latitudes than at high latitudes. The internal-cycle variation is inferred as the result of both the latitudinal migration of the surface torsional pattern and the repression of strong magnetic activity in differentiation.

WHY IS THE SOLAR CONSTANT NOT A CONSTANT?

K. J. **Li**1,2, W. Feng3, J. C. Xu1,4, P. X. Gao1, L. H. Yang1,4, H. F. Liang5 and L. S. Zhan
2012 ApJ 747 135

In order to probe the mechanism of variations of the solar constant on the inter-solar-cycle scale, the total solar irradiance (TSI; the so-called solar constant) in the time interval of 1978 November 7 to 2010 September 20 is decomposed into three components through empirical mode decomposition and time-frequency analyses. The first component is the rotation signal, counting up to 42.31% of the total variation of TSI, which is understood to be mainly caused by large magnetic structures, including sunspot groups. The second is an annual-variation signal, counting up to 15.17% of the total variation, the origin of which is not known at this point in time. Finally, the third is the inter-solar-cycle signal, counting up to 42.52%, which is inferred to be caused by the network magnetic elements in quiet regions, whose magnetic flux ranges from (4.27-38.01) × 1019 Mx.

Solar winds along curved magnetic field lines

B. **Li**1,2, L. D. Xia1 and Y. Chen1
A&A 529, A148 (**2011**)

Context. Both remote-sensing measurements using the interplanetary scintillation (IPS) technique and in-situ measurements by the Ulysses spacecraft show a bimodal structure for the solar wind at solar minimum conditions. At present it still remains to address why the fast wind is fast and the slow wind is slow. While a robust empirical correlation exists between the coronal expansion rate fc of the flow tubes and the speeds v measured in situ, a more detailed data analysis suggests that v depends on more than just fc.
Aims. We examine whether the non-radial shape of field lines, which naturally accompanies any non-radial expansion, could be an additional geometrical factor.
Methods. We solved the transport equations incorporating the heating from turbulent Alfvén waves for an electron-proton solar wind along curved field lines given by an analytical magnetic field model, which is representative of a solar minimum corona.
Results. The field line shape is found to influence the solar wind parameters substantially, reducing the asymptotic speed by up to ~130 km s-1 or by ~28% in relative terms, compared with the case where the field line curvature is neglected. This effect was interpreted in the general framework of energy addition in the solar wind: compared to the straight case, the field line curvature enhances the effective energy deposition to the subsonic flow, which results in a higher proton flux and a lower terminal proton speed.
Conclusions. Our computations suggest that the field line curvature could be a geometrical factor which, in addition to the tube expansion, substantially influences the solar wind speed. Furthermore, although the field line curvature is unlikely to affect the polar fast solar wind at solar minima, it does help make the wind at low latitudes slow, which in turn helps better reproduce the Ulysses measurements.

VARIATIONS OF SOLAR ROTATION AND SUNSPOT ACTIVITY

K. J. **Li**1,2, X. J. Shi1,3, H. F. Liang4, L. S. Zhan5, J. L. Xie1,3 and W. Feng6
2011 ApJ 730 49

The continuous wavelet transformation is used to study the temporal variations of the rotational cycle length of daily sunspot numbers from 1849 January 1 to 2010 February 28, from a global point of view. The rotational cycle length of the Sun is found to have a secular trend, which statistically shows a linear decrease by about 0.47 days during the time interval considered. The empirical mode decomposition analysis of the temporal variations of the rotational cycle length shows an acceleration trend for the surface rotation rate from cycles 11 to 19, but a deceleration trend from the beginning of cycle 20 onward. We cannot determine whether the rotation rate around the maximum times of the Schwable cycles should be faster or slower than that around the minimum times, implying no Schwable cycle in the long-term variations of rotation. The results obtained are compared to those from the literature. It is inferred that the variation of the rotational cycle length may be related to the variation of sunspot activity in the long run.

High-precision Multichannel Solar Image Registration Using Image Intensity

Bo **Liang**1, Xi Chen1, Lan Yu2, Song Feng6,1, Yangfan Guo1, Wenda Cao3,4, Wei Dai1, Yunfei Yang1, and Ding Yuan5
2022 ApJS 261 10

https://iopscience.iop.org/article/10.3847/1538-4365/ac7232/pdf

Solar images observed in different channels with different instruments are crucial to the study of solar activity. However, the images have different fields of view, causing them to be misaligned. It is essential to accurately register the images for studying solar activity from multiple perspectives. Image registration is described as an optimizing problem from an image to be registered to a reference image. In this paper, we proposed a novel coarse-to-fine solar image registration method to register the multichannel solar images. In the coarse registration step, we used the regular step gradient descent algorithm as an optimizer to maximize the normalized cross correlation metric. The fine registration step uses the Powell–Brent algorithms as an optimizer and brings the Mattes mutual

information similarity metric to the minimum. We selected five pairs of images with different resolutions, rotation angles, and shifts to compare and evaluate our results to those obtained by scale-invariant feature transform and phase correlation. The images are observed by the 1.6 m Goode Solar Telescope at Big Bear Solar Observatory and the Helioseismic and Magnetic Imager on board the Solar Dynamics Observatory. Furthermore, we used the mutual information and registration time criteria to quantify the registration results. The results prove that the proposed method not only reaches better registration precision but also has better robustness. Meanwhile, we want to highlight that the method can also work well for the time-series solar image registration. **2012 May 22, 2014 August 5, 2015 January 5, 2015 May 21, 2015 July 14**

Time-distance helioseismology of solar Rossby waves

Zhi-Chao **Liang**, Laurent Gizon, Aaron C. Birch, Thomas L. Duvall Jr
A&A 626, A3 **2018**
https://arxiv.org/pdf/1812.07413.pdf
https://www.aanda.org/articles/aa/pdf/2019/06/aa34849-18.pdf
Context. Solar equatorial Rossby waves (r modes) have recently been observed in the horizontal flow field near the solar surface. This discovery used the techniques of granulation-tracking and ring-diagram analysis applied to six years of SDO/HMI data.
Aims. Here we apply time-distance helioseismology to the SOHO/MDI and SDO/HMI data, which cover 21 years of observations from May 1996 to April 2017. The goal of this study is to provide an independent confirmation of the solar r modes over two solar cycles and in deeper layers of the Sun.
Methods. We measure south-north helioseismic travel times along the equator, which are sensitive to subsurface north-south flows. To reduce noise, the travel times are averaged over travel distances from 6∘ to 30∘; the mean distance corresponds to a p-mode lower turning point of 0.91 R⊙. The 21-year time series of travel-time measurements is split into three seven-year subsets and transformed to obtain power spectra in a co-rotating frame.
Results. The power spectra from the three data subsets all show peaks near the frequencies of the classical Rossby waves. The mode frequencies and linewidths of the modes with azimuthal wavenumbers in the range $3 \le m \le 9$ are consistent with a previous study; however, modes with $m \ge 10$ shift toward less negative frequencies by 10--20 nHz. While most of these modes have e-folding lifetimes on the order of a few months, the longest lived mode, m=3, has a e-folding lifetime of almost two years. The rms north-south flow speed associated with r modes along the equator is estimated to be in the range of 1--3 m s^{-1}, with the largest values for m=10 and m=11. No evidence for the m=2 mode is found in the power spectrum, implying that the rms velocity of this mode is below ∼0.5 m s^{-1}.
HMI Science Nuggets #127 **2019** http://hmi.stanford.edu/hminuggets/?p=2936

Solar meridional circulation from twenty-one years of SOHO/MDI and SDO/HMI observations: Helioseismic travel times and forward modeling in the ray approximation

Zhi-Chao **Liang** (1), Laurent Gizon (1,2,3), Aaron C. Birch (1), Thomas L. Duvall Jr. (1), S. P. Rajaguru (4) ((1) Max-Planck-Institut für Sonnensystemforschung, (2) Institut für Astrophysik, Georg-August-Universität Göttingen, (3) Center for Space Science, New York University Abu Dhabi, (4) Indian Institute of Astrophysics)
A&A 619, A99 **2018**
https://arxiv.org/pdf/1808.08874.pdf
sci-hub.tw/10.1051/0004-6361/201833673
The south-north travel-time differences are measured by applying time-distance helioseismology to the MDI and HMI medium-degree Dopplergrams covering May 1996-April 2017. Our data analysis corrects for several sources of systematic effects: P-angle error, surface magnetic field effects, and center-to-limb variations. An interpretation of the travel-time measurements is obtained using a forward-modeling approach in the ray approximation. The travel-time differences are similar in the southern hemisphere for cycles 23 and 24. However, they differ in the northern hemisphere between cycles 23 and 24. Except for cycle 24's northern hemisphere, the measurements favor a single-cell meridional circulation model where the poleward flows persist down to ∼0.8 R⊙, accompanied by local inflows toward the activity belts in the near-surface layers. Cycle 24's northern hemisphere is anomalous: travel-time differences are significantly smaller when travel distances are greater than 20∘. This asymmetry between northern and southern hemispheres during cycle 24 was not present in previous measurements (e.g., Rajaguru & Antia 2015), which assumed a different P-angle error correction where south-north travel-time differences are shifted to zero at the equator for all travel distances. In our measurements, the travel-time differences at the equator are zero for travel distances less than ∼30∘, but they do not vanish for larger travel distances. This equatorial offset for large travel distances need not be interpreted as a deep cross-equator flow; it could be due to the presence of asymmetrical local flows at the surface near the end points of the acoustic ray paths.

Comparison of acoustic travel-time measurement of solar meridional circulation from SDO/HMI and SOHO/MDI

Zhi-Chao **Liang** (1), Aaron C. Birch (1), Thomas L. Duvall Jr. (1), Laurent Gizon (1 and 2), Jesper Schou
A&A 601, A46 **2017**
https://arxiv.org/pdf/1704.00475.pdf

Time-distance helioseismology is one of the primary tools for studying the solar meridional circulation. However, travel-time measurements of the subsurface meridional flow suffer from a variety of systematic errors, such as a center-to-limb variation and an offset due to the P-angle uncertainty of solar images. Here we apply the time-distance technique to contemporaneous medium-degree Dopplergrams produced by SOHO/MDI and SDO/HMI to obtain the travel-time difference caused by meridional circulation throughout the solar convection zone. The P-angle offset in MDI images is measured by cross-correlating MDI and HMI images. The travel-time measurements in the south-north and east-west directions are averaged over the same observation period for the two data sets and then compared to examine the consistency of MDI and HMI travel times after correcting the systematic errors.
The offsets in the south-north travel-time difference from MDI data induced by the P-angle error gradually diminish with increasing travel distance. However, these offsets become noisy for travel distances corresponding to waves that reach the base of the convection zone. This suggests that a careful treatment of the P-angle problem is required when studying a deep meridional flow. After correcting the P-angle and the removal of the center-to-limb effect, the travel-time measurements from MDI and HMI are consistent within the error bars for meridional circulation covering the entire convection zone. The fluctuations observed in both data sets are highly correlated and thus indicate their solar origin rather than an instrumental origin. Although our results demonstrate that the ad hoc correction is capable of reducing the wide discrepancy in the travel-time measurements from MDI and HMI, we cannot exclude the possibility that there exist other systematic effects acting on the two data sets in the same way.

Probing Magnetic Fields at the Base of the Solar Convection Zone with Meridional Flows

Zhi-Chao **Liang** and Dean-Yi Chou
2015 ApJ 809 150

Solar magnetic fields are responsible for most of the activities on the Sun. Many theories predict that it is generated by a dynamo near the base of the convection zone (BCZ), located at $0.71R_{\odot}$. In this study, we use the solar-cycle variations of the meridional flow to probe magnetic field variations near the BCZ. A helioseismic time-distance method is used to measure the travel-time difference between opposite directions in meridional planes, which reflects the meridional flow at different depths. Two systematic effects, the surface magnetic effect and the center-to-limb effect, are removed. Using Solar and Heliospheric Observatory/Michelson Doppler Imager data, we measure the latitudinal distribution of travel-time difference for different travel distances, corresponding to meridional flow signals in the solar interior down to $0.54R_{\odot}$, over 15 years, including two solar minima and one maximum. The travel-time differences at the maximum and the minimum behave differently in three different depth ranges. The travel-time difference at the maximum is greater than that at the minimum above the BCZ, while it is smaller around the BCZ; both are close to zero below the BCZ. The difference in the travel-time difference between the maximum and the minimum changes about 0.1 s from the region above the BCZ to the region around the BCZ, corresponding to a change in flow velocity of about 10 m s−1 around the BCZ. We tend to attribute this change in the meridional flow to the variation in the magnetic field from the minimum to the maximum near the BCZ.

Effects of Solar Surface Magnetic Fields on the Time-Distance Analysis of Solar Subsurface Meridional Flows

Zhi-Chao **Liang** and Dean-Yi Chou
2015 ApJ 805 165

The solar meridional flow in the deep convection zone can be measured with time–distance analysis. The difference between northward and southward acoustic wave travel times relates to the speed of meridional flow in the solar convection zone. We study the effects of surface magnetic field on the measured travel time difference in time–distance analysis by comparing the results using data with and without removing surface magnetic regions. Two results are significantly different if the field strength threshold used to remove magnetic regions is small enough, such as 50 G. The difference represents the surface magnetic effects. This difference strongly correlates with the sunspot number. The range of travel distance in this study is 7°–75°, corresponding to a depth range of $0.54-0.96\ R_{\odot}$. The difference depends on the travel time distance, and is greatest for the travel distance of $11°-20°$. The study with different field strength thresholds indicates that a threshold of about 50 G can remove most surface magnetic effects. The measured surface magnetic effects can be explained by an effective downflow inside magnetic regions. These signals are not related to the large-scale meridional flow; they need to be considered in the measured travel time difference even when activity is low, if the travel time difference is used to infer meridional flow signals.

Nonstandard interactions in solar neutrino oscillations with Hyper-Kamiokande and JUNO

Jiajun **Liao**, Danny Marfatia, Kerry Whisnant

2017

https://arxiv.org/pdf/1704.04711.pdf

Measurements of the solar neutrino mass-squared difference from KamLAND and solar neutrino data are somewhat discrepant, perhaps due to nonstandard neutrino interactions in matter. We show that the zenith angle distribution of solar neutrinos at Hyper-Kamiokande and the energy spectrum of reactor antineutrinos at JUNO can conclusively confirm the discrepancy and detect new neutrino interactions.

Line formation of He I D3 and He I 10830 Å in a small-scale reconnection event

T. **Libbrecht**, J. P. Bjørgen, J. Leenaarts, J. de la Cruz Rodríguez, V. Hansteen, J. Joshi

A&A 652, A146 (2021)

https://www.aanda.org/articles/aa/pdf/2021/08/aa39788-20.pdf

https://arxiv.org/pdf/2010.15946.pdf

Aims. We aim to explain line formation of He I D3 and He I 10830 Å in small-scale reconnection events.
Methods. We make use of a simulated Ellerman bomb (EB), present in a Bifrost-generated radiative Magnetohydrodynamics (rMHD) snapshot. The resulting He I D3 and He I 10830 Å line intensities are synthesized in 3D using the non-LTE Multi3D code. We compare the synthetic helium spectra with observed SST/TRIPPEL raster scans of EBs in He I 10830 Å\ and He I D3.
Results. Emission in He I D3 and He I 10830 Å is formed in a thin shell around the EB at a height of ∼0.8 Mm while the He I D3 absorption is formed above the EB at ∼4 Mm. The height at which the emission is formed corresponds to the lower boundary of the EB, where the temperature increases rapidly from 6·103 K to 106 K. The opacity in He I D3 and He I 10830 Å is generated via photoionization-recombination driven by EUV radiation that is locally generated in the EB at temperatures in the range of 2·104−2·106 K and electron densities between 1011 and 1013 cm−3. The synthetic emission signals are a result of coupling to local conditions in a thin shell around the EB, with temperatures between 7·103 and 104 K and electron densities ranging from ∼1012 to 1013 cm−3. Hence, both strong non-LTE as well as thermal processes play a role in the formation of He I D3 and He I 10830 Å in the synthetic EB/UV burst that we studied.
Conclusions. In conclusion, the synthetic He I D3 and He I 10830 Å emission signatures are an indicator of temperatures of at least 2·104 K and in this case as high as ∼106 K.

Observations of Ellerman bomb emission features in He i D3 and He i 10 830 Å⋆

Tine **Libbrecht**1, Jayant Joshi1, Jaime de la Cruz Rodríguez1, Jorrit Leenaarts1 and Andrés Asensio Ramos

A&A 598, A33 (**2017**)

Context. Ellerman bombs (EBs) are short-lived emission features, characterised by extended wing emission in hydrogen Balmer lines. Until now, no distinct signature of EBs has been found in the He i 10 830 Å line, and conclusive observations of EBs in He i D3 have never been reported.
Aims. We aim to study the signature of EBs in neutral helium triplet lines.
Methods. The observations consisted of ten consecutive SST/TRIPPEL raster scans close to the limb, featuring the Hβ, He i D3 and He i 10 830 Å spectral regions. We also obtained raster scans with IRIS and made use of the SDO/AIA 1700 Å channel. We used Hazel to invert the neutral helium triplet lines.
Results. Three EBs in our data show distinct emission signatures in neutral helium triplet lines, most prominently visible in the He i D3 line. The helium lines have two components: a broad and blueshifted emission component associated with the EB, and a narrower absorption component formed in the overlying chromosphere. One of the EBs in our data shows evidence of strong velocity gradients in its emission component. The emission component of the other two EBs could be fitted using a constant slab. Our analysis hints towards thermal Doppler motions having a large contribution to the broadening for helium and IRIS lines. We conclude that the EBs must have high temperatures to exhibit emission signals in neutral helium triplet lines. An order of magnitude estimate places our observed EBs in the range of T ∼ 2 × 104−105 K.

In-flight validation of Metis Visible-light Polarimeter Coronagraph on board Solar Orbiter

A. **Liberatore**, S. Fineschi, M. Casti, G. Capobianco, L. Abbo, V. Andretta, V. Da Deppo, M. Fabi, F. Frassati, G. Jerse, F. Landini, D. Moses, G. Naletto, G. Nicolini, M. Pancrazzi, M. Romoli, G. Russano, C. Sasso, D. Spadaro, M. Stangalini, R. Susino, D. Telloni, L. Teriaca, M. Uslenghi

A&A **2023**

https://arxiv.org/pdf/2302.07308.pdf

Context. The Metis coronagraph is one of the remote-sensing instruments of the ESA/NASA Solar Orbiter mission. Metis is aimed at the study of the solar atmosphere and solar wind by simultaneously acquiring images of the solar corona at two different wavelengths; visible-light (VL) within a band ranging from 580 nm to 640 nm, and in the HI Ly-alpha 121.6 +/- 10 nm ultraviolet (UV) light. The visible-light channel includes a polarimeter with electro-optically modulating Liquid Crystal Variable Retarders (LCVRs) to measure the linearly polarized brightness of the K-corona to derive the electron density.
Aims. In this paper, we present the first in-flight validation results of the Metis polarimetric channel together with a comparison to the on-ground calibrations. It is the validation of the first use in deep space (with hard radiation environment) of an electro-optical device: a liquid crystal-based polarimeter.
Methods. We used the orientation of the K-corona's linear polarization vector during the spacecraft roll maneuvers for the in-flight calibration.
Results. The first in-flight validation of the Metis coronagraph on-board Solar Orbiter shows a good agreement with the on-ground measurements. It confirms the expected visible-light channel polarimetric performance. A final comparison between the first pB obtained by Metis with the polarized brightness (pB) obtained by the space-based coronagraph LASCO and the ground-based coronagraph KCor shows the consistency of the Metis calibrated results.

Topological plasma oscillations in the solar tachocline

Ruben **Lier**, Richard Green, Jan de Boer, Jay Armas
2024
https://arxiv.org/pdf/2401.07622.pdf
We study the properties of plasma oscillations in the solar tachocline using shallow-water magnetohydrodynamic equations. These oscillations are expected to correlate with solar activity. We find new qualitative features in the equatorial spectrum of magnetohydrodynamic oscillations associated with magneto-Rossby and magneto-Yanai waves. By studying this spectrum in terms of band theory, we find that magneto-Kelvin and magneto-Yanai waves are topologically protected. This highlights the important role of these two classes of waves, as robust features of the plasma oscillation spectrum, in the interpretation of helioseismological observations.

Comparison of Helioseismic Far-side Active Region Detections with STEREO Far-Side EUV Observations of Solar Activity

P. C. **Liewer**, J. Qiu, C. Lindsey
Solar Phys. 292:146 **2017**
https://arxiv.org/ftp/arxiv/papers/1709/1709.07801.pdf
Seismic maps of the Sun's far hemisphere, computed from Doppler data from the Helioseismic and Magnetic Imager (HMI) on board the Solar Dynamics Observatory (SDO) are now being used routinely to detect strong magnetic regions on the far side of the Sun (http:/jsoc.stanford.edu/data/farside/). To test the reliability of this technique, the helioseismically inferred active region detections are compared with far-side observation of solar activity from the Solar TErrestrial RElations Observatory (STEREO), using brightness in extreme ultraviolet light (EUV) as a proxy for magnetic fields. Two approaches are used to analyze nine months of STEREO and HMI data. In the first approach, we determine whether or not new large east-limb active regions are detected seismically on the far side before they appear Earth side and study how the detectability of these regions relates to their EUV intensity. We find that, while there is a range of EUV intensities for which far-side regions may or may not be detected seismically, there appears to be an intensity level above which they are almost always detected and an intensity level below which they are never detected. In the second approach, we analyze concurrent extreme ultraviolet and helioseismic far-side observations. We find that 100% (22) of the far-side seismic regions correspond to an extreme ultraviolet plage; 95% of these either became a NOAA-designated magnetic region when reaching the east limb or were one before crossing to the far side. A low but significant correlation is found between the seismic signature strength and the EUV intensity of a farside region. **2011, 2012**
HMI Science Nuggets #75 Dec **2017** http://hmi.stanford.edu/hminuggets/?p=2041

Testing the Reliability of Predictions of Far-Side Active Regions from Helioseismology Using STEREO Far-Side Observations of Solar Activity

P. C. **Liewer**, I. González Hernández, J. R. Hall, C. Lindsey, X. Lin
Solar Physics, October **2014**, Volume 289, Issue 10, pp 3617-3640
We test the reliability of helioseismic far-side active-region predictions, made using Dopplergrams from both the Helioseismic and Magnetic Imager (HMI) onboard the Solar Dynamics Observatory (SDO) and the Global Oscillation Network Group (GONG), by comparison with far-side observation of solar activity from the Solar TErrestrial RElations Observatory (STEREO). Both GONG and HMI produce seismic Carrington maps that show strong magnetic-field regions, labeling predictions of far-side active regions that have a probability ≥ 70 %. By visual comparison of these prediction maps with STEREO extreme ultraviolet (EUV) Carrington maps, we determine whether or not solar activity, as evidenced as brightness in EUV, is observed at the predicted locations.

We analyzed nine months of data from 2011 and 2012. For both GONG and HMI, we find that for approximately 90 % of the active-region predictions, activity/brightness is observed in EUV at the predicted location. We also investigated the success of GONG and HMI at predicting large active regions before they appear at the east limb as viewed from Earth. Of the 27 identified large east-limb active regions in the nine months of data analyzed, GONG predicted 15 (55 %) at least once within the week prior to Earth-side appearance and HMI predicted 13 (48 %). Based on the STEREO far-side EUV observations, we suggest that 9 of the 27 active regions were probably too weak to be predicted while on the far side. Overall, we conclude that HMI and GONG have similar reliability using the current data-processing procedures.

Comparison of Far-Side STEREO Observations of Solar Activity and Active Region Predictions from GONG

P. C. **Liewer**, I. González Hernández, J. R. Hall, W. T. Thompson, A. Misrak
Solar Physics, November **2012**, Volume 281, Issue 1, pp 3-20

On 6 February 2011, the two Solar TErrestrial Relations Observatory (STEREO) spacecraft reached 180° separation and began imaging the entire far-side hemisphere of the Sun in extreme ultraviolet light (EUV). Here, we compare STEREO's observations of far-side solar activity, as evidenced by bright regions in the EUV images, to predictions of far-side active regions from helioseismology using National Solar Observatory Global Oscilla-tion Network Group (GONG) observations. GONG produces seismic Carrington maps of strong magnetic field regions, labeling far-side regions with a probability ≥ 70%. By visual comparison of these GONG maps with STEREO EUV Carrington maps, we determine whether or not solar activity is observed at the locations of the predicted active regions. For data from February – June 2011, we find that for 139 of 157 comparisons activity is observed in EUV at the predicted site, yielding an 89% success rate. For 18 comparisons, no activity was seen at the predicted region (11% false predictions). We also investigated GONG's success at predicting large active regions before they appear at the east limb as viewed from Earth. Of 15 such east-limb active regions, eight were predicted by GONG at least once in the seven days preceding their Earth-side appearance. STEREO B observations of activity in the days preceding the appearance of the other seven large East-limb active regions indicated that, while three were possibly too small for GONG to make a prediction, four seemed as large and active as other active regions that had been predicted successfully by GONG.

A New Broadening Technique of the Numerically Unresolved Solar Transition Region and Its Effect on the Spectroscopic Synthesis Using Coronal Approximation

Haruhisa **Iijima**1,2 and Shinsuke Imada1
2021 ApJ 917 65
https://doi.org/10.3847/1538-4357/ac07a5

The transition region is a thin layer of the solar atmosphere that controls the energy loss from the solar corona. Large numbers of grid points are required to resolve this thin transition region fully in numerical modeling. In this study, we propose a new numerical treatment, called LTRAC, which can be easily extended to the multidimensional domains. We have tested the proposed method using a one-dimensional hydrodynamic model of a coronal loop in an active region. The LTRAC method enables modeling of the transition region with a numerical grid size of 50–100 km, which is about 1000 times larger than the physically required value. We used the velocity differential emission measure to evaluate the possible effects on the optically thin emission. Lower-temperature emissions were better reproduced by the LTRAC method than by previous methods. Doppler shift and nonthermal width of the synthesized line emission agree with those from a high-resolution reference simulation within an error of several kilometers per second above the formation temperature of 105

Undersampling effects on observed periods of coronal oscillations

Daye **Lim**, Tom Van Doorsselaere, Valery M. Nakariakov, Dmitrii Y. Kolotkov, Yuhang Gao, David Berghmans
A&A Letter **2024**
https://arxiv.org/pdf/2409.12095

Context. Recent observations of decayless transverse oscillations have shown two branches in the relationship between periods and loop lengths. One is a linear relationship, interpreted as a standing mode. The other shows almost no correlation and has not yet been interpreted conclusively. Aims. We investigated the undersampling effect on observed periods of decayless oscillations. Methods. We considered oscillating coronal loops that closely follow the observed loop length distribution. Assuming that all oscillations are standing waves, we modeled a signal that represents decayless oscillations where the period is proportional to the loop length and the amplitude and phase are randomly drawn. A downsampled signal was generated from the original signal by considering different sample rates that mimic temporal cadences of telescopes, and periods for sampled signals were analysed using the fast Fourier transform. Results. When the sampling cadence is getting closer to the actual oscillation period, a tendency for overestimating periods in short loops is enhanced. The relationship between loop lengths and periods of the

sampled signals shows the two branches as in the observation. Conclusions. We find that long periods of decayless oscillations occurring in short loops could be the result of undersampling.

The Role of High-frequency Transverse Oscillations in Coronal Heating

Daye **Lim**1,2, Tom Van Doorsselaere1, David Berghmans2, Richard J. Morton3, Vaibhav Pant4, and Sudip Mandal5
2023 ApJL 952 L15
https://arxiv.org/pdf/2308.03657
https://iopscience.iop.org/article/10.3847/2041-8213/ace423/pdf
Transverse oscillations that do not show significant damping in solar coronal loops are found to be ubiquitous. Recently, the discovery of high-frequency transverse oscillations in small-scale loops has been accelerated by the Extreme Ultraviolet Imager on board Solar Orbiter. We perform a meta-analysis by considering the oscillation parameters reported in the literature. Motivated by the power law of the velocity power spectrum of propagating transverse waves detected with CoMP, we consider the distribution of energy fluxes as a function of oscillation frequencies and the distribution of the number of oscillations as a function of energy fluxes and energies. These distributions are described as a power law. We propose that the power-law slope ($\delta = -1.40$) of energy fluxes depending on frequencies could be used for determining whether high-frequency oscillations dominate the total heating ($\delta < 1$) or not ($\delta > 1$). In addition, we found that the oscillation number distribution depending on energy fluxes has a power-law slope of $\alpha = 1.00$, being less than 2, which means that oscillations with high energy fluxes provide the dominant contribution to the total heating. It is shown that, on average, higher energy fluxes are generated from higher-frequency oscillations. The total energy generated by transverse oscillations ranges from about 1020 to 1025 erg, corresponding to the energies for nanoflare (1024–1027 erg), picoflare (1021–1024 erg), and femtoflare (1018–1021 erg). The respective slope results imply that high-frequency oscillations could provide the dominant contribution to total coronal heating generated by decayless transverse oscillations.

Selection of Three (Extreme)Ultraviolet Channels for Solar Satellite Missions by Deep Learning

Daye **Lim**1, Yong-Jae Moon1,2, Eunsu Park1, and Jin-Yi Lee1
2021 ApJL 915 L31
https://doi.org/10.3847/2041-8213/ac0d54
We address the question of which combination of channels can best translate other channels in ultraviolet (UV) and extreme UV (EUV) observations. For this, we compare the image translations among the nine channels of the Atmospheric Imaging Assembly (AIA) on board the Solar Dynamics Observatory (SDO) using a deep-learning (DL) model based on conditional generative adversarial networks. In this study, we develop 170 DL models: 72 models for single-channel input, 56 models for double-channel input, and 42 models for triple-channel input. All models have a single-channel output. Then we evaluate the model results by pixel-to-pixel correlation coefficients (CCs) within the solar disk. Major results from this study are as follows. First, the model with 131 Å shows the best performance (average CC = 0.84) among single-channel models. Second, the model with 131 and 1600 Å shows the best translation (average CC = 0.95) among double-channel models. Third, among the triple-channel models with the highest average CC (0.97), the model with 131, 1600, and 304 Å is suggested in that the minimum CC (0.96) is the highest. Interestingly, they represent coronal, upper photospheric, and chromospheric channels, respectively. Our results may be used as a secondary perspective in addition to primary scientific purposes in selecting a few channels of an UV/EUV imaging instrument for future solar satellite missions.

Sausage oscillations in a plasma cylinder with a surface current

Daye **Lim**, Valery M.NakariakovabYong-JaeMoona
Journal of Atmospheric and Solar-Terrestrial Physics Volume 175, October **2018**, Pages 49-55
https://reader.elsevier.com/reader/sd/20B6A973A30F8641D49C2790117D08A1F2ED2BE23B5C4F20C1BB47F342AB9EAEB068EB308BA53123FBB7883BC457313E
Linear sausage oscillations of a cylinder embedded in a plasma with an azimuthal magnetic field, created by a current on the surface of the cylinder, are studied. Such a plasma configuration could be applied to modelling flaring loops, and magnetic ropes in coronal mass ejections. The plasma is assumed to be cold everywhere. Dispersion relations demonstrate that the lowest radial harmonic of the sausage mode is in the trapped regime for all values of the parallel wave number. In the long-wavelength limit, phase and group speeds of this mode are equal to the Alfvén speed in the external medium. It makes the oscillation period to be determined by the ratio of the parallel wavelength, e.g. double the length of an oscillating loop, to the external Alfvén speed, allowing for its seismological estimations. The application of the results obtained to the interpretation of long-period (longer than a minute) oscillations of emission intensity detected in solar coronal structures, gives reasonable estimations of the external Alfvén speed. Cutoff values of the parallel wavenumber for higher radial harmonics are determined analytically. Implications of this finding to the observational signatures of fast magnetoacoustic wave trains guided by cylindrical plasma non-uniformities are discussed.

Evolutionary Relationship between Sunspot Groups and Soft X-Ray Flares over Solar Cycles 21–25

Jiaqi **Lin** (林家琪)1,2, Feng Wang (王锋)1,2, Linhua Deng (邓林华)3,4, Hui Deng (邓辉)1,2, Ying Mei (梅盈)1,2, and Xiaojuan Zhang

2023 ApJ 958 1

https://iopscience.iop.org/article/10.3847/1538-4357/ad0469/pdf

Studying the interaction between solar flares and sunspot groups (SGs) is crucial for understanding and predicting solar activity. We examined the distribution, correlation, and flaring rates in the northern and southern hemispheres to reveal the relationship between different classes of soft X-ray (SXR) flares and different magnetic classifications of SGs. We discovered a significant north–south asymmetry in SXR flares and SG distribution over Solar Cycles (SC) 21–25. In the rising phase of SC24, the northern hemisphere's activity is significantly excessive. In the declining phase of SC24, the southern hemisphere's activity becomes significantly excessive. The total numbers of various SXR flares and SGs vary between the northern and southern hemispheres over the solar cycle. B-class flares are negatively correlated with all SGs at maximum but positively correlated at minimum. C-class flares correlate best with α and β SGs. M-class flares correlate best with βγδ and β SGs. X-class flares correlate highest with βγδ SGs. The flaring rate of each flare class is lowest for α SGs and highest for βγδ SGs. The flaring rates are higher in the southern hemisphere than in the northern hemisphere. Our results demonstrate that solar flares originate from different sources of solar active regions; the high-energy flares tend to be caused by more complex magnetic fields.

Development of Integral Field Spectrographs to Revolutionize Spectroscopic Observations of Solar Flares and other Energetic Solar Eruptions

Haosheng **Lin** (Institute for Astronomy, University of Hawaii), Tetsu Anan (National Solar Observatory), Gianna Cauzzi (National Solar Observatory), Lyndsay Fletcher (University of Glasgow, University of Oslo), Pei Huang (Ball Aerospace), Adam Kowalski (University of Colorado), Maxim Kramar (Institute for Astronomy, University of Hawaii), Jiong Qiu (Montana State University), Jenna Samra (Center for Astrophysics, Harvard & Smithsonian), Constance Spittler (Ball Aerospace), Takashi Sukegawa (Canon, Inc., Japan), Gregory Wirth (Ball Aerospace)

White Paper submitted for **2022**

https://arxiv.org/pdf/2209.00788.pdf

The Sun's proximity offers us a unique opportunity to study in detail the physical processes on a star's surface; however, the highly dynamic nature of the stellar surface -- in particular, energetic eruptions such as flares and coronal mass ejections -- presents tremendous observational challenges. Spectroscopy probes the physical state of the solar atmosphere, but conventional scanning spectrographs and spectrometers are unable to capture the full evolutionary history of these dynamic events with a sufficiently wide field of view and high spatial, spectral, and temporal resolution. Resolving the physics of the dynamic sun requires gathering simultaneous spectra across a contiguous area over the full duration of these events, a goal now tantalizingly close to achievable with continued investment in developing powerful new Integral Field Spectrographs to serve as the foundation of both future ground- and space-based missions. This technology promises to revolutionize our ability to study solar flares and CMEs, addressing NASA's strategic objective to "understand the Sun, solar system, and universe." Since such events generate electromagnetic radiation and high-energy particles that disrupt terrestrial electric infrastructure, this investment not only advances humanity's scientific endeavors but also enhances our space weather forecasting capability to protect against threats to our technology-reliant civilization.

Chinese Sunspot Drawing and Its Digitization-(I) Parameter Archives

G.H. **Lin**, X.F. Wang, S. Liu, X. Yang, G.F. Zhu, Y.Y. Deng, H.S. Ji, T.H. Zhou, L.N. Sun, Y.L. Feng, Z.Z. Liu, J.P. Tao, M.X. Ben, J. Lin, M.D. Ding, Z. Li, S. Zheng, S.G. Zeng, H.L. He, X.Y. Zeng, Y. Shu, X.B. Sun

2019 Solar Phys. 294:79

https://arxiv.org/pdf/1904.12316.pdf

https://link.springer.com/content/pdf/10.1007%2Fs11207-019-1456-0.pdf

Based on the Chinese historical sunspots drawings, a data set consisting of the scanned images and all their digitized parameters from 1925 to 2015 have been constructed. In this paper, we briefly describe the developmental history of sunspots drawings in China. This paper describes the preliminary processing processes that strat from the initial data (inputing to the scanning equipment) to the parameters extraction, and finally summarizes the general features of this dataset. It is the first systematic project in Chinese solar-physics community that the historical observation of sunspots drawings were digitized. Our data set fills in an almost ninety years historical gap, which span 60 degrees from east to west and 50 degrees from north to south and have no continuous and detailed digital sunspot

observation information. As a complementary to other sunspots observation in the world, our dataset provided abundant information to the long term solar cycles solar activity research.

Solar Open Flux Migration from Pole to Pole: Magnetic Field Reversal

Chia-Hsien **Lin**

HMI Science Nuggets #101 June **2018** http://hmi.stanford.edu/hminuggets/?p=2516

Solar open magnetic flux (OMF) regions are the regions with magnetic field lines extending far away from the Sun. They represent the largest-scale magnetic-field structure of the Sun. Their “open” magnetic field configuration allows plasma to flow into the interplanetary space. Therefore, they are major source regions for high-speed solar wind streams (HSS), which can cause significant geomagnetic activity at the Earth[1]. Observed in soft X-ray and certain extreme ultraviolet (EUV) wavelength, OMF regions often appear dark, and are called coronal holes[2]/sup>.

Solar-Cycle Variations of Meridional Flows in the Solar Convection Zone with Helioseismic Methods

Chia-Hsien **Lin**1 & Dean-Yi Chou

2018 ApJ 860 48

The solar meridional flow is an axisymmetric flow in solar meridional planes, extending through the convection zone. Here we study its solar-cycle variations in the convection zone using SOHO/MDI helioseismic data from 1996 to 2010, including two solar minima and one maximum. The travel-time difference between northward and southward acoustic waves is related to the meridional flow along the wave path. Applying the ray approximation and the SOLA inversion method to the travel-time difference measured in a previous study, we obtain the meridional flow distributions in $0.67 \leq r \leq 0.96R \odot$ at the minimum and maximum. At the minimum, the flow has a three-layer structure: poleward in the upper convection zone, equatorward in the middle convection zone, and poleward again in the lower convection zone. The flow speed is close to zero within the error bar near the base of the convection zone. The flow distribution changes significantly from the minimum to the maximum. The change above $0.9R \odot$ shows two phenomena: first, the poleward flow speed is reduced at the maximum; second, an additional convergent flow centered at the active latitudes is generated at the maximum. These two phenomena are consistent with the surface meridional flow reported in previous studies. The change in flow extends all the way down to the base of the convection zone, and the pattern of the change below $0.9R \odot$ is more complicated. However, it is clear that the active latitudes play a role in the flow change: the changes in flow speed below and above the active latitudes have opposite signs. This suggests that magnetic fields could be responsible for the flow change.

HMI Science Nuggets #98 may **2018**

http://hmi.stanford.edu/hminuggets/?p=2468

The Formation of IRIS Diagnostics. IX. The Formation of the C i 135.58 NM Line in the Solar Atmosphere

Hsiao-Hsuan **Lin**1, Mats Carlsson1, and Jorrit Leenaarts

2017 ApJ 846 40

https://arxiv.org/pdf/1708.09426.pdf

The C i 135.58 nm line is located in the wavelength range of NASA's Interface Region Imaging Spectrograph (IRIS) small explorer mission. We study the formation and diagnostic potential of this line by means of non local-thermodynamic-equilibrium modeling, employing both 1D and 3D radiation-magnetohydrodynamic models. The C i/C ii ionization balance is strongly influenced by photoionization by Lyα emission. The emission in the C i 135.58 nm line is dominated by a recombination cascade and the line forming region is optically thick. The Doppler shift of the line correlates strongly with the vertical velocity in its line forming region, which is typically located at 1.5 Mm height. With IRIS, the C i 135.58 nm line is usually observed together with the O i 135.56 nm line, and from the Doppler shift of both lines, we obtain the velocity difference between the line forming regions of the two lines. From the ratio of the C i/O i line core intensity, we can determine the distance between the C i and the O i forming layers. Combined with the velocity difference, the velocity gradient at mid-chromospheric heights can be derived. The C i/O i total intensity line ratio is correlated with the inverse of the electron density in the mid-chromosphere. We conclude that the C i 135.58 nm line is an excellent probe of the middle chromosphere by itself, and together with the O i 135.56 nm line the two lines provide even more information, which complements other powerful chromospheric diagnostics of IRIS such as the Mg ii h and k lines and the C ii lines around 133.5 nm.

mxCSM: A 100-slit, 6-Wavelength Wide-Field Coronal Spectropolarimeter for the Study of the Dynamics and the Magnetic Fields of the Solar Corona

Haosheng **Lin**

Front. Astron. Space Sci., 3:9. **2016** |

https://www.frontiersin.org/articles/10.3389/fspas.2016.00009/full
https://doi.org/10.3389/fspas.2016.00009
Tremendous progress has been made in the field of observational coronal magnetometry in the first decade of the Twenty-First century. With the successful construction of the Coronal Multichannel Magnetometer (CoMP) instrument, observations of the linear polarization of the coronal emission lines (CELs), which carry information about the azimuthal direction of the coronal magnetic fields, are now routinely available. However, reliable and regular measurements of the circular polarization signals of the CELs remain illusive. The CEL circular polarization signals allow us to infer the magnetic field strength in the corona, and is critically important for our understanding of the solar corona. Current telescopes and instrument can only measure the coronal magnetic field strength over a small field of view. Furthermore, the observations require very long integration time that preclude the study of dynamic events even when only a small field of view is required. This paper describes a new instrument concept that employs large-scale multiplexing technology to enhance the efficiency of current coronal spectropolarimeter by more than two orders of magnitude. This will allow for the instrument to increase the integration time at each spatial location by the same factor, while also achieving a large field of view coverage. We will present the conceptual design of a 100-slit coronal spectropolarimeter that can observe six CELs simultaneously. Instruments based on this concept will allow us to study the evolution of the coronal magnetic field even with coronagraphs with modest aperture.

Soft X-ray irradiance measured by the Solar Aspect Monitor on the Solar Dynamic Observatory Extreme ultraviolet Variability Experiment

C. Y. **Lin**, S. M. Bailey, A. Jones, D. Woodraska, A. Caspi, T. N. Woods, F. G. Eparvier, S. R. Wieman, L. V. Didkovsky
JGR 121, 3648 **2016**
http://arxiv.org/pdf/1605.01444v1.pdf
The Solar Aspect Monitor (SAM) is a pinhole camera on the Extreme-ultraviolet Variability Experiment (EVE) aboard the Solar Dynamics Observatory (SDO). SAM projects the solar disk onto the CCD through a metallic filter designed to allow only solar photons shortward of 7 nm to pass. Contamination from energetic particles and out-of-band irradiance is, however, significant in the SAM observations. We present a technique for isolating the 0.01--7 nm integrated irradiance from the SAM signal to produce the first results of broadband irradiance for the time period from May 2010 to May 2014. The results of this analysis agree with a similar data product from EVE's EUV SpectroPhotometer (ESP) to within 25%. We compare our results with measurements from the Student Nitric Oxide Explorer (SNOE) Solar X-ray Photometer (SXP) and the Thermosphere Ionosphere Mesosphere Energetics and Dynamics (TIMED) Solar EUV Experiment (SEE) at similar levels of solar activity. We show that the full-disk SAM broadband results compare well to the other measurements of the 0.01--7 nm irradiance. We also explore SAM's capability toward resolving spatial contribution from regions of solar disk in irradiance and demonstrate this feature with a case study of several strong flares that erupted from active regions on **March 11, 2011**.

Automatic detection method, forecast and alert of solar proton events

Ganghua **Lin**
Solar and Stellar Variability: Impact on Earth and Planets, Proceedings IAU Symposium No. 264, **2009**, p. 105-108, A.G. Kosovichev, A.H. Andrei & J.-P. Rozelot, eds.
Y:\obridko\otchet09
The methods of automatic solar active phenomenon or event detection have been researched and explored by people for many years, which have gone into actual services. The paper analyzes the relationship between these methods of automatic detection and the forecast or alert, using the solar short-term proton events predictions as an example. Using automatic method to conduct forecast or alert is under thinking.

Time variations of the non-potential and volume-threading magnetic helicities

Luis **Linan**, Étienne Pariat, Kostas Moraitis, Gherardo Valori, James E. Leake
ApJ **865** 52 **2018**
https://arxiv.org/pdf/1809.03765.pdf
https://sites.lesia.obspm.fr/helisol/files/2018/09/Flux_Hj_Hpj.pdf
sci-hub.tw/10.3847/1538-4357/aadae7
Relative magnetic helicity is a gauge invariant quantity suitable for the study of the magnetic helicity content of heliospheric plasmas. Relative magnetic helicity can be decomposed uniquely into two gauge invariant quantities, the magnetic helicity of the non-potential component of the field, and a complementary volume-threading helicity. Recent analysis of numerical experiments simulating the generation of solar eruptions have shown that the ratio of the non-potential helicity to the total relative helicity is a clear marker of the eruptivity of the magnetic system, and that the high value of that quantity could be a sufficient condition for the onset of the instability generating the

eruptions. The present study introduces the first analytical examination of the time variations of these non-potential and volume-threading helicities. The validity of the analytical formulas derived are confirmed with analysis of three-dimensional (3D) magnetohydrodynamics (MHD) simulations of solar coronal dynamics. Both the analytical investigation, and the numerical application show that, unlike magnetic helicity, the non-potential and the volume-threading helicities are not conserved quantities, even in the ideal MHD regime. A term corresponding to the transformation between the non-potential and volume-threading helicities frequently dominates their dynamics. This finding has an important consequence for their estimation in the solar corona: unlike with relative helicity, their volume coronal evolution cannot be ascertained by the flux of these quantities through the volume's boundaries. Only techniques extrapolating the 3D coronal field will enable both the proper study of the non-potential and volume-threading helicities, and the observational analysis of helicity-based solar-eruptivity proxies.

First Observations of Solar Disk Gamma Rays over a Full Solar Cycle

Tim **Linden**, John F. Beacom, Annika H. G. Peter, Benjamin J. Buckman, Bei Zhou, Guanying Zhu
PHYSICAL REVIEW D (PRD) **2020**
https://arxiv.org/pdf/2012.04654.pdf
The solar disk is among the brightest gamma-ray sources in the sky. It is also among the most mysterious. No existing model fully explains the luminosity, spectrum, time variability, and morphology of its emission. We perform the first analysis of solar-disk gamma rays over a full 11-year solar cycle, utilizing a powerful new method to differentiate solar signals from astrophysical backgrounds. We produce: (i) a robustly measured spectrum from 100 MeV to 100 GeV, reaching a precision of several percent in the 1-10 GeV range, (ii) new results on the anti-correlation between solar activity and gamma-ray emission, (iii) strong constraints on short-timescale variability, ranging from hours to years, and (iv) new detections of the equatorial and polar morphologies of high-energy gamma rays. Intriguingly, we find no significant energy dependence in the time variability of solar-disk emission, indicating that strong magnetic-field effects close to the solar surface, rather than modulation throughout the heliosphere, must primarily control the flux and morphology of solar-disk emission.

Using the Butterfly Effect to Probe How the Sun Generates Acoustic Noise

Charles **Lindsey**, Matthias Rempel
Solar Physics February **2020**, 295:26
https://doi.org/10.1007/s11207-020-1580-x
A major encumbrance to recognition of individual episodes of noise emission is the accumulation over hours of other noise emitted long before. This is true in simulations just as it is in the solar environment itself. The composite seismic signature of acoustic radiation accumulated over preceding hours drowns out the signature of newly emitted "acoustic pings." This problem could be alleviated in simulations by periodically damping the accumulated acoustic radiation – if this can be done benignly, i.e. in such a way that the onset transient of the damping (and its subsequent termination) does not emit its own acoustic noise. We introduce a way of doing this based upon a study of the butterfly effect in compressible radiative MHD simulations of convection that excites p-modes. This gives us an encouraging preview of what further development of this utility offers for an understanding of the character of p-mode generation in convective atmospheres.

Risks for Life on Habitable Planets from Superflares of Their Host Stars

Manasvi **Lingam**1,2 and Abraham Loeb
2017 ApJ 848 41
http://sci-hub.cc/10.3847/1538-4357/aa8e96
We explore some of the ramifications arising from superflares on the evolutionary history of Earth, other planets in the solar system, and exoplanets. We propose that the most powerful superflares can serve as plausible drivers of extinction events, and that their periodicity corresponds to certain patterns in the terrestrial fossil diversity record. On the other hand, weaker superflares may play a positive role in enabling the origin of life through the formation of key organic compounds. Superflares could also prove to be quite detrimental to the evolution of complex life on present-day Mars and exoplanets in the habitable zone of M- and K-dwarfs. We conclude that the risk posed by superflares has not been sufficiently appreciated, and that humanity might potentially witness a superflare event in the next $\sim 10^3$ years, leading to devastating economic and technological losses. In light of the many uncertainties and assumptions associated with our analysis, we recommend that these results should be viewed with due caution.

Solar Activity Parameters and Associated Forbush Decreases During the Minimum Between Cycles 23 and 24 and the Ascending Phase of Cycle 24

D. **Lingri**, H. Mavromichalaki , A. Belov, E. Eroshenko, V. Yanke, A. Abunin, M. Abunina
Solar Phys. Volume 291, Issue 3, pp 1025-1041 **2016**
We study the Forbush decreases in cosmic-ray intensity from January 2008 to December 2013, covering the minimum between Solar Cycles 23 and 24 and the ascending phase of Cycle 24. We performed a statistical analysis

of 617 events and concentrated on three of the most important ones. We used the IZMIRAN database of Forbush effects obtained by processing the data of the worldwide neutron monitor network using the global survey method. The first event occurred on **18 February 2011** with a ~5 % decrease of cosmic rays with 10 GV rigidity, the second on **8 March 2012** with an amplitude of ~12 %, and the third on **14 July 2012** with an amplitude of ~6 %. For these three events, we also studied the events that occurred on the Sun and the way that these affected the interplanetary space, and finally provoked the decreases of the galactic cosmic rays near Earth. We found that each neutron monitor records these decreases, which depend on the cut-off rigidity of the station. We carried out a statistical analysis of the amplitude of the cosmic-ray decreases with solar and geomagnetic parameters.

Global MHD Simulations of the Time-Dependent Corona

Roberto **Lionello**, CooperDowns, Emily I. Mason, Jon A. Linker, Ronald M. Caplan, Pete Riley, Viacheslav S.Titov, Marc L. DeRosa

ApJ **959** 77 **2023**

https://arxiv.org/pdf/2306.12551.pdf

https://iopscience.iop.org/article/10.3847/1538-4357/ad00be/pdf

We describe, test, and apply a technique to incorporate full-sun, surface flux evolution into an MHD model of the global solar corona. Requiring only maps of the evolving surface flux, our method is similar to that of Lionello et al. (2013), but we introduce two ways to correct the electric field at the lower boundary to mitigate spurious currents. We verify the accuracy of our procedures by comparing to a reference simulation, driven with known flows and electric fields. We then present a thermodynamic MHD calculation lasting one solar rotation driven by maps from the magnetic flux evolution model of Schrijver & DeRosa (2003). The dynamic, time-dependent nature of the model corona is illustrated by examining the evolution of the open flux boundaries and forward modeled EUV emission, which evolve in response to surface flows and the emergence and cancellation flux. Although our main goal is to present the method, we briefly investigate the relevance of this evolution to properties of the slow solar wind, examining the mapping of dipped field lines to the topological signatures of the "S-Web" and comparing charge state ratios computed in the time-dependently driven run to a steady state equivalent. Interestingly, we find that driving on its own does not significantly improve the charge states ratios, at least in this modest resolution run that injects minimal helicity. Still, many aspects of the time-dependently driven model cannot be captured with traditional steady-state methods, and such a technique may be particularly relevant for the next generation of solar wind and CME models.

Characteristics of the Heliospheric Current Sheets at the Sector Boundaries: Wind Observations from 1995–2020

Kan **Liou**1 and Chin-Chun Wu2

2021 ApJ 920 39

https://iopscience.iop.org/article/10.3847/1538-4357/ac1586/pdf

https://doi.org/10.3847/1538-4357/ac1586

We report results of a statistical study of 1197 heliospheric current sheet (HCS) events associated with the sector boundaries observed by the Wind spacecraft between 1995 and 2020. The average property of the HCS events can be characterized as follows: (1) The width of the current sheets ranges between ~600 km and 1.1 × 106 km, with an average width of 1.06 ± 2.37 × 105 km; (2) The longitude (in Geocentric Solar-Ecliptic coordinate) of the HCS normal shows a large peak at ~210° (0° sunward pointing) and a longer tail at smaller angles; (3) The latitudinal angle (inclination) of the HCS normal shows a near symmetric distribution (peak and average ~0°); (4) The yearly occurrence rate is relatively constant (~46 or 3.4 events per solar rotation), without showing a clear solar cycle dependence; (5) There are solar cycle variations in the properties of the plasma and field within the current sheets and these variations follow closely with the background solar wind plasma and field; (6) A mild (~10%) proton temperature increase within the HCS, suggesting that heating of the solar wind proton can occur within the current sheet; and (7) A sudden decrease in the proton temperature anisotropy (T∥/T⊥) toward unity within ~3 hr of the HCS was identified. These results suggest that on the large scale the HCS at 1 au is a relatively stable and persistent solar wind structure throughout the solar cycle. On the small scale the HCS property is probably controlled by the dynamics of the current system, which is still poorly known. **1995 January 1–28**

A Possible Cause of the Diminished Solar Wind During the Solar Cycle 23 – 24 Minimum

Kan **Liou**, Chin-Chun Wu

Solar Phys. **2016**

http://link.springer.com/article/10.1007/s11207-016-0989-8

Interplanetary magnetic field and solar wind plasma density observed at 1 AU during Solar Cycle 23 – 24 (SC-23/24) minimum were significantly smaller than those during its previous solar cycle (SC-22/23) minimum. Because the Earth's orbit is embedded in the slow wind during solar minimum, changes in the geometry and/or content of the slow wind region (SWR) can have a direct influence on the solar wind parameters near the Earth. In this study, we

analyze solar wind plasma and magnetic field data of hourly values acquired by Ulysses. It is found that the solar wind, when averaging over the first (1995.6 – 1995.8) and third (2006.9 – 2008.2) Ulysses' perihelion (\({\sim}\,1.4~\mbox{AU}\)) crossings, was about the same speed, but significantly less dense (\({\sim}\,34~\%\)) and cooler (\({\sim}\,20~\%\)), and the total magnetic field was \({\sim}\,30~\%\) weaker during the third compared to the first crossing. It is also found that the SWR was \({\sim}\,50~\%\) wider in the third (\({\sim}\,68.5^{\circ}\) in heliographic latitude) than in the first (\({\sim}\,44.8^{\circ}\)) solar orbit. The observed latitudinal increase in the SWR is sufficient to explain the excessive decline in the near-Earth solar wind density during the recent solar minimum without speculating that the total solar output may have been decreasing. The observed SWR inflation is also consistent with a cooler solar wind in the SC-23/24 than in the SC-22/23 minimum. Furthermore, the ratio of the high-to-low latitude photospheric magnetic field (or equatorward magnetic pressure force), as observed by the Mountain Wilson Observatory, is smaller during the third than the first Ulysses' perihelion orbit. These findings suggest that the smaller equatorward magnetic pressure at the Sun may have led to the latitudinally-wider SRW observed by Ulysses in SC-23/24 minimum.

Analytical description of nonlinear acoustic waves in the solar chromosphere

Yuri E. **Litvinenko**1 and Jongchul Chae
A&A 599, A15 (**2017**) 10.1051/0004-6361/201629568
Aims. Vertical propagation of acoustic waves of finite amplitude in an isothermal, gravitationally stratified atmosphere is considered.
Methods. Methods of nonlinear acoustics are used to derive a dispersive solution, which is valid in a long-wavelength limit, and a non-dispersive solution, which is valid in a short-wavelength limit. The influence of the gravitational field on wave-front breaking and shock formation is described. The generation of a second harmonic at twice the driving wave frequency, previously detected in numerical simulations, is demonstrated analytically.
Results. Application of the results to three-minute chromospheric oscillations, driven by velocity perturbations at the base of the solar atmosphere, is discussed. Numerical estimates suggest that the second harmonic signal should be detectable in an upper chromosphere by an instrument such as the Fast Imaging Solar Spectrograph installed at the 1.6-m New Solar Telescope of the Big Bear Observatory.

Five-minute oscillations of photospheric and chromospheric swirls

Jiajia **Liu** (刘佳佳)1,2,3, David Jess2,4, Robert Erdélyi5,6,7 and Mihalis Mathioudakis2
A&A 674, A142 (**2023**)
https://www.aanda.org/articles/aa/pdf/2023/06/aa45373-22.pdf
Context. Swirls are ubiquitous in the solar atmosphere. They are thought to be related to the excitation of different modes of magnetohydrodynamic waves and pulses, as well as spicules. However, statistical studies of their collective behaviour are rare.
Aims. We aim to study the collective as well as the individual behaviour of photospheric and chromospheric swirls detected by the automated swirl detection algorithm (ASDA) from observations obtained by the Swedish 1-m Solar Telescope and the Hinode satellite.
Methods. We performed a detailed analysis of six different parameters of photospheric and chromospheric swirls with the wavelet analysis. Two clusters with periods with significant wavelet power, one from 3 − 8 min and the other from 10 − 14 min, were found. The former coincides with the dominant period of the global p-mode spectrum. The wavelet and fast Fourier transform analysis of example swirls also revealed similar periods.
Results. These results suggest that global p-modes might be important in triggering photospheric and thus chromospheric swirls. A novel scenario of global p-modes providing energy and mass fluxes to the upper solar atmosphere via generating swirls, Alfvén pulses, and spicules is then proposed.

Solar Toroidal Field Evolution Spanning Four Sunspot Cycles Seen by the Wilcox Solar Observatory, the Solar and Heliospheric Observatory/Michelson Doppler Imager, and the Solar Dynamics Observatory/Helioseismic and Magnetic Imager

Allison L. **Liu**1 and Philip H. Scherrer2
2022 ApJL 927 L2
https://iopscience.iop.org/article/10.3847/2041-8213/ac52ae/pdf
Forty-four years of Wilcox Solar Observatory, 14 years of Michelson Doppler Imager on the Solar and Heliospheric Observatory, and 11 years of Helioseismic and Magnetic Imager on the Solar Dynamics Observatory magnetic field data have been studied to determine the east–west inclination—the toroidal component—of the magnetic field. Maps of the zonal averaged inclination show that each toroidal field cycle begins at around the same time at high latitudes in the northern and southern hemispheres, and ends at the equator. Observation of these maps also shows that each instance of a dominant toroidal field direction starts at high latitudes near sunspot maximum and is still visible near the equator well past the minimum of its cycle, indicating that the toroidal field cycle spans

approximately two sunspot cycles. The length of the extended activity cycle is measured to be approximately 16.8 yr.

Solar Toroidal Field Evolution Spanning Four Sunspot Cycles Seen By WSO, SOHO/MDI, and SDO/HMI

Allison L. **Liu**1 , P. H. Scherrer2
HMI Science Nuggets #170 **2021** http://hmi.stanford.edu/hminuggets/?p=3767

Investigations of Sizes and Dynamical Motions of Solar Photospheric Granules by a Novel Granular Segmenting Algorithm

Liu Yanxiao, Jiang Chaowei, Yuan Ding, Zuo Pingbing, Wang Yi, Cao Wenda
ApJ **2021**
https://arxiv.org/pdf/2110.03951.pdf
Granules observed in solar photosphere are believed to be convective and turbulent, but the physical picture of granular dynamical process remains unclear. Here we performed an investigation of granular dynamical motions of full length scales based on data obtained by the 1-meter New Vacuum Solar Telescope (NVST) and the 1.6-meter Goode Solar Telescope (GST). We developed a new granule segmenting method, which can detect both small faint and large bright granules. A large number of granules were detected and two critical sizes, 265 km and 1420 km, were found to separate the granules into three length ranges. The granules with sizes above 1420 km follow Gaussian distribution, and demonstrate "flat" in flatness function, which shows that they are non-intermittent and thus are dominated by convective motions. Small granules with sizes between 265 and 1420 km are fitted by a combination of power law function and Gauss function, and exhibit non-linearity in flatness function, which reveals that they are in the mixing motions of convection and turbulence. Mini granules with sizes below 265 km follow power law distribution and demonstrate linearity in flatness function, indicating that they are intermittent and strongly turbulent. These results suggest that a cascade process occurs: large granules break down due to convective instability, which transport energy into small ones; then turbulence is induced and grows, which competes with convection and further causes the small granules to continuously split. Eventually, the motions in even smaller scales enter in a turbulence-dominated regime.

Electromagnetic Proton Beam Instabilities in the Inner Heliosphere: Energy Transfer Rate, Radial Distribution, and Effective Excitation

Wen **Liu**, Jinsong Zhao, Huasheng Xie, Yuhang Yao, Dejin Wu, L. C. Lee
ApJS **2021**
https://arxiv.org/pdf/2107.12883.pdf
Differential flows among different ion species are often observed in the solar wind, and such ion differential flows can provide the free energy to drive Alfvén/ion-cyclotron and fast-magnetosonic/whistler instabilities. Previous works mainly focused on the ion beam instability under the parameters representative of the solar wind nearby 1 au. In this paper we further study the proton beam instability using the radial models of the magnetic field and plasma parameters in the inner heliosphere. We explore a comprehensive distribution of the proton beam instability as functions of the heliocentric distance and the beam speed. We also perform a detailed analysis of the energy transfer between unstable waves and particles and quantify how much the free energy of the proton beam flows into unstable waves and other kinds of particle species (i.e., proton core, alpha particle and electron). This work clarifies that both parallel and perpendicular electric field are responsible for the excitation of oblique Alfvén/ion-cyclotron and oblique fast-magnetosonic/whistler instabilities. Moreover, this work proposes an effective growth length to estimate whether the instability is efficiently excited or not. It shows that the oblique Alfvén/ion-cyclotron instability, oblique fast-magnetosonic/whistler instability and oblique Alfvén/ion-beam instability can be efficiently driven by proton beams drifting at the speed ∼600−1300 km/s in the solar atmosphere. In particular, oblique Alfvén/ion-cyclotron waves driven in the solar atmosphere can be significantly damped therein, leading to the solar corona heating. These results are helpful for understanding the proton beam dynamics in the inner heliosphere and can be verified through in situ satellite measurements.

Predicting Sunspot Numbers Based on Inverse Number and Intelligent Fixed Point

Zhi **Liu**, Tie Zhang & Hongxu Wang
Solar Physics volume 296, Article number: 83 (**2021**)
https://link.springer.com/content/pdf/10.1007/s11207-021-01835-z.pdf
https://doi.org/10.1007/s11207-021-01835-z
This article proposes a new model for predicting sunspot activity based on the inverse number and intelligent fixed point. Firstly, in the training phase, the optimal parameters of the model are selected by the inverse-number formula and intelligent fixed-point algorithm. Secondly, in the validation phase, the model is verified by the data. Finally, the

model is applied to the prediction of monthly mean sunspot number (MSN). The model's predictions are compared with those of autoregressive models (AR) and the National Oceanic and Atmospheric Administration (NOAA) predictions. The results show that the prediction accuracy of the proposed method is higher than that of previous methods. The method is then used to predict the 13-month smoothed monthly total sunspot number (MSSN13), and a higher prediction accuracy is obtained. The model proposed in this article is theoretically complete and robust.

New Vacuum Solar Telescope Fringe Removal Based on "Fringes Flat Field"

Dejian **Liu**, Sheng Zheng, Yao Huang & Yongyuan Xiang
Solar Physics volume 296, Article number: 28 (**2021**)
https://link.springer.com/content/pdf/10.1007/s11207-021-01775-8.pdf
The solar chromosphere data products of the New Vacuum Solar Telescope (NVST) have been affected by the interference fringes since its first operation. These fringes have a serious impact on the quality of NVST high-resolution data, which are reconstructed by short-exposure data. In order to improve the quality of NVST high-resolution data, this article proposes a method based on "Fringes Flat Field" to remove the interference fringes in NVST short-exposure data. We made the "Fringes Flat Field" using Adaptive Wavelet Transform (AWT) and Butterworth low-pass filter. The results of the experiments are satisfactory, and the method cannot only remove the fringes effectively, but keep the solar structures from being lost.

Co-spatial velocity and magnetic swirls in the simulated solar photosphere

Jiajia **Liu**, Mats Carlsson, Chris J Nelson, Robert Erdélyi
A&A 632, A97 **2019**
https://arxiv.org/pdf/1911.10923.pdf
https://doi.org/10.1051/0004-6361/201936882
Context. Velocity or intensity swirls have now been shown to be widely present throughout the photosphere and chromosphere. It has been suggested that these events could contribute to the heating of the upper solar atmosphere, via exciting Alfvén pulses, which could carry significant amounts of energy. However, the conjectured necessary physical conditions for their excitation, that the magnetic field rotates co-spatially and co-temporally with the velocity field, has not been verified. Aims. We aim to understand whether photospheric velocity swirls exist co-spatially and co-temporally with photospheric magnetic swirls, in order to demonstrate the link between swirls and pulses. Methods. The automated swirl detection algorithm (ASDA) is applied to the photospheric horizontal velocity and vertical magnetic fields obtained from a series of realistic numerical simulations using the RMHD code Bifrost. The spatial relationship between the detected velocity and magnetic swirls is further investigated via a well-defined correlation index (CI) study. Results. On average, there are ~63 short-lived photospheric velocity swirls (with lifetimes mostly less than 20 s, and average radius of ~37 km and rotating speeds of ~2.5 km/s) detected in a field of view (FOV) of 6\times6 Mm^{-2}, implying a total population of velocity swirls of ~1.06\times10^7 in the solar photosphere. More than 80% of the detected velocity swirls are found to be accompanied by local magnetic concentrations in intergranular lanes. On average, ~71% of the detected velocity swirls have been found to co-exist with photospheric magnetic swirls with the same rotating direction. Conclusions. The co-temporal and co-spatial rotation in the photospheric velocity and magnetic fields provide evidence that the conjectured condition for the excitation of Alfvén pulses by photospheric swirls is fulfilled.

Prediction of the Sunspot Number with a New Model Based on the Revised Data

Jinhuo **Liu**, Juan Zhao, Haibo Lin
Solar Physics October **2019**, 294:157
https://link.springer.com/content/pdf/10.1007%2Fs11207-019-1536-1.pdf
Sunspot-number prediction plays a very important role in space-weather forecasts and environmental research. In 2015, the international relative sunspot-number publisher released a new version of the data. Compared with the old version, the new data changed enough to influence sunspot-prediction methods that were based on the old data. The aim of this study is to propose a new prediction method based on the new data, and improve prediction accuracy as much as possible. A modified gaussian function, which has four parameters, was used in our method to describe each single cycle. Via four relationships among the four parameters, we found the most probable values and their uncertainties for the four parameters, and then we obtained the sunspot-number variation curve and its range for Solar Cycle 24. The results showed that the peak value should be 113.3 (the real value was 116.4), at the 57th month (between the two real peak at the 39th and the 64th month). A range of peak values was also given by this method, which range from 91 (less than the real value by 25) to 134 (greater than the real value by 18).

Standard Magnetic Field Production at Huairou Solar Observing Station

Suo **Liu**1,2 & Ganghua Lin1,2 & Xiao Yang1,2 & Xiaofan Wang1,2 & Jiangtao Su1,2 & Yuanyong Deng1,2

Proceedings IAU Symposium No. 340, **2018**
https://arxiv.org/pdf/1902.00344.pdf
The regular solar observations are operated at Huairou Solar Observing Station (HSOS) since 1987, which make the construction of long-term magnetic field datasets available to understand solar magnetic field and cycles. There exist some inconveniences for solar physicist to use these data, because the data storage medium and format at HSOS experienced some changes. Additionally, the processes of magnetic field calibration are not easy to deal with for who are not familiar with these data. Here shows that the magnetic field of HSOS are further processed toward international standards, in order to explore HSOS observations data for scientific research.

Toward Standard Data Production for Magnetic Field Observations at Huairou Solar Observing Station

S. **Liu**, X. Yang, C. Zhao, G.H. Lin
Astronomical Data Analysis Software and Systems XXV 2017
http://adsabs.harvard.edu/abs/**2017**ASPC..512..539L
https://arxiv.org/pdf/1902.00338.pdf
The productions of data with internationally agreed standards are the common pursuits for all astronomical observation instruments both ground and spacebased undoubtedly, Since standard data to facilitate the use of scientific research. The routine solar observations are available at Huairou Solar Observing Station (HSOS) since 1987, which should be regarded as one main solar observations in the world. The data storage medium and format at HSOS experienced several changes, so there exist some inconveniences for solar physicist. This paper shows that the observations data of HSOS are further processed both for storage medium and format toward international standards, in order to explore HSOS observations data for scientific research.

Mingguang Liu

The HMI Vector Magnetic Field Synoptic Charts

Yang **Liu**1, J. Todd Hoeksema1, Xudong Sun1, & Keiji Hayashi
HMI Science Nuggets #59 Sept **2016**
http://hmi.stanford.edu/hminuggets/?p=1689
HMI vector magnetic field synoptic charts are now available through the JSOC website at hmi.b_synoptic. Here we describe the procedure to produce the synoptic charts and the disambiguation method we choose to solve the 180-degree ambiguity of the azimuth in vector magnetic field measurement. The procedure to produce vector magnetic field synoptic charts is described below.

On the Parallel and Perpendicular Propagating Motions Visible inPolar Plumes: An Incubator For (Fast) Solar Wind Acceleration?

Jiajia **Liu**1,2, Scott W. McIntosh2, Ineke De Moortel3, and Yuming Wang
2015 ApJ 806 273
We combine observations of the Coronal Multi-channel Polarimeter and the Atmospheric Imaging Assembly on board the Solar Dynamics Observatory to study the characteristic properties of (propagating) Alfvénic motions and quasi-periodic intensity disturbances in polar plumes. This unique combination of instruments highlights the physical richness of the processes taking place at the base of the (fast) solar wind. The (parallel) intensity perturbations with intensity enhancements around 1% have an apparent speed of 120 km s−1 (in both the 171 and 193 Å passbands) and a periodicity of 15 minutes, while the (perpendicular) Alfvénic wave motions have a velocity amplitude of 0.5 km s−1, a phase speed of 830 km s−1, and a shorter period of 5 minutes on the samestructures. These observations illustrate a scenario where the excited Alfvénic motions are propagating along an inhomogeneously loaded magnetic field structure such that the combination could be a potential progenitor of the magnetohydrodynamic turbulence required to accelerate the fast solar wind.

On the Parallel and Perpendicular Propagating Motions Visible in Polar Plumes: An Incubator For (Fast) Solar Wind Acceleration?

Jiajia **Liu**, Scott W. McIntosh, Ineke De Moortel, Yuming Wang
2015
http://arxiv.org/pdf/1507.00143v1.pdf
We combine observations of the Coronal Multi-channel Polarimeter (CoMP) and the Atmospheric Imaging Assembly (AIA) onboard the Solar Dynamics Observatory (SDO) to study the characteristic properties of (propagating) Alfvenic motions and quasi-periodic intensity disturbances in polar plumes. This unique combination of instruments highlights the physical richness of the processes taking place at the base of the (fast) solar wind. The (parallel) intensity perturbations with intensity enhancements around 1% have an apparent speed of 120 km/s (in

both the 171A and 193A passbands) and a periodicity of 15 minutes, while the (perpendicular) Alfvenic wave motions have a velocity amplitude of 0.5 km/s, a phase speed of 830 km/s, and a shorter period of 5 minutes on the same structures. These observations illustrate a scenario where the excited Alfvenic motions are propagating along an inhomogeneously loaded magnetic field structure such that the combination could be a potential progenitor of the magnetohydrodynamic turbulence required to accelerate the fast solar wind. **December 30, 2011**

New Vacuum Solar Telescope and Observations with High Resolution

Zhong **Liu**, Jun Xu, Bo-Zhong Gu, Sen Wang, Jian-Qi You, Long-Xiang Shen, Ru-Wei Lu, Zhen-Yu Jin, Lin-Fei Chen, Ke Lou, Zhi Li, Guang-Qian Lu, Zhi Xu, Chang-Hui Rao, Qi-Qian Hu, Ru-Feng Li, Hao-Wen Fu, Men-Xian Bao, Ming-Chan Wu, Bo-Rong Zhang
Research in Astronomy and Astrophysics, **2014**
http://arxiv.org/pdf/1403.6896v1.pdf
The New Vacuum Solar Telescope (NVST) is a 1 meter vacuum solar telescope that aims to observe the fine structures on the Sun. The main tasks of NVST are high resolution imaging and spectral observations, including the measurements of solar magnetic field. NVST is the primary ground-based facility of Chinese solar community in this solar cycle. It is located by the Fuxian Lake of southwest China, where the seeing is good enough to perform high resolution observations. In this paper, we first introduce the general conditions of Fuxian Solar Observatory and the primary science cases of NVST. Then, the basic structures of this telescope and instruments are described in detail. Finally, some typical high resolution data of solar photosphere and chromosphere are also shown.

Testing Hemispheric Rule of Helicity with HMI Data

Y. **Liu**, J. T. Hoeksema, X. Sun
HMI Science Nuggets, No. 2, Jan **2014**
http://hmi.stanford.edu/hminuggets/?p=361
Hemispheric helicity preference in groups of active regions with different properties suggests different origins of magnetic twist.

Test of the Hemisphere Rule of Magnetic Twist in Solar Active Regions Using the Helioseismic and Magnetic Imager (HMI) Vector Magnetic Field Data

Y. **Liu**, J. T. Hoeksema, X. Sun
E-print, Jan **1014**; **2014** ApJ 783 L1
http://soi.stanford.edu/~yliu/papers/testofHemRule.pdf
Magnetic twist in solar active regions has been found to have a hemispheric preference in sign (hemisphere rule): negative in the northern hemisphere and positive in the southern. The preference reported in previous studies ranges greatly, from ~ 58\% to 82\%. In this study, we examine this hemispheric preference using vector magnetic field data taken by HMI and find that 75\% pm 7\% of 151 active regions studied obey the hemisphere rule, well within the preference range in previous studies. If the sample is divided into two groups,--,active regions having magnetic twist and writhe of the same sign and having opposite signs,--,the strength of the hemispheric preference differs substantially: (64\% pm 11\%) for the former group and (87\% pm 8\%) for the latter. This difference becomes even more significant in a sub-sample of 82 active regions having a simple bipole magnetic configuration: (56\% pm 16\%) for the active regions having the same signs of twist and writhe, and 93\% with lower and upper confidence bounds of 80\% and 98\% for the active regions having the opposite signs. The error reported here is a 95\% confidence interval. This may suggest that, prior to emergence of magnetic tubes, either the sign of twist does not have a hemispheric preference or the twist is relatively weak.

A new solar signal: Average maximum sunspot magnetic fields independent of activity cycle

William **Livingston**, Fraser Watson
Geophys. Res. Lett. **2015**, 42, 9185-9188
http://arxiv.org/pdf/1604.03050v1.pdf
Over the past five years, 2010-2015, we have observed, in the near infrared (IR), the maximum magnetic field strengths for 4145 sunspot umbrae. Herein we distinguish field strengths from field flux. (Most solar magnetographs measure flux). Maximum field strength in umbrae is co-spatial with the position of umbral minimum brightness (Norton and Gilman, 2004). We measure field strength by the Zeeman splitting of the Fe 15648.5 A spectral line. We show that in the IR no cycle dependence on average maximum field strength (2050 G) has been found +/- 20 Gauss. A similar analysis of 17,450 spots observed by the Helioseismic and Magnetic Imager onboard the Solar Dynamics Observatory reveal the same cycle independence +/- 0.18 G., or a variance of 0.01%. This is found not to

change over the ongoing 2010-2015 minimum to maximum cycle. Conclude the average maximum umbral fields on the Sun are constant with time.

Restoration of the K and F Components of the Solar Corona from LASCO-C2 Images over 24 Years [1996--2019]

Antoine **Llebaria** (1), Philippe Lamy (2), Hugo Gilardy (2), Brice Boclet (1), Jean Loirat (1)
Solar Phys. 296, Article number: 53 **2021**
https://arxiv.org/pdf/2011.12920.pdf
https://link.springer.com/content/pdf/10.1007/s11207-021-01800-w.pdf
https://doi.org/10.1007/s11207-021-01800-w
We present a photometrically accurate restitution of the K and F coronae from white-light images obtained over 24 Years [1996--2019] by the Large-Angle Spectrometric COronagraph "LASCO-C2" onboard the Solar and Heliospheric Observatory (SOHO). The procedure starts with the data set coming from the polarimetric separation of images of 512 x 512 pixels in which the F-corona and the instrumental stray light are entangled. Disentangling these components proceeds in three stages, each composed of several steps. Stage 1 establishes the distinct variations of the radiance of these components with the Sun--SOHO distance and generate a new data set of median images calculated for each Carrington rotation. Stage 2 achieves the restitution of a set of 36 stray light images reflecting its temporal variation and the periodic rolls of SOHO which started in 2003. Stage 3 achieves the restitution of the F-corona and a time series of daily images is generated. These results allowed us processing the whole set of routine LASCO-C2 images of 1024 x 1024 pixels (approximately 626000 images) and producing calibrated, high resolution images of the K-corona. We extend our past conclusions that the temporal variation of the integrated radiance of the K-corona tracks the solar activity over two solar cycles 23 and 24 and that it is highly correlated with the temporal variation of the total magnetic field. The behaviours of the integrated radiance during the last few years of the declining phases of solar cycles 23 and 24 are remarkably similar, reaching the same floor level and leading to a duration of 11.0 year for the latter cycle, in agreement with the sunspot determination.

Thermodynamic Structure of the Solar Corona: Tomographic Reconstructions and MHD Modeling

Diego G. **Lloveras**, Alberto M. Vásquez, Federico A. Nuevo, Cecilia Mac Cormack, Nishtha Sachdeva, Ward Manchester IV, Bartholomeus Van der Holst & Richard A. Frazin
Solar Physics volume 295, Article number: 76 (**2020**)
https://link.springer.com/content/pdf/10.1007/s11207-020-01641-z.pdf
We carry out a study of the global three-dimensional (3D) structure of the electron density and temperature of the quiescent inner solar corona ($r<1.25R_\odot r<1.25R_\odot$) by means of tomographic reconstructions and magnetohydrodynamic simulations. We use differential emission measure tomography (DEMT) and the Alfvén Wave Solar Model (AWSoM), in their latest versions. Two target rotations were selected from the solar minimum between Solar Cycles (SCs) 23 and 24 and the declining phase of SC 24. We report in quantitative detail on the 3D thermodynamic structure of the core and outer layers of the streamer belt, and of the high latitude coronal holes (CH), as revealed by the DEMT analysis. We report on the presence of two types of structures within the streamer belt, loops with temperature decreasing/increasing with height (dubbed down/up loops), as reported first in previous DEMT studies. We also estimate the heating energy flux required at the coronal base to keep these structures stable, found to be of order $105\ \mathrm{erg cm^{-2} s^{-1}} 105\ \mathrm{erg cm^{-2} s^{-1}}$, consistently with previous DEMT and spectroscopic studies. We discuss how these findings are consistent with coronal dissipation of Alfvén waves. We compare the 3D results of DEMT and AWSoM in distinct magnetic structures. We show that the agreement between the products of both techniques is the best so far, with an overall agreement $\lesssim 20\% \lesssim 20\%$, depending on the target rotation and the specific coronal region. In its current implementation the ASWsoM model cannot reproduce down loops though. Also, in the source region of the fast and slow components of the solar wind, the electron density of the AWSoM model increases with latitude, opposite to the trend observed in DEMT reconstructions. **CR 2082 , CR 2208**

Comparative Study of the Three-Dimensional Thermodynamical Structure of the Inner Corona of Solar Minimum Carrington Rotations 1915 and 2081

Diego G. **Lloveras**, Alberto M. Vásquez, Federico A. Nuevo, Richard A. Frazin
Solar Physics October **2017**, 292:153
https://link.springer.com/content/pdf/10.1007%2Fs11207-017-1179-z.pdf
Using differential emission measure tomography (DEMT) based on time series of EUV images, we carry out a quantitative comparative analysis of the three-dimensional (3D) structure of the electron density and temperature of the inner corona ($r<1.25R_\odot r<1.25R_\odot$) between two specific rotations selected from the last two solar minima, namely Carrington Rotations (CR)1915 and CR-2081. The analysis places error bars on the results because of the systematic uncertainty of the sources. While the results for CR-2081 are characterized by a remarkable north–south symmetry, the southern hemisphere for CR-1915 exhibits higher densities and temperatures than the northern hemisphere. The core region of the streamer belt in both rotations is found to be populated by structures whose

temperature decreases with height (called “down loops” in our previous articles). They are characterized by plasma $\beta \gtrsim 1 \beta \gtrsim 1$, and may be the result of the efficient dissipation of Alfvén waves at low coronal heights. The comparative analysis reveals that the low latitudes of the equatorial streamer belt of CR-1915 exhibit higher densities than for CR-2081. This cannot be explained by the systematic uncertainties. In addition, the southern hemisphere of the streamer belt of CR-1915 is characterized by higher temperatures and density scale heights than for CR-2081. On the other hand, the coronal hole region of CR-1915 shows lower temperatures than for CR-2081. The reported differences are in the range $\approx 10\text{--}25\% \approx 10\text{--}25\%$, depending on the specific physical quantity and region that is compared, as fully detailed in the analysis. For other regions and/or physical quantities, the uncertainties do not allow assessing the thermodynamical differences between the two rotations. Future investigation will involve a DEMT analysis of other Carrington rotations selected from both epochs, and also a comparison of their tomographic reconstructions with magnetohydrodynamical simulations of the inner corona.
1996, 15 October through 11 November; 2009, 9 March through 5 April

Separating He II and Si XI Emission Components in Off-limb 304 Å Observations

Ivan **Loboda**, Anton Reva, Sergey Bogachev, Alexey Kirichenko & Artem Ulyanov
Solar Phys. 298, Article number: 136 (**2023**)
https://doi.org/10.1007/s11207-023-02230-6
Solar extreme ultraviolet (EUV) imaging instruments usually have a channel centered at 304 Å to observe the strong He II 303.8 Å line, which is valuable for studying the dynamics of chromospheric and transition-region structures. In off-limb regions where He II is weak, however, the coronal Si XI 303.3 Å line becomes significant and provides a background haze that reduces the contrast of He II structures such as jets and macrospicules, complicating the interpretation of the observations. Generally, the separation of this background would require spectroscopic observations. In this article, we take an alternate approach by reconstructing the differential emission measure (DEM) of the quiescent corona to obtain synthetic radial emission profiles in the Si XI 303.3 Å line and show that at altitudes above 20 Mm it makes the major contribution to the background. We also find the silicon abundance to be significantly, by around 80%, lower in the quiet Sun than in the coronal hole. Based on the DEM profiles, we propose a physical model for the off-limb radial intensity profile in the Si XI 303.3 Å line. The model’s main advantage is the possibility to estimate and subtract the background of the quiescent corona using observations in the 304 Å channel alone, which may be of use for future studies of small-scale solar activity.

Plasma dynamics in solar macrospicules from high-cadence EUV observations

I.P. **Loboda**, S.A. Bogachev
A&A 597, A78 **2017**
https://arxiv.org/pdf/1610.07536v1.pdf
Macrospicules are relatively large spicule-like formations found mainly over the polar coronal holes when observing in the transition region spectral lines. In this study, we took advantage of the two short series of observations in the He II 304 \r{A} line obtained by the TESIS solar observatory with a cadence of up to 3.5 s to study the dynamics of macrospicules in unprecedented detail. We used a one-dimensional hydrodynamic method based on the assumption of their axial symmetry and on a simple radiative transfer model to reconstruct the evolution of the internal velocity field of 18 macrospicules from this dataset. Besides the internal dynamics, we studied the motion of the apparent end points of the same 18 macrospicules and found 15 of them to follow parabolic trajectories with high precision which correspond closely to the obtained velocity fields. We found that in a clear, unperturbed case these macrospicules move with a constant deceleration inconsistent with a purely ballistic motion and have roughly the same velocity along their entire axis, with the obtained decelerations typically ranging from 160 to 230 m/s^2, and initial velocities from 80 to 130 km/s. We also found a propagating acoustic wave for one of the macrospicules and a clear linear correlation between the initial velocities of the macrospicules and their decelerations, which indicates that they may be driven by magneto-acoustic shocks. Finally, we inverted our previous method by taking velocities from the parabolic fits to give rough estimates of the percentage of mass lost by 12 of the macrospicules. We found that typically from 10 to 30% of their observed mass fades out of the line (presumably being heated to higher coronal temperatures) with three exceptions of 50% and one of 80%.

Reconstruction of Carrington Rotation Means of Open Solar Flux over the Past 154 Years.

Lockwood, M., Owens, M.
Sol Phys 299, 28 (**2024**).
https://doi.org/10.1007/s11207-024-02268-0
https://link.springer.com/content/pdf/10.1007/s11207-024-02268-0.pdf
We generate reconstructions of signed open solar flux (OSF) for the past 154 years using observations of geomagnetic activity. Previous reconstructions have been limited to annual resolution, but this is here increased by a factor of more than 13 by using averages over Carrington rotation (CR) intervals. We use two indices of geomagnetic activity, the homogeneous aa index, aaH, and the IDV(1d) index; a combination of the two is fitted to OSF estimates from near-Earth interplanetary satellite data. For 1995 – 2022, these are corrected for excess flux (i.e. orthogardenhose flux and switchbacks) using strahl electrons. For 1970 – 2022, we also use the absolute values of

the radial component of the near-Earth interplanetary magnetic field |Brτ |CR,, where the excess flux is allowed for by adopting the optimum averaging interval τ of 20 h. However, in the interval 1970 – 1995, data gaps in the interplanetary data are a serious problem. The errors that these missing data cause in CR averages of OSF are evaluated by synthetically masking data for CRs that have a full complement, using the same number and time series of data gaps as for the CR in question. Given the potential for missing data to generate large errors, we use the near-continuous 1995 – 2022 data to derive the best-fit combination of the geomagnetic data and employ the 1970 – 1995 data for testing in which we can readily allow for the errors caused by data gaps. Errors caused by inaccuracies in the geomagnetic data are shown to be considerably smaller than the uncertainties due to the polynomial fitting. It is shown that the new reconstructions are consistent with the previous annual estimates and that there is considerable variability in the OSF values from one CR to the next; in particular, in high-activity solar cycles, there can be individual CRs in which the OSF exceeds that for adjacent CRs by a factor as large as two.

Application of historic datasets to understanding Open Solar Flux and the 20 th -century Grand Solar Maximum. 2. Solar observations **Review**

Mike **Lockwood**, Mathew Owens, Stephanie Yardley, Iiro Virtanen, Anthony Yeates, and Andres Munoz-Jaramillo

Front. Astron. Space Sci., 9:976444. **2022**

doi: 10.3389/fspas.2022.976444
https://www.frontiersin.org/articles/10.3389/fspas.2022.976444/pdf

We study historic observations of solar activity from the 20th-century rise towards the peak of the Modern Grand Solar Maximum (MGSM) and compare with observations of the decline that has occurred since. The major difference in available solar observations of the rise and of the fall are accurate magnetograms from solar magnetographs: we here use synthetic magnetograms to interpret the rise and employ historic observations of Polar Crown Filaments to test them and verify their use. We show that eclipse images at sunspot minimum reveal the long-term variation of open flux deduced from geomagnetic observations in Paper 1 (Lockwood et al., 2022). We also make use of polar coronal hole fluxes derived from historic white light images of polar faculae, but have to consider the implications of the fact that these facular images do not tell us the polarity of the field. Given this caveat, the agreement between the polar coronal hole fluxes and the values derived from open flux continuity modelling based on sunspot numbers is extremely good. This comparison indicates that one possible solution to the "open flux problem" is open flux within the streamer belt that potential-based modelling of coronal fields from photospheric fields is not capturing. We take a detailed look at the solar cycle at the peak of the MGSM, cycle 19, and show the variation of the polar coronal hole fluxes and the inferred poleward flux surges are predictable from the asymmetries in flux emergence in the two hemispheres with implied transequatorial flux transfer and/or "anti-Hale" (or more general "rogue" active region flux) emergence late in the sunspot cycle.

Application of historic datasets to understanding Open Solar Flux and the 20th century Grand Solar Maximum. 1. Geomagnetic, ionospheric and sunspot observations

Mike **Lockwood**, Mathew Owens, Luke Barnard, Chris Scott, Anna Frost, Bingkun Yu, and Yutian Chi

Front. Astron. Space Sci. 9:960775. 2022

https://www.frontiersin.org/articles/10.3389/fspas.2022.960775/pdf

We updated annual mean reconstructions of near-Earth interplanetary conditions and (signed) open solar flux FS for the past 186 years. Furthermore, we added observations for solar cycle 24 to refine regressions and improved allowance for orthogardenhose and folded (a.k.a., switchback) heliospheric flux from studies using strahl electrons. We also improved the allowance made for the annual mean gardenhose angle of the interplanetary magnetic field. We used both multiple regression with interplanetary magnetic field B and solar wind speed VSW and linear regression with the function BVnSWBVSWn and demonstrated that the latter gives correlations that are not significantly lower than those given by the former. We conducted a number of tests of the geomagnetic indices used, of which by far the most important is that all four usable pairings of indices produce almost identical results for B, VSW, and FS. All reconstructions were given full 2σ uncertainties using a Monte Carlo technique that generates an ensemble of 1 million members for each pairing of indices. The long-term variations of near-Earth interplanetary field B and open solar flux FS were found to closely match those of the international sunspot numbers but VSW show a significantly different variation. This result explains why of the two peaks of 20th-century grand solar maximum, the range geomagnetic indices give a larger second peak, whereas the diurnal variation indices give a first peak that is larger, as it is for sunspots. We found that the increase in solar cycle averages of FS was between 2.46 × 1014 Wb in 1906 and 4.10 × 1014 Wb in 1949, the peak of the grand maximum, and hence, the rise in open flux was by a factor of 67%.

Space climate and space weather over the past 400 years: 2. Proxy indicators of geomagnetic storm and substorm occurrence

Mike **Lockwood**, Mathew J. Owens, Luke A. Barnard, Chris J. Scott, Clare E. Watt and Sarah Bentley
J. Space Weather Space Clim. **2018**, 8, A12
https://www.swsc-journal.org/articles/swsc/pdf/2018/01/swsc170036.pdf
Using the reconstruction of power input to the magnetosphere presented in Paper 1 Lockwood et al. [J Space Weather Space Clim 7 (2017a)], we reconstruct annual means of the geomagnetic Ap and AE indices over the past 400 years to within a 1-sigma error of ±20%. In addition, we study the behaviour of the lognormal distribution of daily and hourly values about these annual means and show that we can also reconstruct the fraction of geomagnetically-active (storm-like) days and (substorm-like) hours in each year to accuracies of to accuracies of ~50%, including the large percentage uncertainties in near-zero values. The results are the first physics-based quantification of the space weather conditions in both the Dalton and Maunder minima. Looking to the future, the weakening of Earth's magnetic moment means that the terrestrial disturbance levels during a future repeats of the solar Dalton and Maunder minima will be weaker and we here quantify this effect for the first time.

Coronal and heliospheric magnetic flux circulation and its relation to open solar flux evolution

Mike **Lockwood**, Mathew J. Owens,Suzanne M. Imber, Matthew K. James, Emma J. Bunce, Timothy K. Yeoman
JGR Volume 122, Issue 6 Pages 5870–5894 **2017**
http://onlinelibrary.wiley.com/doi/10.1002/2016JA023644/pdf
Solar cycle 24 is notable for three features that can be found in previous cycles but which have been unusually prominent: (1) sunspot activity was considerably greater in the northern/southern hemisphere during the rising/declining phase; (2) accumulation of Open Solar Flux (OSF) during the rising phase was modest, but rapid in the early declining phase; (3) the Heliospheric Current Sheet (HCS) tilt showed large fluctuations. We show these features had a major influence on the progression of the cycle. All flux emergence causes a rise then a fall in OSF, but only OSF with footpoints in opposing hemispheres progresses the solar cycle via the evolution of the polar fields. Emergence in one hemisphere, or symmetric emergence without some form of footpoint exchange across the heliographic equator, causes poleward-migrating fields of both polarities in one or both (respectively) hemispheres which temporarily enhance OSF but do not advance the polar field cycle. The heliospheric field observed near Mercury and Earth reflects the asymmetries in emergence. Using magnetograms, we find evidence that the poleward magnetic flux transport (of both polarities) is modulated by the HCS tilt, revealing an effect on OSF loss rate. The declining phase rise in OSF was caused by strong emergence in the southern hemisphere with an anomalously low HCS tilt. This implies the recent fall in the southern polar field will be sustained and that the peak OSF has limited implications for the polar field at the next sunspot minimum and hence for the amplitude of cycle 25.

An Assessment of Sunspot Number Data Composites over 1845-2014

Mike **Lockwood**, Mathew J. Owens, Luke A. Barnard, Ilya G. Usoskin
ApJ **824** 54 **2016**
http://arxiv.org/pdf/1604.04538v1.pdf
New sunspot data composites, some of which are radically different in the character of their long-term variation, are evaluated over the interval 1845-2014. The method commonly used to calibrate historic sunspot data, relative to modern-day data, is "daisy-chaining", whereby calibration is passed from one data subset to the neighbouring one, usually using regressions of the data subsets for the intervals of their overlap. Recent studies have illustrated serious pitfalls in these regressions and the resulting errors can be compounded by their repeated use as the data sequence is extended back in time. Hence the recent composite data series by Usoskin et al. (2016), RUEA, is a very important advance because it avoids regressions, daisy-chaining and other common, but invalid, assumptions: this is achieved by comparing the statistics of "active day" fractions to those for a single reference dataset. We study six sunspot data series including RUEA and the new "backbone" data series RBB, recently generated by Svalgaard and Schatten (2016) by employing both regression and daisy-chaining. We show that all six can be used with a continuity model to reproduce the main features of the open solar flux variation for 1845-2014, as reconstructed from geomagnetic activity data. However, some differences can be identified that are consistent with tests using a basket of other proxies for solar magnetic fields. Using data from a variety of sunspot observers, we illustrate problems with the method employed in RBB which cause it to increasingly overestimate sunspot numbers going back in time and we recommend using RUEA because it employs more robust procedures that avoid such problems.

Tests of sunspot number sequences: 4. Discontinuities around 1946 in various sunspot number and sunspot group number reconstructions

Mike **Lockwood**, Mathew J. Owens, Luke A. Barnard
Solar Phys. Volume 291, Issue 9, pp 2843–2867 **2016**
http://arxiv.org/pdf/1605.05149v1.pdf
We use 5 test data series to quantify putative discontinuities around 1946 in 5 annual-mean sunspot number or group number sequences. The series tested are: the original and new versions of the Wolf/Zurich/International sunspot

number composite [RISNv1 and RISNv2] ; the corrected version of RISNv1 [RC]; the backbone group number [RBB]; and the group number composite [RUEA]. The test data are: the group number NG and total sunspot area AG from the RGO photoheliographic data; the CaK index from re-analysis of MWO CaII K spectroheliograms; the group number from the MWO sunspot drawings, NMWO; and ionospheric critical frequencies at Slough [foF2]. The test data all vary with sunspot numbers, in some cases non-linearly. Tests use both before-and-after fit-residual comparison and correlation methods, applied to intervals iterated to minimise errors and eliminate the effect of the discontinuity date. It is not assumed that the correction required is by a constant factor, nor even linear in sunspot number. A non-linear correction is required by RC, RBB and RISNv1, but not by RISNv2 or RUEA. The test datasets give very similar results in all cases. By multiplying the probability distribution functions together we obtain the optimum correction for each data series that must be applied to pre-discontinuity data to make them consistent with the post-discontinuity data. It is shown that, on average, values for 1932-1943 are too small (relative to later values) by about 12.3% for RISNv1 but are too large for RISNv2 and RBB by 3.8% and 5.2%. The correction applied to generate RC from RISNv1 reduces this average factor to 0.5% but does not remove the non-linear variation, and other errors remain uncorrected. A test is provided by RUEA, which is identical to the RGO NG values over the interval used.

Tests of Sunspot Number Sequences: 3. Effects of Regression Procedures on the Calibration of Historic Sunspot Data

Mike **Lockwood**, Mathew J. Owens, Luke A. Barnard, I. G. Usoskin
Solar Phys. Volume 291, Issue 9, pp 2829–2841 **2016**

We use sunspot-group observations from the Royal Greenwich Observatory (RGO) to investigate the effects of intercalibrating data from observers with different visual acuities. The tests are made by counting the number of groups [RB][RB] above a variable cut-off threshold of observed total whole spot area (uncorrected for foreshortening) to simulate what a lower-acuity observer would have seen. The synthesised annual means of RBRB are then re-scaled to the full observed RGO group number [RA][RA] using a variety of regression techniques. It is found that a very high correlation between RARA and RBRB (rAB>0.98rAB>0.98) does not prevent large errors in the intercalibration (for example sunspot-maximum values can be over 30 % too large even for such levels of rABrAB). In generating the backbone sunspot number [RBB][RBB], Svalgaard and Schatten (*Solar Phys.*, 2016) force regression fits to pass through the scatter-plot origin, which generates unreliable fits (the residuals do not form a normal distribution) and causes sunspot-cycle amplitudes to be exaggerated in the intercalibrated data. It is demonstrated that the use of Quantile–Quantile ("Q–Q") plots to test for a normal distribution is a useful indicator of erroneous and misleading regression fits. Ordinary least-squares linear fits, not forced to pass through the origin, are sometimes reliable (although the optimum method used is shown to be different when matching peak and average sunspot-group numbers). However, other fits are only reliable if non-linear regression is used. From these results it is entirely possible that the inflation of solar-cycle amplitudes in the backbone group sunspot number as one goes back in time, relative to related solar–terrestrial parameters, is entirely caused by the use of inappropriate and non-robust regression techniques to calibrate the sunspot data.

Tests of Sunspot Number Sequences: 2. Using Geomagnetic and Auroral Data

Mike **Lockwood**, Mathew J. Owens, Luke A Barnard, Chris J. Scott, Ilya G. Usoskin, Heikki Nevanlinna
Solar Phys. Volume 291, Issue 9, pp 2811–2828 **2016**
http://arxiv.org/pdf/1605.01948v1.pdf

We compare four sunspot-number data sequences against geomagnetic and terrestrial auroral observations. The comparisons are made for the original SIDC composite of Wolf-Zurich-International sunspot number [RISNv1], the group sunspot number [RG] by Hoyt and Schatten (Solar Phys., 1998), the new "backbone" group sunspot number [RBB] by Svalgaard and Schatten (Solar Phys., 2016), and the "corrected" sunspot number [RC] by Lockwood at al. (J.G.R., 2014). Each sunspot number is fitted with terrestrial observations, or parameters derived from terrestrial observations to be linearly proportional to sunspot number, over a 30-year calibration interval of 1982-2012. The fits are then used to compute test sequences, which extend further back in time and which are compared to RISNv1, RG, RBB, and RC. To study the long-term trends, comparisons are made using averages over whole solar cycles (minimum-to-minimum). The test variations are generated in four ways: i) using the IDV(1d) and IDV geomagnetic indices (for 1845-2013) fitted over the calibration interval using the various sunspot numbers and the phase of the solar cycle; ii) from the open solar flux (OSF) generated for 1845 - 2013 from four pairings of geomagnetic indices by Lockwood et al. (Ann. Geophys., 2014) and analysed using the OSF continuity model of Solanki at al. (Nature, 2000) which employs a constant fractional OSF loss rate; iii) the same OSF data analysed using the OSF continuity model of Owens and Lockwood (J.G.R., 2012) in which the fractional loss rate varies with the tilt of the heliospheric current sheet and hence with the phase of the solar cycle; iv) the occurrence frequency of low-latitude aurora for 1780-1980 from the survey of Legrand and Simon (Ann. Geophys., 1987). For all cases, RBB exceeds the test terrestrial series by an amount that increases as one goes back in time.

Tests of Sunspot Number Sequences: 1. Using Ionosonde Data

M. **Lockwood** , C. J. Scott, M. J. Owens, L. Barnard, D. M. Willis

Solar Phys. Volume 291, Issue 9, pp 2785–2809 **2016** Open Access
http://link.springer.com/article/10.1007/s11207-016-0855-8

More than 70 years ago, it was recognised that ionospheric F2-layer critical frequencies [foF2] had a strong relationship to sunspot number. Using historic datasets from the Slough and Washington ionosondes, we evaluate the best statistical fits of foF2 to sunspot numbers (at each Universal Time [UT] separately) in order to search for drifts and abrupt changes in the fit residuals over Solar Cycles 17 – 21. This test is carried out for the original composite of the Wolf/Zurich/International sunspot number [*R*], the new "backbone" group sunspot number [*R*BB], and the proposed "corrected sunspot number" [*R*C]. Polynomial fits are made both with and without allowance for the white-light facular area, which has been reported as being associated with cycle-to-cycle changes in the sunspot-number–foF2 relationship. Over the interval studied here, *R*, *R*BB, and *R*C largely differ in their allowance for the "Waldmeier discontinuity" around 1945 (the correction factor for which for *R*, *R*BB, and *R*C is, respectively, zero, effectively over 20 %, and explicitly 11.6 %). It is shown that for Solar Cycles 18 – 21, all three sunspot data sequences perform well, but that the fit residuals are lowest and most uniform for *R*BB. We here use foF2 for those UTs for which *R*, *R*BB, and *R*C all give correlations exceeding 0.99 for intervals both before and after theWaldmeier discontinuity. The error introduced by the Waldmeier discontinuity causes *R* to underestimate the fitted values based on the foF2 data for 1932 – 1945, but *R*BB overestimates them by almost the same factor, implying that the correction for the Waldmeier discontinuity inherent in *R*BB is too large by a factor of two. Fit residuals are smallest and most uniform for *R*C, and the ionospheric data support the optimum discontinuity multiplicative correction factor derived from the independent Royal Greenwich Observatory (RGO) sunspot group data for the same interval.

Centennial variations in sunspot number, open solar flux and streamer belt width: 3. Modelling

M. **Lockwood** and M.J. Owens

JGR, Volume 119, Issue 7, pages 5193–5209, **2014**

From the variation of near-Earth interplanetary conditions, reconstructed for the mid-19th century to the present day using historic geomagnetic activity observations, Lockwood and Owens [2014] have suggested that Earth remains within a broadened streamer belt during solar cycles when the Open Solar Flux (OSF) is low. From this they propose that the Earth was immersed in almost constant slow solar wind during the Maunder minimum (c. 1650-1710). In this paper, we extend continuity modelling of the OSF to predict the streamer belt width using both group sunspot numbers and corrected international sunspot numbers to quantify the emergence rate of new OSF. The results support the idea that the solar wind at Earth was persistently slow during the Maunder minimum because the streamer belt was broad.

CENTENNIAL VARIATIONS IN SUNSPOT NUMBER, OPEN SOLAR FLUX AND STREAMER BELT WIDTH: 2. COMPARISON WITH THE GEOMAGNETIC DATA

M. **Lockwood**, M.J. Owens and L. Barnard

JGR, Volume 119, Issue 7, pages 5183–5192, **2014**

We investigate the relationship between interdiurnal variation geomagnetic activity indices, IDV and IDV(1d), corrected sunspot number, RC, and the group sunspot number RG. RC uses corrections for both the "Waldmeier discontinuity", as derived in Paper 1 [Lockwood et al., 2014c], and the "Wolf discontinuity" revealed by Leussu et al. [2013]. We show that the simple correlation of the geomagnetic indices with RCn or RGn masks a considerable solar cycle variation. Using IDV(1d) or IDV to predict or evaluate the sunspot numbers, the errors are almost halved by allowing for the fact that the relationship varies over the solar cycle. The results indicate that differences between RC and RG have a variety of causes and are highly unlikely to be attributable to errors in either RG alone, as has recently been assumed. Because it is not known if RC or RG is a better predictor of open flux emergence before 1874, a simple sunspot number composite is suggested which, like RG, enables modelling of the open solar flux for 1610 onwards in Paper 3, but maintains the characteristics of RC.

CENTENNIAL VARIATIONS IN SUNSPOT NUMBER, OPEN SOLAR FLUX AND STREAMER BELT WIDTH:
1. CORRECTION OF THE SUNSPOT NUMBER RECORD SINCE 1874

M. **Lockwood**, M.J. Owens and L. Barnard
JGR, Volume 119, Issue 7, pages 5172–5182, **2014**
We analyse the widely-used international/ Zürich sunspot number record, R, with a view to quantifying a suspected calibration discontinuity around 1945 (which has been termed the “Waldmeier discontinuity” [Svalgaard, 2011]). We compare R against the composite sunspot group data from the Royal Greenwich Observatory (RGO) network and the Solar Optical Observing Network (SOON), using both the number of sunspot groups, NG, and the total area of the sunspots, AG. In addition, we compare R with the recently developed interdiurnal variability geomagnetic indices IDV and IDV(1d). In all four cases, linearity of the relationship with R is not assumed and care is taken to ensure that the relationship of each with R is the same before and after the putative calibration change. It is shown the probability that a correction is not needed is of order 10−8 and that R is indeed too low before 1945. The optimum correction to R for values before 1945 is found to be 11.6%, 11.7%, 10.3% and 7.9% using AG, NG, IDV, and IDV(1d), respectively. The optimum value obtained by combining the sunspot group data is 11.6% with an uncertainty range 8.1-14.8% at the 2σ level. The geomagnetic indices provide an independent yet less stringent test but do give values that fall within the 2σ uncertainty band with optimum values are slightly lower than from the sunspot group data. The probability of the correction needed being as large as 20%, as advocated by Svalgaard [2011], is shown to be 1.6×10^{-5}.

Reconstruction and Prediction of Variations in the Open Solar Magnetic Flux and Interplanetary Conditions **Review**

Mike **Lockwood**
Living Rev. Solar Phys. 10 (**2013**), 4
http://www.livingreviews.org/lrsp-2013-4
Historic geomagnetic activity observations have been used to reveal centennial variations in the open solar flux and the near-Earth heliospheric conditions (the interplanetary magnetic field and the solar wind speed). The various methods are in very good agreement for the past 135 years when there were sufficient reliable magnetic observatories in operation to eliminate problems due to site-specific errors and calibration drifts. This review underlines the physical principles that allow these reconstructions to be made, as well as the details of the various algorithms employed and the results obtained. Discussion is included of: the importance of the averaging timescale; the key differences between ``range"□ and ``interdiurnal variability" geomagnetic data; the need to distinguish source field sector structure from heliospherically-imposed field structure; the importance of ensuring that regressions used are statistically robust; and uncertainty analysis. The reconstructions are exceedingly useful as they provide calibration between the in-situ spacecraft measurements from the past five decades and the millennial records of heliospheric behaviour deduced from measured abundances of cosmogenic radionuclides found in terrestrial reservoirs. Continuity of open solar flux, using sunspot number to quantify the emergence rate, is the basis of a number of models that have been very successful in reproducing the variation derived from geomagnetic activity. These models allow us to extend the reconstructions back to before the development of the magnetometer and to cover the Maunder minimum. Allied to the radionuclide data, the models are revealing much about how the Sun and heliosphere behaved outside of grand solar maxima and are providing a means of predicting how solar activity is likely to evolve now that the recent grand maximum (that had prevailed throughout the space age) has come to an end.

Solar Elemental Abundances **Review**

Katharina **Lodders**
The Oxford Research Encyclopedia of Planetary Science, Oxford University Press.**2019**
https://arxiv.org/ftp/arxiv/papers/1912/1912.00844.pdf
Review of the history of solar system elemental abundances with a new assessment of elemental and isotopic abundances from CI-chondrites and solar data. Solar elemental abundances, or solar system elemental abundances refer to the complement of chemical elements in the entire solar system. The sun contains more than 99-percent of the mass in the solar system and therefore the composition of the sun is a good proxy for the composition of the overall solar system. The solar system composition can be taken as the overall composition of the molecular cloud within the interstellar medium from which the solar system formed 4.567 billion years ago. Active research areas in astronomy and cosmochemistry model collapse of a molecular cloud of solar composition into a star with a planetary system, and the physical and chemical fractionation of the elements during planetary formation and differentiation. The solar system composition is the initial composition from which all solar system objects (the sun, terrestrial planets, gas giant planets, planetary satellites and moons, asteroids, Kuiper-belt objects, and comets) were derived.

Synoptic maps from two viewpoints

Preparing for maps from SDO/HMI and SO/PHI data

P. **Loeschl**1,2, J. Hirzberger1, S. K. Solanki1, J. Schou1 and G. Valori1
A&A 682, A108 (**2024**)
https://www.aanda.org/articles/aa/pdf/2024/02/aa46044-23.pdf

Context. Over recent decades, various kinds of magnetic synoptic chart products have seen major improvements in observation cadence, resolution, and processing, but their creation is still limited by the 27.27 day rotation rate of the solar surface.
Aims. Co-observation from a second vantage point away from the Earth–Sun line with SO/PHI enables the creation of combined magnetic synoptic maps from observation periods that are significantly shorter than a typical Carrington rotation, and therefore provides a data product with magnetic information that is temporally more consistent.
Methods. We upgraded the SDO/HMI synoptic map pipeline in order for it to be compatible with SO/PHI observations at variable distances and a much lower and variable observation cadence. This enabled us to produce combined magnetic synoptic maps using SO/PHI data taken from the far side of the Sun.
Results. We present a pipeline to produce combined magnetic synoptic maps from simultaneous SO/PHI and SDO/HMI observations. Depending on the orbital position of SO/PHI, our combined synoptic maps can be produced up to 13 days faster than any other comparable data product currently available. This strongly reduces the time-lag between the observations that are used to build the map and thereby provides a more consistent map of the magnetic field across the solar surface.

Convective blueshifts in the solar atmosphere: III. High-accuracy observations of spectral lines in the visible

Johannes **Löhner-Böttcher**, Wolfgang Schmidt, Rolf Schlichenmaier, Tilo Steinmetz, Ronald Holzwarth
A&A 624, A57 **2019**
https://arxiv.org/pdf/1901.07606.pdf

Convective motions in the solar atmosphere cause spectral lines to become asymmetric and shifted in wavelength. For photospheric lines, this differential Doppler shift varies from the solar disk center to the limb. Precise and comprehensive observations of the convective blueshift and its center-to-limb variation improve our understanding of the atmospheric hydrodynamics and ensuing line formation, and provide the basis to refine 3D models of the solar atmosphere. We performed systematical spectroscopic measurements of the convective blueshift of the quiet Sun with the Laser Absolute Reference Spectrograph (LARS) at the German Vacuum Tower Telescope. The spatial scanning of the solar disk covered four radial (meridional and equatorial) axes. The high-resolution spectra of 26 photospheric to chromospheric lines in the visible range were calibrated with a laser frequency comb to absolute wavelengths at the 1m/s accuracy. Applying ephemeris and reference corrections, the bisector analysis provided line asymmetries and Doppler shifts with an uncertainty of only few m/s. To allow for a comparison with other observations, we convolved the results to lower spectral resolutions. Typically, a blueshifted "C"-shaped curve at disk center transforms into a less blueshifted "\"-shape toward the solar limb. The comparison of all lines reveals the systematic dependence of the convective blueshift on the line depth. Synthetic models yield considerable deviations from the observed center-to-limb variation. The obtained Doppler shifts of the quiet Sun can serve as an absolute reference for other observations, the relative calibration of Dopplergrams, and the necessary refinement of atmospheric models. Based on this, the development of high-precision models of stellar surface convection will advance the detection of (potentially habitable) exoplanets by radial velocity measurements.

Convective blueshifts in the solar atmosphere, I. Absolute measurements with LARS of the spectral lines at 6302 Å

Johannes **Löhner-Böttcher**, Wolfgang Schmidt, Franziska Stief, Tilo Steinmetz, Ronald Holzwarth
A&A 611, A4 **2018**
https://arxiv.org/pdf/1712.07059.pdf

The solar convection manifests as granulation and intergranulation at the solar surface. In the photosphere, convective motions induce differential Doppler shifts to spectral lines. The observed convective blueshift varies across the solar disk. We focus on the impact of solar convection on the atmosphere and aim to resolve its velocity stratification in the photosphere. We performed high-resolution spectroscopic observations of the solar spectrum in the 6302\,\AA\ range with the Laser Absolute Reference Spectrograph (LARS) at the Vacuum Tower Telescope. A laser frequency comb enabled the calibration of the spectra to an absolute wavelength scale with an accuracy of 1ms−1. We systematically scanned the Quiet Sun from disk center to the limb at ten selected heliocentric positions. The analysis included 99 time sequences of up to 20\,min in length. By means of ephemeris and reference corrections, we translated wavelength shifts into absolute line-of-sight velocities. A bisector analysis on the line profiles yielded the shapes and convective shifts of seven photospheric lines. At disk center, the bisector profiles of the iron lines feature a pronounced C-shape with maximum convective blueshifts of up to −450ms−1 in the spectral line wings. Toward the solar limb, the bisectors change into a \textbackslash-shape with a saturation in the line core at a redshift of +100ms−1. The center-to-limb variation of the line core velocities shows a slight increase in blueshift

when departing the disk center for larger heliocentric angles. This increase in blueshift is more pronounced for the magnetically less active meridian than for the equator. Toward the solar limb, the blueshift decreases and can turn into a redshift. Best spectroscopic measurements enabled the accurate determination of absolute convective shifts in the solar photosphere.

Correlations between sunspots and their moat flows

Johannes **Löhner-Böttcher**
HMI Science Nuggets #18, **2014**
http://hmi.stanford.edu/hminuggets/?p=793

Identifying plasma fractionation processes in the chromosphere using IRIS

David M. **Long** , 1, 2 Deborah Baker , 3 Andy S. H. To , 4 Lidia van Driel-Gesztelyi , +++
ApJ **2024**
https://arxiv.org/pdf/2403.06711.pdf
The composition of the solar corona differs from that of the photosphere, with the plasma thought to fractionate in the solar chromosphere according to the First Ionisation Potential (FIP) of the different elements. This produces a FIP bias, wherein elements with a low FIP are preferentially enhanced in the corona compared to their photospheric abundance, but direct observations of this process remain elusive. Here we use a series of spectroscopic observations of Active Region AR 12759 as it transited the solar disc over a period of 6 days from 2-7 April 2020 taken using the Hinode Extreme ultraviolet Imaging Spectrometer (EIS) and Interface Region Imaging Spectrograph (IRIS) instruments to look for signatures of plasma fractionation in the solar chromosphere. Using the Si X/S X and Ca XIV/Ar XIV diagnostics, we find distinct differences between the FIP bias of the leading and following polarities of the active region. The widths of the IRIS Si IV lines exhibited clear differences between the leading and following polarity regions, indicating increased unresolved wave activity in the following polarity region compared to the leading polarity region, with the chromospheric velocities derived using the Mg II lines exhibiting comparable, albeit much weaker, behaviour. These results are consistent with plasma fractionation via resonant/non-resonant waves at different locations in the solar chromosphere following the ponderomotive force model, and indicate that IRIS could be used to further study this fundamental physical process. **2020-April-3, 7**

Measuring the magnetic field of a trans-equatorial loop system using coronal seismology

David M. **Long**, Gherardo Valori, David Pérez-Suárez, Richard J. Morton, Alberto Marcos Vásquez
A&A 603, A101 **2017**
https://arxiv.org/pdf/1703.10020.pdf **File**
"EIT waves" are freely-propagating global pulses in the low corona which are strongly associated with the initial evolution of coronal mass ejections (CMEs). They are thought to be large-amplitude, fast-mode magnetohydrodynamic waves initially driven by the rapid expansion of a CME in the low corona. An "EIT wave" was observed on **6 July 2012** to impact an adjacent trans-equatorial loop system which then exhibited a decaying oscillation as it returned to rest. Observations of the loop oscillations were used to estimate the magnetic field strength of the loop system by studying the decaying oscillation of the loop, measuring the propagation of ubiquitous transverse waves in the loop and extrapolating the magnetic field from observed magnetograms. Observations from the Atmospheric Imaging Assembly onboard the Solar Dynamics Observatory (SDO/AIA) and the Coronal Multi-channel Polarimeter (CoMP) were used to study the event. An Empirical Mode Decomposition analysis was used to characterise the oscillation of the loop system in CoMP Doppler velocity and line width and in AIA intensity. The loop system was shown to oscillate in the 2nd harmonic mode rather than at the fundamental frequency, with the seismological analysis returning an estimated magnetic field strength of ~5.5±1.5 G. This compares to the magnetic field strength estimates of ~1-9 G and ~3-9 G found using the measurements of transverse wave propagation and magnetic field extrapolation respectively.
Erratum A&A 607, C3 (**2017**)

Relating magnetic reconnection to coronal heating

Dana W. **Longcope**, Lucas A. Tarr
Phil. Trans. Royal Soc. A, **2015**
http://arxiv.org/pdf/1501.06546v1.pdf
It is clear that the solar corona is begin heated and that coronal magnetic fields undergo reconnection all the time. Here we attempt to show that these two facts are in fact related - i.e. coronal reconnection generates heat. This attempt must address the fact that topological change of field lines does not automatically generate heat. We present one case of flux emergence where we have measured the rate of coronal magnetic reconnection and the rate of energy dissipation in the corona. The ratio of these two, $P/\dot{\Phi}$, is a current comparable to the amount of current expected to flow along the boundary separating the emerged flux from the pre-existing flux overlying it. We can generalize this relation to the overall corona in quiet Sun or in active regions. Doing so yields estimates for the

contribution to corona heating from magnetic reconnection. These estimated rates are comparable to the amount required to maintain the corona at its observed temperature.

The Sun: Light Dark Matter and Sterile Neutrinos

Ilídio **Lopes**1,2
2020 ApJ 905 22
https://doi.org/10.3847/1538-4357/abbfb6
Next-generation experiments allow for the possibility of testing the neutrino flavor oscillation model to very high levels of accuracy. Here, we explore the possibility that the dark matter in the current universe is made of two particles, a sterile neutrino and a very light dark matter particle. By using a 3+1 neutrino flavor oscillation model, we study how such a type of dark matter imprints the solar neutrino fluxes, spectra, and survival probabilities of electron neutrinos. The current solar neutrino measurements allow us to define an upper limit for the ratio of the mass of a light dark matter particle m ϕ and the Fermi constant G ϕ , such that G ϕ /m ϕ must be smaller than 1030 G F eV−1 to be in agreement with current solar neutrino data from the Borexino, Sudbury Neutrino Observatory, and Super-Kamiokande detectors. Moreover, for models with a very small Fermi constant, the amplitude of the time variability must be lower than 3% to be consistent with current solar neutrino data. We also found that solar neutrino detectors like Darwin, able to measure neutrino fluxes in the low-energy range with high accuracy, will provide additional constraints to this class of models that complement the ones obtained from the current solar neutrino detectors.

New neutrino physics and the altered shapes of solar neutrino spectra

Ilídio **Lopes**
Phys. Rev. D **2017**
https://arxiv.org/pdf/1702.00447v1.pdf
Neutrinos coming from the Sun's core are now measured with a high precision, and fundamental neutrino oscillations parameters are determined with a good accuracy. In this work, we estimate the impact that a new neutrino physics model, the so-called generalized Mikheyev-Smirnov-Wolfenstein (MSW) oscillation mechanism, has on the shape of some of leading solar neutrino spectra, some of which will be partially tested by the next generation of solar neutrino experiments. In these calculations, we use a high-precision standard solar model in good agreement with helioseismology data. We found that the neutrino spectra of the different solar nuclear reactions of the proton-proton chains and carbon-nitrogen-oxygen cycle have quite distinct sensitivities to the new neutrino physics. The HeP and 8B neutrino spectra are the ones for which their shapes are more affected when neutrinos interact with quarks in addition to electrons. The shape of the 15O and 17F neutrino spectra are also modified, although in these cases the impact is much smaller. Finally, the impact in the shape of the PP and 13N neutrino spectra is practically negligible.

Looking for Granulation and Periodicity Imprints in the Sunspot Time Series

Ilídio **Lopes**1,2 and Hugo G. Silva
2015 ApJ 804 120
http://arxiv.org/pdf/1505.04835v1.pdf
The sunspot activity is the end result of the cyclic destruction and regeneration of magnetic fields by the dynamo action. We propose a new method to analyze the daily sunspot areas data recorded since 1874. By computing the power spectral density of daily data series using the Mexican hat wavelet, we found a power spectrum with a well-defined shape, characterized by three features. The first term is the 22 yr solar magnetic cycle, estimated in our work to be 18.43 yr. The second term is related to the daily volatility of sunspots. This term is most likely produced by the turbulent motions linked to the solar granulation. The last term corresponds to a periodic source associated with the solar magnetic activity, for which the maximum power spectral density occurs at 22.67 days. This value is part of the 22–27 day periodicity region that shows an above-average intensity in the power spectra. The origin of this 22.67 day periodic process is not clearly identified, and there is a possibility that it can be produced by convective flows inside the star. The study clearly shows a north–south asymmetry. The 18.43 yr periodical source is correlated between the two hemispheres, but the 22.67 day one is not correlated. It is shown that toward the large timescales an excess occurs in the northern hemisphere, especially near the previous two periodic sources. To further investigate the 22.67 day periodicity, we made a Lomb–Scargle spectral analysis. The study suggests that this periodicity is distinct from others found nearby.

Detecting gravity modes in the solar neutrino flux

Ilídio **Lopes**, Sylvaine Turck-Chièze
ApJ, **2014**
http://arxiv.org/pdf/1408.6671v1.pdf

The detection of gravity modes produced in the solar radiative zone has been a challenge in modern astrophysics for more than 30 yr and their amplitude in the core is not yet determined. In this Letter, we develop a new strategy to look for standing gravity modes through solar neutrino fluxes. We note that due to a resonance effect, the gravity modes of low degree and low order have the largest impact on the 8B neutrino flux. The strongest effect is expected to occur for the dipole mode with radial order 2, corresponding to periods of about 1.5 hr. These standing gravity waves produce temperature fluctuations that are amplified by a factor of 170 in the boron neutrino flux for the corresponding period, in consonance with the gravity modes. From current neutrino observations, we determine that the maximum temperature variation due to the gravity modes in the Sun's core is smaller than 5.8×10−4. This study clearly shows that due to their high sensitivity to the temperature, the 8B neutrino flux time series is an excellent tool to determine the properties of gravity modes in the solar core. Moreover, if gravity mode footprints are discovered in the 8B neutrino flux, this opens a new line of research to probe the physics of the solar core as non-standing gravity waves of higher periods cannot be directly detected by helioseismology but could leave their signature on boron neutrino or on other neutrino fluxes.

Oscillator Models of the Solar Cycle : Towards the development of inversion methods

Ilídio **Lopes**, Dário Passos, Melinda Nagy, Kristof Petrovay
Space Science Reviews, July **2014**
http://arxiv.org/pdf/1407.4918v1.pdf
This article reviews some of the leading results obtained in solar dynamo physics by using temporal oscillator models as a tool to interpret observational data and dynamo model predictions. We discuss how solar observational data such as the sunspot number is used to infer the leading quantities responsible for the solar variability during the last few centuries. Moreover, we discuss the advantages and difficulties of using inversion methods (or backward methods) over forward methods to interpret the solar dynamo data. We argue that this approach could help us to have a better insight about the leading physical processes responsible for solar dynamo, in a similar manner as helioseismology has helped to achieve a better insight on the thermodynamic structure and flow dynamics in the Sun’s interior.

Short- and Mid-term Periodicities Observed in Neutron Monitor Counting Rates throughout Solar Cycles 20–24

A. **López-Comazzi**1 and J. J. Blanco1
2022 ApJ 927 155
https://iopscience.iop.org/article/10.3847/1538-4357/ac4e19/pdf
This paper examines the short- and mid-term periodicities (≲2 yr) in the cosmic-ray flux along 55 yr, from 1964 to 2019. The cosmic-ray flux has been computed by averaging the counting rates, in typified units, of a set of selected neutron monitors. This builds a representative virtual neutron monitor, named the global neutron monitor. The relevant discovered periodicities are ∼13.5, ∼27, ∼46–64, ∼79–83 day; Rieger-type (∼134–190 days); ∼225–309 day; and ∼1.06–1.15, ∼1.31–1.40, and ∼1.75–2.20 yr periods. The same analyses have been applied to the sunspot number (SSN) with the aim to compare the discovered periodicities and look for possible origins of these periodicities. Two main results have been achieved: the periodicities of 77–83 days, 134–190 days (Rieger type), 225–309 days, ∼1.3 yr, and ∼1.7 yr could be related to the solar dynamo, and an inversely linear relationship has been found between the average of the SSN versus the duration time for each solar cycle of the ∼1.75–2.20 yr period.

Short-Term Periodicities Observed in Neutron Monitor Counting Rates

A. **López-Comazzi** & J. J. Blanco
Solar Physics volume 295, Article number: 81 (**2020**)
https://link.springer.com/content/pdf/10.1007/s11207-020-01649-5.pdf
Neutron monitor counting rates and solar wind velocity, interplanetary magnetic field, sunspot number and total solar irradiance measurements from 2013 to 2018 corresponding to the end of solar maximum and the decreasing phase of the Solar Cycle 24 have been used. The main objective is to check whether the periodicities observed in the cosmic rays are affected by the magnetic rigidity or the height at which the neutron monitors are placed. A Global Neutron Monitor (GNM) has been defined as representative of the neutron monitor global network. This GNM is constructed by averaging the counting rates of a set of selected neutron monitors. The selection process is based on the combination of three new data quality criteria, which are applied to neutron monitors in the Neutron Monitor Data Base giving a final pool of 22 selected neutron monitors. Morlet wavelet analysis is applied to the GNM and the selected solar activity parameters to find the common periodicities. Short-term periodicities of 13.5, 27, 48, 92, 132 and 298 days have been observed in cosmic ray intensity. A clear inverse relationship between rigidity and spectral power has been obtained for the 13.5-, 48-, 92-, 132-day periods. A not so clear but still observed direct relationship between the height of the neutron monitors and the spectral power for the 48-, 92-, 132-day periods has been also found. The periodicity of 92 days is the one which shows the highest dependence with rigidity cutoff and height. As far as we know, this is the first time that these dependencies are reported. We think that these

observations could be explained by assuming some cosmic ray intensity energy dependence in such periodicities and a competitive effect between rigidity and height.

Symmetric wave modes in coronal flux tubes with magnetically twisted layer

Igor P **Lopin**

MNRAS, Volume 505, Issue 2, August **2021**, Pages 1878–1890,

https://doi.org/10.1093/mnras/stab1355

The properties of axisymmetric magnetohydrodynamic wave modes are studied for the model of coronal magnetic tube, consisting of a central cord with homogeneous axial magnetic field, surrounded by an annulus with twisted magnetic field. This model mimics the coronal loops with radially localized magnetic twist. The derived dispersion relation is solved numerically. A number of limiting cases are examined analytically. The two families of axisymmetric modes are found to exist in the model. The first one includes an infinite number of fast-sausage modes (FSMs), modified by the twist and the second one is a set of modes with frequencies, lying in a narrow band, closed to Alfvén frequency of a twisted layer ωA0. The fundamental FSM (the mode of the lowest radial order) exists as a trapped mode for the entire range of axial wavenumbers. Its phase speed is always below the Alfvén speed of a magnetically twisted layer. This mode has a weak dispersion in the range of long and intermediate wavelengths. The higher radial order FSMs were found to be less sensitive to the presence of the magnetic twist. Both the fundamental FSM in the case of a weak magnetic twist and a set of symmetric modes for arbitrary twist have very similar frequencies, which are nearly equal to ωA0. This property implies that aforementioned wave modes behave like Alfvén torsional modes in the twisted annulus and like the radial modes in the untwisted core and environment, moreover they are strongly coupled. The main results of the study are discussed in the framework of their applications to coronal seismology.

Oscillations of a coronal plasma slab excited by an external source

I **Lopin**, I Nagorny

Monthly Notices of the Royal Astronomical Society, Volume 496, Issue 3, August **2020**, Pages 3035–3042,

https://doi.org/10.1093/mnras/staa1654

The dispersive properties of fast oscillations in a coronal plasma slab are studied. These oscillations are assumed to be generated by an external source, located at a finite distance from the slab. It is shown that the problem reduces to examination of the normal modes of a system, consisting of a slab cavity and a finitely distant rigid boundary. The relation that governs the eigenfrequencies of the system is derived. Both the kink and the sausage modes are excited. The main finding indicates that the principal kink mode is trapped not for all axial wavenumbers. It has a non-zero cut-off wavenumber and can exist either as a trapped mode or as a leaky mode. This cut-off tends to zero for infinitely distant sources, in accordance with the well-known result from the normal mode analysis. The expressions for the frequency and damping rate of the leaky principal kink mode are derived. The effect of a finitely distant rigid boundary on the higher transverse-order kink modes and all the sausage modes is found to be only minor, when the distance between the source and the slab is much more than the transverse size of the slab. The applications of the obtained results in coronal seismology are discussed.

Global-scale equatorial Rossby waves as an essential component of solar internal dynamics

Björn **Löptien**, Laurent Gizon, Aaron C. Birch, Jesper Schou, Bastian Proxauf, Thomas L. Duvall Jr., Richard S. Bogart, Ulrich R. Christensen

Nature Astronomy **2018**

https://arxiv.org/pdf/1805.07244.pdf

The Sun's complex dynamics is controlled by buoyancy and rotation in the convection zone and by magnetic forces in the atmosphere and corona. While small-scale solar convection is well understood, the dynamics of large-scale flows in the solar convection zone is not explained by theory or simulations. Waves of vorticity due to the Coriolis force, known as Rossby waves, are expected to remove energy out of convection at the largest scales. Here we unambiguously detect and characterize retrograde-propagating vorticity waves in the shallow subsurface layers of the Sun at angular wavenumbers below fifteen, with the dispersion relation of textbook sectoral Rossby waves. The waves have lifetimes of several months, well-defined mode frequencies below 200 nHz in a co-rotating frame, and eigenfunctions of vorticity that peak at the equator. Rossby waves have nearly as much vorticity as the convection at the same scales, thus they are an essential component of solar dynamics. We find a transition from turbulence-like to wave-like dynamics around the Rhines scale of angular wavenumber of twenty; this might provide an explanation for the puzzling deficit of kinetic energy at the largest spatial scales.

Measuring solar active region inflows with local correlation tracking of granulation

B. **Löptien**, A. C. Birch, T. L. Duvall Jr., L. Gizon, B. Proxauf, J. Schou

A&A 606, A28 **2017**
https://arxiv.org/pdf/1705.08833.pdf

Context. Local helioseismology has detected spatially extended converging surface flows into solar active regions. These play an important role in flux-transport models of the solar dynamo.
Aims. We aim to validate the existence of the inflows by deriving horizontal flow velocities around active regions with local correlation tracking of granulation.
Methods. We generate a six-year long-time series of full-disk maps of the horizontal velocity at the solar surface by tracking granules in continuum intensity images provided by the Helioseismic and Magnetic Imager (HMI) onboard the Solar Dynamics Observatory (SDO).
Results. On average, active regions are surrounded by inflows extending up to 10 deg from the center of the active region of magnitudes of 20-30 m/s, reaching locally up to 40 m/s, which is in agreement with results from local helioseismology. By computing an ensemble average consisting of 243 individual active regions, we show that the inflows are not azimuthally symmetric but converge predominantly towards the trailing polarity of the active region with respect to the longitudinally and temporally averaged flow field.

The shrinking Sun: a systematic error in local correlation tracking of solar granulation

B. **Löptien**, A. C. Birch, T. L. Duvall Jr., L. Gizon, J. Schou
A&A 590, A130 **2016**
http://arxiv.org/pdf/1604.04469v1.pdf

Context. Local correlation tracking of granulation (LCT) is an important method for measuring horizontal flows in the photosphere. This method exhibits a systematic error that looks like a flow converging towards disk center, also known as the shrinking-Sun effect.
Aims. We aim at studying the nature of the shrinking-Sun effect for continuum intensity data and at deriving a simple model that can explain its origin.
Methods. We derived LCT flow maps by running the local correlation tracking code FLCT on tracked and remapped continuum intensity maps provided by the Helioseismic and Magnetic Imager (HMI) onboard the Solar Dynamics Observatory. We also computed flow maps from synthetic continuum images generated from STAGGER code simulations of solar surface convection. We investigated the origin of the shrinking-Sun effect by generating an average granule from synthetic data from the simulations.
Results. The LCT flow maps derived from HMI and from the simulations exhibit a shrinking-Sun effect of comparable magnitude. The origin of this effect is related to the apparent asymmetry of granulation originating from radiative transfer effects when observing with a viewing angle inclined from vertical. This causes, in combination with the expansion of the granules, an apparent motion towards disk center.

Data compression for local correlation tracking of solar granulation

Björn **Löptien**, Aaron C. Birch, Tom L. Duvall Jr., Laurent Gizon, Jesper Schou
A&A 587, A9 **2016**
http://arxiv.org/pdf/1512.03243v1.pdf

Context. Several upcoming and proposed space missions, such as Solar Orbiter, will be limited in telemetry and thus require data compression.
Aims. We test the impact of data compression on local correlation tracking (LCT) of time-series of continuum intensity images. We evaluate the effect of several lossy compression methods (quantization, JPEG compression, and a reduced number of continuum images) on measurements of solar differential rotation with LCT.
Methods. We apply the different compression methods to tracked and remapped continuum intensity maps obtained by the Helioseismic and Magnetic Imager (HMI) onboard the Solar Dynamics Observatory. We derive 2D vector velocities using the local correlation tracking code FLCT and determine the additional bias and noise introduced by compression to differential rotation.
Results. We find that probing differential rotation with LCT is very robust to lossy data compression when using quantization. Our results are severely affected by systematic errors of the LCT method and the HMI instrument. The sensitivity of LCT to systematic errors is a concern for Solar Orbiter.

Helioseismology with Solar Orbiter **Review**

Björn **Löptien**, Aaron C. Birch, Laurent Gizon, Jesper Schou, Thierry Appourchaux, Julián Blanco Rodríguez, Paul S. Cally, Carlos Dominguez-Tagle, Achim Gandorfer, Frank Hill, Johann Hirzberger, Philip H. Scherrer, Sami K. Solanki
Space Science Reviews, Volume 196, Issue 1, pp 251-283 **2015**
http://arxiv.org/pdf/1406.5435v1.pdf

The Solar Orbiter mission, to be launched in July 2017, will carry a suite of remote sensing and in-situ instruments, including the Polarimetric and Helioseismic Imager (PHI). PHI will deliver high-cadence images of the Sun in intensity and Doppler velocity suitable for carrying out novel helioseismic studies. The orbit of the Solar Orbiter spacecraft will reach a solar latitude of up to 21 deg (up to 34 deg by the end of the extended mission) and thus will enable the first local helioseismology studies of the polar regions. Here we consider an array of science objectives to be addressed by helioseismology within the baseline telemetry allocation (51 Gbit per orbit, current baseline) and within the science observing windows (baseline 3 x 10 days per orbit). A particularly important objective is the measurement of large-scale flows at high latitudes (rotation and meridional flow), which are largely unknown but play an important role in flux transport dynamos. The full range of Earth-Sun-spacecraft angles provided by the orbit will enable helioseismology from two vantage points by combining PHI with another instrument: stereoscopic helioseismology will allow the study of the deep solar interior and a better understanding of the physics of solar oscillations in both quiet Sun and sunspots. We have used a model of the PHI instrument to study its performance for helioseismology applications. As input we used a 6 hr time-series of realistic solar magneto-convection simulation (Stagger code) and the SPINOR radiative transfer code to synthesize the observables. The simulated power spectra of solar oscillations show that the instrument is suitable for helioseismology. In particular, the specified point spread function, image jitter, and photon noise are no obstacle to a successful mission.

Image compression in local helioseismology

Björn **Löptien**, Aaron C. Birch, Laurent Gizon, Jesper Schou
Astronomy & Astrophysics **2014**
http://arxiv.org/pdf/1409.4176v1.pdf
Context. Several upcoming helioseismology space missions are very limited in telemetry and will have to perform extensive data compression. This requires the development of new methods of data compression.
Aims. We give an overview of the influence of lossy data compression on local helioseismology. We investigate the effects of several lossy compression methods (quantization, JPEG compression, and smoothing and subsampling) on power spectra and time-distance measurements of supergranulation flows at disk center.
Methods. We applied different compression methods to tracked and remapped Dopplergrams obtained by the Helioseismic and Magnetic Imager onboard the Solar Dynamics Observatory. We determined the signal-to-noise ratio of the travel times computed from the compressed data as a function of the compression efficiency.
Results. The basic helioseismic measurements that we consider are very robust to lossy data compression. Even if only the sign of the velocity is used, time-distance helioseismology is still possible. We achieve the best results by applying JPEG compression on spatially subsampled data. However, our conclusions are only valid for supergranulation flows at disk center and may not be valid for all helioseismology applications.

The Role of Subsurface Flows in Solar Surface Convection: Modeling the Spectrum of Supergranular and Larger Scale Flows

J. W. **Lord**, R. H. Cameron, M. P. Rast, M. Rempel, T. Roudier
2014 ApJ 793 24
http://arxiv.org/pdf/1407.2209v1.pdf
We model the solar horizontal velocity power spectrum at scales larger than granulation using a two-component approximation to the mass continuity equation. The model takes four times the density scale height as the integral (driving) scale of the vertical motions at each depth. Scales larger than this decay with height from the deeper layers. Those smaller are assumed to follow a Kolomogorov turbulent cascade, with the total power in the vertical convective motions matching that required to transport the solar luminosity in a mixing length formulation. These model components are validated using large scale radiative hydrodynamic simulations. We reach two primary conclusions: 1. The model predicts significantly more power at low wavenumbers than is observed in the solar photospheric horizontal velocity spectrum. 2. Ionization plays a minor role in shaping the observed solar velocity spectrum by reducing convective amplitudes in the regions of partial helium ionization. The excess low wavenumber power is also seen in the fully nonlinear three-dimensional radiative hydrodynamic simulations employing a realistic equation of state. This adds to other recent evidence suggesting that the amplitudes of large scale convective motions in the Sun are significantly lower than expected. Employing the same feature tracking algorithm used with observational data on the simulation output, we show that the observed low wavenumber power can be reproduced in hydrodynamic models if the amplitudes of large scale modes in the deep layers are artificially reduced. Since the large scale modes have reduced amplitudes, modes on the scale of supergranulation and smaller remain important to convective heat flux even in the deep layers, suggesting that small scale convective correlations are maintained through the bulk of the solar convection zone.

The ancient main-sequence solar proxy HIP 102152 unveils the activity and rotational fate of our Sun

Diego **Lorenzo-Oliveira**, Jorge Meléndez, Geisa Ponte, Jhon Yana Galarza

MNRAS **2020**
https://arxiv.org/pdf/2003.13871.pdf
We present a detailed analysis of the possible future Sun's rotational evolution scenario based on the 8 Gyr-old solar twin HIP 102152. Using HARPS high-cadence observations (and TESS light curves), we analyzed the modulation of a variety of activity proxies (Ca II, HI Balmer, and Na I lines), finding a strong rotational signal of 35.7 ± 1.4 days (logBfactor~70, in the case of Ca II K line). This value matches with the theoretical expectations regarding the smooth rotational evolution of the Sun towards the end of the main-sequence, validating the use of gyrochronology after solar age.

Plasma Diagnostics From Active Region and Quiet Sun Spectra Observed by Hinode/EIS: Quantifying the Departures from a Maxwellian Distribution

Juraj **Lörinčík**, Jaroslav Dudík, Giulio del Zanna, Elena Dzifčáková, Helen E. Mason
ApJ **893** 34 **2020**
https://arxiv.org/pdf/2003.07091.pdf
https://doi.org/10.3847/1538-4357/ab8010
We perform plasma diagnostics, including that of the non-Maxwellian κ-distributions, in several structures observed in the solar corona by the Extreme-Ultraviolet Imaging Spectrometer (EIS) onboard the Hinode spacecraft. To prevent uncertainties due to the in-flight calibration of EIS, we selected spectral atlases observed shortly after the launch of the mission. One spectral atlas contains an observation of an active region, while the other is an off-limb quiet Sun region. To minimize the uncertainties of the diagnostics, we rely only on strong lines and we average the signal over a spatial area within selected structures. Multiple plasma parameters are diagnosed, such as the electron density, differential emission measure, and the non-Maxwellian parameter κ. To do that, we use a simple, well-converging iterative scheme based on refining the initial density estimates via the DEM and κ. We find that while the quiet Sun spectra are consistent with a Maxwellian distribution, the coronal loops and moss observed within active region are strongly non-Maxwellian with $\kappa \lessapprox 3$. These results were checked by calculating synthetic ratios using DEMs obtained as a function of κ. Ratios predicted using the DEMs assuming κ-distributions converged to the ratios observed in the quiet Sun and coronal loops. To our knowledge, this work presents a strong evidence of a presence of different electron distributions between two physically distinct parts of the solar corona.
Hinode/EIS Nuggets June **2020** http://solarb.mssl.ucl.ac.uk/SolarB/eisnuggets.jsp

Magnetic bipoles in rotating turbulence with coronal envelope

I. R. **Losada**, J. Warnecke, A. Brandenburg, N. Kleeorin, I. Rogachevskii
A&A 621, A61 (**2019**)
https://arxiv.org/pdf/1803.04446.pdf
The formation of sunspots and starspots is not yet fully understood and is therefore one of the major open problems in solar and stellar physics. Magnetic flux concentrations can be produced by the negative effective magnetic pressure instability (NEMPI). This instability is strongly suppressed by rotation. However, the presence of an outer coronal envelope was previously found to strengthen the flux concentrations and make them more prominent. It also allows for the formation of bipolar regions (BRs). We want to know whether the presence of an outer coronal envelope also changes the excitation conditions and the rotational dependence of NEMPI. We use direct numerical simulations and mean-field simulations. We adopt a simple two-layer model of turbulence that mimics the jump between the convective turbulent and coronal layers below and above the surface of a star, respectively. The computational domain is Cartesian and located at a certain latitude of a rotating sphere. We investigate the effects of rotation on NEMPI by changing the Coriolis number, the latitude, and the box resolution. Rotation has a strong impact on the process of BR formation. Even rather slow rotation is found to suppress their formation. However, increasing the imposed magnetic field strength also makes the structures stronger and alleviates the rotational suppression somewhat. The presence of a coronal layer itself does not significantly alleviate the effects of rotational suppression.

The association of the Hale Sector Boundary with RHESSI solar flares and active longitudes

K. **Loumou**, I. G. Hannah, H. S. Hudson
A&A 618, A9 **2018**
https://arxiv.org/pdf/1808.05866.pdf
sci-hub.tw/10.1051/0004-6361/201731050
The heliospheric magnetic field (HMF) is structured into large sectors of positive and negative polarity. The parts of the boundary between these sectors where the change in polarity matches that of the leading-to-following sunspot polarity in that solar hemisphere, are called Hale Sector Boundaries (HSB). We investigate the flare occurrence rate near HSBs and the association between HSBs and active longitudes. Previous work determined the times HSBs were at solar central meridian, using the detection of the HMF sector boundary crossing at the Earth. In addition to this, we use a new approach which finds the HSB locations at all times by determining them from Potential Field

Source Surface (PFSS) extrapolations of photospheric magnetograms. We use the RHESSI X-ray flare list for comparison to the HSB as it provides accurate flare locations over 14 years, from February 2002 to February 2016, covering both Cycles 23 and 24. For the active longitude positions we use previously published work based on sunspot observations. We find that the two methods of determining the HSB generally agree and that 41% (Cycle 23) and 47% (Cycle 24) of RHESSI flares occur within 30◦ of the PFSS determined-HSB. The behaviour of the HSBs varies over the two Cycles studied, and as expected they swap in hemisphere as the Cycles change. The HSBs and active longitudes do overlap but not consistently. They often move at different rates relative to each other (and the Carrington solar rotation rate) and these vary over each Cycle. The HSBs provide a useful additional activity indicator, particularly during periods when active longitudes are difficult to determine.

Testing the accuracy of Coimbra Astronomical Observatory solar filament historical series (1929-1941)

Ana **Lourenço**, Ricardo Gafeira, Vitor Bonifacio, Teresa Barata, Joao Fernandes, Eva Silva
Solar Phys. **2021**
https://arxiv.org/ftp/arxiv/papers/2108/2108.05978.pdf
The present work aims to validate the positions of solar filaments published in the Annals of Coimbra University Astronomical Observatory, currently the Geophysical and Astronomical Observatory of the University of Coimbra, corresponding to years 1929 to 1941. The published Stonyhurst positions were obtained by an original method devised in the early 20th century that used a spherical calculator instrument, a wood-made model of the sun. We used the digital images of the original spectroheliograms to measure the positions of the filaments, and heliographic coordinates were determinate with the routines implemented on python package Sunpy. The correlation coefficients between both sets of coordinates are positive and highly significant. The results validate the method used at the Coimbra observatory and the data published. We conclude that Coimbra solar filaments catalogues are reliable and can therefore be considered for future solar activity studies.

Chapter 6 - Coronal Magnetism as a Universal Phenomenon **Review**

B.C. **Low**
In: ***The Sun as a Guide to Stellar Physics*** ***Book***
Eds. Oddbjørn Engvold, Jean-Claude Vial, and Andrew Skumanich
Elsevier , November **2018**
https://www.sciencedirect.com/book/9780128143346/the-sun-as-a-guide-to-stellar-physics
In the 60 years after E. N. Parker's prediction of the existence of the solar wind and the magnetic origin of coronal heating, space-borne and ground-based observations have built a conceptually complete phenomenology of the corona as a fully ionized hydromagnetic atmosphere responding in step to the global magnetic reversals of the Sun in 11-year cycles. This phenomenology is reviewed with the theoretical ideas it motivated, describing the photospheric emergence of new-cycle magnetic fluxes of a reversed polarity into the corona, ubiquitous coronal heating, hydromagnetic self-organization, explosive energy release, and the breaking of self-confinement into flows of expansion winds and episodic ejections of magnetic structures. High electrical and thermal conductivities at coronal million-degree temperatures have central roles. The corona obeys a hemispherical rule independent of magnetic cycle, that self-organized structures have a statistical preference for left- and right-handed magnetic twists, respectively, in the northern and southern hemispheres relative to the rotational axis. It is pointed out, perhaps for the first time, that this hemispherical rule is a hydromagnetic implication of the Parker (1955a,b) dynamo, straightforward to deduce graphically from his book Cosmical Magnetic Fields (1979). Solar physics has reached a broad-brush physical understanding of the corona solar-wind system as the prototype of a universal astrophysical phenomenon.

Periodic Coronal Rain Driven by Self-consistent Heating Process in a Radiative Magnetohydrodynamic Simulation

Zekun **Lu**, Feng Chen, J. H. Guo, M. D. Ding, Can Wang, Haocheng Yu, Y. W. Ni, Chun Xia
ApJL **2024**
https://arxiv.org/pdf/2408.16988
The periodic coronal rain and in-phase radiative intensity pulsations have been observed in multiple wavelengths in recent years. However, due to the lack of three-dimensional coronal magnetic fields and thermodynamic data in observations, it remains challenging to quantify the coronal heating rate that drives the mass cycles. In this work, based on the MURaM code, we conduct a three-dimensional radiative magnetohydrodynamic simulation spanning from the convective zone to the corona, where the solar atmosphere is heated self-consistently through dissipation resulting from magneto-convection. For the first time, we model the periodic coronal rain in an active region. With a high spatial resolution, the simulation well resembles the observational features across different extreme ultraviolet wavelengths. These include the realistic interweaving coronal loops, periodic coronal rain and periodic intensity pulsations, with two periods of 3.0~h and 3.7~h identified within one loop system. Moreover, the simulation allows for a detailed three-dimensional depiction of coronal rain on small scales, revealing adjacent shower-like rain

clumps ~500~km in width and showcasing their multi-thermal internal structures. We further reveal that these periodic variations essentially reflect the cyclic energy evolution of the coronal loop under thermal non-equilibrium state. Importantly, as the driver of the mass circulation, the self-consistent coronal heating rate is considerably complex in time and space, with hour-level variations in one order of magnitude, minute-level bursts, and varying asymmetry reaching ten times between footpoints. This provides an instructive template for the ad hoc heating function, and further enhances our understanding of the coronal heating process.

A Novel Bimodal Forecasting Model for Solar Cycle 25

J. Y. **Lu**1, Y. T. Xiong1, K. Zhao1, M. Wang1, J. Y. Li1, G. S. Peng1, and M. Sun1
2022 ApJ 924 59
https://iopscience.iop.org/article/10.3847/1538-4357/ac3488/pdf
In this paper, a novel bimodal model to predict a complete sunspot cycle based on comprehensive precursor information is proposed. We compare the traditional 13 month moving average with the Gaussian filter and find that the latter has less missing information and can better describe the overall trend of the raw data. Unlike the previous models that usually only use one precursor, here we combine the implicit and geometric information of the solar cycle (peak and skewness of the previous cycle and start value of the predicted cycle) with the traditional precursor method based on the geomagnetic index and adopt a multivariate linear approach with a higher goodness of fit (>0.85) in the fitting. Verifications for cycles 22–24 demonstrate that the model has good performance in predicting the peak and peak occurrence time. It also successfully predicts the complete bimodal structure for cycle 22 and cycle 24, showing a certain ability to predict whether the next solar cycle is unimodal or bimodal. It shows that cycle 25 is a single-peak structure and that the peak will come in 2024 October with a peak of 145.3.

New Space Companies Meet a "Normal" Solar Maximum

Noé **Lugaz**, Huixin Liu, Brett A. Carter, Jennifer Gannon, Shasha Zou, Steven K. Morley
Space Weather Volume21, Issue9 e2023SW003702 **2023**
https://doi.org/10.1029/2023SW003702
https://agupubs.onlinelibrary.wiley.com/doi/epdf/10.1029/2023SW003702
The monthly mean sunspot number has been larger in June–July 2023 than the double peak of solar cycle 24 (146 in February 2014 and 139 in November 2011) and brings us back to the sunspot level of solar cycle 23. However, the number of rocket launches, satellites in orbit and private space companies has increased dramatically in the past 20 years. Additionally, there is a growing interest for space exploration beyond Earth's orbit, to the Moon and beyond, which comes with higher risk of being affected by space weather. Here, we discuss some of these trends and the role of the journal to improve awareness of space weather impacts.

Centennial evolution of monthly solar wind speeds: Fastest monthly solar wind speeds from long-duration coronal holes†

R. **Lukianova**, L. Holappa, K. Mursula
JGR **2017**
High speed solar wind streams (HSSs) are very efficient drivers of geomagnetic activity at high latitudes. In this paper we use a recently developed ΔH parameter of geomagnetic activity, calculated from the night-side hourly magnetic field measurements of the Sodankylä observatory, as a proxy for solar wind (SW) speed at monthly time resolution in 1914-2014 (solar cycles 15-24). The seasonal variation in the relation between monthly ΔH and solar wind speed is taken into account by calculating separate regressions between ΔH and SW speed for each month. Thereby, we obtain a homogeneous series of proxy values for monthly solar wind speed for the last 100 years. We find that the strongest HSS-active months of each solar cycle occur in the declining phase, in years 1919, 1930, 1941, 1952, 1959, 1973, 1982, 1994 and 2003. Practically all these years are the same or adjacent to the years of annual maximum solar wind speeds. This implies that the most persistent coronal holes, lasting for several solar rotations and leading to the highest annual SW speeds, are also the sources of the highest monthly SW speeds. Accordingly, during the last 100 years, there were no coronal holes of short duration (of about one solar rotation) that would produce faster monthly (or solar rotation) averaged solar wind than the most long-living coronal holes in each solar cycle produce.

Self-Similar Approach for Rotating Magnetohydrodynamic Solar and Astrophysical Structures

Manuel **Luna**, Eric Priest, Fernando Moreno-Insertis
ApJ Volume 863, Issue 2, article id. 147 **2018**
https://arxiv.org/pdf/1807.02473.pdf
https://iopscience.iop.org/article/10.3847/1538-4357/aad093/pdf
Rotating magnetic structures are common in astrophysics, from vortex tubes and tornados in the Sun all the way to jets in different astrophysical systems. The physics of these objects often combine inertial, magnetic, gas pressure and gravitational terms. Also, they often show approximate symmetries that help simplify the otherwise rather

intractable equations governing their morphology and evolution. Here we propose a general formulation of the equations assuming axisymmetry and a self-similar form for all variables: in spherical coordinates (r,θ,ϕ), the magnetic field and plasma velocity are taken to be of the form: $B=f(\theta)/rn$ and $v=g(\theta)/rm$, with corresponding expressions for the scalar variables like pressure and density. Solutions are obtained for potential, force-free, and non-force-free magnetic configurations. Potential-field solutions can be found for all values of~n. Non-potential force-free solutions possess an azimuthal component $B\phi$ and exist only for $n\geq 2$; the resulting structures are twisted and have closed field lines but are not collimated around the system axis. In the non-force free case, including gas pressure, the magnetic field lines acquire an additional curvature to compensate for an outward pointing pressure gradient force. We have also considered a pure rotation situation with no gravity, in the zero-β limit: the solution has cylindrical geometry and twisted magnetic field lines. The latter solutions can be helpful in producing a collimated magnetic field structure; but they exist only when $n<0$ and $m<0$: for applications they must be matched to an external system at a finite distance from the origin.

Spatial incoherence of solar granulation: a global analysis using BiSON 2B data

Mikkel N. **Lund**, William J. Chaplin, Steven J. Hale, Guy R. Davies, Yvonne P. Elsworth, Rachel Howe
MNRAS **2017**
https://arxiv.org/pdf/1709.01329.pdf

Assessing and calibrating these effects is therefore of great importance. Here we study the spatial coherence of granulation noise and oscillation modes in the Sun, with the aim of exploiting any incoherence to beat-down observed granulation noise, hence improving the detection of low-frequency p-modes. Using data from the BiSON 2B instrument, we assess the coherence between different atmospheric heights and between different surface regions. We find that granulation noise from the different atmospheric heights probed is largely incoherent; frequency regions dominated by oscillations are almost fully coherent. We find a randomised phase difference for the granulation noise, and a near zero difference for the evanescent oscillations. A reduction of the incoherent granulation noise is shown by application of the cross-spectrum.

The signature of granulation in a solar power spectrum as seen with CO5BOLD

Mia S. **Lundkvist** (1 and 2), Hans-Günter Ludwig (2), Remo Collet (1), Thomas Straus
MNRAS **2020**
https://arxiv.org/pdf/2011.10045.pdf

The granulation background seen in the power spectrum of a solar-like oscillator poses a serious challenge for extracting precise and detailed information about the stellar oscillations. Using a 3D hydrodynamical simulation of the Sun computed with CO5BOLD, we investigate various background models to infer, using a Bayesian methodology, which one provides the best fit to the background in the simulated power spectrum. We find that the best fit is provided by an expression including the overall power level and two characteristic frequencies, one with an exponent of 2 and one with a free exponent taking on a value around 6. We assess the impact of the 3D hydro-code on this result by repeating the analysis with a simulation from Stagger and find that the main conclusion is unchanged. However, the details of the resulting best fits differ slightly between the two codes, but we explain this difference by studying the effect of the spatial resolution and the duration of the simulation on the fit. Additionally, we look into the impact of adding white noise to the simulated time series as a simple way to mimic a real star. We find that, as long as the noise level is not too low, the results are consistent with the no-noise case.

The Sun's Magnetic Power Spectra over Two Solar Cycles. II. Cycle Dependence of Active Region, Magnetic Network, and Their Relation

Yukun **Luo**, Jie Jiang, Ruihui Wang
ApJ **970** 76 **2024**
https://arxiv.org/pdf/2406.08141
https://iopscience.iop.org/article/10.3847/1538-4357/ad5677/pdf

The multi-scaled solar magnetic field consists of two major components: active regions (ARs) and magnetic network. Unraveling the cycle-dependent properties and interrelations of these components is crucial for understanding the evolution of the solar magnetic field. In this study, we investigate these components using magnetic power spectra derived from high-resolution and continuous synoptic magnetograms since cycle 23 onwards. Our results show that the size of the magnetic network ranges from 26 Mm to 41 Mm without dependence on the solar cycle. The power of the network field (PNW) accounts for approximately 20\% of the total power during any phase of solar cycles. In contrast to the AR power (PAR), PNW displays a weaker cycle dependence, as described by the relationship $PNW \approx 0.6* PAR + 40$. The power-law index between AR sizes and magnetic network sizes presents a strong anti-correlation with the activity level. Additionally, our study indicates that in the absence of sunspots on the solar disc, the magnetic power spectra remain time-independent, consistently exhibiting similarity in both shape and power. This study introduces a new method to investigate the properties of the magnetic network and

provides magnetic power spectra for high-resolution simulations of the solar magnetic field at the surface at various phases of solar cycles.

Long-term evolution of solar activity and prediction of the following solar cycles

Peixin **Luo** (1 and 2), Baolin Tan
Research in Astron. Astrophys. **2024**
https://arxiv.org/pdf/2402.13173.pdf
Solar activities have a great impact on modern high-tech systems, such as human aerospace, satellite communication and navigation, deep space exploration, and related scientific research. Therefore, studying the long - term evolution trend of solar activity and accurately predicting the future solar cycles is highly anticipated. Based on wavelet transform and empirical function fitting of the longest recorded data of the annual average relative sunspot number (ASN) series of 323 years to date, this work decisively verified the existence of the solar century cycles and confirmed that its length is about 104.0 years, and the magnitude has a slightly increasing trend on the time scale of several hundreds of years. Based on this long-term evolutionary trend, we predicted solar cycle 25 and 26 by using phase similar prediction methods. As for the solar cycle 25, its maximum ASN will be about 146.7±33.40, obviously stronger than solar cycle 24. The peak year will occur approximately in 2024, and the period is about 11±1 years. As for the solar cycle 26, it will start around 2030, reach the maximum between 2035 and 2036, with maximum ASN of about 133.0±3.200, and the period is about 10 years.

The Sun's Magnetic Power Spectra Over Two Solar Cycles. I. Calibration Between SDO/HMI And SOHO/MDI Magnetograms

Yukun **Luo**, Jie Jiang, Ruihui Wang
ApJ **954** 199 **2023**
https://arxiv.org/pdf/2308.07530.pdf
https://iopscience.iop.org/article/10.3847/1538-4357/acec77/pdf
The Sun's magnetic field is strongly structured over a broad range of scales. The magnetic spatial power spectral analysis provides a powerful tool to understand the various scales of magnetic fields and their interaction with plasma motion. We aim to investigate the power spectra using spherical harmonic decomposition of high-resolution SOHO/MDI and SDO/HMI synoptic magnetograms covering three consecutive solar cycle minima in a series of papers. As the first of the series, we calibrate and analyze the power spectra based on co-temporal SDO/HMI and SOHO/MDI data in this paper. For the first time, we find that the calibration factor r between SOHO/MDI and SDO/HMI varies with the spatial scale l of the magnetic field, where l is the degree of a spherical harmonics. The calibration factor satisfies $r(l)=-0.021l0.64+2-----------\sqrt{}(5<l\leq539)$. With the calibration function, most contemporaneous SOHO/MDI and SDO/HMI magnetograms show consistent power spectra from about 8 Mm to the global scales over about 3 orders of magnitudes. Moreover, magnetic power spectra from SOHO/MDI and SDO/HMI maps show peaks/knees at $l\approx120$ corresponding to the typical supergranular scale (about 35 Mm) constrained from direct velocimetric measurements. This study paves the way for investigating the solar-cycle dependence of supergranulation and magnetic power spectra in subsequent studies.

Signs of Cycle 25 Seen in the Surface Toroidal Field

William **Ma** and Philip H. Scherrer
HMI Science Nuggets #58 Sept **2016**
http://hmi.stanford.edu/hminuggets/?p=1657
Analyzing the toroidal field component from data collected by the Solar Dynamics Observatory/Helioseismic Magnetic Imager (SDO/HMI) and Wilcox Solar Observatory (WSO), we see signs of the next solar cycle have already appeared at high latitudes. WSO has provided data for the past four sunspot cycles, while HMI has been observing for six years.

Accurately constraining velocity information from spectral imaging observations using machine learning techniques

Conor D. **MacBride**, David B. Jess, Samuel D. T. Grant, Elena Khomenko, Peter H. Keys, Marco Stangalini
Philosophical Transactions of the Royal Society A **2020**
https://arxiv.org/pdf/2007.07904.pdf
Determining accurate plasma Doppler (line-of-sight) velocities from spectroscopic measurements is a challenging endeavour, especially when weak chromospheric absorption lines are often rapidly evolving and, hence, contain multiple spectral components in their constituent line profiles. Here, we present a novel method that employs machine learning techniques to identify the underlying components present within observed spectral lines, before subsequently constraining the constituent profiles through single or multiple Voigt fits. Our method allows active and quiescent components present in spectra to be identified and isolated for subsequent study. Lastly, we employ a Ca II 8542 Å spectral imaging dataset as a proof-of-concept study to benchmark the suitability of our code for

extracting two-component atmospheric profiles that are commonly present in sunspot chromospheres. Minimisation tests are employed to validate the reliability of the results, achieving median reduced $\chi 2$ values equal to 1.03 between the observed and synthesised umbral line profiles.

Energy Input Flux in the Global Quiet-Sun Corona

C. **Mac Cormack**, A. M. Vásquez, M. López Fuentes, F. A. Nuevo, E. Landi, R. A. Frazin

2017 *ApJ* **843** 70

https://arxiv.org/pdf/1706.00365.pdf

We present first results of a novel technique that provides, for the first time, constraints on the energy input flux at the coronal base (r∼1.025R⊙) of the quiet-Sun at a global scale. By combining differential emission measure tomography (DEMT) of EUV images, with global models of the coronal magnetic field, we estimate the energy input flux at the coronal base that is required to maintain thermodynamically stable structures. The technique is described in detail and first applied to data provided by the Extreme Ultraviolet Imager (EUVI) instrument, on board the Solar TErrestrial RElations Observatory (STEREO) mission, and the Atmospheric Imaging Assembly (AIA) instrument, on board the Solar Dynamics Observatory (SDO) mission, for two solar rotations with different levels of activity. Our analysis indicates that the typical energy input flux at the coronal base of magnetic loops in the quiet-Sun is in the range ∼0.5−2.0×105(ergsec−1cm−2), depending on the structure size and level of activity. A large fraction of this energy input, or even its totality, could be accounted for by Alfv\'en waves, as shown by recent independent observational estimates derived from determinations of the non-thermal broadening of spectral lines in the coronal base of quiet-Sun regions. This new tomography product will be useful for validation of coronal heating models in magnetohydrodinamic simulations of the global corona.

Magnetic winding -- a key to unlocking topological complexity in flux emergence

David **MacTaggart**, Chris Prior

J. Phys. Conf. Ser. (IC-Msquared conference) **2020**

https://arxiv.org/pdf/2009.11712.pdf

Magnetic helicity is an invariant of ideal magnetohydrodynamics (MHD) that encodes information on the topology of magnetic field lines. It has long been appreciated that magnetic topology is an important constraint for the evolution of magnetic fields in MHD. In applications to the solar atmosphere, understanding magnetic topology is crucial for following the evolution and eruption of magnetic fields. At present, magnetic helicity flux can be measured in solar observations but the interpretation of results is difficult due to the combination of confounding factors. We propose that a renormalization of helicity flux, the \emph{magnetic winding}, can be used to detect more detailed topological features in magnetic fields and thus provide a more reliable signature for predicting the onset of solar eruptions.

Solar activity simulation and forecast with a flux-transport dynamo

Alejandro **Macario-Rojas**, Katharine L. Smith, Peter C. E. Roberts

MNRAS Volume 479, Issue 3, 21, Pages 3791–3803, **2018**

https://arxiv.org/pdf/1806.10733.pdf

We present the assessment of a diffusion-dominated mean field axisymmetric dynamo model in reproducing historical solar activity and forecast for solar cycle 25. Previous studies point to the Sun's polar magnetic field as an important proxy for solar activity prediction. Extended research using this proxy has been impeded by reduced observational data record only available from 1976. However, there is a recognised need for a solar dynamo model with ample verification over various activity scenarios to improve theoretical standards. The present study aims to explore the use of helioseismology data and reconstructed solar polar magnetic field, to foster the development of robust solar activity forecasts. The research is based on observationally inferred differential rotation morphology, as well as observed and reconstructed polar field using artificial neural network methods via the hemispheric sunspot areas record. Results show consistent reproduction of historical solar activity trends with enhanced results by introducing a precursor rise time coefficient. A weak solar cycle 25, with slow rise time and maximum activity −14.4%(±19.5%) with respect to the current cycle 24 is predicted.

Different Modes of Star Formation II: Gas Accretion Phase of Initially Subcritical Star-Forming Clouds

Masahiro N. **Machida**, Shantanu Basu

MNRAS **2020**

https://arxiv.org/pdf/2003.03078.pdf

The accretion phase of star formation is investigated in magnetically-dominated clouds that have an initial subcritical mass-to-flux ratio. We employ nonideal magnetohydrodynamic simulations that include ambipolar diffusion and ohmic dissipation. During the early prestellar phase the mass-to-flux ratio rises toward the critical value for collapse, and during this time the angular momentum of the cloud core is reduced significantly by

magnetic braking. Once a protostar is formed in the core, the accretion phase is characterized by the presence of a small amount of angular momentum but a large amount of magnetic flux in the near-protostellar environment. The low angular momentum leads to a very small (or even nonexistent) disk and weak outflow, while the large magnetic flux can lead to an interchange instability that rapidly removes flux from the central region. The effective magnetic braking in the early collapse phase can even lead to a counter-rotating disk and outflow, in which the rotation direction of the disk and outflow is opposite to that of the infalling envelope. The solutions with a counter-rotating disk, tiny disk, or nonexistent disk (direct collapse) are unique outcomes that are realized in collapse from magnetically-dominated clouds with an initial subcritical mass-to-flux ratio.

Magnetic Helicity Condensation and the Solar Cycle

Duncan H. **Mackay**1, C. Richard DeVore2, Spiro K. Antiochos2, and Anthony R. Yeates3
2018 ApJ 869 62 https://doi.org/10.3847/1538-4357/aaec7c
sci-hub.tw/10.3847/1538-4357/aaec7c

Solar filaments exhibit a global chirality pattern where dextral/sinistral filaments, corresponding to negative/positive magnetic helicity, are dominant in the northern/southern hemisphere. This pattern is opposite to the sign of magnetic helicity injected by differential rotation along east–west oriented polarity inversion lines, posing a major conundrum for solar physics. A resolution of this problem is offered by the magnetic helicity-condensation model of Antiochos. To investigate the global consequences of helicity condensation for the hemispheric chirality pattern, we apply a temporally and spatially averaged statistical approximation of helicity condensation. Realistic magnetic field configurations in both the rising and declining phases of the solar cycle are simulated. For the helicity-condensation process, we assume convective cells consisting of positive/negative vorticities in the northern/southern hemisphere that inject negative/positive helicity. The magnitude of the vorticity is varied as a free parameter, corresponding to different rates of helicity injection. To reproduce the observed percentages of dominant and minority filament chiralities, we find that a vorticity of magnitude $2.5 \times 10{-}6\ s{-}1$ is required. This rate, however, is insufficient to produce the observed unimodal profile of chirality with latitude. To achieve this, a vorticity of at least $5 \times 10{-}6\ s{-}1$is needed. Our results place a lower limit on the small-scale helicity injection required to dominate differential rotation and reproduce the observed hemispheric pattern. Future studies should aim to establish whether the helicity injection rate due to convective flows and/or flux emergence across all latitudes of the Sun is consistent with our results.

SCSS-Net: solar corona structures segmentation by deep learning

Šimon **Mackovjak**, Martin Harman, Viera Maslej-Krešňáková, Peter Butka
MNRAS, Volume 508, Issue 3, December **2021**, Pages 3111–3124,
https://doi.org/10.1093/mnras/stab2536

Structures in the solar corona are the main drivers of space weather processes that might directly or indirectly affect the Earth. Thanks to the most recent space-based solar observatories, with capabilities to acquire high-resolution images continuously, the structures in the solar corona can be monitored over the years with a time resolution of minutes. For this purpose, we have developed a method for automatic segmentation of solar corona structures observed in the EUV spectrum that is based on a deep-learning approach utilizing convolutional neural networks. The available input data sets have been examined together with our own data set based on the manual annotation of the target structures. Indeed, the input data set is the main limitation of the developed model's performance.
Our *SCSS-Net* model provides results for coronal holes and active regions that could be compared with other generally used methods for automatic segmentation. Even more, it provides a universal procedure to identify structures in the solar corona with the help of the transfer learning technique. The outputs of the model can be then used for further statistical studies of connections between solar activity and the influence of space weather on Earth.

Differential emission measure analysis of active region cores and quiet Sun for the non-Maxwellian κ-distributions

Š. **Mackovjak**1,2, E. Dzifčáková2 and J. Dudík
A&A 564, A130 (**2014**)

Context. The non-Maxwellian κ-distributions have been detected in the solar wind and can explain intensities of some transition region lines. Presence of such distributions in the outer layers of the solar atmosphere influences the ionization and excitation equilibrium and widens the line contribution functions. This behavior may be reflected on the reconstructed differential emission measure (DEM).
Aims. We aim to investigate the influence of κ-distributions on the reconstructed DEMs.
Methods. We perform DEM reconstruction for three active region cores and a quiet Sun region using the Withbroe-Sylwester method and the regularization method.
Results. We find that the reconstructed DEMs depend on the value of κ. The DEMs of the active region cores show similar behavior with decreasing κ, or an increasing departure from the Maxwellian distribution. For lower κ, the peaks of the DEMs are typically shifted to higher temperatures and the DEMs themselves become more concave. This is caused by the less steep high-temperature slopes for lower κ. However, the low-temperature slopes do not

change significantly even for extremely low κ. The behavior of the quiet-Sun DEM distribution is different. It becomes progressively less multithermal for lower κ with the EM-loci plots that indicate near-isothermal plasma for $\kappa = 2$.
Conclusions. The κ-distributions can influence the reconstructed DEMs. The slopes of the DEM, however, do not change with κ significantly enough to produce different constraints on the heating mechanism in terms of frequency of coronal heating events.

Sunquake survey of X-class flares for the current solar cycle

Connor **Macrae** & Sergei Zharkov
UKSP Nuggets #74 Nov **2016**
http://spd.aas.org/SolarNews/2016/20161201.html
Improved detection methods unearth more sunquakes from the current solar cycle
2013-11-10
Table 1 – Summary of suitable X-class flare candidates with presence of detected seismic signatures (SQ)

Helicity and winding fluxes as indicators of twisted flux emergence

David **MacTaggart**, Chris Prior
Geophysical and Astrophysical Fluid Dynamics Vol. 00, No. 00, 2012, 1–26 **2019**
https://arxiv.org/pdf/1909.01071.pdf
Evidence for the emergence of twisted flux tubes into the solar atmosphere has, so far, come from indirect signatures. In this work, we investigate directly the topological input of twisted flux tube emergence by studying helicity and winding fluxes. In magnetohydrodynamic simulations with domains spanning from the top of the convection zone to the lower corona, we simulate the emergence of twisted flux tubes with a range of different initial field strengths. One important feature of this work is the inclusion of a convectively unstable layer beneath the photosphere. We find approximately self-similar behaviour in the helicity input for the different field strengths considered. As the tubes rise and reach the photosphere, there is a strong input of negative helicity since we consider left-handed twisted tubes. This phase is then followed by a reduction of the negative input and, for low initial field strengths, a net positive helicity input. This phase corresponds to the growing influence of convection on the field and the development of serpentine field structures during emergence. The winding flux can be used to detect when the twisted cores of the tubes reach the photosphere but this signature does not exhibit self-similar behaviour across the range of initial field strengths. In short, the helicity and winding fluxes can provide much information about how a magnetic field emerges that is not directly available from other sources, such as magnetograms.

The magnetic structure of surges in small-scale emerging flux regions

MacTaggart, D., Guglielmino, S.L., Haynes, A.L., Simitev, R., and Zuccarello, F.
A&A, 2015
http://eprints.gla.ac.uk/102318/1/102318.pdf
Aims. To investigate the relationship between surges and magnetic reconnection during the emergence of small-scale active regions. In particular, to examine how the large-scale geometry of the magnetic field, shaped by different phases of reconnection, guides the flowing of surges. Methods. We present three flux emergence models. The first model, and the simplest, consists of a region emerging into a horizontal ambient field that is initially parallel to the top of the emerging region. The second model is the same as the first but with an extra smaller emerging region which perturbs the main region. This is added to create a more complex magnetic topology and to test how this complicates the development of surges compared to the first model. The last model has a non-uniform ambient magnetic field to model the effects of emergence near a sunspot field and impose asymmetry on the system through the ambient magnetic field. At each stage, we trace the magnetic topology to identify the locations of reconnection. This allows for field lines to be plotted from different topological regions, highlighting how their geometry affects the development of surges. Results. In the first model, we identify distinct phases of reconnection. Each phase is associated with a particular geometry for the magnetic field and this determines the paths of the surges. The second model follows a similar pattern to the first but with a more complex magnetic topology and extra eruptions. The third model highlights how an asymmetric ambient field can result in preferred locations for reconnection, subsequently guiding the direction of surges. Conclusions. Each of the identified phases highlights the close connection between magnetic field geometry, reconnection and the flow of surges. These phases can now be detected observationally and may prove to be key signatures in determining whether or not an emerging region will produce a large-scale (CME-type) eruption.

Modelling Persistent Cycles in Solar Activity

Federico **Maddanu** & Tommaso Proietti
Solar Physics volume 297, Article number: 13 (**2022**)
https://link.springer.com/content/pdf/10.1007/s11207-021-01943-w.pdf

Solar activity at decadal time scales is characterised by persistent periodic patterns with global effects on the Earth's climate. This article deals with the analysis and prediction of the revised monthly sunspot numbers, adopting a recently proposed time-series model for long-range dependent cycles. The methodology is based on the maximum-likelihood estimate of the model parameters and provides optimal signal extraction filters for cycle estimation and prediction. The analysis suggests the presence of stationary cyclical long memory in the sunspot-generating process. Moreover, our formulation provides a reliable method for solar-cycle predictions, yielding forecasts of the future Cycle 25. In particular, we claim a main peak will occur in early 2024 with an amplitude of 114 and an end of the cycle in early 2030.

Coronal magnetic field and emission properties of small-scale bright and faint loops in the quiet Sun

Maria S. **Madjarska**, Thomas Wiegelmann, Pascal Démoulin, Klaus Galsgaard
A&A 690, A242 **2024**
https://arxiv.org/pdf/2407.09769
https://www.aanda.org/articles/aa/pdf/2024/10/aa50343-24.pdf

The present study provides statistical information on the coronal magnetic field and intensity properties of small-scale bright and faint loops in the quiet Sun. We aim to quantitatively investigate the morphological and topological properties of the coronal magnetic field in bright and faint small-scale loops, with the former known as coronal bright points (CBPs). We analyse 126 small-scale loops using quasi-temporal imaging and line-of-sight magnetic field observations. We employ a recently developed automatic tool that uses a linear magneto-hydro-static model to compute the magnetic field in the solar atmosphere and automatically match individual magnetic field lines with small-scale loops. For most of the loops, we automatically obtain an excellent agreement of the magnetic field lines from the LMHS model and the loops seen in AIA 193 A. One stand-out result is that the magnetic field is non-potential. We obtain the typical ranges of loop heights, lengths, intensities, mean magnetic field strength along the loops and at loop tops, and magnetic field strength at loop footpoints. We find that loops below the classic chromospheric height of 1.5 Mm are flatter suggesting that non-magnetic forces (one of which is the plasma pressure) play an important role below this height. We find a strong correlation (Pearson coefficient of 0.9) between loop heights and lengths. The average intensity along the loops correlates stronger with the average magnetic field along the loops than with the field strength at loop tops. The latter correlation indicates that the energy release in the loops is more likely linked to the average magnetic field along the loops than the field strength on the loop tops. In other words, the energy is probably released all along the loops, but not just at the loop top. This result is consistent with the recent benchmarking radiative 3D MHD model of Nóbrega-Siberio etal.

Photospheric magnetic flux and coronal emission properties of small-scale bright and faint loops in the quiet Sun⋆

Maria S. **Madjarska**1,2, Klaus Galsgaard3 and Thomas Wiegelmann1
A&A 678, A32 (**2023**)
https://www.aanda.org/articles/aa/pdf/2023/10/aa47058-23.pdf

Context. The study explores the photospheric magnetic properties of bright and faint small-scale loop systems in the solar atmosphere of the quiet Sun, also known as X-ray or coronal bright points.
Aims. To understand how plasma confined in small-scale loops is heated to million degrees, the loop-associated photospheric and coronal magnetic flux properties should be known because the magnetic field is generally assumed to be the main energy source or waveguide. This and follow-up studies aim to provide a qualitative and quantitative investigation of these magnetic properties and their impact on the heating of plasma to million degrees.
Methods. We used quasi-temporal imaging observations taken in the 193 Å channel of the Atmospheric Imaging Assembly (AIA) and line-of-sight magnetograms from the Helioseismic Magnetic Imager (HMI) on board the Solar Dynamics Observatory. The observations cover 48 h of data at a 6 min cadence with a field of view of 400″ × 400″, from which 90 loop systems (of which 83 are CBPs) were extracted and analysed in full detail.
Results. We obtain the evolution properties of both faint and bright small-scale loop systems (SSLSs) related to either magnetic flux emergence or magnetic flux coalescence and a chance encounter of magnetic fluxes. We estimate the lifetimes of the two loop systems and the impact of the magnetic flux evolution on their life span. The photospheric magnetic flux associated with SSLSs confining plasma heated to coronal temperatures is found to cover at least two orders of magnitude from 3.0 × 1018 Mx to 1.8 × 1020 Mx. The analysis of the maximum intensity of SSLSs during their lifetime shows numerous spikes of intensity that are identified as small (a few AIA pixels) compact brightenings associated with cancelling magnetic fluxes. Most of them are identified as microflares. The intensity flux range of these spikes is reported. The coronal intensity flux evolution of SSLSs is strongly correlated with the total unsigned photospheric magnetic flux evolution when there is little or no contamination in the selected field of view of the SSLSs by unrelated magnetic fluxes or intensity features. We report on the footpoint separation and change during the lifetime of the faint and bright SSLSs. The magnetic flux emergence and decay rates of some of the SSLSs are also provided in this study.
Conclusions. The power-law index α of the logarithm of the total unsigned magnetic flux and the total intensity for the full lifetime of SSLSs is 1.10 ± 0.02, compared with 1.14 ± 0.03 for a previous study of the whole disc in the

same intensity range (Fe XII 193–195 Å). This indicates that the emission of the corona of the quiet Sun at ~1.25 MK is mostly confined to small-scale loops (some brighter, others fainter). Therefore, it is imperative to understand the mechanism that heats the plasma in these loops.

Coronal Plasma Characterization via Coordinated Infrared and Extreme Ultraviolet Observations of a Total Solar Eclipse

Chad A. **Madsen**, Jenna E. Samra, Giulio Del Zanna, Edward E. DeLuca
ApJ **2019**
https://arxiv.org/pdf/1901.10425.pdf
We present coordinated coronal observations of the **August 21, 2017** total solar eclipse with the Airborne Infrared Spectrometer (AIR-Spec) and the Extreme-ultraviolet Imaging Spectrometer (EIS). These instruments provide an unprecedented view of the solar corona in two disparate wavelength regimes, the near to mid infrared (IR) and the extreme ultraviolet (EUV), opening new pathways for characterizing the complex coronal plasma environment. During totality, AIR-Spec sampled coronal IR spectra near the equatorial west limb, detecting strong sources of Fe IX, Mg VIII, S XI, Si IX, and Si X in two passbands encompassing 1.4 - 4 μm. We apply emission measure (EM) loci analysis to these IR emission lines to test their capacity as coronal temperature diagnostics. The density-sensitive Fe XII 186.9 Å/192.4 Å line pair supplies spatially resolved, line-of-sight electron densities, supporting the EM loci analysis. From this, we find EM loci intersections at temperatures of 106.13 K at 30 arcsec from the limb and 106.21 K at 100 arcsec. Applying the same EM loci analysis to 27 EIS emission lines associated with seven ion species (Fe X-XIV, S X, and Si X) confirms these results, displaying strong evidence of isothermal plasma throughout the region. However, the IR EM loci analysis suffers from moderate uncertainties. The likely sources include: poor signal, infrared contamination from a prominence, and photoexcitation by continuum radiation. Regardless, we demonstrate that EUV spectral data are valuable constraints to coronal infrared emission models, and will be powerful supplements for future IR solar observatories, particularly DKIST.

Aggregation Characteristics of the Sun's Large-Scale Magnetic Field Associated with a Global Magnetic Anomaly in the Last Extended Solar Cycle

Tetsuya **Magara**, Junmo An, Hwanhee Lee & Jihye Kang
Solar Physics volume 296, Article number: 41 (**2021**)
https://doi.org/10.1007/s11207-021-01782-9
The solar cycle represents the Sun's periodically changing magnetic state, which is potentially subject to global magnetic anomalies emerging on it. What the characteristics are of the Sun's large-scale magnetic field playing roles in these anomalies is a key to clarifying how the Sun deviates from its normal magnetic state. This article reports aggregation characteristics of the large-scale magnetic field associated with a global magnetic anomaly that emerged when the Sun went through one of the longest solar cycles in two hundred years. The characteristics were identified by extracting cluster feature values of solar surface magnetic fields via a population ecological method from synoptic maps, obtained by the longest homogeneous series of magnetic field observations for the past several decades. We found that the anomaly was due to the uneven clustering of positive and negative surface magnetic fields that occurred during the solar minimum leading to the last extended solar cycle. Our findings may provide new insight into magnetic field characteristics peculiar to a solar minimum with an extended cycle length.

Observational constraints on the origin of the elements. IV: The standard composition of the Sun

Ekaterina **Magg**, Maria Bergemann, Aldo Serenelli, Manuel Bautista, Bertrand Plez, Ulrike Heiter, Jeffrey M. Gerber, Hans-Günter Ludwig, Sarbani Basu, Jason W. Ferguson, Helena Carvajal Gallego, Sébastien Gamrath, Patrick Palmeri, Pascal Quinet
A&A **2022**
https://arxiv.org/pdf/2203.02255
The chemical composition of the Sun is requested in the context of various studies in astrophysics, among them in the calculation of the standard solar models (SSMs), which describe the evolution of the Sun from the pre-main-sequence to its present age. In this work, we provide a critical re-analysis of the solar chemical abundances and corresponding SSMs. For the photospheric values, we employ new high-quality solar observational data collected with the IAG facility, state-of-the art non-equilibrium modelling, new oscillator strengths, and different atmospheric models, including the MARCS model, but also averages based on Stagger and CO5BOLD 3D radiation-hydrodynamics simulations of stellar convection. We perform new calculations of oscillator strengths for transitions in O I and N I. For O I - the critical element for the interior models - calculations are carried out using several independent methods. We find unprecedented agreement between the new estimates of transition probabilities, thus supporting our revised solar oxygen abundance. We also provide new estimates of the noble gas Ne abundance. We investigate our results in comparison with the previous estimates. We discuss the consistency of our photospheric measurements with meteoritic values taking into account systematic and correlated errors. Finally, we provide

revised chemical abundances, leading to a new value of the solar photospheric present-day metallicity Z/X=0.0225, and employ them in the calculations of the SSM. We find that the puzzling mismatch between the helioseismic constraints on the solar interior structure and the model is resolved with the new chemical composition.

Surface-effect corrections for the solar model

Zazralt **Magic**, Achim Weiss
A&A **2016**
http://arxiv.org/pdf/1606.01030v1.pdf

Solar p-mode oscillations exhibit a systematic offset towards higher frequencies due to shortcomings in the 1D stellar structure models, especially, the lack of turbulent pressure in the superadiabatic layers just below the optical surface, arising from the convective velocity field. We study the influence of the turbulent expansion, chemical composition, and magnetic fields on the stratification in the upper layers of the solar models in comparison with solar observations. Furthermore, we test alternative <3D> averages for improved results on the oscillation frequencies. We appended temporally and spatially averaged <3D> stratifications to 1D models to compute adiabatic oscillation frequencies that we then tested against observations. We also developed depth-dependent corrections for the solar 1D model, for which we expanded the geometrical depth to match the pressure stratification of the solar <3D> model, and we reduced the density that is caused by the turbulent pressure. We obtain the same results with our <3D> models as have been reported previously. Our depth-dependent corrected 1D models match the observations to almost a similar extent as the <3D> model. We find that correcting for the expansion of the geometrical depth and the reducing of the density are both equally necessary. Interestingly, the influence of the adiabatic exponent Gam1 is less pronounced than anticipated. The turbulent elevation directly from the <3D> model does not match the observations properly. Considering different reference depth scales for the <3D> averaging leads to very similar frequencies. Solar models with high metal abundances in their initial chemical composition match the low-frequency part much better. We find a linear relation between the p-mode frequency shift and the vertical magnetic field strength with dvnl = 26.21Bz microHz/kG, which is able to render the solar activity cycles correctly.

Standing kink waves in sigmoid solar coronal loops: implications for coronal seismology

N. **Magyar**, V. M. Nakariakov
2020 *ApJL* **894** L23
https://arxiv.org/pdf/2004.14083.pdf
https://doi.org/10.3847/2041-8213/ab8e36

Using full three-dimensional magnetohydrodynamic numerical simulations, we study the effects of magnetic field sigmoidity or helicity on the properties of the fundamental kink oscillation of solar coronal loops. Our model consists of a single denser coronal loop, embedded in a plasma with dipolar force-free magnetic field with a constant alpha-parameter. For the loop with no sigmoidity, we find that the numerically determined oscillation period of the fundamental kink mode matches the theoretical period calculated using WKB theory. In contrast, with increasing sigmoidity of the loop, the actual period is increasingly smaller than the one estimated by WKB theory. Translated through coronal seismology, increasing sigmoidity results in magnetic field estimates which are increasingly shifting towards higher values, and even surpassing the average value for the highest alpha value considered. Nevertheless, the estimated range of the coronal magnetic field value lies within the mimimal/maximal limits, proving the robustness coronal seismology. We propose that the discrepancy in the estimations of the absolute value of the force-free magnetic field could be exploited seismologically to determine the free energy of coronal loops, if averages of the internal magnetic field and density can be reliably estimated by other methods.

Assessing the Capabilities of Dynamic Coronal Seismology of Alfvénic Waves through Forward Modeling

N. **Magyar**1 and T. Van Doorsselaere
2018 ApJ 856 144
http://sci-hub.tw/http://iopscience.iop.org/0004-637X/856/2/144/
https://arxiv.org/pdf/1804.02175.pdf

Coronal seismology is a diagnostic tool used in solar physics for measuring parameters that are otherwise hard to measure; of these parameters, magnetic field values are arguably the most important. The parameters are inferred by combining observations of waves with magnetohydrodynamic (MHD) wave theory. To date, coronal seismology has successfully been applied to various single-oscillation events. Such events are relatively rare, resulting in rare occasions to use diagnostics. Ubiquitous waves in the solar atmosphere might, however, allow for the possibility of dynamic coronal seismology, which involves the continuous inversions of coronal parameters and would constitute a huge leap forward in many areas of solar physics. In this paper, we investigate the robustness and accuracy of magnetic field diagnostics applied to forward-modeled 3D MHD simulations of propagating Alfvénic waves. We find that the seismologically measured magnetic field values are reassuringly close to the input value (within ≈20%) for a range of setups studied, providing encouragement and confidence for the further development of dynamic coronal seismology.

Damping of nonlinear standing kink oscillations: a numerical study

N. **Magyar** and T. Van Doorsselaere

A&A 595, A81 (**2016**)

Aims. We aim to study the standing fundamental kink mode of coronal loops in the nonlinear regime, investigating the changes in energy evolution in the cross-section and oscillation amplitude of the loop which are related to nonlinear effects, in particular to the development of the Kelvin-Helmholtz instability (KHI).
Methods. We run ideal, high-resolution three-dimensional (3D) magnetohydrodynamic (MHD) simulations, studying the influence of the initial velocity amplitude and the inhomogeneous layer thickness. We model the coronal loop as a straight, homogeneous magnetic flux tube with an outer inhomogeneous layer, embedded in a straight, homogeneous magnetic field.
Results. We find that, for low amplitudes which do not allow for the KHI to develop during the simulated time, the damping time agrees with the theory of resonant absorption. However, for higher amplitudes, the presence of KHI around the oscillating loop can alter the loop's evolution, resulting in a significantly faster damping than predicted by the linear theory in some cases. This questions the accuracy of seismological methods applied to observed damping profiles, based on linear theory.

The Sun's Large-Scale Flows I: Measurements of Differential Rotation & Torsional Oscillation.

Mahajan, S.S., Upton, L.A., Antia, H.M. et al.

Sol Phys 299, 38 (**2024**).

https://doi.org/10.1007/s11207-024-02282-2
https://link.springer.com/content/pdf/10.1007/s11207-024-02282-2.pdf

We have developed a comprehensive catalog of the variable differential rotation measured near the solar photosphere. This catalog includes measurements of these flows obtained using several techniques: direct Doppler, granule tracking, magnetic pattern tracking, global helioseismology, as well as both time-distance and ring-diagram methods of local helioseismology. We highlight historical differential rotation measurements to provide context, and thereafter provide a detailed comparison of the MDI-HMI-GONG-Mt. Wilson overlap period (April 2010 – Jan 2011) and investigate the differences between velocities obtained from different techniques and attempt to explain discrepancies. A comparison of the rotation rate obtained by magnetic pattern tracking with the rotation rates obtained using local and global helioseismic techniques shows that magnetic pattern tracking measurements correspond to helioseismic flows located at a depth of 25 to 28 Mm. In addition, we show the torsional oscillation from Sunspot Cycles 23 and 24 and discuss properties that are consistent across measurement techniques. We find that acceleration derived from torsional oscillation is a better indicator of long-term trends in torsional oscillation compared to the residual velocity magnitude. Finally, this analysis will pave the way toward understanding systematic effects associated with various flow measurement techniques and enable more accurate determination of the global patterns of flows and their regular and irregular variations.

Removal of Active Region Inflows Reveals a Weak Solar Cycle Scale Trend in the Near-surface Meridional Flow

Sushant S. **Mahajan**1,2, Xudong Sun (孙旭东)1, and Junwei Zhao

2023 ApJ 950 63

https://iopscience.iop.org/article/10.3847/1538-4357/acc839/pdf

Using time–distance local helioseismology flow maps within 1 Mm of the solar photosphere, we detect inflows toward activity belts that contribute to solar-cycle scale variations in the near-surface meridional flow. These inflows stretch out as far as 30° away from the active region centroids. If active region neighborhoods are excluded, the solar-cycle-scale variation in the background meridional flow diminishes to below 2 m s−1, but still shows systematic variations in the absence of active regions between sunspot cycles 24 and 25. We therefore propose that the near-surface meridional flow is a three-component flow made up of a constant baseline flow profile that can be derived from quiet-Sun regions, variations due to inflows around active regions, and solar-cycle-scale variation of about 2 m s−1. Torsional oscillation, on the other hand, is found to be a global phenomenon, i.e., exclusion of active region neighborhoods does not significantly affect its magnitude or phase. This nonvariation in torsional oscillation with distance away from active regions and the three-component breakdown of the near-surface meridional flow serve as vital constraints for solar dynamo models and surface flux-transport simulations.

Improved Measurements of the Sun's Meridional Flow and Torsional Oscillation from Correlation tracking on MDI \& HMI magnetograms

Sushant S. **Mahajan**, David H. Hathaway, Andrés Muñoz-Jaramillo, Petrus C. Martens

ApJ **917** 100 **2021**

https://arxiv.org/pdf/2107.07731.pdf

https://doi.org/10.3847/1538-4357/ac0a80
The Sun's axisymmetric flows, differential rotation and meridional flow, govern the dynamics of the solar magnetic cycle and variety of methods are used to measure these flows, each with its own strengths and weaknesses. Flow measurements based on cross-correlating images of the surface magnetic field have been made since the 1970s which require advanced numerical techniques that are capable of detecting movements of less than the pixel size in images of the Sun. We have identified several systematic errors in addition to the center-to-limb effect that influence previous measurements of these flows and propose numerical techniques that can minimize these errors by utilizing measurements of displacements at several time-lags. Our analysis of line-of-sight magnetograms from the {\em Michelson Doppler Imager} (MDI) on the ESA/NASA {\em Solar and Heliospheric Observatory} (SOHO) and {\em Helioseismic and Magnetic Imager} (HMI) on the NASA {\em Solar Dynamics Observatory} (SDO) shows long-term variations in the meridional flow and differential rotation over two sunspot cycles from 1996 to 2020. These improved measurements can serve as vital inputs for solar dynamo and surface flux transport simulations.
HMI Science Nuggets, **#165**, **2021** http://hmi.stanford.edu/hminuggets/?p=3685

Torsional Oscillations in the Suns rotation contribute to the Waldmeier-effect in Solar Cycles

Sushant S. **Mahajan**, Dibyendu Nandy, H.M. Antia, B.N. Dwivedi
ApJ **2018**
https://arxiv.org/pdf/1803.07758.pdf
Temporal variations in the Suns internal velocity field with a periodicity of about 11 years have been observed over the last four decades. The period of these torsional oscillations and their latitudinal propagation roughly coincides with the period and equatorward propagation of sunspots which originate from a magnetohydrodynamic dynamo mechanism operating in the Suns interior. While the solar differential rotation plays an important role in this dynamo mechanism by inducting the toroidal component of magnetic field, the impact of torsional oscillations on the dynamo mechanism and hence the solar cycle is not well understood. Here, we include the observed torsional oscillations into a flux transport dynamo model of the solar cycle to investigate their effect. We find that the overall amplitude of the solar cycle does not change significantly on inclusion of torsional oscillations. However, all the characteristics of the Waldmeier effect in the sunspot cycle are qualitatively reproduced by varying only the amplitude of torsional oscillations. The Waldmeier effect, first noted in 1935, includes the important characteristic that the amplitude of sunspot cycles is anti-correlated to their rise time; cycles with high initial rise rate tend to be stronger. This has implications for solar cycle predictions. Our results suggest that the Waldmeier effect could be a plausible outcome of cycle to cycle modulation of torsional oscillations and provides a physical basis for sunspot cycle forecasts based on torsional oscillation observations. We also provide a theoretical explanation based on the magnetic induction equation thereby connecting two apparently disparate phenomena.

Neutrinos from the Sun can discover dark matter-electron scattering

Tarak Nath **Maity**, Akash Kumar Saha, Sagnik Mondal, Ranjan Laha
2023
https://arxiv.org/pdf/2308.12336.pdf
We probe dark matter-electron scattering using high-energy neutrino observations from the Sun. Dark matter (DM) interacting with electrons can get captured inside the Sun. These captured DM may annihilate to produce different Standard Model (SM) particles. Neutrinos produced from these SM states can be observed in IceCube and DeepCore. Although there is no excess of neutrinos from the Solar direction, we find that the current data-sets of IceCube and DeepCore set the strongest constraint on DM-electron scattering cross section in the DM mass range 10GeV to 105GeV. Our work implies that future observations of the Sun by neutrino telescopes have the potential to discover DM-electron interaction.

The Coronal Veil

A. **Malanushenko**, M.C.M. Cheung, C.E. DeForest, J.A. Klimchuk, M. Rempel
ApJ **2021**
https://arxiv.org/pdf/2106.14877.pdf
Coronal loops, seen in solar coronal images, are believed to represent emission from magnetic flux tubes with compact cross-sections. We examine the 3D structure of plasma above an active region in a radiative magnetohydrodynamic simulation to locate volume counterparts for coronal loops. In many cases, a loop cannot be linked to an individual thin strand in the volume. While many thin loops are present in the synthetic images, the bright structures in the volume are fewer, and of complex shape. We demonstrate that this complexity can form impressions of thin bright loops, even in the absence of thin bright plasma strands. We demonstrate the difficulty of discerning from observations whether a particular loop corresponds to a strand in the volume, or a projection artifact. We demonstrate how apparently isolated loops could deceive observers, even when observations from multiple viewing angles are available.
While we base our analysis on a simulation, the main findings are independent from a particular simulation setup

and illustrate the intrinsic complexity involved in interpreting observations resulting from line-of-sight integration in an optically thin plasma.
We propose alternative interpretation for strands seen in EUV images of the corona. The "coronal veil" hypothesis is mathematically more generic, and naturally explains properties of loops that are difficult to address otherwise -- such as their constant cross section and anomalously high density scale height. We challenge the paradigm of coronal loops as thin magnetic flux tubes, offering new understanding of solar corona and, by extension, of other magnetically confined bright, hot plasmas.

Electron Heating by Kinetic Alfvén Waves in Coronal Loop Turbulence

Francesco **Malara**1, Giuseppina Nigro1, Francesco Valentini1, and Luca Sorriso-Valvo
2019 ApJ 871 66
sci-hub.tw/10.3847/1538-4357/aaf168
A test-particle model describing the energization of electrons in a turbulent plasma is presented. Parameters are chosen to represent turbulence in a magnetic structure of the solar corona. A fluctuating electric field component parallel to the background magnetic field, with properties similar to those of Kinetic Alfvén Waves, is assumed to be present at scales of the order of the proton Larmor radius. Electrons are stochastically accelerated by multiple interactions with such fluctuations, reaching energies of the order of 102 eV within tens to hundreds of seconds, depending on the turbulence amplitude. For values of the large-scale plasma velocity fluctuation of the order of tens of kilometers per second, the power absorbed by electrons per surface unit is of the order of that typically necessary to heat the corona. The power that electrons absorb from fluctuations is proportional to the third power of the large-scale velocity amplitude, and is comparable with the power associated with the turbulent cascade. Therefore, this mechanism can be considered as an equivalent kinetic dissipation for turbulence, and it can play a relevant role in the heating of electrons in the corona.

Temporal evolution and correlations of optical activity indicators measured in Sun-as-a-star observations

J. **Maldonado**, D. F. Phillips, X. Dumusque, A. Collier Cameron, R. D. Haywood, ...
A&A 627, A118 **2019**
https://arxiv.org/pdf/1906.03002.pdf
We perform a detailed study of the main optical activity indicators (Ca II H & K, Balmer lines, Na I D1 D2, and He I D3) measured for the Sun using the data provided by the HARPS-N solar-telescope feed at the Telescopio Nazionale Galileo. The value of the solar rotation period is found in all the activity indicators, with the only exception being Hδ. The derived values vary from 26.29 days (Hγ line) to 31.23 days (He I). From an analysis of sliding periodograms we find that in most of the activity indicators the spectral power is split into several "bands" of periods around 26 and 30 days, that might be explained by the migration of active regions between the equator and a latitude of ∼ 30∘, spot evolution or a combination of both effects. In agreement with previous works a typical lifetime of active regions of ∼ ten rotation periods is inferred from the pooled variance diagrams. We find that Hα, Hβ, Hγ, Hϵ, and He I show a significant correlation with the S index. Significant correlations between the contrast, bisector span, and the heliocentric radial velocity with the activity indexes are also found. We show that the full width at half maximum, the bisector, and the disc-integrated magnetic field correlate with the radial velocity variations. The correlation of the S index and Hα changes with time, increasing with larger sun spot numbers and solar irradiance. A similar tendency with the S index - radial velocity correlation is also present in the data. Our results are consistent with a scenario in which higher activity favours the correlation between the S index and the Hα activity indicators and between the S index and radial velocity variations.

In pursuit of the Sun, from Jules Janssen to the present day Historical Review

Jean-Marie **Malherbe**
2024
https://arxiv.org/pdf/2401.15998.pdf
The Sun has been observed through a telescope for four centuries. However, its study made a prodigious leap at the end of the nineteenth century with the appearance of photography and spectroscopy, then at the beginning of the following century with the invention of the coronagraph and monochromatic filters, and finally in the second half of the twentieth century with the advent of space exploration (satellites, probes). This makes it possible to observe the radiations hidden by the Earth's atmosphere (Ultra Violet, X-rays, γ) and to carry out "in situ" measurements in the solar environment. This article retraces the major stages of this fantastic epic in which renowned scientists such as Janssen, Deslandres, d'Azambuja, Lyot and Dollfus entered the scene, giving the Paris-Meudon Observatory a pioneering role in the history of solar physics until 1960. After this golden age, space exploration required large resources shared between nations, which could no longer be implemented within teams or even individual institutes. The development of numerical simulation, a new research tool, also required the pooling of supercomputers.

Optical characteristics and capabilities of the successive versions of Meudon spectroheliograph (1908-2023)

Jean-Marie **Malherbe**

2023

https://arxiv.org/ftp/arxiv/papers/2303/2303.10952.pdf

The spectroheliograph is a spectroscopic instrument designed to produce monochromatic images of the photosphere (the visible layer) and the chromosphere of the Sun. It was invented at the same time (1892), but independently, by Hale in the USA and Deslandres in France and was dedicated to long-term surveys of the solar cycles. For that purpose, systematic observations of the CaII K and Hα lines started in Meudon observatory in 1908 and continue today, so that a huge collection of more than 100000 spectroheliograms, spanning 115 years of solar activity, was recorded. We present in this paper the optical characteristics and the capabilities of the successive versions of the instrument, from 1908 to now.

130 years of spectroheliograms at Paris-Meudon observatories (1892-2022)

Jean-Marie **Malherbe**

2023

https://arxiv.org/ftp/arxiv/papers/2301/2301.11105.pdf

Broad-band observations of the solar photosphere began in Meudon in 1875 under the auspices of Jules Janssen. For his part, Henri Deslandres initiated imaging spectroscopy in 1892 at Paris observatory. He invented, concurrently with George Hale in Kenwood (USA) but quite independently, the spectroheliograph designed for monochromatic imagery of the solar atmosphere. Deslandres developed two kinds of spectrographs: the "spectroh{é}liographe des formes", i.e. the narrow bandpass instrument to reveal chromospheric structures (such as filaments, prominences, plages and active regions); and the "spectroh{é}liographe des vitesses", i.e. the section spectroheliograph to record line profiles of cross sections of the Sun with a 20"-30" spatial step. This second apparatus was intended to measure the velocities (more exactly the Dopplershifts) of dynamic features. Deslandres moved to Meudon in 1898 with his instruments and tested various combinations, in order to improve the spectral and spatial resolutions, leading to the final large quadruple spectroheliograph in 1908. CaII K systematic observations started at this date and were followed in 1909 by Hα. The service was organized by Lucien d'Azambuja and continues today. Optical and mechanical parts were revisited in 1989 and the digital technology was introduced in 2002. Full line profiles are registered for all pixels of the Sun since 2018, so that the instrument produces now data-cubes. The collection is one of the longest available (more than 100 000 observations). It contains sporadic images from 1893 to 1907 (during the development phase) and systematic observations along 10 solar cycles since 1908, in Hα and CaII K lines. This paper summarizes 130 years of observations, instrumental research and technical advances.

Monitoring fast solar chromospheric activity: the MeteoSpace project

Jean-Marie **Malherbe**, Thierry Corbard, Gaële Barbary, Frédéric Morand, Claude Collin, Daniel Crussaire, Florence Guitton

Experimental Astronomy, **2022**, pp.1-22

https://arxiv.org/pdf/2301.13480.pdf

We present in this reference paper an instrumental project dedicated to the monitoring of solar activity during solar cycle 25. It concerns the survey of fast evolving chromospheric events implied in Space Weather, such as flares, coronal mass ejections, filament instabilities and Moreton waves. Coronal waves are produced by large flares around the solar maximum and propagate with chromospheric counterparts; they are rare, faint, difficult to observe, and for that reason, challenging. They require systematic observations with automatic, fast and multi-channel optical instruments. MeteoSpace is a high cadence telescope assembly specially designed for that purpose. The large amount of data will be freely available to the solar community. We describe in details the optical design, the qualification tests and capabilities of the telescopes, and show how waves can be detected. MeteoSpace will be installed at Calern observatory (C{ô}te d'Azur, 1270 m) and will be in full operation in 2023.

The Solar Line Emission Dopplerometer project

J.-M. **Malherbe**, P. Mein, F. Sayede, P. Rudawy, K. Phillips, F. Keenan, J. Rybak

2021

https://arxiv.org/pdf/2110.01645.pdf

Observations of the dynamics of solar coronal structures are necessary to investigate space weather phenomena and global heating of the corona. The profiles of high temperature lines emitted by the hot plasma are usually integrated by narrow band filters or recorded by classical spectroscopy. We present in this paper details of a new transportable instrument (under construction) for imaging spectroscopy: the Solar Line Emission Dopplerometer (SLED). It uses the Multi-channel Subtractive Double Pass (MSDP) technique, which combines the advantages of both filters and narrow slit spectrographs, i.e. high temporal, spatial and spectral resolutions. The SLED will measure at high cadence (1 Hz) the line-of-sight velocities (Doppler shifts) of hot coronal loops, in the forbidden lines of FeX 637. nm and FeXIV 530.3 nm. It will follow the dynamics of fast evolving events of solar activity such as flares or

Coronal Mass Ejections (CMEs), and also study coronal heating by short period waves. Observations will be performed with the coronagraph at the Lomnicky Stit Observatory (LSO, in Slovakia) or during total eclipses. The SLED will also observe the dynamics of solar prominences in Halpha 656.3 nm or HeD3 587.6 nm lines when mounted on the Bialkow coronagraph (near Wroclaw, Poland). It is fully compatible with polarimetric measurements by various techniques.

Optical instrumentation for chromospheric monitoring during solar cycle 25 at Paris and Côte d'Azur observatories

Jean-Marie **Malherbe**1*, Thierry Corbard2 and Kevin Dalmasse3
J. Space Weather Space Clim. **2020**, 10, 31
https://www.swsc-journal.org/articles/swsc/pdf/2020/01/swsc200027.pdf
We present the observing program proposed by Paris and Côte d'Azur Observatories for monitoring solar activity during the upcoming cycle 25 and providing near real time images and movies of the chromosphere for space-weather research and applications. Two optical instruments are fully dedicated to this task and we summarize their capabilities. Short-term and fast-cadence observations of the chromosphere will be performed automatically at Calern observatory (Côte d'Azur), where dynamic events, as flare development, Moreton waves, filament instabilities and Coronal Mass Ejections onset, will be tracked. This new set of telescopes will operate in 2021 with narrow bandpass filters selecting Hα and CaII K lines. We present the instrumental design and a simulation of future images. At Meudon, the Spectroheliograph is well adapted to the long-term and low-cadence survey of chromospheric activity by recently improved and optimized spectroscopic means. Surface scans deliver daily (x, y, λ) datacubes of Hα, CaII K and CaII H line profiles. We describe the nature of available data and emphasize the new calibration method of spectra.

The New 2018 Version of the Meudon Spectroheliograph

J.-M. **Malherbe**, K. Dalmasse
Solar Phys. **2020**
https://arxiv.org/pdf/2001.02638.pdf
Daily full-disk observations of the solar photosphere and chromosphere started at Meudon Observatory in 1908. After a review of the scientific context and the historical background, we describe the instrumental characteristics and capabilities of the new version operating since 2018. The major change is the systematic recording of full line profiles over the entire solar disk providing 3D data cubes. Spectral and spatial sampling are both improved. Classical 2D images of the Sun at fixed wavelength are still delivered. We summarize the different processing levels of on-line data and briefly review the new scientific perspectives. **November 13, 2013, 20 June 2018**

Meteospace, a New Instrument for Solar Survey at the Calern Observatory

J.-M. **Malherbe**, Th. Corbard, K. Dalmasse, The Meteospace team
Solar Physics November **2019**, 294:177
https://link.springer.com/content/pdf/10.1007%2Fs11207-019-1569-5.pdf
https://arxiv.org/pdf/2001.02162.pdf
High-cadence observations of solar activity (active regions, flares, filaments) in the Hα line were performed at Meudon and Haute Provence Observatories from 1956 to 2004. More than 7 million images were recorded, mainly on 35 mm films. After a review of the scientific interest of solar surveys at high temporal resolution and the historical background, we describe the new instrument which will operate automatically in 2020 at the Calern station of the Côte d'Azur observatory (1270 m). It will replace the former heliographs with improved cadence, seeing and time coverage. We summarize the capabilities of the optical design and present new scientific perspectives in terms of flare onset and Moreton wave detection.

The New 2018 Version of the Meudon Spectroheliograph

J.-M. **Malherbe**, K. Dalmasse
Solar Physics May **2019**, 294:52
Daily full-disk observations of the solar photosphere and chromosphere started at the Meudon Observatory in 1908. After a review of the scientific context and the historical background, we describe the instrumental characteristics and capabilities of the new version operating since 2018. The major change is the systematic recording of full line profiles over the entire solar disk providing 3D data cubes. Spectral and spatial sampling are both improved. Classical 2D images of the Sun at fixed wavelength are still delivered. We summarize the different processing levels of on-line data and briefly review the new scientific perspectives.

Dynamics of Trees of Fragmenting Granules in the Quiet Sun: Hinode/SOT Observations Compared to Numerical Simulation

J.-M. **Malherbe**, T. Roudier, R. Stein, Z. Frank

Solar Physics January **2018**, 293:4
https://link.springer.com/content/pdf/10.1007%2Fs11207-017-1225-x.pdf
https://arxiv.org/pdf/1804.01870.pdf
We compare horizontal velocities, vertical magnetic fields, and the evolution of trees of fragmenting granules (TFG, also named families of granules) derived in the quiet Sun at disk center from observations at solar minimum and maximum of the Solar Optical Telescope (SOT on board Hinode) and results of a recent 3D numerical simulation of the magneto-convection. We used 24-hour sequences of a 2D field of view (FOV) with high spatial and temporal resolution recorded by the SOT Broad band Filter Imager (BFI) and Narrow band Filter Imager (NFI). TFG were evidenced by segmentation and labeling of continuum intensities. Horizontal velocities were obtained from local correlation tracking (LCT) of proper motions of granules. Stokes V provided a proxy of the line-of-sight magnetic field (BLOS). The MHD simulation (performed independently) produced granulation intensities, velocity, and magnetic field vectors. We discovered that TFG also form in the simulation and show that it is able to reproduce the main properties of solar TFG: lifetime and size, associated horizontal motions, corks, and diffusive index are close to observations. The largest (but not numerous) families are related in both cases to the strongest flows and could play a major role in supergranule and magnetic network formation. We found that observations do not reveal any significant variation in TFG between solar minimum and maximum.

Families of Granules, Flows, and Acoustic Events in the Solar Atmosphere from Hinode Observations

J.-M. **Malherbe**, T. Roudier, Z. Frank, M. Rieutord
Solar Phys. February **2015**, Volume 290, Issue 2, pp 321-333
We investigate the relationship between trees of fragmenting granules (TFG), horizontal and vertical flows, and acoustic events (AE) in the photospheric network. AE are spatially concentrated and short-duration locations of acoustic energy flux. We performed observations at disk center of a 2D field of view (FOV) with high spatial and temporal resolutions provided by the Solar Optical Telescope onboard Hinode. Line profiles of Fe i 557.6 nm were recorded by the Narrow-band Filter Imager on an 80″×36″ FOV during five hours with a cadence of 22 seconds and 0.08″ pixel size. Vertical velocities were derived at two atmospheric levels allowing the determination of the energy flux at the acoustic frequency of 3.3 mHz. Families of granules and horizontal velocities were obtained from local correlation tracking (LCT) after segmentation and labeling of either continuum intensities or granular Doppler shifts. AE exhibit durations in the range 0.25 to 1 hour compatible with the lifetime of families (80 % do not last more than two hours). High-energy AE have the shortest lifetimes. We found that most AE occur in intergranular lanes located in or close to the boundaries between different families (called inter families) in regions with predominantly downward vertical motions and horizontal converging flows. In contrast, diverging flows are observed inside families, with a few AE in the intergranules. At the beginning of the sequence, when families are not yet detected, the distribution of AE is not uniform and is already organized at spatial lengths related to the mesogranular scale, with maximum contribution in the range 5″ to 10″, fully compatible with the scale of the maximum contribution of families in the TFG space. Although all sizes and durations seem to exist for families, their number decreases with increasing size and lifetime.

Solar neutrinos and neutrino physics **Review**

Michele **Maltoni**, Alexei Yu. Smirnov
European Journal of Physics (EJP) issue on "The Solar Neutrinos" **2015**
http://arxiv.org/pdf/1507.05287v1.pdf
Solar neutrino studies triggered and largely motivated the major developments in neutrino physics in the last 50 years. Theory of neutrino propagation in different media with matter and fields has been elaborated. It includes oscillations in vacuum and matter, resonance flavor conversion and resonance oscillations, spin and spin-flavor precession, etc. LMA MSW has been established as the true solution of the solar neutrino problem. Parameters theta12 and Delta_m21^2 have been measured; theta13 extracted from the solar data is in agreement with results from reactor experiments. Solar neutrino studies provide a sensitive way to test theory of neutrino oscillations and conversion. Characterized by long baseline, huge fluxes and low energies they are a powerful set-up to search for new physics beyond the standard 3nu paradigm: new neutrino states, sterile neutrinos, non-standard neutrino interactions, effects of violation of fundamental symmetries, new dynamics of neutrino propagation, probes of space and time. These searches allow us to get stringent, and in some cases unique bounds on new physics. We summarize the results on physics of propagation, neutrino properties and physics beyond the standard model obtained from studies of solar neutrinos.

Differential rotation of the solar corona: A new data-adaptive multiwavelength approach

S. **Mancuso**, S. Giordano, D. Barghini, D. Telloni
A&A 644, A18 **2020**

https://arxiv.org/pdf/2010.06353.pdf
https://www.aanda.org/articles/aa/pdf/2020/12/aa39094-20.pdf
For the purpose of investigating the differential rotation of the solar corona, we analyzed ultraviolet (UV) spectral line observations acquired on both the east and west limbs at 1.7 R⊙ by SOHO/UVCS during the solar minimum preceding solar cycle 23. To obtain a reliable and statistically robust picture of the rotational profile, we used a set of simultaneous 400-day long spectral line intensities of five different spectral lines: O VI 1032 A, O VI 1037 A, Si XII 499 A, Si XII 521 A, and H I 1216 A, which are routinely observed by UVCS. The data were analyzed by means of two different techniques: the generalized Lomb-Scargle periodogram (GLS) and a multivariate data-adaptive technique called multichannel singular spectrum analysis (MSSA). Among many other positive outcomes, this latter method is unique in its ability to recognize common oscillatory modes between the five time series observed at both limbs. The latitudinal rotation profile obtained in this work emphasizes that the low-latitude region of the UV corona (about ±20∘ from the solar equator) exhibits differential rotation, while the higher-latitude structures do rotate quasi-rigidly. The differential rotation rate of the solar corona as evinced at low-latitudes is consistent with the rotational profile of the near-surface convective zone of the Sun, suggesting that the rotation of the corona at 1.7 R⊙ is linked to intermediate-scale magnetic bipole structures anchored near 0.99 R⊙. The quasi-rigid rotation rate found at mid and high latitudes is instead attributed to the influence of large-scale coronal structures linked to the rigidly rotating coronal holes. We further suggest that the methodology presented in this paper could represent a milestone for future investigations on differential rotation rates when dealing with simultaneous multiwavelength data.

Spatio-Temporal Evolution and North–South Asymmetry of Quasi-Biennial Oscillations in the Coronal Fe xiv Emission

S. **Mancuso**, T. S. Lee, C. Taricco, S. Rubinetti
Solar Physics August **2018**, 293:124
https://arxiv.org/pdf/1808.10255.pdf
https://link.springer.com/content/pdf/10.1007%2Fs11207-018-1346-x.pdf
In this work, we apply multichannel singular spectrum analysis (MSSA), a data-adaptive, multivariate, non-parametric technique that simultaneously exploits the spatial and temporal correlations of the input data to extract common modes of variability, to investigate the intermediate quasi-periodicities of the Fe xiv green coronal emission line at 530.3 nm for the period between 1944 and 2008. Our analysis reveals several significant mid-term periodicities in a range from about one to four years that are consistent with the so-called quasi-biennial oscillations (QBOs), which have been detected by several authors using different data sets and analysis methods. These QBOs display amplitudes varying significantly with time and latitude over the six solar cycles (18 to 23) covered by this study. A clear North–South asymmetry is detected both in their intensity and period distribution, with a net predominance of spectral power in the active-region belt of the northern hemisphere. On the other hand, while the QBOs with periods ≳1.7≳1.7 years are particularly intense around the polar regions and therefore related to the global magnetic field, the ones with shorter periods are mainly generated at mid-latitudes, in correspondence with the emergence of active regions. Our findings indicate that the North–South asymmetry manifested in the uneven latitudinal distribution of QBOs is a fundamental, albeit puzzling, characteristic of solar activity.

Long-term evolution of the heliospheric magnetic field inferred from cosmogenic 44Ti activity in meteorites

S. **Mancuso**, C. Taricco, P. Colombetti, S. Rubinetti, N. Sinha, N. Bhandari
A&A 610, A28 **2018**
https://arxiv.org/pdf/1801.01311.pdf
Typical reconstructions of historic heliospheric magnetic field (HMF) BHMF are based on the analysis of the sunspot activity, geomagnetic data or on measurement of cosmogenic isotopes stored in terrestrial reservoirs like trees (14C) and ice cores (10Be). The various reconstructions of BHMF are however discordant both in strength and trend. Cosmogenic isotopes, which are produced by galactic cosmic rays (GCRs) impacting on meteoroids and whose production rate is modulated by the varying HMF convected outward by the solar wind, may offer an alternative tool for the investigation of the HMF in the past centuries. In this work, we aim to evaluate the long-term evolution of BHMF over a period covering the past twenty-two solar cycles by using measurements of the cosmogenic 44Ti activity (τ1/2=59.2±0.6 yr) measured in 20 meteorites which fell between 1766 and 2001. Within the given uncertainties, our result is compatible with a HMF increase from 4.87+0.24−0.30 nT in 1766 to 6.83+0.13−0.11 nT in 2001, thus implying an overall average increment of 1.96+0.43−0.35 nT over 235 years since 1766 reflecting the modern Grand maximum. The BHMF trend thus obtained is then compared with the most recent reconstructions of the near-Earth heliospheric magnetic field strength based on geomagnetic, sunspot number and cosmogenic isotope data.

Doppler-shift oscillations in the H i Lyα coronal emission line: spectroscopic signature of propagating kink waves?

S. **Mancuso**1 and J. C. Raymond
A&A 573, A33 (**2015**)
We report the first detection of long-period, slowly decaying Doppler-shift oscillations in the H I Lyα (1215.67 Å) coronal emission line with the Ultraviolet Coronagraph Spectrometer (UVCS) onboard the Solar and Heliospheric Observatory (SOHO) satellite. The UV spectral data were collected at 1.43 $R_{\odot}$ above the eastern limb of the Sun during a special high-cadence sit-and-stare observation on 1997 December 14. Time-series analyses with different spectral techniques clearly show highly significant Doppler-shift oscillations in a portion with a size of 154″ of the UVCS slit that lasted for several cycles. A period of $P = 14.3 \pm 0.4$ min was established with a confidence of better than 99.9% in the Lomb-Scargle periodogram. On average, the Doppler-shift amplitude of 3.7 ± 0.7 km s^{-1} was estimated for the most significant oscillations, roughly corresponding to a displacement of 800 ± 150 km. The origin of the regular H I Lyα Doppler-shift oscillations is most probably due to the excitation of propagating fast magnetoacoustic kink waves along a narrow, jet-like ejection observed higher up in the white-light corona. However, different mechanisms, such as low-amplitude coherent kink oscillations of a bundle of loops along the line of sight or quasi-periodic outflows caused by oscillatory magnetic reconnection in the low corona cannot be ruled out.

Helioseismic Properties of Dynamo Waves in the Variation of Solar Differential Rotation

Krishnendu **Mandal**, Alexander G. Kosovichev, Valery V. Pipin
ApJ **973** 36 **2024**
https://arxiv.org/pdf/2402.15647.pdf
https://iopscience.iop.org/article/10.3847/1538-4357/ad5f2c/pdf
Solar differential rotation exhibits a prominent feature: its cyclic variations over the solar cycle, referred to as zonal flows or torsional oscillations, are observed throughout the convection zone. Given the challenge of measuring magnetic fields in subsurface layers, understanding deep torsional oscillations becomes pivotal in deciphering the underlying solar dynamo mechanism. In this study, we address the critical question of identifying specific signatures within helioseismic frequency-splitting data associated with the torsional oscillations. To achieve this, a comprehensive forward modeling approach is employed to simulate the helioseismic data for a dynamo model that, to some extent, reproduces solar-cycle variations of magnetic fields and flows. We provide a comprehensive derivation of the forward modeling process utilizing generalized spherical harmonics, as it involves intricate algebraic computations. All estimated frequency-splitting coefficients from the model display an 11-year periodicity. Using the simulated splitting coefficients and realistic noise, we show that it is possible to identify the dynamo wave signal present in the solar zonal flow from the tachocline to the solar surface. By analyzing observed data, we find similar dynamo wave patterns in the observational data from MDI, HMI, and GONG. This validates the earlier detection of dynamo waves and holds potential implications for the solar dynamo theory models.

Evolution of dynamic fibrils from the cooler chromosphere to the hotter corona

Sudip **Mandal**, Hardi Peter, Lakshmi Pradeep Chitta, Sami K. Solanki, +++
A&A **2023**
Dynamic fibrils (DFs) are commonly observed chromospheric features in solar active regions. Recent observations from the Extreme Ultraviolet Imager (EUI) aboard the Solar Orbiter have revealed unambiguous signatures of DFs at the coronal base, in extreme ultraviolet (EUV) emission. However, it remains unclear if the DFs detected in the EUV are linked to their chromospheric counterparts. Simultaneous detection of DFs from chromospheric to coronal temperatures could provide important information on their thermal structuring and evolution through the solar atmosphere. In this paper, we address this question by using coordinated EUV observations from the Atmospheric Imaging Assembly (AIA), Interface Region Imaging Spectrograph (IRIS), and EUI to establish a one-to-one correspondence between chromospheric and transition region DFs (observed by IRIS) with their coronal counterparts (observed by EUI and AIA). Our analysis confirms a close correspondence between DFs observed at different atmospheric layers, and reveals that DFs can reach temperatures of about 1.5 million Kelvin, typical of the coronal base in active regions. Furthermore, intensity evolution of these DFs, as measured by tracking them over time, reveals a shock-driven scenario in which plasma piles up near the tips of these DFs and, subsequently, these tips appear as bright blobs in coronal images. These findings provide information on the thermal structuring of DFs and their evolution and impact through the solar atmosphere.

Signatures of dynamic fibrils at the coronal base: Observations from Solar Orbiter/EUI

Sudip **Mandal**, Hardi Peter, Lakshmi Pradeep Chitta, Regina A. Cuadrado, Udo Schühle, Luca Teriaca, Sami K. Solanki, Louise Harra, David Berghmans, Frédéric Auchère, Susanna Parenti, Andrei N. Zhukov, Éric Buchlin, Cis Verbeeck, Emil Kraaikamp, Luciano Rodriguez, David M. Long, Conrad Schwanitz, Krzysztof Barczynski, Gabriel Pelouze, Philip J. Smith, Wei Liu, Mark C. Cheung
A&A Letters **2022**
https://arxiv.org/pdf/2212.05025.pdf

The solar chromosphere hosts a wide variety of transients, including dynamic fibrils (DFs) that are characterised as elongated, jet-like features seen in active regions, often through Hα diagnostics. So far, these features have been difficult to identify in coronal images primarily due to their small size and the lower spatial resolution of the current EUV imagers. Here we present the first unambiguous signatures of DFs in coronal EUV data using high-resolution images from the Extreme Ultraviolet Imager (EUI) on board Solar Orbiter. Using the data acquired with the 174~Å High Resolution Imager (HRIEUV) of EUI, we find many bright dot-like features (of size 0.3-0.5 Mm) that move up and down (often repeatedly) in the core of an active region. In a space-time map, these features produce parabolic tracks akin to the chromospheric observations of DFs. Properties such as their speeds (14 km~s−1), lifetime (332~s), deceleration (82 m~s−2) and lengths (1293~km) are also reminiscent of the chromospheric DFs. The EUI data strongly suggest that these EUV bright dots are basically the hot tips (of the cooler chromospheric DFs) that could not be identified unambiguously before because of a lack of spatial resolution. **2022-03-07**

Propagating brightenings in small loop-like structures in the quiet Sun corona: Observations from Solar Orbiter/EUI

Sudip **Mandal**, Hardi Peter, Lakshmi Pradeep Chitta, Sami K. Solanki, Regina Aznar Cuadrado, Luca Teriaca, Udo Schühle, David Berghmans, Frèdèric Auchère
A&A Letters **2021**
https://arxiv.org/pdf/2111.08106.pdf
Brightenings observed in the solar extreme-ultraviolet (EUV) images are generally interpreted as signatures of micro- or nanoflares occurring at the transition region or coronal temperatures. Recent observations with the Extreme Ultraviolet Imager (EUI) on board Solar Orbiter have revealed the smallest of such brightenings (termed campfires) in the quiet-Sun corona. Analyzing EUI 174 Å data at a resolution of about 400 km on the Sun with a cadence of 5 s from **30-May-2020**, we report here a number of cases where these campfires exhibit propagating signatures along their apparent small (3-5 Mm) loop-like structures. Measured propagation speeds are generally between 25 km s−1 and 60 km s−1. These apparent motions would be slower than the local sound speed if the loop plasma is assumed to be at a million Kelvin. Furthermore, these brightenings exhibit non-trivial propagation characteristics such as bifurcation, merging, reflection and repeated plasma ejections. We suggest that these features are manifestations of the internal dynamics of these small-scale magnetic structures and could provide important insights into the dynamic response (∼40 s) of the loop plasma to the heating events as well as into the locations of the heating events themselves.

Detection of Rossby modes with even azimuthal orders using helioseismic normal-mode coupling

K. **Mandal**, S. M. Hanasoge, L. Gizon
A&A 652, A96 **2021**
https://arxiv.org/pdf/2106.03971.pdf
https://www.aanda.org/articles/aa/pdf/2021/08/aa41044-21.pdf
https://doi.org/10.1051/0004-6361/202141044
Retrograde Rossby waves, measured to have significant amplitudes in the Sun, likely have notable implications for various solar phenomena. Rossby waves create small-amplitude, very-low frequency motions (on the order of the rotation rate and lower), which in turn shift the resonant frequencies and eigenfunctions of the acoustic modes of the Sun. The detection of even azimuthal orders Rossby modes using mode coupling presents additional challenges and prior work therefore only focused on odd orders. Here, we successfully extend the methodology to measure even azimuthal orders as well. We analyze 4 and 8 years of Helioseismic and Magnetic Imager (HMI) data and consider coupling between different-degree acoustic modes (of separations 1 and 3 in harmonic degree). The technique uses couplings between different frequency bins to capture the temporal variability of the Rossby modes. We observe significant power close to the theoretical dispersion relation for sectoral Rossby modes (where the azimuthal order is same as harmonic degree, $s = |t|$). Our results are consistent with prior measurements of Rossby modes with azimuthal orders over the range $t = 4$ to 16 with maximum power occurring at mode $t = 8$. The amplitudes of these modes vary from 1 to 2 m/s. We place an upper bound of 0.2 m/s on the sectoral $t = 2$ mode, which we do not detect in our measurements. This effort adds credence to the mode-coupling methodology in helioseismology

Sunspot area catalogue revisited: Daily cross-calibrated areas since 1874

Sudip **Mandal**, Natalie A. Krivova, Sami K. Solanki, Nimesh Sinha, Dipankar Banerjee
A&A 640, A78 **2020**
https://arxiv.org/pdf/2004.14618.pdf
https://www.aanda.org/articles/aa/pdf/2020/08/aa37547-20.pdf
Long and consistent sunspot area records are important for understanding the long-term solar activity and variability. Multiple observatories around the globe have regularly recorded sunspot areas, but such individual records only cover restricted periods of time. Furthermore, there are also systematic differences between them, so that these records need to be cross-calibrated before they can be reliably used for further studies. We produce a

cross-calibrated and homogeneous record of total daily sunspot areas, both projected and corrected, covering the period between 1874 and 2019. A catalogue of calibrated individual group areas is also generated for the same period. We have compared the data from nine archives: Royal Greenwich Observatory (RGO), Kislovodsk, Pulkovo, Debrecen, Kodaikanal, Solar Optical Observing Network (SOON), Rome, Catania, and Yunnan Observatories, covering the period between 1874 and 2019. Mutual comparisons of the individual records have been employed to produce homogeneous and inter-calibrated records of daily projected and corrected areas. As in earlier studies, the basis of the composite is formed by the data from RGO. After 1976, the only datasets used are those from Kislovodsk, Pulkovo and Debrecen observatories. This choice was made based on the temporal coverage and the quality of the data. In contrast to the SOON data used in previous area composites for the post-RGO period, the properties of the data from Kislovodsk and Pulkovo are very similar to those from the RGO series. They also directly overlap the RGO data in time, which makes their cross-calibration with RGO much more reliable. We have also computed and provide the daily Photometric Sunspot Index (PSI) widely used, e.g., in empirical reconstructions of solar irradiance.

Properties of solar Rossby waves from normal mode coupling and characterizing its systematics

Krishnendu **Mandal**, Shravan Hanasoge
2020 *ApJ* **891** 125
https://arxiv.org/pdf/1908.05890.pdf
https://doi.org/10.3847/1538-4357/ab7227
Rossby waves play an important role in mediating the angular momentum of rotating spherical fluids, creating weather on Earth and tuning exoplanet orbits in distant stellar systems (Ogilvie 2014). Their recent discovery in the solar convection zone provides an exciting opportunity to appreciate the detailed astrophysics of Rossby waves. Large-scale Rossby waves create subtle drifts in acoustic oscillations in the convection zone, which we measure using helioseismology to image properties of Rossby waves in the interior. We analyze 20 years of space-based observations, from 1999 to 2018, to measure Rossby-mode frequencies, line-widths, and amplitudes. Spatial leakage affects the measurements of normal model coupling and complicates the analysis of separating out specific harmonic degree and the azimuthal number of features on the Sun. Here we demonstrate a novel approach to overcome this difficulty and test it by performing synthetic tests. We find that the root-mean-square velocity of the modes is of the order of 0.5 m/s at the surface.

Helioseismic inversion to infer depth profile of solar meridional flow using spherical Born kernels

K. **Mandal**, S. M. Hanasoge, S. P. Rajaguru, H. M. Antia
ApJ *ApJ* **863** 39 **2018**
https://arxiv.org/pdf/1807.00314.pdf
Accurate inference of solar meridional flow is of crucial importance for the understanding of solar dynamo process. Wave travel times, as measured on the surface, will change if the waves encounter perturbations e.g. in the sound speed or flows, as they propagate through the solar interior. Using functions called sensitivity kernels, we may image the underlying anomalies that cause measured shifts in travel times. The inference of large-scale structures e.g meridional circulation requires computing sensitivity kernels in spherical geometry. Mandal et al. (2017) have computed such spherical kernels in the limit of the first-Born approximation. In this work, we perform an inversion for meridional circulation using travel-time measurements obtained from 6 years of SDO/HMI data and those sensitivity kernels. We enforce mass conservation by inverting for a stream function. The number of free parameters is reduced by projecting the solution on to cubic B-splines in radius and derivatives of the Legendre-polynomial basis in latitude, thereby improving the condition number of the inverse problem. We validate our approach for synthetic observations before performing the actual inversion. The inversion suggests a single-cell profile with the return-flow occurring at depths below 0.78 R$\odot$.

An Overview of Science Results Obtained From Kodaikanal Digitized White-Light Data Archive: 1921-2011

Sudip **Mandal**, Dipankar Banerjee
Proceedings IAU Symposium No. 340, **2018**
https://arxiv.org/pdf/1805.04816.pdf
In this proceeding, we present a summary of the recent scientific results that have been derived using the newly digitized whit-light (WL) data obtained from the Kodaikanal Solar Observatory.

A Statistical Study on The Frequency-Dependent Damping of Slow-mode Waves in Polar Plumes and Interplumes

Sudip **Mandal**, S.Krishna Prasad, Dipankar Banerjee
ApJ **853** 134 **2017**
https://arxiv.org/pdf/1712.03673.pdf
We perform a statistical study on the frequency-dependent damping of slow waves propagating along polar plumes and interplumes in the solar corona. Analysis of a large sample of extreme ultraviolet (EUV) imaging data with high spatial and temporal resolutions obtained from AIA/SDO suggests an inverse power-law dependence of the damping length on the periodicity of slow waves (i.e., the shorter period oscillations exhibit longer damping lengths), in agreement with the previous case studies. Similar behavior is observed in both plume and interplume regions studied in AIA 171 \AA\ and AIA 193 \AA\ passbands. It is found that the short-period (2--6 min) waves are relatively more abundant than their long period (7--30 min) counterparts in contrast to the general belief that the polar regions are dominated by the longer-period slow waves. We also derived the slope of the power spectra (α, the power-law index) statistically to better understand the characteristics of turbulence present in the region. It is found that the α values and their distributions are similar in both plume and interplume structures across the two AIA passbands. At the same time, the spread of these distributions also indicates the complexity of the underlying turbulence mechanism. **2 Feb 2017**

Latitude Distribution of Sunspots: Analysis Using Sunspot Data and A Dynamo Model

Sudip **Mandal,** Bidya Binay Karak, Dipankar Banerjee
ApJ **851** 70 **2017**
https://arxiv.org/pdf/1711.00222.pdf
http://iopscience.iop.org.sci-hub.tw/0004-637X/851/1/70/
In this paper, we explore the evolution of sunspot latitude distribution and explore its relations with the cycle strength. With the progress of the solar cycle, the distributions in two hemispheres from mid-latitudes propagate toward the equator and then (before the usual solar minimum) these two distributions touch each other. By visualizing the evolution of the distributions in two hemispheres, we separate the solar cycles by excluding this hemispheric overlap. From these isolated solar cycles in two hemispheres, we generate latitude distributions for each cycle, starting from cycle 8 to cycle 23. We find that the parameters of these distributions, namely, the central latitude (C), width (δ) and height (H) evolve with the cycle number and they show some hemispheric asymmetries. Although the asymmetries in these parameters persist for a few successive cycles, they get corrected within a few cycles and the new asymmetries appear again. In agreement with the previous study, we find that distribution parameters are correlated with the strengths of the cycles, although these correlations are significantly different in two hemispheres. The general trend that stronger cycles begin sunspot eruptions at relatively higher latitudes and have wider bands of sunspot emergence latitudes are confirmed when combining the data from two hemispheres. We explore these features using a flux transport dynamo model with stochastic fluctuations. We find that these features are correctly reproduced in this model. The solar cycle evolution of the distribution center is also in good agreement with observations. Possible explanations of the observed features based on this dynamo model are presented.

Association Of Supergranule Mean Scales with Solar Cycle Strengths and Total Solar Irradiance

Sudip **Mandal**, Subhamoy Chatterjee, Dipankar Banerjee
ApJ **844** 24 **2017**
https://arxiv.org/pdf/1705.11171.pdf
We analyze the long-term behavior of supergranule scale parameter, in active and quiet regions (AR, QR), using the Kodaikanal digitized data archive. This database provides century-long daily full disc observations of the Sun in Ca-II K wavelength. In this paper, we study the distributions of the supergranular scales, over the whole data duration, which show identical shape in these two regimes. We found that the AR mean scale values are always higher than that of the QR for every solar cycle. The mean scale values are highly correlated with the sunspot number cycle amplitude and also with total solar irradiance (TSI) variations. Such correlation establishes the cycle-wise mean scale as a potential calibrator for the historical data reconstructions. We also see an upward trend in the mean scales, as already been reported in TSI. This may provide new input for climate forcing models. These results also give us insight into the different evolutionary scenarios of the supergranules in the presence of strong (AR) and weak (QR) magnetic fields.

Finite-frequency sensitivity kernels in spherical geometry for time-distance helioseismology

Krishnendu **Mandal**, Jishnu Bhattacharya, Samrat Halder, Shravan Hanasoge
ApJ **842** 89 **2017**
https://arxiv.org/pdf/1705.04020.pdf

The inference of internal properties of the Sun from surface measurements of wave travel times is the goal of time-distance helioseismology. A critical step toward the accurate interpretation of travel-time shifts is the computation of sensitivity functions linking seismic measurements to internal structure. Here we calculate finite-frequency sensitivity kernels in spherical geometry for two-point travel-time measurements. We numerically build Green's function by solving for it at each frequency and spherical-harmonic degree and summing over all these pieces. These computations are performed in parallel ("embarrassingly"), thereby achieving significant speedup in wall-clock time. Kernels are calculated by invoking the first-order Born approximation connecting deviations in the wavefield to perturbations in the operator. Validated flow kernels are shown to produce travel times within 0.47% of the true value for uniform flows up to 750 m/s. We find that travel-time can be obtained with errors of 1 millisecond or less for flows having magnitudes similar to meridional circulation. Alongside flows, we also compute and validate sensitivity kernel for sound-speed perturbations. These accurate sensitivity kernels might improve the current inferences of sub-surface flows significantly.

Association of Plages With Sunspots: A multi wavelength Study Using Kodaikanal Ca II K and Greenwich sunspot area Data

Sudip **Mandal**, Subhamoy Chatterjee, Dipankar Banerjee
ApJ 835 158 **2017**
https://arxiv.org/pdf/1612.05711v1.pdf
Plages are the magnetically active chromospheric structures prominently visible in Ca II K line (3933.67 \r{A}). A plage may or may not be associated with a sunspot which is a magnetic structure visible in the solar photosphere. In this study we explore this aspect of association of plages with sunspots using the newly digitized Kodaikanal Ca II K plage data and the Greenwich sunspot area data. Instead of using the plage index or fractional plage area and their comparison with the sunspot number, we use, to our knowledge for the first time, the individual plage areas and compared it with the sunspot area time series. Our analysis shows that these two structures formed at two different layers are highly correlated with each other on a time scale comparable to the solar cycle. The area and the latitudinal distributions of plages are also similar to that of the sunspots. Different area thresholdings on the `Butterfly diagram' reveal that plages with ≥4 arcmin2 are mostly associated with a sunspot in the photosphere. Apart from this, we found that the cyclic properties change when different sized plages are considered separately. These results may help us to better understand the generation and the evolution of the magnetic structures in different layers of the solar atmosphere.

Solar Active Longitudes From Kodaikanal White-light Digitized Data

Sudip **Mandal**, Subhamoy Chatterjee, Dipankar Banerjee
2017 ApJ 835 62
https://arxiv.org/pdf/1611.07637v1.pdf
The study of solar active longitudes has generated a great interest in the recent years. In this work we have used an unique continuous sunspot data series obtained from Kodaikanal observatory and revisited the problem. Analysis of the data shows a persistent presence of the active longitude during the whole 90 years of data duration. We compare two well studied analysis methods and presented their respective results. The separation between the two most active longitudes is found be roughly 180{\deg} for majority of time. Additionally, we also find a comparatively weaker presence of separations at 90{\deg} and 270{\deg}. Migration pattern of these active longitudes as revealed from our data is found to be consistent with the solar differential rotation curve. We also study the periodicities in the active longitudes and found two dominant periods of ≈1.3 years and ≈2.2 years. These periods, also found in other solar proxies, indicate their relation with the global solar dynamo mechanism.

Sunspot Sizes and The Solar Cycle: Analysis Using Kodaikanal White-light Digitized Data

Sudip **Mandal**, Dipankar Banerjee
ApJL **2016**
https://arxiv.org/pdf/1610.02531v1.pdf
Sizes of the sunspots vary in a wide range during the progression of a solar cycle. Long-term variation study of different sunspot sizes are key to better understand the underlying process of sunspot formation and their connection to the solar dynamo. Kodaikanal white-light digitized archive provides daily sunspot observations for a period of 90 years (1921-2011). Using different size criteria on the detected individual sunspots, we have generated yearly averaged sunspot area time series for the full Sun as well as for the individual hemispheres. In this paper, we have used the sunspot area values instead of sunspot numbers used in earlier studies. Analysis of these different time series show that different properties of the sunspot cycles depend on the sunspot sizes. The `odd-even rule', double peaks during the cycle maxima and the long-term periodicities in the area data are found to be present for specific sunspot sizes and are absent or not so prominent in other size ranges. Apart from that, we also find a range of periodicities in the asymmetry index which have a dependency on the sunspot sizes. These statistical differences in the different size ranges may indicate that a complex dynamo action is responsible for the generation and dynamics of sunspots with different sizes.

Kodaikanal Digitized White-light Data Archive (1921-2011): Analysis of various solar cycle features

Sudip **Mandal**, Manjunath Hegde, Tanmoy Samanta, Gopal Hazra, Dipankar Banerjee, Ravindra B

A&A **2016**

http://arxiv.org/pdf/1608.04665v1.pdf

Long-term sunspot observations are key to understand and predict the solar activities and its effects on the space weather.Consistent observations which are crucial for long-term variations studies,are generally not available due to upgradation/modifications of observatories over the course of time. We present the data for a period of 90 years acquired from persistent observation at the Kodaikanal observatory in India. We use an advanced semi-automated algorithm to detect the sunspots form each calibrated white-light image. Area, longitude and latitude of each of the detected sunspots are derived. Implementation of a semi-automated method is very necessary in such studies as it minimizes the human bias in the detection procedure. Daily, monthly and yearly sunspot area variations obtained from the Kodaikanal, compared well with the Greenwich sunspot area data. We find an exponentially decaying distribution for the individual sunspot area for each of the solar cycles. Analyzing the histograms of the latitudinal distribution of the detected sunspots, we find Gaussian distributions, in both the hemispheres, with the centers at ∼15◦ latitude. The height of the Gaussian distributions are different for the two hemispheres for a particular cycle. Using our data, we show clear presence of Waldmeier effect which correlates the rise time with the cycle amplitude. Using the wavelet analysis, we explored different periodicities of different time scales present in the sunspot area times series.

On the Origin of Solar Hemispheric Helicity Rules: Rise of 3D Magnetic Flux Concentrations through a Background Magnetic Field

Bhishek **Manek**, Nicholas Brummell

ApJ **2024**

https://arxiv.org/pdf/2406.13104

https://iopscience.iop.org/article/10.3847/1538-4357/ad5993/pdf

Sunspots and active regions observed on the solar surface are widely believed to be manifestations of compact predominantly-toroidal magnetic field structures (``flux tubes") that emerge by magnetic buoyancy from the deeper interior of the Sun. Much work has examined the evolution of such magnetic structures, typically considering them as idealized isolated magnetic entities and not as more realistic magnetic concentrations in a volume-filling background magnetic field. Here, we report results that explore the buoyant rise dynamics of magnetic concentrations in a volume-filling field in the full three dimensions. Earlier 2.5D work in this series (arXiv:1805.08806, arXiv:2101.03472, arXiv:2204.13078) established the remarkable fact that the twist orientation of a flux concentration relative to the background field affected it's likelihood to rise and emerge, regardless of whether the buoyant rise took place in the absence or presence of convection. The contrasting dynamics between structures with differing orientations leads to a selection mechanism that reproduces characteristics of the ``solar hemispheric helicity rule(s)" (SHHR) observations strikingly well. Here, we show that this two-dimensional selection mechanism persists in the face of the added complexity of three-dimensional dynamics. Arching of the magnetic structure in the third dimension, as might be expected in the solar application, is introduced. The role of tension force leading to this selection mechanism is elucidated and subtle differences that arise due to the three-dimensional geometry are discussed.

On the origin of the solar hemispherical helicity rules: Simulations of the rise of magnetic flux concentrations in a background field

Bhishek **Manek**, Nicholas Brummell

ApJ **909** 72 **2021**

https://arxiv.org/pdf/2101.03472.pdf

https://doi.org/10.3847/1538-4357/abd859

Solar active regions and sunspots are believed to be formed by the emergence of strong toroidal magnetic flux from the solar interior. Modeling of such events has focused on the dynamics of compact magnetic entities, colloquially known as "flux tubes", often considered to be isolated magnetic structures embedded in an otherwise field-free environment. In this paper, we show that relaxing such idealized assumptions can lead to surprisingly different dynamics. We consider the rise of tube-like flux concentrations embedded in a large-scale volume-filling horizontal field in an initially quiescent adiabatically-stratified compressible fluid. In a previous letter, we revealed the unexpected major result that concentrations that have their twist aligned with the background field at the bottom of the tube are more likely to rise than the opposite orientation (for certain values of the parameters). This bias leads to a selection rule which, when applied to solar dynamics, is in agreement with the observations known as the solar hemispheric helicity rule(s) (SHHR). Here, we examine this selection mechanism in more detail than was possible in the earlier letter. We explore the dependence on the parameters via simulations, delineating the Selective Rise

Regime (SRR), where the bias operates. We provide a theoretical model to predict and explain the simulation dynamics. Furthermore, we create synthetic helicity maps from Monte Carlo simulations to mimic the SHHR observations and demonstrate that our mechanism explains the observed scatter in the rule and its variation over the solar cycle.

The Rise of a Magnetic Flux Tube in a Background Field: Solar Helicity Selection Rules

Bhishek **Manek**, Nicholas Brummell, Dongwook Lee

ApJL **859** L27 **2018**

https://arxiv.org/pdf/1805.08806.pdf

The buoyant transport of magnetic fields from the solar interior towards the surface plays an important role in the emergence of active regions, the formation of sunspots and the overall solar dynamo. Observations suggest that toroidal flux concentrations often referred to as "flux tubes", rise from their region of initiation likely in the solar tachocline towards the solar surface due to magnetic buoyancy. Many studies have assumed the existence of such magnetic structures and studied the buoyant rise of an isolated flux tube in a quiescent, field-free environment. Here, motivated by their formation (Cline et al. 2003; Brummell et al. 2002), we relax the latter assumption and study the rise of a toroidal flux tube embedded in a large-scale poloidal background magnetic field. We find that the presence of the large-scale background field severely affects the dynamics of the rising tube. A relatively weak background field, as low as 6% of the tube strength, can destroy the rise of a tube that would otherwise rise in the absence of the background field. Surprisingly, the rise of tubes with one sign of the twist is suppressed by a significantly weaker background field than the other. This demonstrates a potential mechanism for the selection of the preferred helicity of rising and emerging tubes for the solar case that is commensurate with many features of the hemispherical rule.

Multifluid modeling of magnetosonic wave propagtion in the solar chromosphere -- effects of impact ionization and radiative recombination

Yana G. **Maneva**, Alejandro A. Laguna, Andrea Lani, Stefaan Poedts

2016

https://arxiv.org/pdf/1611.08439v1.pdf

In order to study chromospheric magnetosonic wave propagation including, for the first time, the effects of ion-neutral interactions in the partially ionized solar chromosphere, we have developed a new multi-fluid computational model, accounting for ionization and recombination reactions in gravitationally stratified magnetized collisional media. The two-fluid model used in our 2D numerical simulations treats neutrals as a separate fluid and considers charged species (electrons and ions) within the resistive MHD approach with Coulomb collisions and anisotropic heat flux determined by Braginskii's transport coefficients. The electromagnetic fields are evolved according to the full Maxwell equations and the solenoidality of the magnetic field is enforced with a hyperbolic divergence cleaning scheme. The initial density and temperature profiles are similar to VAL III chromospheric model in which dynamical, thermal and chemical equilibrium are considered to ensure comparison to existing MHD models and avoid artificial numerical heating. In this initial setup we include simple homogeneous flux tube magnetic field configuration and an external photospheric velocity driver to simulate the propagation of MHD waves in the partially ionized reactive chromosphere. In particular, we investigate the loss of chemical equilibrium and the plasma heating related to the steepening of fast magnetosonic wave fronts in the gravitationally stratified medium.

Magnetic flux in the Sun emerges unaffected by supergranular-scale surface flows

Prasad **Mani**, Chris S. Hanson, Siddarth Dhanpal, Shravan Hanasoge, Srijan Bharati Das, Matthias Rempel

ApJ **2024**

https://arxiv.org/pdf/2403.00295.pdf

Magnetic flux emergence from the convection zone into the photosphere and beyond is a critical component of the behaviour of large-scale solar magnetism. Flux rarely emerges amid field-free areas at the surface, but when it does, the interaction between magnetism and plasma flows can be reliably explored. Prior ensemble studies identified weak flows forming near emergence locations, but the low signal-to-noise required averaging over the entire dataset, erasing information about variation across the sample. Here, we apply deep learning to achieve improved signal-to-noise, enabling a case-by-case study. We find that these associated flows are dissimilar across instances of emergence and also occur frequently in the quiet convective background. Our analysis suggests diminished influence of supergranular-scale convective flows and magnetic buoyancy on flux rise. Consistent with numerical evidence, we speculate that small-scale surface turbulence and / or deep-convective processes play an outsize role in driving flux emergence.

Imaging the Sun's Near-surface Flows Using Mode-coupling Analysis

Prasad **Mani**1, Chris S. Hanson2, and Shravan Hanasoge1,2

2022 ApJ 926 127

https://iopscience.iop.org/article/10.3847/1538-4357/ac474e/pdf

The technique of normal-mode coupling is a powerful tool with which to seismically image non-axisymmetric phenomena in the Sun. Here we apply mode coupling in the Cartesian approximation to probe steady, near-surface flows in the Sun. Using Doppler cubes obtained from the Helioseismic and Magnetic Imager on board the Solar Dynamics Observatory, we perform inversions on mode-coupling measurements to show that the resulting divergence and radial vorticity maps at supergranular length scales (~30 Mm) near the surface compare extremely well with those obtained using the local correlation tracking method. We find that the Pearson correlation coefficient is ≥0.9 for divergence flows, while ≥0.8 is obtained for the radial vorticity. **2017 November 14**

Investigating toroidal flows in the Sun using normal-mode coupling

Prasad **Mani**, Shravan Hanasoge

ApJ **920** 36 **2021**

https://arxiv.org/pdf/2108.01426.pdf

https://doi.org/10.3847/1538-4357/ac1ad6

Helioseismic observations have provided valuable datasets with which to pursue the detailed investigation of solar interior dynamics. Among various methods to analyse these data, normal-mode coupling has proven to be a powerful tool, used to study Rossby waves, differential rotation, meridional circulation, and non-axisymmetric multi-scale subsurface flows. Here, we invert mode-coupling measurements from Helioseismic Magnetic Imager (HMI) and Michelson Doppler Imager (MDI) to obtain mass-conserving toroidal convective flow as a function of depth, spatial wavenumber, and temporal frequency. To ensure that the estimates of velocity magnitudes are proper, we also evaluate correlated realization noise, caused by the limited visibility of the Sun. We benchmark the near-surface inversions against results from Local Correlation Tracking (LCT). Convective power likely assumes greater latitudinal isotropy with decrease in spatial scale of the flow. We note an absence of a peak in toroidal-flow power at supergranular scales, in line with observations that show that supergranulation is dominantly poloidal in nature.

Capabilities of bisector analysis of the Si I 10827 A line for estimating line-of-sight velocities in the quiet Sun

S.J. González **Manrique** (1), C. Quintero Noda (2,3), C. Kuckein (4), B. Ruiz Cobo (5,6), M. Carlsson (A&A **2020**

https://arxiv.org/pdf/2001.00508.pdf

We examine the capabilities of a fast and simple method to infer line-of-sight (LOS) velocities from observations of the photospheric Si I 10827 A line. This spectral line is routinely observed together with the chromospheric He I 10830 A triplet as it helps to constrain the atmospheric parameters. We study the accuracy of bisector analysis and a line core fit of Si I 10827 A. We employ synthetic profiles starting from the Bifrost enhanced network simulation. The profiles are computed solving the radiative transfer equation, including non-local thermodynamic equilibrium effects on the determination of the atomic level populations of Si I. We found a good correlation between the inferred velocities from bisectors taken at different line profile intensities and the original simulation velocity at given optical depths. This good correlation means that we can associate bisectors taken at different line-profile percentages with atmospheric layers that linearly increase as we scan lower spectral line intensities. We also determined that a fit to the line-core intensity is robust and reliable, providing information about atmospheric layers that are above those accessible through bisectors. Therefore, by combining both methods on the Si I 10827 A line, we can seamlessly trace the quiet-Sun LOS velocity stratification from the deep photosphere to higher layers until around $\log\tau=-3.5$ in a fast and straightforward way. This method is ideal for generating quick-look reference images for future missions like the Daniel K. Inoue Solar Telescope and the European Solar Telescope, for example.

Capabilities of bisector analysis of the Si I 10 827 Å line for estimating line-of-sight velocities in the quiet Sun

S. J. González **Manrique**1, C. Quintero Noda2,3, C. Kuckein4, B. Ruiz Cobo5,6 and M. Carlsson2,3 A&A 634, A19 (**2020**)

https://doi.org/10.1051/0004-6361/201937274

We examine the capabilities of a fast and simple method to infer line-of-sight (LOS) velocities from observations of the photospheric Si I 10 827 Å line. This spectral line is routinely observed together with the chromospheric He I 10 830 Å triplet as it helps to constrain the atmospheric parameters. We study the accuracy of bisector analysis and a line core fit of Si I 10 827 Å. We employ synthetic profiles starting from the Bifrost enhanced network simulation. The profiles are computed solving the radiative transfer equation, including non-local thermodynamic equilibrium effects on the determination of the atomic level populations of Si I. We found a good correlation between the inferred velocities from bisectors taken at different line profile intensities and the original simulation velocity at given optical depths. This good correlation means that we can associate bisectors taken at different line-profile percentages with atmospheric layers that linearly increase as we scan lower spectral line intensities. We also determined that a fit to the line-core intensity is robust and reliable, providing information about atmospheric layers that are above those accessible through bisectors. Therefore, by combining both methods on the Si I 10 827 Å line, we can seamlessly trace the quiet-Sun LOS velocity stratification from the deep photosphere to higher layers until

around logτ = −3.5 in a fast and straightforward way. This method is ideal for generating quick-look reference images for future missions like the Daniel K. Inoue Solar Telescope and the European Solar Telescope, for example.

Flows along arch filaments observed in the GRIS 'very fast spectroscopic mode'
S. J. González **Manrique**, C. Denker, C. Kuckein, A. Pastor Yabar, M. Collados, M. Verma, H. Balthasar, A. Diercke, C. E. Fischer, P. Gömöry, N. Bello González, R. Schlichenmaier, M. Cubas Armas, T. Berkefeld, A. Feller, S. Hoch, A. Hofmann, A. Lagg, H. Nicklas, D. Orozco Suárez, D. Schmidt, W. Schmidt, M. Sigwarth, M. Sobotka, S.K. Solanki, D. Soltau, J. Staude, K.G. Strassmeier, R. Volkmer, O. von der Lühe, T. Waldmann
Conference proceedings of the IAUS 327: "Fine Structure and Dynamics of the Solar Atmosphere" **2017**
https://arxiv.org/pdf/1701.02206v1.pdf
A new generation of solar instruments provides improved spectral, spatial, and temporal resolution, thus facilitating a better understanding of dynamic processes on the Sun. High-resolution observations often reveal multiple-component spectral line profiles, e.g., in the near-infrared He I 10830 \AA\ triplet, which provides information about the chromospheric velocity and magnetic fine structure. We observed an emerging flux region, including two small pores and an arch filament system, on **2015 April 17** with the 'very fast spectroscopic mode' of the GREGOR Infrared Spectrograph (GRIS) situated at the 1.5-meter GREGOR solar telescope at Observatorio del Teide, Tenerife, Spain. We discuss this method of obtaining fast (one per minute) spectral scans of the solar surface and its potential to follow dynamic processes on the Sun. We demonstrate the performance of the 'very fast spectroscopic mode' by tracking chromospheric high-velocity features in the arch filament system.

Fitting peculiar spectral profiles in He I 10830 Å absorption features
S. J. González **Manrique**, C. Kuckein, A. Pastor Yabar, M. Collados C. Denker, C. E. Fischer, P. Gömöry, …
Astron. Nachr. as a part of special edition of the 12th Potsdam Thinkshop, **2016**
http://arxiv.org/pdf/1603.00679v1.pdf
The new generation of solar instruments provides better spectral, spatial, and temporal resolution for a better understanding of the physical processes that take place on the Sun. Multiple-component profiles are more commonly observed with these instruments. Particularly, the He I 10830 \r{A} triplet presents such peculiar spectral profiles, which give information on the velocity and magnetic fine structure of the upper chromosphere. The purpose of this investigation is to describe a technique to efficiently fit the two blended components of the He I 10830 \r{A} triplet, which are commonly observed when two atmospheric components are located within the same resolution element. The observations used in this study were taken on 2015 April 17 with the very fast spectroscopic mode of the GREGOR Infrared Spectrograph (GRIS) attached to the 1.5-meter GREGOR solar telescope, located at the Observatorio del Teide, Tenerife, Spain. We apply a double-Lorentzian fitting technique using Levenberg-Marquardt least-squares minimization. This technique is very simple and much faster than inversion codes. Line-of-sight Doppler velocities can be inferred for a whole map of pixels within just a few minutes. Our results show sub- and supersonic downflow velocities of up to 32 km/s for the fast component in the vicinity of footpoints of filamentary structures. The slow component presents velocities close to rest.

Helium Fluxes Measured by the PAMELA Experiment from the Minimum to the Maximum Solar Activity for Solar Cycle 24
N. **Marcelli**1,2, M. Boezio3,4, A. Lenni3,4,5, W. Menn6, R. Munini3,4, O. P. M. Aslam7, D. Bisschoff7, M. D. Ngobeni7, M. S. Potgieter8, O. Adriani9,10Show full author list
2022 ApJL 925 L24
https://iopscience.iop.org/article/10.3847/2041-8213/ac4787/pdf
Time-dependent energy spectra of galactic cosmic rays (GCRs) carry fundamental information regarding their origin and propagation. When observed at the Earth, these spectra are significantly affected by the solar wind and the embedded solar magnetic field that permeates the heliosphere, changing significantly over an 11 yr solar cycle. Energy spectra of GCRs measured during different epochs of solar activity provide crucial information for a thorough understanding of solar and heliospheric phenomena. The PAMELA experiment collected data for almost 10 years (2006 June 15–2016 January 23), including the minimum phase of solar cycle 23 and the maximum phase of solar cycle 24. In this paper, we present new spectra for helium nuclei measured by the PAMELA instrument from 2010 January to 2014 September over a three-Carrington-rotation time basis. These data are compared to the PAMELA spectra measured during the previous solar minimum, providing a picture of the time dependence of the helium-nuclei fluxes over a nearly full solar cycle. Time and rigidity dependencies are observed in the proton-to-helium flux ratios. The force-field approximation of the solar modulation was used to relate these dependencies to the shapes of the local interstellar proton and helium-nuclei spectra.

Relationship between Total Solar Irradiance and Magnetic Flux during Solar Minima

Sergey V. **Marchenko**1,2, Judith L. Lean3, and Matthew T. DeLand1,2
2022 ApJ 936 158
https://iopscience.iop.org/article/10.3847/1538-4357/ac8a98/pdf
What drives the small total solar irradiance (TSI) changes of ∼50–100 parts per million (compared with >1000 ppm solar-cycle amplitudes) during a deep solar minimum, i.e., in the practical absence of detectable sunspots and long-lasting active regions? We consider the epoch 2008 June–October and investigate multiple data sets (TSI; various Mg ii line-activity indices, extreme ultraviolet fluxes, and full-disk magnetograms) to show that variations in TSI closely follow changes in total magnetic flux from sources with |B| > 80 G (up to ∼600 G) that persist even during extended periods with no detectable sunspots. These sources comprise the populations of (a) short-lived (<20 minutes), small-scale (predominantly a single 2" MDI pixel), ∼evenly distributed regions, and (b) on average, more extended (a few MDI pixels) and longer-lived (140–260 minutes median lifetimes) magnetic areas. We ascribe the latter to ephemeral regions, finding them clustering on ∼200 Mm scales. We speculate that the short-lived MDI sources are linked to the ubiquitous magnetic bright points. Our analysis of magnetic flux variations during solar cycle 23 shows that the magnetic regions present during this deep solar minimum elevate the total magnetic flux above the total flux in just the Gaussian "cores," fitted to histogram distributions of the full-disk flux. This suggests that solar irradiance during more extended, even deeper minima, such as the Maunder Minimum, may be lower than in 2008.

Solar activity and responses observed in Balmer lines

S. **Marchenko**1,2, S. Criscuoli3, M. T. DeLand1,2, D. P. Choudhary4 and G. Kopp5
A&A 646, A81 (**2021**)
https://doi.org/10.1051/0004-6361/202037767
https://www.aanda.org/articles/aa/pdf/2021/02/aa37767-20.pdf
Context. Many stars show Sun-like magnetic activity cycles, which are frequently observed by tracking changes in the chromospherically sensitive CaII H&K doublet. However, relationships between the line profile changes related to the magnetic activity seen in strong spectral transitions in other portions of a stellar spectrum are yet to be understood.
Aims. We follow variability patterns in various solar lines in order to relate them to the emergence, passage, and decay of active solar regions.
Methods. The line activity indices (core-to-wing ratio) for the upper Balmer lines – Hβ, Hγ, and Hδ – are constructed from the near-daily solar measurements acquired by the Ozone Monitoring Instrument and the TROPOspheric Monitoring Instrument.
Results. On solar rotation timescales, the upper Balmer line activity indices closely follow variations in the total solar irradiance, $r \sim -(0.6 - 0.7)$, and thus frequently deviate from the behavior of the line activity indices that track chromospheric activity levels (e.g., the CH 430 nm band used in this study), specifically during passages of big sunspot groups.

Solar Spectral Irradiance Variability in Cycle 24: Observations and Models

S. V. **Marchenko**, M. T. DeLand, J. L. Lean
Journal of Space Weather and Space Climate (SWSC) **2016**
https://arxiv.org/pdf/1610.08001v1.pdf
http://www.swsc-journal.org/articles/swsc/pdf/2016/01/swsc160006.pdf
Utilizing the excellent stability of the Ozone Monitoring Instrument (OMI), we characterize both short-term (solar rotation) and long-term (solar cycle) changes of the solar spectral irradiance (SSI) between 265-500 nm during the on-going Cycle 24. We supplement the OMI data with concurrent observations from the GOME-2 and SORCE instruments and find fair-to-excellent, depending on wavelength, agreement among the observations and predictions of the NRLSSI2 and SATIRE-S models.

Solar Spectral Irradiance Changes during Cycle 24

S. V. **Marchenko**1 and M. T. DeLand
2014 ApJ 789 117
We use solar spectra obtained by the Ozone Monitoring Instrument (OMI) on board the Aura satellite to detect and follow long-term (years) and short-term (weeks) changes in the solar spectral irradiance (SSI) in the 265-500 nm spectral range. During solar Cycle 24, in the relatively line-free regions the SSI changed by ~0.6% ± 0.2% around 265 nm. These changes gradually diminish to 0.15% ± 0.20% at 500 nm. All strong spectral lines and blends, with the notable exception of the upper Balmer lines, vary in unison with the solar "continuum." Besides the lines with strong chromospheric components, the most involved species include Fe I blends and all prominent CH, NH, and CN spectral bands. Following the general trend seen in the solar "continuum," the variability of spectral lines also decreases toward longer wavelengths. The long-term solar cycle SSI changes are closely, to within the quoted 0.1%-0.2% uncertainties, matched by the appropriately adjusted short-term SSI variations derived from the 27 day

rotational modulation cycles. This further strengthens and broadens the prevailing notion about the general scalability of the UV SSI variability to the emissivity changes in the Mg II 280 nm doublet on timescales from weeks to years. We also detect subtle deviations from this general rule: the prominent spectral lines and blends at λ 350 nm show slightly more pronounced 27 day SSI changes when compared to the long-term (years) trends. We merge the solar data from Cycle 21 with the current Cycle 24 OMI and GOME-2 observations and provide normalized SSI variations for the 170-795 nm spectral region.

On-Orbit Sensitivity Evolution of the EUV Imaging Spectrometer on Hinode

J. T. **Mariska**

Solar Physics , February **2013**, Volume 282, Issue 2, pp 629-639

Since its launch on 22 September 2006, the EUV Imaging Spectrometer onboard the Hinode satellite has exhibited a gradual decay in sensitivity. Using spectroheliograms taken in the Fe viii 185.21 Å and Si vii 275.35 Å emission lines in quiet regions near Sun center we characterize that decay. For the period from December 2006 to March 2012, the decline in the sensitivity can be characterized as an exponential decay with an average time constant of 7358±1030 days (20.2±2.8 years). Emission lines formed at temperatures ≳ 106.1 K in the quiet Sun data exhibit solar-cycle effects.

Hard X-Ray Constraints on Small-Scale Coronal Heating Events

Andrew J. **Marsh**, David M. Smith, Lindsay Glesener, James A. Klimchuk, Stephen J. Bradshaw, Juliana Vievering, Iain G. Hannah, Steven Christe, Shin-nosuke Ishikawa, Sam Krucker

ApJ **864** 5 **2018**

https://arxiv.org/pdf/1808.02630.pdf

http://sci-hub.tw/http://iopscience.iop.org/article/10.3847/1538-4357/aad380/meta

Much evidence suggests that the solar corona is heated impulsively, meaning that nanoflares may be ubiquitous in quiet and active regions (ARs). Hard X-ray (HXR) observations with unprecedented sensitivity >3~keV are now enabled by focusing instruments. We analyzed data from the \textit{Focusing Optics X-ray Solar Imager (FOXSI)} rocket and the \textit{Nuclear Spectroscopic Telescope Array (NuSTAR)} spacecraft to constrain properties of AR nanoflares simulated by the EBTEL field-line-averaged hydrodynamics code. We generated model X-ray spectra by computing differential emission measures for homogeneous nanoflare sequences with heating amplitudes H0, durations τ, delay times between events tN, and filling factors f. The single quiescent AR observed by \textit{FOXSI-2} on 2014 December 11 is well fit by nanoflare sequences with heating amplitudes 0.02 erg cm−3 s−1 < H0 < 13 erg cm−3 s−1 and a wide range of delay times and durations. We exclude delays between events shorter than ∼900 s at the 90\% confidence level for this region. Three of five regions observed by {\nustar} on **2014 November 1** are well fit by homogeneous nanoflare models, while two regions with higher fluxes are not. Generally, the {\nustar} count spectra are well fit by nanoflare sequences with smaller heating amplitudes, shorter delays, and shorter durations than the allowed \textit{FOXSI-2} models. These apparent discrepancies are likely due to differences in spectral coverage between the two instruments and intrinsic differences among the regions. Steady heating (tN = τ) was ruled out with >99\% confidence for all regions observed by either instrument.

Hemispheric Patterns in Filament Chirality and Sigmoid Shape over the Solar Cycle, (Invited Review)

Petrus C. **Martens**, Anthony R. Yeates, and Karthik G. Pillai, Proceedings of IAU Symposion 300, 122-125, **2014**

"Nature of solar prominences and their role in Space Weather", Paris, France, June 10-14, 2013,

B. B. Schmieder, J.-M. Malherbe & S. T. Wu, eds.

http://solar.physics.montana.edu/martens/papers/IAU300-Martens-proofs.pdf

The motivation for our research was to study the correlation between the chirality of filaments and the handedness (S- or Z-shape) of sigmoids. It was assumed that sigmoids would mostly coincide with filaments and that the S-shaped sigmoids would correlate well with filaments of sinistral chirality, which we found that to be at best a very weak relation. Since we had a full solar cycle of filament metadata at hand it was easy to verify the supposedly known hemispheric preference of filament chirality. We discovered that the hemispheric chirality rule was confirmed for the epoch where a thorough manual study had been performed, but that at other phases of the solar cycle the rule seems to disappear and sometimes even reverse.

Observations key to understanding solar cycles: a review

Sara F. **Martin***

Front. Astron. Space Sci. 10:1177097. **2024**

doi: 10.3389/fspas.2023.1177097
https://www.frontiersin.org/articles/10.3389/fspas.2023.1177097/pdf
A paradigm shift is taking place in the conception of solar cycles. In the previous conception, the changing numbers of sunspots over intervals of 9–14 years have been regarded as the fundamental solar cycle although two average 11-year cycles were necessary to account for the complete magnetic cycle. In the revised picture, sunspots are a phase in the middle of two 22-year overlapping solar cycles that operate continuously with clock-like precision. More than 20 researchers have contributed to the initial research articles from 2014 through 2021 which are dramatically altering the perception of solar cycles. The two 22-year cycles overlap in time by 11 years. This overlap is coincidentally the same average duration as the sunspot phase in each 22-year cycle. This coincidence and the relative lack of knowledge of the large numbers of small active regions without sunspots is what led to the previous paradigm in which the 11-year sunspot phases were misinterpreted as a single fundamental solar cycle. The combination of the two 22-year solar cycles, with their large numbers of short-lived active regions and ephemeral active regions are now understood to be the fundamental cycle with the proposed name "The Hale Solar Cycle." The two 22-year solar cycles each occupy separate but adjacent bands in latitude. The orientations of the majority of bipolar magnetic regions in the two adjacent bands differ from each other by ∼180°. Both bands continuously drift from higher to lower latitudes as has been known for sunspot cycles. However, the polarity reversal occurs at the start of each 22-year cycle and at higher latitudes than it does for the sunspot cycles. This paradigm shift in the concept of solar cycles has resulted in major reconsiderations of additional topics on solar cycles in this review. These are 1) the large role of ephemeral active regions in the origin of solar cycles, 2) the depth of the origin of active regions and sunspots, 3) the mechanisms of how areas of unipolar magnetic network migrate to the solar poles every 11 years, and 4) the nature of the polarity reversal in alternate 22-year cycles rather than 11-year cycles.

Observational Evidence of Shallow Origins for the Magnetic Fields of Solar Cycles Review

Sara F. **Martin**
Front. Astron. Space Sci., 5:17 **2018** |
https://doi.org/10.3389/fspas.2018.00017
https://www.frontiersin.org/articles/10.3389/fspas.2018.00017/full
Observational evidence for the origin of active region magnetic fields has been sought from published information on extended solar cycles, statistical distributions of active regions and ephemeral regions, helioseismology results, positional relationships to supergranules, and fine-scale magnetic structure of active regions and their sunspots during their growth. Statistical distributions of areas of ephemeral and active regions blend together to reveal a single power law. The shape of the size distribution in latitude of all active regions is independent of time during the solar cycle, yielding further evidence that active regions of all sizes belong to the same population. Elementary bipoles, identified also by other names, appear to be the building blocks of active regions; sunspots form from elementary bipoles and are therefore deduced to develop from the photosphere downward, consistent with helioseismic detection of downflows to 3–4 Mm below sunspots as well as long-observed downflows from chromospheric/coronal arch filaments into sunspots from their earliest appearance. Time-distance helioseismology has been effective in revealing flows related to sunspots to depths of 20 Mm. Ring diagram analysis shows a statistically significant preference for upflows to precede major active region emergence and downflows after flux emergence but both are often observed together or not detected. From deep-focus helioseismic techniques for seeking magnetic flux below the photosphere prior major active regions, there is evidence of acoustic travel-time perturbation signatures rising in the limited range of depths of 42–75 Mm but these have not been verified or found at more shallow depths by helioseismic holographic techniques. The development of active regions from clusters of elementary bipoles appears to be the same irrespective of how much flux an active region eventually develops. This property would be consistent with the magnetic fields of large active regions being generated in the same way and close the same depth as small active regions in a shallow zone below the photosphere. All evidence considered together, understanding the origins of the magnetic fields of solar cycles boils down to learning how and where elementary bipoles are generated beneath the photosphere.

Questioning Many Mysteries MEMOIRS Review

Sara F. **Martin**
Solar Phys. 290(4) :1011–1080 **2015**
https://link.springer.com/content/pdf/10.1007%2Fs11207-015-0668-1.pdf
The first section of this memoir queries my formative years. Indirectly I address the question, did my childhood and early years make a difference in my choice of career? Why and how did I begin my journey to becoming a scientist? Did I choose the field of solar astronomy or did circumstances dictate it for me? In the second section, I travel through my work environments and experiences, talking about interactions and aspects of being a scientist that do not appear in our research papers. What parts of my research were happenstances and what parts did I plan? What does it feel like to be on scientific quests? Using examples in my journey, I also turn to questions that have intrigued me throughout my sojourn as a solar astronomer. How do scientific discoveries come about? What factors lead to little discoveries? And what factors lead to major exciting discoveries? Are there timely questions we do not think to ask? How can small, seemingly scattered pieces of knowledge suddenly coalesce into a deeper understanding – what

is called the “Aha!” experience – the times when our mental light switches on, and with child-like wonder we behold a “big picture”?

Evolution of the Sun's non-axisymmetric toroidal field

David **Martin-Belda**, Robert H. Cameron
A&A 603, A53 **2017**
https://arxiv.org/pdf/1703.10075.pdf

Aims. We aim to infer the sub-surface distribution of the Sun's non-axisymmetric azimuthal magnetic flux from observable quantities, such as the surface magnetic field and the large scale plasma flows.
Methods. We have built a kinematic flux transport model of the solar dynamo based on the Babcock-Leighton framework. We constructed the source term for the poloidal field using SOLIS magnetograms spanning three solar cycles. Based on this source we calculated the azimuthal flux below the surface. The flux transport model has two free parameters which we constrain using sunspot observations from cycle 22. We compared the model results with observations from cycle 23.
Results. The structure of the azimuthal field is mainly axisymmetric. The departures from axisymmetry represent, on average, ~3% of the total azimuthal flux. Owing to its relative weakness, the non-axisymmetric structure of the azimuthal field does not have a significant impact on the location in which the emergences appear or on the amount of flux contained in them. We find that the probability of emergence is a function of the ratio between the flux content of an active region and the underlying azimuthal flux.

Inflows towards active regions and the modulation of the solar cycle: a parameter study

David **Martin-Belda**, Robert H. Cameron
A&A 597, A21 **(2017)**
http://arxiv.org/pdf/1609.01199v1.pdf

Aims: We aim to investigate how converging flows towards active regions affect the surface transport of magnetic flux, as well as their impact on the generation of the Sun's poloidal field. The inflows constitute a potential non-linear mechanism for the saturation of the global dynamo and may contribute to the modulation of the solar cycle in the Babcock-Leighton framework.
Methods: We build a surface flux transport code incorporating a parametrized model of the inflows and run simulations spanning several cycles. We carry out a parameter study to assess how the strength and extension of the inflows affect the build-up of the global dipole field. We also perform simulations with different levels of activity to investigate the potential role of the inflows in the saturation of the global dynamo.
Results: We find that the interaction of neighbouring active regions can lead to the occasional formation of single-polarity magnetic flux clumps inconsistent with observations. We propose the darkening caused by pores in areas of high magnetic field strength as a plausible mechanism preventing this flux-clumping. We find that inflows decrease the amplitude of the axial dipole moment by a ∼30%, relative to a no-inflows scenario.
Stronger (weaker) inflows lead to larger (smaller) reductions of the axial dipole moment. The relative amplitude of the generated axial dipole is about 9% larger after very weak cycles than after very strong cycles. This supports the inflows as a non-linear mechanism capable of saturating the global dynamo and contributing to the modulation of the solar cycle within the Babcock-Leighton framework.

Large ion-neutral drift velocities and plasma heating in partially ionized coronal rain blobs

David **Martínez-Gómez**, Ramón Oliver, Elena Khomenko, Manuel Collados
ApJL **940** L47 **2022**
https://arxiv.org/pdf/2211.05493.pdf
https://iopscience.iop.org/article/10.3847/2041-8213/aca0a1/pdf

In this paper we present a numerical study of the dynamics of partially ionized coronal rain blobs. We use a two-fluid model to perform a high-resolution 2D simulation that takes into account the collisional interaction between the charged and neutral particles contained in the plasma. We follow the evolution of a cold plasma condensation as it falls through an isothermal vertically stratified atmosphere that represents the much hotter and lighter solar corona. We study the consequences of the different degrees of collisional coupling that are present in the system. On the one hand, we find that at the dense core of the blob there is a very strong coupling and the charged and neutral components of the plasma behave as a single fluid, with negligible drift velocities (of a few cm s^-1). On the other hand, at the edges of the blob the coupling is much weaker and larger drift velocities (of the order of 1 km s^-1) appear. In addition, frictional heating causes large increases of temperature at the transition layers between the blob and the corona. For the first time we show that such large drift velocities and temperature enhancements can develop as a consequence of ion-neutral decoupling associated to coronal rain dynamics. This can lead to enhanced emission coming from the plasma at the coronal rain-corona boundary, which possesses transition region temperature.

Two-dimensional simulations of coronal rain dynamics. I. Model with vertical magnetic field and an unbounded atmosphere

David **Martínez-Gómez**, Ramón Oliver, Elena Khomenko, Manuel Collados
A&A 634, A36 **2020**
https://arxiv.org/pdf/1911.06638.pdf

https://doi.org/10.1051/0004-6361/201937078
Aims. We aim to improve the understanding of the physical mechanisms behind the slower than free-fall motion and the two-stage evolution (an initial phase of acceleration followed by an almost constant velocity phase) detected in coronal rain events.
Methods. Using the Mancha3D code, we solve the 2D ideal MHD equations. We represent the solar corona as an isothermal vertically stratified atmosphere with a uniform vertical magnetic field and the plasma condensation as a density enhancement described by a 2D Gaussian profile. We analyse the temporal evolution of the descending plasma and study its dependence on parameters such as density and magnetic field strength.
Results. We confirm previous findings that the pressure gradient is the main force that opposes the action of gravity and slows down the blob descent and that larger densities require larger pressure gradients to reach the constant speed phase. We find that the shape of a condensation with a horizontal variation of density is distorted as it falls, due to the denser parts of the blob falling faster than the lighter ones. This is explained by the fact that the duration of the initial acceleration phase, and therefore the maximum falling speed attained by the plasma, increases with the ratio of blob to coronal density. We also find that the magnetic field plays a fundamental role in the evolution of the descending condensations. A strong enough magnetic field (greater than 10 G in our simulations) forces each plasma element to follow the path given by a particular field line, which allows to describe the evolution of each vertical slice of the blob in terms of 1D dynamics, without influence of the adjacent slices. In addition, under the typical conditions of the coronal rain events, the magnetic field prevents the development of the Kelvin-Helmholtz instability.

Multi-fluid approach to high-frequency waves in plasmas: I. Small-amplitude regime in fully ionized medium

David **Martínez-Gómez**, Roberto Soler, Jaume Terradas
ApJ **2016**
http://arxiv.org/pdf/1609.06190v1.pdf
Ideal MHD provides an accurate description of low-frequency Alfv\'en waves in fully ionized plasmas. However, higher frequency waves in many plasmas of the solar atmosphere cannot be correctly described by ideal MHD and a more accurate model is required. Here, we study the properties of small-amplitude incompressible perturbations in both the low and the high frequency ranges in plasmas composed of several ionized species. We use a multi-fluid approach and take into account the effects of collisions between ions and the inclusion of Hall's term in the induction equation. Through the analysis of the corresponding dispersion relations and numerical simulations we check that at high frequencies ions of different species are not as strongly coupled as in the low frequency limit. Hence, they cannot be treated as a single fluid. In addition, elastic collisions between the distinct ionized species are not negligible for high frequency waves since an appreciable damping is obtained. Furthermore, Coulomb collisions between ions remove the cyclotron resonances and the strict cut-off regions that are present when collisions are not taken into account. The implications of these results for the modelling of high-frequency waves in solar plasmas are discussed.

Chromospheric Heating from Local Magnetic Growth and Ambipolar Diffusion under Nonequilibrium Conditions

Juan **Martínez-Sykora1**,2,3,4, Jaime de la Cruz Rodríguez5, Milan Gošić1,2, Alberto Sainz Dalda1,2, Viggo H. Hansteen1,2,3,4, and Bart De Pontieu1,3,4
2023 ApJL 943 L14
https://iopscience.iop.org/article/10.3847/2041-8213/acafe9/pdf
The heating of the chromosphere in internetwork regions remains one of the foremost open questions in solar physics. In the present study, we tackle this old problem by using a very-high-spatial-resolution simulation of quiet-Sun conditions performed with radiative MHD numerical models and interface region imaging spectrograph (IRIS) observations. We have expanded a previously existing 3D radiative MHD numerical model of the solar atmosphere, which included self-consistently locally driven magnetic amplification in the chromosphere, by adding ambipolar diffusion and time-dependent nonequilibrium hydrogen ionization to the model. The energy of the magnetic field is dissipated in the upper chromosphere, providing a large temperature increase due to ambipolar diffusion and nonequilibrium ionization (NEQI). At the same time, we find that adding the ambipolar diffusion and NEQI in the simulation has a minor impact on the local growth of the magnetic field in the lower chromosphere and its dynamics. Our comparison between synthesized Mg ii profiles from these high-spatial-resolution models, with and without ambipolar diffusion and NEQI, and quiet-Sun and coronal hole observations from IRIS now reveal a slightly better correspondence. The intensity of profiles is increased, and the line cores are slightly broader when

ambipolar diffusion and NEQI effects are included. Therefore, the Mg ii profiles are closer to those observed than in previous models, though some differences still remain.

On the velocity drift between ions in the solar atmosphere

Juan **Martínez-Sykora**, Mikolaj Szydlarski, Viggo H. Hansteen, Bart De Pontieu
ApJ **900** 101 **2020**
https://arxiv.org/pdf/2008.00069.pdf
https://doi.org/10.3847/1538-4357/ababa3
The solar atmosphere is composed of many species which are populated at different ionization and excitation levels. The upper chromosphere, transition region, and corona are nearly collisionless. Consequently, slippage between, for instance, ions and neutral particles, or interactions between separate species, may play important roles. We have developed a 3D multi-fluid and multi-species numerical code (Ebysus) to investigate such effects. Ebysus is capable of treating species (e.g., hydrogen, helium, etc) and fluids (neutrals, excited and ionized elements) separately, including non-equilibrium ionization, momentum exchange, radiation, thermal conduction, and other complex processes in the solar atmosphere. Treating different species as different fluids leads to drifts between different ions and an electric field that couples these motions. The coupling for two ionized fluids can lead to an anti-phase rotational motion between them. Different ionized species and momentum exchange can dissipate this velocity drift, i.e., convert wave kinetic energy into thermal energy. High frequency Alfvén waves driven by, e.g., reconnection thought to occur in the solar atmosphere, can drive such multi-ion velocity drifts.

Ion–neutral Interactions and Nonequilibrium Ionization in the Solar Chromosphere

Juan **Martínez-Sykora**1,2,4,5, Jorrit Leenaarts3, Bart De Pontieu2,4,5, Daniel Nóbrega-Siverio4,5, Viggo H. Hansteen1,2,4,5, Mats Carlsson4,5, and Mikolaj Szydlarski
2020 ApJ 889 95
https://doi.org/10.3847/1538-4357/ab643f
The thermal structure of the chromosphere is regulated through a complex interaction of various heating processes, radiative cooling, and the ionization degree of the plasma. Here, we study the impact on the thermal properties of the chromosphere when including the combined action of nonequilibrium ionization (NEI) of hydrogen and helium and ion–neutral interaction effects. We have performed a 2.5D radiative magnetohydrodynamic simulation using the Bifrost code. This model includes ion–neutral interaction effects by solving the generalized Ohm' s law (GOL) as well as NEI for hydrogen and helium. The GOL equation includes ambipolar diffusion and the Hall term. We compare this simulation with another simulation that computes the ionization in local thermodynamic equilibrium (LTE) including ion–neutral interaction effects. Our numerical models reveal substantial thermal differences in magneto-acoustic shocks, the wake behind the shocks, spicules, low-lying magnetic loops, and the transition region. In particular, we find that heating through ambipolar diffusion in shock wakes is substantially less efficient, while in the shock fronts themselves it is more efficient, under NEI conditions than when assuming LTE.

On the origin of the magnetic energy in the quiet solar chromosphere

Juan **Martinez-Sykora**, Viggo H. Hansteen, Boris Gudiksen, Mats Carlsson, Bart De Pontieu, Milan Govsic
ApJ **878** 40 **2019**
https://arxiv.org/pdf/1904.04464.pdf
sci-hub.se/10.3847/1538-4357/ab1f0b
The presence of magnetic field is crucial in the transport of energy through the solar atmosphere. Recent ground-based and space-borne observations of the quiet Sun have revealed that magnetic field accumulates at photospheric heights, via a local dynamo or from small-scale flux emergence events. However, most of this small-scale magnetic field may not expand into the chromosphere due to the entropy drop with height at the photosphere. Here we present a study that uses a high resolution 3D radiative MHD simulation of the solar atmosphere with non-grey and non-LTE radiative transfer and thermal conduction along the magnetic field to reveal that: 1) the net magnetic flux from the simulated quiet photosphere is not sufficient to maintain a chromospheric magnetic field (on average), 2) processes in the lower chromosphere, in the region dominated by magneto-acoustic shocks, are able to convert kinetic energy into magnetic energy, 3) the magnetic energy in the chromosphere increases linearly in time until the r.m.s. of the magnetic field strength saturates at roughly 4 to 30 G (horizontal average) due to conversion from kinetic energy, 4) and that the magnetic features formed in the chromosphere are localized to this region.

Impact of Type II Spicules in the Corona: Simulations and Synthetic Observables

Juan **Martínez-Sykora**, Bart De Pontieu, Ineke De Moortel, Viggo H. Hansteen, Mats Carlsson
ApJ **860** 116 **2018**
https://arxiv.org/pdf/1805.06475.pdf
The role of type II spicules in the corona has been a much debated topic in recent years. This paper aims to shed light on the impact of type II spicules in the corona using novel 2.5D radiative MHD simulations including ion-

neutral interaction effects with the Bifrost code. We find that the formation of simulated type II spicules, driven by the release of magnetic tension, impacts the corona in various manners. Associated with the formation of spicules, the corona exhibits 1) magneto-acoustic shocks and flows which supply mass to coronal loops, and 2) transversal magnetic waves and electric currents that propagate at Alfv\'en speeds. The transversal waves and electric currents, generated by the spicule's driver and lasting for many minutes, are dissipated and heat the associated loop. These complex interactions in the corona can be connected with blue shifted secondary components in coronal spectral lines (Red-Blue asymmetries) observed with Hinode/EIS and SOHO/SUMER, as well as the EUV counterpart of type II spicules and propagating coronal disturbances (PCDs) observed with the 171~\AA\ and 193~\AA\ SDO/AIA channels.

On the generation of solar spicules and Alfvénic waves

Juan **Martínez-Sykora**, Bart De Pontieu, Viggo H. Hansteen, Luc Rouppe van der Voort, Mats Carlsson, Tiago M. D. Pereira

2017

https://arxiv.org/ftp/arxiv/papers/1710/1710.07559.pdf

In the lower solar atmosphere, the chromosphere is permeated by jets known as spicules, in which plasma is propelled at speeds of 50 to 150 kilometers per second into the corona. The origin of the spicules is poorly understood, although they are expected to play a role in heating the million-degree corona and are associated with Alfv\'enic waves that help drive the solar wind. We compare magnetohydrodynamic simulations of spicules with observations from the Interface Region Imaging Spectrograph and the Swedish 1-m Solar Telescope. Spicules are shown to occur when magnetic tension is amplified and transported upward through interactions between ions and neutrals or ambipolar diffusion. The tension is impulsively released to drive flows, heat plasma (through ambipolar diffusion), and generate Alfv\'enic waves. **26- June-2015**

Two-dimensional Radiative Magnetohydrodynamic Simulations of Partial Ionization in the Chromosphere. II. Dynamics and Energetics of the Low Solar Atmosphere

Juan **Martínez-Sykora**, Bart De Pontieu, Mats Carlsson, Viggo H. Hansteen, Daniel Nóbrega-Siverio,Boris V. Gudiksen

ApJ **847** 36 **2017**

https://arxiv.org/pdf/1708.06781.pdf

We investigate the effects of interactions between ions and neutrals on the chromosphere and overlying corona using 2.5D radiative MHD simulations with the Bifrost code. We have extended the code capabilities implementing ion-neutral interaction effects using the Generalized Ohm's Law, i.e., we include the Hall term and the ambipolar diffusion (Pedersen dissipation) in the induction equation. Our models span from the upper convection zone to the corona, with the photosphere, chromosphere and transition region partially ionized. Our simulations reveal that the interactions between ionized particles and neutral particles have important consequences for the magneto-thermodynamics of these modeled layers: 1) ambipolar diffusion increases the temperature in the chromosphere; 2) sporadically the horizontal magnetic field in the photosphere is diffused into the chromosphere due to the large ambipolar diffusion; 3) ambipolar diffusion concentrates electrical currents leading to more violent jets and reconnection processes, resulting in 3a) the formation of longer and faster spicules, 3b) heating of plasma during the spicule evolution, and 3c) decoupling of the plasma and magnetic field in spicules. Our results indicate that ambipolar diffusion is a critical ingredient for understanding the magneto-thermo-dynamic properties in the chromosphere and transition region. The numerical simulations have been made publicly available, similar to previous Bifrost simulations. This will allow the community to study realistic numerical simulations with a wider range of magnetic field configurations and physics modules than previously possible.

Misalignment between chromospheric features and magnetic field

Juan **Martínez-Sykora**, Bart De Pontieu, Mats Carlsson, Viggo Hansteen

ApJL 831 L1 **2016**

http://arxiv.org/pdf/1607.02551v1.pdf

Observations of the upper chromosphere shows an enormous amount of intricate fine structure. Much of this comes in the form of linear features which are most often assumed to be well aligned with the direction of the magnetic field in the low plasma beta regime thought to dominate the upper chromosphere. We use advanced radiative MHD simulations including the effects of ion-neutral interactions (using the generalized Ohm's law) in the partially ionized chromosphere to show that the magnetic field is often not well aligned with chromospheric features. This occurs where the ambipolar diffusion is large, i.e., ions and neutral populations decouple as the ion-neutral collision frequency drops allowing the field to slip through the neutral population, currents perpendicular to the field are strong, and thermodynamic timescales are longer than or similar to the those of ambipolar diffusion. We find this often happens in dynamic spicule or fibril-like features at the top of the chromosphere. This has important consequences for field extrapolation methods which increasingly use such upper chromospheric features to help

constrain the chromospheric magnetic field: our results invalidate the underlying assumption that these features are aligned with the field. In addition, our results cast doubt on results from 1D hydrodynamic models, which assume that plasma remains on the same field lines. Finally, our simulations show that ambipolar diffusion significantly alters the amount of free energy available in the coronal part of our simulated volume, which is likely to have consequences for studies of flare initiation.

The Role of Partial Ionization Effects in the Chromosphere

Juan **Martinez-Sykora**, Bart De Pontieu, Viggo H. Hansteen, Mats Carlsson
2015
http://arxiv.org/pdf/1503.02723v1.pdf
The energy for the coronal heating must be provided from the convection zone. The amount and the method by which this energy is transferred into the corona depends on the properties of the lower atmosphere and the corona itself. We review: 1) how the energy could be built in the lower solar atmosphere; 2) how this energy is transferred through the solar atmosphere; and 3) how the energy is finally dissipated in the chromosphere and/or corona. Any mechanism of energy transport has to deal with the various physical processes in the lower atmosphere. We will focus on a physical process that seems to be highly important in the chromosphere and not deeply studied until recently: the ion-neutral interaction effects (INIE) in the chromosphere. We review the relevance and the role of the partial ionization in the chromosphere and show that this process actually impacts considerably the outer solar atmosphere. We include analysis of our 2.5D radiative MHD simulations with the Bifrost code (Gudiksen et al. 2011) including the partial ionization effects on the chromosphere and corona and thermal conduction along magnetic field lines. The photosphere, chromosphere and transition region are partially ionized and the interaction between ionized particles and neutral particles has important consequences on the magneto-thermodynamics of these layers. The INIE are treated using generalized Ohm's law, i.e., we consider the Hall term and the ambipolar diffusion in the induction equation. The interaction between the different species affects the modeled atmosphere as follows: 1) the ambipolar diffusion dissipates magnetic energy and increases the minimum temperature in the chromosphere; 2) the upper chromosphere may get heated and expanded over a greater range of heights. These processes reveal appreciable differences between the modeled atmospheres of simulations with and without INIE.

Internetwork chromospheric bright grains observed with IRIS

Juan **Martínez-Sykora**, Luc Rouppe van der Voort, Mats Carlsson et al.
ApJ, **803** 44 **2015**
http://arxiv.org/pdf/1502.03490v1.pdf
The Interface Region Imaging Spectrograph (IRIS) reveals small-scale rapid brightenings in the form of bright grains all over coronal holes and the quiet sun. These bright grains are seen with the IRIS 1330 \AA, 1400 \AA\ and 2796 \AA\ slit-jaw filters. We combine coordinated observations with IRIS and from the ground with the Swedish 1-m Solar Telescope (SST) which allows us to have chromospheric (Ca II 8542 \AA, Ca II H 3968 \AA, H\alpha, and Mg II k 2796 \AA), and transition region (C II 1334 \AA, Si IV 1402) spectral imaging, and single-wavelength Stokes maps in Fe I 6302 \AA at high spatial (0.33"), temporal and spectral resolution. We conclude that the IRIS slit-jaw grains are the counterpart of so-called acoustic grains, i.e., resulting from chromospheric acoustic waves in a non-magnetic environment. We compare slit-jaw images with spectra from the IRIS spectrograph. We conclude that the grain intensity in the 2796 \AA\ slit-jaw filter comes from both the Mg II k core and wings. The signal in the C II and Si IV lines is too weak to explain the presence of grains in the 1300 and 1400 \AA\ slit-jaw images and we conclude that the grain signal in these passbands comes mostly from the continuum. Even though weak, the characteristic shock signatures of acoustic grains can often be detected in IRIS C II spectra. For some grains, spectral signature can be found in IRIS Si IV. This suggests that upward propagating acoustic waves sometimes reach all the way up to the transition region. 2013 September 22

WHAT DO SPECTRAL LINE PROFILE ASYMMETRIES TELL US ABOUT THE SOLAR ATMOSPHERE?

Juan **Martínez-Sykora**1,2, Bart De Pontieu1, Viggo Hansteen2 and Scott W. McIntosh
2011 ApJ 732 84
Recently, analysis of solar spectra obtained with the EUV Imaging Spectrograph (EIS) onboard the Hinode satellite has revealed the ubiquitous presence of asymmetries in transition region (TR) and coronal spectral line profiles. These asymmetries have been observed especially at the footpoints of coronal loops and have been associated with strong upflows that may play a significant role in providing the corona with hot plasma. Here, we perform a detailed study of the various processes that can lead to spectral line asymmetries, using both simple forward models and state-of-the-art three-dimensional radiative MHD simulations of the solar atmosphere using the Bifrost code. We describe a novel technique to determine the presence and properties of faint secondary components in the wings of spectral line profiles. This method is based on least-squares fitting of observed so-called R(ed)B(lue) asymmetry profiles with pre-calculated RB asymmetry profiles for a wide variety of secondary component properties. We

illustrate how this method could be used to perform reliable double Gaussian fits that are not over- or under-constrained. We also find that spectral line asymmetries appear in TR and coronal lines that are synthesized from our three-dimensional MHD simulations. Our models show that the spectral asymmetries are a sensitive measure of the velocity gradient with height in the TR of coronal loops. The modeled TR shows a large gradient of velocity that increases with height: this occurs as a consequence of ubiquitous, episodic heating at low heights in the model atmosphere. We show that the contribution function of spectral lines as a function of temperature is critical for sensitivity to velocity gradients and thus line asymmetries: lines that are formed over a temperature range that includes most of the TR are the most sensitive. As a result, lines from lithium-like ions (e.g., O VI) are found to be the most sensitive to line asymmetries. We compare the simulated line profiles directly with line profiles observed in the quiet Sun with SOHO/SUMER and Hinode/EIS and find that the shape of the profiles is very similar. In addition, the simulated profiles with the strongest blueward asymmetry occur in footpoint regions of coronal loops, which is similar to what we observe with SUMER and EIS. There is however a significant discrepancy between the simulations and observations: the simulated RB asymmetries are an order of magnitude smaller than the observations. We discuss the possible reasons for this discrepancy. In summary, our analysis shows that observations of spectral line asymmetries can provide a powerful new diagnostic to help constrain coronal heating models.

Proton Fluxes Measured by the PAMELA Experiment from the Minimum to the Maximum Solar Activity for Solar Cycle 24

M. **Martucci**1,2, R. Munini3, M. Boezio3, V. Di Felice4,5, O. Adriani6,7, G. C. Barbarino8,9,G. A. Bazilevskaya …

2018 ApJL 854 L2

http://sci-hub.tw/10.3847/2041-8213/aaa9b2

Precise measurements of the time-dependent intensity of the low-energy (<50 GeV) galactic cosmic rays (GCRs) are fundamental to test and improve the models that describe their propagation inside the heliosphere. In particular, data spanning different solar activity periods, i.e., from minimum to maximum, are needed to achieve comprehensive understanding of such physical phenomena. The minimum phase between solar cycles 23 and 24 was peculiarly long, extending up to the beginning of 2010 and followed by the maximum phase, reached during early 2014. In this Letter, we present proton differential spectra measured from 2010 January to 2014 February by the PAMELA experiment. For the first time the GCR proton intensity was studied over a wide energy range (0.08–50 GeV) by a single apparatus from a minimum to a maximum period of solar activity. The large statistics allowed the time variation to be investigated on a nearly monthly basis. Data were compared and interpreted in the context of a state-of-the-art three-dimensional model describing the GCRs propagation through the heliosphere.

Detection of the solar internal flows with numerical simulation and machine learning

Hiroyuki **Masaki**, Hideyuki Hotta

Publications of the Astronomical Society of Japan **2024**

https://arxiv.org/pdf/2410.06487

The solar interior is filled with turbulent thermal convection, which plays a key role in the energy and momentum transport and the generation of the magnetic field. The turbulent flows in the solar interior cannot be optically detected due to its significant optical depth. Currently, helioseismology is the only way to detect the internal dynamics of the Sun. However, long-duration data with a high cadence is required and only the temporal average can be inferred. To address these issues effectively, in this study, we develop a novel method to infer the solar internal flows using a combination of radiation magnetohydrodynamic numerical simulations and machine/deep learning. With the application of our new method, we can evaluate the large-scale flow at 10 Mm depth from the solar surface with three snapshots separated by an hour. We also apply it to the observational data. Our method is highly consistent with the helioseismology, whereas the amount of input data is significantly reduced.

Solar horizontal flow evaluation using neural network and numerical simulation with snapshot data

Hiroyuki **Masaki**, Hideyuki Hotta, Yukio Katukawa, Ryohtaroh T. Ishikawa

Publ. Astron. Soc. Japan **2023**

https://arxiv.org/pdf/2308.16424.pdf

We suggest a method that evaluates the horizontal velocity in the solar photosphere with easily observable values using a combination of neural network and radiative magnetohydrodynamics simulations. All three-component velocities of thermal convection on the solar surface have important roles in generating waves in the upper atmosphere. However, the velocity perpendicular to the line of sight (LoS) is difficult to observe. To deal with this problem, the local correlation tracking (LCT) method, which employs the difference between two images, has been widely used, but LCT has several disadvantages. We develop a method that evaluates the horizontal velocity from a snapshot of the intensity and the LoS velocity with a neural network. We use data from numerical simulations for training the neural network. While two consecutive intensity images are required for LCT, our network needs just

one intensity image at only a specific moment for input. From these input array, our network outputs a same-size array of two-component velocity field. With only the intensity data, the network achieves a high correlation coefficient between the simulated and evaluated velocities of 0.83. In addition, the network performance can be improved when we add LoS velocity for input, enabling achieving a correlation coefficient of 0.90. Our method is also applied to observed data.

MinXSS-2 CubeSat mission overview: Improvements from the successful MinXSS-1 mission

James Paul **Mason**, Thomas N. Woods, Phillip C. Chamberlin, Andrew Jones, Rick Kohnert, Bennet Schwab, Robert Sewell, Amir Caspi, Christopher S. Moore, Scott Palo, Stanley C. Solomon, Harry Warren

Advances in Space Research 66, 3 **2020**

https://arxiv.org/pdf/1905.01345.pdf

The second Miniature X-ray Solar Spectrometer (MinXSS-2) CubeSat, which begins its flight in late 2018, builds on the success of MinXSS-1, which flew from 2016-05-16 to 2017-05-06. The science instrument is more advanced -- now capable of greater dynamic range with higher energy resolution. More data will be captured on the ground than was possible with MinXSS-1 thanks to a sun-synchronous, polar orbit and technical improvements to both the spacecraft and the ground network. Additionally, a new open-source beacon decoder for amateur radio operators is available that can automatically forward any captured MinXSS data to the operations and science team. While MinXSS-1 was only able to downlink about 1 MB of data per day corresponding to a data capture rate of about 1%, MinXSS-2 will increase that by at least a factor of 6. This increase of data capture rate in combination with the mission's longer orbital lifetime will be used to address new science questions focused on how coronal soft X-rays vary over solar cycle timescales and what impact those variations have on the earth's upper atmosphere.

Solving 3D Magnetohydrostatics with RBF-FD: Applications to the Solar Corona

Nathaniel H. **Mathews**, Natasha Flyer, Sarah E. Gibson

Journal of Computational Physics **2021**

https://arxiv.org/pdf/2112.04561

We present a novel magnetohydrostatic numerical model that solves directly for the force-balanced magnetic field in the solar corona. This model is constructed with Radial Basis Function Finite Differences (RBF-FD), specifically 3D polyharmonic splines plus polynomials, as the core discretization. This set of PDEs is particularly difficult to solve since in the limit of the forcing going to zero it becomes ill-posed with a multitude of solutions. For the forcing equal to zero there are no numerically tractable solutions. For finite forcing, the ability to converge onto a physically viable solution is delicate as will be demonstrated. The static force-balance equations are of a hyperbolic nature, in that information of the magnetic field travels along characteristic surfaces, yet they require an elliptic type solver approach for a sparse overdetermined ill-conditioned system. As an example, we reconstruct a highly nonlinear analytic model designed to represent long-lived magnetic structures observed in the solar corona.

Uncertainty Quantification in Sunspot Counts

Sophie **Mathieu**1, Rainer von Sachs1, Christian Ritter1, Véronique Delouille2, and Laure Lefèvre2

2019 ApJ 886 7

https://doi.org/10.3847/1538-4357/ab4990

Observing and counting sunspots constitutes one of the longest-running scientific experiments, with first observations dating back to Galileo (around 1610). Today the sunspot number (SN) time series acts as a benchmark of solar activity in a large range of physical models. An appropriate statistical modeling, adapted to the time series' complex nature, is, however, still lacking. In this work, we provide the first comprehensive uncertainty quantification analysis of sunspot counts. We study three components: the number of sunspots (N s), the number of sunspot groups (N g), and the composite N c , defined as $N_c := N_s + 10N_g$. Those are reported by a network of observatories around the world and are corrupted by errors of various types. We use a multiplicative framework to provide, for these three components, an estimation of their error distribution in various regimes (short-term, long-term, minima of solar activity). We also propose a robust estimator for the underlying solar signal and fit density distributions that take into account intrinsic characteristics such as overdispersion, excess of zeros, and multiple modes. The estimation of the solar signal underlying the composite N c may be seen as a robust version of the International Sunspot Number (ISN), widely used as a proxy of solar activity. Therefore, our results on N c may help characterize the uncertainty on ISN as well. Our results pave the way for a future monitoring of the observatories in quasi-real time, with the aim of alerting the observers when they start deviating from the network and preventing large drifts from occurring.

Properties of shock waves in the quiet Sun chromosphere

Harsh Mathur, Jayant Joshi, K. Nagaraju, Luc Rouppe van der Voort, Souvik Bose
A&A **2022**
https://arxiv.org/pdf/2210.01045.pdf
Short-lived (100s or less), sub-arcsec to a couple of arcsec size features of enhanced brightenings in the narrowband images at the H2V and K2V positions of the Ca II H and K lines in the quiet Sun are known as bright grains. With simultaneous observations of a quiet Sun internetwork region in the Fe I 6173 Å, Ca II 8542 {AA}, and Ca II K lines acquired by the CRisp Imaging Spectro-Polarimeter and the CHROMospheric Imaging Spectrometer instruments on the Swedish 1-m Solar Telescope, we performed multi-line non-local thermodynamic equilibrium inversions using the STockholm inversion Code to infer the time-varying stratified atmosphere's physical properties such as the temperature, line-of-sight (LOS) velocity, and microturbulence.
The Ca II K profiles of bright grains show enhancement in the K2V peak intensities with absence of the K2R features. At the time of maximum enhancement in the K2V peak intensities, we found average enhancements in temperature at lower chromospheric layers (at $\log\tau500 \simeq -4.2$) of about 1.1 kK with maximum enhancement of about 4.5 kK. These temperature enhancements are colocated with upflows, as strong as -6 kms-1, in the direction of the LOS. The LOS velocities at upper chromospheric layers at $\log\tau500 < -4.2$ show consistent downflows greater than +8 kms-1. The retrieved value of microturbulence in the atmosphere of bright grains is negligible at chromospheric layers.
The study provides observational evidence to support the interpretation that the bright grains observed in narrowband images at the H2V and K2V positions of the Ca II H and K lines are manifestations of upward propagating acoustic shocks against a background of downflowing atmospheres. **2019-06-06**

Confinement of the Solar Tachocline by a Non-Axisymmetric Dynamo
Loren I. **Matilsky**, Nicholas H. Brummell, Bradley W. Hindman, Juri Toomre
ApJ **2023**
https://arxiv.org/pdf/2311.10202.pdf
We recently presented the first 3D numerical simulation of the solar interior for which tachocline confinement was achieved by a dynamo-generated magnetic field. In this followup study, we analyze the degree of confinement as the magnetic field strength changes (controlled by varying the magnetic Prandtl number) in a coupled radiative zone (RZ) and convection zone (CZ) system. We broadly find three solution regimes, corresponding to weak, medium, and strong dynamo magnetic field strengths. In the weak-field regime, the large-scale magnetic field is mostly axisymmetric with regular, periodic polarity reversals (reminiscent of the observed solar cycle), but fails to create a confined tachocline. In the strong-field regime, the large-scale field is mostly non-axisymmetric with irregular, quasi-periodic polarity reversals, and creates a confined tachocline. In the medium-field regime, the large-scale field resembles a strong-field dynamo for extended intervals, but intermittently weakens to allow temporary epochs of strong differential rotation. In all regimes, the amplitude of poloidal field strength in the RZ is very well explained by skin-depth arguments, wherein the oscillating field that gives rise to the skin depth (in the medium- and strong-field cases) is a non-axisymmetric field structure rotating with respect to the RZ. These new simulations reaffirm that tachocline confinement by the solar dynamo (the so-called fast magnetic confinement scenario) is possible, but suggest a new picture in which non-axisymmetric field components rotating with respect to the RZ play the primary role, instead of the regularly reversing axisymmetic field associated with the 22-year cycle.

Confinement of the Solar Tachocline by Dynamo Action in the Radiative Interior
Loren I. **Matilsky**1, Bradley W. Hindman1,2, Nicholas A. Featherstone3, Catherine C. Blume1, and Juri Toomre1
2022 ApJL 940 L50
https://iopscience.iop.org/article/10.3847/2041-8213/ac93ef/pdf
A major outstanding problem in solar physics is the confinement of the solar tachocline, the thin shear layer that separates nearly solid-body rotation in the radiative interior from strong differential rotation in the convection zone. Here, we present the first 3D, global solar simulation that displays a magnetically confined tachocline. The nonaxisymmetric magnetism is initially built in the convection zone and then diffusively imprints downward, similar to the proposed fast magnetic confinement scenario by the Sun's cyclic dynamo field. Additionally, the field is locally amplified throughout the radiative interior by vigorous horizontal motions that seem to arise from a combination of equatorial Rossby waves and shear, magnetic, and buoyancy instabilities. Our work thus supports prior studies proposing dynamo action in the radiative interior, and suggests that horizontal motions could play a key role in driving this deep dynamo.

Full compressible 3D magnetohydrodynamic simulation of solar wind
Takuma **Matsumoto**
MNRAS **2020**

https://arxiv.org/pdf/2009.03770
Identifying the heating mechanisms of the solar corona and the driving mechanisms of solar wind are key challenges in understanding solar physics. A full three-dimensional compressible magnetohydrodynamic (MHD) simulation was conducted to distinguish between the heating mechanisms in the fast solar wind above the open field region. Our simulation describes the evolution of the Alfvénic waves, which includes the compressible effects from the photosphere to the heliospheric distance s of 27 solar radii ($R_\odot$). The hot corona and fast solar wind were reproduced simultaneously due to the dissipation of the Alfvén waves. The inclusion of the transition region and lower atmosphere enabled us to derive the solar mass loss rate for the first time by performing a full three-dimensional compressible MHD simulation. The Alfvén turbulence was determined to be the dominant heating mechanism in the solar wind acceleration region ($s>1.3R_\odot$), as suggested by previous solar wind models. In addition, shock formation and phase mixing are important below the lower transition region ($s<1.03R_\odot$) as well.

Spontaneous Formation of Surface Magnetic Structure from Large-scale Dynamo in Strongly-stratified Convection

Youhei **Masada**, Takayoshi Sano
ApJL **822** L22 **2016**
http://arxiv.org/pdf/1604.05374v1.pdf
We report the first successful simulation of spontaneous formation of surface magnetic structures from a large-scale dynamo by strongly-stratified thermal convection in Cartesian geometry. The large-scale dynamo observed in our strongly-stratified model has physical properties similar to those in earlier weakly-stratified convective dynamo simulations, indicating that the α2-type mechanism is responsible for it. Additionally to the large-scale dynamo, we find that large-scale structures of the vertical magnetic field are spontaneously formed in the convection zone surface only for the case of strongly-stratified atmosphere. The organization of the vertical magnetic field proceeds in the upper convection zone within tens of convective turn-over time and band-like bipolar structures are recurrently-appeared in the dynamo-saturated stage. We examine possibilities of several candidates as the origin of the surface magnetic structure formation, and then suggest the existence of an as-yet-unknown mechanism for the self-organization of the large-scale magnetic structure, which should be inherent in the strongly-stratified convective atmosphere.

Cross-Referenced NOAA Active Region List for Multi-Rotation Active Regions, 2011-2019 Now Available

Emily **Mason**1, Kara Kniezewski2, David Fritz3
HMI Science Nuggets #195 **2023**
http://hmi.stanford.edu/hminuggets/?p=4161
The National Oceanic and Atmospheric Administration (NOAA) identifies and tracks active regions (ARs) due to their role in producing geoeffective space weather, numbering every AR that appears or rotates into view as the Sun rotates. NOAA does not, however, track which ARs persist for multiple solar rotations. This becomes a challenge for researchers looking to study the life cycle of ARs, as older ARs are given new numbers that don't relate to their previous designations. We have constructed a database of linked NOAA AR numbers for the years 2011 – 2019 to lower the barrier for long-term AR study.
Active Regions with Multiple NOAA Numbers, 2011-2019
https://zenodo.org/record/8336354

Time-Dependent Dynamics of the Corona

Emily I. **Mason**, Roberto Lionello, Cooper Downs, Jon A. Linker, Ronald M. Caplan
ApJ **2023**
https://arxiv.org/pdf/2306.11956.pdf
We present in this Letter the first global comparison between traditional line-tied steady state magnetohydrodynamic models and a new, fully time-dependent thermodynamic magnetohydrodynamic simulation of the global corona. The maps are scaled to the approximate field distributions and magnitudes around solar minimum using the Lockheed Evolving Surface-Flux Assimilation Model to incorporate flux emergence and surface flows over a full solar rotation, and include differential rotation and meridional flows. Each time step evolves the previous state of the plasma with a new magnetic field input boundary condition. We find that this method is a significant improvement over steady-state models, as it closely mimics the constant photospheric driving on the Sun. The magnetic energy levels are higher in the time-dependent model, and coronal holes evolve more along the following edge than they do in steady-state models. Coronal changes, as illustrated with forward-modeled emission maps, evolve on longer timescales with time-dependent driving. We discuss implications for active and quiet Sun scenarios, solar wind formation, and widely-used steady state assumptions like potential field source surface calculations.

Coronal Heating as Determined by the Solar Flare Frequency Distribution Obtained by Aggregating Case Studies

James Paul **Mason**, Alexandra Werth, Colin G. West, Allison A. Youngblood, Donald L. Woodraska, Courtney Peck, +++++

ApJ **948** 71 **2023**

https://arxiv.org/pdf/2305.05687.pdf

https://iopscience.iop.org/article/10.3847/1538-4357/accc89/pdf

Flare frequency distributions represent a key approach to addressing one of the largest problems in solar and stellar physics: determining the mechanism that counter-intuitively heats coronae to temperatures that are orders of magnitude hotter than the corresponding photospheres. It is widely accepted that the magnetic field is responsible for the heating, but there are two competing mechanisms that could explain it: nanoflares or Alfvén waves. To date, neither can be directly observed. Nanoflares are, by definition, extremely small, but their aggregate energy release could represent a substantial heating mechanism, presuming they are sufficiently abundant. One way to test this presumption is via the flare frequency distribution, which describes how often flares of various energies occur. If the slope of the power law fitting the flare frequency distribution is above a critical threshold, $\alpha=2$ as established in prior literature, then there should be a sufficient abundance of nanoflares to explain coronal heating. We performed >600 case studies of solar flares, made possible by an unprecedented number of data analysts via three semesters of an undergraduate physics laboratory course. This allowed us to include two crucial, but nontrivial, analysis methods: pre-flare baseline subtraction and computation of the flare energy, which requires determining flare start and stop times. We aggregated the results of these analyses into a statistical study to determine that $\alpha=1.63\pm0.03$. This is below the critical threshold, suggesting that Alfvén waves are an important driver of coronal heating. **2016-07-24, 2016-11-29, 2017-02-22**

MinXSS-2 CubeSat mission overview: Improvements from the successful MinXSS-1 mission

James Paul **Mason**, Thomas N. Woods, Phillip C. Chamberlin, Andrew Jones, Rick Kohnert, Bennet Schwab, Robert Sewell, Amir Caspi, Christopher S. Moore, Scott Palo, Stanley C. Solomon, Harry Warren

2020, Adv. Space Res., 66, 3; DOI: 10.1016/j.asr.2019.02.011

https://www.sciencedirect.com/science/article/pii/S0273117719301152?via%3Dihub

The second Miniature X-ray Solar Spectrometer (MinXSS-2) CubeSat, which begins its flight in late 2018, builds on the success of MinXSS-1, which flew from 2016-05-16 to 2017-05-06. The science instrument is more advanced – now capable of greater dynamic range with higher energy resolution. More data will be captured on the ground than was possible with MinXSS-1 thanks to a sun-synchronous, polar orbit and technical improvements to both the spacecraft and the ground network. Additionally, a new open-source beacon decoder for amateur radio operators is available that can automatically forward any captured MinXSS data to the operations and science team. While MinXSS-1 was only able to downlink about 1 MB of data per day corresponding to a data capture rate of about 1%, MinXSS-2 will increase that by at least a factor of 6. This increase of data capture rate in combination with the mission's longer orbital lifetime will be used to address new science questions focused on how coronal soft X-rays vary over solar cycle timescales and what impact those variations have on the earth's upper atmosphere.

MinXSS-1 CubeSat On-Orbit Pointing and Power Performance: The First Flight of the Blue Canyon Technologies XACT 3-axis Attitude Determination and Control System

James P. **Mason**, Matt Baumgart, Bryan Rogler, Chloe Downs, Margaret Williams, Thomas N. Woods, Scott Palo, Phillip C. Chamberlin, Stanley Solomon, Andrew Jones, Xinlin Li, Rick Kohnert, Amir Caspi

J. Small Satellites, 6(3), 651, **2017**

https://jossonline.com/wp-content/uploads/2018/01/Mason-Final-MinXSS-1-CubeSat-On-Orbit-Pointing-and-Power-Performance.pdf

The Miniature X-ray Solar Spectrometer (MinXSS) is a three-unit (3U) CubeSat designed for a three-month mission to study solar soft X-ray spectral irradiance. The first of the two flight models was deployed from the International Space Station in May 2016, and operated for one year before its natural deorbiting. This was the first flight of the Blue Canyon Technologies XACT 3-axis attitude determination and control system ? a commercially available, high-precision pointing system. The performance of the pointing system on orbit was characterized, including performance at low altitudes where drag torque builds up. It was found that the pointing accuracy was 0.0042? - 0.0117? (15" - 42", 3 sigma, axis dependent) consistently from 190 km - 410 km, slightly better than the specification sheet states. Peak-to-peak jitter was estimated to be 0.0073? (10 s-1) - 0.0183? (10 s-1) (26" (10 s-1) - 66" (10 s-1), 3 sigma). The system was capable of dumping momentum until an altitude of 185 km. Small amounts of sensor degradation were found in the star tracker and coarse sun sensor. The mission profile did not require high-agility maneuvers, so it was not possible to characterize this metric. Without a GPS receiver, it was necessary to periodically upload ephemeris information to update the orbit propagation model and maintain pointing. At 400 km,

these uploads were required once every other week; at ~270 km, they were required every day. The power performance of the electric power system was also characterized, including use of a novel pseudo-peak power tracker ? a resistor that limited the current draw from the battery on the solar panels. With 19 30% efficient solar cells and an 8 W system load, the power balance had 65% of margin on orbit. The current paper presents several recommendations to other CubeSat programs throughout.

MEM_GE: a new maximum entropy method for image reconstruction from solar X-ray visibilities

Paolo **Massa**, Richard Schwartz, A Kim Tolbert, Anna Maria Massone, Brian R Dennis, Michele Piana, Federico Benvenuto

ApJ **894** 46 **2020**

https://arxiv.org/pdf/2002.07921v1.pdf

https://doi.org/10.3847/1538-4357/ab8637

Maximum Entropy is an image reconstruction method conceived to image a sparsely occupied field of view and therefore particularly appropriate to achieve super-resolution effects. Although widely used in image deconvolution, this method has been formulated in radio astronomy for the analysis of observations in the spatial frequency domain, and an Interactive Data Language (IDL) code has been implemented for image reconstruction from solar X-ray Fourier data. However, this code relies on a non-convex formulation of the constrained optimization problem addressed by the Maximum Entropy approach and this sometimes results in unreliable reconstructions characterized by unphysical shrinking effects.

This paper introduces a new approach to Maximum Entropy based on the constrained minimization of a convex functional. In the case of observations recorded by the Reuven Ramaty High Energy Solar Spectroscopic Imager (RHESSI), the resulting code provides the same super-resolution effects of the previous algorithm, while working properly also when that code produces unphysical reconstructions. Results are also provided of testing the algorithm with synthetic data simulating observations of the Spectrometer/Telescope for Imaging X-rays (STIX) in Solar Orbiter. The new code is available in the {\em{HESSI}} folder of the Solar SoftWare (SSW)tree.

Compressed sensing and Sequential Monte Carlo for solar hard X-ray imaging

Anna Maria Massone, Federica Sciacchitano, Michele Piana, Alberto Sorrentino

'Nuovo Cimento' as proceeding SOHE3 **2018**

https://arxiv.org/pdf/1812.08413.pdf

We describe two inversion methods for the reconstruction of hard X-ray solar images. The methods are tested against experimental visibilities recorded by the Reuven Ramaty High Energy Solar Spectroscopic Imager (RHESSI) and synthetic visibilities based on the design of the Spectrometer/Telescope for Imaging X-rays (STIX).

First Observations from the Multi-Application Solar Telescope (MAST) Narrow-Band Imager

Shibu K. **Mathew**, Ankala Raja Bayanna, Alok Ranjan Tiwary, Ramya Bireddy…

Solar Physics August **2017**, 292:106

The *Multi-Application Solar Telescope* is a 50 cm off-axis Gregorian telescope recently installed at the Udaipur Solar Observatory, India. In order to obtain near-simultaneous observations at photospheric and chromospheric heights, an imager optimized for two or more wavelengths is being integrated with the telescope. Two voltage-tuneable lithium-niobate Fabry–Perot etalons along with a set of interference blocking filters have been used for developing the imager. Both of the etalons are used in tandem for photospheric observations in Fe I 6173 Å and chromospheric observation in Hαα 6563 Å spectral lines, whereas only one of the etalons is used for the chromospheric Ca II line at 8542 Å. The imager is also being used for spectropolarimetric observations. We discuss the characterization of the etalons at the above wavelengths, detail the integration of the imager with the telescope, and present a few sets of observations taken with the imager set-up.

Nonparametric monitoring of sunspot number observations: a case study

Sophie **Mathieu**, Laure Lefèvre, Rainer von Sachs, Véronique Delouille, Christian Ritter, Frédéric Clette

2021

https://arxiv.org/pdf/2106.13535.pdf

Solar activity is an important driver of long-term climate trends and must be accounted for in climate models. Unfortunately, direct measurements of this quantity over long periods do not exist. The only observation related to solar activity whose records reach back to the seventeenth century are sunspots. Surprisingly, determining the number of sunspots consistently over time has remained until today a challenging statistical problem. It arises from the need of consolidating data from multiple observing stations around the world in a context of low signal-to-noise ratios, non-stationarity, missing data, non-standard distributions and many kinds of errors. The data from some

stations experience therefore severe and various deviations over time. In this paper, we propose the first systematic and thorough statistical approach for monitoring these complex and important series. It consists of three steps essential for successful treatment of the data: smoothing on multiple timescales, monitoring using block bootstrap calibrated CUSUM charts and classifying of out-of-control situations by support vector techniques. This approach allows us to detect a wide range of anomalies (such as sudden jumps or more progressive drifts), unseen in previous analyses. It helps us to identify the causes of major deviations, which are often observer or equipment related. Their detection and identification will contribute to improve future observations. Their elimination or correction in past data will lead to a more precise reconstruction of the world reference index for solar activity: the International Sunspot Number.

Uncertainty quantification in sunspot counts

Sophie **Mathieu**, Véronique Delouille, Laure Lefèvre, Christian Ritter, Rainer von Sachs
The Astrophysical Journal 886(1):7 **2019**
https://sci-hub.st/10.3847/1538-4357/ab4990
https://arxiv.org/pdf/2009.09810.pdf
Observing and counting sunspots constitutes one of the longest-running scientific experiment, with first observations dating back to Galileo and the invention of the telescope around 1610. Today the sunspot number (SN) time series acts as a benchmark of solar activity in a large range of physical models. An appropriate statistical modelling, adapted to the time series' complex nature, is however still lacking. In this work, we provide the first comprehensive uncertainty quantification analysis of sunspot counts. Our interest lies in the following three components: the number of spots (Ns), the number of sunspot groups (Ng), and the composite Nc, defined as Nc:=Ns+10Ng. Those are reported by a network of observatories around the world, and are corrupted by errors of various types. We use a multiplicative framework to provide, for each of the three components, an estimation of their error distribution in various regimes (short-term, long-term, minima of solar activity). We also propose a robust estimator for the underlying solar signal and fit a density distribution that takes into account intrinsic characteristics such as over-dispersion, excess of zeros, and multiple modes. The estimation of the solar signal underlying the composite Nc may be seen as a robust version of the International Sunspot Number (ISN), a quantity widely used as a proxy of solar activity. Therefore our results on Nc may serve to characterize the uncertainty on ISN as well. Our results paves the way for a future monitoring of the observatories in quasi-real time, with the aim to alert the observers when they start deviating from the network and prevent large drifts from occurring in the network.

Study of cosmic ray intensity in relation to the interplanetary magnetic field and geomagnetic storms for solar cycle 24

Chandni **Mathpal**, Lalan Prasad, Meena Pokharia, Chandrashekhar Bhoj
Astrophysics and Space Science August **2018**, 363:177
http://sci-hub.tw/10.1007/s10509-018-3390-2
In the present study, we investigate the association of cosmic ray intensity (CRI) with various solar wind parameters (i.e. solar wind speed V, plasma proton temperature, plasma proton density), interplanetary magnetic field (IMF B), geomagnetic storms (GSs), averaged planetary A-index (Ap index) and sun spot number (SSN) for the period 2009–2016 (solar cycle 24) by using their daily mean average. To find the association of CRI with various solar wind parameters, GSs, IMF B, Ap index and SSN, we incorporate the analysis technique by superposed-epoch method. We have observed that CRI decreases with the increase in IMF B. Moreover the time-lag analysis has been performed by the method of correlation coefficient and observed a time lag of 0 to 2 day between the decrease in CRI and increase in IMF B. In addition, we show that the CRI is found to decrease in a similar pattern to disturbance storm time (Dst index) for most of the period of solar cycle 24. The high and positive correlation is found between CRI and Dst index. The CRI and Ap index are better anti-correlated to each other than CRI and IMF. CRI and SSN are positively correlated with each other. Solar wind parameters such as solar wind speed V is a CR-effective parameter while plasma proton temperature and plasma proton density are not CR-effective parameters. The indicated parameters such as Dst index, Ap index, IMF B and solar wind parameters such as solar wind speed V, plasma proton temperature, plasma proton density shows a kind of irregular variations for solar cycle 23 and 24 while CRI and SSN shows distinct behaviour for the two cycle.

Solar Tachocline Confinement by the Nonaxisymmetric Modes of a Dynamo Magnetic Field

Loren I. **Matilsky**4,1, Nicholas H. Brummell1, Bradley W. Hindman2,3, and Juri Toomre3
2024 ApJ 962 189
https://iopscience.iop.org/article/10.3847/1538-4357/ad18b2/pdf
We recently presented the first 3D numerical simulation of the solar interior for which tachocline confinement was achieved by a dynamo-generated magnetic field. In this follow-up study, we analyze the degree of confinement as the magnetic field strength changes (controlled by varying the magnetic Prandtl number) in a coupled radiative zone (RZ) and convection zone (CZ) system. We broadly find three solution regimes, corresponding to weak, medium,

and strong dynamo magnetic field strengths. In the weak-field regime, the large-scale magnetic field is mostly axisymmetric with regular, periodic polarity reversals (reminiscent of the observed solar cycle) but fails to create a confined tachocline. In the strong-field regime, the large-scale field is mostly nonaxisymmetric with irregular, quasi-periodic polarity reversals and creates a confined tachocline. In the medium-field regime, the large-scale field resembles a strong-field dynamo for extended intervals but intermittently weakens to allow temporary epochs of strong differential rotation. In all regimes, the amplitude of poloidal field strength in the RZ is very well explained by skin-depth arguments, wherein the oscillating field that gives rise to the skin depth (in the medium- and strong-field cases) is a nonaxisymmetric field structure at the base of the CZ that rotates with respect to the RZ. These simulations suggest a new picture of solar tachocline confinement by the dynamo, in which nonaxisymmetric, very long-lived (effectively permanent) field structures rotating with respect to the RZ play the primary role, instead of the regularly reversing axisymmetric field associated with the 22 yr cycle.

Confinement of the Solar Tachocline by Dynamo Action in the Radiative Interior

Loren I. **Matilsky**, Bradley W. Hindman, Nicholas A. Featherstone, Catherine C. Blume, Juri Toomre
ApJL **2022**
https://arxiv.org/pdf/2206.12920
A major outstanding problem in solar physics is the confinement of the solar tachocline, the thin shear layer that separates nearly solid-body rotation in the radiative interior from strong differential rotation in the convection zone. Here, we present the first 3-D, global solar simulation in which a tachocline is confined by a self-excited dynamo. The non-axisymmetric magnetism is initially built in the convection zone and then diffusively imprints downward. Additionally, the field is locally amplified throughout the radiative interior by vigorous horizontal motions that arise from equatorial Rossby waves and possibly shear instabilities. Our work thus challenges the long-held notion that the Sun's dynamo magnetic field is amplified only as deep as the tachocline and stored in a quiescent radiative interior.

Building and Maintaining a Solar Tachocline through Convective Dynamo Action

Loren I. **Matilsky**, Juri Toomre
In the 20.5th Cambridge Workshop on Cool Stars, Stellar Systems, and the Sun, edited by Scott J. Wolk **2021**
https://arxiv.org/pdf/2105.05412.pdf
For more than thirty years, the dynamical maintenance of the thin solar tachocline has remained one of the central outstanding problems of stellar astrophysics. Three main theories have been developed to explain the tachocline's thinness, but so far none of them has been shown to work convincingly in the extreme parameter regime of the solar interior. Here, we present a rotating, 3D, spherical-shell simulation of a combined solar-like convection zone and radiative zone that achieves a tachocline built and maintained by convective dynamo action. Because of numerical constraints, the dynamo prevents the viscous spread of the tachocline instead of the Eddington-Sweet-time-scale radiative spread believed to occur in the Sun. Nonetheless, our simulation supports the scenario of tachocline confinement via the cyclic solar dynamo, and is the first time one of the main confinement scenarios has been realized in a global, 3D, spherical-shell geometry including nonlinear fluid motions and a self-consistently generated dynamo.

Revisiting the Sun's Strong Differential Rotation along Radial Lines

Loren I. **Matilsky**, Bradley W. Hindman, Juri Toomre
ApJ **898** 111 **2020**
https://arxiv.org/pdf/2004.00208.pdf
https://iopscience.iop.org/article/10.3847/1538-4357/ab9ca0/pdf
Current state-of-the-art models of the solar convection zone consist of solutions to the Navier-Stokes equations in rotating, 3D spherical shells. Such models are highly sensitive to the choice of boundary conditions. Here we present two suites of simulations differing only in their outer thermal boundary condition, which is either one of fixed-entropy or fixed-entropy-gradient. We find that the resulting differential rotation is markedly different between the two sets. The fixed-entropy-gradient simulations have strong differential rotation contrast and isocontours tilted along radial lines (in good agreement with the Sun's interior rotation revealed by helioseismology), while the fixed-entropy simulations have weaker contrast and contours tilted in the opposite sense. We examine in detail the force balances leading to the different rotation profiles and find that the poleward transport of heat by Busse columns plays a key role. We conclude that the Sun's strong differential rotation along radial lines may result from the solar emissivity being invariant with latitude (which is similar to the fixed-entropy-gradient condition in our models) and the poleward transport of heat by Busse columns. In future work on convection in the solar context, we strongly advise modelers to use a fixed-gradient outer boundary condition.

Exploring Bistability in the Cycles of the Solar Dynamo through Global Simulations

Loren **Matilsky**, Juri Toomre
2020 *ApJ* **892** 106
https://iopscience.iop.org/article/10.3847/1538-4357/ab791c/pdf
https://arxiv.org/pdf/1912.08158.pdf
The calling card of solar magnetism is the sunspot cycle, during which sunspots regularly reverse their polarity sense every 11 years. However, a number of more complicated time-dependent behaviors have also been identified. In particular, there are temporal modulations associated with active longitudes and hemispheric asymmetry, when sunspots appear at certain solar longitudes or else in one hemisphere preferentially. So far, a direct link between between this asymmetric temporal behavior and the underlying solar dynamo has remained elusive. In this work, we present results from global, 3D magnetohydrodynamic (MHD) simulations, which for the first time display both behavior reminiscent of the sunspot cycle (regular polarity reversals and equatorward migration of internal magnetic field) and asymmetric, irregular behavior that in the simulations we interpret as active longitudes and hemispheric asymmetry. The simulations are thus bistable, in that the turbulent convection can stably support two distinct flavors of magnetism at different times, in superposition, or with smooth transitions from one state to the other. We discuss this new family of dynamo models in the context of the extensive observations of the Sun's surface magnetic field with the Solar and Heliospheric Observatory (SOHO) and the Solar Dynamics Observatory (SDO), as well as earlier observations of sunspot number and synoptic maps. We suggest that the solar dynamo itself may be bistable in nature, exhibiting two types of temporal behavior in the magnetic field.

Exploring the Influence of Density Contrast on Solar Near-Surface Shear

Loren I. **Matilsky**, Bradley W. Hindman, Juri Toomre
https://arxiv.org/pdf/1811.00665.pdf
The 20th Cambridge Workshop on Cool Stars, Stellar Systems, and the Sun, edited by Scott J. **2018**
https://arxiv.org/pdf/1811.00665.pdf
The advent of helioseismology has determined in detail the average rotation rate of the Sun as a function of radius and latitude. These data immediately reveal two striking boundary layers of shear in the solar convection zone (CZ): a tachocline at the base, where the differential rotation of the CZ transitions to solid-body rotation in the radiative zone, and a 35-Mm-thick near-surface shear layer (NSSL) at the top, where the rotation rate slows by about 5% with increasing radius. Though asteroseismology cannot probe the differential rotation of distant stars to the same level of detail that helioseismology can achieve for the Sun, it is possible that many cool stars with outer convective envelopes possess similar differential rotation characteristics, including both a tachocline and a NSSL. Here we present the results of 3D global hydrodynamic simulations of spherical-shell convection for a Sun-like star at different levels of density contrast across the shell. The simulations with high stratification possess characteristics of near-surface shear, especially at low latitudes. We discuss in detail the dynamical balance of torques giving rise to the NSSL in our models and interpret what these balances imply for the real Sun. We further discuss the dynamical causes that may serve to wipe out near-surface shear at high latitudes, and conclude by offering some theories as to how this problem might be tackled in future work.

The Role of Downflows in Establishing Solar Near-Surface Shear

Loren I. **Matilsky**, Bradley W. Hindman, J. Toomre
ApJ **871** 217 **2019**
https://arxiv.org/pdf/1810.00115.pdf
https://iopscience.iop.org/article/10.3847/1538-4357/aaf647/pdf
The dynamical origins of the Sun's tachocline and near-surface shear layer (NSSL) are still not well understood. We have attempted to self-consistently reproduce a NSSL in numerical simulations of a solar-like convection zone by increasing the density contrast across rotating, 3D spherical shells. We explore the hypothesis that high density contrast leads to near-surface shear by creating a rotationally unconstrained layer of fast flows near the outer surface. Although our high-contrast models do have near-surface shear, it is confined primarily to low latitudes (between ±15◦). Two distinct types of flow structures maintain the shear dynamically: rotationally constrainedBusse columns aligned with the rotation axis and fast, rotationally unconstrained downflow plumes that deplete angular momentum from the outer fluid layers. The plumes form at all latitudes, and in fact are more efficient at transporting angular momentum inward at high latitudes. The presence of Busse columns at low latitudes thus appears essential to creating near-surface shear in our models. We conclude that a solar-like NSSL is unobtainable from a rotationally unconstrained outer fluid layer alone. In numerical models, the shear is eliminated through the advection of angular momentum by the meridional circulation. Therefore, a detailed understanding how the solar meridional circulation is dynamically achieved will be necessary to elucidate the origin of the Sun's NSSL.

Thermal responses in a coronal loop maintained by wave heating mechanisms

Takuma **Matsumoto**

Monthly Notices of the Royal Astronomical Society, Volume 476, Issue 3, 21 May **2018**, Pages 3328–3335,
http://sci-hub.tw/https://academic.oup.com/mnras/article-abstract/476/3/3328/4907980?
A full 3-dimensional compressible magnetohydrodynamic (MHD) simulation is conducted to investigate the thermal responses of a coronal loop to the dynamic dissipation processes of MHD waves. When the foot points of the loop are randomly and continuously forced, the MHD waves become excited and propagate upward. Then, 1-MK temperature corona is produced naturally as the wave energy dissipates. The excited wave packets become non-linear just above the magnetic canopy, and the wave energy cascades into smaller spatial scales. Moreover, collisions between counter-propagating Alfvén wave packets increase the heating rate, resulting in impulsive temperature increases. Our model demonstrates that the heating events in the wave-heated loops can be nanoflare-like in the sense that they are spatially localized and temporally intermittent.

Competition between shock and turbulent heating in coronal loop system

Takuma **Matsumoto**
MNRAS **2016**
http://arxiv.org/pdf/1606.06019v1.pdf
2.5-dimensional magnetohydrodynamic (MHD) simulations are performed with high spatial resolution in order to distinguish between competing models of the coronal heating problem. A single coronal loop powered by Alfv\'{e}n waves excited in the photosphere is the target of the present study. The coronal structure is reproduced in our simulations as a natural consequence of the transportation and dissipation of Alfv\'{e}n waves. Further, the coronal structure is maintained as the spatial resolution is changed from 25 to 3 km, although the temperature at the loop top increases with the spatial resolution. The heating mechanisms change gradually across the magnetic canopy at a height of 4 Mm. Below the magnetic canopy, both the shock and the MHD turbulence are dominant heating processes. Above the magnetic canopy, the shock heating rate reduces to less than 10 % of the total heating rate while the MHD turbulence provides significant energy to balance the radiative cooling and thermal conduction loss or gain. The importance of compressibility shown in the present study would significantly impact on the prospects of successful MHD turbulence theory in the solar chromosphere.

The European Solar Telescope

Sarah **Matthews**, Mihalis Mathioudakis, Robertus von Fay-Siebenburgen
UKSP nugget #73, Oct **2016**
http://www.uksolphys.org/uksp-nugget/73-the-european-solar-telescope/
The European Solar Telescope (EST) is a pan-European 4m ground-based solar telescope planned for construction in the Canaries, with first-light in 2026. The EST consortium consists of 27 partners from 14 European countries

Searching for the Origin of Sun-quakes

Sarah **Matthews**, Sergei Zharkov & Valentina Zharkova
UKSP nugget, May **2011**, http://www.uksolphys.org/?p=2414
What launches a sunquake – particles, heating, or something completely different?

Neural Network for Solar Irradiance Modeling (NN-SIM)

Steffen **Mauceri**, Odele Coddington, Danielle Lyles, Peter Pilewskie
Solar Physics October **2019**, 294:160
https://link.springer.com/content/pdf/10.1007%2Fs11207-019-1555-y.pdf
An understanding of solar variability over a broad range of wavelengths and timescales is needed by scientists studying Earth's climate. While the current understanding of solar irradiance from measurements and models is maturing, there remain notable areas of discrepancy that highlight a lack of understanding of the variability in solar spectral irradiance (SSI) on 27-day solar-rotational timescales and longer, and in total solar irradiance (TSI) at solar-cycle timescales and longer. The sources of instrumental noise and instability suspected behind differences in independent measurement records are actively debated. Furthermore, estimates from solar-irradiance empirical-proxy models and semi-empirical models also differ from each other and from the observations by varying degrees. To investigate whether models and observations can be brought into closer agreement we developed a novel, data-driven, solar-irradiance model using an ensemble of feed-forward artificial neural networks. Key features of our model architecture include a non-linear relationship between solar-activity proxy and irradiance with a high degree of freedom that comes from the incorporation of a greater number of solar-activity proxies than previous proxy models. Furthermore, we utilize a recent re-analysis of solar spectral irradiance (SSI) observations, stemming from a new degradation-correction methodology, to develop our model. Our approach, the Neural Network for Solar Irradiance Modeling (NN-SIM), reconstructs total solar irradiance and SSI from 205 nm to 2300 nm and from 1979 to the present day. We find close agreement between NN-SIM and various observational records as well as independent models. NN-SIM is available at lasp.colorado.edu/lisird/.

Revision of the Sun's Spectral Irradiance as Measured by SORCE SIM

Steffen **Mauceri** Peter Pilewskie Erik Richard Odele Coddington Jerald Harder Tom Woods
Solar Physics December **2018**, 293:161

The Spectral Irradiance Monitor (SIM) instrument on board the Solar Radiation and Climate Experiment (SORCE) performs daily measurements of the solar spectral irradiance (SSI) from 200 to 2400 nm. Both temporal and spectral corrections for instrument degradation have been built on physical models based on comparison of two independent channels with different solar exposure. The present study derives a novel correction for SIM degradation using the total solar irradiance (TSI) measurements from the Total Irradiance Monitor (TIM) on SORCE. The correction is applied to SIM SSI data from September 2004 to October 2012 over the wavelength range from 205 nm to 2300 nm. The change in corrected, integrated SSI agrees within 0.1 Wm−20.1 Wm−2(1σ1σ) with SORCE TIM TSI and independently shows agreement with the SATIRE-S and NRLSSI2 solar models within measurement uncertainties.

Magnetic and Velocity Field Topology in Active Regions of Descending Phase of the Solar Cycle 23

R. A. **Maurya**, A. Ambastha
Solar Phys. **295**, Article number: 106 **2020**
https://arxiv.org/pdf/2006.13602.pdf
https://link.springer.com/content/pdf/10.1007/s11207-020-01666-4.pdf

We analyse the topology of photospheric magnetic fields and sub-photospheric flows of several active regions (ARs) that are observed during the peak to descending phase of the solar cycle 23. Our analysis shows clear evidence of hemispheric preferences in all the topological parameters such as the magnetic, current and kinetic helicities, and the 'curl-divergence'. We found that 68\%(67\%) ARs in the northern (southern) hemisphere with negative (positive) magnetic helicities. Same hemispheric preference sign is found for the current helicities in 68\%(68\%) ARs. The hemispheric preferences are found to exist statistically for all the time except in few ARs observed during the peak and the end phases of the solar cycle. This means that magnetic fields are dominantly left(right)-helical in scales smaller than individual ARs of northern(southern) hemisphere. We found that magnetic and current helicities parameters show equator-ward propagation similar to the sunspot cycle. The kinetic helicity showed similar hemispheric trend to that of magnetic and current helicity parameters. There are 65\%(56\%) ARs with negative (positive) kinetic helicity as well as divergence-curl, at the depth of 2.4\,Mm, in the northern (southern) hemisphere. The hemispheric distribution of the kinetic helicity becomes more evident at larger depths, e.g., 69\%(67\%) at the depth of 12.6\,Mm. Similar hemispheric trend of kinetic helicity to that of the current helicity supports the mean field dynamo model. We also found that the hemispheric distribution of all the parameters increases with the field strength of ARs. The topology of photospheric magnetic fields and near surface sub-photospheric flow fields did not show good association but the correlation between them enhances with depths which could be indicating more aligned flows at deeper layers of ARs.

Degradation Correction of TSIS SIM

Steffen **Mauceri**, Erik Richard, Peter Pilewskie, Dave Harber, Odele Coddington, Stephane Béland, Michael Chambliss & Steve Carson
Solar Physics volume 295, Article number: 152 (**2020**)
https://link.springer.com/content/pdf/10.1007/s11207-020-01707-y.pdf

An understanding of solar variability over a broad spectral range and broad range of timescales is needed by scientists studying Earth's climate. The Total and Spectral Solar Irradiance Sensor (TSIS) Spectral Irradiance Monitor (SIM), is designed to measure solar spectral irradiance (SSI) with unprecedented accuracy from 200 nm to 2400 nm. SIM started daily observations in March 2018. To maintain its accuracy over the course of its anticipated 5-year mission and beyond, TSIS SIM needs to be corrected for optical degradation, common for solar viewing instruments. The differing long-term trends of various independent solar-irradiance records attest to the challenge at hand.

The correction of TSIS SIM for optical degradation is based on piecewise linear fits that bring the three instrument channels into agreement. It is fundamentally different to the correction applied to the TSIS SIM predecessor on SORCE. The correction facilitates reproducibility, uncertainty estimation and is measurement-based. Corrected, integrated TSIS SIM SSI agrees with independent observations of total solar irradiance to within 45 ppm as well as various solar-irradiance models. TSIS SIM SSI is available at: http://lasp.colorado.edu/lisird/.

Magnetic and Velocity Field Topology in Active Regions of Descending Phase of the Solar Cycle 23

R. A. **Maurya** and A. Ambastha
Solar Phys. **2020**

https://arxiv.org/pdf/2006.13602.pdf
We analyse the topology of photospheric magnetic fields and sub-photospheric flows of several active regions (ARs) that are observed during the peak to descending phase of the solar cycle 23. Our analysis shows clear evidence of hemispheric preferences in all the topological parameters such as the magnetic, current and kinetic helicities, and the 'curl-divergence'. We found that 68%(67%) ARs in the northern (southern) hemisphere with negative (positive) magnetic helicities. Same hemispheric preference sign is found for the current helicities in 68%(68%) ARs. The hemispheric preferences are found to exist statistically for all the time except in few ARs observed during the peak and the end phases of the solar cycle. This means that magnetic fields are dominantly left(right)-helical in scales smaller than individual ARs of northern(southern) hemisphere. We found that magnetic and current helicities parameters show equator-ward propagation similar to the sunspot cycle. The kinetic helicity showed similar hemispheric trend to that of magnetic and current helicity parameters. There are 65%(56%) ARs with negative (positive) kinetic helicity as well as divergence-curl, at the depth of 2.4 Mm, in the northern (southern) hemisphere. The hemispheric distribution of the kinetic helicity becomes more evident at larger depths, e.g., 69%(67%) at the depth of 12.6 Mm. Similar hemispheric trend of kinetic helicity to that of the current helicity supports the mean field dynamo model. We also found that the hemispheric distribution of all the parameters increases with the field strength of ARs. The topology of photospheric magnetic fields and near surface sub-photospheric flow fields did not show good association but the correlation between them enhances with depths which could be indicating more aligned flows at deeper layers of ARs.

Do the solar flares' locations illustrate the boundaries of the solar inner layers?

Ramy **Mawad**

2022

https://arxiv.org/pdf/2209.04755.pdf

The angular distance of the solar flares from their position to the projection point of the center of the Sun on the solar disk has been studied during the periods 1975−2021 for GOES events and 2002−2021 for RHESSI events. This distribution by the number of events of flare importance gives a specific curvature shape, that remains the same without significant changes, with the different GOES classifications, and with different observational satellites. during each solar cycle. The curvature of the distance distribution has four peaks, which are denoted by the four central rings around the center of the solar disk that look like the solar inner layers in the background. 1) The core circle [0 − 15∘]: it is a projection of the solar core onto the solar disk. 2) Radiative ring [15∘ − 45∘]. 3) The convection ring [45∘ − 55∘]. The limb ring [80∘ − 90∘]. A large number of solar flares occurred in the radiative and convection rings. While we have a few events in the core and limb rings.

Solar cycle and 27-day variations of the diurnal anisotropy of cosmic rays during the solar cycle 23

H. **Mavromichalaki**, Ch. Papageorgiou & M. Gerontidou

Astrophysics and Space Science February **2016**, 361:69

The diurnal anisotropy of cosmic-ray intensity observed over the period 1997–2006, which coincides with the solar cycle 23, has been analyzed using cosmic ray data from Athens and Oulu neutron monitor stations. In this analysis it was observed that the time of the diurnal variation maximum shifted to earlier hours than the corotation direction from 1997 to 2000, where the polarity state of the magnetic field was positive (qA>0) and to later hours from 2001 to 2006 where the polarity state was negative (qA<0).

Moreover the 27-day variation of the cosmic-ray diurnal anisotropy in connection with the 27-day variation of the interplanetary magnetic field has been studied. In this study six groups of ten Bartel rotations each one have been analyzed (2232–2241, 2249–2258, 2275–2284, 2286–2295, 2328–2337, 2356–2365). It is remarkable that the 27-day variation of cosmic- ray intensity is characterized by the well known sector structure and it is well correlated with the BXY component of the interplanetary magnetic field. These findings during the last solar cycle confirm once again the close relation of the diurnal variation of cosmic ray intensity and the interplanetary magnetic field.

Solar Cycle Evolution of Filaments over a Century: Investigations with the Meudon and McIntosh Hand-drawn Archives

Rakesh **Mazumder**, Subhamoy Chatterjee, Dibyendu Nandy, Dipankar Banerjee

ApJ 2021

https://arxiv.org/pdf/2106.04320.pdf

Hand-drawn synoptic maps from the Meudon Observatory (1919 onwards) and the McIntosh archive (1967 onwards) are two important sources of long-term, manually recorded filament observations. In this study, we calibrate the Meudon maps and subsequently identify filaments through an automated method. We extract physical parameters from this filament database and perform a comparative study of their long-term evolution focusing on the cotemporal period of McIntosh and Meudon observations. The spatio-temporal evolution of filaments manifests in the form of a filament butterfly diagram, indicating further that they are intimately related to the large-scale solar

cycle. Physical descriptors such as the number and length of filaments, which are tracers of solar surface magnetic field, have cycles which are phase-locked with the 11 year sunspot cycle. The tilt angle distribution of filaments - both near or distant from active region locations - indicates that their origin is due to either large-scale surface magnetic field or inter-active region field evolution. This study paves the way for constructing a composite series of hand-drawn filament data with minimal gaps stretching the time span of solar filament observations to a century. On the one hand, this would serve as useful constraints for models of magnetic field emergence and evolution on the Sun's surface over multiple solar cycles, and on the other hand, this filament database may be used to guide the reconstruction of filament-prominence associated eruptive events before the space age

Properties of filament in Solar cycle 20-23 from McIntosh database

Rakesh **Mazumder**
Research in Astron. Astrophys. **2018**
https://arxiv.org/pdf/1812.02489.pdf
Filament is a cool, dense structure suspended in the solar corona. The eruption of a filament is often associated with coronal mass ejection (CME), which has an adverse effect on space weather. Hence, the study of filament has attracted much attention in the recent past. The tilt angle of active region (AR) magnetic bipoles is a crucial parameter in the context of the solar dynamo. It governs the conversion efficiency of the toroidal magnetic field to poloidal magnetic field. The filament always forms over the Polarity Inversion Lines (PILs). So the study of tilt angles of the filament can provide valuable information about generation of magnetic field in the Sun. We study the tilt angle of filaments and other properties of it using McIntosh archive data. We fit a straight line to each filament to estimate its tilt angle. We study the variation of mean tilt angle with time. The latitude distribution of positive tilt angle filaments and negative tilt angle filaments reveal that there is a dominance of positive tilt angle filaments in the southern hemisphere and negative tilt angle filaments dominate in the northern hemisphere. We study the variation of the mean tilt angle for low and high latitude separately. Study of temporal variation of filament number reveals that total filament number and low latitude filament number varies cyclically, in phase with the solar cycle. The number of filaments in high latitude is less, and they also show a cyclic pattern in temporal variation. We also study the north-south asymmetry of filament for different latitude criteria.

The Association of Filaments, Polarity Inversion Lines, and Coronal Hole Properties with the Sunspot Cycle: An Analysis of the McIntosh Database

Rakesh **Mazumder**, Prantika Bhowmik, Dibyendu Nandy
ApJ **868** 52 **2018**
https://arxiv.org/pdf/1810.02133.pdf
sci-hub.tw/10.3847/1538-4357/aae68a
Filaments and coronal holes, two principal features observed in the solar corona are sources of space weather variations. Filament formation is closely associated with polarity inversion lines (PIL) on the solar photosphere which separate positive and negative polarities of the surface magnetic field. The origin of coronal holes is governed by large-scale unipolar magnetic patches on the photosphere from where open magnetic field lines extend to the heliosphere. We study properties of filaments, PILs and coronal holes in solar cycles 20, 21, 22 and 23 utilizing the McIntosh archive. We detect a prominent cyclic behavior of filament length, PIL length, and coronal hole area with significant correspondence with the solar magnetic cycle. The spatio-temporal evolution of the geometric centers of filaments shows a butterfly-like structure and distinguishable pole-ward migration of long filaments during cycle maxima. We identify this rush to the poles of filaments to be co-temporal with the initiation of polar field reversal as gleaned from Mount Wilson and Wilcox Solar Observatory polar field observations and quantitatively establish their temporal correspondence. We analyze the filament tilt angle distribution to constrain their possible origins. Majority of the filaments exhibit negative and positive tilt angles in the northern and the southern hemispheres, respectively -- strongly suggesting that their formation is governed by the overall large-scale magnetic field distribution on the solar photosphere and not by the small-scale intra-active region magnetic field configurations. We also investigate the hemispheric asymmetry in filaments, PILs, and coronal holes. We find that the hemispheric asymmetry in filaments and PILs are positively correlated -- whereas coronal hole asymmetry is uncorrelated -- with sunspot area asymmetry.

Differential Rotation Rates of Recurrent Sunspot Groups Lasting Two or Three Passages in the Debrecen Photoheliographic Data Catalogue.

McCann, A.D., Cadavid, A.C., Parthibhan, S. et al.
Sol Phys 299, 138 (**2024**).
https://doi.org/10.1007/s11207-024-02376-x
We investigate the angular rotation velocities of stable recurrent sunspot groups characterized by a leading unipolar sunspot with an initially well-developed penumbra, similar to the H or J types in the Zürich classification. These structures are tracked for two (class I) or three (class II) solar rotations. The Debrecen Photoheliographic Data sunspot catalogue (1977 – 2017) used in this study provides the daily positions and areas of observable sunspots and

sunspot groups with great precision. This allows the calculation of the angular rotation synodic velocities from a least-squares fit to the sunspot positions over a given disk passage. After converting to sidereal coordinates, the velocities were used to obtain the solar rotation parameters via a least-squares fit to the solar differential rotation law. Comparison is made with the solar differential rotation laws obtained in two previous studies considering the same classes of sunspot groups, and over comparable time periods, using the data from the Greenwich Photoelectric Results (GPR) catalogue. We find that, on average, the sunspots exhibit a braking tendency, aligning with previous findings. The common results across the three studies, when examined in the context of simulations for sunspot formation and evolution, suggest a scenario in which recurrent unipolar sunspots are anchored at a shallow subsurface layer. The observed braking effect is attributed to gradual fragmentation, leading to disconnection and a transition to dynamics increasingly influenced by surface flows.

Re-examining Sunspot Tilt Angle to Include Anti-Hale Statistics

B. H. **McClintock**1, A. A. Norton2, and J. Li
2014 ApJ 797 130
https://iopscience.iop.org/article/10.1088/0004-637X/797/2/130/pdf
Sunspot groups and bipolar magnetic regions (BMRs) serve as an observational diagnostic of the solar cycle. We use Debrecen Photohelographic Data (DPD) from 1974-2014 that determined sunspot tilt angles from daily white light observations, and data provided by Li & Ulrich that determined sunspot magnetic tilt angle using Mount Wilson magnetograms from 1974-2012. The magnetograms allowed for BMR tilt angles that were anti-Hale in configuration, so tilt values ranged from 0 to 360? rather than the more common ?90?. We explore the visual representation of magnetic tilt angles on a traditional butterfly diagram by plotting the mean area-weighted latitude of umbral activity in each bipolar sunspot group, including tilt information. The large scatter of tilt angles over the course of a single cycle and hemisphere prevents Joy's law from being visually identified in the tilt-butterfly diagram without further binning. The average latitude of anti-Hale regions does not differ from the average latitude of all regions in both hemispheres. The distribution of anti-Hale sunspot tilt angles are broadly distributed between 0 and 360? with a weak preference for east-west alignment 180? from their expected Joy's law angle. The anti-Hale sunspots display a log-normal size distribution similar to that of all sunspots, indicating no preferred size for anti-Hale sunspots. We report that 8.4% ? 0.8% of all bipolar sunspot regions are misclassified as Hale in traditional catalogs. This percentage is slightly higher for groups within 5? of the equator due to the misalignment of the magnetic and heliographic equators.

Flaring Rates and the Evolution of Sunspot Group McIntosh Classifications

Aoife E. **McCloskey** , Peter T. Gallagher, D. Shaun Bloomfield
Solar Phys. Volume 291, Issue 6, pp 1711–1738 **2016**
http://arxiv.org/pdf/1607.00903v1.pdf
http://link.springer.com/article/10.1007/s11207-016-0933-y
Sunspot groups are the main source of solar flares, with the energy to power them being supplied by magnetic-field evolution (e.g. flux emergence or twisting/shearing). To date, few studies have investigated the statistical relation between sunspot-group evolution and flaring, with none considering evolution in the McIntosh classification scheme. Here we present a statistical analysis of sunspot groups from Solar Cycle 22, focusing on 24-hour changes in the three McIntosh classification components. Evolution-dependent ≥C1.0, ≥M1.0, and ≥X1.0 flaring rates are calculated, leading to the following results: i) flaring rates become increasingly higher for greater degrees of upward evolution through the McIntosh classes, with the opposite found for downward evolution; ii) the highest flaring rates are found for upward evolution from larger, more complex, classes (e.g. Zurich D- and E-classes evolving upward to F-class produce ≥C1.0 rates of 2.66±0.28 and 2.31±0.09 flares per 24 hours, respectively); iii) increasingly complex classes give higher rates for all flare magnitudes, even when sunspot groups do not evolve over 24 hours. These results support the hypothesis that injection of magnetic energy by flux emergence (i.e. increasing in Zurich or compactness classes) leads to a higher frequency and magnitude of flaring.

Doppler Events in the Solar Photosphere: The Coincident Superposition of Fast Granular Flows and p-mode Coherence Patches

R. Lee **McClure**, Mark P. Rast, Valentin MartınezPillet
Solar Phys. 294:18 **2019**
https://arxiv.org/pdf/1811.08944.pdf
Observations of the solar photosphere show spatially-compact large-amplitude Doppler velocity events with short lifetimes. In data from the Imaging Magnetograph eXperiment (IMaX) on the first flight of the Sunrise balloon in 2009, events with velocities in excess of 4σ from the mean can be identified in both intergranular downflow lanes and granular upflows. We show that the statistics of such events are consistent with the random superposition of strong convective flows and p-mode coherence patches. Such coincident superposition has implications for the interpretation of acoustic wave sources in the solar photosphere, and may be important to the interpretation of spectral line profiles formed in solar photosphere.

Weakest Solar Wind of the Space Age and the Current "Mini" Solar Maximum

D. J. **McComas**1,2, N. Angold1, H. A. Elliott1, G. Livadiotis1, N. A. Schwadron3, R. M. Skoug4, and C. W. Smith

2013 ApJ 779 2

The last solar minimum, which extended into 2009, was especially deep and prolonged. Since then, sunspot activity has gone through a very small peak while the heliospheric current sheet achieved large tilt angles similar to prior solar maxima. The solar wind fluid properties and interplanetary magnetic field (IMF) have declined through the prolonged solar minimum and continued to be low through the current mini solar maximum. Compared to values typically observed from the mid-1970s through the mid-1990s, the following proton parameters are lower on average from 2009 through day 79 of 2013: solar wind speed and beta (~11%), temperature (~40%), thermal pressure (~55%), mass flux (~34%), momentum flux or dynamic pressure (~41%), energy flux (~48%), IMF magnitude (~31%), and radial component of the IMF (~38%). These results have important implications for the solar wind's interaction with planetary magnetospheres and the heliosphere's interaction with the local interstellar medium, with the proton dynamic pressure remaining near the lowest values observed in the space age: ~1.4 nPa, compared to ~2.4 nPa typically observed from the mid-1970s through the mid-1990s. The combination of lower magnetic flux emergence from the Sun (carried out in the solar wind as the IMF) and associated low power in the solar wind points to the causal relationship between them. Our results indicate that the low solar wind output is driven by an internal trend in the Sun that is longer than the ~11 yr solar cycle, and they suggest that this current weak solar maximum is driven by the same trend.

The Annual Cosmic-Radiation Intensities 1391 – 2014; The Annual Heliospheric Magnetic Field Strengths 1391 – 1983, and Identification of Solar Cosmic-Ray Events in the Cosmogenic Record 1800 – 1983

K. G. **McCracken** , J. Beer

Solar Phys. Volume 290, Issue 10, pp 3051-3069 **201**5

The annual cosmogenic 10Be ice-core data from Dye 3 and the North Greenland Ice-core Project (NGRIP), and neutron-monitor data, 1951 – 2014, are combined to yield a record of the annual cosmic-ray intensity, 1391 – 2014. These data were then used to estimate the intensity of the heliospheric magnetic field (HMF), 1391 – 1983. All of these annual data are provided in the Electronic Supplementary Material. Analysis of these annual data shows that there were significant impulsive increases in 10Be production in the year following the very large solar cosmic-ray events of 1942, 1949, and 1956. There was an additional enhancement that we attribute to six high-altitude nuclear explosions in 1962. All of these enhancements result in underestimates of the strength of the HMF. An identification process is defined, resulting in a total of seven impulsive 10Be events in the interval 1800 – 1942 prior to the first detection of a solar cosmic-ray event using ionization chambers. Excision of the 10Be impulsive enhancements yields a new estimate of the HMF, designated B(PCR-2). Five of the seven 10Be enhancements prior to 1941 are well correlated with the occurrence of very great geomagnetic storms. It is shown that a solar cosmic-ray event similar to that of 25 July 1946, and occurring in the middle of the second or third year of the solar cycle, may merge with the initial decreasing phase of the 11-year cycle in cosmic-ray intensity and be unlikely to be detected in the 10Be data. It is concluded that the occurrence rate for solar energetic-particle (SEP) events such as that on 23 February 1956 is about seven per century, and that there is an upper limit to the size of solar cosmic-ray events.

Evidence for Planetary Forcing of the Cosmic Ray Intensity and Solar Activity Throughout the Past 9400 Years

K. G. **McCracken**, J. Beer, F. Steinhilber

Solar Physics, Volume 289, Issue 8, pp 3207-3229 **2014**

Paleo-cosmic-ray (PCR) records based on cosmogenic 10Be and 14C data are used to study the variations in cosmic-ray intensity and solar activity over the past 9400 years. There are four strong correlations with the motion of the Jovian planets; the probability of occurring by chance being < 10−5. They are i) the PCR periodicities at 87, 350, 510, and 710 years, which closely approximate integer multiples of half the Uranus–Neptune synodic period; ii) eight periodicities in the torques calculated to be exerted by the planets on an asymmetric tachocline that approximate the periods observed in the PCR; iii) the maxima of the long-term PCR variations are coincident with syzygy (alignment) of the four Jovian planets in 5272 and 644 BP; and iv) in the time domain, the PCR intensity decreases during the first 60 years of the ≈ 172 year Jose cycle (Jose, Astron. J. 70, 193, 1965) and increases in the remaining ≈ 112 years in association with barycentric anomalies in the distance between the Sun and the center of mass of the solar system. Furthermore, sunspot and neutron-monitor data show that three anomalous sunspot cycles (4th, 7th, and 20th) and the long sunspot minimum of 2006 – 2009 CE coincided with the first and second

barycentric anomalies of the 58th and 59th Jose cycles. Phase lags between the planetary and heliospheric effects are ≤ five years. The 20 largest Grand Minima during the past 9400 years coincided with the latter half of the Jose cycle in which they occurred. These correlations are not of terrestrial origin, nor are they due to the planets' contributing directly to the cosmic-ray modulation process in the heliosphere. Low cosmic-ray intensity (higher solar activity) occurred when Uranus and Neptune were in superior conjunction (mutual cancellation), while high intensities occurred when Uranus–Neptune were in inferior conjunction (additive effects). Many of the prominent peaks in the PCR Fourier spectrum can be explained in terms of the Jose cycle, and the occurrence of barycentric anomalies.

Comparison of the extended solar minimum of 2006-9 with the Spoerer, Maunder, and Dalton Grand Minima in solar activity in the past.†

K.G. **McCracken**1,* and J. Beer

JGR, Volume 119, Issue 4, pages 2379–2387, **2014**

We use cosmic radiation records (neutron monitor and the cosmogenic radionuclides, 10Be and 14C) as a proxy to compare the solar activity during the extended solar minimum 2006-9, with that during the Grand Solar Minima and Maxima that occurred between 1391-2010. The inferred cosmic ray intensities during the Spoerer, Maunder, and Dalton Grand Minima were significantly greater than those during 2006-9. The onset phases of the three Grand Minima extended over between two and five Schwabe (sunspot) cycles, the cosmic ray intensity at the Schwabe minima increasing from a value approximating that of 2006-9, to substantially higher values later in the Grand Minimum. The minimum estimated strengths of the heliospheric magnetic field near Earth during the Grand Minima were 2.4nT (Spoerer); <2.0nT(Maunder) and 2.6 nT (Dalton), compared to 3.9nT in 2009. We conclude that the periods of highest solar activity during the Maunder Minimum approximated those near the sunspot minima between 1954 and 1996. The average ratio of the maximum to minimum estimated HMF in the six Schwabe cycles in the Maunder Minimum is 1.54 (range 1.30-1.85) compared to 1.52 (1.31-1.63) for the modern epoch suggesting similar operation of the solar dynamo in both intervals. The onset phase of the Maunder Minimum extending over five Schwabe cycles, and the large increase in cosmic ray flux (and decrease in estimated heliospheric magnetic field), leads us to speculate that the magnetohydrodynamic amplification in the solar dynamo exhibits a relaxation time well in excess of the 11 year period of the Schwabe cycle.

Complexity Heliophysics: A Lived and Living History of Systems and Complexity Science in Heliophysics. Review

McGranaghan, R.M.

Space Sci Rev 220, 52 (**2024**).

https://doi.org/10.1007/s11214-024-01081-2

https://link.springer.com/content/pdf/10.1007/s11214-024-01081-2.pdf

This review examines complexity science in the context of Heliophysics, describing it not as a discipline, but as a paradigm. In the context of Heliophysics, complexity science is the study of a star, interplanetary environment, magnetosphere, upper and terrestrial atmospheres, and planetary surface as interacting subsystems. Complexity science studies entities in a system (e.g., electrons in an atom, planets in a solar system, individuals in a society) and their interactions, and is the nature of what emerges from these interactions. It is a paradigm that employs systems approaches and is inherently multi- and cross-scale. Heliophysics processes span at least 15 orders of magnitude in space and another 15 in time, and its reaches go well beyond our own solar system and Earth's space environment to touch planetary, exoplanetary, and astrophysical domains. It is an uncommon domain within which to explore complexity science. After first outlining the dimensions of complexity science, the review proceeds in three epochal parts: 1) A pivotal year in the Complexity Heliophysics paradigm: 1996; 2) The transitional years that established foundations of the paradigm (1996-2010); and 3) The emergent literature largely beyond 2010. This review article excavates the lived and living history of complexity science in Heliophysics. It identifies five dimensions of complexity science, some enjoying much scholarship in Heliophysics, others that represent relative gaps in the existing research. The history reveals a grand challenge that confronts Heliophysics, as with most physical sciences, to understand the research intersection between fundamental science (e.g., complexity science) and applied science (e.g., artificial intelligence and machine learning (AI/ML)). A risk science framework is suggested as a way of formulating the grand scientific and societal challenges in a way that AI/ML and complexity science converge. The intention is to provide inspiration, help researchers think more coherently about ideas of complexity science in Heliophysics, and guide future research. It will be instructive to Heliophysics researchers, but also to any reader interested in or hoping to advance the frontier of systems and complexity science.

Heliophysics Discovery Tools for the 21st Century: Data Science and Machine Learning Structures and Recommendations for 2020-2050

R. M. **McGranaghan**, B. Thompson, E. Camporeale, J. Bortnik, M. Bobra, G. Lapenta, S. Wing, B. Poduval, S. Lotz, S. Murray, M. Kirk, T. Y. Chen, H. M. Bain, P. Riley, B. Tremblay, M. Cheung, V. Delouille

Heliophysics 2050 White Paper **2022**

https://arxiv.org/ftp/arxiv/papers/2212/2212.13325.pdf

Three main points: 1. Data Science (DS) will be increasingly important to heliophysics; 2. Methods of heliophysics science discovery will continually evolve, requiring the use of learning technologies [e.g., machine learning (ML)] that are applied rigorously and that are capable of supporting discovery; and 3. To grow with the pace of data, technology, and workforce changes, heliophysics requires a new approach to the representation of knowledge.

Deciphering Solar Magnetic Activity: Some (Unpopular) Thoughts On the Coupling of the Sun's "Weather" and "Climate"

Scott W. **McIntosh**, Robert J. Leamon

Frontiers **2024**

https://arxiv.org/pdf/2408.10354

The Sun exhibits episodic surges of magnetic activity across a range of temporal and spatial scales, the most prominent of which is the 11-ish year modulation of sunspot production. Beside the ~170 (min to max) decadal variation in sunspot production there is a less-explored quasi-annual variation in the range of 25-50 sunspots/year in magnitude. In addition, there is there is a slower, ~80 year period, 10-50 variation in the sunspot number, that is commonly referred to as the 'Gleissberg Cycle.' Using a suite of contemporary and historical observations we will illustrate these elements of our star's episodic behavior and present a hypothesis that may provide a consistent physical link between the observed 'climatic', 'decadal' and 'seasonal' magnetic variation of our star.

Deciphering Solar Magnetic Activity: The (Solar) Hale Cycle Terminator of 2021

Scott W **McIntosh**, Robert J. Leamon, R. Egeland

Front. Astron. Space Sci. 10: 1050523. **2023**

doi: 10.3389/fspas.2023.1050523

https://arxiv.org/pdf/2209.10577

https://www.frontiersin.org/articles/10.3389/fspas.2023.1050523/pdf

McIntosh and colleagues identified an event in the solar timeline that appeared to play a role in how Sunspot Cycle 23 (SC23) transitioned into Sunspot Cycle 24 (SC24). The timeframe for this transition was rapid, taking place in as short as time as a solar rotation. M2014 inferred that the transition observed was a critical episode for the Sun's global-scale magnetic field that was being manifest in the spatially and temporally overlapping and magnetic systems belonging to the Sun's 22-year (Hale) magnetic cycle. These events have been dubbed as Hale Cycle terminations, or `terminators' for short. Further exploration revealed a relationship between terminator separation (as a measure of overlap in the Hale Cycles) and the upcoming sunspot cycle amplitude. McIntosh and colleagues extrapolated upon this relationship to identify the termination of the SC24 carrying Hale Cycle band in Mid-2020 and inferred that this would result in a very large Sunspot Cycle 25 (SC25). This paper presents observational analysis of the end of SC24 and the initial months of SC25 growth following a terminator that occurred in mid-December 2021 (approximately 12/13/2021). We use the December 2021 terminator to finalize the forecast of SC25 amplitude 184 (±17 with 95\% confidence, and ±63 with 68\% confidence). Finally, we use other terminator-related superposed epoch analyses to project the timing of SC25 maxima in late 2023 to mid 2024.

Uniting The Sun's Hale Magnetic Cycle and `Extended Solar Cycle' Paradigms

Scott W. **McIntosh**, Phillip H. Scherrer, Leif Svalgaard, Robert J. Leamon

Frontiers in Solar and Stellar Physics 9:923049. **2022**

https://arxiv.org/pdf/2208.09026

https://www.frontiersin.org/articles/10.3389/fspas.2022.923049/pdf

https://doi.org/10.3389/fspas.2022.923049

Through meticulous daily observation of the Sun's large-scale magnetic field the Wilcox Solar Observatory (WSO) has catalogued two magnetic (Hale) cycles of solar activity. Those two (~22-year long) Hale cycles have yielded four (11-year long) sunspot cycles (numbers 21 through 24). Recent research has highlighted the persistence of the ``Extended Solar Cycle" (ESC) and its connection to the fundamental Hale Cycle - albeit through a host of proxies resulting from image analysis of the solar photosphere, chromosphere and corona. This short manuscript presents the correspondence of the ESC, the surface toroidal magnetic field evolution, and the evolution of the Hale Cycle. As Sunspot Cycle 25 begins, interest in observationally mapping the Hale and Extended cycles could not be higher given potential predictive capability that synoptic scale observations can provide.

Deciphering Solar Magnetic Activity: 140 Years Of The `Extended Solar Cycle' -- Mapping the Hale Cycle

Scott W. **McIntosh**, Robert J. Leamon, Ricky Egeland, Mausumi Dikpati, Richard C. Altrock, Dipankar Banerjee, Subhamoy Chatterjee, Edward Cliver, Abhishek K. Srivastava, Marco Velli

Solar Phys. **296**, Article number: 189 **2021**

https://arxiv.org/pdf/2010.06048.pdf

https://link.springer.com/content/pdf/10.1007/s11207-021-01938-7.pdf

https://doi.org/10.1007/s11207-021-01938-7

We investigate the occurrence of the “extended solar cycle” (ESC) as it occurs in a host of observational data spanning 140 years. Investigating coronal, chromospheric, photospheric, and interior diagnostics, we develop a consistent picture of solar activity migration linked to the 22-year Hale (magnetic) cycle using superposed epoch analysis (SEA) and previously identified Hale cycle termination events as the key time for the SEA. Our analysis shows that the ESC and Hale cycle, as highlighted by the terminator-keyed SEA, is strongly recurrent throughout the entire observational record studied, some 140 years. Applying the same SEA method to the sunspot record confirms that Maunder’s butterfly pattern is a subset of the underlying Hale cycle, strongly suggesting that the production of sunspots is not the fundamental feature of the Hale cycle, but the ESC is. The ESC (and Hale cycle) pattern highlights the importance of 55∘ latitude in the evolution, and possible production, of solar magnetism.

The Extended Solar Cycle (ESC)

Solar Filaments

Overlapping Magnetic Activity Cycles and the Sunspot Number: Forecasting Sunspot Cycle 25 Amplitude

Scott W. **McIntosh**, Sandra C. Chapman, Robert J. Leamon, Ricky Egeland, Nicholas W. Watkins

Solar Physics volume 295, Article number: 163 **2020**

https://arxiv.org/pdf/2006.15263.pdf

https://link.springer.com/content/pdf/10.1007/s11207-020-01723-y.pdf

The Sun exhibits a well-observed modulation in the number of sunspots over a period of about 11 years. From the dawn of modern observational astronomy sunspots have presented a challenge to understanding - their quasi-periodic variation in number, first noted 160 years ago, stimulates community-wide interest to this day. A large number of techniques are able to explain the temporal landmarks, (geometric) shape, and amplitude of sunspot "cycles," however forecasting these features accurately in advance remains elusive. Recent observationally-motivated studies have illustrated a relationship between the Sun's 22-year (Hale) magnetic cycle and the production of the sunspot cycle landmarks and patterns, but not the amplitude of the cycle. Using (discrete) Hilbert transforms on 270 years of (monthly) sunspot numbers to robustly identify the so-called "termination"' events, landmarks marking the start and end of sunspot and magnetic activity cycles, we extract a relationship between the temporal spacing of terminators and the magnitude of sunspot cycles. Given this relationship and our prediction of a terminator event in 2020, we deduce that sunspot cycle 25 will have a magnitude that rivals the top few since records began. This outcome would be in stark contrast to the community consensus estimate of sunspot cycle 25 magnitude.

What the sudden death of solar cycles can tell us about the nature of the solar interior

Scott W. **McIntosh**, Robert J. Leamon, Mausumi Dikpati, Yuhong Fan, Matthias Rempel

ApJ 294:88 **2019**

https://arxiv.org/pdf/1901.09083.pdf

sci-hub.se/10.1007/s11207-019-1474-y

We observe the abrupt end of solar activity cycles at the Sun's equator by combining almost 140 years of observations from ground and space. These "terminator" events appear to be very closely related to the onset of magnetic activity belonging to the next sunspot cycle at mid-latitudes and the polar-reversal process at high-latitudes. Using multi-scale tracers of solar activity we examine the timing of these events in relation to the excitation of new activity and find that the time taken for the solar plasma to communicate this transition is of the order of one solar rotation, but could be shorter. Utilizing uniquely comprehensive solar observations from the Solar Terrestrial Relations Observatory (STEREO), and Solar Dynamics Observatory (SDO) we see that this transitional event is strongly longitudinal in nature. Combined, these characteristics imply that magnetic information is communicated through the solar interior rapidly. A range of possibilities exist to explain such behavior: the presence of magnetic reconnection in the deep interior, internal gravity waves on the solar tachocline, or that the magnetic fields present in the Sun's convection zone could be very large, with a poloidal field strengths reaching 50k - considerably larger than conventional explorations of solar and stellar dynamos estimate. Regardless of mechanism responsible, the rapid timescales demonstrated by the Sun's global magnetic field reconfiguration present strong constraints on first-principles numerical simulations of the solar interior and, by extension, other stars.

The Heliospheric Meteorology Mission: A Mission to DRIVE our Understanding of Heliospheric Variability

Scott W. **McIntosh**, and Robert J. Leamon
Front. Astron. Space Sci., 5:21 **2018** |
https://www.frontiersin.org/articles/10.3389/fspas.2018.00021/full
https://doi.org/10.3389/fspas.2018.00021
To make transformational scientific progress with the space weather enterprise the Sun, Earth, and heliosphere must be studied as a coupled system, comprehensively. Rapid advances were made in the study, and forecasting, of terrestrial meteorology half a century ago that accompanied the dawn of earth observing satellites. Those assets provided a global perspective on the Earth's weather systems and the ability to look ahead of the observer's local time and to. From a heliospheric, or space, weather perspective we have the same fundamental limitation as the terrestrial meteorologists had—by far the majority of our observing assets are tied to the Sun-Earth line—our planet's "local time" with respect to the Sun. This perspective intrinsically limits our ability to "see what is coming around the solar limb" far less to gain any insight into the global patterns of solar weather and how they guide weather throughout the heliosphere. We propose a mission concept—the Heliospheric Meteorology Mission (HMM)—to sample the complete magnetic and thermodynamic state of the heliosphere inside 1AU using a distributed network of deep space hardened smallsats that encompass the Sun. The observations and in situ plasma measurements made by the fleet of HMM smallsats would be collected, and assimilated into current operational space weather models. Further, the HMM measurements would also being used in an nationally coordinated research effort—at the frontier of understanding the coupled heliospheric system—as a means to develop the next generation models required to provide seamless prediction for the geospace environment to protect vital infrastructure and human/robotic explorers throughout the solar system. The HMM mission concept naturally allows for research-motivated technology development that can improve forecast skill.

Deciphering Solar Magnetic Activity: Spotting Solar Cycle 25

Scott W. **McIntosh**, Robert J. Leamon
Front. Astron. Space Sci., **2017**
https://arxiv.org/pdf/1702.04414.pdf
https://doi.org/10.3389/fspas.2017.00004
https://www.frontiersin.org/articles/10.3389/fspas.2017.00004/full
We present observational signatures of solar cycle 25 onset. Those signatures are visibly following a migratory path from high to low latitudes. They had starting points that are asymmetrically offset in each hemisphere at times that are 21-22 years after the corresponding, same polarity, activity bands of solar cycle 23 started their migration. Those bands define the so-called "extended solar cycle." The four magnetic bands currently present in the system are approaching a mutually cancelling configuration, and solar minimum conditions are imminent. Further, using a tuned analysis of the daily band latitude-time diagnostics, we are able to utilize the longitudinal wave number (m=1) variation in the data to more clearly reveal the presence of the solar cycle 25 bands. This clarification illustrates that prevalently active longitudes (different in each hemisphere) exist at mid-latitudes presently, lasting many solar rotations, that can be used for detailed study over the next several years with instruments like the Spectrograph on IRIS, the Spectropolarimeter on Hinode, and, when they come online, similar instruments on the Daniel K. Inouye Solar Telescope (DKIST) as we watch those bands evolve following the cancellation of the solar cycle 24 activity bands at the equator late in 2019.

Deciphering Solar Magnetic Activity: On Grand Minima in Solar Activity

Scott W. **McIntosh**, Robert J. Leamon
2015
http://arxiv.org/pdf/1505.02326v1.pdf
The Sun provides the energy necessary to sustain our existence. While the Sun provides for us, it is also capable of taking away. The weather and climatic scales of solar evolution and the Sun-Earth connection are not well understood. There has been tremendous progress in the century since the discovery of solar magnetism - magnetism that ultimately drives the electromagnetic, particulate and eruptive forcing of our planetary system. There is contemporary evidence of a decrease in solar magnetism, perhaps even indicators of a significant downward trend, over recent decades. Are we entering a minimum in solar activity that is deeper and longer than a typical solar minimum, a "grand minimum"? How could we tell if we are? What is a grand minimum and how does the Sun recover? These are very pertinent questions for modern civilization. In this paper we present a hypothetical demonstration of entry and exit from grand minimum conditions based on a recent analysis of solar features over the past 20 years and their possible connection to the origins of the 11(-ish) year solar activity cycle.

The solar magnetic activity band interaction and instabilities that shape quasi-periodic variability

Scott W. **McIntosh**1 , Robert J. Leamon2, Larisza D. Krista3, Alan M. Title4, Hugh S. Hudson5, Pete Riley6, Jerald W. Harder7, Greg Kopp7, Martin Snow7, Thomas N. Woods7, Justin C. Kasper8,9, Michael L. Stevens8 & Roger K. Ulrich10
Nature Communications, Volume 6, id. 6491 (**2015**).
sci-hub.si/10.1038/ncomms7491
Solar magnetism displays a host of variational timescales of which the enigmatic 11-year sunspot cycle is most prominent. Recent work has demonstrated that the sunspot cycle can be explained in terms of the intra- and extra-hemispheric interaction between the overlapping activity bands of the 22-year magnetic polarity cycle. Those activity bands appear to be driven by the rotation of the Sun's deep interior. Here we deduce that activity band interaction can qualitatively explain the 'Gnevyshev Gap'—a well-established feature of flare and sunspot occurrence. Strong quasi-annual variability in the number of flares, coronal mass ejections, the radiative and particulate environment of the heliosphere is also observed. We infer that this secondary variability is driven by surges of magnetism from the activity bands. Understanding the formation, interaction and instability of these activity bands will considerably improve forecast capability in space weather and solar activity over a range of timescales.

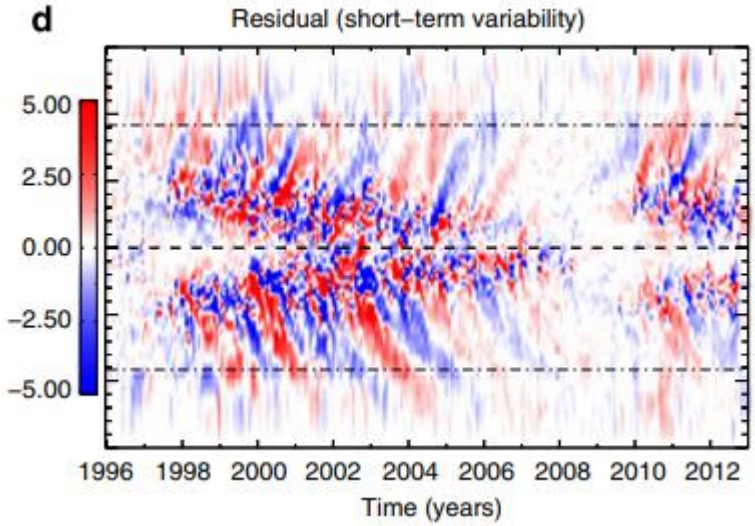

On Magnetic Activity Band Overlap, Interaction, and the Formation of Complex Solar Active Regions

Scott W. **McIntosh**, Robert J. Leamon
ApJL **2014**
http://arxiv.org/pdf/1410.6411v1.pdf
Recent work has revealed an phenomenological picture of the how the ~11-year sunspot cycle of Sun arises. The production and destruction of sunspots is a consequence of the latitudinal-temporal overlap and interaction of the toroidal magnetic flux systems that belong to the 22-year magnetic activity cycle and are rooted deep in the Sun's convective interior. We present a conceptually simple extension of this work, presenting a hypothesis on how complex active regions can form as a direct consequence of the intra- and extra-hemispheric interaction taking place in the solar interior. Furthermore, during specific portions of the sunspot cycle we anticipate that those complex active regions may be particular susceptible to profoundly catastrophic breakdown---producing flares and coronal mass ejections of most severe magnitude.

Deciphering Solar Magnetic Activity I: On The Relationship Between The Sunspot Cycle And The Evolution Of Small Magnetic Features

Scott W. **McIntosh**, Xin Wang, Robert J. Leamon, Alisdair R. Davey, Rachel Howe, Larisza D. Krista, Anna V. Malanushenko, Jonathan W. Cirtain, Joseph B. Gurman, Michael J.
E-print, March **2014**; ApJ, 792 12, **2014**
Sunspots are a canonical marker of the Sun's internal magnetic field which flips polarity every ~22-years. The principal variation of sunspots, an ~11-year variation in number, modulates the amount of magnetic field that pierces the solar surface and drives significant variations in our Star's radiative, particulate and eruptive output over that period. This paper presents observations from the Solar and Heliospheric Observatory and Solar Dynamics Observatory indicating that the 11-year sunspot variation is intrinsically tied it to the spatio-temporal overlap of the activity bands belonging to the 22-year magnetic activity cycle. Using a systematic analysis of ubiquitous coronal brightpoints, and the magnetic scale on which they appear to form, we show that the landmarks of sunspot cycle 23

can be explained by considering the evolution and interaction of the overlapping activity bands of the longer scale variability.

HEMISPHERIC ASYMMETRIES OF SOLAR PHOTOSPHERIC MAGNETISM: RADIATIVE, PARTICULATE, AND HELIOSPHERIC IMPACTS

Scott W. **McIntosh**1, Robert J. Leamon2, Joseph B. Gurman3, Jean-Philippe Olive4, Jonathan W. Cirtain5, David H. Hathaway5, Joan Burkepile1, Mark Miesch1, Robert S. Markel1, and Leonard Sitongia

2013 ApJ 765 146

Among many other measurable quantities, the summer of 2009 saw a considerable low in the radiative output of the Sun that was temporally coincident with the largest cosmic-ray flux ever measured at 1 AU. Combining measurements and observations made by the Solar and Heliospheric Observatory (SOHO) and Solar Dynamics Observatory (SDO) spacecraft we begin to explore the complexities of the descending phase of solar cycle 23, through the 2009 minimum into the ascending phase of solar cycle 24. A hemispheric asymmetry in magnetic activity is clearly observed and its evolution monitored and the resulting (prolonged) magnetic imbalance must have had a considerable impact on the structure and energetics of the heliosphere. While we cannot uniquely tie the variance and scale of the surface magnetism to the dwindling radiative and particulate output of the star, or the increased cosmic-ray flux through the 2009 minimum, the timing of the decline and rapid recovery in early 2010 would appear to inextricably link them. These observations support a picture where the Sun's hemispheres are significantly out of phase with each other. Studying historical sunspot records with this picture in mind shows that the northern hemisphere has been leading since the middle of the last century and that the hemispheric "dominance" has changed twice in the past 130 years. The observations presented give clear cause for concern, especially with respect to our present understanding of the processes that produce the surface magnetism in the (hidden) solar interior—hemispheric asymmetry is the normal state—the strong symmetry shown in 1996 was abnormal. Further, these observations show that the mechanism(s) which create and transport the magnetic flux are slowly changing with time and, it appears, with only loose coupling across the equator such that those asymmetries can persist for a considerable time. As the current asymmetry persists and the basal energetics of the system continue to dwindle we anticipate new radiative and particulate lows coupled with increased cosmic-ray fluxes heading into the next solar minimum.

3D WKB solution for fast magnetoacoustic wave behaviour around an X-line

J. A. **McLaughlin**, G. J. J. Botha, S. Régnier and D. L. Spoors

A&A 591, A103 (**2016**)

Context. We study the propagation of a fast magnetoacoustic wave in a 3D magnetic field created from two magnetic dipoles. The magnetic topology contains an X-line.

Aims. We aim to contribute to the overall understanding of MHD wave propagation within inhomogeneous media, specifically around X-lines.

Methods. We investigate the linearised, 3D MHD equations under the assumptions of ideal and cold plasma. We utilise the WKB approximation and Charpit's method during our investigation.

Results. It is found that the behaviour of the fast magnetoacoustic wave is entirely dictated by the local, inhomogeneous, equilibrium Alfvén speed profile. All parts of the wave experience refraction during propagation, where the magnitude of the refraction effect depends on the location of an individual wave element within the inhomogeneous magnetic field. The X-line, along which the Alfvén speed is identically zero, acts as a focus for the refraction effect. There are two main types of wave behaviour: part of the wave is either trapped by the X-line or escapes the system, and there exists a critical starting region around the X-line that divides these two types of behaviour. For the set-up investigated, it is found that 15.5% of the fast wave energy is trapped by the X-line.

Conclusions. We conclude that linear, $\beta = 0$ fast magnetoacoustic waves can accumulate along X-lines and thus these will be specific locations of fast wave energy deposition and thus preferential heating. The work here highlights the importance of understanding the magnetic topology of a system. We also demonstrate how the 3D WKB technique described in this paper can be applied to other magnetic configurations.

The Great Solar Active Region NOAA 12192: Helicity Transport, Filament Formation, and Impact on the Polar Field

Tyler C. **McMaken**1,2 and Gordon J. D. Petrie

2017 ApJ 840 100

http://sci-hub.cc/10.3847/1538-4357/aa6d0b

The solar active region (AR), NOAA 12192, appeared in **2014 October** as the largest AR in 24 years. Here we examine the counterintuitive nature of two diffusion-driven processes in the region: the role of helicity buildup in the formation of a major filament, and the relationship between the effects of supergranular diffusion and meridional flow on the AR and on the polar field. Quantitatively, calculations of current helicity and magnetic twist from

Helioseismic and Magnetic Imager (HMI) vector magnetograms indicate that, though AR 12192 emerged with negative helicity, positive helicity from subsequent flux emergence, consistent with the hemispheric sign-preference of helicity, increased over time within large-scale, weak-field regions such as those near the polarity inversion line (PIL). Morphologically, Atmospheric Imaging Assembly observations of filament barbs, sigmoidal patterns, and bases of Fe xii stalks initially exhibited signatures of negative helicity, and the long filament that subsequently formed had a strong positive helicity consistent with the helicity buildup along the PIL. We find from full-disk HMI magnetograms that AR 12192's leading positive flux was initially closer to the equator but, owing either to the region's magnetic surroundings or to its asymmetric flux density distribution, was transported poleward more quickly on average than its trailing negative flux, contrary to the canonical pattern of bipole flux transport. This behavior caused the AR to have a smaller effect on the polar fields than expected and enabled the formation of the very long neutral line where the filament formed.

Phase mixing of propagating Alfv{é}n waves in a single-fluid partially ionized solar plasma

Max **McMurdo**, Istvan Ballai, Gary Verth, Abdulaziz Alharbi, Viktor Fedun
ApJ **958** 81 **2023**
https://arxiv.org/pdf/2311.02989.pdf
https://iopscience.iop.org/article/10.3847/1538-4357/ad0364/pdf
Phase mixing of Alfven waves is one of the most promising mechanisms for heating of the solar atmosphere. The damping of waves in this case requires small transversal scales, relative to the magnetic field direction. Here this requirement is achieved by considering a transversal inhomogeneity in the equilibrium plasma density profile. Using a single fluid approximation of a partially ionized chromospheric plasma we study the effectiveness of the damping of phase mixed shear Alfven waves and investigate the effect of varying the ionization degree on the dissipation of waves. Our results show that the dissipation length of shear Alfven waves strongly depends on the ionization degree of the plasma, but more importantly, in a partially ionized plasma, the damping length of shear Alfven waves is several orders of magnitude shorter than in the case of a fully ionized plasma, providing evidence that phase mixing could be a large contributor to heating the solar chromosphere. The effectiveness of phase mixing is investigated for various ionization degrees, ranging from very weakly to very strongly ionized plasmas. Our results show that phase mixed propagating Alfven waves in a partially ionized plasma with ionization degrees in the range 0.518 to 0.657, corresponding to heights of 1916 to 2150 km above the solar surface, can provide sufficient heating to balance chromospheric radiative losses in the quiet Sun.

Observation of a propagating slow magnetoacoustic wave in a coronal plasma fan with SDO/AIA and SolO/EUI

Rebecca L **Meadowcroft**, Sihui Zhong, Dmitrii Y Kolotkov, Valery M Nakariakov
MNRAS, Volume 527, Issue 3, January **2024**, Pages 5302–5310,
https://doi.org/10.1093/mnras/stad3506
https://academic.oup.com/mnras/article-pdf/527/3/5302/53961559/stad3506.pdf
Simultaneous observations of a propagating disturbance of EUV intensity, with SDO/AIA at 171 Å and SolO/EUI-HRIEUV at 174 Å, are investigated. The disturbance moves outwards along a plasma fan structure in active region AR 12941 on February 7th 2022, at 12:45–14:15 UT. The spacecraft line-of-sight separation is 19°. The variation of the EUV intensity resembles an almost harmonic wave with an oscillation period of $2.7^{-0.2}_{+0.1}$ and $2.6^{-0.1}_{+0.1}$ min for AIA and HRIEUV, respectively. Over 30 oscillation cycles are detected. The wave originated at the footpoint of the fan, anchored in a sunspot. The projected phase speeds are 60.5 ± 5.2 and 74.4 ± 6.2 km s^{-1} in the AIA and HRIEUV data, respectively, determined by the cross-correlation technique. The observed parameters of the propagating EUV disturbance suggest its interpretation as a slow magnetoacoustic wave. Observations with AIA show that the wave decays with height, with a calculated *e*-folding length of $6.9^{-0.8}_{+1.3}$ Mm. In contrast, in the HRIEUV data, the propagating EUV disturbance is also seen much higher, with the *e*-folding length of $12.8^{-1.7}_{+1.1}$ Mm. This observation demonstrates, for the first time, that the apparent spatial damping of propagating slow waves depends on the observational instrument. Moreover, our work shows that the study of slow waves can be advanced with the use of HRIEUV, and multiple instruments with non-parallel lines of sight.

Updated values of solar gravitational moments J2n using HMI helioseismic inference of internal rotation

Redouane **Mecheri** (1), Mustapha Meftah (2)
MNRAS Volume 506, Issue 2, September **2021**, Pages 2671–2676,
https://doi.org/10.1093/mnras/stab1827
https://arxiv.org/pdf/2107.10575.pdf
The solar gravitational moments J2n are important astronomical quantities whose precise determination is relevant for solar physics, gravitational theory and high precision astrometry and celestial mechanics. Accordingly, we

propose in the present work to calculate new values of J2n (for n=1,2,3,4 and 5) using recent two-dimensional rotation rates inferred from the high resolution SDO/HMI helioseismic data spanning the whole solar activity cycle 24. To this aim, a general integral equation relating J2n to the solar internal density and rotation is derived from the structure equations governing the equilibrium of slowly rotating stars. For comparison purpose, the calculations are also performed using rotation rates obtained from a recently improved analysis of SoHO/MDI heliseismic data for solar cycle 23. In agreement with earlier findings, the results confirmed the sensitivity of high order moments (n>1) to the radial and latitudinal distribution of rotation in the convective zone. The computed value of the quadrupole moment J2 (n=1) is in accordance with recent measurements of the precession of Mercury's perihelion deduced from high precision ranging data of the MESSENGER spacecraft. The theoretical estimate of the related solar oblateness $\Delta\odot$ is consistent with the most accurate space-based determinations, particularly the one from RHESSI/SAS.

SOLAR-v: A new solar spectral irradiance dataset based on SOLAR/SOLSPEC observations during solar cycle 24

M. **Meftah**1, M. Snow2, L. Damé1, D. Bolseé3, N. Pereira3, G. Cessateur3, S. Bekki1, P. Keckhut1, A. Sarkissian1 and A. Hauchecorne1

A&A 645, A2 (**2021**)
https://doi.org/10.1051/0004-6361/202038422
https://www.aanda.org/articles/aa/pdf/2021/01/aa38422-20.pdf

Context. Solar spectral irradiance (SSI) is the wavelength-dependent energy input to the top of the Earth's atmosphere. Solar ultraviolet (UV) irradiance represents the primary forcing mechanism for the photochemistry, heating, and dynamics of the Earth's atmosphere. Hence, both temporal and spectral variations in solar UV irradiance represent crucial inputs to the modeling and understanding of the behavior of the Earth's atmosphere. Therefore, measuring the long-term solar UV irradiance variations over the 11-year solar activity cycle (and over longer timescales) is fundamental. Thus, each new solar spectral irradiance dataset based on long-term observations represents a major interest and can be used for further investigations of the long-term trend of solar activity and the construction of a homogeneous solar spectral irradiance record.
Aims. The main objective of this article is to present a new solar spectral irradiance database (SOLAR-v) with the associated uncertainties. This dataset is based on solar UV irradiance observations (165−300 nm) of the SOLAR/SOLSPEC space-based instrument, which provides measurements of the full-disk SSI during solar cycle 24.
Methods. SOLAR/SOLSPEC made solar acquisitions between April 5, 2008 and February 10, 2017. During this period, the instrument was affected by the harsh space environment that introduces instrumental trends (degradation) in the SSI measurements. A new method based on an adaptation of the Multiple Same-Irradiance-Level (MuSIL) technique was used to separate solar variability and any uncorrected instrumental trends in the SOLAR/SOLSPEC UV irradiance measurements.
Results. A new method for correcting degradation has been applied to the SOLAR/SOLSPEC UV irradiance records to provide new solar cycle variability results during solar cycle 24. Irradiances are reported at a mean solar distance of 1 astronomical unit (AU). In the 165−242 nm spectral region, the SOLAR/SOLSPEC data agrees with the observations (SORCE/SOLSTICE) and models (SATIRE-S, NRLSSI 2) to within the 1-sigma error envelope. Between 242 and 300 nm, SOLAR/SOLSPEC agrees only with the models.

A New Version of the SOLAR-ISS Spectrum Covering the 165 – 3000 nm Spectral Region

M. **Meftah**1 · L. Damé1 · D. Bolsée2 · N. Pereira2 · M. Snow3 · M. Weber4 · K. Bramstedt4 · T. Hilbig4 · G. Cessateur2 · M.-Y. Boudjella1,5 · M. Marchand1 · F. Lefèvre1 · R. Thiéblemont1 · A. Sarkissian1 · A. Hauchecorne1 · P. Keckhut1 · S. Bekki1

Solar Physics volume 295, Article number: 14 (**2020**)
https://link.springer.com/content/pdf/10.1007/s11207-019-1571-y.pdf

The accurate measurement of the solar spectrum at the top of the atmosphere and its variability are fundamental inputs for solar physics (Sun modeling), terrestrial atmospheric photochemistry, and Earth's climate (climate's modeling). These inputs were the prime objective set in 1996 for the SOLAR International Space Station (ISS). The SOLAR package represents a set of three solar instruments measuring the total and spectral absolute irradiance from 16 nm to 3088 nm. SOLAR was launched with the European Columbus space laboratory in February 2008 aboard the NASA Space Shuttle Atlantis. SOLAR on the ISS tracked the Sun until it was decommissioned in February 2017. The SOLar SPECtrum (SOLSPEC) instrument of the SOLAR payload allowed the measurement of solar spectra in the 165 – 3000 nm wavelength range for almost a decade. Until the end of its mission, SOLAR/SOLSPEC was pushed to its limits to test how it was affected by space environmental effects (external thermal factors) and to better calibrate the space-based spectrometer. To that end, a new solar reference spectrum (SOLAR-ISS – V1.1) representative of the 2008 solar minimum was obtained from the measurements made by the SOLAR/SOLSPEC instrument and its calibrations. The main purpose of this article is to improve the SOLAR-ISS reference spectrum (between 165 and 180 nm in the far ultraviolet, between 216.9 and 226.8 nm in the middle ultraviolet, and between

2400 and 3000 nm in the near-infrared). SOLAR-ISS has a resolution better than 0.1 nm between 165 and 1000 nm, and 1 nm in the 1000 – 3000 nm wavelength range. Finally, a first comparison is made between the new SOLAR-ISS spectrum (V2.0) and the Total and Spectral solar Irradiance Sensor (TSIS-1) spectrum obtained from its first observations from the ISS. Indeed, the launch of TSIS in December 2017 provides a new light on the absolute determination of the solar spectrum and especially in the infrared region of the spectrum.

Solar radius determined from PICARD/SODISM observations and extremely weak wavelength dependence in the visible and the near-infrared

M. **Meftah**1, T. Corbard2, A. Hauchecorne1, F. Morand2, R. Ikhlef2, B. Chauvineau2, C. Renaud2, A. Sarkissian1 and L. Damé1

A&A 616, A64 (**2018**)

http://www.aanda.org/articles/aa/pdf/2018/08/aa32159-17.pdf

Context. In 2015, the International Astronomical Union (IAU) passed Resolution B3, which defined a set of nominal conversion constants for stellar and planetary astronomy. Resolution B3 defined a new value of the nominal solar radius ($R_{\odot}^{N}$ = 695 700 km km) that is different from the canonical value used until now (695 990 km). The nominal solar radius is consistent with helioseismic estimates. Recent results obtained from ground-based instruments, balloon flights, or space-based instruments highlight solar radius values that are significantly different. These results are related to the direct measurements of the photospheric solar radius, which are mainly based on the inflection point position methods. The discrepancy between the seismic radius and the photospheric solar radius can be explained by the difference between the height at disk center and the inflection point of the intensity profile on the solar limb. At 535.7 nm (photosphere), there may be a difference of ∼330 km between the two definitions of the solar radius.

Aims. The main objective of this work is to present new results of the solar radius in the near-ultraviolet, the visible, and the near-infrared from PICARD space-based and ground-based observations. Simulations show the strong influence of atmosphere effects (refraction and turbulence) on ground-based solar radius determinations and highlight the interest of space-based solar radius determinations, particularly during planet transits (Venus or Mercury), in order to obtain more realistic and accurate measurements.

Methods. Solar radius observations during the 2012 Venus transit have been made with the SOlar Diameter Imager and Surface Mapper (SODISM) telescope on board the PICARD spacecraft. We used the transit of Venus as an absolute calibration to determine the solar radius accurately at several wavelengths. Our results are based on the determination of the inflection point position of the solar limb-darkening function (the most common solar radius definition). A realistic uncertainty budget is provided for each solar radius obtained with the PICARD space-based telescope during the 2012 Venus transit. The uncertainty budget considers several sources of error (detection of the centers of Venus and Sun in PICARD images, positions of Sun and Venus from ephemeris (planetary theory), PICARD on-board timing, PICARD spacecraft position, and optical distortion correction from PICARD images).

Results. We obtain new values of the solar radius from the PICARD mission at several wavelengths and in different solar atmosphere regions. The PICARD spacecraft with its SODISM telescope was used to measure the radius of the Sun during the Venus transit in 2012. At 535.7 nm, the solar radius is equal to 696 134 ± 261 km (combined standard uncertainty based (ξ) on the uncertainty budget). At 607.1 nm, the solar radius is equal to 696 156 ± 145 km (ξ), and the standard deviation of the solar radius mean value is ±22 km. At 782.2 nm, the solar radius is equal to 696 192 ± 247 km (ξ). The PICARD space-based results as well as PICARD ground-based results show that the solar radius wavelength dependence in the visible and the near-infrared is extremely weak. The differences in inflection point position of the solar radius at 607.1 nm, 782.2 nm, and 1025.0 nm from a reference at 535.7 nm are less than 60 km for the different PICARD measurements.

SOLAR-ISS: A new reference spectrum based on SOLAR/SOLSPEC observations★

M. **Meftah**1, L. Damé1, D. Bolsée2, A. Hauchecorne1, N. Pereira2, D. Sluse2, G. Cessateur2, A. Irbah1, J. Bureau3, M. Weber3, K. Bramstedt3, T. Hilbig3, R. Thiéblemont1, M. Marchand1, F. Lefèvre1, A. Sarkissian1 and S. Bekki1

A&A 611, A1 (**2018**)

https://www.aanda.org/articles/aa/pdf/2018/03/aa31316-17.pdf

Context. Since April 5, 2008 and up to February 15, 2017, the SOLar SPECtrometer (SOLSPEC) instrument of the SOLAR payload on board the International Space Station (ISS) has performed accurate measurements of solar spectral irradiance (SSI) from the middle ultraviolet to the infrared (165 to 3088 nm). These measurements are of primary importance for a better understanding of solar physics and the impact of solar variability on climate. In particular, a new reference solar spectrum (SOLAR-ISS) is established in April 2008 during the solar minima of cycles 23–24 thanks to revised engineering corrections, improved calibrations, and advanced procedures to account for thermal and aging corrections of the SOLAR/SOLSPEC instrument.

Aims. The main objective of this article is to present a new high-resolution solar spectrum with a mean absolute uncertainty of 1.26% at 1σ from 165 to 3000 nm. This solar spectrum is based on solar observations of the SOLAR/SOLSPEC space-based instrument.

Methods. The SOLAR/SOLSPEC instrument consists of three separate double monochromators that use concave holographic gratings to cover the middle ultraviolet (UV), visible (VIS), and infrared (IR) domains. Our best ultraviolet, visible, and infrared spectra are merged into a single absolute solar spectrum covering the 165–3000 nm domain. The resulting solar spectrum has a spectral resolution varying between 0.6 and 9.5 nm in the 165–3000 nm wavelength range. We build a new solar reference spectrum (SOLAR-ISS) by constraining existing high-resolution spectra to SOLAR/SOLSPEC observed spectrum. For that purpose, we account for the difference of resolution between the two spectra using the SOLAR/SOLSPEC instrumental slit functions.
Results. Using SOLAR/SOLSPEC data, a new solar spectrum covering the 165–3000 nm wavelength range is built and is representative of the 2008 solar minimum. It has a resolution better than 0.1 nm below 1000 nm and 1 nm in the 1000–3000 nm wavelength range. The new solar spectrum (SOLAR-ISS) highlights significant differences with previous solar reference spectra and with solar spectra based on models. The integral of the SOLAR-ISS solar spectrum yields a total solar irradiance of 1372.3 ± 16.9 Wm−2 at 1σ, that is yet 11 Wm−2 over the value recommended by the International Astronomical Union in 2015.

A New Solar Spectrum from 656 to 3088 nm

M. **Meftah**, L. Damé, D. Bolsée, N. Pereira, D. Sluse…
Solar Physics August **2017**, 292:101
The solar spectrum is a key parameter for different scientific disciplines such as solar physics, climate research, and atmospheric physics. The SOLar SPECtrometer (SOLSPEC) instrument of the Solar Monitoring Observatory (SOLAR) payload onboard the International Space Station (ISS) has been built to measure the solar spectral irradiance (SSI) from 165 to 3088 nm with high accuracy. To cover the full wavelength range, three double-monochromators with concave gratings are used. We present here a thorough analysis of the data from the third channel/double-monochromator, which covers the spectral range between 656 and 3088 nm. A new reference solar spectrum is therefore obtained in this mainly infrared wavelength range (656 to 3088 nm); it uses an absolute preflight calibration performed with the blackbody of the Physikalisch-Technische Bundesanstalt (PTB). An improved correction of temperature effects is also applied to the measurements using in-flight housekeeping temperature data of the instrument. The new solar spectrum (SOLAR–IR) is in good agreement with the ATmospheric Laboratory for Applications and Science (ATLAS 3) reference solar spectrum from 656 nm to about 1600 nm. However, above 1600 nm, it agrees better with solar reconstruction models than with spacecraft measurements. The new SOLAR/SOLSPEC measurement of solar spectral irradiance at about 1600 nm, corresponding to the minimum opacity of the solar photosphere, is 248.08 ± 4.98 mW m−2 nm−1 (1 σσ), which is higher than recent ground-based evaluations.

Total solar irradiance as measured by the SOVAP radiometer onboard PICARD

Mustapha **Meftah**1*, André Chevalier2, Christian Conscience2 and Stijn Nevens
J. Space Weather Space Clim., 6, A34 (**2016**)
http://www.swsc-journal.org/articles/swsc/pdf/2016/01/swsc160004.pdf
From the SOlar VAriability PICARD (SOVAP) space-based radiometer, we obtained a new time series of the total solar irradiance (TSI) during Solar Cycle 24. Based on SOVAP data, we obtained that the TSI input at the top of the Earth's atmosphere at a distance of one astronomical unit from the Sun is 1361.8 ± 2.4 W m−2 (1σ) representative of the 2008 solar minimum period. From 2010 to 2014, the amplitude of the changes has been of the order of ± 0.1%, corresponding to a range of about 2.7 W m−2. To determine the TSI from SOVAP, we present here an improved instrument equation. A parameter was integrated from a theoretical analysis that highlighted the thermo-electrical non-equivalence of the radiometric cavity. From this approach, we obtained values that are lower than those previously provided with the same type of instrument. The results in this paper supersede the previous SOVAP analysis and provide the best SOVAP-based TSI-value estimate and its temporal variation.

Solar Irradiance from 165 to 400 nm in 2008 and UV Variations in Three Spectral Bands During Solar Cycle 24

M. **Meftah**, D. Bolsée, L. Damé, A. Hauchecorne, N. Pereira, A. Irbah, S. Bekki, G. Cessateur, T. Foujols, R. Thiéblemont
Solar Phys. Volume 291, Issue 12, pp 3527–3547 **2016**
Accurate measurements of the solar spectral irradiance (SSI) and its temporal variations are of primary interest to better understand solar mechanisms, and the links between solar variability and Earth's atmosphere and climate. The SOLar SPECtrum (SOLSPEC) instrument of the Solar Monitoring Observatory (SOLAR) payload onboard the International Space Station (ISS) has been built to carry out SSI measurements from 165 to 3088 nm. We focus here on the ultraviolet (UV) part of the measured solar spectrum (wavelengths less than 400 nm) because the UV part is

potentially important for understanding the solar forcing of Earth's atmosphere and climate. We present here SOLAR/SOLSPEC UV data obtained since 2008, and their variations in three spectral bands during Solar Cycle 24. They are compared with previously reported UV measurements and model reconstructions, and differences are discussed.

Total solar irradiance as measured by the SOVAP radiometer onboard PICARD

Mustapha **Meftah**1*, André Chevalier2, Christian Conscience2 and Stijn Nevens
J. Space Weather Space Clim., 6, A34 (**2016**)
http://www.swsc-journal.org/articles/swsc/pdf/2016/01/swsc160004.pdf
From the SOlar VAriability PICARD (SOVAP) space-based radiometer, we obtained a new time series of the total solar irradiance (TSI) during Solar Cycle 24. Based on SOVAP data, we obtained that the TSI input at the top of the Earth's atmosphere at a distance of one astronomical unit from the Sun is 1361.8 ± 2.4 W m−2 (1σ) representative of the 2008 solar minimum period. From 2010 to 2014, the amplitude of the changes has been of the order of ± 0.1%, corresponding to a range of about 2.7 W m−2. To determine the TSI from SOVAP, we present here an improved instrument equation. A parameter was integrated from a theoretical analysis that highlighted the thermo-electrical non-equivalence of the radiometric cavity. From this approach, we obtained values that are lower than those previously provided with the same type of instrument. The results in this paper supersede the previous SOVAP analysis and provide the best SOVAP-based TSI-value estimate and its temporal variation.

Solar Spectral Irradiance at 782 nm as Measured by the SES Sensor OnboardPicard

M. **Meftah**, A. Hauchecorne, A. Irbah, G. Cessateur, S. Bekki, L. Damé, D. Bolsée, N. Pereira
Solar Phys. Volume 291, Issue 4, pp 1043-1057 **2016**
Picard is a satellite dedicated to the simultaneous measurement of the total and solar spectral irradiance, the solar diameter, the solar shape, and to the Sun's interior through the methods of helioseismology. The satellite was launched on June 15, 2010, and pursued its data acquisitions until March 2014. A Sun Ecartometry Sensor (SES) was developed to provide the stringent pointing requirements of the satellite. The SES sensor produced an image of the Sun at 782±2.5 nm782±2.5 nm. From the SES data, we obtained a new time series of the solar spectral irradiance at 782 nm from 2010 to 2014. During this period of Solar Cycle 24, the amplitude of the changes has been of the order of ± 0.08 %, corresponding to a range of about 2×10−3 Wm−2nm−12×10−3 Wm−2nm−1. SES observations provided a qualitatively consistent evolution of the solar spectral irradiance variability at 782 nm. SES data show similar amplitude variations with the semi-empirical model Spectral And Total Irradiance REconstruction for the Satellite era (SATIRE-S), whereas the Spectral Irradiance Monitorinstrument (SIM) onboard the SOlar Radiation and Climate Experiment satellite (SORCE) highlights higher amplitudes.

On the Constancy of the Diameter of the Sun during the Rising Phase of Solar Cycle 24

M. **Meftah**1, A. Hauchecorne1, A. Irbah1, T. Corbard2, R. Ikhlef2, F. Morand2, C. Renaud2, F. Riguet3, and F. Prada
2015 ApJ 808 4
The potential relationship between solar activity and changes in solar diameter remains the subject of debate and requires both models and measurements with sufficient precision over long periods of time. Using the PICARD instruments, we carried out precise measurements of variations in solar diameter during the rising phase of solar cycle 24. From new correction methods we found changes in PICARD space telescope solar radius amplitudes that were less than ±20 mas (i.e. ±14.5 km) for the years 2010–2011. Moreover, PICARD ground-based telescope solar radius amplitudes are smaller than ±50 mas from 2011 to 2014. Our observations could not find any direct link between solar activity and significant fluctuations in solar radius, considering that the variations, if they exist, are included within this range of values. Further, the contribution of solar radius fluctuations is low with regard to variations in total solar irradiance. Indeed, we find a small variation of the solar radius from space measurements with a typical periodicity of 129.5 days, with ±6.5 mas variation.

On the Determination and Constancy of the Solar Oblateness

M. **Meftah**, A. Irbah, A. Hauchecorne, et al.
Solar Physics March **2015**, Volume 290, Issue 3, pp 673-687,
The equator-to-pole radius difference (Δr=R eq−R pol) is a fundamental property of our star, and understanding it will enrich future solar and stellar dynamical models. The solar oblateness (Δ⊙) corresponds to the excess ratio of the equatorial solar radius (R eq) to the polar radius (R pol), which is of

great interest for those working in relativity and different areas of solar physics. Δr is known to be a rather small quantity, where a positive value of about 8 milli-arcseconds (mas) is suggested by previous measurements and predictions. The Picard space mission aimed to measure Δr with a precision better than 0.5 mas. The Solar Diameter Imager and Surface Mapper(SODISM) onboard Picard was a Ritchey–Chrétien telescope that took images of the Sun at several wavelengths. The SODISM measurements of the solar shape were obtained during special roll maneuvers of the spacecraft by 30° steps. They have produced precise determinations of the solar oblateness at 782.2 nm. After correcting measurements for optical distortion and for instrument temperature trend, we found a solar equator-to-pole radius difference at 782.2 nm of 7.9±0.3 mas (5.7±0.2 km) at one σ. This measurement has been repeated several times during the first year of the space-borne observations, and we have not observed any correlation between oblateness and total solar irradiance variations.

Cycle dependency of a quasi-biennial variability in the solar interior

T. **Mehta**, K. Jain, S. C. Tripathy, R. Kiefer, D. Kolotkov, A.-M. Broomhall

MNRAS Volume 515, Issue 2, Pages 2415–2429, **2022**

https://arxiv.org/pdf/2207.14560

https://doi.org/10.1093/mnras/stac1943

https://watermark.silverchair.com/stac1943.pdf

We investigated the solar cycle dependency on the presence and periodicity of the Quasi-Biennial Oscillation (QBO). Using helioseismic techniques, we used solar oscillation frequencies from the Global Oscillations Network Group (GONG), Michelson Doppler Imager (MDI) and Helioseismic & Magnetic Imager (HMI) in the intermediate-degree range to investigate the frequency shifts over Cycles 23 and 24. We also examined two solar activity proxies, the F10.7 index and the MgII index, for the last four solar cycles to study the associated QBO. The analyses were performed using Empirical Mode Decomposition (EMD) and the Fast Fourier Transform (FFT). We found that the EMD analysis method is susceptible to detecting statistically significant Intrinsic Mode Functions (IMFs) with periodicities that are overtones of the length of the dataset under examination. Statistically significant periodicites, which were not due to overtones, were detected in the QBO range. We see a reduced presence of the QBO in Cycle 24 compared to Cycle 23. The presence of the QBO was not sensitive to the depth to which the p-mode travelled, nor the average frequency of the p-mode. The analysis further suggested that the magnetic field responsible for producing the QBO in frequency shifts of p-modes is anchored above approximately 0.95 solar radii.

On midrange periodicities in solar radio flux and sunspot areas

Y. **Mei**, H. Deng,F. Wang

Astrophysics and Space Science April **2018**, 363:84

https://link.springer.com/content/pdf/10.1007%2Fs10509-018-3306-1.pdf

https://arxiv.org/pdf/1811.04650.pdf

Using the Hilbert-Huang transform technique, we investigate the midrange periodicities in solar radio flux at 2800 MHz (F10.7) and sunspot areas (SAs) from February 1, 1947 to September 30, 2016. The following prominent results are found: (1) The quasi-periodic oscillations of both data sets are not identical, such as the rotational cycle, the midrange periodicities, and the Schwabe cycle. In particular, the midrange periodicities ranging from 37.9 days to 297.3 days are related to the magnetic Rossby-type waves; (2) The 1.3-year and 1.7-year fluctuations in solar activity indicators are surface manifestations (from photosphere to corona) of magnetic flux changes generated deep inside the Sun; (3) At the timescale of the Schwabe cycle, the complicated phase relationships in the three intervals (1947–1958, 1959–1988, and 1989–2016) agree with the produced periodicities of the magnetic Rossby-type waves. The findings indicate that the magnetic Rossby-type waves are the possible physical mechanism behind the midrange periodicities of solar activity indicators. Moreover, the significant change in the relationship between photospheric and coronal activity took place after the maximum of solar cycle 22 could be interpreted by the magnetic Rossby-type waves.

A Machine Learning Enhanced Approach for Automated Sunquake Detection in Acoustic Emission Maps

Vanessa **Mercea**, Alin Razvan Paraschiv, Daniela Adriana Lacatus, Anca Marginean, Diana Besliu-Ionescu

Solar Phys. **2022**

https://arxiv.org/pdf/2212.06717.pdf

Sunquakes are seismic emissions visible on the solar surface, associated with some solar flares. Although discovered in 1998, they have only recently become a more commonly detected phenomenon. Despite the availability of several manual detection guidelines, to our knowledge, the astrophysical data produced for sunquakes is new to the field of Machine Learning. Detecting sunquakes is a daunting task for human operators and this work aims to ease and, if possible, to improve their detection. Thus, we introduce a dataset constructed from acoustic

egression-power maps of solar active regions obtained for Solar Cycles 23 and 24 using the holography method. We then present a pedagogical approach to the application of machine learning representation methods for sunquake detection using AutoEncoders, Contrastive Learning, Object Detection and recurrent techniques, which we enhance by introducing several custom domain-specific data augmentation transformations. We address the main challenges of the automated sunquake detection task, namely the very high noise patterns in and outside the active region shadow and the extreme class imbalance given by the limited number of frames that present sunquake signatures. With our trained models, we find temporal and spatial locations of peculiar acoustic emission and qualitatively associate them to eruptive and high energy emission. While noting that these models are still in a prototype stage and there is much room for improvement in metrics and bias levels, we hypothesize that their agreement on example use cases has the potential to enable detection of weak solar acoustic manifestations.
Table 1. Sunquake events between 09 July 1996 and 15 January 2005 from SC23 and between 15 February 2011 and 07 September 2017 from SC24. E

Magnetically coupled atmosphere, fast sausage MHD waves, and forced magnetic field reconnection during the SOL2014-09-10T17:45 flare

Hana **Meszarosova**, Peter Gomory
A&A 643, A140 **2020**
https://arxiv.org/pdf/2010.01527.pdf
https://doi.org/10.1051/0004-6361/202038388
https://www.aanda.org/articles/aa/pdf/2020/11/aa38388-20.pdf
We study the physical properties and behavior of the solar atmosphere during the GOES X1.6 solar flare on **2014 September 10**. The steady plasma flows and the fast sausage MHD waves were analysed with the wavelet separation method. The magnetically coupled atmosphere and the forced magnetic field reconnection were studied with the help of the Vertical-Current Approximation Non-linear Force-Free Field code. We studied a mechanism of MHD wave transfer from the photosphere without dissipation or reflection before reaching the corona and a mechanism of the wave energy distribution over the solar corona. We report a common behavior of (extreme)ultraviolet steady plasma flows (speed of 15.3 -> 10.9 km/s) and fast sausage MHD waves (Alfven speed of 13.7 -> 10.3 km/s and characteristic periods of 1 587 -> 1 607 s), propagating in cylindrical plasma waveguides of the individual atmospheric layers (photosphere -> corona) observed by SDO/AIA/HMI and IRIS space instruments. A magnetically coupled solar atmosphere by a magnetic field flux tube above a sunspot umbra and a magnetic field reconnection forced by the waves were analysed. The solar seismology with trapped, leakage, and tunnelled modes of the waves, dissipating especially in the solar corona, is discussed with respect to its possible contribution to the outer atmosphere heating. We demonstrate that a dispersive nature of fast sausage MHD waves, which can easily generate the leaky and other modes propagating outside of their waveguide, and magnetic field flux tubes connecting the individual atmospheric layers can distribute the magnetic field energy across the active region. This mechanism can contribute to the coronal energy balance and to our knowledge on how the coronal heating is maintained.

The Magnetic Mid-life Crisis of the Sun

Travis **Metcalfe**1, Jennifer van Saders2, Ricky Egeland
HMI Science Nuggets # 72 Sept **2017**
http://hmi.stanford.edu/hminuggets/?p=1977
Astronomers have known for a long time that the Sun is a typical star near the middle of its main-sequence lifetime. What we didn't appreciate until recently is that all Sun-like stars experience a fundamental shift in their rotation and magnetism around middle-age. We have now identified the manifestation of this unexpected transition in the best available data on stellar cycles[1]. The observations suggest that the solar cycle will grow longer over a few billion years before the global dynamo shuts down.

Magnetic Evolution and the Disappearance of Sun-like Activity Cycles

Travis S. **Metcalfe** and Jennifer van Saders
Solar Phys. 292:126 **2017**
https://arxiv.org/pdf/1705.09668.pdf
After decades of effort, the solar activity cycle is exceptionally well characterized but it remains poorly understood. Pioneering work at the Mount Wilson Observatory demonstrated that other sun-like stars also show regular activity cycles, and suggested two possible relationships between the rotation rate and the length of the cycle. Neither of these relationships correctly describe the properties of the Sun, a peculiarity that demands explanation. Recent discoveries have started to shed light on this issue, suggesting that the Sun's rotation rate and magnetic field are currently in a transitional phase that occurs in all middle-aged stars. Motivated by these developments, we identify the manifestation of this magnetic transition in the best available data on stellar cycles. We propose a

reinterpretation of previously published observations to suggest that the solar cycle may be growing longer on stellar evolutionary timescales, and that the cycle might disappear sometime in the next 0.8-2.4 Gyr. Future tests of this hypothesis will come from ground-based activity monitoring of Kepler targets that span the magnetic transition, and from asteroseismology with the TESS mission to determine precise masses and ages for bright stars with known cycles.

Stellar Evidence of a Solar Dynamo in Transition

Travis S. **Metcalfe**, Ricky Egeland, Jennifer van Saders
ApJL **2016**
http://arxiv.org/pdf/1606.01926v1.pdf

Precise photometry from the Kepler space telescope allows not only the measurement of rotation in solar-type field stars, but also the determination of reliable masses and ages from asteroseismology. These critical data have recently provided the first opportunity to calibrate rotation-age relations for stars older than the Sun. The evolutionary picture that emerges is surprising: beyond middle-age the efficiency of magnetic braking is dramatically reduced, implying a fundamental change in angular momentum loss beyond a critical Rossby number (Ro~2). We compile published chromospheric activity measurements for the sample of Kepler asteroseismic targets that were used to establish the new rotation-age relations. We use these data along with a sample of well characterized solar analogs from the Mount Wilson HK survey to develop a qualitative scenario connecting the evolution of chromospheric activity to a fundamental shift in the character of differential rotation. We conclude that the Sun is in a transitional evolutionary phase, and that its magnetic cycle may represent a special case of stellar dynamo theory.

Four Decades of Advances from MSDP to S4I and SLED Imaging Spectrometers

P. **Mein**, J.-M. Malherbe, F. Sayède, P. Rudawy, K. J. H. Phillips & F. P. Keenan
Solar Physics volume 296, Article number: 30 (**2021**)
https://link.springer.com/content/pdf/10.1007/s11207-021-01766-9.pdf

The Multichannel Subtractive Double Pass (MSDP) is an imaging spectroscopy technique, which allows observations of spectral line profiles over a 2D field of view with high spatial and temporal resolution. It has been intensively used since 1977 on various spectrographs (Meudon, Pic du Midi, the German Vacuum Tower Telescope, THEMIS, Wrocław). We summarize previous developments and describe the capabilities of a new design that has been developed at Meudon and that has higher spectral resolution and increased channel number: Spectral Sampling with Slicer for Solar Instrumentation (S4I), which can be combined with a new and fast polarimetry analysis. This new generation MSDP technique is well adapted to large telescopes. Also presented are the goals of a derived compact version of the instrument, the Solar Line Emission Dopplerometer (SLED), dedicated to dynamic studies of coronal loops observed in the forbidden iron lines, and prominences. It is designed for observing total solar eclipses, and for deployment on the Wrocław and Lomnicky peak coronagraphs respectively for prominence and coronal observations.

A Machine Learning Enhanced Approach for Automated Sunquake Detection in Acoustic Emission Maps

Vanessa **Mercea**, Alin Razvan Paraschiv, Daniela Adriana Lacatus, Anca Marginean & Diana Besliu-Ionescu
Solar Physics volume 298, Article number: 4 (**2023**)
https://link.springer.com/content/pdf/10.1007/s11207-022-02081-7.pdf

Sunquakes are seismic emissions visible on the solar surface, associated with some solar flares. Although discovered in 1998, they have only recently become a more commonly detected phenomenon. Despite the availability of several manual detection guidelines, to our knowledge, the astrophysical data produced for sunquakes is new to the field of machine learning. Detecting sunquakes is a daunting task for human operators, and this work aims to ease and, if possible, to improve their detection. Thus, we introduce a dataset constructed from acoustic egression-power maps of solar active regions obtained for Solar Cycles 23 and 24 using the holography method. We then present a pedagogical approach to the application of machine-learning representation methods for sunquake detection using autoencoders, contrastive learning, object detection and recurrent techniques, which we enhance by introducing several custom, domain-specific data augmentation transformations. We address the main challenges of the automated sunquake-detection task, namely the very high noise patterns in and outside the active region shadow and the extreme class imbalance given by the limited number of frames that present sunquake signatures. With our trained models, we find temporal and spatial locations of peculiar acoustic emission and qualitatively associate them to eruptive and high energy emission. While noting that these models are still in a prototype stage, and there is much room for improvement in metrics and bias levels, we hypothesize that their agreement on example use cases has the potential to enable detection of weak solar acoustic manifestations.

Solar chromospheric emission and magnetic structures from plages to intranetwork: Contribution of the very quiet Sun

Nadège **Meunier**

A&A 615, A87 **2018**

https://arxiv.org/pdf/1804.00869.pdf

We need to establish a correspondence between the magnetic structures generated by models and usual stellar activity indexes to simulate radial velocity time series for stars less active than the Sun. This is necessary to compare the outputs of such models with observed radial velocity jitters and is critical to better understand the impact of stellar activity on exoplanet detectability. We propose a coherent picture to describe the relationship between magnetic activity, including the quiet Sun regions, and the chromospheric emission using the Sun as a test-bench and a reference. We analyzed a time series of MDI magnetograms jointly with chromospheric emission time series obtained at Sacramento Peak and Kitt Peak observatories. This has allowed us to study the variability in the quiet Sun over the solar cycle, and then, based on available relations between magnetic fields in active structures and chromospheric emission, to propose an empirical reconstruction of the solar chromospheric emission based on all contributions. We show that the magnetic flux covering the solar surface, including in the quieted regions, varies in phase with the solar cycle, suggesting a long-term relationship between the global dynamo and the contribution of all components of solar activity. We have been able to propose a reconstruction of the solar S-index, including a relationship between the weak field component and its chomospheric emission, which is in good agreement with the literature. This allows us to explain that stars with a low average chromospheric emission level exhibit a low variability. We conclude that weak flux regions significantly contribute to the chromospheric emission; these regions should be critical in explaining the lower variability associated with the lower average activity level in other stars as compared to the Sun and estimated from their chromospheric emission.

Association between tornadoes and hosting prominence instability

Irakli **Mghebrishvili**, Teimuraz V. Zaqarashvili, Vasil Kukhianidze, David Kuridze, David Tsiklauri, Bidzina M. Shergelashvili, Stefaan Poedts

ApJ 861, Issue 2, article id. 112, **2018**

https://arxiv.org/pdf/1807.01345.pdf

https://iopscience.iop.org/article/10.3847/1538-4357/aac823/pdf

We studied the dynamics of all prominence tornadoes detected by the Solar Dynamics Observatory/Atmospheric Imaging Assembly from 2011 January 01 to December 31. In total, 361 events were identified during the whole year, but only 166 tornadoes were traced until the end of their lifetime. Out of 166 tornadoes, 80 (48%) triggered CMEs in hosting prominences, 83 (50%) caused failed coronal mass ejections (CMEs) or strong internal motion in the prominences, and only 3 (2%) finished their lifetimes without any observed activity. Therefore, almost all prominence tornadoes lead to the destabilization of their hosting prominences and half of them trigger CMEs. Consequently, prominence tornadoes may be used as precursors for CMEs and hence for space weather predictions.

2011 April 29, 2011-07-05, 2011.10.10-13

Table 2. A catalog of prominence tornadoes during the year 2011

Magnetic Flux Conservation in the Heliosheath Including Solar Cycle Variations of Magnetic Field Intensity

A. T. **Michael**1, M. Opher1, E. Provornikova2, J. D. Richardson3, and G. Tóth

2015 ApJ 803 L6

In the heliosheath (HS), Voyager 2 has observed a flow with constant radial velocity and magnetic flux conservation. Voyager 1, however, has observed a decrease in the flow's radial velocity and an order of magnitude decrease in magnetic flux. We investigate the role of the 11 yr solar cycle variation of the magnetic field strength on the magnetic flux within the HS using a global 3D magnetohydrodynamic model of the heliosphere. We use time and latitude-dependent solar wind velocity and density inferred fromSolar and Heliospheric Observatory/SWAN and interplanetary scintillations data and implemented solar cycle variations of the magnetic field derived from 27 day averages of the field magnitude average of the magnetic field at 1 AU from the OMNI database. With the inclusion of the solar cycle time-dependent magnetic field intensity, the model matches the observed intensity of the magnetic field in the HS along both Voyager 1 and 2. This is a significant improvement from the same model without magnetic field solar cycle variations, which was over a factor of two larger. The model accurately predicts the radial velocity observed by Voyager2; however, the model predicts a flow speed ~100 km s−1 larger than that derived from LECP measurements at Voyager 1. In the model, magnetic flux is conserved along both Voyager trajectories, contrary to observations. This implies that the solar cycle variations in solar wind magnetic field observed at 1 AU does not cause the order of magnitude decrease in magnetic flux observed in the Voyager 1 data.

Solar luminosity bounds on mirror matter

Erez **Michaely**, Itzhak Goldman, Shmuel Nussinov

MNRAS **2019**

https://arxiv.org/pdf/1905.12643.pdf

We present bounds on mirror dark matter scenario derived by using the effect of mirror matter on the luminosity of the Sun. In the perturbative regime where the mirror matter concentration is small relative to the ordinary matter we estimate the heat transfer from ordinary matter to the mirror sector by simple analytic consideration. That amount of heat transfer is radiated via mirror photons and increases the required energy production in order to maintain the observed luminosity. We then present more detailed numerical calculations of the total amount of this energy transfer.

Evolution of Kelvin-Helmholtz Instability in the Fan-Spine Topology

Sudheer K. **Mishra**, Balveer Singh, A.K. Srivastava, Pradeep Kayshap, B.N. Dwivedi

ApJ **2021**

https://arxiv.org/pdf/2109.11416.pdf

We use multiwavelength imaging observations from the Atmospheric Imaging Assembly (AIA) onboard the Solar Dynamics Observatory (SDO) to study the evolution of Kelvin-Helmholtz (K-H) instability in a fan-spine magnetic field configuration. This magnetic topology exists near an active region AR12297 and is rooted in a nearby sunspot. In this magnetic configuration, two layers of cool plasma flow in parallel and interact with each other inside an elongated spine. The slower plasma flow (5 kms−1) is the reflected stream along the spine field lines from the top, which interacts with the impulsive plasma upflows (114-144 km s−1) from below. This process generates a shear motion and subsequent evolution of the K--H instability. The amplitude and characteristic wavelength of the K-H unstable vortices increase, satisfying the criterion of the fastest growing mode of this instability. We also describe that the velocity difference between two layers and velocity of K-H unstable vortices are greater than the Alfven speed in the second denser layer, which also satisfies the criterion of the growth of K-H instability. In the presence of the magnetic field and sheared counter streaming plasma as observed in the fan-spine topology, we estimate the parametric constant, $\Lambda \geq 1$, that confirms the dominance of velocity shear and the evolution of the linear phase of the K-H instability. This observation indicates that in the presence of complex magnetic field structuring and flows, the fan-spine configuration may evolve into rapid heating, while the connectivity changes due to the fragmentation via the K-H instability.

Long-term Evolution of the Solar Corona Using PROBA2 Data

Marilena **Mierla**, Jan Janssens, Elke D'Huys, Laurence Wauters, Matthew J. West, Daniel B. Seaton, David Berghmans, Elena Podladchikova

Solar Phys. **295**, Article number: 66 **2020**

https://arxiv.org/pdf/2004.09785.pdf

https://link.springer.com/content/pdf/10.1007/s11207-020-01635-x.pdf

We use The Sun Watcher with Active Pixel System detector and Image Processing (SWAP) imager onboard the Project for Onboard Autonomy 2 (PROBA2) mission to study the evolution of large-scale EUV structures in the solar corona observed throughout Solar Cycle 24 (from 2010 to 2019). We discuss the evolution of the on-disk coronal features and at different heights above the solar surface based on EUV intensity changes. We also look at the evolution of the corona in equatorial and polar regions and compare them at different phases of the solar cycle, as well as with sunspot number evolution and with the PROBA2/Lyman-Alpha Radiometer (LYRA) signal. The main results are as follows: The three time series (SWAP on-disk average brightness, sunspot number and LYRA irradiance) are very well correlated, with correlation coefficients around 0.9. The average rotation rate of bright features at latitudes of +15, 0, and -15 degrees was around 15 degree/day throughout the period studied. A secondary peak in EUV averaged intensity at the Poles was observed on the descending phase of SC24. These peaks (at North and South poles respectively) seem to be associated with the start of the development of the (polar) coronal holes. Large-scale off-limb structures were visible from around March 2010 to around March 2016, meaning that they were absent at the minimum phase of solar activity. A fan at the North pole persisted for more than 11 Carrington rotations (February 2014 to March 2015), and it could be seen up to altitudes of 1.6 Rs.

Magnetic Helicity Reversals in a Cyclic Convective Dynamo

Mark S. **Miesch** (HAO/NCAR, USA), Mei Zhang (National Astronomical Observatories, China), Kyle C. Augustson

ApJL 824 L15 **2016**

http://arxiv.org/pdf/1605.09687v1.pdf

We investigate the role of magnetic helicity in promoting cyclic magnetic activity in a global, 3D, magnetohydrodynamic (MHD) simulation of a convective dynamo. This simulation is characterized by coherent bands of toroidal field that exist within the convection zone, with opposite polarities in the northern and southern

hemispheres. Throughout most of the cycle, the magnetic helicity in these bands is negative in the northern hemisphere and positive in the southern hemisphere. However, during the declining phase of each cycle, this hemispheric rule reverses. We attribute this to a global restructuring of the magnetic topology that is induced by the interaction of the bands across the equator. This band interaction appears to be ultimately responsible for, or at least associated with, the decay and subsequent reversal of both the toroidal bands and the polar fields. We briefly discuss the implications of these results within the context of solar observations, which also show some potential evidence for toroidal band interactions and helicity reversals.

A Three-Dimensional Babcock-Leighton Solar Dynamo Model: Initial Results with Axisymmetric Flows

Mark S. **Miesch**, Kinfe Teweldebirhan

Special issue of Advances in Space Research on "Solar Dynamo Frontiers" **201**5

http://arxiv.org/pdf/1511.03613v1.pdf

The main objective of this paper is to introduce the STABLE (Surface flux Transport And Babcock-LEighton) solar dynamo model. STABLE is a 3D Babcock-Leighton/Flux Transport dynamo model in which the source of poloidal field is the explicit emergence, distortion, and dispersal of bipolar magnetic regions (BMRs). Here we describe the STABLE model in more detail than we have previously and we verify it by reproducing a 2D mean-field benchmark. We also present some representative dynamo simulations, focusing on the special case of kinematic magnetic induction and axisymmetric flow fields. Not all solutions are supercritical; it can be a challenge for the BL mechanism to sustain the dynamo when the turbulent diffusion near the surface is ≥1012cm2 s−1. However, if BMRs are sufficiently large, deep, and numerous, then sustained, cyclic, dynamo solutions can be found that exhibit solar-like features. Furthermore, we find that the shearing of radial magnetic flux by the surface differential rotation can account for most of the net toroidal flux generation in each hemisphere, as has been recently argued for the Sun by Cameron & Schussler (2015).

Intriguing Plasma Composition Pattern in a Solar Active Region: a Result of Non-Resonant Alfvén Waves?

Teodora **Mihailescu**, David H. Brooks, J. Martin Laming, Deborah Baker, Lucie M. Green, Alexander W. James, David M. Long, Lidia van Driel-Gesztelyi, Marco Stangalini

ApJ **959** 72 **2023**

https://arxiv.org/pdf/2310.13677.pdf

https://iopscience.iop.org/article/10.3847/1538-4357/ad05bf/pdf

The plasma composition of the solar corona is different from that of the solar photosphere. Elements that have a low first ionisation potential (FIP) are preferentially transported to the corona and, therefore, show enhanced abundances in the corona compared to the photosphere. The level of enhancement is measured using the FIP bias parameter. In this work, we use data from the EUV Imaging Spectrometer (EIS) on Hinode to study the plasma composition in an active region following an episode of significant new flux emergence into the pre-existing magnetic environment of the active region. We use two FIP bias diagnostics: Si X 258.375 A/S X 264.233 A (temperature of approximately 1.5 MK) and Ca XIV 193.874 A/Ar XIV 194.396 A (temperature of approximately 4 MK). We observe slightly higher FIP bias values with the Ca/Ar diagnostic than Si/S in the newly emerging loops, and this pattern is much stronger in the preexisting loops (those that had been formed before the flux emergence). This result can be interpreted in the context of the ponderomotive force model, which proposes that the plasma fractionation is generally driven by Alfvén waves. Model simulations predict this difference between diagnostics using simple assumptions about the wave properties, particularly that the fractionation is driven by resonant/non-resonant waves in the emerging/preexisting loops. We propose that this results in the different fractionation patterns observed in these two sets of loops. **2017 July 9**

Hinode/EIS Science Nugget June **2024** https://solarb.mssl.ucl.ac.uk/SolarB/nuggets/nugget_2024bjune.jsp

What determines active region coronal plasma composition?

Teodora **Mihailescu**, Deborah Baker, Lucie M. Green, Lidia van Driel-Gesztelyi, David M. Long, David H. Brooks, Andy S. H. To

ApJ **933** 245 **2022**

https://arxiv.org/pdf/2205.05027.pdf

https://iopscience.iop.org/article/10.3847/1538-4357/ac6e40/pdf

The chemical composition of the solar corona is different from that of the solar photosphere, with the strongest variation being observed in active regions (ARs). Using data from the Extreme Ultraviolet (EUV) Imaging

Spectrometer (EIS) on Hinode, we present a survey of coronal elemental composition as expressed in the first ionisation potential (FIP) bias in 28 ARs of different ages and magnetic flux content, which are at different stages in their evolution. We find no correlation between the FIP bias of an AR and its total unsigned magnetic flux or age. However, there is a weak dependence of FIP bias on the evolutionary stage, decreasing from 1.9-2.2 in ARs with spots to 1.5-1.6 in ARs that are at more advanced stages of the decay phase. FIP bias shows an increasing trend with average magnetic flux density up to 200 G but this trend does not continue at higher values. The FIP bias distribution within ARs has a spread between 0.4 and 1. The largest spread is observed in very dispersed ARs. We attribute this to a range of physical processes taking place in these ARs including processes associated with filament channel formation. These findings indicate that, while some general trends can be observed, the processes influencing the composition of an AR are complex and specific to its evolution, magnetic configuration or environment. The spread of FIP bias values in ARs shows a broad match with that previously observed in situ in the slow solar wind.

Acoustic Waves in a High-Temperature Plasma II. Damping and Instability

B. B. **Mikhalyaev**, S. B. Derteev, N. K. Shividov, M. E. Sapraliev & D. B. Bembitov
Solar Physics volume 298, Article number: 102 (**2023**)
https://doi.org/10.1007/s11207-023-02196-5
In this article we study the properties of acoustic waves in the rarefied high-temperature plasma of the solar corona, assuming that the heating and cooling of the plasma has a well-defined description. We consider a constant heating function supposing that the heating processes are generally established. For the radiative-loss function, a number of values are taken, which have been found using the CHIANTI code. On their basis, an analytical expression of the function in the form of a cubic interpolation has been worked out. We analyze the dispersion relation for linear acoustic waves. The heating and cooling function, introduced along with the classical expression of the thermal conductivity, allows us to obtain some specific results about their properties. In other words, a model of non-adiabatic acoustic waves with field-aligned thermal conduction, CHIANTI-based radiative cooling and constant heating function is constructed. Using the available observational data on compression waves, we can set the problem of finding the parameters of the coronal plasma. The model allows to specify the temperature range at which the thermal instability of waves is possible and to draw some conclusions about their damping. The coronal temperatures considered can be divided into intervals from 0.5 to 0.98 MK and from 4.57 to 8.38 MK, where the radiation function increases, and intervals from 0.98 to 4.57 MK and from 8.38 to 10 MK, where the radiation function decreases. With constant heating, at large wavelengths, acoustic waves can be unstable in the decreasing interval from 1.38 to 3.15 MK. In the increasing intervals, they may have a zero real part of the oscillation frequency and thus become non-propagating, also subject to a large wavelength. In some cases, the plasma density has a significant effect on the damping of acoustic oscillations due to heating and cooling. A change in density within the same order can lead to the fact that the heating and cooling effects prevail over the effect of thermal conductivity on long-wave perturbations.

The Hidden Cycle of the Solar Tesseral-Quadrupole Magnetic Field

V. P. **Mikhaylutsa**
Solar Physics volume 295, Article number: 67 (**2020**)
https://link.springer.com/content/pdf/10.1007/s11207-020-01636-w.pdf
Based on the Stanford harmonic coefficients of the solar magnetic fields and on the results of Shannon entropy transfer technique applied to magnetic mode intensities (Mikhaylutsa in J. Astrophys. Astron.40, 22, 2019), we have found that most of the medium and small-scale solar magnetic modes (order l>3l>3; degree m>0m>0) must be interdependent. The features and physical sense of these dependencies are analyzed and suggest that an unknown process in the Sun may control clusters of dependent magnetic modes according to some underlying physical scenario. The scenario may be revealed by studying the spatial distribution of the global surface magnetic field. We find that the tesseral-quadrupole (l=2l=2; m=1m=1) polarity distribution reappears periodically over four solar cycles. The periodicity (T≈72T≈72 solar rotations) is synchronized with the phases of modulation of the Shannon entropy transfer from the tesseral-quadrupole mode. An unknown process (twice per sunspot cycle) organizes a recurring cluster of interconnected magnetic modes that restore the global structure of the tesseral-quadrupole polarity, as a kind of “template.” This cycle is hidden in traditional methods of analysis, but its spatial-phase origin is made clear by the Shannon entropy transfer technique. Investigation of the “template” rotation rate suggests a probable coincidence with the 27-day Bartels rotation period.

Shannon entropy transfer between solar magnetic modes

Mikhaylutsa, V. P.
Journal of Astrophysics and Astronomy, Volume 40, Issue 3, article id. 22, **2019**
https://link.springer.com/article/10.1007%2Fs12036-019-9594-1
Based on Shannon entropy transfer estimation technique and Stanford's solar global magnetic field harmonic coefficients, several new facts about solar magnetic modes have been found. The entropy transferring between most

of the modes has been subjected to a steady modulation with a period near 72 solar rotations (5.38 years). As a rule, the amplitudes of entropy transferring modulation were less or equal to 0.1 bit/solar rotation. These modulations had no relations with intensity or configuration of the solar magnetic fields. Besides, Shannon entropy exchanges have been found between some modes—the sign of dependencies of them. Such modes had sector nature. The influence of a magnetic mode on another is strongest with the delay time between the two modes being twenty to forty solar rotations. Special properties have been revealed for zonal modes also.
HMI Science Nuggets, #132 Oct **2019** http://hmi.stanford.edu/hminuggets/?p=3116

Estimating Magnetic Filling Factors from Simultaneous Spectroscopy and Photometry: Disentangling Spots, Plage, and Network

T. W. **Milbourne**1,2, D. F. Phillips2, N. Langellier1,2, A. Mortier3,4, R. D. Haywood20,2,5, S. H. Saar2, H. M. Cegla21,6,7, A. Collier Cameron8, X. Dumusque9, D. W. Latham2Show full author list
2021 ApJ 920 21
https://doi.org/10.3847/1538-4357/ac1266
State-of-the-art radial velocity (RV) exoplanet searches are limited by the effects of stellar magnetic activity. Magnetically active spots, plage, and network regions each have different impacts on the observed spectral lines and therefore on the apparent stellar RV. Differentiating the relative coverage, or filling factors, of these active regions is thus necessary to differentiate between activity-driven RV signatures and Doppler shifts due to planetary orbits. In this work, we develop a technique to estimate feature-specific magnetic filling factors on stellar targets using only spectroscopic and photometric observations. We demonstrate linear and neural network implementations of our technique using observations from the solar telescope at HARPS-N, the HK Project at the Mt. Wilson Observatory, and the Total Irradiance Monitor onboard SORCE. We then compare the results of each technique to direct observations by the Solar Dynamics Observatory. Both implementations yield filling factor estimates that are highly correlated with the observed values. Modeling the solar RVs using these filling factors reproduces the expected contributions of the suppression of convective blueshift and rotational imbalance due to brightness inhomogeneities. Both implementations of this technique reduce the overall activity-driven rms RVs from 1.64 to 1.02 m s−1, corresponding to a 1.28 m s−1 reduction in the rms variation. The technique provides an additional 0.41 m s−1 reduction in the rms variation compared to traditional activity indicators.

HARPS-N Solar Radial-Velocity Variations Are Dominated By Large, Bright Magnetic Regions

T. W. **Milbourne** (1 and 2), R. D. Haywood (2), D. F. Phillips et al.
ApJ **2019**
https://arxiv.org/pdf/1902.04184.pdf
State of the art radial-velocity (RV) exoplanet searches are currently limited by RV signals arising from stellar magnetic activity. We analyze solar observations acquired over a 3-year period during the decline of Carrington Cycle 24 to test models of RV variation of Sun-like stars. A purpose-built solar telescope at the High Accuracy Radial velocity Planet Searcher for the Northern hemisphere (HARPS-N) provides disk-integrated solar spectra, from which we extract RVs and logR′HK. The Solar Dynamics Observatory (SDO) provides disk-resolved images of magnetic activity. The Solar Radiation and Climate Experiment (SORCE) provides near-continuous solar photometry, analogous to a Kepler light curve. We verify that the SORCE photometry and HARPS-N logR′HKcorrelate strongly with the SDO-derived magnetic filling factor, while the HARPS-N RV variations do not. To explain this discrepancy, we test existing models of RV variations. We estimate the contributions of the suppression of convective blueshift and the rotational imbalance due to brightness inhomogeneities to the observed HARPS-N RVs. We investigate the time variation of these contributions over several rotation periods, and how these contributions depend on the area of active regions. We find that magnetic active regions smaller than 60 Mm2 do not significantly suppress convective blueshift. Our area-dependent model reduces the amplitude of activity-induced RV variations by a factor of two. The present study highlights the need to identify a proxy that correlates specifically with large, bright magnetic regions on the surfaces of exoplanet-hosting stars.

Diffuse solar coronal features and their spicular footpoints

Nikolina **Milanović**, Lakshmi Pradeep Chitta, Hardi Peter
A&A **2023**
https://arxiv.org/pdf/2303.13161.pdf
In addition to a component of the emission that originates from clearly distinguishable coronal loops, the solar corona also exhibits extreme-ultraviolet (EUV) and X-ray ambient emission that is rather diffuse and is often considered undesirable background. Importantly, unlike the generally more structured transition region and chromosphere, the diffuse corona appears to be rather featureless. The magnetic nature of the diffuse corona, and in particular, its footpoints in the lower atmosphere, are not well understood. We study the origin of the diffuse corona above the quiet-Sun network on supergranular scales. We identified regions of diffuse EUV emission in the coronal

images from the SDO/AIA. To investigate their connection to the lower atmosphere, we combined these SDO/AIA data with the transition region spectroscopic data from the IRIS and with the underlying surface magnetic field information from the SDO/HMI. The region of the diffuse emission is of supergranular size and persists for more than five hours, during which it shows no obvious substructure. It is associated with plasma at about 1 MK that is located within and above a magnetic canopy. The canopy is formed by unipolar magnetic footpoints that show highly structured spicule-like emission in the overlying transition region. Our results suggest that the diffuse EUV emission patch forms at the base of long-ranging loops, and it overlies spicular structures in the transition region. Heated material might be supplied to it by means of spicular upflows, conduction-driven upflows from coronal heating events, or perhaps by flows originating from the farther footpoint. Therefore, the question remains open how the diffuse EUV patch might be sustained. Nevertheless, our study indicates that heated plasma trapped by long-ranging magnetic loops might substantially contribute to the featureless ambient coronal emission. **21 July 2014**

Mimicking spectropolarimetric inversions using convolutional neural networks

I. **Milić**1,2,3 and R. Gafeira4,5
A&A 644, A129 (**2020**)
https://doi.org/10.1051/0004-6361/201936537

Context. Interpreting spectropolarimetric observations of the solar atmosphere takes much longer than the acquiring the data. The most important reason for this is that the model fitting, or "inversion", used to infer physical quantities from the observations is extremely slow, because the underlying models are numerically demanding.
Aims. We aim to improve the speed of the inference by using a neural network that relates input polarized spectra to the output physical parameters.
Methods. We first select a subset of the data to be interpreted and infer physical quantities from corresponding spectra using a standard minimization-based inversion code. Taking these results as reliable and representative of the whole data set, we train a convolutional neural network to connect the input polarized spectra to the output physical parameters (nodes, in context of spectropolarimetric inversion). We then apply the neural network to the various other data, previously unseen to the network. As a check, we apply the referent inversion code to the unseen data and compare the fit quality and the maps of the inferred parameters between the two inversions.
Results. The physical parameters inferred by the neural network show excellent agreement with the results from the inversion, and are obtained in a factor of 105 less time. Additionally, substituting the results of the neural network back in the forward model, shows excellent agreement between inferred and original spectra.

Conclusions. The method we present here is very simple for implementation and extremely fast. It only requires a training data set, which can be obtained by inverting a representative subset of the observed data. Applying these (and similar) machine learning techniques will yield orders of magnitude acceleration in the routine interpretation of spectropolarimetric data.

Using the infrared iron lines to probe solar subsurface convection

Ivan **Milic**, Smitha Narayanamurthy, Andreas Lagg
A&A 630, A133 **2019**
https://arxiv.org/pdf/1904.07306.pdf
https://www.aanda.org/articles/aa/pdf/2019/10/aa35126-19.pdf

Studying the properties of the solar convection using high-resolution spectropolarimetry began in the early 90's with the focus on observations in the visible wavelength regions. Its extension to the infrared (IR) remains largely unexplored. The IR iron lines around 15600\,$\rm{\AA}$, most commonly known for their high magnetic sensitivity, also have a non-zero response to line-of-sight velocity below log(τ)=0.0. In this paper we aim to tap this potential to explore the possibility of using them to measure sub-surface convective velocities. By assuming a snapshot of a three-dimensional magnetohydrodynamic simulation to represent the quiet Sun, we investigate how well the iron IR lines can reproduce the LOS velocity in the cube and up to what depth. We use the recently developed spectropolarimetric inversion code SNAPI and discuss the optimal node placements for the retrieval of reliable results from these spectral lines. We find that the IR iron lines can measure the convective velocities down to log(τ)=0.5, below the photosphere, not only at original resolution of the cube but also when degraded with a reasonable spectral and spatial PSF and stray light. Meanwhile, the commonly used Fe~{\sc i} 6300\,\AA{} line pair performs significantly worse. Our investigation reveals that the IR iron lines can probe the subsurface convection in the solar photosphere. This paper is a first step towards exploiting this diagnostic potential.

Line response functions in nonlocal thermodynamic equilibrium
Isotropic case

I. **Milić** and M. van Noort
A&A 601, A100 (**2017**)

Context. Response functions provide us with a quantitative measure of sensitivity of the emergent spectrum to perturbations in the solar atmosphere and are thus the method of choice for interpreting spectropolarimetric observations. For the lines formed in the solar chromosphere, it is necessary to compute these responses taking into account nonlocal thermodynamic equilibrium (NLTE) effects.
Aims. We show how to analytically compute the response of the level populations in NLTE to a change of a given physical quantity at a given depth in the atmosphere. These responses are then used to compute opacity and emissivity responses, which are then propagated to obtain the response of the emergent intensity.
Methods. Our method is based on the derivative of the rate equations, where we explicitly incorporate spatial coupling in the radiative rate terms. After considering and collecting all interdependencies, the problem reduces to a linear system of equations with a dimension equal to the product of the number of spatial points and the number of energy levels.
Results. We compare analytically computed response functions with those obtained using a finite difference approach and find very good agreement. In addition, a more accurate way of propagating opacity and emissivity perturbations through the numerical solution of the radiative transfer equation was developed.
Conclusions. This method allows for the fast evaluation of the response of the emergent spectrum to perturbations of a given quantity at a given depth, and thus is a significant step towards more efficient NLTE inversions.

Latitudinal dependence of variations in the frequencies of solar oscillations above the acoustic cut-off

Laura Jade **Millson**, Anne-Marie Broomhall, Tishtrya Mehta
Solar Phys. **2024**
https://arxiv.org/pdf/2409.03574
Known as the pseudo-modes, their frequencies have been shown to vary in anti-phase with solar magnetic activity. In this work, we determined temporal variations in these frequencies across the solar disc, with the aim of identifying any potential latitudinal dependence of pseudo-mode frequency shifts. We utilised nearly 22 years of spatially resolved GONG data for all azimuthal orders, m, for harmonic degrees $0 \leq l \leq 200$, and determined shifts using the resampled periodogram method. Periodogram realisations were created from overlapping, successive 216d-long segments in time, and cropped to 5600-6800μHz. Cross-correlation functions were then repeatedly generated between these realisations to identify any variation in frequency and the uncertainty. We categorised each mode by its latitudinal sensitivity and used this categorisation to produce average frequency shifts for different latitude bands (15◦ and 5◦ in size) which were compared to magnetic proxies, the F10.7 index and GONG synoptic maps. Morphological differences in the pseudo-mode shifts between different latitudes were found, which were most pronounced during the rise to solar maximum where shifts reach their minimum values. At all latitudes, shift behaviour was strongly in anti-correlation with the activity proxy. Additionally, periodicities shorter than the 11-year cycle were observed. Wavelet analysis was used to identify a periodicity of four years at all latitudes.

Recent results on pp-chain solar neutrinos with the Borexino detector

Lino **Miramonti** (on behalf of Borexino Collaboration)
Proceeding for NuPhys **2019**
Measuring all neutrino components is the most direct way to test the standard solar model (SSM). Despite the great results obtained so far, important questions such as the solar metallicity remain open. A precise measurement of the solar pp chain and the CNO cycle would settle this controversy between high (HZ) and low (LZ) metallicity compositions of the Sun. Solar neutrinos allow the determination of oscillation parameters, in particular the θ12 mixing angle and, to a lesser degree the Δm212mass splitting. Furthermore the measurement of the electron neutrino survival probability Pee as a function of neutrino energy allows one to directly probe the MSW-LMA mechanism of neutrino oscillations In this work I will report the first simultaneous precision spectroscopic measurement of the complete pp-chain and its implications for both solar and neutrino physics with the Borexino detector.

Analyzing the variation of Lyapunov exponents of solar and geomagnetic activity indices during coronal mass ejections

Mirmomeni, M.; Lucas, C.
Space Weather, Vol. 7, No. 7, S07002, **2009**
http://dx.doi.org/10.1029/2008SW000454
Hostile space weather is one of the principal threats to modern human technology because of the dependency of our lives on satellites. Solar coronal mass ejections, solar flares, and high-speed solar wind streams often cause some sequences of damaging disturbances within the Earth's magnetosphere, in the atmosphere, and even on the Earth's surface. The time-varying Sun, as the main source of space weather causes geomagnetic storms and substorms in many ways with coronal mass ejections (CME) being possibly the most harmful among them. CMEs cause transient

magnetized plasma flows as interplanetary consequences, which drive the geomagnetic storms and substorms in the Earth's magnetosphere. It is shown that the cyclic solar activity has chaotic characteristics. It seems that the chaotic modeling of solar and geomagnetic activity indices is an important approach for analysis and prediction of the solar extreme events. This is particularly useful for engineers and designers interested in space weather prediction and its applications. One of the most important tools for eliciting the chaotic trends is the “Lyapunov exponents,” which is a useful measure of the stability of a dynamic system. This paper analyzes the variation of Lyapunov exponents (LE) for three solar and geomagnetic activity indices during CMEs: the sunspot number, disturbance storm time, and proton temperature. The analysis has been carried out using the technique of adaptive LE estimation adopted from previous works; the suitable window for which has been determined via trial and error. It is shown that the LE of these solar and geomagnetic activity indices varies rapidly during CMEs. The variation in LEs creates a pattern as a precursor for the forthcoming CME. This precursor, which is an oscillation in the values of Les, begins several steps sooner than the CME's occurrence. Then, during the CME, the LEs decrease to a small positive or a negative value, which demonstrates that during an anomaly such as a CME the chaotic characteristics of solar and geomagnetic activity indices decrease and solar and geomagnetic activity indices follow more regular dynamics.

Mechanism of heating the Solar Corona in the splitting of Massive Photon Pairs

I.K.**Mirzoeva**, S.G.Chefranov

2019

https://arxiv.org/ftp/arxiv/papers/1904/1904.03022.pdf

Data obtained in the framework of the INTERBALL-Tail Probe (1995-2000) and RHESSI (from 2002 to the present) projects have revealed variations in the X-ray intensity of the solar corona in the photon energy range of 2-15 keV during the period of the quiet Sun. Previously, a hypothesis was proposed that this phenomenon could be associated with the effect of coronal heating. In the present study, a new mechanism of coronal plasma heating is proposed on the basis of the experimental data and the quantum theory of photon pairs that are produced from vacuum in the course of the Universe's expansion. A similar mechanism based on the splitting of photon pairs in the interplanetary and intergalactic space is also proposed to explain the observed microwave background radiation.

Differential Rotation of the Solar Chromosphere using multidecadal Ca II K Spectroheliograms

Dibya Kirti **Mishra**, Srinjana Routh, Bibhuti Kumar Jha, Subhamoy Chatterjee, Dipankar Banerjee

Proceedings of IAUS 365 **2023**

https://arxiv.org/pdf/2311.09629.pdf

The study of the differential rotation in the chromosphere of the Sun is of significant importance as it provides valuable insights into the rotational behaviour of the solar atmosphere at higher altitudes and the coupling mechanism between the various layers of the solar atmosphere. In this work, we employed the image correlation technique, explicitly focusing on plages, intending to estimate the chromospheric differential rotation. For this purpose, we have utilized Ca II K spectroheliograms (1907-2007) from the Kodaikanal Solar Observatory (KoSO), recently calibrated with a better technique to ensure accuracy. Our analysis indicates that plages in the chromosphere exhibit faster rotation and a smaller latitudinal gradient when compared to the rotation rate obtained through sunspot tracking. Furthermore, we investigate the temporal analysis of the chromospheric differential rotation parameters across various solar cycles.

Mass Loss via Solar Wind and Coronal Mass Ejections During Solar Cycle 23 and 24

Wageesh **Mishra**, Nandita Srivastava, Yuming Wang, Zavkiddin Mirtoshev, Jie Zhang, Rui Liu

MNRAS **2019**

https://arxiv.org/pdf/1904.09898.pdf

Similar to the Sun, other stars shed mass and magnetic flux via ubiquitous quasi-steady wind and episodic stellar coronal mass ejections (CMEs). We investigate the mass loss rate via solar wind and CMEs as a function of solar magnetic variability represented in terms of sunspot number and solar X-ray background luminosity. We estimate the contribution of CMEs to the total solar wind mass flux in the ecliptic and beyond, and its variation over different phases of the solar activity cycles. The study exploits the number of sunspots observed, coronagraphic observations of CMEs near the Sun by SOHO/LASCO, in situ observations of the solar wind at 1 AU by WIND, and GOES X-ray flux during solar cycle 23 and 24. We note that the X-ray background luminosity, occurrence rate of CMEs and ICMEs, solar wind mass flux, and associated mass loss rates from the Sun do not decrease as strongly as the sunspot number from the maximum of solar cycle 23 to the next maximum. Our study confirms a true physical increase in CME activity relative to the sunspot number in cycle 24. We show that the CME occurrence rate and associated mass loss rate can be better predicted by X-ray background luminosity than the sunspot number. The solar wind mass loss rate which is an order of magnitude more than the CME mass loss rate shows no obvious dependency on cyclic variation in sunspot number and solar X-ray background luminosity. These results have implications to the study of solar-type stars.

Long-Term Modulation of Cosmic-Ray Intensity and Correlation Analysis Using Solar and Heliospheric Parameters

V. K. **Mishra**, A. P. Mishra

Solar Physics October **2018**, 293:141

https://link.springer.com/content/pdf/10.1007%2Fs11207-018-1357-7.pdf

Based on the monthly sunspot numbers (SSNs), the solar-flare index (SFI), grouped solar flares (GSFs), the tilt angle of heliospheric current sheet (HCS), and cosmic-ray intensity (CRI) for Solar Cycles 21 – 24, a detailed correlation study has been performed using the cycle-wise average correlation (with and without time lag) method as well as by the "running cross-correlation" method. It is found that the slope of regression lines between SSN and SFI, as well as between SSN and GSF, is continuously decreasing from Solar Cycle 21 to 24. The length of regression lines has significantly decreased during Cycles 23 and 24 in comparison to Cycles 21 and 22. The cross-correlation coefficient (without time lag) between SSN–CRI, SFI–CRI, and GSF–CRI has been found to be almost the same during Cycles 21 and 22, while during Cycles 23 and 24 it is significantly higher between SSN–CRI and HCS–CRI than for SFI–CRI and GSF–CRI. Considering time lags of 1 to 20 months, the maximum correlation coefficient (negative) amongst all of the sets of solar parameters is observed with almost the same time lags during Cycles 21 – 23, whereas exceptional behaviour of the time lag has been observed during Cycle 24, as the correlation coefficient attains its maximum value with two time lags (four and ten months) in the case of the SSN–CRI relationship. A remarkably large time lag (22 months) between HCS and CRI has been observed during the odd-numbered Cycle 21, whereas during another odd cycle, Cycle 23, the lag is small (nine months) in comparison to that for other solar/flare parameters (13 – 15 months). On the other hand, the time lag between SSN–CRI and HCS–CRI has been found to be almost the same during even-numbered Solar Cycles 22 and 24. A similar analysis has been performed between SFI and CRI, and it is found that the correlation coefficient is maximum at zero time lag during the present solar cycle. The GSFs have shown better maximum correlation with CRI as compared to SFI during Cycles 21 to 23, indicating that GSF could also be used as a significant solar parameter to study the cosmic-ray modulation. Furthermore, the running cross-correlation coefficient between SSN–CRI and HCS–CRI, as well as between solar-flare activity parameters (SFI and GSF) and CRI is observed to be strong during the ascending and descending phases of solar cycles. The level of cosmic-ray modulation during the period of investigation shows the appropriateness of different parameters in different cycles, and even during the different phases of a particular solar cycle. We have also studied the galactic cosmic-ray modulation in relation to combined solar and heliospheric parameters using the empirical model suggested by Paouris et al. (Solar Phys.280, 255, 2012). The proposed model for the calculation of the modulated cosmic-ray intensity obtained from the combination of solar and heliospheric parameter gives a very satisfactory value of standard deviation as well as R2R2 (the coefficient of determination) for Solar Cycles 21 – 24.

Kelvin–Helmholtz Instability in the Solar Atmosphere, Solar Wind and Geomagnetosphere

V. V. **Mishin** V. M. Tomozov **Review**

Solar Physics November **2016**, Volume 291, Issue 11, pp 3165–3184

Modern views on the nature of the Kelvin–Helmholtz (KH) instability and its manifestations in the solar corona, in the interplanetary medium, and at the geomagnetospheric boundary are under consideration. We briefly describe the main theoretical results of the KH instability obtained in the linear approximation. Analysis of observational data, confirming the occurrence of the KH instability in magnetic formations of the solar coronal plasma and on the daytime magnetopause, was mainly performed in the approximation of incompressibility. We show that the Rayleigh–Taylor instability can significantly enhance the KH instability in the above regions due to interface accelerations or its curvature. Special attention is focused on the compressibility effect on the supersonic shear flow instability in the solar wind (SW) and at the geomagnetic tail boundary where this instability is usually considered to be ineffective. We have shown that the phase velocity of oblique perturbations is substantially less than the flow velocity, and values of the growth rate and frequency range are considerably higher than when only taking velocity-aligned disturbances into account. We emphasize that the magnetic field and plasma density inhomogeneity which weaken the KH instability of subsonic shear flows, in the case of a supersonic velocity difference weaken the stabilizing effect of the medium compressibility, and can significantly increase the instability. Effective generation of oblique disturbances by the supersonic KH instability explains the observations of magnetosonic waves and the formation of diffuse shear flows in the SW and on the distant magnetotail boundary, as well as the SW-magnetosphere energy and impulse transfer.

Differential Rotation of the Solar Chromosphere: A Century-long Perspective from Kodaikanal Solar Observatory Ca II K Data

Dibya Kirti **Mishra**, Srinjana Routh, Bibhuti Kumar Jha, Theodosios Chatzistergos, Judhajeet Basu, Subhamoy Chatterjee, Dipankar Banerjee, Ilaria Ermolli

ApJ **2023**

https://arxiv.org/pdf/2311.18800.pdf

Chromospheric differential rotation is a key component in comprehending the atmospheric coupling between the chromosphere and the photosphere at different phases of the solar cycle. In this study, we therefore utilize the newly calibrated multidecadal Ca II K spectroheliograms (1907-2007) from the Kodaikanal Solar Observatory (KoSO) to investigate the differential rotation of the solar chromosphere using the technique of image cross-correlation. Our analysis yields the chromospheric differential rotation rate $\Omega(\theta)=(14.61\pm0.04-2.18\pm0.37\sin2\theta-1.10\pm0.61\sin4\theta)^{\circ}$/day. These results suggest the chromospheric plages exhibit an equatorial rotation rate 1.59% faster than the photosphere when compared with the differential rotation rate measured using sunspots and also a smaller latitudinal gradient compared to the same. To compare our results to those from other observatories, we have applied our method on a small sample of Ca II K data from Rome, Meudon, and Mt. Wilson observatories, which support our findings from KoSO data. Additionally, we have not found any significant north-south asymmetry or any systematic variation in chromospheric differential rotation over the last century.

Solar cycle variation of coronal mass ejections contribution to solar wind mass flux

Wageesh **Mishra**, Nandita Srivastava, Zavkiddin Mirtoshev, Yuming Wang
Proceedings IAU Symposium No. 340, **2018**
https://arxiv.org/pdf/1805.07593.pdf
Coronal Mass Ejections (CMEs) contributes to the perturbation of solar wind in the heliosphere. Thus, depending on the different phases of the solar cycle and the rate of CME occurrence, contribution of CMEs to solar wind parameters near the Earth changes. In the present study, we examine the long term occurrence rate of CMEs, their speeds, angular widths and masses. We attempt to find correlation between near sun parameters, determined using white light images from coronagraphs, with solar wind measurements near the Earth from in-situ instruments. Importantly, we attempt to find what fraction of the averaged solar wind mass near the Earth is provided by the CMEs during different phases of the solar cycles.

Solar cycle dependence of Wind/EPACT protons, solar flares and coronal mass ejections

Miteva, R. 1 , Samwel, S. W. 2 , Costa-Duarte, M. V. 3 , Malandraki, O. E. 4
Sun and Geosphere, **2017**; 12/1: 11 -19
http://newserver.stil.bas.bg/SUNGEO//00SGArhiv/SG_v12_No1_2017-pp-11-19.pdf
The aim of this work is to compare the occurrence and overall properties of solar energetic particles (SEPs), solar flares and coronal mass ejections (CMEs) over the first seven years in solar cycles (SCs) 23 and 24. For the case of SEP events, we compiled a new proton event catalog using data from the Wind/EPACT instrument. We confirm the previously known reduction of high energy proton events in SC24 compared to the same period in SC23; our analysis shows a decrease of 25–50 MeV protons by about 30%. The similar trend is found for X to C-class solar flares which are less by about 40% and also for faster than 1000 km/s CMEs, which are reduced by about 45%. In contrast, slow CMEs are more numerous in the present solar cycle. We discuss the implications of these results for the population of SEP-productive flares and CMEs. **2013-03-04, 2013-04-11**,

Spatial and Temporal Distribution of Nanoflare Heating During Active Region Evolution

Biswajit **Mondal**, James A Klimchuk, Amy R. Winebarger, P. S. Athiray, Jiayi Liu
ApJ **2024**
https://arxiv.org/pdf/2412.20348
Nanoflares are believed to be key contributors to heating solar non-flaring active regions, though their individual detection remains challenging. This study uses a data-driven field-aligned hydrodynamic model to examine nanoflare properties throughout the lifecycle of AR12758. We simulate coronal loop emissions, where each loop is heated by random nanoflares depending on the loop parameters derived from photospheric magnetograms observed by SDO/HMI. Simulated X-ray flux and temperature can reproduce the temporal variations observed by Chandrayaan-2/XSM. Our findings show that high-frequency nanoflares contribute to cool emissions across the AR, while low- and intermediate- frequency primarily contribute to hot emissions. During the emerging phase, energy deposition is dominated by low-frequency events. Post-emergence, energy is deposited by both low- and intermediate-frequency nanoflares, while as the AR ages, the contribution from intermediate- and high-frequency nanoflares increases. The spatial distribution of heating frequencies across the AR reveals a clear pattern: the core of the active region spends most of its time in a low-frequency heating state, the periphery is dominated by high-frequency heating, and the region between the core and periphery experiences intermediate-frequency heating. **6-15 Mar 2020**

Solar X-ray Monitor On Board the Chandrayaan-2 Orbiter: In-flight Performance and Science Prospects

N. P. S. **Mithun**, Santosh V. Vadawale, Aveek Sarkar, M. Shanmugam, Arpit R. Patel, Biswajit Mondal, Bhuwan Joshi, Janardhan P., Hiteshkumar L. Adalja, Shiv Kumar Goyal, Tinkal Ladiya, Neeraj Kumar Tiwari, Nishant Singh, Sushil Kumar, Manoj K. Tiwari, M. H. Modi, Anil Bhardwaj

Solar Phys. **295**, Article number: 139 **2020**

https://arxiv.org/pdf/2009.09759.pdf

https://link.springer.com/content/pdf/10.1007/s11207-020-01712-1.pdf

The Solar X-ray Monitor (abbreviated as XSM) on board India's Chandrayaan-2 mission is designed to carry out broadband spectroscopy of the Sun from lunar orbit. It observes the Sun as a star and measures the spectrum every second in the soft X-ray band of 1 - 15 keV with an energy resolution better than 180 eV at 5.9 keV. The primary objective of the XSM is to provide the incident solar spectrum for the X-ray fluorescence spectroscopy experiment on the Chandrayaan-2 orbiter, which aims to generate elemental abundance maps of the lunar surface. However, observations with the XSM can independently be used to study the Sun as well. The Chandrayaan-2 mission was launched on 22 July 2019, and the XSM began nominal operations, in lunar orbit, from September 2019. The in-flight observations, so far, have shown that its spectral performance has been identical to that on the ground. Measurements of the effective area from ground calibration were found to require some refinement, which has been carried out using solar observations at different incident angles. It also has been shown that the XSM is sensitive enough to detect solar activity well below A-class. This makes the investigations of microflares and the quiet solar corona feasible in addition to the study of the evolution of physical parameters during intense flares. This article presents the in-flight performance and calibration of the XSM instrument and discusses some specific science cases that can be addressed using observations with the XSM.

Data Processing Software for Chandrayaan-2 Solar X-ray Monitor

N. P. S. **Mithun**, Santosh V. Vadawale, Arpit R. Patel, M. Shanmugam, D. Chakrabarty, Partha Konar, Tejas N. Sarvaiya, Girish D. Padia, Aveek Sarkar, Prashant Kumar, Prashant Jangid, Aaditya Sarda, Manan S. Shah, Anil Bhardwaj

Astronomy and Computing **2020**

https://arxiv.org/pdf/2007.11371.pdf

Solar X-ray Monitor (XSM) instrument of India's Chandrayaan-2 lunar mission carries out broadband spectroscopy of the Sun in soft X-rays. XSM, with its unique features such as low background, high time cadence, and high spectral resolution, provides the opportunity to characterize transient and quiescent X-ray emission from the Sun even during low activity periods. It records the X-ray spectrum at one-second cadence, and the data recorded on-board are downloaded at regular intervals along with that of other payloads. During ground pre-processing, the XSM data is segregated, and the level-0 data is made available for higher levels of processing at the Payload Operations Center (POC). XSM Data Analysis Software (XSMDAS) is developed to carry out the processing of the level-0 data to higher levels and to generate calibrated light curves and spectra for user-defined binning parameters such that it is suitable for further scientific analysis. A front-end for the XSMDAS named XSM Quick Look Display (XSMQLD) is also developed to facilitate a first look at the data without applying calibration. XSM Data Management-Monitoring System (XSMDMS) is designed to carry out automated data processing at the POC and to maintain an SQLite database with relevant information on the data sets and an internal web application for monitoring data quality and instrument health. All XSM raw and calibrated data products are in FITS format, organized into day-wise files, and the data archive follows Planetary Data System-4 (PDS4) standards. The XSM data will be made available after a lock-in period along with the XSM Data Analysis Software from ISRO Science Data Archive (ISDA) at Indian Space Science Data Center(ISSDC). Here we discuss the design and implementation of all components of the software for the XSM data processing and the contents of the XSM data archive.

Ground Calibration of Solar X-ray Monitor On-board Chandrayaan-2 Orbiter

N. P. S. **Mithun**, Santosh V. Vadawale, M. Shanmugam, Arpit R. Patel, Neeraj Kumar Tiwari, Hiteshkumar L. Adalja, Shiv Kumar Goyal, Tinkal Ladiya, Nishant Singh, Sushil Kumar, Manoj K. Tiwari, M. H. Modi, Biswajit Mondal, Aveek Sarkar, Bhuwan Joshi, P. Janardhan, Anil Bhardwaj

Experimental Astronomy **2020**

https://arxiv.org/pdf/2007.07326.pdf

Chandrayaan-2, the second Indian mission to the Moon, carries a spectrometer called the Solar X-ray Monitor (XSM) to perform soft X-ray spectral measurements of the Sun while a companion payload measures the fluorescence emission from the Moon. Together these two payloads will provide quantitative estimates of elemental abundances on the lunar surface. XSM is also expected to provide significant contributions to the solar X-ray studies with its highest time cadence and energy resolution spectral measurements. For this purpose, the XSM employs a Silicon Drift Detector and carries out energy measurements of incident photons in the 1 -- 15 keV range with a resolution of less than 180 eV at 5.9 keV, over a wide range of solar X-ray intensities. Extensive ground calibration experiments have been carried out with the XSM using laboratory X-ray sources as well as X-ray beam-line facilities to determine the instrument response matrix parameters required for quantitative spectral analysis. This includes measurements of gain, spectral redistribution function, and effective area, under various observing

conditions. The capability of the XSM to maintain its spectral performance at high incident flux as well as the dead-time and pile-up characteristics have also been investigated. The results of these ground calibration experiments of the XSM payload are presented in this article.

Radial Distribution of Compressive Waves in the Solar Corona Revealed by Akatsuki Radio Occultation Observations

Mayu **Miyamoto**1, Takeshi Imamura2, Munetoshi Tokumaru3, Hiroki Ando2, Hiroaki Isobe4, Ayumi Asai4, Daikou Shiota3, Tomoaki Toda2, Bernd H?usler5, Martin P?tzold6, Alexander Nabatov7, and Masato Nakamur

2014 ApJ 797 51

Radial variations of the amplitude and the energy flux of compressive waves in the solar corona were explored for the first time using a spacecraft radio occultation technique. By applying wavelet analysis to the frequency time series taken at heliocentric distances of 1.5-20.5?RS (solar radii), quasi-periodic density disturbances were detected at almost all distances. The period ranges from 100 to 2000?s. The amplitude of the fractional density fluctuation increases with distance and reaches ~30% around 5?RS , implying that nonlinearity of the wave field is potentially important. We further estimate the wave energy flux on the assumption that the observed periodical fluctuations are manifestations of acoustic waves. The energy flux increases with distance below ~6?RS and seems to saturate above this height, suggesting that the acoustic waves do not propagate from the low corona but are generated in the extended corona, probably through nonlinear dissipation of Alfv?n waves. The compressive waves should eventually dissipate through shock generation to heat the corona.

Scaling Features of Diurnal Variation of Galactic Cosmic Rays

Renata **Modzelewska**, Agata Krasińska, Anna Wawrzaszek & Agnieszka Gil

Solar Physics volume 296, Article number: 125 (**2021**)

https://link.springer.com/content/pdf/10.1007/s11207-021-01866-6.pdf

https://doi.org/10.1007/s11207-021-01866-6

We analyze the scaling properties of the diurnal variation of galactic cosmic rays (GCRs) in Solar Cycle 24 and the solar minima between Solar Cycles 23/24 and 24/25 for 2007 – 2019 based on the count rates of the Oulu, Newark, Hermanus, and Potchefstroom neutron monitors. The scaling features of the GCR diurnal variation are studied by evaluating the Hurst exponent, a quantitative parameter used as an indicator of the state of the randomness of a time series. We estimate the Hurst exponents for GCR diurnal-variation parameters amplitude and phase using structure-function and detrended-fluctuation-analysis methods. Results show that the Hurst exponents for the GCR diurnal variation vary in the range from ≈0.3≈0.3 to ≈0.9≈0.9, with a general tendency of being systematically above 0.5. It suggests that the GCR diurnal variation reveals a more persistent structure than Brownian motion. However, the time series of GCR diurnal-variation amplitude and phase evolve from a more persistent structure in the solar minimum between Solar Cycles 23/24 in 2007 – 2009 to a more random character in and near the solar maximum 2012 – 2014. This observation seems to be in agreement with the general configuration of the heliosphere through the 11-year solar-activity cycle. Moreover, the temporal profile of the Hurst exponent for GCR diurnal amplitude and phase around the beginning of the solar minimum between Solar Cycles 24/25 (2018 – 2019) differs from the solar minimum between Solar Cycles 23/24 in 2007 – 2009, suggesting a dependence on solar-magnetic polarity. These findings could shed more light on GCR particle transport in the turbulent heliosphere over the solar cycle.

Features of the Galactic Cosmic Ray Anisotropy in Solar Cycle 24 and Solar Minima 23/24 and 24/25

R. **Modzelewska**, K. Iskra, W. Wozniak, M. Siluszyk, M. V. Alania

Solar Physics October **2019**, 294:148

https://link.springer.com/content/pdf/10.1007%2Fs11207-019-1540-5.pdf

We study the role of the drift effect in the temporal changes of the anisotropy of galactic cosmic rays (GCRs) and the influence of the sector structure of the heliospheric magnetic field on it. We analyze the GCR anisotropy in Solar Cycle 24 and solar minimum 23/24 with negative polarity (qA<0qA<0) for the period of 2007 – 2009 and near minimum 24/25 with positive polarity (qA>0qA>0) in 2017 – 2018 using data of the global network of Neutron Monitors. We use the harmonic analysis method to calculate the radial and tangential components of the anisotropy of GCRs for different sectors (‘+’ corresponds to the positive and ‘−’ to the negative directions) of the heliospheric magnetic field. We compare the analysis of GCR anisotropy using different evaluations of the mean GCRs rigidity related to Neutron Monitor observations. Then the radial and tangential components are used for characterizing the GCR modulation in the heliosphere. We show that in the solar minimum 23/24 in 2007 – 2009 when qA<0qA<0, the drift effect is not visibly evident in the changes of the radial component, i.e. the drift effect is found to produce ≈4≈4% change in the radial component of the GCR anisotropy for 2007 – 2009. Hence the diffusion dominated model of GCR transport is more acceptable in 2007 – 2009. In turn, near the solar minimum 24/25 in 2017 – 2018 when qA>0qA>0, the drift effect is evidently visible and produces ≈40% change in the radial

component of the GCR anisotropy for 2017 – 2018. So in the period of 2017 – 2018 a diffusion model with noticeably manifested drift is acceptable. The results of this work are in good agreement with the drift theory of GCR modulation, according to which, during negative (positive) polarity cycles, a drift stream of GCRs is directed toward (away from) the Sun, thus giving rise to a 22-year cycle variation of the radial GCR anisotropy.

Quasi-periodic changes in the 3D solar anisotropy of Galactic cosmic rays for 1965–2014

R. **Modzelewska**1 and M. V. Alania
A&A 609, A32 (**2017**)
https://www.aanda.org/articles/aa/pdf/2018/01/aa31697-17.pdf
Aims. We study features of the 3D solar anisotropy of Galactic cosmic rays (GCR) for 1965−2014 (almost five solar cycles, cycles 20−24). We analyze the 27-day variations of the 2D GCR anisotropy in the ecliptic plane and the north-south anisotropy normal to the ecliptic plane. We study the dependence of the 27-day variation of the 3D GCR anisotropy on the solar cycle and solar magnetic cycle. We demonstrate that the 27-day variations of the GCR intensity and anisotropy can be used as an important tool to study solar wind, solar activity, and heliosphere.
Methods. We used the components Ar, Aϕ and At of the 3D GCR anisotropy that were found based on hourly data of neutron monitors (NMs) and muon telescopes (MTs) using the harmonic analyses and spectrographic methods. We corrected the 2D diurnal (~24-h) variation of the GCR intensity for the influence of the Earth magnetic field. We derived the north-south component of the GCR anisotropy based on the GG index, which is calculated as the difference in GCR intensities of the Nagoya multidirectional MTs.
Results. We show that the behavior of the 27-day variation of the 3D anisotropy verifies a stable long-lived active heliolongitude on the Sun. This illustrates the usefulness of the 27-day variation of the GCR anisotropy as a unique proxy to study solar wind, solar activity, and heliosphere. We distinguish a tendency of the 22-yr changes in amplitude of the 27-day variation of the 2D anisotropy that is connected with the solar magnetic cycle. We demonstrate that the amplitudes of the 27-day variation of the north-south component of the anisotropy vary with the 11-yr solar cycle, but a dependence of the solar magnetic polarity can hardly be recognized. We show that the 27-day recurrences of the GG index and the At component are highly positively correlated, and both are highly correlated with the By component of the heliospheric magnetic field.

On the 27-day Variations of Cosmic Ray Intensity in Recent Solar Minimum 23/24

R. **Modzelewska**, M.V. Alania
Solar Phys. **2013**
http://arxiv.org/pdf/1504.00180v1.pdf
We have studied the 27-day variations and their harmonics of the galactic cosmic ray (GCR) intensity, solar wind velocity, and interplanetary magnetic field (IMF) components in the recent prolonged solar minimum 23 24. The time evolution of the quasi-periodicity in these parameters connected with the Suns rotation reveals that their synodic period is stable and is aprox 26-27 days. This means that the changes in the solar wind speed and IMF are related to the Suns near equatorial regions in considering the differential rotation of the Sun. However, the solar wind parameters observed near the Earths orbit provide only the conditions in the limited local vicinity of the equatorial region in the heliosphere (within in latitude). We also demonstrate that the observed period of the GCR intensity connected with the Suns rotation increased up to aprox 33-36 days in 2009. This means that the process driving the 27-day variations of the GCR intensity takes place not only in the limited local surroundings of the equatorial region but in the global 3-D space of the heliosphere, covering also higher latitude regions. A relatively long period (aprox 34 days) found for 2009 in the GCR intensity gives possible evidence of the onset of cycle 24 due to active regions at higher latitudes and rotating slowly because of the Suns differential rotation. We also discuss the effect of differential rotation on the theoretical model of the 27-day variations of the GCR intensity.

Dependence of the 27-Day Variation of Cosmic Rays on the Global Magnetic Field of the Sun

R. **Modzelewska**, M.V. Alania
Advances in Space Research (**2012**)
http://arxiv.org/ftp/arxiv/papers/1504/1504.00924.pdf
We show that the higher range of the heliolongitudinal asymmetry of the solar wind speed in the positive polarity period (Apos) than in the negative polarity period (Aneg) is one of the important reasons of the larger amplitudes of the 27-day variation of the galactic cosmic ray (GCR) intensity in the period of 1995-1997 (Apos) than in 1985-1987 (Aneg). Subsequently, different ranges of the heliolongitudinal asymmetry of the solar wind speed jointly with equally important corresponding drift effect are general causes of the polarity dependence of the amplitudes of the 27-day variation of the GCR intensity. At the same time, we show that the polarity dependence is feeble for the last unusual minimum epoch of solar activity 2007-2009 (Aneg); the amplitude of the 27-day variation of the GCR intensity shows only a tendency of the polarity dependence. We present a three dimensional (3-D) model of the 27-day variation of GCR based on the Parkers transport equation. In the 3-D model is implemented a longitudinal

variation of the solar wind speed reproducing in situ measurements and corresponding divergence-free interplanetary magnetic field (IMF) derived from the Maxwells equations. We show that results of the proposed 3-D modeling of the 27-day variation of GCR intensity for different polarities of the solar magnetic cycle are in good agreement with the neutron monitors experimental data. To reach a compatibility of the theoretical modeling with observations for the last minimum epoch of solar activity 2007-2009 (Aneg) a parallel diffusion coefficient was increased by 40 percent

Lenslet Array and Fabry–Pérot-Based Hyperspectral Imaging

R. **Mohanakrishna**, K. Sankarasubramanian
Solar Physics July 2018, 293:**108**
Snapshot spectroscopic imagers/instruments (SSI) are a class of spectroscopic instruments that are capable of acquiring spectral information of a given field of view in a single frame. Standard spectroscopic instruments like a grating-based spectrograph or a Fabry–Pérot-based spectrograph obtain two dimensional data of 2D space or 1D space and 1D wavelength. But SSIs have three dimensional data of 2D space and wavelength embedded in two dimensional detector/image plane. So standard data reduction techniques are not applicable. Lenslet array spectroscope is a novel SSI which images the object on to a hybrid spatio-spectral image plane. A procedure to extract the spatial and spectral information of the field of view from this hyperplane is presented. We demonstrate the snapshot capabilities of this instrument to study dynamic activities of the Sun as inferred from two measurements: (i) Evershed flow in a sunspot in NOAA 12526 at Fe i 6301.5 Å and (ii) oscillations in a quiescent prominence at Hαα6562.8 Å. This instrument can be used for large or small scale structures, making it efficient for studying a wide range of dynamic activities like helioseismology, Moreton waves, prominence oscillation etc.

Constraining the systematics of (acoustic) wave heating estimates in the solar chromosphere

Momchil E. **Molnar**, Kevin P. Reardon, Steven R. Cranmer, Adam F. Kowalski, Ivan Milic
ApJ **945** 154 **2023**
https://arxiv.org/pdf/2302.04253
https://iopscience.iop.org/article/10.3847/1538-4357/acbc75/pdf
Acoustic wave heating is believed to contribute significantly to the missing energy input required to maintain the solar chromosphere in its observed state. We studied the propagation of waves above the acoustic cutoff in the upper photosphere into the chromosphere with ultraviolet and optical spectral observations interpreted through comparison with three dimensional radiative magnetohydrodynamic (rMHD) \emph{Bifrost} models to constrain the heating contribution from acoustic waves in the solar atmosphere. Sit-and-stare observations taken with the Interface Region Imaging Spectrograph (IRIS) and data from the Interferometric BIdimensional Spectrograph (IBIS) were used to provide the observational basis of this work. We compared the observations with synthetic observables derived from the Bifrost solar atmospheric model. Our analysis of the \emph{Bifrost} simulations show that internetwork and enhanced network regions exhibit significantly different wave propagation properties, which are important for the accurate wave flux estimates. The inferred wave energy fluxes based on our observations are not sufficient to maintain the solar chromosphere. We point out that the systematics of the modeling approaches in the literature lead to differences which could determine the conclusions of this type of studies, based on the same observations.
IRIS Nugget May 2023 https://iris.lmsal.com/nugget

Solar Chromospheric Temperature Diagnostics: a joint ALMA-Hα analysis

Momchil E. **Molnar**, Kevin P. Reardon, Yi Chai, Dale Gary, Han Uitenbroek, Gianna Cauzzi, Steven R. Cranmer
ApJ **881** 99 **2019**
https://arxiv.org/pdf/1906.08896.pdf
https://doi.org/10.3847/1538-4357/ab2ba3
We present the first high-resolution, simultaneous observations of the solar chromosphere in the optical and millimeter wavelength ranges, obtained with ALMA and the IBIS instrument at the Dunn Solar Telescope. In this paper we concentrate on the comparison between the brightness temperature observed in ALMA Band 3 (3 mm; 100 GHz) and the core width of the Hα 656.3 nm line, previously identified as a possible diagnostic of the chromospheric temperature. We find that in the area of plage, network and fibrils covered by our FOV the two diagnostics are well correlated, with similar spatial structures observed in both. The strength of the correlation is remarkable, given that the source function of the mm-radiation obeys local thermodynamic equilibrium, while the Hα line has a source function that deviates significantly from the local Planck function. The observed range of ALMA brightness temperatures is sensibly smaller than the temperature range that was previously invoked to explain the observed width variations in Hα. We employ analysis from forward modeling with the RH code to argue that the strong correlation between Hα width and ALMA brightness temperature is caused by their shared dependence on the population number n2 of the first excited level of hydrogen. This population number drives millimeter opacity through hydrogen ionization via the Balmer continuum, and Hα width through a curve-of-

growth-like opacity effect. Ultimately, the n2 population is regulated by the enhancement or lack of downward Lyα flux, which coherently shifts the formation height of both diagnostics to regions with different temperature, respectively. **April 23, 2017**

Evolution of dynamic fibrils from the cooler chromosphere to the hotter corona⋆

Sudip **Mandal**1, Hardi Peter1, Lakshmi Pradeep Chitta1, Sami K. Solanki1,2, +++
A&A 678, L5 (**2023**)
https://www.aanda.org/articles/aa/pdf/2023/10/aa47343-23.pdf
Dynamic fibrils (DFs) are commonly observed chromospheric features in solar active regions. Recent observations from the Extreme Ultraviolet Imager (EUI) aboard the Solar Orbiter have revealed unambiguous signatures of DFs at the coronal base in extreme ultraviolet (EUV) emission. However, it remains unclear if the DFs detected in the EUV are linked to their chromospheric counterparts. Simultaneous detection of DFs from chromospheric to coronal temperatures could provide important information on their thermal structuring and evolution through the solar atmosphere. In this paper, we address this question by using coordinated EUV observations from the Atmospheric Imaging Assembly (AIA), Interface Region Imaging Spectrograph (IRIS), and EUI to establish a one-to-one correspondence between chromospheric and transition region DFs (observed by IRIS) with their coronal counterparts (observed by EUI and AIA). Our analysis confirms a close correspondence between DFs observed at different atmospheric layers and reveals that DFs can reach temperatures of about 1.5 million Kelvin, typical of the coronal base in active regions. Furthermore, the intensity evolution of these DFs, as measured by tracking them over time, reveals a shock-driven scenario in which plasma piles up near the tips of these DFs and, subsequently, these tips appear as bright blobs in coronal images. These findings provide information on the thermal structuring of DFs and their evolution and impact through the solar atmosphere. **2022-03-17**

Differential Rotation of the Solar Chromosphere: A Century-long Perspective from Kodaikanal Solar Observatory Ca ii K Data

Dibya Kirti **Mishra**1,2, Srinjana Routh1,2, Bibhuti Kumar Jha3, Theodosios Chatzistergos4, Judhajeet Basu5, Subhamoy Chatterjee3, Dipankar Banerjee1,5,6, and Ilaria Ermolli7
2024 ApJ 961 40
https://iopscience.iop.org/article/10.3847/1538-4357/ad1188/pdf
Chromospheric differential rotation is a key component in comprehending the atmospheric coupling between the chromosphere and the photosphere at different phases of the solar cycle. In this study, we therefore utilize the newly calibrated multidecadal Ca ii K spectroheliograms (1907–2007) from the Kodaikanal Solar Observatory (KoSO) to investigate the differential rotation of the solar chromosphere using the technique of image cross-correlation. Our analysis yields the chromospheric differential rotation rate $\Omega(\theta) = (14.61 \pm 0.04–2.18 \pm 0.37 \sin2\theta–1.10\pm0.61\sin4\theta)^\circ$ day−1. These results suggest the chromospheric plages exhibit an equatorial rotation rate 1.59% faster than the photosphere when compared with the differential rotation rate measured using sunspots and also a smaller latitudinal gradient compared to the same. To compare our results to those from other observatories, we have applied our method on a small sample of Ca ii K data from Rome, Meudon, and Mount Wilson observatories, which support our findings from KoSO data. Additionally, we have not found any significant north–south asymmetry or any systematic variation in chromospheric differential rotation over the last century.

Determining the nanoflare heating frequency of an X-ray Bright Point observed by MaGIXS

Biswajit **Mondal**, P. S. Athiray, Amy R. Winebarger, Sabrina L. Savage, +++
ApJ **967** 23 **2024**
https://arxiv.org/pdf/2402.05036.pdf
https://iopscience.iop.org/article/10.3847/1538-4357/ad2766/pdf
Nanoflares are thought to be one of the prime candidates that can heat the solar corona to its multi-million kelvin temperature. Individual nanoflares are difficult to detect with the present generation instruments, however their presence can be inferred by comparing simulated nanoflare-heated plasma emissions with the observed emission. Using HYDRAD coronal loop simulations, we model the emission from an X-ray bright point (XBP) observed by the Marshall Grazing Incidence X-ray Spectrometer (MaGIXS), along with nearest-available observations from the Atmospheric Imaging Assembly (AIA) onboard Solar Dynamics Observatory (SDO) and X-Ray Telescope (XRT) onboard Hinode observatory. The length and magnetic field strength of the coronal loops are derived from the linear-force-free extrapolation of the observed photospheric magnetogram by Helioseismic and Magnetic Imager (HMI) onboard SDO. Each loop is assumed to be heated by random nanoflares, whose magnitude and frequency are determined by the loop length and magnetic field strength. The simulation results are then compared and matched against the measured intensity from AIA, XRT, and MaGIXS. Our model results indicate the observed emissions from the XBP under study could be well matched by a distribution of nanoflares with average delay times 1500 s to

3000 s, which suggest that the heating is dominated by high-frequency events. Further, we demonstrate the high sensitivity of MaGIXS and XRT to diagnose the heating frequency using this method, while AIA passbands are found to be the least sensitive. **2021-07-30**

2.5-D MHD Simulation of the Formation and Evolution of Plasmoids in Coronal Current Sheets

Sripan **Mondal**, Abhishek K Srivastava, David I. Pontin, Ding Yuan, Eric R. Priest

ApJ **2024**

https://arxiv.org/pdf/2401.07048.pdf

In the present paper, using MPI-AMRVAC, we perform a 2.5-D numerical MHD simulation of the dynamics and associated thermodynamical evolution of an initially force-free Harris current sheet subjected to an external velocity perturbation under the condition of uniform resistivity. The amplitude of the magnetic field is taken to be 10 Gauss, typical of the solar corona. We impose a Gaussian velocity pulse across this current sheet mimicking the interaction of fast magnetoacoustic waves with a current sheet in corona. This leads to a variety of dynamics and plasma processes in the current sheet, which is initially quasi-static. The initial pulse interacts with the current sheet and splits into a pair of counter-propagating wavefronts, which forms a rarefied region and leads to inflow and a thinning of the current sheet. The thinning results in Petschek-type magnetic reconnection followed by tearing instability and plasmoid formation. The reconnection outflows containing outward-moving plasmoids have accelerated motions with velocities ranging from 105-303 km/s. The average temperature and density of the plasmoids are found to be 8 MK and twice the background density of the solar corona, respectively. These estimates of velocity, temperature and density of plasmoids are similar to values reported from various solar coronal observations. Therefore, we infer that the external triggering of a quasi-static current sheet by a single velocity pulse is capable of initiating magnetic reconnection and plasmoid formation in the absence of a localized enhancement of resistivity in the solar corona.

Reconnection generated plasma flows in the quasi-separatrix layer in localised solar corona

Sripan **Mondal**, A.K. Srivastava, Sudheer K. Mishra, K. Sangal, Pradeep Kayshap, Yang Guo, David I. Pontin, Vadim M. Uritsky, Leon Ofman, T.-J. Wang, Ding Yuan

ApJ **2023**

https://arxiv.org/pdf/2305.02277.pdf

Multiwavelength observations of the propagating disturbances (PDs), discovered by Atmospheric Imaging Assembly (AIA) onboard Solar Dynamics Observatory (SDO), are analyzed to determine its driving mechanism and physical nature. Two magnetic strands in the localised corona are observed to approach and merge with each other followed by the generation of brightening, which further propagates in a cusp-shaped magnetic channel. Differential emission measure analysis shows an occurrence of heating in this region-of-interest (ROI). We extrapolate potential magnetic field lines at coronal heights from observed Helioseismic and Magnetic Imager (HMI) vector magnetogram via Green's function method using MPI-AMRVAC. We analyze the field to locate magnetic nulls and quasi-separatrix layers (QSLs) which are preferential locations for magnetic reconnection. Dominant QSLs including a magnetic null are found to exist and match the geometry followed by PDs, therefore, it provides conclusive evidence of magnetic reconnection. In addition, spectroscopic analysis of Interface Region Imaging Spectrograph (IRIS) Si IV 1393.77 Å line profiles show a rise of line-width in the same time range depicting presence of mass motion in the observed cusp-shaped region. PDs are observed to exhibit periodicities of around four minutes. The speeds of PDs measured by Surfing Transform Technique are almost close to each other in four different SDO/AIA bandpasses, i.e., 304, 171, 193 and 131 Å excluding the interpretation of PDs in terms of slow magnetoacoustic waves. We describe comprehensively the observed PDs as quasi-periodic plasma flows generated due to periodic reconnection in vicinity of a coronal magnetic null. **17 April 2021.**

Multifrequency microwave imaging of weak transients from the quiet solar corona

Surajit **Mondal**, Bin Chen, Sijie Yu

ApJ **953** 4 **2023**

https://arxiv.org/pdf/2301.07840.pdf

https://iopscience.iop.org/article/10.3847/1538-4357/acdf4f/pdf

Understanding the dynamics of the quiet solar corona is important for answering key questions including the coronal heating problem. Multiple studies have suggested small-scale magnetic reconnection events may play a crucial role. These reconnection events are expected to involve accelerating electrons to suprathermal energies, which can then produce nonthermal observational signatures. However, due to the paucity of sensitive high-fidelity observations capable of probing these nonthermal signatures, most studies were unable to quantify their nonthermal nature. Here we use joint radio observations from the Very Large Array (VLA) and the Expanded Owens Valley Solar Array (EOVSA) to detect transient emissions from the quiet solar corona in the microwave (GHz) domain. While similar transients have been reported in the past, their nonthermal nature could not be adequately quantified due to the

unavailability of broadband observations. Using a much larger bandwidth available now with the VLA and EOVSA, in this study, we are able to quantify the nonthermal energy associated with two of these transients. We find that the total nonthermal energy associated with some of these transients can be comparable to or even larger than the total thermal energy of a nanoflare, which underpins the importance of nonthermal energy in the total coronal energy budget. **February 1, 2020**

Role of small-scale impulsive events in heating the X-ray bright points of the quiet Sun

Biswajit **Mondal**, James A Klimchuk, Santosh V. Vadawale, Aveek Sarkar, Giulio Del Zanna, P.S. Athiray, N. P. S. Mithun, Helen E. Mason, A. Bhardwaj

ApJ **945** 37 **2023**

https://arxiv.org/pdf/2301.02519

https://iopscience.iop.org/article/10.3847/1538-4357/acb8bb/pdf

Small-scale impulsive events, known as nanoflares, are thought to be one of the prime candidates that can keep the solar corona hot at its multi-million Kelvin temperature. Individual nanoflares are difficult to detect with the current generation instruments; however, their presence can be inferred through indirect techniques such as a Differential Emission Measure (DEM) analysis. Here we employ this technique to investigate the possibility of nanoflare heating of the quiet corona during the minimum of solar cycle 24. During this minimum, active regions (ARs) were absent on the solar-disk for extended periods. In the absence of ARs, X-ray bright points (XBP) are the dominant contributor to disk-integrated X-rays. We estimate the DEM of the XBPs using observations from the Solar X-ray Monitor (XSM) onboard the Chandrayaan-2 orbiter and the Atmospheric Imaging Assembly (AIA) onboard the Solar Dynamic Observatory. XBPs consist of small-scale loops associated with bipolar magnetic fields. We simulate such XBP loops using the EBTEL hydrodynamic code. The lengths and magnetic field strengths of these loops are obtained through a potential field extrapolation of the photospheric magnetogram. Each loop is assumed to be heated by random nanoflares having an energy that depends on the loop properties. The composite nanoflare energy distribution for all the loops has a power-law slope close to -2.5. The simulation output is then used to obtain the integrated DEM. It agrees remarkably well with the observed DEM at temperatures above 1 MK, suggesting that the nanoflare distribution, as predicted by our model, can explain the XBP heating.

Contribution of spicules to solar coronal emission

Shanwlee Sow **Mondal**, James A. Klimchuk, Aveek Sarkar

ApJ **937** 71 **2022**

https://arxiv.org/pdf/2208.05240.pdf

https://iopscience.iop.org/article/10.3847/1538-4357/ac879b/pdf

Recent high-resolution imaging and spectroscopic observations have generated renewed interest in spicules' role in explaining the hot corona. Some studies suggest that some spicules, often classified as type II, may provide significant mass and energy to the corona. Here we use numerical simulations to investigate whether such spicules can produce the observed coronal emission without any additional coronal heating agent. Model spicules consisting of a cold body and hot tip are injected into the base of a warm (0.5 MK) equilibrium loop with different tip temperatures and injection velocities. Both piston- and pressure-driven shocks are produced. We find that the hot tip cools rapidly and disappears from coronal emission lines such as Fe XII 195 and Fe XIV 274. Prolonged hot emission is produced by pre-existing loop material heated by the shock and by thermal conduction from the shock. However, the shapes and Doppler shifts of synthetic line profiles show significant discrepancies with observations. Furthermore, spatially and temporally averaged intensities are extremely low, suggesting that if the observed intensities from the quiet Sun and active regions were solely due to type II spicules, one to several orders of magnitude more spicules would be required than have been reported in the literature. This conclusion applies strictly to the ejected spicular material. We make no claims about emissions connected with waves or coronal currents that may be generated during the ejection process and heat the surrounding area.

A Search for the Counterparts of Quiet-Sun Radio Transients in Extreme Ultraviolet Data

Surajit **Mondal**

Solar Physics volume 296, Article number: 131 (**2021**)

https://arxiv.org/pdf/2107.04525.pdf

https://link.springer.com/content/pdf/10.1007/s11207-021-01877-3.pdf

https://doi.org/10.1007/s11207-021-01877-3

Nonthermal radio transients from the quiet Sun have been recently discovered and it has been hypothesized using rough calculations that they might be important for coronal heating. It is well realized that energy calculations using coherent emissions are often subject to poorly constrained parameters and hence have large uncertainties. However, energy estimates using observations in the extreme ultraviolet (EUV) and soft X-ray bands are routinely done and the techniques are pretty well established. This work presents the first attempt to identify the EUV counterparts of these radio transients and then use them to estimate the energy deposited into the corona during the event. I show that the group of radio transients studied here is associated with a brightening observed in the EUV waveband and is

produced by an energy release of ≈1025≈1025 ergs. The fact that the flux density of the radio transient is only ≈2≈2 mSFU suggests that it might be possible to do large statistical studies in the future for understanding the relationship between these radio transients and other EUV and X-ray counterparts, as well as for understanding their importance in coronal heating. **November 27, 2017**

First radio evidence for impulsive heating contribution to the quiet solar corona

Surajit **Mondal**, Divya Oberoi, Atul Mohan
ApJL **895** L39 **2020**
https://arxiv.org/pdf/2004.04399.pdf
https://doi.org/10.3847/2041-8213/ab8817
This letter explores the relevance of nanoflare based models for heating the quiet sun corona. Using metrewave data from the Murchison Widefield Array, we present the first successful detection of impulsive emissions down to flux densities of ∼mSFU, about two orders of magnitude weaker than earlier attempts. These impulsive emissions have durations ≲1s and are present throughout the quiet solar corona. The fractional time occupancy of these impulsive emissions at a given region is ≲10%. The histograms of these impulsive emissions follow a powerlaw distribution and show signs of clustering at small timescales. Our estimate of the energy which must be dumped in the corona to generate these impulsive emissions is consistent with the coronal heating requirements. Additionally, the statistical properties of these impulsive emissions are very similar to those recently determined for magnetic switchbacks by the Parker Solar Probe (PSP). We hope that this work will lead to a renewed interest in relating these weak impulsive emissions to the energy deposited in the corona, the quantity of physical interesting from a coronal heating perspective, and explore their relationship with the magnetic switchbacks observed by the PSP. **November 27, 2017**

Quantifying the evidence for resonant damping of coronal waves with foot-point wave power asymmetry

M. **Montes-Solís**, I. Arregui
A&A 640, L17 **2020**
https://arxiv.org/pdf/2008.03004.pdf
https://www.aanda.org/articles/aa/pdf/2020/08/aa37237-19.pdf
We use Coronal Multi-channel Polarimeter (CoMP) observations of propagating waves in the solar corona and Bayesian analysis to assess the evidence of models with resonant damping and foot-point wave power asymmetries. Two nested models are considered. The reduced model considers resonant damping as the sole cause of the measured discrepancy between outward and inward wave power. The larger model contemplates an extra source of asymmetry with origin at the foot-points. We first compute probability distributions of parameters conditional on the models and the observed data. The obtained constraints are then used to calculate the evidence for each model in view of data. We find that we need to consider the larger model to explain CoMP data and to accurately infer the damping ratio, hence, to better assess the possible contribution of the waves to coronal heating.

Data Fusion of Total Solar Irradiance Composite Time Series Using 41 Years of Satellite Measurements

Jean-Philippe **Montillet**, Wolfgang Finsterle, Gael Kermarrec, Rok Sikonja, Margit Haberreiter, Werner Schmutz, Thierry Dudok de Wit
JGR Atmospheres; in Special Section: Monitoring the Earth radiation budget and its implication to climate simulations: **2022**
https://arxiv.org/pdf/2207.04926
Since the late 1970s, successive satellite missions have been monitoring the sun's activity and recording the total solar irradiance (TSI). Some of these measurements have lasted for more than a decade. In order to obtain a seamless record whose duration exceeds that of the individual instruments, the time series have to be merged. Climate models can be better validated using such long TSI time series which can also help to provide stronger constraints on past climate reconstructions (e.g., back to the Maunder minimum). We propose a 3-step method based on data fusion, including a stochastic noise model to take into account short and long-term correlations. Compared with previous products scaled at the nominal TSI value of 1361 W/m2, the difference is below 0.2 W/m2 in terms of solar minima. Next, we model the frequency spectrum of this 41-year TSI composite time series with a Generalized Gauss-Markov model to help describe an observed flattening at high frequencies. It allows us to fit a linear trend into these TSI time series by joint inversion with the stochastic noise model via a maximum-likelihood estimator. Our results show that the amplitude of such trend is ∼ -0.004 +/- 0.004 W/(m2yr) for the period 1980 - 2021. These results are compared with the difference of irradiance values estimated from two consecutive solar minima. We conclude that the trend in these composite time series is mostly an artifact due to the colored noise.

Prospective Implications of EUV Coronal Plumes for Magnetic-network Genesis of Coronal Heating, Coronal-hole Solar Wind, and Solar-wind Magnetic-field Switchbacks

Ronald L. **Moore**, Sanjiv K. Tiwari, Navdeep K. Panesar, Alphonse C. Sterling

ApJL **945** L16 **2023**

https://arxiv.org/pdf/2303.00097

https://iopscience.iop.org/article/10.3847/2041-8213/acbe46/pdf

We propose that coronal heating in EUV coronal plumes is weaker, not stronger, than in adjacent non-plume coronal magnetic funnels. This expectation stems from (i) the observation that an EUV plume is born as the magnetic flux at the foot of the plume's magnetic funnel becomes tightly packed together, and (ii) the observation that coronal heating in quiet regions increases in proportion to the coast-line length of the underlying magnetic network. We do not rule out the possibility that coronal heating in EUV plumes might be stronger, not weaker, but we point out how the opposite is plausible. We reason that increasing coronal heating during plume birth would cause co-temporal increasing net upward mass flux in the plume, whereas decreasing coronal heating during plume birth would cause co-temporal net downward mass flux in quiet-region plumes and co-temporal decrease in net upward mass flux or even net downward mass flux in coronal-hole plumes. We further reason that conclusive evidence of weaker coronal heating in EUV plumes would strengthen the possibility that magnetic twist waves from fine-scale magnetic explosions at the edges of the magnetic network (1) power much of the coronal heating in quiet regions, and (2) power most of the coronal heating and solar wind acceleration in coronal holes, with many twist waves surviving to become magnetic-field switchbacks in the solar wind from coronal holes.

On Making Magnetic-Flux-Rope Ω Loops for Solar Bipolar Magnetic Regions of All Sizes by Convection Cells

Ronald L. **Moore**, Sanjiv K. Tiwari, Navdeep K. Panesar, Alphonse C. Sterling

ApJL **2020**

https://arxiv.org/pdf/2009.13694.pdf

We propose that the flux-rope Ω loop that emerges to become any bipolar magnetic region (BMR) is made by a convection cell of the Ω-loop's size from initially-horizontal magnetic field ingested through the cell's bottom. This idea is based on (1) observed characteristics of BMRs of all spans (~ 1000 km to ~ 200,000 km), (2) a well-known simulation of the production of a BMR by a supergranule-size convection cell from horizontal field placed at cell bottom, and (3) a well-known convection-zone simulation. From the observations and simulations, we (1) infer that the strength of the field ingested by the biggest convection cells (giant cells) to make the biggest BMR Ω loops is ~ 103 G, (2) plausibly explain why the span and flux of the biggest observed BMRs are ~ 200,000 km and ~ 1022 Mx, (3) suggest how giant cells might also make "failed-BMR" Ω loops that populate the upper convection zone with horizontal field, from which smaller convection cells make BMR Ω loops of their size, (4) suggest why sunspots observed in a sunspot cycle's declining phase tend to violate the hemispheric helicity rule, and (5) support a previously-proposed amended Babcock scenario for the sunspot cycle's dynamo process. Because the proposed convection-based heuristic model for making a sunspot-BMR Ω loop avoids having ~ 105 G field in the initial flux rope at the bottom of the convection zone, it is an appealing alternative to the present magnetic-buoyancy-based standard scenario and warrants testing by high-enough-resolution giant-cell magnetoconvection simulations.

The Instruments and Capabilities of the Miniature X-ray Solar Spectrometer (MinXSS) CubeSats

Christopher S. **Moore** (1, 2 and 3), Amir Caspi (4), Thomas N. Woods (2), Phillip C. Chamberlin (2 and 5),Brian R. Dennis (5), Andrew R. Jones (2), James P. Mason (2 and 5), Richard A. Schwartz (5 and 6),Anne K. Tolbert

Solar Phys. 293:21 **2018**

https://arxiv.org/pdf/1801.01261.pdf

https://link.springer.com/content/pdf/10.1007%2Fs11207-018-1243-3.pdf

The Miniature X-ray Solar Spectrometer (MinXSS) CubeSat is the first solar science oriented CubeSat mission flown for the NASA Science Mission Directorate, with the main objective of measuring the solar soft X-ray (SXR) flux and a science goal of determining its influence on Earth's ionosphere and thermosphere. These observations can also be used to investigate solar quiescent, active region, and flare properties. The MinXSS X-ray instruments consist of a spectrometer, called X123, with a nominal 0.15 keV full-width-half-maximum (FWHM) resolution at 5.9 keV and a broadband X-ray photometer, called XP. Both instruments are designed to obtain measurements from 0.5 - 30 keV at a nominal time cadence of 10 seconds. A description of the MinXSS instruments, performance capabilities, and relation to the Geostationary Operational Environmental Satellite (GOES) 0.1 - 0.8 nm flux are discussed in this article. Early MinXSS results demonstrate the capability to measure variations of the solar spectral SXR flux between 0.8 - 12 keV from at least GOES A5 - M5 (5×10^{-8}- 5×10^{-5} W m^{-2}) levels and infer physical properties (temperature and emission measure) from the MinXSS data alone. Moreover, coronal elemental

abundances can be inferred, specifically Fe, Ca, Si, Mg, S, Ar, and Ni, when there is sufficiently high count rate at each elemental spectral feature. Additionally, temperature response curves and emission measure loci demonstrate the MinXSS sensitivity to plasma emission at different temperatures. MinXSS observations coupled with those from other solar observatories can help address some of the most compelling questions in solar coronal physics. Finally, simultaneous observations by MinXSS and Reuven Ramaty High Energy Solar Spectroscopic Imager (RHESSI) can provide the most spectrally complete soft X-ray solar flare photon flux measurements to date.

Babcock Redux: An Ammendment of Babcock's Schematic of the Sun's Magnetic Cycle

Ronald L. **Moore**, J. W. Cirtain, Alphonse C. Sterling

2016

http://arxiv.org/pdf/1606.05371v1.pdf

We amend Babcock's original scenario for the global dynamo process that sustains the Sun's 22-year magnetic cycle. The amended scenario fits post-Babcock observed features of the magnetic activity cycle and convection zone, and is based on ideas of Spruit and Roberts (1983) about magnetic flux tubes in the convection zone. A sequence of four schematic cartoons lays out the proposed evolution of the global configuration of the magnetic field above, in, and at the bottom of the convection zone through sunspot Cycle 23 and into Cycle 24. Three key elements of the amended scenario are: (1) as the net following-polarity field from the sunspot-region omega-loop fields of an ongoing sunspot cycle is swept poleward to cancel and replace the opposite-polarity polar-cap field from the previous sunspot cycle, it remains connected to the ongoing sunspot cycle's toroidal source-field band at the bottom of the convection zone; (2) topological pumping by the convection zone's free convection keeps the horizontal extent of the poleward-migrating following-polarity field pushed to the bottom, forcing it to gradually cancel and replace old horizontal field below it that connects the ongoing-cycle source-field band to the previous-cycle polar-cap field; (3) in each polar hemisphere, by continually shearing the poloidal component of the settling new horizontal field, the latitudinal differential rotation low in the convection zone generates the next-cycle source-field band poleward of the ongoing-cycle band. The amended scenario is a more-plausible version of Babcock's scenario, and its viability can be explored by appropriate kinematic flux-transport solar-dynamo simulations.

Dynamics of internetwork chromospheric fibrils: Basic properties and MHD kink waves

K. **Mooroogen**, R. J. Morton, V. Henriques

A&A 607, A46 **2017**

https://arxiv.org/pdf/1708.03500.pdf

Using the spectroscopic imaging capabilities of the Swedish Solar Telescope, we aim to provide the first investigation on the nature and dynamics of elongated absorption features (fibrils) observed in Hα in the internetwork. We observe and identify a number of internetwork fibrils, which form away from the kilogauss, network magnetic flux, and we provide a synoptic view on their behaviour. The internetwork fibrils are found to support wave-like behaviour, which we interpret as Magnetohydrodynamic (MHD) kink waves. The properties of these waves, that is, amplitude, period, and propagation speed, are measured from time-distance diagrams and we attempt to exploit them via magneto-seismology in order to probe the variation of plasma properties along the wave-guides. We found that the Internetwork (IN) fibrils appear, disappear, and re-appear on timescales of tens of minutes, suggesting that they are subject to repeated heating. No clear photospheric footpoints for the fibrils are found in photospheric magnetograms or Hα wing images. However, we suggest that they are magnetised features as the majority of them show evidence of supporting propagating MHD kink waves, with a modal period of 120~s. Additionally, one IN fibril is seen to support a flow directed along its elongated axis, suggesting a guiding field. The wave motions are found to propagate at speeds significantly greater than estimates for typical chromospheric sound speeds. Through their interpretation as kink waves, the measured speeds provide an estimate for local average Alfv\'en speeds. Furthermore, the amplitudes of the waves are also found to vary as a function of distance along the fibrils, which can be interpreted as evidence of stratification of the plasma in the neighbourhood of the IN fibril.

Directional Time-Distance Probing of Model Sunspot Atmospheres

H. **Moradi**, P. S. Cally, D. Przybylski, S. Shelyag

MNRAS, **2015**

http://arxiv.org/pdf/1503.04270v1.pdf

A crucial feature not widely accounted for in local helioseismology is that surface magnetic regions actually open a window from the interior into the solar atmosphere, and that the seismic waves leak through this window, reflect high in the atmosphere, and then re-enter the interior to rejoin the seismic wave field normally confined there. In a series of recent numerical studies using translation invariant atmospheres, we utilised a "directional time-distance helioseismology" measurement scheme to study the implications of the returning fast and Alfv\'en waves higher up in the solar atmosphere on the seismology at the photosphere (Cally & Moradi 2013; Moradi & Cally 2014). In this study, we extend our directional time-distance analysis to more realistic sunspot-like atmospheres to better

understand the direct effects of the magnetic field on helioseismic travel-time measurements in sunspots. In line with our previous findings, we uncover a distinct frequency-dependant directional behaviour in the travel-time measurements, consistent with the signatures of MHD mode conversion. We found this to be the case regardless of the sunspot field strength or depth of its Wilson depression. We also isolated and analysed the direct contribution from purely thermal perturbations to the measured travel times, finding that waves propagating in the umbra are much more sensitive to the underlying thermal effects of the sunspot.

Energy and helicity evolution in a flux emergence simulation

K. **Moraitis**1,⋆, V. Archontis1 and G. Chouliaras2
A&A, 690, A181 (**2024**)
https://doi.org/10.1051/0004-6361/202450924
https://www.aanda.org/articles/aa/pdf/2024/10/aa50924-24.pdf
Aims. The main aim of this work is to study the evolution of the recently introduced relative helicity of the magnetic polarity inversion line (PIL) in a magnetohydrodynamics simulation.
Methods. The simulation used is a typical flux emergence simulation in which there is additionally an oblique, pre-existing magnetic field. The interaction of the emerging and ambient fields produces intense coronal activity, with four jets standing out. The 3D magnetic field allows us to compute various energies and helicities, and to study their evolution during the simulation, especially around the identified jets. We examine the evolution of all quantities in three different regions: in the whole volume, in three separate subvolumes of the whole volume, and in a 2D region around the PIL on the photosphere.
Results. We find that the helicities are in general more responsive to the jets, followed by the free energy. The eruptivity index, the ratio of the current-carrying helicity to the relative helicity, does not show the typical behaviour it has in other cases, as its variations do not follow the production of the jets. By considering the subvolumes we find that the magnetic field gets more potential and less helical with height. The PIL relative helicity confirms the recent results it showed in observed active regions, exhibiting stronger variations during the jets compared to the standard relative helicity. Moreover, the current-carrying helicity around the PIL has a similar behaviour to the PIL relative helicity, and so this quantity could be equally useful in solar eruptivity studies.

Computation of Relative Magnetic Helicity in Spherical Coordinates

K. **Moraitis**, É. Pariat, A. Savcheva, G. Valori
Solar Phys. 293:92 **2018**
https://arxiv.org/pdf/1806.03011.pdf
https://link.springer.com/content/pdf/10.1007%2Fs11207-018-1314-5.pdf
Magnetic helicity is a quantity of great importance in solar studies because it is conserved in ideal magneto-hydrodynamics. While many methods to compute magnetic helicity in Cartesian finite volumes exist, in spherical coordinates, the natural coordinate system for solar applications, helicity is only treated approximately. We present here a method to properly compute relative magnetic helicity in spherical geometry. The volumes considered are finite, of shell or wedge shape, and the three-dimensional magnetic field is considered fully known throughout the studied domain. Testing of the method with well-known, semi-analytic, force-free magnetic-field models reveals that it has excellent accuracy. Further application to a set of nonlinear force-free reconstructions of the magnetic field of solar active regions, and comparison with an approximate method used in the past, indicates that the proposed methodology can be significantly more accurate, thus making our method a promising tool in helicity studies that employ the spherical geometry. Additionally, the range of applicability of the approximate method is determined and discussed.

An observationally-driven kinetic approach to coronal heating

K. **Moraitis**1, A. Toutountzi2, H. Isliker2, M. Georgoulis1, L. Vlahos2 and G. Chintzoglou3
A&A 596, A56 (**2016**)
Aims. Coronal heating through the explosive release of magnetic energy remains an open problem in solar physics. Recent hydrodynamical models attempt an investigation by placing swarms of “nanoflares” at random sites and times in modeled one-dimensional coronal loops. We investigate the problem in three dimensions, using extrapolated coronal magnetic fields of observed solar active regions.
Methods. We applied a nonlinear force-free field extrapolation above an observed photospheric magnetogram of NOAA active region (AR) 11 158. We then determined the locations, energy contents, and volumes of “unstable” areas, namely areas prone to releasing magnetic energy due to locally accumulated electric current density. Statistical distributions of these volumes and their fractal dimension are inferred, investigating also their dependence on spatial resolution. Further adopting a simple resistivity model, we inferred the properties of the fractally distributed electric fields in these volumes. Next, we monitored the evolution of 105 particles (electrons and ions) obeying an initial Maxwellian distribution with a temperature of 10 eV, by following their trajectories and energization when subjected to the resulting electric fields. For computational convenience, the length element of

the magnetic-field extrapolation is 1 arcsec, or ~725 km, much coarser than the particles' collisional mean free path in the low corona (0.1−1 km).
Results. The presence of collisions traps the bulk of the plasma around the unstable volumes, or current sheets (UCS), with only a tail of the distribution gaining substantial energy. Assuming that the distance between UCS is similar to the collisional mean free path we find that the low active-region corona is heated to 100−200 eV, corresponding to temperatures exceeding 2 MK, within tens of seconds for electrons and thousands of seconds for ions.
Conclusions. Fractally distributed, nanoflare-triggening fragmented UCS in the active-region corona can heat electrons and ions with minor enhancements of the local resistivity. This statistical result is independent from the nature of the extrapolation and the spatial resolution of the modeled active-region corona. This finding should be coupled with a complete plasma treatment to determine whether a quasi-steady temperature similar to that of the ambient corona can be maintained, either via a kinetic or via a hybrid, kinetic and fluid, plasma treatment. The finding can also be extended to the quiet solar corona, provided that the currently undetected nanoflares are frequent enough to account for the lower (compared to active regions) energy losses in this case.

Evolution of the Sun's activity and the poleward transport of remnant magnetic flux in Cycles 21--24

Alexander V. **Mordvinov**, Bidya Binay Karak, Dipankar Banerjee, Elena M. Golubeva, Anna I. Khlystova, Anastasiya V. Zhukova, Pawan Kumar

MNRAS Volume 510, Issue 1, February **2022**, Pages 1331–1339,
https://doi.org/10.1093/mnras/stab3528
https://arxiv.org/pdf/2111.15585

Detailed study of the solar magnetic field is crucial to understand its generation, transport and reversals. The timing of the reversals may have implications on space weather and thus identification of the temporal behavior of the critical surges that lead to the polar field reversals is important. We analyze the evolution of solar activity and magnetic flux transport in Cycles 21--24. We identify critical surges of remnant flux that reach the Sun's poles and lead to the polar field reversals. We reexamine the polar field buildup and reversals in their causal relation to the Sun's low-latitude activity. We further identify the major remnant flux surges and their sources in the time-latitude aspect. We find that special characteristics of individual 11-year cycles are generally determined by the spatiotemporal organization of emergent magnetic flux and its unusual properties. We find a complicated restructuring of high-latitude magnetic fields in Cycle~21. The global rearrangements of solar magnetic fields were caused by surges of trailing and leading polarities that occurred near the activity maximum. The decay of non-Joy and anti-Hale active regions resulted in the remnant flux surges that disturbed the usual order in magnetic flux transport. We finally show that the leading-polarity surges during cycle minima sometimes link the following cycle and a collective effect of these surges may lead to secular changes in solar activity. The magnetic field from a Babcock--Leighton dynamo model generally agrees with these observations.

Long-Term Evolution of the Sun's magnetic field during Cycles 15--19 based on their proxies from Kodaikanal Solar Observatory

Alexander V. **Mordvinov**, Bidya Binay Karak, Dipankar Banerjee, Subhamoy Chatterjee, Elena M. Golubeva, Anna I. Khlystova

ApJL **902** L15 **2020**
https://arxiv.org/pdf/2009.11174.pdf
https://doi.org/10.3847/2041-8213/abba80

The regular observation of the solar magnetic field is available only for about last five cycles. Thus, to understand the origin of the variation of the solar magnetic field, it is essential to reconstruct the magnetic field for the past cycles, utilizing other datasets. Long-term uniform observations for the past 100 years as recorded at the Kodaikanal Solar Observatory (KoSO) provide such opportunity. We develop a method for the reconstruction of the solar magnetic field using the synoptic observations of the Sun's emission in the Ca II K and Hα lines from KoSO for the first time. The reconstruction method is based on the facts that the Ca II K intensity correlates well with the unsigned magnetic flux, while the sign of the flux is derived from the corresponding Hα map which provides the information of the dominant polarities. Based on this reconstructed magnetic map, we study the evolution of the magnetic field in Cycles 15--19. We also study bipolar magnetic regions (BMRs) and their remnant flux surges in their causal relation. Time-latitude analysis of the reconstructed magnetic flux provides an overall view of magnetic field evolution: emergent magnetic flux, its further transformations with the formation of unipolar magnetic regions (UMRs) and remnant flux surges. We identify the reversals of the polar field and critical surges of following and leading polarities. We found that the poleward transport of opposite polarities led to multiple changes of the dominant magnetic polarities in poles. Furthermore, the remnant flux surges that occur between adjacent 11-year cycles reveal physical connections between them.

Evolution of the Sun's Polar-fields and the Poleward Transport of Remnant Magnetic Flux

A. V. **Mordvinov**, L. L. Kitchatinov
Solar Phys. 294:21 **2019**
https://arxiv.org/pdf/1902.00199.pdf
https://link.springer.com/content/pdf/10.1007%2Fs11207-019-1410-1.pdf
Synoptic magnetograms and relevant proxy data were analyzed to study the evolution of the Sun's polar magnetic fields. Time-latitude analysis of large-scale magnetic fields demonstrates cyclic changes in their zonal structure and the polar-field buildup. The time-latitude distributions of the emergent and remnant magnetic flux enable us to examine individual features of recent cycles. The poleward transport of predominantly following polarities contributed much of the polar flux and led to polar-field reversals. Multiple reversals of dominant polarities at the Sun's poles were identified in Cycles 20 and 21. Three-fold reversals were caused by remnant flux surges of following and leading polarities. Time-latitude analysis of solar magnetic fields in Cycles 20--24 revealed zones which are characterized by a predominance of negative (non-Joy's) tilts and appearance of active regions which violate Hale's polarity law. The decay of non-Joy's and anti-Hale's active regions result in remnant flux surges which disturb the usual order in magnetic flux transport and sometimes lead to multiple reversals of polar fields. The analysis of local and large-scale magnetic fields in their causal relation improved our understanding of the Sun's polar field weakening.

The reversal of the Sun's magnetic field in cycle 24

Alexander V. **Mordvinov**, Alexei A. Pevtsov, Luca Bertello, Gordon J.D. Petrie
JASTP **2016**
http://arxiv.org/pdf/1602.02460v1.pdf
Analysis of synoptic data from the Vector Stokes Magnetograph (VSM) of the Synoptic Optical Long-term Investigations of the Sun (SOLIS) and the NASA/NSO Spectromagnetograph (SPM) at the NSO/Kitt Peak Vacuum Telescope facility shows that the reversals of solar polar magnetic fields exhibit elements of a stochastic process, which may include the development of specific patterns of emerging magnetic flux, and the asymmetry in activity between northern and southern hemispheres. The presence of such irregularities makes the modeling and prediction of polar field reversals extremely hard if possible. In a classical model of solar activity cycle, the unipolar magnetic regions (UMRs) of predominantly following polarity fields are transported polewards due to meridional flows and diffusion. The UMRs gradually cancel out the polar magnetic field of the previous cycle, and re-build the polar field of opposite polarity setting the stage for the next cycle. We show, however, that this deterministic picture can be easily altered by the developing of a strong center of activity, or by the emergence of an extremely large active region, or by a "strategically placed" coronal hole. We demonstrate that the activity occurring during the current cycle 24 may be the result of this randomness in the evolution of the solar surface magnetic field. **2010/07/20-30**

Evolution of sunspot activity and inversion of the Sun’s polar magnetic field in the current cycle

A.V. **Mordvinov**, , , V.M. Grigoryev, , D.V. Erofeev,
Advances in Space Research, Volume 55, Issue 11, 1 June **2015**, Pages 2739–2743
A spatiotemporal analysis of the Sun’s magnetic field was carried out to study the polar-field inversion in the current cycle in relation to sunspot activity. The causal relationship between these phenomena was demonstrated in a time-latitude aspect. After decay of long-lived activity complexes their magnetic fields were redistributed into the surrounding photosphere and formed unipolar magnetic regions which were transported to high latitudes. Zones of intense sunspot activity during 2011/2012 produced unipolar magnetic regions of the following polarities, whose poleward drift led to the inversion of the Sun’s polar fields at the North and South Poles. At the North Pole the polar field reversal was completed by May 2013. It was demonstrated that mixed magnetic polarities near the North Pole resulted from violations of Joy’s law at lower latitudes. Later sunspot activity in the southern hemisphere has led to a delay in magnetic polarity reversal at the South Pole. Thus, the north–south asymmetry of sunspot activity resulted in asynchronous polar field reversal in the current cycle.

Reversals of the Sun's polar magnetic fields in relation to activity complexes and coronal holes

A.V. **Mordvinov** and S.A. Yazev
E-print, Dec **2013**; Solar Physics, June **2014**, Volume 289, Issue 6, pp 1971-1981
A spatiotemporal analysis of long-term measurements of the Sun?s magnetic field was carried out to study changes in its zonal structure and reversals of the polar fields in Cycles 21 ? 24. A causal relationship between activity

complexes, their remnant magnetic fields, and high-latitude magnetic fields has been demonstrated in the current cycle. The appearance of unipolar magnetic regions near the poles is largely determined by the decay of preceding long-lived activity complexes. The nonuniform distribution of sunspot activity and its north?south asymmetry result in the asymmetry of remnant fields that are transported poleward due to meridional circulation. The asymmetry of high-latitude magnetic fields leads to an asynchrony of polar-field reversals in both hemispheres. The interaction of highlatitude unipolar magnetic regions with the polar fields affects the embedded coronal holes. The evolution of large-scale magnetic fields was also studied in a time?latitude aspect. It is shown that regular reversals of the Sun?s polar fields resulted from cyclic changes in highlatitude magnetic fields. A triple polarity reversal of the polar fields in Cycle 21 and shortterm polarity alternations at the poles were interpreted taking into account the interaction of the remnant fields with the Sun?s polar fields.

Observations and mode identification of sausage waves in a magnetic pore⋆

M. G. **Moreels**1, N. Freij2, R. Erdélyi2, T. Van Doorsselaere1 and G. Verth
A&A 579, A73 (**2015**)
Aims. We aim to determine the phase speed of an oscillation in a magnetic pore using only intensity images at one height. The observations were obtained using the CRisp Imaging SpectroPolarimeter at the Swedisch 1-m Solar Telescope and show variations in both cross-sectional area and intensity in a magnetic pore.
Methods. We have designed and tested an observational method to extract the wave parameters that are important for seismology. We modelled the magnetic pore as a straight cylinder with a uniform plasma both inside and outside the flux tube and identify different wave modes. Using analytic expressions, we are able to distinguish between fast and slow modes and obtain the phase speed of the oscillations.
Results. We found that the observed oscillations are slow modes with a phase speed around 5 km s-1. We also have strong evidence that the oscillations are standing harmonics.

An Improved Method for Estimating the Velocity Field of Coronal Propagating Disturbances

Huw **Morgan** & Marianna B. Korsós
Solar Physics volume 297, Article number: 102 (**2022**)
https://link.springer.com/content/pdf/10.1007/s11207-022-02033-1.pdf
The solar corona is host to a continuous flow of propagating disturbances (PD). These are continuous and ubiquitous across broad regions of the corona, including the quiet Sun. The aim of this article is to present an improved, efficient method to create velocity vector field maps based on the direction and magnitude of the PD as observed in time series of extreme ultraviolet (EUV) images. The method presented here is for use with the Atmospheric Imaging Assembly (AIA)/Solar Dynamics Observatory (SDO) EUV channels and takes as input ≈2≈2 hours of images at the highest 12 s cadence. Data from a region near disc centre is extracted, and a process called time normalisation is applied to the co-aligned data. Following noise reduction using à trous decomposition, the PD are effectively revealed. A modified Lucas–Kanade algorithm is then used to map the velocity field. The method described here runs comfortably on a desktop computer in a few minutes and offers an order of magnitude improvement in efficiency compared to a previous implementation. As applied to a region of the quiet Sun, we find that the velocity field describes a mosaic of cells of coherent outwardly-diverging PD flows of typical size 50 to 100″100″ (36 to 72 Mm). The flows originate from points and narrow corridors in the cell centres and end in the narrow boundaries between cells. Visual comparison with ultraviolet AIA images shows that the flow sources are correlated with the bright photospheric supergranular network boundaries. Assuming that the PD follow the local magnetic field, the velocity flow field is a proxy for the plane-of-sky distribution of the coronal magnetic field, and therefore the maps offer a unique insight into the topology of the corona. These are particularly valuable for quiet Sun regions where the appearance of structures in EUV images is hard to interpret. **6 November 2019**

Tracing the magnetic field topology of the quiet corona using propagating disturbances

Huw **Morgan**, Marianna Korsos
ApJ **2022**
https://arxiv.org/pdf/2206.11077.pdf
The motion of faint propagating disturbances (PD) in the solar corona reveals an intricate structure which must be defined by the magnetic field. Applied to quiet Sun observations by the Atmospheric Imaging Assembly (AIA)/Solar Dynamics Observatory (SDO), a novel method reveals a cellular network, with cells of typical diameters 50\arcsec\ in the cool 304Å channel, and 100\arcsec\ in the coronal 193Å channel. The 193Å cells can overlie several 304Å\ cells, although both channels share common source and sink regions. The sources are points, or narrow corridors, of divergence that occupy the centres of cells. They are significantly aligned with photospheric network features and enhanced magnetic elements. This shows that the bright network is important to the production of PDs, and confirms that the network is host to the source footpoint of quiet coronal loops. The other footpoint, or the sinks of the PDs, form the boundaries of the coronal cells. These are not significantly aligned with the photospheric network - they are generally situated above the dark internetwork photosphere. They form compact

points or corridors, often without an obvious signature in the underlying photosphere. We argue that these sink points can either be concentrations of closed field footpoints associated with minor magnetic elements in the internetwork, or concentrations of upward-aligned open field. The link between the coronal velocity and magnetic fields is strengthened by a comparison with a magnetic extrapolation, which shows several general and specific similarities, thus the velocity maps offer a valuable additional constraint on models. **2018 October 27**

SITES: Solar Iterative Temperature Emission Solver for differential emission measure inversion of EUV observations

Huw **Morgan**, James Pickering
Solar Phys. 294:135 **2019**
https://arxiv.org/pdf/1908.07773.pdf
https://link.springer.com/content/pdf/10.1007%2Fs11207-019-1525-4.pdf
Extreme UltraViolet (EUV) images of the optically-thin solar corona in multiple spectral channels give information on the emission as a function of temperature through differential emission measure (DEM) inversions. The aim of this paper is to describe, test, and apply a new DEM method named the Solar Iterative Temperature Emission Solver (SITES). The method creates an initial DEM estimate through a direct redistribution of observed intensities across temperatures according to the temperature response function of the measurement, and iteratively improves on this estimate through calculation of intensity residuals. It is simple in concept and implementation, is non-subjective in the sense that no prior constraints are placed on the solutions other than positivity and smoothness, and can process a thousand DEMs per second on a standard desktop computer. The resulting DEMs replicate model DEMs well in tests on Atmospheric Imaging Assembly (AIA) synthetic data. The same tests show that SITES performs less well on very narrow DEM peaks, and should not be used for temperature diagnostics below ~0.5MK in the case of AIA observations. The SITES accuracy of inversion compares well with two other established methods. A simple yet powerful new method to visualise DEM maps is introduced, based on a fractional emission measure (FEM). Applied to a set of AIA full-disk images, the SITES method and FEM visualisation show very effectively the dominance of certain temperature regimes in different large-scale coronal structures. The method can easily be adapted for any multi-channel observations of optically-thin plasma and, given its simplicity and efficiency, will facilitate the processing of large existing and future datasets.

An Atlas of Coronal Electron Density at 5R ⊙. II. A Spherical Harmonic Method for Density Reconstruction

Huw **Morgan**
2019 ApJS 242 3
https://iopscience.iop.org/article/10.3847/1538-4365/ab125d/pdf
This is the second of a series of three papers that present a methodology with the aim of creating a set of maps of the coronal density over a period of many years. This paper describes a method for reconstructing the coronal electron density based on spherical harmonics. By assuming a radial structure to the corona at the height of interest, line-of-sight integrations can be made individually on each harmonic basis prior to determining coefficients, i.e., the computationally expensive integrations are calculated only once during initialization. This approach reduces the problem to finding the set of coefficients that best match the observed brightness using a regularized least-squares approach and is very efficient. The method is demonstrated on synthetic data created from both a simple and an intricate coronal density model. The quality of reconstruction is found to be reasonable in the presence of noise and large gaps in the data. The method is applied to both Large Angle and Spectrometric Coronagraph Experiment C2 and SolarTerrestrial Relations Observatory Cor2 coronagraph observations from 2009 March 20, and the results from both spacecraft compared. Future work will apply the method to large data sets.

Ubiquitous and Continuous Propagating Disturbances in the Solar Corona

Huw **Morgan** and Joseph Hutton
2018 ApJ 853 145
http://sci-hub.tw/http://iopscience.iop.org/0004-637X/853/2/145/
A new processing method applied to Atmospheric Imaging Assembly/Solar Dynamic Observatoryobservations reveals continuous propagating faint motions throughout the corona. The amplitudes are small, typically 2% of the background intensity. An hour's data are processed from four AIA channels for a region near disk center, and the motions are characterized using an optical flow method. The motions trace the underlying large-scale magnetic field. The motion vector field describes large-scale coherent regions that tend to converge at narrow corridors. Large-scale vortices can also be seen. The hotter channels have larger-scale regions of coherent motion compared to the cooler channels, interpreted as the typical length of magnetic loops at different heights. Regions of low mean and high time variance in velocity are where the dominant motion component is along the line of sight as a result of a largely vertical magnetic field. The mean apparent magnitude of the optical velocities are a few tens of km s−1, with different distributions in different channels. Over time, the velocities vary smoothly between a few km s−1 to 100 km s−1 or higher, varying on timescales of minutes. A clear bias of a few km s−1 toward positive x-velocities is due

to solar rotation and may be used as calibration in future work. All regions of the low corona thus experience a continuous stream of propagating disturbances at the limit of both spatial resolution and signal level. The method provides a powerful new diagnostic tool for tracing the magnetic field, and to probe motions at sub-pixel scales, with important implications for models of heating and of the magnetic field. **2015-03-21**

AN ATLAS OF CORONAL ELECTRON DENSITY AT 5R⊙. I. DATA PROCESSING AND CALIBRATION

Huw **Morgan**
2015 ApJS 219 23
https://iopscience.iop.org/article/10.1088/0067-0049/219/2/23/pdf
Tomography of the solar corona can provide cruicial constraints for models of the low corona, unique information on changes in coronal structure and rotation rates, and a valuable boundary condition for models of the heliospheric solar wind. This is the first of a series of three papers which aim to create a set of maps of the coronal density over an extended period (1996-present). The papers will describe the data processing and calibration (this paper), the tomography method (Paper II), and the resulting atlas of coronal electron density at a height of 5 R⊙ between years 1996–2014 (Paper III). This first paper presents a detailed description of data processing and calibration for the Large-Angle and Spectrometric Coronagraph (LASCO) C2 instrument on board the Solar and Heliospheric Observatory (SOHO) and the COR2 instruments of the Sun Earth Connection Coronal and Heliospheric Investigation (SECCHI) package on board the Solar Terrestial Relations Observatory (STEREO) A and B spacecraft. The methodology includes noise suppression, background subtraction, separation of large dynamic events, conversion of total brightness to K-coronal brightness, and simple functions for cross-calibration between C2/LASCO and COR2/SECCHI. Comparison of the brightness of stars between LASCO C2 total and polarized brightness (pB) observations provide in-flight calibration factors for the pBobservations, resulting in considerable improved agreement between C2 and COR2 A, and elimination of curious artifacts in the C2 pB images. The cross-calibration between LASCO C2 and the STEREO coronagraphs allows, for the first time, the potential use of multi-spacecraft coronagraph data for tomography and for coronal mass ejection analysis.

Multi-Scale Gaussian Normalization for Solar Image Processing

Huw **Morgan**, Miloslav Druckmüller
Solar Physics, August **2014**, Volume 289, Issue 8, pp 2945-2955,
Extreme ultra-violet images of the corona contain information over a wide range of spatial scales, and different structures such as active regions, quiet Sun, and filament channels contain information at very different brightness regimes. Processing of these images is important to reveal information, often hidden within the data, without introducing artefacts or bias. It is also important that any process be computationally efficient, particularly given the fine spatial and temporal resolution of Atmospheric Imaging Assembly on the Solar Dynamics Observatory (AIA/SDO), and consideration of future higher resolution observations. A very efficient process is described here, which is based on localised normalising of the data at many different spatial scales. The method reveals information at the finest scales whilst maintaining enough of the larger-scale information to provide context. It also intrinsically flattens noisy regions and can reveal structure in off-limb regions out to the edge of the field of view. We also applied the method successfully to a white-light coronagraph observation.

Spatio-temporal analysis of chromospheric heating in a plage region

R. **Morosin**, J. de la Cruz Rodríguez, C.J. Díaz Baso, J. Leenaarts
A&A 664, A8 **2022**
https://arxiv.org/pdf/2203.01688.pdf
https://www.aanda.org/articles/aa/pdf/2022/08/aa43461-22.pdf
Our knowledge of the heating mechanisms that are at work in the chromosphere of plage regions remains highly unconstrained from observational studies. The purpose of our study is to estimate the chromospheric heating terms from a plage dataset, characterize their spatio-temporal distribution and set constraints on the heating processes that are at work. We make use of NLTE inversions to infer a model of the photosphere and chromosphere of a plage dataset acquired with the Swedish 1-m Solar Telescope. We use this model atmosphere to calculate the chromospheric radiative losses from H i, Ca ii and Mg ii atoms. We approximate the chromospheric heating terms by the net radiative losses predicted by the inverted model. In order to make the analysis of time-series over a large field-of-view computationally tractable, we make use of a neural network. In the lower chromosphere, the contribution from the Ca ii lines is dominant and located in the surroundings of the photospheric footpoints. In the upper chromosphere, the H i contribution is dominant. Radiative losses in the upper chromosphere form an homogeneous patch that covers the plage region. The net radiative losses can be split in a periodic component with an average amplitude of ampQ = 7.6 kW m^{-2} and a static (or very slowly evolving) component with a mean value of -26.1 kW m^{-2}. Our interpretation is that in the lower chromosphere, the radiative losses are tracing the sharp lower edge of the hot magnetic canopy, where the electric current is expected to be large. In the upper chromosphere, both the magnetic field and the distribution of net radiative losses are room-filling, whereas the

amplitude of the periodic component is largest. Our results suggest that acoustic wave heating may be responsible for one third of the energy deposition in the upper chromosphere, whereas other heating mechanisms must be responsible for the rest. **14 Sep 2016**

Stratification of canopy magnetic fields in a plage region. Constraints from a spatially-coupled weak-field approximation method

R. **Morosin**, J. de la Cruz Rodriguez, G. J. M. Vissers, R. Yadav
A&A 642, A210 **2020**
https://arxiv.org/pdf/2006.14487.pdf
https://doi.org/10.1051/0004-6361/202038754
https://sci-hub.st/https://www.aanda.org/articles/aa/abs/2020/10/aa38754-20/aa38754-20.html
The role of magnetic fields in the chromospheric heating problem remains greatly unconstrained. Most theoretical predictions from numerical models rely on a magnetic configuration, field strength and connectivity whose details have not been well established with observational studies. High-resolution studies of chromospheric magnetic fields in plage are very scarce or non-existent in general. Our aim is to study the stratification of the magnetic field vector in plage regions. We use high-spatial resolution full-Stokes observations acquired with CRISP instrument at the Swedish 1-m Solar Telescope in the Mg I λ5173, Na I λ5896 and Ca II λ8542 lines. We have developed a spatially-constrained weak-field approximation (WFA) method based on the idea of spatial regularization. This method allows for a fast computation of magnetic field maps for an extended field of view. The fidelity of this new technique has been assessed using a snapshot from a realistic 3D magnetohydrodynamics simulation. We have derived the depth-stratification of the line-of-sight component of the magnetic field from the photosphere to the chromosphere in a plage region. The magnetic fields are concentrated in the intergranular lanes in the photosphere and expand horizontally toward the chromosphere, filling all the space and forming a canopy. Our results suggest that the lower boundary of this canopy must be located around 400-600 km from the photosphere. The mean canopy total magnetic field strength in the lower chromosphere ($z\approx760$ km) is 658 G. At $z=1160$ km we estimate $\langle B_\parallel \rangle \approx 417$ G. We propose a modification to the WFA that improves its applicability to data with worse signal-to-noise ratio. These methods provide a quick and reliable way of studying multi-layer magnetic field observations without the many difficulties inherent to other inversion methods.

Comparison of Solar UV Spectral Irradiance from SUSIM and SORCE

J. S. **Morrill**, L. Floyd, D. McMullin
Solar Phys., 2014, Volume 289, Issue 10, pp 3641-3661, **2014**
Knowledge of solar spectral irradiance (SSI) is important in determining the impact of solar variability on climate. Observations of UV SSI have been made by the Solar Ultraviolet Spectral Irradiance Monitor (SUSIM) on the Upper Atmosphere Research Satellite (UARS), the Solar-Stellar Irradiance Comparison Experiment (SOLSTICE), and the Solar Irradiance Monitor (SIM), both on the Solar Radiation and Climate Experiment (SORCE) satellite. Measurements by SUSIM and SORCE overlapped from 2003 to 2005.
SUSIM and SORCE observations represent ~ 20 years of absolute UV SSI. Unfortunately, significant differences exist between these two data sets. In particular, changes in SORCE UV SSI measurements, gathered at moderate and minimum solar activity, are a factor of two greater than the changes in SUSIM observations over the entire solar cycle. In addition, SORCE UV SSI have a substantially different relationship with the Mg ii index than did earlier UV SSI observations. Acceptance of these new SORCE results impose significant changes on our understanding of UV SSI variation. Alternatively, these differences in UV SSI observations indicate that some or all of these instruments have changes in instrument responsivity that are not fully accounted for by the current calibration.
In this study, we compare UV SSI changes from SUSIM with those from SIM and SOLSTICE. The primary results are that (1) long-term observations by SUSIM and SORCE generally do not agree during the overlap period (2003 – 2005), (2) SUSIM observations during this overlap period are consistent with an SSI model based on Mg ii and early SUSIM SSI, and (3) when comparing the spectral irradiance for times of similar solar activity on either side of solar minimum, SUSIM observations show slight differences while the SORCE observations show variations that increase with time between spectra. Based on this work, we conclude that the instrument responsivity for SOLSTICE and SIM need to be reevaluated before these results can be used for climate-modeling studies.

The Solar Benchmark: Rotational Modulation of the Sun Reconstructed from Archival Sunspot Records

Brett M. **Morris**, James R.A. Davenport, Helen A.C. Giles, Leslie Hebb, Suzanne L. Hawley, Ruth Angus, Peter A. Gilman, Eric Agol
MNRAS Volume 484, Issue 3, Pages 3244–3250 **2019**
https://arxiv.org/pdf/1901.04557.pdf
http://sci-hub.tw/10.1093/mnras/stz199
We use archival daily spot coverage measurements from Howard et al. (1984) to study the rotational modulation of the Sun as though it were a distant star. A quasi-periodic Gaussian process measures the solar rotation

period Prot=26.3±0.1 days, and activity cycle period Pcyc=10.7±0.3 years. We attempt to search for evidence of differential rotation in variations of the apparent rotation period throughout the activity cycle and do not detect a clear signal of differential rotation, consistent with the null results of the hare-and-hounds exercise of Aigrain et al. (2015). The full reconstructed solar light curve is available online.

Alfvénic waves in the inhomogeneous solar atmosphere **Review**

R. J. **Morton**, R. Sharma, E. Tajfirouzhe, H. Miriyala

Journal of Modern Plasma Physics **2022**

https://arxiv.org/pdf/2208.05222

The solar atmosphere is known to be replete with magneto-hydrodynamic wave modes, and there has been significant investment in understanding how these waves propagate through the Sun's atmopshere and deposit their energy into the plasma. The waves' journey is made interesting by the vertical variation in plasma quantities that define the solar atmosphere. In addition to this large-scale inhomogeneity, a wealth of fine-scale structure through the chromosphere and corona has been brought to light by high-resolution observations over the last couple of decades. This fine-scale sturcture represents inhomogeneity that is thought to be perpendicular to the local magnetic fields. The implications of this form of inhomogeneity on wave propagation is still being uncovered, but is known to fundamentally change the nature of MHD wave modes. It also enables interesting physics to arise including resonances, turbulence and instabilities. Here we review some of the key insights into how the inhomogeneity influences Alfvénic wave propagation through the Sun's atmosphere, discussing both inhomogeneities parallel and perpendicular to the magnetic field.

Weak damping of propagating MHD kink waves in the quiescent corona

Richard J. **Morton**, Ajay K. Tiwari, Tom Van Doorsselaere, James A. McLaughlin

ApJ **923** 225 **2021**

https://arxiv.org/pdf/2105.11924.pdf

https://iopscience.iop.org/article/10.3847/1538-4357/ac324d/pdf

https://doi.org/10.3847/1538-4357/ac324d

Propagating transverse waves are thought to be a key transporter of Poynting flux throughout the Sun's atmosphere. Recent studies have shown that these transverse motions, interpreted as the propagating magnetohydrodynamic kink mode, are prevalent throughout the corona. The associated energy estimates suggest the waves carry enough energy to meet the demands of the coronal radiative losses in the quiescent Sun. However, it is still unclear how the waves deposit their energy into the coronal plasma. We present the results from a large-scale study of propagating kink waves in the quiescent corona using data from the Coronal Multi-channel Polarimeter (CoMP). The analysis reveals that the kink waves appear to be weakly damped, which would imply low rates of energy transfer from the large-scale transverse motions to smaller-scales via either uni-turbulence or resonant absorption. This raises questions about how the observed kink modes would deposit their energy into the coronal plasma. Moreover, these observations, combined with the results of Monte Carlo simulations, lead us to infer that the solar corona displays a spectrum of density ratios, with a smaller density ratio (relative to the ambient corona) in quiescent coronal loops and a higher density ratio in active region coronal loops.

Transverse motions in sunspot super-penumbral fibrils

R. J. **Morton**, K. Mooroogen, V. M. J. Henriques

Special Issue of the Philosophical Transactions of the Royal Society A **2020**

https://arxiv.org/pdf/2012.07394.pdf

Sunspots have played a key role in aiding our understanding of magnetohydrodynamic (MHD) wave phenomenon in the Sun's atmosphere, and it is well known they demonstrate a number of wave phenomenon associated with slow MHD modes. Recent studies have shown that transverse wave modes are present throughout the majority of the chromosphere. Using high-resolution Ca II 8542 Å observations from the Swedish Solar Telescope, we provide the first demonstration that the chromospheric super-penumbral fibrils, which span out from the sunspot, also show ubiquitous transverse motions. We interpret these motions as transverse waves, in particular the MHD kink mode. We compile the statistical properties of over 2000 transverse motions to find distributions for periods and amplitudes, finding they are broadly consistent with previous observations of chromospheric transverse waves in quiet Sun fibrils. The very presence of the waves in super-penumbral fibrils raises important questions about how they are generated, and could have implications for our understanding of how MHD wave energy is transferred through the atmosphere of a sunspot. **28 July 2014**

A basal contribution from p-modes to the Alfvénic wave flux in the Sun's corona

R. J. **Morton**, M. Weberg, J. A. McLaughlin

Nature Astronomy **3, 223** **2019**

https://arxiv.org/ftp/arxiv/papers/1902/1902.03811.pdf

Many cool stars possess complex magnetic fields [1] that are considered to undertake a central role in the structuring and energising of their atmospheres [2]. Alfvénic waves are thought to make a critical contribution to energy transfer along these magnetic fields, with the potential to heat plasma and accelerate stellar winds [3] [4] [5]. Despite Alfvénic waves having been identified in the Sun's atmosphere, the nature of the basal wave energy flux is poorly understood. It is generally assumed that the associated Poynting flux is generated solely in the photosphere and propagates into the corona, typically through the continuous buffeting of magnetic fields by turbulent convective cells [4] [6] [7]. Here we provide evidence that the Sun's internal acoustic modes also contribute to the basal flux of Alfvénic waves, delivering a spatially ubiquitous input to the coronal energy balance that is sustained over the solar cycle. Alfvénic waves are thus a fundamental feature of the Sun's corona. Acknowledging that internal acoustic modes have a key role in injecting additional Poynting flux into the upper atmospheres of Sun-like stars has potentially significant consequences for the modelling of stellar coronae and winds.
UKSP Nugget: #102 July **2019**
http://www.uksolphys.org/uksp-nugget/102-do-p-modes-power-the-corona-of-cool-stars/

Probing the corona through infrared observations

Richard **Morton**
UKSP Nugget #75 **2017**
http://www.uksolphys.org/uksp-nugget/75-probing-the-corona-through-infrared-observations/
More recently, the Coronal Multi-channel Polarimeter (CoMP) has extended our range, providing spectroscopic imaging in the infrared (Fe XIII 10747 Å) and some of its first results uncovered a potentially key component for understanding the dynamics of the corona.
https://www2.hao.ucar.edu/mlso/instruments/mlso-comp-polarimeter

Exploring Coronal Dynamics: A Next Generation Solar Physics Mission white paper

R. J. **Morton**, E. Scullion, D. S. Bloomfield, J. A. McLaughlin, S. Regnier, S. W. McIntosh, S. Tomczyk, P. Young
2016
https://arxiv.org/pdf/1611.06149v1.pdf
Determining the mechanisms responsible for the heating of the coronal plasma and maintaining and accelerating the solar wind are long standing goals in solar physics. There is a clear need to constrain the energy, mass and momentum flux through the solar corona and advance our knowledge of the physical process contributing to these fluxes. Furthermore, the accurate forecasting of Space Weather conditions at the near-Earth environment and, more generally, the plasma conditions of the solar wind throughout the heliosphere, require detailed knowledge of these fluxes in the near-Sun corona. Here we present a short case for a space-based imaging-spectrometer coronagraph, which will have the ability to provide synoptic information on the coronal environment and provide strict constraints on the mass, energy, and momentum flux through the corona. The instrument would ideally achieve cadences of ~10~s, spatial resolution of 1" and observe the corona out to 2~$R_{\sun}$. Such an instrument will enable significant progress in our understanding of MHD waves throughout complex plasmas, as well as potentially providing routine data products to aid Space Weather forecasting.

A global view of velocity fluctuations in the corona below 1.3 R⊙with CoMP

R. J. **Morton**, S. Tomczyk, R. F. Pinto
ApJ 828 89 **2016**
http://arxiv.org/pdf/1608.01831v1.pdf
The Coronal Multi-channel Polarimeter (CoMP) has previously demonstrated the presence of Doppler velocity fluctuations in the solar corona. The observed fluctuations are thought to be transverse waves, i.e. highly incompressible motions whose restoring force is dominated by the magnetic tension, some of which demonstrate clear periodicity. We aim to exploit CoMP's ability to provide high cadence observations of the off-limb corona to investigate the properties of velocity fluctuations in a range of coronal features, providing insight into how(if) the properties of the waves are influenced by the varying magnetic topology in active regions, quiet Sun and open fields regions. An analysis of Doppler velocity time-series of the solar corona from the 10,747~{\AA} Iron XIII line is performed, determining the velocity power spectra and using it as a tool to probe wave behaviour. Further, the average phase speed and density for each region are estimated and used to compute the spectra for energy density and energy flux. In addition, we assess the noise levels associated with the CoMP data, deriving analytic formulae for the uncertainty on Doppler velocity measurements and providing a comparison by estimating the noise from the data. It is found that the entire corona is replete with transverse wave behaviour. The corresponding power spectra indicates that the observed velocity fluctuations are predominately generated by stochastic processes, with the

spectral slope of the power varying between the different magnetic regions. Most strikingly, all power spectra reveal the presence of enhanced power occurring at ~3~mHz, potentially implying that the excitation of coronal transverse waves by p-modes is a global phenomenon. **27 March 2012**

Model fitting of kink waves in the solar atmosphere: Gaussian damping and time-dependence

R. J. **Morton**, K. Mooroogen
A&A 593, A59 **2016**
http://arxiv.org/pdf/1607.05905v1.pdf
{Observations of the solar atmosphere have shown that magnetohydrodynamic waves are ubiquitous throughout. Improvements in instrumentation and the techniques used for measurement of the waves now enables subtleties of competing theoretical models to be compared with the observed waves behaviour. Some studies have already begun to undertake this process. However, the techniques employed for model comparison have generally been unsuitable and can lead to erroneous conclusions about the best model. The aim here is to introduce some robust statistical techniques for model comparison to the solar waves community, drawing on the experiences from other areas of astrophysics. In the process, we also aim to investigate the physics of coronal loop oscillations. } {The methodology exploits least-squares fitting to compare models to observational data. We demonstrate that the residuals between the model and observations contain significant information about the ability for the model to describe the observations, and show how they can be assessed using various statistical tests. In particular we discuss the Kolmogorov-Smirnoff one and two sample tests, as well as the runs test. We also highlight the importance of including any observational trend line in the model-fitting process.} {To demonstrate the methodology, an observation of an oscillating coronal loop undergoing standing kink motion is used. The model comparison techniques provide evidence that a Gaussian damping profile provides a better description of the observed wave attenuation than the often used exponential profile. This supports previous analysis from Pascoe et al. (2016). Further, we use the model comparison to provide evidence of time-dependent wave properties of a kink oscillation, attributing the behaviour to the thermodynamic evolution of the local plasma.}

Investigating Alfvénic wave propagation in coronal open-field regions

R. J. **Morton**, S. Tomczyk & R. Pinto
Nature Communications 6, Article number: 7813 **2015**
http://www.nature.com/ncomms/2015/150727/ncomms8813/full/ncomms8813.html
The physical mechanisms behind accelerating solar and stellar winds are a long-standing astrophysical mystery, although recent breakthroughs have come from models invoking the turbulent dissipation of Alfvén waves. The existence of Alfvén waves far from the Sun has been known since the 1970s, and recently the presence of ubiquitous Alfvénic waves throughout the solar atmosphere has been confirmed. However, the presence of atmospheric Alfvénic waves does not, alone, provide sufficient support for wave-based models; the existence of counter-propagating Alfvénic waves is crucial for the development of turbulence. Here, we demonstrate that counter-propagating Alfvénic waves exist in open coronal magnetic fields and reveal key observational insights into the details of their generation, reflection in the upper atmosphere and outward propagation into the solar wind. The results enhance our knowledge of Alfvénic wave propagation in the solar atmosphere, providing support and constraints for some of the recent Alfvén wave turbulence models.

Coupled MHD -- Hybrid Simulations of Space Plasmas

S. P. **Moschou**, I. V. Sokolov, O. Cohen, G. Toth, J. J. Drake, Z. Huang, C. Garraffo, J. D. Alvarado-Gómez, T. Gombosi
ASTRONUM 2019 - the 14th International Conference on Numerical Modeling of Space Plasma Flows at Paris, France, 1-5 July, **2019**.
https://arxiv.org/pdf/1911.08660.pdf
Heliospheric plasmas require multi-scale and multi-physics considerations. On one hand, MHD codes are widely used for global simulations of the solar-terrestrial environments, but do not provide the most elaborate physical description of space plasmas. Hybrid codes, on the other hand, capture important physical processes, such as electric currents and effects of finite Larmor radius, but they can be used locally only, since the limitations in available computational resources do not allow for their use throughout a global computational domain. In the present work, we present a new coupled scheme which allows to switch blocks in the block-adaptive grids from fluid MHD to hybrid simulations, without modifying the self-consistent computation of the electromagnetic fields acting on fluids (in MHD simulation) or charged ion macroparticles (in hybrid simulation). In this way, the hybrid scheme can refine the description in specified regions of interest without compromising the efficiency of the global MHD code.

Simulating coronal condensation dynamics in 3D

S.P. **Moschou**a, b, , , R. Keppensb, C. Xiab, X. Fang

Advances in Space Research Volume 56, Issue 12, 15 December **2015**, Pages 2738–2759

http://www.sciencedirect.com/science/article/pii/S0273117715003336

We present numerical simulations in 3D settings where coronal rain phenomena take place in a magnetic configuration of a quadrupolar arcade system. Our simulation is a magnetohydrodynamic simulation including anisotropic thermal conduction, optically thin radiative losses, and parametrised heating as main thermodynamical features to construct a realistic arcade configuration from chromospheric to coronal heights. The plasma evaporation from chromospheric and transition region heights eventually causes localised runaway condensation events and we witness the formation of plasma blobs due to thermal instability, that evolve dynamically in the heated arcade part and move gradually downwards due to interchange type dynamics. Unlike earlier 2.5D simulations, in this case there is no large scale prominence formation observed, but a continuous coronal rain develops which shows clear indications of Rayleigh–Taylor or interchange instability, that causes the denser plasma located above the transition region to fall down, as the system moves towards a more stable state. Linear stability analysis is used in the non-linear regime for gaining insight and giving a prediction of the system's evolution. After the plasma blobs descend through interchange, they follow the magnetic field topology more closely in the lower coronal regions, where they are guided by the magnetic dips.

Parity fluctuations in stellar dynamos

D. L. **Moss**, D.D. Sokoloff

2017

https://arxiv.org/pdf/1705.08853.pdf

Observations of the solar butterfly diagram from sunspot records suggest persistent fluctuation in parity, away from the overall, approximately dipolar structure. We use a simple mean-field dynamo model with a solar-like rotation law, and perturb the α-effect. We find that the parity of the magnetic field with respect to the rotational equator can demonstrate what we describe as resonant behaviour, while the magnetic energy behaves in a more or less expected way. We discuss possible applications of the phenomena in the context of various deviations of the solar magnetic field from dipolar symmetry, as reported from analysis of archival sunspot data. We deduce that our model produces fluctuations in field parity, and hence in the butterfly diagram, that are consistent with observed fluctaions in solar behaviour.

Prediction of the in situ coronal mass ejection rate for solar cycle 25: Implications for Parker Solar Probe in situ observations

Christian **Möstl**, Andreas J. Weiss, Rachel L. Bailey, Martin A. Reiss, Ute V. Amerstorfer, Tanja Amerstorfer, Jürgen Hinterreiter, Maike Bauer, Scott W. McIntosh, Noé Lugaz, David Stansby

ApJ **903** 92 **2020**

arxiv.org/pdf/2007.14743.pdf

https://iopscience.iop.org/article/10.3847/1538-4357/abb9a1/pdf

The Parker Solar Probe (PSP) and Solar Orbiter missions are designed to make groundbreaking observations of the Sun and interplanetary space within this decade. We show that a particularly interesting in situ observation of an interplanetary coronal mass ejection (ICME) by PSP may arise during close solar flybys (<0.1 AU). During these times, the same magnetic flux rope inside an ICME could be observed in situ by PSP twice, by impacting its frontal part as well as its leg. Investigating the odds of this situation, we forecast the ICME rate in solar cycle 25 based on 2 models for the sunspot number (SSN): (1) the consensus prediction of an expert panel in 2019 (maximum SSN = 115), and (2) a prediction by McIntosh et al. (2020, maximum SSN = 232). We link the SSN to the observed ICME rates in solar cycles 23 and 24 with the Richardson and Cane list and our own ICME catalog with a linear fit. We calculate that between 2 and 7 ICMEs will be observed by PSP at heliocentric distances <0.1 AU until 2025, including 1σ uncertainties. We then model the potential flux rope signatures of such a double-crossing event with the semi-empirical 3DCORE flux rope model, showing a telltale elevation of the radial magnetic field component BR and a sign reversal in the component BN normal to the solar equator, which is in contrast to the classic field rotation in the first encounter. This holds considerable promise to determine the structure of CMEs close to their origin in the solar corona.

Eleven-year, 22-year and ~90-year solar cycles discovered in nitrate concentrations in a Dome Fuji (Antarctica) ice core

Yuko **Motizuki**, Yoichi Nakai, Kazuya Takahashi, Takashi Imamura, Hideaki Motoyama

Proceedings of the Japan Academy, Series B **2022**

https://arxiv.org/pdf/2209.11330.pdf

Ice cores are known to yield information about astronomical phenomena as well as information about past climate. We report time series analyses of annually resolved nitrate variations in an ice core, drilled at the Dome Fuji station

in East Antarctica, corresponding to the period from CE 1610 to 1904. Our analyses revealed clear evidence of ~11, ~22, and ~90 year periodicities, comparable to the respective periodicities of the well-known Schwabe, Hale, and Gleissberg solar cycles. Our results show for the first time that nitrate concentrations in an ice core can be used as a proxy for past solar activity on decadal to multidecadal time scales. Furthermore, 11-year and 22-year periodicities were detected in nitrate variations even during the Maunder Minimum (1645-1715), when sunspots were almost absent. This discovery may support cyclic behavior of the solar dynamo during the grand solar minimum.

An Analysis of Solar Global Activity

Zadig **Mouradian**

Solar Physics, February **2013**, Volume 282, Issue 2, pp 553-564

This article proposes a unified observational model of solar activity based on sunspot number and the solar global activity in the rotation of the structures, both per 11-year cycle. The rotation rates show a variation of a half-century period and the same period is also associated to the sunspot amplitude variation. The global solar rotation interweaves with the observed global organisation of solar activity. An important role for this assembly is played by the Grand Cycle formed by the merging of five sunspot cycles: a forgotten discovery by R. Wolf. On the basis of these elements, the nature of the Dalton Minimum, the Maunder Minimum, the Gleissberg Cycle, and the Grand Minima are presented.

Empirical Constructs and Cartoons

Forrest **Mozer**.

RHESSI Nuggets, No. 222, **2014**

http://sprg.ssl.berkeley.edu/~tohban/wiki/index.php/Empirical_Constructs_and_Cartoons

How our mental images may relate to what's really going on.

A Sunspot from Cycle 25 for sure

Tomek **Mrozek** & Hugh Hudson

RHESSI Science Nuggets #321 **2018**

http://sprg.ssl.berkeley.edu/~tohban/wiki/index.php/A_Sunspot_from_Cycle_25_for_sure

Study of Dynamo Action in Three Dimensional Magnetohydrodynamic Plasma with Arnold-Beltrami-Childress Flow

Rupak **Mukherjee**, Rajaraman Ganesh

2019

https://arxiv.org/pdf/1901.09610.pdf

For a three dimensional magnetohydrodynamic (MHD) plasma the dynamo action with ABC flow as initial condition has been studied. The study delineates crucial parameter that gives a transition from coherent nonlinear oscillation to dynamo. Further, for both kinematic and dynamic models at magnetic Prandtl number equal to unity the dynamo action is studied for driven ABC flows. The magnetic resistivity has been chosen at a value where the fast dynamo occurs and the growth rate shows no further variation with the change of magnetic Reynold's number. The exponent of growth of magnetic energy increases, indicating a faster dynamo, if a higher wave number is excited compared to the one with a lower wave number. The result has been found to hold good for both kinematic and externally forced dynamic dynamos where the backreaction of magnetic field on the velocity field is no more negligible. In case of an externally forced dynamic dynamo, the super Alfvenic flows have been found to excite strong dynamos giving rise to the growth of magnetic energy of seven orders of magnitude. The back-reaction of magnetic field on the velocity field through Lorentz force term has been found to affect the dynamics of the velocity field and in turn the dynamics of magnetic field, leading to a saturation, when the dynamo action is very prominent.

The Solar Orbiter SPICE instrument - An extreme UV imaging spectrometer

Daniel **Mueller**, The SPICE Consortium

A&A **2019**

https://sci-hub.se/https://doi.org/10.1051/0004-6361/201935574

The Spectral Imaging of the Coronal Environment (SPICE) instrument is a high-resolution imaging spectrometer operating at extreme ultraviolet (EUV) wavelengths. In this paper, we present the concept, design, and pre-launch performance of this facility instrument on the ESA/NASA Solar Orbiter mission. The goal of this paper is to give prospective users a better understanding of the possible types of observations, the data acquisition, and the sources that contribute to the instrument's signal. The paper discusses the science objectives, with a focus on the SPICE-specific aspects, before presenting the instrument's design, including optical, mechanical, thermal, and electronics aspects. This is followed by a characterisation and calibration of the instrument's performance. The paper concludes with descriptions of the operations concept and data processing. The performance measurements of the various

instrument parameters meet the requirements derived from the mission's science objectives. The SPICE instrument is ready to perform measurements that will provide vital contributions to the scientific success of the Solar Orbiter mission.

JHelioviewer - Time-dependent 3D visualisation of solar and heliospheric data

D. **Mueller**, B. Nicula, S. Felix, F. Verstringe, B. Bourgoignie, A. Csillaghy, D. Berghmans, P. Jiggens, J. P. Garcia-Ortiz, J. Ireland, S. Zahniy, B. Fleck

A&A **2017 File**

https://arxiv.org/pdf/1705.07628.pdf

Context. Solar observatories are providing the world-wide community with a wealth of data, covering large time ranges, multiple viewpoints, and returning large amounts of data. In particular, the large volume of SDO data presents challenges: it is available only from a few repositories, and full-disk, full-cadence data for reasonable durations of scientific interest are difficult to download practically due to their size and download data rates available to most users. From a scientist's perspective this poses three problems: accessing, browsing and finding interesting data as efficiently as possible.
Aims. To address these challenges, we have developed JHelioviewer, a visualisation tool for solar data based on the JPEG2000 compression standard and part of the open source ESA/NASA Helioviewer Project. Since the first release of JHelioviewer, the scientific functionality of the software has been extended significantly, and the objective of this paper is to highlight these improvements.
Methods. The JPEG2000 standard offers useful new features that facilitate the dissemination and analysis of high-resolution image data and offers a solution to the challenge of efficiently browsing petabyte-scale image archives. The JHelioviewer software is open source, platform independent and extendable via a plug-in architecture.
Results. With JHelioviewer, users can visualise the Sun for any time period between September 1991 and today. They can perform basic image processing in real time, track features on the Sun and interactively overlay magnetic field extrapolations. The software integrates solar event data and a time line display. As a first step towards supporting science planning of the upcoming Solar Orbiter mission, JHelioviewer offers a virtual camera model that enables users to set the vantage point to the location of a spacecraft or celestial body at any given time.

Solar Orbiter: Exploring the Sun-heliosphere connection A Review

D. **Mueller**, R.G. Marsden, O.C. StCyr, H.R. Gilbert for the Solar Orbiter Team

E-print, July **2012**, **File**; Solar Phys. July **2013**, Volume 285, Issue 1-2, pp 25-70

The heliosphere represents a uniquely accessible domain of space, where fundamental physical processes common to solar, astrophysical and laboratory plasmas can be studied under conditions impossible to reproduce on Earth and unfeasible to observe from astronomical distances. Solar Orbiter, the first mission of ESA's Cosmic Vision 2015-2025 programme, will address the central question of heliophysics: How does the Sun create and control the heliosphere? In this paper, we present the scientific goals of the mission and provide an overview of the mission implementation.

The Solar Orbiter mission -- Science overview Review

D. **Müller**, O.C. St. Cyr, I. Zouganelis, H.R. Gilbert, R. Marsden, T. Nieves-Chinchilla, E. Antonucci, F. Auchère, D. Berghmans, T. Horbury, R.A. Howard, S. Krucker, M. Maksimovic, C.J. Owen, P. Rochus, J. Rodriguez-Pacheco, M. Romoli, S.K. Solanki, R. Bruno, M.Carlsson, A. Fludra, L. Harra, D.M. Hassler, S. Livi, P. Louarn, H. Peter, U. Schühle, L. Teriaca, J.C. del Toro Iniesta, R.F. Wimmer-Schweingruber, E. Marsch, M. Velli, A. De Groof, A. Walsh, D. Williams

A&A 642, A1 **2020**

https://arxiv.org/pdf/2009.00861.pdf **File**

https://www.aanda.org/articles/aa/pdf/2020/10/aa38467-20.pdf

Solar Orbiter, the first mission of ESA's Cosmic Vision 2015-2025 programme and a mission of international collaboration between ESA and NASA, will explore the Sun and heliosphere from close up and out of the ecliptic plane. It was launched on 10 February 2020 04:03 UTC from Cape Canaveral and aims to address key questions of solar and heliospheric physics pertaining to how the Sun creates and controls the Heliosphere, and why solar activity changes with time. To answer these, the mission carries six remote-sensing instruments to observe the Sun and the solar corona, and four in-situ instruments to measure the solar wind, energetic particles, and electromagnetic fields. In this paper, we describe the science objectives of the mission, and how these will be addressed by the joint observations of the instruments onboard. The paper first summarises the mission-level science objectives, followed by an overview of the spacecraft and payload. We report the observables and performance figures of each instrument, as well as the trajectory design. This is followed by a summary of the science operations concept. The paper concludes with a more detailed description of the science objectives. Solar Orbiter will combine in-situ measurements in the heliosphere with high-resolution remote-sensing observations of the Sun to address

fundamental questions of solar and heliospheric physics. The performance of the Solar Orbiter payload meets the requirements derived from the mission's science objectives. Its science return will be augmented further by coordinated observations with other space missions and ground-based observatories.

Does the solar granulation change with the activity cycle?

R. **Muller**1, A. Hanslmeier2, D. Utz2 and K. Ichimoto3
A&A 616, A87 (**2018**)
https://www.aanda.org/articles/aa/pdf/2018/08/aa32085-17.pdf
Context. Knowledge of the variation of the solar granulation properties (contrast and scale) with the 11-yr activity cycle is useful for a better understanding of the interaction between magnetic field and convection at global or local scales. A varying granulation may also contribute to irradiance variations and affect the p-mode damping rates and lifetimes.
Aims. HINODE/SOT blue continuum images taken in the frame of the synoptic program at the disk center on a daily basis between November 2006 and February 2016 are used. This period covers the minimum of activity between cycles 23 and 24 and the maximum of cycle 24.
Methods. The sharpness of a significant number of images was reduced because of instrumental aberrations or inaccurate focusing. Only the sharpest images were selected for this investigation.
Results. To be detectable with HINODE/SOT images, the variation of the granulation contrast and of the granulation scale at the disk center should have been larger than 3%. As it is not the case, it is concluded that they varied by less than 3% through the weak cycle 24.

Latitude dependence of the solar granulation during the minimum of activity in 2009

R. **Muller**1, A. Hanslmeier2 and D. Utz
A&A 598, A6 (**2017**)
Context. Knowledge of the latitude variation of the solar granulation properties (contrast and scale) is useful to better understand interactions between magnetic field, convection, differential rotation, and meridional circulation in the solar atmosphere.
Aims. We investigated the latitude dependence of the contrast and scale of the solar granulation, with the help of HINODE/SOT blue continuum images taken in the frame of the HOP 79 program, along the central meridian and along the equator on a monthly basis in 2009 during the last solar minimum of activity.
Methods. We selected the sharpest images in latitude and longitude intervals. The selected images in all the N-S and E-W scans taken in 2009 were combined to get statistically reliable results.
Results. The contrast of the solar granulation decreases towards the poles and the scale increases, but not regularly since a perturbation occurs at around 60° where both quantities return close to their values at the disk center.
Conclusions. Such a latitude variation in a period of minimum of activity (2009), is probably not due to magnetic field, neither the quiet magnetic field at the surface, nor the strong magnetic flux tubes associated with active regions, which could be embedded more or less deeply in the convection zone before they reach the surface. The decrease in contrast and increase in scale towards the pole seem to be related to the differential rotation and the perturbation around 60° to the meridional circulation.

Solar Orbiter: **Exploring the Sun–Heliosphere Connection**

Müller, D., Marsden, R. G., St. Cyr, O. C., & Gilbert, H. R.
2013, Sol. Phys., 285, 25-70
https://link.springer.com/content/pdf/10.1007%2Fs11207-012-0085-7.pdf
The heliosphere represents a uniquely accessible domain of space, where fundamental physical processes common to solar, astrophysical and laboratory plasmas can be studied under conditions impossible to reproduce on Earth and unfeasible to observe from astronomical distances. Solar Orbiter, the first mission of ESA's Cosmic Vision 2015 – 2025 programme, will address the central question of heliophysics: How does the Sun create and control the heliosphere? In this paper, we present the scientific goals of the mission and provide an overview of the mission implementation.

Solar Physics with SunPy

Stuart **Mumford** and Andrew Leonard
UKSP Nuggets of **2016** #67
http://www.uksolphys.org/uksp-nugget/67-solar-physics-with-sunpy/

SunPy - Python for Solar Physics

The SunPy Community, S. J. **Mumford**; S. Christe; D. P?rez-Su?rez; J. Ireland; A. Y. Shih; A. R. Inglis; S. Liedtke; R. J. Hewett; F. Mayer; K. Hughitt; N. Freij; T. Meszaros; S. M. Bennett; M. Malocha; J. Evans; A. Agrawal; A. J. Leonard; T. P. Robitaille; B. Mampaey; J. Iv?n Campos-Rozo; M. S. Kirk
Computational Science & Discovery, **2015**
http://arxiv.org/pdf/1505.02563v1.pdf
This paper presents SunPy (version 0.5), a community-developed Python package for solar physics. Python, a free, cross-platform, general-purpose, high-level programming language, has seen widespread adoption among the scientific community, resulting in the availability of a large number of software packages, from numerical computation (NumPy, SciPy) and machine learning (scikit-learn) to visualisation and plotting (matplotlib). SunPy is a data-analysis environment specialising in providing the software necessary to analyse solar and heliospheric data in Python. SunPy is open-source software (BSD licence) and has an open and transparent development workflow that anyone can contribute to. SunPy provides access to solar data through integration with the Virtual Solar Observatory (VSO), the Heliophysics Event Knowledgebase (HEK), and the HELiophysics Integrated Observatory (HELIO) webservices. It currently supports image data from major solar missions (e.g., SDO, SOHO, STEREO, and IRIS), time-series data from missions such as GOES, SDO/EVE, and PROBA2/LYRA, and radio spectra from e-Callisto and STEREO/SWAVES. We describe SunPy's functionality, provide examples of solar data analysis in SunPy, and show how Python-based solar data-analysis can leverage the many existing tools already available in Python. We discuss the future goals of the project and encourage interested users to become involved in the planning and development of SunPy.

Generation of Magnetohydrodynamic Waves in Low Solar Atmospheric Flux Tubes by Photospheric Motions

S. J. **Mumford**1, V. Fedun1,2, and R. Erdélyi
2015 ApJ 799 6
Recent ground- and space-based observations reveal the presence of small-scale motions between convection cells in the solar photosphere. In these regions, small-scale magnetic flux tubes are generated via the interaction of granulation motion and the background magnetic field. This paper studies the effects of these motions on magnetohydrodynamic (MHD) wave excitation from broadband photospheric drivers. Numerical experiments of linear MHD wave propagation in a magnetic flux tube embedded in a realistic gravitationally stratified solar atmosphere between the photosphere and the low choromosphere (above $\beta = 1$) are performed. Horizontal and vertical velocity field drivers mimic granular buffeting and solar global oscillations. A uniform torsional driver as well as Archimedean and logarithmic spiral drivers mimic observed torsional motions in the solar photosphere. The results are analyzed using a novel method for extracting the parallel, perpendicular, and azimuthal components of the perturbations, which caters to both the linear and non-linear cases. Employing this method yields the identification of the wave modes excited in the numerical simulations and enables a comparison of excited modes via velocity perturbations and wave energy flux. The wave energy flux distribution is calculated to enable the quantification of the relative strengths of excited modes. The torsional drivers primarily excite Alfvén modes ($\approx$60% of the total flux) with small contributions from the slow kink mode, and, for the logarithmic spiral driver, small amounts of slow sausage mode. The horizontal and vertical drivers primarily excite slow kink or fast sausage modes, respectively, with small variations dependent upon flux surface radius.

Photospheric Logarithmic Velocity Spirals as MHD Wave Generation Mechanisms

S. J. **Mumford**, R. Erdélyi
2015 Mon. Not. R. Astron. Soc.
http://arxiv.org/pdf/1501.01871v1.pdf
High-resolution observations of the solar photosphere have identified a wide variety of spiralling motions in the plasma. These spirals vary in properties, but are observed to be abundant on the solar surface. In this work these spirals are studied for their potential as magnetohydrodynamic (MHD) wave generation mechanisms. The inter-granular lanes, where these spirals are commonly observed, are also regions where the magnetic field strength is higher than average. This combination of magnetic field and spiralling plasma is a recipe for the generation of Alfv\'en waves and other MHD waves.
This work employs numerical simulations of a self-similar magnetic flux tube embedded in a realistic, gravitationally stratified, solar atmosphere to study the effects of a single magnetic flux tube perturbed by a logarithmic velocity spiral driver. The expansion factor of the logarithmic spiral driver is varied, multiple simulations are run for a range of values of the expansion factor centred around observational data.
The simulations are analysed using `flux surfaces' constructed from the magnetic field lines so that the vectors perpendicular, parallel and azimuthal to the local magnetic field vector can be calculated. The results of this analysis show that the Alfv\'en wave is the dominant wave for lower values of the expansion factor, whereas, for the higher values the parallel component is dominant. This transition occurs within the range of the observational constraints,

meaning that spiral drivers, as observed in the solar photosphere, have the potential to generate a variety of MHD wave modes.

Solar Anti-Hale Bipolar Magnetic Regions: A Distinct Population with Systematic Properties

Andrés **Muñoz-Jaramillo**1, Benjamín Navarrete2, and Luis E. Campusano2
2021 ApJ 920 31
https://doi.org/10.3847/1538-4357/ac133b
Besides their causal connection with long and short-term magnetic variability, solar bipolar magnetic regions are our chief source of insight into the location, size, and properties of large-scale toroidal magnetic structures in the solar interior. The great majority of these regions (≈95%) follow a systematic east–west polarity orientation (Hale's law) that reverses in opposite hemispheres and across even and odd cycles. These regions also present a systematic north–south polarity orientation (Joy's law) that helps build the poloidal field that seeds the new cycle. Exceptions to Hale's law are rare and difficult to study due to their low numbers. Here, we present a statistical analysis of the inclination (tilt) with respect to the equator of Hale versus anti-Hale regions spanning four solar cycles, considering two complementary tilt definitions adopted in previous studies. Our results show that anti-Hale regions belong to a separate population than Hale regions, suggesting a different originating mechanism. However, we find that anti-Hale region tilts present similar systematic tilt properties and similar latitudinal distributions to Hale regions, implying a strong connection between the two. We see this as evidence that they belong to a common toroidal flux system. We speculate that anti-Hale regions originate from poloidal field sheared and strengthened on the spot after the emergence of Hale regions with very strong poloidal contribution. Thus, they are not in contradiction with the idea of largely coherent toroidal flux systems inside the solar interior.

The Minimum of Solar Cycle 23: As Deep as It Could Be?

Andrés **Muñoz-Jaramillo**1,2,3, Ryan R. Senkpeil4, Dana W. Longcope1, Andrey G. Tlatov5, Alexei A. Pevtsov6, Laura A. Balmaceda7,8, Edward E. DeLuca9, and Petrus C. H. Martens
ApJ 804 68 **2015**.
http://arxiv.org/pdf/1508.01222v1.pdf
In this work we introduce a new way of binning sunspot group data with the purpose of better understanding the impact of the solar cycle on sunspot properties and how this defined the characteristics of the extended minimum of cycle 23. Our approach assumes that the statistical properties of sunspots are completely determined by the strength of the underlying large-scale field and have no additional time dependencies. We use the amplitude of the cycle at any given moment (something we refer to as activity level) as a proxy for the strength of this deep-seated magnetic field. We find that the sunspot size distribution is composed of two populations: one population of groups and active regions and a second population of pores and ephemeral regions. When fits are performed at periods of different activity level, only the statistical properties of the former population, the active regions, are found to vary. Finally, we study the relative contribution of each component (small-scale versus large-scale) to solar magnetism. We find that when hemispheres are treated separately, almost every one of the past 12 solar minima reaches a point where the main contribution to magnetism comes from the small-scale component. However, due to asymmetries in cycle phase, this state is very rarely reached by both hemispheres at the same time. From this we infer that even though each hemisphere did reach the magnetic baseline, from a heliospheric point of view the minimum of cycle 23 was not as deep as it could have been.

The Photospheric Size-Flux Distribution and its Relationship with the Small-Scale and Global Components of the Solar Dynamo

Andrés **Muñoz-Jaramillo**
HMI Science Nuggets 31, **2014**.
http://hmi.stanford.edu/hminuggets/?p=1016
Taking advantage of 11 different databases, we use statistical analysis to probe the nature of photospheric magnetic structures. We find evidence of two separate mechanisms at play, and propose that they are directly connected to the global and small-scale components of the solar dynamo.

SOLAR CYCLE PROPAGATION, MEMORY, AND PREDICTION: INSIGHTS FROM A CENTURY OF MAGNETIC PROXIES

Andrés **Muñoz-Jaramillo**1,2,3, María Dasi-Espuig4, Laura A. Balmaceda5, and Edward E. DeLuca
2013 ApJ 767 L25
The solar cycle and its associated magnetic activity are the main drivers behind changes in the interplanetary environment and Earth's upper atmosphere (commonly referred to as space weather). These changes have a direct impact on the lifetime of space-based assets and can create hazards to astronauts in space. In recent years there has

been an effort to develop accurate solar cycle predictions (with aims at predicting the long-term evolution of space weather), leading to nearly a hundred widely spread predictions for the amplitude of solar cycle 24. A major contributor to the disagreement is the lack of direct long-term databases covering different components of the solar magnetic field (toroidal versus poloidal). Here, we use sunspot area and polar faculae measurements spanning a full century (as our toroidal and poloidal field proxies) to study solar cycle propagation, memory, and prediction. Our results substantiate predictions based on the polar magnetic fields, whereas we find sunspot area to be uncorrelated with cycle amplitude unless multiplied by area-weighted average tilt. This suggests that the joint assimilation of tilt and sunspot area is a better choice (with aims to cycle prediction) than sunspot area alone, and adds to the evidence in favor of active region emergence and decay as the main mechanism of poloidal field generation (i.e., the Babcock-Leighton mechanism). Finally, by looking at the correlation between our poloidal and toroidal proxies across multiple cycles, we find solar cycle memory to be limited to only one cycle.

Observation of Alfvén Wave Reflection in the Solar Chromosphere: Ponderomotive Force and First Ionization Potential Effect

Mariarita **Murabito**, Marco Stangalini, J. Martin Laming, Deborah Baker, Andy S. H. To, David M. Long, David H. Brooks, Shahin Jafarzadeh, David B. Jess, Gherardo Valori

Physical review Letters; **2024**

https://arxiv.org/pdf/2404.08305

We investigate the propagation of Alfvén waves in the solar chromosphere, distinguishing between upward and downward propagating waves. We find clear evidence for the reflection of waves in the chromosphere and differences in propagation between cases with waves interpreted to be resonant or nonresonant with the overlying coronal structures. This establishes the wave connection to coronal element abundance anomalies through the action of the wave ponderomotive force on the chromospheric plasma, which interacts with chromospheric ions but not neutrals, thereby providing a novel mechanism of ion-neutral separation. This is seen as a "First Ionization Potential Effect" when this plasma is lifted into the corona, with implications elsewhere on the Sun for the origin of the slow speed solar wind and its elemental composition.

Investigating the origin of magnetic perturbations associated with the FIP Effect⋆

M. **Murabito**, M. Stangalini, D. Baker, G. Valori, D. B. Jess, S. Jafarzadeh, D. H. Brooks, I. Ermolli, F. Giorgi, S. D. T. Grant, D. M. Long, L. van Driel-Gesztelyi

A&A 656, A87 **2021**

https://arxiv.org/pdf/2108.11164.pdf

https://www.aanda.org/articles/aa/pdf/2021/12/aa41504-21.pdf

https://doi.org/10.1051/0004-6361/202141504

In \citet{Stangalini20} and \citet{Deb20}, magnetic oscillations were detected in the chromosphere of a large sunspot and found to be linked to the coronal locations where a First Ionization Potential (FIP) effect was observed. In an attempt to shed light onto the possible excitation mechanisms of these localized waves, we further investigate the same data by focussing on the relation between the spatial distribution of the magnetic wave power and the overall field geometry and plasma parameters obtained from multi-height spectropolarimetric non-local thermodynamic equilibrium (NLTE) inversions of IBIS data. We find that, in correspondence with the locations where the magnetic wave energy is observed at chromospheric heights, the magnetic fields have smaller scale heights, meaning faster expansions of the field lines, which ultimately results in stronger vertical density stratification and wave steepening. In addition, the acoustic spectrum of the oscillations at the locations where magnetic perturbations are observed is broader than that observed at other locations, which suggests an additional forcing driver to the p-modes. Analysis of the photospheric oscillations in the sunspot surroundings also reveals a broader spectrum in between the two opposite polarities of the active region (the leading spot and the trailing opposite polarity plage), and on the same side where magnetic perturbations are observed in the umbra. We suggest that strong photospheric perturbations in between the two polarities are responsible for this broader spectrum of oscillations, with respect to the p-mode spectrum, resulting in locally-excited acoustic waves that, after crossing the equipartition layer, located close to the umbra-penumbra boundary at photopheric heights, are converted into magnetic-like waves and steepen due to the strong density gradient.

Unveiling the magnetic nature of chromospheric vortices

Mariarita **Murabito**, Juie Shetye, Marco Stangalini, Erwin Verwichte, Tony Arber, Ilaria Ermolli, Fabrizio Giorgi, Tom Goffrey

A&A 639, A59 **2020**

https://arxiv.org/pdf/2006.13776.pdf

https://www.aanda.org/articles/aa/pdf/2020/07/aa38360-20.pdf

Vortex structures in the Sun's chromosphere are believed to channel energy between different layers of the solar atmosphere. We investigate the nature and dynamics of two small-scale quiet-Sun rotating structures in the

chromosphere. We analyse two chromospheric structures that show clear rotational patterns in spectropolarimetric observations taken with the Interferometric Bidimensional Spectrometer (IBIS) at the Ca II 8542 Å~ line. We present the detection of spectropolarimetric signals that manifest the magnetic nature of rotating structures in the chromosphere. Our observations show two long-lived structures of plasma that each rotate clockwise inside a 10 arcsec2~ quiet-Sun region. Their circular polarization signals are 5-10 times above the noise level. Line-of-sight Doppler velocity and horizontal velocity maps from the observations reveal clear plasma flows at and around the two structures. An MHD simulation shows these two structures are plausibly magnetically connected. Wave analysis suggests that the observed rotational vortex pattern could be due to a combination of slow actual rotation and a faster azimuthal phase speed pattern of a magneto-acoustic mode. Our results imply that the vortex structures observed in the Sun's chromosphere are magnetic in nature and that they can be connected locally through the chromosphere. **May 1, 2015**
European Solar Physics Nugget #4 Dec **2021** https://est-east.eu/nuggets/46-espn/1116-espn-4-first-detection-of-the-magnetic-field-in-solar-vortices

Formation of the penumbra and start of the Evershed flow

M. **Murabito**, P. Romano, S. L. Guglielmino, F. Zuccarello, S.K. Solanki
ApJ **2016**
http://arxiv.org/pdf/1604.05610v1.pdf
We studied the variations of line-of-sight photospheric plasma flows during the formation phase of the penumbra around a pore in Active Region NOAA 11490. We used a high spatial, spectral, and temporal resolution data set acquired by the Interferometric BIdimensional Spectrometer (IBIS) operating at the NSO/Dunn Solar Telescope as well as data taken by the Helioseismic and Magnetic Imager onboard the Solar Dynamics Observatory satellite (SDO/HMI). Before the penumbra formed we observed a redshift of the spectral line in the inner part of the annular zone surrounding the pore as well as a blueshift of material associated with opposite magnetic polarity further away from the pore. We found that the onset of the classical Evershed flow occurs in a very short time scale -- 1-3 hours -- while the penumbra is forming. During the same time interval we found changes in the magnetic field inclination in the penumbra, with the vertical field actually changing sign near the penumbral edge, while the total magnetic field showed a significant increase, about 400 G. To explain these and other observations related to the formation of the penumbra and the onset of the Evershed flow we propose a scenario in which the penumbra is formed by magnetic flux dragged down from the canopy surrounding the initial pore. The Evershed flow starts when the sinking magnetic field dips below the solar surface and magnetoconvection sets in. **2012May 28-29**

Application of Coupled Harmonic Oscillator model to Solar Activity and El Niño Phenomena

Yasushi **Muraki**
Proceeding of the 35th ICRC at Busan **2017**
https://arxiv.org/ftp/arxiv/papers/1706/1706.09105.pdf
The solar activity provides an important impact not only on the intensity of cosmic rays but also on the earth environment. In this paper, a coupled oscillator model is proposed to explain the solar activity. By this model the 89 year Gleissberg cycle can be naturally reduced. Furthermore as an application of the coupled oscillator model we try to apply it to the El Nino-La Nina phenomena (ENSO). The 26 year oscillation of the Pacific Ocean is naturally explained. Finally we search a possible substance of the coupled oscillators in actual solar activities.

Connection Between Solar Hemispheric Toroidal Cycles and Geomagnetic Variations

Judit **Muraközy**
Solar Physics April **2019**, 294:46
sci-hub.se/10.1007/s11207-019-1438-2
The solar activity has hemispheric asymmetries. The levels of activity are different on the two hemispheres on intermediate and longer time scales. During four Schwabe cycles the progress of the northern hemispheric activity precedes the southern one, while in the next four cycles the southern cycle takes over the preceding role (Muraközy and Ludmány, Mon. Not. Roy. Astron. Soc.419, 3624, 2012; Muraközy, Astrophys. J.826, 145, 2016). The interplanetary magnetic field is formed by the distribution of the solar magnetic fields and the outward-streaming solar wind. The present study intends to show how the solar-hemispheric predominance affects the interplanetary and geophysical magnetic field. The interplanetary and geophysical data sets have been chosen from various sources such as the components of the interplanetary magnetic field [BB], cosmic-ray data, Ap, aa, and Dst geomagnetic indices, while the solar-hemispheric asymmetry has been examined by using sunspot data from Greenwich Photoheliographic Results (GPR) and Debrecen Photoheliographic Data (DPD).

Phase relationships of solar hemispheric toroidal and poloidal cycles

Judit **Muraközy**

2016 *ApJ* **826** 145
http://arxiv.org/pdf/1605.08230v1.pdf
The solar northern and southern hemispheres exhibit differences between the intensities and time profiles of the activity cycles. The time variation of these properties has been studied in a previous article on the data of Cycles 12-23. The hemispheric phase lags exhibited a characteristic variation: the leading role has been exchanged between the hemispheres by four cycles. The present work extends the investigation of this variation with the data of Schwabe and Staudacher in Cycles 1-4 and 7-10 as well as Sp\"orer's data in cycle 11. The previously found variation can not be clearly recognized using the data of Staudacher, Schwabe and Sp\"orer. However, it is more interesting that the phase lags of the reversals of the magnetic fields at the poles follow the same variation as that of the hemispheric cycles in Cycles 12-23, i.e. in four cyles one of the hemispheres leads and the leading role jumps to the opposite hemisphere in the next four cycles. This means that this variation is a long term property of the entire solar dynamo mechanism, both the toroidal and poloidal fields, that hints at an unidentified component of the process responsible for the long term memory.

An alternative measure of solar activity from detailed sunspot datasets

Muraközy, J.; Baranyi, T.; Ludmány, A.
Solar Phys. **2016**
http://arxiv.org/pdf/1603.05870v1.pdf
The sunspot number is analyzed by using detailed sunspot data, including aspects of observability, sunspot sizes, and proper identification of sunspot groups as discrete entities of the solar activity. The tests show that besides the subjective factors there are also objective causes of the ambiguities in the series of sunspot numbers. To introduce an alternative activity measure the physical meaning of the sunspot number has to be reconsidered. It contains two components whose numbers are governed by different physical mechanisms, this is one source of the ambiguity. This article suggests an activity index, which is the amount of emerged magnetic flux. The only long-term proxy measure is the detailed sunspot area dataset with proper calibration to the magnetic flux amount. The Debrecen sunspot databases provide an appropriate source for the establishment of the suggested activity index.

Phase lags of solar hemispheric cycles

J. **Murakozy**, A. Ludmany
E-print, Sept **2013**, MNRAS (**2012**) Vol. 419 3624-3630
The North-South asymmetry of solar activity is variable in time and strength. We analyse the long-term variation of the phase lags of hemispheric cycles and check a conjectured relationship between these phase lags and the hemispheric cycle strengths. Sunspot data are used from cycles 12-23 in which the separation of northern and southern hemispheres is possible. The centers of mass of the hemispheric cycle profiles were used to study the phase relations and relative strengths of the hemispheric cycles. This approach considers a cycle as a whole and disregards the short-term fluctuations of the cycle time profile. The phase of the hemispheric cycles shows an alternating variation: the northern cycle leads in 4 cycles and follows in 4 cycles. No significant relationship is found between the phase and strength differences of the hemispheric cycles. The period of 4+4 cycles appears to be close to the Gleissberg cycle and may provide a key to its physical background. It may raise a new aspect in the solar dynamo mechanism because it needs a very long memory.

Exploring possibilities for solar irradiance prediction from solar photosphere images using recurrent neural networks

Amita **Muralikrishna**, Rafael Duarte Coelho dos Santos and Luis Eduardo Antunes Vieira
J. Space Weather Space Clim. **2022**, 12, 19
https://www.swsc-journal.org/articles/swsc/pdf/2022/01/swsc210045.pdf
Studies of the Sun and the Earth's atmosphere and climate consider solar variability as an important driver, and its constant monitoring is essential for climate models. Solar total and spectral irradiance are among the main relevant parameters. Physical semi-empirical and empirical models have been developed and made available, and they are crucial for the reconstruction of irradiance during periods of data failure or their absence. However, ionospheric and climate models would also benefit from solar irradiance prediction through prior knowledge of irradiance values hours or days ahead. This paper presents a neural network-based approach, which uses images of the solar photosphere to extract sunspot and active region information and thus generate inputs for recurrent neural networks to perform the irradiance prediction. Experiments were performed with two recurrent neural network architectures for short- and long-term predictions of total and spectral solar irradiance at three wavelengths. The results show good quality of prediction for total solar irradiance (TSI) and motivate further effort in improving the prediction of each type of irradiance considered in this work. The results obtained for spectral solar irradiance (SSI) point out that photosphere images do not have the same influence on the prediction of all wavelengths tested but encourage the bet on new spectral lines prediction.

Detecting Asymmetric Dark Matter in the Sun with Neutrinos

Kohta **Murase**, Ian M. Shoemaker
2016
http://arxiv.org/pdf/1606.03087v1.pdf
Dark Matter (DM) may have a relic density that is in part determined by a particle/antiparticle asymmetry, much like baryons. If this is the case, it can accumulate in stars like the Sun to sizable number densities and annihilate to Standard Model (SM) particles including neutrinos. We show that the combination of neutrino telescope and direct detection data can be used in conjunction to determine or constrain the DM asymmetry from data. Depending on the DM mass, the current neutrino data from Super-K and IceCube give powerful constraints on asymmetric DM unless its fractional asymmetry is $\lesssim 10^{-2}$. Future neutrino telescopes and detectors like Hyper-K and KM3NeT can search for the resulting signal of high-energy neutrinos from the center of the Sun. The observation of such a flux yields information on both the DM-nucleus cross section but also on the relative abundances of DM and anti-DM.

Two-fluid numerical model of chromospheric heating and plasma outflows in a quiet-Sun

K. **Murawski**, Z.E. Musielak, S. Poedts, A.K. Srivastava, L.H.S. Kadowaki
Nature **2022**
https://arxiv.org/pdf/2211.12289.pdf
\textbf{Purpose:} This paper addresses long-standing solar physics problems, namely, the heating of the solar chromosphere and the origin of the solar wind. Our aim is to reveal the related mechanisms behind chromospheric heating and plasma outflows in a quiet-Sun. \textbf{Methods:} The approach is based on a two-fluid numerical model that accounts for thermal non-equilibrium (ionization/recombination), non-adiabatic, and non-ideal dynamics of protons+electrons and hydrogen atoms. The model is applied to numerically simulate the propagation and dissipation of granulation-generated waves in the chromosphere and plasma flows inside a quiet region. \textbf{Results:} The obtained results demonstrate that collisions between protons+electrons and hydrogen atoms supplemented by plasma viscosity, magnetic resistivity, and recombination lead to thermal energy release, which compensates radiative and thermal losses in the chromosphere, and sustains the atmosphere with vertical profiles of averaged temperature and periods of generated waves that are consistent with recent observational data. \textbf{Conclusion:} Our model conjectures a most robust and global physical picture of granulation-generated wave motions, plasma flows, and subsequent heating, which form and dynamically couple the various layers of the solar atmosphere.

3D Numerical Simulations of Solar Quiet Chromosphere Wave Heating

K. **Murawski**1, Z. E. Musielak2,3, and D. Wójcik1
2020 ApJL 896 L1
https://doi.org/10.3847/2041-8213/ab94a9
Despite numerous observational and theoretical attempts, the heating problem of the solar chromosphere still remains unsolved. We develop a novel 3D two-fluid model that accounts for dynamics of charged species and neutrals, and use it to perform the numerical simulations of granulation driven jets and associated waves in a quiet region of the solar chromosphere. The energy carried by the waves is dissipated through ion–neutral collisions, which are sufficient to balance radiative energy losses and to sustain the quasi-stationary atmosphere whose ion and neutral number densities, ionization fraction, and temperature profiles are relatively close to the observationally based semi-empirical model. Additional verification of our results is provided by a good fit of the numerically predicted waveperiod variations with height to the recent observational data. These observational validations of the numerical results demonstrate that the wave heating problem of a quiet region of the chromosphere may be solved.

Magnetic swirls and associated fast magnetoacoustic kink waves in a solar chromospheric flux tube

K. **Murawski**, P. Kayshap, A. K. Srivastava, D. J. Pascoe, P. Jelínek, B. Kuźma, V. Fedun
MNRAS **2017**
https://arxiv.org/pdf/1710.08179.pdf
We perform numerical simulations of impulsively generated magnetic swirls in an isolated flux tube which is rooted in the solar photosphere. These swirls are triggered by an initial pulse in a horizontal component of the velocity. The initial pulse is launched either: (a) centrally, within the localized magnetic flux tube; or (b) off-central, in the ambient medium. The evolution and dynamics of the flux tube is described by three-dimensional, ideal magnetohydrodynamic equations. These equations are numerically solved to reveal that in case (a) dipole-like swirls associated with the fast magnetoacoustic kink and m=1 Alfvén waves are generated. In case (b), the fast magnetoacoustic kink and m=0 Alfvén modes are excited. In both these cases, the excited fast magnetoacoustic kink and Alfvén waves consist of similar flow pattern and magnetic shells are also generated with clockwise and counter-clockwise rotating plasma within them, which can be the proxy of dipole-shaped chromospheric swirls. The complex dynamics of vortices and wave perturbations reveals the channelling of sufficient amount of energy to

fulfill energy losses in the chromosphere (~ 104 W m-1) and in the corona (~ 102 W m-1). Some of these numerical findings are reminiscent of signatures in recent observational data.

Randomly driven acoustic-gravity waves in the solar atmosphere: cutoff period and its observational verification

K. **Murawski**1, Z.E. Musielak2;3
Mon. Not. R. Astron. Soc. **2016**
http://kft.umcs.lublin.pl/kmur/download/papers/2016/cutt-off-HD-full-paper.pdf
We study the propagation of acoustic-gravity waves in the solar atmosphere. The waves are excited by a space- and time-dependent random driver, whose action mimics turbulence in the upper part of the solar convection zone. Our main goal is to find vertical variations of wave periods of these waves and compare the obtained results to the recent observations of Wi\'sniewska et al. (2016). We solve numerically the hydrodynamic equations in the solar atmosphere whose temperature is given by the semi-empirical model of Avrett & Loeser (2008). The obtained numerical results show that wave periods vary along vertical direction in agreement with the recent observational data. We discuss physical consequences of our theoretical results.

Variation of acoustic cutoff period with height in the solar atmosphere: theory versus observations

K. **Murawski**, Z.E. Musielak, P. Konkol, A. Wiśniewska
Astrophysical Journal, 827:37 (3pp), **2016**
http://arxiv.org/pdf/1608.02748v1.pdf
Recently Wi\'sniewska et al. demonstrated observationally how the acoustic cutoff frequency varies with height in the solar atmosphere including the upper photosphere and the lower and middle chromosphere, and showed that the observational results cannot be accounted for by the existing theoretical formulas for the acoustic cutoff. In order to reproduce the observed variation of the cutoff with atmospheric height, numerical simulations of impulsively generated acoustic waves in the solar atmosphere are performed, and the spectral analysis of temporal wave profiles is used to compute numerically changes of the acoustic cutoff with height. Comparison of the numerical results with the observational data shows good agreement, which clearly indicates that the obtained results may be used to determine the structure of the background solar atmosphere.

A Numerical Model of MHD Waves in a 3D Twisted Solar Flux Tube

K. **Murawski**, A. Solov'ev, J. Kraśkiewicz
Solar Physics July **2015**, Volume 290, Issue 7, pp 1909-1922
We generalize our analytical and numerical models of the solar flux tube on twisted magnetic-field lines. The basic equations and numerical methods have much in common with those of Murawskiet al. (Astron. Astrophys. 577, A126, 2015); the new and important issue is the twisted magnetic-field component that couples explored torsional Alfvén and magnetoacoustic waves. In these models we specify a magnetic-flux function and derive general analytical formulas for the equilibrium mass density and a gas pressure. We use the developed models, which can be adopted for any axisymmetric structure with twisted and untwisted magnetic lines, to simulate the MHD waves. These waves are excited by a localized pulse in the azimuthal velocity component that is launched at the top of the solar photosphere. Their propagation through the solar chromosphere and transition region to the solar corona reveals a complex scenario of twisted magnetic-field lines and flows associated with torsional Alfvén and magnetoacoustic waves.

Multi-shell Magnetic Twisters as a New Mechanism for Coronal Heating and Solar Wind Acceleration

K. **Murawski**1, A. K. Srivastava2, Z. E. Musielak3,4, and B. N. Dwivedi
2015 ApJ 808 5
We perform numerical simulations of impulsively generated Alfvén waves in an isolated photospheric flux tube and explore the propagation of these waves along such magnetic structure that extends from the photosphere, where these waves are triggered, to the solar corona, and we analyze resulting magnetic shells. Our model of the solar atmosphere is constructed by adopting the temperature distribution based on the semi-empirical model and specifying the curved magnetic field lines that constitute the magnetic flux tube that is rooted in the solar photosphere. The evolution of the solar atmosphere is described by 3D, ideal MHD equations that are numerically solved by the FLASH code. Our numerical simulations reveal, based on the physical properties of the multi-shell magnetic twisters and the amount of energy and momentum associated with them, that these multi-shell magnetic

twisters may be responsible for the observed heating of the lower solar corona and for the formation of solar wind. Moreover, it is likely that the existence of these twisters can be verified by high-resolution observations.

Torsional Alfven Waves in Solar Magnetic Flux Tubes of Axial Symmetry

K. **Murawski**, A. Solov'ev, Z.E. Musielak, A.K. Srivastava, J. Kraskiewicz
A&A, **2015**
http://arxiv.org/pdf/1501.00252v1.pdf
Aims: Propagation and energy transfer of torsional Alfv\'en waves in solar magnetic flux tubes of axial symmetry is studied. Methods: An analytical model of a solar magnetic flux tube of axial symmetry is developed by specifying a magnetic flux and deriving general analytical formulae for the equilibrium mass density and a gas pressure. The main advantage of this model is that it can be easily adopted to any axisymmetric magnetic structure. The model is used to simulate numerically the propagation of nonlinear Alfv\'en waves in such 2D flux tubes of axial symmetry embedded in the solar atmosphere. The waves are excited by a localized pulse in the azimuthal component of velocity and launched at the top of the solar photosphere, and they propagate through the solar chromosphere, transition region, and into the solar corona. Results: The results of our numerical simulations reveal a complex scenario of twisted magnetic field lines and flows associated with torsional Alfv\'en waves as well as energy transfer to the magnetoacoustic waves that are triggered by the Alfv\'en waves and are akin to the vertical jet flows. Alfv\'en waves experience about 5 % amplitude reflection at the transition region. Magnetic (velocity) field perturbations experience attenuation (growth) with height is agreement with analytical findings. Kinetic energy of magnetoacoustic waves consists of 25 % of the total energy of Alfv\'en waves. The energy transfer may lead to localized mass transport in the form of vertical jets, as well as to localized heating as slow magnetoacoustic waves are prone to dissipation in the inner corona.

Transition to a weaker Sun: Changes in the solar atmosphere during the decay of the Modern Maximum

K. **Mursula**, A. A. Pevtsov, T. Asikainen, I. Tähtinen, A. R. Yeates
A&A 685, A170 **2024**
https://arxiv.org/ftp/arxiv/papers/2403/2403.08047.pdf
https://www.aanda.org/articles/aa/pdf/2024/05/aa49231-24.pdf
The Sun experienced a period of unprecedented activity during the 20th century, now called the Modern Maximum (MM). The decay of the MM after cycle 19 has changed the Sun, the heliosphere, and the planetary environments in many ways. However, studies disagree on whether this decay has proceeded synchronously in different solar parameters or not. One key issue is if the relation between two long parameters of solar activity, the sunspot number and the solar 10.7cm radio flux, has remained the same during this decay. A recent study argues that there is an inhomogeneity in the 10.7cm radio flux in 1980, which leads to a step-like jump ("1980 jump") in this relation. Here we show that the relation between sunspot number and 10.7cm radio flux varies in time, not due to an inhomogeneous radio flux but due to physical changes in the solar atmosphere. We used radio fluxes at four different wavelengths measured in Japan, and studied their long-term relation with the sunspot number and the 10.7cm radio flux. We also used two other solar parameters, the MgII index and the number of active regions. We find that the 1980 jump is only the first of a series of 1-2-year "humps" that mainly occur during solar maxima. All radio fluxes increase with respect to the sunspot number from the 1970s to 2010s. These results reestablish the 10.7cm flux as a homogeneous measure of solar activity. The fluxes of the longer radio waves are found to increase with respect to the shorter waves, which suggests a long-term change in the solar radio spectrum. We also find that the MgII index and the number of active regions also increased with respect to the sunspot number, further verifying the difference in the long-term evolution in chromospheric and photospheric parameters. Our results provide evidence for important structural changes in solar magnetic fields and the solar atmosphere during the decay of the MM.

Hale cycle in solar hemispheric radio flux and sunspots: Evidence for a northward shifted relic field

Kalevi **Mursula**
A&A **2023**
https://arxiv.org/pdf/2305.01030.pdf
Solar and heliospheric parameters can depict notable differences between the northern and southern hemisphere. Although hemispheric asymmetries of some heliospheric parameters vary systematically with Hale cycle, this is not common for solar parameters. Also, no physical mechanism exists which can explain systematic hemispheric asymmetries. We use a novel method of high heliolatitudes to increase the fraction of one hemisphere in solar 10.7cm radio fluxes and sunspot numbers. We calculate sets of hemispheric high-latitude radio fluxes and sunspot numbers with increasing heliographic latitude during the last 75 years. We also normalise these fluxes by yearly means in order to study their continuous variation. We find that cycle maximum radio fluxes and sunspot numbers in each odd cycle (19, 21, 23) are larger at northern high latitudes, while in all even cycles (18, 20, 22 24) they are

larger at southern latitudes. This alternation indicates a new form of Hale cycle variation in solar activity. Hemispheric differences at cycle maxima are 15% for radio flux and 23% for sunspot numbers. The difference is largest during cycle 19 and smallest in cycle 24. Continuous fluxes depict a Hale cycle in both hemispheres, with an opposite phase and amplitude of 5% in north and 4% in south. Hemispheric Hale cycle can be explained if there is a northward directed relic magnetic field, which is shifted northward. In odd cycles, the northern hemisphere is enhanced more than the southern hemisphere and, in even cycles, the northern hemisphere is reduced more than the southern hemisphere. The decrease of asymmetry during the 7 cycles can be explained if the relic shift oscillates at the 210-year Suess/deVries period. Gleissberg cycle consists of one off-equator excursion of the relic. Relic field in the Sun also offers a possibility for century-scale forecasting of solar activity.

Spatial–temporal evolution of photospheric weak-field shifts in solar cycles 21–24

K. **Mursula**, T. Getachew and I. I. Virtanen
A&A 645, A47 (**2021**)
https://doi.org/10.1051/0004-6361/201936917
Context. Weak magnetic field elements make a dominant contribution to the total magnetic field on the solar surface. Even so, little is known of their long-term occurrence.
Aims. We study the long-term spatial–temporal evolution of the weak-field shift and skewness of the distribution of photospheric magnetic field values during solar cycles 21−24 in order to clarify the role and relation of the weak field values to the overall magnetic field evolution.
Methods. We used Wilcox Solar Observatory (WSO) and the Synoptic Optical Long-term Investigations of the Sun Vector SpectroMagnetograph synoptic maps to calculate weak-field shifts for each latitude bin of each synoptic map, and thereby constructed a time–latitude butterfly diagram for shifts. We also calculated butterfly diagrams for skewness for all field values and for weak field values only.
Results. The weak-field shifts and (full-field) skewness depict a similar spatial–temporal solar cycle evolution to that of the large-scale surface magnetic field. The field distribution has a systematic non-zero weak-field shift and a large skewness already at (and after) the emergence of the active region, even at the highest resolution. We find evidence for coalescence of opposite-polarity fields during the surge evolution. This is clearly more effective at the supergranulation scale. However, a similar dependence of magnetic field coalescence on spatial resolution was not found in the unipolar regions around the poles.
Conclusions. Our results give evidence for the preference of even the weakest field elements toward the prevailing magnetic polarity since the emergence of an active region, and for a systematic coalescence of stronger magnetic fields of opposite polarities to produce weak fields during surge evolution and at the poles. We also find that the supergranulation process is reduced or turned off in the unipolar regions around the poles. These observations improve the understanding not only of the development of the weakest magnetic field elements, but also of the dynamics of magnetic fields at large, and even of processes below the solar surface.

Seasonal solar wind speeds for the last 100 years: Unique coronal hole structures during the peak and demise of the Grand Modern Maximum

Kalevi **Mursula**, Lauri Holappa, Renata Lukianova
2016
https://arxiv.org/pdf/1612.04941v1.pdf
Solar coronal holes are sources of high-speed solar wind streams, which cause persistent geomagnetic activity especially at high latitudes. Here we estimate seasonal solar wind speeds at 1 AU for the last 100 years using high-latitude geomagnetic measurements and show that they give information on the long-term evolution of important structures of the solar large-scale magnetic field, such as persistent coronal holes. We find that the centennial evolution of solar wind speed at 1 AU is different for equinoxes and solstices, reflecting differences in the evolution of polar coronal hole extensions and isolated low-latitude coronal holes. Equinoctial solar wind speeds had their centennial maximum in 1952, during the declining phase of solar cycle 18, verifying that polar coronal holes had exceptionally persistent extensions just before the peak of the Grand Modern Maximum of solar activity. On the other hand, solstice speeds had their centennial maximum during the declining phase of solar cycle 23 due to large low-latitude coronal holes. A similar configuration of seasonal speeds as in cycle 23 was not found earlier, not even during the less active cycles of early 20th century. Therefore the exceptional occurrence of persistent, isolated low-latitude coronal holes in cycle 23 is not related to the absolute level of sunspot activity but, most likely, to the demise of the Grand Modern Maximum.

Occurrence of high-speed solar wind streams over the Grand Modern Maximum

Kalevi **Mursula**, Renata Lukianova, Lauri Holappa
2015 *ApJ* **801** 30
http://arxiv.org/pdf/1501.05010v1.pdf

In the declining phase of the solar cycle, when the new-polarity fields of the solar poles are strengthened by the transport of same-signed magnetic flux from lower latitudes, the polar coronal holes expand and form non-axisymmetric extensions toward the solar equator. These extensions enhance the occurrence of high-speed solar wind streams (HSS) and related co-rotating interaction regions in the low-latitude heliosphere, and cause moderate, recurrent geomagnetic activity in the near-Earth space. Here, using a novel definition of geomagnetic activity at high (polar cap) latitudes and the longest record of magnetic observations at a polar cap station, we calculate the annually averaged solar wind speeds as proxies for the effective annual occurrence of HSS over the whole Grand Modern Maximum (GMM) from 1920s onwards. We find that a period of high annual speeds (frequent occurrence of HSS) occurs in the declining phase of each solar cycle 16-23. For most cycles the HSS activity clearly maximizes during one year, suggesting that typically only one strong activation leading to a coronal hole extension is responsible for the HSS maximum. We find that the most persistent HSS activity occurred in the declining phase of solar cycle 18. This suggests that cycle 19, which marks the sunspot maximum period of the GMM, was preceded by exceptionally strong polar fields during the previous sunspot minimum. This gives interesting support for the validity of solar dynamo theory during this dramatic period of solar magnetism.

Kink instability of flux ropes in partially-ionised plasmas

Giulia **Murtas**, Andrew Hillier, Ben Snow
ApJ **2024**
https://arxiv.org/pdf/2409.06901
In the solar atmosphere, flux ropes are subject to current driven instabilities that are crucial in driving plasma eruptions, ejections and heating. A typical ideal magnetohydrodynamics (MHD) instability developing in flux ropes is the helical kink, which twists the flux rope axis. The growth of this instability can trigger magnetic reconnection, which can explain the formation of chromospheric jets and spicules, but its development has never been investigated in a partially-ionised plasma (PIP). Here we study the kink instability in PIP to understand how it develops in the solar chromosphere, where it is affected by charge-neutral interactions. Partial ionisation speeds up the onset of the non-linear phase of the instability, as the plasma β of the isolated plasma is smaller than the total plasma β of the bulk. The distribution of the released magnetic energy changes in fully and partially-ionised plasmas, with a larger increase of internal energy associated to the PIP cases. The temperature in PIP increases faster also due to heating terms from the two-fluid dynamics. PIP effects trigger the kink instability on shorter time scales, which is reflected in a more explosive chromospheric flux rope dynamics. These results are crucial to understand the dynamics of small-scale chromospheric structures - mini-filament eruptions - that this far have been largely neglected but could significantly contribute to chromospheric heating and jet formation.

Coalescence Instability in Chromospheric Partially Ionised Plasmas

Giulia **Murtas**, Andrew Hillier, Ben Snow
Physics of Plasmas **2021**
https://arxiv.org/pdf/2102.01630.pdf
Fast magnetic reconnection plays a fundamental role in driving explosive dynamics and heating in the solar chromosphere. The reconnection time scale of traditional models is shortened at the onset of the coalescence instability, which forms a turbulent reconnecting current sheet through plasmoid interaction. In this work we aim to investigate the role of partial ionisation on the development of fast reconnection through the study of the coalescence instability of plasmoids. Unlike the processes occurring in fully ionised coronal plasmas, relatively little is known about how fast reconnection develops in partially ionised plasmas of the chromosphere. We present 2.5D numerical simulations of coalescing plasmoids in a single fluid magnetohydrodynamic (MHD) model, and a two-fluid model of a partially ionised plasma (PIP). We find that in the PIP model, which has the same total density as the MHD model but an initial plasma density two orders of magnitude smaller, plasmoid coalescence is faster than the MHD case, following the faster thinning of the current sheet and secondary plasmoid dynamics. Secondary plasmoids form in the PIP model where the effective Lundquist number S=7.8·103, but are absent from the MHD case where S=9.7·103: these are responsible for a more violent reconnection. Secondary plasmoids also form in linearly stable conditions as a consequence of the non-linear dynamics of the neutrals in the inflow. In the light of these results we can affirm that two-fluid effects play a major role on the processes occurring in the solar chromosphere.

The Revised Sunspot Record in Comparison to Cosmogenic Radionuclide-Based Solar Activity Reconstructions

Raimund **Muscheler**, Florian Adolphi, Konstantin Herbst, Andreas Nilsson
Solar Phys. **2016**
Recent revisions in the sunspot records illustrate the challenges related to obtaining a 400-year-long observational record of past solar-activity changes. Cosmogenic radionuclides offer the possibility of obtaining an alternative and completely independent record of solar variability. Here, we illustrate that these records offer great potential for quantitative solar-activity reconstructions far back into the past, and we provide updated radionuclide-based solar-

activity reconstructions for the past 2000 years. However, cosmogenic-radionuclide records are also influenced by processes independent of solar activity, leading to the need for critical assessment and correction for the non-solar influences. Independent of these uncertainties, we show a very good agreement between the revised sunspot records and the 10Be records from Antarctica and, in particular, the 14C-based solar-activity reconstructions. This comparison offers the potential of identifying remaining non-solar processes in the radionuclide-based solar-activity reconstructions, but it also helps identifying remaining biases in the recently revised sunspot records.

An improved multi-ridge fitting method for ring-diagram helioseismic analysis

Kaori **Nagashima**, Aaron C. Birch, Jesper Schou, Bradley W. Hindman, Laurent Gizon
A&A 633, A109 **2020**
https://arxiv.org/pdf/1911.07772.pdf
https://www.aanda.org/articles/aa/pdf/2020/01/aa36662-19.pdf
Context: There is a wide discrepancy in current estimates of the strength of convection flows in the solar interior obtained using different helioseismic methods applied to observations from SDO/HMI. The cause for these disparities is not known. Aims: As one step in the effort to resolve this discrepancy, we aim to characterize the multi-ridge fitting code for ring-diagram helioseismic analysis that is used to obtain flow estimates from local power spectra of solar oscillations. Methods: We updated the multi-ridge fitting code developed by Greer et al.(2014) to solve several problems we identified through our inspection of the code. In particular, we changed the merit function to account for the smoothing of the power spectra, model for the power spectrum, and noise estimates. We used Monte Carlo simulations to generate synthetic data and to characterize the noise and bias of the updated code by fitting these synthetic data. Results: The bias in the output fit parameters, apart from the parameter describing the amplitude of the p-mode resonances in the power spectrum, is below what can be measured from the Monte-Carlo simulations. The amplitude parameters are underestimated; this is a consequence of choosing to fit the logarithm of the averaged power. We defer fixing this problem as it is well understood and not significant for measuring flows in the solar interior. The scatter in the fit parameters from the Monte-Carlo simulations is well-modeled by the formal error estimates from the code. Conclusions: We document and demonstrate a reliable multi-ridge fitting method for ring-diagram analysis. The differences between the updated fitting results and the original results are less than one order of magnitude and therefore we suspect that the changes will not eliminate the aforementioned orders-of-magnitude discrepancy in the amplitude of convective flows in the solar interior.

The amplitude of the cross-covariance function of solar oscillations as a diagnostic tool for wave attenuation and geometrical spreading

Kaori **Nagashima**, Damien Fournier, Aaron C. Birch, Laurent Gizon
A&A 599, A111 (**2017**)
https://arxiv.org/pdf/1612.08991v1.pdf
Context. In time-distance helioseismology, wave travel times are measured from the two-point cross-covariance function of solar oscillations and are used to image the solar convection zone in three dimensions. There is, however, also information in the amplitude of the cross-covariance function, for example about seismic wave attenuation. Aims. Here we develop a convenient procedure to measure the amplitude of the cross-covariance function of solar oscillations. Methods. In this procedure, the amplitude of the cross-covariance function is linearly related to the cross-covariance function and can be measured even for high levels of noise. Results. As an example application, we measure the amplitude perturbations of the seismic waves that propagate through the sunspot in active region NOAA 9787. We can recover the amplitude variations due to the scattering and attenuation of the waves by the sunspot and associated finite-wavelength effects. Conclusions. The proposed definition of cross-covariance amplitude is robust to noise, can be used to relate measured amplitudes to 3D perturbations in the solar interior under the Born approximation, and will provide independent information from the travel times.

Statistics of the two-point cross-covariance function of solar oscillations

Kaori **Nagashima**, Takashi Sekii, Laurent Gizon, Aaron C. Birch
A&A 593, A41 **2016**
http://arxiv.org/pdf/1606.06497v1.pdf
Context: The cross-covariance of solar oscillations observed at pairs of points on the solar surface is a fundamental ingredient in time-distance helioseismology. Wave travel times are extracted from the cross-covariance function and are used to infer the physical conditions in the solar interior. Aims: Understanding the statistics of the two-point cross-covariance function is a necessary step towards optimizing the measurement of travel times. Methods: By modeling stochastic solar oscillations, we evaluate the variance of the cross-covariance function as function of time-lag and distance between the two points. Results: We show that the variance of the cross-covariance is independent of both time-lag and distance in the far field, i.e., when they are large compared to the coherence scales of the solar oscillations. Conclusions: The constant noise level for the cross-covariance means that the signal-to-noise ratio for the cross-covariance is proportional to the amplitude of the expectation value of the cross-covariance. This observation is important for planning data analysis efforts.

Solar Cycle Pairing and Prediction of Cycle 25

Yu. A. **Nagovitsyn**, V. G. Ivanov

Solar Phys. 298, Article number: 37 **2023**

https://arxiv.org/pdf/2208.00101.pdf

In addition to the Gnevyshev-Ohl rule (GOR), the relation of the odd cycle with the subsequent even one in the 22-year Hale solar cycle was found. It is shown that 3 years before the 11-year minimum m, the value of the relative sunspot number SN in an odd cycle is closely related to the value of the maximum in the next even cycle (correlation coefficient ρ=0.94), and the same relation of an odd cycle with the previous even one is weaker. Like GOR, cycles are linked in pairs, but opposite to the Rule.

Based on this result, we propose to use SNm−3 on the descending phase of the previous odd cycle as a precursor of the subsequent EVEN cycle (Figure 3a) -- a precursor called MI3E. For the prediction of an odd cycle or a prediction without consideration of parity (as in the article by Brajša et al., 2022), this method gives less reliable results.

To predict the amplitude of an ODD cycle, we propose to use the precursor of the seventh year to its maximum M MA7O -- SNM−7 on the descending phase of the previous even cycle (Figure 3b). It turned out that in this case, we can also predict the years near the maximum with a high correlation coefficient (ρ=0.90−0.94).

Thus, the proposed approaches allow us to predict cycles of different parity. According to our prediction, the current solar Cycle 25 in 2023 will reach a maximum of 154 units with a prediction error of ±25 (68% confidence) and ±53 (95% confidence). In 2024, SN will be almost as high as in 2023 -- 147 units, so with smaller time averaging scales, the maximum will fall at the end of 2023.

Average annual total sunspot area in the last 410 years: The most probable values and limits of their uncertainties

Yury A. **Nagovitsyn**, Aleksandra A. Osipova

MNRAS Volume 505, Issue 1, Pages 1206–1212, **2021**

https://arxiv.org/pdf/2105.06519.pdf

https://doi.org/10.1093/mnras/stab1328

The aim of this work is to create a long (410 years) series of average annual total sunspot areas AR - physically-based index of sunspot activity. We used telescopic observations of the AR index in 1832-1868 and 1875-2020, as well as the relationship between AR and long series of sunspot indices SN (ISN version 2.0) and sunspot groups GN (Svalgaard and Schatten (2016) GSN version). The Royal Greenwich observatory series after 1976 is extended by the Kislovodsk Mountain Astronomical Station data. When reconstructing AR from SN, it is taken into account that the function AR = f (SN) has a nonlinear systematic character and uncertainty associated with the heterogeneity of these indices. Therefore, in addition to modeling the most probable AR values, predictive limits of reconstruction uncertainty are determined. In the interval 1610-1699 the reconstruction we carried out on the basis of the GN series using the previously proposed decomposition in pseudo-phase space method (DPS). The resulting series NO21y is freely available online. We show that for this series the empirical Gnevyshev-Ohl rule and Waldmeier effect are fulfilled. Wavelet analysis reveals periodicities of 8.4-13.8 years for the main cycle (with a sharp decrease of the period before the global Maunder and Dalton minima) and a two-component Gleissberg cycle with typical periods of 50-60 years and 90-110 years.

“Generative” Indices of Sunspot Solar Activity: 145-Year Composite Series

Y. A. **Nagovitsyn**, A. A. Osipova & E. Y. Nagovitsyna

Solar Physics volume 296, Article number: 32 (**2021**)

https://link.springer.com/content/pdf/10.1007/s11207-021-01772-x.pdf

Traditional indices, which we call apparent indices, describe the current state of solar activity and are very important for understanding the influence of the Sun on Earth. To study the productivity of the solar dynamo, however, we need a different index that would describe each magnetic region once – at the moment of its maximum area. We refer to such indices as generative ones. The aim of this work is to produce such a generative series improving the procedure by Nagovitsyn et al. (Geomagn. Aeron. 58, 1170, 2018). We use sunspot group data from two archives – Royal Greenwich Observatory (1875 – 1976) and Kislovodsk Mountain Astronomical Station (1955 – 2019). We produce generative indices with annual values of sunspot group areas AA, and counts of sunspot groups CC. Unified 145-year series of these indices were compiled. We study the characteristics of the indices AA and CC, and indices derived from them for two sunspot group populations – large long-living groups and small short-living groups according to Nagovitsyn and Pevtsov (Astrophys. J. 833, 94, 2016) – for the northern and southern hemispheres separately. We find a 50-year variation in several indices on the 145-year interval, and detect a similar phase variation in the north-south asymmetry taken with the opposite sign. Perhaps this indicates the existence of another secular cycle along with the Gleissberg cycle on the Sun. The obtained series of indices AA and CC can be useful for studying the long-term properties of the solar dynamo.

Duffing Oscillator Model of Solar Cycles

Yury A. **Nagovitsyn**1,2 and Alexei A. Pevtsov

2020 ApJL 888 L26

https://doi.org/10.3847/2041-8213/ab6335

We propose that the solar cycle variability could be described in the framework of an external quasi-sinusoidal influence on an oscillator with cubic nonlinearity and linear damping (Duffing oscillator). To demonstrate this, we compare the empirical amplitude–frequency dependence with the theoretical one obtained by the Krylov–Bogolyubov averaging method. The empirical data are a composite time series of 2.0 version of sunspot number series, which starts in 1700, and the sunspot group number series by Svalgaard & Schatten, scaled to sunspot number, for 1610–1699 interval. We find that while this interpretation of solar cycle is a mathematical approximation, it explains several properties of solar cycle variability.

ON THE PRESENCE OF TWO POPULATIONS OF SUNSPOTS

Yury A. **Nagovitsyn**1,3 and Alexei A. Pevtsov2,4

2016 ApJ 833 94 **File**

http://sci-hub.cc/doi/10.3847/1538-4357/833/1/94#

Using historical (1894–1976) and more modern (1977–2014) observations, we investigate statistical properties of distributions of sunspot areas and their long-term variations. We confirm the presence of two populations of sunspots with smaller and larger areas, and show that sunspot/group lifetime can be used to separate the two populations on small short-lived sunspot groups (SSG) and large long-lived groups (LLG). The area properties of LLG are nearly constant over the entire period of observations, while the SSGs show significant long-term variations. Based on the presence of long-term variations in one component and the absence of those in the other, we suggest that the production of two populations of sunspots (SSG and LLG) may be affected by different processes.

Long-term variations in sunspot magnetic field - area relation

Yury A. **Nagovitsyn**, Alexei A. Pevtsov, Aleksandra A. Osipova

Astron. Nachrichten **2016**

http://arxiv.org/pdf/1608.01132v1.pdf

Using observations of sunspot magnetic field strengths (H) from the Crimean Astrophysical Observatory (CrAO) and area (S) of sunspots from the Kislovodsk Mountain Astronomical Station of Pulkovo Observatory, we investigate the changes in the relation between H and S over the period of about two solar cycles (1994-2013). The data were fitted by H = A + B log S, where A = (778+/-46) and B = (778+/-25). We show that the correlation between H and S varies with the phase of solar cycle, and A coefficient decreases significantly after year 2001, while B coefficient does not change significantly. Furthermore, our data confirm the presence of two distinct populations in distribution of sunspots (small sunspots with weaker field strength and large sunspots with stronger field). We show that relative contribution of each component to the distribution of sunspots by their area changes with the phase of solar cycle and on longer-then-cycle periods. We interpret these changes as a signature of a long-term (centennial) variations in properties of sunspots.

The Upper Limit of Sunspot Activity as Observed over a Long Time Interval

Yu. A. **Nagovitsyn**, V. N. Obridko, A. I. Kuleshova

Solar Phys. Volume 290, Issue 4, pp 1285-1294 **2015**

After analyzing the observational manifestations of the α- and ω-effects of the dynamo theory and using the modified Waldmeier rule, we show that the annual mean Wolf numbers at the maximum of the 11-year cycle that are likely to occur a time interval of 104 years have an upper limit amounting approximately to W EXTR~230 – 240. Similar values were also obtained using the results by Usoskin et al. (2014, Astron. Astrophys. 562, L10), who considered the probability of various activity levels by reconstructing the variations of solar activity over three thousand years. As an additional result, the predicted maximum of Cycle 24 is refined and is shown to be W M=72 – 132 with a 95 % confidence.

Impact of nonlinear surface inflows into activity belts on the solar dynamo

Melinda **Nagy**1*, Alexandre Lemerle2,3 and Paul Charbonneau3

J. Space Weather Space Clim. **2020**, 10, 62

https://doi.org/10.1051/swsc/2020064

https://www.swsc-journal.org/articles/swsc/pdf/2020/01/swsc200060.pdf

We examine the impact of surface inflows into activity belts on the operation of solar cycle models based on the Babcock–Leighton mechanism of poloidal field regeneration. Towards this end we introduce in the solar cycle model of Lemerle & Charbonneau (2017. ApJ 834: 133) a magnetic flux-dependent variation of the surface

meridional flow based on the axisymmetric inflow parameterization developped by Jiang et al. (2010. ApJ 717: 597). The inflow dependence on emerging magnetic flux thus introduces a bona fide nonlinear backreaction mechanism in the dynamo loop. For solar-like inflow speeds, our simulation results indicate a decrease of 10–20% in the strength of the global dipole building up at the end of an activity cycle, in agreement with earlier simulations based on linear surface flux transport models. Our simulations also indicate a significant stabilizing effect on cycle characteristics, in that individual cycle amplitudes in simulations including inflows show less scatter about their mean than in the absence of inflows. Our simulations also demonstrate an enhancement of cross-hemispheric coupling, leading to a significant decrease in hemispheric cycle amplitude asymmetries and temporal lag in hemispheric cycle onset. Analysis of temporally extended simulations also indicate that the presence of inflows increases the probability of cycle shutdown following an unfavorable sequence of emergence events. This results ultimately from the lower threshold nonlinearity built into our solar cycle model, and presumably operating in the sun as well.

Towards an algebraic method of solar cycle prediction II. Reducing the need for detailed input data with ARDoR

Melinda **Nagy**, Kristóf Petrovay, Alexandre Lemerle, Paul Charbonneau
Journal of Space Weather and Space Climate **10**, 46 **2020**
https://arxiv.org/pdf/2009.02300.pdf
https://www.swsc-journal.org/articles/swsc/pdf/2020/01/swsc200046.pdf
An algebraic method for the reconstruction and potentially prediction of the solar dipole moment value at sunspot minimum (known to be a good predictor of the amplitude of the next solar cycle) was suggested in the first paper in this series. The method sums up the ultimate dipole moment contributions of individual active regions in a solar cycle: for this, detailed and reliable input data would in principle be needed for thousands of active regions in a solar cycle. To reduce the need for detailed input data, here we propose a new active region descriptor called ARDoR (Active Region Degree of Rogueness). In a detailed statistical analysis of a large number of activity cycles simulated with the 2×2D dynamo model we demonstrate that ranking active regions by decreasing ARDoR, for a good reproduction of the solar dipole moment at the end of the cycle it is sufficient to consider the top N regions on this list explicitly, where N is a relatively low number, while for the other regions the ARDoR value may be set to zero. E.g., with N=5 the fraction of cycles where the dipole moment is reproduced with an error exceeding ±30% is only 12%, significantly reduced with respect to the case N=0, i.e. ARDoR set to zero for all active regions, where this fraction is 26%. This indicates that stochastic effects on the intercycle variations of solar activity are dominated by the effect of a low number of large ``rogue" active regions, rather than the combined effect of numerous small ARs. The method has a potential for future use in solar cycle prediction.

Impact of rogue active regions on hemispheric asymmetry

Melinda **Nagy** Alexandre Lemerleb Paul Charbonneau
Advances in Space Research Volume 63, Issue 4, 15 February **2019**, Pages 1425-1433
https://arxiv.org/pdf/1909.07672.pdf
The solar dipole moment at activity minimum is a good predictor of the strength of the subsequent solar cycle. Through a systematic analysis using a state-of-the-art 2×2D solar dynamo model, we found that bipolar magnetic regions (BMR) with atypical characteristics can modify the strength of the next cycle via their impact on the buildup of the dipole moment as a sunspot cycle unfolds. In addition to summarizing these results, we present further effects of such “rogue” BMRs. These have the ability to generate hemispheric asymmetry in the subsequent sunspot cycle, since they modify the polar cap flux asymmetry of the ongoing cycle. We found strong correlation between the polar cap flux asymmetry of cycle i and the total pseudo sunspot number asymmetry of cycle i+1. Good correlation also appears in the case of the time lag of the hemispheres of cycle i+1.

The Effect of “Rogue” Active Regions on the Solar Cycle

Melinda **Nagy**, Alexandre Lemerle, François Labonville, Kristóf Petrovay, Paul Charbonneau
Solar Physics November **2017**, 292:167
https://link.springer.com/content/pdf/10.1007%2Fs11207-017-1194-0.pdf
https://arxiv.org/pdf/1712.02185.pdf
The origin of cycle-to-cycle variations in solar activity is currently the focus of much interest. It has recently been pointed out that large individual active regions with atypical properties can have a significant impact on the long-term behavior of solar activity. We investigate this possibility in more detail using a recently developed 2×2D2×2D dynamo model of the solar magnetic cycle. We find that even a single “rogue” bipolar magnetic region (BMR) in the simulations can have a major effect on the further development of solar activity cycles, boosting or suppressing the amplitude of subsequent cycles. In extreme cases, an individual BMR can completely halt the dynamo, triggering a grand minimum. Rogue BMRs also have the potential to induce significant hemispheric asymmetries in the solar cycle. To study the effect of rogue BMRs in a more systematic manner, a

series of dynamo simulations were conducted, in which a large test BMR was manually introduced in the model at various phases of cycles of different amplitudes. BMRs emerging in the rising phase of a cycle can modify the amplitude of the ongoing cycle, while BMRs emerging in later phases will only affect subsequent cycles. In this model, the strongest effect on the subsequent cycle occurs when the rogue BMR emerges around cycle maximum at low latitudes, but the BMR does not need to be strictly cross-equatorial. Active regions emerging as far as 20∘20∘ from the equator can still have a significant effect. We demonstrate that the combined effect of the magnetic flux, tilt angle, and polarity separation of the BMR on the dynamo is viatheir contribution to the dipole moment, δDBMRδDBMR. Our results indicate that prediction of the amplitude, starting epoch, and duration of a cycle requires an accurate accounting of a broad range of active regions emerging in the previous cycle.

Oscillator Models of the Solar Cycle and the Waldmeier Effect

M. **Nagy**, K. Petrovay
Astronomische Nachrichten, 334, 964-967 (**2013**)
http://arxiv.org/pdf/1404.3668v1.pdf
We study the behaviour of the van der Pol oscillator when either its damping parameter μ or its nonlinearity parameter ξ is subject to additive or multiplicative random noise. Assuming various power law exponents for the relation between the oscillating variable and the sunspot number, for each case we map the parameter plane defined by the amplitude and the correlation time of the perturbation and mark the parameter regime where the sunspot number displays solar-like behaviour. Solar-like behaviour is defined here as a good correlation between the rise rate and cycle amplitude {\it and} the lack of a good correlation between the decay rate and amplitude, together with significant ($\ga 10$\,%) r.m.s. variation in cycle lengths and cycle amplitudes. It is found that perturbing μ alone the perturbed van der Pol oscillator does not show solar-like behaviour. When the perturbed variable is ξ, solar-like behaviour is displayed for perturbations with a correlation time of about 3--4 years and significant amplitude. Such studies may provide useful constraints on solar dynamo models and their parameters.

Transition from decaying to decayless kink oscillations of solar coronal loops

Valery M. **Nakariakov**, Yu Zhong, Dmitrii Y. Kolotkov
MNRAS **2024**
https://arxiv.org/pdf/2406.07490
The transition of an impulsively excited kink oscillation of a solar coronal loop to an oscillation with a stationary amplitude, i.e., the damping pattern, is determined using the low-dimensional self-oscillation model. In the model, the decayless kink oscillations are sustained by the interaction of the oscillating loop with an external quasi-steady flow. The analytical solution is based on the assumption that the combined effect of the effective dissipation, for example, by resonant absorption, and interaction with an external flow, is weak. The effect is characterised by a dimensionless coupling parameter. The damping pattern is found to depend upon the initial amplitude and the coupling parameter. The approximate expression shows a good agreement with a numerical solution of the self-oscillation equation. The plausibility of the established damping pattern is demonstrated by an observational example. Notably, the damping pattern is not exponential, and the characteristic decay time is different from the time determined by the traditionally used exponential damping fit. Implications of this finding for seismology of the solar coronal plasmas are discussed. In particular, it is suggested that a very rapid, in less than the oscillation period, decay of the oscillation to the stationary level, achieved for larger values of the coupling parameter, can explain the relative rareness of the kink oscillation events. **May 30, 2012**

Diagnostics of the solar coronal plasmas by magnetohydrodynamic waves: Magnetohydrodynamic seismology

Valery M. **Nakariakov**, Sihui Zhong, Dmitrii Y. Kolotkov, Rebecca L. Meadowcroft, Yu Zhong, Ding Yuan
Reviews of Modern Plasma Physics **2024**
https://arxiv.org/pdf/2404.00105.pdf
Macroscopic wave and oscillatory phenomena ubiquitously detected in the plasma of the corona of the Sun are interpreted in terms of magnetohydrodynamic theory. Fast and slow magnetoacoustic waves are clearly distinguished in observations. Properties of coronal magnetohydrodynamic waves are determined by local parameters of the plasma, including the field-aligned filamentation typical for the corona. It makes coronal magnetohydrodynamic waves reliable probes of the coronal plasma structures by the method of magnetohydrodynamic seismology. For example, propagating slow waves indicate the local direction of the guiding magnetic field. Standing, sloshing and propagating slow waves can be used for probing the coronal heating function and the polytropic index. Kink oscillations of coronal plasma loops provide us with the estimations of the absolute value of the magnetic field in oscillating plasma loops. This **tutorial** introduces several techniques of magnetohydrodynamic seismology of solar coronal plasmas. It includes the description of practical steps in the data

acquisition, pre-processing, and processing using the open-access data of the Atmospheric Imaging Assembly on the Solar Dynamics Observatory spacecraft, and elaborated data analysis techniques of motion magnification and Bayesian statistics.

Oscillatory Processes in Solar and Stellar Coronae ***Reviews***

Space Sci. Rev Topical collection

*Ed. by Valery M. **Nakariakov**, Dipankar Banerjee, Bo Li, Tongjiang Wang, Ivan Zimovets and Maurizio Falanga*

http://link.springer.com/journal/11214/topicalCollection/AC_b5bf4ca939ef807534e522d3c54d129f

Editorial to the Topical Collection: Oscillatory Processes in Solar and Stellar Coronae.

Nakariakov, V.M., Banerjee, D., Li, B. et al.

Space Sci Rev 218, 13 (**2022**).

https://doi.org/10.1007/s11214-022-00888-1

Properties of slow magnetoacoustic oscillations of solar coronal loops by multi-instrumental observations

Nakariakov, V. M., Kosak, M. K., Kolotkov, D. Y., Anfinogentov, S. A., Kumar, P., Moon, Y.-J.

ApJL **2019**

https://warwick.ac.uk/fac/sci/physics/research/cfsa/people/valery/Nakariakov_rev5.pdf

Rapidly decaying oscillations of the thermal emission detected in the decay phase of solar and stellar flares are usually interpreted as standing or sloshing (reflecting) slow magnetoacoustic oscillations. We determine the scalings of the oscillation periods, damping times and amplitudes with the temperature, considering both standing and sloshing oscillations detected with different instruments. In addition, the time evolution of different spatial harmonics of a sloshing oscillation is considered. Parameters of slow oscillations observed in the EUV, X-ray, and microwave bands, and published in the literature, are used. The damping time of slow oscillations is found to scale almost linearly with the oscillation period, as the period to 0.87± 0.1, giving the average Q-factor determined as the ratio of the damping time to the period, of about 1. The Q-factor is found to scale with the relative amplitude to the power of 0.33+0.10-0.11 with 95 % confidence. The amplitudes of different spatial harmonics forming a sloshing pulse show similar time evolution, suggesting that the period-dependent dissipation is counteracted by another mechanism. The results obtained indicate that the damping of slow oscillations depends on the oscillation amplitude, and that the competition of nonlinear and dissipative effects could allow for the existence of wave pulses of a sustained shape. **2012 May 7**

Non-stationary quasi-periodic pulsations in solar and stellar flares **Review**

Nakariakov, V.M., Kolotkov, D., Kupriyanova, E.G., Mehta, T., Pugh, C.E., Lee, D.-H., Broomhall, A.M.

Plasma Physics and Controlled Fusion **2018**

https://warwick.ac.uk/fac/sci/physics/research/cfsa/people/valery/research/eprints/NakariakovPPCF18.pdf

Often the enhanced electromagnetic radiation generated in solar and stellar flares shows a pronounced (quasi)-oscillatory pattern ? quasi-periodic pulsations (QPP), with characteristic periods ranging from a fraction of a second to several tens of minutes. We review recent advances in the empirical study of QPP in solar and stellar flares, addressing the intrinsic non-stationarity of the signal, i.e. the variation of its amplitude, period or phase with time. This non-stationarity could form a basis for a classification of QPP, necessary for revealing specific physical mechanisms responsible for their appearance. We could identify two possible classes of QPP, decaying harmonic oscillations, and trains of symmetric triangular pulsations. Apparent similarities between QPP and irregular geomagnetic pulsations Pi offer a promising avenue for the knowledge transfer in both analytical techniques and theory. Attention is also paid to the effect of the flare trend on the detection and analysis of QPP. **2014- 10-27, 2017-09-04**

Preface to Topical Issue: Waves in the Solar Corona: From Microphysics to Macrophysics

V. M. **Nakariakov**, D. J. Pascoe, R. Sych, L. van Driel-Gesztely

Solar Phys. Volume 291, Issue 11, pp 3139–3142 **2016**

http://link.springer.com/article/10.1007/s11207-016-1020-0

Effect of local thermal equilibrium misbalance on long-wavelength slow magnetoacoustic waves

Nakariakov, V.M., Afanasyev, A.N., Kumar, S., Moon, Y.-J.

ApJ 849:62, **2017**

https://www2.warwick.ac.uk/fac/sci/physics/research/cfsa/people/valery/research/eprints/Nakariakov_2017_ApJ_849_62.pdf
Evolution of slow magnetoacoustic waves guided by a cylindrical magnetic flux tube that represents a coronal loop or plume, is modelled accounting for the effects of finite gas pressure, weak nonlinearity, dissipation by thermal conduction and viscosity, and the misbalance between the cooling by optically thin radiation and unspecified heating of the plasma. An evolutionary equation of the Burgers-Malthus type is derived. It is shown that the cooling/heating misbalance, determined by the derivatives of the combined radiative cooling and heating function, with respect to the density, temperature and magnetic field at the thermal equilibrium affect the wave rather strongly. This effect may either cause additional damping, or counteract it, or lead to the gradual amplification of the wave. In the latter case the coronal plasma acts as an active medium for the slow magnetoacoustic waves. The effect of the cooling/heating misbalance could be important for coronal slow waves, and could be responsible for certain discrepancies between theoretical results and observations, in particular the increased or decreased damping lengths and times, detection of the waves at certain heights only, and excitation of compressive oscillations. The results obtained open up a possibility for the diagnostics of the coronal heating function by slow magnetoacoustic waves.

Magnetohydrodynamic Oscillations in the Solar Corona and Earth's Magnetosphere: Towards Consolidated Understanding Review

V. M. **Nakariakov** , V. Pilipenko, B. Heilig, P. Jelínek, M. Karlický, D. Y. Klimushkin, D. Y. Kolotkov, D.-H. Lee, G. Nisticò and 3 more
Space Sci. Revs. April **2016**, Volume 200, Issue 1, pp 75-203
http://www2.warwick.ac.uk/fac/sci/physics/research/cfsa/people/valery/research/eprints/s11214-015-0233-0.pdf
Magnetohydrodynamic (MHD) oscillatory processes in different plasma systems, such as the corona of the Sun and the Earth's magnetosphere, show interesting similarities and differences, which so far received little attention and remain under-exploited. The successful commissioning within the past ten years of THEMIS, Hinode, STEREO and SDO spacecraft, in combination with matured analysis of data from earlier spacecraft (Wind, SOHO, ACE, Cluster, TRACE and RHESSI) makes it very timely to survey the breadth of observations giving evidence for MHD oscillatory processes in solar and space plasmas, and state-of-the-art theoretical modelling. The paper reviews several important topics, such as Alfvénic resonances and mode conversion; MHD waveguides, such as the magnetotail, coronal loops, coronal streamers; mechanisms for periodicities produced in energy releases during substorms and solar flares, possibility of Alfvénic resonators along open field lines; possible drivers of MHD waves; diagnostics of plasmas with MHD waves; interaction of MHD waves with partly-ionised boundaries (ionosphere and chromosphere). The review is mainly oriented to specialists in magnetospheric physics and solar physics, but not familiar with specifics of the adjacent research fields.

"Coronal Waves and Oscillations" Review

Valery M. **Nakariakov** and Erwin Verwichte
http://www.livingreviews.org/lrsp-2005-3
Wave and oscillatory activity of the solar corona is confidently observed with modern imaging and spectral instruments in the visible light, EUV, X-ray and radio bands, and interpreted in terms of magnetohydrodynamic (MHD) wave theory. The **review** reflects the current trends in the observational study of coronal waves and oscillations (standing kink, sausage and longitudinal modes, propagating slow waves and fast wave trains, the search for torsional waves), theoretical modelling of interaction of MHD waves with plasma structures, and implementation of the theoretical results for the mode identification. Also the use of MHD waves for remote diagnostics of coronal plasma - MHD coronal seismology - is discussed and the applicability of this method for the estimation of coronal magnetic field, transport coefficients, fine structuring and heating function is demonstrated.

Exploring the Solar Poles: The Last Great Frontier of the Sun as a Review

Dibyendu **Nandy**, Dipankar Banerjee, Prantika Bhowmik, Allan Sacha Brun, Robert H. Cameron, S. E. Gibson, Shravan Hanasoge, Louise Harra, Donald M. Hassler, Rekha Jain, Jie Jiang, Laurène Jouve, Duncan H. Mackay, Sushant S. Mahajan, Cristina H. Mandrini, Mathew Owens, Shaonwita Pal, Rui F. Pinto, Chitradeep Saha, Xudong Sun, Durgesh Tripathi, Ilya G. Usoskin
White Paper **2023**
https://arxiv.org/ftp/arxiv/papers/2301/2301.00010.pdf
Despite investments in multiple space and ground-based solar observatories by the global community, the Sun's polar regions remain unchartered territory - the last great frontier for solar observations. Breaching this frontier is fundamental to understanding the solar cycle - the ultimate driver of short-to-long term solar activity that encompasses space weather and space climate. Magnetohydrodynamic dynamo models and empirically observed relationships have established that the polar field is the primary determinant of the future solar cycle amplitude. Models of solar surface evolution of tilted active regions indicate that the mid to high latitude surges of magnetic flux govern dynamics leading to the reversal and build-up of polar fields. Our theoretical understanding and numerical models of this high latitude magnetic field dynamics and plasma flows - that are a critical component of

the sunspot cycle - lack precise observational constraints. This limitation compromises our ability to observe the enigmatic kilo Gauss polar flux patches and constrain the polar field distribution at high latitudes. The lack of these observations handicap our understanding of how high latitude magnetic fields power polar jets, plumes, and the fast solar wind that extend to the boundaries of the heliosphere and modulate solar open flux and cosmic ray flux within the solar system. Accurate observation of the Sun's polar regions, therefore, is the single most outstanding challenge that confronts Heliophysics. This paper argues the scientific case for novel out of ecliptic observations of the Sun's polar regions, in conjunction with existing, or future multi-vantage point heliospheric observatories. Such a mission concept can revolutionize the field of Heliophysics like no other mission concept has - with relevance that transcends spatial regimes from the solar interior to the heliosphere.

Sunspot Cycle 25 is Brewing: Early Signs Herald its Onset

Dibyendu **Nandy**1,2, Aditi Bhatnagar1,2, and Sanchita Pal1
2020 Res. Notes AAS 4 30
https://iopscience.iop.org/article/10.3847/2515-5172/ab79a1
We conclude that the sunspot-forming toroidal field belt of solar cycle 25 is brewing in the Sun's convection zone and the magnetic regions we identify are harbingers of the next solar cycle. We shall have a sunspot cycle 25!

Progress in Solar Cycle Predictions: Sunspot Cycles 24-25 in Perspective **Review**

Dibyendu **Nandy**
Solar Phys. **296**, Article number: 54 **2021**
https://arxiv.org/pdf/2009.01908.pdf
https://link.springer.com/content/pdf/10.1007/s11207-021-01797-2.pdf
https://doi.org/10.1007/s11207-021-01797-2
The dynamic activity of the Sun -- sustained by a magnetohydrodynamic dynamo mechanism working in its interior -- modulates the electromagnetic, particulate and radiative environment in space. While solar activity variations on short timescale create space weather, slow long-term modulation forms the basis of space climate. Space weather impacts diverse space-reliant technologies while space climate influences planetary atmospheres and climate. Having prior knowledge of the Sun's activity is important in these contexts. However, forecasting solar-stellar magnetic activity has remained an outstanding challenge. In this review, predictions for sunspot cycle 24 and the upcoming cycle 25 are summarized, and critically assessed. The analysis demonstrates that while predictions based on diverse techniques disagree across solar cycles 24--25, physics-based predictions for solar cycle 25 have converged and indicates a weak sunspot cycle 25. It is argued that this convergence in physics-based predictions is indicative of progress in the fundamental understanding of solar cycle predictability. Based on this understanding, resolutions to several outstanding questions related to solar cycle predictions are discussed. These questions include: is it possible to predict the solar cycle, what is the best proxy for predictions, how early can we predict the solar cycle and how many cycles into the future can we predict relying on our current understanding? Based on our analysis, we also suggest a rigorous pathway towards generating and disseminating a “consensus forecast” by any solar cycle prediction panels tasked with such a challenge.

The Large-scale Coronal Structure of the 2017 August 21 Great American Eclipse: An Assessment of Solar Surface Flux Transport Model Enabled Predictions and Observations

Dibyendu **Nandy**1,2, Prantika Bhowmik1, Anthony R. Yeates3, Suman Panda1,2, Rajashik Tarafder1, and Soumyaranjan Dash1
2018 ApJ 853 72 10.3847/1538-4357/aaa1eb
On 2017 August 21, a total solar eclipse swept across the contiguous United States, providing excellent opportunities for diagnostics of the Sun's corona. The Sun's coronal structure is notoriously difficult to observe except during solar eclipses; thus, theoretical models must be relied upon for inferring the underlying magnetic structure of the Sun's outer atmosphere. These models are necessary for understanding the role of magnetic fields in the heating of the corona to a million degrees and the generation of severe space weather. Here we present a methodology for predicting the structure of the coronal field based on model forward runs of a solar surface flux transport model, whose predicted surface field is utilized to extrapolate future coronal magnetic field structures. This prescription was applied to the 2017 August 21 solar eclipse. A post-eclipse analysis shows good agreement between model simulated and observed coronal structures and their locations on the limb. We demonstrate that slow changes in the Sun's surface magnetic field distribution driven by long-term flux emergence and its evolution governs large-scale coronal structures with a (plausibly cycle-phase dependent) dynamical memory timescale on the order of a few solar rotations, opening up the possibility for large-scale, global corona predictions at least a month in advance.

Twisted solar active region magnetic fields as drivers of space weather: Observational and theoretical investigations

Dibyendu **Nandy**, Duncan H. Mackay, Richard C. Canfield and P.C.H. Martens
Journal of Atmospheric and Solar-Terrestrial Physics
Volume 70, Issues 2-4, February **2008**, Pages 605-613

The properties and dynamics of magnetic fields on the Sun's photosphere and outer layers—notably those within solar active regions—govern the eruptive activity of the Sun. These photospheric magnetic fields also act as the evolving lower boundary of the Sun–Earth coupled system. Quantifying the physical attributes of these magnetic fields and exploring the mechanisms underlying their influence on the near-Earth space environment are of vital importance for forecasting and mitigating adverse space weather effects. In this context, we discuss here a novel technique for measuring twist in the magnetic field lines of solar active regions that does not invoke the force-free field assumption. Twist in solar active regions can play an important role in flaring activity and the initiation of CMEs via the kink instability mechanism; we outline a procedure for determining this solar active region eruptive potential. We also discuss how twist in active region magnetic fields can be used as inputs in simulations of the coronal and heliospheric fields; specifically, we explore through simulations, the formation, evolution and ejection of magnetic flux ropes that originate in twisted magnetic structures. The results and ideas presented here are relevant for exploring the role of twisted solar active region magnetic fields and flux ropes as drivers of space weather in the Sun–Earth system.

Power distribution of oscillations in the atmosphere of a plage region: Joint observations with ALMA, IRIS and SDO

Nancy **Narang**, Kalugodu Chandrashekhar, Shahin Jafarzadeh, Bernhard Fleck, Mikołaj Szydlarski, Sven Wedemeyer
A&A **2022**
https://arxiv.org/pdf/2202.11547.pdf

We present a statistical analysis of power distribution of oscillations in a plage region in active region NOAA AR12651, observed jointly with ALMA (Atacama Large Millimeter/Submillimeter Array), IRIS (Interface Region Imaging Spectrograph), and SDO (Solar Dynamics Observatory). We employ coordinated ALMA Band-6 (1.25 mm) brightness temperature maps, IRIS Slit-Jaw Images in 2796 Å passband, and observations in six passbands (1600 Å, 304 Å, 131 Å, 171 Å, 193 Å and 211 Å) of AIA (Atmospheric Imaging Assembly) onboard SDO. We perform Lomb-Scargle transforms to study the distribution of oscillation power over the observed region by means of dominant period maps and power maps. We study spatial association of oscillations through the atmosphere mapped by the different passbands, with focus on the correlation of power distribution of ALMA oscillations with others. We do not observe any significant association of ALMA oscillations with IRIS and AIA oscillations. While the global behavior of ALMA dominant oscillations shows similarity with that of transition region and coronal passbands of AIA, the ALMA dominant period maps and power maps do not show any correlation with those from the other passbands. The spatial distribution of dominant periods and power in different period intervals of ALMA oscillations is uncorrelated with any other passband. We speculate the non-association of ALMA oscillations with those of IRIS and AIA be due to significant variations in the height of formation of the millimeter continuum observed by ALMA. Additionally, the fact that ALMA directly maps the brightness temperature, in contrast to the intensity observations by IRIS and AIA, can result in the very different intrinsic nature of the ALMA oscillations compared to the IRIS and AIA oscillations.

High-frequency dynamics of active region moss as observed by IRIS

Nancy **Narang**, Vaibhav Pant, Dipankar Banerjee, Tom Van Doorsselaere
Front. Astron. Space Sci **2019**
https://arxiv.org/pdf/1905.00722.pdf
sci-hub.se/10.3389/fspas.2019.00036

The high temporal, spatial and spectral resolution of Interface Region Imaging Spectrograph (IRIS) has provided new insights into the understanding of different small-scale processes occurring at the chromospheric and transition region (TR) heights. We study the dynamics of high-frequency oscillations of active region (AR 2376) moss as recorded by simultaneous imaging and spectral data of IRIS. Wavelet transformation, power maps generated from slit-jaw images in the Si IV 1400\AA passband, and sit-and-stare spectroscopic observations of the Si IV 1403\AA spectral line reveal the presence of high-frequency oscillations with ∼1-2 minute periods in the bright moss regions. The presence of such low periodicities is further confirmed by intrinsic mode functions (IMFs) as obtained by the empirical mode decomposition (EMD) technique. We find evidence of the presence of slow waves and reconnection-like events, and together they cause the high-frequency oscillations in the bright moss regions. **2015-07-05**

Association of calcium network bright points with underneath photospheric magnetic patches

Nancy **Narang**, Dipankar Banerjee, Kalugodu Chandrashekhar, Vaibhav Pant
Solar Phys. **2019**
https://arxiv.org/pdf/1902.03764.pdf
Recent dedicated Hinode polar region campaigns revealed the presence of concentrated kilogauss patches of magnetic field in the polar regions of the Sun which are also shown to be correlated with facular bright points at the photospheric level. In this work, we demonstrate that this spatial intermittency of the magnetic field persists even up to the chromospheric heights. The small-scale bright elements visible in the bright network lanes of solar network structure as seen in the Ca ii H images are termed as network bright points. We use special Hinode campaigns devoted to observe polar regions of the Sun to study the polar network bright points during the phase of last extended solar minimum. We use Ca ii H images of chromosphere observed by Solar Optical Telescope (SOT). For magnetic field information, level 2 data of spectro-polarimeter (SP) is used. We observe a considerable association between the polar network bright points and magnetic field concentrations. The intensity of such bright points is found to be correlated well with the photospheric magnetic field strength underneath with a linear relation existing between them. **2007-11-08, 2008-12-04, 2008-12-05, 2009-04-01, 2010-05-14, 2012-03-18**

Coronal Elemental Abundance: New Results from Soft X-ray Spectroscopy of the Sun

S. **Narendranath**, P. Sreekumar, Netra S Pillai, S. Panini, K. Sankarasubramanian, Juhani Huovelin
Solar Phys. **297**, Article number: 107 **2020**
https://arxiv.org/pdf/2011.08584.pdf
https://doi.org/10.1007/s11207-022-02038-w
Elemental abundances in the solar corona are known to be different from those observed in the solar photosphere. The ratio of coronal to photospheric abundance shows a dependence on the first ionisation potential (FIP) of the element. We estimate FIP bias from direct measurements of elemental abundances from soft X-ray spectra using data from multiple space missions covering a range of solar activity levels. This comprehensive analysis shows clear evidence for a decrease in FIP bias around maximum intensity of the X-ray flare with coronal abundances briefly tending to photospheric values and a slow recovery as the flare decays. The departure from coronal abundances are larger for the low FIP elements Ca, Fe and Si than for S which have a mid FIP value. These changes in the degree of fractionation might provide inputs to model wave propagation through the chromosphere during flares.

Response to Comment on “Tidally Synchronized Solar Dynamo: A Rebuttal”

Henri-Claude **Nataf**
Solar Physics volume 298, Article number: 33 (**2023**)
https://doi.org/10.1007/s11207-023-02128-3
The core of my article (Nataf in Solar Phys. 297, 107, 2022) was about a flaw in the reasoning used by Stefani, Giesecke, and Weier (Solar Phys. 294, 60, 2019) to demonstrate that the ∼11∼11-year Schwabe cycle is “clocked”. To give some background and point out other difficulties, I displayed tidal signals built from a very simple four-planet model. Nicola Scafetta criticizes this simplified tidal model because it assumes circular orbits. This is correct. It seems that he did not notice that I referred to the article of Okal and Anderson (Nature, 253, 511, 1975), who were the first to construct a tidal model that takes into account the actual orbits of these four planets. His comment gives me the opportunity to be more explicit on this question. The main conclusion of my original article does not change: no support for a planetary influence on solar cycles.

Tidally synchronized solar dynamo: a rebuttal

Henri-Claude **Nataf**
Solar Phys. 297, 107 **2022**
https://arxiv.org/pdf/2206.14809.pdf
The idea of a planetary origin for the solar cycle dates back to the nineteenth century. Despite unsurmounted problems, it is still advocated by some. Stefani, Giesecke, and Weier (2019) thus recently proposed a scenario based on this idea. A key argument they put forward is evidence that the ∼11 years-solar cycle is clocked. Their demonstration rests upon the computation of a ratio proposed by Dicke (1978) applied to the solar cycle time series of Schove (1955). I show that their demonstration is invalid, because the assumptions used by Schove to build his time series force a clocked behaviour. I also show that instabilities in a magnetized fluid can produce fluctuation time series that are close to being clocked.
See Comment https://link.springer.com/content/pdf/10.1007/s11207-023-02118-5.pdf

Thermal conduction effects on formation of chromospheric solar tadpole-like jets

Anamaría **Navarro**, F. D. Lora-Clavijo K. Murawski, Stefaan Poedts
MNRAS **2020**

https://arxiv.org/pdf/2011.02006.pdf
We measure the effects of non-isotropic thermal conduction on generation of solar chromospheric jets through numerical simulations carried out with the use of one fluid MHD code MAGNUS. Following the work of Srivastava et al. (2018), we consider the atmospheric state with a realistic temperature model and generate the ejection of plasma through a gas pressure driver operating in the top chromosphere. We consider the magnetic field mimicking a flux tube and perform parametric studies by varying the magnetic field strength and the amplitude of the driver. We find that in the case of thermal conduction the triggered jets exhibit a considerably larger energy and mass fluxes and their shapes are more collimated and penetrate more the solar corona than for the ideal MHD equations. Low magnetic fields allow these jets to be more energetic, and larger magnetic fields decrease the enhancement of mass and energy due to the inclusion of the thermal conductivity.

Feasibility of Ion-cyclotron Resonant Heating in the Solar Wind

Roberto E. **Navarro**1, Víctor Muñoz2, Juan A. Valdivia2, and Pablo S. Moya2,3
2020 ApJL 898 L9
https://doi.org/10.3847/2041-8213/aba0ae
Wave–particle interactions are believed to be one of the most important kinetic processes regulating the heating and acceleration of solar wind plasma. One possible explanation for the observed preferential heating of alpha (He+2) ions relies on a process similar to a second-order Fermi acceleration mechanism. In this model, heavy ions are able to resonate with multiple counter-propagating ion-cyclotron waves, while protons can encounter only single resonances, resulting in the subsequent preferential energization of minor ions. In this work, we address and test this idea by calculating the number of plasma particles that are resonating with ion-cyclotron waves propagating parallel and antiparallel to an ambient magnetic field $\boldsymbol{B}_0$ in a proton/alpha plasma with cold electrons. Resonances are calculated through the proper kinetic multispecies dispersion relation of Alfvén waves. We show that 100% of the alpha population can resonate with counter-propagating waves below a threshold $|\Delta U_{\alpha p}/v_A| < U_0 + a(\beta_p + \beta_0)^b$ in the differential streaming between protons and He+2 ions, where U 0 = −0.532, a = 1.211, β 0 = 0.0275, and b =0.348 for isotropic ions. This threshold seems to match with constraints of the observed ΔU αp in the solar wind for low values of the plasma beta (β p). Finally, it is also shown that this process is limited by the growth of plasma kinetic instabilities, a constraint that could explain alpha-to-proton temperature ratio observations in the solar wind at 1 au.

Study of the effects of magnetic braking on the lithium abundances of the Sun and solar-type stars

R. Caballero **Navarro**, A. García Hernández, A. Ayala, J.C. Suárez
MNRAS **2020**
https://arxiv.org/pdf/2006.01899.pdf
The study of lithium (Li) surface abundance in the Sun and young stellar globular clusters which are seemingly anomalous in present-day scenarios, as well as the influence of rotation and magnetic braking (MB) on its depletion during pre-main sequence (PMS) and main sequence (MS). In this work, the effects of rotational mixing and of the rotational hydrostatic effects on Li abundances are studied by simulating several grids of PMS and MS rotating and non-rotating models. Those effects are combined with the additional impact of the MB (with magnetic field intensities ranging between 3.0 and 5.0 G). The data obtained from simulations are confronted by comparing different stellar parameters. The results show that the surface Li abundance for the Sun like models at the end of the PMS and throughout the MS decreases when rotational effects are included, i.e. the Li depletion rate for rotating models is higher than for non-rotating ones. This effect is attenuated when the MB produced by a magnetic field is present. This physical phenomena impacts also the star effective temperature (Teff) and its location in the HR diagram. The impact of MB in Li depletion is sensitive to the magnetic field intensity: the higher it is, the lower the Li destruction. A direct link between the magnetic fields and the convective zone (CZ) size is observed: stronger magnetic fields produce shallower CZ's. This result suggests that MB effect must be taken into consideration during PMS if we aim to reproduce Li abundances in young clusters.

A Multicomponent Approach for Strongly Collisional Plasmas in the Solar Atmosphere

Anatoly K. **Nekrasov**
Solar Phys. February **2015**, Volume 290, Issue 2, pp 389-397
A simple collisional three-component plasma model consisting of electrons, ions, and neutrals with arbitrary collision frequencies and dynamic time scales is considered. For the partially ionized plasma with a strong collisional coupling of neutrals with ions, magnetosonic and Alfvén waves modified by neutrals are obtained. It is shown that the magnetic diffusivity appears for magnetosonic waves as a result of the ion transverse collision current connected with the field E 1⊥ and for Alfvén waves because both the ion transverse collision current and the electron longitudinal collision current are connected with E 1z at the angular propagation of perturbations relative to the background magnetic field.

The model can be applied to different parts of the solar atmosphere and prominences.

Spatial distributions of EUV brightenings in the quiet-Sun

C. J. **Nelson**, L. A. Hayes, D. Müller, S. Musset, N. Freij, F. Auchère, R. Aznar Cuadrado, K. Barczynski, E. Buchlin, L. Harra, D. M. Long, S. Parenti, H. Peter, U. Schühle, P. Smith, L. Teriaca, C. Verbeeck, A. N. Zhukov, D. Berghmans

A&A **2024**

https://arxiv.org/pdf/2411.00467

The identification of large numbers of localised transient EUV brightenings, with small spatial scales, in the quiet-Sun corona has been one of the key early results from Solar Orbiter. However, much is still unknown about these events. Here, we aim to better understand EUV brightenings by investigating their spatial distributions, specifically whether they occur co-spatial with specific line-of-sight magnetic field topologies in the photospheric network. EUV brightenings are detected using an automated algorithm applied to a high-cadence (3 s) dataset sampled over ~30 min on **8 March 2022** by the Extreme Ultraviolet Imager's 17.4 nm EUV High Resolution Imager. Data from the Solar Dynamics Observatory's Helioseismic and Magnetic Imager and Atmospheric Imaging Assembly are used to provide context about the line-of-sight magnetic field and for alignment purposes. We found a total of 5064 EUV brightenings within this dataset that are directly comparable to events reported previously in the literature. These events occurred within around 0.015-0.020 % of pixels for any given frame. We compared eight different thresholds to split the EUV brightenings into four different categories related to the line-of-sight magnetic field. Using our preferred threshold, we found that 627 EUV brightenings (12.4 %) occurred co-spatial with Strong Bipolar configurations and 967 EUV brightenings (19.1 %) occurred in Weak Field regions. Fewer than 10 % of EUV brightenings occurred co-spatial with Unipolar line-of-sight magnetic field no matter what threshold was used. Of the 627 Strong Bipolar EUV Brightenings, 54 were found to occur co-spatial with cancellation whilst 57 occurred co-spatial with emergence. EUV brightenings preferentially occur co-spatial with the strong line-of-sight magnetic field in the photospheric network. They do not, though, predominantly occur co-spatial with (cancelling) bi-poles.

EUV brightenings in the quiet-Sun: Signatures in spectral and imaging data from the Interface Region Imaging Spectrograph

C. J. **Nelson**, F. Auchère, R. Aznar Cuadrado, K. Barczynski, E. Buchlin, L. Harra, D. M. Long, S. Parenti, H. Peter, U. Schühle, C. Schwanitz, P. Smith, L. Teriaca, C. Verbeeck, A. N. Zhukov, D. Berghmans

A&A 676, A64 **2023**

https://arxiv.org/pdf/2306.05190

https://www.aanda.org/articles/aa/pdf/2023/08/aa46144-23.pdf

Localised transient EUV brightenings, sometimes named `campfires', occur throughout the quiet-Sun. However, there are still many open questions about such events, in particular regarding their temperature range and dynamics. In this article, we aim to determine whether any transition region response can be detected for small-scale EUV brightenings and, if so, to identify whether the measured spectra correspond to any previously reported bursts in the transition region, such as Explosive Events (EEs). EUV brightenings were detected in a ~29.4 minute dataset sampled by Solar Orbiter's Extreme Ultraviolet Imager on **8 March 2022** using an automated detection algorithm. Any potential transition region response was inferred through analysis of imaging and spectral data sampled through coordinated observations conducted by the Interface Region Imaging Spectrograph (IRIS). EUV brightenings display a range of responses in IRIS slit-jaw imager (SJI) data. Some events have clear signatures in the Mg II and Si IV SJI filters, whilst others have no discernible counterpart. Both extended and more complex EUV brightenings are found to, sometimes, have responses in IRIS SJI data. Examples of EUI intensities peaking before, during, and after their IRIS counterparts were found in lightcurves constructed co-spatial to EUV brightenings. Importantly, therefore, it is likely that not all EUV brightenings are driven in the same way, with some seemingly being magnetic reconnection driven and others not. A single EUV brightening occurred co-spatial to the IRIS slit, with its spectra matching the properties of EEs. EUV brightenings is a term used to describe a range of small-scale event in the solar corona. The physics responsible for all EUV brightenings is likely not the same and, therefore, more research is required to assess their importance towards global questions in the field, such as coronal heating.

IRIS Nugget 14 Feb **2024** https://iris.lmsal.com/nugget

Oscillations in the line-of-sight magnetic field strength in a pore observed by the GREGOR Infrared Spectrograph (GRIS)

C. J. **Nelson**, R. J. Campbell and M. Mathioudakis

A&A 654, A50 (**2021**)

https://www.aanda.org/articles/aa/pdf/2021/10/aa41368-21.pdf

Context. Numerous magnetohydrodynamic oscillations have been reported within solar pores over the past few decades, including in line-of-sight (LOS) velocities, intensities, and magnetic field strengths.

Aims. Our aim is to identify whether high-amplitude oscillations in the LOS magnetic field strength can be detected within a pore located in Active Region 12748 and to investigate which physical mechanisms could be responsible for them.
Methods. A solar pore was observed on **1 September 2019** using the GREGOR Infrared Spectrograph instrument for around one hour. Full-Stokes vectors were sampled in a 37 Å window containing the Fe I 15 648.52 Å line (effective Landé g factor of 3). The LOS magnetic field strength was inferred using the strong-field approximation. Additionally, the Stokes Inversion based on Response functions code was used to gain a more complete understanding of the physical properties of the solar atmosphere at the locations of these oscillations.
Results. Oscillations of more than 100 G are observed in the LOS magnetic field in the period window between 600 and 1272 s at three localised (> 1″2) regions. These oscillations have coherence across individual regions, indicating that jitter cannot account for their occurrence. Longer-period amplitude variations, amplitudes over 200 G, are also detected, but they have periods outside of the cone-of-influence. Numerical inversions confirm both oscillations in the LOS magnetic field strength at optical depths of around log $\tau 5000 = -0.5$ (potentially caused by compression) and other effects (e.g. changes in the optical depth or the inclination of the magnetic field) may account for these changes.
Conclusions. The oscillations in the separations of the Stokes-V lobes of the 15 648.52 Å line appear to be solar in nature. Future work will be required to understand whether these are truly oscillations in the magnetic field strength at a specific depth in the solar atmosphere or whether other effects are responsible for these signatures.

Driving Solar Giant Cells through the Self-Organization of Near-Surface Plumes

Nicholas J. **Nelson**, Nicholas A. Featherstone, Mark S. Miesch, Juri Toomre
ApJ **2018**
https://arxiv.org/pdf/1804.01166.pdf
Global 3D simulations of solar giant-cell convection have provided significant insight into the processes which yield the Sun's observed differential rotation and cyclic dynamo action. However, as we move to higher resolution simulations a variety of codes have encountered what has been termed the convection conundrum. As these simulations increase in resolution and hence the level of turbulence achieved, they tend to produce weak or even anti-solar differential rotation patterns associated with a weak rotational influence (high Rossby number) due to large convective velocities. One potential culprit for this convection conundrum is the upper boundary condition applied in most simulations which is generally impenetrable. Here we present an alternative stochastic plume boundary condition which imposes small-scale convective plumes designed to mimic near-surface convective downflows, thus allowing convection to carry the majority of the outward solar energy flux up to and through our simulated upper boundary. The use of a plume boundary condition leads to significant changes in the convective driving realized in the simulated domain and thus to the convective energy transport, the dominant scale of the convective enthalpy flux, and the relative strength of the strongest downflows, the downflow network, and the convective upflows. These changes are present even far from the upper boundary layer. Additionally, we demonstrate that in spite of significant changes, giant cell morphology in the convective patterns is still achieved with self-organization of the imposed boundary plumes into downflow lanes, cellular patterns, and even rotationally-aligned banana cells in equatorial regions. This plume boundary presents an alternative pathway for 3D global convection simulations where driving is non-local and may provide a new approach towards addressing the convection conundrum.

IRIS Burst Spectra Co-spatial to a Quiet-Sun Ellerman-like Brightening

C. J. **Nelson**1,2, N. Freij3, A. Reid2, R. Oliver3,4, M. Mathioudakis2, and R. Erdélyi
2017 ApJ 845 16
http://iopscience.iop.org/article/10.3847/1538-4357/aa7e7a/pdf
Ellerman bombs (EBs) have been widely studied over the past two decades; however, only recently have the counterparts of these events been observed in the quiet-Sun. The aim of this article is to further understand small-scale quiet-Sun Ellerman-like brightenings (QSEBs) through research into their spectral signatures, including investigating whether the hot signatures associated with some EBs are also visible co-spatial to any QSEBs. We combine Hαand Ca ii 8542 Å line scans at the solar limb with spectral and imaging data sampled by the Interface Region Imaging Spectrograph (IRIS). Twenty-one QSEBs were identified with average lifetimes, lengths, and widths measured to be around 120 s, $0\overset{''}{.}63$, and $0\overset{''}{.}35$, respectively. Three of these QSEBs displayed clear repetitive flaring through their lifetimes, comparable to the behavior of EBs in active regions. Two QSEBs in this sample occurred co-spatial to increased emission in SDO/AIA 1600 Å and IRIS slit-jaw imager 1400 Å data; however, these intensity increases were smaller than those reported co-spatially with EBs. One QSEB was also sampled by the IRIS slit during its lifetime, displaying increases in intensity in the Si iv 1393 Å and Si iv1403 Å cores, as well as the C ii and Mg ii line wings, analogous to IRIS bursts (IBs). Using RADYN simulations, we are unable to reproduce the observed QSEB Hα and Ca ii 8542 Å line profiles, leaving the question of the temperature

stratification of QSEBs open. Our results imply that some QSEBs could be heated to transition region temperatures, suggesting that IB profiles should be observed throughout the quiet-Sun. **2016 June 9**

On The Relationship Between Magnetic Cancellation and UV Burst Formation

C. J. **Nelson**, J. G. Doyle, R. Erdelyi
MNRAS **2016**
http://arxiv.org/pdf/1608.06505v1.pdf
Burst-like events with signatures in the UV are often observed co-spatial to strong line-of-sight photospheric magnetic fields. Several authors, for example, have noted the spatial relationship between Ellerman bombs (EBs) and Moving Magnetic Features (MMFs), regions of flux which disconnect from a sunspot or pore before propagating away in the moat flow and often displaying evidence of cancellation. In this article, data collected by the Solar Dynamics Observatory's Helioseismic and Magnetic Imager and Atmospheric Imaging Assembly are analysed in an attempt to understand the potential links between such cancellation and UV burst formation. Two MMFs from AR 11579, three bi-poles from AR 11765, and six bi-poles (four of which were co-spatial to IRIS bursts) in AR 11850 were identified for analysis. All of these cancellation features were found to have lifetimes of the order hours and cancellation rates of the order 10^14-10^15 Mx s^-1. H-alpha line wing data from the Dunn Solar Telescope's Interferometric BIdimensional Spectrometer were also available for AR 11579 facilitating a discussion of links between MMFs and EBs. Using an algebraic model of photospheric magnetic reconnection, the measured cancellation rates are then used to ascertain estimates of certain quantities (such as up-flow speeds, jet extents, and potential energy releases) which compared reasonably to the properties of EBs reported within the literature. Our results suggest that cancellation rates of the order measured here are capable of supplying enough energy to drive certain UV bursts (including EBs), however, they are not a guaranteeing condition for burst formation. **30th September 2012**

Small-scale Structuring of Ellerman Bombs at the Solar Limb

C. J. **Nelson**1,2, E. M. Scullion3,4, J. G. Doyle1, N. Freij2, and R. Erdélyi
2015 ApJ 798 19
Ellerman bombs (EBs) have been widely studied in recent years due to their dynamic, explosive nature and apparent links to the underlying photospheric magnetic field implying that they may be formed by magnetic reconnection in the photosphere. Despite a plethora of researches discussing the morphologies of EBs, there has been a limited investigation of how these events appear at the limb, specifically, whether they manifest as vertical extensions away from the disk. In this article, we make use of high-resolution, high-cadence observations of an Active Region at the solar limb, collected by the CRisp Imaging SpectroPolarimeter (CRISP) instrument, to identify EBs and infer their physical properties. The upper atmosphere is also probed using the Solar Dynamic Observatory's Atmospheric Imaging Assembly (SDO/AIA). We analyze 22 EB events evident within these data, finding that 20 appear to follow a parabolic path away from the solar surface at an average speed of 9 km s–1, extending away from their source by 580 km, before retreating back at a similar speed. These results show strong evidence of vertical motions associated with EBs, possibly explaining the dynamical "flaring" (changing in area and intensity) observed in on-disk events. Two in-depth case studies are also presented that highlight the unique dynamical nature of EBs within the lower solar atmosphere. The viewing angle of these observations allows for a direct linkage between these EBs and other small-scale events in the Hα line wings, including a potential flux emergence scenario. The findings presented here suggest that EBs could have a wider-reaching influence on the solar atmosphere than previously thought, as we reveal a direct linkage between EBs and an emerging small-scale loop, and other near-by small-scale explosive events. However, as previous research found, these extensions do not appear to impact upon the Hα line core, and are not observed by the SDO/AIA EUV filters.

Exploring the solar paradigm to explain stellar variability **Thesis-Review**

Nina-Elisabet **Nèmec**
2021
https://arxiv.org/pdf/2106.13183.pdf
The unprecedented precision of broadband stellar photometry achieved with the planet-hunting missions CoRoT and \textit{Kepler} initiated a new era in examining the magnetically-driven brightness variations of hundreds of thousands of stars. Such brightness variations are well studied and understood for the Sun. The plethora of data allows to accurately compare solar and stellar brightness variations. An intriguing question is whether the observed trends in the stellar photometric variability (e.g. the dependence of the variability on the stellar rotation period) can be explained by utilising the solar paradigm, in particular the physical concepts of brightness variations learnt from the Sun. The goal of this work is to find out, through comparison of observational and simulated data, if any physical concepts of solar brightness variability have to be altered to reproduce the distribution of Sun-like stars variabilities.

Connecting measurements of solar and stellar brightness variations

N.-E. **Nèmec** (1), E. Işık (2, 1), A. I. Shapiro (1), S. K. Solanki (1, 3), N. A. Krivova (1), Y. Unruh (4)
A&A 638, A56 **2020**
https://arxiv.org/pdf/2004.06974.pdf
https://www.aanda.org/articles/aa/pdf/2020/06/aa38054-20.pdf
Comparing solar and stellar brightness variations is hampered by the difference in spectral passbands used in observations as well as by the possible difference in the inclination of their rotation axes from the line of sight. We calculate the rotational variability of the Sun as it would be measured in passbands used for stellar observations. In particular, we consider the filter systems used by the CoRoT, Kepler, TESS, and Gaia space missions. We also quantify the effect of the inclination of the rotation axis on the solar rotational variability. We employ the Spectral And Total Irradiance REconstructions (SATIRE) model to calculate solar brightness variations in different filter systems as observed from the ecliptic plane. We then combine the simulations of the surface distribution of the magnetic features at different inclinations using a surface flux transport model (SFTM) with the SATIRE calculations to compute the dependence of the variability on the inclination. For an ecliptic-bound observer, the amplitude of the solar rotational variability, as observed in the total solar irradiance (TSI) is 0.68 mmag (averaged over solar cycles 21-24). We obtained corresponding amplitudes in the Kepler (0.74 mmag), CoRoT (0.73 mmag), TESS (0.62 mmag), Gaia (0.74 mmag), Gaia GRP (0.62 mmag), and), Gaia GBP (0.86 mmag) passbands. Decreasing the inclination of the rotation axis decreases the rotational variability. For a sample of randomly inclined stars, the variability is on average 15% lower in all filter systems considered in this work. This almost compensates for the difference in the amplitudes of the variability in TSI and Kepler passbands, making the amplitudes derived from the TSI records an ideal representation of the solar rotational variability for comparison to Kepler stars with unknown inclinations.

Power spectra of solar brightness variations at different inclinations

N.-E. **Nèmec** (1), A. I. Shapiro (1), N. A. Krivova (1), S. K. Solanki (1,2), R. V. Tagirov (1,3), R. H. Cameron (1), S. Dreizler
A&A **2020**
https://arxiv.org/pdf/2002.10895.pdf
Magnetic features on the surfaces of cool stars cause variations of their brightness. Such variations have been extensively studied for the Sun. Recent planet-hunting space telescopes allowed measuring brightness variations in hundred thousands of other stars. The new data posed the question of how typical is the Sun as a variable star. Putting solar variability into the stellar context suffers, however, from the bias of solar observations being made from its near-equatorial plane, whereas stars are observed at all possible inclinations. We model solar brightness variations at timescales from days to years as they would be observed at different inclinations. In particular, we consider the effect of the inclination on the power spectrum of solar brightness variations. The variations are calculated in several passbands routinely used for stellar measurements. We employ the Surface Flux Transport Model (SFTM) to simulate the time-dependent spatial distribution of magnetic features on both near- and far-sides of the Sun. This distribution is then used to calculate solar brightness variations following the SATIRE (Spectral And Total Irradiance REconstruction) approach. We have quantified the effect of the inclination on solar brightness variability at timescales down to a day. Thus, our results allow making solar brightness records directly comparable to those obtained by the planet-hunting space telescopes. Furthermore, we decompose solar brightness variations into the components originating from the solar rotation and from the evolution of magnetic features.

Can the long-term hemispheric asymmetry of solar activity result from fluctuations in dynamo parameters?

Alexander **Nepomnyashchikh**, Sudip Mandal, Dipankar Banerjee, Leonid Kitchatinov
A&A 625, A37 **2019**
https://arxiv.org/pdf/1903.10707.pdf
The hemispheric asymmetry of sunspot activity observed possesses a regular component varying on a time scale of several solar cycles whose origin and properties are currently debated. This paper addresses the question of whether the long-term hemispheric asymmetry can result from random variations of solar dynamo parameters in time and latitude. Scatter in the observed tilt angles of sunspot groups is estimated to infer constraints on fluctuations in the dynamo mechanism for poloidal field regeneration. A dynamo model with fluctuations in the Babcock-Leighton type α-effect is designed in accordance with these constraints and then used to compute a large number of magnetic cycles for statistical analyses of their hemispheric asymmetry. Hemispheric asymmetry in the simulated dynamo results from the presence of an equator-symmetric part in the oscillating magnetic field. The subdominant quadrupolar oscillations are stochastically forced by dominant dipolar oscillations via the equator-symmetric part of the fluctuating α-effect. The amplitude and sense of the asymmetry of individual cycles varies on a time scale of the order of four dynamo-cycle periods. The variations are irregular, i.e. not periodic. The model suggests that asymmetry in the polar magnetic fields in the solar minima can be used as a precursor for asymmetry of sunspot activity in the following solar cycle.

Auto-Calibration of Remote Sensing Solar Telescopes with Deep Learning

Brad **Neuberg**, Souvik Bose, Valentina Salvatelli, Luiz F.G. dos Santos, Mark Cheung, Miho Janvier, Atilim Gunes Baydin, Yarin Gal, Meng Jin

NeurIPS 2019 Workshop ML4PS **2019**

https://arxiv.org/pdf/1911.04008.pdf

As a part of NASA's Heliophysics System Observatory (HSO) fleet of satellites,the Solar Dynamics Observatory (SDO) has continuously monitored the Sun since2010. Ultraviolet (UV) and Extreme UV (EUV) instruments in orbit, such asSDO's Atmospheric Imaging Assembly (AIA) instrument, suffer time-dependent degradation which reduces instrument sensitivity. Accurate calibration for (E)UV instruments currently depends on periodic sounding rockets, which are infrequent and not practical for heliophysics missions in deep space. In the present work, we develop a Convolutional Neural Network (CNN) that auto-calibrates SDO/AIA channels and corrects sensitivity degradation by exploiting spatial patterns in multi-wavelength observations to arrive at a self-calibration of (E)UV imaging instruments. Our results remove a major impediment to developing future HSOmissions of the same scientific caliber as SDO but in deep space, able to observe the Sun from more vantage points than just SDO's current geosynchronous orbit.This approach can be adopted to perform autocalibration of other imaging systems exhibiting similar forms of degradation

Reconstructed sunspot positions in the Maunder Minimum based on the correspondence of Gottfried Kirch

R. **Neuhäuser**, R. Arlt, S. Richter

Astronomische Nachrichten - Astronomical Notes **2018**

https://arxiv.org/pdf/1807.10241.pdf

We present reconstructed sunspot positions based on observations reported in letters between Gottfried Kirch and other contemporary astronomers from AD 1680 to 1709, i.e. in the last decades of the Maunder Minimum. The letters were compiled and edited by Herbst (2006). The letters (and observations) from Kirch are mostly by Gottfried Kirch, but some also by his 2nd wife Maria M. Kirch (married 1692) and their son Christfried Kirch (born 1694). Using excerpts from the letters, some with drawings, we found some 35 sunspot groups (often for several days in a row or with interruptions) by Kirch and/or his letter partners (in three cases, only the month is given: 1704 Jan, Feb, 1707 Mar, otherwise always the exact dates) - usually one group at a time. We also found 17 explicit spotless days, several of them new (previously without any known observations). We could constrain the heliographic latitude by Bayesian inference for 19 sunspot groups - five of them completely new (one group 1680 May 20-22 from Kirch and Ihle, one to two groups 1680 Jun 15-23 for Kirch, one group 1684 May 6 from Ihle, and one group 1688 Dec 14-15 from Kirch), while the others mostly agree (within 2sigma) with previously published values for those dates by others. With these data, we then amend the butterfly diagram for the Maunder Minimum. By comparison of our data with the sunspot group catalog in Hoyt & Schatten (1998), we noticed a number of discrepancies, e.g. that dates for British observers in the Maunder Minimum (Flamsteed, Caswell, Derham, Stannyan, Gray, and Sharp) as listed in Hoyt & Schatten (1998) are their original Julian dates, not converted to the Gregorian calendar (10-11 day offset in Hoyt & Schatten). Most of these modifications also apply to the modified sunspot group catalog in Vaquero et al. (2016). We also present two aurorae observed by the Kirchs in 1707 and 1716.

New sunspots and aurorae in the historical Chinese text corpus? Comments on uncritical digital search applications

D.L. **Neuhaeuser**, R. Neuhaeuser , J. Chapman

Astron. Nachr. / AN 999, No. 88, 1 – 20 (**2018**)

https://arxiv.org/pdf/1711.05132.pdf

We review some applications of the method of electronic searching for historical observations of sunspots and aurorae in the Chinese text corpus by Hayakawa et al. etc. However, we show strong shortcomings in the digital search technique as applied by them: almost all likely true sunspot and aurora records were presented before (e.g. Xu et al. 2000), which is not mentioned in those papers; the remaining records are dubious and often refer to other phenomena, neither spots nor aurorae (this also applies to Hayakawa et al. 2017c). Most of the above publications include very few Chinese texts and translations, and their tables with abbreviated keywords do not allow the reader to consider alternative interpretations (the tables also do not specify which records mention night-time). We have compared some of their event tables with previously published catalogs and found various discrepancies. There are also intrinsic inconsistencies, misleading information (lunar phase for day-time events), and dating errors. We present Chinese texts and translations for some of their presumable new aurorae: only one can be considered a likely true aurora (AD 604 Jan); some others were selected on the sole basis of the use of the word "light" or "rainbow". Several alleged new aurorae present observations beside the Sun during day-time. There are well-known comets among their presumable aurorae. We also discuss, (i) whether "heiqi ri pang" can stand for black spot(s) "on one side of" or "beside" the sun, (ii) aurora color confusion in Hayakawa et al. (2015, 2016), and (iii) whether "white" and "unusual rainbows" can be aurorae.

Sunspot numbers based on historic records in the 1610s - early telescopic observations by Simon Marius and others

Ralph **Neuhaeuser**, Dagmar L. Neuhaeuser
Astronomical Notes **2016**
http://arxiv.org/pdf/1604.03724v1.pdf
Hoyt & Schatten (1998) claim that Simon Marius would have observed the sun from 1617 Jun 7 to 1618 Dec 31 (Gregorian calendar) all days, except three short gaps in 1618, but would never have detected a sunspot -- based on a quotation from Marius in Wolf (1857), but misinterpreted by Hoyt & Schatten. Marius himself specified in early 1619 that "for one and a half year ... rather few or more often no spots could be detected ... which was never observed before" (Marius 1619). The generic statement by Marius can be interpreted such that the active day fraction was below 0.5 (but not zero) from fall 1617 to spring 1619 and that it was 1 before fall 1617 (since August 1611). Hoyt & Schatten cite Zinner (1952), who referred to Zinner (1942), where observing dates by Marius since 1611 are given, but which were not used by Hoyt & Schatten. We present all relevant texts from Marius where he clearly stated that he observed many spots in different form on and since 1611 Aug 3 (Julian) = Aug 13 (Greg.) (on the first day together with Ahasverus Schmidnerus), 14 spots on 1612 May 30 (Julian) = Jun 9 (Greg.), which is consistent with drawings by Galilei and Jungius for that day, the latter is shown here for the first time, at least one spot on 1611 Oct 3 and/or 11 (Julian), i.e. Oct 13 and/or 21 (Greg.), when he changed his sunspot observing technique, he also mentioned that he has drawn sunspots for 1611 Nov 17 (Julian) = Nov 27 (Greg.), in addition to those clearly datable detections, there is evidence in the texts for regular observations. ... Sunspots records by Malapert from 1618 to 1621 show that the last low-latitude spot was seen in Dec 1620, while the first high-latitude spots were noticed in June and Oct 1620, so that the Schwabe cycle turnover (minimum) took place around that time, ..

Newly found sunspot observations by Peter Becker from Rostock for 1708, 1709, and 1710

Ralph **Neuhaeuser** (U Jena), Rainer Arlt (AIP Potsdam), Elvira Pfitzner (Rostock), Susanne Richter
Astron. Nachr. / AN 999, No. 88, 789 – 799 (**2011**)
http://arxiv.org/pdf/1508.05798v1.pdf
We present a few newly found old sunspot observations from the years AD 1708, 1709, and 1710, which were obtained by Peter Becker from Rostock, Germany. For 1709, Becker gave a detailed drawing: he observed a sunspot group made up of two spots on Jan 5, 6, and 7, and just one of the two spots was observed on Jan 8 and 9. We present his drawing and his explanatory text. We can measure the latitude and longitude of these two spots and estimate their sizes for all five days. While the spots and groups in 1708 and the spot on four of the five days in January 1709 were known before from other observers (e.g. Hoyt & Schatten 1998), the location of the spots in early January 1709 were not known before, so that they can now be considered in reconstructed butterfly diagrams. The sunspots detected by Becker on 1709 Jan 5 and 1710 Sep 10 were not known before at all, as the only observer known for those two dates, La Hire, did not detect that spot (group). We estimate new group sunspot numbers for the relevant days, months, and years. The time around 1708--1710 is important, because it documents the recovery of solar activity towards the end of the Maunder Grand Minimum. We also show two new spot observations from G. Kirch for 1708 Sep 13 \& 14 as described in his letter to Wurzelbaur (dated Berlin AD 1708 Dec 19).

Solar activity around AD 775 from aurorae and radiocarbon

Ralph **Neuhaeuser**, Dagmar L. Neuhaeuser
Astron. Nachr. / AN **999**, No. 88, 789 – 812 (**2011**)
http://arxiv.org/pdf/1503.01581v1.pdf
A large variation in 14 C around AD 775 has been considered to be caused by one or more solar super-flares within one year. We critically review all known aurora reports from Europe as well as the Near, Middle, and Far East from AD 731 to 825 and find 39 likely true aurorae plus four more potential aurorae and 24 other reports about halos, meteors, thunderstorms etc., which were previously misinterpreted as aurorae or misdated; we assign probabilities for all events according to five aurora criteria. We find very likely true aurorae in AD 743, 745, 762, 765, 772, 773, 793, 796, 807, and 817. There were two aurorae in the early 770s observed near Amida (now Diyarbakir in Turkey near the Turkish-Syrian border), which were not only red, but also green-yellow - being at a relatively low geo-magnetic latidude, they indicate a relatively strong solar storm. However, it cannot be argued that those aurorae (geo-magnetical latitude 43 to 50 deg, considering five different reconstructions of the geo-magnetic pole) could be connected to one or more solar super-flares causing the 14 C increase around AD 775: There are several reports about low- to mid-latitude aurorae at 32 to 44 deg geo-magnetical latitude in China and Iraq; some of them were likely observed (quasi-)simultaneously in two of three areas (Europe, Byzantium/Arabia, East Asia), one lasted several nights, and some indicate a particulary strong geo-magnetic storm (red colour and dynamics), namely in AD 745, 762, 793, 807, and 817 - always without 14 C peaks. We use 39 likely true aurorae as well as historic reports

about sunspots together with the radiocarbon content from tree rings to reconstruct solar activity: From about AD 733 to 823, we see at least nine Schwabe cycles ...

CNO Solar Neutrinos in Next-Generation Dark Matter Experiments

Jayden L. **Newstead**, Louis E. Strigari, Rafael F. Lang
2018
https://arxiv.org/pdf/1807.07169.pdf
We study the prospects for measuring the low-energy components of the solar neutrino flux in future direct dark matter detection experiments. We show that for a depletion of 136Xe by a factor of 100 relative to its natural abundance, and an extension to electron recoil energies of ~ MeV, future xenon experiments with exposure ~200 ton-yr can detect the CNO component of the solar neutrino flux at ~3σ significance. A CNO detection will provide important insight into metallicity of the solar interior. Precise measurement of low-energy solar neutrinos, including as pp, 7Be, and pep components, will further improve constraints on the "neutrino luminosity" of the Sun, thereby providing constraints on alternative sources of energy production. We find that a measurement of Lν/L⊙ of order one percent is possible with the above exposure, improving on current bounds from a global analysis of solar neutrino data by a factor of about seven.

Coronal Mass Ejections, Solar Cycles and Magnetic Poles Reversal,

Kim Kwee **Ng**,
American Journal of Astronomy and Astrophysics. Vol. 7, No. 1, **2019**, pp. 10-17.
10.11648.j.ajaa.20190701.12.pdf
The magnitude of the measured geomagnetic index increases when the Coronal Mass Ejections occur on the Sun's surface. The abrupt increase in the geomagnetic index has seriously impacted the accuracy in the forecast of the activity of the next solar cycle. A method is proposed to filter the effect from the Coronal Mass Ejections. The correlation between the geomagnetic index and the activity of the subsequent solar cycle is found to have drastically improved with the proposed scheme. A strong correlation between the maximum amplitude RN of a solar cycle N and its pre-cycle coronal mass ejections adjusted monthly geomagnetic activity index has been qualitatively determined, as illustrated by an impressive correlation coefficient of 0.91+0.09-0.12, with its statistical significance estimated at 4.3 σ. The corrected data have significantly improved the correlation between the observed variables from their original un-corrected case of 0.63 ± 0.23. Our result indicates that the upcoming solar cycle, estimated at R25 = 147 ± 30, would be stronger than the current waning solar cycle 24. In a related calculation, the magnetic poles reversals occurring in the solar cycles 21 and 22 are reproduced numerically from Maxwell's electromagnetic equations.

Inferring solar differential rotation and viscosity via passive imaging with inertial waves

Tram Thi Ngoc **Nguyen**, Thorsten Hohage, Damien Fournier, Laurent Gizon
WAVES **2024**, Berlin, Germany
https://arxiv.org/pdf/2403.00488.pdf
The recent discovery of inertial waves on the surface of the Sun offers new possibilities to learn about the solar interior. These waves are long-lived with a period on the order of the Sun rotation period (~27 days) and are sensitive to parameters deep inside the Sun. They are excited by turbulent convection, leading to a passive imaging problem. In this work, we present the forward and inverse problem of reconstructing viscosity and differential rotation on the Sun from cross-covariance observations of these inertial waves.

Power-law energy distributions of small-scale impulsive events on the active Sun: Results from IRIS

Nived Vilangot **Nhalil**, Chris J. Nelson, Mihalis Mathioudakis, J. Gerry Doyle, Gavin Ramsay
MNRAS Volume 499, Issue 1, Pages 1385–1394, **2020**
https://arxiv.org/pdf/2009.03123.pdf
https://doi.org/10.1093/mnras/staa2897
Numerous studies have analysed inferred power-law distributions between frequency and energy of impulsive events in the outer solar atmosphere in an attempt to understand the predominant energy supply mechanism in the corona. Here, we apply a burst detection algorithm to high-resolution imaging data obtained by the Interface Region Imaging Spectrograph to further investigate the derived power-law index, γ, of bright impulsive events in the transition region. Applying the algorithm with a constant minimum event lifetime (of either 60 s or 110 s) indicated that the target under investigation, such as Plage and Sunspot, has an influence on the observed power-law index. For regions dominated by sunspots, we always find $\gamma<2$; however, for datasets where the target is a plage region, we often find that $\gamma>2$ in the energy range [~1023, ~1026] erg. Applying the algorithm with a minimum event lifetime of three timesteps indicated that cadence was another important factor, with the highest cadence datasets returning $\gamma>2$ values. The estimated total radiative power obtained for the observed energy distributions is typically 10-25 % of what would be required to sustain the corona indicating that impulsive events in this energy range are

not sufficient to solve coronal heating. If we were to extend the power-law distribution down to an energy of 1021 erg, and assume parity between radiative energy release and the deposition of thermal energy, then such bursts could provide 25-50 % of the required energy to account for the coronal heating problem. **August 31 2013** **Table** 1. Details of the IRIS SJI observations studied here (2013-2016)

Plausibility of ultraviolet burst generation in the low solar chromosphere

Lei **Ni**, Guanchong Cheng, Jun Lin
A&A 665, A116 **2022**
https://arxiv.org/pdf/2206.13080.pdf
https://www.aanda.org/articles/aa/pdf/2022/09/aa43304-22.pdf
Ultraviolet (UV) bursts and Ellerman bombs (EBs) are small-scale magnetic reconnection events taking place in the highly stratified, low solar atmosphere. It is still not clear whether UV bursts have to be generated at a higher atmospheric layer than EBs or whether both UV bursts and EBs can occur in the low chromosphere. We numerically studied the low β magnetic reconnection process around the solar temperature minimum region (TMR). The time-dependent ionization degrees of hydrogen and helium are included in the MHD code, which lead to a more realistic magnetic diffusion caused by electron-neutral collision and ambipolar diffusion. A more realistic radiative cooling model from Carlsson & Leenaarts 2012 is included in the simulations. Our results in high resolution indicate that the plasmas in the reconnection region are heated up to more than 20,000 K if the reconnecting magnetic field is as strong as 500 G, which suggests that UV bursts can be generated in the dense low chromosphere. The dominant mechanism for producing the UV burst in the low chromosphere is heating, as a result of the local compression in the reconnection process. The thermal energy occurring in the reconnection region rapidly increases after the turbulent reconnection mediated by plasmoids is invoked. The average power density of the generated thermal energy in the reconnection region can reach over 1000 erg cm−3 s−1, which is comparable to the average power density accounting for a UV burst. With the strength of the reconnecting magnetic field exceeding 900 G, the width of the synthesized Si IV 1394 A line profile with multiple peaks can reach up to 100 km s−1, which is consistent with observations.

A Magnetic Reconnection model for Hot Explosions in the Cool Atmosphere of the Sun

Lei **Ni**, Yajie Chen, Hardi Peter, Hui Tian, Jun Lin
A&A 646, A88 **2021**
https://arxiv.org/pdf/2011.07692.pdf
UV bursts and Ellerman bombs are transient brightenings observed in the low solar atmospheres of emerging flux regions. Observations have discovered the cospatial and cotemporal EBs and UV bursts, and their formation mechanisms are still not clear. The multi-thermal components with a large temperature span in these events challenge our understanding of magnetic reconnection and heating mechanisms in the low solar atmosphere. We have studied magnetic reconnection between the emerging and back ground magnetic fields. The initial plasma parameters are based on the C7 atmosphere model. After the current sheet with dense photosphere plasma is emerged to 0.5 Mm above the solar surface, plasmoid instability appears. The plasmoids collide and coalesce with each other, which makes the plasmas with different densities and temperatures mixed up in the turbulent reconnection region. Therefore, the hot plasmas corresponding to the UV emissions and colder plasmas corresponding to the emissions from other wavelenghts can move together and occur at about the same height. In the meantime, the hot turbulent structures basically concentrate above 0.4 Mm, whereas the cool plasmas extend to much lower heights to the bottom of the current sheet. These phenomena are consistent with the observations of Chen et al. 2019, ApJL. The synthesized Si IV line profiles are similar to the observed one in UV bursts, the enhanced wing of the line profiles can extend to about 100 km s−1. The differences are significant among the numerical results with different resolutions, which indicate that the realistic magnetic diffusivity is crucial to reveal the fine structures and realistic plasmas heating in these reconnection events. Our results also show that the reconnection heating contributed by ambipolar diffusion in the low chromosphere around the temperature minimum region is not efficient.

Onset of secondary instabilities and plasma heating during magnetic reconnection in strongly magnetized regions of the low solar atmosphere

Lei **Ni**, Vyacheslav S. Lukin
2018 (v1), last revised 25 Oct 2018 (this version, v2))
https://arxiv.org/pdf/1810.09874.pdf
We numerically study magnetic reconnection on different spatial scales and at different heights in the weakly ionized plasma of the low solar atmosphere (around 300−800~km above the solar surface) within a reactive 2.5 D multi-fluid plasma-neutral model. We consider a strongly magnetized plasma (β~6%) evolving from a force-free magnetic configuration and perturbed to initialize formation of a reconnection current sheet. On large scales, the resulting current sheets are observed to undergo a secondary 'plasmoid' instability. A series of simulations at different scales demonstrate a cascading current sheet formation process that terminates for current sheets with

width of ~2m and length of ~100~m, corresponding to the critical current sheet aspect ratio of ~50. We also observe that the plasmoid instability is the primary physical mechanism accelerating the magnetic reconnection in this plasma parameter regime. After plasmoid instabilities appear, the reconnection rate sharply increases to a value of ~ 0.035, observed to be independent of the Lundquist number. These characteristics are very similar to magnetic reconnection in fully ionized plasmas. In this low βguide field reconnection regime, both the recombination and collisionless effects are observed to have a small contribution to the reconnection rate. The simulations show that it is difficult to heat the dense weakly ionized photospheric plasmas to above 2×104~K during the magnetic reconnection process. However, the plasmas in the low solar chromosphere can be heated above 3×104~K with reconnection magnetic fields of 500~G or stronger.

Magnetic reconnection in the low solar chromosphere with a more realistic radiative cooling model

Lei **Ni**, Vyacheslav S. Lukin, Nicholas A. Murphy, Jun Lin
2018
https://arxiv.org/pdf/1804.05631.pdf
Magnetic reconnection is the most likely mechanism responsible for the high temperature events that are observed in strongly magnetized locations around the temperature minimum in the low solar chromosphere. This work improves upon our previous work ["Magnetic Reconnection in Strongly Magnetized Regions of the Low Solar Chromosphere", The Astrophysical Journal 852, 95 (2018)] by using a more realistic radiative cooling model computed from the OPACITY project and the CHIANTI database. We find that the rate of ionization of the neutral component of the plasma is still faster than recombination within the current sheet region. For low β plasmas, the ionized and neutral fluid flows are well-coupled throughout the reconnection region resembling the single-fluid Sweet-Parker model dynamics. Decoupling of the ion and neutral inflows appears in the higher β case with $\beta_0=1.46$, which leads to a reconnection rate about three times faster than the rate predicted by the Sweet-Parker model. In all cases, the plasma temperature increases with time inside the current sheet, and the maximum value is above 2×10^4~K when the reconnection magnetic field strength is greater than 500~G. While the more realistic radiative cooling model does not result in qualitative changes of the characteristics of magnetic reconnection, it is necessary for studying the variations of the plasma temperature and ionization fraction inside current sheets in strongly magnetized regions of the low solar atmosphere. It is also important for studying energy conversion during the magnetic reconnection process when the hydrogen-dominated plasma approaches full ionization.

Magnetic Reconnection in Strongly Magnetized Regions of the Low Solar Chromosphere

Lei **Ni**1,2, Vyacheslav S. Lukin3,5, Nicholas A. Murphy4, and Jun Lin1,2
2018 ApJ 852 95
Magnetic reconnection in strongly magnetized regions around the temperature minimum region of the low solar atmosphere is studied by employing MHD-based simulations of a partially ionized plasma within a reactive 2.5D multi-fluid model. It is shown that in the absence of magnetic nulls in a low β plasma, the ionized and neutral fluid flows are well-coupled throughout the reconnection region. However, non-equilibrium ionization–recombination dynamics play a critical role in determining the structure of the reconnection region, leading to much lower temperature increases and a faster magnetic reconnection rate as compared to simulations that assume plasma to be in ionization–recombination equilibrium. The rate of ionization of the neutral component of the plasma is always faster than recombination within the current sheet region even when the initial plasma β is as high as $\beta_0 = 1.46$. When the reconnecting magnetic field is in excess of a kilogauss and the plasma β is lower than 0.0145, the initially weakly ionized plasmas can become fully ionized within the reconnection region and the current sheet can be strongly heated to above 2.5×10^4 K, even as most of the collisionally dissipated magnetic energy is radiated away. The Hall effect increases the reconnection rate slightly, but in the absence of magnetic nulls it does not result in significant asymmetries or change the characteristics of the reconnection current sheet down to meter scales.

Heating mechanisms in the low solar atmosphere through magnetic reconnection in current sheets

Lei **Ni**, Jun Lin, Ilia I. Roussev, Brigitte Schmieder
2016 ApJ 832 195
https://arxiv.org/pdf/1611.01746v1.pdf
We simulate several magnetic reconnection processes in the low solar chromosphere/photosphere, the radiation cooling, heat conduction and ambipolar diffusion are all included. Our numerical results indicate that both the high temperature(≳8×104~K) and low temperature(~104~K) magnetic reconnection events can happen in the low solar atmosphere (100~600~km above the solar surface). The plasma β controlled by plasma density and magnetic fields is one important factor to decide how much the plasma can be heated up. The low temperature event is formed in a high β magnetic reconnection process, Joule heating is the main mechanism to heat plasma and the maximum temperature increase is only several thousand Kelvin. The high temperature explosions can be generated in a low β

magnetic reconnection process, slow and fast-mode shocks attached at the edges of the well developed plasmoids are the main physical mechanisms to heat the plasma from several thousand Kelvin to over 8×104~K. Gravity in the low chromosphere can strongly hinder the plasmoind instability and the formation of slow-mode shocks in a vertical current sheet. Only small secondary islands are formed; these islands, however, are not well developed as those in the horizontal current sheets. This work can be applied for understanding the heating mechanism in the low solar atmosphere and could possibly be extended to explain the formation of common low temperature EBs (~104~K) and the high tenperature IRIS bombs (≳8×104) in the future.

Topological Structures of Velocity and Electric Field in the Vicinity of a Cusp-type Magnetic Null Point

Dieter H. **Nickeler**, Marian Karlický, and Michaela Kraus
2019 ApJ 873 41
https://doi.org/10.3847/1538-4357/ab020b
Topological characteristics reveal important physical properties of plasma structures and astrophysical processes. Physical parameters and constraints are linked with topological invariants, which are important for describing magnetic reconnection scenarios. We analyze stationary nonideal Ohm's law concerning the Poincaré classes of all involved physical fields in two dimensions by calculating the corresponding topological invariants of their Jacobian (here: particularly the eigenvalues) or Hessian matrices. The magnetic field is assumed to have a cusp structure, and the stagnation point of the plasma flow coincides with the cusp. We find that the stagnation point must be hyperbolic. Furthermore, the functions describing both the resistivity and the ohmic heating have a saddle-point structure, being displaced with respect to the cusp point. These results imply that there is no monotonous relation between current density and anomalous resistivity in the case of a two-dimensional standard magnetic cusp.

Electric current filamentation induced by 3D plasma flows in the solar corona

Dieter H. **Nickeler**, Thomas Wiegelmann, Marian Karlicky, Michaela Kraus
ApJ 837 104 **2017**
https://arxiv.org/pdf/1702.03986.pdf
Many magnetic structures in the solar atmosphere evolve rather slowly so that they can be assumed as (quasi-)static or (quasi-)stationary and represented via magneto-hydrostatic (MHS) or stationary magneto-hydrodynamic (MHD) equilibria, respectively. While exact 3D solutions would be desired, they are extremely difficult to find in stationary MHD. We construct solutions with magnetic and flow vector fields that have three components depending on all three coordinates. We show that the non-canonical transformation method produces quasi-3D solutions of stationary MHD by mapping 2D or 2.5D MHS equilibria to corresponding stationary MHD states, i.e., states that display the same field line structure as the original MHS equilibria. These stationary MHD states exist on magnetic flux surfaces of the original 2D MHS states. Although the flux surfaces and therefore also the equilibria have a 2D character, these stationary MHD states depend on all three coordinates and display highly complex currents. The existence of geometrically complex 3D currents within symmetric field-line structures provide the base for efficient dissipation of the magnetic energy in the solar corona by Ohmic heating. We also discuss the possibility of maintaining an important subset of non-linear MHS states, namely force-free fields, by stationary flows. We find that force-free fields with non-linear flows only arise under severe restrictions of the field-line geometry and of the magnetic flux density distribution.

Determining the Kappa Distributions of Space Plasmas from Observations in a Limited Energy Range

G. **Nicolaou**1,2, G. Livadiotis3, C. J. Owen1, D. Verscharen1,4, and R. T. Wicks1
2018 ApJ 864 3
http://iopscience.iop.org/article/10.3847/1538-4357/aad45d/pdf
Spacecraft observations allow us to reconstruct the velocity distributions of space plasmas, which fully describe the kinetic state of the plasma. Space plasmas often exist in stationary states out of equilibrium, which are typically described by kappa distributions. Thus, the kappa index and temperature that govern these distributions are parameters that need to be determined for a full and accurate description of these plasmas. In this study, we demonstrate a novel and reliable way to determine the kappa index and temperature of plasma distribution functions constructed from counts observed in a narrow energy range by typical electrostatic sensors. Our method applies to cases in which the high-energy tail of the plasma is observed with significant uncertainty, or not observed at all. For the validation of our method, we produce pseudo-observations for typical input plasma parameters, specifically considering the design of the ion plasma instrument SWA-PAS on board the Solar Orbiter mission. Our method reliably estimates the relevant plasma parameters by fitting the angular spread of the distribution in a narrow energy range around the core bulk energy. We compare the output of our technique with the input parameters used to generate artificial data for a selected range of the kappa index and the temperature, and for a bulk energy typical for the solar wind. In addition, we study the effects of Poisson errors on the instrument's counting statistics, test our method against Helios 2 measurements, and discuss its potential applications and limitations.

Impulsively generated two-fluid magnetoacoustic-gravity waves: Solar chromosphere heating and plasma outflows

R. **Niedziela**1, K. Murawski1, L. Kadowaki1, T. Zaqarashvili2,3,5 and S. Poedts4,1
A&A 668, A32 (**2022**)
https://www.aanda.org/articles/aa/pdf/2022/12/aa44844-22.pdf

Context. We use a two-fluid model to study the heating of the solar chromosphere by magnetoacoustic and magnetoacoustic-gravity waves. In the model, we include energy dissipation as a result of ion–neutral collisions.
Aims. The aim of this paper is to study impulsively generated two-fluid magnetoacoustic and magnetoacoustic-gravity waves and to quantify their contribution to chromosphere heating and the generation of plasma outflows.
Methods. We consider a 2D model of the gravitationally stratified and partially ionized solar atmosphere that is permeated by a vertical magnetic field. To describe the dynamics of the atmosphere, we use a set of two-fluid equations which we solve numerically with the use of the JOANNA code.
Results. We show that large-amplitude impulsively generated magnetoacoustic-gravity waves can efficiently heat the chromosphere and generate plasma outflows in the low solar corona. The chromosphere is heated by ion–neutral collisions, which are most effective at the top of this atmospheric layer. Wider and larger amplitude pulses heat the atmosphere more effectively and generate faster plasma outflows.
Conclusions. Large-amplitude, impulsively generated two-fluid magnetoacoustic-gravity waves have the potential to contribute to the solar chromosphere heating and plasma outflows in the low corona.

Chromospheric heating and generation of plasma outflows by impulsively generated two-fluid magnetoacoustic waves

R. **Niedziela**, K. Murawski, S. Poedts
A&A 652, A124 **2021**
https://arxiv.org/pdf/2107.12050.pdf
https://www.aanda.org/articles/aa/pdf/2021/08/aa41027-21.pdf
https://doi.org/10.1051/0004-6361/202141027

Context. The origin of the heating of the solar atmosphere is still an unsolved problem. As the photosphere and chromosphere radiate more energy than the solar corona, it is challenging but important to reveal all the mechanisms that contribute to plasma heating there. Ion-neutral collisions could play an important role. Aims. We aim to investigate the impulsively generated two-fluid magnetoacoustic waves in the partially ionized solar chromosphere and to study the associated heating and plasma outflows, which higher up may result in nascent solar wind. Methods. To describe the plasma dynamics, we applied a two-fluid model in which ions+electrons and neutrals are treated as separate fluids. We solved the two-fluid equations numerically using the JOANNA code. Results. We show that magnetoacoustic waves triggered in the photosphere by localised velocity pulses can steepen into shocks which heat the chromosphere through ion-neutral collisions. Pulses of greater amplitude heat plasma more effectively and generate larger plasma outflows. Rising the altitude at which the pulse is launched results in opposite effects, mainly in local cooling of the chromosphere and slower plasma outflows. Conclusions. Even a solitary pulse results in a train of waves. These waves can transform into shock waves and release thermal energy, heating the chromosphere significantly. A pulse can drive vertical flows which higher up can result in the origin of the solar wind.

Solar Line Asymmetries: Modelling the Effect of Granulation on the Solar Spectrum

Timo A. **Nieminen**
PhD thesis, The University of Queensland, Brisbane, Australia, 1995 **2017**
https://arxiv.org/ftp/arxiv/papers/1708/1708.06408.pdf

A parametric model of granulation employing a small number of parameters was developed. Synthetic spectra calculated using this model closely match observed spectra and, in particular, reproduce the asymmetries observed in spectral lines. Both the microturbulent motions and the large-scale flow velocity decrease exponentially with a scale height of 368 km as the height within the photosphere increases. The model agrees with observations of the solar granulation (from which it was derived).
The horizontal motions associated with granulation were found and used to calculate spectra emergent away from disk centre. These calculated spectra were compared to observed spectra, with the agreement supporting the accuracy of the granular model.
Also in the course of this work, the Brueckner-O'Mara damping theory was found to predict damping constants

accurately. The photospheric abundances of a number of elements were determined. The abundance obtained for iron agrees with the meteoric iron abundance. Astrophysical f-values for some lines were also determined.

Differences in the solar cycle variability of simple and complex active regions during 1996-2018

Shabnam **Nikbakhsh**, Eija Tanskanen, Maarit Käpylä, Thomas Hackman
A&A 629, A45 **2019**
https://arxiv.org/pdf/1908.02226.pdf
Aims. Our aim is to examine the solar cycle variability of magnetically simple and complex active region. Methods. We studied simple (α and β) and complex (βγ and βγδ) active regions based on the Mount Wilson magnetic classification by applying our newly developed daily approach. We analyzed the daily number of the simple active regions (SARs) and compared that to the abundance of the complex active regions (CARs) over the entire solar cycle 23 and cycle 24 until December 2018. Results. We show that CARs evolve differently over the solar cycle from SARs. The time evolution of SARs and CARs on different hemispheres also shows differences, even though on average their latitudinal distributions are shown to be similar. The time evolution of SARs closely follows that of the sunspot number, and their maximum abundance was observed to occur during the early maximum phase, while that of the CARs was seen roughly two years later. We furthermore found that the peak of CARs was reached before the latitudinal width of the activity band starts to decease. Conclusions. Our results suggest that the active region formation process is a competition between the large-scale dynamo (LSD) and the small-scale dynamo (SSD) near the surface, the former varying cyclically and the latter being independent of the solar cycle. During solar maximum, LSD is dominant, giving a preference to SARs, while during the declining phase the relative role of SSD increases. Therefore, a preference for CARs is seen due to the influence of the SSD on the emerging flux.

The Sun at GeV--TeV Energies: A New Laboratory for Astroparticle Physics

M.U. **Nisa**, J.F. Beacom, S.Y. BenZvi, R.K. Leane, T. Linden, K.C.Y. Ng, A.H.G. Peter, B. Zhou
Astro2020 Decadal Survey on Astronomy and Astrophysics **2019**
https://arxiv.org/pdf/1903.06349.pdf
The Sun is an excellent laboratory for astroparticle physics but remains poorly understood at GeV--TeV energies. Despite the immense relevance for both cosmic-ray propagation and dark matter searches, only in recent years has the Sun become a target for precision gamma-ray astronomy with the Fermi-LAT instrument. Among the most surprising results from the observations is a hard excess of GeV gamma-ray flux that strongly anti-correlates with solar activity, especially at the highest energies accessible to Fermi-LAT. Most of the observed properties of the gamma-ray emission cannot be explained by existing models of cosmic-ray interactions with the solar atmosphere. GeV--TeV gamma-ray observations of the Sun spanning an entire solar cycle would provide key insights into the origin of these gamma rays, and consequently improve our understanding of the Sun's environment as well as the foregrounds for new physics searches, such as dark matter. These can be complemented with new observations with neutrinos and cosmic rays. Together these observations make the Sun a new testing ground for particle physics in dynamic environments.

Probing the Density Fine Structuring of the Solar Corona with Comet Lovejoy

Giuseppe **Nisticò**, Gaetano Zimbardo, Silvia Perri, Valery M. Nakariakov, Timothy J. Duckenfield, Miloslav Druckmueller
ApJ **2022**
https://arxiv.org/pdf/2209.04051.pdf
The passage of sungrazing comets in the solar corona can be a powerful tool to probe the local plasma properties. Here, we carry out a study of the striae pattern appearing in the tail of sungrazing Comet Lovejoy, as observed by the Atmospheric Imaging Assembly (AIA) aboard the Solar Dynamics Observatory (SDO) during the inbound and outbound phases of the comet orbit. We consider the images in EUV in the 171 Å bandpass, where emission from oxygen ions O4+ and O5+ is found. The striae are described as due to a beam of ions injected along the local magnetic field, with the initial beam velocity decaying because of collisions. Also, ion collisional diffusion contributes to ion propagation. Both the collision time for velocity decay and the diffusion coefficient for spatial spreading depend on the ambient plasma density. A probabilistic description of the ion beam density along the magnetic field is developed, where the beam position is given by the velocity decay and the spreading of diffusing ions is described by a Gaussian probability distribution. Profiles of emission intensity along the magnetic field are computed and compared with the profiles along the striae observed by AIA, showing a good agreement for most considered striae. The inferred coronal densities are then compared with a hydrostatic model of the solar corona. The results confirm that the coronal density is strongly spatially structured. **December 15–16, 2011**

Data-Constrained Solar Modeling with GX Simulator

Gelu M. **Nita**, Gregory D. Fleishman, Alexey A. Kuznetsov, Sergey A. Anfinogentov, Alexey G. Stupishin, Eduard P. Kontar, Samuel J. Schonfeld, James A. Klimchuk, Dale E. Gary

ApJS **267** 6 **2023**

https://arxiv.org/pdf/2301.00795.pdf

https://iopscience.iop.org/article/10.3847/1538-4365/acd343/pdf

To facilitate the study of solar active regions and flaring loops, we have created a modeling framework, the freely distributed GX Simulator IDL package, that combines 3D magnetic and plasma structures with thermal and non-thermal models of the chromosphere, transition region, and corona. The package has integrated tools to visualize the model data cubes, compute multi-wavelength emission maps from them, and quantitatively compare the resulting maps with observations. Its object-based modular architecture, which runs on Windows, Mac, and Unix/Linux platforms, offers capabilities that include the ability to either import 3D density and temperature distribution models, or to assign numerically defined coronal or chromospheric temperatures and densities, or their distributions to each individual voxel. The application integrates FORTRAN and C++ libraries for fast calculation of radio emission (free-free, gyroresonance, and gyrosynchrotron emission) along with soft and hard X-ray and EUV codes developed in IDL. To facilitate the creation of models, we have developed a fully automatic model production pipeline that downloads the required SDO/HMI vector magnetic field data and (optionally) the contextual SDO/AIA images, performs potential or nonlinear force free field extrapolations, populates the magnetic field skeleton with parameterized heated plasma coronal models that assume either steady-state or impulsive plasma heating, and generates non-LTE density and temperature distribution models of the chromosphere that are constrained by photospheric measurements. The standardized models produced by this pipeline may be further customized through a set of interactive tools provided by the graphical user interface. Here we describe the GX Simulator framework and its applications.

CESRA #3579 **2023** https://www.astro.gla.ac.uk/users/eduard/cesra/?p=3579

Dressing the Coronal Magnetic Extrapolations of Active Regions with a Parameterized Thermal Structure

Gelu M. **Nita**1, Nicholeen M. Viall2, James A. Klimchuk2, Maria A. Loukitcheva1,3,Dale E. Gary1, Alexey A. Kuznetsov4, and Gregory D. Fleishman

2018 ApJ 853 66 10.3847/1538-4357/aaa4bf

The study of time-dependent solar active region (AR) morphology and its relation to eruptive events requires analysis of imaging data obtained in multiple wavelength domains with differing spatial and time resolution, ideally in combination with 3D physical models. To facilitate this goal, we have undertaken a major enhancement of our IDL-based simulation tool, GX_Simulator, previously developed for modeling microwave and X-ray emission from flaring loops, to allow it to simulate quiescent emission from solar ARs. The framework includes new tools for building the atmospheric model and enhanced routines for calculating emission that include new wavelengths. In this paper, we use our upgraded tool to model and analyze an AR and compare the synthetic emission maps with observations. We conclude that the modeled magneto-thermal structure is a reasonably good approximation of the real one.

Implications of spicule activity on coronal loop heating and catastrophic cooling

V.N. **Nived**, E. Scullion, J. G. Doyle, R. Susino, P. Antolin, D. Spadaro, C. Sasso, S. Sahin, M. Mathioudakis

MNRAS **2021**

https://arxiv.org/pdf/2111.07967.pdf

We report on the properties of coronal loop foot-point heating with observations at the highest resolution, from the CRisp Imaging Spectro-Polarimeter (CRISP) located at the Swedish 1-m Solar Telescope (SST) and co-aligned NASA Solar Dynamics Observatory (SDO) observations, of Type II spicules in the chromosphere and their signatures in the EUV corona. Here, we address one important issue, as to why there is not always a one-to-one correspondence, between Type II spicules and hot coronal plasma signatures, i.e. beyond TR temperatures. We do not detect any difference in their spectral properties in a quiet Sun region compared to a region dominated by coronal loops. On the other hand, the number density close to the foot-points in the active region is found to be an order of magnitude higher than in the quiet Sun case. A differential emission measure analysis reveals a peak at ∼5×105 K on the order of 1022∼cm−5∼K−1. Using this result as a constraint, we conduct numerical simulations and show that with an energy input of 1.25×1024 erg (corresponding to ∼10 RBEs contributing to the burst) we manage to reproduce the observation very closely. However, simulation runs with lower thermal energy input do not reproduce the synthetic AIA 171Å signatures, indicating that there is a critical number of spicules required in order to account for the AIA 171Å signatures in the simulation. Furthermore, the higher energy (1.25×1024 ergs) simulations reproduce catastrophic cooling with a cycle duration of ∼5 hours, matching a periodicity we observe in the EUV observations.

The global modulation of Galactic and Jovian electrons in the heliosphere

Rendani R. **Nndanganeni**, Marius S. Potgieter
Astrophysics and Space Science July **2018**, 363:156
http://sci-hub.tw/10.1007/s10509-018-3377-z
A full three-dimensional, numerical model is used to study the modulation of Jovian and Galactic electrons from 1 MeV to 50 GeV, and from the Earth into the heliosheath. For this purpose the very local interstellar spectrum and the Jovian electron source spectrum are revisited. It is possible to compute the former with confidence at kinetic energies E<50 MeVsince Voyager 1 crossed the heliopause in 2012 at ∼122 AU, measuring Galactic electrons at these energies. Modeling results are compared with Voyager 1 observations in the outer heliosphere, including the heliosheath, as well as observations at or near the Earth from the ISSE3 mission, and in particular the solar minimum spectrum from the PAMELA space mission for 2009, also including data from Ulysses for 1991 and 1992, and observations above 1 MeV from SOHO/EPHIN. Making use of the observations at or near the Earth and the two newly derived input functions for the Jovian and Galactic electrons respectively, the energy range over which the Jovian electrons dominate the Galactic electrons is determined so that the intensity of Galactic electrons at Earth below 100 MeV is calculated. The differential intensity for the Galactic electrons at Earth for E=1 MeV is ∼4 electrons m−2s−1sr−1MeV−1, whereas for Jovian electrons it is ∼350 electrons m−2s−1sr−1MeV−1. At E=30 MeV the two intensities are the same; above this energy the Jovian electron intensity quickly subsides so that the Galactic intensity completely dominates. At 6 MeV, in the equatorial plane the Jovian electrons dominate but beyond ∼15 AU the Galactic intensity begins to exceed the Jovian intensity significantly.

Small-scale magnetic flux emergence preceding a chain of energetic solar atmospheric events

D. **Nóbrega-Siverio**, I. Cabello, S. Bose, L. H. M. Rouppe van der Voort, R. Joshi, C. Froment, V. M. J. Henriques
A&A 686, A218 **2024**
https://arxiv.org/pdf/2403.11652
https://www.aanda.org/articles/aa/pdf/2024/06/aa48894-23.pdf
Advancements in instrumentation have revealed a multitude of small-scale EUV events in the solar atmosphere. Our aim is to employ high-resolution magnetograms to gain a detailed understanding of the magnetic origin of such phenomena. We have used coordinated observations from SST, IRIS, and SDO to analyze an ephemeral magnetic flux emergence episode and the following chain of small-scale energetic events. These unique observations clearly link these phenomena together. The high-resolution (0."057/pixel) magnetograms obtained with SST/CRISP allows us to reliably measure the magnetic field at the photosphere and detect the emerging bipole that causes the subsequent eruptive atmospheric events. Notably, this small-scale emergence episode remains indiscernible in the lower resolution SDO/HMI magnetograms (0."5/pixel). We report the appearance of a dark bubble in Ca II K related to the emerging bipole, a sign of the canonical expanding magnetic dome predicted in flux emergence simulations. Evidences of reconnection are also found: first through an Ellerman bomb, and later by the launch of a surge next to a UV burst. The UV burst exhibits a weak EUV counterpart in the coronal SDO/AIA channels. By calculating DEM, its plasma is shown to reach a temperature beyond 1 MK and have densities between the upper chromosphere and transition region. Our study showcases the importance of high-resolution magnetograms to unveil the mechanisms triggering phenomena such as EBs, UV bursts, and surges. This could hold implications for small-scale events akin to those recently reported in EUV using Solar Orbiter. The finding of temperatures beyond 1 MK in the UV burst plasma strongly suggests that we are examining analogous features. Therefore, we signal caution regarding drawing conclusions from full-disk magnetograms that lack the necessary resolution to reveal their true magnetic origin.

Deciphering the solar coronal heating: Energizing small-scale loops through surface convection

D. **Nóbrega-Siverio**, F. Moreno-Insertis, K Galsgaard, K. Krikova, L. Rouppe van der Voort, R. Joshi, M. S. Madjarska
ApJL **958** L38 **2023**
https://arxiv.org/pdf/2311.11912.pdf
https://iopscience.iop.org/article/10.3847/2041-8213/ad0df0/pdf
The solar atmosphere is filled with clusters of hot small-scale loops commonly known as Coronal Bright Points (CBPs). These ubiquitous structures stand out in the Sun by their strong X-ray and/or extreme-ultraviolet (EUV) emission for hours to days, which makes them a crucial piece when solving the solar coronal heating puzzle. In addition, they can be the source of coronal jets and small-scale filament eruptions. Here we present a novel 3D numerical model using the Bifrost code that explains the sustained CBP heating for several hours. We find that

stochastic photospheric convective motions alone significantly stress the CBP magnetic field topology, leading to important Joule and viscous heating concentrated around the CBP's inner spine at a few megameters above the solar surface. We also detect continuous upflows with faint EUV signal resembling observational dark coronal jets and small-scale eruptions when Hα fibrils interact with the reconnection site. We validate our model by comparing simultaneous CBP observations from SDO and SST with observable diagnostics calculated from the numerical results for EUV wavelengths as well as for the Hα line using the Multi3D synthesis code. Additionally, we provide synthetic observables to be compared with Hinode, Solar Orbiter, and IRIS. Our results constitute a step forward in the understanding of the many different facets of the solar coronal heating problem.

Ambipolar diffusion in the Bifrost code

Nóbrega-Siverio, D.; Martínez-Sykora, J.; Moreno-Insertis, F.; Carlsson, M.
Astronomy & Astrophysics, Volume 638, id.A79, **2020**
https://arxiv.org/pdf/2004.11927.pdf
https://www.aanda.org/articles/aa/pdf/2020/06/aa37809-20.pdf
Context. Ambipolar diffusion is a physical mechanism related to the drift between charged and neutral particles in a partially ionized plasma that is key to many different astrophysical systems. However, understanding its effects is challenging due to basic uncertainties concerning relevant microphysical aspects and the strong constraints it imposes on the numerical modeling.
Aims: Our aim is to introduce a numerical tool that allows us to address complex problems involving ambipolar diffusion in which, additionally, departures from ionization equilibrium are important or high resolution is needed. The primary application of this tool is for solar atmosphere calculations, but the methods and results presented here may also have a potential impact on other astrophysical systems.
Methods: We have developed a new module for the stellar atmosphere Bifrost code that improves its computational capabilities of the ambipolar diffusion term in the generalized Ohm's law. This module includes, among other things, collision terms adequate to processes in the coolest regions in the solar chromosphere. As the main feature of the module, we have implemented the super time stepping (STS) technique, which allows an important acceleration of the calculations. We have also introduced hyperdiffusion terms to guarantee the stability of the code.
Results: We show that to have an accurate value for the ambipolar diffusion coefficient in the solar atmosphere it is necessary to include as atomic elements in the equation of state not only hydrogen and helium, but also the main electron donors like sodium, silicon, and potassium. In addition, we establish a range of criteria to set up an automatic selection of the free parameters of the STS method that guarantees the best performance, optimizing the stability and speed for the ambipolar diffusion calculations. We validate the STS implementation by comparison with a self-similar analytical solution.

Nonequilibrium ionization and ambipolar diffusion in solar magnetic flux emergence processes

D. **Nóbrega-Siverio**, F. Moreno-Insertis, J. Martínez-Sykora, M. Carlsson, M. Szydlarski
A&A 633, A66 (**2020**)
https://arxiv.org/pdf/1912.01015.pdf
https://doi.org/10.1051/0004-6361/201936944
Magnetic flux emergence has been shown to be a key mechanism for unleashing a wide variety of solar phenomena. However, there are still open questions concerning the rise of the magnetized plasma through the atmosphere, mainly in the chromosphere, where the plasma departs from local thermodynamic equilibrium (LTE) and is partially ionized. We aim to investigate the impact of the nonequilibrium (NEQ) ionization and recombination and molecule formation of hydrogen, as well as ambipolar diffusion, on the dynamics and thermodynamics of the flux emergence process. Using the Bifrost code, we performed 2.5D numerical experiments of magnetic flux emergence from the convection zone up to the corona. The experiments include the NEQ ionization and recombination of atomic hydrogen, the NEQ formation and dissociation of H2 molecules, and the ambipolar diffusion term of the Generalized Ohm's Law. Our experiments show that the LTE assumption substantially underestimates the ionization fraction in most of the emerged region, leading to an artificial increase in the ambipolar diffusion and, therefore, in the heating and temperatures as compared to those found when taking the NEQ effects on the hydrogen ion population into account. We see that LTE also overestimates the number density of H2 molecules within the emerged region, thus mistakenly magnifying the exothermic contribution of the H2 molecule formation to the thermal energy during the flux emergence process. We find that the ambipolar diffusion does not significantly affect the amount of total unsigned emerged magnetic flux, but it is important in the shocks that cross the emerged region, heating the plasma on characteristic times ranging from 0.1 to 100 s. We also briefly discuss the importance of including elements heavier than hydrogen in the equation of state so as not to overestimate the role of ambipolar diffusion in the atmosphere.

Surges and Si IV bursts in the solar atmosphere. Understanding IRIS and SST observations through RMHD experiments

D. **Nóbrega-Siverio**, J. Martínez-Sykora, F. Moreno-Insertis, L. Rouppe van der Voort

ApJ **2017**

https://arxiv.org/pdf/1710.08928.pdf

Surges often appear as a result of the emergence of magnetized plasma from the solar interior. Traditionally, they are observed in chromospheric lines such as Hα 6563 \AA and Ca II 8542 \AA. However, whether there is a response to the surge appearance and evolution in the Si IV lines or, in fact, in many other transition region lines has not been studied. In this paper we analyze a simultaneous episode of an Hα surge and a Si IV burst that occurred on **2016 September 03** in active region AR12585. To that end, we use coordinated observations from the Interface Region Imaging Spectrograph (IRIS) and the Swedish 1-m Solar Telescope (SST). For the first time, we report emission of Si IV within the surge, finding profiles that are brighter and broader than the average. Furthermore, the brightest Si IV patches within the domain of the surge are located mainly near its footpoints. To understand the relation between the surges and the emission in transition region lines like Si IV, we have carried out 2.5D radiative MHD (RMHD) experiments of magnetic flux emergence episodes using the Bifrost code and including the non-equilibrium ionization of silicon. Through spectral synthesis we explain several features of the observations. We show that the presence of Si IV emission patches within the surge, their location near the surge footpoints and various observed spectral features are a natural consequence of the emergence of magnetized plasma from the interior to the atmosphere and the ensuing reconnection processes.

The European Solar Telescope

C. Quintero **Noda**, R. Schlichenmaier, L. R. Bellot Rubio, M. G. Löfdahl, E. Khomenko, J. Jurcak, J. Leenaarts, C. Kuckein, S. J. González Manrique, S. Gunar, C. J. Nelson, J. de la Cruz Rodríguez, K. Tziotziou, G. Tsiropoula, G. Aulanier, M. Collados, the EST team

A&A **2022**

https://arxiv.org/ftp/arxiv/papers/2207/2207.10905.pdf

The European Solar Telescope (EST) is a project aimed at studying the magnetic connectivity of the solar atmosphere, from the deep photosphere to the upper chromosphere. Its design combines the knowledge and expertise gathered by the European solar physics community during the construction and operation of state-of-the-art solar telescopes operating in visible and near-infrared wavelengths: the Swedish 1m Solar Telescope (SST), the German Vacuum Tower Telescope (VTT) and GREGOR, the French Télescope Héliographique pour l'Étude du Magnétisme et des Instabilités Solaires (THÉMIS), and the Dutch Open Telescope (DOT). With its 4.2 m primary mirror and an open configuration, EST will become the most powerful European ground-based facility to study the Sun in the coming decades in the visible and near-infrared bands. EST uses the most innovative technological advances: the first adaptive secondary mirror ever used in a solar telescope, a complex multi-conjugate adaptive optics with deformable mirrors that form part of the optical design in a natural way, a polarimetrically compensated telescope design that eliminates the complex temporal variation and wavelength dependence of the telescope Mueller matrix, and an instrument suite containing several (etalon-based) tunable imaging spectropolarimeters and several integral field unit spectropolarimeters. This publication summarises some fundamental science questions that can be addressed with the telescope, together with a complete description of its major subsystems.

Diagnostic capabilities of spectropolarimetric observations for understanding solar phenomena I. Zeeman-sensitive photospheric lines

C. Quintero **Noda**, P. S. Barklem, R. Gafeira, B. Ruiz Cobo, M. Collados, M. Carlsson, V. Martínez Pillet, D. Orozco Suárez, H. Uitenbroek, Y. Katsukawa

A&A 652, A161 **2021**`

https://arxiv.org/pdf/2106.05084.pdf

https://www.aanda.org/articles/aa/pdf/2021/08/aa37735-20.pdf

https://doi.org/10.1051/0004-6361/202037735

Future ground-based telescopes will expand our capabilities for simultaneous multi-line polarimetric observations in a wide range of wavelengths, from the near-ultraviolet to the near-infrared. This creates a strong demand to compare candidate spectral lines to establish a guideline of the lines that are most appropriate for each observation target. We focused in this first work on Zeeman-sensitive photospheric lines in the visible and infrared. We first examined their polarisation signals and response functions using a 1D semi-empirical atmosphere. Then we studied the spatial distribution of the line core intensity and linear and circular polarisation signals using a realistic 3D numerical simulation. We ran inversions of synthetic profiles, and we compared the heights at which we obtain a high correlation between the input and the inferred atmosphere. We also used this opportunity to revisit the atomic information we have on these lines and computed the broadening cross-sections due to collisions with neutral hydrogen atoms for all the studied spectral lines. The results reveal that four spectral lines stand out from the rest for quiet-Sun and network conditions: Fe I 5250.2, 6302, 8468, and 15648 A. The first three form higher in the atmosphere, and the last line is mainly sensitive to the atmospheric parameters at the bottom of the photosphere.

However, as they reach different heights, we strongly recommend using at least one of the first three candidates together with the Fe I 15648 A line to optimise our capabilities for inferring the thermal and magnetic properties of the lower atmosphere.

Solar polarimetry in the K I D2 line : A novel possibility for a stratospheric balloon

C. Quintero **Noda**1, G. L. Villanueva2, Y. Katsukawa3, S. K. Solanki4,5, D. Orozco Suárez6, B. Ruiz Cobo7,8, T. Shimizu1, T. Oba1,9, M. Kubo3, T. Anan10, K. Ichimoto3,10 and Y. Suematsu
A&A 610, A79 (**2018**)
https://www.aanda.org/articles/aa/pdf/2018/02/aa32111-17.pdf
Of the two solar lines, K I D1 and D2, almost all attention so far has been devoted to the D1 line, as D2 is severely affected by an O2 atmospheric band. This, however, makes the latter appealing for balloon and space observations from above (most of) the Earth's atmosphere. We estimate the residual effect of the O2 band on the K I D2 line at altitudes typical for stratospheric balloons. Our aim is to study the feasibility of observing the 770 nm window. Specifically, this paper serves as a preparation for the third flight of the Sunrise balloon-borne observatory. The results indicate that the absorption by O2 is still present, albeit much weaker, at the expected balloon altitude. We applied the obtained O2 transmittance to K I D2 synthetic polarimetric spectra and found that in the absence of line-of-sight motions, the residual O2 has a negligible effect on the K I D2 line. On the other hand, for Doppler-shifted K I D2 data, the residual O2 might alter the shape of the Stokes profiles. However, the residual O2 absorption is sufficiently weak at stratospheric levels that it can be divided out if appropriate measurements are made, something that is impossible at ground level. Therefore, for the first time with Sunrise III, we will be able to perform polarimetric observations of the K I D2 line and, consequently, we will have improved access to the thermodynamics and magnetic properties of the upper photosphere from observations of the K I lines.

Chromospheric polarimetry through multi-line observations of the 850 nm spectral region III: Chromospheric jets driven by twisted magnetic fields

C. Quintero **Noda**, H. Iijima, Y. Katsukawa, T. Shimizu, M. Carlsson, J. de la Cruz Rodríguez, B. Ruiz Cobo, D. Orozco Suárez, T. Oba, T. Anan, M. Kubo, Y. Kawabata, K. Ichimoto, Y. Suematsu
MNRAS Volume 486, Issue 3, Pages 4203–4215 **2019**
https://arxiv.org/pdf/1904.09151.pdf
We investigate the diagnostic potential of the spectral lines at 850 nm for understanding the magnetism of the lower atmosphere. For that purpose, we use a newly developed 3D simulation of a chromospheric jet to check the sensitivity of the spectral lines to this phenomenon as well as our ability to infer the atmospheric information through spectropolarimetric inversions of noisy synthetic data. We start comparing the benefits of inverting the entire spectrum at 850 nm versus only the Ca II 8542 A spectral line. We found a better match of the input atmosphere for the former case, mainly at lower heights. However, the results at higher layers were not accurate. After several tests, we determined that we need to weight more the chromospheric lines than the photospheric ones in the computation of the goodness of the fit. The new inversion configuration allows us to obtain better fits and consequently more accurate physical parameters. Therefore, to extract the most from multi-line inversions, a proper set of weights needs to be estimated. Besides that, we conclude again that the lines at 850 nm, or a similar arrangement with Ca II 8542 A plus Zeeman sensitive photospheric lines, poses the best observing configuration for examining the thermal and magnetic properties of the lower solar atmosphere.

Chromospheric polarimetry through multi-line observations of the 850 nm spectral region II: A magnetic flux tube scenario

C. Quintero **Noda**, Y. Kato, Y. Katsukawa, T. Oba, J. de la Cruz Rodríguez, M. Carlsson, T. Shimizu, D. Orozco Suárez, B. Ruiz Cobo, M. Kubo, T. Anan, K. Ichimoto, Y. Suematsu
MNRAS **2017**
https://arxiv.org/pdf/1708.01333.pdf
In this publication we continue the work started in Quintero Noda et al. (2017) examining this time a numerical simulation of a magnetic flux tube concentration. Our goal is to study if the physical phenomena that take place in it, in particular, the magnetic pumping, leaves a specific imprint on the examined spectral lines. We find that the profiles from the interior of the flux tube are periodically dopplershifted following an oscillation pattern that is also reflected in the amplitude of the circular polarization signals. In addition, we analyse the properties of the Stokes profiles at the edges of the flux tube discovering the presence of linear polarization signals for the Ca II lines, although they are weak with an amplitude around 0.5% of the continuum intensity. Finally, we compute the response functions to perturbations in the longitudinal field and we estimate the field strength using the weak field approximation. Our results indicate that the height of formation of the spectral lines changes during the magnetic pumping process which makes the interpretation of the inferred magnetic field strength and its evolution more difficult. These results complement those from previous works demonstrating the capabilities and limitations of the 850 nm spectrum for chromospheric Zeeman polarimetry in a very dynamic and complex atmosphere.

Chromospheric polarimetry through multi-line observations of the 850 nm spectral region

C. Quintero **Noda**, T. Shimizu, Y. Katsukawa, J. de la Cruz Rodriguez, M. Carlsson, T. Anan, T. Oba, K. Ichimoto, Y. Suematsu

MNRAS **2016**

https://arxiv.org/pdf/1610.06651v1.pdf

Future solar missions and ground-based telescopes aim to understand the magnetism of the solar chromosphere. We performed a supporting study in Quintero Noda et al. (2016) focused on the infrared Ca II 8542 A line and we concluded that is one of the best candidates because it is sensitive to a large range of atmospheric heights, from the photosphere to the middle chromosphere. However, we believe that it is worth to try improving the results produced by this line observing additional spectral lines. In that regard, we examined the neighbour solar spectrum looking for spectral lines that could increase the sensitivity to the atmospheric parameters. Interestingly, we discovered several photospheric lines that greatly improve the photospheric sensitivity to the magnetic field vector. Moreover, they are located close to a second chromospheric line that also belongs to the Ca II infrared triplet, i.e. the Ca II 8498 A line, and enhances the sensitivity to the atmospheric parameters at chromospheric layers. We conclude that the lines in the vicinity of the Ca II 8542 A line not only increase its sensitivity to the atmospheric parameters at all layers, but also they constitute an excellent spectral window for chromospheric polarimetry.

Analysis of spatially deconvolved polar faculae

C. Quintero **Noda**, Y. Suematsu, B. Ruiz Cobo, T. Shimizu, A. Asensio Ramos

MNRAS **2016**

http://arxiv.org/pdf/1605.00330v1.pdf

Polar faculae are bright features that can be detected in solar limb observations and they are related to magnetic field concentrations. Although there is a large number of works studying them, some questions about their nature as their magnetic properties at different heights are still open. Thus, we aim to improve the understanding of solar polar faculae. In that sense, we infer the vertical stratification of the temperature, gas pressure, line of sight velocity and magnetic field vector of polar faculae regions. We performed inversions of the Stokes profiles observed with Hinode/SP after removing the stray light contamination produced by the spatial point spread function of the telescope. Moreover, after solving the azimuth ambiguity, we transform the magnetic field vector to local solar coordinates. The obtained results reveal that the polar faculae are constituted by hot plasma with low line of sight velocities and single polarity magnetic fields in the kilogauss range that are nearly perpendicular to the solar surface. We also found that the spatial location of these magnetic fields is slightly shifted respect to the continuum observations towards the disc centre. We believe that this is due to the hot wall effect that allows detecting photons that come from deeper layers located closer to the solar limb. **2007 September 6**

Spectropolarimetric capabilities of Ca II 8542 A line

C. Quintero **Noda**, T. Shimizu, J. de la Cruz Rodríguez, Y. Katsukawa, K. Ichimoto, T. Anan, Y. Suematsu

MNRAS **2016**

http://arxiv.org/pdf/1604.04957v1.pdf

The next generation of space and ground-based solar missions aim to study the magnetic properties of the solar chromosphere using the infrared Ca II lines and the He I 10830 {\AA} line. The former seem to be the best candidates to study the stratification of magnetic fields in the solar chromosphere and their relation to the other thermodynamical properties underlying the chromospheric plasma. The purpose of this work is to provide a detailed analysis of the diagnostic capabilities of the Ca II 8542 {\AA} line, anticipating forthcoming observational facilities. We study the sensitivity of the Ca II 8542 {\AA} line to perturbations applied to the physical parameters of reference semi-empirical 1D model atmospheres using response functions and we make use of 3D MHD simulations to examine the expected polarization signals for moderate magnetic field strengths. Our results indicate that the Ca II 8542 {\AA} line is mostly sensitive to the layers enclosed between $\log\tau=[0,-5.5]$, under the physical conditions that are present in our model atmospheres. In addition, the simulated magnetic flux tube generates strong longitudinal signals in its centre and moderate transversal signals, due to the vertical expansion of magnetic field lines, in its edge. Thus, observing the Ca II 8542 {\AA} line we will be able to infer the 3D geometry of moderate magnetic field regions.

High speed magnetized flows in the quiet Sun

C. Quintero **Noda**, J.M. Borrero, D. Orozco Suárez, B. Ruiz Cobo
A&A, **2014**
http://arxiv.org/pdf/1407.7477v1.pdf

We have examined the spatial and polarimetric properties of these events using a variety of data from the Hinode spacecraft. We have also inferred the atmospheric stratification of the physical parameters by means of the inversion of the observed Stokes profiles employing the Stokes Inversion based on Response functions (SIR) code. Finally, we analyzed their evolution using a time series from the same instrument. Blue-shifted events tend to appear over bright regions at the edge of granules, while red-shifted events are seen predominantly over dark regions on intergranular lanes. Large linear polarization signals can be seen in the region that connects them. The magnetic structure inferred from the time series revealed that the structure corresponds to a Ω-loop, with one footpoint always over the edge of a granule and the other inside an intergranular lane. The physical parameters obtained from the inversions of the observed Stokes profiles in both events show an increase with respect to the Harvard-Smithonian reference atmosphere in the temperature at $\log\tau_{500} \in (-1,-3)$ and a strong magnetic field, $B \geq 1$ kG, at the bottom of the atmosphere that quickly decreases upward until vanishing at $\log\tau_{500} \approx -2$. In the blue-shifted events, the line of sight velocities change from upflows at the bottom to downflows at the top of the atmosphere. Red-shifted events display the opposite velocity stratification. The change of sign in line of sight velocity happens at the same optical depth in which the magnetic field becomes zero. The physical mechanism that best explains the inferred magnetic field configuration and flow motions is a siphon flow along an arched magnetic flux tube. Further investigation is required however, as the expected features of a siphon flow cannot be unequivocally identified.

Photospheric downward plasma motions in the quiet-Sun

Carlos Quintero **Noda**, Basilio Ruiz Cobo, David Orozco Suárez
A&A, 566, A139**, 2014**
http://arxiv.org/pdf/1405.1561v1.pdf

We analyze spectropolarimetric data taken with the Hinode spacecraft in quiet solar regions at the disk center. Distorted redshifted Stokes V profiles are found showing a characteristic evolution that always follows the same sequence of phases. We have studied the statistical properties of these events using spectropolarimetric data from Hinode/SP. We also examined the upper photosphere and the low chromosphere using Mg i b2 and Ca ii h data from Hinode. Finally, we have applied the SIRGAUSS inversion code to the polarimetric data in order to infer the atmospheric stratification of the physical parameters. We have also obtained these physical parameters taking into account dynamical terms in the equation of motion.
The Stokes V profiles display a bump that evolves in four different time steps, and the total process lasts 108 seconds. The Stokes I shows a strongly bent red wing and the continuum signal exhibits a bright point inside an intergranular lane. This bright point is correlated with a strong redshift in the Mg i b2 line and a bright feature in Ca ii h images. The model obtained from the inversion of the Stokes profiles is hotter than the average quiet-Sun model, with a vertical magnetic field configuration and field strengths in the range of kG values. It also presents a LOS velocity stratification with a Gaussian perturbation whose center is moving to deeper layers with time.
We have examined a particular type of event that can be described as a plasmoid of hot plasma that is moving downward from the top of the photosphere, placed over intergranular lanes and always related to strong magnetic field concentrations. We argue that the origin of this plasmoid could be a magnetic reconnection that is taking place in the chromosphere. **2007 March 10th and 2007 October 15**

Sunspot Observations by Barnaba Oriani (1778 – 1779)

J. M. **Nogales**, V. M. S. Carrasco, R. Arlt, F. Domínguez-Castro & J. M. Vaquero
Solar Physics volume 295, Article number: 71 (**2020**)
https://link.springer.com/content/pdf/10.1007/s11207-020-01638-8.pdf

We present the sunspot observations made by Barnaba Oriani in 1778 and 1779 at the Brera Observatory (Milan, Italy). We have computed the number of sunspot groups and individual sunspots and extracted the positions of all individual sunspots recorded by Oriani. It must be highlighted that the observations made by Oriani in 1779 are not included in the current sunspot-group number database. The observations made in 1778 were already included, but we have found important deficiencies in these values that underestimated the true level of solar activity. The highest daily number of groups recorded by Oriani was 12 (24 August 1778). Only Horrebow in Solar Cycle 2 observed a higher daily number of groups (up to 16 groups in 1769) in the second half of the 18th century. We have compared the sunspot observations made by Oriani and Staudacher for the common dates. In general, Oriani observed a few more groups than Staudacher, while Staudacher recorded more individual sunspots than Oriani. Furthermore, the sunspot positions recorded by both observers are similar, but some significant differences can be found. Finally, we want to highlight that the sunspot records made in the 18th century will help us to understand better the behavior of

the long-term solar activity. Therefore, we need to improve the observational coverage of the sunspot records carried out in that century.

Coronal voids and their magnetic nature

J. D. **Nölke**1, S. K. Solanki1, J. Hirzberger1, H. Peter1, L. P. Chitta1, F. Kahil1 +++
A&A 678, A196 (**2023**)
https://www.aanda.org/articles/aa/pdf/2023/10/aa46040-23.pdf
https://arxiv.org/pdf/2309.09789.pdf
Context. Extreme ultraviolet (EUV) observations of the quiet solar atmosphere reveal extended regions of weak emission compared to the ambient quiescent corona. The magnetic nature of these coronal features is not well understood.
Aims. We study the magnetic properties of the weakly emitting extended regions, which we name coronal voids. In particular, we aim to understand whether these voids result from a reduced heat input into the corona or if they are associated with mainly unipolar and possibly open magnetic fields, similar to coronal holes.
Methods. We defined the coronal voids via an intensity threshold of 75% of the mean quiet-Sun (QS) EUV intensity observed by the high-resolution EUV channel (HRIEUV) of the Extreme Ultraviolet Imager on Solar Orbiter. The line-of-sight magnetograms of the same solar region recorded by the High Resolution Telescope of the Polarimetric and Helioseismic Imager allowed us to compare the photospheric magnetic field beneath the coronal voids with that in other parts of the QS.
Results. The coronal voids studied here range in size from a few granules to a few supergranules and on average exhibit a reduced intensity of 67% of the mean value of the entire field of view. The magnetic flux density in the photosphere below the voids is 76% (or more) lower than in the surrounding QS. Specifically, the coronal voids show much weaker or no network structures. The detected flux imbalances fall in the range of imbalances found in QS areas of the same size.
Conclusions. We conclude that coronal voids form because of locally reduced heating of the corona due to reduced magnetic flux density in the photosphere. This makes them a distinct class of (dark) structure, different from coronal holes. **2021 February 23**

Statistics of Photospheric Supergranular Cells Observed by SDO/HMI

Majedeh **Noori**, Mohsen Javaherian, Hossein Safari, Hamid Nadjari
Advances in Space Research Volume 64, Issue 2, 15 July **2019**, Pages 504-513
https://arxiv.org/pdf/1807.07479.pdf
sci-hub.se/10.1016/j.asr.2019.04.027
Aims: The statistics of the photospheric granulation pattern are investigated using continuum images observed by Solar Dynamic Observatory (SDO)/Helioseismic and Magnetic Imager (HMI) taken at 6713~\AA.
Methods: The supergranular boundaries can be extracted by tracking photospheric velocity plasma flows. The local ball-tracking method is employed to apply on the HMI data gathered over the years 2011-2015 to estimate the boundaries of the cells. The edge sharpening techniques are exerted on the output of ball-tracking to precisely identify the cells borders. To study the fractal dimensionality (FD) of supergranulation, the box counting method is used.
Results: We found that both the size and eccentricity follow the log-normal distributions with peak values about 330 Mm2 and 0.85, respectively. The five-year mean value of the cells number appeared in half-hour sequences is obtained to be about 60 ± 6 within an area of 350″×350″. The cells orientation distribution presents the power-law behavior.
Conclusions: The orientation of supergranular cells (O) and their size (S) follows a power-law function as |O|∝S9.5. We found that the non-roundish cells with smaller and larger sizes than 600 Mm2 are aligned and perpendicular with the solar rotational velocity on the photosphere, respectively. The FD analysis shows that the supergranular cells form the self-similar patterns.

Impact of anti-solar differential rotation in mean-field solar-type dynamos - Exploring possible magnetic cycles in slowly rotating stars

Q. **Noraz**, A. S. Brun, A. Strugarek and G. Depambour
A&A 658, A144 (**2022**)
https://doi.org/10.1051/0004-6361/202141946
https://www.aanda.org/articles/aa/full_html/2022/02/aa41946-21/aa41946-21.html#top_f
Context. Over the course of their lifetimes, the rotation of solar-type stars goes through different phases. Once they reach the zero-age main sequence, their global rotation rate decreases during the main sequence until at least the solar age, approximately following the empirical Skumanich's law and enabling gyrochronology. Older solar-type stars might then reach a point of transition when they stop braking, according to recent results of asteroseismology. Additionally, recent 3D numerical simulations of solar-type stars show that different regimes of differential rotation can be characterized with the Rossby number. In particular, anti-solar differential rotation (fast poles, slow equator)

may exist for high Rossby number (slow rotators). If this regime occurs during the main sequence and, in general, for slow rotators, we may consider how magnetic generation through the dynamo process might be impacted. In particular, we consider whether slowly rotating stars are indeed subject to magnetic cycles.
Aims. We aim to understand the magnetic field generation of solar-type stars possessing an anti-solar differential rotation and we focus on the possible existence of magnetic cycles in such stars.
Methods. We modeled mean-field kinematic dynamos in solar (fast equator, slow poles) and anti-solar (slow equator, fast poles) differential rotation, using the STELEM code. We consider two types of mean field dynamo mechanisms along with the Ω-effect: the standard α-effect distributed at various locations in the convective envelope and the Babcock-Leighton effect.
Results. We find that kinematic αΩ dynamos allow for the presence of magnetic cycles and global polarity reversals for both rotation regimes, but only if the α-effect is saddled on the tachocline. If it is distributed in the convection zone, solar-type cases still possess a cycle and anti-solar cases do not. Conversely, we have not found any possibility for sustaining a magnetic cycle with the traditional Babcock-Leighton flux-transport dynamos in the anti-solar differential rotation regime due to flux addition. Graphic interpretations are proposed in order to illustrate these cases. However, we find that hybrid models containing both prescriptions can still sustain local polarity reversals at some latitudes.
Conclusions. We conclude that stars in the anti-solar differential rotation regime can sustain magnetic cycles only for very specific dynamo processes. The detection of a magnetic cycle for such a star would therefore be a particularly interesting constraint in working to decipher what type of dynamo is actually at work in solar-type stars.

Perspective on space radiation for space flights in 2020–2040 (Review)

John W. **Norbury**
Advances in Space Research
Volume 47, Issue 4, 15 February **2011**, Pages 611-621
The Sun undergoes several well known periodicities in activity, such as the Schwabe 11 year cycle, the Gleissberg 80–90 year cycle, the Suess 200–210 year cycle and the Halstatt 2200–2300 year cycle. In addition, there is evidence that the 20th century levels of solar activity are unusually high. The years 2020–2040 are expected to coincide with increased activity in human space flight beyond low Earth orbit. The solar cycles and the present level of solar activity are reviewed and their activities during the years 2020–2040 are discussed with a perspective on space radiation and the future program of space flight. It is prudent to prepare for continuing levels of high solar activity as well as for the low levels of the current deep minimum, which has corresponded to high galactic cosmic ray flux.

An Analysis of the Sunspot Groups and Flares of Solar Cycle 23

Donald C. **Norquist**
Solar Phys (**2011**) 269: 111–127
Designing a statistical solar flare forecasting technique can benefit greatly from knowledge of the flare frequency of occurrence with respect to sunspot groups. This study analyzed sunspot groups and H⟨ and X-ray flares reported for the period 1997 – 2007. Annual catalogs were constructed, listing the days that numbered sunspot groups were observed (designated sunspot group-days, SSG-Ds) and for each day a record for each associated H⟨ flare of importance category one or greater and normal or bright brightness and for each X-ray flare of intensity C 5 or higher. The catalogs were then analyzed to produce frequency distributions of SSG-Ds by year, sunspot group class, likelihood of producing at least one flare overall and by sunspot group class, and frequency of occurrence of numbers of flares per day and flare intensity category. Only 3% of SSG-Ds produced a substantial H⟨ flare and 7% had a significant X-ray flare. We found that mature, complex sunspot groups were more likely than simple sunspot groups to produce a flare, but the latter were more prevalent than the former. More than half of the SSG-Ds with flares had a maximum intensity flare greater than the lowest category (C-class of intensity five and higher). The fact that certain sunspot group classes had flaring probabilities significantly higher than the combined probabilities of the intensity categories when all SSG-Ds were considered suggest that it might be best to first predict the flaring probability. For sunspot groups found likely to flare, a separate diagnosis of maximum flare intensity category appears feasible.

Spectral variability of photospheric radiation due to faculae I: The Sun and Sun-like stars

Charlotte M. **Norris**, Benjamin Beeck, Yvonne C. Unruh, Sami K. Solanki, Natalie A. Krivova, Kok Leng Yeo
A&A **2017**
Context. Stellar spectral variability on timescales of a day and longer, arising from magnetic surface features such as dark spots and bright faculae, is an important noise source when characterising extra-solar planets. Current 1D

models of faculae do not capture the geometric properties and fail to reproduce observed solar facular contrasts. Magnetoconvection simulations provide facular contrasts accounting for geometry.
Aims. We calculate facular contrast spectra from magnetoconvection models of the solar photosphere with a view to improve (a) future parameter determinations for planets with early G type host stars and (b) reconstructions of solar spectral variability.
Methods. Regions of a solar twin (G2, log g=4.44) atmosphere with a range of initial average vertical magnetic fields (100 to 500~G) were simulated using a 3D radiation-magnetohydrodynamics code, MURaM, and synthetic intensity spectra were calculated from the ultraviolet (149.5~nm) to the far infrared (160000~nm) with the ATLAS9 radiative transfer code. Nine viewing angles were investigated to account for facular positions across most of the stellar disc.
Results. Contrasts of the radiation from simulation boxes with different levels of magnetic flux relative to an atmosphere with no magnetic field are a complicated function of position, wavelength and magnetic field strength that is not reproduced by 1D facular models. Generally, contrasts increase towards the limb, but at UV wavelengths a saturation and decrease are observed close to the limb. Contrasts also increase strongly from the visible to the UV; there is a rich spectral dependence, with marked peaks in molecular bands and strong spectral lines. At disc centre, a complex relationship with magnetic field was found and areas of strong magnetic field can appear either dark or bright, depending on wavelength. Spectra calculated for a wide variety of magnetic fluxes will also serve to improve total and spectral solar irradiance reconstructions.

Solar Cycle Observations **Review**

Aimee **Norton**, Rachel Howe, Lisa Upton, Ilya Usoskin
Space Science Reviews 219, Article number: 64 **2023**
https://arxiv.org/pdf/2305.19803.pdf
https://link.springer.com/content/pdf/10.1007/s11214-023-01008-3.pdf
We describe the defining observations of the solar cycle that provide constraints for the dynamo processes operating within the Sun. Specifically, we report on the following topics: historical sunspot numbers and revisions; active region (AR) flux ranges and lifetimes; tilt angles; Hale and Joy's law; the impact of rogue ARs on cycle progression; the spatio-temporal emergence of ARs that creates the butterfly diagram; polar fields; large-scale flows including zonal, meridional, and AR in-flows; short-term cycle variability; and helioseismic results including mode parameter changes.

Introducing the SPEAR Catalogue from HMI Data

A.A. **Norton**
HMI Science Nuggets #168 Oct **2021** http://hmi.stanford.edu/hminuggets/?p=3730
In order to make the properties of magnetic features observed by SDO/HMI more accessible, the Solar Photospheric Ephemeral and Active Region (SPEAR) catalogue has been created as an easy-to-read tabulated text file. Both active regions and smaller magnetic features such as ephemeral regions are included in the catalogue from the beginning of HMI science data acquisition, 2010.05.01, until 2020.12.31. More recent data will be added at regular intervals.

Oscillations observed in Umbra, Plage, Quiet-Sun and the Polarity Inversion Line of Active Region 11158 using HMI/SDO Data

A. A. **Norton**, R. B. Stutz, B. T. Welsch
Philisophical Transactions of the Royal Society A, **2021**, 379, 2190
https://arxiv.org/pdf/2101.01349.pdf
Using data from the Helioseismic Magnetic Imager, we report on the amplitudes and phase relations of oscillations in quiet-Sun, plage, umbra and the polarity inversion line (PIL) of an active region NOAA#11158. We employ Fourier, wavelet and cross correlation spectra analysis. Waves with 5-minute periods are observed in umbra, PIL and plage with common phase values of $\phi(v,I)=\pi 2$, $\phi(v,Blos)=-\pi 2$. In addition, $\phi(I,Blos)=\pi$ in plage are observed. These phase values are consistent with slow standing or fast standing surface sausage wave modes. The line width variations, and their phase relations with intensity and magnetic oscillations, show different values within the plage and PIL regions, which may offer a way to further differentiate wave mode mechanics. Significant Doppler velocity oscillations are present along the PIL, meaning that plasma motion is perpendicular to the magnetic field lines, a signature of Alvènic waves. A time-distance diagram along a section of the PIL shows Eastward propagating Doppler oscillations converting into magnetic oscillations; the propagation speeds range between 2−6 km s−1. Lastly, a 3-minute wave is observed in select regions of the umbra in the magnetogram data. **16 Feb 2011**
HMI Science Nuggets **#150** http://hmi.stanford.edu/hminuggets/?p=3439

Hemispheric Coupling: Comparing Dynamo Simulations and Observations **Review**

Aimee A. **Norton**, Paul Charbonneau, Dario Passos

Space Science Reviews, Volume 186, Issue 1-4, pp 251-283, Dec **2014**
http://arxiv.org/pdf/1411.7052v1.pdf
Numerical simulations that reproduce solar-like magnetic cycles can be used to generate long-term statistics. The variations in N-S hemispheric cycle synchronicity and amplitude produced in simulations has not been widely compared to observations. The observed limits on asymmetry show that hemispheric sunspot area production is no more than 20% asymmetric for cycles 12-23 and phase lags do not exceed 20% (2 yrs) of the total cycle period. Independent studies have found a long-term trend in phase values as one hemisphere leads the other for ~four cycles. Such persistence in phase is not indicative of a stochastic phenomenon. We compare the findings to results from a numerical simulation of solar convection recently produced with the EULAG-MHD model. This simulation spans 1600 yrs and generated 40 regular, sunspot-like cycles. While the simulated cycle length is too long and the toroidal bands remain at too high of latitudes, some solar-like aspects of hemispheric asymmetry are reproduced. The model reproduces the synchrony of polarity inversions and onset of cycle as the simulated phase lags do not exceed 20% of the cycle period. Simulated amplitude variations between the N and S hemispheres are larger than observed in the Sun. The simulations show one hemisphere persistently leads the other for several successive cycles, placing an upper bound on the efficiency of transequatorial magnetic coupling mechanisms. These include magnetic diffusion, cross-equatorial mixing within elongated convective rolls and transequatorial meridional flow cells. One or more of these processes may lead to magnetic flux cancellation whereby the oppositely directed fields come in close proximity and cancel each other across the magnetic equator late in the solar cycle. We discuss the discrepancies between model and observations and the constraints they pose on possible mechanisms of hemispheric coupling.

The Biggest Sunspots Produced by Cycle 24

Aimee A. **Norton**
HMI Science Nuggets, No. 3, Jan **2014**
http://hmi.stanford.edu/hminuggets/?p=381
Even though Solar Cycle 24 is weak, it has still produced some large sunspots. **We list the largest sunspots** as observed by HMI and discuss some aspects of the data.

Multimodal Differential Emission Measure in the Solar Corona

Federico A. **Nuevo**, Alberto M. Vásquez, Enrico Landi, Richard Frazin
2015 ApJ 811 128
http://arxiv.org/pdf/1503.02473v1.pdf
The Atmospheric Imaging Assembly (AIA) telescope on board the Solar Dynamics Observatory (SDO) provides coronal EUV imaging over a broader temperature sensitivity range than the previous generations of instruments (EUVI, EIT, and TRACE). Differential emission measure tomography (DEMT) of the solar corona based on AIA data is presented here for the first time. The main product of DEMT is the three-dimensional (3D) distribution of the local differential emission measure (LDEM). While in previous studies, based on EIT or EUVI data, there were 3 available EUV bands, with a sensitivity range ∼0.60−2.70 MK, the present study is based on the 4 cooler AIA bands (aimed at studying the quiet sun), sensitive to the range ∼0.55−3.75 MK. The AIA filters allow exploration of new parametric LDEM models. Since DEMT is better suited for lower activity periods, we use data from Carrington Rotation 2099, when the Sun was in its most quiescent state during the AIA mission. Also, we validate the parametric LDEM inversion technique by applying it to standard bi-dimensional (2D) differential emission measure (DEM) analysis on sets of simultaneous AIA images, and comparing the results with DEM curves obtained using other methods. Our study reveals a ubiquitous bimodal LDEM distribution in the quiet diffuse corona, which is stronger for denser regions. We argue that the nanoflare heating scenario is less likely to explain these results, and that alternative mechanisms, such as wave dissipation appear better supported by our results.

Latitude Survey Investigation of Galactic Cosmic Ray Solar Modulation during 1994-2007

W. **Nuntiyakul**1,2,3, P. Evenson4, D. Ruffolo1,2, A. Sáiz1,2, J. W. Bieber4, J. Clem4, R. Pyle4, M. L. Duldig5, and J. E. Humble
2014 ApJ 795 11
The Galactic cosmic ray spectrum exhibits subtle variations over the 22 yr solar magnetic cycle in addition to the more dramatic variations over the 11 yr sunspot cycle. Neutron monitors are large ground-based detectors that provide accurate measurements of variations in the cosmic ray flux at the top of the atmosphere above the detector. At any given location the magnetic field of the Earth excludes particles below a well-defined rigidity (momentum per unit charge) known as the cutoff rigidity, which can be accurately calculated using detailed models of the geomagnetic field. By carrying a neutron monitor to different locations, e.g., on a ship, the Earth itself serves as a magnet spectrometer. By repeating such latitude surveys with identical equipment, a sensitive measurement of changes in the spectrum can be made. In this work, we analyze data from the 1994 through 2007 series of latitude surveys conducted by the Bartol Research Institute, the University of Tasmania, and the Australian Antarctic Division. We confirm the curious "crossover" in spectra measured near solar minima during epochs of opposite

solar magnetic polarity, and show that it is directly related to a sudden change in the spectral behavior of solar modulation at the time of the polarity reversal, as revealed from contemporaneous variations in the survey data and a fixed station. We suggest that the spectral change and crossover result from the interaction of effects due to gradient/curvature drifts with a systematic change in the interplanetary diffusion coefficient caused by turbulent magnetic helicity.

Role of the Solar Minimum in the Waiting Time Distribution Throughout the Heliosphere

Yosia I. **Nurhan**, Jay R. Johnson, Jonathan R. Homan, Simon Wing

2021

https://arxiv.org/pdf/2105.05939.pdf

We explore the tail of various waiting time datasets of processes that follow a nonstationary Poisson distribution with a sinusoidal driver. Analytically, we find that the distribution of large waiting times of such processes can be described using a power law slope of -2.5. We show that this result applies more broadly to any nonstationary Poisson process driven periodically. Examples of such processes include solar flares, coronal mass ejections, geomagnetic storms, and substorms. We also discuss how the power law specifically relates to the behavior of driver near its minima.

Effects of Plasma Drag on Low Earth Orbiting Satellites due to Heating of Earth's Atmosphere by Coronal Mass Ejections

Nwankwo, Victor U. J.; Chakrabarti, Sandip K.

2013

http://arxiv.org/pdf/1305.0233v1.pdf

Solar events, such as coronal mass ejections (CMEs) and solar flares, heat up the upper atmosphere and near-Earth space environment. Due to this heating and expansion of the outer atmosphere by the energetic ultraviolet, X-ray and particles expelled from the sun, the low Earth-Orbiting satellites (LEOS) become vulnerable to an enhanced drag force by the ions and molecules of the expanded atmosphere. Out of various types of perturbations, Earth directed CMEs play the most significant role. They are more frequent and intense during the active (solar maximum) phase of the sun's approximately 11-year cycle. As we are approaching another solar maximum later in 2013, it may be instructive to analyse the effects of the past solar cycles on the orbiting satellites using the archival data of space environment parameters as indicators. In this paper, we compute the plasma drag on a model LEOS due to the atmospheric heating by CMEs and other solar events as a function of the solar parameters. Using the current forecast on the time and strength of the next solar maximum, we predict how an existing satellite orbit may be affected in the forthcoming years.

Average radial structures of gas convection in the solar granulation

T. **Oba**, Y. Iida, T. Shimizu

ApJ **890** 141 **2020**

https://arxiv.org/pdf/2001.03575.pdf

https://doi.org/10.3847/1538-4357/ab6a90

Gas convection is observed in the solar photosphere as the granulation, i.e., having highly time-dependent cellular patterns, consisting of numerous bright cells called granules and dark surrounding-channels called intergranular lanes. Many efforts have been made to characterize the granulation, which may be used as an energy source for various types of dynamical phenomena. Although the horizontal gas flow dynamics in intergranular lanes may play a vital role, but they are poorly understood. This is because the Doppler signals can be obtained only at the solar limb, where the signals are severely degraded by a foreshortening effect. To reduce such a degradation, we use Hinode's spectroscopic data, which are free from a seeing-induced image degradation, and improve its image quality by correcting for straylight in the instruments. The dataset continuously covers from the solar disk to the limb, providing a multidirectional line-of-sight (LOS) diagnosis against the granulation. The obtained LOS flow-field variation across the disk indicates a horizontal flow speed of 1.8-2.4 km/s. We also derive the spatial distribution of the horizontal flow speed, which is 1.6 km/s in granules and 1.8 km/s in intergranular lanes, and where the maximum speed is inside intergranular lanes. This result newly suggests the following sequence of horizontal flow: A hot rising gas parcel is strongly accelerated from the granular center, even beyond the transition from the granules to the intergranular lanes, resulting in the fastest speed inside the intergranular lanes, and the gas may also experience decelerations in the intergranular lane.

The small-scale structure of photospheric convection retrieved by a deconvolution technique applied to Hinode/SP data

T. **Oba**, T.L. Riethmüller, S. K. Solanki, Y. Iida, C. Quintero Noda, T. Shimizu

ApJ **849** 7 **2017**

https://arxiv.org/pdf/1709.06933.pdf

Solar granules are bright patterns surrounded by dark channels called intergranular lanes in the solar photosphere and are a manifestation of overshooting convection. Observational studies generally find stronger upflows in granules and weaker downflows in intergranular lanes. This trend is, however, inconsistent with the results of numerical simulations in which downflows are stronger than upflows through the joint action of gravitational acceleration/deceleration and pressure gradients. One cause of this discrepancy is the image degradation caused by optical distortion and light diffraction and scattering that takes place in an imaging instrument. We apply a deconvolution technique to Hinode/SP data in an attempt to recover the original solar scene. Our results show a significant enhancement in both, the convective upflows and downflows, but particularly for the latter. After deconvolution, the up- and downflows reach maximum amplitudes of -3.0 km/s and +3.0 km/s at an average geometrical height of roughly 50 km, respectively. We found that the velocity distributions after deconvolution match those derived from numerical simulations. After deconvolution the net LOS velocity averaged over the whole FOV lies close to zero as expected in a rough sense from mass balance.

Height-dependent velocity structure of photospheric convection in granules and intergranular lanes with Hinode/SOT

T. **Oba**, Y. Iida, T. Shimizu
2017 ApJ 836 40
https://arxiv.org/pdf/1612.06175v1.pdf

The solar photosphere is the visible surface of the Sun, where many bright granules, surrounded by narrow dark intergranular lanes, are observed everywhere. The granular pattern is a manifestation of convective motion at the photospheric level, but its velocity structure in the height direction is poorly understood observationally. Applying bisector analysis to a photospheric spectral line recorded by the Hinode Solar Optical Telescope, we derived the velocity structure of the convective motion in granular regions and intergranular lanes separately. The amplitude of motion of the convective material decreases from 0.65 to 0.40 km/s as the material rises in granules, whereas the amplitude of motion increases from 0.30 to 0.50 km/s as it descends in intergranular lanes. These values are significantly larger than those obtained in previous studies using bisector analysis. The acceleration of descending materials with depth is not predicted from the convectively stable condition in a stratified atmosphere. Such convective instability can be developed more efficiently by radiative cooling and/or a gas pressure gradient, which can control the dynamical behavior of convective material in intergranular lanes. Our analysis demonstrated that bisector analysis is a useful method for investigating the long-term dynamic behavior of convective material when a large number of pixels is available. In addition, one example is the temporal evolution of granular fragmentation, in which downflowing material develops gradually from a higher layer downward.

Is There a Synchronizing Influence of Planets on Solar and Stellar Cyclic Activity?

V.N. **Obridko**, M.M. Katsova, D.D. Sokoloff, N.V. Emelianov
Solar Phys. **299**, 124 **2024**
https://arxiv.org/pdf/2408.15499
https://doi.org/10.1007/s11207-024-02365-0

This work continues our research of connection between the long-term activity of stars and their planets. We analyze new data on the previously considered two dozen solar-type stars with identified cycles, adding the results of studying the long-term variability of two more solar-type G stars and 15 cooler M dwarfs with planets. If the cyclic activity is determined by a strong tidal influence of the planet, then the cycle duration of the star should be synchronized with the period of orbital revolution of the planet. We calculate the gravitational effect of planets on their parent stars. The results obtained confirm the earlier conclusion that exoplanets do not influence the formation of the stellar cycle. We examine the change in the position of the barycenter of the solar system relative to the center of the Sun over 420 years. A comparison of these data with the most reliable 120-year SSN (sunspot number) series as the index of solar activity has shown that they are not synchronized.

Gnevyshev gap in the large-scale magnetic field

V.N. **Obridko**, A.S. Shibalova, D.D. Sokoloff
Solar Phys. **299**, 60 **2024**
https://arxiv.org/pdf/2403.18568.pdf
https://doi.org/10.1007/s11207-024-02292-0

The phenomenon of the Gnevyshev gap was first identified in the solar-corona irradiance data (green line). Later, it was studied in the sunspot, coronal, and heliospheric data. We have investigated the Gnevyshev gap in the magnetic field data and have arrived at the conclusion that it reflects the behavior of the large-scale magnetic field. The Gnevyshev gap occurs at the polarity reversal of the solar magnetic field at the photosphere level. The presence of the Gnevyshev gap in sunspot data at the photosphere level is disguised by non-global structures that retain dependence on both latitude and longitude (the accepted mathematical term is tessaral, see below for more details). However, it is clearly visible in the magnetic field data at the photosphere level and is even more pronounced at the source surface (i.e., in the corona).

Cyclic variations of the structure and energetics of solar magnetic fields

V.N. **Obridko**, A.S. Shibalova, D.D. Sokoloff

MNRAS Volume 529, Issue 3, April 2024, Pages 2846–2853, **2024**

https://arxiv.org/pdf/2403.06293.pdf

https://doi.org/10.1093/mnras/stae685

https://academic.oup.com/mnras/article-pdf/529/3/2846/57055422/stae685.pdf

The solar cycle is a complex phenomenon, a comprehensive understanding of which requires the study of various tracers. Here, we consider the solar cycle as manifested in the harmonics of the solar large-scale surface magnetic field, including zonal, sectorial and tesseral harmonics, divided into odd and even relative to the solar equator. In addition to considering the amplitudes of the harmonics, we analyze their contribution to the magnetic energy. It turns out that the relative contribution of different types of harmonics to the magnetic energy is virtually independent of the cycle height. We identify different phases of the activity cycle using harmonics of different symmetries. A possible way to incorporate the obtained result into the solar dynamo theory is proposed.

The Structure of the Solar Cycle and of the Activity Cycles of Late-Type Stars

V.N. **Obridko**, D.D. Sokoloff, M.M. Katsova

Astronomy Reports (**2023**)

https://arxiv.org/pdf/2311.00472.pdf

It is shown that the description of the solar cycle that takes into account the odd zonal harmonic of the solar magnetic field allows us to deepen our knowledge of two important aspects of the solar activity. First, to clarify and expand predictions of the evolution of the cyclic activity of the Sun in the near future. Second, to develop a program for monitoring the spectrophotometric characteristics of radiation of the solar-type stars aimed at obtaining new information about their magnetic fields.

Estimates of the Height and Date of the 25th Cycle of Solar Activity

V.N. **Obridko**, D.D. Sokoloff, M.M. Katsova

ASTRONOMICHESKII TSIRKULYAR 1658 (**2023**) 1-4

https://arxiv.org/pdf/2307.05725.pdf

Further development of the work of Obridko et al. [1] based on recent data confirms the assumption that the 25th cycle of solar activity is a medium-low cycle. Its height is expected to be 125.2±5.6, and the expected date of the maximum phase is the end of 2023 or the first quarter of 2024.

The Extended Solar Cycle and Asymmetry of the Large-Scale Magnetic Field

V.N. **Obridko**, A.S. Shibalova, D.D. Sokoloff

MNRAS **2023**

https://arxiv.org/pdf/2305.19427.pdf

Traditionally, the solar activity cycle is thought as an interplay of the main dipole component of the solar poloidal magnetic field and the toroidal magnetic field. However, the real picture as presented in the extended solar-cycle models is much more complicated. Here, we develop the concept of the extended solar cycle clarifying what zonal harmonics are responsible for the equatorward and polarward propagating features in the surface activity tracers. We arrive at a conclusion that the zonal harmonics with L = 5 play a crucial role in separating the phenomena of both types, which are associated with the odd zonal harmonics. Another objective of our analysis is the role of even zonal harmonics, which prove to be rather associated with the North-South asymmetry of the solar activity than with its 11-year solar periodicity.

Solar and stellar activity cycles -- no synchronization with exoplanets

V.N. **Obridko**, M.M. Katsova, D.D. Sokoloff

MNRAS Volume 523, Issue 1, July **2023**, Pages 982–990,

https://arxiv.org/pdf/2208.06190.pdf

https://doi.org/10.1093/mnras/stad1515

Cyclic activity on the Sun and stars is primarily explained by generation of the magnetic field by a dynamo mechanism, which converts the energy of the poloidal field into the energy of the toroidal component due to differential rotation. There is, however, an alternative point of view, which explains the field generation by gravitational influence of the planetary system and, first of all, Jupiter. This hypothesis can be verified by comparing the characteristics of exoplanets with the activity variations on their associated stars. We have performed such a comparison and have drawn a negative conclusion. No relationship between the gravitational influence of the exoplanets and cycle of the host star could be found in any of the cases considered. Moreover, there are reasons to believe that a strong gravitational influence may completely eliminate cyclic variation in stellar activity.

Zonal harmonics of solar magnetic field for solar cycle forecast

V.N. **Obridko**, D.D. Sokoloff, V.V. Pipin, A.S. Shibalvaa, I.M. Livshits

J(A)STP **2021**

https://arxiv.org/pdf/2108.10527.pdf

According to the scheme of action of the solar dynamo, the poloidal magnetic field can be considered a source of production of the toroidal magnetic field by the solar differential rotation. From the polar magnetic field proxies, it is natural to expect that solar Cycle 25 will be weak as recorded in sunspot data. We suggest that there are parameters of the zonal harmonics of the solar surface magnetic field, such as the magnitude of the ℓ=3 harmonic or the effective multipole index, that can be used as a reasonable addition to the polar magnetic field proxies. We discuss also some specific features of solar activity indices in Cycles 23 and 24.

Solar large-scale magnetic field and cycle patterns in solar dynamo

V.N. **Obridko**, V.V. Pipin, D.D. Sokoloff, A.S. Shibalova

MNRAS Volume 504, Issue 4, Pages 4990–5000, **2021**

https://arxiv.org/pdf/2104.06808.pdf

https://doi.org/10.1093/mnras/stab1062

We compare spectra of the zonal harmonics of the large-scale magnetic field of the Sun using observation results and solar dynamo models. The main solar activity cycle as recorded in these tracers is a much more complicated phenomenon than the eigen solution of solar dynamo equations with the growth saturated by a back reaction of the dynamo-driven magnetic field on solar hydrodynamics. The nominal 11(22)-year cycle as recorded in each mode has a specific phase shift varying from cycle to cycle; the actual length of the cycle varies from one cycle to another and from tracer to tracer. Both the observation and the dynamo model show an exceptional role of the axisymmetric ℓ5 mode. Its origin seems to be readily connected with the formation and evolution of sunspots on the solar surface. The results of observations and dynamo models show a good agreement for the low ℓ1 and ℓ3 modes. The results for these modes do not differ significantly for the axisymmetric and nonaxisymmetric models. Our findings support the idea that the sources of the solar dynamo arise as a result of both the distributed dynamo processes in the bulk of the convection zone and the surface magnetic activity.

Magnetic Coupling of the Solar Hemispheres During the Solar Cycle

V. N. **Obridko**, V. G. Fainshtein, Y. S. Zagainova & G. V. Rudenko

Solar Physics volume 295, Article number: 149 (**2020**)

https://link.springer.com/content/pdf/10.1007/s11207-020-01716-x.pdf

This work is devoted to the study of peculiarities in the magnetic coupling of the solar hemispheres over a solar activity cycle. Two approaches have been used. We have studied (i) the magnetic coupling of active regions (ARs) located in different hemispheres in the vicinity of the central meridian and, simultaneously, in the vicinity of the equator and (ii) the properties and time variation of the meridional component of the equatorial magnetic field derived from a potential-field source surface (PFSS) reconstruction at the heliocentric distance of 1.1 solar radii. In the first case, it was shown that most of the ARs in the selected pairs were magnetically connected by field lines in their leading parts. In the second case, the magnetic field monthly mean meridional component, $B\theta B\theta$, in the equatorial plane, which magnetically connects the two hemispheres, displayed a cyclic time variation. In the process, the extreme values of $B\theta B\theta$ (both positive and negative) coincided in time with the sunspot maxima, and the amplitude of the $B\theta B\theta$ extreme values decreased with decreasing height of the sunspot activity cycle. The sign of the $B\theta B\theta$ extreme value was opposite to the sign of the forthcoming extreme value of the polar field, while the sign of $B\theta B\theta$ coincided with that of the field lines connecting the leading spots. This means that the polar field is indeed generated by the trailing spots of ARs, and the magnetic flux of the leading spots closes through the equator.

3 August 2013, 7 October 2013, 12 December 2014, 16 June 2015,

Table 1 List of AR pairs located near the central meridian and, simultaneously, near the equator in the opposite hemispheres.

Differential rotation of the solar corona and its importance for helioseismology

Vladimir **Obridko** and Olga Badalyan

EGU2020-3710 May **2020**

https://meetingorganizer.copernicus.org/EGU2020/displays/36057

It is shown that the solar corona rotates differentially at all heliocentric distances up to the source surface. As the distance increases, the differential rotation gradient decreases, and the rotation becomes more and more rigid. At small distances, the corona at latitudes above $\approx \pm 40^{\circ}$ rotates faster than the photosphere at the same latitudes. The type of the rotation depends also on the phase of the activity cycle. The differential rotation gradient is the largest in the vicinity of the cycle minimum. It is shown that time variations in the coronal rotation characteristics are associated with the tilt of the magnetic equator of the Sun. Based on the concept that the

differential rotation of the corona reflects the rotation of deep subphotospheric layers, we compared the changes in the coronal rotation characteristics with distance with the helioseismic data and showed their satisfactory agreement. The results obtained allow us to suggest that the rotation of the solar corona can be used as indicator of the differential rotation of subphotospheric layers and calculate the nature of some current sheets in heliosphere.
Presentation #3710 https://presentations.copernicus.org/EGU2020/presentations-ST1.7.zip

Cyclic variations in the main components of the solar large-scale magnetic field

V. N. **Obridko** (1), D. D. Sokoloff (1 and 2), B. D. Shelting (1), A. S. Shibalova (1 and 2), I. M. Livshits (1 and 3)
MNRAS Volume 492, Issue 4, March **2020**, Pages 5582–5591,
https://doi.org/10.1093/mnras/staa147
https://arxiv.org/pdf/2001.05433.pdf
We considered variations the dipole and the quadrupole components of the solar large-scale magnetic field. Both the axial and the equatorial dipoles exhibit a systematic decrease in the past four cycles in accordance with the general decrease of solar activity. The transition of the pole of a dipole from the polar region to mid latitudes occurs rather quickly, so that the longitude of the pole changes little. With time, however, this inclined dipole region shifts to larger longitudes, which suggests an acceleration of the dipole rotation. The mean rotation rate exceeds the Carrington velocity by 0.6%. The behavior of the quadrupole differs dramatically. Its decrease over last four cycles was much smaller than that of the dipole moment. The ratio of the quadrupole and dipole moments has increased for four cycles more than twice in contrast to the sunspot numbers, which displayed a twofold decrease for the same time interval. What about quadrupole rotation, the mean longitude of the poles of one sign decreased by 600 degrees over four cycles, which suggests that the mean rotation rate was lower than the Carrington velocity by 0.28%. We do not see however any conclusive evidence that, in the period under discussion, a mode of quadrupole symmetry was excited on the Sun along with the dipole mode.

Solar activity in the following decades **Review**

V.**Obridko**, K.Georgieva
Journal of Atmospheric and Solar-Terrestrial Physics Volume 176, September **2018**, Pages 1-4
sci-hub.tw/10.1016/j.jastp.2018.08.001

On the history of the solar wind discovery **Review**

V. N. **Obridko** & O. L. Vaisberg
Solar System Research March **2017**, Volume 51, Issue 2, pp 165–169
http://download.springer.com/static/pdf/608/art%253A10.1134%252FS0038094617020058.pdf?originUrl=http%3A%2F%2Flink.springer.com%2Farticle%2F10.1134%2FS0038094617020058&token2=exp=1490688542~acl=%2Fstatic%2Fpdf%2F608%2Fart%25253A10.1134%25252FS0038094617020058.pdf%3ForiginUrl%3Dhttp%253A%252F%252Flink.springer.com%252Farticle%252F10.1134%252FS0038094617020058*~hmac=6c50cbd1e1d1cedcabbcd1c14d70abfee414eb0ec76501a3141ddc47c43bd29c
The discovery of the solar wind has been an outstanding achievement in heliophysics and space physics. The solar wind plays a crucial role in the processes taking place in the Solar System. In recent decades, it has been recognized as the main factor that controls the terrestrial effects of space weather. The solar wind is an unusual plasma laboratory of giant scale with a fantastic diversity of parameters and operating modes, and devoid of influence from the walls of laboratory plasma systems. It is also the only kind of stellar wind accessible for direct study. The history of this discovery is quite dramatic. Like many remarkable discoveries, it had several predecessors. However, the honor of a discovery usually belongs to a scientist who was able to more fully explain the phenomenon. Such a man is deservedly considered the US theorist Eugene Parker, who discovered the solar wind, as we know it today, almost "with the point of his pen". In 2017, we will celebrate the 90th anniversary birthday of Eugene Parker.

North–South Asymmetry in the Distribution of Solar Background Magnetic Field

V. N. **Obridko**, V. E. Chertoprud, K. M. Kuzanyan
Solar Physics, Volume 289, Issue 8, pp 2867-2878 **2014**
The aim of this article is to investigate how the background magnetic field of the Sun behaves in different hemispheres. We used SOHO/MDI data obtained during a period of eight years from 2003 to 2011 to analyze the intensity distribution of the background magnetic field over the solar surface. We find that the background fields of both polarities (signs) are more intense in the southern than in the northern hemisphere. Mixed polarities are observed in the vicinity of the equator. In addition to the main field, a weaker field of opposite polarity is always present in the polar regions. In the declining phase of the cycle, the main field dominates, but at the minimum and in the rising phase of the cycle, it is gradually replaced by the growing stronger secondary field.

Global complexes of activity

V. N. **Obridko**, B. D. Shelting

Astronomy Reports, October **2013**, Volume 57, Issue 10, pp 786-796

Astronomicheskii Zhurnal, **2013**, Vol. 90, No. 10, pp. 857–868.

A new concept of "Global Complexes of Activity" on the Sun is presented, which brings together objects associated with both global and local fields in a single framework. Activity complexes have traditionally been identified purely from observations of active regions. We show here that a global complex also includes coronal holes and active regions. Our analysis is based on a large dataset on magnetic fields on various scales, SOHO/MDI observations of active regions and magnetic fields, and UV observations of coronal holes. It is shown that the evolution of coronal holes and active regions are parts of a single process. The relationships between the fields on different scales during the generation of the cycle is discussed.

'Active Longitudes' in the Heliomagnetic Reference Frame

V. N. **Obridko**, V. E. Chertoprud and E. V. Ivanov

Solar Physics, Volume 272, Number 1, 59-71, **2011**

A new coordinate system – heliomagnetic reference frame – has been proposed in which the great circle passes through the solar pole and the north pole of the magnetic dipole is considered as the central meridian. It is shown that, in the new coordinate system, the active longitudes are defined much more clearly, are more stable in time, and are interlaced every 11 years.

CAFE-AMR: A computational MHD Solar Physics simulation tool that uses AMR

Ricardo **Ochoa-Armenta**, Francisco S. Guzmán

MNRAS Volume 525, Issue 1, Pages 667–682, **2023**

https://arxiv.org/pdf/2307.15238.pdf

https://doi.org/10.1093/mnras/stad2342

The study of our Sun holds significant importance in Space Weather research, encompassing a diverse range of phenomena characterized by distinct temporal and spatial scales. To address these complexities, we developed CAFE-AMR, an implementation of an Adaptive Mesh Refinement (AMR) strategy coupled with a Magnetohydrodynamics (MHD) equation solver, aiming to tackle Solar Physics-related problems. CAFE-AMR employs standard fluid dynamics methods, including Finite Volume discretization, HLL and Roe class flux formulas, linear order reconstructors, second-order Runge-Kutta, and Corner Transport Upwind time stepping. In this paper, we present the core structure of CAFE-AMR, discuss and evaluate mesh refinement criteria strategies, and conduct various tests, including simulations of idealized Solar Wind models, relevant for Space Weather applications.

THE EFFECTS OF SPATIAL SMOOTHING ON SOLAR MAGNETIC HELICITY PARAMETERS AND THE HEMISPHERIC HELICITY SIGN RULE

Stella Koch **Ocker**1,2 and Gordon Petrie

2016 ApJ 832 162

The hemispheric preference for negative/positive helicity to occur in the northern/southern solar hemisphere provides clues to the causes of twisted, flaring magnetic fields. Previous studies on the hemisphere rule may have been affected by seeing from atmospheric turbulence. Using Hinode/SOT-SP data spanning 2006–2013, we studied the effects of two spatial smoothing tests that imitate atmospheric seeing: noise reduction by ignoring pixel values weaker than the estimated noise threshold, and Gaussian spatial smoothing. We studied in detail the effects of atmospheric seeing on the helicity distributions across various field strengths for active regions (ARs) NOAA 11158 and NOAA 11243, in addition to studying the average helicities of 179 ARs with and without smoothing. We found that, rather than changing trends in the helicity distributions, spatial smoothing modified existing trends by reducing random noise and by regressing outliers toward the mean, or removing them altogether. Furthermore, the average helicity parameter values of the 179 ARs did not conform to the hemisphere rule: independent of smoothing, the weak-vertical-field values tended to be negative in both hemispheres, and the strong-vertical-field values tended to be positive, especially in the south. We conclude that spatial smoothing does not significantly affect the overall statistics for space-based data, and thus seeing from atmospheric turbulence seems not to have significantly affected previous studies' ground-based results on the hemisphere rule.

Wave Modeling of the Solar Wind **Review**

Leon **Ofman**

Living Reviews in Solar Physics, PUB.NO. lrsp-**2010**-4; REVISED: **2013**-11-28
http://www.livingreviews.org/lrsp-2010-4
The acceleration and heating of the solar wind have been studied for decades using satellite observations and models. However, the exact mechanism that leads to solar wind heating and acceleration is poorly understood. In order to improve the understanding of the physical mechanisms that are involved in these processes a combination of modeling and observational analysis is required. Recent models constrained by satellite observations show that wave heating in the low-frequency (MHD), and high-frequency (ion-cyclotron) range may provide the necessary momentum and heat input to coronal plasma and produce the solar wind. This review is focused on the results of several recent solar modeling studies that include waves explicitly in the MHD and the kinetic regime. The current status of the understanding of the solar wind acceleration and heating by waves is reviewed.

The Spörer minimum was deep

M.G.**Ogurtsov**
Advances in Space Research Volume 64, Issue 5, 1 September **2019**, Pages 1112-1116
https://sci-hub.se/10.1016/j.asr.2019.06.011
Seventeen reconstructions of past solar activity, based on cosmogenic isotope and auroral data, were analyzed for the time interval CE 1402–1850 covering three prolonged periods of weak solar activity – the Spoerer, Maunder and Dalton minima. The information contained in these proxies has been generalized and sunspot number reconstructed. It was shown that from the point of view of solar paleoastrophysics the Spoerer minimum (15th–16th centuries) was a prolonged (ca 140 years) period of very quiet Sun with a mean solar activity level lower than that during the minimum of Maunder.

Solar Activity during the Maunder Minimum: Comparison with the Dalton Minimum

M. G. **Ogurtsov**
Astronomy Letters April **2018**, Volume 44, Issue 5, pp 278–288
The solar modulation potential has been reconstructed from data on the 10Be concentration in south and central Greenland ice over more than 500 last years. These two reconstructions, along with fourteen others obtained by various authors from data on the cosmogenic isotopes14C and 10Be, have been investigated in the time interval 1630–1840 encompassing the Maunder and Dalton minima. The information contained in these sixteen paleoreconstructions has been generalized. The available data on the concentration of cosmogenic isotopes in terrestrial archives suggest that the solar activity in the first part of theMaunder minimum (1645–1680) was lower than that at the Dalton minimum (1792–1827), while in the second part (1680–1715) it was considerably lower. At the same time, at the beginning of theMaunder minimum (1645–1660) the solar activity could reach levels exceeding noticeably the estimates based on telescopic observations. Possible causes of these discrepancies and the directions of further research are discussed.

Variations in Solar Parameters and Cosmic Rays with Solar Magnetic Polarity

S. **Oh**1 and Y. Yi
2017 ApJ 840 14
http://sci-hub.cc/10.3847/1538-4357/aa6c62
The sunspot number varies with the 11-year Schwabe cycle, and the solar magnetic polarity reverses every 11 years approximately at the solar maximum. Because of polarity reversal, the difference between odd and even solar cycles is seen in solar activity. In this study, we create the mean solar cycle expressed by phase using the monthly sunspot number for all solar cycles 1–23. We also generate the mean solar cycle for sunspot area, solar radio flux, and cosmic ray flux within the allowance of observational range. The mean solar cycle has one large peak at solar maximum for odd solar cycles and two small peaks for most even solar cycles. The odd and even solar cycles have the statistical difference in value and shape at a confidence level of at least 98%. For solar cycles 19–23, the second peak in the even solar cycle is larger than the first peak. This result is consistent with the frequent solar events during the declining phase after the solar maximum. The difference between odd and even solar cycles can be explained by a combined model of polarity reversal and solar rotation. In the positive/negative polarity, the polar magnetic field introduces angular momentum in the same/opposite direction as/to the solar rotation. Thus the addition/subtraction of angular momentum can increase/decrease the motion of plasma to support the formation of sunspots. Since the polarity reverses at the solar maximum, the opposite phenomenon occurs in the declining phase.

Impact of flux distribution on elementary heating events

J. P. **O'Hara** and I. De Moortel
A&A 594, A67 (**2016**)
Context. The complex magnetic field on the solar surface has been shown to contain a range of sizes and distributions of magnetic flux structures. The dynamic evolution of this magnetic carpet by photospheric flows

provides a continual source of free magnetic energy into the solar atmosphere, which can subsequently be released by magnetic reconnection.
Aims. We investigate how the distribution and number of magnetic flux sources impact the energy release and locations of heating through magnetic reconnection driven by slow footpoint motions.
Methods. 3D magnetohydrodynamic (MHD) simulations using Lare3D are carried out, where flux tubes are formed between positive and negative sources placed symmetrically on the lower and upper boundaries of the domain, respectively. The flux tubes are subjected to rotational driving velocities on the boundaries and are forced to interact and reconnect.
Results. Initially, simple flux distributions with two and four sources are compared. In both cases, central current concentrations are formed between the flux tubes and Ohmic heating occurs. The reconnection and subsequent energy release is delayed in the four-source case and is shown to produce more locations of heating, but with smaller magnitudes. Increasing the values of the background field between the flux tubes is shown to delay the onset of reconnection and increases the efficiency of heating in both the two- and four-source cases. The cases with two flux tubes are always more energetic than the corresponding four flux tube cases, however the addition of the background field makes this disparity less significant. A final experiment with a larger number of smaller flux sources is considered and the field evolution and energetics are shown to be remarkably similar to the two-source case, indicating the importance of the size and separation of the flux sources relative to the spatial scales of the velocity driver.

Dynamics of Quasi-Biennal Variations of Cosmic Rays and Solar Activity

V. P. **Okhlopkov**
Cosmic Research March **2018**, Volume 56, Issue 2, pp 101–107
Kosmicheskie Issledovaniya, **2018**, Vol. 56, No. 2, pp. 111–118.
https://doi.org/10.1134/S0010952518020065
The quasi-biennial variations in the flux of galactic cosmic rays (GCRs) have been studied based on the data of stratospheric sensing and measurements by neutron monitors, as well as in various manifestations of solar activity and interplanetary medium parameters. It has been shown that quasi-biennial GCR variations are caused by variations with the same period in the mean magnetic field of the Sun that coincide with them over time and have been identified in the anti-phase, which respond to the sign of this field. The variations in the quasi-biennial cosmic ray are caused by quasi-biennial variations in the mean magnetic field of the Sun via the quasi-biennial variations in the interplanetary magnetic field.

On the Relationships Between Sunspot Number and Solar Radio Flux at 10.7 Centimeters

Daniel **Okoh** & Eucharia Okoro
Solar Physics volume 295, Article number: 1 (**2020**)
https://doi.org/10.1007/s11207-019-1566-8
Regression analysis and neural network training procedures are used to study the relationship between sunspot number (SSN) and solar flux at 10.7 cm (F10.7). Measurements of SSN and F10.7 for the periods from December 1963 to January 2019 (including the periods from Solar Cycles 20 to 24) were used. The value of correlation coefficient between SSN and F10.7 for the entire data used in the study is 0.95, showing that the parameters are well correlated. Results from the study reveal that there are remarkable differences on the relationship between SSN and F10.7 during the four solar cycle phases of low (-activity), high (-activity), ascending, and descending. The relationships are identical for the ascending and descending phases when the SSNs are lower than about 150, but the regression curves diverge as the SSNs increase beyond that limit. A conspicuously changed relationship between SSN and F10.7 is also observed for years 2014 and 2015 in which the annual SSN-versus-F10.7 plots for those years are visibly above those of the prior years. The results indicate that F10.7 values can be predicted from SSNs using neural networks, with root-mean-square errors of about 13.68 solar flux units. Results from the neural network procedure also indicate that a newly introduced solar cycle phase index (defined to indicate the phase of the solar cycle in which given observations belong) was effective in improving the neural network predictions.

A Hybrid Regression-Neural Network (HR-NN) Method for Forecasting the Solar Activity

D. I. **Okoh**, G. K. Seemala, A. B. Rabiu, J. Uwamahoro, J. B. Habarulema, M. Aggarwal
Space Weather Volume16, Issue9 September **2018** Pages 1424-1436
sci-hub.tw/10.1029/2018SW001907
The Sun is the major driver of space weather events, and as a result, most applications requiring modeling/forecasting of space weather phenomena depend largely on the activities of Sun. Accurate modeling of solar activity parameters like the sunspot number (SSN) is therefore considered significant for the quantitative modeling of space weather phenomena. Sunspot number forecasts are applied in ionospheric models like the International Reference Ionosphere model and in several other projects requiring prediction of space weather phenomena. A method called Hybrid Regression-Neural Network that combines regression analysis and neural

network learning is used for forecasting the SSN. Considering the geomagnetic Ap index during the end of the previous cycle (known as the precursor Ap index) as a reliable measurement, we predict the end of solar cycle 24 to be in March 2020 (±7 months), with monthly SSN 5.4 (±5.5). Using an estimated value of precursor Ap index as 5.6 nT for solar cycle 25, we predict the maximum SSN to be 122.1 (±18.2) in January 2025 (±6 months) and the minimum to be 6.0 (±5.5) in April 2031 (±5 months). We found from the model that on changing the assumed value of precursor Ap index (5.6 nT) by ±1 nT, the predicted peak of solar cycle 25 changes by about 11 sunspots for every 1-nT change in the assumed precursor Ap index.

Dynamics of coronal rain and descending plasma blobs in solar PROMINENCES: II. PARTIALLY IONIZED CASE

Oliver, R., Soler, R., Terradas, J., Zaqarashvili, T. V.

2015

http://solar.uib.es/media/RO/FallingBlobs-PIP/ms.pdf

Coronal rain clumps and prominence knots are dense condensations with chromospheric to transition region temperatures that fall down in the much hotter corona. Their typical speeds are in the range 30--150~km~s-1 and of the order of 10--30~km~s-1, respectively, i.e., they are considerably smaller than free fall velocities. These cold blobs contain a mixture of ionized and neutral material that must be dynamically coupled in order to fall together, as observed. We investigate this coupling by means of hydrodynamic simulations in which the coupling arises from the friction between ions and neutrals. The numerical simulations presented here are an extension of those of oliver2014} to the partially ionized case. We find that, although the relative drift speed between the two species is smaller than 1~m~s^{-1 at the blob center, it is sufficient to produce the forces required to strongly couple charged particles and neutrals. The ionization degree has no discernible effect on the main results of our previous work for a fully ionized plasma: the condensation has an initial acceleration phase followed by a period with roughly constant velocity and, in addition, the maximum descending speed is clearly correlated with the ratio of initial blob to environment density.

Propagation and dispersion of sausage wave trains in magnetic flux tubes

R. **Oliver**, M. S. Ruderman, J. Terradas

2015

http://arxiv.org/pdf/1502.01330v1.pdf

A localized perturbation of a magnetic flux tube produces a pair of wave trains that propagate in opposite directions along the tube. These wave packets disperse as they propagate, where the extent of dispersion depends on the physical properties of the magnetic structure, on the length of the initial excitation, and on its nature (e.g., transverse or axisymmetric). In Oliver et al. (2014) we considered a transverse initial perturbation, whereas the temporal evolution of an axisymmetric one is examined here. In both papers we use a method based on Fourier integrals to solve the initial value problem. Previous studies on wave propagation in magnetic wave guides have emphasized that the wave train dispersion is influenced by the particular dependence of the group velocity on the longitudinal wavenumber. Here we also find that long initial perturbations result in low amplitude wave packets and that large values of the magnetic tube to environment density ratio yield longer wave trains. To test the detectability of propagating transverse or axisymmetric wave packets in magnetic tubes of the solar atmosphere (e.g., coronal loops, spicules, or prominence threads) a forward modelling of the perturbations must be carried out. This is left for a future work.

Grand Activity Minima and Maxima via Dual Dynamos

Deniz **Ölçek**, Paul Charbonneau, Alexandre Lemerle, Gabriel Longpré, Florence Boileau

Solar Physics July **2019**, 294:99

sci-hub.se/10.1007/s11207-019-1492-9

Reconstructions of past solar activity based on cosmogenic radioisotopes have reavealed that the Sun spends a significant fraction (≈20≈20%) of its time in aperiodically recurring states of so-called Grand Minima or Grand Maxima, namely epochs of strongly supressed and markedly above-average levels of magnetic activity, respectively. The physical origin of these episodes is not yet understood. In this article we present a dual-dynamo model of the solar cycle, combining a dominant dynamo based on differential-rotation shear and surface decay of bipolar active regions, and a weak, deep-seated turbulent dynamo. The resulting dynamo simulations are found to exhibit the equivalent of observed Grand Minima and Maxima. By adjusting the magnitude and saturation level of the secondary turbulent dynamo, we can reproduce well the duration and waiting-time distributions of Grand Minima and Maxima inferred from the cosmogenic-isotope record. The exit from Grand Minima episodes is typically characterized by strong hemispheric asymmetries, in agreement with sunspot observations during the 1645 – 1715 Maunder Minimum. In these simulations, Grand Maxima can be unambiguously identified as a distinct dual-dynamo state resulting from constructive interference between the two dynamos mechanisms operating within the simulation. This interaction leads to the autonomous production of long quasi-periodicities in the millennial range, commensurate with the Halstatt cycle. Such a quasi-periodic modulation, readily produced through dynamical

backreaction on large-scale flows in non-kinematic dynamo models, is quite uncommon in a purely kinematic solar-cycle model such as the one developed herein. We argue that these long periodicities are set by the long diffusion time of magnetic field accumulating in the stable layers underlying the turbulent convection zone.

Investigating the Behavior and Spatiotemporal Variations of Green Line Emission in the Solar Corona

Jacob **Oloketuyi** , Yu Liu , Linhua Deng , Abouazza Elmhamdi +++
Astrophysical Journal Supplement Series, 275:3 (21pp), **2024**
https://arxiv.org/pdf/2411.16980
Understanding coronal structure and dynamics can be facilitated by analyzing green-line emission, which enables the investigation of diverse coronal structures such as coronal loops, streamers, coronal holes, and various eruptions in the solar atmosphere. In this study, we investigated the spatiotemporal behaviors of green-line emissions in both low and high latitudes across nine solar cycles, ranging from cycle 17 to the current cycle 25, using the Modified Homogeneous Data Set (MHDS). We employed methodologies such as cross-correlation, power spectral density (PSD), and wavelet transform techniques for this analysis. We found distinct behaviors in green line energy across various latitudinal distributions in the solar atmosphere. The trends observed at higher latitudes differ from those at lower latitudes. The emission behaviors show a close association with other solar phenomena like solar flares, sunspots, and coronal mass ejections (CMEs) throughout the solar cycles. The observed variations exhibit harmonic periods. The emission activity is significantly higher in the low latitudes, accounting for over 70 percent of the emissions, while the higher latitudes contribute less than 30 percent. The emissions exhibit asymmetric behavior between the northern and southern hemispheres, leading to a 44-year cycle of solar hemispheric dominance shifts. Various factors, such as Alfvén waves, solar magnetic fields, sunspots, differential rotation, and reconnection events, influence the observed differences in behavior between lower and higher latitudes, suggesting the existence of potential underlying phenomena contributing to deviations in properties, intensity, temporal dynamics, and spatiotemporal lifetime.

Turbulent convection in the Sun: modeling in unstructured meshes

Vyacheslav **Olshevsky**, Chunlei Liang, Frank Ham
Solar Phys. **2015**
http://arxiv.org/pdf/1412.7318v1.pdf
We adopted an unstructured hydrodynamical solver CharLES to the problem of global convection in the Sun. With the aim to investigate the properties of solar turbulent convection and reproduce differential rotation pattern. We performed simulations in two spherical shells, with 1.3 and 10 million cells. In the first, coarse mesh, the solution does not reproduce realistic convection, and is dominated by numerical effects. In the second mesh, thermal conduction leads to cooling of bottom layers, that could not be compensated by solar irradiance. More simulations in the 10M cells mesh should be performed to investigate the influence of transport coefficients and numerical effects. Our estimate of the code performance suggests, that realistic simulations in even finer grids could be performed for reasonable computational cost.

The Heliosphere: What Did We Learn in Recent Years and the Current Challenges **Review**

M. **Opher**
Space Science Reviews April **2016**, Volume 200, Issue 1, pp 475-494
sci-hub.si/10.1007/s11214-015-0186-3
As the Sun moves through the interstellar medium it carves a bubble called the heliosphere. A fortunate confluence of missions has provided a treasury of data that will likely not be repeated for decades The measurements in-situ by the Voyager spacecrafts, combined with the all-sky images of the heliospheric boundaries by the Interstellar Boundary Explorer and CASSINI missions have transformed our understanding of heliosphere. In particular one of the first surprises was that both Voyager spacecrafts found no evidence for the acceleration of the anomalous cosmic rays (ACRs) at the termination shock as expected for approximately 25 years. Another challenge are the energetically particles intensities and the plasma flows that are dramatically different at Voyager 1 and 2. There are several other observations that are key challenges to the heliospheric models that indicate that the nature of the heliosheath (the region where the solar wind is subsonic) is much more complex than thought, such as (a) Why the azimuthal magnetic flux is not conserved along the Voyager 1 trajectory? (b) What causes the flow stagnation region seen at Voyager 1? (c) What causes the unexpected observation of a depletion-region beginning in 2012 at Voyager 1? These observations point to the need to move past the standard description of the heliosphere. In this paper, I will review the state-of-the art of our understanding of this “new heliosphere”. In late 2012 Voyager 1 observed several events that indicated a magnetic connectivity between the heliosheath magnetic field and the interstellar medium magnetic field; where the energetic particles of the heliosheath leaked out while the galactic cosmic rays penetrated the heliosheath. With the radio observations confirming densities of the interstellar medium, there is a consensus that Voyager 1 left the heliosphere in September 2012 and entered the interstellar medium. We

will review as well our current understanding of the nature of the heliopause. The knowledge gain from the edge of the heliosphere will have consequences for other astrospheres and astrosheaths where the magnetic nature of the winds could be much more complex that previously thought.

Newly Discovered Source of Turbulence and Heating in the Solar Chromosphere

Meers **Oppenheim**1, Yakov Dimant1, William Longley1,2,3, and Alex C. Fletcher4
2020 ApJL 891 L9
https://doi.org/10.3847/2041-8213/ab75bc
Above the Sun's luminous photosphere lies the solar chromosphere, where the temperature increases from below 4000 K to over 1 million K. Though physicists do not understand the origin of these increases, they know it powers the solar wind with enormous consequences for the entire solar system. This report describes a set of simulations and analytical theory showing that solar atmospheric flows originating in the photosphere will frequently drive a previously unidentified thermal plasma instability that rapidly develops into turbulence. Though this turbulence is small scale (centimeters to a few meters), it will modify the conductivity, temperatures, and energy flows through much of the chromosphere. Incorporating the effects of this turbulence, and other small-scale turbulence, into large-scale models of solar and stellar atmospheres will improve physicists' ability to model energy flows with important consequences for the predicted temperatures and radiation patterns.

Alfvén Wave Turbulence as a Coronal Heating Mechanism: Simultaneously Predicting the Heating Rate and the Wave-induced Emission Line Broadening

R. **Oran**1, E. Landi2, B. van der Holst2, I. V. Sokolov2, and T. I. Gombosi
2017 ApJ 845 98
We test the predictions of the Alfvén Wave Solar Model (AWSoM), a global wave-driven magnetohydrodynamic (MHD) model of the solar atmosphere, against high-resolution spectra emitted by the quiescent off-disk solar corona. AWSoM incorporates Alfvén wave propagation and dissipation in both closed and open magnetic field lines; turbulent dissipation is the only heating mechanism. We examine whether this mechanism is consistent with observations of coronal EUV emission by combining model results with the CHIANTI atomic database to create synthetic line-of-sight spectra, where spectral line widths depend on thermal and wave-related ion motions. This is the first time wave-induced line broadening is calculated from a global model with a realistic magnetic field. We used high-resolution SUMER observations above the solar west limb between 1.04 and 1.34 R ⊙ at the equator, taken in 1996 November. We obtained an AWSoM steady-state solution for the corresponding period using a synoptic magnetogram. The 3D solution revealed a pseudo-streamer structure transversing the SUMER line of sight, which contributes significantly to the emission; the modeled electron temperature and density in the pseudo-streamer are consistent with those observed. The synthetic line widths and the total line fluxes are consistent with the observations for five different ions. Further, line widths that include the contribution from the wave-induced ion motions improve the correspondence with observed spectra for all ions. We conclude that the turbulent dissipation assumed in the AWSoM model is a viable candidate for explaining coronal heating, as it is consistent with several independent measured quantities.

SOLAR ATMOSPHERIC MAGNETIC ENERGY COUPLING: BROAD PLASMA CONDITIONS AND SPECTRUM REGIMES

N. Brice **Orange**1,2, David L. Chesny1,3, Bruce Gendre2,4,5, David C. Morris2,4, and Hakeem M. Oluseyi3
2016 ApJ 833 257
Solar variability investigations that include magnetic energy coupling are paramount to solving many key solar/stellar physics problems, particularly for understanding the temporal variability of magnetic energy redistribution and heating processes. Using three years of observations from the Solar Dynamics Observatory's Atmospheric Imaging Assembly and Heliosemic Magnetic Imager, we measured radiative and magnetic fluxes from gross features and at full-disk scales, respectively. Magnetic energy coupling analyses support radiative flux descriptions via the plasma heating connectivity of dominant (magnetic) and diffuse components, specifically of the predominantly closed-field corona. Our work shows that this relationship favors an energetic redistribution efficiency across large temperature gradients, and potentially sheds light on the long-standing issue of diffuse unresolved low corona emission. The close connection between magnetic energy redistribution and plasma conditions revealed by this work lends significant insight into the field of stellar physics, as we have provided possible means for probing distant sources in currently limited and/or undetectable radiation distributions.

OBSERVATIONS OF AN ENERGETICALLY ISOLATED QUIET SUN TRANSIENT: EVIDENCE OF QUASI-STEADY CORONAL HEATING

N. Brice **Orange**1,2, David L. Chesny1,3, and Hakeem M. Oluseyi
2015 ApJ 810 98

Increasing evidence for coronal heating contributions from cooler solar atmospheric layers, notably quiet Sun (QS) conditions, challenges standard solar atmospheric descriptions of bright transition region (TR) emission. As such, questions about the role of dynamic QS transients in contributing to the total coronal energy budget are raised. Using observations from the Atmospheric Imaging Assembly and Heliosemic Magnetic Imager on board the Solar Dynamics Observatory, and numerical model extrapolations of coronal magnetic fields, we investigate a dynamic QS transient that is energetically isolated to the TR and extrudes from a common footpoint shared with two heated loop arcades. A non-causal relationship is established between episodic heating of the QS transient and widespread magnetic field re-organization events, while evidence is found favoring a magnetic topology that is typical of eruptive processes. Quasi-steady interchange reconnection events are implicated as a source of the transient's visibly bright radiative signature. We consider the QS transient's temporally stable (≈35 minutes) radiative nature to occur as a result of the large-scale magnetic field geometries of the QS and/or relatively quiet nature of the magnetic photosphere, which possibly act to inhibit energetic build-up processes that are required to initiate a catastrophic eruption phase. This work provides insight into the QS's thermodynamic and magnetic relation to eruptive processes that quasi-steadily heat a small-scale dynamic and TR transient. This work explores arguments of non-negligible coronal heating contributions from cool atmospheric layers in QS conditions and contributes evidence to the notion that solar wind mass feeds off of dynamic transients therein.

Temporal Pointing Variations of The Solar Dynamics Observatory's HMI and AIA Instruments on Sub-Weekly Time Scales

N. Brice **Orange**, Hakeem M. Oluseyi, David L. Chesny, Maulik Patel, Patrick Champey, Katie Hesterly, Dylan Anthony, Robert Treen

2015

http://arxiv.org/pdf/1501.05000v1.pdf

Achieving sub-arcsecond co-registration across varying time-lines of multi-wavelength and instrument images is not trivial, and requires accurate characterization of instrument pointing jitter. In this work we have investigated internal pointing errors, on daily and yearly time-scales, occurring across the \textit{Solar Dynamics Observatory}'s (SDO) {\it Atmospheric Imaging Assembly} (AIA) and { \it Helioseismic Magnetic Imager} (HMI). Using cross-correlation techniques on AIA 1700\,{\AA} passband and HMI line-of-sight (LOS) magnetograms, from three years of observational image pairs at approximately three day intervals, internal pointing errors are quantified. Pointing variations of ±\,0.26$\arcsec$ (jitter limited) and ±\,0.50$\arcsec$ in the solar East-West (x) and North-South (y) directions, respectively, are measured. AIA observations of the Venus June 2012 transit are used to measure existing coalignment offsets in all passbands. We find AIA passband pointing variations are <ΔXCO>\,=\, 1.10$\arcsec$\,±\,1.41$\arcsec$ and <ΔYCO>\,=\, 1.25$\arcsec$\,±\,1.24$\arcsec$, when aligned to HMI's nominal image center, referred to herein as the CutOut technique (CO). Minimal long-term pointing variations found between limb and correlation derived pointings provide evidence that image center positions provided by the instrument teams achieve single pixel accuracy on time-scales below their characterization. However, daily AIA passband pointing variations of ≲\,1.18$\arcsec$ indicate autonomous sub-arcsecond co-registration is not yet fully achievable.

A New Component from the Quiet Sun from Radio to Gamma Rays: Synchrotron Radiation by Galactic Cosmic-Ray Electrons

Elena **Orlando**1,2, Vahe' Petrosian2, and Andrew Strong3

2023 ApJ 943 173

https://arxiv.org/pdf/2212.01364.pdf

https://iopscience.iop.org/article/10.3847/1538-4357/acad75/pdf

The quiet Sun, i.e., in its nonflaring state or nonflaring regions, emits thermal radiation from radio to ultraviolet. The quiet Sun also produces nonthermal radiation observed in gamma rays due to interactions of Galactic cosmic rays (GCRs) with the solar atmosphere and photons. We report on a new component: the synchrotron emission by GCR electrons in the solar magnetic field. To the best of our knowledge this is the first time this emission has been theoretically claimed and modeled. We find that the measured GCR electrons with energies from tens of GeV to a few TeV produce synchrotron emission in X-rays, which is a few orders of magnitude lower than current upper limits of the quiet Sun set by RHESSI and FOXSI, with no energy losses included. For a radially decreasing solar magnetic field we find the expected synchrotron intensity to be almost constant in the solar disk, to peak in the close proximity of the Sun, and to quickly drop away from the Sun. We also estimate the synchrotron emission from radio to gamma rays, and we compare it with current observations, especially with LOFAR. While it is negligible from radio to UV compared to the solar thermal radiation, this emission can potentially be observed at high energies with NuSTAR and more promising future FOXSI observations. This could potentially allow for constraining GCR densities and magnetic-field intensities at the Sun. This study provides a more complete description and a possible new way for understanding the quiet Sun and its environment.

Ellerman bombs and UV bursts: reconnection at different atmospheric layers

Ada **Ortiz**, Viggo H. Hansteen, Daniel Nóbrega-Siverio, Luc Rouppe van der Voort
A&A **2019**
https://arxiv.org/pdf/1910.10736.pdf
The emergence of magnetic flux into the solar atmosphere produces, among other phenomena, Ellerman bombs (EBs), which are observed in H alpha and are due to magnetic reconnection in the photosphere below the chromospheric canopy. Signs of reconnection are also observed in other spectral lines, typical of the chromosphere or the transition region. An example are the UV bursts observed in the transition region lines of Si IV and the upper chromospheric lines of Mg II. In this work we analyze high cadence, high resolution coordinated observations between the Swedish 1-m Solar Telescope (SST) and the Interface Region Imaging Spectrograph (IRIS) spacecraft. H alpha images from the SST provide us with the positions, timings and trajectories of EBs in an emerging flux region. Simultaneous, co-aligned IRIS slit-jaw images at 133 (C II, transition region), 140 (Si IV, transition region) and 279.6 (Mg II k, core, upper chromosphere) nm, as well as spectroscopy in the far and near ultraviolet from the fast spectrograph raster, allow us to study the possible chromospheric/transition region counterparts of those EBs. Our main goal is to study the possible temporal and spatial relationship between several reconnection events at different layers in the atmosphere (namely EBs and UV bursts), the timing history between them, and the connection of these dynamical phenomena to the ejection of surges in the chromosphere. We also investigate the properties of an extended UV burst and their variations across the burst domain. Our results suggest a scenario where simultaneous and co-spatial EBs and UV bursts are part of the same reconnection system occurring sequentially along a vertical or nearly vertical current sheet. Heating and bidirectional jets trace the location where reconnection takes place. These results support and expand those obtained from recent numerical simulations of magnetic flux emergence. **September 3-5 2016**

Emergence of granular-sized magnetic bubbles through the solar atmosphere. III. The path to the transition region

Ada **Ortiz**, Viggo Hansteen, Luis Ramon Bellot Rubio,
Jaime de la Cruz **Rodriguez**, Bart De Pontieu, Mats Carlsson, Luc Rouppe van der Voort
ApJ **2016**
http://arxiv.org/pdf/1604.00302v1.pdf
We study the ascent of granular-sized magnetic bubbles from the solar photosphere through the chromosphere into the transition region and above, for the first time. Such events occurred in a flux emerging region in NOAA 11850 on **September 25, 2013**. During that time, the first co-observing campaign between the Swedish 1-m Solar Telescope and the IRIS spacecraft was carried out. Simultaneous observations of the chromospheric Hα 656.28 nm and \ion{Ca}{2} 854.2 nm lines, plus the photospheric \ion{Fe}{1} 630.25 nm line, were made with the CRISP spectropolarimeter at the SST reaching a spatial resolution of 0."14. At the same time, IRIS was performing a four-step dense raster of the said emerging flux region, taking slit-jaw images at 133 (C~{\sc ii}, transition region), 140 (\ion{Si}{4}, transition region), 279.6 (\ion{Mg}{2} k, core, upper chromosphere), and 283.2 nm (\ion{Mg}{2} k, wing, photosphere). Spectroscopy of several lines was performed by the IRIS spectrograph in the far and near ultraviolet, of which we have used the \ion{Si}{4} 140.3 and the \ion{Mg}{2} k 279.6 nm lines. Coronal images from the Atmospheric Imaging Assembly of the Solar Dynamics Observatory were used to investigate the possible coronal signatures of the flux emergence events. The photospheric and chromospheric properties of small-scale emerging magnetic bubbles have been described in detail in Ortiz et al. (2014). Here we are able to follow such structures up to the transition region. We describe the properties, including temporal delays, of the observed flux emergence in all layers. We believe this may be an important mechanism of transporting energy and magnetic flux from subsurface layers to the transition region and corona.

Statistical Analysis of Current Helicity and Twist in Solar Active Regions over the Phases of the Solar Cycle Using the Spectro-Polarimeter Data of Hinode

Kenichi **Otsuji**, Takashi Sakurai and Kirill Kuzanyan
2014
http://jp.arxiv.org/pdf/1410.7532
Current helicity and twist of solar magnetic fields are important quantities to characterize the dynamo mechanism working in the convection zone of the Sun. We have carried out a statistical study on the current helicity of solar active regions observed with the Spectro-Polarimeter (SP) of Hinode Solar Optical Telescope (SOT). We used SOT-SP data of 558 vector magnetograms of a total of 80 active regions obtained from 2006 to 2012. We have applied spatial smoothing and division of data points into weak and strong field ranges to compare the contributions from different scales and field strengths. We found that the current helicity follows the so-called hemispheric sign rule when the weak magnetic fields (absolute field strength < 300 gauss) are considered and no smoothing is applied. On the other hand, the pattern of current helicity fluctuates and violates the hemispheric sign rule when stronger magnetic fields are considered and the smoothing of 2.0 arcsec (mimicking ground-based observations) is applied. Furthermore, we found a tendency that the weak and inclined fields better conform to and the strong and vertical fields tend to violate the hemispheric sign rule. These different properties of helicity through the strong and weak

magnetic field components give important clues to understanding the solar dynamo as well as the mechanism of formation and evolution of solar active regions.

CHIRALITY AND MAGNETIC CONFIGURATIONS OF SOLAR FILAMENTS

Y. **Ouyang** (欧阳雨)1,2, Y. H. Zhou (周雨昊)1,3, P. F. Chen (陈鹏飞)1,3, and C. Fang (方成)1,3
2017 ApJ 835 94 DOI 10.3847/1538-4357/835/1/94
http://sci-hub.cc/10.3847/1538-4357/835/1/94
https://arxiv.org/pdf/1612.01054v1.pdf

It has been revealed that the magnetic topology in the solar atmosphere displays hemispheric preference, i.e., helicity is mainly negative/positive in the northern/southern hemispheres, respectively. However, the strength of the hemispheric rule and its cyclic variation are controversial. In this paper, we apply a new method based on the filament drainage to 571 erupting filaments from 2010 May to 2015 December in order to determine the filament chirality and its hemispheric preference. It is found that 91.6% of our sample of erupting filaments follows the hemispheric rule of helicity sign. It is also found that the strength of the hemispheric preference of the quiescent filaments decreases slightly from ~97% in the rising phase to ~85% in the declining phase of solar cycle 24, whereas the strength of the intermediate filaments keeps a high value around 96 ± 4% at all times. Only the active-region filaments show significant variations. Their strength of the hemispheric rule rises from ~63% to ~95% in the rising phase, and keeps a high value of 82% ± 5% during the declining phase. Furthermore, during a half-year period around the solar maximum, their hemispheric preference totally vanishes. Additionally, we also diagnose the magnetic configurations of the filaments based on our indirect method and find that in our sample of erupting events, 89% are inverse-polarity filaments with a flux rope magnetic configuration, whereas 11% are normal-polarity filaments with a sheared arcade configuration. **10 Feb 2012, 29 Oct 2015**

A link between solar events and congenital malformations: Is ionizing radiation enough to explain it?†

Andrew C. **Overholt**1,*, Adrian L. Melott2 and Dimitra Atri
JGR **2015**

Cosmic rays are known to cause biological effects directly and through ionizing radiation produced by their secondaries. These effects have been detected in airline crews and other specific cases where members of the population are exposed to above average secondary fluxes. Recent work has found a correlation between solar proton events (SPEs) and congenital malformations. In this work we use the results of computational simulations to approximate the ionizing radiation from such events as well as longer term increases in cosmic ray flux. We find that the amounts of ionizing radiation produced by these events are insufficient to produce congenital malformations under the current paradigm regarding muon ionizing radiation. We believe further work is needed to determine the correct ionizing radiation contribution of cosmogenic muons. We suggest that more extensive measurements of muon radiation effects may show a larger contribution to ionizing radiation dose than currently assumed.

Reconstructing Sunspot Number by Forward-Modelling Open Solar Flux

Mathew J. **Owens**, Mike Lockwood, Luke A. Barnard, Ilya Usoskin, Hisashi Hayakawa, Benjamin J. S. Pope & Ken McCracken
Solar Phys. Volume 299, article number 3, (**2024**)
https://link.springer.com/content/pdf/10.1007/s11207-023-02241-3.pdf

The open solar flux (OSF) is the integrated unsigned magnetic flux leaving the top of the solar atmosphere to form the heliospheric magnetic field. As the OSF modulates the intensity of galactic cosmic rays at Earth, the production rate of cosmogenic isotopes – such as 14C and 10Be stored in tree rings and ice sheets – is closely related to the OSF. Thus on the basis of cosmogenic isotope data, OSF can be reconstructed over millennia. As sunspots are related to the production of OSF, this provides the possibility of reconstructing sunspot number (SSN) and hence properties of the solar cycles prior to the first sunspot telescopic observations in 1610. However, while models exist for estimating OSF on the basis of SSN, the hysteresis present in OSF and the lack of a priori knowledge of the start/end dates of individual solar cycles means that directly inverting these models is not possible. We here describe a new method that uses a forward model of OSF to estimate SSN and solar cycle start/end dates through a Monte Carlo approach. The method is tested by application to geomagnetic reconstructions of OSF over the period 1845-present, and compared to the known SSN record for this period. There is a substantial improvement in reconstruction of both the SSN time series and the solar cycle start/end dates compared with existing OSF-SSN regression methods. This suggests that more accurate solar-cycle information can be extracted from cosmogenic isotope records by forward modelling, and also provides a means to assess the level of agreement between independent SSN and OSF reconstructions. We find the geomagnetic OSF and observed SSN agree very well after

1875, but do differ during the early part of the geomagnetic record, though still agree within the larger observational uncertainties.

Extreme Space-Weather Events and the Solar Cycle

Mathew J. **Owens**, Mike Lockwood,Luke A. Barnard,Chris J. Scott, Carl Haines & Allan Macneil
Solar Physics volume 296, Article number: 82 (**2021**)
https://link.springer.com/content/pdf/10.1007/s11207-021-01831-3.pdf
https://doi.org/10.1007/s11207-021-01831-3

Space weather has long been known to approximately follow the solar cycle, with geomagnetic storms occurring more frequently at solar maximum than solar minimum. There is much debate, however, about whether the most hazardous events follow the same pattern. Extreme events – by definition – occur infrequently, and thus establishing their occurrence behaviour is difficult even with very long space-weather records. Here we use the 150-year aaHaaH record of global geomagnetic activity with a number of probabilistic models of geomagnetic-storm occurrence to test a range of hypotheses. We find that storms of all magnitudes occur more frequently during an active phase, centred on solar maximum, than during the quiet phase around solar minimum. We also show that the available observations are consistent with the most extreme events occurring more frequently during large solar cycles than small cycles. Finally, we report on the difference in extreme-event occurrence during odd- and even-numbered solar cycles, with events clustering earlier in even cycles and later in odd cycles. Despite the relatively few events available for study, we demonstrate that this is inconsistent with random occurrence. We interpret this finding in terms of the overlying coronal magnetic field and enhanced magnetic-field strengths in the heliosphere, which act to increase the geoeffectiveness of sheath regions ahead of extreme coronal mass ejections. Putting the three "rules" together allows the probability of extreme event occurrence for Solar Cycle 25 to be estimated, if the magnitude and length of the coming cycle can be predicted. This highlights both the feasibility and importance of solar-cycle prediction for planning and scheduling of activities and systems that are affected by extreme space weather.

The Maunder minimum and the Little Ice Age: an update from recent reconstructions and climate simulations

Mathew J. **Owens**, Mike Lockwood, Ed Hawkins, Ilya Usoskin, Gareth S. Jones, Luke Barnard, Andrew Schurer and John Fasullo
J. Space Weather Space Clim. **2017**, 7, A33
https://www.swsc-journal.org/articles/swsc/pdf/2017/01/swsc170014.pdf

The Maunder minimum (MM) was a period of extremely low solar activity from approximately AD 1650 to 1715. In the solar physics literature, the MM is sometimes associated with a period of cooler global temperatures, referred to as the Little Ice Age (LIA), and thus taken as compelling evidence of a large, direct solar influence on climate. In this study, we bring together existing simulation and observational studies, particularly the most recent solar activity and paleoclimate reconstructions, to examine this relation. Using northern hemisphere surface air temperature reconstructions, the LIA can be most readily defined as an approximately 480 year period spanning AD 1440–1920, although not all of this period was notably cold. While the MM occurred within the much longer LIA period, the timing of the features are not suggestive of causation and should not, in isolation, be used as evidence of significant solar forcing of climate. Climate model simulations suggest multiple factors, particularly volcanic activity, were crucial for causing the cooler temperatures in the northern hemisphere during the LIA. A reduction in total solar irradiance likely contributed to the LIA at a level comparable to changing land use.

Near-Earth heliospheric magnetic field intensity since 1750: 2. Cosmogenic radionuclide reconstructions

M.J. **Owens**, E. Cliver, K.G. McCracken, J. Beer, L. Barnard, M. Lockwood, A. Rouillard, D. Passos, P. Riley, I. Usoskin and Y-M. Wang

JGR Volume 121, Issue 7 Pages 6064–6074 **2016**
http://onlinelibrary.wiley.com/doi/10.1002/2016JA022550/epdf

This is Part 2 of a study of the near-Earth heliospheric magnetic field strength, *B*, since 1750. Part 1 produced composite estimates of *B* from geomagnetic and sunspot data over the period 1750–2013. Sunspot-based reconstructions can be extended back to 1610, but the paleocosmic ray (PCR) record is the only data set capable of providing a record of solar activity on millennial timescales. The process for converting ^{10}Be concentrations measured in ice cores to *B* is more complex than with geomagnetic and sunspot data, and the uncertainties in *B* derived from cosmogenic nuclides (~20% for any individual year) are much larger. Within this level of uncertainty, we find reasonable overall agreement between PCR-based *B* and the geomagnetic- and sunspot number-based series. This agreement was enhanced by excising low values in PCR-based *B* attributed to high-energy solar proton events. Other discordant intervals, with as yet unspecified causes remain included in our analysis. Comparison of 3 year averages centered on sunspot minimum yields reasonable agreement between the three

estimates, providing a means to investigate the long-term changes in the heliospheric magnetic field into the past even without a means to remove solar proton events from the records.

Near-Earth Heliospheric Magnetic Field Intensity since 1750. Part 1: Sunspot and Geomagnetic Reconstructions

M.J. **Owens**, E. Cliver, K.G. McCracken, J. Beer, L. Barnard, M. Lockwood, A. Rouillard, D. Passos, P. Riley, I. Usoskin and Y-M. Wang

JGR Volume 121, Issue 7 Pages 6048–6063 **2016**

http://onlinelibrary.wiley.com/doi/10.1002/2016JA022529/epdf

We present two separate time series of the near-Earth heliospheric magnetic field strength (B) based on geomagnetic data and sunspot number (SSN). The geomagnetic-based B series from 1845-2013 is a weighted composite of two series that employ the interdiurnal variability index; this series is highly correlated with in situ spacecraft measurements of B (correlation coefficient, r = 0.94; mean square error, MSE = 0.16 nT2). The SSN-based estimate of B, from 1750-2013, is a weighted composite of eight time series derived from two separate reconstruction methods applied to four different SSN time series, allowing determination of the uncertainty from both the underlying sunspot records and the B-reconstruction methods. The SSN-based composite is highly correlated with direct spacecraft measurements of B and with the composite geomagnetic B time series from 1845-2013 (r = 0.91; MSE = 0.24 nT2), demonstrating that B can accurately reconstructed by both geomagnetic and sunspot-based methods. The composite sunspot and geomagnetic B time series, with uncertainties, are provided as supplementary electronic material.

The heliospheric Hale cycle over the last 300 years and its implications for a “lost” late 18th century solar cycle

Mathew J. **Owens**1*, Ken G. McCracken2, Mike Lockwood1 and Luke Barnard

J. Space Weather Space Clim., 5, A30 (**2015**)

A Hale cycle, one complete magnetic cycle of the Sun, spans two complete Schwabe cycles (also referred to as sunspot and, more generally, solar cycles). The approximately 22-year Hale cycle is seen in magnetic polarities of both sunspots and polar fields, as well as in the intensity of galactic cosmic rays reaching Earth, with odd- and even-numbered solar cycles displaying qualitatively different waveforms. Correct numbering of solar cycles also underpins empirical cycle-to-cycle relations which are used as first-order tests of stellar dynamo models. There has been much debate about whether the unusually long solar cycle 4 (SC4), spanning 1784–1799, was actually two shorter solar cycles combined as a result of poor data coverage in the original Wolf sunspot number record. Indeed, the group sunspot number does show a small increase around 1794–1799 and there is evidence of an increase in the mean latitude of sunspots at this time, suggesting the existence of a cycle “4b”. In this study, we use cosmogenic radionuclide data and associated reconstructions of the heliospheric magnetic field (HMF) to show that the Hale cycle has persisted over the last 300 years and that data prior to 1800 are more consistent with cycle 4 being a single long cycle (the “no SC4b” scenario). We also investigate the effect of cycle 4b on the HMF using an open solar flux (OSF) continuity model, in which the OSF source term is related to sunspot number and the OSF loss term is determined by the heliospheric current sheet tilt, assumed to be a simple function of solar cycle phase. The results are surprising; Without SC4b, the HMF shows two distinct peaks in the 1784–1799 interval, while the addition of SC4b removes the secondary peak, as the OSF loss term acts in opposition to the later rise in sunspot number. The timing and magnitude of the main SC4 HMF peak is also significantly changed by the addition of SC4b. These results are compared with the cosmogenic isotope reconstructions of HMF and historical aurora records. These data marginally favour the existence of SC4b (the “SC4b” scenario), though the result is less certain than that based on the persistence of the Hale cycle. Thus while the current uncertainties in the observations preclude any definitive conclusions, the data favour the “no SC4b” scenario. Future improvements to cosmogenic isotope reconstructions of the HMF, through either improved modelling or additional ice cores from well-separated geographic locations, may enable questions of the existence of SC4b and the phase of Hale cycle prior to the Maunder minimum to be settled conclusively.

Solar cycle evolution of dipolar and pseudostreamer belts and their relation to the slow solar wind†

M.J. **Owens**1,*, N.U. Crooker2, M. Lockwood

JGR, **2014**

Dipolar streamers are coronal structures formed by open solar flux converging from coronal holes of opposite polarity. Thus the dipolar streamer belt traces the coronal foot print of the heliospheric current sheet (HCS), and it is strongly associated with the origin of slow solar wind. Pseudostreamers, on the other hand, separate converging regions of open solar flux from coronal holes of the same polarity and do not contain current sheets. They have

recently received a great deal of interest as a possible additional source of slow solar wind. Here we add to that growing body of work by using the potential-field source-surface model to determine the occurrence and location of dipolar and pseudostreamers over the last three solar cycles. In addition to providing new information about pseudostreamer morphology, the results help explain why the observations taken during the first Ulysses perihelion pass in 1995 showed noncoincidence between dipolar streamer belt and the locus of slowest flow. We find that Carrington rotation averages of the heliographic latitudes of dipolar and pseudostreamer belts are systematically shifted away from the equator, alternately in opposite directions, with a weak solar cycle periodicity, thus keeping slow wind from the web of combined streamer belts approximately symmetric about the equator. The largest separation of dipolar and pseudostreamer belts occurred close to the Ulysses pass, allowing a unique opportunity to see that slow wind from pseudostreamer belts north of the southward-displaced dipolar belt was responsible for the noncoincident pattern.

The Heliospheric Magnetic Field **Review**

Owens, Mathew J. and Forsyth, Robert J.
Living Reviews in Solar Physics, PUB.NO. lrsp-**2013**-5
http://www.livingreviews.org/lrsp-2013-5
The heliospheric magnetic field (HMF) is the extension of the coronal magnetic magnetic carried by the solar wind. It is the means by which the Sun interacts with planetary magnetospheres and channels charged particles propagating through the heliosphere. As the HMF remains rooted at the solar photosphere as the Sun rotates, the large-scale HMF traces out an Archimedean spiral. This pattern is distorted by the the interaction of fast and slow solar wind streams, as well as the interplanetary manifestations of coronal mass ejections. On the smaller scale, the HMF exhibits an array of waves, discontinuities and turbulence, which give hints to the solar wind formation process. This review aims to summarise observations and theory of the small- and large-scale structure of the HMF. Solar-cycle and cycle-to-cycle evolution of the HMF is discussed in terms of recent spacecraft observations and pre-spaceage proxies for the HMF in geomagnetic and galactic cosmic ray records.

How is open solar magnetic flux lost over the solar cycle?

M. J. **Owens**, N. U. Crooker, M. Lockwood
JOURNAL OF GEOPHYSICAL RESEARCH, VOL. 116, A04111, 13 PP., **2011**
The Sun's open magnetic field, magnetic flux dragged out into the heliosphere by the solar wind, varies by approximately a factor of 2 over the solar cycle. We consider the evolution of open solar flux in terms of a source and loss term. Open solar flux creation is likely to proceed at a rate dependent on the rate of photospheric flux emergence, which can be roughly parameterized by sunspot number or coronal mass ejection rate, when available. The open solar flux loss term is more difficult to relate to an observable parameter. The supersonic nature of the solar wind means open solar flux can only be removed by near-Sun magnetic reconnection between open solar magnetic field lines, be they open or closed heliospheric field lines. In this study we reconstruct open solar flux over the last three solar cycles and demonstrate that the loss term may be related to the degree to which the heliospheric current sheet (HCS) is warped, i.e., locally tilted from the solar rotation direction. This can account for both the large dip in open solar flux at the time of sunspot maximum as well as the asymmetry in open solar flux during the rising and declining phases of the solar cycle. The observed cycle-to-cycle variability is also well matched. Following Sheeley et al. (2001), we attribute modulation of open solar flux by the degree of warp of the HCS to the rate at which opposite polarity open solar flux is brought together by differential rotation.

Formation of Chromospheric Spicules in Magnetic Bright Points: An Analytical Approach Using Cartesian Slab Geometry

William **Oxley**1, Joseph Scalisi1, Michael S. Ruderman1,2, and Róbert Erdélyi1,3,4
2020 ApJ 905 168
https://doi.org/10.3847/1538-4357/abcafe
We aim to provide insight into chromospheric spicules by suggesting a new formation mechanism. A magnetic field boundary condition is imposed, generating an Alfvén wave that shears a magnetic slab and propagates up the slab. The resulting Lorentz force accelerates material vertically, potentially nonlinearly driving a jet-like feature. This formation mechanism is applied to take place in a magnetic bright point embedded in the photosphere, providing motivation to use the simplifying assumption of a zero-β plasma. After deriving an analytical expression describing the vertical mass flux that constitutes the spicular jet, further understanding is gained by examining a model example of a magnetic field boundary condition in terms of standard functions. By visualizing the vertical mass flux through 3D plots, we demonstrate that the jet properties capture the observed properties of chromospheric spicules during their formation. This vindicates the model and simplifying assumptions used. Although we do not provide insight into the full evolution of a spicule, we show that the role of Alfvén waves triggered by shear in fact could be a viable formation mechanism for at least some chromospheric spicules. Consequently, we provide a starting point for

further studies of this formation mechanism, which will lead to a greater understanding of the vast variety of chromospheric jets.

Standing MHD Waves in a Magnetic Slab Embedded in an Asymmetric Magnetic Plasma Environment: Surface Waves

William **Oxley**, Noémi Kinga Zsámberger, Róbert Erdélyi
ApJ **2020**
https://arxiv.org/pdf/2006.05425.pdf
Building on a previous study that analyses surface waves in magnetic slabs embedded in a non-magnetic external environment, in this study the model is generalised and external magnetic fields are added. The slab is assumed to be thin, with weak magnetic asymmetry. The frequencies of the standing harmonic modes are derived to leading-order in the small quantities representing the thin slab width and the weak asymmetry. It is found that the frequencies are more prone to changes to the width of the slab than changes in the magnetic asymmetry. The frequency ratio of the first harmonic to the fundamental mode is derived, along with the amplitude difference between the two sides of the slab, as these may be observable quantities that can be compared with observational results and applied to carry out solar magneto-seismology.

Effects of Hysteresis Between Maximum CME Speed Index and Typical Solar Activity Indicators During Cycle 23

A. **Özgüç**, A. Kilcik, J. P. Rozelot
Solar Physics, December **2012**, Volume 281, Issue 2, pp 839-846
Using the smoothed time series of maximum CME speed index for solar cycle 23, it is found that this index, analyzed jointly with six other solar activity indicators, shows a hysteresis phenomenon. The total solar irradiance, coronal index, solar radio flux (10.7 cm), Mg ii core-to-wing ratio, sunspot area, and Hα flare index follow different paths for the ascending and the descending phases of solar cycle 23, while a saturation effect exists at the maximum phase of the cycle. However, the separations between the paths are not the same for the different solar activity indicators used: the Hα flare index and total solar irradiance depict broad loops, while the Mg ii core-to-wing ratio and sunspot area depict narrow hysteresis loops. The lag times of these indices with respect to the maximum CME speed index are discussed, confirming that the hysteresis represents a clue in the search for physical processes responsible for changing solar emission.

An Unusual Pattern of Cosmic-Ray Modulation During Solar Cycles 23 and 24

A. A. **Pacini**, I. G. Usoskin
Solar Phys. Volume 290, Issue 3, pp 943-950 **2015**
By means of an analysis of data from eight neutron monitor (NM) stations with different geomagnetic cutoff rigidities, we found an unusual latitudinal effect observed in the cosmic-ray (CR) modulation during the last solar cycles. Since the beginning of the ground-based cosmic-ray monitoring, it is known that the solar-cycle modulation is more evident in data from high latitude than from the medium and low latitudes, showing an expected geomagnetic cutoff rigidity effect. However, a more detailed look shows a new latitudinal effect in cycle 24: while the magnitude of the solar modulation in the low-latitude data remains the same for the last three solar minima, the last solar minimum caused a more intense peak in the polar NM data than in the previous cycles. After correcting the data for the geomagnetic changes of the period, we found an anomalous solar modulation in the last cycle. This suggests a weaker heliospheric modulation at low-energy particles (responsible for the NM counting in polar sites) now than in the previous cycles, while there is no significant difference of the modulation for the more energetic part of the CR spectrum. Our result can be associated with changes of the solar wind turbulence, which would corroborate some recent studies about the last solar minimum phase, and indicates that this new solar modulation feature is still present in the current solar maximum stage.

Effect of Coronal Loop Structure on Wave Heating by Phase Mixing

P. **Pagano**, I. De Moortel, R. J. Morton
2020 A&A 643, A73
https://arxiv.org/pdf/2009.04366.pdf
https://doi.org/10.1051/0004-6361/202039209
The mechanism behind coronal heating still elude direct observation and modelling of viable theoretical processes and the subsequent effect on coronal structures is one of the key tools available to assess possible heating mechanisms. Wave-heating via phase-mixing of Magnetohydrodynamics (MHD) transverse waves has been proposed as a possible way to convert magnetic energy into thermal energy but increasingly, MHD models suggest this is not a sufficiently efficient mechanism. We model heating by phase-mixing of transverse MHD waves in various configurations, to investigate whether certain circumstances can enhance the heating sufficiently to sustain the million degree solar corona and to assess the impact of the propagation and phase-mixing of transverse MHD waves on the structure of the boundary shell of coronal loops. We use 3D MHD simulations of a pre-existing density

enhancement in magnetised medium and a boundary driver to trigger the propagation of transverse waves with the same power spectrum as measured by the COmP. We consider different density structures, boundary conditions at the non-drive footpoint, characteristics of the driver, and different forms of magnetic resistivity. We find that different initial density structures affect the evolution of the boundary shell and some driver configurations enhance the heating generated from the dissipation of the MHD waves. In particular, drivers coherent on a larger spatial scale and higher dissipation coefficients generate significant heating, although it is still insufficient. We conclude that while phase-mixing of transverse MHD waves is unlikely to sustain the thermal structure of the corona, there are configurations that allow for an enhanced efficiency of this mechanism. We provide possible signatures to identify the presence of such configurations, such as the location of where the heating is deposited along the coronal loop

MHD simulations of the in-situ generation of kink and sausage waves in the solar corona by collision of dense plasma clumps

P. **Pagano**, H.J. Van Damme, P. Antolin, I. De Moortel
A&A 626, A53 **2019**
https://arxiv.org/pdf/1905.03749.pdf
MHD waves are ubiquitous in the solar corona where the highly structured magnetic fields provide efficient wave guides for their propagation. While MHD waves have been observed originating from lower layers of the solar atmosphere, recent studies have shown that some can be generated in-situ by the collision of dense counter propagating flows. In this theoretical study, we analyse the mechanism that triggers the propagation of kink and sausage modes in the solar corona, following the collision of counter-propagating flows and how the properties of the flows affect the properties of the generated waves. In order to study in detail such a mechanism we run a series of ideal 2D and 3D MHD simulations where we vary the properties of the counter-propagating flows and by means of a simple technique to estimate the amplitudes of the kink and sausage modes, we investigate their role on the generation and propagation of the MHD waves. We find that the amplitude of the waves is largely dependent on the kinetic energy of the flows and that the onset of kink or sausage modes depends on the asymmetries between the colliding blobs. Moreover, the initial wavelength of the MHD waves is associated with the magnetic configuration resulting from the collision of the flows. We also find that genuine 3D systems respond with smaller wave amplitudes. In this study, we present a parameter space description of the mechanism that leads to the generation of MHD waves from the collision of flows in the corona. Future observations of these waves can be used to understand the properties of the plasma and magnetic field of the solar corona.

Contribution of observed multi frequency spectrum of Alfvén waves to coronal heating

Paolo **Pagano**, Ineke De Moortel
A&A 623, A37 **2019**
https://arxiv.org/pdf/1901.02310.pdf
https://doi.org/10.1051/0004-6361/201834158
Whilst there are observational indications that transverse MHD waves carry enough energy to maintain the thermal structure of the solar corona, it is not clear whether such energy can be efficiently and effectively converted into heating. Phase-mixing of Alfvén waves is considered a candidate mechanism, as it can develop transverse gradient where magnetic energy can be converted into thermal energy. However, phase-mixing is a process that crucially depends on the amplitude and period of the transverse oscillations, and only recently have we obtained a complete measurement of the power spectrum for transverse oscillations in the corona. We aim to investigate the heating generated by phase-mixing of transverse oscillations triggered by buffeting of a coronal loop that follows from the observed coronal power spectrum as well as the impact of these persistent oscillations on the structure of coronal loops. We consider a 3D MHD model of an active region coronal loop and we perturb its footpoints with a 2D horizontal driver that represents a random buffeting motion of the loop footpoints. Our driver is composed of 1000 pulses superimposed to generate the observed power spectrum. We find that the heating supply from the observed power spectrum in the solar corona through phase mixing is not sufficient to maintain the million degree active region solar corona. We also find that the development of Kelvin-Helmholtz instabilities could be a common phenomenon in coronal loops that could affect their apparent life time. This study concludes that is unlikely that phase-mixing of Alfvén waves resulting from an observed power spectrum of transverse coronal loop oscillations can heat the active region solar corona. However, transverse waves could play an important role in the development of small scale structures.

Contribution of phase-mixing of Alfvén waves to coronal heating in multi-harmonic loop oscillations

P. **Pagano**1, D. J. Pascoe2,3 and I. De Moortel1
A&A 616, A125 (**2018**)
Context. Kink oscillations of a coronal loop are observed and studied in detail because they provide a unique probe into the structure of coronal loops through magnetohydrodynamics (MHD) seismology and a potential test of coronal heating through the phase mixing of Alfvén waves. In particular, recent observations show that standing

oscillations of loops often involve higher harmonics in addition to the fundamental mode. The damping of these kink oscillations is explained by mode coupling with Alfvén waves.
Aims. We investigate the consequences for wave-based coronal heating of higher harmonics and which coronal heating observational signatures we may use to infer the presence of higher harmonic kink oscillations.
Methods. We performed a set of non-ideal MHD simulations in which we modelled the damping of the kink oscillation of a flux tube via mode coupling. We based our MHD simulation parameters on the seismological inversion of an observation for which the first three harmonics are detected. We studied the phase mixing of Alfvén waves, which leads to the deposition of heat in the system, and we applied seismological inversion techniques to the MHD simulation output.
Results. We find that the heating due to phase mixing of Alfvén waves triggered by the damping of kink oscillation is relatively small. We can however illustrate how the heating location drifts from subsequent damping of lower order harmonics. We also address the role of higher order harmonics and the width of the boundary shell in the energy deposition.
Conclusions. We conclude that the coronal heating due to phase mixing does not seem to provide enough energy to maintain the thermal structure of the solar corona even when multi-harmonic oscillations are included; these oscillations play an inhibiting role in the development of smaller scale structures.

Contribution of mode-coupling and phase-mixing of Alfvén waves to coronal heating

P. **Pagano** and I. De Moortel
A&A 601, A107 (**2017**)
https://arxiv.org/pdf/1703.05707.pdf
Context. Phase-mixing of Alfvén waves in the solar corona has been identified as one possible candidate to explain coronal heating. While this scenario is supported by observations of ubiquitous oscillations in the corona carrying sufficient wave energy and by theoretical models that have described the concentration of energy in small-scale structures, it is still unclear whether this wave energy can be converted into thermal energy in order to maintain the million-degree hot solar corona.
Aims. The aim of this work is to assess how much energy can be converted into thermal energy by a phase-mixing process triggered by the propagation of Alfvénic waves in a cylindric coronal structure, such as a coronal loop, and to estimate the impact of this conversion on the coronal heating and thermal structure of the solar corona.
Methods. To this end, we ran 3D MHD simulations of a magnetised cylinder where the Alfvén speed varies through a boundary shell, and a footpoint driver is set to trigger kink modes that mode couple to torsional Alfvén modes in the boundary shell. These Alfvén waves are expected to phase-mix, and the system allows us to study the subsequent thermal energy deposition. We ran a reference simulation to explain the main process and then we varied the simulation parameters, such as the size of the boundary shell, its structure, and the persistence of the driver.
Results. When we take high values of magnetic resistivity and strong footpoint drivers into consideration, we find that i) phase-mixing leads to a temperature increase of the order of 105 K or less, depending on the structure of the boundary shell; ii) this energy is able to balance the radiative losses only in the localised region involved in the heating; and iii) we can determine the influence of the boundary layer and the persistence of the driver on the thermal structure of the system.
Conclusions. Our conclusion is that as a result of the extreme physical parameters we adopted and the moderate impact on the heating of the system, it is unlikely that phase-mixing can contribute on a global scale to the heating of the solar corona.

Algebraic Quantification of the Contribution of Active Regions to the Sun's Dipole Moment: Applications to Polar Field Estimates and Solar Cycle Forecasting

Shaonwita **Pal**, Dibyendu Nandy
MNRAS Volume 531, Issue 1, June 2024, Pages 1546–1553,
https://doi.org/10.1093/mnras/stae1205
https://arxiv.org/pdf/2312.15703.pdf
https://scholar.google.com/scholar_url
The solar cycle is generated by a magnetohydrodynamic dynamo mechanism, which involves the induction and recycling of the toroidal and poloidal components of the Sun's magnetic field. Recent observations indicate that the Babcock-Leighton mechanism -- mediated via the emergence and evolution of tilted bipolar active regions -- is the primary contributor to the Sun's large-scale dipolar field. Surface flux transport models and dynamo models have been employed to simulate this mechanism, which also allows for physics-based solar cycle forecasts. Recently, an alternative analytic method has been proposed to quantify the contribution of individual active regions to the Sun's dipole moment. Utilizing solar cycle observations spanning a century, here we test the efficacy of this algebraic approach. Our results demonstrate that the algebraic quantification approach is reasonably successful in estimating dipole moments at solar minima over the past century -- providing an independent verification of the Babcock-Leighton mechanism as the primary contributor to the Sun's dipole field variations. We highlight that this algebraic methodology stands as an independent approach for estimating the dipole moment at the minima of solar cycles,

relying on characteristics of the sunspot cycle. We also show how this method may be utilized for solar cycle predictions; our estimate of the Sun's dipole field at the end of cycle 24 using this approach indicates that solar cycle 25 would be a moderately weak cycle, ranging between solar cycle 20 and cycle 24.

Impact of Anomalous Active Regions on the Large-scale Magnetic Field of the Sun

Shaonwita **Pal**, Prantika Bhowmik2, Sushant S. Mahajan3, and Dibyendu Nandy1,4
2023 ApJ 953 51
https://iopscience.iop.org/article/10.3847/1538-4357/acd77e/pdf
One of the major sources of perturbation in the solar cycle amplitude is believed to be the emergence of anomalous active regions that do not obey Hale's polarity law and Joy's law of tilt angles. Anomalous regions containing high magnetic flux that disproportionately impact the polar field are sometimes referred to as "rogue regions." In this study, utilizing a surface flux transport model, we analyze the large-scale dipole moment buildup due to the emergence of anomalous active regions on the solar surface. Although these active regions comprise a small fraction of the total sunspot number, they can substantially influence the magnetic dipole moment buildup and subsequent solar cycle amplitude. Our numerical simulations demonstrate that the impact of "anti-Joy" regions on the solar cycle is similar to those of "anti-Hale" regions. We also find that the emergence time, emergence latitude, relative number, and flux distribution of anomalous regions influence the large-scale magnetic field dynamics in diverse ways. We establish that the results of our numerical study are consistent with the algebraic (analytic) approach to explaining the Sun's dipole moment evolution. Our results are relevant for understanding how anomalous active regions modulate the Sun's large-scale dipole moment buildup and its reversal timing within the framework of the Babcock–Leighton dynamo mechanism—now believed to be the primary source of solar cycle variations.

Flux erosion of magnetic clouds by reconnection with the Sun's open flux

Sanchita **Pal**, Soumyaranjan Dash, Dibyendu Nandy
Geophysical Research Letters,47, Issue 8, e2019GL086372, **2020**
https://arxiv.org/pdf/2103.05990.pdf
https://doi.org/10.1029/2019GL086372
Magnetic clouds (MCs) are flux-rope magnetic structures forming a subset of solar coronal mass ejections which have significant space weather impacts. The geoeffectiveness of MCs depends on their properties which evolve during their interplanetary passage. Based on an analysis of observations spanning two solar cycles we establish that MCs interacting with the ambient solar wind magnetic field (i.e., heliospheric open flux) lose a substantial amount of their initial magnetic flux via magnetic reconnection, which in some cases, reduce their geoeffectiveness. We find a linear correlation between the eroded flux of MCs and solar open flux which is consistent with the scenario that MC erosion is mediated via the local heliospheric magnetic field draping around an MC during its interplanetary propagation. The solar open flux is governed by the sunspot cycle. This work therefore uncovers a hitherto unknown pathway for solar cycle modulation of the properties of MCs. **30 Sep 2002, 29 Jun 2014**

Solar observatory Einstein Tower -- Data release of the digitized solar full-disk photographic plate archive

Partha S. **Pal**, M. Verma, J. Rendtel, S. J. González Manrique, H. Enke, C. Denker
2020
https://arxiv.org/pdf/2007.14744.pdf
We present solar full-disk observations, which were recorded at the Einstein Tower during the years 1943 - 1991 (Solar Cycles 18 - 22). High-school students from Potsdam and Berlin digitized more than 3500 full-disk images during two- to three-week internships at AIP. The digital images cover a 15 cm × 15 cm region on photographic plates, which were scanned at a resolution of 7086 × 7086 pixels. The raw data are monochromatic 8-bit images in the Tagged Image File Format (TIFF). These images were calibrated and saved with improved photometric precision as 16-bit images with 2048 × 2048 pixels in the Flexible Image Transport System (FITS) format, which contains extensive headers describing the full-disk images and the observations. The various calibration steps include, for example, accurate measurements of the solar radius, determination of the limb-darkening function, and establishing an accurate coordinate system. The contrast-enhanced and limb-darkening corrected images as well as the raw data are freely available to researchers and the general public in publicly accessible repository. The data are published as a special data release of the Archives of Photographic PLates for Astronomical USE (APPLAUSE) project.

Multi-wavelength observations of vortex-like flows in the photosphere using ground-based and space-borne telescopes

J. **Palacios**, S. Vargas Domínguez, L. A. Balmaceda, I. Cabello, V. Domingo
ASP Conference Series, **2016**, Volume 504: Ground-based solar observations in the space instrumentation era **2017**
https://arxiv.org/pdf/1704.00660.pdf

In this work we follow a series of papers on high-resolution observations of small-scale structures in the solar atmosphere \citep[][Cabello et al., in prep]{Balmaceda2009, Balmaceda2010, Vargas2011, Palacios2012, Domingo2012, Vargas2015}, combining several multi-wavelength data series. These were acquired by both ground-based (SST) and space-borne (Hinode) instruments during the joint campaign of the Hinode Operation Program 14, in September 2007. Diffraction-limited SST data were taken in the G-band and G-cont, and were restored by the MFBD technique. Hinode instruments, on the other hand, provided multispectral data from SOT-FG in the CN band, and Mg~{\sc I} and Ca {\sc II}~lines, as well as from SOT-SP in the Fe~{\sc I} line. In this series of works we have thoroughly studied vortex flows and their statistical occurrences, horizontal velocity fields by means of Local Correlation Tracking (LCT), divergence and vorticity. Taking advantage of the high-cadence and high spatial resolution data, we have also studied bright point statistics and magnetic field intensification, highlighting the importance of the smallest-scale magnetic element observations.

Helioseismology: Observations and Space Missions **Review**

P.L. **Palle**, T. Appourchaux, J. Christensen-Dalsgaard, R.A. Garcia
Chapter 2 of the book Extraterrestrial Seismology **2018**
https://arxiv.org/pdf/1802.00674.pdf

The great success of Helioseismology resides in the remarkable progress achieved in the understanding of the structure and dynamics of the solar interior. This success mainly relies on the ability to conceive, implement, and operate specific instrumentation with enough sensitivity to detect and measure small fluctuations (in velocity and/or intensity) on the solar surface that are well below one meter per second or a few parts per million. Furthermore the limitation of the ground observations imposing the day-night cycle (thus a periodic discontinuity in the observations) was overcome with the deployment of ground-based networks --properly placed at different longitudes all over the Earth-- allowing longer and continuous observations of the Sun and consequently increasing their duty cycles. In this chapter, we start by a short historical overview of helioseismology. Then we describe the different techniques used to do helioseismic analyses along with a description of the main instrumental concepts. We in particular focus on the instruments that have been operating long enough to study the solar magnetic activity. Finally, we give a highlight of the main results obtained with such high-duty cycle observations (>80%) lasting over the last few decades.

Viscous Heating and Instabilities in the Partially Ionized Solar Atmosphere

B.P. **Pandey**, Mark Wardle
MNRAS **2024**
https://arxiv.org/pdf/2411.08242

In weak magnetic fields ($\lesssim$50G), parallel and perpendicular viscosities, mainly from neutrals, may exceed magnetic diffusivities (Ohm, Hall, ambipolar) in the middle and upper chromosphere. Ion-driven gyroviscosity may dominate in the upper chromosphere and transition region. In strong fields ($\gtrsim$100G), viscosities primarily exceed diffusivities in the upper chromosphere and transition region. Parallel and perpendicular viscosities, being similar in magnitude, dampen waves and potentially compete with ambipolar diffusion in plasma heating, potentially inhibiting Hall and ambipolar instabilities when equal. The perpendicular viscosity tensor has two components, $\nu1$ and $\nu2$, which differ slightly and show weak dependence on ion magnetization. Their differences, combined with shear, may destabilize waves, though magnetic diffusion introduces a cutoff for this instability. In configurations with a magnetic field B having vertical (bz=Bz/|B|) and azimuthal (by=By/|B|) components, and a wavevector k with radial ($\kx=k_x/|\bf{k}|$) and vertical ($\kz=k_z/|\bf{k}|$) components, parallel viscosity and Hall diffusion can generate the viscous-Hall instability. Gyroviscosity further destabilizes waves in the upper regions. These findings indicate that the solar atmosphere may experience various viscous instabilities, revealing complex interactions between viscosity, magnetic fields, and plasma dynamics across different atmospheric regions.

Latitude character and evolution of Gnevyshev gap

K. K. **Pandey**, K. M. Hiremath & G. Yellaiah
Astrophys Space Sci (**2017**) 362: 106.
http://sci-hub.cc/10.1007/s10509-017-3083-2

The time interval, between two highest peaks of the sunspot maximum, during which activity energy substantially absorbed is called Gnevyshev gap. In this study we focus on mysterious evolution of the Gnevyshev gap by analyzing and comparing the integrated (over the whole Sun) characteristics of magnetic field strength of sunspot groups, soft x-ray flares, filaments or prominences and polar faculae. The time latitude distribution of these solar activities from photosphere to coronal height, for the low ($\leq$50$\circ\leq$50$\circ$) and high ($\geq$50$\circ\geq$50$\circ$) latitudes, shows the way Gnevyshev gap is evolved. The presence of double peak structure is noticed in high latitude ($\geq$50$\circ\geq$50$\circ$) activity. During activity maximum the depression (or valley) appearing, in different activity processes, probably due to shifting, spreading, and transfer of energy from higher to lower latitudes with the progress of solar cycle. The morphology of successive lower latitude zones, considering it as a wave pulse, appears to be modified/scattered, by certain degree due to shifting of magnetic energy to empower higher or lower latitudes.

Latitudinal distribution of soft X-ray flares and dispairty in butterfly diagram

K. K. **Pandey**, G. Yellaiah, K. M. Hiremath

Astrophysics and Space Science, April **2015**, Volume 356, Issue 2, pp 215-224

We present statistical analysis of about 63000 soft X-ray flare (class≥C) observed by geostationary operational environmental satellite (GOES) during the period 1976–2008. Class wise occurrence of soft X-ray (SXR) flare is in declining trend since cycle 21. The distribution pattern of cycle 21 shows the transit of hemispheric dominance of flare activity from northern to southern hemisphere and remains there during cycle 22 and 23. During the three cycles, 0–100, 21–300 latitude belts in southern hemisphere (SH) and 31–400 latitude belt in northern hemisphere (NH) are mightier. The 11–200 latitude belt of both hemisphere is mightiest. Correlation coefficient between consecutive latitude appears to be increasing from equator to poleward in northern hemisphere whereas pole to equatorward in southern hemisphere. Slope of the regression line fitted with asymmetry time series of daily flare counts is negative in all three cycles for different classes of flares. The yearly asymmetry curve fitted by a sinusoidal function varies from 5.6 to 11 years period and depends upon the intensity of flare. Variation, of curve fitted with wings of butterfly diagram, from first to second order polynomial suggests that latitudinal migration of flare activity varies from cycle to cycle, northern to southern hemisphere. The variation in slope of the butterfly wing of different flare class indicates the non uniform migration of flare activity.

The Magnetic Origin of Solar Campfires

Navdeep K. **Panesar**, Sanjiv K. Tiwari, David Berghmans, Mark C. M. Cheung, Daniel Muller, Frederic Auchere, Andrei Zhukov

ApJL **921** L20 **2021**

https://arxiv.org/pdf/2110.06846.pdf

https://iopscience.iop.org/article/10.3847/2041-8213/ac3007/pdf

https://doi.org/10.3847/2041-8213/ac3007

Solar campfires are fine-scale heating events, recently observed by Extreme Ultraviolet Imager (EUI), onboard Solar Orbiter. Here we use EUI 174Å\ images, together with EUV images from SDO/AIA, and line-of-sight magnetograms from SDO/HMI to investigate the magnetic origin of 52 randomly selected campfires in the quiet solar corona. We find that (i) the campfires are rooted at the edges of photospheric magnetic network lanes; (ii) most of the campfires reside above the neutral line between majority-polarity magnetic flux patch and a merging minority-polarity flux patch, with a flux cancelation rate of ∼1018Mx hr−1; (iii) some of the campfires occur repeatedly from the same neutral line; (iv) in the large majority of instances, campfires are preceded by a cool-plasma structure, analogous to minifilaments in coronal jets; and (v) although many campfires have `complex' structure, most campfires resemble small-scale jets, dots, or loops. Thus, `campfire' is a general term that includes different types of small-scale solar dynamic features. They contain sufficient magnetic energy (∼1026-1027 erg) to heat the solar atmosphere locally to 0.5--2.5MK. Their lifetimes range from about a minute to over an hour, with most of the campfires having a lifetime of <10 minutes. The average lengths and widths of the campfires are 5400±2500km and 1600±640km, respectively. Our observations suggest that (a) the presence of magnetic flux ropes may be ubiquitous in the solar atmosphere and not limited to coronal jets and larger-scale eruptions that make CMEs, and (b) magnetic flux cancelation is the fundamental process for the formation and triggering of most campfires. **20-May-2020, 30-May-2020**

Network Jets as the Driver of Counter-Streaming Flows in a Solar Filament/Filament Channel

Navdeep K. **Panesar**, Sanjiv K. Tiwari, Ronald L. Moore, Alphonse C. Sterling

ApJL Volume 897, Issue 1, id.L2, **2020**

https://arxiv.org/pdf/2006.04249.pdf

https://ui.adsabs.harvard.edu/link_gateway/2020ApJ...897L...2P/PUB_PDF

Counter-streaming flows in a small (100" -long) solar filament/filament channel are directly observed in high-resolution SDO/AIA EUV images of a region of enhanced magnetic network. We combine images from SDO/AIA, SDO/HMI and IRIS to investigate the driving mechanism of these flows. We find that: (i) counter-streaming flows are present along adjacent filament/filament channel threads for about 2 hours, (ii) both ends of the filament/filament channel are rooted at the edges of magnetic network flux lanes along which there are impinging fine-scale opposite-polarity flux patches, (iii) recurrent small-scale jets (known as network jets) occur at the edges of the magnetic network flux lanes at the ends of the filament/filament channel, (iv) the recurrent network jet eruptions clearly drive the counter-streaming flows along threads of the filament/filament channel, (v) some of the network jets appear to stem from sites of flux cancelation, between network flux and merging opposite-polarity flux, and (vi) some show brightening at their bases, analogous to the base brightening in coronal jets. The average speed of the counter-streaming flows along the filament/filament channel threads is 70 km/s. The average widths of the AIA filament/filament channel and the Halpha filament are 4" and 2.5", respectively, consistent with the earlier findings that filaments in EUV images are wider than in Halpha images. Thus, our observations show that the continually

repeated counter-streaming flows come from network jets, and these driving network-jet eruptions are possibly prepared and triggered by magnetic flux cancelation. **8 Jan 2016**

Onset of the Magnetic Explosion in Solar Coronal Jets in Quiet Regions on the Central Disk

Navdeep K. **Panesar**, Ronald L. Moore, Alphonse C. Sterling
ApJ Volume 894, Issue 2, id.104, **2020**
https://arxiv.org/pdf/2006.04253.pdf
https://ui.adsabs.harvard.edu/link_gateway/2020ApJ...894..104P/PUB_PDF
We examine the initiation of 10 coronal jet eruptions in quiet regions on the central disk, thereby avoiding near-limb spicule-forest obscuration of the slow-rise onset of the minifilament eruption. From the SDO/AIA 171A 12-second-cadence movie of each eruption, we (1) find and compare the start times of the minifilament's slow rise, the jet-base bright point, the jet-base interior brightening, and the jet spire, and (2) measure the minifilament's speed at the start and end of its slow rise. From (a) these data, (b) prior observations showing that each eruption was triggered by magnetic flux cancelation under the minifilament, and (c) the breakout-reconnection current sheet observed in one eruption, we confirm that quiet-region jet-making minifilament eruptions are miniature versions of CME-making filament eruptions, and surmise that in most quiet region jets: (1) the eruption starts before runaway reconnection starts, (2) runaway reconnection does not start until the slow-rise speed is at least about 1 km/s, and (3) at and before eruption onset there is no current sheet of appreciable extent. We therefore expect: (i) many CME-making filament eruptions are triggered by flux cancelation under the filament, (ii) emerging bipoles seldom, if ever, directly drive jet production because the emergence is seldom, if ever, fast enough, and (iii) at a separatrix or quasi-separatrix in any astrophysical setting of magnetic field in low-beta plasma, a current sheet of appreciable extent can be built only dynamically by a magnetohydrodynamic convulsion of the field, not by quasi-static gradual converging of the field.
2012 Mar 22, 2012 Sep 21, 2012 Nov 13
Table 1. Key Data for our 10 Central-Disk Quiet-Region Jet Eruption Onsets (2012)

Hi-C 2.1 Observations of Jetlet-like Events at Edges of Solar Magnetic Network Lanes

Navdeep K. **Panesar**1,2,3,15, Alphonse C. Sterling3, Ronald L. Moore ...
2019 ApJL 887 L8
https://ui.adsabs.harvard.edu/link_gateway/2019ApJ...887L...8P/PUB_PDF
We present high-resolution, high-cadence observations of six, fine-scale, on-disk jet-like events observed by the High-resolution Coronal Imager 2.1 (Hi-C 2.1) during its sounding-rocket flight. We combine the Hi-C 2.1 images with images from the Solar Dynamics Observatory (SDO)/Atmospheric Imaging Assembly (AIA) and the Interface Region Imaging Spectrograph (IRIS), and investigate each event's magnetic setting with co-aligned line-of-sight magnetograms from the SDO/Helioseismic and Magnetic Imager (HMI). We find that (i) all six events are jetlet-like (having apparent properties of jetlets), (ii) all six are rooted at edges of magnetic network lanes, (iii) four of the jetlet-like events stem from sites of flux cancelation between majority-polarity network flux and merging minority-polarity flux, and (iv) four of the jetlet-like events show brightenings at their bases reminiscent of the base brightenings in coronal jets. The average spire length of the six jetlet-like events (9000 ± 3000 km) is three times shorter than that for IRIS jetlets (27,000 ± 8000 km). While not ruling out other generation mechanisms, the observations suggest that at least four of these events may be miniature versions of both larger-scale coronal jets that are driven by minifilament eruptions and still-larger-scale solar eruptions that are driven by filament eruptions. Therefore, we propose that our Hi-C events are driven by the eruption of a tiny sheared-field flux rope, and that the flux rope field is built and triggered to erupt by flux cancelation.

The Coronal Flattening Index at the 20 April 2023 Total Solar Eclipse and the Prediction of Solar Cycle 25.

Pangestu, A.D., Yusuf, A.A., Prastyo, H.A. et al.
Sol Phys 299, 58 (**2024**).
https://doi.org/10.1007/s11207-024-02307-w
The Ludendorff coronal flattening index is a quantitative parameter to analyze the global structure and shape of the corona. This index plays a crucial role in identifying solar magnetic activity and estimating the phase of the solar cycle. We observed a total solar eclipse on 20 April 2023 in Timor-Leste and obtained a Ludendorff coronal flattening index of 0.109±0.025 by analyzing isophotes in white-light coronal images. Based on the composite image of the corona, streamers and plumes were observed extending in various directions across the solar disk, indicating that the Sun was in the ascending phase of its cycle. To establish the relationship between the coronal flattening index and the solar cycle phase, historical total solar eclipse data (1893 – 2013) were analyzed, focusing on smoothed sunspot numbers and flattening indices during the ascending phase. Two datasets, designated as “full” and “conservative”, were constructed considering temporal constraints relative to solar maxima and minima. The coronal morphology observed during the 20 April 2023 total solar eclipse corresponded to a premaximum phase, with values of 0.673±0.172 and 0.613±0.171 for the full and conservative datasets, respectively. We also developed

a multilinear correlation and polynomial regression of second order models to predict the peak amplitude of the current solar cycle using both datasets. The full dataset predicted a peak on 3 December 2024 with amplitudes of 173±23 and 163±21 for the respective models. Conversely, the conservative dataset predicted a peak on 30 May 2025 with amplitudes of 180±24 and 180±25 for the respective models. These findings suggest that Solar Cycle 25 will likely be stronger than Solar Cycle 24.

Forecasting of Sunspot Time Series Using a Hybridization of ARIMA, ETS and SVM Methods

Sibarama **Panigrahi**, Radha Mohan Pattanayak, Prabira Kumar Sethy & Santi Kumari Behera
Solar Physics volume 296, Article number: 6 (**2021**)
https://link.springer.com/content/pdf/10.1007/s11207-020-01757-2.pdf
Solar activity directly influences the heliospheric environment and lives on the Earth. Sunspot number (SN) is one of the most crucial and commonly predicted solar activity indices. The prediction of SN time series is a challenging problem owing to its non-stationary, non-Gaussian and nonlinear nature. Therefore, improving the forecasting accuracy of SN time series is an important and challenging task. Motivated from this, in this paper, we have proposed a hybridization of the autoregressive integrated moving average (ARIMA); exponential smoothing with error, trend and seasonality (ETS); and support vector machine (SVM) to predict monthly and yearly SN time series. In this method, first ARIMA, ETS and SVM with linear kernel function are applied to the SN time series and the maximum of forecasts are determined to obtain the forecasts on linear component. Then the residual series is obtained by subtracting the forecasts on linear component from SN time series. The residual series is considered as nonlinear and modeled using SVM with Gaussian kernel function. Then the forecasts on linear component are added with the forecasts on nonlinear component to obtain the final forecasts. To evaluate the efficiency of the proposed method, three constituent models, one of the most popular deep learning models long short-term memory (LSTM), four hybrid methods, four ensemble methods are considered. Furthermore, two horizons, monthly and yearly sunspot time series are considered to evaluate the robustness of the proposed method. Results indicate the statistical superiority of the proposed methods over different horizons considering different accuracy measures.

Revisiting the relation between nonthermal line widths and transverse MHD wave amplitudes

Vaibhav **Pant**, Tom Van Doorsselaere
ApJ **899** 1 **2020**
https://arxiv.org/pdf/2007.02836.pdf
https://doi.org/10.3847/1538-4357/aba429
Observations and 3D MHD simulations of the transverse MHD waves in the solar corona have established that true wave energies hide in the nonthermal line widths of the optically thin emission lines. This displays the need for a relation between the nonthermal line widths and transverse wave amplitudes for estimating the true wave energies. In the past decade, several studies have assumed that the root mean square (rms) wave amplitudes are larger than nonthermal line widths by a factor of 2–√. However, a few studies have ignored this factor while estimating rms wave amplitudes. Thus there appears to exist a discrepancy in this relation. In this study, we investigate the dependence of nonthermal line widths on wave amplitudes by constructing a simple mathematical model followed by 3D MHD simulations. We derive this relation for the linearly polarised, circularly polarised oscillations, and oscillations excited by multiple velocity drivers. We note a fairly good match between mathematical models and numerical simulations. We conclude that the rms wave amplitudes are never greater than the nonthermal line widths which raises questions about earlier studies claiming transverse waves carry enough energy to heat the solar corona.

Investigating `dark' energy in the solar corona using forward modeling of MHD waves

Vaibhav **Pant**, Norbert Magyar, Tom Van Doorsselaere, Richard J. Morton
ApJ **881** 95 **2019**
https://arxiv.org/pdf/1906.10941.pdf
sci-hub.se/10.3847/1538-4357/ab2da3
It is now well established that the Alfvénic waves are ubiquitous in the solar corona. However, the Alfvénic wave energy estimated from the Doppler velocity measurements in the corona was found to be four orders of magnitude less than that estimated from non-thermal line widths. McIntosh & De Pontieu (2012) suggested that this discrepancy in energy might be due to the line-of-sight (LOS) superposition of the several oscillating structures, which can lead to an underestimation of the Alfvénic wave amplitudes and energies. McIntosh & De Pontieu (2012) termed this coronal `dark' or `hidden' energy. However, their simulations required the use of an additional, unknown source of Alfvénic wave energy to provide agreement with measurements of the coronal non-thermal line widths. In this study, we investigate the requirement of this unknown source of additional `dark' energy in the solar corona using gravitationally stratified 3D magnetohydrodynamic (MHD) simulations of propagating waves. We excite the

transverse MHD waves and generate synthetic observations for the Fe XIII emission line. We establish that the LOS superposition greatly reduces the Doppler velocity amplitudes and increases the non-thermal line widths. Importantly, our model generates the observed wedge-shaped correlation between Doppler velocities and non-thermal line widths. We find that the observed wave energy is only 0.2-1\% of the true wave energy which explains 2-3 orders of magnitude of the energy discrepancy. We conclusively establish that the true wave energies are hidden in the non-thermal line widths. Hence, our results rule out the requirement for an additional `dark' energy in the solar corona.

Dynamics of on-disk plumes as observed with Interface Region Imaging Spectrograph, Atmospheric Imaging Assembly and Helioseismic and Magnetic Imager

Vaibhav **Pant**, Laurent Dolla, Rakesh Mazumder, Dipankar Banerjee, S. Krishna Prasad, Vemareddy Panditi

ApJ **807** 71 **2015**

http://arxiv.org/pdf/1505.04473v1.pdf

We examine the role of small-scale transients in the formation and evolution of solar coronal plumes. We study the dynamics of plume footpoints seen in the vicinity of a coronal hole using the Atmospheric Imaging Assembly (AIA) images, the Helioseismic and Magnetic Imager (HMI) magnetogram on board the Solar Dynamics Observatory (SDO) and spectroscopic data from the Interface Region Imaging Spectrograph (IRIS). Quasi-periodic brightenings are observed in the base of the plumes and are associated with magnetic flux changes. With the high spectral and spatial resolution of IRIS, we identify the sources of these oscillations and try to understand what role the transients at the foot points can play in sustaining the coronal plumes. IRIS sit and stare observation provide a unique opportunity to study the evolution of foot points of the plumes. We notice enhanced line width, intensity and large deviation from the average Doppler shift in the line profiles at specific instances which indicate the presence of flows at the foot points of plumes. We propose that outflows (jet-like features) as a result of small scale reconnections affect the line profiles. These jet-like features may be also responsible for the generation of propagating disturbances within the plumes which are observed to be propagating to larger distances as recorded from multiple AIA channels. These propagating disturbances can be explained in terms of slow magnetoacoustic waves. **12 July 2014**

MHD Seismology of a loop-like filament tube by observed kink waves

V. **Pant**, A.K. Srivastava, D. Banerjee, M. Goossens, P.F. Chen, N.C. Joshi, Y.H. Zhou

RAA, **2015**

http://arxiv.org/pdf/1503.02281v1.pdf

We report and analyze the observational evidence of global kink oscillations in a solar filament as observed in H alpha by National Solar Observatory (NSO)/Global Oscillation Network Group (GONG) instrument. An M1.1-class flare in active region 11692 on **2013 March 15** induced a global kink mode in the filament lying in the south-west of AR11692.We find periods of about 61 - 67 minutes and damping times of 92 - 117 minutes at three vertical slice positions chosen in and around the filament apex. We find that the waves are damped. From the observed global kink mode period and damping time scale using the theory of resonant absorption we perform prominence seismology. We estimate a lower cut-off value for the inhomogeneity length-scale to be around 0.34 - 0.44 times the radius of the filament cross-section.

Flows and Waves in Braided Solar Coronal Magnetic Structures

V. **Pant**1, A. Datta1,2, and D. Banerjee

ApJ 801 L2 **2015**

We study the high frequency dynamics in the braided magnetic structure of an active region (AR 11520) moss as observed by the High-Resolution Coronal Imager (Hi-C). We detect quasi-periodic flows and waves in these structures. We search for high frequency dynamics while looking at power maps of the observed region. We find that shorter periodicities (30–60 s) are associated with small spatial scales which can be resolved by Hi-C only. We detect quasi-periodic flows with a wide range of velocities, from 13–185 km s−1, associated with braided regions. This can be interpreted as plasma outflows from reconnection sites. We also find short period and large amplitude transverse oscillations associated with the braided magnetic region. Such oscillations could be triggered by reconnection or such oscillations may trigger reconnection.

Galactic Cosmic Ray Modulation and the Last Solar Minimum

E. **Paouris**, H. Mavromichalaki, A. Belov, R. Gushchina and V. Yanke

Solar Physics, Volume 280, Number 1 (**2012**), 255-271

In this work the galactic cosmic ray modulation in relation to solar activity indices and heliospheric parameters during the years 1996 – 2010 covering solar cycle 23 and the solar minimum between cycles 23 and 24 is studied. A new perspective of this contribution is that cosmic ray data with a rigidity of 10 GV at the top of the atmosphere obtained from many ground-based neutron monitors were used. The proposed empirical relation gave much better results than those in previous works concerning the hysteresis effect. The proposed models obtained from a combination of solar activity indices and heliospheric parameters give a standard deviation < 10 % for all the cases. The correlation coefficient between the cosmic ray variations of 10 GV and the sunspot number reached a value of r=−0.89 with a time lag of 13.6±0.4 months. The best reproduction of the cosmic ray intensity is obtained by taking into account solar and interplanetary indices such as sunspot number, interplanetary magnetic field, CME index, and heliospheric current sheet tilt. The standard deviation between the observed and calculated values is about 7.15 % for all of solar cycle 23; it also works very well during the different phases of the cycle. Moreover, the use of the cosmic ray intensity of 10 GV during the long minimum period between cycles 23 and 24 is of special interest and is discussed in terms of cosmic ray intensity modulation.

Asteroseismic Signature of a Large Active Region

Emanuele **Papini**, Laurent Gizon

Frontiers in Astronomy and Space Sciences 6:72. **2019**

https://arxiv.org/pdf/1911.11812.pdf

sci-hub.se/10.3389/fspas.2019.00072

Axisymmetric magnetic activity on the Sun and Sun-like stars increases the frequencies of the modes of acoustic oscillation. However, it is unclear how a corotating patch of activity affects the oscillations, since such a perturbation is unsteady in the frame of the observer. In this paper we qualitatively describe the asteroseismic signature of a large active region in the power spectrum of the dipole and quadrupole p modes. In the corotating frame of the active region, the perturbations due to (differential) rotation and the active region completely lift the $(2\ell+1)$-fold azimuthal degeneracy of the frequency spectrum of modes with harmonic degree ℓ. In the frame of the observer, the unsteady nature of the perturbation leads to the appearance of $(2\ell+1)2$ peaks in the power spectrum of a multiplet. These peaks blend into each other to form asymmetric line profiles. In the limit of a small active region, we approximate the power spectrum of a multiplet in terms of $2\times(2\ell+1)$ peaks, whose amplitudes and frequencies depend on the latitude of the active region and the inclination angle of the star's rotation axis. In order to check the results and to explore the nonlinear regime, we also perform numerical simulations using the 3D time-domain pseudo-spectral linear pulsation code GLASS.

Mean field solar surface dynamo in the presence of partially ionized plasmas and sub-surface shear layer

B S **Paradkar**, S M Chitre, V Krishan

MNRAS 488, Issue 3, September **2019**, Pages 4329–4337

sci-hub.se/10.1093/mnras/stz2008

A non-linear $\alpha - \Omega$ dynamo in the partially ionized turbulent plasma in the presence of sub-surface velocity shear is studied with mean-field electrodynamics. Such a dynamo is probably operational in the near-surface region of the Sun, where the presence of both neutrals and the velocity shear (due to sub-surface shear layer in the rotation profile) is observationally well established. In particular, we show that the inclusion of ambipolar diffusion leads to a saturation of magnetic field amplitudes in the $\alpha - \Omega$ dynamo. We also demonstrate that the temporal evolution of large-scale global magnetic fields follows the well-known pattern similar to the 'butterfly' diagram displayed by sunspots. As usual the velocity shear converts part of the poloidal into the toroidal magnetic field which in turn is regenerated largely by the combined kinetic plus Hall helicity, thus closing the dynamo loop. In addition, by allowing temporal variation in the helicity and ambipolar diffusion coefficient we are able to reproduce the grand-minimum type behaviour of the solar dynamo. Details of theoretical model along with numerical computations of dynamo equations in the partially ionized plasma are outlined. The solar surface dynamo model envisaged in this work could operate in conjunction with the global dynamo present in the bulk of the convection zone.

Physical properties of solar polar jets: A statistical study with Hinode XRT data

A. R. **Paraschiv**1,3⋆, A. Bemporad1 and A. C. Sterling

A&A 579, A96 (**2015**)

Aims. The target of this work is to investigate the physical nature of polar jets in the solar corona and their possible contribution to coronal heating and solar wind flow based on the analysis of X-ray images acquired by the Hinode XRT telescope. We estimate the different forms of energy associated with many of these small-scale eruptions, in particular the kinetic energy and enthalpy.

Methods. Two Hinode XRT campaign datasets focusing on the two polar coronal holes were selected to analyze the physical properties of coronal jets; the analyzed data were acquired using a series of three XRT filters. Typical kinematical properties (e.g., length, thickness, lifetime, ejection rate, and velocity) of 18 jets are evaluated from the observed sequences, thus providing information on their possible contribution to the fast solar wind flux escaping

from coronal holes. Electron temperatures and densities of polar-jet plasmas are also estimated using ratios of the intensities observed in different filters.
Results. We find that the largest amount of energy eventually provided to the corona is thermal. The energy due to waves may also be significant, but its value is comparatively uncertain. The kinetic energy is lower than thermal energy, while other forms of energy are comparatively low. Lesser and fainter events seem to be hotter, thus the total contribution by polar jets to the coronal heating could have been underestimated so far. The kinetic energy flux is usually around three times smaller than the enthalpy counterpart, implying that this energy is converted into plasma heating more than in plasma acceleration. This result suggests that the majority of polar jets are most likely not escaping from the Sun and that only cooler ejections could possibly have enough kinetic energy to contribute to the total solar wind flow.

Spectroscopy of very hot plasma in non-flaring parts of a solar limb active region: spatial and temporal properties

Susanna **Parenti**, Giulio del Zanna, Antonino Petralia, Fabio Reale, Luca Teriaca, Paola Testa, Helen E. Mason

2017 *ApJ* **846** 25

https://arxiv.org/pdf/1707.08445.pdf

In this work we investigate the thermal structure of an off-limb active region in various non-flaring areas, as it provides key information on the way these structures are heated. In particular, we concentrate in the very hot component (>3 MK) as it is a crucial element to discriminate between different heating mechanisms. We present an analysis using Fe and Ca emission lines from both SOHO/SUMER and HINODE/EIS. A dataset covering all ionization stages from Fe X to Fe XIX has been used for the thermal analysis (both DEM and EM). Ca XIV is used for the SUMER-EIS radiometric cross-calibration.
We show how the very hot plasma is present and persistent almost everywhere in the core of the limb AR. The off-limb AR is clearly structured in Fe XVIII. Almost everywhere, the EM analysis reveals plasma at 10 MK (visible in Fe XIX emission) which is down to 0.1% of EM of the main 3 MK plasma. We estimate the power law index of the hot tail of the EM to be between -8.5 and -4.4. However, we leave an open question on the possible existence of a small minor peak at around 10 MK. The absence in some part of the AR of Fe XIX and Fe XXIII lines (which fall into our spectral range) enables us to determine an upper limit on the EM at such temperatures. Our results include a new Ca XIV 943.59 \AA~ atomic model. **27 and 28 April 2012**

Short story of stratospheric and ground-based observations of solar photosphere with high angular resolution in the 70s of the XX century at the Pulkovo Observatory

L.D.**Parfinenko**

2020

https://arxiv.org/ftp/arxiv/papers/2007/2007.00348.pdf

In the 70s of the last century, the stratospheric solar observatory "Saturn" with a 100cm telescope was launched at Pulkovo Observatory. The photographs and spectra obtained on it for more than 45 years remained record-breaking in angular resolution. Then, for ground-based observations of Sun fine structure in Pamir at an altitude of 4.5 km, a 50 cm open-type Pulkovo mobile telescope was installed. Photographs and spectra obtained with the Saturn telescope for the visible range were an important step in the development of high spatial resolution technologies in heliophysics. However, to date, the details of these studies remain unknown to the global scientific community. In this paper, an attempt is made to partially fill this gap.

Supergranulation Velocity Field from the MDI (SOHO) Data

L. D. **Parfinenko**, V. I. Efremov, A. A. Solovev

*Geomagnetism and Aeronomy, **2014**, Vol. 54, No. 8, pp. 1–6.*

http://arxiv.org/ftp/arxiv/papers/1412/1412.2065.pdf

Long (up to 100 hours) time series of SOHO/MDI Doppler data are analyzed. The power spectrum of radial velocity time series in the quiet photosphere is observed to have, along with the known 5-min mode, a stable strong mode with a period of about 32 h, which is close to the supergranulation cell lifetime. The spatial distribution of the amplitudes of these oscillations also coincides with the characteristic size scale of supergranulation (~35 Mm).

A model for straight and helical solar jets: II. Parametric study of the plasma beta

E. **Pariat**, K. Dalmasse, C.R. DeVore, S.K. Antiochos, J.T. Karpen

A&A **2016**

http://arxiv.org/pdf/1609.08825v1.pdf

Jets are dynamic, impulsive, well-collimated plasma events that develop at many different scales and in different layers of the solar atmosphere. Jets are believed to be induced by magnetic reconnection, a process central to many astrophysical phenomena. Within the solar atmosphere, jet-like events develop in many different environments, e.g.,

in the vicinity of active regions as well as in coronal holes, and at various scales, from small photospheric spicules to large coronal jets. In all these events, signatures of helical structure and/or twisting/rotating motions are regularly observed. The present study aims to establish that a single model can generally reproduce the observed properties of these jet-like events. In this study, using our state-of-the-art numerical solver ARMS, we present a parametric study of a numerical tridimensional magnetohydrodynamic (MHD) model of solar jet-like events. Within the MHD paradigm, we study the impact of varying the atmospheric plasma β on the generation and properties of solar-like jets.
The parametric study validates our model of jets for plasma β ranging from 10−3 to 1, typical of the different layers and magnetic environments of the solar atmosphere. Our model of jets can robustly explain the generation of helical solar jet-like events at various β≤1. This study introduces the new result that the plasma β modifies the morphology of the helical jet, explaining the different observed shapes of jets at different scales and in different layers of the solar atmosphere.
Our results allow us to understand the energisation, triggering, and driving processes of jet-like events. ***Our model allows us to make predictions of the impulsiveness and energetics of jets as determined by the surrounding environment, as well as the morphological properties of the resulting jets.***

Model for straight and helical solar jets. I. Parametric studies of the magnetic field geometry

E. **Pariat**, K. Dalmasse, C.R. DeVore, S.K. Antiochos, J.T. Karpen
A&A 573, id.A130, 15 pp. **2016**
http://www.aanda.org/articles/aa/pdf/2015/01/aa24209-14.pdf
Context. Jets are dynamic, impulsive, well-collimated plasma events developing at many different scales and in different layers of the solar atmosphere.
Aims: Jets are believed to be induced by magnetic reconnection, a process central to many astrophysical phenomena. Studying their dynamics can help us to better understand the processes acting in larger eruptive events (e.g., flares and coronal mass ejections) as well as mass, magnetic helicity, and energy transfer at all scales in the solar atmosphere. The relative simplicity of their magnetic geometry and topology, compared with larger solar active events, makes jets ideal candidates for studying the fundamental role of reconnection in energetic events.
Methods: In this study, using our recently developed numerical solver ARMS, we present several parametric studies of a 3D numerical magneto-hydrodynamic model of solar-jet-like events. We studied the impact of the magnetic field inclination and photospheric field distribution on the generation and properties of two morphologically different types of solar jets, straight and helical, which can account for the observed so-called standard and blowout jets.
Results: Our parametric studies validate our model of jets for different geometric properties of the magnetic configuration. We find that a helical jet is always triggered for the range of parameters we tested. ***This demonstrates that the 3D magnetic null-point configuration is a very robust structure for the energy storage and impulsive release characteristic of helical jets.*** In certain regimes determined by magnetic geometry, a straight jet precedes the onset of a helical jet. We show that the reconnection occurring during the straight-jet phase influences the triggering of the helical jet.
Conclusions: Our results allow us to better understand the energization, triggering, and driving processes of straight and helical jets. Our model predicts the impulsiveness and energetics of jets in terms of the surrounding magnetic field configuration. Finally, we discuss the interpretation of the observationally defined standard and blowout jets in the context of our model, as well as the physical factors that determine which type of jet will occur.

Magnetic Helicity Flux across Solar Active Region Photospheres: II. Association of Hemispheric Sign Preference with Flaring Activity during Solar Cycle 24

Sung-Hong **Park**, K. D. Leka, Kanya Kusano
ApJ **911** 79 **2021**
https://arxiv.org/pdf/2102.13331.pdf
ttps://doi.org/10.3847/1538-4357/abea13
In our earlier study of this series (Park et al. 2020, Paper I), we examined the hemispheric sign preference (HSP) of magnetic helicity flux dH/dt across photospheric surfaces of 4802 samples of 1105 unique active regions (ARs) observed during solar cycle 24. Here, we investigate any association of the HSP, expressed as a degree of compliance, with flaring activity, analyzing the same set of dH/dt estimates as used in Paper I. The AR samples under investigation are assigned to heliographic regions (HRs) defined in the Carrington longitude-latitude plane with a grid spacing of 45◦ in longitude and 15◦ in latitude. For AR samples in each of the defined HRs, we calculate the degree of HSP compliance and the average soft X-ray flare index. The strongest flaring activity is found to be in one distinctive HR with an extremely low HSP compliance of 41% as compared to the mean and standard deviation of 62% and 7%, respectively, over all HRs. This sole HR shows an anti-HSP (i.e., less than 50%) and includes the highly flare-productive AR NOAA 12673, however this AR is not uniquely responsible for the HR's low HSP. We also find that all HRs with the highest flaring activity are located in the southern hemisphere, and they tend to have

lower degrees of HSP compliance. These findings point to the presence of localized regions of the convection zone with enhanced turbulence, imparting a greater magnetic complexity and a higher flaring rate to some rising magnetic flux tubes.

Magnetic Helicity Flux across Solar Active Region Photospheres: I. Hemispheric Sign Preference in Solar Cycle 24

Sung-Hong **Park**, K. D. Leka, Kanya Kusano

ApJ **904** 6 **2020**

https://arxiv.org/pdf/2010.06134.pdf

https://doi.org/10.3847/1538-4357/abbb93

A hemispheric preference in the dominant sign of magnetic helicity has been observed in numerous features in the solar atmosphere: i.e., left-handed/right-handed helicity in the northern/southern hemisphere. The relative importance of different physical processes which may contribute to the observed hemispheric sign preference (HSP) of magnetic helicity is still under debate. Here, we estimate magnetic helicity flux (dH/dt) across the photospheric surface for 4,802 samples of 1,105 unique active regions (ARs) that appeared over an 8-year period from 2010 to 2017 during solar cycle 24, using photospheric vector magnetic field observations by the Helioseismic and Magnetic Imager (HMI) onboard the Solar Dynamics Observatory (SDO). The estimates of dH/dt show that 63% and 65% of the investigated AR samples in the northern and southern hemispheres, respectively, follow the HSP. We also find a trend that the HSP of dH/dt increases from ~50-60% up to ~70-80% as ARs (1) appear at the earlier inclining phase of the solar cycle or higher latitudes; (2) have larger values of |dH/dt|, the total unsigned magnetic flux, and the average plasma flow speed. These observational findings support the enhancement of the HSP mainly by the Coriolis force acting on a buoyantly rising and expanding flux tube through the turbulent convection zone. In addition, the differential rotation on the solar surface as well as the tachocline α-effect of flux-transport dynamo may reinforce the HSP for ARs at higher latitudes.

HMI Science Nuggets #151 March **2021** http://hmi.stanford.edu/hminuggets/?p=3450

Negative Magnetic Diffusivity β Replacing the α Effect in the Helical Dynamo

Kiwan **Park**

2020 ApJ 898 112

https://doi.org/10.3847/1538-4357/ab9b89

In the Sun, the converting process of a poloidal magnetic field (B pol) from a toroidal field (B tor) is essential to sustaining the solar magnetic fields. However, the converting process, dominated by α and β effects, is not yet clearly understood. Conventional theories expect that the α effect should be quenched as the magnetic field grows. Also, plasma kinetic energy is thought to diffuse magnetic energy (positive β effect). Then, B pol is supposed to decay resulting in the dissipation of B tor, followed by the diminishing dynamo process. But the solar magnetic field evolves periodically, as is observed. To solve this inconsistency between the theory and real nature, we first need to check if the α and β effects indeed evolve as the conventional theories expect. However, these effects are theoretically or conceptually inferred quantities, and their exact expressions are not yet known. So, instead of their incomplete formulas, we used more practical representations composed of large-scale magnetic helicity $\overline{H}_M$ $(\equiv \overline{A} \cdot \overline{B})$ and energy $\overline{E}_M$ $(\equiv \overline{B}^2/2)$. We verified that the α effect quenches as the conventional theory expects. However, we also found that the β effect can be negative. This negative β apparently looks inconsistent with the conventional conclusion, but it can be a promising substitution for the decaying α effect. We discuss their physical bases and mechanisms using a field structure model supported by an analytic method. The model shows that the interaction between the poloidal velocity component (U pol) and nonlocally transferred magnetic field (B ∙ ∇ U) induces a current density j ind along with the magnetic field. Their combined structure yields magnetic helicity to the system, which is the α effect. However, U pol can also interact with the locally transferred magnetic field, i.e., U pol × (− U ∙ ∇ B) inducing a current density j diff. This current density can produce additional magnetic helicity (negative β effect) to the system. Simultaneously, the toroidal component U tor with − U ∙ ∇ B leads to the usual positive β effect, which diffuses the magnetic field. Finally, using the negative β effect, we show how the plasma motion is suppressed in a helically forced dynamo system where Lorentz force (J × B) apparently looks negligible.

An Observational Test of Solar Plasma Heating by Magnetic Flux Cancellation

Sung-Hong **Park**

ApJ **897** 49 **2020**

https://arxiv.org/pdf/2005.07953.pdf

https://doi.org/10.3847/1538-4357/ab93ca

Recent observations suggest that magnetic flux cancellation may play a crucial role to heat the Sun's upper atmosphere (chromosphere, transition region, corona). Here, we intended to validate an analytic model for magnetic

reconnection and consequent coronal heating, driven by a pair of converging and cancelling magnetic flux sources of opposite polarities. For this test, we analyzed photospheric magnetic field and multi-wavelength UV/EUV observations of a small-scale flux cancellation event in a quiet-Sun internetwork region over a target interval of 5.2 hr. The observed cancellation event exhibits a converging motion of two opposite-polarity magnetic patches on the photosphere and red-shifted Doppler velocities (downflows) therein consistently over the target interval, with a decrease in magnetic flux of both polarities at a rate of 1015 Mx s−1. Several impulsive EUV brightenings, with DEM values peaked at 1.6-2.0 MK, are also observed in the shape of arcades with their two footpoints anchored in the two patches. The rate of magnetic energy released as heat at the flux cancellation region is estimated to be in the range of (0.2-1)×1024 erg s−1 over the target interval, which can satisfy the requirement of previously reported heating rates for the quiet-Sun corona. Finally, both short-term (a few to several tens of minutes) variations and long-term (a few hours) trends in the magnetic energy release rate are clearly shown in the estimated rate of radiative energy loss of electrons at temperatures above 2.0 MK. All these observational findings support the validity of the investigated reconnection model for plasma heating in the upper solar atmosphere by flux cancellation. **2017 November 7**

Generation of Solar UV and EUV Images from SDO/HMI Magnetograms by Deep Learning

Eunsu **Park**1, Yong-Jae Moon1, Jin-Yi Lee2, Rok-Soon Kim3,4, Harim Lee2, Daye Lim1, Gyungin Shin1, and Taeyoung Kim1,5
2019 ApJL 884 L23
https://doi.org/10.3847/2041-8213/ab46bb
In this Letter, we apply deep-learning methods to the image-to-image translation from solar magnetograms to solar ultraviolet (UV) and extreme UV (EUV) images. For this, We consider two convolutional neural network models with different loss functions, one (Model A) is with L1 loss (L 1), and the other (Model B) is with L 1 and cGAN loss (L cGAN). We train the models using pairs of Solar Dynamics Observatory (SDO)/Atmospheric Imaging Assembly (AIA) nine-passband (94, 131, 171, 193, 211, 304, 335, 1600, and 1700 Å) UV/EUV images and their corresponding SDO/Helioseismic and Magnetic Imager (HMI) line-of-sight (LOS) magnetograms from 2011 to 2016. We evaluate the models by comparing pairs of SDO/AIA images and the corresponding ones generated in 2017. Our main results from this study are as follows. First, the models successfully generate SDO/AIA-like solar UV and EUV images from SDO/HMI LOS magnetograms. Second, in view of three metrics (pixel-to-pixel correlation coefficient, relative error, and the percentage of pixels having errors less than 10%), the results from Model A are mostly comparable or slightly better than those from Model B. Third, in view of the rms contrast measure, the generated images by Model A are much more blurred than those by Model B because of L cGAN specialized for generating realistic images.

First simultaneous SST/CRISP and IRIS observations of a small-scale quiet Sun vortex

S.-H. **Park**, G. Tsiropoula, I. Kontogiannis, K. Tziotziou, E. Scullion, J.G. Doyle
A&A 586, A25 **2016**
http://arxiv.org/pdf/1512.06032v1.pdf
Context. Ubiquitous small-scale vortices have recently been found in the lower atmosphere of the quiet Sun in state-of-the-art solar observations and in numerical simulations.
Aims. We investigate the characteristics and temporal evolution of a granular-scale vortex and its associated upflows through the photosphere and chromosphere of a quiet Sun internetwork region.
Methods. We analyzed high spatial and temporal resolution ground- and spaced-based observations of a quiet Sun region. The observations consist of high-cadence time series of wideband and narrowband images of both Hα 6563 A and Ca II 8542 A lines obtained with the CRisp Imaging SpectroPolarimeter (CRISP) instrument at the Swedish 1-m Solar Telescope (SST), as well as ultraviolet imaging and spectral data simultaneously obtained by the Interface Region Imaging Spectrograph (IRIS).
Results. A small-scale vortex is observed for the first time simultaneously in Hα, Ca II 8542 A, and Mg II k lines. During the evolution of the vortex, Hα narrowband images at −0.77A and Ca II 8542 A narrowband images at −0.5A, and their corresponding Doppler Signal maps, clearly show consecutive high-speed upflow events in the vortex region. These high-speed upflows with a size of 0.5–1Mm appear in the shape of spiral arms and exhibit two distinctive apparent motions in the plane of sky for a few minutes: (1) a swirling motion with an average speed of 13 km/s and (2) an expanding motion at a rate of 4–6 km/s. Furthermore, the spectral analysis of Mg II k and Mg II subordinate lines in the vortex region indicates an upward velocity of up to ∼8 km/s along with a higher temperature compared to the nearby quiet Sun chromosphere.
Conclusions. The consecutive small-scale vortex events can heat the upper chromosphere by driving continuous high-speed upflows through the lower atmosphere. **June 7, 2014**

Reminiscing my sixty year pursuit of the physics of the Sun and the Galaxy

Parker, Eugene N.

Research in Astronomy and Astrophysics, Volume 14, Issue 1, article id. 1-14 (**2014**)
http://iopscience.iop.org/1674-4527/14/1/001/pdf/1674-4527_14_1_001.pdf
Reminiscing begins with childhood and passes on to student days through graduate school and the first real contact with research. Then early academic positions and stumbling efforts to pursue my ideas. The first significant progress came as a research associate with Prof. W. M. Elsasser at the University of Utah, beginning with an introduction to magnetohydrodynamics and the generation of the geomagnetic field through induction in the liquid metal core of Earth. A move to the University of Chicago to work with Prof. J. A. Simpson, on the implications of cosmic ray variations and interplanetary magnetic fields, led to the theory of coronal expansion and the solar wind and then to exploring the dynamical effects of cosmic rays on the galactic magnetic field. Spontaneous current sheets and intrinsic rapid reconnection in interlaced magnetic field line topologies were the next big project, leading up to retirement. Finally, it is a pleasure to recall my many associates, whose fresh thinking helped stimulate the daily research activities.

A contemporary view of coronal heating **Review**

Parnell,C.E. and De Moortel, I.
2012, Philosophical Transactions of the Royal Society A: Mathematical, Physical and Engineering Sciences, 370, 3217-3240
http://sci-hub.tw/10.1098/rsta.2012.0113
Determining the heating mechanism (or mechanisms) that causes the outer atmosphere of the Sun, and many other stars, to reach temperatures orders of magnitude higher than their surface temperatures has long been a key problem. For decades, the problem has been known as the coronal heating problem, but it is now clear that 'coronal heating' cannot be treated or explained in isolation and that the heating of the whole solar atmosphere must be studied as a highly coupled system. The magnetic field of the star is known to play a key role, but, despite significant advancements in solar telescopes, computing power and much greater understanding of theoretical mechanisms, the question of which mechanism or mechanisms are the dominant supplier of energy to the chromosphere and corona is still open. Following substantial recent progress, we consider the most likely contenders and discuss the key factors that have made, and still make, determining the actual (coronal) heating mechanism (or mechanisms) so difficult.

Propagating Alfvén waves in open structures with random structuring

D J **Pascoe**, I De Moortel, P Pagano, T A Howson
MNRAS, Volume 516, Issue 2, October **2022**, Pages 2181–2188,
https://doi.org/10.1093/mnras/stac2294
https://scholar.google.com/scholar_url?url=https://academic.oup.com/mnras/article-pdf/516/2/2181/45787623/stac2294.pdf
We consider the behaviour of Alfvén waves propagating in a medium with random density perturbations. The imposed density perturbations have a broad-band spectrum and their characteristic spatial scale may be defined according to the peak in the spectrum. The interaction of the boundary driven Alfvén waves with the medium generates reflections most efficiently when their wavelength is comparable to the spatial scale of the density perturbations. For our monotonic driver, this leads to the generation of quasi-periodic oscillations. The periods of oscillation of the propagating Alfvén waves is no longer only associated with the driver. Additional periodicities may be associated with one or more characteristic spatial scales in the density profile, or with beating between other spectral components. Multiple wave reflections cause oscillatory power to be retained at low altitudes, increasing opportunities to contribute to heating at those locations.

Coronal Seismology Using Damping of Propagating Kink Waves

D. J. **Pascoe**1, T. Van Doorsselaere2, and I. De Moortel1,3
2022 ApJ 929 101
https://iopscience.iop.org/article/10.3847/1538-4357/ac5e30/pdf
We consider the use of propagating kink waves, such as those observed by the Coronal Multi-channel Polarimeter, as a diagnostic technique. The transverse structuring of the plasma may be inferred by the frequency-dependent wave damping, which is attributed to resonant absorption. We include the effect of reflection of waves at the loop footpoints, which leads to the asymmetry parameter, describing the ratio of driven wave power at the footpoints becoming weakly constrained. The classical model of resonant absorption based on an exponential damping profile significantly overestimates the damping rate in coronal loops with low density contrast ratios. The use of the exponential profile in an analysis of observations therefore leads to underestimates for the density contrast ratio and associated parameters such as the heating rate following phase mixing.

Coronal Density and Temperature Profiles Calculated by Forward Modeling EUV Emission Observed by SDO/AIA

D. J. **Pascoe**, A. Smyrli, T. Van Doorsselaere

ApJ **2020**
https://arxiv.org/pdf/2003.13497.pdf
We present a model for the intensity of optically thin EUV emission for a plasma atmosphere. We apply our model to the solar corona as observed using the six optically thin EUV channels of the SDO/AIA instrument. The emissivity of the plasma is calculated from the density and temperature using CHIANTI tables and the intensity is then determined by integration along the line of sight. We consider several different profiles for the radial density and temperature profiles, each of which are constrained by the observational data alone with no further physical assumptions. We demonstrate the method first by applying it to a quiet region of the corona, and then use it as the background component of a model including coronal holes, allowing the plasma densities and temperatures inside and outside the hole to be estimated. We compare our results with differential emission measure (DEM) inversions. More accurate estimates for the coronal density and temperature profiles have the potential to help constrain plasma properties such as the magnetic field strength when used in combination with methods such as seismology.

Coronal Density and Temperature Profiles Calculated by Forward Modeling EUV Emission Observed by SDO/AIA

D. J. **Pascoe**1, A. Smyrli2, and T. Van Doorsselaere1
2019 ApJ 884 43
https://doi.org/10.3847/1538-4357/ab3e39
We present a model for the intensity of optically thin extreme ultraviolet (EUV) emission for a plasma atmosphere. We apply our model to the solar corona as observed using the six optically thin EUV channels of the Solar Dynamics Observatory/Atmospheric Imaging Assembly instrument. The emissivity of the plasma is calculated from the density and temperature using CHIANTI tables and the intensity is then determined by integration along the line of sight. We consider several different profiles for the radial density and temperature profiles, each of which are constrained by the observational data alone with no further physical assumptions. We demonstrate the method first by applying it to a quiet region of the corona, and then use it as the background component of a model including coronal holes, allowing the plasma densities and temperatures inside and outside the hole to be estimated. We compare our results with differential emission measure inversions. More accurate estimates for the coronal density and temperature profiles have the potential to help constrain plasma properties such as the magnetic field strength when used in combination with methods such as seismology.

Coronal loop seismology using damping of standing kink oscillations by mode coupling II. additional physical effects and Bayesian analysis

D. J. **Pascoe**, S. Anfinogentov, G. Nistico, C. R. Goddard, and V. M. Nakariakov
A&A 600, A78 **2017**
http://www2.warwick.ac.uk/fac/sci/physics/staff/research/davidpascoe/mc2.pdf
The strong damping of kink oscillations of coronal loops can be explained by mode coupling. The damping envelope depends on the transverse density profile of the loop. Observational measurements of the damping envelope have been used to determine the transverse loop structure which is important for understanding other physical processes such as heating. The general damping envelope describing the mode coupling of kink waves consists of a Gaussian damping regime followed by an exponential damping regime. Recent observational detection of these damping regimes has been employed as a seismological tool. We extend the description of the damping behaviour to account for additional physical effects, namely a time-dependent period of oscillation, the presence of additional longitudinal harmonics, and the decayless regime of standing kink oscillations. We examine four examples of standing kink oscillations observed by the Atmospheric Imaging Assembly (AIA) onboard the Solar Dynamics Observatory (SDO). We use forward modelling of the loop position and investigate the dependence on the model parameters using Bayesian inference and Markov Chain Monte Carlo (MCMC) sampling. Our improvements to the physical model combined with the use of Bayesian inference and MCMC produce improved estimates of model parameters and their uncertainties. Calculation of the Bayes factor also allows us to compare the suitability of different physical models. We also use a new method based on spline interpolation of the zeroes of the oscillation to accurately describe the background trend of the oscillating loop. This powerful and robust method allows for accurate seismology of coronal loops, in particular the transverse density profile, and potentially reveals additional physical effects.

Spatially resolved observation of the fundamental and second harmonic standing kink modes using SDO/AIA

D. J. **Pascoe**, C. R. Goddard, and V. M. Nakariakov
A&A **2016**
http://wrap.warwick.ac.uk/79792/1/WRAP_1273366-px-230616-ms_accepted.pdf
We consider a coronal loop kink oscillation observed by the Atmospheric Imaging Assembly (AIA) of the Solar Dynamics Observatory (SDO) which demonstrates two strong spectral components. The period of the lower

frequency component being approximately twice that of the shorter frequency component suggests the presence of harmonics. We examine the presence of two longitudinal harmonics by investigating the spatial dependence of the loop oscillation. The time-dependent displacement of the loop is measured at 15 locations along the loop axis. For each position the detrended displacement is fitted as the sum of two damped sinusoids, having periods P1 and P2, and a damping time τ. The shorter period component exhibits anti-phase oscillations in the loop legs. We interpret the observation in terms of the first (global or fundamental) and second longitudinal harmonics of the standing kink mode. The strong excitation of the second harmonic appears connected to the preceding coronal mass ejection (CME) which displaced one of the loop legs. The oscillation parameters found are P1 = 5.00 " 0.62 minutes, P2 = 2.20 " 0.23 minutes, P1/2P2 = 1.15 " 0.22, and τ/P = 3.35 " 1.45. **9 February 2011**

Meridional Circulation Dynamics in a Cyclic Convective Dynamo

D. **Passos**, M. Miesch, G. Guerrero, P. Charbonneau
A&A **2017**
https://arxiv.org/pdf/1702.02421.pdf

Surface observations indicate that the speed of the solar meridional circulation in the photosphere varies in anti-phase with the solar cycle. The current explanation for the source of this variation is that inflows into active regions alter the global surface pattern of the meridional circulation. When these localized inflows are integrated over a full hemisphere, they contribute to the slow down of the axisymmetric poleward horizontal component. The behavior of this large scale flow deep inside the convection zone remains largely unknown. Present helioseismic techniques are not sensitive enough to capture the dynamics of this weak large scale flow. Moreover, the large time of integration needed to map the meridional circulation inside the convection zone, also masks some of the possible dynamics on shorter timescales. In this work we examine the dynamics of the meridional circulation that emerges from a 3D MHD global simulation of the solar convection zone. Our aim is to assess and quantify the behavior of meridional circulation deep inside the convection zone, where the cyclic large-scale magnetic field can reach considerable strength. Our analyses indicate that the meridional circulation morphology and amplitude are both highly influenced by the magnetic field, via the impact of magnetic torques on the global angular momentum distribution. A dynamic feature induced by these magnetic torques is the development of a prominent upward flow at mid latitudes in the lower convection zone that occurs near the equatorward edge of the toroidal bands and that peaks during cycle maximum. Globally, the dynamo-generated large-scale magnetic field drives variations in the meridional flow, in stark contrast to the conventional kinematic flux transport view of the magnetic field being advected passively by the flow.

Meridional circulation dynamics from 3D MHD global simulations of solar convection

Dario **Passos**, Paul Charbonneau, Mark Miesch
ApJL 800 L18 **2015**
http://arxiv.org/pdf/1502.01154v1.pdf

The form of the solar meridional circulation is a very important ingredient for mean field flux transport dynamo models. Yet a shroud of mystery still surrounds this large-scale flow, given that its measurement using current helioseismic techniques is challenging. In this work we use results from 3D global simulations of solar convection to infer the dynamical behavior of the established meridional circulation. We make a direct comparison between the meridional circulation that arises in these simulations and the latest observations. Based on our results we argue that there should be an equatorward flow at the base of the convection zone at mid latitudes, below the current maximum depth helioseismic measures can probe (0.75 R). We also provide physical arguments to justify this behaviour. The simulations indicate that the meridional circulation undergoes substantial changes in morphology as the magnetic cycle unfolds. We close by discussing the importance of these dynamical changes for current methods of observation that involve long averaging periods of helioseismic data. Also noteworthy is the fact that these topological changes indicate a rich interaction between magnetic fields and plasma flows, which challenges the ubiquitous kinematic approach used in the vast majority of mean field dynamo simulations.

Characteristics of magnetic solar-like cycles in a 3D MHD simulation of solar convection⋆

D. **Passos**1, 2, 3 and P. Charbonneau
A&A 568, A113 (**2014**)

We analyse the statistical properties of the stable magnetic cycle unfolding in an extended 3D magnetohydrodynamic simulation of solar convection produced with the EULAG-MHD code. The millennium simulation spans over 1650 years, in the course of which forty polarity reversals take place on a regular ~40 yr cadence, remaining well-synchronized across solar hemispheres. In order to characterize this cycle and facilitate its comparison with measures typically used to represent solar activity, we build two proxies for the magnetic field in the simulation mimicking the solar toroidal field and the polar radial field. Several quantities that characterize the cycle are measured (period, amplitudes, etc.) and correlations between them are computed. These are then compared

with their observational analogs. From the typical Gnevyshev-Ohl pattern, to hints of Gleissberg modulation, the simulated cycles share many of the characteristics of their observational analogs even though the simulation lacks poloidal field regeneration through active region decay, a mechanism nowadays often considered an essential component of the solar dynamo. Some significant discrepancies are also identified, most notably the in-phase variation of the simulated poloidal and toroidal large-scale magnetic components, and the low degree of hemispheric coupling at the level of hemispheric cycle amplitudes. Possible causes underlying these discrepancies are discussed.

A solar dynamo model driven by mean-field alpha and Babcock-Leighton sources: fluctuations, grand-minima-maxima, and hemispheric asymmetry in sunspot cycles

D. **Passos**1,2,3, D. Nandy4, 5, S. Hazra4 and I. Lopes
A&A 563, A18 (**2014**)

Context. Extreme solar activity fluctuations and the occurrence of solar grand minima and maxima episodes, such as the Maunder minimum and Medieval maximum are well-established, observed features of the solar cycle. Nevertheless, such extreme activity fluctuations and the dynamics of the solar cycle during Maunder minima-like episodes remain ill understood.
Aims. We explore the origin of such extreme solar activity fluctuations and the role of dual poloidal field sources, namely the Babcock-Leighton mechanism and the mean-field α effect in the dynamics of the solar cycle. We mainly concentrate on entry and recovery from grand minima episodes such as the Maunder minimum and the dynamics of the solar cycle, including the structure of solar butterfly diagrams during grand minima episodes.
Methods. We use a kinematic solar dynamo model with a novel set-up in which stochastic perturbations force two different poloidal sources. We explore different regimes of operation of these poloidal sources with distinct operating thresholds to identify the importance of each. The perturbations are implemented independently in both hemispheres which allows the study of the level of hemispheric coupling and hemispheric asymmetry in the emergence of sunspots.
Results. From the simulations performed we identify a few different ways in which the dynamo can enter a grand minima episode. While fluctuations in any of the α effects can trigger intermittency, in keeping with results from a mathematical time-delay model we find that the mean-field α effect is crucial for the recovery of the solar cycle from a grand minima episode, which a Babcock-Leighton source alone fails to achieve. Our simulations also demonstrate many types of hemispheric asymmetries, including grand minima and failed grand minima where only one hemisphere enters a quiescent state.
Conclusions. We conclude that stochastic fluctuations in two interacting poloidal field sources working with distinct operating thresholds is a viable candidate for triggering episodes of extreme solar activity and that the mean-field α effect capable of working on weak, sub-equipartition fields is critical to the recovery of the solar cycle following an extended solar minimum. Based on our results, we also postulate that solar activity can exhibit significant parity shifts and hemispheric asymmetry, including phases when only one hemisphere is completely quiescent while the other remains active, to, successful grand minima like conditions in both hemispheres.

A Simple Radial Gradient Filter for Batch-Processing of Coronagraph Images

Ritesh **Patel**, Satabdwa Majumdar, Vaibhav Pant, Dipankar Banerjee
Solar Phys. **297**, Article number: 27 **2022**
https://arxiv.org/pdf/2201.13043.pdf
https://link.springer.com/content/pdf/10.1007/s11207-022-01957-y.pdf

Images of the extended solar corona, as observed by white-light coronagraphs as observed by different white-light coronagraphs include the K- and F-corona and suffer from a radial variation in intensity. These images require separation of the two coronal components with some additional image-processing to reduce the intensity gradient and analyse the structures and processes occurring at different heights in the solar corona within the full field of view. To process these bulk coronagraph images with steep radial-intensity gradients, we have developed an algorithm: Simple Radial Gradient Filter (SiRGraF). This algorithm is based on subtracting a minimum background (F-corona) created using long-duration images and then dividing the resultant by a uniform intensity gradient image to enhance the K-corona. We demonstrate the utility of this algorithm to bring out the short time-scale transient structures of the corona. SiRGraF could be used to reveal and analyse such structures. It is not suitable for quantitative estimations based on intensity. We have successfully tested the algorithm on images of the LASCO-C2 onboard the Solar and Heliospheric Observatory (SOHO), and COR-2A onboard the STEREO with good signal to noise ratio (SNR) along with low-SNR images of STEREO/COR-1A and the KCoronagraph. We also compared the performance of SiRGraF with Normalising Radial Gradient Filter (NRGF). We found that when hundreds of images have to be processed, SiRGraF works faster than NRGF, providing similar brightness and contrast in the images and separating the transient features. Moreover, SiRGraF works better on low-SNR images of COR-1A than NRGF, providing better identification of dynamic coronal structures throu,ghout the field of view. We discuss the advantages and limitations of the algorithm. **07 July 2001, 01 August 2010, 03 April 2014, 02 July 2015,**

Characterizing Spectral Channels of Visible Emission Line Coronagraph of Aditya-L1

Ritesh **Patel**, Megha A., Arpit Kumar Shrivastav, Vaibhav Pant, M. Vishnu, Sankarasubramanian K., Dipankar Banerjee
Frontiers in Astronomy and Space Sciences **2021**
https://arxiv.org/pdf/2105.05880.pdf
Aditya-L1 is India's first solar mission with Visible Emission Line Coronagraph (VELC) consisting of three spectral channels taking high-resolution spectroscopic observations of the inner corona up to 1.5 Rsun at 5303 Å, 7892 Å, and 10747 Å. In this work, we present the strategy for the slit width optimization for the VELC using synthetic line profiles by taking into account the instrument characteristics and coronal conditions for log(T) varying from 6 to 6.5. The synthetic profiles are convolved with simulated instrumental scattered light and noise to estimate the signal-to-noise ratio (SNR), which will be crucial to design the future observation plans. We find that the optimum slit width for VELC turns out to be 50 microns providing sufficient SNR for observations in different solar conditions. We also analyzed the effect of plasma temperature on the SNR at different heights in the VELC field of view for the optimized slit width. We also studied the expected effect of the presence of a CME on the spectral channel observations. This analysis will help to plan the science observations of VELC in different solar conditions.

The First Survey of Quiet Sun Features Observed in Hard X-Rays With NuSTAR

Sarah **Paterson**, Iain G. Hannah, Brian W. Grefenstette, Hugh Hudson, Säm Krucker, Lindsay Glesener, Stephen M. White, David M. Smith
Solar Phys. **298**, Article number: 47 (**2023**)
https://arxiv.org/pdf/2210.01544.pdf
https://link.springer.com/content/pdf/10.1007/s11207-023-02135-4.pdf
We present the first survey of quiet Sun features observed in hard X-rays (HXRs), using the the Nuclear Spectroscopic Telescope ARray (NuSTAR), a HXR focusing optics telescope. The recent solar minimum combined with NuSTAR's high sensitivity has presented a unique opportunity to perform the first HXR imaging spectroscopy on a range of features in the quiet Sun. By studying the HXR emission of these features we can detect or constrain the presence of high temperature (>5 MK) or non-thermal sources, to help understand how they relate to larger more energetic solar phenomena, and determine their contribution to heating the solar atmosphere. We report on several features observed in the 28 September 2018 NuSTAR full-disk quiet Sun mosaics, the first of the NuSTAR quiet Sun observing campaigns, which mostly include steady features of X-ray bright points and an emerging flux region which later evolved into an active region, as well as a short-lived jet. We find that the features' HXR spectra are well fitted with isothermal models with temperatures ranging between 2.0-3.2 MK. Combining the NuSTAR data with softer X-ray emission from Hinode/XRT and EUV from SDO/AIA we recover the differential emission measures, confirming little significant emission above 4 MK. The NuSTAR HXR spectra allow us to constrain the possible non-thermal emission that would still be consistent with a null HXR detection. We found that for only one of the features (the jet) was there a potential non-thermal upper limit capable of powering the heating observed. However, even here the non-thermal electron distribution had to be very steep (effectively mono-energetic) with a low energy cut-off between 3-4 keV. The higher temperature or non-thermal sources in the typical quiet Sun features found in this September 2018 data are therefore found to be very weak, if present at all. **28 September 2018**

The cyclic behaviour in the N–S asymmetry of sunspots and solar plages for the period 1910 to 1937 using data from Ebro catalogues

V de **Paula**, J J Curto, R Oliver
Monthly Notices of the Royal Astronomical Society, Volume 512, Issue 4, June **2022**, Pages 5726–5742,
https://doi.org/10.1093/mnras/stac424
The heliophysics catalogues published by the Ebro Observatory during 1910–1937 have been converted into a digital format in order to provide the data for computational processing. This has allowed us to study in detail the North–South (N–S) asymmetry of solar activity in that period, focusing on two different structures located at two different layers of the solar atmosphere: sunspots (Photosphere) and solar plages (Chromosphere). The examination of the absolute and normalized N–S asymmetry indices in terms of their monthly sum of occurrences and areas has made possible to find out a cyclic behaviour in the solar activity, in which the preferred hemisphere changes systematically with a global period of 7.9±0.2 yr7.9±0.2 yr. In order to verify and quantify accurately this periodicity and study its prevalence in time, we employed the Royal Greenwich Observatory-United States Air Force/National Oceanic and Atmospheric Administration sunspot data series during 1874–2016. Then, we examined each absolute asymmetry index time series through different techniques as the power-spectrum analysis, the Complete Ensemble Empirical Mode Decomposition With Adaptive Noise algorithm or the Morlet wavelet transform. The combined results reveal a cyclic behaviour at different time-scales, consisting in two quite stable periodicities of 1.47±0.02 yr1.47±0.02 yr and 3.83±0.06 yr3.83±0.06 yr, which co-exist with another three discontinuous components with more marked time-varying periods with means of 5.4±0.2 yr5.4±0.2 yr, 9.0±0.2 yr9.0±0.2 yr, and 12.7±0.3 yr12.7±0.3 yr. Moreover, during 1910–1937, only two dominant signals with averaged periods of 4.10±0.04 yr4.10±0.04 yr and 7.57±0.03 yr7.57±0.03 yr can be clearly observed. Finally, in both signals, periods are slightly longer for plages in comparison with sunspots.

Sunspot group tilt angle measurements from historical observations

V. Senthamizh **Pavai**, R. Arlt, A. Diercke, C. Denker, J.M. Vaquero
Advances in Space Research **2016**
http://arxiv.org/pdf/1603.02510v1.pdf
Sunspot positions from various historical sets of solar drawings are analysed with respect to the tilt angles of bipolar sunspot groups. Data by Scheiner, Hevelius, Staudacher, Zucconi, Schwabe, and Spoerer deliver a series of average tilt angles spanning a period of 270 years, additional to previously found values for 20th-century data obtained by other authors. We find that the average tilt angles before the Maunder minimum were not significantly different from the modern values. However, the average tilt angles of a period 50 years after the Maunder minimum, namely for cycles 0 and 1, were much lower and near zero. The normal tilt angles before the Maunder minimum suggest that it was not abnormally low tilt angles which drove the solar cycle into a grand minimum.

Sunspot group tilt angle measurements from historical observations

V. Senthamizh **Pavai**, R. Arlt, A. Diercke, C. Denker, J.M. Vaquero
Advances in Space Research **2016**
http://arxiv.org/pdf/1603.02510v1.pdf
Sunspot positions from various historical sets of solar drawings are analysed with respect to the tilt angles of bipolar sunspot groups. Data by Scheiner, Hevelius, Staudacher, Zucconi, Schwabe, and Spoerer deliver a series of average tilt angles spanning a period of 270 years, additional to previously found values for 20th-century data obtained by other authors. We find that the average tilt angles before the Maunder minimum were not significantly different from the modern values. However, the average tilt angles of a period 50 years after the Maunder minimum, namely for cycles 0 and 1, were much lower and near zero. The normal tilt angles before the Maunder minimum suggest that it was not abnormally low tilt angles which drove the solar cycle into a grand minimum.

Sunspot areas and tilt angles for solar cycles 7-10

V. Senthamizh **Pavai**, R. Arlt, M. Dasi-Espuig, N. Krivova, S. Solanki
A&A 584, A73 **2015**
http://arxiv.org/pdf/1508.07849v1.pdf
Extending the knowledge about the properties of solar cycles into the past is essential for understanding the solar dynamo. This paper aims at estimating areas of sunspots observed by Schwabe in 1825-1867 and at calculating the tilt angles of sunspot groups. The sunspot sizes in Schwabe's drawings are not to scale and need to be converted into physical sunspot areas. We employed a statistical approach assuming that the area distribution of sunspots was the same in the 19th century as it was in the 20th century. Umbral areas for about 130,000 sunspots observed by Schwabe were obtained, as well as the tilt angles of sunspot groups assuming them to be bipolar. There is, of course, no polarity information in the observations. The annually averaged sunspot areas correlate reasonably with sunspot number. We derived an average tilt angle by attempting to exclude unipolar groups with a minimum separation of the two alleged polarities and an outlier rejection method which follows the evolution of each group and detects the moment it turns unipolar at its decay. As a result, the tilt angles, although displaying considerable scatter, place the leading polarity on average 5.85+-0.25 closer to the equator, in good agreement with tilt angles obtained from 20th-century data sets. Sources of uncertainties in the tilt angle determination are discussed and need to be addressed whenever different data sets are combined. The sunspot area and tilt angle data are provided online.

Solar off-limb emission of the O i 7772 Å line

H. **Pazira**, D. Kiselman and J. Leenaarts
A&A 604, A49 (**2017**)
Aims. The aim of this paper is to understand the formation of the O i line at 7772 Å in the solar chromosphere.
Methods. We used SST/CRISP observations to observe O i 7772 Å in several places around the solar limb. We compared the observations with synthetic spectra calculated with the RH code in the one-dimension spherical geometry mode. New accurate hydrogen collisional rates were included for the RH calculations.
Results. The observations reveal a dark gap in the lower chromosphere, which is caused by variations in the line opacity as shown by our models. The lower level of the 7772 Å transition is populated by a downward cascade from the continuum. We study the effect of Lyman-β pumping and hydrogen collisions between the triplet and quintet system in O i. Both have a small but non-negligible influence on the line intensity.

Long Term Sunspot Cycle Phase Coherence with Periodic Phase Disruptions

Gerald E. **Pease**, Gregory S. Glenn
2016
https://arxiv.org/pdf/1610.03553v1.pdf
In 1965 Paul D. Jose published his discovery that both the motion of the Sun about the center of mass of the solar system and periods comprised of eight Hale magnetic sunspot cycles with a mean period of ~22.375 years have a matching periodicity of ~179 years. We have investigated the implied link between solar barycentric torque cycles and sunspot cycles and have found that the unsigned solar torque values from 1610 to 2058 are consistently phase and magnitude coherent in ~179 year Jose Cycles. We are able to show that there is also a surprisingly high degree of sunspot cycle phase coherence for times of minima in addition to magnitude correlation of peaks between the nine Schwabe sunspot cycles of 1878 through 1976 (SC12 through SC20) and those of 1699 through 1797 (SC[-5] through SC4). We further identify subsequent subcycles of predominantly non-coherent sunspot cycle phase. In addition we have analyzed the empirical solar motion triggers of both sunspot cycle phase coherence and phase coherence disruption, from which we boldly predict a future return to sunspot cycle phase coherence at times of minima with SC12 to SC20 for SC28 to SC36. The resulting predicted start times, +/- 1 year, 1 sigma, of future sunspot cycles SC28 to SC36 are tabulated.

The Solar Photospheric Continuum Brightness as a Function of Mean Magnetic Flux Density. I. The Role of the Magnetic Structure Size Distribution

C. L. **Peck**1,2,3, M. P. Rast2,4, S. Criscuoli3, and M. Rempel
2019 ApJ 870 89
sci-hub.tw/10.3847/1538-4357/aaf289
Solar irradiance models indicate that irradiance variations are dominated by changes in the disk-coverage of magnetic structures, whose brightness is thought to be determined by their size and average magnetic flux density. Recent results suggest that the brightness of small-scale magnetic structures also depends on the mean magnetic flux of the extended region surrounding them due to reduced convective vigor. Low spatial resolution, however, may limit the ability to distinguish the role of magnetic structure size distributions from that of the mean magnetic flux. Using high-resolution 3D MHD simulations, we investigate the brightness of magnetic structures embedded in regions characterized by different mean magnetic flux. In agreement with previous results, we find reduced brightness with increasing mean magnetic flux when comparing the pixel-by-pixel continuum brightness versus magnetic field strength. Evaluating equivalently sized magnetic structures, however, we find no significant dependence of the magnetic structure brightness on the mean magnetic flux of the region in which they are embedded. Rather, we find that simulations with larger mean magnetic flux generate larger, and therefore darker, magnetic structures whose contributions result in an overall darkening of the region. The differences in magnetic structure size distributions alone can explain the reduced brightness of regions with larger mean magnetic flux. This implies that, for the range of mean magnetic flux of the simulations, convective suppression plays at most a secondary role in determining radiative output of magnetized regions. Quantifying the role of convective transport over a wider range of mean magnetic flux is the subject of the second paper in this series.

Influence of speckle image reconstruction on photometric precision for large solar telescopes

C. L. **Peck**1,2, F. Wöger3 and J. Marino3
A&A 607, A83 (**2017**)
https://www.aanda.org/articles/aa/pdf/2017/11/aa31275-17.pdf
Context. High-resolution observations from large solar telescopes require adaptive optics (AO) systems to overcome image degradation caused by Earth's turbulent atmosphere. AO corrections are, however, only partial. Achieving near-diffraction limited resolution over a large field of view typically requires post-facto image reconstruction techniques to reconstruct the source image.
Aims. This study aims to examine the expected photometric precision of amplitude reconstructed solar images calibrated using models for the on-axis speckle transfer functions and input parameters derived from AO control data. We perform a sensitivity analysis of the photometric precision under variations in the model input parameters for high-resolution solar images consistent with four-meter class solar telescopes.
Methods. Using simulations of both atmospheric turbulence and partial compensation by an AO system, we computed the speckle transfer function under variations in the input parameters. We then convolved high-resolution numerical simulations of the solar photosphere with the simulated atmospheric transfer function, and subsequently deconvolved them with the model speckle transfer function to obtain a reconstructed image. To compute the resulting photometric precision, we compared the intensity of the original image with the reconstructed image.
Results. The analysis demonstrates that high photometric precision can be obtained for speckle amplitude reconstruction using speckle transfer function models combined with AO-derived input parameters. Additionally, it shows that the reconstruction is most sensitive to the input parameter that characterizes the atmospheric distortion, and sub-2% photometric precision is readily obtained when it is well estimated.

Photometric Trends in the Visible Solar Continuum and Their Sensitivity to the Center-to-Limb Profile

Courtney **Peck**, Mark Rast

ApJ **808** 192 **2015**

http://arxiv.org/pdf/1502.06308v1.pdf

Solar irradiance variations over solar rotational time-scales are largely determined by the passage of magnetic structures across the visible solar disk. Variations on solar cycle time scales are thought to be similarly due to changes in surface magnetism with activity. Understanding the contribution of magnetic structures to total solar irradiance and solar spectral irradiance requires assessing their contributions as a function of disk position. Since only relative photometry is possible from the ground, the contrasts of image pixels are measured with respect to a center-to-limb intensity profile. Using nine years of full-disk red and blue continuum images from the Precision Solar Photometric Telescope at the Mauna Loa Solar Observatory (PSPT/MLSO), we examine the sensitivity of continuum contrast measurements to the center-to-limb profile definition. Profiles which differ only by the amount of magnetic activity allowed in the pixels used to determine them yield oppositely signed solar cycle length continuum contrast trends; either agreeing with the result of Preminger et al. (2011) showing negative correlation with solar cycle or disagreeing and showing positive correlation with solar cycle. Changes in the center-to-limb profile shape over the solar cycle are responsible for the contradictory contrast results, and we demonstrate that the lowest contrast structures, internetwork and network, are most sensitive to these. Thus the strengths of the full-disk, internetwork, and network photometric trends depend critically on the magnetic flux density used in the quiet-sun definition. We conclude that the contributions of low contrast magnetic structures to variations in the solar continuum output, particularly to long-term variations, are difficult, if not impossible, to determine without the use of radiometric imaging.

A Critical Comment on "Can Solar Cycle 25 Be a New Dalton Minimum?"

J. C. **Peguero** & V. M. S. Carrasco

Solar Physics volume 298, Article number: 48 (**2023**)

https://link.springer.com/content/pdf/10.1007/s11207-023-02140-7.pdf

The sunspot number is the most used solar-activity index to study the behavior of solar activity. In this work, we reproduce the methodology of Coban, Raheem, and Cavus (Solar Phys. 296, 156, 2021) using a long short-term memory model with daily data from the American Association of Variable Star Observers (AAVSO) to predict the maximum amplitude of Solar Cycle 25. We have also used that same methodology with daily values from the official sunspot number (Version 2) of the Sunspot Index and Long-term Solar Observations (SILSO). The objective of this work is to analyze if the predictions obtained from that methodology agree with the observed values available for the current Solar Cycle 25. Thus, we conclude that the predictions are not reproducing well the behavior of the Solar Cycle 25 in its rising phase. Moreover, contrary to the previous prediction, no minor peak occurred in February 2022, and we also conclude that it seems unlikely that the combination of the solar-activity level of Solar Cycle 24 and 25 constitutes a new Dalton-type Minimum, such as Coban, Raheem, and Cavus (2021) proposed.

Origin of the solar wind: A novel approach to link in situ and remote observations - A study for SPICE and SWA on the upcoming Solar Orbiter mission A24

Thies **Peleikis**, Martin Kruse, Lars Berger and Robert Wimmer-Schweingruber

A&A 602, A24 (**2017**)

https://www.aanda.org/articles/aa/pdf/2017/06/aa29727-16.pdf

Context. During the last decades great progress has been achieved in understanding the properties and the origin of the solar wind. While the sources for the fast solar wind are well understood, the sources for the slow solar wind remain elusive.

Aims. The upcoming Solar Orbiter mission aims to improve our understanding of the sources of the solar wind by establishing the link between in situ and remote sensing observations. In this paper we aim to address the problem of linking in situ and remote observations in general and in particular with respect to ESA's Solar Orbiter mission.

Methods. We have used a combination of ballistic back mapping and a potential field source surface model to identify the solar wind source regions at the Sun. As an input we use in situ measurements from the Advanced Composition Explorer and magnetograms obtained from the Michelson Doppler Interferometer on board the Solar Heliospheric Observatory. For the first time we have accounted for the travel time of the solar wind above and also below the source surface.

Results. We find that a prediction scheme for the pointing of any remote sensing instrumentation is required to capture a source region not only in space but also in time. An ideal remote-sensing instrument would cover up to ≈50% of all source regions at the right time. In the case of the Spectral Imaging of the Coronal Environment instrument on Solar Orbiter we find that ≈25% of all source regions would be covered.

Conclusions. To successfully establish a link between in situ and remote observations the effects of the travel time of the solar wind as well as the magnetic displacement inside the corona cannot be neglected. The predictions needed cannot be based solely on a model, nor on observations alone, only the combination of both is sufficient.

Solar chromosphere heating and generation of plasma outflows by impulsively generated two fluid Alfven waves

M. **Pelekhata**, K. Murawski, S. Poedts
A&A 652, A114 **2021**
https://arxiv.org/pdf/2107.12032.pdf
https://doi.org/10.1051/0004-6361/202141262
https://www.aanda.org/articles/aa/pdf/2021/08/aa41262-21.pdf
Aims. We attempt to detect variations in ion temperature and vertical plasma flows, which are driven by impulsively excited two-fluid Alfvén waves. We aim to investigate the possible contribution of these waves to solar chromosphere heating and plasma outflows. Methods. We performed numerical simulations of the generation and evolution of Alfvén waves with the use of the JOANNA code, which solves the two-fluid equations for ions+electrons and neutrals, coupled by collision terms.
Results. We confirm that the damping of impulsively generated small-amplitude Alfvén waves slightly affects the temperature of the chromosphere and generates slow plasma flows. In contrast, the Alfvén waves generated by large-amplitude pulses increase the chromospheric plasma temperature more significantly and result in faster plasma outflows. The maximum heating occurs when the pulse is launched from the central photosphere, and the magnitude of the related plasma flows grows with the amplitude of the pulse.
Conclusions. Large-amplitude two-fluid Alfvén waves can contribute significantly to the heating of the solar chromosphere and to the generation of plasma outflows.

Interchange reconnection dynamics in a solar coronal pseudo-streamer⋆

T. **Pellegrin-Frachon**1, S. Masson1,2, É. Pariat1, P. F. Wyper3 and C. R. DeVore4
A&A 675, A55 (**2023**)
https://www.aanda.org/articles/aa/pdf/2023/07/aa45611-22.pdf
Context. The generation of the slow solar wind remains an open problem in heliophysics. One of the current theories among those aimed at explaining the injection of coronal plasma in the interplanetary medium is based on interchange reconnection. It assumes that the exchange of magnetic connectivity between closed and open fields allows the injection of coronal plasma in the interplanetary medium to travel along the newly reconnected open field. However, the exact mechanism underlying this effect is still poorly understood.
Aims. Our objective is to study this scenario in a particular magnetic structure of the solar corona: a pseudo-streamer. This topological structure lies at the interface between open and closed magnetic field and is thought to be involved in the generation of the slow solar wind.
Methods. We performed innovative 3D magnetohydrodynamic (MHD) simulations of the solar corona with a pseudo-streamer, using the Adaptively Refined MHD Solver (ARMS). By perturbing the quasi-steady ambient state with a simple photospheric, large-scale velocity flow, we were able to generate a complex dynamics of the open-and-closed boundary of the pseudo-streamer. We studied the evolution of the connectivity of numerous field lines to understand its precise dynamics.
Results. We witnessed different scenarios of opening of the magnetic field initially closed under the pseudo-streamer: one-step interchange reconnection dynamics, along with more complex scenarios, including a coupling between pseudo-streamer and helmet streamer, as well as back-and-forth reconnections between open and closed connectivity domains. Finally, our analysis revealed large-scale motions of a newly opened magnetic field high in the corona that may be explained by slipping reconnection.
Conclusions. By introducing a new analysis method for the magnetic connectivity evolution based on distinct closed-field domains, this study provides an understanding of the precise dynamics underway during the opening of a closed field, which enables the injection of closed-field, coronal plasma in the interplanetary medium. Further studies shall provide synthetic observations for these diverse outgoing flows, which could be measured by Parker Solar Probe and Solar Orbiter.

The role of asymmetries in coronal rain formation during thermal non-equilibrium cycles

Gabriel **Pelouze**, Frédéric Auchère, Karine Bocchialini, Clara Froment, Zoran Mikić, Elie Soubrié, Alfred Voyeux
A&A 658, A71 **2022**
https://arxiv.org/pdf/2110.09975.pdf
https://doi.org/10.1051/0004-6361/202140477
https://www.aanda.org/articles/aa/pdf/2022/02/aa40477-21.pdf
Context: Thermal non-equilibrium (TNE) produces several observables that can be used to constrain the spatial and temporal distribution of solar coronal heating. Its manifestations include prominence formation, coronal rain, and long-period intensity pulsations in coronal loops. The recent observation of abundant periodic coronal rain

associated with intensity pulsations by Auchère et al. allows to unify these two phenomena as the result of TNE condensation and evaporation cycles. On the other hand, many intensity pulsation events observed by Froment et al. show little to no coronal rain formation. Aims: Our goal is to understand why some TNE cycles produce such abundant coronal rain, while others produce little to no rain. Methods: We reconstruct the geometry of the event reported by Auchère et al., using images from STEREO/SECCHI/EUVI and magnetograms from SDO/HMI. We then perform 1D hydrodynamic simulations of this event, for different heating parameters and variations of the loop geometry (9000 simulations in total). We compare the resulting behaviour to simulations of TNE cycles by Froment et al. that do not produce coronal rain. Results: Our simulations show that both prominences and TNE cycles (with and without coronal rain) can form within the same magnetic structure. We show that the formation of coronal rain during TNE cycles depends on the asymmetry of the loop and of the heating. Asymmetric loops are overall less likely to produce coronal rain, regardless of the heating. In symmetric loops, coronal rain forms when the heating is also symmetric. In asymmetric loops, rain forms only when the heating compensates the asymmetry.

Comprehensive Determination of the Hinode/EIS Roll Angle

Gabriel **Pelouze**, Frédéric Auchère, Karine Bocchialini, Louise Harra, Deborah Baker, Harry P. Warren, David H. Brooks, John T. Mariska
Solar Phys. 294:59 **2019**
https://arxiv.org/pdf/1903.11923.pdf
We present a new coalignment method for the EUV Imaging Spectrometer (EIS) on board the Hinode spacecraft. In addition to the pointing offset and spacecraft jitter, this method determines the roll angle of the instrument, which has never been systematically measured, and is therefore usually not corrected. The optimal pointing for EIS is computed by maximizing the cross-correlations of the Fe XII 195.119 Å line with images from the 193 Å band of the Atmospheric Imaging Assembly (AIA) on board the Solar Dynamics Observatory (SDO). By coaligning 3336 rasters with high signal-to-noise ratio, we estimate the rotation angle between EIS and AIA and explore the distribution of its values. We report an average value of $(-0.387 \pm 0.007)°$. We also provide a software implementation of this method that can be used to coalign any EIS raster.

Method of frequency dependent correlations: investigating the variability of total solar irradiance

Jaan **Pelt**, Maarit Käpylä, Nigul Olspert
A&A 600, A9 **2017**
https://arxiv.org/pdf/1612.07494v1.pdf
This paper contributes to the field of modeling and hindcasting of the total solar irradiance (TSI) based on different proxy data that extend further back in time than the TSI that is measured from satellites.
We introduce a simple method to analyze persistent frequency-dependent correlations (FDCs) between the time series and use these correlations to hindcast missing historical TSI values. We try to avoid arbitrary choices of the free parameters of the model by computing them using an optimization procedure. The method can be regarded as a general tool for pairs of data sets, where correlating and anticorrelating components can be separated into non-overlapping regions in frequency domain.
Our method is based on low-pass and band-pass filtering with a Gaussian transfer function combined with de-trending and computation of envelope curves.
We find a major controversy between the historical proxies and satellite-measured targets: a large variance is detected between the low-frequency parts of targets, while the low-frequency proxy behavior of different measurement series is consistent with high precision. We also show that even though the rotational signal is not strongly manifested in the targets and proxies, it becomes clearly visible in FDC spectrum.
The application of the new method to solar data allows us to obtain important insights into the different TSI modeling procedures and their capabilities for hindcasting based on the directly observed time intervals.

Spectropolarimetry of Atomic and Molecular Lines near 4135 nm

Matthew James **Penn**, Han Uitenbroek, Alan Clark, Roy Coulter, Phil Goode, Wenda Cao
Solar Phys. **2016**
New spatially scanned spectropolarimetry sunspot observations are made of photospheric atomic and molecular absorption lines near 4135 nm. The relative splittings among several atomic lines are measured and shown to agree with values calculated with configuration interaction and intermediate coupling. Large splitting is seen in a line identified with Fe i at 4137 nm, showing multiple Stokes V components and an unusual linear polarization. This line will be a sensitive probe of quiet-Sun magnetic fields, with a magnetic sensitivity of 2.5 times higher than that of the well-known 1565 nm Fe i line.

Infrared Solar Physics **A Review**

M **Penn**

E-print, May **2014**; Living Reviews in Solar Physics

http://www.noao.edu/noao/staff/mpenn/article_revised.pdf

http://www.livingreviews.org/lrsp-2014-2

The infrared solar spectrum contains a wealth of physical data about our Sun, and is explored using modern detectors and technology with new ground-based solar telescopes. The scientific motivation behind exploring these wavelengths is presented, along with a brief look at the rich history of observations here. Several avenues of solar physics research exploiting and benefiting from observations at infrared wavelengths from roughly 1000nm to 12400nm are discussed, and the instrument and detector technology driving this research is briefly summarized. Finally, goals for future work at infrared wavelengths are presented in conjunction with ground and space-based observations.

Conversion and Smoothing of MHD Shocks in Atmospheres with Open and Closed Magnetic Field and Neutral Points

Jamon D. **Pennicott** & Paul S. Cally

Solar Physics volume 296, Article number: 97 (**2021**)

https://link.springer.com/content/pdf/10.1007/s11207-021-01829-x.pdf

Planar acoustically dominated magnetohydrodynamic waves are initiated at the high-β base of a simulated 2D isothermal stratified atmosphere with potential magnetic field exhibiting both open and closed field regions as well as neutral points. They shock on their way upward toward the Alfvén–acoustic equipartition surface a=c, where aa and cc are the Alfvén and sound speeds, respectively. Expanding on recent 1.5D findings that such shocks mode-convert to fast shocks and slow smoothed waves on passing through a=c, we explore the implications for these more complex magnetic geometries. It is found that the 1.5D behaviour carries over to the more complex case, with the fast shocks strongly attracted to neutral points, which are disrupted producing extensive fine structure. It is also observed that shocks moving in the opposite direction, from a>ca>c to a<ca<c, split into fast and slow components too, and that again it is the slow component that is smoothed.

Reconstruction of the Total Solar Irradiance during the last Millenium

Valentina **Penza**, Luca Bertello, Matteo Cantoresi, Serena Criscuoli, Lorenza Lucaferri, Raffaele Reda, Simone Ulzega, Francesco Berrilli

ApJ **976** 11 **2024**

https://arxiv.org/pdf/2409.12648

https://iopscience.iop.org/article/10.3847/1538-4357/ad7c49/pdf

Solar irradiance variations across various timescales, from minutes to centuries, represents a potential natural driver of past regional and global climate cold phases. To accurately assess the Sun's effect on climate, particularly during periods of exceptionally low solar activity known as grand minima, an accurate reconstruction of solar forcing is essential. While direct measurements of Total Solar Irradiance (TSI) only began in the late 1970s with the advent of space radiometers, indirect evidence from various historical proxies suggests that the Sun's magnetic activity has undergone possible significant fluctuations over much longer timescales. Employing diverse and independent methods for TSI reconstruction is essential to gaining a comprehensive understanding of this issue. This study employs a semi-empirical model to reconstruct TSI over the past millennium. Our approach uses an estimated open solar magnetic field (Fo), derived from cosmogenic isotope data, as a proxy for solar activity. We reconstruct the cyclic variations of TSI, due to the solar surface magnetic features, by correlating Fo with the parameter of active region functional form. Instead, we obtain the long-term TSI trend by applying the Empirical Mode Decomposition (EMD) algorithm to the reconstructed Fo to filter out the 11-year and 22-year solar variability. We prepare a reconstructed TSI record, spanning 971 to 2020 CE. The estimated departure from modern TSI values occurred during the Spörer Minimum (around 1400 CE), with a decrease of approximately 2.3 Wm−2. A slightly smaller decline of 2.2 Wm−2 is reported during the Maunder Minimum, between 1645 and 1715 CE.

Total Solar Irradiance during the Last Five Centuries

V. **Penza**, F. Berrilli, L. Bertello, M. Cantoresi, S. Criscuoli, P. Giobbi

ApJ **937** 84 **2022**

https://arxiv.org/pdf/2209.10115.pdf

https://iopscience.iop.org/article/10.3847/1538-4357/ac8a4b/pdf

The total solar irradiance (TSI) varies on timescales of minute to centuries. On short timescales it varies due to the superposition of intensity fluctuations produced by turbulent convection and acoustic oscillations. On longer scale times, it changes due to photospheric magnetic activity, mainly because of the facular brightenings and dimmings caused by sunspots. While modern TSI variations have been monitored from space since 1970s, TSI variations over much longer periods can only be estimated using either historical observations of magnetic features, possibly

supported by flux transport models, or from the measurements of the cosmogenic isotope (e.g., ^{14}C or ^{10}Be) concentrations in tree rings and ice cores. The reconstruction of the TSI in the last few centuries, particularly in the 17th/18th centuries during the Maunder minimum, is of primary importance for studying climatic effects. To separate the temporal components of the irradiance variations, specifically the magnetic cycle from secular variability, we decomposed the signals associated with historical observations of magnetic features and the solar modulation potential Φ by applying an Empirical Mode Decomposition algorithm. Thus, the reconstruction is empirical and does not require any feature contrast or field transport model. The assessed difference between the mean value during the Maunder minimum and the present value is ≃2.5Wm−2. Moreover it shows, in the first half of the last century, a growth of ≃1.5Wm−2 which stops around the middle of the century to remain constant for the next 50 years, apart from the modulation due to the solar cycle.

Prediction of sunspot and plage coverage for Solar Cycle 25

Valentina **Penza**, Francesco Berrilli, Luca Bertello, Matteo Cantoresi, Serena Criscuoli
ApJL **2021**
https://arxiv.org/pdf/2111.02928.pdf
Solar variability occurs over a broad range of spatial and temporal scales, from the Sun's brightening over its lifetime to the fluctuations commonly associated with magnetic activity over minutes to years. The latter activity includes most prominently the 11-year sunspot solar cycle and its modulations. Space weather events, in the form of solar flares, solar energetic particles, coronal mass ejections, and geomagnetic storms, have long been known to approximately follow the solar cycle occurring more frequently at solar maximum than solar minimum. These events can significantly impact our advanced technologies and critical infrastructures, making the prediction for the strength of future solar cycles particularly important.
Several methods have been proposed to predict the strength of the next solar cycle, cycle 25, with results that are generally not always consistent. Most of these methods are based on the international sunspot number time series, or other indicators of solar activity. We present here a new approach that uses more than 100 years of measured fractional areas of the visible solar disk covered by sunspots and plages and an empirical relationship for each of these two indices of solar activity in even-odd cycles. We anticipate that cycle 25 will peak in 2024 and will last for about 12 years, slightly longer than cycle 24. We also found that, in terms of sunspot and plage areas coverage, the amplitude of cycle 25 will be substantially similar or slightly higher than cycle 24.

The dynamic chromosphere: pushing the boundaries of observations and models **Review**

Tiago M. D. **Pereira**
Advances in Space Research, special issue "Solar Physics Advances from the Interior to the Heliosphere"
Volume 63, Issue 4, 15 February **2019**, Pages 1434-1442
https://arxiv.org/pdf/1809.04077.pdf
http://sci-hub.tw/https://www.aanda.org/articles/aa/abs/2018/09/aa32792-18/aa32792-18.html
The interface between the bright solar surface and the million-degree corona continues to hold the key to many unsolved problems in solar physics. Advances in instrumentation now allow us to observe the dynamic structures of the solar chromosphere down to less than 0.1" with cadences of just a few seconds and in multiple polarisation states. Such observational progress has been matched by the ever-increasing sophistication of numerical models, which have become necessary to interpret the complex observations. With an emphasis on the quiet Sun, I will review recent progress in the observation and modelling of the chromosphere. Models have come a long way from 1D static atmospheres, but their predictions still fail to reproduce several key observed features. Nevertheless, they have given us invaluable insight into the physical processes that energise the atmosphere. With more physics being added to models, the gap between predictions and observations is narrowing. With the next generation of solar observatories just around the corner, the big question is: will they close the gap?

Chromospheric counterparts of solar transition region unresolved fine structure loops

Tiago M. D. **Pereira**, Luc Rouppe van der Voort, Viggo H. Hansteen, Bart De Pontieu
A&A 612, L6 **2018**
https://arxiv.org/pdf/1803.04415.pdf
Low-lying loops have been discovered at the solar limb in transition region temperatures by the Interface Region Imaging Spectrograph (IRIS). They do not appear to reach coronal temperatures, and it has been suggested that they are the long-predicted unresolved fine structures (UFS). These loops are dynamic and believed to be visible during both heating and cooling phases. Making use of coordinated observations between IRIS and the Swedish 1-m Solar Telescope, we study how these loops impact the solar chromosphere. We show for the first time that there is indeed a chromospheric signal of these loops, seen mostly in the form of strong Doppler shifts and a conspicuous lack of chromospheric heating. In addition, we find that several instances have a inverse Y-shaped jet just above the loop, suggesting that magnetic reconnection is driving these events. Our observations add several puzzling details to the

current knowledge of these newly discovered structures; this new information must be considered in theoretical models. **17 June 2014**

The Appearance of Spicules in High Resolution Observations of Ca II H and H-alpha

Tiago M. D. **Pereira**, Luc Rouppe van der Voort, Mats Carlsson
ApJ 824 65 **2016**
http://arxiv.org/pdf/1604.03116v1.pdf
https://www.aanda.org/articles/aa/pdf/2018/03/aa32762-18.pdf
Solar spicules are chromospheric fibrils that appear everywhere on the Sun, yet their origin is not understood. Using high resolution observations of spicules obtained with the Swedish 1-m Solar Telescope we aim to understand how spicules appear in filtergrams and Dopplergrams, how they compare in Ca II H and H-alpha, and what can make them appear and disappear. We find spicules display a rich and detailed spatial structure, and show a distribution of transverse velocities that when aligned with the line of sight can make them appear at different H-alpha wing positions. They become more abundant at positions closer to the line core, reflecting a distribution of Doppler shifts and widths. In H-alpha width maps they stand out as bright features both on disk and off-limb, reflecting their large Doppler motions and possibly higher temperatures than in the typical H-alpha formation region. Spicule lifetimes measured from narrowband images at only a few positions will be an underestimate because Doppler shifts can make them disappear prematurely from such images; for such cases width maps are a more robust tool. In H-alpha and Ca II H filtergrams, off-limb spicules have essentially the same properties, appearance, and evolution. We find that the sudden appearance of spicules can be explained by Doppler shifts from their transverse motions, and does not require other convoluted explanations.

The Formation of IRIS Diagnostics. IV. The Mg II Triplet Lines as a New Diagnostic for Lower Chromospheric Heating

Tiago M. D. **Pereira**1, Mats Carlsson1, Bart De Pontieu1,2, and Viggo Hansteen
2015 ApJ 806 14
A triplet of subordinate lines of Mg ii exists in the region around the h&k lines. In solar spectra these lines are seen mostly in absorption, but in some cases can become emission lines. The aim of this work is to study the formation of this triplet, and investigate any diagnostic value they can bring. Using 3D radiative magnetohydrodynamic simulations of quiet Sun and flaring flux emergence, we synthesize spectra and investigate how spectral features respond to the underlying atmosphere. We find that emission in the lines is rare and is typically caused by a steep temperature increase in the lower chromosphere (above 1500 K, with electron densities above 1017 m−3). In both simulations the lines are sensitive to temperature increases taking place at column masses $\gtrsim 5 \cdot 10^{-4}$ g cm−2. Additional information can also be inferred from the peak-to-wing ratio and shape of the line profiles. Using observations from NASA's Interface Region Imaging Spectrograph we find both absorption and emission line profiles with similar shapes to the synthetic spectra, which suggests that these lines represent a useful diagnostic that complements the Mg iih&k lines.

An Interface Region Imaging Spectrograph first view on Solar Spicules

T. M. D. **Pereira**, B. De Pontieu, M. Carlsson, V. Hansteen, T. D. Tarbell, J. Lemen, A. Title, P. Boerner, N. Hurlburt, J. P. Wülser, J. Martínez-Sykora, L. Kleint, L. Golub, S. McKillop, K. K. Reeves, S. Saar, P. Testa, H. Tian, S. Jaeggli, C. Kankelborg
ApJL, 792 L15 **2014**
http://arxiv.org/pdf/1407.6360v1.pdf
Solar spicules have eluded modelers and observers for decades. Since the discovery of the more energetic type II, spicules have become a heated topic but their contribution to the energy balance of the low solar atmosphere remains unknown. Here we give a first glimpse of what quiet Sun spicules look like when observed with NASA's recently launched Interface Region Imaging Spectrograph (IRIS). Using IRIS spectra and filtergrams that sample the chromosphere and transition region we compare the properties and evolution of spicules as observed in a coordinated campaign with Hinode and the Atmospheric Imaging Assembly. Our IRIS observations allow us to follow the thermal evolution of type II spicules and finally confirm that the fading of Ca II H spicules appears to be caused by rapid heating to higher temperatures. The IRIS spicules do not fade but continue evolving, reaching higher and falling back down after 500-800 s. Ca II H type II spicules are thus the initial stages of violent and hotter events that mostly remain invisible in Ca II H filtergrams. These events have very different properties from type I spicules, which show lower velocities and no fading from chromospheric passbands. The IRIS spectra of spicules show the same signature as their proposed disk counterparts, reinforcing earlier work. Spectroheliograms from spectral rasters also confirm that quiet Sun spicules originate in bushes from the magnetic network. Our results

suggest that type II spicules are indeed the site of vigorous heating (to at least transition region temperatures) along extensive parts of the upward moving spicular plasma. **9 October 2013 , 2014 February 21**

Temporal Defocusing as a Depth Diagnostic of Submerged Sources of Transient Acoustic Emission from Solar Flares

Savannah **Perez-Piel**, Juan Camilo Buitrago-Casas, Juan Carlos Martínez Oliveros & Charles Lindsey
Solar Physics volume 298, Article number: 77 (**2023**)
https://link.springer.com/content/pdf/10.1007/s11207-023-02163-0.pdf
Helioseismic holography applied to HMI observations of a sunquake associated with the SOL**20140207**T10:29M1.9 flare hosted by NOAA AR11968 shows the signature of a compact submerged acoustic source. In the 9 – 11-mHz bandpass, this source appears to be at a depth of 2 Mm. This is nearly double the depth of the highly impulsive acoustic transient, referred to as an ultra-impulsive transient source recently found in the SOL**20110730**T02:09M9.3 flare, emerging from NOAA AR11261 in 2011. The latter source was compound, having multiple surface components overlaying a single submerged component. Many of the sources observed have evidence of being constituted of multiple components, some of which are staggered in depth. The helioseismic source of the flare of 2014-02-07 is distinguished by the apparent absence of a strong shallow compact overlying source component matching the character of those apparent in the flare of **2011-07-30**. This suggests that the volume several Mm beneath active-region photospheres could possibly harbor many more ultra-impulsive transient acoustic sources than the rarities that have so far appeared in familiar surface-focal-plane diagnostics. Based on weak surface signatures that appear in place of the strong ones, we find a temporal delay between weak surface and strong submerged sources similar to that found between surface-and-submerged sources in the flare of 2011-07-30. While it remains highly speculative based on the limited statistics we have at this point, this temporal delay supports a model in which the submerged source is perturbed by some presently invisible triggering disturbance that propagates downward from the flaring outer atmosphere at ~ 5 km s^{-1}. This is slower than the sound speed anywhere in the 0 – 2-Mm depth range. However, this potentially could be an Alfvèn speed if submerged magnetic flux densities along which the trigger propagates are as high as possible. The standard local-helioseismic diagnostics we have used in the past have been heavily reinforced in this study by a powerful new control resource found in the recognition of temporal defocusing of compact transient sources. In particular, its tight relationship to the standard spatial defocusing upon which helioseismic holography has capitalized from its early advent.

Unbiased CLEAN for STIX in Solar Orbiter

Emma **Perracchione1**, Fabiana Camattari1,2, Anna Volpara3, Paolo Massa4, Anna Maria Massone3, and Michele Piana3,5
2023 ApJS 268 68
https://iopscience.iop.org/article/10.3847/1538-4365/acf669/pdf
CLEAN is an iterative deconvolution method for radio and hard-X-ray solar imaging. In a specific step of its pipeline, CLEAN requires the convolution between an idealized version of the instrumental point-spread function (PSF), and a map collecting point sources located at positions from where most of the flaring radiation is emitted. This step has highly heuristic motivations and the shape of the idealized PSF, which depends on the user's choice, impacts the shape of the reconstruction. This study introduces a user-independent release of CLEAN for image reconstruction from observations recorded by the Spectrometer/Telescope for Imaging X-rays (STIX) on board Solar Orbiter. Specifically, we show here that this unbiased release of CLEAN outperforms the standard version of the algorithm, with reconstructions in line with the ones offered by other imaging methods developed in the STIX framework.

Visibility Interpolation in Solar Hard X-Ray Imaging: Application to RHESSI and STIX

Emma **Perracchione**1, Paolo Massa2, Anna Maria Massone1, and Michele Piana1
2021 ApJ 919 133
https://doi.org/10.3847/1538-4357/ac158d
Space telescopes for solar hard X-ray imaging provide observations made of sampled Fourier components of the incoming photon flux. The aim of this study is to design an image reconstruction method relying on enhanced visibility interpolation in the Fourier domain. The interpolation-based method is applied to synthetic visibilities generated by means of the simulation software implemented within the framework of the Spectrometer/Telescope for Imaging X-rays (STIX) mission on board Solar Orbiter. An application to experimental visibilities observed by the Reuven Ramaty High Energy Solar Spectroscopic Imager (RHESSI) is also considered. In order to interpolate these visibility data, we have utilized an approach based on Variably Scaled Kernels (VSKs), which are able to realize feature augmentation by exploiting prior information on the flaring source and which are used here, for the first time, in the context of inverse problems. When compared to an interpolation-based reconstruction algorithm previously introduced for RHESSI, VSKs offer significantly better performance, particularly in the case of STIX imaging, which is characterized by a notably sparse sampling of the Fourier domain. In the case of RHESSI data, this novel approach is particularly reliable when the flaring sources are either characterized by narrow, ribbon-like

shapes or high-resolution detectors are utilized for observations. The use of VSKs for interpolating hard X-ray visibilities allows remarkable image reconstruction accuracy when the information on the flaring source is encoded by a small set of scattered Fourier data and when the visibility surface is affected by significant oscillations in the frequency domain.

The dynamo-wind feedback loop: Assessing their non-linear interplay

Barbara **Perri**, Allan Sacha Brun, Antoine Strugarek, Victor Réville
IAUS 354 **2019**
https://arxiv.org/pdf/1912.01271.pdf
Though generated deep inside the convection zone, the solar magnetic field has a direct impact on the Earth space environment via the Parker spiral. It strongly modulates the solar wind in the whole heliosphere, especially its latitudinal and longitudinal speed distribution over the years. However the wind also influences the topology of the coronal magnetic field by opening the magnetic field lines in the coronal holes, which can affect the inner magnetic field of the star by altering the dynamo boundary conditions. This coupling is especially difficult to model because it covers a large variety of spatio-temporal scales. Quasi-static studies have begun to help us unveil how the dynamo-generated magnetic field shapes the wind, but the full interplay between the solar dynamo and the solar wind still eludes our understanding.
We use the compressible magnetohydrodynamical (MHD) code PLUTO to compute simultaneously in 2.5D the generation and evolution of magnetic field inside the star via an alpha-Omega dynamo process and the corresponding evolution of a polytropic coronal wind over several activity cycles for a young Sun. A multi-layered boundary condition at the surface of the star connects the inner and outer stellar layers, allowing both to adapt dynamically. Our continuously coupled dynamo-wind model allows us to characterize how the solar wind conditions change as a function of the cycle phase, and also to quantify the evolution of integrated quantities such as the Alfvén radius. We further assess the impact of the solar wind on the dynamo itself by comparing our results with and without wind feedback.

Simulations of solar wind variations during an 11-year cycle and the influence of north-south asymmetry

Barbara **Perri**, Allan Sacha Brun, Victor Réville, Antoine Strugarek
Journal of Plasma Physics, **2018**, vol. 84, issue 5
https://arxiv.org/pdf/1809.03205.pdf
We want to study the connections between the magnetic field generated inside the Sun and the solar wind impacting Earth, especially the influence of north-south asymmetry on the magnetic and velocity fields. We study a solar-like 11-year cycle in a quasi-static way: an asymmetric dynamo field is generated through a 2.5-dimensional (2.5-D) flux-transport model with the Babcock-Leighton mechanism, and then is used as bottom boundary condition for compressible 2.5-D simulations of the solar wind. We recover solar values for the mass loss rate, the spin-down time scale and the Alfv\'en radius, and are able to reproduce the observed delay in latitudinal variations of the wind and the general wind structure observed for the Sun. We show that the phase lag between the energy of the dipole component and the total surface magnetic energy has a strong influence on the amplitude of the variations of global quantities. We show in particular that the magnetic torque variations can be linked to topological variations during a magnetic cycle, while variations in the mass loss rate appear to be driven by variations of the magnetic energy.

An Interesting Correlation Between the Peak Slope and Peak Value of a Sunspot Cycle.

Pesnell, W.D.
Sol Phys 299, 14 (**2024**).
https://doi.org/10.1007/s11207-024-02256-4
https://link.springer.com/content/pdf/10.1007/s11207-024-02256-4.pdf
The maximum slope of the sunspot number during the rising phase of a sunspot cycle has an excellent correlation with the maximum value of the sunspot number during that cycle. This is demonstrated using a Savitzky–Golay filter to both smooth and calculate the derivative of the sunspot-number data. Version 2 of the International Sunspot Number (S) is used to represent solar activity. The maximum of the slope during the rising phase of each cycle was correlated against the peaks of solar activity. Using three different correlation fits, the average predicted amplitude for Solar Cycle 25 is 130.7 ± 0.5, among the best correlations in solar predictions. A possible explanation for this correlation is given by the similar behavior of a shape function representing the time variation of the sunspot number. This universal function also provides the timing of the solar maximum by the time from the slope maximum to the peak in the function as late 2023 or early 2024. A Hilbert transform gives similar results, which are caused by the dominance of the 11-yr sunspot-cycle period in a Fourier fit of the sunspot number.

Lessons learned from predictions of Solar Cycle 24

W. Dean **Pesnell***

J. Space Weather Space Clim. **2020**, 10, 60
https://doi.org/10.1051/swsc/2020060
https://www.swsc-journal.org/articles/swsc/pdf/2020/01/swsc200057.pdf
Solar Cycle 24 has almost faded and the activity of Solar Cycle 25 is appearing. We have learned much about predicting solar activity in Solar Cycle 24, especially with the data provided by SDO and STEREO. Many advances have come in the short-term predictions of solar flares and coronal mass ejections, which have benefited from applying machine learning techniques to the new data. The arrival times of coronal mass ejections is a mid-range prediction whose accuracy has been improving, mostly due to a steady flow of data from SoHO, STEREO, and SDO. Longer term (greater than a year) predictions of solar activity have benefited from helioseismic studies of the plasma flows in the Sun. While these studies have complicated the dynamo models by introducing more complex internal flow patterns, the models should become more robust with the added information. But predictions made long before a sunspot cycle begins still rely on precursors. The success of some categories of the predictions of Solar Cycle 24 will be examined. The predictions in successful categories should be emphasized in future work. The SODA polar field precursor method, which has accurately predicted the last three cycles, is shown for Solar Cycle 25. Shape functions for the sunspot number and F10.7 are presented. What type of data is needed to better understand the polar regions of the Sun, the source of the most accurate precursor of long-term solar activity, will be discussed.

Effects of Version 2 of the International Sunspot Number on Naïve Predictions of Solar Cycle 25

W. Dean **Pesnell**
Space Weather 16?, 12, 1997-1203 **2018**
http://sci-hub.tw/10.1029/2018SW002080
The recalibration of the International Sunspot Number brings new challenges to predictions of Solar Cycle 25. One is that the list of extrema for the original series is no longer usable because the values of all maxima and minima are different for the new version of the sunspot number. Timings of extrema are less sensitive to the recalibration but are a natural result of the calculation. Predictions of Solar Cycle 25 published before 2016 must be converted to the new version of the sunspot number. Any prediction method that looks across the entire time span will have to be reconsidered because values in the nineteenth century were corrected by a larger factor than those in the twentieth century. We report a list of solar maxima and minima values and timings based on the recalibrated sunspot number. Naïve forecasts that depend only on the current values of the time series are common in economic studies. Several naïve predictions of Solar Cycle 25, the climatological average (180 ± 60), two versions of the inertial forecast, and two versions of the even-odd forecast, are derived from that table. The climatological average forecast is the baseline for more accurate predictions and the initial forecast in assimilative models of the Sun. It also provides the error estimate for Monte Carlo techniques that anticipate the long-term effects on the terrestrial environment. The other four predictions are shown to be statistically insignificant.

An Early Prediction of the Amplitude of Solar Cycle 25

W. Dean **Pesnell**, Kenneth H. Schatten
Solar Physics July **2018**, 293:112
http://sci-hub.tw/https://link.springer.com/article/10.1007/s11207-018-1330-5
A “Solar Dynamo” (SODA) Index prediction of the amplitude of Solar Cycle 25 is described. The SODA Index combines values of the solar polar magnetic field and the solar spectral irradiance at 10.7 cm to create a precursor of future solar activity. The result is an envelope of solar activity that minimizes the 11-year period of the sunspot cycle. We show that the variation in time of the SODA Index is similar to several wavelet transforms of the solar spectral irradiance at 10.7 cm. Polar field predictions for Solar Cycles 21 – 24 are used to show the success of the polar field precursor in previous sunspot cycles. Using the present value of the SODA index, we estimate that the next cycle’s smoothed peak activity will be about 140±30140±30 solar flux units for the 10.7 cm radio flux and a Version 2 sunspot number of 135±25135±25. This suggests that Solar Cycle 25 will be comparable to Solar Cycle 24. The estimated peak is expected to occur near 2025.2±1.52025.2±1.5 year. Because the current approach uses data prior to solar minimum, these estimates may improve as the upcoming solar minimum draws closer.

Predictions of Solar Cycle 24: How are we doing?

William Dean **Pesnell**
Space Weather Volume 14, Issue 1 January **2016** Pages 10–21
http://onlinelibrary.wiley.com/doi/10.1002/2015SW001304/full
Predictions of solar activity are an essential part of our Space Weather forecast capability. Users are requiring usable predictions of an upcoming solar cycle to be delivered several years before solar minimum. A set of predictions of

the amplitude of Solar Cycle 24 accumulated in 2008 ranged from zero to unprecedented levels of solar activity. The predictions formed an almost normal distribution, centered on the average amplitude of all preceding solar cycles. The average of the current compilation of 105 predictions of the annual-average sunspot number is 106 ± 31, slightly lower than earlier compilations but still with a wide distribution. Solar Cycle 24 is on track to have a below-average amplitude, peaking at an annual sunspot number of about 80. Our need for solar activity predictions and our desire for those predictions to be made ever earlier in the preceding solar cycle will be discussed. Solar Cycle 24 has been a below-average sunspot cycle. There were peaks in the daily and monthly averaged sunspot number in the Northern Hemisphere in 2011 and in the Southern Hemisphere in 2014. With the rapid increase in solar data and capability of numerical models of the solar convection zone we are developing the ability to forecast the level of the next sunspot cycle. But predictions based only on the statistics of the sunspot number are not adequate for predicting the next solar maximum. I will describe how we did in predicting the amplitude of Solar Cycle 24 and describe how solar polar field predictions could be made more accurate in the future.

Predicting Solar Cycle 24 Using a Geomagnetic Precursor Pair

W. Dean **Pesnell**

Solar Physics, June **2014**, Volume 289, Issue 6, pp 2317-2331,

We describe using Ap and F10.7 as a geomagnetic-precursor pair to predict the amplitude of Solar Cycle 24. The precursor is created by using F10.7 to remove the direct solar-activity component of Ap. Four peaks are seen in the precursor function during the decline of Solar Cycle 23. A recurrence index that is generated by a local correlation of Ap is then used to determine which peak is the correct precursor. The earliest peak is the most prominent but coincides with high levels of non-recurrent solar activity associated with the intense solar activity of October and November 2003. The second and third peaks coincide with some recurrent activity on the Sun and show that a weak cycle precursor closely following a period of strong solar activity may be difficult to resolve. A fourth peak, which appears in early 2008 and has recurrent activity similar to precursors of earlier solar cycles, appears to be the “true” precursor peak for Solar Cycle 24 and predicts the smallest amplitude for Solar Cycle 24. To determine the timing of peak activity it is noted that the average time between the precursor peak and the following maximum is ≈ 6.4 years. Hence, Solar Cycle 24 would peak during 2014. Several effects contribute to the smaller prediction when compared with other geomagnetic-precursor predictions. During Solar Cycle 23 the correlation between sunspot number and F10.7 shows that F10.7 is higher than the equivalent sunspot number over most of the cycle, implying that the sunspot number underestimates the solar-activity component described by F10.7. During 2003 the correlation between aa and Ap shows that aa is 10 % higher than the value predicted from Ap, leading to an overestimate of the aa precursor for that year. However, the most important difference is the lack of recurrent activity in the first three peaks and the presence of significant recurrent activity in the fourth. While the prediction is for an amplitude of Solar Cycle 24 of 65±20 in smoothed sunspot number, a below-average amplitude for Solar Cycle 24, with maximum at 2014.5±0.5, we conclude that Solar Cycle 24 will be no stronger than average and could be much weaker than average.

Solar Cycle Predictions (Invited Review)

W. Dean **Pesnell**

Solar Physics, November **2012**, Volume 281, Issue 1, pp 507-532

Solar cycle predictions are needed to plan long-term space missions, just as weather predictions are needed to plan the launch. Fleets of satellites circle the Earth collecting many types of science data, protecting astronauts, and relaying information. All of these satellites are sensitive at some level to solar cycle effects. Predictions of drag on low-Earth orbit spacecraft are one of the most important. Launching a satellite with less propellant can mean a higher orbit, but unanticipated solar activity and increased drag can make that a Pyrrhic victory as the reduced propellant load is consumed more rapidly. Energetic events at the Sun can produce crippling radiation storms that endanger all assets in space. Solar cycle predictions also anticipate the shortwave emissions that cause degradation of solar panels. Testing solar dynamo theories by quantitative predictions of what will happen in 5 – 20 years is the next arena for solar cycle predictions. A summary and analysis of 75 predictions of the amplitude of the upcoming Solar Cycle 24 is presented. The current state of solar cycle predictions and some anticipations of how those predictions could be made more accurate in the future are discussed.

Plasmoid-mediated reconnection in solar UV bursts

H. **Peter**, Y.-M. Huang, L. P. Chitta, P. R. Young

A&A 628, A8 **2019**

https://arxiv.org/pdf/1907.04335.pdf

https://www.aanda.org/articles/aa/pdf/2019/08/aa35820-19.pdf

UV bursts are transients in the solar atmosphere with an increased impulsive emission in the extreme UV lasting for one to several tens of minutes. They often show spectral profiles indicative of a bi-directional outflow in response to magnetic reconnection. To understand UV bursts, we study how motions of magnetic elements at the surface can

drive the self-consistent formation of a current sheet resulting in plasmoid-mediated reconnection. In particular, we want to study the role of the height of the reconnection in the atmosphere. We conducted numerical experiments solving the 2D MHD equations from the solar surface to the upper atmosphere. Motivated by observations, we drove a small magnetic patch embedded in a larger system of magnetic field of opposite polarity. This configuration creates an X-type neutral point in the initial potential field. The models are characterized by the plasma-beta at the height of this X point. The driving at the surface stretches the X-point into a current sheet, where plasmoids appear, and a bi-directional jet forms. This is consistent with what is expected for UV bursts or explosive events, and we provide a self-consistent model of the formation of the reconnection region in such events. The gravitational stratification gives an explanation for why explosive events are restricted to a temperature range around a few 0.1 MK, and the presence of plasmoids in the reconnection process provides an understanding of the observed variability during the transient events on a timescale of minutes. Our numerical experiments provide a comprehensive understanding of UV bursts and explosive events, in particular of how the atmospheric response changes if the reconnection happens at different plasma-beta, that is, at different heights in the atmosphere. This analysis also gives new insight into how UV bursts might be related to the photospheric Ellerman bombs**. 2013 October 22**

Hot Explosions in the Cool Atmosphere of the Sun

H. **Peter**, H. Tian, W. Curdt, D. Schmit, D. Innes, B. De Pontieu, J. Lemen, A. Title, P. Boerner, N. Hurlburt, T. D. Tarbell, J. P. Wuelser, J. Martínez-Sykora, L. Kleint, L. Golub, S. McKillop, K. K. Reeves, S. Saar, P. Testa, C. Kankelborg, S. Jaeggli, M. Carlsson, V. Hansteen
Science, 346, 1255726 (**2014**),
http://arxiv.org/pdf/1410.5842v1.pdf
The solar atmosphere was traditionally represented with a simple one-dimensional model. Over the past few decades, this paradigm shifted for the chromosphere and corona that constitute the outer atmosphere, which is now considered a dynamic structured envelope. Recent observations by IRIS (Interface Region Imaging Spectrograph) reveal that it is difficult to determine what is up and down even in the cool 6000-K photosphere just above the solar surface: this region hosts pockets of hot plasma transiently heated to almost 100,000 K. The energy to heat and accelerate the plasma requires a considerable fraction of the energy from flares, the largest solar disruptions. These IRIS observations not only confirm that the photosphere is more complex than conventionally thought, but also provide insight into the energy conversion in the process of magnetic reconnection.
Movie S1 (http://www2.mps.mpg.de/data/outgoing/peter/papers/2014-iris-eb/fig1-movie.mov)

Predictions for solar flares activity in solar cycle 25

Eleni **Petrakou**
2019
https://arxiv.org/ftp/arxiv/papers/1907/1907.06545.pdf
A forecast for the evolution of solar cycle 25 in terms of solar flares activity is presented. The forecast is derived from an existing phenomenological model based on the coupling of an internal solar component and a planetary component. In addition to sufficient temporal resolution, the predictions are characterized by features which both differentiate the model from other methods for space climate prediction and make it falsifiable.

Reprint of A deterministic model for forecasting long-term solar activity☆

Eleni **Petrakou**
Journal of Atmospheric and Solar-Terrestrial Physics Volume 176, September **2018**, Pages 51-56
http://sci-hub.tw/10.1016/j.jastp.2018.06.010
A phenomenological model is presented for the quantitative description of individual solar cycles' features, such as onset, intensity, evolution, in terms of the number of M and X-class solar flares. The main elements of the model are the relative ecliptic motion of the planets Jupiter and Saturn, and its synergy with a quasi-periodic component of solar activity. Using as input the temporal distribution of flares during cycle 21, the general evolution of cycles 22–24 is reproduced in notable agreement with the observations, including the resurgence of activity in the last months of 2017, and further predictions are provided for cycle 25. This deterministic description could contribute to elucidating the responsible physical mechanisms and forecasting space weather.

A deterministic model for forecasting long-term solar activity

Eleni **Petrakou**
Journal of Atmospheric and Solar-Terrestrial Physics Volume 175, October **2018**, Pages 18-23
https://arxiv.org/pdf/1702.00641v1.pdf
https://reader.elsevier.com/reader/sd/1EABC1B9CE911486561C760859882D992B5F114ACB348EBAE97031ABF0785E515E46F4F6C6296AAD66362E1CBDC48C3D

A phenomenological model is presented for the quantitative description of individual solar cycles' features, such as onset, intensity, evolution, in terms of the number of M and X-class solar flares. The main elements of the model are the relative eclipticmotion of the planets Jupiter and Saturn, and its synergy with a quasi-periodic component of solar activity. Using as input the temporal distribution of flares during cycle 21, the general evolution of cycles 22–24 is reproduced in notable agreement with the observations, including the resurgence of activity in the last months of 2017, and further predictions are provided for cycle 25. This deterministic description could contribute to elucidating the responsible physical mechanisms and forecasting space weather.

Guided flows in coronal magnetic flux tubes

A. **Petralia**, F. Reale, P. Testa
A&A 609, A18 **2017**
https://arxiv.org/pdf/1711.04641.pdf
There is evidence for coronal plasma flows to break down into fragments and to be laminar. We investigate this effect by modeling flows confined along magnetic channels. We consider a full MHD model of a solar atmosphere box with a dipole magnetic field. We compare the propagation of a cylindrical flow perfectly aligned to the field to that of another one with a slight misalignment. We assume a flow speed of 200 km/s, and an ambient magnetic field of 30 G. We find that while the aligned flow maintains its cylindrical symmetry while it travels along the magnetic tube, the misaligned one is rapidly squashed on one side, becoming laminar and eventually fragmented because of the interaction and backreaction of the magnetic field. This model could explain an observation of erupted fragments that fall back as thin and elongated strands and end up onto the solar surface in a hedge-like configuration, made by the Atmospheric Imaging Assembly on board the Solar Dynamics Observatory. The initial alignment of plasma flow plays an important role in determining the possible laminar structure and fragmentation of flows while they travel along magnetic channels. **4 November 2015**

Magnetic shuffling of coronal downdrafts

A. **Petralia**, F. Reale, S.Orlando
A&A 598, L8 **(2017)**
https://arxiv.org/pdf/1701.05752v1.pdf
Channelled fragmented downflows are ubiquitous in magnetized atmospheres, and have been recently addressed from an observation after a solar eruption. We study the possible back-effect of the magnetic field on the propagation of confined flows. We compare two 3D MHD simulations of dense supersonic plasma blobs downfalling along a coronal magnetic flux tube. In one, the blobs move strictly along the field lines; in the other, the initial velocity of the blobs is not perfectly aligned to the magnetic field and the field is weaker. The aligned blobs remain compact while flowing along the tube, with the generated shocks. The misaligned blobs are disrupted and merged by the chaotic shuffling of the field lines, and structured into thinner filaments; Alfven wave fronts are generated together with shocks ahead of the dense moving front. Downflowing plasma fragments can be chaotically and efficiently mixed if their motion is misaligned to field lines, with broad implications, e.g., disk accretion in protostars, coronal eruptions and rain.

Dispersion and spatial structure of the coupled Alfvén and slow magnetosonic oscillations in the Solar corona

Aleksandr V **Petrashchuk**, S A Anfinogentov, V V Fedenev, P N Mager, D Yu Klimushkin
Monthly Notices of the Royal Astronomical Society, Volume 525, Issue 4, **2023**, Pages 5669–5676,
https://doi.org/10.1093/mnras/stad2635
Numerical and analytical analysis of the magnetohydrodynamic (MHD) waves in Solar coronal arcades is performed. A semicylinder slab model of arcade is used where the field lines are represented by half-circles intersecting the photosphere, the magnetic shells are represented by nested coaxial semicylinders. The finite plasma pressure is taken into account. The ‘corrugational’ perturbations are considered, that is, the perturbations with short wavelength in the direction along the arcade. In this limit, there are two oscillation modes, the Alfvén and slow magnetosonic modes, coupled due to the field line curvature. The transverse dispersion of the modes, that is, the dependence of the radial wave vector’s component kr on the wave frequency ω, is considered. It was found that the wave is concentrated in two regions of mode’s existence, where $k_{2r}>0$: the Alfvén and magnetosonic transparent regions. On one side, each of them is bounded by the resonance surface, where $k_{2r}\to\infty$. On the resonance surface, the wave’s frequency is determined by the Alfvén and slow magnetosonic modes dispersion relations, respectively. On the other side, the transparent regions are bounded by cut-off frequencies where $k_{2r}=0$. In both transparent regions, the perturbations have both transverse electric field (characteristic for the Alfvén mode) and field aligned velocity (characteristic for the slow mode). The wave structure along the field line for several models of plasma parameters is calculated.

Global solar photospheric and coronal magnetic field over activity cycles 21–25

Gordon J. D. **Petrie***
J. Space Weather Space Clim. **2024**, 14, 5
https://www.swsc-journal.org/articles/swsc/pdf/2024/01/swsc230030.pdf
The evolution of the global solar magnetic field from the beginning of cycle 21 (mid-1970s) until the currently-ascending cycle 25 is described using photospheric full-disk and synoptic magnetograms from NSO Kitt Peak Vacuum Telescope (KPVT) 512-channel and Spectromagnetograph (SPMG) and the Synoptic Optical Long-term Investigation of the Sun (SOLIS) Vector Spectro-Magnetograph (VSM) and Global Oscillations Network Group (GONG), and Stanford University's Wilcox Solar Observatory (WSO). The evolving strength and symmetry of the global coronal field are described by potential-field source-surface models decomposed into axisymmetric and non-axisymmetric, and even- and odd-ordered magnetic multipoles. The overall weakness of the global solar magnetic field since cycle 23 splits the 50-year observing window into the stronger, simpler, more hemispherically symmetric cycles 21 and 22 and the weaker, more complex cycles 23 and 24. An anomalously large decrease in the global solar field strength occurred during cycles 23, and an anomalously weak axial/polar field resulted from that cycle, accompanied by an anomalously weak radial interplanetary magnetic field (IMF) during cycle 23 activity minimum and a weakened radial IMF overall since cycle 23. The general long-term decline in solar field strength and the development during cycle 24 of strong swings of hemispheric and polar asymmetry are analyzed in detail, including their transfer through global coronal structural changes to dominate mean in situ interplanetary field measurements for several years. Although more symmetric than cycle 24, the rise phase of cycle 25 began with the southern leading the northern hemisphere, but the north has recovered to lead this cycle's polar field reversal. The mean polar flux (poleward of ±60°) has reversed at each pole, so far more symmetrically than the cycle 23 and 24 polar reversals.

Polar Photospheric Magnetic Field Evolution and Global Flux Transport

Gordon J. D. **Petrie**
Solar Physics volume 298, Article number: 43 (**2023**)
https://doi.org/10.1007/s11207-023-02134-5
The Sun's polar magnetic fields are of paramount importance in structuring the heliosphere and in seeding the activity cycle, but they are difficult to observe from the ecliptic plane. However, they are formed by observable active-region magnetic-flux decay and transport processes. We give an observational description of photospheric flux transport and polar field evolution using the >40>40 yr series (1974 – 2017) of full-disk line-of-sight photospheric magnetograms from the NSO Kitt Peak Vacuum Telescope (KPVT) 512-channel and Spectromagnetograph (SPMG) and the Synoptic Optical Long-term Investigation of the Sun (SOLIS) Vector Spectro-Magnetograph (VSM). An analytical technique introduced by Durrant, Turner, and Wilson (Solar Physics, 222, 345, 2004). is adapted to analyze time series of full-disk magnetograms to estimate global photospheric flux transport self-consistently. The major hemispheric flux changes, due to cancellation or transport of leading-polarity flux across the equator, occur around activity maximum in each cycle, when peak levels of flux emerge ≥10∘≥10∘ from the equator. This highlights the efficiency of flux cancellation and transport within each hemisphere, allowing peak levels of leading-polarity flux to reach the equator at this time, letting peak trailing-polarity flux surge poleward. Polar flux evolution follows the hemispheric flux closely each cycle, but with temporal variations dampened by lower-latitude flux cancellation. Major net hemispheric flux change ceased early during Cycle 23, producing weakened polar fields. Cycle 24 was distinguished by large hemispheric flux fluctuations forming a three-part structure: (i) dominant northern activity and north polar flux decrease toward zero; (ii) dominant southern activity peak, swift south polar field decrease, polarity reversal, and growth while the north pole was stalled; and (iii) southern activity decline, north again dominant, north polar flux growth with reversed polarity. Recent global photospheric field evolution and polar field changes are described using Global Oscillations Network Group (GONG, 2006 – present) and Solar Dynamics Observatory Helioseismic and Magnetic Imager (SDO/HMI) line-of-sight magnetograms.

On the enhanced coronal mass ejection detection rate since the solar cycle 23 polar field reversal

Gordon **Petrie**
ApJ MS **2015**
http://arxiv.org/pdf/1508.06729v1.pdf
Coronal mass ejections (CMEs) with angular width >30∘ have been observed to occur at a higher rate during solar cycle 24 compared to cycle 23, per sunspot number. This result is supported by data from three independent databases constructed using Large Angle and Spectrometric Coronagraph Experiment (LASCO) coronagraph images, two employing automated detection techniques and one compiled manually by human observers. According to the two databases that cover a larger field of view, the enhanced CME rate actually began shortly after the cycle 23 polar field reversal, in 2004, when the polar fields returned with a 40\% reduction in strength and interplanetary radial magnetic field became ≈30% weaker. This result is consistent with the link between anomalous CME expansion and heliospheric total pressure decrease recently reported by Gopalswamy et al.

Polar Field Reversals and Active Region Decay **Review**

Gordon **Petrie**, Sophie Ettinger

Space Science Reviews **2015**

We study the relationship between polar field reversals and decayed active region magnetic flux. Photospheric active region flux is dispersed by differential rotation and turbulent diffusion, and is transported poleward by meridional flows and diffusion. We summarize the published evidence from observation and modeling of the influence of meridional flow variations and decaying active region flux's spatial distribution, such as the Joy's law tilt angle. Using NSO Kitt Peak synoptic magnetograms covering cycles 21–24, we investigate in detail the relationship between the transport of decayed active region flux to high latitudes and changes in the polar field strength, including reversals in the magnetic polarity at the poles. By means of stack plots of low- and high-latitude slices of the synoptic magnetograms, the dispersal of flux from low to high latitudes is tracked, and the timing of this dispersal is compared to the polar field changes. In the most abrupt cases of polar field reversal, a few activity complexes (systems of active regions) are identified as the main cause. The poleward transport of large quantities of decayed trailing-polarity flux from these complexes is found to correlate well in time with the abrupt polar field changes. In each case, significant latitudinal displacements were found between the positive and negative flux centroids of the complexes, consistent with Joy's law bipole tilt with trailing-polarity flux located poleward of leading-polarity flux. The activity complexes of the cycle 21 and 22 maxima were larger and longer-lived than those of the cycle 23 and 24 maxima, and the poleward surges were stronger and more unipolar and the polar field changes larger and faster. The cycle 21 and 22 polar reversals were dominated by only a few long-lived complexes whereas the cycle 23 and 24 reversals were the cumulative effects of more numerous, shorter-lived regions. We conclude that sizes and lifetimes of activity complexes are key to understanding the diversity of polar reversals.

Solar Polar Fields and the 22-Year Activity Cycle: Observations and Models **Review**

G. J. D. **Petrie**, K. Petrovay, K. Schatten

Space Science Reviews, December **2014**, Volume 186, Issue 1-4, pp 325-357

We explore observations and models of the interacting, cyclical behavior of the active regions and the polar magnetic fields of the Sun. We focus on observational evidence of these fields interacting across the corridor between active and polar latitudes. We present observations of diverse magnetic signatures on, above and beneath the solar surface, and find much evidence of phenomena migrating in both directions across this corridor in each hemisphere, including photospheric fields, ephemeral bipoles, interior torsional oscillations, high-latitude filaments, and coronal green line intensity. Together these observations produce a complex physical picture of high-latitude solar magnetic field evolution in the photosphere, atmosphere and interior, and demonstrate their essential role in the solar cycle. The picture presented by these collected observations is consistent with the Babcock-Leighton phenomenological model for the cycle, and we discuss related efforts to predict cycle amplitudes based on polar field strengths and on combining activity and polar-field information in a single phase-independent, slowly-evolving index. We also briefly review related work on magnetic flux transport models for the solar cycle, with particular reference to the interaction between flux emergence patterns and meridional flows.

High frequency decayless waves with significant energy in Solar Orbiter/EUI observations

Elena **Petrova**, Norbert Magyar, Tom Van Doorsselaere, David Berghmans

ApJ **946** 36 **2023**

https://arxiv.org/pdf/2205.05319.pdf

https://iopscience.iop.org/article/10.3847/1538-4357/acb26a/pdf

High-frequency wave phenomena present a great deal of interest as one of the possible candidates to contribute to the energy input required to heat the corona as a part of the AC heating theory. However, the resolution of imaging instruments up until the Solar Orbiter have made it impossible to resolve the necessary time and spatial scales. The present paper reports on high-frequency transverse motions in a small loop located in a quiet Sun region of the corona. The oscillations were observed with the HRIEUV telescope (17.4 nm) of the EUI instrument onboard the Solar Orbiter. We detect two transverse oscillations in short loops with lengths of 4.5 Mm and 11 Mm. The shorter loop displays an oscillation with a 14 s period and the longer a 30 s period. Despite the high resolution, no definitive identification as propagating or standing waves is possible. The velocity amplitudes are found to be equal to 72 km/s and 125 km/s, respectively, for the shorter and longer loop. Based on that, we also estimated the values of the energy flux contained in the loops - the energy flux of the 14 s oscillation is 1.9 kW m^-2 and of the 30 s oscillation it is 6.5 kW m^-2 . While these oscillations have been observed in the Quiet Sun, their energy fluxes are of the same order as the energy input required to heat the active solar corona. Numerical simulations were performed in order to reproduce the observed oscillations. The correspondence of the numerical results to the observations provide support to the energy content estimates for the observations. Such high energy densities have not yet been observed in

decayless coronal waves, and this is promising for coronal heating models based on wave damping. **2021 February 23**

Towards an algebraic method of solar cycle prediction I. Calculating the ultimate dipole contributions of individual active regions

Kristóf **Petrovay**, Melinda Nagy, Anthony R. Yeates
Journal of Space Weather and Space Climate 10, 50 **2020**
https://arxiv.org/pdf/2009.02299.pdf
https://www.swsc-journal.org/articles/swsc/pdf/2020/01/swsc200044.pdf
We discuss the potential use of an algebraic method to compute the value of the solar axial dipole moment at solar minimum, widely considered to be the most reliable precursor of the activity level in the next solar cycle. The method consists of summing up the ultimate contributions of individual active regions to the solar axial dipole moment \revtwo{at the end of the cycle}. A potential limitation of the approach is its dependence on the underlying surface flux transport (SFT) model details. We demonstrate by both analytical and numerical methods that the factor relating the initial and ultimate dipole moment contributions of an active region displays a Gaussian dependence on latitude with parameters that only depend on details of the SFT model through the parameter $\eta/\Delta u$ where η is supergranular diffusivity and Δu is the divergence of the meridional flow on the equator. In a comparison with cycles simulated in the 2×2D dynamo model we further demonstrate that the inaccuracies associated with the algebraic method are minor and the method may be able to reproduce the dipole moment values in a large majority of cycles.

Optimization of surface flux transport models for the solar polar magnetic field

K. **Petrovay**, M. Talafha
A&A **2019**
https://arxiv.org/pdf/1909.06125.pdf
The choice of free parameters in surface flux transport (SFT) models describing the evolution of the large-scale poloidal magnetic field of the Sun is critical for the correct reproduction of the polar magnetic flux built up during a solar cycle, which in turn is known to be a good predictor of the amplitude of the upcoming cycle. For an informed choice of parameters it is important to understand the effect and interplay of the various parameters and to optimize the models for the polar magnetic field. Here we present the results of a large-scale systematic study of the parameter space in an SFT model where the source term representing the net effect of tilted flux emergence was chosen to represent a typical, average solar cycle as described by observations. Comparing the results with observational constraints on the spatiotemporal variation of the polar magnetic field, as seen in magnetograms for the last four solar cycles, we mark allowed and excluded regions in the 3D parameter space defined by the flow amplitude u0, the magnetic diffusivity eta and the decay time scale tau, for three different assumed meridional flow profiles. Without a significant decay term in the SFT equation (i.e., for tau >10 yr) the global dipole moment reverses too late in the cycle for all flow profiles and parameters, providing independent supporting evidence for the need of a decay term, even in the case of identical cycles. An allowed domain is found to exist for tau values in the 5-10 yr range for all flow profiles considered. Generally higher values of eta (500-800 km^2/s) are preferred though some solutions with lower eta are still allowed.

Solar cycle prediction **Review**

Kristof **Petrovay**
Living Reviews in Solar Physics **17,** 2 (**2020**)
https://arxiv.org/pdf/1907.02107.pdf
https://link.springer.com/content/pdf/10.1007/s41116-020-0022-z.pdf
A review of solar cycle prediction methods and their performance is given, including early forecasts for cycle 25. The review focuses on those aspects of the solar cycle prediction problem that have a bearing on dynamo theory. The scope of the review is further restricted to the issue of predicting the amplitude (and optionally the epoch) of an upcoming solar maximum no later than right after the start of the given cycle.
In their overall performance during the course of the last few solar cycles, precursor methods have clearly been superior to extrapolation methods. One method that has yielded predictions consistently in the right range during the past few solar cycles is the polar field precursor. Nevertheless, some extrapolation methods may still be worth further study. Model based forecasts are quickly coming into their own, and, despite not having a long proven record, their predictions are received with increasing confidence by the community.

Precursors of an upcoming solar cycle at high latitudes from coronal green line data

K.**Petrovay** M.Nagy T.Gerják L.Juhászb
Journal of Atmospheric and Solar-Terrestrial Physics Volume 176, September **2018**, Pages 15-20

http://sci-hub.tw/10.1016/j.jastp.2017.12.011
After reviewing potential early indicators of an upcoming solar cycle at high latitudes, we focus attention on the rush–to-the-poles (RTTP) phenomenon in coronal green line emission. Considering various correlations between properties of the RTTP with the upcoming solar cycle we find a correlation between the rate of the RTTP and the time delay until the maximum of the next solar cycle. On the basis of this correlation and the known internal regularities of the sunspot number series we predict that, following a minimum in 2019, cycle 25 will peak in late 2024 at an amplitude of about 130 (in terms of smoothed monthly revised sunspot numbers). This slightly exceeds the amplitude of cycle 24 but it would still make cycle 25 a fairly weak cycle.

Rogue active regions and the inherent unpredictability of the solar dynamo

K. **Petrovay**, M. Nagy
Proc. IAU Symp. 340. **2018**
https://arxiv.org/pdf/1804.03427.pdf
New developments in surface flux transport modeling and theory of flux transport dynamos have given rise to the notion that certain large active regions with anomalous properties (location, tilt angle and/or Hale/non-Hale character) may have a major impact on the course of solar activity in subsequent years, impacting also on the amplitude of the following solar cycles. Here we discuss our current understanding of the role of such "rogue" active regions in cycle-to-cycle variations of solar activity.

Precursors of an upcoming solar cycle at high latitudes from coronal green line data

K. **Petrovay**, M. Nagy, T. Gerják, L. Juhász
J. Atm. Sol.-Terr. Phys **2018**
https://arxiv.org/pdf/1802.05628.pdf
After reviewing potential early indicators of an upcoming solar cycle at high latitudes, we focus attention on the rush-to-the-poles (RTTP) phenomenon in coronal green line emission. Considering various correlations between properties of the RTTP with the upcoming solar cycle we find a correlation between the rate of the RTTP and the time delay until the maximum of the next solar cycle. On the basis of this correlation and the known internal regularities of the sunspot number series we predict that, following a minimum in 2019, cycle 25 will peak in late 2024 at an amplitude of about 130 (in terms of smoothed monthly revised sunspot numbers). This slightly exceeds the amplitude of cycle 24 but it would still make cycle 25 a fairly weak cycle.

Solar Cycle Prediction **Review**

Krist/of **Petrovay**
Living Rev. Solar Phys., 7, (2010), 6
http://www.livingreviews.org/lrsp-2010-6
A review of solar cycle prediction methods and their performance is given, including forecasts for cycle 24. The review focuses on those aspects of the solar cycle prediction problem that have a bearing on dynamo theory. The scope of the review is further restricted to the issue of predicting the amplitude (and optionally the epoch) of an upcoming solar maximum no later than right after the start of the given cycle.
Prediction methods form three main groups. Precursor methods rely on the value of some measure of solar activity or magnetism at a specified time to predict the amplitude of the following solar maximum. Their implicit assumption is that each numbered solar cycle is a consistent unit in itself, while solar activity seems to consist of a series of much less tightly intercorrelated individual cycles. Extrapolation methods, in contrast, are based on the premise that the physical process giving rise to the sunspot number record is statistically homogeneous, i.e., the mathematical regularities underlying its variations are the same at any point of time and, therefore, it lends itself to analysis and forecasting by time series methods. Finally, instead of an analysis of observational data alone, model based predictions use physically (more or less) consistent dynamo models in their attempts to predict solar activity.
In their overall performance during the course of the last few solar cycles, precursor methods have clearly been superior to extrapolation methods. Nevertheless, most precursor methods overpredicted cycle 23, while some extrapolation methods may still be worth further study. Model based forecasts have not yet had a chance to prove their skills. One method that has yielded predictions consistently in the right range during the past few solar cycles is that of K. Schatten et al., whose approach is mainly based on the polar field precursor.
The incipient cycle 24 will probably mark the end of the Modern Maximum, with the Sun switching to a state of less strong activity. It will therefore be an important testbed for cycle prediction methods and, by inference, for our understanding of the solar dynamo.

Helio2024 Science White Paper: ngGONG -- Future Ground-based Facilities for Research in Heliophysics and Space Weather Operational Forecast

Alexei A. **Pevtsov**, V. Martinez-Pillet, H. Gilbert, A. G. de Wijn, M. Roth, S. Gosain, L. A. Upton, Y. Katsukawa, J. Burkepile, Jie Zhang, K. P. Reardon, L. Bertello, K. Jain, S. C. Tripathy, K.D. Leka
White paper submitted to Decadal Survey for Solar and Space Physics (Heliophysics) 2024-2033 **2022**
https://arxiv.org/pdf/2211.06712.pdf
Long-term synoptic observations of the Sun are critical for advancing our understanding of Sun as an astrophysical object, understanding the solar irradiance and its role in solar-terrestrial climate, for developing predictive capabilities of solar eruptive phenomena and their impact on our home planet, and heliosphere in general, and as a data provider for the operational space weather forecast. We advocate for the development of a ground-based network of instruments provisionally called ngGONG to maintain critical observing capabilities for synoptic research in solar physics and for the operational space weather forecast.

Long-term studies of photospheric magnetic fields on the Sun **Review**

Alexei A. **Pevtsov**1*, Luca Bertello1, Yury A. Nagovitsyn2,3, Andrey G. Tlatov4 and Valery V. Pipin5
J. Space Weather Space Clim. **2021**, 11, 4
https://doi.org/10.1051/swsc/2020069
Long-term studies of photospheric magnetic fields on the Sun (swsc-journal.org)
We briefly review the history of observations of magnetic fields on the Sun, and describe early magnetograps for full disk measurements. Changes in instruments and detectors, the cohort of observers, the knowledge base etc may result in non-uniformity of the long-term synoptic datasets. Still, such data are critical for detecting and understanding the long-term trends in solar activity. We demonstrate the value of historical data using studies of active region tilt (Joy's law) and the evolution of polar field and its reversal. Using the longest dataset of sunspot field strength measurements from Mount Wilson Observatory (1917-present) supplemented by shorter datasets from Pulkovo (1956–1997) and Crimean (1956-present) observatories we demonstrate that the magnetic properties of sunspots did not change over the last hundred years. We also show that the relationship between the sunspot area and its magnetic flux can be used to extend the studies of magnetic field in sunspots to periods with no direct magnetic field measurements. Finally, we show how more recent full disk observations of the vector magnetic field can be used to study the long-term (solar cycle) variations in magnetic helicity on the Sun.

Reconstructing solar magnetic fields from historical observations V. Sunspot magnetic field measurements at Mount Wilson Observatory

Alexei A. **Pevtsov**, Kseniya A. Tlatova, Alexander A. Pevtsov, Elina Heikkinen, Ilpo Virtanen, Nina V. Karachik, Luca Bertello, Andrey G. Tlatov, Roger Ulrich, Kalevi Mursula
A&A **2019**
https://arxiv.org/pdf/1907.06492.pdf
Context. Systematic observations of magnetic field strength and polarity in sunspots began at Mount Wilson Observatory (MWO), USA in early 1917. Except for a few brief interruptions, this historical dataset continues till present. Aims. The sunspot field strength and polarity observations are critical in our project of reconstructing the solar magnetic field over the last hundred years. Here we provide a detailed description of the newly digitized dataset of drawings of sunspot magnetic field observations. Methods. The digitization of MWO drawings is based on a software package develope d by us. It includes a semi-automatic selection of solar limbs and other features of the drawing, and a manual entry of the time of observations, the measured field strength and other notes hand-written on each drawing. The data are preserved in a MySQL database. Results. We provide a brief history of the project and describe the results from digitizing this historical dataset. We also provide a summary of the final dataset, and describe its known limitations. Finally, we compare the sunspot magnetic field measurements with other instruments, and demonstrate that, if needed, the dataset could be continued using modern observations such as, for example, Vector Stokes Magnetograph (VSM) on Synoptic Optical Long-term Investigations of the Sun (SOLIS) platform.

The Vorticity of Solar Photospheric Flows on the Scale of Granulation

A.A. **Pevtsov**
Geomagnetism and Aeronomy **2016**
http://arxiv.org/pdf/1606.01390v1.pdf
We employ time sequences of images observed with a G-band filter (4305{\AA}) by the Solar Optical Telescope (SOT) on board of Hinode spacecraft at different latitude along solar central me-ridian to study vorticity of granular flows in quiet Sun areas during deep minimum of solar activity. Using a feature correlation tracking (FCT) technique, we calculate the vorticity of granular-scale flows. Assuming the known pattern of vertical flows (upward in granules and downward in inter-granular lanes), we infer the sign of kinetic helicity of these flows. We show that the kinetic helicity of granular flows and intergranular vortices exhibits a weak hemispheric preference, which is in

agreement with the action of the Coriolis force. This slight hemispheric sign asymmetry, however, is not statistically significant given large scatter in the average vorticity. The sign of the current he-licity density of network magnetic fields computed using full disk vector magnetograms from the Synoptic Optical Long-term Investigations of the Sun (SOLIS) does not show any hemispheric preference. The combination of these two findings suggests that the photospheric dynamo operating on the scale of granular flows is non-helical in nature.

Reconstructing solar magnetic fields from historical observations I. Renormalized Ca K spectroheliograms and pseudo-magnetograms

Alexei A. **Pevtsov**1, Ilpo Virtanen2, Kalevi Mursula2, Andrey Tlatov3 and Luca Bertello4
A&A 585, A40 (**2016**)

Aims. The present work is the first in a series of articles that develop a new proxy to represent the evolution of magnetic activity in past solar cycles by combining the information from historical Ca II K line spectroheliograms and sunspot magnetic field measurements.
Methods. We use synoptic (Carrington) maps from 1915–1985 that were derived from daily Ca K line observations at Mount Wilson Observatory to identify the chromospheric plages and to create synoptic pseudo-magnetograms. We use historical observations of sunspot magnetic fields from 1917 to the present to assign polarity to pixels situated within plages. The original Ca K spectroheliograms are nonuniform in their brightness, and we develop a novel approach to re-normalize their intensities.
Results. We show that a homogeneous long-term series of pseudo-magnetograms can be successfully constructed by combining sunspot field measurements and plages with renormalized intensities. In our tests, about 80% of pixels situated within plages showed the same magnetic polarity as the synoptic magnetograms taken with the Kitt Peak Vacuum Telescope. Finally, we discuss possible approaches to further improve the agreement between observed and pseudo-magnetograms.

Magnetic Helicity, Tilt, and Twist **Review**

Alexei A. **Pevtsov**, Mitchell A. Berger, Alexander Nindos, Aimee A. Norton, Lidia van Driel-Gesztelyi
Space Science Reviews, December **2014**, Volume 186, Issue 1-4, pp 285-324

Since its introduction to astro- and solar physics, the concept of helicity has proven to be useful in providing critical insights into physics of various processes from astrophysical dynamos, to magnetic reconnection and eruptive phenomena. Signature of helicity was also detected in many solar features, including orientation of solar active regions, or Joy's law. Here we provide a summary of both solar phenomena and consider mutual relationship and its importance for the evolution of solar magnetic fields.

Cyclic and Long-Term Variation of Sunspot Magnetic Fields

Alexei A. **Pevtsov**, Luca Bertello, Andrey G. Tlatov, Ali Kilcik, Yury A. Nagovitsyn, Edward W. Cliver
Solar Physics February **2014**, Volume 289, Issue 2, pp 593–602

Measurements from the Mount Wilson Observatory (MWO) were used to study the long-term variations of sunspot field strengths from 1920 to 1958. Following a modified approach similar to that presented in Pevtsov et al. (Astrophys. J. Lett.742, L36, 2011), we selected the sunspot with the strongest measured field strength for each observing week and computed monthly averages of these weekly maximum field strengths. The data show the solar cycle variation of the peak field strengths with an amplitude of about 500 – 700 gauss (G), but no statistically significant long-term trends. Next, we used the sunspot observations from the Royal Greenwich Observatory (RGO) to establish a relationship between the sunspot areas and the sunspot field strengths for cycles 15 – 19. This relationship was used to create a proxy of the peak magnetic field strength based on sunspot areas from the RGO and the USAF/NOAA network for the period from 1874 to early 2012. Over this interval, the magnetic field proxy shows a clear solar cycle variation with an amplitude of 500 – 700 G and a weaker long-term trend. From 1874 to around 1920, the mean value of magnetic field proxy increases by about 300 – 350 G, and, following a broad maximum in 1920 – 1960, it decreases by about 300 G. Using the proxy for the magnetic field strength as the reference, we scaled the MWO field measurements to the measurements of the magnetic fields in Pevtsov et al. (2011) to construct a combined data set of maximum sunspot field strengths extending from 1920 to early 2012. This combined data set shows strong solar cycle variations and no significant long-term trend (the linear fit to the data yields a slope of -0.2 ± 0.8 G year-1). On the other hand, the peak sunspot field strengths observed at the minimum of the solar cycle show a gradual decline over the last three minima (corresponding to cycles 21 – 23) with a mean downward trend of ≈ 15 G year-1.

SOLIS: reconciling disk-integrated and disk-resolved spectra from the Sun

Alexei **Pevtsov**, Luca Bertello, Brian Harker, Mark Giampapa, Andrew Marble

18th Cambridge Workshop on Cool Stars, Stellar Systems, and the Sun, Proceedings of Lowell Observatory (**2014**), pp. 871-878
http://arxiv.org/pdf/1411.7266v1.pdf
Unlike other stars, the surface of the Sun can be spatially resolved to a high degree of detail. But the Sun can also be observed as if it was a distant star. The availability of solar disk-resolved and disk-integrated spectra offers an opportunity to devise methods to derive information about the spatial distribution of solar features from Sun-as-a-star measurements. Here, we present an update on work done at the National Solar Observatory to reconcile disk-integrated and disk-resolved solar spectra from the Synoptic Optical Long-term Investigation of the Sun (SOLIS) station. The results of this work will lead to a new approach to infer the information about the spatial distribution of features on other stars, from the overall filling factor of active regions to, possibly, the latitude/longitude distribution of features.

Velocity-intensity asymmetry reversal of solar radial p-modes

J. **Philidet**, K. Belkacem, H.-G. Ludwig, R. Samadi, C. Barban
A&A **2020**
https://arxiv.org/pdf/2011.02439.pdf
The development of space-borne missions has significantly improved the quality of the measured spectra of solar-like oscillators. Their p-mode line profiles can now be resolved, and the asymmetries inferred for a variety of stars other than the Sun. However, it has been known for a long time that the asymmetries of solar p-modes are reversed between the velocity and the intensity spectra. Understanding the origin of this reversal is necessary in order to use asymmetries as a tool for seismic diagnosis. For stars other than the Sun, only the intensity power spectrum is sufficiently resolved to allow for an estimation of mode asymmetries. We recently developed an approach designed to model and predict these asymmetries in the velocity power spectrum of the Sun and to successfully compare them to their observationally derived counterparts. In this paper we expand our model and predict the asymmetries featured in the intensity power spectrum. We find that the shape of the mode line profiles in intensity is largely dependent on how the oscillation-induced variations of the radiative flux are treated, and that modelling it realistically is crucial to understanding asymmetry reversal. Perturbing a solar-calibrated grey atmosphere model, and adopting the quasi-adiabatic framework as a first step, we reproduce the asymmetries observed in the solar intensity spectrum for low-frequency modes. We conclude that, unlike previously thought, it is not necessary to invoke an additional mechanism (e.g. non-adiabatic effects, coherent non-resonant background signal) to explain asymmetry reversal. This additional mechanism is necessary, however, to explain asymmetry reversal for higher-order modes.

Modelling the asymmetries of the Sun's radial p-mode line profiles

J. **Philidet**, K. Belkacem, R. Samadi, C. Barban, H.-G. Ludwig
A&A **2020**
https://arxiv.org/pdf/2001.10271.pdf
In this paper, we aim to develop a predictive model for solar radial p-mode line profiles in the velocity spectrum. Unlike the approach favoured by prior studies, this model is not described by free parameters and we do not use fitting procedures to match the observations. Instead, we use an analytical turbulence model coupled with constraints extracted from a 3D hydrodynamic simulation of the solar atmosphere. We then compare the resulting asymmetries with their observationally derived counterpart.
We find that stochastic excitation localised beneath the mode upper turning point generates negative asymmetry for $\nu<\nu_{max}$ and positive asymmetry for $\nu>\nu_{max}$. On the other hand, stochastic excitation localised above this limit generates negative asymmetry throughout the p-mode spectrum. As a result of the spatial extent of the source of excitation, both cases play a role in the total observed asymmetries. By taking this spatial extent into account and using a realistic description of the spectrum of turbulent kinetic energy, both a qualitative and quantitative agreement can be found with solar observations perfoemed by the GONG network. We also find that the impact of the correlation between acoustic noise and oscillation is negligible for mode asymmetry in the velocity spectrum.

Case study on the identification and classification of small-scale flow patterns in flaring active region

E. **Philishvi**, B.M. Shergelashvili, S. Buitendag, J. Raes, S. Poedts, M.L. Khodachenko
A&A **2020**
https://arxiv.org/pdf/2011.07634.pdf
We propose a novel methodology to identity flows in the solar atmosphere and classify their velocities as either supersonic, subsonic, or sonic. The proposed methodology consists of three parts. First, an algorithm is applied to the Solar Dynamics Observatory (SDO) image data to locate and track flows, resulting in the trajectory of each flow over time. Thereafter, the differential emission measure inversion method is applied to six AIA channels along the trajectory of each flow in order to estimate its background temperature and sound speed. Finally, we classify each

flow as supersonic, subsonic, or sonic by performing simultaneous hypothesis tests on whether the velocity bounds of the flow are larger, smaller, or equal to the background sound speed. The proposed methodology was applied to the SDO image data from the 171 Å spectral line for the date **6 March 2012** from 12:22:00 to 12:35:00 and again for the date **9 March 2012** from 03:00:00 to 03:24:00. Eighteen plasma flows were detected, 11 of which were classified as supersonic, 3 as subsonic, and 3 as sonic at a 70% level of significance. Out of all these cases, 2 flows cannot be strictly ascribed to one of the respective categories as they change from the subsonic state to supersonic and vice versa. We labelled them as a subclass of transonic flows. The proposed methodology provides an automatic and scalable solution to identify small-scale flows and to classify their velocities as either supersonic, subsonic, or sonic. We identified and classified small-scale flow patterns in flaring loops. The results show that the flows can be classified into four classes: sub-, super-, trans-sonic, and sonic. The detected flows from AIA images can be analyzed in combination with the other high-resolution observational data, such as Hi-C 2.1 data, and be used for the development of theories of the formation of flow patterns.

GRID-SITES: Gridded Solar Iterative Temperature Emission Solver for Fast DEM Inversion

James **Pickering**, Huw Morgan
Solar Physics October **2019**, 294:136
https://link.springer.com/content/pdf/10.1007%2Fs11207-019-1526-3.pdf
The increasing size of solar datasets demands highly efficient and robust analysis methods. This paper presents an approach that can increase the computational efficiency of differential emission measure (DEM) inversions by an order of magnitude or higher, with the efficiency factor increasing with the size of the input dataset. The method, named the Gridded Solar Iterative Temperature Emission Solver (Grid-SITES) is based on grouping pixels according to the similarity of their intensities in multiple channels, and solving for one DEM per group. This is shown to be a valid approach, given a sufficiently high number of grid bins for each channel. The increase in uncertainty arising from the quantisation of the input data is small compared to the general measurement and calibration uncertainties. In this paper, we use the Solar Iterative Temperature Emission Solver (SITES) as the core method for the DEM inversion, although Grid-SITES provides a general framework which may be used with any DEM inversion method, or indeed any large multi-dimensional data inversion problem. The method is particularly efficient for processing larger images, offering a factor of 30 increase in speed for a 10 megapixel image. For a time series of observations, the gridded results can be passed sequentially to each new image, with new populated bins added as required. This process leads to increasing efficiency with each new image, with potential for a ≈100≈100 increase in efficiency dependent on the size of the images.

Coronal heating and solar wind acceleration for electrons, protons and minor ions obtained from kinetic models based on Kappa distributions†

V. **Pierrard**1,2,* andM. Pieters
JGR, Volume 119, Issue 12, pages 9441–9455, December **2014**
http://onlinelibrary.wiley.com/doi/10.1002/2014JA020678/pdf
Astrophysical and space plasmas are commonly found to be out of thermal equilibrium, i.e., the velocity distribution functions (VDF) of their particles are not well described by Maxwellian distributions. They generally have more suprathermal particles in the tail of the distribution. The Kappa distribution provides a generalization to successfully describe such plasmas with tails decreasing as a power law of the velocity. In the present work, we improve the solar wind model developed on the basis of such Kappa distributions by incorporating azimuthally varying 1 AU boundary conditions to produce a spatially structured view of the solar wind expansion. By starting from the top of the chromosphere to the heliosphere and by applying relevant boundary conditions in the ecliptic plane, a global model of the corona and the solar wind is developed for each particle species. The model includes the natural heating of the solar corona automatically appearing when an enhanced population of suprathermal particles is present at low altitude in the solar (or stellar) atmosphere. This applies not only for electrons and protons, but also for the minor ions which have then a temperature increase proportional to their mass. Moreover, the presence of suprathermal electrons contributes to the acceleration of the solar wind to high bulk velocities when Coulomb collisions are neglected. The results of the model are illustrated in the solar corona and in solar wind for the different particles species and can now be directly compared in two dimensions with spacecraft observations in the ecliptic plane.

Inference of the chromospheric magnetic field configuration of solar plage using the Ca II 8542 Å line

A.G.M. **Pietrow**, D. Kiselman, J. de la Cruz Rodríguez, C. J. Díaz Baso, A. Pastor Yabar, R. Yadav
A&A 644, A43 **2020**
https://arxiv.org/pdf/2006.14486.pdf
https://doi.org/10.1051/0004-6361/202038750

Context: It has so far proven impossible to reproduce all aspects of the solar plage chromosphere in quasi-realistic numerical models. The magnetic field configuration in the lower atmosphere is one of the few free parameters in such simulations. The literature only offers proxy-based estimates of the field strength, as it is difficult to obtain observational constraints in this region. Sufficiently sensitive spectro-polarimetric measurements require a high signal-to-noise ratio, spectral resolution and cadence, which are at the limit of current capabilities. Aims: We use critically sampled spectro-polarimetric observations of the Ca II λ 8542 line obtained with the CRISP instrument of the Swedish 1-m Solar Telescope, to study the strength and inclination of the chromospheric magnetic field of a plage region. This will provide direct physics-based estimates of these values, which could aid modellers to put constraints on plage models. Methods: We increased the signal-to-noise ratio of the data by applying several methods including deep learning and PCA. We reach a noise level of 6·10−4Ic. We then use STiC, a non-local thermodynamic equilibrium (NLTE) inversion code to infer the atmospheric structure and magnetic field pixel by pixel. Results: We are able to infer a magnetic field strength and inclination for a plage region and for fibrils in the surrounding canopy. In the plage we report an absolute field strength of |B|=405±90 G, with an inclination of 9∘±6∘ with respect to the local vertical. This value for |B| is roughly double of what was reported previously, while the inclination matches previous studies done in the photosphere. In the fibrillar region we found |B|=290±50 G, with an inclination of 49∘±16∘. **June 15th 2018**

Solar physics in the 2020s: DKIST, parker solar probe, and solar orbiter as a multi-messenger constellation **Review**

V. Martinez **Pillet**, A. Tritschler, L. Harra, V. Andretta, A. Vourlidas …

2020

https://arxiv.org/ftp/arxiv/papers/2004/2004.08632.pdf

The National Science Foundation (NSF) Daniel K. Inouye Solar Telescope (DKIST) is about to start operations at the summit of Haleakala (Hawaii). DKIST will join the early science phases of the NASA and ESA Parker Solar Probe and Solar Orbiter encounter missions. By combining in-situ measurements of the near-sun plasma environment and detail remote observations of multiple layers of the Sun, the three observatories form an unprecedented multi-messenger constellation to study the magnetic connectivity inside the solar system. This white paper outlines the synergistic science that this multi-messenger suite enables.

Astro2020 Science White Paper: Synoptic Studies of the Sun as a Key to Understanding Stellar Astrospheres

Valentin Martinez **Pillet**, Frank Hill, Heidi Hammel, Dr. Alfred G. de Wijn, Sanjay Gosain, Joan Burkepile, Carl J. Henney, James R. T. McAteer, Hazel M. Bain, Ward B. Manchester IV, Haosheng Lin, Markus Roth, Kiyoshi Ichimoto, Yoshinori Suematsu

2019

https://arxiv.org/ftp/arxiv/papers/1903/1903.06944.pdf

Ground-based solar observations provide key contextual data (i.e., the 'big picture') to produce a complete description of the only astrosphere we can study in situ: our Sun's heliosphere. The next decade will see the beginning of operations of the Daniel K. Inouye Solar Telescope (DKIST). DKIST will join NASA's Parker Solar Probe and the NASA/ESA Solar Orbital mission, which together will study our Sun's atmosphere with unprecedented detail. This white paper outlines the current paradigm for ground-based solar synoptic observations, and indicates those areas that will benefit from focused attention.

Amplitude of solar gravity modes generated by penetrative plumes

C. **Pinçon**, T. Appourchaux, G. Buldgen

A&A **2021**

https://arxiv.org/pdf/2103.03760.pdf

The detection of gravity modes is expected to give us unprecedented insights into the inner dynamics of the Sun. Within this framework, predicting their amplitudes is essential to guide future observational strategies and seismic studies. In this work, we predict the amplitude of low-frequency asymptotic gravity modes generated by penetrative convection at the top of the radiative zone. The result is found to depend critically on the time evolution of the plumes inside the generation region. Using a solar model, we compute the GOLF apparent surface radial velocity of low-degree gravity modes in the frequency range 10 μHz≤ν≤100 μHz. In case of a Gaussian plume time evolution, gravity modes turn out to be undetectable because of too small surface amplitudes. This holds true despite a wide range of values considered for the parameters of the model. In the other limiting case of an exponential time evolution, plumes are expected to drive gravity modes in a much more efficient way because of a much higher temporal coupling between the plumes and the modes than in the Gaussian case. Using reasonable values for the plume parameters based on semi-analytical models, the apparent surface velocities in this case turn out to be one order of magnitude smaller than the 22-years GOLF detection threshold and than the previous estimates considering

turbulent pressure as the driving mechanism, with a maximum value of 0.05 cm s−1 for ℓ=1 and ν≈100 μHz. When accounting for uncertainties on the plume parameters, the apparent surface velocities in the most favorable plausible case become comparable to those predicted with turbulent pressure, and the GOLF observation time required for a detection at ν≈100 μHz and ℓ=1 is reduced to about 50 yrs.

Flux-tube geometry and wind speed during an activity cycle

R. F. **Pinto**, A. S. Brun, A. P. Rouillard
A&A **2016**
http://arxiv.org/pdf/1603.09251v1.pdf
The solar wind speed at 1 AU shows variations in latitude and in time which reflect the evolution of the global background magnetic field during the activity cycle. It is commonly accepted that the terminal wind speed in a magnetic flux-tube is anti-correlated with its expansion ratio, which motivated the definition of widely-used semi-empirical scaling laws relating one to the other. In practice, such scaling laws require ad-hoc corrections. A predictive law based solely on physical principles is still missing. We test whether the flux-tube expansion is the controlling factor of the wind speed at all phases of the cycle and at all latitudes using a very large sample of wind-carrying open magnetic flux-tubes. We furthermore search for additional physical parameters based on the geometry of the coronal magnetic field which have an influence on the terminal wind flow speed. We use MHD simulations of the corona and wind coupled to a dynamo model to provide a large statistical ensemble of open flux-tubes which we analyse conjointly in order to identify relations of dependence between the wind speed and geometrical parameters of the flux-tubes which are valid globally (for all latitudes and moments of the cycle). Our study confirms that the terminal speed of the solar wind depends very strongly on the geometry of the open magnetic flux-tubes through which it flows. The total flux-tube expansion is more clearly anti-correlated with the wind speed for fast rather than for slow wind flows, and effectively controls the locations of these flows during solar minima. Overall, the actual asymptotic wind speeds attained are also strongly dependent on field-line inclination and magnetic field amplitude at the foot-points. We suggest ways of including these parameters on future predictive scaling-laws for the solar wind speed.

Solar poloidal magnetic field generation rate from observations and mean-field dynamos

V.V. **Pipin**
Solar Phys. **299**, 111 **2024**
https://arxiv.org/pdf/2408.04934
https://doi.org/10.1007/s11207-024-02357-0
To estimate the hemispheric flux generation rate of the large-scale radial magnetic field in the Solar Cycles 23 and 24, we use the photospheric observations of the solar magnetic fields and results of the mean-field dynamo models. Results of the dynamo model show the strong impact of the radial turbulent diffusion on the surface evolution of the large-scale poloidal magnetic field and on the hemispheric magnetic flux generation rate. To process the observational data set we employ the parameters of the meridional circulation and turbulent diffusion from the Surface Flux-Transport (SFT) models. We find that the observed evolution of the axisymmetric vector potential contains the time--latitude patterns which can result from the effect of turbulent diffusion of the large-scale poloidal magnetic field in the radial direction. We think that, the SFT models can reconcile the observed rate of hemispheric magnetic flux generation by considering radial turbulent diffusion and lower values of the diffusion coefficient.

Toroidal Magnetic Flux Budget in Mean-field Dynamo Model of Solar Cycles 23 and 24

Valery V. **Pipin**1 and Alexander G. Kosovichev2,3
2024 ApJ 962 25
https://iopscience.iop.org/article/10.3847/1538-4357/ad1590/pdf
We study the toroidal magnetic flux budget of the axisymmetric part of a data-driven 3D mean-field dynamo model of Solar Cycles 23 and 24. The model simulates the global solar dynamo that includes the effects of the formation and evolution of bipolar magnetic regions (BMRs) emerging on the solar surface. By applying Stokes's theorem to the dynamo induction equation, we show that the hemispheric magnitude of the net axisymmetric toroidal magnetic field generation rate in the bulk of the convection zone can only partially be estimated from the surface parameters of the differential rotation and the axisymmetric radial magnetic field. The contribution of the radial integral along the equator, which is mostly due to the rotational radial shear at the bottom of the convection zone, has the same magnitude and is nearly in phase with the effect of the surface latitudinal differential rotation. Also, the toroidal field generation rate estimate strongly depends on the latitudinal profile of the surface radial magnetic field near the poles. This profile in our dynamo models significantly deviates from the polar magnetic field distribution observed during the minima of Solar Cycles 22, 23, and 24. The cause of this discrepancy requires further observational and theoretical studies. Comparing the 2D axisymmetric and the 3D nonaxisymmetric dynamo models, we find an increase in the toroidal field generation rate in the 3D model due to the surface effects of BMRs, resulting in an increase in the axisymmetric poloidal magnetic field magnitude.

Magnetic Flux Budget in Mean-Field Dynamo Model of Solar Cycles 23 and 24

V. V. **Pipin**, A. G. Kosovichev

ApJ **2023**

https://arxiv.org/pdf/2306.04124.pdf

We investigate the magnetic flux budget in a previously developed dynamo model of Solar Cycles 23 and 24. The mean-field 3D MHD model simulates the global dynamo process and the magnetic buoyancy instability that leads to the formation of bipolar magnetic regions (BMR) on the solar surface. The initial perturbations of the instability correspond to the distribution of active regions observed during the solar cycles. The toroidal and poloidal flux budgets are calculated by applying the Stokes theorem. The results are compared with a baseline 2D dynamo model without bipolar magnetic regions and with the synoptic observations from Kitt Peak Observatory and SoHO (Solar and Heliospheric Observatory) and SDO (Solar Dynamics Observatory) space missions. We find that while the regions of the high radial rotational shear at the boundaries of the convection zone are important for maintaining the dynamo process, the toroidal magnetic flux that results in the formation of BMR is generated by the latitudinal differential rotation. The toroidal flux generation reaches the maximum at the poles during the solar minima, which explains the correlation between the polar field strength and the subsequent sunspot maximum. However, we find that the generation rate of this flux strongly depends on the radial magnetic field distribution near the solar poles. Our results suggest that while the surface magnetic activity contributes to the poloidal magnetic flux budget, a significant part of the poloidal flux is generated in the deep convection zone, contrary to the Babcock-Leighton solar cycle scenario.

Effects of Emerging Bipolar Magnetic Regions in Mean-field Dynamo Model of Solar Cycles 23 and 24

V. V. **Pipin**1, A. G. Kosovichev2, and V. E. Tomin1

2023 ApJ 949 7

https://iopscience.iop.org/article/10.3847/1538-4357/acaf69/pdf

We model the physical parameters of Solar Cycles 23 and 24 using a nonlinear dynamical mean-field dynamo model that includes the formation and evolution of bipolar magnetic regions (BMRs). The Parker-type dynamo model consists of a complete MHD system in the mean-field formulation: the 3D magnetic induction equation, and 2D momentum and energy equations in the anelastic approximation. The initialization of BMRs is modeled in the framework of Parker's magnetic buoyancy instability. It defines the depths of BMR injections, which are typically located at the edge of the global dynamo waves. The distribution with longitude and latitude and the size of the initial BMR perturbations are taken from the NOAA database of active regions. The modeling results are compared with various observed characteristics of the solar cycles. Only the BMR perturbations located in the upper half of the convection zone lead to magnetic active regions on the solar surface. While the BMRs initialized in the lower part of the convection zone do not emerge on the surface, they still affect the global dynamo process. Our results show that BMRs can play a substantial role in the dynamo processes and affect the strength of the solar cycles. However, the data driven model shows that the BMR's effect alone cannot explain the weak Cycle 24. This weak cycle and the prolonged preceding minimum of magnetic activity were probably caused by a decrease of the turbulent helicity in the bulk of the convection zone during the decaying phase of Cycle 23.

On effects of surface bipolar magnetic regions on the convection zone dynamo

V.V. **Pipin**

MNRAS **2021**

https://arxiv.org/pdf/2112.09460.pdf

We investigate the effect of the surface tilted bipolar magnetic regions (BMR) on the large-scale dynamo distributed in the bulk of the convection zone. The study employs the nonlinear 3D mean-field dynamo model. The emergence of the BMR on the surface is modeled by means of the nonaxisymmetric magnetic buoyancy effect which acts on the large-scale toroidal magnetic field in the upper half of the convection zone. The nonaxisymmetric magnetic field which results from this mechanism is shallow. At the surface the effect of the BMR on the magnetic field generation is dominant. However, because of the shallow BMR distribution, its effect on the global dynamo is moderate. The most dynamo effect of the surface BMR is due to their evolution and the convective zone α effect. The fluctuations of the BMR's tilt affect the equatorial symmetry of the dynamo-generated magnetic field. In agreement with the solar observations, the emerging BMRs result in the negative magnetic helicity density of the large-scale nonaxisymmetric magnetic fields in the northern hemisphere of the star.

Solar dynamo cycle variations with a rotational period

V V **Pipin**

Monthly Notices of the Royal Astronomical Society, Volume 502, Issue 2, April **2021**, Pages 2565–2581,

https://doi.org/10.1093/mnras/stab033

Using non-linear mean-field dynamo models, we calculate magnetic cycle parameters, such as the dynamo cycle period, the amplitude of the total magnetic energy and the Poynting flux luminosity from the surface, for solar analogues with rotation periods in the range of 1–30 d. We perform simulations for both kinematic and non-kinematic dynamo models. The kinematic dynamo models, which take into account the non-linear α-effect and the loss of the magnetic flux due to magnetic buoyancy, show a decrease of the magnetic cycle with the decrease of the stellar rotation period. Stars with a rotational period of fewer than 10 d show non-stationary long-term variations of magnetic activity. The non-kinematic dynamo models take into account the magnetic field feedback on the large-scale flow and heat transport inside the convection zone. They show the non-monotonic variation of the dynamo period with the rotation rate. The models for rotational periods fewer than 10 d show non-stationary evolution with a slight increase in the primary dynamo period with the increase of the rotation rate. The non-kinematic models show the growth of the dynamo-generated magnetic flux with the increase of the rotation rate. There is a dynamo saturation for a star rotating with a period of 2 d or less. The saturation of the magnetic activity parameters is accompanied by a depression of the differential rotation.

The magnetic helicity density patterns from non-axisymmetric solar dynamo

V.V. **Pipin**

J. Plasma Phys. **2020**

https://arxiv.org/pdf/2006.01982.pdf

In the paper we study the helicity density patterns which can result from the emerging bipolar regions. Using the relevant dynamo model and the magnetic helicity conservation law we find that the helicity density pattern around the bipolar regions depends on the configuration of the ambient large-scale magnetic field, and in general they show the quadrupole distribution. The position of this pattern relative to the equator can depend on the tilt of the bipolar region. We compute the time-latitude diagrams of the helicity density evolution. The longitudinally averaged effect of the bipolar regions show two bands of sign for the density distribution in each hemisphere. Similar helicity density patterns are provided by the helicity density flux from the emerging bipolar regions subjected to the surface differential rotation. Examining effect of helicity fluxes from the bipolar regions on the large-scale dynamo we find that its effect to the dynamo saturation is negligible.

Torsional Oscillations in Dynamo Models with Fluctuations and Potential for Helioseismic Predictions of the Solar Cycles

Valery V**. Pipin**1 and Alexander G. Kosovichev2,3,4

2020 ApJ 900 26

https://doi.org/10.3847/1538-4357/aba4ad

Using a nonlinear mean-field solar dynamo model, we study relationships between the amplitude of the "extended" mode of migrating zonal flows ("torsional oscillations") and magnetic cycles, and investigate whether properties the torsional oscillations in subsurface layers and in the deep convection zone can provide information about the future solar cycles. We consider two types of dynamo models: models with regular variations of the α-effect, and models with stochastic fluctuations, simulating "long-memory" and "short-memory" types of magnetic activity variations. It is found that torsional oscillation parameters, such the zonal acceleration, show a considerable correlation with the magnitude of the subsequent cycles with a time lag of 11–20 yr. The sign of the correlation and the time-lag parameters can depend on the depth and latitude of the torsional oscillations as well as on the properties of long-term ("centennial") variations of the dynamo cycles. The strongest correlations are found for the zonal acceleration at high latitudes at the base of the convection zone. The model results demonstrate that helioseismic observations of the torsional oscillations can be useful for advanced prediction of the solar cycles, 1–2 sunspot cycles ahead.

Torsional oscillations and magnetic cycles in dynamo models with fluctuations

V.V. **Pipin**, A.G. Kosovichev

ApJ **2020**

https://arxiv.org/pdf/2004.08537.pdf

Using a nonlinear mean-field dynamo model, we study relationships between amplitude of the "extended" mode of migrating zonal flows ("torsional oscillations") and magnetic cycles, and investigate whether the torsional oscillations can be used for solar cycle prediction. We consider two types of dynamo models: models with regular variations of the alpha-effect, and models with stochastic variations. The regular dynamo models show the two different relationships for the growing and decaying stages of the magnetic cycle variations on centennial time scales. For the dynamo models with fluctuations, these relations are merged. We find that for both types of models the amplitude of solar cycles correlates well with the integral amplitude of the zonal harmonic ℓ=9 of the torsional acceleration waves of the preceding cycles in subsurface layers and with the ℓ=3 harmonic at the bottom of the convection zone. While these relationships are weaker than the previously known relationship of the cycle magnitude with the poloidal field in the preceding minima, the prediction horizon of the torsional oscillations is greater and may reach the full 11-year activity cycle. In addition, we find that the amplitude of the asymmetric about

the equator components of the torsional oscillations can be used as a precursor in forecasts of the hemispheric asymmetry of magnetic activity.

On the Origin of Solar Torsional Oscillations and Extended Solar Cycle

V.V. **Pipin**, A.G. Kosovichev
ApJ **887** 215 **2019**
https://arxiv.org/pdf/1908.04525.pdf
https://doi.org/10.3847/1538-4357/ab5952
We present a nonlinear mean-field model of the solar interior dynamics and dynamo, which reproduces the observed cyclic variations of the global magnetic field of the Sun, as well as the differential rotation and meridional circulation. Using this model, we explain, for the first time, the extended 22-year cycle of the solar torsional oscillations, observed as propagation of zonal variations of the angular velocity from high latitudes to the equator during the time equal to the full dynamo cycle. Our results show that the torsional oscillations result from an overlay of dynamo waves propagating in the bulk of the convection zone. The oscillations are driven by a combinations of magnetic field effects acting on turbulent angular momentum transport the dynamo-induced variations of meridional circulation and the large-scale Lorentz force. They are the primary drivers of the torsional oscillations, and provide necessary conditions for the extended solar-cycle phenomenon.

Evolution of Magnetic Helicity in Solar Cycle 24

Valery V. **Pipin**, Alexei A. Pevtsov, Yang Liu, Alexander G. Kosovichev
2019 *ApJL* **877** L36
https://arxiv.org/pdf/1905.00772.pdf
We propose a novel approach to reconstruct the surface magnetic helicity density on the Sun or sun-like stars. The magnetic vector potential is determined via decomposition of vector magnetic field measurements into toroidal and poloidal components. The method is verified using data from a non-axisymmetric dynamo model. We apply the method to vector field synoptic maps from Helioseismic and Magnetic Imager (HMI) onboard of Solar Dynamics Observatory (SDO) to study evolution of the magnetic helicity density during solar cycle 24. It is found that the mean helicity density of the non-axisymmetric magnetic field of the Sun evolves in a way which is similar to that reported for the current helicity density of the solar active regions. It has predominantly the negative sign in the northern hemisphere, and it is positive in the southern hemisphere. Also, the hemispheric helicity rule for the non-axisymmetric magnetic field showed the sign inversion at the end of cycle 24. Evolution of magnetic helicity density of large-scale axisymmetric magnetic field is different from that expected in dynamo theory. On one hand, the mean large- and small-scale components of magnetic helicity density display the hemispheric helicity rule of opposite sign at the beginning of cycle 24. However, later in the cycle, the two helicities exhibit the same sign in contrast with the theoretical expectations.
HMI Science Nuggets #128 **2019** http://hmi.stanford.edu/hminuggets/?p=2984

Does Nonaxisymmetric Dynamo Operate in the Sun?

V. V. **Pipin**1 and A. G. Kosovichev
2018 ApJ 867 145
sci-hub.tw/10.3847/1538-4357/aae1fb
We explore effects of random nonaxisymmetric perturbations of kinetic helicity (the α effect) and diffusive decay of bipolar magnetic regions on generation and evolution of large-scale nonaxisymmetric magnetic fields on the Sun. Using a reduced 2D nonlinear mean-field dynamo model and assuming that bipolar regions emerge due to magnetic buoyancy in situ of the large-scale dynamo action, we show that fluctuations of the α effect can maintain the nonaxisymmetric magnetic fields through a solar-type α 2Ω dynamo process. It is found that diffusive decay of bipolar active regions is likely to be the primary source of nonaxisymmetric magnetic fields observed on the Sun. Our results show that nonaxisymmetric dynamo models with stochastic perturbations of the α effect can explain periods of extremely high activity ("super-cycle" events) as well as periods of deep decline of magnetic activity. We compare the models with synoptic observations of solar magnetic fields for the last four activity cycles and discuss implications of our results for interpretation of observations of stellar magnetic activity.

The Nature of Variations in Anomalies of the Chemical Composition of the Solar Corona with the 11-Year Cycle

V. V. **Pipin** & V. M. Tomozov
Astronomy Reports April **2018**, Volume 62, Issue 4, pp 281–287
Astronomicheskii Zhurnal, **2018**, Vol. 95, No. 4, pp. 299–306.
Evidence that the distribution of the abundances of admixtures with low first-ionization potentials (FIP < 10 eV) in the lower solar corona could be associated with the typology of the largescale magnetic field is presented. Solar observations show an enhancement in the abundances of elements with low FIPs compared to elements with high

FIPs (>10 eV) in active regions and closed magnetic configurations in the lower corona. Observations with the ULYSSES spacecraft and at the Stanford Solar Observatory have revealed strong correlations between the manifestation of the FIP effect in the solar wind, the strength of the open magnetic flux (without regard to sign), and the ratio of the large-scale toroidal and poloidal magnetic fields at the solar surface. Analyses of observations of the Sun as a star show that the enhancement of the abundances of admixtures with low FIPs in the corona compared to their abundances in the photosphere (the FIP effect) is closely related to the solar-activity cycle and also with variations in the topology of the large-scale magnetic field. A possible mechanism for the relationship between the FIP effect and the spectral type of a star is discussed in the framework of solar–stellar analogies.

Nonkinematic solar dynamo models with double-cell meridional circulation

V.V. **Pipin**

JASTP 179 185-201 **2018**

https://arxiv.org/pdf/1803.09459.pdf

https://reader.elsevier.com/reader/sd/438B0064CEC8B99B7C8D5945A5F7723C0B543CA5DCCBD0433BC555AF0825DAF66BDF824E7FAA7ED7AF88C12BB045E89E

Employing the standard solar interior model as input we construct a dynamically-consistent nonlinear dynamo model that takes into account the detailed description of the \Lambda- effect, turbulent pumping, magnetic helicity balance, and magnetic feedback on the differential rotation and meridional circulation. The background mean-field hydrodynamic model of the solar convection zone accounts the solar-like angular velocity profile and the double-cell meridional circulation. We investigate an impact of the nonlinear magnetic field generation effects on the long-term variability and properties of the magnetic cycle. The nonlinear dynamo solutions are studied in the wide interval of the \alpha effect parameter from a slightly subcritical to supercritical values. It is found that the magnetic cycle period decreases with the increasing cycle's magnitude. The periodic long-term variations of the magnetic cycle are excited in case of the overcritical \alpha effect. These variations result from the hemispheric magnetic helicity exchange. It depends on the magnetic diffusivity parameter and the magnetic helicity production rate. The large-scale magnetic activity modifies the distribution of the differential rotation and meridional circulation inside convection zone. It is found that the magnetic feedback on the global flow affects the properties of the long-term magnetic cycles. We confront our findings with solar and stellar magnetic activity observations.

On the Origin of the Double-cell Meridional Circulation in the Solar Convection Zone

V. V. **Pipin**1,2 and A. G. Kosovichev

2018 ApJ 854 67

http://iopscience.iop.org/article/10.3847/1538-4357/aaa759/pdf

Recent advances in helioseismology, numerical simulations and mean-field theory of solar differential rotation have shown that the meridional circulation pattern may consist of two or more cells in each hemisphere of the convection zone. According to the mean-field theory the double-cell circulation pattern can result from the sign inversion of a nondiffusive part of the radial angular momentum transport (the so-called Λ-effect) in the lower part of the solar convection zone. Here, we show that this phenomenon can result from the radial inhomogeneity of the Coriolis number, which depends on the convective turnover time. We demonstrate that if this effect is taken into account then the solar-like differential rotation and the double-cell meridional circulation are both reproduced by the mean-field model. The model is consistent with the distribution of turbulent velocity correlations determined from observations by tracing motions of sunspots and large-scale magnetic fields, indicating that these tracers are rooted just below the shear layer.

HMI Science Nuggets, #91 March **2018** http://hmi.stanford.edu/hminuggets/?p=2351

Meridional circulation and torsional oscillations in a self-consistent solar dynamo model

V.V. **Pipin**, A.G. Kosovichev

2017

https://arxiv.org/pdf/1708.03073.pdf

Recent advances in helioseismology, numerical simulations and mean-field theory of the solar differential rotation have shown that the meridional circulation pattern may consist of two or more cells in each hemisphere of the convection zone. Accordingly, to the mean-field theory, the double-cell circulation pattern can result from inversion of the sign of non-diffusive part of the radial angular momentum transport (called the Lambda - effect) in the lower part of the solar convection zone. Here, we argue that this effect results from the radial gradients of the Coriolis force acting on convective flows. Employing the standard solar interior model as input we construct a dynamically self-consistent nonlinear dynamo model that takes into account the detailed description of the Lambda - effect, turbulent pumping, magnetic helicity balance, and magnetic feedback on the differential rotation and meridional circulation. The model explains the observed solar-cycle variations of the differential rotation ('torsional oscillations') as a manifestation of Lorentz forces associated with magnetic dynamo wave.

Nonlinear regimes in mean-field full-sphere dynamo

V.V. **Pipin**

2016

http://arxiv.org/pdf/1609.00906v1.pdf

The mean-field dynamo model is employed to study the non-linear dynamo regimes in a fully convective star of mass 0.3M⊙ rotating with period of 10 days. The differential rotation law was estimated using the mean-field hydrodynamic and heat transport equations. For the intermediate parameter of the turbulent magnetic Reynolds number, PmT=3 we found the oscillating dynamo regimes with period about 40Yr. The higher PmT results to longer dynamo periods. The meridional circulation has one cell per hemisphere. It is counter-clockwise in the Northen hemisphere. The amplitude of the flow at the surface around 1 m/s. Tne models with regards for meridional circulation show the anti-symmetric relative to equator magnetic field. If the large-scale flows is fixed we find that the dynamo transits from axisymmetric to non-axisymmetric regimes for the overcritical parameter of the αeffect. The change of dynamo regime occurs because of the non-axisymmetric non-linear α-effect. The situation persists in the fully non-linear dynamo models with regards of the magnetic feedback on the angular momentum balance and the heat transport in the star. It is found that the large-scale magnetic field quenches the latitudinal shear in the bulk of the star. However, the strong radial shear operates in the subsurface layer of the star. In the nonlinear case the profile of the angular velocity inside the star become close to the spherical surfaces. This supports the equator-ward migration of the axisymmetric magnetic field dynamo waves. Results of the nonlinear model suggest that, the magnetic configuration of the star dominates by the regular non-axisymmetric mode m=1, forming Yin Yang magnetic polarity pattern (at the plan perpendicular to the rotation axis) with the strong (>500 G) poloidal magnetic field in polar regions.

Effects of large-scale non-axisymmetric perturbations in the mean-field solar dynamo

V.V. **Pipin**, A.G. Kosovichev

2015 ApJ 813 134

http://arxiv.org/pdf/1505.00219v1.pdf

We explore a response of the non-linear non-axisymmetric mean-field solar dynamo model to the shallow non-axisymmetric perturbations with the strength of 1G. The amplitude of the non-axisymmetric field depends on the initial condition, helicity conservation, the depth of perturbation. It is found that perturbation which is anchored at the 0.9R have a profound effect and it produce the transient magnetic cycle of the axisymmetric magnetic field if it is initiated at the growing phase of the cycle. The non-symmetric about equator perturbation results the hemispheric asymmetry of the magnetic activity. The evolution of the axisymmetric and non-axisymmetric field depends on how well the magnetic helicity is conserved. In the range of Rm=10^{4-6} the evolution returns to the normal course in the next cycle and the non-axisymmetric field is generated due to non-linear alpha-effect and the magnetic buoyancy. In the stationary state of evolution the large-scale magnetic field demonstrate, the phenomena of the "active longitude" and the cyclic 180 degree flip-flop of the orientation of the large-scale magnetic field. We do not use any assumptions about the non-axisymmetric distribution of the turbulent parameters. The flip-flop effect is demonstrated for the first time in the solar type dynamo model. This effect disappears in the model which includes meridional circulation. The rotation periods of the equatorial dipole evolves from the period of 25.2 days during the relaxation epoch to the period of 27 days at the stationary state of evolution.

Magnetic Helicity of the Global Field in Solar Cycles 23 and 24

V. V. **Pipin**1,2 and A. A. Pevtsov

2014 ApJ 789 21

For the first time we reconstruct the magnetic helicity density of the global axisymmetric field of the Sun using the method proposed by Brandenburg et al. and Pipin et al. To determine the components of the vector potential, we apply a gauge which is typically employed in mean-field dynamo models. This allows for a direct comparison of the reconstructed helicity with the predictions from the mean-field dynamo models. We apply this method to two different data sets: the synoptic maps of the line-of-sight magnetic field from the Michelson Doppler Imager (MDI) on board the Solar and Heliospheric Observatory (SOHO) and vector magnetic field measurements from the Vector Spectromagnetograph (VSM) on the Synoptic Optical Long-term Investigations of the Sun (SOLIS) system. Based on the analysis of the MDI/SOHO data, we find that in solar cycle 23 the global magnetic field had positive (negative) magnetic helicity in the northern (southern) hemisphere. This hemispheric sign asymmetry is opposite to the helicity of the solar active regions, but it is in agreement with the predictions of mean-field dynamo models. The data also suggest that the hemispheric helicity rule may have reversed its sign during the early and late phases of cycle 23. Furthermore, the data indicate an imbalance in magnetic helicity between the northern and southern hemispheres. This imbalance seems to correlate with the total level of activity in each hemisphere in cycle 23. The magnetic helicity for the rising phase of cycle 24 is derived from SOLIS/VSM data, and qualitatively its latitudinal pattern is similar to the pattern derived from SOHO/MDI data for cycle 23.

On Polar Magnetic Field Reversal in Solar Cycles 21, 22, 23, and 24

Mykola I. **Pishkalo**

Solar Phys. 294:137 **2019**

https://arxiv.org/ftp/arxiv/papers/1909/1909.00055.pdf

https://link.springer.com/content/pdf/10.1007%2Fs11207-019-1520-9.pdf

The Sun's polar magnetic fields change their polarity near the maximum of sunspot activity. We analyzed the polarity reversal epochs in Solar Cycles 21 to 24. There was a triple reversal in the N-hemisphere in Solar Cycle 24 and single reversals in the rest of cases. Epochs of the polarity reversal from measurements of the Wilcox Solar Observatory (WSO) are compared with ones when the reversals were completed in the N- and S-hemispheres. The reversal times were compared with hemispherical sunspot activity and with the Heliospheric Current Sheet (HCS) tilts, too. It was found that reversals occurred at the epoch of the sunspot activity maximum in Cycles 21 and 23, and after the corresponding maxima in Cycles 22 and 24, and one-two years after maximal HCS tilts calculated in WSO. Reversals in Solar Cycles 21, 22, 23, and 24 were completed first in the N-hemisphere and then in the S-hemisphere after 0.6, 1.1, 0.7, and 0.9 years, respectively. The polarity inversion in the near-polar latitude range \pm(55-90)^\circ occurred from 0.5 to 2.0 years earlier that the times when the reversals were completed in corresponding hemisphere. Using the maximal smoothed WSO polar field as precursor we estimated that amplitude of Solar Cycle 25 will reach 116 \pm 12 in values of smoothed monthly sunspot numbers and will be comparable with the current cycle amplitude equaled to 116.4.

Solar surveillance with CLIMSO: instrumentation, database and on-going developments

Frédéric **Pitout**1*, Laurent Koechlin1, Arturo López Ariste1, Luc Dettwiller2 and Jean-Michel Glorian1

J. Space Weather Space Clim. **2020**, 10, 47

https://doi.org/10.1051/swsc/2020039

https://www.swsc-journal.org/articles/swsc/pdf/2020/01/swsc200034.pdf

CLIMSO is a suite of solar telescopes installed at Pic du Midi observatory in the southwest of France. It consists of two refractors that image the full solar disk in Hα and CaII K, and two coronagraphs that capture the prominences and ejections of chromospheric matter in Hα and HeI. Synoptic observations are carried out since 2007 and they follow those of previous instruments. CLIMSO, together with its predecessors, offer a temporal coverage of several solar cycles. With a direct access to its images, CLIMSO contributes to real time monitoring of the Sun. For that matter, the national research council for astrophysics (CNRS/INSU) has labelled CLIMSO as a national observation service for “surveillance of the Sun and the terrestrial space environment”. Products, under the form of images, movies or data files, are available via the CLIMSO DataBase. In this paper, we present the current instrumental configuration; we detail the available products and show how to access them; we mention some possible applications for solar and space weather; and finally, we evoke developments underway, both numerical to valorise our data, and instrumental to offer more and better capabilities.

The solar cycle variation of topological structures in the global solar corona

S. J. **Platten**, C. E. Parnell, A. L. Haynes, E. R. Priest and D. H. Mackay

A&A 565, A44 (**2014**)

http://arxiv.org/pdf/1406.5333v1.pdf

Context. The complicated distribution of magnetic flux across the solar photosphere results in a complex web of coronal magnetic field structures. To understand this complexity, the magnetic skeleton of the coronal field can be calculated. The skeleton highlights the (separatrix) surfaces that divide the field into topologically distinct regions, allowing open-field regions on the solar surface to be located. Furthermore, separatrix surfaces and their intersections with other separatrix surfaces (i.e., separators) are important likely energy release sites.

Aims. The aim of this paper is to investigate, throughout the solar cycle, the nature of coronal magnetic-field topologies that arise under the potential-field source-surface approximation. In particular, we characterise the typical global fields at solar maximum and minimum.

Methods. Global magnetic fields are extrapolated from observed Kitt Peak and SOLIS synoptic magnetograms, from Carrington rotations 1645 to 2144, using the potential-field source-surface model. This allows the variations in the coronal skeleton to be studied over three solar cycles.

Results. The main building blocks which make up magnetic fields are identified and classified according to the nature of their separatrix surfaces. The magnetic skeleton reveals that, at solar maximum, the global coronal field involves a multitude of topological structures at all latitudes criss-crossing throughout the atmosphere. **Many open-field regions exist originating anywhere on the photosphere.** At solar minimum, the coronal topology is heavily influenced by the solar magnetic dipole. A strong dipole results in a simple large-scale structure involving just two large polar open-field regions, but, at short radial distances between ± 60° latitude, the small-scale topology is complex. If the solar magnetic dipole if weak, as in the recent minimum, then the low-latitude quiet-sun magnetic fields may be globally significant enough to create many disconnected open-field regions between ± 60° latitude, in addition to the two polar open-field regions.

High-fidelity 3D Reconstruction of Solar Coronal Physics with the Updated CROBAR Method

Joseph **Plowman** (1), Daniel B. Seaton (1), Amir Caspi (1), J. Marcus Hughes (1), Matthew J. West (1)
ApJ **2023**
https://arxiv.org/pdf/2309.08053.pdf
We present an extension of the Coronal Reconstruction Onto B-Aligned Regions (CROBAR) method to Linear Force Free Field (LFFF) extrapolations, and apply it to the reconstruction of a set of AIA, MDI, and STEREO EUVI data. The results demonstrate that CROBAR can not only reconstruct coronal emission structures, but also that it can help constrain the coronal field extrapolations via the LFFF's helicity α parameter. They also provide a real-world example of how CROBAR can easily incorporate information from multiple perspectives to improve its reconstructions, and we also use the additional perspectives to help validate the reconstructions. We furthermore touch on the use of real-world emission passbands rather than idealized power-law type ones using DEMs. We conclude with a comparison of CROBAR generated emission to observed emission and those produced with idealized DEM based power-laws. These results further illustrate the promise of CROBAR for real-world applications, and we make available a preliminary release of the software available for download. **2010-07-25**

Three-dimensional Reconstruction of Coronal Plasma Properties from a Single Perspective

Joseph **Plowman**
ApJ **2021**
https://arxiv.org/pdf/2103.02028.pdf
Much of our understanding of the state of coronal plasmas comes from observations that are optically thin. This means that light travels freely through the corona without being materially affected by it, which allows it to be easily seen through, but also results in a line-of-sight degeneracy which has previously thwarted attempts to recover the three-dimensional structure of the coronal plasma. However, although the corona is disorganized in the line-of-sight direction, it is highly organized in the field-aligned direction. This paper demonstrates how to exploit this organization to resolve the line-of-sight degeneracy in the plasma properties using a suitable magnetic field structure. A preliminary investigation with a potential field is shown, finding a solution which clearly resembles the real solar data, even with a single perspective. The results indicate that there is ample information in the resulting residuals that can be used to refine the magnetic field structure, allowing, for the first time, the optically thin plasma observations to speak directly to the magnetic field extrapolations.

A Fast, Simple, Robust Algorithm for Coronal Temperature Reconstruction

Joseph **Plowman**1 and Amir Caspi2
2020 ApJ 905 17
https://doi.org/10.3847/1538-4357/abc260
We describe a new algorithm for reconstruction of differential emission measures (DEMs) in the solar corona. Although a number of such algorithms currently exist, they can have difficulty converging for some cases and can be complex, slow, or idiosyncratic in their output (i.e., their inversions can have features that are a result of the inversion code and instrument response, not of the solar source); we will document some of these issues in this paper. The new algorithm described here significantly reduces these drawbacks and is particularly notable for its simplicity; it is reproduced here, in full, on a single page. After we describe the algorithm, we compare its performance and fidelity with some prevalent methods. Although presented here for extreme-ultraviolet data, the algorithm is robust and extensible to any other wavelengths (e.g., X-rays) where the DEM treatment is valid.

Calibrating GONG Magnetograms with End-to-End Instrument Simulation III: Comparison, Calibration, and Results

Joseph E. **Plowman** & Thomas E. Berger
Solar Physics volume 295, Article number: 144 (**2020**)
https://link.springer.com/content/pdf/10.1007/s11207-020-01683-3.pdf
This is the last of three papers describing an ‘absolute’ calibration of the GONG magnetograph using and end-to-end simulation of its measurement process. The simulation begins with a MURaM 3D MHD datacube and ends with a ‘synthetic magnetogram’ of the corresponding magnetic field values as they would be observed by GONG. We determine a calibration by comparing the synthetic magnetic field measurements with the MURaM magnetic field values that produced them. The previous two papers have described the GONG measurement process (both instrument and data processing), our simulation of it, and the theory of magnetogram comparison and calibration. In this paper, we address some final points on calibration, combine all of this work into a set of calibration curves, and consider the results. We also review the results of the previous two papers for locality of reference. Our calibration indicates that GONG magnetograms underestimate weak flux by a factor of ∼2∼2 near disk center, but that factor decreases to ∼1as the line-of-sight approaches the limb. A preliminary investigation of the generalizability of these results suggests other instruments will be affected in a similar way. We also find that some differences in previous magnetograph comparisons are artifacts of instrumental resolution which do not reflect an intrinsic calibration

difference, and the measurements are more similar than sometimes thought. These results are directly applicable to question of solar wind prediction model accuracies, particularly in the search for the cause of the common discrepancy between predicted solar wind magnetic flux at 1 AU and values measured in situ by current satellite missions.

Calibrating GONG Magnetograms with End-to-End Instrument Simulation II: Theory of Calibration

Joseph E. **Plowman** & Thomas E. Berger
Solar Physics volume 295, Article number: 142 (**2020**)
https://link.springer.com/content/pdf/10.1007/s11207-020-01709-w.pdf
This is the second of three papers describing an 'absolute' calibration of the GONG magnetograph using an end-to-end simulation of its measurement process. In the first paper, we described the GONG instrument and our 'end-to-end' simulation of its measurement process. In this paper, we consider the theory of calibration, and magnetograph comparison in general, identifying some of the significant issues and pitfalls. The calibration of a magnetograph is a function of whether or not it preserves flux, independent of its spatial resolution. However, we find that the one-dimensional comparison methods most often used for magnetograph calibration and comparison will show dramatic differences between two magnetograms with differing spatial resolution, even if they both preserve flux. Some of the apparent disagreement between magnetograms found in the literature are likely a result of these instrumental resolution differences rather than any intrinsic calibration differences. To avoid them, spatial resolution must be carefully matched prior to comparing magnetograms or making calibration curves. In the third paper, we apply the lessons learned here to absolute calibration of GONG using our 'end-to-end' measurement simulation.

Calibrating GONG Magnetograms with End-to-end Instrument Simulation I: Background, the GONG Instrument, and End-to-end Simulation

Joseph E. **Plowman** & Thomas E. Berger
Solar Physics volume 295, Article number: 143 (**2020**)
https://link.springer.com/content/pdf/10.1007/s11207-020-01682-4.pdf
This is the first of three papers describing an 'absolute' calibration of the GONG magnetograph using an end-to-end simulation of its measurement process. The input to this simulation is a MURaM 3D MHD photospheric simulation and the output is the corresponding set of simulated data numbers which would be recorded by the GONG detectors. These simulated data numbers are then used to produce 'synthetic magnetograms' which can be compared with the simulation inputs. This paper describes the GONG instrument, the MURaM datacube, our instrument simulator, and calculation of synthetic magnetograms, setting the stage for the subsequent two papers. These will first lay groundwork for calibration (and magnetogram comparison in general), then apply them to calibration of GONG using the simulation results.

A Fast, Simple, Robust Algorithm for Coronal Temperature Reconstruction

Joseph **Plowman**, Amir Caspi
ApJ **2020**
https://arxiv.org/pdf/2006.06828.pdf
We describe a new algorithm for reconstruction of Differential Emission Measures (DEMs) in the solar corona. Although a number of such algorithms currently exist, they can have difficulty converging for some cases, and can be complex, slow, or idiosyncratic in their output (i.e., their inversions can have features that are a result of the inversion code and instrument response, not of the solar source); we will document some of these issues in this paper. The new algorithm described here significantly reduces these drawbacks and is particularly notable for its simplicity; it is reproduced here, in full, on a single page. After we describe the algorithm, we compare its performance and fidelity with some prevalent methods. Although presented here for extreme ultraviolet (EUV) data, the algorithm is robust and extensible to any other wavelengths (e.g., X-rays) where the DEM treatment is valid.
2010-08-01, 2010-08-14

A center-median filtering method for detection of temporal variation in coronal images

Joseph **Plowman***
J. Space Weather Space Clim., 6, A8 (**2016**)
http://www.swsc-journal.org/articles/swsc/pdf/2016/01/swsc150009.pdf
http://arxiv.org/pdf/1511.04481v1.pdf
Events in the solar corona are often widely separated in their timescales, which can allow them to be identified when they would otherwise be confused with emission from other sources in the corona. Methods for cleanly separating such events based on their timescales are thus desirable for research in the field. This paper develops a technique for identifying time-varying signals in solar coronal image sequences which is based on a per-pixel running median filter and an understanding of photon-counting statistics. Example applications to "EIT waves" (named after EIT, the EUV Imaging Telescope on the Solar and Heliospheric Observatory) and small-scale dynamics are shown, both

using 193 Å data from the Atmospheric Imaging Assembly (AIA) on the Solar Dynamics Observatory. The technique is found to discriminate EIT waves more cleanly than the running and base difference techniques most commonly used. It is also demonstrated that there is more signal in the data than is commonly appreciated, finding that the waves can be traced to the edge of the AIA field of view when the data are rebinned to increase the signal-to-noise ratio. **2013-04-11**

Maximal growth rate of the ascending phase of a sunspot cycle for predicting its amplitude

Tatiana **Podladchikova**, Shantanu Jain, Astrid M. Veronig, Olga Sutyrina, Mateja Dumbovic, Frederic Clette, Werner Poetzi

A&A **2022**

https://arxiv.org/pdf/2206.12606

Forecasting the solar cycle amplitude is important for a better understanding of the solar dynamo as well as for many space weather applications. We demonstrated a steady relationship between the maximal growth rate of sunspot activity in the ascending phase of a cycle and the subsequent cycle amplitude on the basis of four data sets of solar activity indices: total sunspot numbers, hemispheric sunspot numbers from the new catalogue from 1874 onwards, total sunspot areas, and hemispheric sunspot areas. For all the data sets, a linear regression based on the maximal growth rate precursor shows a significant correlation. Validation of predictions for cycles 1-24 shows high correlations between the true and predicted cycle amplitudes reaching r = 0.93 for the total sunspot numbers. The lead time of the predictions varies from 2 to 49 months, with a mean value of 21 months. Furthermore, we demonstrated that the sum of maximal growth rate indicators determined separately for the north and the south hemispheric sunspot numbers provides more accurate predictions than that using total sunspot numbers. The advantages reach 27% and 11% on average in terms of rms and correlation coefficient, respectively. The superior performance is also confirmed with hemispheric sunspot areas with respect to total sunspot areas. The maximal growth rate of sunspot activity in the ascending phase of a solar cycle serves as a reliable precursor of the subsequent cycle amplitude. Furthermore, our findings provide a strong foundation for supporting regular monitoring, recording, and predictions of solar activity with hemispheric sunspot data, which capture the asymmetric behaviour of the solar activity and solar magnetic field and enhance solar cycle prediction methods.

Stereoscopic Measurements of Coronal Doppler Velocities

O. **Podladchikova**, L. Harra, K.Barczynski, C.H. Mandrini, F. Auchere, D. Berghmans, E. Buchlin, L. Dolla, M. Mierla, S. Parenti, L. Rodriguez

A&A 655, A57 **2021**

https://arxiv.org/pdf/2108.02280.pdf

https://www.aanda.org/articles/aa/pdf/2021/11/aa40457-21.pdf

https://doi.org/10.1051/0004-6361/202140457

The Solar Orbiter mission, with an orbit outside the
Sun Earth line and leaving the ecliptic plane, opens up opportunities for the combined analysis of measurements obtained by solar imagers and spectrometers. For the first time, different space spectrometers will be located at wide angles to each other, allowing three-dimensional (3D) spectroscopy of the solar atmosphere. The aim of this work is to prepare the methodology to facilitate the reconstruction of 3D vector velocities from two stereoscopic LOS Doppler velocity measurements using the Spectral Imaging of the Coronal Environment (SPICE) onboard the Solar Orbiter and the near-Earth spectrometers, while widely separated in space. We develop the methodology using the libraries designed earlier for the STEREO mission but applied to spectroscopic data from the Hinode mission and the Solar Dynamics Observatory. We use well-known methods of static and dynamic solar rotation stereoscopy and the methods of EUV stereoscopic triangulation for optically thin coronal EUV plasma emissions. We develop new algorithms using analytical geometry in space to determine the 3D velocity in coronal loops. We demonstrate our approach with the reconstruction of 3D velocity vectors in plasma flows along "open" and "closed" magnetic loops. This technique will be applied to an actual situation of two spacecraft at different separations with spectrometers onboard (SPICE versus the Interface Region Imaging Spectrograph (IRIS) and Hinode imaging spectrometer) during the Solar Orbiternominal phase. We summarise how these observations can be coordinated.

Sunspot Number Second Differences as a Precursor of the Following 11-year Sunspot Cycle

Tatiana **Podladchikova**1, Ronald Van der Linden2, and Astrid M. Veronig3

2017 ApJ 850 81

http://sci-hub.cc/http://iopscience.iop.org/0004-637X/850/1/81/

https://arxiv.org/pdf/1712.05782.pdf

Forecasting the strength of the sunspot cycle is highly important for many space weather applications. Our previous studies have shown the importance of sunspot number variability in the declining phase of the current 11-year sunspot cycle to predict the strength of the next cycle when the minimum of the current cycle has been observed. In this study we continue this approach and show that we can remove the limitation of having to know the minimum

epoch of the current cycle, and that we can already provide a forecast of the following cycle strength in the early stage of the declining phase of the current cycle. We introduce a method to reliably calculate sunspot number second differences (SNSD) in order to quantify the short-term variations of sunspot activity. We demonstrate a steady relationship between the SNSD dynamics in the early stage of the declining phase of a given cycle and the strength of the following sunspot cycle. This finding may bear physical implications on the underlying dynamo at work. From this relation, a relevant indicator is constructed that distinguishes whether the next cycle will be stronger or weaker compared to the current one. We demonstrate that within 24–31 months after reaching the maximum of the cycle, it can be decided with high probability (0.96) whether the next cycle will be weaker or stronger. We predict that sunspot cycle 25 will be weaker than the current cycle 24.

AI-ready Data in Space Science and Solar Physics: Problems, Mitigation and Action Plan

Bala **Poduval**, Robert McPherron, Raymond Walker, +++
Front. Astron. Space Sci., 10: 1203598 **2023**
https://www.frontiersin.org/articles/10.3389/fspas.2023.1203598/pdf
In the domain of space science, numerous ground-based and space-borne data of various phenomena have been accumulating rapidly, making analysis and scientific interpretation challenging. However, recent trends in the application of artificial intelligence (AI) have been shown to be promising in the extraction of information or knowledge discovery from these extensive data sets. Coincidentally, preparing these data for use as inputs to the AI algorithms, referred to as AI-readiness, is one of the outstanding challenges in leveraging AI in space science. Preparation of AI-ready data includes, among other aspects: 1) collection (accessing and downloading) of appropriate data representing the various physical parameters associated with the phenomena under study from different repositories; 2) addressing data formats such as conversion from one format to another, data gaps, quality flags and labeling; 3) standardizing metadata and keywords in accordance with NASA archive requirements or other defined standards; 4) processing of raw data such as data normalization, detrending, and data modeling; and 5) documentation of technical aspects such as processing steps, operational assumptions, uncertainties, and instrument profiles. Making all existing data AI-ready within a decade is impractical and data from future missions and investigations exacerbates this. This reveals the urgency to set the standards and start implementing them now. This article presents our perspective on the AI-readiness of space science data and mitigation strategies including definition of AI-readiness for AI applications; prioritization of data sets, storage, and accessibility; and identifying the responsible entity (agencies, private sector, or funded individuals) to undertake the task.

Editorial: Applications of Statistical Methods and Machine Learning in the Space Sciences

Bala **Poduval**, Karly Pitman, Olga Verkhoglyadova, and Peter Wintoft
Editorial: Applications of statistical methods and machine learning in the space sciences.
Front. Astron. Space Sci. 10:1163530. **2023**
doi: 10.3389/fspas.2023.1163530
https://www.frontiersin.org/articles/10.3389/fspas.2023.1163530/pdf
The fully virtual conference, Applications of Statistical Methods and Machine Learning in the Space Sciences, hosted by Space Science Institute's (SSI) Center for Data Science (CDS) and sponsored by the National Science Foundation (NSF), was held during 17–21 May 2021 (http://spacescience.org/workshops/mlconference2021.php). This event brought together experts in various disciplines of the space sciences (such as solar physics and aeronomy, planetary and exoplanetary sciences, geology, astrobiology, and astronomy) and industry to leverage the advancements in statistics, data science, methods of artificial intelligence (AI), and information theory with the aim of improving the analytic models and their predictive capabilities utilizing the enormous volume of data in these fields.
See http://spacescience.org/workshops/mlconference2021.php

POINT-SPREAD FUNCTIONS FOR THE EXTREME-ULTRAVIOLET CHANNELS OF SDO/AIA TELESCOPES

B. **Poduval**1, C. E. DeForest1, J. T. Schmelz2, and S. Pathak
2013 ApJ 765 144
We present the stray-light point-spread functions (PSFs) and their inverses we characterized for the Atmospheric Imaging Assembly (AIA) EUV telescopes on board the Solar Dynamics Observatory (SDO) spacecraft. The inverse kernels are approximate inverses under convolution. Convolving the original Level 1 images with them produces images with improved stray-light characteristics. We demonstrate the usefulness of these PSFs by applying them to two specific cases: photometry and differential emission measure (DEM) analysis. The PSFs consist of a narrow Gaussian core, a diffraction component, and a diffuse component represented by the sum of a Gaussian-truncated Lorentzian and a shoulder Gaussian. We determined the diffraction term using the measured geometry of the diffraction pattern identified in flare images and the theoretically computed intensities of the principal maxima of the first few diffraction orders. To determine the diffuse component, we fitted its parameterized model using iterative forward-modeling of the lunar interior in the SDO/AIA images from the 2011 March 4 lunar transit. We

find that deconvolution significantly improves the contrast in dark features such as miniature coronal holes, though the effect was marginal in bright features. On a percentage-scattering basis, the PSFs for SDO/AIA are better by a factor of two than that of the EUV telescope on board the Transition Region And Coronal Explorer mission. A preliminary analysis suggests that deconvolution alone does not affect DEM analysis of small coronal loop segments with suitable background subtraction. We include the derived PSFs and their inverses as supplementary digital materials.

Modeling Magnetic Flux Emergence in Bipolar Active Regions

Mariano **Poisson**, Marcelo López Fuentes, Cristina H. Mandrini, Pascal Démoulin, Francisco Grings
Solar Phys. **2024**
https://arxiv.org/pdf/2405.12208
Active regions (ARs) appear in the solar atmosphere as a consequence of the emergence of magnetic flux-ropes (FR). In this study, we use Bayesian methods to analyze line-of-sight magnetograms of emerging ARs. We employ a FR model consisting of a half-torus field structure based on eight parameters. The goal is to derive constrained physical parameters of the originating FR which are consistent with the observations. Specifically, we aim to obtain a precise estimation of the AR tilt angle and magnetic twist at different stages of the emergence process. To achieve this, we propose four temporal methods that correlate the field parameter evolutions with a single coherent FR. These methods differ from each other in the size of the explored parameter space. We test the methods on four bipolar ARs observed with the Michelson Doppler Imager on board the Solar and Heliospheric Observatory. We find that tilt angles are typically consistent between the temporal methods, improving previous estimations at all stages of the emergence. The twist sign derived from the temporal methods is consistent with previous estimations. The standard errors of all the methods used are similar, indicating that they model the observations equally well. These results indicate that the proposed methods can be used to obtain global magnetic parameters of ARs during their early evolution. The derived parameters contribute to a better understanding of the formation of FRs, and the role of ARs in the magnetic recycling process along the solar cycle.

Bayesian approach for modeling solar active region global magnetic parameters

M. **Poisson**, F. Grings, C.H. Mandrini, M. López-Fuentes, P. Démoulin
A&A **2022**
https://arxiv.org/pdf/2207.05900.pdf
Context. Active regions (ARs) appear in the solar atmosphere as a consequence of the emergence of magnetic flux tubes. The presence of elongated magnetic polarities in line-of-sight (LOS) magnetograms indicates the existence of twist in the flux tubes forming them. These polarity elongations, called magnetic tongues, bias the measurement of AR characteristics obtained during their emergence phase (e.g. their tilt angle and magnetic flux, among others). In particular, obtaining a good estimation of the tilt angle evolution plays a key role in constraining flux-transport dynamo models. Aims. In this work we aim to estimate the intrinsic properties of the twisted flux tubes, or flux ropes, that form ARs by quantitatively comparing observed LOS magnetograms with synthetic ones derived from a toroidal magnetic flux tube model. Methods. For this reason, we develop a Bayesian inference method to obtain the statistical distributions of the inferred model parameters. As an example, we apply the method to NOAA AR 10268. Next, we test the results using a synthetic-AR generator to quantify the effect of small scale perturbations over the inferred parameter distributions. Results. We conclude that this method can significantly remove the effects of magnetic tongues on the derived AR global characteristics, providing a better knowledge of the intrinsic properties of the emerging flux rope. Conclusions. These results provide a framework for future analysis of the physical properties of emerging ARs using Bayesian statistics.

Properties of Magnetic Tongues over a Solar Cycle

Mariano **Poisson** , Pascal Démoulin, Marcelo López Fuentes, Cristina H. Mandrini
Solar Phys. Volume 291, Issue 6, pp 1625–1646 **2016**
http://arxiv.org/pdf/1609.00329v1.pdf
The photospheric spatial distribution of the main magnetic polarities of bipolar active regions (ARs) present during their emergence deformations are known as magnetic tongues. They are attributed to the presence of twist in the toroidal magnetic-flux tubes that form the ARs. The aim of this article is to study the twist of newly emerged ARs from the evolution of magnetic tongues observed in photospheric line-of-sight magnetograms. We apply the procedure described by Poisson et al. (Solar Phys. 290, 727, 2015a) to ARs observed over the full Solar Cycle 23 and the beginning of Cycle 24. Our results show that the hemispherical rule obtained using the tongues as a proxy of the twist has a weak sign dominance (53 % in the southern hemisphere and 58 % in the northern hemisphere). By defining the variation of the tongue angle, we characterize the strength of the magnetic tongues during different phases of the AR emergence. We find that there is a tendency of the tongues to be stronger during the beginning of the emergence and to become weaker as the AR reaches its maximum magnetic flux. We compare this evolution with the emergence of a toroidal flux-rope model with non-uniform twist. The variety of evolution of the tongues in the analyzed ARs can only be reproduced when using a broad range of twist profiles, in particular having a large variety of twist gradients in the direction vertical to the photosphere. Although the analytical model used is a special

case, selected to minimize the complexity of the problem, the results obtained set new observational constraints to theoretical models of flux-rope emergence that form bipolar ARs.

Study of Geomagnetic Storms and Solar and Interplanetary Parameters for Solar Cycles 22 and 24

Meena **Pokharia**, Lalan Prasad, Chandrashekhar Bhoj, Chandni Mathpal
Solar Physics September **2018**, 293:126
https://link.springer.com/article/10.1007/s11207-018-1345-y
http://sci-hub.tw/https://link.springer.com/article/10.1007/s11207-018-1345-y
The aim of this paper is to investigate the association of geomagnetic storms with the component of the *interplanetary magnetic field (IMF) perpendicular to the ecliptic (BzBz), the solar wind speed (VV), the* product of solar wind speed and BzBz (VBz), the Kp index, and the sunspot number (SSN) for two consecutive even solar cycles, Solar Cycles 22 (1986 – 1995) and 24 (2009 – 2017). A comparative study has been done using the superposed epoch method (Chree analysis). The results of the present analysis show that BzBz is a geoeffective parameter. The correlation coefficient between Dst and BzBz is found to be 0.8 for both Solar Cycles 22 and 24, which indicates that these two parameters are highly correlated. Statistical relationships between Dst and Kp are established and it is shown that for the two consecutive even solar cycles, Solar Cycles 22 and 24, the patterns are strikingly similar. The correlation coefficient between Dst and Kp is found to be the same for the two solar cycles (−0.8), which clearly indicates that these parameters are well anti-correlated. For the same studied period we found that the SSN does not show any relationship with Dst and Kp, while there exists an inverse relation between Dst and the solar wind speed, with some time lag. We have also found that VBz is a more relevant parameter for the production of geomagnetic storms, as compared to VV and BzBz separately. In addition, we have found that in Solar Cycles 22 and 24 this combined parameter is more relevant during the descending phase as compared to the ascending phase.

Solar Coronal Plumes **Review**

Giannina **Poletto**
Living Reviews in Solar Physics PUB.NO. lrsp-**2015**-7
http://solarphysics.livingreviews.org/Articles/lrsp-2015-7/download/lrsp-2015-7Color.pdf
Polar plumes are thin long ray-like structures that project beyond the limb of the Sun polar regions, maintaining their identity over distances of several solar radii. Plumes have been first observed in white-light (WL) images of the Sun, but, with the advent of the space era, they have been identified also in X-ray and UV wavelengths (XUV) and, possibly, even in in situ data. This review traces the history of plumes, from the time they have been first imaged, to the complex means by which nowadays we attempt to reconstruct their 3-D structure. Spectroscopic techniques allowed us also to infer the physical parameters of plumes and estimate their electron and kinetic temperatures and their densities. However, perhaps the most interesting problem we need to solve is the role they cover in the solar wind origin and acceleration: Does the solar wind emanate from plumes or from the ambient coronal hole wherein they are embedded? Do plumes have a role in solar wind acceleration and mass loading? Answers to these questions are still somewhat ambiguous and theoretical modeling does not provide definite answers either. Recent data, with an unprecedented high spatial and temporal resolution, provide new information on the fine structure of plumes, their temporal evolution and relationship with other transient phenomena that may shed further light on these elusive features.

Cosmogenic Isotope Variability During the Maunder Minimum: Normal 11-year Cycles Are Expected

S. V. **Poluianov**, I. G. Usoskin, G. A. Kovaltsov
Solar Phys., **2014**
The amplitude of the 11-year cycle measured in the cosmogenic isotope 10Be during the Maunder Minimum is comparable to that during the recent epoch of high solar activity. Because of the virtual absence of the cyclic variability of sunspot activity during the Maunder Minimum this seemingly contradicts an intuitive expectation that lower activity would result in smaller solar-cycle variations in cosmogenic radio-isotope data, or in none, leading to confusing and misleading conclusions. It is shown here that large 11-year solar cycles in cosmogenic data observed during periods of suppressed sunspot activity do not necessarily imply strong heliospheric fields. Normal-amplitude cycles in the cosmogenic radio-isotopes observed during the Maunder Minimum are consistent with theoretical expectations because of the nonlinear relation between solar activity and isotope production. Thus, cosmogenic-isotope data provide a good tool to study solar-cycle variability even during grand minima of solar activity.

IRIS observations of the low-atmosphere counterparts of active region outflows

Vanessa **Polito**, Bart De Pontieu, Paola Testa, David H. Brooks, Viggo Hansteen

2020 *ApJ* **903** 68

https://arxiv.org/pdf/2010.15945.pdf

https://doi.org/10.3847/1538-4357/abba1d

Active region (AR) outflows have been studied in detail since the launch of \textit{Hinode}/EIS and are believed to provide a possible source of mass and energy to the slow solar wind. In this work, we investigate the lower atmospheric counterpart of AR outflows using observations from the \textit{Interface Region Imaging Spectrograph} (\textit{IRIS}). We find that the \textit{IRIS} \siiv, \cii\ and \mgii\ transition region (TR) and chromospheric lines exhibit different spectral features in the outflows as compared to neighboring regions at the footpoints ("moss") of hot AR loops. The average redshift of \siiv\ in the outflows region (≈ 5.5~km s−1) is smaller than typical moss (≈ 12--13 km~s−1) and quiet Sun (≈ 7.5 km~s−1) values, while the \cii~line is blueshifted (≈ -1.1--1.5 km~s−1), in contrast to the moss where it is observed to be redshifted by about ≈ 2.5 km~s−1. Further, we observe that the low atmosphere underneath the coronal outflows is highly structured, with the presence of blueshifts in \siiv\ and positive \mgii\ k2 asymmetries (which can be interpreted as signatures of chromospheric upflows) which are mostly not observed in the moss. These observations show a clear correlation between the coronal outflows and the chromosphere and TR underneath, which has not been shown before. Our work strongly suggests that these regions are not separate environments and should be treated together, and that current leading theories of AR outflows, such as the interchange reconnection model, need to take into account the dynamics of the low atmosphere. **2017-08-26, 2018-06-17**

Density diagnostics derived from the O iv and S iv intercombination lines observed by IRIS⋆

V. **Polito**1, G. Del Zanna1, J. Dudík2, H. E. Mason1, A. Giunta3 and K. K. Reeves

A&A 594, A64 (**2016**)

The intensity of the O iv 2s2 2p 2P–2s2p24P and S iv 3 s2 3p 2P–3s 3p24 P intercombination lines around 1400 Å observed with the Interface Region Imaging Spectrograph (IRIS) provide a useful tool to diagnose the electron number density (Ne) in the solar transition region plasma. We measure the electron number density in a variety of solar features observed by IRIS, including an active region (AR) loop, plage and brightening, and the ribbon of the 22-June-2015 M 6.5 class flare. By using the emissivity ratios of O iv and S iv lines, we find that our observations are consistent with the emitting plasma being near isothermal (logT[K] ≈ 5) and iso-density (Ne ≈ 1010.6 cm-3) in the AR loop. Moreover, high electron number densities (Ne ≈ 1013 cm-3) are obtained during the impulsive phase of the flare by using the S iv line ratio. We note that the S iv lines provide a higher range of density sensitivity than the O iv lines. Finally, we investigate the effects of high densities (Ne ≳ 1011 cm-3) on the ionization balance. In particular, the fractional ion abundances are found to be shifted towards lower temperatures for high densities compared to the low density case. We also explored the effects of a non-Maxwellian electron distribution on our diagnostic method.

Solar energetic particles and galactic cosmic rays over millions of years as inferred from data on cosmogenic 26Al in lunar samples

S. **Poluianov**1,2, G. A. Kovaltsov3 and I. G. Usoskin1

A&A 618, A96 (**2018**)

sci-hub.ru/10.1051/0004-6361/201833561

Aims. Lunar soil and rocks are not protected by a magnetic field or an atmosphere and are continuously irradiated by energetic particles that can produce cosmogenic radioisotopes directly inside rocks at different depths depending on the particle's energy. This allows the mean fluxes of solar and galactic cosmic rays to be assessed on the very long timescales of millions of years.

Methods. Here we show that lunar rocks can serve as a very good particle integral spectrometer in the energy range 20–80 MeV. We have developed a new method based on precise modeling, that is applied to measurements of 26Al (half-life ≈0.7 megayears) in lunar samples from the Apollo mission, and present the first direct reconstruction (i.e., without any a priori assumptions) of the mean energy spectrum of solar and galactic energetic particles over a million of years.

Results. We show that the reconstructed spectrum of solar energetic particles is totally consistent with that over the last decades, despite the very different levels of solar modulation of galactic cosmic rays ($\phi = 496 \pm 40$ MV over a million years versus ($\phi = 660 \pm 20$ MV for the modern epoch). We also estimated the occurrence probability of extreme solar events and argue that no events with the F(>30 MeV) fluence exceeding 5×1010 and 1011 cm−2 are expected on timescales of a thousand and million years, respectively.

Conclusions. We conclude that the mean flux of solar energetic particles hardly depends on the level of solar activity, in contrast to the solar modulation of galactic cosmic rays. This puts new observational constraints on solar physics and becomes important for assessing radiation hazards for the planned space missions.

Critical Analysis of a Hypothesis of the Planetary Tidal Influence on Solar Activity

S. **Poluianov**, I. Usoskin

Solar Physics, June **2014**, Volume 289, Issue 6, pp 2333-2342

The present work is a critical revision of the hypothesis of the planetary tidal influence on solar activity published by Abreu et al. (Astron. Astrophys. 548, A88, 2012; called A12 here). A12 describes the hypothesis that planets can have an impact on the solar tachocline and therefore on solar activity. We checked the procedure and results of A12, namely the algorithm of planetary tidal torque calculation and the wavelet coherence between torque and heliospheric modulation potential. We found that the claimed peaks in long-period range of the torque spectrum are artefacts caused by the calculation algorithm (viz. aliasing effect). Also the statistical significance of the results of the wavelet coherence is found to be overestimated by an incorrect choice of the background assumption of red noise. Using a more conservative non-parametric random-phase method, we found that the long-period coherence between planetary torque and heliospheric modulation potential becomes insignificant. Thus we conclude that the considered hypothesis of planetary tidal influence on solar activity is not based on a solid ground.

See: Response to: "Critical Analysis of a Hypothesis of the Planetary Tidal Influence on Solar Activity" by S. Poluianov and I. Usoskin

J. A. **Abreu**, C. Albert, J. Beer, A. Ferriz-Mas, K. G. McCracken, F. Steinhilber

Solar Physics, June **2014**, Volume 289, Issue 6, pp 2343-2344

On the Claim of Modulations in 36Cl Beta Decay and Their Association with Solar Rotation

S. **Pommé**, K. Kossert, O. Nähle

Solar Physics November **2017**, 292:162

https://link.springer.com/content/pdf/10.1007%2Fs11207-017-1187-z.pdf

Recently, claims were made by Sturrock et al. (Astropart. Phys.42, 62, 2013), Sturrock, Fischbach, and Scargle (Solar Phys.291, 3467, 2016; arXiv, 2017) that beta decay can be induced by interaction of the nucleus with solar neutrinos and that cyclic modulations in decay rates are indicative of the dynamics of the solar interior. Transient modulations in residuals from a purely exponential decay curve were observed at frequencies near 11 a−111 a−1 and 12.7 a−112.7 a−1 in repeated activity measurements of a 36Cl source by Alburger, Harbottle, and Norton (Earth Planet Sci. Lett.78, 168, 1986) at Brookhaven National Laboratory in a period from 1984 to 1985. Sturrock et al. have speculatively associated them with rotational influence on the solar neutrino flux. In this work, more accurate 36Cl decay-rate measurements – performed at the Physikalisch-Technische Bundesanstalt Braunschweig in the period 2010 – 2013 by means of the triple-to-double coincidence ratio measurement technique – are scrutinised. The residuals from an exponential decay curve were analysed by a weighted Lomb–Scargle periodogram. The existence of modulations in the frequency range between 0.2 a−10.2 a−1 and 20 a−120 a−1 could be excluded down to an amplitude of about 0.0016%. The invariability of the 36Cl decay constant contradicts the speculations made about the deep solar interior on the basis of instabilities in former activity measurements.

Probing the Physics of the Solar Atmosphere with the Multi-slit Solar Explorer (MUSE). I. Coronal Heating

Bart De **Pontieu**1,2,3, Paola Testa4, Juan Martínez-Sykora1,2,3,5, Patrick Antolin6, Konstantinos Karampelas6,7, Viggo Hansteen1,2,3,5, Matthias Rempel8, Mark C. M. Cheung1, Fabio Reale9,10, Sanja Danilovic11Show full author list

2022 ApJ 926 52

https://iopscience.iop.org/article/10.3847/1538-4357/ac4222/pdf

The Multi-slit Solar Explorer (MUSE) is a proposed mission composed of a multislit extreme ultraviolet (EUV) spectrograph (in three spectral bands around 171 Å, 284 Å, and 108 Å) and an EUV context imager (in two passbands around 195 Å and 304 Å). MUSE will provide unprecedented spectral and imaging diagnostics of the solar corona at high spatial ($\leq 0\farcs5$) and temporal resolution (down to ~0.5 s for sit-and-stare observations), thanks to its innovative multislit design. By obtaining spectra in four bright EUV lines (Fe ix 171 Å, Fe xv 284 Å, Fe xix–Fe xxi 108 Å) covering a wide range of transition regions and coronal temperatures along 37 slits simultaneously, MUSE will, for the first time, "freeze" (at a cadence as short as 10 s) with a spectroscopic raster the evolution of the dynamic coronal plasma over a wide range of scales: from the spatial scales on which energy is released ($\leq 0\farcs5$) to the large-scale (~170" × 170") atmospheric response. We use numerical modeling to showcase how MUSE will constrain the properties of the solar atmosphere on spatiotemporal scales ($\leq 0\farcs5$, ≤20 s) and the large field of view on which state-of-the-art models of the physical processes that drive coronal heating, flares, and coronal mass ejections (CMEs) make distinguishing and testable predictions. We describe the synergy between MUSE, the single-slit, high-resolution Solar-C EUVST spectrograph, and ground-based observatories (DKIST and others), and the critical role MUSE plays because of the multiscale nature of the physical processes involved. In this first paper, we focus on coronal heating mechanisms. An accompanying paper focuses on flares and CMEs.

A New View of the Solar Interface Region from the Interface Region Imaging Spectrograph (IRIS)

Bart De **Pontieu**, Vanessa Polito, Viggo Hansteen, Paola Testa, Katharine K. Reeves, Patrick Antolin, Daniel Elias Nóbrega-Siverio, Adam F. Kowalski, Juan Martinez-Sykora, Mats Carlsson, Scott W. McIntosh, Wei Liu, Adrian Daw & Charles C. Kankelborg

Solar Physics volume 296, Article number: 84 (**2021**)

https://link.springer.com/content/pdf/10.1007/s11207-021-01826-0.pdf

https://doi.org/10.1007/s11207-021-01826-0

The Interface Region Imaging Spectrograph (IRIS) has been obtaining near- and far-ultraviolet images and spectra of the solar atmosphere since July 2013. IRIS is the highest resolution observatory to provide seamless coverage of spectra and images from the photosphere into the low corona. The unique combination of near- and far-ultraviolet spectra and images at sub-arcsecond resolution and high cadence allows the tracing of mass and energy through the critical interface between the surface and the corona or solar wind. IRIS has enabled research into the fundamental physical processes thought to play a role in the low solar atmosphere such as ion–neutral interactions, magnetic reconnection, the generation, propagation, and dissipation of waves, the acceleration of non-thermal particles, and various small-scale instabilities. IRIS has provided insights into a wide range of phenomena including the discovery of non-thermal particles in coronal nano-flares, the formation and impact of spicules and other jets, resonant absorption and dissipation of Alfvénic waves, energy release and jet-like dynamics associated with braiding of magnetic-field lines, the role of turbulence and the tearing-mode instability in reconnection, the contribution of waves, turbulence, and non-thermal particles in the energy deposition during flares and smaller-scale events such as UV bursts, and the role of flux ropes and various other mechanisms in triggering and driving CMEs. IRIS observations have also been used to elucidate the physical mechanisms driving the solar irradiance that impacts Earth's upper atmosphere, and the connections between solar and stellar physics. Advances in numerical modeling, inversion codes, and machine-learning techniques have played a key role. With the advent of exciting new instrumentation both on the ground, e.g. the Daniel K. Inouye Solar Telescope (DKIST) and the Atacama Large Millimeter/submillimeter Array (ALMA), and space-based, e.g. the Parker Solar Probe and the Solar Orbiter, we aim to review new insights based on IRIS observations or related modeling, and highlight some of the outstanding challenges.

The Multi-slit Approach to Coronal Spectroscopy with the Multi-slit Solar Explorer (MUSE)

Bart De **Pontieu**, Juan Martinez-Sykora, Paola Testa, Amy Winebarger, Adrian Daw, Viggo Hansteen, Mark C.M. Cheung, Patrick Antolin, the MUSE team

ApJ **2019**

https://arxiv.org/pdf/1909.08818.pdf

The Multi-slit Solar Explorer (MUSE) is a proposed mission aimed at understanding the physical mechanisms driving the heating of the solar corona and the eruptions that are at the foundation of space weather. MUSE contains two instruments, a multi-slit EUV spectrograph and a context imager. It will simultaneously obtain EUV spectra (along 37 slits) and context images with the highest resolution in space (0.33-0.4 arcsec) and time (1-4 s) ever achieved for the transition region and corona. The MUSE science investigation will exploit major advances in numerical modeling, and observe at the spatial and temporal scales on which competing models make testable and distinguishable predictions, thereby leading to a breakthrough in our understanding of coronal heating and the drivers of space weather. By obtaining spectra in 4 bright EUV lines (Fe IX 171A, Fe XV 284A, Fe XIX-XXI 108A) covering a wide range of transition region and coronal temperatures along 37 slits simultaneously, MUSE will be able to "freeze" the evolution of the dynamic coronal plasma. We describe MUSE's multi-slit approach and show that the optimization of the design minimizes the impact of spectral lines from neighboring slits, generally allowing line parameters to be accurately determined. We also describe a Spectral Disambiguation Code to resolve multi-slit ambiguity in locations where secondary lines are bright. We use simulations of the corona and eruptions to perform validation tests and show that the multi-slit disambiguation approach allows accurate determination of MUSE observables in locations where significant multi-slit contamination occurs.

Coronal Heating and Solar Wind Generation by Flux Cancellation Reconnection

D. I. **Pontin**1, E. R. Priest2, L. P. Chitta3, and V. S. Titov4

2024 ApJ 960 51

https://iopscience.iop.org/article/10.3847/1538-4357/ad03eb/pdf

https://arxiv.org/pdf/2401.11643.pdf

In this paper, we propose that flux cancellation on small granular scales (≲1000 km) ubiquitously drives reconnection at a multitude of sites in the low solar atmosphere, contributing to chromospheric/coronal heating and the generation of the solar wind. We analyze the energy conversion in these small-scale flux cancellation events

using both analytical models and three-dimensional, resistive magnetohydrodynamic (MHD) simulations. The analytical models—in combination with the latest estimates of flux cancellation rates—allow us to estimate the energy release rates due to cancellation events, which are found to be on the order 106–107 erg cm−2 s−1, sufficient to heat the chromosphere and corona of the quiet Sun and active regions, and to power the solar wind. The MHD simulations confirm the conversion of energy in reconnecting current sheets, in a geometry representing a small-scale bipole being advected toward an intergranular lane. A ribbon-like jet of heated plasma that is accelerated upward could also escape the Sun as the solar wind in an open-field configuration. We conclude that through two phases of atmospheric energy release—precancellation and cancellation—the cancellation of photospheric magnetic flux fragments and the associated magnetic reconnection may provide a substantial energy and mass flux contribution to coronal heating and solar wind generation.

The Parker problem: existence of smooth force-free fields and coronal heating **Review**

David I. **Pontin** & Gunnar Hornig
Living Reviews in Solar Physics volume 17, Article number: 5 (**2020**)
https://link.springer.com/content/pdf/10.1007/s41116-020-00026-5.pdf
Parker (Astrophys J 174:499, 1972) put forward a hypothesis regarding the fundamental nature of equilibrium magnetic fields in astrophysical plasmas. He proposed that if an equilibrium magnetic field is subjected to an arbitrary, small perturbation, then—under ideal plasma dynamics—the resulting magnetic field will in general not relax towards a smooth equilibrium, but rather, towards a state containing tangential magnetic field discontinuities. Even at astrophysical plasma parameters, as the singular state is approached dissipation must eventually become important, leading to the onset of rapid magnetic reconnection and energy dissipation. This topological dissipation mechanism remains a matter of debate, and is a key ingredient in the nanoflare model for coronal heating. We review the various theoretical and computational approaches that have sought to prove or disprove Parker's hypothesis. We describe the hypothesis in the context of coronal heating, and discuss different approaches that have been taken to investigating whether braiding of magnetic field lines is responsible for maintaining the observed coronal temperatures. We discuss the many advances that have been made, and highlight outstanding open questions.

Non-thermal line broadening due to braiding-induced turbulence in solar coronal loops

D. I. **Pontin**1,2, H. Peter3 and L. P. Chitta3
A&A 639, A21 (**2020**)
https://www.aanda.org/articles/aa/pdf/2020/07/aa37582-20.pdf
Aims. Emission line profiles from solar coronal loops exhibit properties that are unexplained by current models. We investigate the non-thermal broadening associated with plasma heating in coronal loops that is induced by magnetic field line braiding.
Methods. We describe the coronal loop by a 3D magnetohydrodynamic model of the turbulent decay of an initially-braided magnetic field. From this, we synthesised the Fe XII line at 193 Å that forms around 1.5 MK.
Results. The key features of current observations of extreme ultraviolet (UV) lines from the corona are reproduced in the synthesised spectra: (i) Typical non-thermal widths range from 15 to 20 km s−1. (ii) The widths are approximately independent of the size of the field of view. (iii) There is a correlation between the line intensity and non-thermal broadening. (iv) Spectra are found to be non-Gaussian, with enhanced power in the wings of the order of 10–20%.
Conclusions. Our model provides an explanation that self-consistently connects the heating process to the observed non-thermal line broadening. The non-Gaussian nature of the spectra is a consequence of the non-Gaussian nature of the underlying velocity fluctuations, which is interpreted as a signature of intermittency in the turbulence.

Observable Signatures of Energy Release in Braided Coronal Loops

D. I. **Pontin**1, M. Janvier2, S. K. Tiwari3,4, K. Galsgaard5, A. R. Winebarger3, and J. W. Cirtain3
2017 ApJ 837 108
http://c.brightcove.com/article/10.3847/1538-4357/aa5ff9/pdf
We examine the turbulent relaxation of solar coronal loops containing non-trivial field line braiding. Such field line tangling in the corona has long been postulated in the context of coronal heating models. We focus on the observational signatures of energy release in such braided magnetic structures using MHD simulations and forward modeling tools. The aim is to answer the following question: if energy release occurs in a coronal loop containing braided magnetic flux, should we expect a clearly observable signature in emissions? We demonstrate that the presence of braided magnetic field lines does not guarantee a braided appearance to the observed intensities. Observed intensities may—but need not necessarily—reveal the underlying braided nature of the magnetic field, depending on the degree and pattern of the field line tangling within the loop. However, in all cases considered, the evolution of the braided loop is accompanied by localized heating regions as the loop relaxes. Factors that may influence the observational signatures are discussed. Recent high-resolution observations from Hi-C have claimed

the first direct evidence of braided magnetic fields in the corona. Here we show that both the Hi-C data and some of our simulations give the appearance of braiding at a range of scales.

Three-dimensional magnetic reconnection regimes: A review

D.I. **Pontin**

Advances in Space Research, Volume 47, Issue 9, 3 May **2011**, Pages 1508-1522; **File**

The magnetic field in many astrophysical plasmas – such as the solar corona and Earth's magnetosphere – has been shown to have a highly complex, three-dimensional structure. Recent advances in theory and computational simulations have shown that reconnection in these fields also has a three-dimensional nature, in contrast to the widely used two-dimensional (or 2.5-dimensional) models. Here we discuss the underlying theory of three-dimensional magnetic reconnection. We also review a selection of new models that illustrate the current state of the art, as well as highlighting the complexity of energy release processes mediated by reconnection in complicated three-dimensional magnetic fields.

On a role of quadruple component of magnetic field in defining solar activity in grand cycles

Popova, E., Zharkova V.V., Shepherd S.J. and Zharkov S.I.

Journal of Atmospheric and Solar-Terrestrial Physics, Volume 176 Pages 61-68 **2018**

http://computing.unn.ac.uk/staff/slmv5/kinetics/popova_zhark_jastp17.pdf

http://sci-hub.tw/10.1016/j.jastp.2017.05.006

In this paper we revise our prediction of solar activity using a solar background magnetic field as a proxy by the inclusion of eigen vectors of solar magnetic waves produced by quadruple magnetic sources, in addition to the principal eigen modes generated by two-layer dipole sources (Zharkova et al., 2015). By considering the interference of two dipole and one quadruple waves we produce the revised summary curve for the last 400 years accounting for the additional minima of solar activity occurred at the beginning of 19th (Dalton minimum) and 20th centuries. Using the dynamo model with meridional circulation and selecting the directions of circulation for quadruple waves, we estimate the parameters of quadrupole waves best fitting the observations in the past grand cycle. The comparison shows that the quadruple wave has to be generated in the inner layer of the solar convective zone, in order to provide the additional minima observed in 19 and 20 centuries, thus, naturally accounting for Gleissberg centennial cycle. The dynamo wave simulated for the dipole and quadruple sources reveals much closer correspondence of the resulting summary curve derived from the principal components of magnetic field variations to the solar activity oscillations derived from the average sunspot numbers in the current grand cycle.

See: **Usoskin**, I. (**2017**). Comment on the paper by Popova et al. On a role of quadruple component of magnetic field in defining solar activity in grand cycles, J. Atmosph. Solar-Terr. Phys., 176, 69-71, **2018**

http://sci-hub.tw/10.1016/j.jastp.2017.09.018

See: Reply to comment by Usoskin (2017) on the paper "On a role of quadruple component of magnetic field in defining solar activity in grand cycles"

Zharkova V.V., Popova E., Shepherd S.J. and Zharkov S.

J. Atmosph. Solar-Terr. Phys., 176, 72-82, **2018**

http://computing.unn.ac.uk/staff/slmv5/kinetics/zharkova_etal_reply_jastp17.pdf

http://sci-hub.tw/10.1016/j.jastp.2017.09.019

Review of Image Quality Measures for Solar Imaging

Adam **Popowicz**, Krystian Radlak, Krzysztof Bernacki, Valeri Orlov

Solar Physics December **2017**, 292:187

https://link.springer.com/content/pdf/10.1007%2Fs11207-017-1211-3.pdf

Observations of the solar photosphere from the ground encounter significant problems caused by Earth's turbulent atmosphere. Before image reconstruction techniques can be applied, the frames obtained in the most favorable atmospheric conditions (the so-called lucky frames) have to be carefully selected. However, estimating the quality of images containing complex photospheric structures is not a trivial task, and the standard routines applied in nighttime lucky imaging observations are not applicable. In this paper we evaluate 36 methods dedicated to the assessment of image quality, which were presented in the literature over the past 40 years. We compare their effectiveness on simulated solar observations of both active regions and granulation patches, using reference data obtained by the Solar Optical Telescope on theHinode satellite. To create images that are affected by a known degree of atmospheric degradation, we employed the random wave vector method, which faithfully models all the seeing characteristics. The results provide useful information about the method performances, depending on the average seeing conditions expressed by the ratio of the telescope's aperture to the Fried parameter, D/r0D/r0. The comparison identifies three methods for consideration by observers: Helmli and Scherer's mean, the median filter gradient similarity, and the discrete cosine transform energy ratio. While the first method requires less

computational effort and can be used effectively in virtually any atmospheric conditions, the second method shows its superiority at good seeing (D/r0<4D/r0<4). The third method should mainly be considered for the post-processing of strongly blurred images.

MODULATION OF GALACTIC ELECTRONS IN THE HELIOSPHERE DURING THE UNUSUAL SOLAR MINIMUM OF 2006–2009: A MODELING APPROACH

M. S. **Potgieter**1, E. E. Vos1, R. Munini2, M. Boezio2, and V. Di Felice
2015 ApJ 810 141

The last solar minimum activity period, and the consequent minimum modulation conditions for cosmic rays, was unusual. The highest levels of Galactic protons were recorded at Earth in late 2009 in contrast to expectations. A comprehensive model was used to study the proton modulation for the period from 2006 to 2009 in order to determine what basic processes were responsible for solar modulation during this period and why it differs from proton modulation during previous solar minimum modulation periods. This established model is now applied to studying the solar modulation of electron spectra as observed for 80 MeV–30 GeV by the PAMELA space detector from mid-2006 to the end of 2009. Over this period the heliospheric magnetic field had decreased significantly until the end of 2009 while the waviness of the heliospheric current sheet decreased moderately and the observed electron spectra increased by a factor of ~1.5 at 1.0 GeV to ~3.5 at 100 MeV. In order to reproduce the modulation evident from seven consecutive semesters, the diffusion coefficients had to increase moderately while maintaining the basic rigidity dependence. It is confirmed that the main diffusion coefficients are independent of rigidity below ~0.5 GV, while the drift coefficient had to be reduced below this value. The 2006–2009 solar minimum epoch indeed was different than previously observed minima, at least since the beginning of the space exploration era. This period could be called "diffusion-dominated" as was also found for the modulation of protons.

Forced magnetic reconnection and plasmoid coalescence: I - MHD Simulations

Max **Potter**, Philippa Browning, Mykola Gordovskyy
A&A **2019**
https://arxiv.org/pdf/1901.02392.pdf

Forced magnetic reconnection, a reconnection event triggered by external perturbation, should be ubiquitous in the solar corona. Energy released during such cases can be much greater than that which was introduced by the perturbation. It is unclear how the properties of the external perturbation and the initial current sheet affect the reconnection region properties, and thereby the reconnection dynamics and energy release profile. We investigate the effect of the form of the external perturbation and initial current sheet on the evolution of the reconnection region and the energy release process. Chiefly we explore the non-linear interactions between multiple, simultaneous perturbations, which represent more realistic scenarios. Future work will use these results in test particle simulations to investigate particle acceleration over multiple reconnection events. Simulations are performed using Lare2d, a 2.5D Lagrangian-remap solver for the visco-resistive MHD equations. The model of forced reconnection is extended to include superpositions of sinusoidal driving disturbances, including localised Gaussian perturbations. A transient perturbation is applied to the boundaries of a region containing a force-free current sheet. The simulation domain is sufficiently wide to allow multiple magnetic islands to form and coalesce. Island coalescence contributes significantly to energy release and involves rapid reconnection. Long wavelength modes in perturbations dominate the evolution, without the presence of which reconnection is either slow, as in the case of short wavelength modes, or the initial current sheet remains stable, as in the case of noise perturbations. Multiple perturbations combine in a highly non-linear manner: reconnection is typically faster than when either disturbance is applied individually, with multiple low-energy events contributing to the same total energy release.

Kanzelhöhe Observatory: instruments, data processing and data products

Werner **Pötzi**, Astrid Veronig, Robert Jarolim, Jenny Marcela Rodríguez Gómez, Tatiana Podlachikova, Dietmar Baumgartner, Heinrich Freislich, Heinz Strutzmann
Solar Phys. **296**, Article number: 164 **2021**
https://arxiv.org/pdf/2111.03176.pdf
https://link.springer.com/content/pdf/10.1007/s11207-021-01903-4.pdf
https://doi.org/10.1007/s11207-021-01903-4

Kanzelhöhe Observatory for Solar and Environmental Research (KSO) of the University of Graz (Austria) is in continuous operation since its foundation in 1943. Since the beginning its main task was the regular observation of the Sun in full disc. In this long time span covering almost seven solar cycles, a substantial amount of data was collected, which is made available online. In this paper we describe the separate processing steps from data acquisition to high level products for the different observing wavelengths. First of all we work out in detail the quality classification, which is important for further processing of the raw images. We show how we construct

centre-to-limb variation (CLV) profiles and how we remove large scale intensity variations produced by the telescope optics in order to get images with uniform intensity and contrast. Another important point is an overview of the different data products from raw images to high contrast images with heliographic grids overlaid. As the data products are accessible via different sources we also present how to get information about the availability and how to obtain these data. Finally, in an appendix, we describe in detail the information in the FITS headers, the file naming and the data hierarchy.
Correction Solar Physics volume 297, Article number: 1 (**2022**)
https://link.springer.com/content/pdf/10.1007/s11207-021-01944-9.pdf

70 Years of Sunspot Observations at the Kanzelhöhe Observatory: Systematic Study of Parameters Affecting the Derivation of the Relative Sunspot Number

Werner **Pötzi** , Astrid M. Veronig, Manuela Temmer, Dietmar J. Baumgartner, Heinrich Freislich, Heinz Strutzmann
Solar Phys. **2016**
The Kanzelhöhe Observatory (KSO) was founded during World War II by the Deutsche Luftwaffe (German Airforce) as one station of a network of observatories that were set up to provide information on solar activity in order to better assess the actual conditions of the Earth's ionosphere in terms of radio-wave propagation. Solar observations began in 1943 with photographs of the photosphere and drawings of sunspots, plage regions, and faculae, as well as patrol observations of the solar corona. At the beginning, all data were sent to Freiburg (Germany). After WW II, international cooperation was established and the data were sent to Zurich, Paris, Moscow, and Greenwich. Relative sunspot numbers have been derived since 1944. The agreement between relative sunspot numbers derived at KSO and the new International Sunspot Number (ISN) (SILSO World Data Center in International Sunspot Number Monthly Bulletin and online catalogue, 1945 – 2015) lies within ≈10 %. However, revisiting the historical data, we also find periods with larger deviations. The reasons for the deviations were twofold: On the one hand, a major instrumental change took place during which the instrument was relocated and modified. On the other hand, a period of frequent replacements of personnel caused significant deviations; this clearly shows the importance of experienced observers. In the long term, the instrumental improvements led to better image quality. Additionally, we find a long-term trend towards better seeing conditions that began in 2000.

Contribution of flows around active regions to the north-south helioseismic travel-time measurements

Paul-Louis **Poulier**, Zhi-Chao Liang, Damien Fournier, Laurent Gizon
A&A **2022**
https://arxiv.org/pdf/2206.10751.pdf
Context. In local helioseismology, the travel times of acoustic waves propagating in opposite directions along the same meridian inform us about horizontal flows in the north-south direction. The longitudinal averages of the north-south helioseismic travel-time shifts vary with the sunspot cycle. Aims. We aim to study the contribution of inflows into solar active regions to this solar-cycle variation. Methods. To do so, we identify the local flows around active regions in the horizontal flow maps obtained from correlation tracking of granulation in SDO/HMI continuum images. We compute the forward-modeled travel-time perturbations caused by these inflows using 3D sensitivity kernels. In order to compare with the observations, we average these forward-modeled travel-time perturbations over longitude and time in the same way as the measured travel times. Results. The forward-modeling approach shows that the inflows associated with active regions may account for only a fraction of the solar-cycle variations in the north-south travel-time measurements. Conclusions. The travel-time perturbations caused by the large-scale inflows surrounding the active regions do not explain in full the solar-cycle variations seen in the helioseismic measurements of the meridional circulation.

Acoustic wave propagation through solar granulation: Validity of effective-medium theories, coda waves

P.-L. **Poulier**, D. Fournier, L. Gizon, T. L. Duvall Jr
A&A 643, A168 **2020**
https://arxiv.org/pdf/2010.01174.pdf
https://www.aanda.org/articles/aa/pdf/2020/11/aa39201-20.pdf
https://doi.org/10.1051/0004-6361/202039201

Context. The frequencies, lifetimes, and eigenfunctions of solar acoustic waves are affected by turbulent convection, which is random in space and in time. Since the correlation time of solar granulation and the periods of acoustic waves (∼5 min) are similar, the medium in which the waves propagate cannot a priori be assumed to be time independent. Aims. We compare various effective-medium solutions with numerical solutions in order to identify the approximations that can be used in helioseismology. For the sake of simplicity, the medium is one dimensional. Methods. We consider the Keller approximation, the second-order Born approximation, and spatial homogenization to obtain theoretical values for the effective wave speed and attenuation (averaged over the realizations of the medium). Numerically, we computed the first and second statistical moments of the wave field over many thousands of realizations of the medium (finite-amplitude sound-speed perturbations are limited to a 30 Mm band and have a zero mean). Results. The effective wave speed is reduced for both the theories and the simulations. The attenuation of the coherent wave field and the wave speed are best described by the Keller theory. The numerical simulations reveal the presence of coda waves, trailing the coherent wave packet. These late arrival waves are due to multiple scattering and are easily seen in the second moment of the wave field. Conclusions. We find that the effective wave speed can be calculated, numerically and theoretically, using a single snapshot of the random medium (frozen medium); however, the attenuation is underestimated in the frozen medium compared to the time-dependent medium. Multiple scattering cannot be ignored when modeling acoustic wave propagation through solar granulation.

Comparison of Travel-Time and Amplitude Measurements for Deep-Focusing Time--Distance Helioseismology

Majid **Pourabdian**, Damien Fournier, Laurent Gizon
2018 Solar Phys. 293:66
https://arxiv.org/pdf/1804.02311.pdf
The purpose of deep-focusing time--distance helioseismology is to construct seismic measurements that have a high sensitivity to the physical conditions at a desired target point in the solar interior. With this technique, pairs of points on the solar surface are chosen such that acoustic ray paths intersect at this target (focus) point. Considering acoustic waves in a homogeneous medium, we compare travel-time and amplitude measurements extracted from the deep-focusing cross-covariance functions. Using a single-scattering approximation, we find that the spatial sensitivity of deep-focusing travel times to sound-speed perturbations is zero at the target location and maximum in a surrounding shell. This is unlike the deep-focusing amplitude measurements, which have maximum sensitivity at the target point. We compare the signal-to-noise ratio for travel-time and amplitude measurements for different types of sound-speed perturbations, under the assumption that noise is solely due to the random excitation of the waves. We find that, for highly localized perturbations in sound speed, the signal-to-noise ratio is higher for amplitude measurements than for travel-time measurements. We conclude that amplitude measurements are a useful complement to travel-time measurements in time--distance helioseismology.

Characteristics of the Solar Coronal Line Profiles from Fabry-Perot Interferometric Observations

Maya **Prabhakar**, K.P. Raju, T. Chandrasekhar
Solar Phys. 294:26 **2019**
https://arxiv.org/pdf/1901.11328.pdf
This article reports the analysis of a set of Fabry-Perot interferograms that were studied to probe the physical parameters of the inner solar corona. The observations were carried out in the coronal green line, Fe XIV 5302.86 {\AA}, during the total solar eclipse of **21 June 2001** which occurred in Lusaka, Zambia. The study was performed in the radial range of 1.1-1.5 Ro and examines the Doppler velocity, halfwidth, centroid and asymmetry and their correlations with each other at various points in the corona. It is found that 59 % of the line profiles are blueshifted, 34 % of them are single components and only 7 % of them are redshifted. The variations of halfwidth and Doppler velocity with respect to coronal height have a large scatter and shows no significant changes. It has been found that the variations of halfwidth with Doppler velocity or centroid follow a parabolic trend with a weak correlation, whereas the relation between halfwidth and the asymmetry is inconclusive. These results may provide more insight to the coronal dynamics and help in understanding the coronal physical problems.

Inferring magnetic helicity spectrum in spherical domains: the method and example applications

A. P. **Prabhu**, N. K. Singh, M. J. Käpylä, A. Lagg
A&A 654, A3 654, A3 **2021**
https://arxiv.org/pdf/2104.07588.pdf
https://www.aanda.org/articles/aa/pdf/2021/10/aa41101-21.pdf
https://doi.org/10.1051/0004-6361/202141101

Obtaining observational constraints on the role of turbulent effects for the solar dynamo is a difficult, yet crucial, task. Without such knowledge, the full picture of the operation mechanism of the solar dynamo cannot be formed. The magnetic helicity spectrum provides important information about the α effect. Here we demonstrate a formalism in spherical geometry to infer magnetic helicity spectra directly from observations of the magnetic field, taking into account the sign change of magnetic helicity across the Sun's equator. Using an angular correlation function of the magnetic field, we develop a method to infer spectra for magnetic energy and helicity. The retrieval of the latter relies on a fundamental definition of helicity in terms of linkage of magnetic flux. We apply the two-scale approach, previously used in Cartesian geometry, to spherical geometry for systems where a sign reversal of helicity is expected across the equator at both small and large scales. We test the method by applying it to an analytical model of a fully helical field, and to magneto-hydrodynamic simulations of a turbulent dynamo. The helicity spectra computed from the vector potential available in the models are in excellent agreement to the spectra computed solely from the magnetic field using our method. In a next test, we use our method to obtain the helicity spectrum from a synoptic magnetic field map corresponding to a Carrington rotation. We observe clear signs of a bihelical spectrum of magnetic helicity. Our formalism makes it possible to infer magnetic helicity in spherical geometry, without the necessity of computing the magnetic vector potential. This has the advantage of being gauge invariant. It has many applications in solar and stellar observations, but can also be used to analyze global magnetoconvection models of stars and compare them with observations.

Helicity proxies from linear polarisation of solar active regions

A. **Prabhu**, A. Brandenburg, M. J. Käpylä, A. Lagg
A&A 641, A46 **2020**
https://arxiv.org/pdf/2001.10884.pdf
https://www.aanda.org/articles/aa/pdf/2020/09/aa37614-20.pdf
The alpha effect is believed to play a key role in the generation of the solar magnetic field. A fundamental test for its significance in the solar dynamo is to look for magnetic helicity of opposite signs in the two hemispheres, and at small and large scales. However, measuring magnetic helicity is compromised by the inability to fully infer the magnetic field vector from observations of solar spectra, caused by what is known as the "pi ambiguity" of spectropolarimetric observations. We decompose linear polarisation into parity-even and parity-odd E and B polarisations, which are not affected by the "pi ambiguity". Furthermore, we study whether the correlations of spatial Fourier spectra of B and parity-even quantities such as E or temperature T are a robust proxy for magnetic helicity of solar magnetic fields. We analyse polarisation measurements of active regions observed by the Helioseismic and Magnetic Imager on board the Solar Dynamics observatory. Theory predicts the magnetic helicity of active regions to have, statistically, opposite signs in the two hemispheres. We then compute the parity-odd E B and T B correlations, and test for systematic preference of their sign based on the hemisphere of the active regions. We find that: (i) E B and T B correlations are a reliable proxy for magnetic helicity, when computed from linear polarisation measurements away from spectral line cores, and (ii) E polarisation reverses its sign close to the line core. Our analysis reveals Faraday rotation to not have a significant influence on the computed parity-odd correlations. The EB decomposition of linear polarisation appears to be a good proxy for magnetic helicity independent of the "pi ambiguity". This allows us to routinely infer magnetic helicity directly from polarisation measurements.

Recurring coronal holes and their rotation rates during the solar cycles 22–24

K. **Prabhu**, B. Ravindra, Manjunath Hegde & Vijayakumar H. Doddamani
Astrophysics and Space Science May **2018**, 363:108
http://sci-hub.tw/10.1007/s10509-018-3307-0
Coronal holes (CHs) play a significant role in making the Earth geo-magnetically active during the declining and minimum phases of the solar cycle. In this study, we analysed the evolutionary characteristics of the Recurring CHs from the year 1992 to 2016. The extended minimum of Solar Cycle 23 shows unusual characteristics in the number of persistent coronal holes in the mid- and low-latitude regions of the Sun. Carrington rotation maps of He 10830 Å and EUV 195 Å observations are used to identify the Coronal holes. The latitude distribution of the RCHs shows that most of them are appeared between ±20∘±20∘ latitudes. In this period, more number of recurring coronal holes appeared in and around 100∘100∘ and 200∘200∘ Carrington longitudes. The large sized coronal holes lived for shorter period and they appeared close to the equator. From the area distribution over the latitude considered, it shows that more number of recurring coronal holes with area <1021 cm2<1021 cm2 appeared in the southern latitude close to the equator. The rotation rates calculated from the RCHs appeared between ±60∘±60∘ latitude shows rigid body characteristics. The derived rotational profiles of the coronal holes show that they have anchored to a depth well below the tachocline of the interior, and compares well with the helioseismology results.

A Linear Analysis of Torsional Alfvén Waves in Open Twisted Divergent Magnetic Flux Tubes for Coronal Heating.

Pradhan, B., Mishra, G.C., Karmakar, P.K. et al.

Sol Phys 299, 127 (**2024**).
https://doi.org/10.1007/s11207-024-02372-1
https://link.springer.com/content/pdf/10.1007/s11207-024-02372-1.pdf
The torsional Alfvén wave is highly regarded as the carrier of the energy from the photosphere to the corona in the solar atmosphere. This paper presents a comprehensive linear analysis of the wave behavior and energy transfer within an open, twisted, divergent magnetic flux tube configuration, considering the impact of wave guide structure on the propagation of these waves using the magneto-hydrodynamic approach. The study shows that waves with frequencies between 0.001 Hz and 1 Hz can effectively penetrate the transition region, with the most efficient energy transfer occurring in the 0.1 Hz to 1 Hz frequency range. The research findings suggest that waves with certain intermediate frequencies are able to transmit energy to the coronal region of the Sun, contributing to its active heating.

Measuring relative abundances in the solar corona with optimised linear combinations of spectral lines

Natalia Zambrana **Prado** and Éric Buchlin
A&A 632, A20 (**2019**)
https://www.aanda.org/articles/aa/pdf/2019/12/aa34735-18.pdf
Context. Elemental abundances in some coronal structures differ significantly from photospheric abundances, with a dependence on the first ionization potential (FIP) of the element. Measuring these FIP-dependent abundance biases is important for coronal and heliospheric physics.
Aims. We aim to build a method for optimal determination of FIP biases in the corona from spectroscopic observations in a way that is in practice independent from differential emission measure (DEM) inversions.
Methods. We optimised linear combinations of spectroscopic lines of low-FIP and high-FIP elements so that the ratio of the corresponding radiances yields the relative FIP bias with good accuracy for any DEM in a small set of typical DEMs.
Results. These optimised linear combinations of lines allow retrieval of a test FIP bias map with good accuracy for all DEMs in the map. The results also compare well with a FIP bias map obtained from observations using a DEM-dependent method.
Conclusions. The method provides a convenient, fast, and accurate way of computing relative FIP bias maps. It can be used to optimise the use of existing observations and the design of new observations and instruments.

An Improved Prediction of Solar Cycle 25 Using Deep Learning Based Neural Network

Amrita **Prasad**, Soumya Roy, Arindam Sarkar, Subhash Chandra Panja & Sankar Narayan Patra
Solar Physics volume 298, Article number: 50 (**2023**)
https://doi.org/10.1007/s11207-023-02129-2
A deep-learning Vanilla, or single layer, Long Short-Term Memory model is proposed for improving the prediction of Solar Cycle 25. WDC-SILSO the Royal Observatory of Belgium, Brussels provides the 13-month smoothed sunspot-number data that were used to make this prediction. The root mean square error (RMSE) obtained by the proposed model, which is improved in comparison to the existing stacked LSTM model, lies within the range of 1.65 – 4.92, according to analysis on a number of temporal intervals taken into consideration in this study. The model performance has been validated by forecasting the peak amplitude of Solar Cycles 21 – 24. It is shown that for Cycles 21 and 22, the prediction error in estimating the peak is 1.159% and 0.423%, while the RMSE is estimated to be 4.149 and 3.274, respectively. For Cycle 23, the relative error and RMSE are 1.054% and 2.985, respectively, whereas for Cycle 24 they are 1.117% and 3.406, respectively. The current proposed model has exactly predicted the timing when the SSN reached its maximum for Cycle 23. While for Cycle 21, the prediction has a 1-month delay from the actual timing. For Cycles 22 and 24, the year during which the SSN reached maximum coincides with the observed year, although their month of peak occurrence showed a difference of three months and one month, respectively. The current proposed model suggests that the Cycle 25 will peak in April 2023 with an amplitude value of 136.9, which will be approximately 17.68% stronger compared with Cycle 24.

The magnetic topology of the inverse Evershed flow

A. **Prasad**, M. Ranganathan, C. Beck, D. P. Choudhary and Q. Hu
A&A 662, A25 (**2022**)
https://www.aanda.org/articles/aa/pdf/2022/06/aa42585-21.pdf
Context. The inverse Evershed flow (IEF) is a mass motion towards sunspots at chromospheric heights.
Aims. We combined high-resolution observations of NOAA 12418 from the Dunn Solar Telescope and vector magnetic field measurements from the Helioseismic and Magnetic Imager (HMI) to determine the driver of the IEF.
Methods. We derived chromospheric line-of-sight (LOS) velocities from spectra of Hα and Ca II IR. The HMI data were used in a non-force-free magnetic field extrapolation to track closed field lines near the sunspot in the active region. We determined their length and height, located their inner and outer foot points, and derived flow velocities along them.

Results. The magnetic field lines related to the IEF reach on average a height of 3 megameter (Mm) over a length of 13 Mm. The inner (outer) foot points are located at 1.2 (1.9) sunspot radii. The average field strength difference ΔB between inner and outer foot points is +400 G. The temperature difference ΔT is anti-correlated with ΔB with an average value of −100 K. The pressure difference Δp is dominated by ΔB and is primarily positive with a driving force towards the inner foot points of 1.7 kPa on average. The velocities predicted from Δp reproduce the LOS velocities of 2–10 km s−1 with a square-root dependence.
Conclusions. We find that the IEF is driven along magnetic field lines connecting network elements with the outer penumbra by a gas pressure difference that results from a difference in field strength as predicted by the classical siphon flow scenario. **16 Sep 2015**
HMI Science Nuggets , #182, Jul **2022** http://hmi.stanford.edu/hminuggets/?p=3933

Role of Non-Ideal Dissipation with Heating-Cooling Misbalance on the Phase Shifts of Standing Slow Magnetohydrodynamic Waves

Abhinav **Prasad**, A.K. Srivastava, Tongjiang Wang, Kartika Sangal
Solar Phys. **2021**
https://arxiv.org/pdf/2112.04995.pdf
We analyse the phase shifts of standing, slow magnetohydrodynamic (MHD) waves in solar coronal loops using a linear MHD model taking into account the role of thermal conductivity, compressive viscosity, radiative losses, and heating-cooling misbalance. We estimate the phase shifts in time and space of density and temperature perturbations with respect to velocity perturbations and also calculate the phase difference between density and temperature perturbations. The overall significance of compressive viscosity is found to be negligible for most of the loops considered in the study. For loops with high background density and/or low background temperature, the role of radiative losses (with heating-cooling misbalance) is found to be more significant. Also the effect of heating-cooling misbalance with a temperature- and density-dependent heating function is found to be more significant in the case of longer loop lengths (L=500\, Mm). We derived a general expression for the polytropic index [γeff] and found that under linear MHD the effect of compressive viscosity on polytropic index is negligible. The radiative losses with constant heating lead to a monotonic increase of γeff with increasing density whereas the consideration of an assumed heating function [H(ρ,T)∝ρaTb, where a=−0.5 and b=−3] makes the γeff peak at a certain loop density. We also explored the role of different heating functions by varying the free parameters a and b for a fixed loop of ρ0=10−11\, kg m−3, T0=6.3\, MK and loop length L=180\, Mm. We find that the consideration of different heating functions [H(ρ,T)] leads to a significant variation in the phase difference between density and temperature perturbations; however, the polytropic index remains close to a value of 1.66.

Effect of Thermal Conductivity, Compressive Viscosity and Radiative Cooling on the Phase Shift of Propagating Slow Waves with and Without Heating–Cooling Imbalance

Abhinav **Prasad**, A. K. Srivastava & Tongjiang Wang
Solar Physics volume 296, Article number: 105 (**2021**)
https://link.springer.com/content/pdf/10.1007/s11207-021-01846-w.pdf
https://doi.org/10.1007/s11207-021-01846-w
We study the phase shifts of propagating slow magnetoacoustic waves in solar coronal loops invoking the effects of thermal conductivity, compressive viscosity, radiative losses, and heating–cooling imbalance. We derive the general dispersion relation and solve it to determine the phase shifts of density and temperature perturbations relative to the velocity and their dependence on the equilibrium parameters of the plasma such as the background density [ρ0] and temperature [T0]. We estimate the phase difference [ΔϕΔϕ] between density and temperature perturbations and its dependence on ρ0 and T0. The role of radiative losses, along with the heating–cooling imbalance for an assumed specific heating function [H(ρ,T)∝ρ−0.5T−3], in the estimation of the phase shifts is found to be significant for the high-density and low-temperature loops. Heating–cooling imbalance can significantly increase the phase difference (Δϕ≈140∘) for the low-temperature loops compared to the constant-heating case (Δϕ≈30∘). We derive a general expression for the polytropic index [γeff] using the linear MHD model. We find that in the presence of thermal conduction alone, γeff remains close to its classical value 5/3 for all the considered ρ0 and T0 observed in typical coronal loops. We find that the inclusion of radiative losses (with or without heating–cooling imbalance) cannot explain the observed polytropic index under the considered heating and cooling models. To make the expected γeff match the observed value of 1.1±0.02 in typical coronal loops, the thermal conductivity needs to be enhanced by an order of magnitude compared to the classical value. However, this conclusion is based on the presented model and needs to be confirmed further by considering more realistic radiative functions. We also explore the role of different heating functions for typical coronal parameters and find that although the γeffγeff remains close to 5/3, but the phase difference is highly dependent on the form of the heating function.
Correction: Solar Physics volume 296, Article number: 110 (**2021**) https://doi.org/10.1007/s11207-021-01860-y

Role of Compressive Viscosity and Thermal Conductivity on the Damping of Slow Waves in Coronal Loops with and Without Heating–Cooling Imbalance

Abhinav **Prasad**, A. K. Srivastava & T. J. Wang
Solar Physics volume 296, Article number: 20 (**2021**)
https://link.springer.com/content/pdf/10.1007/s11207-021-01764-x.pdf
In the present article, we derive a new dispersion relation for slow magnetoacoustic waves invoking the effect of thermal conductivity, compressive viscosity, radiation, and an unknown heating term along with the consideration of heating–cooling imbalance from linearized MHD equations. We solve the general dispersion relation to understand the role of compressive viscosity and thermal conductivity in the damping of slow waves in coronal loops with and without heating–cooling imbalance. We have analyzed the wave damping for the range of loop length L=50--500 MmL=50--500 Mm, temperature T=5--30 MK, and density ρ=10−11--10−9 kgm−3. It was found that the inclusion of compressive viscosity along with thermal conductivity significantly enhances the damping of the fundamental mode oscillations in shorter (e.g. L=50 Mm) and super-hot (T>10 MK) loops. However, the role of viscosity in the damping is insignificant in longer (e.g. L=500 Mm) and hot loops (T≤10 MK) where, instead, thermal conductivity along with the presence of heating–cooling imbalance plays a dominant role. For shorter loops at a super-hot regime of temperature, the increment in the loop density substantially enhances the damping of the fundamental modes due to thermal conductivity when viscosity is absent, however, when the compressive viscosity is added the increase in density substantially weakens the damping. Thermal conductivity alone is found to play a dominant role in longer loops at lower temperatures (T≤10 MK), while compressive viscosity dominates the damping at super-hot temperatures (T>10 MK) in shorter loops. The predicted scaling law between damping time (τ) and wave period (P) is found to better match the observed SUMER (Solar Ultraviolet Measurements of Emitted Radiation) oscillations when the heating–cooling imbalance is taken into account in addition to thermal conductivity and compressive viscosity for the damping of the fundamental slow mode oscillations.

The polytropic index of solar coronal plasma in sunspot fan loops and its temperature dependence

S. Krishna **Prasad**, J. O. Raes, T. Van Doorsselaere, N. Magyar, D. B. Jess
ApJ 868 149 **2018**
https://arxiv.org/pdf/1810.08449.pdf
sci-hub.tw/10.3847/1538-4357/aae9f5
Observations of slow magneto-acoustic waves have been demonstrated to possess a number of applications in coronal seismology. Determination of the polytropic index (γ) is one such important application. Analysing the amplitudes of oscillations in temperature and density corresponding to a slow magneto-acoustic wave, the polytropic index in the solar corona has been calculated and based on the obtained value it has been inferred that thermal conduction is highly suppressed in a very hot loop in contrast to an earlier report of high thermal conduction in a relatively colder loop. In this study, using SDO/AIA data, we analysed slow magneto-acoustic waves propagating along sunspot fan loops from 30 different active regions and computed polytropic indices for several loops at multiple spatial positions. The obtained γ values vary from 1.04±0.01 to 1.58±0.12 and most importantly display a temperature dependence indicating higher γ at hotter temperatures. This behaviour brings both the previous studies to agreement and perhaps implies a gradual suppression of thermal conduction with increase in temperature of the loop. The observed phase shifts between temperature and density oscillations, however, are substantially larger than that expected from a classical thermal conduction and appear to be influenced by a line-of-sight integration effect on the emission measure.

Heating in the Solar Atmosphere at a Fin Current Sheet Driven by Magnetic Flux Cancellation

Eric R. **Priest**, David I. Pontin
MNRAS olume 534, Issue 4, Pages 3133–3142, **2024**
https://arxiv.org/pdf/2410.11204
https://doi.org/10.1093/mnras/stae2294
https://scholar.google.com/scholar_url
Magnetic reconnection before flux cancellation in the solar photosphere when two opposite-polarity photospheric magnetic fragments are approaching one another is usually modelled by assuming that a small so-called "floating current sheet" forms about a null point or separator that is situated in the overlying atmosphere. Here instead we consider the reconnection that is initiated as soon as the fragments become close enough that their magnetic fields interact. The resulting current sheet, which we term a "fin sheet" extends up from the null point or separator that is initially located in the solar surface. We develop here nonlinear analyses for finite-length models of both fin and floating current sheets that extend the previous models that were limited to short floating current sheets. These enable the length of the current sheet to be calculated in both cases as functions of the separation distance of the sources and the reconnection rate, as well as the rate of heating. Usually, the fin current sheet liberates more energy than a floating current sheet.

Chromospheric and coronal heating and jet acceleration due to reconnection driven by flux cancellation. I. At a three-dimensional current sheet

E. R. **Priest**, P. Syntelis
A&A 647, A31 **2021**
https://arxiv.org/pdf/2101.04600.pdf
https://doi.org/10.1051/0004-6361/202038917
Context. The recent discovery of much greater magnetic flux cancellation taking place at the photosphere than previously realised has led us in our previous works to suggest magnetic reconnection driven by flux cancellation as the cause of a wide range of dynamic phenomena, including jets of various kinds and solar atmospheric heating. Aims. Previously, the theory considered energy release at a two-dimensional current sheet. Here we develop the theory further by extending it to an axisymmetric current sheet in three dimensions without resorting to complex variable theory. Methods. We analytically study reconnection and treat the current sheet as a three-dimensional structure. We apply the theory to the cancellation of two fragments of equal but opposite flux that approach each another and are located in an overlying horizontal magnetic field. Results. The energy release occurs in two phases. During Phase 1, a separator is formed and reconnection is driven at it as it rises to a maximum height and then moves back down to the photosphere, heating the plasma and accelerating a plasma jet as it does so. During Phase 2 the fluxes cancel in the photosphere and accelerate a mixture of cool and hot plasma upwards.

Chapter 7 - Magnetohydrodynamics and Solar Dynamo Action **Review**

E.R. **Priest**
In: ***The Sun as a Guide to Stellar Physics*** ***Book***
Eds. Oddbjørn Engvold, Jean-Claude Vial, and Andrew Skumanich
Elsevier , November **2018**
https://www.sciencedirect.com/book/9780128143346/the-sun-as-a-guide-to-stellar-physics
Magnetohydrodynamics (MHD) describes the complex interaction between magnetic fields and plasmas that are responsible for much dynamic behavior in the Sun and many other cosmic objects. This chapter introduces the fundamental equations and their physical effects, including the basic physics inherent in the equations of induction and motion and the key process of magnetic reconnection for converting magnetic energy into other forms. MHD is important in astrophysical processes such as magnetoconvection, magnetic flux emergence, flux ropes, spots, atmospheric heating, wind acceleration, flares, and eruptions. In particular, the focus is on the generation of magnetic fields by dynamo action.

A Cancellation Nanoflare Model for Solar Chromospheric and Coronal Heating

E.R. **Priest**, L.P. Chitta, P. Syntelis
2018
https://arxiv.org/pdf/1807.08161.pdf
Nanoflare models for heating the solar corona usually assume magnetic braiding and reconnection as the source of the energy. However, recent observations at record spatial resolution from the {\sc Sunrise} balloon mission suggest that photospheric magnetic flux cancellation is much more common than previously realised. We therefore examine the possibility of three-dimensional reconnection driven by flux cancellation as a cause of chromospheric and coronal heating. In particular, we estimate how the heights and amount of energy release produced by flux cancellation depend on flux size, flux cancellation speed and overlying field strength. **2013 June 12**

Our dynamic sun: Hannes Alfvén Medal lecture at the EGU **Review**

Eric **Priest**
Ann. Geophys., 35, 805–816, **2017**
http://www.ann-geophys.net/35/805/2017/angeo-35-805-2017.pdf
A review is given of major progress towards addressing unsolved fundamental puzzles about the Sun. The solar magnetic field is generated by dynamo action in the solar interior. Several mechanisms may heat the corona to 106 K and drive the solar wind. Occasionally, giant flux ropes (prominences) erupt and produce huge CMEs and solar flares. A new theory is presented for the origin of the twist observed in erupting prominences and the nature of reconnection in the rise phase of a flare or CME.
This lecture summarises how our understanding of many aspects of the Sun has been revolutionised over the past few years by new observations and models. Much of the dynamic behaviour of the Sun is driven by the magnetic field since, in the outer atmosphere, it represents the largest source of energy by far.
The interior of the Sun possesses a strong shear layer at the base of the convection zone, where sunspot magnetic fields are generated. A small-scale dynamo may also be operating near the surface of the Sun, generating magnetic fields that thread the lowest layer of the solar atmosphere, the turbulent photosphere. Above the photosphere lies the highly dynamic fine-scale chromosphere, and beyond that is the rare corona at high temperatures exceeding

1 million degrees K. Possible magnetic mechanisms for heating the corona and driving the solar wind (two intriguing and unsolved puzzles) are described.
Other puzzles include the structure of giant flux ropes, known as prominences, which have complex fine structure. Occasionally, they erupt and produce huge ejections of mass and magnetic fields (coronal mass ejections), which can disrupt the space environment of the Earth. When such eruptions originate in active regions around sunspots, they are also associated with solar flares, in which magnetic energy is converted to kinetic energy, heat and fast-particle energy. A new theory will be presented for the origin of the twist that is observed in erupting prominences and for the nature of reconnection in the rise phase of an eruptive flare or coronal mass ejection.

The Chemical Composition of the Solar Surface

Carlos Allende **Prieto**
Journal of Astrophysics and Astronomy, **2020**, Volume 41, Issue 1, article id.41
https://arxiv.org/pdf/2106.10750.pdf
The Sun provides a standard reference against which we compare the chemical abundances found anywhere else in the Universe. Nevertheless, there is not a unique 'solar' composition, since the chemical abundances found in the solar interior, the photosphere, the upper atmosphere, or the solar wind, are not exactly the same. The composition of the solar photosphere, usually preferred as a reference, changes with time due to diffusion, convection, and probably accretion. In addition, we do not know the solar photospheric abundances, inferred from the analysis of the solar spectrum using model atmospheres, with high accuracy, and uncertainties for many elements exceed 25%. This paper gives an overview of the methods and pitfalls of spectroscopic analysis, and discusses the chemistry of the Sun in the context of the solar system.

Solar and stellar photospheric abundances **Review**

Carlos Allende **Prieto**
Living Rev. Sol. Phys. (**2016**) 13: 1,
http://link.springer.com/article/10.1007%2Fs41116-016-0001-6
The determination of photospheric abundances in late-type stars from spectroscopic observations is a well-established field, built on solid theoretical foundations. Improving those foundations to refine the accuracy of the inferred abundances has proven challenging, but progress has been made. In parallel, developments on instrumentation, chiefly regarding multi-object spectroscopy, have been spectacular, and a number of projects are collecting large numbers of observations for stars across the Milky Way and nearby galaxies, promising important advances in our understanding of galaxy formation and evolution. After providing a brief description of the basic physics and input data involved in the analysis of stellar spectra, a review is made of the analysis steps, and the available tools to cope with large observational efforts. The paper closes with a quick overview of relevant ongoing and planned spectroscopic surveys, and highlights of recent research on photospheric abundances.

Magnetic winding: what is it and what is it good for?

Chris **Prior**, David MacTaggart
Proc. R. Soc. A **2020**
https://arxiv.org/pdf/2009.11708.pdf
Magnetic winding is a fundamental topological quantity that underpins magnetic helicity and measures the entanglement of magnetic field lines. Like magnetic helicity, magnetic winding is also an invariant of ideal magnetohydrodynamics. In this article we give a detailed description of what magnetic winding describes, how to calculate it and how to interpret it in relation to helicity. We show how magnetic winding provides a clear topological description of magnetic fields (open or closed) and we give examples to show how magnetic winding and helicity can behave differently, thus revealing different and imporant information about the underlying magnetic field.

Spatial Scales and Locality of Magnetic Helicity: Part 1

Christopher **Prior**, Gareth Hawkes, Mitch Berger
A&A 635, A95 (**2020**)
https://arxiv.org/pdf/1909.07838.pdf
https://doi.org/10.1051/0004-6361/201936675
Context. Magnetic helicity is approximately conserved in resistive magnetohydrodynamic models. It quantifies the entanglement of the magnetic field within the plasma. The transport and removal of helicity is crucial in both dynamo development in the solar interior and active region evolution in the solar corona. This transport typically leads to highly inhomogeneous distributions of entanglement.
Aims. There exists no consistent systematic means of decomposing helicity over varying spatial scales and in localised regions. Spectral helicity decompositions can be used in periodic domains and is fruitful for the analysis of

homogeneous phenomena. This paper aims to develop methods for analysing the evolution of magnetic field topology in non-homogeneous systems.
Methods. The method of multi-resolution wavelet decomposition is applied to the magnetic field. It is demonstrated how this decomposition can further be applied to various quantities associated with magnetic helicity, including the field line helicity. We use a geometrical definition of helicity, which allows these quantities to be calculated for fields with arbitrary boundary conditions.
Results. It is shown that the multi-resolution decomposition of helicity has the crucial property of local additivity. We demonstrate a general linear energy-topology conservation law, which significantly generalises the two-point correlation decomposition used in the analysis of homogeneous turbulence and periodic fields. The localisation property of the wavelet representation is shown to characterise inhomogeneous distributions, which a Fourier representation cannot. Using an analytic representation of a resistive braided field relaxation, we demonstrate a clear correlation between the variations in energy at various length scales and the variations in helicity at the same spatial scales. Its application to helicity flows in a surface flux transport model show how various contributions to the global helicity input from active region field evolution and polar field development are naturally separated by this representation.

Statistical analysis on Dynamic Fibrils observed from NST/BBSO observations

T G **Priya**, Su Jiangtao, Jie Chen, Deng Yuanyong, Debi Prasad Choudhury
Research in Astron. Astrophys. (2012?) **2017**
https://arxiv.org/pdf/1711.06381.pdf
We present the results obtained from the analysis of dynamic fibrils in NOAA active region (AR) 12132, using high resolution Hα observations from New Solar Telescope operating at BBSO. The dynamic fibrils are seen to be moving up and down, and most of these dynamic fibrils are periodic and have jet like appearance. We found from our observations that the fibrils follows perfect parabolic paths at the most in many cases. A statistical measure on the properties of the parabolic paths showing an analysis on deceleration, maximum velocity, duration and kinetic energy of these fibrils is presented here. We found the average maximum velocity to be around 15 km s−1 and mean deceleration to be around 100 m s−2. The deceleration observed appears to be a fraction of gravity of sun and is not compatible with the path of ballistic at the gravity of sun. We found positive correlation between the deceleration and the maximum velocity. This correlation is consistent with the simulations done earlier on magnetoacoustic shock waves propagating upward. **2014 August 5**

Periodic and Quasi-Periodic Variations in the Ca K Index During the 20th Century Using Kodaikanal Data

Muthu **Priyal**, Jagdev Singh, B. Ravindra, Chandar Shekar B
Solar Physics September **2019**, 294:131
https://link.springer.com/content/pdf/10.1007%2Fs11207-019-1522-7.pdf
We have digitized the Ca K images obtained at Kodaikanal Observatory with a pixel resolution of 0.86 arcsec and 16-bit readout to achieve better spatial and photometric accuracy. In addition to the general photometric analysis procedure carried out on the data, we have corrected these digitized images for instrumental effects. Then, we have normalized all the images considering their intensity distribution. Afterwards, we separate the images into two groups considering the width of the intensity distribution and their visual quality. Group I contains uniform time series of images taken at the center of the Ca K line and the other group contains the remaining images. We study the variation in the Ca K index with time for both data sets. Comparing the results we find that it is necessary to select the images to generate uniform time series to investigate periodic variations. We find that uniform time series termed as “Good” shows well-defined 11-year periodicity in the Ca K average intensity. In addition, the fast Fourier transform and wavelet analysis of the data show a quasi-periodicity of ≈ 3 years that may be due to the duration of the active phase of the solar cycle. The time series with non-uniform images termed as “Okay” shows a large scatter in the average intensity and affects the amplitude of the activity. This series also shows a number of mid-term quasi-periodicities of short duration in the wavelet analysis, probably due to the non-uniform quality of the images. This methodology will be also useful to combine the data from different observatories and generate a uniform time series with less gaps in the data.

Long-term Variations in the Intensity of Plages and Networks as Observed in Kodaikanal Ca-K Digitized Data

Muthu **Priyal**, Jagdev Singh, Ravindra Belur…
Solar Physics July **2017**, 292:85
https://arxiv.org/pdf/1707.00411.pdf
In our previous article (Priyal et al. in Solar Phys.289, 127, 2014) we have discussed the details of observations and methodology adopted to analyze the Ca-K spectroheliograms obtained at the Kodaikanal Observatory (KO) to study the variation of Ca-K plage areas, enhanced network (EN), and active network (AN) for Solar Cycles, namely 19, 20, and 21. Now, we have derived the areas of chromospheric features using KO Ca-K spectroheliograms to study

the long-term variations of Solar Cycles 14 to 21. The comparison of the derived plage areas from the data obtained at the KO observatory for the period 1906 – 1985 with that of MWO, NSO for the period 1965 – 2002, earlier measurements made by Tlatov, Pevtsov, and Singh (Solar Phys.255, 239, 2009) for KO data, and the SIDC sunspot numbers shows a good correlation. The uniformity of the data obtained with the same instrument remaining with the same specifications provided a unique opportunity to study long-term intensity variations in plages and network regions. Therefore, we have investigated the variation of the intensity contrast of these features with time at a temporal resolution of six months assuming that the quiet-background chromosphere remains unchanged during the period 1906 – 2005 and found that the average intensity of the AN, representing the changes in small-scale activity over solar surface, varies with solar cycle being less during the minimum phase. In addition, the average intensity of plages and EN varies with a very long period having a maximum value during Solar Cycle 19, which was the strongest solar cycle of twentieth century.

Polar Network Index as a magnetic proxy for the solar cycle studies

Muthu **Priyal**, Dipankar Banerjee, Bidya Binay Karak, Andres Munoz-Jaramillo, B. Ravindra, Arnab Rai Choudhuri, Jagdev Singh

ApJL, ApJ 793 L4 **2014**

http://arxiv.org/pdf/1407.4944v1.pdf

The Sun has a polar magnetic field which oscillates with the 11 year sunspot cycle. This polar magnetic field is an important component of the dynamo process which is operating in the solar convection zone and produces the sunspot cycle. We have systematic direct measurements of the Sun's polar magnetic field only from about mid 1970s. There are, however, indirect proxies which give us information about this field at earlier times. The Ca K spectroheliograms taken in Kodaikanal Solar Observatory during 1904 - 2007 have now been digitized with the 4k x 4k CCD and have higher resolution (0.86 arcsec) than the other available historical datasets. From these Ca-K spectroheliograms, we have developed a completely new proxy (Polar Network Index, PNI) for the Sun's polar magnetic field. We calculate the PNI from the digitized images using an automated algorithm and calibrate our measured PNI against the polar field as measured by the Wilcox Solar Observatory for the period of 1976 - 1990. This calibration allows us to estimate polar fields for the earlier period up to 1904. The dynamo calculations done with this proxy as input data reproduce the Sun's magnetic behavior for the past century reasonably well.

Shape Parameters of 1991 to 2016 Solar Corona

Rhorom **Priyatikanto**

Research in Astron. Astrophys. (RAA) **2016**

http://arxiv.org/pdf/1607.07928v1.pdf

The global structure of solar corona observed in optical window is governed by the global magnetic field with different characteristics over solar activity cycle. Ludendorff flattening index becomes a popular measure of the global structure of solar corona as observed during eclipse. In this study, 15 digital images of solar corona from 1991 to 2016 were analyzed in order to construct the coronal flattening profiles as a function of radius. In most of the cases, the profile can be modeled with 2nd order polynomial function so that the radius with maximum flattening index (Rmax) can be determined. Along with this value, Ludendorff index (a+b) was also calculated. Both Ludendorff index and Rmax show anti-correlation with monthly sunspot number, though the Rmax values are more scattered. The variation of Rmax can be regarded as the impact of changing coronal brightness profile over equator.

Investigating the damping rate of phase-mixed Alfven waves

A. P. K. **Prokopyszyn**, A. W. Hood

A&A 632, A93 **2019**

https://arxiv.org/pdf/1910.12510.pdf

https://doi.org/10.1051/0004-6361/201936658

Context: This paper investigates the effectiveness of phase mixing as a coronal heating mechanism. A key quantity is the wave damping rate, γ, defined as the ratio of the heating rate to the wave energy.

Aims: We investigate whether or not laminar phase-mixed Alfvén waves can have a large enough value of γ to heat the corona. We also investigate the degree to which the γ of standing Alfvén waves which have reached steady-state can be approximated with a relatively simple equation. Further foci of this study are the cause of the reduction of γ in response to leakage of waves out of a loop, the quantity of this reduction, and how increasing the number of excited harmonics affects γ.

Results: We find that at observed frequencies γ is too small to heat the corona by approximately three orders of magnitude. Therefore, we believe that laminar phase mixing is not a viable stand-alone heating mechanism for coronal loops. We show that γ is largest at resonance. We find our simple equation provides a good estimate for the damping rate (within approximately 10% accuracy) for resonant field lines. However, away from resonance, the equation provides a poor estimate, predicting γ to be orders of magnitude too large. We find that leakage acts to reduce γ but plays a negligible role if γ is of the order required to heat the corona. If the wave energy follows a power spectrum with slope -5/3 then γ grows logarithmically with the number of excited harmonics. If the number

of excited harmonics is increased by much more than 100, then the heating is mainly caused by gradients that are parallel to the field rather than perpendicular to it. Therefore, in this case, the system is not heated mainly by phase mixing.

Phase mixing of nonlinear Alfven waves

Alexander **Prokopyszyn**, Alan Hood, Ineke De Moortel
A&A 624, A90 **2019**
https://arxiv.org/pdf/1903.08093.pdf
Aims: This paper presents 2.5D numerical experiments of Alfvén wave phase mixing and aims to assess the effects of nonlinearities on wave behaviour and dissipation. In addition, this paper aims to quantify how effective the model presented in this work is at providing energy to the coronal volume.
Methods: The model is presented and explored through the use of several numerical experiments which were carried out using the Lare2D code. The experiments study footpoint driven Alfvén waves in the neighbourhood of a two-dimensional x-type null point with initially uniform density and plasma pressure. A continuous sinusoidal driver with a constant frequency is used. Each experiment uses different driver amplitudes to compare weakly nonlinear experiments with linear experiments.
Results: We find that the wave trains phase-mix owing to variations in the length of each field line and variations in the field strength. The nonlinearities reduce the amount of energy entering the domain, as they reduce the effectiveness of the driver, but they have relatively little effect on the damping rate (for the range of amplitudes studied). The nonlinearities produce density structures which change the natural frequencies of the field lines and hence cause the resonant locations to move. The shifting of the resonant location causes the Poynting flux associated with the driver to decrease. Reducing the magnetic diffusivity increases the energy build-up on the resonant field lines, however, it has little effect on the total amount of energy entering the system. From an order of magnitude estimate, we show that the Poynting flux in our experiments is comparable to the energy requirements of the quiet Sun corona. However a (possibly unphysically) large amount of magnetic diffusion was used however and it remains unclear if the model is able to provide enough energy under actual coronal conditions.

Reflection of Fast Magnetosonic Waves near a Magnetic Reconnection Region

E. **Provornikova**1,2, J. M. Laming2, and V. S. Lukin3
2018 ApJ 860 138 https://doi.org/10.3847/1538-4357/aac1c1
Magnetic reconnection in the solar corona is thought to be unstable with the formation of multiple interacting plasmoids, and previous studies have shown that plasmoid dynamics can trigger MHD waves of different modes propagating outward from the reconnection site. However, variations in plasma parameters and magnetic field strength in the vicinity of a coronal reconnection site may lead to wave reflection and mode conversion. In this paper we investigate the reflection and refraction of fast magnetoacoustic waves near a reconnection site. Under a justified assumption of an analytically specified Alfvén speed profile, we derive and solve analytically the full wave equation governing the propagation of fast-mode waves in a non-uniform background plasma without recourse to the small wavelength approximation. We show that the waves undergo reflection near the reconnection current sheet due to the Alfvén speed gradient and that the reflection efficiency depends on the plasma-βparameter, as well as on the wave frequency. In particular, we find that waves are reflected more efficiently near reconnection sites in a low-β plasma, which is typical under solar coronal conditions. Also, the reflection is larger for lower-frequency waves while high-frequency waves propagate outward from the reconnection region almost without the reflection. We discuss the implications of efficient wave reflection near magnetic reconnection sites in strongly magnetized coronal plasma for particle acceleration, and also the effect this might have on first ionization potential (FIP) fractionation by the ponderomotive force of these waves in the chromosphere.

Observations of large-scale solar flows

Bastian **Proxauf**
Thesis **2021**
https://arxiv.org/pdf/2106.07251.pdf
In this dissertation, several components of large-scale solar flows are studied observationally: solar equatorial Rossby waves (waves of radial vorticity), large-scale convection, and surface flows around active regions. Maps of horizontal flows are derived from photospheric observations by the Helioseismic and Magnetic Imager (HMI) aboard the Solar Dynamics Observatory (SDO) using two different techniques: granulation tracking and local helioseismology. First, the eigenfunctions of solar Rossby waves are measured from helioseismic ring-diagram flow maps with a correlation method and a spectral analysis. Down to 9 Mm below the surface, the dependence of the radial vorticity with radius r is consistent with rm−1, for a given longitudinal wavenumber m. At the surface, the eigenfunctions are complex-valued. The real part decreases away from the equator and switches sign around ±20−30∘. The imaginary part is small, but nonzero, and may be due to wave attenuation. This may have implications for the transport of angular momentum in the latitudinal direction. Second, we revisit previous measurements of power spectra of longitudinal velocities near the solar surface, obtained from time-distance and

ring-diagram helioseismology. Several issues in these past helioseismic analyses are identified and corrected. The corrections are not sufficient to remove the discrepancy between the measurements. I thus present new velocity power spectra from granulation tracking and ring-diagram helioseismology. The two new measurements are close to each other near the solar surface, and the corresponding kinetic energy decreases with increasing spatial scale.

Exploring the latitude and depth dependence of solar Rossby waves using ring-diagram analysis

B. **Proxauf**, L. Gizon, B. Löptien, J. Schou, A. C. Birch, R. S. Bogart
A&A 634, A44 **2020**
https://arxiv.org/pdf/1912.02056.pdf
https://www.aanda.org/articles/aa/pdf/2020/02/aa37007-19.pdf
Global-scale Rossby waves have recently been unambiguously identified on the Sun. Here we study the latitude and depth dependence of the Rossby wave eigenfunctions. By applying helioseismic ring-diagram analysis and granulation tracking to SDO/HMI observations, we compute maps of the radial vorticity of flows in the upper solar convection zone (down to depths of more than 16 Mm). We use a Fourier transform in longitude to separate the different azimuthal orders m in the range $3 \leq m \leq 15$. At each m we obtain the phase and amplitude of the Rossby waves as a function of depth using the helioseismic data. At each m we also measure the latitude dependence of the eigenfunctions by calculating the covariance between the equator and other latitudes. We then study the horizontal and radial dependences of the radial vorticity eigenfunctions. The horizontal eigenfunctions are complex. As observed previously, the real part peaks at the equator and switches sign near $\pm 30^\circ$, thus the eigenfunctions show significant non-sectoral contributions. The imaginary part is smaller than the real part. The phase of the radial eigenfunctions varies by only roughly $\pm 5^\circ$ over the top 15 Mm. The amplitude of the radial eigenfunctions decreases by about 10% from the surface down to 8 Mm (the region where ring-diagram analysis is most reliable, as seen by comparing with the rotation rate measured by global-mode seismology). The radial dependence of the radial vorticity eigenfunctions deduced from ring-diagram analysis is consistent with a power-law down to 8 Mm and is unreliable at larger depths. However, the observations provide only weak constraints on the power-law exponents. For the real part, the latitude dependence of the eigenfunctions is consistent with previous work (using granulation tracking). The imaginary part is smaller than the real part but significantly nonzero.

Nominal values for selected solar and planetary quantities: IAU 2015 Resolution B3

Andrej **Prsa**, Petr Harmanec, Guillermo Torres, et al.
AJ **2016**
http://arxiv.org/pdf/1605.09788v1.pdf
In this brief communication we provide the rationale for, and the outcome of the International Astronomical Union (IAU) resolution vote at the XXIX-th General Assembly in Honolulu, Hawaii, in 2015, on recommended nominal conversion constants for selected solar and planetary properties. The problem addressed by the resolution is a lack of established conversion constants between solar and planetary values and SI units: a missing standard has caused a proliferation of solar values (e.g., solar radius, solar irradiance, solar luminosity, solar effective temperature and solar mass parameter) in the literature, with cited solar values typically based on best estimates at the time of paper writing. As precision of observations increases, a set of consistent values becomes increasingly important. To address this, an IAU Working Group on Nominal Units for Stellar and Planetary Astronomy formed in 2011, uniting experts from the solar, stellar, planetary, exoplanetary and fundamental astronomy, as well as from general standards fields to converge on optimal values for nominal conversion constants. The effort resulted in the IAU 2015 Resolution B3, passed at the IAU General Assembly by a large majority. The resolution recommends the use of nominal solar and planetary values, which are by definition exact and are expressed in SI units. These nominal values should be understood as conversion factors only, not as the true solar/planetary properties or current best estimates. Authors and journal editors are urged to join in using the standard values set forth by this resolution in future work and publications to help minimize further confusion.

On the nature of the transition region between the solar corona and chromosphere

O. V. **Ptitsyna**, B. V. Somov
Astronomy Letters, December **2012**, Volume 38, Issue 12, pp 801-812
Pis'ma v Astronomicheskiı Zhurnal, **2012**, Vol. 38, No. 12, pp. 892–903.
We have calculated an equilibrium temperature distribution over the column depth of plasma in the transition region between the solar corona and chromosphere by assuming the plasma in the transition region and the chromosphere to be heated by the heat flux from the corona and the energy fluxes from the convective zone, respectively. The corona-chromosphere transition region is shown to be actually a stable, very thin layer in which, however, the standard collision approximation is well applicable for describing the heat flux. The solution we found explains well the currently available results of satellite observations of extreme ultraviolet (EUV) radiation from the transition region.

On the relation between transition region network jets and coronal plumes

Youqian **Qi**, Zhenghua Huang, Lidong Xia, Bo Li, Hui Fu, Weixin Liu, Mingzhe Sun, Zhenyong Hou
Solar Phys. 294:92 **2019**
https://arxiv.org/pdf/1906.10353.pdf
sci-hub.se/10.1007/s11207-019-1484-9

Both coronal plumes and network jets are rooted in network lanes. The relationship between the two, however, has yet to be addressed. For this purpose, we perform an observational analysis using images acquired with the Atmospheric Imaging Assembly (AIA) 171{\AA} passband to follow the evolution of coronal plumes, the observations taken by the Interface Region Imaging Spectrograph (IRIS) slit-jaw 1330{\AA} to study the network jets, and the line-of-sight magnetograms taken by the Helioseismic and Magnetic Imager (HMI) to overview the the photospheric magnetic features in the regions. Four regions in the network lanes are identified, and labeled ``R1--R4". We find that coronal plumes are clearly seen only in ``R1"&"R2" but not in ``R3"&``R4", even though network jets abound in all these regions. Furthermore, while magnetic features in all these regions are dominated by positive polarity, they are more compact (suggesting stronger convergence) in ``R1"&``R2" than that in ``R3"&``R4". We develop an automated method to identify and track the network jets in the regions. We find that the network jets rooted in ``R1"&``R2" are higher and faster than that in ``R3"&``R4",indicating that network regions producing stronger coronal plumes also tend to produce more dynamic network jets. We suggest that the stronger convergence in ``R1"&``R2" might provide a condition for faster shocks and/or more small-scale magnetic reconnection events that power more dynamic network jets and coronal plumes. **2015 December 4**

Three Types of Solar Coronal Rain during Magnetic Reconnection between Open and Closed Magnetic Structures

Fangfang **Qiao**1, Leping Li2,3,4, Hui Tian1,3, Zhenyong Hou1, Hongqiang Song5, Kaifan Ji6, and Zheng Sun1
2024 ApJ 973 57
https://iopscience.iop.org/article/10.3847/1538-4357/ad6770/pdf

Coronal rain (CR) is a crucial part of the mass cycle between the corona and chromosphere. It includes flare-driven CR and two types of quiescent CR, along nonflaring active region closed loops and along open structures, separately, labeled as type I, type II, and type III CR, respectively. Among them, type I and type III CR are generally associated with magnetic reconnection. In this study, employing data taken by the Solar Dynamics Observatory and the Solar Upper Transition Region Imager on **2022 October 11**, we report three types of CR during an interchange reconnection between open and closed magnetic field structures above the southeastern solar limb. The open and closed structures converge, with the formation of the current sheet at the interface, and reconnect. The newly formed closed and open structures then recede from the reconnection region. During the reconnection, coronal condensation occurs along the reconnecting closed loops and falls toward the solar surface along both loop legs, as type II CR. Subsequently, condensation happens in the newly formed closed loops and moves down toward the solar surface along both loop legs, as type I CR. Magnetic dips of the reconnecting open structures form during the reconnection. In the dips, condensation occurs and propagates along the open structures toward the solar surface as type III CR. Our results suggest that the reconnection rate may be crucial for the formation of type I and type III CR during reconnection.

A Model of Sunspot Number with Modified Logistic Function

G. **Qin**, S.-S. Wu
2018 *ApJ* **869** 48
https://arxiv.org/pdf/1804.03617.pdf
sci-hub.tw/10.3847/1538-4357/aaec08

Solar cycles are studied with the new (version 2) monthly smoothed international sunspot number, the variations of which are found to be well represented by the modified logistic differential equation with four parameters: maximum cumulative sunspot number or total sunspot number xm, initial cumulative sunspot number x0, maximum emergence rate r0, and asymmetry α. A two-parameter function can be obtained by taking the parameters α and r0 as fixed value. In addition, it is found that the two parameters xm and x0 can be well determined at the start of a cycle based on the analysis of solar cycles 1−23. Therefore, a prediction model of the sunspot number variations of solar cycles is established based on the two-parameter function. The prediction for cycles 4−23 shows that the solar maximum can be predicted with relative error being 9\% at the start of the cycle, which is better than that of other fitting functions in the literature. Besides, our model can predict the cycle length with the relative error being 10\%. Furthermore, we predict the sunspot number variations of solar cycle 24 with the relative errors of the solar maximum and that of the ascent time being 8\% and 7\%, respectively, we also predict that the length of cycle 24 is 10.90±1.09 years. The comparison to the observation of cycle 24 shows that our prediction model has good effectiveness.

Cool matter distribution in inner solar corona from 2023 total solar eclipse observation

Z.Q. **Qu**, H. Su, Y. Liang, Z. Xu, R.Y. Zhou

2024

https://arxiv.org/pdf/2404.18563

Solar corona has been judged to consist of free electrons and highly ionized ions with extremely high temperature as a widely accepted knowledge. This view is changed by our eclipse observations. Distributions of cool matter represented by neutral iron atoms in hot inner solar corona are presented via derived global maps of solar Fraunhofer(F-) and Emission(E-) coronae, compared with those of continuum(Kontinuierlich, K-) corona formed by free electrons. The maps are obtained from simultaneous observations of dual filtering bands centered respectively at 659.4nm and 660.1nm, performed from twin telescopes during the total solar eclipse on **April 20, 2023** at Com town of East Timor, assisted for judgement via spectral images obtained by a portable spectrograph. They show respectively presences of these neutral iron atoms yielding 659.3nm and 659.4nm lines in both the quiet sun and active regions. The distribution of the cool matter in form of line depression forms an inner F-corona, different from that of the cool matter in form of line enhancement. Both the distributions show a crucial difference from that of the free electrons represented by the K-corona map. It is also found that intensities of the F-corona and the E-corona induced by these neutral atoms are only small fractions of the K-corona, and the diffusion can be seen clearly in all these maps. They uncover also that the coronal heating resources do not distribute pervasively but likely form a thermodynamic griddle where minor photospheric neutral atoms can escape from the heating into the corona globally.

High-order Harmonics of a Kink Wave and a Narrow Quasiperiodic Fast-propagating Wave Train Excited Simultaneously in a Plasma Resonator

Zhining **Qu**1, Xinping Zhou1, Jie Zheng2, Linqiao Jiang3, Hongbo Li4, and Hang Yang1

2023 ApJ 955 89

https://iopscience.iop.org/article/10.3847/1538-4357/acef10/pdf

We present the observations of multimode kink waves and a narrow quasiperiodic fast-propagating (QFP) wave train in association with a jet on **2011 December 11**. The jet impinged on a loop, which excited a propagating kink mode transitioning into a standing kink mode and also excited a QFP wave train away from the jet. Motion magnification is used to fit the higher harmonic standing wave oscillation profile with three periods at three different spatial locations. The periods have the ratio 6:3:2. The ratio of the fundamental mode to the second harmonic of the standing wave is about 1.95, suggesting that the magnetic field strength variation effect is strong enough to cancel out the density stratification. The differential emission measure is used to estimate the loop's plasma property at these three points, and it found the density and the temperature are roughly constant. The magnetic field strength, $B = 51 \pm 16$ G, is derived by the coronal seismology using the fundamental kink mode. It is striking to find that the the ratio of the second harmonic to the third harmonic of the kink wave coincides with that of the periods of the QFP wave train, and the ratio of periods is about 1.5 in both cases. We propose that the excitation of the high-order harmonics and the QFP wave train could be the nonlinear response of the steep density-gradient plasma interacting with electromagnetic field in the southwest foot region. This region, like a resonator, might play an important role in energy reservoir capture and act as a frequency filter to generate propagating waves of particular frequencies.

Complexity of the Upper Solar Atmosphere Revealed from Spectropolarimetry during a Solar Eclipse

Z. Q. **Qu**1,2, L. Chang1,2, G. T. Dun1, Z. Xu1, X. M. Cheng1,3, L. H. Deng1, X. Y. Zhang1, and Y. H. Jin1,2

2022 ApJ 940 150

https://iopscience.iop.org/article/10.3847/1538-4357/ac9af4/pdf

We analyze linear polarimetric spectrum data of solar emission lines with different formation temperatures in a visible light band from 516.3–532.6 nm, obtained during the 2013 Gabon solar eclipse using the prototype Fiber Arrayed Solar Optical Telescope. Complexities are found from the chromosphere through the transition zone to the corona at the spatial resolution limit of 2" and temporal resolution of seconds. The observations show irregular spatial and spectral variations in linear polarization amplitudes, directions, and profile shapes. Within the observational band, spectral lines with different formation temperatures can have comparable polarization amplitudes in one spatial volume but one order difference in another, and at the same spatial volume, the amplitudes can differ by one order at different lines. The polarization amplitudes do not consistently increase with elongation in local regions. The variation in the direction of the polarization along the elongation is found from the green coronal line and the transition zone line more frequently than from the chromospheric lines. Such a variation in orientation is not synchronous for the different lines. Finally, Stokes Q/I profiles of the broad lines, such as the magnesium triplet and the green coronal line, show very diverse and complicated patterns. After pixel binning, we show that some of

the complexity may be caused by the integration over different polarization sources at subresolution scales and/or along the line of sight in the optically thin layers with complex geometric corrugations. **2013 November 2**

Spectro-Imaging Polarimetry of the Local Corona During Solar Eclipse

Z. Q. **Qu**, G. T. Dun, L. Chang, G. Murray, X. M. Cheng, X. Y. Zhang, L. H. Deng
Solar Physics February **2017**, 292:37
Results are presented from spectro-imaging polarimetry of radiation from the local solar corona during the 2013 total solar eclipse in Gabon. This polarimetric observation was performed from 516.3 nm to 532.6 nm using a prototype Fiber Arrayed Solar Optical Telescope (FASOT). A polarimetric noise level on the order of 10−310−3 results from a reduced polarimetric optical switching demodulation (RPOSD) procedure for data reduction. It is revealed that the modality of fractional linear polarization profiles of the green coronal line shows a diversity, which may indicate complex mechanisms. The polarization degree can approach 3.2 % above the continuum polarization level on a scale of 1500 km, and the nonuniform spatial distribution in amplitude and polarization direction is found even within a small field of view of 7500 km. All of this implies that the coronal polarization is highly structured and complex even on a small scale. **November 2, 2013**

On the Variation of Solar Radius in Rotation Cycles

Z. N. **Qu**1,2,3, D. F. Kong1,2,3, N. B. Xiang1,2,3, and W. Feng
2015 ApJ 798 113
The Date Compensated Discrete Fourier Transform and CLEANest algorithm are used to study the temporal variations of the solar radius observed at Rio de Janeiro Observatory from 1998 March 2 to 2009 November 6. The CLEANest spectra show several significant periodicities around 400, 312, 93.5, 86.2, 79.4, 70.9, 53.2, and 26.3 days. Then, combining the data on the daily solar radius measured at Calern Observatory and Rio de Janeiro Observatory and the corresponding daily sunspot areas, we study the short-term periodicity of the solar radius and the role of magnetic field in the variation of the solar radius. The rotation period of the daily solar radius is determined to be statistically significant. Moreover, its temporal evolution is anti-phase with that of sunspot activity, and it is found anti-phase with solar activity. Generally, the stronger solar activity is, the more obvious is the anti-phase relation of radius with solar activity. This indicates that strong magnetic fields have a greater inhibitive effect than weak magnetic fields on the variation of the radius.

Estimation of the Eclipse Solar Radius by Flash Spectrum Video Analysis

Luca **Quaglia**, John Irwin, Konstantinos Emmanouilidis, Alessandro Pessi
ApJ **2021**
https://arxiv.org/pdf/2107.09416.pdf
The value of the eclipse solar radius during the **2017 August 21** total solar eclipse was estimated to be S⊙=(959.95±0.05)" at 1au with no significant dependence on wavelength. The measurement was obtained from the analysis of a video of the eclipse flash spectrum recorded at the southern limit of the umbral shadow path. Our analysis was conducted by extracting light curves from the flash spectrum and comparing them to simulated light curves. Simulations were performed by integrating the limb darkening function (LDF) over the exposed area of photosphere. These numerical integrations relied upon very precise computations of the relative movement of the lunar and solar limbs.

The Effect of Anisotropic Viscosity on the Nonlinear Kink Instability

James **Quinn**, David MacTaggart, Radostin Simitev
Communications in Nonlinear Science and Numerical Simulation, 105131 **2019**
https://arxiv.org/pdf/1912.01076.pdf
The kink instability of magnetohydrodynamics is believed to be fundamental to many aspects of the dynamic activity of the solar atmosphere, such as the initiation of flares and the heating of the solar corona. In this work, we investigate the importance of viscosity on the kink instability. In particular, we focus on two forms of viscosity; isotropic viscosity (independent of the magnetic field) and anisotropic viscosity (with a preferred direction following the magnetic field). Through the detailed analysis of magnetohydrodynamic simulations of the kink instability with both types of viscosity, we show that the form of viscosity has a significant effect on the nonlinear dynamics of the instability. The different viscosities allow for different flow and current structures to develop, thus affecting the behaviour of magnetic relaxation, the formation of secondary instabilities and the Ohmic and viscous heating produced. Our results have important consequences for the interpretation of solar observations of the kink instability.

The Chromospheric Response to the Sunquake generated by the X9.3 Flare of NOAA 12673

Sean **Quinn**, Aaron Reid, Mihalis Mathioudakis, Christopher Nelson, S. Krishna Prasad, Sergei Zharkov
2019
https://arxiv.org/pdf/1906.08545.pdf
Active region NOAA 12673 was extremely volatile in 2017 September, producing many solar flares, including the largest of solar cycle 24, an X9.3 flare of **06 September 2017**. It has been reported that this flare produced a number of sunquakes along the flare ribbon (Sharykin & Kosovichev 2018; Zhao & Chen 2018). We have used co-temporal and co-spatial Helioseismic and Magnetic Imager (HMI) line-of-sight (LOS) and Swedish 1-m Solar Telescope observations to show evidence of the chromospheric response to these sunquakes. Analysis of the Ca II 8542 \AA\space line profiles of the wavefronts revealed that the crests produced a strong blue asymmetry, whereas the troughs produced at most a very slight red asymmetry. We used the combined HMI, SST datasets to create time-distance diagrams and derive the apparent transverse velocity and acceleration of the response. These velocities ranged from 4.5 km s−1 to 29.5 km s−1 with a constant acceleration of 8.6 x 10−3 km s−2. We employed NICOLE inversions, in addition to the Center-of-Gravity (COG) method to derive LOS velocities ranging 2.4 km s−1 to 3.2 km s−1. Both techniques show that the crests are created by upflows. We believe that this is the first chromospheric signature of a flare induced sunquake.

Effect of Anisotropic Collisions on Solar Scattering Polarization

Saleh **Qutub**, Moncef Derouich, Badruddin Zaheer Ahmad
Research in Astronomy and Astrophysics **2020**
https://arxiv.org/pdf/2010.06982.pdf
Scattering of anisotropic radiation by atoms, ions or molecules is sufficient to generate linear polarization observable in stars and planets atmospheres, circumstellar environments, and in particular in the Sun's atmosphere. This kind of polarization is called scattering polarization (SP) or second solar spectrum (SSS) if it is formed near the limb of the solar photosphere. Generation of linear SP can typically be reached more easily than circular SP. Interestingly, the later is often absent in observations and theories. Intrigued by this, we propose to demonstrate how circular SP can be created by anisotropic collisions if a magnetic field is present. We also demonstrate how anisotropic collisions can result in the creation of circular SP if the radiation field is anisotropic. We show that under certain conditions, linear SP creation is accompanied by the emergence of circular SP which can be useful for diagnostics of solar and astrophysical plasmas. We treat an example and calculate the density matrix elements of tensorial order k=1 which are directly associated with the presence of circular SP. This work should encourage theoretical and observational research to be increasingly oriented towards circular SP profiles in addition to linear SP in order to improve our analysis tools of astrophysical and solar observations.

Statistical Analysis of Acoustic Wave Power and Flows around Solar Active Regions

M. Cristina **Rabello-Soares**1, Richard S. Bogart2, and Philip H. Scherrer2
2018 ApJ 859 7
We analyze the effect of a sunspot in its quiet surroundings applying a helioseismic technique on almost three years of Helioseismic and Magnetic Imager (HMI) observations obtained during solar cycle 24 to further study the sunspot structure below the solar surface. The attenuation of acoustic waves with frequencies lower than 4.2 mHz depends more strongly on the wave direction at a distance of 6°–7° from the sunspot center. The amplification of higher frequency waves is highest 6° away from the active region and is largely independent of the wave's direction. We observe a mean clockwise flow around active regions, the angular speed of which decreases exponentially with distance and has a coefficient close to −0.7 degree−1. The observed horizontal flow in the direction of the nearby active region agrees with a large-scale circulation around the sunspot in the shape of cylindrical shell. The center of the shell seems to be centered around 7° from the sunspot center, where we observe an inflow close to the surface down to ~2 Mm, followed by an outflow at deeper layers until at least 7 Mm.

Benchmarking Hall-Induced Magnetoacoustic to Alfvén Mode Conversion in the Solar Chromosphere

Abbas **Raboonik**, Paul Cally
MNRAS **2021**
https://arxiv.org/pdf/2108.02396.pdf
A 2.5D numerical model of magnetoacoustic-Alfvén linear mode conversions in the partially ionised low solar atmosphere induced by the Hall effect is surveyed, varying magnetic field strength and inclination, and wave frequency and horizontal wave number. It is found that only the magnetic component of wave energy is subject to Hall-mediated conversions to Alfvén wave-energy via a process of polarisation rotation. This strongly boosts direct mode conversion between slow magneto\-acoustic and Alfvén waves in the quiet low chromosphere, even at mHz frequencies. However, fast waves there, which are predominantly acoustic in nature, are only subject to Hall-induced conversion via an indirect two-step process: (i) a geometry-induced fast-slow transformation near the Alfvén-acoustic equipartition height zeq; and (ii) Hall-rotation of the fast wave in z>zeq. Thus, for the two-stage process to yield upgoing Alfvén waves, zeq must lie below or within the Hall-effective window $0 \lesssim z \lesssim 700$ km.

Magnetic field strengths over 100 G are required to achieve this. Since the potency of this Hall effect varies inversely with the field strength but directly with the wave frequency, only frequencies above about 100 mHz are significantly affected by the two-stage process. Increasing magnetic field inclination θ generally strengthens the Hall convertibility, but the horizontal wavenumber kx has little effect. The direct and indirect Hall mechanisms both have implications for the ability of MHD waves excited at the photosphere to reach the upper chromosphere, and by implication the corona.

Hall-coupling of Slow and Alfvén Waves at Low Frequencies in the Lower Solar Atmosphere

Abbas **Raboonik**, Paul S. Cally
Solar Physics October **2019**, 294:147
https://link.springer.com/content/pdf/10.1007%2Fs11207-019-1544-1.pdf
The Hall effect due to weak ionization in the lower solar atmosphere is shown to produce significant coupling between slow magneto-acoustic and Alfvén waves, especially in highly inclined magnetic fields, and even at low frequencies (≈5≈5 mHz and above). Based on the exact magneto-acoustic linear wave solutions in a 2D isothermal model atmosphere, a perturbation approach is used to calculate the coupling to Alfvén waves polarized in the third dimension. First, a fast wave is injected at the bottom and is partially and often strongly reflected/converted to a down-going slow wave at the Alfvén-acoustic equipartition height, depending on magnetic field inclination, frequency, and wave number. This slow wave then couples strongly to the down-going Alfvén wave via the Hall effect for realistic Hall parameters. The coupling is strongest for horizontal wavenumbers oriented opposite to the field inclination, and magnetic fields around 100 G, for which large values of the Hall parameter are co-spatial with the region where slow and Alfvén waves have almost identical wave forms. Second, a slow wave is injected at the bottom, and found to couple even more strongly to up-going Alfvén waves in certain regions of the wavenumber–frequency plane where acoustic-gravity waves are evanescent. These results contrast with those for Hall-mediated fast-Alfvén coupling, which occurs higher in the atmosphere and is evident only at much higher frequencies.

The High-Resolution Coronal Imager, Flight 2.1

Laurel A. **Rachmeler** (1), Amy R. Winebarger (1), Sabrina L. Savage (1), Leon Golub (2) ....
Solar Phys. **294**, Article number: 174 **2019**
https://arxiv.org/pdf/1909.05942.pdf
https://link.springer.com/content/pdf/10.1007/s11207-019-1551-2.pdf
The third flight of the High-Resolution Coronal Imager (Hi-C 2.1) occurred on **May 29, 2018**, the Sounding Rocket was launched from White Sands Missile Range in New Mexico. The instrument has been modified from its original configuration (Hi-C 1) to observe the solar corona in a passband that peaks near 172 Angstrom and uses a new, custom-built low-noise camera. The instrument targeted Active Region 12712, and captured 78 images at a cadence of 4.4 sec (18:56:22 - 19:01:57 UT; 5 min and 35 sec observing time). The image spatial resolution varies due to quasi-periodic motion blur from the rocket; sharp images contain resolved features of at least 0.47 arcsec. There are coordinated observations from multiple ground- and space-based telescopes providing an unprecedented opportunity to observe the mass and energy coupling between the chromosphere and the corona. Details of the instrument and the data set are presented in this paper.

Patterns of Variation for the Sun and Sun-like Stars

Richard R. **Radick**1, G. Wesley Lockwood2, Gregory W. Henry3, Jeffrey C. Hall2, and Alexei A. Pevtsov4
2018 ApJ 855 75
http://sci-hub.tw/http://iopscience.iop.org/0004-637X/855/2/75/
We compare patterns of variation for the Sun and 72 Sun-like stars by combining total and spectral solar irradiance measurements between 2003 and 2017 from the SORCE satellite, Strömgren b, y stellar photometry between 1993 and 2017 from Fairborn Observatory, and solar and stellar chromospheric Ca ii H+K emission observations between 1992 and 2016 from Lowell Observatory. The new data and their analysis strengthen the relationships found previously between chromospheric and brightness variability on the decadal timescale of the solar activity cycle. Both chromospheric H+K and photometric b, y variability among Sun-like stars are related to average chromospheric activity by power laws on this timescale. Young active stars become fainter as their H+K emission increases, and older, less active, more Sun-age stars tend to show a pattern of direct correlation between photometric and chromospheric emission variations. The directly correlated pattern between total solar irradiance and chromospheric Ca ii emission variations shown by the Sun appears to extend also to variations in the Strömgren b, y portion of the solar spectrum. Although the Sun does not differ strongly from its stellar age and spectral class mates in the activity and variability characteristics that we have now studied for over three decades, it may be somewhat unusual in two respects: (1) its comparatively smooth, regular activity cycle, and (2) its rather low

photometric brightness variation relative to its chromospheric activity level and variation, perhaps indicating that facular emission and sunspot darkening are especially well-balanced on the Sun.

The explanation for the mysterious hot solar corona

Anil Narayan **Raghav**
2020
https://arxiv.org/pdf/2003.10326.pdf
The coronal heating has remained a puzzle for decades since its observation in 1940. Several space missions have been planned to resolve this conundrum in the past and many more intend to target this issue in the future. The unfolding of this issue will not only advance the fundamentals of astrophysical science but also promise an improvement in space weather prediction. Its origin has been debated without complete convergence; the acoustic waves, magneto-hydrodynamic waves, and micro/nano-flares are the strongest candidates so far to explain the mystery of coronal heating. However, none of these processes significantly justifies the million-degree temperature of the solar corona and the problem remains unsolved to date. Here, we propose a new physical mechanism to explain the observed heating of the solar corona. The statistical energy created during the interaction of the spin magnetic moment of the plasma particles with the turbulent and continuously evolving coronal magnetic field could substantiate the observed million-degree coronal temperature.

Conditions for Chromospheric Plasma Acceleration or Trigger of Chromospheric Mass Ejections by Magnetic-field-aligned Electric Fields

B. R. **Ragot**
2020 ApJ 897 76
https://sci-hub.tw/https://iopscience.iop.org/article/10.3847/1538-4357/ab910a
https://doi.org/10.3847/1538-4357/ab910a
Backward-propagating or reverse fluctuations in Alfvénic turbulence were recently found to produce magnetic-field-aligned (MFA) electric fields that can easily transfer their energy to the plasma, either in the form of heat (or electron beams that quickly dissipate their energy as heat) if electrons absorb most of the MFA energy, or in the form of translational motion of the plasma if the ions absorb most of the MFA energy. Conditions for the direct proton acceleration (jet formation) in the quiet chromosphere included a temperature ≤104 K and a magnetic field between about 10 and 100 G, conditions very similar to those under which chromospheric plasma jets or dynamic jet-like spicules are observed with the Interface Region Imaging Spectrograph. Here the conditions for direct ion acceleration by MFA electric fields are determined for a much broader range of electron densities and plasma temperatures, to include both quiet and flaring conditions of the chromospheric plasma. For the higher chromospheric electron densities of solar flaring conditions, direct ion and therefore plasma acceleration by MFA electric fields is found to be possible in the much stronger (kG) magnetic fields of active regions, provided the plasma temperature remains less than about 105 K. Under flaring conditions, the MFA electric fields may cause the acceleration or at least trigger the upward motion of dense (>1012–1013 cm−3) chromospheric plasma. It is also suggested that chromospheric nonresonant MFA acceleration, by producing local electron beams, may eliminate the need for electron beams to propagate from the flaring corona down to the denser chromosphere.

Solar Cycles and Covid-19 Pandemic Paradoxes.

Ragulskaya, M.V.
Geomagn. Aeron. 63, 984–995 (**2023**).
https://doi.org/10.1134/S0016793223070198
This article discusses different-scale cycles of solar activity, from 11-year to quasi-millennial, and the manifestation of their combinatorics in epidemiological dynamics. It is shown that a significant change in the dynamics of the number of infectious diseases during an 11-year cycle is associated with solar activity, and not with its geophysical manifestations. Covid-19 pandemic paradoxes to began under conditions of a simultaneous minimum of 11-year solar activity (SA) and a minimum of the quasi-secular solar cycle are considered. It is assumed that under the conditions of the global SA minimum, genetic population characteristics played a decisive role in the development of local coronavirus epidemics, and also played a significant role in the effectiveness of mass vaccination in various countries. The highest relative mortality was observed in haplogroup R1b (values 20–35) versus values 5–8 in haplogroup R1a, and values 2–4 in haplogroup N. Vaccination efficiency is also maximum in haplogroup R1b. The estimated height of the cycles during which viral pandemics can develop both at the maximum and at the minimum of 11-year SA cycles fluctuates around the value of 100–110 average annual Wolf numbers. Basically, this binary phenomenon is observed in the phase of growth and decline of the SA quasi-centennial cycle. Under conditions of a long global minimum of solar activity with a cycle amplitude of 90 to 120, a doubling of the number of viral pandemics can be observed, with a significant contribution of the genetic characteristics of the population to the dynamics of local epidemics.

Evidence from Galactic Cosmic Rays That the Sun Has Likely Entered A Secular Minimum in Solar Activity

F. **Rahmanifard**,A. P. Jordan,W. C. de Wet,N. A. Schwadron,J. K. Wilson,M. J. Owens,H. E. Spence,P. Riley

Space weather **Volume20, Issue2** e2021SW002796 **2022**

https://agupubs.onlinelibrary.wiley.com/doi/epdf/10.1029/2021SW002796

https://doi.org/10.1029/2021SW002796

Since the beginning of the space age, the Sun has been in a multi-cycle period of elevated activity (secular maximum). This secular maximum is the longest in the last 9300 years. Since the end of solar cycle 21 (SC21), however, the Sun has shown a decline in overall activity, which has remarkably increased the fluxes of galactic cosmic rays (GCRs). Here, we investigate the correlation between the modulation of GCRs, the heliospheric magnetic field, and solar wind speed for the last 24 solar cycles to find trends that can potentially be used to predict future solar activity. Specifically, we develop a tool for predicting future magnetic field intensity, based on the hysteresis in the GCR variation, during the last phases of the current cycle. This method estimates that SC25 will be as weak as or weaker than SC24. This would mean that the Sun has likely entered a secular minimum, which, according to historical records, should last for another two cycles (SC25 and SC26).

Inferring the Heliospheric Magnetic Field Back through Maunder Minimum

Fatemeh **Rahmanifard**1,2, Nathan A. Schwadron1,2, Charles W. Smith1,2, Kenneth G. McCracken3, Katharine A. Duderstadt2, Noé Lugaz1,2, and Molly L. Goelzer

2017 ApJ 837 165

Recent solar conditions include a prolonged solar minimum (2005–2009) and a solar maximum that has not fully recovered in terms of the Heliospheric Magnetic Field (HMF) strength when compared to the previous maximum values. These anomalies may indicate that we are entering an era of lower solar activity than observed at other times during the space age. We study past solar grand minima, especially the Maunder period (1645–1715) to gain further insight into grand minima. We find the timescale parameters associated with three processes attributed to the magnetic flux balance in the heliosphere using chi-square analysis. We use HMF time series reconstructed based on geomagnetic data and near-Earth spacecraft measurements (OMNI) data to find the fundamental timescales that influence heliospheric field evolution through conversion or opening of magnetic flux from coronal mass ejections (CMEs) into the ambient heliospheric field, removal or loss of the ambient heliospheric field through magnetic reconnection, and interchange reconnection between CME magnetic flux and ambient heliospheric magnetic flux. We also investigate the existence of a floor in the heliospheric magnetic flux, in the absence of CMEs, and show that a floor $\leqslant 1.49$ nT is sufficient to successfully describe the HMF evolution. The minimum value for the HMF at 1 au in the model-predicted historic record is 3.13 ± 0.35 nT. Our model results favorably reproduce paleocosmic data and near-Earth spacecraft measurements data and show how the HMF may evolve through periods of extremely low activity.

Global Solar Magnetic-field and Interplanetary Scintillations During the Past Four Solar Cycles

K. Sasikumar **Raja**, P. Janardhan, Susanta Kumar Bisoi, Madhusudan Ingale, Prasad Subramanian, K. Fujiki, Milan Maksimovic

Solar Phys. 294:123 **2019**

https://arxiv.org/pdf/1908.09134.pdf

sci-hub.se/10.1007/s11207-019-1514-7

The extended minimum of Solar Cycle 23, the extremely quiet solar-wind conditions prevailing and the mini-maximum of Solar Cycle 24 drew global attention and many authors have since attempted to predict the amplitude of the upcoming Solar Cycle 25, which is predicted to be the third successive weak cycle; it is a unique opportunity to probe the Sun during such quiet periods. Earlier work has established a steady decline, over two decades, in solar photospheric fields at latitudes above 45∘ and a similar decline in solar-wind micro-turbulence levels as measured by interplanetary scintillation (IPS) observations. However, the relation between the photospheric magnetic fields and those in the low corona/solar-wind are not straightforward. Therefore, in the present article, we have used potential force-free source-surface (PFSS) extrapolations to deduce global magnetic-fields using synoptic magnetograms observed with National Solar Observatory (NSO), Kitt Peak, USA (NSO/KP) and Solar Optical Long-term Investigation of the Sun (NSO/SOLIS) instruments during 1975-2018. Furthermore, we have measured the normalized scintillation index [m] using the IPS observations carried out at the Institute of Space Earth Environment Research (ISEE), Japan during 1983-2017. From these observations, we have found that, since the mid-1990s, the magnetic-field over different latitudes at 2.5 R⊙ and 10 R⊙(extrapolated using PFSS method) has decreased by ≈11.3−22.2%. In phase with the declining magnetic-fields, the quantity m also declined by ≈23.6%. These observations emphasize the inter-relationship among the global magnetic-field and various turbulence parameters in the solar corona and solar wind.

Time-Distance Helioseismology of Deep Meridional Circulation

S.P. **Rajaguru** (1), H.M. Antia

Astrophysics and Space Science Proceedings of "Dynamics of the Sun & Stars: Honoring the Life & Work of Michael Thompson" (**2020**)

https://arxiv.org/pdf/2004.12708.pdf

A key component of solar interior dynamics is the meridional circulation (MC), whose poleward component in the surface layers has been well observed. Time-distance helioseismic studies of the deep structure of MC, however, have yielded conflicting inferences. Here, following a summary of existing results we show how a large center-to-limb systematics (CLS) in the measured travel times of acoustic waves affect the inferences through an analysis of frequency dependence of CLS, using data from the Helioseismic and Doppler Imager (HMI) onboard Solar Dynamics Observatory (SDO). Our results point to the residual systematics in travel times as a major cause of differing inferences on the deep structure of MC.

Magnetic fields and low-frequency acoustic wave-energy supply to the solar chromosphere

S.P. **Rajaguru** (1), C.R. Sangeetha (2), Durgesh Tripathi

ApJ **871** 155 **201**9

https://arxiv.org/pdf/1812.05322.pdf

The problem of solar chromospheric heating remains a challenging one with wider implications for stellar physics. Several studies in the recent past have shown that small-scale inclined magnetic field elements channel copious amount of energetic low-frequency acoustic waves, that are normally trapped below the photosphere. These magneto-acoustic waves are expected to shock at chromospheric heights contributing to chromospheric heating. In this work, exploiting simultaneous photospheric vector magnetic field, Doppler, continuum and line-core intensity (of FeI 6173 Å) observations from the Helioseismic and Magnetic Imager (HMI) and lower-atmospheric UV emission maps in the 1700 Å and 1600 Å channels of the Atmospheric Imaging Assembly (AIA), both onboard the Solar Dynamics Observatory (SDO) of NASA, we revisit the relationships between magnetic field properties (inclination and strength) and the acoustic wave propagation (phase travel time). We find that the flux of acoustic energy, in the 2 - 5 mHz frequency range, between the upper photosphere and lower chromosphere is in the range of 2.25 - 2.6 kW m−2, which is about twice the previous estimates. We identify that the relatively less-inclined magnetic field elements in the quiet-Sun channel a significant amount of waves of frequency lower than the theoretical minimum for acoustic cut-off frequency due to magnetic inclination. We also derive indications that these waves steepen and start to dissipate within the heights ranges probed, while those let out due to inclined magnetic fields pass through. We explore connections with existing theoretical and numerical results that could explain the origin of these waves.

HMI Science Nuggets #120 Feb **2019** http://hmi.stanford.edu/hminuggets/?p=2836

Solar supergranular fractal dimension dependence on the Solar cycle phase

G. **Rajani**, G. M. Sowmya, U. Paniveni, R. Srikanth

Res. Astron. Astrophys. **2022**

https://arxiv.org/pdf/2202.00447.pdf

We study the complexity of the supergranular network through fractal dimension by using Ca II K digitized data archive obtained from Kodaikanal solar observatory. The data consists of 326 visually selected supergranular cells spread across the 23rd solar cycle. Only cells that were well-defined were chosen for the analysis and we discuss the potential selection effect thereof, mainly that it favors cells of a smaller size (< 20 Mm). Within this sample, we analyzed the fractal dimension of supergranules across the Solar cycle and find that it is anticorrelated with the activity level.

Energetics of the solar atmosphere

Abhishek **Rajhans**

Thesis **2023**

https://arxiv.org/pdf/2302.09259

The excess temperature of the solar corona over the photosphere poses a challenge. Multiple energetic events contribute to maintaining the corona at such high temperatures. The energy released in different events can vary across several orders of magnitude. Large energy events of geomagnetic importance like flares and coronal mass ejections (CMEs) contribute little to the global energetics of the solar corona. Therefore, events with several (9-10) orders of magnitudes of lower energy, with much higher frequency of occurrence, need to be studied in great detail. Observations suggest that these impulsive events with different energies follow a power-law distribution, indicating a common underlying mechanism. We perform observation-motivated modeling of coronal loops (magnetic flux tubes) to understand the energetics of these small transient events and their similarity with impulsive events like flares. This thesis uses the EBTEL code based on the 0D hydrodynamical description of coronal loops. This approach is appropriate for getting quick estimates of the energetics of the system over a wide range of parameters. We then discuss the improvement of EBTEL to make it suitable over a broader range of parameters. This is

followed by using improved EBTEL to explore the possibility of simulating impulsive events of different energy generated using a single power-law distribution. Comparison between observed emissions from various components of multi-thermal plasma and hydrodynamical models suggest the heating to be impulsive. Since field-aligned flows induced due to impulsive events are a crucial part of our modeling of coronal loops, we discuss the implications of such flows in the context of transition region heating.

Hydrodynamics of small transient brightenings in Solar corona

Abhishek **Rajhans**, Durgesh Tripathi, Vinay L. Kashyap

ApJ **917** 29 **2021**

https://arxiv.org/pdf/2105.08800.pdf

https://doi.org/10.3847/1538-4357/ac03bb

Small scale transients occur in the Solar corona at much higher frequencies than flares and play a significant role in coronal dynamics. Here we study three well-identified transients discovered by Hi-C and also detected by the EUV channels of Atmospheric Imaging Assembly (AIA) on board Solar Dynamics Observatory (SDO). We use 0-D enthalpy-based hydrodynamical simulations and produce synthetic light curves to compare with AIA observations. We have modeled these transients as loops of ~ 1.0~Mm length depositing energies ~ 10^23 ergs in ~ 50 seconds. The simulated synthetic light curves show reasonable agreement with the observed light curves. During the initial phase, conduction flux from the corona dominates over the radiation, like impulsive flaring events. Our results further show that the time-integrated net enthalpy flux is positive, hence into the corona. The fact that we can model the observed light curves of these transients reasonably well by using the same physics as those for nanoflares, microflares, and large flares, suggests that these transients may have a common origin. **2012 July 11**

Correlation between Supergranular Lane Widths and Sunspot Number; A Simple Way to Predict the Amplitude of Sunspot Cycle

K P **Raju**1, Jagdev Singh1, Belur Ravindra1, and Muthu Priyal1

2023 ApJL 959 L24

https://iopscience.iop.org/article/10.3847/2041-8213/ad13e9/pdf

The network structure seen in the solar images is the outline of supergranulation, which is the large-scale convection in the Sun with a size of about 30 Mm and a lifetime of 24 hr. We have obtained the supergranulation lane widths from the autocorrelation function of image windows from the Ca ii K spectroheliograms. The images are obtained from the 100 yr Kodaikanal data, which contains information on more than nine solar cycles. The lane widths are known to show a positive correlation with the sunspot number. It is now found that the lane widths, obtained near the mid-latitudes during the sunspot cycle minima, are strongly correlated to the following sunspot number maxima. A straight-line fit adequately describes the variation. It is also found that the correlation is weak or insignificant at other times. The strong correlation of the two parameters thus provides a simple way to predict the maximum sunspot number about 4–5 yr in advance. The results are important in space weather predictions and solar irradiance variations.

Asymmetry in the Length Scales of the Solar Supergranulation Network

K. P. **Raju**

2020 ApJL 899 L35

https://doi.org/10.3847/2041-8213/abacb7

Supergranulation is the horizontal velocity pattern on the solar surface with a typical size of 30,000 km and a lifetime of 24 hr. The network structure seen in chromospheric lines, such as Ca ii K 3934 Å, is the manifestation of supergranulation. The network seen in the extreme-ultraviolet lines like He ii 304 Å is the extension of the chromospheric network into the upper solar atmosphere. We have obtained the length scales of the supergranulation network from the autocorrelation function of calcium ii K spectroheliograms from the Kodaikanal archival data. The behavior of the length scales in the horizontal (parallel to the direction of rotation) and vertical (perpendicular to the direction of rotation) have been obtained in different latitudes for a period of about 100 yr. The time-averaged length scales show a nearly symmetric variation in the northern and southern hemispheres. The length scales also show a profound asymmetry in the horizontal and vertical directions, which is dependent on solar latitude. A comparison reveals that both length scales are almost equal near the equatorial latitudes, but the vertical length scales relatively become smaller toward higher latitudes. The asymmetry is independently verified from He ii 304 Å images from the Solar Dynamic Observatory/Atmospheric Imaging Assembly. As the length scales are related to the width of the network, the results point to the asymmetry in the supergranular cell boundary. Supergranulation is one of the basic length scales of solar convection, hence these results can have implications for the convection in Sun-like stars.

Variation in the Width of Transition Region Network Boundaries

K. P. **Raju**

Solar Phys. Volume 291, Issue 12, pp 3519–3526 **2016**

The transition region network seen in solar extreme ultraviolet (EUV) lines is the extension of the chromospheric network. The network appears as an irregular web-like pattern over the solar surface outside active regions. The average width of transition region network boundaries is obtained from the two-dimensional autocorrelation function of SOlar and Heliospheric Observatory (SOHO)/Coronal Diagnostic Spectrometer (CDS) synoptic images of the Sun in two emission lines, He i 586 Å and O v 630 Å during 1996 – 2012. The width of the network boundaries is found to be roughly correlated with the solar cycle variation with a lag of about ten months. A comparison of the widths in the two emission lines shows that they are larger for the He i line. The SOHO/CDS data also show large asymmetry in boundary widths in the horizontal (x) and vertical (y) image directions, which is shown to be caused by image distortions that are due to instrumental effects. Since the network boundary widths are related to the magnetic flux concentration along the boundaries, the results are expected to have implications on the flux transport on the solar surface, solar cycle, and the mass and energy budget of network loops and jets.

Transition Region Brightening in a Moss Region and Their Relation with Lower Atmospheric Dynamics

Bhinva **Ram**1,2, Tanmoy Samanta1, Yajie Chen2, Alphonse C. Sterling3, Jayant Joshi1, Vasyl Yurchyshyn4, Lakshmi Pradeep Chitta2, and Vaibhav Pant5
2024 ApJ 977 25
https://iopscience.iop.org/article/10.3847/1538-4357/ad84e1/pdf
Small-scale brightenings (SBs) are commonly observed in the transition region (TR) that separates the solar chromosphere from the corona. These brightenings, omnipresent in active region patches known as "moss" regions, could potentially contribute to the heating of active region plasma. In this study, we investigate the properties of SB events in a moss region and their associated chromospheric dynamics, which could provide insights into the underlying generation mechanisms of the SBs. We analyzed the data sets obtained by coordinated observations using the Interface Region Imaging Spectrograph and the Goode Solar Telescope at Big Bear Solar Observatory. We studied 131 SB events in our region of interest and found that 100 showed spatial and temporal matches with the dynamics observed in the chromospheric Hα images. Among these SBs, 98 of them were associated with spicules that are observed in Hα images. Furthermore, detailed analysis revealed that one intense SB event corresponded to an Ellerman bomb (EB), while another SB event consisted of several recurring brightenings caused by a stream of falling plasma. We observed that Hα far wings often showed flashes of strong brightening caused by the falling plasma, creating an Hα spectral profile similar to an EB. However, 31 of the 131 investigated SB events showed no noticeable spatial and temporal matches with any apparent features in Hα images. Our analysis indicated that the predominant TR SB events in moss regions are associated with chromospheric phenomena primarily caused by spicules. Most of these spicules display properties akin to dynamic fibrils. **2017 May 27**

Transverse MHD waves as signatures of braiding-induced magnetic reconnection in coronal loops

A. **Ramada**. C. Sukarmadji, Patrick Antolin
ApJL **2024**
https://arxiv.org/pdf/2401.07678.pdf
A major coronal heating theory based on magnetic reconnection relies on the existence of braided magnetic field structures in the corona. In this small-angle reconnection scenario, numerical simulations indicate that the reconnected magnetic field lines are driven sideways by magnetic tension and can overshoot from their new rest position, thereby leading to low-amplitude transverse MHD waves. This provides an efficient mechanism for transverse MHD wave generation, and the direct causality also constitutes substantial evidence of reconnection from braiding. However, this wave-generation mechanism has never been directly observed. Recently, the telltale signature of small-angle reconnection in a sheared coronal structure has been identified through nanojets, which are small, short-lived, and fast jet-like bursts in the nanoflare range transverse to the guide-field. We present for the first time IRIS and SDO observations of transverse MHD waves in a coronal loop that directly result from braiding-induced reconnection. The reconnection is identified by the presence of nanojets at the loop apex which release nanoflare-range energy. We find that the oscillations have an energy flux on the order of 106−108~erg~cm−2~s−1, which is within the budget to power active region loops. The estimated kinetic and thermal energy from the nanojets is also sufficient to power the transverse waves and sustain the observed heating at the loop apex. This discovery provides major support to (a) existing theories that transverse MHD waves can be a signature of reconnection, (b) the existence of braiding in coronal structures and (c) the coronal reconnection scenario identified by nanojets. **29 Oct 2014**
IRIS Nugget June 2024 https://iris.lmsal.com/nugget

Sunspot data collection of Specola Solare Ticinese in Locarno

Renzo **Ramelli**, Marco Cagnotti, Sergio Cortesi, Michele Bianda, Andrea Manna
IAU Symposium No. 340 **2018**

https://arxiv.org/pdf/1805.09202.pdf
Sunspot observations and counting are carried out at the Specola Solare Ticinese in Locarno since 1957 when it was built as an external observing station of the Zurich observatory. When in 1980 the data center responsibility was transferred from ETH Zurich to the Royal Observatory of Belgium in Brussels, the observations in Locarno continued and Specola Solare Ticinese got the role of pilot station. The data collected at Specola cover now the last 6 solar cycles.
The aim of this presentation is to discuss and give an overview about the Specola data collection, the applied counting method and the future archiving projects. The latter includes the publication of all data and drawings in digital form in collaboration with the ETH Zurich University Archives, where a parallel digitization project is ongoing for the document of the former Swiss Federal Observatory in Zurich collected since the time of Rudolph Wolf.

Atlas of the solar intensity spectrum and its center to limb variation

R. **Ramelli**, M. Setzer, M. Engelhard, M. Bianda, F. Paglia, J. O. Stenflo, G. Küveler, R. Plewe
Proceedings of the Solar Polarization Workshop 8, held in Florence (I), September, 12-16 2017 **2017**
https://arxiv.org/pdf/1708.03284.pdf
The solar limb darkening function is well known and is widely employed in models of the solar atmosphere. However, there has been a lack of systematic spectrally resolved measurements. Therefore we recently decided to start an observing campaign with the Gregory Coud\'e Telescope at IRSOL in Locarno in order to produce a spectral atlas obtained at 10 different heliocentric angles θ, chosen so that μ=cosθ covers the interval from 0.1 to 1.0 in step of 0.1. The measurements carried out till now include the spectral range from 439 nm to 666 nm. The collected data provide information about the anisotropy of the emergent radiation field on the solar surface, allowing a better modeling of the Second Solar Spectrum. In addition the data give observational constraints that should be taken into account when modeling the solar atmosphere.

Measurement of the evolution of the magnetic field of the quiet photosphere during a solar cycle

Renzo **Ramelli**, Michele Bianda, Svetlana Berdyugina, Luca Belluzzi, Lucia Kleint
Proceedings of the Solar Polarization Workshop 8, held in Florence (I), September, 12-16 2017 **2017**
https://arxiv.org/pdf/1708.03287.pdf
The solar photosphere is filled by a magnetic field which is tangled on scales much smaller than the resolution capability of solar telescopes. This hidden magnetic field can be investigated via the Hanle effect. In 2007 we started a synoptic program to explore if the magnetic flux of the quiet photosphere varies with the solar cycle. For this purpose we applied a differential Hanle effect technique based on observations of scattering polarization in C2 molecular lines around 514.0 nm, taken generally every month. Our results now span almost one complete solar cycle.

Radio, X-Ray, and Extreme-ultraviolet Observations of Weak Energy Releases in the "Quiet" Sun

R. **Ramesh**1, C. Kathiravan1, N. P. S. Mithun2, and S. V. Vadawale2
2021 ApJL 918 L18
https://doi.org/10.3847/2041-8213/ac1da3
We analyzed ground-based low frequency (<100 MHz) radio spectral and imaging data of the solar corona obtained with the facilities in the Gauribidanur observatory during the same time as the very weak soft X-ray flares (sub-A-class, flux <10−7Wm−2 in the 1–8 Å wavelength range) from the quiet Sun observed with the X-ray Solar Monitor (XSM) on board Chandrayaan-2 during the recent solar minimum. Nonthermal type I radio burst activity was noticed in close temporal association with the X-ray events. The estimated brightness temperature (Tb) of the bursts at a typical frequency like 80 MHz is ≈3 × 105 K. Extreme-ultraviolet (EUV) observations at 94 Å with the Atmospheric Imaging Assembly (AIA) on board the Solar Dynamics Observatory (SDO) revealed a brightening close to the same location and time as the type I radio bursts. As far as we know reports of simultaneous observations of X-ray and/or EUV counterpart to weak transient radio emission at low frequencies from the quiet Sun in particular are rare. Considering this and the fact that low frequency radio observations are sensitive to weak energy releases in the solar atmosphere, the results indicate that coordinated observations of similar events would be useful to understand transient activities in the quiet Sun.

Machine learning in solar physics **Review**

A. Asensio **Ramos**, M. C. M. Cheung, I. Chifu, R. Gafeira
Living Review in Solar Physics (LRSP) **20**, Article number: 4 **2023**
https://arxiv.org/pdf/2306.15308.pdf
https://link.springer.com/content/pdf/10.1007/s41116-023-00038-x.pdf

The application of machine learning in solar physics has the potential to greatly enhance our understanding of the complex processes that take place in the atmosphere of the Sun. By using techniques such as deep learning, we are now in the position to analyze large amounts of data from solar observations and identify patterns and trends that may not have been apparent using traditional methods. This can help us improve our understanding of explosive events like solar flares, which can have a strong effect on the Earth environment. Predicting hazardous events on Earth becomes crucial for our technological society. Machine learning can also improve our understanding of the inner workings of the sun itself by allowing us to go deeper into the data and to propose more complex models to explain them. Additionally, the use of machine learning can help to automate the analysis of solar data, reducing the need for manual labor and increasing the efficiency of research in this field.

Real-time multiframe blind deconvolution of solar images

A. Asensio **Ramos** (1,2), J. de la Cruz Rodriguez (3), A. Pastor Yabar (1,2,4)
A&A 620, A73 **2018**
https://arxiv.org/pdf/1806.07150.pdf

The quality of images of the Sun obtained from the ground are severely limited by the perturbing effect of the turbulent Earth's atmosphere. The post-facto correction of the images to compensate for the presence of the atmosphere require the combination of high-order adaptive optics techniques, fast measurements to freeze the turbulent atmosphere and very time consuming blind deconvolution algorithms. Under mild seeing conditions, blind deconvolution algorithms can produce images of astonishing quality. They can be very competitive with those obtained from space, with the huge advantage of the flexibility of the instrumentation thanks to the direct access to the telescope. In this contribution we leverage deep learning techniques to significantly accelerate the blind deconvolution process and produce corrected images at a peak rate of ~100 images per second. We present two different architectures that produce excellent image corrections with noise suppression while maintaining the photometric properties of the images. As a consequence, polarimetric signals can be obtained with standard polarimetric modulation without any significant artifact. With the expected improvements in computer hardware and algorithms, we anticipate that on-site real-time correction of solar images will be possible in the near future.

DeepVel: deep learning for the estimation of horizontal velocities at the solar surface

A. Asensio **Ramos** (1,2), I. S. Requerey (1,2), N. Vitas (1,2) ((1) Instituto de Astrofisica de Canarias, (2) Universidad de La Laguna)
A&A 604, A11 **2017**
https://arxiv.org/pdf/1703.05128.pdf

Many phenomena taking place in the solar photosphere are controlled by plasma motions. Although the line-of-sight component of the velocity can be estimated using the Doppler effect, we do not have direct spectroscopic access to the components that are perpendicular to the line-of-sight. These components are typically estimated using methods based on local correlation tracking. We have designed DeepVel, an end-to-end deep neural network that produces an estimation of the velocity at every single pixel and at every time step and at three different heights in the atmosphere from just two consecutive continuum images. We confront DeepVel with local correlation tracking, pointing out that they give very similar results in the time- and spatially-averaged cases. We use the network to study the evolution in height of the horizontal velocity field in fragmenting granules, supporting the buoyancy-braking mechanism for the formation of integranular lanes in these granules. We also show that DeepVel can capture very small vortices, so that we can potentially expand the scaling cascade of vortices to very small sizes and durations.

Inference of the chromospheric magnetic field orientation in the Ca ii 8542 Å line fibrils

A. Asensio **Ramos**1,2, J. de la Cruz Rodríguez3, M. J. Martínez González1,2 and H. Socas-Navarro
A&A 599, A133 (**2017**)

Context. Solar chromospheric fibrils, as observed in the core of strong chromospheric spectral lines, extend from photospheric field concentrations suggesting that they trace magnetic field lines. These images have been historically used as proxies of magnetic fields for many purposes.
Aims. Use statistical analysis to test whether the association between fibrils and magnetic field lines is justified.
Methods. We use a Bayesian hierarchical model to analyze several tens of thousands of pixels in spectro-polarimetric chromospheric images of penumbrae and chromospheric fibrils. We compare the alignment between the field azimuth inferred from the linear polarization signals through the transverse Zeeman effect and the direction of the fibrils in the image.
Results. We conclude that, in the analyzed fields of view, fibrils are often well aligned with the magnetic field azimuth. Despite this alignment, the analysis also shows that there is a non-negligible dispersion. In penumbral filaments, we find a dispersion with a standard deviation of ~ 16°, while this dispersion goes up to ~ 34° in less magnetized regions.

Automated analysis of oscillations in coronal bright points

Brad **Ramsey**, Erwin Verwichte, Huw Morgan

A&A **2023**

https://arxiv.org/pdf/2309.14863.pdf

Coronal bright points (BPs) are numerous, bright, small-scale dynamical features found in the solar corona. Bright points have been observed to exhibit intensity oscillations across a wide range of periodicities and are likely an important signature of plasma heating and/or transport mechanisms. We present a novel and efficient wavelet-based method that automatically detects and tracks the intensity evolution of BPs using images from the Atmospheric Imaging Assembly (AIA) on board the Solar Dynamics Observatory (SDO) in the 193Å bandpass. Through the study of a large, statistically significant set of BPs, we attempt to place constraints on the underlying physical mechanisms. We used a continuous wavelet transform (CWT) in 2D to detect the BPs within images. One-dimensional CWTs were used to analyse the individual BP time series to detect significant periodicities. We find significant periodicity at 4, 8-10, 17, 28, and 65 minutes. Bright point lifetimes are shown to follow a power law with exponent -1.13 ± 0.07. The relationship between the BP lifetime and maximum diameter similarly follows a power law with exponent 0.129 ± 0.011. Our wavelet-based method successfully detects and extracts BPs and analyses their intensity oscillations. Future work will expand upon these methods, using larger datasets and simultaneous multi-instrument observations. **1-3 Jan 2020**

Path-lengths in the quiet Sun transition region using O IV lines from IRIS

Yamini K **Rao**, Giulio Del Zanna, Helen E Mason, Roger Dufresne

MNRAS, Volume 517, Issue 1, November **2022**, Pages 1422–1435,

https://doi.org/10.1093/mnras/stac2772

We use spectroscopic diagnostics to determine different plasma parameters in the transition region of the quiet Sun. The electron number density from O IV lines using high-resolution spectral observations from the Interface Region Imaging Spectrograph (IRIS) are estimated to be around 1010 cm−3, in agreement with literature values and our re-analysis of earlier observations from HRTS and SUMER. We also find a large scatter in the densities obtained from IRIS and SUMER. We use these densities to estimate the size of the emitting region (the path-length) using an isothermal assumption. We find evidence for some centre-to-limb variations, with median values of path-lengths for disc centre and near the limb from IRIS O IV being 10 and 31 km, respectively. These values are close to those obtained from HRTS. We also use new atomic models for the quiet Sun, which include electron density effects, photoionization, and charge transfer, to find path-lengths from Si IV and C IV in close agreement with those from O IV. Finally, we estimate the emission measure from HRTS data to show that the isothermal assumption overestimates the path-lengths by factors of 5–8. Such small path-lengths should be taken into account when modelling the transition region for the interpretation of observations from e.g. IRIS and the Solar Orbiter SPICE spectrometer.

IRIS Nugget Nov 2022 https://iris.lmsal.com/nugget

The Center-to-Limb Variation of Non-Thermal Velocities using IRIS Si IV

Yamini K. **Rao**, Giulio Del Zanna, Helen E. Mason

MNRAS, **2022**

https://arxiv.org/pdf/2201.07290.pdf

We study the non-thermal velocities in the quiet-sun using various high spatial, temporal, and spectral resolution observations from the Interface Region Imaging Spectrograph (IRIS). We focus our analysis on the transition region using the optically thin line (Si IV 1393.7 Å), and select line profiles that are nearly Gaussian. We find evidence of a centre-to-limb variation using different observations having different exposure times, ranging from 5-30 s. The distribution of non-thermal velocities close to the limb are observed to peak around 20 km s−1 while the disc observations show a peak around 15 km s−1. The distributions are also different. The overall variation in the non-thermal velocities are correlated with the intensity of the line, as found previously. The on-disc velocities are smaller than most previous observations. In general, we find that the non-thermal velocities are independent of the selected exposure times. The Si IV lines didn't seem to exhibit any significant opacity effects. We conclude that these Doppler motions are mostly transverse to the radial direction. The possibility of swaying/torsional motions leading to such variations are validated from these IRIS observations. **22 Jan 2014, 25 Feb 2014**

Table 2. Non-thermal velocities observed for different IRIS observations at different locations

Impulsive plasma outflows due to wave driven magnetic reconnection

Yamini K. **Rao**, A.K. Srivastava, J.G. Doyle and Bhola N. Dwivedi

MNRAS **2017**

http://star.arm.ac.uk/preprints/2017/690.pdf

We study an impulsive plasma outflow in the quiet-Sun using multi-wavelength observations from the Atmospheric Imaging Assembly (AIA) onboard the Solar Dynamics Observatory (SDO) on **2011 March 30**. The outflow rises to the upper solar atmosphere with a high terminal speed of 1250 km s-1. Emissions from multiple SDO/AIA channels (log T (K) = 4.7 to log T (K) = 7.0), peak at the same time indicating its highly impulsive origin. We obtain the line-of-sight differential emission measure (DEM) maps and find that the outflow is made up of multi-temperature plasma. Investigation of SDO/HMI magnetic field data at its foot-point shows that the emerging flux of negative polarity is oscillating at the period of 416 sec. The oscillations are also observed in the intensity of 1600A almost co-temporally near the base of the outflow with the almost same period (~442 sec). The ~7.0 min periodicity respectively in the magnetic flux at the photosphere and 1600A flux at the chromosphere/TR height is present both prior to and during the onset, and even after the outflows for the duration of ~1 hr. This indicates that the waves are generated and present at the base of the outflow interacting with the localised small-scale current-sheet thus leading to magnetic reconnection and the impulsive outflows. Observed magnetoacoustic waves may see the discontinuity at the X-point which may develop into fast oblique magnetic shocks leading to the local heating due to the reconnection and compression at the X-point and forming a shock-cusp enabling hot plasma outflows.

INSTRUMENT DESCRIPTION AND PERFORMANCE EVALUATION OF A HIGH-ORDER ADAPTIVE OPTICS SYSTEM FOR THE 1 m NEW VACUUM SOLAR TELESCOPE AT FUXIAN SOLAR OBSERVATORY

Changhui **Rao**1,2, Lei Zhu1,2,4, Xuejun Rao1,2, Lanqiang Zhang1,2, Hua Bao1,2, Lin Kong1,2,3, Youming Guo1,2, Libo Zhong1,2, Xue'an Ma1,2, Mei Li1 …

2016 ApJ 833 210

A high-order solar adaptive optics (AO) system including a fine tracking loop and a high-order wavefront correction loop has been installed at the 1 m New Vacuum Solar Telescope of the Fuxian Solar Observatory, in routine operation since 2016. The high-order wavefront correction loop consists of a deformable mirror with 151 actuators, a correlating Shack–Hartmann wavefront sensor with 102 subapertures of which the Absolute Difference Square Algorithm is used to extract the gradients, and a custom-built real-time controller based on a Field-Programmable Gate Array (FPGA) and multi-core Digital Signal Processor (DSP). The frame rate of the wavefront sensor is up to 3500 Hz and this is, to our knowledge, the fastest solar AO system. This AO system can work with a Fried parameter r 0, at the 500 nm wavelength, of larger than 3 cm. The first 65 modes of the Zernike aberrations can be efficiently corrected and the Strehl ratio of the corrected TiO image for the solar pore is superior to 0.75 with the Fried parameter r 0 larger than 10 cm. In this paper, the design of the system is described, and high-resolution solar observational images are presented. Furthermore, the performances of the AO system are evaluated according to the data recorded by the real-time controller.

Magnetic Reconnection as the Driver of the Solar Wind

Nour E. **Raouafi**1, G. Stenborg1, D. B. Seaton2, H. Wang3,4,5, J. Wang3,4,5, C. E. DeForest2, S. D. Bale6,7, J. F. Drake8, V. M. Uritsky9,10, J. T. Karpen10Show full author list

2023 ApJ 945 28

https://iopscience.iop.org/article/10.3847/1538-4357/acaf6c/pdf
https://arxiv.org/pdf/2301.00903.pdf

We present EUV solar observations showing evidence for omnipresent jetting activity driven by small-scale magnetic reconnection at the base of the solar corona. We argue that the physical mechanism that heats and drives the solar wind at its source is ubiquitous magnetic reconnection in the form of small-scale jetting activity (a.k.a. jetlets). This jetting activity, like the solar wind and the heating of the coronal plasma, is ubiquitous regardless of the solar cycle phase. Each event arises from small-scale reconnection of opposite-polarity magnetic fields producing a short-lived jet of hot plasma and Alfvén waves into the corona. The discrete nature of these jetlet events leads to intermittent outflows from the corona, which homogenize as they propagate away from the Sun and form the solar wind. This discovery establishes the importance of small-scale magnetic reconnection in solar and stellar atmospheres in understanding ubiquitous phenomena such as coronal heating and solar wind acceleration. Based on previous analyses linking the switchbacks to the magnetic network, we also argue that these new observations might provide the link between the magnetic activity at the base of the corona and the switchback solar wind phenomenon. These new observations need to be put in the bigger picture of the role of magnetic reconnection and the diverse form of jetting in the solar atmosphere. **2019-07-29, 2021-04-28**

Parker Solar Probe: Four Years of Discoveries at Solar Cycle Minimum **Review**

N. E. **Raouafi**, L. Matteini, J. Squire, S. T. Badman, M. Velli, +++

Space Science Reviews article number: 8 **2023** 157 pages, 65 figures

https://arxiv.org/pdf/2301.02727.pdf
https://link.springer.com/content/pdf/10.1007/s11214-023-00952-4.pdf

Launched on 12 Aug. 2018, NASA's Parker Solar Probe had completed 13 of its scheduled 24 orbits around the Sun by Nov. 2022. The mission's primary science goal is to determine the structure and dynamics of the Sun's coronal magnetic field, understand how the solar corona and wind are heated and accelerated, and determine what processes accelerate energetic particles. Parker Solar Probe returned a treasure trove of science data that far exceeded quality, significance, and quantity expectations, leading to a significant number of discoveries reported in nearly 700 peer-reviewed publications. The first four years of the 7-year primary mission duration have been mostly during solar minimum conditions with few major solar events. Starting with orbit 8 (i.e., 28 Apr. 2021), Parker flew through the magnetically dominated corona, i.e., sub-Alfvénic solar wind, which is one of the mission's primary objectives. In this paper, we present an overview of the scientific advances made mainly during the first four years of the Parker Solar Probe mission, which go well beyond the three science objectives that are: (1) Trace the flow of energy that heats and accelerates the solar corona and solar wind; (2) Determine the structure and dynamics of the plasma and magnetic fields at the sources of the solar wind; and (3) Explore mechanisms that accelerate and transport energetic particles. **1 Nov. 2018, 5 Nov. 2018, 11-12 Nov. 2018, 15 Mar. 2019, 2 and 4 Apr. 2019, 20-21 Apr. 2019, 13 Oct. 2019, 20 Jan. 2020, 26-27 Jan. 2020, 25 Jun. 2020, 19 Nov. 2020, 29 Nov. 2020**

Spectra of solar shallow-water waves from bright point observations

B. **Raphaldini**1⋆, M. Dikpati1, S. McIntosh1,2 and A. S. W. Teruya3

A&A 692, A102 (**2024**)
https://www.aanda.org/articles/aa/pdf/2024/12/aa51014-24.pdf
https://doi.org/10.1051/0004-6361/202451014

Context. Rossby waves, large-scale meandering patterns drifting in longitude, detected in the Sun, were recently shown to a play a crucial role in understanding “seasons” of space weather. Unlike Earth’s purely classical atmospheric Rossby waves, the solar counterparts are strongly magnetized and most likely originate in the tachocline. Because of their deeper origin, detecting these magnetized Rossby waves is a challenging task that relies on careful observations of long-lived longitudinally drifting magnetic patterns at the surface and above.
Aims. Here, we have utilized 3 years of global, synchronous observations of coronal bright point densities to obtain empirical signatures of dispersion relations that can be attributed to the simulated waves in the tachocline. By tracking the bright point densities at selected latitudes, we computed their wave-number × frequency spectra.
Methods. Wave-number × frequency spectra were computed utilizing the Wheeler-Kiladis method. This method has been extensively used in the identification of equatorial waves in Earth’s atmosphere by highlighting spectral peaks in the wave-number × frequency space.
Results. Our results are compatible with the predictions of magneto-Rossby waves with typical periods of several months and inertio-gravity waves with typical periods of a few weeks, depending on the background magnetic field’s strength and stratification at the convection zone base. Our analysis suggests that magnetized Rossby waves originate from the tachocline toroidal field of ≲15 kG. Global observations of bright points over extended periods will allow us to better constrain the stratification and magnetic field strength in the tachocline.

Information-theoretic Analysis of Longitude Distribution of Photospheric Magnetic Fields from MDI/HMI Synoptic Maps: Evidence for Rossby Waves

Breno **Raphaldini**1, Mausumi Dikpati1, and Scott W. McIntosh1

2023 ApJ 953 156
https://iopscience.iop.org/article/10.3847/1538-4357/ace320/pdf

Much of the research on the magnetic activity of the Sun has been focused on its axisymmetric component. However, the longitudinal complexity plays a fundamental role in the solar magnetic activity. Rossby waves have recently been proposed as a fundamental mechanism regarding the nonaxisymmetric nature of the solar magnetic fields. Here, we use HMI and MDI magnetic field synoptic maps to evaluate the magnetic field structures' (mainly

active regions) organization and propagation as a function of time and latitude. We demonstrate, using information theory, that the organization of longitudinal structures observed on synoptic maps is proportional to the level of activity at a given latitude. We further show that this organization on the longitudinal structures is persistent and due to long-lived features. The drift velocity of these long-lived photospheric features is inferred and is shown to significantly vary with latitude, and is compatible with the phase speed of tachocline magnetic Rossby waves with a toroidal field in the range of 5–10 kG. Our results suggest that Rossby waves contribute to the organization and propagation of photospheric magnetic features on the timescale of several months and beyond.
HMI Science Nuggets #194 **2023** http://hmi.stanford.edu/hminuggets/?p=4145

A New Mechanism for Maunder-like Solar Minima: Phase Synchronization Dynamics in a Simple Nonlinear Oscillator of Magnetohydrodynamic Rossby Waves

Breno **Raphaldini**1, Everton Medeiros2, Carlos F. M. Raupp1, and Andre Seiji Teruya
2020 ApJL 890 L13
https://doi.org/10.3847/2041-8213/ab71fd
The long-term solar cycle variability and Grand solar minima remain open questions from a theoretical point of view. Recently, a growing basis of evidence points out to the role of the magnetic Rossby waves in the solar cycle. Here we present a simple deterministic model, based on a low-order spectral representation of the barotropic quasi-geostrophic-magnetohydrodynamic equations for the Solar tachocline. This model supports the idea of the long-term behavior of the solar activity as a result of nonlinear interaction of magnetic Rossby modes. Solutions show that Rossby waves undergo irregular switches between periods of high activity and periods of suppressed activity, resembling the Maunder minimum. Low-energy states in the model are associated with the synchronization of the dynamical phases of the waves. These irregular transitions in the amplitudes of the waves are reminiscent of the observed time series of the solar activity. This suggests that Maunder-like states arise from chaotic transitions between regimes with different degrees of organization in the system.

Nonlinear Rossby wave-wave and wave-mean flow theory for long term Solar cycle modulations

Breno **Raphaldini**, André Seiji Teruya, Carlos Frederico Mendonca Raupp, Miguel D. Bustamante
ApJ **887** 1 **2019**
https://arxiv.org/pdf/1908.07056.pdf
https://doi.org/10.3847/1538-4357/ab5067
The Schwabe cycle of solar activity exhibits modulations and frequency fluctuations on slow time scales of centuries and millennia. Plausible physical explanations for the cause of these long-term variations of the solar cycle are still elusive, with possible theories including stochasticity of alpha effect and fluctuations of the differential rotation. It has been suggested recently in the literature that there exists a possible relation between the spatio-temporal structure of Solar cycle and the nonlinear dynamics of magnetohydrodynamic Rossby waves at the solar tachocline, including both wave-wave and wave-mean flow interactions. Here we extend the nonlinear theory of MHD Rossby waves presented in a previous article to take into account long term modulation effects due to a recently discovered mechanism that allows significant energy transfers throughout different wave triads: the precession resonance mechanism. We have found a large number of Rossby-Haurwitz wave triads whose frequency mismatches are compatible with the solar cycle frequency. Consequently, by analyzing the reduced dynamics of two triads coupled by a single mode (five-wave system), we have demonstrated that in the amplitude regime in which precession resonance occurs, the energy transfer throughout the system yields significant long-term modulations on the main ~11yr period associated with intra-triad energy exchanges. We further show that such modulations display an inverse relationship between the characteristic wave amplitude and the period of intra-triad energy exchanges, which is consistent with the Waldmeier's law for the solar cycle. In the presence of a constant forcing and dissipation, the five-wave system in the precession resonance regime exhibits irregular amplitude fluctuations with some periods resembling the Grand Minimum states.

Nonlinear Dynamics of Magnetohydrodynamic Rossby Waves and the Cyclic Nature of Solar Magnetic Activity

Breno **Raphaldini** and Carlos F. M. Raupp
2015 ApJ 799 78
The solar dynamo is known to be associated with several periodicities, with the nearly 11/22 yr cycle being the most pronounced one. Even though these quasiperiodic variations of solar activity have been attributed to the underlying dynamo action in the Sun's interior, a fundamental theoretical description of these cycles is still elusive. Here, we present a new possible direction in understanding the Sun's cycles based on resonant nonlinear interactions among magnetohydrodynamic (MHD) Rossby waves. The WKB theory for dispersive waves is applied to

magnetohydrodynamic shallow-water equations describing the dynamics of the solar tachocline, and the reduced dynamics of a resonant triad composed of MHD Rossby waves embedded in constant toroidal magnetic field is analyzed. In the conservative case, the wave amplitudes evolve periodically in time, with periods on the order of the dominant solar activity timescale (~11 yr). In addition, the presence of linear forcings representative of either convection or instabilities of meridionally varying background states appears to be crucial in balancing dissipation and thus sustaining the periodic oscillations of wave amplitudes associated with resonant triad interactions. Examination of the linear theory of MHD Rossby waves embedded in a latitudinally varying mean flow demonstrates that MHD Rossby waves propagate toward the equator in a waveguide from –35° to 35° in latitude, showing a remarkable resemblance to the structure of the butterfly diagram of the solar activity. Therefore, we argue that resonant nonlinear magnetohydrodynamic Rossby wave interactions might significantly contribute to the observed cycles of magnetic solar activity.

New Results from the Solar Maximum Mission/Bent Crystal Spectrometer

C. G. **Rapley**, J. Sylwester, K. J. H. Phillips
Solar Physics April **2017**, 292:50
http://link.springer.com/article/10.1007/s11207-017-1070-y
The Bent Crystal Spectrometer (BCS) onboard the NASA Solar Maximum Mission was part of the X-ray Polychromator, which observed numerous flares and bright active regions from February to November 1980, when operation was suspended as a result of the failure of the spacecraft fine-pointing system. Observations resumed following the Space Shuttle SMM Repair Mission in April 1984 and continued until November 1989. BCS spectra have been widely used in the past to obtain temperatures, emission measures, and turbulent and bulk flows during flares, as well as element abundances. Instrumental details including calibration factors not previously published are given here, and the in-orbit performance of the BCS is evaluated. Some significant changes during the mission are described, and recommendations for future instrumentation are made. Using improved estimates for the instrument parameters and operational limits, it is now possible to obtain de-convolved calibrated spectra that show finer detail than before, providing the means for improved interpretation of the physics of the emitting plasmas. The results indicate how historical archived data can be re-used to obtain enhanced and new, scientifically valuable results.

Magnetic field line twisting by photospheric vortices: energy storage and release

A. F. **Rappazzo**, M. Velli, R. B. Dahlburg, G. Einaudi
ApJ **883** 148 **2019**
https://arxiv.org/pdf/1905.04420.pdf
https://doi.org/10.3847/1538-4357/ab3c69
We investigate the dynamics of a closed corona cartesian reduced magnetohydrodynamic (MHD) model where photospheric vortices twist the coronal magnetic field lines. We consider two corotating or counter-rotating vortices localized at the center of the photospheric plate, and additionally more corotating vortices that fill the plate entirely. Our investigation is specifically devoted to study the fully nonlinear stage, after the linear stage during which the vortices create laminar and smoothly twisting flux tubes. Our main goal is to understand the dynamics of photospheric vortices twisting the field lines of a coronal magnetic field permeated by finite amplitude broadband fluctuations. We find that depending on the arrangement and handedness of the photospheric vortices an inverse cascade storing a significant amount of magnetic energy may occur or not. In the first case a reservoir of magnetic energy available to large events such as destabilization of a pre-CME configuration develops, while in the second case the outcome is a turbulent heated corona. Although our geometry is simplified our simulations are shown to have relevant implications for coronal dynamics and CME initiation.

Subresolution Activity in Solar and Stellar Coronae from Magnetic Field Line Tangling

A. F. **Rappazzo**, R. B. Dahlburg, G. Einaudi, M. Velli
Monthly Notices of the Royal Astronomical Society, Volume 478, Issue 2, 1 August **2018**, Pages 2257-2266,
https://arxiv.org/pdf/1805.00480.pdf
The heating of coronal loops is investigated to understand the observational consequences in terms of the thermodynamics and radiative losses from the Sun as well as the magnetized coronae of stars with an outer convective envelope. The dynamics of the Parker coronal heating model are studied for different ratios of the photospheric forcing velocity timescale tp to the Alfvén crossing time along a loop tA. It is shown that for tp/tA $\gtrsim$ 10-24 the heating rate and maximum temperature are largest and approximately independent of tp/tA, leading to a strong emission in X-rays and EUV. On the opposite decreasing tp/tA to smaller values leads to lower heating rates and plasma temperatures, and consequently fading high-energy radiative emission once tp/tA $\lesssim$ 1-3. The average volumetric loop heating rate is shown to scale as ℓp up B02/4π L2, where ℓp and up are respectively the convective granule length-scale and velocity, B0 is the intensity of the strong magnetic field threading the loop, and L the loop length. These findings support a recent hypothesis explaining ultracool dwarf observations of stars with similar magnetic field strength but radically different topologies displaying different radiative emission.

Coronal Heating Topology: the Interplay of Current Sheets and Magnetic Field Lines

A. F. **Rappazzo**, W. H. Matthaeus, D. Ruffolo, M. Velli, S. Servidio

ApJ **844** 87 **2017**

https://arxiv.org/pdf/1706.08983.pdf

The magnetic topology and field line random walk properties of a nanoflare-heated and magnetically confined corona are investigated in the reduced magnetohydrodynamic regime. Field lines originating from current sheets form coherent structures, called Current Sheet Connected (CSC) regions, extended around them. CSC field line random walk is strongly anisotropic, with preferential diffusion along the current sheets' in-plane length. CSC field line random walk properties remain similar to those of the entire ensemble but exhibit enhanced mean square displacements and separations due to the stronger magnetic field intensities in CSC regions. The implications for particle acceleration and heat transport in the solar corona and wind, and for solar moss formation are discussed.

PIXEL ANALYSIS OF PHOTOSPHERIC SPECTRAL DATA. I. PLASMA DYNAMICS

Anthony P. **Rasca**1,3,4, James Chen1,4, and Alexei A. Pevtsov

2016 ApJ 832 53

Recent observations of the photosphere using high spatial and temporal resolution show small dynamic features at or below the current resolving limits. A new pixel dynamics method has been developed to analyze spectral profiles and quantify changes in line displacement, width, asymmetry, and peakedness of photospheric absorption lines. The algorithm evaluates variations of line profile properties in each pixel and determines the statistics of such fluctuations averaged over all pixels in a given region. The method has been used to derive statistical characteristics of pixel fluctuations in observed quiet-Sun regions, an active region with no eruption, and an active region with an ongoing eruption. Using Stokes I images from the Vector Spectromagnetograph (VSM) of the Synoptic Optical Long-term Investigations of the Sun (SOLIS) telescope on **2012 March 13**, variations in line width and peakedness of Fe i 6301.5 Å are shown to have a distinct spatial and temporal relationship with an M7.9 X-ray flare in NOAA 11429. This relationship is observed as stationary and contiguous patches of pixels adjacent to a sunspot exhibiting intense flattening in the line profile and line-center displacement as the X-ray flare approaches peak intensity, which is not present in area scans of the non-eruptive active region. The analysis of pixel dynamics allows one to extract quantitative information on differences in plasma dynamics on sub-pixel scales in these photospheric regions. The analysis can be extended to include the Stokes parameters and study signatures of vector components of magnetic fields and coupled plasma properties.

Critical Science Plan for the Daniel K. Inouye Solar Telescope (DKIST)

Mark P. **Rast**, Nazaret Bello González, Luis Bellot Rubio, Wenda Cao, …..

296, Article number: 70 (**2021**)

https://arxiv.org/pdf/2008.08203.pdf

https://link.springer.com/content/pdf/10.1007/s11207-021-01789-2.pdf

https://doi.org/10.1007/s11207-021-01789-2

The Daniel K. Inouye Solar Telescope (DKIST) will revolutionize our ability to measure, understand and model the basic physical processes that control the structure and dynamics of the Sun and its atmosphere. The first-light DKIST images, released publicly on **29 January 2020**, only hint at the extraordinary capabilities which will accompany full commissioning of the five facility instruments. With this Critical Science Plan (CSP) we attempt to anticipate some of what those capabilities will enable, providing a snapshot of some of the scientific pursuits that the Daniel K. Inouye Solar Telescope hopes to engage as start-of-operations nears. The work builds on the combined contributions of the DKIST Science Working Group (SWG) and CSP Community members, who generously shared their experiences, plans, knowledge and dreams. Discussion is primarily focused on those issues to which DKIST will uniquely contribute.

Partial Invariants, Large-scale Dynamo Action, and the Inverse Transfer of Magnetic Helicity

Nicholas M. **Rathmann** and Peter D. Ditlevsen

2019 ApJ 887 95

https://doi.org/10.3847/1538-4357/ab5301

The existence of partially conserved enstrophy-like quantities is conjectured to cause inverse energy transfers to develop embedded in magnetohydrodynamical (MHD) turbulence, in analogy to the influence of enstrophy in two-dimensional nonconducting turbulence. By decomposing the velocity and magnetic fields in spectral space onto helical modes, we identify subsets of three-wave (triad) interactions conserving two new enstrophy-like quantities that can be mapped to triad interactions recently identified with facilitating large-scale α-type dynamo action and the inverse transfer of magnetic helicity. Due to their dependence on interaction scale locality, invariants suggest that the inverse transfer of magnetic helicity might be facilitated by both local- and nonlocal-scale interactions, and is a process more local than the α-dynamo. We test the predicted embedded (partial) energy fluxes by constructing a

shell model (reduced wave-space model) of the minimal set of triad interactions (MTI) required to conserve the ideal MHD invariants. Numerically simulated MTIs demonstrate that, for a range of forcing configurations, the partial invariants are, with some exceptions, indeed useful for understanding the embedded contributions to the total spectral energy flux. Furthermore, we demonstrate that strictly inverse energy transfers may develop if enstrophy-like conserving interactions are favored, a mechanism recently attributed to the energy cascade reversals found in nonconducting three-dimensional turbulence subject to strong rotation or confinement. The presented results have implications for the understanding of the physical mechanisms behind large-scale dynamo action and the inverse transfer of magnetic helicity, processes thought to be central to large-scale magnetic structure formation.

The formation of IRIS diagnostics V. A quintessential model atom of C II and general formation properties of the C II lines at 133.5 nm

Bhavna **Rathore**, Mats Carlsson
ApJ **811** 81 **2015**
http://arxiv.org/pdf/1508.04365v1.pdf
The 133.5 nm lines are important observables for the NASA/SMEX mission Interface Region Imaging Spectrograph (IRIS). To make 3D non-LTE radiative transfer computationally feasible it is crucial to have a model atom with as few levels as possible while retaining the main physical processes. We here develop such a model atom and we study the general formation properties of the C II lines. We find that a nine-level model atom of C I-C III with the transitions treated assuming complete frequency redistribution (CRD) suffices to describe the 133.5 nm lines. 3D scattering effects are important for the intensity in the core of the line. The lines are formed in the optically thick regime. The core intensity is formed in layers where the temperature is about 10kK at the base of the transition region. The lines are 1.2-4 times wider than the atomic absorption profile due to the formation in the optically thick regime. The smaller opacity broadening happens for single peak intensity profiles where the chromospheric temperature is low with a steep source function increase into the transition region, the larger broadening happens when there is a temperature increase from the photosphere to the low chromosphere leading to a local source function maximum and a double peak intensity profile with a central reversal. Assuming optically thin formation with the standard coronal approximation leads to several errors: Neglecting photoionization severly underestimates the amount of C II at temperatures below 16kK, erroneously shifts the formation from 10kK to 25kK and leads to too low intensities.

The formation of IRIS diagnostics VI. The Diagnostic Potential of the C II Lines at 133.5 nm in the Solar Atmosphere

Bhavna **Rathore**, Mats Carlsson, Jorrit Leenaarts, Bart De Pontieu
ApJ **811** 81 **2015**
http://arxiv.org/pdf/1508.04423v1.pdf
We use 3D radiation magnetohydrodynamic models to investigate how the thermodynamic quantities in the simulation are encoded in observable quantities, thus exploring the diagnostic potential of the 133.5 nm lines. We find that the line core intensity is correlated with the temperature at the formation height but the correlation is rather weak, especially when the lines are strong. The line core Doppler shift is a good measure of the line-of-sight velocity at the formation height. The line width is both dependent on the width of the absorption profile (thermal and non-thermal width) and an opacity broadening factor of 1.2-4 due to the optically thick line formation with a larger broadening for double peak profiles. The 133.5 nm lines can be formed both higher and lower than the core of the Mg II k line depending on the amount of plasma in the 14-50 kK temperature range. More plasma in this temperature range gives a higher 133.5 nm formation height relative to the Mg II k line core. The synthetic line profiles have been compared with IRIS observations. The derived parameters from the simulated line profiles cover the parameter range seen in observations but on average the synthetic profiles are too narrow. We interpret this discrepancy as a combination of a lack of plasma at chromospheric temperatures in the simulation box and too small non-thermal velocities. The large differences in the distribution of properties between the synthetic profiles and the observed ones show that the 133.5 nm lines are powerful diagnostics of the upper chromosphere and lower transition region.

Temporal evolutions and quasi-periodic variations present in the sunspot number and group sunspot area data measured at Kodaikanal Observatory for solar cycles 14 to 24

Belur **Ravindra**, Partha Chowdhury, Pratap Chandra Ray, Kumaravel Pichamani
ApJ **940** 43 **2022**
https://arxiv.org/pdf/2211.01651.pdf
https://iopscience.iop.org/article/10.3847/1538-4357/ac98b3/pdf
The Kodaikanal Observatory has made synoptic observations of the Sun in white light since 1904, and these images are sketched on the Stonyhurst grids called sun charts. These continuous hand-drawn data sets are used for long-term studies of the Sun. This article investigates temporal and periodic variations of the monthly hemispheric sunspot number and sunspot group area for 1905--2016, covering solar cycles 14 to 24. We find that the temporal

variations of the sunspot number and group area are different in each hemisphere and peak at different times of the solar cycle in the opposite hemisphere. For both the data sets, Cycle 19 shows maximum amplitude. For the sunspot number time series, Cycle 24 was the weakest, and Cycle 15 for the group area. The existence of double peaks and violation of the ``odd-even rule'' was found in both data sets. We have studied the periodic and quasi-periodic variations in both the time series by wavelet technique. We noticed that along with the fundamental mode of the ~ 11~year cycle and polarity reversal period of 22~years, the sunspot activity data also exhibited several mid-term periodicities in the opposite hemispheres, specifically the Riger group and quasi-biennial periodicities. The temporal evolution of these detected quasi-periodicities also differs in the northern and southern hemispheres. We analyzed the data set statistically to understand the bulk properties and coupling between the opposite hemispheres. The study indicates that the two hemispheric data sets differ, but some dependency could be present.

Solar-Cycle Characteristics in Kodaikanal Sunspot Area: North--South Asymmetry, Phase Distribution and Gnevyshev Gap

B. **Ravindra**, Partha Chowdhury, J. Javaraiah

Solar Phys. **296**, Article number: 2 (**2021**)
https://arxiv.org/pdf/2012.10190.pdf
https://link.springer.com/content/pdf/10.1007/s11207-020-01744-7.pdf

The solar activity is asymmetric in both hemispheres in almost all cycles. This asymmetry is observed both in cycle amplitude and period. We have used about 90~years of sunspot-area data from the Kodaikanal Solar Observatory to study the North--South asymmetry in sunspot activity. The monthly mean sunspot-area showed the northern hemisphere dominated in Solar Cycles 16, 19, and 20, and the southern hemisphere dominated in Cycles 18, 22, and 23. The 13-months smoothed data indicated that in Cycle 17 and 21, the northern and southern hemisphere showed equal amplitude. Cumulative sunspot area showed that the northern hemisphere dominated in Cycles 18, 19, 20, and 21, with a large difference between the two hemispheres in Cycles 19 and 20. The northern hemisphere activity led by 12, 15, and 2 months in Cycles 20, 21, and 22, respectively. No significant phase difference is found between the two hemispheres in Cycles 16, 17, 18, 19, and 23. The wavelet technique is used to find Rieger-type periodicities in the sunspot cycles. The cross-wavelet analysis of these data sets showed several statistically significant common periodicities like the Rieger-type periodicities and Quasi-biennial oscillations. The Gnevyshev gap was found in both the hemispheric data in Cycles 16, 18, 21, 22, and 23. These results are consistent with the earlier reported characteristics of North--South asymmetry in sunspot-area data. These results suggest that the Kodaikanal Observatory data complement the existing sunspot data from other observatories to study solar activity over long and short periods.

Sunspot Drawings at Kodaikanal Observatory: A Representative Results on Hemispheric Sunspot Numbers and Area Measurements

Ravindra B., Kumaravel Pichamani, Selvendran R., Joyce Samuel, Praveen Kumar, Nancy Jassoria, Navneeth R. S

Astrophysics and Space Science **2020**
https://arxiv.org/pdf/2001.02939.pdf

The importance of the periodicity in sunspot appearance was well recognized by the mid of 19th century. Several observatories around the globe have made the record of sunspots in the form of drawings and preserved them safely for posterity. At the Kodaikanal Observatory (KO), the sunspot observations have begun in 1905. In those times observations were recorded on photographic plates and after the development of those plates in the laboratory, the drawings of the same were made on the Stonyhurst grids. In these drawings, called {\em sun charts}, different features on the sun's disk, e.g., sunspots, plages, filaments, prominences, etc. were clearly identified and visually marked with different colors. We have collected 111 years of sunspot drawing spanning over 10 solar cycles. These sunspot drawings were carefully stitched to make bound volumes, each for every 6-months. The drawings are kept at the Kodaikanal library for scientific use and analysis. In this article, we describe briefly the process of drawing, methods of counting sunspot numbers and measurement of sunspot area using square grids. We have collected the data for the Northern and Southern hemispheres separately. From the collected data, we compute the sunspot number and area and compare it with Royal Greenwich Observatory (RGO) and Sunspot Index and Long-term Solar Observations (SILSO) data. The results show that the measurement of the sunspot number is underestimated by about 40\%. The KO monthly averaged sunspot number data of both hemispheres is normalized with the RGO monthly averaged total sunspot number data.

Installation of Solar Chromospheric Telescope at the Indian Astronomical Observatory, Merak

Ravindra B, Prabhu Kesavan, Thulasidharen, K. C., Rajalingam, M., Sagayanathan, K., Kamath, P. U., Namgyal Dorjey, Angchuk Dorjee, Kemkar, P. M. M.,Tsewang Dorjai, Ravinder K. Banyal

Journal of Astrophysics and Astronomy (JOAA) **2018**

https://arxiv.org/pdf/1808.07643.pdf
We report the observations of the solar chromosphere from a newly commissioned solar telescope at the incursion site near Pangong Tso lake in Merak (Leh/Ladakh). This new Hα telescope at the Merak site is identical to the Kodaikanal Hα telescope. The telescope is installed in the month of August, 2017 at the Merak site. A 20-cm doublet lens with additional re-imaging optics makes the telescope. A Lyot filter with 0.5~\AA~passband isolates the Balmer line of the hydrogen spectra to make the observations of the solar chromosphere. The observations made in Hα wavelength delineates the magnetic field directions at the sunspot and the quiet regions. A CCD detector records the images of the chromosphere with a pixel resolution of 0.27″ and covers 9.2′ field-of-view. This telescope has a good guiding system that keeps the FOV in the intended position. We report the development of control software for tuning the filter unit, control detector system, observations, and calibration of the data to make it useful for the scientific community. Some preliminary results obtained from the Merak Hα telescope are also presented. This high altitude facility is a timely addition to regularly available Hα images around the globe.

Full-disk Synoptic Observations of the Chromosphere Using HαTelescope at the Kodaikanal Observatory

B. **Ravindra**, K. Prabhu, K.E. Rangarajan, S.P. Bagare, Singh Jagdev, P.M.M. Kemkar, J.P. Lancelot, K.C. Thulasidharen, F. Gabriel, R. Selvendran

RAA **2016**

This paper reports on the installation and observations of a new solar telescope installed on 7th October, 2014 at the Kodaikanal Observatory. The telescope is a refractive type equipped with a tunable Lyot Hα filter. A CCD camera of 2k×2k size makes the image of the Sun with a pixel size of 1.21″ pixel−1 with a full field-of-view of 41′. The telescope is equipped with a guiding system which keeps the image of the Sun within a few pixels throughout the observations. The FWHM of the Lyot filter is 0.4\AA~and the filter is motorized, capable of scanning the Hα line profile at a smaller step size of 0.01\AA. Partial-disk imaging covering about 10′, is also possible with the help of a relay lens kept in front of the CCD camera. In this paper, we report the detailed specifications of the telescope, filter unit, its installation, observations and the procedures we have followed to calibrate and align the data. We also present preliminary results with this new full-disk telescope.

Kinematics of coronal mass ejections in the LASCO field of view

Anitha **Ravishankar**, Grzegorz Michalek, Seiji Yashiro

Astronomy & Astrophysics, Volume 639, id.A68, 12 pp, July **2020**

https://arxiv.org/pdf/2010.02682.pdf

In this paper we present a statistical study of the kinematics of 28894 coronal mass ejections (CMEs) recorded by the Large Angle and Spectrometric Coronagraph (LASCO) on board the Solar and Heliospheric Observatory spacecraft from 1996 until mid-2017. The initial acceleration phase is characterized by a rapid increase in CME velocity just after eruption in the inner corona. This phase is followed by a non-significant residual acceleration (deceleration) characterized by an almost constant speed of CMEs. We demonstrate that the initial acceleration is in the range 0.24-2616 ms-2 with median (average) value of 57 ms-2 (34 ms-2) and it takes place up to a distance of about 28 solar radius with median (average) value of 7.8 solar radius (6 solar radius). Additionally, the initial acceleration is significant in the case of fast CMEs (V > 900 kms-1), where the median (average) values are about 295 ms-2 (251 ms-2), respectively, and much weaker in the case of slow CMEs (V < 250 kms-1), where the median (average) values are about 18 ms-2 (17 ms-2), respectively. We note that the significant driving force (Lorentz force) can operate up to a distance of 6 solar radius from the Sun during the first 2 hours of propagation. We found a significant anti-correlation between the initial acceleration magnitude and the acceleration duration, whereas the residual acceleration covers a range from -1224 to 0 ms-2 with a median (average) value of -34 ms-2 (-17 ms-2). One intriguing finding is that the residual acceleration is much smaller during the 24th cycle in comparison to the 23rd cycle of solar activity. Our study has also revealed that the considered parameters, initial acceleration (ACC INI), residual acceleration (ACC RES), maximum velocity (V MAX), and time at maximum velocity (Time MAX) mostly follow solar cycles and the intensities of the individual cycle.

Exploring magnetic coupling of solar atmosphere through frequency modulations of 3-min slow magnetoacoustic waves

Ananya **Rawat**, Girjesh Gupta

Bulletin of Liège Royal Society of Sciences (proceedings of the third BINA workshop) **2023**

https://arxiv.org/pdf/2309.02398.pdf

Coronal fan loops rooted in sunspot umbra show outward propagating waves with subsonic phase speed and period around 3-min. However, their source region in the lower atmosphere is still ambiguous. We performed multi-wavelength observations of a clean fan loop system rooted in sunspot observed by Interface Region Imaging Spectrograph (IRIS) and Solar Dynamics Observatory (SDO). We utilised less explored property of frequency modulation of these 3-min waves from the photosphere to corona, and found them to be periodic with the ranges in 14-20 min, and 24-35 min. Based on our findings, we interpret that 3-min slow waves observed in the coronal fan

loops are driven by 3-min oscillations observed at the photospheric footpoints of these fan loops in the umbral region. We also explored any connection between 3-min and 5-min oscillations observed at the photosphere, and found them to be poorly understood. Results provide clear evidence of magnetic coupling of the solar umbral atmosphere through propagation of 3-min waves along the fan loops at different atmospheric heights. **June 16, 2016**

Scaling analysis and model estimation of solar corona index

Samujjwal **Ray**a, Rajdeep Rayb, Mofazzal Hossain Khondekarar, Koushik Ghosh
Advances in Space Research Volume 61, Issue 8, 15 April **2018**, Pages 2214-2226
A monthly average solar green coronal index time series for the period from January 1939 to December 2008 collected from NOAA (The National Oceanic and Atmospheric Administration) has been analysed in this paper in perspective of scaling analysis and modelling. Smoothed and de-noising have been done using suitable mother wavelet as a pre-requisite. The Finite Variance Scaling Method (FVSM), Higuchi method, rescaled range (R/S) and a generalized method have been applied to calculate the scaling exponents and fractal dimensions of the time series. Autocorrelation function (ACF) is used to find autoregressive (AR) process and Partial autocorrelation function (PACF) has been used to get the order of AR model. Finally a best fit model has been proposed using Yule-Walker Method with supporting results ofgoodness of fit and wavelet spectrum. The results reveal an anti-persistent, Short Range Dependent (SRD), self-similar property with signatures of non-causality, non-stationarity and nonlinearity in the data series. The model shows the best fit to the data under observation.

Solar Corona Heating by the Axion Quark Nugget Dark Matter

Nayyer **Raza**, Ludovic van Waerbeke, Ariel Zhitnitsky
Journal of Cosmology and Astroparticle Physics JCAP **2018**
https://arxiv.org/pdf/1805.01897.pdf
Astrophysics faces two 80-year-old mysteries: the nature of dark matter, and the high temperature of the million degree solar corona, radiating an extreme ultraviolet (EUV) excess of 1027 erg/s. The current paradigm is that the corona is heated by hypothetical nano-flares of unknown origin. Recently, in ref. (Zhitnitsky 2017) it was suggested that the nanoflares can be identified with the nuggets from the Axion Quark Nugget (AQN) dark matter model. This model was invented as an explanation of the observed ratio Ωdark∼Ωvisible, and has no free parameter other than the Axion mass. It is proposed that the AQN particles moving through the coronal plasma (and annihilating) can both explain the EUV excess and drastic changes of the temperature in the Transition Region. To test this proposal, we performed detailed numerical simulations with a realistic AQN particle distribution and physical environment. Remarkably, our calculations predict the correct energy budget for the solar corona, and an energy injection altitude in agreement with the temperature and mass density profile of the solar atmosphere. Therefore, we propose that the two 80-year-old mysteries could be two sides of the same coin. We make several predictions based on this proposal that can be tested by the upcoming NASA mission the Parker Solar Probe.

Large-amplitude quasi-periodic pulsations as evidence of impulsive heating in hot transient loop systems detected in the EUV with SDO/AIA

Fabio **Reale**, Paola Testa, Antonino Petralia, Dmitrii Y. Kolotkov
ApJ **2019**
https://arxiv.org/pdf/1909.02847.pdf
Short heat pulses can trigger plasma pressure fronts inside closed magnetic tubes in the corona. The alternation of condensations and rarefactions from the pressure modes drive large-amplitude pulsations in the plasma emission. Here we show the detection of such pulsations along magnetic tubes that brighten transiently in the hot 94A EUV channel of SDO/AIA. The pulsations are consistent with those predicted by hydrodynamic loop modeling, and confirm pulsed heating in the loop system. The comparison of observations and model provides constraints on the heat deposition: a good agreement requires loop twisting and pulses deposited close to the footpoints with a duration of 0.5 min in one loop, and deposited in the corona with a duration of 2.5 min in another loop of the same loop system. **12 November 2015**

Impulsive coronal heating from large-scale magnetic rearrangements: from IRIS to SDO/AIA

Fabio **Reale**, Paola Testa, Antonino Petralia, David R. Graham
ApJ **882** 7 **2019**
https://arxiv.org/pdf/1907.02291.pdf
https://doi.org/10.3847/1538-4357/ab304f
The Interface Region Imaging Spectrograph (IRIS) has observed bright spots at the transition region footpoints associated with heating in the overlying loops, as observed by coronal imagers. Some of these brightenings show significant blueshifts in the Si iv line at 1402.77 A (logT[K] = 4.9). Such blueshifts cannot be reproduced by coronal loop models assuming heating by thermal conduction only, but are consistent with electron beam heating, highlighting for the first time the possible importance of non-thermal electrons in the heating of non-flaring active

regions. Here we report on the coronal counterparts of these brightenings observed in the hot channels of the Atmospheric Imaging Assembly (AIA) on board the Solar Dynamics Observatory. We show that the IRIS bright spots are the footpoints of very hot and transient coronal loops which clearly experience strong magnetic interactions and rearrangements, thus confirming the impulsive nature of the heating and providing important constraints for their physical interpretation.

PLASMA SLOSHING IN PULSE-HEATED SOLAR AND STELLAR CORONAL LOOPS

F. **Reale**

2016 ApJ 826 L20

There is evidence that coronal heating is highly intermittent, and flares are the high energy extreme. The properties of the heat pulses are difficult to constrain. Here, hydrodynamic loop modeling shows that several large amplitude oscillations (~20% in density) are triggered in flare light curves if the duration of the heat pulse is shorter than the sound crossing time of the flaring loop. The reason for this is that the plasma does not have enough time to reach pressure equilibrium during heating, and traveling pressure fronts develop. The period is a few minutes for typical solar coronal loops, dictated by the sound crossing time in the decay phase. The long period and large amplitude make these oscillations different from typical magnetohydrodynamic (MHD) waves. This diagnostic can be applied both to observations of solar and stellar flares and to future observations of non-flaring loops at high resolution.

Disentangling the solar activity-solar wind predictive causality at Space Climate scales

Raffaele **Reda**, Mirko Stumpo, Luca Giovannelli, Tommaso Alberti, Giuseppe Consolini

2023

https://arxiv.org/pdf/2312.01956.pdf

The variability in the magnetic activity of the Sun is the main source of the observed changes in the plasma and electromagnetic environments within the heliosphere. The primary way in which solar activity affects the Earth's environment is via the solar wind and its transients. However, the relationship between solar activity and solar wind is not the same at the Space Weather and Space Climate time scales. In this work, we investigate this relationship exploiting five solar cycles data of Ca II K index and solar wind parameters, by taking advantage of the Hilbert-Huang Transform, which allows to separate the contribution at the different time scales. By filtering out the high frequency components and looking at decennial time scales, we confirm the presence of a delayed response of solar wind to Ca II K index variations, with a time lag of ~ 3.1-year for the speed and ~ 3.4-year for the dynamic pressure. To assess the results in a stronger framework, we make use of a Transfer Entropy approach to investigate the information flow between the quantities and to test the causality of the relation. The time lag results from the latter are consistent with the cross-correlation ones, pointing out the presence of a statistical significant information flow from Ca II K index to solar wind dynamic pressure that peaks at time lag of 3.6-year. Such a result could be of relevance to build up a predictive model in a Space Climate context.

On the time lag between solar wind dynamic parameters and solar activity UV proxies

R. **Reda**, L. Giovannelli, T. Alberti

Advances in Space Research, **2022**, 0273-1177

https://arxiv.org/pdf/2210.07855

The solar activity displays variability and periodic behaviours over a wide range of timescales, with the presence of a most prominent cycle with a mean length of 11 years. Such variability is transported within the heliosphere by solar wind, radiation and other processes, affecting the properties of the interplanetary medium. The presence of solar activity-related periodicities is well visible in different solar wind and geomagnetic indices, although with time lags with respect to the solar one, leading to hysteresis cycles. Here, we investigate the time lag behaviour between a physical proxy of the solar activity, the Ca II K index, and two solar wind parameters (speed and dynamic pressure), studying how their pairwise relative lags vary over almost five solar cycles. We find that the lag between Ca II K index and solar wind speed is not constant over the whole time interval investigated, with values ranging from 6 years to 1 year (average 3.2 years). A similar behaviour is found also for the solar wind dynamic pressure. Then, by using a Lomb-Scargle periodogram analysis we obtain a 10.21-year mean periodicity for the speed and 10.30-year for the dynamic pressure. We speculate that the different periodicities of the solar wind parameters with respect to the solar 11-year cycle may be related to the overall observed temporal evolution of the time lags. Finally, by accounting for them, we obtain empirical relations that link the amplitude of the Ca II K index to the two solar wind parameters.

A Hydrodynamic Model of Alfvénic Wave Heating in a Coronal Loop and its Chromospheric Footpoints

Jeffrey W. **Reep**, Alexander J.B. Russell, Lucas A. Tarr, James E. Leake

ApJ **2017**

https://arxiv.org/pdf/1712.06171.pdf

Alfv\'enic waves have been proposed as an important energy transport mechanism in coronal loops, capable of delivering energy to both the corona and chromosphere and giving rise to many observed features, of flaring and quiescent regions. In previous work, we established that resistive dissipation of waves (ambipolar diffusion) can drive strong chromospheric heating and evaporation, capable of producing flaring signatures. However, that model was based on a simplified assumption that the waves propagate instantly to the chromosphere, an assumption which the current work removes. Via a ray tracing method, we have implemented traveling waves in a field-aligned hydrodynamic simulation that dissipate locally as they propagate along the field line. We compare this method to and validate against the magnetohydrodynamics code Lare3D. We then examine the importance of travel times to the dynamics of the loop evolution, finding that (1) the ionization level of the plasma plays a critical role in determining the location and rate at which waves dissipate; (2) long duration waves effectively bore a hole into the chromosphere, allowing subsequent waves to penetrate deeper than previously expected, unlike an electron beam whose energy deposition rises in height as evaporation reduces the mean-free paths of the electrons; (3) the dissipation of these waves drives a pressure front that propagates to deeper depths, unlike energy deposition by an electron beam.

A Technique to Measure Coronal Electron Density, Temperature, and Velocity Above 2.5 R⊙ from Sun Center Using Polarized Brightness Spectrum

Nelson **Reginald**, Jeffrey Newmark & Lutz Rastaetter
Solar Physics volume 298, Article number: 73 (**2023**)
https://doi.org/10.1007/s11207-023-02160-3

The current model for the polarized brightness (pB) spectrum has a decades-long history of progressively incorporating its dependence on electron density Ne, temperature Te, and flow velocity in the radial direction Ve. The pBNe spectrum follows the exact shape of the photosphere spectrum, which is not smooth, which is expected from the thermal Doppler broadening of the photosphere spectrum due to the high coronal Te; the pBNeTe spectrum is smooth, but the free coronal electrons remain static and unaffected by solar wind, and the pBNeTeVe spectrum is red-shifted by electrons seeing a red-shifted photosphere spectrum as they flow away from the Sun as solar wind, which takes a radial direction above 2.5 R⊙ from Sun center. In this article, we review the progress of the above three model pB spectra in describing the observations and highlight the differences, first by comparing the three model pB spectra against wavelength using a model for Ne and constant values for Te and Ve, and second by generating three model 2D pB maps by integrating over a selected wavelength region in the three model pB spectra along lines of sight passing through the 14 July 2000 (“Bastille Day”) coronal mass ejection (CME) model, which contains 3D information on Ne, Te, and Ve. In this regard, the COronal Diagnostic EXperiment (CODEX) on the International Space Station (ISS) in 2024 will measure Ne, Te, and Ve by matching the measured pB with modeled pBNeTeVe in selected wavelength regions using multiple filters.

Statistical Error Analysis on White-Light Filter Ratio Experiments to Measure Electron Parameters

Nelson **Reginald**, Jeffrey Newmark & Lutz Rastaetter
Solar Physics volume 296, Article number: 146 (**2021**)
https://link.springer.com/content/pdf/10.1007/s11207-021-01887-1.pdf
https://doi.org/10.1007/s11207-021-01887-1

The filter-ratio technique to remotely measure electron temperature and speed using four color filters in visible light and a polarization camera was described in detail in previous works, in which we quantified the systematic error associated with using models of a symmetric corona to interpret results from an asymmetric corona. We also showed the criteria applied to select the bandwidths of filters and the pros and cons of replacing the traditional linear polarizer with a polarization camera to measure pB. What started in the 1990s by ground experiments conducted during total solar eclipses that lasted for a few minutes led to a balloon-borne experiment lasting eight hours in 2019 and will blossom into a space experiment on the International Space Station in 2023. Due to constraints on the bandwidths of the four filters, a successful mission requires quantification of the statistical error using Monte Carlo simulations to generate two feasibility profiles, which are unique to the design parameters of the coronagraph, to comprehend the feasibility to measure temperature and speed within the desired temporal and spatial resolutions. For the statistical error analysis, we use modeled K- and F-corona profiles, representative theoretical diffraction, scattering, and vignetting profiles, assumed efficiencies for lenses, mirrors, and polarizers, assumed detector properties on quantum efficiency, full-well depth, dark noise, and read noise, and assumed instrument properties on aperture diameter, solid angle, and pixel resolution.

Synoptic Measurements of Electron Temperature and Speed in the Solar Corona with Next Generation White-Light Coronagraph

Nelson **Reginald**, Jeffrey Newmark & Lutz Rastaetter
Solar Physics volume 295, Article number: 95 (**2020**)
https://link.springer.com/content/pdf/10.1007/s11207-020-01665-5.pdf

Current white-light coronagraphs measure polarized brightness (pB) of the solar corona using a single bandpass filter to measure the density of electrons. However, future coronagraphs can be modified to take pB images through four bandpass filters to measure density, temperature and speed of electrons. In this article, we use a spherical three dimensional coronal model of the Bastille Day coronal mass ejection to synthetically measure pB through four bandpass filters along lines of sight originating from two observers located diametrically in front (1 AU, 0, 0) and behind (-1 AU, 0, 0) the plane of the sky on the xy-ecliptic plane. The lines of sight pass through 81 positions on a straight line parallel to the solar north–south z-direction in the yz-plane and this line intersects the ecliptic at (0, 1.25 R⊙, 0) from Sun center. The 81 data points are separated in intervals of 0.05 R⊙ and points extend from (0, 1.25 R⊙, -2.0 R⊙) to (0, 1.25 R⊙, 2.0 R⊙). The measured pB ratios are used to measure temperature and speed, then we compare with true temperature and speed in the plane of the sky, and quantify the difference, which is a systematic error associated with using modeled pB ratios, based on a symmetric corona, to compare with measured pB ratios, on an asymmetric corona. This understanding is reached by allowing the coronal model to rotate a full circle in intervals of 1∘1∘ and illuminating the lines of sight with both symmetric and asymmetric coronal atmospheres about the plane of the sky.

Measuring Electron Temperature Using a Linear Polarizer Versus a Polarization Camera

Nelson **Reginald**, Jeffrey Newmark, Lutz Rastaetter
Solar Physics July **2019**, 294:100
sci-hub.se/10.1007/s11207-019-1491-x
Polarized K-coronal brightness (pB) of the solar corona can be measured by taking four successive coronal brightness images through a linear polarizer, by turning it through four successive angles in intervals of 45∘45∘ and using a standard formula to measure pB from the total coronal brightness (TB) that contains both the polarized K- and the unpolarized F-coronal brightness. The question is: will the time-dependent, highly dynamic corona illuminate each pixel with the same brightness during the time it takes to take the four successive images? To mitigate this problem we now have the polarization camera, in which, each super-pixel is made up of four sub-pixels, and built in to these four sub-pixels is a polarization mask that contains four linear polarizers orientated at four angles 45∘45∘ apart. This allows the measurement of pB to be made in a single exposure. Here, the question is: will the variations of the coronal brightness in the four adjacent sub-pixels in a super-pixel be sufficiently negligible to assume that they observe the same part of the corona? This article looks for answers to these two questions by conducting two synthetic experiments to measure the electron temperature in the plane of the sky on a spherically asymmetric model (SAM) corona by first using a linear polarizer, and then replacing it with a polarization camera and use statistical analyses to determine how well the measured temperature matched the true temperature for the two cases.

Dependence of DOLP on Coronal Electron Temperature, Speed, and Structure

Nelson **Reginald**, Lutz Rastaetter
Solar Physics January **2019**, 294:12
The degree of linear polarization (DOLP) is an important measure of the fraction of the total K-coronal brightness due to Thomson scattering of photospheric brightness off the coronal electrons that is linearly polarized. However, the corona is also brightened by the F-coronal brightness due to scattering of photospheric brightness off everything else in the corona except the electrons, which remains totally unpolarized at least up to a coronal height of ≈5 R⊙≈5 R⊙. As a result, to measure the DOLP, the F- and K-coronal brightness need to be separated by taking three consecutive images by turning a linear polarizer through three well-defined angles or with a single image using a polarization camera. In this regard, the theoretically computed DOLP would be a helpful tool to compare with the experimentally measured DOLP on the real corona in order to estimate how well the F-coronal brightness is removed from the total coronal brightness to isolate the K-coronal brightness. This is important because the K-coronal brightness ratios at (410.3 nm/390.0 nm) and (423.3 nm/398.7 nm) can be used to generate maps of electron temperature and speed, respectively, and the individual K-coronal brightness at all four wavelengths can be used independently to generate maps of the electron density in the corona. In this article, for a spherically symmetric model (SSM) corona with assumed temperatures of 1.0 MK and 2.0 MK and radial flow speeds of 0.0 km s−1 and 250.0 km s−1 for the coronal electrons, we have computed the wavelength-dependent DOLP from 370.0 nm to 470.0 nm in intervals of 1.0 nm, and for a spherically asymmetric model (SAM) corona containing a simulation of the Bastille Day coronal mass ejection, streamers, and quiet areas, we have generated maps of DOLP at the four wavelengths 390.0, 398.7, 410.3, and 423.3 nm. Finally, we have used these theoretically computed models of DOLP to compare with the experimentally measured DOLP.

Evaluating Uncertainties in Coronal Electron Temperature and Radial Speed Measurements Using a Simulation of the Bastille Day Eruption

Nelson **Reginald**, Orville St. Cyr, Joseph Davila, Lutz Rastaetter, Tibor Török
Solar Physics May **2018**, 293:82

https://link.springer.com/article/10.1007/s11207-018-1301-x
Obtaining reliable measurements of plasma parameters in the Sun's corona remains an important challenge for solar physics. We previously presented a method for producing maps of electron temperature and speed of the solar corona using K-corona brightness measurements made through four color filters in visible light, which were tested for their accuracies using models of a structured, yet steady corona. In this article we test the same technique using a coronal model of the Bastille Day (**14 July 2000**) coronal mass ejection, which also contains quiet areas and streamers. We use the coronal electron density, temperature, and flow speed contained in the model to determine two K-coronal brightness ratios at (410.3, 390.0 nm) and (423.3, 398.7 nm) along more than 4000 lines of sight. Now assuming that for real observations, the only information we have for each line of sight are these two K-coronal brightness ratios, we use a spherically symmetric model of the corona that contains no structures to interpret these two ratios for electron temperature and speed. We then compare the interpreted (or measured) values for each line of sight with the true values from the model at the plane of the sky for that same line of sight to determine the magnitude of the errors. We show that the measured values closely match the true values in quiet areas. However, in locations of coronal structures, the measured values are predictably underestimated or overestimated compared to the true values, but can nevertheless be used to determine the positions of the structures with respect to the plane of the sky, in front or behind. Based on our results, we propose that future white-light coronagraphs be equipped to image the corona using four color filters in order to routinely create coronal maps of electron density, temperature, and flow speed.

Electron temperature maps of the low solar corona: ISCORE results from the total solar eclipse of 1 August 2008 in China

Nelson L. **Reginald**, Joseph M. Davila, Orville C. St. Cyr, Douglas M. Rabin
JGR Volume 122, Issue 6 June **2017** Pages 5856–5869
We conducted an experiment in conjunction with the total solar eclipse of **1 August 2008** in China to determine the thermal electron temperature in the low solar corona close to the solar limb. The instrument, Imaging Spectrograph of Coronal Electrons (ISCORE), consisted of an 8 inch f/10 Schmidt Cassegrain telescope with a thermoelectrically cooled CCD camera at the focal plane. Results are electron temperatures of 1 MK at 1.08 R⊙ and 1.13 R⊙ from the Sun center in the polar and equatorial regions, respectively. This experiment confirms the results of an earlier experiment conducted in conjunction with the total eclipse of 29 March 2006 in Libya, and results are that at a given coronal height the electron temperature in the polar region is larger than at the equatorial region. In this paper we show the importance of using the correct photospheric spectrum pertinent to the solar activity phase at the time of the experiment, which is a required parameter for modeling the underlying theoretical concept for temperature interpretation of the measured intensity ratios using color filters.

Linking computational models to follow the evolution of heated coronal plasma

J **Reid**, P J Cargill, C D Johnston, A W Hood
MNRAS, Volume 505, Issue 3, August **2021**, Pages 4141–4150,
https://doi.org/10.1093/mnras/stab1255
A 'proof of principle' is presented, whereby the Ohmic and viscous heating determined by a three-dimensional (3D) MHD model of a coronal avalanche are used as the coronal heating input for a series of field-aligned, one-dimensional (1D) hydrodynamic models. Three-dimensional coronal MHD models require large computational resources. For current numerical parameters, it is difficult to model both the magnetic field evolution and the energy transport along field lines for coronal temperatures much hotter than 1MK1MK, because of severe constraints on the time step from parallel thermal conduction. Using the 3D MHD heating derived from a simulation and evaluated on a single field line, the 1D models give coronal temperatures of 1MK1MK and densities 1014--1015m−31014--1015m−3 for a coronal loop length of 80Mm80Mm. While the temperatures and densities vary smoothly along the field lines, the heating function leads to strong asymmetries in the plasma flows. The magnitudes of the velocities in the 1D model are comparable with those seen in 3D reconnection jets in our earlier work. Advantages and drawbacks of this approach for coronal modelling are discussed.

Coronal energy release by MHD avalanches: Heating mechanisms

J. **Reid**1, P. J. Cargill1,2, A. W. Hood1, C. E. Parnell1 and T. D. Arber3
A&A 633, A158 (**2020**)
https://doi.org/10.1051/0004-6361/201937051
The plasma heating associated with an avalanche involving three twisted magnetic threads within a coronal loop is investigated using three-dimensional magnetohydrodynamic simulations. The avalanche is triggered by the kink instability of one thread, with the others being engulfed as a consequence. The heating as a function of both time and location along the strands is evaluated. It is shown to be bursty at all times but to have no preferred spatial location. While there appears to be a level of "background" heating, this is shown to be comprised of individual, small heating events. A comparison between viscous and resistive (Ohmic) heating demonstrates that the strongest heating

events are largely associated with the Ohmic heating that arises when the current exceeds a critical value. Viscous heating is largely (but not entirely) associated with smaller events. Ohmic heating dominates viscous heating only at the time of the initial kink instability. It is also demonstrated that a variety of viscous models lead to similar heating rates, suggesting that the system adjusts to dissipate the same amount of energy.

Determining whether the squashing factor, Q, would be a good indicator of reconnection in a resistive MHD experiment devoid of null points

J. **Reid**1, C. E. Parnell1, A. W. Hood1 and P. K. Browning2
A&A 633, A92 (**2020**)
https://doi.org/10.1051/0004-6361/201936832
The squashing factor of a magnetic field, Q, is commonly used as an indicator of magnetic reconnection, but few studies seek to evaluate how reliable it is in comparison with other possible reconnection indicators. By using a full, self-consistent, three-dimensional, resistive magnetohydrodynamic experiment of interacting magnetic strands constituting a coronal loop, Q and several different quantities are determined. Each is then compared with the necessary and sufficient condition for reconnection, namely the integral along a field line of the component of the electric field parallel to the magnetic field. Among the reconnection indicators explored, we find the squashing factor less successful when compared with alternatives, such as Ohmic heating. In a reconnecting magnetic field devoid of null points, our work suggests that Q, being a geometric measure of the magnetic field, is not a reliable indicator of the onset or a diagnostic of the location of magnetic reconnection in some configurations.

Coronal energy release by MHD avalanches: continuous driving

J. **Reid**1, A. W. Hood1, C. E. Parnell1, P. K. Browning2 and P. J. Cargill1,3
A&A 615, A84 (**2018**)
Previous work has confirmed the concept of a magnetohydrodynamic (MHD) avalanche in pre-stressed threads within a coronal loop. We undertook a series of full, three-dimensional MHD simulations in order to create three threads by twisting the magnetic field through boundary motions until an instability ensues. We find that, following the original instability, one unstable thread can disrupt its neighbours with continued driving. A “bursty” heating profile results, with a series of ongoing energy releases, but no evident steady state. For the first time using full MHD, we show that avalanches are a viable mechanism for the storing and release of magnetic energy in the solar corona, as a result of photospheric motions.

Chromospheric Inversions of a Micro-flaring Region

A. **Reid**1,2, V. Henriques1,3, M. Mathioudakis1, J. G. Doyle2, and T. Ray
2017 ApJ 845 100
We use spectropolarimetric observations of the Ca ii 8542 Å line, taken from the Swedish 1 m Solar Telescope, in an attempt to recover dynamic activity in a micro-flaring region near a sunspot via inversions. These inversions show localized mean temperature enhancements of ~1000 K in the chromosphere and upper photosphere, along with co-spatial bi-directional Doppler shifting of 5–10 km s−1. This heating also extends along a nearby chromospheric fibril, which is co-spatial to 10–15 km s−1 downflows. Strong magnetic flux cancellation is also apparent in one of the footpoints, and is concentrated in the chromosphere. This event more closely resembles that of an Ellerman Bomb, though placed slightly higher in the atmosphere than what is typically observed.

Solar Ellerman Bombs in 1-D Radiative Hydrodynamics

A. **Reid**, M. Mathioudakis, A. Kowalski, J. G. Doyle, J. C. Allred
ApJL **2017**
https://arxiv.org/pdf/1701.04213v1.pdf
Recent observations from the Interface Region Imaging Spectrograph (IRIS) appear to show impulsive brightenings in high temperature lines, which when combined with simultaneous ground based observations in Hα, appear co-spatial to Ellerman Bombs (EBs). We use the RADYN 1-dimensional radiative transfer code in an attempt to try and reproduce the observed line profiles and simulate the atmospheric conditions of these events. Combined with the MULTI/RH line synthesis codes, we compute the Hα, Ca II 8542~\AA, and Mg II h \& k lines for these simulated events and compare them to previous observations. Our findings hint that the presence of superheated regions in the photosphere (>10,000 K) is not a plausible explanation for the production of EB signatures. While we are able to recreate EB-like line profiles in Hα, Ca II 8542~\AA, and Mg II h \& k, we cannot achieve agreement with all of these simultaneously.

Magnetic Flux Cancellation in Ellerman Bombs

A. **Reid**, M. Mathioudakis, J. G. Doyle, E. Scullion, V. Henriques, C. Nelson, T. Ray

ApJ **823** 110 **2016**
http://arxiv.org/pdf/1603.07100v1.pdf
Ellerman Bombs (EBs) are often found co-spatial with bipolar photospheric magnetic fields. We use Hα imaging spectroscopy along with Fe I 6302.5 \AA\ spectro-polarimetry from the Swedish 1-m Solar Telescope (SST), combined with data from the Solar Dynamic Observatory (SDO) to study EBs and the evolution of the local magnetic fields at EB locations. The EBs are found via an EB detection and tracking algorithm. We find, using NICOLE inversions of the spectro-polarimetric data, that on average (3.43 ± 0.49) x 1024 ergs of stored magnetic energy disappears from the bipolar region during the EBs burning. The inversions also show flux cancellation rates of 1014 - 1015 Mx s−1, and temperature enhancements of 200 K at the detection footpoints. We investigate near-simultaneous flaring of EBs due to co-temporal flux emergence from a sunspot, which shows a decrease in transverse velocity when interacting with an existing, stationary area of opposite polarity magnetic flux and the EBs are formed. We also show that these EBs can get fueled further by additional, faster moving, negative magnetic flux regions. **2014 June 5**
See **UKSP Nuggets of 2016 #70**
http://www.uksolphys.org/uksp-nugget/70-magnetic-flux-cancellation-in-ellerman-bombs/

Radial velocity observations of the 2015 Mar 20 eclipse - A benchmark Rossiter-McLaughlin curve with zero free parameters

Ansgar **Reiners**, Ulrike Lemke, Florian Bauer, Benjamin Beeck, Philipp Huke
A&A **2016**
http://arxiv.org/pdf/1609.00535v1.pdf
On **March 20, 2015**, we obtained 159 spectra of the Sun as a star with the solar telescope and the FTS at the Institut f\"ur Astrophysik G\"ottingen, 76 spectra were taken during partial solar eclipse. We obtained RVs using I2 as wavelength reference and determined the RM curve with a peak-to-peak amplitude of almost 1.4 km s−1at typical RV precision better than 1 m s−1. We modeled disk-integrated solar RVs using surface velocities, limb darkening, and information about convective blueshift from 3D magneto-hydrodynamic simulations. We confirm that convective blueshift is crucial to understand solar RVs during eclipse. Our best model reproduced the observations to within a relative precision of 10% with residuals less than 30 m s−1. We cross-checked parameterizations of velocity fields using a Dopplergram from the Solar Dynamics Observatory and conclude that disk-integration of the Dopplergram does not provide correct information about convective blueshift necessary for m s−1 RV work. As main limitation for modeling RVs during eclipses, we identified limited knowledge about convective blueshift and line shape as functions of solar limb angle. We suspect that our model line profiles are too shallow at limb angles larger than μ=0.6 resulting in incorrect weighting of the velocities across the solar disk. Alternative explanations cannot be excluded like suppression of convection in magnetic areas and undiscovered systematics during eclipse observations. Accurate observations of solar line profiles across the solar disk are suggested. We publish our RVs taken during solar eclipse as a benchmark curve for codes calculating the RM effect and for models of solar surface velocities and line profiles.

The IAG solar flux atlas: Accurate wavelengths and absolute convective blueshift in standard solar spectra

Ansgar **Reiners**, Niclas Mrotzek, Ulrike Lemke, Johannes Hinrichs, Klaus Reinsch
A&A **201**5
http://arxiv.org/pdf/1511.03014v1.pdf
We present a new solar flux atlas with the aim to understand wavelength precision and accuracy in solar benchmark data. The atlas covers the wavelength range 405--2300 nm and was observed at the Institut f\"ur Astrophysik, G\"ottingen (IAG) with a Fourier Transform Spectrograph. In contrast to other FTS atlases, the entire visible wavelength range was observed simultaneously using only one spectrograph setting. We compare the wavelength solution of the new atlas to the Kitt Peak solar flux atlases and to the HARPS frequency-comb calibrated solar atlas. Comparison reveals systematics in the two Kitt Peak FTS atlases resulting from their wavelength scale construction, and shows consistency between the IAG and the HARPS atlas. We conclude that the IAG atlas is precise and accurate on the order of ±10 m s−1 in the wavelength range 405--1065 nm while the Kitt Peak atlases show deviations as large as several ten to 100 m s−1. We determine absolute convective blueshift across the spectrum from the IAG atlas and report slight differences relative to results from the Kitt Peak atlas that we attribute to the differences between wavelength scales. We conclude that benchmark solar data with accurate wavelength solution are crucial to better understand the effect of convection on stellar RV measurements, which is one of the main limitations of Doppler spectroscopy at m s−1 precision.

The Sun is less active than other solar-like stars

Timo **Reinhold**, Alexander I. Shapiro, Sami K. Solanki, Benjamin T. Montet, Nathalie A. Krivova, Robert H. Cameron, Eliana M. Amazo-Gomez
Science Vol. 368, Issue 6490, pp. 518-521 DOI: 10.1126/science.aay3821 1 May **2020**
https://arxiv.org/pdf/2005.01401.pdf
https://sci-hub.tw/10.1126/science.aay3821
Magnetic activity of the Sun and other stars causes their brightness to vary. We investigate how typical the Sun's variability is compared to other solar-like stars, i.e. those with near-solar effective temperatures and rotation periods. By combining four years of photometric observations from the Kepler space telescope with astrometric data from the Gaia spacecraft, we measure photometric variabilities of 369 solar-like stars. Most of the solar-like stars with well-determined rotation periods show higher variability than the Sun and are therefore considerably more active. These stars appear nearly identical to the Sun, except for their higher variability. Their existence raises the question of whether the Sun can also experience epochs of such high variability.
Comment: T. Metcalfe, J. van Saders, Comment on Science 368, 518 (2020).
https://arxiv.org/ftp/arxiv/papers/2007/2007.04416.pdf
Reply to the comment: https://arxiv.org/pdf/2007.04817.pdf

A Method for the Estimation of f- and p-mode Parameters and Rotational Splitting Coefficients from Un-averaged Solar Oscillation Power Spectra

J. **Reiter**1, E. J. Rhodes Jr.2,3, A. G. Kosovichev4, P. H. Scherrer5, T. P. Larson5, and S. F. Pinkerton I
2020 ApJ 894 80
https://doi.org/10.3847/1538-4357/ab7a17
We present a new methodology for the fitting of the peaks in solar oscillation power spectra that is equally well-suited for the estimation of low-, medium, and high-degree f- and p-mode parameters and frequency-splitting coefficients. The method can provide accurate input data over a wide portion of the dispersion plane for both structural and rotational inversions. This method, which we call the Multiple-Peak, Tesseral-Spectrum (MPTS) method, operates directly upon of all of the modes in a multiplet (n, l) of radial order n and degree l, and employs a fitting profile that consists of the sum of numerous individual overlapping profiles whose relative amplitudes are determined by the leakage matrix appropriate to the targeted mode. Hence, 2l + 1 sets of modal parameters are obtained simultaneously for each multiplet (n, l). By fitting an appropriate polynomial to the run of the fitted frequencies versus the azimuthal order, frequency-splitting coefficients are also obtained for the same multiplet. Using power spectra obtained from the 66 day long 2010 MDI Dynamics Run, we present sample structural and rotational inversions that employed frequencies and frequency-splitting coefficients from modes in the degree range of 0–1000 and the frequency range of 965–4600 μHz. The structural inversion confirms evidence for a pronounced departure of the sound speed in the outer solar convection zone from the radial sound-speed profile contained in Model S of Christensen-Dalsgaard and his collaborators that we obtained previously using a different fitting method.

A Method for the Estimation of p-Mode Parameters from Averaged Solar Oscillation Power Spectra

J. **Reiter**, E. J. Rhodes Jr.2,4, A. G. Kosovichev3,5, J. Schou3,6, P. H. Scherrer3, and T. P. Larso
2015 ApJ 803 92
http://arxiv.org/pdf/1504.07493v2.pdf
A new fitting methodology is presented that is equally well suited for the estimation of low-, medium-, and high-degree mode parameters from m-averaged solar oscillation power spectra of widely differing spectral resolution. This method, which we call the "Windowed, MuLTiple-Peak, averaged-spectrum" or WMLTP Method, constructs a theoretical profile by convolving the weighted sum of the profiles of the modes appearing in the fitting box with the power spectrum of the window function of the observing run, using weights from a leakage matrix that takes into account observational and physical effects, such as the distortion of modes by solar latitudinal differential rotation. We demonstrate that the WMLTP Method makes substantial improvements in the inferences of the properties of the solar oscillations in comparison with a previous method, which employed a single profile to represent each spectral peak. We also present an inversion for the internal solar structure, which is based upon 6366 modes that we computed using the WMLTP method on the 66 day 2010 Solar and Heliospheric Observatory/MDI Dynamics Run. To improve both the numerical stability and reliability of the inversion, we developed a new procedure for the identification and correction of outliers in a frequency dataset. We present evidence for a pronounced departure of the sound speed in the outer half of the solar convection zone and in the subsurface shear layer from the radial sound speed profile contained in Model S of Christensen-Dalsgaard and his collaborators that existed in the rising phase of Solar Cycle 24 during mid-2010.

Small-scale dynamos: From idealized models to solar and stellar applications **Review**

Matthias **Rempel**, Tanayveer Bhatia, Luis Bellot Rubio, Maarit J. Korpi-Lagg
Space Science Reviews **219**, Article number: 36 **2023**

https://arxiv.org/pdf/2305.02787
https://link.springer.com/content/pdf/10.1007/s11214-023-00981-z.pdf
In this article we review small-scale dynamo processes that are responsible for magnetic field generation on scales comparable to and smaller than the energy carrying scales of turbulence. We provide a review of critical observation of quiet Sun magnetism, which have provided strong support for the operation of a small-scale dynamo in the solar photosphere and convection zone. After a review of basic concepts we focus on numerical studies of kinematic growth and non-linear saturation in idealized setups, with special emphasis on the role of the magnetic Prandtl number for dynamo onset and saturation. Moving towards astrophysical applications we review convective dynamo setups that focus on the deep convection zone and the photospheres of solar-like stars. We review the critical ingredients for stellar convection setups and discuss their application to the Sun and solar-like stars including comparison against available observations.

On the contribution of quiet Sun magnetism to solar irradiance variations: Constraints on quiet Sun variability and grand minimum scenarios

M. **Rempel**

ApJ **894** 140 **2020**

https://arxiv.org/pdf/2004.01795.pdf
https://doi.org/10.3847/1538-4357/ab8633
While the quiet Sun magnetic field shows only little variation with the solar cycle, long-term variations cannot be completely ruled out from first principles. We investigate the potential effect of quiet Sun magnetism on spectral solar irradiance through a series of small-scale dynamo simulations with zero vertical flux imbalance ($\langle Bz\rangle=0$) and varying levels of small-scale magnetic field strength, and one weak network case with an additional flux imbalance corresponding to a flux density of $\langle Bz\rangle=100$ G. From these setups we compute the dependence of the outgoing radiative energy flux on the mean vertical magnetic field strength in the photosphere at continuum optical depth $\tau=1$ ($\langle|Bz|\rangle\tau=1$). We find that a quiet Sun setup with a mean vertical field strength of $\langle|Bz|\rangle\tau=1=69$ G is about 0.6 % brighter than a non-magnetic reference case. We find a linear dependence of the outgoing radiative energy flux on the mean field strength $\langle|Bz|\rangle\tau=1$ with a relative slope of $1.4\cdot10{-}4$ G−1. With this sensitivity, only a moderate change of the quiet Sun field strength by 10% would lead to a total solar irradiance variation comparable to the observed solar cycle variation. While this does provide strong indirect constraints on possible quiet Sun variations during a regular solar cycle, it also emphasizes that potential variability over longer time scales could make a significant contribution to longer-term solar irradiance variations.

Small-scale dynamo simulations: Magnetic field amplification in exploding granules and the role of deep and shallow recirculation

Matthias **Rempel**

ApJ **859** 161 **2018**

https://arxiv.org/pdf/1805.08390.pdf
We analyze recent high resolution photospheric small-scale dynamo simulations that were computed with the MURaM radiative MHD code. We focus the analysis on newly forming downflow lanes in exploding granules since they show how weakly magnetized regions in the photosphere (center of granules) evolve into strongly magnetized regions (downflow lanes). We find that newly formed downflow lanes exhibit initially mostly a laminar converging flow that amplifies the vertical magnetic field embedded in the granule from a few 10 G to field strengths exceeding 800 G. This results in extended magnetic sheets that have a length comparable to granular scales. Field amplification by turbulent shear happens first a few 100 km beneath the visible layers of the photosphere. Shallow recirculation transports the resulting turbulent field into the photosphere within minutes, after which the newly formed downflow lane shows a mix of strong magnetic sheets and turbulent field components. We stress in particular the role of shallow and deep recirculation for the organization and strength of magnetic field in the photosphere and discuss the photospheric and sub-photospheric energy conversion associated with the small-scale dynamo process. While the energy conversion through the Lorentz force depends only weakly on the saturation field strength (and therefore deep or shallow recirculation), it is strongly dependent on the magnetic Prandtl number. We discuss the potential of these findings for further constraining small-scale dynamo models through high resolution observations.

EXTENSION OF THE MURAM RADIATIVE MHD CODE FOR CORONAL SIMULATIONS

M. **Rempel**

2017 ApJ 834 10
We present a new version of the MURaM radiative magnetohydrodynamics (MHD) code that allows for simulations spanning from the upper convection zone into the solar corona. We implement the relevant coronal physics in terms of optically thin radiative loss, field aligned heat conduction, and an equilibrium ionization equation of state. We artificially limit the coronal Alfvén and heat conduction speeds to computationally manageable values using an approximation to semi-relativistic MHD with an artificially reduced speed of light (Boris correction). We present example solutions ranging from quiet to active Sun in order to verify the validity of our approach. We quantify the

role of numerical diffusivity for the effective coronal heating. We find that the (numerical) magnetic Prandtl number determines the ratio of resistive to viscous heating and that owing to the very large magnetic Prandtl number of the solar corona, heating is expected to happen predominantly through viscous dissipation. We find that reasonable solutions can be obtained with values of the reduced speed of light just marginally larger than the maximum sound speed. Overall this leads to a fully explicit code that can compute the time evolution of the solar corona in response to photospheric driving using numerical time steps not much smaller than 0.1 s. Numerical simulations of the coronal response to flux emergence covering a time span of a few days are well within reach using this approach.

Numerical Simulations of Quiet Sun Magnetism: On the Contribution from a Small-scale Dynamo

M. **Rempel**

2014 ApJ 789 132

We present a series of radiative MHD simulations addressing the origin and distribution of the mixed polarity magnetic field in the solar photosphere. To this end, we consider numerical simulations that cover the uppermost 2-6 Mm of the solar convection zone and we explore scales ranging from 2 km to 25 Mm. We study how the strength and distribution of the magnetic field in the photosphere and subsurface layers depend on resolution, domain size, and boundary conditions. We find that 50% of the magnetic energy at the $\tau = 1$ level comes from fields with the less than 500 G strength and that 50% of the energy resides on scales smaller than about 100 km. While the probability distribution functions are essentially independent of resolution, properly describing the spectral energy distribution requires grid spacings of 8 km or smaller. The formation of flux concentrations in the photosphere exceeding 1 kG requires a mean vertical field strength greater than 30-40 G at $\tau = 1$. The filling factor of kG flux concentrations increases with overall domain size as the magnetic field becomes organized by larger, longer-lived flow structures. A solution with a mean vertical field strength of around 85 G at $\tau = 1$ requires a subsurface rms field strength increasing with depth at the same rate as the equipartition field strength. We consider this an upper limit for the quiet Sun field strength, which implies that most of the convection zone is magnetized close to the equipartition. We discuss these findings in view of recent high-resolution spectropolarimetric observations of quiet Sun magnetism.

Sunspot Modeling: From Simplified Models to Radiative MHD Simulations

Matthias **Rempel** and Rolf Schlichenmaier

Living **Review**s in Solar Physics, PUB.NO. lrsp-**2011**-3

We review our current understanding of sunspots from the scales of their fine structure to their large scale (global) structure including the processes of their formation and decay. Recently, sunspot models have undergone a dramatic change. In the past, several aspects of sunspot structure have been addressed by static MHD models with parametrized energy transport. Models of sunspot fine structure have been relying heavily on strong assumptions about flow and field geometry (e.g., flux-tubes, “gaps”, convective rolls), which were motivated in part by the observed filamentary structure of penumbrae or the necessity of explaining the substantial energy transport required to maintain the penumbral brightness. However, none of these models could self-consistently explain all aspects of penumbral structure (energy transport, filamentation, Evershed flow). In recent years, 3D radiative MHD simulations have been advanced dramatically to the point at which models of complete sunspots with sufficient resolution to capture sunspot fine structure are feasible. Here, overturning convection is the central element responsible for energy transport, filamentation leading to fine structure, and the driving of strong outflows. On the larger scale these models are also in the progress of addressing the subsurface structure of sunspots as well as sunspot formation. With this shift in modeling capabilities and the recent advances in high resolution observations, the future research will be guided by comparing observation and theory.

The First Solar Seeing Profile Measurement with Two Apertures and Multiple Guide Regions

Deqing **Ren** Gang Zhao Xin Wang Christian Beck Robert Broadfoot

Solar Physics **2019**, 294:1

Ground-based observations suffer from atmospheric turbulence perturbations, which seriously degrade the image quality. The seeing profile associated with the turbulence is critical to characterize an astronomical site. The optimal design and performance estimation of future solar ground-layer adaptive optics (GLAO) and multi-conjugate adaptive optics (MCAO) heavily rely on our knowledge of the seeing profile at a specific site. Many current optical seeing profile measurement techniques require one to use a large solar telescope for that purpose. The development of a portable instrument to measure and characterize the seeing profile is thus highly needed, in particular for testing potential new sites or for the regularly monitoring of the seeing condition at existing sites. Recently, we proposed the Advanced Multiple Aperture Seeing Profiler (A-MASP), which uses multiple small telescopes and multiple regions of interest (ROIs) on the solar surface to measure the seeing profile up to an altitude of 30 km. Here, we report our recent proof-of-concept observation run of the A-MASP technique with the Dunn Solar Telescope (DST) of the National Solar Observatory (NSO). We found that the Fried parameter, r0r0, was about 12 cm at the observed

wavelength of 630 nm in the early morning and that there were three main turbulence layers. The strongest one was the mix layer near the ground. We observed the evolution of the top of the mix layer and found that it can rise to about 1.5 km in about 18 min, which is consistent with the theory of daytime boundary layer evolution. Another turbulence layer was observed from 8 to 15 km, which is at the top of the convective layer. Comparing an instrument with two sub-apertures with a real A-MASP instrument, we found that they should lead to similar results except for the altitude h=0.

Measurement of Astronomical Seeing Using Long Exposure Solar Images

Sridharan **Rengaswamy** B. Ravindra K. Prabhu
Solar Physics January **2019**, 294:5
https://link.springer.com/content/pdf/10.1007%2Fs11207-019-1393-y.pdf
We extend our modified parameter search method (Sridharan, Dashora, and Venkatakrishnan, Solar Phys.222, 35, 2004) of estimating the Fried parameter (r0r0) from long exposure images to the images obtained from the Hαα-telescope installed at Merak, a cold desert on the Himalayas, with a modified criterion – the contrast ratio of the observed and the deconvolved images – to identify the true r0r0. We validated our new method by applying it to the solar granulation data and found that it is as accurate as our modified parameter search method. The median seeing at Hαα – estimated from the data spanning over 5 months – is ≈ 2 arc-sec and it corresponds to a median r0r0 of 6 cm. About 30% of the estimated values are above r0=7 cmr0=7 cm. The diurnal variation of the seeing is consistent with that expected for a lake-shore site. The significance of our method – extracting the underlying seeing from a single long exposure solar image – lies in the fact that it can be easily adopted to monitor seeing with small Hαα-telescopes that are coveted and eagerly possessed by many solar observatories for patrolling solar flares and filament eruptions.

Persistent magnetic vortex flow at a supergranular vertex★

Iker S. **Requerey**1,2, Basilio Ruiz Cobo1,3, Milan Gošić4,5 and Luis R. Bellot Rubio
A&A 610, A84 (**2018**)
https://www.aanda.org/articles/aa/pdf/2018/02/aa31842-17.pdf
Context. Photospheric vortex flows are thought to play a key role in the evolution of magnetic fields. Recent studies show that these swirling motions are ubiquitous in the solar surface convection and occur in a wide range of temporal and spatial scales. Their interplay with magnetic fields is poorly characterized, however.
Aims. We study the relation between a persistent photospheric vortex flow and the evolution of a network magnetic element at a supergranular vertex.
Methods. We used long-duration sequences of continuum intensity images acquired with Hinode and the local correlation-tracking method to derive the horizontal photospheric flows. Supergranular cells are detected as large-scale divergence structures in the flow maps. At their vertices, and cospatial with network magnetic elements, the velocity flows converge on a central point.
Results. One of these converging flows is observed as a vortex during the whole 24 h time series. It consists of three consecutive vortices that appear nearly at the same location. At their core, a network magnetic element is also detected. Its evolution is strongly correlated to that of the vortices. The magnetic feature is concentrated and evacuated when it is caught by the vortices and is weakened and fragmented after the whirls disappear.
Conclusions. This evolutionary behavior supports the picture presented previously, where a small flux tube becomes stable when it is surrounded by a vortex flow. **2010 November 2–3**

Spectropolarimetric evidence for a siphon flow along an emerging magnetic flux tube

Iker S. **Requerey**, B. Ruiz Cobo, J. C. Del Toro Iniesta, D. Orozco Suárez, J. Blanco Rodríguez, S. K. Solanki, P. Barthol, A. Gandorfer, L. Gizon, J. Hirzberger, T. L. Riethmüller, M. van Noort, W. Schmidt, V. Martínez Pillet, M. Knölker
ApJS **2016**
https://arxiv.org/pdf/1611.06732v1.pdf
We study the dynamics and topology of an emerging magnetic flux concentration using high spatial resolution spectropolarimetric data acquired with the Imaging Magnetograph eXperiment on board the Sunrise balloon-borne solar observatory. We obtain the full vector magnetic field and the line-of-sight (LOS) velocity through inversions of the Fe I line at 525.02 nm with the SPINOR code. The derived vector magnetic field is used to trace magnetic field lines. Two magnetic flux concentrations with different polarity and LOS velocities are found to be connected by a group of arch-shaped magnetic field lines. The positive polarity footpoint is weaker (1100 G) and displays an upflow, while the negative polarity footpoint is stronger (2200 G) and shows a downflow. This configuration is naturally interpreted as a siphon flow along an arched magnetic flux tube. **2013 June 12**

Convectively driven sinks and magnetic fields in the quiet Sun

Iker S. **Requerey**, Jose Carlos Del Toro Iniesta, Luis R. Bellot Rubio, Valentín Martínez Pillet, Sami K. Solanki, Wolfgang Schmidt
ApJS **2016**
https://arxiv.org/pdf/1610.07622v1.pdf
We study the relation between mesogranular flows, convectively driven sinks and magnetic fields using high spatial resolution spectropolarimetric data acquired with the Imaging Magnetograph eXperiment on board Sunrise. We obtain the horizontal velocity flow fields of two quiet-Sun regions (31.2 × 31.2 Mm2) via local correlation tracking. Mesogranular lanes and the central position of sinks are identified using Lagrange tracers. We find 6.7×10−2 sinks per Mm2 in the two observed regions. The sinks are located at the mesogranular vertices and turn out to be associated with (1) horizontal velocity flows converging to a central point and (2) long-lived downdrafts. The spatial distribution of magnetic fields in the quiet Sun is also examined. The strongest magnetic fields are preferentially located at sinks. We find that 40 \% of the pixels with longitudinal component of the magnetic field stronger than 500 G are located in the close neighborhood of sinks. In contrast, the small-scale magnetic loops detected by Mart\'{i}nez Gonz\'{a}lez et al. in the same two observed areas do not show any preferential distribution at mesogranular scales. The study of individual examples reveals that sinks can play an important role in the evolution of quiet-Sun magnetic features.

Kinematic Numerical Simulations of the Solar Dynamo: Dependence on α and Ω Values

S. **Restuccia**, L. Primavera, A. Vecchio, V. Carbone
Solar Physics, March **2014**, Volume 289, Issue 3, pp 693-706
We investigated the generation of dynamo waves in the solar convection zone through a numerical simulation. We integrated the axisymmetric α–Ω kinematic dynamo equations in a spherical geometry, where the α- and Ω-profiles depend on the spatial coordinates. The model results show that the fundamental parameter that determines the behavior of the system is the product between the characteristic intensities of the α and Ω contributions. In particular, we found three different regimes in which the system exhibits different behaviors: a regime without a dynamo effect, one with an exponential amplification of the magnetic field, and one with dynamo waves.

Monochromatic X-Ray Imagers of the Sun Based on the Bragg Crystal Optics

Anton A. **Reva***, Sergey V. Kuzin, Alexey S. Kirichenko, Artem S. Ulyanov, Ivan P. Loboda and Sergey A. Bogachev
Front. Astron. Space Sci., May **2021** |
https://www.frontiersin.org/articles/10.3389/fspas.2021.645062/full
https://doi.org/10.3389/fspas.2021.645062
Investigations of solar activity require information about plasma in a wide range of temperatures. Generally, researchers require observations from telescopes producing monochromatic images of coronal plasma with cool, warm, and hot temperatures. Until now, monochromatic telescopic imaging has been made only in the Mg XII 8.42 Å line with the Mg XII spectroheliograph on board CORONAS-I, CORONAS-F, and CORONAS-PHOTON satellites. The Mg XII spectroheliograph used Bragg crystal optics. Its design is based on two main principles: (1) to select the working wavelength and the crystal in such a way that reflection occurs at small incident angles; (2) to use the aperture of the mirror as a spectral filter. We believe that these design principles can be applied to other spectral lines. In this article, we will review the design of the Mg XII spectroheliograph and present our thoughts on how to apply these principles to the Si XIV 6.18 Å and Si XIII 6.65 Å lines. A combination of the monochromatic Mg XII 8.42 Å, Si XIV 6.18 Å, and Si XIII 6.65 Å images will help us to study the dynamics of the hot plasma in the solar corona.

Global solar magnetic field organization in the outer corona: influence on the solar wind speed and mass flux over the cycle

Victor **Réville**, Allan Sacha Brun
ApJ **2017**
https://arxiv.org/pdf/1710.02908.pdf
The dynamics of the solar wind depends intrinsically on the structure of the global solar magnetic field, which undergoes fundamental changes over the 11-yr solar cycle. For instance, the wind terminal velocity is thought to be anti-correlated with the expansion factor, a measure of how the magnetic field varies with height in the solar corona, usually computed at a fixed height (≈2.5R⊙, the source surface radius which approximates the distance at which all magnetic field lines become open). However, the magnetic field expansion affects the solar wind in a more detailed

way, its influence on the solar wind properties remaining significant well beyond the source surface. We demonstrate this using 3D global MHD simulations of the solar corona, constrained by surface magnetograms over half a solar cycle (1989-2001). A self-consistent expansion beyond the solar wind critical point (even up to 10R⊙) makes our model comply with observed characteristics of the solar wind, namely, that the radial magnetic field intensity becomes latitude independent at some distance from the Sun, and that the mass flux is mostly independent of the terminal wind speed. We also show that near activity minimum, the expansion in the higher corona has more influence on the wind speed than the expansion below 2.5R⊙.

Variation in sunspot properties between 1999 and 2014

R. **Rezaei**1, C. Beck2, A. Lagg3, J. M. Borrero1, W. Schmidt1 and M. Collados
A&A 578, A43 (**2015**)

Aims. We study the variation in the magnetic field strength, area, and continuum intensity of umbrae in solar cycles 23 and 24.
Methods. We analyzed a sample of 374 sunspots observed from 1999 until 2014 with the Tenerife Infrared Polarimeter at the German Vacuum Tower Telescope and the Facility InfRared Spectropolarimeter at the Dunn Solar Telescope. The sample of field strength, area, and intensities was used to trace any long-term or cyclic trend of umbral properties in the last 15 years.
Results. Sunspots are systematically weaker, that is, have a weaker field strength and stronger continuum intensity, toward the end of cycle 23 than they had at the maximum of cycle 23. The linear trend reverses with the onset of cycle 24. We find that the field strength decreases in the declining phase of cycle 23 by about 112 (± 16) G yr-1, while it increases in the rising phase of cycle 24 by about 138 (± 72) G yr-1. The umbral intensity shows the opposite trend: the intensity increases with a rate of 0.7 (± 0.3)% of Ic yr-1 toward the end of cycle 23 and decreases with a rate of 3.8 (± 1.5)% of Ic yr-1 toward the maximum of cycle 24. The distribution of the umbral maximum field strength in cycle 24 is similar to that of cycle 23, but is slightly shifted toward lower values by about 80 G, corresponding to a possible long-term gradient in umbral field strength of about 7 ± 4 G yr-1. If instead of the maximum umbral field we consider the average value over the entire umbra, the distribution shifts by about 44 Gauss.
Conclusions. The umbral brightness decreases in the rising stage of a solar cycle, but increases from maximum toward the end of the cycle. Our results do not indicate a drastic change of the solar cycle toward a grand minimum in the near future.

Comparison of sunspot properties in cycle 24 and 23

Reza **Rezaei**
HMI Science Nuggets, **2014**
http://hmi.stanford.edu/hminuggets/?p=477

We analyze umbral area, magnetic field, and umbral intensity of the sunspots during the rising phase of cycle 24. We do not find a significant variation in either sunspot physical properties or distribution of sunspot umbral area from previous cycles.

Diagnostics of Solar Corona Heating Parameters Using the Observed Gravitational Stratification of the Medium.

Riashchikov, D., Scoptsova, E. & Zavershinskii, D.
Sol Phys 299, 136 (**2024**).
https://doi.org/10.1007/s11207-024-02383-y

The problem of coronal heating is one of the fundamental problems of solar physics. At present, it is again attracting great interest due to the appearance of a large amount of observational data of high spatial and temporal resolution. These data made it possible to diagnose plasma parameters from observations of waves and oscillations in coronal magnetic structures and, moreover, to introduce analytical constraints on the coronal heating function. In this paper, we propose an approach allowing us to impose constraints on the heating function based on data on the gravitational stratification of the solar atmosphere. The developed algorithm is applied to the altitude profiles of temperature and density in several regions of the solar corona obtained from direct modeling of EUV radiation from the Solar Dynamics Observatory/Atmospheric Imaging Assembly (SDO/AIA). Assuming that the heating function is a power function of temperature and density, we determine the domain of power-index constraints allowing us to realize the observed altitude profiles. The obtained results are combined with the conditions of stability for the entropy and magnetoacoustic modes, to narrow the region of possible parameters further.

Recursive Integer Sequences, Detected in Solar-Cycle Periodicities Measured in Numbers of Rigid Rotations of the Sun

Jean-Guillaume **Richard**

Solar Physics volume 295, Article number: 78 (**2020**)
https://link.springer.com/content/pdf/10.1007/s11207-020-01631-1.pdf
Consecutive integers in the recursive number sequences, the Fibonacci sequence (Fn) and the Lucas sequence (Ln), are detected in the lengths of solar-activity variations from ≈ 1 yr to ≈ 12 yr, measured in rigid rotations of the Sun at the helioseismologically determined frequency in the radiative zone, 433 ± 3 nHz. One rotation is denoted by the symbol . Firstly, in the new international sunspot-number record (Ri) the most frequent (modal) sunspot-cycle length, which is also the period defined by autocorrelation for the recurrence of sunspot cycles, has been 144± ≈ 2 (F12 = 144). The most frequent length for a descending leg of the cycle has been 89 ± 2 (F11 = 89), and for an ascending leg 55 ± 1 (F10 = 55). Secondly, there is some observational evidence of Ri spectral peaks at the consecutive Ln numbers of : 18 (≈ 1.3 yr), 29 (≈ 2.1 yr), 47 (≈ 3.4 yr), and 76 (≈ 5.6 yr), which are harmonics of the 144 period divided by the first four Fn > 1: 2, 3, 5, and 8. The numbers of : 144, 89, and 55 may be kinematical thresholds in the dynamo process starting at sunspot maximum, when the poles change polarity and the process is re-set. The ratio of two consecutive Fn or Ln converges to 1+ √5 2 , hence it is suggested that this proportion plays a role in solar behavior over time, described numerically. The length ratio 1+ √5 2 also is characteristic of fivefold symmetry in space. Since the icosahedral group is the link between numerical and spatial expressions of fivefold symmetry, it is proposed that the presence of icosahedral symmetry in the large-scale geometry of the Sun could also be tested.

North/south hemispheric periodicities in the >25 MeV solar proton event rate during the rising and peak phases of solar cycle 24

Ian **Richardson**, Tycho von Rosenvinge, Hilary Cane
Solar Phys. **2016**
http://arxiv.org/pdf/1604.03141v1.pdf **File**
We present evidence that >25 MeV solar proton events show a clustering in time at intervals of ~6 months that persisted during the rising and peak phases of solar cycle 24. This phenomenon is most clearly demonstrated by considering events originating in the northern or southern solar hemispheres separately. We examine how these variations in the solar energetic particle (SEP) event rate are related to other phenomena, such as hemispheric sunspot numbers and areas, rates of coronal mass ejections, and the mean solar magnetic field. Most obviously, the SEP event rate closely follows the sunspot number and area in the same hemisphere. The ~6 month variations are associated with features in many of the other parameters we examine, indicating that they are just one signature of the episodic development of cycle 24. They may be related to the "~150 day" periodicities reported in various solar and interplanetary phenomena during previous solar cycles. The clear presence of ~6 month periodicities in cycle 24 that evolve independently in each hemisphere conflicts with a scenario suggested by McIntosh et al. (2015) for the variational time scales of solar magnetism.

Finding the mechanism of wave energy flux damping in solar pores using numerical simulations

Julia M. **Riedl**, Caitlin A. Gilchrist-Millar, Tom Van Doorsselaere, David B. Jess, Samuel D. T. Grant
A&A 648, A77 **2021**
https://arxiv.org/pdf/2102.12420
https://doi.org/10.1051/0004-6361/202040163
https://www.aanda.org/articles/aa/pdf/2021/04/aa40163-20.pdf
Context. Solar magnetic pores are, due to their concentrated magnetic fields, suitable guides for magnetoacoustic waves. Recent observations have shown that propagating energy flux in pores is subject to strong damping with height; however, the reason is still unclear. Aims. We investigate possible damping mechanisms numerically to explain the observations. Methods. We performed 2D numerical magnetohydrodynamic (MHD) simulations, starting from an equilibrium model of a single pore inspired by the observed properties. Energy was inserted into the bottom of the domain via different vertical drivers with a period of 30s. Simulations were performed with both ideal MHD and non-ideal effects. Results. While the analysis of the energy flux for ideal and non-ideal MHD simulations with a plane driver cannot reproduce the observed damping, the numerically predicted damping for a localized driver closely corresponds with the observations. The strong damping in simulations with localized driver was caused by two geometric effects, geometric spreading due to diverging field lines and lateral wave leakage.

Wave modes excited by photospheric p-modes and mode conversion in a multi-loop system

Julia M. **Riedl**, Tom Van Doorsselaere, Irantzu Calvo Santamaria
A&A 625, A144 **2019**
https://arxiv.org/pdf/1905.01865.pdf
Context. Waves are ubiquitous in the solar corona and there are indications that they are excited by photospheric p-modes. However, it is unclear how p-modes in coronal loops are converted to sausage modes and transverse (kink) modes, which are observed in the corona. Aims. We aim to investigate how those wave modes are excited in the lower corona by photospheric acoustic waves.

Methods. We built 3D magnetohydrostatic loop systems with multiple inclinations spanning from the photosphere to the lower corona. We then simulated these atmospheres with the MANCHA code, in which we perturb the equilibrium with a p-mode driver at the bottom of the domain. By splitting the velocity perturbation into components longitudinal, normal, and azimuthal to the magnetic flux surfaces we can study wave behavior.
Results. In vertical flux tubes, we find that deformed fast sausage surface waves and slow sausage body waves are excited. In inclined flux tubes fast kink surface waves, slow sausage body waves, and either a fast sausage surface wave or a plane wave are excited. In addition, we calculate a wave conversion factor ($0 \leq C \leq 1$) from acoustic to magnetic wave behavior by taking the ratio of the mean magnetic energy flux to the sum of the mean magnetic and acoustic energy flux and compare it to a commonly used theoretical conversion factor. We find that between magnetic field inclinations of 10∘ to 30∘ those two methods lie within 40%. For smaller inclinations the absolute deviation is smaller than 0.1.

Long quasi-periodic oscillations of the faculae and pores

A. **Riehokainen**, P. Strekalova, A. Solov'ev, V. Smirnova, I. Zhivanovich, A. Moskaleva and N. Varun
A&A 627, A10 (**2019**)
DOI: https://doi.org/10.1051/0004-6361/201935629
Aims. The main goal of this work is to analyze the structural and temporal evolution of small-scale magnetic structures (SSMSs) observed in the solar atmosphere, such as solitary faculae and pores, and reveal long quasi-periodic oscillations of these structures.
Methods. The statistical method of regression analysis and the wavelet transform were used to obtain the periods of oscillations and dependences between the parameters of magnetic structures and periods of oscillations.
Results. Long-period oscillations with periods in the interval of 18−260 min are found for the structurally stable phase of SSMSs at the level of the solar photosphere. These long-period oscillations were interpreted as natural oscillations of the structurally stable long-lived magnetic structures around their equilibrium position. These oscillations, which are of similar nature, are observed in the chromospheric bright formations associated with photospheric SSMSs. Dependences between the magnetic field and the continuum intensity of the facula elements were found. It is shown that the continuum intensity of a SSMS decreases when its magnetic field increases.

The potential of many-line inversions of photospheric spectropolarimetric data in the visible and near UV

T. L. **Riethmüller**1 and S. K. Solanki
A&A 622, A36 (**2019**)
Our knowledge of the lower solar atmosphere is mainly obtained from spectropolarimetric observations, which are often carried out in the red or infrared spectral range and almost always cover only a single or a few spectral lines. Here we compare the quality of Stokes inversions of only a few spectral lines with many-line inversions. In connection with this, we have also investigated the feasibility of spectropolarimetry in the short-wavelength range, 3000 Å−4300 Å, where the line density but also the photon noise are considerably higher than in the red, so that many-line inversions could be particularly attractive in that wavelength range. This is also timely because this wavelength range will be the focus of a new spectropolarimeter in the third science flight of the balloon-borne solar observatory SUNRISE. For an ensemble of state-of-the-art magneto-hydrodynamical atmospheres we synthesize exemplarily spectral regions around 3140 Å (containing 371 identified spectral lines), around 4080 Å (328 lines), and around 6302 Å (110 lines). The spectral coverage is chosen such that at a spectral resolving power of 150 000 the spectra can be recorded by a 2K × 2K detector. The synthetic Stokes profiles are degraded with a typical photon noise and afterward inverted. The atmospheric parameters of the inversion of noisy profiles are compared with the inversion of noise-free spectra. We find that significantly more information can be obtained from many-line inversions than from a traditionally used inversion of only a few spectral lines. We further find that information on the upper photosphere can be significantly more reliably obtained at short wavelengths. In the mid and lower photosphere, the many-line approach at 4080 Å provides equally good results as the many-line approach at 6302 Å for the magnetic field strength and the line-of-sight (LOS) velocity, while the temperature determination is even more precise by a factor of three. We conclude from our results that many-line spectropolarimetry should be the preferred option in the future, and in particular at short wavelengths it offers a high potential in solar physics.

Magnetohydrodynamics and Solar Physics **Review**

Michel **Rieutord**
SF2A **2014** annual conference
http://arxiv.org/pdf/1410.3725v2.pdf
In this short review, I present some of the recent progresses on the pending questions of solar physics. These questions let us revisit the solar wind, the solar dynamo problem, the dynamics of the photosphere and finally have a glimpse at other solar type stars. Discussing the use of direct numerical simulations in solar physics, I show that the

full numerical calculation of the flow in a single supergranule would require more electric power than the luminosity of the sun itself with present computer technology.

The Sun's Supergranulation (Review)

Michel **Rieutord** and François Rincon.
Living Reviews in Solar Physics, **2010**
http://solarphysics.livingreviews.org/Articles/lrsp-2010-2/

The Sun's supergranulation refers to a physical pattern covering the surface of the quiet Sun with a typical horizontal scale of approximately 30,000 km and a lifetime of around 1.8 d. Its most noticeable observable signature is as a fluctuating velocity field of 360 m s–1 rms whose components are mostly horizontal. Supergranulation was discovered more than fifty years ago, however explaining why and how it originates still represents one of the main challenges of modern solar physics.

A lot of work has been devoted to the subject over the years, but observational constraints, conceptual difficulties and numerical limitations have all concurred to prevent a detailed understanding of the supergranulation phenomenon so far. With the advent of 21st century supercomputing resources and the availability of unprecedented high-resolution observations of the Sun, a stage at which key progress can be made has now been reached. A unifying strategy between observations and modelling is more than ever required for this to be possible.

The primary aim of this review is therefore to provide readers with a detailed interdisciplinary description of past and current research on the problem, from the most elaborate observational strategies to recent theoretical and numerical modelling efforts that have all taken up the challenge of uncovering the origins of supergranulation. Throughout the text, we attempt to pick up the most robust findings so far, but we also outline the difficulties, limitations and open questions that the community has been confronted with over the years.

In the light of the current understanding of the multiscale dynamics of the quiet photosphere, we finally suggest a tentative picture of supergranulation as a dynamical feature of turbulent magnetohydrodynamic convection in an extended spatial domain, with the aim of stimulating future research and discussions.

MEASUREMENTS OF THE SUN'S HIGH-LATITUDE MERIDIONAL CIRCULATION

Lisa **Rightmire-Upton**1, David H. Hathaway2, and Katie Kosak
2012 ApJ 761 L14

The meridional circulation at high latitudes is crucial to the buildup and reversal of the Sun's polar magnetic fields. Here, we characterize the axisymmetric flows by applying a magnetic feature cross-correlation procedure to high-resolution magnetograms obtained by the Helioseismic and Magnetic Imager (HMI) on board the Solar Dynamics Observatory. We focus on Carrington rotations 2096-2107 (2010 April to 2011 March)—the overlap interval between HMI and the Michelson Doppler Imager (MDI). HMI magnetograms averaged over 720 s are first mapped into heliographic coordinates. Strips from these maps are then cross-correlated to determine the distances in latitude and longitude that the magnetic element pattern has moved, thus providing meridional flow and differential rotation velocities for each rotation of the Sun. Flow velocities were averaged for the overlap interval and compared to results obtained from MDI data. This comparison indicates that these HMI images are rotated counterclockwise by 0075 with respect to the Sun's rotation axis. The profiles indicate that HMI data can be used to reliably measure these axisymmetric flow velocities to at least within 5° of the poles. Unlike the noisier MDI measurements, no evidence of a meridional flow counter-cell is seen in either hemisphere with the HMI measurements: poleward flow continues all the way to the poles. Slight north-south asymmetries are observed in the meridional flow. These asymmetries should contribute to the observed asymmetries in the polar fields and the timing of their reversals.

On the Strength and Duration of Solar Cycle 25: A Novel Quantile-based Superposed Epoch Analysis

Pete **Riley**
Solar Phys. **298**, Article number: 66 (**2023**)
https://arxiv.org/pdf/2210.14384.pdf
https://doi.org/10.1007/s11207-023-02165-y

Sunspot number (SSN) is an important - albeit nuanced - parameter that can be used as an indirect measure of solar activity. Predictions of upcoming active intervals, including the peak and timing of solar maximum can have important implications for space weather planning. Forecasts for the strength of solar cycle 25 have varied considerably, from it being very weak, to one of the strongest cycles in recorded history. In this study, we develop a novel quantile based superposed epoch analysis that can be updated on a monthly basis, and which currently predicts that solar cycle 25 will be a very modest cycle (within the 25th percentile of all numbered cycles), with a monthly-averaged (13-month average) peak of - 130 (110) likely occurring in December, 2024. We validate the model by

performing retrospective forecasts (hindcasts) for the previous 24 cycles, finding that it out performs the baseline (reference) model (the average cycle) 75% of the time.
Correction Solar Physics volume 298, Article number: 80 (**2023**)
https://link.springer.com/content/pdf/10.1007/s11207-023-02181-y.pdf?pdf=button

Using a Heliospheric Upwinding eXtrapolation Technique to Magnetically Connect Different Regions of the Heliosphere

Pete **Riley*** and Opal Issan
Front. Phys., May **2021** |
https://doi.org/10.3389/fphy.2021.679497
Understanding how coronal structure propagates and evolves from the Sun and into the heliosphere has been thoroughly explored using sophisticated MHD models. From these, we have a reasonably good working understanding of the dynamical processes that shape the formation and evolution of stream interaction regions and rarefactions, including their locations, orientations, and structure. However, given the technical expertize required to produce, maintain, and run global MHD models, their use has been relatively restricted. In this study, we refine a simple Heliospheric eXtrapolation Technique (HUX) to include not only forward mapping from the Sun to 1 AU (or elsewhere), but backward mapping toward the Sun. We demonstrate that this technique can provide substantially more accurate mappings than the standard, and often applied "ballistic" approximation. We also use machine learning (ML) methods to explore whether the HUX approximation to the momentum equation can be refined without loss of simplicity, finding that it likely provides the optimum balance. We suggest that HUX can be used, in conjunction with coronal models (PFSS or MHD) to more accurately connect measurements made at 1 AU, Stereo-A, Parker Solar Probe, and Solar Orbiter with their solar sources. In particular, the HUX technique: 1) provides a substantial improvement over the "ballistic" approximation for connecting to the source longitude of streams; 2) is almost as accurate, but considerably easier to implement than MHD models; and 3) can be applied as a general tool to magnetically connect different regions of the inner heliosphere together, as well as providing a simple 3-D reconstruction.

Inferring the Structure of the Solar Corona and Inner Heliosphere During the Maunder Minimum Using Global Thermodynamic Magnetohydrodynamic Simulations

Pete **Riley**1, Roberto Lionello1, Jon A. Linker1, Ed Cliver2, Andre Balogh3, Jürg Beer4, Paul Charbonneau5, Nancy Crooker6, Marc DeRosa7, Mike Lockwood8, Matt Owens8, Ken McCracken9, Ilya Usoskin10, and S. Koutchmy
2015 ApJ 802 105
Observations of the Sun's corona during the space era have led to a picture of relatively constant, but cyclically varying solar output and structure. Longer-term, more indirect measurements, such as from 10Be, coupled by other albeit less reliable contemporaneous reports, however, suggest periods of significant departure from this standard. The Maunder Minimum was one such epoch where: (1) sunspots effectively disappeared for long intervals during a 70 yr period; (2) eclipse observations suggested the distinct lack of a visible K-corona but possible appearance of the F-corona; (3) reports of aurora were notably reduced; and (4) cosmic ray intensities at Earth were inferred to be substantially higher. Using a global thermodynamic MHD model, we have constructed a range of possible coronal configurations for the Maunder Minimum period and compared their predictions with these limited observational constraints. We conclude that the most likely state of the corona during—at least—the later portion of the Maunder Minimum was not merely that of the 2008/2009 solar minimum, as has been suggested recently, but rather a state devoid of any large-scale structure, driven by a photospheric field composed of only ephemeral regions, and likely substantially reduced in strength. Moreover, we suggest that the Sun evolved from a 2008/2009-like configuration at the start of the Maunder Minimum toward an ephemeral-only configuration by the end of it, supporting a prediction that we may be on the cusp of a new grand solar minimum.

A Multi-Observatory Inter-Comparison of Line-of-Sight Synoptic Solar Magnetograms

P. **Riley**, M. Ben-Nun, J. A. Linker, Z. Mikic, L. Svalgaard, J. Harvey, L. Bertello, T. Hoeksema, Y. Liu, R. Ulrich
Solar Physics, March **2014**, Volume 289, Issue 3, pp 769-792
The observed photospheric magnetic field is a crucial parameter for understanding a range of fundamental solar and heliospheric phenomena. Synoptic maps, in particular, which are derived from the observed line-of-sight photospheric magnetic field and built up over a period of 27 days, are the main driver for global numerical models of the solar corona and inner heliosphere. Yet, in spite of 60 years of measurements, quantitative estimates remain elusive. In this study, we compare maps from seven solar observatories (Stanford/WSO, NSO/KPVT, NSO/SOLIS,

NSO/GONG, SOHO/MDI, UCLA/MWO, and SDO /HMI) to identify consistencies and differences among them. We find that while there is a general qualitative consensus, there are also some significant differences. We compute conversion factors that relate measurements made by one observatory to another using both synoptic map pixel-by-pixel and histogram-equating techniques, and we also estimate the correlation between datasets. For example, Wilcox Solar Observatory (WSO) synoptic maps must be multiplied by a factor of 3 – 4 to match Mount Wilson Observatory (MWO) estimates. Additionally, we find no evidence that the MWO saturation correction factor should be applied to WSO data, as has been done in previous studies. Finally, we explore the relationship between these datasets over more than a solar cycle, demonstrating that, with a few notable exceptions, the conversion factors remain relatively constant. While our study was able to quantitatively describe the relationship between the datasets, it did not uncover any obvious "ground truth." We offer several suggestions for how this may be addressed in the future.

The Daniel K. Inouye Solar Telescope – Observatory Overview

Thomas R. **Rimmele**, Mark Warner, […] Charles White
Solar Physics volume 295, Article number: 172 (**2020**)
https://link.springer.com/content/pdf/10.1007/s11207-020-01736-7.pdf
We present an overview of the National Science Foundation's Daniel K. Inouye Solar Telescope (DKIST), its instruments, and support facilities. The 4 m aperture DKIST provides the highest-resolution observations of the Sun ever achieved. The large aperture of DKIST combined with state-of-the-art instrumentation provide the sensitivity to measure the vector magnetic field in the chromosphere and in the faint corona, i.e. for the first time with DKIST we will be able to measure and study the most important free-energy source in the outer solar atmosphere – the coronal magnetic field. Over its operational lifetime DKIST will advance our knowledge of fundamental astronomical processes, including highly dynamic solar eruptions that are at the source of space-weather events that impact our technological society. Design and construction of DKIST took over two decades. DKIST implements a fast (f/2), off-axis Gregorian optical design. The maximum available field-of-view is 5 arcmin. A complex thermal-control system was implemented in order to remove at prime focus the majority of the 13 kW collected by the primary mirror and to keep optical surfaces and structures at ambient temperature, thus avoiding self-induced local seeing. A high-order adaptive-optics system with 1600 actuators corrects atmospheric seeing enabling diffraction limited imaging and spectroscopy. Five instruments, four of which are polarimeters, provide powerful diagnostic capability over a broad wavelength range covering the visible, near-infrared, and mid-infrared spectrum. New polarization-calibration strategies were developed to achieve the stringent polarization accuracy requirement of 5×10−4. Instruments can be combined and operated simultaneously in order to obtain a maximum of observational information. Observing time on DKIST is allocated through an open, merit-based proposal process. DKIST will be operated primarily in "service mode" and is expected to on average produce 3 PB of raw data per year. A newly developed data center located at the NSO Headquarters in Boulder will initially serve fully calibrated data to the international users community. Higher-level data products, such as physical parameters obtained from inversions of spectro-polarimetric data will be added as resources allow.

Dynamo theories **Review**

Francois **Rincon** (CNRS, IRAP, France)
J. Plasma Phys. **2019**
https://arxiv.org/pdf/1903.07829.pdf
These lecture notes are based on a tutorial given in 2017 at a plasma physics winter school in Les Houches. Their aim is to provide a self-contained graduate-student level introduction to the theory and modelling of the dynamo effect in turbulent fluids and plasmas, blended with a review of current research in the field. The primary focus is on the physical and mathematical concepts underlying different (turbulent) branches of dynamo theory, with some astrophysical, geophysical and experimental context disseminated throughout the document. The text begins with an introduction to the rationale, observational and historical roots of the subject, and to the basic concepts of magnetohydrodynamics relevant to dynamo theory. The next two sections discuss the fundamental phenomenological and mathematical aspects of (linear and nonlinear) small- and large-scale MHD dynamos. These sections are complemented by an overview of a selection of current active research topics in the field, including the numerical modelling of the geo- and solar dynamos, shear dynamos driven by turbulence with zero net helicity, and MHD-instability-driven dynamos such as the magnetorotational dynamo. The difficult problem of a unified, self-consistent statistical treatment of small and large-scale dynamos at large magnetic Reynolds numbers is also discussed throughout the text. Finally, an excursion is made into the relatively new but increasingly popular realm of magnetic-field generation in weakly-collisional plasmas. A short discussion of the outlook and challenges for the future of the field concludes the presentation.

The Sun's supergranulation, **Review**

Rincon, F. & Rieutord, M.,
Living Rev Sol Phys (**2018**) 15: 6
link.springer.com/article/10.1007/s41116-018-0013-5

Supergranulation is a fluid-dynamical phenomenon taking place in the solar photosphere, primarily detected in the form of a vigorous cellular flow pattern with a typical horizontal scale of approximately 30 – 35 Mm, a dynamical evolution time of 24 – 48 h, a strong 300 – 400 m/s (rms) horizontal flow component and a much weaker 20 – 30 m/s vertical component. Supergranulation was discovered more than 60 years ago, however, explaining its physical origin and most important observational characteristics has proven extremely challenging ever since, as a result of the intrinsic multiscale, nonlinear dynamical complexity of the problem concurring with strong observational and computational limitations. Key progress on this problem is now taking place with the advent of twenty-first-century supercomputing resources and the availability of global observations of the dynamics of the solar surface with high spatial and temporal resolutions. This article provides an exhaustive review of observational, numerical and theoretical research on supergranulation, and discusses the current status of our understanding of its origin and dynamics, most importantly in terms of large-scale nonlinear thermal convection, in the light of a selection of recent findings.

Supergranulation and multiscale flows in the solar photosphere: Global observations vs. a theory of anisotropic turbulent convection

F. **Rincon** (IRAP Toulouse), T. Roudier (IRAP Toulouse), A. A. Schekochihin (Oxford), M. Rieutord
A&A 599, A69 **2017**
http://arxiv.org/pdf/1609.05785v1.pdf
The Sun provides us with the only spatially well-resolved astrophysical example of turbulent thermal convection. While various aspects of solar photospheric turbulence, such as granulation (one-Megameter horizontal scale), are well understood, the questions of the physical origin and dynamical organization of larger-scale flows, such as the 30-Megameters supergranulation and flows deep in the solar convection zone, remain largely open in spite of their importance for solar dynamics and magnetism. Here, we present a new critical global observational characterization of multiscale photospheric flows and subsequently formulate an anisotropic extension of the Bolgiano-Obukhov scaling theory of hydrodynamic stratified turbulence that may explain several of their distinctive dynamical properties. Our combined analysis suggests that photospheric flows in the horizontal range of scales between supergranulation and granulation have a typical vertical correlation scale of 2.5 to 4 Megameters and operate in a strongly anisotropic, self-similar, nonlinear, buoyant dynamical regime. The theory lends itself to quantitative comparisons with future high-resolution acoustic tomography of subsurface layers and advanced numerical models. Such a validation exercise may also lead to new insights into the asymptotic dynamical regimes in which other, unresolved turbulent anisotropic astrophysical fluid systems supporting waves or instabilities operate.

Methodology for estimating the magnetic Prandtl number and application to solar surface small-scale dynamo simulations

Fabio **Riva**, Oskar Steiner
A&A **2022**
https://arxiv.org/pdf/2202.12115.pdf
Context. A crucial step in the numerical investigation of small-scale dynamos in the solar atmosphere consists of an accurate determination of the magnetic Prandtl number, Prm, stemming from radiative magneto-hydrodynamic (MHD) simulations. Aims. The aims are to provide a reliable methodology for estimating the effective Reynolds and magnetic Reynolds numbers, Re and Rem, and their ratio Prm=Rem/Re (the magnetic Prandlt number), that characterise MHD simulations and to categorise small-scale dynamo simulations in terms of these dimensionless parameters. Methods. The methodology proposed for computing Re and Rem is based on the method of projection on proper elements and it relies on a post-processing step carried out using higher order accurate numerical operators than the ones in the simulation code. A number of radiative MHD simulations with different effective viscosities and plasma resistivities were carried out with the CO5BOLD code, and the resulting growth rate of the magnetic energy and saturated magnetic field strengths were characterised in terms of Re and Rem. Results. Overall, the proposed methodology provides a solid estimate of the dissipation coefficients affecting the momentum and induction equations of MHD simulation codes, and consequently also a reliable evaluation of the magnetic Prandtl number characterising the numerical results. Additionally, it is found that small-scale dynamos are active and can amplify a small seed magnetic field up to significant values in CO5BOLD simulations with a grid spacing smaller than h=12 km, even at Prm=0.65. However, it is also evident that it is difficult to categorise dynamo simulations in terms of Prm alone, because it is not only important to estimate the amplitude of the dissipation coefficients, but also at which scales energy dissipation takes place.

The Dispersion Relation for Waves in a Magnetic Flux Tube.

Roberts, B.
Sol Phys 299, 76 (**2024**).
https://doi.org/10.1007/s11207-024-02320-z
https://link.springer.com/content/pdf/10.1007/s11207-024-02320-z.pdf

A recent discussion (Yelagandula, 2023) of waves in a magnetic flux tube questions the use of the normal velocity continuity condition in the derivation of the standard dispersion relation. We re-assert this condition here.

The SPASE Data Model: A Metadata Standard for Registering, Finding, Accessing, and Using Heliophysics Data Obtained From Observations and Modeling

D. Aaron **Roberts**, James Thieman, Vincent Génot, Todd King, Michel Gangloff, Chris Perry, Chiu Wiegand , Darren De Zeeuw, Shing F. Fung, Baptiste Cecconi, Sébastien Hess

Space Weather **2018**

sci-hub.tw/10.1029/2018SW002038

The Space Physics Archive Search and Extract Consortium has developed and implemented the SPASE Data Model that provides a common language for registering a wide range of Heliophysics data and other products. The Data Model enables discovery and access tools such that any researcher can obtain data easily, thereby facilitating research, including on space weather. The Data Model includes descriptions of Simulation Models and Numerical Output, pioneered by the Integrated Medium for Planetary Exploration (IMPEx) group in Europe, and subsequently adopted by the Community Coordinated Modeling Center (CCMC). The SPASE group intends to register all relevant Heliophysics data resources, including space-, ground-, and model-based. Substantial progress has been made, especially for space-based observational data and associated observatories, instruments, and display data. Legacy product registrations and access go back more than 50 years. Real-time data will be included. The National Aeronautics and Space Administration (NASA) portion of the SPASE group has funding that assures continuity in the upkeep of the Data Model and aids with adding new products. Tools are being developed for making and editing data descriptions. Digital Object Identifiers (DOIs) for Data Products can now be included in the descriptions. The data access that SPASE facilitates is becoming more uniform, and work is progressing on Web Service access via a standard Application Programming Interface. The SPASE Data Model is stable; changes over the past 9 years were additions of terms and capabilities that are backward compatible. This paper provides a summary of the history, structure, use, and future of the SPASE Data Model.

Quiet Sun flux rope formation via incomplete Taylor relaxation

Rebecca **Robinson**, Guillaume Aulanier, Mats Carlsson

A&A **2023**

https://arxiv.org/pdf/2303.11738.pdf

Low-altitude twisted magnetic fields may be relevant to atmospheric heating in the quiet Sun, but the exact role, topology, and formation of these twisted fields remains to be studied. We investigate the formation and evolution of a preflare flux rope in a stratified, 3D MHD simulation. One puzzle is that this modelled flux rope does not form by the usual mechanisms at work in larger flares such as flux emergence, flux cancellation, or tether-cutting. Using Lagrangian markers to trace representative field lines, we follow the spatiotemporal evolution of the flux rope. We isolate flux bundles associated with reconnecting field line pairs by focusing on thin current sheets within the flux system. We also analyze the time-varying distribution of the force-free parameter as the rope relaxes. Lastly, we compare different seeding methods for magnetic fields and discuss their relevance. We show that the modeled flux rope is gradually built from coalescing, current-carrying flux tubes. This occurs through a series of component reconnections that are driven by flows in the underlying convection zone. These reconnections lead to an inverse cascade of helicity from small to larger scales. We also find that the system attempts to relax toward a linear force-free field, but that the convective drivers and eventual nanoflare prevent full relaxation. Using a self-consistently driven simulation of a nanoflare event, we show for the first time an inverse helicity cascade tending toward a Taylor relaxation in the Sun's corona, resulting in a well-ordered flux rope that later reconnects with surrounding fields. This provides clues toward understanding the buildup of nanoflare events in the quiet Sun through incomplete Taylor relaxations when no flux emergence or cancellation is observed.

From incoherent field to coherent reconnection: understanding convection-driven coronal heating in the quiet Sun

Rebecca **Robinson**, Mats Carlsson, Guillaume Aulanier

A&A 668, A177 **2022**

https://arxiv.org/pdf/2211.08364.pdf

https://doi.org/10.1051/0004-6361/202244750

https://www.aanda.org/articles/aa/pdf/2022/12/aa44750-22.pdf

Magnetic reconnection in the quiet Sun is a phenomenon that is consistently observed, and it has recently become feasible to simulate via 3D numerical models of realistically stratified and convection-driven reconnection. We aim to illustrate ways by which quiet Sun fields may contribute to solar atmospheric heating via magnetic reconnection that is driven by convective motion. We also aim to compare our stratified model to earlier idealized coronal models in terms of reconnection drivers and topological conditions. We analyzed a simulation of the quiet Sun in which a complex coronal magnetic field is self-consistently driven by the underlying convection. We employed a selection of Lagrangian markers to trace the spatiotemporal behavior of specific magnetic features that are relevant to

magnetic reconnection and atmospheric heating. A large-scale reconnection-driven heating event occurs in the simulated corona, in a flattened X-shaped feature characterized by a weak field and high current. Relevant features include a smooth overlying horizontal field, an arcade, and a horizontal flux rope which eventually reconnect with the overlying field, raising coronal plasma temperatures up to 1.47 MK. We find that our results are in good agreement with idealized coronal flare models, which demonstrates that the same physical concepts are valid. We also find that the reconnecting flux rope and arcade are neither formed by any obvious coherent flux emergence, nor by any ordered photospheric motion or flux cancellation. Instead, they seem to develop merely from the self-consistent convective driving of pre-existing tangled field lines. This gradual ordering suggests an inverse cascade of magnetic helicity via smaller reconnection events, located at or above photospheric flux concentrations. We suggest that this case is representative of heating events that may be ubiquitous in the real quiet Sun.

Chromospheric observations and magnetic configuration of a supergranular structure

Carolina **Robustini**, Sara Esteban Pozuelo, Jorrit Leenaarts, Jaime de la Cruz Rodrìguez
A&A 621, A6 (**2019**)
https://arxiv.org/pdf/1810.10762.pdf

Unipolar magnetic regions are often associated with supergranular cells. The chromosphere above these regions is regulated by the magnetic field, but the field structure is poorly known. In unipolar regions, the fibrillar arrangement does not always coincide with magnetic field lines, and polarimetric observations are needed to establish the chromospheric magnetic topology. In an active region close to the limb, we observed a unipolar annular network of supergranular size. This supergranular structure harbours a radial distribution of the fibrils converging towards its centre. We observed this structure at different heights by taking data in the FeI 6301-6302 {\AA}, H-\alpha, CaII 8542 \AA\ and the CaII H&K spectral lines with the CRISP and CHROMIS instruments at the Swedish 1-m Solar Telescope. We performed Milne-Eddington inversions of the spectropolarimetric data of FeI and applied the weak field approximation to CaII 8542 \AA\ data to retrieve the magnetic field in the photosphere and chromosphere. We used magnetograms of CRISP, HINODE/SP and HMI to calculate the magnetic flux. We investigated the velocity using the line-of-sight velocities computed from the Milne-Eddington inversion and from Doppler shift of the K3 feature in the CaII K spectral line. To describe the typical spectral profiles characterising the chromosphere above the supergranular structure, we performed a K-mean clustering of the spectra in CaIIK. The photospheric magnetic flux is not balanced. The magnetic field vector at chromospheric heights, retrieved by the weak field approximation, indicates that the field lines within the supegranular cell tend to point inwards, and might form a canopy above the unipolar region. In the centre of the supergranular cell hosting the unipolar region, we observe a persistent chromospheric brightening coinciding with a strong gradient in the line-of-sight velocity. **2017 April 20**

The Solar Orbiter EUI instrument: The Extreme Ultraviolet Imager

P. **Rochus**1, F. Auchère2, D. Berghmans3, L. Harra4, W. Schmutz5 ….
A&A 642, A8 (**2020**)
https://doi.org/10.1051/0004-6361/201936663
https://www.aanda.org/articles/aa/pdf/2020/10/aa36663-19.pdf

Context. The Extreme Ultraviolet Imager (EUI) is part of the remote sensing instrument package of the ESA/NASA Solar Orbiter mission that will explore the inner heliosphere and observe the Sun from vantage points close to the Sun and out of the ecliptic. Solar Orbiter will advance the “connection science” between solar activity and the heliosphere.
Aims. With EUI we aim to improve our understanding of the structure and dynamics of the solar atmosphere, globally as well as at high resolution, and from high solar latitude perspectives.
Methods. The EUI consists of three telescopes, the Full Sun Imager and two High Resolution Imagers, which are optimised to image in Lyman-α and EUV (17.4 nm, 30.4 nm) to provide a coverage from chromosphere up to corona. The EUI is designed to cope with the strong constraints imposed by the Solar Orbiter mission characteristics. Limited telemetry availability is compensated by state-of-the-art image compression, onboard image processing, and event selection. The imposed power limitations and potentially harsh radiation environment necessitate the use of novel CMOS sensors. As the unobstructed field of view of the telescopes needs to protrude through the spacecraft’s heat shield, the apertures have been kept as small as possible, without compromising optical performance. This led to a systematic effort to optimise the throughput of every optical element and the reduction of noise levels in the sensor.
Results. In this paper we review the design of the two elements of the EUI instrument: the Optical Bench System and the Common Electronic Box. Particular attention is also given to the onboard software, the intended operations, the ground software, and the foreseen data products.
Conclusions. The EUI will bring unique science opportunities thanks to its specific design, its viewpoint, and to the planned synergies with the other Solar Orbiter instruments. In particular, we highlight science opportunities brought by the out-of-ecliptic vantage point of the solar poles, the high-resolution imaging of the high chromosphere and corona, and the connection to the outer corona as observed by coronagraphs.

Resonant Instability of Kink Oscillations in Magnetic Flux Tubes with Siphon Flow

Michael S. **Ruderman** & Nikolai S. Petrukhin
Solar Physics volume 296, Article number: 106 (**2021**)
https://link.springer.com/content/pdf/10.1007/s11207-021-01842-0.pdf
https://doi.org/10.1007/s11207-021-01842-0
We study kink oscillations of a straight magnetic tube in the presence of siphon flows. The tube consists of a core and a transitional or boundary layer. The flow velocity is parallel to the tube axis, has constant magnitude, and confined in the tube core. The plasma density is constant in the tube core and it monotonically decreases in the transitional layer to its value in the surrounding plasma. We use the expression for the decrement/increment previously obtained by Ruderman and Petrukhin (Astron. Astrophys. 631, A31, 2019) to study the damping and resonant instability of kink oscillations. We show that, depending on the magnitude of siphon-velocity, resonant absorption can cause either the damping of kink oscillations or their enhancement. There are two threshold velocities: When the flow velocity is below the first threshold velocity, kink oscillations damp. When the flow velocity is above the second threshold velocity, the kink oscillation amplitudes grow. Finally, when the flow velocity is between the two threshold velocities, the oscillation amplitudes do not change. We apply the theoretical result to kink oscillations of prominence threads. We show that, for particular values of thread parameters, resonant instability can excite these kink oscillations.

A method for global inversion of multi-resolution solar data
Jaime de la Cruz **Rodríguez**
A&A 631, A153 (**2019**)
https://doi.org/10.1051/0004-6361/201936635
Understanding the complex dynamics and structure of the upper solar atmosphere strongly benefits from the use of a combination of several diagnostics. Frequently, such diverse diagnostics can only be obtained from telescopes and/or instrumentation operating at widely different spatial resolution. To optimize the utilization of such data, we propose a new method for the global inversion of data acquired at different spatial resolution. The method has its roots in the Levenberg-Marquardt algorithm but involves the use of linear operators to transform and degrade the synthetic spectra of a highly resolved guess model to account for the effects of spatial resolution, data sampling, alignment, and image rotation of each of the datasets. We have carried out a list of numerical experiments to show that our method allows for the extraction of spatial information from two simulated datasets that have gone through two different telescope apertures and that are sampled in different spatial grids. Our results show that each dataset contributes in the inversion by constraining information at the spatial scales that are present in each of the datasets, and no negative effects are derived from the combination of multiple resolution data. This method is especially relevant for chromospheric studies that attempt to combine datasets acquired with different telescopes and/or datasets acquired at different wavelengths. The techniques described in the present study will also help to address the ever increasing resolution gap between space-borne missions and forthcoming ground-based facilities.

Radiative diagnostics in the solar photosphere and chromospheres **Review**
Jaime de la Cruz **Rodríguez**, Michiel van Noort
Space Science Reviews **2016**
http://arxiv.org/pdf/1609.08324v1.pdf
Magnetic fields on the surface of the Sun and stars in general imprint or modify the polarization state of the electromagnetic radiation that is leaving from the star. The inference of solar/stellar magnetic fields is performed by detecting, studying and modeling polarized light from the target star. In this review we present an overview of techniques that are used to study the atmosphere of the Sun, and particularly those that allow to infer magnetic fields. We have combined a small selection of theory on polarized radiative transfer, inversion techniques and we discuss a number of results from chromospheric inversions.

Ionospheric Disturbances and Their Impact on IPS Using MEXART Observations
M. **Rodríguez-Martínez**, H. R. Pérez-Enríquez, A. Carrillo-Vargas…
Solar Physics, July **2014**, Volume 289, Issue 7, pp 2677-2695
We study the impact of ionospheric disturbances on the Earth's environment caused by the solar events that occurred from **20 April to 31 May 2010**, using observations from the Mexican Array Radio Telescope (MEXART). During this period of time, several astronomical sources presented fluctuations in their radio signals. Wavelet analysis, together with complementary information such as the vertical total electron content (vTEC) and the Dst index, were used to identify and understand when the interplanetary scintillation (IPS) could be contaminated by ionospheric disturbances (IOND). We find that radio signal perturbations were sometimes associated with IOND and/or IPS fluctuations; however, in some cases, it was not possible to clearly identify their origin. Our Fourier and

wavelet analyses showed that these fluctuations had frequencies in the range ≈ 0.01 Hz – ≈ 1.0 Hz (periodicities of 100 s to 1 s).

Neutrons and energetic charged particles in the inner heliosphere: Measurements of the MESSENGER neutron spectrometer from 0.3 to 0.85 AU†

Douglas J. **Rodgers**1,*, David J. Lawrence1, William C. Feldman2 andPatrick N. Peplowski
JGR **201**4
http://onlinelibrary.wiley.com/doi/10.1002/2014JA020263/pdf
Energetic charged particle and neutron data from the Neutron Spectrometer (NS) on board the MErcury Surface, Space ENvironment, GEochemistry, and Ranging (MESSENGER) spacecraft have been acquired for solar distances ranging from 0.3 to 0.85 AU. The NS is sensitive to ions with energies greater than 120 MeV/nucleon and has made the first measurements of these energetic ions in the inner heliosphere since the mid 1970s. The high-energy ion measurements are well correlated with Earth-based neutron monitor measurements, which themselves provide a measure of the solar modulation of galactic cosmic rays (GCR). These measurements provide an explicit demonstration of the expected GCR solar modulation for solar distances to 0.3 AU. These NS data also represent the first interplanetary neutron measurements in the inner heliosphere. The time variability of the neutron measurements are driven by two primary effects: time variable production of neutrons from GCRs interacting with local spacecraft material and small count rate changes due to temperature-driven gain changes in the NS instrument. When these time-dependent variations are removed from the neutron measurements, there is no statistically significant variation of neutron count rates versus solar distance. These data are used to derive an upper limit on solar neutron production of 1024 neutrons[0.5<E<9 MeV]•sr-1•s-1 during quiescent periods.

Predicting Solar Cycle 26 Using the Polar Flux as a Precursor, Spectral Analysis, and Machine Learning: Crossing a Gleissberg Minimum?.

Rodríguez, JV., Sánchez Carrasco, V.M., Rodríguez-Rodríguez, I. et al.
Sol Phys 299, 117 (**2024**).
https://doi.org/10.1007/s11207-024-02361-4
https://link.springer.com/content/pdf/10.1007/s11207-024-02361-4.pdf
This study introduces a novel method for predicting the sunspot number (SN) of Solar Cycles 25 (the current cycle) and 26 using multivariate machine-learning techniques, the Sun's polar flux as a precursor parameter, and the fast Fourier transform to conduct a spectral analysis of the considered time series. Using the 13-month running average of the version 2 of the SN provided by the World Data Center—SILSO, we are thus able to present predictive results for the SN until January 2038, giving maximum peak values of 131.4 (in July 2024) and 121.2 (in September 2034) for Solar Cycles 25 and 26, respectively, with a root mean square error of 10.0. These predicted dates are similar to those estimated for the next two polar flux polarity reversals (April 2024 and August 2034). Furthermore, the values for the SN maxima of Solar Cycles 25 and 26 have also been forecasted based on the known correlation between the absolute value of the difference between the polar fluxes of both hemispheres at an SN minimum and the maximum SN of the subsequent cycle, obtaining similar values to those achieved with the previous method: 142.3 ± 34.2 and 126.9 ± 34.2 for Cycles 25 and 26, respectively. Our results suggest that Cycle 25 will have a maximum amplitude that lies below the average and Cycle 26 will reach an even lower peak. This suggests that Solar Cycles 24 (with a peak of 116.4), 25, and 26 would belong to a minimum of the centennial Gleissberg cycle, as was the case in the final years of the 19th and the early 20th centuries (Solar Cycles 12, 13, and 14).

Hemispheric Sunspot Number Prediction for Solar Cycles 25 and 26 Using Spectral Analysis and Machine Learning Techniques.

Rodríguez, JV., Sánchez Carrasco, V.M., Rodríguez-Rodríguez, I. et al.
Sol Phys 299, 116 (**2024**).
https://doi.org/10.1007/s11207-024-02363-2
https://link.springer.com/content/pdf/10.1007/s11207-024-02363-2.pdf
The present study uses machine learning and time series spectral analysis to develop a novel technique to forecast the sunspot number (SN) in both hemispheres for the remainder of Solar Cycle 25 and Solar Cycle 26. This enables us to offer predictions for hemispheric SN until January 2038 (using the 13-month running average). For the Northern hemisphere, we find maximum peak values for Solar Cycles 25 and 26 of 58.5 in April 2023 and 51.5 in November 2033, respectively (root mean square error of 6.1). For the Southern hemisphere, the predicted maximum peak values for Solar Cycles 25 and 26 are 77.0 in September 2024 and 70.1 in November 2034, respectively (root mean square error of 6.8). In this sense, the results presented here predict a Southern hemisphere prevalence over the Northern hemisphere, in terms of SN, for Solar Cycles 25 and 26, thus continuing a trend that began around 1980, after the last period of Northern hemisphere prevalence (which, in turn, started around 1900). On the other hand, for both hemispheres, our findings predict lower maxima for Solar Cycles 25 and 26 than the preceding cycles. This fact implies that, when predicting the total SN as the sum of the two hemispheric forecasts, Solar Cycles 24 – 26 may be

part of a centennial Gleissberg cycle's minimum, as was the case in the final years of the 19th century and the start of the 20th century (Solar Cycles 12, 13, and 14).

A method for global inversion of multi-resolution solar data

J. de la Cruz **Rodríguez**
A&A **2019**
https://arxiv.org/pdf/1909.02604.pdf
Understanding the complex dynamics and structure of the upper solar atmosphere benefits strongly from the use of a combination of several diagnostics. Frequently, such diverse diagnostics can only be obtained from telescopes and/or instrumentation operating at widely different spatial resolution. To optimize the utilization of such data, we propose a new method for the global inversion of data acquired at different spatial resolution. The method has its roots in the Levenberg-Marquardt algorithm but involves the use of linear operators to transform and degrade the synthetic spectra of a highly resolved guess model to account for the the effects of spatial resolution, data sampling, alignment and image rotation of each of the data sets. We have carried out a list of numerical experiments to show that our method allows extracting spatial information from two simulated datasets that have gone through two different telescope apertures and that are sampled in different spatial grids. Our results show that each dataset contributes in the inversion by constraining information at the spatial scales that are present in each of the datasets, without any negative effects derived from the combination of multiple resolution data. This method is especially relevant for chromospheric studies that attempt at combining datasets acquired with different telescopes and/or datasets acquired at different wavelengths, both limiting factors in the resolution of solar instrumentation. The techniques described in the present study will also help addressing the ever increasing resolution gap between space-borne missions and forthcoming ground-based facilities**. 2016-09-14**

Emergence of granular-sized magnetic bubbles through the solar atmosphere. II. Non-LTE chromospheric diagnostics and inversions

Jaime de la Cruz **Rodríguez**, Viggo Hansteen, Luis Bellot-Rubio, Ada Ortiz
ApJ **2015**
http://arxiv.org/pdf/1503.03846v1.pdf
Magnetic flux emergence into the outer layers of the Sun is a fundamental mechanism for releasing energy into the chromosphere and the corona. In this paper, we study the emergence of granular-sized flux concentrations and the structuring of the corresponding physical parameters and atmospheric diagnostics in the upper photo- sphere and in the chromosphere. We make use of a realistic 3D MHD simulation of the outer layers of the Sun to study the formation of the Ca II 8542 line. We also derive semi-empirical 3D models from non-LTE inversions of our observations. These models contain depth-dependent information of the temperature and line-of-sight stratification. Our analysis explains the peculiar Ca II 8542 profiles observed in the flux-emerging region. In addition, we derive detailed temperature and velocity maps describing the ascent of magnetic bubbles from the photosphere to the chromosphere. The inversions suggest that, in active regions, granular-sized bubbles emerge up to the lower chromosphere where the existing large-scale field hinders their ascent. We report hints of heating when the field reaches the chromosphere**. 2009-07-05**

The Plasma β in quiet Sun Regions: Multi-Instrument View

Jenny M. **Rodríguez-Gómez**, Christoph Kuckein, Sergio J. Gonzalez Manrique, Jonas Saqri, Astrid Veronig, Peter Gomöry, Tatiana Podladchikova
2024
https://arxiv.org/ftp/arxiv/papers/2402/2402.00204.pdf
A joint campaign of several space-borne and ground-based observatories, such as the GREGOR solar telescope, the Extreme-ultraviolet Imaging Spectrometer (EIS), and the Interface Region Imaging Spectrograph (Hinode Observing Plan 381, 11-22 October 2019) was conducted to investigate the plasma β in quiet sun regions. In this work, we focus on **October 13, 17, and 19, 2019**, to obtain the plasma β at different heights through the solar atmosphere based on multi-height observational data. We obtained temperature, density and magnetic field estimates from the GREGOR High-resolution Fast Imager (HiFI), and Infrared Spectrograph (GRIS), IRIS, EIS and complementary data from SDO/AIA. Using observational data and models (e.g., FALC and PFSS), we determined the plasma β in the photosphere, chromosphere, transition region and corona. The obtained plasma β values lie inside the expected ranges through the solar atmosphere. However, at EIS and AIA coronal heights (from 1.03 $R_\odot$ to 1.20 $R_\odot$) plasma β values appear in the limit defined by Gary (2001); such behavior was previously reported by Rodríguez Gómez et al. (2019). Additionally, we obtained the plasma β in the solar photosphere at different optical depths from log τ=−1.0 to log τ=−2.0. These values decrease with optical depth. This work provides a complete picture of plasma β in quiet sun regions through the solar atmosphere, which is a pre-requisite of a better understanding of the plasma dynamics at the base of the solar corona.

Turbulent transport of radiation in the solar convective zone

I. **Rogachevskii**, N. Kleeorin

MNRAS Volume 508, Issue 1, Pages 1296–1304 **2021**

https://arxiv.org/pdf/2108.12767.pdf

https://doi.org/10.1093/mnras/stab2595

A turbulent transport of radiation in the solar convective zone is investigated. The mean-field equation for the irradiation intensity is derived. It is shown that due to the turbulent effects, the effective penetration length of radiation can be increased in several times in comparison with the mean penetration length of radiation (defined as an inverse mean absorption coefficient). Using the model of the solar convective zone based on the mixing length theory, where the mean penetration length of radiation is usually much smaller than the turbulent correlation length, it is demonstrated that the ratio of the effective penetration length to the mean penetration length of radiation increases in 2.5 times in the vicinity of the solar surface. The main reason are the compressibility effects that become important in the vicinity of the solar surface where temperature and density fluctuations increase towards the solar surface, enhancing fluctuations of the radiation absorption coefficient and increasing the effective penetration length of radiation.

Lifetimes and Rotation within the Solar Mean Magnetic Field

Eddie **Ross**, William J. Chaplin, Steven J. Hale, Rachel Howe, Yvonne P. Elsworth, Guy R. Davies, Martin Bo Nielsen

MNRAS **2021**

https://arxiv.org/pdf/2102.04743.pdf

We have used very high-cadence (sub-minute) observations of the solar mean magnetic field (SMMF) from the Birmingham Solar Oscillations Network (BiSON) to investigate the morphology of the SMMF. The observations span a period from 1992--2012, and the high-cadence observations allowed the exploration of the power spectrum up to frequencies in the mHz range. The power spectrum contains several broad peaks from a rotationally-modulated (RM) component, whose linewidths allowed us to measure, for the first time, the lifetime of the RM source. There is an additional broadband, background component in the power spectrum which we have shown is an artefact of power aliasing due to the low fill of the data. The sidereal rotation period of the RM component was measured as 25.23±0.11 days and suggests that the signal is sensitive to a time-averaged latitude of ∼12∘. We have also shown the RM lifetime to be 139.6±18.5 days. This provides evidence to suggest the RM component of the SMMF is connected to magnetic flux concentrations (MFCs) and active regions (ARs) of magnetic flux, based both on its lifetime and location on the solar disc.

The behaviour of galactic cosmic ray intensity during solar activity cycle 24

Eddie **Ross**, William J. Chaplin

Solar Phys. 294:8 **2019**

https://arxiv.org/pdf/1812.02125.pdf

https://link.springer.com/content/pdf/10.1007%2Fs11207-019-1397-7.pdf

We have studied long-term variations of galactic cosmic ray (GCR) intensity in relation to the sunspot number (SSN) during the most recent solar cycles. This study analyses the time-lag between the GCR intensity and SSN, and hysteresis plots of the GCR count rate against SSN for solar activity cycles 20-23 to validate a methodology against previous results in the literature, before applying the method to provide a timely update on the behaviour of cycle 24. Cross-plots of SSN vs GCR show a clear difference between the odd-numbered and even-numbered cycles. Linear and elliptical models have been fit to the data with the linear fit and elliptical model proving the more suitable model for even-numbered and odd-numbered solar activity cycles respectively, in agreement with previous literature. Through the application of these methods for the 24th solar activity cycle, it has been shown that cycle 24 experienced a lag of 2-4 months and follows the trend of the preceding activity cycles albeit with a slightly longer lag than previous even-numbered cycles. It has been shown through the hysteresis analysis that the linear fit is a better representative model for cycle 24, as the ellipse model doesn't show a significant improvement, which is also in agreement with previous even-numbered cycles.

On the Detectability of Large-Scale Flows by Asteroseismology **Review**

Markus **Roth*** and Wiebke Herzberg

Front. Astron. Space Sci., 16 October **2020** |

https://doi.org/10.3389/fspas.2020.515227

https://www.frontiersin.org/articles/10.3389/fspas.2020.515227/full

Large-scale convective motions are an integral part of stellar interior dynamics and might play a relevant role in stellar dynamo processes. However, they are difficult to detect or characterize. Stellar oscillations are affected by convective flows due to advection. For the Sun, forward calculations of the advective effect of flows on oscillation modes have already been conducted, but the effect has not yet been examined for other types of stars. Suitable

candidates are subgiant or red giant stars, since they possess extensive outer convection zones, which likely feature large-scale flow cells with strong flow velocities. We investigate the effects of large-scale flows on oscillation modes of subgiant stars by means of forward calculations based on an exemplary subgiant stellar model. We focus in particular on non-axisymmetric cell formations, also referred to as giant cells. The effects are described in the non-rotating and the rotating case. By solving the forward problem, we evaluate, if large-scale flow cells lead to signatures in asteroseismic data that are suitable for the detection of such flows. The influence of flows is calculated by employing perturbation theory as proposed by Lavely and Ritzwoller (1992), where the flow is treated as a perturbation of a 1D equilibrium stellar model. The presence of a flow leads to a coupling of the modes, which results in frequency shifts and a mixing of the mode eigenfunctions. For a non-rotating star, non-axisymmetric flows lead to degeneracies between coupling modes, which cause an asymmetry in the frequency shifts of modes of opposite azimuthal order. If rotation is included, the degeneracy is lifted in first order, but residual degenerate coupling and third order effects can still lead to asymmetries, depending on whether the modes are of p- or of g-type. For rotating stars, the mode mixing induced by non-axisymmetric flows causes the observational signal of a perturbed mode to be multiperiodic, which becomes visible in the power spectrum. An expression for the amplitudes of the signal's different components is derived.

Verification of the helioseismic Fourier-Legendre analysis for meridional flow measurements

Markus **Roth**, Hans-Peter Doerr, Thomas Hartlep
A&A 592, A106 **2016**
http://arxiv.org/pdf/1606.05202v1.pdf
Measuring the Sun's internal meridional flow is one of the key issues of helioseismology. Using the Fourier-Legendre analysis is a technique for addressing this problem. We validate this technique with the help of artificial helioseismic data. The analysed data set was obtained by numerically simulating the effect of the meridional flow on the seismic wave field in the full volume of the Sun. In this way, a 51.2-hour long time series was generated. The resulting surface velocity field is then analyzed in various settings: Two 360◦×90◦ halfspheres, two 120◦×60◦ patches on the front and farside of the Sun (North and South, respectively) and two 120◦×60◦ patches on the northern and southern frontside only. We compare two possible measurement setups: observations from Earth and from an additional spacecraft on the solar farside, and observations from Earth only, in which case the full information of the global solar oscillation wave field was available. We find that, with decreasing observing area, the accessible depth range decreases: the 360◦×90◦ view allows us to probe the meridional flow almost to the bottom of the convection zone, while the 120◦×60◦ view means only the outer layers can be probed. These results confirm the validity of the Fourier-Legendre analysis technique for helioseismology of the meridional flow. Furthermore these flows are of special interest for missions like Solar Orbiter that promises to complement standard helioseismic measurements from the solar nearside with farside observations.

Photospheric downflows observed with SDO/HMI, HINODE, and an MHD simulation

T. **Roudier**, M. Švanda, J. M. Malherbe, J. Ballot, D. Korda, Z. Frank
A&A **2021**
https://arxiv.org/pdf/2103.03077.pdf
Downflows on the solar surface are suspected to play a major role in the dynamics of the convection zone. We investigate the existence of the long-lasting downflows whose effects influence the interior of the Sun and the outer layers. We study the sets of Dopplergrams and magnetograms observed with SDO and Hinode spacecrafts and a MHD simulation. All of the aligned sequences, which were corrected from the satellite motions and tracked with the differential rotation, were used to detect the long-lasting downflows in the quiet-Sun at the disc centre. To learn about the structure of the flows below the solar surface, the time-distance local helioseismology was used.
The inspection of the 3D data cube (x, y, t) of the 24-hour Doppler sequence allowed us to detect 13 persistent downflows. Their lifetimes lie in the range between 3.5 and 20 hours with sizes between 2" and 3" and speeds between -0.25 and -0.72 km/s. These persistent downflows are always filled with the magnetic field with an amplitude of up to 600 G. The helioseismic inversion allows us to describe the persistent downflows and compare them to the other (non-persistent) downflows in the field of view. The persistent downflows seem to penetrate much deeper and, in the case of a well-formed vortex, the vorticity keeps its integrity to the depth of about 5 Mm. In the MHD simulation, only sub-arcsecond downflows are detected with no evidence of a vortex comparable in size to observations at the surface of the Sun.
The long temporal sequences from the space-borne allow us to show the existence of long-persistent downflows together with the magnetic field. They penetrate inside the Sun but are also connected with the anchoring of coronal loops in the photosphere, indicating a link between downflows and the coronal activity. A link suggests that EUV cyclones over the quiet Sun could be an effective way to heat the corona. **2–3 November 2010., 29 November 2018**

Photospheric downflows observed with SDO/HMI, HINODE, and an MHD simulation

T. **Roudier**1, M. Švanda2,3, J. M. Malherbe4,5, J. Ballot1, D. Korda2 and Z. Frank6
A&A 647, A178 (**2021**)
https://www.aanda.org/articles/aa/pdf/2021/03/aa40172-20.pdf
Downflows on the solar surface are suspected to play a major role in the dynamics of the convection zone, at least in its outer part. We investigate the existence of the long-lasting downflows whose effects influence the interior of the Sun but also the outer layers. We study the sets of Dopplergrams and magnetograms observed with Solar Dynamics Observatory and Hinode spacecrafts and an magnetohydrodynamic (MHD) simulation. All of the aligned sequences, which were corrected from the satellite motions and tracked with the differential rotation, were used to detect the long-lasting downflows in the quiet-Sun at the disc centre. To learn about the structure of the flows below the solar surface, the time-distance local helioseismology was used. The inspection of the 3D data cube (x, y, t) of the 24 h Doppler sequence allowed us to detect 13 persistent downflows. Their lifetimes lie in the range between 3.5 and 20 h with a sizes between 2″ and 3″ and speeds between −0.25 and −0.72 km s−1. These persistent downflows are always filled with the magnetic field with an amplitude of up to 600 Gauss. The helioseismic inversion allows us to describe the persistent downflows and compare them to the other (non-persistent) downflows in the field of view. The persistent downflows seem to penetrate much deeper and, in the case of a well-formed vortex, the vorticity keeps its integrity to the depth of about 5 Mm. In the MHD simulation, only sub-arcsecond downflows are detected with no evidence of a vortex comparable in size to observations at the surface of the Sun. The long temporal sequences from the space-borne allows us to show the existence of long-persistent downflows together with the magnetic field. They penetrate inside the Sun but are also connected with the anchoring of coronal loops in the photosphere, indicating a link between downflows and the coronal activity. A links suggests that EUV cyclones over the quiet Sun could be an effective way to heat the corona. **2−3 November 2010, 29 November 2018**

Evolution of exploding granules from coordinated observations by THEMIS, IRIS, SDO/HMI, and HINODE, and a simulation

T. **Roudier**, J.M. Malherbe, B. Gelly, R. Douet, Z. Frank, K. Dalmasse
A&A 641, A50 **2020**
https://arxiv.org/ftp/arxiv/papers/2007/2007.12438.pdf
https://www.aanda.org/articles/aa/pdf/2020/09/aa38132-20.pdf
Exploding granules constitute the strongest horizontal flows on the quiet Sun and contribute to the structure of the surface horizontal velocity fields which build the large-scale organization of the discrete magnetic field. In this work we explore exploding granule expansion through the observations of the ground-based THEMIS telescope, IRIS, SDO, and the Hinode space-borne instruments, and finally with the magnetohydrodynamics simulation. We evaluate the detection and the expansion of exploding granules at several wavelengths and at various spatial and temporal resolutions. To analyze the different temporal sequences, two methods of image segmentation are applied to select the granules. The first allows us to follow individually the exploding granules observed simultaneously by THEMIS, IRIS, and SDO. The second uses long time independent sequences from THEMIS, IRIS, SDO, Hinode, and a simulation. In the first method (called manual) the segmentation isolates the cell of the granules (bright granules and intergranular parts), while in the second method (called statistical) only the bright part of the granules are isolated. The results obtained with simultaneous or distinct temporal observations using the two methods of segmentation are in good agreement. The granule area evolves linearly with an expansion velocity that decreases with the radius. A rapid decrease in the velocity expansion in the first two minutes is observed. The detection and measurement of the dynamics of the explosive granules can be performed from ground- and space-based instruments. Our work reveals the usefulness of SDO data, with low spatial resolution, to study the dynamics of the exploding granules all over the solar surface. **9-14 Sep 2019**

Link between trees of fragmenting granules and deep downflows in MHD simulation

T. **Roudier**, J.M. Malherbe, R. F. Stein, Z.Frank
A&A 622, A112 **2019**
https://arxiv.org/pdf/1901.03255.pdf
Trees of fragmenting granules (TFG) and associated flows are suspected to playa major role in the formation of the network in the quiet Sun. We investigate the counterparts, in terms of dynamics, of surface structures detectable by high resolution observations in deeper layers up to 15 Mm, which are only available from numerical simulations. The first aim is to demonstrate that TFG can be evidenced either from surface intensitites, vertical (Vz), or Doppler (Vdop) velocities. The second is to show that horizontal flows, which are derived from intensities or Vz/Vdop flows, are in good agreement, and that this is the case for observations and numerical simulations. The third objective is to apply this new Vz-based method to a 3D simulation to probe relationships between horizontal surface flows, TFG, and deep vertical motions. The TFG were detected after oscillation filtering of intensities or Vz/Vdop flows, using a segmentation and labelling technique. Surface horizontal flows were derived from local correlation tracking (LCT) and from intensities or Vz/Vdop flows. These methods were applied to Hinode observations, 2D surface results of a first simulation, and 3D Vz data of a second simulation. We find that TFG and horizontal surface flows (provided by the LCT) can be detected either from intensities or Vz/Vdop component, for high resolution observations and

numerical simulations. We apply this method to a 3D run providing the Vz component in depth. This reveals a close relationship between surface TFG (5 Mm mesoscale) and vertical downflows 5 Mm below the surface. We suggest that the dynamics of TFG form larger scales (the 15-20 Mm supergranulation) associated with 15 Mm downflowing cells below the surface. The TFG and associated surface flows seem to be essential to understanding the formation and evolution of the network at the meso and supergranular scale.

Large-scale photospheric motions determined from granule tracking and helioseismology from SDO/HMI data

Th. **Roudier**, M. Svanda, J. Ballot, J.M. Malherbe, M. Rieutord
A&A 611, A92 **2018**
https://arxiv.org/pdf/1712.05255.pdf
Large scale flows in the Sun play an important role in the dynamo process linked to the solar cycle. The important large scale flows are the differential rotation and the meridional circulation with an amplitude of km/s and few m/s , respectively. These flows also have a cycle related components, namely the torsional oscillations. Our attempt is to determine large-scale plasma flows on the solar surface by deriving horizontal flow velocities using the techniques of solar granule tracking, dopplergrams, and time distance helioseismology. Coherent structure tracking (CST) and time distance helioseismology were used to investigate the solar differential rotation and meridional circulation at the solar surface on a 30 day HMI SDO sequence. The influence of a large sunspot on these large scale flows with a specific 7 day HMI SDO sequence has been also studied. The large scale flows measured by the CST on the solar surface and the same flow determined from the same data with the helioseismology in the first 1 Mm below the surface are in good agreement in amplitude and direction. The torsional waves are also located at the same latitudes with amplitude of the same order. We are able to measure the meridional circulation correctly using the CST method with only three days of data and after averaging between + and -15 degrees in longitude. We conclude that the combination of CST and Doppler velocities allows us to detect properly the differential solar rotation and also smaller amplitude flows such as the meridional circulation and torsional waves. The results of our methods are in good agreement with helioseismic measurements.

Dynamics of the photosphere along the solar cycle from SDO/HMI

Th. **Roudier**, J.M. Malherbe, G.M. Mirouh
A&A **2016**
https://arxiv.org/pdf/1611.02152v1.pdf
As the global magnetic field of the Sun has an activity cycle, one expects to observe some variation of the dynamical properties of the flows visible in the photosphere. We investigate the flow field during the solar cycle by analysing SDO/HMI observations of continuum intensity, Doppler velocity and longitudinal magnetic field. We first picked data at disk center during 6 years along the solar cycle with a 48-hour time step in order to study the overall evolution of the continuum intensity and magnetic field. Then we focused on thirty 6-hour sequences of quiet regions without any remnant of magnetic activity separated by 6 months, in summer and winter, when disk center latitude B0 is close to zero. The horizontal velocity was derived from the local correlation tracking technique over a field of view of 216.4Mm x 216.4Mm located at disk center. Our measurements at disk center show the stability of the flow properties between meso- and supergranular scales along the solar cycle. The network magnetic field, produced locally at disk center independently from large scale dynamo, together with continuum contrast, vertical and horizontal flows, seem to remain constant during the solar cycle.

Relation between trees of fragmenting granules and supergranulation evolution

Th. **Roudier**, J.M. Malherbe, M. Rieutord, Z. Frank
A&A 590, A121 **2016**
http://arxiv.org/pdf/1604.04118v1.pdf
Context: The determination of the underlying mechanisms of the magnetic elements diffusion over the solar surface is still a challenge. Understanding the formation and evolution of the solar network (NE) is a challenge, because it provides a magnetic flux over the solar surface comparable to the flux of active regions at solar maximum. Aims: We investigate the structure and evolution of interior cells of solar supergranulation. From Hinode observations, we explore the motions on solar surface at high spatial and temporal resolution. We derive the main organization of the flows inside supergranules and their effect on the magnetic elements. Method: To probe the superganule interior cell, we used the Trees of Fragmenting Granules (TFG) evolution and their relations to horizontal Results: Evolution of TFG and their mutual interactions result in cumulative effects able to build horizontal coherent flows with longer lifetime than granulation (1 to 2 hours) over a scale up to 12\arcsec. These flows clearly act on the diffusion of the intranetwork (IN) magnetic elements and also on the location and shape of the network. Conclusions: From our analysis during 24 hours, TFG appear as one of the major elements of the supergranules which diffuse and advect the magnetic field on the Sun's surface. The strongest supergranules contribute the most to magnetic flux diffusion in the solar photosphere. **29-31 August 2007**

Structure and evolution of solar supergranulation using SDO/HMI data

Th. **Roudier** (1), M. Švanda (2,3), M. Rieutord (1), J.M. Malherbe (4), R. Burston (5), L. Gizon
A&A, 567, A138, **2014**
http://arxiv.org/pdf/1407.0196v1.pdf

Context: Studying the motions on the solar surface is fundamental for understanding how turbulent convection transports energy and how magnetic fields are distributed across the solar surface.
Aims: From horizontal velocity measurements all over the visible disc of the Sun and using data from the Solar Dynamics Observatory/Helioseismic and Magnetic Imager (SDO/HMI), we investigate the structure and evolution of solar supergranulation.
Methods: Horizontal velocity fields were measured by following the proper motions of solar granules using a newly developed version of the coherent structure tracking (CST) code. With this tool, maps of horizontal divergence were computed. We then segmented and identified supergranular cells and followed their histories by using spatio-temporal labelling. With this dataset we derived the fundamental properties of supergranulation, including their motion.
Results: We find values of the fundamental parameters of supergranulation similar to previous studies: a mean lifetime of 1.5 days and a mean diameter of 25~Mm. The tracking of individual supergranular cells reveals the solar differential rotation and a poleward circulation trend of the meridional flow. The shape of the derived differential rotation and meridional flow does not depend on the cell size. If there is a background magnetic field, the diverging flows in supergranules are weaker.
Conclusions: This study confirms that supergranules are suitable tracers that may be used to investigate the large-scale flows of the solar convection as long as they are detectable enough on the surface.

Models and data analysis tools for the Solar Orbiter mission

A. **Rouillard** et al. (MADAWG team)
A&A 642, A2 **2020 (Special issue: The Solar Orbiter Mission)**
https://doi.org/10.1051/0004-6361/201935305
https://www.aanda.org/articles/aa/pdf/forth/aa35305-19.pdf
https://www.aanda.org/articles/aa/pdf/2020/10/aa35305-19.pdf

Context. The Solar Orbiter spacecraft will be equipped with a wide range of remote-sensing (RS) and in-situ (IS) instruments to record novel and unprecedented measurements of the solar atmosphere and the inner heliosphere. To take full advantage of these new datasets, tools and techniques must be developed to ease multi-instrument and multi-spacecraft studies. In particular the currently inaccessible low solar corona below two solar radii can only be observed remotely. Furthermore techniques must be used to retrieve coronal plasma properties in time and in three dimensional (3D) space. Solar Orbiter will run complex observation campaigns that provide interesting opportunities to maximise the likelihood of linking IS data to their source region near the Sun. Several RS instruments can be directed to specific targets situated on the solar disk just days before data acquisition. To compare IS and RS, data we must improve our understanding of how heliospheric probes magnetically connect to the solar disk. Aims. The aim of the present paper is to briefly review how the current modelling of the Sun and its atmosphere can support Solar Orbiter science. We describe the results of a community-led effort by European Space Agency (ESA)'s Modelling and Data Analysis Working Group (MADAWG) to develop different models, tools, and techniques deemed necessary to test different theories for the physical processes that may occur in the solar plasma. The focus here is on the large scales and little is described with regards to kinetic processes. To exploit future IS and RS data fully, many techniques have been adapted to model the evolving 3D solar magneto-plasma from the solar interior to the solar wind. A particular focus in the paper is placed on techniques that can estimate how Solar Orbiter will connect magnetically through the complex coronal magnetic fields to various photospheric and coronal features in support of spacecraft operations and future scientific studies. Methods. Recent missions such as STEREO, provided great opportunities for RS, IS, and multi-spacecraft studies. We summarise the achievements and highlight the challenges faced during these investigations, many of which motivated the Solar Orbiter mission. We present the new tools and techniques developed by the MADAWG to support the science operations and the analysis of the data from the many instruments on Solar Orbiter. Results. This article reviews current modelling and tool developments that ease the comparison of model results with RS and IS data made available by current and upcoming missions. It also describes the modelling strategy to support the science operations and subsequent exploitation of Solar Orbiter data in order to maximise the scientific output of the mission. Conclusions. The on-going community effort presented in this paper has provided new models and tools necessary to support mission operations as well as the science exploitation of the Solar Orbiter data. The tools and techniques will no doubt evolve significantly as we refine our procedure and methodology during the first year of operations of this highly promising mission. **3 June 2008, 2014-08-16**

2. Heritage of the recent STEREO era (Locating coronal and solar wind structures in 3D, Feature tracking and trajectory analysis, Linking CMEs with ICMEs, Linking particle accelerators with SEPs, Linking coronal plasma to the solar wind properties)

Jovian Cosmic-Ray Protons in the Heliosphere: Constraints by Cassini Observations

Elias **Roussos**1, Norbert Krupp1, Konstantinos Dialynas2, Peter Kollmann3, Christopher Paranicas3, Ezequiel Echer4, Donald G. Mitchell3, and Stamatios M. Krimigis2,3

2019 ApJ 871 223

https://doi.org/10.3847/1538-4357/aafb2f

Measurements of >82 MeV Galactic cosmic-ray (GCR) protons at Earth indicate that they may be mixed with protons that leak into the heliosphere from Jupiter's magnetosphere (Jovian cosmic-ray protons (JCRPs)). A ~400 day periodicity in these proton fluxes, which is similar to the synodic period between Jupiter and Earth, and an excess proton flux observed when Jupiter and Earth can be connected through the interplanetary magnetic field were the basis for this claim. Using nearly 13 yr of GCR measurements at Saturn with Cassini's Magnetosphere Imaging Instrument, we show that the ~400 day periodicity is also present in $\gtrsim$100 MeV protons at ~9.6 au, although the synodic period between Saturn and Jupiter is ~20 yr. We also find that the features responsible for this periodicity were convected from 1 au to Saturn's distance with the solar wind velocity. Their origin is therefore heliospheric, not Jovian. We attribute these features to quasi-biennial oscillations, observed in the solar magnetic field and various heliospheric indices. This finding indicates that fluxes of JCRPs at 1 au, if present, are considerably overestimated, because the signal originally attributed to them represents the amplitude of the ~400 day periodic GCR oscillation. This oscillation has to be subtracted before the resulting proton GCR flux residuals are analyzed in the context of a possible Jovian source. A confirmation of the presence of JCRPs over extended regions in the heliosphere and a constraint on their fractional abundance in GCR spectra may therefore require further validation and analysis, and several options are proposed for this purpose.

Exploring the dynamic rotational profile of the hotter solar atmosphere: A multi-wavelength approach using SDO/AIA data

Srinjana **Routh**, Bibhuti Kumar Jha, Dibya Kirti Mishra, Tom Van Doorsselaere, Vaibhav Pant, Subhamoy Chatterjee, Dipankar Banerjee

ApJ **975** 158 **2024**

https://arxiv.org/pdf/2409.03582

https://iopscience.iop.org/article/10.3847/1538-4357/ad7ba2/pdf

Understanding the global rotational profile of the solar atmosphere and its variation is fundamental to uncovering a comprehensive understanding of the dynamics of the solar magnetic field and the extent of coupling between different layers of the Sun. In this study, we employ the method of image correlation to analyze the extensive dataset provided by the Atmospheric Imaging Assembly of the Solar Dynamic Observatory in different wavelength channels. We find a significant increase in the equatorial rotational rate (A) and a decrease in absolute latitudinal gradient (|B|) at all temperatures representative of the solar atmosphere, implying an equatorial rotation up to 4.18% and 1.92% faster and less differential when compared to the rotation rates for the underlying photosphere derived from Doppler measurement and sunspots respectively. In addition, we also find a significant increase in equatorial rotation rate (A) and a decrease in differential nature (|B| decreases) at different layers of the solar atmosphere. We also explore a possible connection from the solar interior to the atmosphere and interestingly found that A at r=0.94R$\odot$,0.965R$\odot$ show an excellent match with 171 Angstrom, 304 Angstrom and 1600 Angstrom, respectively. Furthermore, we observe a positive correlation between the rotational parameters measured from 1600 Angstrom, 131 Angstrom, 193 Angstrom and 211 Angstrom with the yearly averaged sunspot number, suggesting a potential dependence of the solar rotation on the appearance of magnetic structures related to the solar cycle or the presence of cycle dependence of solar rotation in the solar atmosphere.

New Cutoff Frequency for Torsional Alfv'en Waves Propagating along Wide Solar Magnetic flux Tubes

Swati **Routh**, Z.E. Musielak, M.N. Sundar, Sai Sravanthi Joshi, Sree Charan

2020

https://arxiv.org/pdf/2008.03653.pdf

An isolated, isothermal, and wide magnetic flux tube embedded either in the solar chromosphere or in the lower solar corona is considered, and the propagation of linear torsional Alfv'en waves is investigated. It is shown that the wideness of the tube leads to a new cutoff frequency, which is a local quantity that gives the conditions for the wave propagation at different atmospheric heights. The cutoff is used to establish the ranges of frequencies for the propagating and reflected waves in the solar chromosphere and lower solar corona. The obtained results are compared to those previously obtained for thin magnetic flux tubes and the differences are discussed. Moreover, the results are also compared to some current observational data, and used to establish the presence of propagating waves in the data at different atmospheric heights; this has profound implications on the energy and momentum transfer by the waves in the solar atmosphere, and the role of linear torsional Alfv'en waves in the atmospheric heating and wind acceleration.

AI Foundation Model for Heliophysics: Applications, Design, and Implementation

Sujit **Roy**, Talwinder Singh, Marcus Freitag, Johannes Schmude, +++
2024
https://arxiv.org/pdf/2410.10841
Deep learning-based methods have been widely researched in the areas of language and vision, demonstrating their capacity to understand long sequences of data and their usefulness in numerous helio-physics applications. Foundation models (FMs), which are pre-trained on a large-scale datasets, form the basis for a variety of downstream tasks. These models, especially those based on transformers in vision and language, show exceptional potential for adapting to a wide range of downstream applications. In this paper, we provide our perspective on the criteria for designing an FM for heliophysics and associated challenges and applications using the Solar Dynamics Observatory (SDO) dataset. We believe that this is the first study to design an FM in the domain of heliophysics.

Investigation of the Hemispheric Asymmetry in Solar Flare Index During Solar Cycle 21 – 24 from the Kandilli Observatory

Soumya **Roy**, Amrita Prasad, Koushik Ghosh, Subhash Chandra Panja & Sankar Narayan Patra
Solar Physics volume 295, Article number: 100 (**2020**)
https://link.springer.com/content/pdf/10.1007/s11207-020-01656-6.pdf
The hemispheric asymmetry of the solar-flare index during 1976 – 2018 from the Kandilli Observatory is studied in this investigation. The temporal duration covers Solar Cycles 21 – 23 and almost the whole of Solar Cycle 24. Different methodologies, such as cross-correlation analysis, rescaled-range analysis, empirical mode decomposition, and date-compensated discrete Fourier transform, have been used on the hemispheric solar-flare index as well as on absolute asymmetry data to study various inherent characteristics. We observed that: i) the temporal characteristics in the northern and southern hemispheres are different during the progression of a solar cycle; ii) the T-test indicates that Solar Cycles 21 and 23 do not have any dominant hemispheric effect, whereas Solar Cycle 22 and 24 have South-dominated hemispheric characteristics; iii) the southern hemisphere is leading by ten, three, and one months during Solar Cycles 21, 22, and 24, respectively, and for Solar Cycle 23 the hemispheres are in phase; iv) anti-persistence as well as short memory-dependent characteristics are present in both the hemispheric solar-flare index and the absolute asymmetry data; v) all of the time-series data have well-known periods of 11 years and 27 days as well as short-term periods around 7 days and 14 days. Apart from those, several mid-term periodicities such as the Rieger periodicity and quasi-biennial oscillations (QBOs) are also found in both hemispheric solar-flare index as well as absolute asymmetry index data; vi) the Waldmeier effect is also validated using solar-flare-index data. These results will enrich our knowledge about the distribution of hemispheric asymmetry in solar-flare-index data and may reveal some valuable points about asymmetry behaviors.

An outlook on the estimate of the solar quadrupole moment from relativistic gravitation contributions

Jean-Pierre **Rozelot**, Ali Kilcik, Zahra Fazel
2022
https://arxiv.org/ftp/arxiv/papers/2208/2208.06779.pdf
Of all the solar fundamental parameters (mass, diameter, gravity at the surface,...), the gravitational moments have been quite often ignored in the past, mainly due to the great difficulty to get a reliable estimate. Even though the order of magnitude of the solar quadrupole moment J2 is now known to be 10^{-7}, its accurate value is still discussed. Indeed, the expansion in multipoles J(l, l=2,...) of the gravitational potential of a rotating body affects the orbital motion of planets at a relativistic level. We will recall here the recent progresses made in testing General Relativity through the contribution of the first solar quadrupole moment. Using the Eddington-Robertson parameters, we recall the constraints both on a theoretical and experimental point of view. Together with γ, which encodes the amount of curvature of space-time per unit rest-mass, the Post--Newtonian Parameter β contributes to the relativistic precession of planets. The latter parameter encodes the amount of non-linearity in the superposition law of gravitation. Even though in principle, it would be possible to extract J2 from planetary ephemerides, we observe that it is significantly correlated with other solution parameters (semi-major axis of planets, mass of asteroids...). Focusing on the J2 correlations, we show that in general, when $\sim\beta$ and $\sim\gamma$ are freed, the correlations $\sim[\beta,J2]$ and $\sim[\gamma,J2]$ are $\approx 45\%$ and $\approx 55\%$ respectively. Moreover, all the planetary dynamics-based values are biased by the Lense--Thiring effect, which has never been modeled and solved for so far, but can be estimated to $\approx 7\%$. It is thus possible to get a good estimate of the solar quadrupole moment: $1.66\times10^{-7} \leq J2 \leq 2.32\times10^{-7}$.

How big is the Sun: Solar diameter changes over time

J.P. **Rozelot**, A.G. Kosovichev, A. Kilcik
Sun and Geosphere, **2018**, Vol. 13, No 1, pp 63 - 68;
https://arxiv.org/ftp/arxiv/papers/1804/1804.06930.pdf
The measurement of the Sun's diameter has been first tackled by the Greek astronomers from a geometric point of view. Their estimation of ~1800", although incorrect, was not truly called into question for several centuries. The first pioneer works for measuring the Sun's diameter with an astrometric precision were made around the year 1660

by Gabriel Mouton, then by Picard and La Hire. A canonical value of the solar radius of 959".63 was adopted by Auwers in 1891. Despite considerable efforts during the second half of the XXth century, involving dedicated space instruments, no consensus was reached on this issue. However, with the advent of high sensitivity instruments on board satellites, such as the Michelson Doppler Imager (MDI) on Solar and Heliospheric Observatory (SoHO) and the Helioseismic and Magnetic Imager (HMI) aboard NASA's Solar Dynamics Observatory (SDO), it was possible to extract with an unprecedented accuracy the surface gravity oscillation f modes, over nearly two solar cycles, from 1996 to 2017. Their analysis in the range of angular degree l=140-300 shows that the so-called "seismic radius" exhibits a temporal variability in anti-phase with the solar activity. Even if the link between the two radii (photospheric and seismic) can be made only through modeling, such measurements provide an interesting alternative which led to a revision of the standard solar radius by the International Astronomical Union in 2015. This new look on such modern measurements of the Sun's global changes from 1996 to 2017 gives a new way for peering into the solar interior, mainly to better understand the subsurface fields which play an important role in the implementation of the solar cycles.

A brief history of the solar diameter measurements: a critical quality assessment of the existing data

Jean Pierre **Rozelot**, Alexander G. Kosovichev, Ali Kilcik
Proc. International conference on: Variability of the Sun and sun-like stars: from asteroseismology to space weather,Baku, Azerbaijan, 6 - 8 July 2015, ed. J.-P. Rozelot, Lecture Notes in Physics, Springer, **2016**
http://arxiv.org/pdf/1609.02710v1.pdf
The size of the diameter of the Sun has been debated for a very long time. First tackled by the Greek astronomers from a geometric point of view, an estimate, although incorrect, has been determined, not truly called into question for several centuries. The French school of astronomy, under the impetus of Mouton and Picard in the XVIIth century can be considered as a pioneer in this issue. It was followed by the German school at the end of the XIXth century whose works led to a canonical value established at 959".63 (second of arc). A number of ground-based observations has been made in the second half of the XIXth century leading to controversial results mainly due to the difficulty to disentangle between the solar and atmospheric effects. Dedicated space measurements yield to a very faint dependence of the solar diameter with time. New studies over the entire radiation spectrum lead to a clear relationship between the solar diameter and the wavelength, reflecting the height at which the lines are formed. Thus the absolute value of the solar diameter, which is a reference for many astrophysical applications, must be stated according to the wavelength. Furthermore, notable features of the Near Sub-Surface Layer (NSSL), called the leptocline, can be established in relation to the solar limb variations, mainly through the shape asphericities coefficients. The exact relationship has not been established yet, but recent studies encourage further in-depth investigations of the solar subsurface dynamics, both observationally and by numerical MHD simulations.

Photospheric plasma and magnetic field dynamics during the formation of solar AR 11190

J. I. Campos **Rozo**, D. Utz, S. Vargas Dominguez, A. Veronig, T. Van Doorsselaere
A&A 622, A168 **2019**
https://arxiv.org/pdf/1901.02437.pdf
The Sun features on its surface typical flow patterns called the granulation, mesogranulation, and supergranulation. These patterns arise due to convective flows transporting energy from the interior of the Sun to its surface. In this paper we will shed light on the interaction between the convective flows in large-scale cells as well as the large-scale magnetic fields in active regions, and investigate in detail the statistical distribution of flow velocities during the evolution and formation of National Oceanic and Atmospheric Administration (NOAA) active region 11190. To do so, we employed local correlation tracking methods on data obtained by the Solar Dynamics Observatory (SDO) spacecraft in the continuum as well as on processed line-of-sight (LOS) magnetograms. We find that the flow fields in an active region can be modelled by a two-component distribution. One component is very stable, follows a Rayleigh distribution, and can be assigned to the background flows, whilst the other component is variable in strength and velocity range and can be attributed to the flux emergence visible both in the continuum maps as well as magnetograms. Generally, the plasma flows, as seen by the distribution of the magnitude of the velocity, follow a Rayleigh distribution even through the time of formation of active regions. However, at certain moments of large-scale fast flux emergence, a second component featuring higher velocities is formed in the velocity magnitudes distribution. The plasma flows are generally highly correlated to the motion of magnetic elements and vice versa except during the times of fast magnetic flux emergence as observed by rising magnetic elements. At these times, the magnetic fields are found to move faster than the corresponding plasma. **April 11, 2011**

A New Method to Comprehensively Diagnose Shock Waves in the Solar Atmosphere Based on Simultaneous Spectroscopic and Imaging Observations

Wenzhi **Ruan**1,4, Limei Yan2, Jiansen He1, Lei Zhang3, Linghua Wang1, and Yong Wei2

2018 ApJ 860 99
Shock waves are believed to play an important role in plasma heating. The shock-like temporal jumps in radiation intensity and Doppler shift have been identified in the solar atmosphere. However, a quantitative diagnosis of the shocks in the solar atmosphere is still lacking, seriously hindering the understanding of shock dissipative heating of the solar atmosphere. Here, we propose a new method to realize the goal of the shock quantitative diagnosis, based on Rankine–Hugoniot equations and taking the advantages of simultaneous imaging and spectroscopic observations from, e.g., IRIS (Interface Region Imaging Spectrograph). Because of this method, the key parameters of shock candidates can be derived, such as the bulk velocity and temperature of the plasma in the upstream and downstream, the propagation speed and direction. The method is applied to the shock candidates observed by IRIS, and the overall characteristics of the shocks are revealed quantitatively for the first time. This method is also tested with the help of forward modeling, i.e., virtual observations of simulated shocks. The parameters obtained from the method are consistent with the parameters of the shock formed in the model and are independent of the viewing direction. Therefore, the method we proposed here is applicable to the quantitative and comprehensive diagnosis of the observed shocks in the solar atmosphere.

Kinetic Simulation of Slow Magnetosonic Waves and Quasi-periodic Upflows in the Solar Corona

Wenzhi **Ruan**, Jiansen He, Lei Zhang, Christian Vocks, Eckart Marsch, Chuanyi Tu, Hardi Peter, Linghua Wang
2016 ApJ 825 58
http://arxiv.org/pdf/1601.01823v1.pdf
Quasi-periodic disturbances of emission-line parameters are frequently observed in the corona. These disturbances propagate upward along the magnetic field with speeds ∼100 km s−1. This phenomenon has been interpreted as evidence of the propagation of slow magnetosonic waves or argued to be signature of the intermittent outflows superposed on the background plasmas. Here we aim to present a new "wave + flow" model to interpret these observations. In our scenario, the oscillatory motion is a slow mode wave, and the flow is associated with a beam created by the wave-particle interaction owing to Landau resonance. With the help of a Vlasov model, we simulate the propagation of the slow mode wave and the generation of the beam flow. We find that weak periodic beam flows can be generated owing to Landau resonance in the solar corona, and the phase with strongest blueward asymmetry is ahead of that with strongest blueshift by about 1/4 period. We also find that the slow wave damps to the level of 1/e after the transit time of two wave periods, owing to Landau damping and Coulomb collisions in our simulation. This damping time scale is similar to that resulting from thermal-conduction in the magnetohydrodynamics regime. The beam flow is weakened/attenuated with increasing wave period and decreasing wave amplitude since Coulomb collision becomes more and more dominant over the wave action. We suggest that this "wave + flow" kinetic model provides an alternative explanation for the observed quasi-periodic propagating perturbations in various parameters in the solar corona.

Quiet Sun magnetic fields: an observational view **Review**

Luis Bellot **Rubio**, David Orozco Suárez
Living Reviews in Solar Physics, **2019**, 16:1
https://link.springer.com/content/pdf/10.1007%2Fs41116-018-0017-1.pdf
The quiet Sun is the region of the solar surface outside of sunspots, pores, and plages. In continuum intensity it appears dominated by granular convection. However, in polarized light the quiet Sun exhibits impressive magnetic activity on a broad range of scales, from the 30,000 km of supergranular cells down to the smallest magnetic features of about 100 km resolvable with current instruments. Quiet Sun fields are observed to evolve in a coherent way, interacting with each other as they are advected by the horizontal photospheric flows. They appear and disappear over surprisingly short time scales, bringing large amounts of magnetic flux to the solar surface. For this reason they may be important contributors to the heating of the chromosphere. Peering into such fields is difficult because of the weak signals they produce, which are easily affected, and even completely hidden, by photon noise. Thus, their evolution and nature remain largely unknown. In recent years the situation has improved thanks to the advent of high-resolution, high-sensitivity spectropolarimetric measurements and the application of state-of-the-art Zeeman and Hanle effect diagnostics. Here we review this important aspect of solar magnetism, paying special attention to the techniques used to observe and characterize the fields, their evolution on the solar surface, and their physical properties as revealed by the most recent analyses. We identify the main open questions that need to be addressed in the future and offer some ideas on how to solve them.

Decayless Kink Oscillations Excited by Random Driving: Motion in Transitional Layer

M. S. **Ruderman**, N. S. Petrukhin & E. Pelinovsky
Solar Physics volume 296, Article number: 124 (**2021**)
https://link.springer.com/content/pdf/10.1007/s11207-021-01867-5.pdf
https://doi.org/10.1007/s11207-021-01867-5

In this article we study the plasma motion in the transitional layer of a coronal loop randomly driven at one of its footpoints in the thin-tube and thin-boundary-layer (TTTB) approximation. We introduce the average of the square of a random function with respect to time. This average can be considered as the square of the oscillation amplitude of this quantity. Then we calculate the oscillation amplitudes of the radial and azimuthal plasma displacement as well as the perturbation of the magnetic pressure. We find that the amplitudes of the plasma radial displacement and the magnetic-pressure perturbation do not change across the transitional layer. The amplitude of the plasma radial displacement is of the same order as the driver amplitude. The amplitude of the magnetic-pressure perturbation is of the order of the driver amplitude times the ratio of the loop radius to the loop length squared. The amplitude of the plasma azimuthal displacement is of the order of the driver amplitude times Re1/6Re1/6, where Re is the Reynolds number. It has a peak at the position in the transitional layer where the local Alfvén frequency coincides with the fundamental frequency of the loop kink oscillation. The ratio of the amplitude near this position and far from it is of the order of $\ell\ell$, where $\ell\ell$ is the ratio of thickness of the transitional layer to the loop radius. We calculate the dependence of the plasma azimuthal displacement on the radial distance in the transitional layer in a particular case where the density profile in this layer is linear.

Phase mixing of Alfvén waves in two-dimensional magnetic plasma configurations with exponentially decreasing density

Michael S. **Ruderman**2,1 and Nikolai S. Petrukhin3
A&A 620, A44 (**2018**)
We study damping of phase-mixed Alfvén waves propagating in axisymmetric magnetic plasma configurations. We use the linear magnetohydrodynamic (MHD) equations in the cold plasma approximation. The only dissipative process that we take into account is shear viscosity. We reduce the MHD equations describing the Alfvén wave damping to a Klein–Gordon-type equation. We assume that the two terms in this equation, one describing the effect of inhomogeneity and the other the effect of viscosity, are small. Then we use the WKB method to derive the expression describing the wave energy flux attenuation with the height. We apply the general theory to particular equilibria with the exponentially divergent magnetic field lines with the characteristic scale H. The plasma density exponentially decreases with the height with the characteristic scale Hρ. We study the wave damping for typical parameters of coronal plumes and various values of the wave period, the characteristic scale of the magnetic field variation H, and kinematic shear viscosity ν. We show that to have an appreciable wave damping at the height 6H we need to increase shear viscosity by at least six orders of magnitude in comparison with the value given by the classical plasma theory. Another important result is that the efficiency of wave damping strongly depends on the ratio H/Hρ. It increases fast when H/Hρ decreases. We present a physical explanation of this phenomenon.

Nonlinear Generation of Fluting Perturbations by Kink Mode

M. S. **Ruderman**
Solar Physics August **2017**, 292:111
https://link.springer.com/content/pdf/10.1007%2Fs11207-017-1133-0.pdf
We study the excitation of fluting perturbations in a magnetic tube by an initially imposed kink mode. We use the ideal magnetohydrodynamic (MHD) equations in the cold-plasma approximation. We also use the thin-tube approximation and scale the dependent and independent variables accordingly. Then we assume that the dimensionless amplitude of the kink mode is small and use it as an expansion parameter in the regular perturbation method. We obtain the expression for the tube boundary perturbation in the second-order approximation. This perturbation is a superposition of sausage and fluting perturbations. The amplitude of the fluting perturbation takes its maximum at the middle of the tube, and it monotonically decreases with the distance from the middle of the tube.

Compressibility Effect on the Rayleigh–Taylor Instability with Sheared Magnetic Fields

M. S. **Ruderman**
Solar Physics April **2017**, 292:47
http://link.springer.com/article/10.1007/s11207-017-1073-8
We study the effect of plasma compressibility on the Rayleigh–Taylor instability of a magnetic interface with a sheared magnetic field. We assume that the plasma is ideal and the equilibrium quantities are constant above and below the interface. We derive the dispersion equation. Written in dimensionless variables, it contains seven dimensionless parameters: the ratio of plasma densities above and below the interface \(\zeta\), the ratio of magnetic field magnitude squared \(\chi\), the shear angle \(\alpha\), the plasma beta above and below the interface, \(\beta_{2}\) and \(\beta_{1}\), the angle between the perturbation wave number and the magnetic field direction above the interface \(\phi\), and the dimensionless wave number \(\kappa\). Only six of these parameters are independent because \(\chi\), \(\beta_{1}\), and \(\beta_{2}\) are related by the condition of total pressure continuity at the interface. Only perturbations with the wave number smaller than the critical wave number are unstable. The critical wave number depends on \(\phi\), but it is independent of \(\beta_{1}\) and \(\beta_{2}\), and is the same as that in the incompressible plasma approximation. The dispersion equation is solved numerically with \(\zeta= 100\),

$\chi= 1$), and $\beta_{1} = \beta_{2} = \beta$). We obtain the following results. When β) decreases, so does the maximum instability increment. However, the effect is very moderate. It is more pronounced for high values of α). We also calculate the dependence on ϕ) of the maximum instability increment with respect to κ). The instability increment takes its maximum at $\phi= \phi_{\mathrm{m}}$). Again, the decrease of β) results in the reduction of the instability increment. This reduction is more pronounced for high values of $|\phi- \phi_{\mathrm{m}}|$). When both α) and $|\phi- \phi_{\mathrm{m}}|$) are small, the reduction effect is practically negligible. The theoretical results are applied to the magnetic Rayleigh–Taylor instability of prominence threads in the solar atmosphere.

The influence of helical background fields on current helicity and electromotive force of magnetoconvection

G. **Rüdiger** and M. Küker
A&A 592, A73 (**2016**)
Motivated by the empirical finding that the known hemispheric rules for the current helicity at the solar surface are not strict, we demonstrate the excitation of small-scale current helicity by the influence of large-scale helical magnetic background fields on nonrotating magnetoconvection. This is shown within a quasilinear analytic theory of driven turbulence and by nonlinear simulations of magnetoconvection that the resulting small-scale current helicity has the same sign as the large-scale current helicity, while the ratio of both pseudoscalars is of the order of the magnetic Reynolds number of the convection. The same models do not provide finite values of the small-scale kinetic helicity. On the other hand, a turbulence-induced electromotive force is produced including the diamagnetic pumping term, as well as the eddy diffusivity but, however, no α effect. It has thus been argued that the relations for the simultaneous existence of small-scale current helicity and α effect do not hold for the model of nonrotating magnetoconvection under consideration. Calculations for various values of the magnetic Prandtl number demonstrate that, for the considered diffusivities, the current helicity increases for growing magnetic Reynolds number, which is not true for the velocity of the diamagnetic pumping, which is in agreement with the results of the quasilinear analytical approximation.

A Search for High-Frequency Coronal Brightness Variations in the 21 August 2017 Total Solar Eclipse

P. **Rudawy**, K. Radziszewski, A. Berlicki, K.J.H. Phillips, D.B. Jess, P.H. Keys, F.P. Keenan
Solar Phys. 294:48 **2019**
https://arxiv.org/pdf/1903.06076.pdf
We report on a search for short-period intensity variations in the green-line FeXIV 530.3 nm emission from the solar corona during the **21 August 2017** total eclipse viewed from Idaho in the United States. Our experiment was performed with a much more sensitive detection system, and with better spatial resolution, than on previous occasions (1999 and 2001 eclipses), allowing fine details of quiet coronal loops and an active-region loop system to be seen. A guided 200-mm-aperture Schmidt-Cassegrain telescope was used with a state-of-the-art CCD camera having 16-bit intensity discrimination and a field-of-view 0.43 degree x 0.43 degree that encompassed approximately one third of the visible corona. The camera pixel size was 1.55 arcseconds, while the seeing during the eclipse enabled features of approx. 2 arcseconds (1450 km on the Sun) to be resolved. A total of 429 images were recorded during a 122.9 second portion of the totality at a frame rate of 3.49 images per second. In the analysis, we searched particularly for short-period intensity oscillations and travelling waves, since theory predicts fast-mode magneto-hydrodynamic (MHD) waves with short periods may be important in quiet coronal and active-region heating. Allowing first for various instrumental and photometric effects, we used a wavelet technique to search for periodicities in some 404 000 pixels in the frequency range 0.5-1.6 Hz (periods: 2 second to 0.6 second). We also searched for travelling waves along some 65 coronal structures. However, we found no statistically significant evidence in either. This negative result considerably refines the limit that we obtained from our previous analyses, and it indicates that future searches for short-period coronal waves may be better directed towards Doppler shifts as well as intensity oscillations.

Kink Waves in Twisted and Expanding Magnetic Tubes

M. S. **Ruderman**, N. S. Petrukhin
Solar Phys. Volume 298, issue 11, Article: 125, **2023**
https://link.springer.com/content/pdf/10.1007/s11207-023-02219-1.pdf
We study kink and fluting waves in expanding and twisted magnetic flux tubes. We use the thin-tube and zero-beta plasma approximations. The equilibrium magnetic field is force free with a constant proportionality coefficient between the electrical current and the magnetic field. We derive the equation governing the kink and fluting waves in a tube. Using this equation we study the propagation of kink waves in a particular case of a magnetic tube homogeneous in the axial direction. We show that while there is only one propagating kink wave with the phase speed equal to the kink speed in an untwisted tube, in a twisted tube there are two wave modes, accelerated and decelerated. The phase speed of the accelerated wave exceeds the kink speed, while the phase speed of the

decelerated wave is less than the kink speed. We also show that the standing modes are defined by the same eigenvalue problem as that in the case of an untwisted tube. Hence, the frequencies of the standing-wave modes are not affected by the twist. This implies that the seismological results based on the observation of the standing-wave mode frequencies remain valid when the twist is taken into account. The only effect of twist is the variation of the direction of polarisation of the coronal magnetic-loop displacement along the loop. As a result, an apparent node can be detected near the loop apex if only one component of the loop displacement is observed. This can lead to an incorrect conclusion that the observed coronal loop kink oscillation was the first overtone, while in fact it was the fundamental mode.

Angular momentum transport from magnetoconvection and the magnetic modulation of the solar differential rotation

Günther **Rüdiger**, Manfred Küker
A&A **2020**
https://arxiv.org/pdf/2010.13601.pdf
In order to explain the modulation of the solar rotation law during the activity minima and maxima the angular momentum transport by rotating magnetoconvection is numerically simulated when a convective box is penetrated by an inclined azimuthal magnetic field. Turbulence-induced kinetic and magnetic stresses {\em and} the Maxwell stress of the large-scale magnetic background field are the basic transporters. Without rotation the sign of the total stress naturally depends on the signs of the field components as positive (negative) $B\theta B\phi$ transport the angular momentum poleward (equatorward). For fast enough rotation, however, the turbulence-originated Λ effect starts to dominate the transport of the angular momentum. The simulations show that positive angles between the azimuthal field and the two meridional magnetic field components (as expected to be realized by induction of solar-type rotation laws) reduce the inward radial as well as the equatorward latitudinal transport by the rotating magnetoconvection. In accordance with the observations the magnetically influenced rotation law at the solar surface proves to be flatter than the nonmagnetic one even displaying a slightly decelerated equator .

The existence of the Lambda effect in the solar convection zone indicated by SDO observations

Guenther **Ruediger**, Manfred Kueker, Ilya Tereshin
A&A, **2014**
http://arxiv.org/pdf/1408.3837v1.pdf
The empirical finding with data from the Solar Dynamics Observatory (SDO) of positive (negative) horizontal Reynolds stress at the northern (southern) hemisphere for solar giant cells (Hathaway et al. 2013) is discussed for its consequences for the theory of the solar/stellar differential rotation. Solving the nonlinear Reynolds equation for the angular velocity under neglect of the meridional circulation we show that the horizontal Reynolds stress of the northern hemisphere is always negative at the surface but it is positive in the bulk of the solar convection zone by the action of the Lambda effect. The Lambda effect, which describes the angular momentum transport of rigidly rotating anisotropic turbulence and which avoids a rigid-body rotation of the convection zones, is in horizontal direction of cubic power in the rotation rate Ω and it is always equatorwards directed. Theories without Lambda effect which may also provide the observed solar rotation law only by the action of a meridional circulation lead to a horizontal Reynolds stress with the opposite sign as observed.

Estimation of an Upper Limit on the Density of Relic Neutrinos in the Sun via the Solar 8B Neutrino Flux

Tim **Ruhe**, Alexander Sandrock
2020
https://arxiv.org/pdf/2009.11051.pdf
Relic neutrinos from the early universe are predicted to have a relatively large number density, but extremely low energies. Hence, the only possible interaction proceeds via neutrino capture on beta-decaying nuclei. In case relic neutrinos are captured by beta-decaying nuclei in the Sun, the neutrinos normally emerging from the decay of these nuclei will be missing from the overall number of solar neutrinos registered in neutrino experiments. Within the Sun, 8B and three nuclei from the CNO cycle are found to be suitable for this kind of process. Their cross section as well as the possible impact on the observed number of solar neutrinos are discussed. Assuming standard neutrino oscillations, no deviations of neutrino flux measurements from the predictions of the solar standard model are observed and upper limits are derived accordingly.

The Flattening Index of the Eclipse White-Light Corona and Magnetic Fields

V. **Rušin**
Solar Physics January **2017**, 292:24

From observations of the solar white-light corona at 65 eclipses from 1851 to 2015 we confirm earlier findings that the flattening index of the white-light corona depends on the phase, rather than the magnitude of solar cycles, which is in contrast with behavior of other major solar activity indices like the sunspot number, the 2800 MHz radio flux, etc. This indicates that mechanisms responsible for creation and distribution of helmet streamers, the most essential coronal structures influencing the flattening index, could be of different magnetic nature from those of other manifestations of solar surface activity.

Table 1 The flattening index (FI) of the WLC as a function of the phase of solar cycle as derived for the height of two solar radii in the period from 1851 to 2015.

Coronal heating problem solution by means of axion origin photons

V.D. **Rusov**, I.V. Sharph, V.P. Smolyar, M.V. Eingorn, M.E. Beglaryan
Physics of the Dark Universe, Vol. 31, **2021**, 100746
https://arxiv.org/pdf/2011.11415.pdf

In this paper we advocate for the idea that two seemingly unrelated mysteries with almost 90 year history -- the nature of dark matter and the million-degree solar corona -- may be but two sides of the same coin -- the axions of dark matter born in the core of the Sun and photons of axion origin in the million-degree solar corona, whose modulations are controlled by the anticorrelated modulation of the asymmetric dark matter (ADM) density in the solar interior.

Thermomagnetic Ettingshausen-Nernst effect in tachocline, magnetic reconnection phenomenon in lower layers, axion mechanism of solar luminosity variations, coronal heating problem solution and mechanism of DM spike variations around BH **Book**

V.D. **Rusov**, M.V. Eingorn, I.V. Sharph, V.P. Smolyar, M.E. Beglaryan
2019
https://arxiv.org/pdf/1908.06042.pdf

It is shown that the holographic principle of quantum gravity (in the hologram of the Universe, and therefore in our Galaxy, and of course on the Sun!), in which the conflict between the theory of gravitation and quantum mechanics disappears, gives rise to the Babcock-Leighton holographic mechanism. Unlike the solar dynamo models, it generates a strong toroidal magnetic field by means of the thermomagnetic Ettingshausen-Nernst (EN) effect in the tachocline. Hence, it can be shown that with the help of the thermomagnetic EN effect, a simple estimate of the magnetic pressure of an ideal gas in the tachocline of e.g. the Sun can indirectly prove that by using the holographic principle of quantum gravity, the repulsive toroidal magnetic field of the tachocline (BSuntacho=4.1·107 G=−BSuncore) precisely "neutralizes" the magnetic field in the Sun core, since the projections of the magnetic fields in the tachocline and the core have equal values but opposite directions. The basic problem is a generalized problem of the antidynamo model of magnetic flux tubes (MFTs), where the nature of both holographic effects (the thermomagnetic EN~effect and Babcock-Leighton holographic mechanism), including magnetic cycles, manifests itself in the modulation of asymmetric dark matter (WIMP ADM) and, consequently, the solar axion in the Sun interior.

Do Current and Magnetic Helicities Have the Same Sign?

A. J. B. **Russell**1, P. Demoulin2, G. Hornig1, D. I. Pontin1, and S. Candelaresi1
2019 ApJ 884 55
https://doi.org/10.3847/1538-4357/ab40b4

Current helicity, H c , and magnetic helicity, H m , are two main quantities used to characterize magnetic fields. For example, such quantities have been widely used to characterize solar active regions and their ejecta (magnetic clouds). It is commonly assumed that H c and H m have the same sign, but this has not been rigorously addressed beyond the simple case of linear force-free fields. We aim to answer whether H m H c ≥ 0 in general, and whether it is true over some useful set of magnetic fields. This question is addressed analytically and with numerical examples. The main focus is on cylindrically symmetric straight flux tubes, referred to as flux ropes (FRs), using the relative magnetic helicity with respect to a straight (untwisted) reference field. Counterexamples with H m H c < 0 have been found for cylindrically symmetric FRs with finite plasma pressure, and for force-free cylindrically symmetric FRs in which the poloidal field component changes direction. Our main result is a proof that H m H c ≥ 0 is true for force-free cylindrically symmetric FRs where the toroidal field and poloidal field components are each of a single sign, and the poloidal component does not exceed the toroidal component. We conclude that the conjecture that current and magnetic helicities have the same sign is not true in general, but it is true for a set of FRs of importance to coronal and heliospheric physics.

75th Anniversary of `Existence of Electromagnetic-Hydrodynamic Waves' **Review**

Alexander J. B. **Russell**
Solar Phys. May **2018**, 293:83
https://arxiv.org/pdf/1711.04876.pdf

https://link.springer.com/article/10.1007/s11207-018-1296-3
We have recently passed the 75th anniversary of one of the most important results in solar and space physics: Hannes Alfv\'en's discovery of Alfv\'en waves and the Alfv\'en speed. To celebrate the anniversary, this article recounts some major episodes in the history of MHD waves. Following an initially cool reception, Alfv\'en's ideas were propelled into the spotlight by Fermi's work on cosmic rays, the new mystery of coronal heating and, as scientific perception of interplanetary space shifted dramatically and the space race started, detection of Alfv\'en waves in the solar wind. From then on, interest in MHD waves boomed, laying the foundations for modern remote observations of MHD waves in the Sun, coronal seismology and some of today's leading theories of coronal heating and solar wind acceleration. In 1970, Alfv\'en received the Nobel Prize for his work in MHD, including these discoveries. The article concludes with some reflection about what the history implies about the way we do science, especially the advantages and pitfalls of idealised mathematical models.

Sunquake Generation by Coronal Magnetic Restructuring

Alexander J. B. **Russell**, Michaela K. Mooney, James E. Leake, Hugh S. Hudson
ApJ 831 42 **2016**
http://arxiv.org/pdf/1602.08245v1.pdf
Sunquakes are the surface signatures of acoustic waves in the Sun's interior that are produced by some but not all flares and coronal mass ejections (CMEs). This letter explores a mechanism for sunquake generation by the magnetic field changes that occur during flares and CMEs, using MHD simulations with a semiempirical FAL-C atmosphere to demonstrate the generation of acoustic waves in the interior in response to changing magnetic tilt in the corona. We find that Alfv\'en-sound resonance combined with the ponderomotive force produces acoustic waves in the interior with sufficient energy to match sunquake observations when the magnetic field angle changes by the order of 10 degrees in a region where the coronal field strength is a few hundred gauss or more. The most energetic sunquakes are produced when the coronal field is strong, while the variation of magnetic field strength with height and the timescale of the tilt change are of secondary importance.

Quiet-Sun Explosive Events Observed in He ii λ304 with MOSES-06

Thomas **Rust** and Charles C. Kankelborg
2019 ApJ 877 59
sci-hub.se/10.3847/1538-4357/ab12e2
In this paper the unique data from the Multi-Order Solar Extreme-Ultraviolet Spectrograph (MOSES) are used to investigate transition region explosive events in the He ii λ304 spectral line. Particular attention is paid to two example events: one blueshifted jet and one bidirectional jet. Observations suggest that these events consist exclusively of high-velocity (~100 km s−1) plasma. These two and other examples presented here exhibit a striking lack of emission in the line core. No acceleration phase is observed at the onset of either event. In total, 41 examples of explosive events are identified, including 5 blueshifted jets, 2 redshifted jets, and 10 bidirectional jets. The remaining 24 events resist simple classification, but observations indicate compact, highly Doppler-shifted emission. Event spatial scales and lifetimes are consistent with published explosive event characteristics. Data from the Michelson Doppler Imager provide magnetic context to the MOSES observations. Bidirectional jets lacking line core emission are interesting because they are predicted in models of Petschek reconnection in the transition region. **8 Feb 2006**

Cornelis de Jager: In Memoriam

Robert J. **Rutten**, Oddbjørn Engvold & Adrianus C. T. Nieuwenhuizen
Solar Physics volume 297, Article number: 15 (**2022**)
https://link.springer.com/content/pdf/10.1007/s11207-021-01946-7.pdf
Cornelis (“Kees”) de Jager, the co-founder of the journal Solar Physics, passed away on 27 May 2021. He was an exemplary human being, a great scientist, and he had a large impact on our field. In this tribute, we first briefly summarize his life and career and then describe some of his solar activities, from his Ph.D. thesis on the hydrogen lines in 1952 to the book on cycle–climate relations that he completed last year.

Small-scale solar surface magnetism

Robert J. **Rutten**
Brief review in monograph "Solar Magnetic Variability and Climate" by C. de Jager, S. Duhau, A.C.T. Nieuwenhuizen, 2020, Stip Media, Alkmaar **2021**
https://arxiv.org/pdf/2105.14533.pdf
This contribution to "Solar Magnetic Variability and Climate" reviews small-scale magnetic features on the solar surface, in particular the strong-field but tiny magnetic concentrations that constitute network and plage and represent most magnetism outside sunspots and filaments. Where these are mostly of the same polarity, as in active-region plage, their occurrence varies with the activity variations measured by the sunspot number, but when they

appear bipolar-mixed on small scales they can also result from granular-scale dynamo action that does not vary with the cycle. **April 29 2015, April 29 2019**

Compendium solar spectrum formation **Review**

Robert J. **Rutten**
Lingezicht Astrophysics Report 2 **2021**
https://arxiv.org/pdf/2103.02369.pdf
The solar spectrum conveys most of our diagnostics to find out how our star works. They must be understood for utilization, but solar spectrum formation is complex because the interaction of matter and radiation within the solar atmosphere suffers non-local control in space, wavelength, and time. These complexities are summarized and illustrated with classic literature.

SolO campfires in SDO images

Robert J. **Rutten**
Lingezicht Astrophysics Reports 1 **2020**
https://arxiv.org/pdf/2009.00376.pdf
I present the appearance of Solar Orbiter "campfires" in simultaneous images from the Solar Dynamics Observatory where most are visible although less sharp. I also show such features elsewhere in the SDO database. I show them in detail and discuss their nature.

Solar H-alpha features with hot onsets. IV. Network fibrils

Robert J. **Rutten**, Luc H. M. Rouppe van der Voort, Bart De Pontieu
A&A **2019**
https://arxiv.org/pdf/1908.09315.pdf
Even in quiet areas underneath coronal holes the solar chromosphere contains ubiquitous heating events. They tend to be small scale and short lived, hence difficult to identify. Here we do not address their much-debated contribution to outer-atmosphere heating, but their aftermaths. We performed a statistical analysis of high-resolution observations in the Balmer H-alpha line to suggest that many slender dark H-alpha fibrils spreading out from network represent cooling gas that outlines tracks of preceding rapid type II spicule events or smaller similar but as yet unresolved heating agents in which the main gas constituent, hydrogen, ionizes at least partially. Subsequent recombination then causes dark H-alpha fibrils enhanced by nonequilibrium overopacity. We suggest that the extraordinary fibrilar appearance of the H-alpha chromosphere around network results from intermittent, frequent small-scale prior heating.

Non-Equilibrium Spectrum Formation Affecting Solar Irradiance **Review**

Robert J. **Rutten**
Solar Phys. 294:165 **2019**
https://arxiv.org/pdf/1908.04624.pdf
https://link.springer.com/content/pdf/10.1007%2Fs11207-019-1535-2.pdf
This is an overview of non-equilibrium aspects of the formation of solar continua and lines affecting the contributions by magnetic network and plage to spectrally resolved solar irradiance. After a brief summary of these contributions and a compact refresher of solar spectrum formation, the emphasis is on graphical exposition. Major obstacles for simulation-based irradiance studies are how to cope with NLTE scattering in the violet and ultraviolet line haze and how to cope with retarded hydrogen opacities in infrared and mm radiation.

Solar ALMA predictions: tutorial

Robert J. **Rutten**
Proceedings IAU Symposium 327, **2016**
https://arxiv.org/pdf/1611.05308v1.pdf
I have proposed that long Halpha fibrils are caused by heating events of which the tracks are afterwards outlined by contrails of cooling gas with extraordinary Halpha opacity and yet larger opacity at the ALMA wavelengths. Here I detail the radiative transfer background.

H-alpha features with hot onsets. II. A contrail fibril

R.J. **Rutten**, L.H.M. Rouppe van der Voort
A&A 597, A138 (**2017**)
http://arxiv.org/pdf/1609.07616v1.pdf
The solar chromosphere observed in H-alpha consists mostly of narrow fibrils. The longest typically originate in network or plage and arch far over adjacent internetwork. We use data from multiple telescopes to analyze one well-

observed example in a quiet area. It resulted from the earlier passage of an accelerating disturbance in which the gas was heated to high temperature as in the spicule-II phenomenon. After this passage a dark H-Halpha fibril appeared as a contrail. We use Saha-Boltzmann extinction estimation to gauge the onset and subsequent visibilities in various diagnostics and conclude that such H-alpha fibrils can indeed be contrail phenomena, not indicative of the thermodynamic and magnetic environment when they are observed but of more dynamic happenings before. They do not connect across internetwork cells but represent launch tracks of heating events and chart magnetic field during launch, not at present. **June 21, 2014**

H-alpha features with hot onsets III. Fibrils in Lyman-alpha and with ALMA

Robert J. **Rutten**
A&A **2016**
http://arxiv.org/pdf/1609.01122v1.pdf
In H-alpha most of the solar surface is covered by a dense canopy of long opaque fibrils, but predictions for quiet-Sun observations with ALMA have ignored this fact. Comparison with Ly-alpha suggests that the large opacity of H-alpha fibrils is caused by hot precursor events. Application of a recipe that assumes momentary Saha-Boltzmann extinction during their hot onset to millimeter wavelengths suggests that ALMA will observe the H-alpha fibril canopy, not acoustic shocks underneath, and will yield data more interesting than if this canopy were transparent.

H-alpha features with hot onsets. I. Ellerman bombs

R. J. **Rutten**
A&A 590, A124 **2016**
http://arxiv.org/pdf/1601.03280v1.pdf
Ellerman bombs are transient brightenings of the wings of the Balmer lines that uniquely mark reconnection in the solar photosphere. They are also bright in strong Ca II and ultraviolet lines and in ultraviolet continua, but they are not visible in the optical continuum and the Na I D and Mg I b lines. These discordant visibilities invalidate all published Ellerman bomb modeling. I argue that the assumption of Saha-Boltzmann lower-level populations is informative to estimate bomb-onset opacities for these diverse diagnostics, even and especially for H-alpha, and employ such estimates to gauge the visibilities of Ellerman bomb onsets in all of them. They constrain Ellerman bomb formation to temperatures 10,000 - 20,000 K and hydrogen densities around 10^15 cm^-3. Similar arguments likely hold for H-alpha visibility in other transient phenomena with hot and dense onsets.

Ellerman bombs at high resolution. IV. Visibility in Na I and Mg I

R. J. **Rutten**, L. H. M. Rouppe van der Voort, G. J. M. Vissers
ApJ **808** 133 **2015**
http://arxiv.org/pdf/1506.04426v1.pdf
Ellerman bombs are transient brightenings of the wings of the solar Balmer lines that mark reconnection in the photosphere. Ellerman noted in 1917 that he did not observe such brightenings in the Na I D and Mg I b lines. This non-visibility should constrain EB interpretation, but has not been addressed in published bomb modeling. We therefore test Ellerman's observation and confirm it using high-quality imaging spectrometry with the Swedish 1-m Solar Telescope. However, we find diffuse brightness in these lines that seems to result from prior EBs. We tentatively suggest this is a post-bomb hot-cloud phenomenon also found in recent EB spectroscopy in the ultraviolet. **2013 July 4**

On the Periodicities in Solar Rotation and Activity Determined from Sunspot-Group Data and Possible Connection with Rossby-Like Waves

Domagoj **Ruždjak**, Roman Brajša, Ivica Skokić, Davor Sudar & Arnold Hanslmeier
Solar Physics volume 298, Article number: 39 (**2023)**
https://doi.org/10.1007/s11207-023-02114-9
Analyses of solar rotation and activity, and their variations, can improve the understanding of the formation and interaction of the solar-activity bands and therefore give important observational constraints on the modelling of the solar dynamo and improve the forecast capability in solar activity and space weather. Sunspot-position data obtained from the Greenwich and Debrecen Photoheliographic data for the years 1874 to 2016 were used to calculate the rotational and meridional velocities of the solar plasma. The velocities were calculated from daily shifts of sunspot groups. By analysing the rotation-rate residuals, covariance of meridional velocities and rotation-rate residuals, as well as daily total sunspot number, taken from WDC-SILSO, for periodicity in the range of periods larger than two days, significant periods of their changes were found. It was demonstrated that the frequencies of the quasi-annual variations of solar activity, with periods from 230 to 400 days, match those of classical Rossby modes with $m \geq 17$. There is no match between the frequencies of Rossby modes and the peaks in the rotation-rate residual and horizontal component of the Reynolds-stress-tensor periodograms. These variations are most probably connected

with the existence of active longitudes. It was demonstrated that the algorithms for detecting periodic signals should be used with caution when analysing complex periodic data.

Meridional Motions and Reynolds Stress Determined by Using Kanzelhöhe Drawings and White Light Solar Images from 1964 to 2016

Domagoj **Ruždjak**, Davor Sudar, Roman Brajša, Ivica Skokić…
Solar Physics April **2018**, 293:59
https://arxiv.org/pdf/1804.01344.pdf
Sunspot position data obtained from Kanzelhöhe Observatory for Solar and Environmental Research (KSO) sunspot drawings and white light images in the period 1964 to 2016 were used to calculate the rotational and meridional velocities of the solar plasma. Velocities were calculated from daily shifts of sunspot groups and an iterative process of calculation of the differential rotation profiles was used to discard outliers. We found a differential rotation profile and meridional motions in agreement with previous studies using sunspots as tracers and conclude that the quality of the KSO data is appropriate for analysis of solar velocity patterns. By analyzing the correlation and covariance of meridional velocities and rotation rate residuals we found that the angular momentum is transported towards the solar equator. The magnitude and latitudinal dependence of the horizontal component of the Reynolds stress tensor calculated is sufficient to maintain the observed solar differential rotation profile. Therefore, our results confirm that the Reynolds stress is the dominant mechanism responsible for transport of angular momentum towards the solar equator.

A Relationship between the Solar Rotation and Activity Analysed by Tracing Sunspot Groups

Domagoj **Ruždjak**, Roman Brajša, Davor Sudar, Ivica Skokić, Ivana Poljančić Beljan
Solar Phys. 292:179 **2017**
https://arxiv.org/pdf/1711.03723.pdf
The sunspot position from Greenwich Photoheliographic Results (GPR), US Air Force Solar Optical Observing Network and National Oceanic and Atmospheric Administration (USAF/NOAA), and Debrecen Photoheliographic Data (DPD) data bases in the period 1874 to 2016 were used to calculate yearly values of the solar differential-rotation parameters A and B. The calculated differential-rotation parameters were compared with the solar-activity level. We found that the Sun rotates more differentially at the minimum than at the maximum of activity during the 1977 - 2016 epoch. An inverse correlation between equatorial rotation and solar activity was found using the recently revised sunspot number. The secular decrease of equatorial rotation rate accompanying the increase of activity stopped in the last part of the 20th century. It was noted that when a significant peak of equatorial rotation velocity is observed during minimum of activity, the strength of the next maximum is smaller than the previous one.

Turbulence-induced transport dynamo mechanism

Chang-Mo **Ryu**
Plasma Res. Express 3 (**2021**) 035002
https://arxiv.org/pdf/2110.02433.pdf
The transport dynamo mechanism, which describes the magnetic field generation by diffusion flow is reviewed. In this mechanism, the cross-field transport caused by the random motion of fluid breaks the frozen-flux approximation, and the resulting cross-field diffusion that can generate the magnetic field. Turbulence can play an important role in inducing such random motion. Compared to the conventional dynamo mechanism, this transport mechanism has several special features that the field generation can occur on a very slow time scale because the mechanism is mediated by diffusion and that this mechanism is practically meaningful only when there is density inhomogeneity. Turbulence can significantly enhance cross-field diffusion far beyond collisional transport. The physical meanings of the diffusion-generated magnetic fields are discussed in detail.

How Nonlinearity Changes Different Parameters in the Solar Corona

S. **Sabri**1, S. Poedts2,3, and H. Ebadi1
2023 ApJ 944 72
https://iopscience.iop.org/article/10.3847/1538-4357/acb04e/pdf
We consider different velocity amplitudes of incident waves to study nonlinearity effects on the plasma parameters around a magnetic null point in the solar corona. This could query the seismological methods used to observe and interpret damping profiles of oscillations of magnetic structures, based on linear theory. To this end, initially symmetric fast magnetoacoustic waves with three different amplitudes are applied to the system to pursue the effect of nonlinearity on the resulting plasma heating and flows. The dynamic evolution is investigated by solving the resistive MHD equations in a Cartesian domain by the PLUTO code. The considered magnetic null point is surrounded by an initially constant density and temperature plasma. Pursuing the partition of different energy

components can shed light on our understanding of the energy release mechanisms. It is found that nonlinear behavior could be the reason for the occurring magnetic reconnection and the related excitation of coronal jets. Furthermore, the fully nonlinear simulation run results in a high temperature and a high current density accumulation and less twisting along the wave accumulation direction, which is even higher than the heating at the magnetic null point itself. Moreover, it is found that there is no significant amplification in the velocity profile. This could be related to the fact that there are not any clear correlations between jets and flares. Furthermore, it is illustrated that the period of the oscillations depends on the amplitude of the initial perturbation, obtaining a shorter period for the fully nonlinear case.

Plasma heating by magnetoacoustic wave propagation in the vicinity of a 2.5D magnetic null-point

S. **Sabri**1,2,⋆, S. Poedts1 and H. Ebadi2,3
A&A 623, A81 (**2019**)
Context. Magnetohydrodynamic (MHD) waves have significant potential as a plasma heating mechanism. Finding a suitable wave dissipation mechanism is a very tough task, given the many observational constraints on the models, and this has resulted in the development of an important research community in solar physics. The magnetic field structure has an important role in the solar corona heating. Here, we investigate in detail current sheet mode generation via magnetic reconnection and mode conversion releases some of the free magnetic energy and produces heating. In addition, energy conversion is discussed completely. Moreover, nonlinear effects on density variations and, in turn, mode conversion are pursued.
Aims. In order to assess the role of magnetoacoustic waves in plasma heating, we have modeled in detail a fast magneto-acoustic wave pulse near a magnetic null-point in a finite plasma-β. The behavior of the propagation and dissipation of the fast magneto-acoustic wave is investigated in the inhomogeneous magnetically structured solar corona. Particular attention is given to the dissipation of waves and coronal heating and energy transfer in the solar corona, focusing on the energy transfer resulting from the interaction of fast magneto-acoustic waves with 2.5D magnetic null-points.
Methods. The shock−capturing Godunov−type PLUTO code was used to solve the ideal MHD set of equations in the context of wave-plasma energy transfer.
Results. It is shown that magneto-acoustic waves could be a viable candidate to contribute significantly to the heating of the solar corona and maintain the solar corona at a temperature of a few million degrees. The temperature is not constant in the corona. Coronal heating occurs near magnetic null points. It is found that magnetic reconnection, phase mixing and mode conversion contribute to the heating. Moreover, nonlinear fast and slow magnetoacoustic waves are decoupled except in $\beta = 1$ layer.

Validation of the Alfvén Wave Solar atmosphere Model (AWSoM) with Observations from the Low Corona to 1 AU

N. **Sachdeva**, B. van der Holst, W. B. Manchester, G. Tóth, Y. Chen, D. G. Lloveras, A. M. Vásquez, Philippe Lamy, Julien Wojak, B. V. Jackson, H.-S. Yu, C. J. Henney
ApJ **887** 83 **2019**
https://arxiv.org/pdf/1910.08110.pdf
https://doi.org/10.3847/1538-4357/ab4f5e
We perform a validation study of the latest version of the Alfvén Wave Solar atmosphere Model (AWSoM) within the Space Weather Modeling Framework (SWMF). To do so, we compare the simulation results of the model with a comprehensive suite of observations for Carrington rotations representative of the solar minimum conditions extending from the solar corona to the heliosphere up to the Earth. In the low corona (r<1.25 \Rs), we compare with EUV images from both STEREO-A/EUVI and SDO/AIA and to three-dimensional (3-D) tomographic reconstructions of the electron temperature and density based on these same data. We also compare the model to tomographic reconstructions of the electron density from SOHO/LASCO observations (2.55<r<6.0\Rs). In the heliosphere, we compare model predictions of solar wind speed with velocity reconstructions from InterPlanetary Scintillation (IPS) observations. For comparison with observations near the Earth, we use OMNI data. Our results show that the improved AWSoM model performs well in quantitative agreement with the observations between the inner corona and 1 AU. The model now reproduces the fast solar wind speed in the polar regions. Near the Earth, our model shows good agreement with observations of solar wind velocity, proton temperature and density. AWSoM offers an extensive application to study the solar corona and larger heliosphere in concert with current and future solar missions as well as being well suited for space weather predictions.

IRIS Observational Approach to the Oscillatory and Damping Nature of Network and Internetwork Chromosphere Small-Scale Brightening (SSBs) and Their Unusual Dynamical and Morphological Differences in Different Regions on the Solar Disk.

Sadeghi, R., Tavabi, E.
Sol Phys 299, 106 (**2024**).

https://doi.org/10.1007/s11207-024-02347-2
One of the most exciting benefits of solar small-scale brightening is their oscillations. This study investigated the properties of small-scale brightening (SSBs) in different regions of the Sun and found that there are differences and similarities in the properties of oscillated and non-oscillated SSBs in different regions of the Sun, including quiet Sun (QS), the adjacent to active regions (AAR), and coronal hole (CH).
The damping per period (Q-factor) and maximum Doppler velocity of SSBs varied depending on the region, with the less bright internetwork SSBs in QS having lower damping time (120 seconds) and higher maximum Doppler velocities (47 km s−1) compared to the brighter network SSBs (with 216 seconds & 37 km s−1, respectively), while in AAR, internetwork SSBs tend to have higher damping time (about of 220 seconds) and wider maximum Doppler velocity (10 to 140 km s−1) ranges compared to network SSBs (130 seconds and 10 to 85 km s−1). In CH, both types of SSBs show similar damping time (120 seconds), but internetwork SSBs tend to have higher maximum Doppler velocities (100 km s−1) compared to network SSBs (85 km s−1).
It was also pointed out that the majority of network SSBs in AARs are in the overdamping mode, while in QS, internetwork SSBs demonstrate overdamping behavior and oscillated network SSBs exhibit critical damping behavior. However, it is important to remember that the physical mechanisms underlying the damping of SSBs may vary depending on the local plasma conditions and magnetic environment.

Dampening Long-Period Doppler Shift Oscillations using Deep Machine Learning Techniques in the Solar Network and Internetwork

Rayhaneh **Sadeghi**, Ehsan Tavabi
Advances in Space Research **2024**
https://arxiv.org/pdf/2406.10720
This study explores the Doppler shift at different wavelengths in the Interface Region Imaging Spectrograph (IRIS) solar spectrum and implements a comprehensive consideration of Doppler velocity oscillations in the IRIS channels. This comprehensive consideration reveals a propagating periodic perturbation in a large number of chromosphere and transition region (TR) bright points (BPs). To our knowledge, this is the first investigation of the longitudinal oscillations with damping in BPs using comprehensive consideration of the Doppler velocity at various wavelengths. The phenomena of attenuation in the red and blue Doppler shifts of the solar wavelength range were seen several times during the experiments. We utilized deep learning techniques to examine the statistical properties of damping in network and internetwork BPs, as well as active, quiet areas, and coronal hole areas. Our results revealed varying damping rates across different regions, with 80 percent of network BPs exhibiting damping in quiet areas and 72 in coronal hole areas. In active areas, the figure approached 33. For internetwork BPs, the values were 65, 54, and 63 percent for quiet areas, coronal hole areas, and active regions, respectively. The damping rate in active regions is twice as high at Internetwork's BPs. The damping components in this study were computed, and the findings show that the damping at all points is underdamped. The observed damping process suggests the propagation and leaking of energetic waves out of TR bright points, potentially contributing to the energy transport from the bright magnetic footpoints to the upper chromosphere, transition region, and corona.

The effect of flow on resonant absorption of slow MHD waves in magnetic flux tubes

Mohammad **Sadeghi**1 , Karam Bahari2 , Kayoomars Karami1
2021 *ApJ* **909** 201
https://arxiv.org/pdf/2101.02064.pdf
https://doi.org/10.3847/1538-4357/abdf49
In this paper, we study kink and sausage oscillations in the presence of longitudinal background flow. We study resonant absorption of the kink and sausage modes in the slow continuum under magnetic pore conditions in the presence of flow. we determine the dispersion relation then solve it numerically, and find the frequencies and damping rates of the slow kink and sausage surface modes. We also, obtain analytical solution for the damping rate of the slow surface mode in the long wavelength limit. We show that in the presence of plasma flow, resonance absorption can result in strong damping for forward waves and can be considered as an efficient mechanism to justify the extremely rapid damping of slow surface sausage waves observed in magnetic pores. Also, the plasma flow reduces the efficiency of resonance absorption to damp backward waves. Furthermore, for the pore conditions, the resonance instability is avoided in our model.

The effect of magnetic twist on resonant absorption of slow sausage waves in magnetic flux tubes

Mohammad **Sadeghi**, Kayoomars Karami
2019
https://arxiv.org/pdf/1903.04171.pdf
Observations show that twisted magnetic flux tubes are present throughout the sun's atmosphere. The main aim of this work is to obtain the damping rate of sausage modes in the presence of magnetic twist. Using the connection formulae obtained by Sakurai et al. (1991), we investigate resonant absorption of the sausage modes in the slow

continuum under photosphere conditions. We derive the dispersion relation and solve it numerically and consequently obtain the frequencies and damping rates of the slow surface sausage modes. We conclude that the magnetic twist can result in strong damping in comparison with the untwisted case.

Can Proton Beam Heating Flare Models Explain Sunquakes?

Viacheslav **Sadykov**, John Stefan, Alexander Kosovichev, Joel Allred, Graham S Kerr, Andrey Stejko, Adam Kowalski

2024 *ApJ* **960** 80

https://arxiv.org/pdf/2306.13162.pdf

https://iopscience.iop.org/article/10.3847/1538-4357/ad0cf3/pdf

SDO/HMI observations reveal a class of solar flares with substantial energy and momentum impacts in the photosphere, concurrent with white-light emission and helioseismic responses, known as sunquakes. Previous radiative hydrodynamic modeling has demonstrated the challenges of explaining sunquakes in the framework of the standard flare model of `electron beam' heating. One of the possibilities to explain the sunquakes and other signatures of the photospheric impact is to consider additional heating mechanisms involved in solar flares, for example, via flare-accelerated protons. In this work, we analyze a set of single-loop RADYN+FP simulations where the atmosphere is heated by non-thermal power-law-distributed proton beams which can penetrate deeper than the electron beams into the low atmospheric layers. Using the output of the RADYN models, we calculate synthetic Fe I 6173 A line Stokes profiles and from those the line-of-sight (LOS) observables of the SDO/HMI instrument, as well as the 3D helioseismic response and compare them with the corresponding observational characteristics. These initial results show that the models with proton beam heating can produce the enhancement of the HMI continuum observable and explain qualitatively generation of sunquakes. The continuum observable enhancement is evident in all models but is more prominent in ones with Ec≥500 keV. In contrast, the models with Ec≤100 keV provide a stronger sunquake-like helioseismic impact according to the 3D acoustic modeling, suggesting that low-energy (deka- and hecto-keV) protons have an important role in the generation of sunquakes.

Compression of Solar Spectroscopic Observations: a Case Study of Mg II k Spectral Line Profiles Observed by NASA's IRIS Satellite

Viacheslav M **Sadykov**, Irina N Kitiashvili, Alberto Sainz Dalda, Vincent Oria, Alexander G Kosovichev, Egor Illarionov

CBMI **2021**

https://arxiv.org/pdf/2103.07373.pdf

In this study we extract the deep features and investigate the compression of the Mg II k spectral line profiles observed in quiet Sun regions by NASA's IRIS satellite. The data set of line profiles used for the analysis was obtained on **April 20th, 2020**, at the center of the solar disc, and contains almost 300,000 individual Mg II k line profiles after data cleaning. The data are separated into train and test subsets. The train subset was used to train the autoencoder of the varying embedding layer size. The early stopping criterion was implemented on the test subset to prevent the model from overfitting. Our results indicate that it is possible to compress the spectral line profiles more than 27 times (which corresponds to the reduction of the data dimensionality from 110 to 4) while having a 4 DN average reconstruction error, which is comparable to the variations in the line continuum. The mean squared error and the reconstruction error of even statistical moments sharply decrease when the dimensionality of the embedding layer increases from 1 to 4 and almost stop decreasing for higher numbers. The observed occasional improvements in training for values higher than 4 indicate that a better compact embedding may potentially be obtained if other training strategies and longer training times are used. The features learned for the critical four-dimensional case can be interpreted. In particular, three of these four features mainly control the line width, line asymmetry, and line dip formation respectively. The presented results are the first attempt to obtain a compact embedding for spectroscopic line profiles and confirm the value of this approach, in particular for feature extraction, data compression, and denoising.

Connecting Atmospheric Properties and Synthetic Emission of Shock Waves Using 3D RMHD Simulations of Quiet Sun

Viacheslav M. **Sadykov**, Irina N. Kitiashvili, Alexander G. Kosovichev, Alan A. Wray

ApJ **909** 35 **2021**

https://arxiv.org/pdf/2008.05995.pdf

https://doi.org/10.3847/1538-4357/abd9c7

We analyze the evolution of shock waves in high-resolution 3D radiative MHD simulations of the quiet Sun and their synthetic emission characteristics. The simulations model the dynamics of a 12.8x12.8x15.2 Mm quiet-Sun region (including a 5.2 Mm layer of the upper convection zone and a 10 Mm atmosphere from the photosphere to corona) with an initially uniform vertical magnetic field of 10 G, naturally driven by convective flows. We synthesize the Mg II and C II spectral lines observed by the IRIS satellite and EUV emission observed by the SDO/AIA telescope. Synthetic observations are obtained using the RH1.5D radiative transfer code and temperature

response functions at both the numerical and instrumental resolutions. We found that the Doppler velocity jumps of the C II 1334.5 A IRIS line and a relative enhancement of the emission in the 335 A SDO/AIA channel are the best proxies for the enthalpy deposited by shock waves into the corona (with Kendall's τ correlation coefficients of 0.58 and 0.45, respectively). The synthetic emission of the lines and extreme ultraviolet passbands are correlated with each other during the shock wave propagation. All studied shocks are mostly hydrodynamic (i.e., the magnetic energy carried by horizontal fields is < 2.5% of the enthalpy for all events) and have Mach numbers > 1.0-1.2 in the low corona. The study reveals the possibility of diagnosing energy transport by shock waves into the solar corona, as well as their other properties, by using IRIS and SDO/AIA sensing observations.

Response of SDO/HMI Observables to Heating of the Solar Atmosphere by Precipitating High-energy Electrons

Viacheslav M. **Sadykov1**,2, Alexander G. Kosovichev1,3,4, Irina N. Kitiashvili1,2, and Graham S. Kerr5
2020 ApJ 893 24
https://doi.org/10.3847/1538-4357/ab7b6a
We perform an analysis of the line-of-sight (LOS) observables of the Helioseismic and Magnetic Imager (HMI) on board the Solar Dynamics Observatory (SDO) for models of the solar atmosphere heated by precipitating high-energy electrons during solar flares. The radiative hydrodynamic (RADYN) flare models are obtained from the F-CHROMA database. The Stokes profiles for the Fe 6173 Å line observed by SDO/HMI are calculated using the radiative transfer code RH1.5D, assuming statistical equilibrium for atomic level populations, and imposing uniform background vertical magnetic fields of various strengths. The SDO/HMI observing sequence and LOS data processing pipeline algorithm are applied to derive the observables (continuum intensity, line depth, Doppler velocity, LOS magnetic field). Our results reveal that the strongest deviations of the observables from the actual spectroscopic line parameters are found for the model with a total energy deposited of E total = 1.0 × 1012 erg cm−2, injected with a power-law spectral index of δ = 3 above a low-energy cutoff of E c = 25 keV. The magnitudes of the velocity and magnetic field deviations depend on the imposed magnetic field, and can reach 0.35 km s−1 for LOS velocities, 90 G for LOS magnetic field, and 3% for continuum enhancement for the 1000 G imposed LOS magnetic field setup. For E total ≥ 3.0 × 1011 erg cm−2 models, the velocity and magnetic field deviations are most strongly correlated with the energy flux carried by ~50 keV electrons, and the continuum enhancement is correlated with the synthesized ~55–60 keV hard X-ray photon flux. The relatively low magnitudes of perturbations of the observables and absence of magnetic field sign reversals suggest that the considered RADYN beam heating models augmented with the uniform vertical magnetic field setups cannot explain the strong transient changes found in the SDO/HMI observations.

Using MHD simulations to model H-alpha and UV spectral lines for interpretation of IRIS and NST data

Viacheslav M. **Sadykov**, Alexander G. Kosovichev
2014
http://arxiv.org/pdf/1412.0288v1.pdf
We present results of non-LTE modeling of H-alpha 6563 A and Mg II k&h 2796 A and 2803 A lines. This modeling is important for interpretation of coordinated observations from the recently launched NASA's IRIS mission and from the New Solar Telescope at Big Bear Solar Observatory. Among available codes for the non-LTE modeling, the RH code is chosen as the most appropriate for modeling of the line profiles. The most suitable Hydrogen and Magnesium atomic models are selected by performing several tests of the code. The influence of the ionization degree on the line profiles is also studied. Radiative-MHD simulations of the solar atmosphere, obtained with the Bifrost code, are used as input data for calculation of synthetic spectra of the H-alpha and Mg II h&k lines for particular locations evolving with time. The spectral line variations reveal the presence of MHD waves in the simulation results. We construct oscillation power spectra of the line intensity for different wavelength, and compare these with the corresponding height-dependent power spectra of atmospheric parameters from the simulations. We find correlations between the power spectra of intensities of the line profiles at certain wavelengths and the power spectra of the atmospheric parameters at the tau-unity heights for these wavelengths. These results provide a new diagnostic method of chromospheric oscillations; however, larger amounts of data are needed to confirm these correlations.

Nonlinear mean-field dynamo and prediction of solar activity

N. **Safiullin**, N. Kleeorin, S. Porshnev, I. Rogachevskii, A. Ruzmaikin
J. Plasma Phys. **2017**
https://arxiv.org/pdf/1712.07501.pdf
We apply a nonlinear mean-field dynamo model which includes a budget equation for the dynamics of Wolf numbers to predict solar activity. This dynamo model takes into account the algebraic and dynamic nonlinearities of the alpha effect, where the equation for the dynamic nonlinearity is derived from the conservation law for the magnetic helicity. The budget equation for the evolution of the Wolf number is based on a formation mechanism of

sunspots related to the negative effective magnetic pressure instability. This instability redistributes the magnetic flux produced by the mean-field dynamo. To predict solar activity on the time scale of one month we use a method based on a combination of the numerical solution of the nonlinear mean-field dynamo equations and the artificial neural network. A comparison of the results of the prediction of the solar activity with the observed Wolf numbers demonstrates a good agreement between the forecast and observations.

Understanding Grand Minima in Solar Activity: Confronting Observations with Dynamo Simulations

Chitradeep **Saha**, Dibyendu Nandy
Proceedings IAU Symposium No. 365: Dynamics of Solar and Stellar Convection Zones and Atmospheres, **2024**
https://arxiv.org/pdf/2409.09775
The grand minimum in the Sun's activity is a distinctive mode characterized by a magnetic lull that almost completely lacks the emergence of sunspots on the solar surface for an extended duration. The factors driving this transition of an otherwise magnetically active star into a quiescent phase, the processes occurring within the solar interior and across the heliosphere during this period, and the mechanisms leading to the eventual resurgence of surface magnetic activity remain enigmatic. However, there have been sustained efforts in the past few decades to unravel these mysteries by employing a combination of observation, reconstruction and simulation of solar magnetic variability. Here, we summarize recent research on the solar grand minimum and highlight some outstanding challenges - both intellectual and practical - that necessitate further investigations.

Evidence of persistence of weak magnetic cycles driven by meridional plasma flows during solar grand minima phases

Chitradeep **Saha**, Sanghita Chandra, Dibyendu Nandy
MNRAS Letters Volume 517 Issue 1 November **2022** Pages L36-L40
https://arxiv.org/pdf/2209.14651.pdf
Long-term sunspot observations and solar activity reconstructions reveal that the Sun occasionally slips into quiescent phases known as solar grand minima, the dynamics during which is not well understood. We use a flux transport dynamo model with stochastic fluctuations in the mean-field and Babcock-Leighton poloidal field source terms to simulate solar cycle variability. Our long-term simulations detect a gradual decay of the polar field during solar grand minima episodes. Although regular active region emergence stops, compromising the Babcock-Leighton mechanism, weak magnetic activity continues during minima phases sustained by a mean-field α-effect; surprisingly, periodic polar field amplitude modulation persist during these phases. A spectral analysis of the simulated polar flux time series shows that the 11-year cycle becomes less prominent while high frequency periods and periods around 22 years manifest during grand minima episodes. Analysis of long-term solar open flux observations appears to be consistent with this finding. Through numerical experimentation we demonstrate that the persistence of periodic amplitude modulation in the polar field and the dominant frequencies during grand minima episodes are governed by the speed of the meridional plasma flow -- which appears to act as a clock.

Spatial and Temporal Analysis of Quiescent Coronal Rain over an Active Region

Seray **Şahin**, Patrick Antolin, Clara Froment, Thomas A. Schad
ApJ **950** 171 **2023**
https://arxiv.org/pdf/2305.08775.pdf
https://iopscience.iop.org/article/10.3847/1538-4357/acd44b/pdf
The solar corona produces coronal rain, hundreds of times colder and denser material than the surroundings. Coronal rain is known to be deeply linked to coronal heating, but its origin, dynamics, and morphology are still not well understood. The leading theory for its origin is thermal instability (TI) occurring in coronal loops in a state of thermal non-equilibrium (TNE), the TNE-TI scenario. Under steady heating conditions, TNE-TI repeats in cycles, leading to long-period EUV intensity pulsations and periodic coronal rain. In this study, we investigate coronal rain on the large spatial scales of an active region (AR) and over the long temporal scales of EUV intensity pulsations to elucidate its distribution at such scales. We conduct a statistical study of coronal rain observed over an AR off-limb with IRIS and SDO imaging data, spanning chromospheric to transition region (TR) temperatures. The rain is widespread across the AR, irrespective of the loop inclination, and with minimal variation over the 5.45-hour duration of the observation. Most rain has a downward (87.5%) trajectory; however, upward motions (12.5%) are also ubiquitous. The rain dynamics are similar over the observed temperature range, suggesting that the TR and chromospheric emission are co-located on average. The average clump widths and lengths are similar in the SJI channels and wider in the AIA 304 channel. We find ubiquitous long-period EUV intensity pulsations in the AR. Short-term periodicity is found (16 min) linked to the rain appearance, which constitutes a challenge to explain under the TNE-TI scenario. **2017 June 2**
IRIS Nugget Mar **2024** https://iris.lmsal.com/nugget

Prevalence of Thermal Nonequilibrium over an Active Region

Seray **Şahin**1 and Patrick Antolin1

2022 ApJL 931 L27

https://iopscience.iop.org/article/10.3847/2041-8213/ac6fe9/pdf

https://arxiv.org/pdf/2205.10794.pdf

Recent observations have shown that besides the characteristic multi-million degree component the corona also contains a large amount of cool material called coronal rain, whose clumps are 10 - 100 times cooler and denser than the surroundings and are often organised in larger events termed showers. Thermal instability (TI) within a coronal loop in a state of thermal non-equilibrium (TNE) is the leading mechanism behind the formation of coronal rain but no investigation on showers exists to date. In this study, we conduct a morphological and thermodynamic multi-wavelength study of coronal rain showers observed in an active region (AR) off-limb with IRIS and SDO, spanning chromospheric to transition region and coronal temperatures. Rain showers were found to be widespread across the AR over the 5.45-hour observing time, with average length, width and duration of 27.37±11.95 Mm, 2.14±0.74 Mm, and 35.22±20.35 min, respectively. We find a good correspondence between showers and the cooling coronal structures consistent with the TNE-TI scenario, thereby properly identifying coronal loops in the 'coronal veil', including the strong expansion at low heights and an almost zero expansion in the corona. This agrees with previous work suggesting that the observed zero expansion in the EUV is due to specific cross-field temperature distribution. We estimate the total number of showers to be 155±40, leading to a TNE volume of 4.56±3.71 × 1028cm3, i.e. on the same order of the AR volume. This suggests a prevalence of TNE over the AR indicating strongly stratified and high-frequency heating on average. **2 June 2017**

Grid-based imaging of X-rays and gamma-rays with high angular resolution

Pascal **Saint-Hilaire** ∗ , Albert Y. Shih, Gordon J. Hurford, Brian Dennis

In the 'Handbook of X-ray and Gamma-Ray Astrophysics' **2022**

http://sprg.ssl.berkeley.edu/~shilaire/papers/Grid_imaging_in_X_rays_and_gamma_ray.pdf

This chapter contains an overview of the basic principles of X-ray and gamma-ray imaging for astronomy that achieve high angular resolution with nonfocusing optics. Specific topics include systems with single-grid masks, with pairs of grids known as bi-grid collimators, and with more than two grids known as multigrid collimators. A discussion of each type is given along with advantages and limitations of the various design options and descriptions of actual implementations. **1980 April 30, January 20, 2005, 7-9 May 2021**

Thomson scattering in the lower corona in the presence of sunspots

Pascal **Saint-Hilaire**, Juan-Carlos Martinez Oliveros, Hugh S. Hudson

ApJ **923** 276 **2021**

http://sprg.ssl.berkeley.edu/~shilaire/papers/PSH2021_Thomson_sunspots.pdf

https://iopscience.iop.org/article/10.3847/1538-4357/ac2f9b/pdf

https://doi.org/10.3847/1538-4357/ac2f9b

Polarized scattered light from low (few tens of Mm altitudes) coronal transients has been recently reported in SDO/HMI observations. In a classic paper, Minnaert (1930) provided an analytic theory of polarization via electron scattering in the corona. This work assumed axisymmetric input from the photosphere with a single-parameter limb-darkening function. This diagnostic has recently been used to estimate free electron number and mass of HMI transients near the solar limb, but it applies equally well to any coronal material, at any height. Here we extend this work numerically to incorporate sunspots, which can strongly effect the polarization properties of the scattered light in the low corona.

Sunspot effects are explored first for axisymmetric model cases, and then applied to the full description of two sunspot groups as observed by HMI. We find that, 1) As previously reported by Minnaert, limb darkening has a strong influence, usually increasing the level of linear polarization tangential to the limb; 2) Unsurprisingly, the effects of the sunspot generally increase at the lower scatterer altitudes, the larger the sunspot is, and the closer to their center the scatterer subpoint is; 3) Assuming the Stokes Q>0 basis to be tangential to the limb, sunspots typically decrease the Stokes Q/I polarization and the perceived electron densities below the spotless case, sometimes dramatically; 4) Typically, a sizeable non-zero Stokes U/I polarization component will appear when a sunspot's influence becomes non-negligible. However, that is not true in rare cases of extreme symmetry (e.g. scattering mass at the center of an axisymetric sunspot). The tools developed here are generally applicable to an arbitrary image input.

RHESSI Science Nugget, No. **419**, Nov **2021**

https://sprg.ssl.berkeley.edu/~tohban/wiki/index.php/Thomson_scattering_near_sunspots

Precise Formation-Flying Telescope in Target-Centric Orbit: the Solar Case Pascal

Saint-Hilaire1 ·Jeffrey E. Marchese1

The Journal of the Astronautical Sciences **2020**

https://doi.org/10.1007/s40295-020-00231-2

http://sprg.ssl.berkeley.edu/~shilaire/papers/PSH2020_scopocentricPFFtelescope.pdf
We present the general concept of a telescope with optics and detectors mounted on two separate spacecrafts, in orbit around the telescope's target (scopocentric or target-centric orbit), and using propulsion to maintain the Target-Optics-Detector alignment and Optics-Detector distance. Specifically, we study the case of such a telescope with the Sun as the target, orbiting at ~1 AU. Of prime interest are heliocentric orbits (such as Earth-trailing/leading orbits or Distant Retrograde Orbits), where thrust requirement to maintain formation is primarily in a single direction (either sunward or anti-sunward), can be quite minuscule (a few m/s/year), and preferably met by constant-thrust engines such as solar electric propulsion or even by solar sailing via simple extendable and/or orientable flaps or rudders

Spectropolarimetry of the Solar Mg II h and k Lines

R. Manso **Sainz**, T. del Pino Alemán, R. Casini, S. McIntosh
ApJL **883** L30 **2019**
https://arxiv.org/pdf/1909.05574.pdf
https://doi.org/10.3847/2041-8213/ab412c
We report on spectropolarimetric observations across the Mg II h and k-lines at 2800 angstrom made by the Ultraviolet Spectrometer and Polarimeter onboard the Solar Maximum Mission satellite. Our analysis confirms the strong linear polarization in the wings of both lines observed near the limb, as previously reported, but also demonstrates the presence of a negatively (i.e., radially oriented) polarized signal between the two lines. We find evidence for fluctuations of the polarization pattern over a broad spectral range, resulting in some depolarization with respect to the pure scattering case when observed at very low spatial and temporal resolutions. This is consistent with recent theoretical modeling that predicts this to be the result of redistribution effects, quantum interference between the atomic levels of the upper term, and magneto-optical effects. A first attempt at a quantitative exploitation of these signals for the diagnosis of magnetic fields in the chromosphere is attempted. In active regions, we present observations of circular polarization dominated by the Zeeman effect. We are able to constrain the magnetic field strength in the upper active chromosphere using an analysis based on the magnetograph formula, as justified by theoretical modeling. We inferred a significantly strong magnetic field (~500 G) at the 2.5 sigma level on an exceptionally active, flaring region.

Energy Transfer by Nonlinear Alfvén Waves in the Solar Chromosphere, and Its Effect on Spicule Dynamics, Coronal Heating, and Solar Wind Acceleration

Takahito **Sakaue**, Kazunari Shibata
ApJ **900** 120 **2020**
https://arxiv.org/pdf/2008.00643.pdf
https://doi.org/10.3847/1538-4357/ababa0
Alfvén waves are responsible for the transfer of magnetic energy in the magnetized plasma. They are involved in heating solar atmosphere and driving solar wind through various nonlinear processes. Since the magnetic field configurations directly affect the nonlinearity of Alfvén waves, it is important to investigate how they relate to the solar atmosphere and wind structure through the nonlinear propagation of Alfvén waves. In this study, we carried out the one-dimensional magnetohydrodynamic simulations to realize the above relation. The results show that when the nonlinearity of Alfvén waves in the chromosphere exceeds a critical value, the dynamics of the solar chromosphere (e.g., spicule) and the mass loss rate of solar wind tend to be independent of the energy input from the photosphere. In a situation where the Alfvén waves are highly nonlinear, the strong shear torsional flow generated in the chromosphere ``fractures" the magnetic flux tube. This corresponds to the formation of chromospheric intermediate shocks, which limit the transmission of the Poynting flux into the corona by Alfvén waves and also inhibits the propagation of chromospheric slow shock.

Photospheric activity of the Sun with VIRGO and GOLF: Comparison with standard activity proxies

D. **Salabert**, R.A. García, A Jiménez, L. Bertello, E. Corsaro, P.L. Pallé
A&A 608, A87 **2017**
https://arxiv.org/pdf/1709.05110.pdf
We study the variability of solar activity using new photospheric proxies originally developed for the analysis of stellar magnetism with the CoRoT and Kepler photometric observations. These proxies are obtained by tracking the temporal modulations in the observations associated to the spots and magnetic features as the Sun rotates. We analyze here 21 years, spanning solar cycles 23 and 24, of the observations collected by the space-based photometric VIRGO and radial velocity GOLF instruments on board the SoHO satellite. The photospheric activity proxy Sph is then calculated for each of the three VIRGO photometers as well as the associated Svel proxy from the radial velocity GOLF observations. Comparisons with several standard solar activity proxies sensitive to different layers of the Sun demonstrate that these new activity proxies, Sph and Svel, provide a new manner to monitor solar activity. We show that both the long- and short-term magnetic variabilities respectively associated to the 11-year cycle and the quasi-biennial oscillation are well monitored, and that the magnetic field interaction between the subsurface, the

photosphere, and the chromosphere of the Sun, was modified between Cycle 24 and Cycle 23. Furthermore, the photometric proxies show a wavelength dependence of the response function of the solar photosphere among the three channels of the VIRGO photometers, providing inputs for the study of the stellar magnetism of Sun-like stars.

Seismic sensitivity to sub-surface solar activity from 18 years of GOLF/SoHO observations

D. **Salabert**, R. A. Garcia, S. Turck-Chieze
A&A, 578, A137 **2015**
http://arxiv.org/pdf/1502.07607v1.pdf
Solar activity has significantly changed over the last two Schwabe cycles. After a long and deep minimum at the end of Cycle 23, the weaker activity of Cycle 24 contrasts with the previous cycles. In this work, the response of the solar acoustic oscillations to solar activity is used in order to provide insights on the structural and magnetic changes in the sub-surface layers of the Sun during this on-going unusual period of low activity. We analyze 18 years of continuous observations of the solar acoustic oscillations collected by the Sun-as-a-star GOLF instrument onboard the SoHO spacecraft. From the fitted mode frequencies, the temporal variability of the frequency shifts of the radial, dipolar, and quadrupolar modes are studied for different frequency ranges which are sensitive to different layers in the solar sub-surface interior. The low-frequency modes show nearly unchanged frequency shifts between Cycles 23 and 24, with a time evolving signature of the quasi-biennial oscillation, which is particularly visible for the quadrupole component revealing the presence of a complex magnetic structure. The modes at higher frequencies show frequency shifts 30% smaller during Cycle~24, which is in agreement with the decrease observed in the surface activity between Cycles 23 and 24. The analysis of 18 years of GOLF oscillations indicates that the structural and magnetic changes responsible for the frequency shifts remained comparable between Cycle 23 and Cycle 24 in the deeper sub-surface layers below 1400 km as revealed by the low-frequency modes. The frequency shifts of the higher-frequency modes, sensitive to shallower regions, show that Cycle 24 is magnetically weaker in the upper layers of Sun.

Helioseismic inferences of the solar cycles 23 and 24: GOLF and VIRGO observations

D. **Salabert**, R.A. Garcia, A. Jimenez
Proceedings of the SF2A **2014** Conference
http://arxiv.org/pdf/1411.0396v1.pdf
The Sun-as-a-star helioseismic spectrophotometer GOLF and photometer VIRGO instruments onboard the SoHO spacecraft are collecting high-quality, continuous data since April 1996. We analyze here these unique datasets in order to investigate the peculiar and weak on-going solar cycle 24. As this cycle 24 is reaching its maximum, we compare its rising phase with the rising phase of the previous solar cycle 23.

Generation and Life Cycle of Solar Spicules

Hamid **Saleem**1,2,3 and Zain H. Saleem4
2024 ApJ 967 9
https://iopscience.iop.org/article/10.3847/1538-4357/ad372b/pdf
The physical mechanism for the creation of solar spicules is proposed with three stages of their life cycle. It is assumed that at stage I the density hump is formed locally in the x-y plane in the lower chromosphere in the presence of temperature gradients of electrons and ions along the z-axis (the vertical direction). In this region, the density structure of quasi-neutral ($n_i \simeq n_e = n$) plasma after taking birth is accelerated in the vertical direction owing to the thermal force $F_{th} \propto \nabla n(x, y, t) \times (\nabla T_e + \nabla T_i)$. The exact time-dependent analytical solution of two-fluid plasma equations is presented assuming that density is maximum at the center of the density structure and decays away from it gradually. The 2D density structure is created as a step function H(t) in time at the bottom of the chromosphere, and consequently, the vertical plasma velocity turns out to be the ramp function of time R(t) = tH(t), whereas the source term S(x, y, t) for the density follows the delta function δ(t) form. The upward acceleration $a = a(x, y)\hat{z}$ produced in this density structure is greater than the downward constant solar acceleration $-g_\odot$ in the chromosphere. In the transition region, the temperature gradients are steeper; therefore, the upward acceleration increases in magnitude $g_\odot \ll a$ and the density hump spends less time there. This is stage II of its life cycle. In stage III, the density structure enters into the corona, where the gradients of temperatures vanish and the structure decelerates to zero velocity under the action of the solar gravitational force.

Generation of Short-scale Electrostatic Fields in the Solar Atmosphere and the Role of Helium Ions

H. **Saleem**1,2,3, Shaukat Ali Shan3,4, and A. Rehman3,5,6
2021 ApJ 922 48
https://doi.org/10.3847/1538-4357/ac05cb

Theoretical models are presented to show that expansion of plasma in the radial direction from a denser solar surface to a rarefied upper atmosphere with short-scale inhomogeneous field-aligned flows and currents in the form of thin threads itself is an important source of electrostatic instabilities. Multifluid theory shows that the shear flow–driven purely growing electric fields appear in the transition region. On the other hand, plasma kinetic theory predicts that the short-scale current sheets (or filaments) produce current-driven electrostatic ion acoustic (CDEIA) waves in the hydrogen plasma of the transition region that damp out in the system through wave–particle interactions and increase the temperature. Similar processes take place in the solar corona and act positively for increasing the temperature further and maintaining it. The shear flow–driven instabilities and CDEIA waves have short perpendicular wavelengths of the order of 1 m and low frequencies of the order of 1 or several Hz when the ions' shear flow scale length is considered to be of the order of 1 km. It is pointed out that the purely growing fluid instabilities turn into oscillatory instabilities and the growth rates of kinetic CDEIA wave instabilities are reduced when the dynamics of 10% helium ions is taken into account along with 90% hydrogen ions. Therefore, the role of helium ions should not be ignored in the study of wave dynamics in solar plasma.

Standard solar models: a perspective from updated solar neutrino fluxes and the gravity-mode period spacing

Sébastien **Salmon**, Gaël Buldgen, Arlette Noels, Patrick Eggenberger, Richard Scuflaire, Georges Meynet

A&A **2021**

https://arxiv.org/pdf/2105.00911.pdf

Context: The Sun is by far a privileged target for testing stellar models with unique precision. A recent concern appeared with the progress in the solar surface abundances derivation that has led to a decrease of the solar metallicity. While the ancient high-metallicity models were in fair agreement with other solar observational indicators, it is no longer the case for low-metallicity models. Recent collection of data are however promising to shed a new light on it. For instance, the Borexino collaboration released in 2020 the first-ever complete estimate of neutrinos emitted in the CNO cycle. It has reaffirmed the role of the neutrino constraints in the solar modelling process and its associated issues. In parallel, newly claimed detection of solar gravity modes of oscillations offers another opportunity of probing the stratification in the Sun's central layers. Aims: We propose to combine the diagnoses from neutrinos and helioseismology, both from pressure and gravity modes, for assessing the predictions of solar models. We compare in detail the different physical prescriptions currently at disposal for stellar model computations. Results: The CNO neutrino flux confirms a preference for high-metallicity models. Nevertheless, we found that mild modification of the nuclear screening factors can re-match low-metallicity model predictions to observed fluxes, although it does not restore the agreement with the helioseismic frequency ratios. Neither the high-metallicity or low-metallicity models are able to reproduce the gravity-mode period spacing. The disagreement is huge, more than 100σ to the reported value. Reversely, the family of standard models narrows the expected range of the Sun's period spacing: between ~2150 to ~2190~s. Moreover, we show this indicator can constrain the chemical mixture, opacity, and to a lower extent nuclear reactions in solar models.

Exploring the Limits of Synthetic Creation of Solar EUV Images via Image-to-image Translation

Valentina **Salvatelli**1,2,3, Luiz F. G. dos Santos4, Souvik Bose5,6,7,8, Brad Neuberg1,2,9, Mark C. M. Cheung7, Miho Janvier10, Meng Jin2,7, Yarin Gal11, and Atilim Güneş Baydin12

2022 ApJ 937 100

https://iopscience.iop.org/article/10.3847/1538-4357/ac867b/pdf

The Solar Dynamics Observatory (SDO), a NASA multispectral decade-long mission that has been daily producing terabytes of observational data from the Sun, has been recently used as a use case to demonstrate the potential of machine-learning methodologies and to pave the way for future deep space mission planning. In particular, the idea of using image-to-image translation to virtually produce extreme ultraviolet channels has been proposed in several recent studies, as a way to both enhance missions with fewer available channels and to alleviate the challenges due to the low downlink rate in deep space. This paper investigates the potential and the limitations of such a deep learning approach by focusing on the permutation of four channels and an encoder–decoder based architecture, with particular attention to how morphological traits and brightness of the solar surface affect the neural network predictions. In this work we want to answer the question: can synthetic images of the solar corona produced via image-to-image translation be used for scientific studies of the Sun? The analysis highlights that the neural network produces high-quality images over 3 orders of magnitude in count rate (pixel intensity) and can generally reproduce the covariance across channels within a 1% error. However, the model performance drastically diminishes in correspondence to extremely high energetic events like flares, and we argue that the reason is related to the rareness of such events posing a challenge to model training. **2011-02-10, 2011-02-15**

Using U-Nets to Create High-Fidelity Virtual Observations of the Solar Corona

Valentina **Salvatelli**, Souvik Bose, Brad Neuberg, Luiz F. G. dos Santos, Mark Cheung, Miho Janvier, Atilim Gunes Baydin, Yarin Gal, Meng Jin
NeurIPS 2019 Workshop ML4PS **2019**
https://arxiv.org/pdf/1911.04006.pdf
Understanding and monitoring the complex and dynamic processes of the Sun is important for a number of human activities on Earth and in space. For this reason, NASA's Solar Dynamics Observatory (SDO) has been continuously monitoring the multi-layered Sun's atmosphere in high-resolution since its launch in 2010, generating terabytes of observational data every day. The synergy between machine learning and this enormous amount of data has the potential, still largely unexploited, to advance our understanding of the Sun and extend the capabilities of heliophysics missions. In the present work, we show that deep learning applied to SDO data can be successfully used to create a high-fidelity virtual telescope that generates synthetic observations of the solar corona by image translation. Towards this end we developed a deep neural network, structured as an encoder-decoder with skip connections (U-Net), that reconstructs the Sun's image of one instrument channel given temporally aligned images in three other channels. The approach we present has the potential to reduce the telemetry needs of SDO, enhance the capabilities of missions that have less observing channels, and transform the concept development of future missions.

Generation of Solar Spicules and Subsequent Atmospheric Heating

Tanmoy **Samanta**, Hui Tian, Vasyl Yurchyshyn, Hardi Peter, Wenda Cao, Alphonse Sterling, Robertus Erdélyi, Kwangsu Ahn, Song Feng, Dominik Utz, Dipankar Banerjee, Yajie Chen
Science 366, 890 (**2019**)
https://arxiv.org/ftp/arxiv/papers/2006/2006.02571.pdf
Spicules are rapidly evolving fine-scale jets of magnetized plasma in the solar chromosphere. It remains unclear how these prevalent jets originate from the solar surface and what role they play in heating the solar atmosphere. Using the Goode Solar Telescope at the Big Bear Solar Observatory, we observed spicules emerging within minutes of the appearance of opposite-polarity magnetic flux around dominant-polarity magnetic field concentrations. Data from the Solar Dynamics Observatory showed subsequent heating of the adjacent corona. The dynamic interaction of magnetic fields (likely due to magnetic reconnection) in the partially ionized lower solar atmosphere appears to generate these spicules and heat the upper solar atmosphere.

Evidence for Vortex Shedding in the Sun's Hot Corona

Tanmoy **Samanta**, Hui Tian, Valery M. Nakariakov
Phys. Rev. Lett. 123, 035102 **2019**
https://arxiv.org/pdf/1907.08930.pdf
Vortex shedding is an oscillating flow that is commonly observed in fluids due to the presence of a blunt body in a flowing medium. Numerical simulations have shown that the phenomenon of vortex shedding could also develop in the magnetohydrodynamic (MHD) domain. The dimensionless Strouhal number, the ratio of the blunt body diameter to the product of the period of vortex shedding and the speed of a flowing medium, is a robust indicator for vortex shedding, and, generally of the order of 0.2 for a wide range of Reynolds number. Using an observation from the Atmospheric Imaging Assembly on board the Solar Dynamics Observatory, we report a wavelike or oscillating plasma flow propagating upward against the Sun's gravitational force. A newly formed shrinking loop in the post-flare region possibly generates the oscillation of the upflow in the wake of the hot and dense loop through vortex shedding. The computed Strouhal number is consistent with the prediction from previous MHD simulations. Our observation suggests the possibility of vortex shedding in the solar corona.

The effects of transients on photospheric and chromospheric power distributions

T. **Samanta**, V. M. J. Henriques, D. Banerjee, S. Krishna Prasad, M. Mathioudakis, D. Jess, V. Pant
ApJ **828** 23 **2016**
http://arxiv.org/pdf/1604.06289v1.pdf
We have observed a quiet Sun region with the Swedish 1-meter Solar Telescope (SST) equipped with CRISP Imaging SpectroPolarimeter. High-resolution, high-cadence, Hα line scanning images were taken to observe different layers of the solar atmosphere from the photosphere to upper chromosphere. We study the distribution of power in different period-bands at different heights. Power maps of the upper photosphere and the lower chromosphere show suppressed power surrounding the magnetic-network elements, known as "magnetic shadows". These also show enhanced power close to the photosphere, traditionally referred to as "power halos". The interaction between acoustic waves and inclined magnetic fields is generally believed to be responsible for these two effects. In this study we explore if small-scale transients can influence the distribution of power at different heights. We show that the presence of transients, like mottles, Rapid Blueshifted Excursions (RBEs) and Rapid Redshifted Excursions (RREs), can strongly influence the power-maps. The short and finite lifetime of these events strongly affects all powermaps, potentially influencing the observed power distribution. We show that Doppler-shifted transients like RBEs and RREs that occur ubiquitously, can have a dominant effect on the formation of the power halos in the quiet

Sun. For magnetic shadows, transients like mottles do not seem to have a significant effect in the power suppression around 3 minutes and wave interaction may play a key role here. Our high cadence observations reveal that flows, waves and shocks manifest in presence of magnetic fields to form a non-linear magnetohydrodynamic system.

Detection of high frequency oscillations and damping from multi-slit spectroscopic observations of the corona

T. **Samanta**, J. Singh, G. Sindhuja, D. Banerjee
Solar Physics January **2016**, Volume 291, Issue 1, pp 155-174
http://arxiv.org/pdf/1511.07160v1.pdf
During the total solar eclipse of **11 July 2010**, multi-slit spectroscopic observations of the solar corona were performed from Easter Island, Chile. To search for high-frequency waves, observations were taken at a high cadence in the green line at 5303 A due to [Fe xiv] and the red line at 6374 A due to [Fe x]. The data are analyzed to study the periodic variations in the intensity, Doppler velocity and line width using wavelet analysis. The data with high spectral and temporal resolution enabled us to study the rapid dynamical changes within coronal structures. We find that at certain locations each parameter shows significant oscillation with periods ranging from 6 - 25 s. For the first time, we could detect damping of high-frequency oscillations with periods of the order of 10 s. If the observed damped oscillations are due to magnetohydrodynamic (MHD) waves then they can contribute significantly in the heating of the corona. From a statistical study we try to characterize the nature of the observed oscillations while looking at the distribution of power in different line parameters.

Propagating Disturbances in The Solar Corona and Spicular Connection

Tanmoy **Samanta**, Vaibhav Pant, Dipankar Banerjee
ApJL 815 L16 **2015**
http://arxiv.org/pdf/1511.07354v1.pdf
Spicules are small hairy like structures seen at the solar limb mainly at chromospheric and transition region lines. They generally live for 3-10 minutes. We observe these spicules in a south polar region of the Sun with a coordinated observations using the Interface Region Imaging Spectrograph (IRIS) and the Atmospheric Imaging Assembly (AIA) instruments on board the Solar Dynamics Observatory. Propagating disturbances (PDs) are observed everywhere in the polar off-limb regions of the Sun at coronal heights. From this simultaneous observations we show that the spicules and the PDs may be originated by a common process. From space-time maps we find that the start of the trajectory of PDs is almost co-temporal with the time of the rise of the spicular envelope as seen by IRIS slit-jaw images at 2796 {\deg}A and 1400 A{\deg} . During the return of spicular material, brightenings are seen in AIA 171 {\deg}A and 193 {\deg}A images. The quasi-periodic nature of the spicular activity as revealed by the IRIS spectral image sequences and its relation to coronal PDs as recorded by the coronal AIA channels suggest that they have a common origin. We propose that reconnection like processes generate the spicules and waves simultaneously. The waves escape while the cool spicular material falls back.
21 February 2014

The solar nitrogen abundance under the LTE assumption

Sameh I.S, M. M. Beheary, Abdelrazek M. K. Shaltout
Bulletin of Science Al-Azhar University **2018**
https://arxiv.org/ftp/arxiv/papers/1809/1809.05404.pdf
The solar chemical abundances studied in considerable detail because of discrepant values of solar metallicity inferred from different indicators, where in the present work we have used 28 suitable atomic spectral solar nitrogen lines, relying on new equivalent widths measurements for determining the nitrogen abundance. Corresponding to 28 solar neutral nitrogen lines, we derived a solar abundance of nitrogen using the Holweger and Muller solar model and the measured equivalent widths from the literature. Our study reported the solar nitrogen abundance result to be of 8.05 (sigma = 0.09) using gf-values from Wiese and Fuhr.

New Observations of the IR Emission Corona from the 2019 July 2 Eclipse Flight of the Airborne Infrared Spectrometer

Jenna E. **Samra**1, Chad A. Madsen1, Peter Cheimets1, Edward E. DeLuca1, Leon Golub1, Vanessa Marquez1, and Naylynn Tañón Reyes2
2022 ApJ 933 82
https://iopscience.iop.org/article/10.3847/1538-4357/ac6ce8/pdf
The Airborne Infrared Spectrometer (AIR-Spec) was commissioned during the 2017 total solar eclipse, when it observed five infrared coronal emission lines from a Gulfstream V research jet owned by the National Science

Foundation and operated by the National Center for Atmospheric Research. The second AIR-Spec research flight took place during the 2019 July 2 total solar eclipse across the south Pacific. The 2019 eclipse flight resulted in seven minutes of observations, during which the instrument measured all four of its target emission lines: S xi 1.393 μm, Si x 1.431 μm, S xi 1.921 μm, and Fe ix 2.853 μm. The 1.393 μm S xi line was detected for the first time, and probable first detections were made of Si xi 1.934 μm and Fe x 1.947 μm. The 2017 AIR-Spec detection of Fe ix was confirmed and the first observations were made of the Fe ix line intensity as a function of solar radius. Telluric absorption features were used to calibrate the wavelength mapping, instrumental broadening, and throughput of the instrument. AIR-Spec underwent significant upgrades in preparation for the 2019 eclipse observation. The thermal background was reduced by a factor of 30, providing a 5.5× improvement in signal-to-noise ratio, and the postprocessed pointing stability was improved by a factor of 5 to <10" rms. In addition, two imaging artifacts were identified and resolved, improving the spectral resolution and making the 2019 data easier to interpret.

The Airborne Infrared Spectrometer: Development, Characterization, and the 21 August 2017 Eclipse Observation

Jenna E. **Samra**, Vanessa Marquez, Peter Cheimets, Edward E. DeLuca, Leon Golub, James W. Hannigan, Chad A. Madsen, Alisha Vira

ApJ **2021**

https://arxiv.org/pdf/2105.09419.pdf

On August 21, 2017, the Airborne Infrared Spectrometer (AIR-Spec) observed the total solar eclipse at an altitude of 14 km from aboard the NSF/NCAR Gulfstream V research aircraft. The instrument successfully observed the five coronal emission lines that it was designed to measure: Si X 1.431 μm, S XI 1.921 μm, Fe IX 2.853 μm, Mg VIII 3.028 μm, and Si IX 3.935 μm. Characterizing these magnetically sensitive emission lines is an important first step in designing future instruments to monitor the coronal magnetic field, which drives space weather events as well as coronal heating, structure, and dynamics. The AIR-Spec instrument includes an image stabilization system, feed telescope, grating spectrometer, and slit-jaw imager. This paper details the instrument design, optical alignment method, image processing, and data calibration approach. The eclipse observations are described and the available data are summarized.

Geoeffectiveness of stream interaction regions during 2007–2008

E. **Sanchez-Garcia**, E. Aguilar-Rodriguez, V. Ontiveros, J. A. Gonzalez-Esparza

Space Weather Volume 15, Issue 8 August **2017** Pages 1052–1067

http://sci-hub.cc/10.1002/2016SW001559

The stream interaction regions (SIRs) are generated in the interplanetary medium when a fast solar wind stream overtakes a slower one. If these large-scale phenomena interact with the Earth's magnetosphere, they can give rise to geomagnetic storms (GSs). Their geoeffectivity is measured using magnetic indices at different latitudes. In this study we analyzed the geoeffectiveness of 20 GSs that were generated by SIRs during the period of 2007 to 2008 and observed by the ACE, Wind, and STEREO-A/B spacecraft. We compared the geomagnetic response to the SIRs-magnetosphere interaction employing different geomagnetic indices at low, middle, and high latitudes. The geoeffectiveness was 50%, 55%, and 90% using the criteria of the aa, Kp, and SYM-H indices, respectively. We found that in most cases the maximum intensity of each index was in the weak to moderate range. According to the SYM-H index, a 10%, 60%, and 10% of the forward shocks were followed by quiet, weak, and moderate GSs, respectively. The 10% and 20%, however, were followed by minor and moderate GSs, respectively, according to the Kp index. We analyzed the geoeffective region within the SIRs with respect to the relative position of the stream interface (SI). For 75% of GSs, their maximum intensity occurred during the disturbed fast solar wind (after the passing of the SI), which would be related to the efficiency of a SIR. The time difference Δt between the passing of the SI and the maximum intensity in each index was less than 36 h. **March 7-10, 2008**

Table 3. Shock parameters associated with SIRs registered by WIND, ACE, and/or STEREOA/B observed during the period of 2007 to 2008 (columns 2-9). Date and time of the passing of the SI (columns 10-11). Geoeffectiveness generated by the SIRs-magnetosphere interaction (columns 12-18).

Observational evidence for the associated formation of blobs and raining inflows in the solar Corona

Eduardo **Sanchez-Diaz**, Alexis P. Rouillard, Jackie A. Davies, Benoit Lavraud, Neil R. Sheeley, Rui F. Pinto, Emilia Kilpua, Illya Plotnikov, Vincent Genot

ApJL **2016**

https://arxiv.org/pdf/1612.05487v1.pdf

The origin of the slow solar wind is still a topic of much debate. The continual emergence of small transient structures from helmet streamers is thought to constitute one of the main sources of the slow wind. Determining the height at which these transients are released is an important factor in determining the conditions under which the

slow solar wind forms. To this end, we have carried out a multipoint analysis of small transient structures released from a north-south tilted helmet streamer into the slow solar wind over a broad range of position angles during Carrington Rotation 2137. Combining the remote-sensing observations taken by the Solar-TErrestrial RElations Observatory (STEREO) mission with coronagraphic observations from the Solar and Heliospheric Observatory (SoHO) spacecraft, we show that the release of such small transient structures (often called blobs), which subsequently move away from the Sun, is associated with the concomitant formation of transient structures collapsing back towards the Sun; the latter have been referred to by previous authors as raining inflows. This is the first direct association between outflowing blobs and raining inflows, which locates the formation of blobs above the helmet streamers and gives strong support that the blobs are released by magnetic reconnection. **2013 May 28 to June 06**

Statistical investigation of wave propagation in the quiet-Sun using IRIS spectroscopic observations

Kartika **Sangal**, A.K. Srivastava, P. Kayshap, Ding Yuan, E. Scullion
ApJ **966** 187 **2024**
https://arxiv.org/pdf/2403.10392.pdf
https://iopscience.iop.org/article/10.3847/1538-4357/ad36ca/pdf
In the current analysis, we use spectroscopic observations of the quiet-Sun made by IRIS instrument, and investigate wave propagation. We analyze various spectral lines formed in different atmospheric layers such as the photosphere, chromosphere, and transition region. We examine Doppler velocity time-series at various locations in the quiet-Sun to determine the dominant oscillation periods. Our results executing statistical analysis resemble those of the classical physical scenario, indicating that the photosphere is mainly characterized by the dominant 5-minute period, while the chromosphere is primarily associated with the 3-minute oscillation period. In the transition region, we observe a variety of oscillation periods, with dominant periods of 3, 8, and 12 minutes. We estimate the cut-off frequency by deducing phase difference between two Doppler velocity time-series obtained from spectral line pairs in different atmospheric layers formed at different temperatures. It reveals a significant correlation between 3-minute periods in TR and photospheric oscillations, suggesting that these oscillations in the TR might propagate from the photosphere. Additionally, we analyze the phase difference between chromospheric oscillations and photospheric oscillations, demonstrating that only the 3-minute oscillations propagate upwards. Based on the statistical analyses, we suggest the presence of magnetoacoustic waves in the solar atmosphere in which some are propagating from the lower solar atmosphere upward, while some others are propagating downward. TR carries both long-period oscillations generated in situ, and some photospheric oscillations which are also able to reach there from below.

Spectroscopic study of solar transition region oscillations in the quiet-Sun observed by IRIS using the Si iv spectral line

Kartika **Sangal**, A K Srivastava, P Kayshap, T J Wang, J J González-Avilés, Abhinav Prasad
MNRAS, Volume 517, Issue 1, November **2022**, Pages 458–473,
https://doi.org/10.1093/mnras/stac2649
In this paper, we use the Si IV 1393.755 Å spectral line observed by the Interface Region Imaging Spectrograph (IRIS) in the quiet-Sun (QS) to determine the physical nature of the solar transition region (TR) oscillations. We analyse the properties of these oscillations using wavelet tools (e.g. power, cross-power, coherence, and phase difference) along with the stringent noise model (i.e. power law + constant). We estimate the period of the intensity and Doppler velocity oscillations at each chosen location in the QS and quantify the distribution of the statistically significant power and associated periods in one bright region and two dark regions. In the bright TR region, the mean periods in intensity and velocity are 7 min and 8 min, respectively. In the dark regions, the mean periods in intensity and velocity are 7 min and 5.4 min, respectively. We also estimate the phase difference between the intensity and Doppler velocity oscillations at each location. The statistical distribution of the phase difference is estimated, which peaks at $-119° \pm 13°$, $33° \pm 10°$, $102° \pm 10°$ in the bright region and at $-153° \pm 13°$, $6° \pm 20°$, $151° \pm 10°$ in the dark regions. The statistical distribution reveals that the oscillations are caused by propagating slow magneto-acoustic waves encountered with the TR. Some of these locations may also be associated with standing slow waves. Moreover, in the given time domain, several locations exhibit the presence of both propagating and standing oscillations at different frequencies.

Signatures of Untwisting Magnetic Field in a Small Emerging Bipole in the Solar Photosphere

C. R. **Sangeetha**, Durgesh Tripathi, S. P. Rajaguru
ApJ **895** 67 **2020**
https://arxiv.org/pdf/2004.05615.pdf
https://doi.org/10.3847/1538-4357/ab88a4

We perform a study of fluid motions and its temporal evolution in and around a small bipolar emerging flux region using observations made by the Helioseismic and Magnetic Imager (HMI) on-board the Solar Dynamics Observatory (SDO). We employ local correlation tracking of the Doppler observations to follow horizontal fluid motions and line-of-sight magnetograms to follow the flux emergence. Changes in vertical vorticity and horizontal divergence are used to derive signatures of evolving twists in the magnetic field. Our analysis reveals that the two polarities of the magnetic flux swirl in opposite directions in early stages of flux emergence indicating an unwinding of the pre-emergence twists in the magnetic field. We further find that during the emergence, there is an increase in swirly motions in the neighbouring non-magnetic regions. We estimate the magnetic and kinetic energies and find that magnetic energy is about a factor of ten larger than the kinetic energy. During the evolution, when the magnetic energy decreases, an increase in the kinetic energy is observed indicating transfer of energy from the unwinding of magnetic flux tube to the surrounding fluid motions. Our results thus demonstrate the presence of pre-emergence twists in emerging magnetic field that is important in the context of the hemispheric helicity rule warranting a detailed statistical study in this context. Further, our observations point to a possible widespread generation of torsional waves in emerging flux regions due to the untwisting magnetic field with implications for upward energy transport to the corona. **May 8-11, 2011**

Relationships between fluid vorticity, kinetic helicity and magnetic field at the small-scale (quiet-network) on the Sun

C.R. **Sangeetha**, S.P. Rajaguru
ApJ 824 120 **2016**
http://arxiv.org/pdf/1604.04439v1.pdf
We derive horizontal fluid motions on the solar surface over large areas covering the quiet-Sun magnetic network from local correlation tracking of convective granules imaged in continuum intensity and Doppler velocity by the Helioseismic and Magnetic Imager (HMI) onboard the Solar Dynamics Observatory (SDO). From these we calculate horizontal divergence, vertical component of vorticity, and kinetic helicity of fluid motions. We study the correlations between fluid divergence and vorticity, and that between vorticity (kinetic helicity) and magnetic field. We find that the vorticity (kinetic helicity) around small-scale fields exhibits a hemispherical pattern (in sign) similar to that followed by the magnetic helicity of large-scale active regions (containing sunspots). We identify this pattern to be a result of the Coriolis force acting on supergranular-scale flows (both the outflows and inflows), and is consistent with earlier studies using local helioseismology. Further, we show that the magnetic fields cause transfer of vorticity from supergranular inflow regions to outflow regions, and that they tend to suppress the vortical motions around them when magnetic flux densities exceed about 300 G (HMI). We also show that such action of magnetic fields leads to marked changes in the correlations between fluid divergence and vorticity. These results are speculated to be of importance to local dynamo action if present, and to the dynamical evolution of magnetic helicity at the small-scale.

On the Formation Height of Low-corona and Chromospheric Channels of the Atmospheric Imaging Assembly (AIA) onboard the Solar Dynamics Observatory (SDO)

Y. **Sanjay**1, S. Krishna Prasad2, R. Erdélyi3, M. B. Korsós4, D. Banerjee2, and P. S. Rawat1
2024 ApJ 975 236
https://iopscience.iop.org/article/10.3847/1538-4357/ad7d8c/pdf
The multiwavelength data from the Solar Dynamics Observatory is extensively used in studying the physics of the Sun and its atmosphere. In this study, we estimate the formation heights of low-corona and chromospheric channels of the Atmospheric Imaging Assembly (AIA) over the atmospheres of sunspot umbrae during the quiet condition period within 20 different active regions. The upward propagating slow magnetoacoustic waves of a 3 minute period, which are perpetually present in sunspots, are utilized for this purpose. Employing a cross-correlation technique, the most frequent time lag between different channel pairs is measured. By combining this information with the local sound speed obtained from the characteristic formation temperatures of individual channels, we estimate the respective formation heights. The median values of formation heights obtained across all active regions in our sample are 356, 368, 858, 1180, and 1470 km, respectively, for the AIA 1600, 1700, 304, 131, and 171 Å channels. The corresponding ranges in the formation heights are 247–453, 260–468, 575–1155, 709–1937, and 909–2585 km, respectively. These values are measured with respect to the Helioseismic Magnetic Imager continuum. We find the formation height of UV channels is quite stable (between 250 and 500 km) and displays only a marginal difference between the AIA 1600 and 1700 Å channels during quiet conditions. On the other hand, the formation height of coronal channels is quite variable. **2016 June 16**

The SunPy Project: An interoperable ecosystem for solar data analysis

The **SunPy Community**, Will T. Barnes1,2*†, Steven Christe1†, et al.
Front. Astron. Space Sci. 10:1076726. **2023** doi: 10.3389/fspas.2023.1076726
https://www.frontiersin.org/articles/10.3389/fspas.2023.1076726/full
https://www.frontiersin.org/articles/10.3389/fspas.2023.1076726/pdf

The SunPy Project is a community of scientists and software developers creating an ecosystem of Python packages for solar physics. The project includes the sunpy core package as well as a set of affiliated packages. The sunpy core package provides general purpose tools to access data from different providers, read image and time series data, and transform between commonly used coordinate systems. Affiliated packages perform more specialized tasks that do not fall within the more general scope of the sunpy core package. In this article, we give a high-level overview of the SunPy Project, how it is broader than the sunpy core package, and how the project curates and fosters the affiliated package system. We demonstrate how components of the SunPy ecosystem, including sunpy and several affiliated packages, work together to enable multi-instrument data analysis workflows. We also describe members of the SunPy Project and how the project interacts with the wider solar physics and scientific Python communities. Finally, we discuss the future direction and priorities of the SunPy Project. **2022-03-29**

High frequency generation in the corona: Resonant cavities

I. C. **Santamaria**1,2 and T. Van Doorsselaere1
A&A 611, A10 (**2018**)
Aims. Null points are prominent magnetic field singularities in which the magnetic field strength strongly decreases in very small spatial scales. Around null points, predicted to be ubiquitous in the solar chromosphere and corona, the wave behavior changes considerably. Null points are also responsible for driving very energetic phenomena, and for contributing to chromospheric and coronal heating. In previous works we demonstrated that slow magneto-acoustic shock waves were generated in the chromosphere propagate through the null point, thereby producing a train of secondary shocks escaping along the field lines. A particular combination of the shock wave speeds generates waves at a frequency of 80 MHz. The present work aims to investigate this high frequency region around a coronal null point to give a plausible explanation to its generation at that particular frequency.
Methods. We carried out a set of two-dimensional numerical simulations of wave propagation in the neighborhood of a null point located in the corona. We varied both the amplitude of the driver and the atmospheric properties to investigate the sensitivity of the high frequency waves to these parameters.
Results. We demonstrate that the wave frequency is sensitive to the atmospheric parameters in the corona, but it is independent of the strength of the driver. Thus, the null point behaves as a resonant cavity generating waves at specific frequencies that depend on the background equilibrium model. Moreover, we conclude that the high frequency wave train generated at the null point is not necessarily a result of the interaction between the null point and a shock wave. This wave train can be also developed by the interaction between the null point and fast acoustic-like magneto-acoustic waves, that is, this interaction within the linear regime.

High-frequency waves in the corona due to null points⋆

I. C. **Santamaria**1,2, E. Khomenko1,3,4, M. Collados1,3 and A. de Vicente
A&A 602, A43 (**2017**)
This work aims to understand the behavior of non-linear waves in the vicinity of a coronal null point. In previous works we have shown that high-frequency waves are generated in such a magnetic configuration. This paper studies those waves in detail in order to provide a plausible explanation of their generation. We demonstrate that slow magneto-acoustic shock waves generated in the chromosphere propagate through the null point and produce a train of secondary shocks that escape along the field lines. A particular combination of the shock wave speeds generates waves at a frequency of 80 mHz. We speculate that this frequency may be sensitive to the atmospheric parameters in the corona and therefore can be used to probe the structure of this solar layer.

Simulated interaction of MHD shock waves with a complex network-like region

Irantzu C. **Santamaria**, Elena Khomenko, Manuel Collados, Angel de Vicente
2016
http://arxiv.org/pdf/1604.08783v1.pdf
We provide estimates of the wave energy reaching the solar chromosphere and corona in a network-like magnetic field topology, including a coronal null point. The waves are excited by an instantaneous strong subphotospheric source and propagate through the subphotosphere, photosphere, chromosphere, transition region, and corona with the plasma beta and other atmospheric parameters varying by several orders of magnitude. We compare two regimes of the wave propagation: a linear and nonlinear regime. While the amount of energy reaching the corona is similar in both regimes, this energy is transmitted at different frequencies. In both cases the dominant periods of waves at each height strongly depend on the local magnetic field topology, but this distribution is only in accordance with observations in the nonlinear case.

MHD wave propagation from the sub-photosphere to the corona in an arcade-shaped magnetic field with a null point

Irantzu C. **Santamaria**, Elena Khomenko, Manuel Collados

A&A 577, A70 **2015**

http://arxiv.org/pdf/1503.03094v1.pdf

Aims. The aim of this work is to study the energy transport by means of Magnetohydrodynamic (MHD) waves propagating in quiet-Sun magnetic topology from layers below the surface to the corona. Upwardly propagating waves find obstacles, such as the equipartition layer with plasma $\beta = 1$, the transition region, and null points, and they get transmitted, converted, reflected, and refracted. Understanding the mechanisms by which MHD waves can reach the corona can give us information about the solar atmosphere and the magnetic structures.
Methods. We carried out two-dimensional numerical simulations of wave propagation in a magnetic field structure that consists of two vertical flux tubes with the same polarity separated by an arcade-shaped magnetic field. This configuration contains a null point in the corona, which significantly modifies the behavior of the waves as they pass near it.
Results. We describe in detail the wave propagation through the atmosphere under different driving conditions. We also present the spatial distribution of the mean acoustic and magnetic energy fluxes for the cases where these calculations are possible, as well as the spatial distribution of the dominant frequencies in the whole domain.
Conclusions. We conclude that the energy reaches the corona preferably along almost vertical magnetic fields, that is, inside the vertical flux tubes. This energy is acoustic in nature. Most of the magnetic energy stays concentrated below the transition region owing to the refraction of the magnetic waves and the continuous conversion of acoustic-like waves into fast magnetic waves in the equipartition layer located in the photosphere where plasma $\beta = 1$. However, part of the magnetic energy reaches the low corona when propagating in the region where the arcades are located, but waves are sent back downward into the lower atmosphere at the null-point surroundings. This phenomenon, together with the reflection and refraction of waves in the TR and the lower turning point, act as a re-feeding of the atmosphere, which keeps oscillating during all the simulation time even if a driver with a single pulse was used as initial perturbation. In the frequency distribution, we find that high frequency waves can reach the corona outside the vertical flux tubes.

Magnetic fields in solar plage regions: insights from high-sensitivity spectropolarimetry

J. M. da Silva **Santos**, K. Reardon, G. Cauzzi, T. Schad, V. Martinez Pillet, A. Tritschler, F. Wöger, R. Hofmann, J. Stauffer, H. Uitenbroek

ApJL **2023**

https://arxiv.org/pdf/2308.10983.pdf

Plage regions are patches of concentrated magnetic field in the Sun's atmosphere where hot coronal loops are rooted. While previous studies have shed light on the properties of plage magnetic fields in the photosphere, there are still challenges in measuring the overlying chromospheric magnetic fields, which are crucial to understanding the overall heating and dynamics. Here, we utilize high-sensitivity, spectropolarimetric data obtained by the four-meter Daniel K. Inouye Solar Telescope (DKIST) to investigate the dynamic environment and magnetic field stratification of an extended, decaying plage region. The data show strong circular polarization signals in both plage cores and surrounding fibrils. Notably, weak linear polarization signals clearly differentiate between plage patches and the fibril canopy, where they are relatively stronger. Inversions of the Ca II 8542 A˚ spectra show an imprint of the fibrils in the chromospheric magnetic field, with typical field strength values ranging from $\sim$ 200-300 G in fibrils. We confirm the weak correlation between field strength and cooling rates in the lower chromosphere. Additionally, we observe supersonic downflows and strong velocity gradients in the plage periphery, indicating dynamical processes occurring in the chromosphere. These findings contribute to our understanding of the magnetic field and dynamics within plages, emphasizing the need for further research to explore the expansion of magnetic fields with height and the three-dimensional distribution of heating rates in the lower chromosphere. **3 June 2022**

Heating of the solar chromosphere through current dissipation

J. M. da Silva **Santos**, S. Danilovic, J. Leenaarts, J. de la Cruz Rodríguez, X. Zhu, S. M. White, G. J. M. Vissers, M. Rempel

A&A 661, A59 **2022**

https://arxiv.org/pdf/2202.03955.pdf

https://doi.org/10.1051/0004-6361/202243191

https://www.aanda.org/articles/aa/pdf/2022/05/aa43191-22.pdf

The solar chromosphere is heated to temperatures higher than predicted by radiative equilibrium. This excess heating is larger in active regions where the magnetic field is stronger. We aim to investigate the magnetic topology associated to an area of enhanced millimeter (mm) brightness temperatures in a solar active region mapped by the Atacama Large Millimeter/submillimeter Array (ALMA) using spectropolarimetric coobservations with the 1-m Swedish Solar Telescope (SST). We use Milne-Eddington inversions, nonlocal thermodynamic equilibrium (non-LTE) inversions, and a magnetohydrostatic extrapolation to obtain constraints on the three-dimensional stratification

of temperature, magnetic field, and radiative energy losses. We compare the observations to a snapshot of a magnetohydrodynamics simulation and investigate the formation of the thermal continuum at 3 mm using contribution functions. We find enhanced heating rates in the upper chromosphere of up to ∼5kWm−2 where small-scale emerging loops interact with the overlying magnetic canopy leading to current sheets as shown by the magnetic field extrapolation. Our estimates are about a factor of two higher than canonical values, but they are limited by the ALMA spatial resolution (∼1.2″). Band 3 brightness temperatures reach about ∼104K in the region, and the transverse magnetic field strength inferred from the non-LTE inversions is of the order of ∼500G in the chromosphere. We quantitatively reproduce many of the observed features including the integrated radiative losses in our numerical simulation, and we conclude that the heating is caused by dissipation in current sheets. However, the simulation shows a complex stratification in the flux emergence region where distinct layers may contribute significantly to the emission in the mm continuum. **April 13, 2019**

Multichannel autocalibration for the Atmospheric Imaging Assembly using machine learning

Luiz F. G. dos **Santos**1,2, Souvik Bose3,4, Valentina Salvatelli5,6, Brad Neuberg5,6, Mark C. M. Cheung7, Miho Janvier8, Meng Jin6,7, Yarin Gal9, Paul Boerner7 and Atılım Güneş Baydin10,11
A&A 648, A53 (**2021**)
https://doi.org/10.1051/0004-6361/202040051
https://www.aanda.org/articles/aa/pdf/2021/04/aa40051-20.pdf
Context. Solar activity plays a quintessential role in affecting the interplanetary medium and space weather around Earth. Remote-sensing instruments on board heliophysics space missions provide a pool of information about solar activity by measuring the solar magnetic field and the emission of light from the multilayered, multithermal, and dynamic solar atmosphere. Extreme-UV (EUV) wavelength observations from space help in understanding the subtleties of the outer layers of the Sun, that is, the chromosphere and the corona. Unfortunately, instruments such as the Atmospheric Imaging Assembly (AIA) on board the NASA Solar Dynamics Observatory (SDO), suffer from time-dependent degradation that reduces their sensitivity. The current best calibration techniques rely on flights of sounding rockets to maintain absolute calibration. These flights are infrequent, complex, and limited to a single vantage point, however.
Aims. We aim to develop a novel method based on machine learning (ML) that exploits spatial patterns on the solar surface across multiwavelength observations to autocalibrate the instrument degradation.
Methods. We established two convolutional neural network (CNN) architectures that take either single-channel or multichannel input and trained the models using the SDOML dataset. The dataset was further augmented by randomly degrading images at each epoch, with the training dataset spanning nonoverlapping months with the test dataset. We also developed a non-ML baseline model to assess the gain of the CNN models. With the best trained models, we reconstructed the AIA multichannel degradation curves of 2010–2020 and compared them with the degradation curves based on sounding-rocket data.
Results. Our results indicate that the CNN-based models significantly outperform the non-ML baseline model in calibrating instrument degradation. Moreover, multichannel CNN outperforms the single-channel CNN, which suggests that cross-channel relations between different EUV channels are important to recover the degradation profiles. The CNN-based models reproduce the degradation corrections derived from the sounding-rocket cross-calibration measurements within the experimental measurement uncertainty, indicating that it performs equally well as current techniques.
Conclusions. Our approach establishes the framework for a novel technique based on CNNs to calibrate EUV instruments. We envision that this technique can be adapted to other imaging or spectral instruments operating at other wavelengths.

What future awaits the Sun?

Ângela R. G. **Santos**1, Savita Mathur2,3
Science 01 May **2020**: Vol. 368, Issue 6490, pp. 466-467 DOI: 10.1126/science.abb9208
The Sun and other similar (solar-like) stars have an internal magnetic field that can emerge on the surface, forming features such as dark spots, which drive the so-called magnetic activity. For both the Sun and solar-like stars, magnetic activity varies with time and strongly correlates with photometric (brightness) variability. In the solar and stellar scientific communities, a debate rages about how the magnetic activity of the Sun compares with that of similar stars and whether the Sun will reach very high activity levels or is in a period of transition to a state of reduced magnetic activity. On page 518 of this issue, Reinhold et al. (1) compare the Sun's photometric variability with that of solar-like stars and find the latter to be more active.

The multi-thermal chromosphere: inversions of ALMA and IRIS data

J. M. da Silva **Santos**, J. de la Cruz Rodríguez, J. Leenaarts, G. Chintzoglou, B. De Pontieu, S. Wedemeyer, M. Szydlarski
A&A 634, A56 **2020**

https://arxiv.org/pdf/1912.09886.pdf
https://doi.org/10.1051/0004-6361/201937117
Numerical simulations of the solar chromosphere predict a diverse thermal structure with both hot and cool regions. Observations of plage regions, in particular, feature broader and brighter chromospheric lines, which suggest that they are formed in hotter and denser conditions than in the quiet-Sun, but also imply a non-thermal component whose source is unclear. We revisit the problem of the stratification of temperature and microturbulence in plage now adding millimeter continuum observations provided by ALMA to inversions of near-ultraviolet IRIS spectra as a powerful new diagnostic to disentangle the two parameters. We fit cool chromospheric holes and track the fast evolution of compact mm brightnenings in the plage region. We use the STiC non-LTE inversion code to simultaneously fit real ultraviolet and millimeter spectra in order to infer the thermodynamic parameters of the plasma. We confirm the anticipated constraining potential of ALMA in non-LTE inversions of the solar chromosphere. We find significant differences between the inversion results of IRIS data alone compared to the results of a combination with the mm data: the IRIS+ALMA inversions have increased contrast and temperature range, and tend to prefer lower values of microturbulence in the chromosphere of plage. The average brightness temperature of the plage region at 1.25 mm is 8500 K, but the ALMA maps also show much cooler (∼3000 K) and hotter (∼11000 K) evolving features partially seen in other diagnostics. To explain the former, the inversions require the existence of localized, low temperature regions in the chromosphere where molecules such as CO could form. The hot features could sustain such high temperatures due to non-equilibrium hydrogen ionization effects in a shocked chromosphere - a scenario that is supported by low-frequency shock wave patterns found in the MgII lines probed by IRIS. **22 April 2017**
CESRA #2484 Feb **2020** http://www.astro.gla.ac.uk/users/eduard/cesra/?p=2484

Temperature constraints from inversions of synthetic solar optical, UV and radio spectra

João M. da Silva **Santos**, Jaime de la Cruz Rodríguez, Jorrit Leenaarts
A&A 620, A124 **2018**
https://arxiv.org/pdf/1806.06682.pdf
High-resolution observations of the solar chromosphere at millimeter wavelengths are now possible with the Atacama Large Millimeter Array (ALMA), promising to tackle many open problems in solar physics. Observations from other ground and space-based telescopes will greatly benefit from coordinated endeavors with ALMA, yet the diagnostic potential of combined optical, ultraviolet and mm observations has remained mostly unassessed. In this paper we investigate whether mm-wavelengths could aid current inversion schemes to retrieve a more accurate representation of the temperature structure of the solar atmosphere. We performed several non-LTE inversion experiments of the emergent spectra from a snapshot of 3D radiation-MHD simulation. We included common line diagnostics such as CaII H, K, 8542 \AA and MgII h and k, taking into account partial frequency redistribution effects, along with the continuum around 1.2 mm and 3 mm. We found that including the mm-continuum in inversions allows a more accurate inference of temperature as function of optical depth. The addition of ALMA bands to other diagnostics should improve the accuracy of the inferred chromospheric temperatures between $\log\tau \sim [-6, -4.5]$ where the CaII and MgII lines are weakly coupled to the local conditions. However, we found that simultaneous multi-atom, non-LTE inversions of optical and UV lines present equally strong constraints in the lower chromosphere and thus are not greatly improved by the 1.2 mm band. Nonetheless, the 3 mm band is still needed to better constrain the mid-upper chromosphere.

On the relation between activity-related frequency shifts and the sunspot distribution over the solar cycle 23

A. R. G. **Santos**, M. S. Cunha, P. P. Avelino, W. J. Chaplin, T. L. Campante
Proceedings of the Joint TASC2 - KASC9 Workshop - SPACEINN - HELAS8 Conference "Seismology of the Sun and the Distant Stars 2016: Using Today's Successes to Prepare the Future". To be published by the EPJ Web of Conferences **2016**
https://arxiv.org/pdf/1611.07475v1.pdf
The activity-related variations in the solar acoustic frequencies have been known for 30 years. However, the importance of the different contributions is still not well established. With this in mind, we developed an empirical model to estimate the spot-induced frequency shifts, which takes into account the sunspot properties, such as area and latitude. The comparison between the model frequency shifts obtained from the daily sunspot records and those observed suggests that the contribution from a stochastic component to the total frequency shifts is about 30%. The remaining 70% is related to a global, long-term variation. We also propose a new observable to investigate the short- and mid-term variations of the frequency shifts, which is insensitive to the long-term variations contained in the data. On the shortest time scales the variations in the frequency shifts are strongly correlated with the variations in the total area covered by sunspots. However, a significant loss of correlation is still found, which cannot be fully explained by ignoring the invisible side of the Sun when accounting for the total sunspot area. We also verify that the times when the frequency shifts and the sunspot areas do not vary in a similar way tend to coincide with the times of the maximum amplitude of the quasi-biennial variations found in the seismic data.

A thorough analysis of the short- and mid-term activity-related variations in the solar acoustic frequencies

A. R. G. **Santos**, M. S. Cunha, P. P. Avelino, W. J. Chaplin, T. L. Campante
MNRAS **2016**
https://arxiv.org/pdf/1610.06872v1.pdf

The frequencies of the solar acoustic oscillations vary over the activity cycle. The variations in other activity proxies are found to be well correlated with the variations in the acoustic frequencies. However, each proxy has a slightly different time behaviour. Our goal is to characterize the differences between the time behaviour of the frequency shifts and of two other activity proxies, namely, the area covered by sunspots and the 10.7cm flux. We define a new observable that is particularly sensitive to the short-term frequency variations. We then compare the observable when computed from model frequency shifts and from observed frequency shifts obtained with the Global Oscillation Network Group (GONG) for cycle 23. Our analysis shows that on the shortest time-scales the variations in the frequency shifts seen in the GONG observations are strongly correlated with the variations in the area covered by sunspots. However, a significant loss of correlation is still found. We verify that the times when the frequency shifts and the sunspot area do not vary in a similar way tend to coincide with the times of the maxima of the quasi-biennial variations seen in the solar seismic data. A similar analysis of the relation between the 10.7cm flux and the frequency shifts reveals that the short-time variations in the frequency shifts follow even more closely those of the 10.7cm flux than those of the sunspot area. However, a loss of correlation between frequency shifts and 10.7cm flux variations is still found around the same times.

On the contribution of sunspots to the observed frequency shifts of solar acoustic modes

A. R. G. **Santos**, M. S. Cunha, P. P. Avelino, W. J. Chaplin, T. L. Campante
MNRAS **2016**
http://arxiv.org/pdf/1606.02133v1.pdf

Activity-related variations in the solar oscillation properties have been known for 30 years. However, the relative importance of the different contributions to the observed variations is not yet fully understood. Our goal is to estimate the relative contribution from sunspots to the observed activity-related variations in the frequencies of the acoustic modes. We use a variational principle to relate the phase differences induced by sunspots on the acoustic waves to the corresponding changes in the frequencies of the global acoustic oscillations. From the sunspot properties (area and latitude as a function of time), we are able to estimate the spot-induced frequency shifts. These are then combined with a smooth frequency shift component, associated with long-term solar-cycle variations, and the results compared with the frequency shifts derived from the Global Oscillation Network Group (GONG) data. The result of this comparison is consistent with a sunspot contribution to the observed frequency shifts of roughly 30 per cent, with the remaining 70 per cent resulting mostly from a global, non-stochastic variation, possibly related to the changes in the overall magnetic field. Moreover, analysis of the residuals obtained after the subtraction of the model frequency shifts from the observations indicates the presence of a 1.5-yr periodicity in the data in phase with the quasi-biennial variations reported in the literature.

Spot cycle reconstruction: an empirical tool - Application to the sunspot cycle

A. R. G. **Santos**, M. S. Cunha, P. P. Avelino, T. L. Campante
A&A 580, A62 **2015**
http://arxiv.org/pdf/1506.03014v1.pdf

The increasing interest in understanding stellar magnetic activity cycles is a strong motivation for the development of parameterised starspot models which may be constrained observationally. In this work we develop an empirical tool for the stochastic reconstruction of sunspot cycles, using the average solar properties as a reference. The synthetic sunspot cycle is compared with the sunspot data extracted from the National Geophysical Data Center, in particular using the Kolmogorov-Smirnov test. This tool yields synthetic spot group records, including date, area, latitude, longitude, rotation rate of the solar surface at the group's latitude, and an identification number. Comparison of the stochastic reconstructions with the daily sunspot records (from the National Geophysical Data Center) confirms that our empirical model is able to successfully reproduce the main properties of the solar sunspot cycle. As a by-product of this work, we show that the Gnevyshev-Waldmeier rule, which describes the spots' area-lifetime relation, is not adequate for small groups and we propose an effective correction to that relation which leads to a closer agreement between the synthetic sunspot cycle and the observations.

The Sun's Fast Dynamo Action

D. V. **Sarafopoulos** (Democritus University of Thrace)
2017
https://arxiv.org/pdf/1703.08060.pdf

We provide a synthesis model demonstrating the "fast dynamo" action of the Sun. The latter is essentially accomplished via two toroidal structures presumably formed in the tachocline and placed symmetrically with respect to the equatorial plane. The two tori are characterized by several prominent key-properties as follows: First, in each "Torus" a surplus of negative charge is entrapped for approximately the 11-year sunspot cycle. Second, the net negative charge of Torus, moving with the solar rotational speed, generates a huge toroidal current which, in turn, builds up an intense poloidal magnetic field. Third, each Torus is placed at a specific distance from the Radiative Zone, so that the rotational speed (u) of the entrapped electrons equals the local propagation velocity for an electromagnetic disturbance (v). Thus, two Torus electrons satisfy the condition that the repulsive electrostatic force equals the attractive magnetic force caused from the two elementary currents. Fourth, the surplus negative charge can steadily increase; electrons are systematically attracted inwards. The electrons remain without any "Debye shielding" action in the Torus-core region, while they demonstrate a "Debye anti-shielding effect" closer to the Radiative Zone. Thus, each Torus electron "moves" with zero resistivity and the Torus core region behaves like a gigantic "superconductor" at the extremely high temperatures of tachocline. Fifth, the tori move equatorward drifting on a surface on which the condition u=v is satisfied. Moreover, we present a preliminary 3D solar circuit, for the overall 22-year cycle, with the ability to reverse the magnetic field. If the suggested model is accepted as a workable solution, then many longstanding unresolved questions concerning the powerful CMEs, the flares, the electron acceleration mechanism and the stellar dynamo could be readily addressed.

4.6. The way in which 1036 electrons may be accelerated by a solar flare

4.7. Origination of CMEs

Correction of atmospheric stray light in restored slit spectra

S. **Saranathan**1,2, M. van Noort1 and S. K. Solanki1,3

A&A 653, A17 (**2021**)

https://www.aanda.org/articles/aa/pdf/2021/09/aa37100-19.pdf

https://doi.org/10.1051/0004-6361/201937100

Context. A long-standing issue in solar ground-based observations has been the contamination of data due to stray light, which is particularly relevant in inversions of spectropolarimetric data.

Aims. We aim to build on a statistical method of correcting stray-light contamination due to residual high-order aberrations and apply it to ground-based slit spectra.

Methods. The observations were obtained at the Swedish Solar Telescope, and restored using the multi-frame blind deconvolution restoration procedure. Using the statistical properties of seeing, we created artificially degraded synthetic images generated from magneto-hydrodynamic simulations. We then compared the synthetic data with the observations to derive estimates of the amount of the residual stray light in the observations. In the final step, the slit spectra were deconvolved with a stray-light point spread function to remove the residual stray light from the observations.

Results. The RMS granulation contrasts of the deconvolved spectra were found to increase to approximately 12.5%, from 9%. Spectral lines, on average, were found to become deeper in the granules and shallower in the inter-granular lanes, indicating systematic changes to gradients in temperature. The deconvolution was also found to increase the redshifts and blueshifts of spectral lines, suggesting that the velocities of granulation in the solar photosphere are higher than had previously been observed.

A Revised 27-day Recurrence Index

H. H. **Sargent**

2021

https://arxiv.org/ftp/arxiv/papers/2101/2101.02155.pdf

The original 110 year long 27-day Recurrence Index (original R27) was published more than forty years ago. That index, based on the autocorrelation of consecutive 27-day sets of the geomagnetic aa-index, is a measure of the cycle-to-cycle stability of high speed solar wind structure. During an effort to extend the index, it was discovered that the index could be significantly strengthened by pre-smoothing the geomagnetic aa-index listing used as input. A revised index (revised R27) is presented which clearly shows periods of long term stable solar wind structure toward the end of every sunspot cycle over the last 150 years. The extension of R27 over an interval including the greater part of the space age enables the updating of various studies of long-term solar wind variability based on R27, as well as comparison of R27 with more recently-developed solar-terrestrial parameters.

Science Filter Characterization of the Solar Ultraviolet Imaging Telescope (SUIT) on board Aditya-L1

Janmejoy **Sarkar**, Rushikesh Deogaonkar, Ravi Kesharwani, +++

2024

https://arxiv.org/pdf/2412.11636

The Solar Ultraviolet Imaging Telescope (SUIT) on board the Aditya-L1 mission is designed to observe the Sun across 200-400 nm wavelength. The telescope used 16 dichroic filters tuned at specific wavelengths in various

combinations to achieve its science goals. For accurate measurements and interpretation, it is important to characterize these filters for spectral variations as a function of spatial location and tilt angle. Moreover, we also measured out-of-band and in-band transmission characteristics with respect to the inband transmissions. In this paper, we present the experimental setup, test methodology, and the analyzed results. Our findings reveal that the transmission properties of all filters meet the expected performance for spatial variation of transmission and the transmission band at a specific tilt angle. The out-of-band transmission for all filters is below 1% with respect to in-band, except for filters BB01 and NB01. These results confirm the capabilities of SUIT to effectively capture critical solar features in the anticipated layer of the solar atmosphere.

Chaos and periodicity in solar wind speed: cycle 23

Tushnik **Sarkar**, Rajdeep Ray, Mofazzal H. Khondekar, Koushik Ghosh, Subrata Banerjee
Astrophysics and Space Science May **2015**, 357:128
The solar wind speed time series data from 1st January, 1997 to 28th October, 2003 has been pre-processed using simple exponential smoothing, discrete wavelet transform for denoising to investigate the underneath dynamics of it. Recurrence plot and recurrence quantification analysis has revealed that the time series is non-stationary one with deterministic chaotic behavior. The Hilbert-Huang Transform has been used in search of the underlying periods of the data series. Present investigation has revealed the periods of 21 days, 32.5 days, 43.6 days, 148.86 days, 180.7 days, 355.5 days, 403.2 days, 413.6 days, 490.72 days, 729.6 days, 1086.76 days, 1599.4 days and 1892.6 days.

Cosmic Ray Modulation with the Maximum CME Speed Index During Solar Cycles 23 and 24

Volkan **Sarp**, Ali Kilcik, Vasyl Yurchyshyn, Atila Ozguc, Jean-Pierre Rozelot
Solar Physics July **2019**, 294:86
sci-hub.se/10.1007/s11207-019-1481-z
We analyzed modulation of cosmic-ray intensities (CRIs) during Solar Cycles 23 and 24 by using the international sunspot numbers (ISSN) and the maximum CME speed index (MCMESI) as proxies for solar activity. Temporal variations, cross-correlations, and hysteresis patterns of CRI, MCMESI, and ISSN data were investigated. As a result, we concluded that the MCMESI better describes solar modulation of the CRI as compared to the ISSN. This is mainly because the correlation between CRI and ISSN is caused by the general cyclic trend of solar activity, while the correlation between the CRI and the MCMESI is mainly due to short-term fluctuations related to Forbush decreases. In contrast to the ISSN, there is no time lag between the CRI and the MCMESI variations.

Prediction of solar cycle 25: a non-linear approach

V **Sarp** A Kilcik V Yurchyshyn J P Rozelot A Ozguc
MNRAS 481, Issue 3, 11 December **2018**, Pages 2981–2985
http://sci-hub.tw/10.1093/mnras/sty2470
Predicting the solar activity is an important task for space weather and solar physics. There are various approaches to predict the solar activity and these predictions are used in various areas such as planning space missions, approximating the mechanism of solar dynamo, etc. In this paper, a non-linear prediction algorithm based on delay-time and phase space reconstruction is used to forecast the maximum of Solar Cycle 25. Apart from embedding dimension and delay-time which are the key parameters of such methods, we further found a new parameter (starting point) that should be taken into account to get better solar cycle predictions. This method was tested on last five solar cycles and the results are quite acceptable. We predicted that the maximum of Solar Cycle 25 will be at the year 2023.2±1.12023.2±1.1 with a peak sunspot number of 154±12.154±12. Our results are compared with other available predictions.

The First Flight of the Marshall Grazing Incidence X-ray Spectrometer (MaGIXS)

Sabrina L. **Savage**, Amy R. Winebarger, Ken Kobayashi, +++
ApJ **2022**
https://arxiv.org/pdf/2212.00665.pdf
The Marshall Grazing Incidence X-ray Spectrometer (MaGIXS) sounding rocket experiment launched on **July 30, 2021** from the White Sands Missile Range in New Mexico. MaGIXS is a unique solar observing telescope developed to capture X-ray spectral images, in the 6 - 24 Angstrom wavelength range, of coronal active regions. Its novel design takes advantage of recent technological advances related to fabricating and optimizing X-ray optical systems as well as breakthroughs in inversion methodologies necessary to create spectrally pure maps from overlapping spectral images. MaGIXS is the first instrument of its kind to provide spatially resolved soft X-ray spectra across a wide field of view. The plasma diagnostics available in this spectral regime make this instrument a powerful tool for probing solar coronal heating. This paper presents details from the first MaGIXS flight, the captured observations, the data processing and inversion techniques, and the first science results. **Nov 10, 2011**

Comment on “Tidally Synchronized Solar Dynamo: A Rebuttal” by Nataf (Solar Phys. 297, 107, 2022)

Nicola **Scafetta**

Solar Physics volume 298, Article number: 24 (**2023**)

https://link.springer.com/content/pdf/10.1007/s11207-023-02118-5.pdf

Nataf (Solar Phys. 297, 107, 2022) has recently asserted that the hypothesis that the solar dynamo may be synchronized by planetary tidal forces is unsupported by any evidence. He reached this conclusion by adopting a simplistic tidal model (which was discussed in his Appendix A) that relies solely on the effect of Mercury, Venus, Earth, and Jupiter whose orbits were assumed to be circular. His model was unable to produce tides with periods compatible with those of the Schwabe 11-year solar cycle. I demonstrate here that the modeling in Nataf (2022) is erroneous and that a correct modeling and interpretation of the planetary tidal function, which accounts for all planets and their true orbits, fits well with the spectral requirements of the Schwabe 11-year solar cycle. This result has been already shown and discussed in a substantial body of scholarly research on the subject, which Nataf apparently ignored. A recent and extended review of the empirical and theoretical evidences supporting the planetary synchronized solar dynamo theory was offered by Scafetta and Bianchini (Front. Astron. Space Sci. 9, 937930, 2022).

The Planetary Theory of Solar Activity Variability: A Review.

Scafetta N and Bianchini A

Front. Astron. Space Sci. 9: 937930. (**2022**)

https://www.frontiersin.org/articles/10.3389/fspas.2022.937930/pdf

Commenting the 11-year sunspot cycle, Wolf (1859, MNRAS 19, 85–86) conjectured that “the variations of spot-frequency depend on the influences of Venus, Earth, Jupiter, and Saturn.” The high synchronization of our planetary system is already nicely revealed by the fact that the ratios of the planetary orbital radii are closely related to each other through a scaling-mirror symmetry equation (Bank and Scafetta, Front. Astron. Space Sci. 8, 758184, 2022). Reviewing the many planetary harmonics and the orbital invariant inequalities that characterize the planetary motions of the solar system from the monthly to the millennial time scales, we show that they are not randomly distributed but clearly tend to cluster around some specific values that also match those of the main solar activity cycles. In some cases, planetary models have even been able to predict the time-phase of the solar oscillations including the Schwabe 11-year sunspot cycle. We also stress that solar models based on the hypothesis that solar activity is regulated by its internal dynamics alone have never been able to reproduce the variety of the observed cycles. Although planetary tidal forces are weak, we review a number of mechanisms that could explain how the solar structure and the solar dynamo could get tuned to the planetary motions. In particular, we discuss how the effects of the weak tidal forces could be significantly amplified in the solar core by an induced increase in the H-burning. Mechanisms modulating the electromagnetic and gravitational large-scale structure of the planetary system are also discussed.

Solar Oscillations and the Orbital Invariant Inequalities of the Solar System

Nicola **Scafetta**

Solar Physics volume 295, Article number: 33 (**2020**)

https://link.springer.com/content/pdf/10.1007/s11207-020-01599-y.pdf

Gravitational planetary lensing of slow-moving matter streaming towards the Sun was suggested to explain puzzling solar-flare occurrences and other unexplained solar-emission phenomena (Bertolucci et al. in Phys. Dark Universe17, 13, 2017). If it is actually so, the effect of gravitational lensing of this stream by heavy planets (Jupiter, Saturn, Uranus and Neptune) could be manifested in solar activity changes on longer time scales too where solar records present specific oscillations known in the literature as the cycles of Bray–Hallstatt (2100–2500 yr), Eddy (800–1200 yr), Suess–de Vries (200–250 yr), Jose (155–185 yr), Gleissberg (80–100 year), the 55–65 yr spectral cluster and others. It is herein hypothesized that these oscillations emerge from specific periodic planetary orbital configurations that generate particular waves in the force-fields of the heliosphere which could be able to synchronize solar activity. These harmonics are defined by a subset of orbital frequencies herein labeled as “orbital invariant inequalities” of the solar system that derive from the synodical periods among the Jovian planets. Thus, they are associated with the repeating pattern of planetary alignment relative to the Sun when tidal forcing, interplanetary magnetic couplings and planetary lensing effects could be enhanced. These frequencies are physically relevant also because they are invariant relative to any spinning system centered on the Sun and, therefore, they and their combinations should characterize the spectrum of any forcing able to externally synchronizing the internal dynamics of the solar dynamo. Herein the orbital invariant inequalities of the solar system are determined and are demonstrated to cluster around specific spectral bands that exactly correspond to the above spectrum of solar activity. In particular, the orbital invariant inequality model is shown to predict, both in frequency and phase, the Bray–Hallstatt cycle (2100–2500 yr) found in Δ14CΔ14C and in climate records throughout the Holocene. The result suggests that some kind of planetary forcing is synchronizing solar internal dynamics.

ACRIM total solar irradiance satellite composite validation versus TSI proxy models

Nicola **Scafetta**, Richard C. Willson

http://arxiv.org/pdf/1403.7194v1.pdf

Astrophysics and Space Science 350(2), 421-442, **2014**

The satellite total solar irradiance (TSI) database provides a valuable record for investigating models of solar variation used to interpret climate changes. The 35-year ACRIM TSI satellite composite was updated using corrections to ACRIMSAT/ACRIM3 results derived from recent testing at the Laboratory for Atmospheric and Space Physics/Total solar irradiance Radiometer Facility (LASP/TRF). The corrections lower the ACRIM3 scale by ~5000 ppm, in close agreement with the scale of SORCE/TIM results (solar constant ~1361 W/m^2). Relative variations and trends are not changed. Differences between the ACRIM and PMOD TSI composites, e.g. the decadal trending during solar cycles 21-22, are tested against a set of solar proxy models, including analysis of Nimbus7/ERB and ERBS/ERBE results available to bridge the ACRIM Gap (1989-1992). Our findings confirm: (1) The validity of the TSI peak in the originally published ERB results in early 1979 during solar cycle 21; (2) The correctness of originally published ACRIM1 results during the SMM spin mode (1981-1984); (3) The upward trend of originally published ERB results during the ACRIM Gap; (4) The occurrence of a significant upward TSI trend between the minima of solar cycles 21 and 22 and (5) a decreasing trend during solar cycles 22-23. Our findings do not support: (1) The downward corrections to originally published ERB and ACRIM1 results during solar cycle 21; (2) A step function sensitivity change in ERB results at the end-of-September 1989; (3) the validity of ERBE's downward trend during the ACRIM Gap or (4) the use of ERBE results to bridge the ACRIM Gap. Our analysis provides a first order validation of the ACRIM TSI composite approach and its 0.037%/decade upward trend during solar cycles 21-22. Thus, solar forcing of climate change may be a significantly larger factor than represented in the CMIP5 general circulation climate models.

Reflection and Evolution of Torsional Alfvén Pulses in Zero-beta Flux Tubes

Joseph **Scalisi**1, Michael S. Ruderman1,2,3, and Robertus Erdélyi1,4,5

2021 ApJ 922 118

https://doi.org/10.3847/1538-4357/ac2509

We model the behavior of a torsional Alfvén pulse, assumed to propagate through the chromosphere. Building on our existing model, we utilize the zero-beta approximation appropriate for plasma in an intense magnetic flux tube, e.g., a magnetic bright point. The model is adapted to investigate the connection between these features and chromospheric spicules. A pulse is introduced at the lower, photospheric boundary of the tube as a magnetic shear perturbation, and the resulting propagating Alfvén waves are reflected from an upper boundary, representing the change in density found at the transition region. The induced upward mass flux is followed by the reversal of the flux that may be identified with the rising and falling behavior of certain lower solar atmospheric jets. The ratio of the transmitted and reflected mass flux is estimated and compared with the relative total mass of spicules and the solar wind. An example is used to study the properties of the pulse. We also find that the interaction between the initial and reflected waves may create a localized flow that persists independently from the pulse itself.

Propagation of Torsional Alfvén Pulses in Zero-beta Flux Tubes

Joseph **Scalisi**1, William Oxley1, Michael S. Ruderman1,2,5, and Robertus Erdélyi1,3,4

2021 ApJ 911 39

https://doi.org/10.3847/1538-4357/abe8db

In this study, we investigate analytically the generation of mass flux due to a torsional Alfvén pulse. We derive that the presence of torsional Alfvén waves, which have been observed in, e.g., photospheric magnetic bright points (MBPs), can result in vertical plasma motions. The formation of this mass flux may even be a viable contribution to the generation of chromospheric mass transport, playing potential roles in the form of localized lower solar atmospheric jets. This relationship is studied using a flux tube model, with the waves introduced at the lower boundary of the tube as a magnetic shear perturbation. Due to the nature of MBPs we simplify the model by using the zero-beta approximation for the plasma inside the tube. The analytical results are demonstrated by an example of the type of Alfvén wave perturbation that one might expect to observe, and comparison is made with properties of spicules known from observations. We find that field-aligned plasma flux is formed nonlinearly as a result of the Lorentz force generated by the perturbations, and could be consistent with jet formation, although the current model is not intended to determine the entire evolution of a jet. Critical discussion of the model follows, including suggestions for improvements and for high-resolution proposed observations in order to constrain the driving magnetic and velocity shear.

SOLAR CYCLE VARIABILITY AND SURFACE DIFFERENTIAL ROTATION FROM Ca II K-LINE TIME SERIES DATA

Jeffrey D**. Scargle**1, Stephen L. Keil2, and Simon P. Worden

2013 ApJ 771

Analysis of over 36 yr of time series data from the NSO/AFRL/Sac Peak K-line monitoring program elucidates 5 components of the variation of the 7 measured chromospheric parameters: (a) the solar cycle (period ~ 11 yr), (b) quasi-periodic variations (periods ~ 100 days), (c) a broadband stochastic process (wide range of periods), (d) rotational modulation, and (e) random observational errors, independent of (a)-(d). Correlation and power spectrum analyses elucidate periodic and aperiodic variation of these parameters. Time-frequency analysis illuminates periodic and quasi-periodic signals, details of frequency modulation due to differential rotation, and in particular elucidates the rather complex harmonic structure (a) and (b) at timescales in the range ~0.1-10 yr. These results using only full-disk data suggest that similar analyses will be useful for detecting and characterizing differential rotation in stars from stellar light curves such as those being produced by NASA's Kepler observatory. Component (c) consists of variations over a range of timescales, in the manner of a 1/f random process with a power-law slope index that varies in a systematic way. A time-dependent Wilson-Bappu effect appears to be present in the solar cycle variations (a), but not in the more rapid variations of the stochastic process (c). Component (d) characterizes differential rotation of the active regions. Component (e) is of course not characteristic of solar variability, but the fact that the observational errors are quite small greatly facilitates the analysis of the other components. The data analyzed in this paper can be found at the National Solar Observatory Web site http://nsosp.nso.edu/cak_mon/, or by file transfer protocol at ftp://ftp.nso.edu/idl/cak.parameters.

Polarized Forbidden Coronal Line Emission in the Presence of Active Regions

Thomas **Schad** , Gabriel Dima

Solar Physics volume 296, Article number: 166 (**2021**)

https://link.springer.com/content/pdf/10.1007/s11207-021-01917-y.pdf

https://doi.org/10.1007/s11207-021-01917-y

Photoexcited forbidden lines at visible and infrared wavelengths provide important diagnostics for the coronal magnetic field via scattering induced polarization and the Zeeman effect. In forward models, the polarized formation of these lines is often treated assuming a simplified exciting radiation field consisting only of the photospheric quiet-Sun continuum, which is both cylindrically-symmetric relative to the solar vertical and unpolarized. In particular, this assumption breaks down near active regions, especially due to the presence of sunspots and other surface features that modify the strength and anisotropy of the continuum radiation field. Here we investigate the role of symmetry-breaking on the emergent polarized emission in high resolution models of the active corona simulated with the MURaM code. We treat the full 3D unpolarized continuum radiation field of the photosphere that excites the coronal ions and compare the cases where the symmetry-breaking effects of the photospheric features are included or ignored. Our discussion focuses on the key observables soon to be available by the National Science Foundation’s Daniel K Inouye Solar Telescope. The results indicate that while symmetry breaking can in principle have a large effect, its role is relatively minor for the simulated active region, largely due to the low inherent polarization fraction emitted by forbidden lines in denser active region plasmas.

Forward Synthesis of Polarized Emission in Target DKIST Coronal Lines Applied to 3D MURaM Coronal Simulations

Thomas **Schad** & Gabriel Dima

Solar Physics volume 295, Article number: 98 (**2020**)

https://link.springer.com/content/pdf/10.1007/s11207-020-01669-1.pdf

Self-consistent magnetohydrodynamic simulations of the solar corona with fine (≲10≲10 km) grid scales are now being realized in parallel to advancements in high-resolution coronal spectropolarimetry provided by the National Science Foundation’s Daniel K. Inouye Solar Telescope (DKIST). We investigate the synthesis of polarized emission in the presence of apparent coronal fine structure exhibited by 3D MURaM coronal simulations for the key polarized spectral lines targeted by DKIST, namely Fe XIVλ5303, Fe XIλ7892, Fe XIIIλ10746, Fe XIIIλ10798, Si Xλ14301, and Si IXλ39343. To benchmark our calculations, we provide detailed comparisons between the employed polarized line formation theory and established scalar line synthesis tools provided by the CHIANTI database team. To accelerate polarized synthesis for large simulations, we create efficient lookup tables based on atomic models significantly larger than previous studies. The spectral data cubes we describe provide a useful guide for the new era of multi-spectral DKIST coronal diagnostics as we discuss specific analysis techniques and challenges. Self-consistent magnetohydrodynamic simulations of the solar corona with fine (≲10≲10 km) grid scales are now being realized in parallel to advancements in high-resolution coronal spectropolarimetry provided by the National Science Foundation’s Daniel K. Inouye Solar Telescope (DKIST). We investigate the synthesis of polarized emission in the presence of apparent coronal fine structure exhibited by 3D MURaM coronal simulations for the key polarized spectral lines targeted by DKIST, namely Fe XIVλ5303, Fe XIλ7892, Fe XIIIλ10746, Fe XIIIλ10798, Si Xλ14301, and Si IXλ39343. To benchmark our calculations, we provide detailed comparisons between the employed polarized line formation theory and established scalar line synthesis tools provided by the CHIANTI database team. To accelerate polarized synthesis for large simulations, we create efficient lookup tables based on atomic models significantly larger than previous studies. The spectral data

cubes we describe provide a useful guide for the new era of multi-spectral DKIST coronal diagnostics as we discuss specific analysis techniques and challenges.

Inference of Solar Rotation from Perturbations of Acoustic Mode Eigenfunctions

Ariane **Schad**1,2 and Markus Roth
2020 ApJ 890 32
https://iopscience.iop.org/article/10.3847/1538-4357/ab65ec/pdf
https://arxiv.org/pdf/2002.06114.pdf
Today's picture of the internal solar rotation rate profile results essentially from helioseismic analyses of frequency splittings of resonant acoustic waves. Here we present another, complementary estimation of the internal solar rotation rate using the perturbation of the shape of the acoustic waves. For this purpose, we extend a global helioseismic approach developed previously for the investigation of the meridional flow to work on the components of the differential rotation. We discuss the effect of rotation on mode eigenfunctions and the observables based thereon. Based on a numerical study using a simulated rotation rate profile, we tailor an inversion approach and also consider the case of the presence of an additional meridional flow. This inversion approach is then applied to data from the Michelson Doppler Imager (MDI) on board the Solar Heliospheric Observatory and the Helioseismic and Magnetic Imager (HMI) on board the Solar Dynamics Observatory. In the end, rotation rate profiles estimated from eigenfunction perturbation and frequency splittings are compared.
The rotation rate profiles from the two different approaches are qualitatively in good agreement, especially for the MDI data. Significant differences are obtained at high latitudes >50° and near the subsurface. The result from HMI data shows larger discrepancies between the different methods. We find that the two global helioseismic approaches provide complementary methods for measuring the solar rotation. Comparing the results from different methods may help to reveal systematic influences that affect analyses based on eigenfunction perturbations, like meridional flow measurements.

Neutral Helium Triplet Spectroscopy of Quiescent Coronal Rain with Sensitivity Estimates for Spectropolarimetric Magnetic Field Diagnostics

Thomas A. **Schad**
ApJ **2018**
https://arxiv.org/pdf/1809.02252.pdf
On account of its polarizability and magnetic field sensitivity, as well as the role of neutral helium in partially ionized solar environments, the neutral helium triplet (orthohelium) system provides important, yet under-utilized, diagnostics of solar coronal rain. This work describes off-limb observations of coronal rain in NOAA Active Region 12468 obtained in the He I 10830 $\AA$ triplet using the Massively MultipleXed Imaging Spectrograph experiment at the Dunn Solar Telescope along with co-temporal observations from NASA's Solar Dynamics Observatory and the Interface Region Imaging Spectrograph. We detect rain simultaneously in the IRIS 1400 $\AA$and 2796 $\AA$ channels and in He I 10830 $\AA$. The large degree of spatial coherence present between all channels agrees with previous observations of the multi-thermal nature of coronal rain. A statistical analysis of He I spectral profiles for rain identified via automated detection indicate He I line radiances are, on average, 104ergs cm−2 s−1 sr−1; the average translational velocity is 70 km s−1 and Doppler widths are distributed around 10 km s−1. Based on these results, forward models of expected He I polarized signals allow us to estimate, using synthetic observables and an inversion algorithm including fits for the scattering angle constraining the material's location along-the-line of sight, the magnetic sensitivity of the upcoming National Science Foundation's Daniel K. Inouye Solar Telescope. We predict joint observations of the He I 10830 $\AA$ and 5876 $\AA$ multiplets, using first-light instrumentation, will provide inverted magnetic field errors of ±3.5 G (2σ) for spatial scales of 0.5″ (∼360 km) assuming dynamically-limited integration times of 5.5 seconds. **2015 December 9**

Automated Spatiotemporal Analysis of Fibrils and Coronal Rain Using the Rolling Hough Transform

Thomas **Schad**
Solar Physics September **2017**, 292:132
http://iopscience.iop.org/article/10.1088/0004-637X/739/2/67/pdf
https://arxiv.org/pdf/1809.03635.pdf
A technique is presented that automates the direction characterization of curvilinear features in multidimensional solar imaging datasets. It is an extension of the Rolling Hough Transform (RHT) technique presented by Clark, Peek, and Putman (Astrophys. J.789, 82, 2014), and it excels at rapid quantification of spatial and spatiotemporal feature orientation even for applications with a low signal-to-noise ratio. It operates on a pixel-by-pixel basis within a dataset and reliably quantifies orientation even for locations not centered on a feature ridge, which is used here to derive a quasi-continuous map of the chromospheric fine-structure projection angle. For time-series analysis, a procedure is developed that uses a hierarchical application of the RHT to automatically derive the apparent motion

of coronal rain observed off-limb. Essential to the success of this technique is the formulation presented in this article for the RHT error analysis as it provides a means to properly filter results. **9-10 December 2015**

Recent Developments in Helioseismic Analysis Methods and Solar Data Assimilation

A. **Schad** , L. Jouve, T. L. Duvall Jr., M. Roth, S. Vorontsov **Review**
Space Science Reviews **2016**
http://arxiv.org/pdf/1603.04742v1.pdf
We review recent advances and results in enhancing and developing helioseismic analysis methods and in solar data assimilation. In the first part of this paper we will focus on selected developments in time-distance and global helioseismology. In the second part, we review the application of data assimilation methods on solar data. Relating solar surface observations as well as helioseismic proxies with solar dynamo models by means of the techniques from data assimilation is a promising new approach to explore and to predict the magnetic activity cycle of the Sun.

On the Collective Magnetic Field Strength and Vector Structure of Dark Umbral Cores Measured by the Hinode Spectropolarimeter

T.A. **Schad**
Solar Phys. **2015**
http://arxiv.org/pdf/1505.05581v1.pdf
We study 7530 sunspot umbrae and pores measured by the Hinode Spectropolarimeter (SP) between November 2006 and November 2012. We primarily seek confirmation of the long term secular decrease in the mean magnetic field strength of sunspot umbrae found by Penn and Livingston (2011, IAU Symp. 273,126) between 1998 and 2011. The excellent SP photometric properties and full vector magnetic field determinations from full-Stokes Milne-Eddington inversions are used to address the interrelated properties of the magnetic field strength and brightness temperature for all umbral cores. We find non-linear relationships between magnetic field strength and umbral temperature (and continuum contrast), as well as between umbral radius and magnetic field strength. Using disambiguated vector data, we find that the azimuths measured in the umbral cores reflect an organization weakly influenced by Joy's law. The large selection of umbrae displays a log-normal size spectrum similar to earlier solar cycles. Influenced by the amplitude of the solar cycle and the nonlinear relationship between umbral size and core magnetic field strength, the distribution of core magnetic field strengths, fit most effectively with a skew-normal distribution, shows a weak solar cycle dependence. Yet, the mean magnetic field strength does not show a significant long term trend.

Is the sky the limit? Performance of the revamped Swedish 1-m Solar Telescope and its blue- and red-beam re-imaging systems

Goran **Scharmer**, Mats Lofdahl, Guus Sliepen, Jaime de la Cruz Rodriguez
A&A **2019**
https://arxiv.org/pdf/1905.05588.pdf
We demonstrate that for data recorded with a solar telescope that uses adaptive optics and/or post-processing to compensate for many low- and high-order aberrations, the RMS granulation contrast is directly proportional to the Strehl ratio calculated from the residual (small-scale) wavefront error. We demonstrate that the wings of the high-order compensated PSF for SST are likely to extend to a radius of not more than about 2 arcsec, consistent with earlier conclusions drawn from straylight compensation of sunspot images. We report on simultaneous measurements of seeing and solar granulation contrast averaged over 2 sec time intervals at several wavelengths from 525 nm to 853.6 nm on the red-beam (CRISP beam) and wavelengths from 395 nm to 484 nm on the blue-beam (CHROMIS beam). These data were recorded with the Swedish 1-m Solar Telescope (SST) that has been revamped with an 85-electrode adaptive mirror and a new tip-tilt mirror, both of which were polished to exceptionally high optical quality. The highest 2-sec average image contrast measured in April 2015 through 0.3-0.9 nm interference filters at 525 nm, 557 nm, 630 nm and 853.5 nm with compensation only for the diffraction limited point spread function of SST is 11.8%, 11.8%, 10.2% and 7.2% respectively. Similarly, the highest 2-sec contrast measured at 395 nm, 400 nm and 484 nm in May 2016 through 0.37-1.3 nm filters is 16%, 16% and 12.5% respectively. The granulation contrast observed with SST compares favorably with that of other telescopes. Simultaneously with the above wideband red-beam data, we also recorded narrow-band continuum images with the CRISP imaging spectropolarimeter. We find that contrasts measured with CRISP are entirely consistent with the corresponding wide-band contrasts, demonstrating that any additional image degradation by the CRISP etalons and telecentric optical system is marginal or even insignificant.

A Critical Evaluation of Recent Claims Concerning Solar Rotation

P.H. **Scherrer**, D.O. Gough
ApJ **877** 42 **2019**

https://arxiv.org/pdf/1904.02820.pdf
Fossat et al. (2017) recently reported detecting rotational splitting of g modes indirectly via the interaction with p modes observed directly by the GOLF instrument on SOHO. They concluded that the core of the Sun is rotating 3:8 ? 0:1 times faster than the surrounding radiative envelope. This is startling, partly because such rapid rotation almost contradicts direct inferences from the p-mode rotational splitting inferred from the same data. Moreover, the inferred amplitudes of the g modes appear to exceed the upper bound reported by Appourchaux et al. (2010). It is also suspect because the theory of the procedure implies that the principal modes claimed to have been measured should be undetectable. We point out that there are other interpretations: one leads to a core rotation about twice faster than the surrounding envelope; another, to a core rotating more slowly than the envelope. Here we also report on an independent assessment of the Fossat et al. analysis by applying their procedure to different representations of the GOLF data, expanding on Schunker et al. (2018). We also analyze seismic data obtained from LOI and MDI (both also on SOHO), from HMI (on SDO) and from the ground-based BiSON and GONG, and found the evidence reported by Fossat et al. not to be robust. We also illustrate that merely fitting model spectra to observations, which Fossat et al. do to support their g-mode detections and as Fossat & Schmider (2018) do for extracting additional g-mode splittings, is not necessarily reliable. We are therefore led to doubt the claim.

A Bayesian Approach to Period Searching in Solar Coronal Loops

Bryan **Scherrer**1 and David McKenzie
2017 ApJ 837 24
We have applied a Bayesian generalized Lomb–Scargle period searching algorithm to movies of coronal loop images obtained with the Hinode X-ray Telescope (XRT) to search for evidence of periodicities that would indicate resonant heating of the loops. The algorithm makes as its only assumption that there is a single sinusoidal signal within each light curve of the data. Both the amplitudes and noise are taken as free parameters. It is argued that this procedure should be used alongside Fourier and wavelet analyses to more accurately extract periodic intensity modulations in coronal loops. The data analyzed are from XRT Observation Program #129C: "MHD Wave Heating (Thin Filters)," which occurred during **2006 November 13** and focused on active region 10293, which included coronal loops. The first data set spans approximately 10 min with an average cadence of 2 s, 2" per pixel resolution, and used the Al-mesh analysis filter. The second data set spans approximately 4 min with a 3 s average cadence, 1" per pixel resolution, and used the Al-poly analysis filter. The final data set spans approximately 22 min at a 6 s average cadence, and used the Al-poly analysis filter. In total, 55 periods of sinusoidal coronal loop oscillations between 5.5 and 59.6 s are discussed, supporting proposals in the literature that resonant absorption of magnetic waves is a viable mechanism for depositing energy in the corona.

Segmentation of spectroscopic images of the low solar atmosphere by the self-organizing map technique

F **Schilliro**, P Romano
Monthly Notices of the Royal Astronomical Society, Volume 503, Issue 2, May **2021**, Pages 2676–2687,
https://doi.org/10.1093/mnras/stab507
https://academic.oup.com/mnras/article-pdf/503/2/2676/36742635/stab507.pdf
We describe the application of semantic segmentation by using the self-organizing map technique to an high spatial and spectral resolution data set acquired along the H α line at 656.28 nm by the Interferometric Bi-dimensional Spectrometer installed at the focus plane of the Dunn solar telescope. This machine learning approach allowed us to identify several features corresponding to the main structures of the solar photosphere and chromosphere. The obtained results show the capability and flexibility of this method to identifying and analysing the fine structures which characterize the solar activity in the low atmosphere. This is a first successful application of the SOM technique to astrophysical data sets.

Deep learning image burst stacking to reconstruct high-resolution ground-based solar observations

C. **Schirninger**1⋆, R. Jarolim2, A. M. Veronig1,3 and C. Kuckein4,5,6
A&A, 693, A6 (**2025**)
https://www.aanda.org/articles/aa/pdf/2025/01/aa51850-24.pdf
https://doi.org/10.1051/0004-6361/202451850
Context. Large aperture ground-based solar telescopes allow the solar atmosphere to be resolved in unprecedented detail. However, ground-based observations are inherently limited due to Earth's turbulent atmosphere, requiring image correction techniques.
Aims. Recent post-image reconstruction techniques are based on using information from bursts of short-exposure images. Shortcomings of such approaches are the limited success, in case of stronger atmospheric seeing conditions, and computational demand. Real-time post-image reconstruction is of high importance to enabling automatic processing pipelines and accelerating scientific research. In an attempt to overcome these limitations, we provide a

deep learning approach to reconstruct an original image burst into a single high-resolution high-quality image in real time.
Methods. We present a novel deep learning tool for image burst reconstruction based on image stacking methods. Here, an image burst of 100 short-exposure observations is reconstructed to obtain a single high-resolution image. Our approach builds on unpaired image-to-image translation. We trained our neural network with seeing degraded image bursts and used speckle reconstructed observations as a reference. With the unpaired image translation, we aim to achieve a better generalization and increased robustness in case of increased image degradations.
Results. We demonstrate that our deep learning model has the ability to effectively reconstruct an image burst in real time with an average of 0.5 s of processing time while providing similar results to standard reconstruction methods. We evaluated the results on an independent test set consisting of high- and low-quality speckle reconstructions. Our method shows an improved robustness in terms of perceptual quality, especially when speckle reconstruction methods show artifacts. An evaluation with a varying number of images per burst demonstrates that our method makes efficient use of the combined image information and achieves the best reconstructions when provided with the full-image burst.

Effects of solar evolution on finite acquisition time of Fabry-Perot-Interferometers in high resolution solar physics

Rolf **Schlichenmaier**, Daniel Pitters, Juan Manuel Borrero, Matthias Schubert
A&A **2022**
https://arxiv.org/pdf/2210.15319.pdf
The imaging spectro-polarimeter VTF (Visible Tunable Filter) will be operated at the Daniel K. Inouye Solar Telescope (DKIST). Due to its capability of resolving dynamic fine structure of smaller than 0.05", the finite acquisition time of typically 11 s affects the measurement process and potentially causes errors in deduced physical parameters. We estimate those errors and investigate ways of minimising them.
We mimic the solar surface using a magneto-hydrodynamic simulation with a spatially averaged vertical field strength of 200 G. We simulate the measurement process scanning through successive wavelength points with a temporal cadence of 1 s. We synthesise FeI 617.3 nm. Besides the classical composition of the line profile, we introduce a novel method in which the intensity in each wavelength point is normalised using the simultaneous continuum intensity. Milne-Eddington inversions are used to infer the line-of-sight velocity, v(los), and the vertical (longitudinal) component of the magnetic field, B(los).
We quantify systematic errors, defining the temporal average of the simulation during the measurement as the truth. We find that with the classical composition of the line profiles, errors exceed the sensitivity for v(los) and in filigree regions also for B(los). The novel method that includes normalisation reduces the measurement errors in all cases. Spatial binning without reducing the acquisition time decreases the measurement error slightly.
The evolutionary time-scale in inter-granular lanes, in particular in areas with magnetic features (filigree), is shorter than the time-scale within granules. Hence less accumulations could be used for strong magnetic field in inter-granular lanes and more accumulations could be used for the weak granular magnetic fields. As a key result, we suggest to include the novel method of normalisation in corresponding data pipelines.

Science Requirement Document (SRD) for the European Solar Telescope (EST) (2nd edition, December 2019)

R. **Schlichenmaier** (1), L. R. Bellot Rubio (2), M. Collados (3,4), R. Erdelyi (5,6), A. Feller (7), L. Fletcher (8,13), ...
2nd edition, December **2019** 138 p.
https://arxiv.org/pdf/1912.08650.pdf
The European Solar Telescope (EST) is a research infrastructure for solar physics. It is planned to be an on-axis solar telescope with an aperture of 4 m and equipped with an innovative suite of spectro-polarimetric and imaging post-focus instrumentation. The EST project was initiated and is driven by EAST, the European Association for Solar Telescopes. EAST was founded in 2006 as an association of 14 European countries. Today, as of December 2019, EAST consists of 26 European research institutes from 18 European countries.
The Preliminary Design Phase of EST was accomplished between 2008 and 2011. During this phase, in 2010, the first version of the EST Science Requirement Document (SRD) was published. After EST became a project on the ESFRI roadmap 2016, the preparatory phase started. The goal of the preparatory phase is to accomplish a final design for the telescope and the legal governance structure of EST. A major milestone on this path is to revisit and update the Science Requirement Document (SRD).
The EST Science Advisory Group (SAG) has been constituted by EAST and the Board of the PRE-EST EU project in November 2017 and has been charged with the task of providing with a final statement on the science requirements for EST. Based on the conceptual design, the SRD update takes into account recent technical and scientific developments, to ensure that EST provides significant advancement beyond the current state-of-the-art. The present update of the EST SRD has been developed and discussed during a series of EST SAG meetings. The SRD develops the top-level science objectives of EST into individual science cases. Identifying critical science

requirements is one of its main goals. Those requirements will define the capabilities of EST and the post-focus instrument suite. The technical requirements for the final design of EST will be derived from the SRD.
II Top-level science goals **Review**

HOT PLASMA FROM SOLAR ACTIVE-REGION CORES: CONSTRAINTS FROM THE HINODE X-RAY TELESCOPE

J. T. **Schmelz**1,2,3, G. M. Christian3, and P. O. Matheny
2016 ApJ 833 182
Mechanisms invoked to heat the solar corona to millions of degrees kelvin involve either magnetic waves or magnetic reconnections. Turbulence in the convection zone produces MHD waves, which travel upward and dissipate. Photospheric motions continuously build up magnetic energy, which is released through magnetic reconnection. In this paper, we concentrate on hot non-flaring plasma with temperatures of 5 MK < T < 10 MK because it is one of the few observables for which wave and reconnection models make different predictions. Wave models predict no (or little) hot plasma, whereas reconnection models predict it, although in amounts that are challenging to detect with current instrumentation. We used data from the X-ray Telescope (XRT) and the Atmospheric Imaging Assembly (AIA). We requested a special XRT observing sequence, which cycled through the thickest XRT filter several times per hour so we could average these images and improve the signal-to-noise. We did differential emission measure (DEM) analysis using the time-averaged thick-filter data as well as all available channels from both the XRT and AIA for regions observed on 2014 December 11. Whereas our earlier work was only able to determine that plasma with a temperature greater than 5 MK was *present*, we are now able to find a well-constrained DEM distribution. We have therefore added a strong observational constraint that must be explained by any viable coronal heating model. Comparing state-of-the-art wave and reconnection model predictions, we can conclude that reconnection is heating the hot plasma in these active regions.

What can observations tell us about coronal heating? **Review**

Schmelz,J.T. and Winebarger,A.R.
2015, Phil. Trans A 373, issue 2042, pp. 20140257-20140257
http://sci-hub.tw/10.1098/rsta.2014.0257
The actual source of coronal heating is one of the longest standing unsolved mysteries in all of astrophysics, but it is only in recent years that observations have begun making significant contributions. Coronal loops, their structure and sub-structure, their temperature and density details, and their evolution with time, may hold the key to solving this mystery. Because spatial resolution of current observatories cannot resolve fundamental scale lengths, information about the heating of the corona must be inferred from indirect observations. Loops with unexpectedly high densities and multithermal cross-field temperatures were not consistent with results expected from steady uniform heating models. The hot (T > 5 MK) plasma component of loops may also be a key observation; a new sounding rocket instrument called the Marshall Grazing Incidence X-ray Spectrometer will specifically target this observable. Finally, a loop is likely to be a tangle of magnetic strands. The High Resolution Coronal Imager observed magnetic braids untwisting and reconnecting, dispersing enough energy to heat the surrounding plasma. The existence of multithermal, cooling loops and hot plasma provides observational constraints that all viable coronal heating models will need to explain.

Atmospheric Imaging Assembly Response Functions: Solving the Fe viii Problems with Hinode EIS Bright Point Data

J. T. **Schmelz**, B. S. Jenkins, J. A. Kimble
Solar Physics, April **2013**, Volume 283, Issue 2, pp 325-340
The Atmospheric Imaging Assembly (AIA) onboard the Solar Dynamics Observatory is a state-of-the-art imager with the potential to perform an unprecedented time-dependent multi-thermal analysis at every pixel on scales that are short compared to the radiative and conductive cooling times. Recent results, however, have identified missing spectral lines in the CHIANTI atomic physics database, which is used to construct the instrument response functions. This is not surprising since the wavelength range from 90 Å to 140 Å has rarely been observed with solar spectrometers, and atomic data for many of these ions are simply not available in the literature. We have performed a differential emission measure analysis using simultaneous AIA and Hinode/EIS observations of six X-ray bright points. Our results not only support the conclusion that CHIANTI is incomplete near 131 Å, but more importantly, suggest that the peak temperature of the Fe viii emissivity/response is likely to be closer to log T=5.8 than to the current value of log T=5.7. Using a revised emissivity/response calculation for Fe viii, we find that observed AIA 131-Å flux can be underestimated by ≈ 1.25, lower than previous comparisons. With these adjustments, not only the AIA 131-Å data, but also the EIS Fe viii lines, match the remainder of the bright-point data better. In addition, we find that CHIANTI is reasonably complete in the AIA 171- and 193-Å bands. For the AIA 211-, 335-, and 94-Å channels, we recommend that more work be done with AIA–EIS DEM comparisons using observations of active-

region cores, i.e. coronal structures with more emission measure at warmer temperatures than our bright points. Then a variety of EIS iron lines could be directly compared with AIA data.

SOME LIKE IT HOT: CORONAL HEATING OBSERVATIONS FROM *HINODE* X-RAY TELESCOPE AND *RHESSI*

J. T. **Schmelz**1,2, V. L. Kashyap2, S. H. Saar2, B. R. Dennis3, P. C. Grigis2, L. Lin4, E. E. DeLuca2, G. D. Holman3, L. Golub2, and M. A. Weber2
Astrophysical Journal, 704:863–869, **2009** October
We have used *Hinode* X-Ray Telescope observations and *RHESSI* upper limits together to characterize the differential emission measure (DEM) from a quiescent active region. We find a relatively smooth DEM curve with the expected active region peak at log T = 6.4. We also find a high-temperature component with significant emission measure at log T _ 7. This curve is consistent with previous observations of quiescent active regions in that it does not produce observable Fe xix lines. It is different from that generated with X-Ray Telescope (XRT) data alone—*RHESSI* rules out the possibility of a separate high-temperature component with a peak of approximately log T = 7.4. The strength and position of the high-temperature peak in this XRT-only analysis was, however, poorly determined; adding *RHESSI* flux upper limits in the 4–13 keV energy range provide a strong high-temperature constraint which greatly improves the multi-thermal findings. The results of the present work as well as those from a growing number of papers on this subject imply that our previous understanding of the temperature distribution in active regions has been limited. Hot plasma (log $T \approx 7$) appears to be prevalent, although in relatively small quantities as predicted by nanoflare models. Other models may need to be adjusted or updated to account for these new results.

Reminiscences

Brigitte **Schmieder**
Solar Phys. 294:53 **2019**
https://arxiv.org/pdf/1903.04036.pdf
sci-hub.se/10.1007/s11207-019-1436-4
I would like to thank Solar Physics colleagues for asking me to write this chapter on my professional life. My main interest has always been focused on the Sun, our star, from the heating of the corona, to the dynamics of prominences and their eruptions, ares and coronal mass ejections until their impact on the Earth. I built a new group in solar physics and gave to them my enthusiasm. They brought to me a lot of satisfaction. We have made important advances in solar physics with a step forward to understand the triggers of solar activity and their terrestrial effects. Our avant-garde research and discovery has opened new topics for the solar community. Mixing observations obtained on the ground and in space with theory and numerical simulations brings a new perspective in research.

Magnetic Flux Emergence Along the Solar Cycle **Review**

B. **Schmieder**, V. Archontis, E. Pariat
Space Science Reviews December **2014**, Volume 186, Issue 1-4, pp 227-250
Flux emergence plays an important role along the solar cycle. Magnetic flux emergence builds sunspot groups and solar activity. The sunspot groups contribute to the large scale behaviour of the magnetic field over the 11 year cycle and the reversal of the North and South magnetic polarity every 22 years. The leading polarity of sunspot groups is opposite in the North and South hemispheres and reverses for each new solar cycle. However the hemispheric rule shows the conservation of sign of the magnetic helicity with positive and negative magnetic helicity in the South and North hemispheres, respectively. MHD models of emerging flux have been developed over the past twenty years but have not yet succeeded to reproduce solar observations. The emergence of flux occurs through plasma layers of very high gradients of pressure and changing of modes from a large β to a low β plasma (<1). With the new armada of high spatial and temporal resolution instruments on the ground and in space, emergence of magnetic flux is observed in tremendous detail and followed during their transit through the upper atmosphere. Signatures of flux emergence in the corona depend on the pre-existing magnetic configuration and on the strength of the emerging flux. We review in this paper new and established models as well as the recent observations

Actors of the main activity in large complex centres during the 23 solar cycle maximum

B. Schmieder, , , P. Démoulina, E. Pariata, T. Töröka, 1, G. Molodija, C.H. Mandrinib, S. Dassob, R. Chandrac, W. Uddind, P. Kumard, P.K. Manoharane, P. Venkatakrishnanf and N. Srivastava
Advances in Space Research, Volume 47, Issue 12, 15 June **2011**, Pages 2081-2091, **File**
During the maximum of Solar Cycle 23, large active regions had a long life, spanning several solar rotations, and produced large numbers of X-class flares and CMEs, some of them associated to magnetic clouds (MCs). This is the case for the Halloween active regions in 2003. The most geoeffective MC of the cycle (Dst = −457) had its source

during the disk passage of one of these active regions (NOAA 10501) on 18 November 2003. Such an activity was presumably due to continuous emerging magnetic flux that was observed during this passage. Moreover, the region exhibited a complex topology with multiple domains of different magnetic helicities. The complexity was observed to reach such unprecedented levels that a detailed multi-wavelength analysis is necessary to precisely identify the solar sources of CMEs and MCs. Magnetic clouds are identified using in situ measurements and interplanetary scintillation (IPS) data. Results from these two different sets of data are also compared.

Probing Uncertainties in Diagnostics of a Synthetic Chromosphere

Don **Schmit**1, Juan Martinez-Sykora2, Tiago Pereira3, and Andrés Asensio Ramos4
2021 ApJ 913 71
https://doi.org/10.3847/1538-4357/abf4d2
Effective spectroscopic diagnostics rely on the ability to convert a particular flux measurement into a physical interpretation. Knowledge of uncertainty is a central component of diagnostics. We present data from a simulated solar-like chromosphere, where we have addressed the question of whether degeneracy is a problem in mapping from a non-LTE chromospheric line profile to a particular vertical stratification of atmospheric properties along the line of sight. Our results indicate that stratification degeneracies do exist, at least in our simulated atmosphere. We quantify this effect through the creation of posterior densities for atmospheric properties based on the Mg ii h line profile using the approximate Bayesian computation (ABC) technique. We find that the predictive power of the ABC temperature posterior systematically varies as a function of atmospheric column mass and ground-truth temperature. The ABC posteriors more effectively reproduce the spectral intensity in the Ca ii 8542 Å line than they do temperature stratification, although residual error in the Ca ii line core is common. Our results illustrate that some degeneracies should be alleviated through simultaneous analysis of multiple chromospheric lines.

Understanding the Structure of Rapid Intensity Fluctuations in the Chromosphere with IRIS

D. **Schmit**1,2, B. De Pontieu3,4,5, A. Winebarger6, L. Rachmeler6, and A. Daw2
2020 ApJ 889 112
https://doi.org/10.3847/1538-4357/ab5f6b
Several recent data sets have taken advantage of the unique capabilities of orbital and suborbital spacecraft to image the chromosphere and transition region at a very high cadence. We find that both the chromosphere and transition region exhibit spatially coherent transient features at frequencies above 80 mHz. We have analyzed narrowband imaging data from H i Lyα 1215 Å (provided by CLASP), Mg ii k 2796 Å, and Si iv 1400 Å (provided by the Interface Region Imaging Spectrograph). We categorize the spatial structure of these rapid fluctuations in different magnetic environments. Intensity fluctuations above the noise level are observed in plages in all passbands. We have found jet-like features in 1215 and 1400 Å data that extend from the edges of plages as well as network magnetic concentrations. We have not found any recurrent features that are identified in both 1400 and 1215 Å data. Short loop-like features were only found in 1400 Å data. Temperature minimum grains generate non-propagating features in 1400 Å data. We compare our observations with previous research on dynamic chromospheric phenomena at lower frequencies. Candidate mechanisms, related to both jets and waves, predict chromospheric and transition region intensity fluctuations at high temporal frequencies, which can now be observationally probed.

Comparison of Solar Fine Structure Observed Simultaneously in Ly-α and Mg II h

D.J. **Schmit**, A. V. Sukhorukov, B. De Pontieu, J. Leenaarts, C. Bethge, A. Winebarger, F. Auchère, T. Bando, R. Ishikawa, K. Kobayashi, N. Narukage, J. Trujillo Bueno
ApJ **847** 141 **2017**
https://arxiv.org/pdf/1709.00035.pdf
The Chromospheric Lyman Alpha Spectropolarimeter (CLASP) observed the Sun in H I Lyman-{\alpha} during a suborbital rocket flight on September 3, 2015. The Interface Region Imaging Telescope (IRIS) coordinated with the CLASP observations and recorded nearly simultaneous and co-spatial observations in the Mg II h&k lines. The Mg II h and Ly-{\alpha} lines are important transitions, energetically and diagnostically, in the chromosphere. The canonical solar atmosphere model predicts that these lines form in close proximity to each other and so we expect that the line profiles will exhibit similar variability. In this analysis, we present these coordinated observations and discuss how the two profiles compare over a region of quiet sun at viewing angles that approach the limb. In addition to the observations, we synthesize both line profiles using a 3D radiation-MHD simulation. In the observations, we find that the peak width and the peak intensities are well correlated between the lines. For the simulation, we do not find the same relationship. We have attempted to mitigate the instrumental differences between IRIS and CLASP and to reproduce the instrumental factors in the synthetic profiles. The model indicates that formation heights of the lines differ in a somewhat regular fashion related to magnetic geometry. This variation explains to some degree the lack of correlation, observed and synthesized, between Mg II and Ly-{\alpha}. Our analysis will aid in the definition of future observatories that aim to link dynamics in the chromosphere and transition region.

What Is the Source of Quiet Sun Transition Region Emission?

Donald **Schmit**, Bart De Pontieu

ApJ **2016**

http://arxiv.org/pdf/1608.07620v1.pdf

Dating back to the first observations of the on-disk corona, there has been a qualitative link between the photosphere's magnetic network and enhanced transition-temperature plasma emission. These observations led to the development of a general model that describes emission structures through the partitioning of the atmospheric volume with different magnetic loop geometries that exhibit different energetic equilibria. Does the internetwork produce transition-temperature emission? What fraction of network flux connects to the corona? How does quiet sun emission compare with low-activity Sun-like stars? In this work, we revisit the canonical model of the quiet sun, with high-resolution observations from IRIS and HMI in hand, to address those questions. We use over 900 deep exposures of Si IV 1393A from IRIS along with nearly simultaneous HMI magnetograms to quantify the correlation between transition-temperature emission structures and magnetic field concentrations through a number of novel statistics. Our observational results are coupled with analysis of the Bifrost MHD model and a large-scale potential field model. Our results paint a complex portrait of the quiet sun. We measure an emission signature in the distant internetwork that cannot be attributed to network contribution. We find that the dimmest regions of emission are not linked to the local vertical magnetic field. Using the MHD simulation, we categorize the emission contribution from cool mid-altitude loops and high-altitude coronal loops and discuss the potential emission contribution of spicules. Our results provide new constraints on the coupled solar atmosphere so that we can build on our understanding of how dynamic thermal and magnetic structures generate the observed phenomena in the transition region.

Observed Variability of the Solar Mg II h Spectral Line

Donald **Schmit**, Paul Bryans, Bart De Pontieu, Scott McIntosh, Jorrit Leenaarts, Mats Carlsson

2015

http://arxiv.org/pdf/1508.04714v1.pdf

The Mg II h&k doublet are two of the primary spectral lines observed by the Sun-pointing Interface Region Imaging Spectrograph (IRIS). These lines are tracers of the magnetic and thermal environment that spans from the photosphere to the upper chromosphere. We use a double gaussian model to fit the Mg II h profile for a full-Sun mosaic dataset taken **24-Aug-2014**. We use the ensemble of high-quality profile fits to conduct a statistical study on the variability of the line profile as it relates the magnetic structure, dynamics, and center-to-limb viewing angle. The average internetwork profile contains a deeply reversed core and is weakly asymmetric at h2. In the internetwork, we find a strong correlation between h3 wavelength and profile asymmetry as well h1 width and h2 width. The average reversal depth of the h3 core is inversely related to the magnetic field. Plage and sunspots exhibit many profiles which do not contain a reversal. These profiles also occur infrequently in the internetwork. We see indications of magnetically aligned structures in plage and network in statistics associated with the line core, but these structures are not clear or extended in the internetwork. The center-to-limb variations are compared with predictions of semi-empirical model atmospheres. We measure a pronounced limb darkening in the line core which is not predicted by the model. The aim of this work is to provide a comprehensive measurement baseline and preliminary analysis on the observed structure and formation of the Mg II profiles observed by IRIS.

Making of a solar spectral irradiance dataset I: observations, uncertainties, and methods

Micha **Schöll**1a,*, Thierry Dudok de Wit1a, Matthieu Kretzschmar1a and Margit Haberreiter

J. Space Weather Space Clim., 6, A14 (**2016**)

http://www.swsc-journal.org/articles/swsc/pdf/2016/01/swsc150020.pdf

Context. Changes in the spectral solar irradiance (SSI) are a key driver of the variability of the Earth's environment, strongly affecting the upper atmosphere, but also impacting climate. However, its measurements have been sparse and of different quality. The "First European Comprehensive Solar Irradiance Data Exploitation project" (SOLID) aims at merging the complete set of European irradiance data, complemented by archive data that include data from non-European missions.

Aims. As part of SOLID, we present all available space-based SSI measurements, reference spectra, and relevant proxies in a unified format with regular temporal re-gridding, interpolation, gap-filling as well as associated uncertainty estimations.

Methods. We apply a coherent methodology to all available SSI datasets. Our pipeline approach consists of the pre-processing of the data, the interpolation of missing data by utilizing the spectral coherency of SSI, the temporal re-gridding of the data, an instrumental outlier detection routine, and a proxy-based interpolation for missing and flagged values. In particular, to detect instrumental outliers, we combine an autoregressive model with proxy data.

We independently estimate the precision and stability of each individual dataset and flag all changes due to processing in an accompanying quality mask.
Results. We present a unified database of solar activity records with accompanying meta-data and uncertainties.
Conclusions. This dataset can be used for further investigations of the long-term trend of solar activity and the construction of a homogeneous SSI record.

Transition region contribution to AIA observations in the context of coronal heating

Samuel J. **Schonfeld**, James A. Klimchuk
ApJ **905** 115 **2020**
https://arxiv.org/pdf/2009.06759.pdf
https://doi.org/10.3847/1538-4357/abc3bd
We investigate the relative contributions from the transition region and corona of coronal loops observed by the Atmospheric Imaging Assembly (AIA) on the Solar Dynamics Observatory (SDO). Using EBTEL (Enthalpy-Based Thermal Evolution of Loops) hydrodynamic simulations, we model loops with multiple lengths and energy fluxes heated randomly by events drawn from power-law distributions with different slopes and minimum delays between events to investigate how each of these parameters influences observable loop properties. We generate AIA intensities from the corona and transition region for each realization. The variations within and between models generated with these different parameters illustrate the sensitivity of narrowband imaging to the details of coronal heating. We then analyze the transition region and coronal emission from a number of observed active regions and find broad agreement with the trends in the models. In both models and observations, the transition region brightness is significant, often greater than the coronal brightness in all six "coronal" AIA channels. We also identify an inverse relationship, consistent with heating theories, between the slope of the differential emission measure (DEM) coolward of the peak temperature and the observed ratio of coronal to transition region intensity. These results highlight the use of narrowband observations and the importance of properly considering the transition region in investigations of coronal heating. **2011-08-09**

The Slowly Varying Corona: I --- Daily Differential Emission Measure Distributions Derived from EVE Spectra

Samuel J. **Schonfeld**, Stephen M. White, Rachel A. Hock-Mysliwiec, R. T. James McAteer
ApJ **844** 163 **2017**
https://arxiv.org/pdf/1706.09525.pdf
http://iopscience.iop.org.sci-hub.cc/0004-637X/844/2/163/
The DEMs are calculated using six strong emission features dominated by Fe lines of charge states VIII, IX, XI, XII, XIV, and XVI that sample the non-flaring coronal temperature range 0.3--5 MK. A proxy for the non-XVIII emission in the wavelength band around the 93.9 \AA\ line is demonstrated. There is little variability in the cool component of the corona (T < 1.3 MK) over the four years, suggesting that the quiet-Sun corona does not respond strongly to the solar cycle, whereas the hotter component (T >2.0 MK) varies by more than an order of magnitude. A discontinuity in the behavior of coronal diagnostics in 2011 February--March, around the time of the first X-class flare of cycle 24, suggests fundamentally different behavior in the corona under solar minimum and maximum conditions. This global state transition occurs over a period of several months. The DEMs are used to estimate the thermal energy of the visible solar corona (of order 1031 erg), its radiative energy loss rate (2.5--8 $\times 10^{27}$ erg s^{-1}), and the corresponding energy turnover timescale (about an hour). The uncertainties associated with the DEMs and these derived values are mostly due to the coronal Fe abundance and density and the CHIANTI atomic line database.

Estimating the nonstructural component of the helioseismic surface term using hydrodynamic simulations

J. **Schou**, A. C. Birch
A&A 638, A51 **2020**
https://arxiv.org/pdf/2004.13548.pdf
https://www.aanda.org/articles/aa/pdf/2020/06/aa36530-19.pdf
As the amount of asteroseismic data available continues to grow, the inability to accurately model observed oscillation frequencies is becoming a critical problem for interpreting these frequencies. A major component of this problem is the modeling of the near-surface layers. Our aim is to develop a method to estimate the effect of the near-surface layers on oscillation frequencies. In the proposed method we numerically estimate eigenfunctions in 3D hydrodynamic simulations. We match those to the eigenfunctions calculated from the classic equations applied to the horizontal averages of the structure variables. We use this procedure to calculate the frequency perturbation resulting from the dynamical part of the interaction of the oscillations with near-surface convection. As the last step we scale the numbers to the Sun. To provide a qualitative test of our method we performed a series of simulations, calculated the perturbations using our procedure, and compared them to previously reported residuals relative to

solar models. We find that we can largely reproduce the observed frequency residuals without resorting to poorly justified theoretical models. We find that, while the calculations of Houdek et al. (2017, MNRAS, 464, L124) produce similar frequency perturbations, the density-pressure phase differences computed here do not match those of that work.

Effects of granulation on the visibility of solar oscillations

J. **Schou**
A&A **2015**
http://arxiv.org/pdf/1507.08856v1.pdf
Context. The interaction of solar oscillations with near surface convection is poorly understood. These interactions are likely the cause of several problems in helio- and astero-seismology, including the so-called surface effect and apparently unphysical travel time shifts as a function of center to limb distance. There is thus a clear need for further theoretical understanding and observational tests.
Aims. The aim is to determine how the observed modes are affected by the convection.
Methods. I use HMI velocity and intensity images to construct k-ω diagrams showing how the oscillation amplitude and phase depend on the local granulation intensity.
Results. There is a clear and significant dependence of the observed properties of the oscillations on the local convection state.

A stellar view of the Sun

C.J. (Karel)**Schrijver**
Solar Phys. **298**, Article number: 104 **2023**
https://arxiv.org/pdf/2308.09069.pdf
https://link.springer.com/content/pdf/10.1007/s11207-023-02200-y.pdf
This invited memoir looks back on my scientific career that straddles the solar and stellar branches of astrophysics, with sprinklings of historical context and personal opinion. Except for a description of my life up to my Ph.D. phase, the structure is thematic rather than purely chronological, focusing on those topics that I worked on throughout substantial parts of my life: stars like the Sun and the Sun-as-a-star, surface field evolution, coronal structure and dynamics, heliophysics education, and space weather. Luck and a broadly inquisitive frame of mind shaped a fortunate life on two continents, taking me from one amazing mentor, colleague, and friend to another, working in stimulating settings to interpret data from state-of-the-art space observatories.

Testing the solar activity paradigm in the context of exoplanet transits

Carolus J. **Schrijver**
A & A **2020**
https://arxiv.org/pdf/2001.01093.pdf
Transits of exoplanets across cool stars contain blended information about structures on the stellar surface and about the planetary body and atmosphere. To advance understanding of how this information is entangled, a surface-flux transport code, based on observed properties of the Sun's magnetic field, is used to simulate the appearance of hypothetical stellar photospheres from the visible near 4000 Angstrom to the near-IR at 1.6 micron, by mapping intensities characteristic of faculae and spots onto stellar disks. Stellar appearances are computed for a Sun-like star of solar activity up to a star with mean magnetic flux density ~30 times higher. Simulated transit signals for a Jupiter-class planet are compared with observations. This (1) suggests that the solar paradigm is consistent with observations for stars throughout the activity range explored provided that infrequent large active regions with fluxes up to ~3×1023 Mx are included in the emergence spectrum, (2) quantitatively confirms that for such a model, faculae brighten relatively inactive stars while starspots dim more active stars, (3) suggests that large starspots inferred from transits of active stars are consistent with clusters of more compact spots seen in the model runs, (4) that wavelength-dependent transit-depth effects caused by stellar magnetic activity for the range of activity and the planetary diameter studied here can introduce apparent changes in the inferred exoplanetary radii across wavelengths from a few hundred to a few thousand kilometers, increasing with activity, and (5) that activity-modulated distortions of broadband stellar radiance across the visible to near-IR spectrum can reach several percent.

Publication statistics on Sun and heliosphere **Review**

C.J. **Schrijver**
Solar Phys. Volume 291, Issue 4, pp 1267-1272 **2016**
http://arxiv.org/pdf/1603.08943v1.pdf

The professional literature provides one means to review the evolution and geographic distribution of the scientific communities engaged in solar and heliospheric physics. With help of the Astrophysics Data System (NASA/ADS), I trace the growth of the research community over the past century from a few dozen researchers early in the 20-th Century to over 4,000 names with over refereed 2,000 publications in recent years, with 90% originating from 20 countries, being published in 90 distinct journals. Overall, the lead authors of these publications have their affiliations for 45% in Europe, 29% in the Americas, 24% in Australasia, and 2% in Africa and Arab countries. Publications most frequently appear (in decreasing order) in the Astrophysical Journal, the Journal of Geophysical Research (Space Physics), Solar Physics, Astronomy and Astrophysics, and Advances in Space Research (adding up to 59% of all publications in 2015).

Pathways of large-scale magnetic couplings between coronal events

C.J. **Schrijver**, A.M. Title, A.R. Yeates and M.L. DeRosa
E-print, May **2013, File;** ApJSS
The high-cadence, comprehensive view of the solar corona by SDO/AIA shows many events that are widely separated in space while occurring close together in time. In some cases, sets of coronal events are evidently causally related, while in many other instances indirect evidence can be found. We present case studies to highlight a variety of coupling processes involved in coronal events. We find that physical linkages between events do occur, but concur with earlier studies that these couplings appear to be crucial to understanding the initiation of major eruptive or explosive phenomena relatively infrequently. We note that the post-eruption reconfiguration time scale of the large-scale corona, estimated from the EUV afterglow, is on average longer than the mean time between CMEs, so that many CMEs originate from a corona that is still adjusting from a previous event. We argue that the coronal field is intrinsically global: current systems build up over days to months, the relaxation after eruptions continues over many hours, and evolving connections easily span much of a hemisphere. This needs to be reflected in our modeling of the connections from the solar surface into the heliosphere to properly model the solar wind, its perturbations, and the generation and propagation of solar energetic particles. However, the large-scale field cannot be constructed reliably by currently available observational resources. We assess the potential of high-quality observations from beyond Earth's perspective and advanced global modeling to understand the couplings between coronal events in the context of CMEs and solar energetic particle events. **2010/08/01, 2011/02/14-15, 2011/09/25-26, 2011/11/09, 2011/11/22, 2011/11/30, 2011/12/11, 2011/12/25, 2012/02/09**

Average motion of emerging solar active region polarities II: Joy's law

Hannah **Schunker**, Christian Baumgartner, Aaron C. Birch, Robert H. Cameron, Douglas C. Braun, Laurent Gizon
A&A 640, A116 **2020**
https://arxiv.org/pdf/2006.05565.pdf
https://www.aanda.org/articles/aa/pdf/2020/08/aa37322-19.pdf
The tilt of solar active regions described by Joy's law is essential for converting a toroidal field to a poloidal field in Babcock-Leighton dynamo models. In thin flux tube models the Coriolis force causes Joy's law, acting on east-west flows as they rise towards the surface. Our goal is to measure the evolution of the average tilt angle of hundreds of active regions as they emerge, so that we can constrain the origins of Joy's law. We measured the tilt angle of the primary bipoles in 153 emerging active regions in the Solar Dynamics Observatory Helioseismic Emerging Active Region survey. We used line-of-sight magnetic field measurements averaged over 6 hours to define the polarities and measure the tilt angle up to four days after emergence. We find that at the time of emergence the polarities are on average aligned east-west, and that neither the separation nor the tilt depends on latitude. We do find, however, that ARs at higher latitudes have a faster north-south separation speed than those closer to the equator at the emergence time. After emergence, the tilt angle increases and Joy's law is evident about two days later. The scatter in the tilt angle is independent of flux until about one day after emergence, when higher-flux regions have a smaller scatter in tilt angle than lower-flux regions. Our finding that active regions emerge with an east-west alignment is surprising since thin flux tube models predict that tilt angles of rising flux tubes are generated below the surface. Previously reported tilt angle relaxation of deeply anchored flux tubes can be largely explained by the change in east-west separation. We conclude that Joy's law is caused by an inherent north-south separation speed present when the flux first reaches the surface, and that the scatter in the tilt angle is consistent with buffeting of the polarities by supergranulation.

Fragile detection of solar g modes by Fossat et al.

Hannah **Schunker**, Jesper Schou, Patrick Gaulme, Laurent Gizon
Solar Phys. 293:95 **2018**
https://arxiv.org/pdf/1804.04407.pdf
https://link.springer.com/content/pdf/10.1007%2Fs11207-018-1313-6.pdf

The internal gravity modes of the Sun are notoriously difficult to detect, and the claimed detection of gravity modes presented in Fossat et al. 2017 is thus very exciting. Given the importance of these modes for understanding solar structure and dynamics, the results must be robust. While Fossat et al. 2017 described their method and parameter choices in detail, the sensitivity of their results to several parameters were not presented. Therefore, we test the sensitivity to a selection of them. The most concerning result is that the detection vanishes when we adjust the start time of the 16.5 year velocity time series by a few hours. We conclude that this reported detection of gravity modes is extremely fragile and should be treated with utmost caution.

SDO/HMI survey of emerging active regions for helioseismology

H. **Schunker**, D.C. Braun, A.C. Birch, R.B. Burston, L. Gizon
A&A 595, A107 **2016**
http://arxiv.org/pdf/1608.08005v1.pdf
Observations from the Solar Dynamics Observatory (SDO) have the potential for allowing the helioseismic study of the formation of hundreds of active regions, which would enable us to perform statistical analyses. Our goal is to collate a uniform data set of emerging active regions observed by the SDO/HMI instrument suitable for helioseismic analysis up to seven days before emergence. We restricted the sample to active regions that were visible in the continuum and emerged into quiet Sun largely avoiding pre-existing magnetic regions. As a reference data set we paired a control region (CR), with the same latitude and distance from central meridian, with each emerging active region (EAR). We call this data set, which is currently comprised of 105 emerging active regions observed between May 2010 and November 2012, the SDO Helioseismic Emerging Active Region (SDO/HEAR) survey. To demonstrate the utility of a data set of a large number of emerging active regions, we measure the relative east-west velocity of the leading and trailing polarities from the line-of-sight magnetogram maps during the first day after emergence. The latitudinally averaged line-of-sight magnetic field of all the EARs shows that, on average, the leading (trailing) polarity moves in a prograde (retrograde) direction with a speed of 121 +/- 22 m/s (-70 +/- 13 m/s) relative to the Carrington rotation rate in the first day. However, relative to the differential rotation of the surface plasma, the east-west velocity is symmetric, with a mean of 95 +/- 13 m/s. The SDO/HEAR data set will not only be useful for helioseismic studies, but will also be useful to study other features such as the surface magnetic field evolution of a large sample of EARs.
See HMI Science Nuggets – #60, Oct **2016** http://hmi.stanford.edu/hminuggets/?p=1704

Editorial to the Topical Collection: Solar and Stellar Dynamos: a New Era **to Review**

Manfred **Schüssler**, Robert Cameron, …, Leonid Kitchatinov
Space Sci Rev 220, 2 (**2024**).
https://doi.org/10.1007/s11214-023-01037-y
https://link.springer.com/content/pdf/10.1007/s11214-023-01037-y.pdf
The outcome from the ISSI Workhop "Solar and Stellar Dynamos: a New Era", held 13–17 June 2022, which reviewed and put into perspective the wealth of results from observations, simulations, and simplified models.This collection summarizes the outcome of the workshop in the form of 15 comprehensive review papers covering the whole range of topics discussed during the meeting "Solar and Stellar Dynamos: a New Era"

Origin of the hemispheric asymmetry of solar activity

M. **Schüssler**, R.H. Cameron
A&A 618, A89 **2018**
https://arxiv.org/pdf/1807.10061.pdf
The frequency spectrum of the hemispheric asymmetry of solar activity shows enhanced power for the period ranges around 8.5 years and between 30 and 50 years. This can be understood as the sum and beat periods of the superposition of two dynamo modes: a dipolar mode with a (magnetic) period of about 22 years and aquadrupolar mode with a period between 13 and 15 years. An updated Babcock-Leighton-type dynamo model with weak driving as indicated by stellar observations shows an excited dipole mode and a damped quadrupole mode in the correct range of periods. Random excitation of the quadrupole by stochastic fluctuations of the source term for the poloidal field leads to a time evolution of activity and asymmetry that is consistent with the observational results.

Soft X-Ray Observations of Quiescent Solar Active Regions using Novel Dual-zone Aperture X-ray Solar Spectrometer (DAXSS)
Regions Using the Novel Dual-zone Aperture X-Ray Solar Spectrometer

Bennet D. **Schwab**1,5, Robert H. A. Sewell2,5, Thomas N. Woods2, Amir Caspi3, James Paul Mason2, and Christopher Moore4
2020 ApJ 904 20
https://doi.org/10.3847/1538-4357/abba2a

https://arxiv.org/pdf/2008.11313.pdf
The Dual-zone Aperture X-ray Solar Spectrometer (DAXSS) was flown on **2018 June 18** on the NASA 36.336 sounding rocket flight and obtained the highest resolution to date for solar soft X-ray (SXR) spectra over a broad energy range. This observation was during a time with quiescent (nonflaring) small active regions on the solar disk and when the 10.7 cm radio flux (F10.7) was 75 solar flux units (1 sfu = 10–22 W m−2 Hz−1). The DAXSS instrument consists of a LASP-developed dual-zone aperture and a commercial X-ray spectrometer from Amptek that measures solar full-disk irradiance from 0.5 to 20 keV with a resolving power of 20 near 1 keV. This paper discusses the novel design of the spectrometer and the instrument characterization techniques. Additionally, the solar measurements obtained from the 2018 sounding rocket flight are analyzed using CHIANTI spectral models to fit the temperatures, emission measures, and relative elemental abundances of the solar corona plasma. The abundance of iron was found to be 35% higher than expected in the quiescent Sun's corona suggesting either that our spectral models require additional sophistication or that the underlying atomic database may require updates. Future long-term systematic observations of this spectral range are needed to provide further insight into the sources of coronal heating through modeling the changes of relative elemental abundances during developments of active regions and solar flaring events.

Coronal electron temperature in the protracted solar minimum, the cycle 24 mini maximum, and over centuries

N. A. **Schwadron**1,2, M. L. Goelzer, C. W. Smith1, J. C. Kasper3, K. Korreck3, R. J. Leamon4, S. T. Lepri5, B. A. Maruca6, D. McComas2,7 andM. L. Steven
JGR, Volume 119, Issue 3, pages 1486–1492, March **2014**
Recent in situ observations of the solar wind show that charge states (e.g., the O7+/O6+and C6+/C5+abundance ratios) evolved through the extended, deep solar minimum between solar cycles 23 and 24 (i.e., from 2006 to 2009) reflecting cooler electron temperatures in the corona. We extend previous analyses to study the evolution of the coronal electron temperature through the protracted solar minimum and observe not only the reduction in coronal temperature in the cycles 23–24 solar minimum but also a small increase in coronal temperature associated with increasing activity during the “mini maximum” in cycle 24. We use a new model of the interplanetary magnetic flux since 1749 to estimate coronal electron temperatures over more than two centuries. The reduction in coronal electron temperature in the cycles 23–24 protracted solar minimum is similar to reductions observed at the beginning of the Dalton Minimum (∼1805–1840). If these trends continue to reflect the evolution of the Dalton Minimum, we will observe further reductions in coronal temperature in the cycles 24–25 solar minimum. Preliminary indications in 2013 do suggest a further post cycle 23 decline in solar activity. Thus, we extend our understanding of coronal electron temperature using the solar wind scaling law and compare recent reductions in coronal electron temperature in the protracted solar minimum to conditions that prevailed in the Dalton Minimum.

Magnetic flux balance in the heliosphere

Schwadron, N. A., D. E. Connick, and C. W. Smith
(**2010**), *Astrophys. J.*, , 722, L132−L136.
http://iopscience.iop.org/2041-8205/722/2/L132/fulltext/
Understanding the evolution of magnetic flux in the heliosphere remains an unresolved issue. The current solar minimum between cycles 23 and 24 is anomalously long, which gives rare insight into the long-term evolution of heliospheric magnetic flux when the coronal mass ejection (CME) rate and the flux emergence rate from CMEs were very low. The precipitous drop of heliospheric magnetic flux to levels lower than have ever been observed directly shows that there may be a persistent loss of open magnetic flux through disconnection, the reconnection between opposite polarity heliospheric magnetic field lines relatively near the Sun (beneath the Alfvén point). Here, we develop a model for the levels of magnetic flux in the inner heliosphere balancing new flux injected by CMEs, flux lost through disconnection, and closed flux lost through interchange reconnection near the Sun. This magnetic flux balance is a fundamental property that regulates the plasma and radiation environment of our solar system.

Small-scale EUV features as the drivers of coronal upflows in the quiet Sun⋆

Conrad **Schwanitz**1,2, Louise Harra2,1, Cristina H. Mandrini3, Alphonse C. Sterling4 +++
A&A 674, A219 (**2023**)
https://www.aanda.org/articles/aa/pdf/2023/06/aa46036-23.pdf
Context. Coronal upflows in the quiet Sun are seen in a wide range of features, including jets and filament eruptions. The in situ measurements from Parker Solar Probe within ≈0.2 au have demonstrated that the solar wind is highly structured, showing abrupt and near-ubiquitous magnetic field reversals (i.e., switchbacks) on different timescales. The source of these structures has been associated with supergranular structures on the solar disc. This raises the question of whether there are additional small coronal features that contribute energy to the corona and produce plasma that potentially feeds into the solar wind.

Aims. During the Solar Orbiter first science perihelion, high-resolution images of the solar corona were recorded using the Extreme Ultraviolet High Resolution Imager (HRIEUV) from the Extreme Ultraviolet Imager (EUI). The Hinode spacecraft was also observing at the same location providing coronal spectroscopic measurements. Combining the two datasets allows us to determine the cause of the weak upflows observed in the quiet Sun and the associated activity.
Methods. We used a multi-spacecraft approach to characterise regions of upflows. The upflows were identified in the Fe XII emission line by the Hinode EUV Imaging Spectrometer (EIS). We then used imaging data from the Atmospheric Imaging Assembly on board the Solar Dynamics Observatory (SDO/AIA) and the High Resolution Imagers (HRI) from EUI on board the Solar Orbiter to identify coronal features and magnetic field data from the SDO Helioseismic and Magnetic Imager (HMI). Interface Region Imaging Spectrograph (IRIS) observations were also used to understand the photospheric and chromospheric driving mechanisms.
Results. We have identified two regions of coronal upflows in the quiet Sun, with respective sizes and lifetimes of (20 Mm2, 20 min) and (180 Mm2, several hours), which are contrasting dynamic events. Both examples show weak flux cancellation, indicating that the source of the upflows and enhancements is related to the magnetic field changes. The first event, a larger upflow region, shows velocities of up to −8.6 km s−1 at the footpoint of a complex loop structure. We observe several distinct extreme ultraviolet (EUV) features including frequent loop brightenings and plasma blobs travelling along closed coronal loops. The second upflow region has velocities of up to −7.2 km s−1. Within it, a complex EUV feature that lasts for about 20 min can be seen. This main feature has several substructures. During its appearance, a clear mini-filament eruption takes place at its location, before the EUV feature disappears.
Conclusions. Two features, with contrasting properties, show upflows with comparable magnitudes. The first event, a complex loop structure, shares several similarities with active region upflows. The second one, a complex small-scale feature that could not have been well resolved with previous instruments, triggered a cascade of events, including a mini-filament that lead to a measurable upflow. This is remarkable for an EUV feature that many instruments can barely resolve. The complexity of the two events, including small loop brightenings and travelling plasma blobs for the first and EUV small-scale loops and mini-filament for the second one would not have been identifiable as the sources of upflow without an instrument with the spatial resolution of HRIEUV at this distance to the Sun. These results reinforce the importance of the smallest-scale features in the Sun and their potential relevance for and impact on the solar corona and the solar wind.

Probing Upflowing Regions in the Quiet Sun and Coronal Holes

Conrad **Schwanitz**, Louise Harra, Nour E. Raouafi, Alphonse C. Sterling, Alejandro Moreno Vacas, Jose Carlos del Toro Iniesta, David Orozco Suárez, Hirohisa Hara
Solar Phys. **2021**
https://arxiv.org/pdf/2110.12753.pdf
Recent observations from Parker Solar Probe have revealed that the solar wind has a highly variable structure. How this complex behaviour is formed in the solar corona is not yet known, since it requires omnipresent fluctuations, which constantly emit material to feed the wind. In this article we analysed 14 upflow regions in the solar corona to find potential sources for plasma flow. The upflow regions were derived from spectroscopic data from the EUV Imaging Spectrometer (EIS) onboard Hinode determining their Doppler velocity and defining regions which have blueshifts stronger than −6kms−1. To identify the sources of this blueshift data from the Atmospheric Imaging Assembly (AIA) and the Helioseismic and Magnetic Imager (HMI), onboard the Solar Dynamics Observatory (SDO), and the X-ray Telescope (XRT), onboard Hinode, were used. The analysis revealed that only 5 out of 14 of the upflows were associated with frequent transients, like obvious jets or bright points. In contrast to that, seven events were associated with small-scale features, which show a large variety of dynamics. Some resemble small bright points, while others show an eruptive nature, all of which are faint and only live for a few minutes; we can not rule out that several of these sources may be fainter and, hence, less obvious jets. Since the complex structure of the solar wind is known, this suggests that new sources have to be considered or better methods used to analyse the known sources. This work shows that small and frequent features, which were previously neglected, can cause strong upflows in the solar corona. These results emphasise the importance of the first observations from the Extreme-Ultraviolet Imager (EUI) onboard Solar Orbiter, which revealed complex small-scale coronal structures.
11 Feb-7 Mar 2020
Table 2. The blueshifted events are listed in an ascending number

Scientists tackle a burning question: When will our quiet sun turn violent?

Sarah **Scoles**
2019 ,
https://www.sciencemag.org/news/2019/05/scientists-tackle-burning-question-when-will-our-quiet-sun-turn-violent

The Long-standing Closure Crisis in Coronal Plasmas

J. D. **Scudder**
2019 ApJ 885 148
https://iopscience.iop.org/article/10.3847/1538-4357/ab48e0/pdf
Coronal and solar wind physics have long used plasma fluid models to motivate physical explanations of observations; the hypothesized model is introduced into a fluid simulation to see if observations are reproduced. This procedure is called Verification of Mechanism (VoM) modeling; it is contingent on the self consistency of the closure that made the simulation possible. Inner corona VoMs typically assume weak gradient Spitzer–Braginskii closures. Four prominent coronal VoMs in place for decades are shown to contradict their closure hypotheses, demonstrably shaping coronal and solar wind research. These findings have been possible since 1953. This unchallenged evolution is worth understanding, so that similarly flawed VoMs do not continue to mislead new research. As a first step in this direction, this paper organizes four a posteriori quantitative tests for the purpose of easily screening the physical integrity of a proposed VoM. A fifth screen involving the thermal force, the tandem of the heat flux, has been shown to be mandatory when VoMs involve species-specific energy equations. VoM modeling will soon be required to advance Parker Solar Probe and Solar Orbiter science. Such modeling cannot advance the physical understanding sought by these missions unless the closures adopted (i) are demonstrated to be self consistent for the VoM plasma Knudsen numbers, (ii) are verified a posteriori as possessing nonnegative VDFs throughout the simulated volume, and (iii) include the physical completeness of thermal force physics when the VoM requires species-specific energy equations.

OBSERVING CASCADES OF SOLAR BULLETS AT HIGH RESOLUTION. II.
E. **Scullion**1,2, O. Engvold1, Y. Lin1, and L. Rouppe van der Voort
2015 ApJ 814 123
High resolution observations from the Swedish 1-m Solar Telescope revealed bright, discrete, blob-like structures (which we refer to as solar bullets) in the Hα 656.28 nm line core that appear to propagate laterally across the solar atmosphere as clusters in active regions (ARs). These small-scale structures appear to be field aligned and many bullets become triggered simultaneously and traverse collectively as a cluster. Here, we conduct a follow-up study on these rapidly evolving structures with coincident observations from the Solar Dynamics Observatory/Atmospheric Imaging Assembly. With the co-aligned data sets, we reveal (a) an evolving multithermal structure in the bullet cluster ranging from chromospheric to at least transition region temperatures, (b) evidence for cascade-like behavior and corresponding bidirectional motions in bullets within the cluster, which indicate that there is a common source of the initial instability leading to bullet formation, and (c) a direct relationship between co-incident bullet velocities observed in Hα and He ii 30.4 nm and an inverse relationship with respect to bullet intensity in these channels. We find evidence supporting that bullets are typically composed of a cooler, higher density core detectable in Hα with a less dense, hotter, and fainter co-moving outer sheath. Bullets unequivocally demonstrate the finely structured nature of the AR corona. We have no clear evidence for bullets being associated with locally heated (or cooled), fast flowing plasma. Fast MHD pulses (such as solitons) could best describe the dynamic properties of bullets whereas the presence of a multithermal structure is new.

The Sun's Dynamic Extended Corona Observed in Extreme Ultraviolet
Daniel B. **Seaton**, J. Marcus Hughes, Sivakumara K. Tadikonda, Amir Caspi, Craig DeForest, Alexander Krimchansky, Neal E. Hurlburt, Ralph Seguin, Gregory Slater
https://arxiv.org/ftp/arxiv/papers/2105/2105.08028.pdf
2021
https://arxiv.org/ftp/arxiv/papers/2105/2105.08028.pdf
The "middle corona" is a critical transition between the highly disparate physical regimes of the lower and outer solar corona. Nonetheless, it remains poorly understood due to the difficulty of observing this faint region (1.5-3 solar radii). New observations from the GOES Solar Ultraviolet Imager in August and September 2018 provide the first comprehensive look at this region's characteristics and long-term evolution in extreme ultraviolet (EUV). Our analysis shows that the dominant emission mechanism here is resonant scattering rather than collisional excitation, consistent with recent model predictions. Our observations highlight that solar wind structures in the heliosphere originate from complex dynamics manifesting in the middle corona that do not occur at lower heights. These data emphasize that low-coronal phenomena can be strongly influenced by inflows from above, not only by photospheric motion, a factor largely overlooked in current models of coronal evolution. This study reveals the full kinematic profile of the initiation of several coronal mass ejections, filling a crucial observational gap that has hindered understanding of the origins of solar eruptions. These new data uniquely demonstrate how EUV observations of the middle corona provide strong new constraints on models seeking to unify the corona and heliosphere. **5-9 Sep 2018**

SWAP Observations of the Long-Term, Large-Scale Evolution of the EUV Solar Corona
Seaton, D. B., De Groof, A., Shearer, P., Berghmans, D., Nicula, B.
E-print, Sept **2013**

The Sun Watcher with Active Pixels and Image Processing (SWAP) EUV solar telescope on board the Project for On-Board Autonomy 2 (PROBA2) spacecraft has been regularly observing the solar corona in a bandpass near 17.4 nm since February 2010. With a field-of-view of 54x54 arcmin, SWAP provides the widest-field images of the EUV corona available from the perspective of the Earth. By carefully processing and combining multiple SWAP images it is possible to produce low-noise composites that reveal the structure of the EUV corona to relatively large heights. A particularly important step in this processing was to remove instrumental stray light from the images by determining and deconvolving SWAP's point spread function (PSF) from the observations. In this paper we use the resulting images to conduct the first ever study of the evolution of the large-scale structure of the corona observed in the EUV over a three-year period that includes the complete rise phase of solar cycle 24. Of particular note is the persistence over many solar rotations of bright, diffuse features composed of open magnetic field that overlie polar crown filaments and extend to large heights above the solar surface. These features appear to be related to coronal fans, which have previously been observed in white-light coronagraph images and, at low heights, in the EUV. We also discuss the evolution of the corona at different heights above the solar surface and the evolution of the corona over the course of the solar cycle by hemisphere.

Temporal variation and asymmetry of sunspot and solar plage types from 1930 to 1936

A. **Seguí**, J.J. Curto, V. de Paula, R. Rodríguez-Gasén, J.M. Vaquero
Advances in Space Research Volume 63, Issue 11, 1 June **2019**, Pages 3738-3748
sci-hub.se/10.1016/j.asr.2019.02.018
Using the recently converted to digital format heliophysics catalogues of the Ebro Observatory published in the 1930s, we analyse simultaneously the temporal variation and asymmetry of two different solar structures located at different layers of the solar atmosphere: sunspots and solar plages. In particular, we do the research for all the types of sunspots and plages, including the daily and relative frequencies over the solar cycle. The data were catalogued using the sunspot Cortie classification and a solar plage classification scheme proposed by the Ebro Observatory, which group the phenomena by size and shape. For all types of both sunspots and plages, we observe a decrease in their frequency up to the end of solar cycle 16 and an increase over the beginning of solar cycle 17. Furthermore, we note that small sunspot groups are more likely to happen than bigger groups, although single big spots dominate near the solar minimum. The daily frequency of solar plage occurrences shows that there is not a dominance of compact or scattered solar plages. The North-South occurrence distribution of every type in both sunspots and solar plages shows an asymmetry during the solar cycle: in its declining phase, such asymmetry is directed to the north, while in the beginning of a new cycle is directed to the south.

Future Mission Concepts for Helioseismology

Takashi **Sekii**, Thierry Appourchaux, Bernhard Fleck, Sylvaine Turck-Chièze
Space Science Reviews Volume 196, Issue 1, pp 285-302 **2015**
Future space-mission concepts currently discussed in the helioseismology community are reviewed. One popular idea is to observe the Sun from high latitudes, to explore the polar regions as well as to probe the deep interior using stereoscopic techniques, by combining observations from high latitudes with observations from within the ecliptic plane. Another idea is to stay within the ecliptic plane but still aim for stereoscopic helioseismology for deep layers. A new instrument and a novel mission concept for studying the solar core regions are also discussed.

The 17 GHz active region number

C. L. **Selhorst**, J. E. R. Costa, C. G. Giménez de Castro, A. Valio, A. A. Pacini, K. Shibasaki
ApJ, **2014**
We report the statistics of the number of active regions (NAR) observed at 17 GHz with the Nobeyama Radioheliograph between 1992, near the maximum of cycle 22, and 2013, that also includes the maximum of cycle 24, and we compare with other activity indexes. We find that NAR minima are shorter than those of the sunspot number (SSN) and radio flux at 10.7 cm (F10.7). This shorter NAR minima could reflect the presence of active regions generated by faint magnetic fields or spotless regions, which were a considerable fraction of the counted active regions. The ratio between the solar radio indexes F10.7/NAR shows a similar reduction during the two minima analyzed, which contrasts with the increase of the ratio of both radio indexes in relation to the SSN during the minimum of cycle 23-24. These results indicate that the radio indexes are more sensitive to weaker magnetic fields than those necessary to form sunspots, of the order of 1500 G. The analysis of the monthly averages of the active region brightness temperatures shows that its long term variation mimics the solar cycle, although, due to the gyro-resonance emission, a great number of intense spikes are observed in the maximum temperature study. The decrease, in number, of these spikes is also evident during the current cycle 24, a consequence of the sunspot magnetic field weakening in the last years.

A Combined Study of Photospheric Magnetic and Current Helicities and Subsurface Kinetic Helicities of Solar Active Regions during 2006-2013

Darryl **Seligman**, Gordon Petrie, Rudi Komm
ApJ, 795 113 **2014**
http://arxiv.org/pdf/1409.0764v1.pdf
We compare the average photospheric current helicity Hc, photospheric twist parameter α (a well-known proxy for the full relative magnetic helicity), and subsurface kinetic helicity Hk for 194 active regions observed between 2006-2013. We use 2440 Hinode photospheric vector magnetograms, and the corresponding subsurface fluid velocity data derived from GONG (2006-2012) and HMI (2010-2013) Dopplergrams. We find a significant hemispheric bias in all three parameters. The subsurface kinetic helicity is preferentially positive in the southern hemisphere and negative in the northern hemisphere. The photospheric current helicity and the α parameter have the same bias for strong fields (|B|>1000 G) and no significant bias for weak fields (100 G<|B|<500 G). We find no significant region-by-region correlation between the subsurface kinetic helicity and either the strong-field current helicity or α. Subsurface fluid motions of a given handedness correspond to photospheric helicities of both signs in approximately equal numbers. However, common variations appear in annual averages of these quantities over all regions. Furthermore, in a subset of 77 regions we find significant correlations between the temporal profiles of the subsurface and photospheric helicities. In these cases, the sign of the linear correlation coefficient matches the sign relationship between the helicities, indicating that the photospheric magnetic field twist is sensitive to the twisting motions below the surface.

Solar cycle activity: an early prediction for cycle #25
Stefano **Sello**
2019
https://arxiv.org/pdf/1902.05294.pdf
Solar activity forecasting is an important topic for numerous scientific and technological areas, such as space mission operations, electric power transmission lines, power transformation stations and earth geophysical and climatic impact. Nevertheless, the well-known difficulty is how to accurately predict, on the basis of various recorded solar activity indices, the complete evolution of future solar cycles, due to highly complex dynamical and stochastic processes involved, mainly related to interaction of different components of internal magnetic fields. There are two main distinct classes of solar cycle prediction methods: the precursor-like ones and the mathematical-numerical ones. The main characteristic of precursor techniques, both purely solar and geomagnetic, is their physical basis. Conversely, the non-precursor methods use different mathematical and/or numerical properties of the known temporal evolution of solar activity indices to extract useful information for predicting future activity. For current solar cycle #24 we obtained fairly good statistical performances from both precursor and purely numerical methods, such as the so-called solar precursor and nonlinear ones. To further check the performances of these prediction techniques, we compared the early predictions for the next solar cycle #25. Preliminary results support some coherence of the prediction methods considered and confirm the current trend of a relatively low solar activity.

On the Distinct Periodicities of Sunspot Counts in Flaring and Non-flaring Active Regions
Stefano **Sello**
2017
https://arxiv.org/pdf/1707.01900.pdf
In a recent work, Kilcik et al. (2017), have detected the temporal and periodic behavior of sunspot counts (SSC) in flaring (i.e. C, M, or X class flares), and non-flaring active regions for the last two solar cycles, covering the period: 1996 - 2016. The main results obtained are: 1) The temporal behavior of monthly means of daily total SSC in flaring and non-flaring active regions are different and these differences are also varying from cycle to cycle; 2) The periodicities detected in SSC of flaring and non-flaring active regions are quite different and these variations are also different from one cycle to another; the highest detected period in the flaring active regions is 113 days, while there are much higher periodicities (327, 312, and 256 days) in non-flaring regions. The detection of typical different periodicities in flaring and non-flaring regions can suggests both important differences and physical interpretation in the magneto-hydrodynamic behavior of the Sun. For this reason in the present paper we show a further periodicity analysis of the sunspot counts in flaring and in non-flaring active regions using the same data source of that used by the above cited authors and applying a powerful wavelet analysis tool which is particularly useful to detect multiscale features of complex unsteady and unevenly sampled time series. In order to futher support the differences and similarities found in the time behavior of SSC in flaring and non-flaring regions, we also computed the behavior of the wavelet entropy, a proper time function which allow us to measure the degree of complexity in the dynamics of the related time series.

Solar cycle full-shape predictions: a global error evaluation for cycle 24
Stefano **Sello**
2016
http://arxiv.org/pdf/1606.01675v1.pdf

There are many proposed prediction methods for solar cycles behavior. In a previous paper we updated the full-shape curve prediction of the current solar cycle 24 using a non-linear dynamics method and we compared the results with the predictions collected by the NOAA/SEC prediction panel, using observed data up to October 2010. The aim of the present paper is to give a quantitative evaluation, a posteriori, of the performances of these prediction methods using a specific global error, updated on a monthly basis, which is a measure of the global performance on the predicted shape (both amplitude and phase) of the solar cycle. We suggest also the use of a percent cycle similarity degree, to better evaluate the predicted shape of the solar cycle curve.

On the reduced geoeffectiveness of solar cycle 24: a moderate storm perspective

R. **Selvakumaran**, B. Veenadhari, S. Akiyama, Megha Pandya, N. Gopalswamy, S. Yashiro, Sandeep Kumar, P. Mäkelä, H. Xie

JGR V 121, Is 9 Sept Pages 8188–8202 **2016** **File**

The moderate and intense geomagnetic storms are identified for the first 77 months of solar cycle 23 and 24. The solar sources responsible for the moderate geomagnetic storms are indentified during the same epoch for both the cycles. Solar cycle 24 has shown nearly 80 % reduction in the occurrence of intense storms where as it is only 40 % in case of moderate storms when compared to previous cycle. The solar and interplanetary characteristics of the moderate storms driven by CME are compared for solar cycle 23 and 24 in order to see reduction in geoeffectiveness has anything to do with the occurrence of moderate storm. Though there is reduction in the occurrence of moderate storms, the Dst distribution does not show much difference. Similarly the solar source parameters like CME speed, mass and width did not show any significant variation in the average values as well as the distribution. The correlation between VBz and Dst is determined and it is found to be moderate with value of 0.68 for cycle 23 and 0.61 for cycle 24. The magnetospheric energy flux parameter epsilon (Ɛ) is estimated during the main phase of all moderate storms during solar cycles 23 and 24. The energy transfer decreased in solar cycle 24 when compared to cycle 23. These results are significantly different when all geomagnetic storms are taken in to consideration for both the solar cycles.

3D coupled tearing-thermal evolution in solar current sheets⋆

Samrat **Sen**, Jack Jenkins and Rony Keppens

A&A 678, A132 (**2023**)

https://www.aanda.org/articles/aa/pdf/2023/10/aa47038-23.pdf

Context. The tearing instability plays a major role in the disruption of current sheets, whereas thermal modes can be responsible for condensation phenomena (forming prominences and coronal rain) in the solar atmosphere. However, how current sheets made unstable by combined tearing and thermal instability evolve within the solar atmosphere has received limited attention to date.

Aims. We numerically explore a combined tearing and thermal instability that causes the break up of an idealized current sheet in the solar atmosphere. The thermal component leads to the formation of localized, cool condensations within an otherwise 3D reconnecting magnetic topology.

Methods. We constructed a 3D resistive magnetohydrodynamic simulation of a force-free current sheet under solar atmospheric conditions that incorporates the non-adiabatic influence of background heating, optically thin radiative energy loss, and magnetic-field-aligned thermal conduction with the open source code MPI-AMRVAC. Multiple levels of adaptive mesh refinement reveal the self-consistent development of finer-scale condensation structures within the evolving system.

Results. The instability in the current sheet is triggered by magnetic field perturbations concentrated around the current sheet plane, and subsequent tearing modes develop. This in turn drives thermal runaway associated with the thermal instability of the system. We find subsequent, localized cool plasma condensations that form under the prevailing low plasma-β conditions, and demonstrate that the density and temperature of these condensed structures are similar to more quiescent coronal condensations. Synthetic counterparts at extreme ultraviolet (EUV) and optical wavelengths show the formation of plasmoids (in EUV) and coronal condensations similar to prominences and coronal rain blobs in the vicinity of the reconnecting sheet.

Conclusions. Our simulations imply that 3D reconnection in solar current sheets may well present an almost unavoidable multi-thermal aspect that forms during their coupled tearing-thermal evolution.

How transverse MHD wave-driven turbulence influences the density filling factor in the solar corona?

Samrat **Sen**, Vaibhav Pant

ApJ **923** 178 **2021**

https://arxiv.org/pdf/2110.06844.pdf

https://iopscience.iop.org/article/10.3847/1538-4357/ac3003/pdf

https://doi.org/10.3847/1538-4357/ac3003

It is well established that the transverse MHD waves are ubiquitous in the solar corona. One of the possible mechanisms for heating both open (e.g. coronal holes) and closed (e.g. coronal loops) magnetic field regions of the

solar corona is due to the MHD wave-driven turbulence. In this work, we have studied the variation in the filling factor of overdense structures in the solar corona due to the generation of the transverse MHD wave-driven turbulence. Using 3D MHD simulations, we estimate the density filling factor of an open magnetic structure by calculating the fraction of the volume occupied by the overdense plasma structures to the entire volume of the simulation domain. Next, we perform forward modeling and generate synthetic spectra of Fe XIII 10749 Å and 10800 Å density sensitive line pairs using FoMo. Using the synthetic images, we again estimate the filling factors. The estimated filling factors obtained from both methods are in reasonable agreement. Also, our results match fairly well with the observations of filling factors in coronal holes and loops. Our results show that the generation of turbulence increases the filling factor of the solar corona.

Depth of Ellerman Burst Derived from High-resolution Hαand Ca ii 8542 Å Spectra

Minju **Seo**1, Carlos Quintero Noda2, Jeongwoo Lee3, and Jongchul Chae

2019 ApJ 871 125

High-resolution spectra of an Ellerman burst (EB) sampling the Hα and the Ca ii 8542 Å lines obtained with the Fast Imaging Solar Spectrograph (FISS) installed on the 1.6 m Goode Solar Telescope at the Big Bear Solar Observatory are compared with synthetic line profiles constructed using the RH code for nonlocal thermodynamical equilibrium radiative transfer. The EB heating is modeled by a local temperature hump above the quiet-Sun temperature. Our first finding is that FISS Hα and Ca ii 8542 Å intensity profiles cannot be reproduced simultaneously by a single hump model as far as the hump is thicker than ≥100 km. Simultaneous reproduction of both line profiles is possible when the EB temperature enhancement is confined to a layer as thin as ≤20 km in the photosphere where the Hα wing response is high and that of the Ca ii 8542 Å is not. Moreover, when we examine the EB spectra at different times, we find that the EB at a time of weaker appearance is located at lower heights, ~50 km, and moves upward to ~120 km at the time of maximum intensity. Complementary calculations of the Na i D1 and Mg i b2 lines as well as that of UV continuum at 1600 and 1700 Å with the deduced EB atmosphere are also performed to test the result, which allows us to discuss the shortcomings of this plane–parallel static model atmosphere for understanding the physical properties of EBs.

Implications of solar wind measurements for solar models and composition

Aldo **Serenelli**, Pat Scott, Francesco L. Villante, Aaron C. Vincent, Martin Asplund, Sarbani Basu, Nicolas Grevesse, Carlos Pena-Garay

MNRAS **2016**

http://arxiv.org/pdf/1604.05318v1.pdf

We critically examine recent claims of a high solar metallicity by von Steiger \& Zurbuchen (2016; vSZ16) based on in situ measurements of the solar wind, rather than the standard spectroscopically-inferred abundances (Asplund et al. 2009). We test the claim by Vagnozzi et al. (2016) that a composition based on the solar wind enables one to construct a standard solar model in agreement with helioseismological observations and thus solve the decades-old solar modelling problem. We show that, although some helioseismological observables are improved compared to models computed with established abundances, most are in fact worse. The high abundance of refractory elements leads to an overproduction of neutrinos, with a predicted 8B flux that is nearly twice its observed value, and 7Be and CNO fluxes that are experimentally ruled out at high confidence. A combined likelihood analysis shows that models using the vSZ16 abundances fare much worse than AGSS09 despite a higher metallicity. We also present astrophysical and spectroscopic arguments showing the vSZ16 composition to be an implausible representation of the solar interior, identifying the first ionisation potential in the outer solar atmosphere and wind as the likely culprit.

Alive and well: a short review about standard solar models

Aldo **Serenelli**

European Physical Journal A (EPJ A) **2016** **Review**

http://arxiv.org/pdf/1601.07179v1.pdf

Standard solar models (SSMs) provide a reference framework across a number of research fields: solar and stellar models, solar neutrinos, particle physics the most conspicuous among them. The accuracy of the physical description of the global properties of the Sun that SSMs provide has been challenged in the last decade by a number of developments in stellar spectroscopic techniques. Over the same period of time, solar neutrino experiments, and Borexino in particular, have measured the four solar neutrino fluxes from the pp-chains that are associated with 99\% of the nuclear energy generated in the Sun. Borexino has also set the most stringent limit on CNO energy generation, only ~40% larger than predicted by SSMs. More recently, and for the first time, radiative opacity experiments have been performed at conditions that closely resemble those at the base of the solar convective envelope. In this article, we review these developments and discuss the current status of SSMs, including its intrinsic limitations.

Whistler instabilities from the interplay of electron anisotropies in space plasmas: A quasilinear approach

S.M. **Shaaban**, M. Lazar
MNRAS **2020**
https://arxiv.org/pdf/1912.09283.pdf
Recent statistical studies of observational data unveil relevant correlations between whistler fluctuations and the anisotropic electron populations present in space plasmas, e.g., solar wind and planetary magnetospheres. Locally, whistlers can be excited by two sources of free energy associated with anisotropic electrons, i.e., temperature anisotropies and beaming populations carrying the heat flux. However, these two sources of free energy and the resulting instabilities are usually studied independently preventing a realistic interpretation of their interplay. This paper presents the results of a parametric quasilinear study of the whistler instability cumulatively driven by two counter-drifting electron populations and their anisotropic temperatures. By comparison to individual regimes dominated either by beaming population or by temperature anisotropy, in a transitory regime the instability becomes highly conditioned by the effects of both these two sources of free energy. Cumulative effects stimulate the instability and enhance the resulting fluctuations, which interact with electrons and stimulate their diffusion in velocity space, leading to a faster and deeper relaxation of the beaming velocity associated with a core heating in perpendicular direction and a thermalization of the beaming electrons. In particular, the relaxation of temperature anisotropy to quasi-stable states below the thresholds conditions predicted by linear theory may explain the observations showing the accumulation of these states near the isotropy and equipartition of energy.

Quasilinear Approach of the Whistler Heat-Flux Instability in the Solar Wind

S.M. **Shaaban**, M. Lazar, P.H. Yoon, S. Poedts, R.A. López
MNRAS **2019**
https://arxiv.org/pdf/1903.08005.pdf
The hot beaming (or strahl) electrons responsible for the main electron heat-flux in the solar wind are believed to be self-regulated by the electromagnetic beaming instabilities, also known as the heat-flux instabilities. Here we report the first quasi-linear theoretical approach of the whistler unstable branch able to characterize the long-term saturation of the instability as well as the relaxation of the electron velocity distributions. The instability saturation is not solely determined by the drift velocities, which undergo only a minor relaxation, but mainly from a concurrent interaction of electrons with whistlers that induces (opposite) temperature anisotropies of the core and beam populations and reduces the effective anisotropy. These results might be able to (i) explain the low intensity of the whistler heat-flux fluctuations in the solar wind (although other explanations remain possible and need further investigation), and (ii) confirm a reduced effectiveness of these fluctuations in the relaxation and isotropization of the electron strahl and in the regulation of the electron heat-flux.

An evolutionary computation based algorithm for calculating solar differential rotation by automatic tracking of coronal bright points

Ehsan **Shahamatnia**1,2*, Ivan Dorotovič1,3, Jose M. Fonseca1,2 and Rita A. Ribeiro
J. Space Weather Space Clim., 6, A16 (**2016**)
http://www.swsc-journal.org/articles/swsc/pdf/2016/01/swsc150013.pdf
Developing specialized software tools is essential to support studies of solar activity evolution. With new space missions such as Solar Dynamics Observatory (SDO), solar images are being produced in unprecedented volumes. To capitalize on that huge data availability, the scientific community needs a new generation of software tools for automatic and efficient data processing. In this paper a prototype of a modular framework for solar feature detection, characterization, and tracking is presented. To develop an efficient system capable of automatic solar feature tracking and measuring, a hybrid approach combining specialized image processing, evolutionary optimization, and soft computing algorithms is being followed. The specialized hybrid algorithm for tracking solar features allows automatic feature tracking while gathering characterization details about the tracked features. The hybrid algorithm takes advantages of the snake model, a specialized image processing algorithm widely used in applications such as boundary delineation, image segmentation, and object tracking. Further, it exploits the flexibility and efficiency of Particle Swarm Optimization (PSO), a stochastic population based optimization algorithm. PSO has been used successfully in a wide range of applications including combinatorial optimization, control, clustering, robotics, scheduling, and image processing and video analysis applications. The proposed tool, denoted PSO-Snake model, was already successfully tested in other works for tracking sunspots and coronal bright points. In this work, we discuss the application of the PSO-Snake algorithm for calculating the sidereal rotational angular velocity of the solar corona. To validate the results we compare them with published manual results performed by an expert.

Solar X-ray Monitor (XSM) On-board Chandrayaan-2 Orbiter

M. **Shanmugam**, S. V. Vadawale, Arpit R. Patel, Hitesh Kumar Adalaja, N. P. S. Mithun, Tinkal Ladiya, Shiv Kumar Goyal, Neeraj K. Tiwari, Nishant Singh, Sushil Kumar, Deepak Kumar Painkra, Y.

B. Acharya, Anil Bhardwaj, A. K. Hait, A. Patinge, Abinandhan Kapoor, H. N. Suresh Kumar, Neeraj Satya, Gaurav Saxena, Kalpana Arvind
2019
https://arxiv.org/ftp/arxiv/papers/1910/1910.09231.pdf
Solar X-ray Monitor (XSM) is one of the scientific instruments on-board Chandrayaan-2 orbiter. The XSM along with instrument CLASS (Chandras Large Area Soft x-ray Spectrometer) comprise the remote X-ray fluorescence spectroscopy experiment of Chandrayaan-2 mission with an objective to determine the elemental composition of the lunar surface on a global scale. XSM instrument will measure the solar X-rays in the energy range of 1-15 keV using state-of-the-art Silicon Drift Detector (SDD). The Flight Model (FM) of the XSM payload has been designed, realized and characterized for various operating parameters. XSM provides energy resolution of 180 eV at 5.9 keV with high time cadence of one second. The X-ray spectra of the Sun observed with XSM will also contribute to the study of solar corona. The detailed description and the performance characteristics of the XSM instrument are presented in this paper.

Predicting Maximum Amplitude and Rise Time of Solar Cycle 25 Using Modified Geomagnetic Precursor Technique.

Sharma, K., Rajwanshi, A., Kumar, S. et al.
Sol Phys 299, 167 (**2024**).
https://doi.org/10.1007/s11207-024-02412-w
The present study utilizes the planetary magnetic activity Ap index and the sunspot numbers as geomagnetic precursor pair for predicting the strength of ongoing Cycle 25. The monthly smoothed sunspot number (SSN) and disturbed days (Ap≥25), during the post-peak segments of Sunspot Cycles 17 to 24 are processed through regression analysis and the obtained analytical results are validated by comparing with the observed SSN. Hind casting results show close agreement between predicted and observed maximum amplitudes within a confidence limit of up to 10 percent. The obtained results suggest the maximum sunspot number for Solar Cycle 25 to be ≈112±18. The probable peak time of Cycle 25 may appear within 48±3 months after the commencement of the cycle, i.e., between October 2023 and April 2024.

Differential rotation of the solar transition region from STEREO/EUVI 30.4 nm images

Jaidev **Sharma**, Brajesh Kumar, Anil K Malik, Hari Om Vats
MNRAS **2021**
https://arxiv.org/ftp/arxiv/papers/2107/2107.05244.pdf
The solar photosphere, chromosphere and corona are known to rotate differentially as a function of latitude. To date, it is unclear if the solar transition region also rotates differentially. In this paper, we investigate differential rotational profile of solar transition region as a function of latitude, using solar full disk (SFD) images at 30.4 nm wavelength recorded by Extreme Ultraviolet Imager (EUVI) onboard Solar Terrestrial Relations Observatory (STEREO) space mission for the period from 2008 to 2018 (Solar Cycle 24). Our investigations show that solar transition region rotates differentially. The sidereal rotation rate obtained at +/- 5 degree equatorial band is quite high (~ 14.7 degree/day), which drops to ~ 13.6 degree/day towards both polar regions. We also obtain that the rotational differentiality is low during the period of high solar activity (rotation rate varies from 14.86 to 14.27 degree/day) while it increases during the ascending and the descending phases of the 24th solar cycle (rotation rate varies from 14.56 to 13.56 degree/day in 2008 and 14.6 to 13.1 degree/day in 2018). Average sidereal rotation rate (over SFD) follows the trend of solar activity (maximum ~ 14.97 degree/day during the peak phase of the solar activity, which slowly decreases to minimum ~ 13.9 degree/day during ascending and the descending phases of the 24th solar cycle). We also observe that solar transition region rotates less differentially than the corona.

Dynamic Behavior of Spicules Inferred from Perpendicular Velocity Components

Rahul **Sharma**, Gary Verth, and Robertus Erdélyi
2017 ApJ 840 96
Understanding the dynamic behavior of spicules, e.g., in terms of magnetohydrodynamic (MHD) wave mode(s), is key to unveiling their role in energy and mass transfer from the photosphere to corona. The transverse, torsional, and field-aligned motions of spicules have previously been observed in imaging spectroscopy and analyzed separately for embedded wave-mode identification. Similarities in the Doppler signatures of spicular structures for both kink and torsional Alfvén wave modes have led to the misinterpretation of the dominant wave mode in these structures and is a subject of debate. Here, we aim to combine line- of-sight (LOS) and plane-of-sky (POS) velocity components using the high spatial/temporal resolution Hα imaging-spectroscopy data from the CRisp Imaging SpectroPolarimeter based at the Swedish Solar Telescope to achieve better insight into the underlying nature of these motions as a whole. The resultant three-dimensional velocity vectors and the other derived quantities (e.g., magnetic pressure perturbations) are used to identify the MHD wave mode(s) responsible for the observed spicule motion. We find a number of independent examples where the bulk transverse motion of the spicule is dominant either in the POS or along the LOS. It is shown that the counterstreaming action of the displaced external plasma

due to spicular bulk transverse motion has a similar Doppler profile to that of the m = 0 torsional Alfvén wave when this motion is predominantly perpendicular to the LOS. Furthermore, the inferred magnetic pressure perturbations support the kink wave interpretation of observed spicular bulk transverse motion rather than any purely incompressible MHD wave mode, e.g., the m = 0 torsional Alfvén wave.

The study of variations of low energy cosmic helium's flux (up to 6 MeV) due to solar activity

M. **Shayan**, , P. Davoudifar, Z. Bagheri
Advances in Space Research Volume 59, Issue 8, 15 April **2017**, Pages 2186–2191
In General, the flux of low energy cosmic rays varies with time due to solar activities. The cosmic particle fluxes were studied using data of satellites near the Earth. In this work, first we studied the variations of particle fluxes from 1 Jan to 31 Dec 2000 and 35 events were selected. Then we proposed a relation for cosmic particle flux as a function of time and rigidity in the time of approaching ejecta to the Earth. The coefficients of the relation were calculated using experimental data of particle fluxes from ACE satellite. Finally, we compare time variations of these coefficients for different events.

Solar extreme ultraviolet variability of the quiet Sun

F. **Shakeri**, L. Teriaca, S. K. Solanki
A&A 581, A51 **2015**
http://arxiv.org/pdf/1507.05786v1.pdf
The last solar minimum has been unusually quiet compared to the previous minima (since space-based radiometric measurements are available). The Sun's magnetic flux was substantially lower during this minimum. Some studies also show that the total solar irradiance during the minimum after cycle 23 may have dropped below the values known from the two minima prior to that. For chromospheric and coronal radiation, the situation is less clear-cut. The Sun's 10.7\,cm flux shows a decrease of ~4% during the solar minimum in 2008 compared to the previous minimum, but \ion{Ca}{II} K does not. Here we consider additional wavelengths in the extreme ultraviolet (EUV), specifically transitions of \ion{He}{I} at 584.3\,\AA\ and \ion{O}{V} at 629.7\,\AA , of which the CDS spectrometer aboard SOHO has been taking regular scans along the solar central meridian since 1996. We analysed this unique dataset to verify if and how the radiance distribution undergoes measurable variations between cycle minima. To achieve this aim we determined the radiance distribution of quiet areas around the Sun centre. Concentrating on the last two solar minima, we found out that there is very little variation in the radiance distribution of the chromospheric spectral line \ion{He}{I} between these minima. The same analysis shows a modest, although significant, 4\% variation in the radiance distribution of the transition region spectral line \ion{O}{V}. These results are comparable to those obtained by earlier studies employing other spectral features, and they confirm that chromospheric indices display a small variation, whereas in the TR a more significant reduction of the brighter features is visible.

Occurrence rate of radio-loud and halo CMEs in solar cycle 25: Prediction using their correlation with sunspot numbers

A. **Shanmugaraju**, P. Pappa Kalaivani, Y.-J. Moon, O. Prakash
Solar Phys. **2021**
https://arxiv.org/pdf/2103.13699.pdf
The coronal mass ejections (CMEs) from the Sun are known for their space weather and geomagnetic consequences. Among all CMEs, so-called radio-loud (RL) and halo CMEs are considered the most energetic in the sense that they are usually faster and wider than the general population of CMEs. Hence the study of RL and halo CMEs has become important and the prediction of their occurrence rate in a future cycle will give a warning in advance. In the present paper, the occurrence rates of RL and halo CMEs in solar cycle (SC) 25 are predicted. For this, we obtained good correlations between the numbers of RL and halo CMEs in each year and the yearly mean sunspot numbers in the previous two cycles. The predicted values of sunspot numbers in SC 25 by NOAA/NASA were considered as representative indices and the corresponding numbers of RL and halo CMEs have been determined using linear relations. Our results show that the maximum number of RL and halo CMEs will be around 39 /pm 3 and 45 /pm 4, respectively. Removing backside events, a set of front-side events was also considered separately and the front-side events alone in SC 25 are predicted again. The peak values of front-side RL and halo events have been estimated to be around 31 /pm 3 and 29 /pm 3 respectively. These results are discussed in comparison with the predicted values of sunspots by different authors.

Solar-cycle irradiance variations over the last four billion years

Anna V. **Shapiro**, Alexander I. Shapiro, Laurent Gizon, Natalie A. Krivova, Sami K. Solanki
A&A 636, A83 **2020**

https://arxiv.org/pdf/2002.08806.pdf
https://doi.org/10.1051/0004-6361/201937128
The variability of the spectral solar irradiance (SSI) over the course of the 11-year solar cycle is one of the manifestations of solar magnetic activity. There is a strong evidence that the SSI variability has an effect on the Earth's atmosphere. The faster rotation of the Sun in the past lead to a more vigorous action of solar dynamo and thus potentially to larger amplitude of the SSI variability on the timescale of the solar activity cycle. This could led to a stronger response of the Earth's atmosphere as well as other solar system planets' atmospheres to the solar activity cycle. We calculate the amplitude of the SSI and TSI variability over the course of the solar activity cycle as a function of solar age. We employ the relationship between the stellar magnetic activity and the age based on observations of solar twins. Using this relation we reconstruct solar magnetic activity and the corresponding solar disk area coverages by magnetic features (i.e. spots and faculae) over the last four billion years. These disk coverages are then used to calculate the amplitude of the solar-cycle SSI variability as a function of wavelength and solar age. Our calculations show that the young Sun was significantly more variable than the present Sun. The amplitude of the solar-cycle Total Solar Irradiance (TSI) variability of the 600 Myr old Sun was about 10 times larger than that of the present Sun. Furthermore, the variability of the young Sun was spot-dominated (the Sun being brighter at the activity minimum than in the maximum), i.e. the Sun was overall brighter at activity minima than at maxima. The amplitude of the TSI variability decreased with solar age until it reached a minimum value at 2.8 Gyr. After this point, the TSI variability is faculae-dominated (the Sun is brighter at the activity maximum) and its amplitude increases with age.

Chapter 3 - The Sun's Atmosphere **Review**

Alexander I. **Shapiro**, Hardi Peter and Sami K. Solanki
In: ***The Sun as a Guide to Stellar Physics*** ***Book***
Eds. Oddbjørn Engvold, Jean-Claude Vial, and Andrew Skumanich
Elsevier , November **2018**
https://www.sciencedirect.com/book/9780128143346/the-sun-as-a-guide-to-stellar-physics
The solar atmosphere covers a broad range of temperatures and densities from the solar surface, via the chromosphere and transition region, and to the corona. Although one-dimensional (1D) models of the atmospheric structure have reached a high level of maturity, high–spatial resolution observations have cast some doubt on their validity. Thus, such observations have revealed a richness of highly variable spatial structure, often reaching down to the current resolution limit of 0.1 arcsec, or roughly 70 km on the Sun, in the photosphere and chromosphere. These observational advances have led to a new generation of models that describe the solar atmosphere self-consistently using 3D magnetohydrodynamic approximation simulations, including 3D radiative energy transport for those that cover the lower atmosphere, while simplistically taking into account the complex magnetic structure and energy dissipation processes in the upper atmosphere. These models have achieved considerable success in explaining the best observations, although there are still a number of open questions. Nonetheless, thanks to modern advances, the solar atmosphere now provides an excellent setting to test models of stellar atmospheres critically.
Aug. 17, 2014

The nature of solar noise

A.I. **Shapiro**, S.K. Solanki, N.A. Krivova, R. H. Cameron, K.L. Yeo, W.K. Schmutz
Nature Astronomy **2017**
https://arxiv.org/pdf/1711.04156.pdf
The solar brightness varies on timescales from minutes to decades. Determining the sources of such variations, often referred to as solar noise, is of importance for multiple reasons: a) it is the background that limits the detection of solar oscillations, b) variability in solar brightness is one of the drivers of the Earth's climate system, c) it is a prototype of stellar variability which is an important limiting factor for the detection of extra-solar planets. Here we show that recent progress in simulations and observations of the Sun makes it finally possible to pinpoint the source of the solar noise. We utilise high-cadence observations from the Solar Dynamic Observatory and the SATIRE model to calculate the magnetically-driven variations of solar brightness. The brightness variations caused by the constantly evolving cellular granulation pattern on the solar surface are computed with the MURAM code. We find that surface magnetic field and granulation can together precisely explain solar noise on timescales from minutes to decades, i.e. ranging over more than six orders of magnitude in the period. This accounts for all timescales that have so far been resolved or covered by irradiance measurements. We demonstrate that no other sources of variability are required to explain the data. Recent measurements of Sun-like stars by CoRoT and Kepler uncovered brightness variations similar to that of the Sun but with much wider variety of patterns. Our finding that solar brightness variations can be replicated in detail with just two well-known sources will greatly simplify future modelling of existing CoRoT and Kepler as well as anticipated TESS and PLATO data.

Are solar brightness variations faculae- or spot-dominated?

A.I. **Shapiro**, S.K. Solanki, N.A. Krivova, K.L. Yeo, W.K. Schmutz

A&A **2016**
http://arxiv.org/pdf/1602.04447v1.pdf
Regular spaceborne measurements have revealed that solar brightness varies on multiple timescales, variations on timescales greater than a day being attributed to surface magnetic field. Independently, ground-based and spaceborne measurements suggest that Sun-like stars show a similar, but significantly broader pattern of photometric variability.
To understand whether the broader pattern of stellar variations is consistent with the solar paradigm we assess relative contributions of faculae and spots to solar magnetically-driven brightness variability. We investigate how the solar brightness variability as well as its facular and spot contributions depend on the wavelength, timescale of variability, and position of the observer relative to the ecliptic plane. We perform calculations with the SATIRE model, which returns solar brightness with daily cadence from solar disc area coverages of various magnetic features.
Moving the observer away from the ecliptic plane increases the amplitude of 11-year variability as it would be seen in Str\"omgren (b+y)/2 photometry, but decreases the amplitude of the rotational brightness variations as it would appear in Kepler and CoRoT passbands. The spot and facular contributions to the 11-year solar variability in the Str\"omgren (b+y)/2 photometry almost fully compensate each other so that the Sun appears anomalously quiet with respect to its stellar cohort. Such a compensation does not occur on the rotational timescale.
The rotational solar brightness variability as it would appear in Kepler and CoRoT passband from the ecliptic plane is spot-dominated but the relative contribution of faculae increases for out-of-ecliptic viewing so that the apparent brightness variations are faculae-dominated for inclinations less than about $i=45^{\circ}$.

The role of the Fraunhofer lines in solar brightness variability

A.I. **Shapiro**, S.K. Solanki, N.A. Krivova, R.V. Tagirov, W.K. Schmutz
A&A 581, A116 **2015**
http://arxiv.org/pdf/1507.05437v1.pdf
The solar brightness varies on timescales from minutes to decades. A clear identification of the physical processes behind such variations is needed for developing and improving physics-based models of solar brightness variability and reconstructing solar brightness in the past. This is, in turn, important for better understanding the solar-terrestrial and solar-stellar connections.
We estimate the relative contributions of the continuum, molecular, and atomic lines to the solar brightness variations on different timescales.
Our approach is based on the assumption that variability of the solar brightness on timescales greater than a day is driven by the evolution of the solar surface magnetic field. We calculated the solar brightness variations employing the solar disc area coverage of magnetic features deduced from the MDI/SOHO observations. The brightness contrasts of magnetic features relative to the quiet Sun were calculated with a non-LTE radiative transfer code as functions of disc position and wavelength. By consecutive elimination of molecular and atomic lines from the radiative transfer calculations, we assessed the role of these lines in producing solar brightness variability.
We show that the variations in Fraunhofer lines define the amplitude of the solar brightness variability on timescales greater than a day and even the phase of the total solar irradiance variability over the 11-year cycle. We also demonstrate that molecular lines make substantial contribution to solar brightness variability on the 11-year activity cycle and centennial timescales. In particular, our model indicates that roughly a quarter of the total solar irradiance variability over the 11-year cycle originates in molecular lines. The maximum of the absolute spectral brightness variability on timescales greater than a day is associated with the CN violet system between 380 and 390 nm.

Dynamics of sunspot series on time scales from days to years: correlation of sunspot births, variable lifetimes and evolution of the high-frequency spectral component

A. **Shapoval**, J.-L. Le Mouël, M. Shnirman and V. Courtillot
JGR **2017**
http://onlinelibrary.wiley.com/doi/10.1002/2017JA024430/epdf
This paper explores some features of the dynamics of daily sunspot numbers on scales from days to years. We define higher and lower frequency energy components of the series that are related to periods ranging over 1-6 days and 6 days-2 years respectively. The lower frequency component is found to follow the solar activity, but the maxima of the higher frequency component are unexpectedly lower during the last epoch of high solar activity than during the preceding epoch of low solar activity. We also consider the birthrate of sunspot groups as another indicator of quickly varying components of the solar activity and show that it is the general growth of solar activity in the 1930-1940s which drives up this birthrate. We propose an auto-regressive model that captures the opposite trends exhibited by the two representatives of the high-frequency content, accurately reproduces the evolutions of the lower and higher frequency energy components, and replicates the shape of the curve representing the daily sunspot numbers. The three following hypotheses underlie the model construction: (1) proxy series of

solar activity can be modeled by a random process with a modulated noise; (2) sunspot's birth and disappearance rates, both following the solar cycle, determine properties of this process; (3) the births of sunspots are positively correlated in time during epochs of high solar activity. We find that the mean *birthrate* varies as a power function of the mean *lifetime*. Derived constraints could contribute to narrowing the choice of a proper solar dynamo model.

When Daily Sunspot Births Become Positively Correlated

Alexander **Shapoval** , Jean-Louis Le Mouël, Mikhail Shnirman, Vincent Courtillot
Solar Phys. **2015**, Volume 290, Issue 10, pp 2709-2717

We study the first differences w(t) of the International Sunspot Number (ISSN) daily series for the time span 1850 – 2013. The one-day correlations ρ1 between w(t) and w(t+1) are computed within four-year sliding windows and are found to shift from negative to positive values near the end of Cycle 17 (∼1945). They remain positive during the last Grand Maximum and until ∼2009, when they fall to zero. We also identify a prominent regime change in ∼1915, strengthening previous evidence of major anomalies in solar activity at this date. We test an autoregressive process of order 1 (AR(1)) as a model that can reproduce the high-frequency component of ISSN: we compute ρ1 for this AR(1) process and find that it is negative. Positive values of ρ1 are found only if the process involves positive correlation: this leads us to suggest that the births of successive spots are positively correlated during the last Grand Maximum.

Stochastic Description of the High-frequency Content of Daily Sunspots and Evidence for Regime Changes

A. **Shapoval**1,2,3,4, J.-L. Le Mouël2, M. Shnirman4, and V. Courtillot2
2015 ApJ 799 56

The irregularity index λ is applied to the high-frequency content of daily sunspot numbers ISSN. This λ is a modification of the standard maximal Lyapunov exponent. It is computed here as a function of embedding dimension m, within four-year time windows centered at the maxima of Schwabe cycles. The λ(m) curves form separate clusters (pre-1923 and post-1933). This supports a regime transition and narrows its occurrence to cycle 16, preceding the growth of activity leading to the Modern Maximum. The two regimes are reproduced by a simple autoregressive process AR(1), with the mean of Poisson noise undergoing 11 yr modulation. The autocorrelation a of the process (linked to sunspot lifetime) is a ≈ 0.8 for 1850-1923 and ≈0.95 for 1933-2013. The AR(1) model suggests that groups of spots appear with a Poisson rate and disappear at a constant rate. We further applied the irregularity index to the daily sunspot group number series for the northern and southern hemispheres, provided by the Greenwich Royal Observatory (RGO), in order to study a possible desynchronization. Correlations between the north and south λ(m) curves vary quite strongly with time and indeed show desynchronization. This may reflect a slow change in the dimension of an underlying dynamical system.
The ISSN and RGO series of group numbers do not imply an identical mechanism, but both uncover a regime change at a similar time. Computation of the irregularity index near the maximum of cycle 24 will help in checking whether yet another regime change is under way.

Two Regimes in the Regularity of Sunspot Number

A. **Shapoval**1,2,3,4, J. L. Le Mouël2, V. Courtillot2, and M. Shnirman
2013 ApJ 779 108

Sunspot numbers WN display quasi-periodical variations that undergo regime changes. These irregularities could indicate a chaotic system and be measured by Lyapunov exponents. We define a functional λ (an "irregularity index") that is close to the (maximal) Lyapunov exponent for dynamical systems and well defined for series with a random component: this allows one to work with sunspot numbers. We compute λ for the daily WN from 1850 to 2012 within 4 yr sliding windows: λ exhibit sharp maxima at solar minima and secondary maxima at solar maxima. This pattern is reflected in the ratio R of the amplitudes of the main versus secondary peaks. Two regimes have alternated in the past 150 yr, R1 from 1850 to 1915 (large λ and R values) and R2 from 1935 to 2005 (shrinking difference between main and secondary maxima, R values between 1 and 2). We build an autoregressive model consisting of Poisson noise plus an 11 yr cycle and compute its irregularity index. The transition from R1 to R2 can be reproduced by strengthening the autocorrelation a of the model series. The features of the two regimes are stable for model and WN with respect to embedding dimension and delay. Near the time of the last solar minimum (~2008), the irregularity index exhibits a peak similar to the peaks observed before 1915. This might signal a regime change back from R2 to R1 and the onset of a significant decrease of solar activity.

Periodicity in the Rotation of the Solar Transition Region and Sunspot Numbers.

Sharma, J., Banerjee, S.K., Singh, N.K. et al.
Sol Phys 299, 90 (**2024**).
https://doi.org/10.1007/s11207-024-02335-6
The long-term study of the temporal variation of the rotation period of the solar photosphere, chromosphere, and corona has been widely undertaken. To date it is unclear whether the temporal variation of the rotation period of the solar transition region has a systematic periodicity. In this article we perform a study on the temporal variation of the rotation period of the solar transition region. For this purpose, we use the Lyman α line emission at a wavelength of 121.56 nm corresponding to the solar transition region from the year 1965 to 2019, covering four complete solar cycles (i.e., Cycles 21, 22, 23, 24) as well as descending and ascending phases of Cycles 20 and 25, respectively. An autocorrelation analysis depicts that the average sidereal rotation period of the transition region (from 1965 to 2019) is 24.8 days. Furthermore, we find that a significant periodicity of about 12 years exists in the temporal variation of the sidereal rotation period of the solar transition region. The results indicate that this periodicity is closely linked to the 11-year Schwabe cycle. A cross-correlation analysis between the time series of the sidereal rotation period and sunspot numbers (as a function of lag in years) exhibits a positive correlation between these aforementioned parameters. From this result, we can state that the sidereal rotation period of the solar transition region leads the solar activity by about six months. This correlation again proves the periodicity of about 11 years in the rotation period of the transition region which is closely linked to the 11-year Schwabe cycle. Furthermore, long-term variation of rotation periods also demonstrates a decreasing trend from 1965 to 2019, which is similar to that in the sunspot numbers. From this long-term study, it seems that solar activity is largely driven by solar rotation.

Differential rotation of the solar transition region from STEREO/EUVI 30.4-nm images

Jaidev **Sharma**, Brajesh Kumar, Anil K Malik, Hari Om Vats
Monthly Notices of the Royal Astronomical Society, Volume 506, Issue 4, **2021**, Pages 4952–4959,
https://doi.org/10.1093/mnras/stab1959
The solar photosphere, chromosphere, and corona are known to rotate differentially as a function of latitude. To date, it is unclear whether the solar transition region also rotates differentially. In this work, we investigate the differential rotational profile of the solar transition region as a function of latitude, using solar full-disc (SFD) images at 30.4-nm wavelength recorded by the Extreme Ultraviolet Imager (EUVI) on board the Solar Terrestrial Relations Observatory(STEREO) space mission for the period from 2008–2018 (Solar Cycle 24). Our investigations show that the solar transition region rotates differentially. The sidereal rotation rate obtained in the ±5∘±5∘ equatorial band is quite high (∼14.7 deg day−1), dropping to ∼13.6 deg day−1 towards both polar regions. We also find that rotational differentiality is low during the period of high solar activity (the rotation rate varies from 14.86–14.27 deg day−1), while it increases during the ascending and descending phases of the 24th solar cycle (the rotation rate varies from 14.56 to ∼13.56 deg day−1 in 2008 and 14.6–13.1 deg day−1 in 2018). The average sidereal rotation rate (over SFD) follows the trend of solar activity (maximum ∼14.97 deg day−1 during the peak phase of solar activity, slowly decreasing to a minimum ∼13.9 deg day−1 during ascending and descending phases of the 24th solar cycle). We also observe that the solar transition region rotates less differentially than the corona.

Evidence of strong relationship between hemispheric asymmetry in solar coronal rotation and solar activity during solar cycle 24

Jaidev **Sharma**, Anil K Malik, Brajesh Kumar, Hari Om Vats
MNRAS Volume 499, Issue 4, December **2020**, Pages 5442–5446,
https://doi.org/10.1093/mnras/staa2863
https://arxiv.org/ftp/arxiv/papers/2009/2009.08121.pdf
In this article, we report an evidence of very high and statistically significant relationship between hemispheric asymmetry in solar coronal rotation rate and solar activity. Our approach is based on cross correlation of hemispheric asymmetry index (AI) in rotation rate with annual solar activity indicators. To obtain hemispheric asymmetry in solar rotation rate, we use solar full disc (SFD) images at 30.4 nm, 19.5 nm, and 28.4 nm wavelengths for 24th Solar Cycle i.e., for the period from 2008 to 2018, as recorded by the Solar Terrestrial Relations Observatory (STEREO) space mission. Our analysis shows that hemispheric asymmetry in rotation rate is high during the solar maxima from 2011 to 2014. On the other hand, hemispheric asymmetry drops gradually on both sides (i.e., from 2008 to 2011 and from 2014 to 2018). The results show that asymmetry index (AI) leads sunspot numbers by ~1.56 years. This gives a clear indication that hemispheric asymmetry triggers the formation of sunspots working together with the differential rotation of the Sun.

Wave amplitude modulation in fan loops as observed by AIA/SDO

Aishawnnya **Sharma**1,2, Durgesh Tripathi1, Robertus Erdélyi3,4, Girjesh R. Gupta5 and Gazi A. Ahmed2
A&A 638, A6 (**2020**)

https://www.aanda.org/articles/aa/pdf/2020/06/aa36667-19.pdf
Aims. We perform a detailed analysis to understand the evolution and dynamics of propagating intensity disturbances observed in a fan loop system.
Methods. We performed multiwavelength time-distance analysis of a fan loop system anchored in an isolated sunspot region (AR 12553). The active region was observed by the Atmospheric Imaging Assembly on board the Solar Dynamics Observatory. We measured the phase speeds of the propagating intensity disturbances by employing cross-correlation analysis, and by obtaining the slopes in xt-plots. We obtained original and detrended light curves at different heights of the time-distance maps and characterised them by performing Fourier and wavelet analysis, respectively.
Results. The time-distance maps reveal clear propagation of intensity oscillations in all the coronal extreme ultraviolet (EUV) channels except AIA 94 and 335 Å. We determine the nature of the intensity disturbances as slow magneto-acoustic waves by measuring their phase speeds. The time-distance maps, as well as the detrended light curves, show an increase and decrease in the amplitude of propagating 3 min oscillations over time. The amplitude variations appear most prominently in AIA 171 Å, though other EUV channels also show such signatures. The Fourier power spectrum yields the presence of significant powers with several nearby frequencies in the range of 2–3 min (5–8 mHz), along with many other smaller peaks between 2–4 min. Wavelet analysis shows an increase and decrease of oscillating power around 3 min simultaneous to the amplitude variations. We obtain the modulation period to be in the range of 20–30 min.
Conclusions. Our results provide the viability of occurrence of phenomenon like “Beat” among the nearby frequencies giving rise to the observed amplitude modulation. However, we cannot at this stage rule out the possibility that the modulation may be driven by variability in an underlying unknown source. **June 16, 2016**

On the variation of solar coronal rotation using SDO/AIA observations

Jaidev **Sharma**, Brajesh Kumar, Anil K. Malik, Hari Om Vats
MNRAS Volume 492, Issue 4, March **2020**, Pages 5391–5398,
https://doi.org/10.1093/mnras/staa188
https://arxiv.org/ftp/arxiv/papers/2001/2001.07048.pdf
We report on the variability of rotation periods of solar coronal layers with respect to temperature (or, height). For this purpose, we have used the observations from Atmospheric Imaging Assembly (AIA) telescope on board Solar Dynamics Observatory (SDO) space mission. The images used are at the wavelengths 94 Å, 131 Å, 171 Å, 193 Å, 211 Å, and 335 Å for the period from 2012 to 2018. Analysis of solar full disk images obtained at these wavelengths by AIA is carried out using flux modulation method. Seventeen rectangular strips/bins at equal interval of 10 degrees (extending from 80 degree South to 80 degree North on the Sun) are selected to extract a time series of extreme ultraviolet (EUV) intensity variations to obtain auto-correlation coefficient. The peak of Gaussian fit to first secondary maxima in the autocorrelogram gives synodic rotation period. Our analysis shows the differential rotation with respect to latitude as well as temperature (or, height). In the present study, we find that the sidereal rotation periods of different coronal layers decrease with increasing temperature (or, height). Average sidereal rotation period at the lowest temperature (~ 600000 Kelvin) corresponding to AIA-171 Å which originates from the upper transition region/quiet corona is 27.03 days. The sidereal rotation period decreases with temperature (or, height) to 25.47 days at the higher temperature (~10 million Kelvin) corresponding to the flaring regions of solar corona as seen in AIA-131 Å observations.

Nonlinear Evolution of a 3D Inertial Alfvén Wave and Its Implication in Particle Acceleration

Prachi **Sharma**, Nitin Yadav, R. P. Sharma
Solar Phys. Volume 291, Issue 3, pp 931-939 **2016**
A simulation based on a pseudo-spectral method has been performed in order to study particle acceleration. A model for the acceleration of charged particles by field localization is developed for the low-ββ plasma. For this purpose, a fractional diffusion approach has been employed. The nonlinear interaction between a 3D inertial Alfvén wave and a slow magnetosonic wave has been examined, and the dynamical equations of these two waves in the presence of ponderomotive nonlinearity have been solved numerically. The nonlinear evolution of the inertial Alfvén wave in the presence of slow magnetosonic wave undergoes a filamentation instability and results in field intensity localization. The results obtained show the localization and power spectrum of inertial Alfvén wave due to nonlinear coupling. The scaling obtained after the first break point of the magnetic power spectrum has been used to calculate the formation of the thermal tail of energetic particles in the solar corona.

Role of 3d-dispersive Alfven waves in coronal heating

R. P. **Sharma**, N. Yadav, N. Pathak
Astrophysics and Space Science, May **2014**, Volume 351, Issue 1, pp 75-80
https://link.springer.com/content/pdf/10.1007/s10509-014-1845-7.pdf

Coronal heating is one of the unresolved puzzles in solar physics from decades. In the present paper we have investigated the dynamics of vortices to apprehend coronal heating problem. A three dimensional (3d) model has been developed to study propagation of dispersive Alfvén waves (DAWs) in presence of ion acoustic waves which results in excitation of DAW and evolution of vortices. Taking ponderomotive nonlinearity into account, development of these vortices has been studied. There are observations of such vortices in the chromosphere, transition region and also in the lower solar corona. These structures may play an important role in transferring energy from lower solar atmosphere to corona and result in coronal heating. Nonlinear interaction of these waves is studied in view of recent simulation work and observations of giant magnetic tornadoes in solar corona and lower atmosphere of sun by solar dynamical observatory (SDO).

A Si I atomic model for NLTE spectropolarimetric diagnostics of the 10 827 Å line

N. G. **Shchukina**1,2, A. V. Sukhorukov2,3 and J. Trujillo Bueno
A&A 603, A98 (**2017**)

Aims. The Si i 10 827 Å line is commonly used for spectropolarimetric diagnostics of the solar atmosphere. First, we aim at quantifying the sensitivity of the Stokes profiles of this line to non-local thermodynamic equilibrium (NLTE) effects. Second, we aim at facilitating NLTE diagnostics of the Si i 10 827 Å line. To this end, we propose the use of a relatively simple silicon model atom, which allows a fast and accurate computation of Stokes profiles. The NLTE Stokes profiles calculated using this simple model atom are very similar to those obtained via the use of a very comprehensive silicon model atom.

Methods. We investigate the impact of the NLTE effects on the Si i 10 827 Å line by means of multilevel radiative transfer calculations in a three-dimensional (3D) model atmosphere taken from a state-of-the-art magneto-convection simulation with small-scale dynamo action. We calculate the emergent Stokes profiles for this line at the solar disk center and for every vertical column of the 3D snapshot model, neglecting the effects of horizontal radiative transfer.

Results. We find significant departures from LTE in the Si i 10 827 Å line, not only in the intensity but also in the linearly and circularly polarized profiles. At wavelengths around 0.1 Å, where most of the Stokes Q, U, and V peaks of the Si i 10 827 Å line occur, the differences between the NLTE and LTE profiles are comparable with the Stokes amplitudes themselves. The deviations from LTE increase with increasing Stokes Q, U, and V signals. Concerning the Stokes V profiles, the NLTE effects correlate with the magnetic field strength in the layers where such circular polarization signals are formed.

Conclusions. The NLTE effects should be taken into account when diagnosing the emergent Stokes I profiles as well as the Stokes Q, U, and V profiles of the Si i 10 827 Å line. The sixteen-level silicon model atom proposed here, with six radiative bound-bound transitions, is suitable to account for the physics of formation of the Si i 10 827 Å line and for modeling and inverting its Stokes profiles without assuming LTE.

Sunquakes of Solar Cycle 24

I.N. **Sharykin**, A.G. Kosovichev
2020 *ApJ* **895** 76
https://arxiv.org/pdf/1911.04197.pdf
https://doi.org/10.3847/1538-4357/ab88d1

The paper presents results of a search for helioseismic events (sunquakes) produced by M-X class solar flares during Solar Cycle 24. The search is performed by analyzing photospheric Dopplergrams from Helioseismic Magnetic Imager (HMI). Among the total number of 500 M-X class flares, 82 helioseismic events were detected. This result is quite unexpected, since it was previously thought that sunquakes were very rare and observed mainly in strong flares. However, our analysis has shown that there many strong sunquakes were produced by solar flares of low M class, while in some powerful X-class flares helioseismic waves were not observed or were weak. Our analysis also revealed several active regions characterized by the most efficient generation of helioseismic waves during flares. We found that the sunquake power correlates with the maximum value of soft X-ray flux time derivative better than with the X-ray class, indicating that the sunquake mechanism is associated with high-energy particles. We also show that the seismically active flares are more impulsive than the flares without photospheric and helioseismic perturbations. We present a new catalog of helioseismic solar flares, which opens opportunities for performing statistical studies to better understand physics of sunquakes as well as flare energy release and transport. **October 23, 2012, November 5, 2013**
Table 2011-2017

The impact of surface dynamo magnetic fields on the solar iron abundance⋆

N. **Shchukina**1,2 and J. Trujillo Bueno
A&A 579, A112 (**2015**)

Most chemical abundance determinations ignore that the solar photosphere is significantly magnetized by the ubiquitous presence of a small-scale magnetic field. A recent investigation has suggested that there should be a significant impact on the derived iron abundance, owing to the magnetically induced changes on the photospheric

temperature and density structure (indirect effect). The three-dimensional (3D) photospheric models used in that investigation have non-zero net magnetic flux values and stem from magneto-convection simulations without small-scale dynamo action. Here we address the same problem by instead using 3D models of the quiet solar photosphere that result from a state-of-the-art magneto-convection simulation with small-scale dynamo action, where the net magnetic flux is zero. One of these 3D models has negligible magnetization, while the other is characterized by a mean field strength of 160 Gauss in the low photosphere. With such 3D models we carried out spectral synthesis for a large set of Fe i lines to derive abundance corrections, taking the above-mentioned indirect effect and the Zeeman broadening of the intensity profiles (direct effect) into account. We conclude that if the magnetism of the quiet solar photosphere is mainly produced by a small-scale dynamo, then its impact on the determination of the solar iron abundance is negligible.

Using Polar Faculae to Determine the Sun's High-Latitude Rotation Rate. I. Techniques and Initial Measurements

Neil R. **Sheeley** Jr

ApJ **976** 73 **2024**

https://arxiv.org/pdf/2411.02245

https://iopscience.iop.org/article/10.3847/1538-4357/ad85d0/pdf

This paper describes a new way of determining the high-latitude solar rotation rate statistically from simultaneous observations of many polar faculae. In this experiment, I extracted frames from a movie made previously from flat-fielded images obtained in the 6767 A continuum during February 1997-1998 and used those frames to construct space-time maps from high-latitude slices of the favorably oriented south polar cap. These maps show an array of slanted tracks whose average slope indicates the east-west speed of faculae at that latitude, Ls. When the slopes are measured and plotted as a function of latitude, they show relatively little scatter 0.01-02 km/s from a straight line whose zero-speed extension passes through the Sun's south pole. This means that the speed, v(Ls), and the latitudinal radius, R cos(Ls), approach 0 at the same rate, so that their ratio gives a nearly constant synodic rotation rate 8.6 deg/day surrounding the Sun's south pole. A few measurements of the unfavorably oriented north polar cap are consistent with these measurements near the south pole.

Rotational Components of the Sun's Mean Field

Neil R. **Sheeley** Jr.1

2023 ApJ 959 7

https://iopscience.iop.org/article/10.3847/1538-4357/acfc4a/pdf

This paper uses wavelet transforms to look for the rotational frequencies of the Sun's mean line-of-sight magnetic field. For a sufficiently high wavelet frequency, the spectra of the dipole, quadrupole, and hexapole field components each show a time-dependent fine structure with periods in the range of 26.5–30 days and their harmonics. These maps confirm that a large enhancement of power at 30 days occurred in the dipole field during 1989–1990, as recorded previously using Fourier techniques. In addition, during some years the maps show power at 26.5 days (or its harmonics), which is clearly distinguishable from the rotation period of 26.9–27.0 days at the Sun's equator. In at least one case, the 26.5-day period was a wave phenomenon caused by the systematic eruption of active regions at progressively more western locations in the Carrington coordinate system, as if the flux were emerging from a fixed longitude in a faster-rotating subsurface layer. Based on previous studies of the mean field, I conclude that the enhanced wavelet patterns in this paper are regions where magnetic flux is emerging in configurations that strengthen the Sun's horizontal dipole, quadrupole, and hexapole fields, and (in the case of the more slowly rotating patterns) where this flux is being transported to midlatitudes whose rotation periods are in the range of 28–30 days.

The Sun's Mean Line-of-Sight Field

Neil R. **Sheeley** Jr

ApJ **937** 87 **2022**

https://arxiv.org/pdf/2208.03216

https://iopscience.iop.org/article/10.3847/1538-4357/ac86d6/pdf

We regard the Sun-as-a-star magnetic field (i.e. the mean field) as a filter for the spherical harmonic components of the photospheric field, and calculate the transmission coefficients of this filter. The coefficients for each harmonic, Yml, are listed in three tables according to their dependence on B0, the observer's latitude in the star's polar coordinate system. These coefficients are used to interpret the 46-yr sequence of daily mean-field measurements at the Wilcox Solar Observatory. We find that the non-axisymmetric part of the field originates in the Y11, Y22, and a combination of the Y33 and Y13 harmonic components. The axisymmetric part of the field originates in Y02 plus a B0-dependent combination of the Y01 and Y03 components. The power spectrum of the field has peaks at frequencies corresponding to the ~27-day synodic equatorial rotation period and its second and third harmonics. Each of these peaks has fine structure on its low-frequency side, indicating magnetic patterns that rotate slowly under the influence of differential rotation and meridional flow. The sidebands of the fundamental

mode resolve into peaks corresponding to periods of ~28.5 and ~30 days, which tend to occur at the start of sunspot maximum, whereas the ~27-day period tends to occur toward the end of sunspot maximum. We expect similar rotational sidebands to occur in magnetic observations of other Sun-like stars and to be a useful complement to asteroseismology studies of convection and magnetic fields in those stars.

The Recent Rejuvenation of the Sun's Large-scale Magnetic Field: A Clue for Understanding Past and Future Sunspot Cycles

N. R. **Sheeley** Jr. and Y.-M. Wang
2015 ApJ 809 113
The quiet nature of sunspot cycle 24 was disrupted during the second half of 2014 when the Sun's large-scale field underwent a sudden rejuvenation: the solar mean field reached its highest value since 1991, the interplanetary field strength doubled, and galactic cosmic rays showed their strongest 27-day modulation since neutron-monitor observations began in 1957; in the outer corona, the large increase of field strength was reflected by unprecedentedly large numbers of coronal loops collapsing inward along the heliospheric current sheet. Here, we show that this rejuvenation was not caused by a significant increase in the level of solar activity as measured by the smoothed sunspot number and CME rate, but instead was caused by the systematic emergence of flux in active regions whose longitudinal distribution greatly increased the Sun's dipole moment. A similar post-maximum increase in the dipole moment occurred during each of the previous three sunspot cycles, and marked the start of the declining phase of each cycle. We note that the north–south component of this peak dipole moment provides an early indicator of the amplitude of the next cycle, and conclude that the amplitude of cycle 25 may be comparable to that of cycle 24, and well above the amplitudes obtained during the Maunder Minimum.

Using Running Difference Images to Track Proper Motions of XUV Coronal Intensity on the Sun

N. R. **Sheeley**, Jr., H. P. Warren, J. Lee, S. Chung1, J. Katz2, and M. Namkung
2014 ApJ 797 131
We have developed a procedure for observing and tracking proper motions of faint XUV coronal intensity on the Sun and have applied this procedure to study the collective motions of cellular plumes and the shorter-period waves in sunspots. Our space/time maps of cellular plumes show a series of tracks with the same 5-8 minute repetition times and ~100 km s–1 sky-plane speeds found previously in active-region fans and in coronal hole plumes. By synchronizing movies and space/time maps, we find that the tracks are produced by elongated ejections from the unipolar flux concentrations at the bases of the cellular plumes and that the phases of these ejections are uncorrelated from cell to cell. Thus, the large-scale motion is not a continuous flow, but is more like a system of independent conveyor belts all moving in the same direction along the magnetic field. In contrast, the proper motions in sunspots are clearly waves resulting from periodic disturbances in the sunspot umbras. The periods are ~2.6 minutes, but the sky-plane speeds and wavelengths depend on the heights of the waves above the sunspot. In the chromosphere, the waves decelerate from 35-45 km s–1 in the umbra to 7-8 km s–1 toward the outer edge of the penumbra, but in the corona, the waves accelerate to ~60-100 km s–1. Because chromospheric and coronal tracks originate from the same space/time locations, the coronal waves must emerge from the same umbral flashes that produce the chromospheric waves.

Coronal Inflows during the Interval 1996-2014

N. R. **Sheeley**, Jr. and Y.-M. Wang
2014 ApJ 797 10
We extend our previous counts of coronal inflows from the 5?yr interval 1996-2001 to the 18?yr interval 1996-2014. By comparing stackplots of these counts with similar stackplots of the source-surface magnetic field and its longitudinal gradient, we find that the inflows occur in long-lived streams with counting rates in excess of 18 inflows per day at sector boundaries where the gradient exceeds 0.22?G rad?1. These streams are responsible for the high (86%) correlation between the inflow rate and the longitudinal field gradient. The overall inflow rate was several times larger in sunspot cycle 23 than it has been so far in cycle 24, reflecting the relatively weak source-surface fields during this cycle. By comparison, in cycles 21-22, the source-surface field and its gradient had bursts of great strength, as if large numbers of inflows occurred during those cycles. We find no obvious relation between inflows and coronal mass ejections (CMEs) on timescales of days to weeks, regardless of the speeds of the CMEs, and only a 60% correlation on timescales of months, provided the CMEs are fast (V?> 600?km?s?1). We conclude that most of the flux carried out by CMEs is returned to the Sun via field line reconnection well below the 2.0 R ? inner limit of the LASCO field of view, and that the remainder accumulates in the outer corona for an eventual return at sector boundaries.

Heliospheric Images of the Solar Wind at Earth

N. R. **Sheeley**, Jr., A. D. Herbst, C. A. Palatchi, Y.-M. Wang, R. A. Howard, J. D. Moses, A. Vourlidas, J. S. Newmark, D. G. Socker, S. P. Plunkett, C. M. Korendyke, L. F. Burlaga, J. M. Davila, W. T. Thompson, O. C. St Cyr, R. A. Harrison, C. J. Davis, C. J. Eyles, J. P. Halain, D. Wang et al.
The Astrophysical Journal, Vol. 675, No. 1: 853-862, **2008**.
http://www.journals.uchicago.edu/doi/pdf/10.1086/526422

During relatively quiet solar conditions throughout the spring and summer of 2007, the SECCHI HI2 white-light telescope on the STEREO B solar-orbiting spacecraft observed a succession of wave fronts sweeping past Earth.We have compared these heliospheric images with in situ plasma and magnetic field measurements obtained by near-Earth spacecraft, and we have found a near perfect association between the occurrence of these waves and the arrival of density enhancements at the leading edges of high-speed solar wind streams. Virtually all of the strong corotating interaction regions are accompanied by large-scale waves, and the low-density regions between them lack such waves. Because the Sun was dominated by long-lived coronal holes and recurrent solar wind streams during this interval, there is little doubt that we have been observing the compression regions that are formed at low latitude as solar rotation causes the high-speed wind from coronal holes to run into lower speed wind ahead of it.

Flows and magnetic field structures in reconnection regions of simulations of the solar atmosphere: Do flux pile-up models work?

S. **Shelyag**1, Y. E. Litvinenko2, V. Fedun3, G. Verth4, J. J. González-Avilés5,6 and F. S. Guzmán6
A&A 620, A159 (**2018**)
sci-hub.tw/10.1051/0004-6361/201833752

Aims. We study the process of magnetic field annihilation and reconnection in simulations of magnetised solar photosphere and chromosphere with magnetic fields of opposite polarities and constant numerical resistivity.
Methods. Exact analytical solutions for reconnective annihilations were used to interpret the features of magnetic reconnection in simulations of flux cancellation in the solar atmosphere. We used MURaM high-resolution photospheric radiative magneto-convection simulations to demonstrate the presence of magnetic field reconnection consistent with the magnetic flux pile-up models. Also, a simulated data-driven chromospheric magneto-hydrodynamic simulation is used to demonstrate magnetic field and flow structures, which are similar to the theoretically predicted ones.
Results. Both simulations demonstrate flow and magnetic field structures roughly consistent with accelerated reconnection with magnetic flux pile-up. The presence of standard Sweet–Parker type reconnection is also demonstrated in stronger photospheric magnetic fields.

Heating of the partially ionized solar chromosphere by waves in magnetic structures

S. **Shelyag**, E. Khomenko, A. de Vicente, D. Przybylski
ApJL 819 L11 **2016**
http://arxiv.org/pdf/1602.03373v1.pdf

In this paper, we show a "proof of concept" of the heating mechanism of the solar chromosphere due to wave dissipation caused by the effects of partial ionization. Numerical modeling of non-linear wave propagation in a magnetic flux tube, embedded in the solar atmosphere, is performed by solving a system of single-fluid quasi-MHD equations, which take into account the ambipolar term from the generalized Ohm's law. It is shown that perturbations caused by magnetic waves can be effectively dissipated due to ambipolar diffusion. The energy input by this mechanism is continuous and shown to be more efficient than dissipation of static currents, ultimately leading to chromospheric temperature increase in magnetic structures.

Spectro-polarimetric simulations of the solar limb: absorption-emission FeI 6301.5Å and 6302.5Å line profiles and torsional flows in the intergranular magnetic flux concentrations

S. **Shelyag**
ApJ **801** 46 **2015**
http://arxiv.org/pdf/1501.00870v1.pdf

Using radiative magneto-hydrodynamic simulations of the magnetised solar photosphere and detailed spectro-polarimetric diagnostics with the FeI $6301.5\mathrm{\AA}$ and $6302.5\mathrm{\AA}$photospheric lines in the local thermodynamic equilibrium approximation, we model active solar granulation as if it was observed at the solar limb. We analyse general properties of the radiation across the solar limb, such as the continuum and the line core limb darkening and the granulation contrast. We demonstrate the presence of profiles with both emission and absorption features at the simulated solar limb, and pure emission profiles above the limb. These profiles are associated with the regions of strong linear polarisation of the emergent radiation, indicating the influence of the intergranular magnetic fields on the line formation. We analyse physical origins of the emission wings in the Stokes

profiles at the limb, and demonstrate that these features are produced by localised heating and torsional motions in the intergranular magnetic flux concentrations.

Centre-to-limb spectro-polarimetric diagnostics of simulated solar photospheric magneto-convection: signatures of photospheric Alfven waves

S. **Shelyag**, D. Przybylski

2014

http://arxiv.org/pdf/1405.5954v1.pdf

Using numerical simulations of the magnetised solar photosphere carried out with the radiative magneto-hydrodynamic code, MURaM, and detailed spectro-polarimetric diagnostics of the simulated photospheric 6302A FeI line, spectro-polarimetric signatures of Alfven waves in magnetised intergranular lanes of the simulated solar photosphere were analysed at different positions at the solar disk. The torsional Alfven waves in the intergranular lanes are horizontal plasma motions, which do not have a thermal perturbation counterpart. We find signatures of Alfven waves as small-scale line profile Doppler shifts and Stokes-V area asymmetry enhancements in the simulated off-disk centre observations. These photospheric features disappear when the simulated observations are degraded with a telescope PSF similar to the one of Hinode. We analyse the possibilities for direct observations and confirmation of Alfven wave presence in the solar photosphere.

Macro-microturbulence in the solar photosphere

V. A. **Sheminova**

Kinematics Phys. Celest. Bodies, **1985**, Vol. 1, p. 50-52. In Russian

https://arxiv.org/pdf/2202.06037

The velocity distribution of the large and small-scale motion in solar photosphere has been obtained by crossing method based on fitting the observed and calculated equivalent widths as well as the central depths of the spectral lines at the center of the and the limb of the solar disk. We used about 200 Fe I lines. According to our results the motions in photosphere are anisotropic. The radial component of microturbulent velocity decreases from 1.0 to 0.3 km/s and the tangential one from 1.7 to 1.3 km/c at the photosphere heights from 200 to 500 km (log tau_5 = -1.4 and -3.5). At the same heights the radial component of the macroturbulent velocity decreases from 1.8 to 1.2 km/s and the tangential one from 2.3 to 0.8 km/s.

White-light QFP Wave Train and the Associated Failed Breakout Eruption

Yuandeng **Shen**, Surui Yao, Zehao Tang, Xinping Zhou, Zhining Qu, Yadan Duan, Chengrui Zhou, Song Tan

A&A **2022**

https://arxiv.org/pdf/2207.08110.pdf

Quasi-periodic fast-propagating (QFP) magnetosonic wave trains are commonly observed in the low corona at extreme ultraviolet wavelength bands. Here, we report the first white-light imaging observation of a QFP wave train propagating outwardly in the outer corona ranging from 2 to 4 solar Radii. The wave train was recorded by the Large Angle Spectroscopic Coronagraph on board the Solar and Heliospheric Observatory, and it was associated with a GOES M1.5 flare in NOAA active region AR12172 at the southwest limb of the solar disk. Measurements show that the speed and period of the wave train were about 218 km/s and 26 minutes, respectively. The extreme ultraviolet imaging observations taken by the Atmospheric Imaging Assembly on board the Solar Dynamic Observatory reveals that in the low corona the QFP wave train was associated with the failed eruption of a breakout magnetic system consisting of three low-lying closed loop systems enclosed by a high-lying large-scale one. Data analysis results show that the failed eruption of the breakout magnetic system was mainly because of the magnetic reconnection occurred between the two sided low-lying closed-loop systems. This reconnection enhances the confinement capacity of the magnetic breakout system because the upward-moving reconnected loops continuously feed new magnetic fluxes to the high-lying large-scale loop system. For the generation of the QFP wave train, we propose that it could be excited by the intermittent energy pulses released by the quasi-periodic generation, rapid stretching and expansion of the upward-moving, strongly bent reconnected loops. **2014 October 2**

Calibration of full-disk He I 10830 Å filtergrams of the Chromospheric Telescope

Zili **Shen**, Andrea Diercke, Carsten Denker

Astronomical Notes **2018**

https://arxiv.org/pdf/1812.04404.pdf

The Chromospheric Telescope (ChroTel) is a small 10-cm robotic telescope at Observatorio del Teide on Tenerife (Spain), which observes the entire Sun in Hα, CaII K, and HeI 10830Å. We present a new calibration method that includes limb-darkening correction, removal of non-uniform filter transmission, and determination of HeI Doppler velocities.

Chromospheric full-disk filtergrams are often obtained with Lyot filters, which may display non-uniform transmission

causing large-scale intensity variations across the solar disk. Removal of a 2D symmetric limb-darkening function from full-disk images results in a flat background. However, transmission artifacts remain and are even more distinct in these contrast-enhanced images. Zernike polynomials are uniquely appropriate to fit these large-scale intensity variations of the background. The Zernike coefficients show a distinct temporal evolution for ChroTel data, which is likely related to the telescope's alt-azimuth mount that introduces image rotation. In addition, applying this calibration to sets of seven filtergrams that cover the HeI triplet facilitates determining chromospheric Doppler velocities. To validate the method, we use three data sets with varying levels of solar activity. The Doppler velocities are benchmarked with respect to co-temporal high-resolution spectroscopic data of the GREGOR Infrared Spectrograph (GRIS). Furthermore, this technique can be applied to ChroTel Hα and CaII K data. The calibration method for ChroTel filtergrams can be easily adapted to other full-disk data exhibiting unwanted large-scale variations. The spectral region of the HeI triplet is a primary choice for high-resolution near-infrared spectropolarimetry. Here, the improved calibration of ChroTel data will provide valuable context data.

Three-dimensional MHD Simulation of Solar Wind Using a New Boundary Treatment: Comparison with In Situ Data at Earth

Fang **Shen**1,2,3, Zicai Yang1,2, Jie Zhang4, Wenwen Wei1,2, and Xueshang Feng
2018 ApJ 866 18
http://iopscience.iop.org/article/10.3847/1538-4357/aad806/pdf
Three-dimensional magnetohydrodynamics (MHD) numerical simulation is an important tool in the prediction of solar wind parameters. In this study, we improve our corona interplanetary total variation diminishing MHD model by using a new boundary applicable to all phases of solar cycles. This model uses synoptic magnetogram maps from the Global Oscillation Network Group as the input data. The empirical Wang–Sheeley–Arge relation is used to assign solar wind speed at the lower boundary, while temperature is specified accordingly based on its empirical relation with the solar wind speed. Magnetic field intensity and solar wind density at the boundary are obtained from observational data in the immediate past Carrington rotations, permitting the persistence of these two parameters in a short time period. The boundary conditions depend on only five tunable parameters when simulating the solar wind for different phases of the solar cycle. We apply this model to simulate the background solar wind from 2007 to 2017 and compare the modeled results with the observational data in the OMNI database. Visual inspection shows that our model can capture the time patterns of solar wind parameters well at most times. Statistical analysis shows that the simulated solar wind parameters are all in good agreement with the observations. This study demonstrates that the improved interplanetary total variation diminishing model can be used for predicting all solar wind parameters near the Earth.

Dispersively formed quasi-periodic fast magnetosonic wavefronts due to the eruption of a nearby mini-filament

Yuandeng **Shen**; Tengfei Song; Yu Liu
Monthly Notices of the Royal Astronomical Society: Letters, Volume 477, Issue 1, 11 June **2018**, Pages L6–L10
https://doi.org/10.1093/mnrasl/sly044
Observational analysis is performed to study the excitation mechanism and propagation properties of a quasi-periodic fast-propagating (QFP) magnetosonic wave. The QFP wave was associated with the eruption of a nearby mini-filament and a small B4 Geostationary Operational Environmental Satellite (GOES) flare, which may indicate that the generation of a QFP wave does not require much flare energy. The propagation of the QFP wave was along a bundle of funnel-shaped open loops with a speed of about 1100 ± 78 km s^{-1} and an acceleration of -2.2 ± 1.1 km s^{-2}. Periodicity analysis indicates that the periods of the QFP wave are 43 ± 6 and 79 ± 18 s. For the first time, we find that the periods of the QFP wave and the accompanying flare are inconsistent, which is different from the findings reported in previous studies. We propose that the present QFP wave was possibly caused by the mechanism of dispersive evolution of the initially broad-band disturbance resulting from the nearby mini-filament eruption.

Modulation of Galactic Cosmic Rays in the Inner Heliosphere over Solar Cycles

Z.-N. **Shen**1,2 and G. Qin3
2018 ApJ 854 137
http://sci-hub.tw/http://iopscience.iop.org/0004-637X/854/2/137/
The 11- and 22-year modulation of galactic cosmic rays (GCRs) in the inner heliosphere is studied using a numerical model developed by Qin and Shen in 2017. Based on the numerical solutions of Parker's transport equations, the model incorporates a modified Parker heliospheric magnetic field, a locally static time-delayed heliosphere, and a time-dependent diffusion coefficients model in which an analytical expression of the variation of magnetic turbulence magnitude throughout the inner heliosphere is applied. Furthermore, during solar maximum, the solar magnetic polarity is determined randomly with the possibility of $A > 0$ decided by the percentage of the solar north polar magnetic field being outward and the solar south polar magnetic field being inward. The computed

results are compared at various energies with several GCR observations, e.g., theInterplanetary Monitoring Platform 8 (IMP 8), EPHIN on board the Solar and Heliospheric Observatory (SOHO), Ulysses, and Voyager 1 and 2, and they show good agreement. We show that our model has successfully reproduced the 11- and 22-year modulation cycles.

Time-dependent Ionization in a Steady Flow in an MHD Model of the Solar Corona and Wind

Chengcai **Shen**1, John C. Raymond1, Zoran Mikić2, Jon A. Linker2, Katharine K. Reeves1, andNicholas A. Murphy1

2017 ApJ 850 26

Time-dependent ionization is important for diagnostics of coronal streamers and pseudostreamers. We describe time-dependent ionization calculations for a three-dimensional magnetohydrodynamic (MHD) model of the solar corona and inner heliosphere. We analyze how non-equilibrium ionization (NEI) influences emission from a pseudostreamer during the Whole Sun Month interval (Carrington rotation CR1913, 1996 August 22 to September 18). We use a time-dependent code to calculate NEI states, based on the plasma temperature, density, velocity, and magnetic field in the MHD model, to obtain the synthetic emissivities and predict the intensities of the Lyα, O vi, Mg x, and Si xii emission lines observed by the SOHO/Ultraviolet Coronagraph Spectrometer (UVCS). At low coronal heights, the predicted intensity profiles of both Lyα and O vilines match UVCS observations well, but the Mg x and Si xii emission are predicted to be too bright. At larger heights, the O vi and Mg x lines are predicted to be brighter for NEI than equilibrium ionization around this pseudostreamer, and Si xii is predicted to be fainter for NEI cases. The differences of predicted UVCS intensities between NEI and equilibrium ionization are around a factor of 2, but neither matches the observed intensity distributions along the full length of the UVCS slit. Variations in elemental abundances in closed field regions due to the gravitational settling and the FIP effect may significantly contribute to the predicted uncertainty. The assumption of Maxwellian electron distributions and errors in the magnetic field on the solar surface may also have notable effects on the mismatch between observations and model predictions.

Prediction of Solar Activity from Solar Background Magnetic Field Variations in Cycles 21-23

Simon J. **Shepherd**1, Sergei I. Zharkov2, and Valentina V. Zharkova

2014 ApJ 795 46

A comprehensive spectral analysis of both the solar background magnetic field (SBMF) in cycles 21-23 and the sunspot magnetic field in cycle 23 reported in our recent paper showed the presence of two principal components (PCs) of SBMF having opposite polarity, e.g., originating in the northern and southern hemispheres, respectively. Over a duration of one solar cycle, both waves are found to travel with an increasing phase shift toward the northern hemisphere in odd cycles 21 and 23 and to the southern hemisphere in even cycle 22. These waves were linked to solar dynamo waves assumed to form in different layers of the solar interior. In this paper, for the first time, the PCs of SBMF in cycles 21-23 are analyzed with the symbolic regression technique using Hamiltonian principles, allowing us to uncover the underlying mathematical laws governing these complex waves in the SBMF presented by PCs and to extrapolate these PCs to cycles 24-26. The PCs predicted for cycle 24 very closely fit (with an accuracy better than 98%) the PCs derived from the SBMF observations in this cycle. This approach also predicts a strong reduction of the SBMF in cycles 25 and 26 and, thus, a reduction of the resulting solar activity. This decrease is accompanied by an increasing phase shift between the two predicted PCs (magnetic waves) in cycle 25 leading to their full separation into the opposite hemispheres in cycle 26. The variations of the modulus summary of the two PCs in SBMF reveals a remarkable resemblance to the average number of sunspots in cycles 21-24 and to predictions of reduced sunspot numbers compared to cycle 24: 80% in cycle 25 and 40% in cycle 26.

Categorization model of moving small-scale intensity enhancements in solar active regions

B. M. **Shergelashvili**1,2,3, E. Philishvili2,3, S. Buitendag4, S. Poedts5,6 and M. Khodachenko1,7,8

A&A 662, A30 (**2022**)

https://www.aanda.org/articles/aa/pdf/2022/06/aa42547-21.pdf

Context. The small-scale moving intensity enhancements remotely observed in the extreme ultraviolet images of the solar active regions, which we refer to as active region moving campfires (ARMCs), are related to local plasma temperature and/or density enhancements. Their dynamics is driven by the physical processes in the entire coronal plasma. Our previous study of ARMCs indicates that they have characteristic velocities at around the background sound speed. In the present paper, we further investigate the dynamical and statistical properties of ARMCs.
Aims. The main goal of our work is to carry out a simultaneous analysis of EUV images from two observational missions, SDO/AIA and Hi-C 2.1. The aims of the performed cross-validating analysis of both SDO/AIA and Hi-C 2.1 data were to reveal how the observed moving features are distributed over the studied active region, AR12712, and to perform a statistical hypothesis test of the existence of different groups of ARMCs with distinct physical characteristics.

Methods. We use the statistical model of intensity centroid convergence and tracking that was developed in our previous paper. Furthermore, a Gaussian mixture model fit of the observed complex of moving ARMCs is elaborated to reveal the existence of distinct ARMC groups and to study the physical characteristics of these different groups.
Results. In data from the 171 Å, 193 Å and 211 Å channels of SDO/AIA, we identified several groups of ARMCs with respect to both blob intensity and velocity profiles. The existence of such groups is confirmed by the cross-validation of the 172 Å data sets from Hi-C 2.1.
Conclusions. The ARMCs studied in this paper have characteristic velocities in the range of the typical sound speeds in coronal loops. Hence, these moving objects differ from the well-known rapid Alfvénic velocity jets from magnetic reconnection sites. This is also proven by the fact that ARMCs propagate along the active region magnetic structure (strands). The nature of the discovered statistical grouping of the ARMC events is not known. Further theoretical studies and modeling is required to reveal this nature.

Modeling and removal of optical ghosts in the PROBA-3/ASPIICS externally occulted solar coronagraph

S. V. **Shestov**, A. N. Zhukov, D. B. Seaton
A&A **2018**
https://arxiv.org/pdf/1812.03990.pdf
Context: ASPIICS is a novel externally occulted solar coronagraph, which will be launched onboard the PROBA-3 mission of the European Space Agency. The external occulter will be placed on the first satellite approximately 150 m ahead of the second satellite that will carry an optical instrument. During 6 hours per orbit, the satellites will fly in a precise formation, constituting a giant externally occulted coronagraph. Large distance between the external occulter and the primary objective will allow observations of the white-light solar corona starting from extremely low heights 1.1RSun. Aims: To analyze influence of optical ghost images formed inside the telescope and develop an algorithm for their removal. Methods: We implement the optical layout of ASPIICS in Zemax and study the ghost behaviour in sequential and non-sequential regimes. We identify sources of the ghost contributions and analyze their geometrical behaviour. Finally we develop a mathematical model and software to calculate ghost images for any given input image. Results: We show that ghost light can be important in the outer part of the field of view, where the coronal signal is weak, since the energy of bright inner corona is redistributed to the outer corona. However the model allows to remove the ghost contribution. Due to a large distance between the external occulter and the primary objective, the primary objective does not produce a significant ghost. The use of the Lyot spot in ASPIICS is not necessary.

Influence of misalignments on performance of externally occulted solar coronagraphs. Application to PROBA-3/ASPIICS

S. V. **Shestov**, A. N. Zhukov
A&A **2018**
https://arxiv.org/pdf/1801.04204.pdf
ASPIICS is a novel externally occulted coronagraph that will be launched onboard the PROBA-3 mission of ESA. The external occulter (EO) will be placed on one satellite ~150 m ahead of the second satellite with an optical instrument. During part of each orbit, the satellites will fly in a precise formation, constituting a giant externally occulted coronagraph. Large distance between the EO and the primary objective will allow observations of the white-light solar corona starting already from ~1.1RSun. We analyze influence of shifts of the satellites and misalignments of optical elements on diffracted light. Based on the quantitative influence of misalignments on diffracted light, we will provide a "recipe" for choosing the size of the internal occulter (IO) to achieve a trade-off between the minimal height of observations and sustainability to possible misalignments. We implement a numerical model of the diffracted light and its propagation through the optical system, and compute intensities of diffracted light throughout the instrument. Our numerical model extends axi-symmetrical model of Rougeot et al. 2017 to non-symmetrical cases. The computations fully confirm main properties of the diffracted light obtained from semi-analytical consideration. Results: relative influences of various misalignments are significantly different. We show that: the IO with R=1.1RSun is large enough to compensate possible misalignments in ASPIICS, apodizing the edge of the IO leads to additional suppression of the diffracted light. Conclusions: the most important misalignment is the tilt of the telescope WRT the line connecting the center of the EO and the entrance aperture. Special care should be taken to co-align the EO and the coronagraph, i.e. co-aligning the diffraction fringe from the EO and the IO. We suggest that the best orientation strategy is to point the coronagraph to the center of the EO.

Nonlinear Evolution of Short-wavelength Torsional Alfvén Waves

S. V. **Shestov**1,4, V. M. Nakariakov2,3, A. S. Ulyanov4, A. A. Reva4, and S. V. Kuzin
2017 ApJ 840 64
https://arxiv.org/pdf/1705.02790.pdf

We analyze nonlinear evolution of torsional Alfvén waves in a straight magnetic flux tube filled in with a low-β plasma, and surrounded with a plasma of lower density. Such magnetic tubes model, in particular, a segment of a coronal loop or a polar plume. The wavelength is taken comparable to the tube radius. We perform a numerical simulation of the wave propagation using ideal magnetohydrodynamics. We find that a torsional wave nonlinearly induces three kinds of compressive flows: the parallel flow at the Alfvén speed, which constitutes a bulk plasma motion along the magnetic field, the tube wave, and also transverse flows in the radial direction, associated with sausage fast magnetoacoustic modes. In addition, the nonlinear torsional wave steepens and its propagation speed increases. The latter effect leads to the progressive distortion of the torsional wave front, i.e., nonlinear phase mixing. Because of the intrinsic non-uniformity of the torsional wave amplitude across the tube radius, the nonlinear effects are more pronounced in regions with higher wave amplitudes. They are always absent at the axes of the flux tube. In the case of a linear radial profile of the wave amplitude, the nonlinear effects are localized in an annulus region near the tube boundary. Thus, the parallel compressive flows driven by torsional Alfvén waves in the solar and stellar coronae, are essentially non-uniform in the perpendicular direction. The presence of additional sinks for the wave energy reduces the efficiency of the nonlinear parallel cascade in torsional Alfvén waves.

Fast magnetoacoustic wave trains of sausage symmetry in cylindrical waveguides of the solar corona

S. **Shestov**, V. M. Nakariakov, S. Kuzin
ApJ **2015**
http://arxiv.org/pdf/1510.07908v1.pdf
Fast magnetoacoustic waves guided along the magnetic field by plasma non-uniformities, in particular coronal loops, fibrils and plumes, are known to be highly dispersive, which leads to the formation of quasi-periodic wave trains excited by a broadband impulsive driver, e.g. a solar flare. We investigated effects of cylindrical geometry on the fast sausage wave train formation. We performed magnetohydrodynamic numerical simulations of fast magnetoacoustic perturbations of a sausage symmetry, propagating from a localised impulsive source along a field-aligned plasma cylinder with a smooth radial profile of the fast speed. The wave trains are found to have pronounced period modulation, with the longer instant period seen in the beginning of the wave train. The wave trains have also a pronounced amplitude modulation. Wavelet spectra of the wave trains have characteristic tadpole features, with the broadband large-amplitude heads preceding low-amplitude quasi-monochromatic tails. The mean period of the wave train is about the transverse fast magnetoacoustic transit time across the cylinder. The mean parallel wavelength is about the diameter of the waveguiding plasma cylinder. Instant periods are longer than the sausage wave cutoff period. The wave train characteristics depend on the fast magnetoacoustic speed in both the internal and external media, and the smoothness of the transverse profile of the equilibrium quantities, and also the spatial size of the initial perturbation. If the initial perturbation is localised at the axis of the cylinder, the wave trains contain higher radial harmonics that have shorter periods.

The Nature of High-frequency Oscillations Associated with Short-lived Spicule-type Events

Juie **Shetye**1,2, Erwin Verwichte3, Marco Stangalini4, and J. G. Doyle2
2021 ApJ 921 30
https://iopscience.iop.org/article/10.3847/1538-4357/ac1a12/pdf
https://doi.org/10.3847/1538-4357/ac1a12
https://arxiv.org/pdf/2112.14486
We investigate high-resolution spectroscopic and imaging observations from the CRisp Imaging SpectroPolarimeter (CRISP) instrument to study the dynamics of chromospheric spicule-type events. It is widely accepted that chromospheric fine structures are waveguides for several types of magnetohydrodynamic (MHD) oscillations, which can transport energy from the lower to upper layers of the Sun. We provide a statistical study of 30 high-frequency waves associated with spicule-type events. These high-frequency oscillations have two components of transverse motions: the plane-of-sky (POS) motion and the line-of-sight (LOS) motion. We focus on single isolated spicules and track the POS using time–distance analysis and in the LOS direction using Doppler information. We use moment analysis to find the relation between the two motions. The composition of these two motions suggests that the wave has a helical structure. The oscillations do not have phase differences between points along the structure. This may be the result of the oscillation being a standing mode, or that propagation is mostly in the perpendicular direction. There is evidence of fast magnetoacoustic wave fronts propagating across these structures. To conclude, we hypothesize that the compression and rarefaction of passing magnetoacoustic waves may influence the appearance of spicule-type events, not only by contributing to moving them in and out of the wing of the spectral line but also through the creation of density enhancements and an increase in opacity in the Hα line. **2014 June 5,7**

Multiwavelength High-resolution Observations of Chromospheric Swirls in the Quiet Sun

Juie **Shetye**1, Erwin Verwichte1, Marco Stangalini2,3, Philip G. Judge4, J. G. Doyle5, Tony Arber1, Eamon Scullion6, and Sven Wedemeyer7,8
2019 ApJ 881 83

https://iopscience.iop.org/article/10.3847/1538-4357/ab2bf9/pdf
We report observations of small-scale swirls seen in the solar chromosphere. They are typically 2 Mm in diameter and last around 10 minutes. Using spectropolarimetric observations obtained by the CRisp Imaging Spectro-Polarimeter at the Swedish 1 m Solar Telescope, we identify and study a set of swirls in chromospheric Ca ii 8542 Å and Hα lines as well as in the photospheric Fe i line. We have three main areas of focus. First, we compare the appearance, morphology, dynamics, and associated plasma parameters between the Ca ii and Hα channels. Rotation and expansion of the chromospheric swirl pattern are explored using polar plots. Second, we explore the connection to underlying photospheric magnetic concentration (MC) dynamics. MCs are tracked using the SWAMIS tracking code. The swirl center and MC remain cospatial and share similar periods of rotation. Third, we elucidate the role swirls play in modifying chromospheric acoustic oscillations and found a temporary reduction in wave period during swirls. We use cross-correlation wavelets to examine the change in period and phase relations between different wavelengths. The physical picture that emerges is that a swirl is a flux tube that extends above an MC in a downdraft region in an intergranular lane. The rotational motion of the MC matches the chromospheric signatures. We could not determine whether a swirl is a gradual response to the photospheric motion or an actual propagating Alfvénic wave. **2012 June 21**

Signatures of quiet Sun reconnection events in Ca II, Hα, and Fe I

J **Shetye** S Shelyag A L Reid E Scullion J G Doyle T D Arber
Monthly Notices of the Royal Astronomical Society, Volume 479, Issue 3, 21 September **2018**, Pages 3274–3287
http://sci-hub.tw/10.1093/mnras/sty1548
We use observations of quiet Sun (QS) regions in the Hα 6563 Å, Ca II 8542 Å, and Fe I 6302 Å lines. We observe brightenings in the wings of the Hα and Ca IIcombined with observations of the interacting magnetic concentrations observed in the Stokes signals of Fe I. These brightenings are similar to Ellerman bombs (EBs), i.e. impulsive bursts in the wings of the Balmer lines that leave the line cores unaffected. Such enhancements suggest that these events have similar formation mechanisms to the classical EBs found in active regions, with the reduced intensity enhancements found in the QS regions due to a weaker feeding magnetic flux. The observations also show that the quiet Sun Ellerman bombs are formed at a higher height in the upper photosphere than the photospheric continuum level. Using simulations, we investigate the formation mechanism associated with the events and suggest that these events are driven by the interaction of magnetic field lines in the upper photospheric regions. The results of the simulation are in agreement with observations when comparing the light curves, and in most cases, we found that the peak in the Ca II 8542 Å wing occurred before the peak in Hα wing. Moreover, in some cases, the line profiles observed in Ca II are asymmetrical with a raised core profile. The source of heating in these events is shown by the MURaM simulations and is suggested to occur 430 km above the photosphere. **21 June 2012**

High-frequency transverse oscillations and intensity perturbations in spicular-type events

J. **Shetye**, D. Kuridze, M. Stangalini, J. G. Doyle, E. Scullion, V. Henriques, T. Ray
A&A **2017**
https://star.arm.ac.uk/~jus/outgoing/accepted_papers/fast_features_waves_V12.pdf
https://arxiv.org/pdf/1703.10968.pdf
It is widely accepted that chromospheric fine structures are waveguides for several types of magnetohydrodynamic (MHD) oscillations, which can transport energy from the lower to upper layers of the Sun. Despite a number of recent advances in the field, a detailed study of the properties and physical nature of these oscillations remains a challenging task. Here we aim to study high-frequency transverse oscillations and intensity variations of spicular-type events observed in H α wavelength in an active region. We investigate high resolution spectroscopic and imaging observations from the CRisp Imaging SpectroPolarimeter (CRISP) instrument on the Swedish 1-meter Solar Telescope (SST) to study the dynamics of chromospheric spicular structures. Time-distance analyses are used to examine the characteristics of the transverse (incompressible) and intensity (compressible) perturbations. The relationship between these incompressible and compressible oscillations are also investigated through direct comparisons of the fluctuations. Furhter, we detect transverse oscillations in chromospheric spicules at different positions along their length in both the vertical and horizontal directions with respect to the image plane. We also find a link between intensity perturbations and the horizontal velocity fluctuations of the flux tube. The observed oscillations are interpreted in terms of MHD helical kink waves. The link between intensity and horizontal velocity oscillations can be explained by the coupling of compressive with non-compressive waves and by the interaction of the flux tube with its neighbours. This leads to compressive perturbations correlated to the horizontal displacement of the tube itself. **10 June 2014**.

High--cadence observations of spicular-type events on the Sun

J. **Shetye**, J.G. Doyle, E. Scullion, C. J. Nelson, D. Kuridze, V. Henriques, F. Woeger, T. Ray
A&A 589, A3 **2016**
http://arxiv.org/pdf/1601.08087v1.pdf

Chromospheric observations taken at high cadence and high spatial resolution show a range of spicule like features, including Type I, Type II (as well as RBEs and RREs) and those which seem to appear within a few seconds, which if interpreted as flows would imply mass flow velocities in excess of 1000 km/s. This article seeks to quantify and study rapidly appearing spicular type events. We also compare the MOMFBD and speckle reconstruction techniques in order to understand if such spicules are more favourably observed using a particular technique. We use spectral imaging observations taken with the CRISP on the Swedish 1 m Solar Telescope. Data was sampled at multiple positions within the Halpha line profile for both an ondisk and limb location. The data is host to numerous rapidly appearing features which are observed at different locations within the Halpha line profile. The feature's durations vary between 10 and 20 s and lengths around 3500 km. Sometimes, a time delay in their appearance between the blue and red wings of 3 and 5 s is evident, whereas sometimes they are near simultaneous. In some instances features are observed to fade and then re emerge at the same location several tens of seconds later. We provide the first statistical analysis of these spicules and suggest that these observations can be interpreted as the LOS movement of highly dynamic spicules moving in and out of the narrow 60 mA transmission filter used to observe in different parts of the Halpha line profile. The LOS velocity component of the observed fast chromospheric features, manifested as Doppler shifts, are responsible for their appearance in the red and blue wings of Halpha line. Additional work involving data at other wavelengths is required to investigate

Observations and modelling of North-South asymmetries using a Flux Transport Dynamo

Juie **Shetye**, Durgesh Tripathi, Mausumi Dikpati

ApJ, **799** 220 **2015**

http://arxiv.org/pdf/1412.3245v1.pdf

The peculiar behaviour of the solar cycle 23 and its prolonged minima has been one of the most studied problems over the last few years. In the present paper, we study the asymmetries in active region magnetic flux in the northern and southern hemispheres during complete solar cycle 23 and rising phase of solar cycle 24. During the declining phase of solar cycle 23, we find that the magnetic flux in the southern hemisphere is about 10 times stronger than that in the northern hemisphere during the declining phase of the solar cycle 23 and during the rising phase of cycle 24, however, this trend reversed. The magnetic flux becomes about a factor of 4 stronger in the northern hemisphere to that of southern hemisphere. Additionally, we find that there was significant delay (about 5 months) in change of the polarity in the southern hemisphere in comparison with the northern hemisphere. These results provide us with hints of how the toroidal fluxes have contributed to the solar dynamo during the prolonged minima in the solar cycle 23 and in the rising phase of the solar cycle 24. Using a solar flux-transport dynamo model, we demonstrate that persistently stronger sunspot cycles in one hemisphere could be caused by the effect of greater inflows into active region belts in that hemisphere. Observations indicate that greater inflows are associated with stronger activity. Some other change or difference in meridional circulation between hemispheres could cause the weaker hemisphere to become the stronger one.

Damped kink motions in a system of two solar coronal tubes with elliptic cross sections⋆

Mijie **Shi**1, Bo Li1, Shaoxia Chen1, Hui Yu1 and Mingzhe Guo1,2

A&A, 686, A2 (**2024**)

https://www.aanda.org/articles/aa/pdf/2024/06/aa49319-24.pdf

Aims. This study is motivated by observations of coordinated transverse displacements in neighboring solar active region loops, addressing specifically how the behavior of kink motions in straight two-tube equilibria is impacted by tube interactions and tube cross-sectional shapes.

Methods. We worked with linear, ideal, pressureless magnetohydrodynamics. Axially standing kink motions were examined as an initial value problem for transversely structured equilibria involving two identical, field-aligned, density-enhanced tubes with elliptic cross sections (elliptic tubes). Continuously nonuniform layers were implemented around both tube boundaries. We numerically followed the system response to external velocity drivers, largely focusing on the quasi-mode stage of internal flows to derive the pertinent periods and damping times.

Results. The periods and damping times that we derive for two-circular-tube setups justify the available modal results found with the T-matrix approach. Regardless of cross-sectional shapes, our nonuniform layers feature the development of small-scale shears and energy accumulation around Alfvén resonances, indicative of resonant absorption and phase mixing. As with two-circular-tube systems, our configurational symmetries still make it possible to classify lower-order kink motions by the polarization and symmetric properties of the internal flows; hence, such motions are labeled as Sx and Ax. However, the periods and damping times for two-elliptic-tube setups further depend on cross-sectional aspect ratios, with Ax motions occasionally damped less rapidly than Sx motions. We find uncertainties up to ∼20% (∼50%) for the axial Alfvén time (the inhomogeneity lengthscale) if the periods (damping times) computed for two-elliptic-tube setups are seismologically inverted with canonical theories for isolated circular tubes.

Conclusions. The effects of loop interactions and cross-sectional shapes need to be considered when the periods, and in particular the damping times, are seismologically exploited for coordinated transverse displacements in adjacent coronal loops.

Energy estimation of small-scale jets from the quiet-Sun region

Fanpeng **Shi**, Dong Li, Zongjun Ning, Jun Xu, Yuxiang Song, Yuzhi Yang

A&A **2024**

https://arxiv.org/pdf/2403.16193.pdf

Context. Solar jets play a role in the coronal heating and the supply of solar wind. Aims. This study calculated the energies of 23 small-scale jets emerging from a quiet-Sun region to investigate their contributions for coronal heating. Conclusions. Our observations suggest that although these jets cannot provide sufficient energy for the heating of the whole quiet-Sun coronal region, they are likely to account for a significant portion of the energy demand in the local regions where the jets occur.

AWSoM Magnetohydrodynamic Simulation of a Solar Active Region. II. Statistical Analysis of Alfvén Wave Dissipation and Reflection, Scaling Laws, and Energy Budget on Coronal Loops

Tong **Shi**1, Ward Manchester IV1, Enrico Landi1, Bart van der Holst1, Judit Szente1, Yuxi Chen2, Gábor Tóth1, Luca Bertello3, and Alexander Pevtsov3

2024 ApJ 961 60

https://iopscience.iop.org/article/10.3847/1538-4357/ad0df2/pdf

The coronal heating problem has been a major challenge in solar physics, and a tremendous amount of effort has been made over the past several decades to solve it. In this paper, we aim at answering how the physical processes behind the Alfvén wave turbulent heating adopted in the Alfvén Wave Solar atmosphere Model (AWSoM) unfold in individual plasma loops in an active region (AR). We perform comprehensive investigations in a statistical manner on the wave dissipation and reflection, temperature distribution, heating scaling laws, and energy balance along the loops, providing in-depth insights into the energy allocation in the lower solar atmosphere. We demonstrate that our 3D global model with a physics-based phenomenological formulation for the Alfvén wave turbulent heating yields a heating rate exponentially decreasing from loop footpoints to top, which had been empirically assumed in the past literature. A detailed differential emission measure (DEM) analysis of the AR is also performed, and the simulation compares favorably with DEM curves obtained from Hinode/Extreme-ultraviolet Imaging Spectrometer observations. This is the first work to examine the detailed AR energetics of our AWSoM model with high numerical resolution and further demonstrates the capabilities of low-frequency Alfvén wave turbulent heating in producing realistic plasma properties and energetics in an AR.

The First 3D Coronal Loop Model Heated by MHD Waves against Radiative Losses

Mijie **Shi**, Tom Van Doorsselaere, Mingzhe Guo, Konstantinos Karampelas, Bo Li, Patrick Antolin

ApJ **908** 233 **2021**

https://arxiv.org/pdf/2101.01019.pdf

https://doi.org/10.3847/1538-4357/abda54

In the quest to solve the long-standing coronal heating problem, it has been suggested half a century ago that coronal loops could be heated by waves. Despite the accumulating observational evidence of the possible importance of coronal waves, still no 3D MHD simulations exist that show significant heating by MHD waves. Here we report on the first 3D coronal loop model heating the plasma against radiative cooling. The coronal loop is driven at the footpoint by transverse oscillations and subsequently the induced Kelvin-Helmholtz instability deforms the loop cross-section and generates small-scale structures. Wave energy is transfered to smaller scales where it is dissipated, overcoming the internal energy losses by radiation. These results open up a new avenue to address the coronal heating problem.

Oblique tearing mode instability: guide field and Hall effect

Chen **Shi**, Marco Velli, Fulvia Pucci, Anna Tenerani, Maria Elena Innocenti

ApJ **902** 142 **2020**

https://arxiv.org/pdf/2007.00607.pdf

https://doi.org/10.3847/1538-4357/abb6fa

The tearing mode instability is one important mechanism that may explain the triggering of fast magnetic reconnection in astrophysical plasmas such as the solar corona. In this paper, the linear stability analysis of the tearing mode is carried out for a current sheet in the presence of a guide field, and including the Hall effect. We show that the presence of a strong guide field does not modify the most unstable mode in the two-dimensional wave vector space orthogonal to the current gradient direction, which remains the fastest growing parallel mode. With the Hall effect, the inclusion of a guide field turns the non-dispersive propagation along the guide field direction to a

dispersive one. The oblique modes have a wave-like structure along the normal direction of the current sheet and a strong guide field suppresses this structure while making the eigen-functions asymmetric.

Non-equilibrium Ionization Effects on Extreme-Ultraviolet Emissions Modulated by Standing Sausage Modes in Coronal Loops

Mijie **Shi**, Bo Li, Tom Van Doorsselaere, Shao-Xia Chen, Zhenghua Huang
ApJ **2018**
https://arxiv.org/pdf/1811.08571.pdf
Forward-modeling the emission properties in various passbands is important for confidently identifying magnetohydrodynamic waves in the structured solar corona. We examine how Non-equilibrium Ionization (NEI) affects the Extreme Ultraviolet (EUV) emissions modulated by standing fast sausage modes (FSMs) in coronal loops, taking the Fe IX 171 Å and Fe XII 193 Å emission lines as examples. Starting with the expressions for linear FSMs in straight cylinders, we synthesize the specific intensities and spectral profiles for the two spectral lines by incorporating the self-consistently derived ionic fractions in the relevant contribution functions. We find that relative to the case where Equilibrium Ionization (EI) is assumed, NEI considerably impacts the intensity modulations, but shows essentially no effect on the Doppler velocities or widths. Furthermore, NEI may affect the phase difference between intensity variations and those in Doppler widths for Fe XII 193 Å when the line-of-sight is oblique to the loop axis. While this difference is 180◦ when EI is assumed, it is ∼90◦ when NEI is incorporated for the parameters we choose. We conclude that in addition to viewing angles and instrumental resolutions, NEI further complicates the detection of FSMs in spectroscopic measurements of coronal loops in the EUV passband.

Intermittency of the Solar Magnetic Field and Solar Magnetic Activity Cycle

A. S. **Shibalova**, V. N. Obridko, D. D. Sokoloff
Solar Physics March **2017**, 292:44
Small-scale solar magnetic fields demonstrate features of fractal intermittent behavior, which requires quantification. For this purpose we investigate how the observational estimate of the solar magnetic flux density BB depends on resolution DD in order to obtain the scaling lnBD=−klnD+alnf_0BD=−klnf_0D+a in a reasonably wide range. The quantity kk demonstrates cyclic variations typical of a solar activity cycle. In addition, kk depends on the magnetic flux density, i.e. the ratio of the magnetic flux to the area over which the flux is calculated, at a given instant. The quantity aa demonstrates some cyclic variation, but it is much weaker than in the case of kk. The scaling obtained generalizes previous scalings found for the particular cycle phases. The scaling is typical of fractal structures. In our opinion, the results obtained trace small-scale action in the solar convective zone and its coexistence with the conventional large-scale solar dynamo based on differential rotation and mirror-asymmetric convection.

Long-Term Global Solar Activity Observed by the Nobeyama Radioheliograph

K. **Shibasaki**
Publ. Astron. Soc. Japan 65, No SP1, S17 [6 pages] (**2013**)
http://pasj.asj.or.jp/v65/sp1/65S017/65S017.pdf
The Nobeyama Radioheliograph has been observing the Sun at a frequency of 17 GHz regularly since 1992, providing synthesized full-disk images. This long period of continuous and consistent operation, providing wellcalibrated data of a uniform standard, makes possible long-term studies of solar activity, from full-disk down to the angular resolution of the instrument. By using about 7200 daily, full-disk images, it has been possible to generate a radio version of the butterfly diagram, which differs significantly from the sunspot butterfly diagram. The polar regions are bright at 17 GHz, with their brightness well-correlated with the polar magnetic field strengths. Both are anti-correlated with activity at low latitudes, such as active regions and solar flares. The 17 GHz butterfly diagram shows both high and low-latitude activity. The brightness of both these facets of solar activity shows a significant decline over the 20+ years observations that have been made. In the northern hemisphere, the radio brightnesses at low and high latitudes are strongly anti-correlated. However, this anti-correlation is weak in the southern hemisphere. We find a weakening of the synchronization of activity between the northern and southern hemispheres, and also between high and low latitude activity in the southern hemisphere. Possible causes of polar brightening and the meaning with respect to the general scenario of solar activity are discussed.

Time-Dependent Two-Fluid Magnetohydrodynamic Model and Simulation of the Chromosphere

Qusai Al **Shidi**, Ofer Cohen, Paul Song, Jiannan Tu
Solar Phys. 294:124 **2019**
https://arxiv.org/pdf/1904.01572.pdf
https://doi.org/10.1007/s11207-019-1513-8

The sun's chromosphere is a highly dynamic, partially-ionized region where spicules (hot jets of plasma) form. Here we present a two-fluid MHD model to study the chromosphere, which includes ion-neutral interaction and frictional heating. Our simulation recovers a magnetic canopy shape that forms quickly, but is also quickly disrupted by the formation of a jet. Our simulation produces a shock self-consistently, where the jet is driven by the frictional heating, which is much greater than the ohmic heating. Thus, our simulation demonstrates that the jet could be driven purely by thermal effects due to ion-neutral collisions and not by magnetic reconnection. We plan to improve the model to include photo-chemical effects, neutral radiation and new observations from the Parker Solar Probe mission in the model.

Sustaining high-solar-activity research

Albert Y. **Shih**, Amir Caspi, Jessie Duncan, Lindsay Glesener, Silvina E. Guidoni, Katharine K. Reeves
White paper submitted to the Decadal Survey for Solar and Space Physics (Heliophysics) 2024-2033; **2023**
https://arxiv.org/ftp/arxiv/papers/2306/2306.11776.pdf
Research efforts that require observations of high solar activity, such as multiwavelength studies of large solar flares and CMEs, must contend with the 11-year solar cycle to a degree unparalleled by other segments of heliophysics. While the "fallow" years around each solar minimum can be a great time frame to build the next major solar observatory, the corresponding funding opportunity and any preceding technology developments would need to be strategically timed. Even then, it can be challenging for scientists on soft money to continue ongoing research efforts instead of switching to other, more consistent topics. The maximum of solar cycle 25 is particularly concerning due to the lack of a US-led major mission targeting high solar activity, which could result in significant attrition of expertise in the field. We recommend the development of a strategic program of missions and analysis that ensures optimal science return for each solar maximum while sustaining the research community between maxima.

Fundamentals of impulsive energy release in the corona

Albert Y. **Shih**, Lindsay Glesener, Säm Krucker, Silvina Guidoni, +++
White paper submitted to the Decadal Survey for Solar and Space Physics (Heliophysics) 2024-2033; **2023**
https://arxiv.org/pdf/2306.11777
It is essential that there be coordinated and co-optimized observations in X-rays, gamma-rays, and EUV during the peak of solar cycle 26 (~2036) to significantly advance our understanding of impulsive energy release in the corona. The open questions include: What are the physical origins of space-weather events? How are particles accelerated at the Sun? How is impulsively released energy transported throughout the solar atmosphere? How is the solar corona heated? Many of the processes involved in triggering, driving, and sustaining solar eruptive events -- including magnetic reconnection, particle acceleration, plasma heating, and energy transport in magnetized plasmas -- also play important roles in phenomena throughout the Universe. This set of observations can be achieved through a single flagship mission or, with foreplanning, through a combination of major missions (e.g., the previously proposed FIERCE mission concept).

RHESSI has resumed operations

Albert **Shih**, Brian Dennis, and Sa”m Krucker
RHESSI Science Nugget, No. 276, June 20: **2016**
http://sprg.ssl.berkeley.edu/~tohban/wiki/index.php/RHESSI_has_resumed_operations
2016-05-24

RHESSI Resumes Observations

Albert **Shih**, Säm Krucker
RHESSI Science Nugget, No. 234, **2014**
http://sprg.ssl.berkeley.edu/~tohban/wiki/index.php/RHESSI_Resumes_Observations

Mean-field analysis on large-scale magnetic fields at high Reynolds numbers

Ryota **Shimada**, Hideyuki Hotta, Takaaki Yokoyama
ApJ 2022
https://arxiv.org/pdf/2207.01639
Solar magnetic fields comprise an 11-year activity cycle, represented by the number of sunspots. The maintenance of such a solar magnetic field can be attributed to fluid motion in the convection zone, i.e. a dynamo. This study conducts the mean-field analyses of the global solar dynamo simulation presented by Hotta et al. (2016). Although

the study succeeds in producing coherent large-scale magnetic fields at high Reynolds numbers, the detailed physics of the maintenance of this field have not been fully understood. This study extracts the alpha-tensor and the turbulent magnetic diffusivity tensor through mean-field analyses. The turbulent magnetic diffusivity exhibits a significant decrease towards high Reynolds numbers. The decrease in the turbulent magnetic diffusivity suppresses the energy conversion of large-scale field to small-scale field. This implies that the decrease in the turbulent magnetic diffusivity contributes to the maintenance of a large-scale magnetic field at high Reynolds numbers. A significant downward turbulent pumping is observed; it is enhanced in the weak phase of the large-scale field. This study proposes a cyclic reversal process of a large-scale field which is dominantly driven by the alpha-effect and is possibly triggered by downward pumping.

Estimating the temperature and density of a spicule from 100 GHz data obtained with ALMA

Masumi **Shimojo**, Tomoko Kawate, Takenori J. Okamoto, Takaaki Yokoyama, Noriyuki Narukage, Taro Sakao, Kazumasa Iwai, Gregory D. Fleishman, Kazunari Shibata
2020 *ApJL* **888** L28
https://arxiv.org/pdf/1912.05714.pdf
https://doi.org/10.3847/2041-8213/ab62a5
We succeeded in observing two large spicules simultaneously with the Atacama Large Millimeter/submillimeter Array (ALMA), the Interface Region Imaging Spectrograph (IRIS), and the Atmospheric Imaging Assembly (AIA) onboard the Solar Dynamics Observatory. One is a spicule seen in the IRIS Mg II slit-jaw images and AIA 304Å images (MgII/304A spicule). The other one is a spicule seen in the 100GHz images obtained with ALMA (100GHz spicule). Although the 100GHz spicule overlapped with the MgII/304A spicule in the early phase, it did not show any corresponding structures in the IRIS Mg II and AIA 304A images after the early phase. It suggests that the spicules are individual events and do not have a physical relationship. To obtain the physical parameters of the 100GHz spicule, we estimate the optical depths as a function of temperature and density using two different methods. One is using the observed brightness temperature by assuming a filling factor, and the other is using an emission model for the optical depth. As a result of comparing them, the kinetic temperature of the plasma and the number density of ionized hydrogens in the 100GHz spicule are ~6800 K and 2.2 x 10^10 cm^-3. The estimated values can explain the absorbing structure in the 193A image, which appear as a counterpart of the 100GHz spicule. These results suggest that the 100GHz spicule presented in this paper is classified to a macrospicule without a hot sheath in former terminology. **26 Apr 2017**

Variation of Solar Microwave Spectrum in the Last Half Century

M. **Shimojo**, K. Iwai, A. Asai, S. Nozawa, T. Minamidani, M. Saito
ApJ **2017**
https://arxiv.org/pdf/1709.03695.pdf
The total solar fluxes at 1, 2, 3.75, and 9.4 GHz were observed continuously from 1957 to 1994 at Toyokawa, and from 1994 until now at Nobeyama, Japan with the current Nobeyama Radio Polarimeters. We examined the multi-frequency and long-term datasets, and found that not only the microwave solar flux but also its monthly standard deviation well indicates the long-term variation of solar activity. Furthermore, we found that the microwave spectra at the solar minima of Cycle 20~24 agree with each other. These results show that the average atmospheric structure above the upper chromosphere in the quiet Sun has not varied for half a century, and suggest that the energy input for atmospheric heating from the sub-photosphere to the corona has not changed in the quiet Sun despite significantly differing strengths of magnetic activity in the last five solar cycles.

Unusual Migration of Prominence Activities in the Southern Hemisphere during Cycles 23–24

M. **Shimojo**
Publ. Astron. Soc. Japan 65, No SP1, S16 [6 pages] (**2013**)
http://pasj.asj.or.jp/v65/sp1/65S016/65S016.pdf
The solar activity in Cycles 23–24 shows differences from the previous cycles that were observed with modern instruments, e.g., long cycle duration and a small number of sunspots. To appreciate the anomalies further, we investigated the prominence eruptions and disappearances observed with the Nobeyama Radioheliograph for over 20 years. Consequently, we found that the occurrence of prominence activities in the northern hemisphere is normal because the period of the number variation is 11 years, and the migration of the producing region of the prominence activities traces the migration of 11 years ago. On the other hand, the migration in the southern hemisphere significantly
differs from that in the northern hemisphere and the previous cycles. The prominence activities occurred over _50₁ latitude in spite of the late decay phase of Cycle 23, and the number of prominence activities in the higher

latitude region (over _65₁) is very small, even near the solar maximum of Cycle 24. The results suggest that the anomalies of the global magnetic field distribution started at the solar maximum of Cycle 23. A comparison of the butterfly diagram of the prominence activities with the magnetic butterfly diagram indicates that the timing of "the rush to the pole" and the polar magnetic field closely relates to unusual migration. Considering that the rush to the pole is made of the sunspots, the hemispheric asymmetry of the sunspots and the strength of the polar magnetic fields are essential for understanding the anomalies of the prominence activities.

Vignetting Effect in the Soft X-Ray Telescope Onboard Yohkoh: I. Numerical Simulation

J. **Shin**, T. Sakurai

Solar Phys. Volume 291, Issue 2, pp 705-725 **2015**

Using a numerical simulation method, we examine the vignetting effect in the Soft X-ray Telescope(SXT) onboard Yohkoh. The off-axis variation of the effective area in the field-of-view shows that the vignetting in SXT cannot be described properly with a one-dimensional axisymmetric model. Our model assumes a response function of the X-ray mirror that is symmetric about the optical center, and an effect of occultation due to other telescope structures that is symmetric about the geometrical center; the vignetting is the result of these two contributions. We found that a rotationally non-symmetric distribution of the SXT effective area is mostly due to the offset of the optical center from the geometrical center of the telescope. The deviation from rotational symmetry due to the offset is most noticeable at the outskirts of the field-of-view, which results in the dispersion of effective area when considered as a one-dimensional distribution. The model cannot completely describe the vignetting in SXT because the fitting errors are larger than the measurement errors. We ultimately need a fully two-dimensional model for the vignetting in SXT.

Time-dependent theory of solar meridional flows

James H. **Shirley**

2017

https://arxiv.org/ftp/arxiv/papers/1706/1706.01854.pdf

We explore consequences for the solar dynamo of a newly-developed physical hypothesis describing a weak coupling of the orbital and rotational motions of extended bodies. The coupling is given by - c ((dL/dt) x omega sub alpha) x r, where dL/dt represents the rate of change of barycentric orbital angular momentum, omega sub alpha is the angular velocity of rotation, r is a position vector identifying a particular location in a coordinate system rotating with the Sun, and c is a coupling efficiency coefficient. This form of coupling has no dependence on tides. The coupling expression defines a non-axisymmetric global-scale acceleration field that varies both in space and with time. Meridional components of acceleration typically dominate in equatorial and middle latitudes, while zonal accelerations become increasingly significant at higher latitudes. A comparison of the waveform of the putative dynamical forcing function with the time series for measured solar meridional flow speeds from Sunspot Cycle 23 yields correlations significant at the 99.9% level. We introduce the possibility of a destructive interaction between the predicted large-scale flows (due to orbit-spin coupling) and the dynamo mechanism(s) of the 22-year magnetic activity cycle; observations in recent cycles of higher meridional flow speeds during episodes of reduced solar sunspot activity may be explained as a consequence of differences between the phasing of the magnetic cycle and the phase of the forcing function. Algorithms are provided for calculating meridional and zonal orbit-spin coupling accelerations within the Sun as a function of latitude, longitude, depth, and time.

A Self-consistent Model of the Coronal Heating and Solar Wind Acceleration Including Compressible and Incompressible Heating Processes

Munehito **Shoda**1, Takaaki Yokoyama1, and Takeru K. Suzuki2

2018 ApJ 853 190

http://sci-hub.tw/http://iopscience.iop.org/0004-637X/853/2/190/

We propose a novel one-dimensional model that includes both shock and turbulence heating and qualify how these processes contribute to heating the corona and driving the solar wind. Compressible MHD simulations allow us to automatically consider shock formation and dissipation, while turbulent dissipation is modeled via a one-point closure based on Alfvén wave turbulence. Numerical simulations were conducted with different photospheric perpendicular correlation lengths λ_0, which is a critical parameter of Alfvén wave turbulence, and different root-mean-square photospheric transverse-wave amplitudes δv_0. For the various λ_0, we obtain a low-temperature chromosphere, high-temperature corona, and supersonic solar wind. Our analysis shows that turbulence heating is always dominant when $\lambda_0 \lesssim 1$ Mm. This result does not mean that we can ignore the compressibility because the analysis indicates that the compressible waves and their associated density fluctuations enhance the Alfvén wave reflection and therefore the turbulence heating. The density fluctuation and the cross-helicity are strongly affected by λ_0, while the coronal temperature and mass-loss rate depend weakly on λ_0.

High-frequency spicule oscillations generated via mode conversion

Munehito **Shoda**, Takaaki Yokoyama

ApJ **2018**

https://arxiv.org/pdf/1801.01254.pdf

Spicule oscillations involve high-frequency components with a typical period approximately corresponding to 40−50 s. The typical time scale of the photospheric oscillation is a few minutes, and thus, the origin of this high-frequency component is not trivial. In this study, a one-dimensional numerical simulation is performed to demonstrate that the observed spicule oscillations originate from longitudinal-to-transverse mode conversion that occurs around the equipartition layer in the chromosphere. Calculations are conducted in a self-consistent manner with the exception of additional heating to maintain coronal temperature. The analyses indicate the following features: (1) mode conversion efficiently excites high-frequency transverse waves; (2) the typical period of the high-frequency waves corresponds to the sound-crossing time of the mode conversion region; and (3) simulated root-mean-square velocity of the high-frequency component is consistent with the observed value. These results indicate that the observation of spicule oscillation provides direct evidence of mode conversion in the chromosphere.

Solar rotation and activity for cycle 24 from SDO/AIA observations

Zahra **Shokri**, Nasibe Alipour, Hossein Safari

ApJ **2024**

https://arxiv.org/pdf/2407.17594

The differential rotation plays a crucial role in the dynamics of the Sun. We study the solar rotation and its correlation with solar activity by applying a modified machine learning algorithm to identify and track coronal bright points (CBPs) from the Solar Dynamics Observatory/Atmospheric Imaging Assembly observations at 193 Å during cycle 24. For more than 321,440 CBPs, the sidereal and meridional velocities are computed. We find the occurring height of CBPs about 5627 km above the photosphere. We obtain a rotational map for the corona by tracking CBPs at the formation height of Fe\,{\sc xii} (193 Å) emissions. The equator rotation (14.∘40 to 14.∘54 day−1) and latitudinal gradient of rotation (−3.∘0 to −2.∘64 day−1) show very slightly positive and negative trends with solar activity (sunspots and flares), respectively. For cycle 24, our investigations show that the northern hemisphere has more differential rotation than the southern hemisphere, confirmed by the asymmetry of the midlatitude rotation parameter. The asymmetry (ranked) of the latitudinal gradient of the rotation parameter is concordant with the sunspot numbers for 7 yr within the 9 yr of the cycle; however, for only 3 yr, it is concordant with the flare index. The minimum horizontal Reynolds stress changes from about −2500 m2 s−2 (corresponding to high activity) in 2012 and 2014 to −100 m2 s−2 (corresponding to low activity) in 2019 over 5∘ to 35∘ latitudes within cycle 24. We conclude that the negative horizontal Reynolds stress (momentum transfer toward the Sun's equator) is a helpful indication of solar activity.

Resonant damping of kink oscillations of thin expanding magnetic tubes

A. A. **Shukhobodskiy**1,2 and M. S. Ruderman1,3

A&A 615, A156 (**2018**)

We study the resonant damping of kink oscillations of thin expanding magnetic flux tubes. The tube consists of a core region and a thin transitional region at the tube boundary. The resonance occurs in this transitional layer where the oscillation frequency coincides with the local Alfvén frequency. Our investigation is based on the system of equations that we previously derived. This system is not closed because it contains the jumps of the magnetic pressure perturbation and plasma displacement across the transitional layer. We calculate these jumps and thus close the system. We then use it to determine the decrements of oscillation eigenmodes. We introduce the notion of homogeneous stratification. In accordance with this condition the ratio of densities in the tube core and outside the tube does not vary along the tube, while the density in the transitional layer can be factorised and written as a product of two function, one depending on the variable along the tube and the other on the magnetic flux function. Our main result is that, under the condition of homogeneous stratification, the ratio of the decrement to the oscillation frequency is independent of a particular form of the density variation along the tube. This ratio is also the same for all oscillation eigenmodes.

The Total Solar Irradiance variability in the Evolutionary Timescale and its Impact on the Mean Earth's Surface Temperature

N.T. **Shukure**, S.B Tessema, N. Gopalswamy

ApJ **917** 86 **2021**

https://arxiv.org/pdf/2106.03657.pdf

https://iopscience.iop.org/article/10.3847/1538-4357/ac0894/pdf

https://doi.org/10.3847/1538-4357/ac0894

The Sun is the primary source of energy for the Earth. The small changes in total solar irradiance (TSI) can affect our climate in the longer timescale. In the evolutionary timescale, the TSI varies by a large amount and hence its

influence on the Earth's mean surface temperature (Ts) also increases significantly. We develop a mass-loss dependent analytical model of TSI in the evolutionary timescale and evaluated its influence on the Ts. We determined the numerical solution of TSI for the next 8.23 Gyrs to be used as an input to evaluate the Ts which formulated based on a zero-dimensional energy balance model. We used the present-day albedo and bulk atmospheric emissivity of the Earth and Mars as initial and final boundary conditions, respectively. We found that the TSI increases by 10\% in 1.42 Gyr, by 40\% in about 3.4 Gyrs, and by 120\% in about 5.229 Gyrs from now, while the Ts shows an insignificant change in 1.644 Gyrs and increases to 298.86 K in about 3.4 Gyrs. The Ts attains the peak value of 2319.2 K as the Sun evolves to the red giant and emits the enormous TSI of 7.93×106Wm−2 in 7.676 Gys. At this temperature Earth likely evolves to be a liquid planet. In our finding, the absorbed and emitted flux equally increases and approaches the surface flux in the main sequence, and they are nearly equal beyond the main sequence, while the flux absorbed by the cloud shows opposite trend.

On the Connection between Solar Surface Magnetic Flux and the Total Solar Irradiance

N. T. **Shukure**1,2,3, S. B Tessema1, and N. Gopalswamy4
2021 ApJ 907 39
https://iopscience.iop.org/article/10.3847/1538-4357/abcbf3/pdf
Solar surface magnetic flux evolution plays a dominant role in the variability of total solar irradiance (TSI). Different proxies of magnetic activity have been introduced to correlate solar variability and TSI. We present the daily strong flux densities (SFDs) and weak flux densities (WFDs) defined with three magnetic thresholds calculated from the Solar Dynamic Observatory/Helioseismic Magnetic Imager. TSI measurements are from the radiometers of the Variability of Solar Irradiance and Gravity Oscillations experiment on the Solar and Heliosphere Observatory, and sunspot area (SSA) is from the National Oceanic and Atmospheric Administration. We characterize the influence of the magnetic flux density variation on the TSI using the Pearson, Spearman, and percentage bend correlations and wavelet analysis between the TSI and the flux density. The Pearson's correlation shows that the TSI is negatively and strongly correlated with SFD and moderately with SSA; Spearman and 20% bend correlation shows that the TSI is moderately correlated with SFD and weakly with SSA on solar maximum, but weakly correlated on solar minimum. However, the TSI is not correlated with WFD during solar maximum and minimum. The bootstrapping tests also confirm that the influence of SFD on TSI is more significant than that of SSA. Finally, a wavelet analysis supports the idea that the SFD and TSI have a causality linkage and that the SFD dominantly influences the TSI variability on the rotational timescale.

SIMULATION STUDY OF HEMISPHERIC PHASE-ASYMMETRY IN THE SOLAR CYCLE

D. **Shukuya** and K. Kusano
2017 ApJ 835 84 DOI 10.3847/1538-4357/835/1/84
http://sci-hub.cc/doi/10.3847/1538-4357/835/1/84
Observations of the Sun suggest that solar activities systematically create north–south hemispheric asymmetries. For instance, the hemisphere in which sunspot activity is more active tends to switch after the early half of each solar cycle. Svalgaard & Kamide recently pointed out that the time gaps of polar field reversal between the northern and southern hemispheres are simply consequences of the asymmetry of sunspot activity. However, the mechanism underlying the asymmetric feature in solar cycle activity is not yet well understood. In this paper, in order to explain the cause of the asymmetry from the theoretical point of view, we investigate the relationship between the dipole- and quadrupole-type components of the magnetic field in the solar cycle using the mean-field theory based on the flux transport dynamo model. As a result, we found that there are two different attractors of the solar cycle, in which either the north or the south polar field is first reversed, and that the flux transport dynamo model explains well the phase-asymmetry of sunspot activity and the polar field reversal without any ad hoc source of asymmetry.

The non-Fourier image reconstruction method for the STIX instrument

Marek **Siarkowski** 2 , Tomasz Mrozek 1 , Janusz Sylwester 2 , Michalina Litwicka 2 , and Magdalena Dąbek 3
Open Astronomy Volume 29: Issue 1 220-230 **2020**
https://www.degruyter.com/view/journals/astro/29/1/article-p220.xml
In this work we aimed to develop the image reconstruction algorithm without any analytical simplifications and restrictions. In our method we abandon Fourier's approach to image reconstruction, and instead use the number of counts recorded in each detector pixel, and then reconstruct each image using a classical Richardson-Lucy algorithm. Among similar works performed in the past, our approach is based, for the first time, on the real geometry of STIX. We made a preliminary analysis of expected differences in STIX imaging which may occur due to usage of slightly different geometries. The other difference is that we use single-pixel-response maps. Namely, knowing the instrument geometry we are able to calculate the detector response for point sources covering entire the solar disc. Next, we iteratively combine them with varying weights until the best match between reconstructed and observed detector responses is achieved. Preliminary tests revealed that the developed algorithm reproduces high quality images. The algorithm is moderately fast, but the result comparable to CLEAN algorithm is obtained within

20-50 iteration steps which takes less than 2 seconds on typical portable computer configuration. The location, size and intensity of reconstructed sources are very close to simulated ones. Therefore the algorithm is very well suited for the detailed photometry of the solar HXR sources. Moreover, its simplicity allows to improve photon transmission calculation in case of any grids uncertainties measured after the launch.

ERRATUM: AN UPPER BOUND FROM HELIOSEISMOLOGY ON THE STOCHASTIC BACKGROUND OF GRAVITATIONAL WAVES (2014, ApJ, 784, 88)

Daniel M. **Siegel**[1] and Markus Roth
2015 *ApJ* **810** 84

Cross correlation and time-lag between cosmic ray intensity and solar activity during solar cycles 21, 22 and 23 Review

D. **Sierra-Porta**
Astrophysics and Space Science July **2018**, 363:137
http://sci-hub.se/10.1007/s10509-018-3360-8
https://arxiv.org/pdf/1906.01175.pdf
In the present paper a systematic study is carried out to validate the similarity or co-variability between daily terrestrial cosmic-ray intensity and three parameters of the solar corona evolution, i.e., the number of sunspots and flare index observed in the solar corona and the Ap index for regular magnetic field variations caused by regular solar radiation changes. The study is made for a period including three solar cycles starting with cycle 21 (year 1976) and ending on cycle 23 (year 2008). A cross-correlation analysis was used to establish patterns and dependence of the variables. This study focused on the time lag calculation for these variables and found a maximum of negative correlation over CC1≈0.85CC1≈0.85, CC2≈0.75CC2≈0.75 and CC3≈0.63CC3≈0.63 with an estimation of 181, 156 and 2 days of deviation between maximum/minimum of peaks for the intensity of cosmic rays related with sunspot number, flare index and Ap index regression, respectively.

Visual and H-alpha measurements of solar diameter of 9 may 2016 mercury transit

Costantino **Sigismondi**, Hamed Altafi
GERBERTVS academic journal (www.icra.it/gerbertus) **2018**
https://arxiv.org/ftp/arxiv/papers/1805/1805.09915.pdf
Visual observations of 2016 Mercury transit ingress made in visible light (Rome) and in H-alpha line (Tehran) are compared to evaluate the quote 1.84" of active H-alpha regions at the solar latitude of the transit, without a confirmation of the theory of an oblate Sun at minimum activity. A variation of -0.12" in the photospheric radius, within 0.17" is found.

The opportunity of the 2016 transit of Mercury for measuring the solar diameter and recommendations for the observation

Costantino **Sigismondi**
presented at the congress Solar Metrology, Needs and Methods II 21-23 September 2015 Royal Observatory of Belgium **2016**
http://arxiv.org/pdf/1605.02084v1.pdf
The transit of Mercury occurred two times in this century: 2003, May 7 and 2006, November 8. In 2016 there is another opportunity to observe this phenomenon and measure the solar diameter with the method of comparing the ephemerides with the observations. This method has been presented by I. I. Shapiro in 1980, the data of the observed transits (since 1631) have been re-analyzed by Sveshnikov (2002) and an improvement on the observed data, to avoid the confusion given by the black-drop effect, proposed by C. Sigismondi and collaborators since 2005 exploits the measurement of the chord drawn by the solar limb with the disk of the transiting planet and its extrapolation to zero through the analytic chord fitting the observations before the black drop, in the ingress/egress phases. A network of European observers (IOTA/ES) and observatories (coronograph of Bialkow, PL 56 cm; IRSOL, Locarno CH - 45 cm Gregorian telescope) is active for the 2016 transit. Recommendations to improve the observation of the ingress/egress phases and examples of the data analysis on the 1999 Mercury transit observed by TRACE are also done: the planet should be centered in the field of view of the telescope to avoid optical distortions, and the observations should be prolonged well after the black drop phase, estimated in about 40 seconds and more after the internal contact t2 in the ingress and before the internal contact t3 in egress.

Transits of Venus and Solar diameter measures from ground: method and results from Athens (2004) and Huairou (2012)

Costantino **Sigismondi**, Anthony Ayiomamitis, Xiaofan Wang, Wenbin Xie, Massimo Carinci, Alessio Mimmo
Presented to the PT5 parallel session of the XIV Marcel Grossmann Meeting on General Relativity, Rome Sapienza University, on 17 july **2015**
http://arxiv.org/pdf/1507.03622v1.pdf
The variation of the solar diameter in time and in position angle has implications in astrophysics and in general relativity, as the long series of studies attest. The Transits of Venus in 2004 and 2012 have been carefully studied because of the rarity of the phenomenon and its historical importance due the AU measure and to the discovery of Venus atmosphere. The characterization of Venus atmosphere and the measure of the solar diameter to the milliarcsecond level of precision have been studied also from satellite images. The results of the solar diameter measurements made with the observations in Athens (2004) and at the Huairou Solar Observing Station in China (2012) are presented. The topic of the oblateness of the Sun at sunset and its intrinsic value is drafted to introduce the general public to the relativistic relevance of measuring the solar figure, in the occasion of the International Year of Light 2015.

Modeling the Time Delay Problem of Galactic Cosmic Ray Flux in Solar Cycles 21 and 23

M. **Siluszyk** & K. Iskra
Solar Physics **volume 295**, Article number: 68 (**2020**)
https://link.springer.com/content/pdf/10.1007/s11207-020-01628-w.pdf
We present a 2-dimensional time-dependent simulation based on Parker's transport equation (PTE) describing the propagation of energetic astroparticles – cosmic rays (CR) in the heliosphere. PTE is a second order partial differential equation containing four major processes: diffusion, convection, drift, and adiabatic cooling responsible for modulation of the CR flux in the heliosphere. We implement in the numerical simulation, a few physical parameters as the tilt angle, δδ, of the heliospheric current sheet (HCS), module, BB, of the interplanetary magnetic field (IMF), and variations of drift effect of the CR particles with solar activity (SA). Our approach is the implementation of two independent parameters (proxies), γγ and νν. The parameters γγ and νν are calculated from various independent sources, γγ, from neutron monitors (NM) daily data, and νν, using the IMF hourly data. The solutions of PTE obtained from our numerical model are compared with the variations of the CR flux recorded by NMs. We prove the existence of a varying delay time (DT) between the changes of galactic cosmic ray (GCR) intensity and the parameters characterizing SA. Based on our investigation, we obtained different DTs in Solar Cycles 21 and 23. We conclude that the calculated DTs, after comparison with the observed DTs, are useful parameters for the study of GCR transport in the heliosphere.

Novel Approach to Forecasting Photospheric Emergence of Active Regions

S. S. A. **Silva**1, M. Lennard2, G. Verth2, I. Ballai2, E. L. Rempel3,4, J. Warnecke5, H. Iijima6, H. Hotta7, S.-H. Park8, A. C. Donea9Show full author list
2023 ApJL 948 L24
https://iopscience.iop.org/article/10.3847/2041-8213/acd007/pdf
One key aspect of understanding the solar dynamo mechanism and the evolution of solar magnetism is to properly describe the emergence of solar active regions. In this Letter, we describe the Lagrangian photospheric flows dynamics during a simulated flux emergence that produces an active region formed by pores. We analyze the lower photospheric flow organization prior, during and following the rise of an active region, uncovering the repelling and attracting photospheric structures that act as sources and sinks for magnetic element transport. Our results show that around 10 hr before the simulated emergence, considerable global changes are taking place on mesogranular scales indicated by an increase of the number of regions acting as a source to the multiple and scattered emergences of small-scale magnetic flux. At the location of active region's appearance, the converging flows become weaker and there is an arising of a diverging region 8 hr before the emergence time. Our study also indicates that the strong concentration of magnetic field affects the flow dynamics beyond the area of the actual simulated pores, leading to complex and strongly diverging flows in the neighboring regions. Our findings suggest that the Lagrangian analysis is a powerful tool to describe the changes in the photospheric flows due to magnetic flux emergence.

The importance of horizontal Poynting flux in the solar photosphere

Suzana S. A. **Silva**, Mariarita Murabito, Shahin Jafarzadeh, Marco Stangliani, Gary Verth, Istvan Ballai, Viktor Fedun
ApJ **927** 146 **2022**
https://arxiv.org/pdf/2203.01221.pdf
https://iopscience.iop.org/article/10.3847/1538-4357/ac4601/pdf
The electromagnetic energy flux in the lower atmosphere of the Sun is a key tool to describe the energy balance of the solar atmosphere. Current investigations on energy flux in the solar atmosphere focus primarily on the vertical electromagnetic flux through the photosphere, ignoring the Poynting flux in other directions and its possible

contributions to local heating. Based on a realistic Bifrost simulation of a quiet-Sun (coronal hole) atmosphere, we find that the total electromagnetic energy flux in the photosphere occurs mainly parallel to the photosphere, concentrating in small regions along intergranular lanes. Thereby, it was possible to define a proxy for this energy flux based on only variables that can be promptly retrieved from observations, namely, horizontal velocities of the small-scale magnetic elements and their longitudinal magnetic flux. Our proxy accurately describes the actual Poynting flux distribution in the simulations, with the electromagnetic energy flux reaching 1010 erg\,cm−2\,s−1. To validate our findings, we extended the analysis to SUNRISE/IMaX data. First, we show that Bifrost realistically describes photospheric quiet-Sun regions, as the simulation presents similar distributions for line-of-sight magnetic flux and horizontal velocity field. Second, we found very similar horizontal Poynting flux proxy distributions for the simulated photosphere and observational data. Our results also indicate that the horizontal Poynting flux in the observations is considerably larger than the vertical electromagnetic flux from previous observational estimates. Therefore, our analysis confirms that the electromagnetic energy flux in the photosphere is mainly horizontal and is most intense in localized regions along intergranular lanes.

Solar Vortex Tubes. II. On the Origin of Magnetic Vortices

Suzana S. A. **Silva**1,2, Gary Verth3, Erico L. Rempel4, Sergiy Shelyag5, Luiz A. C. A. Schiavo6, and Viktor Fedun1

2021 ApJ 915 24

https://doi.org/10.3847/1538-4357/abfec2

The solar atmosphere presents a wealth of dynamics due to a constant interplay between the plasma flows and magnetic fields. Twisted flux tubes are an essential magnetic structure, believed to be driven by the rotational surface's motions and linked to plasma heating, jets, and eruptive phenomena. Despite extensive investigations, twisted magnetic flux tubes lack a proper mathematical definition, precluding their automatic detection. This work addresses this issue by defining them as magnetic vortices and introduces a formal definition that is based on a recently developed magnetic vortex detection technique, the integrated averaged current deviation method. We applied this method and a kinetic vortex identification technique to realistic magnetoconvection simulations obtained from the MURaM code. The preferential site for these two types of vortices is the intergranular downflow, but while the magnetic vortices are found mostly in the small areas where plasma-$\beta > 1$, the rotational flow structures (the kinetic vortices), were detected in locations where plasma-$\beta < 1$. The magnetic vortices locally concentrate the magnetic field's vertical components and current, lasting, on average, around a minute. Two types of magnetic vortices are introduced based on their magnetic-to-kinetic energy ratio. For the first type, the magnetic energy prevails, and the magnetic vortices are mostly vertical. The second type of magnetic vortex presents distinct shapes and a lower magnetic-to-kinetic energy ratio. We have found that magnetic vortices may appear if two conditions are simultaneously present: (i) shear flow and (ii) plasma-$\beta > 1$. The presence of rotational motion is not necessary.

Solar Vortex Tubes: Vortex Dynamics in the Solar Atmosphere

Suzana S. A. **Silva**, Viktor Fedun, Gary Verth, Erico L. Rempel,, and Sergiy Shelyag[5]

ApJ **898** 137 **2020**

https://arxiv.org/pdf/2007.04371.pdf

https://doi.org/10.3847/1538-4357/ab99a9

In this work, a state-of-the-art vortex detection method, Instantaneous Vorticity Deviation, is applied to locate three-dimensional vortex tube boundaries in numerical simulations of solar photospheric magnetoconvection performed by the MURaM code. We detected three-dimensional vortices distributed along intergranular regions and displaying coned shapes that extend from the photosphere to the low chromosphere. Based on a well-defined vortex center and boundary, we were able to determine averaged radial profiles and thereby investigate the dynamics across the vortical flows at different height levels. The solar vortex tubes present nonuniform angular rotational velocity, and, at all height levels, there are eddy viscosity effects within the vortices, which slow down the plasma as it moves toward the center. The vortices impact the magnetic field as they help to intensify the magnetic field at the sinking points, and in turn, the magnetic field ends up playing an essential role in the vortex dynamics. The magnetic field was found to be especially important to the vorticity evolution. On the other hand, it is shown that, in general, kinematic vortices do not give rise to magnetic vortices unless their tangential velocities at different height levels are high enough to overcome the magnetic tension.

Nonlocal heat flux effects on temperature evolution of the solar atmosphere

S. S. A. **Silva**1, J. C. Santos2, J. Büchner3 and M. V. Alves1

A&A 615, A32 (**2018**)

Context. Heat flux is one of the main energy transport mechanisms in the weakly collisional plasma of the solar corona. There, rare binary collisions let hot electrons travel over long distances and influence other regions along magnetic field lines. Thus, the fully collisional heat flux models might not describe transport well enough since they consider only the local contribution of electrons. The heat flux in weakly collisional plasmas at high temperatures

with large mean free paths has to consider the nonlocality of the energy transport in the frame of nonlocal models in order to treat energy balance in the solar atmosphere properly.
Aims. We investigate the impact of nonlocal heat flux on the thermal evolution and dynamics of the solar atmosphere by implementing a nonlocal heat flux model in a 3D magnetohydrodynamic simulation of the solar corona.
Methods. We simulate the evolution of solar coronal plasma and magnetic fields considering both a local collision dominated and a nonlocal heat flux model. The initial magnetic field is obtained by a potential extrapolation of the observed line-of-sight magnetic field of AR11226. The system is perturbed by moving the plasma at the photosphere. We compared the simulated evolution of the solar atmosphere in its dependence on the heat flux model.
Results. The main differences for the average temperature profiles were found in the upper chromosphere/transition region. In the nonlocal heat transport model case, thermal energy is transported more efficiently to the upper chromosphere and lower transition region and leads to an earlier heating of the lower atmosphere. As a consequence, the structure of the solar atmosphere is affected with the nonlocal simulations producing on average a smoother temperature profile and the transition region placed about 500 km higher. Using a nonlocal heat flux also leads to two times higher temperatures in some of the regions in the lower corona.
Conclusions. The results of our 3D MHD simulations considering nonlocal heat transport supports the previous results of simpler 1D two-fluid simulations. They demonstrated that it is important to consider a nonlocal formulation for the heat flux when there is a strong energy deposit, like the one observed during flares, in the solar corona.

Rieger-type periodicities on the Sun and the Earth during solar cycles 21 and 22

H. G. **Silva,** I. Lopes
Astrophysics and Space Science March **2017**, 362:44 DOI: 10.1007/s10509-017-3020-4
Rieger-type periods of the magnetic sunspot area time series have been found in two atmospheric time-series variables: neutron monitor count rate and atmospheric electric potential gradient. The data considered comprises two solar cycles (21, 22) and spans from 1978 to 1990. The study reveals the existence of similar and correlated features in sunspot area as well as neutron counts and atmospheric electric potential gradient, favoring the possibility that the Sun's activity affects the Earth's atmosphere and weather at a time scale between 150–300 days. Moreover, five different Rieger-type periods in the sunspot area time series are found, four of which are detected in the neutron monitor count rate, and three in the atmospheric electric potential gradient. These values are consistent with the periods predicted for stationary solar Rossby waves existing inside the Sun. The possibility is discussed that instabilities on the solar magnetic field caused by solar Rossby waves in the Sun's interior might indirectly be affecting the activity of the heliosphere and the Earth's atmosphere.

Comparison of solar radio and EUV synoptic limb charts during the present solar maximum

A. J. Oliveira e **Silva**, C. L. Selhorst, P. J. A. Simões, C. G. Giménes de Castro
A&A 592, A91 **2016**
http://arxiv.org/pdf/1606.03406v1.pdf
The present solar cycle is particular in many aspects: it had a delayed rising phase, it is the weakest of the last 100 years, and it presents two peaks separated by more than one year. To understand the impact of these characteristics on the solar chromosphere and coronal dynamics, images from a wide wavelength range are needed. In this work we use the 17~GHz radio continuum, formed in the upper chromosphere and the EUV lines 304 and 171~{\AA}, that come from the transition region (He II) and the corona (Fe IX, X), respectively. We analyze daily images at 304 and 171~{\AA} obtained by the Atmospheric Imaging Assembly (AIA). The 17~GHz maps were obtained by the Nobeyama Radioheliograph (NoRH). To construct synoptic limb charts, we calculated the mean emission of delimited limb areas with 100" wide and angular separation of 5∘. At the equatorial region, the results show an hemispheric asymmetry of the solar activity. The northern hemisphere dominance is coincident with the first sunspot number peak, whereas the second peak occurs concurrently with the increase in the activity at the south. The polar emission reflects the presence of coronal holes at both EUV wavelengths, moreover, the 17~GHz polar brightenings can be associated with the coronal holes. Until 2013, both EUV coronal holes and radio polar brightenings were more predominant at the south pole. Since then they have not been apparent in the north, but thus appear in the beginning of 2015 in the south as observed in the synoptic charts. This work strengthens the association between coronal holes and the 17~GHz polar brightenings as it is evident in the synoptic limb charts, in agreement with previous case study papers. The enhancement of the radio brightness in coronal holes is explained by the presence of bright patches closely associated with the presence of intense unipolar magnetic fields.

The Dalton Minimum and John Dalton's Auroral Observations

Sam M. **Silverman**, Hisashi Hayakawa

Journal of Space Weather and Space Climate, **2021**
https://arxiv.org/ftp/arxiv/papers/2012/2012.13713.pdf
In addition to the regular Schwabe cycles of approximately 11 y, "prolonged solar activity minima" have been identified through the direct observation of sunspots and aurorae, as well as proxy data of cosmogenic isotopes. Some of these minima have been regarded as grand solar minima, which are arguably associated with the special state of the solar dynamo and have attracted significant scientific interest. In this paper, we review how these prolonged solar activity minima have been identified. In particular, we focus on the Dalton Minimum, which is named after John Dalton. We review Dalton's scientific achievements, particularly in geophysics. Special emphasis is placed on his lifelong observations of auroral displays over approximately five decades in Great Britain. Dalton's observations for the auroral frequency allowed him to notice the scarcity of auroral displays in the early 19th century. We analyze temporal variations in the annual frequency of such displays from a modern perspective. The contemporary geomagnetic positions of Dalton's observational site make his dataset extremely valuable because his site is located in the sub-auroral zone and is relatively sensitive to minor enhancements in solar eruptions and solar wind streams. His data indicate clear solar cycles in the early 19th century and their significant depression from 1798 to 1824. Additionally, his data reveal a significant spike in auroral frequency in 1797, which chronologically coincides with the "lost cycle" that is believed to have occurred at the end of Solar Cycle 4. Therefore, John Dalton's achievements can still benefit modern science and help us improve our understanding of the Dalton Minimum.

Grand Minima in a spherical non-kinematic α2Ω mean-field dynamo model

Corinne **Simard** and Paul Charbonneau
J. Space Weather Space Clim. **2020**, 10, 9
https://www.swsc-journal.org/articles/swsc/pdf/2020/01/swsc190074.pdf
We present a non-kinematic axisymetric α2Ω mean-field dynamo model in which the complete α-tensor and mean differential rotation profile are both extracted from a global magnetohydrodynamical simulation of solar convection producing cycling large-scale magnetic fields. The nonlinear backreaction of the Lorentz force on differential rotation is the only amplitude-limiting mechanism introduced in the mean-field model. We compare and contrast the amplitude modulation patterns characterizing this mean-field dynamo, to those already well-studied in the context of non-kinematic αΩ models using a scalar α-effect. As in the latter, we find that large quasi-periodic modulation of the primary cycle are produced at low magnetic Prandtl number (Pm), with the ratio of modulation period to the primary cycle period scaling inversely with Pm. The variations of differential rotation remain well within the bounds set by observed solar torsional oscillations. In this low-Pm regime, moderately supercritical solutions can also exhibit aperiodic Maunder Minimum-like periods of strongly reduced cycle amplitude. The inter-event waiting time distribution is approximately exponential, in agreement with solar activity reconstructions based on cosmogenic radioisotopes. Secular variations in low-latitude surface differential rotation during Grand Minima, as compared to epochs of normal cyclic behavior, are commensurate in amplitude with historical inferences based on sunspot drawings. Our modeling results suggest that the low levels of observed variations in the solar differential rotation in the course of the activity cycle may nonetheless contribute to, or perhaps even dominate, the regulation of the magnetic cycle amplitude.

Characterisation of the turbulent electromotive force and its magnetically-mediated quenching in a global EULAG-MHD simulation of solar convection

C. **Simard**, P. Charbonneau, C. Dube
Advances in Space Research **2016**
http://arxiv.org/pdf/1604.01533v1.pdf
We perform a mean-field analysis of the EULAG-MHD millenium simulation of global magnetohydrodynamical convection presented in Passos et al. 2014. The turbulent electromotive force operating in the simulation is assumed to be linearly related to the cyclic axisymmetric mean magnetic field and its first spatial derivatives. At every grid point in the simulation's meridional plane, this assumed relationship involves 27 independent tensorial coefficients. Expanding on Racine et al. 2011, we extract these coefficients from the simulation data through a least-squares minimization procedure based on singular value decomposition. The reconstructed alpha-tensor shows good agreement with that obtained by Racine et al. 2011, who did not include derivatives of the mean-field in their fit, as well as with the alpha-tensor extracted by Augustson et al. 2015 from a distinct ASH MHD simulation. The isotropic part of the turbulent magnetic diffusivity tensor beta is positive definite and reaches values of 5.0x10^7 m2s-1 in the middle of the convecting fluid layers. The spatial variations of both alpha_phiphi and beta_phiphi component are well reproduced by expressions obtained under the SOCA, with a good matching of amplitude requiring a turbulent correlation time about five times smaller than the estimated turnover time of the small-scale turbulent flow. We find the magnetic quenching of the alpha-effect to be driven primarily by a reduction of the small-scale flow's kinetic helicity, with variations of the current helicity playing a lesser role in most locations in the simulation domain. Our measurements of turbulent diffusivity quenching are restricted to the beta_phiphi component, but indicate a weaker quenching, by a factor of 1.36, than of the alpha effect, which in our simulation drops by a factor of three between the minimum and maximum phases of the magnetic cycle.

A New Challenge to Solar Dynamo Models from Helioseismic Observations: The Latitudinal Dependence of the Progression of the Solar Cycle

R.**Simoniello**, S.C. Tripathy, K.Jain, F.Hill

ApJ **828** 41 **2016**

http://arxiv.org/pdf/1606.03037v1.pdf

The solar cycle onset at mid-latitudes, the slow down of the sunspot drift toward the equator, the tail-like attachment and the overlap of successive cycles at the time of activity minimum are delicate issues in αΩ dynamo wave and flux transport dynamo models. Very different parameter values produce similar results, making it difficult to understand the origin of these solar cycle properties. We use GONG helioseismic data to investigate the progression of the solar cycle as observed in intermediate-degree global p-mode frequency shifts at different latitudes and subsurface layers, from the beginning of solar cycle 23 up to the maximum of the current solar cycle. We also analyze those for high-degree modes in each hemisphere obtained through the ring-diagram technique of local helioseismology. The analysis highlighted differences in the progression of the cycle below 15\degr\ compared to higher latitudes. While the cycle starts at mid-latitudes and then migrates equatorward/poleward, the sunspot eruptions of the old cycle are still ongoing below 15\degr\ latitude. This prolonged activity causes a delay in the cycle onset and an overlap of successive cycles, whose extension differs in the two hemispheres. Then the activity level rises faster reaching a maximum characterized by a single peak structure compared to the double peak at higher latitudes. Afterwards the descending phase shows up with a slower decay rate. The latitudinal properties of the solar cycle progression highlighted in this study provide useful constraints to discern among the multitude of solar dynamo models.

Study of Meridional Flow Using Ca-K Line Profiles during Solar Cycles 22 and 23

G. **Sindhuja**1,2, Jagdev Singh1, and B. Ravindra

2014 ApJ 792 22

The analysis of Ca-K line spectra as a function of solar latitude and integrated over longitudes taken during the period of 1989-2011 indicates that the K1 width attains maximum amplitude at various latitude belts at different phases of the solar cycle. The FWHM of the K1 distribution at different latitudes shows that its width varies by about 30% for the equatorial belt (<30°) and 11% for the polar region (>70°) latitudes. Interestingly, the K1 width varies by ~6% only in the 40-60° latitude belts during the solar cycle. The analysis of cross-correlation coefficients of the K1 width between the 35° latitude and other latitude belts as a function of phase differences indicates that the activity representing toroidal field shifted at a uniform rate of about 5.1 m s–1 in the northern hemisphere from mid-latitudes toward the equator. In the southern hemisphere, activity shifted at a faster rate, ~14 m s–1, in the beginning of the cycle and the speed decreased with time, yielding an average speed of 7.5 m s–1 toward the equator. The shift of activity in the higher latitude belts showed complex behavior, indicating poleward and equatorward migration. These findings, especially the fewer variations in mid-latitude belts as compared to polar regions, asymmetry in the speed of the shift in the activity in both hemispheres, and complex variation in the direction of the shift in the activity representing poloidal fields in mid-latitude belts, will have an important implication on the modeling of the solar dynamo.

Calcium bright knots and the formation of chromospheric anemone jets on the Sun

Kunwar Alkendra Pratap **Singh**, Keisuke Nishida, Kazunari Shibata

ApJL **2024**

https://arxiv.org/pdf/2401.16319.pdf

Space-based observations show that the solar atmosphere from the solar chromosphere to the solar corona is filled with small-scale jets and is linked with small-scale explosions. These jets may be produced by mechanisms similar to that of large-scale flares and such jets may be related to the heating of corona and chromosphere as well as the acceleration of solar wind. The chromospheric anemone jets on the Sun remain puzzling because their footpoints (or bright knots) have not been well resolved and the formation process of such enigmatic small-scale jets remains unclear. We propose a new model for chromospheric jets using the three-dimensional magnetohydrodynamic (MHD) simulations, which show that the continuous, upward rising of small-scale twisted magnetic flux ropes in a magnetized solar chromosphere drive small-scale magnetic reconnection and the launching of several small-scale jets during the evolution of the chromospheric anemone jets. Our new, self-consistent, three-dimensional computer modeling of small-scale, but ever-changing flux rope emergence in the magnetized solar atmosphere is fully consistent with observations and provides a universal mechanism for nanoflare and jet formation.

A long term multi-frequency study of solar rotation using solar radio flux and its relationship with solar cycles

Vivek Kumar **Singh**, Satish Chandra, Sanish Thomas, Som Kumar Sharma, Hari Om Vats

MNRAS Volume 505, Issue 4, August **2021**, Pages 5228–5237,

https://doi.org/10.1093/mnras/stab1574
https://arxiv.org/pdf/2107.01448.pdf
This paper examines long-term temporal and spatial fluctuations in the solar rotation (more than four solar cycles) by investigating radio emission escapes from various layers of the solar atmosphere during the years 1967-2010. The flux modulation approach can also be used to investigate variations in solar rotation, which is a contentious topic in solar physics. The current study makes use of a time series of radio flux data at different frequencies (245-15400 MHz) obtained at Sagamore Hill Solar Radio Observatory in Massachusetts, USA, and other observatories from 1967 to 2010. The periodicity present in the temporal variation of time series is estimated through Lomb Scargle Periodogram (LSP). The rotation period estimated for five radio emissions (606, 1415, \& 2695 MHz; from corona, and 4995 \& 8800 MHz; from transition region) through statistical approach shows continuous temporal and spatial variation throughout the years. The smoothed rotation period shows the presence of ~ 22-yrs periodic and ~ 11-yrs components in it. The 22-year component could be linked to the reversal of the solar magnetic field (Hale's) cycle, while the 11-yrs component is most likely related to the sunspot (Schwabe's) cycle. Besides these two components, random components are also prominently present in the analyzed data. The cross-correlation between the sunspot number and the rotation period obtained shows a strong correlation with 11-yrs Schwabe's and 22-yr Hale cycle. The corona rotates faster or slower than transition region in different epoch. The swap of faster rotation speed between corona and transition region also follows the 22-yrs cycle.

The Missing Cool Corona in the Flat Magnetic Field around Solar Active Regions

Talwinder **Singh**, Alphonse C. Sterling, Ronald L. Moore
ApJ **909** 57 **2021**
https://arxiv.org/pdf/2012.15406.pdf
https://doi.org/10.3847/1538-4357/abd7f2
SDO/AIA images the full solar disk in several EUV bands that are each sensitive to coronal plasma emissions of one or more specific temperatures. We observe that when isolated active regions (ARs) are on the disk, full-disk images in some of the coronal EUV channels show the outskirts of the AR as a dark moat surrounding the AR. Here we present seven specific examples, selected from time periods when there was only a single AR present on the disk. Visually, we observe the moat to be most prominent in the AIA 171 Angstrom band, which has the most sensitivity to emission from plasma at log10 T = 5.8. By examining the 1D line-of-sight emission measure temperature distribution found from six AIA EUV channels, we find the intensity of the moat to be most depressed over the temperature range log10 T ~ 5.7 - 6.2 for most of the cases. We argue that the dark moat exists because the pressure from the strong magnetic field that splays out from the AR presses down on underlying magnetic loops, flattening those loops -- along with the lowest of the AR's own loops over the moat -- to a low altitude. Those loops, which would normally emit the bulk of the 171 Angstrom emission, are restricted to heights above the surface that are too low to have 171 Angstrom-emitting plasmas sustained in them, according to Antiochos & Noci (1986), while hotter EUV-emitting plasmas are sustained in the overlying higher-altitude long AR-rooted coronal loops. This potentially explains the low-coronal-temperature dark moats surrounding the ARs. **2014 Dec 17, 2018 Feb 11, 2018 Apr 25, 2018 May 30, 2018 Jun 17, 2018 Jul 14, 2019 Feb 20, 2019 Apr 15**

Exploring the outer emission corona spectroscopically by using Visible Emission Line Coronagraph (VELC) on board ADITYA-L1 mission

Jagdev **Singh**, B. Raghavendra Prasad, Suresh Venkata, Amit Kumar
Advances in Space Research Volume 64, Issue 7, 1 October **2019**, Pages 1455-1464
https://sci-hub.se/10.1016/j.asr.2019.07.007
It is very important to make the spectrographic observations of the outer emission corona in number of emission lines simultaneously in view of the results of the observations made in [Fe x] 6374 Å, [Fe xi] 7892 Å, [Fe xiv] 5303 Å and [Fe xiii] 10,747 Å coronal emission lines with the 25 cm coronagraph at Norikura Observatory in Japan. At ground based observatories, availability of number of hours of clear sky for coronagraphic observations is limited due to aerosols scattering and scattering from the internal coronagraph reflections. A space based coronagraph Visible Emission Line Coronagraph (VELC) on board ADITYA-L1 has been planned to perform spectroscopy in 3 out of the 4 emission lines mentioned above. Here, we discuss the various requirements for the parameters of the payload, given the specifications of the satellite, to observe the outer emission corona reliably with good Signal to Noise Ratio (SNR), realize the projected scientific goals and make the mission a great success.

Periodicity Variation of Solar Activity and Cosmic Rays During Solar Cycles 22 – 24

Prithvi Raj **Singh**, C. M. Tiwari, S. L. Agrawal, Tarun Kumar Pant
Solar Physics September **2019**, 294:118
https://link.springer.com/content/pdf/10.1007%2Fs11207-019-1511-x.pdf
sci-hub.se/10.1007/s11207-019-1511-x
The solar radio flux at 2800 MHz (F10.7) and the sunspot number (SSN) are excellent indicators of solar activity. Data from 1986 to 2016 have been used to investigate long-term and mid-term periodicities of the F10.7 solar radio

flux, the sunspot number, and galactic cosmic rays (GCRs) intensity, mainly from Oulu and Moscow, using fast Fourier Transform and Morlet wavelet techniques. The ≈ 148 days period, among other periods, is the one seen prominently in SSN, F10.7, and GCRs throughout Solar Cycles 22 to 24. This period could be the third harmonic of ≈ 1.24 years, i.e. ≈ 444 days period. The period of ≈ 1.24 years, found in SSN, F10.7 flux, and GCRs, is ascribed to the rotation of the convective envelope within the Sun during these cycles. Another period found significantly present in F10.7, SSN, and GCRs, is the Quasi-Biennial Oscillation (QBO), with a period of ≈ 1.94 years. The QBO amplitudes are found to vary significantly from one solar cycle to the other, with a minimum during Solar Cycle 24. The decreasing QBO amplitudes during Solar Cycle 24 in all three datasets are well correlated with the QBOs found in the Earth's atmosphere-ionosphere system reported elsewhere.

Dynamic evolution of current sheets, ideal tearing, plasmoid formation and generalized fractal reconnection scaling relations

Alkendra **Singh**, Fulvia Pucci, Anna Tenerani, Kazunari Shibata, Andrew Hillier, Marco Velli
2019
https://arxiv.org/pdf/1904.00755.pdf
Magnetic reconnection may be the fundamental process allowing energy stored in magnetic fields to be released abruptly, solar flares and coronal mass ejection (CME) being archetypal natural plasma examples. Magnetic reconnection is much too slow a process to be efficient on the large scales, but accelerates once small enough scales are formed in the system. For this reason, the fractal reconnection scenario was introduced (Shibata and Tanuma 2001) to explain explosive events in the solar atmosphere: it was based on the recursive triggering and collapse via tearing instability of a current sheet originally thinned during the rise of a filament in the solar corona. Here we compare the different fractal reconnection scenarios that have been proposed, and derive generalized scaling relations for the recursive triggering of fast, `ideal' - i.e. Lundquist number independent - tearing in collapsing current sheet configurations with arbitrary current profile shapes. An important result is that the Sweet-Parker scaling with Lundquist number, if interpreted as the aspect ratio of the singular layer in an ideally unstable sheet, is universal and does not depend on the details of the current profile in the sheet. Such a scaling however must not be interpreted in terms of stationary reconnection, rather it defines a step in the accelerating sequence of events of the ideal tearing mediated fractal cascade. We calculate scalings for the expected number of plasmoids for such generic profiles and realistic Lundquist numbers.

Study of the Solar Rotational Period and Its Harmonics in Solar Activity, Interplanetary, Geomagnetic, and Cosmic Ray Intensity Indicators During Solar Polarity Reversal Periods

Y. P. **Singh**, Badruddin
Solar Physics March **2019**, 294:27
https://doi.org/10.1007/s11207-019-1413-y
sci-hub.tw/10.1007/s11207-019-1413-y
Short-term variations of interplanetary magnetic field, solar wind speed, solar radio flux, geomagnetic ap index and cosmic ray intensity have been studied during the last five polarity reversal periods in the period from Solar Cycles 20 to 24. Hourly data of all the considered parameters are subject to wavelet analysis exclusively during the polarity reversal periods of these five solar cycles. These solar polarity reversal periods lie during or around the solar maximum of the respective solar cycles. Study reveals a few noteworthy results during these disturbed periods. Periodicities such as the synodic period (≈27.0≈27.0 days), its second (≈13.5≈13.5 days) and third (≈9.1≈9.1-days) harmonics, ≈6.8≈6.8-day, ≈5.5≈5.5-day and ≈4.2≈4.2-day periods are consistently observed during the reversal times with prominent signatures in addition to quasi-periodicities (18.5 days, 16.7 days, 10.6 days, 2.8 days, 2.4 days, and 1.8 days). These significant variations are very strong during reversal periods as they appear in minimum phases of the solar cycles, as reported by Singh and Badruddin (Astrophys. Space Sci.359, 60, 2015a); they could be the higher harmonics (fourth, fifth, and sixth) of the synodic period.

f-mode strengthening from a localized bipolar subsurface magnetic field

Nishant K. **Singh**, Harsha Raichur, Maarit J. Käpylä, Matthias Rheinhardt, Axel Brandenburg, Petri J. Käpylä
Geophysical and Astrophysical Fluid Dynamics (GAFD) special issue on "Physics and Algorithms of the Pencil Code" **2018**
https://arxiv.org/pdf/1808.08904.pdf
Recent numerical work in helioseismology has shown that a periodically varying subsurface magnetic field leads to a fanning of the f-mode, which emerges from the density jump at the surface. In an attempt to model a more realistic situation, we now modulate this periodic variation with an envelope, giving thus more emphasis on localized bipolar magnetic structures in the middle of the domain. Some notable findings are: (i) compared to the purely hydrodynamic case, the strength of the f-mode is significantly larger at high horizontal wavenumbers k, but the fanning is weaker for the localized subsurface magnetic field concentrations investigated here than the periodic ones

studied earlier; (ii) when the strength of the magnetic field is enhanced at a fixed depth below the surface, the fanning of the f-mode in the kω diagram increases proportionally in such a way that the normalized f-mode strengths remain nearly the same in different such cases; (iii) the unstable Bloch modes reported previously in case of harmonically varying magnetic fields are now completely absent when more realistic localized magnetic field concentrations are imposed beneath the surface, thus suggesting that the Bloch modes are unlikely to be supported during most phases of the solar cycle; (iv) the f-mode strength appears to depend also on the depth of magnetic field concentrations such that it shows a relative decrement when the maximum of the magnetic field is moved to a deeper layer. We argue that detections of f-mode perturbations such as those being explored here could be effective tracers of solar magnetic fields below the photosphere before these are directly detectable as visible manifestations in terms of active regions or sunspots.

Bihelical spectrum of solar magnetic helicity and its evolution

Nishant K. **Singh**, Maarit J. Käpylä, Axel Brandenburg, Petri J. Käpylä, Andreas Lagg, Ilpo Virtanen
ApJ **863** 182 **2018**
https://arxiv.org/pdf/1804.04994.pdf
http://iopscience.iop.org/article/10.3847/1538-4357/aad0f2/pdf
Using a recently developed two-scale formalism to determine the magnetic helicity spectrum (Brandenburg et al. 2017), we analyze synoptic vector magnetograms built with data from the Vector Spectromagnetograph (VSM) instrument on the \emph{Synoptic Optical Long-term Investigations of the Sun} (SOLIS) telescope during January 2010-July 2016. In contrast to an earlier study using only three Carrington rotations, our analysis includes 74 synoptic Carrington rotation maps. We recover here bihelical spectra at different phases of solar cycle~24, where the net magnetic helicity in the majority of the data is consistent with a large-scale dynamo with helical turbulence operating in the Sun. More than 20% of the analyzed maps, however, show violations of the expected sign rule.

An early prediction of 25th solar cycle using Hurst exponent

A. K. **Singh**, Asheesh Bhargawa
Astrophysics and Space Science November **2017**, 362:199
The analysis of long memory processes in solar activity, space weather and other geophysical phenomena has been a major issue even after the availability of enough data. We have examined the data of various solar parameters like sunspot numbers, 10.7 cm radio flux, solar magnetic field, proton flux and Alfven Mach number observed for the year 1976–2016. We have done the statistical test for persistence of solar activity based on the value of Hurst exponent (HH) which is one of the most classical applied methods known as rescaled range analysis. We have discussed the efficiency of this methodology as well as prediction content for next solar cycle based on long term memory. In the present study, Hurst exponent analysis has been used to investigate the persistence of above mentioned (five) solar activity parameters and a simplex projection analysis has been used to predict the ascension time and the maximum number of counts for 25th solar cycle. For available dataset of the year 1976–2016, we have calculated H=0.86 and 0.82 for sunspot number and 10.7 cm radio flux respectively. Further we have calculated maximum number of counts for sunspot numbers and F10.7 cm index as 102.8±24.6 and 137.25±8.9 respectively. Using the simplex projection analysis, we have forecasted that the solar cycle 25th would start in the year 2021 (January) and would last up to the year 2031 (September) with its maxima in June 2024.

High-wavenumber solar f-mode strengthening prior to active region formation

Nishant K. **Singh** (1), Harsha Raichur (1), Axel Brandenburg
ApJ 832 120 **2016**
http://arxiv.org/pdf/1601.00629v1.pdf
Using the solar surface mode, i.e. the f-mode, we attempt to predict the emergence of active regions (ARs) in the days before they can be seen in magnetograms. Our study is motivated by earlier numerical findings of Singh et al. (2014) who showed that, in the presence of a nonuniform magnetic field which is concentrated a few scale heights below the surface, the f-mode fans out in the diagnostic kω diagram at high wavenumbers. Here we exploit this property using data from the Helioseismic and Magnetic Imager aboard the Solar Dynamics Observatory, and show for three ARs 11768, 11158 and 12051, that at large latitudinal wavenumbers (corresponding to horizontal scales of around 3000km), the f-mode displays strengthening about two days prior to AR formation and thus provides a new precursor for AR formation. The idea that the f-mode is perturbed days before any visible magnetic activity occurs on the surface can be important in constraining dynamo models aiming at understanding the global magnetic activity of the Sun.

GPS as a Solar observational instrument: Real-time estimation of EUV photons flux rate during strong, medium and weak Solar flares†

Talwinder **Singh**, M. Hernandez-Pajares, Enric Monte, A. Garcia-Rigo, G. Olivares-Pulido

JGR **201**5

In this manuscript, the authors show how the Global Navigation Satellite Systems, GNSS (exemplified in the Global Positioning System, GPS), can be efficiently used for a very different purpose from that for which it was designed; as an accurate Solar observational tool, already operational from the open global GPS measurements available in real-time, and with some advantages regarding dedicated instruments onboard spacecraft. The very high correlation of the solar Extreme Ultraviolet (EUV) photon flux rate in the 26-34 mm spectral band, obtained from the SEM instrument onboard the SOHO spacecraft during Solar flares, is shown with the GNSS Solar Flare Activity Indicator (GSFLAI). The GSFLAI is defined as the gradient of the ionospheric vertical total electron content (VTEC) rate versus the cosine of the Solar zenith angle in the day hemisphere (which filters out non-Solar over-ionization), and it is measured from data collected by a global network of dual frequency GPS receivers (giving in this way continuous coverage). GSFLAI for 60 X class flares, 320 M class flares and 300 C class flares, occurred since 2001, were directly compared with the EUV Solar flux rate data to show existing correlations. It was found that the GSFLAI and EUV flux rate present the same linear relationship for all classes of flares, not only the strong and medium intensity ones, X and M-class, as in previous works, but also for the weakest C-class Solar flares, which is a remarkable result.

Short-Term Variations of Cosmic-Ray Intensity During the Recent Deep Solar Minimum and the Previous Four Solar Minima: A Wavelet Analysis

Y. P. **Singh** , Badruddin

Solar Phys. Volume 290, Issue 10, pp 3071-3079 **2015**

The recent, unusual solar cycle and solar minima between Cycles 23 and 24 have been studied extensively. Wavelet analysis of hourly cosmic-ray intensity during the last five solar minima reveals a number of short-term variations with few temporal shifts in the periods. This study suggests that deviations with a one-solar-rotation period and its harmonics are small during the recent minimum. However, deviations are considerably larger during the other minima. Analysis also demonstrates that the behavior of active regions is nearly the same during the minima of Cycles 19, 20, 21, and 22. The results also suggest that regions outside the streamer stalk are significantly larger in the recent solar minimum as opposed to the other minima.

Reconnection-driven Double Layers in the Stratified Plasma of the Solar Transition Region: Supply of Hot Plasma into the Corona

Nagendra **Singh**

Solar Phys. **2015**

A novel mechanism for the supply of hot plasma into the corona from the chromosphere is suggested here; the mechanism involves collisionless magnetic reconnection (CMR) in the transition region (TR) followed by double layer (DL) formation in the enhanced expansion of the chromospheric cold plasma mixed with CMR-heated hot electrons. It is well known that (i) the CMR produces energetic electrons and (ii) DLs naturally form in expanding dense plasmas containing a minor population of hot electrons. We apply these plasma physics facts to the dynamics of stratified plasma in the TR. In the TR where densities fall below ~1016 m−3, all collisional mean-free paths, electron–ion, ion–neutral, and electron–neutral, become long enough to render plasma collisionless at kinetic scale lengths, making CMR and DL formation possible. The DLs accelerate the chromospheric cold ions to energies comparable to the energy of the hot electrons. When the upflowing energized ions neutralized by the escaping hot electrons thermalize, the resulting hot tenuous plasma supplies an energy flux ~3 × 105 erg cm−2 s−1 = 3 × 102 J m−2 s−1 into the corona. The CMR–DL mechanism introduces sudden transitions in the TR as microstructures in both density and energy. The global transition in the TR could be a fractal structure containing such microscopic features. If not impossible, it is difficult to measure such microstructures, but it seems that the coronal heating begins in the nearly collisionless TR by CMR and DL formation.

Solar activity during first six years of solar cycle 24 and 23: a comparative study

A. K. **Singh**, Apeksha Tonk

Astrophysics and Space Science, **2014**, Volume 353, Issue 2, pp 367-371

Attempt to look into the nature of solar activity and variability have increased importance in recent days because of their terrestrial relationships. In the present work we have attempted to compare the solar activity events during first six years (2008–2013) of the ongoing solar cycle 24 with first six years (1996–2001) of solar cycle 23. To that end, we have considered sunspot numbers, F10.7 cm solar flux, halo CMEs and geomagnetic storms as comparison parameters. Sunspot number during the year 2008–2013 varied from 0 to 96.7 while during the year 1996 to 2001 it was observed from 0.9 to 170.1. Solar radio flux (F10.7 cm index) varied from 65 to 190 during the years 2008–2013 while it was observed from 65 to 283 during the years 1996–2001. 197 cases of halo CMEs (width=360∘) in solar cycle 23 (1996–2001) and 177 cases of halo CMEs (width=360∘) in solar cycle 24 (2008–2013) are investigated. 287 and 104 geomagnetic storm cases (Dst varies between −50 and −350 nT) are analysed during the half period of solar cycle 23 and 24 respectively. Comparative results indicate that solar cycle 23 was more pronounced in comparison of solar cycle 24.

Stochastic Turbulent Acceleration in a fractal environment

Nikos **Sioulas**, Heinz Isliker, Loukas Vlahos

ApJL **895** L14 **2020**

https://arxiv.org/pdf/2005.02668.pdf

https://doi.org/10.3847/2041-8213/ab9092

We analyze the stochastic acceleration of particles inside a fully developed turbulent plasma. It is well known that large-amplitude magnetic fluctuations and coherent structures in such an environment obey a fractal scaling, and our specific aim is to study for the first time the effects of the fractality of these environments on stochastic acceleration. We have shown that an injected Maxwellian energy distribution is heated and forms a high energy tail in a very short time. Using standard parameters for the low solar corona, the injected Maxwellian distribution of electrons gets heated from the initial 100 eV to 10 KeV, and the power-law index of the high energy tail is about -2.3-4.0. The high energy tail starts around 100 keV, and reaches 10 MeV. The index of the power-law tail depends on the system size, and it is in good agreement with observed values for realistic system sizes. The heating and acceleration process is very fast (\sim 2 s). The reason why the acceleration time is so short is that the particles are trapped within small scale parts of the fractal environment, and their scattering mean free path reduces drastically. The presence of small scale activity also pulls easily particles from the thermal pool, so there is no need for a seed population. The mean square displacement in space and energy is superdiffusive for the high energy particles.

Small-scale loops heated to transition region temperatures and their chromospheric signatures in the simulated solar atmosphere

M. **Skan**, S. Danilovic, J. Leenaarts, F. Calvo, M. Rempel

A&A 672, A47 **2023**

https://arxiv.org/pdf/2211.08806.pdf

https://www.aanda.org/articles/aa/pdf/2023/04/aa45390-22.pdf

Recent observations revealed loop-like structures at very small scales visible in observables that sample transition region (TR) and coronal temperatures. Their formation remains unclear.

We study an example of a bipolar system in realistic magnetohydrodynamic simulations and forward synthesis of spectral lines to investigate how these features occur.

Computations are done using the MURaM code to generate model atmospheres. The synthetic Hα and Si IV spectra are calculated at two angles (μ=1, μ=0.66) using the Multi3D code. Magnetic field lines are traced in the model and the evolution of the underlying field topology is examined.

The synthetic Hα dopplergrams reveal loops that evolve dramatically within a few minutes. The synthetic Hα line profiles show observed asymmetries and doppler shifts in the line core. They, however, also show strong emission peaks in the line wings, even at the slated view. The synthetic Si IV emission features partly coincide with structures visible in Hα dopplergrams and partly follow separate magnetic field threads. Some are even visible in the emission measure maps for the lg(T/K)=[5.0,5.5] temperature interval. The emission areas trace out the magnetic field lines rooted in opposite polarities in a bipolar region.

We find that our results largely reproduce the observed features and their characteristics. A bipolar system with footpoints undergoing rapid movement and shuffling can produce many small-scale recurrent events heated to high temperatures. The morphology and evolution of the resulting observable features can vary depending on the viewing angle.

Poynting Flux of MHD Modes in Magnetic Solar Vortex Tubes

Samuel J. **Skirvin**1, Viktor Fedun1, Marcel Goossens2, Suzana S. A. Silva1, and Gary Verth3

2024 ApJ 975 176

https://iopscience.iop.org/article/10.3847/1538-4357/ad7de1/pdf

Magnetic flux tubes in the presence of background rotational flows, known as solar vortex tubes, are abundant throughout the solar atmosphere and may act as conduits for MHD waves to transport magnetic energy to the upper solar atmosphere. We aim to investigate the Poynting flux associated with these waves within solar vortex tubes. We model a solar vortex tube as a straight magnetic flux tube with a background azimuthal velocity component. The MHD wave solutions in the equilibrium configuration of a vortex tube are obtained using the Shooting Eigensolver for SolAr Magnetohydrostatic Equilibria code and we derive an expression for the vertical component of the Poynting flux, Sz, associated with MHD modes. In addition, we present 2D visualizations of the spatial structure of Sz for different MHD modes under different background flow strengths. We show that Sz increases in the presence of a background rotational flow when compared to a flux tube with no rotational flow. When the strength of the background flow is greater than 100 times the strength of the perturbation, the Sz associated with non-axisymmetric ($|m| > 0$) modes increases by over 1000% when compared to a magnetic flux tube in the absence of a background rotational flow. Furthermore, we present a fundamental property of solar vortices, namely that they cannot solely produce an upward Poynting flux in an untwisted tube, meaning that any observed Sz in straight flux tubes must arise from perturbations, such as MHD waves.

Mode conversion and energy flux absorption in the structured solar atmosphere

Samuel **Skirvin**, Tom Van Doorsselaere

A&A 683, A61 **2024**

https://arxiv.org/pdf/2401.02238.pdf

https://www.aanda.org/articles/aa/pdf/2024/03/aa48009-23.pdf

Context. Structuring in the solar atmosphere, in the form of inhomogeneities transverse to the magnetic field, is believed to play a vital role in wave propagation, conversion, and absorption. Aims. We investigated the effect of transverse structuring on the processes of mode conversion and wave energy flux absorption using a 3D ideal magnetohydrodynamic simulation featuring an expanding coronal loop in a gravitationally stratified atmosphere. Methods. Multiple wave drivers were modelled. The location of the driver at the photospheric base was allowed to vary so that we could study how the driven waves interact with the transverse structuring, provided by the magnetic field, as well as with the vertical structuring due to gravity. Results. We find that the transverse structuring acts as a conduit for Alfvén wave energy flux through the transition region and into the solar corona. Moreover, in regions of strong transverse gradients, the reflection of Alfvén waves at the transition region is greatly reduced, supporting results from recent studies. Finally, we investigated the efficiency of the loop structuring at absorbing energy flux from externally driven waves and find that the loop is extremely effective at channelling wave energy flux to the loop apex in the corona; in some cases, it can absorb over a third of the externally driven wave energy flux. Conclusions. These results may have important consequences in the context of decayless loop oscillations as they suggest that the oscillations are driven by acoustic waves outside of the existing loop structure.

Alfvénic Motions Arising from Asymmetric Acoustic Wave Drivers in Solar Magnetic Structures

Samuel J. **Skirvin**1, Yuhang Gao1,2, and Tom Van Doorsselaere1

2023 ApJ 949 38

https://iopscience.iop.org/article/10.3847/1538-4357/acca7d/pdf

Alfvénic motions are ubiquitous in the solar atmosphere and their observed properties are closely linked to those of photospheric p-modes. However, it is still unclear how a predominantly acoustic wave driver can produce these transverse oscillations in the magnetically dominated solar corona. In this study we conduct a 3D magnetohydrodynamic numerical simulation to model a straight, expanding coronal loop in a gravitationally stratified solar atmosphere which includes a transition region and chromosphere. We implement a driver locally at one foot-point corresponding to an acoustic–gravity wave which is inclined by $\theta = 15°$ with respect to the vertical axis of the magnetic structure and is equivalent to a vertical driver incident on an inclined loop. We show that transverse motions are produced in the magnetic loop, which displace the axis of the waveguide due to the breaking of azimuthal symmetry, and study the resulting modes in the theoretical framework of a magnetic cylinder model. By conducting an azimuthal Fourier analysis of the perturbed velocity signals, the contribution from different cylindrical modes is obtained. Furthermore, the perturbed vorticity is computed to demonstrate how the transverse motions manifest themselves throughout the whole non-uniform space. Finally we present some physical properties of the Alfvénic perturbations and present transverse motions with velocity amplitudes in the range 0.2–0.75 km s^{-1} which exhibit two distinct oscillation regimes corresponding to 42 and 364 s, where the latter value is close to the period of the p-mode driver in the simulation.

Dynamic Formation of a Transient Jet from Arched Magnetized Laboratory Plasma

Kamil D. **Sklodowski**1, Shreekrishna Tripathi1, and Troy Carter1

2023 ApJ 953 5

https://iopscience.iop.org/article/10.3847/1538-4357/acdf47/pdf

A laboratory plasma experiment was built to explore the eruptive behavior of arched magnetized plasmas with dimensionless parameters relevant to the Sun's photosphere ($\beta \approx 10^{-3}$, Lundquist number $\approx 10^4$, plasma radius/ion gyroradius ≈ 20, ion–neutral collision frequency $\gg$ ion cyclotron frequency). Dynamic formation of a transient plasma jet was observed in the presence of the strapping magnetic field. The eruption leading to the jet is unintuitive because the arched plasma is both kink- and torus-stable. The jet structure erupts within a few Alfvén transit times from the formation of the arched plasma. Extensive measurements of plasma temperature, density, magnetic field, and flows are presented. In its early stages, the jet plasma flows away from the arch with supersonic speeds (Mach 1.5). This high-speed flow persists up to the resistive diffusion time in the arched plasma and is driven by large gradients in the magnetic and thermal pressures near the birthplace of jets. There are two distinct electric current channels within the jet, one consisting of outgoing electrons and another composed of electrons returning to the anode footpoint. Significant current density around the jet is a consequence of the diamagnetic current produced by a large thermal pressure gradient in the jet. Ion–neutral charge-exchange collisions provide an efficient mechanism to produce the cross-field current and control the dynamics of the complex current channels of the jet.

On the Active Region Bright Grains Observed in the Transition Region Imaging Channels of IRIS

H. **Skogsrud**, L. Rouppe van der Voort, B. De Pontieu

ApJ 817 124 **2016**

http://arxiv.org/pdf/1512.05263v1.pdf

The Interface Region Imaging Spectrograph (IRIS) provides spectroscopy and narrow band slit-jaw (SJI) imaging of the solar chromosphere and transition region at unprecedented spatial and temporal resolution. Combined with high-resolution context spectral imaging of the photosphere and chromosphere as provided by the Swedish 1-m Solar Telescope (SST), we can now effectively trace dynamic phenomena through large parts of the solar atmosphere in both space and time. IRIS SJI 1400 images from active regions, which primarily sample the transition region with the Si IV 1394 and 1403 {\AA} lines, reveal ubiquitous bright "grains" which are short-lived (2-5 min) bright roundish small patches of sizes 0.5-1.7" that generally move limbward with velocities up to about 30 km s−1. In this paper we show that many bright grains are the result of chromospheric shocks impacting the transition region. These shocks are associated with dynamic fibrils (DFs), most commonly observed in H{\alpha}. We find that the grains show strongest emission in the ascending phase of the DF, that the emission is strongest towards the top of the DF and that the grains correspond to a blueshift and broadening of the Si IV lines. We note that the SJI 1400 grains can also be observed in the SJI 1330 channel which is dominated by C II lines. Our observations show that a significant part of the active region transition region dynamics is driven from the chromosphere below rather than from coronal activity above. We conclude that the shocks that drive DFs also play an important role in the heating of the upper chromosphere and lower transition region.

On the temporal evolution of spicules observed with IRIS, SDO and Hinode

H. **Skogsrud**, L. Rouppe van der Voort, B. De Pontieu, T. M. D. Pereira

ApJ **806** 170 **2015**

http://arxiv.org/pdf/1505.02525v1.pdf

Spicules are ubiquitous, fast moving jets observed off-limb in chromospheric spectral lines. Combining the recently-launched Interface Region Imaging Spectrograph with the Solar Dynamics Observatory and Hinode, we have a unique opportunity to study spicules simultaneously in multiple passbands and from a seeing free environment. This makes it possible to study their thermal evolution over a large range of temperatures. A recent study showed that spicules appear in several chromospheric and transition region spectral lines, suggesting that spicules continue their evolution in hotter passbands after they fade from Ca II H. In this follow-up paper we answer some of the questions that were raised in the introductory study. In addition, we study spicules off-limb in C II 1330 {\AA} for the first time. We find that Ca II H spicules are more similar to Mg II 2796 {\AA} spicules than initially reported. For a sample of 54 spicules, we find that 44% of Si IV 1400 {\AA} spicules are brighter toward the top; 56% of the spicules show an increase in Si IV emission when the Ca II H component fades. We find several examples of spicules that fade from passbands other than Ca II H, and we observe that if a spicule fades from a passband, it also generally fades from the passbands with lower formation temperatures. We discuss what these new, multi-spectral results mean for the classification of type I and II spicules.

On the multi-threaded nature of solar spicules

H. **Skogsrud**, L. Rouppe van der Voort, B. De Pontieu

ApJL, 795 L23 **2014**

http://arxiv.org/pdf/1410.1334v1.pdf

A dominant constituent in the dynamic chromosphere are spicules. Spicules at the limb appear as relatively small and dynamic jets that are observed to everywhere stick out. Many papers emphasize the important role spicules might play in the energy and mass balance of the chromosphere and corona. However, many aspects of spicules remain a mystery. In this Letter we shed more light on the multi-threaded nature of spicules and their torsional component. We use high spatial, spectral and temporal resolution observations from the Swedish 1-m Solar Telescope in the H{\alpha} spectral line. The data targets the limb and we extract spectra from spicules far out from the limb to reduce the line-of-sight superposition effect. We discover that many spicules display very asymmetric spectra with some even showing multiple peaks. To quantify this asymmetry we use a double Gaussian fitting procedure and find an average velocity difference between the single Gaussian components to be between 20-30 km s−1 for a sample of 57 spicules. We observe that spicules show significant sub-structure where one spicule consists of many 'threads'. We interpret the asymmetric spectra as line-of-sight superposition of threads in one spicule and therefore have a measure for a perpendicular flow inside spicules which will be important for future numerical model to reproduce. In addition we show examples of {\lambda}-x-slices perpendicular across spicules and find spectral tilts in individual threads providing further evidence for the complex dynamical nature of spicules.

Kinematic Small-Scale Dynamo in Stably Stratified Turbulence

Valentin **Skoutnev**, Jonathan Squire, Amitava Bhattacharjee

2021 *ApJ* **906** 61

https://arxiv.org/pdf/2008.01025.pdf

https://doi.org/10.3847/1538-4357/abc8ee

We present numerical investigations into three principle properties of the kinematic small-scale dynamo in stably stratified turbulence -- the onset criterion, the growth rate, and the nature of the magnetic field anisotropy. Results suggest that all three dynamo properties are controlled by the scale separation between the Ozmidov scale and the viscous or resistive scale. In addition to the critical magnetic Reynolds number, this allows for the definition of critical buoyancy and magnetic buoyancy Reynolds numbers for stratified small-scale dynamo onset in the high and low magnetic Prandtl number regimes, respectively. The presence of a small-scale dynamo in stellar radiative zones could affect dynamics through resulting Maxwell stresses and/or influence large scale dynamo mechanisms in regions of differential rotation. Taking the solar radiative zone as a canonical example and applying the onset criterion, we find that the stratification is strong enough to make the small-scale dynamo marginally active in the solar tachocline.

On the distribution of collisions of a neutrino with nucleons of the Sun

L.M. **Slad**

2020

https://arxiv.org/pdf/2009.01528.pdf

When solving the solar neutrino problem on the basis of the hypothesis of the existence of a new interaction between electron neutrinos and nucleons, carried by a massless pseudoscalar boson, it becomes necessary to find the consequences of the short-term Brownian motion of neutrinos in the Sun. Earlier, when calculating the rates of the observed processes, we conveyed these consequences by the effective number of collisions of a neutrino with nucleons of the Sun and obtained good agreement with experiments. In this paper, we analyze the conveyance of the consequences of the Brownian motion of neutrinos in the Sun by the trial, geometric distribution of collisions. This distribution makes it possible to obtain the ratio of fluxes of left- and right-handed neutrinos near the Earth's surface and confirms the acceptability of the method of the effective number of collisions of a neutrino with nucleons.

Hypothesis about semi-weak interaction and experiments with solar neutrinos. II. Deuteron disintegration by neutral currents

L.M. **Slad**

2018

https://arxiv.org/pdf/1808.05103.pdf

The present work provides one more evidence of that the solar neutrino problem has an elegant solution based on the hypothesis about the existence of a new, semi-weak, interaction. The analysis of the deuteron disintegration by neutral currents of solar neutrinos, generated by both the electroweak and semi-weak interactions, is fulfilled. A good agreement between the theoretical and experimental results for this process is obtained, which is in harmony with the conclusions of the first part of the work on the other four observed processes with solar neutrinos.

Cosmic Rays, Solar Activity and the Climate

T **Sloan**

2013 J. Phys.: Conf. Ser. 409 012020

http://iopscience.iop.org/1742-6596/409/1/012020/pdf/1742-6596_409_1_012020.pdf

Although it is generally believed that the increase in the mean global surface temperature since industrialisation is caused by the increase in green house gases in the atmosphere, some people cite solar activity, either directly or through its effect on cosmic rays, as an underestimated contributor to such global warming. In this paper a simplified version of the standard picture of the role of greenhouse gases in causing the global warming since industrialisation is described. The conditions necessary for this picture to be wholly or partially wrong are then introduced. Evidence is presented from which the contributions of either cosmic rays or solar activity to this warming is deduced. The contribution is shown to be less than 10% of the warming seen in the twentieth century.

Numerical Simulations of Solar Spicule Jets at a Magnetic Null-Point

V. **Smirnova**, P. M. Konkol, A. A. Solov'ev, K. Murawski

Solar Phys. Volume 291, Issue 11, pp 3207–3216 **2016**

Two-dimensional numerical simulations of jet-like structures in the solar atmosphere are performed. These structures result from a pressure pulse that is launched at the null point of a potential magnetic arcade. The plasma jet exhibits a double structure with two components: (a) dense, cool, and short vertical stream and (b) a less dense, hot and tall part of the jet. The upper part of the hot and tall jet may represent a direct response of the system to the pressure pulse launched at the null point, and the second, slower cool and dense part of the jet is formed later through the stretching up of the stream as a result of plasma evacuation from the top of the magnetic arcade. Numerical results show that jet-like structures mimic some properties of both type I and type II spicules, according to the classification provided by De Pontieu et al. (Publ. Astron. Soc. Japan59, S655, 2007).

The influence of NLTE effects in Fe I lines on an inverted atmosphere II. 6301 Å and 6302 Å lines formed in 3D NLTE

H. N. **Smitha**1, R. Holzreuter1,2, M. van Noort1 and S. K. Solanki
A&A 647, A46 (**2021**)
https://doi.org/10.1051/0004-6361/202039107
https://www.aanda.org/articles/aa/pdf/2021/03/aa39107-20.pdf

Context. This paper forms the second part of our study of how neglecting non-local thermodynamic equilibrium (NLTE) conditions in the formation of Fe I 6301.5 Å and the 6302.5 Å lines affects the atmosphere that is obtained by inverting the Stokes profiles of these lines in LTE. The main cause of NLTE effects in these lines is the line opacity deficit that is due to the excess ionisation of Fe I atoms by ultraviolet (UV) photons in the Sun.
Aims. In the first paper, these photospheric lines were assumed to have formed in 1D NLTE and the effects of horizontal radiation transfer (RT) were neglected. In the present paper, the iron lines are computed by solving the RT in 3D. We investigate the effect of horizontal RT on the inverted atmosphere and how it can enhance or reduce the errors that are due to neglecting 1D NLTE effects.
Methods. The Stokes profiles of the iron lines were computed in LTE, 1D NLTE, and 3D NLTE. They were all inverted using an LTE inversion code. The atmosphere from the inversion of LTE profiles was taken as the reference model. The atmospheres from the inversion of 1D NLTE profiles (testmodel-1D) and 3D NLTE profiles (testmodel-3D) were compared with it. Differences between reference and testmodels were analysed and correspondingly attributed to NLTE and 3D effects.
Results. The effects of horizontal RT are evident in regions surrounded by strong horizontal temperature gradients. That is, along the granule boundaries, regions surrounding magnetic elements, and its boundaries with intergranular lanes. In some regions, the 3D effects enhance the 1D NLTE effects, and in some, they weaken these effects. In the small region analysed in this paper, the errors due to neglecting the 3D effects are lower than 5% in temperature. In most of the pixels, the errors are lower than 20% in both velocity and magnetic field strength. These errors also persist when the Stokes profiles are spatially and spectrally degraded to the resolution of the Swedish Solar Telescope (SST) or Daniel K. Inouye Solar Telescope (DKIST).
Conclusions. Neglecting horizontal RT introduces errors not only in the derived temperature, but also in other atmospheric parameters. The error sizes depend on the strength of the local horizontal temperature gradients. Compared to the 1D NLTE effect, the 3D effects are more localised in specific regions in the atmosphere and are weaker overall.

The influence of NLTE effects in Fe I lines on an inverted atmosphere I. 6301 Å and 6302 Å lines formed in 1D NLTE

H. N. **Smitha**1, R. Holzreuter1,2, M. van Noort1 and S. K. Solanki1,3
A&A 633, A157 (**2020**)
https://doi.org/10.1051/0004-6361/201937041

Context. Ultraviolet overionisation of iron atoms in the solar atmosphere leads to deviations in their level populations based on Saha-Boltzmann statistics. This causes their line profiles to form in non-local thermodynamic equilibrium (NLTE) conditions. When inverting such profiles to determine atmospheric parameters, the NLTE effects are often neglected and other quantities are tweaked to compensate for deviations from the LTE.
Aims. We investigate how the routinely employed LTE inversion of iron lines formed in NLTE underestimates or overestimates atmospheric quantities, such as temperature (T), line-of-sight velocity (vLOS), magnetic field strength (B), and inclination (γ) while the earlier papers have focused mainly on T. Our findings has wide-ranging consequences since many results derived in solar physics are based on inversions of Fe I lines carried out in LTE.
Methods. We synthesized the Stokes profiles of Fe I 6301.5 Å and 6302.5 Å lines in both LTE and NLTE using a snapshot of a 3D magnetohydrodynamic simulation. The profiles were then inverted in LTE. We considered the atmosphere inferred from the inversion of LTE profiles as the fiducial model and compared it to the atmosphere resulting from the inversion of NLTE profiles. The observed differences have been attributed to NLTE effects.
Results. Neglecting the NLTE effects introduces errors in the inverted atmosphere. While the errors in T can go up to 13%, in vLOS and B, the errors can go as high as 50% or above. We find these errors to be present at all three inversion nodes. Importantly, they survive degradation from the spatial averaging of the profiles.

Conclusions. We provide an overview of how neglecting NLTE effects influences the values of T, vLOS, B, and γ that are determined by inverting the Fe I 6300 Å line pair, as observed, for example, by Hinode/SOT/SP. Errors are found at the sites of granules, intergranular lanes, magnetic elements, and basically in every region susceptible to NLTE effects. For an accurate determination of the atmospheric quantities and their stratification, it is, therefore, important to take the NLTE effects into account.

Observations of solar chromospheric heating at sub-arcsec spatial resolution

H. N. **Smitha**, L. P. Chitta, T. Wiegelmann, S. K. Solanki
A&A 617, A128 **2018**
https://arxiv.org/pdf/1807.01078.pdf
https://www.aanda.org/articles/aa/pdf/2020/01/aa37041-19.pdf
A wide variety of phenomena such as gentle but persistent brightening, dynamic slender features (~100 km), and compact (~1") ultraviolet (UV) bursts are associated with the heating of the solar chromosphere. High spatio-temporal resolution is required to capture the finer details of the likely magnetic reconnection-driven, rapidly evolving bursts. Such observations are also needed to reveal their similarities to large-scale flares, which are also thought to be reconnection driven, and more generally their role in chromospheric heating. Here we report observations of chromospheric heating in the form of a UV burst obtained with the balloon-borne observatory, SUNRISE. The observed burst displayed a spatial morphology similar to that of a large-scale solar flare with circular ribbon. While the co-temporal UV observations at 1.5" spatial resolution and 24s cadence from the Solar Dynamics Observatory showed a compact brightening, the SUNRISE observations at diffraction-limited spatial resolution of 0.1" at 7s cadence revealed a dynamic sub-structure of the burst that it is composed of extended ribbon-like features and a rapidly evolving arcade of thin (~0.1" wide) magnetic loop-like features, similar to post-flare loops. Such a dynamic sub-structure reveals the small-scale nature of chromospheric heating in these bursts. Furthermore, based on magnetic field extrapolations, this heating event is associated with a complex fan-spine magnetic topology. Our observations strongly hint at a unified picture of magnetic heating in the solar atmosphere from some large-scale flares to small-scale bursts, all being associated with such a magnetic topology. **2013 June 12**

Estimation of the magnetic flux emergence rate in the quiet Sun from Sunrise data

H. N. **Smitha**, L. S. Anusha, S. K. Solanki, T. Riethmueller
ApJS **2016**
https://arxiv.org/pdf/1611.06432v1.pdf
The small-scale internetwork (IN) features are thought to be the major source of fresh magnetic flux in the quiet Sun. During its first science flight in 2009, the balloon-borne observatory Sunrise captured images of the magnetic fields in the quiet Sun at a high spatial resolution. Using these data we measure the rate at which the IN features bring magnetic flux to the solar surface. In a previous paper it was found that the lowest magnetic flux in small-scale features detected using the Sunrise observations is 9 x 10^14 Mx. This is nearly an order of magnitude smaller than the smallest fluxes of features detected in observations from Hinode satellite. In this paper, we compute the flux emergence rate (FER) by accounting for such small fluxes, which was not possible before Sunrise. By tracking the features with fluxes in the range 10^15-10^18 Mx, we measure an FER of 1100 Mx cm^-2 day^-1. The smaller features with fluxes less than or equal to 10^16 Mx are found to be the dominant contributors to the solar magnetic flux. The FER found here is an order of magnitude higher than the rate from Hinode, obtained with a similar feature tracking technique. A wider comparison with the literature shows, however, that the exact technique of determining the rate of the appearance of new flux can lead to results that differ by up to 2 orders of magnitude, even when applied to similar data. The causes of this discrepancy are discussed and first qualitative explanations proposed. **2009 June 9**

Detection of polarization neutral points in observations of the combined corona and sky during the 21 August 2017 total solar eclipse

Frans **Snik**, Steven P. Bos, Stefanie A. Brackenhoff, David S. Doelman, Emiel H. Por, Felix Bettonvil, Michiel Rodenhuis, Dmitry Vorobiev, Laura M. Eshelman, Joseph A. Shaw
Applied Optics Vol. 59, Issue 21, pp. F71-F77 (**2020**)
https://arxiv.org/pdf/2007.12482.pdf
We report the results of polarimetric observations of the total solar eclipse of 21 August 2017 from Rexburg, Idaho (USA). We use three synchronized DSLR cameras with polarization filters oriented at 0°, 60°, and 120° to provide high-dynamic-range RGB polarization images of the corona and surrounding sky. We measure tangential coronal polarization and vertical sky polarization, both as expected. These observations provide detailed detections of polarization neutral points above and below the eclipsed Sun where the coronal polarization is canceled by the sky polarization. We name these special polarization neutral points after Minnaert and Van de Hulst.

SOLar-STellar Irradiance Comparison Experiment II (SOLSTICE II): End-of-Mission Validation of the SOLSTICE Technique

Martin **Snow**, William E. McClintock, Thomas N. Woods & Joshua P. Elliott
Solar Physics volume 297, Article number: 55 (**2022**)
https://link.springer.com/content/pdf/10.1007/s11207-022-01984-9.pdf

The SOLar-STellar Irradiance Comparison Experiment (SOLSTICE: McClintock, Rottman, and Woods, Solar Phys. 230, 225, 2005) onboard the SOlar Radiation and Climate Experiment (SORCE: Rottman, Solar Phys. 230, 7, 2005) observed ultraviolet solar spectral irradiance (SSI) from 2003 – 2020. This article gives an overview of the end-of-mission algorithms and calibration of SOLSTICE. Many of the algorithms were updated after the early mission, either due to an improved understanding of the instrument and the space environment, or due to operational constraints as the spacecraft systems aged. We validate the final official data version (V18) with comparisons to other observations and models. The SOLSTICE observations of the solar-cycle variability in the ultraviolet are compared to model estimates.

Stability of two-fluid partially-ionised slow-mode shock fronts

Ben **Snow**, Andrew Hillier
MNRAS **2021**
https://arxiv.org/pdf/2106.04199.pdf

A magnetohydrodynamic (MHD) shock front can be unstable to the corrugation instability, which causes a perturbed shock front to become increasingly corrugated with time. An ideal MHD parallel shock (where the velocity and magnetic fields are aligned) is unconditionally unstable to the corrugation instability, whereas the ideal hydrodynamic (HD) counterpart is unconditionally stable. For a partially ionised medium (for example the solar chromosphere), both hydrodynamic and magnetohydrodynamic species coexist and the stability of the system has not been studied. In this paper, we perform numerical simulations of the corrugation instability in two-fluid partially-ionised shock fronts to investigate the stability conditions, and compare the results to HD and MHD simulations. Our simulations consist of an initially steady 2D parallel shock encountering a localised upstream density perturbation. In MHD, this perturbation results in an unstable shock front and the corrugation grows with time. We find that for the two-fluid simulation, the neutral species can act to stabilise the shock front. A parameter study is performed to analyse the conditions under which the shock front is stable and unstable. We find that for very weakly coupled or very strongly coupled partially-ionised system the shock front is unstable, as the system tends towards MHD. However, for a finite coupling, we find that the neutrals can stabilise the shock front, and produce new features including shock channels in the neutral species. We derive an equation that relates the stable wavelength range to the ion-neutral and neutral-ion coupling frequencies and the Mach number. Applying this relation to umbral flashes give an estimated range of stable wavelengths between 0.6 and 56 km.

Collisional ionisation, recombination and ionisation potential in two-fluid slow-mode shocks: analytical and numerical results

B. **Snow**, A. Hillier
A&A **2020**
https://arxiv.org/pdf/2010.06303.pdf

Shocks are a universal feature of the lower solar atmosphere which consists of both ionised and neutral species. Including partial ionisation leads to a finite-width existing for shocks, where the ionised and neutral species decouple and recouple. As such, drift velocities exist within the shock that lead to frictional heating between the two species, in addition to the adiabatic temperature changes across the shock. The local temperature enhancements within the shock alter the recombination and ionisation rates and hence change the composition of the plasma. We study the role of collisional ionisation and recombination in slow-mode partially-ionised shocks. In particular we incorporate the ionisation potential energy loss and analyse the consequences of having a non-conservative energy equation. A semi-analytical approach is used to determine the possible equilibrium shock jumps for a two-fluid model with ionisation, recombination, ionisation potential and arbitrary heating. Two-fluid numerical simulations are performed using the (P\underline{I}P) code. Results are compared to the MHD model and semi-analytic solution. Accounting for ionisation, recombination and ionisation potential significantly alters the behaviour of shocks in both substructure and post-shock regions. In particular, for a given temperature, equilibrium can only exist for specific densities due to the radiative losses needing to be balanced by the heating function. A consequence of the ionisation potential is that a compressional shock will lead to a reduction of temperature in the post-shock region, rather than the increase seen for MHD. The numerical simulations pair well with the derived analytic model for shock velocities.

Mode conversion of two-fluid shocks in a partially-ionised, isothermal, stratified atmosphere A97

B. **Snow** and A. Hillier
A&A 637, A97 (**2020**)
https://www.aanda.org/articles/aa/pdf/2020/05/aa37848-20.pdf
Context. The plasma of the lower solar atmosphere consists of mostly neutral particles, whereas the upper solar atmosphere is mostly made up of ionised particles and electrons. A shock that propagates upwards in the solar atmosphere therefore undergoes a transition where the dominant fluid is either neutral or ionised. An upwards propagating shock also passes a point where the sound and Alfvén speed are equal. At this point the energy of the acoustic shock can separated into fast and slow components. The way the energy is distributed between the two modes depends on the angle of magnetic field.
Aims. We aim to investigate the separation of neutral and ionised species in a gravitationally stratified atmosphere. The role of two-fluid effects on the structure of the shocks post-mode-conversion and the frictional heating is quantified for different levels of collisional coupling.
Methods. Two-fluid numerical simulations were performed using the (PIP) code of a wave steepening into a shock in an isothermal, partially-ionised atmosphere. The collisional coefficient was varied to investigate the regimes where the plasma and neutral species are weakly, strongly, and finitely coupled.
Results. The propagation speeds of the compressional waves hosted by neutral and ionised species vary and, therefore, velocity drift between the two species is produced as the plasma attempts to propagate faster than the neutrals. This is most extreme for a fast-mode shock. We find that the collisional coefficient drastically impacts the features present in the system, specifically the mode conversion height, type of shocks present, and the finite shock widths created by the two-fluid effects. In the finitely-coupled regime, fast-mode shock widths can exceed the pressure scale height, which may lead to a new potential observable of two-fluid effects in the lower solar atmosphere.

Intermediate shock substructures within a slow-mode shock occurring in partially ionised plasma

Ben **Snow**, Andrew Hillier
A&A 626, A46 **2019**
https://arxiv.org/pdf/1904.12518.pdf
Slow-mode shocks are important in understanding fast magnetic reconnection, jet formation and heating in the solar atmosphere, and other astrophysical systems. The atmospheric conditions in the solar chromosphere allow both ionised and neutral particles to exist and interact. Under such conditions, fine substructures exist within slow-mode shocks due to the decoupling and recoupling of the plasma and neutral species. We study numerically the fine substructure within slow-mode shocks in a partially ionised plasma, in particular, analysing the formation of an intermediate transition within the slow-mode shock. High-resolution 1D numerical simulations are performed using the (P\underline{I}P) code using a two-fluid approach. We discover that long-lived intermediate (Alfven) shocks can form within the slow-mode shock, where there is a shock transition from above to below the Alfven speed and a reversal of the magnetic field across the shock front. The collisional coupling provides frictional heating to the neutral fluid, resulting in a Sedov-Taylor-like expansion with overshoots in the neutral velocity and neutral density. The increase in density results in a decrease of the Alfven speed and with this the plasma inflow is accelerated to above the Alfven speed within the finite width of the shock leading to the intermediate transition. This process occurs for a wide range of physical parameters and an intermediate shock is present for all investigated values of plasma-β, neutral fraction, and magnetic angle. As time advances the magnitude of the magnetic field reversal decreases since the neutral pressure cannot balance the Lorentz force. The intermediate shock is long-lived enough to be considered a physical structure, independent of the initial conditions.

Magnetic shocks and substructures excited by torsional Alfvén wave interactions in merging expanding flux tubes

B. **Snow**, V. Fedun, F. A. Gent, G. Verth, R. Erdélyi
2018
https://arxiv.org/pdf/1803.06112.pdf
Vortex motions are frequently observed on the solar photosphere. These motions may play a key role in the transport of energy and momentum from the lower atmosphere into the upper solar atmosphere, contributing to coronal heating. The lower solar atmosphere also consists of complex networks of flux tubes that expand and merge throughout the chromosphere and upper atmosphere. We perform numerical simulations to investigate the behaviour of vortex driven waves propagating in a pair of such flux tubes in a non-force-free equilibrium with a realistically modelled solar atmosphere. The two flux tubes are independently perturbed at their footpoints by counter-rotating vortex motions. When the flux tubes merge, the vortex motions interact both linearly and nonlinearly. The linear interactions generate many small-scale transient magnetic substructures due to the magnetic stress imposed by the vortex motions. Thus, an initially monolithic tube is separated into a complex multi-threaded tube due to the photospheric vortex motions. The wave interactions also drive a superposition that increases in amplitude until it exceeds the local Mach number and produces shocks that propagate upwards with speeds of approximately 50 km

s−1. The shocks act as conduits transporting momentum and energy upwards, and heating the local plasma by more than an order of magnitude, with peak temperature approximately 60,000 K. Therefore, we present a new mechanism for the generation of magnetic waveguides from the lower solar atmosphere to the solar corona. This wave guide appears as the result of interacting perturbations in neighbouring flux tubes. Thus, the interactions of photospheric vortex motions is a potentially significant mechanism for energy transfer from the lower to upper solar atmosphere.

Chromospheric seismology above sunspot umbrae

B. **Snow**, G. J. J. Botha, S. Regnier

A&A 580, A107 **2015**

http://arxiv.org/pdf/1507.07371v1.pdf

The acoustic resonator is an important model for explaining the three-minute oscillations in the chromosphere above sunspot umbrae. The steep temperature gradients at the photosphere and transition region provide the cavity for the acoustic resonator, which allows waves to be both partially transmitted and partially reflected. In this paper, a new method of estimating the size and temperature profile of the chromospheric cavity above a sunspot umbra is developed. The magnetic field above umbrae is modelled numerically in 1.5D with slow magnetoacoustic wave trains travelling along magnetic fieldlines. Resonances are driven by applying the random noise of three different colours---white, pink and brown---as small velocity perturbations to the upper convection zone. Energy escapes the resonating cavity and generates wave trains moving into the corona. Line of sight (LOS) integration is also performed to determine the observable spectra through SDO/AIA. The numerical results show that the gradient of the coronal spectra is directly correlated with the chromosperic temperature configuration. As the chromospheric cavity size increases, the spectral gradient becomes shallower. When LOS integrations is performed, the resulting spectra demonstrate a broadband of excited frequencies that is correlated with the chromospheric cavity size. The broadband of excited frequencies becomes narrower as the chromospheric cavity size increases. These two results provide a potentially useful diagnostic for the chromospheric temperature profile by considering coronal velocity oscillations.

Exploring Substructure of the Near-Surface Shear Layer of the Sun

M. Cristina Rabello **Soares**, Sarbani Basu, Richard Bogart

ApJ **967** 143 **2024**

https://arxiv.org/pdf/2404.02321.pdf

https://iopscience.iop.org/article/10.3847/1538-4357/ad3d59/pdf

The gradient of rotation in the near-surface shear layer (NSSL) of the Sun provides valuable insights into the dynamics associated with the solar activity cycle and the dynamo. Results obtained with global oscillation mode-splittings lack resolution near the surface, prompting the use of the local helioseismic ring-diagram method. While the Helioseismic and Magnetic Imager ring-analysis pipeline has been used previously for analyzing this layer, default pipeline parameters limit the accuracy of the near-surface gradients. To address these challenges, we fitted the flow parameters to power spectra averaged over one-year periods at each location, followed by additional averaging over 12 years. We find that the NSSL can be divided into three fairly distinct regions: a deeper, larger region with small shear, steepening towards the surface; a narrow middle layer with a strong shear, with a gradient approximately three times larger; and a layer very close to the surface, where the logarithmic gradient is close to zero but becomes steeper again towards the surface. The middle layer appears to be centered at 3 Mm, but the poor resolution in these layers implies that it is potentially located closer to the surface, around 1.5 Mm deep. While our analysis primarily focused on regions along the central meridian, we also investigated systematic errors at longitudes off the center. The east-west antisymmetric component of the gradient reveals a layer of substantial differences between east and west longitude around at 1.7 Mm, and the amplitude of the differences increases with longitude.

HMI Science Nuggets # 203 **2024** http://hmi.stanford.edu/hminuggets/?p=4276

Effects of flares on solar high-degree helioseismic acoustic mode amplitudes

M. Cristina Rabello **Soares**, Frederic Baudin, Vanessa G. Teixeira

MNRAS Volume 505, Issue 1, Pages 293–303, **2021**

https://arxiv.org/pdf/2102.13181.pdf

https://doi.org/10.1093/mnras/stab1277

Several attempts have been made to observe whether solar flares excite acoustic modes since Wolff (1972) suggested this possibility. Moreover, the rapid progress of asteroseismology and the study of stellar flares makes the study of these phenomena in the Sun important to inform our study of the influence of the more energetic stellar flares on asteroseismic acoustic modes.

We look for the impact of flares on the amplitude of solar acoustic modes and other effects that are also affecting the mode amplitude. Solar acoustic mode amplitudes are known to be sensitive to magnetic fields. As flares usually occur in the presence of strong magnetic fields and most likely are the by-product of magnetic reconnection, we

show how the magnetic field in and around the flaring region affects the mode amplitude. The mode amplitudes were obtained using ring-diagram analysis, which was first applied to a single event, the largest flare in the space age (the `Halloween Flare', SOL**2003-10-28**T11:00), using MDI data. Then, using HMI data, the analysis was applied to the regions corresponding to the flares observed during the high activity phase of cycle 24 and that fall into two groups. These two groups consist of small (10-60 erg cm−2 s−1) and large (>1200 erg cm−2 s−1) peak-flux flares, based on the Heliophysics Event Knowledgebase (HEK).
After applying several corrections in order to take into account several sources of bias, we did not find any amplification in the inferred mode amplitude due to flaring activity, within a 10% uncertainty.
RHESSI Nuggets #408 April **2021**
https://sprg.ssl.berkeley.edu/~tohban/wiki/index.php/Effects_of_Flares_on_Solar_p-modes

On the saturation of acoustic mode frequencies at high solar activity

M. Cristina Rabello **Soares**
MNRAS **2019**
https://arxiv.org/pdf/1904.03452.pdf
Acoustic mode frequencies obtained by applying spherical harmonic decomposition to HMI, MDI and GONG observations were analysed throughout the solar cycle. Evidence of a deviation from a linear relation with solar radio flux was found indicating a saturation effect at high solar activity. The Gompertz model, which is one of the most frequently used sigmoid functions to fit growth data, is used. It is shown that its fitting to MDI and GONG data are statistically significant and a median saturation of four-hundred sfu is estimated. This saturation level is 50% larger than any obtained in the last century, hence the small effect observed in the minimum-to-maximum frequency shift. However, as shown here, it should not be disregarded.

Chromospheric heating by acoustic waves compared to radiative cooling

M. **Sobotka**, P. Heinzel, M. Švanda, J. Jurčák, D. del Moro, F. Berrilli
ApJ **826** 49 **2016**
http://arxiv.org/pdf/1605.04794v1.pdf
Acoustic and magnetoacoustic waves are among the possible candidate mechanisms that heat the upper layers of solar atmosphere. A weak chromospheric plage near a large solar pore NOAA 11005 was observed on **October 15, 2008** in the lines Fe I 617.3 nm and Ca II 853.2 nm with the Interferometric Bidimemsional Spectrometer (IBIS) attached to the Dunn Solar Telescope. Analyzing the Ca II observations with spatial and temporal resolutions of 0.4" and 52 s, the energy deposited by acoustic waves is compared with that released by radiative losses. The deposited acoustic flux is estimated from power spectra of Doppler oscillations measured in the Ca II line core. The radiative losses are calculated using a grid of seven 1D hydrostatic semi-empirical model atmospheres. The comparison shows that the spatial correlation of maps of radiative losses and acoustic flux is 72 %. In quiet chromosphere, the contribution of acoustic energy flux to radiative losses is small, only of about 15 %. In active areas with photospheric magnetic field strength between 300 G and 1300 G and inclination of 20-60 degrees, the contribution increases from 23 % (chromospheric network) to 54 % (a plage). However, these values have to be considered as lower limits and it might be possible that the acoustic energy flux is the main contributor to the heating of bright chromospheric network and plages.

Exploring the Sun's upper atmosphere with neural networks: Reversed patterns and the hot wall effect

Hector **Socas-Navarro**, Andres Asensio Ramos
A&A 652, A78 **2021**
https://arxiv.org/pdf/2101.11445.pdf
https://doi.org/10.1051/0004-6361/202140424
https://www.aanda.org/articles/aa/pdf/2021/08/aa40424-21.pdf
We have developed an inversion procedure designed for high-resolution solar spectro-polarimeters, such as Hinode/SP or DKIST/ViSP. The procedure is based on artificial neural networks trained with profiles generated from random atmospheric stratifications for a high generalization capability. When applied to Hinode data we find a hot fine-scale network structure whose morphology changes with height. In the middle layers this network resembles what is observed in G-band filtergrams but it is not identical. Surprisingly, the temperature enhancements in the middle and upper photosphere have a reversed pattern. Hot pixels in the middle photosphere, possibly associated to small-scale magnetic elements, appear cool at the log(tau_500)=-3 and -4 level, and viceversa. Finally, we find hot arcs on the limb side of magnetic pores, which we interpret as the first direct observational evidence of the "hot wall" effect in temperature.

The Solar Oxygen Abundance from an Empirical Three-Dimensional Model

H. **Socas-Navarro**

A&A , 577, A25 (**2015**)
http://arxiv.org/pdf/1409.6910v1.pdf
The Oxygen abundance in the solar photosphere, and consequently the solar metallicity itself, is still a controversial issue with far-reaching implications in many areas of Astrophysics. This paper presents a new determination obtained by fitting the forbidden OI line at 6300 A with an observational 3D model. The approach presented here is novel because previous determinations were based either on 1D empirical stratifications or on 3D theoretical models. The resulting best-fit abundances are lg E(O)=8.90 and lg E(Ni)=6.15. Nevertheless, introducing minor tweaks in the model and the procedure, it is possible to retrieve very different values, even down to lg E(O)=8.70. This extreme sensitivity of the abundance to possible systematic effects is not something specific to this particular work but probably reflects the real uncertainty inherent to all abundance determinations based on a prescribed model atmosphere.

Shape of solar cycles and mid-term solar activity oscillations

D.D. **Sokoloff**, A.S. Shibalova, V.N. Obridko, V.V. Pipin
MNRAS Volume 497, Issue 4, Pages 4376–4383 **2020**
https://arxiv.org/pdf/2007.14779.pdf
https://doi.org/10.1093/mnras/staa2279
https://sci-hub.st/10.1093/mnras/staa2279
The evolution of the solar activity comprises, apart from the well-known 11-year cycle, various temporal scales ranging from months up to the secondary cycles known as mid-term oscillations. Its nature deserves a physical explanation. In this work, we consider the 5-to-6 year oscillations as derived both from sunspot and from solar magnetic dipole time series. Using the solar dynamo model, we deduced that these variations may be a manifestation of the dynamo nonlinearities and non-harmonic shape of the solar activity cycles. We conclude that the observed mid-term oscillations are related to the nonlinear saturation of the dynamo processes in the solar interior.

Dynamo theory and perspectives of forecasting solar cycles **Review**

Dmitry **Sokoloff**
Journal of Atmospheric and Solar-Terrestrial Physics Volume 176, September **2018**, Pages 10-14
http://sci-hub.tw/10.1016/j.jastp.2017.03.011
Various approaches to forecasting the solar cycle based on solar dynamo models are considered. The importance of separating predictions of catastrophic events such as the Maunder minimum, predictions of general trends in solar activitybetween Grand minima, and forecasts of the next cycle, based on current knowledge of previous cycles is noted. The role of fluctuations of dynamo drivers for the forecast is emphasized. The polar magnetic field in the current cycle is considered as a natural predictor of the amplitude of the following cycle.

The reconstruction of solar activity in the context of solar dynamo modeling

Dmitry **Sokoloff**
Sun and Geosphere, **2017**; 12/1: 20 -22
http://newserver.stil.bas.bg/SUNGEO//00SGArhiv/SG_v12_No1_2017-pp-20-22.pdf
We discuss problems of interpretation of sunspot data for use in solar dynamo modelling. The variety of the current sunspot reconstructions of archival data creates substantial difficulties for such an endeavour. We suggest a possible strategy to avoid these problems. The point is that we have to accept the possibility of several solar activity reconstructions that are contradictory in detail, and have to compare several possible reconstructions with dynamo models. The point is that a given reconstruction may not cover all the time interval of interest because this reconstruction requires information unavailable at earlier or later times.

Solar small-scale dynamo and polarity of sunspot groups

Sokoloff, D.; Khlystova, A.; Abramenko, V.
Monthly Notices of the Royal Astronomical Society, Volume 451, Issue 2, p.1522-1527, **2015**
http://arxiv.org/pdf/1505.01557v1.pdf
In order to clarify a possible role of small-scale dynamo in formation of solar magnetic field, we suggest an observational test for small-scale dynamo action based on statistics of anti-Hale sunspot groups. As we have shown, according to theoretical expectations the small-scale dynamo action has to provide a population of sunspot groups which do not follow the Hale polarity law, and the density of such groups on the time-latitude diagram is expected to be independent on the phase of the solar cycle. Correspondingly, a percentage of the anti-Hale groups is expected to reach its maximum values during solar minima. For several solar cycles, we considered statistics of anti-Hale groups obtained by several scientific teams, including ours, to find that the percentage of anti-Hale groups becomes indeed maximal during a solar minimum. Our interpretation is that this fact may be explained by the small-scale dynamo action inside the solar convective zone.

Threaded-field-line Model for the Low Solar Corona Powered by the Alfvén Wave Turbulence

Igor V. **Sokolov**1, Bart van der Holst1, Ward B. Manchester1, Doga Can Su Ozturk1, Judit Szente1, Aleksandre Taktakishvili2, Gábor Tóth1, Meng Jin3, and Tamas I. Gombosi1

2021 ApJ 908 172
https://doi.org/10.3847/1538-4357/abc000
https://iopscience.iop.org/article/10.3847/1538-4357/abc000/pdf

We present an updated global model of the solar corona, including the transition region. We simulate the realistic three-dimensional (3D) magnetic field using the data from the photospheric magnetic field measurements and assume the magnetohydrodynamic (MHD) Alfvén wave turbulence and its nonlinear dissipation to be the only source for heating the coronal plasma and driving the solar wind. In closed-field regions, the dissipation efficiency in a balanced turbulence is enhanced. In the coronal holes, we account for a reflection of the outward-propagating waves, which is accompanied by the generation of weaker counterpropagating waves. The nonlinear cascade rate degrades in strongly imbalanced turbulence, thus resulting in colder coronal holes. The distinctive feature of the presented model is the description of the low corona as almost-steady-state low-beta plasma motion and heat flux transfer along the magnetic field lines. We trace the magnetic field lines through each grid point of the lower boundary of the global corona model, chosen at some heliocentric distance, R = R b ~ 1.1R ⊙, well above the transition region. One can readily solve the plasma parameters along the magnetic field line from 1D equations for the plasma motion and heat transport together with the Alfvén wave propagation, which adequately describe the physics within the heliocentric distance range R ⊙ < R < R b , in the low solar corona. By interfacing this threaded-field-line model with the full MHD global corona model at r = R b , we find the global solution and achieve a faster-than-real-time performance of the model on ~200 cores.

Generic energy transport solutions to the solar abundance problem -- a hint of new physics

Anton V. **Sokolov**

Journal of Cosmology and Astroparticle Physics (JCAP) **2019**
https://arxiv.org/pdf/1907.06928.pdf

We consider the poorly studied before non-diffusive energy transport solutions to the solar abundance problem. We find the additional energy flux inside the Sun required to reconcile the Standard solar model with helioseismology. An example of an extension of the Standard model is suggested which can provide for this flux.

The Polarimetric and Helioseismic Imager on Solar Orbiter

S.K. **Solanki**, J.C. del Toro Iniesta, J. Woch, et al.

A&A 642, A11 (**2020**)
https://doi.org/10.1051/0004-6361/201935325
https://www.aanda.org/articles/aa/pdf/2020/10/aa35325-19.pdf

This paper describes the Polarimetric and Helioseismic Imager on the Solar Orbiter mission (SO/PHI), the first magnetograph and helioseismology instrument to observe the Sun from outside the Sun-Earth line. It is the key instrument meant to address the top-level science question: How does the solar dynamo work and drive connections between the Sun and the heliosphere? SO/PHI will also play an important role in answering the other top-level science questions of Solar Orbiter, as well as hosting the potential of a rich return in further science. Methods. SO/PHI measures the Zeeman effect and the Doppler shift in the Fe i 617.3 nm spectral line. To this end, the instrument carries out narrow-band imaging spectro-polarimetry using a tunable LiNbO3 Fabry-Perot etalon, while the polarisation modulation is done with liquid crystal variable retarders (LCVRs). The line and the nearby continuum are sampled at six wavelength points and the data are recorded by a 2k × 2k CMOS detector. To save valuable telemetry, the raw data are reduced on board, including being inverted under the assumption of a MilneEddington atmosphere, although simpler reduction methods are also available on board. SO/PHI is composed of two telescopes; one, the Full Disc Telescope (FDT), covers the full solar disc at all phases of the orbit, while the other, the High Resolution Telescope (HRT), can resolve structures as small as 200 km on the Sun at closest perihelion. The high heat load generated through proximity to the Sun is greatly reduced by the multilayer-coated entrance windows to the two telescopes that allow less than 4% of the total sunlight to enter the instrument, most of it in a narrow wavelength band around the chosen spectral line. Results. SO/PHI was designed and built by a consortium having partners in Germany, Spain, and France. The flight model was delivered to Airbus Defence and Space, Stevenage, and successfully integrated into the Solar Orbiter spacecraft. A number of innovations were introduced compared with earlier space-based spectropolarimeters, thus allowing SO/PHI to fit into the tight mass, volume, power and telemetry budgets provided by the Solar Orbiter spacecraft and to meet the (e.g. thermal) challenges posed by the mission's highly elliptical orbit.
2. Science objectives (How does the solar dynamo work and drive connections between the Sun and heliosphere?, What is the structure of the solar rotation ?, What is the structure of the meridional flow?, . How is magnetic flux reprocessed at high solar latitudes? . Is a small-scale turbulent dynamo process acting on the Sun? What drives the

solar wind and where does the coronal magnetic field originate? Pinpoint the origins of the solar wind streams and the heliospheric magnetic field, How do solar transients drive heliospheric variability? Unravel the evolution of coronal mass ejections in the inner heliosphere, How do solar eruptions produce the energetic particle radiation that fills the heliosphere? and others)

The second flight of the SUNRISE balloon-borne solar observatory: overview of instrument updates, the flight, the data and first results

S. K. **Solanki**, T. L. Riethmüller, P. Barthol, S. Danilovic, W. Deutsch, H. P. Doerr, A. Feller, A. Gandorfer,D. Germerott, L. Gizon, B. Grauf, K. Heerlein, J. Hirzberger, M. Kolleck, A. Lagg, R. Meller, G. Tomasch,M. van Noort, J. Blanco Rodríguez, J. L. Gasent Blesa, M. Balaguer Jiménez, J. C. Del Toro Iniesta, A. C. López Jiménez, D. Orozco Suárez, T. Berkefeld, C. Halbgewachs, W. Schmidt, A. Álvarez-Herrero, L. Sabau-Graziati, I. Pérez Grande, V. Martínez Pillet, G. Card, R. Centeno, M. Knölker, A. Lecinski

ApJ **2017**

https://arxiv.org/pdf/1701.01555v1.pdf

The SUNRISE balloon-borne solar observatory, consisting of a 1~m aperture telescope that provided a stabilized image to a UV filter imager and an imaging vector polarimeter, carried out its second science flight in June 2013. It provided observations of parts of active regions at high spatial resolution, including the first high-resolution images in the Mg~{\sc ii}~k line. The obtained data are of very high quality, with the best UV images reaching the diffraction limit of the telescope at 3000~\AA\ after Multi-Frame Blind Deconvolution reconstruction accounting for phase-diversity information. Here a brief update is given of the instruments and the data reduction techniques, which includes an inversion of the polarimetric data. Mainly those aspects that evolved compared with the first flight are described. A tabular overview of the observations is given. In addition, an example time series of a part of the emerging active region NOAA AR~11768 observed relatively close to disk centre is described and discussed in some detail. The observations cover the pores in the trailing polarity of the active region, as well as the polarity inversion line where flux emergence was ongoing and a small flare-like brightening occurred in the course of the time series. The pores are found to contain magnetic field strengths ranging up to 2500~G and, while large pores are clearly darker and cooler than the quiet Sun in all layers of the photosphere, the temperature and brightness of small pores approach or even exceed those of the quiet Sun in the upper photosphere. **2013, June 12**

SUNRISE: INSTRUMENT, MISSION, DATA, AND FIRST RESULTS

S. K. **Solanki**, P. Barthol, S. Danilovic, A. Feller, A. Gandorfer, J. Hirzberger, T. L. Riethmüller, M. Schüssler, J. A. Bonet, V. Martínez Pillet, J. C. del Toro Iniesta, V. Domingo, J. Palacios, M. Knölker, N. Bello González, T. Berkefeld, M. Franz, W. Schmidt and A. M. Title

2010 ApJL 723 L127-L133

The SUNRISE balloon-borne solar observatory consists of a 1 m aperture Gregory telescope, a UV filter imager, an imaging vector polarimeter, an image stabilization system, and further infrastructure. The first science flight of SUNRISE yielded high-quality data that revealed the structure, dynamics, and evolution of solar convection, oscillations, and magnetic fields at a resolution of around 100 km in the quiet Sun. After a brief description of instruments and data, the first qualitative results are presented. In contrast to earlier observations, we clearly see granulation at 214 nm. Images in Ca II H display narrow, short-lived dark intergranular lanes between the bright edges of granules. The very small-scale, mixed-polarity internetwork fields are found to be highly dynamic. A significant increase in detectable magnetic flux is found after phase-diversity-related reconstruction of polarization maps, indicating that the polarities are mixed right down to the spatial resolution limit and probably beyond.

Magnetohydrodynamic waves in the partially ionized solar plasma **Review**

Roberto **Soler**

Philosophical Transactions of the Royal Society A **2024**

https://doi.org/10.1098/rsta.2023.0223

https://royalsocietypublishing.org/doi/pdf/10.1098/rsta.2023.0223

This paper provides a comprehensive review of recent theoretical investigations concerning magnetohydrodynamic (MHD) waves in partially ionized solar plasma. First, we examine the properties of linear MHD waves in a uniform partially ionized plasma and discuss the relevant effects arising from partial ionization. Subsequently, we delve into MHD wave studies in the more intricate settings of the lower solar atmosphere and solar prominences. These investigations involve topics such as MHD waves in magnetic flux tubes, wave excitation, linear and nonlinear mode coupling and wave heating. We outline new challenges that future research should tackle.

Exploring the Ideal MHD Quasi-Modes of a Plasma Interface with a Thick Nonuniform Transition

Roberto **Soler**
Physics, (Special issue in honor of Professor Marcel Goossen) **2022**, *4*(4), 1359-1370;
https://doi.org/10.3390/physics4040087
https://www.mdpi.com/2624-8174/4/4/87
Nonuniform plasma across an imposed magnetic field, such as those present in the solar atmosphere, can support collective Alfvénic oscillations with a characteristic damping time. The damped transverse oscillations of coronal loops are an example of this process. In ideal magnetohydrodynamics (MHD), these transient collective motions are associated with quasi-modes resonant in the Alfvén continuum. Quasi-modes live in a non-principal Riemann sheet of the dispersion relation, and so they are not true ideal MHD eigenmodes. The present study considers the illustrative case of incompressible surface MHD waves propagating on a nonuniform interface between two uniform plasmas with a straight magnetic field parallel to the interface. It is explored how the ideal quasi-modes of this configuration change when the width of the nonuniform transition increases. It is found that interfaces with wide enough transitions are not able to support truly collective oscillations. A quasi-mode that can be related with a resonantly damped surface MHD wave can only be found in interfaces with sufficiently thin transitions.

Resonances in a Coronal Loop Driven by Torsional Alfvén Waves Propagating from the Photosphere

Roberto **Soler**1,2, Jaume Terradas1,2, Ramón Oliver1,2, and José Luis Ballester1,2
2021 ApJ 909 190
https://doi.org/10.3847/1538-4357/abdec5
There is increasing evidence that magnetohydrodynamic waves play an important role in the propagation and dissipation of energy in the solar atmosphere. Here we investigate how torsional Alfvén waves driven at the photosphere can transport energy to an overlying coronal magnetic loop and explore their ability to heat the plasma. We consider a coronal loop whose feet are embedded in the partially ionized chromosphere. A broadband driver at the photosphere excites torsional Alfvén waves that propagate upward to the coronal loop. By means of numerical computations under the stationary-state assumption, we study the transmission of wave energy to the loop and the heating associated with ohmic diffusion and ion–neutral collisions. We find that wave transmission to the loop is heavily affected by the presence of cavity resonances when the frequency of the driver matches an eigenfrequency of the loop. A tremendous amount of wave energy is channeled to the coronal loop for those particular frequencies. The transmitted energy surpasses by many orders of magnitude the requirements to balance thermal radiation. However, dissipation is so weak in the coronal plasma that only a tiny percentage of the energy budget is converted into heat, which is not enough to compensate for radiative losses. Most of the energy simply leaks back to the chromosphere. Conversely, dissipation is much more efficient in the lower atmosphere, and wave heating can locally balance a significant fraction of radiation in the chromosphere. We argue that nonlinear effects such as turbulence triggered by the Kelvin–Helmholtz instability should enhance the heating efficiency at coronal heights.

Transverse waves in coronal flux tubes with thick boundaries: The effect of longitudinal flows

Roberto **Soler**
A&A **2019**
https://arxiv.org/pdf/1901.10785.pdf
Observations show that transverse magnetohydrodynamic (MHD) waves and flows are often simultaneously present in magnetic loops of the solar corona. The waves are resonantly damped in the Alfvén continuum because of plasma and/or magnetic field nonuniformity across the loop. The resonant damping is relevant in the context of coronal heating, since it provides a mechanism to cascade energy down to the dissipative scales. It has been theoretically shown that the presence of flow affects the waves propagation and damping, but most of the studies rely on the unjustified assumption that the transverse nonuniformity is confined to a boundary layer much thinner than the radius of the loop. Here we present a semi-analytic technique to explore the effect of flow on resonant MHD waves in coronal flux tubes with thick nonuniform boundaries. We extend a published method, which was originally developed for a static plasma, in order to incorporate the effect of flow. We allowed the flow velocity to continuously vary within the nonuniform boundary from the internal velocity to the external velocity. The analytic part of the method is based on expressing the wave perturbations in the thick nonuniform boundary of the loop as a Frobenius series that contains a singular term accounting for the Alfvén resonance, while the numerical part of the method consists of solving iteratively the transcendental dispersion relation together with the equation for the Alfvén resonance position. As an application of this method, we investigated the impact of flow on the phase velocity and resonant damping length of MHD kink waves. We consistently recover results in the thin boundary approximation obtained in previous studies. We have extended those results to the case of thick boundaries. We also explored the error associated with the use of the thin boundary approximation beyond its regime of applicability.

Energy transport and heating by torsional Alfvén waves propagating from the photosphere to the corona in the quiet Sun

Roberto **Soler**, Jaume Terradas, Ramon Oliver, Jose Luis Ballester

ApJ **871** 3 **2019**

https://arxiv.org/pdf/1812.01323.pdf

sci-hub.tw/10.3847/1538-4357/aaf64c

In the solar atmosphere, Alfvén waves are believed to play an important role in the transfer of energy from the photosphere to the corona and solar wind, and in the heating of the chromosphere. We perform numerical computations to investigate energy transport and dissipation associated with torsional Alfvén waves propagating in magnetic flux tubes that expand from the photosphere to the corona in quiet-Sun conditions. We place a broadband driver at the photosphere that injects a wave energy flux of 107 erg cm−2 s−1 and consider Ohm's magnetic diffusion and ion-neutral collisions as dissipation mechanisms. We find that only a small fraction of the driven flux,∼105 erg cm−2 s−1, is able to reach coronal heights, but it may be sufficient to partly compensate the total coronal energy loss. The frequency of maximal transmittance is ∼5 mHz for a photospheric field strength of 1 kG and is shifted to smaller/larger frequencies for weaker/stronger fields. Lower frequencies are reflected at the transition region, while higher frequencies are dissipated producing enough heat to balance chromospheric radiative losses. Heating in the low and middle chromosphere is due to Ohmic dissipation, while ion-neutral friction dominates in the high chromosphere. Ohmic diffusion is enhanced by phase mixing because of the expansion of the magnetic field. This effect has the important consequence of increasing the chromospheric dissipation and, therefore, reducing the energy flux that reaches the corona. We provide empirical fits of the transmission coefficient that could be used as input for coronal models.

Fluting Modes in Transversely Nonuniform Solar Flux Tubes

Roberto **Soler**

2017 ApJ 850 114

Magnetohydrodynamic waves of different types are frequently observed in magnetic flux tubes of the solar atmosphere and are often modeled using simple models. In the standard flux tube model made of a straight uniform tube with an abrupt boundary, transverse wave modes are classified according to their azimuthal wavenumber, m. Sausage (m = 0) and kink (m = 1) modes produce pulsations of the cross section and transverse oscillations of tube axis, respectively. Both sausage and kink modes have been observed in the solar atmosphere. Fluting ($m \geqslant 2$) modes produce perturbations that are essentially confined around the boundary of the tube, i.e., they have a strong surface-like character. Unlike sausage and kink modes, the detection of fluting modes remains elusive. Here we show that the inclusion of transverse inhomogeneity in the flux tube model dramatically affects the properties of fluting modes. Even in a thin tube, kink and fluting modes are no longer degenerate in frequency when the tube has a smooth boundary. In addition, fluting modes become heavily damped by resonant absorption in a timescale shorter than the oscillation period. The perturbations loose their global shape and their distinctive surface-like appearance. As a consequence of that, we argue that nonuniform flux tubes with smooth boundaries may not be able to support fluting-like perturbations as coherent, global modes.

Propagation of Torsional Alfvén Waves from the Photosphere to the Corona: Reflection, Transmission, and Heating in Expanding Flux Tubes

Roberto **Soler**1,2, Jaume Terradas1,2, Ramón Oliver1,2, and José Luis Ballester

2017 ApJ 840 20

It has been proposed that Alfvén waves play an important role in the energy propagation through the solar atmospheric plasma and its heating. Here we theoretically investigate the propagation of torsional Alfvén waves in magnetic flux tubes expanding from the photosphere up to the low corona and explore the reflection, transmission, and dissipation of wave energy. We use a realistic variation of the plasma properties and the magnetic field strength with height. Dissipation by ion–neutral collisions in the chromosphere is included using a multifluid partially ionized plasma model. Considering the stationary state, we assume that the waves are driven below the photosphere and propagate to the corona, while they are partially reflected and damped in the chromosphere and transition region. The results reveal the existence of three different propagation regimes depending on the wave frequency: low frequencies are reflected back to the photosphere, intermediate frequencies are transmitted to the corona, and high frequencies are completely damped in the chromosphere. The frequency of maximum transmissivity depends on the magnetic field expansion rate and the atmospheric model, but is typically in the range of 0.04–0.3 Hz. Magnetic field expansion favors the transmission of waves to the corona and lowers the reflectivity of the chromosphere and transition region compared to the case with a straight field. As a consequence, the chromospheric heating due to ion–neutral dissipation systematically decreases when the expansion rate of the magnetic flux tube increases.

Overdamped Alfvén waves due to ion-neutral collisions in the solar chromosphere

R. **Soler**1, J. L. Ballester1 and T. V. Zaqarashvili
A&A 573, A79 (**2015**)
http://arxiv.org/pdf/1411.5887v1.pdf

Alfvénic waves are ubiquitous in the solar atmosphere and their dissipation may play an important role in atmospheric heating. In the partially ionized solar chromosphere, collisions between ions and neutrals are an efficient dissipative mechanism for Alfvén waves with frequencies near the ion-neutral collision frequency. The collision frequency is proportional to the ion-neutral collision cross section for momentum transfer. Here, we investigate Alfvén wave damping as a function of height in a simplified chromospheric model and compare the results for two sets of collision cross sections, namely those of the classic hard-sphere model and those based on recent quantum-mechanical computations. We find important differences between the results for the two sets of cross sections. There is a critical interval of wavelengths for which impulsively excited Alfvén waves are overdamped as a result of the strong ion-neutral dissipation. The critical wavelengths are in the range from 1 km to 50 km for the hard-sphere cross sections, and from 1 m to 1 km for the quantum-mechanical cross sections. Equivalently, for periodically driven Alfvén waves there is an optimal frequency for which the damping is most effective. The optimal frequency varies from 1 Hz to10^2 Hz for the hard-sphere cross sections, and from 10^2 Hz to 10^4 Hz for the quantum-mechanical cross sections. Future observations at sufficiently high spatial or temporal resolution may show the importance of high-frequency Alfvén waves for chromospheric heating. For instance, the Atacama Large Millimeter/submillimeter Array (ALMA) may be able to detect the critical wavelengths and optimal frequencies and so to test the effective collision cross section in the chromospheric plasma.

ON THE SPATIAL SCALES OF WAVE HEATING IN THE SOLAR CHROMOSPHERE

Roberto **Soler**1,2, Marc Carbonell2,3, and Jose Luis Ballester
2015 ApJ 810 146
http://arxiv.org/pdf/1508.01497v1.pdf

Dissipation of magnetohydrodynamic (MHD) wave energy has been proposed as a viable heating mechanism in the solar chromospheric plasma. Here, we use a simplified one-dimensional model of the chromosphere to theoretically investigate the physical processes and spatial scales that are required for the efficient dissipation of Alfvén waves and slow magnetoacoustic waves. We consider the governing equations for a partially ionized hydrogen-helium plasma in the single-fluid MHD approximation and include realistic wave damping mechanisms that may operate in the chromosphere, namely, Ohmic and ambipolar magnetic diffusion, viscosity, thermal conduction, and radiative losses. We perform an analytic local study in the limit of small amplitudes to approximately derive the lengthscales for critical damping and efficient dissipation of MHD wave energy. We find that the critical dissipation lengthscale for Alfvén waves depends strongly on the magnetic field strength and ranges from 10 m to 1 km for realistic field strengths. The damping of Alfvén waves is dominated by Ohmic diffusion for weak magnetic field and low heights in the chromosphere, and by ambipolar diffusion for strong magnetic field and medium/large heights in the chromosphere. Conversely, the damping of slow magnetoacoustic waves is less efficient, and spatial scales shorter than 10 m are required for critical damping. Thermal conduction and viscosity govern the damping of slow magnetoacoustic waves and play an equally important role at all heights. These results indicate that the spatial scales at which strong wave heating may work in the chromosphere are currently unresolved by observations.

Magnetohydrodynamic kink waves in nonuniform solar flux tubes: phase mixing and energy cascade to small scales

Roberto **Soler** and Jaume Terradas
ApJ **803** 43 **2015**
http://arxiv.org/pdf/1502.03949v1.pdf

Magnetohydrodynamic (MHD) kink waves are ubiquitously observed in the solar atmosphere. The propagation and damping of these waves may play relevant roles for the transport and dissipation of energy in the solar atmospheric medium. However, in the atmospheric plasma dissipation of transverse MHD wave energy by viscosity or resistivity needs very small spatial scales to be efficient. Here, we theoretically investigate the generation of small scales in nonuniform solar magnetic flux tubes due to phase mixing of MHD kink waves. We go beyond the usual approach based on the existence of a global quasi-mode that is damped in time due to resonant absorption. Instead, we use a modal expansion to express the MHD kink wave as a superposition of Alfvén continuum modes that are phase mixed as time evolves. The comparison of the two techniques evidences that the modal analysis is more physically transparent and describes both the damping of global kink motions and the building up of small scales due to phase mixing. In addition, we discuss that the processes of resonant absorption and phase mixing are intimately linked. They represent two aspects of the same underlying physical mechanism: the energy cascade from large scales to small scales due to naturally occurring plasma and/or magnetic field inhomogeneities. This process may provide the necessary scenario for efficient dissipation of transverse MHD wave energy in the solar atmospheric plasma.

Nonlinear evolution of fluting oscillations in coronal flux tubes

Roberto **Soler**, Andrew Hillier
A&A **2024**
https://arxiv.org/pdf/2412.09547
Magnetic flux tubes in the solar corona support a rich variety of transverse oscillations, which are theoretically interpreted as magnetohydrodynamic (MHD) modes with a fast and/or Alfvénic character. In the standard flux tube model made of a straight cylindrical tube, these modes can be classified according to their azimuthal wavenumber, m. Sausage m=0 modes produce periodic expansion and contraction of the tube cross section and are observed during solar flares. Kink m=1 modes laterally displace the tube axis and are related to, for example, post-flare global transverse oscillations of coronal loops. Fluting m≥2 modes produce disturbances that are mainly confined to the tube boundary, but their observation remains elusive to date. We use 3D ideal MHD numerical simulations to investigate the nonlinear evolution of fluting modes in coronal flux tubes with transversely nonuniform boundaries. The simulations show that fluting modes are short-lived as coherent, collective motions of the flux tube. Owing to the process of resonant absorption, fluting oscillations become overdamped modes in tubes with wide enough nonuniform boundaries. During the nonlinear evolution, shear flows drive the Kelvin-Helmholtz instability at the tube boundary, which further disrupts the coherent fluting oscillation. For large-enough oscillation amplitudes, baroclinic instabilities of Rayleigh-Taylor type are also present at locations in the boundary where the plasma acceleration is normal to the boundary. The evolution of the instabilities drives turbulence in the flux tube, which may inhibit the resonant damping. However, the oscillations remain strongly damped even in this case. As a result of the combination of the strong damping and the induced instabilities, it is unlikely that coronal flux tubes can support fluting modes as sufficiently enduring coherent oscillations.

Structural features of sun photosphere under high spatial resolution
A. A. **Soloviev**, L. D. Parfinenko, V. I. Efremov, E.A.Kirichek, O.A.Korolkova
2019
https://arxiv.org/ftp/arxiv/papers/1911/1911.02556.pdf
The main small-scale elements observed in the solar photosphere at high resolution are discussed: granules, faculaes, micropores. As a separate element of the fine structure, a continuous network of dark intergranular gaps is considered. The results of image processing of micropores and faculaes knots obtained using modern adaptive telescopes are presented. For intergranular gaps and micropores, a stationary regime of magnetic diffusion is determined, in which horizontal-vertical plasma flows converging to the gap (and micropores) compensate for the dissipative spreading of the magnetic flux on a given scale. A theoretical assessment of the characteristic scales of these structures in the photosphere is obtained: 20-30 km for the thickness of dark intergranular spaces and 200-400 km for the diameter of micropores.

Structure of solar faculae
A A **Solov'ev** E A Kirichek
Monthly Notices of the Royal Astronomical Society, Volume 482, Issue 4, 1 February **2019**, Pages 5290–5301
sci-hub.tw/10.1093/mnras/sty3050
In solar facular regions (plages), three distinct classes of magnetic features are observed: small-scale flux tubes, knots, and pores. Small flux tubes have granular scales; they are in constant motion and can well be simulated numerically according to the concept of magneto-convection. On this dynamic background, one observes quite stable, long-lived. and bright objects called facular knots, with a diameter of 3–8 mm and fine (less than 1 mm) inner filamentary structure. Their magnetic field strength varies in the range from 250 to 1200 G. Our present paper considers only these active formations. The stationary MHD problem is solved and analytical formulae are derived for calculation of the pressure, density, temperature, and Alfven Mach number in the studied configuration from the corresponding magnetic field structure. The facular knot is modelled in a hydrostatic atmosphere defined by the Avrett & Loeser model (2008) and is surrounded by a weak (2 G) external field corresponding to the average global magnetic field strength on the solar surface. The constructed 3D analytical model presents the facular knot as a magnetic ‘fountain’ with numerous slender fibrils and allows solving the following tasks: 1. Calculation of temperature profiles of the knot at any height of the atmosphere; 2. Description of ring brightening and fine azimuthal fibril structure observed in plages at high spatial resolution; 3. New interpretation of Centre-to-Limb Variation problem that fits well with the observational data.

B.V. **Somov**, Moscow State University, Moskva, Russia
Plasma Astrophysics, Part I
Fundamentals and Practice
Series: Astrophysics and Space Science Library, Vol. 391, **2012**
Plasma Astrophysics, Part II
Reconnection and Flares
Series: Astrophysics and Space Science Library, Vol. 392, **2012**

This two-part book is devoted to classic fundamentals and current practices and perspectives of modern plasma astrophysics. This first part uniquely covers all the basic principles and practical tools required for understanding and work in plasma astrophysics. More than 25% of the text is updated from the first edition, including new figures, equations and entire sections on topics such as magnetic reconnection and the Grad-Shafranov equation.
The book is aimed at professional researchers in astrophysics, but it will also be useful to graduate students in space sciences, geophysics, applied physics and mathematics, especially those seeking a unified view of plasma physics and fluid mechanics.

Generation of He i 1083 nm Images from SDO AIA Images by Deep Learning

Jihyeon **Son**1, Junghun Cha2, Yong-Jae Moon1,2, Harim Lee2, Eunsu Park2, Gyungin Shin3, and Hyun-Jin Jeong1
2021 ApJ 920 101
https://doi.org/10.3847/1538-4357/ac16dd
In this study, we generate He i 1083 nm images from Solar Dynamic Observatory (SDO)/Atmospheric Imaging Assembly (AIA) images using a novel deep learning method (pix2pixHD) based on conditional Generative Adversarial Networks (cGAN). He i 1083 nm images from National Solar Observatory (NSO)/Synoptic Optical Long-term Investigations of the Sun (SOLIS) are used as target data. We make three models: single-input SDO/AIA 19.3 nm image for Model I, single-input 30.4 nm image for Model II, and double-input (19.3 and 30.4 nm) images for Model III. We use data from 2010 October to 2015 July except for June and December for training and the remaining one for test. Major results of our study are as follows. First, the models successfully generate He i 1083 nm images with high correlations. Second, Model III shows better results than those with one input image in terms of metrics such as correlation coefficient (CC) and root mean square error (RMSE). CC and RMSE between real and synthetic ones for model III with 4 by 4 binnings are 0.88 and 9.49, respectively. Third, synthetic images show well observational features such as active regions, filaments, and coronal holes. This work is meaningful in that our model can produce He i 1083 nm images with higher cadence without data gaps, which would be useful for studying the time evolution of the chromosphere and transition region.

Solar cycle variation in the properties of photospheric magnetic concentrations

Anchuan **Song**1,2, Quanhao Zhang1,2,4, Yuming Wang1,2,3, Rui Liu1,2,4, Jie Jiang5, Xiaolei Li1,2, Jiajia Liu1,2,4, Shaoyu Lv1,2 and Ruobing Zheng1,2
A&A 682, A87 (**2024**)
https://www.aanda.org/articles/aa/pdf/2024/02/aa46898-23.pdf
It is widely accepted that eruptive phenomena on the Sun are related to the solar magnetic field, which is closely tied to the observed magnetic concentrations (MCs). Therefore, studying MCs is critical in order to understand the origin and evolution of all forms of solar activity. In this paper, we investigate the statistics of characteristic physical parameters of MCs during a whole solar cycle by analyzing magnetograms from 2010 to 2021 observed by the Helioseismic and Magnetic Imager (HMI) on board the Solar Dynamics Observatory (SDO). We discover that there are differences between large- and small-scale MCs in diffenent phases of the solar cycle. By analyzing the distributions of the magnetic flux, area, and magnetic energy of MCs, we find that the small-scale MCs obey a power-law distribution, and that the power indices vary very little with the phases of the solar cycle. However, for the large-scale MCs, although they also obey the power-law distribution, the power indices are clearly modulated by the different phases of the solar cycle. We also investigate the relation between the maximum magnetic field strength (Bmax) and the area of MCs (S) and find the same property. The relation for the large-scale MCs is modulated by the phases of the solar cycle, while it is still independent of the phases of the solar cycle for the small-scale MCs. Our results suggest that small- and large-scale MCs could be generated by different physical mechanisms.

Formation of the Transition Region for the Quiet Sun

Paul **Song**1, Jiannan Tu1, and David B. Wexler1
2023 ApJL 948 L4
https://iopscience.iop.org/article/10.3847/2041-8213/accc27/pdf
We propose a partially ionized collisional two-fluid model of the formation of the transition region between the cool dense chromosphere and hot tenuous corona for the quiet Sun. The chromosphere is treated as an isothermal gravity-bound two-fluid stratified atmosphere without appreciable vertical flow, on average. The different scale heights of the two fluids result in vertical evolution of the ionization state, and the transition region can be defined according to the ionization fraction. The transition region starts at the altitude where the ionization fraction reaches 0.5, the demarcation between the weakly and strongly ionized gas. The upper border of the region is defined as the temperature at which the particles possess enough energy for ionization, i.e., the first ionization potential. Within the transition region is a diffusion process in which the cold chromospheric particles gain energy and ionize through

random collisions with hot coronal particles diffusing upward into the corona, whereas, when colliding with cold chromospheric particles, hot coronal particles lose energy, recombine, and fall into the chromosphere. The type II spicules can be generated when and where the local heating rate is so high that the conditions for a stratified chromosphere are not satisfied; upward flow is formed, penetrating the corona where the chromospheric gas in the spicule is ionized and dispersed. The enhanced radiation via those chromospheric neutral particles cools the coronal gas, and more recombination occurs, producing enhanced downward diffusion. The model reproduces key structural features of the transition region from first principles and a minimum of arbitrary parameters.

Improving the Spatial Resolution of Solar Images Based on an Improved Conditional Denoising Diffusion Probability Model

Wei **Song**1,2,3, Wen Ma1, Ying Ma1, Xiaobing Zhao1,3, and Ganghua Lin2,4
2022 ApJS 263 25
https://iopscience.iop.org/article/10.3847/1538-4365/ac9a4d/pdf
The quality of solar images plays an important role in the analysis of small events in solar physics. Therefore, the improvement of image resolution based on super-resolution (SR) reconstruction technology has aroused the interest of many researchers. In this paper, an improved conditional denoising diffusion probability model (ICDDPM) based on the Markov chain is proposed for the SR reconstruction of solar images. This method reconstructs high-resolution (HR) images from low-resolution images by learning a reverse process that adds noise to HR images. To verify the effectiveness of the method, images from the Goode Solar Telescope at the Big Bear Solar Observatory and the Helioseismic and Magnetic Imager (HMI) on the Solar Dynamics Observatory are used to train a network, and the spatial resolution of reconstructed images is 4 times that of the original HMI images. The experimental results show that the performance based on ICDDPM is better than the previous work in subject judgment and object evaluation indexes. The reconstructed images of this method have higher subjective vision quality and better consistency with the HMI images. And the structural similarity and rms index results are also higher than the compared method, demonstrating the success of the resolution improvement using ICDDPM.

A new post-hoc flat field measurement method for the Solar X-ray and Extreme Ultraviolet Imager onboard the Fengyun-3E satellite

Qiao **Song**, Xianyong Bai, Bo Chen, Xiuqing Hu, Yajie Chen, Zhenyong Hou, Xiaofan Zhang, Lingping He, Kefei Song, Peng Zhang, Jing-Song Wang, Xiaoxin Zhang, Weiguo Zong, Jinping Dun, Hui Tian, Yuanyong Deng
Research in Astronomy and Astrophysics **2022**
https://arxiv.org/pdf/2207.01829.pdf
The extreme ultraviolet (EUV) observations are widely used in solar activity research and space weather forecasting since they can observe both the solar eruptions and the source regions of the solar wind. Flat field processing is indispensable to remove the instrumental non-uniformity of a solar EUV imager in producing high-quality scientific data from original observed data. Fengyun-3E (FY-3E) is a meteorological satellite operated in Sun-synchronous orbit, and the routine EUV imaging data from the Solar X-ray and Extreme Ultraviolet Imager (X-EUVI) onboard FY-3E has the characteristics of concentric rotation. Taking advantage of the concentric rotation, we propose a post-hoc flat field measurement method for its EUV 195 channel in this paper. This method removes small-scale and time-varying component of the coronal activities by taking the median value for each pixel along the time axis of a concentric rotation data cube, and then derives large-scale and invariable component of the quiet coronal radiation, and finally generates a flat field image. Analysis shows that our method is able to measure the instrumental spot-like non-uniformity possibly caused by contamination on the detector, which mostly disappears after the in-orbit self-cleaning process. It can also measure the quasi-periodic grid-like non-uniformity, possibly from the obscuration of the support mesh on the rear filter. After flat field correction, these instrumental non-uniformities from the original data are effectively removed. X-EUVI 195 data after dark and flat field corrections are consistent with the 193 channel data from SDO/AIA, verifying the suitability of the method. Our method is not only suitable for FY-3E/X-EUVI but also a candidate method for the flat field measurement of future solar EUV telescopes.

The Fengyun-3E/Joint Total Solar Irradiance Absolute Radiometer: Instrument Design, Characterization, and Calibration

Baoqi **Song**, Xin Ye, Wolfgang Finsterle, Manfred Gyo, Matthias Gander, Alberto Remesal Oliva, Daniel Pfiffner, Yan Zhao & Wei Fang
Solar Physics volume 296, Article number: 52 (**2021**)
https://doi.org/10.1007/s11207-021-01794-5
https://link.springer.com/content/pdf/10.1007/s11207-021-01794-5.pdf
The Joint Total Solar Irradiance Monitor (JTSIM) is due to fly onboard the Fengyun-3E spacecraft and aims to measure the Total Solar Irradiance (TSI) in orbit. The instruments on the Fengyun-3E/JTSIM include the Digital Absolute Radiometer (DARA) from the Physikalisch Meteorologisches Observatorium, Davos and World Radiation Center (PMOD/WRC) and the Solar Irradiance Absolute Radiometer (SIAR) from the Changchun Institute of

Optics, Fine Mechanics and Physics Chinese Academy of Sciences (CIOMP/CAS). Radiometers from Switzerland and China will monitor the TSI variability on the same pointing system for eight years. The scientific data from JTSIM will support the analysis of potential long-term trends in the Sun's variability. In this article, we describe the sensor box and the electronics box of JTSIM, the measurement principle, and the operation mode of SIAR. Before launch, we accomplished some primary calibrations of SIAR in the CIOMP laboratory, including the aperture area, cavity absorption, non-equivalence, diffraction, etc. Other parameters will be calibrated on orbit. The combined uncertainty of SIAR for characterization is 231 – 233 ppm depending on the measurement channel. The characterization of SIAR is an International System of Units (SI)-native scale calibration. An end-to-end calibration against the World Radiometric Reference (WRR) standard or the Total Irradiance Radiometer Facility (TRF) is a procedure where SIAR is directly calibrated with the WRR reference radiometers. The WRR factor for SIAR is 0.99939 – 1.00092 and the combined measurement uncertainty is 0.074% – 0.099%, depending on the measurement channel.

Correction Solar Physics volume 297, Article number: 77 (**2022**)
https://link.springer.com/content/pdf/10.1007/s11207-022-02028-y.pdf

Automatic Solar Seeing Observations at Mt. Wumingshan in Western China

T. F. **Song**, Y. M. Wen, Y. Liu, A. Elmhamdi, A. S. Kordi, M. Y. Zhao, X. F. Zhang, X. B. Li, J. X. Wang, Y. Fu, X. M. Cheng, F. Y. Xu
Solar Physics February **2018**, 293:37
https://link.springer.com/content/pdf/10.1007%2Fs11207-018-1254-0.pdf

Mountain Wumingshan (Mt. WMS) is located in the southeastern foot of the Tibet Plateau with an altitude of 4,800 m. It is one of the candidate sites to place China's next-generation large-scale solar telescope. A temporary observation platform has been built at Mt. WMS, but there is still a great need of a stable solar-seeing monitoring for long-term observations. Based on the preliminary studies on the Solar Differential Image Motion Monitor (SDIMM) of the Yunnan Observatories, we built an improved version of this early prototype, which is calledWumingshan Mountain Automated Solar Differential Image Motion Monitor (WMA-SDIMM). We develop the automatic system of the WMA-SDIMM, investigate the reliability and precision of our measurements by error analysis and comparison testing, and present the statistical results from October 2016 to September 2017 at Mt. WMS. WMA-SDIMM works very well at Mt. WMS and is quite suitable for long-period daytime seeing observations.

Helioseismic and Neutrino Data Driven Reconstruction of Solar Properties

Ningqiang **Song**, M.C. Gonzalez-Garcia, Francesco L. Villante, Nuria Vinyoles, Aldo Serenelli
MNRAS Volume 477, Issue 1, 11 June **2018**, Pages 1397–1413
https://arxiv.org/pdf/1710.02147.pdf

In this work we use Bayesian inference to quantitatively reconstruct the solar properties most relevant to the solar composition problem using as inputs the information provided by helioseismic and solar neutrino data. In particular, we use a Gaussian process to model the functional shape of the opacity uncertainty to gain flexibility and become as free as possible from prejudice in this regard. With these tools we first readdress the statistical significance of the solar composition problem. Furthermore, starting from a composition unbiased set of standard solar models we are able to statistically select those with solar chemical composition and other solar inputs which better describe the helioseismic and neutrino observations. In particular, we are able to reconstruct the solar opacity profile in a data driven fashion, independently of any reference opacity tables, obtaining a 4% uncertainty at the base of the convective envelope and 0.8% at the solar core. When systematic uncertainties are included, results are 7.5% and 2% respectively. In addition we find that the values of most of the other inputs of the standard solar models required to better describe the helioseismic and neutrino data are in good agreement with those adopted as the standard priors, with the exception of the astrophysical factor S11 and the microscopic diffusion rates, for which data suggests a 1% and 30% reduction respectively. As an output of the study we derive the corresponding data driven predictions for the solar neutrino fluxes.

Effect of Horizontally Inhomogeneous Heating on Flow and Magnetic Field in the Chromosphere of the Sun

P. **Song**1 and V. M. Vasyli?nas
2014 ApJ 796 L23

The solar chromosphere is heated by damped Alfv?n waves propagating upward from the photosphere at a rate that depends on magnetic field strength, producing enhanced heating at low altitudes in the extended weak-field regions (where the additional heating accounts for the radiative losses) between the boundaries of the chromospheric network as well as enhanced heating per particle at higher altitudes in strong magnetic field regions of the network. The resulting inhomogeneous radiation and temperature distribution produces bulk flows, which in turn affect the configuration of the magnetic field. The basic flow pattern is circulation on the spatial scale of a supergranule, with upward flow in the strong-field region; this is a mirror image in the upper chromosphere of

photospheric/subphotospheric convection widely associated with the formation of the strong network field. There are significant differences between the neutral and the ionized components of the weakly ionized medium: neutral flow streamlines can form closed cells, whereas plasma is largely constrained to flow along the magnetic field. Stresses associated with this differential flow may explain why the canopy/funnel structures of the network magnetic field have a greater horizontal extent and are relatively more homogeneous at high altitudes than is expected from simple current-free models.

Differential Rotation of Strong Magnetic Flux During Solar Cycles 21–23

W. B. **Song**, X. S. Feng, F. Shen and J. P. Guo
Solar Physics, Volume 270, Number 1, 35-43, **2011**

In the present investigation we measure the differential rotation of strong magnetic flux during solar cycles 21–23 with the method of wavelet transforms. We find that the cycle-averaged synodic rotation rate of strong magnetic flux can be written as $\omega=13.47-2.58\sin 2\theta$ or $\omega=13.45-2.06\sin 2\theta-1.37\sin 4\theta$, where θ is the latitude. They agree well with the results derived from sunspots. A north–south asymmetry of the rotation rate is found at high latitudes ($28°<\theta<40°$). The strong flux in the southern hemisphere rotates faster than that in the northern hemisphere by 0.2 deg day^{-1}. The asymmetry continued for cycles 21–23 and may be a secular property.

Solar Coronal Heating by Gravity-Induced Resonant Emission

Antony **Soosaleon**
MNRAS **2019**
https://arxiv.org/pdf/1903.11156.pdf
Solar Coronal Heating is a Nonlinear Quantum Mechanical Phenomenon.
Corona is a powerful source of X-rays and ionisations & emissions of such radiations are quantum mechanical and levels are highly unstable to order of femto-seconds. A linear method of energy transfer like collisional ionisation to such levels is practically not feasible. We have proposed gire as the mechanism of this problem and discussed the physics, found it as a nonlinear process of multi photon absorption, similar to the multiple ionisation by ultra fast laser. Here, we are discussing the energy budget for ionisations of all the coronal elements and find gire is sufficient.
Solar coronal heating balances the energy mass condition of the solar system, is a classical thermodynamical problem, but done by a nonlinear quantum mechanical process.

Analysis of EUV Solar Spectrum with Gravity Induced Resonant Emission

Antony **Soosaleon**, Sunitha Ambrose
Solar Phys. **2017**
https://arxiv.org/pdf/1705.09956.pdf
Gravity Induced Resonant Emission (GIRE) is a new phenomenon recently reported; we have analyzed the solar emissions on the basis of GIRE. We have computed the EUV solar spectrum using GIRE wave length as a part of studying coronal heating problem. We find all the solar observations converge in GIRE and the GIRE wave length is sufficient to study all the solar emissions.

Two Stream Instability as a Source of Coronal Heating

Antony **Soosaleon**
International Journal of Astronomy and Astrophysics, **2015**, 5, 61-69
https://www.academia.edu/31557354/Two_Stream_Instability_as_a_Source_of_Coronal_Heating
Recent observation of oscillating the two stream instability (TSI) in a solar type III radio bursts and spatial damping of Langmuir oscillations has made this instability as an important candidate to understand the coronal heating problem. This instability has been studied by several authors for cold plasma found to be stable for high frequencies (greater than plasma frequency ωp). In this paper, we prove that this instability is unstable for warm plasma for higher frequencies (greater than plasma frequency ωp) and much suitable to study the solar coronal heating problem. We have derived a general dispersion relation for warm plasma and discussed the various methods analyzing the instability conditions. Also, we derived an expression for the growth rate of TSI and analyzed the growth rate for photospheric and coronal plasmas. A very promising result is that the ion temperature is the source of this instability and shifts the growth rate to high frequency region, while the electron temperature does the reverse. TSI shows a high growth rate for a wide frequency range for photosphere plasma, suggesting that the electron precipitation by magnetic reconnection current, acceleration by flares, may be source of TSI in the photosphere. But for corona,

these waves are damped to accelerate the ions and further growing of such instability is prohibited due to the high conductivity in coronal plasma. The TSI is a common instability; the theory can be easily modifiable for multi-ion plasmas and will be a useful tool to analyze all the astrophysical problems and industrial devices, too.

Supergranular Fractal Dimension and Solar Rotation

Sowmya G. M., Rajani G., U. Paniveni, R. Srikanth
Research in Astronomy and Astrophysics **2022**
https://arxiv.org/pdf/2207.10490
We present findings from an analysis of the fractal dimension of solar supergranulation as a function of latitude, supergranular cell size and solar rotation, employing spectroheliographic data in the Ca II K line of solar cycle no. 23. We find that the fractal dimension tends to decrease from about 1.37 at the equator to about 1 at 20 degree latitude in either hemisphere, suggesting that solar rotation rate has the effect of augmenting the irregularity of supergranular boundaries. Considering that supergranular cell size is directly correlated with fractal dimension, we conclude that the mechanism behind our observation is that solar rotation influences the cell outflow strength, and thereby cell size, with the latitude dependence of the supergranular fractal dimension being a consequence thereof.

Magnetized supersonic downflows in the chromosphere

K. **Sowmya**, A. Lagg, S. K. Solanki, J. S. Castellanos Durán
A&A 661, A122 **2022**
https://arxiv.org/pdf/2202.11679.pdf
https://www.aanda.org/articles/aa/pdf/2022/05/aa42850-21.pdf
The chromosphere above active regions (ARs) on the Sun hosts magnetized supersonic downflows. Studies of these supersonic downflows help to decipher the magnetic fine structure and dynamics of the chromosphere. We perform a statistical analysis of the magnetized supersonic downflows in a number of ARs and survey their characteristics. We analyze spectro-polarimetric scans of parts of 13 ARs obtained in the infrared He I 10830 Å triplet formed in the upper chromosphere recorded with the GREGOR Infrared Spectrograph (GRIS) mounted at the GREGOR solar telescope. We retrieve the line-of-sight velocities and the magnetic field vector using the HeLIx+ inversion code that assumes Milne-Eddington atmospheres. We find magnetized supersonic downflows in all the ARs, with larger area coverage by such flows in ARs observed during their emerging phase. The fact that supersonic downflows were detected in all scans, though they cover only a small fraction, 0.2--6.4%, of the observed field-of-view, suggests that they are a common phenomenon in the upper chromospheres of ARs. The supersonic downflows are found to be associated with many AR features such as pores, sunspot umbrae, sunspot penumbrae, light bridges, plages, He I loops as part of arch filament systems characteristic of emerging fields, and filaments. Although several mechanisms are identified to be causing the supersonic downflows, by far the most common one appears to be the draining of plasma along the legs of rising magnetic loops. The loops mainly drain into forming pores. The line-of-sight velocities of the supersonic downflows reach up to 49 kms-1 and the velocity distribution shows multiple populations. Almost 92% of these supersonic downflows coexist with a subsonic flow component. The weaker, more horizontal fields associated with the supersonic component suggests that it is formed above the subsonic component.

POLARIZED SCATTERING OF LIGHT FOR ARBITRARY MAGNETIC FIELDS WITH LEVEL-CROSSINGS FROM THE COMBINATION OF HYPERFINE AND FINE STRUCTURE SPLITTINGS

K. **Sowmya**1, K. N. Nagendra1, M. Sampoorna1, and J. O. Stenflo
2015 ApJ 814 127
Interference between magnetic substates of the hyperfine structure states belonging to different fine structure states of the same term influences the polarization for some of the diagnostically important lines of the Sun's spectrum, like the sodium and lithium doublets. The polarization signatures of this combined interference contain information on the properties of the solar magnetic fields. Motivated by this, in the present paper, we study the problem of polarized scattering on a two-term atom with hyperfine structure by accounting for the partial redistribution in the photon frequencies arising due to the Doppler motions of the atoms. We consider the scattering atoms to be under the influence of a magnetic field of arbitrary strength and develop a formalism based on the Kramers–Heisenberg approach to calculate the scattering cross section for this process. We explore the rich polarization effects that arise from various level-crossings in the Paschen–Back regime in a single scattering case using the lithium atomic system as a concrete example that is relevant to the Sun.

Solar radius and luminosity variations induced by the internal dynamo magnetic fields

F. **Spada**, R. Arlt, M. Kueker, S. Sofia
Astronomische Nachrichten **2018**
https://arxiv.org/pdf/1810.09794.pdf
Although the occurrence of solar irradiance variations induced by magnetic surface features (e.g., sunspots, faculae, magnetic network) is generally accepted, the existence of intrinsic luminosity changes due to the internal magnetic fields is still controversial. This additional contribution is expected to be accompanied by radius variations, and to be potentially significant for the climate of the Earth. We aim to constrain theoretically the radius and luminosity variations of the Sun that are due to the effect of the variable magnetic fields in its interior associated with the dynamo cycle. We have extended a one-dimensional stellar evolution code to include several effects of the magnetic fields on the interior structure. We investigate different magnetic configurations, based on both observational constraints and on the output of state-of-the-art mean field dynamo models. We explore both step-like and simply periodic time dependences of the magnetic field peak strength. We find that the luminosity and radius variations are in anti-phase and in phase, respectively, with the magnetic field strength. For peak magnetic field strengths of the order of tens of kilogauss, luminosity variations ranging between 10^{-6} and 10^{-3} (in modulus) and radius variations between 10^{-6} and 10^{-5} are obtained. Modest but significant radius variations (up to 10^{-5} in relative terms) are obtained for magnetic fields of realistic strength and geometry, providing a potentially observable signature of the intrinsic variations. Establishing their existence in addition to the accepted surface effects would have very important implications for the understanding of solar-induced long-term trends on climate.

Achievements and Lessons Learned from Successful Small Satellite Missions for Space Weather-Oriented Research **Review**

Harlan E. **Spence**, Amir Caspi, Hasan Bahcivan, Jesus Nieves-Chinchilla, +++
Space Weather **2023**
https://arxiv.org/pdf/2206.02968.pdf
When the first CubeSats were launched nearly two decades ago, few people believed that the miniature satellites would likely prove to be a useful scientific tool. Skeptics abounded. However, the last decade has seen the highly successful implementation of space missions that make creative and innovative use of fast-advancing CubeSat and small satellite technology to carry out important science experiments and missions. Several projects now have used CubeSats to obtain first-of-their-kind observations and findings that have formed the basis for high-profile engineering and science publications, thereby establishing without doubt the scientific value and broad utility of CubeSats. In this paper, we describe recent achievements and lessons learned from a representative selection of successful CubeSat missions with a space weather focus. We conclude that these missions were successful in part because their limited resources promoted not only mission focus but also appropriate risk-taking for comparatively high science return. Quantitative analysis of refereed publications from these CubeSat missions and several larger missions reveals that mission outcome metrics compare favorably when publication number is normalized by mission cost or if expressed as a weighted net scientific impact of all mission publications.

The Solar Orbiter SPICE instrument

An extreme UV imaging spectrometer

SPICE Consortium: M. Anderson1 , T. Appourchaux2 , F. Auchère2 , R. Aznar Cuadrado3 , J. Barbay2 , F. Baudin2
A&A **2019**
https://www.aanda.org/articles/aa/pdf/forth/aa35574-19.pdf
Aims. The ***Spectral Imaging of the Coronal Environment (SPICE)*** instrument is a high-resolution imaging spectrometer operating at extreme ultraviolet (EUV) wavelengths. In this paper, we present the concept, design, and pre-launch performance of this facility instrument on the ESA/NASA Solar Orbiter mission. Methods. The goal of this paper is to give prospective users a better understanding of the possible types of observations, the data acquisition, and the sources that contribute to the instrument's signal. Results. The paper discusses the science objectives, with a focus on the SPICE-specific aspects, before presenting the instrument's design, including optical, mechanical, thermal, and electronics aspects. This is followed by a characterisation and calibration of the instrument's performance. The paper concludes with descriptions of the operations concept and data processing. Conclusions. The performance measurements of the various instrument parameters meet the requirements derived from the mission's science objectives. The SPICE instrument is ready to perform measurements that will provide vital contributions to the scientific success of the Solar Orbiter mission.
2. Scientific objectives and opportunities

The magnetic shear-current effect: generation of large-scale magnetic fields by the small-scale dynamo

Jonathan **Squire**, Amitava Bhattacharjee
J. Plasma Phys. **201**5

http://arxiv.org/pdf/1512.04511v1.pdf
A novel large-scale dynamo mechanism, the magnetic shear-current effect, is discussed and explored. The effect relies on the interaction of magnetic fluctuations with a mean shear flow, meaning the saturated state of the small-scale dynamo can drive a large-scale dynamo -- in some sense the inverse of dynamo quenching. The dynamo is nonhelical, with the mean-field α coefficient zero, and is caused by the interaction between an off-diagonal component of the turbulent resistivity and the stretching of the large-scale field by shear flow. Following up on previous numerical and analytic work, this paper presents further details of the numerical evidence for the effect, as well as an heuristic description of how magnetic fluctuations can interact with shear flow to produce the required electromotive force. The pressure response of the fluid is fundamental to this mechanism, which helps explain why the magnetic effect is stronger than its kinematic cousin, and the basic idea is related to the well-known lack of turbulent resistivity quenching by magnetic fluctuations. As well as being interesting for its applications to general high Reynolds number astrophysical turbulence, where strong small-scale magnetic fluctuations are expected to be prevalent, the magnetic shear-current effect is a likely candidate for large-scale dynamo in the unstratified regions of ionized accretion disks. Evidence for this is discussed, as well as future research directions and the challenges involved with understanding details of the effect in astrophysically relevant regimes.

Generation of large-scale magnetic fields by small-scale dynamo in shear flows

Jonathan **Squire**, Amitava Bhattacharjee
2015
http://arxiv.org/pdf/1506.04109v1.pdf
We propose a new mechanism for turbulent mean-field dynamo in which the magnetic fluctuations resulting from a small-scale dynamo drive the generation of large-scale magnetic fields. This is in stark contrast to the common idea that small-scale magnetic fields should be harmful to large-scale dynamo action. These dynamos occur in the presence of large-scale velocity shear and do not require net helicity, resulting from off-diagonal components of the turbulent resistivity tensor as the magnetic analogue of the "shear-current" effect. Given the inevitable existence of non-helical small-scale magnetic fields in turbulent plasmas, as well as the generic nature of velocity shear, the suggested mechanism may help to explain generation of large-scale magnetic fields across a wide range of astrophysical objects.

Chromospheric Heating by MHD Waves and Instabilities **Review**

A.K. **Srivastava**, J.L. Ballester, P.S. Cally, M. Carlsson, M. Goossens, D.B. Jess, E. Khomenko, M. Mathioudakis, K. Murawski, T.V. Zaqarashvili
JGR (The special issue "Solar and Heliospheric Plasma Structures: Waves, Turbulence, and Dissipation") **Volume126, Issue6** e2020JA029097 **2021**
https://agupubs.onlinelibrary.wiley.com/doi/epdf/10.1029/2020JA029097
https://arxiv.org/pdf/2104.02010.pdf
The importance of the chromosphere in the mass and energy transport within the solar atmosphere is now widely recognised. This review discusses the physics of magnetohydrodynamic (MHD) waves and instabilities in large-scale chromospheric structures as well as in magnetic flux tubes. We highlight a number of key observational aspects that have helped our understanding of the role of the solar chromosphere in various dynamic processes and wave phenomena, and the heating scenario of the solar chromosphere is also discussed. The review focuses on the physics of waves and invokes the basics of plasma instabilities in the context of this important layer of the solar atmosphere. Potential implications, future trends and outstanding questions are also delineated.

Editorial on the Research Topic
Data-driven MHD: Novel Applications to the Solar Atmosphere **Review**

A **Srivastava**, Robertus Erdelyi, Stefaan Poedts, Peng-Fei Chen, and Y Yan
Front. Astron. Space Sci., Volume 8, id.140 **2021** |
https://www.frontiersin.org/articles/10.3389/fspas.2021.739264/full
https://doi.org/10.3389/fspas.2021.739264

Velocity Response of the Observed Explosive Events in the Lower Solar Atmosphere: I. Formation of the Flowing Cool Loop System

A.K. **Srivastava**, Yamini K. Rao, P. Konkol, K. Murawski, M. Mathioudakis, Sanjiv K. Tiwari, E. Scullion, J.G. Doyle, B.N. Dwivedi
ApJ **2020**
https://arxiv.org/pdf/2004.02775.pdf
We observe plasma flows in cool loops using the Slit-Jaw Imager (SJI) onboard the Interface Region Imaging Spectrometer (IRIS). Huang et al. (2015) observed unusually broadened Si IV 1403 angstrom line profiles at the footpoints of such loops that were attributed to signatures of explosive events (EEs). We have chosen one such uni-

directional flowing cool loop system observed by IRIS where one of the footpoints is associated with significantly broadened Si IV line profiles. The line profile broadening indirectly indicates the occurrence of numerous EEs below the transition region (TR), while it directly infers a large velocity enhancement /perturbation further causing the plasma flows in the observed loop system. The observed features are implemented in a model atmosphere in which a low-lying bi-polar magnetic field system is perturbed in the chromosphere by a velocity pulse with a maximum amplitude of 200 km/s. The data-driven 2-D numerical simulation shows that the plasma motions evolve in a similar manner as observed by IRIS in the form of flowing plasma filling the skeleton of a cool loop system. We compare the spatio-temporal evolution of the cool loop system in the framework of our model with the observations, and conclude that their formation is mostly associated with the velocity response of the transient energy release above their footpoints in the chromosphere/TR. Our observations and modeling results suggest that the velocity responses most likely associated to the EEs could be one of the main candidates for the dynamics and energetics of the flowing cool loop systems in the lower solar atmosphere. **December 27, 2013**

On the Observations of Rapid Forced Reconnection in the Solar Corona

A. K. **Srivastava**1, S. K. Mishra1, P. Jelínek2, Tanmoy Samanta3, Hui Tian3, Vaibhav Pant4, P. Kayshap2, Dipankar Banerjee5, J. G. Doyle6, and B. N. Dwivedi1
2019 ApJ 887 137
https://doi.org/10.3847/1538-4357/ab4a0c
Using multiwavelength imaging observations from the Atmospheric Imaging Assembly on board the Solar Dynamics Observatory on **2012 May 3**, we present a novel physical scenario for the formation of a temporary X-point in the solar corona, where plasma dynamics are forced externally by a moving prominence. Natural diffusion was not predominant; however, a prominence driven inflow occurred first, forming a thin current sheet, thereafter enabling a forced magnetic reconnection at a considerably high rate. Observations in relation to the numerical model reveal that forced reconnection may rapidly and efficiently occur at higher rates in the solar corona. This physical process may also heat the corona locally even without establishing a significant and self-consistent diffusion region. Using a parametric numerical study, we demonstrate that the implementation of the external driver increases the rate of the reconnection even when the resistivity required for creating normal diffusion region decreases at the X-point. We conjecture that the appropriate external forcing can bring the oppositely directed field lines into the temporarily created diffusion region first via the plasma inflows as seen in the observations. The reconnection and related plasma outflows may occur thereafter at considerably larger rates.

On the rapid forced reconnection in the Sun's corona for its localized heating

A.K. **Srivastava**, P. Jelínek, Sudheer K. Mishra, Tanmoy Samanta, Hui Tian, Vaibhav Pant, P. Kayshap, D. Banerjee, J.G. Doyle, B.N. Dwivedi
2019
https://arxiv.org/pdf/1901.07971.pdf
The million-degree hot solar corona maintains its high temperature and compensates for its radiative losses by continuously acquiring an energy flux of ≈103 W m−2,. Recent studies suggest that energy transport in the solar corona is associated with localized magnetic flux-tubes, which can channel various kinds of magnetohydrodynamic (MHD) waves and shocks as heating candidates. Dissipation of electric current via magnetic reconnection provides an alternate mechanism to heat the solar corona. However, there are various physical conditions that need to be established appropriately in the reconnection region to generate its high rate and subsequent energy release. Using multiwavelength imaging observations from the Atmospheric Imaging Assembly (AIA) onboard the Solar Dynamics Observatory (SDO), we present a novel physical scenario for the formation of a temporary X-point in the solar corona, where plasma dynamics is forced externally by a moving prominence. Natural diffusion was not predominant, however, a prominence driven inflow occurred firstly, forming a thin current sheet and enabling a forced magnetic reconnection at a considerably high rate. Observations vis-á-vis numerical model reveal that forced reconnection may rapidly and efficiently release energy in the solar corona to heat it locally even without establishing a significant and self-consistent diffusion region. **3 May 2012**

The Extended Solar Cycle: Muddying the Waters of Solar/Stellar Dynamo Modeling Or Providing Crucial Observational Constraints? **Review**

A.K. **Srivastava**, S.W. McIntosh, N. Arge, D. Banerjee, E. Cliver, M. Dikpati, B.N. Dwivedi, M. Guhathakurta,B.B. Karak, R.J. Leamon, P. Martens, S.K. Matthew, A. Munoz-Jaramillo, D. Nandi, A. Norton, L. Upton, S. Chatterjee, R. Mazumder, Yamini K. Rao, R. Yadav
Front. Astron. Space Sci., 5:38. **2018** |
https://www.frontiersin.org/articles/10.3389/fspas.2018.00038/full
https://doi.org/10.3389/fspas.2018.00038
https://arxiv.org/pdf/1807.07601.pdf

In 1844 Schwabe discovered that the number of sunspots increased and decreased over a period of about 11 years, that variation became known as the sunspot cycle. Almost eighty years later, Hale described the nature of the Sun's magnetic field, identifying that it takes about 22 years for the Sun's magnetic polarity to cycle. It was also identified that the latitudinal distribution of sunspots resembles the wings of a butterfly showing migration of sunspots in each hemisphere that abruptly start at mid-latitudes towards the Sun's equator over the next 11 years. These sunspot patterns were shown to be asymmetric across the equator. In intervening years, it was deduced that the Sun (and sun-like stars) possess magnetic activity cycles that are assumed to be the physical manifestation of a dynamo process that results from complex circulatory transport processes in the star's interior. Understanding the Sun's magnetism, its origin and its variation, has become a fundamental scientific objective \-- the distribution of magnetism, and its interaction with convective processes, drives various plasma processes in the outer atmosphere. In the past few decades, a range of diagnostic techniques have been employed to systematically study finer scale magnetized objects, and associated phenomena. The patterns discerned became known as the ``Extended Solar Cycle" (ESC). The patterns of the ESC appeared to extend the wings of the activity butterfly back in time, nearly a decade before the formation of the sunspot pattern, and to much higher solar latitudes. In this short review, we describe their observational patterns of the ESC and discuss possible connections to the solar dynamo as we depart on a multi-national collaboration to investigate the origins of solar magnetism through a blend of archived and contemporary data analysis with the goal of improving solar dynamo understanding and modeling.

Polarised kink waves in magnetic elements: evidence for chromospheric helical waves

Marco **Stangalini**, Fabio Giannattasio, Robertus Erdélyi, Shahin Jafarzadeh, Giuseppe Consolini, Serena Criscuoli, Ilaria Ermolli, Salvo Luigi Guglielmino, Francesca Zuccarello

ApJ 840 19 **2017**

https://arxiv.org/pdf/1704.02155.pdf

In recent years, new high spatial resolution observations of the Sun's atmosphere have revealed the presence of a plethora of small-scale magnetic elements down to the resolution limit of current cohort of solar telescopes (∼100−120 km on the solar photosphere). These small magnetic field concentrations, due to the granular buffeting, can support and guide several magneto-hydrodynamics (MHD) wave modes that would eventually contribute to the energy budget of the upper layers of the atmosphere.\\ In this work, exploiting the high spatial and temporal resolution chromospheric data acquired with the Swedish 1-meter Solar Telescope (SST), and applying the empirical mode decomposition (EMD) technique to the tracking of the solar magnetic features, we analyse the perturbations of the horizontal velocity vector of a set of chromospheric magnetic elements. We find observational evidence that suggests a phase relation between the two components of the velocity vector itself, resulting in its helical motion.

Recurrence quantification analysis of two solar cycle indices

Marco **Stangalini**1*, Ilaria Ermolli1, Giuseppe Consolini2 and Fabrizio Giorgi

J. Space Weather Space Clim., 7, A5 (**2017**)

http://www.swsc-journal.org/articles/swsc/pdf/2017/01/swsc150077.pdf

https://arxiv.org/pdf/1701.06802v1.pdf

Solar activity affects the whole heliosphere and near-Earth space environment. It has been reported in the literature that the mechanism responsible for the solar activity modulation behaves like a low-dimensional chaotic system. Studying these kind of physical systems and, in particular, their temporal evolution requires non-linear analysis methods. To this regard, in this work we apply the recurrence quantification analysis (RQA) to the study of two of the most commonly used solar cycle indicators; i.e. the series of the sunspot number (SSN), and the radio flux 10.7 cm, with the aim of identifying possible dynamical transitions in the system; a task which is particularly suited to the RQA. The outcome of this analysis reveals the presence of large fluctuations of two RQA measures: namely the determinism and the laminarity. In addition, large differences are also seen between the evolution of the RQA measures of the SSN and the radio flux. That suggests the presence of transitions in the dynamics underlying the solar activity. Besides it also shows and quantifies the different nature of these two solar indices. Furthermore, in order to check whether our results are affected by dataartefacts, we have also applied the RQA to both the recently recalibrated SSN series and the previous one, unveiling the main differences between the two data sets. The results are discussed in light of the recent literature on the subject.

Non-linear propagation of kink waves to the solar chromosphere

M. **Stangalini**, F. Giannattasio, S. Jafarzadeh

A&A 577, A17 **2015**

http://arxiv.org/pdf/1502.07213v1.pdf

Small-scale magnetic field concentrations (magnetic elements) in the quiet Sun are believed to contribute to the energy budget of the upper layers of the Sun's atmosphere, as they are observed to support a large number of MHD modes. In recent years, kink waves in magnetic elements were observed at different heights in the solar atmosphere, from the photosphere to the corona. However, the propagation of these waves has not been fully evaluated. Our aim is to investigate the propagation of kink waves in small magnetic elements in the solar atmosphere. We analysed spectropolarimetric data of high-quality and long duration of a photospheric quiet Sun region observed near the disk center with the spectropolarimeter CRISP at the Swedish Solar Telescope (SST), and complemented by simultaneous and co-spatial broad-band chromospheric observations of the same region. Our findings reveal a clear upward propagation of kink waves with frequency above 2.6 mHz. Moreover, the signature of a non-linear propagation process is also observed. By comparing photospheric to chromospheric power spectra, no signature of an energy dissipation is found at least at the atmospheric heights at which the data analysed originate. This implies that most of the energy carried by the kink waves (within the frequency range under study <17 mHz) flows to upper layers in the Sun's atmosphere.

Aurora Observations from the Principality of Transylvania from the 16th to the 18th Century CE

Martin **Stangl** & Ulrich Foelsche
Solar Physics volume 296, Article number: 78 (**2021**)
https://link.springer.com/content/pdf/10.1007/s11207-021-01811-7.pdf
https://doi.org/10.1007/s11207-021-01811-7
We focused on the period from about 1500 CE to 1800 CE and present a compilation of 78 different auroral sightings for the period from the geographical area of the former Principality of Transylvania, then part of the Kingdom of Hungary, and we give source quotations in English translation. Of the 78 potential aurorae, 23 are missing from the catalog of Rethly and Berkes (1963) and are introduced here for the first time into the scientific discourse on past solar activity. The region of Transylvania located around 46° northern latitude is a good geographical indicator for an auroral oval extending unusually far towards the Equator. The reports of seven celestial phenomena from Transylvania during the period of the Maunder minimum (1645 – 1715), which are considered genuine northern lights at a medium to very high probability level, suggest that even during this time of greatly reduced solar activity, aurorae penetrated down to near 45° latitude. Three of these potential aurorae, however, fall within the 18th century, when the Sun was already recovering from the deep minimum phase. Comparing the distribution of potential auroral sightings in Transylvania from the 16th to the 18th century clearly shows, in comparison with other aurora catalogs and with reconstructed solar activity, that high selectivity due to the historical-source situation (incomplete chronicles, lost reports, and lack of scientific interest on the part of chroniclers) makes statements about actual long-term distributions almost impossible. Furthermore, the catalog of Rethly and Berkes is shown to be rather incomplete and to contain several doubtful entries.

Solar X-ray variability in terms of a fractional heteroskedastic time series model

Aleksander A **Stanislavsky** Krzysztof Burnecki Joanna Janczura Karol NiczyjAleksander Weron
Monthly Notices of the Royal Astronomical Society, Volume 485, Issue 3, May **2019**, Pages 3970–3980,
https://doi.org/10.1093/mnras/stz656
The Sun is variable in activity with changes on time-scales as short as minutes to as long as a solar cycle. Although the most accurate measurements are limited to the satellite era, the past four decades, looking at the solar variability over this period provides a possible link between complex dynamics of the Sun and the accompanying radiation. Measurements of the latter and their analysis by sophisticated time series methods encourage forecasting future values of the time series. Our data analysis work focuses on the soft X-ray emission observed at the current solar minimum, in 2017 September July. We have found two different (active and inactive) states of the solar activity using a Hidden Markov Model, and we show that in the periods of high-solar activity the energy distribution of soft X-ray solar flares is well described by an ARFIMA-GARCH model, whereas in the case of low-solar activity an ARFIMA model is best fitted. Switching from the inactive state to the active one is caused by explosive phenomena in the Sun. The model describes three effects detected in our empirical studies. One of them is a long-term dependence, the second is variance changing in time, and the third corresponds to heavy-tailed distributions of the X-ray data. Moreover, the model takes into account memory effects in soft X-ray emission due to the Sun's magnetic field evolution. All this together allows us to suggest a statistically justified model for explaining the solar activity variability at the current solar minimum.

Measuring the Flattening of the Outer F-corona Using STEREO-A/HI-1 Images

Johnathan R. **Stauffer**1,1, Guillermo Stenborg2,1, and Russell A. Howard2,1
2018 ApJ 864 29
http://sci-hub.tw/http://iopscience.iop.org/article/10.3847/1538-4357/aad689/meta
The white-light Fraunhofer-corona (F-corona) arises from light scattered by the circumsolar dust. Using weekly minimum background models of ST-A/HI-1 observations, we characterized the flattening of the F-corona between

5° and 24° elongation by measuring the radii of constant-intensity contours along, and at a 25° angle to, the photometric axis. The ratio of these quantities (the pseudo-flattening index $\tilde{f} = R_{\rm eq}/R(25^\circ) - 1$) is analogous to the definition of the flattening index ($f = R_{\rm eq}/R_{\rm pol} - 1$). Measurements of the pseudo-flattening in the north and south hemispheres reveal a periodic asymmetry in the appearance of the F-corona (attributable to changes in polar brightness due to the elevation of the spacecraft from the dust symmetry surface), as well as a north/south asymmetry possibly introduced by the warped dust symmetry surface. The north/south averaged pseudo-flattening was used to infer the flattening for each weekly model. We found that the inferred flattening index (1) varies periodically with spacecraft position, reaching a maximum in the range $262^\circ \lesssim \lambda \lesssim 290^\circ$ due to a brightening along the photometric axis when the spacecraft passes through the surface of maximum dust density, and a minimum at $\lambda \approx 200^\circ$, and (2) slightly varies as a function of time (at least partially due to the displacement of the circumsolar dust with respect to the Sun). Comparison of the flattening index with previous works suggests a cubic dependence of the flattening index with log elongation for $|\epsilon| \lesssim 24^\circ$.

Exploring the Connection between Helioseismic Travel Time Anomalies and the Emergence of Large Active Regions during Solar Cycle 24

John **Stefan**, Alexander Kosovichev

ApJ **948** 1 **2023**

https://arxiv.org/pdf/2212.05959.pdf

https://iopscience.iop.org/article/10.3847/1538-4357/acc836/pdf

We investigate deviations in the mean phase travel time of acoustic waves preceding the emergence of 46 large active regions observed by the Helioseismic and Magnetic Imager (HMI). In our investigation, we consider two different procedures for obtaining the mean phase travel time, by minimizing the difference between cross-correlations and a reference, as well as the Gabor wavelet fitting procedure. We cross-correlate the time series of mean phase travel time deviations with the surface magnetic field and determine the peak correlation time lag. We also compute the perturbation index--the area integrated mean phase travel time deviations exceeding quiet sun thresholds--and compare the time of peak perturbation index with the correlation time lag. We find that the lag times derived from the difference minimization procedure precede the flux emergence for 36 of the 46 active regions, and that this lag time has a noticeable correlation with the maximum flux rate. However, only 28 of the active regions have peak perturbation index times in the range of 24 to 48 hours prior to the flux emergence. Additionally, we examine the relationship between properties of the emerged active regions and the strength of helioseismic signals prior to their emergence.

Analysis and Modeling of High-Frequency Emission and Deep Seismic Sources of Sunquakes

John T. **Stefan**, Alexander G. Kosovichev

ApJ **2022**

https://arxiv.org/pdf/2209.11286.pdf

Recent work published by Lindsey et al find evidence for a deep and compact seismic source for the sunquake associated with the **2011 July 30** M9.3 flare, as well as seismic emission extending up to 10 mHz. We examine the sunquake independently, and a possible wavefront is found in the 8 mHz band, though no wavefront is easily discernible in the 10 mHz band. Additionally, we perform numerical simulations of seismic excitation modeled with the reported parameters and changes in the power spectra with increasing depth of the excitation source are examined. It is found that the peak frequency decreases for increasing depths, but a shallow minimum is indicated between z=0 and z=-840 km. Analysis of the suspected wavefront of the M9.3 sunquake finds that the power spectrum of the reported seismic emission is close to that of background oscillations, though with a peak frequency noticeably lower than the background peak. Additionally, it is found that the amplitude of the source estimated by Lindsey et al is too low to produce the observed wavefront.

Analysis of Time-Distance Helioseismology for Detection of Emerging Active Regions

John T. **Stefan**, Alexander G. Kosovichev, Andrey M. Stejko

ApJ **913** 87 **2021**

https://arxiv.org/pdf/2012.01367.pdf

https://doi.org/10.3847/1538-4357/abf2bf

A time-distance helioseismic technique, similar to the one used by Ilonidis et al (2011), is applied to two independent numerical models of subsurface sound-speed perturbations to determine the spatial resolution and accuracy of phase travel time shift measurements. The technique is also used to examine pre-emergence signatures of several active regions observed by the Michelson Doppler Imager (MDI) and the Helioseismic Magnetic Imager (HMI). In the context of similar measurements of quiet sun regions, three of the five studied active regions show strong phase travel time shifts several hours prior to emergence. These results form the basis of a discussion of noise

in the derived phase travel time maps and possible criteria to distinguish between true and false positive detection of emerging flux.

Estimation of Key Sunquake Parameters through Hydrodynamic Modeling and Cross-Correlation Analysis

John T. **Stefan**, Alexander G. Kosovichev
ApJ **895** 65 **2019**
https://arxiv.org/pdf/1911.06839.pdf
https://doi.org/10.3847/1538-4357/ab88ae
Sunquakes are one of the more distinct secondary phenomena related to solar flares, where energy deposition in the lower layers of the Sun's atmosphere excites acoustic waves easily visible in HMI dopplergrams. We explore two possible sources of sunquakes in the context of the electron beam hypothesis, as an instantaneous transfer of momentum and as a gradual applied force. We model the sunquake excitation and compare with five observed sunquake events using a cross-correlation analysis. We find that at least half the events studied are consistent with the electron beam hypothesis and estimate the energy required to excite the sunquakes to be within the range determined by previous studies. **2012 Oct 23, 2013 Nov 5, 2014 Mar 29, 2015 Sep 30, 2017 Sep 6**

Rieger, Schwabe, Suess-de Vries: The Sunny Beats of Resonance.

Stefani, F., Horstmann, G.M., Klevs, M. et al.
Sol Phys 299, 51 (**2024**).
https://doi.org/10.1007/s11207-024-02295-x
https://link.springer.com/content/pdf/10.1007/s11207-024-02295-x.pdf
We propose a self-consistent explanation of Rieger-type periodicities, the Schwabe cycle, and the Suess-de Vries cycle of the solar dynamo in terms of resonances of various wave phenomena with gravitational forces exerted by the orbiting planets. Starting on the high-frequency side, we show that the two-planet spring tides of Venus, Earth, and Jupiter are able to excite magneto-Rossby waves, which can be linked with typical Rieger-type periods. We argue then that the 11.07-year beat period of those magneto-Rossby waves synchronizes an underlying conventional $\alpha\Omega$-dynamo by periodically changing either the field storage capacity in the tachocline or some portion of the α-effect therein. We also strengthen the argument that the Suess-de Vries cycle appears as an 193-year beat period between the 22.14-year Hale cycle and a spin-orbit coupling effect related with the 19.86-year rosette-like motion of the Sun around the barycenter.

No evidence for absence of solar dynamo synchronization

F. **Stefani**, J. Beer, T. Weier
A&A **2023**
https://arxiv.org/pdf/2303.01154.pdf
Context: The old question of whether the solar dynamo is synchronized by the tidal forces of the orbiting planets has recently received renewed interest, both from the viewpoint of historical data analysis and in terms of theoretical and numerical modelling. Aims: We aim to contribute to the solution of this longstanding puzzle by analyzing cosmogenic radionuclide data from the last millennium. Methods: We reconsider a recent time-series of 14C-inferred sunspot data and compare the resulting cycle minima and maxima with the corresponding conventional series down to 1610 A.D., enhanced by Schove's data before that time. Results: We find that, despite recent claims to the contrary, the 14C-inferred sunspot data are well compatible with a synchronized solar dynamo, exhibiting a relatively phase-stable period of 11.07 years, which points to a synchronizing role of the spring tides of the Venus-Earth-Jupiter system.

Shaken and Stirred: When Bond Meets Suess–de Vries and Gnevyshev–Ohl

F. **Stefani**, R. Stepanov & T. Weier
Solar Physics volume 296, Article number: 88 (**2021**)
https://link.springer.com/content/pdf/10.1007/s11207-021-01822-4.pdf
https://doi.org/10.1007/s11207-021-01822-4
We argue that the most prominent temporal features of the solar dynamo, in particular the Hale cycle, the Suess–de Vries cycle (associated with variations of the Gnevyshev–Ohl rule), Gleissberg-type cycles, and grand minima can all be explained by combined synchronization with the 11.07-year periodic tidal forcing of the Venus–Earth–Jupiter system and the (mainly) 19.86-year periodic motion of the Sun around the barycenter of the solar system. We present model simulations where grand minima, and clusters thereof, emerge as intermittent and non-periodic events on millennial time scales, very similar to the series of Bond events which were observed throughout the Holocene and the last glacial period. If confirmed, such an intermittent transition to chaos would prevent any long-term prediction of solar activity, notwithstanding the fact that the shorter-term Hale and Suess–de Vries cycles are clocked by planetary motion.

Phase coherence and phase jumps in the Schwabe cycle

F. **Stefani**, J. Beer, A. Giesecke, T. Gloaguen, M. Seilmayer, R. Stepanov, T. Weier
Astronomische Nachrichten **2020**
https://arxiv.org/pdf/2004.10028.pdf
Guided by the working hypothesis that the Schwabe cycle of solar activity is synchronized by the 11.07 years alignment cycle of the tidally dominant planets Venus, Earth and Jupiter, we reconsider the phase diagrams of sediment accumulation data in lake Holzmaar, and of methanesulfonate (MSA) data in the Greenland ice core GISP2, which are available for the period 10000-9000 cal. BP. Since the half-cycle phase jumps appearing in the output signals are, very likely, artifacts of applying a biologically substantiated transfer function, the underlying solar input signal with a dominant 11.04 years periodicity can well be considered as mainly phase-coherent over the 1000 years period in the early Holocene. For more recent times, we show that the re-introduction of a hypothesized "lost cycle" at the beginning of the Dalton minimum would lead to a real phase jump. Similarly, by analyzing various series of 14C and 10Be data and comparing them with Schove's historical cycle maxima, we support the existence of another "lost cycle" around 1565, also connected with a phase jump. Viewed synoptically, our results lend greater plausibility to the starting hypothesis of a tidally synchronized solar cycle, which at times can undergo phase jumps, although the competing explanation in terms of a self-synchronizing solar dynamo cannot be completely ruled out.

A Tayler-Spruit model of a tidally synchronized solar dynamo

Frank **Stefani**, André Giesecke, Toma Weier
Solar Phys. **2018**
https://arxiv.org/pdf/1803.08692.pdf
We discuss a solar dynamo model of the Tayler-Spruit type whose Omega-effect is traditionally produced by a solar-like differential rotation but whose alpha-effect is assumed to be periodically modulated by planetary tidal forcing. This resonance-like effect has its rationale in the tendency of the current-driven Tayler instability to undergo intrinsic helicity oscillations which, in turn, can be synchronized by periodic tidal perturbations. Specifically, we focus on the 11.07 years periodicity of the alignment of the tidally dominant planets Venus, Earth, and Jupiter. In the framework of a simple one-dimensional numerical model we prove the subcritical nature of this Tayler-Spruit type dynamo. The typically emerging dynamo modes are dipolar fields, oscillating with a 22.14 years period, but also quadrupolar fields pulsating with a 11.07 years period. Transitions between these field topologies are reminiscent of the observed behaviour during the Maunder minimum. Further interesting features of the model are the emergence of mid-term fluctuations, with periods in the order of one year, and the intermittent appearance of reversed helicities in both hemispheres. With minor model modifications, the correct direction of the butterfly diagram comes out as a robust feature, too.

On the Synchronizability of Tayler–Spruit and Babcock–Leighton Type Dynamos

F. **Stefani**, A. Giesecke, N. Weber, T. Weier
Solar Physics January **2018**, 293:12
https://link.springer.com/content/pdf/10.1007%2Fs11207-017-1232-y.pdf
The solar cycle appears to be remarkably synchronized with the gravitational torques exerted by the tidally dominant planets Venus, Earth and Jupiter. Recently, a possible synchronization mechanism was proposed that relies on the intrinsic helicity oscillation of the current-driven Tayler instability which can be stoked by tidal-like perturbations with a period of 11.07 years. Inserted into a simple αα–ΩΩ dynamo model these resonantly excited helicity oscillations led to a 22.14 years dynamo cycle. Here, we assess various alternative mechanisms of synchronization. Specifically we study a simple time-delay model of Babcock–Leighton type dynamos and ask whether periodic changes of either the minimal amplitude for rising toroidal flux tubes or the ΩΩ effect could eventually lead to synchronization. In contrast to the easy and robust synchronizability of Tayler–Spruit dynamo models, our answer for those Babcock–Leighton type models is less propitious.

Synchronized helicity oscillations: a link between planetary tides and the solar cycle?

F. **Stefani**, A. Giesecke, N. Weber, T. Weier
Solar Phys. 291(8) 2197-2212 **2016**
http://arxiv.org/pdf/1511.09335v1.pdf
Recent years have seen an increased interest in the question whether the gravitational action of planets could have an influence on the solar dynamo. Without discussing the observational validity of the claimed correlations, we ask for a possible physical mechanism which might link the weak planetary forces with solar dynamo action. We focus on the helicity oscillations which were recently found in simulations of the current-driven, kink-type Tayler instability

which is characterized by an m=1 azimuthal dependence. We show how these helicity oscillations can be resonantly excited by some m=2 perturbation that reflects a tidal oscillation. Specifically, we speculate that the 11.07 years tidal oscillation induced by the Venus-Earth-Jupiter system may lead to a 1:1 resonant excitation of the oscillation of the alpha effect. Finally, in the framework of a reduced, zero-dimensional alpha-Omega dynamo model we recover a 22.14 years cycle of the solar dynamo.

Schwabe, Gleissberg, Suess-de Vries: Towards a consistent model of planetary synchronization of solar cycles

F. **Stefani**, A. Giesecke, M. Seilmayer, R. Stepanov, T. Weier
MAGNETOHYDRODYNAMICS Vol. 40 (**2004**), No. 1, pp. 1–10
https://arxiv.org/pdf/1910.10383.pdf
Aiming at a consistent planetary synchronization model of both short-term and long-term solar cycles, we start with an analysis of Schove's historical data of cycle maxima. Their deviations (residuals) from the average cycle duration of 11.07 years show a high degree of regularity, comprising a dominant 200-year period (Suess-de Vries cycle), and a few periods around 100 years (Gleissberg cycle). Encouraged by their robustness, we support previous forecasts of an upcoming grand minimum in the 21st century. To explain the long-term cycles, we enhance our tidally synchronized solar dynamo model by a modulation of the field storage capacity of the tachocline with the orbital angular momentum of the Sun, which is dominated by the 19.86-year periodicity of the Jupiter-Saturn synodes. This modulation of the 22.14 years Hale cycle leads to a 193-year beat period of dynamo activity which is indeed close to the Suess-de Vries cycle. For stronger dynamo modulation, the model produces additional peaks at typical Gleissberg frequencies, which seem to be explainable by the non-linearities of the basic beat process, leading to a bi-modality of the Schwabe cycle. However, a complementary role of beat periods between the Schwabe cycle and the Jupiter-Uranus/Neptune synodic cycles cannot be completely excluded.

Constraining Global Solar Models through Helioseismic Analysis

Andrey M. **Stejko**1, Alexander G. Kosovichev1, Nicholas A. Featherstone2, Gustavo Guerrero1,3, Bradley W. Hindman4,5, Loren I. Matilsky4,5, and Jörn Warnecke6
2022 ApJ 934 161
https://iopscience.iop.org/article/10.3847/1538-4357/ac7a44/pdf
Global hydrodynamic simulations of internal solar dynamics have focused on replicating the conditions for solar-like (equator rotating faster than the poles) differential rotation and meridional circulation using the results of helioseismic inversions as a constraint. Inferences of meridional circulation, however, have provided controversial results showing the possibility of one, two, or multiple cells along the radius. To help address this controversy and develop a more robust understanding of global flow regimes in the solar interior, we apply a "forward-modeling" approach to the analysis of helioseismic signatures of meridional circulation profiles obtained from numerical simulations. We employ the global acoustic modeling code GALE to simulate the propagation of acoustic waves through regimes of mean mass-flows generated by global hydrodynamic and magnetohydrodynamic models: EULAG, the Pencil code, and the Rayleigh code. These models are used to create synthetic Dopplergram data products, used as inputs for local time–distance helioseismology techniques. Helioseismic travel-time signals from solutions obtained through global numerical simulations are compared directly with inferences from solar observations, in order to set additional constraints on global model parameters in a direct way. We show that even though these models are able to replicate solar-like differential rotation, the resulting rotationally constrained convection develops a multicell global meridional circulation profile that is measurably inconsistent with local time–distance inferences of solar observations. However, we find that the development of rotationally unconstrained convection close to the model surface is able to maintain solar-like differential rotation, while having a significant impact on the helioseismic travel-time signal, replicating solar observations within one standard deviation of the error due to noise.

Helioseismic Signatures of One- and Two-Cell Meridional Circulation

Andrey M. **Stejko**, Alexander G. Kosovichev, Valery V. Pipin
ApJ **911** 90 **2021**
https://arxiv.org/pdf/2101.01220.pdf
https://doi.org/10.3847/1538-4357/abec70
Using a 3D global solver of the linearized Euler equations, we model acoustic oscillations over background velocity flow fields of single-cell meridional circulation with deep and shallow return flows as well as a double-cell meridional circulation profile. The velocities are generated using a mean-field hydrodynamic and dynamo model -- moving through the regimes with minimal parameter changes; counter-rotation near the base of the tachocline is induced by sign inversion of the non-diffusive action of turbulent Reynolds stresses (Λ-effect) due to the radial inhomogeneity of the Coriolis number. By mimicking the stochastic excitation of resonant modes in the convective interior, we simulate realization noise present in solar observations. Using deep-focusing to analyze differences in travel-time signatures between the three regimes, as well as comparing to solar observations, we show that current

helioseismology techniques may offer important insights about the location of the return flow, however, that it may not be possible to definitively distinguish between profiles of single-cell or double-cell meridional circulation.
HMI Science Nuggets #157 **2021** http://hmi.stanford.edu/hminuggets/?p=3541

Helioseismic Modeling of Background Flows

Andrey M. **Stejko**, Alexander G. Kosovichev, Nagi N. Mansour
2021 *ApJS* **253** 9
https://arxiv.org/pdf/2011.03131.pdf
https://doi.org/10.3847/1538-4365/abd3fe
We present a 3-dimensional (3D) numerical solver of the linearized compressible Euler equations (3D GLASS -- GLobal Acoustic Solar Simulation), used to model acoustic oscillations throughout the solar interior. The governing equations are solved in conservation form on a fully global spherical mesh ($0 \le \phi \le 2\pi$, $0 \le \theta \le \pi$, $0 \le r \le R\odot$) over a background state generated by the standard Solar Model S. We implement an efficient pseudo-spectral computational method to calculate the contribution of the compressible material derivative dyad to internal velocity perturbations, computing oscillations over arbitrary 3D background velocity fields. This model offers a foundation for a "forward-modeling" approach, using helioseismology techniques to explore various regimes of internal mass flows. We demonstrate the efficacy of the numerical method presented in this paper by reproducing observed solar power spectra, showing rotational splitting due to solid body rotation, and applying local helioseismology techniques to measure travel times created by a simple model of single-cell meridional circulation.

A Heuristic Approach to Remove the Background Intensity on White-light Solar Images. I. STEREO/HI-1 Heliospheric Images

Guillermo **Stenborg** and Russell A. Howard
2017 ApJ 839 68
White-light coronal and heliospheric imagers observe scattering of photospheric light from both dust particles (the F-Corona) and free electrons in the corona (the K-corona). The separation of the two coronae is thus vitally important to reveal the faint K-coronal structures (e.g., streamers, co-rotating interaction regions, coronal mass ejections, etc.). However, the separation of the two coronae is very difficult, so we are content in defining a background corona that contains the F- and as little K- as possible. For both the LASCO-C2 and LASCO-C3 coronagraphs aboard the Solar and Heliospheric Observatory (SOHO) and the white-light imagers of the SECCHI suite aboard the Solar Terrestrial Relationships Observatory (STEREO), a time-dependent model of the background corona is generated from about a month of similar images. The creation of such models is possible because the missions carrying these instruments are orbiting the Sun at about 1 au. However, the orbit profiles for the upcoming Solar Orbiter and Solar Probe Plus missions are very different. These missions will have elliptic orbits with a rapidly changing radial distance, hence invalidating the techniques in use for the SOHO/LASCO and STEREO/SECCHI instruments. We have been investigating techniques to generate background models out of just single images that could be used for the Solar Orbiter Heliospheric Imager and the Wide-field Imager for the Solar Probe Plus packages on board the respective spacecraft. In this paper, we introduce a state-of-the-art, heuristic technique to create the background intensity models of STEREO/HI-1 data based solely on individual images, report on new results derived from its application, and discuss its relevance to instrumental and operational issues.

A FRESH VIEW OF THE EXTREME-ULTRAVIOLET CORONA FROM THE APPLICATION OF A NEW IMAGE-PROCESSING TECHNIQUE

Guillermo **Stenborg**, Angelos Vourlidas and Russell A. Howard
The Astrophysical Journal, 674:1201–1206, **2008** February 20; **File**
http://www.journals.uchicago.edu/doi/pdf/10.1086/525556
The Extreme-ultraviolet Imaging Telescope (EIT) on board the Solar and Heliospheric Observatory (SOHO) has provided (and continues to provide) the solar physics communitywith an unprecedented view of the extreme-ultraviolet (EUV) transition region and corona. In particular, it has observed EUV bright points, coronal holes, loops, and arcades, as well as dynamical events such as flares, EIT waves, and mass ejections. However, the multiscale nature of the observed solar features has not been fully exploited so far. In this paper, we introduce a technique to enhance the EUV features based on their multiscale nature, show a few examples of features not revealed with standard image-processing techniques (and therefore not previously noticed in the EIT data set), and make the solar physics community aware of the availability of the full EIT data set as processed with this novel technique.
See http://lasco-www.nrl.navy.mil/index.php?p=content/wavelet

Transition of the Sunspot Number from Zurich to Brussels in 1980: A Personal Perspective

J. O. **Stenflo**
Solar Phys. Volume 291, Issue 9, pp 2487–2492 **2016**

The Swiss Federal Observatory, which had been founded in 1863 by Rudolf Wolf, was dissolved in connection with the retirement of Max Waldmeier in 1979. The determination of the Zurich sunpot number, which had been a cornerstone activity of the observatory, was then discontinued by ETH Zurich. A smooth transition of the responsibility for the sunspot number from Zurich to Brussels was achieved in 1980, however, through which it was possible to avoid a discontinuity in this important time series. Here we describe the circumstances that led to the termination in Zurich, how Brussels was chosen for the succession, and how the transfer was accomplished.

FTS atlas of the Sun's spectrally resolved center-to-limb variation

J. O. **Stenflo**

A&A 573, A74 **2015**

http://arxiv.org/pdf/1410.8474v1.pdf

The Sun's spectrum varies with center-to-limb distance. This variation is governed by the underlying temperature-density structure of the solar atmosphere. To explore the spectrally resolved center-to-limb variation (CLV) we make use of two spectral atlases recorded with the Fourier transform spectrometer (FTS) at the McMath-Pierce facility at Kitt Peak. One spectral atlas obtained 10 arcsec inside the solar limb was recorded in 1978-79 as part of the first survey of the Second Solar Spectrum, while the other atlas is the well used reference NSO/Kitt Peak FTS atlas for the disk center. Both atlases represent fully resolved spectra without any spectral stray light. We then construct an atlas of the limb/disk-center ratio between the two spectra over the wavelength range 4084-9950 \AA. This ratio spectrum, which expresses the CLV amplitude relative to the continuum, is as richly structured as the intensity spectrum itself, but the line profiles differ greatly in both shape and amplitude. It is as if we are dealing with a new, unfamiliar spectrum of the Sun, distinctly different from both the intensity spectrum (which we here refer to with the acronym SS1) and the linear polarization of the Second Solar Spectrum (for which we use acronym SS2). In analogy we refer to the new ratio spectrum as SS3. While there is hardly any resemblance between SS3 and SS2, we are able to identify a non-linear mapping that can translate SS1 to SS3 in the case of weak to medium-strong spectral lines that are mainly formed in LTE (being directly coupled to the local temperature-density structure). This non-linear mapping is successfully modeled in terms of two free parameters that are found to vary approximately linearly over the entire wavelength range covered. These parameters and the various SS3 line profiles provide a novel, rich set of observational constraints on model atmospheres.

Collapsed, uncollapsed, and hidden magnetic flux on the quiet Sun

J. O. **Stenflo**

A&A 529, A42 (**2011**)

Since the first applications of the Stokes V line ratio in the early 1970s and the Hanle depolarization effect in the early 1980s we have had a dualistic view of quiet-Sun magnetism: intermittent kG flux tubes surrounded by an ocean of turbulent fields with strengths of order 10–100 G. There has been the concern that this dualism could be an artefact of using two mutually almost exclusive diagnostic tools, the Zeeman and Hanle effect. We find however that the Hinode line-ratio data alone, without any reference to the Hanle effect, reveal the existence of two distinct flux populations, representing strong (collapsed) and weak (uncollapsed) flux. The collapsed population is preferentially located in the intergranular lanes, while the uncollapsed population is most visible in the bright cell interiors. From a comparison between the intrinsic field strengths, as derived from the line ratio for the collapsed population, and the corresponding flux densities, we can deduce the size distribution of the flux tubes. The majority of them are found to have sizes in the range 10–70 km. The intrinsic flux tube field strength decreases with diminishing size to become substantially smaller than kG for sizes below about 60 km. Comparison between the average of the unsigned flux density in the Hinode quiet-Sun data set and earlier constraints from the Hanle depolarization effect shows that most of the flux remains invisible at the Hinode resolution scale due to cancellation of the opposite magnetic polarities within the spatial resolution element. We have derived the cancellation function that describes how the visibility of the hidden flux improves with increased spatial resolution. It needs to be extrapolated to extremely small scales before the constraints imposed by the Hanle effect get satified, which suggests that the bulk of the hidden flux resides at scales near the end of the magnetic scale spectrum (of order 10 m).

Global wave patterns in the sun's magnetic field

J. O. **Stenflo**

Astrophysics and Space Science (ISSN 0004-640X), vol. 144, no. 1-2, May **1988**, p. 321-336.

When the observed pattern of solar magnetic fields is decomposed in its spherical-harmonic components and a time series analysis is performed, a resonant global wave pattern is revealed. The power spectrum indicates modes with discrete frequencies, obeying a strict parity selection rule in the case of the zonal, rotationally-symmetric modes. A

more traditional way of looking at the evolution of the zonal magnetic pattern is in the form of isocontours in latitude-time space (as in the "butterfly diagram" of sunspots). It is shown how this pattern can to a good approximation be represented as a superposition of 14 discrete modes, each with a purely sinusoidal time variation. This approach allows to analyse the roles of the individual discrete modes in generating the well-known features in the traditional "butterfly diagrams", e.g., the drift of the sunspot zones towards the equator and the prominence zones towards the poles during the course of the 11 yr cycle. It is shown that these features are accounted for entirely different by the odd parity modes with the single, sinusoidal period of 22 yr.

Three-dimensional Radiative Transfer Simulations of the Scattering Polarization of the Hydrogen Lyα Line in a Magnetohydrodynamic Model of the Chromosphere–Corona Transition Region

J. **Štěpán**1, J. Trujillo Bueno2,3,4, J. Leenaarts5, and M. Carlsson
2015 ApJ 803 65

Probing the magnetism of the upper solar chromosphere requires measuring and modeling the scattering polarization produced by anisotropic radiation pumping in UV spectral lines. Here we apply PORTA (a novel radiative transfer code) to investigate the hydrogen Lyα line in a three-dimensional model of the solar atmosphere resulting from a state of the art magnetohydrodynamic (MHD) simulation. At full spatial resolution the linear polarization signals are very significant all over the solar disk, with a large fraction of the field of view (FOV) showing line-center amplitudes well above the 1% level. Via the Hanle effect the line-center polarization signals are sensitive to the magnetic field of the model's transition region, even when its mean field strength is only 15 G. The breaking of the axial symmetry of the radiation field produces significant forward-scattering polarization in Lyα, without the need of an inclined magnetic field. Interestingly, the Hanle effect tends to decrease such forward-scattering polarization signals in most of the points of the FOV. When the spatial resolution is degraded, the line-center polarization of Lyα drops below the 1% level, reaching values similar to those previously found in one-dimensional (1D) semi-empirical models (i.e., up to about 0.5 %). The center to limb variation (CLV) of the spatially averaged polarization signals is qualitatively similar to that found in 1D models, with the largest line-center amplitudes at $\mu = \cos\theta \approx 0.4$ (θ being the heliocentric angle). These results are important, both for designing the needed space-based instrumentation and for a reliable interpretation of future observations of the Lyα polarization.

Do the Chinese Astronomical Records Dated AD 776 January 12/13 Describe an Auroral Display or a Lunar Halo? A Critical Re-examination

F. Richard **Stephenson**, David M. Willis, Hisashi Hayakawa, Yusuke Ebihara, Christopher J. Scott, Julia Wilkinson, Matthew N. Wild
Solar Physics April **2019**, 294:36
https://link.springer.com/content/pdf/10.1007%2Fs11207-019-1425-7.pdf

The enhancement of carbon-14 in tree rings around AD 774/775 has generated wide interest in solar activity at that time. The historical auroral records have been examined critically. Of particular interest was the “white vapour” observed in China on AD 776 January 12/13. Both Usoskin et al. (Astron. Astrophys.55, L3, 2013; U13) and Stephenson (Adv. Space Res.55, 1537, 2015; S15) interpreted this record as an auroral display. Subsequently, Neuhäuser and Neuhäuser (Astron. Nachr.336, 225, 2015; NN15) proposed five “criteria” for the likeliness of aurorae and on this basis rejected an auroral interpretation. Instead, they interpreted it as a lunar halo, and suggested there were no auroral records as a proxy of solar activity in the interval AD 774 – 785. We consider if their “lunar halo hypothesis” and their auroral criteria could be of use in future researches on historical auroral candidates. We first show a counter-example for the lunar halo hypothesis from a parallel record on 1882 November 17, which was seen as a whitish colour, in the southerly direction, and near the Moon. We then consider NN15’s criteria on colour, direction, and sky brightness and investigate other counter-examples from early-modern auroral observations. We also consider the extension of the white vapour in AD 776 according to the distribution of Chinese asterisms, and show that its large extension was inconsistent with the lunar halo hypothesis. Conversely, the streaks of white vapour penetrating the eight Chinese asterisms can be reproduced if we consider auroral-ray structures at altitudes between 97 km and 170 km, along geomagnetic field lines between the LL-shells L=1.55L=1.55 and 1.64. Our investigations show that we should consider candidate auroral records in historical documents not on the basis of the newly suggested a priori criteria by NN15 but based on all the available observational evidence.

Possible Production of Solar Spicules by Microfilament Eruptions

Alphonse C. **Sterling**, Ronald L. Moore, Tanmoy Samanta, Vasyl Yurchyshyn
ApJ **2020**
https://arxiv.org/pdf/2004.04187.pdf

We examine Big Bear Solar Observatory (BBSO) Goode Solar Telescope (GST) high-spatial resolution (0".06), high-cadence (3.45 s), H-alpha-0.8 Angstrom images of central-disk solar spicules, using data of Samanta et al.

(2019). We compare with coronal-jet chromospheric-component observations of Sterling et al. (2010a). Morphologically, bursts of spicules, referred to as "enhanced spicular activities" by Samanta et al. (2019), appear as scaled-down versions of the jet's chromospheric component. Both the jet and the enhanced spicular activities appear as chromospheric-material strands, undergoing twisting-type motions of ~20---50 km/s in the jet and ~20---30 km/s in the enhanced spicular activities. Presumably, the jet resulted from a minifilament-carrying magnetic eruption. For two enhanced spicular activities that we examine in detail, we find tentative candidates for corresponding erupting microfilaments, but not expected corresponding base brightenings. Nonetheless, the enhanced-spicular-activities' interacting mixed-polarity base fields, frequent-apparent-twisting motions, and morphological similarities to the coronal jet's chromospheric-temperature component, suggest that erupting microfilaments might drive the enhanced spicular activities but be hard to detect, perhaps due to H-alpha opacity. Degrading the BBSO/GST-image resolution with a 1".0-FWHM smoothing function yields enhanced spicular activities resembling the "classical spicules" described by, e.g., Beckers (1968). Thus, a microfilament eruption might be the fundamental driver of many spicules, just as a minifilament eruption is the fundamental driver of many coronal jets. Similarly, a 0".5-FWHM smoothing renders some enhanced spicular activities to resemble previously-reported "twinned" spicules, while the full-resolution features might account for spicules sometimes appearing as 2D-sheet-like structures. **2007 April 1, 2017 June 19**

A MICROFILAMENT-ERUPTION MECHANISM FOR SOLAR SPICULES

Alphonse C. **Sterling**1 and Ronald L. Moore1,2

2016 ApJ 828 L9 DOI 10.3847/2041-8205/828/1/L9

https://arxiv.org/pdf/1612.00430v1.pdf

Recent investigations indicate that solar coronal jets result from eruptions of small-scale chromospheric filaments, called minifilaments; that is, the jets are produced by scaled-down versions of typical-sized filament eruptions. We consider whether solar spicules might in turn be scaled-down versions of coronal jets, being driven by eruptions of microfilaments. Assuming a microfilament's size is about a spicule's width (~300 km), the estimated occurrence number plotted against the estimated size of erupting filaments, minifilaments, and microfilaments approximately follows a power-law distribution (based on counts of coronal mass ejections, coronal jets, and spicules), suggesting that many or most spicules could result from microfilament eruptions. Observed spicule-base Ca ii brightenings plausibly result from such microfilament eruptions. By analogy with coronal jets, microfilament eruptions might produce spicules with many of their observed characteristics, including smooth rise profiles, twisting motions, and EUV counterparts. The postulated microfilament eruptions are presumably eruptions of twisted-core micro-magnetic bipoles that are ~10 wide. These explosive bipoles might be built and destabilized by merging and cancelation of approximately a few to 100 G magnetic-flux elements of size . If, however, spicules are relatively more numerous than indicated by our extrapolated distribution, then only a fraction of spicules might result from this proposed mechanism. **15-Sep-2011**

Convective blueshifts in the solar atmosphere II. High-accuracy observations of the Fe i 6173.3Å line and deviations of full-disk Dopplergrams

Franziska **Stief**, Johannes Löhner-Böttcher, Wolfgang Schmidt, Tilo Steinmetz, Ronald Holzwarth

A&A 622, A34 **2019**

https://arxiv.org/pdf/1811.08685.pdf

Granular convective motions reach into the lower solar atmosphere, typically causing photospheric spectral lines to exhibit a differential line shift. This Doppler shift to shorter wavelength is commonly known as convective blueshift. We performed systematic observations of the quiet Sun with the Laser Absolute Reference Spectrograph (LARS) at the German Vacuum Tower Telescope. The solar disk was scanned along the meridian and the equator, from the disk center toward the limb. The solar spectrum around 6173Å was calibrated with a laser frequency comb on an absolute wavelength scale with an accuracy of a few m/s. We applied a bisector analysis on the spectral lines to reveal the changes of convective blueshift and line asymmetry at different heliocentric positions. Being a signature for convective motions, the bisector curve of Fe i 6173.3Å describes a C-shape at disk center. When approaching the solar limb, the bisector transforms into a \-shape. The analysis of the time- and bisector-averaged line shifts yields three distinct results. Firstly, the center-to-limb variation of Doppler velocities measured with LARS reveals a significant discrepancy (up to 200m/s) to the full-disk Dopplergrams of the Helioseismic and Magnetic Imager (HMI). Secondly, we obtained a significant decrease of convective blueshift toward the solar limb. Thirdly, the line-of-sight effect of solar activity leads to a scatter of up to 100m/s at intermediate heliocentric positions. The accurate observation of the absolute convective blueshift with LARS allows the identification of systematic discrepancy with Doppler velocities measured by HMI. The center-to-limb variation of HMI suffers from an additional blueshift toward the limb that is incompatible with our results. LARS measurements can be taken as reference for the correction of systematic errors in the synoptic HMI Dopplergrams.

Fluctuation Dynamo in a Collisionless, Weakly Magnetized Plasma

Denis A. **St-Onge**1,2 and Matthew W. Kunz
2018 ApJL 863 L25
http://sci-hub.tw/http://iopscience.iop.org/article/10.3847/2041-8213/aad638/meta
Results from a numerical study of fluctuation dynamo in a collisionless, weakly magnetized plasma are presented. The key difference between this dynamo and its magnetohydrodynamic (MHD) counterpart is the adiabatic production of magnetic-field-aligned pressure anisotropy by the amplification of a weak seed field. This, in turn, drives kinetic instabilities on the ion-Larmor scale—namely, firehose and mirror—which sever the adiabatic link between the thermal and magnetic pressures, thereby allowing the dynamo to proceed. After an initial phase of rapid growth driven by these instabilities, the magnetic energy grows exponentially and exhibits a spectrum that peaks near the resistive scale, similar to the large-magnetic-Prandtl-number () MHD dynamo. The magnetic field self-organizes into a folded-sheet topology, with direction reversals at the resistive scale and field lines curved at the parallel scale of the flow. The effective is determined by whether the ion-Larmor scale is above or below the field-reversing scale: in the former case, particles undergo Bohm-like diffusion; in the latter case, particles scatter primarily off of firehose fluctuations residing at the ends of the magnetic folds, and the viscosity becomes anisotropic. The magnetic field ultimately saturates at dynamical strengths, with its spectral peak migrating toward larger scales. This feature, along with an anti-correlation of magnetic-field strength and field-line curvature and a gradual thinning of magnetic sheets into ribbons, resembles the saturated state of the large- dynamo, the primary differences manifesting in firehose/mirror-unstable regions. These results have implications for magnetic-field growth in the weakly collisional intracluster medium of galaxy clusters.

Large-scale Model of the Axisymmetric Dynamo with Feedback Effects

Laura **Sraibman**, Fernando Minotti
Solar Physics January **2019**, 294:14
https://arxiv.org/pdf/1811.00933.pdf
https://link.springer.com/content/pdf/10.1007%2Fs11207-018-1350-1.pdf
A dynamo model is presented, based on a previously introduced kinematic model, in which the reaction of the magnetic field on the mass flow through the Lorentz force is included. Given the base mass flow corresponding to the case with no magnetic field, and assuming that the modification of this flow due to the Lorentz force can be treated as a perturbation, a complete model of the large-scale magnetic field dynamics can be obtained. The input needed consists in the large-scale meridional and zonal flows, the small-scale magnetic diffusivity, and a constant parameter entering the expression of the α-effect. When applied to a solar-like star, the model shows a realistic dynamics of the magnetic field, including cycle duration, consistent field amplitudes with the correct parity, progression of the zonal magnetic field towards the equator, and motion toward the poles of the radial field at high latitudes. Also, the radial and zonal components show a correct phase relation, and, at the surface level, the magnetic helicity is predominantly negative in the northern hemisphere and positive in the southern hemisphere.

No Evidence for Absence of Solar Dynamo Synchronization

F. **Stefani**, J. Beer & T. Weier
Solar Physics volume 298, Article number: 83 (**2023**)
https://link.springer.com/content/pdf/10.1007/s11207-023-02174-x.pdf
The old question of whether the solar dynamo is synchronized by the tidal forces of the orbiting planets has recently received renewed interest, both from the viewpoint of historical data analysis and in terms of theoretical and numerical modeling. We aim to contribute to the solution of this longstanding puzzle by analyzing cosmogenic radionuclide data from the last millennium. We reconsider a recent time series of 14C-inferred sunspot data and compare the resulting cycle minima and maxima with the corresponding conventional series down to 1610 A.D., enhanced by Schove's data before that time. We find that, despite recent claims to the contrary, the 14C-inferred sunspot data are well compatible with a synchronized solar dynamo, exhibiting a relatively phase-stable period of 11.07 years, which points to a synchronizing role of the spring tides of the Venus-Earth-Jupiter system.

A Model of a Tidally Synchronized Solar Dynamo

F. **Stefani**, A. Giesecke, T. Weier
Solar Physics May **2019**, 294:60
sci-hub.se/10.1007/s11207-019-1447-1
We discuss a solar dynamo model of Tayler–Spruit type whose ΩΩ-effect is conventionally produced by a solar-like differential rotation but whose αα-effect is assumed to be periodically modulated by planetary tidal forcing. This resonance-like effect has its rationale in the tendency of the current-driven Tayler instability to undergo intrinsic helicity oscillations which, in turn, can be synchronized by periodic tidal perturbations. Specifically, we focus on the 11.07-years alignment periodicity of the tidally dominant planets Venus, Earth, and Jupiter, whose persistent synchronization with the solar dynamo is briefly touched upon. The typically emerging dynamo modes are dipolar fields, oscillating with a 22.14-years period or pulsating with a 11.07-years period, but also quadrupolar fields with

corresponding periodicities. In the absence of any constant part of αα, we prove the sub-critical nature of this Tayler–Spruit type dynamo. The resulting amplitude of the αα oscillation that is required for dynamo action turns out to lie in the order of 1 ms−11 ms−1, which seems not implausible for the Sun. When starting with a more classical, non-periodic part of αα, even less of the oscillatory αα part is needed to synchronize the entire dynamo. Typically, the dipole solutions show butterfly diagrams, although their shapes are not convincing yet. Phase coherent transitions between dipoles and quadrupoles, which are reminiscent of the observed behavior during the Maunder minimum, can easily be triggered by long-term variations of dynamo parameters, but may also occur spontaneously even for fixed parameters. Further interesting features of the model are the typical second intensity peak and the intermittent appearance of reversed helicities in both hemispheres.

Constraining Global Solar Models through Helioseismic Analysis

Andrey M. **Stejko**, Alexander G. Kosovichev, Nicholas A. Featherstone, Gustavo Guerrero, Bradley W. Hindman, Loren I. Matilsky, Jörn Warnecke

ApJ **2022**

https://arxiv.org/pdf/2204.05207.pdf

Global hydrodynamic simulations of internal solar dynamics have focused on replicating the conditions for solar-like differential rotation and meridional circulation using the results of helioseismic inversions as a constraint. Inferences of meridional circulation, however, have provided controversial results showing the possibility of one, two, or multiple cells along the radius. To resolve this controversy and develop a more robust understanding of global flow regimes in the solar interior, we apply a "forward-modeling" approach to the analysis of helioseismic signatures of meridional circulation profiles obtained from numerical simulations. We employ the global acoustic modeling code GALE to simulate the propagation of acoustic waves through regimes of mean mass flows generated by global hydrodynamic and magnetohydrodynamic models: EULAG, the Pencil Code, and the Rayleigh code. These models are used to create synthetic dopplergram data products, used as inputs for local time-distance helioseismology techniques. Helioseismic travel-time signals from solutions obtained through global numerical simulations are compared directly with inferences from solar observations, in order to set additional constraints on global model parameters in a direct way. We show that even though these models are able to replicate solar-like differential rotation, the resulting rotationally-constrained convection develops a multi-cell global meridional circulation profile that is measurably inconsistent with local time-distance inferences of solar observations. However, we find that the development of rotationally-unconstrained convection close to the model surface is able to maintain solar-like differential rotation, while having a significant impact on the helioseismic travel-time signal, replicating solar observations within one standard deviation of the error due to noise.

HMI Nuggets #188 **2022** http://hmi.stanford.edu/hminuggets/?p=4023

3D MHD Modeling of the Impact of Subsurface Stratification on the Solar Dynamo

Andrey M. **Stejko**, Gustavo Guerrero, Alexander G. Kosovichev, Piotr K. Smolarkiewicz

ApJ **888** 16 **2020**

https://arxiv.org/pdf/1911.09658.pdf

https://doi.org/10.3847/1538-4357/ab5854

Various models of solar subsurface stratification are tested in the global EULAG-MHD solver to simulate diverse regimes of near-surface convective transport. Sub- and superadiabacity are altered at the surface of the model ($r>0.95\ R\odot$) to either suppress or enhance convective flow speeds in an effort to investigate the impact of the near-surface layer on global dynamics. A major consequence of increasing surface convection rates appears to be a significant alteration of the distribution of angular momentum, especially below the tachocline where the rotational frequency predominantly increases at higher latitudes. These hydrodynamic changes correspond to large shifts in the development of the current helicity in this stable layer ($r<0.72R\odot$), significantly altering its impact on the generation of poloidal and toroidal fields at the tachocline and below, acting as a major contributor towards transitions in the dynamo cycle. The enhanced near-surface flow speed manifests in a global shift of the toroidal field ($B\phi$) in the butterfly diagram - from a North-South symmetric pattern to a staggered anti-symmetric emergence.

A novel framework for the three-dimensional NLTE inverse problem

Jiri **Stepan**, Tanausu del Pino Aleman, Javier Trujillo Bueno

A&A **2022**

https://arxiv.org/pdf/2201.01504.pdf

Inversion of spectropolarimetric observations of the solar upper atmosphere is one of the most challenging goals in solar physics. If we account for all relevant ingredients of the spectral line formation process such as three-dimensional (3D) radiative transfer out of local thermodynamic equilibrium (NLTE), the task becomes extremely computationally expensive. Instead of generalizing 1D methods to 3D, we develop a new approach to the inverse

problem. In our meshfree method we do not consider the requirement of 3D NLTE consistency as an obstacle, but as a natural regularization with respect to the traditional pixel-by-pixel methods. This leads to more robust and less ambiguous solutions. We solve the 3D NLTE inverse problem as an unconstrained global minimization problem avoiding repetitive evaluations of the Λ~operator. Apart from 3D NLTE consistency, the method allows to easily include additional conditions of physical consistency such as zero divergence of the magnetic field. Stochastic ingredients make the method less prone to ending up in local minima of the loss function. Our method is capable of solving the inverse problem by orders of magnitude faster than it would be possible using grid-based methods. The method can provide accurate and physically consistent results if sufficient computing time is available, but also approximate solutions in case of very complex plasma structures or limited computing time.

Identifying coronal sources of L1 solar wind disturbances using the Fisk heliospheric magnetic field and potential field extrapolations during three solar minima

P. J. **Steyn**, D. Johnson, G. J. J. Botha, S. Régnier
ApJ **2024**
https://arxiv.org/pdf/2404.11219.pdf
The solar minima between solar cycles 22-23, 23-24 and 24-25 are the best observed minima on record. In situ solar wind and interplanetary magnetic field measurements by the WIND and ACE spacecraft at L1 with one-hour cadence are explored using wavelet analyses for the most quiescent year during each minimum. Times of local peaks in periodicities are identified in the solar wind velocity, magnetic field components, and proton number densities. The measured radial velocities at these times are used to trace magnetic field lines to the photosphere using two models. The first is the Fisk heliospheric magnetic field that traces field lines from L1 to the photosphere. They connect exclusively to solar poles and in 88% instances to locations of polar coronal holes. The second model uses the Parker spiral to trace from L1 to the solar source surface and potential field extrapolations from the source surface to the photosphere. These field lines terminate at equatorial and mid-latitude coordinates of which some are located close to coronal holes. This study connects for the first time coronal hole signatures in the ecliptic plane at L1 with polar coronal holes using the Fisk field. It shows how sources from both the solar equator and poles influence the solar wind at L1 and how the two models compliment each other to identify these sources.

A Generalized Fisk-type HMF: Implications of Spatially Dependent Photospheric Differential Rotation

P. J. **Steyn** and R. A. Burger
2020 ApJ 902 33
https://doi.org/10.3847/1538-4357/abb2a5
The existence of a Fisk-type heliospheric magnetic field (HMF) has been debated ever since Fisk proposed an alternative to the traditional view of the HMF first proposed by Parker. Several modifications of the original Fisk field model have been published in the past, for example, the Schwadron field and the Fisk–Parker hybrid HMF model. This study presents a new generalized Fisk HMF model that implements for the first time a spatially dependent differential rotation rate of the photosphere, by mapping magnetic field lines from the solar wind source surface to the photosphere. Data analysis methods of Forsyth et al. are used to search for a signature of a Fisk-type field during solar minimum conditions, using the magnetic field data from the first solar orbit of the Ulysses spacecraft. The new generalized Fisk field agrees better with the observed magnetic field winding angle than a standard Parker field during the majority of intervals scanned by Ulysses.

Is the Highest Cosmic-Ray Flux Yet to Come?

R. D. **Strauss**, M. S. Potgieter
Solar Physics, Volume 289, Issue 8, pp 3197-3205 **2014**
The recent 2009 solar-minimum period was characterized by a record-setting high Galactic cosmic-ray flux observed at Earth. This, along with the unexpected low heliospheric magnetic-field magnitude, caused this period to be characterized as unusual compared with previous minimum epochs. In this work, selected solar-activity proxies and corresponding cosmic-ray observations for the past five solar cycles are compared with each other, and we identify those that showed unusual behaviour during the 2009 solar-minimum modulation period. Using a state-of-the-art numerical-modulation model, the proton-intensity spectra for the past solar minima are reproduced to establish which of the transport processes might be considered the main cause of this unusually high cosmic-ray flux. It is found that diffusion was more prominent during 2009 so that drift effects on the modulation of cosmic rays in the heliosphere were less evident than during previous solar-polarity epochs. However, particle drifts still occurred and because of these drift effects, the proton spectrum is predicted to be even higher during the coming A>0 solar-minimum period.

Dynamics of the tachocline **Review**

Antoine **Strugarek**, Bernadett Belucz, Allan Sacha Brun, Mausumi Dikpati, Gustavo Guerrero
Space Science Reviews 219, Article number: 87 **2023**

https://arxiv.org/pdf/2311.12648.pdf
The solar tachocline is an internal region of the Sun possessing strong radial and latitudinal shears straddling the base of the convective envelope. Based on helioseismic inversions, the tachocline is known to be thin (less than 5\% of the solar radius). Since the first theory of the solar tachocline in 1992, this thinness has not ceased to puzzle solar physicists. In this review, we lay out the grounds of our understanding of this fascinating region of the solar interior. We detail the various physical mechanisms at stake in the solar tachocline, and put a particular focus on the mechanisms that have been proposed to explain its thinness. We also examine the full range of MHD processes including waves and instabilies that are likely to occur in the tachocline, as well as their possible connection with active region patterns observed at the surface. We reflect on the most recent findings for each of them, and highlight the physical understanding that is still missing and that would allow the research community to understand, in a generic sense, how the solar tachocline and stellar tachocline are formed, are sustained, and evolve on secular timescales.

Influence of Heliolatitudinal Anisotropy of Solar FUV/EUV Emissions on Lyman-alpha Helioglow: SOHO/SWAN Observations and WawHelioGlow Modeling

Marek **Strumik**, Maciej Bzowski, Marzena A. Kubiak
ApJL **919** L18 **2021**
https://arxiv.org/pdf/2109.08095
https://doi.org/10.3847/2041-8213/ac2734
Observations of the Sun's surface suggest a nonuniform radiated flux as related to the presence of bright active regions and darker coronal holes. The variations of the FUV/EUV source radiation can be expected to affect the Lyman-alpha backscatter glow measured by spaceborne instruments. In particular, inferring the heliolatitudinal structure of the solar wind from helioglow variations in the sky can be quite challenging if the heliolatitudinal structure of the solar FUV/EUV radiation is not properly included in the modeling of the heliospheric glow. We present results of analysis of the heliolatitudinal structure of the solar Lyman-alpha radiation as inferred from comparison of SOHO/SWAN satellite observations of the helioglow intensity with modeling results obtained from the recently-developed WawHelioGlow model. We find that in addition to time-dependent heliolatitudinal anisotropy of the solar wind, also time-dependent heliolatitudinal variations of the intensity of the solar Lyman-alpha and photoionizing emissions must be taken into account to reproduce the observed helioglow modulation in the sky. We present a particular latitudinal and temporal dependence of the solar Lyman-alpha flux obtained as a result of our analysis. We analyze also differences between polar-equatorial anisotropies close to the solar surface and seen by an observer located far from the Sun. We discuss the implications of these findings for the interpretation of heliospheric-glow observations.

The Life and Times of a Dissident Scientist MEMOIRS

Peter Andrew **Sturrock**
Solar Physics October **2017**, 292:147
https://link.springer.com/content/pdf/10.1007%2Fs11207-017-1156-6.pdf

Comparative Analyses of Brookhaven National Laboratory Nuclear Decay Measurements and Super-Kamiokande Solar Neutrino Measurements: Neutrinos and Neutrino-Induced Beta-Decays as Probes of the Deep Solar Interior

P. A. **Sturrock**, E. Fischbach, J. D. Scargle
Solar Phys. Volume 291, Issue 12, pp 3467–3484 **2016**
An experiment carried out at the Brookhaven National Laboratory over a period of almost 8 years acquired 364 measurements of the beta-decay rates of a sample of \({}^{32}\mbox{Si}\) and, for comparison, of a sample of \({}^{36}\mbox{Cl}\). The experimenters reported finding “small periodic annual deviations of the data points from an exponential decay … of uncertain origin”. We find that power-spectrum and spectrogram analyses of these datasets show evidence not only of the annual oscillations, but also of transient oscillations with frequencies near 11 year−1 and 12.5 year−1. Similar analyses of 358 measurements of the solar neutrino flux acquired by the Super-Kamiokande neutrino observatory over a period of about 5 years yield evidence of an oscillation near 12.5 year−1 and another near 9.5 year−1. An oscillation near 12.5 year−1 is compatible with the influence of rotation of the radiative zone. We suggest that an oscillation near 9.5 year−1 may be indicative of rotation of the solar core, and that an oscillation near 11 year−1 may have its origin in a tachocline between the core and the radiative zone. Modulation of the solar neutrino flux may be attributed to an influence of the Sun’s internal magnetic field by the Resonant Spin Flavor Precession (RSFP) mechanism, suggesting that neutrinos and neutrino-induced beta decays can provide information about the deep solar interior.

Indications of r-mode Oscillations in SOHO/MDI Solar Radius Measurements

P.A. **Sturrock**, R. Bush, D.O. Gough, J.D. Scargle

ApJ **804** 47 **2015**

Analysis of solar radius measurements acquired by the Michelson Doppler Imager on the SOHO spacecraft supports previously reported evidence of solar internal r-mode oscillations in Mt Wilson radius data and in nuclear-decay data acquired at the Lomonosov Moscow State University. The frequencies of these oscillations are compatible with oscillations in a putative inner tachocline that separates a slowly rotating core from the radiative envelope.

Solar cycle prediction using a combinatorial deep learning model

Xu **Su**, Bo Liang, Song Feng, Yunfang Cai, Wei Dai, Yunfei Yang

MNRAS, Volume 527, Issue 3, January **2024**, Pages 5675–5682,

https://doi.org/10.1093/mnras/stad3451

https://academic.oup.com/mnras/article-pdf/527/3/5675/53980086/stad3451.pdf

The long-term prediction of the solar cycle is of great significance for aerospace, communication, and space missions. For a long time, many studies have used relatively primitive deep learning methods to predict the solar cycle, and most of them do not perform well in the long-term prediction. In this paper, we proposed XG-SN ensemble model. The model used extreme gradient boosting (XGBoost) ensemble learning method, combined with sample convolution and interaction net (SCINet), and neural basis expansion analysis for the interpretable time series (N-BEATS) to make predictions for known solar cycles. 13 months of smoothed monthly total sunspot numbers were selected as the data set. The model performance was evaluated by mean absolute error (MAE), root-mean-square error (RMSE), and mean absolute time lag (MATL) between the predicted and actual values. The first two evaluation metrics measured the prediction deviation from the numerical dimension, and the last one measured the prediction deviation from the temporal dimension. The results show that the model achieves the MAE, RMSE, and MATL values of 13.19, 17.13, and 0.08, respectively, in Solar Cycle 13 to 24. Our model is able to better predict in most cycles, ensuring accurate prediction of peaks with little time lag.

Solar Cycle 25 Prediction Using N-BEATS

Xu **Su**2,1, Bo Liang2,1, Song Feng3,1, Wei Dai1, and Yunfei Yang1

2023 ApJ 947 50

https://iopscience.iop.org/article/10.3847/1538-4357/acc799/pdf

Solar activities lead to Sun variation with an 11 yr periodicity. The periodic variation affects space weather and heliophysics research. So it is important to accurately predict solar cycle variations. In this paper, we predicted the ongoing Solar Cycle 25 using neural basis expansion analysis for the interpretable time series deep learning method. 13 months of smoothed monthly total sunspot numbers taken by sunspot Index and Long-term Solar Observations are selected to train and evaluate our model. We used root mean square error (RMSE) and mean absolute time lag (MATL) to evaluate our model performance. RMSE and MATL measure the difference between our predicted values and the actual values along the Y- and X-axis, respectively. The RMSE value is 26.62 ± 1.56 and the MATL value is 1.34 ± 0.35, demonstrating that our model is able to better predict sunspot number variation. Finally, we predicted the variation of the sunspot numbers for Solar Cycle 25 using the model. The sunspot number of Solar Cycle 25 will peak around 2024 February with an amplitude of 133.9 ± 7.2. This means that Solar Cycle 25 will be slightly more intense than Solar Cycle 24.

Statistical Detection of Slow-mode Waves in Solar Polar Regions with SDO/AIA

J. T. **Su**

ApJ 793 117 **2014**

Observations from the Atmospheric Imaging Assembly (AIA) on board the Solar Dynamics Observatory are utilized to statistically investigate the propagating quasi-periodic oscillations in the solar polar plume and inter-plume regions. On average, the periods are found to be nearly equal in the three coronal channels of AIA 171 Å, 193 Å, and 211 Å, and the wavelengths increase with temperature from 171 Å, 193 Å, and 211 Å. The phase speeds may be inferred from the above parameters. Furthermore, the speed ratios of v 193/v 171 and v 211/v 171 are derived, e.g., 1.4 ± 0.8 and 2.0 ± 1.9 in the plume regions, respectively, which are equivalent to the theoretical ones for acoustic waves. We find that there are no significant differences for the detected parameters between the plume and inter-plume regions. To our knowledge, this is the first time that we have simultaneously obtained the phase speeds of slow-mode waves in the three channels in the open coronal magnetic structures due to the method adopted in the present work, which is able to minimize the influence of the jets or eruptions on wave signals.

Validating inversions for toroidal flows using normal-mode coupling

Prasad **Subramanian**, Shravan Hanasoge

ApJ **2020**

https://arxiv.org/pdf/2008.08834.pdf

Normal-mode coupling is a helioseismic technique that uses measurements of mode eigenfunctions to infer the interior structure of the Sun. This technique has led to insights into the evolution and structure of toroidal flows in the solar interior. Here, we validate an inversion algorithm for normal-mode coupling by generating synthetic seismic measurements associated with input flows and comparing the input and inverted velocities. We study four different cases of input toroidal flows and compute synthetics that take into account the partial visibility of the Sun. We invert the synthetics using Subtractive Optimally Localized Averages (SOLA) and also try to mitigate the systematics of mode leakage. We demonstrate that, ultimately, inversions are only as good as the model we assume for the correlation between flow velocities.

Energetics of Hi-C EUV brightenings

Srividya **Subramanian**1, Vinay L. Kashyap2, Durgesh Tripathi3, Maria S. Madjarska4 and John G. Doyle1

A&A 615, A47 (**2018**)

We study the thermal structure and energetics of the point-like extreme ultraviolet (EUV) brightenings within a system of fan loops observed in the active region AR 11520. These brightenings were simultaneously observed on **2012 July 11** by the High-resolution Coronal (Hi-C) imager and the Atmospheric Imaging Assembly (AIA) on board the Solar Dynamics Observatory (SDO). We identified 27 brightenings by automatically determining intensity enhancements in both Hi-C and AIA 193 Å light curves. The energetics of these brightenings were studied using the Differential Emission Measure (DEM) diagnostics. The DEM weighted temperatures of these transients are in the range log T(K) = 6.2−6.6 with radiative energies ≈1024−25 ergs and densities approximately equal to a few times 109 cm−3. To the best of our knowledge, these are the smallest brightenings in EUV ever detected. We used these results to determine the mechanism of energy loss in these brightenings. Our analysis reveals that the dominant mechanism of energy loss for all the identified brightenings is conduction rather than radiation.

Study of intensive solar flares in the rise phase of solar cycle 23 and 24 and other activities

S. Prasanna **Subramanian** , A. Shanmugaraju

Astrophysics and Space Science, February **2016**, 361:78

We present a statistical study and comparison on the properties of intensive solar flares (>M5.0 X-ray flare), decameter–hectometric (DH) wavelength [frequency, 1–14 MHz] type II radio bursts and solar energetic particle (SEP) events during the rising phase of solar cycles 23 and 24. The period of study is May 1996–November 2000 for solar cycle 23 and December 2008–June 2013 for solar cycle 24. Apart from reported weakness of solar cycle 24 compared to the cycle 23, we noted the following differences between the two cycles on the properties of these activities associated with intensive flares: (i) The reduction in the number of intensive flares (>M5.0 class) in cycle 24 is ∼34 %, similar to the reduction in sunspot number reported by Gopalswamy et al. (2014a); (ii) The slightly higher mean starting-frequency (4.15 MHz) and lower ending frequency (0.58 MHz) in cycle 24 compared to those of cycle 23 (2.63 and 0.89 MHz, respectively) indicate that the radio emission of this cycle started closer to the Sun and the CME-shock travelled farther away from the Sun in cycle 24; (iv) Cycle 23 produced a nearly equal number of SEP events as cycle 24 during the rising phase. The correlation between SEP intensity and CME speed is more prominent in cycle 23 (CC=0.7) than in cycle 24 (
CC=0.3).

Meridional Motion and Reynolds Stress from Debrecen Photoheliographic Data

Davor **Sudar**, Roman Brajša, Ivica Skokić, Ivana Poljančić Beljan…

Solar Physics July **2017**, 292:86

The Debrecen Photoheliographic Data catalogue is a continuation of the Greenwich Photoheliographic Results providing daily positions of sunspots and sunspot groups. We analyse the data for sunspot groups focussing on meridional motions and transfer of angular momentum towards the solar equator. Velocities are calculated with a daily shift method including an automatic iterative process of removing the outliers. Apart from the standard differential rotation profile, we find meridional motion directed towards the zone of solar activity. The difference in measured meridional flow in comparison to Doppler measurements and some other tracer measurements is interpreted as a consequence of different flow patterns inside and outside of active regions. We also find a statistically significant dependence of meridional motion on rotation velocity residuals confirming the transfer of angular momentum towards the equator. Analysis of horizontal Reynolds stress reveals that the transfer of angular momentum is stronger with increasing latitude up to about \(40^{\circ}\), where there is a possible maximum in absolute value.

Steps toward a high precision solar rotation profile: Results from SDO/AIA coronal bright point data

Davor **Sudar**, Ivica Skokić, Roman Brajša, Steven H. Saar

2015 A&A

http://arxiv.org/pdf/1501.01285v1.pdf

Coronal bright points (CBP) are ubiquitous small brightenings in the solar corona associated with small magnetic bipoles. We derive the solar differential rotation profile by tracing the motions of CBPs detected by the Atmospheric Imaging Assembly (AIA) instrument aboard the Solar Dynamics Observatory (SDO). We also investigate problems related to detection of coronal bright points resulting from instrument and detection algorithm limitations. To determine the positions and identification of coronal bright points we used a segmentation algorithm. A linear fit of their central meridian distance and latitude versus time was utilised to derive velocities. We obtained 906 velocity measurements in a time interval of only 2 days. The differential rotation profile can be expressed as ωrot=(14.47±0.10+(0.6±1.0)sin2(b)+(−4.7±1.7)sin4(b))\degr day−1. Our result is in agreement with other work and it comes with reasonable errors in spite of the very short time interval used. This was made possible by the higher sensitivity and resolution of the AIA instrument compared to similar equipment as well as high cadence. The segmentation algorithm also played a crucial role by detecting so many CBPs, which reduced the errors to a reasonable level. Data and methods presented in this paper show a great potential to obtain very accurate velocity profiles, both for rotation and meridional motion and, consequently, Reynolds stresses. The amount of coronal bright point data that could be obtained from this instrument should also provide a great opportunity to study changes of velocity patterns with a temporal resolution of only a few months. Other possibilities are studies of evolution of CBPs and proper motions of magnetic elements on the Sun. **2011-01-01**

Solar Spectral Proxy Irradiance from GOES (SSPRING): a model for solar EUV irradiance

Katherine **Suess**, Martin Snow, Rodney Viereck and Janet Machol
J. Space Weather Space Clim., 6, A10 (**2016**)
http://www.swsc-journal.org/articles/swsc/pdf/2016/01/swsc150034.pdf
Several currently operating instruments are able to measure the full EUV spectrum at sufficient wavelength resolution for use in upper-atmosphere modeling, the effects of space weather, and modeling satellite drag. However, no missions are planned at present to succeed the Thermosphere Ionosphere Mesosphere Energetics and Dynamics (TIMED) and Solar Dynamics Observatory (SDO) missions, which currently provide these data sources. To develop a suitable replacement for these measurements, we use two broadband EUV channels on the NOAA GOES satellites, the magnesium core-to-wing ratio (Mg II index) from the SOlar Radiation and Climate Experiment (SORCE) as well as EUV and Mg II time averages to model the EUV spectrum from 0.1 to 105 nm at 5-nm spectral resolution and daily time resolution. A Levenberg-Marquardt least squares fitting algorithm is used to determine a coefficient matrix that best reproduces a reference data set when multiplied by input data. The coefficient matrix is then applied to model data outside of the fitting interval. Three different fitting intervals are tested, with a variable fitting interval utilizing all days of data before the prediction date producing the best results. The correlation between the model results and the observed spectrum is found to be above 95% for the 0.1–50 nm range, and between 74% and 95% for the 50–105 nm range. We also find a favorable comparison between our results and the Flare Irradiance Spectral Model (FISM). These results provide a promising potential source for an empirical EUV spectral model after direct EUV measurements are no longer available, and utilize a similar EUV modeling technique as the upcoming GOES-R satellites.

Transverse MHD Waves as Signatures of Braiding-induced Magnetic Reconnection in Coronal Loops

A. Ramada C. **Sukarmadji** [1], Patrick Antolin [1]
Astrophysical Journal Letters, Volume 961, Issue 1, id.L17, **2024**
https://iopscience.iop.org/article/10.3847/2041-8213/ad1402/pdf
A major coronal heating theory based on magnetic reconnection relies on the existence of braided magnetic field structures in the corona. In this small-angle reconnection scenario, numerical simulations indicate that the reconnected magnetic field lines are driven sideways by magnetic tension and can overshoot from their new rest position, thereby leading to low-amplitude transverse MHD waves. This provides an efficient mechanism for transverse MHD wave generation, and the direct causality also constitutes substantial evidence of reconnection from braiding. However, this wave-generation mechanism has never been directly observed. Recently, the telltale signature of small-angle reconnection in a sheared coronal structure has been identified through nanojets, which are small, short-lived, and fast jetlike bursts in the nanoflare range transverse to the guide field. We present for the first time Interface Region Imaging Spectrograph and Solar Dynamics Observatory observations of transverse MHD waves in a coronal loop that directly result from braiding-induced reconnection. The reconnection is identified by the presence of nanojets at the loop apex that release nanoflare-range energy. We find that the oscillations have an energy flux on the order of 106-108 erg cm-2 s-1, which is within the budget to power active region loops. The estimated kinetic and thermal energy from the nanojets is also sufficient to power the transverse waves and sustain the observed heating at the loop apex. This discovery provides major support to (a) existing theories that transverse MHD waves can be a signature of reconnection, (b) the existence of braiding in coronal structures, and (c) the coronal reconnection scenario identified by nanojets.

IRIS Nugget Jun **2024** https://iris.lmsal.com/nugget

Partial redistribution in 3D non-LTE radiative transfer in solar-atmosphere models

Andrii V. **Sukhorukov**1,2 and Jorrit Leenaarts1
A&A 597, A46 (**2017**)

Context. Resonance spectral lines such as H i Ly α, Mg ii h&k, and Ca ii H&K that form in the solar chromosphere, are influenced by the effects of 3D radiative transfer as well as partial redistribution (PRD). So far no one has modeled these lines including both effects simultaneously owing to the high computing demands of existing algorithms. Such modeling is, however, indispensable for accurate diagnostics of the chromosphere.
Aims. We present a computationally tractable method to treat PRD scattering in 3D model atmospheres using a 3D non-local thermodynamic equilibrium (non-LTE) radiative transfer code.
Methods. To make the method memory-friendly, we use the hybrid approximation for the redistribution integral. To make the method fast, we use linear interpolation on equidistant frequency grids. We verify our algorithm against computations with the RH code and analyze it for stability, convergence, and usefulness of acceleration using model atoms of Mg ii with the h&k lines and H i with the Ly α line treated in PRD.
Results. A typical 3D PRD solution can be obtained in a model atmosphere with 252 × 252 × 496 coordinate points in 50 000–200 000 CPU hours, which is a factor ten slower than computations assuming complete redistribution. We illustrate the importance of the joint action of PRD and 3D effects for the Mg ii h&k lines for disk-center intensities, as well as the center-to-limb variation.
Conclusions. The proposed method allows for the simulation of PRD lines in a time series of radiation-magnetohydrodynamic models, in order to interpret observations of chromospheric lines at high spatial resolution.

Improved CGEM Electric Field Inversion for HMI Active Regions

Xudong **Sun**1, George Fisher2, and Todd Hoeksema3 (for the CGEM Team)
HMI Science Nuggets, #190 **2023**
http://hmi.stanford.edu/hminuggets/?p=4092

The PDFI_SS software[1], developed by the Coronal Global Evolutionary Model (CGEM) team, derives the photospheric electric field based on a time sequence of vector magnetic field and Doppler velocity maps. It has been applied to the Space-weather HMI Active Region Patch (SHARP) data archive: the electric field maps (cgem.pdfi_output) are now a routine product of the HMI pipeline. As of May 01, 2023, the electric fields have been calculated for 4972 active regions, with a total of 2.9 million snapshots. Details of the software and the data products can be found in ref. [1] and ref. [2]. **2012.07.10**

The Polar Field Reversal of Solar Cycle 24

Xudong **Sun**
HMI Science Nuggets, #32, Dec **2014**
http://hmi.stanford.edu/hminuggets/?p=1030

HMI observations reveal a slow, north-south asymmetric polar magnetic field reversal. Cycle 24 has been weak; an even weaker Cycle 25 seems probable.

On Polar Magnetic Field Reversal and Surface Flux Transport During Solar Cycle 24

Xudong **Sun**, J. Todd Hoeksema, Yang Liu, Junwei Zhao
ApJ **798** 114 **2015**
http://arxiv.org/pdf/1410.8867v1.pdf

As each solar cycle progresses, remnant magnetic flux from active regions (ARs) migrates poleward to cancel the old-cycle polar field. We describe this polarity reversal process during Cycle 24 using four years (2010.33--2014.33) of line-of-sight magnetic field measurements from the Helioseismic and Magnetic Imager. The total flux associated with ARs reached maximum in the north in 2011, more than two years earlier than the south; the maximum is significantly weaker than Cycle 23. The process of polar field reversal is relatively slow, north-south asymmetric, and episodic. We estimate that the global axial dipole changed sign in October 2013; the northern and southern polar fields (mean above 60◦ latitude) reversed in November 2012 and March 2014, respectively, about 16 months apart. Notably, the poleward surges of flux in each hemisphere alternated in polarity, giving rise to multiple reversals in the north. We show that the surges of the trailing sunspot polarity tend to correspond to normal mean AR tilt, higher total AR flux, or slower mid-latitude near-surface meridional flow, while exceptions occur during low magnetic activity. In particular, the AR flux and the mid-latitude poleward flow speed exhibit a clear anti-correlation. We discuss how these features can be explained in a surface flux transport process that includes a field-dependent converging flow toward the ARs, a characteristic that may contribute to solar cycle variability.

The SunPy Project: An Interoperable Ecosystem for Solar Data Analysis

The **SunPy Community**, Will Barnes, Steven Christe, Nabil Freij, Laura Hayes, David Stansby, Jack Ireland, Stuart Mumford, Daniel Ryan, Albert Shih
Frontiers in Astronomy and Space Sciences 10 (**2023**): 29
https://www.frontiersin.org/articles/10.3389/fspas.2023.1076726/pdf
The SunPy Project is a community of scientists and software developers creating an ecosystem of Python packages for solar physics. The project includes the sunpy core package as well as a set of affiliated packages. The sunpy core package provides general purpose tools to access data from different providers, read image and time series data, and transform between commonly used coordinate systems. Affiliated packages perform more specialized tasks that do not fall within the more general scope of the sunpy core package. In this article, we give a high-level overview of the SunPy Project, how it is broader than the sunpy core package, and how the project curates and fosters the affiliated package system. We demonstrate how components of the SunPy ecosystem, including sunpy and several affiliated packages, work together to enable multi-instrument data analysis workflows. We also describe members of the SunPy Project and how the project interacts with the wider solar physics and scientific Python communities. Finally, we discuss the future direction and priorities of the SunPy Project.

A Full-disk Image Standardization of the Chromosphere Observation at Huairou Solar Observing Station

Liu **Suo**
Advances in Space Research **2019**
https://arxiv.org/pdf/1911.06637.pdf
Observations of local features in the solar chromosphere began in 1992 at Huairou Solar Observing Station, while the full-disk chromosphere observations were carried out since 2000. In order to facilitate researchers to use full-disk chromosphere observation, algorithms have been developed to standardize the full-disk images. The algorithms include the determination of the center of the image and size standardization, geometric correction and intensity normalization. The solar limb of each image is determined from a histogram analysis of its intensity distribution. The center and radius are then calculated and the image is corrected for geometric distortions. Images are re-scaled to have a fixed radius of 500 pixels and centered within the 1024×1024 frame. Finally, large-scale variations in intensity, such as limb-darkening, are removed using a median filter. This paper provides a detailed description of these algorithms, and a summary of the properties of these chromosheric full-disk observations to be used for further scientific investigations.

Center to limb observations and modeling of the Ca I 4227 A line

H. D. **Supriya**, H. N. Smitha, K. N. Nagendra, J. O. Stenflo, M. Bianda, R. Ramelli, B. Ravindra, L. S. Anusha
ApJ 793 42 **2014**
http://arxiv.org/pdf/1407.5461v1.pdf
The observed center-to-limb variation (CLV) of the scattering polarization in different lines of the Second Solar Spectrum can be used to constrain the height variation of various atmospheric parameters, in particular the magnetic fields via the Hanle effect. Here we attempt to model non-magnetic CLV observations of the Q/I profiles of the Ca I 4227 A line recorded with the ZIMPOL-3 at IRSOL. For modeling, we use the polarized radiative transfer with partial frequency redistribution with a number of realistic 1-D model atmospheres. We find that all the standard FAL model atmospheres, used by us, fail to simultaneously fit the observed (I, Q/I) at all the limb distances (μ). However, an attempt is made to find a single model which can provide a fit at least to the CLV of the observed Q/I instead of a simultaneous fit to the (I, Q/I) at all μ. To this end we construct a new 1-D model by combining two of the standard models after modifying their temperature structures in the appropriate height ranges. This new combined model closely reproduces the observed Q/I at all the μ, but fails to reproduce the observed rest intensity at different μ. Hence we find that no single 1-D model atmosphere succeeds in providing a good representation of the real Sun. This failure of 1-D models does not however cause an impediment to the magnetic field diagnostic potential of the Ca I 4227 A line. To demonstrate this we deduce the field strength at various μ positions without invoking the use of radiative transfer.

On the Long-Term Modulation of Solar Differential Rotation

M.**Suzuki**
E-print, July **2014**; Solar Phys., Volume 289, Issue 11, pp 4021-4029, **2014**
http://arxiv.org/pdf/1407.5735.pdf
Long-term modulation of solar differential rotation was studied with data from Mt. Wilson and our original observations during Solar Cycles 16 through 23. The results are: i) The global B-value (i.e. latitudinal gradient of differential rotation), is modulated in a period of about six or seven solar cycles. ii) The B-values of the northern and

southern hemispheres are also modulated with a similar period to the global one, but iii) they show quasi-oscillatory behavior with a phase shift between them. We examined the yearly fluctuations of the B-values in every solar cycle with reference to the phase of the sunspot cycle and found that the B-values show high values over the full-cycle years, when the cycle-averaged B-values are high. We discuss the independent long-term behavior of solar differential rotation between the northern and southern solar hemispheres and its implication for the solar dynamo.

Several Populations of Sunspot Group Numbers -- Resolving a Conundrum

Leif **Svalgaard**

2020

https://arxiv.org/ftp/arxiv/papers/2011/2011.05356.pdf

The long-standing disparity between the sunspot number record and the Hoyt and Schatten (1998, H&S) Group Sunspot Number series was initially resolved by the Clette et al. (2014) revision of the sunspot number and the group number series. The revisions resulted in a flurry of dissenting group number series while the revised sunspot number series was generally accepted. Thus, the disparity persisted and confusion reigned, with the choice of solar activity dataset continuing to be a free parameter. A number of workshops and follow-up collaborative efforts by the community have not yet brought clarity. We review here several lines of evidence that validate the original revisions put forward by Clette et al. (2014) and suggest that the perceived conundrum no longer need to delay acceptance and general use of the revised series. We argue that the solar observations constitute several distinct populations with different properties which explain the various discontinuities in the series. This is supported by several proxies: diurnal variation of the geomagnetic field, geomagnetic signature of the strength of the heliomagnetic field, and variation of radionuclides. The Waldmeier effect shows that the sunspot number scale has not changed over the last 270 years and a mistaken scale factor between observers Wolf and Wolfer explains the disparity beginning in 1882 between the sunspot number and the H&S reconstruction of the group number. Observations with replica of 18th century telescopes (with similar optical flaws) validate the early sunspot number scale; while a reconstruction of the group number with monthly resolution (with many more degrees of freedom) validate the size of Solar Cycle 11 given by the revised series that the dissenting series fail to meet.

Prediction of Solar Cycle 25 **Review**

Leif **Svalgaard**

Journal of Space Weather and Space Climate **2020**

https://arxiv.org/ftp/arxiv/papers/2010/2010.02370.pdf

Prediction of solar cycle is an important goal of Solar Physics both because it serves as a touchstone for our understanding of the sun and also because of its societal value for a space faring civilization. The task is difficult and progress is slow. Schatten et al. (1978) suggested that the magnitude of the magnetic field in the polar regions of the sun near solar minimum could serve as a precursor for the evolution and amplitude of the following solar cycle. Since then, this idea has been the foundation of somewhat successful predictions of the size of the last four cycles, especially of the unexpectedly weak solar cycle 24 ("the weakest in 100 years"). Direct measurements of the polar magnetic fields are available since the 1970s and we have just passed the solar minimum prior to solar cycle 25, so a further test of the polar field precursor method is now possible. The predicted size of the new cycle 25 is 128±10 (on the new sunspot number version 2 scale), slightly larger than the previous cycle.

RHESSI Science Nuggets # 390 Oct **2020**

https://sprg.ssl.berkeley.edu/~tohban/wiki/index.php/Prediction_of_Solar_Cycle_25

HMI Science Nuggets # 146 Oct **2020** http://hmi.stanford.edu/hminuggets/?p=3382

Calibration of the Total Solar Irradiance Data Record

Leif **Svalgaard**

2018

https://arxiv.org/ftp/arxiv/papers/1812/1812.09301.pdf

Solar surface magnetic field seems to be able to explain variations in Total Solar Irradiance on timescales from hours to decades. Using magnetograms from spacecraft (MDI and HMI) and ground-based observatories (MWO and WSO) I build a composite dataset of the Total Line-of-Sight Unsigned Magnetic Flux over the solar disk stretching back to 1976, validated by excellent correlations with the solar microwave flux (F10.7) and the Sunspot Group Number. Direct measurements of TSI by space borne sensors have been carried out since late 1978. The early instruments were plagued by scattered light entering the aperture, but this construction flaw can be corrected for. At the AGU 2018 meeting, a new TSI composite has been proposed based on a novel mathematical method vetted by representatives from all current and most past TSI instruments. Although an 'official' release of the dataset has not been offered yet, a preliminary version is available. Anticipating that any last-minute changes might be minor, I compare this new version with the magnetic flux composite. It is clear that we have two TSI populations: values before 1993 that are seriously too low and values from 1993 onwards. I elect to normalize the magnetic flux (the driver of variations of TSI) to a New TSI using the regression equation for the recent population with the smallest

uncertainty. With this normalization, there is now total agreement between the variation of the magnetic flux and of the New TSI as well as with the F10.7 and Group Number proxies. We now have two choices: (1) the Sun underwent a dramatic change in how its magnetic field drives variation of TSI or (2) the New Consensus TSI reconstruction does not work and the new dataset is premature and not useful neither for solar nor for climate research. Following David Hume, we should always believe whatever would be the lesser miracle, which in our case would be choice (2).

Up to Nine Millennia of Multimessenger Solar Activity

Leif **Svalgaard**

2018

https://arxiv.org/ftp/arxiv/papers/1810/1810.11952.pdf

A nine-millennia reconstruction of decadal sunspot numbers derived from 10Be and 14C terrestrial archives for 6755 BC to 1885 AD has been extended to the present using several other messengers (Observed Sunspot Number, Group Number, range of the diurnal variation of the geomagnetic field, and the InterDiurnal Variation of the geomagnetic Ring Current) and scaled to the modern SILSO Version 2 sunspot number. We find that there has been no secular up tick of activity the last three hundred years and that recent activity has not been out of the ordinary. There is a sharp 87.6-year peak in the power spectrum, but no significant power at the Hallstatt 2300-year period. The reconciliation of the cosmogenic record with the modern sunspot record could be an important step to providing a vetted solar activity record for the use in climate research.

A Super-Synoptic Map of HMI Flux Density

Leif Svalgaard

HMI Science Nuggets # 82 **2018**

http://hmi.stanford.edu/hminuggets/?p=2146

25 Cycles of Solar Magnetic Dipole Moments

Leif Svalgaard

HMI Science Nuggets #78 **2018**

http://hmi.stanford.edu/hminuggets/?p=2084

The idea, based on the Babcock model of the cycle, that the solar polar fields near minimum can be used as predictor of the size of the following sunspot cycle1 has proven useful and successful the last four cycles, especially for the critical ‘lowest in a 100 years’ Cycle 242. The ‘Dipole Moment’ (DM), i.e. the difference between the polar fields (using the Wilcox Solar Observatory, WSO, convention that ‘polar fields’ be the average line-of-sight flux density [called the ‘field strength’] above latitudes 55°) in the North and in the South, was taken as a convenient parameter for the purpose of prediction. It was found that the value of DM over the three years preceding the minimum is relatively constant with only a slight decrease over time (due to pole-ward migration of emerging new-cycle flux), sufficiently stable that its average single value was a good precursor at least for the last four sunspot cycles.

Assessment of the Failure of Active Days Fraction Method of Sunspot Group Number Reconstructions

Leif **Svalgaard**, Kenneth H. Schatten

2017

https://arxiv.org/ftp/arxiv/papers/1706/1706.01154.pdf

We identify several pairs of 'equivalent' observers defined as observers with equal or nearly equal 'observational threshold' areas of sunspots on the solar disk as determined by the 'Active Days Fraction' method [e.g. Willamo et al., 2017]. For such pairs of observers, the ADF-method would be expected to map the actually observed sunspot group numbers for the individual observers to two reconstructed series that are very nearly equal and (it is claimed) represent 'real' solar activity without arbitrary choices and deleterious, error-accumulating 'daisy-chaining'. We show that this goal has not been achieved (for the critical period at the end of the 19th century and the beginning of the 20th), rendering the ADF-methodology suspect and not reliable nor useful for studying the long-term variation of solar activity.

Sunspot Group Numbers Since 1900 and Implications for the Long-term Record of Solar Activity

Leif **Svalgaard**, Kenneth H. Schatten

2017

https://arxiv.org/ftp/arxiv/papers/1705/1705.02024.pdf
Recent work on improving and revising estimates of solar activity [Clette et al., 2014] has resulted in renewed interest in what has been called the longest running 'Science Experiment'. We compare four reconstructions of solar activity as reflected in the number of sunspot groups ('active regions') constructed by different authors using very different methods. We concentrate on the period since AD 1900 where the underlying solar and geomagnetic data are plentiful and of sufficient quality and find that all four methods yield essentially the same Sunspot Group Number series. We take that as indicating that protracted and pernicious criticisms of the individual methods are neither fruitful nor helpful and we suggest that future efforts be directed towards understanding the specific reasons why the methods give discordant results for centuries prior to the 20th. The main area of disagreement occurs during the last 25 years of the 19th century and feeds back into the time prior to that. The solar Extreme Ultraviolet flux can be reconstructed since the 1740s [Svalgaard, 2016] and with suitable scaling fits the Svalgaard & Schatten [2016] Sunspot Group Number series since 1865 very well, so we argue that the discordant group series have problems once we move out of the 20th century, and that the community should concentrate on finding out what those are, so a true and useful consensus can emerge.

On the Sunspot Group Number Reconstruction: The Backbone Method

Leif **Svalgaard**, Kenneth H. Schatten
2017
https://arxiv.org/pdf/1704.07061.pdf
We discuss two recent papers very critical of our Group Sunspot Number Series (Svalgaard & Schatten [2016]). Unfortunately, we cannot support any of the concerns they raise. We first show that almost always there is simple proportionality between the counts of different observers and that taking the small, occasional non-linearities into account makes very little difference. Among other examples: we verify that the RGO group count was drifting the first twenty years of observations. We then show that our group count matches the diurnal variation of the geomagnetic field with high fidelity, and that the heliospheric magnetic field derived from geomagnetic data is consistent with our group number series. We evaluate the 'correction matrix' approach [Usoskin et al. 2016] and show that it fails to reproduce the observational data. We clarify the notion of daisy-chaining and point out that our group number series has no daisy-chaining for the period 1794-1996 and therefore no accumulation of errors over that span. We compare with the cosmic ray record for the last 400+ years and find good agreement. We note that the Active Day Fraction method (of Usoskin et al.) has the problem that at sunspot maximum, every day is an 'active day' so ADF is nearly always unity and thus does not carry information about the statistics of high solar activity. This 'information shadow' occurs for even moderate group numbers and thus need to be extrapolated to higher activity. We compare a new application of the correction matrix method utilizing good RGO data after 1900 and find remarkable linear agreement (after correcting for an unphysical offset) with our group series. We conclude that the criticism of Svalgaard & Schatten [2016] is invalid and detrimental to progress in the important field of long-term variation of solar activity, although we would welcome well-reasoned re-examinations of our findings.

The Effect of Sunspot Weighting

Leif **Svalgaard**, Marco Cagnotti, Sergio Cortesi
Solar Physics February **2017**, 292:34
http://arxiv.org/ftp/arxiv/papers/1507/1507.01119.pdf
Although W. Brunner began to weight sunspot counts (from 1926), using a method whereby larger spots were counted more than once, he compensated for the weighting by not counting enough smaller spots in order to maintain the same reduction factor (0.6) as was used by his predecessor A. Wolfer to reduce the count to R. Wolf's original scale, so that the weighting did not have any effect on the scale of the sunspot number. In 1947, M. Waldmeier formalized the weighting (on a scale from 1 to 5) of the sunspot count made at Zurich and its auxiliary station Locarno. This explicit counting method, when followed, inflates the relative sunspot number over that which corresponds to the scale set by Wolfer (and matched by Brunner). Recounting some 60,000 sunspots on drawings from the reference station Locarno shows that the number of sunspots reported was "over counted" by \({\approx}\,44~\%\) on average, leading to an inflation (measured by an effective weight factor) in excess of 1.2 for high solar activity. In a double-blind parallel counting by the Locarno observer M. Cagnotti, we determined that Svalgaard's count closely matches that of Cagnotti, allowing us to determine from direct observation the daily weight factor for spots since 2003 (and sporadically before). The effective total inflation turns out to have two sources: a major one (15 – 18 %) caused by weighting of spots, and a minor source (4 – 5 %) caused by the introduction of the Zürich classification of sunspot groups which increases the group count by 7 – 8 % and the relative sunspot number by about half that. We find that a simple empirical equation (depending on the activity level) fits the observed factors well, and use that fit to estimate the weighting inflation factor for each month back to the introduction of effective inflation in 1947 and thus to be able to correct for the over-counts and to reduce sunspot counting to the Wolfer method in use from 1894 onwards.
Waldmeier in 1947 introduced a weighting (on a scale from 1 to 5) of the sunspot count made at Zurich and its auxiliary station Locarno, whereby larger spots were counted more than once. This counting method inflates the relative sunspot number over that which corresponds to the scale set by Wolfer and Brunner. Svalgaard re-counted

some 60,000 sunspots on drawings from the reference station Locarno and determined that the number of sunspots reported were 'over counted' by 44% on average, leading to an inflation (measured by a weight factor) in excess of 1.2 for high solar activity. In a double-blind parallel counting by the Locarno observer Cagnotti, we determined that Svalgaard's count closely matches that of Cagnotti's, allowing us to determine the daily weight factor since 2003 (and sporadically before). We find that a simple empirical equation fits the observed weight factors well, and use that fit to estimate the weight factor for each month back to the introduction of weighting in 1947 and thus to be able to correct for the over-count and to reduce sunspot counting without weighting to the Wolfer method in use from 1893 onwards.

A Recount of Sunspot Groups on Staudach's Drawings

Leif **Svalgaard**
Solar Phys. January **2017**, 292:4
We have examined the more than 1100 drawings of the solar disk made by the German amateur astronomer Johann Caspar Staudach during 1749 – 1799 and counted the spots on each image. Using the modern perception of how to group spots into active regions, we regrouped the spots as a modern observer would. The resulting number of groups was found to be higher on average by 25 % than the first count of groups performed by Wolf in 1857, which was used by Hoyt and Schatten (Solar Phys. 181, 491, 1998) in their construction of the group sunspot number. Compared to other observers at the time, Staudach's drawings have a very low average number, about two, of spots per group, possibly indicating an inferior telescope that probably suffered from spherical and chromatic aberration, as would be typical of amateur telescopes of the day. We have initiated an ongoing project aiming at observing sunspots with antique telescopes having similar defects in order to determine the factor necessary to bring the Staudach observations onto a modern scale.
Erratum Solar Physics January 2017, 292:14

Reconstruction of Solar Extreme Ultraviolet Flux 1740 – 2015

Leif **Svalgaard**
Solar Phys. **2016**
Solar extreme ultraviolet (EUV) radiation creates the conducting E-layer of the ionosphere, mainly by photo-ionization of molecular oxygen. Solar heating of the ionosphere creates thermal winds, which by dynamo action induce an electric field driving an electric current having a magnetic effect observable on the ground, as was discovered by G. Graham in 1722. The current rises and falls with the Sun, and thus causes a readily observable diurnal variation of the geomagnetic field, allowing us to deduce the conductivity and thus the EUV flux as far back as reliable magnetic data reach. High-quality data go back to the "Magnetic Crusade" of the 1830s and less reliable, but still usable, data are available for portions of the 100 years before that. J.R. Wolf and, independently, J.-A. Gautier discovered the dependence of the diurnal variation on solar activity, and today we understand and can invert that relationship to construct a reliable record of the EUV flux from the geomagnetic record. We compare that to the F10.7F10.7 flux and the sunspot number, and we find that the reconstructed EUV flux reproduces the F10.7F10.7 flux with great accuracy. On the other hand, it appears that the Relative Sunspot Number as currently defined is beginning to no longer be a faithful representation of solar magnetic activity, at least as measured by the EUV and related indices. The reconstruction suggests that the EUV flux reaches the same low (but non-zero) value at every sunspot minimum (possibly including Grand Minima), representing an invariant "solar magnetic ground state".

F10.7 Microwave Flux Matches the Total Disk Unsigned Magnetic Flux from MDI and HMI

Leif **Svalgaard** & Xudong Sun
HMI Science Nuggets #52 Apr **2016**
http://hmi.stanford.edu/hminuggets/?p=1510

Reconstruction of the Sunspot Group Number: The Backbone Method

Leif **Svalgaard**, Kenneth H. Schatten
Solar Phys. Volume 291, Issue 9, pp 2653–2684 **2016**
We have reconstructed the sunspot-group count, not by comparisons with other reconstructions and correcting those where they were deemed to be deficient, but by a re-assessment of original sources. The resulting series is a pure solar index and does not rely on input from other proxies,e.g. radionuclides, auroral sightings, or geomagnetic records. "Backboning" the data sets, our chosen method, provides substance and rigidity by using long-time observers as a stiffness character. Solar activity, as defined by the Group Number, appears to reach and sustain for extended intervals of time the same level in each of the last three centuries since 1700 and the past several decades do not seem to have been exceptionally active, contrary to what is often claimed.

Reconstruction of Solar Extreme Ultraviolet Flux 1740-2015

Leif **Svalgaard**

2015

http://arxiv.org/ftp/arxiv/papers/1506/1506.04408.pdf

Solar Extreme Ultraviolet (EUV) radiation creates the conducting E-layer of the ionosphere, mainly by photo ionization of molecular Oxygen. Solar heating of the ionosphere creates thermal winds which by dynamo action induce an electric field driving an electric current having a magnetic effect observable on the ground, as was discovered by G. Graham in 1722. The current rises and sets with the Sun and thus causes a readily observable diurnal variation of the geomagnetic field, allowing us the deduce the conductivity and thus the EUV flux as far back as reliable magnetic data reach. High-quality data go back to the 'Magnetic Crusade' of the 1830s and less reliable, but still usable, data are available for portions of the hundred years before that. J.R. Wolf and, independently, J.-A. Gautier discovered the dependence of the diurnal variation on solar activity, and today we understand and can invert that relationship to construct a reliable record of the EUV flux from the geomagnetic record. We compare that to the F10.7 flux and the sunspot number, and find that the reconstructed EUV flux reproduces the F10.7 flux with great accuracy. On the other hand, it appears that the Relative Sunspot Number as currently defined is beginning to no longer be a faithful representation of solar magnetic activity, at least as measured by the EUV and related indices. The reconstruction suggests that the EUV flux reaches the same low (but non-zero) value at every sunspot minimum (possibly including Grand Minima), representing an invariant 'solar magnetic ground state'.

Reconstruction of the Sunspot Group Number: the Backbone Method **Review**

Leif **Svalgaard**, Kennuth H. Schatten

Topical Issue of Solar Physics on "Recalibration of the Sunspot Number", **2015**

http://arxiv.org/ftp/arxiv/papers/1506/1506.00755.pdf

We have reconstructed the sunspot group count, not by comparisons with other reconstructions and correcting those where they were deemed to be deficient, but by a re-assessment of original sources. The resulting series is a pure solar index and does not rely on input from other proxies, e.g. radionuclides, auroral sightings, or geomagnetic records. 'Backboning' the data sets, our chosen method, provides substance and rigidity by using long-time observers as a stiffness character. Solar activity, as defined by the Group Number, appears to reach and sustain for extended intervals of time the same level in each of the last three centuries since 1700 and the past several decades do not seem to have been exceptionally active, contrary to what is often claimed.

Solar activity – past, present, future **Review**

Leif **Svalgaard**

J. Space Weather Space Clim. 3 (**2013**) A24

http://www.swsc-journal.org/articles/swsc/abs/2013/01/swsc130003/swsc130003.html

As our civilization depends increasingly on space-borne assets and on a delicate and vulnerable earth-bound infrastructure, solar activity and its potential impact becomes of increasing importance and relevance. In his famous paper on the Maunder Minimum, Eddy (1976) introduced the notion that the Sun is a variable star on long time scales. After the recent decade of vigorous research based on cosmic ray and sunspot data as well as on geomagnetic activity, an emerging consensus reconstruction of solar wind magnetic field strength has been forged for the last century. The consensus reconstruction shows reasonable agreement among the various reconstructions of solar wind magnetic field the past ~ 170 years. New magnetic indices open further possibilities for the exploitation of historic data. The solar wind is a direct result of solar magnetic activity providing an important link to the effects on the Earth's environment. Reassessment of the sunspot series (no Modern Grand Maximum) and new reconstructions of Total Solar Irradiance also contribute to our improved knowledge (or at least best guess) of the environment of the Earth System, with obvious implications for management of space-based technological assets or, perhaps, even climate. Several lines of evidence suggest that the Sun is entering a period of low activity, perhaps even a Grand Minimum. Average space weather might be "milder" with decreased solar activity, but the extreme events that dominate technological effects are not expected to disappear. Prediction of solar activity has a poor track record, but the progression of the current Cycle 24 is in accordance with its behavior predicted from the evolution of the solar polar fields, so perhaps there is hope.

FLARING SOLAR HALE SECTOR BOUNDARIES
L. **Svalgaard**1, I. G. Hannah2 and H. S. Hudson
2011 ApJ 733 49
The sector structure that organizes the magnetic field of the solar wind into large-scale domains has a clear pattern in the photospheric magnetic field as well. The rotation rate, 27-28.5 days, implies an effectively rigid rotation originating deeper in the solar interior than the sunspots. The photospheric magnetic field is known to be concentrated near that portion (the Hale boundary) in each solar hemisphere, where the change in magnetic sector polarity matches that between the leading and following sunspot polarities in active regions in the respective hemispheres. We report here that flares and microflares also concentrate at the Hale boundaries, implying that flux emergence and the creation of free magnetic energy in the corona also have a direct cause in the deep interior.

Iterative construction of the optimal sunspot number series

Michal **Švanda** (1 and 2), Martina Pavelková (1), Jiří Dvořák (3), Božena Solarová (1),
Solar Phys. **2022**
https://arxiv.org/pdf/2211.03332
The relative number of sunspots represents the longest evidence describing the level of solar activity. As such, its use goes beyond solar physics, e.g. towards climate research. The construction of a single representative series is a delicate task which involves a combination of observation of many observers. We propose a new iterative algorithm that allows to construct a target series of relative sunspot number of a hypothetical stable observer by optimally combining series obtained by many observers. We show that our methodology provides us with results that are comparable with recent reconstructions of both sunspot number and group number. Furthermore, the methodology accounts for the possible non-solar changes of observers' time series such as gradually changing observing conditions or slow change in the observers vision. It also provides us with reconstruction uncertainties. We apply the methodology to a limited sample of observations by ČESLOPOL network and discuss its properties and limitations.

Evolution and motions of magnetic fragments during the active region formation and decay: A statistical study

Michal **Švanda**1,2, Michal Sobotka2, Lucia Mravcová2,1 and Tatiana Výbošťoková3
A&A 647, A146 (**2021**)
https://www.aanda.org/articles/aa/pdf/2021/03/aa40127-20.pdf
https://doi.org/10.1051/0004-6361/202040127
Context. The evolution of solar active regions is still not fully understood. The growth and decay of active regions have mostly been studied in case-by-case studies.
Aims. Instead of studying the evolution of active regions case by case, we performed a large-scale statistical study to find indications for the statistically most frequent scenario.
Methods. We studied a large sample of active regions recorded by the Helioseismic and Magnetic Imager instrument. The sample was split into two groups: forming (367 members) and decaying (679 members) active regions. We tracked individual dark features (i.e. those that are assumed to be intensity counterparts of magnetised fragments from small objects to proper sunspots) and followed their evolution. We investigated the statistically most often locations of fragment merging and splitting as well as their properties.
Results. Our results confirm that statistically, sunspots form by merging events of smaller fragments. The coalescence process is driven by turbulent diffusion in a process similar to random-walk, where supergranular flows seem to play an important role. The number of appearing fragments does not seem to significantly correlate with the number of sunspots formed. The formation seems to be consistent with the magnetic field accumulation. Statistically, the merging occurs most often between a large and a much smaller object. The decay of the active region seems to take place preferably by a process similar to the erosion

Exploiting solar visible-range observations by inversion techniques: from flows in the solar subsurface to a flaring atmosphere

Michal **Švanda** (1 and 2), Jan Jurčák (2), David Korda (1), Jana Kašparová (2)
in the book "Reviews in Frontiers of Modern Astrophysics: From Space Debris to Cosmology" (eds Kabath, Jones and Skarka; publisher Springer Nature) **2020**
https://arxiv.org/pdf/2001.03874.pdf
Observations of the Sun in the visible spectral range belong to standard measurements obtained by instruments both on the ground and in the space. Nowadays, both nearly continuous full-disc observations with medium resolution and dedicated campaigns of high spatial, spectral and/or temporal resolution constitute a holy grail for studies that can capture (both) the long- and short-term changes in the dynamics and energetics of the solar atmosphere. Observations of photospheric spectral lines allow us to estimate not only the intensity at small regions, but also various derived data products, such as the Doppler velocity and/or the components of the magnetic field vector. We show that these measurements contain not only direct information about the dynamics of solar plasmas at the surface

of the Sun but also imprints of regions below and above it. Here, we discuss two examples: First, the local time-distance helioseismology as a tool for plasma dynamic diagnostics in the near subsurface and second, the determination of the solar atmosphere structure during flares. The methodology in both cases involves the technique of inverse modelling. **6 Sept 2017**

Polar cap magnetic field reversals during solar grand minima: could pores play a role?

Michal **Švanda**1,2, Allan Sacha Brun3, Thierry Roudier4 and Laurène Jouve
A&A 586, A123 (**2016**)
We study the magnetic flux carried by pores located outside active regions with sunspots and investigate their possible contribution to the reversal of the global magnetic field of the Sun. We find that they contain a total flux of comparable amplitude to the total magnetic flux contained in polar caps. The pores located at distances of 40–100 Mm from the closest active region systematically have the correct polarity of the magnetic field to contribute to the polar cap reversal. These pores can be found predominantly in bipolar magnetic regions. We propose that during grand minima of solar activity, such a systematic polarity trend, which is akin to a weak magnetic (Babcock-Leighton-like) source term, could still be operating but was missed by the contemporary observers because of the limited resolving power of their telescopes.
See HMI Science Nugget #48 Jan 2016
http://hmi.stanford.edu/hminuggets/?p=1380

Issues with time–distance inversions for supergranular flows

Michal **Švanda**
A&A 575, A122 (**2015**)
Aims. Recent studies have shown that time–distance inversions for flows start to be dominated by a random noise at a depth of only a few Mm. It was proposed that the ensemble averaging might be a solution for learning about the structure of the convective flows, e.g. about the depth structure of supergranulation.
Methods. Time–distance inversion is applied to the statistical sample of ∼ 104 supergranules, which allows the inversion cost function to be regularised weakly about the random-noise term and thus provides a much better localisation in space. We compare these inversions at four depths (1.9, 2.9, 4.3, and 6.2 Mm) when using different spatio-temporal filtering schemes in order to gain confidence about these inferences.
Results. The flows inferred by using different spatio-temporal filtering schemes are different (even by the sign) even though the formal averaging kernels and the random-noise levels are very similar. The inverted flows changes its sign several times with depth. I suggest that this is due to the inaccuracies in the forward problem that are possibly amplified by the inversion. It is also possible that other time–distance inversions are affected by this.

Moat Flow System around Sunspots in Shallow Subsurface Layers

Michal **Švanda**1,2, Michal Sobotka1, and Tomáš Bárta
2014 ApJ 790 135
We investigate the subsurface moat flow system around McIntosh H-type symmetrical sunspots and compare it to the flow system within supergranular cells. Representatives of both types of flows are constructed by means of the statistical averaging of flow maps obtained by time-distance helioseismic inversions. We find that moat flows around H-type sunspots replace supergranular flows but there are two principal differences between the two phenomena: the moat flow is asymmetrical, probably due to the proper motion of sunspots with respect to the local frame of rest, while the flow in the supergranular cell is highly symmetrical. Furthermore, the whole moat is a downflow region, while the supergranule contains the upflow in the center, which turns into the downflow at about 60% of the cell radius from its center. We estimate that the mass downflow rate in the moat region is at least two times larger than the mass circulation rate within the supergranular cell.

The response of clouds and aerosols to cosmic ray decreases†

J. **Svensmark**, M. B. Enghoff, N. J. Shaviv, H. Svensmark
JGR Volume 121, Issue 9 September 2016 Pages 8152–8181 **2016** DOI: 10.1002/2016JA022689
A method is developed to rank Forbush Decreases (FDs) in the galactic cosmic ray radiation according to their expected impact on the ionization of the lower atmosphere. Then a Monte Carlo bootstrap based statistical test is formulated to estimate the significance of the apparent response in physical and micro-physical cloud parameters to FDs. The test is subsequently applied to one ground based and three satellite based datasets. Responses (> 95%) to FDs are found in the following parameters of the analyzed datasets. AERONET: Ångström exponent (cloud condensation nuclei changes), SSM/I: liquid water content, ISCCP: total, high and middle, IR detected clouds over the oceans, MODIS: cloud effective emissivity, cloud optical thickness, liquid water, cloud fraction, liquid water path, liquid cloud effective radius. Moreover, the responses in MODIS are found to correlate positively with the strength of the FDs, and the signs and magnitudes of the responses agree with model based expectations. The effect

is mainly seen in liquid clouds. An impact through changes in UV driven photo chemistry is shown to be negligible and an impact via UV absorption in the stratosphere is found to have no effect on clouds. The total solar irradiance has a relative decrease in connection with FDs of the order of 10−3, which is too small to have a thermodynamic impact on timescales of a few days. The results demonstrate that there is a real influence of FDs on clouds probably through ions.

Sixty Years in Solar Physics

Zdenˇek **Švestka**

Solar Phys (**2010**) 267: 235–250, **File**

I recount my career in solar physics beginning at Ondˇrejov Observatory in 1948 and ending with my ~30 year stay at the Laboratory of Space Research in Utrecht.

The reported durations of GOES Soft X-Ray flares in different solar cycles

Bill **Swalwell**, Silvia Dalla, Stephen Kahler, Stephen White, Alan Ling, Rodney Viereck, and Astrid Veronig

Space Weather **2018**

https://arxiv.org/pdf/1805.10246.pdf

The Geostationary Orbital Environmental Satellites (GOES) Soft X-ray (SXR) sensors have provided data relating to, \textit{inter alia}, the time, intensity and duration of solar flares since the 1970s. The GOES SXR Flare List has become the standard reference catalogue for solar flares and is widely used in solar physics research and space weather. We report here that in the current version of the list there are significant differences between the mean duration of flares which occurred before May 1997 and the mean duration of flares thereafter. Our analysis shows that the reported flare timings for the pre-May 1997 data were not based on the same criteria as is currently the case. This finding has serious implications for all those who used flare duration (or fluence, which depends on the chosen start and end times) as part of their analysis of pre-May 1997 solar events, or statistical analyses of large samples of flares, \textit{e.g.} as part of the assessment of a Solar Energetic Particle forecasting algorithm.

The dynamics of 3-minute wavefronts and their relation to sunspot magnetic fields

Robert **Sych**, David B. Jess, Jiangtao Su

Royal Society Philosophical Transactions A **2020**

https://arxiv.org/pdf/2007.09369.pdf

We present a study of wave processes occurring in solar active region NOAA 11131 on **2010 December 10**, captured by the Solar Dynamics Observatory in the 1600A, 304A, and 171A channels. For spectral analysis we employed pixelised wavelet filtering together with a developed digital technique based on empirical mode decomposition. We studied the 3-minute wave dynamics to obtain relationships with the magnetic structuring of the underlying sunspot. We found that during development of wave trains the motion path occurred along a preferential direction, and that the broadband wavefronts can be represented as a set of separate narrowband oscillation sources. These sources become visible as the waves pass through the umbral inhomogeneities caused by the differing magnetic field inclination angles. We found the spatial and frequency fragmentation of wavefronts, and deduced that the combination of narrowband spherical and linear parts of the wavefronts provide the observed spirality. Maps of the magnetic field inclination angles confirm this assumption. We detect the activation of umbral structures as the increasing of oscillations in the sources along the front ridge. Their temporal dynamics are associated with the occurrence of umbral flashes. Spatial localisation of the sources is stable over time and depends on the oscillation period. We propose that these sources are the result of wave paths along the loops extending outwards from the magnetic bundles of the umbra.

Chromospheric Heating from Local Magnetic Growth and Ambipolar Diffusion Under Non-Equilibrium Conditions

Juan Martínez **Sykora**, Jaime de la Cruz Rodríguez, Milan Gošić, Alberto Sainz Dalda, Viggo H. Hansteen, Bart De Pontieu

ApJL **2022**

https://arxiv.org/pdf/2211.08472.pdf

The heating of the chromosphere in internetwork regions remains one of the foremost open questions in solar physics. In the present study we tackle this old problem by using a very high spatial-resolution simulation of quiet-Sun conditions performed with radiative MHD numerical models and IRIS observations. We have expanded a previously existing 3D radiative MHD numerical model of the solar atmosphere, which included self-consistently locally driven magnetic amplification in the chromosphere, by adding ambipolar diffusion and time-dependent non-equilibrium hydrogen ionization to the model. The energy of the magnetic field is dissipated in the upper chromosphere, providing a large temperature increase due to ambipolar diffusion and the non-equilibrium ionization (NEQI). At the same time, we find that adding the ambipolar diffusion and NEQI in the simulation has a minor

impact on the local growth of the magnetic field in the lower chromosphere and its dynamics. Our comparison between synthesized Mg II profiles from these high spatial resolution models, with and without ambipolar diffusion and NEQI, and quiet Sun and coronal hole observations from IRIS now reveal a better correspondence. The intensity of profiles is increased and the line cores are slightly broader when ambipolar diffusion and NEQI effects are included. Therefore, the Mg II profiles are closer to those observed than in previous models, but some differences still remain. **2016 March 25** and **2017 October 15**

Analysis of Quiescent Corona X-ray Spectra from SphinX during the 2009 Solar Minimum

Janusz **Sylwester**, B. Sylwester, M. Siarkowski, K. J. H. Phillips, P. Podgorski, M. Gryciuk

Solar Phys. **294**, Article number: 176 **2019**

https://arxiv.org/pdf/1912.03082.pdf

https://link.springer.com/content/pdf/10.1007/s11207-019-1565-9.pdf

The SphinX X-ray spectrophotometer on the {\em CORONAS-PHOTON}\/ mission observed the 1~--~15\,keV X-ray spectrum of the spatially integrated solar corona during the deep minimum of 2009, when solar activity was exceptionally low. Its sensitivity for energies >1.2\,keV was higher than that of any other solar X-ray spectrometer in orbit at the time, including the detectors on GOES. Using much improved instrumental data than was used previously, we analyzed SphinX spectra in 576 intervals for which there was no discernible activity (NA), 40 intervals when there were X-ray brightenings (B), and sixteen intervals when there were micro-flares with peak emission less than GOES A1 (F). An instrumental background spectrum, formed over 34 hours of spacecraft night-time periods and including electronic noise and particle radiation, was subtracted from the solar spectra. Theoretical spectra were used to deduce temperatures on an isothermal assumption for the NA, B, and F intervals (1.69, 1.81, and 1.86\,MK respectively). Differential emission measure (DEM) analysis for the same spectra revealed a "cooler" component (log\,T=6.2 or T≈1.6\,MK) in each case, but with a second hotter component having a less well-defined peak temperature varying from ≈2.5 to ≈3.5\,MK (log\,T=6.4 and 6.55) and an emission measure between two and three orders smaller than that of the cooler component. These results are similar to those obtained at times just after solar minimum with the EVE instrument. A very hot component that might indicate the signature of nano-flare heating of the corona is not evident in SphinX data.

The soft X-ray spectrometer polarimeter SolpeX

J. **Sylwester**1 · M. Ste¸slicki ´ 1 ·J. Ba¸kała1 · S. Płocieniak1 · Z. Szaforz ˙ 1 · M. Kowalinski ´ 1 ·D. Scisłowski ´ 1 · P. Podgorski ´ 1 · T. Mrozek1 ·J. Barylak1 · A. Makowski1 · M. Siarkowski1 · Z. Kordylewski1 · B. Sylwester1 · S. Kuzin2 · A. Kirichenko2 ·A. Pertsov2 · S. Bogachev2

Experimental Astronomy **2019**

https://doi.org/10.1007/s10686-018-09618-4

https://link.springer.com/content/pdf/10.1007%2Fs10686-018-09618-4.pdf

We present a novel X-ray assembly of functionally related instrument blocks intended to measure solar flare and active region (AR) spectra from within the Russian instrument complex KORTES, to be mounted aboard the International Space Station (ISS). SolpeX consists of three blocks: fast-rotating multiple flat crystal Bragg spectrometer, pin-hole X-ray spectral imager and Bragg polarimeter. This combination of measuring blocks will offer an opportunity to detect/measure possible X-ray polarization in soft X-ray emission lines/continuum and record spectra of solar flares, in particular during their impulsive phases. Polarized Bremsstrahlung and line emission may arise from presence of directed particle beams colliding with denser regions of flares. As a result of evaporation, the X-ray spectral-components are expected to be Doppler shifted, which will also be measured. In this paper, we present details of the construction of three SolpeX blocks and discuss their functionality. Delivery of KORTES with SolpeX to ISS is expected in 2020/2021.

Chromospheric and coronal heating and jet acceleration due to reconnection driven by flux cancellation. II. Cancellation of two magnetic polarities of unequal flux

Syntelis P., Priest E. R

A&A 649, A101 **2021**

https://arxiv.org/pdf/2103.16184.pdf

https://doi.org/10.1051/0004-6361/202140474

Context. Recent observations have shown that magnetic flux cancellation occurs at the photosphere more frequently than previously thought.

Aims. In order to understand the energy release by reconnection driven by flux cancellation, we previously studied a simple model of two cancelling polarities of equal flux. Here, we further develop our analysis to achieve a more general setup where the two cancelling polarities have unequal magnetic fluxes and where many new features are revealed.

Methods. We carried out an analytical study of the cancellation of two magnetic fragments of unequal and opposite flux that approach one another and are located in an overlying horizontal magnetic field.

Results. The energy release as microflares and nanoflares occurs in two main phases. During phase 1a, a separator is

formed and reconnection is driven at it as it rises to a maximum height and then moves back down to the photosphere, heating the plasma and accelerating plasma jets in the process. During phase 1b, once the separator moves back to the photosphere, it bifurcates into two null points. Reconnection is no longer driven at the separator and an isolated magnetic domain connecting the two polarities is formed. During phase 2, the polarities cancel out at the photosphere as magnetic flux submerges below the photosphere and as reconnection occurs at and above the photosphere and plasma jets and a mini-filament eruption can be produced.

A Cancellation Nanoflare Model for Solar Chromospheric and Coronal Heating III. 3D Simulations and Atmospheric Response

P. **Syntelis**, E.R. Priest

ApJ **891** 52 **2020**

https://arxiv.org/pdf/2001.10456.pdf

https://doi.org/10.3847/1538-4357/ab6ffc

Inspired by recent observations suggesting that photospheric magnetic flux cancellation occurs much more frequently than previously thought, we analytically estimated the energy released from reconnection driven by photospheric flux cancellation, and proposed that it can act as a mechanism for chromospheric and coronal heating (Priest et al., 2018). Using two-dimensional simulations we validated the analytical estimates and studied the resulting atmospheric response (Syntelis et al. 2019). In the present work, we set up three-dimensional resistive MHD simulations of two cancelling polarities in a stratified atmosphere with a horizontal external field to further validate and improve upon the analytical estimates. The computational evaluation of the parameters associated with the energy release are in good qualitative agreement with the analytical estimates. The computational Poynting energy flux into the current sheet is in good qualitative agreement with the analytical estimates, after correcting the analytical expression to better account for the horizontal extent of the current sheet. The atmospheric response to the cancellation is the formation of hot ejections, cool ejections, or a combination of both hot and cool ejections, which can appear with a time difference and/or be spatially offset, depending on the properties of the cancelling region and the resulting height of the reconnection. Therefore, during the cancellation, a wide spectrum of ejections can be formed, which can account for the variety of multi-thermal ejections associated with Ellerman bombs, UV bursts and IRIS bombs, and also other ejections associated with small-scale cancelling regions and spicules.

Successful and Failed Flux Tube Emergence in the Solar Interior

P. **Syntelis**, V. Archontis, A. Hood

2019 *ApJ* **874** 15

https://arxiv.org/pdf/1902.07969.pdf

sci-hub.tw/10.3847/1538-4357/ab0959

We report on our three-dimensional (3D) magnetohydrodynamic (MHD) simulations of cylindrical weakly twisted flux tubes emerging from 18 Mm below the photosphere. We perform a parametric study, by varying the initial magnetic field strength (B0), radius (R), twist (α) and length of the emerging part of the flux tube (λ) to investigate how these parameters affect the transfer of the magnetic field from the convection zone to the photosphere. We show that the efficiency of emergence at the photosphere (i.e. how strong the photospheric field will be in comparison to B0) depends not only on the B0 but also the morphology of the emerging field and the twist. We show that parameters such as B0 and magnetic flux cannot alone determine whether a flux tube will emerge to the solar surface. For instance, high-B0(weak-B0) fields may fail (succeed) to emerge at the photosphere, depending on their geometrical properties. We also show that the photospheric magnetic field strength can vary greatly for flux tubes with the same B0 but different geometric properties. Moreover, in some cases we have found scaling laws, whereby the magnetic field strength scales with the local density as $B \propto \rho^{\kappa}$, where $\kappa \approx 1$ deeper in the convection zone and $\kappa < 1$, close to the photosphere. The transition between the two values occurs approximately when the local pressure scale (Hp) becomes comparable to the diameter of the flux tube ($Hp \approx 2R$). We derive forms to explain how and when these scaling laws appear and compare them with the numerical simulations.

A Cancellation Nanoflare Model for Solar Chromospheric and Coronal Heating II. 2D Theory and Simulations

P. **Syntelis**, E.R. Priest, L.P. Chitta

2019 *ApJ* **872** 32

https://arxiv.org/pdf/1901.02798.pdf

Recent observations at high spatial resolution have shown that magnetic flux cancellation occurs on the solar surface much more frequently than previously thought, and so this led Priest et al 2018 to propose magnetic reconnection driven by photospheric flux cancellation as a mechanism for chromospheric and coronal heating. In particular, they estimated analytically the amount of energy released as heat and the height of the energy release during flux cancellation. In the present work, we take the next step in the theory by setting up a two-dimensional resistive MHD simulation of two canceling polarities in the presence of a horizontal external field and a stratified atmosphere in order to check and improve upon the analytical estimates. Computational evaluation of the energy release during

reconnection is found to be in good qualitative agreement with the analytical estimates. In addition, we go further and undertake an initial study of the atmospheric response to reconnection. We find that, during the cancellation, either hot ejections or cool ones or a combination of both hot and cool ejections can be formed, depending on the height of the reconnection location. The hot structures can have the density and temperature of coronal loops, while the cooler structures are suggestive of surges and large spicules.

Simulation Study of Hemispheric Phase-Asymmetry in the Solar Cycle

D. **Syukuya**, K. Kusano
ApJ **2016**
https://arxiv.org/pdf/1612.03294v1.pdf

Observations of the sun suggest that solar activities systematically create north-south hemispheric asymmetries. For instance, the hemisphere in which the sunspot activity is more active tends to switch after the early half of each solar cycle. Svalgaard & Kamide (2013) recently pointed out that the time gaps of polar field reversal between the north and south hemispheres are simply consequences of the asymmetry of sunspot activity. However, the mechanism underlying the asymmetric feature in solar cycle activities is not yet well understood. In this paper, in order to explain the cause of the asymmetry from the theoretical point of view, we investigate the relationship between the dipole- and quadrupole-type components of the magnetic field in the solar cycle using the mean-field theory based on the flux transport dynamo model. As a result, we found that there are two different attractors of the solar cycle, in which either the north or the south polar field is first reversed, and that the flux transport dynamo model well explains the phase-asymmetry of sunspot activity and the polar field reversal without any ad hoc source of asymmetry.

A deep learning virtual instrument for monitoring extreme UV solar spectral irradiance

Alexandre **Szenicer**, David F. Fouhey, Andres Munoz-Jaramillo, Paul J. Wright, ...
Science Advances 02 Oct **2019**: Vol. 5, no. 10, eaaw6548
https://sci-hub.se/10.1126/sciadv.aaw6548

Measurements of the extreme ultraviolet (EUV) solar spectral irradiance (SSI) are essential for understanding drivers of space weather effects, such as radio blackouts, and aerodynamic drag on satellites during periods of enhanced solar activity. In this paper, we show how to learn a mapping from EUV narrowband images to spectral irradiance measurements using data from NASA's Solar Dynamics Observatory obtained between 2010 to 2014. We describe a protocol and baselines for measuring the performance of models. Our best performing machine learning (ML) model based on convolutional neural networks (CNNs) outperforms other ML models, and a differential emission measure (DEM) based approach, yielding average relative errors of under 4.6% (maximum error over emission lines) and more typically 1.6% (median). We also provide evidence that the proposed method is solving this mapping in a way that makes physical sense and by paying attention to magnetic structures known to drive EUV SSI variability.

Coronal Imaging with the Solar UltraViolet Imager

Sivakumara K. **Tadikonda**, Douglas C. Freesland, Robin R. Minor, Daniel B. Seaton, Gustave J. Comeyne, Alexander Krimchansky
Solar Physics March **2019**, 294:28
https://arxiv.org/ftp/arxiv/papers/1901/1901.08531.pdf
https://link.springer.com/content/pdf/10.1007%2Fs11207-019-1411-0.pdf

We investigate the coronal imaging capabilities of the Solar UltraViolet Imager (SUVI) on the Geostationary Operational Environmental Satellite-R series spacecraft. Nominally Sun-pointed, SUVI provides solar images in six Extreme UltraViolet (EUV) wavelengths. On-orbit data indicated that SUVI had sufficient dynamic range and sensitivity to image the corona to the largest heights above the Sun to date while simultaneously imaging the Sun. We undertook a campaign to investigate the existence of the EUV signal well beyond the nominal Sun-centered imaging area of the solar EUV imagers. We off-pointed SUVI line-of-sight by almost one imaging area around the Sun. We present the details of the campaign conducted when the solar cycle is at near the minimum and some results that affirm the EUV presence to beyond three solar radii.

Readdressing the UV solar variability with SATIRE-S: non-LTE effects

R. V. **Tagirov**, A. I. Shapiro, N. A. Krivova, Y. C. Unruh, K. L. Yeo, S. K. Solanki
A&A 631, A178 **2019**
https://arxiv.org/pdf/1909.11736.pdf
https://doi.org/10.1051/0004-6361/201935121

Context. Solar spectral irradiance (SSI) variability is one of the key inputs to models of the Earth's climate. Understanding solar irradiance fluctuations also helps to place the Sun among other stars in terms of their brightness variability patterns and to set detectability limits for terrestrial exo-planets.
Aims. One of the most successful and widely used models of solar irradiance variability is SATIRE-S. It uses

spectra of the magnetic features and surrounding quiet Sun computed with the ATLAS9 spectral synthesis code under the assumption of Local Thermodynamic Equilibrium (LTE). SATIRE-S has been at the forefront of solar variability modelling, but due to the limitations of the LTE approximation its output SSI has to be empirically corrected below 300 nm, which reduces the physical consistency of its results. This shortcoming is addressed in the present paper.
Methods. We replace the ATLAS9 spectra of all atmospheric components in SATIRE-S with the spectra calculated using the non-LTE Spectral Synthesis Code (NESSY). We also use Fontenla et al. (1999) temperature and density stratification models of the solar atmosphere to compute the spectrum of the quiet Sun and faculae.
Results. We compute non-LTE contrasts of spots and faculae and combine them with the SDO/HMI filling factors of the active regions to calculate the total and spectral solar irradiance variability during solar cycle 24.
Conclusions. The non-LTE contrasts result in total and spectral solar irradiance in good agreement with the empirically corrected output of the LTE version. This suggests that empirical correction introduced into SATIRE-S output is well judged and that the corrected total and spectral solar irradiance obtained from the SATIRE-S model in LTE is fully consistent with the results of non-LTE computations.

Reconstructing solar magnetic fields from historical observations X. Effect of magnetic field inclination and boundary structure on AIA 1600 Å emission

Ismo **Tähtinen**, Alexei A. Pevtsov, Timo Asikainen, Kalevi Mursula
A&A **2024**
https://arxiv.org/pdf/2409.17771

The relation between the intensity of chromospheric emissions and the photospheric magnetic field strength has been examined in several studies, but the effect of the magnetic field inclination on chromospheric emissions remains almost unexplored. We study how the inclination of the photospheric magnetic field, as measured by the full 3D magnetic vector from the Helioseismic and Magnetic Imager (HMI), affects the relationship between the magnetic field strength and the far-ultraviolet emission at around 1600 Å observed by the Atmospheric Imaging Assembly (AIA). We also study how these parameters change spatially close to the active region perimeter. We analyzed the mutual dependence of 1168 co-temporal AIA and HMI observations from 2014 to 2017. We focused on magnetically active regions outside sunspots (e.g., plages and network) close to the solar disk center. We studied how the AIA and HMI parameters change with distance from the active region perimeter. The AIA 1600 emission typically decreases with increasing (more horizontal) inclination. For all inclinations, AIA 1600 emission increases with increasing magnetic field strength until saturating at some peak intensity, which depends on the cosine of the inclination, with horizontal regions saturating at lower intensities. In addition, we find that activity clusters have a narrow boundary (< 2 arcseconds) in which the AIA 1600 intensity, magnetic field strength, and inclination distributions and relations differ significantly from those in the inner layers. This study demonstrates the significant effect that magnetic field inclination and activity cluster border regions have on chromospheric emissions. Although the observed effects are likely reduced in low-resolution observations where different regions are averaged together, a detailed study is needed to examine the emission--magnetic field relation at different resolutions.

Straight outta photosphere: Open solar flux without coronal modeling

Ismo **Tähtinen**, Timo Asikainen, Kalevi Mursula
A&A 688, L32 **2024**
https://arxiv.org/pdf/2408.11525
https://www.aanda.org/articles/aa/pdf/2024/08/aa51267-24.pdf

The open solar flux, that is, the total magnetic flux escaping the Sun, is one of the most important parameters connecting solar activity to the Earth. The open solar flux is commonly estimated from photospheric magnetic field measurements by making model assumptions about the solar corona. However, the question in which way the open solar flux is directly related to the distribution of the photospheric magnetic field is still partly unknown. We aim to reconstruct the open solar flux directly from the photospheric magnetic fields without making any assumptions about the corona and without using coronal hole observations, for instance. We modified an earlier vector sum method by taking magnetic field polarities into account and applied the method to the synoptic magnetograms of six instruments to determine the open solar flux from solar cycles 21-24. Results. The modified vector sum method produces a vector of the global solar magnetic field whose magnitude closely matches the open solar flux from the potential field source surface (PFSS) model both by the absolute scale and the overall time evolution for each of the six magnetograms. The latitude of this vector follows the Hale cycle by always pointing toward the dominantly positive-polarity hemisphere, and its longitude coincides with the location of the main coronal holes of the McIntosh Archive. We find multi-year periods during which the longitude of the vector slowly drifts or stays rather stationary in the Carrington frame. These periods are punctuated by times when the longitude moves rapidly in the Carrington frame. By comparing the magnitude of this vector to the open solar flux calculated from the PFSS model with different source surface heights, we find that the best match is produced with a source surface height $R_{ss}=2.4-2.5R_{\odot}$.

Reconstructing solar magnetic fields from historical observations

VIII. AIA 1600 Å contrast as a proxy of solar magnetic fields

I. **Tähtinen**1, I. I. Virtanen1,2, A. A. Pevtsov3 and K. Mursula1
A&A 664, A2 (**2022**)
https://www.aanda.org/articles/aa/pdf/2022/08/aa41164-21.pdf

Context. The bright regions in the solar chromosphere and temperature minimum have a good spatial correspondence with regions of intense photospheric magnetic field. Bright regions are visible in different emission lines and parts of the continuum. Their observation started more than a hundred years ago with the invention of the spectroheliograph. While the historical spectroheliograms are essential for studying the long-term variability of the Sun, the modern satellite-borne observations can help us reveal the nature of chromospheric brightenings in previously unattainable detail.
Aims. Our aim is to improve the understanding of the relation between magnetic fields and radiative structures byf studying modern seeing-free observations of far-ultraviolet (FUV) radiation around 1600 Å and photospheric magnetic fields.
Methods. We used Helioseismic and Magnetic Imager (HMI) observations of photospheric magnetic fields and Atmospheric Imaging Assembly (AIA) observations of FUV contrast around 1600 Å. We developed a robust method to find contrast thresholds defining bright and dark AIA 1600 Å pixels, and we combine them to bright and dark clusters. We investigate the relation of magnetic fields and AIA 1600 Å radiation in bright and dark clusters.
Results. We find that the percentage of bright pixels (ranging from 2% to 10%) almost entirely explains the observed variability of 1600 Å emission. We developed a multilinear regression model based on the percentages of bright and dark pixels, which can reliably predict the magnitude of the disk-averaged unsigned magnetic field. We find that bright and dark clusters closely correspond respectively to the populations of moderate ($B > 55$ G) and strong ($B > 1365$ G) magnetic field HMI clusters. The largest bright clusters have a constant mean unsigned magnetic field, as found previously for Ca II K plages. However, the magnetic field strength of bright clusters is 254.7 ± 0.1 G, which is roughly 100 G larger than found earlier for Ca II K plages.

Relationship between magnetic field properties and statistical flow using numerical simulation and magnetic feature tracking on solar photosphere

K. **Takahata**, H. Hotta, Y. Iida, T. Oba
MNRAS Volume 503, Issue 3, May **2021**, Pages 3610–3616,
https://doi.org/10.1093/mnras/stab710
https://arxiv.org/pdf/2103.03789

We perform radiative magnetohydrodynamic calculations for the solar quiet region to investigate the dependence of statistical flow on magnetic properties and the three-dimensional (3D) structure of magnetic patches in the presence of large-scale flow that mimics differential rotation. It has been confirmed that strong magnetic field patches move faster in the longitudinal direction at the solar surface. Consequently, strong magnetic patches penetrate deeper into the solar interior. The motion of the deep-rooted magnetic patches is influenced by the faster differential rotation in the deeper layer. In this study, we perform realistic radiative magnetohydrodynamic calculations using R2D2 code to validate that stronger patches have deeper roots. We also add large-scale flow to mimic the differential rotation. The magnetic patches are automatically detected and tracked, and we evaluate the depth of 30,000 magnetic patches. The velocities of 2.9 million magnetic patches are then measured at the photosphere. We obtain the dependence of these values on the magnetic properties, such as field strength and flux. Our results confirm that strong magnetic patches tend to show deeper roots and faster movement, and we compare our results with observations using the point spread function of instruments at the Hinode and Solar Dynamics Observatory (SDO). Our result is quantitatively consistent with previous observational results of the SDO.

The Instantaneous Response of Geomagnetic Field, near-Earth IMF and Cosmic-Ray Intensity to Solar Flares

Jouni J. **Takalo**
Sol. Phys. **2024**
https://arxiv.org/pdf/2405.15340

We show using superposed epoch analysis (SEA) that the most energetic protons (greater than 60 MeV) in near-Earth IMF have a peak almost immediately (less than a day) after peak in solar flare index (SFI), while protons greater than 10 MeV peak one day after the SFI and protons greater than 1 MeV two days after the SFI. The geomagnetic indices AU, -AL, PC, Ap and -Dst peak after two to three days in SEAs after the peak in SFI. The auroral electrojet indices AU and -AL, however, have only low peaks. Especially, the response of the eastward electrojet, AU, to SFI is negligible compared to other geomagnetic indices. The SEAs of the SFI and cosmic ray counts (CR) show that the deepest decline in the CR intensity follows also with 2-3 day lag the maximum of the SFI for the Solar Cycles 20-24. The depth of the declines are related to the SFI strength of each cycle, i.e, the average decline is about 5% for the Cycles 21 and 22, but only 3% for the Cycle 24. The strongest Cycle 19, however, differs from the other cycles such that it has double-peaked decline and lasts longer than the decline of the other

cycles. The double superposed epoch analyses show that the response of IMF Bv2, which is about two days, and CR to SFI are quite simultaneous, but sometimes Bv2 may peak somewhat earlier than the decline existing in CR.

Analysis of the Solar Flare Index for Solar Cycles 18 – 24: Extremely Deep Gnevyshev Gap in the Chromosphere

Jouni **Takalo**

Solar Phys. **298**, Article number: 86 **2023**

https://arxiv.org/pdf/2306.04239.pdf

https://doi.org/10.1007/s11207-023-02177-8

We study the solar flare index (SFI) for the solar cycles 18\,--\,24. We find that SFI has deeper Gnevyshev gap (GG) in its first principal component than other atmospheric parameters. The GG is extremely clear especially in the even cycles.

The GG of the SFI appears about a half year later as a drop in the interplanetary magnetic field near the Earth and in the geomagnetic Ap-index. The instantaneous response of the magnetic field to solar flares, however, shows about two to three days after the eruption as a high, sharp peak in the cross-correlation of the SFI and Ap-index and as a lower peak in SFI vs. IMF B cross-correlation. We confirm these rapid responses using superposed-epoch analysis. The most active flare cycles during 1944-2020 are the Cycles 19 and 21. The Cycle 18 has very strong SFI days as much as Cycle 22, but it has least nonzero SFI days in the whole interval. Interestingly Cycle 20 can be compared to the Cycles 23 and 24 in its low flare activity, although it locates between the most active SFI cycles.

Temporal and Latitudinal Variation in Penumbra-Umbra Ratios of the Sunspots: Analyses of RGO, Kodaikanal and Debrecen Databases

Jouni **Takalo**

Solar Phys. **2023**

https://arxiv.org/pdf/2305.10757.pdf

We study the latitudinal distribution and temporal evolution of the sunspot penumbra-umbra ratio (q) for the even and odd Solar Cycles 12-24 of RGO sunspot groups, SC21-SC24 of Debrecen sunspot groups and Kodaikanal sunspot dataset for SC16-SC24. We find that RGO even (odd) Cycles have q-values 5.20 (4.75), Kodaikanal even (odd) cycles have q-values 5.27 (5.43), and Debrecen cycles has q-value 5.74 on the average. We also show that q is at lowest around the Equator of the Sun and increases towards higher latitudes having maximum values at about 10-25 degrees. This is understandable, because smaller sunspots and groups locate nearer to Equator and have smaller q-values than larger sunspots and groups, which maximize at about 10-20 degrees at both hemispheres. The error limits are very wide and thus the confidence of this result is somewhat vague. For Debrecen dataset we find a deep valley in the temporal q-values before the middle of the cycle. We show that this exists simultaneously with the Gnevyshev gap (GG) in the graph of the total and umbral areas of the large sunspot groups. Other databases do not show GG in their q-graphs, although GG exists in their temporal total area and umbral area.

Extracting Hale Cycle Related Components from Cosmic-Ray Data Using Principal Component Analysis

Jouni J. **Takalo**

Solar Phys. **297**, Article number: 113 **2022**

https://arxiv.org/pdf/2206.09350.pdf

https://link.springer.com/content/pdf/10.1007/s11207-022-02048-8.pdf

We decompose the monthly cosmic-ray data, using several neutron monitor count rates, of Cycles 19-24 with principal component analysis (PCA). We show using different cycle limits that the first and second PC of cosmic-ray (CR) data explain 77-79% and 13-15% of the total variation of the Oulu CR Cycles 20-24 (C20- C24), 73-77% and 13-17% of the variation of Hermanus C20-C24, and 74-78% and 17-21% of the Climax C19-C22, respectively. The PC1 time series of the CR Cycles 19-24 has only one peak in its power spectrum at the period 10.95 years, which is the average solar cycle period for the interval SC19-SC24. The PC2 time series of the same cycles has a clear peak at period 21.90 (Hale cycle) and another peak at 1/3 of that period with no peak at the solar cycle period. We show that the PC2 of the CR is essential in explaining the differences in the intensities of the even and odd cycles of the CR. The odd cycles have positive phase in the first half and negative phase in the second half of their PC2. This leads to slow decrease of the intensity in the beginning of the cycle and at minimum for the odd cycles. On the contrary, for the even cycles the phases are vice versa and this leads to faster decrease and more rapid recovery in the CR intensity of the cycle. As a consequence the even cycles have more peak-like structure. The only exceptions of this rule are Cycles 23 and 24 such the former has almost zero line PC2, and the latter has similar PC2 than the earlier odd cycles. These results are confirmed with skewness-kurtosis (S-K) analysis. Furthermore, S-K shows that other even and odd cycles, except Cycle 21, are on the regression line with correlation coefficient 0.85. The Cycles 21 of all calculated eight stations are compactly located in the S -K coordinate system and have smaller skewnesses and higher kurtoses than the odd Cycles 23.

Spatial and Temporal Distribution of Solar Green Line Corona for Solar Cycles 18-24

Jouni J. **Takalo**

Solar Phys. **2022**

https://arxiv.org/pdf/2206.09351.pdf

Homogeneous coronal data set (HCDS) of the green corona (Fe XIV) and coronal index of the solar activity (CI) have been used to study time-latitudinal distribution in solar cycles 18-24 and compared with similar distribution of sunspots, the magnetic fields and the solar radio flux 10.7 cm. The most important results are: (a) distribution of coronal intensities related to the cycle maximum are different for individual cycles, (b) the poleward migration of the HCDS from mid latitudes in each cycle exists, even in extremely weak Cycle 24, and the same is valid for the equatorward migration (c) the overall values of HCDS are slightly stronger for the northern hemisphere than for the southern one, (d) distribution of the HDCS are in coincidence with strongest photospheric magnetic fields (B>50 Gauss) and histogram of the sunspot groups, (e) Gnevyshev gap was confirmed with at least 95% confidence in the CI, however, with different behavior for odd and even cycles. Principal component analysis (PCA) showed that the first and second component account for 87.7% and 7.3% of the total variation of the CI. Furthermore, the PC2 of the green corona was quite different for cycle 21, compared with other cycles.

Separating the aa-index into Solar and Hale Cycle Related Components Using Principal Component Analysis

Jouni **Takalo**

Solar Physics volume 296, Article number: 80 (**2021**)

https://link.springer.com/content/pdf/10.1007/s11207-021-01825-1.pdf

https://doi.org/10.1007/s11207-021-01825-1

We decompose the monthly aa-index of Cycles 10 to 23 using principal component analysis (PCA). We show that the first component (PC1) is related to the 11-year solar cycle, and accounts for 41.5% of the variance of the data. The second component (PC2) is related to 22-year Hale cycle, and explains 23.6% of the variance of the data. The PC1 time series of the aa-index for Cycles 10 – 23 has only one peak in its power spectrum at the period 10.95 years, which is the average solar cycle (SC) period for the interval SC10 – SC23. The PC2 time series of the same cycles has a clear peak at period 21.90 (Hale cycle) and a smaller peak at 3/4 of that period. We also study the principal components of the sunspot number (SSN) for Cycles 10 – 23, and compare the mutual behavior of the PC2 components of the aa-index and SSN PCA analyses. We note that they are in the same phase in all other cycles but Solar Cycles 15 and 20. The aa-index of Cycle 20 also differs from other even aa-index cycles in its shape, especially in anomalously high peaks during its descending phase. Even though there is a coherence in the PC2 time series phases of the aa-index and sunspot number, this effect is too small to be the origin of all the differences between the shape of even and odd aa cycles. We estimate that 30% of the shape of the PC2 component of the aa-index is due to the shape of the PC2 of the sunspot number and the rest to other recurrent events in the Sun and solar wind. The first maximum of the aa-index (typical to odd cycles), during sunspot maximum, has been shown to be related to coronal mass ejections (CME), while the second maximum (typical to even cycles) in the cycle descending phase, is probably related to high-speed streams (HSS). The last events increase the activity level such that the minimum between even and odd cycle pairs is always higher than the minimum between succeeding odd and even cycle pairs.

Comparison of geomagnetic indices during even and odd solar cycles SC17-SC24: Signatures of Gnevyshev gap in geomagnetic activity

Jouni J. **Takalo**

Solar Phys. **296**, Article number: 19 (**2021**)

https://arxiv.org/pdf/2012.05061.pdf

https://link.springer.com/content/pdf/10.1007/s11207-021-01765-w.pdf

We show that the time series of sunspot group areas has a gap, so-called Gnevyshev gap (GG), between ascending and descending phases of the cycle and especially so for the even cycles. For the odd cycles this gap in less obvious, and is only a small decline after the maximum of the cycle. We resample the cycles to have same length of 3945 days (about 10.8 years), and show that the decline is between 1445-1567 days after the start of the cycle for the even cycles, and extending sometimes until 1725 days from the start of the cycle. For the odd cycles the gap is a little earlier 1332-1445 days after the start of the cycles with no extension. We analyze geomagnetic disturbances for solar cycles 17-24 using Dst-index, related Dxt- and Dcx-indices and Ap-index. In all of these time series there is a decline at the time or somewhat after the GG in the solar indices, and as deepest between 1567-1725. The declines are significant at 99 % level for both even and odd cycles of the Dst-index and for Dxt-, Dcx- and Ap-indices for even cycles. For odd cycles of Dxt-index the significance is 95 %, but insignificant for odd cycles of Dcx- and Ap indices. We, however, show that for the cycles 21 and 23, for which Dst exists, the GG is more intense than for the earlier odd cycles. The analyzes of OMNI2 data for 1964-2020 (SC20-SC24) show that these gaps during the maxima of the solar cycles can be seen also in the near-Earth solar wind velocity and IMF magnetic field intensity, and the energy function BV^2.

Temporal Distribution of Solar Cycle 24 Sunspot Groups: Comparison to Cycles 12-23

Jouni J. **Takalo**

ANNALS OF GEOPHYSICS **2020**

https://arxiv.org/ftp/arxiv/papers/2011/2011.12559.pdf

We analyze the temporal distribution of sunspot groups for even and odd cycles in the range SC12-SC24. It seems that cycle 24 is a characteristic even cycle, although with low amplitude. The number of large sunspot groups for cycle 24 is relatively smaller than for the average of both even and odd cycles SC12-SC23, and there is a deep decline of the large groups in the middle of the cycle. Temporal evolution of the sunspot groups of the even cycles is non-synchronous such that the northern hemisphere distribution of groups maximizes earlier that the southern hemisphere groups. This leads to a double-peak structure for the average even cycle. On the other hand, the distributions of the sunspot groups of odd cycles maximize simultaneously. We show that this double-peak structure intensifies the Gnevyshev gap (GG) for the even cycles, but is not its primary cause. On the contrary, we show that the GG exists for even and odd cycles, and separately on both hemispheres. We resample all cycles to have equal number of 3945 days and study the difference in the evolution of average total group area and average group area of the even and odd cycles separately. The analysis shows that there is a decline in both total area and average area in the even cycles 1445 days (about four years) after the beginning of the cycle, which is at least 99 % significant for both total and average area. The odd cycles do not have such a clear decline.

Comparison of the shape and temporal evolution of even and odd solar cycles

Jouni **Takalo** and Kalevi Mursula

A&A 636, A11 (**2020**)

https://www.aanda.org/articles/aa/pdf/2020/04/aa37488-20.pdf

https://arxiv.org/pdf/2004.03855.pdf

We study the difference in the shape of solar cycles for even and odd cycles using the Wolf sunspot numbers and group sunspot numbers of solar cycles 1−23. We furthermore analyse the data of sunspot area sizes for even and odd cycles SC12−SC23 and sunspot group data for even and odd cycles SC8−SC23 to compare the temporal evolution of even and odd cycles.

Methods. We applied the principal component analysis (PCA) to sunspot cycle data and studied the first two components, which describe the average cycle shape and cycle asymmetry. We used a distribution analysis to analyse the temporal evolution of the even and odd cycles and determined the skewness and kurtosis for even and odd cycles of sunspot group data.

Results. The PCA confirms the existence of the Gnevyshev gap (GG) for solar cycles at about 40% from the start of the cycle. The temporal evolution of sunspot area data for even cycles shows that the GG exists at least at the 95% confidence level for all sizes of sunspots. On the other hand, the GG is shorter and statistically insignificant for the odd cycles of aerial sunspot data. Furthermore, the analysis of sunspot area sizes for even and odd cycles of SC12−SC23 shows that the greatest difference is at 4.2−4.6 years, where even cycles have a far smaller total area than odd cycles. The average area of the individual sunspots of even cycles is also smaller in this interval. The statistical analysis of the temporal evolution shows that northern sunspot groups maximise earlier than southern groups for even cycles, but are concurrent for odd cycles. Furthermore, the temporal distributions of odd cycles are slightly more leptokurtic than distributions of even cycles. The skewnesses are 0.37 and 0.49 and the kurtoses 2.79 and 2.94 for even and odd cycles, respectively. The correlation coefficient between skewness and kurtosis for even cycles is 0.69, and for odd cycles, it is 0.90.

Conclusions. The separate PCAs for even and odd sunspot cycles show that odd cycles are more inhomogeneous than even cycles, especially in GSN data. Even cycles, however, have two anomalous cycles: SC4 and SC6. The variation in the shape of the early sunspot cycles suggests that there are too few and/or inaccurate measurements before SC8. According to the analysis of the sunspot area size data, the GG is more distinct in even than odd cycles. This may be partly due to sunspot groups maximizing earlier in the northern than in the southern hemisphere for even cycles. We also present another Waldmeier-type rule, that is, we find a correlation between skewness and kurtosis of the sunspot group cycles.

Comparison of Latitude Distribution and Evolution of Even and Odd Sunspot Cycles

Jouni **Takalo**

Solar Physics volume 295, Article number: 49 (**2020**)

https://link.springer.com/content/pdf/10.1007/s11207-020-01615-1.pdf

https://arxiv.org/pdf/2003.14262.pdf

We study the latitudinal distribution and evolution of sunspot areas of Solar Cycles 12 – 23 (SC12–23) and sunspot groups of Solar Cycles 8 – 23 (SC8–23) for even and odd cycles. The Rician distribution is the best-fit function for both even and odd sunspots group latitudinal occurrence. The mean and variance for even northern/southern butterfly wing sunspots are 14.94/14.76 and 58.62/56.08, respectively, and the mean and variance for odd northern/southern wing sunspots are 15.52/15.58 and 61.77/58.00, respectively. Sunspot groups of even cycle wings

are thus at somewhat lower latitudes on average than sunspot groups of the odd cycle wings, i.e. about 0.6 degrees for northern hemisphere wings and 0.8 degrees for southern hemisphere wings.
The spatial analysis of sunspot areas between SC12–23 shows that the small sunspots are at lower solar latitudes of the Sun than the large sunspots for both odd and even cycles, and also for both hemispheres.
Temporal evolution of sunspot areas shows a lack of large sunspots after four years (exactly between 4.2 – 4.5 years), i.e. about 40% after the start of the cycle, especially for even cycles. This is related to the Gnevyshev gap and is occurring at the time when the evolution of the average sunspot latitudes crosses about 15 degrees. The gap is, however, clearer for even cycles than odd ones. Gnevyshev gap divides the cycle into two disparate parts: the ascending phase/cycle maximum and the declining phase of the sunspot cycle.

Principal component analysis of sunspot cycle shape

Jouni **Takalo**, Kalevi Mursula
A&A 620, A100 **2018**
https://arxiv.org/pdf/1810.08583.pdf
We study the shape of sunspot cycles using the Wolf sunspot numbers and group sunspot numbers of solar cycles 1-23. We determine the most typical "model" cycles and the most asymmetric cycles, and test the validity of the two Waldmeier rules: the anti-correlation between cycle height and the length of its ascending phase (rule 1), and between cycle height and the length of the preceding cycle (rule 2). We applied the principal component analysis to sunspot cycles and studied the first two components, which describe the average cycle shape and cycle asymmetry, respectively. We also calculated their autocorrelation in order to study their recurrence properties. The best model cycles for Wolf numbers are SC12, SC14, and SC16, the successive even cycles from a long period of rather low overall solar activity. We find that the model cycles in eight different analyses using both sunspot series are almost exclusively even cycles. Correspondingly, the most asymmetric cycles are odd cycles. We find that both Waldmeier rules are valid for the whole Wolf number series of 23 cycles. Waldmeier rule 2 is also valid for group number series although its significance is weaker. Waldmeier rule 1 is not significant for the original group number series, but becomes significant for the proxy series. For separate centuries, Waldmeier rules are not always valid for Wolf numbers and very rarely for group numbers. Our results also offer a new interpretation for the Gnevyshev gap. In addition to being a local depression of solar activity, the Gnevyshev gap is a separatrix that divides cycles into two parts whose relative intensities determine the cycle asymmetry. The Gnevyshev gap is the zero value time of PC2, located approximately 33-42% into the cycle after its start.

Measurement of Solar Differential Rotation by Absolutely Calibrated Iodine-Cell Spectroscopy

Yoichi **Takeda**
Solar Phys. **2024**
https://arxiv.org/pdf/2406.18271
The iodine-cell technique, which is known to be efficient in precisely establishing Doppler velocity shifts, was once applied by the author to measuring the solar differential rotation based on full-disk spectroscopic observations (Takeda and Ueno, Sol. Phys. 270, 447, 2011). However, the data reduction procedure (in simple analogy with the stellar case) adopted therein was not necessarily adequate, because specific characteristic involved with the disk-resolved Sun (i.e., center-limb variation of line strengths) was not properly taken into consideration. Therefore, this problem is revisited based on the same data but with an application to theoretical spectrum fitting, which can yield absolute heliocentric radial velocities (v_obs) in a consistent manner as shown in the study of solar gravitational redshift (Takeda and Ueno, Sol. Phys. 281, 551, 2012). Likewise, instead of converting v_obs into omega (angular velocity) at each disk point, which suffers considerable errors especially near the central meridian, omega was derived this time by applying the least squares analysis to a dataset comprising v_obs values at many points. This new analysis resulted in omega (deg/day) = 13.92 (+/- 0.03) -1.69(+/- 0.34)(sin psi)^2 -2.37(+/- 0.62) (sin psi)^4 (psi: the heliographic latitude) along with the gravitational redshift of 675 m/s, which are favorably compared with previous publications. In addition, how the distribution of observing points on the disk affects the result is also examined, which reveals that rotation parameters may suffer appreciable errors depending on cases.

How Solar Soft X-Ray Irradiance Is Affected by the Size of Field of View

Aki **Takeda**1 and Shannon Boland2
2024 ApJ 960 91
https://iopscience.iop.org/article/10.3847/1538-4357/acf9f3/pdf
Soft X-ray images of the Sun obtained with multiple broadband filters provide a simple and useful method to calculate averaged coronal temperature and emission measure, from which we can further calculate solar X-ray irradiance in physical units, e.g., watts per square meter. However, X-ray telescopes are often designed for pursuing high spatial resolution, and thus the field of view (FOV) of full-Sun images is often limited over the limb, extending to only ~1.3 R⊙. This indicates that the irradiance obtained from the limited FOV may underestimate the true full-Sun irradiance by failing to count the contribution from outside the FOV. This work uses Hinode/X-Ray Telescope

(XRT) coronal images observed up to 1.7 R⊙ to investigate the fraction of irradiance excluded from the FOVs limited in size. The analysis indicates that the irradiance obtained within 1.1 R⊙, which is used for XRT irradiance study, excludes ~3.5%/~7% of irradiance relative to the value within 1.2/1.7 R⊙, respectively, for the active corona observed in 2022 July. In contrast, the excluded fraction increases to ~7%/~13%, respectively, for the minimum corona observed in 2009 August. To further investigate the dependence of exclusion fraction on the Sun's activity level, we process mission long Yohkoh/Soft X-ray Telescope full-Sun images to compare the irradiance within 1.1 and 0.9 R⊙ with that obtained from the maximum FOV of 1.2 R⊙. We confirm that the exclusion fraction is the largest in the period around solar minimum. We also find that the average value of exclusion fraction is slightly but measurably larger in the rising phase than the declining phase of the solar cycle.

Center--limb variation of solar photospheric microturbulence

Yoichi **Takeda**

Solar Phys. **297**, Article number: 4 **2022**

https://arxiv.org/pdf/2112.01142.pdf
https://link.springer.com/content/pdf/10.1007/s11207-021-01931-0.pdf
https://doi.org/10.1007/s11207-021-01931-0

Microturbulence (\xi) is a key parameter introduced in stellar spectroscopy to explain the strength of saturated lines by formally incorporating an additional thermal broadening term in the line opacity profile. Although our Sun can serve as an important testing bench to check the usual assumption of constant \xi, the detailed behavior of how \xi varies from the disk center through the limb seems to have never been investigated so far. In order to fill this gap, local \xi values on the solar disk were determined from the equivalent widths of 46 Fe I lines at 32 points from the center to the limb by requiring the consistency between the abundances derived from lines of various strengths. The run of \xi with \theta (angle between line of sight and the surface normal) was found to be only gradual from ~1.0km/s (at sin\theta = 0: disk center) to ~1.3km/s (at sin\theta ~ 0.7: two-thirds of radial distance); but thereafter increasing more steeply up to ~2km/s (at sin\theta = 0.97: limb). This result further suggests that the microturbulence derived from the flux spectrum of the disk-integrated Sun is by ~20% larger than that of the disk-center value, which is almost consistent with the prediction from 3D hydrodynamical model atmospheres.
Table 1. Literature data of solar microturbulence (after 1976)

Solar Cycle Variation of Coronal Temperature, Emission Measure, and Soft X-ray Irradiance Observed with Yohkoh Soft X-ray Telescope

Aki **Takeda**,1 Loren Acton,1 and Nicole Albanese2

ApJ **887** 225 **2019**

http://ylstone.physics.montana.edu/ylegacy/documents/publication/draft_takeda2019.pdf
https://doi.org/10.3847/1538-4357/ab53e3

This paper presents the solar soft X-ray irradiance (0.3-3.0nm) obtained from the mission-long fullSun X-ray images observed with the Soft X-ray Telescope(SXT) of the Yohkoh mission (1991-2001). The irradiance was calculated using filter-ratio temperatures and emission measures from the full-Sun integrated X-ray signals employing a coronal spectrum synthesized with CHIANTI atomic database version 8.0. Dependence of the results on the assumption of elemental abundances is investigated. The SXT irradiance for a shorter wavelength range was also calculated and compared with the low energy flux (0.1-0.8nm) of the X-Ray Sensor(XRS) aboard the GOES satellite. To incorporate the spatial information of the observed corona, we tried the alternative method to derive irradiance by applying the filter ratio method to the images of Northern hemispheric corona instead of spatially integrated signals from there. The emission-measure weighted average of the spatially resolved temperatures turned out to be generally 20 to 30% lower than those derived from the integrated signals, while the total of spatially resolved emission measures are accordingly 1.5 to 2 times higher. This trend is enhanced when solar activity is the lowest in early 1996. The irradiance obtained from the alternative method does not significantly vary from the result from the integrated signals. This provides some validation for the simpler full-Sun integrated method. The temporal variation of the emission measures of cool(2.5MK) components indicates that the ratio of the hot component relative to the medium component is higher in the ascending phase (mid 1998-2001) than the descending phase (1992-1995) of the solar activity cycle.

Solar Center--Limb Variation of the Strengths of Spectral Lines: Classification and Interpretation of Observed Trends

Y. **Takeda**, S. UeNo

Solar Phys. 294:63 **2019**

https://arxiv.org/pdf/1905.02306.pdf

The equivalent widths (W) of 565 spectral lines in the wavelength range of 4690--6870A were evaluated at 31 consecutive points from the solar disk center (mu=cos(theta)=1) to near the limb (mu=0.25) by applying the synthetic spectrum-fitting technique, in order to clarify the nature of their center--limb variations, especially the observed slope differing from line to line and its interpretation in terms of line properties. We found that the

distribution of the gradient beta (= -dlog W/dlog mu) well correlates with that of dlog W/dlog T index, which means that the center-to-limb variation of W is determined mainly by the T-sensitivity of individual lines because the line-forming region shifts towards upper layers of lower T as we go toward the limb. Further, the key to understanding the behavior of dlog W/dlog T (depending on the temperature sensitivity of number population) is whether the considered species is in minor population stage or major population stage, by which the distribution of beta is explained in terms of differences in excitation potential and line strengths. All the center--limb data of equivalent widths (as well as line-of-sight turbulent velocity dispersions, elemental abundances, and mean line-formation depths derived as by-products) along with the solar spectra used for our analysis are made available as on-line materials.

Toward Spectroscopically Detecting the Global Latitudinal Temperature Variation on the Solar Surface

Y. **Takeda**, S. UeNo

Solar Physics September **2017**, 292:123

A very slight rotation-induced latitudinal temperature variation (presumably on the order of several kelvin) on the solar surface is theoretically expected. While recent high-precision solar brightness observations reported its detection, confirmation by an alternative approach using the strengths of spectral lines is desirable, for which reducing the noise due to random fluctuation caused by atmospheric inhomogeneity is critical. Toward this difficult task, we carried out a pilot study of spectroscopically investigating the relative variation of temperature (TT) at a number of points in the solar circumference region near to the limb (where latitude dependence should be detectable, if any exists) based on the equivalent widths (WW) of 28 selected lines in the 5367 – 5393 Å and 6075 – 6100 Å regions. We paid special attention to i) clarifying which types of lines should be employed and ii) how much precision is attainable in practice. We found that lines with strong TT-sensitivity (|logW/logT||logf_0W/logf_0T|) should be used and that very weak lines should be avoided because they inevitably suffer strong relative fluctuations (ΔW/WΔW/W). Our analysis revealed that a precision of ΔT/T≈0.003ΔT/T≈0.003(corresponding to ≈ 15 K) can be achieved at best by a spectral line with comparatively large |logW/logT||logf_0W/logf_0T|, although this can possibly be further improved When a number of lines are used all together. Accordingly, if many such favorable lines could be measured with subpercent precision of ΔW/WΔW/W and by averaging the resulting ΔT/TΔT/T from each line, the random noise would eventually be reduced to ≲ 1 K and detection of a very subtle amount of global TT-gradient might be possible.

The Hinode/XRT Full-Sun Image Corrections and the Improved Synoptic Composite Image Archive

Aki **Takeda**, Keiji Yoshimura, Steven H. Saar

Solar Phys. Volume 291, Issue 1, pp 317-333 **2016**

http://solar.physics.montana.edu/takeda/xrt_synoptics/xrt_scia_final.pdf

The XRT Synoptic Composite Image Archive (SCIA) is a storage and gallery of X-ray full-Sun images obtained through the synoptic program of the X-Ray Telescope (XRT) onboard theHinode satellite. The archived images provide a quick history of solar activity through the daily and monthly layout pages and long-term data for morphological and quantitative studies of the X-ray corona. This article serves as an introduction to the SCIA, i.e., to the structure of the archive and specification of the data products included therein. We also describe a number of techniques used to improve the quality of the archived images: preparation of composite images to increase intensity dynamic range, removal of dark spots that are due to contaminants on the CCD, and correction of the visible stray light contamination that has been detected on the Ti-poly and C-poly filter images since May 2012.

Solar rotation inferred from radial velocities of the sun-as-a-star during the 2012 May 21 eclipse

Yoichi **Takeda**, Osamu Ohshima, Eiji Kambe, Hiroyuki Toda, Hisashi Koyano, Bun'ei Sato, Yasuhisa Nakamura, Norio Narita, Takashi Sekii

Publ. Astron. Soc. Japan, **2014**

http://arxiv.org/pdf/1411.1481v1.pdf

With an aim to examine how much information of solar rotation can be obtained purely spectroscopically by observing the sun-as-a-star during the **2012 May 21** eclipse at Okayama Astrophysical Observatory, we studied the variation of radial velocities (V_r), which were derived by using the iodine-cell technique based on a set of 184 high-dispersion spectra consecutively obtained over the time span of ~4 hours. The resulting V_r(t) was confirmed to show the characteristic variation (Rossiter-McLaughlin effect) caused by time-varying visibility of the solar disk. By comparing the observed V_r(t) curve with the theoretical ones, which were simulated with the latitude (psi) dependent solar rotation law omega(psi) = A + B sin^2(psi) (deg/day), we found that the relation B = -5.5 A + 77 gives the best fit, though separate determinations of A and B were not possible. Since this relationship is consistent with the real values known for the sun (A = 14.5, B = -2.8), we may state that our analysis yielded satisfactory

results. This consequence may provide a prospect of getting useful information on stellar rotation of eclipsing binaries from radial-velocity studies during eclipse, if many spectra of sufficiently high time-resolution are available.

The role of observable nonlinearities in solar cycle modulation

M. **Talafha**, M. Nagy, A. Lemerle, K. Petrovay
A&A 660, A92 **2022**
https://arxiv.org/pdf/2112.14465
https://www.aanda.org/articles/aa/pdf/2022/04/aa42572-21.pdf
Context. Two candidate mechanisms have recently been considered for the nonlinear modulation of solar cycle amplitudes. Tilt quenching (TQ) is a negative feedback between cycle amplitude and the mean tilt angle of bipolar active regions relative to the azimuthal direction; latitude quenching (LQ) consists in a positive correlation between cycle amplitude and average emergence latitude of active regions. Aims. Here we explore the relative importance of and the determining factors behind the LQ and TQ effects. Methods. The degree of nonlinearity induced by TQ, LQ and their combination is systematically probed in a grid of surface flux transport (SFT) models. The role of TQ and LQ is also explored in the successful 2x2D dynamo model optimized to reproduce the statistical behaviour of real solar cycles. Results. The relative importance of LQ vs TQ is found to correlate with the ratio u 0 /{\eta} in the SFT model grid, where u 0 is the meridional flow amplitude and {\eta} is diffusivity. An analytical interpretation of this result is given, further showing that the main underlying parameter is the dynamo effectivity range {\lambda} R which in turn is determined by the ratio of equatorial flow divergence to diffusivity. The relative importance of LQ vs TQ is shown to scale as C 1 +C 2 /{\lambda} 2 R . The presence of a latitude quenching is demonstrated in the 2x2D dynamo, contributing to the nonlinear modulation by an amount comparable to TQ. For other dynamo and SFT models considered in the literature the contribution of LQ to the modulation covers a broad range from being insignificant to being the dominant form of feedback. On the other hand, the contribution of a TQ effect (with the usually assumed amplitude) is never negligible.

Coronal heating in multiple magnetic threads

K. V. **Tam**1,2, A. W. Hood1, P. K. Browning3 and P. J. Cargill
A&A 580, A122 (**2015**)
http://www.aanda.org/articles/aa/pdf/2015/08/aa25995-15.pdf
Context. Heating the solar corona to several million degrees requires the conversion of magnetic energy into thermal energy. In this paper, we investigate whether an unstable magnetic thread within a coronal loop can destabilise a neighbouring magnetic thread.
Aims. By running a series of simulations, we aim to understand under what conditions the destabilisation of a single magnetic thread can also trigger a release of energy in a nearby thread.
Methods. The 3D magnetohydrodynamics code, Lare3d, is used to simulate the temporal evolution of coronal magnetic fields during a kink instability and the subsequent relaxation process. We assume that a coronal magnetic loop consists of non-potential magnetic threads that are initially in an equilibrium state.
Results. The non-linear kink instability in one magnetic thread forms a helical current sheet and initiates magnetic reconnection. The current sheet fragments, and magnetic energy is released throughout that thread. We find that, under certain conditions, this event can destabilise a nearby thread, which is a necessary requirement for starting an avalanche of energy release in magnetic threads.
Conclusions. It is possible to initiate an energy release in a nearby, non-potential magnetic thread, because the energy released from one unstable magnetic thread can trigger energy release in nearby threads, provided that the nearby structures are close to marginal stability.

The Characteristics of Valley Phase as Predictor of the Forthcoming Solar Cycle

Baolin **Tan**
Adv Space Res 63 (**2019**) 617–625
https://arxiv.org/pdf/1808.01417.pdf
Is Solar Cycle 24 anomalous? How do we predict the main features of a forthcoming cycle? In order to reply such questions, this work partitions quantitatively each cycle into valley, ascend, peak, and descend phases, statistically investigate the correlations between valley phase and the forthcoming cycle. We find that the preceding valley phase may dominate and can be predictor of the forthcoming cycle: (1) The growth rate in ascend phase strongly negatively correlates to valley length and strongly positively correlates to cycle maximum. (2) The cycle maximum strongly negatively correlates to valley length, and strongly positively correlates to cycle minimum. (3) The cycle period strongly negatively correlates to the valley variation. Based on these correlations, we conclude that the solar cycle 24 is a relatively weak and long cycle which is obviously weaker than Cycle 23. The similarity analysis also presents the similar result. The Cycle 25 is also inferred possibly to be a weak cycle. These results can help us understanding the physical processes of solar cycles.

Coronal Heating Driven by Magnetic-gradient Pumping Mechanism in Solar Plasmas

Baolin **Tan**

ApJ, **2014**

http://arxiv.org/pdf/1409.6418v1.pdf

The solar coronal heating is a longstanding mystery in astrophysics. Considering that the solar magnetic field is spatially inhomogeneous with considerable magnetic gradient from solar surface to the corona, this work proposes a magnetic gradient pumping (MGP) mechanism and try to explain the formation of hot plasma upflows, such as the hot type II spicules and hot plasma ejections, etc. In MGP mechanism, the magnetic gradients drive the energetic particles to move upwards from the underlying solar atmosphere and form hot upflows. These upflow energetic particles deposit in corona and make it becoming very hot. Roughly estimations indicate that the solar corona can be heated to above 1 million degrees, and the upflow velocity is about 40 km/s in chromosphere and about 130 km/s in the corona. The solar magnetic flux tubes act as pumpers to extract energetic particles from the underlying thermal photosphere, convey them and deposit in the corona. The deposition of energetic particles will make the corona become hot, and their escaping from the photosphere will make the underlying photosphere a bit cold. This mechanism present a natural explanation to the mystery of solar coronal heating.

Changing Relationships Between Sunspot Number, Total Sunspot Area and F10.7 in Cycles 23 and 24

Ken **Tapping**, Carly Morgan

Solar Phys. (**2017**) 292: 73. doi:10.1007/s11207-017-1111-6

This article is an update of a study (Tapping and Valdès in Solar Phys.272, 337, 2011) made in the early part of Cycle 24 using an intercomparison of various solar activity indices (including sunspot number and the 10.7 cm solar radio flux), in which it was concluded that a change in the relationship between photospheric and chromospheric/coronal activity took place just after the maximum of Cycle 23 and continued into Cycle 24. Precursors (short-term variations) were detected in Cycles 21 and 22. Since then the sunspot number index data have been substantially revised. This study is intended to be an update of the earlier study and to assess the impact of the revision of the sunspot number data upon those conclusions. This study compares original and revised sunspot number, total sunspot area, and 10.7 cm solar radio flux. The conclusion is that the transient changes in Cycles 21 and 22, and the more substantial change in Cycle 23, remain evident. Cycle 24 shows indications that the deviation was probably another short-term one.

The Formation and Dissipation of Current Sheets and Shocks due to Compressive Waves in a Stratified Atmosphere Containing a Magnetic Null

Lucas A. **Tarr**1,3,4 and Mark Linton

2019 ApJ 879 127

sci-hub.se/10.3847/1538-4357/ab27c5

We study the propagation and dissipation of magnetohydrodynamic waves in a set of numerical models that each includes a solar-like stratified atmosphere and a magnetic field with a null point. All simulations have the same magnetic field configuration but different transition region heights. Compressive wave packets introduced in the photospheric portion of the simulations refract toward the null and collapse it into a current sheet, which then undergoes reconnection. The collapsed null forms a current sheet owing to a strong magnetic pressure gradient caused by the inability of magnetic perturbations to cross the null. Although the null current sheet undergoes multiple reconnection episodes owing to repeated reflections off the lower boundary, we find no evidence of oscillatory reconnection arising from the dynamics of the null itself. Wave mode conversion around the null generates a series of slow-mode shocks localized near each separatrix. The shock strength is asymmetric across each separatrix, and subsequent shock damping therefore creates a tangential discontinuity across each separatrix, with long-lived current densities. A parameter study of the injected wave energy to reach the null confirms our previous Wentzel–Kramers–Brillouin estimates. Finally, using current estimates of the photospheric acoustic power, we estimate that the shock and ohmic heating we describe may account for ≈1%–10% of the radiative losses from coronal bright points with similar topologies and are similarly insufficient to account for losses from larger structures such as ephemeral regions. At the same time, the dynamics are comparable to proposed mechanisms for generating type II spicules.

On excited frequencies for Alfvén waves in a coronal arcade

Lucas A **Tarr**

ApJ **2017**

https://arxiv.org/pdf/1709.03446.pdf

The normal modes of oscillation for a magnetic arcade are used to analytically solve an initial value problem and estimate the power spectra of wave frequencies generated by a reconnection event in the solar corona. Over a realistic range of parameters, I find that such a disturbance generates a peak power at ∼10smHzfrequencies, but still substantial power up to ∼4Hz. The cadence and sensitivity of current instrumentation does not allow observations of oscillations at these frequencies, but in the near future, new instrumentation will be able to probe this regime, and observationally determine its energetic importance.

Magnetoacoustic Waves in a Stratified Atmosphere with a Magnetic Null Point

Lucas A. **Tarr**, Mark Linton, James Leake
ApJ 837:94 **2017**
https://arxiv.org/pdf/1611.06106v1.pdf
https://iopscience.iop.org/article/10.3847/1538-4357/aa5e4e/pdf
We perform nonlinear MHD simulations to study the propagation of magnetoacoustic waves from the photosphere to the low corona. We focus on a 2D system with a gravitationally stratified atmosphere and three photospheric concentrations of magnetic flux that give rise to a magnetic null point with a magnetic dome topology. We find that a single wavepacket introduced at the lower boundary splits into multiple secondary wavepackets. A portion of the packet refracts towards the null due to the varying Alfv\'en speed. Waves incident on the equipartition contour surrounding the null, where the sound and Alfv\'en speeds coincide, partially transmit, reflect, and mode convert between branches of the local dispersion relation. Approximately 15.5% of the wavepacket's initial energy (Einput) converges on the null, mostly as a fast magnetoacoustic wave. Conversion is very efficient: 70% of the energy incident on the null is converted to slow modes propagating away from the null, 7% leaves as a fast wave, and the remaining 23% (0.036Einput) is locally dissipated. The acoustic energy leaving the null is strongly concentrated along field lines near each of the null's four separatrices. The portion of the wavepacket that refracts towards the null, and the amount of current accumulation, depends on the vertical and horizontal wavenumbers and the centroid position of the wavepacket as it crosses the photosphere. Regions that refract towards or away from the null do not simply coincide with regions of open versus closed magnetic field or the local field orientation. We also modeled wavepacket propagation using a WKB method and found that it agrees qualitatively, though not quantitatively, with the results of the numerical simulation.

Dynamics of Explosive Events Observed by the Interface Region Imaging Spectrograph

E. **Tavabi**, S. Zeighami & M. Heydari
Solar Physics volume 297, Article number: 76 (**2022**)
https://doi.org/10.1007/s11207-022-01990-x
In this research, we investigate Explosive Events (EEs) in the off-limb solar atmosphere, with simultaneous observations from the Si IV, Mg II k, and slit-jaw images (SJI) of the Interface Region Imaging Spectrograph (IRIS), on **17 August 2014, and 19 February**. IRIS data can be investigated to observe the motion of matter, fluctuations, energy absorption, and heat transition of the solar atmosphere. Mechanisms responsible for solar large-scale structures, such as flares and coronal mass ejections, might originate from these small-scale energetic events. Therefore, the study of these events can be helpful for understanding mechanisms in mass and energy transport from the chromosphere toward the transition region and corona. We obtain intensity profiles from spectra in two altitudes, i.e., at the solar limb and 5 arcsec distance from solar limb, and then analyze the EE fluctuations at these two altitudes along the slit. We find that some spectral line profiles show enhancements in blue and red wings indicating upward and downward flows, and some profiles have opposite EEs in both wings. The amplitude of the Doppler velocity in the two data sets of different altitudes was approximated to be about 50 km s−1. We calculated the phase velocity of the oscillations using a technique based on cross-correlation. The phase velocity is obtained as about 220 km s−1. According to the periodic red and blue enhancements in EEs, we suggest that the fluctuations in the EEs with one side enhancement indicate a swaying motions of spicules about their axes, and those EEs observed in both wings indicate a rotational motions of spicules. The swaying and rotational motions are indicative of kink and torsional waves, respectively.

Chromospheric peculiar off-limb dynamical events from IRIS observations

E. **Tavabi**, S. Koutchmy
ApJ **883** 41 **2019**
https://arxiv.org/ftp/arxiv/papers/1907/1907.10960.pdf
https://doi.org/10.3847/1538-4357/ab3730
To study motions and oscillations in the solar chromosphere and at the transition region (TR) level we analyze some extreme Doppler shifts observed off-limb with the Interface Region Imaging Spectrograph (IRIS). Raster scans and slit-jaw imaging observations performed in the near-ultraviolet (NUV) channels were used. Large transverse oscillations are revealed by the far wings profiles after accurately removing the bulk average line profiles of each sequence. Different regions around the Sun are considered. Accordingly, the cool material of spicules is observed in Mg II lines rather dispersed up to coronal heights. In the quiet Sun and especially in a polar coronal hole, we study

dynamical properties of the dispersed spicules-material off-limb using a high spectral, temporal and spatial resolutions IRIS observations. We suggest that numerous small-scale jet-like spicules show rapid twisting and swaying motions evidenced by the large distortion and dispersion of the line profiles, including impressive periodic Doppler shifts. Most of these events repeatedly appear in red- and blue-shifts above the limb throughout the whole interval of the observation datasets with an average swaying speed of order +/-35 kms-1 reaching a maximum value of 50 km s-1 in the polar coronal hole region, well above the 2.2 Mm heights. We identified for the 1st time waves with a short period of order of 100 sec and less and transverse amplitudes of order of +/- 20 to 30 km s-1 with the definite signature of Alfven waves. No correlation exists between brightness and Doppler shift variations; the phase speed of the wave is very large and cannot definitely be determined from the spectral features seen along the quasi-radial features. Even shorter periods waves are evidenced, although their contrast is greatly attenuated by the overlapping effects along the line of sight.

Polar Coronal Plumes as Tornado-like Jets

E. **Tavabi**1,2, S. Koutchmy3, and L. Golub
2018 ApJ 866 35
https://iopscience.iop.org/article/10.3847/1538-4357/aadc64/pdf
We examine the dynamical behavior of white-light polar-plume structures in the inner corona that are observed from the ground during total solar eclipses, based on their extreme ultraviolet (EUV) hot and cool emission line counterparts observed from space. EUV observations from Solar Dynamics Observatory/Atmospheric Imaging Assembly (SDO/AIA) of a sequence of rapidly varying coronal hole structures are analyzed. Evidence of events showing acceleration in the 1.25 Mk line of Fe xii at 193 Å is given. The structures along the plume show an outward velocity of about 140 km s−1that can be interpreted as an upward propagating wave in the 304 Å and 171 Å lines; higher speeds are seen in 193 Å (up to 1000 km s−1). The ejection of the cold He ii plasma is delayed by about 4 minutes in the lowest layer and is delayed more than 12 minutes in the highest level compared to the hot 193 Å behavior. A study of the dynamics using time-slice diagrams reveals that a large amount of fast ejected material originates from below the plume, at the footpoints. The release of plasma material appears to come from a cylinder with quasi-parallel edge-enhanced walls. After the initial phase of a longitudinal acceleration, the speed substantially reduces, and the ejecta disperse into the environment. Finally, the detailed temporal and spatial relationships between the cool and hot components were studied with simultaneous multiwavelength observations, using more AIA data. The outward-propagating perturbation of the presumably magnetic walls of polar plumes supports the suggestion that Alfvén waves propagate outwardly along these radially extended walls. **2010 July 10-11**

Analysis of a Failed Eclipse Plasma Ejection Using EUV Observations

E. **Tavabi**, S. Koutchmy, C. Bazin
Solar Phys. **2018**
https://arxiv.org/ftp/arxiv/papers/1801/1801.09222.pdf
The photometry of eclipse white-light (W-L) images showing a moving blob is interpreted for the first time together with observations from space with the PRoject for On Board Autonomy (PROBA-2) mission (ESA). An off-limb event seen with great details in W-L was analyzed with the SWAP imager (Sun Watcher using Active pixel system detector and image Processing) working in the EUV near 174 A. It is an elongated plasma blob structure of 25 Mm diameter moving above the E-limb with coronal loops under. Summed and co-aligned SWAP images are evaluated using a 20 hours sequence, in addition to the **July 11, 2010** eclipse W-L images taken from several sites. The Atmospheric Imaging Assembly (AIA) instruments on board the Solar Dynamical Observatory (SDO) recorded the event suggesting a magnetic reconnection near a high neutral point; accordingly, we also call it a magnetic plasmoid. The measured proper motion of the blob shows a velocity up to 12 km s^-1. Electron densities of the isolated condensation (cloud or blob or plasmoid) is photometrically evaluated. The typical value is 10^8 cm^-3 at r=1.7 R, superposed on a background corona of 10^7 cm^-3 density. The mass of the cloud near its maximum brightness is found to be 1.6x10^13 gr which is typically 0.6x10^-4 of the overall mass of the corona. From the extrapolated magnetic field the cloud evolves inside a rather broad open region but decelerates, after reaching its maximum brightness. The influence of such small events for supplying material to the ubiquitous slow wind is noticed. A precise evaluation of the EUV photometric data after accurately removing the stray light, suggests an interpretation of the weak 174 A radiation of the cloud as due to resonance scattering in the Fe IX/X lines.

Spicules Intensity Oscillations in SOT/HINODE Observations

E. **Tavabi**, A. Ajabshirizadeh, A. R. Ahangarzadeh Maralani, S. Zeighami
JOAA **2015**
Aims. We study the coherency of solar spicules intensity oscillations with increasing height above the solar limb in quiet Sun, active Sun and active region using observations from HINODE/SOT. Existence of coherency up to

transition region strengthens the theory of the coronal heating and solar wind through energy transport and photospheric oscillations.
Methods. Using time sequences from the HINODE/SOT in Ca II H line, we investigate oscillations found in intensity profiles at different heights above the solar limb. We use the Fourier and wavelet analysis to measure dominant frequency peaks of intensity at the heights, and phase difference between oscillations at two certain heights, to find evidence for the coherency of the oscillations. Finally, we can calculate the energy and the mass transported by spicules providing energy equilibrium, according to density values of spicules at different heights. To extend this work, we can also consider coherent oscillations at different latitudes and suggest to study of oscillations which may be obtained from observations of other satellites.

Alfvenic waves in polar spicules

E. **Tavabi**, S. Koutchmy, A. Ajabshirizadeh, A. R. Ahangarzadeh Maralani, S. Zeighami
A&A, 573, A4, **2015**
http://arxiv.org/pdf/1409.7654v2.pdf
Context. For investigating spicules from the photosphere to coronal heights, the new Hinode/SOT long series of high resolution observations from Space taken in CaII H line emission offers an improved way to look at their remarkable dynamical behavior using images free of seeing effects. They should be put in the context of the huge amount of already accumulated material from ground-based instruments, including high- resolution spectra of off-limb spicules. Results. The surge-like behavior of solar polar region spicules supports the untwisting multi-component interpretation of spicules exhibiting helical dynamics. Several tall spicules are found with (i) upward and downward flows similar at lower and middle-levels, the rate of upward motion being slightly higher at high levels; (ii) the left and right-hand velocities are also increasing with height; (iii) a large number of multi-component spicules show shearing motion of both left-handed and right-handed senses occurring simultaneously, which might be understood as twisting (or untwisting) threads. The number of turns depends on the overall diameter of the structure made of components and changes from at least one turn for the smallest structure to at most two or three turns for surge-like broad structures; the curvature along the spicule corresponds to a low turn number similar to a transverse kink mode oscillation along the threads.

Temporal Variations in Solar Irradiance Since 1947

A. **Tebabal**, B. Damtie, M. Nigussie,E. Yizengaw
Solar Physics August **2017**, 292:112
The study of variations in total solar irradiance (TSI) and spectral irradiance is important for understanding how the Sun affects the Earth's climate. A data-driven approach is used in this article to analyze and model the temporal variation of the TSI and Mg II index back to 1947. In both cases, observed data in the time interval of the satellite era, 1978 – 2013, were used for neural network (NN) model-design and testing. For this particular purpose, the evolution of the solar magnetic field is assumed to be the main driver for the day-to-day irradiance variability. First, we design a model for the Mg II index data from F10.7 cm solar radio-flux using the NN approach in the time span of 1978 through 2013. Results of Mg II index model were tested using various numbers of hidden nodes. The predicted values of the hidden layer with five nodes correspond well to the composite Mg II values. The model reproduces 94% of the variability in the composite Mg II index, including the secular decline between the 1996 and 2008 solar cycle minima. Finally, the extrapolation of the Mg II index was performed using the developed model from F10.7 cm back to 1947. Similarly, the NN model was designed for TSI variability study over the time span of the satellite era using data from the Physikalisch-Meteorologisches Observatorium Davos (PMOD) as a target, and solar activity indices as model inputs. This model was able to reproduce the daily irradiance variations with a correlation coefficient of 0.937 from sunspot and facular measurements in the time span of 1978 – 2013. Finally, the temporal variation of the TSI was analyzed using the designed NN model back to 1947 from the Photometric Sunspot Index (PSI) and the extrapolated Mg IIindex. The extrapolated TSI result indicates that the amplitudes of Solar Cycles 19 and 21 are closely comparable to each other, and Solar Cycle 20 appears to be of lower irradiance during its maximum.

Coronal Heating Rate in the Slow Solar Wind

Daniele **Telloni**1, Marco Romoli2, Marco Velli3, Gary P. Zank4,5, Laxman Adhikari4 +++
2023 ApJL 955 L4
https://iopscience.iop.org/article/10.3847/2041-8213/ace112/pdf
This Letter reports the first observational estimate of the heating rate in the slowly expanding solar corona. The analysis exploits the simultaneous remote and local observations of the same coronal plasma volume, with the Solar Orbiter/Metis and the Parker Solar Probe instruments, respectively, and relies on the basic solar wind magnetohydrodynamic equations. As expected, energy losses are a minor fraction of the solar wind energy flux, since most of the energy dissipation that feeds the heating and acceleration of the coronal flow occurs much closer

to the Sun than the heights probed in the present study, which range from 6.3 to 13.3 R⊙. The energy deposited to the supersonic wind is then used to explain the observed slight residual wind acceleration and to maintain the plasma in a nonadiabatic state. As derived in the Wentzel–Kramers–Brillouin limit, the present energy transfer rate estimates provide a lower limit, which can be very useful in refining the turbulence-based modeling of coronal heating and subsequent solar wind acceleration.
SO Nuggets #20 **2023** https://www.cosmos.esa.int/web/solar-orbiter/-/science-nugget-solar-orbiter-and-parker-solar-probe-jointly-take-a-step-forward-in-understanding-coronal-heating

Energy Budget in the Solar Corona

Daniele **Telloni**1, Marco Romoli2,3, Marco Velli4, Gary P. Zank5,6, Laxman Adhikari5 +++
2023 ApJ 954 108
https://iopscience.iop.org/article/10.3847/1538-4357/aceb64/pdf
This paper addresses the first direct investigation of the energy budget in the solar corona. Exploiting joint observations of the same coronal plasma by Parker Solar Probe and the Metis coronagraph aboard Solar Orbiter and the conserved equations for mass, magnetic flux, and wave action, we estimate the values of all terms comprising the total energy flux of the proton component of the slow solar wind from 6.3 to 13.3 R⊙. For distances from the Sun to less than 7 R⊙, we find that the primary source of solar wind energy is magnetic fluctuations including Alfvén waves. As the plasma flows away from the low corona, magnetic energy is gradually converted into kinetic energy, which dominates the total energy flux at heights above 7 R⊙. It is found too that the electric potential energy flux plays an important role in accelerating the solar wind only at altitudes below 6 R⊙, while enthalpy and heat fluxes only become important at even lower heights. The results finally show that energy equipartition does not exist in the solar corona.

Does Turbulence along the Coronal Current Sheet Drive Ion Cyclotron Waves?

Daniele **Telloni**1, Gary P. Zank2,3, Laxman Adhikari2, Lingling Zhao2 et al./
2023 ApJ 944 227
https://iopscience.iop.org/article/10.3847/1538-4357/acb693/pdf
Evidence for the presence of ion cyclotron waves (ICWs), driven by turbulence, at the boundaries of the current sheet is reported in this paper. By exploiting the full potential of the joint observations performed by Parker Solar Probe and the Metis coronagraph on board Solar Orbiter, local measurements of the solar wind can be linked with the large-scale structures of the solar corona. The results suggest that the dynamics of the current sheet layers generates turbulence, which in turn creates a sufficiently strong temperature anisotropy to make the solar-wind plasma unstable to anisotropy-driven instabilities such as the Alfvén ion cyclotron, mirror-mode, and firehose instabilities. The study of the polarization state of high-frequency magnetic fluctuations reveals that ICWs are indeed present along the current sheet, thus linking the magnetic topology of the remotely imaged coronal source regions with the wave bursts observed in situ. The present results may allow improvement of state-of-the-art models based on the ion cyclotron mechanism, providing new insights into the processes involved in coronal heating.

When the Earth's atmosphere becomes dynamic…

Manuela **Temmer** · Sandro Krauss and Astrid Veronig
RHESSI Science Nugget No. 267 Feb **2016**
http://sprg.ssl.berkeley.edu/~tohban/wiki/index.php/When_the_Earth's_atmosphere_becomes_dynamic…
The results clearly show that the majority of CMEs is able to cause a distinct density enhancement in the thermosphere, with an increase up to a factor of 8 compared to the pre-event level. The highest correlations are derived for the CME Bz component with values greater than 10nT, while the correlation with the CME impact speed is somewhat smaller (see Figure 2). We also find that the density enhancement in the thermosphere is highly correlated to the Dst index (see Figure 3), a standard measure of geomagnetic activity that displays magnetic storms well.

Periodic Appearance of Coronal Holes and the Related Variation of SolarWind Parameters

Manuela **Temmer** · Bojan Vršnak · Astrid M. Veronig
Solar Phys (**2007**) 241: 371–383; **File**
http://www.springerlink.com/content/4764048141351573/fulltext.pdf
Abstract We compared the variability of coronal hole (CH) areas (determined from daily GOES/SXI images) with solar wind (daily ACE data) and geomagnetic parameters for the time span 25 January 2005 until 11 September 2005 (late declining phase of solar cycle 23). Applying wavelet spectral analysis, a clear 9-day period is found in the CH time series.

The GOES/SXI image sequence suggests that this periodic variation is caused by a mutual triangular distribution of CHs ~120° apart in longitude. From solar wind parameters a 9-day periodicity was obtained as well, simultaneously with the 9-day period in the CH area time series. These findings provide strong evidence that the 9-day period in solar wind parameters, showing up as higher harmonic of the solar rotation frequency, is caused by the "periodic" longitudinal distribution of CHs on the Sun recurring for several solar rotations. The shape of the wavelet spectrum from the *Dst* index matches only weakly with that from the CH areas and is more similar to the wavelet spectrum of the solar wind magnetic field magnitude. The distinct 9-day period does not show up in sunspot group areas which gives further evidence that the solar wind modulation is strongly related to CH areas but not to active region complexes. The wavelet power spectra for the whole ACE data range (~1998 – 2006) suggest that the 9-day period is not a singular phenomenon occurring only during a specific time range close to solar minimum but is occasionally also present during the maximum and decay phase of solar cycle 23. The main periods correspond to the solar rotation (27d) as well as to the second (13.5d) and third (9d) harmonic.

Three-dimensional solar active region magnetohydrostatic models and their stability using Euler potentials

Jaume **Terradas**, Thomas Neukirch
A&A **2022**
https://arxiv.org/pdf/2212.04735
Active regions (ARs) are typical magnetic structures found in the solar atmosphere. We calculate several magnetohydrostatic (MHS) equilibrium models that include the effect of a finite plasma-β and gravity and that are representative of these structures in three dimensions. The construction of the models is based on the use of two Euler potentials, α and β, that represent the magnetic field as $B=\nabla\alpha\times\nabla\beta$. The ideal MHS nonlinear partial differential equations are solved numerically using finite elements in a fixed 3D rectangular domain. The boundary conditions are initially chosen to correspond to a potential magnetic field (current-free) with known analytical expressions for the corresponding Euler potentials. The distinctive feature is that we incorporate the effect of shear by progressively deforming the initial potential magnetic field. This procedure is quite generic and allows us to generate a vast variety of MHS models. The thermal structure of the ARs is incorporated through the dependence of gas pressure and temperature on the Euler potentials. Using this method we achieve the characteristic hot and over-dense plasma found in ARs, but we demonstrate that the method can also be applied to study configurations with open magnetic field lines. Furthermore, we investigate basic topologies that include neutral lines. Our focus is on the force balance of the structures and we do not consider the energy balance in the constructed models. In addition, we address the difficult question of the stability of the calculated 3D models. We find that if the plasma is convectively stable, then the system is not prone in general to develop magnetic Rayleigh-Taylor instabilities.

Temporal and Spatial Scales for Coronal Heating by Alfvén Wave Dissipation in Transverse Loop Oscillations

Jaume **Terradas**1,2 and Iñigo Arregui
2018 Res. Notes AAS 2 196
http://iopscience.iop.org/article/10.3847/2515-5172/aaeb26
We address the temporal and spatial scales involved in the process of resonant absorption of magnetohydrodynamic (MHD) waves and their possible role in heating the solar corona by Alfvén wave dissipation.

Effect of Magnetic Twist on Nonlinear Transverse Kink Oscillations of Line-tied Magnetic Flux Tubes

J. **Terradas**1,2, N. Magyar3, and T. Van Doorsselaere3
2018 ApJ 853 35
http://sci-hub.tw/http://iopscience.iop.org/0004-637X/853/1/35/
Magnetic twist is thought to play an important role in many structures of the solar atmosphere. One of the effects of twist is to modify the properties of the eigenmodes of magnetic tubes. In the linear regime standing kink solutions are characterized by a change in polarization of the transverse displacement along the twisted tube. In the nonlinear regime, magnetic twist affects the development of shear instabilities that appear at the tube boundary when it is oscillating laterally. These Kelvin–Helmholtz instabilities (KHI) are produced either by the jump in the azimuthal component of the velocity at the edge of the sharp boundary between the internal and external part of the tube or by the continuous small length scales produced by phase mixing when there is a smooth inhomogeneous layer. In this work the effect of twist is consistently investigated by solving the time-dependent problem including the process of energy transfer to the inhomogeneous layer. It is found that twist always delays the appearance of the shear instability, but for tubes with thin inhomogeneous layers the effect is relatively small for moderate values of twist. On the contrary, for tubes with thick layers, the effect of twist is much stronger. This can have some important implications regarding observations of transverse kink modes and the KHI itself.

Ray Tracing of MHD Rossby waves in the Solar tachocline: meridional propagation and implications for the solar magnetic activity

André **Teruya**, Breno Raphaldini, and Carlos Raupp
Front. Astron. Space Sci. 9:856912 **2022**
https://doi.org/10.3389/fspas.2022.856912
https://www.frontiersin.org/articles/10.3389/fspas.2022.856912/full
Rossby waves have been recently recognised for their role in the large-scale spatio-temporal organisation of the solar magnetic activity. Here, we study the propagation of magnetohydrodynamic Rossby waves in a thin layer, representing the solar tachocline. We consider the waves embedded in a meridionally varying background state characterised by a mean zonal flow, which mimics the differential rotation profile of the Sun, and a toroidal magnetic field. Two anti-symmetric toroidal magnetic fields are utilised: one having a global structure with the maximum at around 50o and the other characterised by a narrow band centered at around 20o. We show that for a global structure toroidal magnetic field, the MHD Rossby modes undergo significant meridional propagation, either equatorward or poleward. In addition, the latitude where the waves exhibit a stationary behaviour is sensitive to the strength of the background magnetic field. On the other hand, a narrow band toroidal magnetic field is shown to work as a waveguide for the fast branch of MHD Rossby waves.

High Resolution Observations of the Low Atmospheric Response to Small Coronal Heating Events in an Active Region Core

Paola **Testa** (1), Helle Bakke (2,3), Luc Rouppe van der Voort (2,3), Bart De Pontieu
ApJ **956** 85 **2023**
https://arxiv.org/pdf/2308.15417.pdf
https://iopscience.iop.org/article/10.3847/1538-4357/acf4f1/pdf
High resolution spectral observations of the lower solar atmosphere (chromosphere and transition region) during coronal heating events, in combination with predictions from models of impulsively heated loops, provide powerful diagnostics of the properties of the heating in active region cores. Here we analyze the first coordinated observations of such events with the Interface Region Imaging Spectrograph (IRIS) and the CHROMospheric Imaging Spectrometer (CHROMIS), at the Swedish 1-m Solar Telescope (SST), which provided extremely high spatial resolution and revealed chromospheric brightenings with spatial dimensions down to ~150km. We use machine learning methods (k-means clustering) and find significant coherence in the spatial and temporal properties of the chromospheric spectra, suggesting, in turn, coherence in the spatial and temporal distribution of the coronal heating. The comparison of IRIS and CHROMIS spectra with simulations suggest that both non-thermal electrons with low energy (low-energy cutoff ~5keV) and direct heating in the corona transported by thermal conduction contribute to the heating of the low atmosphere. This is consistent with growing evidence that non-thermal electrons are not uncommon in small heating events (nano- to micro-flares), and that their properties can be constrained by chromospheric and transition region spectral observations. **2016-09-04**

Coronal Abundances in an Active Region: Evolution and Underlying Chromospheric and Transition Region Properties

Paola **Testa**1, Juan Martínez-Sykora2,3,4,5, and Bart De Pontieu2,4,5
2023 ApJ 944 117
https://iopscience.iop.org/article/10.3847/1538-4357/acb343/pdf
The element abundances in the solar corona and solar wind are often different from those of the solar photosphere, typically with a relative enrichment of elements with low first ionization potential (FIP effect). Here, we study the spatial distribution and temporal evolution of the coronal chemical composition in an active region (AR) over about 10 days, using Hinode/EIS spectra, and we also analyze coordinated IRIS observations of the chromospheric and transition region emission to investigate any evidence of the footprints of the FIP effect in the lower atmosphere. To derive the coronal abundances, we use a spectral inversion method recently developed for the MUSE investigation. We find that, in the studied active region (AR 12738), the coronal FIP bias, as diagnosed by the Si/S abundance ratio, presents significant spatial variations, with its highest values (∼2.5–3.5) in the outflow regions at the boundary of the AR, but typically modest temporal variability. Some moss regions and some regions around the AR sunspot show enhanced FIP bias (∼2–2.5) with respect to the AR core, which has only a small FIP bias of ∼1.5. The FIP bias appears most variable in these moss regions. The IRIS observations reveal that the chromospheric turbulence, as derived from IRIS2 inversions of the Mg ii spectra, is enhanced in the outflow regions characterized by the high FIP bias, providing significant new constraints to both models aimed at explaining the formation of AR outflows and models of chemical fractionation.

The Solar X-ray Corona **Review**

Paola **Testa**, Fabio Reale

Book chapter. To appear in Springer's "Handbook of X-ray and Gamma-ray Astrophysics" (eds. A. Santangelo and C. Bambi), Section "The Sun, Stars & Planets" (eds. G. Micela & B. Stelzer) **2022**
https://arxiv.org/pdf/2206.03530.pdf
The X-ray emission from the Sun reveals a very dynamic hot atmosphere, the corona, which is characterized by a complex morphology and broad range of timescales of variability and spatial structuring. The solar magnetic fields play a fundamental role in the heating and structuring of the solar corona. Increasingly higher quality X-ray solar observations with high spatial (down to subarcsec) and temporal resolution provide fundamental information to refine our understanding of the solar magnetic activity and of the underlying physical processes leading to the heating of the solar outer atmosphere. Here we provide a brief historical overview of X-ray solar observations and we summarize recent progress in our understanding of the solar corona as made possible by state-of-the-art current X-ray observations. **13 January 1992, 8 June 2000, September 13 2011, November 9 2013**

IRIS Observations of Short-term Variability in Moss Associated with Transient Hot Coronal Loops

Testa, Paola ; Polito, Vanessa ; De Pontieu, Bart
The Astrophysical Journal, Volume 889, Issue 2, id.124, 23 pp. (**2020**)
https://iopscience.iop.org/article/10.3847/1538-4357/ab63cf/pdf
We observed rapid variability (≲60 s) at the footpoints of transient, hot (∼8-10 MK) coronal loops in active region cores, with the Interface Region Imaging Spectrograph (IRIS). The high spatial (∼0"33) and temporal (≲5-10 s) resolution of IRIS is often crucial for the detection of this variability. We show how, in combination with 1D RADYN loop modeling, these IRIS spectral observations of the transition region (TR) and chromosphere provide powerful diagnostics of the properties of coronal heating and energy transport (thermal conduction or nonthermal electrons, NTEs). Our simulations of nanoflare-heated loops indicate that emission in the Mg II triplet can be used as a sensitive diagnostic for nonthermal particles. In our events, we observe a large variety of IRIS spectral properties (intensity, Doppler shifts, broadening, chromospheric/TR line ratios, Mg II triplet emission) even for different footpoints of the same coronal events. In several events, we find spectroscopic evidence for NTEs (e.g., TR blueshifts and Mg II triplet emission), suggesting that particle acceleration can occur even for very small magnetic reconnection events, which are generally below the detection threshold of hard X-ray instruments that provide direct detection of emission of nonthermal particles.
IRIS Nugget Jan **2022** https://iris.lmsal.com/nugget?cmd=view-pod&pubDate=2022-01-10

IRIS observations short-term variability in moss associated with transient hot coronal loops

Paola **Testa** , Vanessa Polito , Bart De Pontieu
ApJ **889** 124 **2019**
https://arxiv.org/pdf/1910.08201.pdf
https://doi.org/10.3847/1538-4357/ab63cf
We observed rapid variability (≲60 s) at the footpoints of transient hot (∼8−10 MK) coronal loops in active region cores, with the Interface Region Imaging Spectrograph (IRIS). The high spatial (∼0.33 arcsec) and temporal (≲5-10 s) resolution is often crucial for the detection of this variability. We show how, in combination with 1D RADYN loop modeling, these IRIS spectral observations of the transition region (TR) and chromosphere provide powerful diagnostics of the properties of coronal heating and energy transport (thermal conduction and/or non-thermal electrons (NTE)). Our simulations of nanoflare heated loops indicate that emission in the Mg II triplet can be used as a sensitive diagnostic for non-thermal particles. In our events we observe a large variety of IRIS spectral properties (intensity, Doppler shifts, broadening, chromospheric/TR line ratios, Mg II triplet emission) even for different footpoints of the same coronal events. In several events, we find spectroscopic evidence for NTE (e.g., TR blue-shifts and Mg II triplet emission) suggesting that particle acceleration can occur even for very small magnetic reconnection events which are generally below the detection threshold of hard X-ray instruments that provide direct detection of emission of non-thermal particles. **2014-02-23, 2014-04-10, 2014-09-17-18, 2015-01-29, 2015-11-11-12, 2015-12-24, 2016-01-29**

High spatial resolution FeXII observations of solar active region

Paola **Testa** (1), Bart De Pontieu (2,3), Viggo Hansteen (3), ((1) Harvard-Smithonian Center for Astrophysics, (2) Lockheed-Martin Solar and Astrophysics Laboratory, (3) Institute of Theoretical Astrophysics, University of Oslo)
ApJ **2016**
http://arxiv.org/pdf/1606.04603v1.pdf
We use UV spectral observations of active regions with the Interface Region Imaging Spectrograph (IRIS) to investigate the properties of the coronal FeXII 1349.4A emission at unprecedented high spatial resolution (~0.33"). We find that by using appropriate observational strategies (i.e., long exposures, lossless compression), FeXII

emission can be studied with IRIS at high spatial and spectral resolution, at least for high density plasma (e.g., post-flare loops, and active region moss). We find that upper transition region (moss) FeXII emission shows very small average Doppler redshifts (v_Dop ~3 km/s), as well as modest non-thermal velocities (with an average ~24 km/s, and the peak of the distribution at ~15 km/s). The observed distribution of Doppler shifts appears to be compatible with advanced 3D radiative MHD simulations in which impulsive heating is concentrated at the transition region footpoints of a hot corona. While the non-thermal broadening of FeXII 1349.4A peaks at similar values as lower resolution simultaneous Hinode/EIS measurements of FeXII 195A, IRIS observations show a previously undetected tail of increased non-thermal broadening that might be suggestive of the presence of subarcsecond heating events. We find that IRIS and EIS non-thermal line broadening measurements are affected by instrumental effects that can only be removed through careful analysis. Our results also reveal an unexplained discrepancy between observed 195.1/1349.4A FeXII intensity ratios and those predicted by the CHIANTI atomic database.

Stellar activity and coronal heating: an overview of recent results **Review**

Testa,P., Saar, S. H., & Drake, J. J.

2015, Royal Society of London Philosophical Transactions Series A, 373, p. 20140259

http://sci-hub.tw/10.1098/rsta.2014.0259

http://arxiv.org/pdf/1502.07401v1.pdf

Observations of the coronae of the Sun and of solar-like stars provide complementary information to advance our understanding of stellar magnetic activity, and of the processes leading to the heating of their outer atmospheres. While solar observations allow us to study the corona at high spatial and temporal resolution, the study of stellar coronae allows us to probe stellar activity over a wide range of ages and stellar parameters. Stellar studies therefore provide us with additional tools for understanding coronal heating processes, as well as the long-term evolution of solar X-ray activity. We discuss how recent studies of stellar magnetic fields and coronae contribute to our understanding of the phenomenon of activity and coronal heating in late-type stars.

Inflows towards Bipolar Magnetic Active Regions and Their Nonlinear Impact on a Three-Dimensional Babcock-Leighton Solar Dynamo Model

Kinfe **Teweldebirhan**, Mark Miesch, Sarah Gibson

Solar Phys. **299**, 42 (**2024**)

The changing magnetic fields of the Sun are generated and maintained by a solar dynamo, the exact nature of which remains an unsolved fundamental problem in solar physics. Our objective in this paper is to investigate the role and impact of converging flows toward Bipolar Magnetic Regions (BMR inflows) on the Sun's global solar dynamo. These flows are large scale physical phenomena that have been observed and so should be included in any comprehensive solar dynamo model. We have augmented the Surface flux Transport And Babcock LEighton (STABLE) dynamo model to study the nonlinear feedback effect of BMR inflows with magnitudes varying with surface magnetic fields. This fully 3D realistic dynamo model produces the sunspot butterfly diagram and allows a study of the relative roles of dynamo saturation mechanisms such as tilt angle quenching and BMR inflows. The results of our STABLE simulations show that magnetic field dependent BMR inflows significantly affect the evolution of the BMRs themselves and result in a reduced buildup of the global poloidal field due to local flux cancellation within the BMRs, to an extent that is sufficient to saturate the dynamo. As a consequence, for the first time, we have achieved fully 3D solar dynamo solutions in which BMR inflows alone regulate the amplitudes and periods of the magnetic cycles.

Small-scale dynamos on the solar surface: dependence on magnetic Prandtl number

I. **Thaler**, H.C. Spruit

A&A 578, A54 **2015**

The question of possible small-scale dynamo action in the surface layers of the Sun is revisited with realistic 3D MHD simulations. As in other MHD problems, dynamo action is found to be a sensitive function of the magnetic Prandtl number Pm=ν/η; it disappears below a critical value Pc which is a function of the numerical resolution. At a grid spacing of 3.5 km, Pc based on the hyperdiffusivities implemented in the code (STAGGER) is ≈1, increasing with increasing grid spacing. As in other settings, it remains uncertain whether small scale dynamo action is present in the astrophysical limit where Pm<<1 and magnetic Reynolds number Rm≫1. The question is discussed in the context of the strong effect that external stray fields are observed to have in generating and maintaining dynamo action in other numerical and laboratory systems, and in connection with the type-II hypertransient behavior of dynamo action observed in the absence of such external fields.

Magnetic Helicity Estimations in Models and Observations of the Solar Magnetic Field. IV. Application to Solar Observations

J. K. **Thalmann**1, M. K. Georgoulis2, Y. Liu3, E. Pariat4,5, G. Valori6, S. Anfinogentov7, F. Chen8, Y. Guo8, K. Moraitis9, S. Yang10Show full author list

2021 ApJ 922 41
https://doi.org/10.3847/1538-4357/ac1f93
https://arxiv.org/pdf/2108.08525.pdf
In this ISSI-supported series of studies on magnetic helicity in the Sun, we systematically implement different magnetic helicity calculation methods on high-quality solar magnetogram observations. We apply finite-volume, discrete flux tube (in particular, connectivity-based) and flux-integration methods to data from Hinode's Solar Optical Telescope. The target is NOAA Active Region 10930 during a 1.5-day interval in 2006 December that included a major eruptive flare (SOL**2006-12-13**T02:14X3.4). Finite-volume and connectivity-based methods yield instantaneous budgets of the coronal magnetic helicity, while the flux-integration methods allow an estimate of the accumulated helicity injected through the photosphere. The objectives of our work are twofold: a cross-validation of methods, as well as an interpretation of the complex events leading to the eruption. To the first objective, we find (i) strong agreement among the finite-volume methods, (ii) a moderate agreement between the connectivity-based and finite-volume methods, (iii) an excellent agreement between the flux-integration methods, and (iv) an overall agreement between finite-volume- and flux-integration-based estimates regarding the predominant sign and magnitude of the helicity. To the second objective, we are confident that the photospheric helicity flux significantly contributed to the coronal helicity budget and that a right-handed structure erupted from a predominantly left-handed corona during the X-class flare. Overall, we find that the use of different methods to estimate the (accumulated) coronal helicity may be necessary in order to draw a complete picture of an active region corona, given the careful handling of identified data (preparation) issues, which otherwise would mislead the event analysis and interpretation.

Magnetic helicity budget of solar active regions prolific of eruptive and confined flares

J. K. **Thalmann**, K. Moraitis, L. Linan, E. Pariat, G. Valori, K. Dalmasse
ApJ **2019**
https://arxiv.org/pdf/1910.06563.pdf
We compare the coronal magnetic energy and helicity of two solar active regions (ARs), prolific in major eruptive (AR~11158) and confined (AR~12192) flaring, and analyze the potential of deduced proxies to forecast upcoming flares. Based on nonlinear force-free (NLFF) coronal magnetic field models with a high degree of solenoidality, and applying three different computational methods to investigate the coronal magnetic helicity, we are able to draw conclusions with a high level of confidence. Based on real observations of two solar ARs we checked trends regarding the potential eruptivity of the active-region corona, as suggested earlier in works that were based on numerical simulations, or solar observations. Our results support that the ratio of current-carrying to total helicity, |HJ|/|HV|, shows a strong ability to indicate the eruptive potential of a solar AR. However, |HJ|/|HV| seems not to be indicative for the magnitude or type of an upcoming flare (confined or eruptive). Interpreted in context with earlier observational studies, our findings furthermore support that the total relative helicity normalized to the magnetic flux at the NLFF model's lower boundary, HV/ϕ2, represents no indicator for the eruptivity. **2011 February 14, 2014 October 24**

Solar Photospheric Network Properties and Their Cycle Variation

K. **Thibault**, P. Charbonneau, and M. Béland
2014 ApJ 796 19
We present a numerical simulation of the formation and evolution of the solar photospheric magnetic network over a full solar cycle. The model exhibits realistic behavior as it produces large, unipolar concentrations of flux in the polar caps, a power-law flux distribution with index –1.69, a flux replacement timescale of 19.3 hr, and supergranule diameters of 20 Mm. The polar behavior is especially telling of model accuracy, as it results from lower-latitude activity, and accumulates the residues of any potential modeling inaccuracy and oversimplification. In this case, the main oversimplification is the absence of a polar sink for the flux, causing an amount of polar cap unsigned flux larger than expected by almost one order of magnitude. Nonetheless, our simulated polar caps carry the proper signed flux and dipole moment, and also show a spatial distribution of flux in good qualitative agreement with recent high-latitude magnetographic observations by Hinode. After the last cycle emergence, the simulation is extended until the network has recovered its quiet Sun initial condition. This permits an estimate of the network relaxation time toward the baseline state characterizing extended periods of suppressed activity, such as the Maunder Grand Minimum. Our simulation results indicate a network relaxation time of 2.9 yr, setting 2011 October as the soonest the time after which the last solar activity minimum could have qualified as a Maunder-type Minimum. This suggests that photospheric magnetism did not reach its baseline state during the recent extended minimum between cycles 23 and 24.

The GOES-R EUVS Model for EUV Irradiance Variability

E. M. B. **Thiemann**, F. G. Eparvier, D. Woodraska, P. C. Chamberlin, J. Machol, T. Eden, A. R. Jones, R. Meisner, S. Mueller, M. Snow, R. Viereck, T. N. Woods

Journal of Space Weather and Space Climate **9**, A43 **2019**
https://arxiv.org/pdf/1911.09181.pdf
https://www.swsc-journal.org/articles/swsc/pdf/2019/01/swsc190022.pdf
The Geostationary Operational Environmental Satellite R (GOES-R) series of four satellites are the next generation NOAA GOES satellites. Once on orbit and commissioned, they are renamed GOES 16-19, making critical terrestrial and space weather measurements through 2035. GOES 16 and 17 are currently on orbit, having been launched in 2016 and 2018, respectively. The GOES-R satellites include the EUV and X-ray Irradiance Sensors (EXIS) instrument suite, which measures calibrated solar irradiance in 8 lines or bands between 25 and 285 nm with the Extreme Ultraviolet Sensors (EUVS) instrument. EXIS also includes the X-Ray Sensor (XRS) instrument, which measures solar soft X-ray irradiance at the legacy GOES bands. The EUVS measurements are used as inputs to the EUVS Model, a solar spectral irradiance model for space weather operations that predicts irradiance in twenty-two 5 nm wide intervals from 5 nm to 115 nm, and one 10 nm wide interval from 117 to 127 nm at 30 second cadence. Once fully operational, NOAA will distribute the EUVS Model irradiance with 1 minute latency as a primary space weather data product, ushering in a new era of rapid dissemination and measurement continuity of EUV irradiance spectra. This paper describes the EUVS Model algorithms, data sources, calibration methods and associated uncertainties. Typical model (relative) uncertainties are less than ∼5\% for variability at time-scales longer than 6 hours, and are ∼25\% for solar flare induced variability. The absolute uncertainties, originating from the instruments used to calibrate the EUVS Model, are ∼10\%. Examples of model results are presented at both sub-daily and multi-year timescales to demonstrate the model's capabilities and limitations. Example solar flare irradiances are also modeled.

The spectral impact of magnetic activity on disk-integrated HARPS-N solar observations: exploring new activity indicators

A. P. G. **Thompson**, C. A. Watson, R. D. Haywood, J. C. Costes, ….
MNRAS **2020**
https://arxiv.org/pdf/2004.09830.pdf
Stellar activity is the major roadblock on the path to finding true Earth-analogue planets with the Doppler technique. Thus, identifying new indicators that better trace magnetic activity (i.e. faculae and spots) is crucial to aid in disentangling these signals from that of a planet's Doppler wobble. In this work, we investigate activity related features as seen in disk-integrated spectra from the HARPS-N solar telescope. We divide high-activity spectral echelle orders by low-activity master templates (as defined using both log R'HK and images from the Solar Dynamics Observatory, SDO), creating "relative spectra". With resolved images of the surface of the Sun (via SDO), the faculae and spot filling factors can be calculated, giving a measure of activity independent of, and in addition to, log R'HK. We find pseudo-emission (and pseudo-absorption) features in the relative spectra that are similar to those reported in our previous work on alpha Cen B. In alpha Cen B, the features are shown to correlate better to changes in faculae filling factor than spot filling factor. In this work we more confidently identify changes in faculae coverage of the visible hemisphere of the Sun as the source of features produced in the relative spectra. Finally, we produce trailed spectra to observe the RV component of the features, which show that the features move in a redward direction as one would expect when tracking active regions rotating on the surface of a star.

Current STEREO Status on the Far Side of the Sun

Thompson, William T.; Gurman, Joseph; Ossing, Daniel; Luhmann, Janet; Curtis, David; Schroeder, Peter; Mewaldt, Richard; Davis, Andrew; Wortman, Kristin; Russell, Christopher; and 10 coauthors
Joint American Astronomical Society/American Geophysical Union Triennial Earth-Sun Summit, meeting #1, #402.05, 04/**2015**
The current positions of the two STEREO spacecraft on the opposite side of the Sun from Earth (superior solar conjunction) has forced some significant changes in the spacecraft and instrument operations. No communications are possible when the spacecraft is within 2 degrees of the Sun, requiring that the spacecraft be put into safe mode until communications can be restored. Unfortunately, communications were lost with the STEREO Behind spacecraft on October 1, 2014, during testing for superior solar conjunction operations. We will discuss what is known about the causes of loss of contact, the steps being taken to try to recover the Behind spacecraft, and what has been done to prevent a similar occurrence on STEREO Ahead.We will also discuss the effect of being on the far side of the Sun on the science operations of STEREO Ahead. Starting on August 20, 2014, the telemetry rate from the STEREO Ahead spacecraft has been tremendously reduced due to the need to keep the temperature of the feed horn on the high gain antenna below acceptable limits. However, the amount of telemetry that can be brought down has been highly reduced. Even so, significant science is still possible from STEREO's unique position on the solar far side. We will discuss the science and space weather products that are, or will be, available from each STEREO instrument, when those products will be available, and how they will be used. Some data, including the regular space weather beacon products, are brought down for an average of a few hours each day during the daily real-time passes, while the in situ and radio beacon data are being stored on the onboard recorder to provide a continuous 24-hour coverage for eventual downlink once the spacecraft is back to normal operations.

Grand Challenges in the Physics of the Sun and Sun-like Stars **Review**

Michael J. **Thompson**

2014, Frontiers in Stellar and Solar Physics

The study of stellar structure and evolution is one of the main building blocks of astrophysics, and the Sun has an importance both as the star that is most amenable to detailed study and as the star that has by far the biggest impact on the Earth and near-Earth environment through its radiative and particulate outputs. Over the past decades, studies of stars and of the Sun have become somewhat separate. But in recent years, the rapid advances in asteroseismology, as well as the quest to better understand solar and stellar dynamos, have emphasized once again the synergy between studies of the stars and the Sun. In this article I have selected two "grand challenges" both for their crucial importance and because I thnk that these two problems are tractable to significant progress in the next decade. They are (i) understanding how solar and stellar dynamos generate magnetic field, and (ii) improving the predictability of geo-effective space weather.

Coordinate systems for solar image data

W. T. **Thompson**

2005

http://secchi.nrl.navy.mil/wiki/uploads/Main/coordinates.pdf

A set of formal systems for describing the coordinates of solar image data is proposed. These systems build on current practice in applying coordinates to solar image data. Both heliographic and heliocentric coordinates are discussed. A distinction is also drawn between heliocentric and helioprojective coordinates, where the latter takes the observer's exact geometry into account. The extension of these coordinate systems to observations made from non-terrestial viewpoints is discussed, such as from the upcoming STEREO mission. A formal system for incorporation of these coordinates into FITS files, based on the FITS World Coordinate System, is described, together with examples.

See http://www.jgiesen.de/sunrot/ , http://www.solarphysics.kva.se/LaPalma/turret/node16.html

Present day challenges in understanding the geomagnetic hazard to national power grids

A.W.P. **Thomson**, C.T. Gaunt, P. Cilliers, J.A. Wild, B. Opperman, L.-A. McKinnell, P. Kotze, C.M. Ngwira, S.I. Lotz

Adv. Space Res. Volume 45, Issue 9, Pages 1182-1190, **2010; File**

Power grids and pipeline networks at all latitudes are known to be at risk from the natural hazard of geomagnetically induced currents. At a recent workshop in South Africa, UK and South African scientists and engineers discussed the current understanding of this hazard, as it affects major power systems in Europe and Africa. They also summarised, to better inform the public and industry, what can be said with some certainty about the hazard and what research is yet required to develop useful tools for geomagnetic hazard mitigation.

Can Multi-threaded Flux Tubes in Coronal Arcades Support a Magnetohydrodynamic Avalanche?

J. **Threlfall**, J. Reid & A. W. Hood

Solar Physics volume 296, Article number: 120 (**2021**)

https://link.springer.com/content/pdf/10.1007/s11207-021-01865-7.pdf

https://doi.org/10.1007/s11207-021-01865-7

Magnetohydrodynamic (MHD) instabilities allow energy to be released from stressed magnetic fields, commonly modelled in cylindrical flux tubes linking parallel planes, but, more recently, also in curved arcades containing flux tubes with both footpoints in the same photospheric plane. Uncurved cylindrical flux tubes containing multiple individual threads have been shown to be capable of sustaining an MHD avalanche, whereby a single unstable thread can destabilise many. We examine the properties of multi-threaded coronal loops, wherein each thread is created by photospheric driving in a realistic, curved coronal arcade structure (with both footpoints of each thread in the same plane). We use three-dimensional MHD simulations to study the evolution of single- and multi-threaded coronal loops, which become unstable and reconnect, while varying the driving velocity of individual threads. Experiments containing a single thread destabilise in a manner indicative of an ideal MHD instability and consistent with previous examples in the literature. The introduction of additional threads modifies this picture, with aspects of the model geometry and relative driving speeds of individual threads affecting the ability of any thread to destabilise

others. In both single- and multi-threaded cases, continuous driving of the remnants of disrupted threads produces secondary, aperiodic bursts of energetic release.

Above the Noise: The Search for Periodicities in the Inner Heliosphere

James **Threlfall**, Ineke De Moortel, Thomas Conlon
Solar Physics November **2017**, 292:165
Remote sensing of coronal and heliospheric periodicities can provide vital insight into the local conditions and dynamics of the solar atmosphere. We seek to trace long (one hour or longer) periodic oscillatory signatures (previously identified above the limb in the corona by, e.g., Telloni et al. in Astrophys. J.767, 138, 2013) from their origin at the solar surface out into the heliosphere. To do this, we combined on-disk measurements taken by the Atmospheric Imaging Assembly (AIA) onboard the Solar Dynamics Observatory (SDO) and concurrent extreme ultra-violet (EUV) and coronagraph data from one of the Solar Terrestrial Relations Observatory(STEREO) spacecraft to study the evolution of two active regions in the vicinity of an equatorial coronal hole over several days in early 2011. Fourier and wavelet analysis of signals were performed. Applying white-noise-based confidence levels to the power spectra associated with detrended intensity time series yields detections of oscillatory signatures with periods from 6 – 13 hours in both AIA and STEREO data. As was found by Telloni et al. (2013), these signatures are aligned with local magnetic structures. However, typical spectral power densities all vary substantially as a function of period, indicating spectra dominated by red (rather than white) noise. Contrary to the white-noise-based results, applying global confidence levels based on a generic background-noise model (allowing a combination of white noise, red noise, and transients following Auchère et al. in Astrophys. J.825, 110, 2016) without detrending the time series uncovers only sporadic, spatially uncorrelated evidence of periodic signatures in either instrument. Automating this method to individual pixels in the STEREO/COR coronagraph field of view is non-trivial. Efforts to identify and implement a more robust automatic background noise model fitting procedure are needed.

Solar disc radius determined from observations made during eclipses with bolometric and photometric instruments on board the PICARD satellite

G. **Thuillier**1, P. Zhu2, A. I. Shapiro3, S. Sofia4, R. Tagirov1, M. van Ruymbeke2, J.-M. Perrin5, T. Sukhodolov1 and W. Schmutz1
A&A 603, A28 (**2017**)
Context. Despite the importance of having an accurate measurement of the solar disc radius, there are large uncertainties of its value due to the use of different measurement techniques and instrument calibration. An item of particular importance is to establish whether the value of the solar disc radius correlates with the solar activity level.
Aims. The main goal of this work is to measure the solar disc radius in the near-UV, visible, and near-IR regions of the solar spectrum.
Methods. Three instruments on board the PICARD spacecraft, namely the Bolometric Oscillations Sensor (BOS), the PREcision MOnitoring Sensor (PREMOS), and a solar sensor (SES), are used to derive the solar disc radius using the light curves produced when the Sun is occulted by the Moon. Nine eclipses, from 2010 to 2013, resulted in 17 occultations as viewed from the moving satellite. The calculation of the solar disc radius uses a simulation of the light curve taking into account the center-to-limb variation provided by the Non-local thermodynamic Equilibrium Spectral SYnthesis (NESSY) code.
Results. We derive individual values for the solar disc radius for each viewed eclipse. Tests for a systematic variation of the radius with the progression of the solar cycle yield no significant results during the three years of measurements within the uncertainty of our measurements. Therefore, we derive a more precise radius value by averaging these values. At one astronomical unit, we obtain 959.79 arcseconds (arcsec) from the bolometric experiment; from PREMOS measurements, we obtain 959.78 arcsec at 782 nm and 959.76 arcsec at 535 nm. We found 960.07 arcsec at 210 nm, which is a higher value than the other determinations given the photons at this wavelength originate from the upper photosphere and lower chromosphere. We also give a detailed comparison of our results with those previously published using measurements from space-based and ground-based instruments using the Moon angular radius reference, and different methods.
Conclusions. Our results, which use the Moon as an absolute calibration, clearly show the dependence of the solar disc radius with wavelength in UV, visible and near-IR. Beyond the metrological results, solar disc radius measurements will allow the accuracy of models of the solar atmosphere to be tested. Proposed systematic variations of the solar disc radius during the time of observation would be smaller than the uncertainty of our measurement, which amounts to less than 26 milliarcseconds.

The Infrared Solar Spectrum Measured by the SOLSPEC Spectrometer Onboard the International Space Station

G. **Thuillier**, J. W. Harder, A. Shapiro, T. N. Woods, J.-M. Perrin, M. Snow, T. Sukhodolov, W. Schmutz

Solar Phys., Volume 290, Issue 6, pp 1581-1600 **2015**
A solar spectrum extending from the extreme ultraviolet to the near-infrared is an important input for solar physics, climate research, and atmospheric physics. Ultraviolet measurements have been conducted since the beginning of the space age, but measurements throughout the contiguous visible and infrared (IR) regions are much more sparse. Ageing is a key problem throughout the entire spectral domain, but most of the effort extended to understand degradation was concentrated on the ultraviolet spectral region, and these mechanisms may not be appropriate in the IR. This problem is further complicated by the scarcity of long-term data sets. Onboard the International Space Station, the SOLSPEC spectrometer measured an IR solar spectral irradiance lower than the one given by ATLAS 3, e.g. by about 7 % at 1 700 nm. We here evaluate the consequences of the lower solar spectral irradiance measurements and present a re-analysis of the on-orbit calibration lamp and solar data trend, which lead to a revised spectrum.

See Comment on the Article by Thuillier et al."The Infrared Solar Spectrum Measured by the SOLSPEC Spectrometer onboard the International Space Station"
M. Weber
Solar Physics June 2015, Volume 290, Issue 6, pp 1601-1605

See **Comments to the Article by Thuillier et al. "The Infrared Solar Spectrum Measured by the SOLSPEC Spectrometer Onboard the International Space Station" on the Interpretation of Ground-based Measurements at the Izaña Site**
D. **Bolsée** , N. Pereira, E. Cuevas, R. García, A. Redondas
Solar Phys. Volume 291, Issue 8, pp 2473–2477 **2016**

Solar Spectral Irradiance Variability in November/December 2012: Comparison of Observations by Instruments on the International Space Station and Models

G. **Thuillier**, G. Schmidtke, C. Erhardt, B. Nikutowski, A. I. Shapiro, C. Bolduc, J. Lean, N. Krivova, P. Charbonneau, G. Cessateur, … show all 16
Solar Phys., **2014**
Onboard the International Space Station (ISS), two instruments are observing the solar spectral irradiance (SSI) at wavelengths from 16 to 2900 nm. Although the ISS platform orientation generally precludes pointing at the Sun more than 10 – 14 days per month, in November/December 2012 a continuous period of measurements was obtained by implementing an ISS 'bridging' maneuver. This enabled observations to be made of the solar spectral irradiance (SSI) during a complete solar rotation. We present these measurements, which quantify the impact of active regions on SSI, and compare them with data simultaneously gathered from other platforms, and with models of spectral irradiance variability. Our analysis demonstrates that the instruments onboard the ISS have the capability to measure SSI variations consistent with other instruments in space. A comparison among all available SSI measurements during November–December 2012 in absolute units with reconstructions using solar proxies and observed solar activity features is presented and discussed in terms of accuracy.

See

Comment on the Article by Thuillier et al."The Infrared Solar Spectrum Measured by the SOLSPEC Spectrometer onboard the International Space Station"

M. **Weber**
Solar Phys. **2015**

The Solar Irradiance Spectrum at Solar Activity Minimum Between Solar Cycles 23 and 24

G. **Thuillier**, D. Bolsée, G. Schmidtke, T. Foujols, B. Nikutowski, A. I. Shapiro, R. Brunner, M. Weber, C. Erhardt, M. Hersé, et al.
Solar Physics, June **2014**, Volume 289, Issue 6, pp 1931-1958
On 7 February 2008, the SOLAR payload was placed onboard the International Space Station. It is composed of three instruments, two spectrometers and a radiometer. The two spectrometers allow us to cover the 16 – 2900 nm spectral range. In this article, we first briefly present the instrumentation, its calibration and its performance in orbit. Second, the solar spectrum measured during the transition between Solar Cycles 23 to 24 at the time of the minimum is shown and compared with other data sets. Its accuracy is estimated as a function of wavelength and the solar atmosphere brightness-temperature is calculated and compared with those derived from two theoretical models.

On the periodicity of linear and nonlinear oscillatory reconnection

J.O. **Thurgood**, D.I. Pontin, J.A. McLaughlin
A&A 621, A106 (2019)
https://arxiv.org/pdf/1811.08831.pdf

(Abridged for ArXiv) An injection of energy towards a magnetic null point can drive reversals of current sheet polarity leading to time-dependent Oscillatory Reconnection, which is a possible explanation of how periodic phenomena can be generated when reconnection occurs in the solar atmosphere. However, the details of what controls the period of these oscillations is poorly understood, despite being crucial in assessing whether OR can account for observed periodic behaviour. This paper aims to highlight that different types of reconnection reversal are supported about null points, and that these are distinct from the oscillation on the closed-boundary, linear systems considered in the 1990s. In particular, we explore the features of a nonlinear oscillation local to the null point, and examine the effect of resistivity and perturbation energy on the period, contrasting it to the linear case. It is found that in the linear systems, the inverse Lundquist number dictates the period, provided the perturbation energy is small relative to the inverse Lundquist number defined on the boundary, regardless of the broadband structure of the initial perturbation. However, when the perturbation energy exceeds the threshold required for 'nonlinear' null collapse to occur, a complex oscillation of the magnetic field is produced which is, at best, only weakly-dependent on the resistivity. The resultant periodicity is strongly influenced by the amount of free energy, with more energetic perturbations producing higher-frequency oscillations. Crucially, with regards to typical solar-based and astrophysical-based input energies, we demonstrate that the majority far exceed the threshold for nonlinearity to develop. This substantially alters the properties and periodicity of both null collapse and subsequent OR. Therefore, nonlinear regimes of OR should be considered in solar and astrophysical contexts.

Analysis of Different Solar Spectral Irradiance Reconstructions and Their Impact on Solar Heating Rates

G. **Thuillier**, S. M. L. Melo, J. Lean, N. A. Krivova, C. Bolduc, V. I. Fomichev, P. Charbonneau, A. I. Shapiro, W. Schmutz, D. Bolsée

Solar Physics, April **2014**, Volume 289, Issue 4, pp 1115-1142

Proper numerical simulation of the Earth's climate change requires reliable knowledge of solar irradiance and its variability on different time scales, as well as the wavelength dependence of this variability. As new measurements of the solar spectral irradiance have become available, so too have new reconstructions of historical solar irradiance variations, based on different approaches. However, these various solar spectral irradiance reconstructions have not yet been compared in detail to quantify differences in their absolute values, variability, and implications for climate and atmospheric studies. In this paper we quantitatively compare five different reconstructions of solar spectral irradiance changes during the past four centuries, in order to document and analyze their differences. The impact on atmosphere and climate studies is discussed in terms of the calculation of short wave solar heating rates.

First direct measurements of transverse waves in solar polar plumes using SDO/AIA

J.O. **Thurgood**, R.J Morton, J.A. McLaughlin

2014 ApJ 790 L2

http://arxiv.org/pdf/1406.5348v1.pdf

There is intense interest in determining the precise contribution of Alfv\'enic waves propagating along solar structures to the problems of coronal heating and solar wind acceleration. Since the launch of SDO/AIA, it has been possible to resolve transverse oscillations in off-limb solar polar plumes and recently McIntosh et al. (2011, Nature, 475, 477) concluded that such waves are energetic enough to play a role in heating the corona and accelerating the fast solar wind. However, this result is based on comparisons to Monte Carlo simulations and confirmation via direct measurements is still outstanding. Thus, this letter reports on the first direct measurements of transverse wave motions in solar polar plumes. Over a 4 hour period, we measure the transverse displacements, periods and velocity amplitudes of 596 distinct oscillations observed in the 171 \AA channel of SDO/AIA. We find a broad range of non-uniformly distributed parameter values which are well described by log-normal distributions with peaks at 234 km, 121 s and 8 km s−1, and mean and standard deviations of 407±297 km, 173±118 s and 14±10 km s−1. Within standard deviations, our direct measurements are broadly consistent with previous results. However, accounting for the whole of our observed non-uniform parameter distribution we calculate an energy flux of 9−24 W m−2, which is 4−10 times below the energy requirement for solar wind acceleration. Hence, our results indicate that transverse MHD waves as resolved by SDO/AIA cannot be the dominant energy source for fast solar wind acceleration in the open-field corona.

Upflows in the upper solar atmosphere **Review**

Hui **Tian**, Louise Harra, Deborah Baker, David H. Brooks, Lidong Xia

Solar Phys. **296**, Article number: 47 **2021**

https://link.springer.com/content/pdf/10.1007/s11207-021-01792-7.pdf

https://arxiv.org/pdf/2102.02429.pdf

https://doi.org/10.1007/s11207-021-01792-7

Spectroscopic observations at extreme and far ultraviolet wavelengths have revealed systematic upflows in the solar transition region and corona. These upflows are best seen in the network structures of the quiet Sun and coronal

holes, boundaries of active regions, and dimming regions associated with coronal mass ejections. They have been intensively studied in the past two decades because they are highly likely to be closely related to the formation of the solar wind and heating of the upper solar atmosphere. We present an overview of the characteristics of these upflows, introduce their possible formation mechanisms, and discuss their potential roles in the mass and energy transport in the solar atmosphere. Though past investigations have greatly improved our understanding of these upflows, they have left us with several outstanding questions and unresolved issues that should be addressed in the future. New observations from the Solar Orbiter mission, the Daniel K. Inouye Solar Telescope and the Parker Solar Probe will likely provide critical information to advance our understanding of the generation, propagation and energization of these upflows.

3.4. Connection to the solar wind

4. Upflows from CME-induced dimmings

Are IRIS bombs connected to Ellerman bombs?

Hui **Tian**, Zhi Xu, Jiansen He, Chad Madsen

ApJ **824** 96 **2016**

http://arxiv.org/pdf/1604.05423v1.pdf

Recent observations by the Interface Region Imaging Spectrograph (IRIS) have revealed pockets of hot gas (~2--8 ×104 K) potentially resulting from magnetic reconnection in the partially ionized lower solar atmosphere (IRIS bombs; IBs). Using joint observations between IRIS and the Chinese New Vacuum Solar Telescope, we have identified ten IBs. We find that three are unambiguously and three others are possibly connected to Ellerman bombs (EBs), which show intense brightening of the extended Hα wings without leaving an obvious signature in the Hα core. These bombs generally reveal the following distinct properties: (1) The O~{\sc{iv}}~1401.156\AA{} and 1399.774\AA{} lines are absent or very weak; (2) The Mn~{\sc{i}}~2795.640\AA{} line manifests as an absorption feature superimposed on the greatly enhanced Mg~{\sc{ii}}~k line wing; (3) The Mg~{\sc{ii}}~k and h lines show intense brightening in the wings and no dramatic enhancement in the cores; (4) Chromospheric absorption lines such as Ni~{\sc{ii}}~1393.330\AA{} and 1335.203\AA{} are very strong; (5) The 1700\AA{} images obtained with the Atmospheric Imaging Assembly on board the Solar Dynamics Observatory reveal intense and compact brightenings. These properties support the formation of these bombs in the photosphere, demonstrating that EBs can be heated much more efficiently than previously thought. We also demonstrate that the Mg~{\sc{ii}}~k and h lines can be used to investigate EBs similarly to Hα, which opens a promising new window for EB studies. The remaining four IBs obviously have no connection to EBs and they do not have the properties mentioned above, suggesting a higher formation layer possibly in the chromosphere.

Numerical simulations of Kelvin-Helmholtz instability: a two-dimensional parametric study

Chunlin **Tian**, Yao Chen

ApJ **2016**

http://arxiv.org/pdf/1604.01546v1.pdf

Using two-dimensional simulations, we numerically explore the dependences of Kelvin-Helmholtz instability upon various physical parameters, including viscosity, width of sheared layer, flow speed, and magnetic field strength. In most cases, a multi-vortex phase exists between the initial growth phase and final single-vortex phase. The parametric study shows that the evolutionary properties, such as phase duration and vortex dynamics, are generally sensitive to these parameters except in certain regimes. An interesting result is that for supersonic flows, the phase durations and saturation of velocity growth approach constant values asymptotically as the sonic Mach number increases. We confirm that the linear coupling between magnetic field and Kelvin-Helmholtz modes is negligible if the magnetic field is weak enough. The morphological behaviour suggests that the multi-vortex coalescence might be driven by the underlying wave-wave interaction. Based on these results, we make a preliminary discussion about several events observed in the solar corona. The numerical models need to be further improved to make a practical diagnostic of the coronal plasma properties.

Quantifying Poynting Flux in the Quiet Sun Photosphere

Dennis **Tilipman**1,2, Maria Kazachenko1,2, Benoit Tremblay3, Ivan Milić4,5, Valentin Martínez Pillet1, and Matthias Rempel3

2023 ApJ 956 83

https://iopscience.iop.org/article/10.3847/1538-4357/ace621/pdf

Poynting flux is the flux of magnetic energy, which is responsible for chromospheric and coronal heating in the solar atmosphere. It is defined as a cross product of the electric and magnetic fields, and in ideal MHD conditions it can be expressed in terms of the magnetic field and plasma velocity. Poynting flux has been computed for active regions and plages, but estimating it in the quiet Sun (QS) remains challenging due to resolution effects and

polarimetric noise. However, with the upcoming DKIST capabilities, such estimations will become more feasible than ever before. Here, we study QS Poynting flux in SUNRISE/IMaX observations and MURaM simulations. We explore two methods for inferring transverse velocities from observations—FLCT and a neural network–based method DeepVel—and show DeepVel to be the more suitable method in the context of small-scale QS flows. We investigate the effect of azimuthal ambiguity on Poynting flux estimates, and we describe a new method for azimuth disambiguation. Finally, we use two methods for obtaining the electric field. The first method relies on an idealized Ohm's law, whereas the second is a state-of-the-art inductive electric field inversion method PDFI_SS. We compare the resulting Poynting flux values with theoretical estimates for chromospheric and coronal energy losses and find that some of the Poynting flux estimates are sufficient to match the losses. Using MURaM simulations, we show that photospheric Poynting fluxes vary significantly with optical depth, and that there is an observational bias that results in underestimated Poynting fluxes due to an unaccounted shear term contribution.

Dominance of Bursty over Steady Heating of the 4--8 MK Coronal Plasma in a Solar Active Region: Quantification using Maps of Minimum, Maximum, and Average Brightness

Sanjiv K. **Tiwari**, Lucy A. Wilkerson, Navdeep K. Panesar, Ronald L. Moore, Amy R. Winebarger

ApJ *ApJ* **942** 2 **2023**

https://arxiv.org/pdf/2211.09936.pdf

https://iopscience.iop.org/article/10.3847/1538-4357/aca541/pdf

A challenge in characterizing active region (AR) coronal heating is in separating transient (bursty) loop heating from the diffuse background (steady) heating. We present a method of quantifying coronal heating's bursty and steady components in ARs, applying it to FeXVIII (hot94) emission of an AR observed by SDO/AIA. The maximum, minimum, and average brightness values for each pixel, over a 24 hour period, yield a maximum-brightness map, a minimum-brightness map, and an average-brightness map of the AR. Running sets of such three maps come from repeating this process for each time step of running windows of 20, 16, 12, 8, 5, 3, 1 and 0.5 hours. From each running window's set of three maps, we obtain the AR's three corresponding luminosity light curves. We find: (1) The time-averaged ratio of minimum-brightness-map luminosity to average-brightness-map luminosity increases as the time window decreases, and the time-averaged ratio of maximum-brightness-map luminosity to average-brightness-map luminosity decreases as the window decreases. (2) For the 24-hour window, the minimum-brightness map's luminosity is 5% of the average-brightness map's luminosity, indicating that at most 5% of the AR's hot94 luminosity is from heating that is steady for 24 hours. (3) This upper limit on the fraction of the hot94 luminosity from steady heating increases to 33% for the 30-minute running window. This requires that the heating of the 4--8 MK plasma in this AR is mostly in bursts lasting less than 30 minutes: at most a third of the heating is steady for 30 minutes. **May 29, 2018**

SolO/EUI Observations of Ubiquitous Fine-scale Bright Dots in an Emerging Flux Region: Comparison with a Bifrost MHD Simulation

Sanjiv K. **Tiwari**, Viggo H. Hansteen, Bart De Pontieu, Navdeep K. Panesar, David Berghmans

ApJ **2022**

https://arxiv.org/pdf/2203.06161.pdf

We report on the presence of numerous tiny bright dots in and around an emerging flux region (an X-ray/coronal bright point) observed with SolO's EUI/\hri\ in 174 Å. These dots are roundish, have a diameter of 675±300 km, a lifetime of 50±35 seconds, and an intensity enhancement of 30\% ±10\% above their immediate surroundings. About half of the dots remain isolated during their evolution and move randomly and slowly (<10 \kms). The other half show extensions, appearing as a small loop or surge/jet, with intensity propagations below 30\,\kms. Many of the bigger and brighter \hri\ dots are discernible in SDO/AIA 171 Å channel, have significant emissivity in the temperature range of 1--2 MK, and are often located at polarity inversion lines observed in HMI LOS magnetograms. Although not as pervasive as in observations, Bifrost MHD simulation of an emerging flux region do show dots in synthetic \fe\ images. These dots in simulation show distinct Doppler signatures -- blueshifts and redshifts coexist, or a redshift of the order of 10 \kms\ is followed by a blueshift of similar or higher magnitude. The synthetic images of \oxy\ and \siiv\ lines, which represent transition region radiation, also show the dots that are observed in \fe\ images, often expanded in size, or extended as a loop, and always with stronger Doppler velocities (up to 100 \kms) than that in \fe\ lines. Our observation and simulation results, together with the field geometry of dots in the simulation, suggest that most dots in emerging flux regions form in the lower solar atmosphere (at ≈1 Mm) by magnetic reconnection between emerging and pre-existing/emerged magnetic field. Some dots might be manifestations of magneto-acoustic shocks through the line formation region of \fe\ emission. **May 20, 2020**

Fine-scale explosive energy release at sites of prospective magnetic flux cancellation in the core of the solar active region observed by Hi-C 2.1, IRIS and SDO

Sanjiv K. **Tiwari**, Navdeep K. Panesar, Ronald L. Moore, Bart De Pontieu, Amy R. Winebarger, Leon Golub, Sabrina L. Savage, Laurel A. Rachmeler, Ken Kobayashi, Paola Testa, Harry P. Warren, David H. Brooks, Jonathan W. Cirtain, David E. McKenzie, Richard J. Morton, Hardi Peter, Robert W. Walsh

ApJ **887** 56 **2019**
https://arxiv.org/pdf/1911.01424.pdf
sci-hub.se/10.3847/1538-4357/ab54c1
The second Hi-C flight (Hi-C2.1) provided unprecedentedly-high spatial and temporal resolution (~250km, 4.4s) coronal EUV images of Fe IX/X emission at 172 Å, of AR 12712 on **29-May-2018**, during 18:56:21-19:01:56 UT. Three morphologically-different types (I: dot-like, II: loop-like, III: surge/jet-like) of fine-scale sudden-brightening events (tiny microflares) are seen within and at the ends of an arch filament system in the core of the AR. Although type Is (not reported before) resemble IRIS-bombs (in size, and brightness wrt surroundings), our dot-like events are apparently much hotter, and shorter in span (70s). We complement the 5-minute-duration Hi-C2.1 data with SDO/HMI magnetograms, SDO/AIA EUV images, and IRIS UV spectra and slit-jaw images to examine, at the sites of these events, brightenings and flows in the transition-region and corona and evolution of magnetic flux in the photosphere. Most, if not all, of the events are seated at sites of opposite-polarity magnetic flux convergence (sometimes driven by adjacent flux emergence), implying likely flux cancellation at the microflare's polarity inversion line. In the IRIS spectra and images, we find confirming evidence of field-aligned outflow from brightenings at the ends of loops of the arch filament system. In types I and II the explosion is confined, while in type III the explosion is ejective and drives jet-like outflow. The light-curves from Hi-C, AIA and IRIS peak nearly simultaneously for many of these events and none of the events display a systematic cooling sequence as seen in typical coronal flares, suggesting that these tiny brightening-events have chromospheric/transition-region origin.

Damping of Propagating Kink Waves in the Solar Corona

Ajay K. **Tiwari**, Richard J. Morton, Stephane Régnier, James A. McLaughlin
ApJ **876** 106 **2019**
https://arxiv.org/pdf/1904.08834.pdf
https://iopscience.iop.org/article/10.3847/1538-4357/ab164b/pdf
Alfvénic waves have gained renewed interest since the existence of ubiquitous propagating kink waves were discovered in the corona. {It has long been suggested that Alfvénic} waves play an important role in coronal heating and the acceleration of the solar wind. To this effect, it is imperative to understand the mechanisms that enable their energy to be transferred to the plasma. Mode conversion via resonant absorption is believed to be one of the main mechanisms for kink wave damping, and is considered to play a key role in the process of energy transfer. This study examines the damping of propagating kink waves in quiescent coronal loops using the Coronal Multi-channel Polarimeter (CoMP). A coherence-based method is used to track the Doppler velocity signal of the waves, enabling us to investigate the spatial evolution of velocity perturbations. The power ratio of outward to inward propagating waves is used to estimate the associated damping lengths and quality factors. To enable accurate estimates of these quantities, {we provide the first derivation of a likelihood function suitable for fitting models to the ratio of two power spectra obtained from discrete Fourier transforms. Maximum likelihood estimation is used to fit an exponential damping model to the observed variation in power ratio as a function of frequency.} We confirm earlier indications that propagating kink waves are undergoing frequency dependent damping. Additionally, we find that the rate of damping decreases, or equivalently the damping length increases, for longer coronal loops that reach higher in the corona.

New Evidence that Magnetoconvection Drives Solar–Stellar Coronal Heating

Sanjiv K. **Tiwari**1,2,3,4, Julia K. Thalmann5, Navdeep K. Panesar1, Ronald L. Moore1,2, and Amy R. Winebarger
2017 ApJL 843 L20
http://iopscience.iop.org.sci-hub.cc/2041-8205/843/2/L20/
How magnetic energy is injected and released in the solar corona, keeping it heated to several million degrees, remains elusive. Coronal heating generally increases with increasing magnetic field strength. From a comparison of a nonlinear force-free model of the three-dimensional active region coronal field to observed extreme-ultraviolet loops, we find that (1) umbra-to-umbra coronal loops, despite being rooted in the strongest magnetic flux, are invisible, and (2) the brightest loops have one foot in an umbra or penumbra and the other foot in another sunspot's penumbra or in unipolar or mixed-polarity plage. The invisibility of umbra-to-umbra loops is new evidence that magnetoconvection drives solar-stellar coronal heating: evidently, the strong umbral field at both ends quenches the magnetoconvection and hence the heating. Broadly, our results indicate that depending on the field strength in both feet, the photospheric feet of a coronal loop on any convective star can either engender or quench coronal heating in the loop's body. **2014 April 01/02, 2014 July 07**

Imaging Spectropolarimeter for the Multi-Application Solar Telescope at Udaipur Solar Observatory: Characterization of Polarimeter and Preliminary Observations

Alok Ranjan **Tiwary**, Shibu K. Mathew, A. Raja Bayanna, P. Venkatakrishnan…
Solar Physics April **2017**, 292:49
http://link.springer.com/article/10.1007/s11207-017-1076-5

The Multi-Application Solar Telescope (MAST) is a 50 cm off-axis Gregorian telescope that has recently become operational at the Udaipur Solar Observatory (USO). An imaging spectropolarimeter is being developed as one of the back-end instruments of MAST to gain a better understanding of the evolution and dynamics of solar magnetic and velocity fields. This system consists of a narrow-band filter and a polarimeter. The polarimeter includes a linear polarizer and two sets of liquid crystal variable retarders (LCVRs). The instrument is intended for simultaneous observations in the spectral lines 6173 Å and 8542 Å, which are formed in the photosphere and chromosphere, respectively. In this article, we present results from the characterization of the LCVRs for the spectral lines of interest and the response matrix of the polarimeter. We also present preliminary observations of an active region obtained using the spectropolarimeter. For verification purposes, we compare the Stokes observations of the active region obtained from the Helioseismic Magnetic Imager (HMI) onboard the Solar Dynamics Observatory (SDO) with that of MAST observations in the spectral line 6173 Å. We find good agreement between the two observations, considering the fact that MAST observations are limited by seeing.

Cosmic-Ray Propagation Around the Sun - Investigating the Influence of the Solar Magnetic Field on the Cosmic-Ray Sun Shadow

Julia Becker **Tjus**, Paolo Desiati, Niklas Döpper, Horst Fichtner, Jens Kleimann, Mike Kroll, Frederik Tenholt

A&A 633, A83 (2020)

https://doi.org/10.1051/0004-6361/201936306

https://arxiv.org/pdf/1903.12638.pdf

The cosmic-ray Sun shadow, which is caused by high-energy charged cosmic rays being blocked and deflected by the Sun and its magnetic field, has been observed by various experiments such as Argo-YBJ, HAWC, Tibet, and IceCube. Most notably, the shadow's size and depth was recently shown to correlate with the 11-year solar cycle. The interpretation of such measurements, which help to bridge the gap between solar physics and high-energy particle astrophysics, requires a solid theoretical understanding of cosmic-ray propagation in the coronal magnetic field. It is the aim of this paper to establish theoretical predictions for the cosmic-ray Sun shadow in order to identify observables that can be used to study this link in more detail. To determine the cosmic-ray Sun shadow, we numerically compute trajectories of charged cosmic rays in the energy range of 5 to 316 TeV for five different mass numbers. We present and analyse the resulting shadow images for protons and iron, as well as for typically measured cosmic-ray compositions. We confirm the observationally established correlation between the magnitude of the shadowing effect and both the mean sunspot number and the polarity of the magnetic field during the solar cycle. We also show that during low solar activity, the Sun's shadow behaves similarly to that of a dipole, for which we find a non-monotonous dependence on energy. In particular, the shadow can become significantly more pronounced than the geometrical disk expected for a totally unmagnetized Sun. For times of high solar activity, we instead predict the shadow to depend monotonously on energy, and to be generally weaker than the geometrical shadow for all tested energies. These effects should become visible in energy-resolved measurements of the Sun shadow, and may in the future become an independent measure for the level of disorder in the solar magnetic field.

Near-surface Azimuthal Magnetic Fields and Solar Activity Cycles

A. G. **Tlatov**

Solar Phys. Volume 298, article number 147 **2023**

https://arxiv.org/ftp/arxiv/papers/2309/2309.10381.pdf

https://doi.org/10.1007/s11207-023-02239-x

Variations of the azimuthal magnetic fields of the Sun in the 23-25 activity cycles of the activity cycles are considered. To identify azimuthal magnetic fields, the analysis of daily observations of LOS magnetic fields from the regions near the solar limb was performed. It is shown that with a sufficiently large averaging of the data, large-scale structures are distinguished that can be interpreted by horizontal magnetic fields directed along the East-West line. Azimuthal magnetic fields are visible both in the low-latitude zone and at high latitudes. Azimuthal fields at the same latitudes have opposite directions in the northern and southern hemispheres, and also change sign in even and odd cycles of activity. The mechanism of formation of global azimuthal magnetic fields and their role in the cycle of solar activity is discussed. The near-surface azimuthal magnetic field is closely related to the activity cycle. Apparently, the azimuthal field is formed from U-shaped flux tubes of active regions (AR). Due to the presence of the tilt angle AR during differential rotation, the subsurface magnetic fields are pulled in the azimuthal direction. The role of azimuthal magnetic fields in solar activity cycles is considered. A scheme for generating a magnetic field according to a scheme different from Babcock-Layton dynamo models is proposed.

Ground-based Solar Observations for Space Weather Forecasting

A.G. **Tlatov**, A.A. Pevtsov

2023

https://arxiv.org/ftp/arxiv/papers/2303/2303.01708.pdf

The possibilities of organizing an observation service for solar activity in order to provide space weather forecasting are considered. The most promising at this stage is the creation of a ground-based observation network. Such a network should include solar magnetographs that provide observation of large-scale magnetic fields of the Sun, and patrol optical telescopes designed to detect coronal mass ejections and solar flares. The data of magnetographic observations provide an assessment of recurrent solar winds. Patrol telescopes operating in continuous mode allow detecting the moments of eruption and determining the parameters of coronal mass ejections at the initial stage of acceleration. The network service can be supplemented with other types of observations in the radio and optical bands. The paper considers the composition of observational tools, as well as methods and models for forecasting.
02.10.2014, 20 февраля 2021

Dark Dots on the Photosphere and Their Counting in the Sunspot Index

Andrey G. **Tlatov**
Solar Physics volume 297, Article number: 67 (**2022**)
https://doi.org/10.1007/s11207-022-02002-8
https://arxiv.org/pdf/2205.13142.pdf
A large number of small dark areas can be observed in the continuum with high-spatial resolution in recent satellite observations of the Sun, as well as in high-quality ground-based data. These regions have no penumbra, have a contrast of up to 20%20% and are similar to solar pores. The characteristic area of such structures is from 0.3 to 5 μhm or from 0.5 to 7 Mm typical diameter. The number of such points in one image can be several hundred. The nature of such formations remains unclear.
We have performed a selection of dark regions with a contrast of at least 3%3% of the level of the quiet Sun using data obtained with the Helioseismic and Magnetic Imager (HMI) on board the Solar Dynamcis Observatory (SDO) from 2010 to 2020. We have studied the properties of "dark dots", including their variation with the solar cycle, area distribution, and contrast. We also studied the intensity of the magnetic field of such structures. We found that the number of dark dots with an area of less than 5 μhm, in which the magnetic field is not significant and is less than |B|<30|B|<30 G, is from 60 to 80%80% of the total number of structures of this size. This means that they are not associated with magnetic activity. The existence of such structures can significantly affect the calculations of the sunspot index since they can be mistaken with pores.

The shape of sunspots and solar activity cycles

Andrey **Tlatov**
Solar Physics **volume 297**, Article number: 110
https://arxiv.org/pdf/2203.04722.pdf
https://doi.org/10.1007/s11207-022-02045-x
The paper presents the results of the analysis of the geometric characteristics of sunspots for the period of 19-24 cycles of activity. The shape of sunspots was studied on the basis of the method of normalization of images of sunspots to study the average profile of the spot. The deviation of the shape of sunspots from the axisymmetric configuration is investigated. It was found that the spots, as a rule, have an ellipsoid shape, and the major axis of the ellipse has a predominant inclination to the equator, opposite in the Northern and Southern hemispheres. The angle of inclination of the sunspot axis corresponds to the angle of inclination of the bipoles in the activity cycles. The relationship between the shape of sunspots in the current cycle and the amplitude of the next cycle of activity is found. The greater the elongation along the longitude of the current cycle of spots, the higher the next cycle of activity will be.

On the timing of the next great solar activity minimum

A.G.**Tlatov**. A.A.Pevtsov
Advances in Space Research Volume 60, Issue 5, 1 September **2017**, Pages 1108-1114
http://sci-hub.cc/10.1016/j.asr.2017.05.009
The long-term variations in solar activity are studied using the dataset comprised of sunspot number and 14C radioisotope timeseries. We use a novel S200 index to identify possible past Grand Minima (GM). The Maunder, Oort, Wolf and Spörer Minima fall in phase with the minimum of S200 index. We also show GM develop in clusters, with a separation of about 400–600 years between individual GM. Extending these found similarities to modern solar activity, it is predicted that next grand solar minimum may occur in about ∼2090±20.

Tilt Angles of Solar Filaments over the Period 1919-2014

A. G. **Tlatov**, K.M. Kuzanyan, V.V. Vasil'yeva
Solar Phys. Volume 291, Issue 4, pp 1115-1127 **2016**
http://arxiv.org/pdf/1601.02342v1.pdf
The spatial and temporal distributions of solar filaments were analyzed using data from the Meudon Observatory for the period 1919-2003 and the Kislovodsk Mountain Astronomical Station for the period 1979-2014. We scanned Hα solar synoptic charts on which the filaments were isolated and digitized. The data on each filament comprise its

location, length, area, and other geometrical characteristics. The temporal distributions of the number and total length of the filaments have been obtained. We also found latitudinal migration of filament locations with the solar cycle, and analyzed the longitudinal distribution and asymmetry of filaments in the northern and southern hemispheres, and other properties of their distribution. The tilt angles of filaments with respect the solar equator (τ) were analyzed. On average, the eastern tips of filaments are closer to the poles than the western ones ($\tau \sim 10^\circ$). On the other hand, the filaments in the polar regions ($\theta > 50^\circ$, where θ is the latitude) usually have negative tilts ($\tau < 0^\circ$). The tilt angles vary with the phases of the 11 year sunspot cycle and are at their highest values in the epoch of the activity maximum. In the century-long modulation of the solar activity (Gleissberg cycle), the mean tilt angles of filaments in the mid-latitude zone ($\theta \sim \pm 40^\circ$) were maximum in the middle of the 20th century in solar sunspot cycles 18-19. We hereby propose using the statistical properties of solar filaments as an additional coherent measure of manifestation of the solar cycle which covers all latitudes and for which almost a century long systematically calibrated data series is available.

The change of the solar cyclicity mode ☆

A.G. **Tlatov**

Advances in Space Research, Volume 55, Issue 3, 1 February **2015**, Pages 851–856

http://www.sciencedirect.com/science/article/pii/S027311771400386X

Our analysis of groups of sunspots since the year 1610 till indicates that the Gnevyshev–Ohl rule (GO) displays cycles of inversion with the period of 200 years. The latest inversion occurred in the Hale double cycle 22–23. Due to that, in several subsequent double cycles the odd cycles should be weaker than their preceding even cycles. Gleissberg cycles with the period of about 100 years and variations with the period of 200 years are manifested in variations of physical parameters of sunspots and are interconnected. We suggested that the secular minima of the solar activity occur in the vicinity of the extreme points of the 200-year cycles of inversion of the GO rule. The peak of the next secular minimum is expected between the years 2025÷20352025÷2035. We studied the variations of the physical parameters of sunspots in a Gleissberg cycle. At
the maximum phase of the Gleissberg cycle, the average area of groups and the average number of spots in a group reach their maximum. According to our forecast, the amplitude of the 25th solar activity cycle will be somewhat lower than that of the 24th.

Properties of sunspot umbrae of leading and trailing polarity in 1917–2013

Andrey Georgievich **Tlatov**, , , K.A. Tlatovaa, , V.V. Vasil'evaa, , A.A. Pevtsovb, , K. Mursula

Advances in Space Research, Volume 55, Issue 3, 1 February **2015**, Pages 835–842

http://www.sciencedirect.com/science/article/pii/S0273117714003408

Using the software developed by us, we produced a digitized (tabulated) database of sunspot umbrae and pores observed at Mount Wilson Observatory (MWO) in 1917–2013. The database includes the heliographic coordinates, areas and the polarity and strength of magnetic fields of umbrae and pores in the MWO sunspot drawings. Using this database we study here the properties and long-term variation of sunspot umbrae and pores, separately for leading and trailing polarity spots. We find that the leading sunspots have tendency for larger umbrae and stronger magnetic field strength than the trailing spots. The average field strength and area of sunspot umbrae vary with sunspot cycle. Furthermore, the mean magnetic field strength in sunspot umbrae exhibits a gradual increase from early 1960s to 1990s. The nature of this increase is discussed.

Applying an Automatic Image-Processing Method to Synoptic Observations

Andrey G. **Tlatov**, Valeria V. Vasil'eva, Valentina V. Makarova, Pavel A. Otkidychev

Solar Physics, April **2014**, Volume 289, Issue 4, pp 1403-1412

We used an automatic image-processing method to detect solar-activity features observed in white light at the Kislovodsk Solar Station. This technique was applied to automatically or semi-automatically detect sunspots and active regions. The results of this automated recognition were verified with statistical data available from other observatories and revealed a high detection accuracy. We also provide parameters of sunspot areas, of the umbra, and of faculae as observed in Solar Cycle 23 as well as the **magnetic flux** of these active elements, calculated at the Kislovodsk Solar Station, together with white-light images and magnetograms from the Michaelson Doppler Imager onboard the Solar and Heliospheric Observatory (SOHO/MDI). The ratio of umbral and total sunspot areas during Solar Cycle 23 is ≈ 0.19. The area of sunspots of the leading polarity was approximately 2.5 times the area of sunspots of the trailing polarity.

Bimodal Distribution of Magnetic Fields and Areas of Sunspots

Andrey G. **Tlatov**, Alexei A. Pevtsov

Solar Physics, April **2014**, Volume 289, Issue 4, pp 1143-1152

We applied automatic identification of sunspot umbrae and penumbrae to daily observations from the Helioseismic Magnetic Imager (HMI) on board the Solar Dynamics Observatory (SDO) to study their magnetic flux density (B) and area (A). The results confirm an already known logarithmic relationship between the area of sunspots and their

maximum flux density. In addition, we find that the relation between average magnetic flux density (Bavg) and sunspot area shows a bimodal distribution: for small sunspots and pores (A≤20 millionth of solar hemisphere, MSH), Bavg≈800 G (gauss), and for large sunspots (A≥100 MSH), Bavg is about 600 G. For intermediate sunspots, average flux density linearly decreases from about 800 G to 600 G. A similar bimodal distribution was found in several other integral parameters of sunspots. We show that this bimodality can be related to different stages of sunspot penumbra formation and can be explained by the difference in average inclination of magnetic fields at the periphery of small and large sunspots.

A new dynamo pattern revealed by the tilt angle of bipolar sunspot groups

A.**Tlatov**, E.Illarionov, D.Sokoloff, V.Pipin
E-print, April **2013**, MNRAS
We obtain the latitude-time distribution of the averaged tilt angle of solar bipoles. For large bipoles, which are mainly bipolar sunspot groups, the spatially averaged tilt angle is positive in the Northern solar hemisphere and negative in the Southern, with modest variations during course of the solar cycle. We consider the averaged tilt angle to be a tracer for a crucial element of the solar dynamo, i.e. the regeneration rate of poloidal large-scale magnetic field from toroidal. The value of the tilt obtained crudely corresponds to a regeneration factor corresponding to about 10% of r.m.s. velocity of solar convection. These results develop findings of Kosovichev and Stenflo (2012) concerning Joy's law, and agree with the usual expectations of solar dynamo theory. Quite surprisingly, we find a pronounced deviation from these properties for smaller bipoles, which are mainly solar ephemeral regions. They possess tilt angles of approximately the same absolute value, but of opposite sign compared to that of the large bipoles. Of course, the tilt data for small bipoles are less well determined than those for large bipoles; however they remain robust under various modifications of the data processing.

Tilt of sunspot bipoles in Solar Cycles 15 to 24

Ksenia **Tlatova**, Andrey Tlatov, Alexei Pevtsov, Kalevi Mursula, Valeria Vasil'eva, Elina Heikkinen, Luca Bertello, Alexander Pevtsov, Ilpo Virtanen, Nina Karachik
Solar Phys. 293:118 **2018**
https://arxiv.org/pdf/1807.07913.pdf
We use recently digitized sunspot drawings from Mount Wilson Observatory to investigate the latitudinal dependence of tilt angles of active regions and its change with solar cycle. The drawings cover the period from 1917 to present and contain information about polarity and strength of magnetic field in sunspots. We identify clusters of sunspots of same polarity, and used these clusters to form ``bipole pairs''. The orientation of these bipole pairs was used to measure their tilts. We find that the latitudinal profile of tilts does not monotonically increase with latitude as most previous studies assumed, but instead, it shows a clear maximum at about 25--30 degree latitudes. Functional dependence of tilt (γ) on latitude (φ) was found to be $\gamma=(0.20\pm0.08)\sin(2.80\varphi)+(-0.00\pm0.06)$. We also find that latitudinal dependence of tilts varies from one solar cycle to another, but larger tilts do not seem to result in stronger solar cycles. Finally, we find the presence of a systematic offset in tilt of active regions (non-zero tilts at the equator), with odd cycles exhibiting negative offset and even cycles showing the positive offset.

Understanding the Relationship between Solar Coronal Abundances and F10.7 cm Radio Emission

Andy S. H. **To**1, Alexander W. James1,2, T. S. Bastian3, Lidia van Driel-Gesztelyi1,4,5, David M. Long1,6, Deborah Baker1, David H. Brooks7, Samantha Lomuscio3, David Stansby1, and Gherardo Valori8
2023 ApJ 948 121
https://iopscience.iop.org/article/10.3847/1538-4357/acbc1b/pdf
Sun-as-a-star coronal plasma composition, derived from full-Sun spectra, and the F10.7 radio flux (2.8 GHz) have been shown to be highly correlated (r = 0.88) during solar cycle 24. However, this correlation becomes nonlinear during increased solar magnetic activity. Here we use cotemporal, high spatial resolution, multiwavelength images of the Sun to investigate the underlying causes of the nonlinearity between coronal composition (FIP bias) and F10.7 solar index correlation. Using the Karl G. Jansky Very Large Array, Hinode/EIS (EUV Imaging Spectrometer), and the Solar Dynamics Observatory, we observed a small active region, AR 12759, throughout the solar atmosphere from the photosphere to the corona. The results of this study show that the magnetic field strength (flux density) in active regions plays an important role in the variability of coronal abundances, and it is likely the main contributing factor to this nonlinearity during increased solar activity. Coronal abundances above cool sunspots are lower than in dispersed magnetic plage regions. Strong magnetic concentrations are associated with stronger F10.7 cm gyroresonance emission. Considering that as the solar cycle moves from minimum to maximum, the sizes of sunspots and their field strength increase with the gyroresonance component, the distinctly different tendencies of radio emission and coronal abundances in the vicinity of sunspots is the likely cause of saturation of Sun-as-a-star coronal abundances during solar maximum, while the F10.7 index remains well correlated with the sunspot number and other magnetic field proxies. **2020 April 3, 7**

Two-Station Interplanetary Scintillation Measurements of Solar Wind Speed near the Sun Using the X-band Radio Signal of the Nozomi Spacecraft

M. **Tokumaru**, S. Fujimaki, M. Higashiyama, A. Yokobe, T. Ohmi, K. Fujiki and M. Kojima
Solar Physics, Volume 276, Numbers 1-2, 315-336, **2012**

Interplanetary scintillation (IPS) measurements of the solar wind speed for the distance range between 13 and 37 R S were carried out during the solar conjunction of the Nozomi spacecraft in 2000–2001 using the X-band radio signal. Two large-aperture antennas were employed in this study, and the baseline between the two antennas was several times longer than the Fresnel scale for the X-band. We successfully detected a positive correlation of IPS from the cross-correlation analysis of received signal data during ingress, and estimated the solar wind speed from the time lag corresponding to the maximum correlation by assuming that the solar wind flows radially. The speed estimates range between 200 and 540 km s−1 with the majority below 400 km s−1. We examined the radial variation in the solar wind speed along the same streamline by comparing the Nozomi data with data obtained at larger distances. Here, we used solar wind speed data taken from 327 MHz IPS observations of the Solar-Terrestrial Environment Laboratory (STEL), Nagoya University, and in situ measurements by the Advanced Composition Explorer (ACE) for the comparison, and we considered the effect of the line-of-sight integration inherent to IPS observations for the comparison. As a result, Nozomi speed data were proven to belong to the slow component of the solar wind. Speed estimates within 30 R S were found to be systematically slower by 10–15 % than the terminal speeds, suggesting that the slow solar wind is accelerated between 13 and 30 R S.

Fluctuating Sunspot Numbers Exhibit A Non-Markovian Damped Stochastic Process

Reynan L. **Toledo**, Reinabelle Reyes, Christopher C. Bernido
2023
https://arxiv.org/ftp/arxiv/papers/2306/2306.14151.pdf

The rise and fall in the number of sunspots have served as a lynchpin in many investigations on solar dynamics. Arising from magnetic disturbances in the sun, variations in sunspot numbers have helped define a solar cycle of around eleven years which to date is yet to be fully understood. We model the fluctuation of sunspot numbers as a modulated Brownian motion characterized by a memory parameter {\mu} and a decay parameter \b{eta}. By matching the theoretical and empirical mean square deviation of the sunspot numbers, the values of {\mu} and \b{eta} are determined for each solar cycle. This allows us to obtain an exact form of a probability density function (PDF) which closely matches the dataset for sunspots. This novel PDF for sunspot numbers exhibit a memory behavior from which some insights could be obtained. In particular, the values of {\mu} indicate that consecutive sunspot numbers are negatively correlated for large times. The values of \b{eta}, on the other hand, when viewed as a time series from one solar cycle to another, indicate a positive trend towards increasing values which could possibly suggest a diminishing solar activity.

Evidence for a Time Lag in Solar Modulation of Galactic Cosmic Rays

Nicola **Tomassetti**1, Miguel Orcinha2, Fernando Barão2, and Bruna Bertucci1
2017 ApJL 849 L32
http://iopscience.iop.org/article/10.3847/2041-8213/aa9373/pdf

The solar modulation effect of cosmic rays in the heliosphere is an energy-, time-, and particle-dependent phenomenon that arises from a combination of basic particle transport processes such as diffusion, convection, adiabatic cooling, and drift motion. Making use of a large collection of time-resolved cosmic-ray data from recent space missions, we construct a simple predictive model of solar modulation that depends on direct solar-physics inputs: the number of solar sunspots and the tilt angle of the heliospheric current sheet. Under this framework, we present calculations of cosmic-ray proton spectra, positron/electron and antiproton/proton ratios, and their time dependence in connection with the evolving solar activity. We report evidence for a time lag $\Delta T = 8.1 \pm 1.2$ months, between solar-activity data and cosmic-ray flux measurements in space, which reflects the dynamics of the formation of the modulation region. This result enables us toforecast the cosmic-ray flux near Earth well in advance by monitoring solar activity.

Scientific objectives and capabilities of the Coronal Solar Magnetism Observatory†

S. **Tomczyk**, E. Landi, J. T. Burkepile, R. Casini, E. E. DeLuca, Y. Fan, S. E. Gibson, H. Lin, S. W. McIntosh, S. C. Solomon, G. de Toma, A. G. de Wijn, J. Zhang
JGR Volume 121, Issue 8 August 2016 Pages 7470–7487 **2016**
DOI: 10.1002/2016JA022871

Magnetic influences increase in importance in the solar atmosphere from the photosphere out into the corona, yet our ability to routinely measure magnetic fields in the outer solar atmosphere is lacking. We describe the scientific objectives and capabilities of the **COronal Solar Magnetism Observatory** (**COSMO**), a proposed synoptic facility designed to measure magnetic fields and plasma properties in the large-scale solar atmosphere. COSMO comprises a suite of three instruments chosen to enable the study of the solar atmosphere as a coupled system: 1) a coronagraph with a 1.5-m aperture to measure the magnetic field, temperature, density and dynamics of the corona; 2) an instrument for diagnostics of chromospheric and prominence magnetic fields and plasma properties; and 3) a white-light K-coronagraph to measure the density structure and dynamics of the corona and coronal mass ejections. COSMO will provide a unique combination of magnetic field, density, temperature and velocity observations in the corona and chromosphere that have the potential to transform our understanding of fundamental physical processes in the solar atmosphere and their role in the origins of solar variability and space weather.

Prospects and Challenges for Helioseismology **Review**

J. **Toomre**, M. J. Thompson

Space Science Reviews Volume 196, Issue 1, pp 1-14 **2015**

Helioseismology has advanced considerably our knowledge of the interior of the Sun over the past three decades. Our understanding of the Sun's internal structure, its dynamics, rotation, convection and magnetism, have all been advanced. Yet there are challenges, areas where the results from helioseismology are tantalizing but inconclusive, and aspects where the interpretation of the data has still to be put on a firm footing. In this paper we shall focus on a number of those challenges and give our assessment of where progress needs to be made in the next decade.

Convective Magnetic Flux Emergence Simulations from the Deep Solar Interior to the Photosphere: Comprehensive Study of Flux Tube Twist

Shin **Toriumi**1, Hideyuki Hotta2, and Kanya Kusano2

2024 ApJ 975 209

https://iopscience.iop.org/article/10.3847/1538-4357/ad7e1d/pdf

The emergence of magnetic flux from the deep convection zone plays an important role in solar magnetism, such as the generation of active regions and triggering of various eruptive phenomena, including jets, flares, and coronal mass ejections. To investigate the effects of magnetic twist on flux emergence, we performed numerical simulations of flux tube emergence using the radiative magnetohydrodynamic code R2D2 and conducted a systematic survey on the initial twist. Specifically, we varied the twist of the initial tube both positively and negatively from zero to twice the critical value for kink instability. As a result, regardless of the initial twist, the flux tube was lifted by the convective upflow and reached the photosphere to create sunspots. However, when the twist was too weak, the photospheric flux was quickly diffused and not retained long as coherent sunspots. The degree of magnetic twist measured in the photosphere conserved the original twist relatively well and was comparable to actual solar observations. Even in the untwisted case, a finite amount of magnetic helicity was injected into the upper atmosphere because the background turbulence added helicity. However, when the initial twist exceeded the critical value for kink instability, the magnetic helicity normalized by the total magnetic flux was found to be unreasonably larger than the observations, indicating that the kink instability of the emerging flux tube may not be a likely scenario for the formation of flare-productive active regions.

Universal Scaling Laws for Solar and Stellar Atmospheric Heating: Catalog of Power-law Index between Solar Activity Proxies and Various Spectral Irradiances

Shin **Toriumi**, Vladimir S. Airapetian, Kosuke Namekata, Yuta Notsu

ApJ Supplement Series **262** 46 **2022**

https://arxiv.org/pdf/2208.10511.pdf

https://iopscience.iop.org/article/10.3847/1538-4365/ac8b15/pdf

The formation of extremely hot outer atmospheres is one of the most prominent manifestations of magnetic activity common to the late-type dwarf stars, including the Sun. It is widely believed that these atmospheric layers, the corona, transition region, and chromosphere, are heated by the dissipation of energy transported upwards from the stellar surface by the magnetic field. This is signified by the spectral line fluxes at various wavelengths, scaled with power-law relationships against the surface magnetic flux over a wide range of formation temperatures, which are universal to the Sun and Sun-like stars of different ages and activity levels. This study describes a catalog of power-law indices between solar activity proxies and various spectral line fluxes. Compared to previous studies, we expanded the number of proxies, which now includes the total magnetic flux, total sunspot number, total sunspot area, and the F10.7 cm radio flux, and further enhances the number of spectral lines by a factor of two. This provides the data to study in detail the flux-flux scaling laws from the regions specified by the temperatures of the corona (log(T/K)=6-7) to those of the chromosphere (log(T/K)~4), as well as the reconstruction of various spectral line fluxes of the Sun in the past, F-, G-, and K-type dwarfs, and the modeled stars.

Universal Scaling Laws for the Solar and Stellar Atmospheric Heating

Shin **Toriumi**, Vladimir S. Airapetian

ApJ **927** 179 **2022**

https://arxiv.org/pdf/2202.01232.pdf

https://iopscience.iop.org/article/10.3847/1538-4357/ac5179/pdf

The Sun and sun-like stars commonly host the multi-million-Kelvin coronae and the 10,000-Kelvin chromospheres. These extremely hot gases generate X-ray and Extreme Ultraviolet emissions that may impact the erosion and chemistry of (exo)planetary atmospheres, influencing the climate and conditions of habitability. However, the mechanism of coronal and chromospheric heating is still poorly understood. While the magnetic field most probably plays a key role in driving and transporting energy from the stellar surface upwards, it is not clear if the atmospheric heating mechanisms of the Sun and active sun-like stars can be described in a unified manner. To this end, we report on a systematic survey of the responses of solar and stellar atmospheres to surface magnetic flux over a wide range of temperatures. By analyzing 10 years of multi-wavelength synoptic observations of the Sun, we reveal that the irradiance and magnetic flux show power-law relations with an exponent decreasing from above- to sub-unity as the temperature decreases from the corona to the chromosphere. Moreover, this trend indicating the efficiency of atmospheric heating can be extended to sun-like stars. We also discover that the power-law exponent has a solar cycle dependence, where it becomes smallest at activity maximum, probably due to the saturation of atmospheric heating. Our study provides observational evidence that the mechanism of atmospheric heating is universal among the Sun and sun-like stars, regardless of age or activity.

Sun-as-a-star Spectral Irradiance Observations of Transiting Active Regions

Shin **Toriumi**, Vladimir S. Airapetian, Hugh S. Hudson, Carolus J. Schrijver, Mark C.M. Cheung, Marc L. DeRosa

ApJ **902** 36 **2020**

https://arxiv.org/pdf/2008.04319.pdf

Major solar flares are prone to occur in active region atmospheres associated with large, complex, dynamically-evolving sunspots. This points to the importance of monitoring the evolution of starspots, not only in visible but also in ultra violet (UV) and X-rays, in understanding the origin and occurrence of stellar flares. To this end, we perform spectral irradiance analysis on different types of transiting solar active regions by using a variety of full-disk synoptic observations. The target events are an isolated sunspot, spotless plage, and emerging flux in prolonged quiet-Sun conditions selected from the past decade. We find that the visible continuum and total solar irradiance become darkened when the spot is at the central meridian, whereas it is bright near the solar limb; UV bands sensitive to the chromosphere correlate well with the variation of total unsigned magnetic flux in the photosphere; amplitudes of EUV and soft X-ray increase with the characteristic temperature, whose light curves are flat-topped due to their sensitivity to the optically thin corona; the transiting spotless plage does not show the darkening in the visible irradiance, while the emerging flux produces an asymmetry in all light curves about the central meridian. The multi-wavelength sun-as-a-star study described here indicates that such time lags between the coronal and photospheric light curves have the potential to probe the extent of coronal magnetic fields above the starspots. In addition, EUV wavelengths that are sensitive to the transition-region temperature sometimes show anti-phased variations, which may be used for diagnosing plasmas around starspots. **2018-Feb-01-11, 2018-Jul-04-14, 2019-Jan-14-24, 2019-Nov-27-Dec 07**

Table 1. List of Events Analyzed in This Study (2018-2019)

Analysis of Solar Diameter Measurements Made at the Basilica of San Petronio during and after the Maunder Minimum

I. **Tovar**1, A. J. P. Aparicio1,2, V. M. S. Carrasco1,2, M. C. Gallego1,2, and J. M. Vaquero2,3

2021 ApJ 912 122

https://doi.org/10.3847/1538-4357/abefdb

A series of measurements of the solar diameter taken in the meridian line of the Basilica of San Petronio (Bologna, Italy) between 1655 and 1736 has been analyzed. This series is of interest because the measurement period includes the Maunder Minimum (1645–1715; hereafter MM) when solar activity was abnormally low. Some authors have suggested an increase of the solar diameter during the MM. Trying to detect these changes, statistical analyses comparing measurements taken in San Petronio during the MM (1655–1715) and other ones taken in a subsequent period (1716–1736) have been performed. Mann–Whitney U tests and Student's t-tests indicate that there is no statistically significant difference in the medians and averages of the solar diameter in both periods. In fact, we have found differences around $0''.6$ in the medians and the averages, which are below the mean accuracy of the instrument. Therefore, we conclude that there is no difference between the solar diameter value measured during the MM (1655–1715) and that for the subsequent period 1716–1736. This implies that there has not been an increase in the solar diameter of several arcseconds during the MM as has been speculated by some authors.

The Dark Side of the Sun A Plea for a Next-Generation Opacity Calculation

Regner **Trampedach**
Proceedings of the second Workshop on Astrophysical Opacities (held in Kalamazoo, MI, 2017) **2018**
https://arxiv.org/pdf/1804.03746.pdf
Is the Sun likely to have a more opaque interior than previously thought? The solar oxygen (or abundance) problem can be solved with higher interior opacities, reconciling abundance analyses based on 3D convective atmospheres with the helioseismic structure of the solar interior. This has been known for more than a decade, but last year we learned that the absorption by just iron may contribute 7\% more to the solar opacity at the bottom of the convection zone than predicted by any opacity calculation so far, and by OP05 in particular. I find that artificial changes to the absorption (calibrated against the iron experiment) by other elements in a solar mixture give an opacity increase of a shape and magnitude that can restore agreement between modern abundance analysis and helioseismology. This suggests that improved opacity calculations will solve the solar oxygen problem.

Bayesian Methods for Reconstructing Sunspot Numbers Before and During the Maunder Minimum

Guido **Travaglini**
Solar Physics January **2017**, 292:23
The Maunder Minimum (MM) was an extended period of reduced solar activity in terms of yearly sunspot numbers (SSN) during 1610 – 1715. The reality of this "grand minimum" is generally accepted in the scientific community, but the statistics of the SSN record suggest a need for data reconstruction. The MM data show a nonstandard distribution compared with the entire SSN signal (1610 – 2014). The pattern does not satisfy the weakly stationary solar dynamo approximation, which characterizes many natural events spanning centuries or even millennia, including the Sun and the stars. Over the entire observation period (1610 – 2014), the reported SSN exhibits statistically significant regime switches, departures from autoregressive stationarity, and growing trends. Reconstruction of the SSN during the pre-MM and MM periods is performed using five novel statistical procedures in support of signal analysis. A Bayesian–Monte Carlo backcast technique is found to be most reliable and produces an SSN signal that meets the weak-stationarity requirement. The computed MM signal for this reconstruction does not show a "grand" minimum or even a "semi-grand" minimum.

Inferring depth-dependent plasma motions from surface observations using the DeepVel neural network

Benoit **Tremblay**1,2,3*, Jean-François Cossette3,4, Maria D. Kazachenko2,5, Paul Charbonneau3 and Alain Vincent3
J. Space Weather Space Clim. **2021**, 11, 9
https://www.swsc-journal.org/articles/swsc/pdf/2021/01/swsc200059.pdf
Coverage of plasma motions is limited to the line-of-sight component at the Sun's surface. Multiple tracking and inversion methods were developed to infer the transverse motions from observational data. Recently, the DeepVel neural network was trained with computations performed by numerical simulations of the solar photosphere to recover the missing transverse component at the surface and at two additional optical depths simultaneously from the surface white light intensity in the Quiet Sun. We argue that deep learning could provide additional spatial coverage to existing observations in the form of depth-dependent synthetic observations, i.e. estimates generated through the emulation of numerical simulations. We trained different versions of DeepVel using slices from numerical simulations of both the Quiet Sun and Active Region at various optical and geometrical depths in the solar atmosphere, photosphere and upper convection zone to establish the upper and lower limits at which the neural network can generate reliable synthetic observations of plasma motions from surface intensitygrams. Flow fields inferred in the photosphere and low chromosphere $\tau \in [0.1, 1)$ are comparable to inversions performed at the surface ($\tau \approx 1$) and are deemed to be suitable for use as synthetic estimates in data assimilation processes and data-driven simulations. This upper limit extends closer to the transition region ($\tau \approx 0.01$) in the Quiet Sun, but not for Active Regions. Subsurface flows inferred from surface intensitygrams fail to capture the small-scale features of turbulent convective motions as depth crosses a few hundred kilometers. We suggest that these reconstructions could be used as first estimates of a model's velocity vector in data assimilation processes to nowcast and forecast short term solar activity and space weather.

Inferring Plasma Flows at Granular and Supergranular Scales With a New Architecture for the DeepVel Neural Network

Benoit **Tremblay**, and Raphaël Attie
Front. Astron. Space Sci., **2020** |
https://doi.org/10.3389/fspas.2020.00025
The wealth of observational data available has been instrumental in investigating physical features relevant to solar granulation, supergranulation and Active Regions. Meanwhile, numerical models have attempted to bridge the gap between the physics of the solar interior and such observations. However, there are relevant physical quantities that can be modeled but that cannot be directly measured and must be inferred. For example, direct measurements of

plasma motions at the photosphere are limited to the line-of-sight component. Methods have consequently been developed to infer the transverse plasma motions from continuum images in the case of the Quiet Sun and magnetograms in the case of Active Regions. Correlation-based tracking methods calculate the optical flows by correlating series of images locally while other methods like “Coherent Structure Tracking” or “Balltracking” exploit the coherency of photospheric granules to track them and use the group motions of the granules as a proxy of the average plasma flows advecting them. Recently, neural network computing has been used in conjunction with numerical models of the Sun to be able to recover the full velocity vector in photospheric plasma from continuum images. We experiment with a new architecture for the DeepVel neural network which takes inspiration from the U-Net architecture. Simulation data of the Quiet Sun and Active Regions are then used to evaluate the response at granular and supergranular scales of the aforementioned method.

Reconstruction of Horizontal Plasma Motions at the Photosphere from Intensitygrams: A Comparison Between DeepVel, LCT, FLCT, and CST

Benoit **Tremblay**, Thierry Roudier, Michel Rieutord, Alain Vincent
Solar Physics April **2018**, 293:57
https://link.springer.com/content/pdf/10.1007%2Fs11207-018-1276-7.pdf
Direct measurements of plasma motions in the photosphere are limited to the line-of-sight component of the velocity. Several algorithms have therefore been developed to reconstruct the transverse components from observed continuum images or magnetograms. We compare the space and time averages of horizontal velocity fields in the photosphere inferred from pairs of consecutive intensitygrams by the LCT, FLCT, and CST methods and the DeepVel neural network in order to identify the method that is best suited for generating synthetic observations to be used for data assimilation. The Stein and Nordlund (Astrophys. J. Lett.753, L13, 2012) magnetoconvection simulation is used to generate synthetic SDO/HMI intensitygrams and reference flows to train DeepVel. Inferred velocity fields show that DeepVel performs best at subgranular and granular scales and is second only to FLCT at mesogranular and supergranular scales.

Sensitivity of Global Oscillation Frequencies to Solar Activity on Short Timescales

Sushanta C. **Tripathy**1 and Kiran Jain1
2024 Res. Notes AAS 8 264
https://iopscience.iop.org/article/10.3847/2515-5172/ad85e8
Sun's oscillations frequencies vary with the changing magnetic activity and hold a strong positive correlation. While most of the analysis for global modes have been carried out using time series longer than a solar rotation, only a few studies are available showing their variation on shorter timescales. Using Doppler observations from Global Oscillation Network Group during the period 1995–2024, we analyze oscillation frequencies computed on a timescale of nine days and compare them with those obtained from 108 days. We also study their sensitivity in cycles 23 and 24 to the change in solar activity as represented by the 10.7 cm radio flux.

Probing the Sun's Near Surface Shear Layer using HMI Spherical Harmonic Coefficients

Sushanta C. **Tripathy**, Kiran Jain, Shukurijon Kholikov, Rudolf Komm
Proceedings of the IAU Symposium 365 - Dynamics of Solar and Stellar Convection Zones and Atmospheres, 2023 August 21-25, Yerevan, Armenia **2023**
https://arxiv.org/pdf/2312.11699.pdf
We have measured zonal and meridional components of subsurface flows up to a depth of 30 Mm below the solar surface by applying the technique of ring diagram on Dopplergrams which are constructed from the spherical harmonic (SH) coefficients. The SH coefficients are obtained from the Helioseismic and Magnetic Imager (HMI) full-disk Dopplergrams. We find a good agreement and some differences between the flows obtained in this study with those from the traditional methods using direct Dopplergrams.

Improving the Understanding of Subsurface Structure and Dynamics of Solar Active Regions

S. C. **Tripathy**, K. Jain, D. Braun, P. Cally, M. Dikpati, T. Felipe, R. Jain, S. Kholikov, E. Khomenko, R. Komm, J. Leibacher, V. Martinez-Pillet, A. Pevtsov, S.P. Rajaguru, M. Roth, H. Uitenbroek, J. Zhao
A white paper submitted to the decadal survey for solar and space Physics (Heliophysics) -- SSPH 2024-2033 **2023**
https://arxiv.org/ftp/arxiv/papers/2305/2305.07585.pdf
The goal of helioseismology is to provide accurate information about the Sun's interior from the observations of the wave field at its surface. In the last three decades, both global and local helioseismology studies have made significant advances and breakthroughs in solar physics. However, 3-d mapping of the structure and dynamics of sunspots and active regions below the surface has been a challenging task and are among the longest standing and intriguing puzzles of solar physics due to the complexity of the turbulent and dynamic nature of sunspots. Thus the key problems that need to be addressed during the next decade are: (i) Understanding the wave excitation

mechanisms in the quiet Sun and magnetic regions, (ii) Characterizing the wave propagation and transformation in strong and inclined magnetic field regions and understanding the magnetic portals in the chromosphere, (iii) Improving helioseismology techniques and investigating the whole life cycle of active regions, from magnetic flux emergence to dissipation, and (iv) Detecting helioseismic signature of the magnetic flux of active regions before it becomes visible on the surface so as to provide warnings several days before the emergence. For a transformative progress on these problems require full disk, simultaneous Doppler and vector magnetic field measurements of the photosphere up to the chromosphere with a spatial resolution of about 2 arc-sec as well as large-scale radiative MHD simulations of the plasma dynamics from the sub-photosphere to the chromosphere.

Seismology of Active Regions: Current Status and Perspectives **Review**

Sushanta **Tripathy**

Front. Astron. Space Sci. 10: 1091777 **2023**.

doi: 10.3389/fspas.2023.1091777

https://www.frontiersin.org/articles/10.3389/fspas.2023.1091777/pdf

The goal of helioseismology is to provide accurate information about the Sun's interior from the observations of the wave field at its surface. In the last three decades, both global and local helioseismology studies have made significant advances and breakthroughs in solar physics. However, 3-d mapping of the structure and dynamics of sunspots and active regions below the surface has been a challenging task and is among the long standing and intriguing puzzles in solar physics due to the complexity of the turbulent and dynamic nature of magnetized regions. In this review, I present some of the recent results relevant for helioseismology of sunspots and active regions obtained from high resolution observations, forward modeling and numerical simulations.

Identification of Inertial Modes in the Solar Convection Zone

Santiago A. **Triana**1, Gustavo Guerrero2,3, Ankit Barik4, and Jérémy Rekier1,5

2022 ApJL 934 L4

https://iopscience.iop.org/article/10.3847/2041-8213/ac7dac/pdf

The observation of global acoustic waves (p modes) in the Sun has been key to unveiling its internal structure and dynamics. A different kind of wave, known as sectoral Rossby modes, has been observed and identified, which potentially opens the door to probing internal processes that are inaccessible through p-mode helioseismology. Yet another set of waves, appearing as retrograde-propagating, equatorially antisymmetric vorticity waves, has also been observed but their identification remained elusive. Here, through a numerical model implemented as an eigenvalue problem, we provide evidence supporting the identification of those waves as a class of inertial eigenmodes, distinct from the Rossby-mode class, with radial velocities comparable to the horizontal ones deep in the convective zone but still small compared to the horizontal velocities toward the surface. We also suggest that the signature of tesseral-like Rossby modes might be present in recent observational data.

The Aditya-L1 mission of ISRO

Durgesh **Tripathi**, D. Chakrabarty, B. Raghvendra Prasad, A. Nandi, A. N. Ramaprakash, Nigar Shaji, K. Sankarasubramanian, R. Satheesh Thampi, V. K. Yadav

The Era of Multi-Messenger Solar Physics Proceedings IAU Symposium No. 372, **2022** G. Cauzzi & A. Tritschler, eds.

https://arxiv.org/pdf/2212.13046.pdf

The Aditya-L1 is the first space-based solar observatory of the Indian Space Research Organization (ISRO). The spacecraft will carry seven payloads providing uninterrupted observations of the Sun from the first Lagrangian point. Aditya-L1 comprises four remote sensing instruments, {\it viz.} a coronagraph observing in visible and infrared, a full disk imager in Near Ultra-Violet (NUV), and two full-sun integrated spectrometers in soft X-ray and hard X-ray. In addition, there are three instruments for in-situ measurements, including a magnetometer, to study the magnetic field variations during energetic events. Aditya-L1 is truly a mission for multi-messenger solar astronomy from space that will provide comprehensive observations of the Sun across the electromagnetic spectrum and in-situ measurements in a broad range of energy, including magnetic field measurements at L1.

Coronal heating and solar wind formation in quiet Sun and coronal holes: a unified scenario

Durgesh **Tripathi**, V. N. Nived, Sami K Solanki

ApJ **908** 28 **2021**

https://arxiv.org/pdf/2011.09803.pdf

https://doi.org/10.3847/1538-4357/abcc6b

Coronal holes (CHs) are darker than quiet Sun (QS) when observed in coronal channels. This study aims to understand the similarities and differences between CHs and QS in the transition region using the

\ion{Si}{4}~1394~Å line recorded by the Interface Region Imaging Spectrograph (IRIS) by considering the distribution of magnetic field measured by the Helioseismic and Magnetic Imager (HMI) onboard the Solar Dynamics Observatory (SDO). We find that \ion{Si}{4} intensities obtained in CHs are lower than those obtained in QS for regions with identical magnetic flux densities. Moreover, the difference in intensities between CHs and QS increases with increasing magnetic flux. For the regions with equal magnetic flux density, QS line profiles are more redshifted than those measured in CHs. Moreover, the blue shifts measured in CHs show an increase with increasing magnetic flux density unlike in the QS. The non-thermal velocities in QS, as well as in CHs, show an increase with increasing magnetic flux. However, no significant difference was observed in QS and CHs, albeit a small deviation at small flux densities. Using these results, we propose a unified model for the heating of the corona in the QS and in CHs and the formation of the solar wind. **2014/07/24, 2014/07/26, 2015/10/14**

On the ratios of \ion{Si}{4} lines (λ1394/λ1403) in an emerging flux region

Durgesh **Tripathi**, V. N. Nived, Hiroaki Isobe, J.G. Doyle
ApJ **894** 128 **2020**
https://arxiv.org/pdf/2004.04530.pdf
https://doi.org/10.3847/1538-4357/ab8558
The resonance lines of \ion{Si}{4} formed at λ1394 and 1403 Å are the most critical for the diagnostics of the solar transition region in the observations of the Interface Region Imaging Spectrograph (IRIS). Studying the intensity ratios of these lines (1394Å/1403Å), which under optically thin condition is predicted to be two, helps us to diagnose the optical thickness of the plasma being observed. Here we study the evolution of the distribution of intensity ratios in 31 IRIS rasters recorded for four days during the emergence of an active region. We found that during the early phase of the development, the majority of the pixels show intensity ratios smaller than two. However, as the active region evolves, more and more pixels show the ratios closer to two. Besides, there are a substantial number of pixels with ratio values larger than 2. At the evolved stage of the active region, the pixels with ratios smaller than two were located on the periphery, whereas those with values larger than 2 were in the core. However, for quiet Sun regions, the obtained intensity ratios were close to two irrespective of the location on the disk. Our findings suggest that the \ion{Si}{4} lines observed in active regions are affected by the opacity during the early phase of the flux emergence. The results obtained here could have important implications for the modelling of the solar atmosphere, including the initial stage of the emergence of an active region as well as quiet Sun. **2018 May 22-25**

A Study of Acoustic Halos in Active Region NOAA 11330 using Multi-Height SDO Observations

S. C. **Tripathy**, K. Jain, S. Kholikov, F. Hill, S. P. Rajaguru, P. S. Cally
Advances in Space Research Volume 61, Issue 2, 15 January **2018**, Pages 691-704
https://arxiv.org/pdf/1711.01259.pdf
We analyze data from the Helioseismic Magnetic Imager (HMI) and the Atmospheric Imaging Assembly (AIA) instruments on board the Solar Dynamics Observatory (SDO) to characterize the spatio-temporal acoustic power distribution in active regions as a function of the height in the solar atmosphere. For this, we use Doppler velocity and continuum intensity observed using the magnetically sensitive line at 6173 \AA\ as well as intensity at 1600 \AA\ and 1700 \AA. We focus on the power enhancements seen around AR 11330 as a function of wave frequency, magnetic field strength, field inclination and observation height. We find that acoustic halos occur above the acoustic cutoff frequency and extends up to 10 mHz in HMI Doppler and AIA 1700 \AA\ observations. Halos are also found to be strong functions of magnetic field and their inclination angle. We further calculate and examine the spatially averaged relative phases and cross-coherence spectra and find different wave characteristics at different heights. **27-28 October 2011**

Variations in High Degree Acoustic Mode Frequencies of the Sun during Solar Cycle 23 and 24

S.C. **Tripathy**, K. Jain, F. Hill
ApJ **2015**
http://arxiv.org/pdf/1509.05474v1.pdf
We examine continuous measurements of the high-degree acoustic mode frequencies of the Sun covering the period from 2001 July to June 2014. These are obtained through the ring-diagram technique applied to the full-disk Doppler observations made by the Global Oscillation Network Group (GONG). The frequency shifts in the degree range of 180-1200 are correlated with different proxies of solar activity e.g. 10.7 cm radio flux, the International Sunspot Number and the strength of the local magnetic field. In general, a good agreement is found between the shifts and activity indices, and the correlation coefficients are found to be comparable with intermediate degree mode frequencies. Analyzing the frequency shifts separately for the two cycles, we find that cycle 24 is weaker than cycle 23. Since the magnetic activity is known to be different in the two hemisphere, for the first time, we compute the frequency shifts over the two hemispheres separately and find that the shifts also display hemispheric

asymmetry; the amplitude of shifts in the northern hemisphere peaked during late 2011, more than two years earlier than the south. We further correlate the hemispheric frequency shifts with the hemispheric sunspot number and mean magnetic activity index. Since the frequency shifts and the hemispheric activity indices are found to be significantly correlated, we suggest that the shifts be used as an indicator of hemispheric activity since not many indices are measured over the two hemispheres separately. We also investigate the variation at different latitudinal bands and conclude that the shifts in active latitudes correlate well with the local magnetic activity index.

On the Reflection of Torsional Alfvén Waves from the Solar Transition Region

Yuriy **Tsap** & Yulia Kopylova
Solar Physics volume 296, Article number: 5 (**2021**)
https://link.springer.com/content/pdf/10.1007/s11207-020-01753-6.pdf
On the basis of the two-layer model, we investigate the reflection of linear torsional Alfvén waves propagating in a thin magnetic flux tube from the solar transition region. As distinguished from Hollweg (Astrophys. J. 277, 392, 1984), the density jump across the transition region modeled by a sharp boundary is taken into account. A new expression for the determination of the reflection coefficient is proposed. Weakly damping Alfvén modes with periods from a few tens of seconds to a few minutes can quite effectively penetrate from the chromosphere to the corona and vice versa.

On the Description of Transverse Wave Propagation Along Thin Magnetic Flux Tubes

Yu.T.**Tsap**, A.V.Stepanov, Yu.G.Kopylova
Geomagnetism and Aeronomy, **2018**, V.58, N7, pp.942-946
https://arxiv.org/pdf/1904.03619.pdf
Two approaches are used for description of linear transverse (kink) modes excited in a vertical thin magnetic flux tube. First one is based on the elastic thread model (Spruit, 1981). The second one follows from the the Taylor and Laurent series expansions of wave variables with respect to the tube radius inside and outside of the magnetic flux tube (Lopin and Nagorny, 2013). It has been shown that the main reason of the discrepancy of these approaches is related to the phenomenological equation of plasma motion used in the former case. This suggests that results obtained on the basis of this equation should be revised.

Stratified Solar Photosphere: Hinode Observations and Phase Relationships

Y. T. **Tsap**, A. V. Stepanov, Y. G. Kopylova
Solar Phys. Volume 291, Issue 11, pp 3349–3356 **2016**
Based on the linearized magnetohydrodynamic (MHD) equations within the framework of the thin flux tube approximation, the phase relationships between the disturbed quantities of evanescent acoustic and slow sausage MHD modes excited in the adiabatically stratified solar atmosphere are considered. It has been shown that the sign of the phase differences (equal to \(\pm\pi/2\)) between the velocity and other disturbed quantities such as pressure, density, magnetic field, and temperature, depends on the wave frequency \(\omega\). The obtained phase relationships agree well with SOT/Hinode observations obtained by Fujimura and Tsuneta (Astrophys. J.702, 1443, 2009) when \(\omega\approx\omega_{\mathrm{c}}\), where \(\omega_{\mathrm{c}}\) is the cutoff frequency. The role of various modes excited in the solar atmosphere in the light of the chromospheric and coronal heating problems are discussed.

Frozen-In Magnetic Field Lines and Alfvén Wave Generation in Weakly Ionized Plasma

Y. T. **Tsap**, A. V. Stepanov, Y. G. Kopylova
Solar Phys. Volume 290, Issue 7, pp 1923-1929 **2015**
On the basis of the three-fluid approximation, we consider the generation of linear Alfvén waves with periods $\gtrsim 10^{-3}$ s in the collisional partially ionized plasma of the solar photosphere. The results obtained in previous work (Tsap, Stepanov, and Kopylova in Solar Phys. 270, 205, 2011) are generalized for the case of the arbitrary ratio between the initial velocities of ions and neutral atoms. We find that the ponderomotive force plays an important role during Alfvén wave excitation and propagation. Furthermore, the energy flux of Alfvén waves does not depend on the degree of the plasma ionization if the magnetic field lines are frozen into the charged particles. These modes can be effectively generated in the weakly ionized plasma of the solar photosphere.

Spectral Analysis of Solar and Geomagnetic Parameters in Relation to Cosmic-ray Intensity for the Time Period 1965 – 2018

M. **Tsichla** M. Gerontidou H. Mavromichalaki
Solar Physics January **2019**, 294:15
sci-hub.tw/10.1007/s11207-019-1403-0

https://link.springer.com/content/pdf/10.1007%2Fs11207-019-1403-0.pdf
Spectral analysis of solar and geomagnetic parameters as well as of cosmic-ray intensity was performed aiming to identify possible new periodicities and confirm the well-known ones. Specifically, short-, mid-, and long-term periodicities of these parameters such as sunspot number, Bz-component of the interplanetary magnetic field, geomagnetic Ap index, and cosmic-ray intensity over the time period 1965 – 2018, covering five solar cycles from Cycles 20 to 24, are presented. For this purpose, two different techniques, fast Fourier transformation and wavelet analysis, have been used in order to ensure accuracy in the frequency values and also their localization in the time series. The periodicities resulting from our comprehensive study, including the well-known 11-year and 27-day periods, the harmonics of the 5.5-year and of the 6-, 9-, and 13.9-day periods, respectively, and the ≈ 1.3-year and 1.7-year periods, were found in all of the above parameters except for the Bz-component of the interplanetary magnetic field. New periodicities such as the ≈ 10-month period for sunspot number and cosmic-ray intensity and the ≈ 3-year period for sunspot number, Ap index, and cosmic-ray intensity, were also determined. Furthermore, the newly introduced splitting of the 27-day periodicity into two adjacent peaks was confirmed in the Fourier spectra of the interplanetary magnetic field and the geomagnetic Ap index. It was concluded that several common periodicities appear in solar activity: the Ap index, and the cosmic-ray intensity. This result, in association with the fact that the spectral behavior of geomagnetic-activity parameters, provides invaluable information about the physical processes involved, and indicates that the Ap index might be used as a suitable index for space-weather forecasting.

Electron plasma wake field acceleration in solar coronal and chromospheric plasmas

David **Tsiklauri**
Phys. Plasmas **2017**
https://arxiv.org/pdf/1706.05265.pdf
Three dimensional, particle-in-cell, fully electromagnetic simulations of electron plasma wake field acceleration applicable to solar atmosphere are presented. It is established that injecting driving and trailing electron bunches into solar coronal and chromospheric plasmas, results in electric fields (-(20-5)?106 V/m), leading to acceleration of the trailing bunch up to 52 MeV, starting from initial 36 MeV. The results provide one of potentially important mechanisms for the extreme energetic solar flare electrons, invoking plasma wake field acceleration.

Alfvén wave phase mixing in flows -- why over-dense solar coronal open magnetic field structures are cool?

D. **Tsiklauri**
MNRAS **2015**
http://arxiv.org/pdf/1507.05293v1.pdf
Our magnetohydrodynamic (MHD) simulations and analytical calculations show that, when a background flow is present, mathematical expressions for the Alfv\'en wave (AW) damping via phase mixing are modified by a following substitution C′A(x)→C′A(x)+V′0(x), where CA and V0 are AW phase and the flow speeds and prime denotes derivative in the direction across the background magnetic field. In uniform magnetic field and over-dense plasma structures, in which CA is smaller compared to surrounding plasma, the flow, that is confined to the structure, in the same direction as the AW, reduces the effect of phase mixing, because on the edges of the structure C′A and V′0 have opposite sign. Thus, the wave damps via phase mixing {\it slower} compared to the case without the flow. This is the consequence of the co-directional flow reducing the wave front stretching in the transverse direction. Although, the result is generic and is applicable to different laboratory or astrophysical plasma systems, we apply our finding to address the question why over-dense solar coronal open magnetic field structures (OMFS) are cooler than the background plasma. Observations show that the over-dense OMFS (e.g. solar coronal polar plumes) are cooler than surrounding plasma and that in these structures Doppler broadening of lines is consistent with bulk plasma motions, such as Alfv\'en waves (AW). If over-dense solar coronal OMFS are heated by AW damping via phase mixing, we conjecture that, co-directional with AW, plasma flow in them, reduces the phase mixing induced heating, thus providing an explanation why they appear cooler than the background.

Solar Fine-Scale Structures. I. Spicules and Other Small-Scale, Jet-Like Events at the Chromospheric Level: Observations and Physical Parameters **Review**

G. **Tsiropoula**, K. Tziotziou, I. Kontogiannis, M. S. Madjarska, J. G. Doyle and Y. Suematsu
Space Science Reviews, Volume 169, Numbers 1-4 (**2012**), 181-244,
Over the last two decades the uninterrupted, high resolution observations of the Sun, from the excellent range of telescopes aboard many spacecraft complemented with observations from sophisticated ground-based telescopes have opened up a new world producing significantly more complete information on the physical conditions of the solar atmosphere than before. The interface between the lower solar atmosphere where energy is generated by

subsurface convection and the corona comprises the chromosphere, which is dominated by jet-like, dynamic structures, called mottles when found in quiet regions, fibrils when found in active regions and spicules when observed at the solar limb. Recently, space observations with Hinode have led to the suggestion that there should exist two different types of spicules called Type I and Type II which have different properties. Ground-based observations in the Ca ii H and K filtergrams reveal the existence of long, thin emission features called straws in observations close to the limb, and a class of short-lived events called rapid blue-shifted excursions characterized by large Doppler shifts that appear only in the blue wing of the Ca ii infrared line. It has been suggested that the key to understanding how the solar plasma is accelerated and heated may well be found in the studies of these jet-like, dynamic events. However, while these structures are observed and studied for more than 130 years in the visible, but also in the UV and EUV emission lines and continua, there are still many questions to be answered. Thus, despite their importance and a multitude of observations performed and theoretical models proposed, questions regarding their origin, how they are formed, their physical parameters, their association with the underlying photospheric magnetic field, how they appear in the different spectral lines, and the interrelationship between structures observed in quiet and active regions on the disk and at the limb, as well as their role in global processes has not yet received definitive answers. In addition, how they affect the coronal heating and solar wind need to be further explored. In this review we present observations and physical properties of small-scale jet-like chromospheric events observed in active and quiet regions, on the disk and at the limb and discuss their interrelationship.

Space Plasma Physics: A Review

Bruce T. **Tsurutani** , Gary P. Zank , Veerle J. Sterken , Kazunari Shibata , Tsugunobu Nagai , Anthony J. Mannucci , David M. Malaspina , Gurbax S. Lakhina , Shrikanth G. Kanekal , Keisuke Hosokawa , Richard B. Horne , Rajkumar Hajra , Karl-Heinz Glassmeier , C. Trevor Gaunt , Peng-Fei Chen , and Syun-Ichi Akasofu

IEEE TRANSACTIONS ON PLASMA SCIENCE, VOL. 51, NO. 7, JULY **2023**

https://ieeexplore.ieee.org/stamp/stamp.jsp

Owing to the ever-present solar wind, our vast solar system is full of plasmas. The turbulent solar wind, together with sporadic solar eruptions, introduces various space plasma processes and phenomena in the solar atmosphere all the way to Earth's ionosphere and atmosphere and outward to interact with the interstellar media to form the heliopause and termination shock. Remarkable progress has been made in space plasma physics in the last 65 years, mainly due to sophisticated in situ measurements of plasmas, plasma waves, neutral particles, energetic particles, and dust via space-borne satellite instrumentation. Additionally, high-technology groundbased instrumentation has led to new and greater knowledge of solar and auroral features. As a result, a new branch of space physics, i.e., space weather, has emerged since many of the space physics processes have a direct or indirect influence on humankind. After briefly reviewing the major space physics discoveries before rockets and satellites (Section I), we aim to review all our updated understanding on coronal holes, solar flares, and coronal mass ejections, which are central to space weather events at Earth (Section II), solar wind (Section III), storms and substorms (Section IV), magnetotail and substorms, emphasizing the role of the magnetotail in substorm dynamics (Section V), radiation belts/energetic magnetospheric particles (Section VI), structures and space weather dynamics in the ionosphere (Section VII), plasma waves, instabilities, and waveparticle interactions (Section VIII), long-period geomagnetic pulsations (Section IX), auroras (Section X), geomagnetically induced currents (GICs, Section XI), planetary magnetospheres and solar/stellar wind interactions with comets, moons and asteroids (Section XII), interplanetary discontinuities, shocks and waves (Section XIII), interplanetary dust (Section XIV), space dusty plasmas (Section XV), and solar energetic particles and shocks, including the heliospheric termination shock (Section XVI). This article is aimed to provide a panoramic view of space physics and space weather.

A Study of Alfvén Wave Propagation and Heating the Chromosphere

Jiannan **Tu** and Paul Song

2013 ApJ 777 53

Alfvén wave propagation, reflection, and heating of the chromosphere are studied for a one-dimensional solar atmosphere by self-consistently solving plasma, neutral fluid, and Maxwell's equations with incorporation of the Hall effect and strong electron-neutral, electron-ion, and ion-neutral collisions. We have developed a numerical model based on an implicit backward difference formula of second-order accuracy both in time and space to solve stiff governing equations resulting from strong inter-species collisions. A non-reflecting boundary condition is applied to the top boundary so that the wave reflection within the simulation domain can be unambiguously determined. It is shown that due to the density gradient the Alfvén waves are partially reflected throughout the chromosphere and more strongly at higher altitudes with the strongest reflection at the transition region. The waves are damped in the lower chromosphere dominantly through Joule dissipation, producing heating strong enough to balance the radiative loss for the quiet chromosphere without invoking anomalous processes or turbulences. The heating rates are larger for weaker background magnetic fields below ~500 km with higher-frequency waves subject to heavier damping. There is an upper cutoff frequency, depending on the background magnetic field, above which the waves are completely damped. At the frequencies below which the waves are not strongly damped, the

interaction of reflected waves with the upward propagating waves produces power at their double frequencies, which leads to more damping. The wave energy flux transmitted to the corona is one order of magnitude smaller than that of the driving source.

Solar neutrinos, helioseismology and the solar internal dynamics REVIEW

Sylvaine **Turck-Chièze**1 and Sébastien Couvidat

2011 Rep. Prog. Phys. 74 086901 doi:10.1088/0034-4885/74/8/086901

Neutrinos are fundamental particles ubiquitous in the Universe and whose properties remain elusive despite more than 50 years of intense research activity. This review illustrates the importance of solar neutrinos in astrophysics, nuclear physics and particle physics. After a description of the historical context, we remind the reader of the noticeable properties of these particles and of the stakes of the solar neutrino puzzle. The standard solar model triggered persistent efforts in fundamental physics to predict the solar neutrino fluxes, and its constantly evolving predictions have been regularly compared with the detected neutrino signals. Anticipating that this standard model could not reproduce the internal solar dynamics, a seismic solar model was developed which enriched theoretical neutrino flux predictions with in situ observation of acoustic and gravity waves propagating in the Sun. This seismic model contributed to the stabilization of the neutrino flux predictions. This review recalls the main historical steps, from the pioneering Homestake mine experiment and the GALLEX-SAGE experiments capturing the first proton–proton neutrinos. It emphasizes the importance of the SuperKamiokande and SNO detectors. Both experiments demonstrated that the solar-emitted electron neutrinos are partially transformed into other neutrino flavors before reaching the Earth. This sustained experimental effort opens the door to neutrino astronomy, with long-base lines and underground detectors. The success of BOREXINO in detecting the 7Be neutrino signal alone instills confidence in physicists' ability to detect each neutrino source separately. It justifies the building of a new generation of detectors to measure the entire solar neutrino spectrum in greater detail, as well as supernova neutrinos. A coherent picture has emerged from neutrino physics and helioseismology. Today, new paradigms take shape in these two fields: neutrinos are massive particles, but their masses are still unknown, and the research on the solar interior focuses on the dynamical aspects and on the signature of dark matter. The magnetic moment of the neutrino begins to be an actor in stellar evolution. The third part of the review is dedicated to this prospect. The understanding of the crucial role of both rotation and magnetism in solar physics benefits from SoHO, SDO and PICARD space observations, and from a new prototype, GOLF-NG. The magnetohydrodynamical view of the solar interior is a new way of understanding the impact of the Sun on the Earth's environment and climate. For now, the particle and stellar challenges seem decoupled, but this is only a superficial appearance. The development of asteroseismology—with the COROT and KEPLER spacecraft—and of neutrino physics will both contribute to improvements in our understanding of, for instance, supernova explosions. This shows the far-reaching impact of neutrino and stellar astronomy.

Stochastic Modelling, Analysis, and Simulations of the Solar Cycle Dynamic Process

Douglas C. **Turner**1 and Gangaram S. Ladde2

2018 ApJ 855 108

http://iopscience.iop.org/article/10.3847/1538-4357/aaaf1c

Analytical solutions, discretization schemes and simulation results are presented for the time delay deterministic differential equation model of the solar dynamo presented by Wilmot-Smith et al. In addition, this model is extended under stochastic Gaussian white noise parametric fluctuations. The introduction of stochastic fluctuations incorporates variables affecting the dynamo process in the solar interior, estimation error of parameters, and uncertainty of the α-effect mechanism. Simulation results are presented and analyzed to exhibit the effects of stochastic parametric volatility-dependent perturbations. The results generalize and extend the work of Hazra et al. In fact, some of these results exhibit the oscillatory dynamic behavior generated by the stochastic parametric additative perturbations in the absence of time delay. In addition, the simulation results of the modified stochastic models influence the change in behavior of the very recently developed stochastic model of Hazra et al.

Solar Cycle Slow to Get Going: What Does It Mean for Space Weather?

Turner, Ronald

Space Weather, Vol. 9, No. 4, S04004, **2011**

If you have the sense that the current solar cycle has been slow to build up, maybe it is more than just the “watched pot” failing to boil. A comparison with previous sunspot cycles shows that the current cycle is among the slowest-growing cycles characterized with good historical data. Figure 1 shows the smoothed sunspot number for the period from 2 years before the minimum to 2 years after it for the 24 numbered solar cycles (cycle 1 started in 1755; we are just now entering cycle 24). It illustrates the historically slow increase of the current cycle (shown in red) as of February 2011. Three of the four cycles with slower increases (shown in blue) were during the Dalton Minimum in the early nineteenth century. The fourth is the period leading into cycle 1. The red dots in the figure are cycle 24 monthly average sunspot numbers; these data are too recent to be adjusted by the smoothing algorithm that includes

the influence of monthly averages within 6 months of the smoothed value. Also shown, at the bottom of the figure, for context, are the sunspot data for the first 23 cycles, which also identify the Dalton Minimum.

Vortex Motions in the Solar Atmosphere **Review**

Definitions, Theory, Observations, and Modelling

K. **Tziotziou**, E. Scullion, S. Shelyag, O. Steiner, E. Khomenko, +++

Space Science Reviews volume 219, Article number: 1 (**2023**)

https://link.springer.com/content/pdf/10.1007/s11214-022-00946-8.pdf

Vortex flows, related to solar convective turbulent dynamics at granular scales and their interplay with magnetic fields within intergranular lanes, occur abundantly on the solar surface and in the atmosphere above. Their presence is revealed in high-resolution and high-cadence solar observations from the ground and from space and with state-of-the-art magnetoconvection simulations. Vortical flows exhibit complex characteristics and dynamics, excite a wide range of different waves, and couple different layers of the solar atmosphere, which facilitates the channeling and transfer of mass, momentum and energy from the solar surface up to the low corona. Here we provide a comprehensive review of documented research and new developments in theory, observations, and modelling of vortices over the past couple of decades after their observational discovery, including recent observations in Hα, innovative detection techniques, diverse hydrostatic modelling of waves and forefront magnetohydrodynamic simulations incorporating effects of a non-ideal plasma. It is the first systematic overview of solar vortex flows at granular scales, a field with a plethora of names for phenomena that exhibit similarities and differences and often interconnect and rely on the same physics. With the advent of the 4-m Daniel K. Inouye Solar Telescope and the forthcoming European Solar Telescope, the ongoing Solar Orbiter mission, and the development of cutting-edge simulations, this review timely addresses the state-of-the-art on vortex flows and outlines both theoretical and observational future research directions.

A persistent quiet-Sun small-scale tornado III. Waves

Kostas **Tziotziou**, Georgia Tsiropoula, Ioannis Kontogiannis

A&A 643, A166 **2020**

https://arxiv.org/pdf/2010.06327.pdf

https://doi.org/10.1051/0004-6361/202038951

Vortex flows can foster a variety of wave modes. A recent oscillatory analysis of a persistent 1.7 h vortex flow with a significant substructure has suggested the existence of various types of waves within it. We investigate the nature and characteristics of waves within this quiet-Sun vortex flow to better understand its physics and dynamics. We used a cross-wavelet spectral analysis between pairs of Ha and Ca II 8542 intensity time series at different wavelengths and, hence, atmospheric heights, acquired with CRISP/SST, as well as the derived Ha Doppler velocity and full width at half maximum (FWHM) time series. We constructed halftone frequency-phase difference plots and investigated the existence and propagation characteristics of different wave modes. Our analysis suggests the existence of upwards propagating Alfvenic type waves with phase speeds of ~20-30 km/s. The dominant wave mode seems to be the fast kink wave mode; however, our analysis also suggests the existence of localised Alfvenic torsional waves related to the dynamics of individual chromospheric swirls that characterise the substructure of the vortex flow. The Ha V-I phase difference analysis seems to imply the existence of a standing wave pattern possibly arising from the interference of upwards propagating kink waves with downwards propagating ones that are reflected at the transition region or the corona. Moreover, the results provide further evidence that the central chromospheric swirl drives the dynamics of the vortex flow. This is the first exhaustive phase difference analysis within a vortex flow that explores the nature and dynamics of different wave modes within it. The questions, however, of whether, and how, the dissipation of the derived wave modes occurs and if vortex flows ultimately play a role in the energy budget of the upper layers of the solar atmosphere remain open.

A persistent quiet-Sun small-scale tornado. II. Oscillations

K. **Tziotziou**, G. Tsiropoula, I. Kontogiannis

A&A 623, A160 **2019**

https://arxiv.org/pdf/1903.04796.pdf

https://www.aanda.org/articles/aa/pdf/2019/03/aa34679-18.pdf

Recently, the characteristics, and dynamics of a persistent 1.7 h vortex flow, resembling a small-scale tornado, have been investigated with ground-base and space-based observations and for the first time in the Ha line centre. The vortex flow showed significant substructure in the form of several intermittent chromospheric swirls.

We investigate the oscillatory behaviour of various physical parameters in the vortex area, with a 2D wavelet analysis performed within the vortex flow area and in a quiet-Sun region (for comparison), using the same high spatial and temporal resolution Ha and Ca II 8542 CRISP observations, as well as Doppler velocities and FWHM derived from the Ha line profiles.

The vortex flow shows significant oscillatory power in the 3-5 min range that peaks around 4 min and behaves

differently than the reference quiet-Sun region. Oscillations reflect the cumulative action of different components such as swaying motions, rotation, and waves. The derived swaying motion periods are in the range of 200-220 s, and the rotation periods are ~270 s for Ha and ~215 s for Ca II. Periods increase with atmospheric height and seem to decrease with radial distance from the vortex centre, suggesting a deviation from a rigid rotation. The behaviour of power within the vortex flow as a function of period and height implies the existence of evanescent waves and the excitation of different types of waves, such as magnetoacoustic (e.g. kink) or Alfven waves.
The vortex flow seems to be dominated by two motions: a transverse (swaying) motion, and a rotational motion while oscillations point to the propagation of waves within it. Nearby fibril-like flows could play an important role in the rotational modulation of the vortex flow. Indirect evidence exists that the structure is magnetically supported while the central swirl seems to be acting as a "central engine" to the vortex flow. **June 7, 2014**

A persistent quiet-Sun small-scale tornado
I. Characteristics and dynamics⋆

K. **Tziotziou**1, G. Tsiropoula1, I. Kontogiannis2, E. Scullion3 and J. G. Doyle
A&A 618, A51 (**2018**)
https://www.aanda.org/articles/aa/pdf/2018/10/aa33101-18.pdf
Context. Vortex flows have been extensively observed over a wide range of spatial and temporal scales in different spectral lines, and thus layers of the solar atmosphere, and have been widely found in numerical simulations. However, signatures of vortex flows have only recently been reported in the wings of the Hα, but never so far in the Hα line centre.
Aims. We investigate the appearance, characteristics, substructure, and dynamics of a 1.7 h persistent vortex flow observed from the ground and from space in a quiet-Sun region in several lines/channels covering all atmospheric layers from the photosphere up to the low corona.
Methods. We use high spatial and temporal resolution CRisp Imaging SpectroPolarimeter (CRISP) observations in several wavelengths along the Hα and Ca II 8542 Å line profiles, simultaneous Atmospheric Imaging Assembly (AIA) observations in several Ultraviolet (UV) and Extreme ultraviolet (EUV) channels and Helioseismic and Magnetic Imager (HMI) magnetograms to study a persistent vortex flow located at the south solar hemisphere. Doppler velocities were derived from the Hα line profiles. Our analysis involves visual inspection and comparison of all available simultaneous/near-simultaneous observations and detailed investigation of the vortex appearance, characteristics and dynamics using time slices along linear and circular slits.
Results. The most important characteristic of the analysed clockwise rotating vortex flow is its long duration (at least 1.7 h) and its large radius (~3″). The vortex flow shows different behaviours in the different wavelengths along the Hα and Ca II 8542 Å profiles reflecting the different formation heights and mechanisms of the two lines. Ground-based observations combined with AIA observations reveal the existence of a funnel-like structure expanding with height, possibly rotating rigidly or quasi-rigidly. However, there is no clear evidence that the flow is magnetically driven as no associated magnetic bright points have been observed in the photosphere. Hα and Ca II 8542 Å observations also reveal significant substructure within the flow, manifested as several individual intermittent chromospheric swirls with typical sizes and durations. They also exhibit a wide range of morphological patterns, appearing as dark absorbing features, associated mostly with mean upwards velocities around 3 km s−1 and up to 8 km s−1, and occupying on average ~25% of the total vortex area. The radial expansion of the spiral flow occurs with a mean velocity of ~3 km s−1, while its dynamics can be related to the dynamics of a clockwise rigidly rotating logarithmic spiral with a swinging motion that is, however, highly perturbed by nearby flows associated with fibril-like structures. A first rough estimate of the rotational period of the vortex falls in the range of 200–300 s.
Conclusions. The vortex flow resembles a small-scale tornado in contrast to previously reported short-lived swirls and in analogy to persistent giant tornadoes. It is unclear whether the observed substructure is indeed due to the physical presence of individual intermittent, recurring swirls or a manifestation of wave-related instabilities within a large vortex flow. Moreover, we cannot conclusively demonstrate that the long duration of the observed vortex is the result of a central swirl acting as an “engine” for the vortex flow, although there is significant supporting evidence inferred from its dynamics. It also cannot be excluded that this persistent vortex results from the combined action of several individual smaller swirls further assisted by nearby flows or that this is a new case in the literature of a hydrodynamically driven vortex flow**. June 7, 2014**

SITCoM: SiRGraF Integrated Tool for Coronal dynaMics

Purvi **Udhwani**, Arpit Kumar Shrivastav, Ritesh Patel
Frontiers in Astronomy and Space Sciences 10:1227872 **2023**
https://arxiv.org/pdf/2308.04647.pdf
https://www.frontiersin.org/articles/10.3389/fspas.2023.1227872/pdf
SiRGraF Integrated Tool for Coronal dynaMics (SITCoM) is based on Simple Radial Gradient Filter (SiRGraF) used to filter the radial gradient in the white-light coronagraph images and bring out dynamic structures. SITCoM has been developed in **Python** and integrated with SunPy and can be installed by users with the command pip install sitcom. This enables the user to pass the white-light coronagraph data to the tool and generate radially filtered output with an option to save in various formats as required. We have implemented the functionality of tracking the

transients such as coronal mass ejections (CMEs), outflows, plasma blobs, etc., using height-time plots and deriving their kinematics. In addition, SITCoM also supports oscillation and waves studies such as for streamer waves. This is done by creating a distance-time plot at a user-defined location (artificial slice) and fitting a sinusoidal function to derive the properties of waves, such as time period, amplitude, and damping time (if any). We provide the provision to manually or automatically select the data points to be used for fitting. SITCoM is a tool to analyze some properties of coronal dynamics quickly. We present an overview of the SITCoM with the applications for deriving coronal dynamics' kinematics and oscillation properties. We discuss the limitations of this tool along with prospects for future improvement. **2001-01-07, 06 July 2004, 2005-10-12, 2010-08-01, 2017-09-10, 29 August 2022**

The Magnetic Properties of Heating Events on High-Temperature Active Region Loops

Ignacio **Ugarte-Urra**, Nicholas A. Crump, Harry P. Warren, Thomas Wiegelmann
ApJ **2019**
https://arxiv.org/pdf/1904.11976.pdf
Understanding the relationship between the magnetic field and coronal heating is one of the central problems of solar physics. However, studies of the magnetic properties of impulsively heated loops have been rare. We present results from a study of 34 evolving coronal loops observed in the Fe XVIII line component of AIA/SDO 94 A filter images from three active regions with different magnetic conditions. We show that the peak intensity per unit cross-section of the loops depends on their individual magnetic and geometric properties. The intensity scales proportionally to the average field strength along the loop (Bavg) and inversely with the loop length (L) for a combined dependence of (Bavg/L)0.52±0.13. These loop properties are inferred from magnetic extrapolations of the photospheric HMI/SDO line-of-sight and vector magnetic field in three approximations: potential and two Non Linear Force-Free (NLFF) methods. Through hydrodynamic modeling (EBTEL model) we show that this behavior is compatible with impulsively heated loops with a volumetric heating rate that scales as $\epsilon H \sim B0.3\pm0.2 avg/L0.2\pm0.20.1$. **2011/02/12, 2011/04/15, 2011/11/08**

Modeling Coronal Response in Decaying Active Regions with Magnetic Flux Transport and Steady Heating

Ignacio **Ugarte-Urra**, Harry P. Warren, Lisa A. Upton, Peter R. Young
ApJ **846** 165 **2017**
https://arxiv.org/pdf/1708.04324.pdf
We present new measurements of the dependence of the Extreme Ultraviolet radiance on the total magnetic flux in active regions as obtained from the Atmospheric Imaging Assembly (AIA) and the Helioseismic and Magnetic Imager on board the Solar Dynamics Observatory (SDO). Using observations of nine active regions tracked along different stages of evolution, we extend the known radiance - magnetic flux power-law relationship ($I \propto \Phi\alpha$) to the AIA 335 \AA\ passband, and the Fe XVIII 93.93 \AA\ spectral line in the 94 \AA\ passband. We find that the total unsigned magnetic flux divided by the polarity separation (Φ/D) is a better indicator of radiance for the Fe XVIII line with a slope of $\alpha=3.22\pm0.03$. We then use these results to test our current understanding of magnetic flux evolution and coronal heating. We use magnetograms from the simulated decay of these active regions produced by the Advective Flux Transport (AFT) model as boundary conditions for potential extrapolations of the magnetic field in the corona. We then model the hydrodynamics of each individual field line with the Enthalpy-based Thermal Evolution of Loops (EBTEL) model with steady heating scaled as the ratio of the average field strength and the length ($\bar{B}/L$) and render the Fe XVIII and 335 \AA\ emission. We find that steady heating is able to partially reproduce the magnitudes and slopes of the EUV radiance - magnetic flux relationships and discuss how impulsive heating can help reconcile the discrepancies. This study demonstrates that combined models of magnetic flux transport, magnetic topology and heating can yield realistic estimates for the decay of active region radiances with time. **2013/05-12 – 06-10**

Full Sun monochromatic images

Ignacio **Ugarte-Urra** and Harry Warren
Hinode EIS science nugget 28 Feb **2011**
http://msslxr.mssl.ucl.ac.uk:8080/SolarB/eisnuggets.jsp
While X-ray and EUV imagers take images at a cadence close to the characteristic evolutionary timescales of solar phenomena, narrow slit spectroscopy is better suited for many plasma diagnostics. This improvement in our ability to measure the properties of solar plasmas, however, is often achieved at the expense of longer exposure times and a slower cadence. Wide slit spectroscopy ("overlapograms") is a compromise between both worlds as it produces images of over a relatively large field-of-view in bands as narrow as a single spectral line.
February 2, 2010; December 04, 2010; 2010.11.16

Photospheric Velocities Measured at Mt. Wilson Show Zonal and Sectoral Flows Compose the Torsional Oscillations

Roger K. **Ulrich**, Tham Tran, John Boyden
Solar Phys. 298, Article number: 123 **2023**
https://arxiv.org/pdf/2307.06387
https://link.springer.com/content/pdf/10.1007/s11207-023-02215-5.pdf
The methods for reducing the observations from the 150-foot Tower Telescope on Mt.~Wilson are reviewed and a new method for determining the North/South (sectoral) and the East/West (zonal) velocity components is described and applied. Due to a calibration problem with the data prior to 1983, only observations between 1983 and 2013 are presented at this time. After subtraction of latitude dependent averages over the 30-year period of observation the residual deviations in the sectoral and zonal flow velocities are well synchronized and correspond to what is widely recognized as the Torsional Oscillations. Both flow components need to be included in any model that replicates the Torsional Oscillations.

Heating and dynamics of the Solar atmosphere **Thesis**

Vishal **Upendran**
Thesis presented to IUCAA and JNU **2023**.
https://arxiv.org/pdf/2304.01553
The solar atmosphere shows anomalous variation in temperature, starting from the 5500 K photosphere to the million-degree Kelvin corona. The corona itself expands into the interstellar medium as the free streaming solar wind, which modulates and impacts the near-Earth space weather. The precise source regions of different structures in the solar wind, their formation height, and the heating of the solar atmosphere are inextricably linked and unsolved problems in astrophysics. Observations suggest correlations between Coronal holes (CHs), which are cool, intensity deficit structures in the solar corona, with structures in the solar wind. Observations also suggest the local plasma heating in the corona through power-law distributed impulsive events. In this thesis, we use narrowband photometric, spectroscopic, and disc-integrated emission of the solar atmosphere ranging from Near Ultraviolet to X-rays along with in-situ solar wind measurements to understand (i). the source regions of the solar wind, (ii). the underlying mechanism of solar coronal heating, and (iii). the differentiation in dynamics of CHs with the background Quiet Sun (QS) regions, which do not show any significant signature of the solar wind. We leverage machine learning and numerical modeling tools to develop solar wind forecasting codes using interpretable AI, inversion codes to infer the properties of impulsive events and to understand the differences in the thermodynamics of CHs and QS regions. We finally present a unified scenario of solar wind emergence and heating in the solar atmosphere and discuss the implications of inferences from this thesis.

Nanoflare Heating of the Solar Corona Observed in X-rays

Vishal **Upendran**, Durgesh Tripathi, N.P.S. Mithun, Santosh Vadawale, Anil Bhardwaj
ApJ Letters **940** L38 **2022**
https://arxiv.org/pdf/2211.02324.pdf
https://iopscience.iop.org/article/10.3847/2041-8213/aca078/pdf
The existence of the million-degree corona above the cooler photosphere is an unsolved problem in astrophysics. Detailed study of quiescent corona that exists regardless of the phase of the solar cycle may provide fruitful hints towards resolving this conundrum. However, the properties of heating mechanisms can be obtained only statistically in these regions due to their unresolved nature. Here, we develop a two-step inversion scheme based on the machine learning scheme of Upendran & Tripathi (2021a) for the empirical impulsive heating model of Pauluhn & Solanki (2007), and apply it to disk integrated flux measurements of the quiet corona as measured by the X-ray solar monitor (XSM) onboard Chandrayaan - 2. We use data in three energy passbands, viz., 1 - 1.3 keV, 1.3 - 2.3 keV, and 1 - 2.3 keV, and estimate the typical impulsive event frequencies, timescales, amplitudes, and the distribution of amplitudes. We find that the impulsive events occur at a frequency of ≈25 events per minute with a typical lifetime of ≈10 minutes. They are characterized by a power law distribution with a slope $\alpha \leq 2.0$. The typical amplitudes of these events lie in an energy range of 1021 - 1024 ergs, with a typical radiative loss of about ≈103 erg cm−2 s−1 in the energy range of 1 - 2.3 keV. These results provide further constraints on the properties of sub-pixel impulsive events in maintaining the quiet solar corona.

On the formation of solar wind & switchbacks, and quiet Sun heating

Vishal **Upendran** (1), Durgesh Tripathi (1)
ApJ **2021**
https://arxiv.org/pdf/2111.11668.pdf
The solar coronal heating in quiet Sun (QS) and coronal holes (CH), including solar wind formation, are intimately tied by magnetic field dynamics. Thus, a detailed comparative study of these regions is needed to understand the underlying physical processes. CHs are known to have subdued intensity and larger blueshifts in the corona. This

work investigates the similarities and differences between CHs and QS in the chromosphere using the Mg II h & k, C II lines, and transition region using Si IV line, for regions with identical absolute magnetic flux density (|B|). We find CHs to have subdued intensity in all the ines, with the difference increasing with line formation height and |B|. The chromospheric lines show excess upflows and downflows in CH, while Si IV shows excess upflows (downflows) in CHs (QS), where the flows increase with |B|. We further demonstrate that the upflows (downflows) in Si IV are correlated with both upflows and downflows (only downflows) in the chromospheric lines. CHs (QS) show larger Si IV upflows (downflows) for similar flows in the chromosphere, suggesting a common origin to these flows. These observations may be explained due to impulsive heating via interchange (closed-loop) reconnection in CHs (QS), resulting in bidirectional flows at different heights, due to differences in magnetic field topologies. Finally, the kinked field lines from interchange reconnection may be carried away as magnetic field rotations and observed as switchbacks. Thus, our results suggest a unified picture of solar wind emergence, coronal heating, and near-Sun switchback formation.

IRIS Nugget Feb **2022** https://iris.lmsal.com/nugget

On the Impulsive Heating of Quiet Solar Corona

Vishal **Upendran** (IUCAA, Pune), Durgesh Tripathi (IUCAA, Pune)

ApJ **916** 59 **2021**

https://arxiv.org/pdf/2103.16824.pdf
https://iopscience.iop.org/article/10.3847/1538-4357/abf65a/pdf
https://doi.org/10.3847/1538-4357/abf65a

The solar corona consists of a million-degree Kelvin plasma. A complete understanding of this phenomenon demands the study of Quiet Sun (QS) regions. In this work, we study QS regions in the 171 Å, 193 Å and 211 Å passbands of the Atmospheric Imaging Assembly (AIA) on board the Solar Dynamics Observatory (SDO), by combining the empirical impulsive heating forward model of Pauluhn & Solanki (2007) with a machine-learning inversion model that allows uncertainty quantification. We find that there are {\approx} 2--3 impulsive events per min, with a lifetime of about 10--20 min. Moreover, for all the three passbands, the distribution of power law slope {\alpha} peaks above 2. Our exploration of correlations among the frequency of impulsive events and their timescales and peak energy suggests that conduction losses dominate over radiative cooling losses. All these finding suggest that impulsive heating is a viable heating mechanism in QS corona. **2011-08-14, 2019-05-02**

Solar Cycle Precursors and the Outlook for Cycle 25

Lisa A. **Upton**, David H. Hathaway

JGR **2023**

https://arxiv.org/pdf/2305.06516.pdf

Sunspot Cycle 25 is now over 3 years past the cycle minimum of December 2019. At this point in the cycle, curve-fitting to the activity becomes reliable and now consistently indicates a maximum sunspot number of 135 +/- 10 - slightly larger than Cycle 24's maximum of 116.4, but well below the average of 179. A geomagnetic precursor, the minimum in the aa-index, and the Sun's magnetic precursors, the Sun's polar field strength and its axial dipole moment at the time of minimum, are often used to predict the amplitude of the cycle at (or before) the onset of the cycle. We examine Cycle 25 predictions produced by these precursors. The geomagnetic precursor indicated a Cycle 25 slightly stronger that Cycle 24, with a maximum of 132 +/- 8. The Sun's magnetic precursors indicated that Cycle 25 would be more similar to Cycle 24, with a maximum sunspot number of 120 +/- 10 or 114 +/- 15. Combining the curve-fitting results with the precursor predictions, we conclude that Cycle 25 will have a maximum smoothed sunspot number of 134 +/- 8 with maximum occurring late in the fall of 2024. Models for predicting the Sun's magnetic field ahead of minimum, were generally successful at predicting the polar precursors years in advance. The fact that Sun's magnetic precursors at cycle minimum were successfully predicted years before minimum and that the precursors are consistent with the size of Cycle 25 suggests that we can now reliably predict the solar cycle.

An Updated Solar Cycle 25 Prediction with AFT: The Modern Minimum

Lisa A. **Upton**, David H. Hathaway

Geophysical Research Letters **2018**

https://arxiv.org/pdf/1808.04868.pdf

Over the last decade there has been mounting evidence that the strength of the Sun's polar magnetic fields during a solar cycle minimum is the best predictor of the amplitude of the next solar cycle. Surface flux transport models can be used to extend these predictions by evolving the Sun's surface magnetic field to obtain an earlier prediction for the strength of the polar fields, and thus the amplitude of the next cycle. In 2016, our Advective Flux Transport (AFT) model was used to do this, producing an early prediction for Solar Cycle 25. At that time, AFT predicted that Cycle 25 will be similar in strength to the Cycle 24, with an uncertainty of about 15% . AFT also predicted that the polar fields in the southern hemisphere would weaken in late 2016 and into 2017 before recovering. That AFT prediction was based on the magnetic field configuration at the end of January 2016. We now have 2 more years of observations. We examine the accuracy of the 2016 AFT prediction and find that the new observations track well

with AFT's predictions for the last two years. We show that the southern relapse did in fact occur, though the timing was off by several months. We propose a possible cause for the southern relapse and discuss the reason for the offset in timing. Finally, we provide an updated AFT prediction for Solar Cycle 25 which includes solar observations through January of 2018.

Effects of Meridional Flow Variations on Solar Cycles 23 and 24

Lisa **Upton**, David H. Hathaway
ApJ, ApJ 792 142., **2014**
http://arxiv.org/pdf/1408.0035v1.pdf
The faster meridional flow that preceded the solar cycle 23/24 minimum is thought to have led to weaker polar field strengths, producing the extended solar minimum and the unusually weak cycle 24. To determine the impact of meridional flow variations on the sunspot cycle, we have simulated the Sun's surface magnetic field evolution with our newly developed surface flux transport model. We investigate three different cases: a constant average meridional flow, the observed time-varying meridional flow, and a time-varying meridional flow in which the observed variations from the average have been doubled. Comparison of these simulations shows that the variations in the meridional flow over cycle 23 have a significant impact (~20%) on the polar fields. However, the variations produced polar fields that were stronger than they would have been otherwise. We propose that the primary cause of the extended cycle 23/24 minimum and weak cycle 24 was the weakness of cycle 23 itself - with fewer sunspots, there was insufficient flux to build a big cycle. We also find that any polar counter-cells in the meridional flow (equatorward flow at high latitudes) produce flux concentrations at mid-to-high latitudes that are not consistent with observations.

Are coronal loops projection effects?

Vadim M. **Uritsky**, James A. Klimchuk
ApJ **2023**
https://arxiv.org/pdf/2310.07102.pdf
We report results of an in-depth numerical investigation of three-dimensional projection effects which could influence the observed loop-like structures in an optically thin solar corona. Several archetypal emitting geometries are tested, including collections of luminous structures with circular cross-sections of fixed and random size, light-emitting structures with highly anisotropic cross-sections, as well as two-dimensional stochastic current density structures generated by fully-developed magnetohydrodynamic turbulence. A comprehensive set of statistical signatures is used to compare the line of sight -integrated emission signals predicted by the constructed numerical models with the loop profiles observed by the extreme ultraviolet telescope onboard the flight 2.1 of the High-Resolution Coronal Imager (Hi-C). The results obtained for the Hi-C loops cannot be attributed to randomly oriented quasi-two dimensional emitting structures such as those constituting "coronal veils" (Malanushenko et al., 2022), and they indicate that typical cross-sectional envelopes of loop emission cannot have high eccentricity. The possibility of apparent loop-like projections of very small (close to the resolution limit) or very large (comparable with the size of an active region) light-emitting sheets remains open, but the intermediate range of scales commonly associated with observed loop systems is most likely filled with true quasi-one dimensional (roughly axisymmetric) structures embedded into the three-dimensional coronal volume.

Plumelets: Dynamic Filamentary Structures in Solar Coronal Plumes

V.M. **Uritsky**, C.E. DeForest, J.T. Karpen, C.R. DeVore, P. Kumar, N.E. Raouafi, P.F. Wyper
2021 *ApJ* **907** 1
https://arxiv.org/pdf/2012.05728.pdf
Solar coronal plumes long seemed to possess a simple geometry supporting spatially coherent, stable outflow without significant fine structure. Recent high-resolution observations have challenged this picture by revealing numerous transient, small-scale, collimated outflows ("jetlets") at the base of plumes. The dynamic filamentary structure of solar plumes above these outflows, and its relationship with the overall plume structure, have remained largely unexplored. We analyzed the statistics of continuously observed fine structure inside a single representative bright plume within a mid-latitude coronal hole during **2016 July 2-3**. By applying advanced edge-enhancement and spatiotemporal analysis techniques to extended series of high-resolution images from the Solar Dynamics Observatory's Atmospheric Imaging Assembly, we determined that the plume was composed of numerous time-evolving filamentary substructures, referred to as "plumelets" in this paper, that accounted for most of the plume emission. The number of simultaneously identifiable plumelets was positively correlated with plume brightness, peaked in the fully formed plume, and remained saturated thereafter. The plumelets had transverse widths of 10 Mm and intermittently supported upwardly propagating periodic disturbances with phase speeds of 190-260 km/s and longitudinal wavelengths of 55-65 Mm. The characteristic frequency (3.5 mHz) is commensurate with that of solar p-modes. Oscillations in neighboring plumelets are uncorrelated, indicating that the waves could be driven by p-mode flows at spatial scales smaller than the plumelet separation. Multiple independent sources of outflow within a

single coronal plume should impart significant fine structure to the solar wind that may be detectable by Parker Solar Probe and Solar Orbiter.

Spatiotemporal organization of energy release events in the quiet solar corona

Vadim M. **Uritsky**, Joseph M. Davila
2014 ApJ 795 15
http://arxiv.org/pdf/1404.1086v1.pdf
Using data from STEREO and SOHO spacecraft, we show that temporal organization of energy release events in the quiet solar corona is close to random, in contrast to the clustered behavior of flaring times in solar active regions. The locations of the quiet-Sun events follow the meso- and supergranulation pattern of the underling photosphere. Together with earlier reports of the scale-free event size statistics, our findings suggest that quiet solar regions responsible for bulk coronal heating operate in a driven self-organized critical state, possibly involving long-range Alfv\'{e}nic interactions.

The Steady Global Corona and Solar Wind: A Three-dimensional MHD Simulation with Turbulence Transport and Heating

Arcadi V. **Usmanov**1,2, William H. Matthaeus1, Melvyn L. Goldstein3, and Rohit Chhiber1
2018 ApJ 865 25 https://doi.org/10.3847/1538-4357/aad687
We present a fully three-dimensional magnetohydrodynamic model of the solar corona and solar wind with turbulence transport and heating. The model is based on Reynolds-averaged solar wind equations coupled with transport equations for turbulence energy, cross helicity, and correlation scale. The model includes separate energy equations for protons and electrons and accounts for the effects of electron heat conduction, radiative cooling, Coulomb collisions, Reynolds stresses, eddy viscosity, and turbulent heating of protons and electrons. The computational domain extends from the coronal base to 5 au and is divided into two regions: the inner (coronal) region, 1–30 R ⊙, and the outer (solar wind) region, 30 R ⊙–5 au. Numerical steady-state solutions in both regions are constructed by time relaxation in the frame of reference corotating with the Sun. Inner boundary conditions are specified using either a tilted-dipole approximation or synoptic solar magnetograms. The strength of solar dipole is adjusted, and a scaling factor for magnetograms is estimated by comparison with Ulysses observations. Except for electron temperature, the model shows reasonable agreement with Ulysses data during its first and third fast latitude transits. We also derive a formula for the loss of angular momentum caused by the outflowing plasma. The formula takes into account the effects of turbulence. The simulation results show that turbulence can notably affect the Sun's loss of angular momentum.

Extreme Solar Events: Setting up a Paradigm **Review**

Usoskin, I., Miyake, F., Baroni, M. et al.
Space Sci Rev 219, 73 (**2023**).
https://doi.org/10.1007/s11214-023-01018-1
https://link.springer.com/content/pdf/10.1007/s11214-023-01018-1.pdf **File**
The Sun is magnetically active and often produces eruptive events on different energetic and temporal scales. Until recently, the upper limit of such events was unknown and believed to be roughly represented by direct instrumental observations. However, two types of extreme events were discovered recently: extreme solar energetic particle events on the multi-millennial time scale and super-flares on sun-like stars. Both discoveries imply that the Sun might rarely produce events, called extreme solar events (ESE), whose energy could be orders of magnitude greater than anything we have observed during recent decades. During the years following these discoveries, great progress has been achieved in collecting observational evidence, uncovering new events, making statistical analyses, and developing theoretical modelling. The ESE paradigm lives and is being developed. On the other hand, many outstanding questions still remain open and new ones emerge. Here we present an overview of the current state of the art and the forming paradigm of ESE from different points of view: solar physics, stellar–solar projections, cosmogenic-isotope data, modelling, historical data, as well as terrestrial, technological and societal effects of ESEs. Special focus is paid to open questions and further developments. This review is based on the joint work of the International Space Science Institute (ISSI) team #510 (2020–2022). 7176 BCE and 5259 BCE, **5410 BCE, 1279 CE, 1052 CE,** 774 CE, **1859, 4-6 Dec 2006, 13 Dec 2006**

A history of solar activity over millennia **Review**

Ilya G. **Usoskin**
Living Reviews in Solar Physics volume 20, Article number: 2 (**2023**)
https://link.springer.com/content/pdf/10.1007/s41116-023-00036-z.pdf
Here we review present knowledge of the long-term behaviour of solar activity on a multi-millennial timescale, as reconstructed using the indirect proxy method. The concept of solar activity is discussed along with an overview of

the dedicated indices used to quantify different aspects of variable solar activity, with special emphasis on sunspot numbers. Over long timescales, quantitative information about past solar activity is historically obtained using a method based on indirect proxies, such as cosmogenic isotopes 1414C and 1010Be in natural stratified archives (e.g., tree rings or ice cores). We give a historical overview of the development of the proxy-based method for past solar-activity reconstruction over millennia, as well as a description of the modern state of the art. Special attention is paid to the verification and cross-calibration of reconstructions. It is argued that the method of cosmogenic isotopes makes a solid basis for studies of solar variability in the past on a long timescale (centuries to millennia) during the Holocene (the past ∼∼12 millennia). A separate section is devoted to reconstructions of extremely rare solar eruptive events in the past, based on both cosmogenic-proxy data in terrestrial and lunar natural archives, as well as statistics of sun-like stars. Finally, the main features of the long-term evolution of solar magnetic activity, including the statistics of grand minima and maxima occurrence, are summarized and their possible implications, especially for solar/stellar dynamo theory, are discussed.
This article is a revised version of https://doi.org/10.1007/s41116-017-0006-9 (2017)

Solar cyclic activity over the last millennium reconstructed from annual 14C data

I.G. **Usoskin**, S.K. Solanki, N. Krivova, B. Hofer, G.A. Kovaltsov, L. Wacker, N. Brehm, B. Kromer
A&A 649, A141 **2021**
https://arxiv.org/pdf/2103.15112.pdf
https://www.aanda.org/articles/aa/pdf/2021/05/aa40711-21.pdf
https://doi.org/10.1051/0004-6361/202140711
The 11-year solar cycle is the dominant pattern of solar activity reflecting the oscillatory dynamo mechanism in the Sun. Solar cycles were directly observed since 1700, while indirect proxies suggest their existence over a much longer period of time but generally without resolving individual cycles and their continuity. Here we reconstruct individual cycles for the last millennium using recent 14C data and state-of-the-art models. Starting with the 14C production rate determined from the so far most precise measurements of radiocarbon content in tree rings, solar activity is reconstructed in three physics-based steps: (1) Correction of the 14C production rate for the changing geomagnetic field; (2) Computation of the open solar magnetic flux; and (3) Conversion into sunspot numbers outside of grand minima. Solar activity is reconstructed for the period 971-1900 (85 individual cycles). This more than doubles the number of solar cycles known from direct solar observations. We found that lengths and strengths of well-defined cycles outside grand minima are consistent with those obtained from the direct sunspot observations after 1750. The validity of the Waldmeier rule is confirmed at a highly significant level. Solar activity is found to be in a deep grand minimum when the activity is mostly below the sunspot formation threshold, during about 250 years. Therefore, although considerable cyclic variability in 14C is seen even during grand minima, individual solar cycles can hardly be reliably resolved therein. Three potential solar particle events, ca. 994, 1052 and 1279 AD, are shown. A new about 1000-year long solar activity reconstruction, in the form of annual (pseudo) sunspot numbers with full assessment of uncertainties, is presented based on new high-precision 14C measurements and state-of-the-art models, more than doubling the number of individually resolved solar cycles.
Corrigendum A&A 664, C3 (**2022**) https://www.aanda.org/articles/aa/pdf/2022/08/aa40711e-21.pdf

Robustness of Solar-Cycle Empirical Rules Across Different Series Including an Updated ADF Sunspot Group Series

Ilya **Usoskin**, Gennady Kovaltsov, Wilma Kiviaho
Solar Phys. **296**, Article number: 13 (**2021**)
https://arxiv.org/pdf/2012.08415.pdf
https://link.springer.com/content/pdf/10.1007/s11207-020-01750-9.pdf
Empirical rules of solar cycle evolution form important observational constraints for the solar dynamo theory. This includes the Waldmeier rule relating the magnitude of a solar cycle to the length of its ascending phase, and the Gnevyshev--Ohl rule clustering cycles to pairs of an even-numbered cycle followed by a stronger odd-numbered cycle. These rules were established as based on the "classical" Wolf sunspot number series, which has been essentially revisited recently, with several revised sets released by the research community. Here we test the robustness of these empirical rules for different sunspot (group) series for the period 1749--1996, using four classical and revised international sunspot numbers and group sunspot-number series. We also provide an update of the sunspot group series based on the active-day fraction (ADF) method, using the new database of solar observations. We show that the Waldmeier rule is robust and independent of the exact sunspot (group) series: its classical and n+1 (relating the length of n-th cycle to the magnitude of (n+1)-th cycle) formulations are significant or highly significant for all series, while its simplified formulation (relating the magnitude of a cycle to its full length) is insignificant for all series. The Gnevyshev--Ohl rule was found robust for all analyzed series for Cycles 8--21, but unstable across the Dalton minimum and before it.

Comment on the paper by Popova et al. On a role of quadruple component of magnetic field in defining solar activity in grand cycles,

Usoskin, I.
(**2017**). J. Atmosph. Solar-Terr. Phys., in press.
https://arxiv.org/pdf/1710.05203.pdf
The paper by Popova et al. presents an oversimplified mathematical model of solar activity with a claim of predicting/postdicting it for several millennia ahead/backwards. The work contains several flaws devaluating the results: (1) the method is unreliable from the point of view of signal processing (it is impossible to make harmonic predictions for thousands of years based on only 35 years of data) and lacks quality control, (2) the result of post-diction apparently contradicts the observational data. (3) theoretical speculations make little sense, To summarize, a multi-harmonic mathematical model, hardly related to full solar dynamo theory, is presented, which is not applicable to realistic solar conditions because of the significant chaotic/stochastic intrinsic component and strong non-stationarity of solar activity. The obtained result is apparently inconsistent with the data in the past and thus cannot be trusted for the future predictions.
See: Reply to comment by Usoskin (2017) on the paper "On a role of quadruple component of magnetic field in defining solar activity in grand cycles"
Zharkova V.V., Popova E., Shepherd S.J. and Zharkov S.
2017
http://computing.unn.ac.uk/staff/slmv5/kinetics/zharkova_etal_reply_jastp17.pdf

Heliospheric modulation of cosmic rays during the neutron monitor era: Calibration using PAMELA data for 2006–201†

Ilya G. **Usoskin**, Agnieszka Gil, Gennady A. Kovaltsov, Alexander L. Mishev, Vladimir V. Mikhailov
JGR **Volume 122, Issue 4, pages 3875–3887, April 2017** **2017** DOI: 10.1002/2016JA023819
http://onlinelibrary.wiley.com.sci-hub.cc/doi/10.1002/2016JA023819/abstract;jsessionid=CDE52B06F06C8318AFBC1F81C9C09894.f03t03
A new reconstruction of the heliospheric modulation potential for galactic cosmic rays is presented for the neutron monitor era, since 1951. The new reconstruction is based on an updated methodology in comparison to previous reconstructions: (1) the use of the new-generation neutron monitor yield function; (2) the use of the new model of the local interstellar spectrum, employing in particular direct data from the distant missions; and (3) the calibration of the neutron monitor responses to direct measurements of the cosmic ray spectrum performed by the PAMELA space-borne spectrometer over 47 time intervals during 2006–2010. The reconstruction is based on data from six standard NM64-type neutron monitors (Apatity, Inuvik, Kergulen, Moscow, Newark and Oulu) since 1965, and two IGY-type ground-based detectors (Climax and Mt.Washington) for 1951–1964. The new reconstruction, along with the estimated uncertainties is tabulated in the paper. The presented series forms a benchmark record of the cosmic ray variability (in the energy range between 1–30 GeV) for the last 60 years, and can be used in long-term studies in the fields of solar, heliospheric and solar-terrestrial physics.

A history of solar activity over millennia **Review**

Ilya G. **Usoskin**
Living Reviews in Solar Physics December **2017**, 14:3
https://link.springer.com/content/pdf/10.1007%2Fs41116-017-0006-9.pdf
Presented here is a review of present knowledge of the long-term behavior of solar activity on a multi-millennial timescale, as reconstructed using the indirect proxy method. The concept of solar activity is discussed along with an overview of the special indices used to quantify different aspects of variable solar activity, with special emphasis upon sunspot number. Over long timescales, quantitative information about past solar activity can only be obtained using a method based upon indirect proxies, such as the cosmogenic isotopes 1414C and 1010Be in natural stratified archives (e.g., tree rings or ice cores). We give an historical overview of the development of the proxy-based method for past solar-activity reconstruction over millennia, as well as a description of the modern state. Special attention is paid to the verification and cross-calibration of reconstructions. It is argued that this method of cosmogenic isotopes makes a solid basis for studies of solar variability in the past on a long timescale (centuries to millennia) during the Holocene. A separate section is devoted to reconstructions of strong solar energetic-particle (SEP) events in the past, that suggest that the present-day average SEP flux is broadly consistent with estimates on longer timescales, and that the occurrence of extra-strong events is unlikely. Finally, the main features of the long-term evolution of solar magnetic activity, including the statistics of grand minima and maxima occurrence, are summarized and their possible implications, especially for solar/stellar dynamo theory, are discussed.

An Optical Atmospheric Phenomenon Observed in 1670 over the City of Astrakhan Was Not a Mid-Latitude Aurora

I. G. **Usoskin**, G. A. Kovaltsov, L. N. Mishina, D. D. Sokoloff, J. Vaquero
Solar Physics January **2017**, 292:15
http://link.springer.com/article/10.1007/s11207-016-1035-6

It has recently been claimed (Zolotova and Ponyavin Solar Phys., 291, 2869, 2016; ZP16 henceforth) that a mid-latitude optical phenomenon, which took place over the city of Astrakhan in July 1670, according to Russian chronicles, were a strong aurora borealis. If this were true, it would imply a very strong or even severe geomagnetic storm during the quietest part of the Maunder minimum. However, as we argue in this article, this conclusion is erroneous and caused by a misinterpretation of the chronicle record. As a result of a thorough analysis of the chronicle text, we show that the described phenomenon occurred during the daylight period of the day ("the last morning hour"), in the south ("towards noon"), and its description does not match that of an aurora. The date of the event was also interpreted incorrectly. We conclude that this phenomenon was not a mid-latitude aurora, but an atmospheric phenomenon, the so-called sundog (or parhelion), which is a particular type of solar halo. Accordingly, the claim of a strong mid-latitude aurora during the deep Maunder Minimum is not correct and should be dismissed.

Dependence of the Sunspot-group Size on the Level of Solar Activity and its Influence on the Calibration of Solar Observers

I.G. **Usoskin**, G.A. Kovaltsov, T. Chatzistergos
Solar Phys. Volume 291, Issue 12, pp 3793–3805 **2016**
http://arxiv.org/pdf/1609.00569.pdf

The distribution of the sunspot group size (area) and its dependence on the level of solar activity is studied. It is shown that the fraction of small groups is not constant but decreases with the level of solar activity so that high solar activity is largely defined by big groups. We study the possible influence of solar activity on the ability of a realistic observer to see and report the daily number of sunspot groups. It is shown that the relation between the number of sunspot groups as seen by different observers with different observational acuity thresholds is strongly non-linear and cannot be approximated by the traditionally used linear scaling (k−factors). The observational acuity threshold [Ath] is considered to quantify the quality of each observer, instead of the traditional relative k−factor. A nonlinear c−factor based on Ath is proposed, which can be used to correct each observer to the reference conditions. The method is tested on a pair of principal solar observers, Wolf and Wolfer, and it is shown that the traditional linear correction, with the constant k−factor of 1.66 to scale Wolf to Wolfer, leads to an overestimate of solar activity around solar maxima.

Solar activity during the Holocene: the Hallstatt cycle and its consequence for grand minima and maxima⋆

I. G. **Usoskin**1, Y. Gallet2, F. Lopes2, G. A. Kovaltsov3,4 and G. Hulot2
A&A 587, A150 (**2016**)

Aims. Cosmogenic isotopes provide the only quantitative proxy for analyzing the long-term solar variability over a centennial timescale. While essential progress has been achieved in both measurements and modeling of the cosmogenic proxy, uncertainties still remain in the determination of the geomagnetic dipole moment evolution. Here we aim at improving the reconstruction of solar activity over the past nine millennia using a multi-proxy approach.
Methods. We used records of the 14C and 10Be cosmogenic isotopes, current numerical models of the isotope production and transport in Earth's atmosphere, and available geomagnetic field reconstructions, including a new reconstruction relying on an updated archeo- and paleointensity database. The obtained series were analyzed using the singular spectrum analysis (SSA) method to study the millennial-scale trends.
Results. A new reconstruction of the geomagnetic dipole field moment, referred to as GMAG.9k, is built for the last nine millennia. New reconstructions of solar activity covering the last nine millennia, quantified in terms of sunspot numbers, are presented and analyzed. A conservative list of grand minima and maxima is also provided.
Conclusions. The primary components of the reconstructed solar activity, as determined using the SSA method, are different for the series that are based on 14C and 10Be. This shows that these primary components can only be ascribed to long-term changes in the terrestrial system and not to the Sun. These components have therefore been removed from the reconstructed series. In contrast, the secondary SSA components of the reconstructed solar activity are found to be dominated by a common ≈2400-year quasi-periodicity, the so-called Hallstatt cycle, in both the 14C and 10Be based series. This Hallstatt cycle thus appears to be related to solar activity. Finally, we show that the grand minima and maxima occurred intermittently over the studied period, with clustering near lows and highs of the Hallstatt cycle, respectively.

A New Calibrated Sunspot Group Series Since 1749: Statistics of Active Day Fractions

I. G. **Usoskin** , G. A. Kovaltsov, M. Lockwood, K. Mursula, M. Owens, S. K. Solanki
Solar Phys. Volume 291, Issue 9, pp 2685–2708 **2016**

Although sunspot-number series have existed since the mid-nineteenth century, they are still the subject of intense debate, with the largest uncertainty being related to the "calibration" of the visual acuity of individual observers in the past. A daisy-chain regression method is usually applied to inter-calibrate the observers, which may lead to significant bias and error accumulation. Here we present a novel method for calibrating the visual acuity of the key observers to the reference data set of Royal Greenwich Observatory sunspot groups for the period 1900 – 1976, using the statistics of the active-day fraction. For each observer we independently evaluate their observational thresholds [SS] defined such that the observer is assumed to miss all of the groups with an area smaller than SS and report all the groups larger than SS. Next, using a Monte-Carlo method, we construct a correction matrix for each observer from the reference data set. The correction matrices are significantly non-linear and cannot be approximated by a linear regression or proportionality. We emphasize that corrections based on a linear proportionality between annually averaged data lead to serious biases and distortions of the data. The correction matrices are applied to the original sunspot-group records reported by the observers for each day, and finally the composite corrected series is produced for the period since 1748. The corrected series is provided as supplementary material in electronic form and displays secular minima around 1800 (Dalton Minimum) and 1900 (Gleissberg Minimum), as well as the Modern Grand Maximum of activity in the second half of the twentieth century. The uniqueness of the grand maximum is confirmed for the last 250 years. We show that the adoption of a linear relationship between the data of Wolf and Wolfer results in grossly inflated group numbers in the eighteenth and nineteenth centuries in some reconstructions.

The Maunder minimum (1645--1715) was indeed a Grand minimum: A reassessment of multiple datasets

Ilya G. **Usoskin**, Rainer Arlt, Eleanna Asvestari, Ed Hawkins, Maarit Käpylä, Gennady A. Kovaltsov, Natalie Krivova, Michael Lockwood, Kalevi Mursula, Jezebel O'Reilly, Matthew Owens, Chris J. Scott, Dmitry D. Sokoloff, Sami K. Solanki, Willie Soon, José M. Vaquero
A&A 581, A95 **2015**
http://arxiv.org/pdf/1507.05191v1.pdf

Aims: Although the time of the Maunder minimum (1645--1715) is widely known as a period of extremely low solar activity, claims are still debated that solar activity during that period might still have been moderate, even higher than the current solar cycle #24. We have revisited all the existing pieces of evidence and datasets, both direct and indirect, to assess the level of solar activity during the Maunder minimum.
Methods: We discuss the East Asian naked-eye sunspot observations, the telescopic solar observations, the fraction of sunspot active days, the latitudinal extent of sunspot positions, auroral sightings at high latitudes, cosmogenic radionuclide data as well as solar eclipse observations for that period. We also consider peculiar features of the Sun (very strong hemispheric asymmetry of sunspot location, unusual differential rotation and the lack of the K-corona) that imply a special mode of solar activity during the Maunder minimum.
Results: The level of solar activity during the Maunder minimum is reassessed on the basis of all available data sets.
Conclusions: We conclude that solar activity was indeed at an exceptionally low level during the Maunder minimum. Although the exact level is still unclear, it was definitely below that during the Dalton minimum around 1800 and significantly below that of the current solar cycle #24. Claims of a moderate-to-high level of solar activity during the Maunder minimum are rejected at a high confidence level.

A two-wave dynamo model by Zharkova et al. (2015) disagrees with data on long-term solar variability

I. **Usoskin**, G. Kovaltsov
Sci. Rep **201**5
http://arxiv.org/pdf/1512.05516v1.pdf

A two-wave dynamo model was recently proposed by Zharkova et al. (2015, Zh15 henceforth), which aims at long-term predictions of solar activity for millennia ahead and backwards. Here we confront the backward model predictions for the last 800 years with known variability of solar activity, using both direct sunspot observations since 1610 and reconstructions based on cosmogenic radionuclide data. We show that the Zh15 model fails to reproduce the well-established features of the solar activity evolution during the last millennium. This means that the predictive part for the future is not reliable either.

Evidence for distinct modes of solar activity⋆

I. G. **Usoskin**1, G. Hulot2, Y. Gallet2, R. Roth3, A. Licht2, F. Joos3, G. A. Kovaltsov4, E. Thébault2 and A. Khokhlov
A&A 562, L10 (**2014**)
Aims. The Sun shows strong variability in its magnetic activity, from Grand minima to Grand maxima, but the nature of the variability is not fully understood, mostly because of the insufficient length of the directly observed solar activity records and of uncertainties related to long-term reconstructions. Here we present a new adjustment-free reconstruction of solar activity over three millennia and study its different modes.
Methods. We present a new adjustment-free, physical reconstruction of solar activity over the past three millennia, using the latest verified carbon cycle, 14C production, and archeomagnetic field models. This great improvement allowed us to study different modes of solar activity at an unprecedented level of details.
Results. The distribution of solar activity is clearly bi-modal, implying the existence of distinct modes of activity. The main regular activity mode corresponds to moderate activity that varies in a relatively narrow band between sunspot numbers 20 and 67. The existence of a separate Grand minimum mode with reduced solar activity, which cannot be explained by random fluctuations of the regular mode, is confirmed at a high confidence level. The possible existence of a separate Grand maximum mode is also suggested, but the statistics is too low to reach a confident conclusion.
Conclusions. The Sun is shown to operate in distinct modes – a main general mode, a Grand minimum mode corresponding to an inactive Sun, and a possible Grand maximum mode corresponding to an unusually active Sun. These results provide important constraints for both dynamo models of Sun-like stars and investigations of possible solar influence on Earth's climate.

A History of Solar Activity over Millennia

Ilya G. **Usoskin**
Living Reviews in Solar Physics, March **2013**
http://solarphysics.livingreviews.org/Articles/upcoming.html
Presented here is a review of present knowledge of the long-term behavior of solar activity on a multi-millennial timescale, as reconstructed using the indirect proxy method. The concept of solar activity is discussed along with an overview of the special indices used to quantify different aspects of variable solar activity, with special emphasis upon sunspot number.
Over long timescales, quantitative information about past solar activity can only be obtained using a method based upon indirect proxies, such as the cosmogenic isotopes 14C and 10Be in natural stratified archives (e.g., tree rings or ice cores). We give an historical overview of the development of the proxy-based method for past solar-activity reconstruction over millennia, as well as a description of the modern state. Special attention is paid to the verification and cross-calibration of reconstructions. It is argued that this method of cosmogenic isotopes makes a solid basis for studies of solar variability in the past on a long timescale (centuries to millennia) during the Holocene.
A separate section is devoted to reconstructions of strong solar energetic-particle (SEP) events in the past, that suggest that the present-day average SEP flux is broadly consistent with estimates on longer timescales, and that the occurrence of extra-strong events is unlikely.
Finally, the main features of the long-term evolution of solar magnetic activity, including the statistics of grand minima and maxima occurrence, are summarized and their possible implications, especially for solar/stellar dynamo theory, are discussed.

Temporal relations between magnetic bright points and the solar sunspot cycle

D. **Utz**, R. Muller, T. Van Doorsselaere
proceeding/paper of the 10-years anniversary Hinode conference **2017**
Publ. Astron. Soc. Japan Volume 69, Issue 6, 1 December **2017**, 98,
https://doi.org/10.1093/pasj/psx115
https://arxiv.org/pdf/1710.01678.pdf
The Sun shows a global magnetic field cycle traditionally best visible in the photosphere as a changing sunspot cycle featuring roughly an 11 year period. In addition we know that our host star also harbours small-scale magnetic fields often seen as strong concentrations of magnetic flux reaching kG field strengths. These features are situated in inter-granular lanes where they show up bright as so-called magnetic bright points (MBPs). In this short paper we wish to analyse a homogenous nearly 10 year long synoptic Hinode image data set recorded from November 2006 up to February 2016 in the G-band to inspect the relationship between the number of MBPs at the solar disc centre and the relative sunspot number.
Our findings suggest that indeed the number of MBPs at the solar disc centre is correlated to the relative sunspot number, but with the particular feature of showing two different temporal shifts between the decreasing phase of cycle 23 including the minimum and the increasing phase of cycle 24 including the maximum. While the former is shifted by about 22 months the later is only shifted by less than 12 months. Moreover, we introduce and discuss an

analytical model to predict the number of MBPs at the solar disc centre purely depending on the evolution of the relative sunspot number as well as the temporal change of the relative sunspot number and two background parameters describing a possibly acting surface dynamo as well as the strength of the magnetic field diffusion. Finally, we are able to confirm the plausibility of the temporal shifts by a simplistic random walk model.
The main conclusion to be drawn from this work is that the injection of magnetic flux, coming from active regions as represented by sunspots, happens on faster time scales than the removal of small-scale magnetic flux elements later on.

Long-term trends of magnetic bright points: I. Number of MBPs at disc centre

D. **Utz**, R. Muller, S. Thonhofer, A. Veronig, A. Hanslmeier, M. Bodnárová, M. Bárta, J. C. del Toro Iniesta

A&A A39 (**2016**)

http://arxiv.org/pdf/1511.07767v1.pdf

Context. The Sun shows an activity cycle that is caused by its varying global magnetic field. During a solar cycle, sunspots, i.e. extended regions of strong magnetic fields, occur in activity belts that are slowly migrating from middle to lower latitudes, finally arriving close to the equator during the cycle maximum phase. While this have been well known for centuries, much less is known about the solar cycle evolution of small-scale magnetic fields. Aims. To address this question, we study magnetic bright points (MBPs) as proxies for such small-scale, kG solar magnetic fields. This study is based on a homogeneous data set that covers a period of eight years. Methods. An automated MBP identification algorithm was applied to the synoptic Hinode/SOT G-band data over the period November 2006 to August 2014, i.e. covering the decreasing phase of Cycle 23 and the rise, maximum, and early decrease of Cycle 24. This data set includes, at the moment of investigation, a total of 4 162 images, with about 2.9 million single MBP detections.
Results. After a careful preselection and monthly median filtering of the data, the investigation revealed that the number of MBPs close to the equator is coupled to the global solar cycle but shifted in time by about 2.5 years. Furthermore, the instantaneous number of detected MBPs depends on the hemisphere, with one hemisphere being more prominent, i.e. showing a higher number of MBPs. After the end of Cycle 23 and at the starting point of Cycle 24, the more active hemisphere changed from south to north.
Conclusions. These findings suggest that there is indeed a coupling between the activity of MBPs close to the equator with the global magnetic field. The results also indicate that a significant fraction of the magnetic flux that is visible as MBPs close to the equator originates from the sunspot activity belts.

Observations of the Quiet Sun During the Deepest Solar Minimum of the Past Century with Chandrayaan-2 XSM -- Elemental Abundances in the Quiescent Corona

Santosh V. **Vadawale**, Biswajit Mondal, N. P. S. Mithun, Aveek Sarkar, P. Janardhan, Bhuwan Joshi, Anil Bhardwaj, M. Shanmugam, Arpit R. Patel, Hitesh Kumar L. Adalja, Shiv Kumar Goyal, Tinkal Ladiya, Neeraj Kumar Tiwari, Nishant Singh, Sushil Kumar

ApJL **912** L12 **2021**

https://arxiv.org/pdf/2103.16643.pdf

https://doi.org/10.3847/2041-8213/abf35d

Elements with low First Ionization Potential (FIP) are known to be three to four times more abundant in active region loops of the solar corona than in the photosphere. There have been observations suggesting that this observed "FIP bias" may be different in other parts of the solar corona and such observations are thus important in understanding the underlying mechanism. The Solar X-ray Monitor (XSM) on board the Chandrayaan-2 mission carried out spectroscopic observations of the Sun in soft X-rays during the 2019-20 solar minimum, considered to be the quietest solar minimum of the past century. These observations provided a unique opportunity to study soft X-ray spectra of the quiescent solar corona in the absence of any active regions. By modelling high resolution broadband X-ray spectra from XSM, we estimate the temperature and emission measure during periods of possibly the lowest solar X-ray intensity. We find that the derived parameters remain nearly constant over time with a temperature around 2 MK, suggesting the emission is dominated by X-ray Bright Points (XBPs). We also obtain the abundances of Mg, Al, and Si relative to H, and find that the FIP bias is ~2, lower than the values observed in active regions. **2019-Sep-17, 2019-09-21**

Solar Models in Light of New High Metallicity Measurements from Solar Wind Data

Sunny **Vagnozzi**1, Katherine Freese1,2, and Thomas H. Zurbuchen

2017 ApJ 839 55 DOI 10.3847/1538-4357/aa6931

We study the impact of new metallicity measurements, from solar wind data, on the solar model. The "solar modeling problem" refers to the persisting discrepancy between helioseismological observations and predictions of solar models computed implementing state-of-the-art photospheric abundances. We critically reassess the problem, in particular considering the new set of abundances of von Steiger & Zurbuchen, determined through the in situ

collection of solar wind samples from polar coronal holes. This new set of abundances indicates a solar metallicity , significantly higher than the currently established value. The new values hint at an abundance of volatile elements (i.e., C, N, O, Ne) close to previous results of Grevesse and Sauval, whereas the abundance of refractory elements (i.e., Mg, Si, S, Fe) is considerably increased. Using the Linear Solar Model formalism, we determine the variation of helioseismological observables in response to the changes in elemental abundances, in order to explore the consistency of these new measurements with constraints from helioseismology. We find that for observables that are particularly sensitive to the abundance of volatile elements, in particular the radius of the convective zone boundary (CZB) and the sound speed around the radius of CZB, improved agreement over previous models is obtained. Conversely, the high abundance of refractories correlates with a higher core temperature, resulting in an overproduction of neutrinos and a huge increase in the surface helium abundance. We conclude that the "solar modeling problem" remains unsolved.

New solar metallicity measurements

Sunny **Vagnozzi**

51st Rencontres de Moriond, Cosmology Session, ISBN: 979-10-968-7901-4 **2017**

https://arxiv.org/pdf/1703.10834.pdf

In the past years, a systematic downward revision of the metallicity of the Sun has led to the "solar modelling problem", namely the disagreement between predictions of standard solar models and inferences from helioseismology. Recent solar wind measurements of the metallicity of the Sun, however, provide once more indication for a high-metallicity Sun. Because of the effects of possible residual fractionation, the derived value of the metallicity $Z = 0.0196 \pm 0.0014$ actually represents a lower limit to the true metallicity of Sun.
However, when compared with helioseismological measurements, solar models computed using these new abundances fail to restore agreement, owing to the implausibly high abundance of refractory (Mg, Si, S, Fe) elements, which correlates with a higher core temperature and hence an over-production of solar neutrinos. Moreover, the robustness of these measurements is challenged by possible first ionization potential fractionation processes. In this talk I will discuss these solar wind measurements, which leave the "solar modelling problem" unsolved.

A successful solar model using new solar composition data

Sunny **Vagnozzi**, Katherine Freese, Thomas H. Zurbuchen

2016

http://arxiv.org/pdf/1603.05960v1.pdf

A resolution is proposed to the "solar abundance problem", that is, the discrepancy between helioseismological observations and the predictions of solar models, computed implementing state-of-the-art photospheric abundances. We reassess the problem considering a newly determined set of abundances, which indicate a lower limit to the metallicity of $Z_\odot = 0.0196 \pm 0.0014$, significantly higher than findings during the past decade. Such value for the metallicity is determined in situ, measuring the least fractionated solar winds over the poles of the Sun, rather than spectroscopically. We determine the response of helioseismological observables to the corresponding changes in elemental abundances. Our findings indicate that, taking inversion errors into account, good agreement between models and observations is achieved. The definitive test for these abundances will be measurements of the CNO neutrino fluxes by SNO+ (which we expect to be $\sim$ 30-50\% higher than predictions using abundances based on photospheric spectroscopy). We briefly comment on the implausibility of previously proposed solutions based on dark matter. The results also imply that 3D spectroscopic inversion processes systematically underestimate elemental abundances in the photosphere. Our conclusion is that the solar abundance problem has found a definitive compelling solution.

Why is solar cycle 24 an inefficient producer of high-energy particle events?

Rami **Vainio**, Osku Raukunen, Allan J. Tylka, William F. Dietrich, Alexandr Afanasiev

A&A **2017**

https://arxiv.org/pdf/1707.00485.pdf

The aim of the study is to investigate the reason for the low productivity of high-energy SEPs in the present solar cycle. We employ scaling laws derived from diffusive shock acceleration theory and simulation studies including proton-generated upstream Alfv\'en waves to find out how the changes observed in the long-term average properties of the erupting and ambient coronal and/or solar wind plasma would affect the ability of shocks to accelerate particles to the highest energies. Provided that self-generated turbulence dominates particle transport around coronal shocks, it is found that the most crucial factors controlling the diffusive shock acceleration process are the number density of seed particles and the plasma density of the ambient medium. Assuming that suprathermal populations

provide a fraction of the particles injected to shock acceleration in the corona, we show that the lack of most energetic particle events as well as the lack of low charge-to-mass ratio ion species in the present cycle can be understood as a result of the reduction of average coronal plasma and suprathermal densities in the present cycle over the previous one.

Interaction of Large- and Small-scale Dynamos in Isotropic Turbulent Flows from GPU-accelerated Simulations

Miikka S. **Väisälä**1, Johannes Pekkilä2, Maarit J. Käpylä2,3,4, Matthias Rheinhardt2, Hsien Shang (尚賢)1, and Ruben Krasnopolsky1
2021 ApJ 907 83
https://doi.org/10.3847/1538-4357/abceca
Magnetohydrodynamical (MHD) dynamos emerge in many different astrophysical situations where turbulence is present, but the interaction between large-scale dynamos (LSDs) and small-scale dynamos (SSDs) is not fully understood. We performed a systematic study of turbulent dynamos driven by isotropic forcing in isothermal MHD with magnetic Prandtl number of unity, focusing on the exponential growth stage. Both helical and nonhelical forcing was employed to separate the effects of LSD and SSD in a periodic domain. Reynolds numbers ($\mathrm{Re_M}$) up to ≈250 were examined and multiple resolutions used for convergence checks. We ran our simulations with the Astaroth code, designed to accelerate 3D stencil computations on graphics processing units (GPUs) and to employ multiple GPUs with peer-to-peer communication. We observed a speedup of ≈35 in single-node performance compared to the widely used multi-CPU MHD solver Pencil Code. We estimated the growth rates from both the averaged magnetic fields and their power spectra. At low $\mathrm{Re_M}$ LSD growth dominates, but at high $\mathrm{Re_M}$ SSD appears to dominate in both helically and nonhelically forced cases. Pure SSD growth rates follow a logarithmic scaling as a function of $\mathrm{Re_M}$. Probability density functions of the magnetic field from the growth stage exhibit SSD behavior in helically forced cases even at intermediate $\mathrm{Re_M}$. We estimated mean field turbulence transport coefficients using closures like the second-order correlation approximation (SOCA). They yield growth rates similar to the directly measured ones and provide evidence of α quenching. Our results are consistent with the SSD inhibiting the growth of the LSD at moderate $\mathrm{Re_M}$, while the dynamo growth is enhanced at higher $\mathrm{Re_M}$.

Long-Term and Solar Cycle Variation of Galactic Cosmic Rays: Evidence for Variable Heliospheric Turbulence

Pauli **Väisänen**, Ilya Usoskin, Kalevi Mursula
JGR Volume124, Issue2 February **2019** Pages 804-811
sci-hub.tw/10.1029/2018JA026135
The Sun modulates the flux of galactic cosmic rays (GCR) reaching the Earth's orbit. GCR flux has been measured by ground-based neutron monitors (NMs) for several decades, which provides an interesting long-term monitor of solar activity and the heliospheric magnetic field. Here we study the long-term evolution of the power spectrum of GCR over the last six solar cycles, using the power law slope in the frequency range 5.56·10−6 to 2.14·10−6 Hz (between 50 and 130 hr). We use data from 31 neutron monitors during 1953–2016. We show that the power law slopes vary within the solar cycle, with a Kolmogorov-type slope observed at solar minimum and a random-walk-type slope observed at solar maximum. This implies that the different conditions in the different phases of the solar cycle affect the scaling properties of heliospheric turbulence and, thereby, cosmic ray variability.

Correlations of Sunspot Physical Characteristics during Solar Cycle 23

Adriana **Valio**, Eduardo Spagiari, Mauricio Marengoni & Caius L. Selhorst
Solar Physics volume 295, Article number: 120 (**2020**)
https://link.springer.com/content/pdf/10.1007/s11207-020-01691-3.pdf
The behavior of sunspots is governed by the magnetic dynamo acting deep within the convection zone of the Sun. Therefore, knowledge of sunspot physical characteristics and how they evolve in time during a solar cycle can help to improve our understanding of the solar magnetic behavior. This work analyzes the physical characteristics of sunspots during the Solar Activity Cycle 23, detected using computer vision techniques. The main goal is to derive the relationships between sunspot properties. Images in visible light and magnetograms of the Michelson Doppler Imager (MDI) on board the Solar and Heliospheric Observatory (SOHO) were used to detect sunspots and to extract their characteristics such as area, intensity (or temperature), and magnetic field magnitude. A total of 32,223 sunspots were analyzed, with longitudes between −40∘−40∘ and 40∘40∘, throughout the entire Solar Cycle 23, from May 1996 through April 2008. These spots fell mainly into three categories. Most sunspots (85%) did not exhibit a well defined umbra, with average intensities larger than 0.657 relative to disk center, which corresponds to temperatures greater than 5200 K. A second group comprising less than 12% of the spots, was cooler (temperature less than 5200 K) and with more intense magnetic fields (2000 – 4000 G) and mostly presented a well defined umbra. Lastly, only 3% of the spots had large areas and strong magnetic fields with complex umbrae, but intermediate temperatures. The temporal behavior of sunspot physical characteristics throughout the 11 year cycle

and the relationships between them were verified. Sunspot physical properties presented variations over time during Solar Cycle 23, such that larger, cooler sunspots with stronger magnetic fields occurred more frequently during periods of maximum activity. Linear correlations were found regarding the logarithm of the area and the intensity with extreme magnetic field, and of the temperature (or intensity) with the area; whereas a quadratic relation was found between magnetic field and temperature of spots.

Additivity of relative magnetic helicity in finite volumes

Gherardo **Valori**, Pascal Démoulin, Etienne Pariat, Anthony Yeates, Kostas Moraitis, Luis Linan
A&A **2020**
https://arxiv.org/pdf/2008.00968.pdf
Relative magnetic helicity is conserved by magneto-hydrodynamic evolution even in the presence of moderate resistivity. For that reason, it is often invoked as the most relevant constraint to the dynamical evolution of plasmas in complex systems, such as solar and stellar dynamos, photospheric flux emergence, solar eruptions, and relaxation processes in laboratory plasmas. However, such studies often indirectly imply that relative magnetic helicity in a given spatial domain can be algebraically split into the helicity contributions of the composing subvolumes, i.e., that it is an additive quantity. A limited number of very specific applications have shown that this is not the case. Progress in understanding the non-additivity of relative magnetic helicity requires removal of restrictive assumptions in favour of a general formalism that can be used both in theoretical investigations as well as in numerical applications. We derive the analytical gauge-invariant expression for the partition of relative magnetic helicity between contiguous finite-volumes, without any assumptions on either the shape of the volumes and interface, or the employed gauge. The non-additivity of relative magnetic helicity in finite volumes is proven in the most general, gauge-invariant formalism, and verified numerically. More restrictive assumptions are adopted to derive known specific approximations, yielding a unified view of the additivity issue. As an example, the case of a flux rope embedded in a potential field shows that the non-additivity term in the partition equation is, in general, non-negligible. The relative helicity partition formula can be applied to numerical simulations to precisely quantify the effect of non-additivity on global helicity budgets of complex physical processes.

Magnetic helicity estimations in models and observations of the solar magnetic field. Part I: Finite volume methods **Review**

Gherardo **Valori**, Etienne Pariat, Sergey Anfinogentov, Feng Chen, Manolis K. Georgoulis, Yang Guo, Yang Liu, Kostas Moraitis, Julia K. Thalmann, Shangbin Yang
Space Science Reviews **2016**
https://arxiv.org/pdf/1610.02193v1.pdf
Magnetic helicity is a conserved quantity of ideal magneto-hydrodynamics characterized by an inverse turbulent cascade. Accordingly, it is often invoked as one of the basic physical quantities driving the generation and structuring of magnetic fields in a variety of astrophysical and laboratory plasmas. We provide here the first systematic comparison of six existing methods for the estimation of the helicity of magnetic fields known in a finite volume. All such methods are reviewed, benchmarked, and compared with each other, and specifically tested for accuracy and sensitivity to errors. To that purpose, we consider four groups of numerical tests, ranging from solutions of the three-dimensional, force-free equilibrium, to magneto-hydrodynamical numerical simulations. Almost all methods are found to produce the same value of magnetic helicity within few percent in all tests. In the more solar-relevant and realistic of the tests employed here, the simulation of an eruptive flux rope, the spread in the computed values obtained by all but one method is only 3%, indicating the reliability and mutual consistency of such methods in appropriate parameter ranges. However, methods show differences in the sensitivity to numerical resolution and to errors in the solenoidal property of the input fields. In addition to finite volume methods, we also briefly discuss a method that estimates helicity from the field lines' twist, and one that exploits the field's value at one boundary and a coronal minimal connectivity instead of a pre-defined three-dimensional magnetic-field solution.

Chromospheric evaporation and phase mixing of Alfvén waves in coronal loops

H.J. **Van Damme**, I. De Moortel, P. Pagano, C. D. Johnston
A&A 635, A174 **2020**
https://arxiv.org/pdf/2002.11695.pdf
https://www.aanda.org/articles/aa/pdf/2020/03/aa37266-19.pdf
Phase mixing of Alfvén waves has been studied extensively as a possible coronal heating mechanism but without the full thermodynamic consequences considered self-consistently. It has been argued that in some cases, the thermodynamic feedback of the heating could substantially affect the transverse density gradient and even inhibit the phase mixing process. In this paper, we use MHD simulations with the appropriate thermodynamical terms included to quantify the evaporation following heating by phase mixing of Alfvén waves in a coronal loop and the effect of this evaporation on the transverse density profile. The numerical simulations were performed using the Lare2D code. We set up a 2D loop model consisting of a field-aligned thermodynamic equilibrium and a cross-field

(background) heating profile. A continuous, sinusoidal, high-frequency Alfvén wave driver was implemented. As the Alfvén waves propagate along the field, they undergo phase mixing due to the cross-field density gradient in the coronal part of the loop. We investigated the presence of field-aligned flows, heating from the dissipation of the phase-mixed Alfvén waves, and the subsequent evaporation from the lower atmosphere. We find that phase mixing of Alfvén waves leads to modest heating in the shell regions of the loop and evaporation of chromospheric material into the corona with upflows of the order of only 5-20 m/s. Although the evaporation leads to a mass increase in the shell regions of the loop, the effect on the density gradient and, hence, on the phase mixing process, is insignificant. This paper self-consistently investigates the effect of chromospheric evaporation on the cross-field density gradient and the phase mixing process in a coronal loop. We found that the effects in our particular setup (small amplitude, high frequency waves) are too small to significantly change the density gradient.

Predictions for the First Parker Solar Probe Encounter

B. **van der Holst**1, W. B. Manchester IV1, K. G. Klein2, and J. C. Kasper
2019 ApJL 872 L18
https://doi.org/10.3847/2041-8213/ab04a5
https://arxiv.org/pdf/1902.03921.pdf
We examine Alfvén Wave Solar atmosphere Model (AWSoM) predictions of the first Parker Solar Probe (PSP) encounter. We focus on the 12 day closest approach centered on the first perihelion. AWSoM allows us to interpret the PSP data in the context of coronal heating via Alfvén wave turbulence. The coronal heating and acceleration is addressed via outward-propagating low-frequency Alfvén waves that are partially reflected by Alfvén speed gradients. The nonlinear interaction of these counter-propagating waves results in a turbulent energy cascade. To apportion the wave dissipation to the electron and anisotropic proton temperatures, we employ the results of the theories of linear wave damping and nonlinear stochastic heating as described by Chandran et al. We find that during the first encounter, PSP was in close proximity to the heliospheric current sheet (HCS) and in the slow wind. PSP crossed the HCS two times, at **2018 November 3** UT 01:02 and **2018 November 8** UT 19:09, with perihelion occurring on the south of side of the HCS. We predict the plasma state along the PSP trajectory, which shows a dominant proton parallel temperature causing the plasma to be firehose unstable.

Intermittent reconnection and plasmoids in UV bursts in the low solar atmosphere

L. Rouppe **van der Voort**, B. De Pontieu, G.B. Scharmer, J. de la Cruz Rodriguez, J. Martinez-Sykora, D. Nobrega-Siverio, L.J. Guo, S. Jafarzadeh, T.M.D. Pereira, V.H. Hansteen, M. Carlsson, G. Vissers
ApJL **2017**
https://arxiv.org/pdf/1711.04581.pdf
Magnetic reconnection is thought to drive a wide variety of dynamic phenomena in the solar atmosphere. Yet the detailed physical mechanisms driving reconnection are difficult to discern in the remote sensing observations that are used to study the solar atmosphere. In this paper we exploit the high-resolution instruments Interface Region Imaging Spectrograph (IRIS) and the new CHROMIS Fabry-Perot instrument at the Swedish 1-m Solar Telescope (SST) to identify the intermittency of magnetic reconnection and its association with the formation of plasmoids in so-called UV bursts in the low solar atmosphere. The Si IV 1403A UV burst spectra from the transition region show evidence of highly broadened line profiles with often non-Gaussian and triangular shapes, in addition to signatures of bidirectional flows. Such profiles had previously been linked, in idealized numerical simulations, to magnetic reconnection driven by the plasmoid instability. Simultaneous CHROMIS images in the chromospheric Ca II K 3934A line now provide compelling evidence for the presence of plasmoids, by revealing highly dynamic and rapidly moving brightenings that are smaller than 0.2 arcsec and that evolve on timescales of order seconds. Our interpretation of the observations is supported by detailed comparisons with synthetic observables from advanced numerical simulations of magnetic reconnection and associated plasmoids in the chromosphere. Our results highlight how subarcsecond imaging spectroscopy sensitive to a wide range of temperatures combined with advanced numerical simulations that are realistic enough to compare with observations can directly reveal the small-scale physical processes that drive the wide range of phenomena in the solar atmosphere. **2016 September 3-5**

Heating signatures in the disk counterparts of solar spicules in IRIS observations

L. Rouppe **van der Voort**, B. De Pontieu, T.M.D. Pereira, M. Carlsson, V. Hansteen
ApJL, **799** L3 **2015**
http://arxiv.org/pdf/1412.4531v1.pdf
We use coordinated observations with the Interface Region Imaging Spectrograph (IRIS) and the Swedish 1-m Solar Telescope (SST) to identify the disk counterpart of type II spicules in upper-chromospheric and transition region (TR) diagnostics. These disk counterparts were earlier identified through short-lived asymmetries in chromospheric spectral lines: rapid blue- or red-shifted excursions (RBEs or RREs). We find clear signatures of RBEs and RREs in Mg II h & k, often with excursions of the central h3 and k3 absorption features in concert with asymmetries in co-

temporal and co-spatial H-alpha spectral profiles. We find spectral signatures for RBEs and RREs in C II 1335 and 1336 A and Si IV 1394 and 1403 A spectral lines and interpret this as a sign that type II spicules are heated to at least TR temperatures, supporting other recent work. These C II and Si IV spectral signals are weaker for a smaller network region than for more extended network regions in our data. A number of bright features around extended network regions observed in IRIS slit-jaw imagery SJI 1330 and 1400, recently identified as network jets, can be clearly connected to H-alpha RBEs and/or RREs in our coordinated data. We speculate that at least part of the diffuse halo around network regions in the IRIS SJI 1330 and 1400 images can be attributed to type II spicules with insufficient opacity in the C II and Si IV lines to stand out as single features in these passbands. Movies are available at this http URL **13-23 Sep 2013**

Coronal heating by MHD waves **Review**

Tom **Van Doorsselaere**, Abhishek K. Srivastava, Patrick Antolin, Norbert Magyar, Soheil Vasheghani Farahani, Hui Tian, Dmitrii Y. Kolotkov, Leon Ofman, Mingzhe Guo, Iñigo Arregui, Ineke De Moortel, David Pascoe

Space Science Reviews **216**, Article number: 140 **2020**

https://arxiv.org/pdf/2012.01371.pdf

The heating of the solar chromosphere and corona to the observed high temperatures, imply the presence of ongoing heating that balances the strong radiative and thermal conduction losses expected in the solar atmosphere. It has been theorized for decades that the required heating mechanisms of the chromospheric and coronal parts of the active regions, quiet-Sun, and coronal holes are associated with the solar magnetic fields. However, the exact physical process that transport and dissipate the magnetic energy which ultimately leads to the solar plasma heating are not yet fully understood. The current understanding of coronal heating relies on two main mechanism: reconnection and MHD waves that may have various degrees of importance in different coronal regions. In this review we focus on recent advances in our understanding of MHD wave heating mechanisms. First, we focus on giving an overview of observational results, where we show that different wave modes have been discovered in the corona in the last decade, many of which are associated with a significant energy flux, either generated in situ or pumped from the lower solar atmosphere. Afterwards, we summarise the recent findings of numerical modelling of waves, motivated by the observational results. Despite the advances, only 3D MHD models with Alfvén wave heating in an unstructured corona can explain the observed coronal temperatures compatible with the quiet Sun, while 3D MHD wave heating models including cross-field density structuring are not yet able to account for the heating of coronal loops in active regions to their observed temperature.

Editorial: Magnetohydrodynamic Waves in the Solar Atmosphere: Heating and Seismology **Review**

Tom **Van Doorsselaere**, Valery M. Nakariakov, Bo Li, and Patrick Antolin

Front. Astron. Space Sci., 23 January **2020** | https://doi.org/10.3389/fspas.2019.00079

https://www.frontiersin.org/articles/10.3389/fspas.2019.00079/pdf

THIS ARTICLE IS PART OF THE RESEARCH TOPIC

Energy Propagation by Transverse Waves in Multiple Flux Tube Systems Using Filling Factors

T. **Van Doorsselaere**1, S. E. Gijsen1, J. Andries2, and G. Verth

2014 ApJ 795 18.

https://perswww.kuleuven.be/~u0041608/docs/vd2014fillingfactors.pdf

In the last few years, it has been found that transverse waves are present at all times in coronal loops or spicules. Their energy has been estimated with an expression derived for bulk Alfvén waves in homogeneous media, with correspondingly uniform wave energy density and flux. The kink mode, however, is localized in space with the energy density and flux dependent on the position in the cross-sectional plane. The more relevant quantities for the kink mode are the integrals of the energy density and flux over the cross-sectional plane. The present paper provides an approximation to the energy propagated by kink modes in an ensemble of flux tubes by means of combining the analysis of single flux tube kink oscillations with a filling factor for the tube cross-sectional area. This finally allows one to compare the expressions for energy flux of Alfvén waves with an ensemble of kink waves. We find that the correction factor for the energy in kink waves, compared to the bulk Alfvén waves, is between f and 2f, where f is the density filling factor of the ensemble of flux tubes.

Plasma outflows from active regions: are they sources of the slow solar wind?

Lidia **van Driel-Gesztelyi**, Deb Baker, and Lucie Green

Hinode EIS science nugget for September **2012**

http://msslxr.mssl.ucl.ac.uk:8080/SolarB/nuggets/nugget_2012sep.jsp
Since the discovery of hot plasma upflows from the edges of solar active regions (ARs) by Hinode/XRT (Sakao et al., 2008) and EIS (Harra et al. 2008) it has been suspected that these upflows are in fact outflows, i.e. sources of the slow solar wind (SW). In an article to be published in Solar Physics (van Driel-Gesztelyi et al., 2012) we make an attempt to step beyond anecdotic evidence and show that this is indeed the case - at least for some of the flows.
10 Jan. 2008

Using Bright-Point Shapes to Constrain Wave-Heating of the Solar Corona: Predictions for DKIST

Samuel J. **Van Kooten**, Steven R. Cranmer
ApJ **2024**
https://arxiv.org/pdf/2402.10915.pdf
Magnetic bright points on the solar photosphere mark the footpoints of kilogauss magnetic flux tubes extending toward the corona. Convective buffeting of these tubes is believed to excite magnetohydrodynamic waves, which can propagate to the corona and there deposit heat. Measuring wave excitation via bright-point motion can thus constrain coronal and heliospheric models, and this has been done extensively with centroid tracking, which can estimate kink-mode wave excitation. DKIST is the first telescope to provide well-resolved observations of bright points, allowing shape and size measurements to probe the excitation of other wave modes that have been difficult, if not impossible, to study to date. In this work, we demonstrate a method of automatic bright-point tracking that robustly identifies the shapes of bright points, and we develop a technique for interpreting measured bright-point shape changes as the driving of a range of thin-tube wave modes. We demonstrate these techniques on a MURaM simulation of DKIST-like resolution. These initial results suggest that modes other than the long-studied kink mode could increase the total available energy budget for wave-heating by 50%. Pending observational verification as well as modeling of the propagation and dissipation of these additional wave modes, this could represent a significant increase in the potency of wave-turbulence heating models.

Image restoration of solar spectra

Michiel **van Noort**
A&A **2017**
https://arxiv.org/pdf/1711.09629.pdf
When recording spectra from the ground, atmospheric turbulence causes degradation of the spatial resolution. We present a data reduction method that restores the spatial resolution of the spectra to their undegraded state. By assuming that the point spread function (PSF) estimated from a strictly synchronized, broadband slit-jaw camera is the same as the PSF that spatially degraded the spectra, we can quantify what linear combination of undegraded spectra is present in each degraded data point. The set of equations obtained in this way is found to be generally well-conditioned and sufficiently diagonal to be solved using an iterative linear solver. The resulting solution has regained a spatial resolution comparable to that of the restored slit-jaw images.

Active region upflows I. Multi-instrument observations⋆

K. **Vanninathan**1, M. S. Madjarska2, K. Galsgaard3, Z. Huang4 and J. G. Doyle
A&A 584, A38 (**2015**)
Context. We study upflows at the edges of active regions, called AR outflows, using multi-instrument observations.
Aims. This study intends to provide the first direct observational evidence of whether chromospheric jets play an important role in furnishing mass that could sustain coronal upflows. The evolution of the photospheric magnetic field, associated with the footpoints of the upflow region and the plasma properties of active region upflows is investigated with the aim of providing information for benchmarking data-driven modelling of this solar feature.
Methods. We spatially and temporally combine multi-instrument observations obtained with the Extreme-ultraviolet Imaging Spectrometer on board the Hinode, the Atmospheric Imaging Assembly and the Helioseismic Magnetic Imager instruments on board the Solar Dynamics Observatory and the Interferometric BI-dimensional Spectro-polarimeter installed at the National Solar Observatory, Sac Peak, to study the plasma parameters of the upflows and the impact of the chromosphere on active region upflows.
Results. Our analysis shows that the studied active region upflow presents similarly to those studied previously, i.e. it displays blueshifted emission of 5–20 kms-1 in Fe xii and Fe xiii and its average electron density is 1.8 × 109 cm-3 at 1 MK. The time variation of the density is obtained showing no significant change (in a 3σ error). The plasma density along a single loop is calculated revealing a drop of 50% over a distance of ~20 000 km along the loop. We find a second velocity component in the blue wing of the Fe xii and Fe xiii lines at 105 kms-1 reported only once before. For the first time we study the time evolution of this component at high cadence and find that it is persistent during the whole observing period of 3.5 h with variations of only±15 kms-1. We also, for the first time, study the evolution of the photospheric magnetic field at high cadence and find that magnetic flux diffusion is responsible for the formation of the upflow region. High cadence Hα observations are used to study the chromosphere at the footpoints of the upflow region. We find no significant jet-like (spicule/rapid blue excursion) activity to account for

several hours/days of plasma upflow. The jet-like activity in this region is not continuous and blueward asymmetries are a bare minimum. Using an image enhancement technique for imaging and spectral data, we show that the coronal structures seen in the AIA 193 Å channel are comparable to the EIS Fe xii images, while images in the AIA 171 Å channel reveal additional loops that are a result of contribution from cooler emission to this channel. Conclusions. Our results suggest that at chromospheric heights there are no signatures that support the possible contribution of spicules to active region upflows. We suggest that magnetic flux diffusion is responsible for the formation of the coronal upflows. The existence of two velocity components possibly indicates the presence of two different flows, which are produced by two different physical mechanisms, e.g. magnetic reconnection and pressure-driven jets.

Erratum to: Off-limb (Spicule) DEM Distribution from SoHO/SUMER Observations

K. **Vanninathan**, M. S. Madjarska, E. Scullion, J. G. Doyle
Solar Phys. **2014**
Erratum to: Solar Phys. (**2012**) 280:425–434 DOI10.1007/s11207-012-9986-8

Off-limb (Spicule) DEM Distribution from SoHO/SUMER Observations

K. **Vanninathan**, M. S. Madjarska, E. Scullion, J. G. Doyle
Solar Phys. Volume 280, Issue 2, pp.425-434 **2012**
In the present work we derive a Differential Emission Measure (DEM) distribution from a region dominated by spicules. We use spectral data from the Solar Ultraviolet Measurements of Emitted Radiation (SUMER) spectrometer on-board the Solar Heliospheric Observatory (SoHO) covering the entire SUMER wavelength range taken off-limb in the Northern polar coronal hole to construct this DEM distribution using the CHIANTI atomic database. This distribution is then used to study the thermal properties of the emission contributing to the 171 Å channel in the Atmospheric Imaging Assembly (AIA) on-board the Solar Dynamics Observatory (SDO). From our off-limb DEM we found that the radiance in the AIA 171 Å channel is dominated by emission from the Fe ix 171.07 Å line and has sparingly little contribution from other lines. The product of the Fe ix 171.07 Å line contribution function with the off-limb DEM was found to have a maximum at log T max (K)=5.8 indicating that during spicule observations the emission in this line comes from plasma at transition region temperatures rather than coronal. For comparison, the same product with a quiet Sun and prominence DEM were found to have a maximum at log T max (K)=5.9 and log T max (K)=5.7, respectively. We point out that the interpretation of data obtained from the AIA 171 Å filter should be done with foreknowledge of the thermal nature of the observed phenomenon. For example, with an off-limb DEM we find that only 3.6 % of the plasma is above a million degrees, whereas using a quiet Sun DEM, this contribution rises to 15 %.

A Revised Collection of Sunspot Group Numbers

J. M. **Vaquero**, L. Svalgaard, V. M. S. Carrasco, F. Clette, L. Lefèvre, M. C. Gallego, R. Arlt, A. J. P. Aparicio, J.-G. Richard, R. Howe
Solar Phys. **2016**
http://arxiv.org/pdf/1609.04882v1.pdf
We describe a revised collection of the number of sunspot groups from 1610 to the present. This new collection is based on the work of Hoyt and Schatten (Solar Phys. 179, 189, 1998). The main changes are the elimination of a considerable number of observations during the Maunder Minimum (hereafter, MM) and the inclusion of several long series of observations. Numerous minor changes are also described. Moreover, we have calculated the active-day percentage during the MM from this new collection as a reliable index of the solar activity. Thus, the level of solar activity obtained in this work is greater than the level obtained using the original Hoyt and Schatten data, although it remains compatible with a grand minimum of solar activity. The new collection is available in digital format.

Monitoring the Solar Radius from the Royal Observatory of the Spanish Navy during the Last Quarter-Millennium

J.M. **Vaquero**, M.C. Gallego, J.J. Ruiz-Lorenzo, T. López-Moratalla, V.M.S. Carrasco, A.J.P. Aparicio, F.J. González-González, E. Hernández-García
Solar Phys. Volume 291, Issue 6, pp 1599–1612 **2016**

http://arxiv.org/pdf/1606.03932v1.pdf

The solar diameter has been monitored at the Royal Observatory of the Spanish Navy (today the Real Instituto y Observatorio de la Armada: ROA) almost continuously since its creation in 1753 (i.e. during the last quarter of a millennium). After a painstaking effort to collect data in the historical archive of this institution, we present here the data of the solar semidiameter from 1773 to 2006, making up an extensive new database for solar-radius measurements can be considered. We have calculated the solar semidiameter from the transit times registered by the observers (except values of the solar radius from the modern Danjon astrolabe, which were published by ROA). These data were analysed to reveal any significant long-term trends, but no such trends were found. Therefore, the data sample confirms the constancy of the solar diameter during the last quarter of a millennium (approximately) within instrumental and methodological limits. Moreover, no relationship between solar radius and the new sunspot-number index has been found from measurements of the ROA. Finally, the mean value for solar semidiameter (with one standard deviation) calculated from the observations made in the ROA (1773-2006), after applying corrections by refraction and diffraction, is equal to 958.87" \pm 1.77"

Level and length of cyclic solar activity during the Maunder minimum as deduced from the active day statistics

J.M. **Vaquero**, G. A. Kovaltsov, I.G. Usoskin, V.M.S. Carrasco, M.C. Gallego
A&A 577, A71 **2015**
http://arxiv.org/pdf/1503.07664v1.pdf

The Maunder minimum (MM) of greatly reduced solar activity took place in 1645-1715, but the exact level of sunspot activity is uncertain as based, to a large extent, on historical generic statements of the absence of spots on the Sun. Here we aim, using a conservative approach, to assess the level and length of solar cycle during the Maunder minimum, on the basis of direct historical records by astronomers of that time. A database of the active and inactive days (days with and without recorded sunspots on the solar disc respectively) is constructed for three models of different levels of conservatism (loose ML, optimum MO and strict MS models) regarding generic no-spot records. We have used the active day fraction to estimate the group sunspot number during the MM. A clear cyclic variability is found throughout the MM with peaks at around 1655--1657, 1675, 1684 and 1705, and possibly 1666, with the active day fraction not exceeding 0.2, 0.3 or 0.4 during the core MM, for the three models. Estimated sunspot numbers are found very low in accordance with a grand minimum of solar activity.
We have found, for the core MM (1650-1700), that: (1) A large fraction of no-spot records, corresponding to the solar meridian observations, may be unreliable in the conventional database. (2) The active day fraction remained low (below 0.3-0.4) throughout the MM, indicating the low level of sunspot activity. (3) The solar cycle appears clearly during the core MM. (4) The length of the solar cycle during the core MM appears 9±1 years, but there is an uncertainty in that. (5) The magnitude of the sunspot cycle during MM is assessed to be below 5-10 in sunspot numbers;
A hypothesis of the high solar cycles during the MM is not confirmed.

Sunspot latitudes during the Maunder Minimum: a machine-readable catalogue from previous studies

J. M. **Vaquero**, J. M. Nogales, F. Sánchez-Bajo
Advances in Space Volume 55, Issue 6, Pages 1546–1552 **2015**
http://arxiv.org/ftp/arxiv/papers/1501/1501.05989.pdf
http://www.sciencedirect.com/science/article/pii/S0273117715000204

The Maunder Minimum (1645-1715 approximately) was a period of very low solar activity and a strong hemispheric asymmetry, with most of sunspots in the southern hemisphere. In this paper, two data sets of sunspot latitudes during the Maunder minimum have been recovered for the international scientific community. The first data set is constituted by latitudes of sunspots appearing in the catalogue published by Gustav Sp\"orer nearly 130 years ago. The second data set is based on the sunspot latitudes displayed in the butterfly diagram for the Maunder Minimum which was published by Ribes and Nesme-Ribes almost 20 years ago. We have calculated the asymmetry index using these data sets confirming a strong hemispherical asymmetry in this period. A machine-readable version of this catalogue with both data sets is available in the Historical Archive of Sunspot Observations (this http URL) and in the appendix of this article.

Redefining the limit dates for the Maunder Minimum

J. M. **Vaquero**, R. M. Trigo
2014
http://arxiv.org/pdf/1406.1630v1.pdf

The Maunder Minimum corresponds to a prolonged minimum of solar activity a phenomenon that is of particular interest to many branches of natural and social sciences commonly considered to extend from 1645 until 1715. However, our knowledge of past solar activity has improved significantly in recent years and, thus, more precise dates for the onset and termination of this particularly episode of our Sun can be established. Based on the simultaneous analysis of distinct proxies we propose a redefinition of the Maunder Minimum period with the core "Deep Maunder Minimum" spanning from 1645 to 1700 (that corresponds to the Grand Minimum state) and a wider "Extended Maunder Minimum" for the longer period 1618-1723 that includes the transition periods.

COMPOSITION MOSAICS FROM MARCH 2022

T. **Varesano**1,2,3, D. M. Hassler2, N. Zambrana Prado4, J. Plowman2, G. Del Zanna5, et al.
Solar Orbiter Nugget #34 Aug **2024**
https://www.cosmos.esa.int/web/solar-orbiter/-/science-nugget-composition-mosaics-from-march-2022
We found higher FIP bias values at the footpoints of the loops, indicating that fractionation occurs – even at lower heights below the corona and in the transition region – using sulfur and nitrogen diagnostics. The behavior of the element sulfur is especially interesting because it lies in the “intermediate-FIP” category, meaning that it does not always behave as a high-FIP nor as a low-FIP element. Rather, its behavior depends on the geometry of the magnetic field [9] . From our observations, sulfur behaves as a high-FIP element in closed magnetic loops, but as a low-FIP in the solar wind (open field). **2 Mar 2022**

The role of meridional flow in the generation of solar/stellar magnetic fields and cycles

Vindya **Vashishth**, Bidya Binay Karak
ApJ **974** 6 **2024**
https://arxiv.org/pdf/2407.16620
https://iopscience.iop.org/article/10.3847/1538-4357/ad7027/pdf
Meridional flow is crucial in generating the solar poloidal magnetic field by facilitating the poleward transport of the field from the decayed Bipolar Magnetic Regions (BMRs). As the meridional circulation changes with the stellar rotation rate, the properties of stellar magnetic cycles are expected to be influenced by this flow. In this study, we explore the role of meridional flow in generating magnetic fields in Sun and sun-like stars using STABLE, Surface flux Transport And Babcock-Leighton, dynamo model. We find that a moderate meridional flow increases the polar field by efficiently driving the trailing polarity flux toward the pole, while a strong flow tends to transport both polarities of BMRs poleward, potentially reducing the polar field. Our findings are in perfect agreement with what one can expect from the surface flux transport model. Similarly, the toroidal field initially increases with moderate flow speeds and then decreases after a certain value. This trend is due to the competitive effects of shearing and diffusion. Furthermore, our study highlights the impact of meridional flow on the cycle strength and duration in stellar cycles. By including the meridional flow from a mean-field hydrodynamics model in STABLE, we show that the magnetic field strength initially increases with the stellar rotation rate and then declines in rapidly rotating stars, offering an explanation of the observed variation of stellar magnetic field with rotation rate.

Hysteresis near the transition of the large-scale dynamo in the presence of the small-scale dynamo

Vindya **Vashishth**
Solar Phys. **299**, 115 **2024**
https://arxiv.org/pdf/2407.09042
https://doi.org/10.1007/s11207-024-02360-5
In Sun and solar-type stars, there is a critical dynamo number for the operation of a large-scale dynamo, below which the dynamo ceases to operate. This region is known as the subcritical region. Previous studies showed the possibility of operating the solar-like large-scale (global) dynamo in the subcritical region without a small-scale dynamo. As in the solar convection zone, both large- and small-scale dynamos are expected to operate at the same time and location, we check the robustness of the previously identified subcritical dynamo branch in a numerical model in which both large- and small-scale dynamos are excited. For this, we use the {\sc Pencil Code} and set up an $\alpha\Omega$ dynamo model with uniform shear and helically forced turbulence. We have performed a few sets of simulations at different relative helicity to explore the generation of large-scale oscillatory fields in the presence of small-scale dynamo. We find that in some parameter regimes, the dynamo shows hysteresis behavior, i.e., two dynamo solutions are possible depending on the initial parameters used. A decaying solution when the dynamo was started with a weak field and a strong oscillatory solution if the dynamo was initialized with a strong field. Thus, the existence of the sub-critical branch of the large-scale dynamo in the presence of small-scale dynamo is established. However, the regime of hysteresis is quite narrow with respect to the case without the small-scale dynamo. Our work supports the possible existence of large-scale dynamo in the sub-critical regime of slowly rotating stars.

Bistability in the sunspot cycle

Sumit **Vashishtha**, Katepalli R Sreenivasan

2024
https://arxiv.org/pdf/2406.05289
A direct dynamical test of the sunspot-cycle is carried out which indicates that a stochastically forced non-linear oscillator characterizes its dynamics. The sunspot series is then decomposed into its eigen time-delay coordinates. The analysis of these coordinates reveals that the sunspot series exhibits bistability, and suggests the possibility of modeling the solar cycle as a stochastically and periodically forced bistable oscillator, accounting for the Poloidal and Toroidal modes of the solar magnetic field. Such a representation of the sunspot series in terms of stochastic bistable dynamical system enables us to conjecture stochastic resonance as the key mechanism in amplifying the planetary influence of Jupiter on the sun, and that extreme events, due to turbulent convection noise inside the sun, dictate crucial phases of the sunspot cycle, such as the Maunder minimum.

Subcritical dynamo and hysteresis in a Babcock-Leighton type kinematic dynamo model

Vindya **Vashishth**, Bidya Binay Karak, Leonid Kitchatinov
Research in Astronomy and Astrophysics **2021**
https://arxiv.org/pdf/2107.01546.pdf
In Sun and sun-like stars, it is believed that the cycles of the large-scale magnetic field are produced due to the existence of differential rotation and helicity in the plasma flows in their convection zones (CZs). Hence, it is expected that for each star, there is a critical dynamo number for the operation of a large-scale dynamo. As a star slows down, it is expected that the large-scale dynamo ceases to operate above a critical rotation period. In our study, we explore the possibility of the operation of the dynamo in the subcritical region using the Babcock--Leighton type kinematic dynamo model. In some parameter regimes, we find that the dynamo shows hysteresis behavior, i.e., two dynamo solutions are possible depending on the initial parameters -- decaying solution if started with weak field and strong oscillatory solution (subcritical dynamo) when started with a strong field. However, under large fluctuations in the dynamo parameter, the subcritical dynamo mode is unstable in some parameter regimes. Therefore, our study supports the possible existence of subcritical dynamo in some stars which was previously shown in a mean-field dynamo model with distributed α and MHD turbulent dynamo simulations.

The solar dynamo begins near the surface

Geoffrey M **Vasil**, Daniel Lecoanet, Kyle Augustson, Keaton J Burns, Jeffrey S Oishi, Benjamin P Brown, Nicholas Brummell, Keith Julien
Nature **2024**
https://arxiv.org/pdf/2404.07740
The Sun's magnetic dynamo cycle features a distinct pattern: a propagating region of sunspot emergence appears around 30 degrees latitude and vanishes near the equator every 11 years. Moreover, longitudinal flows called ``torsional oscillations'' closely shadow sunspot migration, undoubtedly sharing a common. Contrary to theories suggesting deep origins for these phenomena, helioseismology pinpoints low-latitude torsional oscillations to the Sun's outer 5-10 percent, the ``Near-Surface Shear Layer''. Within this zone, inwardly increasing differential rotation coupled with a poloidal magnetic field strongly implicates the Magneto-Rotational Instability renowned in accretion-disk theory and observed in laboratory experiments. Together, these two facts prompt the general question: Is it possible that the solar dynamo is a near-surface instability? Here, we report strong affirmative evidence in stark contrast to traditional paradigms focusing on the deeper tachocline. Simple analytic estimates show that the near-surface magneto-rotational instability better explains the spatiotemporal scales of the torsional oscillations and inferred subsurface magnetic field amplitudes. State-of-the-art numerical simulations corroborate these estimates and, strikingly, reproduce hemispherical magnetic current helicity laws. The dynamo resulting from a well-understood near-surface phenomenon improves prospects for accurate predictions of full magnetic cycles and space weather, impacting Earth's electromagnetic infrastructure.

The rotational influence on solar convection

Geoffrey M. **Vasil**, Keith Julien, Nicholas A. Featherstone
2020
https://arxiv.org/pdf/2010.15383.pdf
This paper considers the dominant dynamical, thermal and rotational balances within the solar convection zone. The reasoning is such that: Coriolis forces balance pressure gradients. Background vortex stretching, baroclinic torques and nonlinear advection balance jointly. Turbulent fluxes convey what part of the solar luminosity that radiative diffusion cannot. These four relations determine estimates for the dominant length scales and dynamical amplitudes strictly in terms of known physical quantities. We predict that the dynamical Rossby number for convection is less than unity below the near-surface shear layer, indicating strong rotational constraint. We also predict a characteristic convection length scale of roughly 30 Mm throughout much of the convection zone. These inferences help explain recent observations that reveal weak flow amplitudes at 100-200 Mm scales.

Detecting stellar activity cycles in p-mode travel times: Proof of concept using SOHO/VIRGO solar observations

Valeriy **Vasilyev**, Laurent Gizon

A&A **2023**

https://arxiv.org/pdf/2312.01528.pdf

The eleven year solar cycle is known to affect the global modes of solar acoustic oscillations. In particular, p mode frequencies increase with solar activity. We propose a new method to detect the solar cycle from the p-mode autocorrelation function, and we validate this method using VIRGO/SPM photometric time series from solar cycles 23 and 24. The p-mode autocorrelation function shows multiple wavepackets separated by time lags of ∼123 min. Using a one-parameter fitting method (from local helioseismology), we measure the seismic travel times from each wavepacket up to skip number 40. We find that the travel-time variations due to the solar cycle depend sensitively on the skip number, with the strongest signature in odd skips from 17 to 31. Taking the noise covariance into account, the travel-time perturbations can be averaged over all skip numbers to enhance the signal-to-noise ratio. This method is robust to noise, simpler to implement than peak bagging in the frequency domain, and is promising for asteroseismology. We estimate that the activity cycle of a Sun-like star should be detectable with this new method in Kepler-like observations down to a visual magnitude of mK∼11. However, for fainter stars, activity cycles are easier to detect in the photometric variability on rotational timescales.

Tomography of the Solar Corona with the Wide-Field Imager for the Parker Solar Probe

Alberto M. **Vásquez**, Richard A. Frazin, Angelos Vourlidas, Ward B. ManchesterIV, Bart van der Holst, Russell A. Howard, Philippe Lamy

Solar Physics June **2019**, 294:81

sci-hub.se/10.1007/s11207-019-1471-1

The Wide-field Imager for the Parker Solar Probe (PSP/WISPR) comprises two telescopes that record white-light total brightness [B][B] images of the solar corona. Their fields of view cover a widely changing range of heliocentric heights over the 24 highly eccentric orbits planned for the mission. In this work, the capability of PSP/WISPR data to carry out tomographic reconstructions of the three-dimensional (3D) distribution of the coronal electron density is investigated. Based on the precise orbital information of the mission, BB-images for Orbits 1, 12, and 24 are synthesized from a 3D magnetohydrodynamic model of the corona. For each orbit, the time series of synthetic images is used to carry out a tomographic reconstruction of the coronal electron density and results are compared with the model. As the PSP perihelion decreases, the range of heights that can be tomographically reconstructed progressively shifts to lower values, and the period required to gather the data decreases. For Orbit 1 tomographic reconstruction is not possible. For Orbit 12, tomographic reconstruction is possible in the heliocentric height range ≈5--15 R⊙, over a region spanning up to ≈160∘≈160∘in Carrington longitude, with data gathered over a ≈3.4≈3.4 day-long period. For Orbit 24, tomographic reconstruction is possible in the heliocentric height range ≈3--10 R⊙, over a region spanning up to ≈170∘≈170∘ in Carrington longitude, with data gathered over a ≈2.8≈2.8 day-long period.

Long-Term Trends and Gleissberg Cycles in Aurora Borealis Records (1600 – 2015)

M. **Vázquez**, J. M. Vaquero , M. C. Gallego, T. Roca Cortés, P. L. Pallé

Solar Phys. Vol. 291, Issue 2 **2016**

The long-term spatial and temporal variation of aurora borealis events from 1600 to the present were studied using catalogues and other records of these phenomena. Geographic and geomagnetic coordinates were assigned to approximately 45 000 auroral events with more than 160 000 observations. They were analysed separately for three large-scale areas: i) Europe and North Africa, ii) North America, and iii) Asia. Variations in the cumulative numbers of auroral events with latitude (in both geographic and geomagnetic coordinates) were used to distinguish between the two main solar sources: coronal mass ejections and high-speed streams from coronal holes. We find significant long-term variations in the space-time distribution of auroras. We mainly identify these with four Gleissberg solar activity cycles whose overall characteristics we examine. The Asian observations are crucial in this context, and therefore merit further studies and verifications.

Connection between solar activity cycles and grand minima generation

A. **Vecchio**1, F. Lepreti2, M. Laurenza3, T. Alberti2 and V. Carbone

A&A 599, A58 (**2017**)

Aims. The revised dataset of sunspot and group numbers (released by WDC-SILSO) and the sunspot number reconstruction based on dendrochronologically dated radiocarbon concentrations have been analyzed to provide a deeper characterization of the solar activity main periodicities and to investigate the role of the Gleissberg and Suess cycles in the grand minima occurrence.

Methods. Empirical mode decomposition (EMD) has been used to isolate the time behavior of the different solar activity periodicities. A general consistency among the results from all the analyzed datasets verifies the reliability of the EMD approach.
Results. The analysis on the revised sunspot data indicates that the highest energy content is associated with the Schwabe cycle. In correspondence with the grand minima (Maunder and Dalton), the frequency of this cycle changes to longer timescales of ~14 yr. The Gleissberg and Suess cycles, with timescales of 60−120 yr and ~ 200−300 yr, respectively, represent the most energetic contribution to sunspot number reconstruction records and are both found to be characterized by multiple scales of oscillation. The grand minima generation and the origin of the two expected distinct types of grand minima, Maunder and longer Spörer-like, are naturally explained through the EMD approach. We found that the grand minima sequence is produced by the coupling between Gleissberg and Suess cycles, the latter being responsible for the most intense and longest Spörer-like minima (with typical duration longer than 80 yr). Finally, we identified a non-solar component, characterized by a very long scale oscillation of ~ 7000 yr, and the Hallstatt cycle (~ 2000 yr), likely due to the solar activity.
Conclusions. These results provide new observational constraints on the properties of the solar cycle periodicities, the grand minima generation, and thus the long-term behavior of the solar dynamo.

Understanding the origins of the heliosphere: integrating observations and measurements from Parker Solar Probe, Solar Orbiter, and other space- and ground-based observatories

Review

M. **Velli**1,7, L. K. Harra2,3, A. Vourlidas4, N. Schwadron5, O. Panasenco6 ….
A&A 642, A4 (**2020**)
https://www.aanda.org/articles/aa/pdf/2020/10/aa38245-20.pdf
https://doi.org/10.1051/0004-6361/202038245
Context. The launch of Parker Solar Probe (PSP) in 2018, followed by Solar Orbiter (SO) in February 2020, has opened a new window in the exploration of solar magnetic activity and the origin of the heliosphere. These missions, together with other space observatories dedicated to solar observations, such as the Solar Dynamics Observatory, Hinode, IRIS, STEREO, and SOHO, with complementary in situ observations from WIND and ACE, and ground based multi-wavelength observations including the DKIST observatory that has just seen first light, promise to revolutionize our understanding of the solar atmosphere and of solar activity, from the generation and emergence of the Sun's magnetic field to the creation of the solar wind and the acceleration of solar energetic particles.
Aims. Here we describe the scientific objectives of the PSP and SO missions, and highlight the potential for discovery arising from synergistic observations. Here we put particular emphasis on how the combined remote sensing and in situ observations of SO, that bracket the outer coronal and inner heliospheric observations by PSP, may provide a reconstruction of the solar wind and magnetic field expansion from the Sun out to beyond the orbit of Mercury in the first phases of the mission. In the later, out-of-ecliptic portions of the SO mission, the solar surface magnetic field measurements from SO and the multi-point white-light observations from both PSP and SO will shed light on the dynamic, intermittent solar wind escaping from helmet streamers, pseudo-streamers, and the confined coronal plasma, and on solar energetic particle transport.
Methods. Joint measurements during PSP–SO alignments, and magnetic connections along the same flux tube complemented by alignments with Earth, dual PSP–Earth, and SO-Earth, as well as with STEREO-A, SOHO, and BepiColumbo will allow a better understanding of the in situ evolution of solar-wind plasma flows and the full three-dimensional distribution of the solar wind from a purely observational point of view. Spectroscopic observations of the corona, and optical and radio observations, combined with direct in situ observations of the accelerating solar wind will provide a new foundation for understanding the fundamental physical processes leading to the energy transformations from solar photospheric flows and magnetic fields into the hot coronal plasma and magnetic fields and finally into the bulk kinetic energy of the solar wind and solar energetic particles.
Results. We discuss the initial PSP observations, which already provide a compelling rationale for new measurement campaigns by SO, along with ground- and space-based assets within the synergistic context described above.

Multicomponent Activity Cycles Using Hilbert–Huang Analysis

E. N. **Velloso**1, F. Anthony1, J.-D. do Nascimento Jr.1,2, L. F. Q. Silveira1, J. Hall3, and S. H. Saar2
2023 ApJL 945 L12
https://iopscience.iop.org/article/10.3847/2041-8213/acb8b4/pdf
The temporal analysis of stellar activity evolution is usually dominated by a complex trade-off between model complexity and interpretability, often by neglecting the nonstationary nature of the process. Recent studies appear to indicate that the presence of multiple coexisting cycles in a single star is more common than previously thought. The correct identification of physically meaningful cyclic components in spectroscopic time series is therefore a crucial task, which cannot overlook local behaviors. Here we propose a decomposition technique that adaptively recovers amplitude- and frequency-varying components. We present our results for the solar activity as measured both by the

sunspot number and the K-line emission index, and we consistently recover the Schwabe and Gleissberg cycles as well as the Gnevyshev–Ohl pattern probably related to the Hale cycle. We also recover the known 8 yr cycle for 61 Cygni A, in addition to evidence of a three-cycles-long pattern reminiscent of the Gnevyshev–Ohl rule. This is particularly interesting as we cannot discard the possibility of a relationship between the measured field polarity reversals and this Hale-like periodicity.

Successive injection of opposite magnetic helicity in solar active region NOAA 11928

P. **Vemareddy**1 and P. Démoulin2
A&A 597, A104 (**2017**)
http://www.aanda.org/articles/aa/pdf/2017/01/aa29282-16.pdf
https://arxiv.org/pdf/1611.00699v1.pdf
Aims. Understanding the nature and evolution of the photospheric helicity flux transfer is crucial to revealing the role of magnetic helicity in coronal dynamics of solar active regions.
Methods. We computed the boundary-driven helicity flux with a 12-min cadence during the emergence of the AR 11928 using SDO/HMI photospheric vector magnetograms and the derived flow velocity field. Accounting for the footpoint connectivity defined by nonlinear, force-free magnetic extrapolations, we derived and analyzed the corrected distribution of helicity flux maps.
Results. The photospheric helicity flux injection is found to change sign during the steady emergence of the AR. This reversal is confirmed with the evolution of the photospheric electric currents and with the coronal connectivity as observed in EUV wavelengths with SDO/AIA. During approximately the three first days of emergence, the AR coronal helicity is positive while later on the field configuration is close to a potential field. As theoretically expected, the magnetic helicity cancellation is associated with enhanced coronal activity.
Conclusions. The study suggests a boundary driven transformation of the chirality in the global AR magnetic structure. This may be the result of the emergence of a flux rope with positive twist around its apex while it has negative twist in its legs. The origin of such mixed helicity flux rope in the convective zone is challenging for models. **16-20 Dec 2013**

Recurrent solar density transients in the slow wind observed with the Metis coronagraph⋆

R. **Ventura**1, E. Antonucci2, C. Downs3, P. Romano1, R. Susino2, +++
A&A 675, A170 (**2023**)
https://www.aanda.org/articles/aa/pdf/2023/07/aa46623-23.pdf
Aims We aim to investigate and characterize the morphology and dynamics of small-scale coronal plasma density inhomogeneities detected as brighter, denser features propagating outward through the solar corona in the visible-light images of the Metis coronagraph on board Solar Orbiter on **February 22, 2021**. Our main focus is on investigating their possible origin and contribution to the slow wind variability and dynamics and their dependence on coronal magnetic field configurations and structure.
Methods. The method adopted is based on the computations of autocorrelation and cross-correlation functions applied to temporal and spatial series of total brightness as a function of the heliocentric distance and solar latitudes.
Results. We find that the plasma density inhomogeneities studied here are small-scale structures with typical radial and transverse sizes, as projected on the plane of sky, on the order of 500 Mm and 40 Mm, respectively, and that they are up to 24 times brighter than the ambient solar wind. The brighter density structures exhibit longer lifetime and more stable shape and dimensions as they travel toward the outer edge of the field of view. The enhanced density structures are ejected with a most probable cadence of about 80 min at or below the inner edge of the Metis field of view (within 3.1 R⊙–5.7 R⊙ at the time of observations) in a wide latitudinal region corresponding to the site of a complex web of separatrix and quasi-separatrix layers, as resulting from the simulated magnetohydrodynamic configuration of the west limb of the solar corona. Some of the moving density enhancements clearly show morphological characteristics compatible with the switchback phenomenon, supporting the results indicating that the switchbacks occur at the coronal level. The enhanced density structures were ejected into the ambient slow wind with a mean velocity of about 240 ± 40 km s−1, which is significantly higher than that deduced for the ambient solar wind on the basis of previous Metis observations during the solar minimum of cycle 24. The absence of acceleration observed across the coronagraph field of view suggests that the ejected plasmoids are progressively reaching the expansion rate of the ambient wind.
Conclusions. The results suggest that the quasi-periodic enhanced-density plasmoids might be the consequence of reconnection phenomena occurring in the complex web of the separatrix and quasi-separatrix layers present in the solar corona. Moreover, the structural characteristics of some of the detected plasmoids are in favor of the presence of switchbacks that originate during interchange reconnection processes occurring at or below 3 R⊙ in the S-web. The speed of the plasma ejected in the reconnection process is higher than that of the ambient slow solar wind and is likely to be related to the energy involved in the process generating the propagating structures.

Solar-wind predictions for the Parker Solar Probe orbit

M. S. **Venzmer**, V. Bothmer

A&A **2017**
https://arxiv.org/pdf/1711.07534.pdf
The scope of this study is to model the solar-wind environment for the Parker Solar Probe's unprecedented distances down to 9.86 Rs in its mission phase during 2018-2025. The study is performed within the CGAUSS project which is the German contribution to the PSP mission as part of the WISPR imager on PSP. We present an empirical solar-wind model for the inner heliosphere which is derived from OMNI and Helios data. The sunspot number (SSN) and its predictions are used to derive dependencies of solar-wind parameters on solar activity and to forecast them for the PSP mission. The frequency distributions for the solar-wind key parameters magnetic field strength, proton velocity, density, and temperature, are represented by lognormal functions, considering the velocity distribution's bi-componental shape. Functional relations to the SSN are compiled using OMNI data and based on data from both Helios probes, the parameters' frequency distributions are fitted with respect to solar distance. Thus, an empirical solar-wind model for the inner heliosphere is derived, accounting for solar activity and solar distance. The inclusion of SSN predictions and the extrapolation down to PSP's perihelion region enables us to estimate the solar-wind environment for PSP's planned trajectory during its mission duration. This empirical model yields estimated solar-wind values for PSP's 1st perihelion in 2018 at 0.16 au: 87 nT, 340 km s-1, 214 cm-3 and 503000 K. The estimates for PSP's first closest perihelion, occurring in 2024 at 0.046 au, are 943 nT, 290 km s-1, 2951 cm-3, and 1930000 K. Since the modeled velocity and temperature values below approximately 20 Rs appear overestimated in comparison with existing observations, this suggests that PSP will directly measure solar-wind acceleration and heating processes below 20 Rs as planned.

Classification of High-resolution Solar Hα Spectra using t-distributed Stochastic Neighbor Embedding

Meetu **Verma**, Gal Matijevič, Carsten Denker, Andrea Diercke, Ekaterina Dineva, Horst Balthasar, Robert Kamlah, Ioannis Kontogiannis, Christoph Kuckein, Partha S. Pal
ApJ **907** 54 **2020**
https://arxiv.org/pdf/2011.13214.pdf
https://doi.org/10.3847/1538-4357/abcd95
The H{\alpha} spectral line is a well-studied absorption line revealing properties of the highly structured and dynamic solar chromosphere. This study is based on high-spectral resolution H{\alpha} spectra obtained with the echelle spectrograph of the Vacuum Tower Telescope (VTT) located at Observatorio del Teide (ODT), Tenerife, Spain. The t-distributed Stochastic Neighbor Embedding (t-SNE) is a machine learning algorithm, which is used for nonlinear dimensionality reduction. In this application, it projects H{\alpha} spectra onto a two-dimensional map, where it becomes possible to classify the spectra according to results of Cloud Model (CM) inversions. The CM parameters optical depth, Doppler width, line-of-sight velocity, and source function describe properties of the cloud material. Initial results of t-SNE indicate its strong discriminatory power to separate quiet-Sun and plage profiles from those that are suitable for CM inversions. In addition, a detailed study of various t-SNE parameters is conducted, the impact of seeing conditions on the classification is assessed, results for various types of input data are compared, and the identified clusters are linked to chromospheric features. Although t-SNE proves to be efficient in clustering high-dimensional data, human inference is required at each step to interpret the results. This exploratory study provides a framework and ideas on how to tailor a classification scheme towards specific spectral data and science questions. **11 September 2018**

Long-term variations of the Sun's photospheric magnetic field

E.S. **Vernova**, M.I. Tyasto, D.G. Baranov
Geomagnetism and Aeronomy **63**, 966–974 **2023**
https://arxiv.org/pdf/2307.08009
https://doi.org/10.1134/S0016793223070277
Variations of the weak magnetic fields of the photosphere with periods of the order of the solar magnetic cycle were investigated. Synoptic maps of the photospheric magnetic field produced by NSO Kitt Peak for the period from 1978 to 2016 were used as initial data. In order to study weak magnetic fields, the saturation threshold for synoptic maps was set at 5 G. On the base of transformed synoptic maps the time-latitude chart was built. 18 profiles of the magnetic field evenly distributed along the sine of latitude from the north to the south pole were selected in the diagram for the further analysis. Time dependencies were averaged by sliding smoothing over 21 Carrington rotations. The approximation of averaged time dependencies by the sinusoidal function made it possible to distinguish in weak magnetic fields a cyclic component with a period of about 22 years (the period of the Hale magnetic cycle). The dependence of 22-year variation on latitude was studied. In addition to the well-known 22-year change in the near-polar field, similar variations were found for the fields at all latitudes. The exception was latitudes 26◦ and 33◦ in the northern and 26◦ in the southern hemisphere. These mid-latitude intervals were characterized by a predominance of short-period variations. The amplitude of the long-term variation decreased from the poles to the equator, with the period of variation remaining almost constant (T = 22.3 years).

Ripples and Rush-to-the-Poles in the photospheric magnetic field

Elena S. **Vernova**, Marta I. Tyasto, Dmitrii G. Baranov

Solar Phys. **298**, Article number: 69 **2023**

https://arxiv.org/pdf/2211.01140.pdf

https://doi.org/10.1007/s11207-023-02164-z

The distribution of magnetic fields of positive and negative polarities over the surface of the Sun was studied on the basis of synoptic maps NSO Kitt Peak (1978-2016). To emphasize the contribution of weak fields the following transformation of synoptic maps was made: for each synoptic map only magnetic fields with modulus less than 5 G (|B| < 5 G) were left unchanged on each synoptic map while larger or smaller fields were replaced by the corresponding limiting values +5 G or -5 G. Cyclic variations of the magnetic field polarity have been observed associated with two types of magnetic field flows in the photosphere. Rush-to-the-Poles (RTTP) form near the maximum of solar activity and have the same sign as the following sunspots. The lifetime of RTTP is 3 yrs, during which time they drift from latitudes 30 - 40 deg. to the pole, causing the polarity change of the Sun's polar field. We studied another type of variations which has the form of series of flows with individual flows of 0.5-1 yr and with alternating polarity (ripples). Ripples are located in time between two RTTP and drift from the equator to the latitudes of 50 deg. Magnetic field variations were considered in 6 time intervals along the latitudes +33 deg. in the northern and -33 deg. in the southern hemispheres. The time change of the field strength was approximated by the sinusoidal function. The period of variation of ripples was 1.1 yr for the N-hemisphere and 1.3 yr for the S-hemisphere. The amplitude of variation was higher for the time intervals where the polar field had a positive sign. Within the same flow, fields of positive and negative signs developed in anti-phase.

Nonaxisymmetric Component of Solar Activity: the Vector of the Longitudinal Asymmetry

E. S. **Vernova**, M. I. Tyasto, D. G. Baranov & O. A. Danilova

Solar Physics volume 295, Article number: 86 (**2020**)

https://link.springer.com/content/pdf/10.1007/s11207-020-01651-x.pdf

The vector representation of sunspots is used to study the nonaxisymmetric features of the solar activity distribution (sunspot data from Greenwich–USAF/NOAA, 1874–2016). Each sunspot is represented by a polar vector with modulus equal to the sunspot area and the phase equal to the sunspot heliolongitude. The vector sum of these individual vectors defines both the magnitude of the longitudinal asymmetry and the dominating longitude of the sunspot distribution. These characteristics are to a large extent free from the influence of a stochastic component and emphasize the nonaxisymmetric component of the solar activity. The longitudinal asymmetry follows the 11-year solar cycle with the amplitude three times lower than the sunspot area maximum. Longitudinal asymmetry is mostly determined by large sunspots: 82% of the longitudinal asymmetry is given by sunspots with area from 100 to 2000 MSH. Longitudinal asymmetries of the northern and southern hemispheres are connected only weakly (correlation coefficient R=0.29R=0.29). The longitudinal distribution displays a maximum at the longitude ∼180∘∼180∘ during ascent-maximum and at ∼0∘/360∘∼0∘/360∘ during descent-minimum. The active longitude changes with the reversals of polarity of the local (minimum of solar activity) and global magnetic fields (reversal of polar magnetic field).

Nonaxisymmetric Component of Solar Activity and the Gnevyshev-Ohl Rule

Elena **Vernova**, Marta Tyasto, Dmitrii Baranov, Olga Danilova

Solar Phys. **2019**

https://arxiv.org/pdf/1912.00388.pdf

The vector representation of sunspots is used to study the nonaxisymmetric features of the solar activity distribution (sunspot data from Greenwich - USAF/NOAA, 1874 - 2016).The vector of the longitudinal asymmetry is defined for each Carrington rotation; its modulus characterizes the magnitude of the asymmetry, while its phase points to the active longitude. These characteristics are to a large extent free from the influence of a stochastic component and emphasize the deviations from the axisymmetry. For the sunspot area, the modulus of the vector of the longitudinal asymmetry changes with the 11-year period; however, in contrast to the solar activity, the amplitudes of the asymmetry cycles obey a special scheme. Each pair of cycles from 12 to 23 follows in turn the Gnevyshev - Ohl rule (an even solar cycle is lower than the following odd cycle) or the anti-Gnevyshev - Ohl rule (an odd solar cycle is lower than the preceding even cycle). This effect is observed in the longitudinal asymmetry of the whole disk and the southern hemisphere. Possibly, this effect is a manifestation of the 44-year structure in the activity of the Sun. Northern hemisphere follows the Gnevyshev - Ohl rule in Solar Cycles 12 - 17, while in Cycles 18 - 23 the anti-rule is observed.

Non-axisymmetric component of the photospheric magnetic field

E. S. **Vernova**, **M. I. Tyasto**, **D. G. Baranov**, **O. A. Danilova**

Solar Phys. **2019**

https://arxiv.org/pdf/1904.03034.pdf

The longitudinal asymmetry of the photospheric magnetic field distribution is studied on the basis of the data of the Kitt Peak National Solar Observatory (synoptic maps for the period 1976 - 2016). The method of vector summing of magnetic fields is used, which allows to decrease the influence of the stochastic components uniformly distributed over the whole longitude interval, and to stress a steady non-axisymmetric component of the field. The distributions of magnetic fields of different intensity are considered separately for the strong (B > 50 G), weak (B < 5 G) and medium (50 > B > 5 G) fields. It is shown that the longitudinal asymmetry for all groups of fields changes in phase with the 11-year cycle of solar activity. The asymmetry of strong and medium fields changes in phase with magnetic fluxes of these fields, while the asymmetry of weak fields is in antiphase with the flux of weak fields. The distributions of strong and medium magnetic fields over the longitude are similar in the shape: The maximum of distribution is located at the longitude ~180° during the period of ascent - maximum of solar cycle and at the longitude ~360° during the period of descent - minimum. The weak fields exhibit the opposite picture: the maximum of their distribution is always observed at the longitude, where the strong and medium fields show minimum.

Positive and Negative Photospheric Fields in Solar Cycles 21 - 24

E.S. **Vernova**, M.I. Tyasto, D.G. Baranov, O.A. Danilova
Geomagnetism and Aeronomy **2018**
https://arxiv.org/pdf/1812.03552.pdf
Distribution of the positive and negative photospheric fields is studied on the base of synoptic maps of the photospheric magnetic field produced by the National Solar Observatory Kitt Peak (NSO Kitt Peak) for 1976-2016. In the analysis only the sign of the field irrespective of its strength is taken into account, emphasizing the role of the fields with average and weak strengths.
Time changes in the positive and negative magnetic fields for two hemispheres, for the high latitudes and for the sunspot zone as well as their imbalances are considered. Distributions of fields of opposite polarities, which are defined mostly by the fields of the high latitudes, change with a 22-year cycle. The polarity imbalance in each hemisphere is closely connected with the dipole moment g10.
The imbalance of high latitudes for two hemispheres changes with the 22-year period and coincides with the sign of both the polar field in the southern hemisphere, and the quadrupole moment g20. For the magnetic fields of the sunspot zone during ~75% of time a connection of the magnetic field imbalance with the quadrupole moment taken with the reversed sign −g20 and with the sign of the polar field in the northern hemisphere is observed. The received results testify to cyclic changes in the polarity imbalance.

Polarity imbalance of the photospheric magnetic field

E. S. **Vernova** (1), M. I. Tyasto (1), D. G. Baranov (2), O. A. Danilova (1)
Solar Phys. 293:158 **2018**
https://arxiv.org/pdf/1801.09249.pdf
https://link.springer.com/content/pdf/10.1007%2Fs11207-018-1382-6.pdf
Polarity imbalance of the photospheric magnetic field was studied using synoptic maps of NSO Kitt Peak (1976-2016). Imbalance of positive and negative fluxes was considered for the fields with strength B>50 G in the sunspot zone (5 deg - 40 deg) and for the fields with strength B<50 G at higher latitudes (40 deg - 90 deg). The 22-year periodicity in the imbalance of positive and negative fields was found which maintained itself during four solar cycles. While for the sunspot zone the sign of the imbalance always coincides with the northern hemisphere polarity, for the high latitudes the sign of the imbalance always coincides with the southern hemisphere polarity. Good correspondence of the flux imbalance with the quadrupole moment (g20) of the potential-field source-surface (PFSS) model was observed. The polarity imbalance of the sunspot zone correlates, on one hand, with the asymmetry of the magnetic field of the Sun-as-a-star and, on the other hand, with the sector structure of the interplanetary magnetic field. The obtained results show the close connection of the magnetic fields in active regions with the Sun's polar magnetic field. The weakest fields B<5 G represent quite a special group with the magnetic flux developing in antiphase to the fluxes of the stronger fields.

Photospheric Magnetic Field: Relationship Between North–South Asymmetry and Flux Imbalance

E. S. **Vernova**, M. I. Tyasto, D. G. Baranov
Solar Phys., **2014**
Photospheric magnetic fields were studied using the Kitt Peak synoptic maps for 1976 – 2003. Only strong magnetic fields (B>100 G) of the equatorial region were taken into account. The north–south asymmetry of the magnetic fluxes was considered as well as the imbalance between positive and negative fluxes. The north–south asymmetry displays a regular alternation of the dominant hemisphere during the solar cycle: the northern hemisphere dominated in the ascending phase, the southern one in the descending phase during Solar Cycles 21 – 23. The sign of the imbalance did not change during the 11 years from one polar-field reversal to the next and always coincided with the sign of the Sun’s polar magnetic field in the northern hemisphere. The dominant sign of leading sunspots in one

of the hemispheres determines the sign of the magnetic-flux imbalance. The sign of the north–south asymmetry of the magnetic fluxes and the sign of the imbalance of the positive and the negative fluxes are related to the quarter of the 22-year magnetic cycle where the magnetic configuration of the Sun remains constant (from the minimum where the sunspot sign changes according to Hale's law to the magnetic-field reversal and from the reversal to the minimum). The sign of the north–south asymmetry for the time interval considered was determined by the phase of the 11-year cycle (before or after the reversal); the sign of the imbalance of the positive and the negative fluxes depends on both the phase of the 11-year cycle and on the parity of the solar cycle. The results obtained demonstrate the connection of the magnetic fields in active regions with the Sun's polar magnetic field in the northern hemisphere.

Hemispheric sunspot numbers 1874--2020

Astrid M. **Veronig**, Shantanu Jain, Tatiana Podladchikova, Werner Poetzi, Frederic Clette
A&A 652, A56 **2021**
https://arxiv.org/pdf/2107.00553.pdf
https://www.aanda.org/articles/aa/pdf/2021/08/aa41195-21.pdf
https://doi.org/10.1051/0004-6361/202141195
We create a continuous series of daily and monthly hemispheric sunspot numbers (HSNs) from 1874 to 2020, which will be continuously expanded in the future with the HSNs provided by SILSO. Based on the available daily measurements of hemispheric sunspot areas from 1874 to 2016 from Greenwich Royal Observatory and NOAA, we derive the relative fractions of the northern and southern activity. These fractions are applied to the international sunspot number (ISN) to derive the HSNs. This method and obtained data are validated against published HSNs for the period 1945--2020. We provide a continuous data series and catalogue of daily, monthly mean, and 13-month smoothed monthly mean HSNs for the time range 1874--2020 that are consistent with the newly calibrated ISN. Validation of the reconstructed HSNs against the direct data available since 1945 reveals a high level of consistency, with a correlation of r=0.94 (0.97) for the daily (monthly) data. The cumulative hemispheric asymmetries for cycles 12-24 give a mean value of 16%, with no obvious pattern in north-south predominance over the cycle evolution. The strongest asymmetry occurs for cycle no. 19, in which the northern hemisphere shows a cumulated predominance of 42%. The phase shift between the peaks of solar activity in the two hemispheres may be up to 28 months, with a mean absolute value of 16.4 months. The phase shifts reveal an overall asymmetry of the northern hemisphere reaching its cycle maximum earlier (in 10 out of 13 cases). Relating the ISN and HSN peak growth rates during the cycle rise phase with the cycle amplitude reveals higher correlations when considering the two hemispheres individually, with r = 0.9. Our findings demonstrate that empirical solar cycle prediction methods can be improved by investigating the solar cycle dynamics in terms of the hemispheric sunspot numbers.

MHD wave modes resolved in fine-scale chromospheric magnetic structures **Review**

G. **Verth**, D. B. Jess
AGU/Wiley book "Low-frequency Waves in Space Plasmas", Reviews of Geophysics **2015**
http://arxiv.org/pdf/1505.01155v1.pdf
Within the last decade, due to significant improvements in the spatial and temporal resolution of chromospheric data, magnetohydrodynamic (MHD) wave studies in this fascinating region of the Sun's atmosphere have risen to the forefront of solar physics research. In this review we begin by reviewing the challenges and debates that have manifested in relation to MHD wave mode identification in fine-scale chromospheric magnetic structures, including spicules, fibrils and mottles. Next we go on to discuss how the process of accurately identifying MHD wave modes also has a crucial role to play in estimating their wave energy flux. This is of cardinal importance for estimating what the possible contribution of MHD waves is to solar atmospheric heating. Finally, we detail how such advances in chromospheric MHD wave studies have also allowed us, for the first time, to implement cutting-edge magnetoseismological techniques that provide new insight into the sub-resolution plasma structuring of the lower solar atmosphere.

Excitation and evolution of vertically polarised transverse loop oscillations by coronal rain

E. **Verwichte** and P. Kohutova
A&A 601, L2 (**2017**)
Context. Coronal rain is composed of cool dense blobs that form in solar coronal loops and are a manifestation of catastrophic cooling linked to thermal instability. The nature and excitation of oscillations associated with coronal rain is not well understood.
Aims. We consider observations of coronal rain in a bid to elucidate the excitation mechanism and evolution of wave characteristics.
Methods. We analyse IRIS and Hinode/SOT observations of an oscillating coronal rain event on the 17th Aug. 2014 and determine the wave characteristics as a function of time using tried and tested time-space analysis techniques.

Results. We exploit the seismological capability of the oscillation to deduce the relative rain mass from the oscillation amplitude. This is consistent with the evolution of the oscillation period showing the loop losing a third of its mass due to falling coronal rain in a 10−15 min time period.
Conclusions. We present the first evidence of the excitation of vertically polarised transverse loop oscillations triggered by catastrophic cooling at the loop top and consistent with two thirds of the loop mass being comprised of cool rain mass.

Kinematics of coronal rain in a transversely oscillating loop: Ponderomotive force and rain-excited oscillations

E. **Verwichte**1, P. Antolin2, G. Rowlands1, P. Kohutova1 and T. Neukirch
A&A 598, A57 (**2017**)
http://www.aanda.org/articles/aa/pdf/2017/02/aa29634-16.pdf
Context. Coronal rain is composed of cool dense blobs that form in solar coronal loops and are a manifestation of catastrophic cooling linked to thermal instability. Once formed, rain falls towards the solar surface at sub-ballistic speeds, which is not well understood. Pressure forces seem to be the prime candidate to explain this. In many observations rain is accompanied by transverse oscillations and the interaction between rain and these oscillations needs to be explored.
Aims. Therefore, an alternative kinematic model for coronal rain kinematics in transversely oscillating loops is developed to understand the physical nature of the observed sub-ballistic falling motion of rain. This model explicitly explores the role of the ponderomotive force arising from the transverse oscillation on the rain motion and the capacity of rain to excite wave motion.
Methods. An analytical model is presented that describes a rain blob guided by the coronal magnetic field supporting a one-dimensional shear Alfvén wave as a point mass on an oscillating string. The model includes gravity and the ponderomotive force from the oscillation acting on the mass and the inertia of the mass acting on the oscillation.
Results. The kinematics of rain in the limit of negligible rain mass are explored and falling and trapped regimes are found, depending on wave amplitude. In the trapped regime for the fundamental mode, the rain blob bounces back and forth around the loop top at a long period that is inversely proportional to the oscillation amplitude. The model is compared with several observational rain studies, including one in-depth comparison with an observation that shows rain with up-and-down bobbing motion. The role of rain inertia in exciting transverse oscillations is explored in inclined loops.
Conclusions. It is found that the model requires displacement amplitudes of the transverse oscillation that are typically an order of magnitude larger than observed to explain the measured sub-ballistic motion of the rain. Therefore, it is concluded that the ponderomotive force is not the primary reason for understanding sub-ballistic motion, but it plays a role in cases of large loop oscillations. The appearance of rain causes the excitation of small-amplitude transverse oscillations that may explain observed events and provide a seismological tool to measure rain mass.

Multiheight Observations of Atmospheric Gravity Waves at Solar Disk Center

Oana **Vesa**1, Jason Jackiewicz1, and Kevin Reardon2
2023 ApJ 952 58
https://iopscience.iop.org/article/10.3847/1538-4357/acd930/pdf
Atmospheric gravity waves (AGWs) are low-frequency, buoyancy-driven waves that are generated by turbulent convection and propagate obliquely throughout the solar atmosphere. Their proposed energy contribution to the lower solar atmosphere and sensitivity to atmospheric parameters (e.g., magnetic fields and radiative damping) highlight their diagnostic potential. We investigate AGWs near a quiet-Sun disk center region using multiwavelength data from the Interferometric Bidimensional Spectrometer and the Solar Dynamics Observatory. These observations showcase the complex wave behavior present in the entire acoustic-gravity wave spectrum. Using Fourier spectral analysis and local helioseismology techniques on simultaneously observed line core Doppler velocity and intensity fluctuations, we study both the vertical and horizontal properties of AGWs. Propagating AGWs with perpendicular group and phase velocities are detected at the expected temporal and spatial scales throughout the lower solar atmosphere. We also find previously unobserved, varied phase difference distributions among our velocity and intensity diagnostic combinations. Time–distance analysis indicates that AGWs travel with an average group speed of 4.5 km s−1, which is only partially described by a simple simulation, suggesting that high-frequency AGWs dominate the signal. Analysis of the median magnetic field (4.2 G) suggests that propagating AGWs are not significantly affected by quiet-Sun photospheric magnetic fields. Our results illustrate the importance of multiheight observations and the necessity of future work to properly characterize this observed behavior. **2019 April 25**

The luminosity constraint in the era of precision solar physics

Diego **Vescovi**, Carlo Mascaretti, Francesco Vissani, Luciano Piersanti, Oscar Straniero
JPhG **2020**
https://arxiv.org/pdf/2009.05676.pdf
The luminosity constraint is a very precise relationship linking the power released by the Sun as photons and the solar neutrino fluxes. Such a relation, which is a direct consequence of the physical processes controlling the production and the transport of energy in the solar interior, is of great importance for the studies of solar neutrinos and has a special role for the search of neutrinos from the CNO cycle, whose first detection with a 5σ significance has been recently announced by the Borexino collaboration. Here we revise the luminosity constraint, discussing and validating its underlying hypotheses, in the light of latest solar neutrino and luminosity measurements. We generalize the current formulation of the luminosity constraint relation so that it can be easily used in future analysis of solar neutrino data, and we provide a specific application showing the link between CNO and pp neutrino fluxes.

Solar and Heliospheric Phenomena in October–November 2003: Causes and Effects

I. S. **Veselovsky**, M. I. Panasyuk, S. I. Avdyushin, et al.
*Cosmic Research, Vol. 42, No. 5, **2004**, pp. 435–488. Translated from Kosmicheskie Issledovaniya, Vol. 42, No. 5, 2004, pp. 453–508.*
We present new observational data on the phenomena of extremely high activity on the Sun and in the heliosphere that took place in October–November 2003. A large variety of solar and heliospheric parameters give evidence that the interval under consideration is unique over the entire observation time. Based on these data, comparing them with similar situations in the past and using available theoretical concepts, we discuss possible cause-and-effect connections between the processes observed. The paper includes the first results and conclusions derived by the collaboration “Solar Extreme Events-2003” organized in Russia for detailed investigations of these events. As a result of our consideration, it is beyond question that the physical causes of solar and heliospheric phenomena in October–November 2003 are not exclusively local and do not belong only to the active regions and solar atmosphere above them. The energy reservoirs and driving forces of these processes have a more global nature. In general, they are hidden from an observer, since ultimately their sources lie in the subphotospheric layers of the Sun, where changes that are fast and difficult to predict can sometimes take place (and indeed they do). Solar flares can serve as sufficiently good tracers of these sudden changes and reconstructions on the Sun, although one can still find other diagnostic indicators among the parameters of magnetic fields, motions of matter, and emission characteristics.

The effects of a revised 7Be e−-capture rate on solar neutrino fluxes

D. **Vescovi**, L. Piersanti, S. Cristallo, M. Busso, F. Vissani, S. Palmerini, S. Simonucci, S. Taioli
A&A **2019**
https://arxiv.org/pdf/1902.01826.pdf
The electron-capture rate on 7Be is the main production channel for 7Li in several astrophysical environments. Theoretical evaluations have to account for not only the nuclear interaction, but also the processes in the plasma where 7Be ions and electrons interact. In the past decades several estimates were presented, pointing out that the theoretical uncertainty in the rate is in general of few percents. In the framework of fundamental solar physics, we consider here a recent evaluation for the 7Be+e− rate, not used up to now in the estimate of neutrino fluxes. We analysed the effects of the new assumptions on Standard Solar Models (SSMs) and compared the results obtained by adopting the revised 7Be+e− rate to those obtained by the one reported in a widely used compilation of reaction rates (ADE11). We found that new SSMs yield a maximum difference in the efficiency of the 7Be channel of about -4\% with respect to what is obtained with the previously adopted rate. This fact affects the production of neutrinos from 8B, increasing the relative flux up to a maximum of 2.7\%. Negligible variations are found for the physical and chemical properties of the computed solar models. The agreement with the SNO measurements of the neutral current component of the 8B neutrino flux is improved.

Neutral Hydrogen and its Emission Lines in the Solar Corona

Jean-Claude **Vial**, Martine Chane-Yook
Solar Physics **2016**
http://arxiv.org/pdf/1609.05092v1.pdf
Since the Lalpha rocket observations of (Gabriel, Solar Phys. 21, 392, 1971), it has been realized that the hydrogen (H) lines could be observed in the corona and offer an interesting diagnostic for the temperature, density, and radial velocity of the coronal plasma. Moreover, various space missions have been proposed to measure the coronal magnetic and velocity fields through polarimetry in H lines. A necessary condition for such measurements is to benefit from a sufficient signal-to-noise ratio. The aim of this article is to evaluate the emission in three representative lines of H for three different coronal structures. The computations have been performed with a full non-local thermodynamic equilibrium (non-LTE) code and its simplified version without radiative transfer. Since all collisionnal and radiative quantities (including incident ionizing and exciting radiation) are taken into account, the

ionization is treated exactly. Profiles are presented at two heights (1.05 and 1.9 solar radii, from Sun center) in the corona, and the integrated intensities are computed at heights up to five solar radii.We compare our results with previous computations and observations (e.g. Lalpha from UVCS) and find a rough (model-dependent) agreement. Since the Halpha line is a possible candidate for ground-based polarimetry, we show that in order to detect its emission in various coronal structures, it is necessary to use a very narrow (less than 2 A wide) bandpass filter.

Signatures of Steady Heating in Time Lag Analysis of Coronal Emission

Nicholeen M. **Viall**, James A. Klimchuk

ApJ 828 76 **2016**

http://arxiv.org/pdf/1607.02008v1.pdf

Among the many ways of investigating coronal heating, the time lag method of Viall & Klimchuk (2012) is becoming increasingly prevalent as an analysis technique complementary to those traditionally used. The time lag method cross correlates light curves at a given spatial location obtained in spectral bands that sample different temperature plasmas. It has been used most extensively with data from the Atmospheric Imaging Assembly on the Solar Dynamics Observatory. We have previously applied the time lag method to entire active regions and surrounding quiet Sun and create maps of the results (Viall & Klimchuk 2012; Viall & Klimchuk 2015). We find that the majority of time lags are consistent with the cooling of coronal plasma that has been impulsively heated. Additionally, a significant fraction of the map area has a time lag of zero. This does not indicate a lack of variability. Rather, strong variability must be present, and it must occur in phase in the different channels. We have shown previously that these zero time lags are consistent with the transition region response to coronal nanoflares (Viall & Klimchuk 2015; Bradshaw & Viall 2016), but other explanations are possible. A common misconception is that the zero time lag indicates steady emission resulting from steady heating. Using simulated and observed light curves, we demonstrate here that highly correlated light curves at zero time lag are not compatible with equilibrium solutions. Such light curves can only be created by evolution.

Periodic Density Structures and the Origin of the Slow Solar Wind

Nicholeen M. **Viall**1 and Angelos Vourlidas

2015 ApJ 807 176

The source of the slow solar wind has challenged scientists for years. Periodic density structures (PDSs), observed regularly in the solar wind at 1 AU, can be used to address this challenge. These structures have length scales of hundreds to several thousands of megameters and frequencies of tens to hundreds of minutes. Two lines of evidence indicate that PDSs are formed in the solar corona as part of the slow solar wind release and/or acceleration processes. The first is corresponding changes in compositional data in situ, and the second is PDSs observed in the inner Heliospheric Imaging data on board the Solar Terrestrial Relations Observatory (STEREO)/Sun Earth Connection Coronal and Heliospheric Investigation (SECCHI) suite. The periodic nature of these density structures is both a useful identifier as well as an important physical constraint on their origin. In this paper, we present the results of tracking periodic structures identified in the inner Heliospheric Imager in SECCHI back in time through the corresponding outer coronagraph (COR2) images. We demonstrate that the PDSs are formed around or below 2.5 solar radii—the inner edge of the COR2 field of view. We compute the occurrence rates of PDSs in 10 days of COR2 images both as a function of their periodicity and location in the solar corona, and we find that this set of PDSs occurs preferentially with a periodicity of ~90 minutes and occurs near streamers. Lastly, we show that their acceleration and expansion through COR2 is self-similar, thus their frequency is constant at distances beyond 2.5 solar radii.

SMESE (SMall Explorer for Solar Eruptions): A microsatellite mission with combined solar payload

J.-C. **Vial**, F. Auchère[a], J. Chang[b], C. Fang[c], W.Q. Gan[b], K.-L. Klein[d], J.-Y. Prado[e], F. Rouesnel[a], A. Sémery[d], G. Trottet[d] and C. Wang[f]

Advances in Space Research Volume 41, Issue 1, **2008**, Pages 183-189

The SMESE (SMall Explorer for Solar Eruptions) mission is a microsatellite proposed by France and China. The payload of SMESE consists of three packages: LYOT (a Lyman α imager and a Lyman α coronagraph), DESIR (an Infra-red Telescope working at 35–80 and 100–250 μm), and HEBS (a High Energy Burst Spectrometer working in X- and gamma-rays).

The scientific objectives of the mission are shortly presented. We describe the three instrumental packages and the profile of the mission which accommodates them. With a launch around 2012–2013, the SMESE microsatellite mission will provide a unique tool for detecting and understanding eruptions (flares and coronal mass ejections). Observations should start around solar maximum, and continue in the declining phase of activity, at a time when the Solar Dynamics Observatory (SDO) should still be operating.

Analysis of Pseudo-Lyapunov Exponents of Solar Convection Using State-of-the-Art Observations

Giorgio **Viavattene**, Mariarita Murabito, Salvatore L. Guglielmino, Ilaria Ermolli, Giuseppe Consolini, Fabrizio Giorgi, Shahin Jafarzadeh

Entropy **2021**

DOI: 10.3390/e23040413

https://arxiv.org/pdf/2103.16980.pdf

The solar photosphere and the outer layer of the Sun's interior are characterized by convective motions, which display a chaotic and turbulent character. In this work, we evaluated the pseudo-Lyapunov exponents of the overshooting convective motions observed on the Sun's surface by using a method employed in the literature to estimate those exponents, as well as another technique deduced from their definition. We analyzed observations taken with state-of-the-art instruments at ground- and space-based telescopes, and we particularly benefited from the spectro-polarimetric data acquired with the Interferometric Bidimensional Spectrometer, the Crisp Imaging SpectroPolarimeter, and the Helioseismic and Magnetic Imager. Following previous studies in the literature, we computed maps of four quantities which were representative of the physical properties of solar plasma in each observation, and estimated the pseudo-Lyapunov exponents from the residuals between the values of the quantities computed at any point in the map and the mean of values over the whole map. In contrast to previous results reported in the literature, we found that the computed exponents hold negative values, which are typical of a dissipative regime, for all the quantities derived from our observations. The values of the estimated exponents increase with the spatial resolution of the data and are almost unaffected by small concentrations of magnetic field. Finally, we showed that similar results were also achieved by estimating the exponents from residuals between the values at each point in maps derived from observations taken at different times. The latter estimation technique better accounts for the definition of these exponents than the method employed in previous studies.

Propagation of Leaky MHD Waves at Discontinuities with Tilted Magnetic Field

E.**Vickers**, I. Ballai, R. Erdélyi

Solar Phys. 293:139 **2018**

https://arxiv.org/pdf/1809.03907.pdf

We investigate the characteristics of magneto-acoustic surface waves propagating at a single density interface, in the presence of an inclined magnetic field. For linear wave propagation, dispersion relation is obtained and analytical solutions are derived for small inclination angle. The inclination of the field renders the frequency of waves to be complex, where the imaginary part describes wave attenuation, due to lateral energy leakage.

The magnetic field vector of the Sun-as-a-star.
II. Evolution of the large-scale vector field through activity cycle 24

A. A. **Vidotto** (Trinity College Dublin), L. Lehmann (St Andrews), M. Jardine (St Andrews), A. Pevtsov(NSO)

MNRAS **2018**

https://arxiv.org/pdf/1807.06334.pdf

In the present work, we investigate how the large-scale magnetic field of the Sun, in its three vector components, has evolved during most of cycle 24, from 2010 Jan to 2018 Apr. To filter out the small-scale field of the Sun, present in high-resolution synoptic maps, we use a spherical harmonic decomposition method, which decomposes the solar field in multipoles with different l degrees. By summing together the low-l multipoles, we reconstruct the large-scale field at a resolution similar to observed stellar magnetic fields, which allows the direct comparison between solar and stellar magnetic maps. During cycle 24, the `Sun-as-a-star' magnetic field shows a polarity reversal in the radial and meridional components, but not in the azimuthal component. The large-scale solar field remains mainly poloidal with > 70% of its energy contained in the poloidal component. During its evolution, the large-scale field is more axisymmetric and more poloidal when near minima in sunspot numbers, and with a larger intensity near maximum. There is a correlation between toroidal energy and sunspot number, which indicates that spot fields are major contributors to the toroidal large-scale energy of the Sun. The solar large-scale magnetic properties fit smoothly with observational trends of stellar magnetism reported in See et al. The toroidal (Etor) and poloidal (Epol) energies are related as Etor ~Epol^{1.38 \pm 0.04}. Similar to the stellar sample, the large-scale field of the Sun shows a lack of toroidal non-axisymmetric field.

On the influence of magnetic topology on the propagation of internal gravity waves in the solar atmosphere

G. **Vigeesh**, M. Roth, O. Steiner, B. Fleck

Phil. Trans. R. Soc. A, **2020**

https://arxiv.org/pdf/2010.06926.pdf
The solar surface is a continuous source of internal gravity waves (IGWs). IGWs are believed to supply the bulk of the wave energy for the lower solar atmosphere, but their existence and role for the energy balance of the upper layers is still unclear, largely due to the lack of knowledge about the influence of the Sun's magnetic fields on their propagation. In this work, we look at naturally excited IGWs in realistic models of the solar atmosphere and study the effect of different magnetic field topographies on their propagation. We carry out radiation-magnetohydrodynamic (R-MHD) simulations of a magnetic field free and two magnetic models -- one with an initial, homogeneous, vertical field of 100 G magnetic flux density and one with an initial horizontal field of 100 G flux density. The propagation properties of IGWs are studied by examining the phase-difference and coherence spectra in the kh-ω diagnostic diagram. We find that IGWs in the upper solar atmosphere show upward propagation in the model with predominantly horizontal field similar to the model without magnetic field. In contrast to that the model with predominantly vertical fields show downward propagation. This crucial difference in the propagation direction is also revealed in the difference in energy transported by waves for heights below 0.8 Mm. Higher up, the propagation properties show a peculiar behaviour, which require further study. Our analysis suggests that IGWs may play a significant role in the heating of the chromospheric layers of the internetwork region where horizontal fields are thought to be prevalent.

Synthetic observations of internal gravity waves in the solar atmosphere

G. **Vigeesh**, M. Roth
A&A 633, A140 (**2020**)
https://arxiv.org/pdf/1912.06435.pdf
https://doi.org/10.1051/0004-6361/201936846
We study the properties of internal gravity waves (IGWs) detected in synthetic observations that are obtained from realistic numerical simulation of the solar atmosphere. We used four different simulations of the solar magneto-convection performed using the CO5BOLD code. A magnetic-field-free model and three magnetic models were simulated. The latter three models start with an initial vertical, homogeneous field of 10, 50, and 100 G magnetic flux density, representing different regions of the quiet solar surface. We used the NICOLE code to compute synthetic spectral maps from all the simulated models for the two magnetically insensitive neutral iron lines Fe I 5434 Å and 5576 Å. We find the signatures of the internal gravity waves in the synthetic spectra to be consistent with observations of the real Sun. The phase differences obtained using the spectral lines are significantly different from the phase differences in the simulation. The phase coherency between two atmospheric layers in the gravity wave regime is height dependent and is seen to decrease with the travel distance between the observed layers. We conclude that the energy flux of IGWs determined from the phase difference analysis may be overestimated by an order of magnitude. Spectral lines that are weak and less temperature sensitive may be better suited to detecting internal waves and accurately determining their energy flux in the solar atmosphere.

Internal Gravity Waves in the Magnetized Solar Atmosphere. II. Energy Transport

G. **Vigeesh**, M. Roth, O. Steiner, J. Jackiewicz
ApJ **2019**
https://arxiv.org/pdf/1901.08871.pdf
In this second paper of the series on internal gravity waves (IGWs), we present a study of the generation and propagation of IGWs in a model solar atmosphere with diverse magnetic conditions. A magnetic field free, and three magnetic models that start with an initial, vertical, homogeneous field of 10 G, 50 G, and 100 G magnetic flux density, are simulated using the CO5BOLD code. We find that the IGWs are generated in similar manner in all four models in spite of the differences in the magnetic environment. The mechanical energy carried by IGWs is significantly larger than that of the acoustic waves in the lower part of the atmosphere, making them an important component of the total wave energy budget. The mechanical energy flux (106 - 103 W m−2) is few orders of magnitude larger than the Poynting flux (103 - 101 W m−2). The Poynting fluxes show a downward component in the frequency range corresponding to the IGWs, which confirm that these waves do not propagate upwards in the atmosphere when the fields are predominantly vertical and strong. We conclude that, in the upper photosphere, the propagation properties of IGWs depend on the average magnetic field strength and therefore these waves can be potential candidate for magnetic field diagnostics of these layers. However, their subsequent coupling to Alfvénic waves are unlikely in a magnetic environment permeated with predominantly vertical fields and therefore they may not directly or indirectly contribute to the heating of layers above plasma-β less than 1.

Internal Gravity Waves in the Magnetized Solar Atmosphere. I. Magnetic Field Effects

G. **Vigeesh**1,2, J. Jackiewicz2, and O. Steiner
2017 ApJ 835 148
Observations of the solar atmosphere show that internal gravity waves are generated by overshooting convection, but are suppressed at locations of magnetic flux, which is thought to be the result of mode conversion into magnetoacoustic waves. Here, we present a study of the acoustic-gravity wave spectrum emerging from a realistic,

self-consistent simulation of solar (magneto)convection. A magnetic field free, hydrodynamic simulation and a magnetohydrodynamic (MHD) simulation with an initial, vertical, homogeneous field of 50 G flux density were carried out and compared with each other to highlight the effect of magnetic fields on the internal gravity wave propagation in the Sun's atmosphere. We find that the internal gravity waves are absent or partially reflected back into the lower layers in the presence of magnetic fields and argue that the suppression is due to the coupling of internal gravity waves to slow magnetoacoustic waves still within the high-β region of the upper photosphere. The conversion to Alfvén waves is highly unlikely in our model because there is no strongly inclined magnetic field present. We argue that the suppression of internal waves observed within magnetic flux concentrations may also be due to nonlinear breaking of internal waves due to vortex flows that are ubiquitously present in the upper photosphere and the chromosphere.

Internal Gravity Waves in the Magnetized Solar Atmosphere. I. Magnetic Field Effects

G. **Vigeesh**, J. Jackiewicz, O. Steiner
ApJ **2016**
https://arxiv.org/pdf/1612.04729v1.pdf
Observations of the solar atmosphere show that internal gravity waves are generated by overshooting convection, but are suppressed at locations of magnetic flux, which is thought to be the result of mode conversion into magneto-acoustic waves. Here, we present a study of the acoustic-gravity wave spectrum emerging from a realistic, self-consistent simulation of solar (magneto-)convection. A magnetic field free, hydrodynamic simulation and a magneto-hydrodynamic (MHD) simulation with an initial, vertical, homogeneous field of 50 G flux density were carried out and compared with each other to highlight the effect of magnetic fields on the internal gravity wave propagation in the Sun's atmosphere. We find that the internal gravity waves are absent or partially reflected back into the lower layers in the presence of magnetic fields and argue that the suppression is due to the coupling of internal gravity waves to slow magneto acoustic waves still within the high-beta region of the upper photosphere. The conversion to Alfven waves is highly unlikely in our model because there is no strongly inclined magnetic field present. We argue that the suppression of internal waves observed within magnetic flux-concentrations may also be due to non-linear breaking of internal waves due to vortex flows that are ubiquitously present in the upper photosphere and the chromosphere.

The relevance of nuclear reactions for Standard Solar Models construction **Review**

Francesco L. **Villante**, Aldo Serenelli
Front. Astron. Space Sci. **2021**
https://arxiv.org/pdf/2101.03077.pdf
The fundamental processes by which nuclear energy is generated in the Sun have been known for many years. However, continuous progress in areas such as neutrino experiments, stellar spectroscopy and helioseismic data and techniques requires ever more accurate and precise determination of nuclear reaction cross sections, a fundamental physical input for solar models. In this work, we review the current status of (standard) solar models and present a detailed discussion on the relevance of nuclear reactions for detailed predictions of solar properties. In addition, we also provide an analytical model that helps understanding the relation between nuclear cross sections, neutrino fluxes and the possibility they offer for determining physical characteristics of the solar interior. The latter is of particular relevance in the context of the conundrum posed by the solar composition, the solar abundance problem, and in the light of the first ever direct detection of solar CN neutrinos recently obtained by the Borexino collaboration. Finally, we present a short list of wishes about the precision with which nuclear reaction rates should be determined to allow for further progress in our understanding of the Sun.

An updated discussion of the solar abundance problem **Review**

F.L. **Villante**, A. Serenelli
Proceedings of 5th International Solar Neutrino Conference **2020**
https://arxiv.org/pdf/2004.06365.pdf
We discuss the level of agreement of a new generation of standard solar models (SSMs), Barcelona 2016 or B16 for short, with helioseismic and solar neutrino data, confirming that models implementing the AGSS09met surface abundances, based on refined three-dimensional hydrodynamical simulations of the solar atmosphere, do not not reproduce helioseismic constraints. We clarify that this solar abundance problem can be equally solved by a change of the composition and/or of the opacity of the solar plasma, since effects produced by variations of metal abundances are equivalent to those produced by suitable modifications of the solar opacity profile. We discuss the importance of neutrinos produced in the CNO cycle for removing the composition-opacity degeneracy and the perspectives for their future detection.

The Chemical Composition of the Sun from Helioseismic and Solar Neutrino Data

Francesco L. **Villante**1,2, Aldo M. Serenelli3, Franck Delahaye4, and Marc H. Pinsonneault
2014 ApJ 787 13
We perform a quantitative analysis of the solar composition problem by using a statistical approach that allows us to combine the information provided by helioseismic and solar neutrino data in an effective way. We include in our analysis the helioseismic determinations of the surface helium abundance and of the depth of the convective envelope, the measurements of the 7Be and 8B neutrino fluxes, and the sound speed profile inferred from helioseismic frequencies. We provide all the ingredients to describe how these quantities depend on the solar surface composition, different from the initial and internal composition due to the effects of diffusion and nuclear reactions, and to evaluate the (correlated) uncertainties in solar model predictions. We include error sources that are not traditionally considered such as those from inversion of helioseismic data. We, then, apply the proposed approach to infer the chemical composition of the Sun. Our result is that the opacity profile of the Sun is well constrained by the solar observational properties. In the context of a two-parameter analysis in which elements are grouped as volatiles (i.e., C, N, O, and Ne) and refractories (i.e., Mg, Si, S, and Fe), the optimal surface composition is found by increasing the abundance of volatiles by (45 ± 4)% and that of refractories by (19 ± 3)% with respect to the values provided by Asplund et al. (2009, ARA&A, 47, 481). This corresponds to the abundances $\varepsilon O = 8.85 \pm 0.01$ and $\varepsilon Fe = 7.52 \pm 0.01$, which are consistent at the ~1σ level with those provided by Grevesse & Sauval (1998, SSRv, 85, 161). As an additional result of our analysis, we show that the best fit to the observational data is obtained with values of input parameters of the standard solar models (radiative opacities, gravitational settling rate, and the astrophysical factors S 34 and S 17) that differ at the ~1σ level from those presently adopted.

A new Generation of Standard Solar Models

Núria **Vinyoles**, Aldo M. Serenelli, Francesco L. Villante, Sarbani Basu, Johannes Bergström, M.C. Gonzalez-Garcia, Michele Maltoni, Carlos Peña-Garay, Ningqiang Song
2017 ApJ 835 202
https://arxiv.org/pdf/1611.09867v1.pdf
We compute a new generation of standard solar models (SSMs) that includes recent updates on some important nuclear reaction rates and a more consistent treatment of the equation of state. Models also include a novel and flexible treatment of opacity uncertainties based on opacity kernels, required in the light of recent theoretical and experimental works on radiative opacity. Two large sets of SSMs, each based on a different canonical set of solar abundances with high and low metallicity (Z), are computed to determine model uncertainties and correlations among different observables. We present detailed comparisons of high- and low-Z models against different ensembles of solar observables including solar neutrinos, surface helium abundance, depth of convective envelope and sound speed profile. A global comparison, including all observables, yields a p-value of 2.7σ for the high-Z model and 4.7σ for the low-Z one. When the sound-speed differences in the narrow region of $0.65<r/R_{sun}<0.70$ are excluded from the analysis, results are 0.9σ and 3.0σ for high- and low-Z models respectively. These results show that: high-Z models agree well with solar data but have a systematic problem right below the bottom of the convective envelope linked to steepness of molecular weight and temperature gradients, and that low-Z models lead to a much more general disagreement with solar data. We also show that, while simple parametrizations of opacity uncertainties can strongly alleviate the solar abundance problem, they are insufficient to substantially improve the agreement of SSMs with helioseismic data beyond that obtained for high-Z models due to the intrinsic correlations of theoretical predictions.

New axion and hidden photon constraints from a solar data global fit

Núria **Vinyoles**, Aldo Serenelli, Francesco L. Villante, Sarbani Basu, Javier Redondo, Jordi Isern
2015
http://arxiv.org/pdf/1501.01639v1.pdf
We present a new statistical analysis that combines helioseismology (sound speed, surface helium and convective radius) and solar neutrino observations (boron and beryllium fluxes) to place upper limits to the properties of non standard weakly interacting particles. Our analysis includes theoretical and observational errors, accounts for tensions between input parameters of solar models and can be easily extended to include other observational constraints. We present two applications to test the method: the well studied case of axions and axion-like particles and the more novel case of low mass hidden photons. For axions we obtain an upper limit at 3 sigma for the axion-photon coupling constant of g_a-gamma < 4 x 10^-10 GeV^-1. For hidden photons we obtain the most restrictive upper limit for the product of the kinetic mixing and mass of chi < 1.82 x 10^-12 eV/m at 3 sigma. Both cases improve the previous solar constraints based on the Standard Solar Models showing the power of our global statistical approach.

Periodicity analysis of galactic cosmic rays using Fourier, Hilbert, and higher-order spectral methods

V. **Vipindas**, Sumesh Gopinath, T. E. Girish
Astrophysics and Space Science April **2016**, 361:135
Galactic cosmic rays (GCRs) that traverse the heliosphere, in the energy range from several 100 MeV to a few GeV, are subjected to heliospheric modulation. GCRs interact with varying fields of the heliosphere to produce fluctuations in cosmic-ray intensity with variations in solar activity. The effects of modulation are continuously measured by the well-established world-wide neutron monitor network. Solar activity indices and cosmic-ray neutron monitor rates (at different cut-off rigidities) have been used to compare Fourier, Hilbert, and higher-order spectral (bispectral) features of GCR intensity variations at six stations for a period of nearly 50 years. The present study reveals that GCRs exhibit a number of short- and long-term periodicities that vary between 9 days and 22 years. The bispectral analysis shows the characteristic features of nonlinear coupling and complex phase relationships between various harmonics present in GCRs and solar activity proxies. We also offer possible explanations for the observed periodicities with the help of the previous findings.

Abrupt Shrinking of Solar Corona in the Late 1990s

Ilpo I. **Virtanen**, Jennimari S. Koskela, and Kalevi Mursula
2020 ApJL 889 L28
https://doi.org/10.3847/2041-8213/ab644b
We derive the longest uniform record of rotational intensities solar coronal magnetic field since 1968 and compare it with the heliospheric magnetic field (HMF) observed at the Earth. We scale the Mount Wilson Observatory and Wilcox Solar Observatory observations of the photospheric magnetic field to the level of the Synoptic Optical Long-term Investigations of the Sun/Vector Spectro Magnetograph and apply the potential field source surface model to calculate the coronal magnetic field. We find that the evolution of the coronal magnetic field during the last 50 yr agrees with the HMF observed at the Earth only if the effective coronal size, the distance of the coronal source surface of the HMF, is allowed to change in time. We calculate the optimum source surface distance for each rotation and find that it experienced an abrupt decrease in the late 1990s. The effective volume of the solar corona shrunk to less than one half during a short period of only a few years. We note that this abrupt shrinking coincides with other changes in solar magnetic fields that are likely related to the decrease of the overall solar activity, i.e., the demise of the Grand Modern Maximum.

Reconstructing solar magnetic fields from historical observations - VI. Axial dipole moments of solar active regions in cycles 21−24

I. O. I. **Virtanen**, I. I. Virtanen, A. A. Pevtsov and K. Mursula
A&A 632, A39 (**2019**)
https://sci-hub.se/10.0000/www.aanda.org/articles/aa/abs/2019/12/aa36134-19/aa36134-19.html
Context. The axial dipole moments of emerging active regions control the evolution of the axial dipole moment of the whole photospheric magnetic field and the strength of polar fields. Hale's and Joy's laws of polarity and tilt orientation affect the sign of the axial dipole moment of an active region. If both laws are valid (or both violated), the sign of the axial moment is normal. However, for some active regions, only one of the two laws is violated, and the signs of these axial dipole moments are the opposite of normal. Those opposite-sign active regions can have a significant effect, for example, on the development of polar fields.
Aims. Our aim is to determine the axial dipole moments of active regions identified from magnetographic observations and study how the axial dipole moments of normal and opposite signs are distributed in time and latitude in solar cycles 21−24.
Methods. We identified active regions in the synoptic maps of the photospheric magnetic field measured at the National Solar Observatory (NSO) Kitt Peak (KP) observatory, the Synoptic Optical Long term Investigations of the Sun (SOLIS) vector spectromagnetograph (VSM), and the Helioseismic and Magnetic Imager (HMI) aboard the Solar Dynamics Observatory (SDO), and determined their axial dipole moments.
Results. We find that, typically, some 30% of active regions have opposite-sign axial moments in every cycle, often making more than 20% of the total axial dipole moment. Most opposite-signed moments are small, but occasional large moments, which can affect the evolution of polar fields on their own, are observed. Active regions with such a large opposite-sign moment may include only a moderate amount of total magnetic flux. We find that in cycles 21−23 the northern hemisphere activates first and shows emergence of magnetic flux over a wider latitude range, while the southern hemisphere activates later, and emergence is concentrated to lower latitudes. Cycle 24 differs from cycles 21−23 in many ways. Cycle 24 is the only cycle where the northern butterfly wing includes more active regions than the southern wing, and where axial dipole moment of normal sign emerges on average later than opposite-signed axial dipole moment. The total axial dipole moment and even the average axial moment of active regions is smaller in cycle 24 than in previous cycles.

Reconstructing solar magnetic fields from historical observations - IV. Testing the reconstruction method

I. O. I. **Virtanen**, I. I. Virtanen, A. A. Pevtsov, L. Bertello, A. Yeates and K. Mursula
A&A 627, A11 (**2019**)
DOI: https://doi.org/10.1051/0004-6361/201935606
Aims. The evolution of the photospheric magnetic field has only been regularly observed since the 1970s. The absence of earlier observations severely limits our ability to understand the long-term evolution of solar magnetic fields, especially the polar fields that are important drivers of space weather. Here, we test the possibility to reconstruct the large-scale solar magnetic fields from Ca II K line observations and sunspot magnetic field observations, and to create synoptic maps of the photospheric magnetic field for times before modern-time magnetographic observations.
Methods. We reconstructed active regions from Ca II K line synoptic maps and assigned them magnetic polarities using sunspot magnetic field observations. We used the reconstructed active regions as input in a surface flux transport simulation to produce synoptic maps of the photospheric magnetic field. We compared the simulated field with the observed field in 1975−1985 in order to test and validate our method.
Results. The reconstruction very accurately reproduces the long-term evolution of the large-scale field, including the poleward flux surges and the strength of polar fields. The reconstruction has slightly less emerging flux because a few weak active regions are missing, but it includes the large active regions that are the most important for the large-scale evolution of the field. Although our reconstruction method is very robust, individual reconstructed active regions may be slightly inaccurate in terms of area, total flux, or polarity, which leads to some uncertainty in the simulation. However, due to the randomness of these inaccuracies and the lack of long-term memory in the simulation, these problems do not significantly affect the long-term evolution of the large-scale field.

Reconstructing solar magnetic fields from historical observations
III. Activity in one hemisphere is sufficient to cause polar field reversals in both hemispheres

I. O. I. **Virtanen**1, I. I. Virtanen1, A. A. Pevtsov2,1 and K. Mursula1
A&A 616, A134 (**2018**)
Aims. Sunspot activity is often hemispherically asymmetric, and during the Maunder minimum, activity was almost completely limited to one hemisphere. In this work, we use surface flux simulation to study how magnetic activity limited only to the southern hemisphere affects the long-term evolution of the photospheric magnetic field in both hemispheres. The key question is whether sunspot activity in one hemisphere is enough to reverse the polarity of polar fields in both hemispheres.
Methods. We simulated the evolution of the photospheric magnetic field from 1978 to 2016 using the observed active regions of the southern hemisphere as input. We studied the flow of magnetic flux across the equator and its subsequent motion towards the northern pole. We also tested how the simulated magnetic field is changed when the activity of the southern hemisphere is reduced.
Results. We find that activity in the southern hemisphere is enough to reverse the polarity of polar fields in both hemispheres by the cross-equatorial transport of magnetic flux. About 1% of the flux emerging in the southern hemisphere is transported across the equator, but only 0.1%–0.2% reaches high latitudes to reverse and regenerate a weak polar field in the northern hemisphere. The polarity reversals in the northern hemisphere are delayed compared to the southern hemisphere, leading to a quadrupole Sun lasting for several years.

Photospheric and coronal magnetic fields in six magnetographs
I. Consistent evolution of the bashful ballerina

Ilpo **Virtanen** and Kalevi Mursula
A&A 591, A78 **(2016)**
Aims. We study the long-term evolution of photospheric and coronal magnetic fields and the heliospheric current sheet (HCS), especially its north-south asymmetry. Special attention is paid to the reliability of the six data sets used in this study and to the consistency of the results based on these data sets.
Methods. We use synoptic maps constructed from Wilcox Solar Observatory (WSO), Mount Wilson Observatory (MWO), Kitt Peak (KP), SOLIS, SOHO/MDI, and SDO/HMI measurements of the photospheric field and the potential field source surface (PFSS) model.
Results. The six data sets depict a fairly similar long-term evolution of magnetic fields and the heliospheric current sheet, including polarity reversals and hemispheric asymmetry. However, there are time intervals of several years long, when first KP measurements in the 1970s and 1980s, and later WSO measurements in the 1990s and early 2000s, significantly deviate from the other simultaneous data sets, reflecting likely errors at these times. All of the six magnetographs agree on the southward shift of the heliospheric current sheet (the so-called bashful ballerina phenomenon) in the declining to minimum phase of the solar cycle during a few years of the five included cycles.

We show that during solar cycles 20–22, the southward shift of the HCS is mainly due to the axial quadrupole term, reflecting the stronger magnetic field intensity at the southern pole during these times. During cycle 23 the asymmetry is less persistent and mainly due to higher harmonics than the quadrupole term. Currently, in the early declining phase of cycle 24, the HCS is also shifted southward and is mainly due to the axial quadrupole as for most earlier cycles. This further emphasizes the special character of the global solar field during cycle 23.

North-South Asymmetric Solar Cycle Evolution: Signatures in the Photosphere and Consequences in the Corona

I. I. **Virtanen** and K. Mursula
2014 ApJ 781 99
The heliospheric current sheet is the continuum of the coronal magnetic equator that divides the heliospheric magnetic field into two sectors (polarities). Several recent studies have shown that the heliospheric current sheet is southward shifted during approximately 3 years in the solar declining phase (the so-called bashful ballerina phenomenon). In this article we study the hemispherical asymmetry in the photospheric and coronal magnetic fields using Wilcox Solar Observatory measurements of the photospheric magnetic field since 1976 as well as the potential field source surface model. Multipole analysis of the photospheric magnetic field shows that during the late declining phase of solar cycles since the 1970s, the "bashful ballerina phenomenon" is a consequence of the quadrupole term, signed oppositely to the dipole moment. Surges of new flux transport magnetic field from low latitudes to the poles, thus leading to a systematically varying contribution to the -term from different latitudes. In the case of a north-south asymmetric flux production, this is seen as a quadrupole contribution traveling toward higher latitudes. When the quadrupole term is largest, the main contribution comes from the polar latitudes. At least during the four recent solar cycles, the -term arises because the magnitude of the southern polar field is larger than the magnitude found in the north in the declining phase of the cycle. In the heliosphere this hemispheric asymmetry of the coronal fields is seen as a southward shift of the heliospheric current sheet by about 2°.

Solar Mean Magnetic Field of the Chromosphere

M. **Vishnu**, K. Nagaraju, Harsh Mathur
J. Astrophys. Astr. **2023**
https://arxiv.org/pdf/2302.06924.pdf
The Solar Mean Magnetic Field (SMMF) is the mean value of the line of sight (LOS) component of the solar vector magnetic field averaged over the visible hemisphere of the Sun. So far, the studies on SMMF have mostly been confined to the magnetic field measurements at the photosphere. In this study, we calculate and analyse the SMMF using magnetic field measurements at the chromosphere, in conjunction with that of photospheric measurements. For this purpose, we have used full disk LOS magnetograms derived from spectropolarimetric observations carried out in Fe I 630.15 nm and Ca II 854.2 nm by the Synoptic Optical Long term Investigations of the Sun (SOLIS)/Vector Spectromagnetograph (VSM) instrument during 2010 to 2017. It is found from this study that the SMMF at the chromosphere is weaker by a factor of 0.60 compared to the SMMF at the upper photosphere. The correlation analysis between them gives a Pearson correlation coefficient of 0.80. The similarity and reduced intensity of the chromospheric SMMF with respect to the photospheric SMMF corroborate the idea that it is the source of the Interplanetary Magnetic Field (IMF).

Luminosity constraint and entangled solar neutrino signals

Francesco **Vissani**
Presented at the 5th International Solar Neutrino Conference, Dresden, Germany, June **2018**
https://arxiv.org/pdf/1808.01495.pdf
Now that neutrino propagation phenomena are understood, solar neutrino physics is entering an era when observational progresses indicate new challenges. The luminosity constraint plays a key role for current needs. We present it in a new form, improving the coefficients originally obtained by J. Bahcall, Phys. Rev. C 65 (2002) 025801. It turns out that the PP- and CNO-neutrino signals are entangled: In fact, pp-neutrinos can be extracted from the luminosity constraint only when CNO-neutrinos are quantified; the interpretation of the results of the gallium experiments depends upon both fluxes; a precise knowledge of pep-neutrinos is a precondition to extract the CNO-neutrino signal with Borexino.

Dissecting bombs and bursts: non-LTE inversions of low-atmosphere reconnection in SST and IRIS observations

G. J. M. **Vissers**, J. de la Cruz Rodriguez, T. Libbrecht, L. H. M. Rouppe van der Voort, G. B. Scharmer, M. Carlsson
A&A 627, A101 **2019**
https://arxiv.org/pdf/1905.02035.pdf

Ellerman bombs and UV bursts are transient brightenings that are ubiquitously observed in the lower atmospheres of active and emerging flux regions. Here we present inversion results of SST/CRISP and CHROMIS, as well as IRIS data of such transient events. Combining information from the Mg II h & k, Si IV and Ca II 8542A and Ca II H & K lines, we aim to characterise their temperature and velocity stratification, as well as their magnetic field configuration. We find average temperature enhancements of a few thousand kelvin close to the classical temperature minimum, but localised peak temperatures of up to 10,000-15,000 K from Ca II inversions. Including Mg II generally dampens these temperature enhancements to below 8000 K, while Si IV requires temperatures in excess of 10,000 K at low heights, but may also be reproduced with secondary temperature enhancements of 35,000-60,000 K higher up. However, reproducing Si IV comes at the expense of overestimating the Mg II emission. The line-of-sight velocity maps show clear bi-directional jet signatures and strong correlation with substructure in the intensity images, with slightly larger velocities towards the observer than away. The magnetic field parameters show an enhancement of the horizontal field co-located with the brightenings at similar heights as the temperature increase. We are thus able to largely reproduce the observational properties of Ellerman bombs with UV burst signature with temperature stratifications peaking close to the classical temperature minimum. Correctly modelling the Si IV emission in agreement with all other diagnostics is, however, an outstanding issue. Accounting for resolution differences, fitting localised temperature enhancements and/or performing spatially-coupled inversions is likely necessary to obtain better agreement between all considered diagnostics. **September 3 and 5, 2016**,

Automating Ellerman bomb detection in ultraviolet continua

Gregal J. M. **Vissers**, Luc H. M. Rouppe van der Voort, Robert J. Rutten
A&A 626, A4 **2019**
https://arxiv.org/pdf/1901.07975.pdf
Ellerman bombs are transient brightenings in the wings of H-alpha 6563 {\AA} that pinpoint photospheric sites of magnetic reconnection in solar active regions. Their partial visibility in the 1600 {\AA} and 1700 {\AA} continua registered routinely by the Atmospheric Imaging Assembly (AIA) onboard the Solar Dynamics Observatory (SDO) offers a unique opportunity to inventory such magnetic-field disruptions throughout the AIA database if a reliable recipe for their detection can be formulated. This is done here. We improve and apply an H-alpha Ellerman bomb detection code to ten data sets spanning viewing angles from solar disc centre to the limb. They combine high-quality H-alpha imaging spectroscopy from the Swedish 1-m Solar Telescope with simultaneous AIA imaging around 1600 {\AA} and 1700 {\AA}. A trial grid of brightness, lifetime and area constraints is imposed on the AIA images to define optimal recovery of the 1735 Ellerman bombs detected in H-alpha. The best results when optimising simultaneously for recovery fraction and reliability are obtained from 1700 {\AA} images by requiring 5-sigma brightening above the average 1700 {\AA} nearby quiet-Sun intensity, lifetime above one minute, area of 1-18 AIA pixels. With this recipe 27% of the AIA detections are H-alpha-detected Ellerman bombs while it recovers 19% of these (of which many are smaller than the AIA resolution). Better yet, among the top 10% AIA 1700 {\AA} detections selected with combined brightness, lifetime and area thresholds as many as 80% are H-alpha Ellerman bombs. Automated selection of the best 1700 {\AA} candidates therefore opens the entire AIA database for detecting most of the more significant photospheric reconnection events. This proxy is applicable as flux-dynamics tell-tale in studying any Earth-side solar active region since early 2010 up to the present.

Sunspot periodicity

Claudio **Vita-Finzi**
2022
https://arxiv.org/ftp/arxiv/papers/2212/2212.03249.pdf
The Schwabe (~11 yr) value for the annual sunspot number is sometimes uncritically applied to other measures of solar activity, direct and indirect, including the 10.7 cm radio flux, the inflow of galactic cosmic rays, solar flare frequency, terrestrial weather, and components of space climate, with the risk of a resulting loss of information. The ruling (Babcock) hypothesis and its derivatives link the sunspot cycle to dynamo processes mediated by differential solar rotation, but despite 60 years of observation and analysis the ~11 yr periodicity remains difficult to model; the possible contribution of planetary dynamics is undergoing a revival. The various solar sequences that genuinely display an ~11 yr cycle stand to benefit from an understanding of its periodicity that goes beyond statistical kinship. The outcome could ironically prompt the demotion of sunspots from their dominant historical role in favour of other possible indicators of solar cyclicity, such as the solar wind flux and its isotopic signatures, even if they are less accessible.

Core to solar wind: a stepwise model for heating the solar corona

Claudio **Vita-Finzi**
2021
https://arxiv.org/ftp/arxiv/papers/2101/2101.08251.pdf
Operating experience from fusion research shows how Spitzer resistivity may render ohmic heating in the chromosphere self limiting and thus serve to define the lower margin of the transition region. Its upper margin is at

about 6000 K, where radiative cooling of He:H plasma decelerates sharply. The third and last stage in the proposed scheme is expansion into the tenuous plasma of space, which leads to the acceleration of ions to high energies, long recorded by spacecraft instruments. There is thus dynamic continuity all the way from the solar interior, the energy source for spinning columns in the Rayleigh Benard setting of the convection zone, to the coronal exhalation of the solar wind, a finding which should benefit the analysis of space weather, witness the association between helium in the solar wind and the incidence of coronal mass ejections.

The contribution of the Joule-Thomson effect to solar coronal heating

Claudio **Vita-Finzi**

2016

https://arxiv.org/pdf/1612.07943v1.pdf

Two of the three gases that display isenthalpic Joule-Thomson (J-T) warming under laboratory conditions are hydrogen and helium, the main constituents of the solar plasma, but the temperatures that are attained by this route are at most a few hundred K. Increases in ion temperature by several orders of magnitude are claimed for hydrogen plasmas subject to expansion into a vacuum; modest increases are reported for the shortlived tests of this effect that have been carried out in space in the wakes of artificial satellites and of the Moon. Attempts to calculate the J-T coefficient at very high temperatures using equations of state and thermodynamics remain very preliminary. The potential contribution of plasma expansion to heating of the solar corona must therefore be assessed empirically, but this is consistent with how the J-T effect was first identified. The sunspot record, EUV measurements by the EVE instrument on the SDO satellite, and solar wind fluctuations documented by the ACE satellite indicate broadly coherent periodicity from the photosphere to the outer corona consistent with a non-pulsatory heating process. It comprises three successive stages characterised by induction, the J-T mechanism, and plasma expansion. Astronomical data may therefore be used to derive rather than to test an extension of the J-T effect which could help to explain heating in other solar system bodies and other stellar coronae.

The solar chromosphere as induction disk and the inverse Joule-Thomson effect

Claudio **Vita-Finzi**

2016

https://arxiv.org/ftp/arxiv/papers/1609/1609.00508.pdf

The connection between nuclear fusion in the Sun's core and solar irradiance is obscured among other things by uncertainty over the mechanism of coronal heating. Data for solar wind density and velocity, sunspot number, and EUV flux suggest that electromagnetic energy from the Sun's convection zone is converted by induction through the chromosphere into thermal energy. The helium and hydrogen mixture exhaled by the Sun is then heated by the inverse Joule-Thomson effect when it expands via the corona into space. The almost complete shutdown of the solar wind on **10-11 May 1999** demonstrated that its velocity is a more faithful indicator of solar activity than are sunspots as it reflects short-term variations in coronal heating rather than quasicyclical fluctuations in the Sun's magnetism. Its reconstruction from the cosmic ray flux using isotopes spanning over 800,000 yr should therefore benefit the analysis and long-term forecasting of Earth and space weather.

Hunting down the cause of solar magnetism

M. **Viviani**, A. Prabhu, J. Warnecke, L. Duarte, J. Pekkilä, M. Rheinhardt, M. J. Käpylä

"High Performance Computing Science and Engineering, Garching/Munich, 2020". Editors: P. Bastina, D. Kranzmüller, H. Brëuchle, M. Brehm. ISBN: 978-3-9816675-4-7 **2021**

https://arxiv.org/ftp/arxiv/papers/2102/2102.03168.pdf

To understand solar and stellar dynamos combining local and global numerical modelling with long-term observations is a challenging task: even with state of the art computational methods and resources, the stellar parameter regime remains unattainable. Our goal is to relax some approximations, in order to simulate more realistic systems, and try to connect the results with theoretical predictions and state-of-the-art observations. We present here the first test-field measurements from our higher-resolution runs with improved heat conduction description. They indicate significant changes in the profiles of the most crucial inductive effect related to solar and stellar dynamo mechanisms. Higher resolution runs, currently undertaken, will bring us into an even more turbulent regime, in which we will be able to study, for the first time, the interaction of small- and large-scale dynamos in a quantitative way.

Physically motivated heat-conduction treatment in simulations of solar-like stars: effects on dynamo transitions

M. **Viviani1**,2 and M. J. Käpylä3,2,4

A&A 645, A141 (**2021**)

https://doi.org/10.1051/0004-6361/202038603

https://www.aanda.org/articles/aa/pdf/2021/01/aa38603-20.pdf
Results from global magnetoconvection simulations of solar-like stars are at odds with observations in many respects: simulations show a surplus of energy in the kinetic power spectrum at large scales; anti-solar differential rotation profiles with accelerated poles, and a slow equator for the solar rotation rate; and a transition from axi- to nonaxisymmetric dynamos at a much lower rotation rate than what is observed. Even though the simulations reproduce the observed active longitudes in fast rotators, their motion in the rotational frame (the so-called azimuthal dynamo wave, ADW) is retrograde, in contrast to the prevalent prograde motion in observations.
Aims. We study the effect of a more realistic treatment of heat conductivity in alleviating the discrepancies between observations and simulations.
Methods. We use physically motivated heat conduction by applying Kramers opacity law to a semi-global spherical setup that describes the convective envelopes of solar-like stars, instead of a prescribed heat conduction profile from mixing-length arguments.
Results. We find that some aspects of the results now better correspond to observations: the axi- to nonaxisymmetric transition point is shifted towards higher rotation rates. We also find a change in the propagation direction of ADWs that means that prograde waves are also now found. However, the transition from an anti-solar to solar-like rotation profile is also shifted towards higher rotation rates, leaving the models in an even more unrealistic regime.
Conclusions. Although Kramers-based heat conduction does not help in reproducing the solar rotation profile, it does help in the faster rotation regime, where the dynamo solutions now better match the observations.

Stellar Dynamos in the Transition Regime: Multiple Dynamo Modes and Antisolar Differential Rotation

What drives a cyclic dynamo in a solar-like star with anti-solar differential rotation?

M. **Viviani** (1), M. J. Käpylä (1,2), J. Warnecke (1), P. J. Käpylä (3,2), M. Rheinhardt (2
ApJ **886** 21 **2019**
https://arxiv.org/pdf/1902.04019.pdf
https://doi.org/10.3847/1538-4357/ab3e07
Global and semi-global convective dynamo simulations of solar-like stars are known to show a transition from an anti-solar (fast poles, slow equator) to solar-like (fast equator, slow poles) differential rotation for increasing rotation rate. The dynamo solutions in the latter regime can exhibit regular cyclic modes, whereas in the former regime such cyclic solutions have not been obtained so far. In this paper we present a semi-global dynamo simulation, which for the first time produces clear cyclic magnetic activity in the anti-solar differential rotation regime. We analyze the large-scale flow properties (differential rotation and meridional circulation) together with the turbulent transport coefficients obtained with the test-field method. We find that turbulent dynamo effects play an important role in the dynamics of the system as effective large-scale flows are significantly altered by turbulent pumping. Neither an αΩdynamo wave nor advection-dominated dynamo are able to explain the cycle period and the propagation direction of the mean magnetic field. Furthermore, we find that the α effect is comparable or even larger than the Ω effect in generating the toroidal magnetic field and therefore the dynamo seems to be α2Ω or α2 type.

Transition from axi- to nonaxisymmetric dynamo modes in spherical convection models of solar-like stars

Viviani, M., Warnecke, J., Käpylä, M. J., Käpylä, P. J., Olspert, N., Cole-Kodikara, E. M., Lehtinen, J. J., & Brandenburg, A.
A&A 616, A160 (**2018**)
https://arxiv.org/pdf/1710.10222.pdf
We seek to understand the transition from nearly axisymmetric configurations at solar rotation rates to nonaxisymmetric configurations for rapid rotation using 3D numerical simulations of turbulent convection and considering rotation rates between 1 and 30 times the solar value. We find a transition from axi- to nonaxisymmetric solutions at around 1.8 times the solar rotation rate. This transition coincides with a change in the rotation profile from antisolar- to solar-like differential rotation with a faster equator and slow poles. In the solar-like rotation regime, the field configuration consists of an axisymmetric oscillatory field accompanied by an m=1 azimuthal mode (two active longitudes), which also shows temporal variability. At slow (rapid) rotation, the axisymmetric (nonaxisymmetric) mode dominates. The axisymmetric mode produces latitudinal dynamo waves with polarity reversals, while the nonaxisymmetric mode often exhibits a drift in the rotating reference frame and the strength of the active longitudes changes cyclically over time between the different hemispheres. Most of the obtained dynamo solutions exhibit cyclic variability either caused by latitudinal or azimuthal dynamo waves. In an activity-period diagram, the cycle lengths normalized by the rotation period form two different populations as a function of rotation rate or magnetic activity level. The slowly rotating axisymmetric population lies close to what is called the inactive branch in observations, while the rapidly rotating models are close to the superactive branch with a declining cycle to rotation frequency ratio with increasing rotation rate. We can successfully reproduce the transition from axi- to

nonaxisymmetric dynamo solutions for high rotation rates, but high-resolution simulations are required to limit the effect of rotational quenching of convection at rotation rates above 20 times the solar value.

Are Nanoflares Responsible for Coronal Heating?

Loukas **Vlahos**, Heinz Isliker, Nikos Sioulas
2021
https://arxiv.org/pdf/2108.01722.pdf
Parker (1983) suggested a mechanism for the formation of current sheets (CSs) in the solar atmosphere. His main idea was that the tangling of coronal magnetic field lines by photospheric random flows facilitates the continuous formation of CSs in the solar atmosphere. This part of his idea represents one of the many ways by which the turbulent convection zone drives the formation of coherent structures and CSs in the solar atmosphere. Other mechanisms include emerging magnetic flux, interaction of current filaments, and explosive magnetic structures. However, there are two unproven assumptions in the initial idea of Parker for the coronal heating through nanoflares that must be re-examined. They are related to his suggestion that {ALL CSs formed are led to magnetic reconnection and that magnetic reconnection heats the plasma in the solar atmosphere. Let us discuss these two assumptions briefly in this short comment: (1) Are ALL coherent structures and CSs formed by the turbulent convection zone reconnecting? Does turbulence associated with non-reconnecting CSs play a role in the heating of the corona? (2) Does magnetic reconnection heat the plasma?

Particle Acceleration and Heating in a Turbulent Solar Corona **Review**

Loukas **Vlahos**, Heinz Isliker
Plasma Physics and Controled Fusion (PPCF) **61**, Issue 1, article id. 014020 (**2019**).
https://arxiv.org/pdf/1808.07136.pdf
sci-hub.se/10.1088/1361-6587/aadbe7
Turbulence, magnetic reconnection, and shocks can be present in explosively unstable plasmas, forming a new electromagnetic environment, which we call here turbulent reconnection, and where spontaneous formation of current sheets takes place. We will show that the heating and the acceleration of particles is the result of the synergy of stochastic (second order Fermi) and systematic (first order Fermi) acceleration inside fully developed turbulence. The solar atmosphere is magnetically coupled to a turbulent driver (the convection zone), therefore the appearance of turbulent reconnection in the solar atmosphere is externally driven. Turbulent reconnection, once it is established in the solar corona, drives the coronal heating and particle acceleration.

Suprathermal electron distributions in the solar transition region

C. **Vocks**1, E. Dzifčáková2 and G. Mann1
A&A 596, A41 (**2016**)
https://arxiv.org/pdf/1610.03789v1.pdf
Context. Suprathermal tails are a common feature of solar wind electron velocity distributions, and are expected in the solar corona. From the corona, suprathermal electrons can propagate through the steep temperature gradient of the transition region towards the chromosphere, and lead to non-Maxwellian electron velocity distribution functions (VDFs) with pronounced suprathermal tails.
Aims. We calculate the evolution of a coronal electron distribution through the transition region in order to quantify the suprathermal electron population there.
Methods. A kinetic model for electrons is used, which is based on solving the Boltzmann-Vlasov equation for electrons including Coulomb collisions with both ions and electrons. Initial and chromospheric boundary conditions are Maxwellian VDFs with densities and temperatures based on a background fluid model. The coronal boundary condition has been adopted from earlier studies of suprathermal electron formation in coronal loops.
Results. The model results show the presence of strong suprathermal tails in transition region electron VDFs, starting at energies of a few 10 eV. Above electron energies of 600 eV, electrons can traverse the transition region essentially collision-free.
Conclusions. The presence of strong suprathermal tails in transition region electron VDFs shows that the assumption of local thermodynamic equilibrium is not justified there. This has a significant impact on ionization dynamics, as is shown in a companion paper.

On the possibilities of classical nova identifications among historical Far Eastern guest star observations

Nikolaus **Vogt**, Susanne M. Hoffmann, Claus Tappert
Astronomische Nachrichten **2019**
https://arxiv.org/pdf/1910.13464.pdf
More than 100 guest star observations have been obtained by Chinese, Korean, Japanese and Vietnamese astronomers between ~600 BCE and ~1690 CE. Comparing the coordinates from the information given in old texts

for eight supernova recoveries with modern supernova remnant positions, we estimate a typical positional accuracy of the order of 0.3 to 7 deg for these supernovae. These values turn out to be also a start for the expected deviation angle between a classical nova observed as a guest star and its modern counterpart among known cataclysmic variables (CVs). However, there are considerable disagreements among modern authors in the interpretation of ancient Far Eastern texts, emphasizing the need to consult again the original historic sources, in order to improve the positioning reliability. We also discuss the typical amplitudes of well observed classical novae and find that modern counterparts of nova guest stars should be V = 18 mag and thus easily observable. In this context we also consider the "hibernation scenario" and conclude that it is impossible to decide from currently-available observations whether hibernation is common. In addition to the limiting magnitude around 2 mag for ancient guest star detections mentioned in the literature, we consider the possibility that also fainter guest stars (4-5 mag) could have been detected by ancient observers and give arguments in favor of this possibility. For these limits we compare the expected nova detection rate of ancient naked-eye observers with that during modern times, and conclude that they coincide in order of magnitude, which implies that, indeed, a considerable number of classical nova remnants should be hidden among the Far Eastern guest star reports. Finally, we present a statistical analysis of the probability of casual misidentifications based on frequency and galactic distribution of CVs in the AAVSO-VSX catalogue.

Sunspot Positions and Areas from Observations by Cigoli, Galilei, Cologna, Scheiner, and Colonna in 1612 – 1614

Mikhail **Vokhmyanin**, Rainer Arlt & Nadezhda Zolotova
Solar Physics volume 296, Article number: 4 (**2021**)
https://link.springer.com/content/pdf/10.1007/s11207-020-01752-7.pdf
Digital images of manuscripts stored in the Galilean collection of the Central National Library of Florence are analyzed to obtain sunspot groups, their areas and heliographic positions. Overall, 142 drawings were processed. The way of drawing is usually schematic resulting in area uncertainty which may exceed a factor of two for small sunspots. We suggest that there is an upper limit of a factor of two between sunspot group numbers from the drawings and the actual ones. The computed penumbra-to-umbra ratio is consistent with modern observations. A distribution of sunspot latitudes versus time is reconstructed by means of two methods: exploiting the observation time noted by an observer and minimizing the day-to-day variability of sunspot latitudes.

Sunspot Positions and Areas from Observations by Thomas Harriot

Mikhail **Vokhmyanin**, Rainer Arlt & Nadezhda Zolotova
Solar Physics volume 295, Article number: 39 (**2020**)
https://link.springer.com/content/pdf/10.1007/s11207-020-01604-4.pdf
The reconstruction of sunspot parameters in the early era of telescopic observations extends our knowledge on visual sunspot activity up to 400 years into the past. 200 digital solar images from 18 December 1610 to 28 January 1613 by the English astronomer Thomas Harriot were analyzed to yield sunspot counts, areas and positions. Harriot generally observed in the early morning when the Sun was near the horizon, and he specified the local time of observation, date, place, number of spots, zenith and ecliptic lines, and other information. We assigned 753 sunspots into 293 groups and defined their areas. We developed two approaches to reconstructing the heliographic coordinates of the sunspots. Method I makes use of the time of observation noted by Harriot, and Method II minimizes the day-to-day variability of sunspot latitudes independently of Harriot's notes. The results of the two methods are discussed.

Sunspot Positions and Areas from Observations by Pierre Gassendi

M. V. **Vokhmyanin**, N. V. Zolotova
Solar Physics November **2018**, 293:150
Solar activity behaviour on the eve of the Maunder minimum may provide important information on the period of further suppression of sunspot population. We analyse sunspot positions and areas in the 1630s extracted from rare drawings published by Pierre Gassendi in Opera Omnia. This work was published in two different editions, the first in Lyon and the second almost 70 years later in Florence. The drawings published in Lyon are found to be slightly different from those published in Florence, which produces a discrepancy in the position of spots of a few degrees, while sunspot group areas may differ by a factor of two. We reveal that the orientation of the drawings in the book is not always the same as might be seen in the telescope. We conjecture that the time of Gassendi's observations covers the beginning of a new Schwabe cycle in the southern hemisphere. The differential rotation rate in the 1630s is also assessed and discussed.

Sunspot Positions and Areas from Observations by Galileo Galilei

M. V. **Vokhmyanin**, N. V. Zolotova
Solar Physics February **2018**, 293:31
https://link.springer.com/article/10.1007%2Fs11207-018-1245-1

Sunspot records in the seventeenth century provide important information on the solar activity before the Maunder minimum, yielding reliable sunspot indices and the solar butterfly diagram. Galilei's letters to Cardinal Francesco Barberini and Marcus Welser contain daily solar observations on **3 – 11 May, 2 June – 8 July, and 19 – 21 August 1612**. These historical archives do not provide the time of observation, which results in uncertainty in the sunspot coordinates. To obtain them, we present a method that minimizes the discrepancy between the sunspot latitudes. We provide areas and heliographic coordinates of 82 sunspot groups. In contrast to Sheiner's butterfly diagram, we found only one sunspot group near the Equator. This provides a higher reliability of Galilei's drawings. Large sunspot groups are found to emerge at the same longitude in the northern hemisphere from 3 May to 21 August, which indicates an active longitude.

Long-term Pulses of Dynamic Coupling between Solar Hemispheres

D.M. **Volobuev**, N.G. Makarenko
Solar Phys. 292:68 **2017**
https://arxiv.org/pdf/1704.01330.pdf
North-south (N-S) asymmetry of solar activity is a known statistical phenomenon but its significance is difficult to prove or theoretically explain. Here we consider each solar hemisphere as a separate dynamical system connected with the other hemisphere via an unknown coupling parameter. We use a non-linear dynamics approach to calculate the scale-dependent conditional dispersion (CD) of sunspots between hemispheres. Using daily Greenwich sunspot areas, we calculated the Neumann and Pearson chi-squared distances between CDs as indices showing the direction of coupling. We introduce an additional index of synchronization which shows the strength of coupling and allows us to discriminate between complete synchronization and independency of hemispheres. All indices are evaluated in a four-year moving window showing the evolution of coupling between hemispheres. We find that the driver-response interrelation changes between hemispheres have a few pulses during 130 years of Greenwich data with an at least 40 years-long period of unidirectional coupling. These sharp nearly simultaneous pulses of all causality indices are found at the decay of some 11-year cycles. The pulse rate of this new phenomenon of dynamic coupling is irregular: although the first two pulses repeate after 22-year Hale cycles, the last two pulses repeat after three and four 11-year cycles respectively. The last pulse occurs at the decay phase of Cycle 23 so the next pulse will likely appear during the decay of future Cycle 25 or later. This new phenomenon of dynamic coupling reveals additional constraints for understanding and modeling of the long-term solar activity cycles.

Recent advances in neutrino astrophysics **Review**

Cristina **Volpe**
http://arxiv.org/pdf/1411.6533v1.pdf
Proceedings for the Symposium "Frontiers of Fundamental Physics **2014**", July 15-18, Marseille
Neutrinos are produced by a variety of sources that comprise our Sun, explosive environments such as core-collapse supernovae, the Earth and the Early Universe. The precise origin of the recently discovered ultra-high energy neutrinos is to be determined yet. These weakly interacting particles give us information on their sources, although the neutrino fluxes can be modified when neutrinos traverse an astrophysical environment. Here we highlight recent advances in neutrino astrophysics and emphasise the important progress in our understanding of neutrino flavour conversion in media.

Observations of magnetic reconnection in the deep solar atmosphere in the Hε line⋆

Luc H. M. Rouppe van der **Voort**1,2, Jayant Joshi3 and Kilian Krikova1,2
A&A, 683, A190 (**2024**)
https://www.aanda.org/articles/aa/pdf/2024/03/aa48976-23.pdf
Context. Magnetic reconnection in the deep solar atmosphere can give rise to enhanced emission in the Balmer hydrogen lines, a phenomenon known as Ellerman bombs (EBs). It is most common to observe EBs in the Hα and Hβ spectral lines. High-quality shorter-wavelength Balmer line observations of EBs are rare, but have the potential to provide the most highly resolved view on magnetic reconnection.
Aims. We aim to evaluate the Hε 3970 Å line as an EB diagnostic by analyzing high-quality observations in different Balmer lines.
Methods. Observations of different targets and viewing angles were acquired with the Swedish 1-m Solar Telescope. These observations sample EBs in different environments: active regions, the quiet Sun, and the penumbra and moat of a sunspot. We employed an automated detection method for quiet-Sun EBs based on k-means clustering.
Results. Ellerman bombs in the Hε line show similar characteristics as in the longer-wavelength Balmer lines: a higher intensity than in the surroundings, rapid variability, and a flame-like morphology. In a 24 min quiet-Sun time series, we detected 1674 EBs in the Hε line. This is 1.7 times more EBs than in Hβ. The quiet-Sun EBs measured in Hε are very similar to those in Hβ: They have similar lifetimes and a similar area, brightness, and spatial distribution. Most of the EBs detected in Hε are closer to the limb than their Hβ counterparts because the Hε line core EB emission is formed higher in the atmosphere than the Hβ EB wing emission.

Conclusions. We conclude that the Hε line is well suited for studying EBs, and consequently, for measuring the dynamics of magnetic reconnection in the solar atmosphere at the smallest scales. Our findings suggests that the deep atmosphere in the quiet Sun may host more than 750 000 reconnection events with an EB signature at any time. This is significantly more than what was found in earlier Hβ observations. **2020-08-07-16**

Ultra-high-resolution observations of plasmoid-mediated magnetic reconnection in the deep solar atmosphere⋆

Luc H. M. Rouppe van der **Voort**1,2, Michiel van Noort3 and Jaime de la Cruz Rodríguez4
A&A 673, A11 (**2023**)
https://www.aanda.org/articles/aa/pdf/2023/05/aa45933-23.pdf
Context. Magnetic reconnection in the deep solar atmosphere can give rise to enhanced emission in the Balmer hydrogen lines, a phenomenon referred to as Ellerman bombs.
Aims. To effectively trace magnetic reconnection below the canopy of chromospheric fibrils, we analyzed unique spectroscopic observations of Ellerman bombs in the Hα line.
Methods. We analyzed a 10 min data set of a young emerging active region observed with the prototype of the Microlensed Hyperspectral Imager (MiHI) at the Swedish 1-m Solar Telescope (SST). The MiHI instrument is an integral field spectrograph that is capable of achieving simultaneous ultra-high resolution in the spatial, temporal, and spectral domains. With the combination of the SST adaptive optics system and image restoration techniques, MiHI can deliver diffraction-limited observations if the atmospheric seeing conditions allow. The data set samples the Hα line over 4.5 Å with 10 mÅ pix−1, with 0.″065 pix−1 over a field of view of 8.″6 × 7.″7, and at a temporal cadence of 1.33 s. This constitutes a hyperspectral data cube that measures 132 × 118 spatial pixels, 456 spectral pixels, and 455 time steps.
Results. There were multiple sites with Ellerman bomb activity associated with strong magnetic flux emergence. The Ellerman bomb activity is very dynamic, showing rapid variability and a small-scale substructure. We found a number of plasmoid-like blobs with full-width-half-maximum sizes between 0.″1 and 0.″4 and moving with apparent velocities between 14 and 77 km s−1. Some of these blobs have Ellerman bomb spectral profiles with a single peak at a Doppler offset between 47 and 57 km s−1.
Conclusions. Our observations support the idea that fast magnetic reconnection in Ellerman bombs is mediated by the formation of plasmoids. These MiHI observations demonstrate that a microlens-based integral field spectrograph is capable of probing fundamental physical processes in the solar atmosphere. **24 August 2018, 11 August 2020**

High-resolution observations of the solar photosphere, chromosphere and transition region. A database of coordinated IRIS and SST observations

L.H.M. Rouppe van der **Voort**, B. De Pontieu, M. Carlsson, J. de la Cruz Rodriguez, S. Bose, G. Chintzoglou, A. Drews, C. Froment, M. Gosic, D.R. Graham, V.H. Hansteen, V.M.J. Henriques, S. Jafarzadeh, J. Joshi, L. Kleint, P. Kohutova, T. Leifsen, J. Martinez-Sykora, D. Nobrega-Siverio, A. Ortiz, T.M.D. Pereira, A. Popovas, C. Quintero Noda, A. Sainz Dalda, G.B. Scharmer, D. Schmit, E. Scullion, H. Skogsrud, M. Szydlarski, R. Timmons, G.J.M. Vissers, M.M. Woods, P. Zacharias
A&A **2020**
https://arxiv.org/pdf/2005.14175.pdf
NASA's Interface Region Imaging Spectrograph (IRIS) provides high resolution observations of the solar atmosphere through UV spectroscopy and imaging. Since the launch of IRIS in June 2013, we have conducted systematic observation campaigns in coordination with the Swedish 1-m Solar Telescope (SST) on La Palma. The SST provides complementary high-resolution observations of the photosphere and chromosphere. The SST observations include spectro-polarimetric imaging in photospheric Fe I lines and spectrally-resolved imaging in the chromospheric Ca II 8542 A, H-alpha, and Ca II K lines. We present a database of co-aligned IRIS and SST datasets that is open for analysis to the scientific community. The database covers a variety of targets including active regions, sunspots, plage, quiet Sun, and coronal holes.

Imaging Polarimetry of the 2017 Solar Eclipse with the RIT Polarization Imaging Camera

Dmitry **Vorobiev**, Zoran Ninkov, Lee Bernard, Neal Brock
PASP (Publications of the Astronomical Society of the Pacific?) **2019**
https://arxiv.org/pdf/1909.12785.pdf
In the last decade, imaging polarimeters based on micropolarizer arrays have been developed for use in terrestrial remote sensing and metrology applications. Micropolarizer-based sensors are dramatically smaller and more mechanically robust than other polarimeters with similar spectral response and snapshot capability. To determine the suitability of these new polarimeters for astronomical applications, we developed the RIT Polarization Imaging Camera to investigate the performance of these devices, with a special attention to the low signal-to-noise regime. We characterized the device performance in the lab, by determining the relative throughput, efficiency, and orientation of every pixel, as a function of wavelength. Using the resulting pixel response model, we developed

demodulation procedures for aperture photometry and imaging polarimetry observing modes. We found that, using the current calibration, RITPIC is capable of detecting polarization signals as small as <0.3%. To demonstrate the stability of RITPIC's calibration and its extreme portability, we performed imaging polarimetry of the Solar corona in Madras, Oregon during the total Solar eclipse of 2017. The maximum polarization we measured was ~46%, which agrees well with the maximum value predicted for a Thomson scattering corona. Similarly, we found no strong deviations in the angle of linear polarization from the tangential direction. The relative ease of data collection, calibration, and analysis provided by these sensors suggest than they may become an important tool for a number of astronomical targets. **August 21, 2017**

Modeling Solar Oscillation Power Spectra. III. Spatiotemporal Spectra of Solar Granulation Velocity Field as Seen in HMI Velocity Measurements

Sergei V. **Vorontsov**1,2, Stuart M. Jefferies3, and Timothy P. Larson4,1
2024 ApJ 961 111
https://iopscience.iop.org/article/10.3847/1538-4357/ad12bd/pdf
We suggest a physically motivated model of the uncorrelated background, which can be used to improve the accuracy of helioseismic frequency measurements when the background contributes significantly to the formation of spectral lines of acoustic resonances. The basic assumption of our model is that the correlation length of the convective motions is small compared with the horizontal wavelength $R_\odot/\ell$ of the observations, where ℓ is the degree of the spherical harmonic $Y_\ell^m(\theta, \varphi)$. When applied to solar power spectra at frequencies below acoustic resonances, the model reveals a distinct sensitivity to solar rotation: advection of the convective velocity pattern brings spatial correlations in the apparent stochastic velocity field (temporal correlations in the corotating frame induce spatial correlations in the inertial frame). The induced spatiotemporal correlations manifest themselves as an antisymmetric component in the dependence of the convective noise power on azimuthal order m, which allows us to address the solar differential rotation. With 360 days of data obtained by the Helioseismic and Magnetic Imager on board the Solar Dynamics Observatory, we measure three components of the rotation rate as a function of latitude using only $\ell = 300$. This result indicates that the model suggests a new way of measuring solar subsurface rotation. This approach can complement traditional measurements based on correlation tracking.

Solar Polar Diamond Explorer (SPDEx): Understanding the Origins of Solar Activity Using a New Perspective

A. **Vourlidas**, P. C. Liewer, M. Velli, D. Webb
White paper submitted in response to ideas for the Next Generation Solar Physics Mission Concepts
2018
https://arxiv.org/ftp/arxiv/papers/1805/1805.04172.pdf
Our knowledge of the Sun, its atmosphere, long term activity and space weather potential is severely limited by the lack of good observations of the polar and far-side regions. Observations from a polar vantage point would revolutionize our understanding of the mechanism of solar activity cycles, polar magnetic field reversals, the internal structure and dynamics of the Sun and its atmosphere. Only with extended (many day) observations of the polar regions can the polar flows be determined down to the tachocline where the dynamo is thought to originate. Rapid short period polar orbits, using in situ and remote sensing instrumentation, distributed over a small number of spacecraft, will provide continuous 360o coverage of the solar surface and atmosphere in both longitude and latitude for years on end. This unprecedented full coverage will enable breakthrough studies of the physical connection between the solar interior, the solar atmosphere, the solar wind, solar energetic particles and the inner heliosphere at large. A potential implementation, the Solar Polar Diamond Explorer (SPDEx) built upon the Solar Polar Imager mission design, involves up to four small spacecraft in a 0.48-AU orbit with an inclination of 75o. The orbit is achieved using solar sails or ion engines, both technologies already demonstrated in space.

The Wide-Field Imager for Solar Probe Plus (WISPR)

Angelos **Vourlidas**, Russell A. Howard, Simon P. Plunkett, Clarence M. Korendyke, Arnaud F. . Thernisien, Dennis Wang, Nathan Rich, Michael T. Carter, Damien H. Chua, Dennis G. Socker, …show all 27
Space Science Reviews, Volume 204, Issue 1, pp 83–130 **2016**
http://link.springer.com/journal/11214/204/1?wt_mc=alerts.TOCjournals
The Wide-field Imager for Solar PRobe Plus (WISPR) is the sole imager aboard the Solar Probe Plus (SPP) mission scheduled for launch in 2018. SPP will be a unique mission designed to orbit as close as 7 million km (9.86 solar radii) from Sun center. WISPR employs a 95∘ radial by 58∘transverse field of view to image the fine-scale structure of the solar corona, derive the 3D structure of the large-scale corona, and determine whether a dust-free zone exists near the Sun. WISPR is the smallest heliospheric imager to date yet it comprises two nested wide-field telescopes with large-format (2 K × 2 K) APS CMOS detectors to optimize the performance for their respective fields of view

and to minimize the risk of dust damage, which may be considerable close to the Sun. The WISPR electronics are very flexible allowing the collection of individual images at cadences up to 1 second at perihelion or the summing of multiple images to increase the signal-to-noise when the spacecraft is further from the Sun. The dependency of the Thomson scattering emission of the corona on the imaging geometry dictates that WISPR will be very sensitive to the emission from plasma close to the spacecraft in contrast to the situation for imaging from Earth orbit. WISPR will be the first 'local' imager providing a crucial link between the large-scale corona and the in-situ measurements.

Hurricane Season in the Inner Heliosphere: Observations of Coronal Mass Ejections during Solar Maximum **Review**

A. **Vourlidas**

The 11th Hellenic Astronomical Conference, 8-12 September **2013**, Athens; **Presentation**

7-3-2012, 23-7-2012

Charge exchange in fluid description of partially ionized plasmas

J. **Vranjes**, M. Kono, M. Luna

MNRAS **2015**

http://arxiv.org/pdf/1511.00875v1.pdf

The effects of charge exchange on waves propagating in weakly ionized plasmas are discussed. It is shown that for low-frequency processes, ions and neutrals should be treated as a single fluid with some effective charge on all of them. We have derived a new momentum equation which should be used in such an environment. As a result, the low-frequency magnetic waves can propagate even if particles are not magnetized, which is entirely due to the charge exchange and the fact that it is not possible to separate particles into two different populations as charged and neutral species. So there can be no friction force between ions and neutrals in the usual sense. The mean force per particle is proportional to the ionization ratio n_i/(n_i+ n_n). Regarding the application of the theory to the Alfvén wave propagation in the lower solar atmosphere, the results predict that the plane of displacement of the fluid must change by 90 degrees when an Alfvén wave propagates from the area where particles are un-magnetized (photosphere) to the area where they are magnetized (chromosphere). Because of the most accurate cross sections which we have here, it is possible to very accurately determine altitudes at which such rotation of the Alfvén wave takes place.

Energy in density gradient

J. **Vranjes**, M. Kono

Phys. Plasmas 22, 012105 (**2015**)

http://arxiv.org/pdf/1501.03730v1.pdf

Inhomogeneous plasmas and fluids contain energy stored in inhomogeneity and they naturally tend to relax into lower energy states by developing instabilities or by diffusion. But the actual amount of energy in such inhomogeneities has remained unknown. In the present work the amount of energy stored in a density gradient is calculated for several specific density profiles in a cylindric configuration. This is of practical importance for drift wave instability in various plasmas, and in particular in its application in models dealing with the heating of solar corona because the instability is accompanied with stochastic heating, so the energy contained in inhomogeneity is effectively transformed into heat. It is shown that even for a rather moderate increase of the density at the axis in magnetic structures in the corona by a factor 1.5 or 3, the amount of excess energy per unit volume stored in such a density gradient becomes several orders of magnitude greater than the amount of total energy losses per unit volume (per second) in quiet regions in the corona. Consequently, within the life-time of a magnetic structure such energy losses can easily be compensated by the stochastic drift wave heating.

Alfvén wave coupled with flow-driven fluid instability in interpenetrating plasmas

J. **Vranjes**

Phys. Plasmas 22, 052102 (**2015**)

http://arxiv.org/pdf/1510.05143v1.pdf

The Alfvén wave is analyzed in case of one quasineutral plasma propagating with some constant speed v0 through another static quasineutral plasma. A dispersion equation is derived describing the Alfvén wave coupled with the flow driven mode ω=kv0 and solutions are discussed analytically and numerically. The usual solutions for two oppositely propagating Alfvén waves are substantially modified due to the flowing plasma. More profound is modification of the solution propagating in the negative direction with respect to the magnetic field and the plasma flow. For a large enough flow speed (exceeding the Alfvén speed in the static plasma), this negative solution may become non-propagating, with frequency equal to zero. In this case it represents a spatial variation of the electromagnetic field. For greater flow speed it becomes a forward mode, and it may merge with the positive one. This merging of the two modes represents the starting point for a flow-driven instability, with two complex-

conjugate solutions. The Alfvén wave in interpenetrating plasmas is thus modified and coupled with the flow-driven mode and this coupled mode is shown to be growing when the flow speed is large enough. The energy for the instability is macroscopic kinetic energy of the flowing plasma. The dynamics of plasma particles caused by such a coupled wave still remains similar to the ordinary Alfvén wave. This means that well-known stochastic heating by the Alfvén wave may work, and this should additionally support the potential role of the Alfvén wave in the coronal heating.

Collisions, magnetization, and transport coefficients in the lower solar atmosphere

J. **Vranjes**1,2 and P. S. Krstic
A&A 554, A22 (**2013**)
Context. The lower solar atmosphere is an intrinsically multi-component and collisional environment with electron and proton collision frequencies in the range 108−1010 Hz, which may be considerably higher than the gyro-frequencies for both species. Collisions between different species are altitude dependent because of the variation in density and temperature of all species.
Aims. We aim to provide a reliable quantitative set of data for collision frequencies, magnetization, viscosity, and thermal conductivity for the most important species in the lower solar atmosphere. Having such data at hand is essential for any modeling that is aimed at describing realistic properties of the considered environment.
Methods. The relevant elastic and charge transfer cross sections in the considered range of collision energies are now accepted by the scientific community as known with unprecedented accuracy for the most important species that may be found in the lower solar atmosphere. These were previously calculated using a quantum-mechanical approach and were validated by laboratory measurements. Only with reliable collision data one can obtain accurate values for collision frequencies and coefficients of viscosity and thermal conductivity.
Results. We describe the altitude dependence of the parameters and the different physics of collisions between charged species, and between charged and neutral species. Regions of dominance of each type of collisions are clearly identified. We determine the layers within which either electrons or ions or both are unmagnetized. Protons are shown to be unmagnetized in the lower atmosphere in a layer that is at least 1000 km thick even for a kilo-Gauss magnetic field that decreases exponentially with altitude. In these layers the dynamics of charged species cannot be affected by the magnetic field, and this fact is used in our modeling. Viscosity and thermal conductivity coefficients are calculated for layers where ions are unmagnetized. We compare viscosity and friction and determine the regions of dominance of each of the phenomena.
Conclusions. We provide the most reliable quantitative values for most important parameters in the lower solar atmosphere to be used in analytical modeling and numerical simulations of various phenomena such as waves, transport and magnetization of particles, and the triggering mechanism of coronal mass ejections.

Observed Power and Frequency Variations of Solar Rossby Waves with Solar Cycles

M. **Waidele**, Junwei Zhao
ApJL **954**, L26 **2023**
https://arxiv.org/pdf/2308.07040.pdf
Several recent studies utilizing different helioseismic methods have confirmed the presence of large-scale vorticity waves known as solar Rossby waves within the Sun. Rossby waves are distinct from acoustic waves, typically with longer periods and lifetimes; and their general properties, even if only measured at the surface, may be used to infer properties of the deeper convection zone, such as the turbulent viscosity and entropy gradients which are otherwise difficult to observe. In this study, we utilize 12 years of inverted subsurface velocity fields derived from the SDO/HMI's time--distance and ring-diagram pipelines to investigate the propoerty of the solar equatorial Rossby waves. By covering the maximum and the decline phases of Solar Cycle 24, these datasets enable a systematic analysis of any potential cycle dependence of these waves. Our analysis provides evidence of a correlation between the average power of equatorial Rossby waves and the solar cycle, with stronger Rossby waves during the solar maximum and weaker waves during the minimum. Our result also shows that the frequency of the Rossby waves is lower during the magnetic active years, implying a larger retrograde drift relative to the solar rotation. Although the underlying mechanism that enhances the Rossby wave power and lowers its frequency during the cycle maximum is not immediately known, this observation has the potential to provide new insights into the interaction of large-scale flows with the solar cycle.
HMI Science Nuggets #196 **2023** http://hmi.stanford.edu/hminuggets/?p=4167

On Strengthening of the Solar f-mode Prior to Active Region Emergence Using the Fourier-Hankel Analysis

Matthias **Waidele**, Markus Roth, Nishant Singh, Petri Käpylä
Solar Phys. **2022**
https://arxiv.org/pdf/2202.11236.pdf

Recent results of Singh et al. (2016) show that the emergence of an active region (AR) can be seen in a strengthening of the f-mode power up to two days prior of the region's formation. In the original work, ring diagram analysis was used to estimate the power evolution. In this study, we make use of the Fourier-Hankel method, essentially testing the aforementioned results with an independent method. The data is acquired from SDO/HMI, studying the ARs 11158, 11072, 11105, 11130, 11242 and 11768. Investigating the total power as a function of time, we find a similar behavior to the original work, which is an enhancement of f-mode power about one to three days prior to AR emergence. Analysis of the absorption coefficient α, yielded by a Fourier-Hankel analysis, shows neither absorption ($\alpha>0$) nor emission ($\alpha<0$) of power during the enhancement. Finding no changes of the absorption coefficient (i.e. $\alpha=0$) is an important result, as it narrows down the possible physical interpretation of the original f-mode power enhancement, showing that no directional dependence (in the sense of inward and outward moving waves) is present.

Investigation of surface effects of simple flux tubes using numerical simulations

M. **Waidele**, M. Roth
ApJ, 889, 83 (**2020**)
https://arxiv.org/pdf/2001.11798.pdf
We use the SPARC code for MHD simulations with monolithic flux tubes of varying subsurface topology. Our studies involve the interactions of waves caused by a single source with subsurface magnetic fields. Mode conversion causing acoustic power to trickle downwards along the flux tube has been described before and can be visualized in our simulations. We show that this downward propagation causes the flux tube to act as an isolated source, creating a characteristic surface wavefield. Measuring this wavefield at the surface reveals subsurface properties of the magnetic field topology. Using time distance helioseismology, we demonstrate how to detect such a flux tube signal based on a group travel-time delay of $\Delta t=282.6$ sec due to the wave packet spending time subsurface as a slow mode wave. Although the amplitude is small and generally superimposed by the full wave field, it can be detected if assumptions about Δt are made. We demonstrate this for a simulation with solar like sources. This kind of study has the potential to reveal subsurface information of sunspots based on the analysis of a surface signal.

Coordination of the in situ payload of Solar Orbiter

A. P. **Walsh**1, T. S. Horbury2, M. Maksimovic3, C. J. Owen4, J. Rodríguez-Pacheco5, ….
A&A 642, A5 (**2020**)
https://doi.org/10.1051/0004-6361/201936894
https://www.aanda.org/articles/aa/pdf/2020/10/aa36894-19.pdf
Solar Orbiter's in situ coordination working group met frequently during the development of the mission with the goal of ensuring that its in situ payload has the necessary level of coordination to maximise science return. Here we present the results of that work, namely how the design of each of the in situ instruments (EPD, MAG, RPW, SWA) was guided by the need for coordination, the importance of time synchronisation, and how science operations will be conducted in a coordinated way. We discuss the mechanisms by which instrument sampling schemes are aligned such that complementary measurements will be made simultaneously by different instruments, and how burst modes are scheduled to allow a maximum overlap of burst intervals between the four instruments (telemetry constraints mean different instruments can spend different amounts of time in burst mode). We also explain how onboard autonomy, inter-instrument communication, and selective data downlink will be used to maximise the number of transient events that will be studied using high-resolution modes of all the instruments. Finally, we briefly address coordination between Solar Orbiter's in situ payload and other missions.

Rotation signal on the full disc of the solar chromosphere

M **Wan**, L H Deng, S G Zeng, Z J Yan, J L Xie, T T Xu, Y T Yu
MNRAS, Volume 536, Issue 1, January **2025**, Pages 871–878,
https://doi.org/10.1093/mnras/stae2669
https://watermark.silverchair.com/stae2669.pdf
The rotation signal on the full disc of the solar chromosphere was studied by using the Ca ii K normalized intensity from 938 Carrington rotation (CR) synoptic maps (from CR827 to CR1764) obtained from the Mount Wilson Observatory during the period of 1915 August 10 to 1985 July 7. In this study, our main focus is on the distribution characteristics of the rotation signal on the full disc of the solar chromosphere and its variation with the solar cycle. We found that the chromospheric rotation signal is more pronounced in the latitudinal belt of sunspot activity and tends to extend to higher latitudes, and the trend is essentially the same for each solar cycle. The chromospheric rotation signal is also found to have phase differences in latitudes. The period of the chromospheric rotation signal varies regularly in latitudes, but its phase variation is irregular. In addition, we found that the intensity background is lowest in the latitudinal belt of sunspot drift where the chromospheric rotation signal is generated, but it increases with latitude and tends to extend to higher latitudes. We discussed the possible mechanisms of the above analysis results and thought that the chromospheric rotation signal is mainly caused by sunspots and plages.

Differential rotation: the chromosphere to the quiet chromosphere

M **Wan**, P X Gao, J C Xu, X J Shi, N B Xiang, J L Xie

Monthly Notices of the Royal Astronomical Society, Volume 520, Issue 1, March **2023**, Pages 988–993, https://doi.org/10.1093/mnras/stad192

https://scholar.google.com/scholar_url?url=https://academic.oup.com/mnras/article-pdf/520/1/988/49058086/stad192.pdf

Synoptic maps of Ca II K-normalized intensity at ±40° latitude belt from Carrington rotations 827 (1915 August 10) to 1764 (1985 July 7) are utilized to investigate the long-term variation of the quiet chromospheric differential rotation within solar activity cycles through removing some large values of Ca II-normalized intensity. The equatorial rotation rate of the quiet chromosphere is found to be smaller than that of the chromosphere, and the absolute value of the parameter B is also found to be smaller for the quiet chromosphere than for the chromosphere on the whole, especially during periods of solar cycle maxima. Therefore, we induce that the differential of rotation rate in the quiet chromosphere seems to be enhanced by large-scale magnetic fields. The north–south asymmetry in the solar rotation is also investigated, and the asymmetry coefficients of the chromosphere and the quiet chromosphere are positively correlated in solar cycles 15–17, while they are negatively correlated in solar cycles 18–21.

Solar-cycle-related Variation of Differential Rotation of the Chromosphere

Miao **Wan**1,2 and Peng-xin Gao1,3,4

2022 ApJ 939 111

https://iopscience.iop.org/article/10.3847/1538-4357/ac930d/pdf

Solar-cycle-related variation of the solar chromospheric rotation is studied by analyzing the chromospheric rotation rate of 938 synoptic maps generated from the Ca ii K line at the Mount Wilson Observatory during the period of 1915 August 10 to 1985 July 7. The results obtained are as follows: (1) The parameters A (the equatorial rotation rate) and B (the latitudinal gradient of rotation) in the standard form of differential rotation both show a decreasing trend in the considered time frame, although A has weak statistical significance. (2) There is a significant negative correlation between the level of solar activity and parameter B, indicating that there seems to be a correlation between field strength and chromospheric differential rotation. (3) During solar cycles 15, 16, 19, 20, and 21, the southern hemisphere rotates faster, whereas in cycles 17 and 18, the northern hemisphere rotates faster. (4) There exists a significant negative correlation between the N–S asymmetry of the chromospheric rotation rate and that of solar activity, indicating that differential rotation of the chromosphere seems to be strengthened by stronger magnetic activity in a certain hemisphere. Possible explanations for the above results are given.

1/f Noise in the Heliosphere: A Target for PUNCH Science.

Wang, J., Matthaeus, W.H., Chhiber, R. et al.

Sol Phys 299, 169 (**2024**).

https://doi.org/10.1007/s11207-024-02401-z

https://link.springer.com/content/pdf/10.1007/s11207-024-02401-z.pdf

We present a broad review of 1/f noise observations in the heliosphere, and discuss and complement the theoretical background of generic 1/f models as relevant to NASA's Polarimeter to UNify the Corona and Heliosphere (PUNCH) mission. First observed in the voltage fluctuations of vacuum tubes, the scale-invariant 1/f spectrum has since been identified across a wide array of natural and artificial systems, including heart rate fluctuations and loudness patterns in musical compositions. In the solar wind the interplanetary magnetic field trace spectrum exhibits 1/f scaling within the frequency range from around \unit[2×10−6]Hz to around \unit[10−3]Hz at 1 au. One compelling mechanism for the generation of 1/f noise is the superposition principle, where a composite 1/f spectrum arises from the superposition of a collection of individual power-law spectra characterized by a scale-invariant distribution of correlation times. In the context of the solar wind, such a superposition could originate from scale-invariant reconnection processes in the corona. Further observations have detected 1/f signatures in the photosphere and corona at frequency ranges compatible with those observed at 1 au, suggesting an even lower altitude origin of 1/f spectrum in the solar dynamo itself. This hypothesis is bolstered by dynamo experiments and simulations that indicate inverse cascade activities, which can be linked to successive flux tube reconnections beneath the corona, and are known to generate 1/f noise possibly through nonlocal interactions at the largest scales. Conversely, models positing in situ generation of 1/f signals face causality issues in explaining the low-frequency portion of the 1/f spectrum. Understanding 1/f noise in the solar wind may inform central problems in heliospheric physics, such as the solar dynamo, coronal heating, the origin of the solar wind, and the nature of interplanetary turbulence.

High-resolution Observations of Clustered Dynamic Extreme-Ultraviolet Bright Tadpoles near the Footpoints of Corona Loops

Rui **Wang**, Ying D. Liu, L. P. Chitta, Huidong Hu, Xiaowei Zhao

Research in Astronomy and Astrophysics m **2024**

https://arxiv.org/pdf/2410.15789

An extreme ultraviolet (EUV) close-up view of the Sun offers unprecedented detail of heating events in the solar corona. Enhanced temporal and spatial images obtained by the Solar Orbiter during its first science perihelion enabled us to identify clustered EUV bright tadpoles (CEBTs) occurring near the footpoints of coronal loops. Combining SDO/AIA observations, we determine the altitudes of six distinct CEBTs by stereoscopy, ranging from ~1300 to 3300 km. We then notice a substantial presence of dark, cooler filamentary structures seemingly beneath the CEBTs, displaying periodic up-and-down motions lasting 3 to 5 minutes. This periodic behavior suggests an association of the majority of CEBTs with Type I spicules. Out of the ten selected CEBTs with fast downward velocity, six exhibit corrected velocities close to or exceeding 50 km s−1. These velocities notably surpass the typical speeds of Type I spicules. We explore the generation of such velocities. It indicates that due to the previous limited observations of spicules in the EUV wavelengths, they may reveal novel observational features beyond our current understanding. Gaining insights into these features contributes to a better comprehension of small-scale coronal heating dynamics. **2022-03-30**

An efficient, time-evolving, global MHD coronal model based on COCONUT

H. P. **Wang**, S. Poedts, A. Lani, M. Brchnelova, T. Baratashvili, L. Linan, F. Zhang, D. W. Hou, Y. H. Zhou

A&A **2024**

https://arxiv.org/pdf/2409.02043

Context. Magnetohydrodynamic (MHD) solar coronal models are critical in the Sun-to-Earth model chain and the most complex and computationally intensive component, particularly the time-evolving coronal models, typically driven by a series of time-evolving photospheric magnetograms. There is an urgent need to develop efficient and reliable time-evolving MHD coronal models to further improve our ability to predict space weather. Aims. COCONUT is a rapidly developing MHD coronal model. Adopting the efficient implicit algorithm makes it suitable for performing computationally intensive time-evolving coronal simulations. This paper aims to extend COCONUT to an efficient timeevolving MHD coronal model. Methods. In this MHD model, as usual, an implicit temporal integration algorithm is adopted to avoid the Courant-Friedrichs-Lewy (CFL) stability restriction and increase computational efficiency by large time steps. The Newton iteration method is applied within each time step to enhance the temporal accuracy. The unstructured geodesic mesh is used for flexibility in mesh division and to avoid degeneracy at the poles. Furthermore, an HLL Riemann solver with a self-adjustable dissipation term accommodates both low- and high-speed flows. A series of time-evolving photospheric magnetograms are utilized to drive the evolution of coronal structures from the solar surface to 25 Rs during two Carrington rotations (CRs) around the 2019 eclipse in an inertial coordinate system. It shows that COCONUT can mimic the coronal evolution during a full CR within 9 hours (1080 CPU cores, 1.5M cells). We also compare the simulation results of time-evolving versus quasi-steady-state coronal simulations in the thermodynamic MHD model to validate the time-evolving approach. Additionally, we evaluate the effect of time steps on the simulation results to find an optimal time step that simultaneously maintains high efficiency and necessary numerical stability and accuracy. Results. Consequently, we developed the first fully implicit time-evolving coronal model, and this highly efficient model is promising for timely and accurately simulating the time-evolving corona in practical space weather forecasting.

Toward a live homogeneous database of solar active regions based on SOHO/MDI and SDO/HMI synoptic magnetograms.II.parameters for solar cycle variability

Ruihui **Wang**, Jie Jiang, Yukun Luo

ApJ **971** 110 **2024**

https://arxiv.org/pdf/2405.06224

https://iopscience.iop.org/article/10.3847/1538-4357/ad5b5f/pdf

Solar active regions (ARs) determine solar polar fields and cause solar cycle variability within the framework of the Babcock-Leighton (BL) dynamo. The contribution of an AR to the polar field is measured by its dipole field, which results from flux emergence and subsequent flux transport over the solar surface. The dipole fields contributed by an AR before and after the flux transport are referred to as the initial and final dipole fields, respectively. For a better understanding and prediction of solar cycles, in this paper, we provide a database including AR's initial and final dipole fields and the corresponding results of their bipolar magnetic region (BMR) approximation from 1996 onwards. We also identify the repeated ARs and provide the optimized transport parameters. Based on our database, we find that although the commonly used BMR approximation performs well for the initial dipole field, it exhibits a significant deviation for the final dipole field. To accurately assess an AR's contribution to the polar field, the final dipole field with its real configuration should be applied. Despite the notable contributions of a few rogue ARs, approximately the top 500 ARs ordered by their final dipole fields are necessary to derive the polar field at the cycle minimum. While flux transport may increase or decrease the dipole field for an individual AR, its collective impact over all ARs in a cycle is a reduction in their total dipole field.

The Radial Interplanetary Field Strength at Sunspot Minimum as Polar Field Proxy and Solar Cycle Predictor

Y.-M. **Wang**1

2024 ApJL 961 L27

https://iopscience.iop.org/article/10.3847/2041-8213/ad1c65/pdf

The minimum value of the geomagnetic aa index has served as a remarkably successful predictor of solar cycle amplitude. This value is reached near or just after sunspot minimum, when both the near-Earth solar wind speed and interplanetary magnetic field (IMF) strength fall to their lowest values. At this time, the heliospheric current sheet is flattened toward the heliographic equator and the dominant source of the IMF is the Sun's axial dipole moment, which, in turn, has its source in the polar fields. As recognized previously, the success of aa min as solar cycle precursor provides support for dynamo models in which the sunspots of a given cycle are produced by winding up the poloidal field built up during the previous cycle. Because they are highly concentrated toward the poles by the surface meridional flow, the polar fields are difficult to measure reliably. Here we point out that the observed value of the radial IMF strength at solar minimum can be used to constrain the polar field measurements, and that this parameter, which is directly proportional to the Sun's axial dipole strength, may be an even better solar cycle predictor than geomagnetic activity.

Towards a live homogeneous database of solar active regions based on SOHO/MDI and SDO/HMI synoptic magnetograms. I. Automatic detection and calibration

Ruihui **Wang**, Jie Jiang, Yukun Luo

Astrophysical Journal Supplement Series **2023**

https://arxiv.org/pdf/2308.06914.pdf **File**

Recent studies indicate that a small number of rogue solar active regions (ARs) may have a significant impact on the end-of-cycle polar field and the long-term behavior of solar activity. The impact of individual ARs can be qualified based on their magnetic field distribution. This motivates us to build a live homogeneous AR database in a series of papers. As the first of the series, we develop a method to automatically detect ARs from 1996 onwards based on SOHO/MDI and SDO/HMI synoptic magnetograms. The method shows its advantages in excluding decayed ARs and unipolar regions and being compatible with any available synoptic magnetograms. The identified AR flux and area are calibrated based on the co-temporal SDO/HMI and SOHO/MDI data. The homogeneity and reliability of the database are further verified by comparing it with other relevant databases. We find that ARs with weaker flux have a weaker cycle dependence. Stronger ARs show the weaker cycle 24 compared with cycle 23. Several basic parameters, namely, location, area, and flux of negative and positive polarities of identified ARs are provided in the paper. This paves the way for AR's new parameters quantifying the impact on the long-term behavior of solar activity to be presented in the subsequent paper of the series. The constantly updated database covering more than two full solar cycles will be beneficial for the understanding and prediction of the solar cycle. The database and the detection codes are accessible online.

A comparative study of data-driven MHD simulations of solar coronal evolution with photospheric flows derived from two different approaches.

Xinyi **Wang**, Chaowei Jiang, Xueshang Feng, Boyi Wang, and Bo Chen

Front. Astron. Space Sci. 10: 1157304. **2023**

doi: 10.3389/fspas.2023.1157304

https://www.frontiersin.org/articles/10.3389/fspas.2023.1157304/pdf

Data-driven simulation proves to be a powerful tool in revealing the dynamic process of the solar corona, but it remains challenging to implement the driving boundary conditions in a self-consistent way and match the observables at the photosphere. Here, we test two different photospheric velocity-driven MHD simulations in studying the quasi-static evolution of solar active region NOAA 11158. The two simulations were identically initialized with an MHD equilibrium as relaxed from a non-linear force-free field extrapolation from a vector magnetogram. Then, we energized the MHD system by applying the time series of photospheric velocity at the bottom boundary as derived by two different codes, the DAVE4VM and PDFI, from the observed vector magnetograms. To mimic the small-scale flux cancellation on the photosphere, the magnetic diffusion at the bottom boundary was set to be inversely proportional to the local scale length of the magnetic field. The result shows the evolution curves of the total magnetic energy and unsigned magnetic flux generated by the PDFI velocity match the corresponding curves from the observations much better than those by the DAVE4VM one. The structure of the current layer and synthetic image in PDFI simulation also has a more reasonable consistency with SDO/AIA 131 Å observation. The only shortage of the PDFI velocity is its capability in reproducing the morphology of sunspots, as characterized by a slightly lower correlation coefficient for the bottom magnetic field in simulations and magnetograms. Overall, this study suggests the superiority of each method in the models driven by the bottom velocity, which represents a further step toward the goal of reproducing more realistically the evolution of coronal magnetic fields using data-driven modeling. **15 February 2011**

Implicit Solar Coronal Magnetohydrodynamic (MHD) Modeling with a Low-dissipation Hybridized AUSM-HLL Riemann Solver

Haopeng **Wang**1,2, Changqing Xiang1, Xiaojing Liu1, Jiakun Lv1,2, and Fang Shen1,2
2022 ApJ 935 46
https://iopscience.iop.org/article/10.3847/1538-4357/ac78e0/pdf

In this paper, we develop a 3D implicit single-fluid magnetohydrodynamic (MHD) model to simulate the steady-state solar corona with a wide range of Mach numbers and low plasma β. We employ a low-dissipation advection upstream splitting method (AUSM) to calculate the convective flux in the regions of low Mach numbers for a high resolution, and hybridize the AUSM with Harten-Lax-van Leer Riemann solver in the regions of high Mach numbers to improve the solver's robustness. The inner boundary condition of no backflow is implemented by numerical flux. A reconstruction method based on the divergence-free radial basis function is adopted to enhance the divergence-free constraint of magnetic field. Also, an anisotropic thermal conduction term is considered; the positivity-preserving reconstruction method is used to prevent the presence of negative thermal pressure and plasma density, and the implicit lower-upper symmetric Gauss Seidel method is implemented for a better convergence rate. After establishing the implicit solar wind MHD model, we employ it to simulate steady-state solar coronal structures in Carrington rotations 2177 and 2212. The simulations demonstrate that the MHD model's computational efficiency is desirable, and the modeled results are basically in agreement with the solar coronal observations and the mapped in situ measurements from the OMNI archive. Consequently, this implicit MHD model is promising to simulate a complex plasma environment with high-intensity magnetic field and wide-ranging Mach numbers.

Undetected Minority-polarity Flux as the Missing Link in Coronal Heating

Y.-M. **Wang**
Solar Physics **volume 297**, Article number: 129 **2022**
https://arxiv.org/pdf/2206.11327.pdf
https://link.springer.com/content/pdf/10.1007/s11207-022-02060-y.pdf

During the last few decades, the most widely favored models for coronal heating have involved the in situ dissipation of energy, with footpoint shuffling giving rise to multiple current sheets (the "nanoflare" model) or to Alfv{é}n waves that leak into the corona and undergo dissipative interactions (the wave heating scenario). As has been recognized earlier, observations suggest instead that the energy deposition is concentrated at very low heights, with the coronal loops being filled with hot, dense material from below, which accounts for their overdensities and flat temperature profiles. While an obvious mechanism for footpoint heating would be reconnection with small-scale fields, this possibility seems to have been widely ignored because magnetograms show almost no minority-polarity flux inside active region (AR) plages. Here, we present further examples to support our earlier conclusions (1) that magnetograms greatly underrepresent the amount of minority-polarity flux inside plages and "unipolar" network, and (2) that small loops are a major constituent of \ion{Fe}{9} 17.1 nm moss. On the assumption that the emergence or churning rate of small-scale flux is the same inside plages as in mixed-polarity regions of the quiet Sun, we estimate the energy flux density associated with reconnection with the plage fields to be on the order of 107 erg cm−2 s−1, sufficient to heat the AR corona.
RHESSI Nuggets #432 **2022** https://sprg.ssl.berkeley.edu/~tohban/wiki/index.php/Undetected_Minority-polarity_Flux,_Moss,_and_Coronal_Heating

Variation in Cosmic-Ray Intensity Lags Sunspot Number: Implications of Late Opening of Solar Magnetic Field

Yuming **Wang**1,2,3, Jingnan Guo1,2, Gang Li4, Elias Roussos5, and Junwei Zhao6
2022 ApJ 928 157
https://iopscience.iop.org/article/10.3847/1538-4357/ac5896/pdf

Galactic cosmic rays (GCRs), the highly energetic particles that may raise critical health issues for astronauts in space, are modulated by solar activity, with their intensity lagging behind the variation in sunspot number (SSN) by about one year. Previously, this lag has been attributed to the combined effect of outward convecting solar wind and inward propagating GCRs. However, the lag's amplitude and its solar-cycle dependence are still not fully understood. By investigating the solar surface magnetic field, we find that the source of heliospheric magnetic field—the open magnetic flux on the Sun—already lags behind SSN before it convects into the heliosphere along with the solar wind. The delay during odd cycles is longer than that during sequential even cycles. Thus, we propose that the GCR lag is primarily due to the very late opening of the solar magnetic field with respect to SSN, though solar wind convection and particle transport in the heliosphere also matter. We further investigate the origin of the open flux from different latitudes of the Sun and find that the total open flux is significantly contributed by that from low latitudes, where coronal mass ejections frequently occur and also show an odd–even cyclic pattern. Our findings challenge existing theories, and may serve as the physical basis of long-term forecasts of radiation dose estimates for manned deep-space exploration missions.

Uncovering Intense Ancient Solar Activity from Naked-eye Observations of Egg-like Sunspots

Hongrui **Wang**1 and Huiduan Li1
2021 ApJ 921 159
https://doi.org/10.3847/1538-4357/ac2152
Ancient sunspot records written in classical Chinese provide important information regarding ancient solar activity. The Chinese recorded 14 observations of sunspots that resembled an egg (hereafter, egg record; the word egg is used to represent approximate sunspot sizes) before 1000 CE. However, the egg records in classical Chinese were too short to provide sufficient sunspot details. This study was conducted to decode egg records from 1769 and 1917 through telescopic sunspot observations. The results of our decoding show that egg-like sunspots were generally used by observers in East Asia to represent a very large sunspot group with an approximately elliptical outline. An egg record generally served as a marker of intense solar activity. Three egg records (in 1278, 1769, and 1917) were observed to be close to the solar maxima, with the time difference being smaller than 1 yr. Some egg records could thus be used to identify the solar maxima. The mean time difference between 10 egg records and the nearest solar maxima is 2 yr. Therefore, egg records can provide necessary information for uncovering additional intense solar activity from ancient times.

A New Reconstruction of the Sun's Magnetic Field and Total Irradiance since 1700

Y.-M. **Wang**1 and J. L. Lean3,2
2021 ApJ 920 100
https://doi.org/10.3847/1538-4357/ac1740
We model the Sun's large-scale magnetic field and total solar irradiance (TSI) since 1700 by combining flux transport simulations with empirical relationships between facular brightening, sunspot darkening, and the total photospheric flux. The photospheric field is evolved subject to the constraints that (1) the flux emergence rate scales as the yearly sunspot numbers, and (2) the polar field strength at solar minimum is proportional to the amplitude of the following cycle. Simulations are performed using both the recently revised sunspot numbers and an average of these numbers and the Hoyt–Schatten group numbers. A decrease (increase) in the polar field strength from one cycle to the next is simulated either by increasing (decreasing) the poleward flow speed, or by decreasing (increasing) the average axial tilts of active regions; the resulting photospheric field evolution is very similar whichever parameter is varied. Comparisons between irradiance data and both the simulated and observed photospheric field suggest that TSI and facular brightness increase less steeply with the field strength at solar minimum than at other phases of the cycle, presumably because of the dominance of small-scale ephemeral regions when activity is very low. This relative insensitivity of the irradiance to changes in the large-scale field during cycle minima results in a minimum-to-minimum increase of annual TSI from 1700 to 1964 (2008) of 0.2 (0.06) W m−2, a factor of 2–3 smaller than predicted in earlier reconstructions where the relation between facular brightness and field strength was assumed to be independent of cycle phase.

Naked emergence of an anti-Hale active region
I. Overall evolution and magnetic properties⋆

Jincheng **Wang**1,2,3, Xiaoli Yan1,3, Defang Kong1,3, Zhike Xue1,3, Liheng Yang1,3, Qiaoling Li1,4, Yan Zhang1,4 and Hao Li5,6
A&A 652, A55 (**2021**)
https://arxiv.org/abs/2106.02786
https://www.aanda.org/articles/aa/pdf/2021/08/aa40685-21.pdf
https://doi.org/10.1051/0004-6361/202140685
Aims. In order to understand the emergence of the active region, we investigate the emerging process and magnetic properties of a naked anti-Hale active region during the period between **August 24 to 25, 2018**.
Methods. Using the data from Helioseismic and Magnetic Imager on board the Soar Dynamic Observatory and the New Vacuum Solar Telescope, we calculated different evolving parameters (such as pole separation, tilt angle) and magnetic parameters (such as vertical electric current, force-free parameter, relative magnetic helicity) during the emergence of the active region. With these calculated parameters and some reasonable assumptions, we use two different methods to estimate the twist of the active region.
Results. The magnetic flux and pole separation continue increasing while the tilt angle exhibits a decreasing pattern during the emergence of the active region. The increase of the pole separation is mainly contributed as a result of the enhancement in the longitude direction. A power-law relationship between pole separation and total flux is found during the emergence of the active region. On the other hand, it is found that both the positive and negative electric currents increased equivalently and the average flux-weighted force-free parameter $\tilde{\alpha}$ remains almost consistently positive, on the order of ∼10−8 m−1. The relative magnetic helicity is mainly contributed by the shear term, while the relative magnetic helicity injection flux of the shear term changes its sign at the latter stage of the emergence.

The twist number of the whole active region remains on the order of 10−1 turns during the emergence of the active region.
Conclusions. We find that the magnetic flux tube with low twist also could emerge into the solar atmosphere.

Fast Magnetic Wave Could Heat the Solar Low-beta Chromosphere

Yikang **Wang**1, Takaaki Yokoyama2, and Haruhisa Iijima3,4
2021 ApJL 916 L10
https://arxiv.org/pdf/2107.13722
https://doi.org/10.3847/2041-8213/ac10c7
We perform two-dimensional radiative MHD simulation to investigate the propagation of MHD waves in the quiet region of the solar chromosphere. We identify the mode of the shock waves by using the relationship between gas pressure and magnetic pressure across the shock front and calculate their corresponding heating rate through the entropy jump to obtain a quantitative understanding of the wave-heating process in the chromosphere. Our result shows that the fast magnetic wave is significant in heating the low-beta chromosphere. The low-beta fast magnetic waves are generated from high-beta fast acoustic waves via mode conversion crossing the equipartition layer. Efficient mode conversion is achieved by large attacking angles between the propagation direction of the shock waves and the chromospheric magnetic field.

Algebraic quantification of an active region's contribution to the solar cycle

Zi-Fan **Wang**, Jie Jiang, Jing-Xiu Wang
A&A 650, A87 **2021**
https://arxiv.org/pdf/2104.04307.pdf
https://www.aanda.org/articles/aa/pdf/2021/06/aa40407-21.pdf
https://doi.org/10.1051/0004-6361/202140407
The solar dipole moment at cycle minimum is considered to be the most successful precursor for the amplitude of the subsequent cycle. Numerical simulations of the surface flux transport (SFT) model are widely used to effectively predict the dipole moment at cycle minimum. Recently an algebraic method has been proposed to quickly predict the contribution of an active region (AR) to the axial dipole moment at cycle minimum instead of SFT simulations. However, the method assumes a bipolar magnetic region (BMR) configuration of ARs. Actually most ARs are asymmetric in configuration of opposite polarities, or have more complex configurations. Such ARs evolve significantly differently from that of BMR approximations. We propose a generalized algebraic method to describe the axial dipole contribution of an AR with an arbitrary configuration, and evaluate its effectiveness compared to the BMR-based method. We employ mathematical deductions to obtain the generalized method. We compare the results of the generalized method with SFT simulations of observed ARs, artificially created BMRs, and ARs with more complex configurations. We also compare the results with that from the BMR-based method. The generalized method is equivalent to the SFT model, and precisely predicts the ARs' contributions to the dipole moment. The method has a much higher computational efficiency than SFT simulations. Although the BMR-based method has similar computational efficiency as the generalized method, it is only accurate for symmetric bipolar ARs. The BMR-based method systematically overestimates the dipole contributions of asymmetric bipolar ARs, and randomly miscalculate the contributions of more complex ARs. The generalized method provides a quick and precise quantification of an AR's contribution to the solar cycle evolution, which paves the way for the application into the physics-based solar cycle prediction.

Aurora Sightings Observed in Chinese History Caused by CIRs or Great-storm CMEs

Guowei **Wang**1,2, Shuo Yao1, Yiqun Yu3, Dong Wei3, Fei Di1, Xiujuan Bao1, Shihong Zhang1, and Jianjun Liu2
2021 ApJ 908 187
https://doi.org/10.3847/1538-4357/abd0fe
https://iopscience.iop.org/article/10.3847/1538-4357/abd0fe/pdf
Auroras observed at middle and low geographic latitudes are related to external inputs and varying geomagnetic fields. This work aims to exclude corotating interaction region (CIR) storms and identify strong coronal mass ejection (CME) storms according to historical auroral records when the geomagnetic field varies substantially. An existing catalog of the aurora records in Chinese history reported by Zeng & Jin from 193 B.C. to 1911 A.D. is used. Archaeomagnetic field models are adopted to estimate the variation of the dipole field. According to the empirical relation between the equatorward boundary of the auroral oval, Dst index, and geomagnetic field intensity, the auroras caused by CIRs can be excluded, and those caused by strong CMEs are identified. After 1500 A.D., China's magnetic latitude decreased substantially due to the pole shift. This shift provides a better opportunity to investigate the existence of great-level storms. These great-storm CMEs occurred in both solar maximum and minimum. The space weather modeling framework is used to calculate the cusp area and the downward ion flux through the cusp for varied geomagnetic field and solar wind. For the present solar wind condition and tilt angle <15°, stronger

geomagnetic field tends to generate a larger cusp area and higher ion flux through the cusp. For the weaker solar wind in the Maunder minimum, the ion flux is lower, but the cusp area is similar to that at present.

Slow-Mode Magnetoacoustic Waves in Coronal Loops **Review**

Tongjiang **Wang**, Leon Ofman, Ding Yuan, Fabio Reale, Dmitrii Y. Kolotkov, Abhishek K. Srivastava
Space Science Reviews **2021**
https://arxiv.org/pdf/2102.11376.pdf

Rapidly decaying long-period oscillations often occur in hot coronal loops of active regions associated with small (or micro-) flares. This kind of wave activity was first discovered with the SOHO/SUMER spectrometer from Doppler velocity measurements of hot emission lines, thus also often called "SUMER" oscillations. They were mainly interpreted as global (or fundamental mode) standing slow magnetoacoustic waves. In addition, increasing evidence has suggested that the decaying harmonic type of pulsations detected in light curves of solar and stellar flares are likely caused by standing slow-mode waves. The study of slow magnetoacoustic waves in coronal loops has become a topic of particular interest in connection with coronal seismology. We review recent results from SDO/AIA and Hinode/XRT observations that have detected both standing and reflected intensity oscillations in hot flaring loops showing the physical properties (e.g., oscillation periods, decay times, and triggers) in accord with the SUMER oscillations. We also review recent advances in theory and numerical modeling of slow-mode waves focusing on the wave excitation and damping mechanisms. MHD simulations in 1D, 2D and 3D have been dedicated to understanding the physical conditions for the generation of a reflected propagating or a standing wave by impulsive heating. Various damping mechanisms and their analysis methods are summarized. Calculations based on linear theory suggest that the non-ideal MHD effects such as thermal conduction, compressive viscosity, and optically thin radiation may dominate in damping of slow-mode waves in coronal loops of different physical conditions. Finally, an overview is given of several important seismological applications such as determination of transport coefficients and heating function.

Small-scale Flux Emergence, Coronal Hole Heating, and Flux-tube Expansion: A Hybrid Solar Wind Model

Y.-M. **Wang**
2020 ApJ 904 199
https://doi.org/10.3847/1538-4357/abbda6

Extreme-ultraviolet images from the Solar Dynamics Observatory often show loop-like fine structure to be present where no minority-polarity flux is visible in magnetograms, suggesting that the rate of ephemeral region (ER) emergence inside "unipolar" regions has been underestimated. Assuming that this rate is the same inside coronal holes as in the quiet Sun, we show that interchange reconnection between ERs and open field lines gives rise to a solar wind energy flux that exceeds 105 erg cm−2 s−1 and that scales as the field strength at the coronal base, consistent with observations. In addition to providing ohmic heating in the low corona, these reconnection events may be a source of Alfvén waves with periods ranging from the granular timescale of ~10 minutes to the supergranular/plume timescale of many hours, with some of the longer-period waves being reflected and dissipated in the outer corona. The asymptotic wind speed depends on the radial distribution of the heating, which is largely controlled by the rate of flux-tube expansion. Along the rapidly diverging flux tubes associated with slow wind, heating is concentrated well inside the sonic point (1) because the outward conductive heat-flux density and thus the outer coronal temperatures are reduced, and (2) because the net wave energy flux is dissipated at a rate proportional to the local Alfvén speed. In this "hybrid" solar wind model, reconnection heats the lower corona and drives the mass flux, whereas waves impart energy and momentum to the outflow at greater distances.

Solar modulation of cosmic proton and helium with AMS-02

Bing-Bing **Wang**, Xiao-Jun Bi, Kun Fang, Sujie Lin, Peng-Fei Yin
2020
https://arxiv.org/pdf/2011.12531.pdf

We investigate the solar modulation effect with the long time cosmic ray proton and helium spectrum measured by AMS-02 on the time scale of a Bartels rotation (27 days) between May 2011 and May 2017. The time-span covers the negative heliospheric magnetic field polarity cycle, the polarity reversal period and the positive polarity cycle. The unprecedented accuracy of AMS-02 observation data provide a good opportunity to improve the understanding of the time dependent solar modulation effect. In this work, a two-dimensional solar modulation model is used to compute the propagation of cosmic rays in the heliosphere. Some important ingredients of the model which reflect the global heliospherical environment are taken from the observations. The propagation equation is numerically solved with the pubic Solarprop code. We find that the drift effect is suppressed during the high solar activity period but nearly recovered in the first half of 2017. The time-dependent rigidity dependence of the mean free path is critical to reproduce the observations between August 2012 and October 2015.

Activity Complexes and A Prominent Poleward Surge During Solar Cycle 24

Zi-Fan **Wang**, Jie Jiang, Jie Zhang, Jing-Xiu Wang

ApJ **904** 62 **2020**

https://arxiv.org/pdf/2009.12483.pdf

https://iopscience.iop.org/article/10.3847/1538-4357/abbc1e/pdf

https://doi.org/10.3847/1538-4357/abbc1e

Long-lasting activity complexes (ACs), characterised as a series of closely located, continuously emerging solar active regions (ARs), are considered generating prominent poleward surges from observations. The surges lead to significant variations of the polar field, which are important for the modulation of solar cycles. We aim to study a prominent poleward surge during solar cycle 24 on the southern hemisphere, and analyse its originating ACs and the effect on the polar field evolution. We automatically identify and characterize ARs based on synoptic magnetograms from the Solar Dynamic Observatory. We assimilate these ARs with realistic magnetic configuration into a surface flux transport model, and simulate the creation and migration of the surge. Our simulations well reproduce the characteristics of the surge and show that the prominent surge is mainly caused by the ARs belonging to two ACs during Carrington Rotations 2145-2159 (December 2013-January 2015). The surge has a strong influence on the polar field evolution of the southern hemisphere during the latter half of cycle 24. Without the about one-year-long flux emergence in the form of ACs, the polar field around the cycle minimum would have remained at a low level and even reversed to the polarity at cycle 23 minimum. Our study also shows that the long-lived unipolar regions due to the decay of the earlier emerging ARs cause an intrinsic difficulty of automatically identifying and precisely quantifying later emerging ARs in ACs.

HMI Science Nuggets №149 Dec **2020** http://hmi.stanford.edu/hminuggets/?p=3420

High-resolution Observations of Small-scale Flux Emergence by GST

Jiasheng **Wang**1,2,3, Chang Liu1,2,3, Wenda Cao1,2,3, and Haimin Wang1,2,3

2020 ApJ 900 84

https://doi.org/10.3847/1538-4357/aba696

https://arxiv.org/pdf/2009.06717

Recent observations demonstrated that emerging flux regions, which constitute the early stage of solar active regions, consist of emergence of numerous small-scale magnetic elements. They in turn interact, merge, and form mature sunspots. However, observations of fine magnetic structures on photosphere with subarcsecond resolution are very rare due to limitations of observing facilities. In this work, taking advantage of the high resolution of the 1.6 m Goode Solar Telescope, we jointly analyze vector magnetic fields, continuum images, and Hα observations of NOAA AR 12665 on **2017 July 13**, with the goal of understanding the signatures of small-scale flux emergence, as well as their atmospheric responses as they emerge through multiple heights in the photosphere and chromosphere. Under such a high resolution of $0\farcs1$–$0\farcs2$, our results confirm two kinds of small-scale flux emergence: magnetic flux sheet emergence associated with the newly forming granules, and the traditional magnetic flux loop emergence. With direct imaging in the broadband TiO, we observe that both types of flux emergence are associated with darkening of granular boundaries, while only flux sheets elongate granules along the direction of emerging magnetic fields and expand laterally. With a life span of 10 ~ 15 minutes, the total emerged vertical flux is on the order of 10^{18} Mx for both types of emergence. The magnitudes of the vertical and horizontal fields are comparable in the flux sheets, while the former is stronger in flux loops. Hα observations reveal transient brightenings in the wings in the events of magnetic loop emergence, which are most probably the signatures of Ellerman bombs.

Solar 11-Year Cycle Signal in Stratospheric Nitrogen Dioxide—Similarities and Discrepancies Between Model and NDACC Observations

Shuhui **Wang**, King-Fai Li, Diana Zhu, Stanley P. Sander, Yuk L. Yung, Andrea Pazmino & Richard Querel

Solar Physics volume 295, Article number: 117 (**2020**)

https://link.springer.com/content/pdf/10.1007/s11207-020-01685-1.pdf

NOx (NO2 and NO) plays an important role in controlling stratospheric ozone. Understanding the change in stratospheric NOx and its global pattern is important for predicting future changes in ozone and the corresponding implications on the climate. Stratospheric NOx is mainly produced by the reaction of N2O with the photochemically produced O(1D) and, therefore, it is expected to vary with changes in solar UV irradiance during the solar cycle. Previous studies on this topic, often limited by the relatively short continuous data, show puzzling results. The effect of the 1991 Pinatubo eruption might have caused interference in the data analysis. In this study, we examine the NO2 vertical column density (VCD) data from the Network for the Detection of Atmospheric Composition Change (NDACC). Data collected at 16 stations with continuous long-term observations covering the most recent Solar Cycles 23 and 24 were analyzed. We found positive correlations between changes in NO2 VCD and solar Lyman-αα over nine stations (mostly in the Northern Hemisphere) and negative correlations over three stations

(mostly in the Southern Hemisphere). The other four stations do not show significant NO2 solar-cycle signal. The varying NO2 responses from one location to another are likely due to different geo-locations (latitude and altitude). In particular, two high-altitude stations show the strongest positive NO2 solar-cycle signals. Our 1D chemical-transport model calculations help explain the altitude dependence of NO2 response to the solar cycle. NO2 solar-cycle variability is suggested to play an important role controlling O3 at an altitude range from ≈20 km≈20 km to near 60 km, while OH solar-cycle variability controls O3 at 40 – 90 km. While observations show both positive and negative NO2 responses to solar forcing, the 1D model predicts negative NO2 responses to solar UV changes throughout the middle atmosphere. 3D global model results suggest complex roles of dynamics in addition to photochemistry. The energetic particle-induced NO2 variabilities could also contribute significantly to the NO2 variability during solar cycles.

Concept of the Solar Ring Mission: Overview

Yuming **Wang**, Haisheng Ji, Yamin Wang, Lidong Xia, Chenglong Shen, Jingnan Guo, Quanhao Zhang, Zhenghua Huang, Kai Liu, Xiaolei Li, Rui Liu, Jingxiu Wang, Shui Wang
Science China Technological Sciences, **2020**
https://arxiv.org/pdf/2003.12728.pdf
The concept of the Solar Ring mission was gradually formed from L5/L4 mission concept, and the proposal of its pre-phase study was funded by the National Natural Science Foundation of China in November 2018 and then by the Strategic Priority Program of Chinese Academy of Sciences in space sciences in May 2019. Solar Ring mission will be the first attempt to routinely monitor and study the Sun and inner heliosphere from a full 360-degree perspective in the ecliptic plane. The current preliminary design of the Solar Ring mission is to deploy six spacecraft, grouped in three pairs, on a sub-AU orbit around the Sun. The two spacecraft in each group are separated by about 30 degrees and every two groups by about 120 degrees. This configuration with necessary science payloads will allow us to establish three unprecedented capabilities: (1) determine the photospheric vector magnetic field with unambiguity, (2) provide 360-degree maps of the Sun and the inner heliosphere routinely, and (3) resolve the solar wind structures at multiple scales and multiple longitudes. With these capabilities, the Solar Ring mission aims to address the origin of solar cycle, the origin of solar eruptions, the origin of solar wind structures and the origin of severe space weather events. The successful accomplishment of the mission will advance our understanding of the star and the space environment that hold our life and enhance our capability of expanding the next new territory of human. **3-4 April 2010, 1–2 August 2010, 2014-10-23, 10–16 September 2017**

Simulation of Alfvén Wave Propagation in the Magnetic Chromosphere with Radiative Loss: Effects of Nonlinear Mode Coupling on Chromospheric Heating

Yikang **Wang** and Takaaki Yokoyama
2020 ApJ 891 110
https://doi.org/10.3847/1538-4357/ab70b2
https://arxiv.org/pdf/2003.05796.pdf
We perform magnetohydrodynamic simulations to investigate the propagation of Alfvén waves in the magnetic chromosphere. We use the 1.5D expanding flux tube geometry setting and transverse perturbation at the bottom to generate the Alfvén wave. Compared with previous studies, our expansion is that we include the radiative loss term introduced by Carlsson & Leenaarts. We find that when an observation-based transverse wave generator is applied, the spatial distribution of the time-averaged radiative loss profile in our simulation is consistent with that in the classic atmospheric model. In addition, the energy flux in the corona is larger than the required value for coronal heating in the quiet region. Our study shows that the Alfvén wave-driven model has the potential to simultaneously explain chromospheric heating and how energy is transported to the corona.

Are Large Sunspots Dominant in Naked-eye Sunspot Observations for 1819–1918?

Hongrui **Wang** and Huiduan Li
2020 ApJ 890 134
https://doi.org/10.3847/1538-4357/ab6ddb
This article explores the sizes of sunspots as determined by naked-eye sunspot observations (NSOs). The international sunspot number (ISN), the group sunspot number, and the Greenwich photo-heliographic results (GPR) were utilized. According to the ISN results, 64% of NSOs from 1819 to 1918 have been identified as large sunspots. We found that the sunspot sizes had been considerably underestimated using the ISN data (compared to using the GPR data). About 40% of NSOs from 1819 to 1918 have been identified as giant sunspots, which have ranks of sunspot areas smaller than 5%. The results in this article indicate that the majority of NSOs are large sunspots. This calls into question the previous understanding that NSOs include sunspots of all sizes above the visibility limit.

Do Records of Sunspot Sightings Provide Reliable Indicators of Solar Maxima for 1613 – 1918?

Hongrui **Wang**, Huiduan Li
Solar Physics October **2019**, 294:138
https://link.springer.com/content/pdf/10.1007%2Fs11207-019-1528-1.pdf
Records of Sunspot Sightings (RSS) which were obtained by the naked eye without the aid of the telescope are essential to find the solar activity in the distant past. Intense solar activity or the solar maxima had been identified by using the RSS for several decades. However, the performance of the RSS as the indicators of the solar maxima has rarely been discussed with quantitative analysis. The RSS from 1613 to 1918 are accessed as the indicators of the solar maxima, by using the time difference between each RSS and the specific solar maxima. The results have shown that about 33% of the sunspot sightings were obtained within one year of the solar maxima and about 51% of the sunspot sightings were obtained within 2 years of the solar maxima. The average time error of identifying the solar maxima by the RSS is 2.52 years, during the period 1613 – 1918. If a certain amount of time error could be tolerated for the identification of the solar maxima, the RSS could be generally used as indicators of the solar maxima.

Flat-fielding of Full-disk Solar Images with a Gaussian-type Diffuser

Yiran **Wang**, Xianyong Bai, Siqing Liu, Yuanyong Deng, Zhiyong Zhang, Yueqiang Sun
Solar Physics September **2019**, 294:127
https://link.springer.com/content/pdf/10.1007%2Fs11207-019-1527-2.pdf
Full-disk solar chromospheric and photospheric images are widely used to monitor solar activity. Flat-fielding is a basic step during scientific data production. Here, a Gaussian-type diffuser is used to measure the flat-field of full-disk solar chromospheric and photospheric images. The effectiveness of the method is verified by theoretical simulation and practical measurement. First, the uniformity of the light source generated by the Gaussian diffuser and the sunlight, with a field of view the same as the full-disk solar image, is calculated. The full width at half maximum (FWHM) of the scatter angle of the Gaussian diffuser is one degree, such that the light source presents a Gaussian distribution. After the correction of the Gaussian background, the uniformity of the area light source is 99.6%, which can be regarded as a uniform area light source. Second, experiments are conducted on full-disk solar telescopes at Huairou solar observing station and Yangbajing station. The diffuser covers the entire entrance aperture when taking flat-field frames. Through qualitative and quantitative analysis of experimental results, it is confirmed that a revised flat-field frame can modify uniformity caused by various aspects of the telescope, including vignetting, non-uniformities of filters, and contamination of optical components.

Further Evidence for Looplike Fine Structure inside "Unipolar" Active Region Plages

Y.-M. **Wang**, I. Ugarte-Urra, J. W. Reep
The Astrophysical Journal, 885, 34 (**2019**)
https://arxiv.org/ftp/arxiv/papers/2104/2104.06633.pdf
Earlier studies using extreme-ultraviolet images and line-of-sight magnetograms from the Solar Dynamics Observatory (SDO) have suggested that active region (AR) plages and strong network concentrations often have small, looplike features embedded within them, even though no minority-polarity flux is visible in the corresponding magnetograms. Because of the unexpected nature of these findings, we have searched the SDO database for examples of inverted-Y structures rooted inside "unipolar" plages, with such jetlike structures being interpreted as evidence for magnetic reconnection between small bipoles and the dominant-polarity field. Several illustrative cases are presented from the period 2013--2015, all of which are associated with transient outflows from AR "moss." The triangular or dome-shaped bases have horizontal dimensions of ~2--4 Mm, corresponding to ~1--3 granular diameters. We also note that the spongy-textured Fe IX 17.1 nm moss is not confined to plages, but may extend into regions where the photospheric field is relatively weak or even has mixed polarity. We again find a tendency for bright coronal loops seen in the 17.1, 19.3, and 21.1 nm passbands to show looplike fine structure and compact brightenings at their footpoints. These observations provide further confirmation that present-day magnetograms are significantly underrepresenting the amount of minority-polarity flux inside AR plages and again suggest that footpoint reconnection and small-scale flux cancellation may play a major role in coronal heating, both inside and outside ARs. **2013 April 30, 2013 May 4, 2013 May 5, 2014 September 14, 2014 December 1, 2014 December 13–15, 2015 April 18, 2015 May 5, 2015 October 23, 2015 November 5, 2015 December 19**

Surface Flux Transport and the Evolution of the Sun's Polar Fields **Review**

Y.-M. **Wang**
Space Science Reviews **2017**, Volume 210, Issue 1–4, pp 351–365
The evolution of the polar fields occupies a central place in flux transport (Babcock–Leighton) models of the solar cycle. We discuss the relationship between surface flux transport and polar field evolution, focusing on two main issues: the latitudinal profile of the meridional flow and the axial tilts of active regions. Recent helioseismic observations indicate that the poleward flow speed peaks at much lower latitudes than inferred from magnetic feature tracking, which includes the effect of supergranular diffusion and thus does not represent the actual bulk

flow. Employing idealized simulations, we demonstrate that flow profiles that peak at mid latitudes give rise to overly strong and concentrated polar fields. We discuss the differences between magnetic and white-light measurements of tilt angles, noting the large uncertainties inherent in the sunspot group measurements and their tendency to underestimate the actual tilts. We find no clear evidence for systematic cycle-to-cycle variations in Joy's law during cycles 21–23. Finally, based on the observed evolution of the Sun's axial dipole component and polar fields up to the end of 2015, we predict that cycle 25 will be similar in amplitude to cycle 24.

Variation of Coronal Activity from the Minimum to Maximum of Solar Cycle 24 using Three Dimensional Coronal Electron Density Reconstructions from STEREO/COR1

Tongjiang **Wang**, Nelson L. Reginald, Joseph M. Davila, O. Chris St. Cyr, William T. Thompson
Solar Phys. 292:97 **2017**
https://arxiv.org/pdf/1706.05116.pdf

Three dimensional electron density distributions in the solar corona are reconstructed for 100 Carrington Rotations (CR 2054−2153) during 2007/03−2014/08 using the spherically symmetric method from polarized white-light observations with the STEREO/COR1. These three-dimensional electron density distributions are validated by comparison with similar density models derived using other methods such as tomography and a MHD model as well as using data from SOHO/LASCO-C2. Uncertainties in the estimated total mass of the global corona are analyzed based on differences between the density distributions for COR1-A and -B. Long-term variations of coronal activity in terms of the global and hemispheric average electron densities (equivalent to the total coronal mass) reveal a hemispheric asymmetry during the rising phase of Solar Cycle 24, with the northern hemisphere leading the southern hemisphere by a phase shift of 7−9 months. Using 14-CR (~13-month) running averages, the amplitudes of the variation in average electron density between Cycle 24 maximum and Cycle 23/24 minimum (called the modulation factors) are found to be in the range of 1.6−4.3. These modulation factors are latitudinally dependent, being largest in polar regions and smallest in the equatorial region. These modulation factors also show a hemispheric asymmetry, being somewhat larger in the southern hemisphere. The wavelet analysis shows that the short-term quasi-periodic oscillations during the rising and maximum phases of Cycle 24 have a dominant period of 7−8 months. In addition, it is found that the radial distribution of mean electron density for streamers at Cycle 24 maximum is only slightly larger (by ~30%) than at cycle minimum. **1–15 May 2013**
See Kumari, A., Ramesh, R., Kathiravan, C. et al. Sol Phys (**2017**) 292: 177.
https://link.springer.com/content/pdf/10.1007%2Fs11207-017-1203-3.pdf

Initial In-flight Results: The Total Solar Irradiance Monitor on the FY-3C Satellite, an Instrument with a Pointing System

Hongrui **Wang**, Jin Qi, Huiduan Li, Wei Fang
Solar Physics January **2017**, 292:9

The total solar irradiance (TSI) has been recorded daily since October 2013 by the Total Solar Irradiance Monitor (TSIM) onboard the FY-3C satellite, which is mainly designed for Earth observation. The TSIM has a pointing system to perform solar tracking using a sun sensor. The TSI is measured by two electrical substitution radiometers with traceability to the World Radiation Reference. The TSI value measured with the TSIM on 2 October 2013 is \(1364.88~\mbox{W}\,\mbox{m}^{-2}\) with an uncertainty of \(1.08~\mbox{W}\,\mbox{m}^{-2}\). Short-term TSI variations recorded with the TSIM show good agreement with SOHO/VIRGO and SORCE/TIM. The data quality and accuracy of FY-3C/TSIM are much better than its predecessors on the FY-3A and FY-3B satellites, which operated in a scanning mode.

Instrument Description: The Total Solar Irradiance Monitor on the FY-3C Satellite, an Instrument with a Pointing System

Hongrui **Wang**, Yupeng Wang, Xin Ye, Dongjun Yang, Kai Wang, Huiduan Li, Wei Fang
Solar Physics January **2017**, 292:8

The Total Solar Irradiance Monitor (TSIM) onboard the nadir Feng Yun-3C (FY-3C) satellite provides measurements of the total solar irradiance with accurate solar tracking and sound thermal stability of its heat sink. TSIM/FY-3C mainly consists of the pointing system, the radiometer package, the thermal control system, and the electronics. Accurate solar tracking is achieved by the pointing system, which greatly improves the science data quality when compared with the previous TSIM/FY-3A and TSIM/FY-3B. The total solar irradiance (TSI) is recorded by TSIM/FY-3C about 26 times each day, using a two-channel radiometer package. One channel is used to perform routine observation, and the other channel is used to monitor the degradation of the cavity detector in the routine channel. From the results of the ground test, the incoming irradiance is measured by the routine channel (AR1) with a relative uncertainty of 592 ppm. A general description of the TSIM, including the instrument modules, uncertainty evaluation, and its operation, is given in this article.

Simulation of Quiet-Sun Hard X-rays Related to Solar Wind Superhalo Electrons

Wen **Wang**, Linghua Wang, Säm Krucker, and Iain Hannah
Solar Phys. Volume 291, Issue 5, pp 1357-1367 **2016**
http://arxiv.org/pdf/1605.06339.pdf
In this paper, we propose that the accelerated electrons in the quiet Sun could collide with the solar atmosphere to emit Hard X-rays (HXRs) via non-thermal bremsstrahlung, while some of these electrons would move upwards and escape into the interplanetary medium, to form a superhalo electron population measured in the solar wind. After considering the electron energy loss due to Coulomb collisions and the ambipolar electrostatic potential, we find that the sources of the superhalo could only occur high in the corona (at a heliocentric altitude >~ 1.9 R⊙ (the mean radius of the Sun), to remain a power-law shape of electron spectrum as observed by STEREO at 1AU near solar minimum (Wang et al., 2012). The modeled quiet-Sun HXRs related to the superhalo electrons fit well to a power-law spectrum, f ~ ε^(-γ), with an index γ ≈ 2.0"2.3 (3.3"3.7) at 10?100 keV, for the warm/cold thick-target (thin-target) emissions produced by the downward-traveling (upward-traveling) accelerated electrons. These simulated quiet-Sun spectra are significantly harder than the observed spectra of most solar HXR flares. Assuming that the quiet-Sun sources cover 5% of the solar surface, the modeled thin-target HXRs are more than six orders of magnitude weaker than the RHESSI upper limit for quiet-Sun HXRs (Hannah et al., 2010). Using the thick-target model for the downward-traveling electrons, the RHESSI upper limit restricts the number of downward-traveling electrons to at most ≈3 times the number of escaping electrons. This ratio is fundamentally different from what is observed during solar flares associated with escaping electrons where the fraction of downward-traveling electrons dominates by a factor of 100 to 1000 over the escaping population.

Toward an Understanding of Earth-Affecting Solar Eruptions

Yuming **Wang**
EOS 1 Apr **2016**
Coronal mass ejection forecasting improves with technological developments and increasing availability of data.

Coronal Mass Ejections and the Solar Cycle Variation of the Sun's Open Flux

Y.-M. **Wang** and N. R. Sheeley, Jr.
2015 ApJ 809 L24
The strength of the radial component of the interplanetary magnetic field (IMF), which is a measure of the Sun's total open flux, is observed to vary by roughly a factor of two over the 11 year solar cycle. Several recent studies have proposed that the Sun's open flux consists of a constant or "floor" component that dominates at sunspot minimum, and a time-varying component due to coronal mass ejections (CMEs). Here, we point out that CMEs cannot account for the large peaks in the IMF strength which occurred in 2003 and late 2014, and which coincided with peaks in the Sun's equatorial dipole moment. We also show that near-Earth interplanetary CMEs, as identified in the catalog of Richardson and Cane, contribute at most ~30% of the average radial IMF strength even during sunspot maximum. We conclude that the long-term variation of the radial IMF strength is determined mainly by the Sun's total dipole moment, with the quadrupole moment and CMEs providing an additional boost near sunspot maximum. Most of the open flux is rooted in coronal holes, whose solar cycle evolution in turn reflects that of the Sun's lowest-order multipoles.

Correlation Between CME Occurrence Rate and Current Helicity in the Global Magnetic Field of Solar Cycle 23

Chuanyu **Wang**, Mei Zhang
Solar Phys. **2015**
We investigate the correlation between the occurrence rate of the monthly coronal mass ejection (CME) and the magnitude of the current helicity in global magnetic field on the photosphere of solar cycle 23. We used the technique introduced by Pevtsov and Latushko (Astrophys. J. 528, 999,2000) to retrieve the vector magnetic field from longitudinal full-disk magnetograms, but applied a different method to calculate the current helicity and focused on the evolution of the magnitude of current helicity over a full solar cycle. We found that there is a close relationship between the variation of the current helicity in the global magnetic field and that of the monthly CME occurrence rate. This provides further evidence to support that helicity is an important ingredient for solar eruptions.

Solar Cycle Variation of the Sun's Low-Order Magnetic Multipoles: Heliospheric Consequences **Review**

Y.-M. **Wang**
Space Science Reviews December **2014**, Volume 186, Issue 1-4, pp 387-407
The Sun's dipole and quadrupole components play a central role in the solar cycle evolution of the interplanetary magnetic field (IMF). The long-term variation of the radial IMF component approximately tracks that of the total dipole moment, with additional contributions coming near sunspot maximum from the quadrupole moment and from CMEs. The axial and equatorial components of the dipole vary out of phase with each other over the solar cycle. The equatorial dipole, whose photospheric sources are subject to rotational shearing, decays on a timescale of ∼1 yr and must be continually regenerated by new sunspot activity; its fluctuating strength depends not only on the activity level, but also on the longitudinal phase relationships among the active regions. During cycles 21–23, the equatorial dipole and IMF reached their peak strength ∼2 yrs after sunspot maximum; conversely, large dips or "Gnevyshev gaps" occurred when active regions emerged longitudinally out of phase with each other. The 10Be-inferred phase shift in the IMF variation during the Maunder Minimum may be explained by a decrease in the amplitude of the equatorial dipole relative to the axial dipole, due either to a systematic weakening of the emerging bipoles or to an increase in their tilt angles. In mid-2012, during the polarity reversal of cycle 24, the nonaxisymmetric quadrupole component became so dominant that the heliospheric current sheet (HCS) split into two cylindrical components. Hemispheric asymmetries in sunspot activity give rise to an axisymmetric quadrupole component, which has combined with the axial dipole to produce a systematic southward displacement of the HCS since cycle 20.

Total Solar Irradiance Monitor for the FY-3B Satellite – Space Experiments and Primary Data Corrections

Hongrui **Wang**, Huiduan Li, Jin Qi, Wei Fang
Solar Phys., February **2015**, Volume 290, Issue 2, pp 645-655
We present space experiments of the Total Solar Irradiance Monitor (TSIM) on the FY-3B satellite. The total solar irradiance (TSI) has been measured by TSIM/FY-3B continuously for nearly four years, with some short data gaps. Overlapping measurements of the TSI are provided by the TSIM, with three electrical substitution radiometers that are mounted with different alignment angles onto the leading face of the satellite. TSI measurements are normalized to a distance of 1 AU and zero velocity with respect to the Sun. The relative uncertainty in the TSI measurements is 910 parts per million. TSI values measured with TSIM/FY-3B are around 1365 W m−2, slightly lower than VIRGO/SOHO and higher than TIM/SORCE values. Most of the time, it is found that short time-scale variations in TSI detected by TSIM/FY-3B agree with other space TSI instruments.

Validation of Spherically Symmetric Inversion by Use of a Tomographic Reconstructed Three-Dimensional Electron Density of the Solar Corona

Tongjiang **Wang**, Joseph M. Davila
Solar Phys., 2014
http://arxiv.org/pdf/1404.5925v1.pdf
Determination of the coronal electron density by the inversion of white-light polarized brightness (pB) measurements by coronagraphs is a classic problem in solar physics. An inversion technique based on the spherically symmetric geometry (Spherically Symmetric Inversion, SSI) was developed in the 1950s, and has been widely applied to interpret various observations. However, to date there is no study about uncertainty estimation of this method. In this study we present the detailed assessment of this method using a three-dimensional (3D) electron density in the corona from 1.5 to 4 Rsun as a model, which is reconstructed by tomography method from STEREO/COR1 observations during solar minimum in February 2008. We first show in theory and observation that the spherically symmetric polynomial approximation (SSPA) method and the Van de Hulst inversion technique are equivalent. Then we assess the SSPA method using synthesized pB images from the 3D density model, and find that the SSPA density values are close to the model inputs for the streamer core near the plane of the sky (POS) with differences generally less than a factor of two or so; the former has the lower peak but more spread in both longitudinal and latitudinal directions than the latter. We estimate that the SSPA method may resolve the coronal density structure near the POS with angular resolution in longitude of about 50 degrees. Our results confirm the suggestion that the SSI method is applicable to the solar minimum streamer (belt) as stated in some previous studies. In addition, we demonstrate that the SSPA method can be used to reconstruct the 3D coronal density, roughly in agreement with that by tomography for a period of low solar activity. We suggest that the SSI method is complementary to the 3D tomographic technique in some cases, given that the development of the latter is still an ongoing research effort.

Is Solar Cycle 24 Producing More Coronal Mass Ejections Than Cycle 23?

Y.-M. **Wang** and R. Colaninno
2014 ApJ 784 L27
Although sunspot numbers are roughly a factor of two lower in the current cycle than in cycle 23, the rate of coronal mass ejections (CMEs) appears to be at least as high in 2011-2013 as during the corresponding phase of the previous cycle, according to three catalogs that list events observed with the Large Angle and Spectrometric Coronagraph (LASCO). However, the number of CMEs detected is sensitive to such factors as the image cadence and the tendency (especially by human observers) to under-/overcount small or faint ejections during periods of high/low activity. In contrast to the total number, the total mass of CMEs is determined mainly by larger events. Using the mass measurements of 11,000 CMEs given in the manual CDAW catalog, we find that the mass loss rate remains well correlated with the sunspot number during cycle 24. In the case of the automated CACTus and SEEDS catalogs, the large increase in the number of CMEs during cycle 24 is almost certainly an artifact caused by the near-doubling of the LASCO image cadence after mid-2010. We confirm that fast CMEs undergo a much stronger solar-cycle variation than slow ones, and that the relative frequency of slow and less massive CMEs increases with decreasing sunspot number. We conclude that cycle 24 is not only producing fewer CMEs than cycle 23, but that these ejections also tend to be slower and less massive than those observed one cycle earlier.

On the Strength of the Hemispheric Rule and the Origin of Active-region Helicity

Y.-M. **Wang**
2013 ApJ 775 L46
Vector magnetograph and morphological observations have shown that the solar magnetic field tends to have negative (positive) helicity in the northern (southern) hemisphere, although only ~60%-70% of active regions appear to obey this "hemispheric rule." In contrast, at least ~80% of quiescent filaments and filament channels that form during the decay of active regions follow the rule. We attribute this discrepancy to the difficulty in determining the helicity sign of newly emerged active regions, which are dominated by their current-free component; as the transverse field is canceled at the polarity inversion lines, however, the axial component becomes dominant there, allowing a more reliable determination of the original active-region chirality. We thus deduce that the hemispheric rule is far stronger than generally assumed, and cannot be explained by stochastic processes. Earlier studies have shown that the twist associated with the axial tilt of active regions is too small to account for the observed helicity; here, both tilt and twist are induced by the Coriolis force acting on the diverging flow in the emerging flux tube. However, in addition to this east-west expansion about the apex of the loop, each of its legs must expand continually in cross section during its rise through the convection zone, thereby acquiring a further twist through the Coriolis force. Since this transverse pressure effect is not limited by drag or tension forces, the final twist depends mainly on the rise time, and may be large enough to explain the observed active-region helicity.

ASYMMETRIC SUNSPOT ACTIVITY AND THE SOUTHWARD DISPLACEMENT OF THE HELIOSPHERIC CURRENT SHEET

Y.-M. **Wang**1 and E. Robbrecht
2011 ApJ 736 136
Observations of the interplanetary magnetic field (IMF) have suggested a statistical tendency for the heliospheric current sheet (HCS) to be shifted a few degrees southward of the heliographic equator during the period 1965-2010, particularly in the years near sunspot minimum. Using potential-field source-surface extrapolations and photospheric flux-transport simulations, we demonstrate that this southward displacement follows from Joy's law and the observed hemispheric asymmetry in the sunspot numbers, with activity being stronger in the southern (northern) hemisphere during the declining (rising) phase of cycles 20-23. The hemispheric asymmetry gives rise to an axisymmetric quadrupole field, whose equatorial zone has the sign of the leading-polarity flux in the dominant hemisphere; during the last four cycles, the polarity of the IMF around the equator thus tended to match that of the north polar field both before and after polar field reversal. However, large fluctuations are introduced by the nonaxisymmetric field components, which depend on the longitudinal distribution of sunspot activity in either hemisphere. Consistent with this model, the HCS showed an average northward displacement during cycle 19, when the "usual" alternation was reversed and the northern hemisphere became far more active than the southern hemisphere during the declining phase of the cycle. We propose a new method for determining the north-south displacement of the HCS from coronal streamer observations.

Is there more global solar activity on the Sun?

J. X. **Wang**1, Y.Z. Zhang1, G.P. Zhou1, Y.Y. Wen1 and J. Jiang2

Solar and Stellar Variability: Impact on Earth and Planets, Proceedings IAU Symposium No. 264, **2009**, p. 251-256, A.G. Kosovichev, A.H. Andrei & J.-P. Rozelot, eds.
Y:\obridko\otchet09
There appear indications of more global activity on the Sun which is larger, much beyond the scale of solar active regions (ARs). These indications include formation, flaring and eruption of the trans-equatorial loops seen in EUV and X-rays, formation and eruption of transequatorial filaments, global magnetic connectivity in EUV dimming associated with halo-coronal mass ejections, wide spread of radio burst sources in meter wavelength in the solar corona, and quasi-simultaneous magnetic flux emergence in both hemispheres seen during some major solar events. With examples of a few major events in the last solar cycle we discuss the possibility that there is large or global-scale activity on the Sun. Its spatial scale is many times larger than that of AR and temporal scale is over 10 hours. The exemplified trans-equatorial loops are anchored in ARs and their activity is temporally associated with flares in ARs too. In some sense the flares in ARs appear either as a part of or a precursor of the more global activity. It is likely that the combination of the flares in ARs and the associated global activity is responsible to the major solar-terrestrial events. More efforts in understanding the global activity are undertaken.

Multi-Fluid Simulations of Upper Chromospheric Magnetic Reconnection with Helium-Hydrogen mixture

Q. M. **Wargnier**, J. Martinez-Sykora, V. H. Hansteen, B. De Pontieu
ApJ **2022**
https://arxiv.org/pdf/2211.02157.pdf
Our understanding of magnetic reconnection (MR) under chromospheric conditions remains limited. Recent observations have demonstrated the important role of ion-neutral interactions in the dynamics of the chromosphere. Furthermore, the comparison between spectral profiles and synthetic observations of reconnection events suggest that current MHD approaches appear to be inconsistent with observations. First, collisions and multi-thermal aspects of the plasma play a role in these regions. Second, hydrogen and helium ionization effects are relevant to the energy balance of the chromosphere. This work investigates multi-fluid multi-species (MFMS) effects on MR in conditions representative of the upper chromosphere using the multi-fluid Ebysus code. We compare an MFMS approach based on a helium-hydrogen mixture with a two-fluid MHD model based on hydrogen only. The simulations of MRs are performed in a Lundquist number regime high enough to develop plasmoids and instabilities. We study the evolution of the MR and compare the two approaches including the structure of the current sheet and plasmoids, the decoupling of the particles, the evolution of the heating mechanisms, and the composition. The presence of helium species leads to more efficient heating mechanisms than the two-fluid case. This scenario, which is out of reach of the two-fluid or single-fluid models, can reach transition region temperatures starting from upper chromospheric thermodynamic conditions, representative of a quiet Sun scenario. The different dynamics between helium and hydrogen species could lead to chemical fractionation and, under certain conditions, enrichment of helium in the strongest outflows. This could be of significance for recent observations of helium enrichment in the solar wind in switchbacks and CMEs.

Investigating Global Convective Dynamos with Mean-field Models: Full Spectrum of Turbulent Effects Required

Jörn **Warnecke**1, Matthias Rheinhardt2, Mariangela Viviani1,3, Frederick A. Gent2,4, Simo Tuomisto2, and Maarit J. Käpylä1,2,5
2021 ApJL 919 L13
https://doi.org/10.3847/2041-8213/ac1db5
The role of turbulent effects for dynamos in the Sun and stars continues to be debated. Mean-field (MF) theory provides a broadly used framework to connect these effects to fundamental magnetohydrodynamics. While inaccessible observationally, turbulent effects can be directly studied using global convective dynamo (GCD) simulations. We measure the turbulent effects in terms of turbulent transport coefficients, based on the MF framework, from an exemplary GCD simulation using the test-field method. These coefficients are then used as an input into an MF model. We find a good agreement between the MF and GCD solutions, which validates our theoretical approach. This agreement requires all turbulent effects to be included, even those which have been regarded as unimportant so far. Our results suggest that simple dynamo models, as are commonly used in the solar and stellar community, relying on very few, precisely fine-tuned turbulent effects, may not be representative of the full dynamics of dynamos in global convective simulations and astronomical objects.

Consistent transport properties in multicomponent two-temperature magnetized plasmas *Application to the Sun atmosphere*

Q. **Wargnier**1, A. Alvarez Laguna1,2, J. B. Scoggins1, N. N. Mansour4, M. Massot1 and T. E. Magin1,2,3
A&A 635, A87 (**2020**)
https://www.aanda.org/articles/aa/pdf/2020/03/aa34686-18.pdf
Aims. We present a fluid model that has been developed for multicomponent two-temperature magnetized plasmas in chemical non-equilibrium for the partially to fully ionized collisional regimes. We focus on transport phenomena with the aim of representing the atmosphere of the Sun.
Methods. This study is based on an asymptotic fluid model for multicomponent plasmas derived from kinetic theory, yielding a rigorous description of the dissipative effects. The governing equations and consistent transport properties are obtained using a multiscale Chapman-Enskog perturbative solution to the Boltzmann equation based on a dimensional analysis. The mass disparity between free electrons and heavy particles is accounted for, as well as the influence of the electromagnetic field. We couple this model to the Maxwell equations for the electromagnetic field and derive the generalized Ohm's law for multicomponent plasmas. The model inherits a well-identified mathematical structure leading to an extended range of validity for the Sun's atmospheric conditions. We compute consistent transport properties by means of a spectral Galerkin method using the Laguerre-Sonine polynomial approximation. Two non-vanishing polynomial terms are used when deriving the transport systems for electrons, whereas only one term is retained for heavy particles.
Results. In a simplified framework where the plasma is fully ionized, we compare the transport properties for the lower solar atmosphere to conventional expressions for magnetized plasmas attributed to Braginskii, showing a good agreement between both results. For more general partially ionized conditions, representative of the lower solar atmosphere, we compute the muticomponent transport properties corresponding to the species diffusion velocities, heavy-particle and electron heat fluxes, and viscous stress tensor of the model for a helium-hydrogen mixture in local thermodynamic equilibrium. The model is assessed for the 3D radiative magnetohydrodynamic simulation of a pore at the Sun photosphere. The resistive term is found to dominate mainly the dynamics of the electric field at the pore location. The battery term for heavy particles appears to be higher at the pore location and at some intergranulation boundaries.

Small-scale and large-scale dynamos in global convection simulations of solar-like stars

Jörn **Warnecke**, Maarit J. Korpi-Lagg, Matthias Rheinhard, Mariangela Viviani, Ameya Prabhu
A&A **2024**
https://arxiv.org/pdf/2406.08967
It has been recently shown that a small-scale dynamo (SSD) instability could be possible in solar-like low magnetic Prandtl number Pm plasmas. It has been proposed that the presence of SSD can potentially have a significant impact on the dynamics of the large-scale dynamo (LSD) in the stellar convection zones. Studying these two dynamos, SSD and LSD, together in a global magnetoconvection model requires high-resolution simulations and large amounts of computational resources. Starting from a well-studied global convective dynamo model that produces cyclic magnetic fields, we systematically increased the resolution and lowered the diffusivities to enter the regime of Reynolds numbers that allow for the excitation of SSD on top of the LSD. We studied how the properties of convection, generated differential rotation profiles, and LSD solutions change with the presence of SSD. We performed convective dynamo simulations in a spherical wedge with the Pencil Code. The resolutions of the models were increased in 4 steps by a total factor of 16 to achieve maximal fluid and magnetic Reynolds numbers of over 500. We found that the differential rotation is strongly quenched by the presence of the LSD and SSD. Even though the small-scale magnetic field only mildly decreases increasing Re, the large-scale field strength decreases significantly. We do not find the SSD dynamo significantly quenching the convective flows as claimed recently by other authors; in contrast, the convective flows first grow and then saturate for increasing Re. Furthermore, the angular momentum transport is highly affected by the presence of small-scale magnetic fields, which are mostly generated by LSD. These fields not only change the Reynolds stresses, but also generate dynamically important Maxwell stresses. The LSD evolution in terms of its pattern and field distribution is rather independent of the increase in Rm.

Numerical evidence for a small-scale dynamo approaching solar magnetic Prandtl numbers

Jörn **Warnecke**, Maarit J. Korpi-Lagg, Frederick A. Gent, Matthias Rheinhardt
Nature **2023** (2021)
https://arxiv.org/pdf/2306.03991.pdf
Magnetic fields on small scales are ubiquitous in the universe. Though they can often be observed in detail, their generation mechanisms are not fully understood. One possibility is the so-called small-scale dynamo (SSD). Prevailing numerical evidence, however, appears to indicate that an SSD is unlikely to exist at very low magnetic Prandtl numbers (PrM) such as are present in the Sun and other cool stars. We have performed high-resolution simulations of isothermal forced turbulence employing the lowest PrM values so far achieved. Contrary to earlier findings, the SSD turns out to be not only possible for PrM down to 0.0031, but even becomes increasingly easier to

excite for PrM below ≃0.05. We relate this behaviour to the known hydrodynamic phenomenon referred to as the bottleneck effect. Extrapolating our results to solar values of PrM indicates that an SSD would be possible under such conditions.

Investigating global convective dynamos with mean-field models: full spectrum of turbulent effects required

Jörn **Warnecke**, Matthias Rheinhardt, Mariangela Viviani, Frederick Gent, Simo Tuomisto, Maarit J. Käpylä

ApJL **2021**

https://arxiv.org/pdf/2105.07708.pdf

Turbulent effects are argued to be essential for dynamos in the Sun and stars. While inaccessible observationally, they can be directly studied using global convective dynamo (GCD) simulations. We measure these turbulent effects, in terms of turbulent transport coefficients, from an exemplary GCD simulation using the test-field method. These coefficients are then used as an input into a mean-field (MF) model. We find a good agreement between the MF and GCD solutions, which validates our theoretical approach. This agreement requires all turbulent effects to be included, even those which have been regarded unimportant so far. Our results suggest that simple dynamo models as are commonly used in the solar and stellar community, relying on very few, precisely fine-tuned turbulent effects, may not be representative of the full dynamics of GCDs in astronomical objects.

On the influence of magnetic helicity on X-rays emission of solar and stellar coronae

Jörn **Warnecke**, Hardi Peter, (Max-Planck-Institut für Sonnensystemforschung)

A&A **2019**

https://arxiv.org/pdf/1910.06896.pdf

Observation of solar-like stars show a clear relation between X-ray emission and their rotation. Higher stellar rotation can lead to a larger magnetic helicity production in stars. We aim to understand the relation between magnetic helicity on the surface of a star to their coronal X-ray emission. We use 3D MHD simulations to model the corona of the solar-like stars. We take an observed magnetogram as in photospheric activity input, and inject different values of magnetic helicity. We use synthesis emission to calculate the X-ray emission flux of each simulation and investigate how this scales with injected magnetic helicity. We find that for larger injected magnetic helicities an increase in temperature and an increase in X-ray emission. The X-ray emission scaled cubicly with the injected helicity. We can related this to increase of horizontal magnetic field and therefore higher Poynting flux at the coronal base. Using typical scaling of magnetic helicity production with stellar rotation, we can explain the increase of X-ray emission with rotation only by an increase of magnetic helicity at the surface of a star.

Data-driven model of the solar corona above an active region

Jörn **Warnecke**, Hardi Peter (Max-Planck-Institut f\"ur Sonnensystemforschung)

A&A letters **2019**

https://arxiv.org/pdf/1903.00455.pdf

In this study we aim to reproduce the structure of the corona above a solar active region as seen in the extreme ultraviolet (EUV) using a three-dimensional magnetohydrodynamic (3D MHD) model. The 3D MHD data-driven model solves the induction equation and the mass, momentum and energy balance. To drive the system, we feed the observed evolution of the magnetic field in the photosphere of the active region AR 12139 into the bottom boundary. This creates a hot corona above the cool photosphere in a self-consistent way. We synthesize the coronal EUV emission from the densities and temperatures in the model and compare this to the actual coronal observations. We are able to reproduce the overall appearance and key features of the corona in this active region. The model shows long loops, fan loops, compact loops and diffuse emission forming at the same locations at similar times as in the observation. Furthermore, the low intensity contrast of the model loops in EUV matches the observations. In our model the energy input into the corona is similar as in the scenarios of fieldline-braiding or fluxtube tectonics, i.e. through the driving of the vertical magnetic field by horizontal photospheric motions. The success of our model shows the central role this process plays for the structure, dynamics and heating of the corona. **16 August 2014**

Non-Fourier description of heat flux evolution in 3D MHD simulations of the solar corona

Jörn **Warnecke** (1), Sven Bingert

Geophysical and Astrophysical Fluid Dynamics **2018**

https://arxiv.org/pdf/1811.01572.pdf

The hot loop structures in the solar corona can be well modeled by three dimensional magnetohydrodynamic simulations, where the corona is heated by field line braiding driven at the photosphere. To be able to reproduced the emission comparable to observations, one has to use realistic values for the Spitzer heat conductivity, which puts a large constrain on the time step of these simulations and therefore make them computationally expensive. Here, we present a non-Fourier description of the heat flux evolution, which allow us to speed up the simulations

significantly. Together with the semi-relativistic Boris correction, we are able to limit the time step constrain of the Alfvén speed and speed up the simulations even further. We discuss the implementation of these two methods to the \PC and present their implications on the time step, and the temperature structures, the ohmic heating rate and the emission in simulations of the solar corona. We find that with the use of the non-Fourier description of the heat flux evolution and the Boris correction, we can increase the time step of the simulation significantly without moving far away from the reference solution. However, for too low values of the Alfvén speed limit, the simulation moves away from the reference solution und produces much higher temperatures and stronger emission structures.

Dynamo cycles in global convection simulations of solar-like stars

Jörn **Warnecke** (Max-Planck-Institut für Sonnensystemforschung)

A&A **2017**

https://arxiv.org/pdf/1712.01248.pdf

Several solar-like stars exhibit magnetic activity similar to the Sun. We want to understand the rotational dependency of these activity cycle periods. We use three dimensional magnetohydrodynamical simulations of global convective dynamo models of solar-like stars to investigate the rotational dependency of dynamos. We further apply the test-field method to determine the α effect in these simulations. We find dynamo with clear oscillating mean magnetic fields for moderately and rapidly rotating runs. For slower rotation, the field is constant or exhibit irregular cycles. In the moderately and rapidly rotating regime the cycle periods increase weakly with rotation. This behavior can be well explained with a Parker-Yoshimura dynamo wave traveling equatorward. Even though the α effect becomes stronger for increasing rotation, the shear decreases steeper, causing this weak dependence on rotation. Similar as other numerical studies, we find no indication of activity branches as suggested by Brandenburg et al. (1998). However, our simulation seems to agree more with the transitional branch suggested by Distefano et al. (2017). If the Sun exhibit a dynamo wave similar as we find in our simulations, it would operate deep inside the convection zone.

Influence of a coronal envelope as a free boundary to global convective dynamo simulations

J. **Warnecke**1,2, P. J. Käpylä3,2,1,4, M. J. Käpylä1,2 and A. Brandenburg

A&A 596, A115 (**2016**)

Aims. We explore the effects of an outer stably stratified coronal envelope on rotating turbulent convection, differential rotation, and large-scale dynamo action in spherical wedge models of the Sun.
Methods. We solve the compressible magnetohydrodynamic equations in a two-layer model with unstable stratification below the surface, representing the convection zone, and a stably stratified coronal envelope above. The interface represents a free surface. We compare our model to models that have no coronal envelope.
Results. The presence of a coronal envelope is found to modify the Reynolds stress and the Λ effect resulting in a weaker and non-cylindrical differential rotation. This is related to the reduced latitudinal temperature variations that are caused by and dependent on the angular velocity. Some simulations develop a near-surface shear layer that we can relate to a sign change in the meridional Reynolds stress term in the thermal wind balance equation. Furthermore, the presence of a free surface changes the magnetic field evolution since the toroidal field is concentrated closer to the surface. In all simulations, however, the migration direction of the mean magnetic field can be explained by the Parker-Yoshimura rule, which is consistent with earlier findings.
Conclusions. A realistic treatment of the upper boundary in spherical dynamo simulations is crucial for the dynamics of the flow and magnetic field evolution.

Bipolar region formation in stratified two-layer turbulence

Jörn **Warnecke** (1,2), Illa R. Losada (2,3), Axel Brandenburg (2,3,4,5), Nathan Kleeorin (6,2), Igor Rogachevskii

A&A **2016**

https://arxiv.org/pdf/1502.03799v4.pdf

This work presents an extensive study of the previously discovered formation of bipolar flux concentrations in a two-layer model. We interpret the formation process in terms of negative effective magnetic pressure instability (NEMPI), which is a possible mechanism to explain the origin of sunspots. In our simulations, we use a Cartesian domain of isothermal stratified gas that is divided into two layers. In the lower layer, turbulence is forced with transverse nonhelical random waves, whereas in the upper layer no flow is induced. A weak uniform magnetic field is imposed in the entire domain at all times. In this study we vary the stratification by changing the gravitational acceleration, magnetic Reynolds number, strength of the imposed magnetic field, and size of the domain to investigate their influence on the formation process. Bipolar magnetic structure formation takes place over a large range of parameters. The magnetic structures become more intense for higher stratification until the density contrast becomes around 100 across the turbulent layer. For the Reynolds numbers considered, magnetic flux concentrations are generated at magnetic Prandtl number between 0.1 and 1. The magnetic field in bipolar regions increases with

higher imposed field strength until the field becomes comparable to the equipartition field strength of the turbulence. A larger horizontal extent enables the flux concentrations to become stronger and more coherent. The size of the bipolar structures turns out to be independent of the domain size. In the case of bipolar region formation, we find an exponential growth of the large-scale magnetic field, which is indicative of a hydromagnetic instability. Additionally, the flux concentrations are correlated with strong large-scale downward and converging flows. These findings imply that NEMPI is responsible for magnetic flux concentrations.

Cause of equatorward migration in global convective dynamo simulations

Jörn **Warnecke** (1,2), Petri J. Käpylä (3,2), Maarit J. Käpylä (2), Axel Brandenburg
ApJL, **2014**

We present results from four convectively-driven stellar dynamo simulations in spherical wedge geometry. All of these simulations produce cyclic and migrating mean magnetic fields. Through detailed comparisons we show that the migration direction can be explained by an αΩ dynamo wave following the Parker--Yoshimura rule. We conclude that the equatorward migration in this and previous work is due to a positive (negative) α effect in the northern (southern) hemisphere and a negative radial gradient of Ω outside the inner tangent cylinder of these models. This idea is supported by a strong correlation between negative radial shear and toroidal field strength in the region of equatorward propagation.

A Multicomponent Magnetic Proxy for Solar Activity

Harry P. **Warren**,Linton E. Floyd,Lisa A. Upton
Space Weather **Volume19, Issue12** e2021SW002860 **2021**
https://agupubs.onlinelibrary.wiley.com/doi/epdf/10.1029/2021SW002860
https://doi.org/10.1029/2021SW002860

We present a new, multicomponent magnetic proxy for solar activity derived from full disk magnetograms that can be used in the specification and forecasting of the Sun's radiative output. To compute this proxy we project Carrington maps, such as the synchronic Carrington maps computed with the Advective Flux Transport (AFT) surface flux transport model, to heliographic cartesian coordinates and determine the total unsigned flux as a function of absolute magnetic flux density. Performing this calculation for each day produces an array of time series, one for each flux density interval. Since many of these time series are strongly correlated, we use principal component analysis to reduce them to a smaller number of uncorrelated time series. We show that the first few principal components accurately reproduce widely used proxies for solar activity, such the the 10.7 cm radio flux and the Mg core-to-wing ratio. This suggests that these magnetic time series can be used as a proxy for irradiance variability for emission formed over a wide range of temperatures.

Observation and Modeling of High-temperature Solar Active Region Emission during the High-resolution Coronal Imager Flight of 2018 May 29

Harry P. **Warren**, Jeffrey W. Reep, Nicholas A. Crump, Ignacio Ugarte-Urra, David H. Brooks, Amy R. Winebarger, Sabrina Savage, Bart De Pontieu, Hardi Peter, Jonathan W. Cirtain, Leon Golub, Ken Kobayashi, David McKenzie, Richard Morton, Laurel Rachmeler, Paola Testa, Sanjiv Tiwari, and Robert Walsh
2020 ApJ 896 51
https://doi.org/10.3847/1538-4357/ab917c

Excellent coordinated observations of NOAA active region 12712 were obtained during the flight of the High-resolution Coronal Imager (Hi-C) sounding rocket on **2018 May 29**. This region displayed a typical active region core structure with relatively short, high-temperature loops crossing the polarity inversion line and bright "moss" located at the footpoints of these loops. The differential emission measure (DEM) in the active region core is very sharply peaked at about 4 MK. Further, there is little evidence for impulsive heating events in the moss, even at the high spatial resolution and cadence of Hi-C. This suggests that active region core heating is occurring at a high frequency and keeping the loops close to equilibrium. To create a time-dependent simulation of the active region core, we combine nonlinear force-free extrapolations of the measured magnetic field with a heating rate that is dependent on the field strength and loop length and has a Poisson waiting time distribution. We use the approximate solutions to the hydrodynamic loop equations to simulate the full ensemble of active region core loops for a range of heating parameters. In all cases, we find that high-frequency heating provides the best match to the observed DEM. For selected field lines, we solve the full hydrodynamic loop equations, including radiative transfer in the chromosphere, to simulate transition region and chromospheric emission. We find that for heating scenarios consistent with the DEM, classical signatures of energy release, such as transition region brightenings and chromospheric evaporation, are weak, suggesting that they would be difficult to detect.

Sparse Bayesian Inference and the Temperature Structure of the Solar Corona

Harry P. **Warren**, Jeff M. Byers, Nicholas A. Crump
ApJ **2016**

https://arxiv.org/pdf/1610.05972v1.pdf
Measuring the temperature structure of the solar atmosphere is critical to understanding how it is heated to high temperatures. Unfortunately, the temperature of the upper atmosphere cannot be observed directly, but must be inferred from spectrally resolved observations of individual emission lines that span a wide range of temperatures. Such observations are "inverted" to determine the distribution of plasma temperatures along the line of sight. This inversion is ill-posed and, in the absence of regularization, tends to produce wildly oscillatory solutions. We introduce the application of sparse Bayesian inference to the problem of inferring the temperature structure of the solar corona. Within a Bayesian framework a preference for solutions that utilize a minimum number of basis functions can be encoded into the prior and many ad hoc assumptions can be avoided. We demonstrate the efficacy of the Bayesian approach by considering a test library of 40 assumed temperature distributions.

Transition Region Abundance Measurements During Impulsive Heating Events

Harry P. **Warren**, David H. Brooks, George A. Doschek, Uri Feldman
ApJ 824 56 **2016**
http://arxiv.org/pdf/1512.04447v1.pdf
It is well established that elemental abundances vary in the solar atmosphere and that this variation is organized by first ionization potential (FIP). Previous studies have shown that in the solar corona low-FIP elements, such as Fe, Si, Mg, and Ca, are generally enriched relative to high-FIP elements, such as C, N, O, Ar, and Ne. In this paper we report on measurements of plasma composition made during impulsive heating events observed at transition region temperatures with the Extreme Ultraviolet Imaging Spectrometer (EIS) on Hinode. During these events the intensities of O IV, V, and VI emission lines are enhanced relative to emission lines from Mg V, VI, and VII and Si VI and VII and indicate a composition close to that of the photosphere. Long-lived coronal fan structures, in contrast, show an enrichment of low-FIP elements. We conjecture that the plasma composition is an important signature of the coronal heating process, with impulsive heating leading to the evaporation of unfractionated material from the lower layers of the solar atmosphere and higher frequency heating leading to long-lived structures and the accumulation of low-FIP elements in the corona.

The Effect of the Chromospheric Temperature on Coronal Heating

Haruka **Washinoue**, Munehito Shoda, Takeru K. Suzuki
ApJ **938** 126 **2022**
https://arxiv.org/pdf/2209.10156
https://iopscience.iop.org/article/10.3847/1538-4357/ac91c8/pdf
Recent observational and numerical studies show a variety of thermal structures in the solar chromosphere. Given that the thermal interplay across the transition region is a key to coronal heating, it is worth investigating how different thermal structures of the chromosphere yield different coronal properties. In this work, by MHD simulations of Alfvén-wave heating of coronal loops, we study how the coronal properties are affected by the chromospheric temperature. To this end, instead of solving the radiative transfer equation, we employ a simple radiative loss function so that the chromospheric temperature is easily tuned. When the chromosphere is hotter, because the chromosphere extends to a larger height, the coronal part of the magnetic loop becomes shorter, which enhances the conductive cooling. A larger loop length is therefore required to maintain the high-temperature corona against the thermal conduction. From our numerical simulations we derive a condition for the coronal formation with respect to the half loop length lloop in a simple form: lloop>aTmin+lth, where Tmin is the minimum temperature in the atmosphere and parameters a and lth have negative dependencies on the coronal field strength. Our conclusion is that the chromospheric temperature has a non-negligible impact on coronal heating for loops with small length and weak coronal field. In particular, the enhanced chromospheric heating could prevent the formation of the corona.

Catastrophic cooling in optically thin plasmas

Tim **Waters**, Amanda Stricklan
ApJ **2024**
https://arxiv.org/pdf/2408.15869
The solar corona is the prototypical example of a low density environment heated to high temperatures by external sources. The plasma cools radiatively, and because it is optically thin to this radiation, it becomes possible to model the density, velocity, and temperature structure of the system by modifying the MHD equations to include energy source terms that approximate the local heating and cooling rates. The solutions can be highly inhomogeneous and even multiphase because the well known linear instability associated with these source terms, thermal instability, leads to a catastrophic heating and cooling of the plasma in the nonlinear regime. Here we show that there is a separate, much simpler instance of catastrophic heating and cooling accompanying these source terms that can rival thermal instability in dynamical importance. The linear stability criterion is the isochoric one identified by Parker (1953), and we demonstrate that cooling functions derived from collisional ionization equilibrium are highly prone

to violating this criterion. If catastrophic cooling instability can act locally in global simulations, then it is an alternative mechanism for forming condensations, and due to its nonequilibrium character, it may be relevant to explaining a host of phenomena associated with the production of cooler gas in hot, low density plasmas.

25 Years of Self-organized Criticality: Concepts and Controversies **Review**

Nicholas W. **Watkins** , Gunnar Pruessner, Sandra C. Chapman, Norma B. Crosby, Henrik J. Jensen

Space Science Reviews January **2016**, Volume 198, Issue 1, pp 3-44 **Open Access**

Introduced by the late Per Bak and his colleagues, self-organized criticality (SOC) has been one of the most stimulating concepts to come out of statistical mechanics and condensed matter theory in the last few decades, and has played a significant role in the development of complexity science. SOC, and more generally fractals and power laws, have attracted much comment, ranging from the very positive to the polemical. The other papers (Aschwanden et al. in Space Sci. Rev., 2014, this issue; McAteer et al. in Space Sci. Rev., 2015, this issue; Sharma et al. in Space Sci. Rev. 2015, in preparation) in this special issue showcase the considerable body of observations in solar, magnetospheric and fusion plasma inspired by the SOC idea, and expose the fertile role the new paradigm has played in approaches to modeling and understanding multiscale plasma instabilities. This very broad impact, and the necessary process of adapting a scientific hypothesis to the conditions of a given physical system, has meant that SOC as studied in these fields has sometimes differed significantly from the definition originally given by its creators. In Bak's own field of theoretical physics there are significant observational and theoretical open questions, even 25 years on (Pruessner 2012). One aim of the present review is to address the dichotomy between the great reception SOC has received in some areas, and its shortcomings, as they became manifest in the controversies it triggered. Our article tries to clear up what we think are misunderstandings of SOC in fields more remote from its origins in statistical mechanics, condensed matter and dynamical systems by revisiting Bak, Tang and Wiesenfeld's original papers.

Erratum: Space Science Reviews January **2016**, Volume 198, Issue 1, p 45

Solar Cycle Related Changes in the Helium Ionization Zones of the Sun

Courtney B. **Watson**, Sarbani Basu

ApJL **903** L29 **2020**

https://arxiv.org/pdf/2010.11215.pdf

https://doi.org/10.3847/2041-8213/abc348

Helioseismic data for solar cycles 23 and 24 have shown unequivocally that solar dynamics changes with solar activity. Changes in solar structure have been more difficult to detect. Basu & Mandel (2004) had claimed that the then available data revealed changes in the HeII ionization zone of the Sun. The amount of change, however, indicated the need for larger than expected changes in the magnetic fields. Now that helioseismic data spanning two solar cycles are available, we have redone the analysis using improved fitting techniques. We find that there is indeed a change in the region around the HeII ionization zone that is correlated with activity. Since the data sets now cover two solar cycles, the time variation is easily discernible.

A Multi-instrument Analysis of Sunspot Umbrae

F. T. **Watson**, M. J. Penn, and W. Livingston

2014 ApJ 787 22

The recent solar minimum and rise phase of solar cycle 24 have been unlike any period since the early 1900s. This article examines some of the properties of sunspot umbrae over the last 17 yr with three different instruments on the ground and in space: MDI, HMI and BABO. The distribution of magnetic fields and their evolution over time is shown and reveals that the field distribution in cycle 24 is fundamentally different from that in cycle 23. The annual average umbral magnetic field is then examined for the 17 yr observation period and shows a small decrease of 375 G in sunspot magnetic fields over the period 1996-2013, but the mean intensity of sunspot umbrae does not vary significantly over this time. A possible issue with sample sizes in a previous study is then explored to explain disagreements in data from two of the source instruments. All three instruments show that the relationship between umbral magnetic fields and umbral intensity agrees with past studies in that the umbral intensity decreases as the field strength increases. This apparent contradiction can be explained by the range of magnetic field values measured for a given umbral intensity being larger than the measured 375 G change in umbral field strength over time.

Evolution of sunspot properties during solar cycle 23

F. T. **Watson**1, L. Fletcher1 and S. Marshall

A&A 533, A14 (**2011**)

Context. The long term study of the Sun is necessary if we are to determine the evolution of sunspot properties and thereby inform modeling of the solar dynamo, particularly on scales of a solar cycle.

Aims. We aim to determine a number of sunspot properties over cycle 23 using the uniform database provided by the SOHO Michelson Doppler Imager data. We focus in particular on their distribution on the solar disk, maximum magnetic field and umbral/penumbral areas. We investigate whether the secular decrease in sunspot maximum magnetic field reported in Kitt Peak data is present also in MDI data.
Methods. We have used the Sunspot Tracking And Recognition Algorithm (STARA) to detect all sunspots present in the SOHO Michelson Doppler Imager continuum data giving us 30 084 separate detections. We record information on the sunspot locations, area and magnetic field properties as well as corresponding information for the umbral areas detected within the sunspots, and track them through their evolution.
Results. We find that the total visible umbral area is 20−40% of the total visible sunspot area regardless of the stage of the solar cycle. We also find that the number of sunspots observed follows the Solar Influences Data Centre international sunspot number with some interesting deviations. Finally, we use the magnetic information in our catalogue to study the long term variation of magnetic field strength within sunspot umbrae and find that it increases and decreases along with the sunspot number. However, if we were to assume a secular decrease as was reported in the Kitt Peak data and take into account sunspots throughout the whole solar cycle we would find the maximum umbral magnetic fields to be decreasing by 23.6 ± 3.9 Gauss per year, which is far less than has previously been observed by other studies (although measurements are only available for solar cycle 23). If we only look at the declining phase of cycle 23 we find the decrease in sunspot magnetic fields to be 70 Gauss per year.

LYRA Mid-Term Periodicities

L. **Wauters**, M. Dominique, I. E. Dammasch
Solar Phys. Volume 291, Issue 7, pp 2135–2144 **2016**
The spectra of the PROBA2/LYRA data, similarly to every other solar time series, show predominant periodicities that can be of solar or instrumental origin. In this article, we compare the main periodicities characterizing the LYRA spectrum to those found in the sunspot number, in the 10.7 cm flux, in an X-ray flare index, and in the sunspot area evolution. We focused on the 2010 to 2014 time range, for which the LYRA data are available, although we also briefly address the evolution of the main periodicities in the longer range. The mid-term periodicities at ∼28∼28, ∼44∼44, ∼54∼54, ∼59∼59, ∼100∼100, ∼110∼110, and ∼150∼150 days appear as highly significant in several analyzed datasets. The consistency of distinct periodicities between datasets provides characteristics for the global Sun. This consistency also strengthens the reliability of LYRA data.

The Polar Field Reversal Process over Five Solar Cycles.

Webb, D.F., Emery, B.A., Gibson, S.E. et al.
Sol Phys 299, 27 (**2024**).
https://doi.org/10.1007/s11207-024-02273-3
https://link.springer.com/content/pdf/10.1007/s11207-024-02273-3.pdf
We examine the process during which the solar magnetic field reverses polarity around each solar maximum. We use the McIntosh Archive (McA) of solar synoptic maps over five consecutive solar cycles, SCs 19 – 23, or from 1955 to 2009. This data set allows us to track features such as filaments, polarity inversion lines (PILs), coronal hole (CH) boundaries, and sunspots over many consecutive Carrington rotations (CRs) and solar cycles (SCs). The McA allows tracking of the evolution of the polar magnetic regions and how the rush-to-the-pole (RttP) patterns occur during the period when the polar fields reverse around each activity maximum. We use the McA dataset to determine the timing and lags among these events around the maximum of each SC in each hemisphere: the sunspot number peak, the polarity reversal, the disappearance of the polar crown filaments and PILs, the poleward movement of midlatitude CHs of new-cycle polarity behind the primary PIL, the first appearance of polar CHs of new-cycle polarity, and the earliest persistent complete coverage of each pole by a CH. The goal is to use the RttPs and CH boundary mapping to better constrain solar interior and dynamo models. The end of the PIL RttP, the end of the RttP of the poleward boundary of new-cycle polarity midlatitude CHs, and the first appearance of new-cycle polar CHs are nearly coincident and follow the polarity reversals in each hemisphere by about 1 year. We also show the lag times relative to “terminator” times, which denote when the toroidal magnetic flux built during a given cycle is canceled across the equator, thus beginning the rise of new-cycle flux. This occurs after the start of the RttPs of the polar CH boundaries and near the start of the primary and secondary PIL RttPs. The start of the RttP of the poleward boundary of the new-cycle, midlatitude CH that leads to the new polar CH always occurs later than the terminator time, so the terminator is located near the beginning of the ascending phase.

Global solar magnetic field evolution over 4 solar cycles: Use of the McIntosh archive.

Webb, D.F., Gibson, S.E., Hewins, I.M., McFadden, R.H., Emery, B.A., Malanushenko, A., Kuchar, T.A.:
Front. Astron. Space Sci. 5, 23. **2018**, DOI. ADS.
https://www.frontiersin.org/articles/10.3389/fspas.2018.00023/full
The McIntosh Archive consists of a set of hand-drawn solar Carrington maps created by Patrick McIntosh from 1964 to 2009. McIntosh used mainly Hα, He-I 10830 Å and photospheric magnetic measurements from both

ground-based and NASA satellite observations. With these he traced polarity inversion lines (PILs), filaments, sunspots and plage and, later, coronal holes over a ~45-year period. This yielded a unique record of synoptic maps of features associated with the large-scale solar magnetic field over four complete solar cycles. We first discuss how these and similar maps have been used in the past to investigate long-term solar variability. Then we describe our work in preserving and digitizing this archive, developing a digital, searchable format, and creating a website and an archival repository at NOAA's National Centers for Environmental Information (NCEI). Next we show examples of how the data base can be utilized for scientific applications. Finally, we present some preliminary results on the solar-cycle evolution of the solar magnetic field, including the polar field reversal process, the evolution of active longitudes, and the role of differential solar rotation.

New Views of Global Solar Magnetic Field Evolution Over Four Solar Cycles

D. F. Webb

RHESSI Science Nuggets #331 Sept **2018**

http://sprg.ssl.berkeley.edu/~tohban/wiki/index.php/New_Views_of_Global_Solar_Magnetic_Field_Evolution_Over_Four_Solar_Cycles

A digital archive of Pat McIntosh's 44 years of solar synoptic observations.

Is There a CME Rate Floor? CME and Magnetic Flux Values for the Last Four Solar Cycle Minima

D. F. **Webb**1, R. A. Howard2, O. C. St. Cyr3, and A. Vourlidas4

2017 ApJ 851 142

http://sci-hub.tw/10.3847/1538-4357/aa9b81

The recent prolonged activity minimum has led to the question of whether there is a base level of the solar magnetic field evolution that yields a "floor" in activity levels and also in the solar wind magnetic field strength. Recently, a flux transport model coupled with magneto-frictional simulations has been used to simulate the continuous magnetic field evolution in the global solar corona for over 15 years, from 1996 to 2012. Flux rope eruptions in the simulations are estimated (Yeates), and the results are in remarkable agreement with the shape of the SOlar Heliospheric Observatory/Large Angle and Spectrometric Coronagraph Experiment coronal mass ejection (CME) rate distribution. The eruption rates at the two recent minima approximate the observed-corrected CME rates, supporting the idea of a base level of solar magnetic activity. In this paper, we address this issue by comparing annual averages of the CME occurrence rates during the last four solar cycle minima with several tracers of the global solar magnetic field. We conclude that CME activity never ceases during a cycle, but maintains a base level of 1 CME every 1.5 to ~3 days during minima. We discuss the sources of these CMEs. **1996 May-July, 2008 December - 2009 February**

Preserving a Unique Archive for Long-Term Solar Variability Studies

David F. **Webb**1 , Sarah E. Gibson2 , Ian M. Hewins1,2 , Robert H. McFadden1,2, Barbara A. Emery1,2, William Denig3 , and Patrick S. McIntosh4

Space Weather Volume 15, Issue 11 November **2017** Pages 1442–1446

http://onlinelibrary.wiley.com.sci-hub.tw/doi/10.1002/2017SW001740/abstract;jsessionid=824A0A66CE7483E6AA9C5BB9A47BF94B.f02t02

(**2017**). Space Weather (Quarterly), 15, No. 4, 1442–1446

http://onlinelibrary.wiley.com/doi/10.1002/swq.16/epdf

The McIntosh Archive consists of hand-drawn solar Carrington maps created by Patrick McIntosh from 1964 to 2009, using Hα, He 10830 Å, and photospheric magnetic measurements to trace polarity inversion lines, filaments, sunspots, and plage and coronal holes, yielding a unique 45 year record of the evolution of the solar magnetic field. We discuss our efforts to preserve and digitize this archive.

A Time–Distance Helioseismology Method for Quasi-Linear Geometries

Shea A. Hess **Webber**, W. Dean Pesnell

Solar Physics October **2019**, 294:151

https://link.springer.com/content/pdf/10.1007%2Fs11207-019-1547-y.pdf

Helioseismology is the study of the solar interior, through which we extract flow and wave-speed information from Doppler velocity observations at the surface. Local helioseismology involves the study of small regions on the solar disk and is used to create a detailed picture of the interior in that particular region. Perturbations in the flow and wave-speed results indicate, e.g. magnetic-flux or temperature variations. There are multiple methods used in local-helioseismic research, but all current local-helioseismic techniques assume a point-source perturbation. For this study, we develop a new time–distance (TD) helioseismic methodology that can exploit the quasi-linear geometry of an elongated feature, allowing us to i) improve the signal-to-noise ratio of the TD results, and ii) greatly decrease the number of calculations required and therefore the computing time of the TD analysis. Ultimately, the new method

will allow us to investigate solar features with magnetic-field configurations previously unexplored. We validate our new technique using a simple ff-mode wave simulation, comparing results of point-source and linear perturbations. Results indicate that local-helioseismic analysis is dependent on the geometry of the system and can be improved by taking the magnetic-field configuration into account.

Understanding Active Region Emergence and Origins on the Sun and Other Cool Stars

Review

Maria A. **Weber**, Hannah Schunker, Laurène Jouve, Emre Işık
Space Science Reviews 219, Article number: 63 (**2023**)
https://arxiv.org/pdf/2306.06536.pdf
https://link.springer.com/content/pdf/10.1007/s11214-023-01006-5.pdf
The emergence of active regions on the Sun is an integral feature of the solar dynamo mechanism. However, details about the generation of active-region-scale magnetism and the journey of this magnetic flux to the photosphere are still in question. Shifting paradigms are now developing for the source depth of the Sun's large-scale magnetism, the organization of this magnetism into fibril flux tubes, and the role of convection in shaping active-region observables. Here we review the landscape of flux emergence theories and simulations, highlight the role flux emergence plays in the global dynamo process, and make connections between flux emergence on the Sun and other cool stars. As longer-term and higher fidelity observations of both solar active regions and their associated flows are amassed, it is now possible to place new constraints on models of emerging flux. We discuss the outcomes of statistical studies which provide observational evidence that flux emergence may be a more passive process (at least in the upper convection zone); dominated to a greater extent by the influence of convection and to a lesser extent by buoyancy and the Coriolis force acting on rising magnetic flux tubes than previously thought. We also discuss how the relationship between stellar rotation, fractional convection zone depth, and magnetic activity on other stars can help us better understand flux emergence processes. Looking forward, we identify open questions regarding magnetic flux emergence that we anticipate can be addressed in the next decade with further observations and simulations.
2001.08.11, 2010.05.20-22

Dynamo Processes Constrained by Solar and Stellar Observations

Maria A. **Weber**
Proceedings of IAUS 340 **2018**
https://arxiv.org/pdf/1804.05904.pdf
Our understanding of stellar dynamos has largely been driven by the phenomena we have observed of our own Sun. Yet, as we amass longer-term datasets for an increasing number of stars, it is clear that there is a wide variety of stellar behavior. Here we briefly review observed trends that place key constraints on the fundamental dynamo operation of solar-type stars to fully convective M dwarfs, including: starspot and sunspot patterns, various magnetism-rotation correlations, and mean field flows such as differential rotation and meridional circulation. We also comment on the current insight that simulations of dynamo action and flux emergence lend to our working knowledge of stellar dynamo theory. While the growing landscape of both observations and simulations of stellar magnetic activity work in tandem to decipher dynamo action, there are still many puzzles that we have yet to fully understand.

Comment on the Article by Thuillier et al.“The Infrared Solar Spectrum Measured by the SOLSPEC Spectrometer onboard the International Space Station”

M. **Weber**
Solar Phys. **2015**
Thuillier et al. (Solar Phys., 2015, DOI:10.1007/s11207-015-0704-1) discuss the apparent discrepancy between the ATLAS-3 composite solar spectral irradiances (SSI) covering the ultraviolet/visible/near-infrared (NIR) spectral region with more recent SSI measurements in the NIR. Recent measurements from IRSPERAD, CAVIAR, SCIAMACHY, SOLSPEC/ISS (the SOLAR2 spectrum from 2008), and unadjusted SIM show that above about 1600 nm, SSI is lower by about 8 % with respect to ATLAS-3. A new correction is presented in Thuillier et al. (2015) that leads to SOLSPEC/ISS (SOLAR2rev) which is in better agreement with ATLAS-3. SOLSPEC/ISS SSI underwent a +10 % change from 2008 to 2010, leading to better agreement with ATLAS-3, but it remains unclear which year provided the proper radiometric level, 2008 (SOLAR2) or 2010 (SOLAR2rev) as no link to pre-launch calibration is established. Before interpreting the NIR SSI observations using our current physical understanding (constraints by the total solar irradiance and solar models), the cause for the discrepancy between the early ATLAS-3 and all recent measurements (without a-posteriori adjustments) needs to be understood considering instrument and calibration performance alone.

Flux Tubes in Turbulent Solar-like Convection

M. A. **Weber**, Y. Fan

Solar Phys. **2015**

We study the combined effects of convection and radiative diffusion on the evolution of thin magnetic flux tubes in the solar interior. Radiative diffusion is the primary supplier of heat to convective motions in the lower convection zone, and it results in a heat input per unit volume of magnetic flux tubes that has been ignored by many previous thin flux tube studies. We use a thin flux tube model subject to convection taken from a rotating spherical shell of turbulent, solar-like convection as described by Weber, Fan, and Miesch (Astrophys. J. 741, 11, 2011; Solar Phys. 287, 239, 2013), now taking into account the influence of radiative heating on 1022 Mx flux tubes, corresponding to flux tubes of large active regions. Our simulations show that flux tubes of ≤ 60 kG that are subject to solar-like convective flows do not anchor in the overshoot region, but rather drift upward because of the increased buoyancy of the flux tube earlier in its evolution, which results from including radiative diffusion. Flux tubes of magnetic field strengths ranging from 15 kG to 100 kG have rise times of ≤ 0.2 years and exhibit a Joy's Law tilt-angle trend. Our results suggest that radiative heating is an effective mechanism by which flux tubes can escape from the stably stratified overshoot region. Moreover, flux tubes do not necessarily need to be anchored in the overshoot region to produce emergence properties similar to those of active regions on the Sun.

An Automated Algorithm for Identifying and Tracking Transverse Waves in Solar Images

Micah J. **Weberg**, Richard J. Morton, and James A. McLaughlin

2018 ApJ 852 57

http://sci-hub.tw/10.3847/1538-4357/aa9e4a

https://arxiv.org/ftp/arxiv/papers/1807/1807.04842.pdf

Recent instrumentation has demonstrated that the solar atmosphere supports omnipresent transverse waves, which could play a key role in energizing the solar corona. Large-scale studies are required in order to build up an understanding of the general properties of these transverse waves. To help facilitate this, we present an automated algorithm for identifying and tracking features in solar images and extracting the wave properties of any observed transverse oscillations. We test and calibrate our algorithm using a set of synthetic data, which includes noise and rotational effects. The results indicate an accuracy of 1%–2% for displacement amplitudes and 4%–10% for wave periods and velocity amplitudes. We also apply the algorithm to data from the Atmospheric Imaging Assembly on board the Solar Dynamics Observatory and find good agreement with previous studies. Of note, we find that 35%–41% of the observed plumes exhibit multiple wave signatures, which indicates either the superposition of waves or multiple independent wave packets observed at different times within a single structure. The automated methods described in this paper represent a significant improvement on the speed and quality of direct measurements of transverse waves within the solar atmosphere. This algorithm unlocks a wide range of statistical studies that were previously impractical. **2010 May 23, 2010 Oct 06, 2012 Mar 27**

On the plasma flow inside magnetic tornadoes on the Sun

Sven **WEDEMEYER**1,∗ and Oskar STEINER2,3

Publ. Astron. Soc. Japan (**2014**) 66 (SP1), S10 (1–8)

http://pasj.oxfordjournals.org/content/66/SP1/S10.full.pdf+html

https://watermark.silverchair.com/psu086.pdf

High-resolution observations with the Swedish 1-m Solar Telescope (SST) and the Solar Dynamics Observatory (SDO) reveal rotating magnetic field structures that extend from the solar surface into the chromosphere and the corona. These so-called magnetic tornadoes are primarily detected as rings or spirals of rotating plasma in the Ca II 854.2nm line core (also known as chromospheric swirls). Detailed numerical simulations show that the observed chromospheric plasma motion is caused by the rotation of magnetic field structures, which again are driven by photospheric vortex flows at their footpoints. Under the right conditions, two vortex flow systems are stacked on top of each other.We refer to the lower vortex, which extends from the low photosphere into the convection zone, as intergranular vortex flow (IVF). Once amagnetic field structure is co-located with an IVF, the rotation is mediated into the upper atmospheric layers and an atmospheric vortex flow (AVF, or magnetic tornado) is generated. In contrast to the recent work by Shelyag et al. (2013, ApJ, 776, L4), we demonstrate that particle trajectories in a simulated magnetic tornado indeed follow spirals and argue that the properties of the trajectories decisively depend on the location in the atmosphere and the strength of the magnetic field.

Dynamo induced by time-periodic force

Xing **Wei**

2018 ApJL 855 L7

https://arxiv.org/pdf/1802.08284.pdf
http://sci-hub.tw/http://iopscience.iop.org/2041-8205/855/1/L7/
To understand the dynamo driven by time-dependent flow, e.g. turbulence, we investigate numerically the dynamo induced by time-periodic force in rotating magnetohydrodynamic flow and focus on the effect of force frequency on the dynamo action. It is found that the dynamo action depends on the force frequency. When the force frequency is near resonance the force can drive dynamo but when it is far away from resonance dynamo fails. In the frequency range near resonance to support dynamo, the force frequency at resonance induces a weak magnetic field and magnetic energy increases as the force frequency deviates from the resonant frequency. This is opposite to the intuition that a strong flow at resonance will induce a strong field.

No evidence for synchronization of the solar cycle by a "clock"

E. **Weisshaar**1, R. H. Cameron2 and M. Schüssler2
A&A 671, A87 (**2023**)
https://www.aanda.org/articles/aa/pdf/2023/03/aa44997-22.pdf
The length of the solar activity cycle fluctuates considerably. The temporal evolution of the corresponding cycle phase, that is, the deviation of the epochs of activity minima or maxima from strict periodicity, provides relevant information concerning the physical mechanism underlying the cyclic magnetic activity. An underlying strictly periodic process (akin to a perfect "clock"), with the observer seeing a superposition of the perfect clock and a small random phase perturbation, leads to long-term phase stability in the observations. Such behavior would be expected if cycles were synchronized by tides caused by orbiting planets or by a hypothetical torsional oscillation in the solar radiative interior. Alternatively, in the absence of such synchronization, phase fluctuations accumulate and a random walk of the phase ensues, which is a typical property of randomly perturbed dynamo models. Based on the sunspot record and the reconstruction of solar cycles from cosmogenic 14C, we carried out rigorous statistical tests in order to decipher whether there exists phase synchronization or random walk. Synchronization is rejected at significance levels of between 95% (28 cycles from sunspot data) and beyond 99% (84 cycles reconstructed from 14C), while the existence of random walk in the phases is consistent with all data sets. This result strongly supports randomly perturbed dynamo models with little inter-cycle memory.

Energy goes up... but doesn't come back down! Coronal heating?

Brian **Welsch**
RHESSI Science Nugget, No. 236, Sept **2014**
http://sprg.ssl.berkeley.edu/~tohban/wiki/index.php/Energy_goes_up..._but_doesn't_come_back_down!_Coronal_heating%3F
In a "straightened" corona, the magnetic field runs between two photospheric planes, in which footpoints of the coronal fields are anchored. Photospheric convective motions can braid coronal fields, inducing electric currents in the corona. Such currents imply the presence of free magnetic energy in the corona, i.e, energy that can be released by dissipating the currents.

Did solar flares cook up life on Earth?

Wendel, J.
Eos, 97, doi:10.1029/2016EO052815. 23 May **2016.**
https://eos.org/articles/did-solar-flares-cook-up-life-on-earth
Researchers at NASA have found that when the Sun was half a billion years old, large solar flares—larger than any recorded by humans—could have changed the very chemistry of Earth's atmosphere. What's more, bombardment of the planet by high-energy particles from those jets of superhot solar plasma might have prompted organic molecules considered precursors to life to form from simpler inorganic molecules then abundant on primordial Earth.

Defining the Middle Corona **Review**

Matthew J. **West**, Daniel B. Seaton, David B. Wexler, John C. Raymond, +++
Solar Physics volume 298, Article number: 78 (**2023**)
https://link.springer.com/content/pdf/10.1007/s11207-023-02170-1.pdf
The middle corona, the region roughly spanning heliocentric distances from 1.5 to 6 solar radii, encompasses almost all of the influential physical transitions and processes that govern the behavior of coronal outflow into the heliosphere. The solar wind, eruptions, and flows pass through the region, and they are shaped by it. Importantly, the region also modulates inflow from above that can drive dynamic changes at lower heights in the inner corona. Consequently, the middle corona is essential for comprehensively connecting the corona to the heliosphere and for developing corresponding global models. Nonetheless, because it is challenging to observe, the region has been poorly studied by both major solar remote-sensing and in-situ missions and instruments, extending back to the Solar and Heliospheric Observatory (SOHO) era. Thanks to recent advances in instrumentation, observational processing techniques, and a realization of the importance of the region, interest in the middle corona has increased. Although the region cannot be intrinsically separated from other regions of the solar atmosphere, there has emerged a need to define the region in terms of its location and extension in the solar atmosphere, its composition, the physical

transitions that it covers, and the underlying physics believed to shape the region. This article aims to define the middle corona, its physical characteristics, and give an overview of the processes that occur there. **21 Aug 2017, 29 Apr 2021, 15 Feb 2022**

A Review of the Extended EUV Corona Observed by the Sun Watcher with Active Pixels and Image Processing (SWAP) Instrument

Matthew J. **West**, Daniel B. Seaton, Elke D'Huys, +++
Solar Physics volume 297, Article number: 136 (**2022**)
https://link.springer.com/content/pdf/10.1007/s11207-022-02063-9.pdf
The Sun Watcher with Active Pixels and Image Processing (SWAP) instrument onboard ESA's PRoject for On Board Autonomy 2 (PROBA2) has provided the first uncompressed, high-cadence, continuous, large field-of-view observations of the extended extreme-ultraviolet (EUV) corona for over a complete solar cycle. It has helped shape our understanding of this previously understudied region, and pioneered research into the middle corona. In this article, we present a review of all publications that have utilized these observations to explore the extended EUV corona, highlighting the unique contributions made by SWAP. The review is broadly divided into three main sections of SWAP-based studies about: i) long-lived phenomena, such as streamers, pseudo-streamers, and coronal fans; ii) dynamic phenomena, such as eruptions, jets, EUV waves, and shocks; iii) coronal EUV emission generation. We also highlight SWAP's imaging capabilities, techniques that have been applied to observations to enhance the off-limb observations and its legacy.

LUCI onboard Lagrange, the next generation of EUV space weather monitoring

Matthew J. **West**1,2*, Christian Kintziger3, Margit Haberreiter4, Manfred Gyo4, David Berghmans1, Samuel Gissot1, Valeria Büchel4, Leon Golub5, Sergei Shestov1,6 and Jackie A. Davies
J. Space Weather Space Clim. **2020**, 10, 49
https://www.swsc-journal.org/articles/swsc/pdf/2020/01/swsc200056.pdf
https://doi.org/10.1051/swsc/2020052
Lagrange eUv Coronal Imager (LUCI) is a solar imager in the Extreme UltraViolet (EUV) that is being developed as part of the Lagrange mission, a mission designed to be positioned at the L5 Lagrangian point to monitor space weather from its source on the Sun, through the heliosphere, to the Earth. LUCI will use an off-axis two mirror design equipped with an EUV enhanced active pixel sensor. This type of detector has advantages that promise to be very beneficial for monitoring the source of space weather in the EUV. LUCI will also have a novel off-axis wide field-of-view, designed to observe the solar disk, the lower corona, and the extended solar atmosphere close to the Sun–Earth line. LUCI will provide solar coronal images at a 2–3 min cadence in a pass-band centred on 19.5. Observations made through this pass-band allow for the detection and monitoring of semi-static coronal structures such as coronal holes, prominences, and active regions; as well as transient phenomena such as solar flares, limb coronal mass ejections (CMEs), EUV waves, and coronal dimmings. The LUCI data will complement EUV solar observations provided by instruments located along the Sun–Earth line such as PROBA2-SWAP, SUVI-GOES and SDO-AIA, as well as provide unique observations to improve space weather forecasts. Together with a suite of other remote-sensing and in-situ instruments onboard Lagrange, LUCI will provide science quality operational observations for space weather monitoring.

The need for active region disconnection in 3D kinematic dynamo simulations

T. **Whitbread**, A. R. Yeates, A. Muñoz-Jaramillo
A&A 627, A168 **2019**
https://arxiv.org/pdf/1907.02762.pdf
In this paper we address a discrepancy between the surface flux evolution in a 3D kinematic dynamo model and a 2D surface flux transport model that has been closely calibrated to the real Sun. We demonstrate that the difference is due to the connectivity of active regions to the toroidal field at the base of the convection zone, which is not accounted for in the surface-only model. Initially, we consider the decay of a single active region, firstly in a simplified Cartesian 2D model and subsequently the full 3D model. By varying the turbulent diffusivity profile in the convection zone, we find that increasing the diffusivity - so that active regions are more rapidly disconnected from the base of the convection zone - improves the evolution of the surface field. However, if we simulate a full solar cycle, we find that the dynamo is unable to sustain itself under such an enhanced diffusivity. This suggests that in order to accurately model the solar cycle, we must find an alternative way to disconnect emerging active regions, whilst conserving magnetic flux.

How many active regions are necessary to predict the solar dipole moment?

T. **Whitbread**, A. R. Yeates, A. Muñoz-Jaramillo
ApJ **2018**
https://arxiv.org/pdf/1807.01617.pdf

We test recent claims that the polar field at the end of Cycle 23 was weakened by a small number of large, abnormally oriented regions, and investigate what this means for solar cycle prediction. We isolate the contribution of individual regions from magnetograms for Cycles 21, 22 and 23 using a 2D surface flux transport model, and find that although the top ~10% of contributors tend to define sudden large variations in the axial dipole moment, the cumulative contribution of many weaker regions cannot be ignored. In order to recreate the axial dipole moment to a reasonable degree, many more regions are required in Cycle 23 than in Cycles 21 and 22 when ordered by contribution. We suggest that the negative contribution of the most significant regions of Cycle 23 could indeed be a cause of the weak polar field at the following cycle minimum and the low-amplitude Cycle 24. We also examine the relationship between a region's axial dipole moment contribution and its emergence latitude, flux, and initial axial dipole moment. We find that once the initial dipole moment of a given region has been measured, we can predict the long-term dipole moment contribution using emergence latitude alone.

How Many Active Regions Are Necessary to Predict the Solar Dipole Moment?

T. **Whitbread**1, A. R. Yeates1, and A. Muñoz-Jaramillo
2018 ApJ 863 116
http://sci-hub.tw/http://iopscience.iop.org/article/10.3847/1538-4357/aad17e/meta
We test recent claims that the polar field at the end of Cycle 23 was weakened by a small number of large, abnormally oriented regions, and investigate what this means for solar cycle prediction. We isolate the contribution of individual regions from magnetograms for Cycles 21, 22, and 23 using a 2D surface flux transport model, and find that although the top ~10% of contributors tend to define sudden large variations in the axial dipole moment, the cumulative contribution of many weaker regions cannot be ignored. To recreate the axial dipole moment to a reasonable degree, many more regions are required in Cycle 23 than in Cycles 21 and 22 when ordered by contribution. We suggest that the negative contribution of the most significant regions of Cycle 23 could indeed be a cause of the weak polar field at the following cycle minimum and the low-amplitude Cycle 24. We also examine the relationship between a region's axial dipole moment contribution and its emergence latitude, flux, and initial axial dipole moment. We find that once the initial dipole moment of a given region has been measured, we can predict the long-term dipole moment contribution using emergence latitude alone.
HMI Science Nuggets in September **2018** hmi.stanford.edu/hminuggets/?p=2639

Parameter optimization for surface flux transport models

T. **Whitbread**, A. R. Yeates, A. Muñoz-Jaramillo, G. J. D. Petrie
A&A 607, A76 **2017**
https://arxiv.org/pdf/1708.01098.pdf
Accurate prediction of solar activity calls for precise calibration of solar cycle models. Consequently we aim to find optimal parameters for models which describe the physical processes on the solar surface, which in turn act as proxies for what occurs in the interior and provide source terms for coronal models. We use a genetic algorithm to optimize surface flux transport models using National Solar Observatory (NSO) magnetogram data for Solar Cycle 23. This is applied to both a 1D model that inserts new magnetic flux in the form of idealized bipolar magnetic regions, and also to a 2D model that assimilates specific shapes of real active regions. The genetic algorithm searches for parameter sets (meridional flow speed and profile, supergranular diffusivity, initial magnetic field, and radial decay time) that produce the best fit between observed and simulated butterfly diagrams, weighted by a latitude-dependent error structure which reflects uncertainty in observations. Due to the easily adaptable nature of the 2D model, the optimization process is repeated for Cycles 21, 22, and 24 in order to analyse cycle-to-cycle variation of the optimal solution. We find that the ranges and optimal solutions for the various regimes are in reasonable agreement with results from the literature, both theoretical and observational. The optimal meridional flow profiles for each regime are almost entirely within observational bounds determined by magnetic feature tracking, with the 2D model being able to accommodate the mean observed profile more successfully. Differences between models appear to be important in deciding values for the diffusive and decay terms. In like fashion, differences in the behaviours of different solar cycles lead to contrasts in parameters defining the meridional flow and initial field strength.

Acoustic response in the transition region to transverse oscillations in a solar coronal loop

S. J. **White** and E. Verwichte
A&A 670, A1 (**2023**)
https://www.aanda.org/articles/aa/pdf/2023/02/aa44873-22.pdf
Context. Magnetohydrodynamic (MHD) waves play an important role in the dynamics and heating of the solar corona. Transverse (Alfvénic) oscillations of loops commonly occur in response to solar eruptions and are mostly studied in isolation. However, acoustic coupling has been shown to be readily observable in the form of propagating intensity variations at the loop footpoints.

Aims. We extend the modelling of wave coupling between a transverse loop oscillation and slow magnetoacoustic waves in a structured loop to include a lower atmosphere.
Methods. We achieve this with combined analytical modelling and fully non-linear MHD simulations.
Results. Transverse loop oscillations result in the excitation of propagating slow waves from the top of the transition region and the lower boundary. The rate of excitation for the upward propagating waves at the lower boundary is smaller than for waves at the top of the transition region due to the reduced local sound speed. Additionally, slow waves are found to propagate downwards from the transition region, which reflect at the lower boundary and interfere with the upward propagating waves. Resonances are present in the normal mode analysis but these do not appear in the simulations. Due to the presence of the transition region, additional longitudinal harmonics lead to a narrower slow wave profile. The slow wave field is anti-symmetric in the direction of wave polarisation, which highlights the importance that the loop orientation has on the observability of these waves. The ponderomotive effect must be accounted for when interpreting intensity oscillations. Evidence is found for an additional short-period oscillation, which is likely a hybrid mode.

Sounding Rocket Observations of Active Region Soft X-Ray Spectra Between 0.5 and 2.5 nm Using a Modified SDO/EVE Instrument

Seth **Wieman**, Thomas Woods, Andrew Jones, Christopher Moore
Solar Phys. **2016**

Spectrally resolved measurements of individual solar active regions (ARs) in the soft X-ray (SXR) range are important for studying dynamic processes in the solar corona and their associated effects on the Earth's upper atmosphere. They are also a means of evaluating atomic data and elemental abundances used in physics-based solar spectral models. However, very few such measurements are available. We present spectral measurements of two individual ARs in the 0.5 to 2.5 nm range obtained on the NASA 36.290 sounding rocket flight of **21 October 2013** (at about 18:30 UT) using the *Solar Aspect Monitor* (SAM), a channel of the *Extreme Ultaviolet Variability Experiment* (EVE) payload designed for underflight calibrations of the orbital EVE on the *Solar Dynamics Observatory* (SDO). The EVE rocket instrument is a duplicate of the EVE on SDO, except the SAM channel on the rocket version was modified in 2012 to include a freestanding transmission grating to provide spectrally resolved images of the solar disk with the best signal to noise ratio for the brightest features, such as ARs. Calibrations of the EVE sounding rocket instrument at the *National Institute of Standards and Technology Synchrotron Ultraviolet Radiation Facility* (NIST/SURF) have provided a measurement of the SAM absolute spectral response function and a mapping of wavelength separation in the grating diffraction pattern. We discuss techniques (incorporating the NIST/SURF data) for determining SXR spectra from the dispersed AR images as well as the resulting spectra for NOAA ARs 11877 and 11875 observed on the 2013 rocket flight. In comparisons with physics-based spectral models using the CHIANTI v8 atomic database we find that both AR spectra are in good agreement with isothermal spectra (4 MK), as well as spectra based on an AR differential emission measure (DEM) included with the CHIANTI distribution, with the exception of the relative intensities of strong Fe xvii lines associated with 2p62p6–2p53s2p53s and 2p62p6–2p53d2p53d transitions at about 1.7 nm and 1.5 nm, respectively. The ratio of the Fe xvii lines suggests that the AR 11877 is hotter than the AR 11875. This result is confirmed with analysis of the active regions imaged by *X-ray Telescope* (XRT) onboard *Hinode*.

Resolving Differences in Absolute Irradiance Measurements Between the SOHO/CELIAS/SEM and the SDO/EVE

S. R. **Wieman**, L. V. Didkovsky, D. L. Judg
Solar Physics, Volume 289, Issue 8, pp 2907-2925, **2014**,

The Solar EUV Monitor (SEM) onboard SOHO has measured absolute extreme ultraviolet (EUV) and soft X-ray solar irradiance nearly continuously since January 1996. The EUV Variability Experiment (EVE) on SDO, in operation since April of 2010, measures solar irradiance in a wide spectral range that encompasses the band passes (26−34 nm and 0.1−50 nm) measured by SOHO/SEM. However, throughout the mission overlap, irradiance values from these two instruments have differed by more than the combined stated uncertainties of the measurements. In an effort to identify the sources of these differences and eliminate them, we investigate in this work the effect of reprocessing the SEM data using a more accurate SEM response function (obtained from synchrotron measurements with a SEM sounding-rocket clone instrument taken after SOHO was already in orbit) and time-dependent, measured solar spectral distributions – i.e., solar reference spectra that were unavailable prior to the launch of the SDO. We find that recalculating the SEM data with these improved parameters reduces mean differences with the EVE measurements from about 20 % to less than 5 % in the 26−34 nm band, and from about 35 % to about 15 % for irradiances in the 0.1−7 nm band extracted from the SEM 0.1−50 nm channel.

The Dependence of Joy's Law as a Function of Flux Emergence Phase

Lucy **Will**, Aimee A. Norton, Jon Todd Hoeksema

ApJ **976** 20 **2024**

https://arxiv.org/pdf/2310.20171.pdf

https://iopscience.iop.org/article/10.3847/1538-4357/ad82e3/pdf

Data from the Michelson Doppler Imager (MDI) and Helioseismic and Magnetic Imager (HMI) are analyzed from 1996 to 2023 to investigate tilt angles (γ) of bipolar magnetic regions and Joy's Law for Cycles 23, 24, and a portion of 25. The HMI radial magnetic field (Br) and MDI magnetogram (Blos) data are used to calculate (γ) using the flux-weighted centroids of the positive and negative polarities. Each AR is only sampled once. The analysis includes only Beta (β)-class active regions since computing γ of complex active regions is less meaningful. During the emergence of the ARs, we find that the average tilt angle ($\bar{\gamma}$) increases from 3.30∘±0.75 when 20\% of the flux has emerged to 6.79∘±0.66 when the ARs are at their maximum flux. Cycle 24 had a larger average tilt $\bar{\gamma}24=6.67\pm0.66$ than Cycle 23, $\bar{\gamma}23=5.11\pm0.61$. There are persistent differences in $\bar{\gamma}$ in the hemispheres with the southern hemisphere having higher $\bar{\gamma}$ in Cycles 23 and 24 but the errors are such that these differences are not statistically significant.

A Test of the Active Day Fraction Method of Sunspot Group Number Calibration: Dependence on the Level of Solar Activity

Teemu **Willamo**, Ilya G. Usoskin, Gennady A. Kovaltsov

Solar Phys. 293:69 **2018**

https://arxiv.org/pdf/1803.10501.pdf

The method of active day fraction (ADF) was proposed recently to calibrate different solar observers to the standard observational conditions. The result of the calibration may depend on the overall level of solar activity during the observational period. This dependency is studied quantitatively using data of the Royal Greenwich Observatory, by formally calibrating synthetic pseudo-observers to the full reference dataset. It is shown that the sunspot group number is precisely estimated by the ADF method for periods of moderate activity, may be slightly underestimated by 0.5\,--\,1.5 groups (≤10\,\%) for strong and very strong activity, and is strongly overestimated by up to 2.5 groups (≤30\,\%) for weak--moderate activity. The ADF method becomes unapplicable for the periods of grand minima of activity. In general, the ADF method tends to overestimate the overall level of activity and to reduce the long-term trends.

Updated sunspot group number reconstruction for 1749–1996 using the active day fraction method⋆

T. **Willamo**1, I. G. Usoskin2,3 and G. A. Kovaltsov

A&A 601, A109 (**2017**)

https://arxiv.org/pdf/1705.05109.pdf

Aims. Sunspot number series are composed from observations of hundreds of different observers that require careful normalization to standard conditions. Here we present a new normalized series of the number of sunspot groups for the period 1749–1996.

Methods. The reconstruction is based on the active day fraction (ADF) method, which is slightly updated with respect to previous works, and a revised database of sunspot group observations.

Results. Stability of some key solar observers has been evaluated against the composite series. The Royal Greenwich Observatory dataset appears relatively stable since the 1890s but is approximately 10% too low before that. A declining trend of 10–15% in the quality of Wolfer's observations is found between the 1880s and 1920s, suggesting that using him as the reference observer may lead to additional uncertainties. Wolf (small telescope) appears relatively stable between the 1860s and 1890s, without any obvious trend. The new reconstruction reflects the centennial variability of solar activity as evaluated using the singular spectrum analysis method. It depicts a highly significant feature of the modern grand maximum of solar activity in the second half of the 20th century, being a factor 1.33–1.77 higher than during the 18 and 19th centuries.

Conclusions. The new series of the sunspot group numbers with monthly and annual resolution is provided forming a basis for new studies of the solar variability and solar dynamo for the last 250 yr.

Monthly values of the reconstructed sunspot are available at the CDS via anonymous ftp to cdsarc.u-strasbg.fr (130.79.128.5) or via http://cdsarc.u-strasbg.fr/viz-bin/qcat?J/A+A/601/A109

Evidence for and Analysis of Multiple Hidden Coronal Strands in Cross-Sectional Emission Profiles: Further Results from NASA's High-resolution Solar Coronal Imager

Thomas **Williams**, Robert W. Walsh, Hardi Peter, Amy R. Winebarger
ApJ **902** 90 **2020**
https://arxiv.org/pdf/2009.02210.pdf
https://iopscience.iop.org/article/10.3847/1538-4357/abb60a/pdf
https://doi.org/10.3847/1538-4357/abb60a
Previous work utilising NASA's High-resolution Coronal Imager (Hi-C 2.1) 17.2 nm observations revealed that, even at the increased spatial scales available in the data-set, there may be evidence for coronal structures that are still not fully resolved. In this follow-up study, cross-section slices of coronal strands are taken across the Hi-C 2.1 field-of-view. Following previous loop width studies, the background emission is removed to isolate the coronal strands. The resulting intensity variations are reproduced by simultaneously fitting multiple Gaussian profiles using a non-linear least-squares curve fitting method. In total, 183 Gaussian profiles are examined for possible structures that are hinted at in the data. The full width at half maximum (FWHM) is determined for each Gaussian, which are then collated and analysed. The most frequent structural widths are ≈450-575 km with 47% of the strand widths beneath NASA's Solar Dynamics Observatory Atmospheric Imaging Assembly (AIA) resolving scale (600-1000 km). Only 17% reside beneath an AIA pixel width (435 km) with just 6% of the strands at the Hi-C 2.1 resolving scale (≈220-340 km). These results suggest that non-Gaussian shaped cross-sectional emission profiles observed by Hi-C 2.1 are the result of multiple strands along the integrated line-of-sight that can be resolved, rather than being the result of even finer sub-resolution elements. **29th May 2018**

Is the High-Resolution Coronal Imager Resolving Coronal Strands? Results from AR 12712

Thomas **Williams**, Robert W. Walsh, Amy R. Winebarger, David H. Brooks, Jonathan W. Cirtain, Bart Depontieu, Leon Golub, Ken Kobayashi, David E. Mckenzie, Richard J. Morton, Hardi Peter, Laurel A. Rachmeler, Sabrina L. Savage, Paola Testa, Sanjiv K. Tiwari, Harry P. Warren, Benjamin J. Watkinson
2020 *ApJ* **892** 134
https://arxiv.org/pdf/2001.11254.pdf
https://iopscience.iop.org/article/10.3847/1538-4357/ab6dcf/pdf
Following the success of the first mission, the High-Resolution Coronal Imager (Hi-C) was launched for a third time (Hi-C 2.1) on **29th May 2018** from the White Sands Missile Range, NM, USA. On this occasion, 329 seconds of 17.2 nm data of target active region AR 12712 was captured with a cadence of ~4s, and a plate scale of 0.129"/pixel. Using data captured by Hi-C 2.1 and co-aligned observations from SDO/AIA 17.1 nm we investigate the widths of 49 coronal strands. We search for evidence of substructure within the strands that is not detected by AIA, and further consider whether these strands are fully resolved by Hi-C 2.1. With the aid of Multi-Scale Gaussian Normalization (MGN), strands from a region of low-emission that can only be visualized against the contrast of the darker, underlying moss are studied. A comparison is made between these low-emission strands with those from regions of higher emission within the target active region. It is found that Hi-C 2.1 can resolve individual strands as small as ~202km, though more typical strands widths seen are ~513km. For coronal strands within the region of low-emission, the most likely width is significantly narrower than the high-emission strands at ~388km. This places the low-emission coronal strands beneath the resolving capabilities of SDO/AIA, highlighting the need of a permanent solar observatory with the resolving power of Hi-C.

Fluctuations of Supergranulation Verified Through Spectral Analysis of HMI Doppler Images

Peter E. **Williams**1, W. Dean Pesnell2, John G. Beck3, and Shannon Lee
HMI Science Nuggets #35, Jan **2015**
http://hmi.stanford.edu/hminuggets/?p=1118
We tested the influence of stochastic processes by performing similar analyses on simulated Doppler data and also by producing time series models of the growth and decay of supergranules. While both models exhibited size fluctuations, they did not tend to have a regular 3-5 day oscillation component. So while stochastic mechanisms do influence the variation of supergranule characteristics, our results suggest that an underlying harmonic element is also evident.

Time-Series Analysis of Supergranule Characteristics at Solar Minimum

Peter E. **Williams**, W. Dean Pesnell
Solar Physics, April **2014**, Volume 289, Issue 4, pp 1101-1113
Sixty days of Doppler images from the Solar and Heliospheric Observatory (SOHO) / Michelson Doppler Imager (MDI) investigation during the 1996 and 2008 solar minima have been analyzed to show that certain supergranule characteristics (size, size range, and horizontal velocity) exhibit fluctuations of three to five days. Cross-correlating parameters showed a good, positive correlation between supergranulation size and size range, and a moderate, negative correlation between size range and velocity. The size and velocity do exhibit a moderate, negative

correlation, but with a small time lag (less than 12 hours). Supergranule sizes during five days of co-temporal data from MDI and the Solar Dynamics Observatory (SDO) / Helioseismic Magnetic Imager (HMI) exhibit similar fluctuations with a high level of correlation between them. This verifies the solar origin of the fluctuations, which cannot be caused by instrumental artifacts according to these observations. Similar fluctuations are also observed in data simulations that model the evolution of the MDI Doppler pattern over a 60-day period. Correlations between the supergranule size and size range time-series derived from the simulated data are similar to those seen in MDI data. A simple toy-model using cumulative, uncorrelated exponential growth and decay patterns at random emergence times produces a time-series similar to the data simulations. The qualitative similarities between the simulated and the observed time-series suggest that the fluctuations arise from stochastic processes occurring within the solar convection zone. This behavior, propagating to surface manifestations of supergranulation, may assist our understanding of magnetic-field-line advection, evolution, and interaction.

Comparisons of Supergranule Characteristics During the Solar Minima of Cycles 22/23 and 23/24

Peter E. **Williams** and W. Dean Pesnell

Solar Physics, Volume 270, Number 1, 125-136, **2011**

Supergranulation is a component of solar convection that manifests itself on the photosphere as a cellular network of around 35 Mm across, with a turnover lifetime of 1–2 days. It is strongly linked to the structure of the magnetic field. The horizontal, divergent flows within supergranule cells carry local field lines to the cell boundaries, while the rotational properties of supergranule upflows may contribute to the restoration of the poloidal field as part of the dynamo mechanism, which controls the solar cycle. The solar minimum at the transition from cycle 23 to 24 was notable for its low level of activity and its extended length. It is of interest to study whether the convective phenomena that influence the solar magnetic field during this time differed in character from periods of previous minima. This study investigates three characteristics (velocity components, sizes and lifetimes) of solar supergranulation. Comparisons of these characteristics are made between the minima of cycles 22/23 and 23/24 using MDI Doppler data from 1996 and 2008, respectively. It is found that whereas the lifetimes are equal during both epochs (around 18 h), the sizes are larger in 1996 (35.9 ± 0.3 Mm) than in 2008 (35.0 ± 0.3 Mm), while the dominant horizontal velocity flows are weaker (139 ± 1 m s−1 in 1996; 141 ± 1 m s−1 in 2008). Although numerical differences are seen, they are not conclusive proof of the most recent minimum being inherently unusual.

Linear MHD Wave Propagation in Time-Dependent Flux Tube III. Leaky Waves in Zero-Beta Plasma

A. **Williamson** , R. Erdélyi

Solar Phys. January **2016**, Volume 291, Issue 1, pp 175-185 **Open Access**

In this article, we evaluate the time-dependent wave properties and the damping rate of propagating fast magneto-hydrodynamic (MHD) waves when energy leakage into a magnetised atmosphere is considered. By considering a cold plasma, initial investigations into the evolution of MHD wave damping through this energy leakage will take place. The time-dependent governing equations have been derived previously in Williamson and Erdélyi (2014a, Solar Phys. 289, 899 – 909) and are now solved when the assumption of evanescent wave propagation in the outside of the waveguide is relaxed. The dispersion relation for leaky waves applicable to a straight magnetic field is determined in both an arbitrary tube and a thin-tube approximation. By analytically solving the dispersion relation in the thin-tube approximation, the explicit expressions for the temporal evolution of the dynamic frequency and wavenumber are determined. The damping rate is, then, obtained from the dispersion relation and is shown to decrease as the density ratio increases. By comparing the decrease in damping rate to the increase in damping for a stationary system, as shown, we aim to point out that energy leakage may not be as efficient a damping mechanism as previously thought.

Resonant Damping of Propagating Kink Waves in Time-Dependent Magnetic Flux Tube

A. **Williamson**, R. Erdélyi

Solar Physics November **2014**, Volume 289, Issue 11, pp 4105-4115

We explore the notion of resonant absorption in a dynamic time-dependent magnetised plasma background. Very many works have investigated resonance in the Alfvén and slow MHD continua under both ideal and dissipative MHD regimes. Jump conditions in static and steady systems have been found in previous works, connecting solutions at both sides of the resonant layer. Here, we derive the jump conditions in a temporally dependent, magnetised, inhomogeneous plasma background to leading order in the Wentzel–Kramers–Billouin (WKB) approximation. Next, we exploit the results found in Williamson and Erdélyi (Solar Phys. 289, 899, 2014) to describe the evolution of the jump condition in the dynamic model considered. The jump across the resonant point is

shown to increase exponentially in time. We determined the damping as a result of the resonance over the same time period and investigated the temporal evolution of the damping itself. We found that the damping coefficient, as a result of the evolution of the resonance, decreases as the density gradient across the transitional layer decreases. This has the consequence that in such time-dependent systems resonant absorption may not be as efficient as time progresses.

The Greenwich Photo-heliographic Results (1874 – 1885): Observing Telescopes, Photographic Processes, and Solar Images

D. M. **Willis**, M. N. Wild, G. M. Appleby, L. T. Macdonald

Solar Phys. Volume 291, Issue 9, pp 2553–2586 **2016**

Potential sources of inhomogeneity in the sunspot measurements published by the Royal Observatory, Greenwich, during the early interval 1874 – 1885 are examined critically. Particular attention is paid to inhomogeneities that might arise because the sunspot measurements were derived from solar photographs taken at various contributing solar observatories, which used different telescopes, experienced different seeing conditions, and employed different photographic processes. The procedures employed in the Solar Department at the Royal Greenwich Observatory (RGO), Herstmonceux, during the final phase of sunspot observations provide a modern benchmark for interpreting the early sunspot measurements. The different observing telescopes used at the contributing solar observatories during the interval 1874 – 1885 are discussed in detail, using information gleaned from the official RGO publications and other relevant historical documents. Likewise, the different photographic processes employed at the different solar observatories are reviewed carefully. The procedures used by RGO staff to measure the positions and areas of sunspot groups on photographs of the Sun having a nominal radius of either four or eight inches are described. It is argued that the learning curve for the use of the Kew photoheliograph at the Royal Observatory, Greenwich, actually commenced in 1858, not 1874. The RGO daily number of sunspot groups is plotted graphically and analysed statistically. Similarly, the changes of metadata at each solar observatory are shown on the graphical plots and analysed statistically. It is concluded that neither the interleaving of data from the different solar observatories nor the changes in metadata invalidates the RGO count of the number of sunspot groups, which behaves as a quasi-homogeneous time series. Furthermore, it is emphasised that the correct treatment of days without photographs is quite crucial to the correct calculation of Group Sunspot Numbers.

Re-examination of the Daily Number of Sunspot Groups for the Royal Observatory, Greenwich (1874 – 1885)

D. M. **Willis**, M. N. Wild, J. S. Warburton

Solar Phys. **2016**

The daily number of sunspot groups on the solar disk, as recorded by the programme of sunspot observations performed under the aegis of the Royal Observatory, Greenwich, UK, and subsequently the Royal Greenwich Observatory (RGO), is re-examined for the interval 1874 – 1885. The motivation for this re-examination is the key role that the RGO number of sunspot groups plays in the calculation of Group Sunspot Numbers (Hoyt and Schatten in *Solar Phys.* **179**, 189, 1998a;*Solar Phys.* **181**, 491, 1998b). A new dataset has been derived for the RGO daily number of sunspot groups in the interval 1874 – 1885. This new dataset attempts to achieve complete consistency between the sunspot data presented in the three main sections of the RGO publications and also incorporates all known errata and additions. It is argued that days for which no RGO solar photograph was acquired originally should be regarded, without exception, as being days without meaningful sunspot data. The daily number of sunspot groups that Hoyt and Schatten assign to days without RGO photographs is frequently just a lower limit. Moreover, in the absence of a solar photograph, the daily number of sunspot groups is inevitably uncertain because of the known frequent occurrence of sunspot groups that exist for just a single day. The elimination of days without photographs changes the list of inter-comparison days on which both the primary RGO observer and a specified secondary comparison observer saw at least one sunspot group. The resulting changes in the personal correction factors of secondary observers then change the personal correction factors of overlapping tertiary observers, *etc*. In this way, numerical changes in the personal correction factors of secondary observers propagate away from the interval 1874 – 1885, thereby potentially changing the arithmetical calculation of Group Sunspot Numbers over an appreciably wider time interval.

A Quarter Century of Wind Spacecraft Discoveries **Review**

Wilson, Lynn B., III ; Brosius, Alexandra L. ; Gopalswamy, Natchimuthuk ; Nieves-Chinchilla, Teresa ; Szabo, Adam ; Hurley, Kevin ; Phan, Tai ; Kasper, Justin C. ; Lugaz, Noé ; Richardson, Ian G. ; Chen, Christopher H. K. ; Verscharen, Daniel ; Wicks, Robert T. ; TenBarge, Jason M.
Reviews of Geophysics, Vol. 59, Issue 2, pp. e2020RG000714, **2021**, doi:10.1029/2020RG000714
https://agupubs.onlinelibrary.wiley.com/doi/epdf/10.1029/2020RG000714 **File**
The Wind spacecraft, launched on November 1, 1994, is a critical element in NASA's Heliophysics System Observatory (HSO) - a fleet of spacecraft created to understand the dynamics of the Sun-Earth system. The combination of its longevity (>25 years in service), its diverse complement of instrumentation, and high resolution and accurate measurements has led to it becoming the "standard candle" of solar wind measurements. Wind has over 55 selectable public data products with over ~1,100 total data variables (including OMNI data products) on SPDF/CDAWeb alone. These data have led to paradigm shifting results in studies of statistical solar wind trends, magnetic reconnection, large-scale solar wind structures, kinetic physics, electromagnetic turbulence, the Van Allen radiation belts, coronal mass ejection topology, interplanetary and interstellar dust, the lunar wake, solar radio bursts, solar energetic particles, and extreme astrophysical phenomena such as gamma-ray bursts. This review introduces the mission and instrument suites then discusses examples of the contributions by Wind to these scientific topics that emphasize its importance to both the fields of heliophysics and astrophysics.

Identifying Observables that can Differentiate Between Impulsive and Footpoint Heating: Time Lags and Intensity Ratios

Amy R. **Winebarger**, Roberto Lionello, Cooper Downs, Zoran Mikic, Jon Linker
2018
https://arxiv.org/pdf/1806.05374.pdf
Two potential heating scenarios have been suggested to explain coronal loop observations. One scenario is that the loops are formed of many strands, each heated independently by a series of small-scale impulsive heating events, or nanoflares. Another hypothesis is that the heating is quasi-steady and highly-stratified, i.e., "footpoint heating". The goal of this paper is to identify observables that can be used to differentiate between these two heating scenarios. For footpoint heating, we vary the heating magnitude and stratification, for impulsive heating, we vary the heating magnitude. We use one-dimensional hydrodynamic codes to calculate the resulting temperature and density evolution. We convolve the temperature and density with the response functions of four EUV channels of the Atmospheric Imaging Assembly and one filter channel of Hinode's X-ray Telescope. We consider two principal diagnostics: the time lag between the appearance of the loop in two different channels, and the ratio of the peak intensities of the loop in the two channels. We find 1) that footpoint heating can predict longer time lags than impulsive heating in some channel pairs, 2) that footpoint heating can predict zero or negative time lags in some channel pairs, 3) the intensity ratio expected from impulsive heating is confined to a narrower range than footpoint heating, and 4) the range of temperatures expected in impulsive heating is broader than the range of temperatures expected in footpoint heating. This preliminary study identifies observables that may be useful in discriminating between heating models in future work.

Information Theoretic Approach to Discovering Causalities in the Solar Cycle

Simon **Wing**1, Jay R. Johnson2, and Angelos Vourlidas
2018 ApJ 854 85
http://sci-hub.tw/http://iopscience.iop.org/0004-637X/854/2/85/
The causal parameters and response lag times of the solar cycle dynamics are investigated with transfer entropy, which can determine the amount of information transfer from one variable to another. The causal dependency of the solar cycle parameters is bidirectional. The transfer of information from the solar polar field to the sunspot number (SSN) peaks at lag time (τ) ~ 30–40 months, but thereafter it remains at a persistently low level for at least 400 months (~3 solar cycles) for the period 1906–2014. The latter may lend support to the idea that the polar fields from the last three or more solar cycles can affect the production of the SSN of the subsequent cycle. There is also a similarly long-term information transfer from the SSN to the polar field. Both the meridional flow speed and flux emergence (proxied by the SSN) transfer information to the polar field, but one transfers more information than the other, depending on the lag times. The meridional flow speed transfers more information than the SSN to the polar field at τ ~ 28–30 months and at τ ~ 90–110 months, which may be consistent with some flux transfer dynamo models and some surface flux transport models. However, the flux emergence transfers more information than the meridional flow to the polar field at τ ~ 60–80 months, which may be consistent with a recently developed surface flux transport model. The transfer of information from the meridional flow to the SSN peaks at τ ~ 110–120 months (~1 solar cycle).
HMI Science Nuggets #89 Feb **2018** http://hmi.stanford.edu/hminuggets/?p=2316

Comparing SSN Index to X-ray Flare and Coronal Mass Ejection Rates from Solar Cycles 22-24

Lisa M. **Winter**, Rick Pernak, K.S. Balasubramaniam
Solar Phys. **2016**
http://arxiv.org/pdf/1605.00503v1.pdf
The newly revised sunspot number series allows for placing historical geoeffective storms in the context of several hundred years of solar activity. Using statistical analyses of the Geostationary Operational Environmental Satellites (GOES) X-ray observations from the past ~30 years and the Solar and Heliospheric Observatory (SOHO) Large Angle and Spectrometric Coronagraph (LASCO) Coronal Mass Ejection (CME) catalog (1996-present), we present sunspot-number-dependent flare and CME rates. In particular, we present X-ray flare rates as a function of sunspot number for the past three cycles. We also show that the 1-8 AA X-ray background flux is strongly correlated with sunspot number across solar cycles. Similarly, we show that the CME properties (e.g., proxies related to the CME linear speed and width) are also correlated with sunspot number for SC 23 and 24. These updated rates will enable future predictions for geoeffective events and place historical storms in the context of present solar activity.

Estimate of Solar Maximum using the 1-8 ÅGeostationary Operational Environmental Satellites X-ray Measurements

L.M. **Winter** (AER), K. S. Balasubramaniam
ApJL, 793 L45 **2014**
http://arxiv.org/pdf/1409.2763v1.pdf
We present an alternate method of determining the progression of the solar cycle through an analysis of the solar X-ray background. Our results are based on the NOAA Geostationary Operational Environmental Satellites (GOES) X-ray data in the 1-8 \AAband from 1986 - present, covering solar cycles 22, 23, and 24. The X-ray background level tracks the progression of the solar cycle through its maximum and minimum. Using the X-ray data, we can therefore make estimates of the solar cycle progression and date of solar maximum. Based upon our analysis, we conclude that the Sun reached its hemisphere-averaged maximum in Solar Cycle 24 in late 2013. This is within six months of the NOAA prediction of a maximum in Spring 2013.

OBSERVATIONAL EVIDENCE FOR VARIATIONS OF THE ACOUSTIC CUTOFF FREQUENCY WITH HEIGHT IN THE SOLAR ATMOSPHERE

A. **Wiśniewska**1, Z. E. Musielak1,2, J. Staiger1, and M. Roth
2016 ApJ 819 L23
Direct evidence for the existence of an acoustic cutoff frequency in the solar atmosphere is given by observations performed by using the HELioseismological Large Regions Interferometric DEvice operating on the Vacuum Tower Telescope located on Tenerife. The observational results demonstrate variations of the cutoff with atmospheric heights. The observed variations of the cutoff are compared to theoretical predictions made by using five acoustic cutoff frequencies that have been commonly used in helioseismology and asteroseismology. The comparison shows that none of the theoretical predictions is fully consistent with the observational data. The implication of this finding is far reaching as it urgently requires either major revisions of the existing methods of finding acoustic cutoff frequencies or developing new methods that would much better account for the physical picture underlying the concept of cutoff frequencies in inhomogeneous media.

The Daniel K. Inouye Solar Telescope (DKIST)/Visible Broadband Imager (VBI)

Friedrich **Wöger**, Thomas Rimmele, Andrew Ferayorni, Andrew Beard, Brian S. Gregory, Predrag Sekulic & Steven L. Hegwer
Solar Physics volume 296, Article number: 145 (**2021**)
https://link.springer.com/content/pdf/10.1007/s11207-021-01881-7.pdf
https://doi.org/10.1007/s11207-021-01881-7
The Daniel K. Inouye Solar Telescope (DKIST) is a ground-based observatory for observations of the solar atmosphere featuring an unprecedented entrance aperture of four meters. To address its demanding scientific goals, DKIST features innovative and state-of-the-art instrument subsystems that are fully integrated with the facility and designed to be capable of operating mostly simultaneously. An important component of DKIST's first-light instrument suite is the Visible Broadband Imager (VBI). The VBI is an imaging instrument that aims to acquire images of the solar photosphere and chromosphere with high spatial resolution and high temporal cadence to investigate the to-date smallest detectable features and their dynamics in the solar atmosphere. VBI observations of

unprecedented spatial resolution ultimately will be able to inform modern numerical models and thereby allow new insights into the physics of the plasma motion at the smallest scales measurable by DKIST. The VBI was designed to deliver images at various wavelengths and at the diffraction limit of DKIST. The diffraction limit is achieved by using adaptive optics in conjunction with post-facto image-reconstruction techniques to remove residual effects of the terrestrial atmosphere. The first images of the VBI demonstrate that DKIST's optical system enables diffraction-limited imaging across a large field of view of various layers in the solar atmosphere. These images allow a first glimpse at the exciting scientific discoveries that will be possible with DKIST's VBI.

Wave heating of the solar atmosphere without shocks

D. **Wójcik**, B. Kuźma, K. Murawski and Z. E. Musielak
A&A 635, A28 (**2020**)
https://doi.org/10.1051/0004-6361/201936938
Context. We investigate the wave heating problem of a solar quiet region and present its plausible solution without involving shock formation.
Aims. We aim to use numerical simulations to study wave propagation and dissipation in the partially ionized solar atmosphere, whose model includes both neutrals and ions.
Methods. We used a 2.5D two-fluid model of the solar atmosphere to study the wave generation and propagation. The source of these waves is the solar convection located beneath the photosphere.
Results. The energy carried by the waves is dissipated through ion-neutral collisions, which replace shocks used in some previous studies as the main source of local heating in quiet regions.
Conclusions. We show that the resulting wave dissipation is sufficient to balance radiative and thermal energy losses, and to sustain a quasi-stationary atmosphere whose averaged temperature profile agrees well with the observationally based semi-empirical model of Avrett & Loeser (2008, ApJS, 175, 229).

Partially Ionized Solar Atmosphere: Two-fluid Waves and Their Cutoffs

D. **Wójcik**1, K. Murawski1, and Z. E. Musielak2
2019 ApJ 882 32
https://doi.org/10.3847/1538-4357/ab3224
A novel model of the solar atmosphere that accounts for partially ionized plasma is developed and used to study the propagation of magnetoacoustic-gravity waves, which are generated by solar granulation. The model includes neutrals in otherwise ionized plasma and therefore the considered waves are two-fluid waves. Numerical simulations of these waves allow computing their cutoff period and its variations in the solar atmosphere. The results of these computations are compared to the observational data collected by Wiśniewska et al. and Kayshap et al., and a good agreement between the theory and observations is obtained. This first theoretical confirmation of the observational data profoundly shows the importance of effects caused by partially ionized plasma on the behavior of waves in the solar atmosphere, and on the origin of solar chromospheric oscillations. It is also suggested that theoretically predicted differences between the behavior of ions and neutrals can be verified by some currently operating solar missions.

Two-fluid Numerical Simulations of the Origin of the Fast Solar Wind

D. **Wójcik**1, B. Kuźma1, K. Murawski1, and A. K. Srivastava
2019 ApJ 884 127
https://doi.org/10.3847/1538-4357/ab26b1
With the use of our JOANNA code, which solves radiative equations for ion + electron and neutral fluids, we perform realistic 2.5D numerical simulations of plasma outflows associated with the solar granulation. These outflows exhibit physical quantities that are consistent, to the order of magnitude, with the observational findings for mass and energy losses in the upper chromosphere, transition region, and inner corona, and they may originate the fast solar wind.

Acoustic waves in two-fluid solar atmosphere model: cut-off periods, chromospheric cavity, and wave tunnelling

D **Wójcik** K Murawski Z E Musielak
MNRAS 481, Issue 1, 21 November **2018**, Pages 262–267
We perform numerical simulations of acoustic waves in a two-fluid model of quiet region of the solar atmosphere. The two-fluid model describes partially ionized (non-magnetized) solar plasma, whose main components are neutral atoms, protons, and electrons. The waves are excited by a monochromatic driver, which operates at the bottom of the solar photosphere. Our numerical results show that the driver excites ion and neutral acoustic waves whose propagation is affected by the gravity. As a result, the acoustic waves with periods higher than a local acoustic cut-off period are evanescent, while lower waveperiods are free to reach the solar corona. Acoustic waves, which are evanescent in the photosphere and low chromosphere, tunnel their energy into the upper chromosphere and the

transition region. The wave propagation to the solar corona is affected by partial wave reflection that occurs in the transition region, and is responsible for formation of a cavity, where the waves are trapped. Fourier power analysis of temporal characteristic of plasma quantities reveals that a spectrum of various periods is generated. While oscillations traced in ion and neutral velocities look very similar, dynamics of mass densities of ions and neutrals differs a lot. The obtained results clearly show that the two-fluid model provides new insights into the acoustic wave propagation in a more realistic (partially ionized) quiet region of the solar atmosphere.

Numerical Simulations of Torsional Alfvén Waves in Axisymmetric Solar Magnetic Flux Tubes

D. **Wójcik**, K. Murawski, Z. E. Musielak, P. Konkol, A. Mignone
Solar Physics February **2017**, 292:31
http://link.springer.com/article/10.1007/s11207-017-1058-7
We numerically investigate Alfvén waves propagating along an axisymmetric and non-isothermal solar flux tube embedded in the solar atmosphere. The tube magnetic field is current-free and diverges with height, and the waves are excited by a periodic driver along the tube magnetic field lines. The main results are that the two wave variables, the velocity and magnetic field perturbations in the azimuthal direction, behave differently as a result of gradients of the physical parameters along the tube. To explain these differences in the wave behavior, the time evolution of the wave variables and the resulting cutoff period for each wave variable are calculated and used to determine regions in the solar chromosphere where strong wave reflection may occur.

Solar Irradiance Variability, Influenced by r Modes

Charles L. **Wolff**
2019 ApJ 870 20
A spectrum of the four-decade solar irradiance record has a prominent cluster of power for periodicities near 1 yr. Correlating irradiance with a bandpass filter showed that periodicity values were not constant, but varied sinusoidally with each cycle lasting 14 ± 1 yr. The large modulation amplitude makes solar frequencies ≥1 yr−1 hard to detect at the solar surface. After removing the modulation, a Lomb–Scargle spectrum exposed two true periodicities: 1.006 and 0.920 yr. They are interpreted as the synodic rotation periods of r modes of lowest angular degree ($\ell = 1$). The first propagates in the stable interior and the second in the convective envelope perturbed by its several flow fields. The rotational beat period of the two modes is about 10.9 yr. This is close to the average length of a solar cycle and possibly controls this average. The 1.006 yr periodicity dominates most of the filtered irradiance record but an abrupt change to about 0.8 yr occurs in mid-2010. Also found was evidence for higher-degree r modes ($\ell = 2$ to 8) and a curious sawtooth modulation with a recurrence period of 2.6 yr.

Naked eye observation of the 2017 total solar eclipse: a more complete understanding of the white-light corona

Richard **Woo**
Monthly Notices of the Royal Astronomical Society, Volume 485, Issue 3, May **2019**, Pages 4122–4127,
https://doi.org/10.1093/mnras/stz703
sci-hub.se/10.1093/mnras/stz703
The **2017 August 21** total solar eclipse offered a rare opportunity to scientifically view and capture naked eye observation of the corona. Filling this observational gap has led to a more complete understanding of the white-light corona, because it clarified and reconciled differences in the brightness distributions that are visually observed, imaged (photographed), and measured. Crucial to these new results has been the fortuitous similarity of naked eye observation of the 2017 eclipse to that of 1932. The latter was captured by the unmatched skills of artist–painter Howard Russell Butler in his recently rediscovered painting. Without this remarkable painting, it would not have been possible to either convey confirmation of the illusion or meaningfully explain the role and relevance of naked eye observation to understanding more completely the white-light corona.

First Results for Solar Soft X-Ray Irradiance Measurements from the Third-generation Miniature X-Ray Solar Spectrometer

Thomas N. **Woods**1, Bennet Schwab1, Robert Sewell1, Anant Kumar Telikicherla Kandala2, James Paul Mason +++
2023 ApJ 956 94
https://iopscience.iop.org/article/10.3847/1538-4357/acef13/pdf
Three generations of the Miniature X-ray Solar Spectrometer (MinXSS) have flown on small satellites with the goal "to explore the energy distribution of soft X-ray (SXR) emissions from the quiescent Sun, active regions, and during solar flares, and to model the impact on Earth's ionosphere and thermosphere." The primary science instrument is the Amptek X123 X-ray spectrometer that has improved with each generation of the MinXSS experiment. This

third-generation MinXSS-3 has a higher energy resolution and larger effective area than its predecessors and is also known as the Dual-zone Aperture X-ray Solar Spectrometer (DAXSS). It was launched on the INSPIRESat-1 satellite on **2022 February 14**, and INSPIRESat-1 has successfully completed its 6 month prime mission. The INSPIRESat-1 is in a dawn–dusk, Sun-synchronous orbit and therefore has had 24 hr coverage of the Sun during most of its mission so far. The rise of Solar Cycle 25 has been observed by DAXSS. This paper introduces the INSPIRESat-1 DAXSS solar SXR observations, and we focus the science results here on a solar occultation experiment and multiple flares on **2022 April 24**. One key flare result is that the reduction of elemental abundances appears greatest during the flare impulsive phase, thus highlighting the important role of chromospheric evaporation during flares to inject warmer plasma into the coronal loops. Furthermore, these results are suggestive that the amount of chromospheric evaporation is related to flare temperature and intensity.

Solar-Cycle Variability Results from the Solar Radiation and Climate Experiment (SORCE) Mission

Thomas N. **Woods**, Jerald W. Harder, Greg Kopp & Martin Snow
Solar Physics volume 297, Article number: 43 (**2022**)
https://link.springer.com/content/pdf/10.1007/s11207-022-01980-z.pdf
The Solar Radiation and Climate Experiment (SORCE) was a NASA mission that operated from 2003 to 2020 to provide key climate-monitoring measurements of total solar irradiance (TSI) and solar spectral irradiance (SSI). This 17-year mission made TSI and SSI observations during the declining phase of Solar Cycle 23, during all of Solar Cycle 24, and at the very beginning of Solar Cycle 25. The SORCE solar-variability results include comparisons of the solar irradiance observed during Solar Cycles 23 and 24 and the solar-cycle minima levels in 2008 – 2009 and 2019 – 2020. The differences between these two minima are very small and are not significantly above the estimate of instrument stability over the 11-year period. There are differences in the SSI variability for Solar Cycles 23 and 24, notably for wavelengths longer than 250 nm. Consistency comparisons with SORCE variability on solar-rotation timescales and solar-irradiance model predictions suggest that the SORCE Solar Cycle 24 SSI results might be more accurate than the SORCE Solar Cycle 23 results. The SORCE solar-variability results have been useful for many Sun–climate studies and will continue to serve as a reference for comparisons with future missions studying solar variability.

A Self-consistent Model of the Solar Tachocline

T. S. **Wood**1 and N. H. Brummell2
2018 ApJ 853 97
We present a local but fully nonlinear model of the solar tachocline, using three-dimensional direct numerical simulations. The tachocline forms naturally as a statistically steady balance between Coriolis, pressure, buoyancy, and Lorentz forces beneath a turbulent convection zone. Uniform rotation is maintained in the radiation zone by a primordial magnetic field, which is confined by meridional flows in the tachocline and convection zone. Such balanced dynamics has previously been found in idealized laminar models, but never in fully self-consistent numerical simulations.

Evidence for Large-Scale Subsurface Convection in the Sun

M. F. **Woodard**
MNRAS **2016**
http://arxiv.org/pdf/1605.06192v1.pdf
A helioseismic statistical waveform analysis of subsurface flow was performed on two 720-day time series of SOHO/MDI Medium-l spherical-harmonic coefficients. The time series coincide with epochs of high and low solar activity. Time-dependent coupling-strength coefficients b(s,t;n,l) of modes of the same radial order n and degree l, but different azimuthal order m, were inferred from the waveform analysis. These coefficients are sensitive to flows and general aspherical structure. For odd values of s << l, the coefficient b(s,t;n,l) measures an average over depth of the amplitude of one spherical-harmonic (s,t) component of the toroidal flow velocity field. The depth-dependent weighting function defining the average velocity is the fractional kinetic energy density in radius of modes of the (n,l) multiplet. A mean-square (n,l)-dependent flow velocity was inferred from the b-coefficients for s in the range 5 through 35 for each n and l in the respective ranges 1 through 5 and 120 through 149 for the epochs of high and low activity. A further averaging, over l, yielded a root mean square flow velocity as a function of n for each epoch, which average increases from about 20 m/s at n=1 to 35 m/s at n=5. The inferred velocities are consistent with (though perhaps do not demand) a cellular pattern of flow extending over the vertical range of mode sensitivity, estimated to be about four percent of the solar radius below the photosphere.

The Solar Radiation and Climate Experiment (SORCE) Mission: Final Calibrations and Data Products

Editorial Postface

Thomas N. **Woods** & John W. Leibacher
Solar Physics volume 298, Article number: 25 (**2023**)
https://link.springer.com/content/pdf/10.1007/s11207-023-02125-6.pdf
The Solar Radiation and Climate Experiment (SORCE) was a NASA mission that operated from 2003 to 2020 to provide key climate-monitoring measurements of total solar irradiance (TSI) and solar spectral irradiance (SSI). This topical collection provides an overview of some of the key SORCE science results, an overview of mission operations and how anomalies impacted the science observations, a detailed description of the updated algorithms used in producing the final data products of TSI and SSI from the four SORCE instruments, and results from an underflight calibration-rocket experiment flown in June 2018. The 17-year-long SORCE mission has made many contributions to the climate records of TSI and SSI that date back to the 1970s, and, fortunately, similar observations from the Total and Spectral Solar Irradiance Sensor (TSIS-1) are able to continue these Sun-climate records after SORCE without a gap.

Solar Radiation and Climate Experiment (SORCE) X-Ray Photometer System (XPS): Final Data-Processing Algorithms

Thomas N. **Woods** & Joshua Elliott
Solar Physics volume 297, Article number: 64 (**2022**)
https://link.springer.com/content/pdf/10.1007/s11207-022-01997-4.pdf
The X-ray Photometer System (XPS) is one of four instruments onboard NASA's Solar Radiation and Climate Experiment (SORCE) mission. The SORCE spacecraft operated from 2003 to 2020 to provide key climate-monitoring measurements of total solar irradiance (TSI) and solar spectral irradiance (SSI). The XPS is a set of photometers to measure the solar X-ray ultraviolet (XUV) irradiance shortward of 34 nm and the bright hydrogen emission at 121.6 nm. Each photometer has a spectral bandpass of about 7 nm, and the XPS measurements have an accuracy of about 20%. The updates for the final data-processing algorithms for the XPS solar-irradiance data products are described. These processing updates include improvements for the instrumental corrections for background signal, visible-light signal, and degradation trending. Validation of these updates is primarily with measurements from a very similar XPS instrument onboard NASA's Thermosphere-Ionosphere-Mesosphere-Energetics-Dynamics (TIMED) mission. In addition, the XPS Level 4 spectral model has been improved with new reference spectra derived with recent XUV observations from NASA's Solar Dynamics Observatory (SDO) and Miniature X-ray Solar Spectrometer (MinXSS) cubesat.

Overview of the Solar Radiation and Climate Experiment (SORCE) Seventeen-Year Mission

Thomas N. **Woods**, Jerald W. Harder, Greg Kopp, Debra McCabe, Gary Rottman, Sean Ryan & Martin Snow
Solar Physics volume 296, Article number: 127 (**2021**)
https://link.springer.com/content/pdf/10.1007/s11207-021-01869-3.pdf
https://doi.org/10.1007/s11207-021-01869-3
The Solar Radiation and Climate Experiment (SORCE) was a NASA mission that operated from 2003 to 2020 to provide key climate-monitoring measurements of total solar irradiance (TSI) and solar spectral irradiance (SSI). Three important accomplishments of the SORCE mission are i) the continuation of the 42-year-long TSI climate data record, ii) the continuation of the ultraviolet SSI record, and iii) the initiation of the near-ultraviolet, visible, and near-infrared SSI records. All of the SORCE instruments functioned well over the 17-year mission, which far exceeded its five-year prime mission goal. The SORCE spacecraft, having mostly redundant subsystems, was also robust over the mission. The end of the SORCE mission was a planned passivation of the spacecraft following a successful two-year overlap with the NASA Total and Spectral Solar Irradiance Sensor (TSIS) mission, which continues the TSI and SSI climate records. There were a couple of instrument anomalies and a few spacecraft anomalies during SORCE's long mission, but operational changes and updates to flight software enabled SORCE to remain productive to the end of its mission. The most challenging of the anomalies was the degradation of the battery capacity that began to impact operations in 2009 and was the cause for the largest SORCE data gap (August 2013 – February 2014). An overview of the SORCE mission is provided with a couple of science highlights and a discussion of flight anomalies that impacted the solar observations. Companion articles about the SORCE instruments and their final science data-processing algorithms provide additional details about the instrument measurements over the duration of the mission.

New Solar Irradiance Measurements from the Miniature X-Ray Solar Spectrometer CubeSat

Thomas N. **Woods**, Amir Caspi, Phillip C. Chamberlin, Andrew Jones, Richard Kohnert, James Paul Mason, Christopher S. Moore, Scott Palo, Colden Rouleau, Stanley C. Solomon, Janet Machol, Rodney Viereck

ApJL **2016**
https://arxiv.org/pdf/1610.01936v1.pdf
The goal of the Miniature X-ray Solar Spectrometer (MinXSS) CubeSat is to explore the energy distribution of soft X-ray (SXR) emissions from the quiescent Sun, active regions, and during solar flares, and to model the impact on Earth's ionosphere and thermosphere. The energy emitted in the SXR range (0.1 to 10 keV) can vary by more than a factor of 100, yet we have limited spectral measurements in the SXRs to accurately quantify the spectral dependence of this variability. The MinXSS primary science instrument is an Amptek, Inc. X123 X-ray spectrometer that has an energy range of 0.5-30 keV with a nominal 0.15 keV energy resolution. Two flight models have been built. The first, MinXSS-1, has been making science observations since 2016 June 9, and has observed numerous flares, including 40 C-class and 7 M-class flares. These SXR spectral measurements have advantages over broadband SXR observations, such as providing the capability to derive multiple-temperature components and elemental abundances of coronal plasma, improved irradiance accuracy, and higher resolution spectral irradiance as input to planetary ionosphere simulations. MinXSS spectra obtained during the **M5.0 flare on 2016 July 23** highlight these advantages, and indicate how the elemental abundance changes from primarily coronal to more photospheric during the flare. MinXSS-1 observations are compared to the Geostationary Operational Environmental Satellite (GOES) X-Ray Sensor (XRS) measurements of SXR irradiance and estimated corona temperature. Additionally, a suggested improvement to the calibration of the GOES XRS data is presented.

Solar Models with dynamic screening and early mass loss tested by helioseismic, astrophysical, and planetary constraints

Suzannah R. **Wood**, Katie Mussack, Joyce A. Guzik
Solar Phys. 293:111 **2018**
https://arxiv.org/pdf/1807.03846.pdf
The faint young Sun paradox remains an open question. Presented here is one possible solution to this apparent inconsistency, a more massive early Sun. Based on conditions on early Earth and Mars, a luminosity constraint is set as a function of mass. We examine helioseismic constraints of these alternative mass-losing models. Additionally, we explore a dynamic electron screening correction in an effort to improve helioseismic agreement in the core of the an early mass-losing model.

Towards realistic estimates of solar global oscillation mode-coupling measurement noise

M F **Woodard**
MNRAS, Volume 505, Issue 3, August **2021**, Pages 3433–3441,
https://doi.org/10.1093/mnras/stab1519
Time series of the medium-l spherical-harmonic decomposition of SOHO/MDI Doppler images were used to investigate the noise of solar-oscillation mode-coupling measurements and to reveal the coupling signatures of global-scale Rossby-waves and magnetic activity. A theoretical model of mode-coupling noise was developed starting from the assumption that the Doppler oscillation signal obeys Gaussian statistics. The measured coupling noise was found to agree with the model noise at the level of 20 per cent. The noise of mode-coupling measurements obtained from MDI data turns out to be considerably larger than that of hypothetical, 'ideal' measurements, which could only be obtained from observations with more coverage of the Sun's surface than current instruments provide. The noise analysis was carried out for a simple suboptimal mode-coupling estimation procedure which is described in some detail. A more rigorous, maximum-likelihood, approach to mode-coupling measurement, which generalizes a method currently used to extract global oscillation mode information, is also described and its relationship to the simple mode-coupling analysis is discussed.

New Solar Irradiance Measurements from the Miniature X-Ray Solar Spectrometer Cubesat

Thomas N. **Woods**1, Amir Caspi2, Phillip C. Chamberlin3, Andrew Jones1, Richard Kohnert1, James Paul Mason1, Christopher S. Moore1, Scott Palo1, Colden Rouleau1, Stanley C. Solomon
2017 ApJ 835 122
https://arxiv.org/ftp/arxiv/papers/1610/1610.01936.pdf
The goal of the Miniature X-ray Solar Spectrometer (MinXSS) CubeSat is to explore the energy distribution of soft X-ray (SXR) emissions from the quiescent Sun, active regions, and during solar flares and to model the impact on Earth's ionosphere and thermosphere. The energy emitted in the SXR range (0.1–10 keV) can vary by more than a factor of 100, yet we have limited spectral measurements in the SXRs to accurately quantify the spectral dependence of this variability. The MinXSS primary science instrument is an Amptek, Inc. X123 X-ray spectrometer that has an energy range of 0.5–30 keV with a nominal 0.15 keV energy resolution. Two flight models have been built. The first, MinXSS-1, has been making science observations since 2016 June 9 and has observed numerous flares, including more than 40 C-class and 7 M-class flares. These SXR spectral measurements have advantages over broadband SXR observations, such as providing the capability to derive multiple-temperature components and

elemental abundances of coronal plasma, improved irradiance accuracy, and higher resolution spectral irradiance as input to planetary ionosphere simulations. MinXSS spectra obtained during the M5.0 flare on 2016 July 23 highlight these advantages and indicate how the elemental abundance appears to change from primarily coronal to more photospheric during the flare. MinXSS-1 observations are compared to the Geostationary Operational Environmental Satellite (GOES) X-ray Sensor (XRS) measurements of SXR irradiance and estimated corona temperature. Additionally, a suggested improvement to the calibration of the GOES XRS data is presented.

A Different View of Solar Spectral Irradiance Variations: Modeling Total Energy over Six-Month Intervals

Thomas N. **Woods** , Martin Snow, Jerald Harder, Gary Chapman,
Solar Phys. Volume 290, Issue 10, pp 2649-2676 **2015** **Open Access**
A different approach to studying solar spectral irradiance (SSI) variations, without the need for long-term (multi-year) instrument degradation corrections, is examining the total energy of the irradiance variation during 6-month periods. This duration is selected because a solar active region typically appears suddenly and then takes 5 to 7 months to decay and disperse back into the quiet-Sun network. The solar outburst energy, which is defined as the irradiance integrated over the 6-month period and thus includes the energy from all phases of active region evolution, could be considered the primary cause for the irradiance variations. Because solar cycle variation is the consequence of multiple active region outbursts, understanding the energy spectral variation may provide a reasonable estimate of the variations for the 11-year solar activity cycle. The moderate-term (6-month) variations from the Solar Radiation and Climate Experiment (SORCE) instruments can be decomposed into positive (in-phase with solar cycle) and negative (out-of-phase) contributions by modeling the variations using the San Fernando Observatory (SFO) facular excess and sunspot deficit proxies, respectively. These excess and deficit variations are fit over 6-month intervals every 2 months over the mission, and these fitted variations are then integrated over time for the 6-month energy. The dominant component indicates which wavelengths are in-phase and which are out-of-phase with solar activity. The results from this study indicate out-of-phase variations for the 1400 – 1600 nm range, with all other wavelengths having in-phase variations.

Magnetic Influences on the Solar Wind (Ph.D. Dissertation)

Lauren N. **Woolsey**
Ph.D. Dissertation accepted by Harvard Graduate School of Arts and Sciences **2016**
http://arxiv.org/pdf/1605.04318v1.pdf
The steady, supersonic outflow from the Sun we call the solar wind was first posited in the 1950s and initial theories rightly linked the acceleration of the wind to the existence of the million-degree solar corona. Still today, the wind acceleration mechanisms and the coronal heating processes remain unsolved challenges in solar physics. In this work, I seek to answer a portion of the mystery by focusing on a particular acceleration process: Alfven waves launched by the motion of magnetic field footpoints in the photosphere. The entire corona is threaded with magnetic loops and flux tubes that open up into the heliosphere. I have sought a better understanding of the role these magnetic fields play in determining solar wind properties in open flux tubes. After an introduction of relevant material, I discuss my parameter study of magnetic field profiles and the statistical understanding we can draw from the resulting steady-state wind. In the chapter following, I describe how I extended this work to consider time dependence in the turbulent heating by Alfven waves in three dimensional simulations. The bursty nature of this heating led to a natural next step that expands my work to include not only the theoretical, but also a project to analyze observations of small network jets in the chromosphere and transition region, and the underlying photospheric magnetic field that forms thresholds in jet production. In summary, this work takes a broad look at the extent to which Alfven-wave-driven turbulent heating can explain measured solar wind properties and other observed phenomena. **See Introduction (Review)**

TIME-DEPENDENT TURBULENT HEATING OF OPEN FLUX TUBES IN THE CHROMOSPHERE, CORONA, AND SOLAR WIND

L. N. **Woolsey**1 and S. R. Cranmer
2015 ApJ 811 136
We investigate several key questions of plasma heating in open-field regions of the corona that connect to the solar wind. We present results for a model of Alfvén-wave-driven turbulence for three typical open magnetic field structures: a polar coronal hole, an open flux tube neighboring an equatorial streamer, and an open flux tube near a strong-field active region. We compare time-steady, one-dimensional turbulent heating models against fully time-dependent three-dimensional reduced-magnetohydrodynamic modeling of BRAID. We find that the time-steady results agree well with time-averaged results from BRAID. The time dependence allows us to investigate the variability of the magnetic fluctuations and of the heating in the corona. The high-frequency tail of the power spectrum of fluctuations forms a power law whose exponent varies with height, and we discuss the possible physical

explanation for this behavior. The variability in the heating rate is bursty and nanoflare-like in nature, and we analyze the amount of energy lost via dissipative heating in transient events throughout the simulation. The average energy in these events is 1021.91 erg, within the "picoflare" range, and many events reach classical "nanoflare" energies. We also estimated the multithermal distribution of temperatures that would result from the heating-rate variability, and found good agreement with observed widths of coronal differential emission measure distributions. The results of the modeling presented in this paper provide compelling evidence that turbulent heating in the solar atmosphere by Alfvén waves accelerates the solar wind in open flux tubes.

Partitioning of Magnetic Helicity in Reconnected Flux Tubes

Andrew N. **Wright**
2019 ApJ 878 102
sci-hub.se/10.3847/1538-4357/ab2120
The reconnection of two flux tubes with footpoints anchored to a plane, such as the photosphere, is considered. We focus on properties of the reconnected flux tubes, specifically their twist, which can be quantified using magnetic helicity. If the tubes are of equal flux (Φ) and are initially crossed we find the results are dependent upon the relative positioning of their footpoints: (i) nonequipartition of self-helicity is the typical situation; (ii) the total amount of self-helicity in the reconnected tubes lies between 0 and 2Φ2, corresponding to a total twist of between 0 and 2 turns. If the tubes are initially uncrossed the self-helicity of each reconnected tube depends upon footpoint arrangement. However, care needs to be taken when using these results as bringing the tubes together at the reconnection site can introduce twist or writhe, which will also need to be taken into account. In the case where the tubes are side by side and possess some overlap, reconnection may occur without distorting the tubes. For this situation the reconnected tubes will be crossed: (i) equipartition of self-helicity is never met, but can be approached in the limit of the footpoints being quasi-colinear; (ii) the overlying tube always has a self-helicity whose magnitude >Φ2/2 (it exceeds a half turn); the underling tube's self-helicity magnitude is always <Φ2/2 (less than a half turn). Our results have a broad application in developing models of reconnecting coronal magnetic fields, as well as in interpreting observations and simulations of these fields.

Rotational Characteristics of the Solar Transition Region Using SDO/AIA 304 Å Images

Qian-Rui **Wu**1,2,3, Sheng Zheng1,2, Shu-Guang Zeng1,2, Miao Wan4, Xiang-Yun Zeng1,2, Lin-Hua Deng4, and Yao Huang1,2
2023 ApJ 954 20
https://iopscience.iop.org/article/10.3847/1538-4357/ace623/pdf
To date, the rotational characteristics of the solar transition region remain unclear. In this work, by applying the flux modulation method to the images derived from the Solar Dynamics Observatory/Atmospheric Imaging Assembly between 2011 and 2022 at 304 Å wavelength, we have studied the rotation of the solar transition region, and the results obtained are as follows. The solar transition region rotates differentially, while, from the perspective of the entire time interval, the rotation coefficients A and B are 14.39 (±0.08) and −1.61 (±0.15), respectively, and we find no prominent asymmetry in the average rotation rate of the northern and southern hemispheres. The solar transition region rotates fastest during the solar cycle maximum, and the average rotation rate follows the overall trend of solar activity. Both the equatorial rotation rate (represented by coefficient A) and the latitudinal gradient (represented by coefficient B) of the solar transition region are smaller than that of the solar chromosphere and the corona, indicating the solar transition region rotates more slowly and more rigidly than the other two layers, and we speculate that the solar chromosphere and corona seem to restrain the rotation of the solar transition region at the same

Highly Energetic Electrons Accelerated in Strong Solar Flares as a Preferred Driver of Sunquakes

H. **Wu**, Y. Dai, M. D. Ding
ApJL **943** L6 **2023**
https://arxiv.org/pdf/2301.02865.pdf
https://iopscience.iop.org/article/10.3847/2041-8213/acb0d1/pdf
Sunquakes are enhanced seismic waves excited in some energetic solar flares. Up to now, their origin has still been controversial. In this Letter, we select and study 20 strong flares in Solar Cycle 24, whose impulse phase is fully captured by the \emph{Reuven Ramaty High Energy Solar Spectroscopic Imager} (\emph{RHESSI}). For 11 out of 12 sunquake-active flares in our sample, the hard X-ray (HXR) emission shows a good temporal and spatial correlation with the white-light (WL) enhancement and the sunquake. Spectral analysis also reveals a harder photon spectrum that extends to several hundred keV, implying a considerable population of flare-accelerated nonthermal electrons at high energies. Quantitatively, the total energy of electrons above 300 keV in sunquake-active flares is systematically different from that in sunquake-quiet flares, while the difference is marginal for electrons above 50 keV. All these facts support highly energetic electrons as a preferred driver of the sunquakes. Such an electron-driven scenario can be reasonably accommodated in the framework of a recently proposed selection rule for

sunquake generation. For the remaining one event, the sunquake epicenter is cospatial with a magnetic imprint, i.e., a permanent change of magnetic field on the photosphere. Quantitative calculation shows that the flare-induced downward Lorentz force can do enough work to power the sunquake, acting as a viable sunquake driver for this specific event. **9 Aug 2011, 24 Sep 2011, 2012 October 23, 27 Oct 2014,**
Table 1. List of the Flares under study and the Sunquake Information 2011-2017

Predicting Sunspot Numbers for Solar Cycles 25 and 26

S.-S. **Wu**, G. Qin
ApJ **2021**
https://arxiv.org/pdf/2102.06001.pdf
The prediction of solar activity is important for advanced technologies and space activities. The peak sunspot number (SSN), which can represent the solar activity, has declined continuously in the past four solar cycles (21−24), and the Sun would experience a Dalton-like minimum, or even the Maunder-like minimum, if the declining trend continues in the following several cycles, so that the predictions of solar activity for cycles 25 and 26 are crucial. In Qin & Wu, 2018, ApJ, we established an SSN prediction model denoted as two-parameter modified logistic prediction (TMLP) model, which can predict the variation of SSNs in a solar cycle if the start time of the cycle has been determined. In this work, we obtain a new model denoted as TMLP-extension (TMLP-E). If the start time of a cycle n is already known, TMLP-E can predict the variation of SSNs in the cycle n+1. Cycle 25 is believed to start in December 2019, so that the predictions of cycles 25 and 26 can be made with our models. It is found that the predicted solar maximum, ascent time, and cycle length are 115.1, 4.84 yr, and 11.06 yr, respectively, for cycle 25, and 107.3, 4.80 yr, and 10.97 yr, respectively, for cycle 26. The solar activities of cycles 25 and 26 are predicted to be at the same level as that of cycle 24, but will not decrease further. We therefore suggest that the cycles 24−26 are at a minimum of Gleissberg cycle.

Chromospheric UV Bursts and Turbulent-driven Magnetic Reconnection

Pin **Wu**
2019 ApJ 885 158
https://doi.org/10.3847/1538-4357/ab4a06
We use Interface Region Imaging Spectrograph (IRIS) spacecraft data to study a group of Chromospheric ultraviolet bursts (UVBs) associated with an active region. We classify the UVBs into two types: smaller ones that can only be measured once by the scanning slit, and larger UVBs that are measured twice by the slit. The UVBs' optically thin Si iv 1402.77 Å line profiles are studied intensively. By fitting the smaller UVBs' lines with 1–2 Gaussians, we obtain a variety of line-of-sight flow measurements that hint various 3D orientations of small-scale magnetic reconnections, each associated with a UVB. The larger UVBs are, however, unique in a way that they each have two sets of measurements at two slit locations. This makes it possible to unambiguously detect two oppositely directed heated flows jetting out of a single UVB, a signature of magnetic reconnection operating at the heart of the UVB. Here, we report on the first of such an observation. Additionally, all the optically thin Si iv 1402.77 Å line profiles from those UVBs consistently demonstrate excessive broadening, an order of magnitude larger than would be expected from thermal broadening, suggesting that those small-scale reconnections could be driven by large scale (macroscale) turbulence in the active region.

Solar Cycle Variation of the Heliospheric Plasma Sheet Thickness

Chin-Chun **Wu**, Kan Liou, Ronald P. Lepping
Solar Physics July **2019**, 294:90
https://link.springer.com/content/pdf/10.1007%2Fs11207-019-1464-0.pdf
Past independent studies of the heliospheric plasma sheet (HPS) have shown that the thickness is highly variable, ranging from ≈3.8×105≈3.8×105 to 8.9×1068.9×106 km. Here we conduct a survey of the previous results and find a solar cycle dependence – where the HPS tends to be wider during solar-minimum years and narrower during solar-maximum years. The HPS is thicker near solar minimum than near solar maximum by a factor of 1.6 (in Solar Cycle 23) and 8 (in Solar Cycle 24). We also found that the average HPS thickness in 2007 (near the minimum of Solar Cycle 23/24) was almost ten times larger than that in 1995 (near minimum of Solar Cycle 22/23), and it was associated with a weak polar magnetic field in 2007. Based on the solar-surface-field measurements, we found that the average solar magnetic-field strength [|B||B|] at 2.5 solar radii [R⊙] was ≈40≈40% larger in 1995 than in 2007 (0.22 gauss versus 0.16 gauss). We also found a larger (≈27≈27%) magnetic pressure-gradient force in 1995 than in 2007. Because this magnetic gradient force points toward the Equator in the corona (which is probably also true farther out), a wider HPS is expected to occur in 2007 than in 1995, at least close to the Sun. This result supports the so-called heliospheric plasma-sheet inflation hypothesis, i.e. the HPS is wider if the Sun's polar field is weaker and narrower if the Sun's polar field is stronger.

Chromospheric UV bursts and turbulent driven magnetic reconnection

Pin **Wu**

ApJ **2019**

https://arxiv.org/pdf/1910.00355.pdf

We use Interface Region Imaging Spectrograph (IRIS) spacecraft data to study a group of Chromospheric ultraviolet bursts (UVBs) associated with an active region. We classify the UVBs into two types: smaller ones that can only be measured once by the scanning slit, and larger UVBs that are measured twice by the slit. The UVBs' optically thin Si IV 1402.77 Å line profiles are studied intensively. By fitting the smaller UVBs' lines with 1-2 Gaussians, we obtain a variety of line-of-sight flow measurements that hint various 3-D orientations of small scale magnetic reconnections, each associated with a UVB. The larger UVBs are, however, unique in a way that they each have two sets of measurements at two slit locations. This makes it possible to unambiguously detect two oppositely directed heated flows jetting out of a single UVB, a signature of magnetic reconnection operating at the heart of the UVB. Here we report on the first of such an observation. Additionally, all the optically thin Si IV 1402.77 Å line profiles from those UVBs consistently demonstrate excessive broadening, an order of magnitude larger than would be expected from thermal broadening, suggesting that those small scale reconnections could be driven by large scale (macro-scale) turbulence in the active region. **2017-09-03**

Solar total and spectral irradiance reconstruction over the last 9000 years

C.-J. **Wu**, N. A. Krivova, S. K. Solanki, I. G. Usoskin

A&A 620, A120 **2018**

https://arxiv.org/pdf/1811.03464.pdf

Changes in solar irradiance and in its spectral distribution are among the main natural drivers of the climate on Earth. However, irradiance measurements are only available for less than four decades, while assessment of solar influence on Earth requires much longer records. The aim of this work is to provide the most up-to-date physics-based reconstruction of the solar total and spectral irradiance (TSI/SSI) over the last nine millennia. The concentrations of the cosmogenic isotopes 14C and 10Be in natural archives have been converted to decadally averaged sunspot numbers through a chain of physics-based models. TSI and SSI are reconstructed with an updated SATIRE model. Reconstructions are carried out for each isotope record separately, as well as for their composite. We present the first ever SSI reconstruction over the last 9000 years from the individual 14C and 10Be records as well as from their newest composite. The reconstruction employs physics-based models to describe the involved processes at each step of the procedure. Irradiance reconstructions based on two different cosmogenic isotope records, those of 14C and 10Be, agree well with each other in their long-term trends despite their different geochemical paths in the atmosphere of Earth. Over the last 9000 years, the reconstructed secular variability in TSI is of the order of 0.11%, or 1.5 W/m2. After the Maunder minimum, the reconstruction from the cosmogenic isotopes is consistent with that from the direct sunspot number observation. Furthermore, over the nineteenth century, the agreement of irradiance reconstructions using isotope records with the reconstruction from the sunspot number by Chatzistergos et al. (2017) is better than that with the reconstruction from the WDC-SILSO series (Clette et al. 2014), with a lower chi-square-value.

Solar activity over nine millennia: A consistent multi-proxy reconstruction

Chi Ju **Wu**, I. G. Usoskin, N. Krivova, G. A. Kovaltsov, M. Baroni, E. Bard, S. K. Solanki

A&A 615, A93 **2018**

https://arxiv.org/pdf/1804.01302.pdf

https://www.aanda.org/articles/aa/pdf/2018/07/aa31892-17.pdf

Solar activity in the past millennia can only be reconstructed from cosmogenic radionuclide records in terrestrial archives. However, because of the diversity of the proxy archives, it is difficult to build a homogeneous reconstruction. Here we provide a new consistent multiproxy reconstruction of the solar activity over the last 9000 years, using available long-span datasets of 10Be and 14C in terrestrial archives. A new method, based on a Bayesian approach, was applied for the first time to solar activity reconstruction. A Monte Carlo search for the most probable value of the modulation potential was performed to match data from different datasets for a given time. We used six 10Be series from Greenland and Antarctica, and the global 14C production series. The 10Be series were resampled to match wiggles related to the grand minima in the 14C reference dataset. The GRIP and the EDML 10Be series diverge from each other during the second half of the Holocene, while the 14C series lies between them. A likely reason for this is the insufficiently precise beryllium transport and deposition model for Greenland. A slow 6-millennia variability with lows at ca. 5500 BC and 1500 AD of solar activity is found. Two components of solar activity can be statistically distinguished: the main 'normal' component and a component corresponding to grand minima. A possible existence of a component representing grand maxima is indicated, but it cannot be separated from the main component in a statistically significant manner. A new consistent reconstruction of solar activity over the last nine millennia is presented with the most probable values of decadal sunspot numbers and their realistic

uncertainties. Independent components of solar activity corresponding to the main moderate activity and the grand-minimum state are identified; they may be related to different operation modes of the dynamo.

Instrument Calibration of the Interface Region Imaging Spectrograph (IRIS) Mission

J.-P. **Wülser**, S. Jaeggli, B. De Pontieu, T. Tarbell, P. Boerner, S. Freeland et al.
Solar Physics November **2018**, 293:149
https://link.springer.com/article/10.1007/s11207-018-1364-8
The Interface Region Imaging Spectrograph (IRIS) is a NASA small explorer mission that provides high-resolution spectra and images of the Sun in the 133 – 141 nm and 278 – 283 nm wavelength bands. The IRIS data are archived in calibrated form and made available to the public within seven days of observing. The calibrations applied to the data include dark correction, scattered light and background correction, flat fielding, geometric distortion correction, and wavelength calibration. In addition, the IRIS team has calibrated the IRIS absolute throughput as a function of wavelength and has been tracking throughput changes over the course of the mission. As a resource for the IRIS data user, this article describes the details of these calibrations as they have evolved over the first few years of the mission. References to online documentation provide access to additional information and future updates.

Coronal rain in magnetic bipolar weak fields

Chun **Xia**, Rony Keppens, Xia Fang
A&A 603, A42 **2017**
https://arxiv.org/pdf/1706.01804.pdf
We intend to investigate the underlying physics for the coronal rain phenomenon in a representative bipolar magnetic field, including the formation and the dynamics of coronal rain blobs. With the MPI-AMRVAC code, we performed three dimensional radiative magnetohydrodynamic (MHD) simulation with strong heating localized on footpoints of magnetic loops after a relaxation to quiet solar atmosphere. Progressive cooling and in-situ condensation starts at the loop top due to radiative thermal instability. The first large-scale condensation on the loop top suffers Rayleigh-Taylor instability and becomes fragmented into smaller blobs. The blobs fall vertically dragging magnetic loops until they reach low beta regions and start to fall along the loops from loop top to loop footpoints. A statistic study of the coronal rain blobs finds that small blobs with masses of less than 10^10 g dominate the population. When blobs fall to lower regions along the magnetic loops, they are stretched and develop a non-uniform velocity pattern with an anti-parallel shearing pattern seen to develop along the central axis of the blobs. Synthetic images of simulated coronal rain with Solar Dynamics Observatory Atmospheric Imaging Assembly well resemble real observations presenting dark falling clumps in hot channels and bright rain blobs in a cool channel. We also find density inhomogeneities during a coronal rain "shower", which reflects the observed multi-stranded nature of coronal rain.

Study on the Temporal Evolution of the Radial Differential Rotation of Solar Corona Using Radio Emissions

N. B. **Xiang**, X. H. Zhao, L. H. Deng, F. Y. Li, Y. J. Wang, X. W. Tan
ApJ **2024**
https://arxiv.org/pdf/2411.18105
The daily measurements of the disc-integrated solar radio flux, observed by the Radio Solar Telescope Network (RSTN), at 245, 410, 610, 1415, 2695, 4995, and 8800 MHz during the time interval of 1989 January 1 to 2019 December 17, are used to investigate the temporal evolution of radial differential rotation of solar corona using the methods of Ensemble Empirical Mode Decomposition and wavelet analysis. Overall, the results reveal that over the 30-year period, the rotation rates for the observed solar radio flux within the frequency range of 245\textendash8800 MHz show an increase with frequency. This verifies the existence of the radial differential rotation of the solar corona over long timescales of nearly 3 solar cycles. Based on the radio emission mechanism, to some extent, the results can also serve as an indicator of how the rotation of the solar upper atmosphere varies with altitude within a specific range. From the temporal variation of rotation cycle lengths of radio flux, the coronal rotation at different altitudes from the low corona to approximately 1.3 R⊙ exhibits complex temporal variations with the progression of the solar cycle. However, in this altitude range, over the past 30 years from 1989 to 2019, the coronal rotation consistently becomes gradually slower as the altitude increases. Finally, the EEMD method can extract rotation cycle signals from these highly randomized radio emissions, and so it can be used to investigate the rotation periods for the radio emissions at higher or lower frequencies.

Systematic investigation of mid-term periodicity of the solar full-disk magnetic fields

Nan-Bin **Xiang**
RAA **2019** Vol. 19 No. 9, 131(12pp)
http://www.raa-journal.org/raa/index.php/raa/article/view/4374/4857

The Magnetic Plage Strength Index (MPSI) and the Mount Wilson Sunspot Index (MWSI), which have been measured at Mount Wilson Observatory (MWO) since the 1970s and which indicate weak and strong magnetic field activity on the solar full disk, respectively, are used to systematically investigate midterm periodicities in the solar full-disk magnetic fields. Multitudinous mid-term periodicities are detected in MPSI and MWSI on timescales of 0.3 to 4.5 yr, and these periodicities are found to fluctuate around several typical periodicities within a small amplitude in different solar cycles or phases. The periodicity of 3.44 yr is found in MPSI, and the periodicities of 3.85 and 3.00 yr are detected in MWSI. Our analysis indicates that they reflect the true oscillating signals of solar magnetic field activity. The typical periodicities are 2.8, 2.3 and 1.8 yr in MPSI and MWSI, and possible mechanisms for these periodicities are discussed. A 1.3 yr periodicity is only detected in MPSI, and should be related to meridional flows on the solar surface. The typical annual periodicity of MPSI and MWSI is 1.07 yr, which is not derived from the annual variation of Earth's heliolatitude. Several periodicities shorter than 1 yr found in MPSI and MWSI are considered to be Rieger-type periodicities.

Resonant Mode Conversion of Alfvén Waves to Kinetic Alfvén Waves in an Inhomogeneous Plasma

L. **Xiang**1,2, L. Chen1, and D. J. Wu1
2019 ApJ 881 61
sci-hub.se/10.3847/1538-4357/ab2bf1
Kinetic Alfvén waves (KAWs) are dispersive Alfvén waves (AWs) with a perpendicular wavelength comparable to the ion (ion–acoustic) gyroradius or the electron inertial length and can play an important role in wave energy dissipation and particle energization. In this paper, we investigate the resonant mode conversion of AWs into KAWs for the case of an arbitrary angle α between the density gradient of the ambient plasma and the ambient magnetic field in an inhomogeneous two-temperature magnetoplasma. The results show that the mode conversion sensitively depends on the angle α, the density inhomogeneous gradient kri , and the parallel wavenumber kzri , as well as the ion to electron temperature ratio T T i e. In particular, the excited KAWs are stronger when α is closer to °90° and are hardly excited for 0 < . Moreover, the maximal strength of the excited KAW increases with° a 40 the increase of kzri , but decreases with the increase of kri . Also, the maximal strength of the excited KAW has a °larger value at larger T T i e for 80 90 < . These results are helpful for our comprehensive understanding of° a the resonant mode conversion of AWs into KAWs in solar magnetic atmospheres when AWs originating from the photosphere propagate along solar magnetic fields into the corona.

Photospheric Swirls in a Quiet-Sun Region

Quan **Xie**, Jiajia Liu, Chris J. Nelson, Robert Erdélyi, Yuming Wang
ApJ **2024**
https://arxiv.org/pdf/2412.03816
Swirl-shaped flow structures have been observed throughout the solar atmosphere, in both emission and absorption, at different altitudes and locations, and are believed to be associated with magnetic structures. However, the distribution patterns of such swirls, especially their spatial positions, remain unclear. Using the Automated Swirl Detection Algorithm (ASDA), we identified swirls from the high-resolution photospheric observations, centered on Fe I 630.25 nm, of a quiet region near the Sun's central meridian by the Swedish 1-m Solar Telescope. Through a detailed study of the locations of the detected small-scale swirls with an average radius of ∼300 km, we found that most of them are located in lanes between mesogranules (which have an average diameter of ∼5.4 Mm) instead of the commonly believed intergranular lanes. The squared rotation, expansion/contraction, vector speeds, and proxy kinetic energy are all found to follow Gaussian distributions. Their rotation speed, expansion/contraction speed, and circulation are positively correlated with their radius. These results suggest that photospheric swirls at different scales and locations across the observational 56.5" × 57.5" field-of-view (FOV) could share the same triggering mechanism at preferred spatial and energy scales. A comparison with previous work suggests that the number of photospheric swirls is positively correlated with the number of local magnetic concentrations, stressing the close relation between swirls and local magnetic concentrations:the number of swirls should positively correlate with the number and strength of local magnetic concentrations. **2012 June 21, 2019 July 07**

The data center for the Spectrometer and Telescope for Imaging X-rays (STIX) on board Solar Orbiter **https://datacenter.stix.i4ds.net/stix**

Hualin **Xiao**1, Shane Maloney2, Säm Krucker1, Ewan Dickson3, Paolo Massa4, Erica Lastufka1, Andrea Francesco Battaglia1,5, László Etesi1, Nicky Hochmuth6, Frédéric Schuller7, Daniel F. Ryan1, Olivier Limousin8, Hannah Collier1,5, Alexander Warmuth7 and Michele Piana9,10
A&A 673, A142 (**2023**)
https://www.aanda.org/articles/aa/pdf/2023/05/aa46031-23.pdf

Context. The Spectrometer and Telescope for Imaging X-rays (STIX) on board Solar Orbiter observes solar X-ray emission in the range of 4–150 keV and produces spectra and images of solar flares over a wide range of flare magnitudes. During nominal operation, STIX continuously generates data. A constant data flow requires fully automated data-processing pipelines to process and analyze the data, and a data platform to manage, visualize, and distribute the data products to the scientific community.
Aims. The STIX Data Center has been built to fulfill these needs. In this paper, we outline its main components to help the community better understand the tools and data it provides.
Methods. The STIX Data Center is operated at the University of Applied Sciences and Arts Northwestern Switzerland (FHNW) and consists of automated processing pipelines and a data platform. The pipelines process STIX telemetry data, perform common analysis tasks, and generate data products at different processing levels. They have been designed to operate fully automatically with minimal human intervention. The data platform provides web-based user interfaces and application programmable interfaces for searching and downloading STIX data products.
Results. The STIX Data Center has been operating successfully for more than two years. The platform facilitates instrument operations and provides vital support to STIX data users. 7 Oct 2022, 26 Jan 2023
https://datacenter.stix.i4ds.net/stix

North–South Asymmetry of the Rotation of the Solar Magnetic Field

Jinglan **Xie**1,2,3,4, Xiangjun Shi1,3,4, and Zhining Qu
2018 ApJ 855 84
http://sci-hub.tw/http://iopscience.iop.org/0004-637X/855/2/84/
Using the rotation rates of the solar magnetic field during solar cycles 21 to 23 obtained by Chu et al. by analyzing the synoptic magnetic maps produced by the NSO/Kitt Peak and SOHO/MDI during the years 1975 to 2008, the temporal variation of the equatorial rotation rate (A) and the latitude gradient of rotation (B) in the northern and southern hemispheres are studied separately. The results indicate that the rotation is more differential (about 4.3%) in the southern hemisphere in the considered time frame. It is found that the north–south asymmetry of A and the asymmetry of B show increasing trends in the considered time frame, while the north–south asymmetry of the solar activity shows a decreasing trend. There exists a significant negative correlation (at 95% confidence level) between the asymmetry of B and the asymmetry of the solar activity, and this may be due to stronger magnetic activity in a certain hemisphere that may suppress the differential rotation to some extent. The periodicities in the variation of A and B are also studied, and periods of about 5.0 and 10.5 yr (5.5 and 10.4 yr) can be found for the variation of the northern (southern) hemisphere B. Moreover, the north–south asymmetry of A and the asymmetry of B have similar periods of about 2.6–2.7 and 5.2–5.3 yr. Further, cross-correlation analysis indicates that there exists a phase difference (about eight months) between the northern and southern hemisphere B, and this means that the northern hemisphere B generally leads by about eight months.

Temporal Variation of Solar Coronal Rotation

J. L. **Xie**1,2,3,4, X. J. Shi1,3,4, and J. Zhang
2017 ApJ 841 42
http://sci-hub.cc/10.3847/1538-4357/aa6d7d
In this paper, by applying the wavelet transformation analysis to the data of the daily 10.7 cm radio flux covering the period from 1947 February 14 to 2014 August 31, a significant period of about 27 days can be found, indicating the existence of rotational modulation in the temporal variation of the daily 10.7 cm radio flux. Then, the solar coronal rotation periods are obtained based on the result of the wavelet transformation analysis, and the temporal variation of the coronal rotation is revisited. We find that there exist significant periods of about 2.1, 3.0, 4.5, 6.6, 8.6, and 10.3 yr in the temporal variation of the coronal rotation. A possible period of 22.0 yr can also be found, but its statistical significance is below the 95% confidence level. The coronal rotation seems to show a weak decreasing trend during the considered time. The dependence of the coronal rotation on solar cycle phase is analyzed. The rotation periods are found to be varying with the solar cycle phase, and they are relatively longer around the minimum year of the solar cycle. The result based on the cross-correlation analysis between the rotation periods and the daily 10.7 cm radio flux indicates that there exists a phase difference of about 5.5 yr between them.

Forecasting solar cycle 25 using comprehensive precursor combination and multiple regression technique

Yating **Xiong**, Jianyong Lu, Kai Zhao, Meng Sun, Yang Gao
MNRAS, Volume 505, Issue 1, **2021**, Pages 1046–1052,
https://doi.org/10.1093/mnras/stab1159
In this paper, we propose a new model to predict the complete sunspot cycle based on the comprehensive precursor information (peak, skewness, maximum geomagnetic index aa of the previous cycle, and start value of predicted

cycle). The monthly average sunspot original data are processed by Gaussian smoothing and the new model is validated by the observed sunspots of cycle 24. Compared with the traditional 13-month moving average, the Gaussian filter has less missing information and is better to describe the overall trend of the raw data. Through the permutation and combination of multiple parameters in precursor methods of solar cycle forecasting, the multiple regression technique is used to successfully achieve the peak prediction. The regression coefficient (R) of the empirical model established in this paper can reach 0.95. By adding a new parameter to the original HWR function, we provide a complete solar cycle profile showing unimodal structure. It shows that the peak value of cycle 25 will come in March 2024, with a peak of 140.2.

Data-Driven Forecasting of Sunspot Cycles: Pros and Cons of a Hybrid Approach.

Xu, Q., Jain, R. & Xing, W.
Sol Phys 299, 25 (**2024**).
https://doi.org/10.1007/s11207-024-02270-6
https://link.springer.com/content/pdf/10.1007/s11207-024-02270-6.pdf
Understanding the number of sunspots is crucial for comprehending the Sun's magnetic-activity cycle and its influence on space weather and the Earth. Recent advancements in machine learning have significantly improved the accuracy of time-series predictions, revealing a compelling approach for sunspot forecasts. Our work takes the pioneering work by proposing a hybrid forecasting approach that combines the Seasonal Autoregressive Integrated Moving Average (SARIMA) with machine-learning algorithms like Random Forest and Support Vector Machine, delivering high prediction accuracy. Despite its high accuracy, we highlight the need for caution in deploying machine-learning-based methods for sunspot-number prediction, demonstrated through a detailed case study with only three extra time stamps leading to a dramatic change. More specifically, when making a forecast of monthly averaged sunspot numbers from 2023–2043 based on data from 1749–2023, we found that the observations in June, July, and August 2023 have a significant impact on the forecast, particularly in the long term. Given the multiseasonal and nonstationary nature of the sunspot time series, we conclude that this kind of phenomenon cannot be simply captured by a pure data-driven model, which can be highly sensitive in the forecast in the long term, and requires a more comprehensive approach, possibly with a model that includes physics.

Magnetic field evolution around a fast-moving pore emerging from the quiet Sun⋆

Zhe **Xu**1,2,⋆⋆, Haisheng Ji1, Junchao Hong2, Kaifan Ji2 and Jiayan Yang2
A&A 660, A55 (**2022**)
https://www.aanda.org/articles/aa/pdf/2022/04/aa43021-21.pdf
Context. Solar pores are intense concentrations of magnetic fields on the solar surface and plasma flows have always played a key role in spurring the evolution of the pores.
Aims. In this study, we present the evolution of the magnetic field and plasma velocity around a fast-moving pore. The target pore expands into the quiet Sun area with a sufficiently fast speed after its emergence, while the background magnetic fields around the pore are simple. These characteristics provide us with an excellent opportunity to study the interaction between plasma motions and ambient magnetic fields.
Methods. We analyzed the Helioseismic and Magnetic Imager (HMI) vector magnetograms with a pixel size of 0.5″ and a temporal cadence of 12 min across a duration of 11 h. We also adopted he HMI dopplergrams present the line-of-sight velocities. The horizontal flow fields were obtained using the Differential Affine Velocity Estimator for Vector Magnetograms method.
Results. Pure horizontal magnetic fields are generated in the moving frontwards when the pore is subject to fast movement. The generated magnetic fields occur outside the emerging site and thus can be ruled out as the emerging flux from the interior. Instead, they are highly correlated with the broader downflows and expanding horizontal plasma motions in front of the pore. A magnetic gap can be observed between the magnetic fields inside and outside the pore. The temporal evolution of the generated magnetic fields is related to the speed of the pore, which is also distinguished from the original fields within the pore.
Conclusions. The observations suggest that the plasma flows driven by the fast proper motion of the pore compress and stretch the local magnetic field to a horizontal non-radial direction, ultimately leading to the magnetic field amplification in the front part of the moving pore. **2012 February 6**

Asymmetric Distribution of the Solar Photospheric Magnetic Field Values

Jing-Chen **Xu**, Ke-Jun Li, Peng-Xin Gao
ApJ **919** 102 **2021**
https://arxiv.org/pdf/2107.03548.pdf
https://doi.org/10.3847/1538-4357/ac106e
Understanding the characteristics of the solar magnetic field is essential for interpreting solar activities and dynamo. In this research, we investigated the asymmetric distribution of the solar photospheric magnetic field values, using synoptic charts constructed from space-borne high-resolution magnetograms. It is demonstrated that the Lorentzian function describes the distribution of magnetic field values in the synoptic charts much better than the Gaussian

function, and this should reflect the gradual decay process from strong to weak magnetic fields. The asymmetry values are calculated under several circumstances, and the results generally show two periodicities related to the variation of the solar B0 angle and the solar cycle, respectively. We argue that it is the small-scale magnetic fields, the inclination of the solar axis, the emergence and evolution of magnetic flux, and the polar fields that are responsible for the features of asymmetry values. We further determined the polar field reversal time of solar cycles 23 and 24 with the flip of asymmetry values. Specifically, for cycle 24, we assert that the polar polarities of both hemispheres reversed at the same time - in March 2014; as to cycle 23, the reversal time of the S-hemisphere is March 2001, while the determination of the N-hemisphere is hampered by missing data.

Migration of Solar Polar Crown Filaments in the Past 100 Years

Yan **Xu**1,2, Dipankar Banerjee3,4,5, Subhamoy Chatterjee6, Werner Pötzi7, Ziran Wang8, Xindi Ruan8, Ju Jing1,2, and Haimin Wang1,2
2021 ApJ 909 86
https://doi.org/10.3847/1538-4357/abdc1e
Polar crown filaments (PCFs) are formed above the polarity inversion line, which separates unipolar polar fields and the nearest dispersed fields. They are important features in studying solar polar fields and their cyclical variations. Due to the relatively weak field strength and projection effects, measuring polar magnetic fields is more difficult than obtaining the field strengths concentrated in active regions at lower latitudes. "Rush-to-the-pole" of PCFs represent the progress of unipolar polar fields from the previous solar cycle being canceled by the dispersed fields generated in the current cycle. Such progress is a good indicator of the polarity reversal in the polar areas and a precursor for the solar maximum. In this study, PCFs are identified from a 100 yr archive, covering cycles 16–24. This archive consists of full-disk Hα images obtained from the Kodaikanal Solar Observatory of the Indian Institute of Astrophysics, Kanzelhöhe Solar Observatory, and Big Bear Solar Observatory. The poleward migration speeds are measured and show an obvious asymmetry in the northern and southern hemispheres. In addition, our results show that the PCFs usually reach their highest latitudes first in the northern hemisphere, except cycle 17. Similarly, previous studies show that the magnetic field reversed first at the north pole in six out of nine cycles. We also compare the temporal variations of PCF migration and the latitude gradient factor of the differential rotation, which shows a trend in the southern hemisphere. Moreover, the migration speed of PCFs does not seem to be well correlated with the maximum sunspot numbers.

On the Rotation of the Solar Chromosphere

Jing-Chen **Xu**1,2,3, Peng-Xin Gao1,2,3, and Xiang-Jun Shi1,2,3
2020 ApJ 902 64
https://doi.org/10.3847/1538-4357/abb5b7
https://arxiv.org/pdf/2010.10851
Rotation is a significant characteristic of the Sun and other stars, and it plays an important role in understanding their dynamo actions and magnetic activities. In this study, the rotation of the solar chromospheric activity is investigated from a global point of view with an over 40 yr Mg ii index. We determined the time-varying rotational period lengths (RPLs) with the synchrosqueezed wavelet transform, which provides high temporal and frequency resolution; furthermore, we compared the RPLs with the photospheric and coronal RPLs obtained from the sunspot numbers and the 10.7 cm radio flux data. The significance of the RPLs is taken into consideration. We found that the RPLs of the chromosphere exhibit a downward trend, as do those of the photosphere and corona; in addition, their RPLs at the recent four solar maxima also show a declining trend. This suggests that the rotation of the solar atmosphere has been accelerating during the recent four solar cycles, which is inferred to be caused by the declining strength of solar activity. The variations of the solar atmospheric RPLs show periodicities of multiple harmonics of the solar cycle period, and it is modulated by the solar activity cycle.

Localized Amplification of Magnetic Field in the Solar Photosphere Associated with a Rapid Moving Pore

Zhe **Xu**1,2,3, Haisheng Ji1,3, Kaifan Ji2,3, Yi Bi2,3, Bo Yang2,3, Junchao Hong2,3, and Jiayan Yang2,3
2020 ApJL 900 L17
https://doi.org/10.3847/2041-8213/abb096
https://iopscience.iop.org/article/10.3847/2041-8213/abb096/pdf
In the Sun, the flows of hot plasma drive a dynamo that generates a global magnetic field as well as smaller-scale local fields. The existence of a magnetic field in turn affects the motion of plasma so that complex dynamic characteristics can be observed. In this Letter, we give an analysis on the localized amplification of magnetic fields in front of a moving pore. Moving with the pore, the formation of semicircular penumbra-like structures and enhancement of horizontal fields can be observed simultaneously. The increasing horizontal magnetic fields in a penumbra-like area probably did not come from the pore, since the penumbra-like structures were not connected to the pore and a magnetic gap existed. The possibility of flux emergence can also be safely excluded. We further report that horizontal magnetic fields in the front of a moving pore are amplified in accordance with the MHD

induction equation after necessary yet reasonable simplification. All characteristics show that the flows driven by the moving pore can lead to the amplification of the magnetic fields around its front. The observations are from the Helioseismic and Magnetic Imager on board the Solar Dynamics Observatory. **2016 May 15**

Solar Image Deconvolution by Generative Adversarial Network

Long **Xu**, Wenqing Sun, Yihua Yan, Weiqiang Zhang
Research in Astron. Astrophys. **2020**
https://arxiv.org/pdf/2001.03850.pdf
With Aperture synthesis (AS) technique, a number of small antennas can assemble to form a large telescope which spatial resolution is determined by the distance of two farthest antennas instead of the diameter of a single-dish antenna. Different from direct imaging system, an AS telescope captures the Fourier coefficients of a spatial object, and then implement inverse Fourier transform to reconstruct the spatial image. Due to the limited number of antennas, the Fourier coefficients are extremely sparse in practice, resulting in a very blurry image. To remove/reduce blur, "CLEAN" deconvolution was widely used in the literature. However, it was initially designed for point source. For extended source, like the sun, its efficiency is unsatisfied. In this study, a deep neural network, referring to Generative Adversarial Network (GAN), is proposed for solar image deconvolution. The experimental results demonstrate that the proposed model is markedly better than traditional CLEAN on solar images.

Collective Study of Polar Crown Filaments in the Past Four Solar Cycles

Yan **Xu**, Werner Potzi, Hewei Zhang, Nengyi Huang, Ju Jing, and Haimin Wang
2018 ApJL 862 L23
https://arxiv.org/pdf/1807.11844.pdf
http://sci-hub.tw/10.3847/2041-8213/aad40d
Polar Crown Filaments (PCFs) form above the magnetic polarity inversion line, which separates the unipolar polar fields and the nearest dispersed fields from trailing part of active regions with opposite polarity. The statistical properties of PCFs are correlated with the solar cycle. Therefore, study of PCFs plays an important role in understanding the variation of solar cycle, especially the prolonged cycle 23 and the current "abnormal" solar cycle 24. In this study, we investigate PCFs using full disk Hα data from 1973 to early 2018, recorded by Kanzelhöhe Solar Observatory (KSO) and Big Bear Solar Observatory (BBSO), in digital form from 1997 to 2018 and in 35 mm film (digitized) from 1973 to 1996. PCFs are identified manually because their segmented shape and close-to-limb location were not handled well by automatical detections in several previous studies. Our results show that the PCFs start to move poleward at the beginning of each solar cycle. When the PCFs approach to the maximum latitude, the polar field strength reduces to zero followed by a reversal. The migration rates are about 0.4 to 0.7 degree per Carrington rotation, with clear N-S asymmetric pattern. In cycles 21 and 23, the PCFs in the northern hemisphere migrate faster than those in the southern hemisphere. However, in the "abnormal" cycle 24, the southern PCFs migrate faster, which is consistent with other observations of magnetic fields and radio emission. In addition, there are more days in cycle 23 and 24 without PCFs than in the previous cycles. **2013-March-23**

Modulations of the Surface Magnetic Field on the Intra-cycle Variability of Total Solar Irradiance

J. C. **Xu**, D. F. Kong, F. Y. Li
Astrophysics and Space Science 363:98 **2018**
https://arxiv.org/pdf/1804.06079.pdf
Solar photospheric magnetic field plays a dominant role in the variability of total solar irradiance (TSI). The modulation of magnetic flux at six specific ranges on TSI is characterized for the first time. The daily flux values of magnetic field at four ranges are extracted from MDI/{\sl SOHO}, together with daily flux of active regions (MFar) and quiet regions (MFqr); the first four ranges (MF1−4) are: 1.5--2.9, 2.9--32.0, 32.0--42.7, and 42.7--380.1 (×1018 Mx per element), respectively. Cross-correlograms show that MF4, MFqr, and MFar are positively correlated with TSI, while MF2 is negatively correlated with TSI; the correlations between MF1, MF3 and TSI are insignificant. The bootstrapping tests confirm that the impact of MF4 on TSI is more significant than that of MFar and MFqr, and MFar leads TSI by one rotational period. By extracting the rotational variations in the MFs and TSI, the modulations of the former on the latter at the solar rotational timescale are clearly illustrated and compared during solar maximum and minimum times, respectively. Comparison of the relative amplitudes of the long-term variation show that TSI is in good agreement with the variation of MF4 and MFar; besides, MF2 is in antiphase with TSI, and it lags the latter by about 1.5 years.

Phase Relations between the Sunspot Numbers and Total Solar Irradiance

J. C. **Xu**1,2,3,4, J. L. Xie1,3,4, and Z. N. Qu
2017 ApJ 851 141
http://iopscience.iop.org.sci-hub.tw/0004-637X/851/2/141/

Understanding the effect of sunspot activities on the variations in the total solar irradiance (TSI) is essential for the interpretation of the variability of TSI as well as its reconstruction. Phase relations between the sunspot numbers (SN) and two TSI composite data are investigated. It is found that TSI and SN are positively correlated, and the former lags the latter by about 29 days, which is approximately a solar rotation period; analyses of the data sets in the four individual cycles show that in cycles 21, 23, and 24, TSI lags SN by 28.9–30.3 days, while in cycle 22, the lag is only 21.8–22.3 days. The abnormality in cycle 22 is probably caused by its stronger magnetic field in sunspots compared with its adjacent cycles. The nonlinearity between TSI and SN is confirmed and explained with the different behavior and effect of spots, faculae, and magnetic network. Based on the cross-wavelet transform and wavelet coherence analysis, a common periodicity between TSI and SN at the timescale of the solar cycle is clearly revealed; at timescales longer than about four years, high values of coherence above the 95% confidence level together with a strong phase synchronization feature are exhibited. At timescales shorter than three rotational periods, the relation between TSI and SN indicates low correlations and a noisy behavior with strong phase mixing due to the lifetime of spots and faculae; moreover, if the short-term effect of spots and faculae is smoothed out, then their coherence reaches high values in partial areas at periods from three rotations to about four years.

THE ROTATION OF THE SOLAR PHOTOSPHERIC MAGNETIC FIELD

J. C. **Xu**1,2,3,4 and P. X. Gao

2016 ApJ 833 144

The rotational characteristics of the solar photospheric magnetic field at four flux ranges are investigated together with the total flux of active regions (MFar) and quiet regions (MFqr). The first four ranges (MF1–4) are (1.5–2.9) × 1018, (2.9–32.0) × 1018, (3.20–4.27) × 1019, and (4.27–38.01) × 1019, respectively (the unit is Mx per element). Daily values of the flux data are extracted from magnetograms of the Michelson Doppler Imager on board the Solar and Heliospheric Observatory. Lomb–Scargle periodograms show that only MF2, MF4, MFqr, and MFar exhibit rotational periods. The periods of the first three types of flux are very similar, i.e., 26.20, 26.23, and 26.24 days, respectively, while that of MFar is longer, 26.66 days. This indicates that active regions rotate more slowly than quiet regions on average, and strong magnetic fields tend to repress the surface rotation. Sinusoidal function fittings and cross-correlation analyses reveal that MFar leads MF2 and MF4 by 5 and 1 days, respectively. This is speculated to be related with the decaying of active regions. MF2 and MFar are negatively correlated, while both MF4 and MFqr are positively correlated with MFar. At the timescale of the solar activity cycle, MFar leads (negatively) MF2 by around one year (350 days), and leads MF4 by about 3 rotation periods (82 days). The relation between MF2 and MFar may be explained by the possibility that the former mainly comes from a higher latitude, or emerges from the subsurface shear layer. We conjecture that MF4 may partly come from the magnetic flux of active regions; this verifies previous results that were obtained with indirect solar magnetic indices.

On the Origin of Differences in Helicity Parameters Derived from Data of Two Solar Magnetographs

Haiqing **Xu**, Hongqi Zhang, K. Kuzanyan, T. Sakurai

Solar Phys. Volume 291, Issue 8, pp 2253–2267 **2016**

We analyzed how sensitivity and accuracy in solar magnetic field measurements may affect the values of mean current helicity density hchc and twist parameter αavαav by comparing these values obtained from two magnetographs (SMFT at Beijing and SFT at Mitaka, Tokyo). When we computed the helicity parameters from the SFT data, we replaced the values of the longitudinal field component, transverse field strength, and transverse field azimuth angle with those from the SMFT data and examined the differences. The results show that the correlation coefficient and the fraction of the data that agree in signs of hchc or αavαav increase when an SFT parameter is substituted by the corresponding SMFT parameter because one source of discrepancy is removed. The increase in correlation coefficient is largest when the azimuthal angles and transverse field strengths are set identical in the two instruments; the correlation coefficient of hchc (αavαav) increases from 0.74 (0.56) to 0.86 (0.78), respectively, indicating that the differences in the transverse field strength and its azimuthal angle are the largest source of discrepancy in the values of hchc or αavαav. We found a nonlinear relationship in the components of the magnetic field between the two instruments for some data samples; we conclude that this is due to the discrepancy in the calibration procedure between the two instruments. This nonlinearity can be another source of difference in determining helical parameters between the two instruments.

Current helicity and magnetic field anisotropy in solar active regions

H. **Xu**, R. Stepanov, K. Kuzanyan, D. Sokoloff, H. Zhang, Y. Gao

MNRAS **2015**

http://arxiv.org/pdf/1509.02652v1.pdf

The electric current helicity density $\chi=\langle\epsilon ijkbi\partial bk\partial xj\rangle$ contains six terms, where bi are components of the magnetic field. Due to the observational limitations, only four of the above six terms can be inferred from solar photospheric vector magnetograms. By comparing the results for simulation we distinguished the statistical difference of above six terms for isotropic and anisotropic cases. We estimated the relative degree of anisotropy for three typical active

regions and found that it is of order 0.8 which means the assumption of local isotropy for the observable current helicity density terms is generally not satisfied for solar active regions. Upon studies of the statistical properties of the anisotropy of magnetic field of solar active regions with latitudes and with evolution in the solar cycle, we conclude that the consistency of that assumption of local homogeneity and isotropy requires further analysis in the light of our findings.

Angular Distribution of Solar Wind Magnetic Field Vector at 1 Au

F. **Xu**1,2, G. Li2, L. Zhao2, Y. Zhang1,2, O. Khabarova2,3, B. Miao4, and J. le Roux
2015 ApJ 801 58.

We study the angular distribution of the solar wind magnetic field vector at 1 AU and its solar cycle dependence usingACE observations. A total of twelve 27.27 day (the duration of a solar rotation) intervals during the solar maximum, the solar minimum, as well as the ascending and descending phases of solar cycle 23 are examined. For all selected intervals, we obtain the angular distribution function $f_\tau(\alpha)$, where α is the angle between the instantaneous solar wind magnetic field vector and the average background magnetic field vector, and τ is the period length for the averaging. Our results show that in all periods $f_\tau(\alpha)$has two populations, one at small angles and one at large angles. We suggest that the second population is due to the presence of current sheets in the solar wind. The solar-cycle dependence of $f_\tau(\alpha)$ and a τ-scaling property of the second population of $f_\tau(\alpha)$are discussed. The τ scaling shows a clear dependence on the solar wind type. The implication of $f_\tau(\alpha)$ for particle acceleration at interplanetary shocks driven by coronal mass ejections, such as those in solar energetic particle events, is also discussed.

Simulations of stray light from the surface scattering of the Solar Corona Imager primary mirror

Jianchao **Xue**, Marco Romoli, Federico Landini, Cristian Baccani, Hui Li, Yunqi Wang, Bo Chen
Proceedings of SPIE **2020**
https://arxiv.org/pdf/2012.07367.pdf

The Solar Corona Imager is an internally occulted coronagraph on board the ASO-S mission, which has the advantage of imaging the inner corona in H I {Lyman-\textalpha} (Ly-alpha) and white-light (WL) wavebands. However, scattering of solar disk light by the primary mirror (M1) becomes the main source of stray light. To study the methods of stray light suppression, three scattering models are used to model M1 scattering in Zemax OpticStudio. The ratio of coronal emission to predicted stray light decrease along field of view in both channels. The stray light in Ly-alpha channel is generally lower than coronal emission, but the stray light in WL channel tends to be one order of magnitude higher than coronal signal at 2.5 Rsun. Optimized parameter combinations that suppress the stray light to required level are obtained, which put some limitations on the M1 manufacture. Besides, K-correlation model is recommended to simulate surface scattering.

Inference of electric currents in the solar photosphere

A. Pastor **Yabar**, J.M. Borrero, C. Quintero Noda, B. Ruiz Cobo
A&A 656, L20 **2021**
https://arxiv.org/pdf/2112.04356.pdf
https://www.aanda.org/articles/aa/pdf/2021/12/aa42149-21.pdf
https://doi.org/10.1051/0004-6361/202142149

We aim at demonstrating the capabilities of a newly developed method for determining electric currents in the solar photosphere. We employ three-dimensional radiative magneto-hydrodynamic (MHD) simulations to produce synthetic Stokes profiles in several spectral lines with a spatial resolution similar to what the newly operational 4-meter Daniel K. Inouye Solar Telescope (DKIST) solar telescope should achieve. We apply a newly developed inversion method of the polarized radiative transfer equation with magneto-hydrostatic (MHS) constraints to infer the magnetic field vector in the three-dimensional Cartesian domain, B(x,y,z), from the synthetic Stokes profiles. We then apply Ampere's law to determine the electric currents, j, from the inferred magnetic field, B(x,y,z), and compare the results with the electric currents present in the original MHD simulation. We show that the method employed here is able to attain reasonable reliability (close to 50 % of the cases are within a factor of two, and this increases to 60 %-70 % for pixels with B≥300 G) in the inference of electric currents for low atmospheric heights (optical depths at 500 nm $\tau_5 \in [1, 0.1]$) regardless of whether a small or large number of spectral lines are inverted. Above these photospheric layers, the method's accuracy strongly deteriorates as magnetic fields become weaker and as the MHS approximation becomes less accurate. We also find that the inferred electric currents have a floor value that is related to low-magnetized plasma, where the uncertainty in the magnetic field inference prevents a sufficiently accurate determination of the spatial derivatives. We present a method that allows the inference of the three components of the electric current vector at deep atmospheric layers (photospheric layers) from spectropolarimetric observations.

Photospheric magnetic topology of a north polar region

A. Pastor **Yabar** (1), M. J. Martínez González (2,3), M. Collados

A&A 635, A210 **2020**

https://arxiv.org/pdf/2003.04267.pdf

Aims. We aim to characterise the magnetism of a large fraction of the north polar region close to a maximum of activity, when the polar regions are reversing their dominant polarity.
Methods. We make use of full spectropolarimetric data from the CRisp Imaging Spectro-Polarimeter installed at the Swedish Solar Telescope. The data consist of a photospheric spectral line, which is used to infer the various physical parameters of different quiet Sun regions by means of the solution of the radiative transfer equation. We focus our analysis on the properties found for the north polar region and their comparison to the same analysis applied to data taken at disc centre and low-latitude quiet Sun regions for reference. We also analyse the spatial distribution of magnetic structures throughout the north polar region.
Results. We find that the physical properties of the polar region (line-of-sight velocity, magnetic flux, magnetic inclination and magnetic azimuth) are compatible with those found for the quiet Sun at disc centre and are similar to the ones found at low latitudes close to the limb. Specifically, the polar region magnetism presents no specific features. The structures for which the transformation from a line-of-sight to a local reference frame was possible harbour large magnetic fluxes (>1017 Mx) and are in polarity imbalance with a dominant positive polarity, the largest ones (>1019 Mx) being located below 73◦ latitude.

Wave transformations near a coronal magnetic null-point

Nitin **Yadav**, Rony Keppens

A&A 681, A43 (**2024**)

https://arxiv.org/pdf/2310.17573.pdf

We investigate the viability of MHD waves, in particular acoustic p-modes, in causing strong current accumulation at the null points. We begin with a three-dimensional numerical setup incorporating a gravitationally stratifed solar atmosphere and an axially symmetric magnetic feld including a coronal magnetic null point. To excite waves, we employ wave drivers mimicking global p-modes. We found that most of the vertical velocity transmits through the Alfvén acoustic equipartition layer maintaining acoustic nature while a small fraction generates fast waves via the mode conversion process. The fast waves undergo almost total refection at the transition region due to sharp gradients in density and Alfvén speed. There are only weak signatures of Alfvén wave generation near the transition region due to fast-to-Alfvén mode conversion. Since the slow waves propagate with the local sound speed, they are not much afected by the density gradients at the transition region and undergo secondary mode conversion and transmission at the Alfvén-acoustic equipartition layer surrounding the null point, leading to fast wave focusing at the null point. These fast waves have associated perturbations in current density, showing oscillatory signatures compatible with the second harmonic of the driving frequency which could result in resistive heating and enhanced intensity in the presence of fnite resistivity. We conclude that MHD waves could be a potential source for oscillatory current dissipation around the magnetic null point. We conjecture that besides oscillatory magnetic reconnection, global p-modes could lead to the formation of various quasiperiodic energetic events.

Solar Atmospheric Heating Due to Small-scale Events in an Emerging Flux Region

Rahul **Yadav**, Maria D. Kazachenko, Andrey N. Afanasyev, Jaime de la Cruz Rodríguez, Jorrit Leenaarts

ApJ **958** 54 **2023**

https://arxiv.org/pdf/2309.06452.pdf

https://iopscience.iop.org/article/10.3847/1538-4357/acfd2b/pdf

We investigate the thermal, kinematic and magnetic structure of small-scale heating events in an emerging flux region (EFR). We use high-resolution multi-line observations (including Ca II 8542~Å, Ca II K, and Fe I 6301~Å line pair) of an EFR located close to the disk center from the CRISP and CHROMIS instruments at the Swedish 1-m Solar Telescope. We perform non-LTE inversions of multiple spectral lines to infer the temperature, velocity, and magnetic field structure of the heating events. Additionally, we use the data-driven Coronal Global Evolutionary Model to simulate the evolution of the 3D magnetic field configuration above the events and understand their dynamics. Furthermore, we analyze the differential emission measure to gain insights into the heating of the coronal plasma in the EFR. Our analysis reveals the presence of numerous small-scale heating events in the EFR, primarily located at polarity inversion lines of bipolar structures. These events not only heat the lower atmosphere but also significantly heat the corona. The data-driven simulations, along with the observed enhancement of currents and Poynting flux, suggest that magnetic reconnection in the lower atmosphere is likely responsible for the observed heating at these sites. **September 19, 2016**

Three-dimensional MHD wave propagation near a coronal null point: a new wave mode decomposition approach

N. **Yadav**, Rony Keppens, B. Popescu Braileanu

A&A **2022**
https://arxiv.org/pdf/2201.09704.pdf
We present a new MHD wave decomposition method that overcomes the limitations of existing wave identification methods. Our method allows to investigate the energy fluxes in different MHD modes at different locations of the solar atmosphere as waves generated by vortex flows travel through the solar atmosphere and pass near the magnetic null. We simulate wave dynamics through a coronal null configuration and apply a rotational wave driver at our bottom photospheric boundary. To identify the wave energy fluxes associated with different MHD wave modes, we employ a wave-decomposition method that is able to uniquely distinguish different MHD modes. Our proposed method utilizes the geometry of an individual magnetic field-line in 3D space to separate out velocity perturbations associated with the three fundamental MHD waves. Our method for wave identification is consistent with previous flux-surface-based methods and gives expected results in terms of wave energy fluxes at various locations of the null configuration. We show that ubiquitous vortex flows excite MHD waves that contribute significantly to the Poynting flux in the solar corona. Alfvén wave energy flux accumulates on the fan surface and fast wave energy flux accumulates near the null point. There is a strong current density buildup at the spine and fan surface.The proposed method has advantages over previously utilized wave decomposition methods, since it may be employed in realistic simulations or magnetic extrapolations, as well as in real solar observations, whenever the 3D fieldline shape is known. The enhancement in energy flux associated with magneto-acoustic waves near nulls may have important implications in the formation of jets and impulsive plasma flows.

Slow magneto-acoustic waves in simulations of a solar plage region carry enough energy to heat the chromosphere

Nitin **Yadav**, Robert H. Cameron, Sami K. Solanki
A&A 652, A43 **2021**
https://arxiv.org/pdf/2105.02932.pdf
https://www.aanda.org/articles/aa/pdf/2021/08/aa39908-20.pdf
https://doi.org/10.1051/0004-6361/202039908
We study the properties of slow magneto-acoustic waves that are naturally excited due to turbulent convection and investigate their role in the energy balance of a plage region using three dimensional (3D) radiation-MHD simulations. We calculate the horizontally averaged (over the whole domain) frequency power spectra for both longitudinal and vertical (i.e. the component perpendicular to the surface) components of velocity. To compare our results with the observations we degrade the simulation data with Gaussian kernels having FWHM of 100 km and 200 km, and calculate horizontally averaged power spectra for the vertical component of velocity. The power spectra of the longitudinal component of velocity, averaged over field lines in the core of a kG magnetic flux concentration, reveal that the dominant period of oscillations shifts from around 6.5 minutes in the photosphere to around 4 minutes in the chromosphere. At the same time, the velocity power spectra, averaged horizontally over the whole domain, show that low frequency waves (approximately 6.5 minute period) may reach well into the chromosphere. Importantly, waves with frequencies above 5 mHz propagating along different field lines are found to be out of phase with each other even within a single magnetic concentration. The horizontally averaged power spectra of the vertical component of velocity at various effective resolutions show that the observed acoustic wave energy fluxes are underestimated, by a factor of three even if determined from observations carried out at a high spatial resolution of 200 km. Our results show that longitudinal waves carry (just) sufficient energy to heat the chromosphere in solar plage. We conjecture that current observations (with spatial resolution around 200 km) underestimate the energy flux by roughly a factor of three, or more if the observations have lower spatial resolution.

Vortex Flow Properties in Simulations of Solar Plage Region: Evidence for their role in chromospheric heating

Nitin **Yadav**, Robert H. Cameron, Sami K. Solanki
A&A 645, A3 **2021**
https://arxiv.org/pdf/2010.14971.pdf
Context. Vortex flows exist across a broad range of spatial and temporal scales in the solar atmosphere. Small-scale vortices are thought to play an important role in energy transport in the solar atmosphere. However, their physical properties remain poorly understood due to the limited spatial resolution of the observations.
Aims. We explore and analyze the physical properties of small-scale vortices inside magnetic flux tubes using numerical simulations, and investigate whether they contribute to heating the chromosphere in a plage region.
Methods. Using the three-dimensional radiative magnetohydrodynamic simulation code MURaM, we perform numerical simulations of a unipolar solar plage region. To detect and isolate vortices we use the swirling strength criterion and select the locations where the fluid is rotating with an angular velocity greater than a certain threshold. We concentrate on small-scale vortices as they are the strongest and carry most of the energy. We explore the spatial profiles of physical quantities such as density and horizontal velocity inside these vortices. Moreover, to learn their general characteristics, a statistical investigation is performed.

Results. Magnetic flux tubes have a complex filamentary substructure harboring an abundance of small-scale vortices. At the interfaces between vortices strong current sheets are formed that may dissipate and heat the solar chromosphere. Statistically, vortices have higher densities and higher temperatures than the average values at the same geometrical height in the chromosphere.
Conclusions. We conclude that small-scale vortices are ubiquitous in solar plage regions; they are denser and hotter structures that contribute to chromospheric heating, possibly by dissipation of the current sheets formed at their interfaces.

Simulations Show that Vortex Flows Could Heat the Chromosphere in Solar Plage

Nitin **Yadav**1, R. H. Cameron1, and S. K. Solanki1
2020 ApJL 894 L17
https://doi.org/10.3847/2041-8213/ab8dc5
The relationship between vortex flows at different spatial scales and their contribution to the energy balance in the chromosphere is not yet fully understood. We perform three-dimensional (3D) radiation-magnetohydrodynamic simulations of a unipolar solar plage region at a spatial resolution of 10 km using the MURaM code. We use the swirling-strength criterion that mainly detects the smallest vortices present in the simulation data. We additionally degrade our simulation data to smooth out the smaller vortices, so that also the vortices at larger spatial scales can be detected. Vortex flows at various spatial scales are found in our simulation data for different effective spatial resolutions. We conclude that the observed large vortices are likely clusters of much smaller ones that are not yet resolved by observations. We show that the vertical Poynting flux decreases rapidly with reduced effective spatial resolutions and is predominantly carried by the horizontal plasma motions rather than vertical flows. Since the small-scale horizontal motions or the smaller vortices carry most of the energy, the energy transported by vortices deduced from low-resolution data is grossly underestimated. In full-resolution simulation data, the Poynting flux contribution due to vortices is more than adequate to compensate for the radiative losses in plage, indicating their importance for chromospheric heating.

Three-dimensional magnetic field structure of a flux emerging region in the solar atmosphere

Rahul **Yadav**, J. de la Cruz Rodríguez, C. J. Díaz Baso, Avijeet Prasad, Tine Libbrecht, Carolina Robustini, A. Asensio Ramos
A&A **2019**
https://arxiv.org/pdf/1910.13279.pdf
We analyze high-resolution spectropolarimetric observations of a flux emerging region (FER) in order to understand its magnetic and kinematic structure. Our spectropolarimetric observations in the He I 1083.0 nm spectral region of a FER are recorded with GRIS at the 1.5 m aperture GREGOR telescope. A Milne-Eddington based inversion code was employed to extract the photospheric information of the Si I spectral line, whereas the He I triplet line was analyzed with the Hazel inversion code, which takes into account the joint action of the Hanle and the Zeeman effect. The spectropolarimetric analysis of Si I line displays a complex magnetic structure near the vicinity of FER. Moreover, we find supersonic downflows of 40 km/sec appears near the footpoints of loops connecting two pores of opposite polarity, whereas a strong upflows of 22 km/sec appears near the apex of the loops. Furthermore, non-force-free field extrapolations were performed separately at two layers in order to understand the magnetic field topology of the FER. We determine, using extrapolations from the photosphere and the observed chromospheric magnetic field, that the average formation height of the He triplet line is 2 Mm from the solar surface. The reconstructed loops using photospheric extrapolations along an arch filament system have a maximum height of 10.5 Mm from the solar surface with a foot-points separation of 19 Mm, whereas the loops reconstructed using chromospheric extrapolations are around 8.4 Mm high from the solar surface with a foot-point separation of 16 Mm at the chromospheric height. The magnetic topology in the FER suggests the presence of small-scale loops beneath the large loops. Under suitable conditions, due to magnetic reconnection, these loops can trigger various heating events in the vicinity of the FER. **3 June, 2015**

SPIN: An Inversion Code for the Photospheric Spectral Line

Rahul **Yadav**, Shibu K. Mathew, Alok Ranjan Tiwary
Solar Physics August **2017**, 292:105
Inversion codes are the most useful tools to infer the physical properties of the solar atmosphere from the interpretation of Stokes profiles. In this paper, we present the details of a new Stokes Profile INversion code (SPIN) developed specifically to invert the spectro-polarimetric data of the Multi-Application Solar Telescope (MAST) at Udaipur Solar Observatory. The SPIN code has adopted Milne–Eddington approximations to solve the polarized radiative transfer equation (RTE) and for the purpose of fitting a modified Levenberg–Marquardt algorithm has been employed. We describe the details and utilization of the SPIN code to invert the spectro-polarimetric data. We also present the details of tests performed to validate the inversion code by comparing the results from the other widely

used inversion codes (VFISV and SIR). The inverted results of the SPIN code after its application to Hinode/SP data have been compared with the inverted results from other inversion codes.

Statistical properties of the most powerful solar and heliospheric disturbances

O.S. **Yakovchouk**[a], , I.S. Veselovsky[a, b], and K. Mursula

Advances in Space Research

Volume 43, Issue 4, 16 February **2009**, Pages 634-640

We present and discuss here the first version of a data base of extreme solar and heliospheric events. The data base contains now 87 extreme events mostly since 1940. An event is classified as extreme if one of the three critical parameters passed a lower limit. The critical parameters were the X-ray flux (parameter *R*), solar proton flux (parameter *S*) and geomagnetic disturbance level (parameter *G*). We find that the five strongest extreme events based on four variables (X-rays SEP, Dst, Ap) are completely separate except for the October 2003 event which is one the five most extreme events according to SEP, Dst and Ap. This underlines the special character of the October 2003 event, making it unique within 35 years. We also find that the events based on *R* and *G* are rather separate, indicating that the location of even extreme flares on the solar disk is important for geomagnetic effects. We also find that $S = 3$ events are not extreme in the same sense as $R > 3$ and $G > 3$ events, while $S = 5$ events are missing so far. This suggests that it might be useful to rescale the classification of SEP fluxes.

Effects of Cowling Resistivity in the Weakly-Ionized Chromosphere

Mehmet Sarp **Yalim**, Avijeet Prasad, Nikolai Pogorelov, Gary Zank, Qiang Hu

ApJL **899** L4 **2020**

https://arxiv.org/pdf/2007.12275.pdf

https://doi.org/10.3847/2041-8213/aba69a

The physics of the solar chromosphere is complex from both theoretical and modeling perspectives. The plasma temperature from the photosphere to corona increases from ~5,000 K to ~1 million K over a distance of only ~10,000 km from the chromosphere and the transition region. Certain regions of the solar atmosphere have sufficiently low temperature and ionization rates to be considered as weakly-ionized. In particular, this is true at the lower chromosphere. As a result, the Cowling resistivity is orders of magnitude greater than the Coulomb resistivity. Ohm's law therefore includes anisotropic dissipation. To evaluate the Cowling resistivity, we need to know the external magnetic field strength and to estimate the neutral fraction as a function of the bulk plasma density and temperature. In this study, we determine the magnetic field topology using the non-force-free field (NFFF) extrapolation technique based on SDO/HMI SHARP vector magnetogram data, and the stratified density and temperature profiles from the Maltby-M umbral core model for sunspots. We investigate the variation and effects of Cowling resistivity on heating and magnetic reconnection in the chromosphere as the flare-producing active region (AR) 11166 evolves. In particular, we analyze a C2.0 flare emerging from AR11166 and find a normalized reconnection rate of 0.051. **2011- 03-07-10**

A data-driven MHD model of the weakly-ionized chromosphere

Mehmet Sarp **Yalim**, Avijeet Prasad, Nikolai Pogorelov, Gary Zank, Qiang Hu

Journal of Physics Conference Series - Proceedings of the 19th Annual International Astrophysics **2020**

https://arxiv.org/pdf/2007.12361.pdf

The physics of the solar chromosphere is complex from both theoretical and modeling perspectives. The plasma temperature from the photosphere to corona increases from ~5,000 K to ~1 million K over a distance of only ~10,000 km from the chromosphere and the transition region. Certain regions of the solar atmosphere have sufficiently low temperature and ionization rates to be considered as weakly-ionized. In particular, this is true at the lower chromosphere. In this paper, we present an overview of our data-driven magnetohydrodynamics model for the weakly-ionized chromosphere and show a benchmark result. It utilizes the Cowling resistivity which is orders of magnitude greater than the Coulomb resistivity. Ohm's law therefore includes anisotropic dissipation. We investigate the effects of the Cowling resistivity on heating and magnetic reconnection in the chromosphere as the flare-producing active region (AR) 11166 evolves. In particular, we analyze a C2.0 flare emerging from AR11166 and find a normalized reconnection rate of 0.12. **2011- 03-07-10**

Forecasting Solar Cycle 25 with a Principled Bayesian Two-stage Statistical Model

Youwei **Yan**1, David C. Stenning1, Vinay L. Kashyap2, and Yaming Yu3

2021 Res. Notes AAS 5 192

https://iopscience.iop.org/article/10.3847/2515-5172/ac1ea0

https://doi.org/10.3847/2515-5172/ac1ea0

We update the Bayesian analysis of sunspot numbers (SSNs) developed by Yu et al. prior to the peak of Solar Cycle 24 to account for the recalibration of the SSN index. We show that the model yields an accurate hindcast of Cycle

24 with the revised SSN, and use the data acquired since then to predict the strength and peak of Cycle 25. We predict the behavior of Cycle 25 to be moderate to weak, with a peak SSN of 120±27 to occur c. 2025 July (±7 months).

Research progress based on observations of the New Vacuum Solar Telescope Review

Xiaoli **Yan**, Zhong Liu, Jun Zhang, Zhi Xu
SCIENCE CHINA Technological Sciences **2019**
https://arxiv.org/pdf/1910.09127.pdf

The purpose of this paper is to introduce the main scientific results made by the one-meter New Vacuum Solar Telescope (NVST), which was put into commission on 2010. NVST is one of the large aperture solar telescopes in the world, located on the shore of Fuxian lake of Yunnan province in China, aiming at serving solar physicists by providing them with high resolution photospheric and chromospheric observational data. Based on the data from NVST and complementary observations from space (e.g., Hinode, SDO and IRIS, etc), dozens of scientific papers have been published with a wide range of topics concentrating mainly on dynamics and activities of fine-scale magnetic structures and their roles in the eruptions of active-region filaments and flares. The achievements include dynamic characteristics of photospheric bright points, umbral dots, penumbral waves, and sunspot/light bridge oscillation, observational evidence of small-scale magnetic reconnection, and fine-scale dynamic structure of prominences. All these new results will shed light on the better understanding of solar eruptive activities. Data release, observation proposals, and future research subjects are introduced and discussed.
Bright points. Umbral dot, penumbral wave. Sunspot light bridge. Formation, fine-scale structures, and eruption mechanism of solar filaments. Fine structure of solar prominences. Filament formation. Magnetic structures of active-region filaments. Filament eruption. Small-scale magnetic reconnection in the solar eruptions. Release of twist in a filament by magnetic reconnection. Interchange magnetic reconnection between a filament and nearby open fields. Magnetic reconnection between a twisted arch filament system and coronal loops. Magnetic reconnection between two active-region filaments. Oscillatory magnetic reconnection. Small-scale eruptive activities. Mini-filaments and jets. Formation and trigger mechanism of solar flares

SELF-ABSORPTION IN THE SOLAR TRANSITION REGION

Limei **Yan**1,2, Hardi Peter2, Jiansen He1, Hui Tian3, Lidong Xia4, Linghua Wang1, Chuanyi Tu1, Lei Zhang1, Feng Chen2, and Krzysztof Barczynski2
2015 ApJ 811 48

Transient brightenings in the transition region of the Sun have been studied for decades and are usually related to magnetic reconnection. Recently, absorption features due to chromospheric lines have been identified in transition region emission lines raising the question of the thermal stratification during such reconnection events. We analyze data from the Interface Region Imaging Spectrograph in an emerging active region. Here the spectral profiles show clear self-absorption features in the transition region lines of Si iv. While some indications existed that opacity effects might play some role in strong transition region lines, self-absorption has not been observed before. We show why previous instruments could not observe such self-absorption features, and discuss some implications of this observation for the corresponding structure of reconnection events in the atmosphere. Based on this we speculate that a range of phenomena, such as explosive events, blinkers or Ellerman bombs, are just different aspects of the same reconnection event occurring at different heights in the atmosphere.

Combined Surface Flux Transport and Helioseismic Far-side Active Region Model (FARM)

Dan **Yang**, Stephan G. Heinemann, Robert H. Cameron, Laurent Gizon
Solar Phys. **2024**
https://arxiv.org/pdf/2411.18701

Maps of the magnetic field at the Sun's surface are commonly used as boundary conditions in space-weather modeling. However, continuous observations are only available from the Sun's Earth-facing side. One commonly used approach to mitigate the lack of far-side information is to apply a surface flux transport (SFT) model to model the evolution of the magnetic field as the Sun rotates. Helioseismology can image active regions on the far side using acoustic oscillations, and hence has the potential to improve the modeled surface magnetic field. In this study, we propose a novel approach for estimating magnetic fields of active regions on the Sun's far side based on seismic measurements, and then include them into a SFT model. To calibrate seismic signal to magnetic field, we apply our SFT model to line-of-sight magnetograms from SDO/HMI to obtain reference maps of global magnetic fields. The resulting maps are compared with seismic maps on the Sun's far side computed using helioseismic holography. The spatial structure of the magnetic field within an active region is reflected in the spatial structure of seismic phase shifts. We assign polarities to the unipolar magnetic-field concentrations based on Hale's law and require approximate flux balance between the two polarities. From 2010 to 2024, we modeled 859 active regions, with an average total unsigned flux of 7.84·1021 Mx and an average area of 4.48·1010 km2. Approximately 4.2% of the active regions were found to have an anti-Hale configuration, which we manually corrected. Comparisons between modeled open-field areas and EUV observations reveal a substantial improvement in agreement when far-side active

regions are included. This proof of concept study demonstrates the potential of the ``combined surface flux transport and helioseismic Far-side Active Region Model" (FARM) to improve space-weather modeling. **19 May – 16 June 2010, 25 Mar- 5 Apr 2013, 17 Apr 2013, 3-15 Oct 2013**

Combined Surface Flux Transport and Helioseismic Far-Side Active Region Model (FARM).

Yang, D., Heinemann, S.G., Cameron, R.H. et al.
Sol Phys 299, 161 (**2024**).
https://doi.org/10.1007/s11207-024-02405-9
https://link.springer.com/content/pdf/10.1007/s11207-024-02405-9.pdf
Maps of the magnetic field at the Sun's surface are commonly used as boundary conditions in space-weather modeling. However, continuous observations are only available from the Earth-facing part of the Sun's surface. One commonly used approach to mitigate the lack of far-side information is to apply a surface flux transport (SFT) model to model the evolution of the magnetic field as the Sun rotates. Helioseismology can image active regions on the far side using acoustic oscillations and hence has the potential to improve the modeled surface magnetic field. In this study, we propose a novel approach for estimating magnetic fields of active regions on the Sun's far side based on seismic measurements and then include them into an SFT model. To calibrate the conversion from helioseismic signal to magnetic field, we apply our SFT model to line-of-sight magnetograms from Helioseismic and Magnetic Imager (HMI) on board the Solar Dynamics Observatory (SDO) to obtain reference maps of global magnetic fields (including the far side). The resulting magnetic maps are compared with helioseismic phase maps on the Sun's far side computed using helioseismic holography. The spatial structure of the magnetic field within an active region is reflected in the spatial structure of the helioseismic phase shifts. We assign polarities to the unipolar magnetic-field concentrations based upon Hale's law and require approximate flux balance between the two polarities. From 2010 to 2024, we modeled 859 active regions, with an average total unsigned flux of 7.84·1021 Mx and an average area of 4.48·1010 km2. Approximately 4.2% of the active regions were found to have an anti-Hale configuration, which we manually corrected. Including these far-side active regions resulted in an average increase of 1.2% (up to 25.3%) in the total unsigned magnetogram flux. Comparisons between modeled open-field areas and EUV observations reveal a substantial improvement in agreement when far-side active regions are included. This proof of concept study demonstrates the potential of the "combined surface flux transport and helioseismic Far-side Active Region Model" (FARM) to improve space-weather modeling.

Meridional Flow in the Solar Polar Caps Revealed by Magnetic Field Observation and Simulation

Shuhong **Yang**1,2,7, Jie Jiang3, Zifan Wang1,2,7, Yijun Hou1,2,7, Chunlan Jin1,2,7, Qiao Song4,6, Yukun Luo3, Ting Li1,2,7, Jun Zhang5, Yuzong Zhang1,2,7Show full author list
2024 ApJ 970 183
https://iopscience.iop.org/article/10.3847/1538-4357/ad61e2/pdf
As a large-scale motion on the Sun, the meridional flow plays an important role in determining magnetic structure and strength and solar cycle. However, the meridional flow near the solar poles is still unclear. The Hinode observations show that the magnetic flux density in polar caps decreases from the lower latitudes to the poles. Using a surface flux transport model, we simulate the global radial magnetic field to explore the physical process leading to the observed polar magnetic distribution pattern. For the first time, the high-resolution observations of the polar magnetic fields observed by Hinode are used to directly constrain the simulation. Our simulation reproduces the observed properties of the polar magnetic fields, suggesting the existence of a counter-cell meridional flow in the solar polar caps with a maximum amplitude of about 3 m s−1.
HMI Science Nuggets #204 **2024** http://hmi.stanford.edu/hminuggets/?p=4292

Long-term variation of the solar polar magnetic fields at different latitudes

Shuhong **Yang**1,2,7 , Jie Jiang3 , Zifan Wang1,2,7 , Yijun Hou1,2,7 , Chunlan Jin1,2,7 +++
Research in Astron. Astrophys. **2024** Vol. 24 No. 7, 075015
https://arxiv.org/pdf/2408.15168
The polar magnetic fields of the Sun play an important role in governing solar activity and powering fast solar wind. However, because our view of the Sun is limited in the ecliptic plane, the polar regions remain largely uncharted. Using the high spatial resolution and polarimetric precision vector magnetograms observed by Hinode from 2012 to 2021, we investigate the long-term variation of the magnetic fields in polar caps at different latitudes. The Hinode magnetic measurements show that the polarity reversal processes in the north and south polar caps are non-simultaneous. The variation of the averaged radial magnetic flux density reveals that, in each polar cap, the polarity reversal is completed successively from the 70° latitude to the pole, reflecting a poleward magnetic flux migration therein. These results clarify the polar magnetic polarity reversal process at different latitudes.
HMI Science Nuggets #204 **2024** http://hmi.stanford.edu/hminuggets/?p=4292

Complexity of emerging magnetic flux during lifetime of solar ephemeral regions

Hanlin **Yang**, Chunlan Jin, Zifan Wang, Jingxiu Wang

ApJ **2024**

https://arxiv.org/pdf/2403.18979.pdf

As a relatively active region, ephemeral region (ER) exhibits highly complex pattern of magnetic flux emergence. We aim to study detailed secondary flux emergences (SFEs) which we define as bipoles that they appear close to ERs and finally coalesce with ERs after a period. We study the SFEs during the whole process from emergence to decay of 5 ERs observed by the Helioseismic and Magnetic Imager (HMI) aboard Solar Dynamics Observatory (SDO) . The maximum unsigned magnetic flux for each ER is around 1020 Mx. Each ER has tens of SFEs with an average emerging magnetic flux of approximately 5×1018 Mx. The frequency of normalized magnetic flux for all the SFEs follows a power law distribution with an index of -2.08 . The majority of SFEs occur between the positive and negative polarities of ER , and their growth time is concentrated within one hour. The magnetic axis of SFE is found to exhibit a random distribution in the 5 ERs. We suggest that the relationship between SFEs and ERs can be understood by regarding the photospheric magnetic field observations as cross-sections of an emerging magnetic structure. Tracking the ERs' evolution, we propose that these SFEs in ERs may be sequent emergences from the bundle of flux tube of ERs, and that SFEs are partially emerged Ω-loops.

Direct assessment of SDO/HMI helioseismology of active regions on the Sun's far side using SO/PHI magnetograms

D. **Yang**, L. Gizon, H. Barucq, J. Hirzberger, D. Orozco Suárez, +++

A&A 674, A183 **2023**

https://arxiv.org/pdf/2305.01594.pdf

https://www.aanda.org/articles/aa/pdf/2023/06/aa46030-23.pdf

Earth-side observations of solar p modes can be used to image and monitor magnetic activity on the Sun's far side. Here we use magnetograms of the far side obtained by the Polarimetric and Helioseismic Imager (PHI) onboard Solar Orbiter (SO) to directly assess -- for the first time -- the validity of far-side helioseismic holography. We wish to co-locate the positions of active regions in helioseismic images and magnetograms, and to calibrate the helioseismic measurements in terms of magnetic field strength. We identify three magnetograms on 18 November 2020, 3 October 2021, and 3 February 2022 displaying a total of six active regions on the far side. The first two dates are from SO's cruise phase, the third from the beginning of the nominal operation phase. We compute contemporaneous seismic phase maps for these three dates using helioseismic holography applied to time series of Dopplergrams from the Helioseismic and Magnetic Imager (HMI) on the Solar Dynamics Observatory (SDO). Among the six active regions seen in SO/PHI magnetograms, five active regions are identified on the seismic maps at almost the same positions as on the magnetograms. One region is too weak to be detected above the seismic noise. To calibrate the seismic maps, we fit a linear relationship between the seismic phase shifts and the unsigned line-of-sight magnetic field averaged over the active region areas extracted from the SO/PHI magnetograms. SO/PHI provides the strongest evidence so far that helioseismic imaging provides reliable information about active regions on the far side, including their positions, areas, and mean unsigned magnetic field.

Solar Orbiter nugget #9 2023 https://www.cosmos.esa.int/web/solar-orbiter/science-nuggets/far-side-helioseismology-using-sophi

Imaging individual active regions on the Sun's far side with improved helioseismic holography

Dan **Yang**, Laurent Gizon, Hélène Barucq

A&A **2022**

https://arxiv.org/pdf/2211.07219.pdf

Helioseismic holography is a useful method to detect active regions on the Sun's far side and improve space weather forecasts. We aim to improve helioseismic holography by using a clear formulation of the problem, an accurate forward solver in the frequency domain, and a better understanding of the noise properties. Building on the work of Lindsey et al., we define the forward- and backward-propagated wave fields (ingression and egression) in terms of a Green's function. This Green's function is computed using an accurate forward solver in the frequency domain. We analyse overlapping segments of 31 hr of SDO/HMI dopplergrams, with a cadence of 24 hr. Phase shifts between the ingression and the egression are measured and averaged to detect active regions on the far side. The phase maps are compared with direct EUV intensity maps from STEREO/EUVI. We confirm that medium-size active regions can be detected on the far side with high confidence. Their evolution (and possible emergence) can be monitored on a daily time scale. Seismic maps averaged over 3 days provide an active region detection rate as high as 75% and a false discovery rate only as low as 7%, for active regions with areas above one thousandth of an hemisphere. For a large part, these improvements can be attributed to the use of a complete Green's function (all skips) and to the use

of all observations on the front side (full pupil). Improved helioseismic holography enables the study of the evolution of medium-size active regions on the Sun's far side.

Rotating Solar Models in Agreement with Helioseismic Results and Updated Neutrino Fluxes

Wuming **Yang**

ApJ **939** 61 **2022**

https://arxiv.org/pdf/2209.13483

https://iopscience.iop.org/article/10.3847/1538-4357/ac94cd/pdf

Standard solar models (SSMs) constructed in accordance with old solar abundances are in reasonable agreement with seismically inferred results, but SSMs with new low-metal abundances disagree with the seismically inferred results. The constraints of neutrino fluxes on solar models exist in parallel with those of helioseismic results. The solar neutrino fluxes were updated by Borexino Collaboration. We constructed rotating solar models with new low-metal abundances where the effects of enhanced diffusion and convection overshoot were included. A rotating model using OPAL opacities and the Caffau abundance scale has better sound-speed and density profiles than the SSM with the old solar abundances and reproduces the observed p-mode frequency ratios r02 and r13. The depth and helium abundance of the convection zone of the model agree with the seismically inferred ones at the level of 1σ. The updated neutrino fluxes are also reproduced by the model at the level of 1σ. The effects of rotation and enhanced diffusion not only improve the model's sound-speed and density profiles but bring the neutrino fluxes predicted by the model into agreement with the detected ones. Moreover, the calculations show that OP may underestimate opacities for the regions of the Sun with $T \gtrsim 5\times106$ K by around 1.5%, while OPAL may underestimate opacities for the regions of the Sun with 2×106 K $\lesssim T \lesssim 5\times106$ K by about 1−2%.

Relative Magnetic Helicity Based on a Periodic Potential Field

Kai E. **Yang**, Michael S. Wheatland, Stuart A. Gilchrist

ApJ **894** 151 **2020**

https://arxiv.org/pdf/2004.08590.pdf

https://doi.org/10.3847/1538-4357/ab8810

Magnetic helicity is conserved under ideal magnetohydrodynamics (MHD) and quasi-conserved even under a resistive process. The standard definition for magnetic helicity cannot be applied directly to an open magnetic field in a volume, because it is gauge-dependent. Instead, the relative magnetic helicity is widely used. We find that the energy of a potential magnetic field in a rectangular domain with periodic lateral boundary conditions is less than that of the field with a fixed normal component on all six boundaries. To make use of this lower energy potential field in the analysis of relative magnetic helicity, we introducing a new definition for magnetic helicity for the magnetic field, which involves the periodic potential field. We apply this definition to a sequence of analytic solutions and a numerical simulation. The results show that our new gauge-invariant helicity is very close to the current-carrying part of the relative magnetic helicity of the original magnetic field. We find also that the ratio between the current-carrying helicity and the relative magnetic helicity for the original and our defined relative helicity show different behavior. It seems that the new helicity is more sensitive to the component of the field due to the electric current in the volume, which is the source for instabilities and solar eruptive phenomena.

The origin and effect of hemispheric helicity imbalance in solar dynamo

S. **Yang**, V.V. Pipin, D.D. Sokoloff, K.M. Kuzanyan, H. Zhang

J. Plasma Phys. **2020**

https://arxiv.org/pdf/1912.11285.pdf

In this paper we study the effects of hemispheric imbalance of magnetic helicity density on breaking the equatorial reflection symmetry of the dynamo generated large-scale magnetic field. Our study employs the axisymmetric dynamo model which takes into account the nonlinear effect of magnetic helicity conservation. We find that the evolution of the net magnetic helicity density, in other words, the magnetic helicity imbalance, on the surface follows the evolution of the parity of the large-scale magnetic field. Random fluctuations of the α-effect and the helicity fluxes can inverse the causal relationship, i.e., the magnetic helicity imbalance or the imbalance of magnetic helicity fluxes can drive the magnetic parity breaking. We also found that evolution of the net magnetic helicity of the small-scale fields follows the evolution of the net magnetic helicity of the large-scale fields with some time lag. We interpret this as an effect of the difference of the magnetic helicity fluxes out of the Sun from the large and small scales.

Light Bridge Brightening and Plasma Ejection Driven by a Magnetic Flux Emergence Event

Xu **Yang**1,2, Vasyl Yurchyshyn2, Kwangsu Ahn2, Matt Penn3, and Wenda Cao

2019 ApJ 886 64

sci-hub.se/10.3847/1538-4357/ab4a7d
Observations with the Goode Solar Telescope (GST) are presented here showing that the emergence of 1.91 × 1018 Mx of new magnetic flux occurred at the edge of a filamentary light bridge (LB). This emergence was accompanied by brightness enhancement of a photospheric overturning convection cell (OCC) at the endpoints of the emerging magnetic structure. We present an analysis of the origin and the dynamics of this event using high-resolution GST Fe i 1564.85 nm vector magnetic field data, TiO photospheric, and Hα chromospheric images. The emerged structure was 1.5 × 0.3 Mm in size at the peak of development and lasted for 17 minutes. Doppler observations showed presence of systematic upflows before the appearance of the magnetic field signal and downflows during the decay phase. Changes in the orientation of the associated transverse fields, determined from the differential angle, suggest the emergence of a twisted magnetic structure. A fan-shaped jet was observed to be spatially and temporally correlated with the endpoint of the OCC intruding into the LB. Our data suggest that the emerging fields may have reconnected with the magnetic fields in the vicinity of the LB, which could lead to the formation of the jet. Our observation is the first report of flux emergence within a granular LB with evidence in the evolution of vector magnetic field, as well as photosphere convection motions, and supports the idea that the impulsive jets above the LB are caused by magnetic reconnection. **2016 February 9**

Chromospheric cannonballs on the Sun

Shuhong **Yang**, Jun Zhang, Xiaohong Li, Zhong Liu, Yongyuan Xiang
ApJL **880** L24 **2019**
https://arxiv.org/pdf/1906.10850.pdf
https://iopscience.iop.org/article/10.3847/2041-8213/ab2fe2/pdf
In the highly dynamic chromosphere, there exist many kinds of small-scale activities, such as spicules, surges, and Ellerman bombs. Here, we report the discovery of a new phenomenon in the chromosphere observed with the New Vacuum Solar Telescope at the Fuxian Solar Observatory. In the high tempo-spatial resolution Hα images, some dark or bright structures are found to fly along the curved trajectory, looking like cannonballs. Their average size, mass, and velocity are about 1.5 × 109 km3, 1.5 × 108 kg, and 56 km s−1, respectively. In the simultaneous (extreme-)ultraviolet images obtained by the Solar Dynamics Observatory, these cannonballs appear as brighter features compared to the surrounding area, implying that there exists some kind of heating during this process. The photospheric magnetograms show the magnetic flux emergence and interaction with the pre-existing fields. These observations reveal that the cannonballs are chromospheric material blobs launched due to the magnetic reconnection between emerging magnetic flux and the pre-existing loops. **2017 August 06, 2017 October 28, 2018 May 11**

Rotating Solar Models with Low Metal Abundances as Good as Those with High Metal Abundances

Wuming **Yang**
ApJ **873** 18 **2019**
https://arxiv.org/pdf/1901.11290.pdf
Standard solar models (SSM) constructed in accord with low metal abundances disagree with the seismically inferred results. We constructed rotating solar models with low metal abundances that included enhanced settling and convection overshoot. In one of our rotating models, \textbf{AGSSr2a}, the convection overshoot allowed us to recover the radius of the base of convection zone (CZ) at a level of 1σ. The rotational mixing almost completely counteracts the enhanced settling for the surface helium abundance, but only partially for the surface heavy-element abundance. At the level of 1σ, the combination of rotation and enhanced settling brings the surface helium abundance into agreement with the seismically inferred value of 0.2485±0.0035, and makes the model have better sound-speed and density profiles than SSM constructed in accordance with high metal abundances. The radius of the base of the CZ and the surface helium abundance of \textbf{AGSSr2a} are 0.713 R⊙ and 0.2472, respectively; the absolute values of the relative differences in sound speed and density between it and the Sun are less than 0.0025 and 0.015, respectively. Moreover, predicted neutrino fluxes of our model are comparable with the predictions of previous research works.

Observational Evidence of Magnetic Reconnection Associated with Magnetic Flux Cancellation

Bo **Yang**1,2,3, Jiayan Yang1,2, Yi Bi1,2, Junchao Hong1,2, Haidong Li1,2, Zhe Xu1,2,4, and Hechao Chen
2018 ApJ 861 135 DOI 10.3847/1538-4357/aac37f
Using high spatial and temporal data from the Solar Dynamics Observatory (SDO) and the Interface Region Imaging Spectrograph (IRIS), several observational signatures of magnetic reconnection in the course of magnetic flux cancellation are presented, including two loop–loop interaction processes, multiple plasma blob ejections, and a sheet-like structure that appeared above the flux cancellation sites with a Y-shaped and an inverted Y-shaped end. The IRIS 1400 Å observations show that the plasma blobs were ejected from the tip of the Y-shaped ends of the

sheet-like structure. Obvious photospheric magnetic flux cancellation occurred after the first loop–loop interaction and continued until the end of the observation. Complemented by the nonlinear force-free field extrapolation, we found that two sets of magnetic field lines, which revealed an X-shaped configuration, aligned well with the interacted coronal loops. Moreover, a magnetic null point was found to be situated at about 0.9 Mm height, which was right above the flux cancellation sites and located between the two sets of magnetic field lines. These results suggest that the flux cancellation might be a result of the submergence of magnetic field lines following a magnetic reconnection that occurs in the lower atmosphere of the Sun, and the ejected plasma blobs should be plasmoids created in the sheet-like structure due to the tearing-mode instability. This observation reveals a detailed magnetic field structure and a dynamic process above the flux cancellation sites and will help us to understand magnetic reconnection in the lower atmosphere of the Sun.

Observationally quantified reconnection providing a viable mechanism for active region coronal heating

Kai E. **Yang**, Dana W. Longcope, M. D. Ding & Yang Guo
Nature Communications volume 9, Article number: 692 (**2018**)
https://www.nature.com/articles/s41467-018-03056-8.pdf
The heating of the Sun's corona has been explained by several different mechanisms including wave dissipation and magnetic reconnection. While both have been shown capable of supplying the requisite power, neither has been used in a quantitative model of observations fed by measured inputs. Here we show that impulsive reconnection is capable of producing an active region corona agreeing both qualitatively and quantitatively with extreme-ultraviolet observations. We calculate the heating power proportional to the velocity difference between magnetic footpoints and the photospheric plasma, called the non-ideal velocity. The length scale of flux elements reconnected in the corona is found to be around 160 km. The differential emission measure of the model corona agrees with that derived using multi-wavelength images. Synthesized extreme-ultraviolet images resemble observations both in their loop-dominated appearance and their intensity histograms. This work provides compelling evidence that impulsive reconnection events are a viable mechanism for heating the corona. **11 Feb 2012**
HMI Science Nuggets, #**100**, June **2018** http://hmi.stanford.edu/hminuggets/?p=2495

Automated Segmentation of High-Resolution Photospheric Images of Active Regions

Meng **Yang**, Yu Tian, Changhui Rao
Solar Physics February **2018**, 293:15
https://link.springer.com/content/pdf/10.1007%2Fs11207-017-1236-7.pdf
Due to the development of ground-based, large-aperture solar telescopes with adaptive optics (AO) resulting in increasing resolving ability, more accurate sunspot identifications and characterizations are required. In this article, we have developed a set of automated segmentation methods for high-resolution solar photospheric images. Firstly, a local-intensity-clustering level-set method is applied to roughly separate solar granulation and sunspots. Then reinitialization-free level-set evolution is adopted to adjust the boundaries of the photospheric patch; an adaptive intensity threshold is used to discriminate between umbra and penumbra; light bridges are selected according to their regional properties from candidates produced by morphological operations. The proposed method is applied to the solar high-resolution TiO 705.7-nm images taken by the 151-element AO system and Ground-Layer Adaptive Optics prototype system at the 1-m New Vacuum Solar Telescope of the Yunnan Observatory. Experimental results show that the method achieves satisfactory robustness and efficiency with low computational cost on high-resolution images. The method could also be applied to full-disk images, and the calculated sunspot areas correlate well with the data given by the National Oceanic and Atmospheric Administration (NOAA). **2015-07-08, 12 Jan. 2016, 07 Oct. 2016**

Ghost Images in Helioseismic Holography? Toy Models in a Uniform Medium

Dan **Yang**
Solar Physics 293:17 **2018**
https://arxiv.org/pdf/1801.01759.pdf
https://link.springer.com/content/pdf/10.1007%2Fs11207-018-1246-0.pdf
Helioseismic holography is a powerful technique used to probe the solar interior based on estimations of the 3D wavefield. Porter--Bojarski holography, which is a well-established method used in acoustics to recover sources and scatterers in 3D, is also an estimation of the wavefield, and hence it has the potential to be applied to helioseismology. Here we present a proof of concept study, where we compare helioseismic holography and Porter--Bojarski holography under the assumption that the waves propagate in a homogeneous medium. We consider the problem of locating a point source of wave excitation inside a sphere. Under these assumptions, we find that the two imaging methods have the same capability of locating the source, with the exception that helioseismic holography suffers from "ghost images" (i.e., artificial peaks away from the source location). We conclude that Porter--Bojarski holography may improve the current method used in helioseismology.

Formation of Cool and Warm Jets by Magnetic Flux Emerging from the Solar Chromosphere to Transition Region

Liping **Yang**1,2,3, Hardi Peter4, Jiansen He2,3, Chuanyi Tu2, Linghua Wang2, Lei Zhang1, and Limei Yan2

2018 ApJ 852 16

In the solar atmosphere, jets are ubiquitous at various spatial-temporal scales. They are important for understanding the energy and mass transports in the solar atmosphere. According to recent observational studies, the high-speed network jets are likely to be intermittent but continual sources of mass and energy for the solar wind. Here, we conduct a 2D magnetohydrodynamics simulation to investigate the mechanism of these network jets. A combination of magnetic flux emergence and horizontal advection is used to drive the magnetic reconnection in the transition region between a strong magnetic loop and a background open flux. The simulation results show that not only a fast warm jet, much similar to the network jets, is found, but also an adjacent slow cool jet, mostly like classical spicules, is launched. Differing from the fast warm jet driven by magnetic reconnection, the slow cool jet is mainly accelerated by gradients of both thermal pressure and magnetic pressure near the outer border of the mass-concentrated region compressed by the emerging loop. These results provide a different perspective on our understanding of the formation of both the slow cool jets from the solar chromosphere and the fast warm jets from the solar transition region.

Evolution of Relative Magnetic Helicity: New Boundary Conditions for the Vector Potential

Shangbin **Yang**, Joerg Buechner, Jan Skala, Hongqi Zhang

A&A **2017**

https://arxiv.org/pdf/1712.09219.pdf

We recently proposed a method to calculate the relative magnetic helicity in a finite volume for a given magnetic field which however required the flux to be balanced separately on all the sides of the considered volume. In order to allow finite magnetic fluxes through the boundaries, a Coulomb gauge is constructed that allows for global magnetic flux balance. We tested and verified our method in a theoretical fore-free magnetic field model. We apply the new method to the former calculation data and found a difference of less than 1.2\%. We also applied our method to the magnetic field above active region NOAA 11429 obtained by a new photospheric-data-driven MHD model code GOEMHD3. We analyzed the magnetic helicity evolution in the solar corona using our new method. It was found that the normalized magnetic helicityis equal to -0.038 when fast magnetic reconnection is triggered. This value is comparable to the previous value (-0.029) in the MHD simulations when magnetic reconnection happened and the observed normalized magnetic helicity (-0.036) from the eruption of newly emerging active regions. We found that only 8\% of the accumulated magnetic helicity is dissipated after it is injected through the bottom boundary. This is in accordance with the Woltjer conjecture. Only 2\% of magnetic helicity injected from the bottom boundary escapes through the corona. This is consistent with the observation of magnetic clouds, which could take away magnetic helicity into the interplanetary space, in the case considered here, several halo CMEs and two X-class solar flares origin from this active region. **March 07. 2012**

SCATTERING MATRIX FOR THE INTERACTION BETWEEN SOLAR ACOUSTIC WAVES AND SUNSPOTS. I. MEASUREMENTS

Ming-Hsu **Yang**1, Dean-Yi Chou1, and Hui Zhao

2017 ApJ 835 102

Assessing the interaction between solar acoustic waves and sunspots is a scattering problem. The scattering matrix elements are the most commonly used measured quantities to describe scattering problems. We use the wavefunctions of scattered waves of NOAAs 11084 and 11092 measured in the previous study to compute the scattering matrix elements, with plane waves as the basis. The measured scattered wavefunction is from the incident wave of radial order n to the wave of another radial order n', for $n = 0$–5. For a time-independent sunspot, there is no mode mixing between different frequencies. An incident mode is scattered into various modes with different wavenumbers but the same frequency. Working in the frequency domain, we have the individual incident plane-wave mode, which is scattered into various plane-wave modes with the same frequency. This allows us to compute the scattering matrix element between two plane-wave modes for each frequency. Each scattering matrix element is a complex number, representing the transition from the incident mode to another mode. The amplitudes of diagonal elements are larger than those of the off-diagonal elements. The amplitude and phase of the off-diagonal elements are detectable only for $n - 1 \leqslant n' \leqslant n + 1$ and $-3\Delta k \leqslant \delta k_x \leqslant 3\Delta k$, where δk_x is the change in the transverse component of the wavenumber and $\Delta k = 0.035$ rad Mm^{-1}.

Enhancement of a sunspot light wall with external disturbances

Shuhong **Yang**, Jun Zhang, Robert Erdélyi

ApJL 833 L18 **2016**
https://arxiv.org/pdf/1611.10032v1.pdf
Based on the \emph{Interface Region Imaging Spectrograph} observations, we study the response of a solar sunspot light wall to external disturbances. A flare occurrence near the light wall caused material to erupt from the lower solar atmosphere into the corona. Some material falls back to the solar surface, and hits the light bridge (i.e., the base of the light wall), then sudden brightenings appear at the wall base followed by the rise of wall top, leading to an increase of the wall height. Once the brightness of the wall base fades, the height of the light wall begins to decrease. Five hours later, another nearby flare takes place, a bright channel is formed that extends from the flare towards the light bridge. Although no obvious material flow along the bright channel is found, some ejected material is conjectured to reach the light bridge. Subsequently, the wall base brightens and the wall height begins to increase again. Once more, when the brightness of the wall base decays, the wall top fluctuates to lower heights. We suggest, based on the observed cases, that the interaction of falling material and ejected flare material with the light wall results in the brightenings of wall base and causes the height of the light wall to increase. Our results reveal that the light wall can be not only powered by the linkage of \emph{p}-mode from below the photosphere, but may also be enhanced by external disturbances, such as falling material.

FINE-SCALE PHOTOSPHERIC CONNECTIONS OF ELLERMAN BOMBS

Heesu **Yang**1, Jongchul Chae1, Eun-Kyung Lim2, Donguk Song1, Kyuhyoun Cho1, Hannah Kwak1, Vasyl B Yurchyshyn3, and Yeon-Han Kim2
2016 ApJ 829 100
We investigate the photospheric and magnetic field structures associated with Ellerman bombs (EBs) using the 1.6 m New Solar Telescope at Big Bear Solar Observatory. The nine observed EBs were accompanied by elongated granule-like features (EGFs) that showed transverse motions prior to the EBs with an average speed of about 3.8 km s−1. Each EGF consisted of a sub-arcsecond bright core encircled by a dark lane around its moving front. The bright core appeared in the TiO broadband filter images and in the far wings of the Hα and Ca ii 8542 Å lines. In four EBs, the bi-directional expanding motion of the EGFs was identified in the TiO images. In those cases, the EGFs were found to be accompanied by an emerging flux (EF). In four other EBs, the EGF developed at the edge of a penumbra and traveled in the sunspot's radial direction. The EGFs in these cases were identified as a moving magnetic feature (MMF). Our results show a clear connection among the magnetic elements, photospheric features, and EBs. This result suggests that the EBs result from magnetic reconnection forced by EFs or MMFs that are frequently manifested by EGFs.

Magnetic-reconnection Generated Shock Waves as a Driver of Solar Surges

Heesu **Yang**1, Jongchul Chae1, Eun-Kyung Lim2, Kyoung-sun Lee3, Hyungmin Park1, Dong-uk Song1, and Kyuhyoun Cho
2014 ApJ 790 L4
We found that a surge consists of multiple shock features. In our high-spatiotemporal spectroscopic observation of the surge, each shock is identified with the sudden appearance of an absorption feature at the blue wings of the Ca II 8542 Å line and Hα line that gradually shifts to the red wings. The shock features overlap with one another with the time interval of 110 s, which is much shorter than the duration of each shock feature, 300-400 s. This finding suggests that the multiple shocks might not have originated from a train of sinusoidal waves generated by oscillations and flows in the photosphere. As we found the signature of the magnetic flux cancelations at the base of the surge, we conclude that the multiple shock waves in charge of the surge were generated by the magnetic reconnection that occurred in the low atmosphere in association with the flux cancelation.

Simulation of the Unusual Solar Minimum with 3D SIP-CESE MHD Model by Comparison with Multi-Satellite Observations

Liping **Yang**, Xueshang Feng, Changqing Xiang, Shaohua Zhang and S. T. Wu
Solar Physics, Volume 271, Numbers 1-2, 91-110, **2011**
The observations both near the Sun and in the heliosphere during the activity minimum between solar cycles 23 and 24 exhibit different phenomena from those typical of the previous solar minima. In this paper, we have chosen Carrington rotation 2070 in 2008 to investigate the properties of the background solar wind by using the three-dimensional (3D) Solar–InterPlanetary Conservation Element/Solution Element Magnetohydrodynamic (MHD) model. We also study the effects of polar magnetic fields on the characteristics of the solar corona and the solar wind by conducting simulations with an axisymmetric polar flux added to the observed magnetic field. The numerical results are compared with the observations from multiple satellites, such as the Solar and Heliospheric Observatory (SOHO), Ulysses, Solar Terrestrial Relations Observatory (STEREO), Wind and the Advanced Composition Explorer (ACE). The comparison demonstrates that the first simulation with the observed magnetic

fields reproduces some observed peculiarities near the Sun, such as relatively small polar coronal holes, the presence of mid- and low-latitude holes, a tilted and warped current sheet, and the broad multiple streamers. The numerical results also capture the inconsistency between the locus of the minimum wind speed and the location of the heliospheric current sheet, and predict slightly slower and cooler polar streams with a relatively smaller latitudinal width, broad low-latitude intermediate-speed streams, and globally weak magnetic field and low density in the heliosphere. The second simulation with strengthened polar fields indicates that the weak polar fields in the current minimum play a crucial role in determining the states of the corona and the solar wind.

Investigations of Sizes and Dynamical Motions of Solar Photospheric Granules by a Novel Granular Segmenting Algorithm

Liu **Yanxiao**1, Jiang Chaowei1, Yuan Ding1, Zuo Pingbing1, Wang Yi1, and Cao Wenda2,3
2021 ApJ 923 133
https://doi.org/10.3847/1538-4357/ac2dfd
Granules observed in the solar photosphere are believed to be convective and turbulent, but the physical picture of the granular dynamical process remains unclear. Here we performed an investigation of granular dynamical motions of full length scales based on data obtained by the 1 m New Vacuum Solar Telescope and the 1.6 m Goode Solar Telescope. We developed a new granule segmenting method, which can detect both small faint and large bright granules. A large number of granules were detected, and two critical sizes, 265 and 1420 km, were found to separate the granules into three length ranges. The granules with sizes above 1420 km follow Gaussian distribution, and demonstrate flat in flatness function, which shows that they are non-intermittent and thus are dominated by convective motions. Small granules with sizes between 265 and 1420 km are fitted by a combination of power-law function and Gauss function, and exhibit nonlinearity in flatness function, which reveals that they are in the mixing motions of convection and turbulence. Mini granules with sizes below 265 km follow the power-law distribution and demonstrate linearity in flatness function, indicating that they are intermittent and strongly turbulent. These results suggest that a cascade process occurs: large granules break down due to convective instability, which transports energy into small ones; then turbulence is induced and grows, which competes with convection and further causes the small granules to continuously split. Eventually, the motions in even smaller scales enter in a turbulence-dominated regime.

Surface Flux Transport

Anthony R. **Yeates**, Mark C.M. Cheung, Jie Jiang, Kristof Petrovay, Yi-Ming Wang
Space Science Reviews **2023**
https://arxiv.org/pdf/2303.01209
We review the surface flux transport model for the evolution of magnetic flux patterns on the Sun's surface. Our underlying motivation is to understand the model's prediction of the polar field (or axial dipole) strength at the end of the solar cycle. The main focus is on the "classical" model: namely, steady axisymmetric profiles for differential rotation and meridional flow, and uniform supergranular diffusion. Nevertheless, the review concentrates on recent advances, notably in understanding the roles of transport parameters and - in particular - the source term. We also discuss the physical justification for the surface flux transport model, along with efforts to incorporate radial diffusion, and conclude by summarizing the main directions where researchers have moved beyond the classical model.

Widespread Occurrence of High-Velocity Upflows in Solar Active Regions

S. L. **Yardley**, D. H. Brooks, D. Baker
A&A 650, L10 **2021**
https://arxiv.org/pdf/2106.01396.pdf
https://www.aanda.org/articles/aa/pdf/2021/06/aa41131-21.pdf
https://doi.org/10.1051/0004-6361/202141131
We performed a systematic study of 12 active regions (ARs) with a broad range of areas, magnetic flux and associated solar activity in order to determine whether there are upflows present at the AR boundaries and if these upflows exist, whether there is a high speed asymmetric blue wing component present in the upflows. To identify the presence and locations of the AR upflows we derive relative Doppler velocity maps by fitting a Gaussian function to {\it Hinode}/EIS Fe XII 192.394\,Å line profiles. To determine whether there is a high speed asymmetric component present in the AR upflows we fit a double Gaussian function to the Fe XII 192.394\,Å mean spectrum that is computed in a region of interest situated in the AR upflows. Upflows are observed at both the east and west boundaries of all ARs in our sample with average upflow velocities ranging between -5 to -26~km s−1. A blue wing asymmetry is present in every line profile. The intensity ratio between the minor high speed asymmetric Gaussian component compared to the main component is relatively small for the majority of regions however, in a minority of cases (8/30) the ratios are large and range between 20 to 56~\%. These results suggest that upflows and the high speed asymmetric blue wing component are a common feature of all ARs. **31 Jan 2011, 15 Apr 2011**
Table 1. The NOAA ARs and EIS data used in this study (2010-2011)

Latitude Quenching Nonlinearity in the Solar Dynamo

Anthony R. **Yeates**, Luca Bertello, Alexander A. Pevtsov, Alexei A. Pevtsov
ApJ **2024**
https://arxiv.org/pdf/2412.02312
We compare two candidate nonlinearities for regulating the solar cycle within the Babcock-Leighton paradigm: tilt quenching (whereby the tilt of active regions is reduced in stronger cycles) and latitude quenching (whereby flux emerges at higher latitudes in stronger solar cycles). Digitized historical observations are used to build a database of individual magnetic plage regions from 1923 to 1985. The regions are selected by thresholding in Ca II K synoptic maps, with polarities constrained using Mount Wilson Observatory sunspot measurements. The resulting data show weak evidence for tilt quenching, but much stronger evidence for latitude-quenching. Further, we use proxy observations of the polar field from faculae to construct a best-fit surface flux transport model driven by our database of emerging regions. A better fit is obtained when the sunspot measurements are used, compared to a reference model where all polarities are filled using Hale's Law. The optimization suggests clearly that the "dynamo effectivity range" of the Sun during this period should be less than 10 degrees; this is also consistent with latitude quenching being dominant over tilt quenching.

The Sun's Non-Potential Corona over Solar Cycle 24

Anthony R. **Yeates**
Solar Phys. **299**, 83 **2024**
https://arxiv.org/pdf/2405.14322
https://link.springer.com/content/pdf/10.1007/s11207-024-02328-5.pdf
The global magnetic field in the solar corona is known to contain free magnetic energy and magnetic helicity above that of a current-free (potential) state. But the strength of this non-potentiality and its evolution over the solar cycle remain uncertain. Here we model the corona over Solar Cycle 24 using a simplified magneto-frictional model that retains the magnetohydrodynamic induction equation but assumes relaxation towards force-free equilibrium, driven by solar surface motions and flux emergence. The model is relatively conservative compared to some others in the literature, with free energy approximately 20-25% of the potential field energy. We find that unsigned helicity is about a factor 10 higher at Maximum than Minimum, while free magnetic energy shows an even greater increase. The cycle averages of these two quantities are linearly correlated, extending a result found previously for active regions. Also, we propose a practical measure of eruptivity for these simulations, and show that this increases concurrently with the sunspot number, in accordance with observed coronal mass ejection rates. Whilst shearing by surface motions generates 50% or more of the free energy and helicity in the corona, we show that active regions must emerge with their own internal helicity otherwise the eruptivity is substantially reduced and follows the wrong pattern over time. **2010-09-01, 2010-09-28, 2013-12-29, 2014-12-15, 2019-03-03**

Surface Flux Transport on the Sun

Anthony R. **Yeates**, Mark C. M. Cheung, Jie Jiang, Kristof Petrovay & Yi-Ming Wang
Space Science Reviews volume 219, Article number: 31 (**2023**)
https://link.springer.com/content/pdf/10.1007/s11214-023-00978-8.pdf
We review the surface flux transport model for the evolution of magnetic flux patterns on the Sun's surface. Our underlying motivation is to understand the model's prediction of the polar field (or axial dipole) strength at the end of the solar cycle. The main focus is on the "classical" model: namely, steady axisymmetric profiles for differential rotation and meridional flow, and uniform supergranular diffusion. Nevertheless, the review concentrates on recent advances, notably in understanding the roles of transport parameters and – in particular – the source term. We also discuss the physical justification for the surface flux transport model, along with efforts to incorporate radial diffusion, and conclude by summarizing the main directions where researchers have moved beyond the classical model.

How Good Is the Bipolar Approximation of Active Regions for Surface Flux Transport?

Anthony R. **Yeates**
Solar Physics volume 295, Article number: 119 (**2020**)
https://link.springer.com/content/pdf/10.1007/s11207-020-01688-y.pdf
We investigate how representing active regions with bipolar magnetic regions (BMRs) affects the end-of-cycle polar field predicted by the surface flux transport model. Our study is based on a new database of BMRs derived from the SDO/HMI active region patch data between 2010 and 2020. An automated code is developed for fitting each active region patch with a BMR, matching both the magnetic flux and axial dipole moment of the region and removing repeat observations of the same region. By comparing the predicted evolution of each of the 1090 BMRs with the predicted evolution of their original active region patches, we show that the bipolar approximation leads to a 24% overestimate of the net axial dipole moment, given the same flow parameters. This is caused by neglecting the more

complex multipolar and/or asymmetric magnetic structures of many of the real active regions, and may explain why previous flux transport models had to reduce BMR tilt angles to obtain realistic polar fields. Our BMR database and the Python code to extract it are freely available. **30 September 2017**

Sparse Reconstruction of Electric Fields from Radial Magnetic Data

Anthony R. **Yeates**

2017 ApJ 836 131

Accurate estimates of the horizontal electric field on the Sun's visible surface are important not only for estimating the Poynting flux of magnetic energy into the corona but also for driving time-dependent magnetohydrodynamic models of the corona. In this paper, a method is developed for estimating the horizontal electric field from a sequence of radial-component magnetic field maps. This problem of inverting Faraday's law has no unique solution. Unfortunately, the simplest solution (a divergence-free electric field) is not realistically localized in regions of nonzero magnetic field, as would be expected from Ohm's law. Our new method generates instead a localized solution, using a basis pursuit algorithm to find a sparse solution for the electric field. The method is shown to perform well on test cases where the input magnetic maps are flux balanced in both Cartesian and spherical geometries. However, we show that if the input maps have a significant imbalance of flux—usually arising from data assimilation—then it is not possible to find a localized, realistic, electric field solution. This is the main obstacle to driving coronal models from time sequences of solar surface magnetic maps.

The global distribution of magnetic helicity in the solar corona⋆

A. R. **Yeates**1 and G. Hornig

A&A 594, A98 (**2016**)

By defining an appropriate field line helicity, we apply the powerful concept of magnetic helicity to the problem of global magnetic field evolution in the Sun’s corona. As an ideal-magnetohydrodynamic invariant, the field line helicity is a meaningful measure of how magnetic helicity is distributed within the coronal volume. It may be interpreted, for each magnetic field line, as a magnetic flux linking with that field line. Using magneto-frictional simulations, we investigate how field line helicity evolves in the non-potential corona as a result of shearing by large-scale motions on the solar surface. On open magnetic field lines, the helicity injected by the Sun is largely output to the solar wind, provided that the coronal relaxation is sufficiently fast. But on closed magnetic field lines, helicity is able to build up. We find that the field line helicity is non-uniformly distributed, and is highly concentrated in twisted magnetic flux ropes. Eruption of these flux ropes is shown to lead to sudden bursts of helicity output, in contrast to the steady flux along the open magnetic field lines.

Can a single active region change the course of the solar cycle?

Anthony **Yeates**, Deb Baker, Lidia van Driel-Gesztelyi

UKSP Nugget #63, Nov **2015**

http://www.uksolphys.org/uksp-nugget/63-can-a-single-active-region-change-the-course-of-the-solar-cycle/

Active regions with extreme tilt could limit the predictability of solar activity.

In summary, the evidence is pointing to a limit for how early we can make cycle predictions. We may simply have to wait for most of the active regions to emerge in a given cycle, before we can be sure that no more rogue regions will emerge and change the outcome. It is rather reminiscent of the perils of long-range weather forecasting; perhaps the butterfly diagram and the butterfly effect have more in common than you might think.

Source of a Prominent Poleward Surge During Solar Cycle 24

A.R. **Yeates**, D. Baker, L. van Driel-Gesztelyi

Solar Physics Volume 290, Issue 11, pp 3189-3201 **2015**

http://arxiv.org/pdf/1502.04854v1.pdf

As an observational case study, we consider the origin of a prominent poleward surge of leading polarity, visible in the magnetic butterfly diagram during Solar Cycle 24. A new technique is developed for assimilating individual regions of strong magnetic flux into a surface flux transport model. By isolating the contribution of each of these regions, the model shows the surge to originate primarily in a single high-latitude activity group consisting of a bipolar active region present in Carrington Rotations 2104-05 (November 2010-January 2011) and a multipolar active region in Rotations 2107-08 (February-April 2011). This group had a strong axial dipole moment opposed to Joy's law. On the other hand, the modelling suggests that the transient influence of this group on the butterfly diagram will not be matched by a large long-term contribution to the polar field, because of its location at high latitude. This is in accordance with previous flux transport models.

Asymmetric Latitudinal Gradients of Galactic Cosmic Rays at Low and High Cutoff Rigidities in Two Negative Solar Magnetic Cycles: Solar Cycles 21/22 and 23/24

T. **Yeeram**

Solar Physics September **2019**, 294:132
sci-hub.se/10.1007/s11207-019-1521-8
The south–north asymmetry of the Galactic cosmic-ray (GCR) density [nn] denoted as δnS-N/nδnS-N/n with respect to the heliospheric current sheet (HCS), observed by neutron monitors at low (≈ 1 GV) and high (≈ 13 and ≈ 17 GV) cutoff rigidities [PcPc], is investigated in two negative solar magnetic polarities when the dominant polar field is toward the northern hemisphere of the Sun. Using a new simple correction method for secular changes due to solar activity for the δnS-N/nδnS-N/n reveals that it is inversely rigidity dependent. Annual values of the corrected δnS-N/nδnS-N/n are close to zero in both solar magnetic cycles and exhibit substantial deviations due to their temporal 27-day variations. After corrections for Earth's excursions in helio-latitude for the north–south (NS) differences of HCS tilt angle [αα] as ΔαEN-SΔαN-SE, the number of 27.3-day Carrington rotations that possess correspondences between the corrected δnS-N/nδnS-N/n and ΔαEN-SΔαN-SE in both solar cycles (SCs) is significantly increased. Correlations of the two parameters are considerably increased in both SCs, particularly for SC 21/22. The asymmetric or unidirectional latitudinal gradients [G⊥G⊥] derived from the consistencies between corrected δnS-N/nδnS-N/n and ΔαEN-SΔαN-SE for the low and high PcPc in the SC 21/22 are 1.38% AU−1 and 0.69% AU−1, respectively, which are a few times larger than of SC 23/24. This suggests that asymmetric cosmic-ray modulation by the asymmetric HCS is more pronounced in SC 21/22 than in SC 23/24. Although the corrections also provide results that are fairly consistent with the drift model for the symmetric or bidirectional latitudinal gradient [GzGz], the effects of the SN asymmetric modulation of the GCR density are important as well. It is found that G⊥G⊥, GzGz, and SN asymmetric GCR modulation by NS asymmetric solar-wind speed are also inversely dependent on rigidity. The interplay between SN asymmetric modulation of the GCR density by the asymmetries in HCS and solar-wind speed, together with the effects of diffusion, are discussed for both of the negative solar magnetic cycles.

Reconstruction of total solar irradiance variability as simultaneously apparent from Solar Orbiter and Solar Dynamics Observatory

K.L. **Yeo**, N.A. Krivova, S.K. Solanki, J. Hirzberger, D. Orozco Suárez, K. Albert, +++
A&A 679, A25 **2023**
https://arxiv.org/pdf/2309.16355.pdf
https://www.aanda.org/articles/aa/pdf/2023/11/aa45872-23.pdf
Solar irradiance variability has been monitored almost exclusively from the Earth's perspective. {We present a method to combine the unprecedented observations of the photospheric magnetic field and continuum intensity from outside the Sun-Earth line, which is being recorded by the Polarimetric and Helioseismic Imager on board the Solar Orbiter mission (SO/PHI), with solar observations recorded from the Earth's perspective to examine the solar irradiance variability from both perspectives simultaneously.} Taking SO/PHI magnetograms and continuum intensity images from the cruise phase of the Solar Orbiter mission and concurrent observations from the Helioseismic and Magnetic Imager onboard the Solar Dynamics Observatory (SDO/HMI) as input into the SATIRE-S model, we successfully reconstructed the total solar irradiance variability as apparent from both perspectives. In later stages of the SO mission, the orbital plane will tilt in such a way as to bring the spacecraft away from the ecliptic to heliographic latitudes of up to 33◦. The current study sets the template for the reconstruction of solar irradiance variability as seen from outside the ecliptic from data that SO/PHI is expected to collect from such positions. {Such a reconstruction will be beneficial to factoring inclination into how the brightness variations of the Sun compare to those of other cool stars, whose rotation axes are randomly inclined.

Intensity contrast of solar network and faculae -- II. Implications for solar irradiance modelling

K. L. **Yeo**, N. A. Krivova
A&A **2021**
https://arxiv.org/pdf/2102.09530.pdf
We aim to gain insight into the effect of network and faculae on solar irradiance from their apparent intensity. Taking full-disc observations from the Solar Dynamics Observatory, we examined the intensity contrast of network and faculae in the continuum and core of the Fe I 6173 Å line and 1700 Å, including the variation with magnetic flux density, distance from disc centre, nearby magnetic fields, and time. The brightness of network and faculae is believed to be suppressed by nearby magnetic fields from its effect on convection. The difference in intensity contrast between the quiet-Sun network and active region faculae, noted by various studies, arises because active regions are more magnetically crowded and is not due to any fundamental physical differences between network and faculae. These results highlight that solar irradiance models need to include the effect of nearby magnetic fields on network and faculae brightness. We found evidence that suggests that departures from local thermal equilibrium (LTE) might have limited effect on intensity contrast. This could explain why solar irradiance models that are based on the intensity contrast of solar surface magnetic features calculated assuming LTE reproduce the observed spectral variability even where the LTE assumption breaks down. Certain models of solar irradiance employ chromospheric indices as direct indications of the effect of network and faculae on solar irradiance. Based on past studies of the Ca

II K line and on the intensity contrast measurements derived here, we show that the fluctuations in chromospheric emission from network and faculae are a reasonable estimate of the emission fluctuations in the middle photosphere, but not of those in the lower photosphere. The data set, which extends from 2010 to 2018, indicates that intensity contrast was stable to about 3% in this period.

The Dimmest State of the Sun

K. L. **Yeo**, S. K. Solanki, N. A. Krivova, M. Rempel, L. S. Anusha, A. I. Shapiro, R. V. Tagirov, V. Witzke

Geophysical Research Letters, 47, e2020GL090243 (**2020**)

https://arxiv.org/pdf/2102.09487.pdf

How the solar electromagnetic energy entering the Earth's atmosphere varied since pre-industrial times is an important consideration in the climate change debate. Detrimental to this debate, estimates of the change in total solar irradiance (TSI) since the Maunder minimum, an extended period of weak solar activity preceding the industrial revolution, differ markedly, ranging from a drop of 0.75 Wm-2 to a rise of 6.3 Wm-2. Consequently, the exact contribution by solar forcing to the rise in global temperatures over the past centuries remains inconclusive. Adopting a novel approach based on state-of-the-art solar imagery and numerical simulations, we establish the TSI level of the Sun when it is in its least-active state to be 2.0 +/- 0.7 Wm-2 below the 2019 level. This means TSI could not have risen since the Maunder minimum by more than this amount, thus restricting the possible role of solar forcing in global warming.

How faculae and network relate to sunspots, and the implications for solar and stellar brightness variations

K. L. **Yeo**, S. K. Solanki, N. A. Krivova

A&A 639, A139 **2020**

https://arxiv.org/pdf/2006.14274.pdf

https://www.aanda.org/articles/aa/pdf/2020/07/aa37739-20.pdf

How global faculae and network coverage relates to that of sunspots is relevant to the brightness variations of the Sun and Sun-like stars. We extend earlier studies that found the facular-to-sunspot-area ratio diminishes with total sunspot coverage. Chromospheric indices and the total magnetic flux enclosed in network and faculae, referred to here as 'facular indices', are modulated by the amount of facular and network present. We probed the relationship between various facular and sunspot indices through an empirical model that takes into account how active regions evolve. This model was incorporated into a total solar irradiance (TSI) model. The model presented here replicates most of the observed variability in the facular indices, and is better at doing so than earlier models. Contrary to recent studies, we found the relationship between the facular and sunspot indices to be stable over the past four decades. The model indicates that, like the facular-to-sunspot-area ratio, the ratio of the variation in chromospheric emission and total network and facular magnetic flux to sunspot area decreases with the latter. The TSI model indicates the ratio of the TSI excess from faculae and network to the deficit from sunspots also declines with sunspot area, with the consequence being that TSI rises with sunspot area more slowly than if the two quantities were linearly proportional to one another. The extrapolation of the TSI model to higher activity levels indicates that in the activity range where Sun-like stars are observed to switch from growing brighter with increasing activity to becoming dimmer instead, the activity-dependence of TSI exhibits a similar transition as sunspot darkening starts to rise more rapidly with activity than facular brightening. This bolsters the interpretation of this behavior of Sun-like stars as the transition from a faculae-dominated to a spot-dominated regime.

Corrigendum A&A 642, C2 **(2020)** https://www.aanda.org/articles/aa/pdf/2020/10/aa37739e-20.pdf

Intensity contrast of solar network and faculae
II. Implications for solar irradiance modelling

K. L. **Yeo** and N. A. Krivova

A&A 624, A135 (**2019**)

sci-hub.se/10.1051/0004-6361/201935123

Aims. We aim to gain insight into the effect of network and faculae on solar irradiance from their apparent intensity.
Methods. Taking full-disc observations from the Solar Dynamics Observatory, we examined the intensity contrast of network and faculae in the continuum and core of the Fe I 6173 Å line and 1700 Å, including the variation with magnetic flux density, distance from disc centre, nearby magnetic fields, and time.
Results. The brightness of network and faculae is believed to be suppressed by nearby magnetic fields from its effect on convection. We note that the degree of magnetically crowding of an area also affects the magnetic flux tube sizes and the depth at which magnetic concentrations are embedded in intergranular lanes, such that intensity contrast can be enhanced in magnetically crowded areas at certain flux densities and distances from disc centre. The difference in intensity contrast between the quiet-Sun network and active region faculae, noted by various studies, arises because active regions are more magnetically crowded and is not due to any fundamental physical differences between network and faculae. These results highlight that solar irradiance models need to include the effect of nearby

magnetic fields on network and faculae brightness. We found evidence that suggests that departures from local thermal equilibrium (LTE) might have limited effect on intensity contrast. This could explain why solar irradiance models that are based on the intensity contrast of solar surface magnetic features calculated assuming LTE reproduce the observed spectral variability even where the LTE assumption breaks down. Certain models of solar irradiance employ chromospheric indices as direct indications of the effect of network and faculae on solar irradiance. Based on past studies of the Ca II K line and on the intensity contrast measurements derived here, we show that the fluctuations in chromospheric emission from network and faculae are a reasonable estimate of the emission fluctuations in the middle photosphere, but not of those in the lower photosphere. This is due to the different physical mechanisms that underlie the magnetic intensity enhancement in the various atmospheric regimes, and represents a fundamental limitation of these solar irradiance models. Any time variation in the radiant properties of network and faculae is, of course, relevant to their effect on solar irradiance. The data set, which extends from 2010 to 2018, indicates that their intensity contrast was stable to about 3% in this period.
Conclusions. This study offers new insights into the radiant behaviour of network and faculae, with practical implications for solar irradiance modelling.

Solar Irradiance Variability is Caused by the Magnetic Activity on the Solar Surface

K. L. **Yeo**, S. K. Solanki, C. M. Norris, B. Beeck, Y. C. Unruh, N. A. Krivova
PHYSICAL REVIEW LETTERS **2017**
https://arxiv.org/pdf/1709.00920.pdf
Supplementary Materials; this https URL
The variation in the radiative output of the Sun, described in terms of solar irradiance, is important to climatology. A common assumption is that solar irradiance variability is driven by its surface magnetism. Verifying this assumption has, however, been hampered by the fact that models of solar irradiance variability based on solar surface magnetism have to be calibrated to observed variability. Making use of realistic three-dimensional magnetohydrodynamic simulations of the solar atmosphere and state-of-the-art solar magnetograms from the Solar Dynamics Observatory, we present a model of total solar irradiance (TSI) that does not require any such calibration. In doing so, the modeled irradiance variability is entirely independent of the observational record. (The absolute level is calibrated to the TSI record from the Total Irradiance Monitor.) The model replicates 95% of the observed variability between April 2010 and July 2016, leaving little scope for alternative drivers of solar irradiance variability at least over the time scales examined (days to years). **December 16, 2012**

EMPIRE: A robust empirical reconstruction of solar irradiance variability

K. L. **Yeo**, N. A. Krivova, S. K. Solanki
JGR Volume 122, Issue 4 April 2017 Pages 3888–3914 **2017**
https://arxiv.org/pdf/1704.07652.pdf
We present a new empirical model of total and spectral solar irradiance (TSI and SSI) variability entitled EMPirical Irradiance REconstruction (EMPIRE). As with existing empirical models, TSI and SSI variability is given by the linear combination of solar activity indices. In empirical models, UV SSI variability is usually determined by fitting the rotational variability in activity indices to that in measurements. Such models have to date relied on ordinary least squares regression, which ignores the uncertainty in the activity indices. In an advance from earlier efforts, the uncertainty in the activity indices is accounted for in EMPIRE by the application of an error-in-variables regression scheme, making the resultant UV SSI variability more robust. The result is consistent with observations and unprecedentedly, with that from other modelling approaches, resolving the long-standing controversy between existing empirical models and other types of models. We demonstrate that earlier empirical models, by neglecting the uncertainty in activity indices, underestimate UV SSI variability. The reconstruction of TSI and visible and IR SSI from EMPIRE is also shown to be consistent with observations. The EMPIRE reconstruction is of utility to climate studies as a more robust alternative to earlier empirical reconstructions.

UV solar irradiance in observations and the NRLSSI and SATIRE-S models

K. L. **Yeo**, W. T. Ball, N. A. Krivova, S. K. Solanki, Y. C. Unruh, J. Morrill
J. Geophys. Res. (Space Phys.) v. 120 (**2015**)
http://arxiv.org/pdf/1507.01224v1.pdf
Total solar irradiance and UV spectral solar irradiance have been monitored since 1978 through a succession of space missions. This is accompanied by the development of models aimed at replicating solar irradiance by relating the variability to solar magnetic activity. The NRLSSI and SATIRE-S models provide the most comprehensive reconstructions of total and spectral solar irradiance over the period of satellite observation currently available. There is persistent controversy between the various measurements and models in terms of the wavelength dependence of the variation over the solar cycle, with repercussions on our understanding of the influence of UV solar irradiance variability on the stratosphere. We review the measurement and modelling of UV solar irradiance variability over the period of satellite observation. The SATIRE-S reconstruction is consistent with spectral solar irradiance observations where they are reliable. It is also supported by an independent, empirical reconstruction of

UV spectral solar irradiance based on UARS/SUSIM measurements from an earlier study. The weaker solar cycle variability produced by NRLSSI between 300 and 400 nm is not evident in any available record. We show that although the method employed to construct NRLSSI is principally sound, reconstructed solar cycle variability is detrimentally affected by the uncertainty in the SSI observations it draws upon in the derivation. Based on our findings, we recommend, when choosing between the two models, the use of SATIRE-S for climate studies.

Solar Cycle Variation in Solar Irradiance **Review**

K. L. **Yeo**, N. A. Krivova, S. K. Solanki

Space Science Reviews December **2014**, Volume 186, Issue 1-4, pp 137-167

The correlation between solar irradiance and the 11-year solar activity cycle is evident in the body of measurements made from space, which extend over the past four decades. Models relating variation in solar irradiance to photospheric magnetism have made significant progress in explaining most of the apparent trends in these observations. There are, however, persistent discrepancies between different measurements and models in terms of the absolute radiometry, secular variation and the spectral dependence of the solar cycle variability. We present an overview of solar irradiance measurements and models, and discuss the key challenges in reconciling the divergence between the two.

Analysis and modeling of solar irradiance variations

K. L. **Yeo**

Doctoral thesis, **2014**

http://arxiv.org/pdf/1412.3935v1.pdf

A prominent manifestation of the solar dynamo is the 11-year activity cycle, evident in indicators of solar activity, including solar irradiance. Although a relationship between solar activity and the brightness of the Sun had long been suspected, it was only directly observed after regular satellite measurements became available with the launch of Nimbus-7 in 1978. The measurement of solar irradiance from space is accompanied by the development of models aimed at describing the apparent variability by the intensity excess/deficit effected by magnetic structures in the photosphere. The more sophisticated models, termed semi-empirical, rely on the intensity spectra of photospheric magnetic structures generated with radiative transfer codes from semi-empirical model atmospheres. An established example of such models is SATIRE-S (Spectral And Total Irradiance REconstruction for the Satellite era). One key limitation of current semi-empirical models is the fact that the radiant properties of network and faculae are not adequately represented due to the use of plane-parallel model atmospheres (as opposed to three-dimensional model atmospheres). This thesis is the compilation of four publications, detailing the results of investigations aimed at setting the groundwork necessary for the eventual introduction of three-dimensional atmospheres into SATIRE-S and a review of the current state of the measurement and modelling of solar irradiance. Also presented is an update of the SATIRE-S model. We generated a daily reconstruction of total and spectral solar irradiance, covering 1974 to the present, that is more reliable and, in most cases, extended than similar reconstructions from contemporary models.

Reconstruction of total and spectral solar irradiance from 1974 to 2013 based on KPVT, SoHO/MDI and SDO/HMI observations

K. L. **Yeo**, N. A. Krivova, S. K. Solanki, K. H. Glassmeier

A&A, 570, A85 **2014**

http://arxiv.org/pdf/1408.1229v1.pdf

Total and spectral solar irradiance are key parameters in the assessment of solar influence on changes in the Earth's climate. We present a reconstruction of daily solar irradiance obtained using the SATIRE-S model spanning 1974 to 2013 based on full-disc observations from the KPVT, SoHO/MDI and SDO/HMI. SATIRE-S ascribes variation in solar irradiance on timescales greater than a day to photospheric magnetism. The solar spectrum is reconstructed from the apparent surface coverage of bright magnetic features and sunspots in the daily data using the modelled intensity spectra of these magnetic structures. We cross-calibrated the various data sets, harmonizing the model input so as to yield a single consistent time series as the output. The model replicates 92% of the variability in the PMOD TSI composite including the secular decline between the 1996 and 2008 solar cycle minima. The model also reproduces most of the variability in observed Lyman-alpha irradiance and the Mg II index. The UV solar irradiance measurements from the UARS and SORCE missions are mutually consistent up to about 180 nm before they start to exhibit discrepant rotational and cyclical variability, indicative of unresolved instrumental effects. As a result, the agreement between model and measurement starts to deteriorate above this wavelength. As with earlier similar investigations, the reconstruction cannot reproduce the overall trends in SORCE/SIM SSI. We argue, from the lack of clear solar cycle modulation in the SIM record and the inconsistency between the total flux recorded by the instrument and TSI, that unaccounted instrumental trends are present. The reconstruction is consistent with observations from multiple sources, demonstrating its validity. It also provides further evidence that photospheric magnetism is the prime driver of variation in solar irradiance on timescales greater than a day.

Solar cycle variation in solar irradiance **Review**

K. L. **Yeo**, N. A. Krivova, S. K. Solanki
Space Sci. Rev., (**2014**)
http://arxiv.org/pdf/1407.4249v1.pdf
The correlation between solar irradiance and the 11-year solar activity cycle is evident in the body of measurements made from space, which extend over the past four decades. Models relating variation in solar irradiance to photospheric magnetism have made significant progress in explaining most of the apparent trends in these observations. There are, however, persistent discrepancies between different measurements and models in terms of the absolute radiometry, secular variation and the spectral dependence of the solar cycle variability. We present an overview of solar irradiance measurements and models, and discuss the key challenges in reconciling the divergence between the two.

Solar wind parameters in rising phase of solar cycle 25

Yuri I. **Yermolaev**, Irina G. Lodkina, Alexander A. Khokhlachev, Michael Yu. Yermolaev, Maria O. Riazantseva, Liudmila S. Rakhmanova, Natalia L. Borodkova, Olga V. Sapunova, Anastasiia V. Moskaleva
2023
https://arxiv.org/ftp/arxiv/papers/2304/2304.14707.pdf
Solar activity and solar wind parameters decreased significantly in solar cycles (SCs) 23-24. In this paper, we analyze solar wind measurements at the rising phase of SC 25 and compare them with similar data from the previous cycles. For this purpose, we simultaneously selected the OMNI database data for 1976-2022, both by phases of the 11-year solar cycle and by large-scale solar wind types (in accordance with IKI's catalog, see this http URL), and calculated the mean values of the parameters for the selected datasets. The obtained results testify in favor of the hypothesis that the continuation of this cycle will be similar to the previous cycle 24, i.e. SC 25 will be weaker than SCs 21 and 22.

Drop of solar wind at the end of the 20th century

Yuri I. **Yermolaev**, Irina G. Lodkina, Alexander A. Khokhlachev, Michael Yu. Yermolaev, Maria O. Riazantseva, Liudmila S. Rakhmanova, Natalia L. Borodkova, Olga V. Sapunova, Anastasiia V. Moskaleva
2021
https://arxiv.org/ftp/arxiv/papers/2105/2105.10955.pdf
Variations in the solar wind (SW) parameters with scales of several years are an important characteristic of solar activity and the basis for a long-term space weather forecast. We examine the behavior of interplanetary parameters over 21-24 solar cycles (SCs) on the basis of OMNI database (this https URL). Since changes in parameters can be associated both with changes in the number of different large-scale types of SW, and with variations in the values of these parameters at different phases of the solar cycle and during the transition from one cycle to another, we select the entire study period in accordance with the Catalog of large-scale SW types for 1976-2019 (See the site this http URL, [Yermolaev et al., 2009]), which covers the period from 21 to 24 SCs, and in accordance with the phases of the cycles, and averaging the parameters at selected intervals. In addition to a sharp drop in the number of ICMEs (and associated Sheath types), there is a noticeable drop in the value (by 20-40%) of plasma parameters and magnetic field in different types of solar wind at the end of the 20th century and a continuation of the fall or persistence at a low level in the 23-24 cycles. Such a drop in the solar wind is apparently associated with a decrease in solar activity and manifests itself in a noticeable decrease in space weather factors.

ALMA Observations of the Solar Chromosphere on the Polar Limb

Takaaki **Yokoyama**, Masumi Shimojo, Takenori J. Okamoto, Haruhisa Iijima
ApJ **2018**
https://arxiv.org/pdf/1807.01411.pdf
We report the results of the Atacama Large Millimeter/sub-millimeter Array (ALMA) observations of the solar chromosphere on the southern polar limb. Coordinated observations with the Interface Region Imaging Spectrograph (IRIS) are also conducted. ALMA provided unprecedented high spatial resolution in the millimeter band (≈ 2.0 arcsec) at 100 GHz frequency with a moderate cadence (20 s). The results are as follows: (1) The ALMA 100 GHz images show saw-tooth patterns on the limb, and a comparison with SDO/AIA 171\AA\ images shows a good correspondence of the limbs with each other. (2) The ALMA 100 GHz movie shows a dynamic thorn-like structure elongating from the saw-tooth patterns on the limb, with lengths reaching at least 8 arcsec, thus suggesting jet-like activity in the ALMA microwave range. These **ALMA jets** are in good correspondence with

IRIS jet clusters. (3) A blob ejection event is observed. By comparing with the IRIS Mg II slit-jaw images, the trajectory of the blob is located along the spicular patterns. **2017 April 29**

Which Component of Solar Magnetic Field Drives the Evolution of Interplanetary Magnetic Field over Solar Cycle?

Minami **Yoshida**, Toshifumi Shimizu, Shin Toriumi

ApJ **950** 156 **2023**

https://arxiv.org/pdf/2304.13347.pdf

https://iopscience.iop.org/article/10.3847/1538-4357/acd053/pdf

The solar magnetic structure changes over the solar cycle. It has a dipole structure during solar minimum, where the open flux extends mainly from the polar regions into the interplanetary space. During maximum, a complex structure is formed with low-latitude active regions and weakened polar fields, resulting in spread open field regions. However, the components of the solar magnetic field that is responsible for long-term variations in the interplanetary magnetic field (IMF) are not clear, and the IMF strength estimated based on the solar magnetic field is known to be underestimated by a factor of 3 to 4 against the actual in-situ observations (the open flux problem). To this end, we decomposed the coronal magnetic field into the components of the spherical harmonic function of degree and order (ℓ,m) using the potential field source surface model with synoptic maps from SDO/HMI for 2010 to 2021. As a result, we found that the IMF rapidly increased in December 2014 (seven months after the solar maximum), which coincided with the increase in the equatorial dipole, (ℓ,m)=(1,±1), corresponding to the diffusion of active regions toward the poles and in the longitudinal direction. The IMF gradually decreased until December 2019 (solar minimum) and its variation corresponded to that of the non-dipole component $\ell \geq 2$. Our results suggest that the understanding of the open flux problem may be improved by focusing on the equatorial dipole and the non-dipole component and that the influence of the polar magnetic field is less significant.

High-frequency Wave Propagation Along a Spicule Observed by CLASP

Masaki **Yoshida**, Yoshinori Suematsu, Ryohko Ishikawa, Takenori J. Okamoto, Masahito Kubo, Ryouhei Kano, Noriyuki Narukage, Takamasa Bando, Amy R. Winebarger, Ken Kobayashi, Javier Trujillo Bueno, and Frédéric Auchère

2019 ApJ 887 2

https://doi.org/10.3847/1538-4357/ab4ce7

The Chromospheric Lyman-Alpha Spectro-Polarimeter (CLASP) sounding rocket experiment, launched in 2015 September, observed the hydrogen Lyα line (121.6 nm) in an unprecedented high temporal cadence of 0.3 s. CLASP performed sit-and-stare observations of the quiet Sun near the limb for 5 minutes with a slit perpendicular to the limb and successfully captured an off-limb spicule evolving along the slit. The Lyα line is well suited for investigating how spicules affect the corona because it is sensitive to higher temperatures than other chromospheric lines, owing to its large optical thickness. We found high-frequency oscillations of the Doppler velocity with periods of 20–50 s and low-frequency oscillation of periods of ~240 s on the spicule. From a wavelet analysis of the time sequence data of the Doppler velocity, in the early phase of the spicule evolution, we found that waves with a period of ~30 s and a velocity amplitude of 2–3 km s−1 propagated upward along the spicule with a phase velocity of ~470 km s−1. In contrast, in the later phase, possible downward and standing waves with smaller velocity amplitudes were also observed. The high-frequency waves observed in the early phase of the spicule evolution would be related with the dynamics and the formation of the spicules. Our analysis enabled us to identify the upward, downward, and standing waves along the spicule and to obtain the velocity amplitude of each wave directly from the Doppler velocity for the first time. We evaluated the energy flux by the upward-propagating waves along the spicule, and discussed the impact to the coronal heating.

Difference between even- and odd-numbered cycles in the predictability of solar activity and prediction of the amplitude of cycle 25

A. **Yoshida**

Ann. Geophys., 32, 1035-1042, **2014**

http://www.ann-geophys.net/32/1035/2014/angeo-32-1035-2014.html

It was shown previously that the sunspot number (SSN) at a point 3 years before the minimum is well correlated with the maximum SSN of the succeeding cycle, and a better correlation is obtained when the maximum SSN is replaced by the average SSN over a cycle for which the average SSN is calculated by dividing cycles at a point 3 years before the minimum (Yoshida and Yamagishi, 2010; Yoshida and Sayre, 2012). Following these findings, we demonstrate in this paper that the correlation between the SSN 3 years before the minimum and the amplitude of the coming cycle differs significantly between even-numbered and odd-numbered cycles: the correlation is much better for even-numbered cycles. Further, it is shown that the amplitude of even-numbered cycles is strongly correlated with that of the succeeding odd-numbered cycles, while the correlation between amplitudes of odd-numbered cycles

and those of succeeding even-numbered cycles is very poor. Using the excellent correlations, we estimate the maximum SSN of the current cycle 24 at 81.3 and predict the maximum SSN of cycle 25 to be 115.4 ± 11.9. It is of note, however, that a peak of the SSN has been observed in February 2012 and the peak value 66.9 is considerably smaller than the estimated maximum SSN of cycle 24. We conjecture that the second higher peak of the SSN may appear.

Calibration of Hinode/XRT for Coalignment

Yoshimura, K., McKenzie, David E.
Solar Phys. Volume 290, Issue 8, pp 2355-2372 **2015**
http://ylstone.physics.montana.edu/yosimura/hinode/coalignment/KY_coal_paper_20150706.pdf
We present coalignment calibration procedures for the X-ray Telescope (XRT) onboard the Hinode satellite in this paper. We performed not only an XRT stand-alone calibration, but also cross-calibration using data from the Helioseismic and Magnetic Imager (HMI) and the Atmospheric Imaging Assembly (AIA) onboard the Solar Dynamics Observatory (SDO). Several new methods described herein may also be useful for the coalignment calibration of other instruments. We have developed a database of coalignment coefficients and software to access it, so that all XRT images can be easily and accurately overlaid onto the images from other instruments, especially AIA and HMI. **17-18 Jan 2011,** 28 January 2011. **19 Aug 2011**

Applications of Atomic Data to Studies of the Sun

Peter R. **Young**
European Physical Journal D **2024**
https://arxiv.org/pdf/2409.09166
The Sun is a standard reference object for Astrophysics and also a fascinating subject of study in its own right. X-ray and extreme ultraviolet movies of the Sun's atmosphere show an extraordinary diversity of plasma phenomena, from barely visible bursts and jets to coronal mass ejections that impact a large portion of the solar surface. The processes that produce these phenomena, heat the corona and power the solar wind remain actively studied and accurate atomic data are essential for interpreting observations and making model predictions. For the Sun's interior intense effort is focused on resolving the "solar problem," (a discrepancy between solar interior models and helioseismology measurements) and atomic data are central to both element abundance measurements and interior physics such as opacity and nuclear reaction rates. In this article, topics within solar interior and solar atmosphere physics are discussed and the role of atomic data described. Areas of active research are highlighted and specific atomic data needs are identified.

Properties of EUV Imaging Spectrometer (EIS) Slot Observations

Peter R. **Young** & Ignacio Ugarte-Urra
Solar Physics volume 297, Article number: 87 (**2022**)
https://link.springer.com/content/pdf/10.1007/s11207-022-02014-4.pdf
The Extreme ultraviolet Imaging Spectrometer (EIS) on board the Hinode spacecraft has been operating since 2006, returning high-resolution data in the 170 – 212 and 246 – 292 Å wavelength regions. EIS has four slit options, with the narrow 1″ and 2″ slits used for spectroscopy and the wide 40″ and 266″ slits used for monochromatic imaging. In this article several properties of the 40″ slit (or slot) are measured using the Fe XII 195.12 Å line, which is formed at 1.5 MK. The projected width of the slot on the detector shows a small variation along the slit with an average value of 40.949″. The slot image is tilted on the detector and a quadratic formula is provided to describe the tilt. The tilt corresponds to four pixels on the detector and the slot centroid is offset mostly to the right (longer wavelengths) of the 1″ slit by up to four pixels. Measurement of the intensity decrease at the edge of the slot leads to an estimate of the spatial resolution of the images in the xx-direction. The resolution varies quadratically along the slot, with a minimum value of 2.9″ close to the detector center. Intensities measured from the slot images are found to be on average 14% higher than those measured from the 1″ slit at the same spatial location. Background subtraction is necessary to derive accurate intensities in quiet-Sun and coronal-hole regions. Prescriptions for deriving accurate slot intensities for different types of slot datasets are presented.

An Analysis of Spikes in Atmospheric Imaging Assembly (AIA) Data

Peter R. **Young**, Nicholeen M. Viall, Michael S. Kirk, Emily I. Mason & Lakshmi Pradeep Chitta
Solar Physics volume 296, Article number: 181 (**2021**
https://link.springer.com/content/pdf/10.1007/s11207-021-01929-8.pdf
https://doi.org/10.1007/s11207-021-01929-8
https://arxiv.org/pdf/2108.02624.pdf
The Atmospheric Imaging Assembly (AIA) on the Solar Dynamics Observatory (SDO) returns high-resolution images of the solar atmosphere in seven extreme ultraviolet wavelength channels. The images are processed on the ground to remove intensity spikes arising from energetic particles hitting the instrument, and the despiked images are provided to the community. In this work a three-hour series of images from the 171 A channel obtained on **2017**

February 28 was studied to investigate how often the despiking algorithm gave false positives caused by compact brightenings in the solar atmosphere. The latter were identified through spikes appearing in the same detector pixel for three consecutive frames, and 1096 examples were found from the 900 image frames. These "three-spikes" were assigned to 126 dynamic solar features, and it is estimated that the three-spike method identifies 25% of the total number of features affected by despiking. For any 10 minute sequence of AIA 171 A images there are therefore around 28 solar features that have their intensity modified by despiking. The features are found in active regions, quiet Sun and coronal holes and, in relation to solar surface area, there is a greater proportion within coronal holes. In 96% of the cases, the despiked structure is a compact brightening of size 2 arcsec or less and the remaining 4% have narrow, elongated structures. In all cases, the events are not rendered invisible by the AIA processing pipeline, but the total intensity over the event's lifetimes can be reduced by up to 67%. Scientists are recommended to always restore the original intensities to AIA data when studying short-lived or rapidly-evolving features that exhibit fine-scale structure.

Future Prospects for Solar EUV and Soft X-ray Spectroscopy Missions **Review**

Peter R. **Young**

Frontiers issue on Solar Instrumentation April **2021**

https://arxiv.org/pdf/2102.02943.pdf

https://www.frontiersin.org/articles/10.3389/fspas.2021.662790/full

https://doi.org/10.3389/fspas.2021.662790

Future prospects for solar spectroscopy missions operating in the extreme ultraviolet (EUV) and soft X-ray (SXR) wavelength ranges, 1.2-1600 A, are discussed. NASA is the major funder of Solar Physics missions, and brief summaries of the opportunities for mission development under NASA are given. The methods of observing the Sun in the two wavelength ranges are summarized with a particular focus on imaging spectroscopy techniques. The major spectral features in the EUV and SXR regions are identified, and then the upcoming instruments and concepts are summarized. The instruments range from large spectrometers on dedicated missions, to tiny, low-cost CubeSats launched through rideshare opportunities.

Solar Ultraviolet Bursts **Review**

Peter R. **Young**, Hui Tian, Hardi Peter, Robert J. Rutten, Chris J. Nelson, Zhenghua Huang, ...

Space Science Reviews December **2018**, 214:120

https://link.springer.com/content/pdf/10.1007%2Fs11214-018-0551-0.pdf

The term “ultraviolet (UV) burst” is introduced to describe small, intense, transient brightenings in ultraviolet images of solar active regions. We inventorize their properties and provide a definition based on image sequences in transition-region lines. Coronal signatures are rare, and most bursts are associated with small-scale, canceling opposite-polarity fields in the photosphere that occur in emerging flux regions, moving magnetic features in sunspot moats, and sunspot light bridges. We also compare UV bursts with similar transition-region phenomena found previously in solar ultraviolet spectrometry and with similar phenomena at optical wavelengths, in particular Ellerman bombs. Akin to the latter, UV bursts are probably small-scale magnetic reconnection events occurring in the low atmosphere, at photospheric and/or chromospheric heights. Their intense emission in lines with optically thin formation gives unique diagnostic opportunities for studying the physics of magnetic reconnection in the low solar atmosphere. This paper is a review report from an International Space Science Institute team that met in 2016–2017. **Sep 24, 2013, October 22-23, 2013, 2013 December 6, 13 Feb 2014, 4 March 2014, 2014 June 15, 24 Oct 2014, 26 Oct 2016**

A Si IV/O IV electron density diagnostic for the analysis of IRIS solar spectra

P.R. **Young**, F.P. Keenan, R.O. Milligan, H. Peter

ApJ **857** 5 **2018**

https://arxiv.org/pdf/1803.01721.pdf

Solar spectra of ultraviolet bursts and flare ribbons from the Interface Region Imaging Spectrograph (IRIS) have suggested high electron densities of >1012 cm−3 at transition region temperatures of 0.1 MK, based on large intensity ratios of Si IV λ1402.77 to O IV λ1401.16. In this work a rare observation of the weak O IV λ1343.51 line is reported from an X-class flare that peaked at 21:41 UT on **2014 October 24**. This line is used to develop a theoretical prediction of the Si IV λ1402.77 to O IV λ1401.16 ratio as a function of density that is recommended to be used in the high density regime. The method makes use of new pressure-dependent ionization fractions that take account of the suppression of dielectronic recombination at high densities. It is applied to two sequences of flare kernel observations from the October 24 flare. The first shows densities that vary between 3×1012 to 3×1013 cm−3 over a seven minute period, while the second location shows stable density values of around 2×1012 cm−3 over a three minute period.

Element Abundance Ratios in the Quiet Sun Transition Region

P. R. **Young**

2018 ApJ 855 15

Element abundance ratios of magnesium to neon (Mg/Ne) and neon to oxygen (Ne/O) in the transition region of the quiet Sun have been derived by re-assessing previously published data from the Coronal Diagnostic Spectrometer on board the Solar and Heliospheric Observatory in the light of new atomic data. The quiet Sun Mg/Ne ratio is important for assessing the effect of magnetic activity on the mechanism of the first ionization potential (FIP) effect, while the Ne/O ratio can be used to infer the solar photospheric abundance of neon, which cannot be measured directly. The average Mg/Ne ratio is found to be 0.52 ± 0.11, which applies over the temperature region 0.2–0.7 MK, and is consistent with the earlier study. The Ne/O ratio is, however, about 40% larger, taking the value 0.24 ± 0.05 that applies to the temperature range 0.08–0.40 MK. The increase is mostly due to changes in ionization and recombination rates that affect the equilibrium ionization balance. If the Ne/O ratio is interpreted as reflecting the photospheric ratio, then the photospheric neon abundance is 8.08 ± 0.09 or 8.15 ± 0.10 (on a logarithmic scale for which hydrogen is 12), according to whether the oxygen abundances of M. Asplund et al. or E. Caffau et al. are used. The updated photospheric neon abundance implies a Mg/Ne FIP bias for the quiet Sun of 1.6 ± 0.6.

Solar Analogs as a Tool to Understand the Sun mini Review

Allison **Youngblood**, Steve Cranmer, Sam Van Kooten, James Paul Mason, J. Sebastian Pineda, Kevin France, Dmitry Vorobiev, Frank Eparvier, Yuta Notsu

Heliophysics 2050 Workshop **2020**

https://arxiv.org/ftp/arxiv/papers/2009/2009.05672.pdf

Solar analogs, broadly defined as stars similar to the Sun in mass or spectral type, provide a useful laboratory for exploring the range of Sun-like behaviors and exploring the physical mechanisms underlying some of the Sun's most elusive processes like coronal heating and the dynamo. We describe a series of heliophysics-motivated, but astrophysics-like studies of solar analogs. We argue for a range of stellar observations, including (a) the identification and fundamental parameter determination of new solar analogs, and (b) characterizing emergent properties like activity, magnetism, and granulation. These parameters should be considered in the framework of statistical studies of the dependences of these observables on fundamental stellar parameters like mass, metallicity, and rotation.

Input Selection Based on Information Theory for Constructing Predictor Models of Solar and Geomagnetic Activity Indices

Mohammadmahdi Rezaei **Yousefi** · Babak Salehi Kasmaei · Abdolhossein Vahabie · Caro Lucas · Babak Nadjar Araabi

Solar Phys (**2009**) 258: 297–318

Various phenomena with solar origin and their mutual dependence must be studied in order to predict behaviors in solar – terrestrial system. Linear statistical methods prevalent in analyzing natural systems may not be able to detect nonlinear dependencies among solar and geomagnetic processes. When relations, whether linear or nonlinear, between indices and their changes over time are revealed, better predictions can be made through appropriate modeling techniques. Selection of nonredundant input variables to build suitable models for prediction of solar and geomagnetic activity is of utmost importance. Mutual information is a tool that is capable of capturing all dependencies for detecting nonlinear relations and selecting the best subset of input variables by means of an applicable algorithm that maximizes information about the output and minimizes the shared information between inputs. High generalization power and improved interpretability of the selected inputs are the consequences of this analysis.

Image Desaturation for SDO/AIA Using Deep Learning

Xuexin **Yu**, Long Xu & Yihua Yan

Solar Physics volume 296, Article number: 56 (**2021**)

https://doi.org/10.1007/s11207-021-01808-2

https://link.springer.com/content/pdf/10.1007/s11207-021-01808-2.pdf

The Atmospheric Imaging Assembly (AIA) on board the Solar Dynamics Observatory (SDO) (launched in February 2010) provides uninterrupted full-disk solar images over 10 wavebands. In the case of violent solar flares, saturation would happen to SDO/AIA images in their core regions, which leads to signal loss, hindering us to understand physical mechanism behind solar flares. This paper introduces a deep learning based image restoration model which can recover signal of saturation region by referring to other normal/valid region within an image. The proposed model, namely PCGAN, combines partial convolution (PC) and conditional generative adversarial network (GAN). The PC module was originally designed for image inpainting, for repairing images with scratches and holes. In addition, a new comprehensive loss function consists of an adversarial loss, a pixel reconstruction loss, a gradient loss, a perceptual loss, a style loss and a total variation loss. Moreover, for validating the proposed model, a new dataset consisting of paired saturated and normal SDO/AIA images is established. Experimental results demonstrate

that the proposed PCGAN can get appealing desaturated solar images with respect to both objective and subjective validations. **September 6 2011**

Resonant Damping of Kink Modes in Solar Coronal Slabs

Hui **Yu**, Bo Li, Shaoxia Chen, Mingzhe Guo
Solar Phys. **296**, Article number: 95 **2021**
https://arxiv.org/pdf/2102.00222.pdf
https://link.springer.com/content/pdf/10.1007/s11207-021-01839-9.pdf
We examine resonantly damped kink modes in straight coronal slabs, paying special attention to the effects of the formulation for the transverse density distribution ("profile" for brevity). We work in the framework of pressure-less, gravity-free, resistive magnetohydrodynamics, and adopt the dissipative eigenmode perspective. The density profile is restricted to be one-dimensional, but nonetheless allowed to take a generic form characterized by a continuous transition layer connecting a uniform interior to a uniform exterior. A dispersion relation (DR) is derived in the thin-boundary limit, yielding analytical expressions for the eigenfrequencies that generalize known results in various aspects. We find that the analytical rather than the numerical solutions to the thin-boundary DR serve better the purpose for validating our self-consistent resistive solutions. More importantly, the eigenfrequencies are found to be sensitive to profile specifications, the ratio of the imaginary to the real part readily varying by a factor of two when one profile is used in place of another. Our eigenmode computations are also examined in the context of impulsively excited kink waves, suggesting the importance of resonant absorption for sufficiently oblique components when the spatial scale of the exciter is comparable to the slab half-width.

Excitation of negative energy surface magnetohydrodynamic waves in an incompressible cylindrical plasma

Yu, D.J., Nakariakov, V.M.
ApJ **2020**
https://arxiv.org/pdf/2004.13552.pdf
Negative energy wave phenomena may appear in shear flows in the presence of a wave decay mechanism and external energy supply. We study the appearance of negative energy surface waves in a plasma cylinder in the incompressible limit. The cylinder is surrounded by an axial magnetic field and by a plasma of different density. Considering flow inside and viscosity outside the flux tube, we derive dispersion relations, and obtain analytical solutions for the phase speed and growth rate (increment) of the waves. It is found that the critical speed shear for the occurrence of the dissipative instability associated with negative energy waves (NEWs) and the threshold of Kelvin-Helmholtz instability (KHI) depend on the axial wavelength. The critical shear for the appearance of sausage NEW is lowest for the longest axial wavelengths, while for kink waves the minimum value of the critical shear is reached for the axial wavelength comparable to the diameter of the cylinder. The range between the critical speed of the dissipative instability and the KHI threshold is shown to depend on the difference of the Alfvén speeds inside and outside of the cylinder. For all axial {wavenumbers}, NEW appears for the shear flow speeds lower than the KHI threshold. It is easier to excite NEW in an underdense cylinder than in an overdense one. The negative energy surface waves can be effectively generated for azimuthal number m=0 with a large axial wave number and for higher modes (m>0) with a small axial wave number.

Resonant Absorption of Surface Sausage and Surface Kink Modes under Photospheric Conditions

Dae Jung **Yu**1,2, Tom Van Doorsselaere1, and Marcel Goossens
2017 ApJ 850 44
http://sci-hub.cc/http://iopscience.iop.org/0004-637X/850/1/44/
We study the effect of resonant absorption of surface sausage and surface kink modes under photospheric conditions where the slow surface sausage modes undergo resonant damping in the slow continuum and the surface kink modes in the slow and Alfvén continua at the transitional layers. We use recently derived analytical formulas to obtain the damping rate (time). By considering linear density and linear pressure profiles for the transitional layers, we show that resonant absorption in the slow continuum could be an efficient mechanism for the wave damping of the slow surface sausage and slow surface kink modes while the damping rate of the slow surface kink mode in the Alfvén continuum is weak. It is also found that the resonant damping of the fast surface kink mode is much stronger than that of the slow surface kink mode, showing a similar efficiency as under coronal conditions. It is worth noting that the slow body sausage and kink modes can also resonantly damp in the slow continuum for those linear profiles.
Correction: A&A 626, C2 (**2019**) https://www.aanda.org/articles/aa/pdf/2019/06/aa30355e-16.pdf

Resonant absorption of the slow sausage wave in the slow continuum

D. J. **Yu**, T. Van Doorsselaere and M. Goossens
A&A 602, A108 (**2017**)

Aims. General analytical formulas for the damping rate by resonant absorption of slow sausage modes in the slow (cusp) continuum are derived and the resonant damping of the slow surface mode under photospheric conditions is investigated.
Methods. The connection formula across the resonant layer is used to derive the damping rate for the slow sausage mode in the slow continuum by assuming a thin boundary.
Results. It is shown that the effect of the resonant damping on the slow surface sausage mode in the slow continuum, which has been underestimated in previous interpretations, could be efficient under magnetic pore conditions. A simplified analytical formula for the damping rate of slow surface mode in the long wavelength limit is derived. This formula can be useful for a rough estimation of the damping rate due to resonant absorption for observational wave damping.

Impulsively Generated Wave Trains in Coronal Structures: I. Effects of Transverse Structuring on Sausage Waves in Pressureless Tubes

Hui **Yu**, Bo Li, Shao-Xia Chen, Ming Xiong, Ming-Zhe Guo
ApJ **836** 1 **2017**
https://arxiv.org/pdf/1612.09479v1.pdf
The behavior of the axial group speeds of trapped sausage modes plays an important role in determining impulsively generated wave trains, which have often been invoked to account for quasi-periodic signals with quasi-periods of order seconds in a considerable number of coronal structures. We conduct a comprehensive eigenmode analysis, both analytically and numerically, on the dispersive properties of sausage modes in pressureless tubes with three families of continuous radial density profiles. We find a rich variety of the dependence on the axial wavenumber k of the axial group speed vgr. Depending on the density contrast and profile steepness as well as on the detailed profile description, the vgr−k curves either possess or do not possess cutoff wavenumbers, and they can behave in either a monotonical or non-monotonical manner. With time-dependent simulations, we further show that this rich variety of the group speed characteristics heavily influences the temporal evolution and Morlet spectra of impulsively generated wave trains. In particular, the Morlet spectra can look substantially different from "crazy tadpoles" found for the much-studied discontinuous density profiles. We conclude that it is necessary to re-examine available high-cadence data to look for the rich set of temporal and spectral features, which can be employed to discriminate between the unknown forms of the density distributions transverse to coronal structures.

Impulsively generated sausage waves in coronal tubes with transversally continuous structuring

Hui **Yu**, Bo Li, Shao-Xia Chen, Ming Xiong, Ming-Zhe Guo
ApJ 833 51 **2016**
https://arxiv.org/pdf/1610.04316v1.pdf
The frequency dependence of the longitudinal group speeds of trapped sausage waves plays an important role in determining impulsively generated wave trains, which have often been invoked to account for quasi-periodic signals in coronal loops. We examine how the group speeds (v
gr) depend on angular frequency (ω) for sausage modes in pressureless coronal tubes with continuous transverse density distributions by solving the dispersion relation pertinent to the case where the density inhomogeneity of arbitrary form takes place in a transition layer of arbitrary thickness. We find that in addition to the transverse lengthscale l and density contrast ρi/ρe, the group speed behavior depends also on the detailed form of the density inhomogeneity. For parabolic profiles, vgr always decreases with ω first before increasing again, as happens for the much studied top-hat profiles. For linear profiles, however, the behavior of the ω−v
gr curves is more complex. When ρi/ρe≲6, the curves become monotonical for large values of
l. On the other hand, for higher density contrasts, a local maximum vmaxgr exists in addition to a local minimum vmingr when coronal tubes are diffuse. With time-dependent computations, we show that the different behavior of group speed curves, the characteristic speeds vmingr and vmaxgr in particular, is reflected in the temporal evolution and Morlet spectra of impulsively generated wave trains. We conclude that the observed quasi-periodic wave trains not only can be employed to probe such key parameters as density contrasts and profile steepness, but also have the potential to discriminate between the unknown forms of the transverse density distribution.

Case studies of EUV cyclones and their associated magnetic fields

Xin-Ting **Yu**, Jun Zhang, Ting Li, Shu-Hong Yang
Research in Astronomy and Astrophysics (RAA) Vol 15, No 9 1525-1536 (**2015**)
EUV cyclones are rotating structures in the solar corona, and they are usually rooted in the underlying rotating network magnetic fields in the photosphere. However, their connection with the surrounding magnetic fields remains unknown. Here we report an observational study of four typical cyclones which are rooted in different kinds

of magnetic fields. We use Solar Dynamics Observatory/Atmospheric Imaging Assembly data to investigate the rotation of EUV features in cyclones and Helioseismic and Magnetic Imager data to study the associated magnetic fields. The results show that, (1) an EUV cyclone rooted in a sunspot rotates with the photospheric magnetic field; (2) two EUV cyclones in two faculae of an active region are connected to the same sunspot of the active region but rotate oppositely; (3) an EUV cyclone is rooted in a coronal hole with weak open magnetic fields; (4) a pair of conjugated cyclones is rooted in magnetic fields that have opposite polarity with opposite directions of rotation. The differences in the spatial extent of a cyclone, characteristics of its rotation and underlying fields indicate that cyclones are ubiquitous over the solar atmosphere and that the magnetic structures relevant to the cyclones are more complicated than expected.

Homologous Cyclones in the Quiet Sun

Xinting **Yu**1,2, Jun Zhang1, Ting Li1, Yuzong Zhang1, and Shuhong Yang
2014 ApJ 782 L15
http://iopscience.iop.org/2041-8205/782/2/L15/pdf/apjl_782_2_15.pdf
Through observations with the Solar Dynamics Observatory Atmospheric Imaging Assembly (AIA) and Helioseismic and Magnetic Imager, we tracked one rotating network magnetic field (RNF) near the solar equator. It lasted for more than 100 hr, from **2013 February 23 to 28**. During its evolution, three cyclones were found to be rooted in this structure. Each cyclone event lasted for about 8 to 10 hr. While near the polar region, another RNF was investigated. It lasted for a shorter time (~70 hr), from **2013 July 7 to 9**. There were two cyclones rooted in the RNF and each lasted for 8 and 11 hr, respectively. For the two given examples, the cyclones have a similar dynamic evolution, and thus we put forward a new term: homologous cyclones. The detected brightening in AIA 171 Å maps indicates the release of energy, which is potentially available to heat the corona.

Advanced Γ Method for Small-scale Vortex Detection in the Solar Atmosphere

Yuyang **Yuan**1, Suzana de Souza e Almeida Silva2, Viktor Fedun2, Irina N. Kitiashvili3, and Gary Verth1
2023 ApJS 267 35
https://iopscience.iop.org/article/10.3847/1538-4365/acc835/pdf
Ubiquitous vortical structures are considered to act as a natural source of various solar plasma phenomena, for example, a wide range of magnetohydrodynamic waves and jet excitations. This work aims to develop an advanced vortex detection algorithm based on the Γ method and using a separable convolution kernel technique. This method is applied to detect and analyze the photospheric vortices in 3D realistic magnetoconvection numerical and observational data. We present the advanced Γ method (AGM), and our results indicate that the AGM performs with better accuracy in comparison with the original Γ method. The AGM allows us to identify small- and large-scale vortices with no vortex interposition and without requiring the changing of the threshold. In this way, the nondetection issue is mostly prevented. It was found that the Γ method failed to identify the large and longer-lived vortices, which were detected by the AGM. The size of the detected vortical structures tends to vary over time, with most vortices shrinking toward their end. The vorticity at the center is also not constant, presenting a sharp decay as the vortex ceases to exist. Due to its capability of identifying vortices with minimum nondetection, the vortex properties—such as lifetime, geometry, and dynamics—are better captured by the AGM than by the Γ method. In this era of new high-resolution observation, the AGM can be used as a precise technique for identifying and performing statistical analysis of solar atmospheric vortices.

Multilayered Kelvin–Helmholtz Instability in the Solar Corona

Ding **Yuan**1,2,8, Yuandeng Shen3,8, Yu Liu3, Hongbo Li4, Xueshang Feng1, and Rony Keppens5
2019 ApJL 884 L51
https://doi.org/10.3847/2041-8213/ab4bcd
https://arxiv.org/pdf/1910.05710.pdf
The Kelvin–Helmholtz (KH) instability is commonly found in many astrophysical, laboratory, and space plasmas. It could mix plasma components of different properties and convert dynamic fluid energy from large-scale structure to smaller ones. In this study, we combined the ground-based New Vacuum Solar Telescope (NVST) and the Solar Dynamic Observatories/Atmospheric Imaging Assembly (AIA) to observe the plasma dynamics associated with active region 12673 on **2017 September 9**. In this multitemperature view, we identified three adjacent layers of plasma flowing at different speeds, and detected KH instabilities at their interfaces. We could unambiguously track a typical KH vortex and measure its motion. We found that the speed of this vortex suddenly tripled at a certain stage. This acceleration was synchronized with the enhancements in emission measure and average intensity of the 193 Å data. We interpret this as evidence that KH instability triggers plasma heating. The intriguing feature in this event is that the KH instability observed in the NVST channel was nearly complementary to that in the AIA 193 Å. Such a multithermal energy exchange process is easily overlooked in previous studies, as the cold plasma component is usually not visible in the extreme-ultraviolet channels that are only sensitive to high-temperature plasma emissions.

Our finding indicates that embedded cold layers could interact with hot plasma as invisible matters. We speculate that this process could occur at a variety of length scales and could contribute to plasma heating.

Investigating Sub-Pixel 45-Second Periodic Wobble in SDO/AIA Data from January to August 2012

Ding **Yuan**, Wei Liu, Robert Walsh

Solar Physics October **2018**, 293:147 DOI /10.1007/s11207-018-1368-4

Artifacts could mislead interpretations in astrophysical observations. A thorough understanding of an instrument will help in distinguishing physical processes from artifacts. In this article, we investigate an artifact of the Atmospheric Imaging Assembly (AIA) onboard the Solar Dynamics Observatory. Time-series data and wavelet spectra revealed periodic intensity perturbations in small regions over the entire image in certain AIA extreme ultraviolet (EUV) passbands at a period of about 45 seconds. These artificial intensity variations are prominently detected in regions with sharp intensity contrast, such as sunspot light bridges. This artifact was caused by a periodic pointing wobble of the two AIA telescopes ATA 2 (193 and 211 Å channels) and ATA 3 (171 Å and UV channels), to a lesser extent, while the other two telescopes were not found to be affected. The peak-to-peak amplitude of the wobble was about 0.2 pixel in ATA 2 and 0.1 pixel in ATA 3. This artifact was intermittent and affected the data of seven months from 18 January to 28 August 2012, as a result of a thermal adjustment to the telescopes. We recommend that standard pointing-correction techniques, such as local correlation tracking, should be applied before any detailed scientific analysis that requires sub-pixel pointing accuracy. Specifically, this artificial 45-second periodicity was falsely interpreted as abnormal sub-minute oscillations in a light bridge of a sunspot (Yuan and Walsh in Astron. Astrophys.594, A101, 2016).

Abnormal oscillation modes in a waning light bridge

Ding **Yuan** and Robert W. Walsh

A&A 594, A101 (**2016**)

Context. A sunspot acts as a waveguide in response to the dynamics of the solar interior; the trapped waves and oscillations could reveal its thermal and magnetic structures.
Aims. We study the oscillations in a sunspot intruded by a light bridge, and the details of these oscillations could reveal the fine structure of the magnetic topology.
Methods. We used the Solar Dynamics Observatory/Atmospheric Imaging Assembly data to analyse the oscillations in the emission intensity of light bridge plasma at different temperatures, and we investigated their spatial distributions.
Results. The extreme ultraviolet emission intensity exhibits two persistent oscillations at five-minute and sub-minute ranges. The spatial distribution of the five-minute oscillation follows the spine of the bridge, whereas the sub-minute oscillations overlap with two flanks of the bridge. Moreover, the sub-minute oscillations are highly correlated in spatial domain, however, the oscillations at the eastern and western flanks are asymmetric with regard to the lag time. In the meantime, jet-like activities are only found at the eastern flank.
Conclusions. Asymmetries in the form of oscillatory pattern and jet-like activities are found between two flanks of a granular light bridge. Based on our study and recent findings, we propose a new model of twisted magnetic field for a light bridge and its dynamic interactions with the magnetic field of a sunspot.

Secondary fast magnetoacoustic waves trapped in randomly structured plasmas

Ding **Yuan**, Bo Li, Robert W. Walsh

ApJ **2016**
http://arxiv.org/pdf/1606.06059v1.pdf

Fast magnetoacoustic wave is an important tool for inferring solar atmospheric parameters. We numerically simulate the propagation of fast wave pulses in randomly structured plasmas mimicking the highly inhomogeneous solar corona. A network of secondary waves is formed by a series of partial reflections and transmissions. These secondary waves exhibit quasi-periodicities in both time and space. Since the temporal and spatial periods are related simply through the fast wave speed, we quantify the properties of secondary waves by examining the dependence of the average temporal period ($\bar{p}$) on the initial pulse width (w0) as well as the density contrast ($\delta\rho$) and correlation length (Lc) that characterize the randomness of the equilibrium density profiles. For small-amplitude pulses, $\delta\rho$ does not alter $\bar{p}$ significantly. Large-amplitude pulses, on the other hand, enhance the density contrast when $\delta\rho$ is small but have a smoothing effect when $\delta\rho$ is sufficiently large. We found that $\bar{p}$ scales linearly with Lc and that the scaling factor is larger for a narrower pulse. However, in terms of the absolute values of $\bar{p}$, broader pulses generate secondary waves with longer periods, and this effect is stronger in random plasmas with shorter correlation lengths. Secondary waves carry the signatures of both the leading wave pulse and background plasma, our study may find applications in MHD seismology by exploiting the secondary waves detected in the dimming regions after CMEs or EUV waves.

Stochastic transients as a source of quasi-periodic processes in the solar atmosphere

Ding **Yuan**, Jiangtao Su, Fangran Jiao, Robert W. Walsh

2016 ApJS

http://arxiv.org/pdf/1603.08977v1.pdf

Solar dynamics and turbulence occur at all heights of the solar atmosphere and could be described as stochastic processes. We propose that finite lifetime transients recurring at a certain place could trigger quasi-periodic processes in the associated structures. In this study, we developed a mathematical model for finite lifetime and randomly occurring transients, and found that quasi-periodic processes, with period longer than the time scale of the transients, are detectable intrinsically in form of trains. We simulate their propagation in an empirical solar atmospheric model with chromosphere, transition region and corona. We found that, due to the filtering effect of the chromospheric cavity, only the resonance period of the acoustic resonator is able to propagate to the upper atmosphere, such a scenario is applicable to slow magnetoacoustic waves in sunspots and active regions. If the thermal structure of the atmosphere is less wild and acoustic resonance does not take effect, the long period oscillations could propagate to the upper atmosphere. Such case would be more likely to occur at polar plumes.

Forward Modelling of Standing Kink Modes in Coronal Loops I. Synthetic Views

Ding **Yuan**, Tom Van Doorsselaere

2016

http://arxiv.org/pdf/1603.01632v1.pdf

Kink magnetohydrodynamic (MHD) waves are frequently observed in various magnetic structures of the solar atmosphere. They may contribute significantly to coronal heating and could be used as a tool to diagnose the solar plasma. In this study, we synthesise the \ion{Fe}{9} λ171.073 emission of a coronal loop supporting a standing kink MHD mode. The kink MHD wave solution of a plasma cylinder is mapped into a semi-torus structure to simulate a curved coronal loop. We decompose the solution into a quasi-rigid kink motion and a quadrupole term, which dominate the plasma inside and outside the flux tube, respectively. At the loop edges, the line-of-sight integrates relatively more ambient plasma, and the background emission becomes significant. The plasma motion associated with the quadrupole term causes spectral line broadening and emission suppression. The periodic intensity suppression will modulate the integrated intensity and the effective loop width, which both exhibit oscillatory variations at half of the kink period. The quadrupole term can be directly observed as a pendular motion at front view.

Evolution of fast magnetoacoustic pulses in randomly structured coronal plasmas

D. **Yuan**, D.J. Pascoe, V.M. Nakariakov, B. Li, R. Keppens

2015 *ApJ* **799** 221

http://arxiv.org/pdf/1411.4152v1.pdf

Magnetohydrodynamic waves interact with structured plasmas and reveal the internal magnetic and thermal structures therein, thereby having seismological applications in the solar atmosphere. We investigate the evolution of fast magnetoacoustic pulses in randomly structured plasmas, in the context of large-scale propagating waves in the solar atmosphere. We perform one dimensional numerical simulations of fast wave pulses propagating perpendicular to a constant magnetic field in a low-beta plasma with a random density profile across the field. Both linear and nonlinear regimes are considered. We study how the evolution of the pulse amplitude and width depends on their initial values and the parameters of the random structuring. A randomly structured plasma acts as a dispersive medium for a fast magnetoacoustic pulse, causing amplitude attenuation and broadening of the pulse width. After the passage of the main pulse, secondary propagating and standing fast waves appear in the plasma. Width evolution of both linear and nonlinear pulses can be well approximated by linear functions; however, narrow pulses may have zero or negative broadening. This arises because a narrow pulse is prone to splitting, while a broad pulse usually deviates less from their initial Gaussian shape and form ripple structures on top of the main pulse. A linear pulse decays at almost a constant rate, while a nonlinear pulse decays exponentially. A pulse interacts most efficiently with a random medium which has a correlation length of about half of its initial pulse width. The development of a detailed model of a fast MHD pulse propagating in highly structured medium substantiates the interpretation of EIT waves as fast magnetoacoustic waves. Evolution of a fast pulse provides us with a novel method to diagnose the sub-resolution filamentation of the solar atmosphere.

Multi-height observations of magnetoacoustic cut-off frequency in a sunspot atmosphere

D. **Yuan**1,2, R. Sych2,3, V. E. Reznikova4 and V. M. Nakariakov

A&A 561, A19 (**2014**)
Context. The cut-off frequency of magnetoacoustic gravity (MAG) waves could be decreased by the inclined magnetic field, and therefore, low-frequency waves could penetrate into the upper atmosphere.
Aims. We observe the distribution of the cut-off frequency of compressive waves at various heights and reconstruct the magnetic field inclination, according to the MAG wave theory in a stratified atmosphere permeated by a uniform magnetic field.
Methods. We analysed the emission intensity oscillations of sunspot AR11131 (**08 Dec. 2010**) observed at the 1700 Å, 1600 Å, and 304 Å bandpasses of the Atmospheric Imaging Assembly (AIA) onboard the Solar Dynamics Observatory (SDO), and computed the narrow-band power maps with the pixelised wavelet filtering method. The distribution of the cut-off frequency was defined as the median contour in the azimuthally-averaged oscillation power. The magnetic field inclination was estimated with the local cut-off frequency according to the MAG wave theory in the low-β limit and was compared to the potential field extrapolation.
Results. Shorter period oscillations dominate in the sunspot umbra, while longer period oscillations form an annular shape approximately concentric with the sunspot. Oscillations with longer periods are distributed further away from the sunspot centre. The 5 min oscillations appear to originate at or lower than the photosphere. The magnetic field inclinations determined with the cut-off frequency theory are about 30−40% larger than the values obtained by the potential field extrapolation.
Conclusions. The oscillation power distribution in a sunspot atmosphere reflects its magnetic and thermal structure. The cut-off frequency could be used to probe the magnetic field inclination, however, other factors have to be included to fully understand this phenomenon. The existence of return magnetic flux at the outer penumbra was evidenced by the cut-off frequency distribution.

Leakage of long-period oscillations from the chromosphere to the corona

D. **Yuan**1, V. M. Nakariakov1,2, N. Chorley1 and C. Foullon1
A&A 533, A116 (**2011**)
Long-period oscillations in a coronal diffuse structure are detected with the Transition Region And Coronal Explorer (TRACE). The EUV images of the NOAA active region 8253 are available in 171 Å and 195 Å bandpasses from 30 June to 4 July 1998. The average intensity variation is found to be connected with the CCD temperature, which varies with the orbital motion of the spacecraft. Hence, oscillations with the orbital period and its higher harmonics appear as artifacts in the light curves. After the exclusion of the orbital effects, we identified several long-period oscillations in the diffuse fan-like structure of the active region. Similar periodicities were detected in the radio emission from the chromospheric part of that active region, observed with the ground-based Nobeyama Radioheliograph (NoRH) in the 17 GHz channel. It was found that 0.221, 0.312 and 0.573 mHz oscillations were present in both EUV emission lines in the corona and the radio signal from the sunspot in the chromosphere, just beneath the active region. From the frequency values, the 1st and 3rd detected oscillations could be associated with the $l = 2$, $n = -3$ or $l = 3$, $n = -5$ and $l = 1$ gravity-driven solar interior modes, respectively. The appearance of these oscillations in the coronal part of the active region can be connected with the wave leakage or the evanescence of chromospheric oscillations.

Using Potential Field Extrapolations to Explore the Origin of Type II Spicules

Vasyl **Yurchyshyn**1, Anneliese Schmidt2, Jiasheng Wang2, Xu Yang1, Eun-Kyung Lim3, and Wenda Cao1
2024 ApJ 961 79
https://iopscience.iop.org/article/10.3847/1538-4357/ad0da2/pdf
We used 29 high-resolution line-of-sight magnetograms acquired with the Goode Solar Telescope (GST) in a quiet-Sun area to extrapolate a series of potential field configurations and study their time variations. The study showed that there are regions that consistently exhibit changes in loop connectivity, whereas other vast areas do not show such changes. Analysis of the topological features of the potential fields indicates that the photospheric footprint of the separatrix between open- and closed-loop systems closely matches the roots of rapid blue- and redshifted excursions, which are disk counterparts of type II spicules. There is a tendency for the footpoints of the observed Hα features to be cospatial with the footpoints of the loops that most frequently change their connectivity, while the area occupied by the open fields that did not show any significant and persistent connectivity changes is void of prominent jet and spicular activity. We also detected and tracked magnetic elements using the Southwest Automatic Magnetic Identification Suite and GST magnetograms, which allowed us to construct artificial magnetograms and calculate the corresponding potential field configurations. Analysis of the artificial data showed tendencies similar to those found for the observed data. The present study suggests that a significant amount of chromospheric activity observed in the far wings of the Hα spectral line may be generated by reconnecting closed-loop systems and canopy fields consisting of "open" field lines. **2017 June 19**

Rapid Evolution of Type II Spicules Observed in Goode Solar Telescope On-Disk Hα Images

Vasyl **Yurchyshyn**, 1 Wenda Cao, 1 Valentina Abramenko, 2 Xu Yang, 1 and Kyung-Suk Cho
ApJ **891** L21 **2020**
http://www.bbso.njit.edu/~vayur/spicules2019.pdf
https://doi.org/10.3847/2041-8213/ab7931
https://arxiv.org/pdf/2005.04253.pdf
We analyze ground-based chromospheric data acquired at a high temporal cadence of 2 s in wings of the Hα spectral line using Goode Solar Telescope (GST) operating at the Big Bear Solar Observatory. We inspected a 30 minute long Hα-0.08 nm data set to find that rapid blue-shifted Hα excursions (RBEs), which are a cool component of type II spicules, experience very rapid morphological changes on the time scales of the order of 1 second. Unlike typical reconnection jets, RBEs very frequently appear in situ without any clear evidence of Hα material being injected from below. Their evolution includes inverted "Y", "V", "N", and parallel splitting (doubling) patterns as well as sudden formation of a diffuse region followed by branching. We also find that the same feature may undergo several splitting episodes within about 1 min time interval. **June 7 2019**

Disentangling flows in the solar transition region A110

P. **Zacharias**, V. H. Hansteen, J. Leenaarts, M. Carlsson and B. V. Gudiksen
A&A 614, A110 (**2018**)
Context. The measured average velocities in solar and stellar spectral lines formed at transition region temperatures have been difficult to interpret. The dominant redshifts observed in the lower transition region naturally leads to the question of how the upper layers of the solar (and stellar) atmosphere can be maintained. Likewise, no ready explanation has been made for the average blueshifts often found in upper transition region lines. However, realistic three-dimensional radiation magnetohydrodynamics (3D rMHD) models of the solar atmosphere are able to reproduce the observed dominant line shifts and may thus hold the key to resolve these issues. Aims. These new 3D rMHD simulations aim to shed light on how mass flows between the chromosphere and corona and on how the coronal mass is maintained. These simulations give new insights into the coupling of various atmospheric layers and the origin of Doppler shifts in the solar transition region and corona.
Methods. The passive tracer particles, so-called corks, allow the tracking of parcels of plasma over time and thus the study of changes in plasma temperature and velocity not only locally, but also in a co-moving frame. By following the trajectories of the corks, we can investigate mass and energy flows and understand the composition of the observed velocities.
Results. Our findings show that most of the transition region mass is cooling. The preponderance of transition region redshifts in the model can be explained by the higher percentage of downflowing mass in the lower and middle transition region. The average upflows in the upper transition region can be explained by a combination of both stronger upflows than downflows and a higher percentage of upflowing mass. The most common combination at lower and middle transition region temperatures are corks that are cooling and traveling downward. For these corks, a strong correlation between the pressure gradient along the magnetic field line and the velocity along the magnetic field line has been observed, indicating a formation mechanism that is related to downward propagating pressure disturbances. Corks at upper transition region temperatures are subject to a rather slow and highly variable but continuous heating process.
Conclusions. Corks are shown to be an essential tool in 3D rMHD models in order to study mass and energy flows. We have shown that most transition region plasma is cooling after having been heated slowly to upper transition region temperatures several minutes before. Downward propagating pressure disturbances are identified as one of the main mechanisms responsible for the observed redshifts at transition region temperatures.

On the Verge of a Grand Solar Minimum: A Second Maunder Minimum?

L. **Zachilas**, A. Gkana
Solar Phys. May 2015, Volume 290, Issue 5, pp 1457-1477 **2015**
We analyze the yearly mean sunspot-number data covering the period 1700 to 2012. We show that the yearly sunspot number is a low-dimensional deterministic chaotic system. We perform future predictions trying to forecast the solar activity during the next five years (2013 – 2017). We provide evidence that the yearly sunspot-number data can be used for long-term predictions. To test and prove that our model is able to predict the Maunder Minimum period (1645 – 1715), we perform long-term post-facto predictions comparing them with the observed sunspot-number values. We also perform long-term future predictions trying to forecast the solar activity up to 2102. Our predictions indicate that the present Cycle 24 is expected to be a low-peak cycle. We conclude that the level of solar activity is likely to be reduced significantly during the next 90 years, somewhat resembling theMaunder Minimum period.

On the Role of the Neutral Plasma Component in the Electric Current Dissipation and the Formation of a Transition Region in the Solar Atmosphere.

Zaitsev, V.V., Stepanov, A.V. & Kupriyanova, E.G.

Geomagn. Aeron. 63, 947–952 (**2023**).
https://doi.org/10.1134/S0016793223070319
A mechanism of the formation of a transition region between the chromosphere and the corona, which relies on the dissipation of electric currents in a partially ionized plasma is proposed. It has been demonstrated that the transition region experiences the enhanced level of Joule dissipation due to an increased Cowling resistivity caused by ion-neutral particle collisions. This leads to effective heating of current-carrying open magnetic flux tubes, the type II spicules, which are responsible for the formation of a thin transition layer. An estimation is provided for the width of this transition region, which depends on the power of Joule dissipation, i.e., the magnitude of the electric current.

On the Possibility of Heating the Solar Corona by Heat Fluxes from Coronal Magnetic Structures

V. V. **Zaitsev**, A. V. Stepanov & P. V. Kronshtadtov
Solar Physics volume 295, Article number: 166 (**2020**)
https://link.springer.com/content/pdf/10.1007/s11207-020-01732-x.pdf
We estimate the role of heat flux from hot magnetic loops and open flux tubes into the surrounding corona as a possible source of heating of the corona. We show that hot magnetic-flux tubes (Type-II spicules) provide a more efficient source of coronal heating than hot magnetic loops, as the closed magnetic structure of a loop substantially restricts the heat flux into the corona. In order to compensate for radiation and thermal-conduction losses, approximately 104104 Type-II spicules with a temperature of several million Kelvin are required, which is about 1% of the number of spicules simultaneously observed on the solar disk. Our analysis shows that the principal source of energy that heats the coronal plasma is photospheric convection, which generates electric currents of about 10101010 – 10121012 A in magnetic loops and spicules. Dissipation of the currents increases significantly in the partially ionized plasma, i.e. when ion–atom collisions and the associated Cowling conductivity occur. This results in two important effects: heating of plasma in magnetic structures up to several million Kelvin, and ejection of hot plasma from open magnetic-flux tubes to the corona, replenishing the corona with hot plasma. The ejection of hot plasma results from the heating of the spicule foot-point by electric-current dissipation, which grows with a sporadic increase in the velocity of photospheric convection, for example, due to five-minute oscillations or the Rayleigh–Taylor instability. As a result, the rate of heating the photospheric foot-points of the spicules by ring currents exceeds radiation losses, which leads to a jump in the pressure gradient and the ejection of hot plasma into the corona from the open tips of the magnetic-flux tubes.

Constraining Time Dependent Dark Matter Signals from the Sun

Mohammadreza **Zakeri**, Yu-Feng Zhou
2021
https://arxiv.org/pdf/2109.11662.pdf
Dark matter (DM) particles captured by the Sun can produce high energy electrons outside the Sun through annihilating into meta-stable mediators. The corresponding cosmic-ray electron signals observed by the space-based experiments will be time dependent due to the orbital motion of the space-based detectors. The shape of this time dependence is predictable given the orbital information of the detectors. Since the high-energy CR electron (with energy E>100 GeV) fluxes are expected to be constant in time, non-observation of such time variation can be used to place upper limits on the DM annihilation cross section. We analyze the time dependence of dark matter cosmic-ray signals in three space-based experiments: AMS-02, DAMPE and CALET. Under the assumption that no time dependent signal is observed, we derive the 95% C.L. exclusion limits on the signal strength from the current data. We map our limits onto the parameter space of the dark photon model and find that the constraints are comparable with that derived from the supernova SN1987A.

Contribution of polar plumes to fast solar wind

L. **Zangrilli** and S. M. Giordano
A&A 643, A104 (**2020**)
https://www.aanda.org/articles/aa/pdf/2020/11/aa37653-20.pdf
https://doi.org/10.1051/0004-6361/202037653
Context. Several physical properties of solar polar plumes have been identified by different published studies, however such studies are rare and sometimes in disagreement.
Aims. The purpose of the present work is to analyze a set of SOHO/UVCS data dedicated to the observation of plumes and to obtain a picture of the physical properties of plumes in the intermediate solar corona through a self-consistent analysis.
Methods. We applied the Doppler Dimming technique to data acquired by SOHO/UVCS in **April 1996**, which was during the very early phases of the mission. From this we derived outflow speeds and electron densities. We used SOHO/LASCO images as context data in order to better identify plume and interplume regions in the UVCS field of view.

Results. The results we obtain demonstrate that in three cases out of four plumes expand with outflow speeds comparable to those of interplumes, and in a single case with lower speeds. We estimate that the contribution of plumes to the wind coming from the solar poles is about 20%, and that different plumes provide a different contribution, possibly according to different stages of their evolution.
Conclusions. We conclude that plumes are not static structures, and that they contribute significantly to the wind coming from the solar poles.

Evolution of active region outflows throughout an active region lifetime

L. **Zangrilli**, G. Poletto
A&A 594, A40 **2016**
http://arxiv.org/pdf/1608.07408v1.pdf
We have shown previously that SOHO/UVCS data allow us to detect active region (AR) outflows at coronal altitudes higher than those reached by other instrumentation. These outflows are thought to be a component of the slow solar wind. Our purpose is to study the evolution of the outflows in the intermediate corona from AR 8100, from the time the AR first forms until it dissolves, after several transits at the solar limb. Data acquired by SOHO/UVCS at the time of the AR limb transits, at medium latitudes and at altitudes ranging from 1.5 to 2.3 R_sun, were used to infer the physical properties of the outflows through the AR evolution. To this end, we applied the Doppler dimming technique to UVCS spectra. These spectra include the H I Lyman alpha line and the O VI doublet lines at 1031.9 and 1037.6 A. Plasma speeds and electron densities of the outflows were inferred over several rotations of the Sun. AR outflows are present in the newly born AR and persist throughout the entire AR life. Moreover, we found two types of outflows at different latitudes, both possibly originating in the same negative polarity area of the AR. We also analyzed the behavior of the Si XII 520 A line along the UVCS slit in an attempt to reveal changes in the Si abundance when different regions are traversed. Although we found some evidence for a Si enrichment in the AR outflows, alternative interpretations are also plausible. Our results demonstrate that outflows from ARs are detectable in the intermediate corona throughout the whole AR lifetime. This confirms that outflows contribute to the slow wind.

A SOHO/UVCS study of coronal outflows at the edge of an active region complex

L. **Zangrilli**1 and G. Poletto
A&A 545, A8 (**2012**)
Context. In the past, active regions (ARs) have been suggested as a possible source of the slow solar wind. Their role as solar wind contributors has recently been supported by HINODE observations at low coronal levels.
Aims. Our purpose is to determine whether outflows at the edges of ARs can be detected in higher layers of the corona, supporting the low-corona evidence for the occurrence of wind streams from ARs.
Methods. Data acquired by SOHO/UVCS on January 2, 1998, at altitudes ranging from 1.5 to 2.3 solar radii at mid latitudes, were used to infer the physical properties of an AR complex at the time of its limb passage. To this end, the Doppler dimming technique was applied to UVCS observations of the H i Lyα and O vi doublet lines at 1031.9 and 1037.6 Å.
Results. Outflow speeds (and electron densities) were inferred: outflows, at speeds increasing with height, turn out to be confined within a narrow channel at the edge of closed loop systems within the AR. Our results are compared with those obtained by other authors with different techniques.
Conclusions. Our results support the assumption that ARs are sources of slow wind. To our knowledge these are the first direct measurements of AR flows in the intermediate corona. Tentative profiles of the speed vs. heliocentric altitudes at heliocentric distances between ≈ 1.5 and ≈ 2.3 solar radii show that AR flows are faster than streams from equatorial coronal holes.

Spectral Anisotropy in 2D plus Slab Magnetohydrodynamic Turbulence in the Solar Wind and Upper Corona

G. P. **Zank**1,2, M. Nakanotani1, L.-L. Zhao1, L. Adhikari1, and D. Telloni3
2020 ApJ 900 115
https://doi.org/10.3847/1538-4357/abad30
The 2D + slab superposition model of solar wind turbulence has its theoretical foundations in nearly incompressible magnetohydrodynamics (NI MHD) in the plasma beta ~1 or $\ll 1$ regimes. Solar wind turbulence measurements show that turbulence in the inertial range is anisotropic, for which the superposition model offers a plausible explanation. We provide a detailed theoretical analysis of the spectral characteristics of the Elsässer variables in the 2D + NI/slab model. We find that (1) the majority 2D component has a power spectrum $G^{\infty}(k_{\perp}) \sim k_{\perp}^{-5/3}$ in perpendicular wavenumber k⊥; (2) the strongly imbalanced minority NI/slab turbulence has power spectra $G^{*}(k_{\perp}) \sim k_{\perp}^{-5/3}$ and $G^{*}(k_{z}) \sim k_{z}^{-5/3}$, where kz is aligned with the mean magnetic field; (3) NI/slab turbulence can exhibit a double-power-law spectrum, with the steeper part being G*(k) ~ k−5/3 and corresponding

to strong turbulence and the flatter spectrum satisfying G*(k) ~ k−3/2 and corresponding to weak turbulence; (4) there is a critical balance regime for NI/slab turbulence that satisfies $G^*(k_z) \sim k_z^{-2}$ and $G^*(k_\perp) \sim k_\perp^{-5/3}$; and (5) the forward and backward Elsässer power spectra can have different spectral forms provided that the triple-correlation times for each are different. We use the spectral analysis to compute the total power spectra in frequency parallel to the solar wind flow for the superposition model, showing that strongly imbalanced turbulence yields an f−5/3 spectrum for all angles between the mean flow and magnetic field, and that double power laws are possible when the nonlinear and Alfvén timescales are both finite.

Theory and Transport of Nearly Incompressible Magnetohydrodynamic Turbulence. IV. Solar Coronal Turbulence

G. P. **Zank**, L. Adhikari, P. Hunana, S. K. Tiwari, R. Moore, D. Shiota, R. Bruno, and D. Telloni
2018 ApJ 854 32

A new model describing the transport and evolution of turbulence in the quiet solar corona is presented. In the low plasma beta environment, transverse photospheric convective fluid motions drive predominantly quasi-2D (nonpropagating) turbulence in the mixed-polarity "magnetic carpet," together with a minority slab (Alfvénic) component. We use a simplified sub-Alfvénic flow velocity profile to solve transport equations describing the evolution and dissipation of turbulence from 1 to $15\,R_\odot$ (including the Alfvén surface). Typical coronal base parameters are used, although one model uses correlation lengths derived observationally by Abramenko et al., and the other assumes values 10 times larger. The model predicts that (1) the majority quasi-2D turbulence evolves from a balanced state at the coronal base to an imbalanced state, with outward fluctuations dominating, at and beyond the Alfvén surface, i.e., inward turbulent fluctuations are dissipated preferentially; (2) the initially imbalanced slab component remains imbalanced throughout the solar corona, being dominated by outwardly propagating Alfvén waves, and wave reflection is weak; (3) quasi-2D turbulence becomes increasingly magnetized, and beyond $\sim 6\,R_\odot$, the kinetic energy is mainly in slab fluctuations; (4) there is no accumulation of inward energy at the Alfvén surface; (5) inertial range quasi-2D rather than slab fluctuations are preferentially dissipated within $\sim 3\,R_\odot$; and (6) turbulent dissipation of quasi-2D fluctuations is sufficient to heat the corona to temperatures $\sim 2 \times 10^6$ K within $2\,R_\odot$, consistent with observations that suggest that the fast solar wind is accelerated most efficiently between ~ 2 and $4\,R_\odot$.

Kink instability of triangular jets in the solar atmosphere

T. V. **Zaqarashvili**, S. Lomineishvili, P. Leitner, A. Hanslmeier, P. Gömöry, M. Roth
A&A **2021**
https://arxiv.org/pdf/2102.09952.pdf

It is known that hydrodynamic triangular jets are unstable to antisymmetric kink perturbations. The inclusion of magnetic field may lead to the stabilisation of the jets. Jets and complex magnetic fields are ubiquitous in the solar atmosphere, which suggests the possibility of the kink instability in certain cases. The aim of the paper is to study the kink instability of triangular jets sandwiched between magnetic tubes/slabs and its possible connection to observed properties of the jets in the solar atmosphere. A dispersion equation governing the kink perturbations is obtained through matching of analytical solutions at the jet boundaries. The equation is solved analytically and numerically for different parameters of jets and surrounding plasma. The analytical solution is accompanied by a numerical simulation of fully nonlinear MHD equations for a particular situation of solar type II spicules. MHD triangular jets are unstable to the dynamic kink instability depending on the Alfven Mach number (the ratio of flow to Alfven speeds) and the ratio of internal and external densities. When the jet has the same density as the surrounding plasma, then only super Alfvenic flows are unstable. However, denser jets are unstable also in sub Alfvenic regime. Jets with an angle to the ambient magnetic field have much lower thresholds of instability than field-aligned flows. Growth times of the kink instability are estimated as 6-15 min for type I spicules and 5-60 s for type II spicules matching with their observed life times. Numerical simulation of full nonlinear equations shows that the transverse kink pulse locally destroys the jet in less than a minute in the conditions of type II spicules. Dynamic kink instability may lead to full breakdown of MHD flows and consequently to observed disappearance of spicules in the solar atmosphere.

Dynamic kink instability and transverse motions of solar spicules

T. V. **Zaqarashvili**
ApJL **893** L46 **2020**
https://arxiv.org/pdf/2004.04401.pdf
https://doi.org/10.3847/2041-8213/ab881d

Hydrodynamic jets are unstable to the kink instability (m=1 mode in cylindrical geometry) owing to the centripetal force, which increases the transverse displacement of the jet. When the jet moves along a magnetic field, then the Lorentz force tries to decrease the displacement and stabilises the instability of sub-Alfvenic flows. The threshold of the instability depends on the Alfven Mach number (the ratio of Alfven and jet speeds). We suggest that the dynamic kink instability may be of importance to explain observed transverse motions of type II spicules in the solar

atmosphere. We show that the instability may start for spicules which rise up at the peripheries of vertically expanding magnetic flux tubes owing to the decrease of the Alfven speed in both, the vertical and the radial directions. Therefore, inclined spicules may be more unstable and have more higher transverse speeds. Periods and growth times of unstable modes in the conditions of type II spicules have the values of 30 s and 25-100 s, respectively, which are comparable to the life time of the structures. This may indicate to the interconnection between high speed flow and rapid disappearance of type II spicules in chromospheric spectral lines.

Magneto-Rossby Waves and Seismology of Solar Interior

Teimuraz V. **Zaqarashvili** and Eka Gurgenashvili
Front. Astron. Space Sci. **2018**
https://doi.org/10.3389/fspas.2018.00007
https://doi.org/10.3389/fspas.2018.00007
Eleven-year Schwabe cycle in solar activity is not yet fully understood despite of its almost two century discovery. It is generally interpreted as owing to some sort of magnetic dynamo operating below or inside the convection zone. The magnetic field strength in the dynamo layer may determine the importance of the tachocline in the model which is responsible for the cyclic magnetic field, but the direct measurement is not possible. On the other hand, solar activity also displays short term variations over time scale of months (Rieger-type periodicity), which significantly depend on solar activity level: stronger cycles (or more active hemisphere in each cycle) generally show shorter periodicity and vice versa. The periodicity is probably connected to Rossby-type waves in the dynamo layer, therefore alongside with wave dispersion relations it might be used to estimate the dynamo magnetic field strength. We performed the wavelet analysis of hemispheric sunspot areas during solar cycles 13–24 and corresponding hemispheric values of Rieger-type periodicity are found in each cycle. Two different Rossby-type waves could lead to observed periodicities: spherical fast magneto-Rossby waves and equatorial Poincare-Rossby waves. The dispersion relation of spherical fast magneto-Rossby waves gives the estimated field strength of >40 kG in stronger cycles (or in more active hemisphere) and <40 kG in weaker cycles (or in less active hemisphere). The equatorial Poincare-Rossby waves lead to >20 kG and <15 kG, respectively. Future perspectives of Rieger-type periodicities and Rossby-type waves in testing various dynamo models are discussed.

Long-term variation in the Sun's activity caused by magnetic Rossby waves in the tachocline

T. V. **Zaqarashvili**, R. Oliver, A. Hanslmeier, M. Carbonell, J. L. Ballester, T. Gachechiladze, I. G. Usoskin
ApJL **805** L14 **2015**
http://arxiv.org/pdf/1505.02652v1.pdf
Long-term records of sunspot number and concentrations of cosmogenic radionuclides (10Be and 14C) on the Earth reveal the variation of the Sun's magnetic activity over hundreds and thousands of years. We identify several clear periods in sunspot, 10Be, and 14C data as 1000, 500, 350, 200 and 100 years. We found that the periods of the first five spherical harmonics of the slow magnetic Rossby mode in the presence of a steady toroidal magnetic field of 1200-1300 G in the lower tachocline are in perfect agreement with the time scales of observed variations. The steady toroidal magnetic field can be generated in the lower tachocline either due to the steady dynamo magnetic field for low magnetic diffusivity or due to the action of the latitudinal differential rotation on the weak poloidal primordial magnetic field, which penetrates from the radiative interior. The slow magnetic Rossby waves lead to variations of the steady toroidal magnetic field in the lower tachocline, which modulate the dynamo magnetic field and consequently the solar cycle strength. This result constitutes a key point for long-term prediction of the cycle strength. According to our model, the next deep minimum in solar activity is expected during the first half of this century.

Mixed Properties of Slow Magnetoacoustic and Entropy Waves in a Plasma with Heating/Cooling Misbalance

D. **Zavershinskii**, D. Kolotkov, D. Riashchikov & N. Molevich
Solar Physics volume 296, Article number: 96 (**2021**)
https://link.springer.com/content/pdf/10.1007/s11207-021-01841-1.pdf
The processes of coronal plasma heating and cooling were previously shown to significantly affect the dynamics of slow magnetoacoustic (MA) waves, causing amplification or attenuation, and also dispersion. However, the entropy mode is also excited in such a thermodynamically active plasma and is affected by the heating/cooling misbalance too. This mode is usually associated with the phenomenon of coronal rain and formation of prominences. Unlike adiabatic plasmas, the properties and evolution of slow MA and entropy waves in continuously heated and cooling plasmas get mixed. Different regimes of the misbalance lead to a variety of scenarios for the initial perturbation to evolve. In order to describe properties and evolution of slow MA and entropy waves in various regimes of the misbalance, we obtained an exact analytical solution of the linear evolutionary equation. Using the characteristic

timescales and the obtained exact solution, we identified regimes with qualitatively different behaviour of slow MA and entropy modes. For some of those regimes, the spatio-temporal evolution of the initial Gaussian pulse is shown. In particular, it is shown that slow MA modes may have a range of non-propagating harmonics. In this regime, perturbations caused by slow MA and entropy modes in a low-ββ plasma would look identical in observations, as non-propagating disturbances of the plasma density (and temperature) either growing or decaying with time. We also showed that the partition of the initial energy between slow MA and entropy modes depends on the properties of the heating and cooling processes involved. The exact analytical solution obtained could be further applied to the interpretation of observations and results of numerical modelling of slow MA waves in the corona and the formation and evolution of coronal rain.

Formation of quasi-periodic slow magnetoacoustic wave trains by the heating/cooling misbalance

D. I. **Zavershinskii**, D. Y. Kolotkov, V. M. Nakariakov, N. E. Molevich, D. S. Ryashchikov
Physics of Plasmas **2019**
https://arxiv.org/pdf/1907.08168.pdf
https://warwick.ac.uk/fac/sci/physics/research/cfsa/people/kolotkov/eprints/disp_pop_r1.pdf
Slow magnetoacoustic waves are omnipresent in both natural and laboratory plasma systems. The wave-induced misbalance between plasma cooling and heating processes causes the amplification or attenuation, and also dispersion, of slow magnetoacoustic waves. The wave dispersion could be attributed to the presence of characteristic time scales in the system, connected with the plasma heating or cooling due to the competition of the heating and cooling processes in the vicinity of the thermal equilibrium. We analysed linear slow magnetoacoustic waves in a plasma in a thermal equilibrium formed by a balance of optically thin radiative losses, field-align thermal conduction, and an unspecified heating. The dispersion is manifested by the dependence of the effective adiabatic index of the wave on the wave frequency, making the phase and group speeds frequency-dependent. The mutual effect of the wave amplification and dispersion is shown to result into the occurrence of an oscillatory pattern in an initially broadband slow wave, with the characteristic period determined by the thermal misbalance time scales, i.e. by the derivatives of the combined radiation loss and heating function with respect to the density and temperature, evaluated at the equilibrium. This effect is illustrated by estimating the characteristic period of the oscillatory pattern, appearing because of thermal misbalance in the plasma of the solar corona. It is found that by an order of magnitude the period is about the typical periods of slow magnetoacoustic oscillations detected in the corona.

Evidence for Energy Supply by Active Region Spicules to the Solar Atmosphere

S. **Zeighami**, A. R. Ahangarzadeh Maralani, E. Tavabi, A. Ajabshirizadeh
Solar Phys. Volume 291, Issue 3, pp 847-858 **2016**
http://arxiv.org/pdf/1602.03157v1.pdf
We investigate the role of active region spicules in the mass balance of the solar wind and energy supply for heating the solar atmosphere. We use high cadence observations from the Solar Optical Telescope (SOT) onboard the Hinode satellite in the Ca II H line filter obtained on **26 January 2007**. The observational technique provides the high spatio-temporal resolution required to detect fine structures such as spicules. We apply Fourier power spectrum and wavelet analysis to SOT/Hinode time series of an active region data to explore the existence of coherent intensity oscillations. The presence of coherent waves could be an evidence for energy transport to heat the solar atmosphere. Using time series, we measure the phase difference between two intensity profiles obtained at two different heights, which gives information about the phase difference between oscillations at those heights as a function of frequency. The results of a fast Fourier transform (FFT) show peaks in the power spectrum at frequencies in the range from 2 to 8 mHz at four different heights (above the limb), while the wavelet analysis indicate dominant frequencies similar to those of the Fourier power spectrum results. A coherency study indicates the presence of coherent oscillations at about 5.5 mHz (3 min). We measure mean phase speeds in the range 250 TO 425km/s increasing with height.

Update on Galactic Cosmic Ray Integral Flux Measurements in Lunar Orbit With CRaTER

C. **Zeitlin**,, N. A. Schwadron, H. E. Spence, A. P. Jordan, M. D. Looper, J. Wilson, J. E. Mazur, L. W. Townsend
Space Weather **2019**
sci-hub.se/10.1029/2019SW002223
We report updated measurements of the integral fluxes of energetic protons, helium ions, and heavier ions as measured by the Cosmic Ray Telescope for the Effects of Radiation (CRaTER). CRaTER is a particle telescope that has been operating aboard the Lunar Reconnaissance Orbiter since 2009. In an earlier report, we presented the methodology used to extract linear energy transfer spectra and integral fluxes for particles with sufficient energies to fully penetrate the telescope. Results were presented for the time span from late 2009 to the end of calendar year

2014, a period that encompassed the rise of solar activity from deep solar minimum to the weak maximum of Cycle 24. Here, we update the results with data obtained from that point in time through the end of 2018, in the declining phase of Cycle 24. Fluxes obtained in the most recent data are approaching the peak levels observed in late 2009 and early 2010. The results can be used as input to models of solar modulation of galactic cosmic rays and are also relevant to human exploration of deep space.

Segmentation of photospheric magnetic elements corresponding to coronal features to understand the EUV and UV irradiance variability⋆

J. J. **Zender**1, R. Kariyappa2, G. Giono3, M. Bergmann4, V. Delouille5, L. Damé6, J.-F. Hochedez6,5 and S. T. Kumara

A&A 605, A41 (**2017**)

Context. The magnetic field plays a dominant role in the solar irradiance variability. Determining the contribution of various magnetic features to this variability is important in the context of heliospheric studies and Sun-Earth connection.

Aims. We studied the solar irradiance variability and its association with the underlying magnetic field for a period of five years (January 2011–January 2016). We used observations from the Large Yield Radiometer (LYRA), the Sun Watcher with Active Pixel System detector and Image Processing (SWAP) on board PROBA2, the Atmospheric Imaging Assembly (AIA), and the Helioseismic and Magnetic Imager (HMI) on board the Solar Dynamics Observatory (SDO).

Methods. The Spatial Possibilistic Clustering Algorithm (SPoCA) is applied to the extreme ultraviolet (EUV) observations obtained from the AIA to segregate coronal features by creating segmentation maps of active regions (ARs), coronal holes (CHs) and the quiet sun (QS). Further, these maps are applied to the full-disk SWAP intensity images and the full-disk (FD) HMI line-of-sight (LOS) magnetograms to isolate the SWAP coronal features and photospheric magnetic counterparts, respectively. We then computed full-disk and feature-wise averages of EUV intensity and line of sight (LOS) magnetic flux density over ARs/CHs/QS/FD. The variability in these quantities is compared with that of LYRA irradiance values.

Results. Variations in the quantities resulting from the segmentation, namely the integrated intensity and the total magnetic flux density of ARs/CHs/QS/FD regions, are compared with the LYRA irradiance variations. We find that the EUV intensity over ARs/CHs/QS/FD is well correlated with the underlying magnetic field. In addition, variations in the full-disk integrated intensity and magnetic flux density values are correlated with the LYRA irradiance variations.

Conclusions. Using the segmented coronal features observed in the EUV wavelengths as proxies to isolate the underlying magnetic structures is demonstrated in this study. Sophisticated feature identification and segmentation tools are important in providing more insights into the role of various magnetic features in both the short- and long-term changes in the solar irradiance.

Solar disk center shows scattering polarization in the Sr~{\sc i} 4607~Å~line

Franziska **Zeuner**, Rafael Manso Sainz, Alex Feller, Michiel van Noort, Sami K. Solanki, Francisco A. Iglesias, Kevin Reardon, Valentín Martínez Pillet

ApJ **2020**

https://arxiv.org/pdf/2004.03679.pdf

Magnetic fields in turbulent, convective high-β plasma naturally develop highly tangled and complex topologies---the solar photosphere being the paradigmatic example. These fields are mostly undetectable by standard diagnostic techniques with finite spatio-temporal resolution due to cancellations of Zeeman polarization signals. Observations of resonance scattering polarization have been considered to overcome these problems. But up to now, observations of scattering polarization lack the necessary combination of high sensitivity and high spatial resolution in order to directly infer the turbulent magnetic structure at the resolution limit of solar telescopes. Here, we report the detection of clear spatial structuring of scattering polarization in a magnetically quiet solar region at disk center in the Sr~{\sc i} 4607~Å spectral line on granular scales, confirming theoretical expectations. We find that the linear polarization presents a strong spatial correlation with the local quadrupole of the radiation field. The result indicates that polarization survives the dynamic and turbulent magnetic environment of the middle photosphere and is thereby usable for spatially-resolved Hanle observations. This is an important step towards the long-sought goal of directly observing turbulent solar magnetic fields at the resolution limit and investigating their spatial structure.

Detection of spatially structured scattering polarization of Sr I 4607.3 Åwith the Fast Solar Polarimeter

Franziska **Zeuner**, Alex Feller, Francisco A. Iglesias, Sami K. Solanki

A&A 619, A179 **2018**

https://arxiv.org/pdf/1808.06539.pdf

Scattering polarization in the Sr I 4607.3 \AA line observed with high resolution is an important diagnostic of the Sun's atmosphere and magnetism at small spatial scales. At present, spatially resolved observations of this

diagnostic are rare and have not been reported as close to the disk center as for μ=0.6. Our aim is to measure the scattering polarization in the Sr I line at μ=0.6 and to identify the spatial fluctuations with a statistical approach. Using the Fast Solar Polarimeter (FSP) mounted on the TESOS filtergraph at the German Vacuum Tower Telescope (VTT) in Tenerife, Spain, we measured both the spatially resolved full Stokes parameters of the Sr I line at μ=0.6 and the center-to-limb variation of the spatially averaged Stokes parameters.
We find that the center-to-limb variation of the scattering polarization in the Sr I line measured with FSP is consistent with previous measurements. A statistical analysis of Stokes Q/I (i.e., the linear polarization component parallel to the solar limb), sampled with 0.16" pixel−1 in the line core of Sr I reveals that the signal strength is inversely correlated with the intensity in the continuum. We find stronger linear polarimetric signals corresponding to dark areas (intergranular lanes) in the Stokes I continuum image. In contrast, independent measurements at μ=0.3 show a positive correlation of Q/I with respect to the continuum intensity. We estimate that the patch diameter responsible for the excess Q/I signal is on the order of 0.5"-1". The presented observations and the statistical analysis of Q/I signals at μ=0.6 complement reported scattering polarization observations as well as simulations. **6 May 2015**

Observations of Magnetic Helicity Proxies in Solar Photosphere: Helicity with Solar Cycles

Review

Hongqi **Zhang**, Shangbin Yang, Haiqing Xu, Xiao Yang, Jie Chen, Jihong Liu
2023
https://arxiv.org/pdf/2311.07131.pdf
Observations of magnetic helicity transportation through the solar photosphere reflect the interaction of turbulent plasma movements and magnetic fields in the solar dynamo process. In this chapter, we have reviewed the research process of magnetic helicity inferred from the observed solar magnetic fields in the photosphere and also the solar morphological configurations with solar cycles. After introducing some achievements in the study of magnetic helicity, some key points would like to be summarized.
The magnetic (current) helicity in the solar surface layer presents a statistical distribution similar to that of the sunspot butterfly diagram, but its maximum value is delayed from the extreme value of the sunspot butterfly diagram and corresponds in the phase with the statistical eruption of solar flares. During the spatial transport of magnetic (current) helicity from the interior of the sun into the interplanetary space at the time-space scale of the solar cycle, it shows the statistical distribution and the fluctuation with the hemispheric sign rule. These show that the current helicity and magnetic helicity transport calculation methods are complementary to each other.
We also notice that the study of the inherent relationship between magnetic helicity and the solar cycle still depends on the observed accuracy of the solar magnetic field.

The force-freeness of the solar photosphere: Revisit with new approach and large datasets

Mei **Zhang**, Haocheng Zhang
ApJ Letters **956** L17 **2023**
https://arxiv.org/pdf/2309.15407.pdf
https://iopscience.iop.org/article/10.3847/2041-8213/acfcbd/pdf
Although it is generally believed that the solar photosphere is not magnetically force-free owning to its high plasma β, the estimations of force-freeness using observed magnetograms have produced disputable results. Some studies confirmed that the photosphere is largely not force-free whereas some authors argued that the photosphere is not far away from being force-free. In a previous paper of ours we demonstrated that, due to the fact that the noise levels of the transverse field in the magnetograms are much larger than those of the vertical field, wrong judgements on the force-freeness could be made: a truly force-free field could be judged as being not-force-free and a truly not-force-free field could be judged as being force-free. Here in this letter we propose an approach to overcome this serious problem. By reducing the spatial resolution to lower the noise level, the heavy influence of the measurement noise on the force-freeness judgement can be significantly suppressed. We first use two analytical solutions to show the success and the effectiveness of this approach. Then we apply this new approach to two large datasets of active region magnetograms, obtained with the HMI/SDO and SP/Hinode, respectively. Our analysis shows that the photospheric magnetic fields are actually far away from being force-free. Particularly and most notably, the mean value of Fz/Fp (where Fz the net Lorentz force in the vertical direction and Fp the total Lorentz force) is as low as -0.47, with more than 98% of the active regions having |Fz/Fp|>0.1, when using the SP/Hinode magnetograms of true field strength.

Temporal Variation of the Rotation in the Solar Transition Region

Xiaojuan **Zhang**1,2, Linhua Deng1,2, Yu Fei3, Chun Li3, and Xinan Tian4
2023 ApJL 951 L3
https://iopscience.iop.org/article/10.3847/2041-8213/acd9a3/pdf
The temporal variations of solar rotation in the photosphere, chromosphere, and corona have been widely investigated, whereas the rotation of the solar transition region is rarely studied. Here, we perform a primary study

about the long-term variation of the rotation in the transition region using Lyα irradiance from 1947 February 14 to 2023 February 20. Correlation techniques are used, and the main results are as follows. (1) The sidereal rotation period of the solar transition region varies between 22.24 and 31.49 days, and the mean sidereal rotation period is 25.50 days for the studied time interval 1947–2022. (2) The rotation period of the transition region exhibits a clear downward trend during 1947–2022, which might be caused by the reduced heliospheric pressure and the weaker solar global magnetic fields. (3) Significant periodic signal of the quasi-Schwabe cycle is found in the rotation periods of the transition region. (4) The cross-correlation between the rotation periods of the solar transition region and sunspot activity corroborates a strong correlation with the Schwabe cycle. Possible mechanisms responsible for these results are discussed.

A Potential New Mechanism for the Butterfly Diagram of the Solar Cycle: Latitude-dependent Radial Flux Transport

Zebin **Zhang**, Jie Jiang, Haowei Zhang
ApJL **941** L3 **2022**
https://arxiv.org/pdf/2212.00948
https://iopscience.iop.org/article/10.3847/2041-8213/aca47a/pdf
The butterfly diagram of the solar cycle is the equatorward migration of the emergence latitudes of sunspots as the solar cycle evolves. Revealing the mechanism for the butterfly diagram is essential for understanding the solar and stellar dynamo. The equatorward meridional flow at the base of the convection zone (CZ) was believed to be responsible for the butterfly diagram. However, helioseismological studies indicate controversial forms of the flow, and even present poleward flow at the base of the CZ, which poses a big challenge to the widely accepted mechanism. This motivates us to propose a new mechanism in this study. Using a data-driven Babcock-Leighton-type dynamo model, we carry out numerical simulations to explore how the latitude-dependent radial flux transport affects the latitudinal migration of the toroidal field, under different meridional flow profiles. The results indicate that when the radial transport of the poloidal field at higher latitudes is sufficiently faster, the toroidal fields of a new cycle at higher latitudes are generated earlier than that at lower latitudes, and vice versa. Thus, the butterfly diagram is suggested to correspond to the time- and latitude-dependent regeneration of the toroidal field due to the latitude-dependent radial transport of the poloidal flux.

Propagating and Stationary Bright Knots in the Quiet Sun

Jun **Zhang**1, Yijun Hou2, Yue Fang1, Feng Chen3, Ting Li2 +++
2023 ApJL 942 L2
https://iopscience.iop.org/article/10.3847/2041-8213/aca97b/pdf
The question of what heats the solar chromosphere and corona remains one of the most important puzzles in solar physics and astrophysics. Up to now, two mechanisms are considered to work in heating the chromosphere and corona: magnetic reconnection and wave (turbulent flow) dissipation. But it is still not understood which mechanism is dominant. To solve the heating problem, one important topic at this stage is that we should understand how much energy is contributing from the two mechanisms respectively to the heating. In the quiet Sun, the thermal energy signal is observed as brightenings. Here we report two kinds of bright knots with a total of 3605 in the chromosphere of the quiet Sun, using the data from the New Vacuum Solar Telescope at Yunnan Observatories. The first kind of 1537 bright knots, which is first detected in chromospheric fibrils where waves and their dissipation are ubiquitous, propagates along these fibrils with velocities from 5 to 69 km s−1. The second kind of 2068 knots keeps stationary, and always appears at the footpoints of these fibrils where network magnetic fields exist, suggesting that magnetic reconnection locally produces these stationary knots. Based on the observations of thousands of bright knots, we display the different distribution patterns of the two kinds of bright knots in the quiet Sun, and deduce that half of the energy for heating the chromosphere is supplied by wave dissipation, and the other half by magnetic reconnection. **4 Sep 2019**

Hemispheric asymmetry of long-term sunspot activity: sunspot relative numbers for 1939–2019

X J **Zhang**, L H Deng, Y Fei, C Li, X A Tian, Z J Wan
Monthly Notices of the Royal Astronomical Society, Volume 514, Issue 1, July **2022**, Pages 1140–1147, https://doi.org/10.1093/mnras/stac1231
Hemispheric asymmetry of solar magnetic structures is an important feature of solar cycles, and it involves dynamical processes in the interior of the Sun. For the first time, the data of the monthly sunspot relative numbers derived from the National Astronomical Observatory of Japan (NAOJ) is used to perform a long-term study (1939 March–2019 November) of the north–south asymmetry. The results show the following: (1) the sunspot relative numbers derived from NAOJ/Mitaka observatory are highly correlated with the international sunspot numbers obtained from the World Data Center Sunspot Index and Long-term Solar Observations, which justifies the use of Mitaka sunspot time series for hemispheric variation; (2) the change in the signs of the slopes of the regression lines fitted to the absolute asymmetry index suggest a kind of periodic variation in the hemispheric asymmetry, but the

time interval of the current data base is not long enough to derive 8 or 12 cycles periodicity; and (3) for mid-term periods, there are enhanced powers for the period ranges around 3.7 yr, around 9 yr, between 30 and 50 yr. Our analysis results implicate a possible mechanism responsible for the generation and variation of the hemispheric coupling in the Sun.

A Babcock–Leighton-type Solar Dynamo Operating in the Bulk of the Convection Zone

Zebin **Zhang**1 and Jie Jiang1,2
2022 ApJ 930 30
https://iopscience.iop.org/article/10.3847/1538-4357/ac6177/pdf
The toroidal magnetic field is assumed to be generated in the tachocline in most Babcock–Leighton (BL)-type solar dynamo models, in which the poloidal field is produced by the emergence and subsequent dispersal of sunspot groups. However, magnetic activity of fully convective stars and MHD simulations of global stellar convection have recently raised serious doubts regarding the importance of the tachocline in the generation of the toroidal field. In this study, we aim to develop a new BL-type dynamo model, in which the dynamo operates mainly within the bulk of the convection zone. Our 2D model includes the effect of solar-like differential rotation, one-cell meridional flow, near-surface radial pumping, strong turbulent diffusion, BL-type poloidal source, and nonlinear back-reaction of the magnetic field on its source with a vertical outer boundary condition. The model leads to a simple dipolar configuration of the poloidal field that has the dominant latitudinal component, which is wound up by the latitudinal shear within the bulk of the convection zone to generate the toroidal flux. As a result, the tachocline plays a negligible role in the model. The model reproduces the basic properties of the solar cycle, including (a) approximately 11 yr cycle period and 18 yr extended cycle period; (b) equatorward propagation of the antisymmetric toroidal field starting from high latitudes; and (c) polar field evolution that is consistent with observations. Our model opens the possibility for a paradigm shift in understanding the solar cycle to transition from the classical flux transport dynamo.

Diagnostic of Spectral Lines in Magnetized Solar Atmosphere: Formation of the H\b{eta} Line in Sunspots

Hongqi **Zhang**
SCIENCE CHINA, Physics, Mechanics & Astronomy, November **2020** Vol. 63 No. 11: 119611
https://arxiv.org/pdf/2009.03573.pdf
Formation of the Hβ λ4861.34 Å line is an important topic related to the diagnosis of the basic configuration of magnetic fields in the solar and stellar chromospheres. Specifically, broadening of the Hβ λ4861.34 Å line occurs due to the magnetic and micro-electric fields in the solar atmosphere. The formation of Hβ in the model umbral atmosphere is presented based on the assumption of non-local thermodynamic equilibrium. It is found that the model umbral chromosphere is transparent to the Stokes parameters of the Hβ line, which implies that the observed signals of magnetic fields at sunspot umbrae via the Hβ line originate from the deep solar atmosphere, where $\lg\tau_c \approx -1$ (about 300 km in the photospheric layer for our calculations). This is in contrast to the observed Stokes signals from non-sunspot areas, which are thought to primarily form in the solar chromosphere.

Solar models with convective overshoot, the solar-wind mass loss, and a PMS disk accretion: helioseismic quantities, Li depletion and neutrino fluxes

Qian-Sheng **Zhang**, Yan Li, Jørgen Christensen-Dalsgaard
ApJ 881:103 **2019**
https://arxiv.org/pdf/1907.02166.pdf
https://iopscience.iop.org/article/10.3847/1538-4357/ab2f77/pdf
Helioseismic observations have revealed many properties of the Sun: the depth and the helium abundance of the convection zone, the sound-speed and the density profiles in the solar interior. Those constraints have been used to judge the stellar evolution theory. With the old solar composition (e.g., GS98), the solar standard model is in reasonable agreement with the helioseismic constraints. However, a solar model with revised composition (e.g., AGSS09) with low abundance Z of heavy elements cannot be consistent with those constraints. This is the so-called "solar abundance problem", standing for more than ten years even with the recent upward revised Ne abundance. Many mechanisms have been proposed to mitigate the problem. However, there is still not a low-Z solar model satisfying all helioseismic constraints. In this paper, we report a possible solution to the solar abundance problem. With some extra physical processes that are not included in the standard model, solar models can be significantly improved. Our new solar models with convective overshoot, the solar wind, and an early mass accretion show consistency with helioseismic constraints, the solar Li abundance, and observations of solar neutrino fluxes.

Particle Heating and Energy Partition in Low-β Guide Field Reconnection with Kinetic Riemann Simulations

Qile **Zhang**, J. F. Drake, M. Swisdak
2019

https://arxiv.org/pdf/1904.12922.pdf
Kinetic Riemann simulations have been completed to explore particle heating during guide field reconnection in the low-β environment of the inner heliosphere and the solar corona. The reconnection exhaust is bounded by two rotational discontinuities (RD) and two slow shocks (SS) form within the exhaust as in magnetohydrodynamic (MHD) models. At the RDs, ions are accelerated by the magnetic field tension to drive the reconnection outflow as well as flows in the out-of-plane direction. The out-of-plane flows stream toward the midplane and meet to drive the SSs. The SSs differ greatly from those in the MHD model. The turbulence at the shock fronts and both upstream and downstream is weak so the shocks are laminar and produce little dissipation. Downstream of the SSs the counterstreaming ion beams lead to higher density, which leads to a positive potential between the SSs that acts to confine the downstream electrons to maintain charge neutrality. The potential accelerates electrons from upstream of the SSs to downstream region and traps a small fraction but only modestly increases the downstream electron temperature above the upstream value. In the low-β limit the released magnetic energy is split between bulk flow and ion heating with little energy going to electrons. That the model does not produce strong electron heating nor an energetic electron component as seen in large flares suggests the multiple x-line reconnection scenario is required to explain energetic particle production in flares. The model can be tested with the expected data from the Parker Solar Probe.

Intelligent Recognition of Time Stamp Characters in Solar Scanned Images from Film

JiaFeng **Zhang**, GuangZhong Lin, ShuGuang Zeng, Sheng Zheng, Xiao Yang, GangHua Lin, XiangYun Zeng, HaiMin Wang
Advances in Astronomy **2019**
https://arxiv.org/pdf/1909.00316.pdf
Prior to the availability of digital cameras, the solar observational images are typically recorded on films, and the information such as date and time were stamped in the same frames on film. It is significant to extract the time stamp information on the film so that the researchers can efficiently use the image data. This paper introduces an intelligent method for extracting time stamp information, namely, the Convolutional Neural Network (CNN), which is an algorithm in deep learning of multilayer neural network structures and can identify time stamp character in the scanned solar images. We carry out the time stamp decoding for the digitized data from the National Solar Observatory from 1963 to 2003. The experimental results show that the method is accurate and quick for this application. We finish the time stamp information extraction for more than 7 million images with the accuracy of 98\%.

Solar Kinetic Energy and Cross Helicity Spectra

Hongqi **Zhang**1 and Axel Brandenburg
2018 ApJL 862 L17
https://arxiv.org/pdf/1804.10321.pdf
http://sci-hub.tw/http://iopscience.iop.org/article/10.3847/2041-8213/aad337/meta
We develop a formalism that treats the calculation of solar kinetic energy and cross helicity spectra in an equal manner to that of magnetic energy and helicity spectra. The magnetic helicity spectrum is shown to be equal to the vertical part of the current helicity spectrum divided by the square of the wavenumber. For the cross helicity, we apply the recently developed two-scale approach globally over an entire active region to account for the sign change between the two polarities. Using vector magnetograms and Dopplergrams of NOAA 11158 and 12266, we show that kinetic and magnetic energy spectra have similar slopes at intermediate wavenumbers, where the contribution from the granulation velocity has been removed. At wavenumbers around $0.3\ \mathrm{Mm}^{-1}$, the magnetic helicity is found to be close to its maximal value. The cross helicity spectra are found to be within about 10% of the maximum possible value. Using the two-scale method for NOAA 12266, the global cross helicity spectrum is found to be particularly steep, similarly to what has previously been found in theoretical models of spot generation. In the quiet Sun, by comparison, the cross helicity spectrum is found to be small. **2011 February 14, 2015 January 19**

Evolution of Magnetic Helicity and Energy Spectra of Solar Active Regions

Hongqi **Zhang**, Axel Brandenburg, D.D. Sokoloff
2016 *ApJ* **819** 146
http://arxiv.org/pdf/1503.00846v1.pdf
We adopt an isotropic representation of the Fourier-transformed two-point correlation tensor of the magnetic field for estimating magnetic energy and helicity spectra as well as current helicity spectra of individual active regions and the change of their spectral indices with the solar cycle. The departure of the spectral index of current helicity from 5/3 is analyzed, and it is found that it is lower than that of magnetic energy. There is no obvious relationship between the change of the normalized magnetic helicity and the integral scale of the magnetic field for individual active regions. The evolution of the spectral index reflects the development and distribution of various scales of

magnetic structures in active regions. It is found that around solar maximum the magnetic energy and helicity spectra are steeper. 11-15 February 2011. 30 June - 4 July 2012.

Coronal Heating By the Interaction between Emerging Active Regions and the Quiet Sun Observed By the Solar Dynamics Observatory

Jun **Zhang**1, Bin Zhang1,2, Ting Li1, Shuhong Yang1, Yuzong Zhang1, Leping Li1,3, Feng Chen3, and Hardi Peter

2015 ApJ 799 L27

The question of what heats the solar corona remains one of the most important puzzles in solar physics and astrophysics. Here we report Solar Dynamics Observatory Atmospheric Imaging Assembly observations of coronal heating by the interaction between emerging active regions (EARs) and the surrounding quiet Sun (QS). The EARs continuously interact with the surrounding QS, resulting in dark ribbons which appear at the boundary of the EARs and the QS. The dark ribbons visible in extreme-ultraviolet wavelengths propagate away from the EARs with speeds of a few km s−1. The regions swept by the dark ribbons are brightening afterward, with the mean temperature increasing by one quarter. The observational findings demonstrate that uninterrupted magnetic reconnection between EARs and the QS occurs. When the EARs develop, the reconnection continues. The dark ribbons may be the track of the interface between the reconnected magnetic fields and the undisturbed QS's fields. The propagating speed of the dark ribbons reflects the reconnection rate and is consistent with our numerical simulation. A long-term coronal heating which occurs in turn from nearby the EARs to far away from the EARs is proposed.

Solar surface rotation: N-S asymmetry and recent speed-up

L. **Zhang**, K. Mursula, I. Usoskin

Astron. Astrophys. Lett. 575, L2 **2015**

http://arxiv.org/pdf/1501.02698v1.pdf

Context. The relation between solar surface rotation and sunspot activity still remains open. Sunspot activity has dramatically reduced in solar cycle 24 and several solar activity indices and flux measurements experienced unprecedentedly low levels during the last solar minimum.

Aims. We aim to reveal the momentary variation of solar surface rotation, especially during the recent years of reducing solar activity. Methods. We used a dynamic, differentially rotating reference system to determine the best-fit annual values of the differential rotation parameters of active longitudes of solar X-ray flares and sunspots in 1977-2012.

Results. The evolution of rotation of solar active longitudes obtained with X-ray flares and with sunspots is very similar. Both hemispheres speed up since the late 1990s, with the southern hemisphere rotating slightly faster than the north. Earlier, in 1980s, rotation in the northern hemisphere was considerably faster, but experienced a major decrease in the early 1990s. On the other hand, little change was found in the southern rotation during these decades. This led to a positive asymmetry in north-south rotation rate in the early part of the time interval studied.

Conclusions. The rotation of both hemispheres has been speeding up at roughly the same rate since late 1990s, with the southern hemisphere rotating slightly faster than the north. This period coincides with the start of dramatic weakening of solar activity, as observed in sunspots and several other solar, interplanetary and geomagnetic parameters.

The solar abundance problem: the effect of the turbulent kinetic flux on the solar envelope model

Q.S. **Zhang**

ApJ 787 L28 **2014**

http://arxiv.org/pdf/1404.4996v1.pdf

Recent 3D-simulations have shown that the turbulent kinetic flux (TKF) is significant. We discuss the effects of TKF on the size of convection zone and find that the TKF may help to solve the solar abundance problem. The solar abundance problem is that, with new abundances, the solar convection zone depth, sound speed in the radiative interior, the helium abundance and density in the convective envelope are not in agreement with helioseismic inversions. We have done Monte Carlo simulations on solar convective envelope models with different profile of TKF to test the effects. The solar abundance problem is revealed in the standard solar convective envelope model with AGSS09 composition, which shows significant differences ($\rm{\sim 10 %}$) on density from the helioseicmic inversions, but the differences in the model with old composition GN93 is small ($\rm{\sim 0.5 %}$). In the testing models with different imposed TKF, it is found that the density profile is sensitive to the value of TKF at the base of convective envelope and insensitive to the structure of TKF in the convection zone. Required value of turbulent kinetic luminosity at the base is about $\rm{-13%\sim-19%L_{\odot}}$. Comparing with the 3D-simulations, this value is plausible. This study is for the solar convective envelope only. The evolutionary solar

models with TKF are required for investigating its effects on the solar interior structure below the convection zone and the whole solar abundance problem, but the profile of TKF in the overshoot region is needed.

Consistent long-term variation in the hemispheric asymmetry of solar rotation

L. **Zhang1**,2, K. Mursula1 and I. Usoskin

A&A 552, A84 (**2013**)

Context. Solar active longitudes and their rotation have been studied for a long time using various forms of solar activity. However, the results on the long-term evolution of rotation rates and the hemispheric asymmetry obtained by earlier authors differ significantly from each other.

Aims. We aim to find a consistent result on the long-term migration of active longitudes of sunspots in 1877−2008 separately for the two hemispheres.

Methods. We used a dynamic, differentially rotating reference system to determine the best-fit values of the differential rotation parameters of active longitudes for each year in 1877−2008. With these parameters we determined the momentary rotation rates at the reference latitude of 17° and calculated the non-axisymmetries of active longitudes. We repeated this with five different fit intervals and two weighting methods and compared the results.

Results. The evolution of solar surface rotation in each hemisphere suggests a quasi-periodicity of about 80−90 years. The long-term variations of solar rotation in the northern and southern hemisphere have a close anti-correlation, leading to a significant 80−90-year quasi-periodicity in the north-south asymmetry of solar rotation. The north-south asymmetry of solar rotation is found to have an inverse relationship with the area of large sunspots. The latitudinal contrast of differential rotation is also found to be anti-correlated with the sunspot area. Different fit and weight methods yield similar results.

Conclusions. Our results give strong evidence for the anti-correlation of the rotation of the two solar hemispheres. The long-term oscillation of solar rotation suggests that a systematic interchange of angular momentum takes place between the two hemispheres at a period of about 80−90 years.

Solar cycle variation of the GPS cycle slip occurrence in China low-latitude region

Zhang, D. H.; Cai, L.; Hao, Y. Q.; Xiao, Z.; Shi, L. Q.; Yang, G. L.; Suo, Y. C.

Space Weather, Vol. 8, No. 10, S10D10, **2010**

http://dx.doi.org/10.1029/2010SW000583

Using the Global Positioning System (GPS) cycle slip data detected from the observations of two GPS stations over China low-latitude region from 1999 to 2005, the solar cycle variation of cycle slip occurrence is studied. It is found that the cycle slip occurrence in these two stations varies with solar cycle and shows good temporal correlation; the cycle slip occurs in solar maximum years (1999–2002) much more frequently than that in solar minimum years (2003–2005). In solar maximum years, the seasonal and diurnal dependences of cycle slip occurrence are obvious as shown by previous studies; that is, for seasonal dependence cycle slip mainly occurs in the equinox months and for diurnal dependence cycle slip mainly occurs from 1900 LT to midnight. In solar minimum years, the similar diurnal dependence of cycle slip still exists, nevertheless, the seasonal dependence of cycle slip is not obvious due to small cycle slip occurrence. In the meantime, the spread F occurrence also shows seasonal and diurnal dependence, but there are some differences compared with cycle slip occurrence. During the period from 2000 to 2002, the Q-type spread F mainly occurs in the equinox months; from 2003 to 2005, the Q-type spread F occurs mainly in summer months. As for the diurnal distribution, the Q-type spread F mainly occurs from 2000 LT to sunrise time and lasts much longer than the cycle slip does, and the F-type spread F mainly occurs after midnight and is very different with the cycle slip occurrence. Considering the reasons for cycle slip phenomenon in GPS observations, it is thought that the statistical results of cycle slip occurrence with solar cycle, season, and local time just reflect the temporal distribution of the ionospheric irregularities above a certain intense level over the observing region.

Statistical analysis of corotating interaction regions and their geoeffectiveness during solar cycle 23,

Zhang, Y., W. Sun, X. S. Feng, C. S. Deehr, C. D. Fry, and M. Dryer

J. Geophys. Res., 113, A08106, **2008**

http://dx.doi.org/10.1029/2008JA013095

This is an investigation of the effects of corotating interaction regions (CIRs) in the heliosphere (<1 AU) on geomagnetic disturbances during solar cycle 23 (1996–2005). Three kinds of interplanetary structures, “pure” CIR, interaction of CIR with ICME, and “pure” ICME by transient events, are identified by using the Hakamada-Akasofu-Fry (HAF) solar wind model. Yearly occurrence of 157 “pure” CIRs has a minimum value in 2001 and a peak value in 2003 at the declining phase during the 23rd solar cycle. The maximum correlation coefficient of the

daily sum of *Kp* indices between consecutive Carrington Rotations indicates that recurrent geomagnetic disturbances are dominant during the declining phase near solar minimum. Eighty percent of storms that are related to “pure” CIRs belong to weak and moderate storms. The statistical analysis shows that about 50% of CIRs produce classical interplanetary shocks during the descending phase and 89% of the CIR-related shocks are followed by geomagnetic storms. These results demonstrate that CIR-related shock is not a necessary condition for generating a magnetic storm, but most CIR-related shocks are related to a storm. The *Dst* index that corresponds to CIR-related storms has a better linear relationship with IMF *Bz*, *Ey*, and the coupling function (-динамо с учетом меридиональных потоков. Для полученной системы уравнений генерации магнитного поля построено уравнение Гамильтона Якоби с помощью асимптотического метода, аналогичного методу ВКБ. Это уравнение позволяет аналитически исследовать влияние меридиональных потоков на длительность цикла магнитной активности Солнца и эволюцию волн магнитного поля.

The Extreme Stellar-Signals Project III. Combining Solar Data from HARPS, HARPS-N, EXPRES, and NEID

Lily L. **Zhao**, Xavier Dumusque, Eric B. Ford, Joe Llama, Annelies Mortier, +++
ApJ **2023**
https://arxiv.org/pdf/2309.03762.pdf
We present an analysis of Sun-as-a-star observations from four different high-resolution, stabilized spectrographs -- HARPS, HARPS-N, EXPRES, and NEID. With simultaneous observations of the Sun from four different instruments, we are able to gain insight into the radial velocity precision and accuracy delivered by each of these instruments and isolate instrumental systematics that differ from true astrophysical signals. With solar observations, we can completely characterize the expected Doppler shift contributed by orbiting Solar System bodies and remove them. This results in a data set with measured velocity variations that purely trace flows on the solar surface. Direct comparisons of the radial velocities measured by each instrument show remarkable agreement with residual intra-day scatter of only 15-30 cm/s. This shows that current ultra-stabilized instruments have broken through to a new level of measurement precision that reveals stellar variability with high fidelity and detail. We end by discussing how radial velocities from different instruments can be combined to provide powerful leverage for testing techniques to mitigate stellar signals. **May 25 and June 23, 2021,**

Phase Shifts Measured in Evanescent Acoustic Waves above the Solar Photosphere and Their Possible Impacts on Local Helioseismology

Junwei **Zhao**1, S. P. Rajaguru2, and Ruizhu Chen1
2022 ApJ 933 109
https://iopscience.iop.org/article/10.3847/1538-4357/ac722d/pdf
A set of 464 minutes of high-resolution high-cadence observations were acquired for a region near the Sun's disk center using the Interferometric BI-dimensional Spectrometer installed at the Dunn Solar Telescope. Ten sets of Dopplergrams are derived from the bisector of the spectral line corresponding approximately to different atmospheric heights, and two sets of Dopplergrams are derived using an MDI-like algorithm and center-of-gravity method. These data are then filtered to keep only acoustic modes, and phase shifts are calculated between Doppler velocities of different atmospheric heights as a function of acoustic frequency. The analysis of the frequency- and height-dependent phase shifts shows that, for evanescent acoustic waves, oscillations in the higher atmosphere lead those in the lower atmosphere by an order of 1 s when their frequencies are below about 3.0 mHz, and lags behind by about 1 s when their frequencies are above 3.0 mHz. Nonnegligible phase shifts are also found in areas with systematic upward or downward flows. All these frequency-dependent phase shifts cannot be explained by vertical flows or convective blueshifts, but are likely due to complicated hydrodynamics and radiative transfer in the nonadiabatic atmosphere in and above the photosphere. These phase shifts in the evanescent waves pose great challenges to the interpretation of some local helioseismic measurements that involve data acquired at different atmospheric heights or in regions with systematic vertical flows. More quantitative characterization of these phase shifts is needed so that they can either be removed during measuring processes or be accounted for in helioseismic inversions.
HMI Nuggets #183 Jul **2022** http://hmi.stanford.edu/hminuggets/?p=3951

Long-Term Variation of Helioseismic Far-Side Images and What Causes It

Junwei **Zhao**, Grace Y. Jing, Ruizhu Chen
Solar Phys. **296**, Article number: 186 **2021**
https://arxiv.org/pdf/2112.06985.pdf
https://link.springer.com/content/pdf/10.1007/s11207-021-01937-8.pdf
https://doi.org/10.1007/s11207-021-01937-8
A new time--distance far-side imaging technique was recently developed by utilizing multiple multi-skip acoustic waves. The measurement procedure is applied to 11 years of Doppler observations from the Solar Dynamics Observatory / Helioseismic and Magnetic Imager, and over 8000 far-side images of the Sun have been obtained with

a 12-hour temporal cadence. The mean travel-time shifts in these images unsurprisingly vary with the solar cycle. However, the temporal variation does not show good correlations with the magnetic activity in their respective northern or southern hemisphere, but show very good anti-correlation with the global-scale magnetic activity. We investigate four possible causes of this travel-time variation. Our analysis demonstrates that the acoustic waves that are used for mapping the Sun's far side experience surface reflections around the globe, where they may interact with surface or near-surface magnetic field, and carry travel-time deficits with them. The mean far-side travel-time shifts from these acoustic waves therefore vary in phase with the Sun's magnetic activity.

A New Website Hosting HMI Time-Distance Pipeline Products

Junwei **Zhao** & Ruizhu Chen

HMI Science Nuggets #163 Oct **2021** http://hmi.stanford.edu/hminuggets/?p=3634

A new website was recently developed to host SDO/HMI's time-distance pipeline products, including real-time far-side images, near-real-time full-disk subsurface flow fields, synoptic subsurface flow maps, long-term near-surface zonal and meridional flows, as well as the interior meridional circulation profile. These results or data cover the period starting from 2010 May 1, when the HMI was commissioned, till the present and are ongoing. The website is at: http://jsoc.stanford.edu/data/timed.

Simulating the Solar Minimum Corona in UV Wavelengths with Forward Modeling II. Doppler Dimming and Microscopic Anisotropy Effect

Jie **Zhao**7,1,2, Sarah E. Gibson7,2, Silvano Fineschi3, Roberto Susino3, Roberto Casini7,2, Steven R. Cranmer4, Leon Ofman5,6, and Hui Li

2021 ApJ 912 141

https://doi.org/10.3847/1538-4357/abf143

In ultraviolet (UV) spectropolarimetric observations of the solar corona, the existence of a magnetic field, solar wind velocity, and temperature anisotropies modify the linear polarization associated with resonant scattering. Unlike previous empirical models or global models, which present blended results of the above physical effects, in this work, we forward-model expected signals in the H i Lyα line (121.6 nm) by adopting an analytic model that can be adjusted to test the roles of different effects separately. We find that the impact of all three effects is most evident in the rotation of the linear polarization direction. In particular, (1) for magnetic fields between ~10 and ~100 G, the Hanle effect modifies the linear polarization at low coronal heights, rotating the linear polarization direction clockwise (counterclockwise) when the angle between the magnetic field and the local vertical is greater (less) than the van Vleck angle, which is consistent with the result of Zhao et al.; (2) solar wind velocity, which increases with height, has a significant effect through the Doppler dimming effect at higher coronal heights, rotating the linear polarization direction in an opposite fashion to the Hanle effect; and (3) kinetic temperature anisotropies are most significant at lower heights in open nonradial magnetic field regions, producing tilt opposite to isotropic Doppler dimming. The fact that the three effects operate differently in distinct spatial regimes opens up the possibility for using linear polarization measurements in UV lines to diagnose these important physical characteristics of the solar corona.

Magnetic Helicity Signature and Its Role in Regulating Magnetic Energy Spectra and Proton Temperatures in the Solar Wind

G. Q. **Zhao**1,2, Y. Lin3, X. Y. Wang3, H. Q. Feng1, D. J. Wu4, H. B. Li1, A. Zhao1, and Q. Liu1

2021 ApJ 906 123

https://iopscience.iop.org/article/10.3847/1538-4357/abca3b/pdf

In a previous paper, we found that perpendicular and parallel proton temperatures are clearly associated with the proton-scale turbulence in the solar wind, and magnetic helicity signature appears to be an important indicator in the association. Based on 15 yr of in situ measurements, the present paper further investigates the magnetic helicity of solar wind turbulence and its role in regulating magnetic energy spectra and proton temperatures. Results show that the presence of the helicity signature is very common in solar wind turbulence at scales $0.3 \lesssim k\rho_p \lesssim 1$, with k being the wavenumber and ρ p the proton gyroradius. The sign of the helicity is mostly positive, indicating the dominance of right-handed polarization of the turbulence. The helicity magnitude usually increases with k and $\beta_{\parallel p}$ (the proton parallel beta) when $k\rho_p$ and $\beta_{\parallel p}$ are less than unity. As helicity magnitude increases, the power index of the energy spectrum becomes more negative, and the proton temperatures $T_{\perp p}$ and $T_{\parallel p}$ rise significantly, where $T_{\perp p}$ and $T_{\parallel p}$ are the perpendicular and parallel temperatures with respect to the background magnetic field. In particular, the rise of $T_{\perp p}$ is faster than $T_{\parallel p}$ when $\beta_{\parallel p} < 1$ is satisfied. The faster rise of $T_{\perp p}$ with the helicity magnitude may be interpreted as the result of the preferentially perpendicular heating of solar wind protons by kinetic Alfvén wave turbulence.

Imaging the Sun's Far-Side Active Regions by Applying Multiple Measurement Schemes on Multi-Skip Acoustic Waves

Junwei **Zhao**, Dominick Hing, Ruizhu Chen, Shea Hess Webber
ApJ **887** 216 **2019**
https://arxiv.org/pdf/1912.06736.pdf
https://doi.org/10.3847/1538-4357/ab5951
Being able to image active regions on the Sun's far side is useful for modeling the global-scale magnetic field around the Sun, and for predicting the arrival of major active regions that rotate around the limb onto the near side. Helioseismic methods have already been developed to image the Sun's far-side active regions using near-side high-cadence Doppler-velocity observations; however, the existing methods primarily explore the 3-, 4-, and 5-skip helioseismic waves, leaving room for further improvement in the imaging quality by including waves with more multi-skip waves. Taking advantage of the facts that 6-skip waves have the same target-annuli geometry as 3- and 4-skip waves, and that 8-skip waves have the same target-annuli geometry as 4-skip waves, we further develop a time--distance helioseismic code to include a total of 14 sets of measurement schemes. We then apply the new code on the SDO/HMI-observed Dopplergrams, and find that the new code provides substantial improvements over the existing codes in mapping newly-emerged active regions and active regions near both far-side limbs. Comparing 3 months of far-side helioseismic images with the STEREO/EUVI-observed 304A images, we find that 97.3% of the helioseismically detected far-side active regions that are larger than a certain size correspond to an observed region with strong EUV brightening. The high reliability of the new imaging tool will potentially allow us to further calibrate the far-side helioseismic images into maps of magnetic flux. **2014 February 7-14, 2014 March 13**
HMI Science Nuggets #137 March **2020** http://hmi.stanford.edu/hminuggets/?p=3203

Conditions for Coronal Observations at the Lijiang Observatory in 2011

M. Y. **Zhao**, Y. Liu, A. Elmhamdi, A. S. Kordi, X. F. Zhang, T. F. Song, Z. J. Tian
Solar Physics January **2018**, 293:1
The sky brightness is a critical parameter for estimating the coronal observation conditions for a solar observatory. As part of a site-survey project in Western China, we measured the sky brightness continuously at the Lijiang Observatory in Yunnan province in 2011. A sky brightness monitor (SBM) was adopted to measure the sky brightness in a region extending from 4.5 to 7.0 apparent solar radii based on the experience of the Daniel K. Inouye Solar Telescope (DKIST) site survey. Every month, the data were collected manually for at least one week. We collected statistics of the sky brightness at four bandpasses located at 450, 530, 890, and 940 nm. The results indicate that aerosol scattering is of great importance for the diurnal variation of the sky brightness. For most of the year, the sky brightness remains under 20 millionths per airmass before local Noon. On average, the sky brightness is less than 20 millionths, which accounts for 40.41% of the total observing time on a clear day. The best observation time is from 9:00 to 13:00 (Beijing time). The Lijiang Observatory is therefore suitable for coronagraphs investigating the structures and dynamics of the corona.

Observational Evidence of Magnetic Reconnection for Brightenings and Transition Region Arcades in IRIS observations

Jie **Zhao**, Brigitte Schmieder, Hui Li, Etienne Pariat, Xiaoshuai Zhu, Li Feng, Michalina Grubecka
ApJ **2017**
https://arxiv.org/pdf/1701.08356v1.pdf
By using a new method of forced-field extrapolation, we study the emerging flux region AR 11850 observed by the Interface Region Imaging Spectrograph (IRIS) and Solar Dynamical Observatory (SDO). Our results suggest that the bright points (BPs) in this emerging region have responses in lines formed from the upper photosphere to the transition region, with a relatively similar morphology. They have an oscillation of several minutes according to the Atmospheric Imaging Assembly (AIA) data at 1600 and 1700 Å . The ratio between the BP intensities measured in 1600 Å and 1700 Å filtergrams reveals that these BPs are heated differently. Our analysis of the Helioseismic and Magnetic Imager (HMI) vector magnetic field and the corresponding topology in AR11850 indicates that the BPs are located at the polarity inversion line (PIL) and most of them related with magnetic reconnection or cancelation. The heating of the BPs might be different due to different magnetic topology. We find that the heating due to the magnetic cancelation would be stronger than the case of bald patch reconnection. The plasma density rather than the magnetic field strength could play a dominant role in this process. Based on physical conditions in the lower atmosphere, our forced-field extrapolation shows consistent results between the bright arcades visible in slit-jaw image (SJI) 1400 Å and the extrapolated field lines that pass through the bald patches. It provides a reliable observational evidence for testing the mechanism of magnetic reconnection for the BPs and arcades in emerging flux region, as proposed in simulation works. **September 24, 2013**

Tracing p-Mode Waves from the Photosphere to the Corona in Active Regions

Junwei **Zhao**1, Tobías Felipe2,3, Ruizhu Chen4,1, & Elena Khomenko
HMI Science Nuggets #62 October 30, **2016**
http://hmi.stanford.edu/hminuggets/?p=1745
Through analyzing a suite of space- and ground-based observations, the authors report that above sunspots, helioseismic waves of different frequencies are able to channel up through the chromosphere and transition region into corona. General pictures of how the waves make into corona are also shown. **2013 September 2**

Periodicities in Solar Activity, Solar Radiation and Their Links with Terrestrial Environment

Valentina V. **Zharkova**1,2*, Irina Vasilieva2,3, Simon J. Shepherd2,4, Elena Popova5
Natural Science > Vol.15 No.3, 111-147. **2023**
doi: 10.4236/ns.2023.153010
https://www.scirp.org/journal/paperinformation.aspx?paperid=124007
Solar magnetic activity is expressed via variations of sunspots and active regions varying on different timescales. The most accepted is an 11-year period supposedly induced by the electromagnetic solar dynamo mechanism. There are also some shorter or longer timescales detected: the biennial cycle (2 - 2.7 years), Gleisberg cycle (80 - 100 years), and Hallstatt's cycle (2100 - 2300 years). Recently, using Principal Component Analysis (PCA) of the observed solar background magnetic field (SBMF), another period of 330 - 380 years, or Grand Solar Cycle (GSC), was derived from the summary curve of two eigenvectors of SBMF. In this paper, a spectral analysis of the averaged sunspot numbers, solar irradiance, and the summary curve of eigenvectors of SBMF was carried out using Morlet wavelet and Fourier transforms. We detect a 10.7-year cycle from the sunspots and modulus summary curve of eigenvectors as well a 22-year-cycle and the grand solar cycle of 342 - 350-years from the summary curve of eigenvectors. The Gleissberg centennial cycle is only detected on the full set of averaged sunspot numbers for 400 years or by adding a quadruple component to the summary curve of eigenvectors. Another period of 2200 - 2300 years is detected in the Holocene data of solar irradiance measured from the abundance of 14C isotope. This period was also confirmed with the period of about 2000 - 2100 years derived from a baseline of the solar background magnetic field, supposedly, caused by the solar inertial motion (SIM) induced by the gravitation of large planets. The implication of these findings for different deposition of solar radiation into the northern and southern hemispheres of the Earth caused by the combined effects of the solar activity and solar inertial motion on the terrestrial atmosphere is also discussed.

Comparison of solar activity proxies: eigen vectors versus averaged sunspot numbers

Zharkova V.V, Vasilieva I., Shepherd S.J., Popova E
Monthly Notices of the Royal Astronomical Society, Volume 521, Issue 4, June **2023**, Pages 6247–6265,
https://doi.org/10.1093/mnras/stad1001https://arxiv.org/pdf/2207.14708.pdf
https://watermark.silverchair.com/stad1001.pdf
We attempt to establish links between a summary curve, or modulus summary curve, MSC, of the solar background magnetic field (SBMF) derived from Principal Component Analysis, with the averaged sunspot numbers (SSN). The comparison of MSC with the whole set of SSN reveals rather close correspondence of cycle timings, duration and maxima times for the cycles 12- 24, 6,7 and -4,-3. Although, in 1720-1760 and 1830-1860 there are discrepancies in maximum amplitudes of the cycles, durations and shifts of the maximum times between MSC and SSN curves. The MSC curve reveals pretty regular cycles with double maxima (cycles 1-4), triple maximum amplitude distributions for cycles 0 and 1 and for cycles -1 and -2 just before Maunder minimum. The MSC cycles in 1700-1750 reveal smaller maximal magnitudes in cycles -3 to 0 and in cycle 1-4 than the amplitudes of SSN, while cycles -2 to 0 have reversed maxima with minima with SSN. Close fitting of MSC or Bayesian models to the sunspot curve distorts the occurrences of either Maunder Minimum or/and modern grand solar minimum (2020-2053). These discrepancies can be caused by poor observations and by difference in solar magnetic fields responsible for these proxies. The dynamo simulations of toroidal and poloidal magnetic field in the grand solar cycle (GSC) from 1650 until 2050 demonstrate the clear differences between their amplitude variations during the GSC. The use of eigen vectors of SBMF can provide additional information to that derived from SSN that can be useful for understanding solar activity.

Eigen vectors of solar magnetic field in cycles 21-24 and their links to solar activity indices

Zharkova V.V. and Shepherd S.J.
MNRAS Volume 512, Issue 4, June **2022**, Pages 5085–5099,
https://doi.org/10.1093/mnras/stac781
https://solargsm.com/wp-content/uploads/2022/04/zharkova_shepherd_mnras22.pdf

Using full disk synoptic maps of solar background magnetic field (SBMF) captured from the Wilcox Solar Observatory for 30 latitudinal bands for cycles 21-24 principal components (PCs), or eigen vectors of magnetic oscillations are obtained. The PCs are shown to come in pairs assigned to magnetic waves produced by dipole, quadruple, sextuple and octuple magnetic sources. The first pair is linked to dipole magnetic waves with their summary curve revealing a reasonable fit to the averaged sunspot numbers in cycles 21-24. This verifies the previous results and confirms the summary curve as additional proxy of solar activity decreasing towards grand solar minimum in cycles 25-27. There is also a noticeable asymmetry in latitudinal distributions of these PCs showing an increased activity in northern hemisphere in odd cycles and in southern hemisphere in even ones similar to the N-S asymmetries observed in sunspots. The second pair of PCs linked to quadruple magnetic sources, has 50% smaller amplitudes than the first, while their summary curve correlate closely with SXR fluxes in solar flares. Flare occurrences are also linked to variations of the next two pairs of eigen vectors, quadruple and sextuple components, revealing additional periodicity of about 2.75-3.1 years similar to observed oscillations in flares. Strong latitudinal asymmetries in quadruple and sextuple components are correlating with the N-S asymmetries of flare occurrences skewed to southern hemisphere in even cycles and to northern hemisphere in odd ones. PCA of solar magnetic field raises perspectives for simultaneous prediction of general and flaring solar activity.

Millennial Oscillations of Solar Irradiance and Magnetic Field in 600–2600 Book Chapter

Valentina **Zharkova**

Solar System Planets and Exoplanets **2021**

https://www.intechopen.com/chapters/75534

Daily ephemeris of Sun-Earth distances in two millennia (600–2600) showed significant decreases in February–June by up to 0.005 au in millennium M1 (600– 1600) and 0.011au in millennium M2 (1600–2600). The Earth's aphelion in M2 is shorter because shifted towards mid-July and perihelion longer because shifted to mid-January naturally explaining two-millennial variations (Hallstatt's cycle) of the baseline solar magnetic field measured from Earth. The S-E distance variations are shown imposed by shifts of Sun's position towards the spring equinox imposed by the gravitation of large planets, or solar inertial motion (SIM). Daily variations of total solar irradiance (TSI) calculated with these S-E distances revealed TSI increases in February–June by up to 10–12 W/m^2 in M1 and 14–18 W/m^2 in M2. There is also positive imbalance detected in the annual TSI magnitudes deposited to Earth in millennium M2 compared to millennium M1: up to 1.3 W/m^2, for monthly, and up to 20–25 W/m^2 for daily TSI magnitudes. This imbalance confirms an ascending phase of the current TSI (Hallstatt's) cycle in M2. The consequences for terrestrial atmosphere of this additional solar forcing induced by the annual TSI imbalances are evaluated. The implications of extra solar forcing for two modern grand solar minima in M2 are also discussed.

Solar activity, solar irradiance and terrestrial temperature Book Chapter

Valentina **Zharkova** Daily ephemeris of Sun-Earth distances in two millennia (600–2600) showed significant decreases in February–June by up to 0.005 au in millennium M1 (600– 1600) and 0.011au in millennium M2 (1600–2600). The Earth's aphelion in M2 is shorter because shifted towards mid-July and perihelion longer because shifted to mid-January naturally explaining two-millennial variations (Hallstatt's cycle) of the baseline solar magnetic field measured from Earth. The S-E distance variations are shown imposed by shifts of Sun's position towards the spring equinox imposed by the gravitation of large planets, or solar inertial motion (SIM). Daily variations of total solar irradiance (TSI) calculated with these S-E distances revealed TSI increases in February–June by up to 10–12 W/m^2 in M1 and 14–18 W/m^2 in M2. There is also positive imbalance detected in the annual TSI magnitudes deposited to Earth in millennium M2 compared to millennium M1: up to 1.3 W/m^2, for monthly, and up to 20–25 W/m^2 for daily TSI magnitudes. This imbalance confirms an ascending phase of the current TSI (Hallstatt's) cycle in M2. The consequences for terrestrial atmosphere of this additional solar forcing induced by the annual TSI imbalances are evaluated. The implications of extra solar forcing for two modern grand solar minima in M2 are also discussed.

Zharkova

2020

https://arxiv.org/ftp/arxiv/papers/2008/2008.00439.pdf

In this study we overview recent advances with prediction of solar activity using as a proxy solar background magnetic field and detection of grand solar cycles of about 400 years separated by grand solar minima (GSMs).The previous GSM known as the Maunder minimum was recorded from 1645 to 1715. The terrestrial temperature during Maunder Minimum was reduced by up to 1.0C that led to freezing rivers, cold winters and summers. The modern GSM started in 2020 and will last for three solar cycles until 2053. During this GSM two processes will affect the input of solar radiation: a decrease of solar activity and an increase in total solar irradiance because of solar inertial motion (SIM). For evaluation of the latter this study uses daily ephemeris of the Sun-Earth (SE) distances in two millennia from 600 to 2600 showing significant decreases of SE distances in the first 6 months of a year by 0.005 au in 600 to 1600 and by more than 0.01 au in 1600 to 2600 with consequent increases of SE distances in the second halves of a year. Although, these increases are not fully symmetric in the second millennium (1600 to 2600), during which the longest SE distances are gradually shifted from 21 June to 12 July while the shortest ones from 21 December to 12 January. These distance variations impose significant increases of solar irradiance in the first six months of each year in the two millennia, which are not fully offset by the solar radiation decreases in the last six

months in millennium 1600 to 2600. This misbalance creates an annual surplus of solar radiation to be processed by the terrestrial atmosphere and ocean environments that can lead to an increase of terrestrial temperature. We estimate that decrease of solar activity during GSM combined with its increase imposed by SIM will lead to a reduction of terrestrial temperature during the modern GSM to the levels of 1700.

Oscillations of the baseline of solar magnetic field and solar irradiance on a millennial timescale

V. V. **Zharkova**, S. J. Shepherd, S. I. Zharkov & E. Popova
Scientific Reports volume 9, Article number: 9197, **2019**
sci-hub.se/10.1038/s41598-019-45584-3
https://www.nature.com/articles/s41598-019-45584-3
https://arxiv.org/pdf/2002.06550.pdf

Recently discovered long-term oscillations of the solar background magnetic field associated with double dynamo waves generated in inner and outer layers of the Sun indicate that the solar activity is heading in the next three decades (2019-2055) to a Modern grand minimum similar to Maunder one. On the other hand, a reconstruction of solar total irradiance suggests that since the Maunder minimum there is an increase in the cycle-averaged total solar irradiance (TSI) by a value of about 1?1.5 Wm-2 closely correlated with an increase of the baseline (average) terrestrial temperature. In order to understand these two opposite trends, we calculated the double dynamo summary curve of magnetic field variations backward one hundred thousand years allowing us to confirm strong oscillations of solar activity in regular (11 year) and recently reported grand (350?400 year) solar cycles caused by actions of the double solar dynamo. In addition, oscillations of the baseline (zero-line) of magnetic field with a period of 1950 ? 95 years (a super-grand cycle) are discovered by applying a running averaging filter to suppress large-scale oscillations of 11 year cycles. Latest minimum of the baseline oscillations is found to coincide with the grand solar minimum (the Maunder minimum) occurred before the current super-grand cycle start. Since then the baseline magnitude became slowly increasing towards its maximum at 2600 to be followed by its decrease and minimum at ~3700. These oscillations of the baseline solar magnetic field are found associated with a long-term solar inertial motion about the barycenter of the solar system and closely linked to an increase of solar irradiance and terrestrial temperature in the past two centuries. This trend is anticipated to continue in the next six centuries that can lead to a further natural increase of the terrestrial temperature by more than 2.5-3.0∘C.

Reply to comment by Usoskin (2017) on the paper "On a role of quadruple component of magnetic field in defining solar activity in grand cycles"

Zharkova V.V., Popova E., Shepherd S.J. and Zharkov S.
2017
http://computing.unn.ac.uk/staff/slmv5/kinetics/zharkova_etal_reply_jastp17.pdf

In this communication we provide our answers to the comments by Usoskin (2017) on our recent paper (Popova et al, 2017a). We show that Principal Component Analysis (PCA) allows us to derive eigen vectors with eigen values assigned to variance of solar magnetic field waves from full disk solar magnetograms obtained in cycles 21-23 which came in pairs. The current paper (Popova et al, 2017a) adds the second pair of magnetic waves generated by quadruple magnetic sources. This allows us to recover a centennial cycle, in addition to the grand cycle, and to produce a closer fit to the solar and terrestrial activity features in the past millennium.

Reinforcing the double dynamo model with solar-terrestrial activity in the past three millennia

V.V. **Zharkova**, S.J. Shepherd, E. Popova, S.I Zharkov
2017
https://arxiv.org/pdf/1705.04482.pdf

Using a summary curve of two eigen vectors of solar magnetic field oscillations derived with Principal Components Analysis (PCA) from synoptic maps for solar cycles 21-24 as a proxy of solar activity, we extrapolate this curve backwards three millennia revealing 9 grand cycles lasting 350-400 years each. The summary curve shows a remarkable resemblance to the past sunspot and terrestrial activity: grand minima - Maunder Minimum (1645-1715 AD), Wolf minimum (1280-1350 AD), Oort minimum (1010-1050 AD) and Homer minimum (800-900 BC); grand maxima - modern warm period (1990-2015), medieval warm period (900-1200 AD), Roman warm period (400-10 BC) and others. We verify the extrapolated activity curve by the pre-telescope observations of large sunspots with naked eye, by comparing the observed and simulated butterfly diagrams for Maunder Minimum (MM), by a maximum of the terrestrial temperature and extremely intense terrestrial auroras seen in the past grand cycle occurred in 14-16 centuries. We confirm the occurrence of upcoming Modern grand minimum in 2020-2053, which will have a shorter duration (3 cycles) and, thus, higher solar activity compared to MM. We argue that Sporer minimum (1450-1550) derived from the increased abundances of isotopes 14C and 10Be is likely produced by a strong increase of the terrestrial background radiation caused by the galactic cosmic rays of powerful supernovae.

Can high-mode magnetohydrodynamic waves propagating in a rotating microspicule become unstable against Kelvin--Helmholtz instability?

I. **Zhelyazkov**, R. Chandra

Solar Phys. 294:20 **2019**

https://arxiv.org/pdf/1810.01101.pdf

We investigate the conditions under which high-mode magnetohydrodynamic (MHD) waves propagating in a rotating solar microspicule become unstable against the Kelvin--Helmholtz instability (KHI). We model the microspicule as a weakly twisted cylindrical magnetic flux tube moving along and rotating around its axis. We use the dispersion relation of MHD modes obtained from the linearized MHD equations of incompressible plasma for the jet and cool (zero beta) plasma for its environment by assuming real wave numbers and complex angular wave frequencies/complex wave phase velocities. The dispersion equation is solved numerically at appropriate input parameters to find out an instability region/window that accommodates suitable unstable wavelengths of the order of microspicule's width. It is established that a m=39MHD mode propagating in a microspicule with width of 6~Mm, axial velocity of 75~km\,s−1 and rotating one of 40~km\,s−1 can become unstable against KHI with instability growth times of 3.4 and 0.73~min at 3 and 5~Mm unstable wavelengths, respectively. These growth times are much shorter than the macrospicule lifetime of around 15~min. An increase/decease in the width of the jet would change the KHI growth times remaining more or less of the same order when are evaluated at wavelengths equal to the width/radius of the macrospicule. It is worth noticing that the excited MHD modes are supper-Alfv\'enic waves. A change in the background magnetic field can lead to another MHD mode number m that ensures the required instability window.

Recommending Low-Cost Compact Space Environment and Space Weather Effects Sensor Suites for NASA Missions

Yihua **Zheng**, Michael Xapsos, Insoo Jun, T. P. O'Brien, Linda Parker, Wousik Kim, Justin Likar, Joseph Minow, Thomas Chen, Douglas Rowland

White paper submitted to Decadal Survey for Solar and Space Physics (Heliophysics) 2024-2033 **2023**

https://arxiv.org/ftp/arxiv/papers/2303/2303.11875.pdf

As miniaturized spacecraft (e.g., cubesats and smallsats) and instrumentation become an increasingly indispensable part of space exploration and scientific investigations, it is important to understand their potential susceptibility to space weather impacts resulting from the sometimes volatile space environment. There are multitude of complexities involved in how space environment interacts with different space hardware/electronics. Measurements of such impacts, however, have been lacking. Therefore, we recommend developing and/or procuring low-cost, low-power consumption, and compact sensor suites (mainly for space weather and impact purposes) and flying them on all future NASA (and U.S in general) missions in order to measure and quantify space weather impacts, in addition to the main instrumentation.

Solar Extreme UV radiation and quark nugget dark matter model

Ariel **Zhitnitsky**

2017

https://arxiv.org/pdf/1707.03400.pdf

We advocate the idea that the surprising emission of extreme ultra violet (EUV) radiation and soft x-rays from the Sun are powered externally by incident dark matter (DM) particles. The energy and the spectral shape of this otherwise unexpected solar irradiation is estimated within the quark nugget dark matter model. This model was originally invented as a natural explanation of the observed ratio Ωdark∼Ωvisible when the DM and visible matter densities assume the same order of magnitude values. This generic consequence of the model is a result of the common origin of both types of matter which are formed during the same QCD transition and both proportional to the same fundamental dimensional parameter ΛQCD. We also present arguments suggesting that the transient brightening-like "nano-flares" in the Sun may be related to the annihilation events which inevitably occur in the solar atmosphere within this dark matter scenario.

Discriminating between Babcock-Leighton-type solar dynamo models by torsional oscillations

Congyi **Zhong**, Jie jiang, Zebin Zhang

ApJ **969** 75 **2024**

https://arxiv.org/pdf/2405.17747

https://iopscience.iop.org/article/10.3847/1538-4357/ad4f88/pdf

The details of the dynamo process in the Sun are an important aspect of research in solar-terrestrial physics and astrophysics. The surface part of the dynamo can be constrained by direct observations, but the subsurface part lacks

direct observational constraints. The torsional oscillations, a small periodic variation of the Sun's rotation with the solar cycle, are thought to result from the Lorentz force of the cyclic magnetic field generated by the dynamo. In this study, we aim to discriminate between three Babcock-Leighton (BL) dynamo models by comparing the zonal acceleration of the three models with the observed one. The property that the poleward and equatorward branches of the torsional oscillations originate from about ±55∘ latitudes with their own migration time periods serves as an effective discriminator that could constrain the configuration of the magnetic field in the convection zone. The toroidal field, comprising poleward and equatorward branches separated at about ±55∘ latitudes can generate the two branches of the torsional oscillations. The alternating acceleration and deceleration bands in time is the other property of the torsional oscillations that discriminate between the dynamo models. To reproduce this property, the phase difference between the radial (Br) and toroidal (Bϕ) components of the magnetic field near the surface should be about π/2.

Polarisation of decayless kink oscillations of solar coronal loops

Sihui **Zhong**, Valery M. Nakariakov, Dmitrii Y. Kolotkov, Lakshmi Pradeep Chitta, Patrick Antolin, Cis Verbeeck, David Berghmans

Nature Communications **2023**

https://arxiv.org/pdf/2308.10573.pdf

https://warwick.ac.uk/fac/sci/physics/research/cfsa/people/valery/natcomm23.pdf

Decayless kink oscillations of plasma loops in the solar corona may contain an answer to the enigmatic problem of solar and stellar coronal heating. The polarisation of the oscillations gives us a unique information about their excitation mechanisms and energy supply. However, unambiguous determination of the polarisation has remained elusive. Here, we show simultaneous detection of a 4-min decayless kink oscillation from two non-parallel lines-of-sights, separated by about 104\textdegree, provided by unique combination of the High Resolution Imager on Solar Orbiter and the Atmospheric Imaging Assembly on Solar Dynamics Observatory. The observations reveal a horizontal or weakly oblique linear polarisation of the oscillation. This conclusion is based on the comparison of observational results with forward modelling of the observational manifestation of various kinds of polarisation of kink oscillations. The revealed polarisation favours the sustainability of these oscillations by quasi-steady flows which may hence supply the energy for coronal heating. **1 Apr 2022**

Solar Orbiter nugget #15 2023

https://www.cosmos.esa.int/web/solar-orbiter/-/science-nugget-polarisation-of-decayless-kink-oscillations-of-solar-coronal-loops

30-min Decayless Kink Oscillations in a Very Long Bundle of Solar Coronal Plasma Loops

Sihui **Zhong**, Valery M. Nakariakov, Yuhu Miao, Libo Fu, Ding Yuan

Scientific Reports **2023**

https://arxiv.org/pdf/2308.05479.pdf

https://warwick.ac.uk/fac/sci/physics/research/cfsa/people/valery/Zhong_VLL.pdf

The energy balance in the corona of the Sun is the key to the long-standing coronal heating dilemma, which could be potentially revealed by observational studies of decayless kink oscillations of coronal plasma loops. A bundle of very long off-limb coronal loops with the length of 736±80 Mm and a lifetime of about 2 days are found to exhibit decayless kink oscillations. The oscillations were observed for several hours. The oscillation amplitude was measured at 0.3-0.5 Mm, and the period at 28-33 min. The existence of 30-min periodicity of decayless kink oscillations indicates that the mechanism compensating the wave damping is still valid in such a massive plasma structure. It provides important evidence for the non-resonant origin of decayless kink oscillations with 2-6min periods, i.e., the lack of their link with the leakage of photospheric and chromospheric oscillations into the corona and the likely role of the broadband energy sources. Magnetohydrodynamic seismology based on the reported detection of the kink oscillation, with the assistance of the differential emission measure analysis and a background coronal model provides us with a comprehensive set of plasma and magnetic field diagnostics, which is of interest as input parameters of space weather models. **2022-11-08-10**

The dynamics of AR 12700 in its early emerging phase II: fan-shaped activities relevant to arch filament systems

Sihui **Zhong**, Yijun Hou, Leping Li, Jun Zhang, Yongyuan Xiang

ApJ **882** 110 **2019**

https://arxiv.org/pdf/1907.10345.pdf

The emergence of active regions (ARs) closely relates to the solar dynamo and the dynamical atmospheric phenomena.With high-resolution and long-lasting observations from the New Vacuum Solar Telescope, we report a new dynamic activity phenomenon named "fan-shaped activity (FSA)" in the emerging phase of NOAA AR 12700. The FSAs are clearly observed at Ha wavelength and are closely related to the dynamics of the adjacent arch filament system (AFS), including threads deformation and materials downward motions. On **2018 February 26**, the two most representative FSAs appeared around 05:21 UT and 06:03 UT, respectively, and they firstly ascended and

then decayed in around 10 minutes. At the ascending phase, accompanied by the uplifting of an adjacent AFS, each FSA launches up at one end of the AFS and extends for up to 11 Mm. At the decaying phase, the FSA gradually vanishes, and materials downflows towards the other end of the AFS are detected. After checking the evolution of the magnetic fields of AR 12700, we find that each FSA is located between the end of an AFS and an adjacent magnetic patch with the same polarity and launches at the onset of the collision and compression between these two magnetic patches. We propose that the collision lifts up the AFS, and then the initially compact AFS laterally expands, resulting in the formation of FSA. A cartoon model is proposed to depict the activities.

Frozen-field Modeling of Coronal Condensations with MPI-AMRVAC II: Optimization and application in three-dimensional models

Yuhao **Zhou**, Xiaohong Li, Jack M. Jenkins, Jie Hong, Rony Keppens

ApJ **2024**

https://arxiv.org/pdf/2411.16415

The frozen-field hydrodynamic (ffHD) model is a simplification of the full magnetohydrodynamical (MHD) equations under the assumption of a rigid magnetic field, which significantly reduces computational complexity and enhances efficiency. In this work, we combine the ffHD prescription with hyperbolic thermal conduction (TC) and the Transition Region Adaptive Conduction (TRAC) method to achieve further optimization. A series of two-dimensional tests are done to evaluate the performance of the hyperbolic TC and the TRAC method. The results indicate that hyperbolic TC, while showing limiter-affected numerical dissipation, delivers outcomes comparable to classic parabolic TC. The TRAC method effectively compensates for the underestimation of enthalpy flux in low-resolution simulations, as evaluated on tests that demonstrate prominence formation. We present an application of the ffHD model that forms a three-dimensional prominence embedded in a magnetic flux rope, which develops into a stable slab-like filament. The simulation reveals a prominence with an elongated spine and a width consistent with observations, highlighting the potential of the ffHD model in capturing the dynamics of solar prominences. Forward modeling of the simulation data produces synthetic images at various wavelengths, providing insights into the appearance of prominences and filaments in different observational contexts. The ffHD model, with its computational efficiency and the demonstrated capability to simulate complex solar phenomena, offers a valuable tool for solar physicists, and is implemented in the open-source MPI-AMRVAC framework.

3D Stagger model atmospheres with FreeEOS I. Exploring the impact of microphysics on the Sun

Yixiao **Zhou**, Anish M. Amarsi, Victor Aguirre Børsen-Koch, Klara G. Karlsmose, Remo Collet, Thomas Nordlander

A&A **2023**

https://arxiv.org/pdf/2307.05403.pdf

Three-dimensional radiation-hydrodynamics (3D RHD) simulations of stellar surface convection provide valuable insights into many problems in solar and stellar physics. However, almost all 3D near-surface convection simulations to date are based on solar-scaled chemical compositions, which limit their application on stars with peculiar abundance patterns. To overcome this difficulty, we implement the robust and widely-used FreeEOS equation of state and our Blue opacity package into the Stagger 3D radiation-magnetohydrodynamics code. We present a new 3D RHD model of the solar atmosphere, and demonstrate that the mean stratification as well as the distributions of key physical quantities are in good agreement with those of the latest Stagger solar model atmosphere. The new model is further validated by comparing against solar observations. The new model atmospheres reproduce the observed flux spectrum, continuum centre-to-limb variation, and hydrogen line profiles at a satisfactory level, thereby confirming the realism of the model and the underlying input physics. These implementations open the prospect for studying other stars with different α-element abundance, carbon-enhanced metal-poor stars and population II stars with peculiar chemical compositions using 3D Stagger model atmospheres.

Transition region adaptive conduction (TRAC) in multidimensional magnetohydrodynamic simulations

Yu-Hao **Zhou**, Wen-Zhi Ruan, Chun Xia, Rony Keppens

A&A **2021**

https://arxiv.org/pdf/2102.07549.pdf

In solar physics, a severe numerical challenge for modern simulations is properly representing a transition region between the million-degree hot corona and a much cooler plasma of about 10000 K (e.g., the upper chromosphere or a prominence). In previous 1D hydrodynamic simulations, the transition region adaptive conduction (TRAC) method has been proven to capture aspects better that are related to mass evaporation and energy exchange. We aim to extend this method to fully multidimensional magnetohydrodynamic (MHD) settings, as required for any realistic application in the solar atmosphere. Because modern MHD simulation tools efficiently exploit parallel supercomputers and can handle automated grid refinement, we design strategies for any-dimensional block grid-

adaptive MHD simulations. We propose two different strategies and demonstrate their working with our open-source MPI-AMRVAC code. We benchmark both strategies on 2D prominence formation based on the evaporation--condensation scenario, where chromospheric plasma is evaporated through the transition region and then is collected and ultimately condenses in the corona. A field-line-based TRACL method and a block-based TRACB method are introduced and compared in block grid-adaptive 2D MHD simulations. Both methods yield similar results and are shown to satisfactorily correct the underestimated chromospheric evaporation, which comes from a poor spatial resolution in the transition region. Because fully resolving the transition region in multidimensional MHD settings is virtually impossible, TRACB or TRACL methods will be needed in any 2D or 3D simulations involving transition region physics.

The Relationship between Chirality, Sense of Rotation, and Hemispheric Preference of Solar Eruptive Filaments

Zhenjun **Zhou**, Rui Liu, Xing Cheng, Chaowei Jiang, Yuming Wang, Lijuan Liu, Jun Cui
ApJ **891** 180 **2020**
https://arxiv.org/pdf/2002.05007.pdf
https://iopscience.iop.org/article/10.3847/1538-4357/ab7666/pdf
The orientation, chirality, and dynamics of solar eruptive filaments is a key to understanding the magnetic field of coronal mass ejections (CMEs) and therefore to predicting the geoeffectiveness of CMEs arriving at Earth. However, confusion and contention remain over the relationship between the filament chirality, magnetic helicity, and sense of rotation during eruption. To resolve the ambiguity in observations, in this paper, we used stereoscopic observations to determine the rotation direction of filament apex and the method proposed by Chen et al. (2014) to determine the filament chirality. Our sample of 12 eruptive active-region filaments establishes a strong one-to-one relationship, i.e., during the eruption, sinistral/dextral filaments (located in the southern/northern hemisphere) rotate clockwise/counterclockwise when viewed from above, and corroborates a weak hemispheric preference, i.e., a filament and related sigmoid both exhibit a forward (reverse) S shape in the southern (northern) hemisphere, which suggests that the sigmoidal filament is associated with a low-lying magnetic flux rope with its axis dipped in the middle. As a result of rotation, the projected S shape of a filament is anticipated to be reversed during eruption.
Table 1. Characteristics of 12 selected active-region filaments.

The amplitude of solar p-mode oscillations from three-dimensional convection simulations

Yixiao **Zhou**, Martin Asplund, Remo Collet
ApJ **880** 13 **2019**
https://arxiv.org/pdf/1905.13397.pdf
sci-hub.se/10.3847/1538-4357/ab262c
The amplitude of solar p-mode oscillations is governed by stochastic excitation and mode damping, both of which take place in the surface convection zone. However, the time-dependent, turbulent nature of convection makes it difficult to self-consistently study excitation and damping processes through the use of traditional one-dimensional hydrostatic models. To this end, we carried out \textit{ab initio} three-dimensional, hydrodynamical numerical simulations of the solar atmosphere to investigate how p-modes are driven and dissipated in the Sun. The description of surface convection in the simulations is free from the tuneable parameters typically adopted in traditional one-dimensional models. Mode excitation and damping rates are computed based on analytical expressions whose ingredients are evaluated directly from the three-dimensional model. With excitation and damping rates both available, we estimate the theoretical oscillation amplitude and frequency of maximum power, vmax, for the Sun. We compare our numerical results with helioseismic observations, finding encouraging agreement between the two. The numerical method presented here provides a novel way to investigate the physical processes responsible for mode driving and damping, and should be valid for all solar-type oscillating stars.

Forecasting Solar Cycle 25 Using an Optimized Long Short-term Memory Mode Based on F10.7 and Sunspot Area Data

Hongbing **Zhu**1, Wenwei Zhu2, Haoze Chen2, and Mu He3
2023 ApJS 265 35
https://iopscience.iop.org/article/10.3847/1538-4365/acb650/pdf
In this paper, an optimized long short-term memory model is proposed to deal with the smoothed monthly F10.7 and nonsmoothed monthly sunspot area (SSA) data, aiming to forecast the peak amplitude of both solar activities and the occurring time for Solar Cycle 25 (SC-25), as well as to obtain the maximum amplitude of sunspot number (SSN) and the reaching time according to the relationships between them. The "reforecast" process in the model uses the latest forecast results obtained from the previous forecast as the input for the next forecasting calculation. The forecasting errors between the forecast and observed peak amplitude of F10.7 for SC-23 and SC-24 are 2.87% and 1.09%, respectively. The results of this evaluation indicator of SSA for SC-21 to SC-24 were 8.85%, 4.49%, 2.88%, and 4.57%, respectively, and the errors for the occurring time were all within 6 months. The forecast peak amplitude of F10.7 and SSA for SC-25 is 156.3 and 2562.5 respectively, and the maximum values of SSN are calculated as

147.9 and 213 based on F10.7 and SSA respectively, which implies that SC-25 will be stronger than SC-24, and that SC-25 will reach its peak at the beginning of 2025.

Solar Cycle 25 Prediction Using an Optimized Long Short-Term Memory Mode with F10.7

Hongbing **Zhu**, Wenwei Zhu & Mu He
Solar Physics volume 297, Article number: 157 (**2022**)
https://link.springer.com/content/pdf/10.1007/s11207-022-02091-5.pdf
In this paper, an optimized long short-term memory (LSTM) model is proposed to deal with the smoothed monthly F10.7F10.7 data, aiming to predict the peak amplitude of F10.7 and the occurring time for Solar Cycle 25 (SC-25) to obtain the maximum amplitude of sunspot number (SSN) and the reaching time. The "re-prediction" process in the model uses the latest prediction results obtained from the previous prediction as the input for the next prediction calculation. The prediction errors between the predicted and observed peak amplitude of F10.7 for SC-23 and SC-24 are 2.87% and 1.09%, respectively. The predicted peak amplitude of F10.7 for SC-25 is 156.3, and the maximum value of SSN is calculated as 147.9, which implies that SC-25 will be stronger than SC-24. SC-25 will reach its peak in July 2025.

Fe xii and Fe xiii Line Widths in the Polar Off-limb Solar Corona up to 1.5 R⊙

Yingjie **Zhu**, Judit Szente1, and Enrico Landi1
2021 ApJ 913 74
https://doi.org/10.3847/1538-4357/abf1e3
The nonthermal broadening of spectral lines formed in the solar corona is often used to seek evidence of Alfvén waves propagating in the corona. To have a better understanding of the variation of line widths at different altitudes, we measured the line widths of the strong Fe xii 192.4, 193.5, and 195.1 Å and Fe xiii 202.0 Å in an off-limb southern coronal hole up to 1.5 R⊙ observed by the Extreme Ultraviolet Spectrometer on board the Hinode satellite. We compared our measurements to the predictions from the Alfvén Wave Solar Model (AWSoM) and the SPECTRUM module. We found that the Fe xii and Fe xiii line widths first increase monotonically below 1.1 R⊙ and then keep fluctuating between 1.1 and 1.5 R⊙. The synthetic line widths of Fe xii and Fe xiii below 1.3 R⊙ are notably lower than the observed ones. We found that the emission from a streamer in the line of sight significantly contaminates the coronal hole line profiles even up to 1.5 R⊙ both in observations and simulations. We suggest that either the discrepancy between the observations and simulations is caused by insufficient nonthermal broadening at the streamer in the AWSoM simulation or the observations are less affected by the streamer. Our results emphasize the importance of identifying the origin of the coronal EUV emission in off-limb observations.

A New Approach for the Regression of the Center Coordinates and Radius of the Solar Disk Using a Deep Convolutional Neural Network

Gaofei **Zhu**1,2, Ganghua Lin1, Dongguang Wang1, and Xiao Yang1
2020 ApJ 902 72
https://doi.org/10.3847/1538-4357/abb2a0
This paper presents a new approach for the regression of the center coordinates and radius of the solar disk in Hα solar full-disk images by using a Deep Convolutional Neural Network. We use ~100,000 original Hα solar full-disk images obtained from Huairou Solar Observing Station as the experimental data set. The data set includes two parts: the original image and three numeric values (center coordinates and radius). In order to deal with the uneven distribution of the solar disk position in the original image, we randomly shift the solar disk during image preprocessing. Furthermore, data augmentation is also used to increase the robustness of the model. By evaluating the model with R-square and relative error, the center coordinates and the radius of the solar disk are proved to be effectively regressed. The data sets we constructed and source code are available as open source on GitHub.

On the Extrapolation of Magnetohydrostatic Equilibria on the Sun

Xiaoshuai **Zhu** and Thomas Wiegelmann
2018 ApJ 866 130
sci-hub.tw/10.3847/1538-4357/aadf7f
Modeling the interface region between the solar photosphere and corona is challenging because the relative importance of magnetic and plasma forces change by several orders of magnitude. While the solar corona can be modeled by the force-free assumption, we need to take plasma forces into account (pressure gradient and gravity) in photosphere and chromosphere, here within the magnetohydrostatic (MHS) model. We solve the MHS equations with the help of an optimization principle and use vector magnetogram as the boundary condition. Positive pressure and density are ensured by replacing them with two new basic variables. The Lorentz force during optimization is used to update the plasma pressure on the bottom boundary, which makes the new extrapolation work even without pressure measurements on the photosphere. Our code is tested using a linear MHS model as reference. From the detailed analyses, we find that the newly developed MHS extrapolation recovers the reference model at high

accuracy. The MHS extrapolation is, however, numerically more expensive than the nonlinear force-free field extrapolation and consequently one should limit their application to regions where plasma forces become important, e.g., in a layer of about 2 Mm above the photosphere.

Chirality, extended MHD statistics and solar wind turbulence

Jian-Zhou **Zhu**
MNRAS **2017**
https://arxiv.org/pdf/1703.01705.pdf
We unite the one-flow-dominated-state (OFDS) argument of \citet{MeyrandGaltierPRL12} with the one-chiral-sector-dominated-state \citep[OCSDS:][]{hydrochirality} one to form a nonlinear extended-magnetohydrodynamics (XMHD) theory for the solar wind turbulence (SWT), both in the Hall MHD regime and in the electron inertial MHD regime \citep[modifying the theory of][]{AbdelhamidLingamMahajanAPJ16}. `Degenerate states' in \citet{MiloshevichLingamMorrisonNJP17}'s XMHD absolute equilibria are exposed by helical mode decomposition technique, and the `chiroids absolute equilibria' offer the statistical dynamics basis to replace the linear wave (of infinitesimal or arbitrarily finite amplitudes) arguments of previous theories with OCSDS, suggested here to unite OFDS with careful analyses for the physics of (generalized) helicity and chirality in SWT.

Stereoscopy of extreme UV quiet Sun brightenings observed by Solar Orbiter/EUI

A. N. **Zhukov**, M. Mierla, F. Auchère, S. Gissot, L. Rodriguez, E. Soubrié, W. T. Thompson, B. Inhester, B. Nicula, P. Antolin, S. Parenti, É. Buchlin, K. Barczynski, C. Verbeeck, E. Kraaikamp, P. J. Smith, K. Stegen, L. Dolla, L. Harra, D. M. Long, U. Schühle, O. Podladchikova, R. Aznar Cuadrado, L. Teriaca, M. Haberreiter, A. C. Katsiyannis, P. Rochus, J.-P. Halain, L. Jacques, D. Berghmans
A&A **2021**
https://arxiv.org/pdf/2109.02169.pdf
The 3D fine structure of the solar atmosphere is still not fully understood as most of the available observations are taken from a single vantage point. The goal of the paper is to study the 3D distribution of small-scale brightening events ("campfires") discovered in the EUV quiet Sun by the Extreme Ultraviolet Imager (EUI) aboard Solar Orbiter. We used a first commissioning data set acquired by the EUI's High Resolution EUV telescope on 30 May 2020 in the 174 Å passband and we combined it with simultaneous data taken by the Atmospheric Imaging Assembly (AIA) aboard the Solar Dynamics Observatory in a similar 171 Å passband. The two-pixel spatial resolution of the two telescopes is 400 km and 880 km, respectively, which is sufficient to identify the campfires in both data sets. The two spacecraft had an angular separation of around 31.5 degrees (essentially in heliographic longitude), which allowed for the 3D reconstruction of the campfire position. These observations represent the first time that stereoscopy was achieved for brightenings at such a small scale. Manual and automatic triangulation methods were used to characterize the campfire data. The height of the campfires is located between 1000 km and 5000 km above the photosphere and we find a good agreement between the manual and automatic methods. The internal structure of campfires is mostly unresolved by AIA; however, for a particularly large campfire, we were able to triangulate a few pixels, which are all in a narrow range between 2500 and 4500 km. The low height of EUI campfires suggests that they belong to the previously unresolved fine structure of the transition region and low corona of the quiet Sun. They are probably apexes of small-scale dynamic loops heated internally to coronal temperatures. This work demonstrates that high-resolution stereoscopy of structures in the solar atmosphere has become feasible. **30 May 2020**

Hemispheric analysis of the magnetic flux in regular and irregular solar active regions

A. **Zhukova**
MNRAS Volume 532, Issue 2, August **2024**, Pages 2032–2043,
https://doi.org/10.1093/mnras/stae1604
https://arxiv.org/pdf/2406.18277
https://academic.oup.com/mnras/article-pdf/532/2/2032/58513501/stae1604.pdf
Studying the hemispheric distribution of active regions (ARs) with different magnetic morphology may clarify the features of the dynamo process that is hidden under the photospheric level. The magnetic flux data for 3047 ARs from the CrAO catalog between May 1996 and December 2021 (cycles 23 and 24) were used to study ARs cyclic variations and perform correlation analysis. According to the magneto-morphological classification (MMC) of ARs proposed earlier, subsets of the regular (obeying empirical rules for sunspots) and irregular (violating these rules) ARs were considered separately. Our analysis shows the following. For ARs of each MMC type, in each of the hemispheres, time profiles demonstrate a multi-peak structure. The double-peak structure of a cycle is formed by ARs of both MMC types in both hemispheres. For the irregular ARs, the pronounced peaks occur in the second maxima (close to the polar field reversal). Their significant hemispheric imbalance might be caused by a weakening of the toroidal field in one of the hemispheres due to the interaction between the dipolar and quadrupolar components of the global field, which facilitates the manifestation of the turbulent component of the dynamo. The similarity of the irregular ARs activity that was found in adjacent cycles in different hemispheres also hints at

realization of the mix-parity dynamo solution. For the quadrupolar-like component of the flux (compiled in the simple axisymmetric approximation), signs of oscillations with a period of about 15 years are found, and they are pronounced specifically for the irregular groups. This MMC type ARs might also contribute in α-quenching.

The north-south asymmetry of active regions of different magneto-morphological types in solar cycles 23 and 24 //

Zhukova, A. V., Sokoloff, D. D., Abramenko, V. I., Khlystova, A. I.
Adv. in Space Res., Volume 71, Issue 4, 15 February **2023**, Pages 1984-1994
https://doi.org/10.1016/j.asr.2022.09.013.

We used the elaborated earlier catalog of the magneto-morphological classes (MMC) of active regions (ARs) to study 2046 ARs of the solar cycle (SC) 23 and 1507 ARs of the SC24. According to empiric rules for sunspot groups (Hale's polarity law, Joy's law, etc.) and MMC, all ARs (except for unipolar spots) were sorted out between two categories: A-type – regular bipolar ARs; B-type – all the rest irregular ARs. We found that the number of both regular and irregular ARs follows the cycle with the Pearson's correlation coefficient of 0.92 and 0.78, respectively. The regular ARs are distributed evenly between the two maxima of each cycle. The irregular ARs are also distributed evenly between the two maxima in the SC 23, however their number is enhanced in the second maximum of the SC 24. Both regular and irregular ARs exhibit strong north-south (N-S) asymmetry. The significance of asymmetry is confirmed using Pearson's χ-square test and one more test based on the normal approximation to a binomial distribution. During the two maxima of a cycle, the peaks in two hemispheres for both regular and irregular ARs number do not vary synchronously. This can be explained by the fluctuations in the Babcock-Leighton mechanism. In general, there are more irregular ARs in the S-hemisphere in both cycles, which might be the result of an additional weakening of the toroidal field due to interplay between the dipole and quadrupole components of the global magnetic field.

Synthetic solar cycle for active regions violating the Hale's polarity law

A. **Zhukova**, A. Khlystova, V. Abramenko, D. Sokoloff
MNRAS Volume 512, Issue 1, May 2022, Pages 1365–1370, **2022**
https://arxiv.org/pdf/2203.01274.pdf
https://doi.org/10.1093/mnras/stac597

Long observational series for bipolar active regions (ARs) provide significant information about the mutual transformation of the poloidal and toroidal components of the global solar magnetic field. The direction of the toroidal field determines the polarity of leading sunspots in ARs in accordance with the Hale's polarity law. The vast majority of bipolar ARs obey this regularity, whereas a few percent of ARs have the opposite sense of polarity (anti-Hale ARs). However, the study of these ARs is hampered by their poor statistics. The data for five 11-year cycles (16-18 and 23,24) were combined here to compile a synthetic cycle of unique time length and latitudinal width. The synthetic cycle comprises data for 14838 ARs and 367 of them are the anti-Hale ARs. A specific routine to compile the synthetic cycle was demonstrated. We found that, in general, anti-Hale ARs follow the solar cycle and are spread throughout the time-latitude diagram evenly, which implies their fundamental connection with the global dynamo mechanism and the toroidal flux system. The increase in their number and percentage occurs in the second part of the cycle, which is in favour of their contribution to the polar field reversal. The excess in the anti-Hale ARs percentage at the edges of the butterfly diagram and near an oncoming solar minimum (where the toroidal field weakens) might be associated with strengthening of the influence of turbulent convection and magnetic field fluctuations on the arising flux tubes. The evidence of the misalignment between the magnetic and heliographic equators is also found.

A Catalog of Bipolar Active Regions Violating the Hale Polarity Law, 1989-2018

A. **Zhukova**, A. Khlystova, V. Abramenko, D. Sokoloff
Solar Phys. **295**, Article number: 165 **2020**
https://arxiv.org/pdf/2010.14413.pdf
https://link.springer.com/content/pdf/10.1007/s11207-020-01734-9.pdf

There is no list of bipolar active regions (ARs) with reverse polarity (anti-Hale regions), although statistical investigations of such ARs (bearing the imprint of deep subphotospheric processes) are important for understanding solar-cycle mechanisms. We studied 8606 ARs from 1 January 1989 to 31 December 2018 to detect anti-Hale regions and to compile a catalog. The Solar and Heliospheric Observatory (SOHO) and the Solar Dynamics Observatory (SDO) data, as well as the Debrecen Photoheliographic Data, the Mount Wilson Observatory catalog and drawings, and the USAF/NOAA Solar Region Summary were used. Complex, ambiguous cases related to anti-Hale region identification were analyzed. Two basic and four additional criteria to identify an AR as an anti-Hale region were formulated. The basic criteria assume that: i) dominating features of an AR have to form a bipole of reverse polarity with sunspots/pores of both polarities being present; ii) magnetic connections between the opposite polarities has to be observed. A catalog of anti-Hale regions (275 ARs) is compiled. The catalog contains: NOAA number, date of the greatest total area of sunspots, coordinates, and corrected sunspot area for this date. The tilt and

the most complex achieved Mount Wilson magnetic class are also provided. The percentage of anti-Hale groups meeting the proposed criteria is ~3.0% from all studied ARs, which is close to early estimations by authors who had examined each AR individually: ~2.4% by Hale and Nicholson (Ap.J. 62, 270, 1925) and ~3.1% by Richardson (Ap.J. 107, 78, 1948). The enchancement of the anti-Hale percentage in later research might be related to: i) increasing sensitivity of instruments (considering smaller and smaller bipoles); ii) the ambiguities in the anti-Hale region identification.

Two-dipole model of the asymmetric Sun

Bertalan **Zieger**1,2* and Kalevi Mursula2
J. Space Weather Space Clim. **2020**, 10, 40
https://www.swsc-journal.org/articles/swsc/pdf/2020/01/swsc200015.pdf
The large-scale photospheric magnetic field is commonly thought to be mainly dipolar during sunspot minima, when magnetic fields of opposite polarity cover the solar poles. However, recent studies show that the octupole harmonics contribute comparably to the spatial power of the photospheric field at these times. Also, the even harmonics are non-zero, indicating that the Sun is hemispherically asymmetric with systematically stronger fields in the south during solar minima. We present here an analytical model of two eccentric axial dipoles of different strength, which is physically motivated by the dipole moments produced by decaying active regions. With only four parameters, this model closely reproduces the observed large-scale photospheric field and all significant coefficients of its spherical harmonics expansion, including the even harmonics responsible for the solar hemispheric asymmetry. This two-dipole model of the photospheric magnetic field also explains the southward shift of the heliospheric current sheet observed during recent solar minima.

Chapter 1

Discoveries and Concepts: The Sun's Role in Astrophysics **Review**

Jack B. **Zirker**1 , Oddbjørn Engvold2
In: ***The Sun as a Guide to Stellar Physics*** ***Book***
Eds. Oddbjørn Engvold, Jean-Claude Vial, and Andrew Skumanich
Elsevier , November **2018**
https://www.sciencedirect.com/book/9780128143346/the-sun-as-a-guide-to-stellar-physics
The Sun has had an important role in the development of stellar astrophysics. The discoveries of solar magnetism, solar wind, and global acoustic vibrations, to name only a few, have launched completely new topics for research in stellar physics. In addition, concepts such as magnetic reconnection and neutrino mass first arose in attempts to explain puzzling solar phenomena.
This volume is intended to remind astronomers, physicists, and students of the Sun's key role, which is based in part on its proximity and its commonality with other stars. After a short survey of the subject, successive chapters will describe the status and future progress in several topics in solar physics that are relevant to stellar physics. We begin with the simplest characteristic of the Sun, its luminosity.
Nov. 10, 2010

Indirect solar wind measurements using archival cometary tail observations

N.V. **Zolotova**, Yu.V. Sizonenko, M.V. Vokhmyanin, I.S. Veselovsky
Solar Physics 293:85 **2018**
https://arxiv.org/pdf/1805.04684.pdf
https://link.springer.com/content/pdf/10.1007%2Fs11207-018-1307-4.pdf
The paper addressed to the problem of the solar wind behaviour during the Maunder Minimum. Records on plasma tails of comets would allow to shed light on the physical parameters of the solar wind in the past. We analyse descriptions and drawings of comets to the eighteenth century. To differentiate dust and plasma tails, we address to their color, shape and orientation. Basing on the calculations made by F.A. Bredikhin, we found that deviation of cometary tails from the antisolar direction on average exceeded 10 degrees, that is typical for dust tails. Catalogues of Hevelius and Lubieniecki are also examined. The first indication of plasma tail was revealed only for Great comet C/1769 P1.

How Deep Was the Maunder Minimum?

N. V. **Zolotova**, D. I. Ponyavin
Solar Physics November **2016**, Volume 291, Issue 9, pp 2869–2890
One of the most enigmatic features of the solar history is the Maunder minimum (MM). We analyze reports of solar observers from the group-sunspot-number database. Particular attention is given to short notes that resulted in an underestimation of the sunspot activity. These reports by Derham, Flamsteed, Hevelius, Picard, G.D. Cassini, and Fogel are found to address the absence of sunspots of great significance, which could signify a secular minimum

with a majority of small short-lived spots. Up to Schwabe's discovery of the solar cycle, sunspots were considered as an irregular phenomenon; sunspot observations were not dedicated to the task of sunspot monitoring and counting. Here, we argue that the level of the solar activity in the past is significantly underestimated.

Solar Coronal Heating Fueled by Random Bursts of Fine-scale Magnetic Reconnection in Turbulent Plasma Regions

Jitong **Zou1**, Aohua Mao1,2, Xiaogang Wang1, Yangyang Hua3, and Tianchun Zhou1
2023 ApJ 943 155
https://iopscience.iop.org/article/10.3847/1538-4357/acaec2/pdf
Coronal heating is a longstanding issue in solar physics as well as plasma physics in general. In recent years, significant resolution improvements of satellite observations have contributed to a deeper understanding of small-scale physics, e.g., magnetic reconnection processes on fine scales inside the turbulent geo-magnetosheath. Coronal plasmas feature turbulent complexity of flows and magnetic fields with similar fine scales, and thus electron magnetic reconnection is very likely to be excited in the coronal region working as one of the ways to heat the solar corona, which offers a possible new mechanism for the nanoflare model proposed by Parker. We in this paper simulate and analyze the magnetic reconnection processes on a fine scale of the electron skin depth, with a particle-in-cell treatment, and estimate its contribution to coronal heating. The result shows that the electron magnetic reconnection can provide substantial heating efficiency for heating the corona to its observed temperature, once the reconnection events are reasonably spread.

The Solar Orbiter Science Activity Plan: translating solar and heliospheric physics questions into action **Review**

I. **Zouganelis**, A. De Groof, A. P. Walsh, D. R. Williams, D. Mueller, et al.
A&A 642, A3 **2020**
https://arxiv.org/pdf/2009.10772.pdf
https://www.aanda.org/articles/aa/pdf/2020/10/aa38445-20.pdf
https://doi.org/10.1051/0004-6361/202038445
Solar Orbiter is the first space mission observing the solar plasma both in situ and remotely, from a close distance, in and out of the ecliptic. The ultimate goal is to understand how the Sun produces and controls the heliosphere, filling the Solar System and driving the planetary environments. With six remote-sensing and four in-situ instrument suites, the coordination and planning of the operations are essential to address the following four top-level science questions: (1) What drives the solar wind and where does the coronal magnetic field originate? (2) How do solar transients drive heliospheric variability? (3) How do solar eruptions produce energetic particle radiation that fills the heliosphere? (4) How does the solar dynamo work and drive connections between the Sun and the heliosphere? Maximising the mission's science return requires considering the characteristics of each orbit, including the relative position of the spacecraft to Earth (affecting downlink rates), trajectory events (such as gravitational assist manoeuvres), and the phase of the solar activity cycle. Furthermore, since each orbit's science telemetry will be downloaded over the course of the following orbit, science operations must be planned at mission level, rather than at the level of individual orbits. It is important to explore the way in which those science questions are translated into an actual plan of observations that fits into the mission, thus ensuring that no opportunities are missed. First, the overarching goals are broken down into specific, answerable questions along with the required observations and the so-called Science Activity Plan (SAP) is developed to achieve this. The SAP groups objectives that require similar observations into Solar Orbiter Observing Plans (SOOPs), resulting in a strategic, top-level view of the optimal opportunities for science observations during the mission lifetime.

MHD Wave Propagation and the Kelvin–Helmholtz Instability in an Asymmetric Magnetic Slab System

Noémi Kinga **Zsámberger**1,2,3,4, Yihui Tong5, Balázs Asztalos6, and Róbert Erdélyi1,4,6
2022 ApJ 935 41
https://iopscience.iop.org/article/10.3847/1538-4357/ac7ebf/pdf
Magnetohydrodynamic waves are ubiquitously detected in the finely structured solar atmosphere. At the same time, our Sun is a highly dynamic plasma environment, giving rise to flows of various magnitudes, which can lead to the instability of waveguides. Recent studies have employed the method of introducing waveguide asymmetry to generalize "classical" symmetric descriptions of the fine structuring within the solar atmosphere, with some of them introducing steady flows as well. Building on these recent studies, here we investigate the magnetoacoustic waves guided by a magnetic slab within an asymmetric magnetic environment, in which the slab is under the effect of a steady flow. We provide an analytical investigation of how the phase speeds of the guided waves are changed, and where possible, determine the limiting flow speeds required for the onset of the Kelvin–Helmholtz instability. Furthermore, we complement the study with initial numerical results, which allows us to demonstrate the validity of our approximations and extend the investigation to a wider parameter regime. This configuration is part of a series

of studies aimed to generalize, step-by-step, well-known symmetric waveguide models and understand the additional physics stemming from introducing further sources of asymmetry.

Solar Magneto-seismology of a Magnetic Slab in an Asymmetric Magnetic Environment

Noémi Kinga **Zsámberger**1,2,3 and Róbert Erdélyi1,4,5

2022 *ApJ* **934** 155

https://iopscience.iop.org/article/10.3847/1538-4357/ac7be3/pdf

Diagnosing the solar atmospheric plasma remains one of the major challenges in solar physics. In recent years, new methods have been developed to apply the powerful concept of solar magneto-seismology (SMS) to obtain information about plasma parameters in solar structures guiding magnetohydrodynamic (MHD) waves that would otherwise be difficult to measure. This paper uses the Cartesian model of a magnetic slab placed in an asymmetric magnetic environment to generalize recently discovered SMS techniques. Utilizing the fact that the asymmetric environment changes the character of the classical kink and sausage eigenmodes, we describe two spatial seismology methods built upon this mixed character of quasi-sausage and quasi-kink modes. First, we present the amplitude ratio technique, which compares the oscillation amplitudes measured at the two boundaries of the slab, and we provide expressions to estimate the internal Alfvén speed in the thin slab and in the incompressible plasma approximations. The second main technique relies on the changed distribution of wave power throughout the slab under the effect of waveguide asymmetry. This minimum perturbation shift technique is then also utilized to provide Alfvén speed estimates that depend on the plasma and magnetic parameters of the environment, as well as the measured slab width and oscillation frequency. Finally, we perform a brief investigation of how the amplitude ratio and the minimum perturbation shift depend on the different sources of waveguide asymmetry, and illustrate our findings with numerical results.

Magnetoacoustic Waves in a Magnetic Slab Embedded in an Asymmetric Magnetic Environment. III. Applications to the Solar Atmosphere

Noémi Kinga **Zsámberger**1,2,3 and Róbert Erdélyi1,4,5

2021 ApJ 906 122

https://doi.org/10.3847/1538-4357/abca9d

Analytical and numerical modeling of the behavior of magnetohydrodynamic waves in various magnetic geometries can offer a valuable contribution to the field of solar magnetoseismology. Based on analytical results from our previous studies, here we illustrate a few solar applications of these findings concerning the propagation of magnetoacoustic waves in a magnetic slab embedded in an asymmetric environment. Bearing in mind the simplifying assumptions made, this asymmetric model incorporating external magnetic fields can be used to describe a wide variety of multilayered solar features, some of which are observable and have already been studied in solar structures. Specific potential applications are: prominences, polar plumes and their environment, magnetic bright points, and light bridges, as well as adjacent large-scale layers in the solar atmosphere (e.g., the photosphere—interface region—corona triad, or the chromosphere—transition region—corona group). In these individual cases, the appropriate dispersion relations are derived and solved. The obtained wave propagation solutions may serve (i) not just as impetus to be confirmed by high-resolution observations but (ii) also to be exploited for further diagnostic purposes by solar magnetoseismology of these frequently studied magnetic structures.

Magneto-acoustic waves in a magnetic slab embedded in an asymmetric magnetic environment II: Thin and wide slabs, hot and cold plasmas

Noémi Kinga **Zsámberger**, Róbert Erdélyi

ApJ **894** 123 **2020**

https://arxiv.org/pdf/2004.05584.pdf

https://doi.org/10.3847/1538-4357/ab8791

Wave propagation in magnetically structured atmospheres is a thoroughly studied, yet practically inexhaustible well of investigations in the field of solar magneto-seismology. A simple but powerful example is the examination of wave behaviour in a magnetic slab. Our previous study (Zsámberger, Allcock and Erdélyi, Astrophys. J., 853, p. 136, 2018) used an analytical approach to derive the general dispersion relation for magneto-acoustic waves in a magnetic slab of homogeneous plasma, which was enclosed in an asymmetric magnetic environment. In the present study, we focus on the analysis of wave propagation in various limiting cases applicable to solar and space plasma or astrophysics. The thin- and wide-slab approximations, as well as the limits of low and high plasma-beta values are considered. Utilising the fact that in a weakly asymmetric slab, the dispersion relation can be decoupled, the behaviour of quasi-sausage and quasi-kink modes is studied in further analytical and numerical detail, and their avoided crossings are described. The results highlight how the asymmetry influences the wave properties, e.g. the phase speed of eigenmodes, depending on the ratios of external-to-internal densities and magnetic fields on the two sides. Notably, the phase speeds of surface modes will converge to different values for quasi-sausage and quasi-kink modes in the wide-slab limit, and cut-off frequencies are introduced with respect to both surface and body modes, in

thin as well as wide slabs, beyond which the solutions become leaky. These obtained properties of MHD wave behaviour could be measured with suitable high-resolution instruments in the future.

Magneto-acoustic Waves in a Magnetic Slab Embedded in an Asymmetric Magnetic Environment: The Effects of Asymmetry

Zsámberger, Noémi Kinga; Allcock, Matthew; Erdélyi, Róbert
2018 ApJ...853..136K
https://ui.adsabs.harvard.edu/link_gateway/2018ApJ...853..136K/PUB_PDF
https://iopscience.iop.org/article/10.3847/1538-4357/aa9ffe/pdf
Modeling the behavior of magnetohydrodynamic waves in a range of magnetic geometries mimicking solar atmospheric waveguides, from photospheric flux tubes to coronal loops, can offer a valuable contribution to the field of solar magneto-seismology. The present study uses an analytical approach to derive the dispersion relation for magneto-acoustic waves in a magnetic slab of homogeneous plasma enclosed on its two sides by semi-infinite plasma of different densities, temperatures, and magnetic field strengths, providing an asymmetric plasma environment. This is a step further in the generalization of the classic magnetic slab model, which is symmetric about the slab, was developed by Roberts, and is an extension of the work by Allcock & Erdélyi where a magnetic slab is sandwiched in an asymmetric nonmagnetic plasma environment. In contrast to the symmetric case, the dispersion relation governing the asymmetric slab cannot be factorized into separate sausage and kink eigenmodes. The solutions obtained resemble these well-known modes; however, their properties are now mixed. Therefore we call these modes quasi-sausage and quasi-kink modes. If conditions on the two sides of the slab do not differ strongly, then a factorization of the dispersion relation can be achieved for the further analytic study of various limiting cases representing a solar environment. In the current paper, we examine the incompressible limit in detail and demonstrate its possible application to photospheric magnetic bright points. After the introduction of a mechanical analogy, we reveal a relationship between the external plasma and magnetic parameters, which allows for the existence of quasi-symmetric modes.

Threshold of non-potential magnetic helicity ratios at the onset of solar eruptions

Francesco P. **Zuccarello**, Etienne Pariat, Gherardo Valori, Luis Linan
ApJ **2018**
https://arxiv.org/pdf/1807.00532.pdf
The relative magnetic helicity is a quantity that is often used to describe the level of entanglement of non-isolated magnetic fields, such as the magnetic field of solar active regions.The aim of this paper is to investigate how different kinds of photospheric boundary flows accumulate relative magnetic helicity in the corona and if and how-well magnetic helicity related quantities identify the onset of an eruption. We use a series of three-dimensional, parametric magnetohydrodynamic simulations of the formation and eruption of magnetic flux ropes. All the simulations are performed on the same grid, using the same parameters, but they are characterized by different driving photospheric flows, i.e., shearing, convergence, stretching, peripheral- and central- dispersion flows. For each of the simulations, the instant of the onset of the eruption is carefully identified by using a series of relaxation runs. We find that magnetic energy and total relative helicity are mostly injected when shearing flows are applied at the boundary, while the magnetic energy and helicity associated with the coronal electric currents increase regardless of the kind of photospheric flows. We also find that, at the onset of the eruptions, the ratio between the non-potential magnetic helicity and the total relative magnetic helicity has the same value for all the simulations, suggesting the existence of a threshold in this quantity. Such threshold is not observed for other quantities as, for example, those related to the magnetic energy.

Solar slow magneto-acoustic-gravity waves: an erratum correction and a revisited scenario

E. **Zurbriggen**, M. V. Sieyra, A. Costa, A. Esquivel, G. Stenborg
MNRAS **2020**
https://arxiv.org/pdf/2004.09609.pdf
Slow waves are commonly observed on the entire solar atmosphere. Assuming a thin flux tube approximation, the cut-off periods of slow-mode magneto-acoustic-gravity waves that travel from the photosphere to the corona were obtained in Costa et al. (2018). In that paper, however, a typo in the specific heat coefficient at constant pressure cp value led to an inconsistency in the cut-off calculation, which is only significant at the transition region. Due to the abrupt temperature change in the region, a change of the mean atomic weight (by a factor of approximately two) also occurs, but is often overlooked in analytical models for simplicity purposes. In this paper, we revisit the calculation of the cut-off periods of magneto-acoustic-gravity waves in Costa et al. (2018) by considering an atmosphere in hydrostatic equilibrium with a temperature profile, with the inclusion of the variation of the mean atomic weight and the correction of the inconsistency aforementioned. In addition, we show that the cut-off periods obtained analytically are consistent with the corresponding periods measured in observations of a particular active region.

MHD simulations of coronal supra-arcade downflows including anisotropic thermal conduction

E. **Zurbriggen**, A. Costa, A. Esquivel, M. Schneiter, M. Cécere
ApJ, 832:74, **2016**
https://arxiv.org/pdf/1703.05802.pdf

Coronal supra-arcade downflows (SADs) are observed as dark trails descending towards hot turbulent fan shaped regions. Due to the large temperature values, and gradients in these fan regions the thermal conduction should be very efficient. While several models have been proposed to explain the triggering and the evolution of SADs, none of these scenarios address a systematic consideration of thermal conduction. Thus, we accomplish this task numerically simulating the evolution of SADs within this framework. That is, SADs are conceived as voided (subdense) cavities formed by non-linear waves triggered by downflowing bursty localized reconnection events in a perturbed hot fan. We generate a properly turbulent fan, obtained by a stirring force that permits control of the energy and vorticity input in the medium where SADs develop. We include anisotropic thermal conduction and consider plasma properties consistent with observations. Our aim is to study if it is possible to prevent SADs to vanish by thermal diffusion. We find that this will be the case, depending on the turbulence parameters. In particular, if the magnetic field lines are able to envelope the voided cavities, thermally isolating them from the hot environment. Velocity shear perturbations that are able to generate instabilities of the Kelvin-Helmholtz type help to produce magnetic islands, extending the life-time of SADs.

Segmentation of Coronal Features to Understand the Solar EUV and UV Irradiance Variability III. Inclusion and Analysis of Bright Points

Rens van der **Zwaard**, Matthias Bergmann, Joe Zender, Rangaiah Kariyappa, Gabriel Giono & Luc Damé
Solar Physics volume 296, Article number: 138 (**2021**)
https://link.springer.com/content/pdf/10.1007/s11207-021-01863-9.pdf
https://doi.org/10.1007/s11207-021-01863-9

The study of solar irradiance variability is of great importance in heliophysics, Earth's climate, and space weather applications. These studies require careful identifying, tracking and monitoring of features in the solar photosphere, chromosphere, and corona. Do coronal bright points contribute to the solar irradiance or its variability as input to the Earth atmosphere? We studied the variability of solar irradiance for a period of 10 years (May 2010 – June 2020) using the Large Yield Radiometer (LYRA), the Sun Watcher using APS and image Processing (SWAP) on board PROBA2, and the Atmospheric Imaging Assembly (AIA), and applied a linear model between the segmented features identified in the EUV images and the solar irradiance measured by LYRA. Based on EUV images from AIA, a spatial possibilistic clustering algorithm (SPoCA) is applied to identify coronal holes (CHs), and a morphological feature detection algorithm is applied to identify active regions (ARs), coronal bright points (BPs), and the quiet Sun (QS). The resulting segmentation maps were then applied on SWAP images, images of all AIA wavelengths, and parameters such as the intensity, fractional area, and contribution of ARs/CHs/BPs/QS features were computed and compared with LYRA irradiance measurements as a proxy for ultraviolet irradiation incident to the Earth atmosphere. We modeled the relation between the solar disk features (ARs, CHs, BPs, and QS) applied to EUV images against the solar irradiance as measured by LYRA and the F10.7 radio flux. A straightforward linear model was used and corresponding coefficients computed using a Bayesian method, indicating a strong influence of active regions to the EUV irradiance as measured at Earth's atmosphere. It is concluded that the long- and short-term fluctuations of the active regions drive the EUV signal as measured at Earth's atmosphere. A significant contribution from the bright points to the LYRA irradiance could not be found.

О НЕКОРРЕКТНОСТИ ПРАВИЛА ГНЕВЫШЕВА–ОЛЯ В ОБЪЕДИНЕНИИ ЧЕТНО-НЕЧЕТНЫХ ЦИКЛОВ 11-ЛЕТНЕЙ СОЛНЕЧНОЙ АКТИВНОСТИ В ФИЗИЧЕСКИЕ ПАРЫ И ВЫСОТЕ МАКСИМУМА XXV И XXVI ЦИКЛОВ

Абдусаматов *Х.И.*
АЖ Том: 99Номер: 8 Год: **2022** Страницы: 684-693

Гневышев и Оль, используя ряд с достаточно малой статистикой событий, предложили объединять 11-летние циклы солнечной активности (СА) в отдельные физические пары четный-нечетный, где относительная интенсивность нечетного цикла выше, чем предшествующего четного цикла. Однако данное правило может выполняться только на фазе роста продолжительного и более мощного квазидвухвекового цикла (КДВЦ), когда интенсивность каждого последующего 11-летнего цикла больше интенсивности предыдущего, и нарушаться на фазе спада КДВЦ, когда, наоборот, мощность каждого последующего цикла становится меньше предыдущего. Значительно мощный и более чем на порядок длительный квазидвухвековой цикл определяет и управляет физическими параметрами и последовательными вариациями амплитуды интенсивности коротких и слабых квази-11-летних циклов СА в зависимости от фазы его вариаций. В период фазы спада КДВЦ продолжительность 11-летних циклов солнечной активности последовательно увеличивается, а высота уровня их максимума и относительная интегральная мощность последовательно уменьшаются. Противоположные соотношения наблюдаются в фазе его роста. Впервые утверждается, что правило Гневышева–Оля выполняется как следствие последовательного роста интегральной мощности коротких 11-летних циклов только в течение периода фазы роста квазидвухвекового цикла и нарушается последовательным уменьшением их мощности в течение периода фазы его спада. В XXV и XXVI циклах, развивающихся в период фазы спада КДВЦ, сохранится тенденция последовательного уменьшения

высоты максимума солнечной активности до 110 ± 25 и 60 ± 35 (до 65 ± 15 и 35 ± 20 в версии 1.0 системы подсчета) единиц относительного числа пятен соответственно.

Проявления турбулентной составляющей глобального солнечного динамо
Абраменко В.И.
Сборник трудов XXVI Всероссийской ежегодной конференции по физике Солнца «Солнце и солнечно-земная физика – 2022» ГАО РАН. С. 3-8
http://www.gaoran.ru/russian/solphys/2022/book/conf2022.pdf

ФОРМИРОВАНИЕ УНИФИЦИРОВАННОЙ БАЗЫ ДАННЫХ НАБЛЮДЕНИЙ СОЛНЦА В ЛИНИИ НЕ I 10830 Å, ПОЛУЧЕННЫХ В 1999-2023 ГГ. НА ТЕЛЕСКОПЕ БСТ-2 КРАО
Андреева О.А., Плотников А.А., Малащук В.М.
Изв. КрАО Том: 119Номер: 4 Год: 2023 Страницы: 35-41
На телескопе БСТ-2 накоплен уникальный наблюдательный материал за более чем два солнечных цикла. В период с 1999 г. по настоящее время получено свыше 4500 карт полного диска Солнца в линии Не I 10830 Å , позволяющих исследовать эволюцию и характеристики корональных дыр, волокон и активных областей. В связи с тем, что за этот период процесс наблюдений неоднократно претерпевал модернизацию разной сложности и вносились изменения в программы обработки, мы имеем несколько рядов карт Солнца разного вида. В работе поставлена задача обработать весь наблюдательный материал по единой методике и сформировать унифицированную базу данных наблюдений в линии Не I 10830 Å . Дается краткое описание алгоритма обработки наблюдений, и приводятся фрагменты базы данных.

ЦИКЛИЧЕСКИЕ ВАРИАЦИИ ПЛОЩАДЕЙ КОРОНАЛЬНЫХ ДЫР И СОЛНЕЧНЫХ ПЯТЕН В 2010-2021 ГГ
Андреева *О.А., Абраменко В.И., Малащук В.М.*
ГиА Том: 118Номер: 2 Год: **2022** Страницы: 20-27
https://elibrary.ru/item.asp?id=48749026
В работе исследуется циклическая связь корональных дыр с индексами солнечной активности (solar activity - SA). На основе наблюдательных данных, полученных инструментом AIA/SDO в линии железа Fe XII 19.3 нм в период с 13.05.2010 по 13.05.2021, изучены свойства полярных и неполярных корональных дыр (coronal holes - CHs). Подробно рассмотрены особенности каждой группы, установлена связь площадей корональных дыр с фазой солнечного цикла. В исследуемый период обнаружена северо-южная (N - S) асимметрия полушарий как по индексам солнечной активности, так и по локализации максимальных площадей полярных и неполярных CHs. На протяжении всего цикла выявлена определяющая роль полярных CHs южного и неполярных CHs северного полушария, которая проявилась как в динамике SA полушарий, так и всего диска Солнца в целом.

ПРОСТРАНСТВЕННЫЕ СТРУКТУРЫ СЕВЕРО-ЮЖНОЙ АСИММЕТРИИ В ЗЕЛЕНОЙ КОРОНАЛЬНОЙ ЛИНИИ И В МАГНИТНЫХ ПОЛЯХ
БАДАЛЯН О.Г.
ПАЖ Том: 46Номер: 10 Год: **2020** Страницы: 750-760
Исследуется пространственное распределение северо-южной асимметрии за 1977–2001 гг. Сопоставление распределения и временн\'{\cyr\cyrery }х изменений индекса асимметрии A в зеленой корональной линии 530.3 нм Fe XIV, в полном корональном магнитном поле и в полях малых и больших масштабов показало, что на низких широтах распределение A для полей малых масштабов имеет наибольшее сходство с его распределением в яркости зеленой линии. На широтах выше 40◦ наблюдается антикорреляция между поведением A в зеленой линии и в магнитном поле больших масштабов. Ранее было показано, что широтно-долготные области с преобладанием яркости зеленой линии в одном из полушарий через 14–18 оборотов сменяются похожими по форме областями с преобладанием другого полушария, т.е. карта как бы изменяется на “негативную”. В данной работе этот вывод подтверждается рассмотрением поведения северо-южной асимметрии в напряженности магнитного поля. Изменение карты на негативную наиболее выражено для полей больших масштабов. Северо-южная асимметрия является свидетельством и мерой того, что существуют различия (рассинхронизация) в работе двух полушарий Солнца. Этот факт необходимо учитывать при построении современных теорий динамо.

ДИФФЕРЕНЦИАЛЬНОЕ ВРАЩЕНИЕ СОЛНЕЧНОЙ КОРОНЫ ПО ДАННЫМ О МАГНИТНОМ ПОЛЕ

БАДАЛЯН О.Г.1, ОБРИДКО В.Н.1

АЖ Том: 44Номер: 11 Год: **2018** Страницы: 791-798
Предлагается метод исследования дифференциального вращения солнечной короны с использованием корональных магнитного поля как трассера. Поле рассчитывается в потенциальном приближении по

данным наблюдений на уровне фотосферы. Рассматривается временной интервал с 24.06.1976 по 31.12.2004. Поле рассчитывалось для всех широт от экватора до $\pm 75^{\circ}$ с шагом 5° на расстояниях от основания короны 1.0 $R_{\odot}$ до 2.45 $R_{\odot}$ вблизи поверхности источника. Методом периодограммного анализа определены периоды вращения короны на 14 расстояниях от центра Солнца. Показано, что с увеличением гелиоцентрического расстояния вращение короны становится все менее дифференциальным. При этом даже вблизи поверхности источника оно не становится твердотельным. Рассмотрено изменение периодов вращения короны со временем. Получено, что в минимуме цикла вращение является наиболее дифференциальным, особенно на малых расстояниях от центра Солнца. Изменение вращения короны со временем согласуется с наклоном магнитного экватора Солнца. Результаты, полученные по магнитному полю, сопоставлены с результатами, получаемыми при использовании данных о яркости зеленой корональной линии 530.3 nm Fe XIV. Согласованность этих результатов подтверждает надежность предлагаемого метода изучения вращения короны. Изучение вращения магнитного поля короны позволяет надеяться на возможность использовать этот метод для диагностики дифференциального вращения в подфотосферных слоях.

О СВЯЗИ МЕЖДУ КВАЗИ-ДВУХЛЕТНИМИ ВАРИАЦИЯМИ СОЛНЕЧНОЙ АКТИВНОСТИ, ГЕЛИОСФЕРНОГО МАГНИТНОГО ПОЛЯ И КОСМИЧЕСКИХ ЛУЧЕЙ*

Г. А. **Базилевская**, М. С. Калинин, М. Б. Крайнев, В. С. Махмутов,
А. К. Свиржевская, Н. С. Свиржевский, Ю. И. Стожков КОСМИЧЕСКИЕ ИССЛЕДОВАНИЯ, **2016**, том 54, № 3, с. 181–187 **File**

Квази-двухлетние осцилляции солнечной активности (T ≈ 1–4 года) считаются одними из базовых вариаций солнечной активности, связанных с процессом солнечного динамо. Они передаются в межпланетное пространство открытым магнитным потоком Солнца и порождают КДО в интенсивности космических лучей. В статье обсуждаются наблюдательные характеристики КДО в КЛ, их связь с КДО на Солнце и в межпланетной среде. Время запаздывания КДО в КЛ относительно КДО солнечного и гелиосферного магнитного поля позволяет предположить, что формирование КДО открытого магнитного потока Солнца происходит в течение 3–5 мес. Рассматривается вопрос о выделенной периодичности КЛ (T = 1.6 года), которая превалировала в КЛ и гелиосферном магнитном поле на протяжении более 10 лет, но не была стабильной в течение 60 лет наблюдений. Различия характеристик КДО и долговременных вариаций КЛ предполагают особенности в механизме их образования.

ВАРИАЦИИ КОСМИЧЕСКИХ ЛУЧЕЙ В 23-24 ЦИКЛАХ СОЛНЕЧНОЙ АКТИВНОСТИ ПО ДАННЫМ МИРОВОЙ СЕТИ СТАНЦИЙ КОСМИЧЕСКИХ ЛУЧЕЙ

Белов А.В., Гущина Р.Т., Янке В.Г.
Астрономия-**2018** Том 2 Солнечно-земная физика – современное состояние и перспективы Стр. 27
http://www.izmiran.ru/library/eaas2018/eaas-2018-2.pdf

ИНДЕКС ДОЛГОВРЕМЕННОГО ВЛИЯНИЯ СПОРАДИЧЕСКОЙ СОЛНЕЧНОЙ АКТИВНОСТИ НА МОДУЛЯЦИЮ КОСМИЧЕСКИХ ЛУЧЕЙ

Белов А.В., Гущина Р.Т.
Г и А Том: 58Номер: 1 Год: **2018** Страницы: 3-10

Корональные выбросы вещества не только создают Форбуш-эффекты, но вносят вклад и в долговременную модуляцию космических лучей. Это делает корональные выбросы главным спорадическим проявлением солнечной активности, которое следует учитывать в моделях модуляции. В работе предложен новый вариант CME-индекса, полученный на основе сопоставления данных спутниковых коронографов с Форбуш-эффектами и долговременными вариациями космических лучей.

РАЗЛИЧИЕ ХАРАКТЕРИСТИК СОЛНЕЧНЫХ МАКРОСПИКУЛ НА НИЗКИХ И ВЫСОКИХ ШИРОТАХ

Богачёв С. А., Лобода И. П., Рева А. А., Ульянов А. С., Кириченко А. С.
ПАЖ Том: 48Номер: 1 Год: 2022 Страницы: 52-60

Исследованы 49 солнечных макроспикул, наблюдавшихся в 2010 г., на фазе роста солнечного цикла, на высоких (околополярных) и на низких широтах вблизи солнечного экватора. Мы нашли, что темп формирования макроспикул в пределах точности измерения не зависит от широты и составляет ∼0.1 град$^{-2}$ ч$^{-1}$. Одновременно установлено, что средняя высота макроспикул вблизи экватора и полюсов заметно различается. После устранения эффектов проекции нами получено значение 31.7±0.2 тыс. км для макроспикул на низких широтах и 39.1±0.3 тыс. км для высокоширотных макроспикул.

РЕСТРУКТУРИЗАЦИЯ МАГНИТНЫХ ПОЛЕЙ СОЛНЦА И ЦЕНТРЫ ВСПЫШЕЧНОЙ АКТИВНОСТИ В ЦИКЛЕ 24

БОРОВИК А. В.*1, МОРДВИНОВ А. В.*1, ГОЛУБЕВА Е. М.*

1, ЖДАНОВ А. А.

АЖ Том: 97Номер: 6 Год: **2020** Страницы: 521-528

Выполнен анализ развития магнитной активности Солнца в цикле 24. Показано, что значительная северо-южная асимметрия магнитной активности сопровождалась асинхронной реорганизацией магнитных полей Солнца в северном и южном полушариях. Изучено формирование униполярных магнитных областей после распада центров активности. Показано, что меридиональный перенос униполярных магнитных областей приводит к изменениям зональной структуры магнитного поля Солнца. Установлено, что долгоживущие центры вспышечной активности существовали в периоды перестройки магнитных полей. Показано, что пространственно-временной анализ вспышечного ансамбля дает возможность для диагностики нестационарных процессов в атмосфере Солнца.

Исследования солнечной активности в Байкальской астрофизической обсерватории ИСЗФ СО РАН.

Боровик *А.В., Головко А.А., Поляков В.И., Трифонов В.Д., Язев С.А.*

СОЛНЕЧНО-ЗЕМНАЯ ФИЗИКА Том 5. 2019. № 3. **С.** 21–35

https://naukaru.ru/ru/storage/view/40054

В статье приведены основные результаты исследований Солнца в Байкальской астрофизической обсерватории (БАО) Института солнечно-земной физики Сибирского отделения Российской академии наук за 40 лет существования обсерватории. Кратко изложена история развития обсерватории, упомянуты телескопы, находящиеся на ее территории. Основное внимание уделено Большому солнечному вакуумному телескопу (БСВТ) и хромосферному телескопу полного диска Солнца. Рассказывается о научных задачах, которые решаются с помощью этих инструментов. Представлены некоторые результаты исследований, выполненных на БСВТ и хромосферном телескопе. Приведен список основных публикаций, в которых использованы результаты наблюдений в БАО.

ВОЗМОЖНОСТЬ ДИАГНОСТИКИ НАЧАЛА 25-ГО СОЛНЕЧНОГО ЦИКЛА НА ОСНОВЕ ЕГО ПРЕДВЕСТНИКОВ НА СРЕДНИХ ГЕЛИОШИРОТАХ

ГОЛОВКО А. А.*

Г. И А. Том: 60Номер: 6 Год: 2020 Страницы: 695-703

Geomagnetism and Aeronomy, **2020**, Vol. 60, No. 6, pp. 684–692.

https://link.springer.com/epdf/10.1134/S0016793220060055?sharing_token=WLatUoRla9c51Y77BLjv7UckSORA_DxfnEvY7GoQybbtIrX37QvPuAi0IQvb5eaSUEmCsXkvcLDX24OJQLvnTwSCsT13Zei9fp2wWiMJ5e0WKrdIqfH_fBuBsHOUBfGtq_EhkPifd8Jic7QJrxNDQZLF8gO6XJRMP-sKPJswTJM%3D

Исследована возможность диагностики начала солнечного цикла на основании обнаружения мелкомасштабных магнитных образований — магнитных узлов эфемерных активных областей в зоне средних гелиоширот от 40° до 60°. Магнитные узлы выявлялись на стадии их возникновения методом мультифрактальной сегментации, использованном ранее для фиксации новых магнитных потоков активных областей в зоне низких гелиоширот. Проведены статистические оценки числа магнитных узлов, фиксируемых таким методом, по данным магнитографа SOLIS NSO для 24-го цикла солнечной активности, а также для начала 25-го цикла активности. Обнаружен предвестник 24-го солнечного цикла в виде всплеска числа магнитных узлов в 2007–2008 гг., значительно превышающего его фоновое значение, характерное для периода 2011–2015 гг. Спустя два года началось появление первых активных областей на широтах 30° ± 10°. Аналогичная последовательность фаз начала цикла обнаружена для 25-го цикла. В отличие от ситуации 24-го цикла, массовое появление высокоширотных активных областей 25-го цикла произошло позже всплеска числа узлов эфемерных активных областей примерно на 2.5 года.

Вариации фактора различия и корреляции солнечных магнитных полей в линиях Fe I 525.02 нм и Na I 589.59 нм по измерениям обсерватории Маунт-Вилсон в 2000–2012 гг.

Голубева Елена

Солнечно-земная физика (Том 4 № 2, **2018**)

https://naukaru.ru/ru/nauka/article/20754/view

На основе сопоставления одновременных измерений обсерватории Маунт-Вилсон в двух спектральных линиях анализируются 13-летние вариации фактора различия магнитных полей. Фактор различия и коэффициент корреляции вычисляются как в общем случае, так и в различных диапазонах значений магнитного поля. Рассматриваются изменения обоих параметров. Демонстрируются следующие тенденции: 1) в общем случае имеют место изменения обоих коэффициентов с циклом солнечной активности; 2) зависимости коэффициентов от величины магнитного поля представляют собой нелинейные функции времени, что особенно ярко выражено в поведении фактора различия; 3) анализ общей картины поведения фактора различия дает возможность выделить несколько характерных диапазонов величины магнитного поля.

Обсуждаются соответствия между этими диапазонами и известными структурными объектами солнечной атмосферы. Это позволяет прийти к заключению, что зависимости рассматриваемых коэффициентов от величины поля и от времени определяются разнообразием структурных магнитных элементов и их циклическими перестройками. Представленные результаты могут быть полезны при решении проблем интерпретации измерений солнечных магнитных полей и для взаимной калибровки инструментов. Также они представляют интерес для задач формирования однородных продолжительных рядов солнечных магнитных полей по данным из различных источников.

Активные долготы и структура крупномасштабного магнитного поля в минимуме солнечной активности.

Григорьев В.М., Ермакова Л.В.

СОЛНЕЧНО-ЗЕМНАЯ ФИЗИКА Том 9 № 4 , **2023** С. 30–37.

https://naukaru.ru/ru/storage/viewWindow/138047

По данным каталогов групп солнечных пятен RGO и USAF/NOAA рассмотрены глубокие минимумы 11-летних циклов солнечной активности 13-14, 14-15, 22-23, 23-24, 24-25. Все они имеют большое количество беспятенных дней. Несмотря на это, активные долготы как предпочтительные зоны, где возникают солнечные пятна, проявляются на этой стадии цикла. Анализ синоптических карт и отдельных ежедневных магнитограмм WSO (Wilcox Solar Observatory), отражающих структуру слабого крупномасштабного поля, обнаруживает неосесимметричную компоненту магнитного поля Солнца. В минимуме активности в структуре крупномасштабного магнитного поля наблюдаются вытянутые вдоль меридиана области положительной и отрицательной полярностей, пересекающие экватор. Наиболее заметные из них находятся в зоне активных долгот и часто связаны с полярными магнитными полями. Обсуждается возможная природа меридиональных структур крупномасштабного поля в период минимума активности. Возможно, это связано с гигантскими ячейками конвекции, имеющими структуру банановых ячеек.

Появление активных областей в период завершения 24-го и начала 25-го циклов активности.

Григорьев *В.М., Ермакова Л.В., Хлыстова А.И.*

Солн.-земн. Физика Том 8. **2022**. № 4 С. 29–37.

https://naukaru.ru/ru/storage/viewWindow/105299

Изучение пространственно-временной картины появления активных областей и связи их возникновения со структурой и развитием крупномасштабного магнитного поля (КМП) проводилось в период смены 24-го и 25-го циклов солнечной активности. В этот период не отмечается бурного развития активности и поэтому динамика КМП в процессе появления новых активных областей наиболее заметна. Использовались данные SDO/HMI о продольном магнитном поле для определения времени и гелиографических координат места возникновения активной области и ежедневные карты WSO (Wilcox Solar Observatory) для сравнения со структурой КМП. Получены следующие результаты. В переходный период от одного цикла к другому новые активные области возникали в половине случаев на границе раздела полярностей КМП, причем почти исключительно на хейловских границах в соответствующих полусферах и циклах активности. В остальных случаях местом возникновения были униполярные области КМП без видимого преимущества в расположении областей поля по правилу Хейла. Образование активных областей предваряется или сопровождается изменениями в структуре КМП, при этом в тонкой структуре магнитного поля в фотосфере может наблюдаться усиление сетки магнитного поля на пространственном масштабе размера супергранул и более, а также появление малых областей нового магнитного поля обеих полярностей. Возникающие активные области концентрировались в двух узких долготных зонах, которые покрывали обе полусферы Солнца. Новый цикл начинался в тех же долготных зонах, где затухала активность старого цикла.

КРУПНОМАСШТАБНЫЕ МАГНИТНЫЕ ПОЛЯ СОЛНЦА ПО НАБЛЮДЕНИЯМ В ВИДИМЫХ И ИНФРАКРАСНЫХ ЛИНИЯХ И НЕКОТОРЫЕ ПРОБЛЕМЫ КОСМИЧЕСКОЙ ПОГОДЫ

Демидов М.Л., Ханаока И., Сакураи Т.

Изв. КрАО Том: **119** Номер: **2** Год: **2023**

Одним из наиболее актуальных направлений современной науки, имеющим к тому же важный прикладной аспект, является космическая погода (КП) - исследование и прогноз физических условий в межпланетном космическом пространстве, обусловленных процессами на Солнце. В настоящее время достигнут значительный прогресс в прогнозировании таких важных параметров КП, как скорость и плотность солнечного ветра. Но некоторые проблемы по-прежнему далеки от решения. Одна из таких проблем - противоречие в рассчитанных по различным моделям и наблюдаемых значениях напряженности межпланетного магнитного поля (ММП). Попытки устранить такое различие, например посредством корректировки магнитограмм, носят довольно искусственный характер и не дают стабильного результата. Основной целью настоящей работы, наряду с задачей сопоставления солнечных полнодисковых магнитограмм, получаемых в различных обсерваториях, является попытка разрешения данного противоречия посредством использования новых наблюдений,

выполненных в инфракрасных линиях. Такие линии, как известно, отличаются более высокой чувствительностью к слабым магнитным полям (а именно слабые крупномасштабные магнитные поля определяют параметры ММП), чем линии видимого диапазона. Измерения в инфракрасных линиях Fe i 1564.8 нм, Si i 1082.7 нм, He i 1083.0 нм выполняются на инструменте IRmag (Infrared Stokes spectro-polarimeter) Национальной астрономической обсерватории Японии (NAOJ). Использованные наблюдения в линиях видимого диапазона выполнены на инструментах GONG, SDO/HMI, Wilcox Solar Observatory (WSO), Солнечном телескопе оперативных прогнозов Саянской солнечной обсерватории (СТОП ССО). Обнаружено, что систематические различия в магнитограммах, выполненных в различных линиях, могут быть очень значительными и достигать фактора 2-5. Показано, что при использовании в расчетах ММП наблюдений в линии Si i 1082.7 нм удается в значительной степени устранить противоречие между модельными расчетами и экспериментальными результатами.

О ВОЗМОЖНОСТЯХ И ПРОБЛЕМАХ НАБЛЮДЕНИЙ МАГНИТНЫХ ПОЛЕЙ СОЛНЦА ДЛЯ ПРОГНОЗА КОСМИЧЕСКОЙ ПОГОДЫ

ДЕМИДОВ М.Л.

СОЛНЕЧНО-ЗЕМНАЯ ФИЗИКА Том: 3Номер: 1 Год: **2017** Страницы: 22-33

Важной составной частью актуальной в последние десятилетия проблемы космической погоды является прогноз параметров околоземного космического пространства, состояния ионосферы и геомагнитной активности на основе наблюдений различных явлений на Солнце. Особо значимы измерения магнитных полей, поскольку именно они определяют пространственную структуру внешних слоев солнечной атмосферы и в значительной степени параметры солнечного ветра. Ввиду отсутствия в настоящее время возможностей наблюдений магнитных полей непосредственно в короне практически единственным источником разнообразных моделей количественного расчета параметров гелиосферы являются измеряемые в фотосферных линиях ежедневные магнитограммы и получаемые на их основе синоптические карты. При этом оказывается, что результаты прогноза, в частности, скорости солнечного ветра на орбите Земли и положения гелиосферного токового слоя сильно зависят не только от выбранной модели расчетов, но и от исходного материала, поскольку магнитограммы различных инструментов (а зачастую и наблюдения в разных линиях на одном и том же телескопе) хотя и похожи морфологически, но могут значительно различаться при подробном количественном анализе. Детальному рассмотрению именно этого аспекта проблемы космической погоды посвящена значительная часть настоящей работы.

ИНДЕКСЫ СОЛНЕЧНОЙ АКТИВНОСТИ ДЛЯ ИОНОСФЕРЫ В ЦИКЛАХ 23 И 24: ФОРМА ЦИКЛОВ

Деминов М.Г., Деминов Р.Г., Непомнящая Е.В.

ГиА Том: 62Номер: 1 Год: 2022 Страницы: 75-80

Проведен анализ особенностей формы низких солнечных циклов 23 и 24 для индексов солнечной активности (*F* – потока солнечного радиоизлучения на длине волны 10.7 см, *Rz* и *Ri* – относительного числа солнечных пятен, прежняя и новая версии) и ионосферного индекса этой активности *T*. Для этого анализируемые индексы приведены к шкале *Rz* и рассмотрены сглаженные (с помощью 24-месячного гауссова фильтра) значения этих индексов. Получено, что для циклов 23 и 24 и предыдущих солнечных циклов по индексу *Rz* форма циклов сохранялась, т.е. выполнялась определенная связь между амплитудой цикла и временем наступления максимума цикла. Эта же связь соблюдалась для индекса *Ri*, за исключением цикла 23, когда наблюдаемое время наступления максимума цикла произошло на 7 месяцев позже времени, ожидаемого на основе предыдущих циклов. Для индексов *F* и *T* форма циклов также сохранялась вплоть до цикла 22, но в циклах 23 и 24 наблюдаемые максимумы циклов произошли почти на год позже ожидаемых, что является одним из свойств нового режима продолжительной низкой солнечной активности. В этом режиме нарушается связь между индексами *Ri* и *F*, что и приводит к разным формам циклов для этих индексов.

ИНДЕКСЫ СОЛНЕЧНОЙ АКТИВНОСТИ ДЛЯ ПАРАМЕТРОВ ИОНОСФЕРЫ В ЦИКЛАХ 23 И 24

Деминов М.Г., Непомнящая Е.В., Обридко В.Н.

ГиА Том: 60Номер: 1 Год: **2020**

Проведен анализ особенностей изменений индексов солнечной активности (F – потока солнечного радиоизлучения на длине волны 10.7 см, Ri – относительного числа солнечных пятен, новая версия) и ионосферного индекса этой активности T в солнечных циклах 23 и 24, которые были низкими по амплитуде солнечной и геомагнитной активности. Для этого рассмотрены скользящие средние за 12 мес. и сглаженные (с помощью 24-месячного фильтра) значения этих индексов. Получено, что в среднем связь между индексами T и F оставалась стабильной для этих циклов и не отличалась от предыдущих солнечных циклов. Связь между индексами T и Ri изменялась со временем в циклах 23 и 24 и отличалась от предыдущих циклов. Кроме того, для цикла 24 наблюдался отчетливый эффект гистерезиса в зависимости сглаженных значений T от Ri, когда на фазах роста и спада солнечного цикла фиксированному значению Ri соответствовали разные значения T. Этот эффект отсутствовал в зависимости T от F. Тем самым подтверждено, что индекс F является более точным, чем Ri, индикатором солнечной активности для ионосферы.

ОБ ОДНОМ ИЗ ВОЗМОЖНЫХ МЕХАНИЗМОВ ОБРАЗОВАНИЯ СПИКУЛ В СПОКОЙНЫХ ОБЛАСТЯХ НА СОЛНЦЕ

ДУНИН-БАРКОВСКАЯ О. В.*✉1, СОМОВ Б. В.*✉

ПАЖ ом: 47Номер: 10 Год: **2021** Страницы: 728-732
В качестве источника энергии для образования спикул в хромосфере Солнца рассмотрена гравитационная энергия падающего из короны вещества. Показано, что в спокойном переходном слое между хромосферой и короной направленный вниз поток вещества может порождать ударную волну, которая движется вверх. При этом часть энергии падающего вещества возвращается в корону и дает вклад в ее нагрев. Рассчитаны необходимые для этого скорости падающего вещества. Соответствующий диапазон скоростей хорошо согласуется с современными наблюдениями.

ОБ ЭФФЕКТИВНОМ МЕХАНИЗМЕ ГЕНЕРАЦИИ УДАРНЫХ ВОЛН В СПОКОЙНОМ ПЕРЕХОДНОМ СЛОЕ СОЛНЦА

ДУНИН-БАРКОВСКАЯ О.В.1, СОМОВ Б.В.

ПАЖ Том: 43Номер: 8 Год: **2016** Страницы: 624-630

В проблеме нагрева короны Солнца обычно постулируются две конкурирующие фундаментальные гипотезы: нагрев нановспышками и нагрев волнами. В рамках второй из них предполагается, что из конвективной зоны приходят акустические и магнитогидродинамические возмущения, амплитуда которых нарастает при распространении в среде с падающей плотностью. Формирующиеся при этом ударные волны нагревают корону. В данной работе мы обращаем внимание на еще один весьма эффективный процесс генерации ударных волн, который может реализоваться при определенных условиях, характерных для спокойных областей на Солнце. В приближении стационарной диссипативной гидродинамики нами показано, что в спокойном переходном слое между короной и хромосферой ударная волна может возникать за счет падения вещества из короны в хромосферу. Такая ударная волна направлена вверх, и ее диссипация в короне возвращает часть кинетической энергии падающего вещества в тепловую энергию короны. Обсуждаются перспективы разработки количественной нестационарной модели явления.

ФИЗИЧЕСКИЕ СВОЙСТВА СПОКОЙНОГО ПЕРЕХОДНОГО СЛОЯ МЕЖДУ КОРОНОЙ И ХРОМОСФЕРОЙ СОЛНЦА

ДУНИН-БАРКОВСКАЯ О.В.1, СОМОВ Б.В.

ПАЖ Том: 42Номер: 12 Год: **2016** Страницы: 908
Представлены результаты исследований физических свойств переходного слоя между короной и хромосферой Солнца в спокойных областях. Здесь структура атмосферы Солнца определяется взаимодействием магнитных полей над фотосферой. Они концентрируются в тонкие трубки, внутри которых велика напряженность поля. Исследовано, как в зависимости от скорости плазмы на хромосферной границе переходного слоя меняются распределения температуры, концентрации и скорости плазмы вдоль магнитной трубки, один конец которой находится в хромосфере, а другой - в короне. Рассмотрены два предельных случая: горизонтально и вертикально расположенная магнитная трубка. Для различных концентраций плазмы определены диапазоны скоростей на хромосферной границе переходного слоя, для которых в переходном слое не должны возбуждаться ударные волны. Показано, что наиболее благоприятными для возбуждения ударных волн в переходном слое являются направленные вниз течения плазмы в его основании. Для всех рассчитанных вариантов переходного слоя показано, что перенос тепловой энергии вдоль магнитных трубок может быть хорошо описан в приближении классической электронной столкновительной теплопроводности вплоть до очень больших скоростей в основании переходного слоя. Рассчитанное жесткое ультрафиолетовое (EUV) излучение хорошо согласуется с современными космическими наблюдениями Солнца.

Квазипериодические колебания мелкомасштабных магнитных структур и специальный метод измерения дифференциального вращения Солнца

Живанович И., Риехокайнен А., Соловьев А.А., Ефремов В.И.
СОЛНЕЧНО-ЗЕМНАЯ ФИЗИКА Том 5. **2019**. № 1., 4–12
https://naukaru.ru/upload/7fd3f86c299d8e1ce467f949bdfec858/files/f851f9b299792a475c14162a4da81b56.pdf
Для изучения дифференциального вращения Солнца с помощью эффекта p2p на основе движений мелкомасштабных магнитных структур в фотосфере были использованы данные SDO/HMI с угловым разрешением 1". Показано, что стабильный p2p-артефакт, присущий данным ПЗС-матрицы SDO/HMI, может быть эффективным средством для измерения скорости различных трассеров на Солнце. В частности, в сочетании с анализом Фурье он позволяет исследовать дифференциальное вращение Солнца на различных широтах. Скорости дифференциального вращения, полученные по магнитограммам SDO/HMI с помощью данного метода, хорошо совпадают с полученными ранее из наземных наблюдений.

ПОВЕРХНОСТНЫЕ И ФУНДАМЕНТАЛЬНЫЕ МОДЫ КОЛЕБАНИЙ В ТОНКИХ КОРОНАЛЬНЫХ АРКАХ

ЖУГЖДА Ю. Д.1

ПАЖ ом: 46Номер: 4 Год: **2020** Страницы: 285-291

Рассмотрены колебания в тонких магнитных трубках в солнечной короне. Показано, что основными модами быстрых и медленных колебаний являются поверхностная и фундаментальная моды колебаний. Медленные поверхностная и фундаментальная моды являются волноводными модами. Быстрая поверхностная мода является излучающей модой, в то время как быстрая фундаментальная мода - это волноводная мода. Рассмотренные нами фундаментальные моды существуют только в магнитных трубках, подверженных влиянию окружающей среды. Наше определение фундаментальных мод не совпадает с общепринятым. Современные наблюдения колебаний в корональных арках вряд ли могут зафиксировать медленные сосисочные моды, первая из которых рассматривается как фундаментальная. Быстрые сосисочные моды также не должны наблюдаться при плохом пространственном разрешении. Исключением является первая быстрая сосисочная мода, обычно рассматриваемая как фундаментальная. Однако эта мода отсутствует в тонких магнитных трубках.

ЦИКЛИЧЕСКИЕ ВАРИАЦИИ, МАГНИТНАЯ МОРФОЛОГИЯ И СЛОЖНОСТЬ АКТИВНЫХ ОБЛАСТЕЙ В 23-М И 24-М СОЛНЕЧНЫХ ЦИКЛАХ

ЖУКОВА А. В.[*][1], **СОКОЛОВ Д. Д.**[*][2], **АБРАМЕНКО В. И.**[1], **ХЛЫСТОВА А. И.**[*]

Г. И А. Том: 60Номер: 6 Год: 2020 Страницы: 683-694

Изучены 2046 активных областей 23-го и 1507 – 24-го солнечных циклов с мая 1996 по декабрь 2018 гг. Группы солнечных пятен распределены в соответствии с недавно предложенной магнито-морфологической классификацией. Выделены регулярные активные области, которые подчиняются закону полярностей Хейла, закону Джоя, с лидирующим пятном, преобладающим над основным хвостовым пятном, а также нерегулярные группы солнечных пятен и одиночные пятна. Показано, что основной вклад в развитие цикла вносят регулярные активные области, что согласуется с моделями магнитного цикла. Вклад нерегулярных групп солнечных пятен примерно в 2–5 раз меньше (в максимумах цикла) и сопоставим с вкладом регулярных активных областей в минимумах цикла, что может свидетельствовать о совместном действии глобального динамо среднего поля и флуктуационного динамо. Увеличение количества нерегулярных активных областей в южном полушарии во втором максимуме каждого из исследованных циклов можно объяснить ослаблением тороидального поля (произведенного глобальным динамо) и увеличением вклада флуктуационного динамо в их конкурентном взаимодействии...

СРАВНИТЕЛЬНЫЙ АНАЛИЗ КВАЗИПЕРИОДИЧЕСКИХ ПРОЦЕССОВ В МАГНИТОСФЕРНОМ ТОКОВОМ СЛОЕ И В ТОКОВЫХ СЛОЯХ СОЛНЕЧНОЙ КОРОНЫ

Зимовец И.В., Лукин А.С., Артемьев А.В.

Косм. Исслед. Том: 60Номер: 6 Год: **2022** Страницы: 454-470

Пересоединение магнитных силовых линий представляет собой универсальный процесс высвобождения запасенной энергии магнитного поля и ее трансформации в тепловую энергию плазмы и энергию ускоренных заряженных частиц. Инициализация и протекание процесса магнитного пересоединения существенным образом связана с динамикой пространственно локализованной области сильных плазменных токов – токового слоя. Две наиболее изученные космические магнитоплазменные системы, содержащие токовые слои, – это хвостовая область земной магнитосферы и области с близко расположенными вытянутыми силовыми линиями магнитного поля противоположной полярности в солнечной короне (в частности, лучи корональных стримеров и эруптивные вспышки). Однако, если для земной магнитосферы основным источником информации о структуре и динамике токовых слоев являются многочисленные прямые измерения спутниковых миссий, то для солнечной короны некоторые характеристики токового слоя могут восстанавливаться на основе удаленных наблюдений квазипериодических осцилляций. Как следствие, для прояснения возможных механизмов, ответственных за данные осцилляции, представляется актуальным сопоставление свойств осцилляций токового слоя земной магнитосферы и токовых слоев солнечной короны. Именно такому сравнительному анализу и посвящена данная работа, в которой приводится небольшой обзор имеющейся информации о квазипериодической динамике магнитосферного токового слоя и обсуждается вероятная интерпретация данной динамики в терминах и параметрах наблюдений квазипериодических процессов в токовых слоях солнечной короны.

ИТОГИ И УРОКИ 24 ЦИКЛА – ПЕРВОГО ЦИКЛА ВТОРОЙ ЭПОХИ ПОНИЖЕННОЙ СОЛНЕЧНОЙ АКТИВНОСТИ

Ишков В. Н.

АЖ Том: 99Номер: 1 Год: 2022 Страницы: 54-69

Прошедший 24 цикл солнечной активности реализовался в условиях, когда после переходного 23 цикла фоновые значения общего магнитного поля Солнца уменьшились более чем в два раза, что привело к полной перестройке физических условий на Солнце, и, как следствие, в гелиосфере, и отразилось на состоянии околоземного космического пространства. Он реализовался как цикл низкой величины, пятнообразовательная и вспышечная активность которого существенно ниже всех предыдущих солнечных циклов космической эры, и впервые на достоверном ряде наблюдений солнечных пятен предоставил возможность детально исследовать ход его развития как начального цикла эпохи пониженной солнечной активности.

ЭКСТРЕМАЛЬНЫЕ СОБЫТИЯ КОСМИЧЕСКОЙ ПОГОДЫ В ПЕРВЫЕ ЦИКЛЫ ЭПОХ ПОНИЖЕННОЙ СОЛНЕЧНОЙ АКТИВНОСТИ

Ишков В. Н.

Г и А Том: 61Номер: 6 Год: 2021 Страницы: 704-712

DOI: 10.31857/S0016794021060080
По однородному ряду геомагнитного индекса *Aa* с учетом современной шкалы интенсивности возмущений в околоземном космическом пространстве и сценария солнечной цикличности рассмотрен вопрос о распределении экстремальных и очень больших магнитных бурь, интенсивности (G5, G4), в первых циклах (12 и 24) эпох пониженной солнечной активности. Значительное уменьшение количества таких событий и солнечных активных явлений в последнем цикле может свидетельствовать о том, что пятнообразовательная и вспышечная активность в солнечном цикле 12 была значимо выше, чем в цикле 24, но значительно уступала солнечным циклам эпохи повышенной солнечной активности.

ТЕКУЩИЙ 24 ЦИКЛ СОЛНЕЧНОЙ АКТИВНОСТИ В ФАЗЕ МИНИМУМА: ПРЕДВАРИТЕЛЬНЫЕ ИТОГИ И ОСОБЕННОСТИ РАЗВИТИЯ

ИШКОВ В.Н.

Косм. Исслед. Том: 58Номер: 6 Год: 2020 Страницы: 471-478

Характеристики и ход развития текущего 24 цикла солнечной активности (СА) позволяют отнести его к циклам эпох пониженной СА. Сравнение эволюционных изменений циклов различных эпох в фазах минимума позволило выделить две группы по темпу спада. Первая группа с относительно быстрым спадом (~15 мес.) включает в себя все циклы эпох повышенной СА, переходных периодов и цикл 16 из эпохи пониженной СА. Вторая, с медленным спадом (~40 мес.), остальные циклы эпох пониженной СА, в том числе и текущий 24, минимум которого можно ожидать уже в первой половине 2020.

КОСМИЧЕСКАЯ ПОГОДА И ОСОБЕННОСТИ РАЗВИТИЯ ТЕКУЩЕГО 24-ГО ЦИКЛА СОЛНЕЧНОЙ АКТИВНОСТИ

ИШКОВ В.Н.*

ГиА Том: 58Номер: 6 Год: **2018** Страницы: 785-800

Согласно сценарию цикличности достоверного ряда относительных чисел солнечных пятен 24-й цикл открывает вторую эпоху пониженной солнечной активности (СА). Основной особенностью этой эпохи (5 циклов) – запрет на осуществление высоких солнечных циклов и непременное выполнение основных наблюдательных правил в развитии отдельных циклов. Уменьшение более чем в два раза фоновых значений общего магнитного поля Солнца к концу 23-го цикла привело к полной перестройке физических условий как на Солнце, так и во внутренней гелиосфере, и отразилось на состоянии околоземного космического пространства (ОКП). Текущий 24-й солнечный цикл после 9.2 лет развития стал циклом низкой величины (W* = 81.9) с пониженной вспышечной активностью, с более низкой геоэффективностью солнечных активных явлений, с практическим отсутствием самых мощных солнечных вспышечных явлений, солнечных протонных событий, проявлений геомагнитной активности и ионосферных возмущений.

МОГУТ ЛИ СУПЕРВСПЫШКИ ПРОИСХОДИТЬ НА СОЛНЦЕ? ВЗГЛЯД С ТОЧКИ ЗРЕНИЯ ТЕОРИИ ДИНАМО

Кацова М.М., Кичатинов Л.Л., Лившиц М.А., Мосс Д.Л., Соколов Д.Д., Усоскин И.Г.

АЖ Том: 95Номер: 1 Год: **2018** Страницы: 78-87

Недавние результаты миссии "Kepler" показали, что на звездах, подобных Солнцу, могут происходить супервспышки, которые существенно превосходят по энерговыделению все когда-либо наблюдавшиеся солнечные вспышки. Данные по радионуклидам не дают оснований предполагать наличие супервспышек на Солнце в течение последних 11 тыс. лет. Естественно считать, что механизм динамо на звездах с супервспышками в некотором отношении отличается от солнечного. В работе выявляются управляющие параметры динамо, которые могут описывать различие между Солнцем и звездами с супервспышками. Наша цель состоит в том, чтобы предложить механизм динамо, максимально близкий к обычному солнечному (звездному) динамо, но способный создать существенно больший запас магнитной энергии. Механизм динамо, основанный на совместном действии дифференциального вращения и зеркально асимметричных движений среды, в принципе может приводить к генерации двух типов магнитных конфигураций. Это хорошо известные в физике Солнца волны магнитного поля (динамо-волны). Однако возможен и другой тип решений, при которых магнитное поле сначала растет, а затем стабилизируется. При сопоставимых условиях напряженность магнитных полей второго типа решений существенно больше, чем первого, просто потому, что возможности динамо не тратятся на периодические изменения знака магнитного поля, а целиком расходуются на его усиление. Мы проанализировали имеющиеся результаты наблюдений миссии "Kepler" озвездах с супервспышками, чтобы найти индикаторы аномальной магнитной активности. Отталкиваясь от недавней работы [1], мы приходим к выводу, что антисолнечное дифференциальное вращение или антисолнечный знак зеркальной асимметрии как раз и являются факторами, способными обеспечить необходимую величину магнитного поля в моделях звездного динамо. Мы подтверждаем это представление численными моделями звездного динамо с подобными параметрами. Мы полагаем, что такой механизм может объяснить феномен супервспышек, по крайней мере, для некоторых звезд поздних спектральных классов, включая двойные звезды, субгиганты, маломассивные звезды и молодые быстро вращающиеся звезды.

ПРОИСХОЖДЕНИЕ ПРИПОВЕРХНОСТНОГО СЛОЯ НЕОДНОРОДНОГО ВРАЩЕНИЯ СОЛНЦА

Кичатинов Л.Л.

ПАЖ Том: 49Номер: 11 Год: 2023 Страницы: 829-836

Гелиосейсмология обнаружила возрастание скорости вращения с глубиной в тонком (~30 Мм) приповерхностном слое. Относительная величина неоднородности вращения в этом слое не зависит от широты. Показано, что такое состояние вращения является следствием малого характерного времени приповерхностной конвекции по сравнению с периодом вращения и радиальной анизотропии конвективной турбулентности. Аналитические расчеты в рамках гидродинамики средних полей воспроизводят наблюдаемую величину относительной неоднородности вращения и согласуются с численными экспериментами по радиационной гидродинамике солнечной конвекции. Приповерхностный слой является источником глобального меридионального течения, важного для солнечного динамо.

РАСПАД КРУПНОМАСШТАБНОГО МАГНИТНОГО ПОЛЯ НА ТРУБКИ У ОСНОВАНИЯ КОНВЕКТИВНОЙ ЗОНЫ СОЛНЦА

КИЧАТИНОВ Л.Л.

АЖ Том: 45Номер: 1 Год: **2019** Страницы: 45-54

Подавление турбулентной теплопроводности магнитным полем приводит к неустойчивости крупномасштабного поля с образованием изолированных в пространстве областей усиленного поля. К такому выводу приводит линейный анализ устойчивости в рамках магнитной гидродинамики средних полей с учетом зависимости теплопроводности от напряженности поля. Характерное время развития неустойчивости мало по сравнению с 11-летним периодом солнечной активности. Размер областей усиленного поля составляет десятки тысяч километров. Данная неустойчивость может создавать магнитные неоднородности, всплывание которых на солнечную поверхность создает активные области Солнца. Магнитная энергия образующихся сгустков поля совпадает по порядку величины с энергией активных областей.

АСИММЕТРИЯ СОЛНЕЧНЫХ ЦИКЛОВ КАК СЛЕДСТВИЕ ФЛУКТУАЦИЙ ПАРАМЕТРОВ ДИНАМО

КИЧАТИНОВ Л.Л.1, НЕПОМНЯЩИХ А.А.1

АЖ: Том: 44Номер: 10 Год: **2018** Страницы: 705-712

Длительность ветви роста активности в солнечных циклах в среднем короче длительности ветви спада. Показано, что к такой асимметрии могут приводить флуктуации параметров динамо. Модель солнечного динамо с флуктуациями α -эффекта показывает среднестатистическую асимметрию, которая увеличивается с возрастанием как амплитуды, так и длительности флуктуаций. Предложено объяснение вызванной флуктуациями асимметрии, которое предсказывает корреляцию между величиной асимметрии и временем запаздывания обращений знака полярного поля относительно максимума активности. Такая корреляция подтверждается данными о двенадцати последних солнечных циклах.

К ПОИСКУ НАБЛЮДАТЕЛЬНЫХ ПРОЯВЛЕНИЙ АЛЬВЕНОВСКИХ ВОЛН В СОЛНЕЧНЫХ ФАКЕЛАХ

КОБАНОВ Н.И.1, ЧУПИН С.А.1, ЧЕЛПАНОВ А.А.1

АЖ Том: 43Номер: 12 Год: **2017** Страницы: 925-934

С целью обнаружения крутильных колебаний выполнены исследования периодических вариаций полуширины нескольких спектральных линий в солнечных факелах. Длительность анализируемых серий составляла от 40 до 150 мин. Были определены доминирующие частоты и амплитуды колебаний полуширины, рассмотрены их фазовые связи с колебаниями интенсивности и лучевой скорости. В линии верхней фотосферы Si I 10827 А в факелах уверенно регистрируются пятиминутные колебания полуширины профиля около 10 мЛ (peak-to-peak). Профили хромосферных линий He I 10830 Л и Na показывают вариации величиной около 40-60 мЛ в двух частотных диапазонах 2.5-4 мГц и 1 - 1.9 мГц. В поведении амплитуд этих колебаний не выявлено зависимости центр-лимб, которая, согласно теории, должна сопровождать крутильные колебания. В рамках современных представлений эти вариации не могут быть вызваны периодическими изменениями температуры и магнитного поля. Наши наблюдения также не позволяют объяснить эти вариации и действием "сосисочной" моды (sausage mode), которое должно проявляться на удвоенной частоте.

О ВЕРОЯТНОЙ СМЕНЕ СТАТУСА ТЕКУЩЕГО НЕОРДИНАРНОГО СБОЯ 11-ЛЕТНЕЙ ЦИКЛИЧНОСТИ СОЛНЦА С ЛОКАЛЬНОГО НА ГЛОБАЛЬНЫЙ

КОЗЛОВ В.И.*

КОСМИЧЕСКИЕ ИССЛЕДОВАНИЯ Том: 59Номер: 2 Год: 2021 Страницы: 92-101

Обнаруженное по галактическим космическим лучам (ГКЛ) аномальное увеличение площади солнечного цикла 23 явилось предвестником сбоя 11-летней цикличности: в соответствии с гипотезой автора об инварианте 22-летнего цикла, вслед за увеличением площади 23 цикла последовало уменьшение площади (энергоемкости) следующего 24 цикла. Уменьшение энергоемкости сопровождается уменьшением (относительной вариации) светимости Солнца, которая в 24-цикле уменьшилась до уровня среднего значения трех предыдущих циклов, т.е. практически вдвое. При сохранении инварианта 22-летнего цикла следует ожидать восстановления 11-летней цикличности в 25-м цикле. При нарушении инварианта 22-летнего цикла, уровень радиационного фона ГКЛ в максимуме предстоящего 25 цикла (с 2024 на 2025 гг.) должен быть не ниже уровня фонового излучения в максимуме 24 цикла (2014 г.). В этом случае, состояние неординарного сбоя 23-24-25 циклов изменится с локального на глобальный.

К СУПЕРШТОРМУ ЧЕРЕЗ … «САМООРГАНИЗОВАННУЮ КРИТИЧНОСТЬ»?

В. И. **Козлов**

Наука и техника в Якутии № 1 (36) **2019**

https://www.researchgate.net/profile/Valery_Kozlov/publication/334644071_K_SUPERSTORMU_CEREZ_SAMOORGANIZOVANNUU_KRITICNOST/links/5d37c59ba6fdcc370a5a35b8/K-SUPERSTORMU-CEREZ-SAMOORGANIZOVANNUU-KRITICNOST.pdf?origin=publication_list

Свойства солнечного цикла

АРИТМИЯ СОЛНЦА. В космических лучах

В. И. **Козлов**, В. В. Козлов

Издательство ФГБУН ИМЗ СО РАН г. Якутск **2018**

3-е издание, переработанное и дополненное

https://www.researchgate.net/messages/877872513

ГЛАВНЫЙ АРГУМЕНТ ПРОТИВ ПУЛЬСАЦИЙ СОЛНЦА

Котов В.А.

Изв. КрАО Том: 119Номер: 4 Год: 2023 Страницы: 27-34

Близость периода колебаний Солнца, 0.111 сут, к 9-й гармонике среднесолнечных суток представляется оппонентами в качестве основного аргумента против колебаний. Мы показываем, что на деле он, наоборот, доказывает реальность явления, поскольку суточный период Земли, повидимому, является фундаментальной временн´ой шкалой Солнечной системы, тесно связанной с движениями Солнца, Меркурия, Венеры и Земли. Однако истинная природа солнечных колебаний остается неизвестной.

МАГНИТНЫЕ ЦИКЛЫ СОЛНЦА И РЕЗОНАНСЫ СОЛНЕЧНОЙ СИСТЕМЫ

Котов В.А.

Изв. КрАО Том: 119 Номер: 1 Год: 2023 Страницы: 42-47

Общее магнитное поле Солнца в КрАО, Стэнфорде и пяти других обсерваториях измерялось с 1968 по 2021 гг. (в сумме более 28 тыс. суточных значений). Из этих данных следует, что поле изменяется с циклом Хейла PH ≈ 22 г. и периодом P7 ≈ 7 лет, отношение которых совпадает с приближением Архимеда, 22:7, для числа п. Показано, что в пределах ошибок измеряемых величин (а) орбитальный период Земли PE = (1 - 3/п)PH = (п - 3)P7 = P2$_\odot$/2PD, где P$_\odot$ ≈ 27 сут - синодический период вращения Солнца, а PD - среднесолнечные сутки; (б) связь PE-PH следует также из измерений полярного поля Солнца; (в) шкала PE тесно связана с движением Венеры. Выдвинута гипотеза, что годовой и суточный периоды движения нашей планеты, скорость вращения Солнца и цикл Хейла, объединенные числами 2, 3 и п, имеют космологический смысл и фундаментальное значение для Солнца, Земли и Солнечной системы. Истинная природа связи движений Солнца и Земли с циклом Хейла неизвестна.

ПЯТЬДЕСЯТ ЛЕТ ИССЛЕДОВАНИЯ ПОВЕДЕНИЯ ИНТЕНСИВНОСТИ ГКЛ В ПЕРИОДЫ ИНВЕРСИИ ГЕЛИОСФЕРНОГО МАГНИТНОГО ПОЛЯ. II. ИНВЕРСИЯ ГМП НА ВНУТРЕННЕЙ ГРАНИЦЕ ГЕЛИОСФЕРЫ

КРАЙНЕВ М.Б.[1], **КАЛИНИН М.С.**[1]

СОЛНЕЧНО-ЗЕМНАЯ ФИЗИКА Том: 10 Номер: 3 Год: 2024 Страницы: 40-52

Явления в наружном слое солнечной атмосферы, гелиосфере, включающие сверхзвуковой солнечный ветер, переносимое им гелиосферное магнитное поле (ГМП) и распространяющиеся в гелиосфере космические лучи, важны для многих процессов, происходящих в этом слое. Для некоторых, например геомагнитной активности или распространения космических лучей, важны не только напряженность, но и направление поля. Но если в этом отношении ситуация в периоды низкой пятенной солнечной активности вполне ясна - гелиосфера разделена на два полушария с противоположной полярностью (к Солнцу/от Солнца) - в периоды высокой активности Солнца, когда происходит инверсия ГМП, простой модели этого явления нет. В статье продолжается исследование явления инверсии ГМП и связанных с ним эффектов в интенсивности галактических космических лучей (ГКЛ). Ранее были сформулированы общие представления о 22-летней цикличности в характеристиках Солнца, гелиосферы и космических лучей и подробно обсуждались наблюдаемые эффекты в интенсивности ГКЛ, связываемые нами с

инверсией ГМП. В данной работе рассмотрена модель инверсии ГМП, связанной лишь с эволюцией магнитного поля в слое между фотосферой и основанием гелиосферы из-за изменения распределения фотосферных полей от оборота к обороту Солнца, и показано, что этого недостаточно для объяснения основных эффектов в интенсивности ГКЛ. В указанном слое магнитное поле является основным энергетическим фактором. Более полная модель инверсии ГМП, включающая преобразование его характеристик из-за взаимодействия разноскоростных потоков солнечного ветра в самой гелиосфере, где солнечный ветер является основным энергетическим фактором, будет обсуждаться в следующей статье.

Пятьдесят лет исследования поведения интенсивности ГКЛ в периоды инверсии гелиосферного магнитного поля. I. Наблюдаемые эффекты.

Крайнев М.Б., Базилевская Г.А., Калинин М.С., Михайлов В.В., Свиржевская А.К., Свиржевский Н.С.

СОЛНЕЧНО-ЗЕМНАЯ ФИЗИКА Том 9 № 4 , **2023**, С. 5–20.

https://naukaru.ru/ru/storage/viewWindow/138045

Впервые эффекты 22-летней цикличности солнечных магнитных полей в интенсивности галактических космических лучей (ГКЛ) были замечены группой ФИАН в 1973 г. и интерпретированы как проявления инверсии высокоширотного магнитного поля Солнца в свойствах гелиосферных магнитных полей. С тех пор эти эффекты исследуются уже в течение пятидесяти лет. Для периодов средней и низкой пятенной активности ситуация с гелиосферным магнитным полем (ГМП) понятна: гелиосфера состоит из двух униполярных «полушарий», разделенных волнистым глобальным гелиосферным токовым слоем и характеризующихся общей полярностью A (единичная величина со знаком радиальной компоненты поля в северном полушарии). Однако нет единого мнения, в чем заключается инверсия ГМП и какие явления в ГКЛ с ней связаны. В статье кратко формулируются общие представления о 22-летней цикличности в характеристиках Солнца, гелиосферы и ГКЛ и обсуждаются наблюдаемые эффекты в интенсивности ГКЛ, связываемые нами с инверсией ГМП. Модели этого явления, а также результаты расчетов интенсивности ГКЛ, использующих эти модели, будут обсуждаться в следующей статье.

ПРОЯВЛЕНИЯ В ГЕЛИОСФЕРЕ И В ИНТЕНСИВНОСТИ ГКЛ ДВУХ ВЕТВЕЙ СОЛНЕЧНОЙ АКТИВНОСТИ

Крайнев М.Б.

СОЛНЕЧНО-ЗЕМНАЯ ФИЗИКА Том 5 № 4 ,2019 С 12-25

https://naukaru.ru/ru/storage/viewWindow/43510

Дается представление о процессах в гелиосфере и модуляции галактических космических лучей (ГКЛ) в ней как результатах действия в этом слое Солнца двух ветвей солнечной активности, называемых по топологии солнечных магнитных полей внутри Солнца тороидальной ветвью (активные области, пятна, вспышки, корональные выбросы массы и т. д.) и полоидальной ветвью (высокоширотные магнитные поля, полярные корональные дыры, зональные униполярные магнитные области и т. д.). Формулируется основная причина различного проявления обеих ветвей на поверхности Солнца и в гелиосфере — наличие в основании гелиосферы слоя, в котором основным энергетическим фактором является магнитное поле. При этом преимущество при проникновении в гелиосферу получают более крупномасштабные, хотя и менее интенсивные солнечные магнитные поля полоидальной ветви. Показана связь с полоидальной ветвью солнечной активности гелиосферных характеристик (поле скорости солнечного ветра, размер гелиосферы, форма гелиосферного токового слоя, регулярное гелиосферное магнитное поле и его флуктуации), которые, согласно современным представлениям, определяют распространение в гелиосфере ГКЛ.

НЕЛИНЕЙНАЯ ЗАВИСИМОСТЬ ПОТОКА ИЗЛУЧЕНИЯ СОЛНЦА ОТ ЧИСЕЛ ВОЛЬФА И ЕЕ РАЗЛИЧИЕ ДЛЯ РАЗНЫХ 11-ЛЕТНИХ ЦИКЛОВ

Лаптухов А.И., Лаптухов В.А.

Г и А Том: 61Номер: 5 Год: 2021 Страницы: 547-554

DOI: 10.31857/S0016794021050084

Установлена статистическая нелинейная немонотонная зависимость среднесуточных величин солнечной “постоянной” от суточных чисел Вольфа. Предложен физический механизм этой нелинейной зависимости. Показано, что поток излучения Солнца для 11-летних циклов с высокой и низкой активностью существенно разный и, кроме того, он выше на фазе роста, чем на фазе спада цикла. Эти особенности надо учитывать при восстановлении солнечной “постоянной” на основе суточных чисел Вольфа.

СВЯЗЬ СЕВЕРО-ЮЖНОЙ АСИММЕТРИИ ПЯТНООБРАЗОВАНИЯ С АМПЛИТУДОЙ 11-ЛЕТНИХ ЦИКЛОВ СОЛНЕЧНОЙ АКТИВНОСТИ

ЛАТЫШЕВ С.В.1, ОЛЕМСКОЙ С.В.

ПАЖ Том: 42Номер: 7 Год: **2016** Страницы: 540
По данным о солнечных пятнах RGO/USAF/NOAA установлена связь северо-южной асимметрии пятнообразования с амплитудой 11-летних циклов. Показано, что чем выше амплитуда солнечного цикла, тем меньше абсолютное значение северо-южной асимметрии. Выявленная закономерность исследована в численной модели динамо с нерегулярными изменениями альфа-эффекта.

ФОРМИРОВАНИЕ ВЕКОВОГО РЯДА ДАННЫХ ПО СОЛНЕЧНОЙ ХРОМОСФЕРЕ ДЛЯ ИССЛЕДОВАНИЙ, СВЯЗАННЫХ С СОЛНЕЧНОЙ АКТИВНОСТЬЮ

ГАНХУА **ЛИНЬ**1, СЯО-
ФАНЬ ВАН1, СЯО ЯН1, СО ЛЮ1, МЭЙ ЧЖАН1, ХАЙМИНЬ ВАН2, ЧАН ЛЮ2, ЯНЬ СЮЙ2, Т ЛАТОВ А.Г.3, ДЕМИДОВ М.Л.4, БОРОВИК А.В.4, ГОЛОВКО А.А.4

СОЛНЕЧНО-ЗЕМНАЯ ФИЗИКА Том: 3Номер: 2 Год: **2017** Страницы: 5-9
В статье представлен наш действующий проект «Формирование векового ряда данных по солнечной хромосфере для исследований, связанных с солнечной активностью». Солнечная активность является главным фактором космической погоды, влияющим на жизнь человечества. Некоторые серьезные последствия воздействия космической погоды, например, нарушение космической связи и навигации, угроза безопасности астронавтов и спутников, повреждение электрических систем. Поэтому исследование солнечной активности имеет и научный, и социальный аспекты. Основная база данных формируется из оцифрованных и нормированных данных, полученных в нескольких обсерваториях по всему земному шару, и покрывает более чем 100-летний временной интервал. После тщательной калибровки мы сможем извлечь и получить данные и вместе с полной базой данных предоставить их астрономическому сообществу. Нашей конечной целью является привлечение внимания к нескольким физическим проблемам: поведение волокон в солнечном цикле, аномальный ход 24 цикла, крупномасштабные солнечные эрупции и дистанционно-индуцированные уярчения. Существенный прогресс ожидается в разработке алгоритмов получения данных и программного обеспечения, что поможет научному анализу и в итоге будет способствовать пониманию солнечных циклов.

ПОДТВЕРЖДЕНИЕ "ПОТЕРЯННОГО" ЦИКЛА И ПРАВИЛА ГНЕВЫШЕВА-ОЛЯ В РЯДЕ ПЛОЩАДЕЙ СОЛНЕЧНЫХ ПЯТЕН ЗА 410 ЛЕТ

НАГОВИЦЫН Ю.А.

ПАЖ Том: 50 Номер: 8 Год: 2024 Страницы: 561-566
Правило Гневышева-Оля рассмотрено для нового ряда площадей солнечных пятен на четырехвековой шкале Наговицына и Осиповой (MNRAS 505, 1206, 2021). Принята гипотеза Усоскина и др. (Astron. Astrophys. 370, L31, 2001) о существовании на ветви спада цикла № 4 цюрихской нумерации дополнительного малого цикла. Это приводит к изменению четности циклов ранее № 5. Выделены 11-летние циклы в XVII в. Их средняя продолжительность - от минимума до минимума - составляет T = 8.9 ± 1.4 года. Новые данные и подходы позволили заключить, что правило Гневышева-Оля выполняется для 410-летнего интервала в целом без исключения пары циклов №№ 4-5 цюрихской нумерации, принимаемого в правиле ранее.

ПРАВИЛО ГНЕВЫШЕВА-ОЛЯ: СОВРЕМЕННЫЙ СТАТУС

НАГОВИЦЫН Ю.А.[1,2], **ОСИПОВА А.А.**[1], **ИВАНОВ В.Г.**[1]

АЖ Том: 101Номер: 1 Год: 2024 Страницы: 56-64
Проведено статистическое исследование утверждений, содержащихся в Правиле Гневышева-Оля (ПГО) и в некоторых его толкованиях. Показано, что ПГО в его оригинальной формулировке для индекса суммарной активности за 11-летний цикл SW, фиксирующее тесную связь в паре четный-последующий нечетный цикл (ЧН) и ее отсутствие в противоположной паре (НЧ), строго выполняется для современных наблюдательных данных - версии 2.0 чисел пятен (чисел Вольфа) - при уровне значимости a=0.01. При этом за четным 11-летним циклом следует нечетный с большим S W. Для амплитуд циклов ПГО существует лишь как тенденция, и различие зависимостей пар циклов ЧН и НЧ статистически незначимо. Статистически не подтверждается также чередование величины циклов как для параметра S W, так и для амплитуд. Получено, что различные аспекты ПГО статистически лучше выполняются для новой версии 2.0 относительных чисел пятен - чисел Вольфа, что говорит в пользу ее дальнейшего успешного использования для исследований в солнечной физике.

ЭКСТРЕМАЛЬНЫЕ ЗНАЧЕНИЯ СОЛНЕЧНОЙ ПЯТНООБРАЗОВАТЕЛЬНОЙ ДЕЯТЕЛЬНОСТИ НА ДЛИТЕЛЬНОЙ ВРЕМЕННОЙ ШКАЛЕ

***Наговицын** Ю.А., Осипова А.А.*
ПАЖ Том: 49Номер: 7 Год: **2023** Страницы: 506-514
Рассмотрены экстремальные уровни солнечной активности на временных шкалах 300–400 и 9000 лет. Суммарная площадь солнечных пятен AR — физический индекс активности Солнца — оценена с помощью реконструкции числа солнечных пятен, полученной в работе By и др. (Astron. Astrophys. 615, A93, 2018). Основное исследование проведено именно в терминах этого индекса. Изменения солнечной активности в эпоху последних 300–400 лет достаточно хорошо представляют ее изменения на временах порядка девяти тысячелетий. Максимальный уровень солнечной активности для среднегодовых значений составил AR_M=2930±400 м.д.п. (миллионных долей полусферы). Верхний предел для суточных значений составил AR_M=7500±2200 м.д.п. для традиционных площадей пятен, скорректированных за перспективное искажение, и AR_{OM}=11400±3300 м.д.д. (миллионных долей диска Солнца) для так называемых "наблюдаемых" площадей —

проекций пятен на видимый диск Солнца. Оценены также максимальные среднегодовые значения чисел пятен SN_M=258±38 и чисел групп пятен GN_M=12.3±2.4; 11.3% времени солнечная активность находится на экстремально высоком уровне; 8.5% времени ее уровень соответствует минимуму Дальтона и ниже и 4.5% — крайне низкому. Таким образом, для солнечной активности более вероятны экстремально высокие уровни, чем экстремально низкие.

ДВЕ ПОПУЛЯЦИИ СОЛНЕЧНЫХ ПЯТЕН И ВЕКОВЫЕ ИЗМЕНЕНИЯ ИХ ХАРАКТЕРИСТИК

Ю. А. **Наговицын**1, 2*, А. А. Певцов3, А. А. Осипова1,
А. Г. Тлатов1, Е. В. Милецкий1, Е. Ю. Наговицына1
ПИСЬМА В АСТРОНОМИЧЕСКИЙЖУРНАЛ, **2016**, том 42,№10, с. 773–782
Исследуются магнитные поля и полные площади средне- и низкоширотных солнечных пятен на основе наблюдений в обсерваториях Гринвич, Кисловодск (площади пятен); Маунт-Вилсон, КрАО, Пулково, Урал,ИМИС, Уссурийск,ИЗМИРАН,Шемаха (магнитные поля). Показано, что в линейной форме зависимости логарифма полной площади пятна S от его центрального магнитного поля H коэффициенты изменяются со временем. На двумерной гистограмме встречаемости в осях H − log S выявляются две популяции пятен: мелкие и крупные, разделенные границами log S = 1.6 (S = 40 мдп) и H = 2050 Гс. Рассмотрение пятенного магнитного потока выявляет с высокой степенью достоверности существование двух логнормально распределенных популяций со средней границей между ними Ф = 1021 Мх. В то же время положения максимумов встречаемости значений потока у популяций изменяются на вековой шкале: у мелких пятен в 4.5 раза, у крупных — в 1.15 раза. Подтверждено, что пятна образуют две физически различающиеся популяции, и показано, что свойства этих популяций заметно изменяются со временем. Это согласуется с гипотезой о существовании двух зон генерации пятенного магнитного поля на Солнце в свете пространственно-распределенного динамо.

СТРУКТУРА СОЛНЕЧНОГО ЦИКЛА И ЦИКЛОВ АКТИВНОСТИ ЗВЕЗД ПОЗДНИХ СПЕКТРАЛЬНЫХ ТИПОВ

Обридко В.Н., Соколов Д.Д., Кацова М.М.
АЖ Том: 100Номер: 12 Год: 2023 Страницы: 1311-1321
DOI: 10.31857/S000462992312006X
Показано, что использование описания солнечного цикла, учитывающего нечетную зональную гармонику магнитного поля Солнца, позволяет углубить наши знания о двух важных аспектах солнечной активности: во-первых, уточнить и расширить предсказания на ближайшее будущее эволюции циклической активности Солнца; во-вторых, сформулировать программу мониторинга спектрофотометрических характеристик излучения звезд, подобных Солнцу, нацеленную на получение новой информации об их магнитных полях.

МЕРИДИОНАЛЬНАЯ СОСТАВЛЯЮЩАЯ КРУПНОМАСШТАБНОГО ПОЛЯ В МИНИМУМЕ И ХАРАКТЕРИСТИКИ ПОСЛЕДУЮЩЕГО ЦИКЛА СОЛНЕЧНОЙ АКТИВНОСТИ

ОБРИДКО В.Н.1, ШЕЛЬТИНГ Б.Д.1
ПАЖ Том: 43Номер: 10 Год: **2017** Страницы: 770
Известно, что полярное поле вблизи минимума цикла коррелирует с высотой следующего максимума числа солнечных пятен. Есть основание полагать, что в формировании следующего цикла важную роль может играть взаимодействие полушарий. Одним из индексов связи полушарий может быть меридиональная составляющая крупномасштабного магнитного поля. Для анализа были использованы реконструированные данные о крупномасштабном магнитном поле за 1915□1986 гг. Показано, что в нескольких циклах удается таким образом описать не только высоту, но и общий ход цикла с заблаговременностью около 6 лет. По современным данным с 1976 по 2016 г. такая связь подтвердилась, однако более перспективным оказался параметр отношения меридионального поля к полной абсолютной величине вектора поля. В данной работе он вычислялся на высоте около 70 Мм над фотосферой. Оценка даты предстоящего минимума с использованием этого параметра - середина 2018 г., использование глобального поля в качестве прогностического параметра дает более позднюю дату минимума - начало 2020 г.

ВЛИЯНИЕ ЦИКЛА ГЛЕЙСБЕРГА НА ВАРИАЦИИ ПЕРИОДА 11-ЛЕТНЕГО ЦИКЛА СОЛНЕЧНОЙ АКТИВНОСТИ В 1700–2021 ГГ.

ПТИЦЫНА Н.Г.*[1], **ДЕМИНА И.М.**[1]
ГиА Том: 63Номер: 3 Год: 2023 Страницы: 284-297
При помощи вейвлет-анализа проведено исследование спектрального состава числа солнечных пятен *SN* в течение 1700–2021 гг. Кроме доминирующей 11-летней составляющей, в спектре прослеживаются две мощные составляющие цикла Глейсберга: до 1880 г. ветвь с периодом ~60 лет, с 1850 г. ~115 лет. Найдено, что ряды длины и амплитуды солнечного

цикла в целом находятся в обратной зависимости (коэффициент корреляции $k = -0.5...-0.63$). Лаг между рядами, при котором достигается максимум антикорреляции, зависит от времени. В XVIII–начале XIX века лаг равен одному циклу, в XIX в. – двум циклам, а начиная с 1950 г. и до нашего времени лаг уменьшается до 2 лет. Выделены квазипериодические структуры, которые характерны для длительных периодов пониженной солнечной активности. Такая спектральная особенность в ~1800 г. (минимум Дальтона) вызвана влиянием 60-летней ветви, а формирующаяся с начала XXI в. – более слабым влиянием околостолетней. Поэтому следует ожидать, что ближайшие солнечные циклы будут более высокими и менее длинными, чем в период минимума Дальтона. Показано, что вариации длины солнечного цикла за последние 321 год могут быть описаны в рамках модели, представляющей собой 11-летнее колебание, которое подвергается частотной модуляции ветвями цикла Глейсберга (60 и 115 лет) с изменяющимся во времени влиянием модулятора.

ЧАСТОТНАЯ МОДУЛЯЦИЯ КАК ПРИЧИНА ВОЗНИКНОВЕНИЯ ДОПОЛНИТЕЛЬНЫХ ВЕТВЕЙ ВЕКОВОГО ЦИКЛА ГЛЕЙСБЕРГА В СОЛНЕЧНОЙ АКТИВНОСТИ

Птицына Н.Г., Демина И.М.

ГиА Том: 62Номер: 1 Год: 2022 Страницы: 52-66

Среди цикличностей солнечной активности с периодом более 22 лет вековой цикл, или цикл Глейсберга, привлекает наибольшее внимание исследователей. В данной работе методами Фурье и вейвлет-анализа проведено изучение цикличности солнечной активности, выраженной числом солнечных пятен *SN*, реконструированных из разных источников (длина рядов до ~12 000 лет), в диапазоне периодов цикла Глейсберга. Найдено, что цикл Глейсберга состоит из трех выделенных ветвей со средними периодами 60, 88 и 140 лет. Характер амплитудной вариации всех трех ветвей идентичен, что указывает на то, что они являются частью одного квазипериодического процесса. Анализ показал, что 88-летний цикл является основным. Его источником является солнечное динамо. А 60- и 140-летние циклы являются результатом частотной модуляции основного цикла процессом с периодом 224 года (цикл Зюсса). Построена модель, которая подтверждает и объясняет этот результат. Цикл Зюсса, являющийся частотным модулятором цикла Глейсберга, скорее всего, имеет внесолнечное происхождение. Наши результаты не поддерживают гипотезу о хаотическом Солнце, свидетельствуя о более регулярном квазиопериодическом поведении солнечного динамо.

НЕВИДИМОЕ ДИНАМО В МОДЕЛЯХ СРЕДНЕГО ПОЛЯ

РЕШЕТНЯК М.Ю.

ПАЖ Том: 42Номер: 7 Год: **2016** Страницы: 533

Решена обратная задача в сферической оболочке по нахождению двумерных пространственных распределений -эффекта и дифференциального вращения в модели динамо среднего поля. Полученные распределения приводят к генерации магнитного поля, сконцентрированного внутри конвективной зоны. Показано, что за счет магнитной диффузии магнитное поле за время смены полярности не успевает выйти из области максимальной генерации, расположенной в нижних слоях, к поверхности. Отношение максимальной магнитной энергии в конвективной зоне к ее значению на внешней границе достигает двух порядков и более. Полученный результат важен при интерпретации наблюдаемых звездных и планетарных магнитных полей. Предложенный метод решения обратной задачи нелинейного динамо легко адаптируется для широкого класса задач математической физики.

ФАЗОВОЕ ПРОСТРАНСТВО ДВУМЕРНОЙ МОДЕЛИ ДИНАМО ПАРКЕРА

РЕШЕТНЯК М. Ю.1

АЖ Том: 93 Номер: 2 Год: **2016** Страницы: 254

На примере двумерной модели Паркера в сферическом слое рассмотрены зависимости интенсивности магнитного поля, его вариаций, уровня мультипольности от амплитуд - и -эффектов. Расчеты приведены как для традиционных в астрофизике пространственных распределений и , так и для геострофических режимов, полученных из трехмерного моделирования тепловой конвекции. Приведены двумерные распределения скоростей динамо-волн в зоне генерации магнитного поля. Предложены сопоставления с солнечным и планетарным динамо.

ОСОБЕННОСТИ ДОЛГОТНОГО РАСПРЕДЕЛЕНИЯ ГРУПП СОЛНЕЧНЫХ ПЯТЕН ЗА ПОСЛЕДНИЕ ЧЕТЫРЕ ОДИННАДЦАТИЛЕТНИХ ЦИКЛА

РЫБАК А.Л.

СОЛНЕЧНО-ЗЕМНАЯ ФИЗИКА Том: 2Номер: 2 **2016** Страницы: 22-28

Рассматривается долготное распределение групп солнечных пятен за период 1982-2013 гг. по данным Национального центра геофизических данных (Боулдер, США). Анализируется пространственно-временное распределение групп солнечных пятен по координатным секторам, полученным на основе гелиографических долгот групп. Долготная протяженность координатного сектора сопоставляется со средним размером одной активной области (30-40°). Далее в каждом координатном секторе за все время наблюдения суммируется эволюционная активность групп пятен по классификационной оценке Малдэ. Построенное таким образом долготное распределение групп крупных пятен не показывает отрицательной корреляции между северным и южным полушариями

Солнца в 23-м цикле пятнообразования.

РЕЗУЛЬТАТЫ НАБЛЮДЕНИЙ СОЛНЕЧНОЙ АКТИВНОСТИ В МИРОВОМ ЦЕНТРЕ ДАННЫХ ПО СОЛНЕЧНО-ЗЕМНОЙ ФИЗИКЕ

СЕРГЕЕВА Н.А. 1, ЗАБАРИНСКАЯ Л.П.1, ИШКОВ В.Н.2, КРЫЛОВА Т.А.1

Косм. Исслед. Том: 57Номер: 1 Год: **2019** Страницы: 12-16

В настоящее время экспериментальные данные о солнечной активности находят самое широкое применение в области фундаментальных и прикладных научных исследований – изучении явлений, происходящих на Солнце и в межпланетном пространстве, и их влияния на процессы во внешних и внутренних оболочках Земли. Наиболее ценными являются данные многолетних наблюдений. Мировой центр данных по солнечно-земной физике в Москве обладает представительной коллекцией результатов наблюдений, полученных мировой сетью солнечных и астрономических обсерваторий и на приборах, установленных на космических аппаратах. В статье приводится описание данных о солнечной активности, находящихся в хранилище и опубликованных на веб-сайте Центра в открытом доступе. Центр постоянно совершенствуется, использует новые информационные технологии, обеспечивающие свободный, удобный доступ к данным и возможность цитирования данных, увеличивает информационные ресурсы, доступные в сети Интернет.

НЕКОТОРЫЕ НЕРЕШЕННЫЕ ПРОБЛЕМЫ СОЛНЕЧНОГО ДИНАМО Review

СОКОЛОВ Д.Д.[1,2,3]

Изв. КрАО Том: 118Номер: 1 Год: 2022 Страницы: 12-17
https://www.elibrary.ru/download/elibrary_48073410_55559976.pdf

В изучении работы солнечного динамо сейчас намечается переход к задачам прогноза солнечной активности. При этом важно сохранить тематику изучения основ солнечного динамо. В этой связи дается обзор некоторых задач по выяснению основ работы солнечного динамо, которые остаются до настоящего времени недостаточно исследованными. Эти задачи важны для понимания не только природы магнитной активности Солнца, но и ее эволюционного статуса среди подобных звезд.

ДИНАМО – МЕХАНИЗМ ГЕНЕРАЦИИ МАГНИТНОГО ПОЛЯ В РАЗЛИЧНЫХ ТИПАХ НЕБЕСНЫХ ТЕЛ

Соколов Д.Д.

Астрономия-2018 Том 1 Современная звездная астрономия **2018** Стр. 43

ВЫСШИЕ ИНВАРИАНТЫ СПИРАЛЬНОСТИ И СОЛНЕЧНОЕ ДИНАМО

СОКОЛОВ Д.Д.1,2, ИЛЛАРИОНОВ Е.А.1, АХМЕТЬЕВ П.М.2

ГиА Том: 57Номер: 1 Год: **2017** Страницы: 123-128

Современные модели нелинейного насыщения динамо в небесных телах и, в частности, на Солнце во многом основаны на рассмотрении баланса магнитной спиральности. Эта физическая величина имеет и топологический смысл: она связана с коэффициентом зацепления магнитных трубок. Кроме магнитной спиральности, в магнитной гидродинамике имеется еще ряд топологических интегралов движения, так называемые высшие моменты спиральности. Мы сравнили свойства этих инвариантов со свойствами магнитной спиральности и пришли к выводу, что они вряд ли могут служить в качестве нелинейных ограничений действия динамо.

УЕДИНЕННЫЙ ФАКЕЛЬНЫЙ УЗЕЛ: ФОНТАННАЯ МАГНИТНАЯ СТРУКТУРА И ТЕМПЕРАТУРНЫЙ ПРОФИЛЬ

СОЛОВЬЕВ А. А.1

ПАЖ Том: 46Номер: 11 Год: **2020** Страницы: 792-801

На основе предложенной ранее стационарной 3D-модели солнечного факельного узла развит ее модифицированный вариант, в котором отражен уединенный характер факельного объекта: его магнитное поле резко ограничено в радиальном направлении. Температурный профиль факела, рассчитанный для стационарного состояния такой магнитной структуры, сопоставляется с фильтрограммой высокого разрешения, полученной в фотосферной линии TiO 7057 Å на Big Bear Solar Observatory 19 июня 2017 г. на New Solar Telescope (с апертурой 1.6 м). Снимок изображает две близко расположенных очень темных микропоры с поперечником около 300 км каждая. Микропоры окружены веером тонких, светлых, радиально вытянутых волоконец, напоминающим полутень солнечного пятна. Теоретически рассчитанный T-профиль факельного узла полностью воспроизводит эти морфологические особенности моделируемого объекта.

КОРРЕЛЯЦИЯ ВРЕМЕННЫ́Х РЯДОВ ЧИСЕЛ ВОЛЬФА И ИХ ПРОИЗВОДНЫХ

Старченко С.В., Яковлева С.В.

Г и А Том: 62Номер: 6 Год: 2022 Страницы: 693-701
DOI: 10.31857/S0016794022050169

Приведены результаты исследования корреляции среднегодовых чисел Вольфа W и их временны́х производных W' при сдвигах во времени фрагментов рядов W и W' относительно друг друга. Наиболее значимые (до 0.88 и –0.85) коэффициенты корреляции и антикорреляции получаются при сдвигах на два-три года для фрагментов, охватывающих два 11-летних цикла. Для более длительных фрагментов коэффициенты остаются значимыми (на уровнях около ±0.8) при тех же сдвигах. Поэтому сдвиг по фазе между W и W' составляет примерно четверть солнечного цикла, что физически соответствует преимущественной связи пятен с магнитной энергией. При этом также значим сдвиг на 8–9 лет, которому соответствуют коэффициенты корреляции на уровнях около ±0.75. Обсуждаются прогностические потенциалы полученных корреляционных зависимостей.

ПРОСТЕЙШЕЕ ДИНАМО СОЛНЦА И НОВЫЙ МЕХАНИЗМ СТАБИЛИЗАЦИИ

Старченко С.В.

Г и А Том: 62Номер: 2 Год: 2022 139-143

Показано, что для гидромагнитного динамо Солнца и подобных ему динамо, возможно, значимой является стабилизирующая нелинейность, обратно пропорциональная величине электрического тока. Соответствующая простейшая локальная гидромагнитная модель для магнитной энергии состоит из одного неоднородного линейного обыкновенного дифференциального уравнения, которое детализируется для солнечных пятен. Простейшее же глобальное солнечное динамо может достоверно определяться двумя однородными линейными обыкновенными дифференциальными уравнениями, имитирующими известные альфа-эффект и омега-эффект.

СОЛНЕЧНАЯ АКТИВНОСТЬ ЗА ПОСЛЕДНИЕ 20 ЛЕТ И ЕЕ ПРОГНОЗ НА 25-Й СОЛНЕЧНЫЙ ЦИКЛ

СТОЖКОВ Ю.И.✉1, ХЛОПКОВ В.П.

КОСМИЧЕСКИЕ ИССЛЕДОВАНИЯ Том: 62Номер: 4 Год**: 2024** Страницы: 329-333

Экспериментальные данные о солнечной активности (числе солнечных пятен Rz, индукции полоидального магнитного поля Солнца в полярных шапках Вп и другие), характеристики межпланетной среды и потоки космических лучей свидетельствуют о том, что Солнце вступило в глубокий минимум своей активности, подобный минимуму Дальтона. Обнаружена почти функциональная связь максимальной величины Впmax, наблюдаемой в минимумах солнечной активности, с предстоящим максимумом солнечных пятен. На основе этой связи разработан метод прогнозирования максимального числа солнечных пятен Rzmax и временного хода значений Rz в текущем (в настоящее время 25-ом) цикле солнечной активности.

ВОЛНЫ И КОЛЕБАНИЯ В АТМОСФЕРЕ СОЛНЕЧНЫХ ПЯТЕН: ОБЗОР

СЫЧ Р.А.

Геомагн. и Аэрономия Том: 1Номер: 2 Год: **2015** Страницы: 3-21
Солнечно-земная физика Том: 1Номер: 2 Год: **2015** Страницы: 3-21

Сделан обзор проведенных в последнее время экспериментальных и теоретических исследований источников колебаний и волн в атмосфере солнечных пятен. Представлены результаты наблюдений на наземных и космических инструментах. Показана важная роль механизма частотного обрезания в формировании пространственного распределения узкополосных источников колебаний в атмосфере пятен. Обсуждаются альтернативные методы исследования структуры магнитного поля с использованием полученных гелиосейсмологических результатов. Исследована динамика распространяющихся волновых фронтов с использованием метода попиксельной вейвлет-фильтрации. Проведен анализ параметров колебаний с высотой. Рассмотрена возможность инициации вспышечного энерговыделения МГД-волнами, проникающими из области пятен в область вспышки вдоль магнитных волноводов. Уделено внимание процессам усиления волновой активности в пятнах перед началом вспышки. Дано краткое описание теоретической модели на основе подфотосферного низкочастотного резонатора.

НАПРАВЛЕННАЯ ФИЛЬТРАЦИЯ ДЛЯ ОБРАБОТКИ ИЗОБРАЖЕНИЙ/ВИДЕОИЗОБРАЖЕНИЙ СОЛНЦА

ЛУН **СЮЙ**1, ЙИХУА ЯН1, ЦЗЮНЬ ЧЭН1

Солнечно-земная физика Том: 3Номер: 2 Год: **2017** Страницы: 10-17

В данной работе предлагается новый алгоритм повышения четкости изображений, использующий направленную фильтрацию для улучшения изображений и видеоизображений Солнца, который позволит легко выделять существенные мелкие структуры. Предлагаемый алгоритм может эффективно устранять шумы на изображениях, в том числе гауссовы и импульсные шумы. Кроме того, он может выделять волокнистые структуры на/за солнечным диском. Такие структуры наглядно демонстрируют развитие солнечной вспышки, протуберанца, выброса корональной массы, магнитного поля и т. д. Полученные

экспериментальные результаты показывают, что предложенный алгоритм значительно повышает качество изображений Солнца по сравнению с первоначальными и несколькими классическими алгоритмами улучшения изображений, что облегчит определение **всплесков солнечного радиоизлучения по изображениям/ видеоизображениям Солнца**

Пространственные и временные вариации формы контуров линии K Ca II в различных структурных образованиях солнечной хромосферы. II. Методика определения и корреляционные соотношения между параметрами линии для участков K1 и K2.

Турова И.П., Григорьева С.А., Ожогина О.А.
СОЛНЕЧНО-ЗЕМНАЯ ФИЗИКА Том 6. **2020**. № 4. С. 10–17.
http://ru.iszf.irk.ru/images/3/3f/756238_10-17.pdf
Исследовались две области в атмосфере Солнца, находящиеся в основании корональной дыры. Вычислен ряд параметров линии K Ca II для минимумов интенсивности K_1 и пиков K_2, которые образуются на высотах между верхней фотосферой и нижней хромосферой, и в нижней хромосфере, соответственно. Уточнена методика определения сдвигов контура $\Delta\lambda_{K_{1v}}$ и $\Delta\lambda_{K_{1r}}$, $\Delta\lambda_{K_{2v}}$ и $\Delta\lambda_{K_{2r}}$, включая случаи, когда их прямое нахождение затруднено. Вычислены интенсивности $I_{K_{1v}}$, $I_{K_{1r}}$, $I_{K_{2v}}$, $I_{K_{2r}}$, разделения минимумов K_1 и пиков K_2: $SEP_{K_1}=\Delta\lambda_{K_{1r}}-\Delta\lambda_{K_{1v}}$, $SEP_{K_2}=\Delta\lambda_{K_{2r}}-\Delta\lambda_{K_{2v}}$ соответственно. Построены графики рассеяния и определены корреляционные соотношения между параметрами, относящимися к разным уровням атмосферы. Получены следующие результаты. Интенсивности, которые наблюдаются в нижней и средней хромосфере связаны между собой сильнее, чем интенсивности, относящиеся к верхней фотосфере и средней хромосфере. Структуры с усиленным магнитным полем более яркие на уровне верхней фотосферы и нижней хромосферы по отношению к структурам с более слабым полем. Разделения минимумов K_1 имеют большую величину для структур с усиленным магнитным полем по отношению к структурам с более слабым полем, тогда как для разделения пиков K_2 картина обратная — они меньше для структур с усиленным магнитным полем. Такая зависимость имеет место не только для выбранных структур спокойной области, но и для флоккулов, хотя по флоккулам требуется дополнительная статистика. Зависимость между сдвигами интенсивности минимумов K_1 и пиков K_2 для фиолетового и красного крыльев оказалась слабой. Это может быть связано как с существенным вкладом случайных движений в поле скоростей на уровнях верхней фотосферы и нижней хромосферы, так и с разностью высот образования фиолетового и красного крыльев.

ХАРАКТЕРИСТИКИ ПЕРЕНОСА ЭНЕРГИИ АЛЬВЕНОВСКИХ ВОЛН В АТМОСФЕРЕ СОЛНЦА

Цап Ю.Т., Степанов А.В., Копылова Ю.Г., Ханейчук О.В.
Г и А Том: 60Номер: 4 Год: **2020** Страницы: 463-468
В условиях изотермической атмосферы с учетом амплитудно-фазовых соотношений рассмотрены особенности распространения линейных альвеновских волн с периодами 10–200 с из фотосферы в хромосферу Солнца. Установлено, что с увеличением высоты амплитуда возмущения скорости волн растет, а возмущения магнитного поля – падает, тогда как разность фаз между возмущениями стремится к $\pi/2$. Так называемые точки поворота не могут адекватно характеризовать поток энергии альвеновских волн. Этот вывод свидетельствует о необходимости пересмотра результатов, следующих из анализа осциляционных теорем. Показано, что в пренебрежении диссипативными процессами эффективность переноса волновой энергии с ростом частоты альвеновских мод увеличивается.

МЕЖПЛАНЕТНЫЕ МЕРЦАНИЯ АНСАМБЛЯ РАДИОИСТОЧНИКОВ В МАКСИМУМЕ 24 ЦИКЛА СОЛНЕЧНОЙ АКТИВНОСТИ

ЧАШЕЙ И.В.1, ШИШОВ В.И.1, ТЮЛЬБАШЕВ С.А.1, СУБАЕВ И.А.1
КОСМИЧЕСКИЕ ИССЛЕДОВАНИЯ Том: 54 Номер: 3 Год: **2016** Страницы: 188-194
Представлены результаты наблюдений межпланетных мерцаний, выполненных в период максимума солнечной активности с апреля 2013 г. по апрель 2014 г. на радиотелескопе БСА ФИАН на частоте 111 МГц. Круглосуточно регистрировались флуктуации потока радиоизлучения всех источников с мерцающим потоком более 0.2 Ян, попадающих в полоску неба шириной 50° по склонениям, соответствующую 96-лучевой диаграмме направленности радиотелескопа. Полное число источников, наблюдавшихся в течение суток, достигало 5000. Обработка данных наблюдений проводилась в предположении, что совокупность мерцающих источников представляет собой однородный статистический ансамбль. Ежедневно строились двумерные карты распределения уровня мерцаний, анализ которых показывает сильную нестационарность и крупномасштабную неоднородность пространственного распределения параметров солнечного ветра. По картам распределения уровня мерцаний, усредненным по месячным интервалам, исследована глобальная структура распределения солнечного ветра в период максимума солнечной активности, которая оказалась в среднем близкой к сферически симметричной. Полученные данные показывают, что на сферически

симметричном фоне наблюдается восточно-западная асимметрия, которая свидетельствует о присутствии в солнечном ветре крупномасштабных структур спирального типа.

Обзор и сравнение особенностей МГД-волн на Солнце и в магнитосфере Земли. Review

Челпанов *М.А., Анфиногентов С.А., Костарев Д.В., Михайлова О.С., Рубцов А.В., Феденёв В.В., Челпанов А.А.*

Солн.-земн. Физика Том 8. **2022**. № 4 С. 3–28.

https://naukaru.ru/ru/storage/viewWindow/105436

Магнитогидродинамические (МГД) волны играют ключевую роль в процессах, протекающих в плазменных образованиях в атмосфере Солнца и звезд, а также в магнитосфере Земли и других планет. В настоящий момент известно, что в этих системах имеют место как схожие волновые явления, так и уникальные для каждой из сред. Изучение МГД-волн и сопутствующих явлений в магнитосферной физике и физике Солнца происходит в основном независимо, несмотря на то, что свойства этих сред во многом схожи, а физические основы генерации и распространения волн в них одинаковы. Создание единого подхода к изучению этих явлений на Солнце и в земной магнитосфере открывает перспективы дальнейшего развития и интеграции этих научных направлений. В обзоре рассмотрено текущее состояние исследований МГД-волн в атмосфере Солнца и магнитосфере Земли. Приведены особенности сред, в которых распространяются колебания, их структура, масштабы и типичные параметры. Дано описание основных теоретических моделей, в рамках которых принято изучать поведение волн, их преимущества и ограничения. Сравниваются характеристики различных типов МГД-волн применительно к солнечной атмосфере и земной магнитосфере. Кроме того, представлена информация о методах наблюдений и инструментах, используемых для получения информации о волнах в различных средах.

СОЛНЕЧНЫЙ КВАДРУПОЛЬ В ТЕНЗОРНОМ ОПИСАНИИ

ШИБАЛОВА А. С.*1, ОБРИДКО В. Н.1, СОКОЛОВ Д. Д.1, ПИПИН В. В.2

АЖ Том: 97Номер: 10 Год: **2020** Страницы: 849-857

В работе исследуются циклические вариации квадрупольного компонента магнитного поля Солнца в рамках тензорного описания. Результаты согласуются с классическим описанием квадруполя с помощью сферических функций, а математический аппарат тензорной алгебры позволяет сравнивать наблюдаемые изменения магнитного квадруполя и изменения, предсказываемые теориями магнитного динамо. Мы пришли к выводу, что свойства квадруполя могут быть достаточно хорошо описаны моделями солнечного динамо, предполагающими отклонения от дипольной симметрии без независимого возбуждения мод квадрупольной симметрии.

ФАЗОВЫЙ СДВИГ МЕЖДУ ПОЛУШАРИЯМИ В ЦИКЛЕ СОЛНЕЧНОЙ АКТИВНОСТИ

ШИБАЛОВА А.С.1, ОБРИДКО В.Н.2, СОКОЛОВ Д.Д.

АЖ Том: 93Номер: 10 Год: **2016** Страницы: 918

Исследован сдвиг солнечных циклов активности в северном и южном полушариях Солнца по данным о числе и площадях солнечных пятен. Полученные данные сопоставлены с архивными сведениями об эпизодах существенной асимметрии солнечных циклов. Небольшой фазовый сдвиг между современными циклами активности в северном и южном полушариях Солнца существенно отличается от эпизодов заметных отклонений от дипольной симметрии распределения солнечных пятен, которые с разной степенью достоверности фиксируются по архивным данным об астрономических наблюдениях XVII□XIX вв. В настоящее время временной сдвиг между полушариями невелик и составляет около 6□7 месяцев. В недавней истории солнечной активности этот сдвиг дважды менял знак, что, по-видимому, соответствует его более-менее периодическим изменениям с характерным временем, близким к длительности цикла Гляйсберга.

25-Й ЦИКЛ СОЛНЕЧНОЙ АКТИВНОСТИ: ПЕРВЫЕ ТРИ ГОДА

Язев *С.А., Исаева Е.С., Хос-Эрдэнэ Б.*

СОЛНЕЧНО-ЗЕМНАЯ ФИЗИКА Том: 9Номер: 3 Год: **2023** Страницы: 5-11

Выполнен анализ особенностей текущего 25-го цикла солнечной активности на протяжении первых трех лет развития (2020-2022 гг.). Показано, что по сравнению с предыдущим 24-м циклом текущий превышает его по количеству групп пятен (в 1.5 раза), числу вспышек (в 1.8 раза), суммарному вспышечному индексу (в 1.5 раза). Выявлены различия в распределениях групп пятен в 24-м и 25-м циклах по максимальной достигаемой площади. Показано, что в 25-м цикле наиболее значимо превышение числа групп пятен с площадями до 30

м.д.п. (1 м.д.п.=3.04·106 км^2), а также в интервале от 570 до 1000 м.д.п. В отличие от 24-го цикла, степень северо-южной асимметрии в 25-м цикле существенно понижена. Это позволяет прогнозировать повышенную высоту 25-го цикла (на 20-50 %) в соответствии с правилом Гневышева-Оля, а также возможный одновершинный характер цикла.

Комплексы активности на Солнце в 21-м цикле солнечной активности.

Язев С.А., Ульянова М.М., Исаева Е.С.
СОЛНЕЧНО-ЗЕМНАЯ ФИЗИКА Том 7. **2021**. № 4. С. 3–9
https://naukaru.ru/ru/storage/viewWindow/80807
В работе приведены статистические данные о комплексах активности (КА) на Солнце, наблюдавшихся в 21-м цикле солнечной активности. По синоптическим картам пятенной активности за 1976–1986 гг. выделены области, где пятнообразование наблюдалось как минимум на протяжении трех кэррингтоновских оборотов (CR), — эти области идентифицировались как ядра КА. Составлен каталог КА. Показано, что КА развивались квазипериодично импульсами продолжительностью 15–20 оборотов. Выполнен анализ северо-южной асимметрии расположения КА. Показано, что в 21-м цикле 90 % про-тонных вспышек, влияющих на природную среду, произошли в КА. Для 21–24-го циклов отмечена тенденция к уменьшению активности КА от цикла к циклу, а также проявление правила Гневышева—Оля в свойствах КА.

КОРОНА ВО ВРЕМЯ ПОЛНОГО СОЛНЕЧНОГО ЗАТМЕНИЯ 20 МАРТА 2015 Г.И РАЗВИТИЕ 24-ГО ЦИКЛА

ЯЗЕВ С.А.1,2, МОРДВИНОВ А.В.2, ДВОРКИНА-САМАРСКАЯ А.А.1
СОЛНЕЧНО-ЗЕМНАЯ ФИЗИКА Том: 2Номер: 2 Год: **2016** Страницы: 3-11
Выполнен анализ структуры корональных образований по данным наблюдений полного солнечного затмения **20 марта 2015** г. Индекс Людендорфа, характеризующий форму короны, равен 0.09. Структура короны в северном полушарии соответствует фазе максимума цикла солнечной активности, в южном полушарии - постмаксимальной стадии. Асинхронное развитие магнитной активности в северном и южном полушариях Солнца привело к существенной асимметрии корональных структур, наблюдаемых в период смены знака полярных магнитных полей в текущем цикле. Полярные лучевые структуры в южном полушарии связаны с присутствием полярной корональной дыры, в то время как в северном полушарии полярная дыра еще не сформировалась. Выполнен анализ связи крупномасштабных магнитных полей с расположением высоких корональных структур.

КОМПЛЕКСЫ АКТИВНОСТИ НА СОЛНЦЕ В 24-М ЦИКЛЕ СОЛНЕЧНОЙ АКТИВНОСТИ

ЯЗЕВ С.А.
АЖ Том: 92 Номер: 3 Год: **2015** Страницы: 260
Представлены результаты исследования комплексов активности на Солнце в период с 2009 г. по июль 2014 г. Обсуждается определение комплекса активности, рассмотрены закономерности изменения индексов, описывающих мощность комплексов активности, и закономерности пространственно-временного распределения комплексов активности на солнечной поверхности. Показано, что развитие комплексов активности в 24-м цикле отличается высокой степенью северо-южной асимметрии. Новые комплексы активности имеют тенденцию к возникновению вблизи уже существующих структур (в пределах), формируясь одновременно с последними либо вскоре после их исчезновения (спустя 1 4 кэррингтоновских оборота). Приведены аргументы в пользу того, что именно динамика комплексов активности определяет особенности развития цикла, выраженные в индексах чисел Вольфа.

СТАТИСТИЧЕСКИ-ВЕРОЯТНОСТНЫЕ ХАРАКТЕРИСТИКИ ЧИСЕЛ ВОЛЬФА И ИХ ВРЕМЕННЫ́Х ПРОИЗВОДНЫХ

Яковлева С.В., Старченко С.В.
Г и А Том: 62Номер: 2 Год: 2022 144-154
Предложен результат статистически-вероятностного исследования среднегодовых чисел Вольфа W и их временны́х производных W '. Он состоит в том, что вероятностное распределение W преимущественно экспоненциальное с наиболее вероятным значением, равным 18, при среднеквадратичном 100, медианном 65 и среднем 79. Меньше от нормального распределения отклоняются W ' с наиболее вероятным значением –12/год, медианным –6.1/год, средним –0.02/год, среднеквадратичным 33/год, минимумом –74/год и потенциально недостоверным максимумом 112/год. Отношения средних величин согласуются с характерными временами роста/падения активности в 2.6/3.7 лет и 11-летней цикличностью. Даны оценки полувековой периодичности и скорости течений (~1 м/с), поддерживающих динамо.